Cover Picture

Dennis M. Vriezema, Johan Hoogboom, Kelly Velonia, Ken Takazawa, Peter C. M. Christianen, Jan. C. Maan, Alan E. Rowan,* and Roeland J. M. Nolte*

Enzymes in vesicles are able to catalyze the reaction with substrates that permeate the vesicle membrane. The cover picture shows a vesicle built up from a rigid-rod diblock copolymer that is filled with *Candida antarctica* lipase B enzymes. The thiophene groups in the polymer can be polymerized by the addition of a metal complex, which may result in conducting vesicle membranes thus creating new possibilities in the area of nanoreactors. Further information can be found in the Communication by A. Rowan, R. Nolte et al. on page 772 ff.

Contents

Web Sites

The tmRNA Website ——— 714 | Two in One | *Christian Hammann, Wolfgang Nellen*

Books

Science of Synthesis ——— 715 | Ian Fleming | *reviewed by H. Schmidbaur*

Modern Arene Chemistry ——— 716 | Didier Astruc | *reviewed by S. R. Waldvogel*

Highlights

Medium-Sized Rings by Cycloaddition

M. Murakami* ——— 718 – 720

New Catalyzed Three-Component Cycloadditions for the Synthesis of Eight-Membered Carbocycles

Keywords:
cycloaddition · homogeneous catalysis · medium-sized rings · multicomponent reactions · rhodium

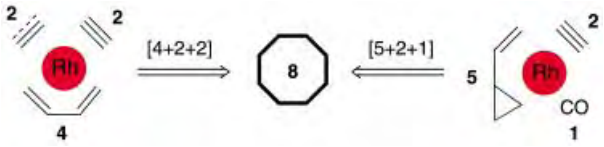

The sum always amounts to eight—Two new three-component [*m*+*n*+*o*] cycloadditions offer novel synthetic routes to eight-membered carbocycles (see scheme; *m*, *n*, *o* = 4, 2, 2 or 5, 2, 1). The rhodium center serves as a template and brings three components into the necessary arrangement for the desired cycloaddition, thus enabling difficult-to-form eight-membered carbocyclic rings to be constructed in a single chemical operation with good atom economy.

Essays

History of Science

L. Jaenicke,
F. W. Lichtenthaler* ——— 722 – 726

A Kaiser Wilhelm Institute for Cologne! Emil Fischer, Konrad Adenauer, and the Meirowsky Endowment

Keywords:
Emil Fischer · history of science · Kaiser Wilhelm Society

It had already been decided by Emil Fischer (left) and Konrad Adenauer (right), but in the end the Kaiser Wilhelm Institute for Physiology was not built in Cologne. The historical background as to why this happened is explained.

Reviews

Biosynthesis of Antibiotics

B. K. Hubbard,*
C. T. Walsh* ——— 730 – 765

Vancomycin Assembly: Nature's Way

Keywords:
antibiotics · biosynthesis · glycopeptides · natural products

All good things come in threes: The synthesis of amino acid monomers, their joining, and their cross-linking are the three phases into which the biosynthesis of glycopeptide antibiotics (here vancomycin (blue) bound to a peptide (orange and red) is shown) can be divided. The elucidation of the reaction mechanism offers fascinating opportunities to make accessible antibiotics with previously unknown properties.

© 2003 Wiley-VCH Verlag GmbH & Co. KGaA, Weinheim

1433-7851/03/4207-0706 $ 20.00+.50/0

Communications

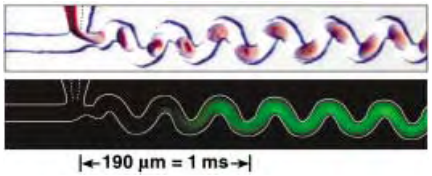

Millisecond mixing and transport with no dispersion are achieved by unsteady flows induced in droplets of about 60 pL that travel through winding microfluidic channels (top). Fluorescence can be used to monitor mixing (bottom) or measure reaction rates. In principle, arbitrarily complex reaction networks can be created by combining and splitting streams of such droplets.

High-Throughput Measurements

H. Song, J. D. Tice,
R. F. Ismagilov* ——— **768 – 772**

A Microfluidic System for Controlling Reaction Networks in Time

Keywords:
analytical methods · kinetics · microfluidics · microreactors · reaction networks

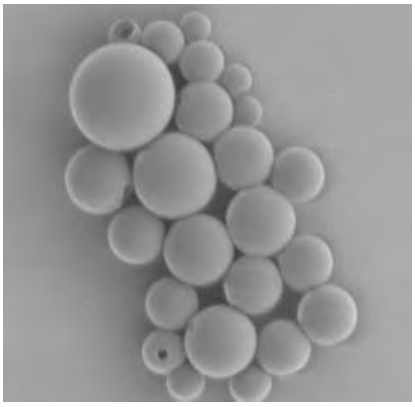

Spontaneous formation of vesicles in both organic solvents and water is observed for new rod–coil-type diblock copolymers containing thiophene groups. The thiophene groups located in the skin of the aggregates can couple to give polymerized vesicles (see picture and cover picture). The vesicles are capable of including enzymes, which results in catalytically active microreactors that are permeable to substrate molecules.

Spontaneously Formed Vesicles

D. M. Vriezema, J. Hoogboom, K. Velonia, K. Takazawa, P. C. M. Christianen, J. C. Maan, A. E. Rowan,* R. J. M. Nolte* ——— **772 – 776**

Vesicles and Polymerized Vesicles from Thiophene-Containing Rod–Coil Block Copolymers

Keywords:
block copolymers · enzymes · polyisocyanides · vesicles

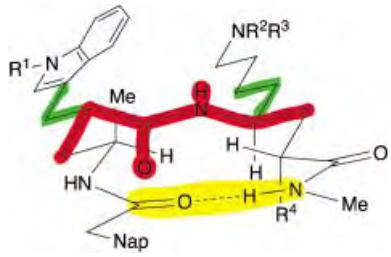

A simple, designed, open-chain γ-dipeptide derivative (see picture; Nap = naphthyl), which contains only three amide bonds, can mimic the 14-amino acid peptide hormone somatostatin. Surprisingly, the highest affinities ($K_D \approx 0.5$ µM) for human receptors are observed when the "mandatory" Trp and Lys side chains on the turn mimic carry bulky substituents.

Somatostatin Mimics

D. Seebach,* L. Schaeffer, M. Brenner, D. Hoyer ——— **776 – 778**

Design and Synthesis of γ-Dipeptide Derivatives with Submicromolar Affinities for Human Somatostatin Receptors

Keywords:
hormones · peptides · peptidomimetics · somatostatin

For the USA and Canada:
ANGEWANDTE CHEMIE International Edition (ISSN 1433-7851) is published weekly by Wiley-VCH PO Box 191161, D 69451 Weinheim, Germany. Air freight and mailing in the USA by Publications Expediting Inc. 200 Meacham Ave., Elmont, NY 11003. Periodicals postage paid at Jamaica NY 11431. US POSTMASTER: send address changes to *Angewandte Chemie*, Wiley-VCH, 111 River Street, Hoboken, NJ 07030. Annual institutional subscription price for institutions: Europe € 2998.00/3148.00. Outside Europe US$ 3718.00/3904.00 (valid for print or electronic/print and electronic delivery); for individuals who are personal members of a national chemical society, or whose institution already subscribes, or who are retired or self-employed consultants, print only (including postage and handling charges): Europe € 248.00/Outside Europe US$ 348.00.

 © 2003 Wiley-VCH Verlag GmbH & Co. KGaA, Weinheim 1433-7851/03/4207-0707 $ 20.00+.50/0

Contents

Controlled Electropolymerization

J. F. Hulvat, S. I. Stupp* ——— 778 – 781

Liquid-Crystal Templating of Conducting Polymers

Keywords:
amphiphiles · electrochemistry · liquid crystals · polymerization · self-assembly

Mimicking the texture and anisotropy of the template, birefringent conducting polymer films (see picture) have been obtained by electropolymerization of 3,4-ethyldioxythiophene (EDOT) within a hexagonal lyotropic liquid crystal. Using a self-assembled template to control molecular orientation in conducting polymers could enhance electronic and optical properties.

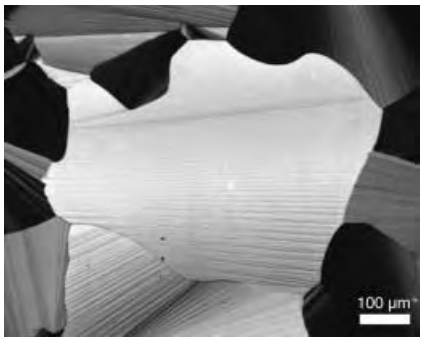

Solid-State Chemosensor for Toluene

Z. Fei, N. Kocher, C. J. Mohrschladt, H. Ihmels, D. Stalke* ——— 783 – 787

Single Crystals of the Disubstituted Anthracene 9,10-$(Ph_2P{=}S)_2C_{14}H_8$ Selectively and Reversibly Detect Toluene by Solid-State Fluorescence Emission

Keywords:
arenes · chromophores · fluorescence spectroscopy · luminescence · phosphanes

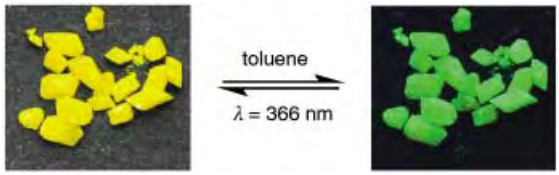

Not π stacking but C–H···π-ring center interactions lead to the fluorescence emission observed for the first time from a heteromolecular excimer complex. In single crystals a toluene molecule is located perpendicular to a $Ph_2P(S)$-disubstituted anthracene chromophore. This toluene complex fluoresces (see picture) but the benzene complex does not.

Chiral Piperidine Derivatives

G. Zech, H. Kunz* ——— 787 – 790

Stereoselective Solid-Phase Synthesis of Chiral Piperidine Derivatives by Using an Immobilized Galactose Auxiliary

Keywords:
carbohydrates · chiral auxiliaries · conjugate addition · nitrogen heterocycles · solid-phase synthesis

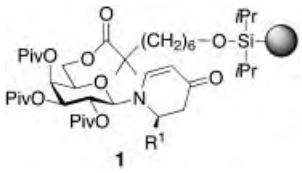

1

The fluoride-labile anchoring of a galactosylamine enabled the first stereoselective solid-phase combinatorial synthesis of didehydropiperidinones **1**. The piperidine derivatives formed by asymmetric domino Mannich–Michael condensation at ambient temperature were isolated after cleavage from the polymeric support in high yield, diastereomeric ratio, and purity (Piv = pivaloyl = *t*BuCO).

Monodentate P Ligands

M. T. Reetz,* T. Sell, A. Meiswinkel, G. Mehler ——— 790 – 793

A New Principle in Combinatorial Asymmetric Transition-Metal Catalysis: Mixtures of Chiral Monodentate P Ligands

Keywords:
asymmetric catalysis · combinatorial chemistry · hydrogenation · phosphorus · rhodium

The right mix!: Surprisingly, the use of the mixture of two different chiral monodentate phosphorus ligands (e.g., a phosphonite/phosphite combination; see schematic representation; cod = 1,5-cyclooctadiene) in Rh-catalyzed olefin hydrogenation leads to significantly higher enantioselectivities than in the case of the pure ligands themselves.

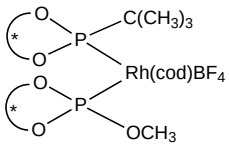

© 2003 Wiley-VCH Verlag GmbH & Co. KGaA, Weinheim
1433-7851/03/4207-0708 $ 20.00+.50/0

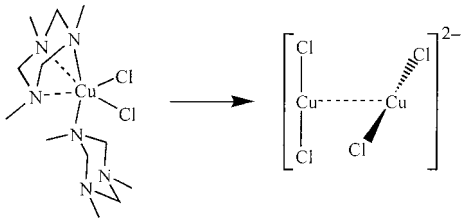

1 2

Cuprophilic interactions are observed between the two copper centers of the unprecedented dimer **2**, the structure of which contains two associated $[Cu^{I}Cl_2]^-$ ions. The surrounding complex is derived from the internal reduction of the Cu^{II} complex **1**, which displays a *cis*-divacant octahedral coordination geometry.

Cu–Cu Interactions

R. D. Köhn,* G. Seifert, Z. Pan, M. F. Mahon, G. Kociok-Köhn ——— **793 – 796**

Reactions of Triazacyclohexanes with $CuCl_2$: Surprising Formation of a Dimer between Two $[CuCl_2]^-$ Ions with an Unsupported Cuprophilic Attraction

Keywords:
copper · heterocycles · N ligands · oxidation · structure elucidation

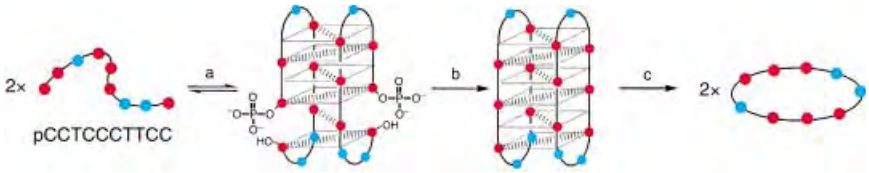

Self-recognition rather than complementarity defines the self-assembly (a) of two cytosine-rich oligodeoxynucleotides in the compact i-motif shown ($C{-}C^+$ base pairs, dark circles). When the 5′-terminal phosphate is activated, phosphodiester bonds form between the termini of the linear sequences, resulting in two circular oligodeoxynucleotides (b), which disassociate on denaturation (c).

Oligonucleotide Rings

D. Liu, J. Chen, A. H. F. Lee, L. M. C. Chow, A. S. C. Chan,* T. Li* ——— **797 – 799**

Small Circular Oligodeoxynucleotides Achieved from Self-Assembling Entities

Keywords:
DNA structures · oligonucleotides · self-assembly

Poly(vinyl alcohol), an inherently amphiphilic material, can act as a superhydrophobic surface when deposited as nanofibers on an aluminum oxide membrane (see picture). The arrangement of the hydrophobic and hydrophilic functional groups, both in the surface and within the interior of the material, has a marked effect on surface activity.

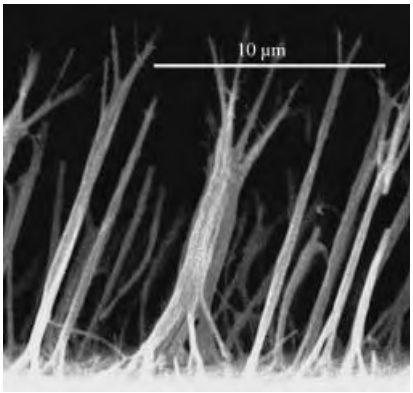

Superhydrophobic Nanofibers

L. Feng, Y. Song, J. Zhai, B. Liu, J. Xu,* L. Jiang,* D. Zhu ——— **800 – 802**

Creation of a Superhydrophobic Surface from an Amphiphilic Polymer

Keywords:
amphiphiles · electron microscopy · nanostructures · surface chemistry · template synthesis

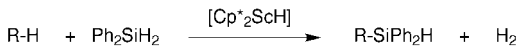

C–H activation with scandium: Reaction of $[Cp^*_2ScCH_3]$ (**1**, $Cp^* = C_5Me_5$) with $MesSiH_3$ ($Mes = 2,4,6\text{-}C_6H_2Me_3$) yielded a new scandium silyl complex $[Cp^*_2ScSiH_2Mes]$ (**2**) by an unusual σ-bond metathesis pathway. Complex **2** activates the C–H bonds of benzene and methane. In the presence of excess Ph_2SiH_2, the catalytic dehydrosilation of saturated and unsaturated hydrocarbons, including methane, was accomplished, with $[Cp^*_2ScH]$ (see scheme; $R = CH_3$, C_3H_5, $CH{=}CMe_2$) which can be formed from **1** or **2**. This appears to be the first example of catalytic methane functionalization by σ-bond metathesis.

Catalytic Methane Activation

A. D. Sadow, T. D. Tilley* ——— **803 – 805**

Catalytic Functionalization of Hydrocarbons by σ-Bond-Metathesis Chemistry: Dehydrosilylation of Methane with a Scandium Catalyst

Keywords:
C–H activation · homogeneous catalysis · methane · scandium · silanes

 © 2003 Wiley-VCH Verlag GmbH & Co. KGaA, Weinheim 1433-7851/03/4207-0709 $ 20.00+.50/0

Contents

Palladium-Catalyzed Addition

C. H. Oh,* H. H. Jung, K. S. Kim, N. Kim ——— 805 – 808

The Palladium-Catalyzed Addition of Organoboronic Acids to Alkynes

Keywords: addition · alkynes · homogeneous catalysis · organoboronic acids · palladium

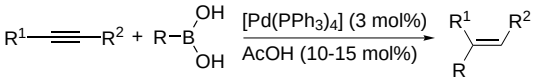

No base is necessary: Excellent yields are produced on addition of organoboronic acids to alkynes under mild reaction conditions when palladium compounds are used as catalysts (see scheme). Unlike the Suzuki-type cross-coupling reaction, the current reaction occurs in an acidic medium.

From Ethene to 1-Hexene

Z.-X. Yu, K. N. Houk* ——— 808 – 811

Why Trimerization? Computational Elucidation of the Origin of Selective Trimerization of Ethene Catalyzed by $[TaCl_3(CH_3)_2]$ and An Agostic-Assisted Hydride Transfer Mechanism

Keywords: ab initio calculations · agostic interactions · alkenes · ethylene trimerization · tantalum

Because only then a relatively rapid agostic-assisted hydrogen shift can help to form the product. This is the answer to the question in the title and it results from a computational analysis of the catalytic cycle shown and its alternatives for dimerization, tetramerization, and higher oligomerization.

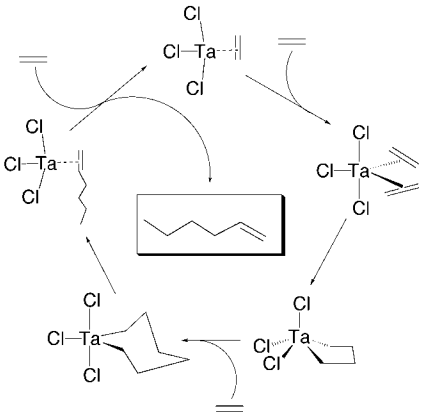

Functional Symmetric Cyclophanes

P. Janvier, M. Bois-Choussy, H. Bienaymé, J. Zhu* ——— 811 – 814

A One-Pot Four-Component (ABC_2) Synthesis of Macrocycles

Keywords: cyclophanes · isocyanide ligands · macrocycles · multicomponent reactions · O ligands

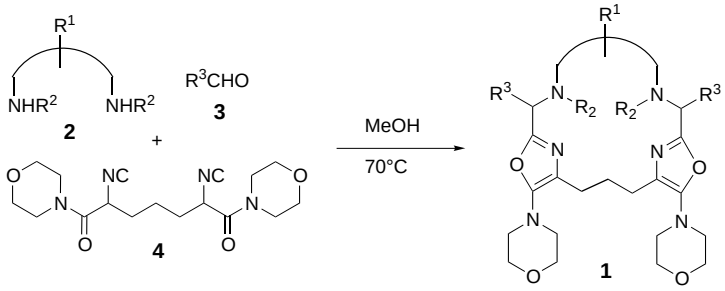

Six bonds are generated in one pot with concomitant creation of two oxazole groups as part of a new macrocycle. Simply mixing a diamine (**2**) and an aldehyde (**3**; 1:2 molar ratio) in MeOH at room temperature, followed by addition of diisocyanoacetamide (**4**) and heating at reflux, provides symmetric cyclophanes in good yield.

Thorium Naphthalene Complexes

I. Korobkov, S. Gambarotta,* G. P. A. Yap ——— 814 – 818

The First Thorium Arene Complex: A Divalent Synthon

Keywords: actinides · arene ligands · macrocyclic ligands · N ligands · thorium

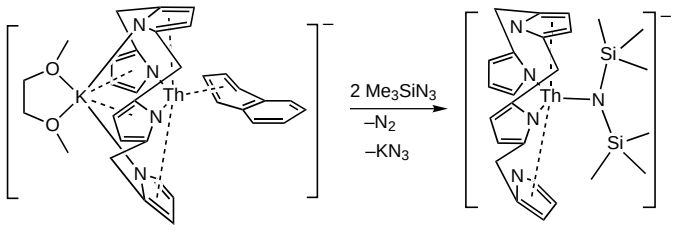

1 **2**

A highly reactive thorium naphthalene complex, namely **1**-$[Li(dme)_3]$ was prepared by reducing a Th^{IV} precursor with Li(naphthalene). The complex behaves as a synthon for Th^{II} and reacts with Me_3SiN_3 to give the thorium silazanate **2**.

© 2003 Wiley-VCH Verlag GmbH & Co. KGaA, Weinheim
1433-7851/03/4207-0710 $ 20.00+.50/0

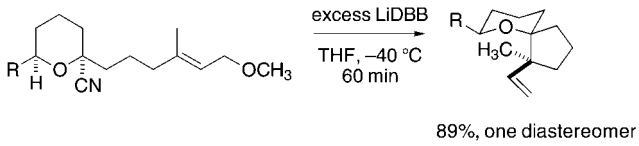

A new ring-forming reaction has been developed in which nitriles act as 1,1-dianion synthons with biselectrophiles. The cyclizations are highly diastereoselective and are capable of forming two adjacent quaternary centers with complete selectivity (see scheme; LiDBB = lithium di-*tert*-butylbiphenylide).

Spiroannulation of THP Rings

S. D. Rychnovsky,*
L. R. Takaoka 818 – 820

Spiroannulation by Alkylation and Reductive Cyclization of Nitriles

Keywords:
annulation · cyclization · diastereoselectivity · reduction · spiro compounds

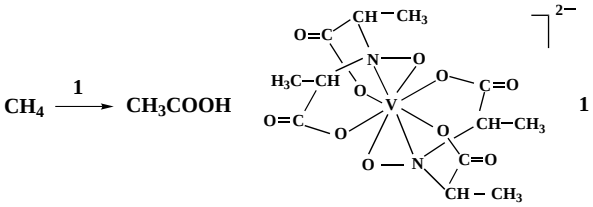

Although its biological function is still unknown, the naturally occurring vanadium complex amavadine may be suitable for industrial applications: This compound (as well as other V^{IV} and V^{V} complexes with N,O and O,O ligands) are shown to act as catalysts for the direct conversion of methane into acetic acid, without requiring CO, under very mild conditions and in high yields (see scheme).

Carboxylation of Methane

P. M. Reis, J. A. L. Silva, A. F. Palavra, J. J. R. Fraústo da Silva,* T. Kitamura, Y. Fujiwara, A. J. L. Pombeiro* 821 – 823

Single-Pot Conversion of Methane into Acetic Acid in the Absence of CO and with Vanadium Catalysts Such As Amavadine

Keywords:
C–H activation · carboxylations · methane · vanadium

Imitating a low-field spectrometer may seem a strange concept, but might be of great help to laboratories that no longer have access to such machines. For example, slowing down the average evolution of the chemical shift during NMR-signal acquisition changes the strength of coupling between spins and the effects of chemical exchange. The spectra of quinine shown were obtained with the NMR technique proposed here.

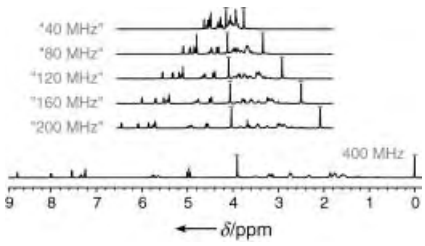

Low-Field NMR Is Back

G. A. Morris,* N. P. Jerome, L.-Y. Lian 823 – 825

Real-Time Chemical-Shift Scaling in High-Resolution NMR Spectroscopy

Keywords:
chemical exchange · NMR spectroscopy · scaling · structure elucidation

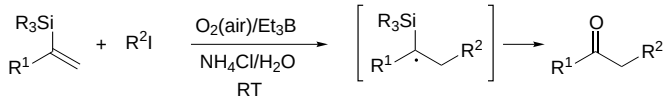

Air and water are required for a tandem intermolecular radical addition–oxidation sequence that converts alkenylsilanes into a variety of ketones. The reaction of 2-silyl-1-alkenes with various carbon-centered radicals (see scheme) provides carbonyl compounds in good yields. This process represents a novel oxidative transformation of organosilicon compounds with molecular oxygen as the oxidant. R_3Si = $MePh_2Si$, Me_2PhSi, R^1 = Me, Ph, CO_2Me, $SiMe_2Ph$, $R^2 = CH_2COR'$ (R′ = OBn, NEt_2, O*n*Bu, Ph), C_6F_{13}.

C–C Coupling

J. Kondo, H. Shinokubo,* K. Oshima* 825 – 827

From Alkenylsilanes to Ketones with Air as the Oxidant

Keywords:
C–C coupling · oxidation · radical reactions · tandem reactions · vinylsilanes

 © 2003 Wiley-VCH Verlag GmbH & Co. KGaA, Weinheim 1433-7851/03/4207-0711 $ 20.00+.50/0

Contents

Organocatalytic Cyclopropanation

C. D. Papageorgiou, S. V. Ley, M. J. Gaunt* ——— 828 – 831

Organic-Catalyst-Mediated Cyclopropanation Reaction

Keywords:
asymmetric synthesis · cyclopropanation · diastereoselectivity · organocatalysis · ylides

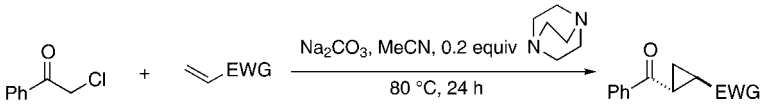

A catalytic ammonium ylide based cyclopropanation process forms *trans*-disubstituted cyclopropanes in good yield upon reaction with electron-deficient alkenes (see scheme; EWG = electron-withdrawing group). The reaction is also highly enantioselective when a stoichiometric amount of a chiral tertiary amine is used.

VIP Communications labeled with this symbol have been judged by two referees as being "very important papers".

The publication of Communications labeled with this symbol has been accelerated because of their topical or highly competitive nature.

Supporting information for articles labeled with this symbol can be found at www.angewandte.org or www.interscience.wiley.com.

Sources

Product and Company Directory

You can start the entry for your company in "Sources" in any issue of *Angewandte Chemie*.

If you would like more information, please do not hesitate to contact us.

Wiley-VCH Verlag – Advertising Department
Tel.: 0 62 01 - 60 65 65
Fax: 0 62 01 - 60 65 50
E-Mail: MSchulz@wiley-vch.de

Service

Keywords ——— *832*

Authors ——— *833*

Angewandte's Sister Journals ——— *834 – 835*

Vacancies ——— *A11*

Preview ——— *837*

Corrigendum

In the Commuication by **T. Mizuta, T. Nakazono, and K. Miyoshi** in Issue 20, 2002, pp. 3897 – 3898, the chemical shift in the ^{31}P NMR data was reported incorrectly. The correct value for compound **4** should be $\delta = 94.9$ ppm and not $\delta = -8.4$ ppm.

 © 2003 Wiley-VCH Verlag GmbH & Co. KGaA, Weinheim 1433-7851/03/4207-0712 $ 20.00+.50/0

Medium-Sized Rings by Cycloaddition

New Catalyzed Three-Component Cycloadditions for the Synthesis of Eight-Membered Carbocycles

*Masahiro Murakami**

Keywords:
cycloaddition · homogeneous catalysis · medium-sized rings · multicomponent reactions · rhodium

The discovery of new reactions is a major focus of research activity in organic chemistry. Many recent examples have been brought into being by the use of transition-metal complexes. Although cycloaddition reactions are prominent methods for the construction of cyclic compounds of structural and functional complexity, assembly modes possible with conventional promoters such as heat, light, and Lewis acids are limited. Transition metals present another valuable class of promoters for these reactions, because of the way they function, and provide a solution to the limitations.[1] A transition-metal complex acts as a template for the unsaturated substrates by bringing them together at the metal center and assembling them in a way which is otherwise difficult or impossible. For example, the two-component [*m*+*n*] mode[2] is most typical for uncatalyzed cycloadditions, while three-component cycloadditions of the [*m*+*n*+*o*] type, such as [2+2+1],[3] [2+2+2],[4] and [4+4+1][5] are accessible by using transition metals. Recently, new rhodium-catalyzed [*m*+*n*+*o*] cycloadditions have been reported, which open up novel synthetic routes to eight-membered carbocycles.

Wender et al. disclosed the first example of a metal-catalyzed intermolecular [5+2+1] cycloaddition reaction.[6] Treatment of vinylcyclopropane **1** with alkyne **2** under CO in the presence of a catalytic amount of [{Rh(CO)$_2$Cl}$_2$] initially leads to the formation of the eight-membered ring adduct **3** (Scheme 1). The ring skeleton is assembled from three components, namely, a C$_5$ unit from vinylcyclopropane **1**, a C$_2$ unit from alkyne **2**, and a single carbon atom from carbon monoxide. Alkynes activated by a carbonyl group are incorporated regioselectively. The intermediate **3** thus formed spontaneously undergoes transannular closure to afford bicyclo[3.3.0]octadiene **4** stereoselectively. Hydrolysis gives diketone **5** in virtually quantitative yield.

In two more recent publications which appeared back-to-back in *J. Am. Chem. Soc.* the research groups of Evans and Gilbertson independently described new three-component cycloadditions. Although both reactions are denoted as [4+2+2]-type cycloadditions,[7] they follow different pathways in assembling difficult-to-form eight-membered carbocycles.

The Evans research group developed the rhodium-catalyzed bimolecular [4+2+2] cycloaddition of the heteroatom-tethered enyne derivative **6** with 1,3-butadiene (Scheme 2).[8] The enyne **6**, which has a C$_2$ unit of an alkyne and another C$_2$ unit of an alkene tethered together through a sulfonamide linkage, is heated in refluxing toluene under an atmosphere of 1,3-butadiene in the presence of a catalytic amount of a modified Wilkinson's complex. Two eight-membered carbocycles (**8** and **9**) adjoining one or two heterocycles are formed. The bicyclic eight-membered ring skeleton of **8** is assembled in a [4+2+2] cycloaddition from the alkyne part, the alkene part, and a C$_4$ unit of 1,3-butadiene. Initially, the tethered enyne **6** coordinates to the metal center to form the metallacycle **7**. Insertion of 1,3-butadiene and ring expansion followed by reductive elimination affords the bicyclic product **8**. Interestingly, 1,3-butadiene is incorporated as a C$_4$ and not as a C$_2$ unit, which would have given the thermodynamically stable six-membered carbocycle. The tricyclic compound **9** is produced by homodimeriza-

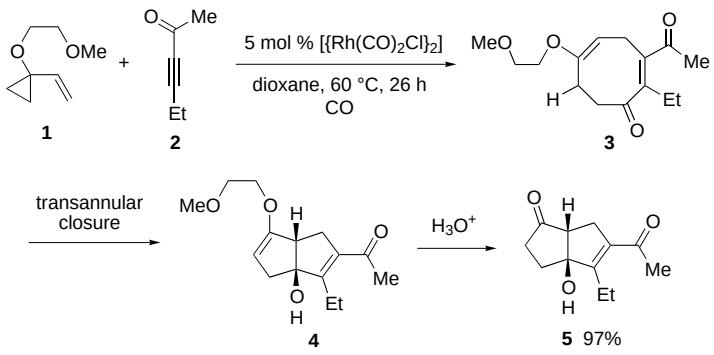

1 2 3 4 **5** 97%

Scheme 1. Rhodium-catalyzed intermolecular [5+2+1] cycloaddition of vinylcyclopropane **1**, alkyne **2**, and carbon monoxide.

[*] Prof. Dr. M. Murakami
Department of Synthetic Chemistry and Biological Chemistry
Kyoto University
Yoshida, Kyoto 606-8501 (Japan)
Fax: (+ 81) 75-753-5668
E-mail: murakami@sbchem.kyoto-u.ac.jp

 © 2003 Wiley-VCH Verlag GmbH & Co. KGaA, Weinheim 1433-7851/03/4207-0718 $ 20.00+.50/0

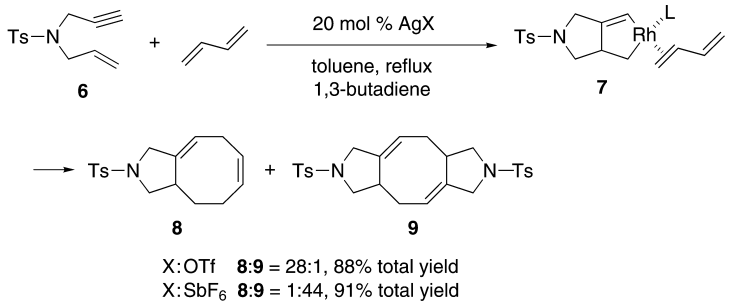

Scheme 2. Rhodium-catalyzed bimolecular [4+2+2] cycloaddition of the heteroatom-tethered enyne derivative **6** with 1,3-butadiene. Ts = 4-toluenesulfonyl.

tion of enyne **6** in a [2+2+2+2] cycloaddition without incorporation of 1,3-butadiene. It is noteworthy that the product selectivity—the desired [4+2+2] cycloadduct **8** and the [2+2+2+2] homodimer **9**—reverses depending on the counterion of the rhodium catalyst employed: the use of silver triflate favors the formation of the [4+2+2] cycloadduct (**8**:**9** = 28:1), while the use of hexafluoroantimonate as the counterion affords homodimer **9** almost exclusively (**8**:**9** = 1:44). In the latter case, 1,3-butadiene is consumed through fast oligomerization prior to participating in the desired three-component cycloaddition.

Although substrates with heteroatom tethers such as ethers and sulfones are effective, the carbon-tethered derivatives lead to mixtures, including the enyne cycloisomerization product. A substituted alkyne was also reactive as a substrate. A high stereoselectivity of $>19{:}1$ is observed in product **11** when **10** (containing a stereogenic center) was used as the substrate (Scheme 3), which demonstrates that this new method is applicable to target-directed synthesis.

The coupling of this new cycloaddition reaction with the rhodium-catalyzed allylic substitution reaction[3b] gave a tandem intermolecular three-component allylic amination/cycloaddition sequence (Scheme 4). An initial rhodium-catalyzed reaction of allyl carbonate **12** with lithium amide **13** at room temperature furnishes tethered enyne **6**, which is then converted into the eight-membered carbocycle **8** on heating at reflux in toluene under an atmosphere of 1,3-butadiene. This sequence eliminated the necessity for prior formation of the enyne.

The Gilbertson research group developed another [4+2+2] mode.[9] The discovery emerged from their previous study on the intramolecular [4+2] cycloaddition reaction of a tethered dieneyne to form a six-membered carbocycle.[10] During this study they identified a minor product **15** that had an eight-membered ring structure (Scheme 5). Compound **15** is constructed in a [4+2+2] cycloaddition by incorporation of an additional C_2 unit from the alkyne portion of a second molecule of **14**. Under the reaction conditions optimized to favor [4+2+2] dimerization, the catalyst is prepared by an elaborated sequential procedure, namely, through mixing $[\{Rh(nbd)Cl\}_2]$, Me-DuPHOS (one molecule per rhodium atom), and $AgSbF_6$ (0.5 molecule per rhodium atom) in THF, exchange of the solvent to a mixed solvent of CH_2Cl_2/AcOEt (6:1), and treatment with dihydrogen gas. The resulting brown heterogeneous material is essential for the formation of the desired product in good yield. Three to four atom tethers containing either ether or sulfonamide functional groups are effective. Carbon tethers in the form of an aromatic ring are also useful. The regioselectivity of the alkyne incorporation is controlled with substrates having an alkyl group at the diene terminus.

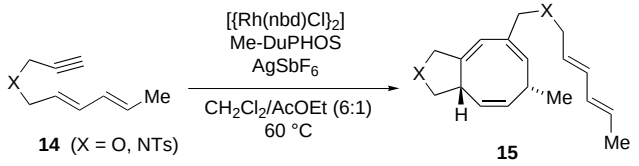

Scheme 5. Rhodium-catalyzed [4+2+2] dimerization of dieneyne **14**. nbd = norbornadiene.

The reaction was further extended to a cross-cycloaddition reaction incorporating a second different alkyne component. The use of five equivalents of propargyl ether **16** in the reaction with dienyne **14** (X = O) furnished the desired cross cycloadduct **17** in 73% yield (Scheme 6). Propargyl ethers are generally preferred as the second alkyne.

Eight-membered carbocycles are often an important structural feature of biologically active compounds. There-

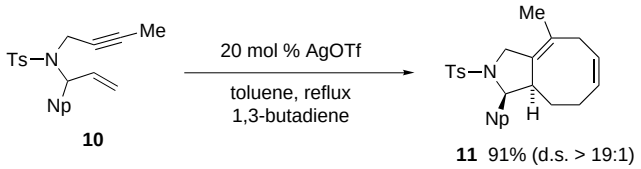

Scheme 3. Stereoselective synthesis of the eight-membered carbocycle **11** with an adjoining heterocycle. Np = 2-naphthyl.

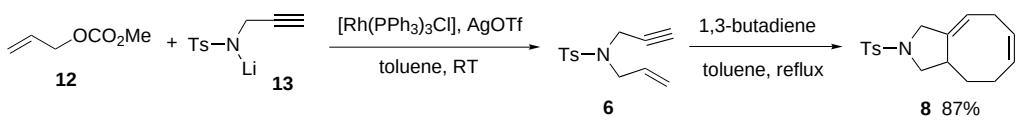

Scheme 4. The tandem intermolecular three-component allylic amination/cycloaddition sequence.

 © 2003 Wiley-VCH Verlag GmbH & Co. KGaA, Weinheim 1433-7851/03/4207-0719 $ 20.00+.50/0

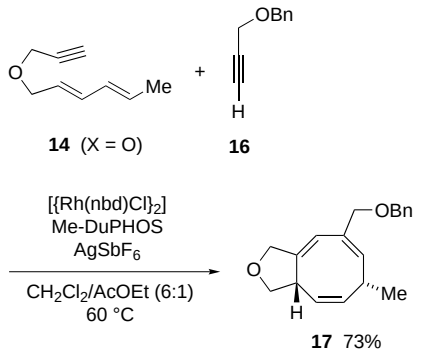

Scheme 6. Rhodium-catalyzed bimolecular [4+2+2] cycloaddition of dieneyne derivative **14** with alkyne **16**.

fore, the development of direct methods for their synthesis has been an important challenge, although a formidable objective. The new catalyzed cycloaddition reactions highlighted herein enable difficult-to-form eight-membered carbocyclic rings to be constructed in a single chemical operation with good atom economy. Rhodium serves as a template to set three components in the correct arrangement for the desired cycloaddition. These studies clearly demonstrate that reactions of the [5+2+1] and [4+2+2] types are viable methods for target-directed synthesis. Although their full potential awaits further exploration, an increase in the existing repertoire of assembly modes and substrate structures expands the synthetic application of cycloaddition reactions.

[1] M. Lautens, W. Klute, W. Tam, *Chem. Rev.* **1996**, *96*, 49.
[2] The variables *m* and *n* simply denote the number of atoms that each component contributes to the ring construction.
[3] a) K. M. Brummond, J. L. Kent, *Tetrahedron* **2000**, *56*, 3263; b) P. A. Evans, J. E. Robinson, *J. Am. Chem. Soc.* **2001**, *123*, 4609, and references therein.
[4] K. P. C. Vollhardt, *Angew. Chem.* **1984**, *96*, 525; *Angew. Chem. Int. Ed. Engl.* **1984**, *23*, 539, and references therein.
[5] M. Murakami, K. Itami, Y. Ito, *Angew. Chem.* **1998**, *110*, 2616; *Angew. Chem. Int. Ed.* **1998**, *37*, 3418.
[6] P. A. Wender, G. G. Caber, R. D. Hubbard, L. Zhang, *J. Am. Chem. Soc.* **2002**, *124*, 2876.
[7] Y. Chen, J. K. Snyder, *J. Org. Chem.* **1998**, *63*, 2060.
[8] P. A. Evans, J. E. Robinson, E. W. Baum, A. N. Fazal, *J. Am. Chem. Soc.* **2002**, *124*, 8782.
[9] S. R. Gilbertson, B. Deboef, *J. Am. Chem. Soc.* **2002**, *124*, 8784.
[10] S. R. Gilbertson, G. S. Hoge, D. Genvf, *J. Org. Chem.* **1998**, *63*, 10077.

History of Science

A Kaiser Wilhelm Institute for Cologne! Emil Fischer, Konrad Adenauer, and the Meirowsky Endowment**

*Lothar Jaenicke and Frieder W. Lichtenthaler**

Dedicated to Professor Klaus Hafner on the occasion of his 75th Birthday

Keywords:
Emil Fischer · history of science · Kaiser Wilhelm Society

The award of the Nobel Prize for Chemistry to Emil Fischer (Figure 1, left) just over 100 years ago,[1] which fell into the year of his 50th birthday, gave many a reason to pay tribute to the personality and scientific legacy of one of the towering figures of our science.[2–5] However, it also presents the opportunity to remember facets of his work other than his scientific achievements.[6,7] It was largely due to his inspiration and untiring energy that the idea of research, free from teaching duties—which he always regarded as an obvious duty but with increasing poor health also as a burden—took shape in the form of institutes established solely for that purpose, and which was realized in 1911 with the foundation of the Kaiser Wilhelm Gesellschaft (KWG), financed through the sponsorship of patrons. The first Kaiser Wilhelm Institutes (KWIs)[1] for Chemistry (Directors Ernst Beckmann, Richard Willstätter) and for Physical Chemistry and Electrochemistry (Director Fritz Haber) were opened with much festivity as early as October 1912.[8] The Institute for Experimental Therapy and Biochemistry (Directors August von Wassermann, Carl Neuberg) followed a year later. The KWI for Coal Research, the first outside the Berlin-Dahlem area, the research profile of which Emil Fischer laid down with determined foresight,[9] opened in 1914 in Mülheim (Ruhr) under the leadership of Franz Fischer. Geographic dispersion and the incorporation of local interests for applied basic research were desired.

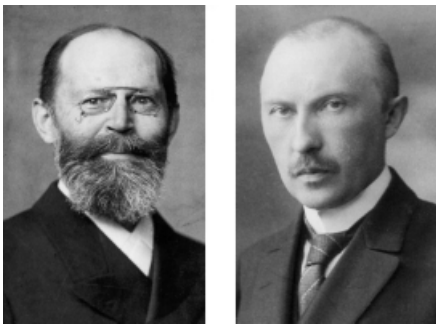

Figure 1. Left: Emil Fischer (around 1915), right: Konrad Adenauer (in 1917).

In March 1914 the Senate of the KWI had decided to set up a KWI for Physiology in Berlin-Dahlem,[10] for which Emil Fischer suggested his long-time collaborator, friend, and colleague Emil Abderhalden, Professor of Physiology at Halle University since 1908, whom he held in high regard.[11] After negotiations throughout April 1914 Abderhalden had agreed to accept the appointment. In public relations and the art of obtaining industrial sponsorship he was a thoroughly modern person, otherwise a child of his time and the Swiss countryside.[12] His research centered around the chemistry and action of protein degradation products which impressed medical doctors and the general public. The KWI for Physiology was intended to provide favorable working conditions for his proximity to practical medicine. This institute was to have been completed in 1914, however, the well-advanced plans were abandoned in 1916 because of the war; instead, from 1917 onwards, annual allowances were paid by the KWG to the "Abderhalden research post" in Halle to promote "comparative biochemical investigations on the structure of proteins", and later, when the terms became established, "vitamins and hormones".[13] Abderhalden, who did not consider himself bound to Halle, was open to offers, even though he put down firm roots there later as the President of the Leopoldina[2].

[*] Prof. Dr. F. W. Lichtenthaler
Institut für Organische Chemie
Technische Universität Darmstadt
Petersenstrasse 22, 64287 Darmstadt (Germany)
Fax: (+ 49) 6151-166-674
E-mail: fwlicht@sugar.oc.chemie.tu-darmstadt.de
Prof. Dr. L. Jaenicke
Institut für Biochemie
Universität zu Köln
Zülpicher Strasse 47, 50674 Cologne (Germany)
Fax: (+ 49) 221-470-6431

[**] We thank Frau Erna Lämmel (Leopoldina Archive, Halle), Dr. R. Rider (Bancroft Library, UC at Berkeley), J. Deres (Historical Archive of the City of Cologne), and T. Müller (University Archive, Cologne), for generously providing information. Picture credits: Edgar Fahs Smith Collection, University of Pennsylvania, Philadelphia (E. Fischer), Stiftung Bundeskanzler-Adenauer-Haus Rhöndorf (K. Adenauer), and ref. [24] (M. Meirowsky).

[1] As the successor organization to the Kaiser Wilhelm Society the Max Planck Society was formed in 1948 as an independent research organization.

[2] Leopoldina: German Academy of Natural Scientists, founded 1652, the first scientific academy world-wide.

 © 2003 Wiley-VCH Verlag GmbH & Co. KGaA, Weinheim 1433-7851/03/4207-0722 $ 20.00+.50/0

From his political contacts in Berlin, the prestige of scientific research and circumstances surrounding the KWI for Physiology were apparently known to Konrad Adenauer (Figure 1, right)[14] and appeared to be of use to him for the benefit of his home town. Since 1908, Adenauer had been the first deputy mayor of the City of Cologne, and from 1917 onwards, at 41, the youngest Lord Mayor of the fourth-largest city in the German Empire and as such a member of the Prussian Herrenhaus (upper house). It is indicative of his ambitious vision that in November 1917 he wanted to use accrued war gains of 1.2 million gold marks donated to the city by an initially anonymous Cologne industrialist to attract a KWI to his city, which in the conception of the benefactor, Max Meirowsky (Figure 2), was to be directed at

Figure 2. Max Meirowsky.

research into human, and in particular children's nutrition, as he had been deeply moved by the misery of the winter of hunger (1916/17) and the suffering of children.

This induced Adenauer, after preliminary discussions with Abderhalden,[15] to a letter to Emil Fischer, the vice-president of the KWG, written in his characteristic administrative style (see letter of May 23, 1918):[16]

This letter obviously initiated probing discussions between Adolf von Harnack, the president of the KWG, and Emil Fischer, as well as between Fischer and Abderhalden. Both clearly came to the conclusion that the City of Cologne had more to do than merely solve the question of the site, especially as the university environment, according to the objectives of the KWG a prerequisite for interactive basic research, was lacking. Cologne university, the oldest

Konrad Adenauer wished to use the money donated by an industrialist for the founding of a KWI in Cologne

For the KWG a university environment was an essential requirement, it promoted interdisciplinary basic research

His Excellency
Director of the Chemical Institute
Member of the Scientific Deputation for Medical Science
Privy Councilor Dr. Fischer
Berlin N.4

Cologne, May 23, 1918

Your Excellency,
On the 10/11 of this month I was in Berlin on a matter concerning the Kaiser Wilhelm Society. I was unable to discuss my suggestion with your Excellency in person, since you were, so I had heard, absent from Berlin. I have therefore taken the liberty of bringing the matter to your Excellency's attention in writing, and I hope also to be able to discuss the matter with you in person during my next visit to Berlin on the occasion of the meeting of the Upper House on the June 5.
A citizen of Cologne is willing to make 1 200 000 M available to the Kaiser Wilhelm Society for the Institute for Physiology planned by the Society on the condition that the Institute is established in Cologne with the leader designate, Professor Abderhalden and is to receive the grants previously planned by the Kaiser Wilhelm Society and the State. As I heard in Berlin, a site is to be made available by the provincial government free of charge for the Institute in Berlin-Dahlem. It became obvious to me that the City of Cologne would also have to make a site available without cost if the Institute were to come to Cologne. To make such a site available would not come up against any obstacle in the City of Cologne, but on the other hand it would not be to the benefactor's liking as he would find it embarrassing that as a result of a donation, planned and given by him to the City of Cologne for reasons of pure philanthropy, the city would be left with a burden. I am sure a way out of this difficulty will be found should it be absolutely necessary, even with consideration of the legitimate sensitivity of the benefactor, although at the moment it is not clear to me how this difficulty can be overcome. Privy councilor Abderhalden, with whom I have discussed this matter, would warmly welcome the establishment of the Institute in Cologne and the increase in resources made possible by this endowment. I assume that he will correspondingly discuss his intentions with your Excellency in person. He has further assured me that constructional and material difficulties would not arise for the Kaiser Wilhelm Society from the separation of the Institute for Physiology from the other institutes to be established in Berlin-Dahlem. The foundation of the Institute within its walls is of considerable interest for the City of Cologne. In the first instance, the reputation of Cologne and its scientific institutions would in this way be fostered, a point upon which I lay great weight, because Kaiser Wilhelm Institutes are also established in Breslau and Düsseldorf, but also, and I put great value upon this, it is of utmost importance for the intellectual life of Cologne with its 650 000 inhabitants to have scientific establishments and prominent men within its walls so that the intellectual life emanating from them will counteract the strongly materialistic features of this large city. I would be especially obliged to your Excellency if you would intercede in favor of the establishment of the Institute in Cologne. I would also add that according to the explicit declaration of the benefactor, should his donation find no acceptance under the above conditions the sum will not be granted for scientific purposes.
I remain, your Excellency's devoted servant
Adenauer
Lord Mayor

 © 2003 Wiley-VCH Verlag GmbH & Co. KGaA, Weinheim 1433-7851/03/4207-0723 $ 20.00+.50/0

German municipal university was founded in 1388, yet converted into French-type central school in 1798 by the French Ministry of Education to which Cologne was subordinate after the annexation of the left border Rhineland; after the "Wars of Freedom", unlike Bonn university, it had not been reopened by the Prussian controlling powers. Chemistry lay fallow, only the business school fostered it,[17] even the Medical Academy had no preclinical foundation.[18] Thus Emil Fischer's perfectly worded reply was, despite all its courteous and diplomatic niceties, quite unambiguous (see letter of June 3, 1918).[19]

In June 1918 the Senate of the KWG decided to give the institute to Cologne

The meeting between Fischer and Adenauer mentioned in this letter took place in Berlin on June 7, 1918. The negotiations progressed sluggishly, but with mutual respect, for in a letter to Abderhalden of June 24[20] Fischer remarked amongst other things: "It may be advisable maintaining towards Lord Mayor Adenauer, who to me appears to be an excellent man, that a budget of 200000 marks will have to be raised."

There are apparently no records of the meetings between Emil Fischer and Konrad Adenauer—a second took place on July 18, 1918—but as early as June 1918 a resolution of the KWG Senate followed,[21] "to move the Institute for Physiology to Cologne on the condition that it is extended by the addition of a Section for Nutritional Science and that the City of Cologne raises the necessary annual operating budget of 200000 Marks—that much is necessary according to the judgment of Excellency Fischer—which means a contribution of 70–80000 Mark to the resources available."

In further negotiations a figure of 153000 Mark was agreed upon, whereafter Konrad Adenauer expressed his gratitude to Emil Fischer on August 14, 1918:[22] "It is with great pleasure that I

Lord Mayor Adenauer
Member of the Upper House

Berlin June 3, 1918

Dear Lord Mayor,
Please accept my apologies that I only today reply to your letter of May 23, but I believed it necessary to refer the matter to my colleague His Excellency von Harnack following an exchange of correspondence with my friend and former student Abderhalden on the offer from the City of Cologne.
It is a pleasant sign of the times that the large German cities desire to see scientific institutes established within their walls, and the Kaiser Wilhelm Society is highly interested in supporting these efforts. It is within this context that I and my colleague Harnack, and presumably all other members of the administrative board and the administrative council of the Kaiser Wilhelm Society, welcome the offer from Cologne. On the other hand there are, however, certain misgivings about relocating the Institute for Physiology from Dahlem to Cologne which I can not conceal and about which Herr Abderhalden has probably already informed you. That is the isolation of the institute because it would be uprooted from intimate connection with the other institutions existing in Dahlem; for physiology is linked by numerous threads to physics, chemistry, and the other biological sciences.
The support of the representatives of the related sciences would be missed by the Biological Institute in Cologne; for the Medical Academy cannot replace it, and even though Bonn University is very close and easy to reach, the possibility of daily interchange is missing. In addition certain difficulties would arise for the younger academics, who the Institute must have, whose choice would be very difficult as they lack the association with the university. As long as Abderhalden, who is an unusually energetic and talented man, remains at the head of the institute these disadvantages would not be so apparent because he is used to overcoming all difficulties through his energy. However, in the future, if a change in personnel becomes necessary, serious attention would have to be given to this problem. Therefore, in the interest of the Institute I consider it necessary that this immense disadvantage is offset by advantages which would accrue to it in Cologne. This includes without doubt the imposing sum of 1.2 million which your anonymous citizen is to make available, from which the interest would be a very welcome increase in operating resources. However, a further idealistic advantage would need to be forthcoming. In my opinion that would be the assurance that the benevolent interest of the citizens of Cologne in the Institute would continue to flourish.
The Kaiser Wilhelm Institutes which have previously been established or are planned in cities without universities have specific practical objectives, I mention in this context the Coal Research Institute in Mülheim/Ruhr, the Iron Institute in Düsseldorf, and finally the planned institute for the textile industry.
It should be possible to give the Institute for Physiology in Cologne a distinctive character which is at the same time evocative of daily life. That would be the nutrition of mankind and animals, which currently occupies the interest of many circles. When one plans such tasks extending beyond the more restricted scope of scientific research then Cologne would be the right place for the Institute, but then considerably larger resources than before would need to be made available to the Institute.
Perhaps you would be so kind, distinguished Lord Mayor, as to take these thoughts into consideration and disseminate them amongst your fellow citizens. One would hope that in this way it would be possible to obtain further donations for the Institute, and move the city government to greater sacrifice than the mere concession of a site.
It would be a particular pleasure to be able to discuss this matter with you personally. As a convalescent from a long and serious illness which I suffered during the Spring I am, however, still spending much of the time in Wannsee, but I am quite willing to come to Berlin for a meeting. Best for me would be the time between 11 and 1 o'clock, or 4.30 to 6.30. I am happy to leave the choice of venue to you. Should you consider it useful we could meet with Harnack at the Royal Library. My telephone number is Wannsee exchange no. 75.
I remain yours sincerely,
Emil Fischer

thank you for your kind letter of the 12th of this month. There was the real risk that the benefactor would change his mind and use the capital for other purposes. I am very pleased that now we can be certain to get this fine Institute to Cologne. You can be assured that I will do my utmost to render possible the very best working conditions. During my next presence to Berlin I shall take the liberty to call upon you in person."

In September of 1918 the loss of the war became obvious and the Empire finally collapsed in November 1918; Emil Fischer's physical suffering increased, presumably a consequence of chronic phenylhydrazine poisoning, and emotional depression from the death of the younger two of his three sons as a result of the war. This all contributed to these plans not being realized, and lastly the donation, raised to three million gold marks by Max Meirowsky in 1919, was forfeited through conflict of interests, mainly in the Lindenburg Clinic, and finally because of inflation.

Despite this sad end to extensive efforts it was indeed the Meirowsky donation which brought together two important personalities—one at the end of his career, the other at the beginning. It can be rightly assumed that these negotiations, particularly Emil Fischer's arguments that in Cologne "connection to the university is lacking for the Director" and, as he wrote to Abderhalden[23] yet presumably also told Adenauer, that the Director there "sits on an isolation stool", were incentives for Adenauer to give further momentum to the much longer-running efforts for reestablishing the University of Cologne and for integrating it into the political vision of the Rhineland as a bridge, especially between Germany and France. Indeed, his roguish extortionate negotiations with the Prussian Ministry of Education led in May 1919 to a contract between the Prussian State Government and the City of Cologne for the establishment of a city-sponsored university. Thus, Emil Fischer had—in an admittedly indirect way—a certain share in the reopening of the University of Cologne in 1919.

Far more tragic—but also very typical of its time is the fate of the Meirowskys. Max Meirowsky (1866–1949) had come to Cologne from East Prussia, and in 1894 he founded a company for the production of insulating material (mica, monazite, feldspar) for the blossoming electrical and motor industries in Porz, close to the military district and later airfield of Wahn, it flourished well and in 1910 was changed into a family stock company the "Meirowsky AG",[24] in which his brother Emil (1876–1940) was also involved. He was a dermatologist and in 1921 Professor for Dermatology at the University of Cologne. As a Jew he was dismissed in 1933, his license to practice medicine was revoked in 1936, and in 1939 he emigrated to the USA via England. His daughter Lisamaria (1904–1942) had an Edith Stein fate:[25] she graduated with a double doctorate in medicine, converted under emotional stress in 1933, became a nun in a nursing order in 1938 in Holland, and in 1941 was porter and medical sister in the Konigsoord Trappist monastery in Brabant. From there she was deported in August 1942 with several companions via Westerbork to Auschwitz, and there immediately sent to the gas chamber. Apart from her dissertation there are no other traces of her existence. The Meirowsky AG was aryanized as Dielektra AG in 1941; Max Meirowsky, its founder, died in exile in Geneva.

The donation of three-million gold marks was forfeited through conflict of interests and finally because of inflation

[1] http:\\www.nobel.se/chemistry/laureates/1902/fischer-bio.html.

[2] "Emil Fischer, his Personality, his Achievements, and his Scientific Progeny": F. W. Lichtenthaler, *Eur. J. Org. Chem.* **2002**, 4095–4122.

[3] "Emil H. Fischer (1852–1919)—Großkophta der Bioorganik": L. Jaenicke, *BIOspektrum* **2002**, *8*, 725–727.

[4] H. Kunz, *Angew. Chem.* **2002**, *114*, 4619–4632; *Angew. Chem. Int. Ed.* **2002**, *41*, 4439–4451.

[5] "Ein Jahrhundertdatum: 1902. Das Geburtsjahr der Peptid-Chemie": L. Jaenicke, *Chem. Unserer Zeit* **2002**, *36*, 338–341.

[6] "Emil Fischer and Franz Hofmeister": J. S. Fruton in *Contrasts in Scientific Style: Research Groups in the Chemical and Biochemical Sciences*, American Philosophical Society, Philadelphia, **1990**, pp. 163–229.

[7] "Die Bedeutung Emil Fischers für die Entwicklung der Organischen Chemie in Ungarn": F. W. Lichtenthaler, *Humboldt Nachrichten Ungarn* **2002**, *22*, 4–12.

[8] "Vom Plan einer chemischen Reichsanstalt zum ersten Kaiser-Wilhelm-Institut: Emil Fischer": J. A. Johnson in *Geschichte und Struktur der Kaiser-Wilhelm-Max-Planck-Gesellschaft* (Eds.: R. Vierhaus, B. vom Brocke), DVA, Stuttgart, **1990**, pp. 486–515.

[9] E. Fischer, "Die Aufgaben des Kaiser-Wilhelm-Instituts für Kohlenforschung zu Mülheim (Ruhr)" ("The Tasks of the Kaiser Wilhelm Institute for Coal Research in Mülheim (Ruhr)"): Lecture on July 29, 1912 in Solbad Raffelberg in Mülheim to representatives of the State, industry, the Kaiser Wilhelm Society, and the city of Mülheim, in *E. Fischer, Untersuchungen aus verschiedenen Gebieten* (Ed.: M. Bergmann), Springer Verlag, Berlin, **1924**, pp. 810–822.

[10] R. Vierhaus, B. vom Brocke, *Forschung im Spannungsfeld von Politik und Gesellschaft. Geschichte und Struktur der Kaiser-Wilhelm-Max-Planck-Gesellschaft (Research in Regions of Political and Social Tension)*, DVA, Stuttgart, **1990**, pp. 147 and 916.

[11] E. Fischer, Letters to E. Abderhalden of December 27, 1913 and January 22, 1914. Copies in *Emil Fischer Papers*, Bancroft Library, UC at Berkeley..

[12] "Sensation, Wissenschaft, Betrug? – Emil Abderhalden und die Geschichte der Abwehrfermente" ("Sensation, Science, Fraud?—Emil Abderhalden and the History of Defense Enzymes"): M. Kaasch, *Acta Historica Leopoldina* **2000**, *36*, 145–210.

[13] KWG Senate resolution of May 11, 1917. The grants of the KWG to Abderhalden amounted to 10.000 Mark per annum, but were later increased. This ruling continued to 1930 (c.f.. ref. [10], p. 241 and 333).

[14] Konrad Adenauer (1876–1967), administration lawyer, Lord Mayor of Cologne 1917, single-mindedly made his city to the economic and cultural capital of the Rhineland through tactical shrewdness and strategic skill: town planning and expansion into the surrounding area, reopening of the university, development of trade fairs. In 1933 driven out of office by the National Socialist regime as a republican catholic and outlawed, was reinstated in 1945, but soon changed to become chairman of the Christian Democratic Party (CDU) co-founded by him. In 1948 President of the Parliamentary

Council, between 1949 and 1963 four times Bundeskanzler (Federal Chancellor). Stabilized bonds with the West and the economic ties of the Federal Republic as well as social conditions until the "Adenauer Era" ended in the revolts of 1968.

[15] On April 18, 1918 a discussion took place between Meirowsky and Abderhalden in his institute in Halle (letters from Meirowsky to Abderhalden of April 13 and April 16, 1918), and on May 11, 1918 a discussion between Adenauer and Abderhalden in the Hotel Adlon, Berlin (Telegram from Adenauer to Abderhalden of May 10, 1918). Documents in Leopoldina Archives, Halle, EA848.

[16] K. Adenauer, letter to E. Fischer, May 23, 1918. Original in *Emil Fischer Papers*, Bancroft Library, UC at Berkeley.

[17] "From Alberti Magni Studium Generale to a Modern University": L. Jaenicke in *Nitrogen Fixation 100 Years After* (Eds.: H. J. Bothe, F. J. de Bruijn, W. E. Newton), G. Fischer, Stuttgart, **1988**, pp. 853 – 868.

[18] "Vor 75 Jahren: Eröffnung des vorklinischen Studiums an der Universität zu Köln" ("75 Years Ago: the Opening of the Preclinical Course at the University of Cologne"): L. Jaenicke in *J. Hoffmann, Dokumentationen*, Köln, **2001**.

[19] E. Fischer, letter to K. Adenauer, June 3, 1918, copy in *Emil Fischer Papers*, Bancroft Library, UC at Berkeley.

[20] E. Fischer, letter to E. Abderhalden, June 24, 1918, Leopoldina Archives, Halle, EA848.

[21] Protocol of the KWG Senate Meeting of June 14, 1918, MPG Archives, Berlin. Extract from a handwritten letter of A. von Harnack to E. Abderhalden of June 21, 1918, Leopoldina Archives, Halle, EA848.

[22] K. Adenauer, letter to E. Fischer, August 14, 1918, Original in *Emil Fischer Papers*, Bancroft Library, UC at Berkeley.

[23] E. Fischer, letter to Abderhalden, May 28, 1918. Leopoldina Archives, Halle, EA848.

[24] "Die Firma Meirowsky & Co., später Dielektra in Porz": H. A. Wessel, *Rechtsrheinisches Köln, Jahrbuch für Geschichte und Landeskunde* **1992**, *16*, 129 – 162.

[25] Edith Stein (1891–1942), from a devout Breslau Jewish family, studied philosophy, mainly with the transcendency phenomenologue Edmund Husserl (1859–1936), whose critical master pupil she became ("Vom Sinn des Seins"). Converted in 1922, taught at different universities until her authorization to teach was revoked by the National Socialist State in 1933. Withdrew as Sister Theresia Benedicta a Cruce into the Carmelite Convent in Cologne to "carry out service to Jews contemplatively". In 1939 she was ordered against her will to the Echt Convent in the Netherlands, where she was betrayed, and for the same reason, and on the same day as Lm. Meirowsky (Sr. Maria Magdalena Dominica) deported to Auschwitz and murdered with Cyclon B; in 1987 beatified as a "Martyr of the Faith", canonized in 1998.

Biosynthesis of Antibiotics

Vancomycin Assembly: Nature's Way

Brian K. Hubbard and Christopher T. Walsh**

Keywords:
antibiotics · biosynthesis · glycopeptides · natural products

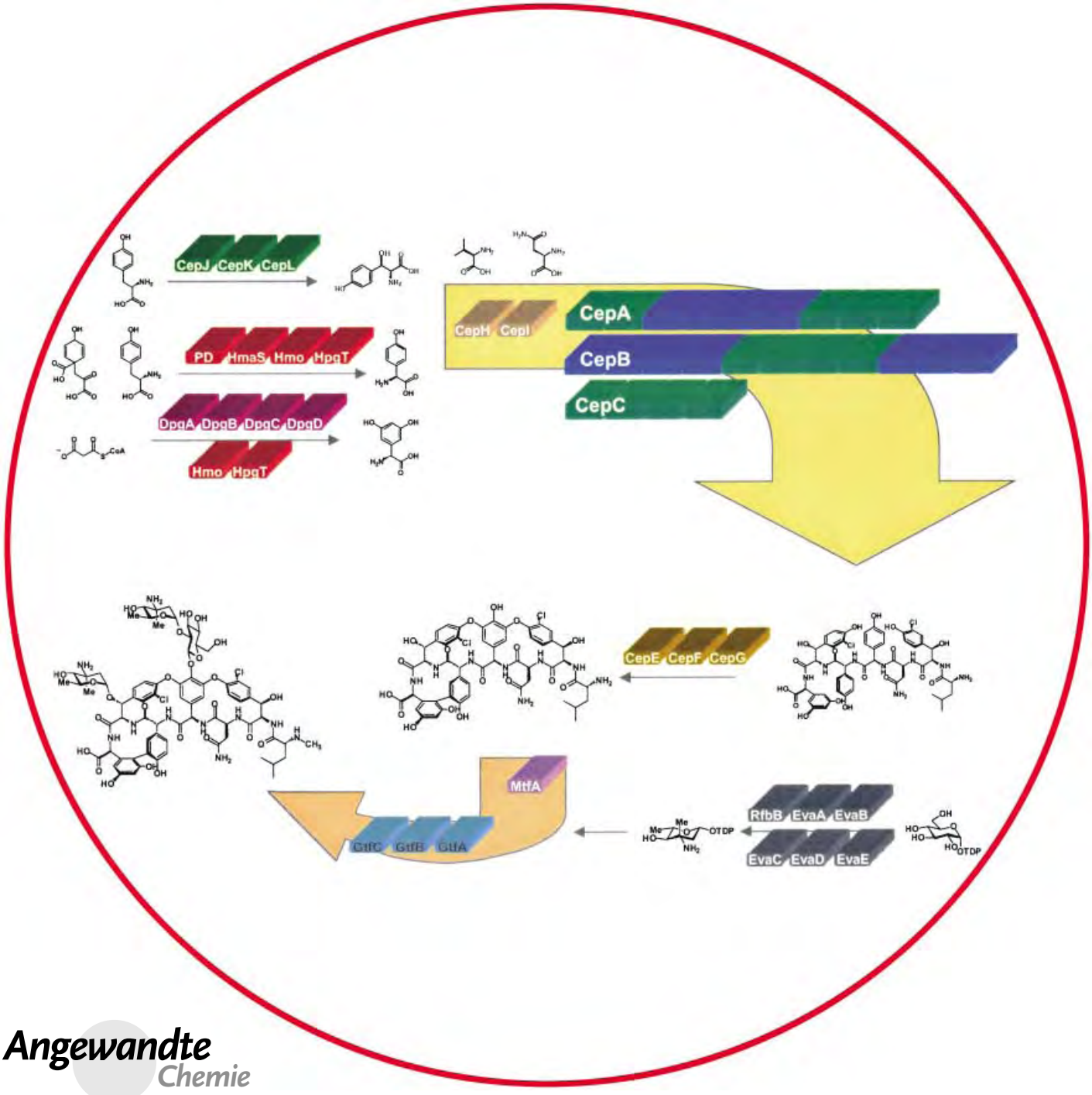

 © 2003 Wiley-VCH Verlag GmbH & Co. KGaA, Weinheim 1433-7851/03/4207-0730 $ 20.00+.50/0

Antibiotics are precious resources in the fight to combat bacterial infections caused by pathogenic organisms. Vancomycin is one of the antibiotics of last resort in the treatment of life-threatening infections by gram-positive bacteria. The rules by which nature assembles the glycopeptide (vancomycin) and lipoglycopeptide (teicoplanin) antibiotics are becoming elucidated and verified: first amino acids are synthesized, then joined together and cross-linked. This knowledge opens up approaches for reprogramming strategies at the level of altered monomers, swapped assembly lines, and different post-assembly tailoring enzymes.

From the Contents

1. Introduction 731
2. Targets for Antibacterial Drugs 731
3. Resistance Development 733
4. Mechanism of Action 733
5. Self-Protection in Organisms 735
6. Molecular Basis of the VanA, VanB, and VanC Phenotypes 736
7. Synthetic Strategies 738
8. Biosynthetic Gene Clusters 739
9. Enzymatic Formation of the Nonproteinogenic Amino Acids 742
10. The Nonribosomal Peptide Synthetase Assembly Line 750
11. Post Assembly Line Tailoring of the Heptapeptide 752
12. Glycosylation: The Thymidinediphospho Sugar Donors 753
13. Gycosylation: Peptide Antibiotic Glycosyl Transferases 758
14. Approaches to Treatment of Vancomycin-Resistant Bacteria 760
15. Conclusions 762

1. Introduction

Antibiotics are precious resources in the fight to combat bacterial infections caused by pathogenic organisms. Vancomycin, the subject of this review, is one of the antibiotics of last resort in the treatment of life-threatening infections by gram-positive bacteria. Table 1 lists a selection of pathogenic gram-positive and gram-negative bacteria and the syndromes or disease states in which these bacteria are common causative agents.[1] These include several bacteria associated with different outbreaks of diarrheal diseases such as *Clostridium difficile, Escherichia coli, Salmonella typhimurium*, and the *Vibrio cholerae* which causes the massive watery diarrhea that is part of the life-threatening syndrome of cholera. In addition to cholera, two other pathogens of long historical standing in human health are the *Yersinia pestis* and *Mycobacterium tuberculosis* strains that cause plague and tuberculosis, respectively.

Many surgical patients are treated prophylactically with antibiotics to reduce the incidence of bacterial infections in the surgical wounds: Staphylococci and Enterococci are the most common bacteria that cause post-surgical infections in US hospitals. Bacteria differ in their degrees of virulence and pathogenicity:[2] *Staphylococcus aureus* and *Streptococcus pneumoniae* can be highly virulent and have been described as professional pathogens, while *Enterococcus faecalis* and *Pseudomonas aeruginosa* are often characterized as opportunistic pathogens which will grow up when other bacteria have been eradicated and when the host defenses are low, for example, in immunosuppressed states.[3]

All these bacterial pathogens have targets in common (see below), which are acted on by the major classes of antibacterial drugs. Antibiotics with a major niche in human therapeutics fall into two categories of origin, natural products and derivatives thereof, and totally synthetic drugs. The synthetic classes include three examples in current therapeutic use: the two agents in bactrim, sulfamethoxazole, and trimethoprim, which inhibit two enzymatic steps in bacterial biosynthesis of folate coenzymes;[4] the fluoroquinolone antibiotics which inhibit DNA topoisomerases;[5] and the recently introduced oxazolidinone linezolid which targets protein synthesis.[6] All the other major classes of antibiotics, the β-lactams, the glycopeptides, the macrolides, the tetracyclines, and aminoglycosides, are natural products or semisynthetic derivatives of natural products.

2. Targets for Antibacterial Drugs

Aside from the bactrim combination of two antifolate drugs, almost all the major antibiotics act against three primary processes in the pathogenic bacteria: cell-wall biosynthesis, protein biosynthesis, and DNA replication and repair (Figure 1).[7,8] Antibiotics directed against cell walls include the β-lactam group of penicillins and cephalosporins as well as the glycopeptide antibiotic class, of which two

[*] Dr. B. K. Hubbard, Prof. Dr. C. T. Walsh
Department of Biological Chemistry and Molecular Pharmacolgy
Harvard Medical School
Boston, MA 02115 (USA)
Fax: (+1) 617-432-0438
E-mail: bhubbard@mpi.com
christopher_walsh@hms.harvard.edu

 © 2003 Wiley-VCH Verlag GmbH & Co. KGaA, Weinheim 1433-7851/03/4207-0731 $ 20.00+.50/0

Table 1: Pathogenic bacteria and the syndromes or disease states in which they are causative agents.

Gram-positive		Gram-negative	
Bacteria	Infection	Bacteria	Infection
Staphylococcus	postsurgical infections	*Escherichia coli*	urinary tract infections, diarrhea
Streptococcus	pneumonia	*Salmonella typhimurium*	diarrhea
Mycobacteriam	tuberculosis	*Pseudomonas aeruginosa*	opportunistic pathogen during cystic fibrosis
Enterococcus	postsurgical infections	*Vibrio cholera*	cholera
Clostridium difficile	diarrhea	*Yersinia pestis*	plague

members, vancomycin and teicoplanin, are approved for clinical use in humans (Table 2). Protein synthesis on bacterial ribosomes offers many steps where antibiotics could disrupt the machinery, and four classes of antibiotics (macrolides, tetracyclines, aminoglycosides and oxazolidinones) act in this pathway. The recent determination of the structure of the 30S and 50S subunits of bacterial ribosomes at atomic resolution will greatly aid in the refinement of mechanistic understanding and the new design of antibiotics targeted to specific sites in the 16S and 23S rRNA components of the ribosome.[9–11] The only class of antibiotics in current use that block DNA replication and repair are the fluoroquinolones that exert their action by blocking the enzyme DNA gyrase and a cognate topoisomerase, TopoIV.[12,13]

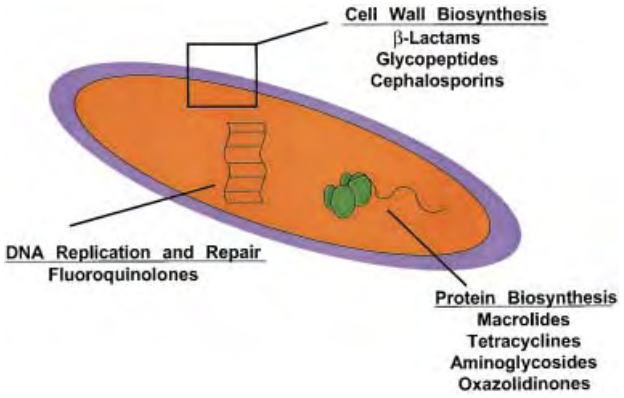

Figure 1. Bacterial targets of antibiotics.

2.1. Targets for β-Lactam and Glycopeptide Antibiotics

Since this review focuses on vancomycin and teicoplanin action to inhibit bacterial peptidoglycan cross-linking in bacterial cell wall biosynthesis, a brief summary of the structure and function of the peptidoglycan layer in bacterial metabolism and physiology is in order. As shown in Figure 2 both gram-negative bacteria (*E. coli, S. typhimurium, P. aeruginosa*) and gram-positive bacteria (*Staph. aureus, S. pneumoniae, Enterococcus faecalis)* have a peptidoglycan layer external to the cytoplasmic membrane. The gram-negative bacteria also have an intact outer membrane that acts as a permeability barrier to drugs such as vancomycin. Thus, vancomycin and teicoplanin cannot penetrate to the peptidoglycan (PG) layer and do not work against gram-negative bacterial infections, only against gram-positive bacteria.

The PG layer, in which the glycan strands are covalently cross-linked through peptide strands (Figure 3a), provides the mechanical strength to the PG network that allows the bacterial cell to withstand changes in osmotic pressure that would otherwise burst the cells. Most of the cross-links are introduced by transpeptidase enzymes, which catalyze the attack of the ε-amino group of lysine at position 3 of a peptide chain onto the carbonyl group of D-Ala_4 in an adjacent chain. The new lys-D-ala isopeptide cross bridge is formed as the D-Ala_4-D-Ala_5 bond cleaves, which result in a net transpeptidation. There are multiple forms of transpeptidases and many of them are the target enzymes for β-lactam antibiotics which mimic the *N*-acyl-D-Ala-D-Ala peptide substrates.[14,15] The transpeptidase starts a catalytic cycle with a penicillin by attacking the β-lactam and creating a more stable acyl enzyme analogue of the normal PG-D-Ala_4-enzyme.[16,17] The slowly hydrolyzing penicilloyl enzyme intermediates effectively inactivate the transpeptidases by tying up their catalytic sites and thereby blocking introduction of the PG isopeptide cross-

Brian K. Hubbard, born in 1972, majored in chemistry at the College of William and Mary and completed his Ph.D. in chemistry with John A. Gerlt at the University of Illinois, Urbana-Champaign. He completed his post-doctoral research with Christopher T. Walsh in 2001. From there he moved to Millennium Pharmaceuticals Inc. in Cambridge MA. His research interests are enzyme mechanisms and novel enzyme classes. A recent focus has been on the role of enzymes as drug targets for the treatment of metabolic diseases.

Christpher T. Walsh, born in 1944, majored in biology at Harvard and completed his PhD in biochemistry in the lab of Fritz Lipmann at Rockefeller Institute of Medical research. He spent 15 years (1972–1987) in the MIT faculty, and since 1987 has been at the Harvard Medical School. He has served as Chair of the Department of Chemistry at MIT (1982–1987) and of the Department of Biology, Chemistry, and Molecular Pharmacology at Harvard Medical School (1987–1995). His research interests are in enzyme mechanisms, the mechanism of inhibitors, and the biosynthesis of nonribosomal peptide antibiotics.

Table 2: Antibiotic targets and resistance mechanisms.

Antibiotic	Target	Resistance mechanism
cell wall		
β-lactams	transpeptidase/transglycosylases (PBPs)	β-lactamases, PBP mutants
vancomycin	D-Ala-D-Ala termini of peptidoglycan and lipid II	reprogramming of D-Ala-D-Ala to D-Ala-D-Lac or D-Ala-D-Ser
teicoplanin	D-Ala-D-Ala termini of peptidoglycan and lipid II	reprogramming of D-Ala-D-Ala to D-Ala-D-Lac or D-Ala-D-Ser
protein synthesis		
erythromycins	peptidyl transferase/ ribosome	rRNA methylation/efflux
tetracyclines	peptidyl transferase	drug efflux
aminoglycosides	peptidyl transferase	drug modification
oxazolidinones	peptidyl transferase	unknown
DNA replication/ repair		
fluoroquinolones	DNA gyrase	gyrase mutations

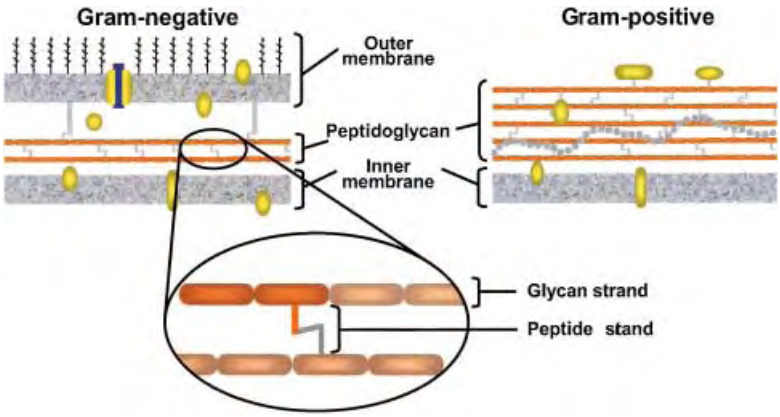

Figure 2. Cell walls of gram-negative and gram-positive bacteria.

bridges and reducing mechanical strength in the PG network (Figure 3b).

A second route to block the formation of the PG cross-bridge is to complex the pentapeptide strands of the free substrate of the transpeptidases and sequester it so it is unavailable for enzymatic cross-linking. That is the mechanism of action of the glycopeptide antibiotics.[18,19] Vancomycin binds to free PG termini with the *N*-Acyl-D-Ala-D-Ala ends as the high affinity binding site. Williams et al. worked out the architecture of the drug–target interaction and established there are five hydrogen bonds from the under surface of the vancomycin to the *N*-acyl-D-Ala-D-Ala PG terminus (Figure 4a).[20,21] The un-cross-linked PG chains are present both in the PG network and attached to the C55-undecaprenol-PP carrier (lipid II) at the outer face of the cytoplasmic membrane (Figure 4b), and both are thought to be targets for binding by vancomycin and teicoplanin.[22,23] Penicillins and vancomycins together block the same step in peptidoglycan cross-linking: one inactivates the enzyme, the other sequesters the substrate.

3. Resistance Development

The introduction of a new antibiotic molecule into widespread human use carries with it an inevitable progression to select for resistant bacteria and to have diminished utility, which ensures the need for new cycles of antibiotics discovery, design, and synthesis. The development of resistance accrues from two facets of bacterial populations: the large number of bacteria in an infection and their mutation frequency. There may be 10^9–10^{10} bacteria in a fulminant infection in an animal or a person. A typical rate of spontaneous mutation that is observed is about one mutant cell in 10^7. At these frequencies there would be about a thousand mutants in a bacterial population of 10^{10}. If each of these mutants had occurred randomly they might be distributed one per gene in each of a thousand genes in the bacterial population. When the bacteria are now exposed to an antibiotic, most will die off. However, if one or more mutants in a particular gene alter the gene product to confer resistance, they will give a selective advantage for the mutant to survive and then grow up in the space vacated by their dying (sensitive) neighbors and dominate the bacterial population. Bacterial resistance to antibiotics is a matter of when, not if, and is almost independent of the structure and type of antibiotic. The resistance could be conferred by the mutation of a single gene or multiple mutations may have to accumulate before significant growth advantage and resistance accrues. In Section 5 it will be shown that five genes had to be collected to reprogram the PG biosynthetic pathway before significant resistance to vancomycin arose in Enterococcal strains in clinical isolates.

4. Mechanism of Action of Glycopeptide Antibiotics

The focus of this review is on the glycopeptide class of antibiotics, natural products produced by the Actinoplanes order of bacteria. Following the discovery of vancomycin in a soil sample collected in Borneo in the 1950s, dozens of related glycopeptide antibiotics have been isolated from soil bacteria both from *Amycolaptosis* and *Streptomyces* strains.[24] The two main subclasses are exemplified by the antibiotics vancomy-

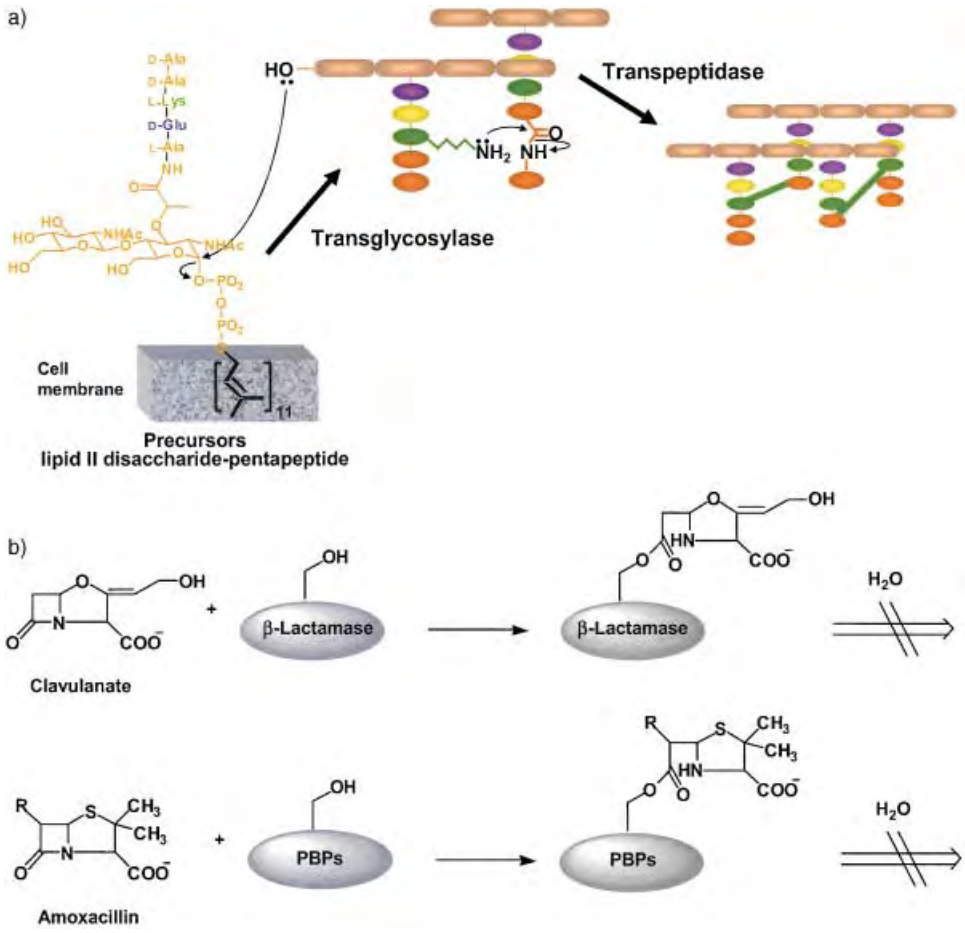

Figure 3. a) Peptidoglycan biosynthesis. b) Mode of inhibition by pencillins.

cin and teicoplanin (Scheme 1), each of which has a heptapeptide moiety that has undergone extensive cross-linking of the aryl side chains of the amino acid residues to impart a rigid dome-shaped architecture to the peptide scaffold. Vancomycin and teicoplanin have the configuration D-D-L-D-D-L-L in the heptapeptide scaffold produced by the action of nonribosomal peptide synthetase, and this configuration is presumed to be crucial for conformations that permit sidechain cyclization. Vancomycin has nonproteinogenic amino acids at residues 4, 5 (4-hydroxyphenylglycine (Hpg)), and 7 (3,5-dihydroxyphenylglyicne (DHpg)) while teicoplanin has an additional Hpg group at residue 1 and a DHpg group at residue 3. Vancomycin has three oxidative cross-links, in the aryl side chains 2–4, 4–6, and 5–7, while teicoplanin, with the additional aryl side chains at residues 1 and 3, has an additional cross-link such that all the side chains are connected.

These are glycopeptide antibiotics. A disaccharide is attached to the phenolic oxygen atom of 4-OH-PheGly$_4$ in vancomycin, whilethere are sugars on residues 4, 6, and 7 in teicoplanin . The disaccharide in vancomycin is a vancosaminyl-1,2-glucosyl moiety where the L-vancosamine is a 2,3,6-trideoxy-3-amino-3-methyl-L-hexose, made just for this antibiotic by the producer cell. Sugars related to vancosamine can be found in vancomycin analogues, including 4-oxo-L-vancosamine in balhimycin and 4-epi-L-vancosamine in chloroeremomycin (Scheme 2). A second L-epivancosamine is found on the β-hydroxy substituent of β-OH-Tyr$_6$ in chloroeremomycin. For a list of additional sugars found in vancomycin family members, see the recent review by Nicolaou et al. and Table 8 (Section 12).[25] In teicoplanin there is an *N*-acyl-D-glucosamine at residues 4 and 6, with a long acyl chain on the D-glucose attached to residue 4 and a more common GlcNAc sugar at residue 6, as well as a mannose group attached to residue 7. There are teicoplanin family members without any sugar groups such as A47934, from *Streptomyces toyocaensis* with a sulfate group on residue 3 (Scheme 2).

Vancomycin, teicoplanin, and other members of these glycopeptide antibiotics with the rigidified cross-linked heptapeptide scaffolds recognize the *N*-acyl-D-Ala$_4$-D-Ala$_5$ terminal D,D-dipeptide of un-cross-linked PG strands and in lipid II molecules to form high affinity complexes through five hydrogen bonds (Figure 4a) from the undersurface of the glycopeptide to the amide and carbonyl groups of the PG terminus. A space-filling model shows the complementary surfaces lead to a tight fit of the antibiotic and the $N_{2,6}$-bis(acyl)-L-Lys-L-Ala-D-Ala ligand. Such a model is shown in Figure 4c where the methyl side chain of D-Ala$_5$ is packed tightly against the antibiotic cavity. The D-Ala$_4$-D-Ala$_5$ amide linkage is sequestered in the complex with the glycopeptide and occluded from recognition by the cross-linking transpeptidases.

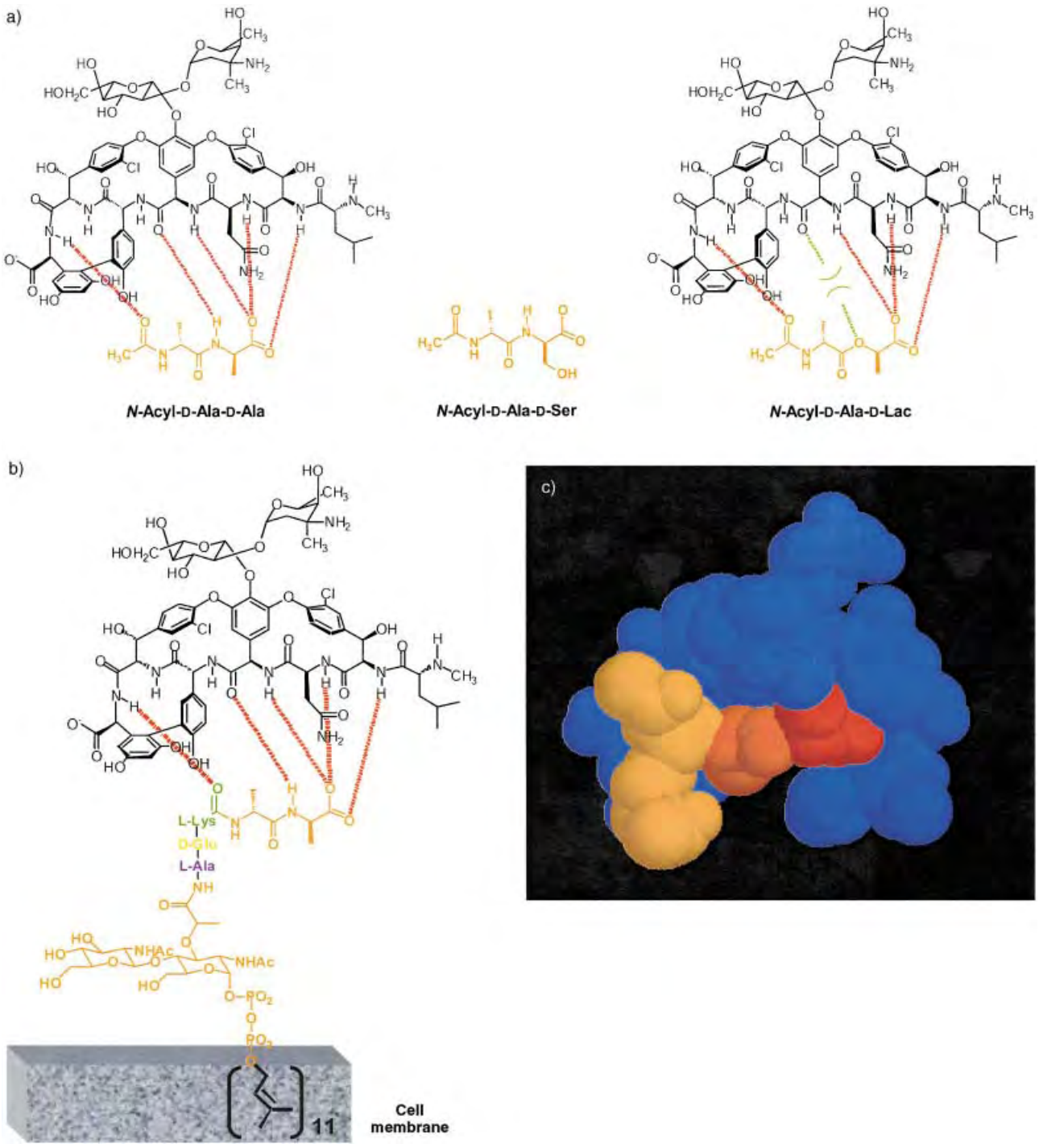

Figure 4. a) Hydrogen bonding in the interaction of vancomycin with *N*-Acyl-D-Ala, *N*-Acyl-D-Ala-D-Lac, and *N*-Acyl-D-Ala-D-Ser. b) Hydrogen bonding in the interaction of vancomycin with the cell-wall intermediate. c) Space-filling model of vancomycin bound to $N_{2,6}$-bis(acyl)-L-Lys-D-Ala-D-Ala. Vancomycin is shown in blue and the peptide shown in orange and red.

5. Self-Protection in Glycopeptide-Producer Organisms

Most bacteria that produce antibiotics have strategies for self-protection and immunity from the action of these chemical weapons. In the nonribosomal peptide antibiotic and polyketide antibiotics where the biosynthetic genes are clustered (see Section 7), there are also immunity-conferring genes. This co-localization of antibiotic production and antibiotic resistance genes enables coordinate regulation. When the antibiotic biosynthetic genes are turned on, so are the resistance genes, and it has been argued that antibiotic production and resistance genes co-evolved.[26] Typical resistance-gene products include transmembrane proteins that serve as efflux pumps, to pump out the nascent antibiotic molecules and keep the intracellular concentration in the

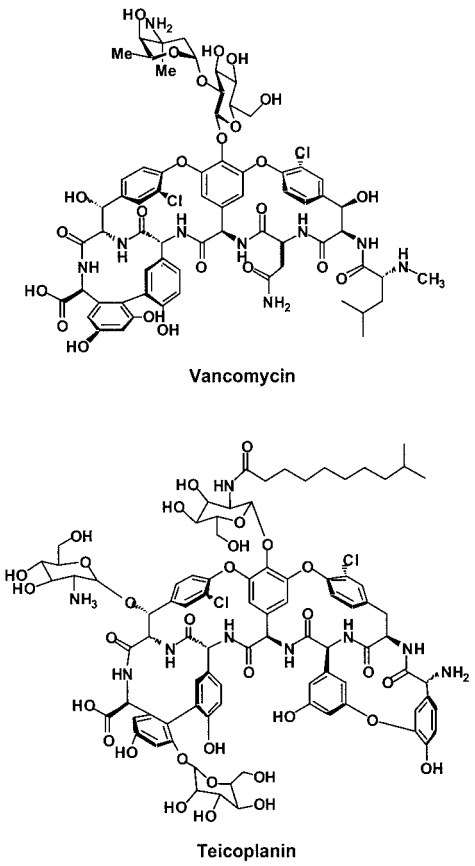

Scheme 1. Structures of vancomycin and teicoplanin.

producing bacteria below some harmful threshold.[27–28] Such antibiotic efflux pumps are found in the glycopeptide biosynthetic clusters.

A more specialized defense mechanism has now been found both in the *Streptomyces toyocaensis* strain that produces A47934 and the teicoplanin-producing *Actinoplanes teichomyceticus*,[29,30] and may have been the source of the resistance genes in pathogenic Enterococci noted below. A three-gene cassette encoding three enzymes that allow reprogramming of the peptidoglycan termini (Figure 5) is expressed when the enzymes that produce the glycopeptide antibiotics become expressed. The first of the three resistance-conferring enzymes (VanH) reduces pyruvate to D-lactate and the second (DdlM) couples that D-lactate with D-alanine to produce the depsipeptide D-Ala-D-Lactate. The third enzyme (VanX) meanwhile hydrolyzes D-Ala-D-Ala

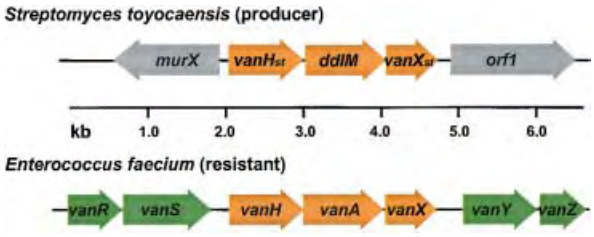

Figure 5. Gene cassettes for vancomycin resistance in the producing organism and resistant strains.

produced by the D-Ala-D-Ala ligase enzyme. The net result is that the concentration of the normal cell-wall precursor D-Ala-D-Ala falls while the new metabolite D-Ala-D-lactate rises. The MurF enzyme, which normally uses D-Ala-D-Ala as a substrate, now cannot find any and substitutes D-Ala-D-lactate in its condensation with UDP-muramyl tripeptide to make the UDP-muramyl-D-Ala-D-*iso*Glu-L-Lys-D-Ala-D-lactate, the depsipeptide analogue of the normal UDP-muramyl pentapeptide.[31] This analogue is glycosylated, transferred to the C55-lipid-PP carrier, translocated to the outer face of the cytoplasmic membrane, and used for PG elongation (Scheme 3). The transpeptidases use the tetrapeptidyl-D-Lac chain for cross-linking, thus disconnecting the D-Ala_4-D-Lac_5 ester bond as the isopeptide cross-link is produced.

The net effect of expression of the three resistance enzymes is to reprogram the cytoplasmic steps of PG assembly to produce D-Ala-D-Lac and carry it through in place of the D-Ala-D-Ala. As noted in the next section the affinity of vancomycin for the PG-D-Ala-D-Lac termini is 1000 fold lower than for the D-Ala-D-Ala termini. The producing bacteria have reprogrammed the biosynthetic pathway of the cell wall to become immune to vancomycin and teicoplanin.

6. Molecular Basis of the VanA, VanB, and VanC Phenotypes in Vancomycin-Resistant Enterococci

As the prevalence of antibiotic resistance spread during the 1980s, especially with the outbreak of methicillin-resistant *Staphylococcus aureus* (MRSA), vancomycin became a more important drug and came into wider use for the treatment of life-threatening gram-positive bacterial infections. It is now front-line therapy for endocarditis, for many bacteremias that occur in cancer patients undergoing cycles of chemotherapy, and became the drug of last resort for the treatment of MRSA infections in hospital wards.[32] With wider use of vancomycin in hospital wards, vancomycin-resistant gram-positive bacterial pathogens emerged, most notably vancomycin-resistant Enterococci (VRE). VRE have been categorized as opportunistic pathogens that are selected for when other bacteria die off.[33] The incidence of VRE rose alarmingly from 0.4% in hospital clinical isolates in 1987 to 16% just six years later,[34] and carried a high mortality rate. About 95% of VRE are *Enterococcus faecalis* strains and about 5% are *Enterococcus faecium* strains. Two main clinical phenotypes have been described as VanA and VanB (Table 3), which are distinguished largely by differential sensitivity to teicoplanin (resistant in VanA, sensitive in VanB).[3,35] A third minor clinical phenotype is categorized as Van C, and more recently variants of the phenotypes A and B have been detected.[36,37]

The VanA and VanB phenotypes of VRE have the same underlying molecular logic and it is the same as that in the glycopeptide antibiotic producer organisms, namely, a reprogramming of the PG termini from D-Ala-D-Ala to D-Ala-D-lactate. A five-gene cassette is required for this inducible enzymatic reprogramming of the PG: *vanR, vanS, vanH, vanA, vanX*, where *vanH* encodes the D-specific pyruvate reductase, *van A* the D-Ala-D-lactate ligase and *vanX* the D-

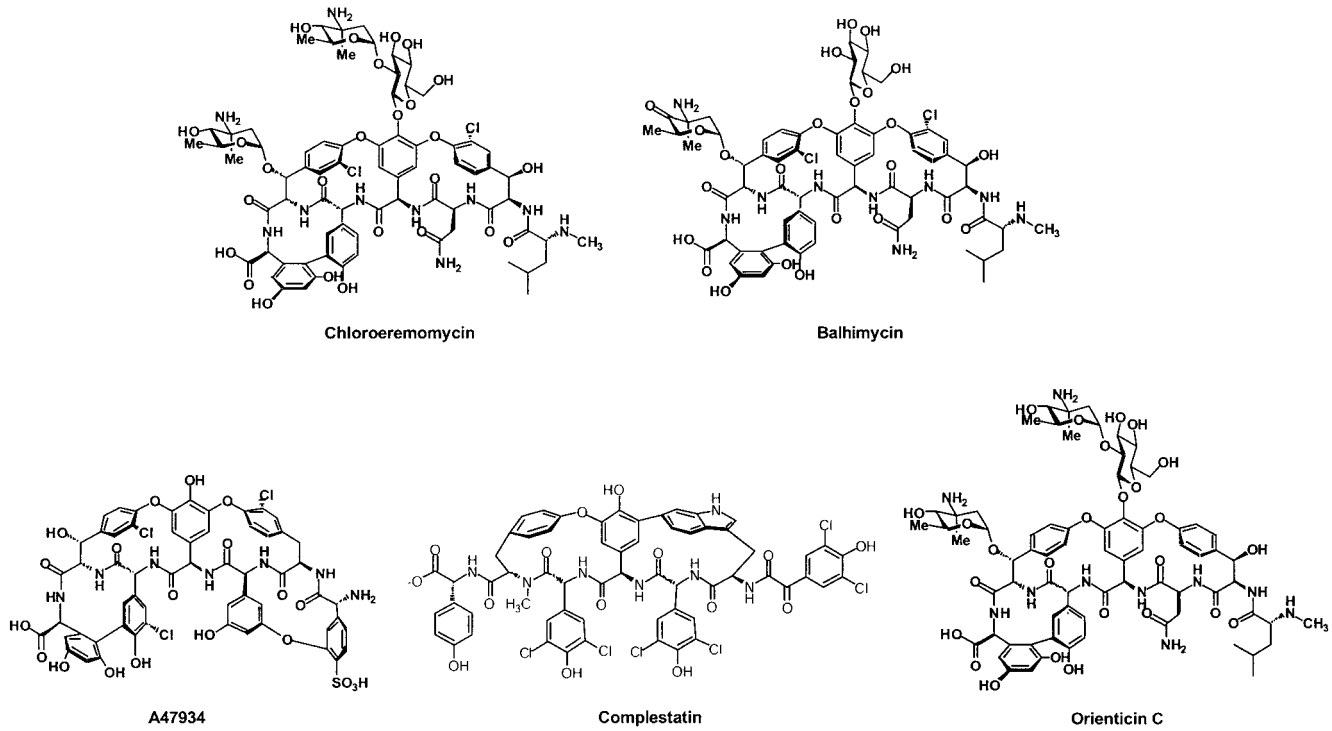

Scheme 2. Structures of chloroeremomycin, balhimycin, A47934, complestatin, and orienticin C.

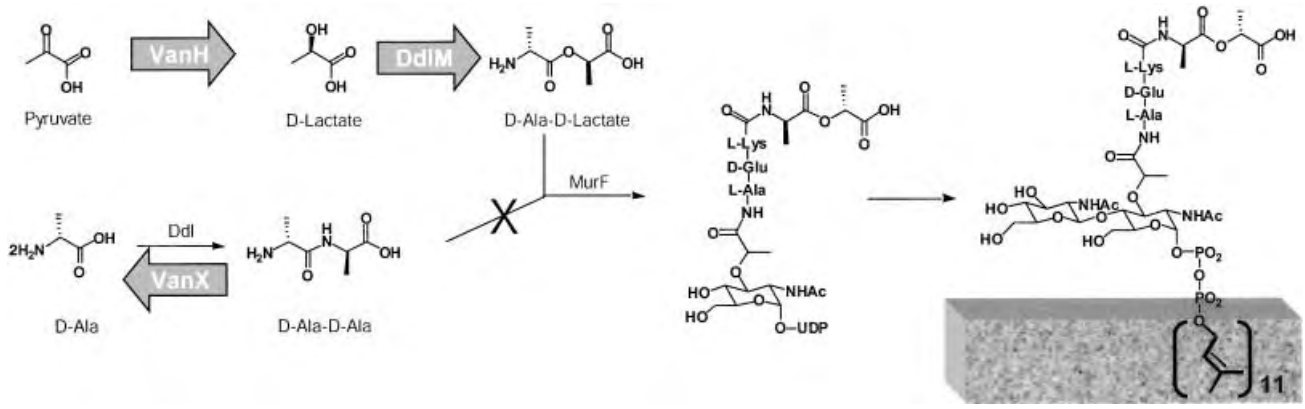

Scheme 3. Biosynthesis and incorporation of the D-Ala-D-Lac terminus of the peptidoglycan.

Ala-D-Ala dipeptidase. This sequence runs along the pathway shown in Figure 5 to produce D-Ala-D-lactate and destroy the normal D-Ala-D-Ala dipeptide selectively.[31,38] The binding of vancomycin to *N*-acyl-D-Ala-D-Lac has been quantitated to be 1000 fold lower in affinity than *N*-Acyl-D-Ala-D-Ala, and accounts fully for the three orders of magnitude higher minimal inhibitory concentrations (MICs; Table 3) seen in VRE clinical isolates of the VanA and VanB phenotypes.[39] Figure 4a shows a schematic representation of complexes of vancomycin with *N*-Acyl-D-Ala_4-D-Ala_5 and *N*-acyl-D-Ala_4-D-Lac_5 in which the one fewer hydrogen bond in the former complex is indicated.[31,35] It is likely there are also ground-state electrostatic repulsions between the vancomycin carbonyl oxygen atom and the ester oxygen atom in the D-Ala-D-Lac bond that contribute to the 1000 fold drop in affinity.

The vancomycin-resistant phenotype in VanA and VanB VRE can be induced by antibiotics, and is mediated by the other two proteins, VanS and VanR, encoded in the five-gene resistance cassette. The VanS and VanR pair form a two-component regulatory system, in which VanS is transmembrane sensor protein kinase and VanR a DNA-binding response regulator (Figure 5).[40] The presence of both vancomycin and teicoplanin at the outer surface of the enterococcal cell in the VanA phenotype, but only vancomycin in the VRE VanB phenotype, induces the VanS transmembrane protein to autophosphorylate itself in its cytoplasmic histidine kinase domain, perhaps by induced dimerization of VanS by an external ligand to bring the cytoplasmic domains together for transphosphorylation.[41] The phosphohistidyl VanS kinase domain can then transfer the phosphate

group to the VanR protein and phosphorylate a conserved aspartyl-β-COOH side chain in the N-terminal "receiver" domain of VanR. The phospho-VanR has a lower binding affinity to its target DNA sequences than VanR, which causes the P-VanR to fall off the promoter regions of the DNA in front of the *vanHAX* genes, thus relieving transcriptional repression.[42] The expression of VanHAX enzymes now starts the peptidoglycan reprogramming that leads to replacement of the D-Ala-D-Ala PG termini by D-Ala-D-Lac.

The continuing sensitivity of VanB-type of VRE to teicoplanin is entirely the result of its failure to be recognized by the $VanS_B$ sensor kinase and failure to turn on the reprogramming trio of enzymes ($VanH_B$, $VanA_B$, $VanX_B$).[43,44] This effect could be demonstrated by mutants that gained resistance to teicoplanin, all of which mapped to amino acid changes in $VanS_B$ that now transmitted the signal to $VanR_B$. These findings are consistent with the glycopeptides, vancomycin ($VanS_A$, $VanS_B$) and teicoplanin ($VanS_A$), being the direct ligands for the external domains of the sensor kinases.

As a generalization of the phenomena that reprogramming the peptidoglycan D-Ala-D-Ala termini is the molecular determinant of vancomycin resistance, *Enterococcus gallinarum* which cause the VanC phenotype produce a D-Ala-D-Ser ligase constitutively.[45,46] Analysis of PG termini show the D-Ala-D-Ser termini with the larger CH_2OH group of D-Ser_5 cause an order of magnitude drop in vancomycin binding affinity and an order of magnitude rise in MIC values (Table 3) relative to that found for termini containing the CH_3 group of D-Ala_5 (Figure 4a). Remarkably, one can even grow *E. faecalis* strains that require vancomycin to survive.[47] These have inactivating mutations in the chromosomal D-Ala-D-Ala ligase and only if the vancomycin-inducible D-Ala-D-lactate ligase (VanA) is expressed can this bacterium make peptidoglycan and survive.

7. Biosynthetic and Synthetic Chemical Strategies

The synthesis and assembly of vancomycin is a formidable challenge both to producer microorganisms and to synthetic chemists. While the main focus of this review is analysis of nature's route to the glycopeptide antibiotics, and the synthetic approaches have been reviewed previously by Nicolaou et al.,[25] it is instructive to compare briefly the successful strategies planned and executed by three synthetic chemistry groups (Evans et al.,[48–51] Nicolaou et al.,[52–56] and Boger et al.) to nature's way.[57] The major difficulty is the introduction of the three cross-links (two aryl ether and one C–C link) that stitch together the five aryl side chains in the vancomycin heptapeptide and all seven of the aryl side chains (three aryl ether and one C–C link) in the teicoplanin subclass.

The first synthesis of a vancomycin-type aglycone was that of the orienticin aglycone (Scheme 2),[50] which differed from the vancomycin aglycone by the absence of chloro substituents on β-hydroxy-Tyr2 and -Tyr6. One starting distinction between the biosynthetic assembly line and the chemical synthesis routes is that the *Amycolaptosis orientalis* bacteria use unprotected amino acid monomers while the chemists build in protective groups (Scheme 4). Nature needs five amino acids, two of which (L-Hpg at residues 4 and 5 and D-Hpg at residue 7) are nonproteinogenic and are biosynthesized just for this purpose. The protected monomers used by the research groups of Evans, Nicolaou, and Boger are listed in Scheme 4 as AA-1-A to AA-7-A (Evans), AA-2-B to AA-7-B (Nicolaou), and AA-3-C and AA-7-C (Boger). The protections at AA-1-A, -3-A, and -7-A are unexceptional, while the other four protection schemes were devised to allow the 2-4, 4-6, and 5-7 cross-links to be introduced. Analogously, the protection manifolds of AA-4-B were devised to enable the double cross-linking (to residue 2 and to residue 6) during the course of the synthesis.

Table 3: Types of resistance mechanisms and their sensitivity to vancomycin and teicoplanin.

Characteristic	Type				
	VanA	VanB	VanC	VanD	VanE*
genetic characteristics	acquired (c.g., Tn1546)	acquired (gene Tn1547)	intrinsic (chromosomally encoded characteristic of the species)	acquired	acquired
terminus of peptidoglycan percursor	D-Ala-D-Lac	D-Ala-D-Lac	D-Ala-D-Ser	D-Ala-D-Ser	D-Ala-D-Ser
minimal inhibitory concentration ($\mu g\,mL^{-1}$)					
vancomycin	64 to >1000	4 to >1000	2 to 32	16 to 64	16
teicoplanin	16 to 512	0.5 to >32	0.5 to 1	2 to 4	0.5
ligase gene	*vanA*	*vanB*	*vanC-1 and vanC-2/vanC-3*	*vanD*	*vanE*
bacteria found to have these genes for resistance in nature	*Enterococcus faecium, E. faecalis, E. durans, E. mundtii, E. avium, E. gallinarum, E. casseliflavus, Bacissuls circulans, Streptococus gallolyticus, corynebacteria, arcanobacteria, lactococci, oerskovia*	*E. faecalis, E. faecium, Streptococcus bovis, S. gallolyticus*	*E. gallinarum and E. casseliflavus/E. favesccus*	*E. faecium*	*E. faecalis*
bacteria to which vancomycin resistance has been transferred in the laboratory setting	*S. sanguis, S. pyogenes, listeria, and Staphylococcus aureus*	*E. faecalis, E. faecium, including transfer with ampicillin resistance*			

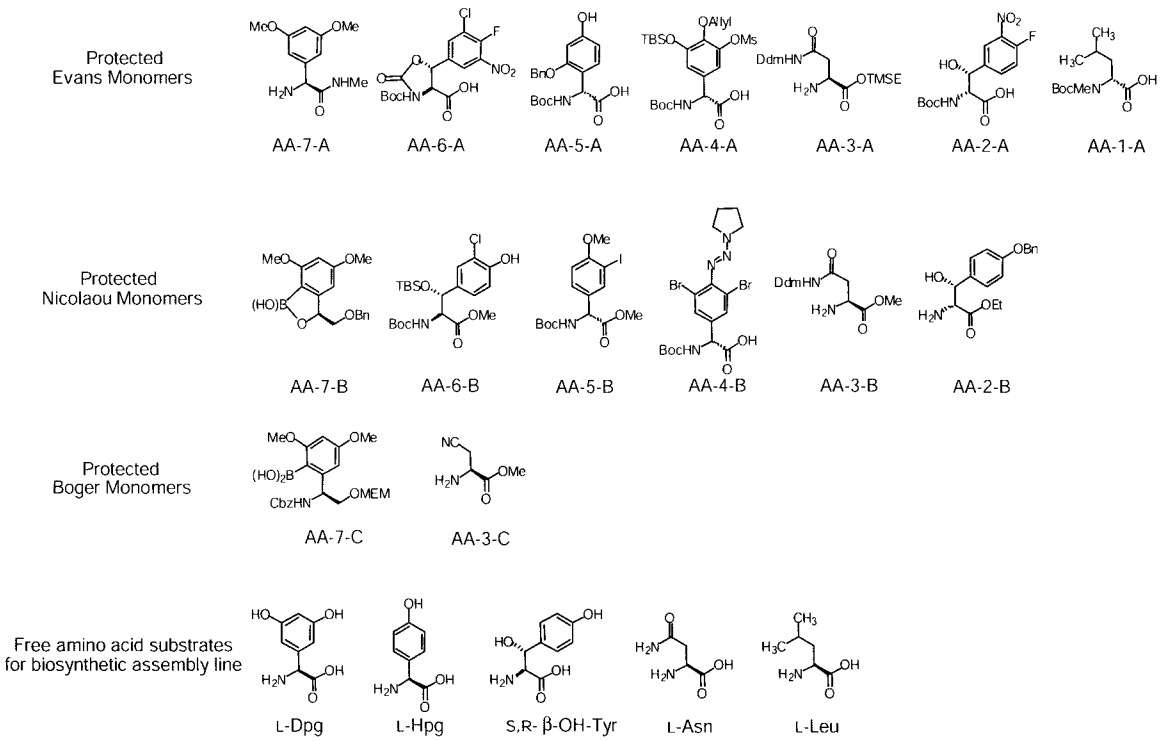

Scheme 4. Monomers used in the chemical and biosynthetic synthesis of vancomycin.

7.1. Timing of Monomer Assembly and Cross-Linking

A retrosynthetic analysis of the three chemical routes to glycopeptide assembly show that the approach of Nicolaou et al. (Scheme 5) differed somewhat from that of Evans et al. and also from that of Boger et al. (Scheme 6). To simplify the overall logic, the protecting groups, which are crucial for the actual implementation of the syntheses, are omitted in these schemes. All three syntheses built the 5–7 C–C cross-link first, then the 4-6, and finally the 2–4 aryl ether linkages to complete the aglycone scaffold. Nicolaou et al. built the 5–7 biaryl cross-link as the first connection then created the 5–6 and 4–5 peptide bonds. The 4–6 aryl ether cross-link was then introduced followed by construction of the 6–7 amide bond to give the macrobicyclic, doubly cross-linked tetrapeptide containing residues 4–7. The tripeptide 1–3 was assembled and coupled to make the 3–4 peptide bond, thereby generating the heptapeptide that lacked only the 2–4 aryl ether cross-link. Its introduction, followed by side-chain deprotections (not shown), completed the synthetic assembly logic to make the three rings of the fully cross-linked heptapeptide.

The routes used by the research groups of Evans and then Boger first assembled the 5–7 tripeptide and then introduced the 5–7 cross-link. Addition of residue 4 through formation of a 4–5 amide bond generated the mono-cross-linked tetrapeptide that was then subjected to 4–6 aryl ether cross-linking. The 1–3 tripeptide unit was then added to produce the equivalent heptapeptide scaffold in which the 2–4 aryl ether cross-link was introduced. All three routes are highly convergent with 28 steps constituting the longest linear synthetic sequence of steps. All three routes put the sugars on after completion of the aglycone scaffold. These are monumental feats of synthetic chemistry. However, the routes are not practical for facile production, averaging 95 steps from readily available starting materials.

A comparable retrosynthetic dissection of nature's logic for vancomycin assembly is shown in Scheme 7. A notable difference, besides the lack of any of the functional group protections noted above, is the assembly of the full linear heptapeptide before any aryl side chain cross-links are introduced. This creates complex problems of conformer control for regiospecific and stereospecific closure of the three rings for the cross-linking enzymes. It is known from gene-knockout studies that the 4–6 aryl ether cross-link is formed first, but the relative timing of the 2–4 and 5–7 cross-links is not yet deciphered.[59] We will discuss the enzymatic machinery for nonproteinogenic amino acid monomers in Section 9 and enzymatic cross-linking in Section 11. The natural route from the start to the fully glycosylated vancomycin involves about 35 steps.

8. Biosynthetic Gene Clusters for the Peptide Scaffold and the Tailoring Enzymes

The availability of the DNA sequence for antibiotic biosynthetic gene clusters illuminates the molecular logic of assembly and allows predictions of the functions of the different open reading frames (orfs) by homology to proteins of known functions and also by location of one orf relative to others within a cluster. Sequence data for the vancomycin group antibiotics has begun to appear. To date, the full cluster

for chloroeremomycin, a vancomycin class member, and for complestatin (Scheme 2), a nonglycosylated molecule, have been reported.[60,61] A partial sequence of the balhimycin cluster has been published, mapping data for the teicoplanin cluster has appeared,[62,30] and the sequence of the A47934 cluster has been reported.[145]

8.1. Chloroeremomycin and Balhimycin

Some 40 contiguous genes from the chloroeremomycin-producing (Cep) *Amycolaptosis orientalis* were sequenced and partially annotated in the 1998 report of van Waginengen et al.[60] Currently it appears that 30 of those Cep orfs can be clearly assigned to genes in the glycopeptide biosynthetic pathway and they are listed in Table 4 as orfs 1–30 in their order of appearance (Figure 6). The protein names are also

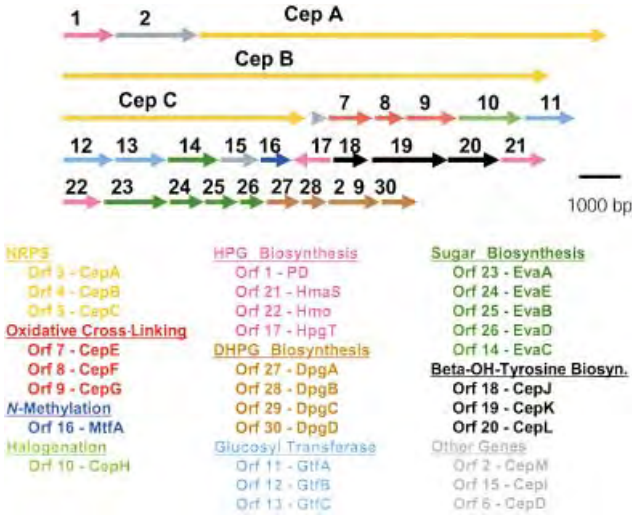

Figure 6. Genes in the chloroeremomycin biosynthetic cluster.

tabulated, together with predicted or known functions and cosubstrates and cofactors for enzyme activity. Analysis of the start and stop codons of those 30 genes indicates there are at least 19 mRNA transcripts, that is, several of the genes are transcribed together and there are overlaps of some stop and start codons, which is typical of translational coupling (as noted in Table 4). Of the 30 gene products, at least 23 have now been purified to substantial purity and their catalytic function established, as will be discussed in the next sections.

Five distinct amino acids are incorporated into the heptapeptide skeleton which is identical for chloroeremomycin, vancomycin, and balhimycin (Scheme 4). Two of these are not found in proteins (Hpg and Dpg), while a third, 3-chloro-β-hydroxytyrosine, is a nonproteinogenic variant of tyrosine. It is anticipated that enzymes devoted to the de novo biosynthesis of Hpg and 3,5-dihydroxyphenylglycine would be found in the cluster. The four orfs 1, 17, 21, and 22 constitute the four-enzyme pathway to Hpg, while the four orfs 27–30 lead to Dpg. The conversion of the common amino acid L-tyrosine to the 3-chloro-β-hydroxy-Tyr found at residues 2 and 6 of the heptapeptide scaffold is proposed to involve the four orfs 10, 18, 19, and 20. The detailed function of these twelve orfs is described in the next sections.

Three Orfs, CepA, CepB, and CepC constitute the nonribosomal peptide synthetase assembly line to produce the heptapeptide. An additional three Orfs, 7, 8, and 9, are heme proteins involved in oxidative cross-linking of the heptapeptide. Eight of the remaining twelve Orfs are involved in producing and attaching the sugar moieties of the glycopeptide. Orfs 14, 23, 24, 25, and 26 produce dTDP-L-epivancosamine from dTDP-D-glucose and orfs 12–14 are three glycosyltransferases that install the one D-glucose and two L-epivancosamine sugars onto the heptapeptide scaffold. Of the remaining four Orfs, Orf 16 is the *N*-methyltransferase that N-methylates the Leu_1 residue.[63] Orf 2 is predicted to be a transporter that is presumed to be the export pump for secretion of chloroeremomycin. Orf 15 has homologies to epimerases, while Orf 6 is the sole gene product with no ascribed function to date.

The partial sequence of the balhimycin cluster has so far revealed seven complete orfs (Table 5) with an almost identical organization to the orfs in the Cep cluster (Table 4).[62] The balhimycin orfs are homologues to Cep orf 6, three hemeproteins are analogous to Cep 7–9, a putative halogenase, three glycosyl transferases, and a partial sequence of a Cep 14 homologue.

8.2. Complestatin

The natural product complestatin (Scheme 2) from *Streptomyces lavendulae* is reported to block protein–protein interactions both in the complement cascade and in gp120–CD4 binding in the HIV life cycle.[64–67] The molecule clearly has similarities to the peptide scaffold of vancomycin, but is not glycosylated. The complestatin biosynthetic gene cluster has now been sequenced (Table 6 and Figure 7).[61] Complestatin is an acyl hexapeptide with all seven residues bearing aromatic side chains. The cross-linking of the electron-rich aryl side chains of residues 2-4-6 mirrors the 2-4-6 pattern found in the vancomycin and teicoplanin classes. Four of the six residues in complestatin are nonproteinogenic and derive from Hpg. The first residue, a *p*-hydroxy-3,5-dichlorobenzoyl formate, could arise by oxidation of *p*-hydroxy-3,5-dichlorophenylglycine, which is found at residues 3 and 5. Complestatin also contains the amino acid tryptophan, which is unique compared to the rest of the vancomycin family members.

Of the 16 genes in the complestatin cluster the four orfs encoding Hpg synthesis are found (orfs 13–16) as homologues to the corresponding *cep* genes. There are four protein subunits for nonribosomal protein synthesis, orfs 3–6, which like the CepA–C subunits have seven recognizable modules for activating the seven monomers. There are two hemeproteins, most likely the cross-linking oxidases orfs 10, 11, and a ferredoxin, orf 12, for electron transport into those hemeproteins. Of the remaining four genes, two appear to be involved in transport, one is a transcriptional regulator, and again one has an as yet unassigned function.

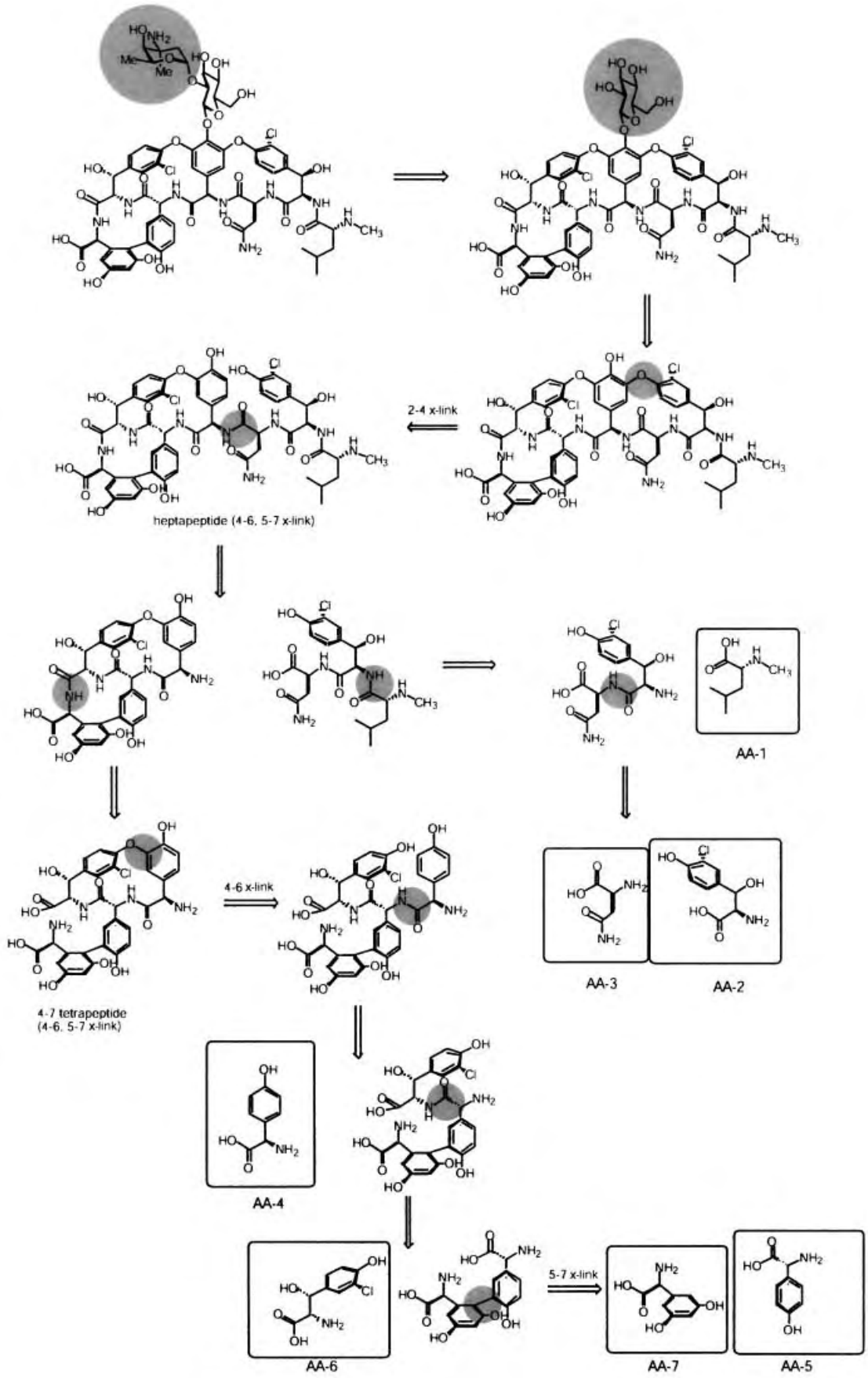

Scheme 5. Retrosynthetic analysis of the chemical synthesis of vancomycin used by Nicolaou et al.

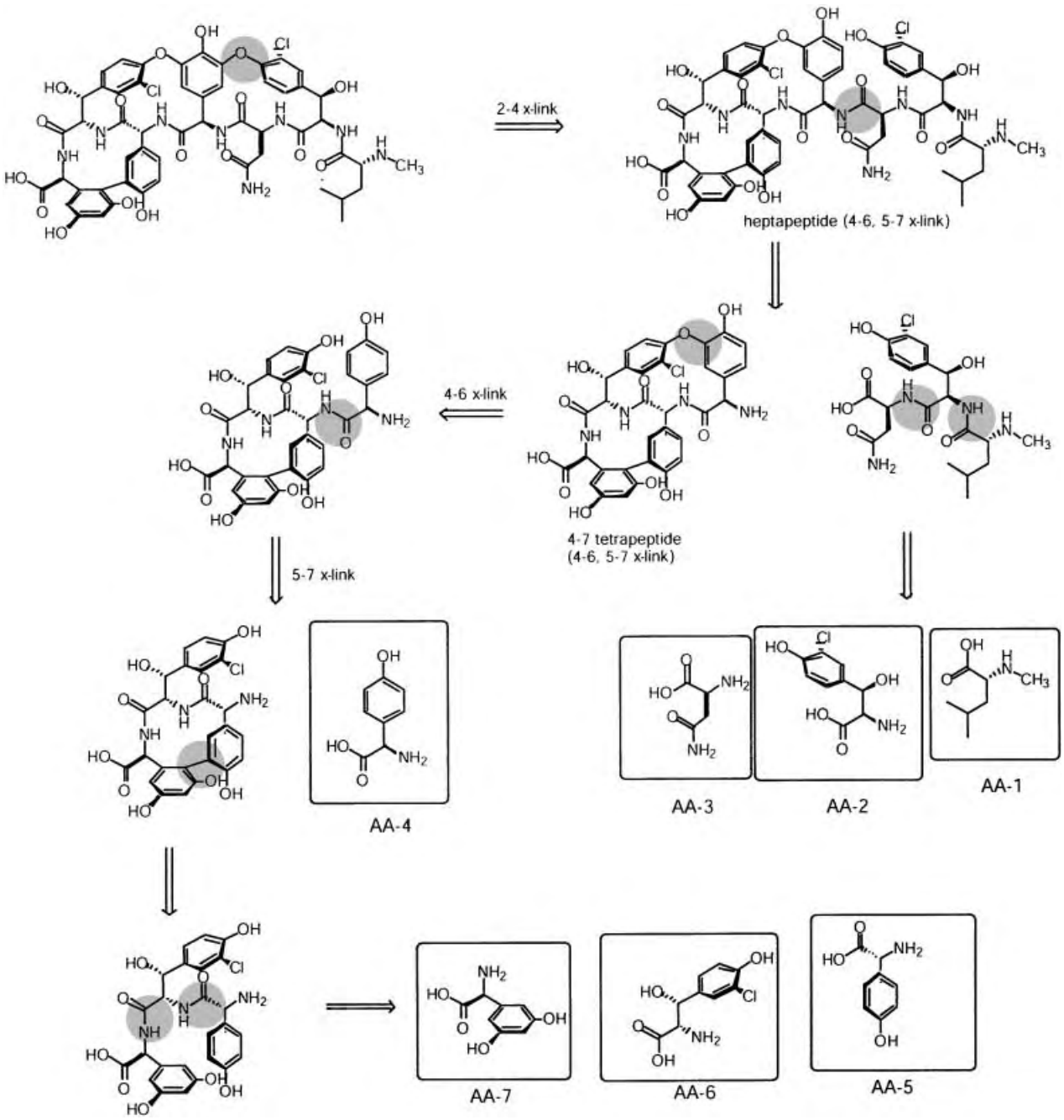

Scheme 6. Retrosynthetic analysis of the chemical synthesis of vancomycin used by Boger et al. and Evans et al.

While the sequences of teicoplanin class glycopeptide antibiotics have begun to emerge, it is highly likely that the above two examples reveal the common molecular logic for synthesis of dedicated amino acid and amino/deoxy sugar monomers;[30] this is, assembly of the nonribosomal peptide scaffold and the halogenation, oxidation, and glycosylation tailoring enzyme strategies for this large class of natural product antibiotics.

9. Enzymatic Formation of the Nonproteinogenic Amino Acid Monomers

9.1. 4-Hydroxyphenylglycine

Every member of the vancomycin and teicoplanin family of glycopeptide antibiotics contains the nonproteinogenic amino acid 4-hydroxyphenylglycine. Each oxidative cross-link in vancomycin and teicoplanin involves one Hpg group, which makes the presence of this amino acid essential to the overall structure of the antibiotic. An understanding of the biosyn-

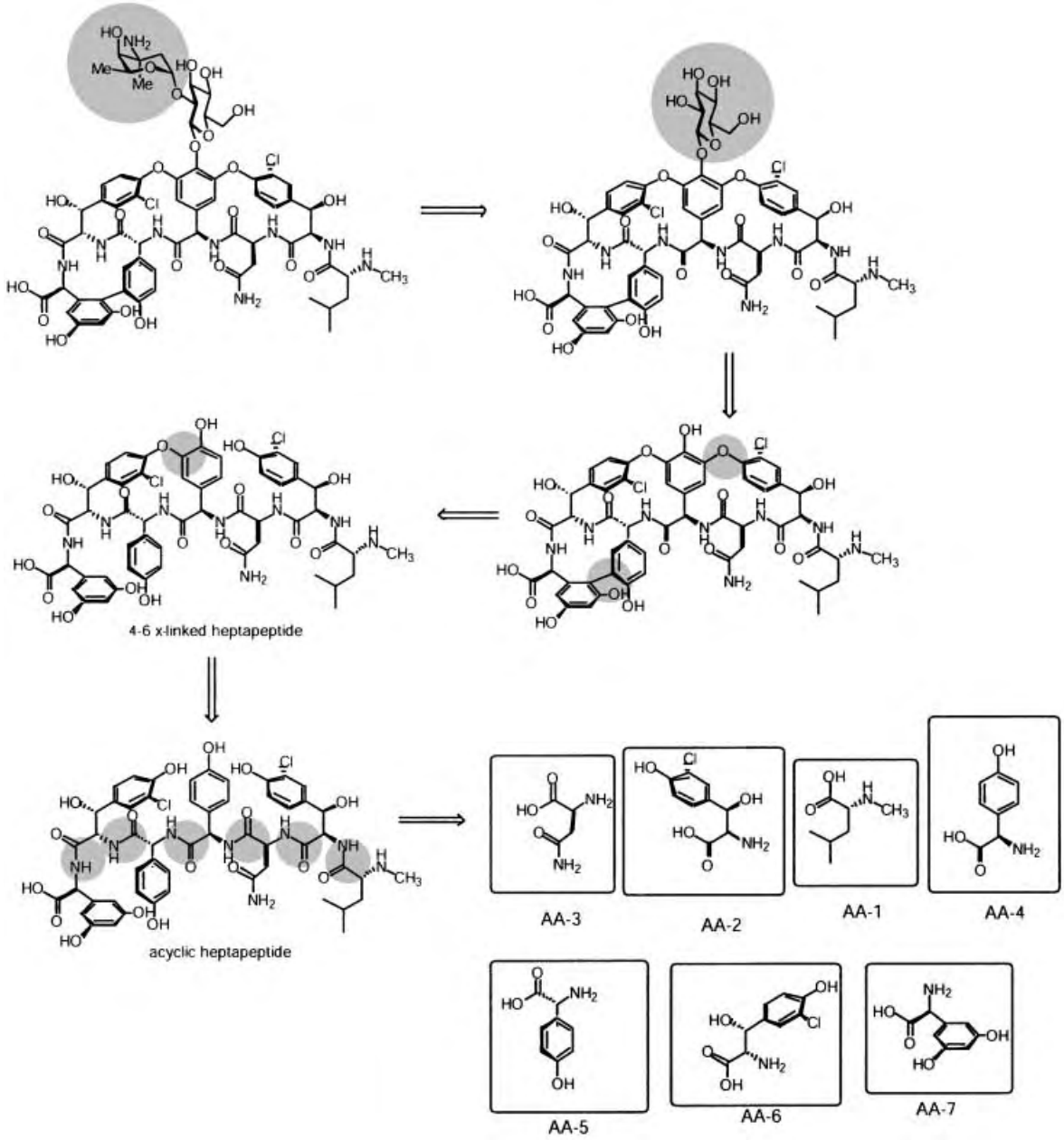

Scheme 7. Retrosynthetic analysis of the biosynthesis of vancomycin.

thesis of this unusual amino acid is essential to understanding how the glycopeptides are assembled.

Early structural studies in vancomycin family members showed that all of the Hpg groups in the mature antibiotics were in the D configuration.[68] Feeding studies also showed that radiolabeled racemic Hpg may serve as monomers for incorporation into the final glycopeptide.[69–71] Feeding experiments with ^{13}C-labeled tyrosine demonstrated that the aromatic ring of Hpg was derived from the aromatic ring of tyrosine and the α-carbon atom of tyrosine forms the carboxylic acid carbon atom of Hpg (Scheme 8).[69,71–73] From these experiments, the linear conversion of tyrosine into 4-hydroxyphenylglycine through 4-hydroxybenxoyl formate was proposed with an unidentified number of steps (Scheme 9).

An examination of the chloroeremomycin gene cluster revealed four orfs that could participate in the biosynthesis of Hpg from prephenate. These orfs comprise homologues to prephenate dehydrogenase (orf 1), hydroxyphenylpyruvate dioxygenase (HppD; orf 21), mandelate oxidase (orf 22), and an aminotranferase (orf 17). These enzymes have been characterized and their predicted functions authenticated.[74,75]

The homologue of hydroxyphenylpyruvate dioxygenase (orf 21) has been assigned as 4-hydroxymandelate synthase (HmaS).[74,75] The enzyme converts 4-hydroxyphenylpyruvate

Table 4: Genes in the chloroeremomycin biosynthetic cluster.

Orf no.	Accession number	Metabolic pathway	Protein name	Predicted function	Cofactors or cosubstrates	Relative start codon	Relative stop codon	No. base pairs	No. amino acids	Transcript number	C[a]	P[b]	A[c]
1	CAA11792.1	Hpg	PD	prephenate dehydrogenase		1	1104	1104	367	1	+	–	–
2	CAA11793.1	transport protein	CepM	ABC transporter	ATP	1308	3260	1953	650	2	–	–	–
3	CAA11794.1	heptapeptide assembly	CepA	NRPS	CoA, ATP	3257	12733	9477	3158	2	+	+	–
4	CAA11795.1	heptapeptide assembly	CepB	NRPS	CoA, ATP	12908	25141	12234	4077	3	+	–	–
5	CAA11796.1	heptapeptide assembly	CepC	NRPS	CoA, ATP	25161	30743	5583	1860	4	+	+	–
6	CAA11799.1	unknown function	CepD			30740	30949	210	69	4	–	–	–
7	CAA11797.1	oxidative cross-linking	CepE	oxidation	NADPH	31044	32246	1203	400	5	+	+	–
8	CAA11798.1	oxidative cross-linking	CepF	oxidation	NADPH	32266	33486	1221	406	6	+	+	–
9	CAA11800.1 CAA11791.1	oxidative cross-linking	CepG	oxidation	NADPH	33525	34892	1368	455	7	+	+	–
10	CAA11780.1	halogenation	CepH	halogenation	NADPH	34954	36429	1476	491	8	+	+	–
11	CAA11774.1	glycosylation	GtfA	attach sugar		36426	37664	1239	412	8	+	+	+
12	CAA11775.1	glycosylation	GtfB	attach sugar		37699	38922	1224	407	9	+	+	+
13	CAA11776.1	glycosylation	GtfC	attach sugar		39002	40300	1299	432	10	+	+	+
14	CAA11777.1	TDP-epivancosamine	EvaC	methylation	SAM	40373	41599	1227	408	11	+	+	+
15	CAA11778.1	epimerization	CepI	epimerase	NADP	41601	42434	834	277	12	+	+	–
16	CAA11779.1	N-methylation	MtfA	methylation	SAM	42431	43309	879	292	12	+	+	+
17	CAA11790.1	Hpg	HpgT	aminotransferase	PLP	44594	43278	1317	438	13	+	+	+
18	CAA11784.1	β-hydroxytyrosine	CepJ	thioesterase		44659	45642	984	327	14	+	+	
19	CAA11773.1	β-hydroxytyrosine	CepK	NRPS	CoA, ATP	45639	47381	1743	580	14	+	+	–
20	CAA11772.1	β-hydroxytyrosine	CepL	hydroxylation	NADPH	47397	48590	1194	397	15	+	+	–
21	CAA11761.1	Hpg	HmaS	diooxygenation	Fe	48766	49908	1143	380	16	+	+	+
22	CAA11762.1	Hpg	Hmo	oxidase	FAD	49905	50978	1074	357	16	+	+	+
23	CAA11763.1	TDP-epivancosamine	EvaA	oxidase	FMN	50978	52393	1416	471	17	+	+	+
24	CAA11764.1	TDP-epivancosamine	EvaE	reductase	NADPH	52395	53372	978	325	18	+	+	+
25	CAA11782.1	TDP-epivancosamine	EvaB	aminotransferase	PLP	53369	54478	1110	369	18	+	+	+
26	CAA11781.1	TDP-epivancosamine	EvaD	epimerase		54475	55119	645	214	18	+	+	+
27	CAA11765.1	L-Dpg	DpgA	PKS Type III		55312	56430	1119	372	19	+	+	–
28	CAA11766.1	L-Dpg	DpgB	isomerase		56427	57230	804	267	19	+	–	–
29	CAA1178.5	L-Dpg	DpgC	thioesterase		57227	58525	1299	432	19	+	+	+
30	CAA11767.1	L-Dpg	DpgD	dehydration		58522	59325	804	267	19	+	+	+

[a] C = clone. [b] P = purified. [c] A = Analyzed. Hpg = 4-hydroxyphenylglycine; ATP = adenosinetriphosphate; NRPS = nonribosomal peptide synthetase; CoA = coenzyme A; NADP = nicotinamide adeninediphosphate (oxidized); NADPH = nicotinamide adeninediphosphate (reduced); SAM = S-adenosyl-L-methionine; PLP = pyridoxal 5′-phosphate; FAD = flavin-adenine-dinucleotide; FMN = flavin mononucleotide; L-Dpg = L-3,5-dihydroxyphenylglycine; PKS = polyketide synthetase.

Table 5: Genes in the partial balhimycin biosynthetic cluster.

Orf no.	Cep homologue (orf no.)	Metabolic pathway	Protein name	Predicted function	Cofactors or cosubstrates	Relative start codon	Relative stop codon	No. base pairs	No. amino acids	Transcript no.	C[a]	P[b]	A[c]
1		regulation	ComG			1	1047	1047	348	1	–	–	–
2	2	transport	ComI	ABC transporter	ATP	1472	3598	2127	708	2	–	–	–
3	3	acylhexapeptide assembly	ComA	NRPS	CoA, ATP	3645	9995	6351	2116	3	+	+	–
4	3	acylhexapeptide assembly	ComB	NRPS	CoA, ATP	9992	14587	4596	1531	3	+	+	–
5	4	acylhexapeptide assembly	ComC	NRPS	CoA, ATP	14686	29382	14697	4898	4	–	–	–
6	5	acylhexapeptide assembly	ComD	NRPS	CoA, ATP	29420	35914	6495	2164	5	+	+	–
7	6	unknown function	ComE			35919	36140	222	73	6	–	–	–
8		regulation	ComF	ion antiporter		36179	37456	1278	425	7	–	–	–
9	10	halogenation	ComH	halogenation	NADPH	37485	38978	1494	497	8	+	+	–
10	8,9	oxidative cross-linking	ComJ	oxidation	NADPH	38996	40189	1194	397	9	+	+	–
11	7	oxidative cross-linking	ComK	oxidation	NADPH	40203	41474	1272	423	10	+	+	–
12		oxidative cross-linking	ComL	ferredoxin	NADPH	41519	41737	219	72	11	+	+	–
13	22	Hpg	Hmo	oxidation	FAD	42933	41815	1119	372	12	+	+	–
14	21	Hpg	HmaS	dioxyenation	Fe	43936	42920	1017	338	13	–	–	–
15	17	Hpg	HpgT	aminotransferase	PLP	44174	45520	1347	448	14	+	–	+
16	1	Hpg	PD	prephenate dehydrogenase		45517	46665	1149	382	15	–	–	–

[a] C = clone. [b] P = purified. [c] A = Analyzed.

Table 6: Genes in the complestatin biosynthetic cluster.

Orf no.	Cep homologue (orf no.)	Metabolic pathway	Protein name	Predicted function	Cofactors or cosubstrates	Relative start codon	Relative stop codon	No. base pairs	No. amino acids	Transcript no.	C[a]	P[b]	A[c]
1	7	oxidative cross-linking	OxyA	oxidation	NADPH	224	1399	1176	391	1	–	–	–
2	8	oxidative cross-linking	OxyB	oxidation	NADPH	1449	2645	1197	398	2	–	–	–
3	9	oxidative cross-linking	OxyC	oxidation	NADPH	2795	4015	1221	406	3	–	–	–
4	10	halogenation	BhaA	halogenation	NADPH	4076	5551	1476	491	4	–	–	–
5	11	glycosylation	BgftA	attach sugar		5634	6824	1191	396	5	–	–	–
6	12	glycosylation	BgtfB	attach sugar		6889	8118	1230	409	6	–	–	–
7	13	glycosylation	BgtfC	attach sugar		8266	9495	1230	409	7	–	–	–
8	14	TDP-ketovancosamine	OrfX′	methylation	SAM	9529	–			8	–	–	–

[a] C = clone. [b] P = purified. [c] A = Analyzed.

into *S*-4-hydroxymandelate (Scheme 10). A mechanism for this enzyme has been proposed based in its homology to HppD (Scheme 11). Both HmaS and its homologue HppD have been shown to be iron-dependent. The initial steps for both enzymes are equivalent and consists of a decarboxylation and oxidation to give 4-hydroxyphenyl acetate and an iron-4-oxo species. At this point the mechanism for HppD and HmaS diverges. In the HppD active site there is an epoxidation of the aromatic ring followed by a side-chain rearrangement to give the product homogentisate. In the HmaS mechanism a radical or cation species could be formed α to the acid group while forming the reactive iron–oxo species. Capture of the iron-3-oxo species occurs regiospecifically at the benzylic carbon to give the final product, *S*-4-hydroxymandelate.

The homologue of mandelate oxidase (orf 22) converts *S*-4-hydroxymandelate into 4-hydroxybenzolyformate and has been designated as 4-hydroxymandelate oxidase (Hmo). Hmo is a flavoenzyme containing a flavin mononucleotide (FMN) cofactor and only accepts substrates of the *S* configuration.[74]

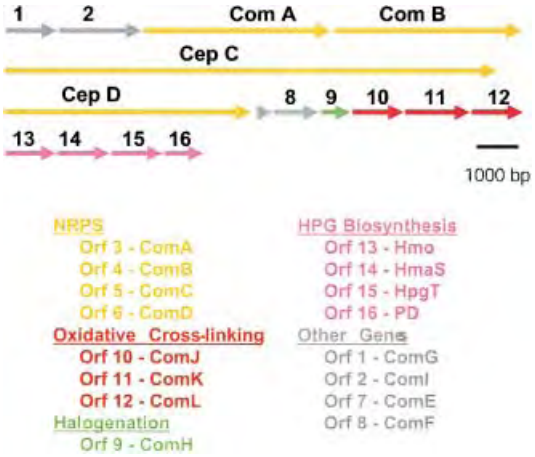

Figure 7. Genes in the complestatin biosynthetic cluster.

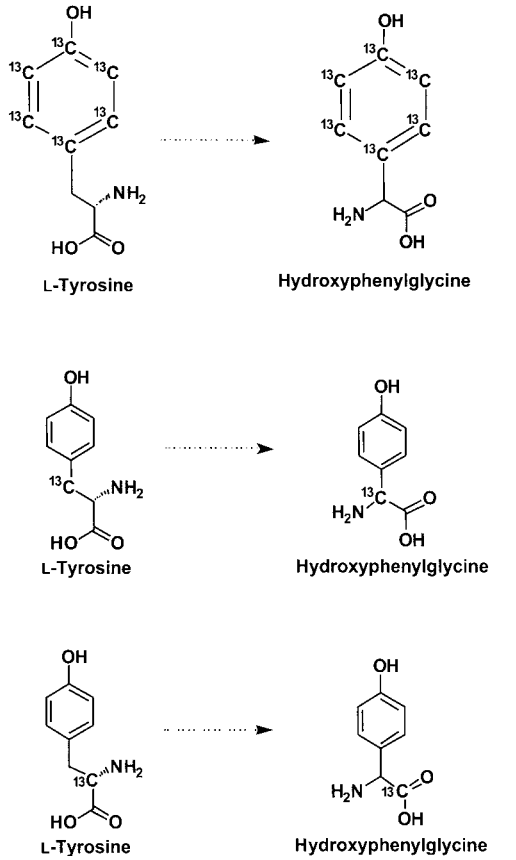

Scheme 8. Radiolabeling experiments in the biosynthesis of 4-hydroxyphenylglycine (Hpg).

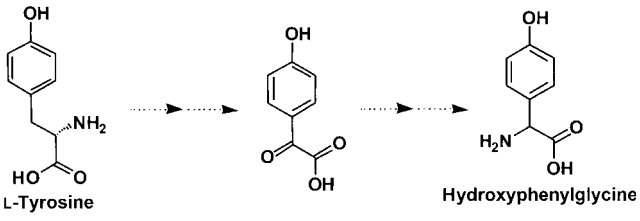

Scheme 9. Initial proposed biosynthesis of Hpg.

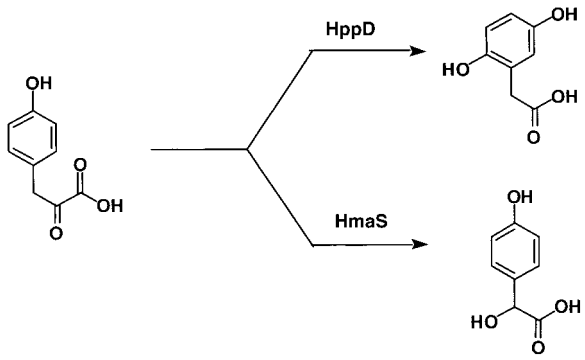

Scheme 10. Comparison of the enzymatic reactions of HppD and HmaS.

The aminotransferase homologue in the chloroeremomycin cluster (orf 17) is a pyridoxal phosphate dependent enzyme that converts 4-hydroxybenzolyformate into L-4-hydroxyphenylglycine, with L-tyrosine as the amino donor.[74] The aminotransferase had been designated L-hydroxyphenylglycine transaminase (HpgT). The use of L-tyrosine by HpgT allows for the conversion of prephenate and L-tyrosine into L-4-hydroxyphenylglycine by the cycle shown in Scheme 12. This cycle is catalytic with respect to prephenate and stoichiometric with respect to L-tyrosine.

The genes that encode for prephenate dehydrogenase (PD), HmaS, Hmo, and HpgT are present in both the calcium-dependent antibiotic (CDA) and complestatin gene clusters. Both of these compounds contain Hpg (Scheme 13). The HpgT enzyme from the complestatin gene cluster has been characterized and shown to utilize both L-Hpg and 3,5-dichloro-L-4-hydroxyphenylglycine in the reverse direction.[61] It is presumed that these four enzymes constitute the pathway by which hydroxyphenylglycine is synthesized for all of the glycopeptide antibiotics as well in other compounds (for example, ramoplanin, nocardicin) that contain Hpg.

9.2. 3,5-Dihydroxyphenylglycine

Vancomycin and teicoplanin contain the nonproteinogenic amino acid 3,5-dihydroxyphenylglycine at residue 7 and at residues 3 and 7, respectively. Initial feeding experiments showed that all of the carbon atoms in 3,5-dihydroxyphenylglycine in avoparcin, vancomycin, aradacin, and ristocetin are derived from acetate and led to the hypothesis that 3,5-dihydroxyphenylglycine was derived from a polyketide synthetase reaction.[69–71,76] However, the method by which the proposed tetraketide was converted into the final amino acid was unclear.

There are four orfs (orf 27, 28, 29, and 30) in the chloroeremomycin cluster that are hypothesized to be involved in the biosynthesis of 3,5-dihydroxyphenylglycine. The protein encoded by gene orf 27 is homologous to chalcone synthase, a member of the Type III polyketide synthase family, and Orfs 28–30 are members of the crotonase superfamily. The mechanism for chalcone synthase, an

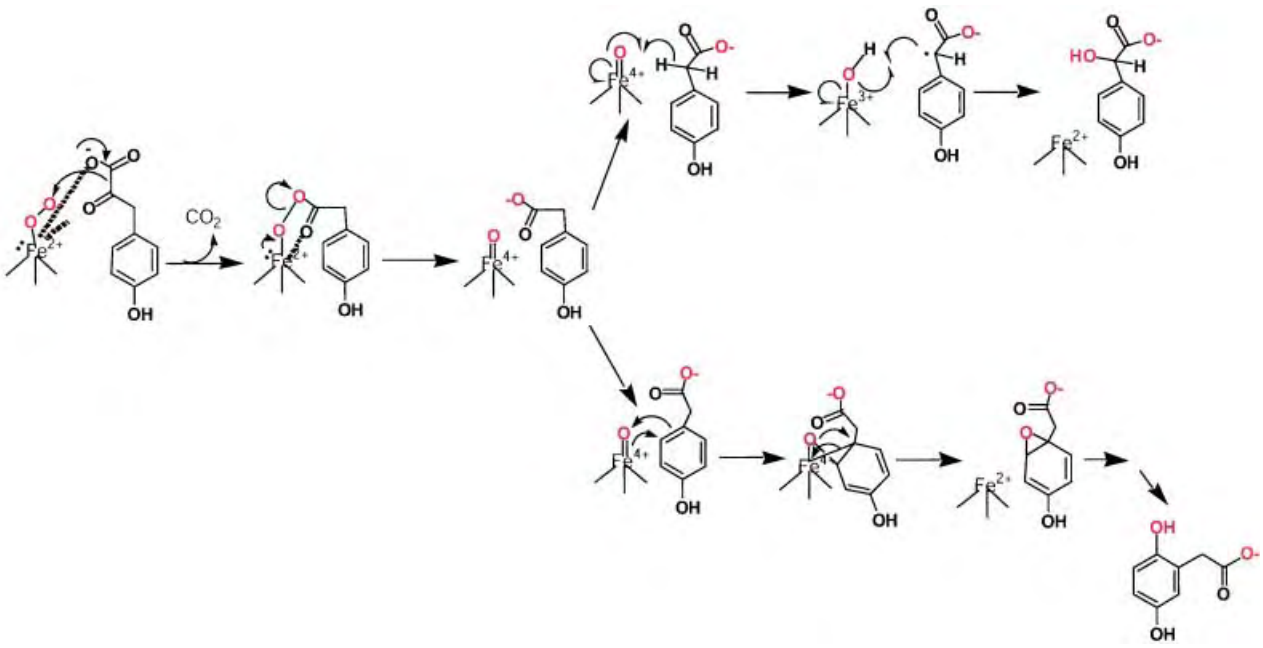

Scheme 11. Comparison of the enzymatic mechanisms of HppD and HmaS.

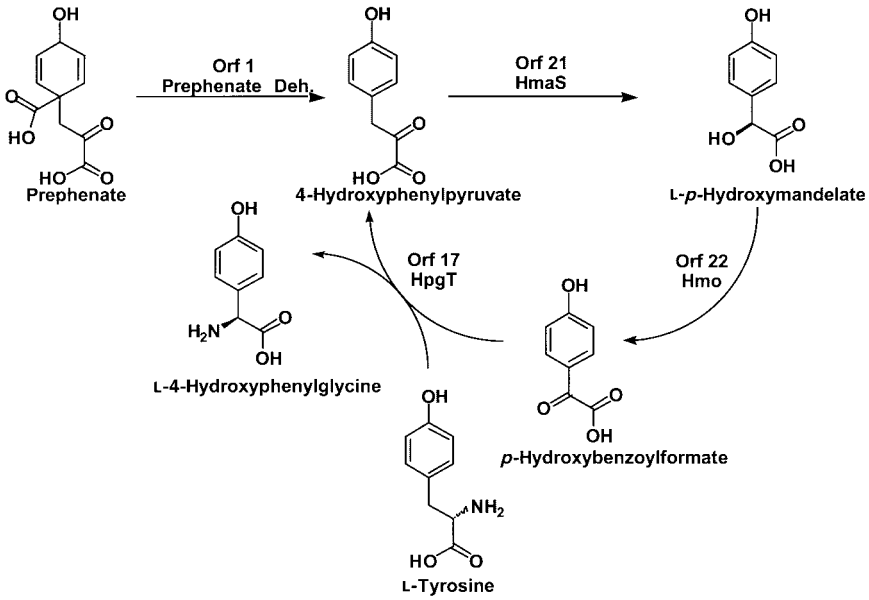

Scheme 12. Biosynthesis of L-Hpg.

Expression of DpgA–D in *E. coli* has allowed purification and initial investigation of the mechanism.[79] Both DpgB and DpgD show enoyl CoA hydratase activity and are likely to function physiologically in the dehydratase direction. When DpgB and D are added to incubations containing DpgA and malonyl CoA, the basal rate of formation of 3,5-dihydroxyphenylacetyl CoA is accelerated more than 30 fold. DpgC is sufficient to convert this intermediate acyl CoA into 3,5-dihydroxyphenylglyoxalate, which is then transaminated by the HpgT enzyme (see Section 9.1) to produce the 3,5-dihydroxyphenylglycine.[78,79] The DpgC reaction involves an O_2-dependent four-electron oxidation of the α-CH_2 group of the phenylacetyl CoA skeleton to the C=O group of phenylglyoxalyl CoA and subsequent thioester hydrolysis to yield the phenylglyoxalate product.[79]

enzyme in plant flavonoid production, serves as precedent for Orf 27. Orfs 28–30 are members of the crotonase superfamily, one of the most diverse enzyme superfamilies, which catalyzes over 15 different reactions.[77] These reactions can consist of hydrations/dehydrations, isomerizations, carbon-bond forming/breaking reactions, and thioesterifications.

The proposal for the biosynthesis of 3,5-dihydroxyphenylglycine is shown in Scheme 14. DpgA (Orf 27) converts four malonyl CoA units into the linear polyketide as well as directing decarboxylation and regiospecific cyclization.[78]

9.3. β-Hydroxytyrosine

Residues 2 and 6 in vancomycin and teicoplanin are β-hydroxytyrosine groups. The 2*R*,3*R*-3-OH diastereomer is found at position 2 while the 2*S*,3*R*-3-OH isomer is found at residue 6. As will be noted in Section 10, the CepA subunit of the nonribosomal peptide synthetase (NRPS) assembly line contains a predicted epimerase (E) domain in module 2, which suggests that a 2*S*,3*R*-3-OH Tyr-S-T_2 acyl enzyme intermediate is epimerized before chain elongation (T = thio-

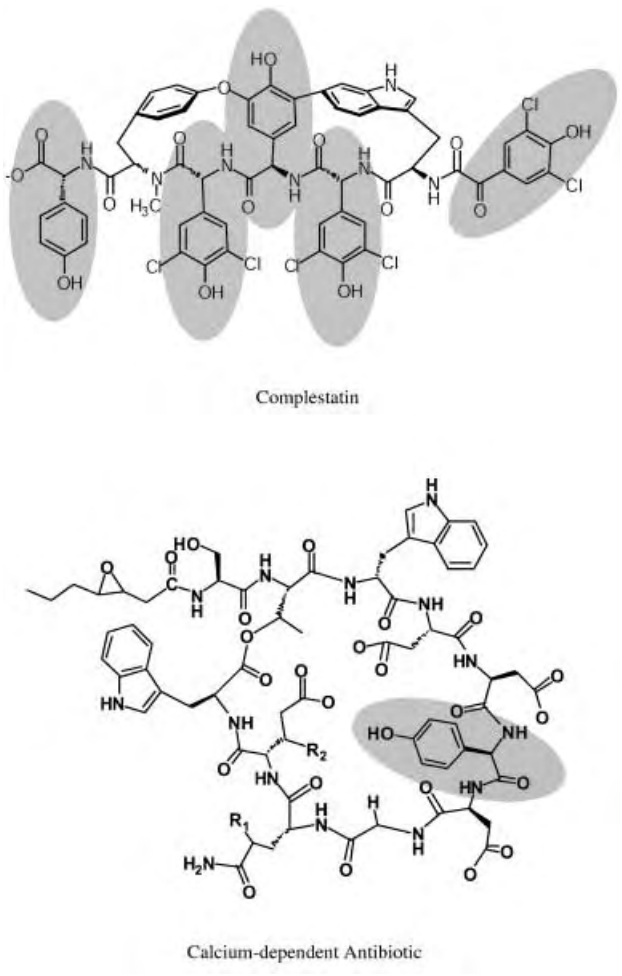

Scheme 13. Presence of Hpg in complestatin and a calcium-dependent antibiotic (chloroeremomycin).

lation domain). In turn this predicts that the A domains in both modules 2 and 6 will activate the L-β-OH-tyrosine (2*S*,3*R*) and focuses attention on how and when the β-oxygenation occurs.

Three orfs, Cep 18, 19, and 20, that are contiguous in the Cep biosynthetic cluster suggest there is a pathway from L-Tyr to L-β-OH-Tyr. Orf 19 is a freestanding adenylation-thiolation (A-T) di-domain subunit, predicted to activate L-Tyr as Tyr-AMP and then install it as the covalent thioester intermediate of the L-Tyr-S-T domain (Scheme 15). Orf 20 is

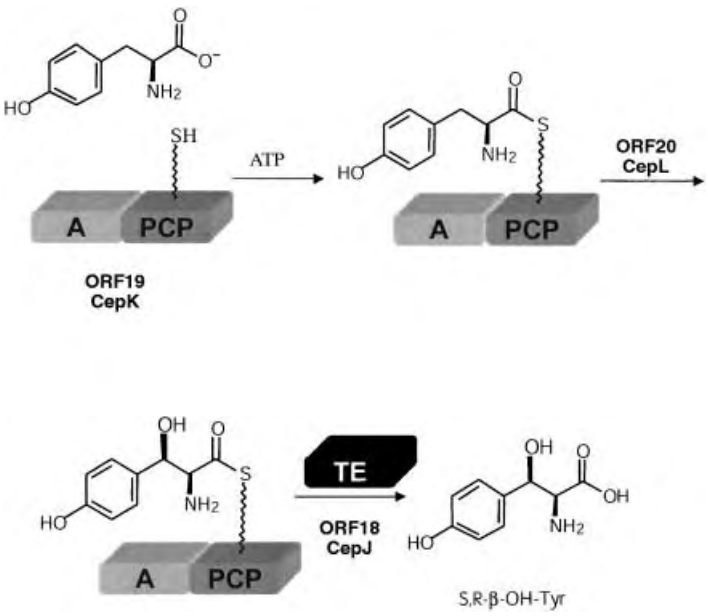

Scheme 15. Proposal for the biosynthesis of *S*,*R*-β-hydroxy-L-tyrosine in chloroeremomycin.

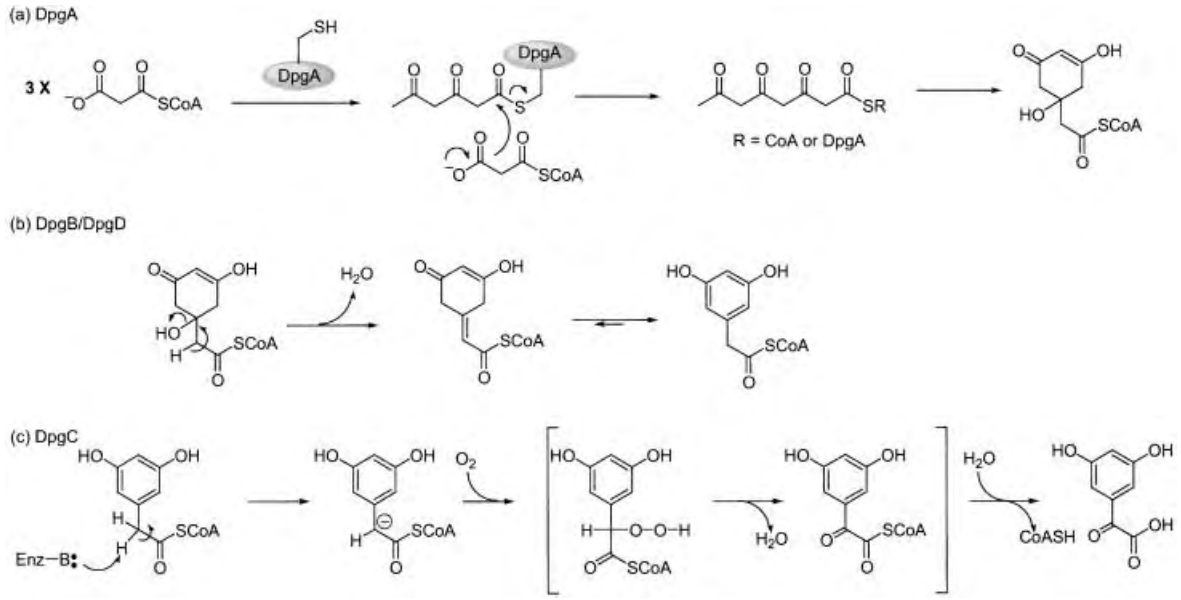

Scheme 14. Proposal for the biosynthesis of L-3,5-dihydroxyphenylglycine (L-Dpg).

predicted by informatic analysis to be a hemeprotein, and that has been validated by expression and purification from *E. coli* (Hubbard and Walsh, unpublished results). Orf 20 is the likely β-hydroxylase, which acts on the tyrosyl thioester of Orf 19 to yield the tethered β-OH-Tyr-S-Orf19 product. Orf 20 is predicted to have thioesterase activity and release the free β-OH-Tyr for use by the CepA and CepB subunits in heptapeptide assembly.

Support for this assignment of Cep 18–20 function is the recent demonstration that two homologues of Orf 19 and 20, NovH and NovI in the novobiocin biosynthetic cluster,[80,81] indeed carry out the first two steps shown in Scheme 16 to generate the 2*S*-3*R*-3-OH-Tyr-S-NovI covalent intermediate on the way to formation of the aminocoumarin ring.[81] There are also three Orfs, NikP1, NikQ, and NikP2, that are homologous to Cep 18–20 in the biosynthetic cluster for the antifungal compound nikkomycin Z[82,83] (Scheme 17). These three nikkomycin proteins have been purified by heterologous expression in *E. coli* and proven to act as predicted above. NikP1 makes a covalent His-S-enzyme on its T domain, the hemeprotein hydroxylase NikQ converts it into β-OH-His-S-NikP1, and NikP2 is a thioesterase generating the free β-hydroxyhistidine.[83]

Thus, Cep 18–20 are a three-enzyme cassette for sequestering some of the L-Tyr pool, regio- and stereospecifically hydroxylating it with O_2, and then releasing the free L-β-OH-Tyr for use by the NRPS assembly line.

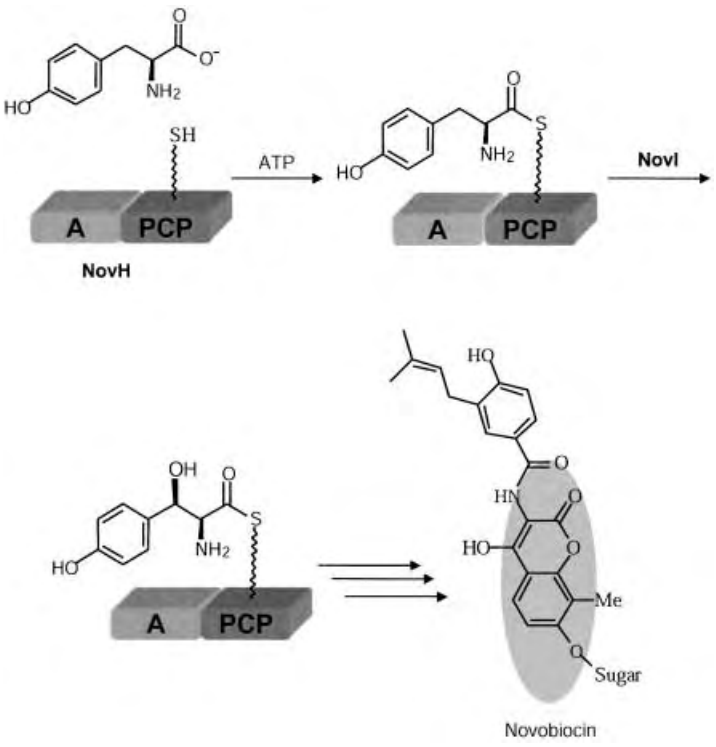

Scheme 16. Biosynthesis of *S,R*-β-hydroxy-L-tyrosine in novobiocin.

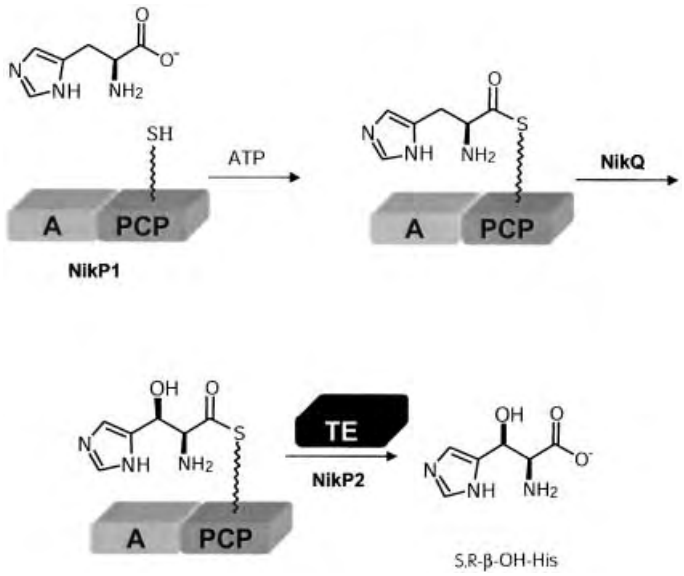

Scheme 17. Biosynthesis of *S,R*-β-hydroxy-L-histidine in nikkomycin X.

9.4. Chlorination of β-Hydroxytyrosines

Each of the two β-hydroxytyrosines at residues 2 and 6 in vancomycin and teicoplanin are chlorinated at position 3 of the aromatic ring, adjacent to the phenol OH group. The cross-linked heptapeptide scaffold of vancomycin is a single atropisomer at both the 2–4 and 4–6 aryl ether linkages. Little is known about the mechanism or timing of the biosynthetic chlorination in this pathway or in the complestatin biosynthesis where 3,5-dichloro-4-hydroxyphenylglycine groups are present in the final cross-linked antibiotic. Both the Cep cluster (Orf 10 or CepH) and the Com cluster (Orf 9, or ComH) have proteins thought to be halogenases, by homology to other non-heme halogenases,[84–86] and most convincingly to a homologue in chlortetracycline biosynthesis.[87] Purified CepH and ComH are yellow, because of a stoichiometric content of bound flavin coenzyme; neither contains any detectable iron (M. Burkart and C. Walsh, unpublished results). If these indeed are catalytic components of an aromatic ring halogenase, then the mechanism advanced by van Pee and co-workers,[88] (Scheme 18) is plausible, with the flavoenzymes acting as epoxidases of the electron-rich phenolic rings of Tyr or Hpg side chains to yield, transiently, the epoxycyclohexadiene that could be opened by chloride ions and then dehydrated to the 3-chlorotyrosine.

Alternatively the $FADH_2$ form of Orf 10 (FAD = flavin-adenine-dinucleotide) could yield a flavin hydroperoxide and then a flavin hypochloride (Fl-OCl) species that could be a direct chlorinating agent. It is unclear when chlorination occurs, whether on the free amino acid (for example, L-β-OH-Tyr), the aminoacyl-S-T domain acyl enzymes in the NRPS assembly line (such as β-OH-Tyr-S-T_2), or at the stage when the linear heptapeptide chain has been assembled, but still on the assembly line, or after release. It is likely that aromatic chlorination precedes the aryl side chain cross-linking steps (discussed in Section 11) since mutants blocked during enzymatic cross-linking accumulate chlorinated linear heptapeptide.[62]

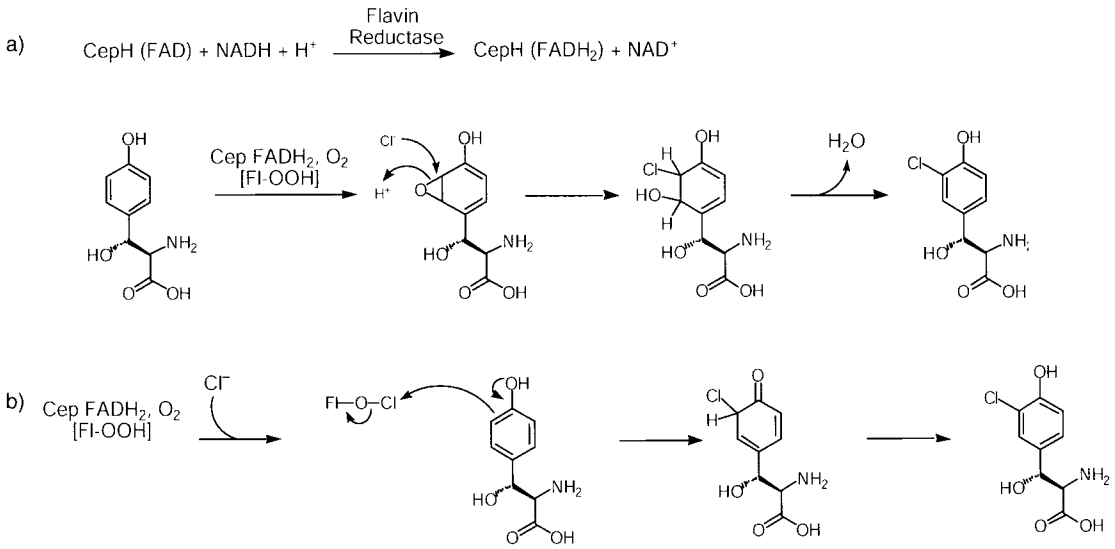

Scheme 18. Possible mechanisms of ComH. a) Direct epoxidation and ring opening with a nucleophilic chloride ion. b) Generation of an electrophilic chloride ion for electrophilic aromatic substitution.

10. The Nonribosomal Peptide Synthetase Assembly Line

Once the nonproteinogenic amino acid monomers needed for the nonribosomal heptapeptide are generated to enable vancomycin biosynthesis to proceed, the nonribosomal peptide synthetase (NRPS) assembly line comes into play. The Cep gene cluster encodes three contiguous, large open reading frames (orfs 3–5) that are the three subunits CepA, CepB, and CepC (Figure 8) that constitute the heptapeptide synthetase. At a presumed stoichiometry of 1:1:1, CepA (336 kDa), CepB (436 kDa), and CepC (200 kDa) comprise almost a megadalton (972 kDa) assembly line (Figure 8). The organizational logic of this NRPS assembly line appears to follow the predictions for thio-templated nonribosomal peptide synthetase logic.[89–91] There are seven amino acids to be activated; one by each of seven adenylation (A) domains, whose placement in the assembly line determines the sequence of the heptapeptide released at the end. All the A domains select a specific amino acid, activate it as the aminoacyl-AMP, and then transfer the aminoacyl moiety to a paired peptidyl carrier protein domain, also known as the thiolation (T) domain because of the post-translationally introduced phosphopantetheinyl arm that ends in a cysteamine thiol moiety which acts as the nucleophile on the aminoacyl-AMP to produce the aminoacyl-S-T domain (Scheme 19). Thus the seven paired A-T domains activate amino acids and install them as covalent aminoacyl-S-enzyme intermediates (Figure 9) In the CepA/CepB/CepC assembly line the seven modules are distributed 3/3/1, with Leu_1, β-OH-Tyr_2, and Asn3 to be activated on CepA, HPG_4 and HPG_5 installed at modules 4 and 5, and β-OH-Tyr_6 at module 6. CepC has the seventh module, which should load $DHPG_7$ as the thioester.

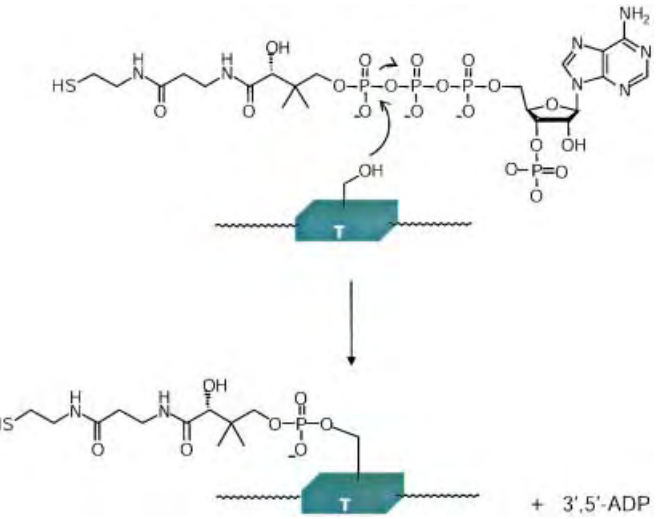

Scheme 19. Phosphopantethenylation of the thiol domain.

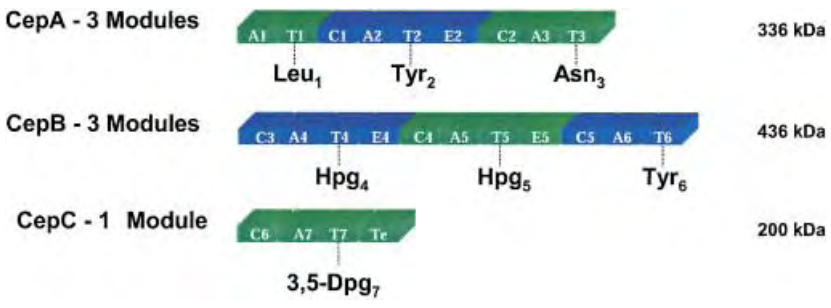

Figure 8. NRPS assembly line in chloroeremomycin.

Six peptide bonds have to be made to form a heptapeptide and there are six condensation (C) domains, two in CepA, three in CepB, and one in CepC. Each time a C domain makes a peptide bond, the growing chain is translocated directionally from the most upstream T domain to the next

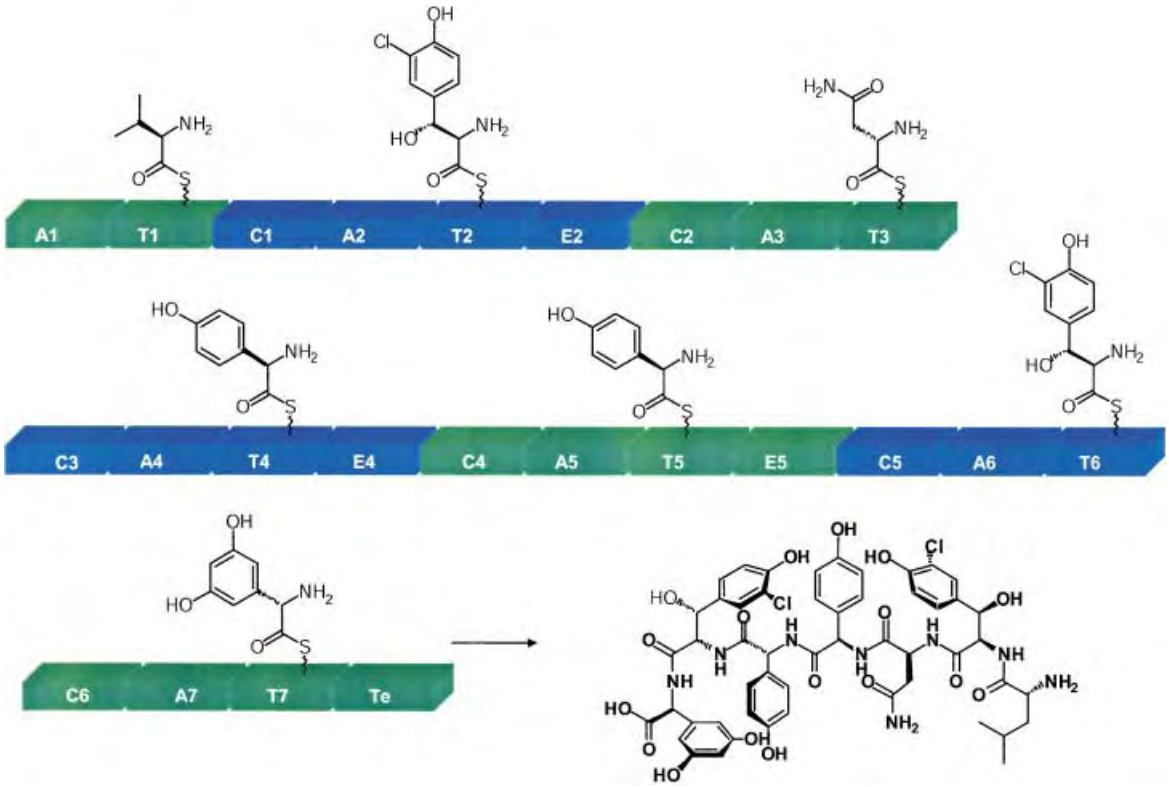

Figure 9. NRPS assembly line in chloroeremomycin with activated amino acids loaded on the thiol domains.

downstream T domain. For example, two chain elongation steps, catalyzed by the C domains in modules 2 and 3, respectively, will generate a tripeptidyl-S-T_3 at the C-terminus of CepA. The next peptide bond-forming step involves transfer of the peptidyl chain *trans* to Hpg-S-T_4 across the interface between the CepA and CepB subunits. Peptidyl chain growth on such NRPS assembly lines involves a cascade of elongating peptidyl-S-enzyme intermediates sequestered along the way from adventitious hydrolysis by water.

The vancomycin and teicoplanin heptapeptides have the configuration D-D-L-D-D-L-L. In general, only L-amino acids are available in substantial concentrations, even in bacterial cells, unless there are dedicated amino acid racemases, as for alanine at the start of peptidoglycan assembly.[92,93] In particular, the Hpg group produced by Orfs 21, 22, and 17 even yields the L isomer of this nonproteinogenic amino acid.[74] The common solution for the generation of D-amino acid residues in nonribosomal peptide antibiotics is the in situ epimerization on the NRPS assembly line by specialized epimerase (E) domains.[94,95] E domains are found in modules where an L-aminoacyl-S-T acyl enzyme domain is epimerized to a L-aminoacyl-S-T domain (Figure 9). This could occur on the free aminoacyl-S-T intermediates before C-domain-mediated peptide bond formation, or after reaction at the C domain, in which case the peptidyl-S-T domain must be epimerized before chain transfer to the next downstream module (Scheme 20). Inspection of the CepA/CepB/CepC assembly line reveals three predicted E domains in modules 2, 4, and 5 in the correct regiospecific placement to account for formation of D-β-OH-Tyr_2, D-Hpg_4, and D-Hpg_5 during chain elongation. However, there is no E domain associated with module 1,[60] which raises the question of how this D configuration is generated. Analysis of the loading of the CepA module 1 heterologously expressed in *E. coli* indicated both L-Leu and D-Leu were activated and installed as the Leu-S-T_1 acyl enzyme species.[96] If this route is operant in the producer *A. orientalis*, it mandates a Leu epimerase, which has not yet been identified.

Once the full-length D-D-L-D-D-L-L-heptapeptidyl chain has arrived at the last thiol way station (T_7), the covalent heptapeptidyl thioester needs to be disconnected for the enzymatic assembly line to proceed through subsequent catalytic cycles. Almost all NRPS assembly lines have a specialized thioesterase (TE) catalytic domain as their most C terminal domain; a TE is indeed the last of the 24 domains in the Cep synthetase, at the C terminus of CepC. All TE domains have serine residues in the active site that act as nucleophiles to transfer the acyl chain and make in this case the heptapeptidyl-O-Ser-TE acyl enzyme (Scheme 21). TE domains can have specific cosubstrates for deacylation, such that macrocyclization can occur with a nucleophilic group internal to the acyl chain, but here intermolecular hydrolysis is the physiologic fate of the acyl-O-TE intermediate, thus releasing the D-D-L-D-D-L-L- heptapeptide acid as the sole product of the assembly line.[97]

Two additional features of this particular NRPS assembly line for the vancomycin/chloroeremomycin heptapeptide scaffold are worth comment. First, is the unresolved question at present of the timing of both β-hydroxylation and ring chlorination of Tyr_2 and Tyr_6. Until modules 2 and 6 are

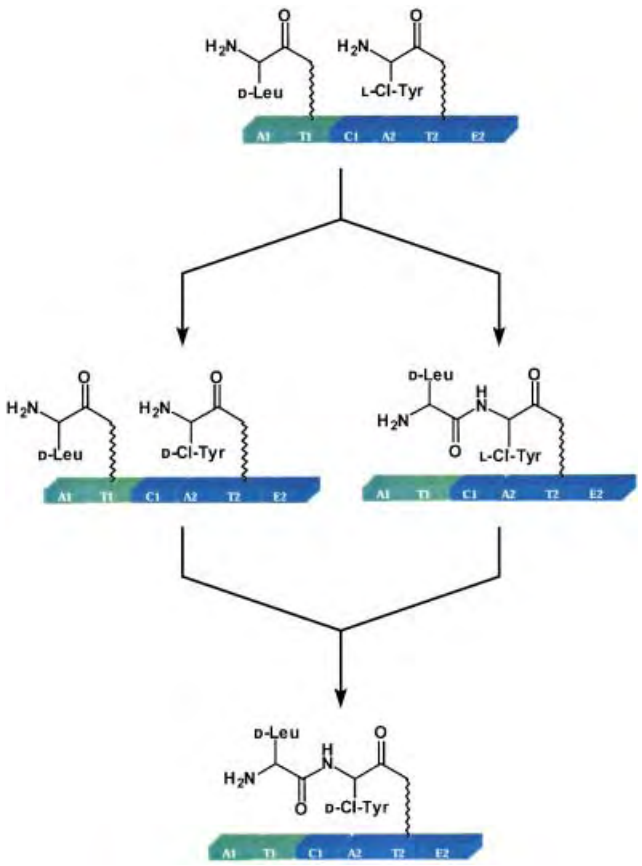

Scheme 20. Two potential routes showing the timing of epimerization. The top route shows epimerization prior to formation of the peptide bond. The bottom route shows formation of the peptide bond followed by epimerization.

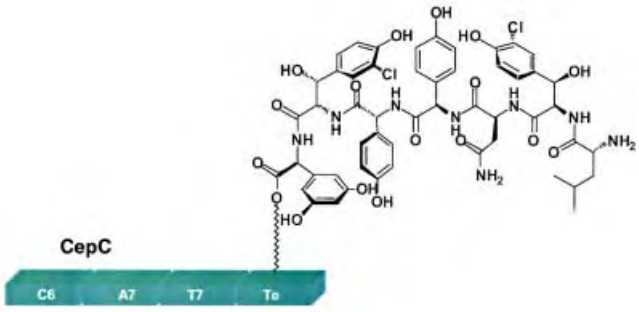

Scheme 21. Capture of the linear chloroeremomycin heptapeptide by formation of a thioester bond in the thiol domain of CepC prior to cleavage.

expressed (heterologously?) and their A domains assayed, it cannot be established whether Tyr is the preferred substrate or whether it is β-OH-Tyr or 3-chloro-Tyr. We commented on the probable hydroxylation of Tyr by Orfs 18, 19, 20 in Section 9.3, and suggested that 2*S*-3*R*-3-OH-Tyr is the substrate for the A_2 and A_6 domains.

Second is the issue of stereospecificity of the C domains as peptide synthetases, but this depends on the timing of the E_2, E_4, and E_5 domains. If the species epimerized are the free amino acyl S-T intermediates (2*S*-3*R*-3-OH-Tyr-S-T_2, 2*S*-HPG-T_4, and 2*S*-HPG-S-T_5) before formation of peptide bonds, then the C_1 peptide synthase domain is D/D specific for donor and acceptor, C_4 is L/D specific, and C_5 is D/D specific (Table 7). If the E domains in modules 2, 4, and 5 work after the C domain condensation steps then C_2 will be D/L specific, C_6 will be L/L specific, and C_5 will be D/L specific. For any combinatorial biosynthetic schemes where libraries of C domains might be made, it is essential to know their stereo preferences for both donor and acceptor. Whatever the timing of the epimerization domains, the C_2 and C_5 domains must be D/L specific, while C_6 is L/L specific. Indeed if C_1 and C_4 would be D/D specific these would be intriguing peptide synthase components in an enzyme library.

Table 7: Specificity of the condensation domains in chloroeremomycin.

Condensation module	Peptidyl donor specificity	Aminoacyl acceptor specificity
C_1	D	D
C_2	D	L
C_3	L	D
C_4	D	D
C_5	D	L
C_6	L	L

11. Post Assembly Line Tailoring of the Heptapeptide

11.1. Cross-Linking of Residues 2-4-6 and 5-7 in Vancomycin

Once the full-length, chlorinated acyclic heptapeptide has been produced by the CepA, CepB, and CepC assembly line it becomes a substrate for side-chain cross-linking and rigidification. It is not yet known whether one or more of the cross-links occurs at the heptapeptidyl-S-CepC acyl enzyme stage or whether chain release precedes recognition by the cross-linking heme proteins. Both the Cep cluster and the partially sequenced balhimycin cluster,[62] which make the identical heptapeptide scaffold, have three contiguous orfs, for example, Cep 7, Cep 8, and Cep 9, which are predicted to be heme proteins by homology to cytochrome P450 enzymes.[60,62] Likewise, sequencing of the A47934 cluster from *S. toyocaensis* reveals that four P450 Orfs are predicted for a teicoplanin-type of heptapeptide scaffold that has a fourth cross-link at residues 1 and 3.[145] Purification of Cep 7, Cep 8, and Cep 9 in *E. coli* expression systems yields fully loaded heme proteins (Hubbard and Walsh, unpublished results). Although in vitro reconstitution of the cross-linking of the aryl side chains at 2–4, 4–6, and 5–7 have not yet been reported, a knockout of the balhimycin orf 7 equivalent (*oxyA*, which corresponds to *cepE*) led to isolation of a partially cyclized aglycone, with the 4–6 cross-link intact (Scheme 22). This result suggests that the aryl ether between the β-OH-3-Cl-Tyr_6 and the 4-OH-$PheGly_4$ is constructed first and that the three hemeprotein oxidases may act regiospecifically and introduce particular cross-links in a given order. This conclusion was validated by subsequent observation that a knockout of oxyC from the balhimycin cluster (equivlent to *cepG*) gave a glycopeptide with two of the three cross-links intact (2–4 and 4–6), which indicates that the 5–7 C–C link is

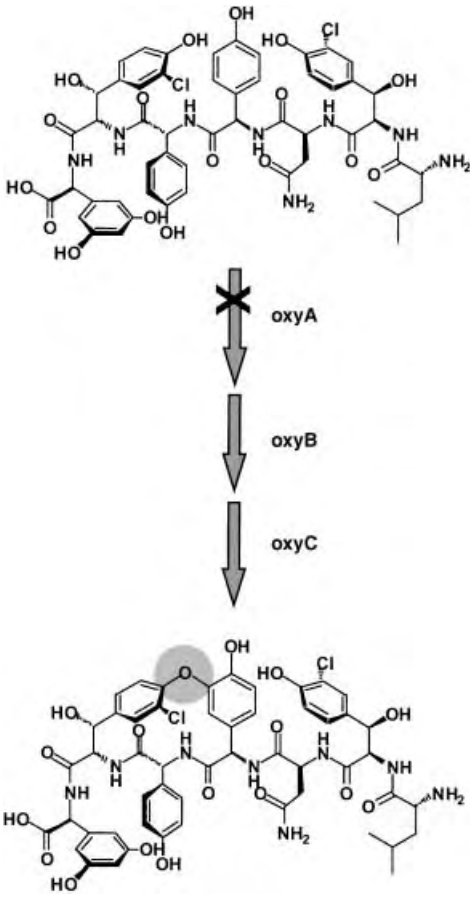

Scheme 22. Generation of a singly cross-linked heptapeptide by the selective knockout of *oxyA* in the balhimycin cluster.

put in last. This allows assignment of a specific order and chemoselectivity to the three heme proteins (Scheme 23). OxyB (CepF equivalent) is the 4–6 cross-linking oxidase, OxyA (CepE) equivalent) the 2–4 cross-linking catalyst, and OxyC (CepG equivalent) the 5–7 phenolic cross-linking catalyst. It is not yet clear what are the determinants of substrate recognition that impose this order to the three heme proteins. It remains to be determined in the teicopoplanin and A47934 cross-linking reactions if the 1–3 cross-link is put in first or last.

The heme cofactors of Cep 7-9 mean that the cross-linking mechanisms are likely to be radical-based, with one-electron oxidations of the electron-rich phenolic rings of the side chains of residues 2, 4, 6, 5, and 7. Scheme 24 shows possible routes for formation of an aryl ether (for example, the 4–6 link) and the direct aryl–aryl coupling (residues 5–7). The heme iron atom in the active site of each oxidase is presumed to be the conduit for passage of two electrons (one from each of the rings being cross-linked) to cosubstrate O_2 for each cross-link generated. The conformer-folding requirements of the linear heptapeptide chain to initiate folding in the active site of the first heme protein oxidase is not yet known, but the β-OH substituents on Tyr_2 and Tyr_6 may provide significant steric constraints essential for populating such conformers. The *N*-Me-Tyr_6 residue in the linear precursor to complestatin may exert a similar role in conformational bias that favors cyclization. The chlorine moieties on the Tyr_2 and Tyr_6 rings may also affect cyclization, for example, by tuning the redox potential to facilitate one-electron pathways in aryl ether formation.

Teicoplanin has one additional cross-link, which is enabled by the substitution of Leu_1 and Asn_3 in vancomycin by 4-OH-$phegly_1$ and 3,5-$(OH)_2$-$PheGly_3$ in the teicoplanin precursor. A fourth heme protein oxidase has indeed been found in the A47934 cluster.[145] There are two hemeproteins in the Com cluster for introducing the two cross-links into the complestatin scaffold (Table 6 and Figure 7).

11.2. N-Methylation of D*-Leu*$_1$

The N-methylation of D-Leu_1 is catalyzed by Orf 16 (MtfA), which has been purified and shown to have N-methyltransferase activity against the aglycone and linear forms (albeit with low specific activities).[63] When mutants in the balhimycin biosynthetic pathway accumulate linear or partially cross-linked precursors they are not yet N-methylated, which suggests this may be a late-stage event, perhaps occurring on the fully cross-linked peptide scaffold, just before glycosylation. The function of N-methylation is not well understood.

12. Glycosylation: The Thymidinediphospho Sugar Donors

The vancomycin and teicoplanin subfamilies are glycopeptides and the glycosylations occur at the last stages of antibiotic maturation, on the cross-linked peptide scaffolds. The placement and identity of the sugars decorating the aglycone scaffold are distinct. In the vancomycin/chloroeremomycin/balhimycin group, there is a glucosyl moiety attached to the phenolic oxygen atom derived from 4-OH-$PheGly_4$ and an L-aminodeoxyhexose of the vancosamine series is then attached in a 1,2-linkage. The 4-substituent of the vancosamine sugar varies, from 4-oxo in balhimycin X to 4-OH (axial) in vancomycin and 4-OH (equtorial) in chloro

eremomycin, which suggests there is a common pathway for biosynthesis (Scheme 25). There are also 3-hydroxy and 3-amino epimeric variants in other glycopeptide members.[98–101] A second L-epivancosamine residue is attached at the benzylic oxygen atom of β-OH-Tyr_6 in chloroeremomycin. There are no comparable amino deoxy sugars in the teicoplanin group, but rather more conventional sugars of primary metabolism, 2-*N*-acetyl-D-glucose (GlcNAc) and D-mannose (Scheme 1). The GlcNAc introduced at the comparable phenolic oxygen atom (4-OH-$PheGly_4$) of the teicoplanin aglycone has the short-chain acetyl replaced by a branched C10 fatty acyl group.

Deoxy sugars and/or amino deoxy sugars are common components of other natural product antibiotics, including the noviose sugar in coumarin inhibitors of DNA gyrase,[80] the macrolide antibiotics (for example, D-desosamine and L-mycarose), and sugars in enediyne and bleomycin classes of antitumor antibiotics (Scheme 26).[102,103] The mixture of

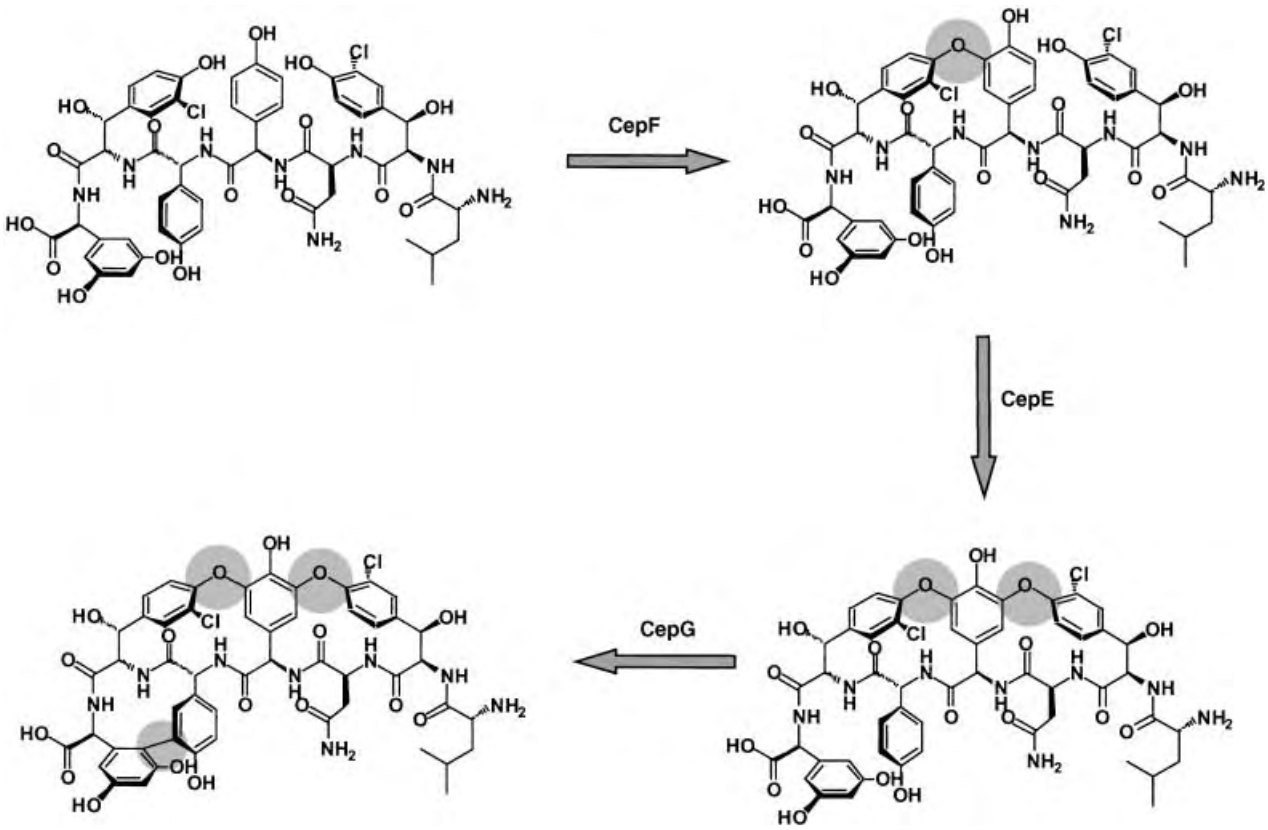

Scheme 23. Potential coupling route of the chloroeremomycin heptapeptide by CepE, CepF, and CepG.

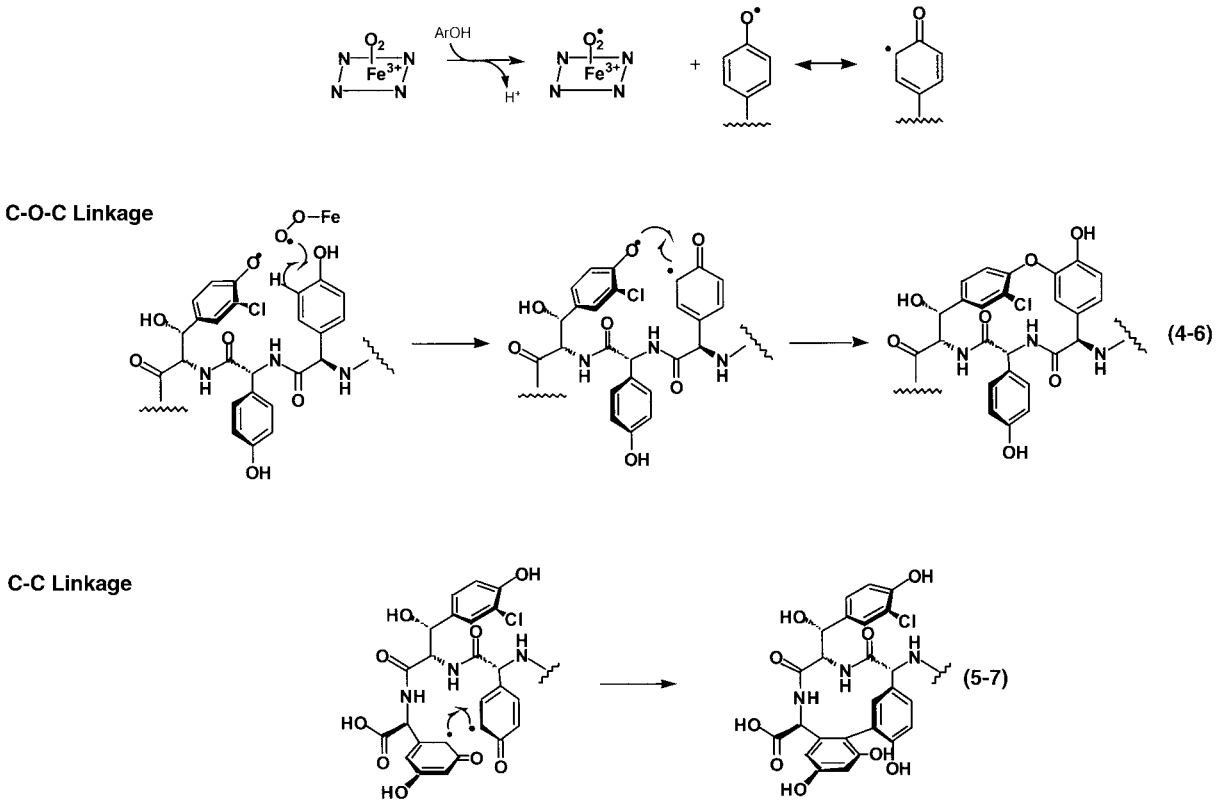

Scheme 24. Potential mechanisms of the heme-catalyzed oxidative couplings performed by CepE, CepF, and CepG.

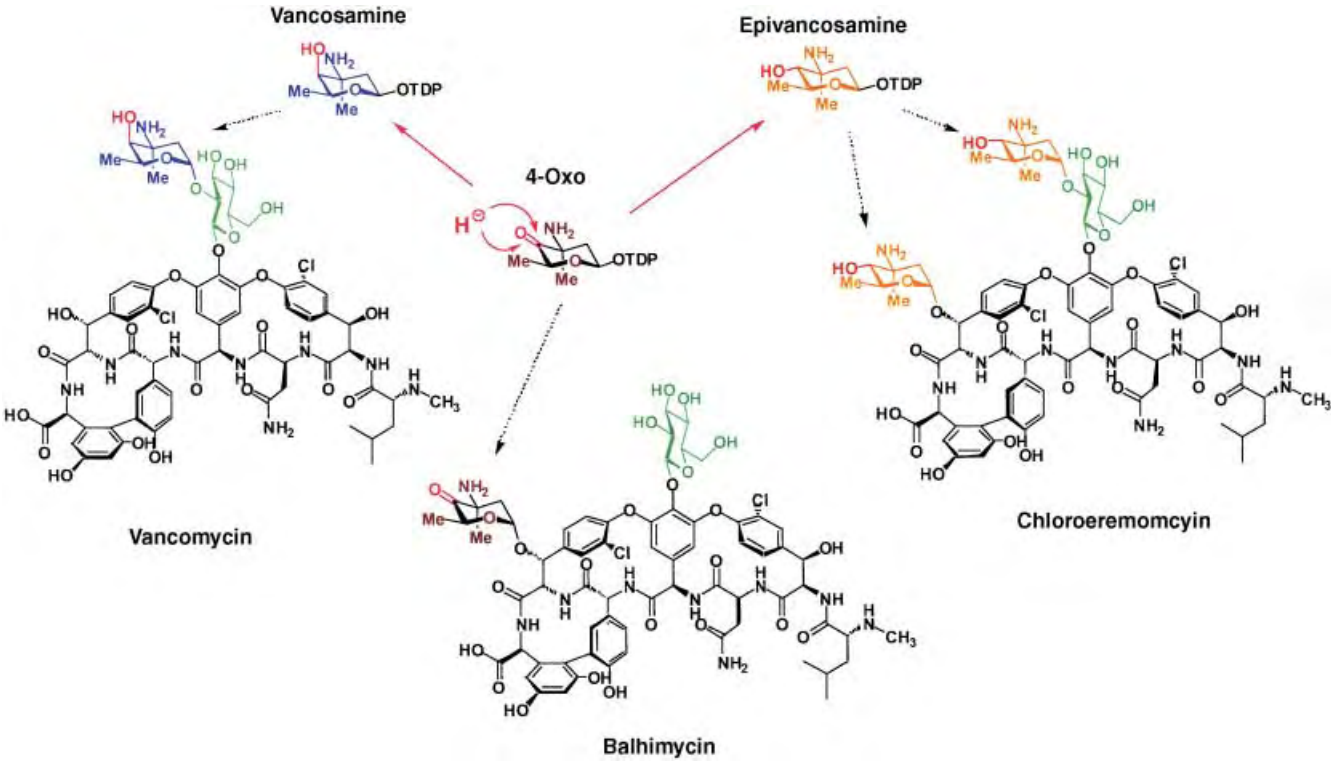

Scheme 25. Biosynthesis of vancosamine and epivancosamine from 4-oxovancosamine and incorporation into vancomycin, chloroeremomycin, and balhimycin.

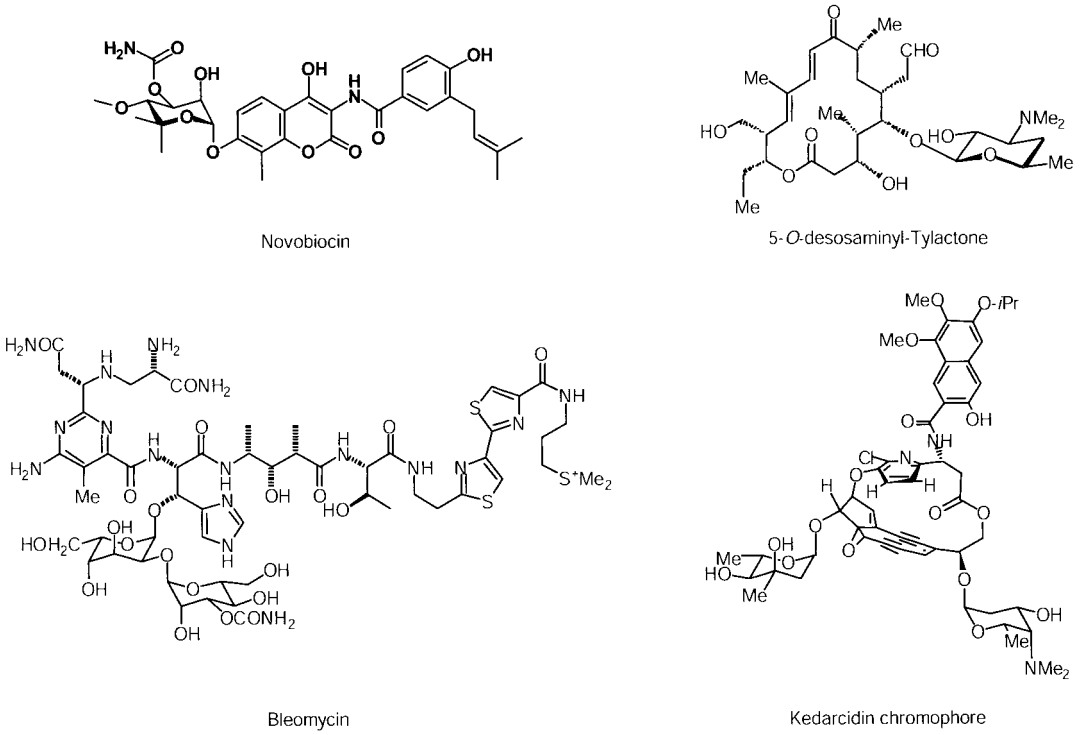

Scheme 26. Structural formulas of novobiocin, 5-*O*-desosaminyl-tylactone, bleomycin, and the kedararcidin chromophore.

deoxy centers, methyl groups, amino groups, and residual hydroxy substituents impart a mixed hydrophobic–hydrophilic character to the deoxy sugar components of antibiotics that may be crucial for recognition. Williams and co-workers have characterized back to back dimerization equilibria with a wide range of K_D values for the glycopeptides (Figure 10).[104,105] These values are dependent on and mediated by hydrogen-bonding interactions through the deoxy sugars, and the authors have argued that these correlate with antibiotic potency. The sugars certainly play a role in conferring water solubility to the hydrophobic aglycones, both in the glycopeptides and in the macrolide antibiotics. The aglycone in the erythromycin biosynthesis has negligible antibiotic activity. Addition of mycarose generates the set of interactions required for binding at the 50S ribosome (Scheme 27) and produces antibiotic activity. It is also likely that glycosylation may be part of the mechanism by which antibiotic-producing bacteria engage in self-protection as extra glycosylation occurs during oleandromycin biosynthesis, thus leading to inactive macrolide, which is activated only after export and extracellular glycosidase action.[106] Partially cyclized peptide intermediates accumulating in mutants of the balhimycin producer are adventitiously glycosylated, perhaps for self-protection and/or to facilitate export.[59]

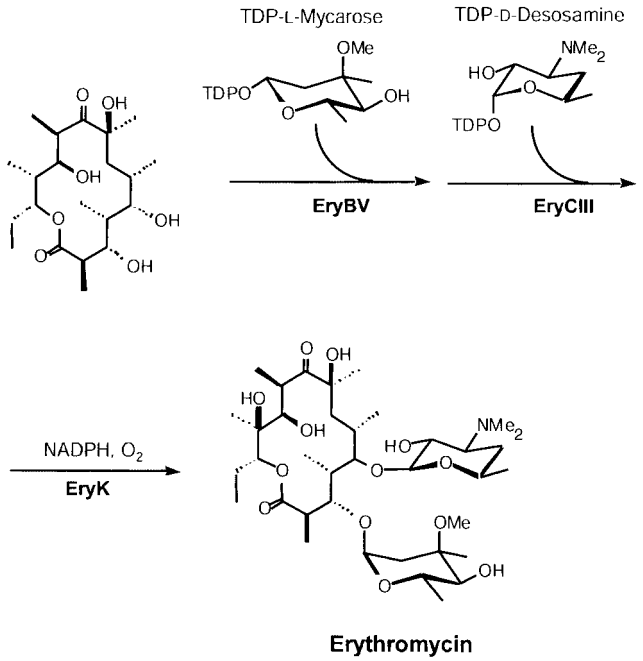

Scheme 27. Attachment of thymidinediphosphate sugars (TDP-sugars) in the biosynthesis of erythromycin.

The general strategy for the biosynthesis of deoxy and amino/deoxy sugar components of antibiotics is now well understood.[107–109] First, all the modified hexoses are built as nucleoside diphospho sugars (NDP sugars) with the pyrophosphate linkage of the NDP attached to C_1 of the hexose, thus activating it for attack by some cosubstrate nucleophile in subsequent glycosyl transferase catalysis. The NDP deoxy sugars are UDP or thymidinediphospho (TDP) sugars in the Streptomycete and Actinoplanes antibiotic producers. All the enzymatic manipulations to generate TDP-deoxy sugars dedicated to antibiotic maturation start from the readily available, activated sugar TDP-glucose. Scheme 28 lists the enzymatic transformations for conversion of TDP-glucose into TDP-L-β-epivancosamine, and indicates the adjustment of the redox state and/or substituent and configuration at each carbon site (C_2–C_6) to emphasize the exquisite tailoring of the TDP-sugar donor. The other general feature of the biosynthetic pathways to antibiotic sugars is that the encoding genes, for example, for the transformations of Scheme 28, are clustered with the other glycopeptide biosynthetic genes (Figure 6 and Table 4). In the Cep gene cluster the five open reading frames, orf 23, 25, 14, 26, and 24, act sequentially in that order to convert TDP-4-keto-6-deoxyglucose into TDP-L-epivancosamine (Scheme 29).[110,111] The clustering of the biosynthetic NDP-deoxy sugar genes in antibiotic operons enables coordinate regulation and just-in-time biosynthesis of these key monomer units during antibiotic production.

Scheme 29 delineates the specific enzymatic steps that have been elucidated for the five committed Orfs of Figure 6, by purification of each of the five enzymes, now known as EvaA, EvaB, EvaC, EvaD, and EvaE (Eva = 4-L-epivancosamine). The enzyme catalyzing the first step, that is, conversion of TDP-glucose to the 4-keto compound, followed

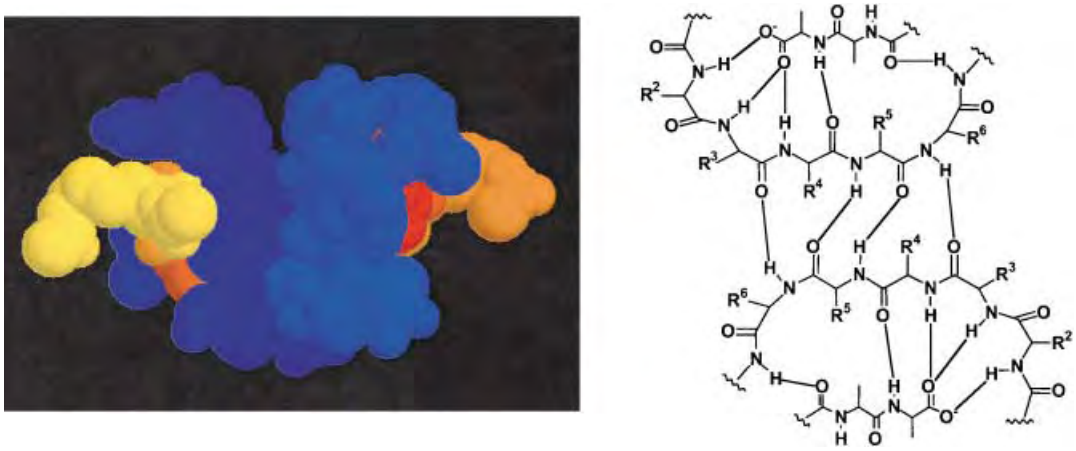

Figure 10. Back to back dimerization of vancomycin, shown as a space-filling model (bound to to $N_{2,6}$-bis-acyl-L-Lys-D-Ala-D-Ala and the hydrogen-bonding network).

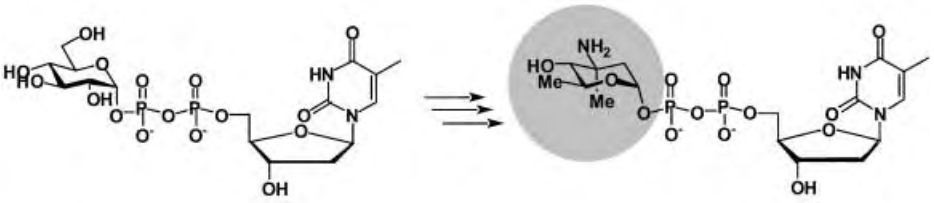

Position	Change	Type	Gene
Conformation	ring-flip	$^4C_1 \rightarrow {}^1C_4$	EvaD
C-2	deoxygenation	-OH → -H	EvaA
C-3	methylation	-H → -Me	EvaC
C-3	amination	-OH → NH_2	EvaB
C-4	epimerzation	S → R	EvaE
C-5	epimerization	R → S	
C-6	deoxygenation	-OH → H	RfbB

Scheme 28. Transformations in the biosynthesis of TDP-L-epivancosamine from TDP-glucose.

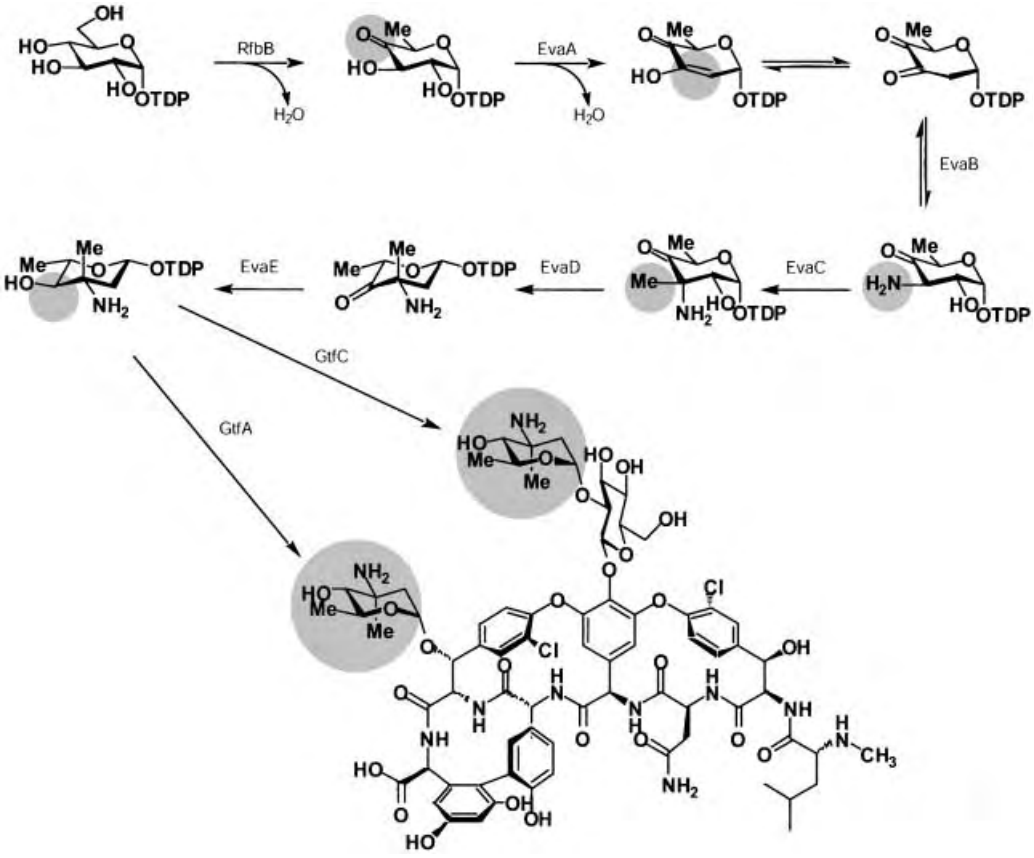

Scheme 29. Biosynthesis of TDP-L-epivancosamine and its attachment in the assembly of chloroeremomycin.

by dehydration to the 4-keto-6-ene and reduction of the conjugated olefin to the 6-methyl sugar to produce the TDP-4-keto-6-deoxyglucose substrate for EvaA, is not encoded in the Cep cluster. This is a well-known and well-studied enzymatic transformation. It is likely that it initiates several pathways and is a more general housekeeping enzyme for sugar metabolism in bacterial cells, and so is not part of the specialized, dedicated antibiotic gene cluster.[112,108]

EvaA acts to create the 3,4-diketo sugar as part of the strategy to deoxygenate C2, by abstraction of the C3-H, acidification by its adjacency to the 4-keto group, and elimination of the C2-OH group. The resulting 2,3-ene is the enol form of the 3,4-diketo-6-deoxy sugar nucleotide. The 3-keto group is reductively aminated by EvaB, a pyridoxal phosphate-dependent aminotransferase, which acts with regio- and stereoselectivity to introduce the amino group in an equatorial arrangement in position 3. EvaC is an *S*-adenosylmethionine-dependent C-methyl transferase, which introduces the methyl group with inversion of stereochemistry when attacked by the carbanion of the C3 amino sugar. Now, C3 has

Table 8: Some sugars found in the vancomycin family.

Sugar	Structure	Antibiotic
L-olivose		orienticin B
L-rhodinose	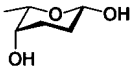	UK69542
L-acosamine	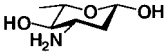	actinoidin A, MM47767, MM55256
L-actinosamine	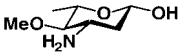	actinoidin, MM47767, MM55256
L-ristosamin	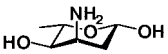	actaplanin, avoparcin, chloropolysporin A–C, galacardin, symnonicin A–C, helvecardin, ristocetin A, B
L-vancosamine	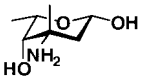	A42867, A51568 B, dechlorovancomycin, demethylvancomycin, M43, vancomycin CDP-I, vancomycin
3-epi-L-vancosamine	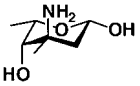	A35512 B
L-eremonsamine	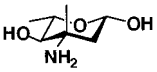	chloroorienticin, dechloroeremomycin, eremomycin, MM47761, MM49721, orenticin
4-oxovacosamine	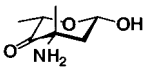	A83850, balhimycin, balhimycin V, dechlorobalhimycin V, deglucobalhimycin, demethylbalhimycin, methylbalhimycin

been both aminated and C-methylated and its configuration fixed. At this point EvaD, a member of the TDP-sugar 3- and 5-epimerase family, acts. Only C5 bears an acidic hydrogen atom so it can be enolized by EvaD and equilibrated to the L stereochemistry at C5, thus creating the TDP-L-β-4-oxovancosamine. This is presumed to be the 4-oxovancosamine donor in balhimycin biosynthesis (Scheme 2). Finally, EvaE catalyzes the stereospecific reduction of the 4-oxo group (by hydride addition from NADPH) to yield the equatorial 4-OH group of TDP-epivancosamine, thus completing the transformation of TDP-glucose (Scheme 29). In TDP-L-β-vancosamine biogenesis, only the last step will be distinct; a homologue of EvaE that introduces a hydride ion from the opposite face of the 4-keto group yields the 4-OH group in an axial orientation.

Comparable enzymes that process NDP sugars (C_2, C_3, and C_6 deoxygenation, C_3 amination and methylation, and epimerization of the C_3 and C_5 hydroxy configuration) are likely for other sugars found in the vancomycin family (Table 8), and are well-precedented in the TDP-D-desosamine, TDP-L-mycarose, and TDP-daunosamine biosynthetic pathways.[113–115]

13. Glycosylation: Peptide Antibiotic Glycosyl Transferases

13.1. GtfA, GftB, and GftC in Cep; GtfD and GftE in Van Clusters

As shown in Figure 6 and Table 4 there are three contiguous genes (encoding orfs 11–13) in the Cep gene cluster that have homologies to glycosyl transferases. After heterologous expression and purification to homogeneity the three proteins have been proved to be the glycosyl transferases GtfA, GtfB, and GtfC, respectively.[60,116] Scheme 30 shows the specificity of the three Cep Gtf proteins: GtfA uses TDP-L-β-epivancosamine as a glycosyl donor and the benzylic oxygen atom of the 2*S*-3*R*-3-OH-Tyr_6 as the nucleophilic substrate. GtfB is the glucosyl transferase, which attaches the activated C1 of TDP-glucose onto the attacking phenolic oxygen atom of the 4-OH-$Phegly_4$ residue in the cross-linked aglycone. GtfC, like GtfA, recognizes the TDP-L-β-epivancosamine, but now transfers it to a different site on the antibiotic, in this case the 2-OH group of the glucosyl residue to create the epivancosaminyl-1,2-glucosyl disaccharide moiety. It is known that pure GtfB works on the aglycone and GtfC on the monoglucosyl product (Scheme 31), but the timing of GtfA action,[116] first or last, is not yet resolved. By analogy, vancomycin has two sugars; there are two glycosyl

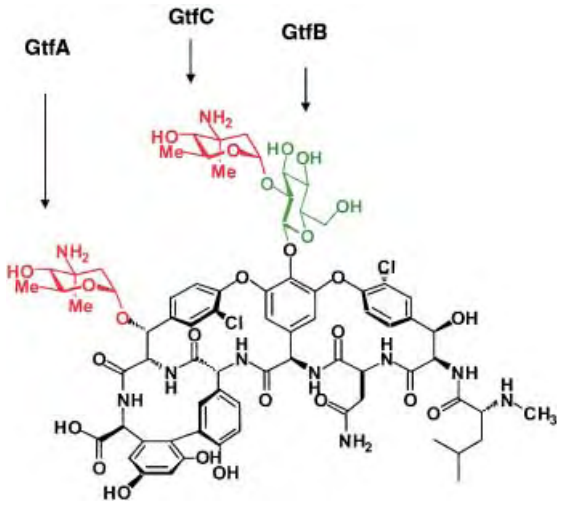

Scheme 30. Function of GtfA, GtfB, and GtfC.

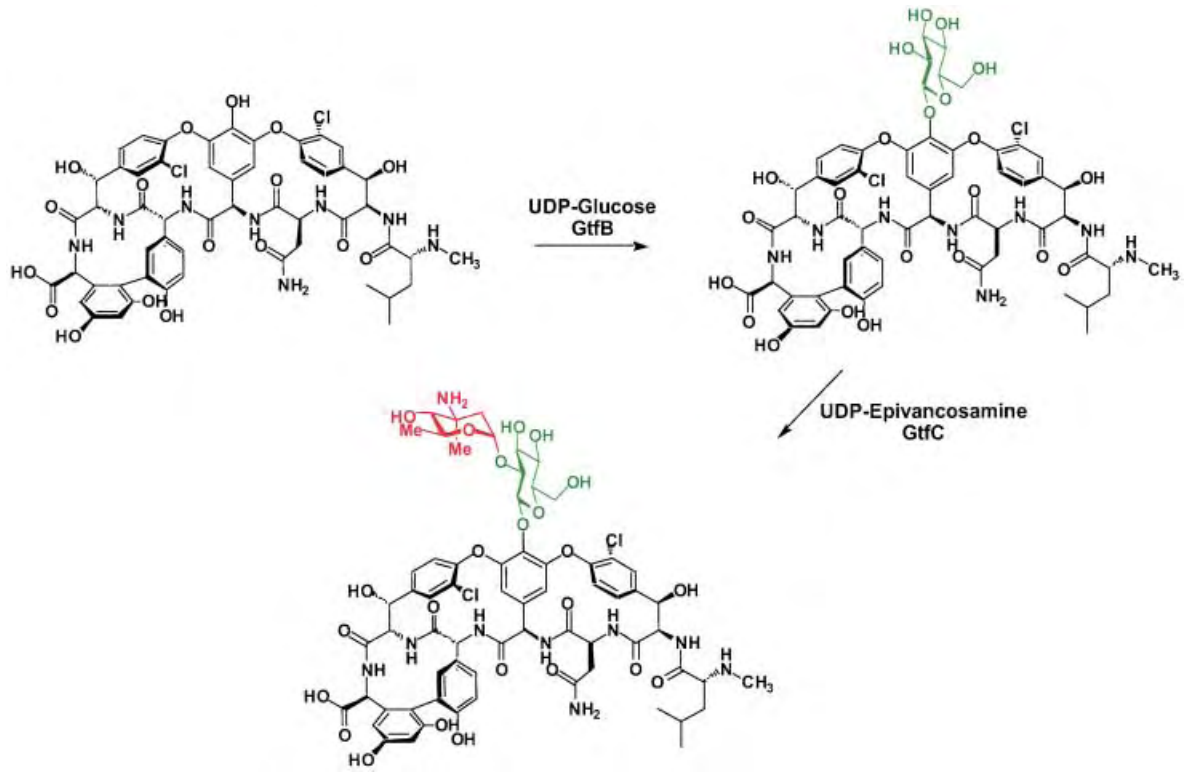

Scheme 31. Order of addition of uridinediphosphate glucose (UDP-glucose) and UDP-L-epivancosamine by GtfB and GtfC, respectively.

transferases, GtfD and GtfE, which are homologues of GtfB and GtfC, respectively, and they utilize TDP-glucose and TDP-L-β-vancosamine, respectively,[117,60] to create the comparable vancosaminyl-1,2-glucose disaccharide moiety at 4-OH-Phegly$_4$ of the cross-linked aglycone scaffold. The X-ray structure of GtfB has been determined (Figure 11): it reveals a two-lobed enzyme with only a single strand connecting the two domains. GtfB has architectural similarity to the MurG transglycosylase in peptidoglycan biosynthesis and to a phage DNA glucosyl transferase.[118–120] GtfA, GtfC, GtfD, GtfE, and other antibiotic glycosyl transferases show sequence homology to GtfB, thus making it likely they will all be part of the same architectural super family.[62]

The corresponding two or three Gtfs in the teicoplanin pathway (one enzyme could transfer a GlcNAc to both residue 4 and 6) have not yet been characterized. Since the TDP sugars are more prosaic, it will be of interest to see how homologous the teicoplanin Gtfs will be to the above Gtfs in the vancomycin subfamily. The timing of acylation of the glucosamine in teicoplanin by the 10-methylundecanoyl group is not known, nor has the acyl transferase been identified. A possible precedent is the two-step enzymatic conversion of GlcNAc residues during lipid A biosynthesis to long-chain 3-OH acyl derivatives, where a zinc-dependent deacetylase generates the free amino group, which is then reacylated by an enzyme using a 3-OH-myryistoyl-S-acyl carrier protein (CP) substrate.[121] In the teicoplanin case, a 10-methylundecanoyl-S-ACP could be an acyl thioester intermediate rerouted from normal fatty acid biosynthesis in the teicoplanin producer.

Figure 11. Crystal structure of GtfB.

The glycol transferases in clusters of other types of antibiotics have been assigned largely by homology and knockout or complementation studies. In the maturation of

the erythronolide aglycone the L-mycarosyl unit is added first to the C3-OH group by EryBV and then the D-desosamine by Ery CIII (Scheme 27). A third sugar is present at the C6-OH in the polyketide macrolide megalomycin.[122] Analogous Gtfs have been detected in, for example, the novobiocin, the bleomycin, and the daunomycin clusters.[80,103,123]

14. Approaches to Treatment of Vancomycin-Resistant Bacteria

14.1. Inhibitors of VanS, VanR, VanH, VanA, and VanX

With the molecular principle of vancomycin resistance in the VanA and VanB clinical phenotypes of VRE revealed, there is a pressing need for new drugs that work against VRE and an opportunity for rational design efforts to reverse the phenotype. One approach is to produce inhibitors to any of the five proteins, the two component regulatory pair VanS and VanR, and the three enzymes VanH, VanA, and VanX.[40,41] X-ray structures (Figure 12) of the VanA D-Ala-D-Ala ligase with a phosphanylphosphate analogue of the D-D-dipeptide substrate bound and of the VanX D-D-dipeptidase with a phosphinate inhibitor bound have been reported to aid ligand design.[124,125] While the phosphinate is a potent inhibitor of VanX and a substrate analogue of VanA (which generates the tightly bound phosphanylphosphate), bacterial cells are impermeable to the anionic phosphinate so there is no activity against intact bacteria. A mechanism-based inactivator of VanX has also been described that reveals a reactive group on cleavage of the peptide bond by the peptidase (Scheme 32).[126] No inhibitors of response regulators have yet been reported, but compounds described as inhibitors of other two-component sensor systems have been described.[127,128] However, it is likely those were acting as membrane perturbants and/or nonspecific surface agents that disrupt the transmembrane sensor. Given that the intracellular domain of VanS and other sensor proteins of bacterial two-component regulatory systems are histidine autokinases, it should be possible to build on the increasing number of protein kinase inhibitors that compete against ATP to find leads against this feature of VanS.[129]

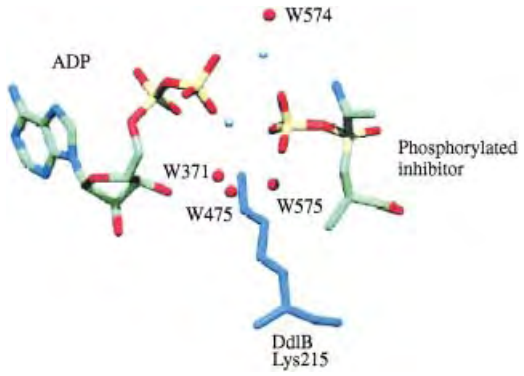

Figure 12. Crystal structure of VanA bound to a phosphinate inhibitor.

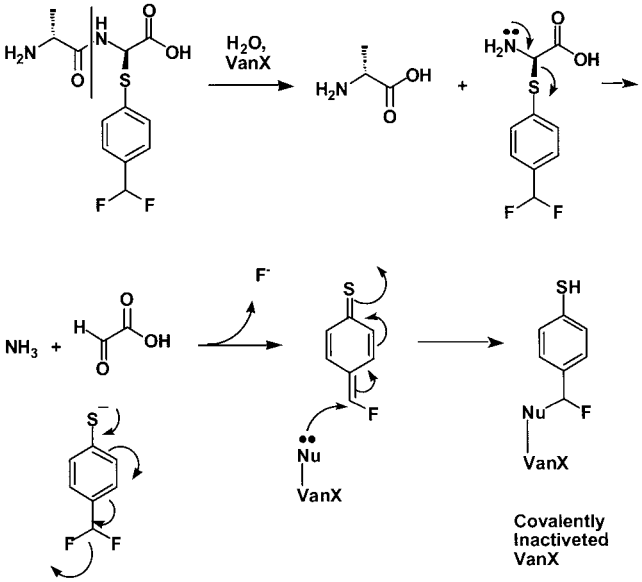

Scheme 32. Inactivation of VanX by a mechanistic-based inhibitor.

14.2. Antibiotics Active Against VRE

Two recently approved antibiotics have shown some efficacy against VRE during clinical development. The first is synercid, a combination of synergizing pristinamycins I and II (Scheme 33). This compound belongs to a class of antibiotics also known historically as virginiamycins and streptogramins. The pristinamycins are produced by *Streptomyces pristinaespiralis*, with pristinamycin I (trade name dalfoprustin) and pristinamycin II (trade name quinopristin) as semisynthetic variants modified to improve the water solubility. Pristinamycin II is a nonribosomally generated hexapeptide,

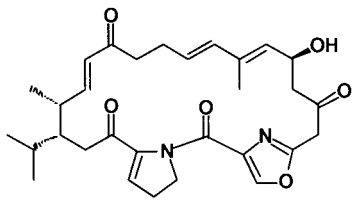

Pristinamycin I

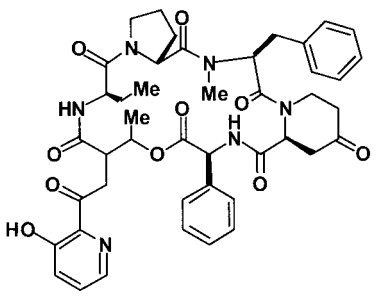

Pristinamycin II

Scheme 33. Structure of pristinamycin I and pristinamycin II.

while pristinamycin I is a hybrid of a polyketide synthase assembly line and three NRPS modules.[130–131] Both pristinamycin components act on the same site of the 50S ribosome subunit as erythromycin and block protein biosynthesis.[132]

The second antibiotic active against VRE is linezolid. Linezolid is the first example of a new class of synthetic antibacterial compounds, the oxazolidinones, that also act at the ribosome to block protein biosynthesis.[133]

14.3. Semisynthetic Glycopeptides Active Against VRE

When the clinical isolates of VRE strain began to appear, they were used to screen for new antibacterial agents that would be active against both sensitive and resistant strains of enterococci. Semisynthetic derivatives of vancomycins and chloroeremomycins with lipids attached to the amino group of the vancosamine or epivancosamine were active against VRE (Scheme 34). One representative compound, an *N*-chlorobiphenyl derivative of chloroeremomycin known as LY333328, recovered about 80 fold of the 1000 fold loss of activity against VRE and has proceeded into clinical trials.[134,135] This and related *N*-aryl and *N*-alkyl substituents are introduced by reductive alkylation of the 3-amino groups of vancosamine and epivancosamine. They are reminiscent of the *N*-acyl chain in teicoplanin and may act to preconcentrate the lipoglycopeptides at the outer surface of the cytoplasmic membrane in the vicinity of both the lipid II substrate and the transpeptidase and transglycosylase enzymes that catalyze the last stages of peptidoglucan assembly. Moving the lipophilic chlorobiphenyl group around on the disaccharyl tail of vancomycin-group antibiotics maintained the gain in activity towards VRE. For example, when a 6-aminoglucosyl analogue of the vancomycin disaccharide unit was constructed synthetically from the aglycone and N-arylated, this regioisomer had good VRE activity,[136] which suggests it is the lipid anchor rather than a specific structure on the lipodisaccharide that produces activity.

No enhanced affinity was observed when LY333328 and analogues are measured in binding assays against *N*-acyl-D-Ala-D-Lac, which suggests that the regain of activity in VRE may proceed at least in part by a distinct mechanism. This was further supported by retention of VRE activity in chlorobiphenyl analogues in which the binding site for *N*-acyl-D-Ala-D-Ala was destroyed by removal of *N*-methyl-D-Leu1.[136] Kahne and co-workers suggested membrane-localized transglycosylases (Figure 13) may be the targets for these impaired lipoglycopeptides.[136,137] If this proposal turns out to be generally valid it offers new targets and new structure–activity relationships to reverse clinical VRE phenotypes in life-threatening infections.

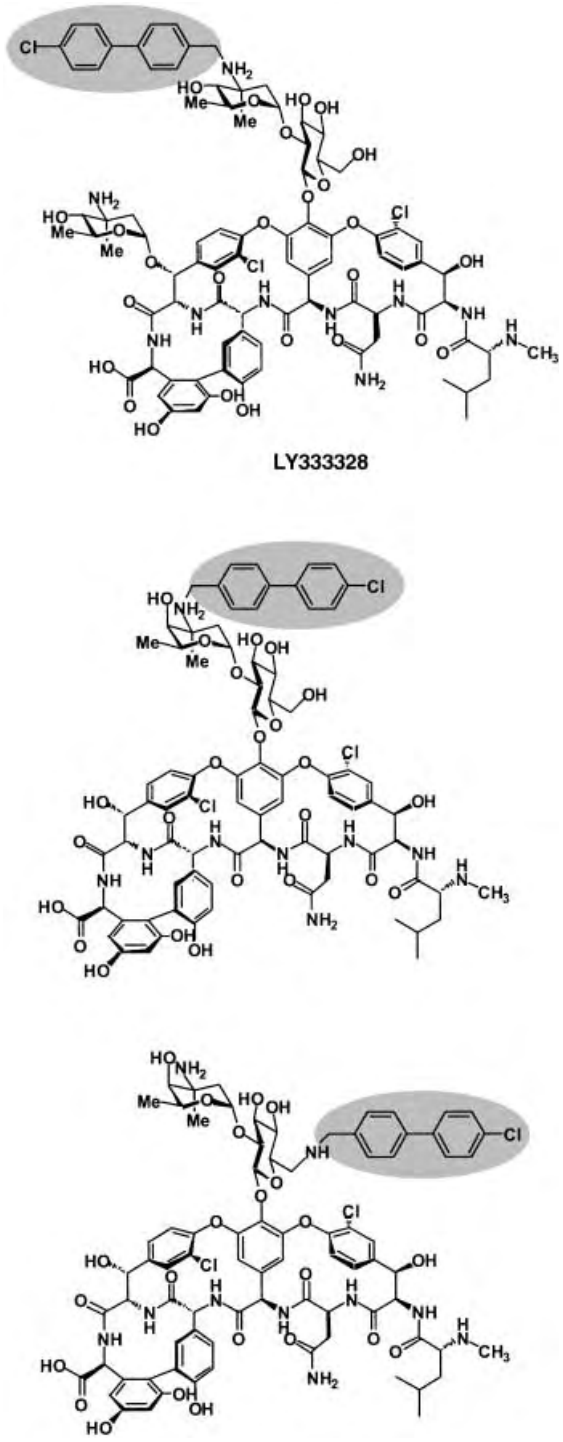

Scheme 34. Semisynthetic derivatives of vancomycin that are active against VRE.

14.4. Combinatorial Biosynthesis of Glycopeptide Antibiotics

A potential complement to synthetic efforts to modify the natural glycopeptide skeletons to generate new useful properties in glycopeptide antibiotics would be a combinatorial biosynthesis approach. This would build on the information summarized in Sections 8–13 of this review. One route would be to provide alternative amino acid monomers for incorporation into the heptapeptide scaffold by the producer organism. This could be done by classical feeding of alternate amino acids, especially nonproteinogenic ones, but suffers from an undetermined ease of access and uptake of the amino acid variants. An alternative is to import the biosynthetic pathway for the de novo construction of a desired amino acid and to express this pathway at higher concentrations. The

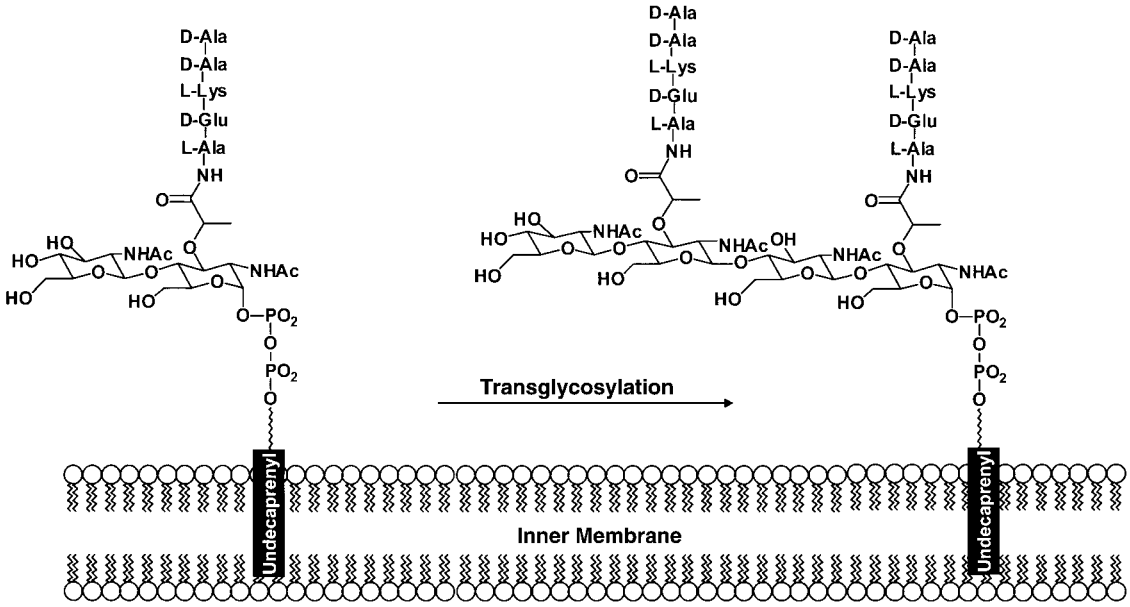

Figure 13. Proposed membrane-localized transglycosylases as targets for impaired lipglycopeptides.

producing actinoplanes may not be very user friendly for such transformations, but *Streptomyces toyocaensis*, the producer of A47934, would be more tractable.[29]

A second stage for reprogramming the biosynthetic pathway would be at the heptapeptide NRPS assembly line. Two kinds of approaches are now feasible. One is to alter the selectivity of any of the adenylation domains by mutation of a small number of side chains that control the selection and activation of amino acids.[138,139] For example, one could reprogram module 1 and/or 3 to select an amino acid other than Leu1 or Asn3. These are the two side chains not involved in cross-linking. Whether one would need to supply a D-amino acid at residue 1 remains to be determined. The VanC-VRE variants elaborate a serine racemase and the encoding *vanT* gene could be introduced into such a mutant producer to encode Ser at position 1 or 3.[140] A variant of this approach would be to inactivate the E domain in modules 2, 3, or 4 by mutation of a highly conserved histidine residue.[94] For example, would an E_5 mutant still make the full-length heptapeptide chain, now D-D-L-D-L-L-L, and would that still be cross-linked and glycosylated and retain antibiotic activity? A second approach is to swap domains or modules to alter identity and placement of any of the seven amino acids. Linne and Marahiel have begun to elaborate rules for both domain and module swaps in the tyrocidine synthetase assembly line, and those could be applied in the Cep, Van, and Teicoplanin NRPS assembly lines.[141] For example, would a replacement of the DHpg-activating module 3 in teicoplanin synthetase or A47934 synthetase by Hpg lead to a full-length teicoplanin analogue?

A third stage of intervention for reprogramming would be in the tailoring enzyme steps after the NRPS assembly line, and includes N-methylation, β-hydroxylation of tyrosine, or the cross-linking of P450 hemeprotein genes.

A fourth stage for reprogramming is to swap or replace enzymes in the TDP-deoxy sugar pathway. It is likely that the oxovancosamine sugar in the balhimycins is such a natural experiment where the final reductase is defective or absent. Would TDP-daunosamine or TDP-mycarose be made in the glycopeptide producers and utilized by the Gtfs? There is now good precedent in the polyketide macrolide pathways for reprogramming of the deoxy sugar biosynthesis and utilization by the Gtfs to produce final products with altered glycosyl moieties.[142–144] This strategy for changing the glycosyl moieties depends on Gtfs such as GtfA–E being sufficiently promiscuous to use alternate TDP-deoxyhexoses and for GtfB/C or D/E to act in series on the altered substrates and intermediates. We have shown this is possible by using GtfB and GtfC to make epivancomycin, and more intriguingly to utilize the teicoplanin aglycone and introduce the epivancosaminyl-1,2-glucosyl chain,[116] which has never been seen on this scaffold in nature (Scheme 35). In this connection, it may be possible to construct chimeras of such antibiotic-modifying Gtfs if they all have the two-lobed structure of GtfB (Figure 11) where the top lobe recognizes the TDP-sugar and the bottom lobe the aglycone. Combinatorial chimerization of such Gtfs might generate libraries of Gtfs able to mix and match new aglycones with TDP-deoxy and amino sugars for efficient glycosylation.

15. Conclusions

Bacterial genomics has now revealed dozens of gene clusters for nonribosomal peptide antibiotics, polyketide, and hybrid peptide/polyketide antibiotics, and revealed the logic used by nature for templated assembly. The strategy can now be deciphered from bioinformatics-based predictions and validated by experiment, even for antibiotics as complex as chloroeremomycin and vancomycin.

The clustering of all or almost all of the genes needed to encode a dedicated metabolic pathway to a secondary metabolite allows coordinate regulation of gene transcription, protein production, and construction of small molecules to

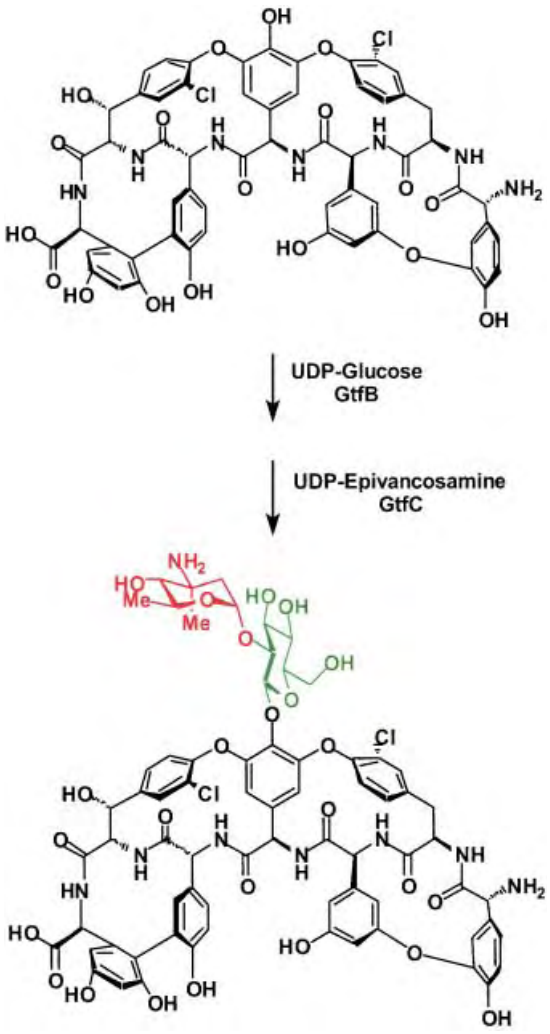

Scheme 35. Novel functions of GtfB and GtfC to add UDP-glucose and UDP-L-epivancosamine to the teicoplanin aglycone.

provide the dedicated building blocks. The 29 genes in the chloroeremomycin cluster segregate into three functional phases, typical for these classes of bioactive natural products.

The first phase, pre-assembly line, is enzymatic creation of a pool of dedicated small-molecule monomers, in a "just in time" inventory control, to serve as substrates for the assembly line process. In the vancomycin class of glycopeptide antibiotics this means creation of three nonproteinogenic amino acids, of the five amino acids in the heptapeptide scaffold. Some 12 of the 29 genes are assignable to production of these three amino acids. The other dedicated monomer is the activated L-amino deoxy sugar nucleotide TDP-L-β-epivancosamine, and five more genes generate this specific substrate.

Phase II is the assembly line process. The NRPS assembly line for these glycoheptapeptide antibiotics has 24 domains distributed over three protein subunits. The identity and placement of each domain controls monomer selection and activation in chain elongation, chain elongation involving four of the seven D residues, and then hydrolytic chain termination. Growth of the peptide chain is directional, from the N- to the C-termini of the assembly line, by an elongation cascade of covalently tethered aminoacyl- and peptidyl-S-enzyme intermediates.

The third phase, post assembly line, is the tailoring of the released heptapeptide. Oxidations and glycosylations are typical and N-methylations are not uncommon. All three types of transformations occur here, through seven dedicated enzymes. The most striking architectural and chemical feature of the vancomycin/teicoplanin classes of antibiotics are the side-chain phenolic cross-links. The inventory of cross-linking heme protein oxidases is now apparent, although the timing, specificity, and mechanisms remain to be worked out.

The rules by which nature assembles the glycopeptide (vancomycin) and lipoglycopeptide (teicoplanin) antibiotics are becoming elucidated and verified. This situation opens up approaches for reprogramming strategies, at the level of altered monomers, swapped assembly lines, and different batteries of post assembly tailoring enzymes.

Received: July 16, 2001 [A486]

[1] E. M. Scholar, W. B. Pratt, *The Antimicrobial Drugs, 2nd ed*, Oxford University Press, New York, **2000**, 7–10.
[2] *Antimicrobial Chemotherapy, 4th ed*, (Ed.: H. Greenwood), Oxford University Press, New York **, 2000,** 223–387.
[3] H. S. Gold, R. C. Moellering, Jr., *N. Engl. J. Med.* **1996**, *335*, 1445–1453.
[4] A. J. Salter, *Rev. Infect Dis.* **1982**, *4*, 196–236.
[5] E. M. Scholar, W. B. Pratt, *The Antimicrobial Drugs, 2nd ed*, Oxford University Press, New York **, 2000,** chapt. 7.
[6] P. Kloss, L. Xiong, D. L. Shinabarger, A. S. Mankin, *J. Mol. Biol.* **1999**, *294*, 93–101.
[7] H. C. Neu, *Science* **1992**, *257*, 1064–1073.
[8] C. Walsh, *Nature* **2000**, *406*, 775–781.
[9] N. Ban, P. Nissen, J. Hansen, P. B. Moore, T. A. Steitz, *Science* **2000**, *289*, 905–920.
[10] D. E. Brodersen, W. M. Clemons, Jr., A. P. Carter, R. J. Morgan-Warren, B. T. Wimberly, V. Ramakrishnan, *Cell* **2000**, *103*, 1143–1154.
[11] P. Nissen, J. Hansen, N. Ban, P. B. Moore, T. A. Steitz, *Science* **2000**, *289*, 920–930.
[12] A. Maxwell, *Trends Microbiol.* **1997**, *5*, 102–109.
[13] L. Ferrero, B. Cameron, J. Crouzet, *Antimicrob. Agents Chemother.* **1995**, *39*, 1554–1558.
[14] B. G. Spratt, *Science* **1994**, *264*, 388–393.
[15] B. G. Spratt, K. D. Cromie, *Rev. Infect. Dis.* **1988**, *10*, 699–711.
[16] J. M. Ghuysen, *Annu. Rev. Microbiol.* **1991**, *45*, 37–67.
[17] J. R. Knox, P. C. Moews, J. M. Frere, *Chem. Biol* **1996**, *3*, 937–947.
[18] D. H. Williams, *Nat. Prod. Rep.* **1996**, *13*, 469–477.
[19] D. H. Williams, B. Bardsley, *Angew. Chem.* **1999**, *111*, 1264–1286; *Angew. Chem. Int. Ed.* **1999**, *38*, 1172–1193.
[20] D. H. Williams, M. P. Williamson, D. W. Butcher, S. J. Hammond, *J. Am. Chem. Soc* **1983**, *105*, 1332–1339.
[21] J. C. Barna, D. H. Williams, *Annu. Rev. Microbiol.* **1984**, *38*, 339–357.
[22] *Bacterial Cell Wall* (Eds.: J.-M. Ghuysen, R. Hakenbeck), Elsevier, Amsterdam **, 1994**.
[23] K. K. Wong, D. L. Pompliano, *Adv. Exp. Med. Biol.* **1998**, *456*, 197–217.
[24] *Glycopeptide Antibiotics* (Ed.: R. Nagarajan), Marcel Dekker, New York **, 1994**.
[25] K. C. Nicolaou, C. N. C. Boddy, S. Brase, N. Winssinger, *Angew Chem.* **1999**, *111*, 2230–2287; *Angew Chem. Int. Ed.* **1999**, *38*, 2096–2152.
[26] J. Davies, *Science* **1994**, *264*, 375–382.

[27] I. T. Paulsen, M. H. Brown, R. A. Skurray, *Microbiol. Rev.* **1996**, *60*, 575 – 608.
[28] M. Putman, H. W. van Veen, W. N. Konings, *Microbiol. Mol. Biol. Rev.* **2000**, *64*, 672 – 693.
[29] C. G. Marshall, I. A. Lessard, I. Park, G. D. Wright, *Antimicrob. Agents Chemother.* **1998**, *42*, 2215 – 2220.
[30] M. Sosio, A. Bianchi, E. Bossi, S. Donadio, *Antonie Van Leeuwenhoek* **2000**, *78*, 379 – 384.
[31] C. T. Walsh, S. L. Fisher, I. S. Park, M. Prahalad, Z. Wu, *Chem. Biol.* **1996**, *3*, 21 – 28.
[32] M. N. Swartz, *Proc. Natl. Acad. Sci. USA* **1994**, *91*, 2420 – 2427.
[33] B. E. Murray, *N. Engl. J. Med.* **2000**, *342*, 710 – 721.
[34] D. Hoeffler, U. Zimmermann, *Lancet* **1997**, *350*, 739.
[35] M. Arthur, P. Courvalin, *Antimicrob. Agents Chemother.* **1993**, *37*, 1563 – 1571.
[36] S. Dutka-Malen, C. Molinas, M. Arthur, P. Courvalin, *Gene* **1992**, *112*, 53 – 58.
[37] M. Fines, B. Perichon, P. Reynolds, D. F. Sahm, P. Courvalin, *Antimicrob. Agents Chemother.* **1999**, *43*, 2161 – 2164.
[38] V. L. Healy, I. A. Lessard, D. I. Roper, J. R. Knox, C. T. Walsh, *Chem. Biol.* **2000**, *7*, R109 – 119.
[39] T. D. Bugg, G. D. Wright, S. Dutka-Malen, M. Arthur, P. Courvalin, C. T. Walsh, *Biochemistry* **1991**, *30*, 10408 – 10415.
[40] M. Arthur, C. Molinas, P. Courvalin, *J. Bacteriol.* **1992**, *174*, 2582 – 2591.
[41] T. R. Holman, Z. Wu, B. L. Wanner, C. T. Walsh, *Biochemistry* **1994**, *33*, 4625 – 4631.
[42] A. Haldimann, S. L. Fisher, L. L. Daniels, C. T. Walsh, B. L. Wanner, *J. Bacteriol.* **1997**, *179*, 5903 – 5913.
[43] M. Arthur, F. Depardieu, P. Reynolds, P. Courvalin, *Mol. Microbiol.* **1996**, *21*, 33 – 44.
[44] M. Baptista, F. Depardieu, P. Courvalin, M. Arthur, *Antimicrob. Agents Chemother.* **1996**, *40*, 2291 – 2295.
[45] I. S. Park, C. H. Lin, C. T. Walsh, *Proc. Natl. Acad. Sci. USA* **1997**, *94*, 10040 – 10044.
[46] F. Navarro, P. Courvalin, *Antimicrob. Agents Chemother.* **1994**, *38*, 1788 – 1793.
[47] N. Mani, P. Sancheti, Z. D. Jiang, C. McNaney, M. DeCenzo, B. Knight, M. Stankis, M. Kuranda, D. M. Rothstein, P. Sanchet, B. Knighti, *J. Antibiot.* **1998**, *51*, 471 – 479.
[48] D. A. Evans, C. J. Dinsmore, A. M. Ratz, D. A. Evrard, J. C. Barrow, *J. Am. Chem. Soc.* **1997**, *119*, 3417 – 3418.
[49] D. A. Evans, C. J. Dinsmore, A. M. Ratz, *Tetrahedron Lett.* **1997**, *38*, 3189 – 3192.
[50] D. A. Evans, J. C. Barrow, P. S. Watson, A. M. Ratz, C. J. Dinsmore, D. A. Evrard, K. M. DeVries, *J. Am. Chem. Soc.* **1997**, *119*, 3419 – 3420.
[51] D. A. Evans, M. R. Wood, B. W. Trotter, T. I. Richardson, J. C. Barrow, J. L. Katz, *Angew. Chem.* **1998**, *110*, 2868 – 2872; *Angew. Chem. Int. Ed.* **1998**, *37*, 2704 – 2708.
[52] K. C. Nicolaou, S. Natarajan, H. Li, N. F. Jain, R. Hughes, M. E. Solomon, J. M. Ramanjulu, C. N. C. Boddy, M. Takayanagi, *Angew. Chem.* **1998**, *110*, 2872 – 2878; *Angew. Chem. Int. Ed.* **1998**, *37*, 2708 – 2714.
[53] K. C. Nicolaou, N. F. Jain, S. Natarajan, R. Hughes, M. E. Solomon, H. Li, J. M. Ramanjulu, M. Takayanagi, A. E. Koumbis, T. Bando, *Angew. Chem.* **1998**, *110*, 2879 – 2881; *Angew. Chem. Int. Ed.* **1998**, *37*, 2714 – 2717.
[54] K. C. Nicolaou, M. Takayanagi, N. F. Jain, S. Natarajan, A. E. Koumbis, T. Bando, J. M. Ramanjulu, *Angew. Chem.* **1998**, *110*, 2881 – 2883; *Angew. Chem. Int. Ed.* **1998**, *37*, 2717 – 2719.
[55] K. C. Nicolaou, H. J. Mitchell, N. F. Jain, N. Winssinger, R. Hughes, T. Bando, *Angew. Chem.* **1999**, *111*, 253 – 255; *Angew. Chem. Int. Ed.* **1999**, *38*, 240 – 244.
[56] K. C. Nicolaou, H. J. Mitchell, N. F. Jain, T. Bando, R. Hughes, N. Winssinger, S. Natarajan, A. E. Koumbis, *Chem. Eur. J.* **1999**, *5*, 2648 – 2667.
[57] D. L. Boger, S. Miyazaki, S. H. Kim, J. H. Wu, O. Loiseleur, S. L. Castle, *J. Am. Chem. Soc.* **1999**, *121*, 3226 – 3227.
[58] D. Bischoff, S. Pelzer, A. Holtzel, G. J. Nicholson, S. Stockert, W. Wohlleben, G. Jung, R. D. Süßmuth, *Angew. Chem.* **2001**, *113*, 1736 – 1739; *Angew. Chem. Int. Ed.* **2001**, *40*, 1693 – 1696.
[59] D. Bischoff, S. Pelzer, B. Bister, G. J. Nicholson, S. Stockert, W. Wohlleben, G. Jung, R. D. Süßmuth, *Angew. Chem.* **2001**, *113*, 4824 – 4827; *Angew. Chem. Int. Ed.* **2001**, *40*, 4688 – 4691.
[60] A. M. van Wageningen, P. N. Kirkpatrick, D. H. Williams, B. R. Harris, J. K. Kershaw, N. J. Lennard, M. Jones, S. J. Jones, P. J. Solenberg, *Chem. Biol.* **1998**, *5*, 155 – 162.
[61] H.-T. Chiu, B. K. Hubbard, A. N. Shah, J. Eide, R. A. Fredenburg, C. T. Walsh, C. Khosla, *Proc. Natl. Acad. Sci. USA* **2001**, *98*, 8548 – 8553.
[62] S. Pelzer, R. Süßmuth, D. Heckmann, J. Recktenwald, P. Huber, G. Jung, W. Wohlleben, *Antimicrob. Agents Chemother.* **1999**, *43*, 1565 – 1573.
[63] D. P. O'Brien, P. N. Kirkpatrick, S. W. O'Brien, T. Staroske, T. I. Richardson, D. A. Evans, A. Hopkinson, J. B. Spencer, D. H. Williams, *Chem. Commun.* **2000**, 103 – 104.
[64] H. Seto, T. Fujioka, K. Furihata, I. Kaneko, S. Takahashi, *Tetrahedron Lett.* **1989**, *30*, 4987 – 4990.
[65] K. Matsuzaki, H. Ikeda, T. Ogino, A. Matsumoto, H. B. Woodruff, H. Tanaka, S. Omura, *J. Antibiot.* **1994**, *47*, 1173 – 1174.
[66] K. Matsuzaki, T. Ogino, T. Sunazuka, H. Tanaka, S. Omura, *J. Antibiot.* **1997**, *50*, 66 – 69.
[67] K. Tachikawa, K. Hasumi, A. Endo, *Thromb. Haemostasis* **1997**, *77*, 137 – 142.
[68] C. M. Harris, T. M. Harris, *J. Am. Chem. Soc.* **1982**, *104*, 4293 – 4295.
[69] S. J. Hammond, M. P. Williamson, D. H. Williams, L. D. Boeck, G. G. Marconi, *J. Chem. Soc. Chem. Commun.* **1982**, 344 – 346.
[70] S. J. Hammond, D. H. Williams, R. V. Nielsen, *J. Chem. Soc. Chem. Commun.* **1983**, 116 – 117.
[71] M. J. Zmijewski, Jr., B. Briggs, R. Logan, L. D. Boeck, *Antimicrob. Agents Chemother.* **1987**, *31*, 1497 – 1501.
[72] S. K. Chung, P. Taylor, Y. K. Oh, C. DeBrosse, P. W. Jeffs, *J. Antibiot.* **1986**, *39*, 642 – 651.
[73] T. I. Nicas, R. D. G. Cooper in *Biotechnology of Antibiotics* (Ed.: W. R. Strohl), Marcel Dekker, New York, **1997**, pp. 363 – 392.
[74] B. K. Hubbard, M. G. Thomas, C. T. Walsh, *Chem. Biol.* **2000**, *7*, 931 – 942.
[75] O. W. Chorba, D. H. Williams, J. B. Spencer, *J. Am. Chem. Soc.* **2000**, *122*, 5389 – 5390.
[76] W. J. McGahren, J. H. Martin, G. O. Morton, R. T. Hargreaves, R. A. Leese, F. M. Lovell, G. A. Ellestad, E. O'Brien, J. S. E. Holker, *J. Am. Chem. Soc.* **1980**, *102*, 1671 – 1684.
[77] H. M. Holden, M. M. Benning, T. Haller, J. A. Gerlt, *Acc. Chem. Res.* **2001**, *34*, 145 – 157.
[78] V. Pfeifer, G. J. Nicholson, J. Ries, J. Recktenwald, A. B. Schefer, R. M. Shawky, J. Schröder, W. Wohlleben, S. Pelzer, *J. Biol. Chem.* **2001**, *276*, 38370 – 38377.
[79] H. Chen, C. C. Tseng, B. K. Hubbard, C. T. Walsh, *Proc. Natl. Acad. Sci USA*, **2001**, *98*, 14901 – 14906.
[80] M. Steffensky, A. Muhlenweg, Z. X. Wang, S. M. Li, L. Heide, *Antimicrob. Agents Chemother.* **2000**, *44*, 1214 – 1222.
[81] H. Chen, C. T. Walsh, *Chem. Biol.* **2001**, *8*, 301 – 312.
[82] B. Lauer, R. Russwurm, C. Bormann, *Eur. J. Biochem.* **2000**, *267*, 1698 – 1706; B. Lauer, R. Russwurm, W. Schwarz, A. Kalmanczhelyi, C. Bruntner, A. Rosemeier, C. Bormann, *Mol. Gen. Genet.* **2001**, *264*, 662 – 673.
[83] H.-W. Chen, B. K. Hubbard, S. O. O'Connor, C. T. Walsh, unpublished results.
[84] S. Kirner, S. Krauss, G. Sury, S. T. Lam, J. M. Ligon, K. H. van Pee, *Microbiology* **1996**, *142*, 2129 – 2135.

[85] P. E. Hammer, D. S. Hill, S. T. Lam, K.-H. van Pee, J. M. Ligon, *Appl. Environ. Microbiol.* **1997**, *63*, 2147 – 2154.
[86] K. Hohaus, A. Altmann, W. Burd, I. Fischer, P. E. Hammer, D. S. Hill, J. M. Ligon, K.-H. van Pee. , *Angew. Chem.* **1997**, *109*, 2102 – 2104; *Angew. Chem. Int. Ed. Engl.* **1997**, *36*, 2012 – 2013.
[87] T. Dairi, T. Nakano, K. Aisaka, R. Katsumata, M. Hasegawa, *Biosci. Biotechnol. Biochem.* **1995**, *59*, 1099 – 1106.
[88] S. Keller, T. Wage, K. Hohaus, M. Holzer, E. Eichhorn, K.-H. van Pee, *Angew. Chem.* **2000**, *112*, 2380 – 2382; *Angew. Chem. Int. Ed.* **2000**, *39*, 2300 – 2302.
[89] M. A. Marahiel, T. Stachelhaus, H. D. Mootz, *Chem. Rev.* **1997**, *97*, 2651 – 2673.
[90] H. von Doehren, U. Keller, J. Vater, R. Zocher, *Chem. Rev.* **1997**, *97*, 2675 – 2705.
[91] T. Stein, J. Vater, V. Kruft, A. Otto, B. Wittmann-Liebold, P. Franke, M. Panico, R. McDowell, H. R. Morris, *J. Biol. Chem.* **1996**, *271*, 15428 – 15435.
[92] C. T. Walsh, *J. Biol. Chem.* **1989**, *264*, 2393 – 2396.
[93] K. Hoffmann, E. Schneider-Scherzer, H. Kleinkauf, R. Zocher, *J. Biol. Chem.* **1994**, *269*, 12710 – 12714.
[94] T. Stachelhaus, C. T. Walsh, *Biochemistry* **2000**, *39*, 5775 – 5787.
[95] L. Luo, C. T. Walsh, *Biochemistry* **2001**, *40*, 5329 – 5337.
[96] J. W. Trauger, C. T. Walsh, *Proc. Natl. Acad. Sci. USA* **2000**, *97*, 3112 – 3117.
[97] J. W. Trauger, R. M. Kohli, H. D. Mootz, M. A. Marahiel, C. T. Walsh, *Nature* **2000**, *407*, 215 – 218.
[98] A. Klemer, H. Wilbers, *Liebigs Ann. Chem.* **1987**, 815 – 823.
[99] G. Fronza, C. Fuganti, P. Grasseli, G. Pedrocchi-Fantoni, *J. Charbohydr. Chem.* **1983**, *2*, 5073 – 5076.
[100] G. Fronza, C. Fuganti, P. Grasseli, G. Pedrocchi-Fantoni, *J. Carbohydr. Chem.* **1983**, *2*, 5073 – 5076.
[101] R. Greven, P. Jutten, H.-D. Scharf, *Carbohydr. Res.* **1995**, *275*, 83 – 93.
[102] J. Thorson, B. Shen, R. Whitman, H.-w. Liu, Y. Li, J. Ahlert, *Bioorg. Chem.* **1999**, *27*, 172 – 188.
[103] L. Du, C. Sanchez, M. Chen, D. J. Edwards, B. Shen, *Chem. Biol.* **2000**, *7*, 623 – 642.
[104] J. P. Mackay, U. Gerhard, D. A. Beauregard, R. A. Maplestone, D. H. Williams, *J. Am. Chem. Soc.* **1994**, *116*, 4573 – 4580.
[105] U. Gerhard, J. P. Mackay, R. A. Maplestone, D. H. Williams, *J. Am. Chem. Soc.* **1993**, *115*, 232 – 237.
[106] L. M. Quiros, I. Aguirrezabalaga, C. Olano, C. Mendez, J. A. Salas, *Mol. Microbiol.* **1998**, *28*, 1177 – 1185.
[107] R. Kornfeld, S. Kornfeld, *Annu. Rev. Biochem.* **1985**, *54*, 631 – 664.
[108] H. W. Liu, J. S. Thorson, *Annu. Rev. Microbiol.* **1994**, *48*, 223 – 256.
[109] A. Kirschning, A. F.-W. Becthold, J. Rohr, *Top. Curr. Chem.* **1997**, *188*, 1 – 84.
[110] H. Chen, M. G. Thomas, B. K. Hubbard, H. C. Losey, C. T. Walsh, M. D. Burkart, *Proc. Natl. Acad. Sci. USA* **2000**, *97*, 11942 – 11947.
[111] P. N. Kirkpatrick, W. Scaife, T. M. Hallis, H.-w. Liu, J. B. Spencer, D. H. Williams, *Chem. Commun.* **2000**, 1565 – 1566.
[112] A. D. Hegeman, J. W. Gross, P. A. Frey, *Biochemistry* **2001**, *40*, 6598 – 6610.
[113] S. Gaisser, G. A. Bohm, J. Cortes, P. F. Leadlay, *Mol. Gen. Genet.* **1997**, *256*, 239 – 251.
[114] S. Gaisser, G. A. Bohm, M. Doumith, M. C. Raynal, N. Dhillon, J. Cortes, P. F. Leadlay, *Mol. Gen. Genet.* **1998**, *258*, 78 – 88.
[115] L. Katz, S. Donadio, *Genetics and Biochemistry of Antibiotic Production*, Butterworth-Heinemann, Boston, **1995**, pp. 385 – 420.
[116] H. C. Losey, M. W. Peczuh, Z. Chen, U. S. Eggert, S. D. Dong, I. Pelczer, D. Kahne, C. T. Walsh, *Biochemistry* **2001**, *40*, 4745 – 4755.
[117] P. J. Solenberg, P. Matsushima, D. R. Stack, S. C. Wilkie, R. C. Thompson, R. H. Baltz, *Chem. Biol.* **1997**, *4*, 195 – 202.
[118] A. M. Mulichak, H. C. Losey, C. T. Walsh, R. M. Garvito, *Structure* **2001**, *9*, 547 – 557.
[119] S. Ha, D. Walker, Y. Shi, S. Walker, *Protein Sci.* **2000**, *9*, 1045 – 1052.
[120] A. Vrielink, W. Ruger, H. P. Driessen, P. S. Freemont, *EMBO J.* **1994**, *13*, 3413 – 3422.
[121] J. E. Jackman, C. R. Raetz, C. A. Fierke, *Biochemistry* **1999**, *38*, 1902 – 1911.
[122] Y. Volchegursky, Z. Hu, L. Katz, R. McDaniel, *Mol. Microbiol.* **2000**, *37*, 752 – 762.
[123] C. R. Hutchinson, *Chem. Rev.* **1997**, *97*, 2525 – 2535.
[124] D. I. Roper, T. Huyton, A. Vagin, G. Dodson, *Proc. Natl. Acad. Sci. USA* **2000**, *97*, 8921 – 8925.
[125] D. E. Bussiere, S. D. Pratt, L. Katz, J. M. Severin, T. Holzman, C. H. Park, *Mol. Cell* **1998**, *2*, 75 – 84.
[126] R. Araoz, E. Anhalt, L. Rene, M. A. Badet-Denisot, P. Courvalin, B. Badet, *Biochemistry* **2000**, *39*, 15971 – 15979.
[127] J. F. Barrett, J. A. Hoch, *Antimicrob. Agents Chemother.* **1998**, *42*, 1529 – 1536.
[128] K. Stephenson, Y. Yamaguchi, J. A. Hoch, *J. Biol. Chem.* **2000**, *275*, 38900 – 38904.
[129] G. McMahon, L. Sun, C. Liang, C. Tang, *Curr. Opin. Drug Discov. Dev.* **1998**, *1*, 131 – 146.
[130] N. Bamas-Jacques, S. Lorenzon, F. Massey, G. deSwetschin, I. DeCourty, G. Sezonov, J. L. Permodet, A. Friedmann, M. Vuilhorgne, M. Couder, D. Thabaut, J. F. Desnotes, *Xth International Symposium on Biology of Actinomycetes. Abstract 2P11.*, Bejing, **1997**.
[131] L. Du, C. Sanchez, B. Shen, *Metab. Eng.* **2001**, *3*, 78 – 95.
[132] C. Cocitto, *Microbiol. Rev.* **1979**, *43*, 145 – 198.
[133] P. Kloss, L. Xiong, D. L. Shinabarger, A. S. Mankin, *J. Mol. Biol.* **1999**, *294*, 93 – 101.
[134] F. Biavasco, C. Vignaroli, R. Lupidi, E. Manso, B. Facinelli, P. E. Varaldo, *Antimicrob. Agents Chemother.* **1997**, *41*, 2165 – 2172.
[135] E. Hershberger, J. R. Aeschlimann, T. Moldovan, M. J. Rybak, *Antimicrob. Agents Chemother.* **1999**, *43*, 717 – 721.
[136] R. Kerns, S. D. Dong, S. Fukuzawa, J. Carbeck, J. Kohler, L. Silver, D. Kahne, *J. Am. Chem. Soc.* **2000**, *122*, 12608 – 12609.
[137] R. C. Goldman, E. R. Baizman, C. B. Longley, A. A. Branstrom, *FEMS Microbiol. Lett.* **2000**, *183*, 209 – 214.
[138] T. Stachelhaus, H. D. Mootz, M. A. Marahiel, *Chem. Biol.* **1999**, *6*, 493 – 505.
[139] G. L. Challis, J. Ravel, C. A. Townsend, *Chem. Biol.* **2000**, *7*, 211 – 224.
[140] C. A. Arias, M. Martin-Martinez, T. L. Blundell, M. Arthur, P. Courvalin, P. E. Reynolds, *Mol. Microbiol.* **1999**, *31*, 1653 – 1664.
[141] U. Linne, M. A. Marahiel, *Biochemistry* **2000**, *39*, 10439 – 10447.
[142] S. Gaisser, J. Reather, G. Wirtz, L. Kellenberger, J. Staunton, P. F. Leadlay, *Mol. Microbiol.* **2000**, *36*, 391 – 401.
[143] H. Yamase, L. Zhao, H.-w. Liu, *J. Am. Chem. Soc.* **2000**, *122*, 12397 – 12398.
[144] L. Zhao, J. Ahlant, Y. Zue, J. S. Thorson, D. H. Shermann, H.-w. Liu, *J. Am. Chem. Soc.* **1999**, *121*, 9881 – 9882.
[145] J. Pootoolal, M. G. Thomas, C. G. Marshall, J. M. Neu, B. K. Hubbard, C. T. Walsh, G. D. Wright, *Proc. Natl. Acad. Sci.* **2002**, *99*, 8962 – 8967.

Communications

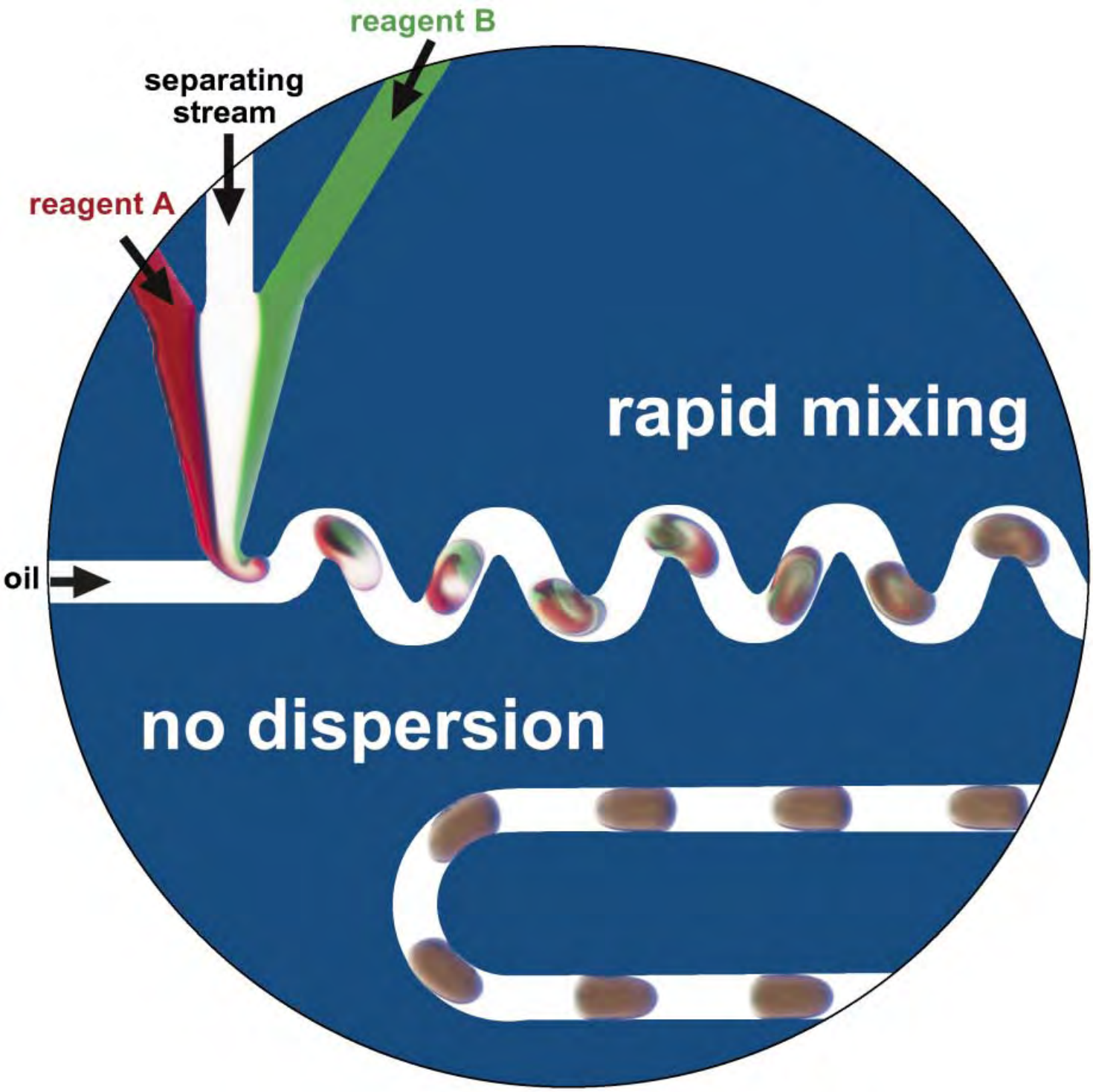

Aqueous droplets of 250 pL formed in a microfluidic channel in a continuous flow of a water-immiscible fluid act as microreactors that mix the reagents rapidly and transport them with no dispersion. These droplets may also be used to control chemical reaction networks on millisecond time scale. For more information see the following publication by R. F. Ismagilov et al.

 © 2003 Wiley-VCH Verlag GmbH & Co. KGaA, Weinheim 1433-7851/03/4207-0767 $ 20.00+.50/0

High-Throughput Measurements

A Microfluidic System for Controlling Reaction Networks in Time**

*Helen Song, Joshua D. Tice, and Rustem F. Ismagilov**

We present here a microfluidic system that may be used to control networks of many chemical reactions on the millisecond scale. It allows to control when each reaction begins, for how long each reaction evolves before it is separated or combined with other reactions, and when each reaction is analyzed or quenched. The system uses flow of fluids to linearly transform space (length of capillaries) into time (reaction time). For a chemical reaction in an open system this transformation is simple and well known: A solution of reagent A and a solution of reagent B are injected as steady streams into a microfluidic channel at initial point $d = 0$ where the reaction between them begins ($t = 0$). As the reaction mixture is transported by the fluid stream at a constant velocity U, every spatial point d corresponds to a time point t, the reaction time, where $t = d/U$. If such a system is implemented, interactions of multiple chemical reactions in time could be controlled simply by creating a network of converging and diverging channels carrying reaction mixtures, and varying flow velocities to adjust reaction and interaction times. If the reactions are accompanied by an optical signal (e.g. changes in fluorescence or absorption), time-resolved measurements of the reactions in the entire network could be obtained from a single spatially resolved optical image.

Networks of microfluidic channels[1–3] are especially attractive for this distance-to-time transformation because they can be easily fabricated and used to manipulate small volumes of reagents; they are becoming essential for chemical and biological analysis and synthesis.[1–3] Flow in microfluidic devices is laminar; it occurs at low values of the Reynolds number, Re (~0.01–100). Re is defined as $lU\rho/\mu$, where l [m] is the diameter of the capillary, U [m s^{-1}] the velocity of the flow, ρ [kg m^{-3}] the density, and μ [kg m^{-1} s^{-1}] the viscosity of the fluid.[4] This laminar flow makes it difficult to implement the distance-to-time transformation in microfluidic devices for two reasons (Figure 1a). First, mixing is slow—two streams injected into a channel flow side-by-side with mixing only by diffusion,[4–6] therefore $d = 0$ does not correspond to a well-defined starting point ($t = 0$) of the reaction. Significant research efforts have been devoted to solving this problem of slow mixing.[2,3,7] Turbulent flows provide both rapid mixing and low dispersion,[8] but turbulence occurs at values of $Re > 2000$ reached in microchannels only at high flow rates (~10 m s^{-1}). Achieving such flow velocities requires undesirably high sample consumption (~1 mL s^{-1}) and high pressures. Second, the dispersion of solutes along the channel is large—the flow profile is parabolic, and the reagents are transported at a range of velocities.[4] Therefore, a given distance d corresponds to a range of reaction times $t = d/U$.

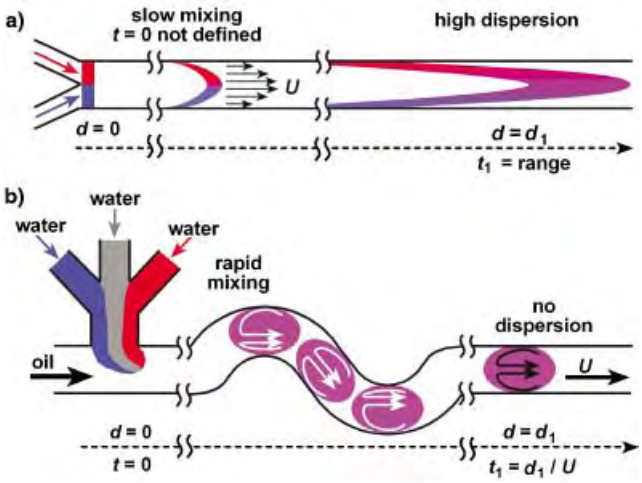

Figure 1. Schematic comparison of a reaction A + B conducted in a standard pressure-driven microfluidic system device (a) and in the microfluidic device described here (b). a) Reaction time $t \neq d/U$. b) Reaction time $t = d/U$. Two aqueous reagents (red, A and blue, B) can form laminar streams separated by a gray "divider" aqueous stream in a microchannel. When the three streams enter the channel with a flowing immiscible fluid, they form droplets (plugs). The reagents come into contact as the contents of the droplets are rapidly mixed. Internal recirculation within plugs flowing through channels of different geometries is shown schematically by arrows.

We developed a simple microfluidic system that overcomes both problems—it transports solutions with rapid mixing and no dispersion (Figure 1b). This system uses networks of microchannels with rectangular cross sections and hydrophobic surfaces fabricated using rapid prototyping in polydimethylsiloxane (PDMS).[9] We controlled the volumetric flow rates through each channel using syringe pumps. Dispersion was eliminated by localizing the reagents within aqueous plugs (droplets large enough to block the channel) separated by a water-immiscible oil. Immiscible fluids have been used to localize reagents in both commercial[10] and laboratory[11–13] systems. Here we describe methods for forming plugs of multiple solutions of reagents, for using chaotic advection to achieve especially rapid (~2 ms) mixing within the plugs, and for splitting and merging these plugs in order to create complex microfluidic networks.

To form droplets from two solutions of reagents without bringing the reagents into prior contact we flowed these

[*] Prof. R. F. Ismagilov, H. Song, J. D. Tice
Department of Chemistry
The University of Chicago
5735 S. Ellis Avenue, Chicago, IL 60637 (USA)
Fax: (+1) 773-702-0805
E-mail: r-ismagilov@uchicago.edu

[**] This work was supported by the Camille and Henry Dreyfus New Faculty Award Program, the Searle Scholars Program, an award from Research Corporation, the Chicago MRSEC funded by the NSF. H.S. was supported by a Predoctoral Training Grant of the NIH (GM 08720). We thank our colleagues at the University of Chicago for invaluable discussions and suggestions. We thank Prof. Sidney Nagel, in addition, for an equipment loan and Ian Hawkins for measuring surface tensions. Photolithography was performed by H.S. at MAL of the University of Illinois at Chicago. Microscopy was conducted at the University of Chicago Cancer Center Digital Light Microscopy Facility.

 © 2003 Wiley-VCH Verlag GmbH & Co. KGaA, Weinheim 1433-7851/03/4207-0768 $ 20.00+.50/0

solutions in a microchannel as two laminar streams,[14] and used an inert center stream to separate them. These three streams were continuously injected into a flow of water-immiscible perfluorodecaline (PFD) in the main microchannel, where they spontaneously broke up into streams of plugs (~500 pL) separated and surrounded by PFD (Figure 2). Diffusion through the central stream was too slow for the reagents in the two side streams to interact prior to the formation of a plug. Plugs of three or more reagents could be formed in the same manner. PFD is an attractive choice of carrier fluid because it is inert, immiscible with water and organic solvents, and does not swell PDMS. Emulsions of perfluorocarbons such as PFD are used as blood substitutes in humans during surgeries[15] and should be compatible with a range of biological molecules. We controlled the wetting of PDMS by PFD by adding 9% v/v of $C_6F_{11}C_2H_4OH$ to PFD. Water-in-oil emulsions are known to form in pressure-driven flow in microchannels,[16,17] often at high values of the dimensionless capillary number, Ca ($Ca = U\mu/\gamma$, γ [$N\,m^{-1}$]: surface tension at the PFD/water interface).[18] Our system was operated at low values of Ca because at high values of Ca, the shear flow broke up the aqueous phase into small droplets that did not block the channels and were not transported reliably over long distances. Complex behavior in this latter regime has been carefully characterized.[16]

A plug moving in a straight channel generates a steady, recirculating flow.[19] This flow mixes the fluid within the left and the right (along the direction of the flow) halves of the plug (black arrows in Figure 1b, right), but not between the two halves. Laminar flow is preserved during plug formation that occurs at low Re; the reagent solutions end up in the two halves of the plug, and internal recirculation within elongated plugs enhances mixing only moderately (Figure 2).

Chaotic advection accelerates mixing by using unsteady fluid flow to stretch and fold a volume of fluid. Stretching and folding leads to a rapid, exponential decrease of the striation length—distance over which mixing has to occur by diffusion. At intermediate Re ($Re \sim 70$), chaotic advection can be generated in three-dimensional microfluidic systems.[20] An elegant system used asymmetric ridges on the floor of a microchannel to induce chaotic advection at both low and intermediate values of Re ($Re = 0$–100).[7] Here we show how the principles of chaotic advection can be applied to mixing inside plugs.

The principle of chaotic advection has been illustrated with flow-cavity experiments.[21] In a flow cavity, motion of the top and bottom walls induces flow within a volume of fluid. Simultaneous motion of these walls induces steady flow that mixes solutions slowly (Figure 3a). Time-periodic, alternating motion of the walls induces unsteady, chaotic flow that mixes solutions rapidly (Figure 3b). Crossing of streamlines in this time-periodic flow is a necessary condition for chaos.[21]

Fluid flow in a flow cavity is similar to fluid flow in a plug moving inside a channel, except for the frame of reference—in a flow cavity walls move relative to the fluid, and in a plug fluid moves relative to the walls. Steady flow in a flow cavity is similar to steady, recirculating flow in plugs moving in a straight channel (black arrows in Figure 1b right). For arbitrary initial conditions, mixing by this steady flow is inefficient (efficiency decreases as $1/t$)[19,21] because solutes become trapped on the streamlines that do not cross.[21] For example, this flow mixes the contents within the left and right halves of the plug, but not between the two halves (Figure 2). The two-dimensional component of this flow responsible for mixing of the solutions can be envisioned as two counter-rotating vortices located in the left and right halves of the plug (white arrows in Figure 1b). In the flow cavity shown in Figure 3 the two vortices are co-rotating.

Pairs of co-[22–24] and counter-rotating[24,25] vortices both generate chaos in periodic time-dependent flow. We induced such a flow in plugs by replacing a straight channel with a winding channel (Figure 4). A plug moving through a curved part of the winding channel is moving at different velocities relative to the two walls, similar to fluid in a flow cavity of Figure 3b. We have deduced the streamlines shown by the

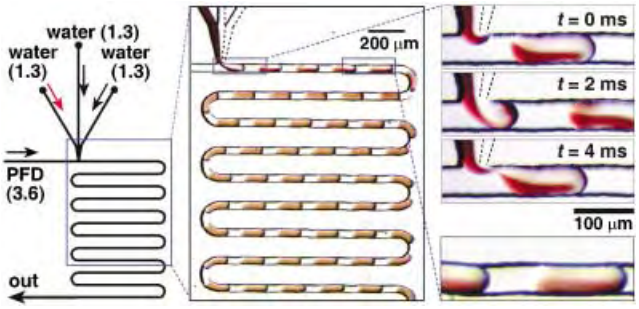

Figure 2. Spontaneous formation of uniform plugs out of multiple aqueous streams. Left: Schematic diagram of the microchannel network. Volumetric flow rates for all streams (in $\mu L\,min^{-1}$) are given in parenthesis. Middle: Microphotograph (10 μs exposure) of plug formation and transport. Right: Magnified microphotographs (10 μs exposure) of the plug-forming region at different time points. All microchannels had $50 \times 50\ \mu m^2$ cross sections. Total flow rate in the main channel: $7.5\ \mu L\,min^{-1}$ ($50\ mm\,s^{-1}$ average flow velocity); $Re \sim 2.5$ (water), ~0.93 (PFD). PFD here stands for a 10:1 mixture of perfluorodecaline and $C_6F_{11}C_2H_4OH$. Red stream: solution of $[Fe(SCN)_x]^{(3-x)+}$ prepared by mixing 0.067 M $Fe(NO_3)_3$ with 0.2 M KSCN; colorless streams: 0.2 M KNO_3.

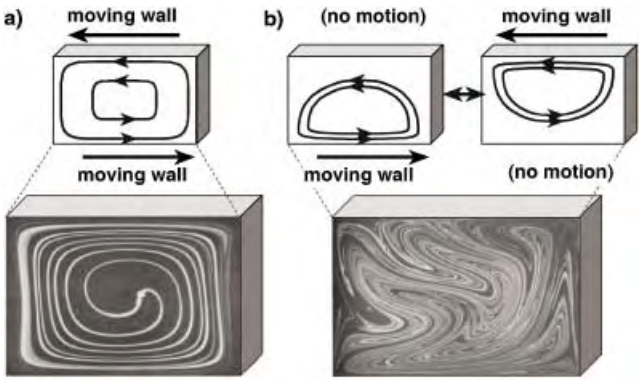

Figure 3. Mixing by steady (a) and time-periodic (b) flows in flow cavities. a, b) Top: Schematic illustration of the flow cavity. The vertical walls are stationary and the horizontal walls move as shown. Bottom: Images (reprinted with permission of Cambridge University Press from ref. [21]) that illustrate the flow patterns. For details, see text.

 © 2003 Wiley-VCH Verlag GmbH & Co. KGaA, Weinheim 1433-7851/03/4207-0769 $ 20.00+.50/0

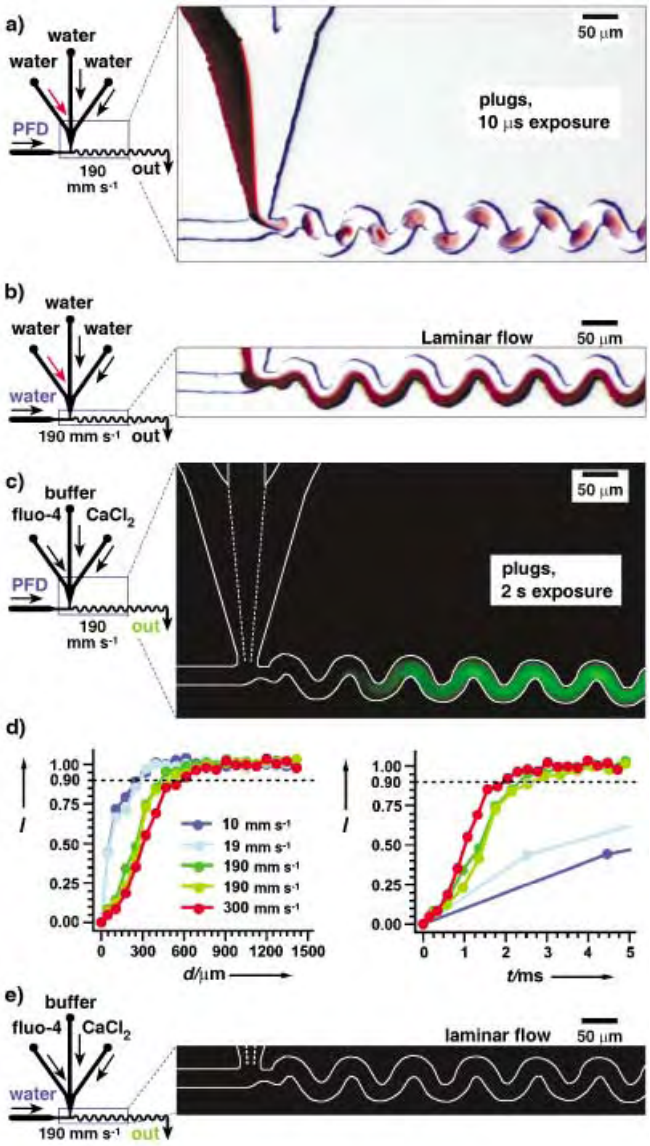

Figure 4. a), b) Microphotographs (10 µs exposure) illustrating rapid mixing inside plugs (a) and negligible mixing in a laminar flow (b) moving through winding channels at the same total flow velocity; same solutions as for Figure 2. c) A false-color microphotograph (2 s exposure, individual plugs are invisible) showing time-averaged fluorescence arising from rapid mixing inside plugs of solutions of Fluo-4 (54 µM) and $CaCl_2$ (70 µM) in aqueous sodium morpholine propanesulfonate buffer (20 mM, pH 7.2); this buffer was also used as the middle aqueous stream. d) Relative normalized intensity (I) of fluorescence obtained from images such as shown in (c) as a function of distance (left) traveled by the plugs and of time required to travel that distance (right) at a given flow rate. The total intensity across the width of the channel was measured. Total PFD/water volumetric flow rates (in $\mu L\,min^{-1}$) were ● 0.6:0.3, ● 1.0:0.6, ● 12.3:3.7, ● 10:6, ● 20:6. e) A false-color microphotograph (2 s exposure) of the weak fluorescence arising from negligible mixing in a laminar flow of the solutions used in (c). All channels were 45 µm deep; inlet channels were 50 µm and winding channels 28 µm wide; $Re \sim 5.3$ (water), ~ 2.0 (PFD).

white arrows in Figure 1b by observing asymmetric plugs traveling through curved channels; these streamlines are similar to those shown in Figure 3b. In plugs moving through winding channels we observed flow patterns that corresponded to very rapid mixing (Figure 4a). These flow patterns were reproducible, and were similar for plugs moving at different speeds, except for some blurring by diffusion at lower speeds. At these low values of Re, winding channels did not accelerate mixing in laminar flow in the absence of PFD (Figure 4b).

In Figure 4c,d we show that this system can be used to measure the rates of chemical reactions on the millisecond time scale, and that these rates can be used to quantify mixing.[6] This was done by measuring the rate of rapid binding ($k_{on} = 7.1 \times 10^8\,M^{-1}\,s^{-1}$)[26] of Ca^{2+} ions to the calcium-sensitive dye fluo-4 (Figure 4c). Fluo-4 is weakly fluorescent in the absence of calcium whereas the complex fluo-4·Ca^{2+} shows strong fluorescence; accordingly, increase in fluorescence corresponds to mixing. At every flow rate we obtained a complete time-resolved reaction profile by acquiring a single spatially resolved long-exposure image of the fluorescence.[8] Each image was integrated over two seconds to give the average fluorescence intensity of hundreds of moving plugs (~60 pL in volume) and non-fluorescent PFD, and consumed less than 50 nL of fluo-4 solution. For the laminar flow of these solutions in the absence of PFD only weak fluorescence was observed (Figure 4e) consistent with negligible mixing shown in Figure 4b. Mixing of $CaCl_2$ and fluo-4 solutions in the plugs was achieved within a short distance (~500 µm, Figure 4d), which was not very sensitive to the PFD/water ratio, and was weakly dependent on flow velocity. At higher flow rates it corresponded to mixing in about 2 ms (Figure 4d).

These facts and the flow patterns in Figure 4a are consistent with chaotic mixing, but detailed modeling would be required to identify the chaotic regions within the plugs. Such modeling would have to account for the three-dimensional recirculation within both aqueous plugs and PFD in a given geometry and should suggest the geometry of the winding channels—symmetric or asymmetric, regular or random—required for most efficient mixing.

A key attractive feature of microfluidics is the possibility of creating large fluidic networks.[27] To demonstrate how, in principle, a network with complex connectivity could be created with this system we designed methods for combining two streams of plugs into a single stream in a main channel (merging plugs), and for dividing one stream of plugs into two streams (splitting plugs). Merging was rare when the main channel was of the same width as the channels in which the plugs formed as plugs merged only if they entered the main channel simultaneously (in phase). Plugs that entered out of phase continued through the main channel separated by PFD because they all moved at the same constant velocity. By contrast, merging was achieved in a wide main channel, even for streams of plugs that were out of phase (Figure 5a). We formed small and large plugs in 30-µm and 60-µm wide channels, respectively. These plugs did not block the expanded 100-µm wide main channel and could move at two different velocities until they coalesced.[28] Small droplets moved more slowly than large droplets;[16] this effect is well known and is the basis of hydrodynamic chromatography.[29] Sufficiently large fluctuations in the relative flow rates in the two channels disrupted merging, but more than 95% of the plugs merged

 © 2003 Wiley-VCH Verlag GmbH & Co. KGaA, Weinheim 1433-7851/03/4207-0770 $ 20.00+.50/0

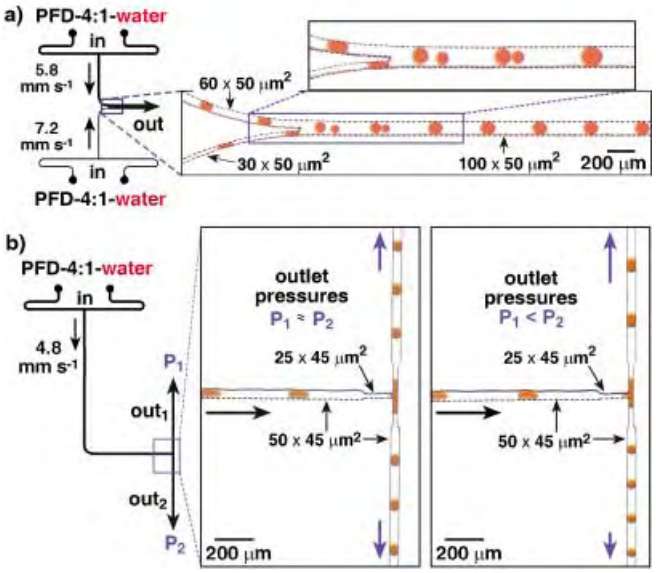

Figure 5. a) Spontaneous merging of pairs of plugs into single plugs. Left: schematic diagram of the microfluidic network; right: microphotograph of two streams of plugs merging in a main microchannel. b) Spontaneous splitting of plugs at a branching point in a microchannel. Left: schematic diagram of the microchannel network and the experimental conditions used. Middle: microphotograph showing splitting of a stream of plugs into plugs of approximately one-half the volume of the initial plugs. The outlet pressures were equal for the two channels. Right: asymmetric splitting of both aqueous and PFD plugs occurred when hydrostatic pressure of about 6 kPa was applied to the second outlet. a), b) Volumetric PFD/water flow rate ratios, flow velocities, and cross-sectional dimensions of the channels (width × height) are also shown.

correctly when flows were simply driven with pressure of compressed air from a house line, regulated manually.

Reliable splitting of plugs at branching points of microchannels was achieved by constricting the channels at the branching points. When the channels were not constricted, short rounded plugs often showed a complicated behavior dominated by the surface tension at the PFD/water interfaces. In constricted channels the plugs became long and narrow and behaved simply like laminar flows subjected to pressure gradients (Figure 5b). The size of the split plugs was proportional to the relative flow rates in the two outlet channels; we controlled these flow rates by varying the relative hydrostatic pressures at the two outlets. Splitting and subsequent merging of plugs could become useful for high-throughput parallel measurements. These methods of merging and splitting rely on a simple control of widths of channels and should become especially useful in combination with advanced methods of pumping.[30]

Overall, the phenomena described here allow us to construct a microfluidic system that linearly converts distance into time by achieving millisecond mixing and transport with no dispersion. We believe that it will be useful for both chemical analysis and synthesis, and for studies of complex reaction networks.[31] The system is easy to fabricate and operate, has no active or moving components, and can be controlled simply by varying the rates of fluid flow. The uncertainty of the distance-to-time transformation is limited by the mixing distance. Both short (ms) and long (min) time scales can be accessed in the same microfluidic device simply by varying the flow velocity. Sub-millisecond time scales should be accessible by decreasing the size of the channels, and by increasing the flow rate (as long as the capillary number remains small). In a serpentine microfluidic network an entire time course of a chemical reaction can be obtained with millisecond resolution by analyzing fluorescence from a single image. Because the flows are steady this image does not have to be time-resolved[8] and can be obtained with long exposures of a CCD or even a photographic camera. This system consumes samples at a rate about 10000 times lower ($\mu L\,min^{-1}$) than devices that rely on turbulence for mixing ($mL\,s^{-1}$). It may serve a broad community of chemists, biochemists, and biophysicists as an inexpensive compliment to stop-flow instruments. In addition to a planar, trivial to fabricate, disposable plastic chip it only requires equipment already present in most laboratories: a source of pressure, such as a syringe pump or a cylinder of compressed gas, and a microscope with a CCD camera. We believe that this system for conducting reactions in sub-nanoliter plugs will also become valuable in traditional areas of microfluidics where miniaturization and speed are important—for example, high-throughput screening, combinatorial synthesis, analysis, and diagnostics—both as a self-contained platform, and in combination with the existing technologies, especially those using flows of immiscible fluids.[32,33]

Received: September 6, 2002 [Z50110]

[1] M. A. Burns, *Science* **2002**, *296*, 1818.
[2] P.-A. Auroux, D. Iossifidis, D. R. Reyes, A. Manz, *Anal. Chem.* **2002**, *74*, 2623.
[3] P.-A. Auroux, D. Iossifidis, D. R. Reyes, A. Manz, *Anal. Chem.* **2002**, *74*, 2637.
[4] R. B. Bird, W. E. Stewart, E. N. Lightfoot, *Transport Phenomena*, Wiley, New York, **2002**.
[5] A. E. Kamholz, P. Yager, *Sens. Actuators B* **2002**, *82*, 117.
[6] R. F. Ismagilov, A. D. Stroock, P. J. A. Kenis, G. Whitesides, H. A. Stone, *Appl. Phys. Lett.* **2000**, *76*, 2376.
[7] A. D. Stroock, S. K. W. Dertinger, A. Ajdari, I. Mezic, H. A. Stone, G. M. Whitesides, *Science* **2002**, *295*, 647.
[8] M. C. R. Shastry, S. D. Luck, H. Roder, *Biophys. J.* **1998**, *74*, 2714.
[9] J. C. McDonald, D. C. Duffy, J. R. Anderson, D. T. Chiu, H. K. Wu, O. J. A. Schueller, G. M. Whitesides, *Electrophoresis* **2000**, *21*, 27.
[10] D. D. Cunningham, *Anal. Chim. Acta* **2001**, *429*, 1.
[11] M. A. Burns, B. N. Johnson, S. N. Brahmasandra, K. Handique, J. R. Webster, M. Krishnan, T. Sammarco, P. M. Man, D. Jones, D. Heldsinger, C. H. Mastrangelo, D. T. Burke, *Science* **1998**, *282*, 484.
[12] K. Handique, D. T. Burke, C. H. Mastrangelo, M. A. Burns, *Anal. Chem.* **2001**, *73*, 1831.
[13] K. Hosokawa, T. Fujii, I. Endo, *Anal. Chem.* **1999**, *71*, 4781.
[14] P. J. A. Kenis, R. F. Ismagilov, G. M. Whitesides, *Science* **1999**, *285*, 83.
[15] J. E. Squires, *Science* **2002**, *295*, 1002.
[16] T. Thorsen, R. W. Roberts, F. H. Arnold, S. R. Quake, *Phys. Rev. Lett.* **2001**, *86*, 4163.
[17] S. Sugiura, M. Nakajima, M. Seki, *Langmuir* **2002**, *18*, 5708.

 © 2003 Wiley-VCH Verlag GmbH & Co. KGaA, Weinheim 1433-7851/03/4207-0771 $ 20.00+.50/0

[18] The viscosity of PFD is 5.10×10^{-3} kg m^{-3} s^{-1}, the surface tension at the interface between water and fluorinated phase was 13×10^{-3} N m^{-1}. We have shown that this system can be operated at values of *Ca* up to about 0.1 (at 300 mm s^{-1}). As the value of *Ca* increases above about 0.2, the formation of plugs becomes irregular.
[19] K. Handique, M. A. Burns, *J. Micromech. Microeng.* **2001**, *11*, 548.
[20] R. H. Liu, M. A. Stremler, K. V. Sharp, M. G. Olsen, J. G. Santiago, R. J. Adrian, H. Aref, D. J. Beebe, *J. Microelectromech. Syst.* **2000**, *9*, 190.
[21] J. M. Ottino, *The Kinematics of Mixing: Stretching, Chaos, and Transport*, Cambridge University Press, Cambridge, **1989**.
[22] H. Aref, *J. Fluid Mech.* **1984**, *143*, 1.
[23] W. L. Chien, H. Rising, J. M. Ottino, *J. Fluid Mech.* **1986**, *170*, 355.
[24] S. C. Jana, G. Metcalfe, J. M. Ottino, *J. Fluid Mech.* **1994**, *269*, 199.
[25] T. H. Solomon, J. P. Gollub, *Phys. Rev. A* **1988**, *38*, 6280.
[26] M. Naraghi, *Cell Calcium* **1997**, *22*, 255.
[27] T. Thorsen, S. J. Maerkl, S. R. Quake, *Science* **2002**, *298*, 580.
[28] J. Eggers, J. R. Lister, H. A. Stone, *J. Fluid Mech.* **1999**, *401*, 293.
[29] H. Small, M. A. Langhorst, *Anal. Chem.* **1982**, *54*, A892.
[30] M. A. Unger, H. P. Chou, T. Thorsen, A. Scherer, S. R. Quake, *Science* **2000**, *288*, 113.
[31] A. Arkin, P. D. Shen, J. Ross, *Science* **1997**, *277*, 1275.
[32] B. Zhao, N. O. L. Viernes, J. S. Moore, D. J. Beebe, *J. Am. Chem. Soc.* **2002**, *124*, 5284.
[33] M. Tokeshi, T. Minagawa, K. Uchiyama, A. Hibara, K. Sato, H. Hisamoto, T. Kitamori, *Anal. Chem.* **2002**, *74*, 1565.

 © 2003 Wiley-VCH Verlag GmbH & Co. KGaA, Weinheim 1433-7851/03/4207-0772 $ 20.00+.50/0

Spontaneously Formed Vesicles

Vesicles and Polymerized Vesicles from Thiophene-Containing Rod–Coil Block Copolymers**

Dennis M. Vriezema, Johan Hoogboom, Kelly Velonia, Ken Takazawa, Peter C. M. Christianen, Jan. C. Maan, Alan E. Rowan, and Roeland J. M. Nolte**

In recent years the self-assembly of block copolymers has received considerable attention, which has resulted in many exciting discoveries.[1] By careful selection of the type of blocks employed, the properties of these polymers can be readily tuned, making them potentially interesting systems from both an academic and industrial point of view. When a good solvent is chosen for only one of the blocks, aggregation will occur, thus leading to phase separation. A great number of parameters can be varied, which alter the aggregation architecture, namely, temperature, solvent, block length, ratio of one block to another, concentration, and pH.[2] Consequently, a wide variety of morphologies has been reported for this type of self-assembled macromolecules, for example, spheres, rods, lamellae, films, and patterned surfaces,[3] which have a considerable potential in a wide range of applications in the fields of optoelectronics and biomedicine.[4]

Rod–coil diblock copolymers, consisting of a flexible and a rigid block, constitute a special class of block copolymers.[2,3] Recently, we have shown that polyisocyanopeptides can be used as the rigid component in such systems.[5,6] These isocyanide polymers have a very high persistence length, which originates from the well-defined helical β-sheet arrangement of the polymer side chains.[7] Charged diblock copolymers of styrene and isocyano-L-alanyl-L-alanine, and of styrene and isocyano-L-alanyl-L-histidine have also been prepared and found to self-assemble in water to form a variety of structures such as vesicles, multilayers and even helical aggregates.[5]

Herein, we describe the aggregation behavior of a rod–coil diblock copolymer derived from an isocyanoamino acid containing a thiophene group. This diblock copolymer consists of 40 styrene and 50 3-(isocyano-L-alanyl-amino-ethyl)-thiophene (PS-PIAT) units and is an amphiphile in both organic and aqueous solvents because of only a slight difference in polarity between the two blocks (Figure 1a, b). The thiophene rings in PS-PIAT are present as functional groups that can be polymerized after aggregation,[8] to form stable polymerized morphologies with possibly interesting applications, for example, as conducting materials.

PS-PIAT was synthesized and characterized following procedures previously reported by us.[5] As a result of the amide functional groups in the PIAT side chains the thiophene groups are arranged in four stacks, which run parallel to the helical polymer backbone (Figure 1c). When PS-PIAT is dissolved in $CHCl_3$ it forms vesicles as was shown by transmission electron microscopy (TEM).[9] Upon drying, the spherical shape of the vesicles was not retained, as we concluded from the collapsed structures that were visible after platinum shadowing of the TEM grids (Figure 2a, inset I). Aggregation of the diblock copolymer molecules is induced by the poor solubility of the polyisocyanide block in $CHCl_3$. The formed vesicles have a high polydispersity, with diameters varying between 2 and 22 μm, with an average diameter of 7 μm, and an average membrane thickness, as determined from the TEM images, of 27 ± 5 nm, which is approximately twice the length of a single, stretched, PS-PIAT molecule. We propose that the vesicle membrane is composed of a bilayer, in which the polyisocyanide blocks are located in the center of the membrane and the polystyrene blocks are directed towards the solvent (Figure 2b). In separate experiments PS-PIAT was added to a dispersion of ($FeCl_3$) in $CHCl_3$ to polymerize the thiophene groups of the

[*] Dr. A. E. Rowan, Prof. Dr. R. J. M. Nolte, D. M. Vriezema, J. Hoogboom, Dr. K. Velonia
Department of Organic Chemistry
University of Nijmegen
Toernooiveld, 6525ED Nijmegen (The Netherlands)
Fax: (+31) 24-365-2929
E-mail: rowan@sci.kun.nl
nolte@sci.kun.nl
Dr. K. Takazawa, Dr. P. C. M. Christianen, Prof. Dr. J. C. Maan
High Field Magnet Laboratory
University of Nijmegen
Toernooiveld, 6525ED Nijmegen (The Netherlands)

[**] We thank Dr. J. J. L. M. Cornelissen for discussions, J. M. Hannink for making the drawings, and H. P. M. Geurts and Dr. E. S. Pierson for their help with electron and optical microscopy experiments.

 © 2003 Wiley-VCH Verlag GmbH & Co. KGaA, Weinheim 1433-7851/03/4207-0772 $ 20.00+.50/0

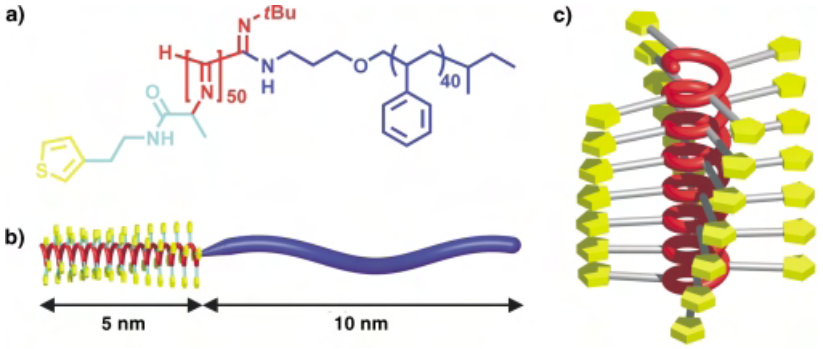

Figure 1. a) Chemical structure of PS-PIAT. b) Schematic representation of PS-PIAT. c) Schematic representation of the PIAT block showing the stacks of thiophene groups.

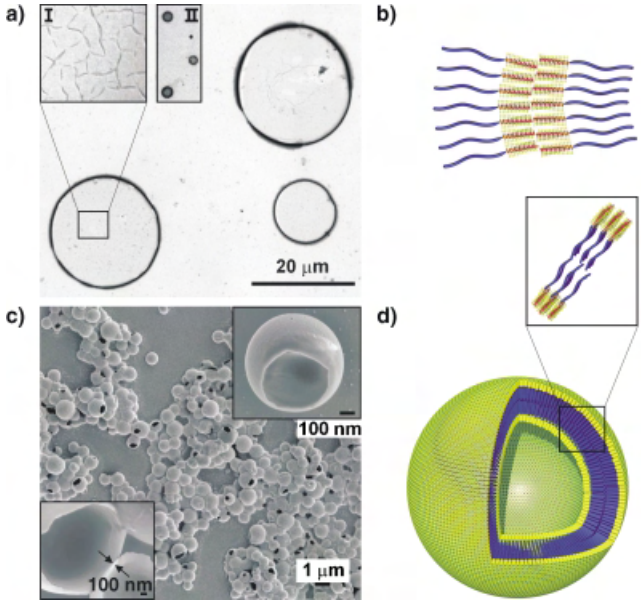

Figure 2. a) Transmission electron micrograph of PS-PIAT vesicles formed in $CHCl_3$ (concentration = 0.1 g L^{-1}) and dried on a carbon-coated copper grid (Pt shadowed). The inset I shows the middle section of the collapsed vesicles and inset II shows vesicles containing $FeCl_3$ (without Pt shadowing). b) Schematic representation of the vesicle wall in $CHCl_3$. c) Scanning electron micrograph of PS-PIAT vesicles formed in THF/water. The inset top right shows a close-up of a vesicle, and the inset bottom left shows the membrane thickness, indicated by arrows. d) Schematic representation of a PS-PIAT vesicle formed in water with a close-up of the vesicle membrane showing the proposed bilayer structure.

aggregates. However, no polymerization occurred and only smaller vesicles were formed, which contained entrapped metal complexes. TEM studies on these samples revealed that there was a high concentration of $FeCl_3$ located near or in the membrane of the vesicles (inset II in Figure 2a).

The aggregation behavior of PS-PIAT was subsequently studied in water by injecting a PS-PIAT solution in THF (0.5 g L^{-1}) into ultra-pure water, which gave a final water/THF ratio of 5:1 (v/v).[9] After the solution was allowed to equilibrate over two days, the morphology of the aggregates was examined by cryogenic scanning-electron microscopy (cryo-SEM) and SEM (Figure 2c). In both the SEM and cryo-SEM images spherical particles were visible. A number of these particles contained holes, which shows that they had a hollow interior. From this evidence, it was concluded that the aggregates were vesicular in nature. Inclusion experiments with the water-soluble fluorescence probe ethidium bromide, followed by size-exclusion chromatography, also indicated that the spherical particles were vesicles.[10] Fluorescence microscopy studies of these filled vesicles and of vesicles filled with methylene blue support the vesicular nature of the spheres. Their membranes had a thickness of 30 ± 10 nm (see bottom-left inset in Figure 2c), which corresponds to twice the length of a single PS-PIAT molecule. The most likely membrane structure of the vesicles in water is therefore a bilayer of PS-PIAT molecules in which the polystyrene blocks are pointed towards the center of the membrane and the polyisocyanide blocks towards the solvent (Figure 2d).[2]

The SEM images revealed that upon drying the formed PS-PIAT vesicles retained their shape. These vesicles have therefore a much higher stability than the vesicles formed in $CHCl_3$, which arises from the different constitutions of their vesicle membranes. In pure water, or when only a small amount of organic solvent is present, the polystyrene blocks are in their glassy state, and consequently, there is no reorganization after evaporation of the solvent water, so the vesicles preserve their shape. In $CHCl_3$ the polystyrene blocks are in direct contact with the solvent, which gives them a high degree of flexibility, allowing the vesicles to collapse when the $CHCl_3$ evaporates.

The vesicles in THF/water (1:5 v/v) were found to fuse when left to stand to yield particles that had increased in size by a factor of 20. Fusion of the vesicles of diblock copolymers has been reported,[11] but the increase in size of these aggregates was not as dramatic as shown here. Directly after preparation the average vesicle diameter was 80 nm (Figure 3a), but a few hours after preparation larger vesicles were seen amongst the vesicles that still had a diameter of 80 nm (Figure 3b). After 50 h only large vesicles, with an average diameter of 1.5 μm, were present (Figure 3c). The growth curve of the vesicles was determined by measuring the average vesicle diameter at several intervals of time after the initial injection into water, as observed by SEM images (Figure 3d). The driving force behind the fusion process is the release of strain in the initially formed vesicles, which have a high curvature and a large number of membrane defects. By fusing into larger vesicles, the curvature energy decreases, thus leading to a thermodynamically more stable state.[12] A factor that facilitates the fusion process is the presence of THF, which gives the PS-PIAT molecules the mobility to reorganize by solvation of the polystyrene blocks. Indeed, dialysis against ultra-pure water of the PS-PIAT vesicles prepared in THF/water directly after preparation, showed that the vesicles remained small, but many vesicles were seen that were in an intermediate stage of fusion (Figure 3e, f). Even after the vesicles were allowed to stand in pure water for

 © 2003 Wiley-VCH Verlag GmbH & Co. KGaA, Weinheim 1433-7851/03/4207-0773 $ 20.00+.50/0

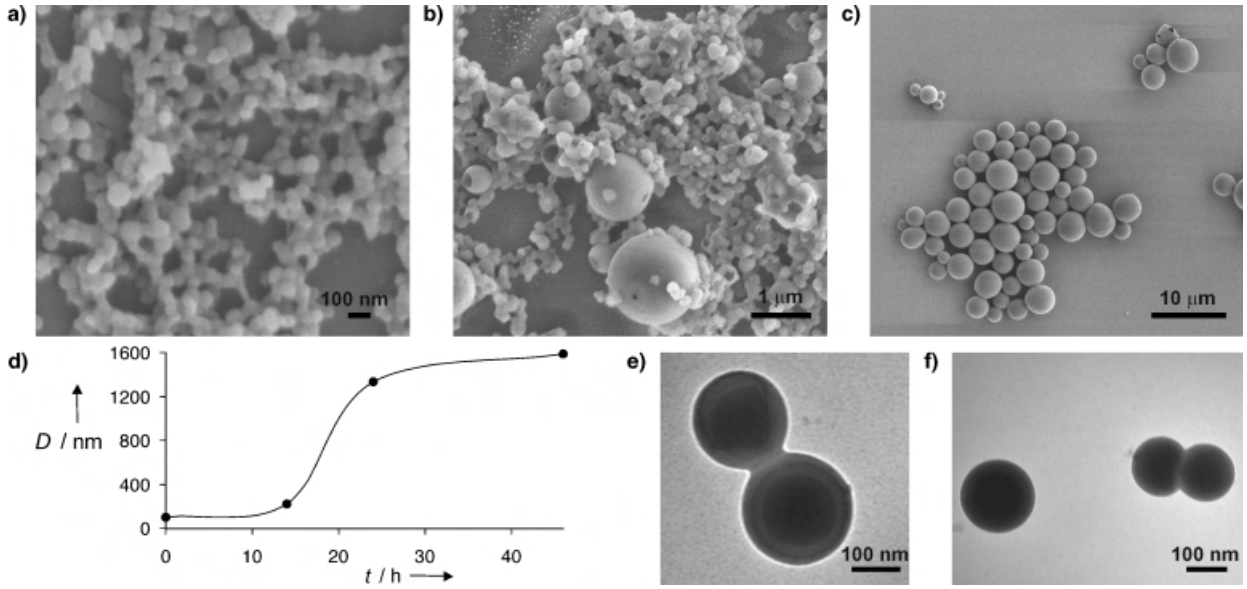

Figure 3. Fusion of PS-PIAT vesicles. a) Freshly prepared vesicles. b) Vesicles 19 h after preparation. c) Vesicles 50 h after preparation. d) Average vesicle diameter (D) as a function of time. e), and f) Intermediate stages of vesicle fusion as recorded in a dialyzed solution.

two weeks, their size remained unchanged. Therefore, THF is a necessary component for the vesicles to fuse.

Polymerization of the thiophene functional groups in the skin of PS-PIAT vesicles formed in water was investigated by electrochemical oxidation. Blank experiments with precursors of PIAT were carried out to estimate the oxidation potential necessary for thiophene polymerization inside vesicles; this potential amounted to 1.55 V (versus ferrocene/ferrocenium; Fc/Fc^+). Electrochemical polymerization was subsequently carried out by drying a drop of PS-PIAT vesicles in THF/water (1:5 v/v) on an indium-tin oxide (ITO) plate.[13] The results of SEM studies on the ITO plate after polymerization showed that the vesicles were very deformed because of intervesicular cross linking, and therefore the polymerization of the thiophene groups occurred readily, but not very selectively (Figure 4a).[14] To have more control during the polymerization, we tried chemical oxidation. Polymerization by use of $FeCl_3$ (see above), was not successful, but we found that the complex [bis(2,2′-bipyridine)ruthenium(II)-bis(pyrazolyl)] (BRP)[15] can act as a chemical oxidant.[16] In water, one of the pyrazolyl groups of BRP is protonated and the resulting species $[(bpy)_2Ru(pz)(pzH)]^+$ (BRP-H) has an oxidation potential of 1.60 V (versus Fc/Fc^+), thus making it suitable to polymerize the thiophene groups in PS-PIAT. Vesicles of PS-PIAT were prepared by injecting a 0.5 g L^{-1} solution of the diblock copolymer in THF into a solution of 2×10^{-7} M BRP in ultra-pure water at 70 °C. After the sample was allowed to stand for three days, SEM studies were carried out, the results of which showed that the vesicles were not deformed and had retained their original spherical shape (Figure 4b). The presence of polythiophene was investigated

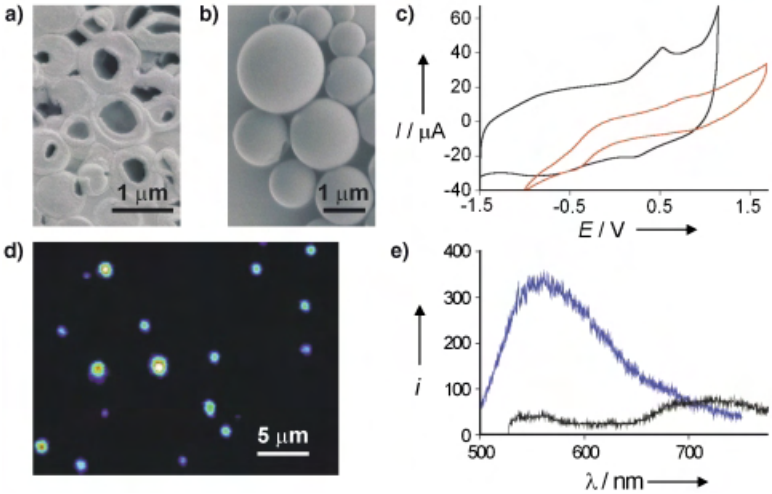

Figure 4. Polymerization of the thiophene groups of PS-PIAT vesicles. a) ITO plate containing PS-PIAT vesicles after electrochemical treatment. b) Vesicles polymerized by BRP-H. c) Cyclic voltammograms of unpolymerized vesicles (red), and of vesicles polymerized by BRP-H (black), scan-rate 250 mV s^{-1} (potential versus Fc/Fc^+). d) Fluorescence micrograph of polymerized vesicles excited with laser light at 460 nm. e) Fluorescence spectra of (excitation at 460 nm) a single unpolymerized vesicle (blue) and a single vesicle polymerized with BRP-H (black).

by electrochemical measurements on a sample of dried-in vesicles. This sample showed a new oxidation wave at 0.523 V (versus Fc/Fc^+), and a broad reduction wave at 0.23 V ($E^{1/2}=$ 0.38 V), indicative of polymerized thiophene groups (Figure 4c).[17] Infrared studies on the same sample revealed a vibration at 802 cm^{-1}, which also confirms the presence of polymerized thiophene groups.[18] To definitively prove the formation of polymerized vesicles, fluorescence experiments were carried out on single vesicles formed with and without BRP-H.[19] The polymerized vesicles are observed as fluorescent spheres upon excitation at 460 nm (Figure 4d). The emission spectrum of a single vesicle polymerized by use of

 © 2003 Wiley-VCH Verlag GmbH & Co. KGaA, Weinheim 1433-7851/03/4207-0774 $ 20.00+.50/0

the ruthenium complex displays a maximum at 725 nm (Figure 4e, black curve), which does not arise from the ruthenium complex, and is in agreement with the presence of polymerized thiophene groups.[17,20] Interestingly, a single vesicle without BRP-H has an emission spectrum with a maximum at 550 nm (Figure 4e, blue curve). We attribute the signal at 550 nm to the highly organized stacks of thiophene groups in PIAT (Figure 1c).

A potentially interesting application of the vesicles of PS-PIAT would be their use as microreactors. To this end, vesicles of PS-PIAT were loaded with *Candida antarctica* Lipase B (CAL B) enzymes.[21] When this sample was examined by TEM, dark and light vesicles were seen (Figure 5a). The same experiment was carried out with CAL B enzymes labeled with the fluorescent dye Alexa Fluor 488. Fluorescence microscopy experiments again showed that two types of vesicles were present: vesicles with, and without fluorescence (Figure 5b). From the results of these combined experiments, it was concluded that the dark vesicles in the TEM images contain entrapped enzymes and the light vesicles are empty. The activity of the entrapped enzymes was tested by adding the substrate 6,8-difluoro-4-methylumbelliferyl octanoate (DiFMU octanoate) to the mixture. This compound fluoresces when the DiFMU group is cleaved upon hydrolysis, which is catalyzed by the enzyme CAL B. After 30 min a significant increase in fluorescence intensity from the single vesicles could be detected, compared to the normal intensity arising from the auto-hydrolysis of the DiFMU octanoate (Figure 5c). This proves that the entrapped enzymes were still active and that the substrate can permeate through the vesicle membrane. Interestingly, the resulting more polar product does not permeate the vesicle.

In summary, we have synthesized new diblock copolymers that are uniquely able to form aggregates in both water and organic solvents. In THF/water (1:5 v/v) the initially formed vesicles fuse to form aggregates with a diameter 20× larger than that of the original vesicles. The thiophene groups located in the skin of the aggregates can be coupled to give polymerized vesicles. The vesicles are capable of including enzymes, thus resulting in catalytically active microreactors, which are permeable to substrate molecules. The combination of polymerizable vesicle-forming diblock copolymers with the inclusion of enzymes opens the possibility to create stable micrometer-sized reaction vessels. The presence of the thiophene functional groups in the diblock copolymers additionally enables the construction of conducting vesicles with potentially tunable properties.

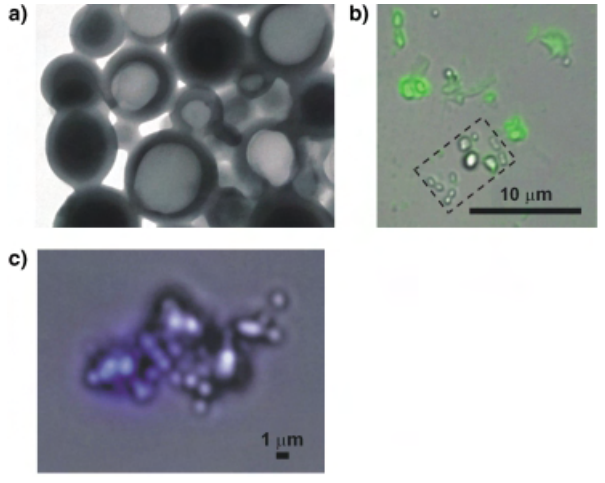

Figure 5. Inclusion of CAL B enzymes inside vesicles of PS-PIAT in THF/water. a) TEM micrograph of a dried drop of this mixture on a carbon-coated copper grid. b) Superposition of an optical micrograph and a fluorescence micrograph excited at 488 nm of the same region of the sample showing a distribution of both empty PS-PIAT vesicles and vesicles containing Alexa Fluor 488 labeled enzymes. Vesicles without enzymes are indicated by a rectangle. c) Fluorescent emission of product formed from DiFMU octanoate hydrolysis by CAL B entrapped in PS-PIAT vesicles.

Received: September 12, 2002 [Z50150]

[1] a) M. Lee, B.-K. Cho, W.-C. Zin, *Chem. Rev.* **2001**, *101*, 3869; b) B. M. Discher, D. A. Hammer, F. S. Bates, D. E. Discher, *Curr. Opin. Colloid Interface Sci.* **2000**, *5*, 125.
[2] N. S. Cameron, M. K. Corbierre, A. Eisenberg, *Can. J. Chem.* **1999**, *77*, 1311.
[3] a) L. Zhang, K. Yu, A. Eisenberg, *Science* **1996**, *272*, 1777; b) S. A. Jenekhe, X. L. Chen, *Science* **1998**, *279*, 1903.
[4] a) J. Liu, E. Sheina, T. Kowalewski, R. D. McCullough, *Angew. Chem.* **2002**, *114*, 339; *Angew. Chem. Int. Ed.* **2002**, *41*, 329; b) B. de Boer, U. Stalmach, H. Nijland, G. Hadziioannou, *Adv. Mater.* **2000**, *12*, 1581; c) B. Jeong, Y. H. Bae, D. S. Lee, S. W. Kim, *Nature* **1997**, *388*, 860.
[5] J. J. L. M. Cornelissen, M. Fischer, N. A. J. M. Sommerdijk, R. J. M. Nolte, *Science* **1998**, *280*, 1427.
[6] J. J. L. M. Cornelissen J. J. J. M. Donners, R. de Gelder, W. S. Graswinckel, G. A. Metselaar, A. E. Rowan, N. A. J. M. Sommerdijk, R. J. M. Nolte, *Science* **2001**, *293*, 676.
[7] P. Samorí, C. Ecker, I. Gössl, P. A. J. de Witte, J. J. L. M. Cornelissen, G. A. Metselaar, M. B. J. Otten, A. E. Rowan, R. J. M. Nolte, J. P. Rabe, *Macromolecules* **2002**, *35*, 5290.
[8] Polymerized vesicles were prepared from low-molecular-weight surfactants, for a review see: H. Ringsdorf, B. Schlarb, J. Venzmer, *Angew. Chem.* **1988**, *100*, 117; *Angew. Chem. Int. Ed. Engl.* **1988**, *27*, 113.
[9] During the preparation no extra energy, for example, from stirring or sonication, was put into the suspension.
[10] A PS-PIAT solution of 0.5 g L^{-1} in THF was injected into a solution of 10^{-4} M ethidium bromide in water, with a final THF/water ratio of 1:5 (v/v). This mixture was allowed to equilibrate over 50 h before purification by Sephadex gel chromatography. A fluorescence detector at 280 nm was used to monitor the fractions. The vesicles with entrapped ethidium bromide had a retention time of 3 h; the nonincluded dye had a retention time of 56 h.
[11] a) L. Luo, A. Eisenberg, *Langmuir* **2001**, *17*, 6804; b) M. Maskos, J. R. Harris, *Macromol. Rapid Commun.* **2001**, *22*, 271.
[12] J.-K. Lee, B. R. Lentz, *Biochemistry* **1997**, *36*, 6251.
[13] An electrochemical cell, fitted with a $Ag/AgNO_3$ reference electrode, a platinum counter electrode, and an ITO plate as the working electrode, was used for the electrochemical polymerizations. Acetonitrile served as the solvent and tetrabutylammoniumhexafluorophosphate was added as the electrolyte. The polymerization was carried out under an inert atmosphere of nitrogen.
[14] In acetonitrile, in which the electrochemical experiments were conducted, the vesicles shrink, but do not collapse or fall apart.
[15] B. P. Sullivan, D. J. Salmon, T. J. Meyer, J. Peedin, *Inorg. Chem.* **1979**, *18*, 3369.

 © 2003 Wiley-VCH Verlag GmbH & Co. KGaA, Weinheim 1433-7851/03/4207-0775 $ 20.00+.50/0

[16] We found that BRP-H is also a polymerization catalyst for other thiophenes, for example, 3-dodecyl-thiophene.
[17] *Handbook of Oligo- and Polythiophenes* (Ed.: D. Fichou), Wiley-VCH, Weinheim, **1999**.
[18] D. Dini, F. Decker, F. Andreani, E. Salatelli, P. Hapiot, *Polymer* **2000**, *41*, 6473.
[19] In the measurement setup an argon ion laser beam was focused by a 25× microscope objective to a 50 μm diameter spot on the sample. The fluorescence emission was imaged by a 50× objective on a CCD camera.
[20] No UV/Vis spectrum could be recorded from a single vesicle, nor from a suspension of vesicles, because of scattering problems.
[21] A 0.5 $g L^{-1}$ solution of PS-PIAT dissolved in THF was injected into a 30 $mg L^{-1}$ solution of CAL B enzymes; the final water/THF ratio was 12:1 (v/v). After the mixture was left for two days to equilibrate, it was dialyzed to dispose of all nonincluded enzymes.

 © 2003 Wiley-VCH Verlag GmbH & Co. KGaA, Weinheim 1433-7851/03/4207-0776 $ 20.00+.50/0

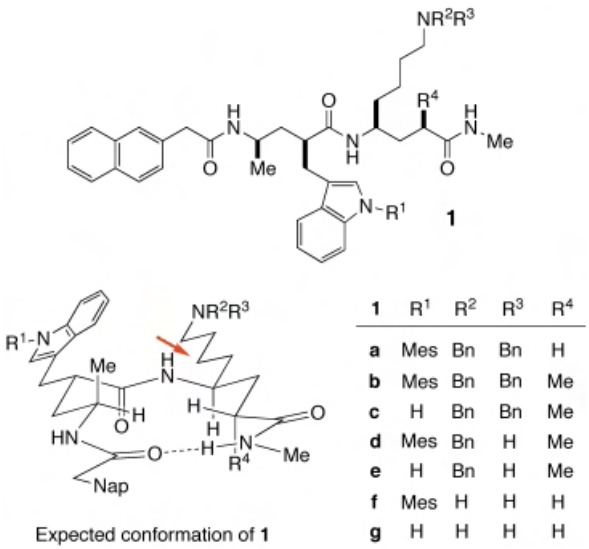

1	R^1	R^2	R^3	R^4
a	Mes	Bn	Bn	H
b	Mes	Bn	Bn	Me
c	H	Bn	Bn	Me
d	Mes	Bn	H	Me
e	H	Bn	H	Me
f	Mes	H	H	H
g	H	H	H	H

Scheme 1. Structural formulae of the γ-peptides **1**. In the expected conformation of **1** the red arrow points to a CH_2 group of the $H_2N(CH_2)_4$ unit, which is placed inside the shielding cone of the aromatic indole ring. Mes = mesitylenesulfonyl, Bn = benzyl, Nap = naphthyl.

Somatostatin Mimics

Design and Synthesis of γ-Dipeptide Derivatives with Submicromolar Affinities for Human Somatostatin Receptors

Dieter Seebach, Laurent Schaeffer, Meinrad Brenner, and Daniel Hoyer*

In a previous paper we have shown that simple *N*-acyl-γ-dipeptide amides that resemble a βII′ turn of an α-peptide can be designed to form a turn structure in solution (NMR) and in the solid state (X-ray).[1,2] To see whether such a turn could also be used to mimic a peptide, the biological activity of which rests upon a turn structure carrying functionalized side chains, we have now synthesized compounds **1a–g** (Scheme 1), with the side chain of tryptophan in the γ^2 position of the first and of lysine in the γ^4 position of the second γ-amino acid, and have tested their affinities for the human somatostatin receptors $hsst_{1-5}$.[3–6]

The synthesis of γ-dipeptide derivatives **1** commenced with the *N*-Boc-γ-lactams **2** and **3** (Boc = *tert*-butoxycarbonyl), readily available from the corresponding commercial (*R*)-Ala and (*S*)-Lys acids by known procedures.[1,7] Ring opening (with the Lys derivative after change of side-chain protection, →**4**), and esterification with $Me_3Si(CH_2)_2OH$ provided the (*R*)-Boc-γ^4-hhAla and Boc-γ^4-hhLys(Bn_2) esters, which were

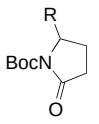

(*R*)-**2**, R = Me
(*S*)-**3**, R = $(CH_2)_4$NH(2-Cl-Z)
(*S*)-**4**, R = $(CH_2)_4NBn_2$

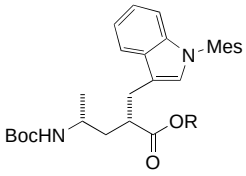

5, R = $(CH_2)_2SiMe_3$
6, R = H

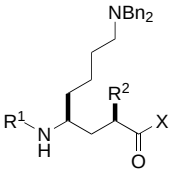

7, R^1 = Boc, R^2 = Me, X = $O(CH_2)_2SiMe_3$
8, R^1 = R^2 = H, X = NHMe
9, R^1 = H, R^2 = Me, X = NHMe

doubly deprotonated and alkylated with 1-mesitylenesulfonyl-3-bromomethylindole and MeI to give the *unlike* $\gamma^{2,4}$-amino acid derivatives **5** and **7**, respectively. The ester group in compound **5** with Trp side chain was cleaved (Bu_4NF, →**6**), and the lysine-derived esters were converted to the methylamides **8** and **9** without and with 2-methyl substitution, respectively (1. Bu_4NF, 2. $MeNH_2$, 3. F_3CCO_2H). Coupling of the two γ-amino acid derivatives (**6** + **8** and **6** + **9**), removal of the Boc groups, and acylation with 2-naphthylacetic acid[8] (4-methylmorpholine, 1-hydroxy-1*H*-benzotriazole, 1-ethyl-3-(3-dimethylaminopropyl)carbodiimide) produced the side-chain-protected *N*-acyl-dipeptide amides **1a** and **1b**. Deprotection procedures ($MeSO_3H$, F_3CCO_2H, and Pd/C, H_2) led to the various partially or fully deprotected γ-dipeptide derivatives **1c–1g**. All compounds were purified and fully characterized by elemental analyses, specific optical rotations, circular dichroism (CD), IR, and NMR spectroscopy, and mass spectrometry.

[*] Prof. Dr. D. Seebach, Dr. L. Schaeffer, Dr. M. Brenner
Laboratorium für Organische Chemie
Eidgenössische Technische Hochschule
ETH Hönggerberg, 8093 Zürich (Switzerland)
Fax: (+41) 1-632-11-44
E-mail: seebach@org.chem.ethz.ch
Dr. D. Hoyer
Novartis Pharma AG
Nervous System Research
S-386-745, 4002 Basel (Switzerland)

 © 2003 Wiley-VCH Verlag GmbH & Co. KGaA, Weinheim 1433-7851/03/4207-0776 $ 20.00+.50/0

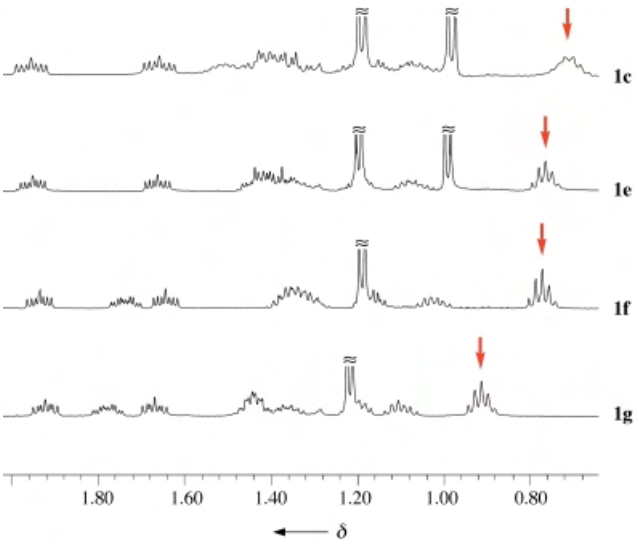

Figure 1. High-field part of the 500 MHz ^{1}H NMR spectra of the γ-dipeptides **1c, 1e, 1f**, and **1g** in CD_3OD. The red arrows point to high-field-shifted $N(CH_2)_4$ resonances.

A typical feature of the turn structure in somatostatin and its analogues is the juxtaposition of the tryptophan and lysine side chains, which places CH_2 groups of the $H_2N(CH_2)_4$ unit inside the shielding cone of the aromatic indole ring (NMR shifts between $\delta = 0.8$ and 0.3 ppm are observed).[9] High-field sections of the NMR spectra of four γ-dipeptide amides, shown in Figure 1, in which CH_2 signals appear between $\delta = 0.9$ and 0.6 ppm, confirm the proximity between the corresponding side chains, and are thus compatible with a turn conformation of these compounds. The CD spectra of the *N*-naphthylacetyl dipeptide amides **1** exhibit an intensive negative Cotton effect near 200 nm ([Θ] up to 70000 deg cm^2 dmol^{-1}), with a weaker and broader peak near 220 nm ([Θ] up to 30000 deg cm^2 dmol^{-1}) (Figure 2); this CD pattern may be taken as another piece of evidence for the presence of a secondary structure.

Probably the most stringent test of the γ-dipeptide structure is the affinity for somatostatin receptors. Binding affinities for the five cloned human receptors $hsst_{1-5}$, expressed in CCL-39 cell lines, were determined by displacement of [^{125}I]LTT-$SRIF_{28}$ from these receptor proteins.[10] While the fully protected γ-dipeptide **1d** binds to $hsst_1$ and $hsst_3$ with remarkable K_D values of 0.55 and 1.00 μM, respectively, the partially and the fully deprotected γ-dipeptide derivatives **1f** and **1g** bind to $hsst_5$ with K_D values of 0.51 and 0.87 μM, respectively (Table 1). Intriguingly, the highest affinities (**1d**/$hsst_1$, **1f**/$hsst_5$) are observed when the side chain functional groups (3-indolylmethyl and $(CH_2)_4NH_3^+$) are protected by bulky aromatic moieties (*N*-mesitylenesulfonyl and/or -benzyl)!

The results presented here are confirmative, surprising, and promising; they demonstrate that a 14-amino-acid cyclic disulfide hormone, somatostatin, can be mimicked by a simple, designed, low-molecular-weight, open-chain γ-dipeptide derivative (cf. **1g**) that contains only three amide bonds; they suggest that hitherto unknown hydrophobic pockets are present in the receptors ($hsst_1$, $hsst_3$, and $hsst_5$), which supposedly house the turn-bound Trp and Lys side chains (cf. **1c, 1d, 1f**); and they promise a potential of γ-peptides for the development of peptidase-resistant[11] peptidomimetic drugs.

Table 1: pK_D Values for γ-peptides **1b–1g** at the five hsst receptors expressed in CCL-39 cells and measured by radioligand binding assays with [^{125}I]LTT-$SRIF_{28}$ as radioligand.[a],[10]

Receptor	1b	1c	1d	1e	1f	1g	Octreotide[b]	$SRIF_{14}$[c]
$hsst_1$	5.47	6.06	6.26	5.61	5.98	4.73	6.45	9.08
$hsst_2$	< 5	< 5	5.17	< 5	5.01	2.81	9.11	10.06
$hsst_3$	5.53	5.89	6.00	5.73	5.67	5.42	8.60	9.67
$hsst_4$	4.67	5.74	5.92	5.66	5.79	5.44	5.76	8.39
$hsst_5$	4.49	5.01	5.87	5.14	6.29	6.06	7.31	9.01

[a] Submicromolar affinities are highlighted in red. [b] Sandostatin. [c] Somatostatin.

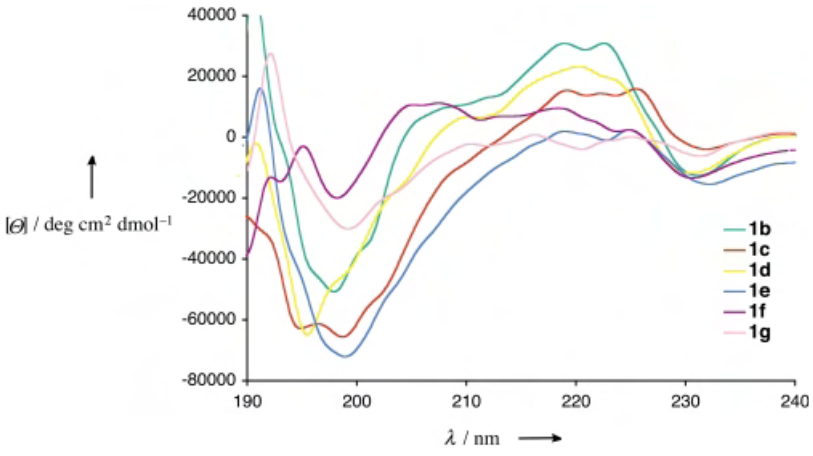

Figure 2. Nonnormalized CD spectra in MeOH (0.2 mM) of the γ-dipeptide derivatives **1b–1g**.

Received: September 25, 2002 [Z50242]

[1] M. Brenner, D. Seebach, *Helv. Chim. Acta* **2001**, *84*, 2155–2166.
[2] For a non-peptidic analogue, see: R. W. Hoffmann, *Angew. Chem.* **2000**, *112*, 2134–2150; *Angew. Chem. Int. Ed.* **2000**, *39*, 2054–2070.
[3] For β-tetrapeptides mimicking somatostatin with nanomolar affinities for $hsst_4$, see: K. Gademann, M. Ernst, D. Hoyer, D. Seebach, *Angew. Chem.* **1999**, *111*, 1302–1304; *Angew. Chem. Int. Ed.* **1999**, *38*, 1223–1226; K. Gademann, M. Ernst, D. Seebach, D. Hoyer, *Helv. Chim. Acta* **2000**, *83*, 16–33; K. Gademann, T. Kimmerlin, D. Hoyer, D. Seebach, *J. Med. Chem.* **2001**, *44*, 2460–2468; D. Seebach, M. Rueping, P. I. Arvidsson, T. Kimmerlin, P.

 © 2003 Wiley-VCH Verlag GmbH & Co. KGaA, Weinheim 1433-7851/03/4207-0777 $ 20.00+.50/0

Micuch, C. Noti, D. Langenegger, D. Hoyer, *Helv. Chim. Acta* **2001**, *84*, 3503 – 3510.
[4] For a review on somatostatin receptors, see: D. Hoyer, H. Luebbert, C. Bruns, *Naunyn-Schmiedeberg's Arch. Pharmacol.* **1994**, *350*, 441 – 453; J. P. Hannon, C. Nunn, B. Stolz, C. Bruns, G. Weckbecker, I. Lewis, T. Troxler, K. Hurth, D. Hoyer, *J. Mol. Neurosci.* **2002**, *18*, 15 – 27. Classification and nomenclature of somatostatin receptors: D. Hoyer, G. I. Bell, M. Berelowitz, J. Epelbaum, W. Feniuk, P. P. Humphrey, A. M. O'Carroll, Y. C. Patel, A. Schonnbrunn, J. E. Taylor, T. Reisine, *Trends Pharmacol. Sci.* **1995**, *16*, 86 – 88.
[5] For a review on somatostatin analogues, see: A. Janecka, M. Zubrzycka, T. Janecki, *J. Pept. Res.* **2001**, *58*, 91 – 107.
[6] Methyl groups in the γ^4 position of the first and in the γ^2 position of the second γ-amino acid do stabilize the turn (see ref. [1] for more details).
[7] M. Smreina, P. Majer, E. Majerova, T. A. Guerassina, M. A. Eissanstat, *Tetrahedron* **1997**, *53*, 12867 – 12874; S. Hanessian, R. Schaum, *Tetrahedron Lett.* **1997**, *38*, 163 – 166; T. Hintermann, K. Gademann, B. Jaun, D. Seebach, *Helv. Chim. Acta* **1998**, *81*, 983 – 1002.
[8] The choice of a 2-naphthylacetyl group at the *N*-terminus was inspired by previous observations: The naphthyl group may be considered to mimic the benzyl side chain of a Phe residue, which precedes the Trp in the peptide chain of somatostatin: S. J. Hocart, R. Jain, W. A. Murphy, J. E. Taylor, B. Morgan, D. H. Coy, *J. Med. Chem.* **1998**, *41*, 1146 – 1154; A. J. Souers, A. A. Virgilio, A. Rosenquist, W. Fenuik, J. A. Ellman, *J. Am. Chem. Soc.* **1999**, *121*, 1817 – 1825.
[9] B. H. Arison, R. Hirschmann, D. F. Veber, *Bioorg. Chem.* **1978**, *7*, 447 – 451; R. M. Freidinger, D. S. Perlow, W. C. Randall, R. Saperstein, B. H. Arison, D. F. Veber, *Int. J. Pept. Protein Res.* **1984**, *23*, 142 – 150; C. Wynants, D. Tourwe, W. Kazmierski, V. J. Hruby, G. Van Binst, *Eur. J. Biochem.* **1989**, *185*, 371.
[10] J. P. Hannon, C. Petrucci, D. Fehlmann, C. Viollet, J. Epelbaum, D. Hoyer, *Neuropharmacology* **2002**, *42*, 396 – 413. CCL-39 stands for *C*hinese hamster *l*ung fibroblast *c*ells No. 39. [^{125}I]LTT-SRIF$_{28}$ is a somatostatin dimer containing three mutations (*L*eu^8, D-Trp^{22}, ^{125}I-*T*yr), and SRIF is the acronym for *s*omatostatin *r*elease *i*nhibiting *f*actor, 28 refers to the numbere of amino acids in the physiologically active form of the hormone.
[11] J. Franckenpohl, P. I. Arvidsson, J. V. Schreiber, D. Seebach, *ChemBioChem* **2001**, *2*, 445 – 455.

 © 2003 Wiley-VCH Verlag GmbH & Co. KGaA, Weinheim 1433-7851/03/4207-0778 $ 20.00+.50/0

Controlled Electropolymerization

Liquid-Crystal Templating of Conducting Polymers**

*James F. Hulvat and Samuel I. Stupp**

In organic electronics, conducting polymers have a number of advantages over small molecules, particularly because of their stability, mechanical properties, and ease of processing.[1,2] However, performance of some conducting polymers is limited by their high degree of disorder.[3,4] Molecular ordering improves carrier mobility in organic field-effect transistors and enhances charge injection in organic light-emitting diodes (OLEDs).[5] For this reason, vapor-sublimated crystalline films of small molecules are often used,[3] but alternative strategies to obtain molecular ordering would reduce cost and simplify fabrication of organic electronic devices. One possible way to achieve this is through molecular self-organization. Toward this goal we developed an aqueous, low-temperature technique for preparing conducting polymer films in a self-organized template.

Films of poly(3,4-ethyldioxythiophene) (PEDOT) are commonly used as hole injection layers in OLEDs. PEDOT can be polymerized in organic solvents or in an aqueous suspension with a soluble copolymer or surfactant, leading to amorphous films.[6] We have studied here the formation of PEDOT films by electropolymerization within a liquid crystalline template.

The well-known hexagonal (H1) lyotropic liquid crystal (LC) consists of cylindrical hydrophobic cores parallel to one another and separated by a hydrophilic continuum (see Figure 1 in the Supporting Information).[7] LCs have been used by us and others to template inorganic minerals as well as in the formation of mesoporous silica.[8] With regard to conducting polymers, template chemistry has been used to incorporate chains within the channels of mesoporous silica[9] or in aqueous channels of an inverse hexagonal LC.[10] These approaches, however, are limited to soluble, chemically polymerized polymers or to water-soluble monomers such as aniline or pyrrole. Our approach described here is novel in two key respects. First, polymerization occurs in the hydrophobic domain of the LC, allowing use of less polar

[*] Prof. S. I. Stupp, J. F. Hulvat
Department of Materials Science and Engineering
Department of Chemistry
Feinberg School of Medicine
Northwestern University
Evanston, IL 60208-3108 (USA)
Fax: (+1) 847-491-3010
E-mail: s-stupp@northwestern.edu

[**] This work made use of the Electron Probe Instrumentation Center at Northwestern University and was funded by a DoE grant (DE-FG02-00ER45810/A001). J.F.H. is supported by an NDSEG fellowship. We thank M. Kern for assistance with XRD and Prof. I. Koltover for helpful discussions.

Supporting information for this article is available on the WWW under http://www.angewandte.org or from the author.

 © 2003 Wiley-VCH Verlag GmbH & Co. KGaA, Weinheim 1433-7851/03/4207-0778 $ 20.00+.50/0

monomers with potentially more useful electronic properties, such as 3,4-ethyldioxythiophene (EDOT) and bithiophene.[2,11] In addition, the polymers formed within the template need not be soluble since the nanoscale distribution of monomers in the LC is locked-in during polymerization. Incorporation of bulky substituents to solubilize the polymer is avoided, simplifying preparation and possibly improving electronic properties.[12]

Poly(oxyethylene)–alkyl amphiphiles form various LC phases in water.[13] Poly(oxyethylene)$_n$–oleyl ether ($n \sim 10$) (Scheme 1) forms a self-supporting gel at concentrations in water in the range of 35—60 wt %. This gel is a hexagonal LC

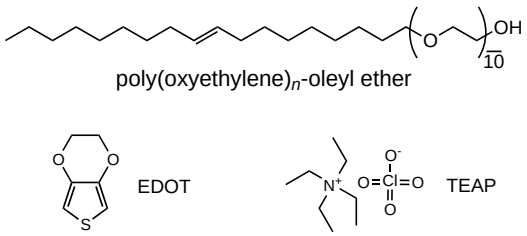

Scheme 1. Amphiphile, monomer, and supporting electrolyte for liquid crystal templating system.

with 3 nm hydrophobic cores spaced 7.7 nm apart, as determined by small-angle X-ray diffraction (XRD) (see Figure 2 in the Supporting Information). The aliphatic cores solublize hydrophobic molecules such as EDOT, which is only sparingly soluble in water (< 0.002 M), but up to 0.25 M EDOT can be incorporated in the hexagonal LC phase. This strongly suggests that the monomer becomes localized within the 3 nm hydrophobic cores. We use tetraethylammonium perchlorate (TEAP) as a supporting electrolyte to facilitate electropolymerization in the LC. Small-angle XRD shows no significant change in LC structure upon incorporation of 0.2 M EDOT and TEAP (see Figure 2 in the Supporting Information). Differential scanning calorimetry (DSC) indicates that EDOT- and TEAP-doped gels are thermally stable with an isotropization point (T_i) of 46 °C compared with 49 °C for undoped gels (see Figure 3 in the Supporting Information).

We polymerized EDOT-doped gels potentiostatically on gold- or ITO(indium-tin oxide)-coated glass substrates. In this procedure, the electrochemical cell is sealed, heated to 60 °C, cooled slowly (0.03 °C min^{-1}), and annealed just below T_i. This allows the LC to self-organize forming large, uniaxial domains ~500 μm in size. EDOT electropolymerizes anodically at 1.3 V versus Ag/AgCl in the LC template, with a mean current density of 2.0 mA cm^{-2}. After polymerization, the LC gel is removed by washing in water, acetone, and CH_2Cl_2. Heating to 110 °C in vacuum (~10 mbar) removes any remaining solvent.

Figure 1a shows the polymer thickness t obtained as a function of time at different potentials, as measured by profilometry. Film growth in the LC is shown to be diffusion-limited given the observed quadratic growth rate, whereas in isotropic solutions it follows a linear, reaction-limited rate (Figure 1b). This is likely due to the confinement of EDOT molecules in the hydrophobic cores of the LC template. Figure 1c shows cyclic voltammetry of the EDOT- and

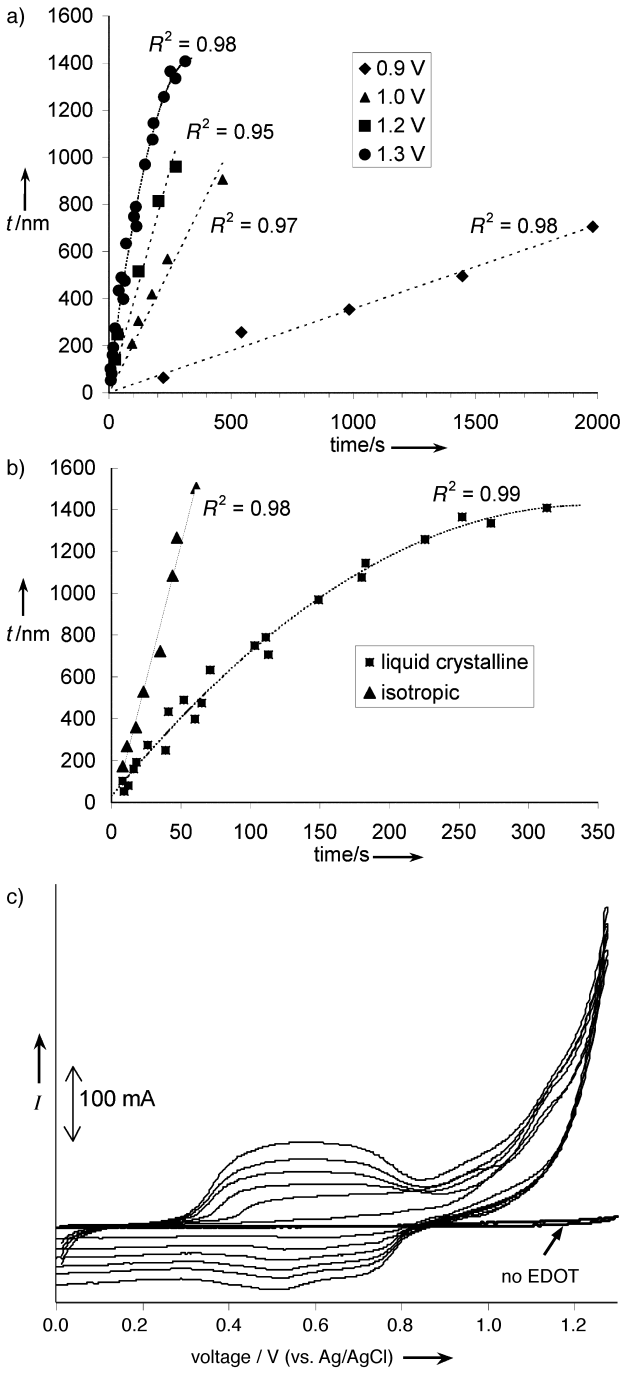

Figure 1. EDOT electropolymerization: a) PEDOT film thickness t as a function of time and potential. b) Film growth within the liquid crystalline template and in an isotropic solution of similar composition (at 1.3 V versus Ag/AgCl). Quadratic behavior (dashed line) indicates diffusion-limited growth. c) Cyclic voltammetry of EDOT and TEAP in LC gel of **1**. Arrow indicates LC gel without EDOT.

TEAP-doped LC. The electrochemical behavior is similar to that described in the literature for PEDOT polymerization.[14]

We observed in situ the film formed during electropolymerization using a two-electrode setup with transparent ITO glass sandwiched around a teflon spacer filled with LC gel. Blue domains of PEDOT grow commensurate with domains of the LC template (Figure 2), and polymer thick-

 © 2003 Wiley-VCH Verlag GmbH & Co. KGaA, Weinheim 1433-7851/03/4207-0779 $ 20.00+.50/0

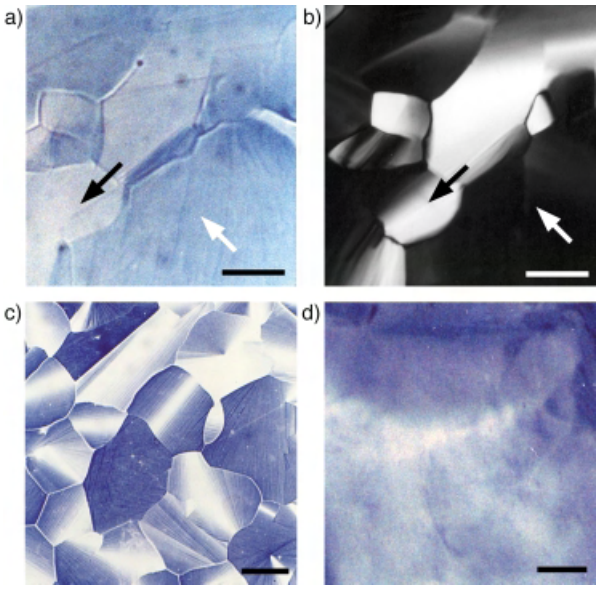

Figure 2. Optical micrographs of PEDOT electropolymerized on ITO (bars = 100 μm): a) nonpolarized and b) cross-polarized images of PEDOT in LC template during polymerization. Black arrows show a domain with director parallel to the substrate (slow PEDOT growth), and white arrows point to domains with director normal to substrate (rapid growth). c) Domain structure of a similarly grown PEDOT film after the LC template is removed. d) PEDOT polymerized in isotropic solution has no domain structure.

ness was found to vary with LC director orientation. Domains with director orientation parallel to the substrate result in less polymer growth, while those with a director oriented normal to the electrode surface exhibit the most rapid and thickest polymer growth. This indicates that the anisotropic LC environment mediates polymerization, that is, if monomer diffusion is confined to hydrophobic cores, the polymer should grow fastest in cores aligned normal to the substrate, that is, parallel to the electric field.

After the LC template is washed away, PEDOT films remain adhered to the electrode with no change in microstructure. Interestingly, these polymeric films essentially "copy" the LC texture, revealing birefringent domains that match those of the LC medium (Figure 3). We propose that polymerization within the confined nanoscale environment of hydrophobic cores produces polymer chains oriented parallel to the director of the LC. Thus, the optical anisotropy of the LC template is transferred to the PEDOT film during polymerization. Anisotropy is of course locked-in due to the polymer's insolubility. Similar films prepared from EDOT and TEAP in CH_3CN or in an LC mixture heated above the isotropization temperature (Figure 2d) lead to amorphous films with no domain structure or birefringence, confirming that the optical anisotropy of the PEDOT arises directly from the self-organized nature of the LC template. Figure 4 shows scanning electron microscopy (SEM) images of the PEDOT film after removal of the LC gel. Templated films show a texture consisting of ~50 nm nodules (Figure 4a–c) the size and height of which creates the observed domain structure. Amorphous films (Figure 4d,e) show no similar features. We propose that the structure observed in the templated films

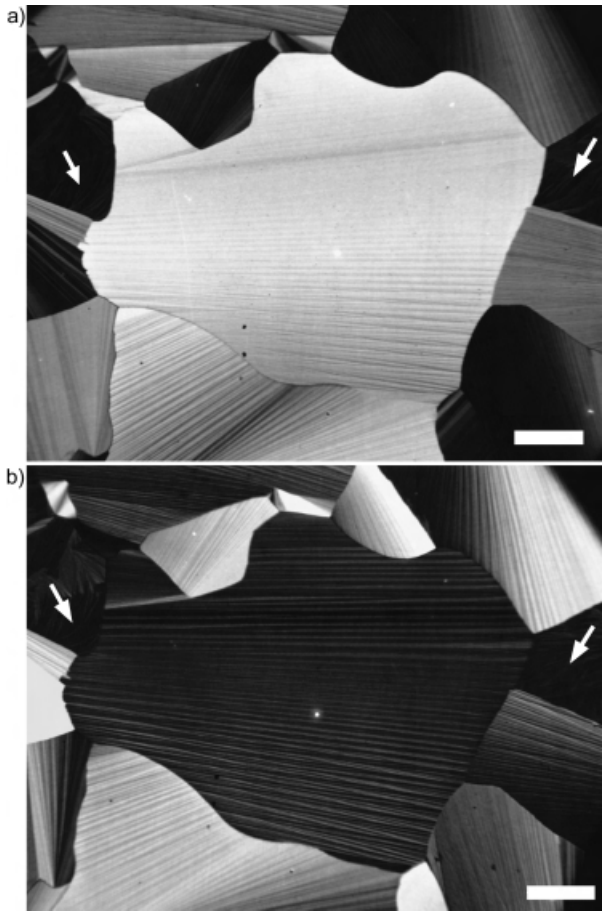

Figure 3. Polarized optical micrographs showing birefringence of templated PEDOT film after removing the LC template (bar = 100 μm). Center domain has its optical axis oriented parallel to the substrate: a) 45° relative to polarizer, b) 0° relative to polarizer. Arrows indicate domains with their optical axis oriented normal to the substrate.

results from a directed aggregation of oriented polymer chains that collapse together when the LC template is removed (Figure 4f).

The method reported here offers a simple, novel way to control and lock-in molecular orientation in conducting polymers using a self-assembled medium of surfactant molecules. EDOT electropolymerization in an organized template yields films exhibiting optical anisotropy commensurate with the LC template. Molecular alignment in these films might be used to improve charge injection from conducting polymer layers in OLEDs or otherwise enhance film properties in organic electronic devices.

Experimental Section

LC gels were prepared by dissolving 0.1M EDOT (99%, Bayer AG) and 0.1M TEAP (95%, Acros Organics) in poly(oxyethylene)$_n$–oleyl ether (1.0 g; 95%, Aldrich, $n \sim 10$). Deionized water (1.0 g) was added. Samples were heated in a closed vial to 80°C, vigorously mixed, and cooled, forming a transparent gel.

Electrode substrates were either e-beam evaporated (40 nm Au/10 nm Ti/glass) at $\sim 10^{-6}$ Torr or on an ITO glass (120 nm thick, Applied Thin Films). Substrates were cleaned by sonication (15 min) in acetone, CH_2Cl_2, CH_3OH, 6N HCl (30 s), and deionized water.

 © 2003 Wiley-VCH Verlag GmbH & Co. KGaA, Weinheim 1433-7851/03/4207-0780 $ 20.00+.50/0

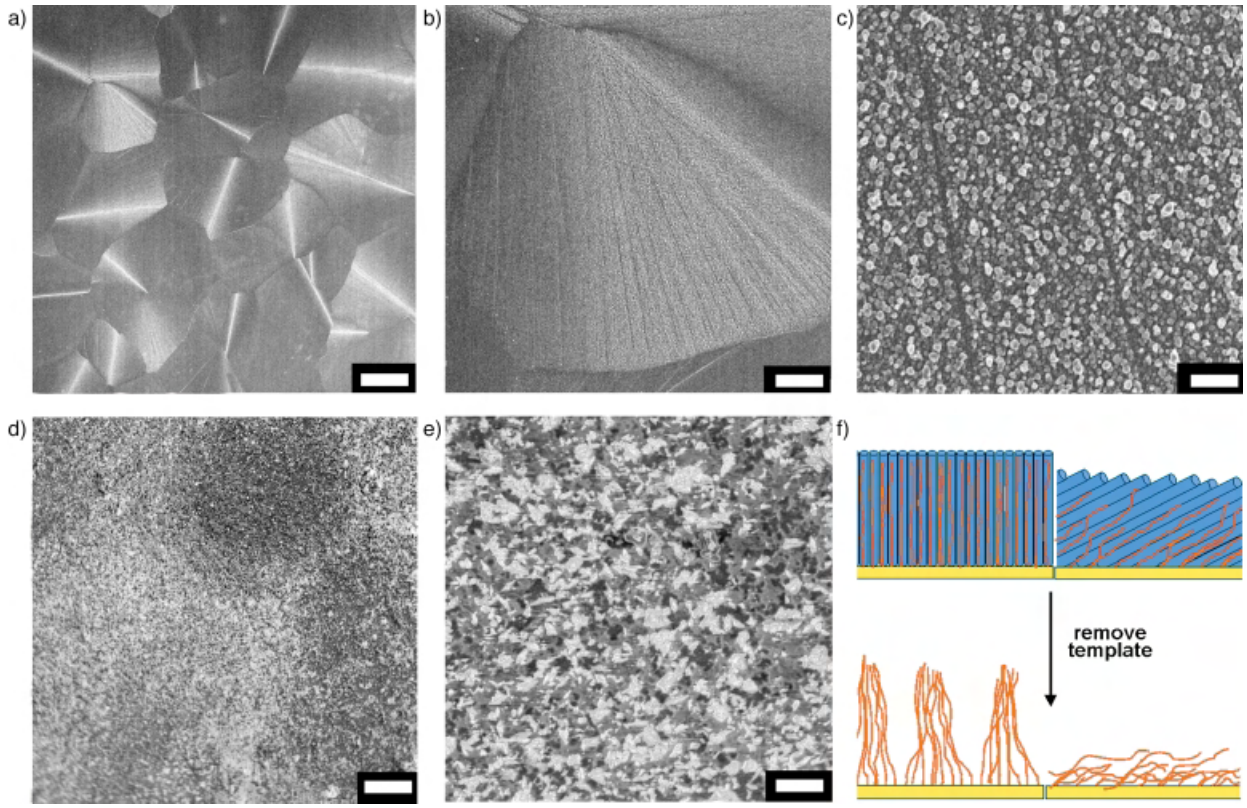

Figure 4. SEM images of PEDOT film after removal of the LC template. Templated polymer films have textures similar to focal conic textures of liquid crystals: bar = a) 50 μm, b) 10 μm, c) 1 μm. Nontemplated film grown from isotropic solution d) bar = 50 μm, e) bar = 5 μm. f) Schematic diagram depicting directed aggregation of oriented conducting polymer chains.

1.0 cm^2 substrates were placed in a glass cell 5 mm from a Pt counter electrode with a Ag/AgCl reference electrode (BAS Inc. model RE-5B). Electropolymerization and cyclic voltammetry used an E&G Princeton Applied Research potentiostat model 263A. For cyclic voltammetry, the potential was swept 0.0 to 1.3 V at 50 $mV\,s^{-1}$.

Small-angle XRD was performed in transmission geometry by sealing LC gel (~5 mg) in a polycarbonate holder using a Rigaku $Cu_{K\alpha}$ source and a 2D Bruker CCD detector calibrated with silver behenate. T_i of the LC was measured by using a TA Instruments 2920 diferential scanning calorimeter. For this purpose, 10 mg was hermetically sealed in Al pans and cycled at $5\,^{\circ}C\,min^{-1}$. The thickness of the PEDOT film was measured with a Tencor P10 profilometer, and five measurements per sample were averaged. Optical micrographs were prepared by using a Leitz Laborlux 12POL polarizing microscope with a heating stage and either a 35 mm film camera or a Sony XC-ST70 CCD camera. SEM was performed on a Hitachi S-4500FE operating at 2 kV. PEDOT films conducted sufficiently and therefore did not require any coating prior to imaging.

Received: October 29, 2002 [Z50457]

[1] a) J. Pei, W. L. Yu, W. Huang, A. J. Heeger, *Macromolecules* **2000**, *33*, 2462; b) L. J. Rothberg, A. J. Lovinger, *J. Mater. Res.* **1996**, *11*, 3174; c) H. Sirringhaus, T. Kawase, R. H. Friend, T. Shimoda, M. Inbasekaran, W. Wu, E. P. Woo, *Science* **2000**, *290*, 2123.

[2] K. Gurunathan, A. Vadivel Murugan, R. Marimuthu, U. P. Mulik, D. P. Amalanerkar, *J. Mater. Chem.* **1999**, *61*, 173.

[3] Z. N. Bao, J. A. Rogers, H. E. Katz, *J. Mater. Chem.* **1999**, *9*, 1895.

[4] T. M. Brown, J. S. Kim, R. H. Friend, F. Cacialli, R. Daik, W. J. Feast, *Appl. Phys. Lett.* **1999**, *75*, 1679.

[5] a) R. Osterbacka, C. P. An, X. M. Jiang, Z. V. Vardeny, *Science* **2000**, *287*, 839; b) P. Markart, E. Zojer, S. Tasch, R. Smith, D. Gin, G. Leising, *Synth. Met.* **1999**, *102*, 1155; c) P. K. H. Ho, J. S. Kim, J. H. Burroughes, H. Becker, S. F. Y. Li, T. M. Brown, F. Cacialli, R. H. Friend, *Nature* **2000**, *404*, 481.

[6] B. L. Groenendaal, F. Jonas, D. Freitag, H. Pielartzik, J. R. Reynolds, *Adv. Mater.* **2000**, *12*, 481.

[7] P. J. Collins, *Liquid Crystals*, Princeton University Press, Princeton, NJ, **1990**.

[8] a) P. V. Braun, P. Osenar, V. Tohver, S. B. Kennedy, S. I. Stupp, *J. Am. Chem. Soc.* **1999**, *121*, 7302; b) A. Sayari, S. Hamoudi, *Chem. Mater.* **2001**, *13*, 3151.

[9] a) T. Q. Nguyen, J. J. Wu, V. Doan, B. J. Schwartz, S. H. Tolbert, *Science* **2000**, *288*, 652; b) J. J. Wu, A. F. Gross, S. H. Tolbert, *J. Phys. Chem. B* **1999**, *103*, 2374.

[10] a) D. Gin, R. Smith, H. Deng, G. Leising, *Synth. Met.* **1999**, *101*, 52; b) L. M. Huang, Z. B. Wang, H. T. Wang, X. L. Cheng, A. Mitra, Y. X. Yan, *J. Mater. Chem.* **2002**, *12*, 388; c) X. H. Li, X. G. Zhang, H. L. Li, *J. Appl. Polym. Sci.* **2001**, *81*, 3002.

[11] A. Greiner, *Polym. Adv. Technol.* **1998**, *9*, 371.

[12] a) M. A. Sato, M. A. Sakamoto, M. Miwa, M. Hiroi, *Polymer* **2000**, *41*, 5681; b) O. Stephan, P. Schottland, P. Y. Le Gall, C. Chevrot, C. Mariet, M. Carrier, *J. Electroanal. Chem.* **1998**, *443*, 217.

[13] H. Kunieda, G. Umizu, Y. Yamaguchi, *J. Colloid Interface Sci.* **1999**, *218*, 88.

[14] a) Q. B. Pei, G. Zuccarello, M. Ahlskog, O. Inganas, *Polymer* **1994**, *35*, 1347; b) M. Dietrich, J. Heinze, G. Heywang, F. Jonas, *J. Electroanal. Chem.* **1994**, *369*, 87.

 © 2003 Wiley-VCH Verlag GmbH & Co. KGaA, Weinheim 1433-7851/03/4207-0781 $ 20.00+.50/0

Solid-State Chemosensor for Toluene

Single Crystals of the Disubstituted Anthracene 9,10-$(Ph_2P{=}S)_2C_{14}H_8$ Selectively and Reversibly Detect Toluene by Solid-State Fluorescence Emission**

*Zhaofu Fei, Nikolaus Kocher, Christian J. Mohrschladt, Heiko Ihmels, and Dietmar Stalke**

Anthracene derivatives are key compounds in the design of luminescent materials[1] both in solution and in the solid state, for example, for phosphors and lasers.[2] Chemosensors containing an anthracene unit as the fluorophore are designed either to detect alkali, alkaline-earth,[3] and transition-metal[4] cations or, more recently, even anions[5] like halides, acetate, and dihydrogenphosphate.[6] The basic strategy in the construction of these sensor molecules is to substitute the anthracene chromophore moiety in the 9-position or in the 9- and 10-positions (Scheme 1) with remote chelating groups

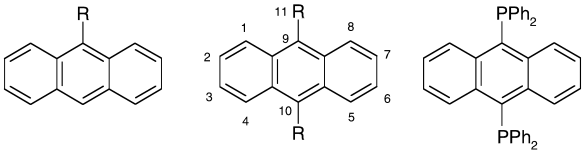

1 2 3

Scheme 1. Mono- and disubstituted anthracenes. $R = (CH_2)_nE(H)R'$, $(CH_2)_nER'_2$ with E = N, P.

that are capable of complexing cations or anions by means of hydrogen bonds or electrostatic interactions with the neutral or positively charged sensor molecules.[7] Disubstituted anthracene derivatives of type **2** are important building blocks in crystal engineering[8] and in asymmetric synthesis.[9] However, research on 9,10-heterodisubstituted anthracenes **2** has so far been limited mainly to nitrogen- and silicon-substituted species. Since some exhibit photoluminescence,[10] electroluminescence, and triboluminescence[10b,f] in the solid state, they may have potential applications in light-emitting and electroluminescent devices.[11]

[*] Prof. Dr. D. Stalke, Dr. Z. Fei, N. Kocher
Institut für Anorganische Chemie, Universität Würzburg
Am Hubland, 97074 Würzburg (Germany)
Fax: (+49) 931-888-4619
E-mail: dstalke@chemie.uni-wuerzburg.de
Dipl.-Chem. C. J. Mohrschladt, Priv.-Doz. Dr. H. Ihmels
Institut für Organische Chemie, Universität Würzburg
Am Hubland, 97074 Würzburg (Germany)

[**] This work was supported by the Deutsche Forschungsgemeinschaft (Graduiertenkolleg 690: Elektronendichte) and the Fonds der Chemischen Industrie. We thank Bruker Nonius, Karlsruhe, and CHEMETALL, Frankfurt/Main, for their support.

Supporting information for this article is available on the WWW under http://www.angewandte.org or from the author.

Reports on diphosphorus-substituted anthracenes still are rare. Schmutzler et al. synthesized the first monophosphorus derivative substituted in the 9-position,[12] and subsequently its properties as a ligand for d-block metals were investigated.[13a,b] Upon irradiation with light the compound underwent [4+4] dimerization.[13a,c] 1,8-Bis(diphenylphosphanyl)anthracene serves as a neutral chelating donor ligand in transition-metal chemistry,[14] and recently the synthesis of 9,10-bis(diphenylphosphanyl)anthracene (**3**) was reported. Upon complexation of gold(I) ions, a fluorescent $[\{Au[(Ph_2P)_2C_{14}H_8]\}_3]^{3+}$ trimeric ring is formed.[15]

Here we report the synthesis and structure determinations of the parent $(Ph_2P)_2C_{14}H_8$ (**3**), and of the oxidized species $(Ph_2P{=}O)_2C_{14}H_8$ (**4**), $(Ph_2P{=}S)_2C_{14}H_8$ (**5**), and $(Ph_2P{=}Se)_2C_{14}H_8$ (**6**). Compound **3** was synthesized by literature methods.[15] Chemically, **3** behaves similarly to triphenylphosphane; thus, we expected oxidation with $H_2O_2{\cdot}(NH_2)_2C{=}O$, elemental sulfur, and selenium to give the corresponding oxidized compounds **4**–**6** in high yields (Scheme 2). At 0 °C

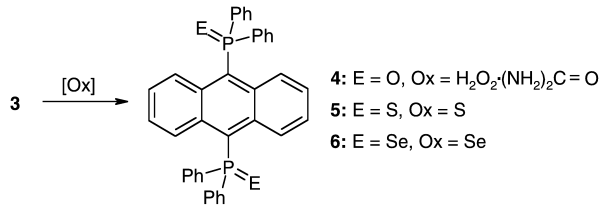

Scheme 2. Synthesis of compounds **4**–**6**.

the oxidation of **3** with the mild oxidizing agent $H_2O_2{\cdot}(NH_2)_2C{=}O$ in $CDCl_3$ proved to be a stepwise process, which could be monitored by ^{31}P NMR spectroscopy. All attempts to stop the reaction after the first oxidation were unsuccessful. The reaction of **3** with elemental sulfur and selenium in toluene at reflux gave compounds **5** and **6**, respectively. The $\delta(^{31}P)$ chemical shifts of the phosphorus atoms in **3**–**6** are comparable with those of $Ph_3P{=}E$ (E = lone pair, O, S, Se).[16,17] Interestingly, all of the products **4**–**6** are significantly more soluble than **3** in common organic solvents.

We found that solutions of **4** in common organic solvents show strong luminescence on irradiation with UV light (λ = 366 nm), whereas solutions of **5** and **6** do not. Figure 1a depicts toluene solutions of **4** (left), **5** (middle), and **6** (right) in daylight; the same samples are shown in Figure 1b on exposure to UV light. Interestingly, only single crystals of **5** emit light on UV irradiation (Figures 1c and d). Crystals of **5** that are ground to a powder retain keep this feature and only lose it when the sample is vacuum-dried (Figure 1e). Addition of a small amount of toluene restores the luminescence of the powder while other common organic solvents (including benzene) do not have this effect (Figure 1f). In this context it is important to note that **5** is perfectly air-stable and easy to synthesize from readily accessible, inexpensive materials. Single crystals of suitable size (up to cm dimensions) can be grown from solution. They are hard and robust enough to be ground in any required shape. Even lenses of a defined optical profile are feasible.

 © 2003 Wiley-VCH Verlag GmbH & Co. KGaA, Weinheim 1433-7851/03/4207-0783 $ 20.00+.50/0

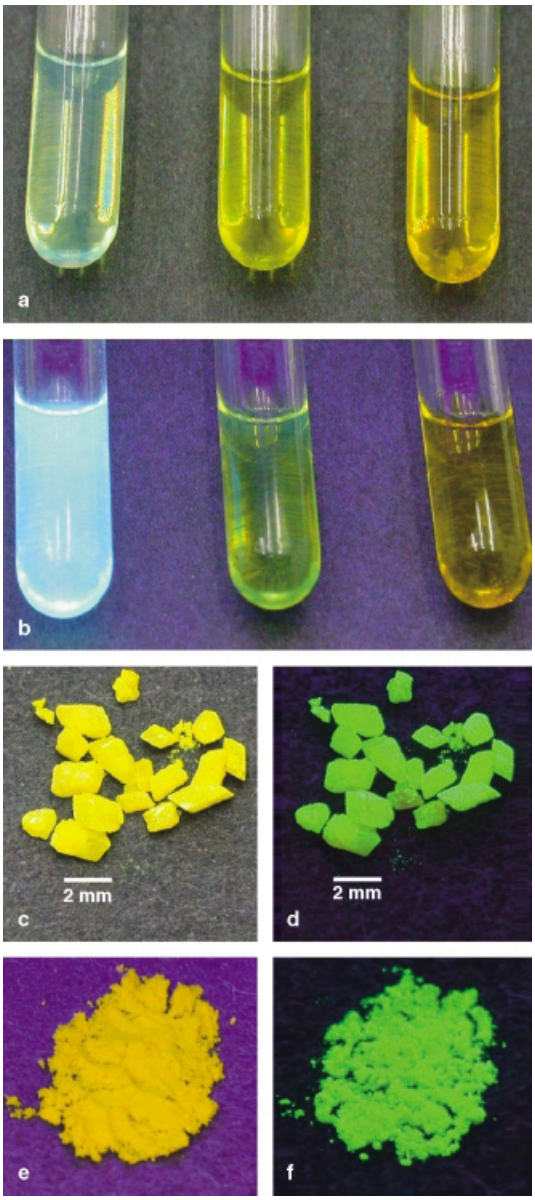

Figure 1. Luminescence properties of compounds **4**–**6** (see text for details).

The results of the structure determinations of **3**–**6** are shown in Figure 2. The asymmetric unit of each compound contains half a molecule, except the structure of **6**, in which two half-molecules are present. For all the compounds the complete molecules are generated by a center of inversion in the middle C_6 perimeter of the anthracene chromophore. In the asymmetric units of **5** and **6** a toluene molecule is present in the crystal lattice. Hence, the ratio of lattice solvent molecules to anthracene molecules is 2:1 in **5** and 1:1 in **6**. Molecules of **3** and **4** have the same conformation with a *transoid* orientation of the Ph_2P and Ph_2P=O substituents, respectively, relative to the anthracene plane. The arene plane bisects the Ph-P-Ph bond angle of on average 107°. The lone pair at the phosphorus atom in **3** and the oxygen atom in **4** are almost in plane with the anthracene perimeter (O-P-C-C torsion angle 23.6°).

The conformation of **5** and **6** is different from that of **3** and **4**. The two phenyl substituents are oriented above and below the aromatic core (Figure 2c and d). The torsion angle S-P-C-C in **5** is 84.7°, while the angle Se-P-C-C in **6** is 80.9°. Although the molecules are isomorphous, **5** and **6** are not isostructural. While **5** crystallizes in the monoclinic space group $P2_1/n$, **6** crystallizes in the triclinic space group $P\bar{1}$. Apparently the presence of the lattice toluene is essential for the luminescence behavior. The orientation of the phenyl substituents above and below the C_{14} chromophore in **4** and **5** precludes cocrystallization of the solvent. Excimer fluorescence (excimer = *exci*ted di*mer*) cannot take place. Only the orientation of the sulfur atom in **5** and of the selenium atom in **6** above and below the chromophore plane provides a suitable groove in which a toluene molecule can be in close proximity to the middle ring center of the anthracene moiety. In **5** the shortest intermolecular distance of 295 pm is found between the anthracene center and one *ortho* hydrogen atom of both toluene molecules (*meta*-H–outer ring 320, methyl-H–outer ring 367 and 398 pm). In **6** this distance is only 366 pm, presumably because the radius of a selenium atom in a covalent bond (116 pm) is larger than that of sulfur (102 pm). In contrast to **6,** in **5** the orientation of the lattice solvent is fixed relative to the chromophore due to the appreciable C–H···π-ring center interaction. The two anthracene chromophores are well separated from each other (1075 pm) such that formation of a topochemical excimer upon irradiation is most unlikely.

Moreover, for **5** crystallization in the monoclinic space group results in an almost orthogonal arrangement of the C_6 perimeter of toluene relative to the inner ring of anthracene (70.9°). This arrangement of the excimer complex is much more effective than in **6**. Crystallization of **6** in the centrosymmetric triclinic space group causes a considerably more acute angle (48.7°). This arrangement is somewhat reminiscent of that of a coplanar π-stacked excimer. However, the π–π interaction would be considerably weaker than the orthogonal C–H···π-ring center interaction.

The absorption spectra of the anthracene derivatives **4**–**6** in methanol show an intense, broad β band (S_0–S_3 transition; $\lambda_{max} = 265$ nm) and a broad p band (S_0–S_1 transition; $\lambda = 350$–450 nm). The UV/Vis spectrum of **4** in acetonitrile is shown in Figure 3a. In solution, only compound **4** exhibits a detectable emission, which is slightly solvent dependent (Figure 3a). Apparently the stabilizing effect of different solvents on the ground and excited states of the anthracene derivative is rather weak.[18] Most notably **5**, which does not emit in solution, shows a very intense fluorescence in the solid state at $\lambda = 508$ nm. Single crystals of **4** emit at $\lambda = 482$ nm, albeit significantly more weakly and with a much broader emission band than **5** (Figure 3b). The selenium derivative **6** shows essentially no emission in the solid state.

Compound **5** is a striking example of a molecule whose emission properties are drastically influenced by the surrounding medium. In contrast to most fluorophores, which emit in solution but show essentially no solid-state fluorescence, **5** exhibits just the opposite behavior. In crystals it displays a relatively sharp emission band that is significantly red-shifted relative to the fluorescence maximum of common

 © 2003 Wiley-VCH Verlag GmbH & Co. KGaA, Weinheim 1433-7851/03/4207-0784 $ 20.00+.50/0

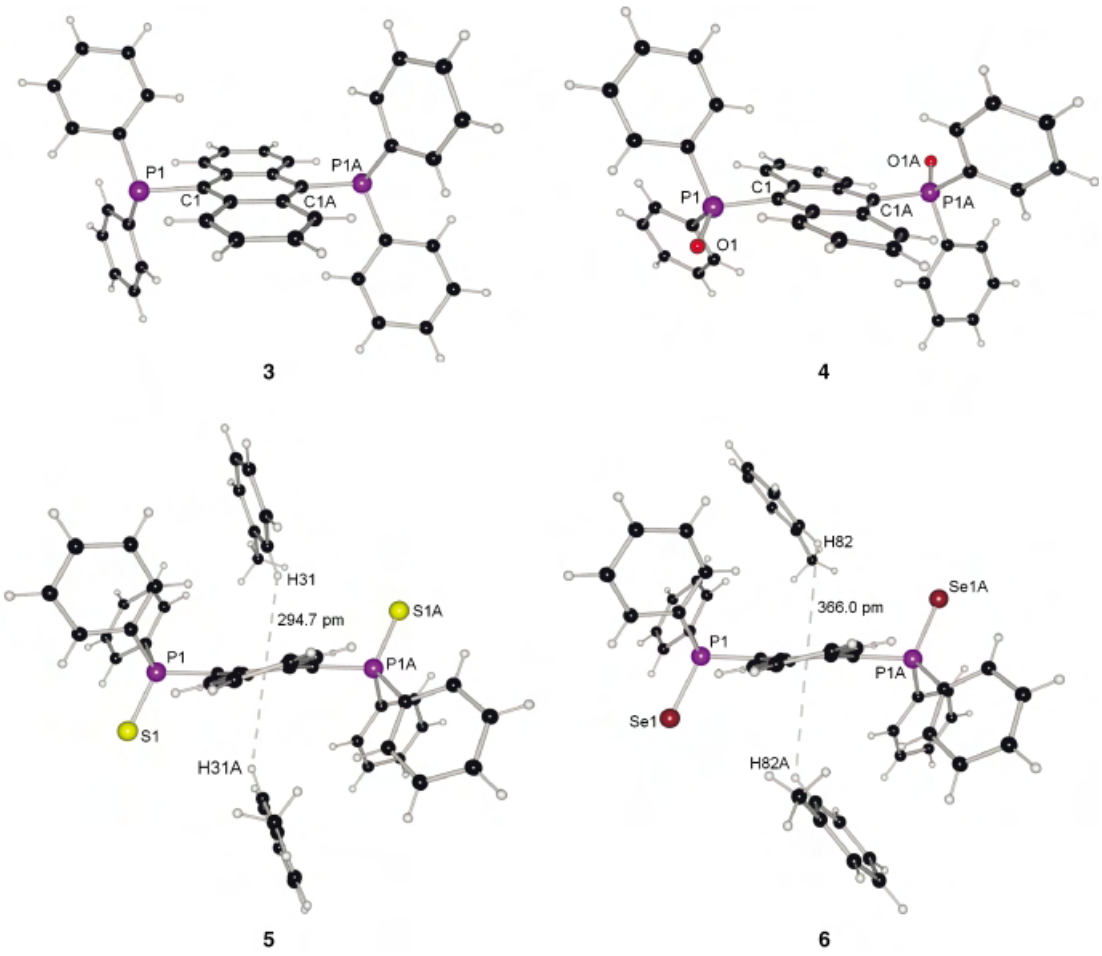

Figure 2. X-ray crystal structures of **3**–**6**. For **6** the molecule depicted accommodates two toluene molecules, the second present in the lattice is toluene-free.

anthracene derivatives, for example, **4**. Therefore it is most likely that this emission is not due to monomer fluorescence. Such drastic shifts of the emission maximum upon a change from solution to the solid state are frequently caused when one excited molecule associates with a ground-state molecule to form a fluorescent complex (excimer).[19] Although weak in the ground state,[20] the T-shaped C–H···π-ring center interaction has been observed in excited complexes of toluene–benzene[21] and toluene–anthracene.[22] The latter complexes rearrange prior to emission to give π-stacked exciplexes or excimers. Because of the ideal preorganization of **5** and toluene in the crystal, a T-shaped exciplex may also form on excitation in the solid state. Moreover, the steric constraints in the crystal prevent the rearrangement to a π-stacked exciplex, and the emission takes place from the T-shaped excited state. This is further substantiated by the fact that vacuum-drying of the ground crystals led to a significant decrease of the emission (Figure 1e and f and spectrum **H** in Figure 3b), and its intensity is re-established upon exposure to toluene. In **6** the orientation of the toluene and the anthracene chromophore is an incipient π-stacked coplanar arrangement. Thus, the observed solid-state emission may result from a sandwich-type excimer. However, the resulting weak fluorescence band is blue-shifted and also much broader than that of **5**. This behavior may be explained by the rather large separation between the molecular planes and the resulting weak overlap of the two π systems.

In conclusion, molecules of $(Ph_2P{=}S)_2C_{14}H_8$ (**5**) form single crystals which have a groove suitable for binding toluene reversibly to the anthracene chromophore by means of C–H···π-ring center interactions. Hence, crystalline **5** is the first solid-state excimer that can serve as a chemosensor to detect toluene selectively. In the related compounds $(Ph_2P{=}O)_2C_{14}H_8$ (**4**) and $(Ph_2P{=}Se)_2C_{14}H_8$ (**6**) the T-shaped orientation of the anthracene and toluene molecules is prevented either by substituents shielding the chromophore (as in **4**) or by crystallization in a unsuitable space group (as in **6**).[23]

Experimental Section

All manipulations were performed under dry nitrogen with Schlenk techniques. Solvents were dried over Na/K alloy and distilled prior to use. NMR spectra were obtained in $CDCl_3$ on a Bruker DMX 300 instrument with the external standards $SiMe_4$ (^{1}H NMR), 85 % H_3PO_4 (^{31}P NMR), and Me_2Se (^{77}Se NMR). EI mass spectra were recorded on a Finnigan Mat 2000 instrument (70 eV). Elemental analyses were carried out by the Institut für Anorganische Chemie, Universität Würzburg. UV spectra were recorded on a Hitachi U-3200 spectrophotometer, fluorescence spectra on a Perkin-Elmer LS50 spectrom-

 © 2003 Wiley-VCH Verlag GmbH & Co. KGaA, Weinheim 1433-7851/03/4207-0785 $ 20.00+.50/0

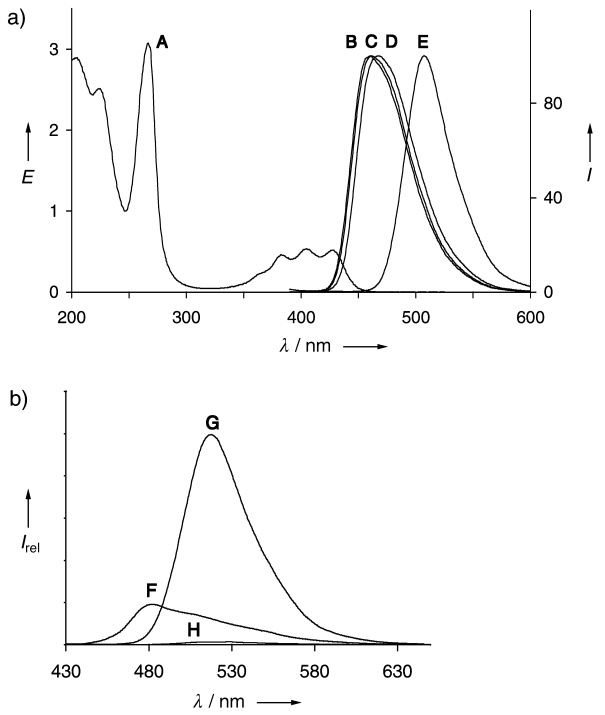

Figure 3. a) Absorption (**A**) and normalized emission (**B**–**D**) spectra of **4** in solution (**A**: $c(\mathbf{4}) = 10^{-4}$ M, **B**–**D**: $c(\mathbf{4}) = 10^{-5}$ M; $\lambda_{ex} = 380$ nm; **B**: in acetonitrile; **C**: in benzene; **D**: in methanol) and in the solid state (**E**). b) Solid-state fluorescence spectra of **4** (**F**) and **5** (**G** and **H**); ($\lambda_{ex} = 380$ nm; emission spectra determined under identical conditions; **G**: single crystals of **5** containing toluene as lattice solvent; **H**: vacuum-dried powder of **5** obtained from ground single crystals).

eter. Fluorescence spectra of solids were recorded with a front surface accessory from Perkin-Elmer. Emission spectra were recorded with an excitation wavelength close to the absorption maximum of the S_0–S_1 transition ($\lambda = 380$ nm). The relative fluorescence quantum yields were determined by standard methods[24] with quinine sulfate in 1N H_2SO_4 as a reference ($\phi_{Fl} = 0.546$[25]). Solid-state fluorescence spectra of ground crystals were determined with a front surface accessory from Perkin-Elmer ($\lambda = 380$ nm, excitation slit: 2.5; emission slit: 2.5).

4: An excess of $H_2O_2{\cdot}(NH_2)_2C{=}O$ (200 mg) was added to a solution of **3** (137 mg, 0.25 mmol) in dichloromethane (20 mL) at 0°C. The reaction mixture was stirred at 0°C for 1 h and then filtered. The filtrate was washed with H_2O (2×5 mL) and dried with $MgSO_4$ overnight. After filtration and removal of the solvent, the product was obtained by recrystallization from toluene. Yield: 131 mg (91%); m.p. 264°C; ^{1}H NMR: $\delta = 8.50$–7.30 ppm (unresolved multiplets); ^{31}P NMR: $\delta = 31.3$ ppm (s); EI-MS: m/z (%): 578 $[M]^+$ (100), 377 $[M-P(O)(C_6H_5)_2]^+$ (58); elemental analysis (%) calcd for $C_{38}H_{28}P_2O_2$: C 78.88, H 4.88; found: C 72.94, H 5.02; UV (MeOH): λ_{max} ($\lg\varepsilon$) = 210 (4.69), 224 (4.71), 387 (3.96), 409 (4.02), 431 (4.00); (MeCN): 203 (4.76), 224 (4.70), 267 (4.88), 383 (3.97), 405 (4.03), 428 (4.02); (C_6H_6): 279 (4.38), 384 (3.91), 407 (3.98), 430 nm (3.98).

5: Elemental sulfur (16 mg, 0.5 mmol) was added to a solution of **3** (137 mg, 0.25 mmol) in toluene (15 mL). The reaction mixture was then heated at reflux for 4 h. The product was obtained when the reaction mixture was allowed to cool to room temperature. Yield: 116 mg (88%); m.p. 260°C; ^{1}H NMR: $\delta = 8.20$–6.90 (unresolved multiplets); ^{31}P NMR: $\delta = 34.9$ ppm (s); EI-MS: m/z (%): 610 $[M]^+$ (32), 578 $[M-S]^+$ (20), 546 $[M-2S]^+$ (8); elemental analysis (%) calcd for $C_{38}H_{28}P_2S_2$: C 74.72, H 4.62; found: C 74.84, H 4.78; UV (MeOH): λ_{max} ($\lg\varepsilon$) = 207 (4.81), 269 (4.66), 392 (3.76), 420 (3.89), 442 (3.91); (MeCN): 269 (4.75), 391 (3.82), 420 (3.96), 442 (3.97); (C_6H_6): 278 (4.44), 394 (3.69), 423 (3.81), 447 nm (3.82).

6: This compound was prepared in analogy to **5** from **3** (137 mg, 0.25 mmol) and gray selenium (39 mg, 0.5 mmol). Yield: 147 mg (84%); m.p. 238°C; ^{1}H NMR: $\delta = 8.10$ (m, 4H; H3-H6 and H3′-H6′ (centrosymmetric numbering), 7.82–7.00 (m, 20H; Ph), 7.0 ppm (m, 4H; H4-H5 and H4′-H5′); ^{31}P NMR: $\delta = 25.7$ ppm (s); ^{77}Se NMR: $\delta = -259.0$ ppm (d, ^1J(P,Se) = 732.4 Hz); EI-MS: m/z (%): 704 $[M]^+$ (5), 626 $[M-Se]^+$ (25), 546 $[M-2Se]^+$ (100); elemental analysis (%) calcd for $C_{38}H_{28}P_2Se_2$: C 64.79, H 4.01; found: C 65.04%, H 4.42; UV (MeOH): λ_{max} ($\lg\varepsilon$) = 211 (4.64), 272 (4.48), 395 (3.54), 450 (3.81); (MeCN): 272 (4.40), 395 (3.57), 452 (3.83); (C_6H_6): 278 (4.70), 395 (3.87), 458 nm (4.14).

X-ray crystal structure analyses of **3**–**6:** The data sets were collected from oil-coated, shock-cooled crystals on a Bruker smart-apex diffractometer with a D8 goniometer (graphite-monochromated $Mo_{K\alpha}$ radiation, $\lambda = 0.71073$ Å) in ω-scan mode at 130(2) K (**3**) and 173(2) K (**4**–**6**).[26] The data were integrated with SAINT,[27] and an empirical absorption correction was applied. The structures were solved by direct methods (SHELXS-97)[28] and refined by full-matrix least-squares methods against F^2. CCDC-189388 (**3**), CCDC-189389 (**4**), CCDC-189390 (**5**), and CCDC-189391 (**6**) contain the supplementary crystallographic data for this paper. These data can be obtained free of charge via www.ccdc.cam.ac.uk/conts/retrieving.html (or from the Cambridge Crystallographic Data Centre, 12, Union Road, Cambridge CB2 1EZ, UK; fax: (+44) 1223-336-033; or deposit@ccdc.cam.ac.uk).

Received: October 2, 2002 [Z50285]

[1] a) H. B. Rosenstock, *J. Chim. Phys. Phys.-Chim. Biol.* **1968**, *48*, 532; b) A. Matsui, K. Mizuno, M. Kobayashi, *J. Phys. Colloq.* **1985**, *7*, 19.

[2] R. C. Ropp, N. J. Warren, *Luminescence and the Solid State,* Elsevier, Amsterdam, **1991**.

[3] M. Montalti, L. Prodi, N. Zaccheroni, *J. Fluoresc.* **2000**, *10*, 71.

[4] S. Alves, F. Pina, M. T. Albelda, E. Garcia-España, C. Soriano, S. V. Luis, *Eur. J. Inorg. Chem.* **2001**. 405.

[5] P. D. Beer, P. A. Gale, *Angew. Chem.* **2001**, *113*, 502; *Angew. Chem. Int. Ed.* **2001**, *40*, 2556.

[6] T. Gunnlaugsson, A. P. Davis, M. Glynn, *Chem. Commun.* **2001**, 2556.

[7] Reviews: a) A. W. Czarnik, *Acc. Chem. Res.* **1994**, *27*, 302; b) A. P. de Silva, H. Q. N. Gunaratne, T. Gunnlaugsson, A. J. M. Huxley, C. P. McCoy, J. T. Rademacher, T. E. Rice, *Chem. Rev.* **1997**, *97*, 1515; c) inverse crowns ethers: R. E. Mulvey, *Chem. Commun.* **2001**, 1049; d) inverse podands: B. Walfort, S. K. Pandey, D. Stalke, *Chem. Commun.* **2001**, 1640.

[8] a) E. Weber, T. Hens, T. H. Brehmer, I. Csöregh, *J. Chem. Soc. Perkin Trans. 2* **2000**, 235; b) T. H. Brehmer, P. P. Korkas, E. Weber, *Sens. Actuators A* **1997**, *44*, 595; c) H. Bock, M. Ansari, N. Nagel, R. F. C. Claridge, *J. Organomet. Chem.* **1996**, *521,* 51.

[9] A. Port, M. Moragas, X. Sánchez-Ruiz, C. Jaime, A. Virgili, A. Alvarez-Larena, J. F. Piniella, *J. Org. Chem.* **1997**, *62*, 899.

[10] a) H. Ihmels, D. Leusser, M. Pfeiffer, D. Stalke, *Tetrahedron* **2000**, *56*, 6867; b) L. M. Sweeting, A. L. Rheingold, J. M. Gingerich, A. W. Rutter, R. A. Spence, C. D. Cox, T. J. Kim, *Chem. Mater.* **1997**, *9*, 1103; c) J. M. Bruss, M. R. V. Sahyun, M. R. V. Schmidt, D. K. Sharma, *J. Polym. Sci. Part A* **1993**, *31*, 987; d) E.-Z. M. Ebeid, A. M. Donia, *J. Phys. Chem. Solids* **1988**, *49*, 263; e) E. Heller, G. M. Schmidt, *Isr. J. Chem.* **1971**, *9*, 449; f) N. W. Mitzel, C. Lustig, R. J. F. Berger, N. Runeberg, *Angew. Chem.* **2002**, *114*, 2629; *Angew. Chem. Int. Ed.* **2002**, *41*, 2519.

[11] Patents: a) C. Hosokawa, M. Funehashi, H. Kawamura, H. Arai, H. Koga, H. Ikeda, Idemitsu Kosan Co. Ltd. Japan, Japanese Patent, WO 0039247 A1 **2000**; b) H. Higashi, T. Sakai, C.

 © 2003 Wiley-VCH Verlag GmbH & Co. KGaA, Weinheim 1433-7851/03/4207-0786 $ 20.00+.50/0

Hosokawa, Idemitsu Kosan Co. Ltd. Japan, Japanese Patent, WO 0005927 A1 **2000**.
[12] L. Heuer, R. Schmutzler, *J. Fluorine Chem.* **1988**, *39*, 197.
[13] a) J. Wesemann, P. G. Jones, D. Schomburg, L. Heuer, R. Schmutzler, *Chem. Ber.* **1992**, *125*, 2187; b) T. E. Müller, J. C. Green, D. M. P. Mingos, C. M. McPartlin, C. Whittingham, D. J. Williams, T. Woodroffe, *J. Organomet. Chem.* **1998**, *551*, 313; c) L. Heuer, D. Schomburg, R. Schmutzler, *Chem. Ber.* **1989**, *122*, 1473.
[14] a) M. W. Haenel, D. Jakubik. C. Krüger, P. Betz, *Chem. Ber.* **1991**, *124*, 333; b) M. W. Haenel, S. Oevers, J. Bruckmann, J. Kuhnigk, C. Krüger, *Synlett* **1998**, *3*, 301; c) R. H. Laitinen, V. Heikkinen, M. Haukka, A. M. P. Koskinen, J. Pursiainen, *J. Organomet. Chem.* **2000**, *598*, 235.
[15] a) J. H. K. Yip, J. Prabhavathy, *Angew. Chem.* **2001**, *113*, 2217; *Angew. Chem. Int. Ed.* **2001**, *40*, 2159.
[16] S. Berger, S. Braun, H.-O. Kalinowski, *NMR-Spektroskopie von Nichtmetallen, Vol. 3,* Georg Thieme, Stuttgart, New York, **1993**.
[17] D. W. Allen, *J. Chem. Soc. Dalton Trans.* **1982**, 51.
[18] P. Suppan, N. Ghoneim, *Solvatochromism*, RSC, London, **1997**, chap. 4.
[19] a) D. Sandman, G. J. Lopez, *Mol. Cryst. Liq. Cryst.* **1996**, *277*, 28; b) I. Ortmann, S. Werner, C. Krüger, S. Mohr, K. Schaffner, *J. Am. Chem. Soc.* **1992**, *114*, 5048; c) Y. Yakot, M. D. Cohen, Z. Ludmer, *Adv. Photochem.* **1979**, *11*, 241; d) B. Stevens, *Spectrochim. Acta* **1962**, *18*, 439.
[20] T. Steiner, *Angew. Chem.* **2002**, *114*, 50; *Angew. Chem. Int. Ed.* **2002**, *41*, 48.
[21] H. Saigusa, M. Morohoshi, S. Tsuchiya, *J. Phys. Chem. A* **2001**, *105*, 7334.
[22] a) T. Chakraborty, E. C. Lim, *J. Phys. Chem.* **1993**, *97*, 11151; b) H. Saigusa, E. C. Lim, *J. Phys. Chem.* **1995**, *99*, 15738.
[23] While this manuscript was in prepration, a publication appeared describing a *syn* isomer of a dinuclear platinum(II) complex, which shows similar behavior upon exposure to MeCN and EtOH. Unfortunately the solvent molecules could not be located in the lattice unambiguously but are most likely disordered in intermolecular channels; M. Kato, A. Omura, A. Toshikawa, S. Kishi, Y. Sugimoto, *Angew. Chem.* **2002**, *114*, 3315; *Angew. Chem. Int. Ed.* **2002**, *41*, 3183.
[24] J. N. Demas, G. A. Crosby, *J. Phys. Chem.* **1971**, *75*, 991.
[25] D. F. Eaton, *Pure Appl. Chem.* **1988**, *60*, 1108.
[26] a) D. Stalke, *Chem. Soc. Rev.* **1998**, *27*, 171; b) T. Kottke, R. J. Lagow, D. Stalke, *J. Appl. Crystallogr.* **1996**, *29*, 465; c) T. Kottke, D. Stalke, *J. Appl. Crystallogr.* **1993**, *26*, 615.
[27] Bruker-Nonius, SAINT-NT, Madison WI 2000.
[28] G. M. Sheldrick, *Acta Crystallogr. Sect. A* **1990**, *46*, 467.

 © 2003 Wiley-VCH Verlag GmbH & Co. KGaA, Weinheim 1433-7851/03/4207-0787 $ 20.00+.50/0

Chiral Piperidine Derivatives

Stereoselective Solid-Phase Synthesis of Chiral Piperidine Derivatives by Using an Immobilized Galactose Auxiliary**

*Gernot Zech and Horst Kunz**

Drug development[1] has significantly been accelerated by exploiting combinatorial solid-phase synthetic methodologies.[2] Although enantiomerically pure compounds[3] are of major interest for the pharmaceutical industry only few stereoselective syntheses on the solid-phase have been reported so far. Besides polymer-bound chiral ligands and catalysts[4] some immobilized chiral auxiliaries and their application in aldol condensations,[5] conjugate additions,[6] 1,3-dipolar cycloadditions,[7] or radical allylations[8] have been described.

Recently, we reported on the synthesis of an immobilized galactosylamine as auxiliary and its employment in stereoselective Ugi reactions on the solid-phase.[9] Within this approach a galactosyl azide as precursor was coupled to hydroxyfunctionalized polymers, for example Wang resin, through the sterically demanding α,α,α′,α′-tetramethyl azelaic acid and subsequently reduced to the galactosylamine on the solid-phase. Major disadvantages of this anchoring for application in other solid-phase reactions lay in the acid lability of the Wang anchor and in the low loading of the polymer with the galactosylamine.

Herein, we report diastereoselective domino Mannich–Michael condensations[10] performed with an immobilized glycosylamine as the auxiliary, allowing reactions with Lewis acids and organometallic reagents. Thus, a polymer-bound chlorodiisopropylsilane[11,12] was attached to the carbohydrate auxiliary through a hydroxyfunctionalized spacer unit, which enabled facile cleavage of reaction products from the solid-phase by mild fluoridolysis.[13] Linkages of substrates through sterically demanding silyl ethers have proven stable towards a variety of organometallic reagents. Similar strategies have been applied for the synthesis of oligosaccharides,[14] polyketides,[15] and prostaglandins.[16]

For the assembly of the galactose auxiliary 1,6-hexanediol was monosilylated with *tert*-butyldiphenylsilyl chloride, the remaining hydroxy function was transformed to bromide to give **1** under Appel conditions. Compound **1** was then allowed to react with isobutyric acid dianion to give α,α-branched octanoic acid **2** (Scheme 1). The acid chloride obtained from **2** was regioselectively esterified with the primary hydroxy function of galactosyl azide **3**. After pivaloylation[17] of the

[*] Prof. Dr. H. Kunz, Dipl.-Chem. G. Zech
Institut für Organische Chemie der Universität Mainz
Duesbergweg 10-14, 55128 Mainz (Germany)
Fax: (+49) 6131-39-24786
E-mail: hokunz@mail.uni-mainz.de

[**] This work was supported by the Deutsche Forschungsgemeinschaft and the Fonds der Chemischen Industrie (FCI). G.Z. is grateful to the FCI for a Doktorandenstipendium.

 © 2003 Wiley-VCH Verlag GmbH & Co. KGaA, Weinheim 1433-7851/03/4207-0787 $ 20.00+.50/0

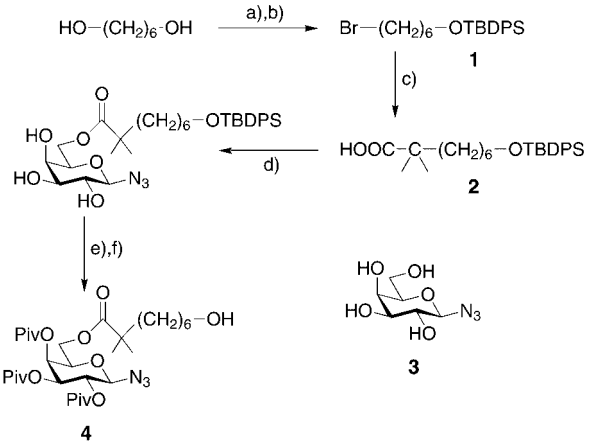

Scheme 1. Solution synthesis of **4**. a) TBDPSCl, imidazole, DMF, 20 °C, 88 %; b) CBr_4, PPh_3, CH_2Cl_2, 0 °C→20 °C, 85 %; c) $Me_2C{=}C(OLi)_2$, THF, −20→40 °C, 77 %; d) 1. $C_2O_2Cl_2$, CH_2Cl_2, 20 °C, 2. β-D-galactopyranosyl azide (**3**), pyridine, DMAP, 60 °C, 49 %; e) PivCl, pyridine, 60 °C, 85 %; f) TBAF·3 H_2O, THF, 20 °C, 85 %. TBDPS = *tert*-butyldiphenylsilyl, DMAP = 4-(*N*,*N*-dimethylamino)pyridine, Piv = pivaloyl (*t*BuCO), TBAF = tetra-*n*-butylammonium fluoride, DMF = dimethylformamide.

remaining hydroxy groups and removal of the silyl protecting groups, galactosyl azide **4** was coupled to the polymer-bound chlorosilane **5** through a hexamethylene spacer (Scheme 2). Owing to the high loading (ca. 2 mmol g^{-1}) of **5** (see ref. [11] for synthesis) almost complete coupling was observed when 0.25 equivalents of galactosyl azide **4** were subjected to etherification. Methanolysis of the unreacted chlorosilane groups furnished polymer-bound galactosyl azide **6** with a loading of about 0.38 mmol g^{-1}, which corresponds to an average substitution of every tenth styrene unit with the carbohydrate moiety (Scheme 2).[18] Reduction of the galactosyl azide with ten equivalents each of 1,3-propanedithiol and triethylamine in DMF gave immobilized galactosylamine **7** quantitatively and without anomerization. Both the coupling with the glycosyl azide ($\tilde{\nu}_{C=O} = 1742\ cm^{-1}$, $\tilde{\nu}_{azide} = 2116\ cm^{-1}$) and the azide reduction were monitored by IR spectroscopy.

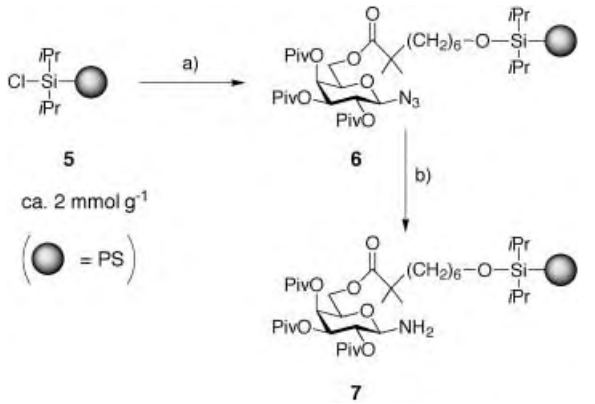

Scheme 2. Synthesis of the immobilized galactosylamine. a) 1. imidazole, **4** (0.25 equiv), CH_2Cl_2, 20 °C, 12 h, 2. addition of MeOH, 24 h; b) 1,3-propanedithiol, NEt_3 (each 10 equiv), DMF, 20 °C, 12 h. PS = polystyrene.

To optimize reaction and cleavage conditions with this system we initially performed model Ugi reactions using the galactosylamine **7**. Fluoridolysis with tetra-*n*-butylammonium fluoride (TBAF) gave the corresponding Ugi condensation products in high yields and in diastereomeric ratios (80–92 % *de*) comparable to those obtained for analogous syntheses in solution[19] and on the solid-phase.[9]

Encouraged by these results we employed galactosylamine **7** for the stereoselective synthesis of heterocycles. The domino Mannich–Michael condensation of glycosyl imines with the electron-rich Danishefsky's diene opens up a stereoselective access to 2-substituted *N*-galactosyl-5,6-dehydropiperidin-4-ones,[10] which are valuable synthons for the synthesis of nitrogen heterocycles.[20]

So far, only three combinatorial syntheses of didehydropiperidin-4-ones have been reported, all of them based on different methodologies, but all giving racemic products.[21] Herein we describe the first stereoselective synthesis of chiral dehydropiperidinones on the solid-phase. The immobilized galactosylamine auxiliary **7** was transformed to the corresponding galactosyl imines **8** with high *E*-isomeric and β-anomeric purity by acid-catalyzed condensation (Scheme 3).

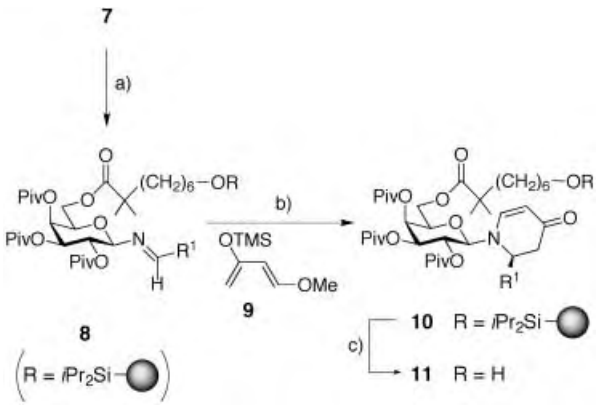

Scheme 3. Solid-phase synthesis of didehydropiperidinones. a) R^1CHO (5 equiv), AcOH (10 equiv), toluene, 20 °C, 6 h; b) Danishefsky's diene **9** (10 equiv), $ZnCl_2$ (5 equiv), THF, 20 °C, 48 h; c) TBAF·3 H_2O (5 equiv based on silyl units), AcOH (1.7 equiv), THF, 20 °C, 48 h.

It is noteworthy that analogous conditions applied to the solution process led to an irreversible anomerization giving the thermodynamically more stable and less reactive α-imines. According to IR spectroscopy trimethyl orthoformate[22] was found to be an unsuitable dehydrating agent. Subsequent domino Mannich–Michael condensation at room temperature with Danishefsky's diene **9** gave resin-bound didehydropiperidinones **10**, which could be cleaved from the polymeric support with TBAF (1 M solution in THF, buffered with AcOH). The LC-MS analysis of the resulting crude products **11**[23] showed that they were formed in high purity, yield, and diastereoselectivity (Table 1), despite the relatively high temperature (22 °C). The diastereomeric excesses of the 2-alkyl didehydropiperidinones **11l–o** and **11q** were found to be lower than those of the 2-aryl analogues. Only a slight increase of the diastereomeric ratio was observed when the reaction was performed at lower temperature.

 © 2003 Wiley-VCH Verlag GmbH & Co. KGaA, Weinheim 1433-7851/03/4207-0788 $ 20.00+.50/0

Table 1: Diastereoselective synthesis of didehydropiperidinones on the solid-phase according to Scheme 3.

Compound	R	Yield [%][a]	Purity [%][b]	d.r.[b]
11a	C_6H_5	77	98	97:3
11b	*p*-Cl-C_6H_4	77	92	97:3
11c	*p*-O_2N-C_6H_4	40	80	94:6
11d	*p*-F-C_6H_4	73	97	98:2
11e	*m*-F-C_6H_4	n.d.	91	100:0
11f	*p*-NC-C_6H_4	75	93	99:1
11g	*p*-F_3C-C_6H_4	81	97	98:2
11h	2-Cl-6-F-C_6H_3	49	89	93:7
11i	*m*-Br-C_6H_4	57	95	99:1
11j	*p*-Br-C_6H_4	n.d.	97	96:4
11k	*p*-MeO-C_6H_4	80	98	98:2
11l	CH_2CH_2-C_6H_5	50	83	90:10
11m	*n*-C_7H_{15}	57	74	89:11
11n	*n*-C_5H_{11}	76	95	87:13
11o	CH_2-$CH(CH_3)_2$	61	88	84:16
11p	$CH(CH_3)_2$	70	92	98:2
11q	CH_3	73	90	80:20

[a] Yield of crude product (four steps); based on initial loading of **6**. [b] Determined by LC-MS (evaporative light scattering (ELS) /UV detection). n.d. not determined.

For further functionalization resin-bound enaminones **10** were subjected to conjugate addition reactions. The reaction with L-selectride as hydride donor under different reaction conditions only gave mixtures of 1,2- and 1,4-reduced products. The reduction in the presence of the oxygenophilic Lewis acid methylaluminum bis[2,6-di-*tert*-butyl-4-methylphenoxide] (MAD),[24] however, after cleavage from resins **12a–e** yielded the chemoselectively 1,4-reduced piperidinones **13a–e** (Scheme 4, Table 2). As shown for the release of

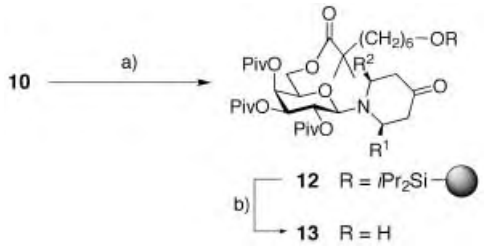

Scheme 4. Conjugate hydride and cuprate addition to polymer-bound enones **10**. a) For R^2 = H: L-Selectride (10 equiv), MAD (20 equiv), THF/toluene, −20 °C, 4 h; for R^2 = alkyl: $(R^2)_2Cu(CN)Li_2$ (15 equiv), $BF_3{\cdot}OEt_2$ (15 equiv), THF, −60 °C→−15 °C, 14 h; b) TBAF·3 H_2O (5 equiv based on silyl units), AcOH (1.7 equiv), THF, 20 °C, 48 h.

the corresponding piperidinone from resin **12c**, cleavage from the polymer-bound auxiliary can be accomplished by treatment with dilute trifluoroacetic acid in the presence of dimethyl sulfide and water giving rise to the corresponding piperidine trifluoroacetate. In this case, the piperidine derivative was isolated in 53% yield. The conditions chosen are so mild that the acid-sensitive anchoring of the auxiliary to the solid-phase is not affected all. Piperidinones can be released from *N*-galactosyl derivatives **13** according to the previously reported methodology.[10]

Table 2: Conjugate hydride and cuprate addition to polymer-bound enones according to Scheme 4.

Compound	R^1	R^2	Yield [%][a]	Purity [%][b]	*cis*/*trans*[b]
13a	*p*-Cl-C_6H_4	H	34	65	–
13b	*m*-F-C_6H_4	H	53	95	–
13c	*p*-F_3C-C_6H_4	H	n.d.	83	–
13d	*p*-Br-C_6H_4	H	38	82	–
13e	$CH(CH_3)_2$	H	60	70	–
13f	*m*-F-C_6H_4	*n*Bu	75	49	98:2
13g	*p*-F_3C-C_6H_4	*n*Bu	76	61	93:7
13h	*m*-Br-C_6H_4	*n*Bu	71	78	95:5
13i	2-Cl-6-F-C_6H_3	Me	67	78	96:4

[a] Yield of crude product (five steps); based on initial loading of **6**. [b] Determined by LC-MS (ELS/UV detection). n.d. not determined.

As 2,6-disubstituted piperidines are a widespread structural motif in natural products we are also interested in a stereoselective solid-phase approach to this class of compounds. Among many cuprate reagents tested cyano-modified Gilman reagents (Lipshutz cuprates)[25] in the presence of $BF_3{\cdot}OEt_2$ were found to be the reagents of choice for the conjugate cuprate addition to polymer-bound enones **10**. Cleavage from the polymeric support gave *N*-galactosylated 2,6-disubstituted piperidinones **13f–i** in high yields and excellent *cis* selectivity (Scheme 4, Table 2).

The fluoride-labile anchoring strategy of the galactosylamine as immobilized auxiliary described herein and its application in domino Mannich–Michael condensations leads to almost diastereomerically pure products even at room temperature. The products are obtained in high purity without the necessity for tedious separation procedures. The dehydropiperidinones formed stereoselectively on the solid-phase can be subjected to further functionalization as was shown by conjugate addition reactions. Consequently, the methodology presented herein enables rapid combinatorial access to structurally diverse chiral piperidine derivatives.

Received: August 27, 2002 [Z50054]

[1] a) R. G. Franzén, *J. Comb. Chem.* **2000**, *2*, 195–214; b) R. E. Dolle, *J. Comb. Chem.* **2001**, *3*, 477–517; c) R. E. Dolle, *J. Comb. Chem.* **2002**, *4*, 369–418; d) B. Lou, *Drug Discovery Today* **2001**, *6*, 1288–1294; e) A. Ganesan, *Drug Discovery Today* **2002**, *7*, 47–55.

[2] a) *Combinatorial Chemistry—Synthesis, Analysis, Screening* (Ed.: G. Jung), Wiley-VCH, Weinheim, **1999**; b) *Solid-Phase Organic Synthesis* (Ed.: K. Burgess), Wiley, New York, **1999**; c) F. Zaragoza Dörwald, *Organic Synthesis on Solid Phase*, Wiley-VCH, Weinheim, **2000**; d) P. Seneci, *Solid-Phase Synthesis and Combinatorial Technologies*, Wiley, New York, **2000**; e) *Solid-Phase Organic Syntheses, Vol. 1* (Ed.: A. W. Czarnik), Wiley, New York, **2001**; f) *Handbook of Combinatorial Chemistry* (Eds.: K. C. Nicolaou, R. Hanko, W. Hartwig), Wiley-VCH, Weinheim, **2002**.

[3] a) S. C. Stinson, *Chem. Eng. News* **2001**, *79*(20), 45–56; b) A. M. Rouhi, *Chem. Eng. News* **2002**, *80*(23), 43–50.

[4] Reviews: a) S. J. Shuttleworth, S. M. Allin, R. D. Wilson, D. Nasturica, *Synthesis* **2000**, 1035–1074; b) Y. R. de Miguel, *J. Chem. Soc. Perkin Trans. 1* **2000**, 4213–4221.

 © 2003 Wiley-VCH Verlag GmbH & Co. KGaA, Weinheim 1433-7851/03/4207-0789 $ 20.00+.50/0

[5] A. V. Purandare, S. Natarajan, *Tetrahedron Lett.* **1997**, *38*, 8777 – 8780.
[6] C. W. Phoon, C. Abell, *Tetrahedron Lett.* **1998**, *39*, 2655 – 2658.
[7] G. Faita, A. Paio, P. Quadrelli, F. Rancati, P. Seneci, *Tetrahedron Lett.* **2000**, *41*, 1265 – 1269.
[8] E. J. Enholm, M. E. Gallagher, S. Jiang, W. A. Batson, *Org. Lett.* **2000**, *2*, 3355 – 3357.
[9] K. Oertel, G. Zech, H. Kunz, *Angew. Chem.* **2000**, *112*, 1489 – 1491; *Angew. Chem. Int. Ed.* **2000**, *39*, 1431 – 1433.
[10] a) H. Kunz, W. Pfrengle, *Angew. Chem.* **1989**, *101*, 1041 – 1042; *Angew. Chem. Int. Ed. Engl.* **1989**, *28*, 1067 – 1068; b) M. Weymann, W. Pfrengle, D. Schollmeyer, H. Kunz, *Synthesis* **1997**, 1151 – 1160.
[11] The polymer-bound chlorosilane is easily prepared with a loading capacity of about 2 mmol g^{-1} by direct lithiation of commercially available polystyrene resin (crosslinked with 1% divinylbenzene, 100–200 mesh) with *n*BuLi and subsequent treatment with dichlorodiisopropylsilane (see also ref. [12]).
[12] M. J. Farrall, J. M. J. Fréchet, *J. Org. Chem.* **1976**, *41*, 3877 – 3882.
[13] This enables the direct analysis of diastereomeric *N*-galactosylated products and of potential side products and facilitates the analysis of complex reaction sequences on the solid-phase.
[14] a) S. J. Danishefsky, K. F. McClure, J. T. Randolph, R. B. Ruggeri, *Science* **1993**, *260*, 1307 – 1309; b) J. T. Randolph, K. F. McClure, S. J. Danishefsky, *J. Am. Chem. Soc.* **1995**, *117*, 5712 – 5719.
[15] a) C. Gennari, S. Ceccarelli, U. Piarulli, K. Aboutayab, M. Donghi, I. Paterson, *Tetrahedron* **1998**, *54*, 14999 – 15016; b) I. Paterson, M. Donghi, K. Gerlach *Angew. Chem.* **2000**, *112*, 3453 – 3457; *Angew. Chem. Int. Ed.* **2000**, *39*, 3315 – 3319.
[16] a) L. A. Thompson, F. L. Moore, Y.-C. Moon, J. A. Ellman, *J. Org. Chem.* **1998**, *63*, 2066 – 2067; b) D. R. Dragoli, L. A. Thompson, J. O'Brien, J. A. Ellman, *J. Comb. Chem.* **1999**, *1*, 534 – 539.
[17] The presence of the pivaloyl group at C-2 is necessary for effective diastereofacial differentiation of glycosyl imines (review: K. Rück, H. Kunz, *Angew. Chem.* **1993**, *105*, 355 – 377; *Angew. Chem. Int. Ed. Engl.* **1993**, *32*, 336 – 358); the other hydroxy functions are pivaloyl or pseudopivaloyl (as at C-6 in **4**) protected, to increase the stability of the auxiliary against organometallic reagents.
[18] The loading capacity was calculated from the nitrogen content of a resin sample that was washed thoroughly and dried for 48 h at 40 °C under high vacuum.
[19] H. Kunz, W. Pfrengle, *J. Am. Chem. Soc.* **1988**, *110*, 651 – 652.
[20] H. Kunz, M. Weymann, M. Follmann, P. Allef, K. Oertel, M. Schultz-Kukula, A. Hofmeister, *Pol. J. Chem.* **1999**, *73*, 15 – 27. *N*-Carbamoyl-5,6-didehydropiperidin-4-ones and their functionalization have been studied extensively by Comins et al.: D. L. Comins, *J. Heterocycl. Chem.* **1999**, *36*, 1491 – 1500.
[21] a) Y. Wang, S. R. Wilson, *Tetrahedron Lett.* **1997**, *38*, 4021 – 4024; b) M. W. Creswell, G. L. Bolton, J. C. Hodges, M. Meppen, *Tetrahedron* **1998**, *54*, 3983 – 3998; c) B. Munoz, C. Chen, I. A. McDonald, *Biotechnol. Bioeng.* **2000**, *71*, 78 – 84.
[22] G. C. Look, M. M. Murphy, D. A. Campbell, M. A. Gallop, *Tetrahedron Lett.* **1995**, *36*, 2937 – 2940.
[23] After evaporation of the combined cleavage and washing solutions, the residue was subjected to filtration through a short plug of silica, the crude product was eluted with petroleum ether/ethyl acetate (1/1), and after removal of the solvent the residue was analyzed by HPLC-MS.
[24] K. Maruoka, K. Nonoshita, H. Yamamoto, *Tetrahedron Lett.* **1987**, *28*, 5723 – 5726.
[25] B. H. Lipshutz, R. S. Wilhelm, D. M. Floyd, *J. Am. Chem. Soc.* **1981**, *103*, 7672 – 7674.

 © 2003 Wiley-VCH Verlag GmbH & Co. KGaA, Weinheim 1433-7851/03/4207-0790 $ 20.00+.50/0

Monodentate P Ligands

A New Principle in Combinatorial Asymmetric Transition-Metal Catalysis: Mixtures of Chiral Monodentate P Ligands**

Manfred T. Reetz, Thorsten Sell, Andreas Meiswinkel, and Gerlinde Mehler*

Successful ligand optimization in the area of enantioselective transition-metal catalysis requires rational design, intuition, and experience, but also some degree of trial and error.[1,2] Combinatorial asymmetric catalysis was recently developed to speed up and/or to complement the process of optimization.[3,4] All of the examples thus far involve the generation and screening of libraries of chiral ligands whose modular construction allows structural diversity and therefore increases the chance of finding a "hit".

We describe a new concept in the area of combinatorial enantioselective transition-metal catalysis. The basic idea concerns the use of mixtures of chiral monodentate ligands. The method is relevant whenever in the transition state of the reaction at least two monodentate ligands (L) are coordinated to the metal (M) of the active catalyst ML_x. For example, in the case of a mixture of two such ligands L^a and L^b, three different catalysts exist in equilibrium with one another, namely the two homocombinations ML^aL^a and ML^bL^b as well as the heterocombination ML^aL^b.[5] Many examples for homocombinations are known in the literature,[1a,6] for example, the recently reported BINOL-based modular monophosphonites **1**,[7] monophosphites **2**,[8] and the monophosphoramidite **3**,[9] which often (but not always) lead to high

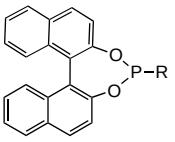

1 **a** R = CH_3
b R = C_2H_5
c R = *c*-C_6H_{11}
d R = $C(CH_3)_3$
e R = C_6H_5
f R = Cl

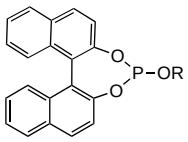

2 **a** R = CH_3
b R = C_2H_5
c R = *c*-C_6H_{11}
d R = $C(CH_3)_3$
e R = C_6H_5
f R = 2,6-$(CH_3)_2$-C_6H_5
g R = $CH(CH_3)_2$
h R = 9-Fluorenyl

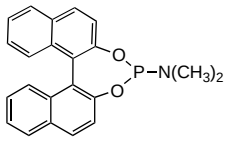

3

enantioselectivities when used as ligands in Rh-catalyzed olefin hydrogenation (BINOL = 2,2′-dihydroxy-1,1′-binaphthyl). In contrast, nothing has been reported about the use of heterocombinations ML^aL^b as catalysts. Since rapid

[*] Prof. M. T. Reetz, Dipl.-Chem. T. Sell, Dipl.-Chem. A. Meiswinkel, G. Mehler
Max-Planck-Institut für Kohlenforschung
Kaiser-Wilhelm-Platz 1, 45470 Mülheim an der Ruhr (Germany)
Fax: (+49) 208-306-2985
E-mail: reetz@mpi-muelheim.mpg.de

[**] This work was supported by the Fonds der Chemischen Industrie.

 © 2003 Wiley-VCH Verlag GmbH & Co. KGaA, Weinheim 1433-7851/03/4207-0790 $ 20.00+.50/0

ligand exchange is likely in most systems, the preparation of ML^aL^b in pure form in solution is not expected to be possible. However, the mixture of all three catalysts may well lead to enhanced enantioselectivity provided ML^aL^b is more active and more selective than either of the traditional catalysts ML^aL^a or ML^bL^b. Moreover, the relative amounts of the ligands L^a and L^b used may also influence the stereochemical outcome.

The Rh-catalyzed hydrogenation of the acetamidoacrylate **4a** in dichloromethane was chosen as the test reaction. Initially the ratio $Rh:L^a:L^b$ was kept constant at 1:1:1. Although not all of the theoretically possible combinations of L^a/L^b were tested, the results summarized in Table 1 uncover some remarkable trends, which need to be compared to the most enantioselective homocombinations [Eq. (1)].

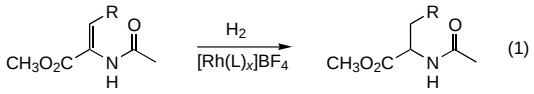

4a R = H
b R = Ph

5a R = H
b R = Ph

(1)

It is apparent that certain ligand combinations L^a/L^b lead to notably high enantioselectivities. In the case of two different phosphonites (Table 1, entries 15–19) enantioselectivity in the test reaction **4**→**5** is nearly complete (*ee* = 98%) whenever one component bears a small substituent R at the phosphorus center (e.g., methyl as in **1a**) and the other is characterized by steric bulk (Table 1, entries 16 and 17). The results constitute significant improvements relative to the use of the corresponding homocombinations which lead to *ee* values of only 92–94% (Table 1, entries 1, 3, 4). The chloro derivative **1f** fails to afford high enantioselectivity, irrespective of its use as a homocombination (Table 1, entry 6) or as a heterocombination (Table 1, entry 20). Acceptable *ee* values occur in the phosphite series (Table 1, entries 21–36), but improvements upon using heterocombinations are in most cases not significant. The greatest effect results when going from the homocombinations **2a** (76.6% *ee*) and **2f** (32.4% *ee*) to the heterocombination based on the same ligands **2a**/**2f** (84.6% *ee*) (Table 1, entry 25). In contrast, upon using proper combinations of phosphonites **1** and phosphites **2**, pronounced enhancements in enantioselectivity are observed, especially if a bulky phosphonite (e.g., **1c** or **1d**) is combined with the sterically least demanding phosphite **2a** (Table 1, entries 40, 42).

In the case of the hydrogenation of **4b** the combinatorial search was restricted to mixtures of phosphonites **1**. Again, significant improvements in the *ee* values were accomplished ((*R*)-**1a**/(*R*)-**1c**: 96.7% *ee* (*S*); (*R*)-**1a**/(*R*)-**1d**: 99.2% *ee* (*S*); (*R*)-**1b**/(*R*)-**1d**: 94.6% *ee* (*S*) relative to (*R*)-**1a**/(*R*)-**1a**: 89.9% *ee* (*S*); (*R*)-**1b**/(*R*)-**1b**: 89.2% *ee* (*S*); (*R*)-**1d**/(*R*)-**1d**: 69.1% *ee* (*S*)).

We next studied the hydrogenation of the *N*-acyl enamine **6a**[10] which led to the formation of the chiral amine **7a** (Rh:**6a** = 1:250; 1.5 bar H_2; 22 h; CH_2Cl_2; [Eq. (2)]). Once again application of the method led to significantly enhanced enantioselectivities. Upon carrying out only 30 hydrogenation experiments, several highly selective combinations were identified, among them (*R*)-**1a**/(*R*)-**1d** (96.1% *ee* (*S*)). In contrast, the respective homocombinations deliver mediocre or poor enantioselectivities ((*R*)-**1a**/(*R*)-**1a**: 75.6% *ee* (*S*);

Table 1: Rh-catalyzed hydrogenation of **4a**.[a]

Entry	Ligands	*ee* [%] (config.)
	Homocombinations	
1	(*R*)-**1a**/(*R*)-**1a**	91.8 (*S*)
2	(*R*)-**1b**/(*R*)-**1b**	94.4 (*S*)
3	(*R*)-**1c**/(*R*)-**1c**	92.0 (*S*)
4	(*R*)-**1d**/(*R*)-**1d**	93.3 (*S*)
5	(*R*)-**1e**/(*R*)-**1e**	72.8 (*S*)
6[b]	(*R*)-**1f**/(*R*)-**1f**	7.4 (*S*)
7	(*S*)-**2a**/(*S*)-**2a**	76.6 (*R*)
8	(*S*)-**2b**/(*S*)-**2b**	83.6 (*R*)
9	(*R*)-**2c**/(*R*)-**2c**	94.6 (*S*)
10	(*S*)-**2d**/(*S*)-**2d**	95.4 (*R*)
11[c]	(*S*)-**2e**/(*S*)-**2e**	78.6 (*R*)
12[d]	(*S*)-**2f**/(*S*)-**2f**	32.4 (*R*)
13	(*S*)-**2g**/(*S*)-**2g**	94.4 (*R*)
14	(*S*)-**2h**/(*S*)-**2h**	92.4 (*R*)
	Heterocombinations	
15	(*R*)-**1a**/(*R*)-**1b**	92.6 (*S*)
16	(*R*)-**1a**/(*R*)-**1c**	97.9 (*S*)
17	(*R*)-**1a**/(*R*)-**1d**	97.8 (*S*)
18	(*R*)-**1c**/(*R*)-**1d**	94.1 (*S*)
19	(*R*)-**1d**/(*R*)-**1e**	75.8 (*S*)
20	(*R*)-**1d**/(*R*)-**1f**	racemic
21	(*R*)-**2a**/(*R*)-**2b**	80.0 (*S*)
22	(*R*)-**2a**/(*R*)-**2c**	76.6 (*S*)
23	(*R*)-**2a**/(*R*)-**2d**	89.0 (*S*)
24	(*R*)-**2a**/(*R*)-**2e**	77.4 (*S*)
25	(*R*)-**2a**/(*R*)-**2f**	84.6 (*S*)
26	(*R*)-**2a**/(*R*)-**2g**	87.2 (*S*)
27	(*R*)-**2b**/(*R*)-**2c**	79.0 (*S*)
28	(*R*)-**2b**/(*R*)-**2d**	91.2 (*S*)
29	(*R*)-**2b**/(*R*)-**2e**	80.8 (*S*)
30	(*R*)-**2b**/(*R*)-**2g**	90.0 (*S*)
31	(*R*)-**2d**/(*R*)-**2c**	94.2 (*S*)
32	(*R*)-**2d**/(*R*)-**2e**	92.2 (*S*)
33	(*R*)-**2e**/(*R*)-**2c**	85.6 (*S*)
34	(*R*)-**2g**/(*R*)-**2c**	94.6 (*S*)
35	(*R*)-**2g**/(*R*)-**2d**	94.8 (*S*)
36	(*R*)-**2g**/(*R*)-**2e**	91.2 (*S*)
37	(*R*)-**1a**/(*R*)-**2a**	81.9 (*S*)
38	(*R*)-**1a**/(*R*)-**2c**	94.4 (*S*)
39	(*R*)-**1a**/(*R*)-**2d**	93.0 (*S*)
40	(*R*)-**1c**/(*R*)-**2a**	96.4 (*S*)
41	(*R*)-**1c**/(*R*)-**2d**	91.8 (*S*)
42	(*R*)-**1d**/(*R*)-**2a**	98.0 (*S*)
43	(*R*)-**1d**/(*R*)-**2c**	94.6 (*S*)
44	(*R*)-**1d**/(*R*)-**2h**	97.2 (*S*)
45	(*R*)-**1c**/(*R*)-**2h**	95.6 (*S*)

[a] Rh/substrate ratio 1:1000; Rh/P ratio 1:2; solvent: CH_2Cl_2; $p(H_2) = 1.3$ bar; $T = 20°C$; reaction time: 20 h; conversion: 100%.
[b] Conversion: 1%. [c] Conversion: 93%. [d] Conversion: 62%.

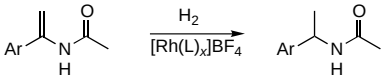

6a Ar = Ph
b Ar = *p*-Cl-Ph
c Ar = 2-Naphthyl

7a Ar = Ph
b Ar = *p*-Cl-Ph
c Ar = 2-Naphthyl

(2)

 © 2003 Wiley-VCH Verlag GmbH & Co. KGaA, Weinheim 1433-7851/03/4207-0791 $ 20.00+.50/0

(*R*)-**1d**/(*R*)-**1d**: 13.2% *ee* (*S*)). Moreover, by using (*R*)-**1a**/(*R*)-**1d** product **7b**, which is of interest in plant protection, was obtained enantioselectively (95.0% *ee* (*S*)). Finally, this particular catalyst system (again the mixture of all three catalysts) allowed the enantioselective hydrogenation of **6c** (97.0% *ee* (*S*)), whereas the pure homocombinations led to inferior results (78.2% *ee* (*S*) and <3% *ee*, respectively).

To study the possible influence of the relative amounts of the two ligands used, appropriate mixtures of **1a** and **1d** were employed in the Rh-catalyzed hydrogenation of **6a** (Rh:P ligand = 1:2). The results summarized in Table 2 show that precise adjustment of the ratio is not necessary. However, when the relative amount of the methyl phosphonite **1a** dominates strongly, then the *ee* value drops significantly.

Table 2: Influence of the ratio **1a**:**1d** on the enantioselectivity of the hydrogenation of **6a**.[a]

Entry	Ligands (*R*)-**1a**/(*R*)-**1d**	*ee* [%] (config.)
1[b]	1:5	95.4 (*S*)
2	1:3	97.4 (*S*)
3	1:2	97.2 (*S*)
4	1:1	96.4 (*S*)
5	2:1	88.8 (*S*)
6	3:1	85.0 (*S*)
7	5:1	81.2 (*S*)

[a] In all cases the ratio Rh/((*R*)-**1a**/(*R*)-**1d**)was kept constant at 1:2 and the Rh/substrate ratio at 1:500; solvent: CH_2Cl_2; $p(H_2) = 1.5$ bar; $T = 20$°C; reaction time: 1 h; conversion: 100%. [b] Conversion: 95%.

Finally, the hydrogenation of dimethyl itaconate (**8**) was studied [Eq. (3)], the combinatorial search being restricted mainly to phosphonites. Table 3 shows that in the list of homocombinations the methyl derivative (*R*)-**1a** is by far the most enantioselective (90.2% *ee* (*R*)), whereas the *tert*-butyl ligand (*R*)-**1d** leads to an *ee* value of only 57.3% (*R*). In contrast, the heterocombination (*R*)-**1a**/(*R*)-**1d** constitutes by far the best catalyst system (96.4% *ee*, Table 3, entry 8). Upon varying the ratio of (*R*)-**1a** to (*R*)-**1d** from 1:3 to 2:1, the *ee* value remained approximately constant (95.8% and 96.6%, respectively). In the case of (*R*)-**1a**:(*R*)-**1d** = 1:1, the performance of the catalyst system was explored by successively reducing the Rh/substrate ratio. The *ee* value remained nearly constant at quantitative conversion (Rh/**8** = 1:6000, 95.8% *ee* (*R*); Rh/**8** = 1:10000, 95.4% *ee* (*R*); Rh/**8** = 1:20000, 94.6% *ee* (*R*)).

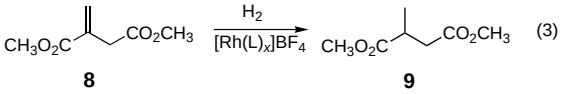

8 **9** (3)

Table 3: Rh-catalyzed hydrogenation of **8**.[a]

Entry	Ligands	*ee* [%] (config.)
	homocombinations	
1	(*R*)-**1a**/(*R*)-**1a**	90.2 (*R*)
2	(*R*)-**1b**/(*R*)-**1b**	71.4 (*R*)
3	(*R*)-**1c**/(*R*)-**1c**	21.9 (*R*)
4	(*R*)-**1d**/(*R*)-**1d**	57.3 (*R*)
5	(*R*)-**1e**/(*R*)-**1e**	28.8 (*R*)
	heterocombinations	
6	(*R*)-**1a**/(*R*)-**1b**	82.4 (*R*)
7	(*R*)-**1a**/(*R*)-**1c**	88.6 (*R*)
8	(*R*)-**1a**/(*R*)-**1d**	96.4 (*R*)
9	(*R*)-**1b**/(*R*)-**1d**	92.2 (*R*)
10	(*R*)-**1c**/(*R*)-**1d**	69.1 (*R*)
11	(*R*)-**1c**/(*R*)-**1e**	50.0 (*R*)
12	(*R*)-**1d**/(*R*)-**1e**	57.4 (*R*)

[a] In all cases the ratio Rh/P was kept constant at 1:2 and the Rh/substrate ratio at 1:1000; solvent: CH_2Cl_2; $p(H_2) = 1.3$ bar; $T = 20$°C; reaction time: 20 h; conversion: 100%.

Our results illustrate a new principle in the area of combinatorial asymmetric transition-metal catalysis.[11] Accordingly, it makes sense to consider the use of mixtures of chiral monodentate ligands in asymmetric transition metal catalysis, inspite of the fact that systems of this kind contain at least three different catalysts or precatalysts. For example, the NMR spectrum of the mixture of **1a, 1d**, and $[Rh(cod)_2]BF_4$ (cod = 1,5-cyclooctadiene) shows the presence of $[Rh(\mathbf{1a})_2(cod)]BF_4$, $[Rh(\mathbf{1d})_2(cod)]BF_4$ and $[Rh(\mathbf{1a})(\mathbf{1d})(cod)]BF_4$ in a ratio of about 20:20:60.[12] Initial kinetic studies indicate that this mixture is a more *active* catalyst system than the respective homocombinations $[Rh(\mathbf{1a})_2(cod)]BF_4$ or $[Rh(\mathbf{1d})_2(cod)]BF_4$. Additional studies are necessary to identify the source of increased enantioselectivity. The question whether the general concept is also valid in other types of asymmetric reactions, and whether mixtures of achiral ligands enhance catalyst performance in achiral transformations, also needs to be addressed.

Experimental Section

General procedure for the hydrogenation of **4** and **8** using mixtures of monodentate P ligands: A dry 50-mL Schlenk flask under an atmosphere of argon was charged with a mixture of a 1.7 mM solution of the first ligand (0.6 mL) and a 1.7 mM solution of the second ligand (0.6 mL) in dry dichloromethane. The solution was treated with a 2.0 mM solution of $[Rh(cod)_2]BF_4$ (0.5 mL) in dichloromethane and stirred for 5 min at room temperature. Then a 0.112 M solution of the substrate in dichloromethane (9 mL) was added. Vacuum was applied three times until the solvent began to evaporate gently, and hydrogen was introduced. Hydrogenation was carried out at 1.3 bar for the periods given. Following dilution, conversion was determined by gas chromatography (GC). To determine the *ee* values, about 1.5 mL of the reaction solution was passed through a small amount of silica gel prior to the GC or HPLC analysis. The hydrogenation experiments were carried out in a parallel manner using 20 or more flasks.

Received: September 16, 2002 [Z50171]

[1] a) W. S. Knowles, *Angew. Chem.* **2002**, *114*, 2096–2107; *Angew. Chem. Int. Ed.* **2002**, *41*, 1998–2007; b) R. Noyori, *Angew. Chem.* **2002**, *114*, 2108–2123; *Angew. Chem. Int. Ed.* **2002**, *41*, 2008–2022; c) K. B. Sharpless, *Angew. Chem.* **2002**, *114*, 2126–2135; *Angew. Chem. Int. Ed.* **2002**, *41*, 2024–2032.

[2] *Comprehensive Asymmetric Catalysis, Vol. I–III* (Eds.: E. N. Jacobsen, A. Pfaltz, H. Yamamoto), Springer, Berlin, **1999**.

[3] See, for example: a) M. B. Francis, E. N. Jacobsen, *Angew. Chem.* **1999**, *111*, 987–991; *Angew. Chem. Int. Ed.* **1999**, *38*, 937–941; b) S. R. Gilbertson, C.-W. T. Chang, *Chem. Commun.* **1997**,

 © 2003 Wiley-VCH Verlag GmbH & Co. KGaA, Weinheim 1433-7851/03/4207-0792 $ 20.00+.50/0

975 – 976; c) C. Gennari, S. Ceccarelli, U. Piarulli, C. A. G. N. Montalbetti, R. F. W. Jackson, *J. Org. Chem.* **1998**, *63*, 5312 – 5313; d) K. Burgess, H.-J. Lim, A. M. Porte, G. A. Sulikowski, *Angew. Chem.* **1996**, *108*, 192 – 194; *Angew. Chem. Int. Ed. Engl.* **1996**, *35*, 220 – 222; e) C. A. Krueger, K. W. Kuntz, C. D. Dzierba, W. G. Wirschun, J. D. Gleason, M. L. Snapper, A. H. Hoveyda, *J. Am. Chem. Soc.* **1999**, *121*, 4284 – 4285; f) J. Long, J. Hu, X. Shen, B. Ji, K. Ding, *J. Am. Chem. Soc.* **2002**, *124*, 10 – 11; g) A. Berkessel, R. Riedl, *J. Comb. Chem.* **2000**, *2*, 215 – 219; h) S. Dahmen, S. Bräse, *Synthesis* **2001**, 1431 – 1449.

[4] Reviews of combinatorial and evolutionary methods for the generation of enantioselective (bio)catalysts as well as high-throughput screening systems: a) M. T. Reetz, *Angew. Chem.* **2001**, *113*, 292 – 320; *Angew. Chem. Int. Ed.* **2001**, *40*, 284 – 310; b) M. T. Reetz, *Angew. Chem.* **2002**, *114*, 1391 – 1394; *Angew. Chem. Int. Ed.* **2002**, *41*, 1335 – 1338.

[5] Of course, transition-metal catalysts with two different types of ligands are known, for example, Noyori's Ru catalysts for asymmetric ketone reduction, composed of BINAP and a chiral diamine (whose proton is transferred onto the substrate).[1b] Both in the matched and mismatched case discrete diastereomeric catalyst systems having two different chelating ligands are involved. The corresponding BINAP-free and diamine-free Ru complexes are not catalytically active.[1b] In contrast, we employ two different mono-P ligands having the same absolute configuration with formation of three structurally different (not diastereomeric!) active catalysts which are in equilibrium with one another, the reactivity and selectivity of which differ.

[6] I. V. Komarov, A. Börner, *Angew. Chem.* **2001**, *113*, 1237 – 1240; *Angew. Chem. Int. Ed.* **2001**, *40*, 1197 – 1200.

[7] a) M. T. Reetz, T. Sell, *Tetrahedron Lett.* **2000**, *41*, 6333 – 6336; b) C. Claver, E. Fernandez, A. Gillon, K. Heslop, D. J. Hyett, A. Martorell, A. G. Orpen, P. G. Pringle, *Chem. Commun.* **2000**, 961 – 962.

[8] M. T. Reetz, G. Mehler, *Angew. Chem.* **2000**, *112*, 4047 – 4049; *Angew. Chem. Int. Ed.* **2000**, *39*, 3889 – 3890.

[9] a) M. van den Berg, A. J. Minnaard, E. P. Schudde, J. van Esch, A. H. M. de Vries, J. G. de Vries, B. L. Feringa, *J. Am. Chem. Soc.* **2000**, *122*, 11539 – 11540; b) A. J. Minnaard, M. van den Berg, E. P. Schudde, J. van Esch, A. H. M. de Vries, J. G. de Vries, B. L. Feringa, *Chim. Oggi* **2001**, *19*, 12 – 13.

[10] Synthesis and hydrogenation of *N*-acyl enamines: a) M. J. Burk, G. Casy, N. B. Johnson, *J. Org. Chem.* **1998**, *63*, 6084 – 6085; b) X. Jia, R. Guo, X. Li, X. Yao, A. S. C. Chan, *Tetrahedron Lett.* **2002**, *43*, 5541 – 5544; c) A.-G. Hu, Y. Fu, J.-H. Xie, H. Zhou, L.-X. Wang, Q.-L. Zhou, *Angew. Chem.* **2002**, *114*, 2454 – 2456; *Angew. Chem. Int. Ed.* **2002**, *41*, 2348 – 2350; d) W. Tang, X. Zhang, *Angew. Chem.* **2002**, *114*, 1682 – 1684; *Angew. Chem. Int. Ed.* **2002**, *41*, 1612 – 1614; e) S.-G. Lee, Y. J. Zhang, C. E. Song, J. K. Lee, J. H. Choi, *Angew. Chem.* **2002**, *114*, 875 – 877; *Angew. Chem. Int. Ed.* **2002**, *41*, 847 – 849; f) M. T. Reetz, G. Mehler, A. Meiswinkel, T. Sell, *Tetrahedron Lett.* **2002**, 43, 7941 – 7943.

[11] M. T. Reetz, T. Sell, A. Meiswinkel, G. Mehler, patent application, DE-A 10247633.0 (11.10.2002).

[12] In this heterocombination (60% of total catalyst system) NMR spectroscopy shows the presence of two different species (R. Mynott, unpublished results). Detailed NMR studies are in progress.

 © 2003 Wiley-VCH Verlag GmbH & Co. KGaA, Weinheim 1433-7851/03/4207-0793 $ 20.00+.50/0

Cu–Cu Interactions

Reactions of Triazacyclohexanes with $CuCl_2$: Surprising Formation of a Dimer between Two $[CuCl_2]^-$ Ions with an Unsupported Cuprophilic Attraction**

Randolf D. Köhn, Guido Seifert, Zhida Pan, Mary F. Mahon, and Gabriele Kociok-Köhn*

The variation in both the coordination number and the geometry of complexes containing copper centers in either the +1 or +2 oxidation states has attracted much attention owing to the extent to which control over the coordination geometry influences the redox properties that are perfected in many biological enzymes.[1] Another area of current interest concerns the possibility of strong closed-shell interactions between two Cu^I ions, where the origin, strength, or even existence of such interactions is highly controversial (cuprophilicity, in analogy to the less-controversial aurophilicity).[2] Crystallographic evidence for close Cu–Cu interactions is often ambiguous because of bridging ligands or electrostatic interactions.[3] Unambiguous experimental evidence for a cuprophilic interaction would entail the isolation of a dimer containing two equally charged ions connected only through a Cu–Cu interaction. Hence, we report herein that the simple system of **1a**/$CuCl_2$ can demonstrate the destabilization of Cu^{II}, in comparison with Cu^I, through coordination geometry, as well as produce the first evidence for a cuprophilic interaction between two $[CuCl_2]^-$ ions (Scheme 1).

Over recent years we have been developing the coordination chemistry of the readily available *N*-substituted triazacyclohexanes **1** with transition metals.[4] Compared to the larger triazacyclononanes, an unusual coordination geometry is enforced with acute N-metal-N bond angles of approximately 60° and misdirected nitrogen lone pairs in κ^3 complexes. We have previously reported that $CuCl_2$ reacts with **1** to give the dinuclear complex **3a** (R = Me) or the mononuclear complex **2c** (R = *i*Pr).[5] We also found that **3a** is dimeric in a different crystal environment[6] and that by using the slightly larger Et substituent, a mononuclear structure is obtained for **2b**,[6] which is similar to that of **2c** (Figure 1). However, UV/Vis spectra of "**3a**" in CH_2Cl_2 are modestly dependent on concentration, and can be interpreted as an

[*] Dr. R. D. Köhn, Dr. G. Seifert, Dr. Z. Pan, Dr. M. F. Mahon, Dr. G. Kociok-Köhn
Department of Chemistry
University of Bath
Bath BA2 7AY (UK)
Fax: (+44) 1225-386231
E-mail: r.d.kohn@bath.ac.uk

[**] The Chemistry of 1,3,5-Triazacyclohexane Complexes, Part 11. This work was supported by the Deutsche Forschungsgemeinschaft (G.S.) and the EPSRC (UK) (Z.P.). We thank Prof. H. Schumann (TU Berlin) for support and Prof. A. C. Filippou (HU Berlin) for diffractometer time. Part 10, see ref. [4d].

Supporting information for this article is available on the WWW under http://www.angewandte.org or from the author.

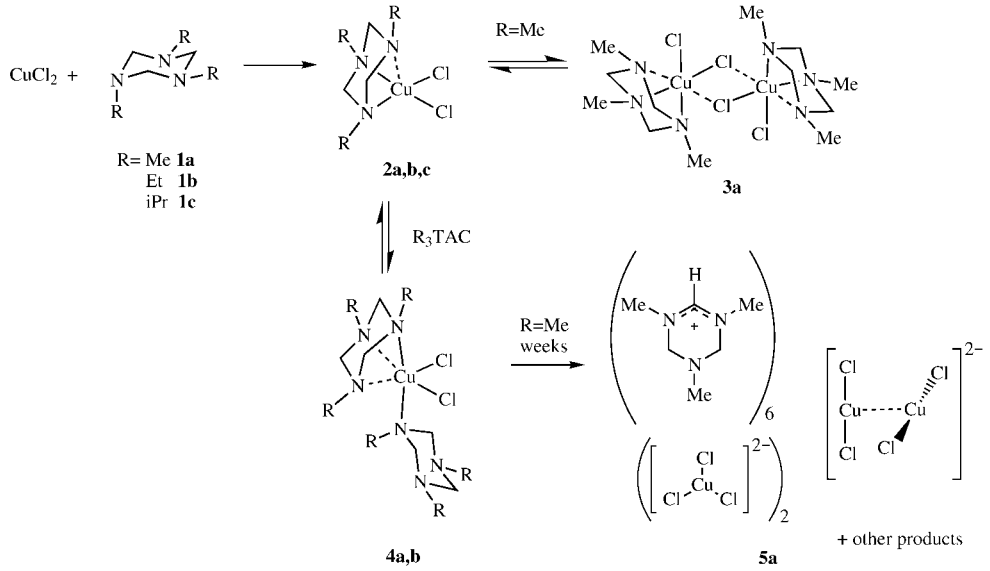

Scheme 1. Syntheses of the complexes (see Supporting Information for details).

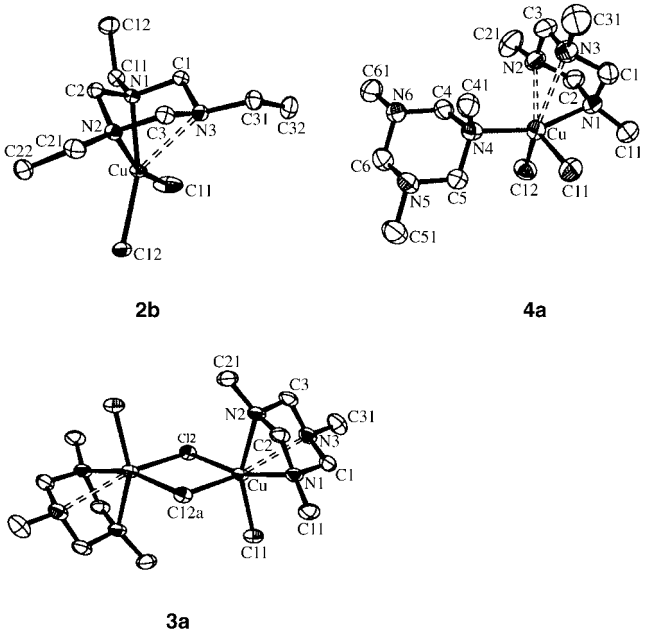

Figure 1. Molecular structures of **2b, 3a**, and **4a**.[6] Selected bond lengths [Å] for **2b** [**3a**] {**4a**}: Cu-N1 2.0706(12) [2.0657(16)] {2.017(4)}, Cu-N2 2.0952(13) [2.1303(16)] {2.509(4)}, Cu-N3 2.5218(13) [2.6073(18)] {2.618(4)}, Cu-Cl1 2.2122(5) [2.2428(5)] {2.3193(13)}, Cu-Cl2 2.2166(4) [2.2646(5)] {2.3342(13)}, Cu-Cl2a [2.7083(5)], Cu-N4 {2.027(4)} (ellipsoids at the 50% probability level).

equilibrium between **2a** and **3a**, with **2a** being the predominant species in solutions of about 10^{-3} M. Solutions of **2a** and **2b** react with excess **1a** and **1b**, respectively, to yield the bis(triazacyclohexane) complexes **4a** and **4b**. The equilibrium between the green complex **2** and the yellow complex **4** at different [Cu]/[**1**] ratios was studied by UV/Vis spectroscopy in CH_2Cl_2, and can be described by $K = [\mathbf{4}]/([\mathbf{2}] \times [\mathbf{1}])$ ($K = 850$ (R = Me) and $30\ M^{-1}$ (R = Et)). Compound **4a** was isolated in the solid state from **3a** in neat **1a**, while the less stable and more soluble **4b** could not be isolated.

Crystals of **4a** revealed an octahedral coordination geometry for the Cu^{II} center, with two long Cu–N bonds of 2.51 and 2.62 Å in a *cis* orientation.[6] The other Cu–N bonds (2.02 and 2.03 Å) are significantly shorter, while the Cu–Cl bonds (2.32 and 2.33 Å) are significantly longer than the corresponding bonds in **3a** and **2b**. The coordination geometry of the four short bonds is much closer to tetrahedral than square-planar, as seen from the average angle (θ) of the two largest bond angles[7] (ideal tetrahedron 109.5°, **4a** 136.7°, **3a** 158.9°, **2b** 161.5°, ideal square plane 180°) or the dihedral angle (Δ) between the N-Cu-N and Cl-Cu-Cl planes[8] (ideal tetrahedron 90°, **4a** 89.0°, **3a** 15.4°, **2b** 12.9°, ideal square plane 0°). Thus, the Cu^{II} center in **4a** should be more susceptible towards reduction to Cu^{I}.[1]

A solution comprising mostly **4a** in neat **1a** completely decolorized after a few weeks when left in a tightly sealed flask under argon, and eventually yielded colorless crystals. The X-ray single-crystal structure of **5a** showed that ligand **1a** had been oxidized to the amidinium ion, probably by the Cu^{II} center, which was subsequently converted to Cu^{I}, which appears in the structure of **5a** in the form of $[CuCl_3]^{2-}$ and $([CuCl_2]^-)_2$ ions (Figure 2). The oxidation of triazacyclohexanes to amidinium ions, along with the production of one equivalent of a protonated triazacyclohexane, has been observed before in the reaction with I_2.[9] Whereas the trigonal-planar $[CuCl_3]^{2-}$ ion is known,[10] the $[CuCl_2]^-$ ion is only observed as a monomeric unit,[11] or in chloride-bridged dimeric units ($[ClCu(\mu\text{-}Cl)_2CuCl]^{2-}$).[12] However, the $[CuCl_2]^-$ ion in the crystal structure[6] of **5a** is present as a dimer with a Cu–Cu separation of 2.92 Å, without any bridging chloride ions.

Thus, attractions that can compensate the electrostatic repulsion between the two $[CuCl_2]^-$ ions must arise from the weak Cu–Cu interaction and the crystal field. The dianion in the structure is surrounded by a sphere of cations with weak $Cl\cdots H_{amidinium}$ contacts of 3–4 Å, but with no obvious "bridging" unit; there are closer Cl···H contacts to CH_2 and

 © 2003 Wiley-VCH Verlag GmbH & Co. KGaA, Weinheim 1433-7851/03/4207-0794 $ 20.00+.50/0

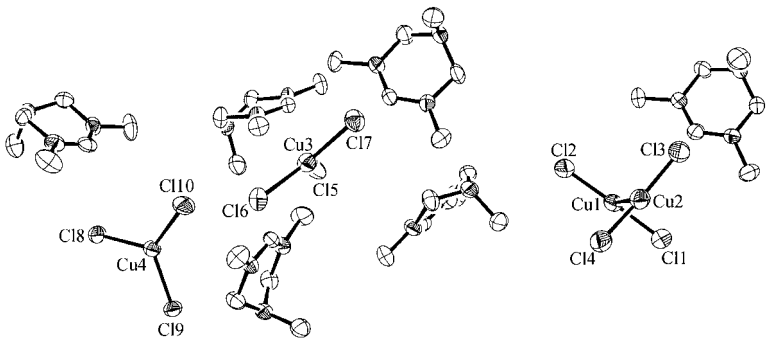

Figure 2. Structure of **5a**.[6] (ellipsoids at the 50% probability level).

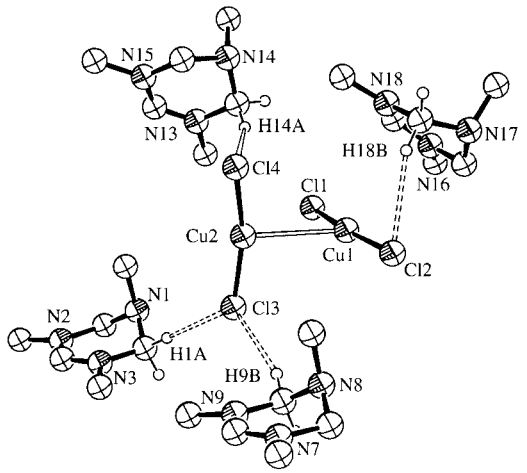

Figure 3. Structure of the $([CuCl_2]^-)_2$ dimer in **5a** with the closest associated cations. Bond lengths [Å] and angles [°]: Cu1-Cu2 2.9217(17), Cu-Cl 2.110–2.116(3); Cl1-Cu1-Cl2 171.46(11), Cl3-Cu2-Cl4 164.98(11), Cl1-Cu1-Cu2 78.62(8), Cl2-Cu1-Cu2 109.91(8), Cl3-Cu2-Cu1 95.46(9), Cl4-Cu2-Cu1 98.44(9); separations involving crystallographic hydrogen atoms: Cl2-H18B 2.79, Cl3-H1A 2.68, Cl3-9B 2.76, Cl4-H14A 2.67.

CH_3 groups with no formal charge. The dimer with the four closest cations (with Cl···H contacts up to 2.8 Å) is shown in Figure 3. The next-nearest anions are more than 7 Å distant, and are not found in positions along the Cu–Cu axis that might serve to push the two $[CuCl_2]^-$ units closer together. There is, therefore, no obvious reason why the two $[CuCl_2]^-$ units should be close to each other, yet the nearly linear anions are distorted, with the copper atoms bent towards each other resulting in Cl-Cu-Cl angles of 165 and 172°.

To date, the best evidence for cuprophilic interactions has been found in the structures of the cuprates $[t\text{BuCu}\{\text{CNLi}(\text{OEt}_2)_2\}]_\infty$[13] and $[\{(\text{Me}_3\text{SiCH}_2)_2\text{CuLi}\}_2(\text{Et}_2\text{O})_3]$.[14] Similar to the case of **5a**, two nearly linear [R-Cu-R] anions form almost perpendicular dimers with Cu–Cu separations of 2.71 and 2.83 Å, and with R-Cu-R angles of 170 and 172°. However, these structures do contrast with **5a**, as lithium ions are closely associated to the anions therein, which results in an overall neutral dimer. The bonding within these dimers was recently treated theoretically for $[\text{RCuX}]_2$ (R = Me, H, Cl; X = a variety of neutral ligands).[15] The results indicate a small attractive interaction of around 4 kcal mol^{-1} between the copper atoms, with a shallow potential for Cu–Cu separations ranging from 2.5 to 3.2 Å. Experimentally determined close Cu–Cu separations range from 2.35[16] to 3.45 Å.[17] Thus, the observed Cu–Cu separation in **5a** falls well within the range of cuprophilic interactions, and is to our knowledge the first case of an isolated dimer between two anionic copper units.

The stoichiometry of the reaction that yields **5a** from **4a** demands that there must be other soluble products. However, we were unable to identify these products as the highly air-sensitive colorless solution returned to the greenish color of **3a** immediately after opening the flask, even under a stream of argon. NMR spectra of the resulting paramagnetic solution could not be interpreted and the reaction could not be repeated in solvents other than neat **1a**. However, in a sealed flask, the solution became colorless again after a few weeks, and this cycle of oxidation by traces of air followed by slow reduction could be repeated several times, eventually yielding crystals identical to **5a** once again. Thus, the copper complex appears to slowly catalyze the oxidation of **1a** to the amidinium ion with dioxygen. Preliminary results show that the stoichiometric oxidant PhCOOO*t*Bu can oxidize **1a** catalytically to give the amidinium ion in **5a**. We are currently investigating this reaction further.

In summary, the reactions of **1** with $CuCl_2$ result in the formation of the complex **4a** with *cis*-divacant octahedral geometry that is susceptible to internal reduction of Cu^{II} to Cu^{I}. The crystal structure of the product **5a** revealed the first example of an isolated dimer consisting of two anionic $[CuCl_2]^-$ units that are solely connected through a cuprophilic Cu–Cu interaction.

Received: September 18, 2002 [Z50187]

[1] P. Comba, *Coord. Chem. Rev.* **2000**, *200*, 217–245; R. K. Szilagyi, E. I. Solomon, *Curr. Opin. Chem. Biol.* **2002**, *6*, 250–258, and references therein.

[2] P. Pyykkö, *Chem. Rev.* **1997**, *97*, 597–636.

[3] A case similar to **5a**, $[CuL_2]^+[CuCl_2]^-$ (U. Siemeling, U. Vorfeld, B. Neumann, H.-G. Stammler, *Chem. Commun.* **1997**, 1723–1724) was later dismissed as mostly electrostatic: J.-M. Poblet, M. Bénard, *Chem. Commun.* **1998**, 1179–1180.

[4] a) R. D. Köhn, G. Kociok-Köhn, *Angew. Chem.* **1994**, *106*, 1958–1960; *Angew. Chem. Int. Ed. Engl.* **1994**, *33*, 1877–1879; b) R. D. Köhn, M. Haufe, S. Mihan, D. Lilge, *Chem. Commun.* **2000**, 1927–1928; c) R. D. Köhn, M. Haufe, G. Kociok-Köhn, S. Grimm, P. Wasserscheid, W. Keim, *Angew. Chem.* **2000**, *112*, 4519–4521; *Angew. Chem. Int. Ed.* **2000**, *39*, 4337–4339; d) R. D. Köhn, Z. Pan, G. Kociok-Köhn, M. F. Mahon, *J. Chem. Soc. Dalton Trans.* **2002**, 2344–2347, and references therein.

[5] R. D. Köhn, G. Seifert, G. Kociok-Köhn, *Chem. Ber.* **1996**, *129*, 1327–1333.

[6] Crystal data for $\mathbf{3a}\cdot(CH_2Cl_2)_{1/3}$ and **2b** can be found in the Supporting Information. Crystal data of $\mathbf{4a}\cdot(\text{toluene})_{0.5}$: crystal size $0.15\times0.15\times0.08$ mm, monoclinic, space group $P2_1/c$ (no. 14), $Z=4$, $a=8.7484(10)$, $b=13.3152(16)$, $c=18.634(2)$ Å, $\beta=95.538(10)°$, $V=2160.5(4)$ Å^3, $M_W=434.90$, $\rho_{calcd}=1.337$ g cm^{-3}, $F(000)=912$, $T=210(2)$ K, Stoe IPDS area detec-

tor, $2.20 \le \theta \le 24.46°$, ($\lambda(Mo_{K\alpha}) = 0.71073$ Å, $\mu = 1.247\ mm^{-1}$), 14033 reflections collected, 3518 unique ($R_{int} = 0.0422$), structure solution by direct methods (SHELXS-86) and refinement of the 236 parameters by least-squares optimization against F^2 (SHELXL-97), $R_1(I > 2\sigma(I)) = 0.0524$, $wR_2 = 0.1212$, GOF = 0.924, max/min residual electron density 0.46/−0.73 e Å^{-3}, $\chi = 0.0073(9)$ for secondary extinction. Crystal data of **5a**: crystal size $0.38 \times 0.11 \times 0.08$ mm, orthorhombic, space group $Pna2_1$ (no. 33), $Z = 4$, $a = 43.680(10)$, $b = 16.730(4)$, $c = 8.335(3)$ Å, $V = 6091(3)$ Å^3, $M_W = 1377.91$, $\rho_{calcd} = 1.503\ Mg\,m^{-3}$, $F(000) = 2848$, $T = 170$ K, Stoe IPDS area detector, $2.23 \le \theta \le 26.13°$, ($\lambda(Mo_{K\alpha}) = 0.71073$ Å, $\mu = 1.829\ mm^{-1}$), 71501 reflections collected, 12039 unique, ($R_{int} = 0.1584$), direct methods (SHELXS-86) and refinement of the 613 parameters by least-squares optimization against F^2 (SHELXL-97), $R_1(I > 2\sigma(I)) = 0.069$, $wR_2 = 0.1503$, GOF = 1.027, max/min residual electron density 0.545/−0.583 e Å^{-3}, Flack parameter = −0.02(2). CCDC-193015 (**3a**), CCDC-193014 (**2b**), CCDC-193012 (**4a**), and CCDC-193013 (**5a**) contain the supplementary crystallographic data for this paper. These data can be obtained free of charge via www.ccdc.cam.ac.uk/conts/retrieving.html (or from the Cambridge Crystallographic Data Centre, 12, Union Road, Cambridge CB21EZ, UK; fax: (+44) 1223-336-033; or deposit@ccdc.cam.ac.uk).

[7] R. L. Harlow, W. J. Wells, G. W. Watt, S. H. Siminsen, *Inorg. Chem.* **1975**, *14*, 1768–1773; R. D. Willett, J. A. Haugen, J. Lebsack, J. Morrey, *Inorg. Chem.* **1974**, *13*, 2510–2513.

[8] L. P. Battaglia, A. B. Corradi, G. Marcotrigiano, L. Menabue, *Inorg. Chem.* **1979**, *18*, 148–152; A. M. W. Cargill Thompson, I. Blandford, H. Redfearn, J. C. Jeffrey, M. D. Ward, *J. Chem. Soc. Dalton Trans.* **1997**, 2661–2665.

[9] H. Stegemann, A. Oprea, K.-F. Tebbe, *Z. Anorg. Allg. Chem.* **1995**, *621*, 871–876; H. Stegemann, A. Oprea, K.-F. Tebbe, *Z. Anorg. Allg. Chem.* **1995**, *623*, 89–103.

[10] C. Clegg, J. R. Nicholson, D. Collison, C. D. Garner, *Acta Crystallogr. Sect. C* **1988**, *44*, 453–461.

[11] M. Asplund, S. Jagner, M. Nilson, *Acta Chem. Scand. Sect. A* **1983**, *37*, 57–62.

[12] L. Escriche, N. Lucena, J. Casabó, F. Teixidor, R. Kivekäs, R. Sillanpää, *Polyhedron* **1995**, *14*, 649–654; J. G. Haasnoot, T. L. F. Favre, W. Hinrichs, J. Reedijk, *Angew. Chem.* **1988**, *100*, 884–885; *Angew. Chem. Int. Ed. Engl.* **1988**, *27*, 856–858.

[13] G. Boche, F. Bosold, M. Marsch, K. Harms, *Angew. Chem.* **1998**, *110*, 1779–1781; *Angew. Chem. Int. Ed.* **1998**, *37*, 1684–1686.

[14] M. John, C. Aurel, C. Behrens, M. Marsch, K. Harms, F. Bosold, R. M. Geschwind, P. R. Rajamohanan, G. Boche, *Chem. Eur. J.* **2000**, *6*, 3060–3068.

[15] H. L. Hermann, G. Boche, P. Schwerdtfeger, *Chem. Eur. J.* **2001**, *7*, 5333–5342; L. Magnko, M. Schweizer, G. Rauhut, M. Schutz, H. Stoll, H. J. Werner, *Phys. Chem. Chem. Phys.* **2002**, *4*, 1006–1013.

[16] J. Beck, J. Strähle, *Angew. Chem.* **1985**, *97*, 419–420; *Angew. Chem. Int. Ed. Engl.* **1985**, *24*, 409–410.

[17] M. R. Churchill, K. L. Kalra, *J. Am. Chem. Soc.* **1973**, *95*, 5772–5773.

 © 2003 Wiley-VCH Verlag GmbH & Co. KGaA, Weinheim 1433-7851/03/4207-0796 $ 20.00+.50/0

Oligonucleotide Rings

Small Circular Oligodeoxynucleotides Achieved from Self-Assembling Entities**

Dongsheng Liu, Jian Chen, Alex H. F. Lee, Larry M. C. Chow, Albert S. C. Chan, and Tianhu Li**

Over the past decade circular oligodeoxynucleotides[1,2] have emerged as useful molecular tools for hybridization, diagnostics, and sequence-specific inhibition of gene expression because their DNA-binding affinity, sequence selectivity, and exonuclease resistance are better than that of the corresponding linear sequences.[3,4] As a result of advances in solid-phase technology[5] circular oligodeoxynucleotides can now be synthesized efficiently and without any sequence restriction. Most importantly, the size of circular oligodeoxynucleotides constructed by these convenient solid-phase methodologies can be varied easily from 2 to 20 nucleotides.[5] Conversely, the template-directed synthesis of circular oligodeoxynucleotides of comparable size has been unachievable so far.[1] With the aim of probing the size limit of circular oligodeoxynucleotides constructed by self-assembly, we recently fabricated some very short ones. Here we report a new type of spatial arrangement of the i-motif,[10] through which the size of the circular oligonucleotides can be reduced to only nine nucleotides, the smallest circular unit ever achieved by means of self-assembling entities of nucleic acids. Unlike the self-assemblies identified previously for fabricating circular oligodeoxynucleotides,[6–8] the characteristics of the newly designed entity of the i-motif are self-recognition at the oligodeoxynucleotide level, rather than complementarity, and the mutual templating that guides the alignment of two separate strands in the formation of dimeric complexes (**b** in Figure 1). The present work accordingly defines a new size limit for circular oligodeoxynucleotides synthesized through self-assembling entities.[4]

The term i-motif describes a structural entity composed of two parallel-stranded DNA duplexes zipped together in an antiparallel orientation and held together by hemiprotonated C–C$^+$ base pairs.[10] Mainly through NMR investigations, it has been established that the same C-rich strands of oligodeoxynucleotides can form intercalated structural entities of the i-motif that differ essentially in their intercalation and loop topologies.[11] Based on this well-established principle for the formation of the i-motif,[11,12] we selected oligodeoxynucleotide pCCTCCCTTC (**a** in Figure 1), anticipating that this sequence would self-assemble into a dimeric complex (**b**) through self-recognition and that the two termini of this linear sequence would be aligned in a head-to-tail fashion through mutual templating. It should be pointed out that the i-motif formed by pCCTCCCTTC could exist in two or more isomeric forms with different intercalation and loop topologies; **b** represents only one of these possible configurations. In addition, certain constraints from the phosphate–sugar backbone must be present within this assembly of the i-motif, since only one or two nucleotides were required to sustain the hairpin loops. Consequently, an equilibrium could exist between the assembled entity **b** and unstructured form **a** of the linear sequence. Once the dimeric complex **b** is generated, covalent linkage between the two open termini would lead to the desired circular oligodeoxynucleotides with a preferred orientation (**c** and **d** in Figure 1).

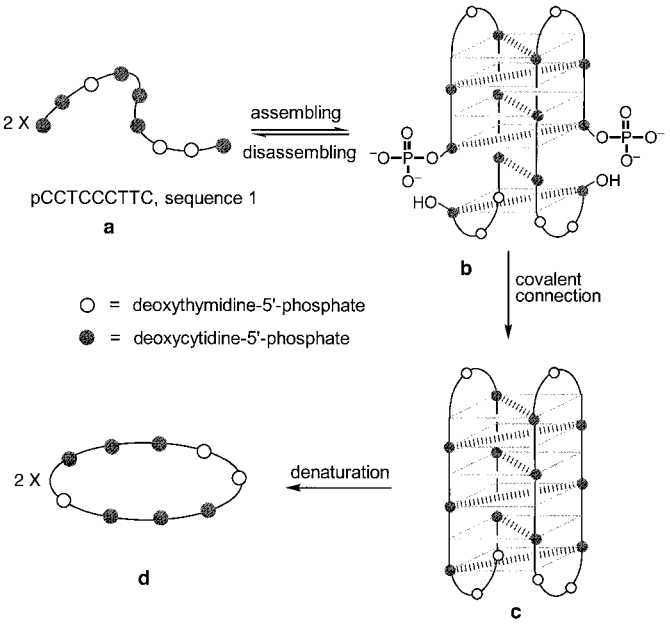

Figure 1. Representation of our strategy for constructing very short circular oligodeoxynucleotides through bimolecular assembly of the i-motif (**b**).

Following the strategy outlined in Figure 1, we first incubated the 9-mer linear sequence pCCTCCCTTC (sequence 1) in pH 5 buffer to generate the desired assembly of the i-motif[11,12] (**a**→**b**). The 5′-terminal phosphate was subsequently activated by the addition of *N*-cyanoimidazole[13] to promote formation of the phosphodiester bonds between the 5′- and 3′-termini of this linear sequence (**b**→**c**). The products of this circularization course were then analyzed by denaturing polyacrylamide gel electrophoresis (PAGE). As apparent on the autoradiograms, a new product was generated in 43 % yield from the circularization reaction (Figure 2a, lane 3), which was deduced by quantifying the radioactivities of both linear and circular products using PhosphoImager SI (Molecular Dynamics). This new product, which has a greater mobility shift than its linear precursor,[9] was identified as the corresponding circular oligodeoxynucleotide

[*] A. S. C. Chan, T. Li, D. Liu, J. Chen, A. H. F. Lee, L. M. C. Chow
Department of Applied Biology and Chemical Technology
The Hong Kong Polytechnic University
Hung Hom, Kowloon, Hong Kong SAR (P.R. China)
Fax: (+852) 2364-9932
E-mail: bctli@polyu.edu.hk

[**] We thank The Hong Kong Research Grants Council (Grant No. PolyU 5302/01P to T. L.), The Hong Kong Polytechnic University ASD Fund, and the Hong Kong UGC Area of Excellence Fund (Project No. AoE P/10-01) for financial support of this study and Dr. Alan Nadin (Merck, UK) for helpful discussions.

 © 2003 Wiley-VCH Verlag GmbH & Co. KGaA, Weinheim 1433-7851/03/4207-0797 $ 20.00+.50/0

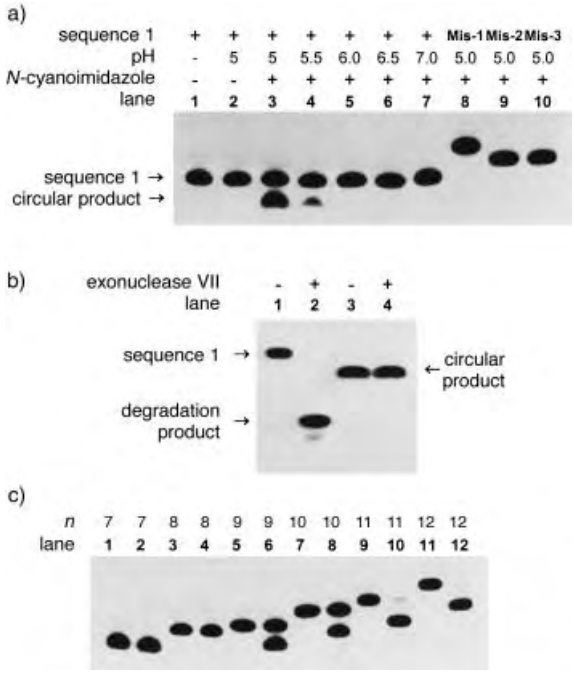

Figure 2. Analysis of the oligodeoxynucleotides obtained in circularization experiments. For details see text and Experimental Section.
a) Lanes 1 and 2 are control experiments. b) Treatment with exonuclease VII. Lanes 1 and 3 are control experiments. Lanes 2 and 4 show the different behavior of sequence 1 and the purified (by the "crush-and-soak" method) circular product with the faster mobility shift (see the lower spot in lane 3, Figure 2a).[15] c) Results of experiments to synthesize differently sized circular oligodeoxynucleotides. Lanes 1, 3, 5, 7, 9, and 11: the *n*-mers alone. Lanes 2, 4, 6, 8, 10, and 11: reaction mixtures of the *n*-mers.

⟨CCTCCCTTC⟩. The efficiency of the reaction was found to be strongly pH-dependent. Circularization at pH 5.0 (lane 3), 5.5 (lane 4), and 6.0 (lane 5) proceeded in yields of 43, 17, and 4%, respectively, and at pH 6.5 (lane 6) and 7.0 (lane 7) no product from the reaction was observed. This pH dependency is consistent with the necessity for the formation of base pairs between cytosine and protonated cytosine ($C{-}C^+$).[10–12] Moreover, we examined the correlation of this circularization course with the structural intactness of the i-motif by using three "mismatched" sequences—pCTACTTGCA (Mis-1), pGCTCCCTTC (Mis-2), and pCCTCCCTTG (Mis-3)—in which one or more cytosines of sequence 1 were replaced with guanine, thymine, and adenine, respectively. According to the rule for the generation of the i-motif,[10,11] these three sequences should be incapable of supporting the correct conformation of the i-motif because they do not have the correct number of cytosines for proper $C{-}C^+$ base pairing. As expected, none of the sequences of Mis-1 (lane 8), Mis-2 (lane 9), and Mis-3 (lane 10) gave rise to a circular product under the same reaction conditions as described for sequence 1.

With the aim of confirming the circular nature of the phosphate–sugar backbone, we purified the newly formed product (lane 3 in Figure 2b) by PAGE and digested it with exonuclease VII, an exodeoxyribonuclease that hydrolyzes nucleotides from both the 3′- and 5′-ends of single-stranded DNA.[7,14] As expected, no degradation was observed from this digestion reaction (lane 4). As a control, the linear sequence of pCCTCCCTTC was also hydrolyzed under the same reaction conditions, which accordingly gave rise to products of lower molecular weight quantitatively (lane 2). The identified circular product was also digested with exonuclease I and alkaline phosphatase (data not shown). Again, no degradation products were observed from these digestion reactions. These results strongly suggest that the phosphate–sugar backbone of this newly formed product is indeed circular in nature.[7,14]

The bimolecular assembly of the i-motif as an intermediate entity is also suitable for the fabrication of circular oligonucleotides over nine nucleotides in length. For example, when the linear sequences of 10-mer (pCCTTCCCTTC, lane 8 in Figure 2c), 11-mer (pCCTTCCCCTCC, lane 10), and 12-mer (pCCTTCCCCTTCC, lane 12) were incubated under the same conditions as described for sequence 1 (9-mer, lane 6), the corresponding circular oligodeoxynucleotides were generated in yields of 48%, 84%, and 93%, respectively. Conversely, within experimental limits, no circular products were evident when the linear sequences of 7-mer (pCTCCTTC , lane 2) and 8-mer (pCTTCCTTC, lane 4) were incubated under the standard circularization conditions, which implies that these two oligodeoxynucleotides are too short to sustain a steady bimolecular assembly of the i-motif.

In conclusion, by manipulating the dimeric structure of the i-motif, we have synthesized 9- to 12-membered circular oligonucleotides, which are far smaller than the previous smallest circular sequences (20 nucleotides in length)[9] achieved via self-assembling entities. Illustration of the extraordinarily compact conformation of the i-motif (**b** in Figure 1) attainable by nucleic acids may be beneficial to the elucidation of the structures and roles of cytosine-rich sequences in biological processes (e.g. the centromeric region and at the telomeric end).[10]

Experimental Section

Oligodeoxynucleotides were supplied by Operon Technologies, Inc. and phosphorylated at their 5′-ends with T_4 polynucleotide kinase and [γ-^{32}P]ATP. The circularization products were analyzed by 20% PAGE and visualized by autoradiography. The autoradiograms in Figure 2a show the influence of pH and oligonucleotide length on the formation of circular oligodeoxynucleotides. For lane 3, a stock solution of sequence 1 was prepared by incubation of 100 mM 2-(*N*-morpholino)ethanesulfonic acid (MES, pH 5), 50 mM NaCl, and 10 μM sequence 1 at 4°C for 12 h for the formation of bimolecular complexes of the i-motif. The reaction mixture consisting of 5 μM sequence 1 taken from the stock solution, 100 mM MES (pH 5), 25 mM NaCl, 50 mM $NiCl_2$, and 50 mM *N*-cyanoimidazole in a total volume of 20 μL was then incubated at 4°C for 12 h. The reaction was terminated by refrigeration and further analyzed by PAGE. For the experiments in Figure 2b, a reaction mixture of 1 × exonuclease VII buffer (100 mM Tris-HCl, 100 mM potassium phosphate, 16.6 mM ethylenediamine tetraacetic acid, and 20 mM 2-sulfanylethanol, pH 7.9), 10 units of exonuclease VII, and sequence 1 in a total volume of 20 μL was prepared and incubated at 37°C for 2 h. The reaction mixtures for Figure 2c were prepared in the same way as the

 © 2003 Wiley-VCH Verlag GmbH & Co. KGaA, Weinheim 1433-7851/03/4207-0798 $ 20.00+.50/0

one loaded in Figure 2a, lane 3, except for replacing sequence 1 with oligodeoxynucleotides of different lengths.

Received: June 14, 2002
Revised: October 29, 2002 [Z19480]

[1] E. T. Kool, *Annu. Rev. Biophys. Biomol. Struct.* **1996**, *25*, 1–28.
[2] a) E. T. Kool, *Acc. Chem. Res.* **1998**, *31*, 502–510; b) E. T. Kool in *Comprehensive Natural Product Chemistry, Vol. 7* (Ed.: E. T. Kool), Elsevier, Amsterdam, **1999**, pp. 341–369; c) C. Giovannangeli, J.-S. Sun, C. Hélène in *Comprehensive Supramolecular Chemistry, Vol. 4* (Ed.: Y. Murakami), Elsevier, Oxford, **1996**, pp. 177–192; d) J. Liu, J.-S. Taylor, *Nucleic Acids Res.* **1998**, *26*, 3300–3304; e) S. A. Kuznetsova, I. N. Merenkova, I. E. Kanevsky, Z. A. Shabarova, M. Blumenfeld, *Antisense Nucleic Acid Drug Dev.* **1999**, *9*, 95–100; f) D. E. Wemmer, A. S. Benight, *Nucleic Acids Res.* **1985**, *13*, 8611–8621; g) H. Kuhn, V. V. Demidov, M. D. Frank-Kamenetskii, *Angew. Chem.* **1999**, *111*, 1544–1547; *Angew. Chem. Int. Ed.* **1999**, *38*, 1446–1449; h) L. Wang, D. E. Ruffner, *Nucleic Acids Res.* **1998**, *26*, 2502–2504; i) Z. Chen, D. E. Ruffner, *Nucleic Acids Res.* **1998**, *26*, 1126–1127; j) D. A. Erie, R. A. Jones, W. K. Olson, N. K. Sinha, K. J. Breslauer, *Biochemistry* **1989**, *28*, 268–273; k) M. L. Capobianco, A. Carcuro, L. Tondelli, A. Garbesi, G. M. Bonora, *Nucleic Acids Res.* **1990**, *18*, 2661–2669; l) L. De Napoli, A. Messere, D. Montesarchio, G. Piccialli, C. Santacroce, *Nucleosides Nucleotides* **1993**, *12*, 21–30.
[3] a) Y.-G. Gao, H. Robinson, Y. Guan, Y.-C. Liaw, J. H. van Boom, G. A. van der Marel, A. H.-J. Wang, *J. Biomol. Struct. Dyn.* **1998**, *16*, 69–76; b) S. A. Salisbury, S. E. Wilson, H. R. Powell, O. Kennard, P. Lubini, G. M. Sheldrick, N. Escaja, E. Alazzouzi, A. Grandas, E. Pedroso, *Proc. Natl. Acad. Sci. USA* **1997**, *94*, 5515–5518; c) C. González, N. Escaja, M. Rico, E. Pedroso, *J. Am. Chem. Soc.* **1998**, *120*, 2176–2177; d) M. Frieden, E. Pedroso, E. T. Kool, *Angew. Chem.* **1999**, *111*, 3870–3874; *Angew. Chem. Int. Ed.* **1999**, *38*, 3654–3657; e) R. Micura, *Chem. Eur. J.* **1999**, *5*, 2077–2082.
[4] a) S. Wang, E. T. Kool, *Nucleic Acids Res.* **1994**, *22*, 2326–2333; b) S. Rumney IV, E. T. Kool, *Angew. Chem.* **1992**, *104*, 1686–1689; *Angew. Chem. Int. Ed. Engl.* **1992**, *31*, 1617–1619; c) A. Fire, S. Q. Xu, *Proc. Natl. Acad. Sci. USA* **1995**, *92*, 4641–4645; d) S. L. Daubendiek, K. Ryan, E. T. Kool, *J. Am. Chem. Soc.* **1995**, *117*, 7818–7819; e) D. Liu, S. L. Daubendiek, M. A. Zillman, K. Ryan, E. T. Kool, *J. Am. Chem. Soc.* **1996**, *118*, 1587–1594; f) C. Escudé, T. Garestier, C. Hélène, *Proc. Natl. Acad. Sci. USA* **1999**, *96*, 10603–10607; g) T. Roulon, C. Hélène, C. Escudé, *Angew. Chem.* **2001**, *113*, 1571–1574; *Angew. Chem. Int. Ed.* **2001**, *40*, 1523–1526; h) A. V. Maksimenko, E. M. Volkov, J.-R. Bertrand, H. Porumb, C. Malvy, Z. A. Shabarova, M. B. Gottikh, *Eur. J. Biochem.* **2000**, *267*, 3592–3603; i) M. Nilsson, H. Malmgren, M. Samiotaki, M. Kwiatkowski, B. P. Chowdhary, U. Landegen, *Science* **1994**, *265*, 2085–2088.
[5] E. Alazzouzi, N. Escaja, A. Grandas, E. Pedroso, *Angew. Chem.* **1997**, *109*, 1564–1567; *Angew. Chem. Int. Ed. Engl.* **1997**, *36*, 1506–1508.
[6] a) M. J. Doktycz, R. F. Goldstein, T. M. Paner, F. J. Gallo, A. S. Benight, *Biopolymers* **1992**, *32*, 849–864; b) D. Rentzeperis, J. Ho, L. A. Marky, *Biochemistry* **1993**, *32*, 2564–2572; c) K. D. James, A. R. Boles, D. Henckel, A. D. Ellington, *Nucleic Acids Res.* **1998**, *26*, 5203–5211; d) K. Zhang, J.-S. Taylor, *J. Am. Chem. Soc.* **1999**, *121*, 11579–11580; e) J. Selvasekaran, K. D. Turnbull, *Nucleic Acids Res.* **1999**, *27*, 624–627.
[7] a) E. T. Kool, *J. Am. Chem. Soc.* **1991**, *113*, 6265–6266; b) G. Prakash, E. T. Kool, *J. Chem. Soc. Chem. Commun.* **1991**, *17*, 1161–1163; c) G. Prakash, E. T. Kool, *J. Am. Chem. Soc.* **1992**, *114*, 3523–3527; d) J. Selvasekaran, K. D. Turnbull, *Nucleic Acids Res.* **1999**, *27*, 624–627.
[8] T. Li, D. Liu, J. Chen, A. H. F. Lee, J. Qi, A. S. C. Chan, *J. Am. Chem. Soc.* **2001**, *123*, 12901–12902.
[9] G. W. Ashley, D. M. Kushlan, *Biochemistry* **1991**, *30*, 2927–2933.
[10] a) K. Gehring, J.-L. Leroy, M. Guéron, *Nature* **1993**, *363*, 561–564; b) C. Kang, I. Berger, C. Lockshin, R. Ratliff, R. Moyzis, A. Rich, *Proc. Natl. Acad. Sci. USA* **1995**, *92*, 3874–3878; c) J.-L. Leroy, K. Gehring, A. Kettani, M. Guéron, *Biochemistry* **1993**, *32*, 6019–6031; d) O. N. Voloshin, A. G. Veselkov, B. P. Belotserkovskii, O. N. Danilevskaya, M. N. Pavlova, V. N. Dobrynin, M. D. Frank-Kamenetskii, *J. Biomol. Struct. Dyn.* **1992**, *9*, 643–652; e) L. Lacroix, J.-L. Mergny, J.-L. Leroy, C. Hélène, *Biochemistry* **1996**, *35*, 8715–8722; f) J.-L. Mergny, *Biochemistry* **1999**, *38*, 1573–1581; g) K. Snoussi, S. Nonin-Lecomte, J.-L. Leroy, *J. Mol. Biol.* **2001**, *309*, 139–153; h) M. Gueron, J.-L. Leroy, *Curr. Opin. Struct. Biol.* **2000**, *10*, 326–331; i) D. E. Gilbert, J. Feigon, *Curr. Opin. Struct. Biol.* **1999**, *9*, 305–314; j) O. Y. Fedoroff, A. Rangan, V. V. Chemeris, L. H. Hurley, *Biochemistry* **2000**, *39*, 15083–15090; k) J.-L. Mergny, L. Lacroix, X. Han, J.-L. Leroy, C. Hélène, *J. Am. Chem. Soc.* **1995**, *117*, 8887–8898; l) J. L. Leroy, M. Gueron, J. L. Mergny, C. Hélène, *Nucleic Acids Res.* **1994**, *22*, 1600–1606; m) J. Gallego, S.-H. Chou, B. R. Reid, *J. Mol. Biol.* **1997**, *273*, 840–856.
[11] A. T. Phan, M. Gueron, J.-L. Leroy, *J. Mol. Biol.* **2000**, *299*, 123–144.
[12] a) S. Nonin, A. T. Phan, J.-L. Leroy, *Structure* **1997**, *5*, 1231–1246; b) S. Ahmed, A. Kintanar, E. Henderson, *Nat. Struct. Biol.* **1994**, *1*, 83–88; c) D. J. Patel, S. Bouaziz, A. Kettani, Y. Wang in *Oxford Handbook of Nucleic Acid Structure* (Ed.: S. Neidle), Oxford University Press, Oxford, **1999**, pp. 389–453.
[13] a) K. J. Luebke, P. B. Dervan, *J. Am. Chem. Soc.* **1989**, *111*, 8733–8735; b) K. J. Luebke, P. B. Dervan, *J. Am. Chem. Soc.* **1991**, *113*, 7447–7448; c) G. F. Joyce, L. E. Orgel, *J. Mol. Biol.* **1986**, *188*, 433–441; d) E. Kanaya, H. Yanagawa, *Biochemistry* **1986**, *25*, 7423–7430; e) J. P. Ferris, C. H. Huang, W. J. Hagan, Jr., *Nucleosides Nucleotides* **1989**, *8*, 407–414; f) H. J. Giesemann, *Prakt. Chem.* **1955**, *1*, 345–348.
[14] N. G. Dolinnaya, M. Blumenfeld, I. N. Merenkova, T. S. Oretskaya, N. F. Krynetskaya, M. G. Ivanovskaya, M. Vasseur, Z. A. Shabarova, *Nucleic Acids Res.* **1993**, *21*, 5403–5407.
[15] J. Sambrook, E. F. Fritsch, T. Maniatis, *Molecular Cloning: A Laboratory Manual*, Cold Spring Harbor Laboratory Press, New York, **1989**, pp. 646–648.

 © 2003 Wiley-VCH Verlag GmbH & Co. KGaA, Weinheim 1433-7851/03/4207-0799 $ 20.00+.50/0

Superhydrophobic Nanofibers

Creation of a Superhydrophobic Surface from an Amphiphilic Polymer**

Lin Feng, Yanlin Song, Jin Zhai, Biqian Liu, Jian Xu, Lei Jiang,* and Daoben Zhu*

Superhydrophobic surfaces, with a water contact angle (CA) greater than 150°, have attracted great interest for both fundamental research and practical applications.[1] Conventionally, superhydrophobic surfaces are fabricated by combining appropriate surface roughness with low-surface-energy materials (hydrophobic materials, CA greater than 90°).[2–18] It has been commonly acknowledged that it is impossible to obtain superhydrophobic surfaces from amphiphilic materials. Herminghaus reported that it was theoretically possible to construct a water-repellent surface from a material with a CA less than 90°,[19] however, this has never been proven by experimental results. Herein, we report the creation of a superhydrophobic surface (CA = 171.2°) consisting of nanofibers fabricated from amphiphilic poly(vinyl alcohol) (PVA). The PVA nanofibers were prepared using the template-based extrusion method,[2] namely, the extrusion of a PVA precursor solution through a template composed of a nanoporous anodic aluminum oxide membrane. This phenomenon is attributable to the rearrangement of PVA molecules during the initial stage of the extrusion process, which is accompanied by the reorientation of hydrophobic groups ($-CH_2-$) at the air/solid interface. This method can be extended to prepare superhydrophobic surfaces using many types of materials.

The templates of anodic aluminum oxide membranes were prepared by a published route,[20] with pore diameters in the range of 20–500 nm. Control of the diameters and densities of the prepared PVA nanofibers can be easily achieved by using templates with different pore diameters. In the present study, a template with an average pore diameter of 68.7 nm, and a density of approximately 1.23×10^{10} pores per square centimeter was used. Figure 1a shows a typical scanning electron microscopy (SEM) image of the substrate, as viewed from above, coated with well-spaced PVA nanofibers. The average diameter of the nanofiber tips is 72.1 nm, which is in good agreement with the pore diameter of the template. The average interfiber distance is 361.8 nm, while the nanofiber density is approximately 7.07×10^8 fibers per square centimeter. Figure 1b shows a cross-sectional SEM image of the as-synthesized PVA nanofibers, which shows that the length of the fibers is approximately 14.3 μm. The ends of the aligned nanofibers are very sharp, although there are often some aggregations along their length.

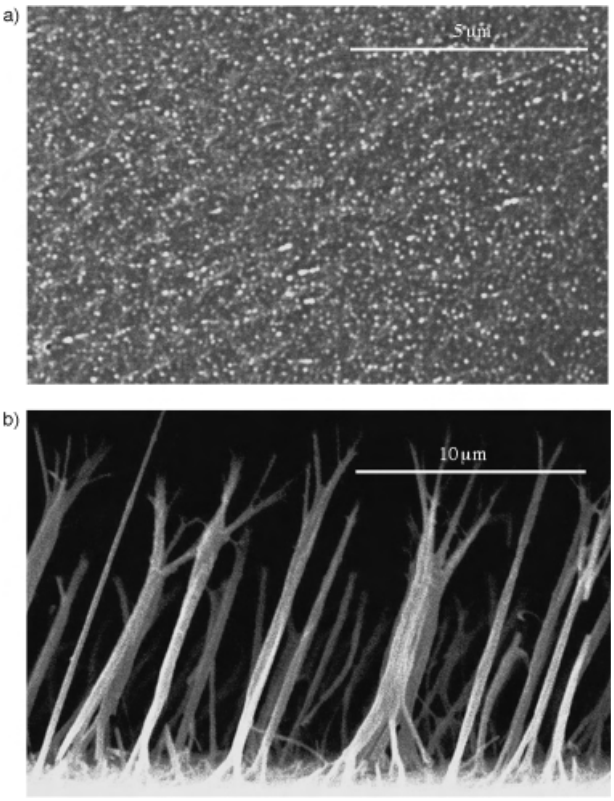

Figure 1. a) SEM image of a substrate coated with PVA nanofibers, as viewed from above; b) cross-sectional SEM image of the as-synthesized PVA nanofibers.

PVA is an amphiphilic material, with a water contact angle on native PVA films with smooth surfaces of only 72.1 ± 1.1° (Figure 2a). However, the PVA nanofibers reported herein have rough surfaces, and can be shown to be superhydrophobic. Figure 2b shows the shape of a water droplet on the surface of a PVA nanofiber, where the water contact angle is 171.2 ± 1.6°. These results confirm that nanostructure has a profound effect on superhydrophobic properties.

There have been numerous reports over the past 60 years describing the preparation of superhydrophobic surfaces using hydrophobic materials ($\theta > 90°$).[2–18] For example, Onda et al.[7] have demonstrated a superhydrophobic fractal surface formed from an alkylketene dimer (AKD, $\theta = 109°$), while Öner and McCarthy reported the preparation of a rough surface that exhibited superhydrophobic properties, through the silanization of silicon wafers ($\theta_A = 107°$, $\theta_R = 109°$; θ_A and θ_R are the advancing and receding contact angles, respectively).[8] We have also prepared a superhydrophobic surface of aligned nanofibers using polyacrylonitrile (PAN, $\theta = 100.8°$) as the precursor.[2] In addition, there have been many other reports concerning the preparation of

[*] Prof. J. Xu, Prof. L. Jiang, Dr. L. Feng, Prof. Y. Song, Dr. J. Zhai, B. Liu, Prof. D. Zhu
Center of Molecular Sciences
Institute of Chemistry, Chinese Academy of Sciences
Beijing 100080 (P. R. China)
Fax: (+86) 10-8262-7566
E-mail: jxu@infoc3.icas.ac.cn
jianglei@infoc3.icas.ac.cn

[**] The authors thank the State Key Project for Fundamental Research (G1999064504) and the Special Research Foundation of the National Nature Science Foundation of China (29992530 and 20125102) for continuing financial support.

Supporting information for this article is available on the WWW under http://www.angewandte.org or from the author.

 © 2003 Wiley-VCH Verlag GmbH & Co. KGaA, Weinheim 1433-7851/03/4207-0800 $ 20.00+.50/0

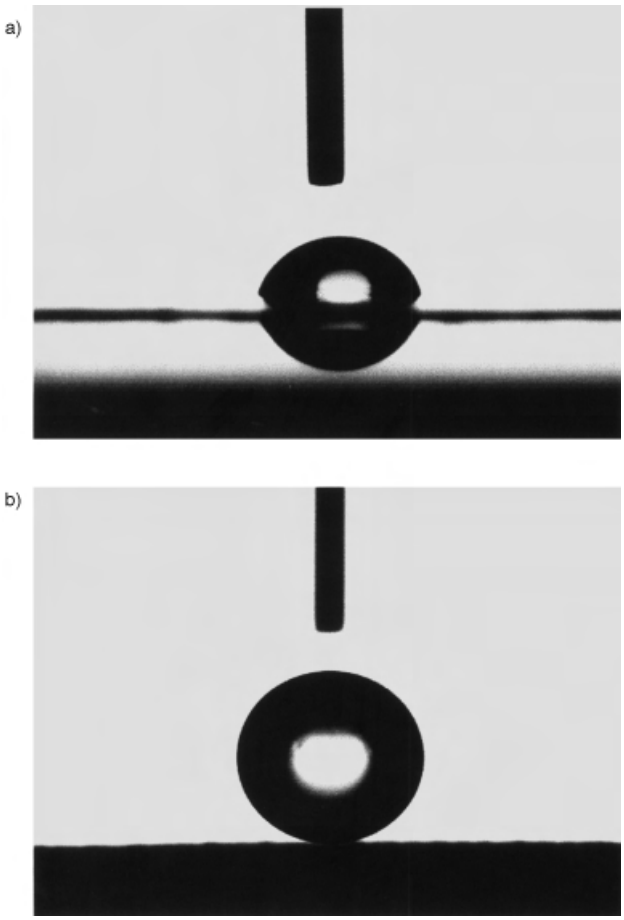

Figure 2. Pictures showing the water contact angles of a native PVA film with a smooth surface (a) and the synthesized PVA nanofibers with a rough surface (b).

superhydrophobic surfaces that have been modified by hydrophobic materials, such as polytetrafluoroethylene (PTFE, $\theta = 108°$)[9,10] and various fluoroalkylsilanes (FASs, $\theta = 107°$).[11–18] Wenzel[3] first derived Equation (1) to show

$$\cos\theta_r = r\cos\theta \quad (1)$$

the relationship between the contact angle of a liquid on a smooth surface (θ) and on a rough surface (θ_r) made of the same material, where r is the roughness factor.

This equation indicates that a rough surface can be superhydrophobic when the surface is composed of hydrophobic materials. From this point of view, it is very surprising that superhydrophobic surfaces can be synthesized from an amphiphilic polymer. We know that PVA is an amphiphilic molecule composed of both hydrophilic (−OH) and hydrophobic ($-CH_2-$) groups. It has been proposed that when the precursor of the PVA solution is compressed into the nanometer-scale pores of the template, strong orientation of the PVA molecules can be induced, and intermolecular hydrogen bonds are created.[21–25] Furthermore, most of the hydrophobic groups may be exposed at the surface, which would minimize the free energy of the system. Figure 3 represents the possible conformation of PVA molecules at the air/solid interface, where $-CH_2-$ groups are present at the

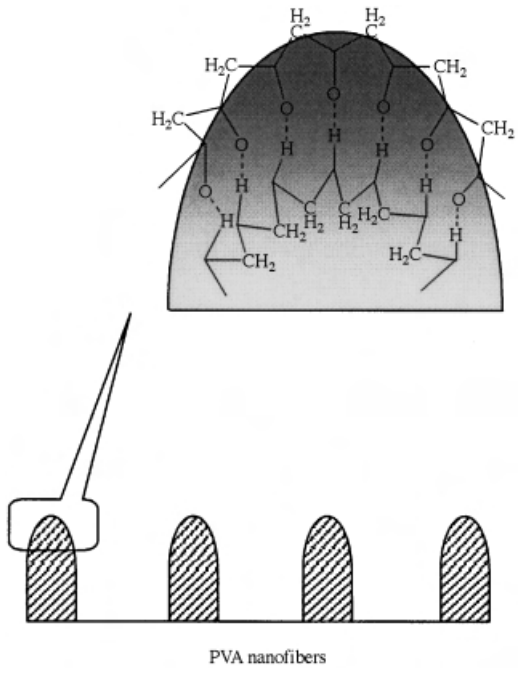

Figure 3. Possible conformation modes of the PVA molecules at the air/solid interface.

surface, and hydrogen bonds are formed in the interior. It has been shown that angle-resolved X-ray photoelectron spectroscopy (XPS) can provide useful information about the conformation of the polymer at the surface.[26] Figure 4a shows the results of an angle-resolved XPS study of the PVA nanofiber/air interface, where the detection angles are 5, 30, 60, and 90°, respectively. Figure 4b shows the effect of varying the detection angle on the ratio of carbon (both $-CH_2-$ and $>CH-$) to oxygen atoms that were detected. The ratio of $-CH_2-$:O decreases while that of $>CH-$:O increases as the detection angle is increased. Since the detected thickness will be greater upon increasing detection angle, it can be deduced that the PVA backbone at the surface is mainly composed of $-CH_2-$ groups. As a result, the surface free energy of the PVA nanofibers decreases. In contrast, angle-resolved XPS results of native PVA films (See Supporting Information) indicate that the content of hydrophobic and hydrophilic groups is almost the same in the surface as in the interior, which is a result of the free arrangement of PVA molecules at the initiation of the spin-coating process. These results demonstrate that the conformation of molecules at the surface plays the most important role in surface activity.

In conclusion, a superhydrophobic surface of aligned PVA nanofibers has been prepared, even though the PVA molecule is inherently amphiphilic. We believe that a reorientation of the PVA molecules occurs when they are confined to a nanosized space. Since the hydrophobic groups in this case are located at a rough surface, the surface free energy decreases. This is the first example of an amphiphilic material being used to prepare a superhydrophobic surface. The method might successfully be used to prepare superhydrophobic surfaces from a wide variety of materials.

 © 2003 Wiley-VCH Verlag GmbH & Co. KGaA, Weinheim 1433-7851/03/4207-0801 $ 20.00+.50/0

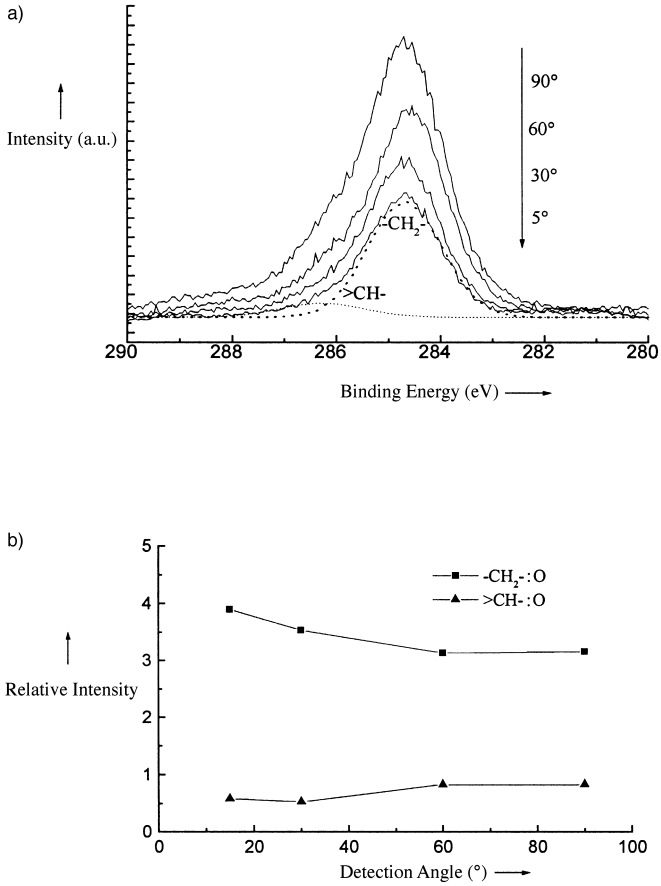

Figure 4. a) X-ray photoelectron spectra illustrating the dependence of the detection angle for the C_{1s}-core spectra of PVA nanofibers (—— real XPS spectra; ----- fit to a Gauss–Lorenz function); b) chart showing the relation between the $-CH_2-$:O and $>CH-$:O ratio to the detection angle.

Experimental Section

The precursor was prepared by dissolving polyvinylalcohol (8.823 g, atactic, $M_W = 1750 \pm 15$) in stirred deionised and deaerated water (50 mL) at 90 °C, which formed a 15 wt % aqueous polyvinylalcohol solution. Aqueous solutions of sodium sulfate (400 g L^{-1}) were prepared for use as the solidifying solution. A commercial anodic aluminum oxide membrane with a pore diameter of 68.7 nm was used as the template. The synthesis and characterization process were the same as that reported in Ref. [2]. The native PVA film was prepared by spin-coating the PVA solution on a clean glass slide. XPS results were recorded using a VG ESCALAB MKII spectrometer with an $Al_{K\alpha}$ monochromatic X-ray source.

Received: July 23, 2002
Revised: November 4, 2002 [Z19807]

[1] a) L. Jiang, R. Wang, B. Yang, T. J. Li, D. A. Tryk, A. Fujishima, K. Hashimoto, D. B. Zhu, *Pure Appl. Chem.* **2000**, *72*, 73; b) P. Aussillous, D. Quéré, *Nature* **2001**, *411*, 924; c) A. Nakajima, K. Hashimoto, T. Watanabe, *Monatsh. Chem.* **2001**, *132*, 31; d) L. Feng, S. H. Li, Y. S. Li, H. J. Li, L. J. Zhang, J. Zhai, Y. L. Song, B. Q. Liu, L. Jiang, D. B. Zhu, *Adv. Mater.* **2003**, in press.
[2] L. Feng, S. H. Li, H. J. Li, J. Zhai, Y. L. Song, L. Jiang, D. B. Zhu, *Angew. Chem.* **2002**, *114*, 1269; *Angew. Chem. Int. Ed.* **2002**, *41*, 1221.
[3] R. N. Wenzel, *Ind. Eng. Chem.* **1936**, *28*, 988.
[4] A. B. D. Cassie, *Discuss. Faraday Soc.* **1948**, *3*, 11.
[5] G. Wolansky, A. Marmur, *Langmuir* **1998**, *14*, 5292.
[6] P. S. Swain, R. Lipowsky, *Langmuir* **1998**, *14*, 6772.
[7] a) T. Onda, S. Shibuichi, N. Satoh, K. Tsujii, *Langmuir* **1996**, *12*, 2125; b) S. Shibuichi, T. Onda, N. Satoh, K. Tsujii, *J. Phys. Chem.* **1996**, *100*, 19512; c) S. Shibuichi, T. Yamamoto, T. Onda, K. Tsujii, *J. Colloid Interface Sci.* **1998**, *208*, 287.
[8] D. Öner, T. J. McCarthy, *Langmuir* **2000**, *16*, 7777.
[9] a) W. Chen, A. Y. Fadeev, M. C. Heieh, D. Öner, J. Youngblood, T. J. McCarthy, *Langmuir* **1999**, *15*, 3395; b) J. P. Youngblood, T. J. McCarthy, *Macromolecules* **1999**, *32*, 6800.
[10] S. Veeramasuneni, J. Drelich, J. D. Miller, G. Yanauchi, *Prog. Org. Coat.* **1997**, *31*, 265.
[11] a) A. Nakajima, K. Abe, K. Hashimoto, T. Watanabe, *Thin Solid Films* **2000**, *376*, 140; b) A. Nakajima, C. Saiki, K. Hashimoto, T. Watanabe, *J. Mater. Sci. Lett.* **2001**, *20*, 1975; c) A. Nakajima, A. Fujishima, K. Hashimoto, T. Watanabe, *Adv. Mater.* **1999**, *11*, 1365.
[12] A. Hozumi, O. Takai, *Thin Solid Films* **1997**, *303*, 222.
[13] a) K. Tadanaga, N. Katata, T. Minami, *J. Am. Ceram. Soc.* **1997**, *80*, 1040; b) K. Tadanaga, N. Katata, T. Minami, *J. Am. Ceram. Soc.* **1997**, *80*, 3213; c) K. Tadanaga, K. Kitamuro, J. Morinaga, Y. Kotani, A. Matsuda, T. Minani, *Chem. Lett.* **2000**, 864.
[14] J. Bico, C. Marzolin, D. Quéré, *Europhys. Lett.* **1999**, *47*, 220.
[15] Y. Wu, H. Sugimura, Y. Inoue, O. Takai, *Chem. Vap. Deposition* **2002**, *8*, 47.
[16] H. Tada, H. Nagayama, *Langmuir* **1995**, *11*, 136.
[17] T. Nishino, M. Meguro, K. Nakamae, M. Matsushita, Y. Ueda, *Langmuir* **1999**, *15*, 4321.
[18] H. J. Li, X. B. Wang, Y. L. Song, Y. Q. Liu, Q. S. Li, L. Jiang, D. B. Zhu, *Angew. Chem.* **2001**, *113*, 1793; *Angew. Chem. Int. Ed.* **2001**, *40*, 1743.
[19] S. Herminghaus, *Europhys. Lett.* **2000**, *52*, 165.
[20] H. Masuda, K. Fukuda, *Science* **1995**, *268*, 1466.
[21] G. Hummer, J. G. Rasaiah, J. P. Noworyta, *Nature* **2001**, *414*, 188.
[22] K. Koga, G. T. Gao, H. Tanaka, X. C. Zeng, *Nature* **2001**, *412*, 802.
[23] B. Zhao, J. S. Moore, D. J. Beebe, *Science* **2001**, *291,* 1023.
[24] J. H. K. Ky Hirschberg, L. Brunsveld, A. Ramzi, J. A. J. M. Vekemans, R. P. Sijbesma, E. W. Meijer, *Nature* **2000**, *407*, 167.
[25] N. Nandi, B. Bagchi, *J. Am. Chem. Soc.* **1996**, *118*, 11208.
[26] a) J. Xu, L. H Shi, M. L. Ye, *J. Polym. Sci. Part B* **1997**, *35*, 827; b) J. Xu, L. H Shi, M. L. Ye, *J. Polym. Sci. Part B* **1999**, *37*, 2297; c) L. Li, C. M. Chan, L. T. Weng, *Polymer* **1998**, *39*, 2355.

 © 2003 Wiley-VCH Verlag GmbH & Co. KGaA, Weinheim 1433-7851/03/4207-0802 $ 20.00+.50/0

Catalytic Methane Activation

Catalytic Functionalization of Hydrocarbons by σ-Bond-Metathesis Chemistry: Dehydrosilylation of Methane with a Scandium Catalyst**

*Aaron D. Sadow and T. Don Tilley**

The selective, catalytic functionalization of saturated hydrocarbons represents one of the most important challenges in chemical research.[1] While some progress has been made,[2–5] there are very few processes which allow conversion of the cheapest and most abundant hydrocarbon, methane. A few homogeneous catalytic conversions of methane have been developed, but none of these are efficient enough to be employed in routine chemical syntheses. One type of homogeneous catalytic system, originally described by Shilov and co-workers,[1a] features a platinum-group-metal complex as the catalyst and converts methane into simple derivatives of the type MeX (X = Cl, OH, OSO_3H, O_2CCF_3) under acidic conditions.[1,3] Metal oxo complexes, such as $[NBu_4]VO_3$ with pyrazine-2-carboxylic acid and methane monooxygenase, have also been found to catalyze selective oxidations of methane with O_2 and/or peroxides in protic solvents to yield methanol or its derivatives.[4] Although several stoichiometric reactions of transition-metal complexes with methane are known,[1,5] this reactivity has not yet provided useful catalytic processes.

New approaches to the development of catalysts for methane conversion might involve σ-bond metathesis steps. Indeed, the first reports of stoichiometric, homogeneous methane activation, by $[Cp^*_2MMe]$ (M = Sc (**3**), Y, Lu; Cp* = η^5-C_5Me_5) complexes, suggest the reaction proceeds via such transition states [Eq. (1)].[6] Despite this early breakthrough involving the degenerate exchange of methyl groups, productive reactions of methane by σ-bond metathesis have not been reported. A possible limitation to the development of such processes (e.g., carbon–carbon coupling) is the apparent restriction that carbon cannot adopt the position β to the metal center in a four-centered transition state.[7] In contrast, a few catalytic processes involving d^0 (and f^nd^0) metal catalysts and silane substrates have been discovered (e.g., olefin hydrosilation and silane dehydropolymerization).[8,9] Mechanistic investigations indicate that this reactivity is possibly the result of the ability of silicon, unlike carbon, to adopt the β position of a four-centered transition state.[10]

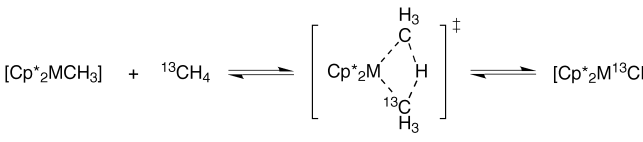

(1)

The recent discovery of arene C–H activation by a cationic, hafnium silyl complex suggests that hydrocarbon conversions might be based on catalysts that possess highly reactive metal–silicon bonds [Eq. (2)].[11] The possibility that scandocene–silicon bonds might be highly reactive in this sense was suggested by the similarity between the electron

(2)

count and ionic radius of the metal center in the complexes $[Cp'_2HfSiR_3]^+$ and $[Cp'_2ScSiR_3]$,[12] and by the known ability of $[Cp^*_2Sc]$ derivatives to activate hydrocarbons by σ-bond metathesis.[6b]

Methods for the generation of d^0-metal–silicon bonds have involved σ-bond metathesis reactions of hydrosilanes with hydride or silyl derivatives.[10] However, d^0-metal alkyl derivatives generally react with hydrosilanes by alkyl transfer to silicon and formation of a metal hydride.[8,13] It was surprising, then, to discover that $[Cp^*_2ScMe]$ (**1**) reacted with 1.2 equivalents of $MesSiH_3$ (Mes = 2,4,6-$C_6H_2Me_3$) with elimination of methane to produce a bright-yellow solution of $[Cp^*_2ScSiH_2Mes]$ [**2**; 3 h, room temperature, $[D_{12}]$cyclohexane; Eq. (3)]. The competitive formation of $[Cp^*_2ScH]$ (**3**) and

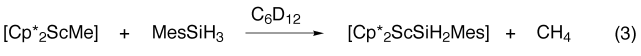

1 **2**

(3)

$MesMeSiH_2$ (ca. 5%) was also observed, but addition of a slight excess of $MesSiH_3$ converted the by-product **3** into **2** (an optimized preparation of **2** is given in the Experimental Section).

Complex **2** reacted in $[D_6]$benzene at 65 °C to form the scandium phenyl complex $[Cp^*_2ScC_6D_5]$ ($[D_5]$**4**; ca. 70% after 60 min at 90% conversion, by ^{1}H NMR spectroscopy). The primary by-product in this reaction is the hydride $[D_1]$**3** (ca. 12% after 60 mins at 65 °C), which may form by reaction of a $[Cp^*_2ScR]$ species with hydrogen or $MesSiH_3$, or by the thermal decomposition of **2** ($t_{1/2}$ = 8.5 h at 50 °C in $[D_{12}]$cyclohexane; 95% yield of **3**). A ^{2}H NMR spectrum of the reaction mixture (in $[D_6]$benzene) indicates that $MesSiD_3$ is the major silane product, but also reveals the presence of a trace amount (< 5%) of the dehydrocoupling product $MesD_2SiSiD_2Mes$; there is no evidence for the formation of $[([D_n]Cp^*)_2ScC_6D_5]$. The conversion of **2** into the phenyl complex **4** in benzene is approximately two-times faster than it is in $[D_6]$benzene, which indicates that CH bond activation is involved in the rate-determining step. Plots of [**2**] versus time reveal that the reaction rate increases as the thermolysis proceeds, which suggests that a product or intermediate promotes the reaction. A reasonable mechanism

[*] Prof. T. D. Tilley, A. D. Sadow
Department of Chemistry
University of California, Berkeley
Berkeley, CA 94720-1460 (USA)
Fax: (+1) 510-642-8940
E-mail: tilley@cchem.berkeley.edu

[**] Acknowledgment is made to the National Science Foundation for their generous support of this work, and to Dr. Richard Andersen, Dr. John Bercaw, and Dr. Mark Thompson for helpful discussions.

for this reaction, involving hydrogen as a catalyst, is analogous to that proposed for the reaction of $[Cp^*_2SmCH(SiMe_3)_2]$ with $H_2Si(SiMe_3)_2$.[14]

Reaction of **2** with methane (14 equiv) in $[D_{12}]$cyclohexane occurred slowly at room temperature over four days to give $MesSiH_3$ and $MesMeSiH_2$ (85% and 15%, respectively, by GC-MS), and **3** (42%) as the major scandium-containing product [Eq. (4)]. At intermediate stages of the reaction the methyl complex **1** was observed in trace quantities. As

$$\underset{\mathbf{2}}{[Cp^*_2ScSiH_2Mes]} + CH_4 \rightleftharpoons \underset{\mathbf{1}}{[Cp^*_2ScCH_3]} + MesSiH_3 \rightleftharpoons \underset{\mathbf{3}}{[Cp^*_2ScH]} + MesMeSiH_2 \quad (4)$$

described above, **1** reacted with $MesSiH_3$ to give **2** and CH_4 as the primary kinetic products. Taken together, these results indicate the existence of the coupled equilibria of Equation (4), for which the thermodynamic products are $MesMeSiH_2$ and the scandium hydride **3**. However, just as in the metalation of benzene discussed above, it is not clear whether the C–H activation step involves **2** or **3**.

The observed behavior of methane as a methylating reagent suggested that catalytic methane functionalization might be possible with the appropriate organosilane [Eq. (2)], where $RH = CH_4$). A screening of several silanes with the catalyst **3** revealed that Ph_2SiH_2 provided the best results in terms of the minimization of competitive side reactions (e.g., dehydrocoupling and redistribution). A mixture of **3** and 10 equivalents of Ph_2SiH_2 in $[D_{12}]$cyclohexane reacted under approximately 7 atm of CH_4 in a Young's tube at 80°C to yield Ph_2MeSiH (by GC-MS and NMR spectroscopy) in substoichiometric quantities (ca. 0.4 equiv after 1 week). The reaction rate is dependent on methane concentration; heating a cyclohexane solution of Ph_2SiH_2 and **1** to 80°C under 150 atm of methane produced five equivalents of Ph_2MeSiH after 1 week, one equivalent of which was derived directly from **1** [Eq. (5)]. Increasing the amount of added Ph_2SiH_2 to

$$Ph_2SiH_2 + 150\ atm\ CH_4 \xrightarrow[C_6H_{12},\ 80\ °C,\ 7\ days]{10\%\ \mathbf{1}} Ph_2MeSiH + H_2 \quad (5)$$

20 equivalents did not substantially affect the rate of reaction, as approximately five equivalents of Ph_2MeSiH were detected after a week in both cases. Apparently, the rate-limiting step in the catalytic cycle is C–H bond activation. Though the methane conversion is slow, the reaction is reasonably selective with 75% of the consumed Ph_2SiH_2 being converted into Ph_2MeSiH. It seems likely that some of the Ph_2SiH_2 reacts by competitive Si–Ph hydrogenolysis and silane dehydropolymerization, but no other products were detected by GC after the catalyst had been removed by an aqueous workup. Increasing the temperature to 100°C decreased the amount of Ph_2MeSiH produced (< 1 turnover, by NMR spectroscopy), apparently as a result of rapid decomposition of the catalyst **3** at this temperature.

The composition of the catalytic reaction mixture was probed by ^1H NMR spectroscopy at low methane pressures (ca. 8 atm), but attempts to study the mechanism of the catalysis were complicated by the presence of several species in the reaction mixture. The solution remained homogeneous over the course of the reaction and precipitation of insoluble species, such as $[\{(\eta^1{:}\eta^5\text{-}C_5Me_4CH_2)(\eta^5\text{-}Cp^*)Sc\}_2]$,[6b] did not occur. As **3** was depleted over the course of the reaction (because of slow decomposition), the rate of formation of Ph_2MeSiH decreased, which suggests that **3** is involved in the catalytic cycle.

Mechanistic investigations of the catalytic functionalization of methane with Ph_2SiH_2 have thus far focused separately on the Si–C bond formation and C–H activation steps. The mechanism of Si–C bond formation could proceed via a four-centered transition state in which a Sc–Me derivative reacts with Ph_2SiH_2 to yield **3** and Ph_2MeSiH (methyl transfer), or by reaction of a scandium silyl species with methane (silyl transfer). The methylation of Ph_2SiH_2 by **1** to give Ph_2MeSiH and **3** in $[D_6]$benzene or $[D_{12}]$cyclohexane ($t_{1/2} \approx 45$ min at 25°C) was readily observed; note the sharp contrast between this reaction and that of **1** with $MesSiH_3$, which produced methane and **2** (see above; [Eq. (2)]).[15] In contrast, the reaction of **2** with a large excess of methane was significantly slower and less efficient than the reaction of **1** with Ph_2SiH_2. These observations lead us to favor methyl transfer from Sc to Si as the Si–C bond-forming step in the catalysis outlined in Equation (5).

Attempts to directly detect the activation of methane by **3** have been unsuccessful. Heating $[D_{12}]$cyclohexane solutions of **3** under 7–150 atm of CH_4 to 80°C for 4 days, followed by release of the pressure, did not produce observable quantities of **1** (by ^1H NMR spectroscopy). Note, however, that a reaction between $[Cp^*_2ScD]$ ($[D_1]$**3**) and CH_4 is implied by the observed incorporation of deuterium into methane in the presence of excess D_2 or $[D_6]$benzene.[6b] The possible participation of $[Cp^*_2ScSiHPh_2]$ (**5**) in methane activation is suggested by the observed reactions of isoelectronic $[Cp_2Hf(SiHMes_2)]^+$ ($Cp = \eta\text{-}C_5H_5$) with the C–H bonds of both benzene and toluene.[11] However, **5** could not be detected under catalytic conditions, and attempts to isolate it have failed.

The dehydrogenative silylation of other hydrocarbons can also be mediated by $[Cp^*_2Sc]$ derivatives. For example, the vinyl complex $[Cp^*_2ScCHCMe_2]$ slowly catalyzed the coupling of Ph_2SiH_2 (8 equiv) with isobutylene (18 equiv) at 50°C to produce the vinyl silane $Ph_2(Me_2CCH)SiH$ (ca. 2 turnovers after 20 days in $[D_{12}]$cyclohexane).[6b] With $PhSiH_3$ and isobutylene, a mixture of hydrosilation ($Me_2HCCH_2SiH_2Ph$) and dehydrosilation ($Me_2CCHSiH_2Ph$) products (3:2 ratio; 3 turnovers, 2 days in $[D_{12}]$cyclohexane), as well as minor amounts of dehydrocoupling products, were observed. Compound **3** also catalyzed the dehydrocoupling of cyclopropane and Ph_2SiH_2 in $[D_{12}]$cyclohexane at 80°C (2.5 turnovers, 20 days). Interestingly, benzene and pentane were not suitable substrates for this dehydrosilation process.

Herein we described a new approach for the selective, catalytic conversion of methane. The catalytic cycles reported (for hydrocarbon dehydrosilations) are believed to involve only σ-bond-metathesis steps. Such mechanisms are therefore quite analogous to those previously proposed for d^0-metal-

 © 2003 Wiley-VCH Verlag GmbH & Co. KGaA, Weinheim 1433-7851/03/4207-0804 $ 20.00+.50/0

catalyzed dehydropolymerizations of silanes and stannanes.[10,16] Jordan and Taylor have reported the 1,2-addition of a C–H bond of picoline to an olefin (hydroalkylation), which is catalyzed by a cationic d^0 bis(Cp) zirconium complex by a mechanism involving σ-bond metathesis and olefin insertion.[17] Dehydrogenative silation of terminal alkynes has been observed as a competitive process to hydrosilation.[18] Note that the ability of $[Cp^*_2ScH]$ (**3**) to catalyze hydrocarbon dehydrosilation requires that competitive processes, such as silane polymerization and redistribution, are slow relative to C–H bond activation. This characteristic of the scandium system described here is unusual, and further investigations will address mechanistic issues related to this selectivity.

Experimental Section

All manipulations were performed either on a Schlenk line under an Ar atmosphere or in a N_2-filled drybox (M. Braun). All solvents and reagents were purified by standard procedures.

2: Neat $MesSiH_3$ (0.120 g, 0.798 mmol) was added to solid $[Cp^*_2ScMe]$ (**1**; 0.0485 g, 0.1468 mmol). The bright-yellow solid which formed was washed with cold pentane (3 × 2 mL), yielding **2**. The washings were cooled to −30 °C from which additional compound could be isolated: yield 0.030 g, 44 %, m.p. 175 °C, elemental analysis: calcd (%) for $C_{29}H_{43}ScSi$: C 74.96, H 9.33; found: C 74.98, H 9.31; ^{1}H NMR (500 MHz, [D$_6$]Benzene, 25 °C, TMS): $\delta = 6.988$ (s, 2H, $C_6H_2Me_3$), 4.345 (s, 2H, SiH), 2.581 (s, 6H, *o*-$C_6H_2Me_3$), 2.295 (s, 3H, *p*-$C_6H_2Me_3$), 1.814 ppm (s, 30H, C_5Me_5); ^{13}C{^{1}H} NMR (125 MHz): $\delta = 160.70$ ($C_6H_2Me_3$), 143.98 ($C_6H_2Me_3$), 141.56 ($C_6H_2Me_3$), 135.83 ($C_6H_2Me_3$), 123.00 (C_5Me_5), 26.45 (*o*-$C_6H_2Me_3$), 21.71 (*p*-$C_6H_2Me_3$), 11.86 ppm (C_5Me_5); ^{29}Si{^{1}H} NMR (99 MHz): $\delta = -71.0$ ppm ($^1J_{SiH} = 135$ Hz); IR (KBr): $\tilde{\nu} = 2014$ cm^{-1} (Si-H).

Received: August 26, 2002 [Z50046]

[1] a) J. A. Labinger, J. E. Bercaw, *Nature* **2002**, *417*, 507; b) R. H. Crabtree, *J. Chem. Soc. Dalton Trans.* **2001**, 2437; c) A. Sen, *Acc. Chem. Res.* **1998**, *31*, 550; d) S. S. Stahl, J. A. Labinger, J. E. Bercaw, *Angew. Chem.* **1998**, *110*, 2298; *Angew. Chem. Int. Ed.* **1998**, *37*, 2180; e) A. E. Shilov, G. B. Shul'pin, *Chem. Rev.* **1997**, *97*, 2879; f) B. A. Arndtsen, R. G. Bergman, T. A. Mobley, T. H. Peterson, *Acc. Chem. Res.* **1995**, *28*, 154.

[2] Some recent representative examples of catalytic hydrocarbon functionalizations: a) H. Chen, S. Schlecht, T. C. Semple, J. F. Hartwig, *Science* **2000**, *287*, 1995; b) J.-Y. Cho, M. K. Tse, D. Holmes, R. E. Maleczka, M. R. Smith, *Science* **2002**, *295*, 305; c) C. Jia, D. Piao, J. Oyamada, W. Lu, T. Kitamura, Y. Fujiwara, *Science* **2000**, *287*, 1992; d) F. Liu, E. B. Pak, B. Singh, C. M. Jensen, A. S. Goldman, *J. Am. Chem. Soc.* **1999**, *121*, 4086.

[3] R. A. Periana, D. J. Taube, S. Gamble, H. Taube, T. Satoh, H. Fujii, *Science* **1998**, *280*, 560.

[4] a) G. V. Nizova, G. Suss-Fink, G. B. Shul'pin, *Chem. Commun.* **1997**, 397; b) M. N. Vargaftik, I. P. Stolarov, I. I. Moiseev, *J. Chem. Soc. Chem. Commun.* **1990**, 1049; c) M. Merkx, D. A. Kopp, M. H. Sazinsky, J. L. Blazyk, J. Müller, S. J. Lippard, *Angew. Chem.* **2001**, *113*, 2860; *Angew. Chem. Int. Ed.* **2001**, *40*, 2782.

[5] R. H. Crabtree, *Chem. Rev.* **1995**, *95*, 987, and references therein.

[6] a) P. L. Watson, G. W. Parshall, *Acc. Chem. Res.* **1985**, *18*, 51; b) M. E. Thompson, S. M. Baxter, A. R. Bulls, B. J. Burger, M. C. Nolan, B. D. Santarsiero, W. P. Schaefer, J. E. Bercaw, *J. Am. Chem. Soc.* **1987**, *109*, 203; c) C. M. Fendrick, T. J. Marks, *J. Am. Chem. Soc.* **1986**, *108*, 425.

[7] W. E. Piers, P. J. Shapiro, E. E. Bunel, J. E. Bercaw, *Synlett* **1990**, 74.

[8] a) P.-F. Fu, L. Brard, Y. Li, T. J. Marks, *J. Am. Chem. Soc.* **1995**, *117*, 7157, and references therein; b) T. I. Gountchev, T. D. Tilley, *Organometallics* **1999**, *18*, 5661; c) G. A. Molander, M. Julius, *J. Am. Chem. Soc.* **1995**, *117*, 4415; d) A. K. Dash, I. Gourevich, J. Q. Wang, J. Wang, M. Kapon, M. S. Eisen, *Organometallics* **2001**, *20*, 5084.

[9] a) C. T. Aitken, J. F. Harrod, E. Samuel, *J. Am. Chem. Soc.* **1986**, *108*, 4059; b) J. Y. Corey, X.-H. Zhu, T. C. Bedard, L. D. Lange, *Organometallics*, **1991**, *10*, 115; c) T. D. Tilley, *Acc. Chem. Res.* **1993**, *26*, 22.

[10] a) H.-G. Woo, J. F. Walzer, T. D. Tilley, *J. Am. Chem. Soc.* **1992**, *114*, 7047; b) G. L. Casty, C. G. Lugmair, N. S. Radu, T. D. Tilley, J. F. Walzer, D. Zargarian, *Organometallics* **1997**, *16*, 8; c) N. S. Radu, T. D. Tilley, *J. Am. Chem. Soc.* **1992**, *114*, 8293.

[11] A. D. Sadow, T. D. Tilley, *J. Am. Chem. Soc.* **2002**, *124*, 6814.

[12] M. E. Thompson, J. E. Bercaw, *Pure Appl. Chem.* **1984**, *56*, 1.

[13] A. Z. Voskoboynikov, I. N. Parshina, A. K. Shestakova, K. P. Butin, I. P. Beletskaya, L. G. Kuz'mina, J. A. K. Howard, *Organometallics* **1997**, *16*, 4041.

[14] N. S. Radu, T. D. Tilley, *J. Am. Chem. Soc.* **1995**, *117*, 5863.

[15] Reactions of **1** with organosilanes are highly sensitive to the nature of substituents at silicon; A. D. Sadow, T. D. Tilley, unpublished results.

[16] T. Imori, V. Lu, H. Cai, T. D. Tilley, *J. Am. Chem. Soc.* **1995**, *117*, 9931.

[17] R. F. Jordan, D. F. Taylor, *J. Am. Chem. Soc.* **1989**, *111*, 778.

[18] A. K. Dash, J. Q. Wang, M. S. Eisen, *Organometallics* **1999**, *18*, 4727.

Palladium-Catalyzed Addition

The Palladium-Catalyzed Addition of Organoboronic Acids to Alkynes**

Chang Ho Oh, Hyung Hoon Jung, Ki Seong Kim, and Nakjoong Kim*

Palladium-catalyzed cross-coupling of organoboronic acids with organic halides or their equivalents has long been the subject of intensive work in the area of transition-metal chemistry.[1] The Suzuki reaction is now one of the most

[*] Prof. Dr. C. H. Oh, H. H. Jung, K. S. Kim, N. Kim
Department of Chemistry
Hanyang University
Sungdong-Gu, Seoul 131-791 (Korea)
Fax: (+82) 2-2299-0762
E-mail: changho@hanyang.ac.kr

[**] We wish to acknowledge the financial support of KOSEF (2001-1-123-001-5) and the Center for Molecular Design and Synthesis (CMDS, R11-1999-05601).

Supporting information for this article is available on the WWW under http://www.angewandte.org or from the author.

 © 2003 Wiley-VCH Verlag GmbH & Co. KGaA, Weinheim 1433-7851/03/4207-0805 $ 20.00+.50/0

general reactions used to synthesize stereodefined biaryls,[2] alkadienes,[3] and trienes.[4] Since a variety of organoboron compounds have now become readily available, much attention has been devoted to develop a new aspect of organoboron chemistry.

Miyaura and co-workers reported the rhodium-catalyzed 1,4-conjugated addition of organoboronic acids to α,β-unsaturated ketones through a sequence of boron–rhodium transmetalation reactions.[5] The use of the chiral binap–rhodium (binap = 2,2′-bis(diphenylphosphanyl)-1,1′-binaphthyl) catalyst enabled asymmetric additions of organoboronic acids to aldehydes,[6] *N*-sulfonyl imines,[7] α,β-unsaturated enones,[8] and α,β-unsaturated esters to be achieved.[9] The rhodium-catalyzed additions of aryl boronic acids to unactivated alkenes and alkynes were also accomplished.[10] The well-accepted catalytic cycle for the hydroarylation of unactivated alkynes involves the addition of aryl–rhodium intermediates (Ar-Rh-L), formed by oxidative addition of the rhodium catalyst to the $ArB(OH)_2$ species, to the π bond of the substrate.[11] Similar hydroarylations have also been attained by nickel-catalyzed additions of aryl magnesium or aryl zinc reagents to alkynes or by titanium-catalyzed hydrozincations of alkynes.[12] Here we report the first example of palladium-catalyzed hydroarylations of alkynes with organoboronic acids and a mechanistic interpretation based on a isotope-labeling study.

The palladium-catalyzed additions of a series of organoboronic acids (**2i**–**2o**) to various alkynes (**1a**–**1h**) were examined (Scheme 1, Table 1). The reaction of 5-hexyn-1-ol (**1a**) with phenylboronic acid (**2i**) was first examined in a variety of solvents (such as 1,4-dioxane, THF, and toluene) in the presence of a catalytic amount of formic or acetic acid. The optimal yield of 5-phenyl-5-hexen-1-ol (**3ai**) was obtained (entry 1) when a mixture of **1a, 2i** (1.2 equiv), acetic acid (0.10–0.15 equiv), and $[Pd(PPh_3)_4]$ (3 mol% relative to **1a**) in 1,4-dioxane was heated at 80 °C for 10 h. The reaction took place very slowly (several days), even in the absence of an acid additive.

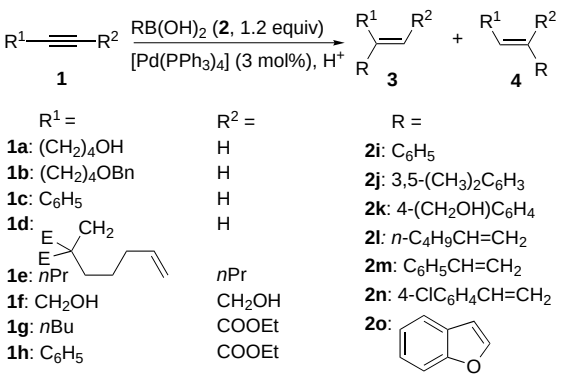

Scheme 1.

Table 1: Pd-catalyzed hydroalkylation of alkynes **1** with organoboronic acids **2**.[a]

Entry	Alkyne	$RB(OH)_2$	*T* [°C]	*t* [h]	Products	Yield [%]
1	**1a**	**2i**	80	10	**3ai**	93
2	**1a**	**2j**	70	4	**3aj**	96
3	**1a**	**2k**	70	5	**3ak**	65
4	**1a**	**2l**	40	12	**3al**	88
5	**1a**	**2m**	60	6	**3am**	83
6	**1a**	**2n**	70	12	**3an**	83
7	**1a**	**2o**	70	12	**3ao**	92
8	**1b**	**2i**	60	2	**3bi**	90
9	**1b**	**2l**	60	3	**3bl**	88
10	**1c**	**2i**	80	12	**3ci**	91
11	**1c**	**2l**	80	12	**3cl**	75
12	**1d**	**2i**	50	15	**3di**	85
13	**1d**	**2l**	60	5	**3dl**	78
14	**1e**	**2i**	60	48	**3ei**	99
15	**1e**	**2l**	80	24	**3el**	89
16	**1f**	**2i**	80	6	**3fi**	94
17	**1f**	**2l**	80	4	**3fl**	72
18	**1g**	**2i**	80	8	**3gi, 4gi**	80 (4:1)[b]
19	**1g**	**2l**	80	8	**3gl, 4gl**	85 (3:1)[b]
20	**1h**	**2i**	80	4	**3hi, 4hi**	84 (4:1)[b]
21	**1h**	**2l**	80	4	**3hl, 4hl**	78 (1:1)[b]

[a] The reaction was carried out with **1** and organoboronic acid **2** (1.2 equiv) in 1.0 mL of 1,4-dioxane in the presence of 3 mol% of $[Pd(PPh_3)_4]$ and acetic acid (0.10–0.15 equiv). [b] The combined yields and isomeric ratios were determined by ^1H NMR spectral analysis.

Both 3,5-dimethylphenylboronic acid (**2j**) and 4-(hydroxymethyl)phenylboronic acid (**2k**) added to the alkyne **1a** under the optimal conditions to give the hydroarylation products **3aj** and **3ak** in yields of 96 and 65%, respectively (entries 2 and 3). In addition, *trans*-1-hexenylboronic acid (**2l**), *trans*-2-phenylvinylboronic acid (**2m**), *trans*-2-(4-chlorophenyl)vinylboronic acid (**2n**), and 2-benzofuranylboronic acid (**2o**) added to the alkyne **1a** to give the corresponding dienes **3al, 3am, 3an**, and **3ao** in yields of 88, 83, 83, and 92%, respectively (entries 4–7). Next, the palladium-catalyzed addition of organoboronic acids to various terminal alkynes was tested. As expected, both aryl and alkenylboronic acids **2i** and **2l** added to the alkynes **1b–d** to give the corresponding products **3bi, 3bl, 3ci, 3cl, 3di**, and **3dl**, respectively, in excellent yields (entries 8–13). Two internal alkynes, 4-octyne (**1e**) and 2-butyne-1,4-diol (**1f**), also underwent hydroarylation with organoboronic acids (**2i** and **2l**) in excellent yields, although 4-octyne (**1e**) required a relatively long reaction time for completion (entries 14–17). Finally, the two alkynes **1g** and **1h** conjugated with electron-withdrawing groups were treated with boronic acids (**2i** and **2l**) under the same conditions. As expected, the reactions were very facile but gave a mixture of regioisomers of the addition products **3** and **4**.

To gain more insight into the mechanism of the present reaction the reaction of alkyne **1a** with phenylboronic acid was conducted using deuterated acetic acid (DOAc; Scheme 2). Only 40% of the deteurium-incorporated product

 © 2003 Wiley-VCH Verlag GmbH & Co. KGaA, Weinheim 1433-7851/03/4207-0806 $ 20.00+.50/0

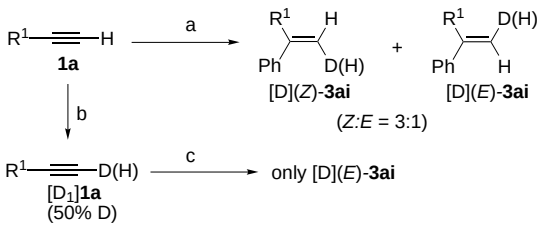

a) 3 mol% $[Pd(PPh_3)_4]$, 3 equiv DOAc, 1.2 equiv **2i**, 1,4-dioxane, 80 °C, 5 h.
b) 3 mol% $[Pd(PPh_3)_4]$, 3 equiv DOAc, 1,4-dioxane, 80 °C, 2 h.
c) 3 mol% $[Pd(PPh_3)_4]$, 3 mol% HOAc, 1.2 equiv **2i**, 1,4-dioxane, 80 °C, 5 h.

Scheme 2.

[D]**3ai** was isolated in a *Z*:*E* ratio of 3:1 as evident by ^{1}H NMR analysis when 3.0 equivalents of deuterated acetic acid were used. This result indicated that there was some stereochemical scrambling or deuterium exchange between the alkyne-H and AcOD prior to the addition of D-Pd-OAc to the triple bond.[13] In fact, the 50% deuterated alkyne $[D_1]$**1a** was obtained when alkyne **1a** was exposed to similar conditions in the absence of phenyboronic acid. When the reaction of the 50% deuterated alkyne $[D_1]$**1a** with **2i** was examined in the presence of a catalytic amount of acetic acid, $[D_1]$(*E*)-**3ai** was obtained exclusively without any loss of deuterium.[14]

A proposed mechanism based on the deuterium-labeling study is shown in Scheme 3. The *syn* addition of the H-Pd-OAc species into the triple bond would form the alkenylpalladium intermediate **I**. The reaction was complete even in the presence of a catalytic amount of the acid, which suggests that a proton source for the hydropalladation reaction could be the organoboronic acid. The organic group can transfer from the metal–boron species to the metal–palladium species to form the intermediates (**II**) containing two organic ligands in the coordination sphere of the palladium center, acetic acid, and a boric acid derivative such as metaboric acid. It has been well-documented that the high oxophilicity of the boron center and the electron richness of palladium(0) and platinum(0) complexes would induce transmetalation, whereby organic groups on the boron atom readily transfer to $Pd(OAc)_2$,[15] $[\eta^3\text{-}C_3H_5PdOAc]_2$,[16] $[\eta^3\text{-}C_3H_5Pd(acac)]$ (acacH = acetylacetone),[17] $[Pd(OR)L_2]$ (R = H, Me, Ac), and $[Pt(OR)(S)L_2]$ (R = H, Me; S = solvent) under neutral conditions. The reductive elimination of the intermediate **II** would form the desired products (**3** and **4**) and the eliminated Pd^0 species.

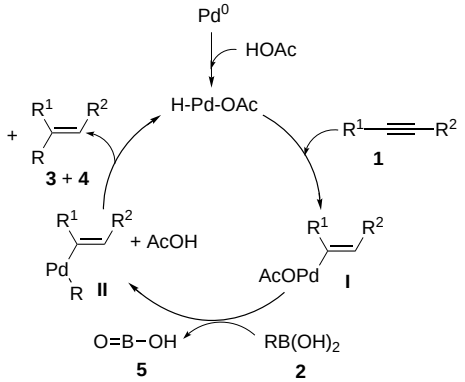

Scheme 3.

The presence of a mineral base has been generally believed to be fundamental for the success of the Suzuki-type cross-coupling. The present study shows importantly that the alkenylpalladium intermediates **I** could be smoothly cross-coupled with organoboronic acids even in acidic media. It is noteworthy that no base is involved in the catalytic cycle.

In conclusion, we have shown for the first time that palladium compounds can catalyze the addition of organoboronic acids to alkynes. The ready availability of alkynes and organoboronic acids combined with the excellent chemical yields and mild reaction conditions of this process suggest that the present reaction should find wide application in organic synthesis.

Received: August 29, 2002
Revised: November 5, 2002 [Z50062]

[1] a) N. Miyaura, A. Suzuki, *Chem. Rev.* **1995**, *95*, 2457; b) A. Suzuki, *J. Organomet. Chem.* **1999**, *576*, 147.
[2] a) T. Hayashi, S. Niizuma, T. Kamikawa, N. Suzuki, Y. Uozumi, *J. Am. Chem. Soc.* **1995**, *117*, 9101; b) T. Kamikawa, T. Hayashi, *Tetrahedron* **1999**, *55*, 3455.
[3] a) M. J. Burk, J. G. Allen, W. F. Kiesman, *J. Am. Chem. Soc.* **1998**, *120*, 657; b) N. Hénaff, A. Whiting, *J. Chem. Soc. Perkin Trans. 1* **2000**, 395.
[4] a) W. R. Roush, K. J. Moriarty, B. B. Brown, *Tetrahedron Lett.* **1990**, *31*, 6509; b) J. Uenishi, R. Kawahama, O. Yonemitsu, J. Tsuji, *J. Org. Chem.* **1996**, *61*, 5716.
[5] M. Sakai, H. Hayashi, N. Miyaura, *Organometallics* **1997**, *16*, 4229.
[6] a) M. Sakai, M. Ueda, N. Miyaura, *Angew. Chem.* **1998**, *110*, 3475; *Angew. Chem. Int. Ed.* **1998**, *37*, 3279; b) M. Ueda, N. Miyaura, *J. Org. Chem.* **2000**, *65*, 4450.
[7] M. Ueda, N. Miyaura, *J. Organomet. Chem.* **2000**, *595*, 31.
[8] a) T. Hayashi, T. Senda, Y. Takaya, M. Ogasawara, *J. Am. Chem. Soc.* **1999**, *121*, 11591; b) Y. Takaya, M. Ogasawara, T. Hayashi, *Tetrahedron Lett.* **1998**, *39*, 8479; c) Y. Takaya, M. Ogasawara, T. Hayashi, M. Sakai, N. Miyaura, *J. Am. Chem. Soc.* **1998**, *120*, 5579.
[9] S. Sakuma, M. Sakai, R. Itooka, N. Miyaura, *J. Org. Chem.* **2000**, *65*, 5951.
[10] a) K. Oguma, M. Miura, T. Satoh, M. Nomura, *J. Am. Chem. Soc.* **2000**, *122*, 10464; b) M. Lautens, A. Roy, K. Fukuoka, K. Fagnou, B. Martin-Matute, *J. Am. Chem. Soc.* **2001**, *123*, 5358; c) M. Lautens, M. Yoshida, *Org. Lett.* **2002**, *4*, 123.
[11] T. Hayashi, K. Inoue, N. Taniguchi, M. Ogasawara, *J. Am. Chem. Soc.* **2001**, *123*, 9918.
[12] a) For a review on the Ni-catalyzed addition, see I. N. Houpis, J. Lee, *Tetrahedron* **2000**, *56*, 817; b) for a review on the organozinc reagents, see P. Knochel, J. J. Almena Perea, P. Jones, *Tetrahedron* **1998**, *54*, 8275; c) for a review on the organotitanium reagents, see F. Sato, H. Urabe, S. Okamoto, *Chem. Rev.* **2000**, *100*, 2835.
[13] B. M. Trost, D. L. Romero, F. Rise, *J. Am. Chem. Soc.* **1994**, *116*, 4268.
[14] Some representative ^{1}H signals were observed at $\delta = 5.25$ ppm for H^1, $\delta = 5.04$ ppm for H^2, and the ^{13}C NMR signal for the

terminal olefinic carbon atom was observed at $\delta = 111.89$ ppm (t, $J = 24$ Hz) in the NMR spectra.
[15] H. A. Dieck, R. F. Heck, *J. Org. Chem.* **1975**, *40*, 1083.
[16] N. Miyaura, K. Yamada, H. Suginome, A. Suzuki, *J. Am. Chem. Soc.* **1985**, *107*, 972.
[17] A. Suzuki in *Metal-Catalyzed Cross-Coupling Reactions* (Eds.: F. Diederich, P. J. Stang), VCH, Weinheim, **1988**; p. 49.

 © 2003 Wiley-VCH Verlag GmbH & Co. KGaA, Weinheim 1433-7851/03/4207-0808 $ 20.00+.50/0

From Ethene to 1-Hexene

Why Trimerization? Computational Elucidation of the Origin of Selective Trimerization of Ethene Catalyzed by $[TaCl_3(CH_3)_2]$ and An Agostic-Assisted Hydride Transfer Mechanism**

*Zhi-Xiang Yu and K N. Houk**

Transition-metal-catalyzed alkene oligomerizations usually yield mixtures of alkenes in the C_4–C_{26} range.[1] It is tedious to separate these mixtures into pure compounds. Consequently, much effort from both industrial and academic communities has been devoted to the search for more efficient catalysts that will produce terminal alkenes of specific lengths. The trimerization of ethene to 1-hexene is of special industrial significance since 1-hexene is an important comonomer in the preparation of linear low-density polyethylene.[2] Most catalysts known today are based on chromium compounds.[3,4] Recently, Sen and co-workers discovered that $[TaCl_3R_2]$, generated in situ by the reaction of $TaCl_5$ with alkyl metal compounds such as CH_3Li, can also function as trimerization catalysts under mild conditions (47.6 atm, 40–60 °C).[5] It has been postulated that metallacycles are involved in alkene trimerizations,[3e,f,6–8] but there has not been detailed information about the potential energy surfaces (PESs) and the structures of the transition states (TSs) and intermediates. Here we report MP2 and B3LYP calculations on the detailed mechanism of the olefin trimerization catalyzed by Sen's catalyst $[TaCl_3(CH_3)_2]$.[9,15] We also explored why this catalyst selectively trimerizes rather than dimerizes or polymerizes alkenes, and have uncovered a novel mechanism for the decomposition of dialkyl complexes of tantalum.

Dialkyltantalum complexes $[TaCl_3(R^1)(R^2)]$ (R^1 and R^2 are alkyl groups) are most stable as trigonal bipyramids with two electronegative Cl ligands in the axial positions (TB-1 conformation, see **1** in Figure 1 and Supporting Information). The TSs and intermediates (except **9**, see below) involved in the trimerization process adopt similar TB-1 conformations.

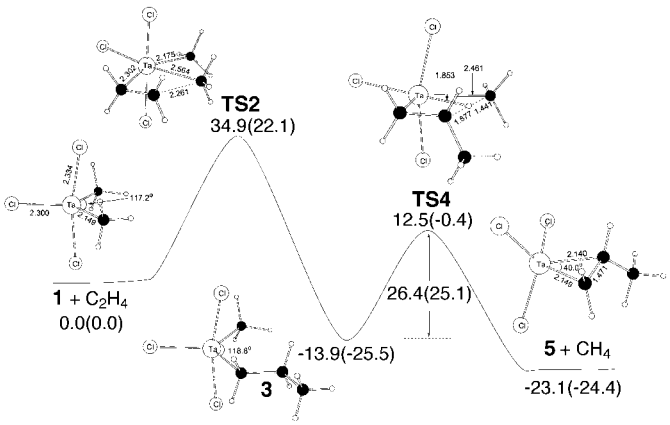

Figure 1. Free energy (ΔG_{298}) surface for the generation of catalytic precursor **5**. Potential energies (ΔE_0) are in parentheses. Energies in kcal mol^{-1}, distances in Å.

The insertion of ethene into **1** proceeds directly via **TS2** to give **3** (Figure 1). No complex of ethene with **1** was found, in contrast to the usual Cossee mechanism.[16] The lack of ethene complexation may be explained by the crowded TB-1 conformation, the coordinately saturated Ta center of **1**, and the lone-pair–π repulsion between Cl ligands and the incoming ethene. Subsequently, **3** undergoes β elimination to afford **5** with liberation of methane. This step is a novel agostic-assisted hydride shift (see below), and no minimum for a metal-hydride intermediate could be found. A similar mechanism was proposed by Negishi et al. for the transformation of dialkylzirconocenes to zirconocene–alkene complexes.[17a,b]

The catalytic cycle shown in Figure 2 starts with the coordination of a second ethene molecule to the tantalum–ethylene complex **6**, producing **7**. Subsequently, facile ring closure via **TS8** transforms **7** to a tantalacyclopentane intermediate, which initially has the TB-1 conformation of **9*** but easily converts into the more stable **9** with a pseudo-square-pyramidal structure. Intermediate **9** is transformed to tantalacycloheptane **11** by ethene insertion via **TS10**. The activation energy (in terms of ΔE_0) of this step is 13.0 kcal mol^{-1} (25.6 kcal mol^{-1} in terms of ΔG_{298}). **TS10** is 14.6 kcal mol^{-1} higher than **TS8** in terms of ΔG_{298}, suggesting that **6, 7**, and **9** can all equilibrate before they are irreversibly converted to tantalacycloheptane **11**. Because of this equilibrium process, ligand exchange reactions between $[TaCl_3(alkene)]$ complexes and ethene (Scheme 1) favor $[TaCl_3(ethene)]$, **6**, that can enter the trimerization cycle. Complex **6** is more stable than **5** and **13** ($\Delta G_{298}/\Delta E_0$ for Equations (1) and (2) are −0.7/0.3 and −2.8/−1.5 kcal mol^{-1}, respectively).

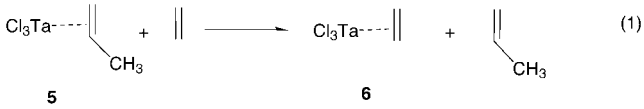

[*] Prof. Dr. K. N. Houk, Dr. Z.-X. Yu
Department of Chemistry and Biochemistry
University of California
Los Angeles, CA 90095-1569 (USA)
Fax: (+1) 310-206-1843
E-mail: houk@chem.ucla.edu

[**] We are grateful to the National Science Foundation for financial support of this research.

Supporting information for this article is available on the WWW under http://www.angewandte.org or from the author.

 © 2003 Wiley-VCH Verlag GmbH & Co. KGaA, Weinheim 1433-7851/03/4207-0808 $ 20.00+.50/0

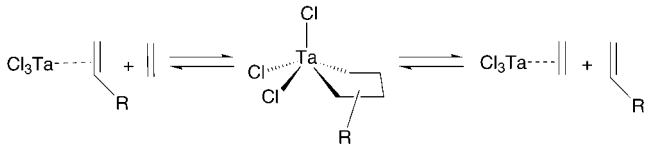

Scheme 1. Ligand exchange reactions between [$TaCl_3$(alkene)] and ethene.

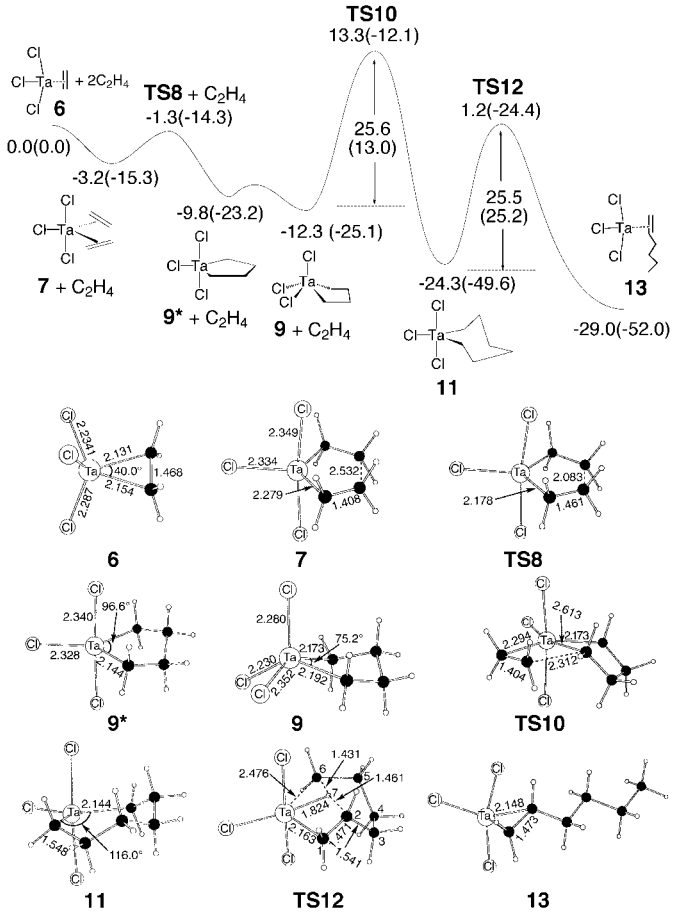

Figure 2. Top: ΔG_{298} surface for the trimerization of ethene; ΔE_0 values in parentheses. Bottom: B3LYP optimized structures of the stationary points involved in this trimerization. Energies in kcal mol^{-1}, distances in Å.

The preference of the ethene–$TaCl_3$ complex over the terminal alkene–$TaCl_3$ is of steric origin. Similar ready ligand-exchange reactions have been observed by Negishi

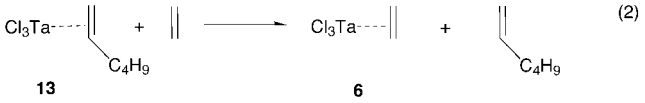

(2)

13 6

and co-workers in the Zr system.[17] Consequently, **6** is readily generated from precursor **5** to initiate the trimerization, and it is readily regenerated from **13** upon completion of one catalytic cycle. As shown in Figure 2, the activation free energies for the ligand exchange processes are estimated to be about 12.3 kcal mol^{-1} (**9**→**6** + C_2H_4), which is significantly less than that (25.6 kcal mol^{-1}) for the insertion of ethene into tantalacyclopentane **9**. This preference of ethene coordination to $TaCl_3$ contributes to the selective generation of 1-hexene instead of branched oligomers.

The barrier for ethene addition to **9** is about 9 kcal mol^{-1} lower than for ethene addition to **1**, because of the ring strain in **9**. The ideal 120° of the C-Ta-C angle in [$TaCl_3R_2$] cannot be achieved in **9** and **9***, but an angle near this is found in **11**. This is a key element that favors trimerization; conversion of **9** into **11** is much more facile than formation of higher complexes. The reaction of **11** with a fourth ethene molecule to form a tetramer requires an activation energy of 23.1 (see Figure 3) instead of the 13.0 kcal mol^{-1} for the formation of the trimer.

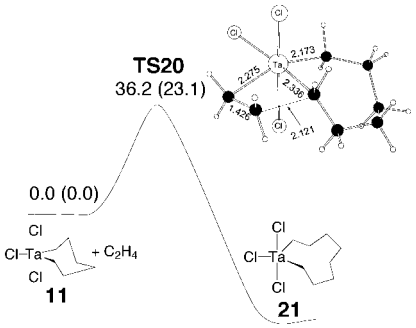

Figure 3. ΔG_{298} surface and calculated TS for the tetramerization of ethene; ΔE_0 values in parentheses. Energies in kcal mol^{-1}, distances in Å.

By contrast to the activation free energy of 36.2 kcal mol^{-1} for the formation of **21**, the conversion of **11** into **13** occurs as a concerted process with an activation free energy of only 25.5 kcal mol^{-1}.[18] This is a novel hydrogen shift related to the well-known metal–hydrogen interaction called β-agostic interaction. The reaction involving **TS12** is called an agostic-assisted hydride shift. Intrinsic reaction coordinate (IRC)[19] calculations demonstrate that distorted geometries of **11** involve a β-agostic interaction of C-H with Ta. These structures are not minima of **11** since too much ring strain is required to achieve the appropriate geometry. But nevertheless this interaction facilitates the conversion of **11** into **13**.[20] The alternate two-step process involving β-H abstraction and reductive elimination, which has been proposed for the Cr and Pt systems,[21,22] requires a higher activation energy to form the metastable intermediate, and a very unfavorable second reductive elimination step (Figure 4a). The overall trimerization cycle from **6** to **13** is highly exothermic and has activation free energies around 26 kcal mol^{-1} for the two most difficult steps.

The agostic-assisted hydride shift leading to reductive elimination requires the dihedral angle H7-C2-C1-Ta to be near 0°, as shown by **TS12** (Figure 2 bottom). The geometry required for the TS of the concerted reductive elimination could not be achieved in **9**. Instead, only a two-step mechanism was found for the transformation of tantalacyclopentane **9** to 1-butene (Figure 4b). The PES of this process is very similar to that shown in Figure 4a, implying that dimerization is disfavored not because of the ring strain in **9**, but because of the nonexistence of a concerted reductive elimination process in the smaller ring size.

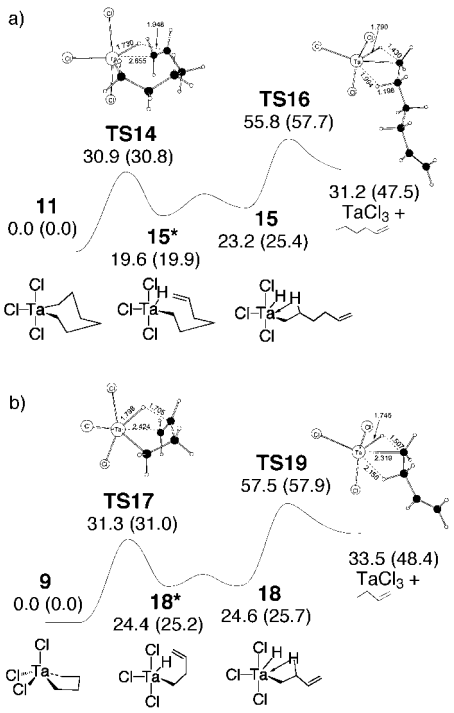

Figure 4. ΔG_{298} surfaces of the β-H abstraction and reductive elimination processes from a) **11** and b) **9**; ΔE_0 values in parentheses. Energies in kcal mol^{-1}, distances in Å.

These theoretical results confirm the intermediacy of tantalacycloalkanes in the trimerization process. The convertion of tantalacycloheptane **11** to tantalum–(1-hexene) complex **13** is a novel concerted process. The dimerization is disfavored by the nonexistence of this kind of concerted reductive elimination process for the tantalacyclopentane, whereas the bimolecular processes of tetramerization and possible higher oligomerization cannot compete with the facile reductive elimination. A similar trimerization mechanism is likely to be shared by the Cr-based catalysts and is under investigation.

Received: August 30, 2002 [Z50075]

[1] a) J. Skupinska, *Chem. Rev.* **1991**, *91*, 613; b) T. Ruther, N. Braussaud, K. J. Cavell, *Organometallics* **2001**, *20*, 1247; c) S. A. Svejda, M. Brookhart, *Organometallics* **1999**, *18*, 65; d) D. Jones, K. J. Cavell, W. Keim, *J. Mol. Catal. A* **1999**, *138*, 37; e) B. L. Small, M. Brookhart, *J. Am. Chem. Soc.* **1998**, *120*, 7143; f) C. M. Killian, L. K. Johnson, M. Brookhart, *Organometallics* **1997**, *16*, 2005; g) M. Peuckert, W. Keim, *Organometallics* **1983**, *2*, 594.

[2] a) *Hydrocarbon Processing, Vol. 3* (Ed.: W. Weirauch), **1998**; b) A. H. Tullo, *Chem. Eng. News* **2000**, *78*(32), 35; c) P. M. Morse, *Chem. Eng. News* **1999**, *77*(11), 19.

[3] a) R. D. Köhn, M. Haufe, G. Kociok-Köhn, S. Grimm, P. Wasserscheid, W. Keim, *Angew. Chem.* **2000**, *112,* 4519; *Angew. Chem. Int. Ed.* **2000**, *39*, 4337; b) M. E. Lashier, Phillips Petroleum Company, EP0 780353 **1995** [*Chem. Abstr.* **1997**, *127,* P50277g]; c) J. R. Briggs, *J. Chem. Soc. Chem. Commun.* **1989**, 674; d) A. Carter, S. A. Cohen, N. A. Cooley, A. Murphy, J. Scutt, D. F. Wass, *Chem. Commun.* **2002**, 858; e) R. M. Manyik, W. E. Walker, T. P. Wilson, *J. Catal.* **1977**, *47*, 197; f) W. K. Reagen, B. Kconroy Phillips Petroleum Company, EP 416304 **1990** [*Chem. Abstr.* **1992**, *116*, 60189]; g) M. Tamura, K. Uchida, K. Iwanaga, Y. Ito Sumitomo Chemical, EP 699648 **1995** [*Chem. Abstr.* **1996**, *124*, 344431]; h) Y. Araki, H. Nakamura, Y. Nanba, T. Okano Mitsubishi Chemical, US-A 5856612 **1997** [*Chem. Abstr.* **1997**, *127*, 161493].

[4] Catalysts based on Ti systems have also been found to trimerize ethene to 1-hexene, see: a) C. Pellecchia, D. Pappalardo, L. Oliva, M. Mazzeo, G.-J. Gruter, *Macromolecules* **2000**, *33*, 2807; b) P. J. W. Deckers, B. Hessen, J. H. Teuben, *Angew. Chem.* **2001**, *113*, 2584; *Angew. Chem. Int. Ed.* **2001**, *40*, 2516.

[5] C. Andes, S. Harkins, S. Murtuza, K. Oyler, A. Sen, *J. Am. Chem. Soc.* **2001**, *123*, 7423.

[6] N. Meijboom, C. Schaveien, A. G. Orpen, *Organometallics* **1990**, *9*, 774.

[7] R. Emrich, O. Heinemann, P. W. Jolly, C. Krüger, G. P. W. Verhovnik, *Organometallics* **1997**, *16*, 1511.

[8] K. H. Theopold, *Eur. J. Inorg. Chem.* **1988**, 15.

[9] All stationary points were located and vibrational analyses were performed using the B3LYP hybrid functional.[10] Single-point energy calculations on these geometries were conducted with the MP2[11,12] method. For C and H, the 6-31G* basis set was applied,[13] while for Ta and Cl, the basis set used is LANL2DZ including a set of polarization functions (LANL2DZp).[14] MP2//B3LYP instead of B3LYP//B3LYP was used because the latter gives a very high activation barrier for the insertion of ethene into $[TaCl_3(Me)_2]$ (**1**), while the MP2//B3LYP method affords the activation energy close to that obtained by the CCSD(T)//B3LYP method (see Figure S1 in the Supporting Information).[12] The zero-point energies (ZPEs) and thermal corrections from the B3LYP vibrational analyses were used, without scaling, to convert the MP2 electronic energies to free energies at 1 atm, 298 K (G_{298}). E_0 is the ZPE corrected energy.

[10] a) A. D. Becke, *J. Chem. Phys.* **1993**, *98,* 5648; b) C. Lee, W. Yang, R. G. Parr, *Phys. Rev. B* **1988**, *37,* 785; c) B. Miehlich, A. Savin, H. Stoll, H. Preuss, *Chem. Phys. Lett.* **1989**, *157*, 200.

[11] C. Møller, M. S. Plesset, *Phys. Rev.* **1934**, *46*, 618.

[12] Møller–Plesset pertubation methods have been shown to give reliable results for systems involving second- and third-row transition metals, see: S. Niu, M. B. Hall, *Chem. Rev.* **2000**, *100,* 353, and references therein.

[13] W. J. Hehre, L. Radom, P. von R. Schleyer, J. A. Pople, *Ab initio Molecular Orbital Theory*, Wiley, New York, **1986**.

[14] For the LANL2DZp basis set, see: a) P. J. Hay, W. R. Wadt, *J. Chem. Phys.* **1985**, *82*, 299; b) T. H. Dunning, Jr., P. J. Hay in *Modern Theoretical Chemistry* (Ed.: H. F. Schaefer III), Plenum, New York, **1977**, pp. 1–28; for polarization functions, see: c) S. Huzinaga, J. Anzelm, M. Klobukowski, E. Radzio-Andzelm, Y. Sakai, H. Tatewaki, *Gaussian Basis Sets for Molecular Calculations*, Elsevier, Amsterdam, **1984**.

[15] All calculations were performed with the Gaussian 98 program: Gaussian 98 (Revision A.7), M. J. Frisch, G. W. Trucks, H. B. Schlegel, G. E. Scuseria, M. A. Robb, J. R. Cheeseman, V. G. Zakrzewski, J. A. Montgomery, R. E. Stratmann, J. C. Burant, S. Dapprich, J. M. Millam, A. D. Daniels, K. N. Kudin, M. C. Strain, O. Farkas, J. Tomasi, V. Barone, M. Cossi, R. Cammi, B. Mennucci, C. Pomelli, C. Adamo, S. Clifford, J. Ochterski, G. A. Petersson, P. Y. Ayala, Q. Cui, K. Morokuma, D. K. Malick, A. D. Rabuck, K. Raghavachari, J. B. Foresman, J. Cioslowski, J. V. Ortiz, B. B. Stefanov, G. Liu, A. Liashenko, P. Piskorz, I. Komaromi, R. Gomperts, R. L. Martin, D. J. Fox, T. Keith, M. A. Al-Laham, C. Y. Peng, A. Nanayakkara, C. Gonzalez, M. Challacombe, P. M. W. Gill, B. G. Johnson, W. Chen, M. W. Wong, J. L. Andres, M. Head-Gordon, E. S. Replogle, J. A. Pople, Gaussian, Inc., Pittsburgh, PA, **1998**.

[16] a) P. Cossee, *J. Catal.* **1964**, *3*, 80; b) E. J. Arlman, P. Cossee, *J. Catal.* **1964**, *3,* 99.

 © 2003 Wiley-VCH Verlag GmbH & Co. KGaA, Weinheim 1433-7851/03/4207-0810 $ 20.00+.50/0

[17] a) E. Negishi, T. Takahashi, *Bull. Chem. Soc. Jpn.* **1998**, *71*, 755; b) E. Negishi, T. Takahashi, *Acc. Chem. Res.* **1994**, *27*, 124; c) D. R. Swanson, E. Negishi, *Organometallics* **1991**, *10*, 825.
[18] Since the tetramerization step is mainly disfavored by entropy, higher oligomerization could compete at very high ethene pressure.
[19] K. Fukui, *J. Phys. Chem.* **1970**, *74*, 4161.
[20] The relationship of β-agostic interaction to alkyl migration to a metal center in homogenous systems was noted earlier: G. F. Schmidt, M. Brookhart, *J. Am. Chem. Soc.* **1985**, *107*, 1443.
[21] a) J. X. McDermott, J. F. White, G. M. Whitesides, *J. Am. Chem. Soc.* **1973**, *95*, 4451; b) J. X. McDermott, J. F. White, G. M. Whitesides, *J. Am. Chem. Soc.* **1976**, *98*, 6521.
[22] Preliminary calculations indicate that in the Pt^{II} and Cr^{III} systems, the transformation of the metallaheptane to a metal–(1-hexene) complex is a two-step process involving β-hydride abstraction and reductive elimination: Z.-X. Yu, unpublished results.

 © 2003 Wiley-VCH Verlag GmbH & Co. KGaA, Weinheim 1433-7851/03/4207-0811 $ 20.00+.50/0

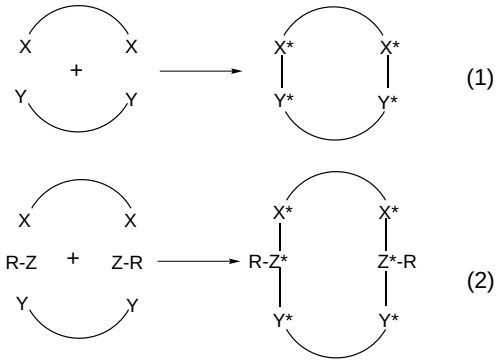

Scheme 1. Schematic representation of cyclodimerization [Eq. (1)] and multicomponent (ABC_2) synthesis [Eq. (2)] of macrocycles.

Functional Symmetric Cyclophanes

A One-Pot Four-Component (ABC_2) Synthesis of Macrocycles**

*Pierre Janvier, Michèle Bois-Choussy, Hugues Bienaymé, and Jieping Zhu**

Macrocycles, by virtue of their widespread occurrence in nature and their intrinsic three-dimensional structure, have found numerous applications in areas such as drug development, material science, and supramolecular chemistry.[1] Not surprisingly, the challenging problem of macrocyclization has attracted attention of synthetic chemists and provided impetus for the development of new technologies.[2] Among many existing methodologies, one-step synthesis of targeted macrocycles is a particularly attractive strategy.[3] Indeed, the cyclodimerization of two bifunctional monomers ([Eq. (1)], Scheme 1) has been successfully developed and applied in the synthesis of natural products[4] as well as non-natural molecules.[5] We report herein a novel four-component (ABC_2) synthesis of symmetric cyclophanes (see schematic representation in Equation (2) in Scheme 1).

Multicomponent reactions (MCRs) are based on a cascade of bond-forming events that are kinetically favored when the reaction is performed at high concentration.[6] On the other hand, macrocyclization has to be generally carried out at high dilution for it involves entropically disfavored end-to-end cyclization.[7] The projected transformation shown in Equation (2) in Scheme 1 comprises a sequence of one three-component process, one bimolecular reaction, and finally one intramolecular reaction. To help circumvent the problems associated with concentration and to make the overall process successful, we decided to incorporate a structural unit that could reduce the conformational mobility of the linear precursor, which assembles in situ during the MCR. The rigidifying effect of aromatic heterocycles is well known, we therefore considered that the recently developed three-component synthesis of oxazole[8] might be applicable for the synthesis of macrocycles **1** according to Scheme 2.

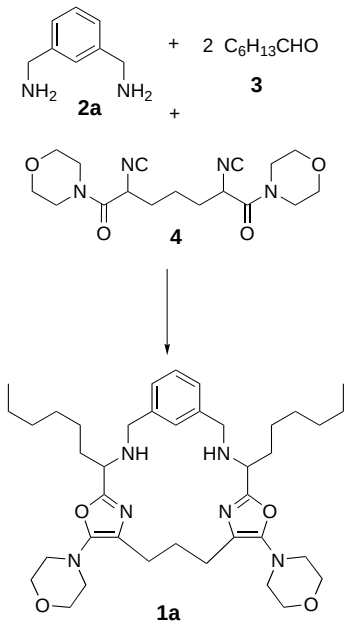

Scheme 2. A four-component (ABC_2) synthesis of macrocycle **1a**. Variations of the reaction conditions are given in Table 1.

[*] Dr. J. Zhu, P. Janvier, M. Bois-Choussy
Institut de Chimie des Substances Naturelles
CNRS, 91198 Gif-sur-Yvette Cedex (France)
Fax: (+33) 1-69-07-72-47
E-mail: zhu@icsn.cnrs-gif.fr
Dr. H. Bienaymé
Chrysalon, 11, Avenue A. Einstein
69100 Villeurbanne (France)

[**] Financial support from CNRS and Rhodia (doctoral fellowship to P.J.) is gratefully acknowledged. We thank Marie-Thérèse Adeline of this institute for carrying out the LC/MS experiment.

 © 2003 Wiley-VCH Verlag GmbH & Co. KGaA, Weinheim 1433-7851/03/4207-0811 $ 20.00+.50/0

Interestingly, double Ugi-4CR (formally one intermolecular and one intramolecular Ugi-4CR)[9] has been observed as an undesired side reaction during a search for macrocyclization substrates based on the cyclization strategy pioneered by Ugi and co-workers.[10]

Initial experiments employed *m*-xylylenediamine (**2a**), *n*-heptanal (**3**), and 2,6-diisocyanoheptanedioic acid bismorpholinylamide (**4**).[11] Stirring a solution of **2a** and **3** (molar ratio 1/2, 0.01M) in toluene for 30 min in the presence of lithium bromide followed by addition of **4** provided **1a** (70 °C, 4 h) in 15% yield as a mixture of inseparable diastereomers. Although only one set of peaks was observed in the ^{1}H NMR spectrum of **1a**, the presence of two diastereomers (*dl* and *meso* forms in a 1:1 ratio) of the purified material is readily seen from the ^{13}C NMR spectrum.

These promising results prompted a more detailed examination of the reaction conditions (Table 1). Methanol was found to be a better solvent than toluene leading to **1a** in an improved yield of 31% (Table 1, entry 2). Interestingly, increasing the concentration from 0.01M to 0.1M further improved the yield of **1a** (52%, Table 1 entry 3).[12] The template effect was examined by adding various salts to the reaction mixture.[13] However, it was observed that none of the salts used, including antimony methoxide,[14] led to an improved yield for this multicomponent process (Table 1, entries 5–7).

Table 1: Survey of reaction conditions for the one-pot four-component synthesis of macrocycle **1**.[a]

Entry	Solvent	*T*	Additive	Conc. [M]	Yield [%][b]
1	toluene	70 °C	LiBr	0.01	15
2	MeOH	reflux	non	0.01	31
3	MeOH	reflux	non	0.1	52
4	MeOH	reflux	CSA[c]	0.1	48
5	MeOH	reflux	LiBr	0.1	29
6	MeOH	reflux	NaBr	0.1	35
7	MeOH	reflux	$Sb(OMe)_3$	0.1	43

[a] Reaction time: 4 h. [b] Yield of isolated product. [c] CSA = camphorsulfonic acid.

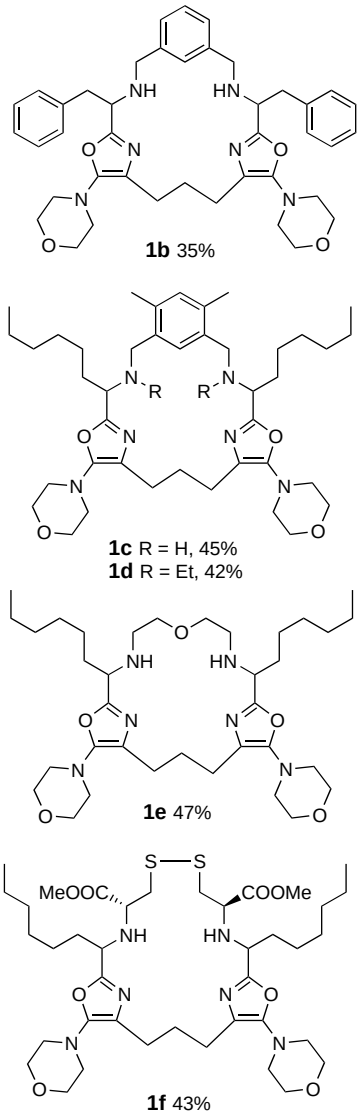

Scheme 3. Structures of macrocycles synthesized.

With these results in hand, the potential and generality of this one-pot multicomponent synthesis of macrocycles were examined under optimized conditions (MeOH, 0.1M, reflux). We initially focused on the structural tolerance of the diamine employed since a wider variety of this component was more readily available than derviatives of the bis(isonitrile) **4**, and it was considered the diamine would have more impact than the aldehyde **3** on the outcome of the reaction. To examine whether the steric buttressing effect[15] as well as intramolecular hydrogen bonds[16] could have any effect on the macrocyclization step, 1,3-bis(aminomethyl)-4,6-dimethylbenzene (**2c**) and its *N,N′*-diethyl derivative (**2d**) were synthesized[17] and submitted to the MCR conditions. The yields of resulting macrocycles **1c** and **1d** (Scheme 3) were similar to that of **1a**, indicating that both effects are minimal, if they exist at all. In the case of **1d**, two diastereomers (1:1 ratio) were isolated and characterized, although their relative stereochemistry remained unknown. Besides the rigid *m*-xylylenediamine, aliphatic diamines such as 1,5-diamino-3-oxapentane (**2e**) and cystine dimethyl ester (**2f**) were shown to participate in this process leading to the macrocycles **1e** and **1f**, respectively (Scheme 3). The formation of macrocycles at such a high concentration (0.1M) is unique and intriguing. It may indicate that the intermediate, assembled in situ by MCR, was preorganized into a folded conformer that is conducive to cyclization.[18]

Although compound **1** is of interest in its own right (e.g., as a pincer ligand for metal complex),[19] it could also serve as a useful chemical platform for the production of new structures by taking advantage of the rich chemistry of oxazole.[8,20] One such example is shown in Scheme 4. Hydrolysis of **1a** under standard conditions (THF–H_2O–TFA (8/2/1))[21] afforded the corresponding macrocyclic amide **5** in over 85% yield. All six possible diastereomers were readily separated and identified by LC/MS. Interestingly, the retention time of these diastereomers differed

 © 2003 Wiley-VCH Verlag GmbH & Co. KGaA, Weinheim 1433-7851/03/4207-0812 $ 20.00+.50/0

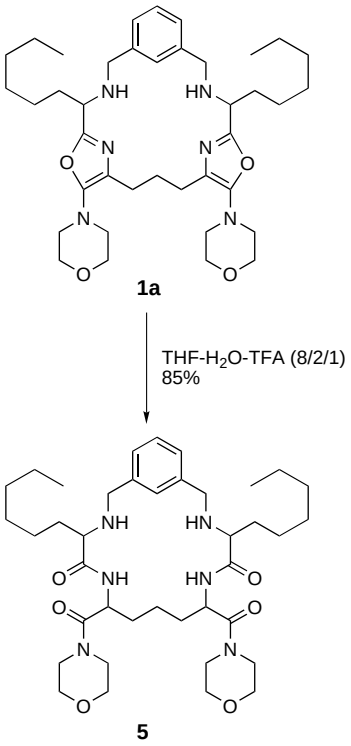

Scheme 4. Transformation of cyclophane **1a**: selective hydrolysis of oxazole groups to give **5**.

significantly, ranging from 2.2 min to 26.3 min (column: Symmetry C-18, gradient H_2O/MeCN = 2/3, then MeCN). This result confirmed the earlier observation that stereochemistry can have an impact on the hydrophobicity and consequently, may modulate the pharmacological properties of small bioactive molecules.[22]

In summary, we have developed a novel one-pot multicomponent synthesis that delivers at least three elements of diversity into the final macrocycles. The overall process leads to the creation of six chemical bonds with the concomitant formation of two oxazole groups as part of a new macrocycle, and thus involves a large increase in molecular complexity.[23] The synthesis is ecologically benign and atom economic since only two molecules of water are lost in this rather complex bond-forming process.[24]

Experimental Section

Typical procedure: A solution of diamine **2a** (95.0 μmol) and aldehyde **3** (209.0 μmol, 2.2 equiv) in anhydrous methanol (0.45 mL) was stirred at room temperature for 30 min. The diisocyanide **4** (114.0 μmol, 1.2 equiv) in anhydrous methanol (0.5 mL) was added and the reaction mixture was heated to reflux. When the reaction was deemed complete by TLC analysis (typically 4 h), the reaction mixture was cooled to room temperature and the volatile components were removed under reduced pressure. The crude reaction mixture was purified by either preparative TLC (silica gel) or flash chromatography (alumina gel). Compound **1a** (pale yellow oil, yield 52%, two diastereomers, preparative TLC on silica gel, eluent: CH_2Cl_2/MeOH = 95/5). IR ($CHCl_3$): $\tilde{\nu}$ = 3692, 3438, 3017, 2957, 2929, 2859, 1666, 1603, 1455, 1376, 1264, 1212, 1115, 910 cm^{-1}; ^1H NMR ($CDCl_3$, 250 MHz): δ = 7.40–7.27 (m, 4H), 3.83 (m, 8H), 3.65 (q, J = 7.1 Hz, 2H), 3.54 (m, 4H), 3.07 (m, 8H), 2.51 (m, 4H), 2.09 (m, 4H), 1.74 (m, 4H), 1.25 (m, 16H), 0.86 ppm (t, J = 6.5 Hz, 6H); ^{13}C NMR ($CDCl_3$, 75 MHz): δ = 162.1 (161.8), 151.5 (151.3), 140.1 (139.9), 131.3 (131.1), 128.9 (128.8), 128.2 (128.1), 126.1 (125.9), 67.4, 57.0 (56.7), 52.8 (52.6), 51.8, 35.4 (35.1), 32.0, 29.4, 29.0 (28.9), 26.3, 25.2 (25.1), 22.9, 14.4 ppm; MS (ES, positive mode): m/z $[M+H]^+$ 677.

Received: September 6, 2002 [Z50114]

[1] a) Y. Z. Shu, *J. Nat. Prod.* **1998**, *61*, 1053–1071; b) F. M. Raymo, J. F. Stoddart, *Chem. Rev.* **1999**, *99*, 1643–1663.

[2] Recent examples, see: a) B. Lipshutz, F. Kayser, Z. P. Liu, *Angew. Chem.* **1994**, *106,* 1962–1964; *Angew. Chem. Int. Ed. Engl.* **1994**, *33*, 1842–1844; b) S. Saito, M. M. Salter, V. Gevorgyan, N. Tsuboya, K. Tando, Y. Yamamoto, *J. Am. Chem. Soc.* **1996**, *118*, 3970–3971; c) M. P. Doyle, C. S. Peterson, M. N. Protopopova, A. B. Marnett, D. L. Parker, Jr., D. G. Ene, V. Lynch, *J. Am. Chem. Soc.* **1997**, *119*, 8826–8837; d) H. Wang, W. D. Wulff, A. L. Rheingold, *J. Am. Chem. Soc.* **2000**, *122*, 9862–9863; e) A. C. Carbonnelle, J. Zhu, *Org. Lett.* **2000**, *2*, 3477–3480; f) A. F. Moretto, H. C. Zhang, B. E. Maryanoff, *J. Am. Chem. Soc.* **2001**, *123*, 3157–3158; g) G. Zhao, X. Sun, H. Bienaymé, J. Zhu, *J. Am. Chem. Soc.* **2001**, *123*, 6700–6701; h) D. R. Spring, S. Krishnan, H. E. Blackwell, S. L. Schreiber, *J. Am. Chem. Soc.* **2002**, *124*, 1354–1363; i) C. W. Lee, T.-L. Choi, R. H. Grubbs, *J. Am. Chem. Soc.* **2002**, *124*, 3224–3225, and references therein.

[3] For a recent review, see: K. E. Krakowiak, R. M. Izatt, J. S. Bradshaw, *J. Heterocycl. Chem.* **2001**, *38*, 1239–1248.

[4] a) T. R. Hoye, P. E. Humpal, B. Moon, *J. Am. Chem. Soc.* **2000**, *122*, 4982–4983; b) A. B. Smith III, S. A. Kozmin, C. M. Adams, D. V. Paone, *J. Am. Chem. Soc.* **2000**, *122*, 4984–4985, and references therein.

[5] a) S. J. Rowan, D. G. Hamilton, P. A. Brady, J. K. M. Sanders, *J. Am. Chem. Soc.* **1997**, *119*, 2578–2579; b) D. Ranganathan, V. Haridas, K. P. Madhusudanan, R. Roy, R. Nagaraj, G. B. John, *J. Am. Chem. Soc.* **1997**, *119*, 11578–11584; c) Y. Singh, N. Sokolenko, M. J. Kelso, L. R. Gahan, G. Abbenante, D. P. Fairlie, *J. Am. Chem. Soc.* **2001**, *123*, 333–334.

[6] a) A. Domling, I. Ugi, *Angew. Chem.* **2000**, *112*, 3300–3344; *Angew. Chem. Int. Ed.* **2000**, *39*, 3168–3210; b) H. Bienaymé, C. Hulme, G. Oddon, P. Schmitt, *Chem. Eur. J.* **2000**, *6*, 3321–3329; c) L. Weber, K. Illgen, M. Almstetter, *Synlett* **1999**, 366–374; d) R. W. Armstrong, A. P. Combs, P. A. Tempest, S. D. Brown, T. A. Keating, *Acc. Chem. Res.* **1996**, *29*, 123–131; e) G. H. Posner, *Chem. Rev.* **1986**, *86*, 831–844.

[7] a) C. J. Roxburgh, *Tetrahedron* **1995**, *51*, 9767–9822; b) R. H. Grubbs, S. J. Miller, G. C. Fu, *Acc. Chem. Res.* **1995**, *28*, 446–452; c) J. Zhu, *Synlett* **1997**, 133–144; d) A. Fürstner, *Angew. Chem.* **2000**, *112*, 3140–3172; *Angew. Chem. Int. Ed.* **2000**, *39*, 3012–3043.

[8] a) X. Sun, P. Janvier, G. Zhao, H. Bienaymé, J. Zhu, *Org. Lett.* **2001**, *3*, 877–880; b) P. Janvier, X. Sun, H. Bienaymé, J. Zhu, *J. Am. Chem. Soc.* **2002**, *124*, 2560–2567.

[9] A. Failli, H. Immer, M. Götz, *Can. J. Chem.* **1979**, *57*, 3257–3261.

[10] For reviews, see ref [6a] and I. Ugi, *Angew. Chem.* **1982**, *94*, 826–835; *Angew. Chem. Int. Ed. Engl.* **1982**, *21*, 810–819.

[11] Synthesized from commercially available 2,6-diaminopimelic acid.

[12] Since half of the starting materials were consumed in the first "intermolecular" three-component reaction, the actual concentration at the cyclization step should be 0.005 and 0.05 M, respectively.

[13] C. Seel, F. Vogtle, *Chem. Eur. J.* **2000**, *6*, 21–24.

 © 2003 Wiley-VCH Verlag GmbH & Co. KGaA, Weinheim 1433-7851/03/4207-0813 $ 20.00+.50/0

[14] K. Ishihara, Y. Kuroki, N. Hanaki, S. Ohara, H. Yamamoto, *J. Am. Chem. Soc.* **1996**, *118*, 1569 – 1570.
[15] For a review, see: P. G. Sammes, D. J. Weller, *Synthesis* **1995**, 1205 – 1222.
[16] F. J. Carver, C. A. Hunter, R. J. Shannon, *J. Chem. Soc. Chem. Commun.* **1994**, 1277 – 1280.
[17] C. L. Parris, R. M. Christenson, *J. Org. Chem.* **1960**, *25*, 1888 – 1893.
[18] Synthesis of porphyrins by ABC_2 approach, see: A. Wiehe, C. Ryppa, M. O. Senge, *Org. Lett.* **2002**, *4*, 3807 – 3809. The yield of macrocycle ranges from 2 to 11 %.
[19] a) For a review, see: M. H. P. Rietveld, D. M. Grove, G. Van Koten, *New J. Chem.* **1997**, *21*, 751 – 771; for recent examples, see: b) D. Salvemini, Z.-Q. Wang, J. L. Zweier, A. Samouilov, H. Macarthur, T. P. Misko, M. G. Currie, S. Cuzzocrea, J. A. Silkorski, D. P. Riley, *Science* **1999**, *286*, 304 – 306; c) M. Gerisch, J. R. Krumper, R. G. Bergman, T. D. Tilley, *J. Am. Chem. Soc.* **2001**, *123*, 5818 – 5819.
[20] a) P. A. Jacobi, *Advances in Heterocyclic Natural Product Synthesis, Vol. 2* (Ed.: W. H. Pearson), JAI, Greenwich, CT, **1992**, pp. 251 – 298; b) A. Hassner, B. Fischer, *Heterocycles* **1993**, *35*, 1441 – 1465; c) G. Zhao, X. Sun, H. Bienaymé, J. Zhu, *J. Am. Chem. Soc.* **2001**, *123*, 5818 – 5819; d) E. González-Zamora, A. Fayol, M. Bois-Choussy, A. Chiaroni, J. Zhu, *Chem. Commun.* **2001**, 1684 – 1685; general discussion on branching pathway e) S. L. Schreiber, *Science* **2000**, *287*, 1964 – 1969; f) P. Arya, D. T. H. Chou, M.-G. Baek, *Angew. Chem.* **2001**, *113,* 351 – 358; *Angew. Chem. Int. Ed.* **2001**, *40*, 339 – 346.
[21] a) D. Clerin, J. P. Fleury, *Bull. Soc. Chim. Fr.* **1973**, 3127 – 3142; b) D. Clerin, J. P. Fleury, *Tetrahedron* **1974**, *30*, 469 – 474; c) B. H. Lipshutz, R. W. Hungate, K. E. McCarthy, *Tetrahedron Lett.* **1983**, *24*, 5155 – 5158.
[22] Stereochemistry as diversity element, selected examples: a) I. Paterson, J. A. Channon, *Tetrahedron Lett.* **1992**, *33*, 797 – 800; b) D. A. Annis, O. Helluin, E. N. Jacobsen, *Angew. Chem.* **1998**, *110,* 2010 – 2012; *Angew. Chem. Int. Ed.* **1998**, *37*, 1907 – 1909; c) T. M. Gierasch, M. Chytil, M. T. Didiuk, J. Y. Park, J. J. Urban, S. P. Nolan, G. L. Verdine, *Org. Lett.* **2000**, *2*, 3999 – 4002.
[23] Macrocyclization with concurrent creation of heterocycles by way of multiple cycloadditiion reactions, see: B. H. Kim, E. J. Jeong, G. T. Hwang, N. Venkatesan, *Synthesis* **2001**, 2191 – 2202.
[24] B. M. Trost, *Angew. Chem.* **1995**, *107*, 285 – 307; *Angew. Chem. Int. Ed. Engl.* **1995**, *34*, 259 – 281.

 © 2003 Wiley-VCH Verlag GmbH & Co. KGaA, Weinheim 1433-7851/03/4207-0814 $ 20.00+.50/0

Thorium Naphthalene Complexes

The First Thorium Arene Complex: A Divalent Synthon**

Ilia Korobkov, Sandro Gambarotta, and Glenn P. A. Yap*

Very strong reducing power[1] and a marked inclination toward performing cooperative attack on the same substrate[2] are the basis of the distinctive reactivity of divalent f-block metals.[3] In spite of the great interest in this field, divalent actinides remain basically unknown, possibly as a result of an intrinsic instability of this oxidation state. Moreover, the significance of the low oxidation states remains questionable, since the f electrons are expected to be more likely engaged in backbonding with the ligand rather than being metal-centered, nonbonding electrons. As a consequence, even simple salts such as UI_2[4] and ThI_2[5] are regarded as divalent only from the point of view of formula, since the f electrons are believed to be located in a type of conduction band. Nevertheless, the electron-rich nature of these species raises expectations for high reactivity and strong reducing power. This idea is substantiated by the chemical behavior of the two known U^{II} synthons,[6] and by some recent findings that a trivalent calix-tetrapyrrolide uranium compound resulted, upon reduction, in a complex series of transformations including dinitrogen cleavage, solvent deoxygenation, and depolymerization of silicone grease.[7] For thorium such chemistry is limited to a handful of trivalent compounds or synthons.[8]

Given this scenario, we became interested in exploring the chemistry of divalent Th complexes, most likely synthons, with the dual purpose of: 1) probing the stability of an oxidation state unknown for thorium and 2) preparing potent two-electron reductants for further reactivity studies. For this purpose, we focused on pyrrole-based polyanions as ligands. These species have proved their ability both to stabilize low oxidation states in large cluster structures[9] and to increase the high reactivity of the low-valent compounds even further.[3f–n] Here we describe the reduction of a tetravalent polypyrrolide thorium complex, which resulted in both solvent fragmentation and formation of the first divalent synthon thorium arene complex.

The reactions of $[\{(Et_8\text{-calix[4]tetrapyrrole})Th(\mu\text{-}Cl)\}_2][K(dme)]_2$[10] (dme = 1,2-dimethoxyethane) with two equivalents of M(naphthalene) (M = K, Li) in DME afforded dark

[*] Prof. S. Gambarotta, Dr. I. Korobkov, Dr. G. P. A. Yap
Department of Chemistry
University of Ottawa
Ottawa, Ontario, K1N 6N5 (Canada)
Fax: (+1) 613-5672-5170
E-mail: sgambaro@science.uottawa.ca

[**] This work was supported by the Natural Sciences and Engineering Council of Canada (NSERC).

Supporting information for this article is available on the WWW under http://www.angewandte.org or from the author.

 © 2003 Wiley-VCH Verlag GmbH & Co. KGaA, Weinheim 1433-7851/03/4207-0814 $ 20.00+.50/0

brown solutions from which very similar diamagnetic compounds **1a** and **1b** were obtained in good yield as dark brown, extremely air sensitive crystals (see Scheme 1).

$[\{(Et_8\text{-calix[4]tetrapyrrole})Th\}\{K(dme)\}(\eta^4\text{-}C_{10}H_8)][Li(dme)_3]$ **1a**

$[\{(Et_8\text{-calix[4]tetrapyrrole})Th\}\{K(dme)\}(\mu\text{-}\eta^4 : \eta^6\text{-}C_{10}H_8)(\mu\text{-}K)]_n$ **1b**

The formulations were provided by X-ray crystal structures (Figures 1 and 2). In both structures the Th and K atoms are located on either side of the calix[4]tetrapyrrole tetraanion. While the K atom adopts the usual bonding mode with two π- and two σ-bonded pyrrolyl rings, the coordination of the Th atom is rather unusual in comparison with other U and lanthanide complexes of the same ligand system.[11] While two rings are σ-bonded as usual, only one of the other two rings is symmetrically π-bonded. The remaining ring, located on the opposite side of the ligand, displays considerable slippage due to η^4 coordination of thorium by one ring of a naphthalene molecule.

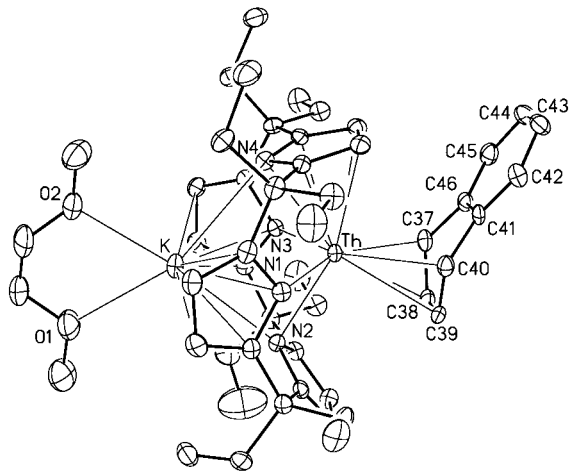

Figure 1. Thermal ellipsoid plot of the anionic moiety of **1a**. Selected bond lengths [Å]: Th-C37 2.704(6), Th-C38 2.761(6), Th-C39 2.754(6), Th-C40 2.675(6), C37-C38 1.445(9), C38-C39 1.378(9), C39-C40 1.457(9), Th-N1 2.544(5), Th-N2 2.569(5), Th-N3 2.533(5), Th-N4 2.729(5), K-N1 3.195(5), K-N2 3.024(5), K-N3 3.242(5), K-N4 3.214(5).

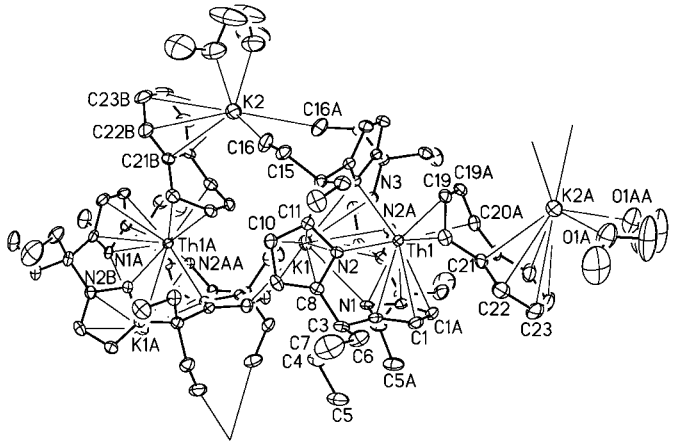

Figure 2. Thermal ellipsoid plot of **1b**. Selected bond lengths [Å]: Th-C19 2.775(4), Th-C20 2.684(5), C19-C20 1.446(6), C19-C19A 1.375(8), Th-N1 2.690(5), Th-N2 2.529(5), Th-N3 2.545(4), K1-N1 3.126(5), K1-N2 3.169(4), K1-N3 3.054(6), K2A-C21 2.982(5), K2A-C22 3.197(6), K2A-C23 3.428(6).

The major structural difference between **1a** and **1b** is determined by the second alkali-metal cation. In **1a**, an Li cation is solvated by three molecules of DME and is unconnected with the Th-containing anion. In **1b**, a second potassium atom is coordinated η^6 to the other naphthalene ring without perturbing its planarity. This second potassium atom is also engaged in substantial agostic interactions with two methyl groups of the ethyl substituents of a second molecule, and a polymeric framework is thus assembled. However, the fact that **1a** and **1b** display nearly identical NMR spectra (apart from the higher content of dme in **1a**) clearly indicates that both the agostic interactions and the polymeric structure are unlikely to be preserved in solution. Furthermore, only two signals of equal intensity are observed for the pyrrolyl rings, in agreement with two different bonding modes (σ and π), that is, slippage of one of the two π-bonded rings is rapidly averaged with the other. The naphthalene ligand shows four double doublets. The ethyl groups produced only one slightly broad triplet for the terminal methyl groups coupled to two different resonances in the ^{13}C NMR spectrum and four partly overlapping quadruplets for the methylene protons, each coupled to one ^{13}C resonance.

We observed that formation of **1b** is occasionally accompanied by tiny amount of colorless, air-sensitive, crystalline solid. The crystal quality was sufficient to allow a crystallographic structural determination. The complex is formulated as **2** (Figure 3).

$[\{(Et_8\text{-calix[4]tetrapyrrole})Th\}_2(\mu\text{-O})(\mu\text{-Me})\{K(dme)\}(\mu\text{-K})\{K(dme)_4\}]_n$ **2**

In the dinuclear moiety two $\{(Et_8\text{-calix[4]tetrapyrrole})Th\}$ units are bridged by one oxo and one methyl ligand. In each unit, a potassium atom is both σ- and π-bonded to the ligand system. For one of them, the potassium coordination sphere is completed by one molecule of dme, and in the other the alkali metal atom interacts with one of the pyrrolyl rings of a second dinuclear unit and thus forms an infinite array. A third K atom, solvated by four molecules of DME, is unconnected to the Th-containing moiety. Regrettably, the presence of **2** in

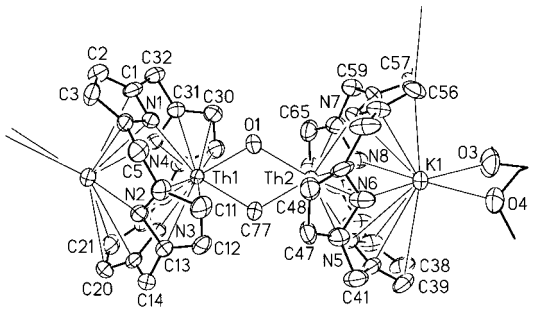

Figure 3. Thermal ellipsoid plot of the anionic moiety of **2**. Selected bond lengths [Å]: Th1-O1 2.24(2), Th2-O1 2.15(2), Th1-C77 2.50(3), Th2-C77 2.43(4), Th1-N1 2.583(9), Th1-N2 2.752(11), Th1-N3 2.610(9), Th1-N4 2.767(10), K2-N1 3.179(10), K2-N2 3.017(9), K2-N3 3.049(11), K2-N4 2.937(10), K2A-C56 3.280(14), K2A-C57 3.074(14).

 © 2003 Wiley-VCH Verlag GmbH & Co. KGaA, Weinheim 1433-7851/03/4207-0815 $ 20.00+.50/0

the reaction mixture was not always reproducible, and the very low yield prevented satisfactory characterization. Nevertheless, the presence of the bridging methyl group was conclusively indicated by NMR spectroscopy: one sharp ^1H resonance at $\delta = -2.68$ ppm with the appropriate intensity ratio, coupled with a resonance at $\delta = 7.52$ ppm in the ^{13}C NMR spectrum. The formation of **2** is most likely the result of solvent fragmentation, which is a recurrent feature in the chemistry of low-valent f-block metals.[2a,b,3j,3k,7,11a] However, since **1a** and **1b** do not react with DME even on prolonged reflux, the occasional formation of **2** indicates that intermediate species, generated during reduction, are sufficiently reactive to attack the solvent.

Complexes **1** are the first thorium arene complexes to be added to the small family of actinide arene compounds.[1,6,12] Although the connectivity may imply a formal divalent oxidation state, the folding of the naphthalene ring, closely reminiscent of the bonding mode of butadiene to Cp_2Th moieties[13] or of that observed in $Ln(\eta^4\text{-}C_{10}H_8)$ complexes,[14] clearly indicate that the f-electrons are primarily engaged in backbonding to the aromatic ring. These observations, in addition to the diamagnetism, indicate that it is unlikely this species contains the metal in the oxidation state $+2$. Nevertheless, **1** reacts as a Th^{II} synthon. An unusual reaction was observed on treatment of **1a** with Me_3SiN_3, which required two equivalents for the complete disappearance of **1a** (Scheme 1). After an induction period of about 15 s, vigorous gas evolution took place and a colorless suspension formed. A small amount of residual solid was identified as a DME-solvated form of KN_3 on the basis of its intense absorption at 2115 cm^{-1} in the IR spectrum, the presence of K, and the absence of the SiN band. The reaction mother liquor afforded, upon layering with heptane, the new diamagnetic and colorless complex **3** in high yield.

[(Et_8-calix[4]tetrapyrrole)Th{$N(SiMe_3)_2$}][$Li(dme)_3$] **3**

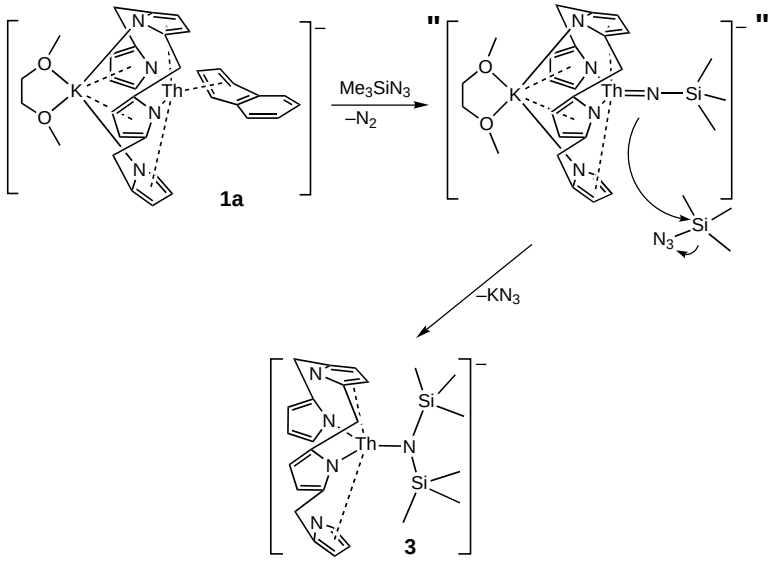

Scheme 1. Reaction of **1a** with Me_3SiN_3.

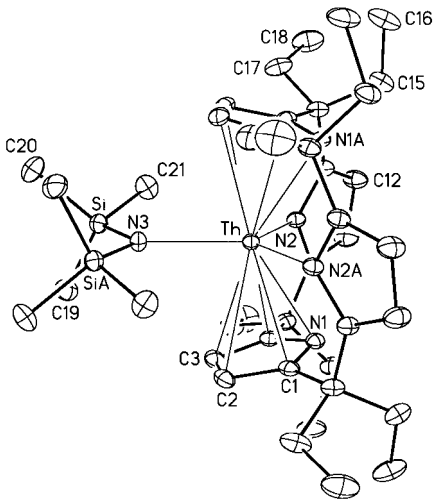

Figure 4. Thermal ellipsoid plot of the anionic moiety of **3**. Selected bond lengths [Å] and angles [°]: Th-N1 2.6640(19), Th-N2 2.4968(19), Th-N3 2.398(3), Th-C1 2.817(2), Th-C2 2.969(2), Th-C4 2.780(2); N2-Th-N2A 126.11(9), N2-Th-N3 116.94(4), Th-N3-Si 121.02(8).

The crystal structure (Figure 4) showed the ligand adopting the usual arrangement with two rings π- and two σ-bonded to the metal atom. A silazanate group is σ-bonded to the Th atom in a coplanar arrangement characteristic of metal amides. An Li atom solvated by three molecules of DME and unconnected with the Th anion completes the structure. The NMR data were in complete agreement with the crystal structure, showing two different pyrrolyl ring resonances and two sharp triplets for the eight methyl groups in accordance with their positions with respect to the silazanate group. The resonances of the methylene protons consist of four partly overlapping pseudoquadruplets coupled to only two ^{13}C NMR resonances, that is, geminal inequivalency.

The formation of **3** clearly indicates that **1a** acts as a two-electron reductant Th^{II} synthon. The first step (Scheme 1) is likely the decomposition of azide to form an imido derivative, most likely mononuclear. As usual, this process is accompanied by N_2 evolution. The final formation of **3** necessarily requires intervention of a second azide to transfer the Me_3Si group to the imide N atom and to form the silazanate group and KN_3. Further work to clarify the promising behavior of mononuclear imide derivatives is in progress.

Experimental Section

1a: In a glove box, a dark-green solution of Li(napthalene), prepared in situ by stirring Li foil (0.007 g, 1.023 mmol) and naphthalene (0.132 g, 1.030 mmol) in DME (5 mL) was rapidly added to a colorless solution of [{(Et_8-calix[4]tetrapyrrole)Th(μ-Cl)}$_2$][K(dme)]$_2$[10] (0.501 g, 0.512 mmol) in DME (7 mL). The color of the reaction mixture changed to dark brown-red, and stirring was continued at room temperature for 6 h. A small amount of insoluble material was separated by filtration. The resulting solution was concentrated to about 5 mL and layered with heptane (10 mL). After the mixture had been left

 © 2003 Wiley-VCH Verlag GmbH & Co. KGaA, Weinheim 1433-7851/03/4207-0816 $ 20.00+.50/0

to stand for two days at room temperature, the mother liquor was placed in a freezer at −37 °C. After 12 h, dark-brown prisms of **1a** separated (0.427 g, 0.328 mmol, 64 %). Elemental analysis (%) calcd for $C_{62}H_{96}N_4O_8ThLiK$: C 57.13, H 7.42, N 4.30, found: C 57.01, H 7.37, N 4.25. ^{1}H NMR (500 MHz, [D$_8$]THF): $\delta = 6.27$, 5.57 (s, each 4H, CH pyrrolyl), 1.93–1.62 (4q, overlapping, 16H, CH_2 ethyl), 0.51 (t, 24H, CH_3 ethyl), 5.96, 5.39, 4.56, 2.18 (dd, each 2H, CH naphthalene), 3.27 (s, 24H, CH_3 dme), 3.41 ppm (s, 16H, CH_2 dme); ^{13}C NMR (125.72 MHz, [D$_8$]THF): $\delta = 115.79$, 101.94 (CH pyrrole), 34.73, 32.66, 31.93, 31.09 (CH_2 ethyl), 10.01, 9.65 (CH_3 ethyl), 125.75, 119.56, 114.95, 94.42 (CH naphthalene), 59.06 (CH_3 dme), 72.94 (CH_2 dme), 149.87, 128.75, 47.86, 47.27 ppm (quaternary C).

1b: Yield 79 % at room temperature. Elemental analysis (%) calcd for $C_{50}H_{66}N_4O_2ThK_2$: C 56.37, H 6.24, N 5.26; found: C 56.01, H 6.07, N 5.15. ^{1}H NMR (500 MHz, [D$_8$]THF): $\delta = 6.31$, 5.60 (s, each 4H, CH pyrrolyl), 2.03–1.81 (4q, overlapping, 16H, CH_2 ethyl), 0.52 (2t, overlapping, 24H, CH_3 ethyl), 6.03, 5.43, 4.60, 2.20 (br s, each 2H, CH naphthalene), 3.27 (s, 6H, CH_3 dme), 3.43 ppm (s, 4H, CH_2 dme); ^{13}C NMR (125.72 MHz, [D$_8$]THF): $\delta = 116.02$, 102.23 (CH pyrrole), 34.72, 31.86, 30.91, 29.61 (CH_2 ethyl), 9.95, 9.78, 9.67, 9.51 (CH_3 ethyl), 126.65, 120.40, 115.32, 92.80 (CH naphthalene), 59.07 (CH_3 dme), 72.94 (CH_2 DME), 149.78, 128.75, 47.89, 47.21 ppm (quaternary C).

3: A dark brown-red solution of **1a** (0.400 g, 0.307 mmol) in DME (5 mL) was treated with neat $(CH_3)_3SiN_3$ (0.071 g, 0.62 mmol) dropwise at room temperature. After about 15 s vigorous gas evolution was observed, accompanied by complete decoloration of the solution. The reaction mixture was stirred at room temperature for 2 h. A small amount of colorless insoluble material was separated by filtration, and the resulting solution was concentrated to about 2 mL and layered with 8 mL of heptane. After 2 d at room temperature colorless crystals of **3** separated (0.301 g, 0.25 mmol, 81 %). Elemental analysis (%) calcd for $C_{54}H_{96}N_5O_6Si_2ThLi$: C 53.76, H 8.02, N 5.80; found: C 53.68, H 7.98, N 5.75. ^{1}H NMR (500 MHz, [D$_8$]THF): $\delta = 6.48$, 5.55 (s, each 4H, CH pyrrolyl), 2.12–1.85 (8q, overlapping, 16H, CH_2 ethyl), 0.82, 0.46 (2t, each 12H, CH_3 ethyl), 3.27 (s, 24H, CH_3 dme), 3.42 (s, 16H, CH_2 dme), 0.14 ppm (s, 18H, Me_3Si); ^{13}C NMR (125.72 MHz, [D$_8$]THF): $\delta = 116.14$, 102.95 (CH pyrrole), 30.69, 28.60 (CH_2 ethyl), 9.62, 9.86 (CH_3 ethyl), 6.38 (Me_3Si), 59.04 (CH_3 dme), 72.90 (CH_2 dme), 159.00, 151.96, 46.70 ppm (quaternary C).

Crystal data: **1a**: $C_{62}H_{96}N_4O_8ThKLi$, $M_r = 1303.51$, triclinic, $P\bar{1}$, $a = 13.1970(18)$, $b = 13.1904(18)$, $c = 18.966(3)$ Å, $\alpha = 105.855(2)$, $\beta = 94.643(2)$, $\gamma = 92.688(2)°$, $V = 32056.2(7)$ Å^3, $Z = 2$, $\rho_{calcd} = 1.351$ Mg m^{-3}. Absorption coefficient 2.444 mm^{-1}, $F(000) = 1344$, reflections collected 24688, independent reflections 14011, GOF 1.007, $R = 0.0499$, $wR_2 = 0.1132$. **1b**: $C_{50}H_{66}N_4O_2ThK_2$, $M_r = 1065.31$, orthorhombic, *Pnma*, $a = 15.6699(18)$, $b = 13.202(2)$, $c = 16.3768(19)$ Å, $V = 4927.6(10)$ Å^3, $Z = 4$, $\rho_{calcd} = 1.436$ Mg m^{-3}. Absorption coefficient 3.236 mm^{-1}, $F(000) = 2152$, reflections collected 34524, independent reflections 6198, GOF 1.030, $R = 0.0429$, $wR_2 = 0.0594$. **2**: $C_{93}H_{149}N_8O_{11}Th_2K_3$, $M_r = 2136.58$, monoclinic, $P2(1)/c$, $a = 13.5302(7)$, $b = 25.3219(13)$, $c = 30.8345(18)$ Å, $\beta = 99.350(2)°$, $V = 10423.9(10)$ Å^3, $Z = 4$, $\phi_{calcd} = 1.361$ Mg m^{-3}. Absorption coefficient 3.025 mm^{-1}, $F(000) = 4352$, reflections collected 30504, independent reflections 21644, GOF 1.040, $R = 0.0916$, $wR_2 = 0.2099$. **3**: $C_{54}H_{196}N_5O_6ThLiSi_2$, $M_r = 1206.52$, monoclinic, $C2/c$, $a = 18.503(3)$, $b = 17.592(3)$, $c = 19.194(3)$ Å, $\beta = 103.046(2)°$, $V = 6086.5(16)$ Å^3, $Z = 4$, $\phi_{calcd} = 1.317$ Mg m^{-3}. Absorption coefficient 2.536 mm^{-1}, $F(000) = 2496$, reflections collected 22358, independent reflections 7136, GOF = 1.019, $R = 0.0223$, $wR_2 = 0.0620$. CCDC-193482, -193483, -193484, and -193485 contains the supplementary crystallographic data for this paper. These data can be obtained free of charge via www.ccdc.cam.ac.uk/conts/retrieving.html (or from the Cambridge Crystallographic Data Centre, 12, Union Road, Cambridge CB2 1EZ, UK; fax: (+44) 1223-336-033; or deposit@ccdc.cam.ac.uk).

Received: September 16, 2002 [Z50163]

[1] See for example a) W. J. Evans, N. T. Allen, J. W. Ziller, *J. Am. Chem. Soc.* **2001**, *123*, 7927; b) W. J. Evans, N. T. Allen, J. W. Ziller, *Angew. Chem.* **2002**, *114*, 369; *Angew. Chem. Int. Ed.* **2002**, *41*, 359; c) W. J. Evans, L. A. Hughes, T. P. Hanusa, *Organometallics* **1986**, *5*, 1285; d) W. J. Evans, L. A. Hughes, T. P. Hanusa, *J. Am. Chem. Soc.* **1984**, *106*, 4270; e) W. J. Evans, T. A. Ulibarri, J. W. Ziller, *J. Am. Chem. Soc.* **1988**, *110*, 6877; f) W. J. Evans, D. K. Drummond, J. W. Grate, H. Zhang, J. L. Atwood, *J. Am. Chem. Soc.* **1987**, *109*, 3928; g) W. J. Evans, J. W. Grate, R. J. Doedens, *J. Am. Chem. Soc.* **1985**, *107*, 1671; h) W. J. Evans, T. A. Ulibarri, *J. Am. Chem. Soc.* **1987**, *109*, 4292; i) W. J. Evans, D. K. Drummond, *J. Am. Chem. Soc.* **1988**, *110*, 2772; j) W. J. Evans, D. K. Drummond, L. R. Chamberlain, R. J. Doedens, S. G. Bott, H. Zhang, J. L. Atwood, *J. Am. Chem. Soc.* **1988**, *110*, 4983; k) W. J. Evans, D. K. Drummond, *J. Am. Chem. Soc.* **1986**, *108*, 7440.

[2] See for example: a) W. J. Evans, J. W. Grate, L. A. Hughes, H. Zhang, J. L. Atwood, *J. Am. Chem. Soc.* **1985**, *107*, 3728; b) H. Schumann, *Angew. Chem.* **1984**, *96*, 475; *Angew. Chem. Int. Ed. Engl.* **1984**, *23*, 474; c) K. G. Wang, E. D. Stevens, S. P. Nolan, *Organometallics* **1992**, *11*, 1011; d) W. J. Evans, D. K. Drummond, S. G. Bott, J. L. Atwood, *Organometallics* **1986**, *5*, 2389; e) W. J. Evans, D. K. Drummond, *J. Am. Chem. Soc.* **1989**, *111*, 3329; f) T. Dubé, J. Guan, S. Gambarotta, G. P. A. Yap, *Chem. Eur. J.* **2001**, *7*, 374; g) T. Dubé, S. Gambarotta, G. P. A. Yap, *Organometallics* **2000**, *19*, 817; h) T. Dubé, S. Gambarotta, G. P. A. Yap, *Organometallics* **2000**, *19*, 121; i) J. Guan, T. Dubé, S. Gambarotta, G. P. A. Yap, *Organometallics* **2000**, *19*, 4820; j) J. Jubb, S. Gambarotta, *J. Am. Chem. Soc.* **1994**, *116*, 4477; k) T. Dubé, S. Gambarotta, G. P. A. Yap, *Angew. Chem.* **1999**, *111*, 1507; *Angew. Chem. Int. Ed.* **1999**, *38*, 1432; l) T. Dubé, S. Conoci, S. Gambarotta, G. P. A. Yap, G. Vasapollo, *Angew. Chem.* **1999**, *111*, 3890; *Angew. Chem. Int. Ed.* **1999**, *38*, 3657; m) T. Dubé, S. Conoci, S. Gambarotta, G. P. A. Yap, *Organometallics* **2000**, *19*, 3716; n) M. Ganesan, M. P. Lalonde, S, Gambarotta, G. P. A. Yap, *Organometallics* **2001**, *20*, 2443.

[3] See for example F. T. Edelmann in *Comprehensive Organometallic Chemistry*, 2nd ed. (Eds.: E. W. Abel, F. G. A. Stone, G. Wilkinson), Pergamon, Oxford, **1995**.

[4] a) H. P. Beck, H. Schuster, *Z. Anorg. Allg. Chem.* **1993**, *619*, 690; b) S. G. Bratsch, J. J. Lagowski, *J. Phys. Chem.* **1986**, *90*, 307.

[5] L. J. Guggenberger, R. A. Jacobson, *Inorg. Chem.* **1968**, *7*, 2257.

[6] The term "synthon" was forged by Corey and used to define "a structural unit within a molecule related to a possible synthetic operation". In coordination and organometallic chemistry, it can be also attributed to molecules that behave as synthetic equivalents of species that unlikely exist. a) P. Diaconescu, P. L. Arnold, T. Baker, D. Mindiola, C. C. Cummins, *J. Am. Chem. Soc.* **2000**, *122*, 6108; b) B. P. Warner, B. L. Scott, C. J. Burns, *Angew. Chem.* **1998**, *110*, 1005; *Angew. Chem. Int. Ed.* **1998**, *37*, 959; c) P. J. Fagan, J. M. Manriquez, T. J. Marks, C. S. Day, S. H. Vollmer, V. W. Day, *Organometallics* **1982**, *1*, 170.

[7] I. Khorobkov, S. Gambarotta, G. P. A. Yap, *Angew. Chem.* **2002**, *114*, 3583; *Angew. Chem. Int. Ed.* **2002**, *41*, 3433.

[8] a) J. S. Parry, G. F. N. Cloke, S. J. Cole, M. B. Hursthouse, *J. Am. Chem. Soc.* **1999**, *121*, 6867, and references therein; b) B. Kannellakopulos, E. Dornberger, F. Baumgaertner, *Inorg. Nucl. Chem. Lett.* **1974**, *10*, 155; c) P. C. Blake, M. F. Lappert, J. L. Atwood, H. Zhang, *J. Chem. Soc. Chem. Commun.* **1986**, 1148; d) M. R. Spirlet, J. Rebizant, J. Goffart, *Acta Crystallogr. Sect. B* **1982**, *38*, 2400.

[9] a) D. M. M. Freckmann, T. Dubé, C. D. Bérubé, S. Gambarotta, G. P. A. Yap, *Organometallics* **2002**, *21*, 1240; b) M. Ganesan, S. Gambarotta, G. P. A. Yap, *Angew. Chem.* **2001**, *113*, 766; *Angew. Chem. Int. Ed.* **2001**, *40*, 788; c) T. Dube, D. M. M. Freckmann, S.

Conoci, S. Gambarotta, G. P. A. Yap, *Organometallics* **2000**, *19*, 209.
[10] I. Khorobkov, S. Gambarotta, G. P. A. Yap, unpublished results.
[11] See for example: a) I. Korobkov, S. Gambarotta, G. P. A. Yap, *Organometallics* **2001**, *20*, 2552; b) I. Korobkov, G. Aharonian, S. Gambarotta, G. P. A. Yap, *Organometallics*, in press.
[12] F. A. Cotton, *Inorg. Chem.* **2002**, *41*, 643.
[13] a) M. D. Fryzuk, L. Jafarpour, F. M. Kerton, J. B. Love, S. J. Rettig, *Angew. Chem.* **2000**, *112*, 783; *Angew. Chem. Int. Ed.* **2000**, *39*, 767; b) M. M. Bocharev, *Chem. Rev.* **2002**, *102*, 2089.
[14] a) G. Erker, T. Mühlenbernd, R. Benn, A. Rufinska, *Organometallics* **1986**, *5*, 402; b) G. M. Smith, H. Suzuki, D. C. Sonnenberger, V. W. Day, T. J. Marks, *Organometallics* **1986**, *5*, 549.

 © 2003 Wiley-VCH Verlag GmbH & Co. KGaA, Weinheim 1433-7851/03/4207-0818 $ 20.00+.50/0

Spiroannulation of THP Rings

Spiroannulation by Alkylation and Reductive Cyclization of Nitriles**

Scott D. Rychnovsky and Leo R. Takaoka*

Annulation reactions occupy a central role in synthetic chemistry. Alkyllithium cyclizations onto alkenes or other electrophiles have been studied by a number of groups,[1] but have only rarely been applied to complex synthetic targets because of the limitations of the reaction.[2] In particular, unactivated alkene cyclizations work well only with terminal alkenes to form five-membered rings. A related S_N2' cyclization onto allylic alkoxy groups shows broader scope.[1b,3] Synthesis of the cyclization precursor also can be tedious. We report a new approach to alkyllithium cyclizations that takes advantage of the unique reactivity of nitriles. Nitriles can be alkylated efficiently to introduce functionalized alkyl chains. Tertiary nitriles can be reductively cleaved to form alkyllithium reagents[4] that cyclize in the presence of an internal electrophile. The combination of an alkylation and reductive cyclization results in a facile and unusual annulation reaction. Herein we describe the development of this strategy for the spiroannulation of tetrahydropyran rings, including an example in which two adjacent quaternary centers are formed with complete stereoselectivity.

Our interest in this spiroannulation strategy was piqued by a surprisingly facile alkyllithium cyclization onto a tethered alkene.[5] A diastereoselective version of this cyclization is outlined in Scheme 1. The 2-cyanotetrahydropyran **2** was prepared by reductive acetylation[6] of δ-decanolactone followed by treatment with trimethylsilyl cyanide (TMSCN) and a Lewis acid. Alkylation with 5-iodo-1-pentene produced the cyclization precursor **3**. In each of the alkylations of **2** reported herein, the selectivity was $>99{:}1$ in favor of the axial nitrile. Addition of **3** to excess lithium di-*tert*-butylbiphenylide (LiDBB)[7] in THF at $-78\,^{\circ}C$ and warming immediately to $-42\,^{\circ}C$ led to cyclization of the alkyllithium intermediate **4**. Trapping the alkyllithium product with CO_2 and working up the reaction with CH_2N_2 produced the spirocyclic ester **5** as a single diastereomer in 75% yield. The configuration of the quaternary center was assigned by NOE measurements. The configuration of the other new center was assigned by correlation with alkene **9** (vide infra). Reductive decyanation generated an axial lithium reagent,[4] that cyclized onto the alkene with retention of configuration.[8] The alkyllithium cyclized onto only one face of the alkene and led to a single diastereomer with the alkyllithium chain *cis* to the tetrahydropyran (THP) oxygen atom. This annulation reaction was carried out in two steps from cyanotetrahydropyran **2** and introduced two new stereogenic centers with high selectivity.

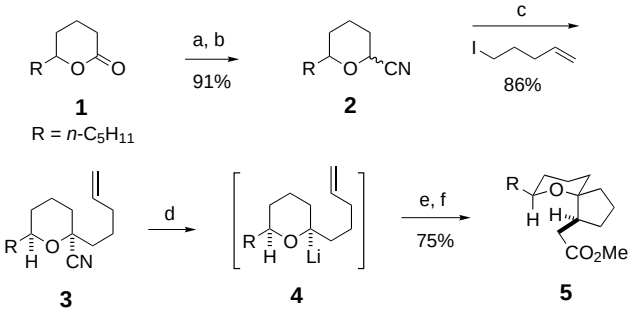

Scheme 1. Reagents and conditions: a) 1. DIBAL-H, $-78\,^{\circ}C$; 2. Ac_2O, DMAP, pyridine; b) TMSCN, $BF_3{\cdot}OEt_2$; c) LDA, $-40\,^{\circ}C$, THF, DMPU then iodide; d) add to excess LiDBB in THF, $-78\,^{\circ}C$, then warm to $-42\,^{\circ}C$; e) add CO_2 gas; f) CH_2N_2. DIBAL-H = diisobutylaluminum hydride.

We investigated the spirocyclization of a THP alkyllithium reagent with a TMS-alkyne and the results are shown in Scheme 2. Bailey and co-workers have shown that alkyllithium reagents cyclize efficiently onto alkynes with a net *cis* RLi addition across the alkyne.[9] The precursor for our study was prepared by alkylation of nitrile **2**. Reductive cyclization at $-40\,^{\circ}C$ delivered the spirocycle **7** in 58% yield, accompanied by reductive decyanation and alkyne reduction side products. The alkene geometry was determined by NOE measurements and was consistent with the precedent from Bailey and coworkers.

Allylic methoxyalkenes will participate as electrophiles in S_N2' alkyllithium cyclizations.[1b,3] They are more reactive than simple alkenes and have been used to form both five- and six-membered rings. The reductive cyclization of methoxyalkene substrates is illustrated in Scheme 3. The methoxyalkene side

[*] S. D. Rychnovsky, L. R. Takaoka
Department of Chemistry
University of California, Irvine
516 Rowland Hall, Irvine, CA 92697-2025 (USA)
Fax: (+1) 949-824-6379
E-mail: srychnov@uci.edu

[**] This work was supported by the National Institute of General Medical Sciences (GM-65338).

Supporting information for this article is available on the WWW under http://www.angewandte.org or from the author.

 © 2003 Wiley-VCH Verlag GmbH & Co. KGaA, Weinheim 1433-7851/03/4207-0818 $ 20.00+.50/0

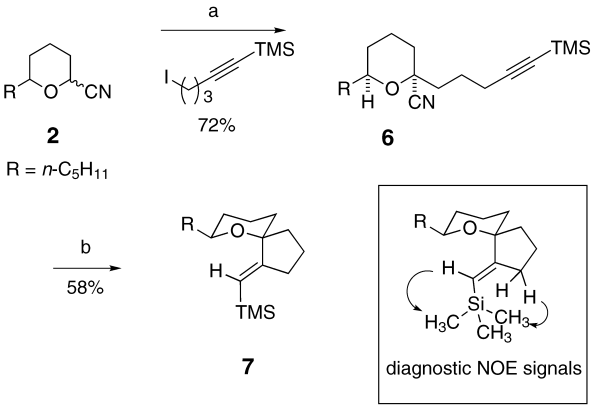

Scheme 2. Reagents and conditions: a) LDA, −40 °C, THF, DMPU then iodide; b) add to excess LiDBB in THF, −40 °C, 20 min, and then quench with MeOH. DMPU = *N*,*N*-dimethylpropyleneurea.

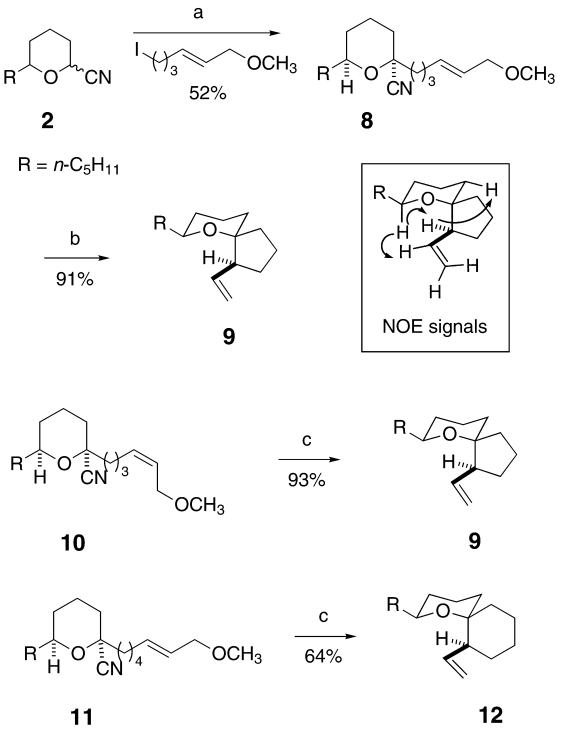

Scheme 3. Reagents and conditions: a) LDA, −40 °C, THF, DMPU then iodide; b) add to excess LiDBB in THF, −78 °C, 20 min, and then quench with MeOH; c) add to excess LiDBB in THF, −42 °C, 60 min, and then quench with MeOH.

chains were introduced by alkylation of cyanotetrahydropyran **2**. Cyclization of the *E* alkene **8** took place on addition to excess LiDBB at −78 °C. Spirocycle **9** was isolated in 91% yield as a single diastereomer. Its configuration was assigned by NOE experiments. The structure of ester **5** was confirmed by correlation with alkene **9**.[10] The *Z* alkene **10** was prepared by alkylation of **2** in 76% yield. Reductive cyclization gave moderate yields at −78 °C, but conducting the cyclization at −42 °C for 60 min led to an excellent yield of same spirocycle **9**. None of the diastereomeric product with the alkene *trans* to the oxygen atom was detected in the cyclization of either the *E* or *Z* alkene. The substrate for the six-membered ring cyclization, (*E*)-**11**, was prepared by alkylation of **2** in 77% yield. Reductive cyclization of **12** once again required the more forcing conditions to proceed efficiently. At −42 °C the cyclization gave **12** as a single isomer in 64% yield. The corresponding *Z* alkene (not shown) did not cyclize efficiently under these conditions. Cyclizations with methoxyalkenes produce both five- and six-membered rings efficiently and with excellent diastereoselectivity.

Reductive cyclization onto a trisubstituted alkene has the potential to form two adjacent quaternary centers, a challenging problem for synthetic chemists. We investigated this possibility with the methoxyalkene substrate **14** (Scheme 4).

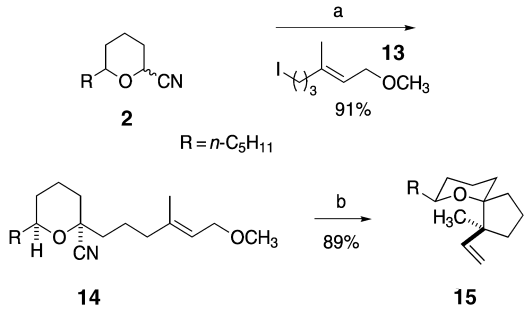

Scheme 4. Reagents and conditions: a) LDA, −40 °C, THF, DMPU then iodide **13**; b) add to excess LiDBB in THF, −40 °C, 60 min, and then quench with MeOH.

Once again, the cyclization substrate was prepared by alkylation of nitrile **2** with iodide **13**. Addition of nitrile **14** to excess LiDBB at −40 °C in THF produced spirocycle **15** in 89% yield as a single diastereomer after workup. The configuration of **15** was assigned by NOE measurements.[11] The alkene ends up *cis* to the oxygen atom as was found with the methoxyalkene cyclizations in Scheme 3. This surprisingly efficient cyclization generates two new quaternary stereocenters with complete stereoselectivity.

Electrophiles that reduce more slowly than nitriles would be expected to cyclize in the reductive decyanation reaction. Grierson and co-workers reported the reductive cyclization of an aminonitrile phosphate using potassium and [18]crown-6.[12] Several cyclizations with halide and phosphate electrophiles are shown in Scheme 5. The cyclization substrates **16, 18**, and **19** were prepared by alkylation of nitrile **2** with alkyl iodides. Chloronitrile **16** cyclizes very efficiently on addition to excess LiDBB in THF at −78 °C. Formation of the spirocycle **17** demonstrates that the cyanohydrin functional group is reduced more rapidly than an alkyl chloride. Reductive cyclization of cyanophosphate **18** was even more efficient and led to a nearly quantitative yield of **17**. Formation of the six-membered ring **20** was problematic. Addition of **19** to excess LiDBB gave a mixture of spirocycle **20** and reduced product **21** in a 66:34 ratio. Spirocycle **20** was isolated in 41% yield. Attempts to improve the ratio by varying temperature, order of addition, and equivalents of LiDBB were unsuccessful. Cyclization of the phosphate corresponding to **19** led to reductive decyanation and

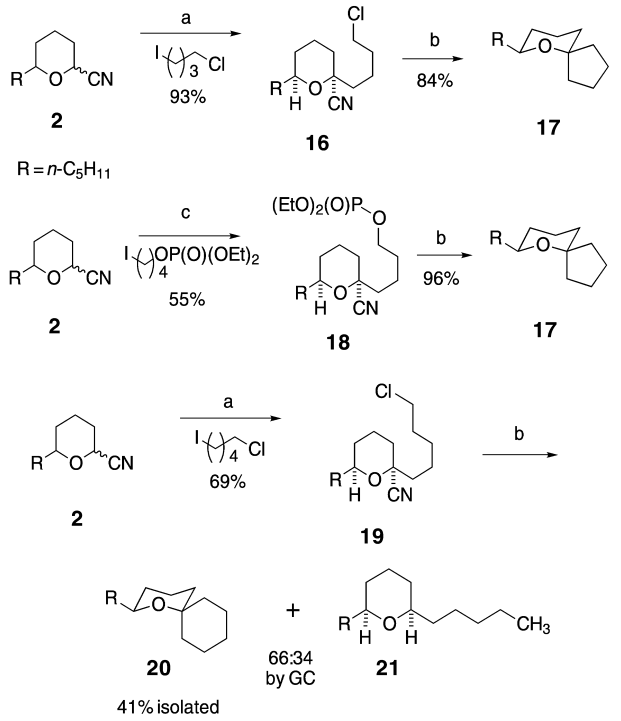

Scheme 5. Reagents and conditions: a) LDA, −40 °C, THF, DMPU then iodide; b) add to excess LiDBB in THF, −78 °C, 20–30 min, and then quench with MeOH; c) LDA, −40 °C, THF, then iodide.

essentially no cyclization. These spiroannulations are very efficient for the five-membered ring cases but produce six-membered rings with modest yields.

For each of the alkene cyclizations we found that the diastereomer with the alkyl chain *cis* to the THP oxygen atom was formed exclusively.[5] We have previously shown that these reductive decyanation cyclizations take place through an anionic cyclization rather than a radical cyclization.[5] Bailey, Wiberg, and co-workers proposed a model for the cyclization of alkyllithium reagents based on computational modeling.[1d] We have adapted their model to the cyclization of alkyllithium **4**; the competing cyclization transition states are **22**, with the alkene *cis* to the oxygen atom, and **24**, with the alkene *trans* to the oxygen atom. We propose that **22** should

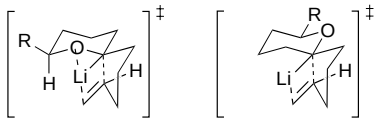

22 **24**

be favored over **24** because it allows continuous coordination of the Li atom with the oxygen atom, whereas cyclization to the disfavored *trans* product requires that the strong Li–O dative bond be lost along the reaction coordinate. The same *cis* selectivity was observed with alkene cyclizations and methoxyalkene S_N2' cyclizations. The *cis* alkene–oxygen selectivity is a dependable feature of these cyclizations and the Li–O dative bond is a plausible rationale for this selectivity.

We have shown that spirocyclic rings are easily prepared from 2-cyanotetrahydropyrans. The key feature of this method is the use of a nitrile to facilitate alkylation and as a precursor to an alkyllithium reagent. The two-step sequence, alkylation and reductive cyclization, is successful with a variety of biselectrophiles, generates five- and six-membered rings, and is highly stereoselective. The axial alkyllithium reacts with retention of configuration, leading to axial attack of the internal electrophile. Alkene cyclizations strongly favor products with the alkene *cis* to the THP ring oxygen atom. This strategy even can be used to produce adjacent quaternary centers with excellent selectivity. We expect this reductive cyclization methodology to be a powerful new tool in organic synthesis.

Received: September 19, 2002 [Z50194]

[1] a) D. G. Farnum, T. Monego, *Tetrahedron Lett.* **1983**, *24,* 1361–1364; b) W. F. Bailey, T. T. Nurmi, J. J. Patricia, W. Wang, *J. Am. Chem. Soc.* **1987**, *109,* 2442–2448; c) A. R. Chamberlin, S. H. Bloom, L. A. Cervini, C. H. Fotsch, *J. Am. Chem. Soc.* **1988**, *110,* 4788–4796; d) W. F. Bailey, A. D. Khanolkar, K. Gavaskar, T. V. Ovaska, K. Rossi, Y. Thiel, K. B. Wiberg, *J. Am. Chem. Soc.* **1991**, *113,* 5720–5727; e) W. F. Bailey, A. D. Khanolkar, K. V. Gavaskar, *J. Am. Chem. Soc.* **1992**, *114,* 8053–8060; f) W. F. Bailey, M. W. Carson, *J. Org. Chem.* **1998**, *63,* 361–365; g) A. Deiters, D. Hoppe, *J. Org. Chem.* **2001**, *66,* 2842–2849; h) W. F. Bailey, M. J. Mealy, *J. Am. Chem. Soc.* **2000**, *122,* 6787–6788; i) M. J. Mealy, W. F. Bailey, *J. Organomet. Chem.* **2002**, *646,* 59–67.

[2] a) W. F. Bailey, X.-L. Jiang, C. E. McLeod, *J. Org. Chem.* **1995**, *60,* 7791–7795; b) W. F. Bailey, X.-L. Jiang, *J. Org. Chem.* **1996**, *61,* 2596–2597; c) E. Coldham, R. Hufton, D. J. Snowden, *J. Am. Chem. Soc.* **1996**, *118,* 5322–5323; d) A. Deiters, D. Hoppe, *Angew. Chem.* **1999**, *111,* 529–532; *Angew. Chem. Int. Ed.* **1999**, *38,* 546–548.

[3] a) C. A. Broka, W. J. Lee, T. Shen, *J. Org. Chem.* **1988**, *53,* 1336–1338; b) C. A. Broka, T. Shen, *J. Am. Chem. Soc.* **1989**, *111,* 2981–2984; c) A. E. Harms, J. R. Stille, S. K. Taylor, *Organometallics* **1994**, *13,* 1456–1464.

[4] S. D. Rychnovsky, J. P. Powers, T. J. Lepage, *J. Am. Chem. Soc.* **1992**, *114,* 8375–8384.

[5] S. D. Rychnovsky, T. Hata, A. I. Kim, A. J. Buckmelter, *Org. Lett.* **2001**, *3,* 807–810.

[6] D. J. Kopecky, S. D. Rychnovsky, *J. Org. Chem.* **2000**, *65,* 191–198.

[7] P. K. Freeman, L. L. Hutchinson, *J. Org. Chem.* **1980**, *45,* 1924–1930.

[8] K. Tomooka, N. Komine, T. Nakai, *Tetrahedron Lett.* **1997**, *38,* 8939–8942.

[9] a) W. F. Bailey, T. V. Ovaska, T. K. Leipert, *Tetrahedron Lett.* **1989**, *30,* 3901–3904; b) W. F. Bailey, T. V. Ovaska, *J. Am. Chem. Soc.* **1993**, *115,* 3080–3090; c) W. F. Bailey, N. M. Wachter-Jurcsak, M. R. Pineau, T. V. Ovaska, R. R. Warren, C. E. Lewis, *J. Org. Chem.* **1996**, *61,* 8216–8228.

[10] Alkene **9** was converted to ester **5** and shown to be identical by ^{1}H NMR, ^{13}C NMR, and HRMS. Conditions: a) 1. 9-borabicyclo[3.3.1]nonane (9-BBN); 2. NaOH, H_2O_2; b) 2,2,6,6-tetramethyl-1-piperidinyloxy (TEMPO), NaOCl, $NaClO_2$; c) CH_2N_2.

[11] See Supporting Information.

[12] a) E. Zeller, H. Sajus, D. S. Grierson, *Synlett* **1991**, 44–46; b) E. Zeller, D. S. Grierson, *Synlett* **1991**, 878–880.

 © 2003 Wiley-VCH Verlag GmbH & Co. KGaA, Weinheim 1433-7851/03/4207-0820 $ 20.00+.50/0

Carboxylation of Methane

Single-Pot Conversion of Methane into Acetic Acid in the Absence of CO and with Vanadium Catalysts Such as Amavadine**

Patrícia M. Reis, José A. L. Silva, António F. Palavra, João J. R. Fraústo da Silva, Tsugio Kitamura, Yuzo Fujiwara, and Armando J. L. Pombeiro**

Despite current interest in the biological roles of vanadium, its application in catalysis is still an underdeveloped field of research.[1] We have already reported that amavadine, a natural vanadium complex present in some *Amanita* fungi and whose biological function is still unknown, can exhibit haloperoxidase- and peroxidase-type activities and act as a catalyst for the oxidation of some biological thiols,[2] as well as for the peroxidative halogenation, hydroxylation, and oxo-functionalization of alkanes and aromatic compounds.[3] Following this work, we have been searching for other reactions that could be catalyzed by this and related V complexes, in particular the conversion of methane—the main component of natural gas and the most abundant and least reactive alkane—into functionalized products with added commercial value.[4] Recently attention has focused on the metal-catalyzed transformation of CH_4 and CO into acetic acid,[5–11] as well as the formation of carbonylated products without requiring the use of noxious CO, such as the conversion of CH_4 into methyl esters[12] and into acetic acid (and methanol).[9] The latter, the reaction of CH_4 and CO_2 catalyzed by $NaVO_3$/pyrazine-2-carboxylic acid (in the presence of H_2O_2 in aqueous solution), occurs in very low yield based on CH_4 (ca. 0.01 %) and at a considerable pressure (50 bar) of this gas, although at low temperature (40 °C).[9] The reaction also proceeds with CO, which apparently is the carbonylating agent even when CO_2 is used (CO is then formed by reduction of CO_2 by methyl and/or hydroxyl radicals).[9] We now report the unprecedented (to our knowledge) conversion of CH_4 into CH_3COOH in the absence of either CO or CO_2, in a novel single-pot catalytic reaction [Eq. (1)] under considerably mild conditions and in high yields.

$$CH_4 \xrightarrow[K_2S_2O_8,\ CF_3COOH]{\text{V cat.}} CH_3COOH \qquad (1)$$

[*] Prof. J. J. R. Fraústo da Silva, Prof. A. J. L. Pombeiro, P. M. Reis, Dr. J. A. L. Silva, Prof. A. F. Palavra
Centro de Química Estrutural, Complexo I
Instituto Superior Técnico
Av. Rovisco Pais, 1049-001 Lisboa (Portugal)
Fax: (+351) 21-846-4455
E-mail: pcd1950@popsrv.ist.utl.pt
pombeiro@ist.utl.pt
Prof. T. Kitamura, Prof. Y. Fujiwara
Department of Chemistry and Biochemistry
Graduate School of Engineering
Kyushu University, Fukuoka, 812-8581 (Japan)

[**] This work was supported in part by the Fundação para a Ciência e a Tecnologia (FCT) and the POCTI Programme, Portugal.

The catalytic systems are based on a V^{IV} or V^{V} complex with poly- or bidentate N,O or O,O ligands in the presence of the peroxodisulfate salt $K_2S_2O_8$ as the oxidizing agent and in trifluoroacetic acid as the solvent. The V catalysts include: oxovanadium(v) complexes **1** and **2** of the type [VO(*N,O*-L)];

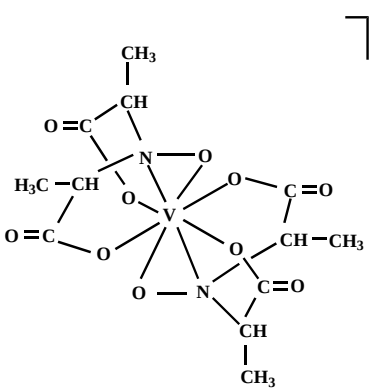

3

synthetic amavadine **3** and its model **4**, which are Ca^{2+} salts of V^{IV} complexes with N,O ligands; and V^{IV} vanadyl complexes **5–9** of the type [VO(*O,O*-L)$_2$]. Turnover numbers (TONs, moles of acetic acid per mol of metal catalyst) and yields (based on methane) are given in Table 1, and typical conditions include conducting the reaction in CF_3COOH at 80 °C with molar ratios of CH_4:V catalyst and $K_2S_2O_8$:V catalyst of 46:1 (corresponding to CH_4 pressure of 5 atm) and 200:1, respectively. Usually the yields were determined after a reaction time of 20 h, but often much shorter times were sufficient to attain close values (see entries 1 and 11 for yields obtained after 2 h; the former is 92 % of that in entry 2 obtained after 20 h).

$[VO(N(CH_2CH_2O)_3)]$ **1**

$[VO(N(CH_2CH_2O)_2(CH_2COO)]$ **2**

$Ca[V(ON(CH(CH_3)COO)_2)_2]$ **3**

$Ca[V(ON(CH_2COO)_2)_2]$ **4**

$[VO(maltolate)_2]$ **5**
(maltolate = basic form of 3-hydroxy-2-methyl-4-pyrone)

$[VO(HOCH_2CH_2N(CH_2CO_2)_2)]$ **6**

$[VO(CF_3COO)_2]$ **7**

$[VO(CF_3SO_3)_2]$ **8**

$VOSO_4$ **9**

The most active catalysts, which can give yields over 50 % and TONs close to 30, are complex **1** within the type [VO(*N,O*-L)], both amavadine (**3**) and its model **4** of the [V(*N,O*-L) salts, and complexes **5, 7**, and **8** of the type [VO(*O,O*-L)$_2$]. In contrast **2, 6**, and **9** exhibit much lower

 © 2003 Wiley-VCH Verlag GmbH & Co. KGaA, Weinheim 1433-7851/03/4207-0821 $ 20.00+.50/0

Table 1: Conversion of methane into acetic acid.[a]

Entry	Cat.	$p(CH_4)$ [atm][b]	$p(CO)$ [atm][b]	t [h]	TON[c]	Yield [%][d]
1	**1**	5	–	2	9.2	19.7
2	**1**	5	–	20	10.0	21.4
3	**1**	5	5	20	10.9	23.5
4	**1**	5	15	20	10.4	22.2
5	**1**	3	15	20	5.1	18.5
6	**1**	8	15	20	24.7	33.7
7	**1**	12	15	20	28.2	25.6
8[e]	**1**	5	15	20	10.4	35.3
9[f]	**1**	5	5	20	3.9	42.7
10	**2**	5	–	20	2.2	4.8
11	**3**	5	–	2	7.0	15.3
12	**3**	5	–	20	13.4	29.4
13	**3**	5	5	20	9.7	21.2
14	**3**	5	15	20	8.1	17.3
15[g]	**3**	5	15	20	12.0	54.3
16	**4**	5	–	20	9.6	20.9
17	**4**	5	15	20	9.6	20.6
18	**4**	12	15	20	27.9	25.4
19[h]	**4**	5	15	20	5.4	24.5
20	**5**	5	–	20	6.8	14.9
21	**5**	5	15	20	8.2	17.6
22	**6**	5	–	20	2.0	4.5
23	**7**	5	–	20	1.8	3.8
24	**7**	5	5	20	10.5	23.0
25	**7**	5	20	20	8.8	19.0
26	**8**	5	–	20	6.7	14.6
27	**8**	5	5	20	10.1	22.1
28	**8**	5	20	20	12.1	29.0
29	**9**	5	–	20	1.0	2.2
30	**9**	5	20	20	2.3	5.0

[a] Reaction conditions (unless stated otherwise): metal complex catalyst (0.0625 mmol), $K_2S_2O_8$ (12.5 mmol, i.e. 200:1 molar ratio of $K_2S_2O_8$ to metal catalyst), CF_3COOH (23 mL), 80 °C, in an autoclave (39-mL capacity). Amounts of CH_4 or CO gas correspond to 0.572 mol atm^{-1}, with pressure measured at 25 °C; for example, 2.86 and 8.58 mmol gas for pressures of 5 and 15 atm, respectively. The catalyst complexes were prepared according to the literature: **1**,[14] **3**,[15] **4**,[15] **5**,[16] **8**.[17] New complexes **2, 6**, and **7** were prepared by processes similar to those for **1**, of[18], and for **8**, respectively, but with the appropriate ligand. $VOSO_4$, CF_3COOH, and $K_2S_2O_8$ were purchased from Merck or Aldrich.
[b] Measured at 25 °C. [c] Turnover number (moles of acetic acid per mol of metal catalyst) determined by GLC or GC-MS; the reaction mixture, with an internal standard, was filtered to remove the ionic species and the metal complex, diethyl ether was added (which leads to further precipitation), and the reaction mixture was filtered again. [d] Molar yield [%] based on CH_4, i.e. moles of acetic acid per 100 moles of methane. [e] Less CH_4 was used (1.84 mmol) than in the conditions described in footnote [a] by using a higher volume of CF_3COOH (28 mL). [f] Five times more metal catalyst (0.312 mmol) was used. [g] Less CH_4 was used (1.02 mmol) than in the conditions described in footnote [a] by using a smaller reactor (23.5 mL): metal catalyst (0.046 mmol), $K_2S_2O_8$ (9.2 mmol i.e. 200:1 molar ratio of $K_2S_2O_8$ to metal catalyst), CF_3COOH (17 mL). [h] Less CH_4 was used (1.02 mmol) than in the conditions described in footnote [a] by using a higher volume of CF_3COOH (32 mL).

activities. Of the oxo-V complexes with aminoalcohol ligands (basic forms), **1** is the most active, whereas the activity decreases on replacement of alcoholato by carboxylato groups; that is, **2** and **6** are less active than **1** (Table 1, entries 10, 22, 2). The active species, at least for the [VO(*N,O*-L)] and [V(*N,O*-L)]$^{2-}$ types, are believed to have the metal in the +5 oxidation state (the starting blue V^{IV} complexes **3** and **4** are oxidized by $K_2S_2O_8$ to the respective red V^{V} forms).

Interestingly, the carboxylation of CH_4 does not require CO. With amavadine (**3**) and its model **4**, as well as with complex **1**, yields of acetic acid within the 20–30% range (TON ca. 10–13) are commonly obtained under standard conditions (entries 12, 16, and 2). CH_4 is the carbon source for the methyl group of acetic acid as we demonstrated by using ^{13}C-labeled CH_4. The product, $^{13}CH_3COOH$, was determined by the $^{13}C\{^1H\}$ and ^{13}C NMR spectra of the reaction solution. The carbon source of the carboxylic acid group, in the absence of CO, is CF_3COOH, which is known[4d] to undergo radical reactions with $K_2S_2O_8$ derivatives to form, for example, CO_2. However, our reactions do not appear to proceed via a free CO_2 intermediate or free CH_3OH, since the former does not promote the carboxylation and the latter is not converted into the acid under our experimental conditions.

Although the mechanistic details are still unknown, the carboxylation of methane may possibly involve the formation of the methyl radical and the derived methyl cation (upon hydrogen abstraction from CH_4 followed by oxidation, for example, by a V^{V}-oxo or V^{V}-peroxo species) which would react[12] with CF_3COOH. The role of the chelating N,O and O,O ligands still remains unclear, but one can postulate their involvement (upon decoordination of a single N or O atom of the ligand) in proton-transfer steps, for example, among oxo- or hydroxo-V species and CF_3COOH or $K_2S_2O_8$ (which, acting as an oxidant, can give[12] HSO_4^- and $HSO_4^{\bullet}$). A related role in promoting proton transfer from coordinated H_2O_2 to oxo ligands has been suggested[13] for some vanadium systems such as nBu$_4$NVO$_3$/H_2O_2/O_2, whose activity towards alkane oxygenation requires[9,13] particular N,O additives as cocatalysts (e.g. heteroaromatic aminocarboxylic acids like pyrazine-2-carboxylic acid). Moreover, in amavadine (**3**) and its model **4**, the hydroxyimino(1−) groups of the ligands, η^2-(O-N<)$^-$, are isoelectronic with peroxo(2−), and their possible behavior as peroxo-like ligands also deserves consideration.

The formation of CH_3COOH from CH_4 can be enhanced by the presence of CO at sufficiently low pressures, which suggests that CO can behave as a carboxylating agent, as was clearly observed for **7** (Table 1, entries 23–25) and **8** (entries 26–28). For **1** this enhancing effect is very small (Figure 1), whereas for **3** and **4** (entries 12–14 and 16, 17) it was not detected at all. Moreover, higher CO pressures often result in an inhibiting effect (Figure 1 for **1** and entries 23–25 for **7**), conceivably because ligation of CO lowers the activity of the catalyst; we are investigating this possibility.

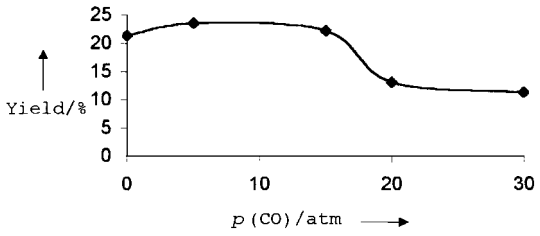

Figure 1. Effect of CO pressure on the yield of acetic acid derived from methane (at 5 atm) by using catalyst **1** and $K_2S_2O_8$ in CF_3COOH (see Table 1).

 © 2003 Wiley-VCH Verlag GmbH & Co. KGaA, Weinheim 1433-7851/03/4207-0822 $ 20.00+.50/0

The increase of CH_4 pressure (up to 12 atm in our work) can have a notorious enhancing effect on the TONs (entries 5–7 and 17, 18), whereas the yield tends to decrease after reaching a maximum (entries 5–7). Higher yields can be obtained when less CH_4 is used but at the same pressure (e.g., entry 8 vs. 4 and entry 15 vs. 14), or when more metal catalyst is employed (entry 9 vs. 3).

The reaction does not occur in the absence of $K_2S_2O_8$, CF_3COOH (which is replaced by ethanol or water as the solvent), or the V catalyst. Related complexes with other metals, even of the same periodic group, display little or no catalytic activity. The carboxylation by CO is also strongly hampered when acetonitrile is used instead of CF_3COOH.

This direct one-pot synthesis of CH_3COOH from CH_4 without required CO is a process whose simplicity and low energy requirements contrast with the features of the industrial route.[4e] The established synthesis involves three separate stages: the metal-catalyzed high-temperature steam-reforming of CH_4, conversion of the derived synthesis gas to CH_3OH, and final carboxylation of CH_3OH with CO and either an expensive Rh catalyst (Monsanto process) or an Ir catalyst (BP–Amoco modified process). The route we now report has also the advantage of requiring a cheap V catalyst, but we are still searching for less expensive solvents, carboxylating agents, and oxidants. The V catalysts used in this work are also effective in the carboxylation of other alkanes apart from CH_4 to give the corresponding carboxylic acids, and the study of these catalytic reactions is underway. Of particular interest is the behavior of amavadine, whose catalytic activity is now extended to such interesting reactions. Can they take place in natural conditions and also be of biological significance?

Received: September 24, 2002 [Z50224]

[1] a) J. J. R. Fraústo da Silva, R. J. P. Williams, *The Biological Chemistry of the Elements*, 2nd ed., Clarendon Press, Oxford, **2001**; b) "Vanadium Compounds": *ACS Symp. Ser.* **1998**, *711*; c) D. Rehder, *Coord. Chem. Rev.* **1999**, *182*, 297.

[2] a) C. M. M. Matoso, A. J. L. Pombeiro, J. J. R. Fraústo da Silva, M. F. C. G. da Silva, J. A. L. Silva, J. L. Baptista-Ferreira, F. Pinho-Almeida, *ACS Symp. Ser.* **1998**, *711*, 241–247; b) M. F. C. G. da Silva, J. A. L. Silva, J. J. R. Fraústo da Silva, A. J. L. Pombeiro, C. Amatore, J.-N. Verpeaux, *J. Am. Chem. Soc.* **1996**, *118*, 7568.

[3] P. M. Reis, J. A. L. Silva, J. J. R. Fráusto da Silva, A. J. L. Pombeiro, *Chem. Commun.* **2000**, 1845.

[4] a) C. Jia, T. Kitamura, Y. Fujiwara, *Acc. Chem. Res.* **2001**, *34*, 633; b) R. H. Crabtree, *J. Chem. Soc. Dalton Trans.* **2001**, 2437; c) A. E. Shilov, G. B. Shul'pin, *Chem. Rev.* **1997**, *97*, 2879; d) Y. Fujiwara, K. Takaki, Y. Taniguchi, *Synlett* **1996**, 591; e) *Catalytic Activation and Functionalisation of Light Alkanes* (Eds.: E. G. Derouane, J. Haber, F. Lemos, F. R. Ribeiro, M. Guisnet), Kluwer, Dordrecht, **1998**; e) R. H. Crabtree, *The Organometallic Chemistry of the Transition Metals*, Wiley, New York, **2001**, chap. 12.

[5] Y. Taniguchi, T. Hayashida, H. Shibasaki, D.-G. Piao, T. Kitamura, T. Yamaji, Y. Fujiwara, *Org. Lett.* **1999**, *1*, 557.

[6] a) T. Nishiguchi, K. Nakata, K. Takaki, Y. Fujiwara, *Chem. Lett.* **1992**, 1141; b) M. Asadullah, Y. Taniguchi, T. Kitamura, Y. Fujiwara, *Appl. Catal. A* **2000**, *194–195*, 443.

[7] a) M. Asadullah, T. Kitamura, Y. Fujiwara, *Angew. Chem.* **2000**, *112*, 2609; *Angew. Chem. Int. Ed.* **2000**, *39*, 2475; b) M. Asadullah, T. Kitamura, Y. Fujiwara, *Appl. Organomet. Chem.* **1999**, *13*, 539.

[8] M. Asadullah, T. Kitamura, Y. Fujiwara, *Chem. Lett.* **1999**, 449.

[9] G. V. Nizova, G. Süss-Fink, S. Stanislas, G. B. Shul'pin, *Chem. Commun.* **1998**, 1885.

[10] a) M. Lin, A. Sen, *Nature* **1994**, *368*, 613; b) M. Lin, A. Sen, *J. Chem. Soc. Chem. Commun.* **1992**, 892.

[11] A. Bagno, J. Bukala, G. A. Olah, *J. Org. Chem.* **1990**, *55*, 4284.

[12] a) D.-G. Piao, K. Inoue, H. Shibasaki, Y. Taniguchi, T. Kitamura, Y. Fujiwara, *J. Organomet. Chem.* **1999**, *574*, 116; b) G. Yin, D.-G. Piao, T. Kitamura, Y. Fujiwara, *Appl. Organomet. Chem.* **2000**, *14*, 438.

[13] a) G. B. Shul'pin, *J. Mol. Catal. A* **2002**, *189*, 39; b) G. B. Shul'pin, Y. N. Kozlov, G. V. Nizova, G. Süss-Fink, S. Stanislas, A. Kitaygorodskiy, V. S. Kulikova, *J. Chem. Soc. Perkin Trans. 2* **2001**, 1351.

[14] D. C. Crans, H. Chen, O. P. Anderson, M. M. Miller, *J. Am. Chem. Soc.* **1993**, *115*, 6769.

[15] R. E. Berry, E. M. Armstrong, R. L. Beddoes, D. Collison, S. N. Ertok, M. Helliwell, C. D. Garner, *Angew. Chem.* **1999**, *111*, 871; *Angew. Chem. Int. Ed.* **1999**, *38*, 795.

[16] P. Caravan, L. Gelmini, N. Glover, F. G. Herring, H. Li, J. H. McNeill, S. J. Rettig, I. A. Setyawati, E. Shuter, Y. Sun, A. S. Tracey, V. G. Yuen, C. Orvig, *J. Am. Chem. Soc.* **1995**, *117*, 12759.

[17] C. T. Chen, J. H. Kuo, C. H. Li, N. B. Barhate, S. W. Hon, T. W. Li, S. D. Chao, C. C. Liu, Y. C. Li, I. H. Chang, J. S. Lin, C. J. Liu, Y. C. Chou, *Org. Lett.* **2001**, *3*, 3729.

[18] B. J. Hamstra, A. L. P. Houseman, G. J. Colpas, J. W. Kampf, R. LoBrutto, W. D. Frasch, V. L. Pecoraro, *Inorg. Chem.* **1997**, *36*, 4866.

Low-Field NMR is Back

Real-Time Chemical-Shift Scaling in High-Resolution NMR Spectroscopy

Gareth A. Morris, Neil P. Jerome, and Lu-Yun Lian*

Superconducting magnets have brought many blessings to NMR spectroscopy, but these are not entirely unmixed. Problems arise particularly with systems undergoing chemical exchange, since linewidth is proportional to the square of the field strength in the fast exchange limit; here, lower-field spectra can show both higher sensitivity and higher resolution. Unfortunately, relatively few laboratories now have

[*] Prof. G. A. Morris, N. P. Jerome
Department of Chemistry
University of Manchester
Oxford Road, Manchester M13 9PL (UK)
Fax: (+44) 161-275-4598
E-mail: g.a.morris@man.ac.uk
Prof. L.-Y. Lian
Department of Biomolecular Sciences
UMIST
P.O. Box 88, Manchester M60 1QD (UK)

 © 2003 Wiley-VCH Verlag GmbH & Co. KGaA, Weinheim 1433-7851/03/4207-0823 $ 20.00+.50/0

access to low-field NMR instrumentation. A new technique, real-time chemical-shift scaling (δ scaling) is proposed which causes the apparent chemical-shift to be scaled down during signal acquisition, allowing the effects of chemical exchange and scalar coupling on spectra to be controlled.

The selective scaling of NMR parameters such as chemical shifts and scalar and dipolar couplings has been exploited extensively in solid-state NMR spectroscopy.[1] Applications to high-resolution NMR spectroscopy have been more limited, although scaling has been used with success in indirect (parameter time) dimensions in multidimensional NMR spectroscopy.[2] Heteronuclear J scaling in high-resolution NMR spectroscopy has been carried out in parameter time[3,4] and in real time,[5] but since its first proposal[6] and one subsequent refinement,[7] only a single application of real-time δ scaling in high-resolution NMR spectroscopy appears to have been reported.[8] Paradoxically, this last report made no use of the scaling effect, rather exploiting the sensitivity to imperfections of the pulse sequence to achieve spatial localization. A special case of real-time δ scaling, refocussed acquisition, has however been used in the past to improve sensitivity in parameter time experiments for J scaling[3] and for the spectroscopy of systems with inhomogeneously broadened signals,[9] and recently in multiple-quantum NMR spectroscopy.[10]

A new approach to real-time δ scaling is proposed here, based on repeated refocussing[3] rather than phase-alternated pulses of variable flip angle.[6,7] Figure 1 shows one practical

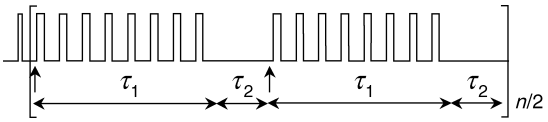

Figure 1. Prototype pulse sequence for the measurement of a spectrum with δ scaling. Narrow boxes indicate 90°, broad boxes 180° pulses; vertical arrows indicate acquisition of one complex data point. The phases of successive 180° pulses follow the *XY*-16 supercycle $x,y,x,y,y,x,y,x,-x,-y,-x,-y,-y,-x,-y,-x$, with a total of n complex points being acquired.

realization. The signal elicited by a simple 90° pulse is repeatedly refocussed by alternate sequences of 180° pulses forming the two *XY*-8 subcycles of an *XY*-16 supercycle,[11] with one complex data point measured at the end of the precession delay τ_2 following each subcycle. *XY*-16 refocussing has previously been used successfully for chemical-shift suppression ($\lambda = 0$) in the INEPT[12] sections of two-dimensional ^{15}N-correlated NOESY experiments,[13] and there is an interesting parallel in the use of windowed acquisition during DIPSI-2 heteronuclear Hartmann–Hahn transfer by Luy and Glaser.[14] Many other configurations of refocussing blocks, phase sequences, precession intervals and data sampling are possible. The average effect of the chemical shift is scaled down by a factor $\lambda = \tau_2/(\tau_1 + \tau_2)$ for shifts within the spectral window. The use of a phase sequence such as *XY*-16 is essential if the cumulative effect of pulse imperfections is not to result in the rapid attenuation of any transverse magnetization components orthogonal to the radiofrequency pulse axis. The phase sequence is remarkably effective; even with conventional hardware, signals survive several thousand refocussing steps, allowing high resolution to be achieved. All experiments were carried out using a Varian INOVA 400 spectrometer with no relevant hardware modifications. A 5 mm broadband probe with pulsed field gradient inverse geometry was used, with a 90° pulse width of 5 μs.

Figure 2 shows the scaling of a typical high-resolution proton spectrum using the sequence of Figure 1. A clean straightforward scaling of the chemical shifts is achieved; as

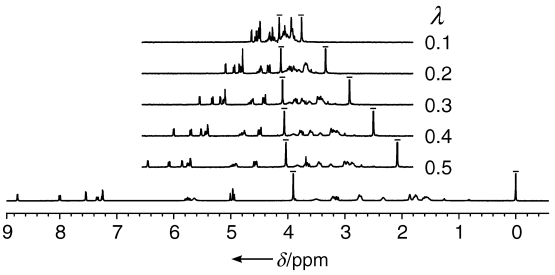

Figure 2. 400 MHz proton NMR spectra of quinine in $CDCl_3$, acquired using (bottom) a single 90° pulse, and (remainder) the sequence of Figure 1 with different scaling factors λ.

expected, the relative signal intensities change as the spin systems become more strongly coupled. Figure 3 illustrates the potential of δ scaling for manipulating the spectra of dynamic systems. The result of applying the pulse sequence of Figure 1 with different scaling factors λ to a simple two-site proton-exchange system (CD_3OH and HDO) which is in the

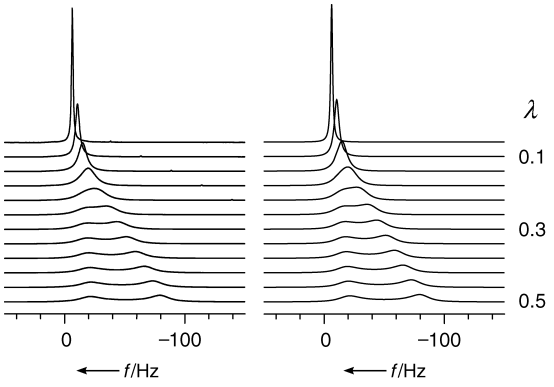

Figure 3. Left: 400 MHz proton NMR spectra of a solution of H_2O in CD_3OD at 40 °C, measured with the sequence of Figure 1. Right: spectra calculated for this spin system with chemical shifts scaled down by the factor λ.

slow-exchange regime under normal conditions ($\lambda = 1$) is compared with the behavior expected from theory.[15] As λ decreases, the system first shows coalescence, then moves into the fast exchange limit, with the peak intensity increasing as the inverse square of the scaling factor. δ scaling is also of potential use in the analysis of spin systems, where it is unclear whether a particular splitting is caused by chemical shift or

 © 2003 Wiley-VCH Verlag GmbH & Co. KGaA, Weinheim 1433-7851/03/4207-0824 $ 20.00+.50/0

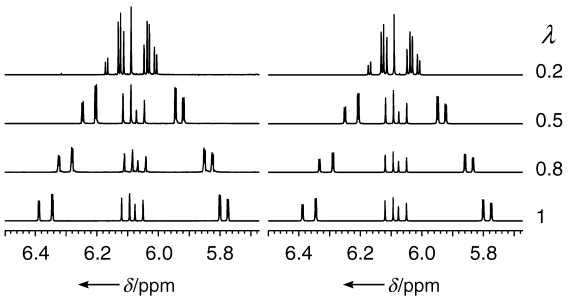

Figure 4. Left: 400 MHz proton NMR spectra of a solution of methyl acrylate in $CDCl_3$, measured with the sequence of Figure 1 (top three spectra) and with a single 90° pulse (bottom spectrum). Right: spectra calculated for this spin system with chemical shifts scaled down by the factor λ and unchanged coupling constants.

homonuclear coupling, or where the relative signs of coupling constants are required. Figure 4 shows scaled spectra for a simple three-spin system, methyl acrylate, comparing theory and experiment.

Real-time δ scaling gives the experimenter considerable freedom to control the apparent chemical-shift scale of a spectrum while retaining close to the full sensitivity of a high-field instrument; the principal drawback is the high radio-frequency power required. The method presented here appears both efficient and much more robust than preceding methods, and is relatively easy to implement on modern spectrometers. Potential applications include the scaling of spectra to improve the sensitivity of signals lost through exchange broadening, the investigation of chemical exchange processes, distinguishing between homogeneous and inhomogeneous broadening, and the analysis of spin systems. Complete scaling ($\lambda = 0$) may be used to reduce by one the dimensionality of multidimensional experiments where proton chemical-shift resolution is either impossible (e.g. because of inhomogeneous broadening in heterogeneous samples) or unnecessary (as for example in some applications of multiple-quantum NMR spectroscopy), while retaining high sensitivity; the use of *XY*-16 or similar phase sequences greatly improves the efficacy of such techniques.

Particularly promising is the application to biomolecules such as proteins. Chemical-shift heterogeneity in biological systems can arise from conformational exchange (e.g. exchange between free and complexed forms), proteins containing flexible or conformationally dynamic regions, and exchange between folded and unfolded forms. Often the exchange is on the microsecond to millisecond timescale, causing a modulation of the isotropic chemical shifts and leading to deterioration of the NMR spectrum. In many cases, resonances from important protein residues are not detectable, ironically rendering the NMR method unsuitable for obtaining the very type of structural and dynamic information that NMR spectroscopy can best provide. Hence, ways need to be found to recover the missing resonances. δ scaling, possibly combined with parameter-time scaling, should be able to restore sensitivity even in cases of severe broadening.

Received: October 7, 2002 [Z50305]

[1] M. Mehring, *High Resolution NMR in Solids*, Springer, New York, **1983**, chap. 3.
[2] R. V. Hosur, *Prog. Nucl. Magn. Reson. Spectrosc.* **1990**, *22*, 1 – 53.
[3] R. Freeman, G. A. Morris, *J. Magn. Reson.* **1978**, *29*, 173 – 176.
[4] G. A. Morris, R. Freeman, *J. Am. Chem. Soc.* **1978**, *100*, 6763 – 6764.
[5] a) W. P. Aue, R. R. Ernst, *J. Magn. Reson.* **1978**, *31*, 533 – 538; b) W. P. Aue, D. P. Burum, R. R. Ernst, *J. Magn. Reson.* **1980**, *38*, 375 – 380; c) G. A. Morris, G. L. Nayler, A. J. Shaka, J. Keeler, R. Freeman, *J. Magn. Reson.* **1984**, *58*, 155 – 160; d) A. J. Shaka, J. Keeler, R. Freeman, G. A. Morris, G. L. Nayler, *J. Magn. Reson.* **1984**, *58*, 161 – 166.
[6] J. D. Ellett, J. S. Waugh, *J. Chem. Phys.* **1969**, *51*, 2851 – 2858.
[7] J. A. DiVerdi, S. J. Opella, *J. Chem. Phys.* **1982**, *75*, 5594 – 5595.
[8] M. Nuss, E. T. Olejniczak, *J. Magn. Reson.* **1986**, *69*, 542 – 545.
[9] G. A. Morris, A. Gibbs, *J. Magn. Reson.* **1988**, *78*, 594 – 596.
[10] K. H. Lim, T. Nguyen, T. Mazur, D. E. Wemmer, A. Pines, *J. Magn. Reson.* **2002**, *157*, 160 – 162.
[11] T. Gullion, D. B. Baker, M. S. Conradi, *J. Magn. Reson.* **1990**, *89*, 479 – 484.
[12] G. A. Morris, R. Freeman, *J. Am. Chem. Soc.* **1979**, *101*, 760 – 762; G. A. Morris, *J. Am. Chem. Soc.* **1980**, *102*, 428 – 429.
[13] L. Mueller, P. Legault, A. Pardi, *J. Am. Chem. Soc.* **1995**, *117*, 11 043 – 11 048.
[14] B. Luy, S. J. Glaser, *J. Magn. Reson.* **1999**, *138*, 187 – 190.
[15] J. Sandström, *Dynamic NMR Spectroscopy*, Academic Press, London, **1982**, chap. 2.

 © 2003 Wiley-VCH Verlag GmbH & Co. KGaA, Weinheim 1433-7851/03/4207-0825 $ 20.00+.50/0

C–C Coupling

From Alkenylsilanes to Ketones with Air as the Oxidant**

Junichi Kondo, Hiroshi Shinokubo, and Koichiro Oshima**

The Tamao–Kumada–Fleming oxidation is not only a fundamental transformation of organosilicon compounds but also a method of great importance for the synthesis of alcohols.[1] This oxidation typically exploits hydrogen peroxide as the oxidant. On the other hand, oxidative cleavage of silicon–-

[*] Dr. H. Shinokubo, Prof. Dr. K. Oshima, J. Kondo
Department of Material Chemistry
Graduate School of Engineering
Kyoto University
Yoshida, Sakyo-ku, Kyoto 606–8501 (Japan)
Fax: (+81) 75-753-4863
E-mail: shino@fm1.kuic.kyoto-u.ac.jp
oshima@fm1.kuic.kyoto-u.ac.jp

[**] This work was supported by a Grant-in-Aid for Scientific Research (No. 14703026) from the Ministry of Education, Culture, Sports, Science, and Technology, Japan. We thank Prof. Tamejiro Hiyama for helpful discussions.

Supporting information for this article is available on the WWW under http://www.angewandte.org or from the author.

 © 2003 Wiley-VCH Verlag GmbH & Co. KGaA, Weinheim 1433-7851/03/4207-0825 $ 20.00+.50/0

carbon bonds with molecular oxygen has not been well investigated.[2] We have recently reported a synthesis of acylsilanes through aerobic oxidation of 1,1-disilylalkylcopper compounds.[3] We then envisaged that a silyl hydroperoxide **1**—generated from a carbon-centered radical and molecular oxygen[4]—would yield a carbonyl compound (Scheme 1). If this were the case, this oxidation of a Si–C

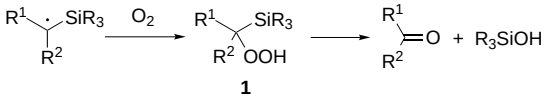

Scheme 1. Formation of carbonyl compounds from silyl hydroperoxides.

bond could be combined with a variety of radical processes. Herein we wish to report what amounts effectively to the oxidative cleavage of a Si–C bond with air. A tandem radical addition–oxidation sequence which converts alkenylsilanes into ketones is also described.

At the outset of this research, we examined the reaction of α-silylalkyl iodides **3** with a radical mediator in air (Scheme 2). The iodide **3a** employed can be easily prepared

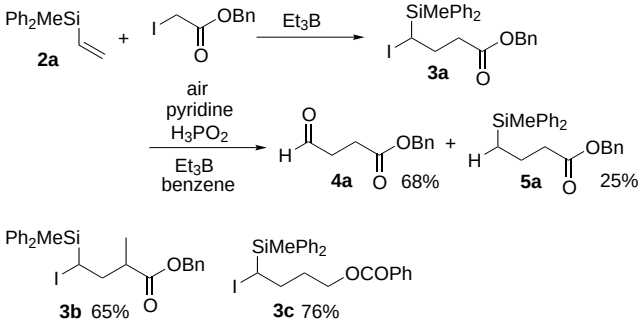

Scheme 2. Aldehyde formation from α-iodosilanes.

from vinylsilane **2a** in an iodine-atom-transfer radical reaction.[5] To a mixture of iodide **3a**, H_3PO_2,[6] and pyridine in benzene, a solution of Et_3B[7] (3.0 equiv) in hexane was added in five portions at intervals of 1 h at room temperature. To our delight, aldehyde **4a** was obtained in 68% yield after purification. The use of **3b** or **3c** as the iodide also furnished the corresponding aldehydes in good yields. Phosphinic acid as the radical chain carrier is a crucial component: tris(trimethylsilyl)silane instead of phosphinic acid provided the reduction product **5a** exclusively. The choice of the silyl group in **3** is also important, and the reaction of a trimethylsilyl analog of **3a** provided aldehyde **4a** in only 49% yield along with **5a** in 35% yield.

We next turned our attention toward the synthesis of ketones from alkenylsilanes. In the preparation of the starting alkyl iodide **3d**[8] through an iodine-atom transfer reaction with 2-silylpropene **2b**, we came across the formation of methyl ketone **4d** as a byproduct (22% yield, Scheme 3). Obviously, ketone **4d** is nothing but the desired product in the

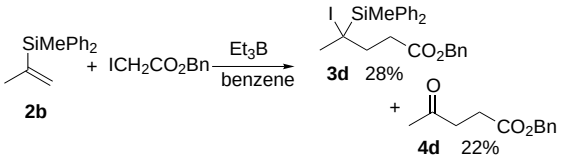

Scheme 3. Formation of a methyl ketone.

oxidation of **3d** in air. Consequently, we then focused on a tandem radical addition–oxidation reaction with 2-silyl-1-alkenes. The use of an excess amount of triethylborane (2.0 equiv) in air afforded methyl ketone **4d** as the major product. After several experiments, we found that water is an excellent solvent to provide **4d** in 80% yield (see Table 1, entry 1).[9,10] The addition of ammonium chloride is important as without it, the yield of **4d** lowered to 62%, and vinylsilane **2b** was recovered in 11%.

Table 1 summarizes the results of the tandem radical addition–oxidation reactions of Scheme 4. This process can convert vinylsilanes into α-substituted ketones in one step.[11]

Table 1: Synthesis of carbonyl compounds according to Scheme 4.[a]

Entry	R^1	R^2I	Product		Yield [%]
1	Me (**2b**)	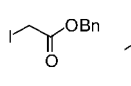	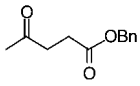	**4d**	80
2	Me (**2b**)	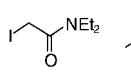	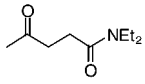	**4e**	51[b]
3	Ph (**2c**)	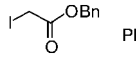	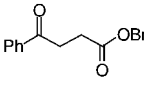	**4f**	77
4	Ph (**2c**)	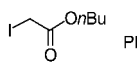	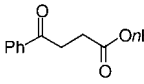	**4g**	74
5	Ph (**2c**)	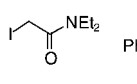	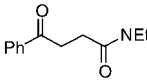	**4h**	60
6	Ph (**2c**)	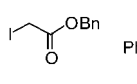	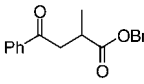	**4i**	40
7	Ph (**2c**)	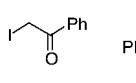	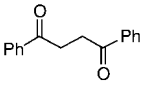	**4j**	84[b]
8	Ph (**2c**)	$C_6F_{13}I$	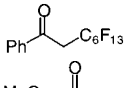	**4k**	81
9	CO_2Me (**2d**)	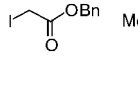	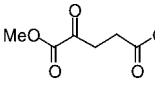	**4l**	61
10	$PhMe_2Si$ (**2e**)	$C_6F_{13}I$	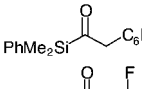	**4m**	64[b,c]
			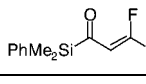	**4n**	58[d]

[a] Reaction conditions: alkenylsilane **2** (0.5 mmol), iodide (0.75 mmol), H_2O (5 mL), NH_4Cl (15 mmol), Et_3B (5×0.2 mmol), air atmosphere, room temperature (RT), 5 h. [b] Iodide (1.5 mmol) and Et_3B (5×0.4 mmol) were employed. [c] Yield determined by NMR spectroscopy with dibenzyl ether as the internal standard. [d] Yield after purification over a silica gel column.

 © 2003 Wiley-VCH Verlag GmbH & Co. KGaA, Weinheim 1433-7851/03/4207-0826 $ 20.00+.50/0

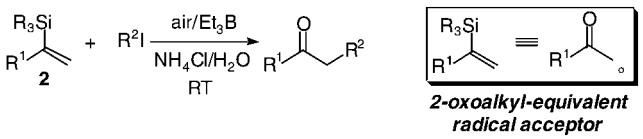

Scheme 4. Synthesis of carbonyl compounds from alkenylsilanes **2** as 2-oxoalkyl-equivalent radical acceptors. **2b,c,d**: $R_3Si = Ph_2MeSi$, **2e**: $R_3Si = Me_2PhSi$. For details see Table 1.

One can hence regard vinylsilanes as a 2-oxoalkyl-equivalent radical acceptor. Several characteristics of this process are noteworthy: 1) The reaction of α-silylstyrene **2c** also afforded the desired ketones in good yields. 2) The reaction can employ iodo ketones as a radical source (entry 7). However, concurrent reduction of the iodo ketone via a water-unstable boron enolate occurred,[12] and the use of excess iodo ketone (3.0 equiv) was required. 3) The reaction allows efficient introduction of a perfluoroalkyl group at the α position of ketones (entries 8 and 10). 4) Direct oxidation of the iodide can lower the yield of ketone (entry 6; the undesired oxidation product is 2-hydroxypropionate).[4b] 5) Acylsilanes can be prepared from 1,1-disilylethene **2e**. The product **4m** was converted into α,β-unsaturated acylsilane **4n** during purification over silica gel (entry 10). 6) In all cases, silanol was obtained as a byproduct.

We propose the reaction pathway for the sequential radical addition–oxidation reaction as illustrated in Scheme 5. Addition of a radical **6** to alkenylsilane **2** provides an α-silyl radical **7**, which then reacts with oxygen to afford peroxy

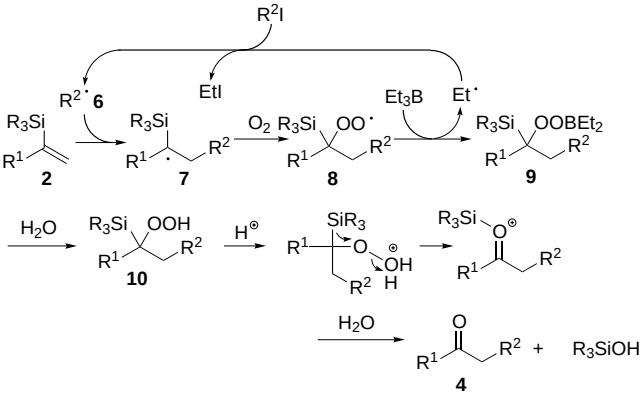

Scheme 5. Proposed reaction pathway for the sequential radical addition–oxidation reaction studied.

radical **8**. The reaction of radical **8** with Et_3B furnishes peroxyborane **9**. Hydroperoxide **10**, derived from the peroxyborane by hydrolysis, is eventually converted into the carbonyl product **4** through migration of the silyl group to the internal oxygen atom.[13] The ethyl radical which results from reaction **8**→**9** regenerates an alkyl radical from R^2I.

In conclusion, we have achieved the synthesis of aldehydes and ketones from alkenylsilanes under radical conditions with air as the oxidant. A tandem intermolecular radical addition–oxidation sequence can convert vinylsilanes into ketones in good yields. This process demonstrates novel utility of vinylsilanes in organic synthesis. Further research on the oxidation of organosilicon compounds with molecular oxygen is currently under way in our laboratory.

Received: October 10, 2002 [Z50337]

[1] a) I. Fleming, *Chemtracts: Org. Chem.* **1996**, *9*, 1; b) K. Tamao, N. Ishida, Y. Ito, M. Kumada, *Org. Synth. Col. Vol.* **1993**, *8*, 315.

[2] K. Kato, T. Mukaiyama, *Chem. Lett.* **1989**, 2233.

[3] A. Inoue, J. Kondo, H. Shinokubo, K. Oshima, *J. Am. Chem. Soc.* **2001**, *123*, 11109.

[4] For the reaction of carbon-centered radicals with molecular oxygen, see: a) C. Ollivier, P. Renaud in *Radicals in Organic Synthesis, Vol. 2* (Eds.: P. Renaud, M. P. Sibi), Wiley-VCH, Weinheim, **2001**, p. 93; b) N. Kihara, C. Ollivier, P. Renaud, *Org. Lett.* **1999**, *1*, 1419, and references therein.

[5] For reviews on atom-transfer radical reactions, see: J. Byers in *Radicals in Organic Synthesis, Vol. 1* (Eds.: P. Renaud, M. P. Sibi), Wiley-VCH, Weinheim, **2001**, p. 72.

[6] For the use of phosphinic acid as a radical chain carrier, see: a) D. H. R. Barton, D. O. Jang, J. C. Jaszberenyi, *J. Org. Chem.* **1993**, *58*, 6838; b) R. McCague, R. G. Pritchard, R. J. Stoodley, D. S. Williamson, *Chem. Commun.* **1998**, 2691; c) S. R. Graham, J. A. Murphy, D. Coates, *Tetrahedron Lett.* **1999**, *40*, 2414; d) H. Tokuyama, T. Yamashita, M. T. Reding, Y. Kaburagi, T. Fukuyama, *J. Am. Chem. Soc.* **1999**, *121*, 3791; e) M. T. Reding, T. Fukuyama, *Org. Lett.* **1999**, *1*, 973; f) C. G. Martin, J. A. Murphy, C. R. Smith, *Tetrahedron Lett.* **2000**, *41*, 1833; g) D. O. Jang, S. H. Song, *Tetrahedron Lett.* **2000**, *41*, 247; h) H. Yorimitsu, H. Shinokubo, K. Oshima, *Bull. Chem. Soc. Jpn.* **2001**, *74*, 225; i) H. Yorimitsu, H. Shinokubo, K. Oshima, *Chem. Lett.* **2000**, 104.

[7] For reviews on Et_3B as a radical initiator, see: a) C. Ollivier, P. Renaud, *Chem. Rev.* **2001**, *101*, 3415; b) H. Yorimitsu, K. Oshima in *Radicals in Organic Synthesis, Vol. 1* (Eds.: P. Renaud, M. P. Sibi), Wiley-VCH, Weinheim, **2001**, p. 11.

[8] α-Iodosilane **3d** is stable in water at room temperature. None of the hydrolyzed alcohol could be detected.

[9] **Caution**: The addition of Et_3B in methanol to an aqueous mixture in air may be flammable. Accordingly, the solution of Et_3B was introduced under argon atmosphere, and then the reaction flask was connected to a balloon filled with air. See Supporting Information.

[10] For radical reactions in aqueous media, see: H. Yorimitsu, H. Shinokubo, K. Oshima, *Synlett* **2002**, 674.

[11] Unfortunately, the reaction with 1-substituted vinylsilanes was unsuccessful. No addition reaction proceeded. The reaction with **2a** in the one-pot procedure mainly provided α-silylalkyl iodides **3**.

[12] For the formation of boron enolates from α-iodo ketones, see: a) K. Nozaki, K. Oshima, K. Utimoto, *Tetrahedron Lett.* **1988**, *29*, 1041; b) K. Nozaki, K. Oshima, K. Utimoto, *Bull. Chem. Soc. Jpn.* **1991**, *64*, 403.

[13] We carried out DFT calculations on the migration of the silyl group of a silylated hydroperoxide. See ref. [3].

 © 2003 Wiley-VCH Verlag GmbH & Co. KGaA, Weinheim 1433-7851/03/4207-0827 $ 20.00+.50/0

Organocatalytic Cyclopropanation

Organic-Catalyst-Mediated Cyclopropanation Reaction**

*Charles D. Papageorgiou, Steven V. Ley, and Matthew J. Gaunt**

Cyclopropane units are a fundamental class of functional group that are the focus of many organic synthesis programs and perform a key structural role in a range of bioactive natural and nonnatural molecules.[1] The importance of cyclopropanes is reflected in the enormous effort that has been invested in their diastereo- and enantioselective synthesis.[1,2]

Recently, a strong emphasis has been placed on the development of catalytic methods to generate cyclopropanes. While there have been significant advances in the development of catalytic versions of the Simmons–Smith and carbene transfer reactions, there are few reports of catalytic methods based on the reaction of ylides with electron-deficient alkenes.[2] The use of ylides as cyclopropanation reagents dates back to work by Corey et al.[3] Of the many developments that have since been reported, the contributions from the groups of Hanessian,[4] Dai and Tang,[5] and Aggarwal[6] deserve special mention. In these processes, however, the ylide precursor is usually generated in a separate step and there is only one reported process that is catalytic in the ylide species.[6,7]

We were interested in utilizing a nitrogen ylide to effect a cyclopropanation reaction. Surprisingly, there are relatively few examples that employ nitrogen-derived ylides.[8,9] An ammonium ylide based reaction becomes an attractive target for a general diastereo- and enantioselective cyclopropanation process owing to the vast range of tertiary amines that are commercially available. In this communication we describe the development of a stoichiometric "one-pot" ammonium ylide based cyclopropanation process and our initial studies towards an enantioselective reaction. We also report the development of the first catalytic cyclopropanation reaction involving ammonium ylides where the catalyst is a tertiary amine.

We began our study by investigating the reactivity of preformed quaternary ammonium salts such as **1** as nitrogen ylide precursors. Treatment of salt **1** with base followed by *tert*-butyl acrylate (**2a**) formed cyclopropane **3a** in varying yields depending on the conditions employed; the best results are highlighted in Table 1. Of crucial importance was the temperature, with little or no reaction observed at room temperature. However, at 80 °C the reaction produced the highest yield of *trans*-disubstituted cyclopropane. It is important to note that the corresponding reaction between phenacyl chloride (instead of salt **1**) and acrylate **2a** does not form the cyclopropane.[10]

Table 1: Optimization of reaction conditions.[a]

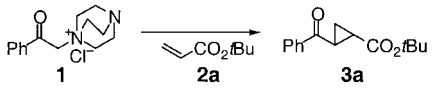

1 2a 3a

Solvent	Base	*t* [h]	Yield[b]	d.r. (*trans*:*cis*)[c]
MeCN	**NaOH**	**6**	**96%**	**>95:5**
THF	NaOH	3.5	66%	15:1
DCE	NaOH	19	73%	>95:5
DMSO	NaOH	1.5	54%	>95:5
CH_2Cl_2[d]	NaOH	4.5	65%	>95:5
MeCN	KOH	4.5	68%	15:1
MeCN	**Na_2CO_3**	**25**	**79%**	**>95:5**
MeCN	**DBU**	**16**	**87%**	**>95:5**
MeCN	DABCO[e]	24	5%	>95:5
MeCN	Et_3N	24	10%	>95:5

[a] Salt **1**, acrylate **2a** (1 equiv), base (2 equiv), solvent (0.25 M), 80 °C (oil bath temperature). [b] Yield of isolated product after chromatography. [c] Determined by ^{1}H NMR spectroscopy. [d] Reaction stirred at 45 °C. [e] 2.5 equiv of DABCO was used. DABCO = 1,4-diazobicyclo[2.2.2]octane, DCE = 1,2-dichloroethane, DBU = 1,8-diazabicyclo[5.4.0]undec-7-ene.

To increase the efficiency of this process we investigated the development of a stoichiometric "one-pot" cyclopropanation reaction, in which the ammonium salt and hence the ylide could be generated in situ from readily available starting materials. Accordingly, DABCO (**5**) was added to phenacyl chloride (**4**) in acetonitrile followed by the base and alkene **2a**, and the reaction mixture was stirred at 80 °C. After 18 h, cyclopropane **3a** was isolated in 79% yield after chromatography as a single diastereoisomer (Scheme 1).[11] It is noteworthy that the reaction proceeds without the formation of byproducts, and simple aqueous workup affords pure cyclopropane (^{1}H NMR spectroscopy, LCMS) that does not necessarily require further purification.

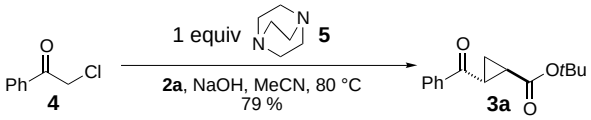

Scheme 1. One-pot cyclopropanation.

A stoichiometric "one-pot" cyclopropanation reaction offers significant advantages over other similar methods as it precludes the necessity to generate and isolate the ylide precursor (**1**) in a separate step. The general utility of this

[*] Dr. M. J. Gaunt, C. D. Papageorgiou, Prof. Dr. S. V. Ley
University Chemical Laboratory
Lensfield Road, Cambridge, CB2 1EW (UK)
Fax: (+44) 1223-336-442
E-mail: mjg32@cam.ac.uk

[**] We gratefully acknowledge financial support from the EPSRC and Pfizer Global Research and Development (Sandwich, UK) for Industrial Case Award (to C.D.P.), the Novartis Research Fellowship (to S.V.L.), and the British Ramsay Memorial Trust and Magdalene College for Research Fellowship (to M.J.G.). We also thank Dr. A. J. Morrison for helpful advice and discussion.

Supporting information for this article is available on the WWW under http://www.angewandte.org or from the author.

 © 2003 Wiley-VCH Verlag GmbH & Co. KGaA, Weinheim 1433-7851/03/4207-0828 $ 20.00+.50/0

Table 2: Scope of reaction.

Entry	α-Chloro-carbonyl	Acceptor	Conditions[a]	Yield[b]	Product	d.r. (*trans*:*cis*)[c]
1	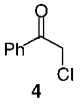 **4**	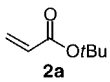 **2a**	NaOH, MeCN	79%	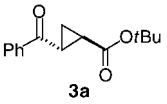 **3a**	>95:5
2	**4**	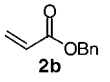 **2b**	Na_2CO_3, MeCN	77%	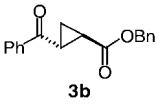 **3b**	>95:5
3	**4**	**2c**	Na_2CO_3, MeCN	96%	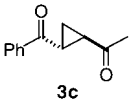 **3c**	>95:5
4	**4**	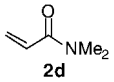 **2d**	NaOH, THF	73%	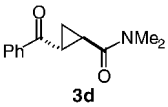 **3d**	>95:5
5	**4**	**2e**	NaOH, MeCN	81%	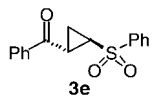 **3e**	>95:5
6	**4**	**2f**	Na_2CO_3, THF/DMSO	78%	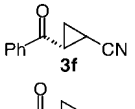 **3f**	2.3:1
7	**4**	**2g**	Na_2CO_3, MeCN	40%	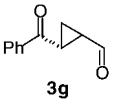 **3g**	4.3:1
8	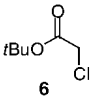 **6**	**2c**	Na_2CO_3, MeCN	70%	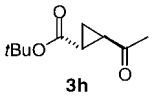 **3h**	>95:5
9[d]	**7**	**2c**	Na_2CO_3, MeCN	70%	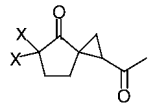 X = CH_2CH_2COMe **3i**	>95:5

[a] α-Chlorocarbonyl, DABCO (1.0 equiv), MeCN (0.25 M), room temperature, 30 min, then alkene (1 equiv), base (1.5 equiv), 80 °C. [b] Yield of isolated product after chromatography. [c] Determined by ^{1}H NMR spectroscopy. [d] Preformed salt **1** was used in this reaction.

process was demonstrated across a range of substrates which established the efficacy of this new and versatile cyclopropane methodology (Table 2). The reaction worked well for a range of alkenes, with acrylates **2a** and **2b**, enone **2c**, acrylamide **2d**, and vinyl sulfone **2e** all forming only the *trans*-substituted 1,2-cyclopropanes **3a**–**3e** in good to excellent yield.[12] Acrylonitrile (**2f**) gave a mixture of cyclopropanes (**3f**; 2.3:1, *trans*:*cis*) in good yield, although some polymerization was observed. Acrolein (**2g**) also gave a separable mixture of cyclopropanes (**3g**; 4.3:1, *trans*:*cis*) in 40% yield when the preformed salt **1** was used. Ammonium ylide species bearing other functional groups were also investigated and produced cyclopropanes in good yield (entries 8 and 9, Table 2). Ketone **7** formed spiro[2.4]heptane derivative **3i** as a single diastereomer when reacted with 3 equivalents of **2c**.

The simplicity of the one-pot ammonium ylide approach to cyclopropanation should allow the use of any tertiary amine.[13] DABCO (**5**) was chosen as a model tertiary amine to mimic the core structure of the cinchona alkaloids because they are a potential source of chirality for an enantioselective cyclopropanation reaction. The chiral quaternary ammonium salt **11** was readily formed in situ from the addition of phenacyl bromide (**8**) to amine **9**.[14] Subsequent addition of acrylate **2a** and sodium hydroxide (2 equiv), and stirring the reaction at 80 °C for 24 h generated cyclopropane (+)-**3a** in 61% yield (Table 3). The enantiomeric ratio (e.r.) from this initial reaction was 91.5:8.5 (83% *ee*), as determined by chiral HPLC.[15] While this result displayed excellent enantioselectivity we were concerned for the enantiomeric integrity of the cyclopropane in the reaction mixture. By monitoring the e.r. over the course of the reaction, we observed an erosion in the enantiomeric purity of the cyclopropane (Table 3, entry 1). However, reducing the amount of base in the reaction to 1.3 equivalents generated (+)-**3a** in 57% yield with an e.r. of 97:3 (94% *ee*). Furthermore, using dihydrocinchonine derivative **10** under our modified reaction conditions formed the opposite enantiomer, (−)-**3a**, in 58% yield and an e.r. of 97:3 (94% *ee*). To the best of our knowledge these are the first examples of an enantioselective cyclopropanation reaction based on a chiral ammonium ylide. We are currently screening the range of alkenes and other chiral tertiary

Table 3: One-pot enantioselective cyclopropanation.

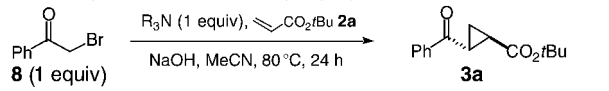

8 (1 equiv) → **3a**

Entry[a]	Chiral amine	equiv NaOH	*t* [h]	Yield[b]	e.r. (*ee*)[c]
1	**9**	2	8	10%	97:3 (94) (+)
			16	46%	92:8 (84) (+)
			24	61%	91.5:8.5 (83) (+)
2	**9**	1.3	24	57%	97:3 (94) (+)
3	**10**	1.3	24	58%	97:3 (94) (−)

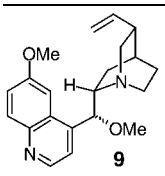
9

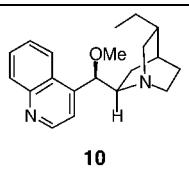
10

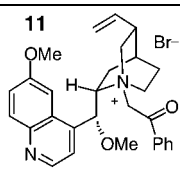
11

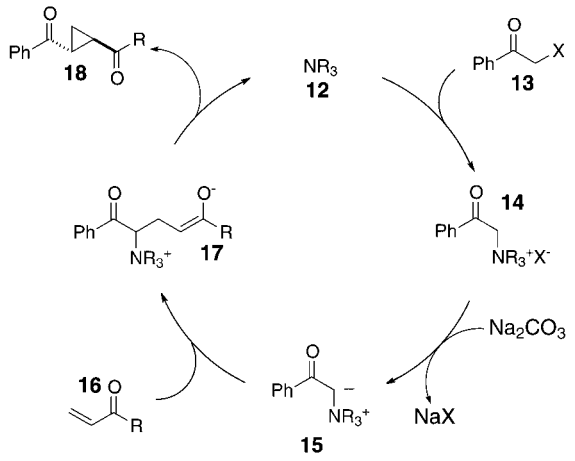

Scheme 2. Proposed catalytic cycle for cyclopropanation.

amines to investigate the scope of this new enantioselective process.

With an efficient stoichiometric one-pot cyclopropanation reaction in hand, we next investigated a catalytic process. Examination of a possible reaction mechanism suggests that the amine **12** should be released at the end of the reaction when the cyclopropane ring forms (Scheme 2).[16] Thus, in principle it should be possible to use the tertiary amine in catalytic quantities without fear of a competing background reaction. Accordingly, stirring a mixture of phenacyl chloride (**4**), **2c** (3 equiv),[17] sodium carbonate (1.2 equiv) and DABCO (0.2 equiv) in acetonitrile at 80 °C for 24 h produced cyclopropane **3c** in 82 % yield. *tert*-Butyl acrylate (**2a**) and vinyl sulfone **2e** also produce cyclopropanes **3a** and **3e**, respectively, under catalytic conditions (Table 4). In the absence of DABCO little or no reaction takes place which proves that the tertiary amine is required as a catalyst. We are currently exploring the scope of the reaction to develop a general catalytic cyclopropanation reaction based on ammonium ylides.

In summary, we have developed a practical and general "one-pot" cyclopropanation process, mediated by a tertiary amine via an ammonium ylide intermediate, by using readily available starting materials. We have demonstrated that this reaction is both diastereo- and enantioselective and that the reaction can be made catalytic.[18] We are currently exploring the scope of an asymmetric process with the goal of developing a catalytic enantioselective cyclopropanation reaction. Furthermore, application of this methodology to an intramolecular cyclopropanation system and to the synthesis of small-ring heterocycles is also being explored.

Table 4: Initial results for a catalytic cyclopropanation.[a]

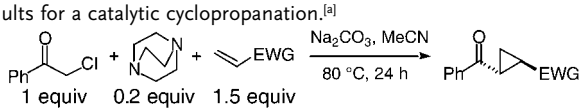

α-Chlorocarbonyl	Acceptor	Yield[b]	Product	d.r. (*trans*:*cis*)[c]
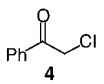 **4**	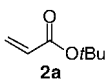 **2a**	69	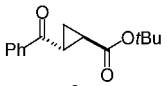 **3a**	> 95:5
4	**2c**	82[d]	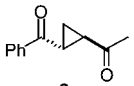 **2c**	> 95:5
4	**2e**	63	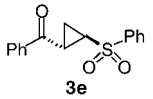 **3e**	> 95:5

[a] Phenacyl chloride, DABCO (0.2 equiv), alkene (1.5 equiv), Na_2CO_3 (1.2 equiv), MeCN (0.25 M), 80 °C, 24 h. [b] Yield of isolated product after chromatography. [c] Determined by ^{1}H NMR spectroscopy. [d] 3 equiv Of **2c** was used.

Received: October 14, 2002 [Z50353]

[1] For reviews, see: a) J. Salaun, *Chem. Rev.* **1989**, *89*, 1247; b) A.-H. Li, L.-X. Dai, V. K. Aggarwal, *Chem. Rev.* **1997**, *97*, 2341; c) A. Pfaltz in *Comprehensive Asymmetric Catalysis II* (Eds.: E. N. Jacobsen, A. Pfaltz, H. Yammamoto), Springer, Berlin, **1999**, pp. 513 – 538.

[2] For recent developments, see: W. A. Donaldson, *Tetrahedron* **2001**, *57*, 8589, and references therein. For other examples see ref. [1].

[3] E. J. Corey, M. Chaykovsky, *J. Am. Chem. Soc.* **1965**, *87*, 1353; E. J. Corey, M. Jautelat, *J. Am. Chem. Soc.* **1967**, *89*, 3912.

[4] S. Hanessian, D. Andreotti, A. Gomtsyan, *J. Am. Chem. Soc.* **1995**, *117*, 10393.

[5] S. Ye, Z.-Z. Huang, C.-A. Xia, Y. Tang, L.-X. Dai, *J. Am. Chem. Soc.* **2002**, *124*, 2432.

[6] V. K. Aggarwal, A. Thompson, R. V. H. Jones, *Chem. Commun.* **1997**, 1785 and ref. [7]. See also A. Solladie-Cavallo, A. Diep-Vohuule, T. Isarno, *Angew. Chem.* **1998**, *110*, 1824; *Angew. Chem. Int. Ed.* **1998**, *37*, 1689.

[7] a) V. K. Aggarwal, E. Alonso, G. Fang, M. Ferrara, G. Hynd, M. Porcelloni, *Angew. Chem.* **2001**, *113*, 1482; *Angew. Chem. Int. Ed.* **2001**, *40*, 1433; b) V. K. Aggarwal, H. W. Smith, G. Hynd, R. V. H. Jones, R. Fieldhouse, S. E. Spey, *J. Chem. Soc. Perkin Trans. 1* **2000**, 3267.

[8] I. Zugravescu, M. Petrovanu, *N-Ylid Chemistry*, McGraw-Hill, New York, **1976**.

[9] a) S. S. Bhattacarjee, H. Ila, H. Junjappa, *Synthesis* **1982**, 301; b) A. Jonczyk, A. Konarska, *Synlett* **1999**, 1085; for other examples, see c) N. H. Vo, C. J. Eyermann, C. N. Hodge, *Tetrahedron Lett.* **1997**, *38*, 7951; d) A. M. Shestopalov, V. P. Litvinov, L. A. Rodinovskaya, Y. A. Sharanin, *Zh. Org. Khim.* **1991**, *27*, 146.

[10] When Na_2CO_3 is used as the base, no reaction is observed. When NaOH is used, decomposition is observed.

[11] All compounds were characterized by ^{1}H and ^{13}C NMR spectroscopy, high-resolution mass spectrometry and infrared spectroscopy.

[12] *trans*-Stereochemistry was confirmed in **3a** by hydrolysis of the *tert*-butyl ester and comparison with an authentic sample, and in **3e** by X-ray crystal-structure analysis.

[13] We also found that using quinuclidine in place of DABCO produced **3a** in similar yield.

[14] Phenacyl chloride did not react with the more hindered chiral amine.

[15] See supporting information for details chiral HPLC analysis.

[16] No cyclopropane formation was observed when the reaction was

 © 2003 Wiley-VCH Verlag GmbH & Co. KGaA, Weinheim 1433-7851/03/4207-0830 $ 20.00+.50/0

carried out with styrene instead of the electron-deficient alkenes which suggests that the reaction does not proceed through a carbene mechanism.

[17] In the case of methyl vinyl ketone, 3.0 equiv was used because of its volatility. In the other cases only 1.5 equiv of the alkene was used.

[18] For an overview of organocatalysis, see: P. I. Dalko, L. Moisan, *Angew. Chem.* **2001**, *113*, 3840; *Angew. Chem. Int. Ed.* **2001**, *40*, 3726.

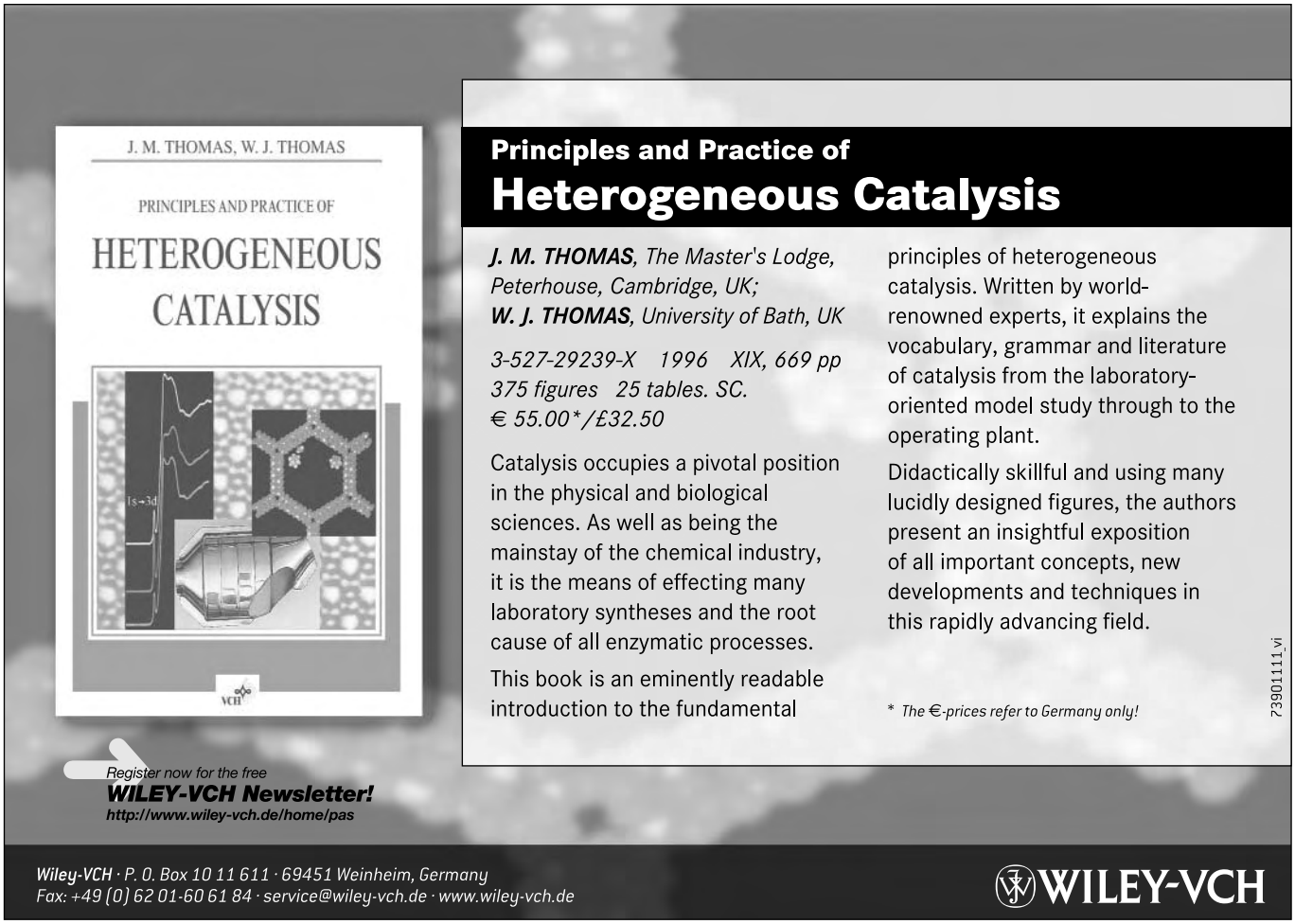

Cover Picture

Zhong-Ze Gu, Hiroshi Uetsuka, Kazuyuki Takahashi, Rie Nakajima, Hiroshi Onishi, Akira Fujishima, and Osamu Sato*

Learning from nature to design the materials of the future. The cover picture shows the Morpho butterfly, whose wings displays structural color, and lotus leaves, which exhibit hydrophobicity. To mimic these natural products, materials were prepared that utilize the unique structural properties of an inverse opal film, which displays uniform structural colors and a surface with well-ordered bumps that aid hydrophobicity. Modification leads to a superhydrophobic surface with a large water-contact angle. For more information see the Communication by O. Sato et al. on page 894 ff.

Contents

Obituary

Harry Georg Drickamer (1918–2002) — 850

Electronic Phenomena in Condensed Matter at High Pressure — *F. Hensel*

News

H. Kessler Receives Philip Morris Award — 851

T. Fukuyama and P. Wipf Recognized for Heterocyclic Chemistry — 851

H. Wiezer New Member of the Editorial Board — 851

Books

Titanium and Zirconium in Organic Synthesis — 852 — Ilan Mark — *edited by R. Mahrwald*

Peptides: Chemistry and Biology — 853 — Norbert Sewald, Hans-Dieter Jakubke — *edited by B. Merrifield*

Highlights

Aromatic Substitution

D. Lenoir* — 854–857

The Electrophilic Substitution of Arenes: Is the π Complex a Key Intermediate and What is Its Nature?

Keywords:
ab initio calculations · arenes · aromatic substitutions · electrophilic additions · reaction mechanisms

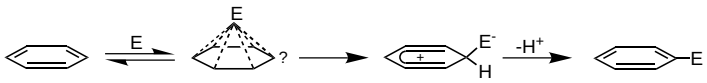

Aromatic substitution in detail: How does one prove that the intermediate charge-transfer (CT) complex (see scheme, where E = electrophile) is a key intermediate in the electrophilic substitution of arenes, and what is the structure, nature, and significance of this intermediate? On the basis of recent experimental findings these questions and others will be examined.

Cross-Aldol Reactions of Aldehydes

B. Alcaide,* P. Almendros* — 858–860

The Direct Catalytic Asymmetric Cross-Aldol Reaction of Aldehydes

Keywords:
aldol reactions · asymmetric catalysis · asymmetric synthesis · C–C coupling · enantioselectivity

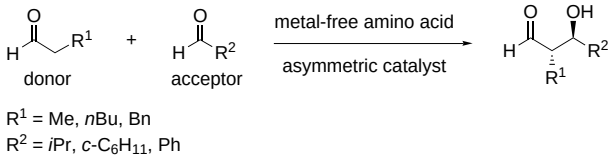

R^1 = Me, *n*Bu, Bn
R^2 = *i*Pr, *c*-C_6H_{11}, Ph

Although the more elegant and most economically attractive way to introduce chirality into a molecule is by using a catalytic amount of chiral controller to induce chiral transformation without the need for any other activation of the starting materials, the first report of chemical catalysis for the direct catalytic asymmetric cross-aldol reaction of aldehydes has only recently appeared (see scheme).

© 2003 Wiley-VCH Verlag GmbH & Co. KGaA, Weinheim

1433-7851/03/4208-0842 $ 20.00+.50/0

Reviews

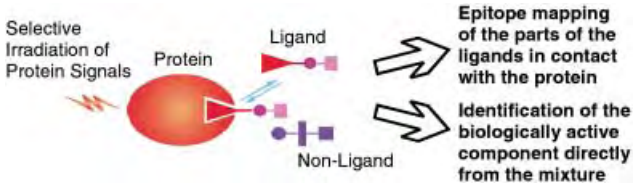

Picking the locks of protein binding: NMR spectroscopic techniques for the characterization of binding processes have recently gained much attention. Binding epitopes on the ligands and on the protein can be identified easily without the aid of crystal structures (see scheme). Hereby, rational design of new drugs has become more accessible.

NMR Spectroscopy of Proteins

B. Meyer,* T. Peters* _____ **864 – 890**

NMR Spectroscopy Techniques for Screening and Identifying Ligand Binding to Protein Receptors

Keywords:
drug design · ligand–protein interactions · NMR spectroscopy · proteins · screening

Communications

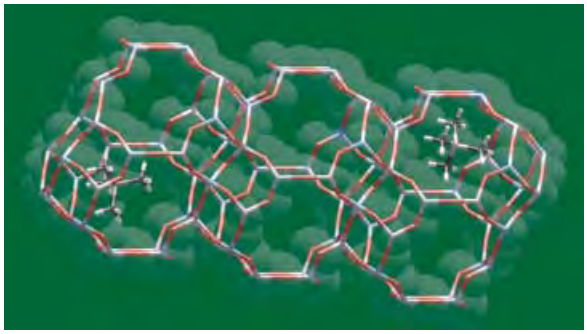

Active phosphate flotsam: Tetramethylphosphonium cations can be prepared in the cages of HSAPO-34 catalysts from PH_3 and methanol by using a ship-in-a-bottle approach (see picture). Calcination of this material leaves phosphate debris in some of the cages, which produces an active methanol-to-olefin catalyst with improved ethylene selectivity.

Methanol-to-Olefin Catalyst

W. Song, J. F. Haw* _____ **892 – 894**

Improved Methanol-to-Olefin Catalyst with Nanocages Functionalized through Ship-in-a-Bottle Synthesis from PH_3

Keywords:
heterogeneous catalysis · hydrocarbons · microporous materials · nanostructures · NMR spectroscopy

Dry and bright: To mimic the wings of the displayed Morpho butterfly, a new decorative material that exhibits both structural color and superhydrophobicity (the "lotus effect") was developed by taking advantage of the unique structural properties of an inverse opal film, which was fabricated by the self-assembly of polystyrene spheres and silica nanoparticles.

Surface Effects from Nanostructure

Z.-Z. Gu, H. Uetsuka, K. Takahashi, R. Nakajima, H. Onishi, A. Fujishima, O. Sato* _____ **894 – 897**

Structural Color and the Lotus Effect

Keywords:
colloids · nanostructures · self-assembly · structural color · wettability

For the USA and Canada:
ANGEWANDTE CHEMIE International Edition (ISSN 1433-7851) is published weekly by Wiley-VCH PO Box 191161, D 69451 Weinheim, Germany. Air freight and mailing in the USA by Publications Expediting Inc. 200 Meacham Ave., Elmont, NY 11003. Periodicals postage paid at Jamaica NY 11431. US POSTMASTER: send address changes to *Angewandte Chemie*, Wiley-VCH, 111 River Street, Hoboken, NJ 07030. Annual institutional subscription price for institutions: Europe € 2998.00/3148.00. Outside Europe US$ 3718.00/3904.00 (valid for print or electronic/print and electronic delivery); for individuals who are personal members of a national chemical society, or whose institution already subscribes, or who are retired or self-employed consultants, print only (including postage and handling charges): Europe € 248.00/Outside Europe US$ 348.00.

 © 2003 Wiley-VCH Verlag GmbH & Co. KGaA, Weinheim 1433-7851/03/4208-0843 $ 20.00+.50/0

Contents

Liquid-Crystal Molecular Design

S.-W. Tam-Chang,* W. Seo, I. K. Iverson, S. M. Casey ——— **897 – 900**

Ionic Quaterrylenebis(dicarboximide): A Novel Mesogen and Long-Wavelength Polarizing Material

Keywords:
aggregation · liquid crystals · polarization · supramolecular chemistry · thin films

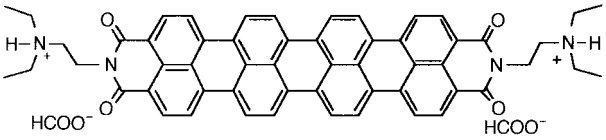

An absorbing study: The displayed quaterrylenebis(dicarboximide) was imparted with lyotropic liquid-crystalline properties by molecular design. The ability of the molecule to self-organize in solution allows for the subsequent control of its orientation in thin solid films. Induced orientation of the liquid-crystalline domains of the molecule under a shearing force results in highly anisotropically ordered films that serve as dichroic polarizers of light at wavelengths greater than 600 nm.

Pentalene Bonding in Fullerenes

M. M. Olmstead, H. M. Lee, J. C. Duchamp, S. Stevenson, D. Marciu, H. C. Dorn,* A. L. Balch* ——— **900 – 903**

$Sc_3N@C_{68}$: Folded Pentalene Coordination in an Endohedral Fullerene that Does Not Obey the Isolated Pentagon Rule

Keywords:
fullerenes · isomers · nitrogen · scandium · structure elucidation

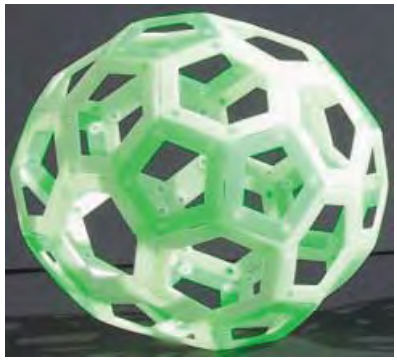

Breaking the rule: The structure of $Sc_3N@C_{68}\cdot[Ni^{II}(OEP)]\cdot 2\,C_6H_6$ has been determined by single-crystal X-ray diffraction. The fullerene cage exists as an isomer with D_3 symmetry (see picture), as initially predicted by density functional calculations. The scandium atoms are located over the centers of three pentalene units within the three-cornered carbon cage, which cannot obey the isolated pentagon rule. OEP = Octaethylporphyrinate.

Multiparallel Organic Synthesis

S. A. Kozmin,* Y. Wang ——— **903 – 905**

A Three-Dimensional Array for Multiparallel Synthesis

Keywords:
combinatorial chemistry · multiparallel synthesis · peptides · synthetic methods

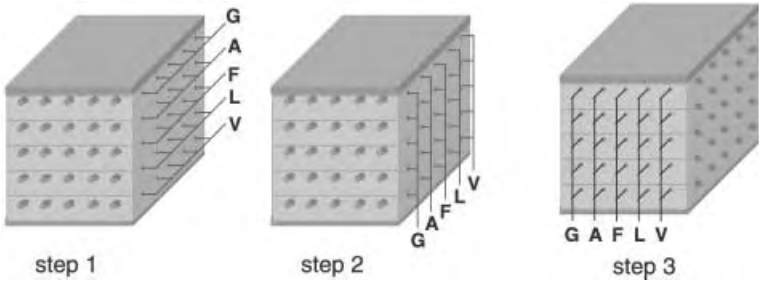

An operationally simple and general technique for multiparallel organic synthesis is based on the three-dimensional delivery of reactants to an array of interconnected reaction wells. This technology can be readily adapted to the design of substantially large arrays, or multiple copies of interconnected arrays, thus allowing the necessary flexibility for the synthesis and screening of a wide range of chemical libraries.

© 2003 Wiley-VCH Verlag GmbH & Co. KGaA, Weinheim
1433-7851/03/4208-0844 $ 20.00+.50/0

Detection and characterization of unstable and complex DNA species, including hyperstranded DNA species such as the forklike structure of replicating DNA (see picture), is made possible by cold-spray ionization mass spectrometry.

DNA Structure

S. Sakamoto, K. Yamaguchi* ——— 905 – 908

Hyperstranded DNA Architectures Observed by Cold-Spray Ionization Mass Spectrometry

Keywords:
DNA structures · hydrogen bonds · mass spectrometry · supramolecular chemistry

$$\begin{array}{l} CH_4 + H_2O \rightleftharpoons CO + 3\,H_2 \\ CO + H_2O \rightleftharpoons CO_2 + H_2 \\ \hline CH_4 + 2\,H_2O \rightleftharpoons CO_2 + 4\,H_2 \end{array}$$

More rapidly to the target: Screening experiments in a miniautoclave demonstrate the different effects of catalytically active additives such as Raney nickel and basic alkali-metal compounds on the reaction of methane in supercritical water. Accordingly, this opens up the possibility to convert methane into hydrogen and carbon dioxide with water in a single process step without the need to pass through the intermediate carbon monoxide stage which is currently necessary in industrial set ups (see scheme).

Reactions in Supercritical Water

A. Kruse,* E. Dinjus ——— 909 – 911

Hydrogen from Methane and Supercritical Water

Keywords:
high-pressure chemistry · hydrogen · methane · reforming · supercritical fluids

Starting from germanium(I) bromide, which can be obtained by preparative co-condensation, the first polyhedral Ge cluster $[Ge_8\{N(SiMe_3)_2\}_6]$ (see picture) has been synthesized in which the average oxidation state of all the Ge atoms in the cluster core lies between 0 and +1.

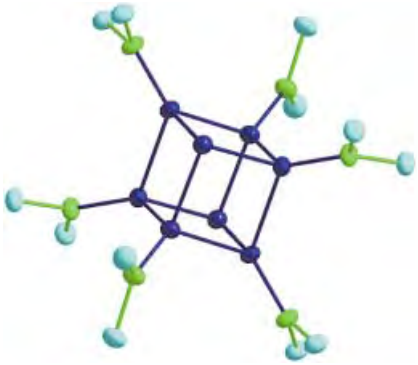

Clusters with Ge^0 Atoms

A. Schnepf,* R. Köppe ——— 911 – 913

$[Ge_8\{N(SiMe_3)_2\}_6]$: A Ligand-Stabilized Ge Cluster Compound with Formally Zero-Valent Ge Atoms

Keywords:
bond theory · cluster compounds · density functional calculations · disproportionation · germanium

The Rh-catalyzed asymmetric hydrogenation of β-aryl-substituted (*E*)-β-acylaminoacrylates, which were isolated for the first time, with, for example $[Rh\{(R,R)\text{-(Et-FerroTANE)}\}(nbd)]^+$ as catalyst (see picture) proceeds under very mild conditions (25 °C, normal pressure) and high substrate/catalyst ratios with very good enantioselectivity (Et-FerroTANE = (+)-1,1′-bis(2,4-diethylphosphyltane)ferrocene, nbd = 3,5-norbornadiene).

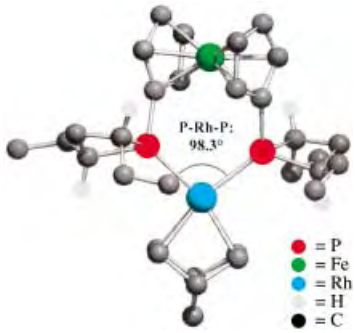

Asymmetric Hydrogenation

J. You, H.-J. Drexler, S. Zhang, C. Fischer, D. Heller* ——— 913 – 916

Preparation and Asymmetric Hydrogenation of β-Aryl-Substituted β-Acylaminoacrylates

Keywords:
amino acids · asymmetric catalysis · hydrogenation · P ligands · rhodium

 © 2003 Wiley-VCH Verlag GmbH & Co. KGaA, Weinheim 1433-7851/03/4208-0845 $ 20.00+.50/0

Contents

Synthesis of Lipoteichoic Acids

A. Stadelmaier, S. Morath, T. Hartung, R. R. Schmidt* ——— 916 – 920

Synthesis of the First Fully Active Lipoteichoic Acid

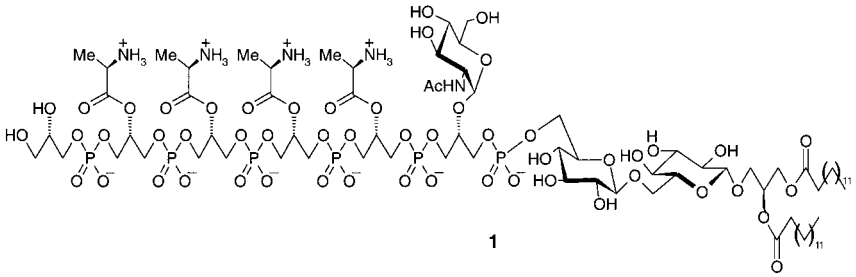

1

Keywords:
biological activity · glycolipids · lipoteichoic acid · natural products · synthetic methods

Nature outfoxed! Owing to the sensitivity of lipoteichoic acids (LTAs) to hydrolysis their biological activity could not be ascertained thus far. The chemical synthesis of LTA of *Staphylococcus aureus* **1**, which contains hydrolytically labile D-alanine residues in the required ratio with other substituents, resulted in the same activity as exhibited by the natural product obtained by a new isolation procedure. Thus, the biological activity of LTA could be ascertained for the first time.

Stable Spirobis(radical cation)

A. Ito, M. Urabe, K. Tanaka* ——— 921 – 924

A Spiro-Fused Triarylaminium Radical Cation with a Triplet Ground State

Keywords:
EPR spectroscopy · magnetic properties · radical ions · spiro compounds

Novel spirobis(radical cation) 1^{2+} was prepared to examine the magnetic interaction between the two radical centers. The dication 1^{2+} was found to be a robust triplet diradical on the basis of the ESR spectrum, magnetic susceptibility measurements, which indicated ferromagnetic interaction between the radical centers (i.e., $J > 0$), and quantum chemical calculations.

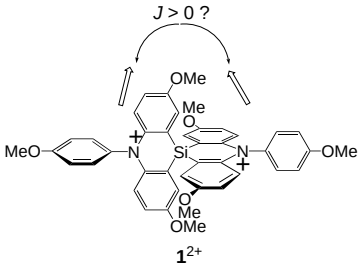

1^{2+}

Redox-Switchable Lithium Trap

M. Scheibitz, R. F. Winter, M. Bolte, H.-W. Lerner, M. Wagner* ——— 924 – 927

[1.1]Diborataferrocenophane: A Highly Efficient Li^+ Scavenger

Keywords:
boron · electrochemistry · lithium · metal–metal interactions · sandwich complexes

A naked lithium cation is efficiently trapped within the [1.1]diborataferrocenophane dianion $[\mathbf{1}]^{2-}$, but released upon electrochemical oxidation of the ferrocene moieties. The complex [**1**-Li]Li([12]crown-4)$_2$ provides the first experimental evidence for a theoretically predicted ferrocene···Li^+ complex in which the Li^+ ion is laterally bound to the Fe atom.

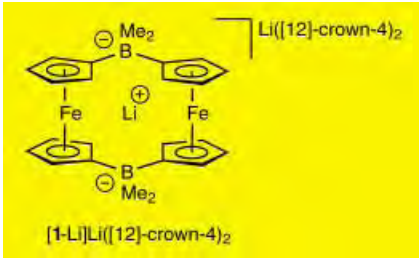

Li-Intercalated Oxometallocubanes

J. Gracia, A. Martín, M. Mena,* M. d. C. Morales-Varela, J.-M. Poblet, C. Santamaría ——— 927 – 930

Intercalation of Alkali Metal Cations into Layered Organotitanium Oxides

Keywords:
alkali metals · cyclopentadienyl ligands · density functional calculations · oxo ligands · titanium

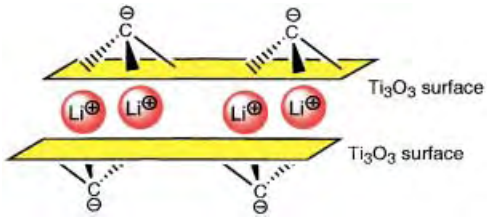

Deprotonation of the complex [{Ti(η^5-C_5Me_5)(μ-O)}$_3$(μ_3-CH)] with different alkali metal alkyl and amide reagents provides a method for the intercalation of alkali-metal ions into layered organometallic titanium oxides (see picture). The process and the structures were analyzed by DFT calculations.

© 2003 Wiley-VCH Verlag GmbH & Co. KGaA, Weinheim
1433-7851/03/4208-0846 $ 20.00+.50/0

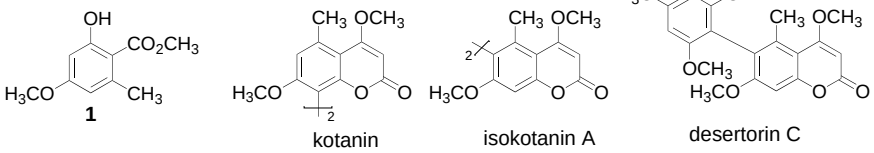

One monomeric orsellinate (1) suffices for a highly efficient total synthesis of the dimeric coumarins kotanin, isokotanin A, and desertorin C. The reason is the unselective course of its oxidative phenolic coupling, which leads to three regioisomeric biaryls as precursors of the dimers.

Unselectivity as an Advantage

D. Drochner, W. Hüttel, M. Nieger, M. Müller* ——— **931 – 933**

Unselective Phenolic Coupling of Methyl 2-Hydroxy-4-methoxy-6-methylbenzoate—A Valuable Tool for the Total Synthesis of Natural Product Families

Keywords:
atropisomerism · biaryls · biomimetic synthesis · molecular diversity · total synthesis

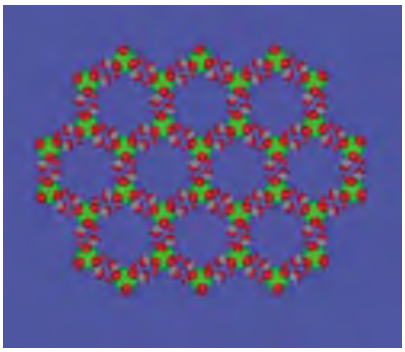

Large pores comprising 48-membered rings characterize the isostructural lanthanide–transition-metal coordination polymers $[\{[Ln(dipic)_3Mn_{1.5}(H_2O)_3]\cdot n H_2O\}_\infty]$, H_2dipic = pyridine-2,6-dicarboxylic acid; Ln = Pr, $n = 2$ (shown here); Ln = Gd, $n = 3.5$; Ln = Er, $n = 3$. Many water molecules are trapped in the nanotubular structure, and the framework remains intact on removal of the uncoordinated water molecules.

3d-4f Metal Coordination Polymers

B. Zhao, P. Cheng,* Y. Dai, C. Cheng, D.-Z. Liao,* S.-P. Yan, Z.-H. Jiang, G.-L. Wang ——— **934 – 936**

A Nanotubular 3D Coordination Polymer Based on a 3d–4f Heterometallic Assembly

Keywords:
coordination polymers · lanthanides · self-assembly · transition metals · zeolite analogues

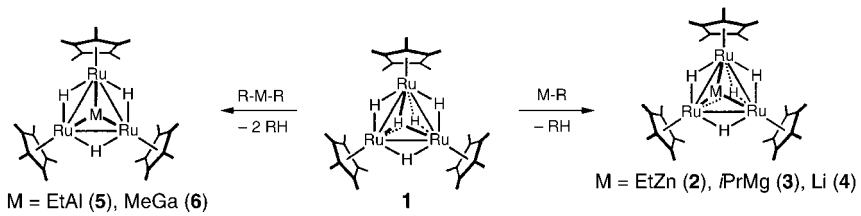

The cluster's clever cap: Treatment of **1** with an equimolar amount of diethylzinc yields the cluster **2** together with the elimination of ethane (see scheme). The pentahydride **1** also reacts with metal alkyls, such as $MgiPr_2$, MeLi, $AlEt_3$, and $GaMe_3$, to yield complexes **3**–**6** analogous to **2** that contain a triply bridged metal ligand. The effect of these ligands on reactivity is evaluated by means of cyclic voltammetry.

Capped Metal Polyhydride Clusters

M. Ohashi, K. Matsubara, T. Iizuka, H. Suzuki* ——— **937 – 940**

Trinuclear Ruthenium Polyhydride Complexes with a Triply Bridging Ligand: $[\{(\eta^5\text{-}C_5Me_5)Ru\}_3(\mu_3\text{-}M)(\mu\text{-}H)_3(\mu_3\text{-}H)]$ (M = Li, Mg*i*Pr, and ZnEt) and $[\{(\eta^5\text{-}C_5Me_5)Ru\}_3(\mu_3\text{-}M)(\mu\text{-}H)_3]$ (M = AlEt and GaMe)

Keywords:
cluster compounds · cyclic voltammetry · hydride ligands · ruthenium · trinuclear complexes

 © 2003 Wiley-VCH Verlag GmbH & Co. KGaA, Weinheim 1433-7851/03/4208-0847 $ 20.00+.50/0

Contents

Epoxidation

N. Makita, Y. Hoshino, H. Yamamoto* ——— 941 – 943

Asymmetric Epoxidation of Homoallylic Alcohols and Application in a Concise Total Synthesis of (−)-α-Bisabolol and (−)-8-*epi*-α-Bisabolol

Keywords: bisabolol · epoxidation · homoallylic alcohols · hydroxamic acids · vanadium

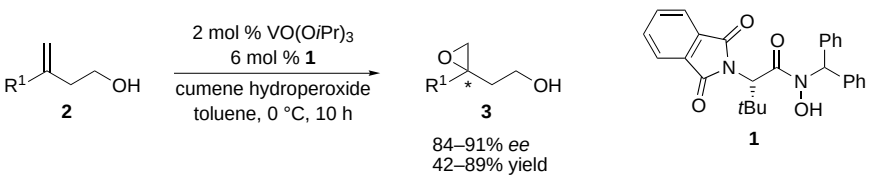

Vanadium triisopropoxide oxide and an α-amino acid-based hydroxamic acid (e.g. **1**) form the catalyst for the asymmetric epoxidation of homoallylic alcohols presented here. 3-Substituted alcohols **2** were epoxidized to the corresponding epoxy alcohols **3** with good *ee* values. In addition, a concise total synthesis of (−)-α- and (−)-8-*epi*-α-bisabolol was achieved.

Catalytic Asymmetric Hydrogenation

W. Tang, W. Wang, X. Zhang* ——— 943 – 946

Phospholane–Oxazoline Ligands for Ir-Catalyzed Asymmetric Hydrogenation

Keywords: asymmetric catalysis · hydrogenation · iridium · ligand design · N,P ligands

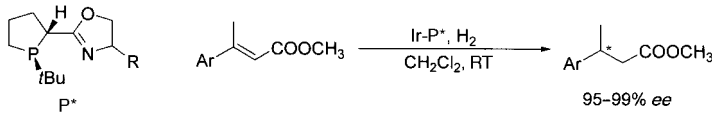

A new class of chiral phospholane–oxazoline ligands P* was developed for Ir-catalyzed asymmetric hydrogenation (see scheme, e.g. R = Ph; Ar = *m*-$CH_3C_6H_4$). High enantioselectivities (up to 99% *ee*) were obtained for the hydrogenation of methylstilbene derivatives and (*E*)-β-methylcinnamic esters.

Allylation of Aldehydes

K. Kubota, J. L. Leighton* ——— 946 – 948

A Highly Practical and Enantioselective Reagent for the Allylation of Aldehydes

Keywords: aldehydes · allylation · asymmetric synthesis · chiral auxiliaries · homoallylic alcohols

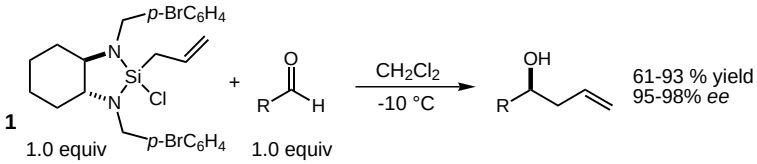

Strain at silicon is the key to success of reagent **1** since this strain, which is induced by the diazasilacyclopentane ring, determines its reactivity. This practical and general new reagent for the highly enantioselective allylation of aldehydes is easily prepared as an air-stable solid and may be stored without significant decomposition.

One-Step Route to Tetrahydrofurans

T. J. Donohoe,* S. Butterworth ——— 948 – 951

A General Oxidative Cyclization of 1,5-Dienes Using Catalytic Osmium Tetroxide

Keywords: cyclization · heterocycles · osmium · oxidation · synthetic methods

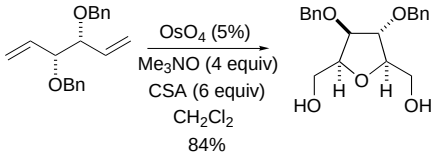

(1)

Dihydroxylation of 1,5-dienes under acidic conditions is sufficient to induce an efficient oxidative cyclization that produces stereochemically defined tetrahydrofurans in one step [Eq. (1)]. This method is very general and efficient for a range of dienes and shows complete stereoselectivity for formation of the 2,5-*cis* diastereoisomers. Bn = benzyl, CSA = camphorsulfonic acid.

© 2003 Wiley-VCH Verlag GmbH & Co. KGaA, Weinheim
1433-7851/03/4208-0848 $ 20.00+.50/0

Communications labeled with this symbol have been judged by two referees as being "very important papers".

The publication of Communications labeled with this symbol has been accelerated because of their topical or highly competitive nature.

Supporting information for articles labeled with this symbol can be found at www.angewandte.org or www.interscience.wiley.com.

News in *Angewandte Chemie*?

The aim of this section is to bring the scientific community closer together. The focus will be on international and interdisciplinary events, moves and awards. News items will include references to current articles in our family of journals.

Service

Keywords ____ 952

Authors ____ 953

Preview ____ 955

Corrigendum

In the Meeting Reviews "The 50th Birthday of the Organocuprates" by Norbert Krause in Issue 4, **2003**, the lecture by Gernot Boche was wrongly cited. Instead of "…and it could be shown that Michael additions of organocuprates proceed via *solvent-separated* ion pairs" it should say "…that Michael additions of organocuprates proceed via contact ion pairs" (see also Boche et al., *Chem. Eur. J.* **2002**, *6*, 3060–3068). The author apologises for this error.

40 Years of Chemistry History

★ The basis for a **journey of discovery** through all the important developments in chemistry and related disciplines

★ The **authors** and **keywords** of all the reviews that have appeared in ***Angewandte Chemie*** in the last 40 years

★ ***Now available at a special price of € 19.80*** (including postage)

Only available directly from:
Angewandte Chemie
Postfach 10 11 61
69451 Weinheim (Germany)
Telephone: (+49) 6201-606-265
Fax: (+49) 6201-606-331
E-mail: angewandte@wiley-vch.de

 © 2003 Wiley-VCH Verlag GmbH & Co. KGaA, Weinheim 1433-7851/03/4208-0849 $ 20.00+.50/0

Figure 1. Harry G. Drickamer (Copyright Dept. Chemical Engineering, University of Illinois, Urbana, IL, USA).

Harry George Drickamer (1918–2002): Electronic Phenomena in Condensed Matter at High Pressure

Over the past forty years, the application of high pressures has proven to be a powerful and nearly indispensable tool in chemistry, physics, geology, and biology research. Ever-increasing sophistication in experimental high-pressure techniques coupled with new theoretical developments have resulted in important advances in the understanding of the molecular structures, electronic properties, dynamics, and reactivity of condensed matter. One of the towering pioneers of this development was Harry G. Drickamer (Figure 1), Professor of Chemical Engineering, Chemistry and Physics at the University of Illinois in Urbana-Champaign, who died of a stroke on May 6, 2002 in Urbana, Illinois, at the age of 83.

Harry Drickamer was born on November 19, 1918 in Cleveland, Ohio. After graduating from high school he attended Indiana University for a short period. He then transferred to the University of Michigan, where he received his bachelor's degree in 1941, his master's degree in chemical engineering in 1942, and his doctorate in chemical engineering in 1946. That same year he joined the University of Illinois in Urbana-Champaign, where he was appointed, in recognition of the breadth of his research, Center of Advanced Study Professor of Chemical Engineering, Chemistry, and Physics, the highest accolade bestowed by the University on its faculty members.

During his more than 50 years of research in Urbana, he developed the concept that pressure can change the chemical and physical properties of condensed matter by its effect on the electronic orbitals, a method he called "Pressure Tuning Spectroscopy". Exploitation of this method led to his discovery in the late 1950s of a wide variety of electronic transitions in solids, including insulator–metal transitions for six elements and more than 30 covalent and ionic compounds, metal–semiconductor transitions for the elements calcium, strontium, and ytterbium, (which are metals at one atmosphere and which become semiconductors at high pressure), and s–d or 4f–5d transitions of the conducting electrons in alkali and rare-earth metals, respectively. In the 1970s he also investigated closely related pressure-induced changes to magnetic properties, such as high-spin–low-spin transitions and paramagnetic–ferromagnetic transitions in ferrous compounds and in iron. Furthermore, he discovered electronic transitions with chemical consequences, such as the stabilization of reactive charge-transfer states of electron donor–acceptor complexes at high pressures and the pressure-induced conversion of photochromic into thermochromic materials. In the 1980s his research expanded to high-pressure investigations in protein chemistry, organic photochemistry, and the efficiency of luminescence devices.

Harry Drickamer's style of experimental research kept him in close contact with theoretical work. In this way, he was able to provide clear-cut and unequivocal tests for a large number of theories, including the ligand-field theory, van Vleck's theory of spin-flip transitions, Mulliken's theory of bonding in electron donor–acceptor complexes, the Förster–Dexter theory of energy transfer in phosphors, and van Vleck's theory of high-spin–low-spin transitions. He also developed successful tests for theories on the efficiency of phosphor and laser materials, including II-VI and III-V compounds with zinc-blende structure, rare-earth oxides, chelates, and organic phosphors.

The list of his awards and honors is too long to relate in full, and reflects not only universal respect and admiration for his scientific research, but also the remarkable breadth of his activities. The 27 awards he received were for both research and teaching, and were from organizations in physics, chemistry, and chemical engineering. Among them were the Oliver E. Buckley Prize in Condensed Matter Physics from the American Physical Society (1967), the Irving Langmuir Award in Chemical Physics (1974), the Peter Debeye Award of the American Chemical Society (1987), the first P. W. Bridgman Award of the International Association for the Advancement of High-Pressure Science and Technology (1977), and a Research Award from the Alexander von Humboldt Foundation of the Federal Republic of Germany (1986). In 1989, President George H. W. Bush awarded him the National Medal of Science.

Drickamer's laboratory in Urbana attracted scientists and students from many places around the world. His passionate interest in high-pressure research continued after his retirement in 1989. Even then, he did not change his research schedule, but continued to maintain an active and successful research group and was in the laboratory six days a week. The results of 56 years of high-pressure research were published in more than 450 original contributions to the scientific literature. A summary, in Drickamer's own words, of the impact of "Pressure Tuning Spectroscopy", can be found in Annual Reviews Materials Science **1990**, 1–17. Insight into his research can be found in his review on "Electronic Transitions in Transition Metal Compounds at High Pressure" (*Angew. Chem.* **1974**, *86*, 61–79; *Angew. Chem. Int. Ed. Engl.* **1974**, *13*, 39–47).

Dickamer's scientific work has affected high-pressure research in an important way and will continue to do so in the future. Those who have been fortunate and privileged enough to work with him as students, colleagues, or friends owe him a great debt of gratitude. We will miss him.

Friedrich Hensel (Marburg)

 © 2003 Wiley-VCH Verlag GmbH & Co. KGaA, Weinheim 1433-7851/03/4208-0850 $ 20.00+.50/0

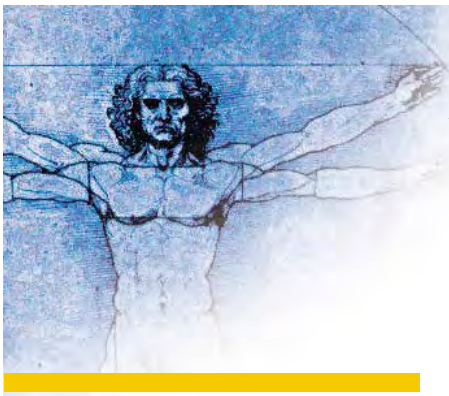

Horst Kessler Receives Philip Morris Research Award

Editorial Board Chairman Horst Kessler (Technical University of Munich) is one of four winners of this year's Philip Morris Research Award worth 100 000 €. He was recognized for his contributions to structure elucidation of proteins by means of NMR spectroscopy. He has investigated small peptides and their interactions in natural environments and the results are important to the understanding of biocatalysis and inhibition. As a result, artificial surfaces may be stabilized to become biocompatible.

H. Kessler

Kessler obtained his doctorate from the University of Tübingen (Germany) in 1966 under the guidance of Eugen Müller for work on copper salt catalysis. During his habilitation, his interest was first attracted to NMR spectroscopy: Monitoring intramolecular mobility by means of NMR spectroscopy. In 1971, he became a Professor of Organic Chemistry in Frankfurt (Germany) and moved to Munich in 1989. He is also a member the Editorial Board of *Angewandte*'s sister journal *ChemBioChem*.

See his Minireview on "The Structures of Integrins and Integrin–Ligand Complexes: Implications for Drug Design and Signal Transduction."[1]

R. B. Williams Hosts Heterocyclic Chemistry Conference, T. Fukuyama and P. Wipf To Give Award Lectures

Robert B. Williams (Colorado State University, USA) chairs the organizing committee of the 19th International Congress of Heterocyclic Chemistry (August 10–15, 2003, Ft. Collins, CO). The program includes award lectures by two distinguished scientists:

- Tohru Fukuyama will receive the 2003 International Award in Heterocyclic Chemistry. After graduation from Nagoya University, he obtained his PhD in 1977 under the direction of Y. Kishi (Harvard University). After a postdoctoral time there, he joined the faculty of Rice University (Houston, TX) and became a professor of pharmaceutical sciences at the University of Tokyo in 1995. His research is devoted to the total synthesis of complex natural products, such as the "Facile Construction of *N*-Hydroxybenzazocine: Enantioselective Total Synthesis of (+)-FR900482".[2]

T. Fukuyama

- Peter Wipf will receive the 2003 International Junior Award in Heterocyclic Chemistry, also known as the Katritzky Award. Wipf received his doctorate from the University of Zurich (Switzerland) in 1987 and is currently the director of the Combinatorial Chemistry Center at Pittsburgh University. Besides heterocyclic, organometallic, and combinatorial chemistry, the research of his group is focused on total syntheses of marine natural products; an example thereof is the "Total Synthesis of a Stereoisomer of Bistramide C and Assignment of Configuration of the Natural Product."[3] Their development of zirconium-based organometallic methods is summarized in a recent Concept entitled "Novel Applications of Alkenyl Zirconocenes".[4]

P. Wipf

Angewandte will publish a review on the "Chemistry and Biology of Biosynthetic Diels–Alder Reactions" by Williams in the near future.

H. Wiezer Member of the Editorial Board of Angewandte Chemie

The members of *Angewandte*'s Editorial Board serve a four-year term advising the Editors on all aspects of the journal's contents and policies. The group represents chemistry in its broadest meaning as found in universities, research institutes, and industry. Major decisions are subject to approval by the German Chemical Society (GDCh).

H. Wiezer

When Axel Kleemann (formerly ASTA Medica) retired from the Editorial Board of *Angewandte*, a seat became available. Following an invitation of the Board of the German Chemical Society, Hartmut Wiezer will succeed him.

Wiezer received his doctorate in 1974 from the University of Göttingen (Germany) in the group of H.-W. Roesky. His thesis deals with organometallic–inorganic heterocyclic compounds. In the following year, he started work at Hoechst on polymer additives. When the specialty chemicals division was taken over by Clariant in 1997, he was the head of the fine-chemicals division. He has overseen research and development at Clariant since 2000.

[1] K.-E. Gottschalk, H. Kessler, *Angew. Chem.* **2002**, *114*, 3919; *Angew. Chem. Int. Ed.* **2002**, *41*, 3767.
[2] M. Suzuki, M. Kambe, H. Tokuyama, T. Fukuyama, *Angew. Chem.* **2002**, *114*, 4880; *Angew. Chem. Int. Ed.* **2002**, *41*, 4686.
[3] P. Wipf, Y. Uto, S. Yoshimura, *Chem. Eur. J.* **2002**, *8*, 1670.
[4] P. Wipf, C. Kendall, *Chem. Eur. J.* **2002**, *8*, 1778.

 © 2003 Wiley-VCH Verlag GmbH & Co. KGaA, Weinheim 1433-7851/03/4208-0851 $ 20.00+.50/0

Aromatic Substitution

The Electrophilic Substitution of Arenes: Is the π Complex a Key Intermediate and What is Its Nature?

*Dieter Lenoir**

Keywords:
ab initio calculations · arenes · aromatic substitutions · electrophilic additions · reaction mechanisms

> *"Chemistry is the science of the elemental metamorphosis of matter. Its fundamental principle is not the existing substance, but rather its past and future."*
> Kekulé, 1861

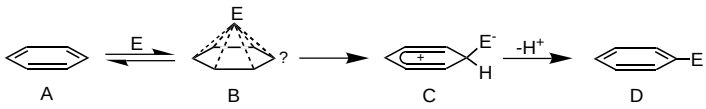

Scheme 1. Textbook perception of the course of electrophilic substitution reactions.

1. The Nature of the Problem

Organic chemical reactions can be divided into a readily comprehensible number of mechanistic types. Electrophilic substitution reactions of electrophiles, such as H^+, Cl_2, Br_2, NO^+, NO_2^+, SO_3, alkyl, or acyl cations, with arenes belong to the repertoire of preparative and mechanistic organic chemistry.[1] Every student learns the difference between the initially formed intermediates, the so-called π and σ complexes (arenium ion or Wheland intermediate, Scheme 1).

π-Complex stability was determined in 1950 from the relative equilibrium states of the reactions of alkyl-substituted arenes with HCl. The energetic differences between benzene and pentamethylbenzene are relatively small, k_{rel} varies between 0.61 and 1.67. σ-Complex stability was derived from the relative basicities of arenes towards HF, the relative differences vary between 0.09 and 29900.[2] In most substitution reactions the overall rate is highly dependent upon the nature of the substituent, which indicates that the formation of the intermediate arenium ion is the rate-determining step. By using the concepts developed by Mulliken for electron-donor/-acceptor (EDA) complexes[3] Benesi and Hildebrand (in 1949) first established π or charge-transfer (CT) complexes in the reaction of benzene with electrophiles, such as bromine and iodine, from the characteristic CT bands in the UV/Vis spectrum.[4] On the basis of a single-crystal X-ray structural analysis by Hassel and Strømme[5] the aromatic CT complex from benzene and bromine was assigned a centrosymmetric over-ring structure which has entered the textbooks (structure B in Scheme 1). Even today it has still not been explained whether the CT complex in equilibrium with substrate A lies on the side or main reaction coordinate.

In the last decade the CT complexes formed in the electrophilic addition reactions (halogenations) of alkenes, allenes, and alkynes have been investigated. Initially the reaction takes place analogously to aromatic substitution: formation of a CT complex with subsequent dissociation to the halonium ion which then adds a nucleophile.[6] The cardinal question for both types of reaction is: how can it be proved that the transient CT complex is a key intermediate, that is, it lies on the main not the side reaction coordinate? And how can the structure, nature, and the significance of this intermediate be established? New approaches have been developed for both types of reaction to answer these questions.

2. Electrophilic Substitutions on Arenes

The new results of Kochi et al.[7] are a very important contribution to organic chemistry. They demonstrate the existence of CT complexes as a key intermediate in the bromination of benzene and toluene.[7] By using a special technique the Kochi group succeeded in isolating different arene–bromine CT complexes and determining their structure by X-ray crystal structural analysis at very low temperatures (−150 °C). The preparation of the benzene–bromine complex in a glass capillary is an experimental master stroke: "The equimolar mixture of benzene and bromine remained liquid at −30 °C, but crystal nucleation was readily initiated by carefully brushing liquid nitrogen over the capillary with a cotton applicator. By a series of local (manual) warming all but one small crystal was alternatively dissolved/melted, and the remaining single crystal was allowed to grow along the capillary axis at −40 °C." It is probable that by this ingenious method imperfections in the crystal were avoided. The structures determined at −150 °C show an unsymmetrical "over-bond" structure for benzene and toluene (Figure 1),

[*] Prof. Dr. D. Lenoir
Institut für Ökologische Chemie
GSF-Forschungszentrum für Umwelt und Gesundheit, Postfach 1129
85764 Neuherberg (Germany)
Fax: (+49) 89-3187-4047
E-mail: lenoir@gsf.de

 © 2003 Wiley-VCH Verlag GmbH & Co. KGaA, Weinheim 1433-7851/03/4208-0854 $ 20.00+.50/0

in contradiction to the old, symmetric over-ring structures. Two isomeric CT complexes are obtained for toluene. The structure determinations carried out earlier by Hassel and Strømme were undertaken at higher temperatures (ca. −40 °C) which could have led to erroneous structural assignments as a result of disorder and thermal movement of the atoms in the crystal lattice. These structures may be described by the hapticity.[7b] The Br_2 molecule in the CT complex is nearly perpendicular and situated asymmetrically over one edge (bond) of the benzene or toluene ring (see Figure 1). The Br_2 unit is tilted by 6.1° relative to the C_6 axis of the benzene and the distances to the carbon atoms of the ring are distinctly different.

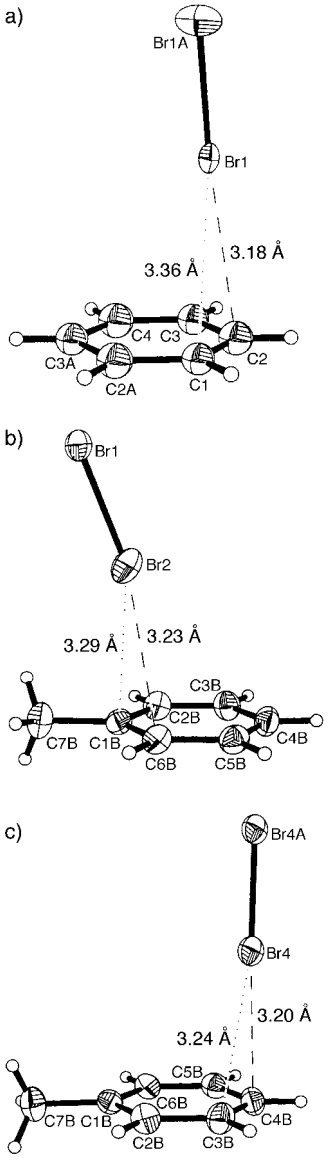

Figure 1. Results of the single-crystal X-ray structural analysis of the CT complex of benzene (a) and toluene (b and c) with bromine (ORTEP diagram). Reproduced with permission from The Royal Society of Chemistry from ref. [7c].

With bromine Kochi et al. were able to convert the CT complexes from benzene or toluene into bromobenzene or bromotoluene and HBr, respectively, in the solid state at low temperature (from −30 to −78 °C). The reaction followed first-order kinetics. Thus, for the first time they were able to demonstrate directly the existence of an aromatic CT complex as a key intermediate. The regioselectivity of the bromination of toluene, that is, the *o*/*p* ratio of about 1:2 found in acetic acid, is also observed in the solid state. It is noticeable that in the solid state too the reaction also occurs via an ionic intermediate without solvent stabilization. It must also be mentioned here that according to Kaupp[21] the Wagner–Meerwein rearrangement of camphene hydrochloride to isobornyl chloride also occurs in the crystalline state at 25 °C, a remarkable effect of "solvation" of an ionic intermediate without solvent in the crystal. Kochi refers to this occurrence as topochemical control of a solid-state reaction.

In the bromination of hexamethylbenzene under similar conditions a deep red salt is obtained of formula $C_6(CH_3)_6Br^+Br_3^-$. The structure shows that it is the σ complex (arenium ion), the rearrangement of the preceding CT complex probably has a low barrier. The salt in the crystal with Br_3^- as the anion is slightly disordered, this does not occur with SbF_6^- as the anion (Figure 2).

The structure and electronic nature of the CT complexes of benzene and toluene with bromine can be derived from ab initio (MP2/6-311 + G**) and DFT calculations.[8] The structure thus calculated corresponds essentially to the values determined experimentally by Kochi et al., and is shown in Figure 3 for the benzene–bromine complex. It is noticeable that the calculated energy of complexation (Table 1) expressed as ΔE

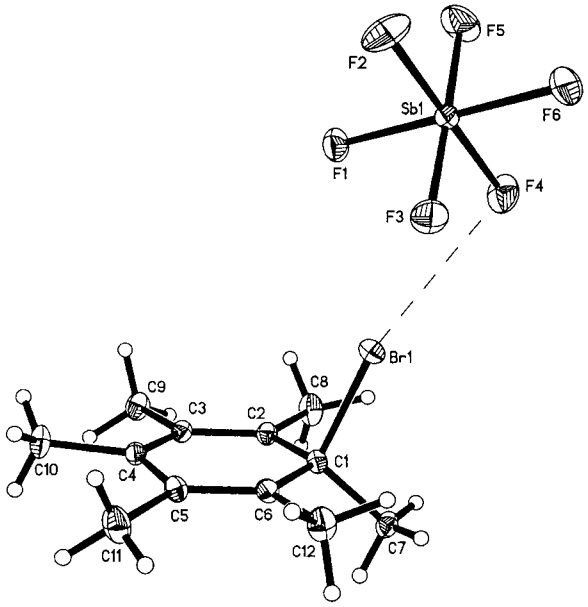

Figure 2. Result of the X-ray crystal analysis (ORTEP diagram) of the product from hexamethylbenzene and bromine with SbF_6^- as anion. Reproduced with permission from The Royal Society of Chemistry from ref. [7c].

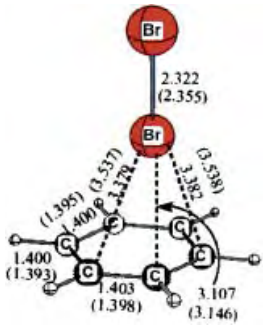

Figure 3. Calculated CT complex from benzene with bromine.[8] For further details of the methods used and the parameters calculated see ref. [9].

is considerably greater than the value calculated by the same method for the bromine complexes from ethylene, ethyne, and allene.[9] It is possible that the structure contribution of radical ions postulated by Kochi et al. plays a larger role in aromatic complexes than in aliphatic bromine CT complexes.

The relative stability of the centrosymmetric over-ring structure to the over-bond coordinated structure and to the arenium ion depends both on the nature of the electrophile and on the choice of arene. It is noteworthy that Kochi et al. had already derived a sym-

 © 2003 Wiley-VCH Verlag GmbH & Co. KGaA, Weinheim 1433-7851/03/4208-0855 $ 20.00+.50/0

Table 1: Calculated thermodynamic parameters for the CT complex from benzene and bromine.[8]

Parameter[a]	Benzene:Br_2	Basis sets
ΔE	−5.46 (−1.74)	MP2/6-311+G** (B3LYP/6-311+G**)
ΔE_{ZPE}	−5.74 (−2.05)	MP2/6-311+G**+ ZPE//MP2/6-31G* (B3LYP/6-311+G**+ ZPE//B3LYP/6-31G*)
$\Delta(\Delta G)$	1.20 (4.58)	MP2/6-31G* (B3LYP/6-31G*)
$\Delta(\Delta S)$	−24.3 (−29.7)	

[a] At 298.15 K. Values for energies are in kcal mol^{-1}; for entropies in e.u.

metrical over-ring structure for the complex from mesitylene and NO in 1991.[7b]

The corresponding CT and σ complexes have also been investigated experimentally and theoretically for the reaction of arenes with other electrophiles, such as H^+,[10] secondary and tertiary alkyl cations,[11] and SO_3.[12] The existence of a symmetrical over-ring structure can be excluded in these cases as energetically it lies much higher than the other configurations. In the case of protonated benzene, $C_6H_7^+$, the σ complex can be detected as the most stable species with high-resolution IR spectroscopy (band analysis of the C–H vibration at 2800 cm^{-1}) by the photodissociation of the complexes formed with argon or nitrogen in the gas phase.[10] This result agrees with calculations according to which the over-edge protonated form and the symmetric over-ring structure are more energy rich, by 6.4 kcal mol^{-1} and 49.3 kcal mol^{-1}, respectively, than the benzenium ion structure. This result also agrees with the NMR spectroscopic investigations of Olah et al. who have investigated this species in superacid solution. Here the over-bond protonated structures are transition states of the sixfold degenerate rearrangement.[13]

The alkylation of benzene with *tert*-butyl, 2-propyl, and methyl cations as electrophiles has been investigated theoretically (MP2/6-31+G**) by Heidrich. Only in the reaction with the tertiary carbocation is a minimum found on the energy hypersurface which corresponds to a CT complex with an over-edge structure.[11] In addition to an over-edge structure with C_s symmetry, a "face" structure (C_3) and three "quasi-face" structures (C_s) with similar energy content are found. The almost planar cation can move relatively freely over the π-electron belt of the benzene to change into the approximately 6 kcal mol^{-1} more stable σ complex through a transition state with C_1 symmetry (see Figure 4). In contrast, the reaction with the primary and secondary carbocation leads directly to the corresponding alkylbenzenium ion. This result correlates with the general scale of Mayr et al. for the prediction of the reactivity of electrophile–nucleophile reactions.[14] The *tert*-butyl cation with benzene as its nucleophilic reaction partner lies in the "green" region of the scale. Reaction should thus take place between them with a reasonable rate at 20°C. In comparison to the *tert*-butyl cation the 2-propyl cation lies, according to the results of Pezacki et al.,[15] about five units of the electrophile parameter (E) higher, and thus lies in the "yellow-red" region of the scale: a stable CT complex is therefore kinetically less likely. The reaction of toluene with SO_3 in solution has been investigated experimentally and calculated theoretically with less rigorous basis sets (4-31G/S*).[12] Here corner-coordinated (atom-coordinated) π and σ complexes

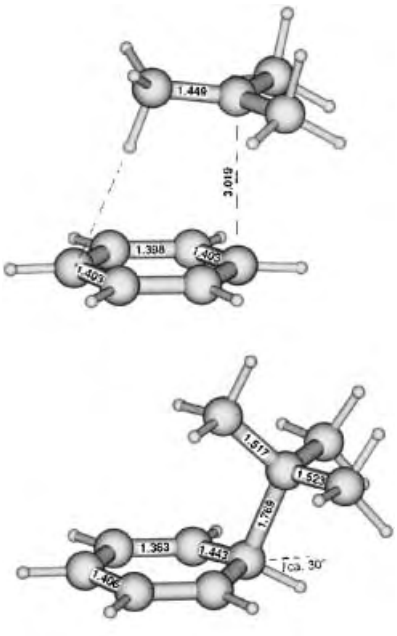

Figure 4. π (top) and σ complex (bottom) from benzene and the *tert*-butyl cation. Bond lenghts [Å], angles [°], reproduced from ref. [11].

with arene–SO_3–SO_3 structures are found, the experimentally determined reactivities of which can be predicted well theoretically. Herges has calculated the complex from benzene and NO_2^+ at the B3LYP/6-31+G* level.[16] The species is edge-coordinated through the nitrogen atom to benzene, the oxygen atoms lie along-side it, and by rotation of the NO_2 unit through of 90° the species is converted into the σ complex (Figure 5).

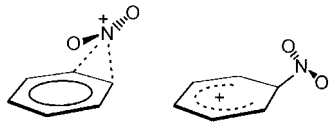

Figure 5. Calculated π and σ complexes from benzene and the NO_2^+ ion.[16]

3. CT Complexes in the Bromination of Aliphatic Multiple Bonds: A Comparison with Aromatic Complexes

Hitherto it has not been possible to isolate CT complexes in the electrophilic bromination of aliphatic multiple bonds. They are detected indirectly from their kinetic and thermodynamic parameters through measurement of the CT band (in 1,2-dichloroethane) at about 280 nm in the UV spectrum.[6d] The confirmation of these complexes as key intermediates may be derived kinetically: negative apparent activation energies (E_a) have been found for the overall reaction in the bromination of strained alkenes (bromination of aliphatic multiple bond systems in dichloroethane). This situation is characteristic of reactions with an established equilibrium, A⇌B→C, where the intermediate B represents the CT complex. The ΔG values and the preferred structures have been calculated for ethylene, ethyne, and allene in the gas phase by ab initio methods (MP2/6-311+G**).[9] The enthalpy values measured in solution correlate well if the entropic contributions of the solvent are taken into consideration. The geometric parameters found for the "T-shaped" structure of the ethylene–bromine complex agree with the results of the structure determined in the gas phase by Legon with microwave spectroscopy (Fabry–Perot

rotation spectrum).[17] The CT complexes of bromine with aliphatic multiple-bond compounds show a series of similarities with the aromatic bromine complexes, but a number of significant differences also exist.[6d] For example, unlike the aromatic complexes, in the bromination of strained alkenes no good correlation of the measured equilibrium constants of the complexes with the calculated ionization potentials is found.

4. Summary and Outlook

"Tempora mutantur, nos et mutamur in illis"[*]—this is also valid for the theory of the electrophilic substitution reaction. Because of the predetermined geometric structure of the species, relatively small exothermic enthalpy values of approximately -5 kcal mol^{-1} during the formation of CT complexes from benzene or ethylene with bromine have a large effect on the overall reaction. Kochi et al. have drawn attention to the general importance of the species as highly structured complexes in the equilibrium,[7b] which can be important in other bimolecular reactions. An important role is attributed to the 1:2 CT complexes which are formed by the addition of a second bromine molecule to the outer bromine atom of the "T-shaped" 1:1 complex. Because of the principle of the "least motion pathway"[18] this complex can readily eject linear Br_3^- as the anion, and because of the special stability of the anion the process is exothermic by approximately -40 kcal, thus facilitating the formation of the subsequent cationic intermediate.[19] This is a special case of autocatalysis of an electrophile. CT complexes formed from substrate and enzyme can also be important in enzymatic reactions.[20] It is becoming increasingly clear that ground state and the primarily formed van der Waals complexes play an important role in the reaction of biomolecules.

[1] a) K. P. C. Vollhardt, N. E. Schore, *Organische Chemie*, 3. ed., Wiley-VCH, Weinheim, **2000**; b) M. B. Smith, J. March, *March's Advanced Organic Chemistry, Reactions, Mechanisms, and Structure*, Wiley, New York, **2001**, chap. 11; c) R. Taylor, *Electrophilic Aromatic Substitution*, Wiley, Chichester, **1990**.

[2] a) M. J. S. Dewar, *Electronic Theory of Organic Chemistry*, Clarendon, Oxford, **1949**; b) M. Kilpatrick, F. E. Luborskyi, *J. Am. Chem. Soc.* **1953**, *75*, 577–584; c) H. C. Brown, J. D. Brady, *J. Am. Chem. Soc.* **1952**, *74*, 3570–3582.

[3] a) R. S. Mulliken, *J. Am. Chem. Soc.* **1952**, *74*, 811–824; b) R. S. Mulliken, W. B. Berson, *Molecular Complexes*, Wiley, New York, **1969**, and references therein.

[4] H. A. Benisi, J. H. Hildebrand, *J. Am. Chem. Soc.* **1949**, *71*, 2703–2707.

[5] a) O. Hassel, K. O. Strømme, *Acta Chem. Scand.* **1958**, *12*, 1146–1147; b) O. Hassel, K. O. Strømme, *Acta Chem. Scand.* **1959**, *13*, 1781–1786.

[6] Reviews: a) M.-F. Ruasse, *Adv. Phys. Org. Chem.* **1993**, *28*, 207–291; b) R. Herges, *Angew. Chem.* **1995**, *107*, 57–59; *Angew. Chem. Int. Ed. Engl.* **1995**, *34*, 51–52; c) R. S. Brown, *Acc. Chem. Res.* **1997**, *30*, 131–147; d) D. Lenoir, C. Chiappe, *Chem. Eur. J.* **2003**, *9*, 1036–1044.

[7] a) A. V. Vasilyev, S. V. Lindeman, J. K. Kochi, *Chem. Commun.* **2001**, 909–910; b) S. V. Rosokha, J. K. Kochi, *J. Org. Chem.* **2002**, *67*, 1727–1737; c) A. V. Vasilyev, S. V. Lindeman, J. K. Kochi, *New J. Chem.* **2002**, *26*, 582–592.

[8] P. von R. Schleyer, C. Wannere, personal communication. I thank Prof. Schleyer and Chait Wannere for the calculations.

[9] C. Chiappe, A. De Rubertis, H. Detert, D. Lenoir, C. S. Wannere, P. von R. Schleyer, *Chem. Eur. J.* **2002**, *8*, 967–978.

[10] N. Solcà, O. Dopfer, *Angew. Chem.* **2002**, *114*, 3781–3784; *Angew. Chem. Int. Ed.* **2002**, *41*, 3628–3631.

[11] D. Heidrich, *Angew. Chem.* **2002**, *114*, 3343–3346; *Angew. Chem. Int. Ed.* **2002**, *41*, 3208–3210.

[12] J. O. Morley, D. W. Roberts, S. P. Watson, *J. Chem. Soc. Perkin Trans. 2* **2002**, 538–544.

[13] G. A. Olah, J. S. Staral, G. Asencio, G. Liang, D. A. Forsyth, G. D. Mateescu, *J. Am. Chem. Soc.* **1978**, *100*, 6299–6308.

[14] R. Lucius, R. Loos, H. Mayr, *Angew. Chem.* **2002**, *114*, 97–102; *Angew. Chem. Int. Ed.* **2002**, *41*, 91–95. The scheme discussed in the text is found in the frontispiece of this article on p. 97 and. p. 91, respectively.

[15] J. P. Pezacki, D. Shukla, J. Lusztyk, J. Warentin, *J. Am. Chem. Soc.* **1999**, *121*, 6589–6598.

[16] R. Herges, personnal communication.

[17] a) A. C. Legon, *Chem. Eur. J.* **1998**, *4*, 1890–1897; b) A. C. Legon, *Angew. Chem.* **1999**, *111*, 2850–2880; *Angew. Chem. Int. Ed.* **1999**, *38*, 2688–2714; c) A. C. Legon, J. M. A. Thumwood, *Phys. Chem. Chem. Phys.* **2001**, *3*, 1397–1402.

[18] a) J. Hine, *J. Org. Chem.* **1966**, *31*, 1236–1244; b) J. Hine, *Adv. Phys. Org. Chem.* **1977**, *15*, 1–61.

[19] a) R. Bianchini, C. Chiappe, D. Lenoir, P. Lemmen, R. Herges, J. Grunenberg, *Angew. Chem.* **1997**, *109*, 1340–1343; *Angew. Chem. Int. Ed. Engl.* **1997**, *36*, 1284–1287; b) R. Bianchini, C. Chiappe, G. Lo Moro, D. Lenoir, P. Lemmen, N. Goldberg, *Chem. Eur. J.* **1999**, *5*, 1570–1580.

[20] R. Boyer, *Concepts in Biochemistry*, S. Brooks/Cole, Monterey, **1999**, pp. 154–158.

[21] G. Kaupp, personal communication; see also G. Kaupp, J. Schmeyers, J. Boy, *Chemosphere*, **2001**, *43*, 55–62.

[*] "Times change, and we change with them."

Cross-Aldol Reactions of Aldehydes

The Direct Catalytic Asymmetric Cross-Aldol Reaction of Aldehydes

Benito Alcaide and Pedro Almendros**

Keywords:
aldol reactions · asymmetric catalysis · asymmetric synthesis · C–C coupling · enantioselectivity

The aldol reaction, in addition to being an effective method for the formation of C–C bonds in organic synthesis,[1] is also a critical biological reaction in the context of metabolism. The classical aldol reaction is highly atom-economic but suffers from problems with selectivity, notably, with respect to chemo- and regioselectivity. A further challenge is to perform these reactions asymmetrically.[2] Stimulated by this challenge, it is not surprising that great effort is currently being made in the search for elegant and practical solutions to the structural and stereochemical problems presented by the aldol motif. Impressive achievements in asymmetric aldol methodology have been made which, in general, rely on the use of chiral auxiliaries, ligands, and catalysts as the main stereochemical controllers.[3] The importance of asymmetric catalysis is undisputed, as evidenced, among other things, by the award of the 2001 Nobel Prize for Chemistry to K. Barry Sharpless, Ryoji Noyori, and William S. Knowles. Undoubtedly, the more elegant and most economically attractive way to introduce chirality into a molecule is by using a catalytic amount of a chiral controller to induce the chiral transformation. The two main options available to chemists are the use of biochemical catalysts or the use of chemical catalysts, such as homogeneous transition-metal catalysts or nonmetallic small organic molecules. In metal-mediated enantioselective catalytic reactions, the metal plays an organizational role by translating chiral information and activating the reagents. In the absence of a metal, the well-organized transition state, which is required for the enantioselective transformation, can be formed either by passive or dynamic interactions, as is the case in biological systems. Small organic molecules are more in keeping with enzyme- or antibody-catalyzed reactions than with organometallic processes. Indeed, these small organic molecules are often also known as artificial enzymes or enzyme mimetics, because they show some characteristic features of bioorganic reactions.

A remarkable enhancement of the efficiency of the aldol reaction would be achieved if a chemical chiral catalyst were found that did not require the pregeneration of enolates or enolate-like species, and which acts both directly and asymmetrically.[4] Biological-type catalysts (enzymes and antibodies) have had selected successes.[5] The first report of the use of chemical catalysis for a direct catalytic enantioselective aldol reaction appeared just five years ago from Shibasaki and co-workers.[6] This group developed the multifunctional catalyst (*R*)-LLB-**1** which promotes the direct asymmetric aldol reaction of aldehydes **2** with unmodified ketones **3** by employing 20 mol% of the compound (*R*)-LLB-**1** (Scheme 1). The heterobimetallic complex **1** can be regarded as an enzyme mimic of the metal-containing aldolases of type II (with a zinc cofactor).

Organocatalysis,[7] and in particular aminocatalysis,[8] is a biomimetic strategy used for important enzymes such as class I aldolases (enamine catalysis) and ketoacid decarboxylases (iminium catalysis). Applications in asymmetric organic synthesis are relatively rare despite the well-known Hajos–Parrish–Eder–Sauer–Wiechert reaction,[9] an intramolecular proline-catalyzed process (Scheme 2).

The direct aldol reaction facilitated by chiral nonracemic amines is a challenging new dimension to this powerful method of forming C–C bonds. In this respect, List, Lerner, and Barbas III

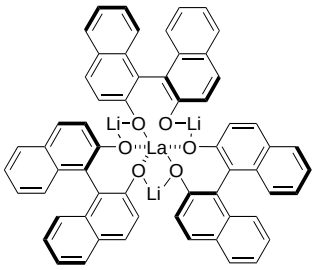

(*R*)-LLB-**1**

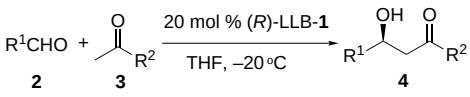

2 **3** **4**

R^1 = $Ph(CH_2)_2$, *c*-C_6H_{11}, *i*Pr, *t*Bu
R^2 = Me, Et, Ph, 1-naphthyl

(53–90%)
(44–94% *ee*)

Scheme 1. Direct asymmetric aldol reaction between aldehydes and unmodified ketones catalyzed by (*R*)-LLB-**1**.

[*] Prof. Dr. B. Alcaide
Departamento de Química Orgánica I
Facultad de Química
Universidad Complutense de Madrid
28040 Madrid (Spain)
Fax: (+34) 91-394-4103
E-mail: alcaideb@quim.ucm.es
Dr. P. Almendros
Instituto de Química Orgánica General
Consejo Superior de Investigaciones Científicas
Juan de la Cierva 3, 28006 Madrid (Spain)
Fax: (+34) 91-564-4853
E-mail: iqoa392@iqog.csic.es

 © 2003 Wiley-VCH Verlag GmbH & Co. KGaA, Weinheim 1433-7851/03/4208-0858 $ 20.00+.50/0

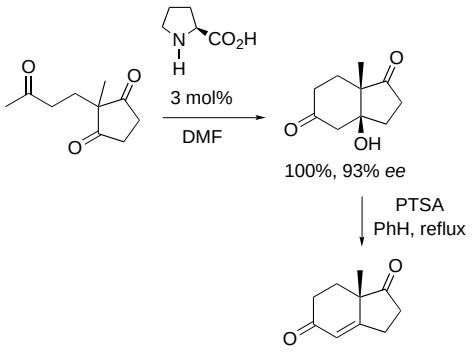

Scheme 2. L-Proline-catalyzed asymmetric Robinson annulation: the Hajos–Parrish–Eder–Sauer–Wiechert reaction. PTSA = *p*-toluenesulfonic acid.

have identified L-proline as a metal-free organocatalyst for the direct enantioselective aldol addition of acetone and a variety of aldehydes (Scheme 3).[10] This result constitutes the first low-molecular-weight amine-catalyzed direct asymmetric aldol reaction, which represents a promising alternative catalytic concept to the commonly used metal-containing catalysts.[11] This catalyst can therefore be regarded as an enzyme mimic of a metal-free type I aldolase. Unlike the proline-catalyzed intramolecular aldol, this reaction does not exhibit a nonlinear effect, consistent with the involvement of only one equivalent of catalyst in the transition state.

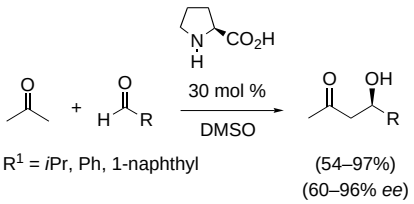

Scheme 3. L-Proline-catalyzed direct enantioselective aldol reaction of acetone and aldehydes.

Even at such an advanced stage of modern enolate chemistry, the stereoselectively controlled self-aldol reaction of aldehydes has found no general solution.[12] The problems associated with the above-mentioned reaction include: 1) polyaldolization, which results from secondary additions to the aldehyde products, 2) dehydration of the product, which enables Michael-type additions, 3) Tishchenko-type processes, and 4) oligomerization of the product. In 2001, Denmark and Ghosh reported the first catalytic enantioselective cross-aldol reaction of aldehydes, promoted by the phosphoramide **5**.[13] The use of this dimeric chiral nonracemic Lewis base as the catalyst was critical in achieving useful enantioselectivities. Geometrically defined trichlorosilyl enolates of aldehydes undergo high-yield diastereoselective additions to a wide range of aldehyde acceptors with good, albeit highly variable, enantioselectivities (Scheme 4). The cross-aldol products were isolated as stable dimethyl acetals on quenching the reaction with dry methanol.

Nevertheless, stoichiometric amounts of base and/or adjunct reagents (such as silylating agents to form the enol silyl ethers) are required, which decreases the atom efficiency of the process. Therefore, efforts should be devoted to the development of the direct catalytic enantioselective cross-aldol reaction of aldehydes, where there is no need for any other activation of the starting materials. Inspired by the good results obtained by the L-proline-promoted direct enantioselective aldol condensation between acetone and aldehydes, MacMillan was interested in examining the capacity of proline to catalyze the asymmetric cross-aldol reactions of aldehydes. However, this reaction had been restricted to ketones, which by reaction with the chiral amine generates an enamine intermediate, which reacts with another carbonyl compound. It should be noted that the use of aldehydes in direct catalytic enantioselective aldol reactions is very challenging, when compared to such reactions with ketones, as a result of the comparatively low reactivity of the enamine intermediate that is generated from aldehydes. Fortunately, the scope of the Hajos–Parrish–Barbas–List methodology has been enhanced remarkably by the very recent use of aldehyde substrates for direct asymmetric crossed-aldol reactions by MacMillan's research group.[14] This group have described the first example of a direct enantioselective aldehyde-dimerization through the exposure of propionaldehyde to catalytic quantities of L-proline in DMF. The desired aldol adduct was obtained with *anti*-aldol selectivity, and with excellent levels of enantiocontrol (Scheme 5).

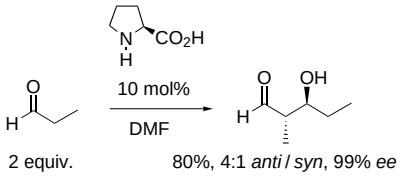

Scheme 5. Direct enantioselective aldehyde–aldehyde dimerization catalyzed by L-proline.

The high reaction efficiency that was observed in the proline-induced asymmetric aldehyde dimerization prompted MacMillan's group to evaluate if L-proline could also catalyze the enantioselective cross-aldol reaction between nonequivalent aldehydes, an elusive transformation. The fundamental problem is that the catalyst must differentiate between the α protons of the acceptor and donor aldehydes, as deprotonation of both aldehydes may lead to undesirable self-aldolization products. However, only a single regioisomer of the cross-aldol product was obtained in good yield and in excellent enantioselectivity (Scheme 6).[14] Interestingly, syringe-pump addition of the aldehyde donor to a series of aldehyde acceptors in the

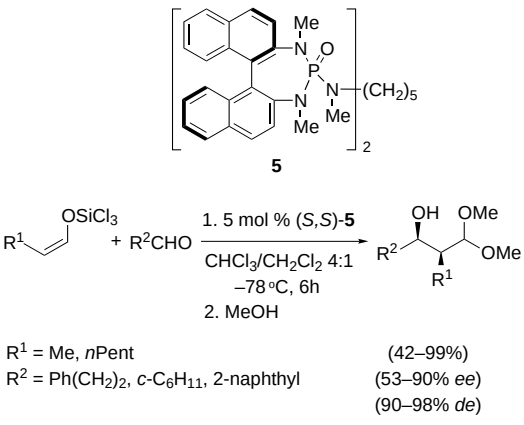

Scheme 4. Catalytic nondirect enantioselective cross-aldol reaction of aldehydes promoted by a dimeric phosphoramide.

 © 2003 Wiley-VCH Verlag GmbH & Co. KGaA, Weinheim 1433-7851/03/4208-0859 $ 20.00+.50/0

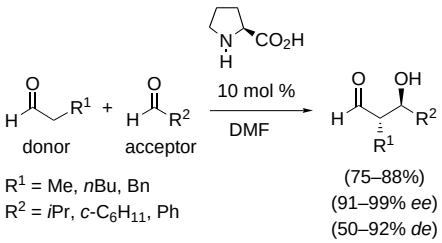

Scheme 6. Direct catalytic asymmetric cross-aldol reactions between nonequivalent aldehydes induced by L-proline.

presence of L-proline effectively suppressed homodimerization of the donor aldehyde. A drawback of the ketone-based proline-catalyzed aldol reactions was the large quantity of catalyst required (30 mol%). Fortunately, there were no similar concerns with the cross-aldol reaction of aldehydes, where it was possible to use much lower catalyst loadings (typically around 10 mol%) without producing a loss in the reaction efficiency.

It should be noted that both the absolute and relative configurations of the aldol product were in good agreement with previously proposed models of proline-catalyzed aldol reactions.[15] According to this proposal, proline functions as a microaldolase, with the secondary amine acting as a nucleophilic enamine catalyst and the carboxylic acid moiety as a general Brønsted cocatalyst. The observed stereochemistry can be explained by invoking a metal-free Zimmerman–Traxler-like transition state (Figure 1). A bifurcated hydrogen bond involving the carboxylate, enamine, and aldehyde moieties, organizes the transition state. Steric interactions between the aldehyde and enamine substituents may be the most important, which would account for the excellent *anti*-enantiofacial selectivity exhibited by this reaction.

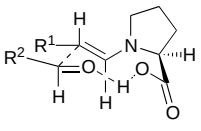

Figure 1. Proposed transition state for the direct cross-aldol reaction catalyzed by L-proline.

However, there are unsolved problems in the area of the formation of *syn*-products, and also in expanding the number and type of aldehydes that may be used. At the moment, it appears that only branched aldehydes may be used as the R^2-aldehydes, with the exception of homodimerization reactions.

In summary, this new method for an elusive transformation, namely, the direct catalytic asymmetric cross-aldol reaction of aldehydes, constitutes a significant advancement of synthetic methodology, which allows straightforward enantioselective access to important synthons in polypropionate and polyacetate natural products. The search for small, metal-free organic molecules that can be utilized for more-broadly applicable and more-selective catalysts should yield new information in this exciting area.

[1] a) T. Mukaiyama, *Org. React.* **1982**, *28*, 203; b) C. H. Heathcock in *Asymmetric Synthesis, Vol. 3* (Ed.: J. D. Morrison), Academic Press, New York, **1984**, chap. 2; c) B. M. Kim, S. F. Williams, S. Masamune in *Comprehensive Organic Synthesis, Vol. 2* (Eds.: B. M. Trost, I. Fleming, C. H. Heathcock), Pergamon, Oxford, **1991**, chap. 1.7.

[2] For a recent overwiew, see: C. Palomo, M. Oiarbide, J. M. García, *Chem. Eur. J.* **2002**, *8*, 37.

[3] For a review on the catalytic asymmetric aldol reaction, see: T. D. Machajewski, C.-H. Wong, *Angew. Chem.* **2000**, *112*, 1406; *Angew. Chem. Int. Ed.* **2000**, *39*, 1352.

[4] For a recent review, see: B. Alcaide, P. Almendros, *Eur. J. Org. Chem.* **2002**, 1595.

[5] a) B. List, D. Shabat, C. F. Barbas III, R. A. Lerner, *Chem. Eur. J.* **1998**, *4*, 881; b) T. Hoffmann, G. Zhong, B. List, D. Shabat, J. Anderson, S. Gramatikova, R. A. Lerner, C. F. Barbas III, *J. Am. Chem. Soc.* **1998**, *120*, 2768; c) H. J. M. Gijsen, L. Qiao, W. Fitz, C.-H. Wong, *Chem. Rev.* **1996**, *96*, 443; d) W.-D. Fessner, G. Sinerius, A. Schneider, M. Dreyer, G. E. Schulz, J. Badia, J. Aguilar, *Angew. Chem.* **1991**, *103*, 596; *Angew. Chem. Int. Ed. Engl.* **1991**, *30*, 555.

[6] Y. M. A. Yamada, N. Yoshikawa, H. Sasai, M. Shibasaki, *Angew. Chem.* **1997**, *109*, 1942; *Angew. Chem. Int. Ed. Engl.* **1997**, *36*, 1871.

[7] P. I. Dalko, L. Moisan, *Angew. Chem.* **2001**, *113*, 3840; *Angew. Chem. Int. Ed.* **2001**, *40*, 3726.

[8] E. R. Jarvo, S. J. Miller, *Tetrahedron* **2002**, *58*, 2481.

[9] a) U. Eder, G. Sauer, R. Wiechert, *Angew. Chem.* **1971**, *83*, 492; *Angew. Chem. Int. Ed. Engl.* **1971**, *10*, 496; b) Z. G. Hajos, D. R. Parrish, *J. Org. Chem.* **1974**, *39*, 1615.

[10] B. List, R. A. Lerner, C. F. Barbas III, *J. Am. Chem. Soc.* **2000**, *122*, 2395.

[11] It has been reported recently that both isomers of nornicotine were tested for the direct asymmetric aldol reaction. However, only a small amount of asymmetric induction (20%) was observed with either enantiomer: T. J. Dickerson, K. D. Janda, *J. Am. Chem. Soc.* **2002**, *124*, 3220.

[12] For the problems inherent in this construction, see: a) C. H. Heathcock in *Comprehensive Organic Synthesis, Vol. 2, Part 2* (Eds.: B. M. Trost, I. Flemming, C. H. Heathcock), Pergamon, Oxford, **1991**, p. 133. For the enzyme-catalyzed aldol reaction of acetaldehyde and propanal with various aldehyde acceptors, see: b) H. J. M. Gijsen, C.-H. Wong, *J. Am. Chem. Soc.* **1995**, *117*, 7585.

[13] S. E. Denmark, S. K. Ghosh, *Angew. Chem.* **2001**, *113*, 4895; *Angew. Chem. Int. Ed.* **2001**, *40*, 4759.

[14] A. B. Northrup, D. W. C. MacMillan, *J. Am. Chem. Soc.* **2002**, *124*, 6798.

[15] S. Kandasamy, W. Notz, T. Bui, C. F. Barbas III, *J. Am. Chem. Soc.* **2001**, *123*, 5260.

NMR Spectroscopy of Proteins

NMR Spectroscopy Techniques for Screening and Identifying Ligand Binding to Protein Receptors

Bernd Meyer and Thomas Peters**

Keywords:
drug design · ligand–protein interactions · NMR spectroscopy · proteins · screening

Dedicated to Professor Hans Paulsen on the occasion of his 80th birthday

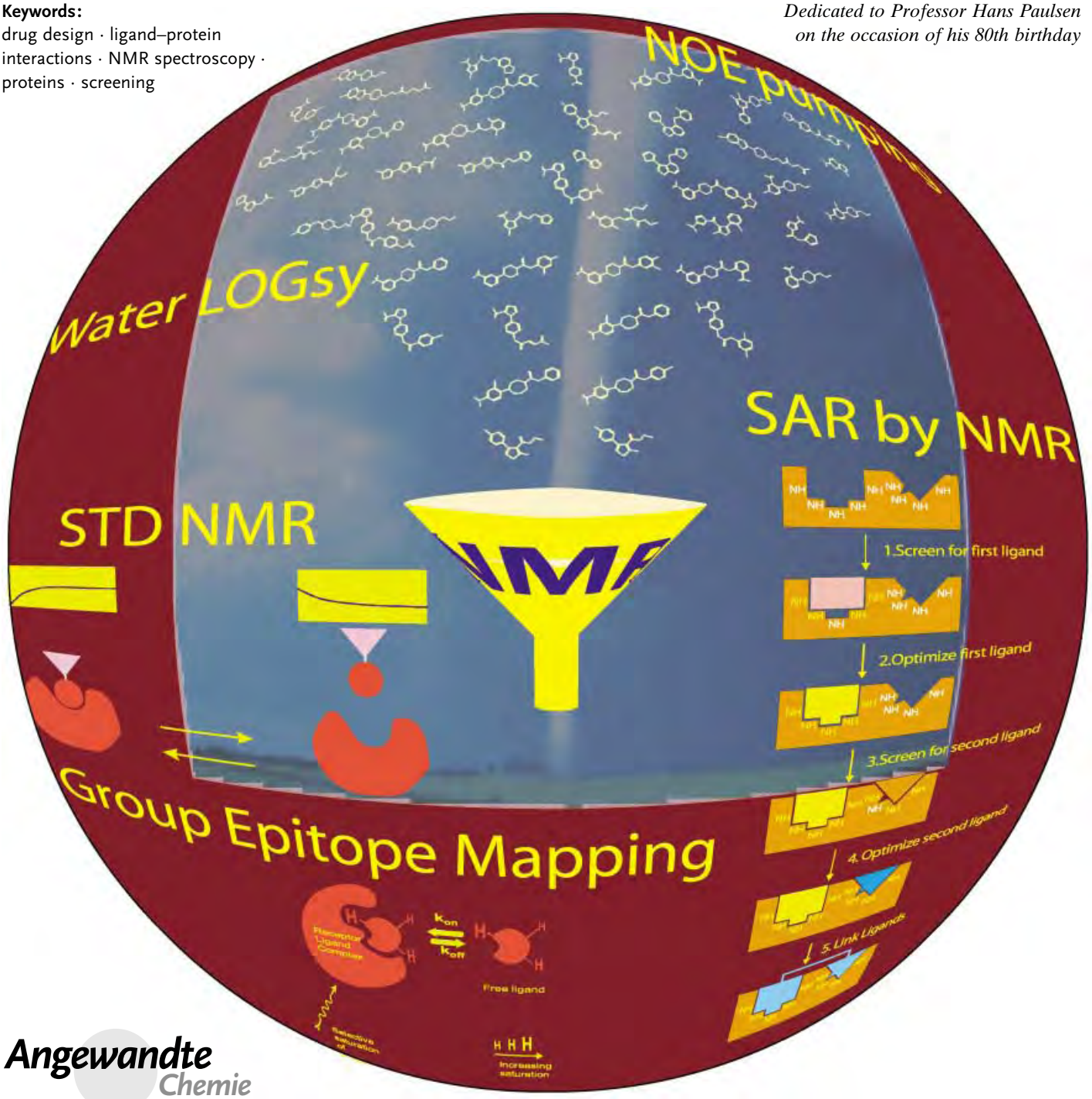

© 2003 Wiley-VCH Verlag GmbH & Co. KGaA, Weinheim
1433-7851/03/4208-0864 $ 20.00+.50/0

Binding events of ligands to receptors are the key for an understanding of biological processes. Gaining insight into protein–protein and protein–ligand interactions in solution has recently become possible on an atomic level by new NMR spectroscopic techniques. These experiments identify binding events either by looking at the resonance signals of the ligand or the protein. Ideally, both techniques together deliver a complete picture of ligand binding to a receptor. The approaches discussed in this review allow screening of compound libraries as well as a detailed identification of the groups involved in the binding events. Also, characterization of the binding strength and kinetics is possible, competitive binding as well as allosteric effects can be identified, and it has even been possible to identify ligand binding to intact viruses and membrane-bound proteins.

From the Contents

1. Introduction 865
2. Use of the Transferred NOE Effect for Detecting and Characterizing Ligand Binding 866
3. Using Chemical-Shift Changes To Identify Ligand Binding and the Binding Pocket of the Receptor 881
4. Use of Relaxation Times To Identify Ligand Binding 886
5. Use of Diffusion To Identify Ligand Binding 887
6. Conditions for NMR Spectroscopy Screening and Characterization of Binding 888

1. Introduction

In general, the biological function of a protein depends on its interaction with ligand molecules. Examples are the interaction of hormone receptors with hormones, that trigger complicated signal cascades, or the interaction of certain proteins with nucleic acid sequences to regulate gene replication, transcription, or translation, or the highly specific interaction of cell-surface antigens with receptors located on other cells. This list of arbitrary examples may be continued almost infinitely. It is clear that understanding biological function requires a precise knowledge about the underlying protein–ligand recognition events at an atomic level. Therefore, there have been many attempts aimed at accurately characterizing such processes with a variety of biophysical methods.

Of special interest are certainly those protein–ligand interactions that play a key role for the development of severe disease states, such as HIV or cancer. Understanding the principles of how a certain protein receptor interacts with biological, that is, natural ligands, allows the development of other more potent substances that may then serve as drug candidates. The process of identifying and optimizing such drug candidates is usually a very time consuming task, and consists of several steps. One major step comprises the identification of substances with binding activity for the protein receptor under investigation from which to generate so-called leads. This discovery process requires the screening of a very large number of compounds, often more than 10^6. Classically, this screening step is performed utilizing biological assay formats, such as the enzyme-linked immunoadsorbent assay (ELISA). Recently, several novel NMR spectroscopic techniques have emerged as powerful techniques to understand the binding process at a molecular level and to utilize them for identification of new bioactive substances. As these methods become increasingly important, several review articles with varying focus have been published during recent years.[1–13] It will be the purpose of this review to give a comprehensive overview about different NMR spectroscopic methods to identify and to characterize the binding activity of ligands with receptor proteins. Subsequent steps that involve the analysis of the bioactive conformations of ligands and the epitope mapping of ligand molecules will also be discussed.

Theoretically, all NMR spectroscopic parameters may serve as a gauge for the binding activity of a ligand to a protein. In practice, however, only parameters that can be obtained easily and with high sensitivity are of significance. For example, chemical-shift changes, changes in relaxation times, changes of diffusion constants, changes of NOEs, or exchange of saturation serve as measures of binding. In general, two main experimental approaches exist. The first focuses on the NMR signals of the ligand and usually utilizes NOE effects between protein and ligand (Section 2). The second approach focuses on chemical-shift changes of the target protein upon binding of the ligand (Section 3). As will become clear in the following, the two approaches are complementary and have different advantages. Other approaches utilize changes in relaxation or diffusion behavior of the ligand upon binding to a protein (Sections 4 and 5).

[*] Prof. Dr. T. Peters
Institute for Chemistry
University of Lübeck
Ratzeburger Allee 160, 23538 Lübeck (Germany)
Fax: (+49) 451-500-4241
E-mail: thomas.peters@chemie.mu-luebeck.de
Prof. Dr. B. Meyer
Institute for Organic Chemistry
University of Hamburg
Martin Luther King Platz 6, 20146 Hamburg (Germany)
Fax: (+49) 451-500-4241
E-mail: bernd.meyer@sgi1.chemie.uni-hamburg.de

 © 2003 Wiley-VCH Verlag GmbH & Co. KGaA, Weinheim 1433-7851/03/4208-0865 $ 20.00+.50/0

2. Use of the Transferred NOE Effect for Detecting and Characterizing Ligand Binding

It is well established that NOE effects (NOEs) are extremely useful in determining the 3D structure of molecules in solution.[14] The method has been especially successful for the structural analysis of proteins.[15–20] When ligand molecules bind to receptor proteins the NOEs undergo drastic changes leading to the observation of transferred NOEs (trNOEs). These changes are the basis for a variety of experimental schemes that are designed to detect and characterize binding activity.

The principles of trNOEs were originally observed and described more than twenty years ago[21–25] and have since then found widespread use in the determination of the 3D structures of ligands bound to receptor proteins.[26–30] The observation of trNOEs relies on different tumbling times τ_c of free and bound molecules. Low- or medium-molecular-weight molecules ($M_W < 1000$–2000) have a short correlation time τ_c and, as a consequence, such molecules exhibit positive NOEs, no NOEs, or very small negative NOEs depending on their molecular weight, shape, and the field strength. Large molecules, however, exhibit strongly negative NOEs. When a small molecule (ligand) is bound to a large-molecular-weight protein (the protein receptor molecule) it behaves as a part of the large molecule and adopts the corresponding NOE behavior, that is, it shows strong negative NOEs, so-called trNOEs. These trNOEs reflect the bound conformation of the ligand. Binding of a ligand to a receptor protein can thus easily be distinguished by looking at the sign and size of the observed NOEs. Furthermore, the discrimination between trNOEs originating from the bound state and NOEs of the ligand in solution can also be achieved by the build-up rate, that is, the time required to achieve maximum intensity, which for trNOEs is in the range of 50 to 100 ms, whereas for nonbinding molecules it is four- to ten-times as long. Therefore, the maximum enhancement for trNOEs is observed at significantly shorter mixing times τ_{mix} than for isolated small molecules in solution. Various experimental implementations have been explored in the last two decades, ranging from 1D selective steady-state experiments to 1D and 2D transient NOE experiments.[14] Also, several schemes have been developed that allow a quantitative interpretation of trNOEs and, thus, yield more reliable information about the conformation of bound ligands.[26,27,30]

In general, one can observe inter- and intramolecular trNOEs. Whereas intramolecular trNOEs are the key to define bound-ligand conformations, intermolecular trNOEs occur between a ligand and a receptor protein, and therefore, in principle, allow the determination of the orientation of bound ligands in protein binding pockets.[31,32]

In the following we will present experimental schemes that rely on the trNOE phenomenon, and that have been used to detect and characterize binding activities in combinatorial libraries and other complex compound mixtures.

2.1. Saturation-Transfer-Difference (STD) NMR Spectroscopy Experiments

Saturation-transfer NMR spectroscopy has been used for many years to characterize binding in tightly bound ligand—receptor complexes. If a ligand shows two different signals because of a slow exchange between the bound state and the free state a transfer of saturation is possible between the free and the bound state. By irradiating, for example, signals of the free ligand, the signals of the bound ligand may be identified. In addition to the assignment of resonance signals of the bound ligand the saturation-transfer method has been employed to analyze the binding kinetics of ligand–protein complex formation.[33–51]

The technique has also been applied to analyze the binding of carbohydrate ligands to proteins.[52,53] However, the enormous potential of saturation-transfer NMR experiments to screen compound mixtures for binding activity was only realized recently. We have developed a method based on the transfer of saturation from the protein to the bound ligands which in turn, by exchange, is moved into solution where it is detected (Figure 1, Scheme 1).[54,55] By utilizing the power of difference spectra the method can easily be used for homonuclear spectroscopy, especially proton NMR experiments, to obtain well-resolved spectra of the ligand alone. Subtracting a spectrum in which the protein is saturated from one without protein saturation produces a difference spec-

Bernd Meyer obtained his Ph.D. in chemistry at the University of Hamburg in 1979. Then, he was a postdoctoral fellow with Prof. Dr. Klaus Bock, at the Technical University of Lyngby in Denmark. In 1986 he obtained his Habilitation in Organic Chemistry at the University of Oldenburg, and shortly thereafter moved as an Assistant Professor to the Complex Carbohydrate Research Center in Athens, Georgia, USA. In 1992 he received tenure and became Associate Professor. In 1993 he returned to the University of Hamburg, Germany, as professor of chemistry. His research interests are structural NMR spectroscopic analysis of glycoproteins, glycopeptide synthesis, screening of combinatorial libraries for binding affinity, and the rational design of ligands and inhibitors for proteins and the HIV infection.

Thomas Peters received his Ph.D. at the University of Hamburg in 1986. He was a post doctoral fellow with Prof. Dr. David R. Bundle, at the National Research Council, Ottawa, Canada. In 1993 he obtained his Habilitation in biophysical chemistry at the University of Frankfurt. In 1994 he became professor at the Medical University of Lübeck. With his strong background in NMR spectroscopy he is working on the theoretical and experimental determination of the 3D structure of oligosaccharides and the analysis of ligand binding to fully functional native viruses and the analysis of viral proteins.

Box 1: Kinetics and thermodynamics of the binding of small-molecule ligands to large receptor proteins—relevance to NMR spectroscopy binding experiments

The binding of small-molecule ligands to large receptor proteins in its simplest form follows a bimolecular association reaction with second-order kinetics. For the association of a ligand L to a receptor protein P to give the complex PL the equilibrium in Equation (1) ex-

$$P + L \underset{k_{off}}{\overset{k_{on}}{\rightleftharpoons}} PL \quad (1)$$

ists with k_{on} and k_{off} being the on (association) and off (dissociation) rate constants.

The dissociation constant K_D is then given in Equation (2).

$$K_D = \frac{[P]\,[L]}{[PL]} = \frac{k_{off}}{k_{on}} \quad (2)$$

Estimates for k_{off} may be obtained by assuming a diffusion controlled association (on rates) where k_{on} is about $10^7\ s^{-1}\,M^{-1}$. From this the dissociation rates (off rates) are calculated as shown in Table 1.

Table 1:

K_D	k_{off} [s^{-1}]
1 mM	10000
1 μM	10
1 nM	0.01

However, k_{on} can vary from less than 10^4 to 10^{11} giving rise to variations in off rates of more than seven orders of magnitude. The on rate is typically slow if large conformational rearrangements of either ligand or receptor occur upon binding. Off rates larger than 10^7 are observed for very small ligands, for example, H_2CO_3.

Estimates for k_{off} become important for the interpretation of NMR binding experiments (see Box 5) in which different conditions can be found:

a) fast exchange on the chemical-shift time scale [Eq. (3)]

$$k_{off} \gg '''\omega \quad (3)$$

b) intermediate exchange on the chemical-shift time scale [Eq. (4)]

$$k_{off} \approx \omega \quad (4)$$

c) slow exchange on the chemical-shift time scale [Eq. (5)]

$$k_{off} \ll '''\omega \quad (5)$$

Where $\Delta\omega = 2\pi\Delta\nu$ is the chemical-shift difference [Hz] of signals in the bound and free state. "Exchange" here relates to the exchange between free and bound states of the ligand.

For NMR binding experiments which are based on chemical-shift differences, such as structure–activity relationships (SAR) by NMR, the intermediate exchange regime may be reached even at micromolar values of K_D, depending on the chemical-shift difference expected. For example, if a chemical-shift difference of $\Delta\nu = 20$ Hz is observed for the difference between the signal for the free ligand and that of the bound ligand, then a K_D of 12 μM, which corresponds to a k_{off} value of 125 s^{-1}, would yield intermediate exchange and thus very broad signals of low intensity.

At faster k_{off} values, signals appear at the position corresponding to the weighted-average of the chemical shifts of the signals from the bound and free ligand. At slower k_{off} values two separate signals will be found, one for the ligand-bound and one for ligand-free state.

In many cases it will be important to estimate the fraction of molecules bound to a receptor protein. With $[P]_0$ and $[L]_0$ being the total protein and the total ligand concentration, respectively, Equation (2) can be transformed into a quadratic equation with the solution given in Equation (6).

$$[PL] = 1/2(K_D + [P]_0 + [L]_0) - \sqrt{1/4(K_D + [P]_0 + [L]_0)^2 - [L]_0\,[P]_0} \quad (6)$$

At a given concentration of $[L]_0$ and $[P]_0$ and a given value of K_D the actual concentration of the complex PL can be calculated with Equation (6) and from this the fraction of ligand and protein bound can be easily determined as f_{LB} in Equation (7) and f_{PB} Equation (8),

$$f_{LB} = [PL]/[L]_0 \quad (7)$$

$$f_{PB} = [PL]/[P]_0 \quad (8)$$

respectively.

The f_{LB} fraction is important to estimate the observed line widths of ligand signals. The f_{PB} fraction is used to assess the availability of free binding sites for competition studies.

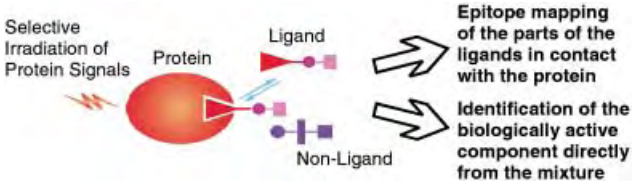

Scheme 1. Representation of STD NMR spectroscopy. When a protein becomes saturated, ligands that are in exchange between a bound and the free form become saturated when bound to the protein. By exchange that saturation is carried into solution where it is detected. By subtraction of this spectrum from a spectrum without protein irradiation an NMR spectrum is obtained in which the only signals are from molecules that bind to the protein. Resonance signals from nonbinders do not show up in the difference spectrum. The receptor protein is saturated with a selective saturation pulse. In general, the saturation pulse consists of a cascade of Gauss-shaped pulses. The duration of saturation times typically ranges from 1 to 2 s. The ligand is normally used in an approximately 100-fold molar excess over the protein, allowing low μM protein concentrations to be used.

trum in which only the signals of the ligand(s) remain. The irradiation frequency is set to a value where only resonances from the protein nuclei and no resonances from ligand nuclei are located. Therefore, in the on-resonance experiment selective saturation of the signals of the protein nuclei is achieved. For the on-resonance irradiation frequency values around −1 ppm are practical because no ligand nuclei resonances are found in this spectral region whereas the significant line width of protein signals still allows selective saturation. If the ligands show no resonance signals in the aromatic proton spectral region the saturation frequency may also be placed here or even further downfield ($\delta = 11$–12 ppm). In order to achieve the desired selectivity and to avoid side-band irradiation, shaped pulses are employed for the saturation of the protein signals (Figure 2).

One of the major advantages of the new STD technique is that the STD method may be combined with any NMR spectroscopy pulse sequence generating a whole suite of STD NMR experiments such as STD TOCSY or STD HSQC.[54,56]

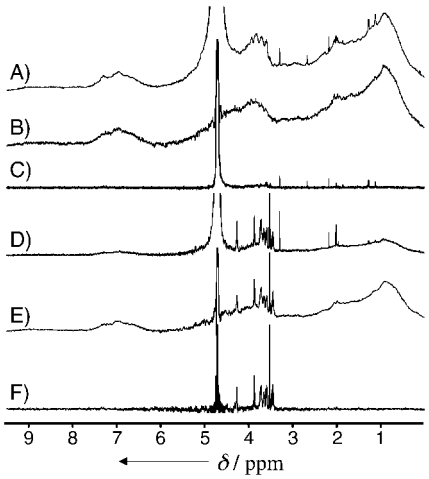

Figure 1. A) Reference 1D NMR spectrum of the 120 kDa protein RCA_{120} (binding site concentration 50 μM) displaying the very broad signals normal for a protein this size. The few sharp resonance signals arise from low-molecular-weight impurities. B) Corresponding STD NMR spectrum showing that by irradiating at $\delta = -2$ ppm the entire protein is saturated uniformly and can therefore be efficiently used for the STD NMR technique. One can also see, that the impurities contained in the spectrum (A) are effectively subtracted and therefore do not give rise to signals in the difference STD spectrum. C) 1D NMR spectrum recorded with a $T_{1\rho}$ filter (a 30 ms spin-lock pulse), to eliminate the broad resonance signals of the protein. Only those resonance signals of the low-molecular-weight impurities remain in the spectrum. D) Reference 1D NMR spectrum of RCA_{120} (binding site concentration 40 μM) in presence of 1.2 mM β-GalOMe, without the $T_{1\rho}$ filter. E) Corresponding STD NMR spectrum, which shows the β-GalOMe resonance signals and therefore that β-GalOMe binds to the receptor. F) STD NMR spectrum as in (E) but with the $T_{1\rho}$ filter eliminating all protein background signals.

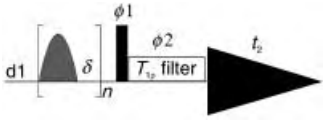

Figure 2. Pulse sequence for 1D STD NMR spectroscopy. The subtraction is performed after every scan by phase cycling. The on and off resonance frequency of the selective pulse is therefore switched between −0.4 ppm and 30 ppm after every scan. Phases are $\phi_1 = (x,-x,-x,x,y,-y,-y,y,-x,x,x,-x,-y,y,y,-y)$; $\phi_2 = 2(y,-y),2(-x,x)$; and $\phi_{rec} = 2(x),2(-x),2(y),2(-y),2(-x),2(x),2(-y),2(y)$. The length of the selective pulse is 50 ms and the delay δ between the pulses is 1 ms, the duration of the presaturation period is adjusted by the number of pulses n (typically $n = 40$), d1 is an additional short relaxation delay. The intensity of the selective saturation Gauss pulses is about $\gamma B_1 = 86$ Hz.

The STD experiment was first applied to screen a library of carbohydrate molecules for binding activity towards a carbohydrate binding protein, wheat-germ agglutinin (WGA). At the same time it was also shown that STD NMR is an excellent technique for determining the binding epitope of the ligand, information that is of prime importance for the directed development of drugs.[54] This will be discussed in more detail further below (see Section 2.1.4).

Box 2: Parameters affecting STD effects

The Scheme shows the situation of a solution containing ligand and receptor after the initial saturation time of typically 50 to 200 ms. Assuming a large excess of ligand over protein, the rebinding of already saturated ligands can be neglected. (r.f.: radio frequency for saturation; τ_{sat}: saturation time; τ_{res}: residence time of ligand in the binding site; P*: saturated protein; L: unsaturated ligand; L*: saturated

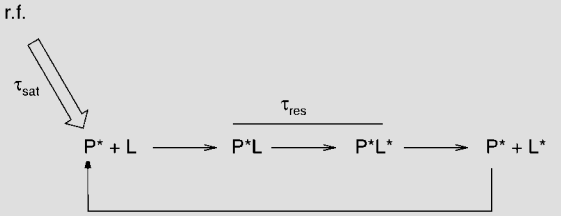

ligand.)During the saturation time τ_{sat} the binding site of the protein is consecutively occupied by n ligand molecules with $n = f_{PB} * \tau_{sat}/\tau_{res}$, where f_{PB} is the fraction of occupied binding sites (see Box 1). This turnover is responsible for the amplification of the information resulting from the saturated protein. A large excess of ligands allows for the maximum effect to be observed.

A recent paper describes the application of full-relaxation matrix theory to the calculation of theoretical STD effects taking into account the binding kinetics and thermodynamics as well as all protons of the binding site.[128]

Box 3: Techniques for selective excitation

Radio-frequency pulses with a selective excitation profile are very important tools in NMR spectroscopy. Selectivity of pulses in general is achieved by reducing the B_1 intensity and at the same time increasing the pulse duration. Rectangular pulses are rarely used for selective excitation because of their unfavorable excitation profile, which is a sinc function. The sidebands that are associated are responsible for unwanted excitation of signals. Therefore, other pulse shapes have been devised. One of the most effective shaping functions for this purpose is the Gaussian envelope [Eq. (9)] where t_0 is the center

$$S(t) = \exp[-a(t-t_0)^2] \qquad (9)$$

of the pulse envelope, S is the intensity of the pulse, a comprises the pulse duration and thus determines the pulse width, and t is the time.

The Fourier transform of the Gaussian envelope is also a Gaussian function which reduces the side-band problem to a large extent. The family of BURP pulses has been especially devised for NMR experiments where pure phase spectra are expected and where uniform excitation of a region of signals is required.[127] For the purposes of the saturation-transfer-difference experiments described in this review it is usually fully sufficient to use Gaussian-shaped pulses. Instead of a long Gaussian pulse (saturation times are usually in the range of 1 to 2 s) a train of Gaussian pulses, each 50 ms long with a spacing of 1 ms, is applied. This ensures a bandwidth of the irradiation in the order of 40 Hz.

In the following, experimental guide lines for STD NMR spectroscopy are summarized utilizing the original study as an example.[54] Ligands are added to a solution of the receptor protein and one ^{1}H NMR spectroscopy experiment is performed where the protein is selectively irradiated at a frequency at least 700 Hz away from the closest ligand signal (on-resonance experiment). Usually such regions are easily

identified depending on the chemical nature of the ligands. At 500 MHz usually −1.5 ppm is a generally good choice. Even though the irradiation is highly selective and has usually only a band width of a few Hz irradiation at such frequencies still yields full saturation of the protein by efficient spin diffusion within about 50–200 ms.

A ligand that binds to the protein will also be saturated. The degree of ligand saturation naturally depends on the residence time of the ligand in the protein binding pocket. The dissociation of the ligand will then transfer this saturation into solution where the free ligand again gives rise to resonance signals with narrow line widths. For those ligand protons that interact with protein protons through an intermolecular trNOE a decrease in intensity is observed. However, in the presence of other molecules such as impurities and other nonbinding components it is not usually possible to identify such attenuated signals.

Therefore, in a second experiment the irradiation frequency is set at a value that is far from any signal, ligand or protein, for example, 40 ppm (off-resonance spectrum). The spectrum is recorded and yields a normal NMR spectrum of the mixture. Subtraction of the on-resonance from the off-resonance spectra leads to a difference spectrum, in which only signals of protons are visible that were attenuated by saturation transfer. All molecules without binding activity are cancelled out.

Saturation of protein and bound ligand is very fast (about 100 ms). Therefore, a fast off rate of the ligand transfers the information about saturation quickly into solution. If a large excess of the ligand is present one binding site can be used to saturate many ligand molecules in a few seconds. Ligands in solution loose their information by normal T_1/T_2 relaxation which is in the order of about one second for small molecules. Thus, the proportion of saturated ligands in solution increases during the saturation time, and so the information about the bound state resulting from the saturated protein is amplified, which means a relatively small amount of protein is required. The STD principle is shown in Scheme 1.

On the other hand, if binding is very tight, and consequentially off rates are in the range of 0.1–0.01 Hz, the saturation transfer to ligand molecules is not very efficient. This is usually the case for K_D values less than 1 nM. If the K_D values are 100 nM or larger fast exchange of free and bound ligands leads to a very efficient build up of saturation of the ligand molecules in solution.

It is clear that the observed intensity of the signals arising from the ligand in the STD NMR spectrum are not proportional to the binding strength. STD NMR effects depend largely on the off rate. As outlined above, larger off rates should result in larger STD signals. However, when binding becomes very weak the probability of the ligand being in the receptor site becomes very low which results in weak STD signals. STD NMR spectroscopy can be used from very tight binding up to a K_D of about 10 mM.

As seen in the pulse scheme in Figure 2 it is an advantage to apply a spin-lock filter after the detection pulse to suppress the background of protein signals. Usually, spin-lock pulses of 10–20 ms are sufficient to achieve efficient signal suppression.

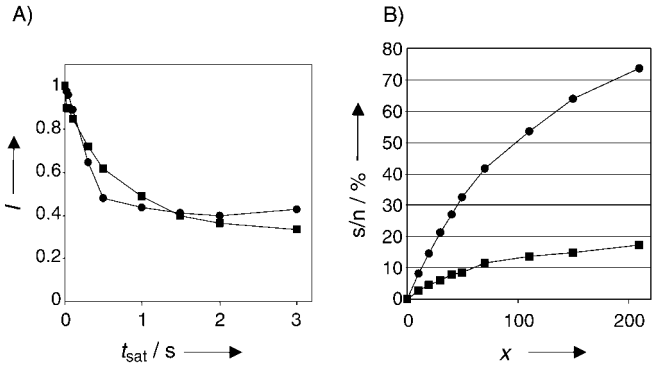

Figure 3. A) Normalized integral values (*I*) of selected ^{1}H NMR spectroscopy signals (● *O*-methyl group of FucOMe, ■ H6-methyl group of FucOMe) as a function of saturation time (t_{sat}). The ligand was *O*-methyl-α-L-fucose (FucOMe), the protein was *Aleuria aurantia* agglutinin (AAA). FucOMe was used with 30-fold molar excess over AAA. It is clear that the decrease of intensity levels out at about 60% of the original intensity. B) Signal-to-noise ratio (s/n) of STD spectra at 500 MHz as a function of ligand molar excess (*x*; GlcNAc: ● *N*-acetyl group, ■ H1) over protein (WGA).

When using labeled ligands it is of course possible to achieve this effect by utilizing isotope-edited experiments instead.

The intensity of the STD signals depends, among other things, on the irradiation time/saturation time and on the excess of ligand molecules used (Figure 3). The more ligand that is used and the longer the irradiation time the stronger the STD signal is. It is seen that both curves in Figure 3 asymptotically approach a maximum value. In general, an irradiation time of 2 s and a 100-fold excess of ligand give good results. The excess of the ligand results in a stronger STD signal—even though a smaller proportion of the ligands become saturated. Upon dissociation, the saturation of the ligand is transported into solution where it accumulates as a result of the slow decline of the saturation by relaxation processes in solution. Before ligands in solution have lost their saturation the process of association followed by dissociation can occur many times and thus put many more saturated ligands into solution. The maximum net effect of saturation on ligand protons occurs if a large excess of ligand is used because it is very unlikely that a ligand with saturation re-enters the binding site. From the high ligand:protein ratios it is clear that the amount of protein required for the measurements is very small. At 500 MHz an amount of approximately 0.3 nmol of protein is sufficient to record STD spectra. At a molecular weight of 50 kDa this translates into about 15 μg.

Using 1D STD spectra the compound *N*-acetylglucosamine (GlcNAc) was identified as the only one with binding affinity for WGA. All the other molecules showed no response in the STD spectra. As mentioned above the STD principle can be combined with any NMR pulse sequence, and one rather powerful experiment is the STD TOCSY experiment. Especially in cases where the library is more complex the additional deconvolution of signals brought about by the second dimension is very helpful. The STD TOCSY experiment was also shown to be ideally suited for mapping the binding epitope of ligands.[54,57–59]

By using the STD TOCSY method it was possible to screen a library of like carbohydrates to identify functional groups involved in binding. A library of randomly methylated derivatives of D-galactose, D-glucose, and D-mannose was tested for binding to a lectin from elderberry, *Sambucus nigra* agglutinin (SNA).[56] The subfraction of the 20 dimethylated monosaccharides was subjected to a binding analysis by STD NMR. A clear and easy identification of binding components was straightforward using STD TOCSY spectra (Figure 4). Only components in the β-D-galacto configuration with the 3- and 4-OH groups free showed binding affinity. With conventional screening technology, the identification of the compound with binding activity directly from the mixture would have been inherently difficult, as it would require the clean separation of all the different compounds. Therefore, all 20 components of the library would have had to be synthesized individually and investigated in a step-by-step screening process.

Also, it was shown that with little chemical effort, a randomly *O*-methylated library of *O*-methyl-β-D-galactoside, in which only *O*-methyl groups are ^{13}C labeled, can be obtained. The presence of the labels allows HMQC and HMBC STD experiments to readily reveal those hydroxy groups of the sugar that are essential for binding to the protein. Using standard binding assays this task would normally require considerable synthetic effort. The STD NMR spectroscopy variant allows the fast identification of hydroxy and carboxy groups involved in binding even if a very complex mixture of methylated ligands is obtained.

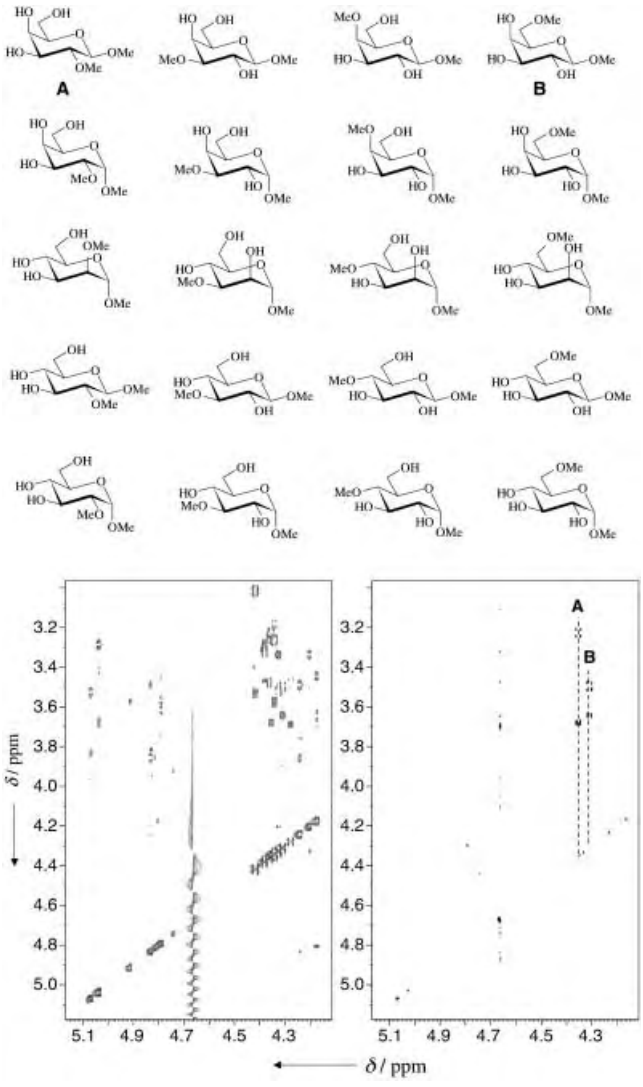

Figure 4. Left: 500 MHz TOCSY spectrum of the compound mixture shown (top). Only the portion of the spectrum containing the resonance signals of the anomeric protons of the monosaccharide derivatives is shown. Right: STD TOCSY spectrum of the same mixture in the presence of the lectin SNA (ca. 50-fold molar excess of ligands) showing that only the two β-D-galactose derivatives **A** and **B** bind to the protein.

2.1.1. *Using STD NMR Spectroscopy for Characterizing Ligand Binding to Immobilized Proteins*

Many interesting targets in drug design are membrane-bound proteins, and therefore are inherently difficult to investigate. When devoid of their natural membrane environment these proteins often loose their structure and hence their functionality. The only way to solve this problem is to study these proteins in a biological membrane. For high-resolution NMR spectroscopy this poses many problems, and therefore structural work on membrane-bound proteins has been confined to magic-angle spinning (MAS) NMR spectroscopy to date. STD NMR spectroscopy has the significant advantage that binding to membrane-bound proteins can be studied even within the natural membrane environment without causing any problems.

In a pilot experiment, WGA was immobilized on glass particles containing pores of specific size (controlled pore glass particles; CPG), and the binding of carbohydrate derivatives to the immobilized WGA was studied by STD NMR utilizing high-resolution magic-angle spinning NMR spectroscopy (HRMAS).[60] The resulting STD NMR spectra clearly indicated the binding of only the expected compound in the mixture.

This technique of immobilizing proteins on solid particles can also be used to recover the protein more quickly, by simple filtration, from the mixture of ligands and protein, therefore, facilitating a high-throughput screening method for scarce proteins (Scheme 2).

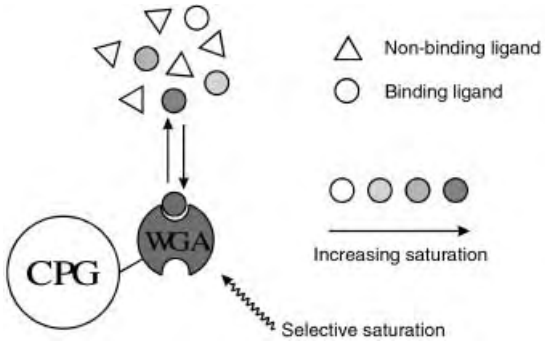

Scheme 2. Identification of ligands from binding to immobilized protein by HRMAS NMR spectroscopy.

2.1.2. *Using STD NMR Spectroscopy for Characterizing Ligand Binding to Membrane-Integrated Proteins*

To study membrane-bound proteins in their native environment, we have studied the binding properties of integrins embedded in liposomes by STD NMR.[61] Many membrane-bound proteins can be stabilized in solution by detergents. The solubilized integrin $\alpha_{IIb}\beta_3$ was integrated into liposome membranes formed of dimyrystyl phosphatidyl cholin (DMPC) and dimyrystyl phosphatidyl glycerol (DMPG). These liposomes have a diameter of about 200 nm and 50 % of the integrins are orientated towards the inside and 50 % towards the outside. It is known that integrins bind to peptides containing the RGD-motif (Arg-Gly-Asp). Binding of such peptides to the liposome-integrated integrins was assayed in homogenous solution by STD NMR spectroscopy. It was found that a clear distinction could be made between peptides with binding properties and peptides that do not show binding. Also stronger-binding ligands could be clearly discriminated from weaker-binding ones in that the stronger completely displaced the weaker from the binding site.

We could show that about 0.25 nmol of the integrin is sufficient to assay its binding specificity. The cyclic peptide cyclo(RGDfV) developed by Kessler and co-workers[62] to be a specific inhibitor of integrin $\alpha_V\beta_3$ has also binding affinity to the integrin $\alpha_{IIb}\beta_3$ with a dissociation constant of about 5 μM. This cyclic peptide displaced the open-chain peptide RGD from the binding site (Figure 5). The binding of the peptides to the integrin embedded into liposomes is specific up to a concentration of about 20 $\mu mol\,L^{-1}$. Beyond that an unspecific binding or potentially a low-affinity binding site on the integrin is being used by the peptides. It was shown clearly in a control experiment that no unspecific binding of the peptide ligand was occurring to the protein-free liposomes.

Further, the binding epitope of the cyclic peptide cyclo(RGDfV) to liposome integrated integrins was determined by STD NMR spectroscopy. The major factor in binding is the phenyl ring of the phenyl alanin groups whereas the aspartate and arginin groups have a weaker but still strong contact with the protein. In the case of the aspartate, the contact is through the carboxy group whereas in the case of the arginin it is a hydrophobic contact. The valin also participates in binding (Figure 6).

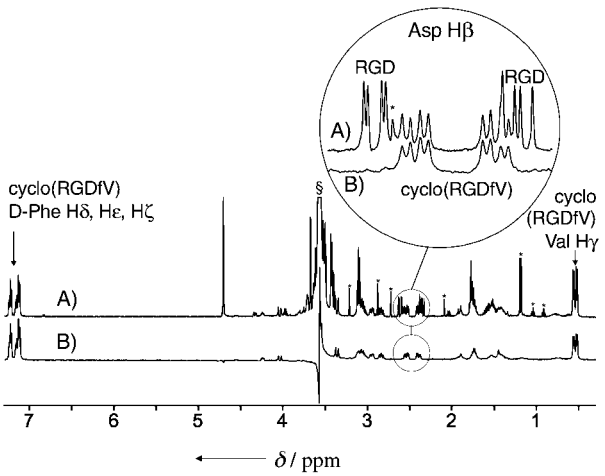

Figure 5. ^{1}H NMR spectra of 274 μM RGD and 264 μM cyclo(RGDfV) with integrin $\alpha_{IIb}\beta_3$ which is integrated into liposomes. A) Normal ^{1}H NMR spectrum displaying signals of both ligands. The inset shows the expanded region containing the resonance signals of two diastereopic aspartate β protons. The other signals are from the buffer TRIS, and an impurity ⋆) B) STD NMR spectrum showing only STD effects of the tight-binding cyclopeptide ligand. The inset shows only signals from the tight binding cyclopeptide (cyclo(RGDfV)).

binding constants for Integrins in solution are about a factor of 100 weaker than the same receptor-ligand interaction in membrane-integrated form. Therefore, it is important to study and understand the interaction of membrane-bound proteins with their ligands in a form close to the native environment.

2.1.3. *Using STD NMR Spectroscopy for Characterizing Ligand Binding to Viruses*

Currently, new compounds that inhibit virus infections by hindering the virus from entering the host cell are being developed, the so-called entry inhibitors. Entry inhibitors that

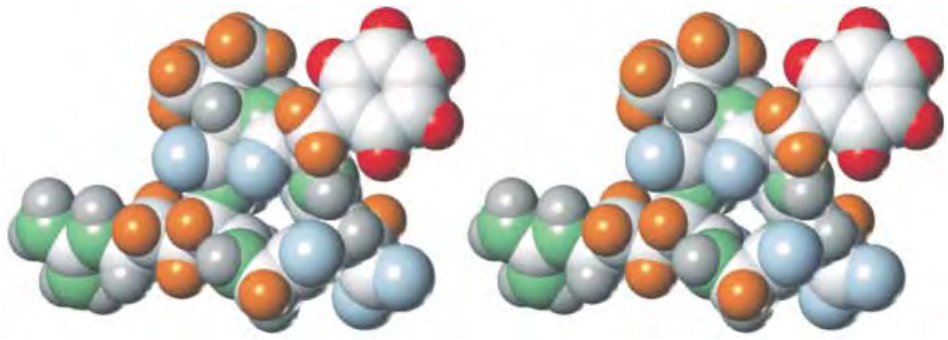

Figure 6. Stereo representation of the binding epitope of cyclo(RGDfV). Shown is the 3D structure of cyclo(RGDfV) in DMSO determined by Aumailley et al.,[122] based on NMR spectroscopy and MD simulations. The STD-NMR-derived binding epitope of the cyclic ligand is in orange and red. The aromatic protons of D-Phe show strong STD effects indicating closest contacts to the integrin (red). The medium STD intensities (orange) of the protons: Val-Hγ, Arg-Hα, Arg-Hβ, and Arg-Hγ, lead to important binding epitopes. Other sections of the molecule giving rise to medium STD intensity are D-Phe-Hβ, one Asp-Hβ, one Gly-Hα proton (orange).

specifically target the virus whilst not affecting the host are promising because they may deliver therapies that are free of side effects. To find leads for the design of such entry inhibitors knowledge about the composition and shape of the viral coat is desirable. For some human rhinoviruses (HRV) that are the cause of the common cold a complete structural analysis has been possible by means of X-ray crystallography.[63–68] On the basis of these results a class of inhibitors, the so-called WIN compounds **1**, (named after the company

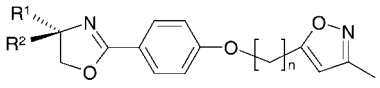

1

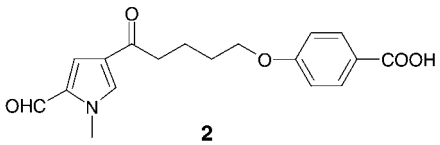

2

Winthorp Sterling) has been synthesized that bind to the canyon binding site on the virus surface thereby inhibiting the virus from infecting the host. One of these compounds, pleconaril, is currently in phase III of clinical trials.[69,70]

It is possible to subject native viruses to NMR spectroscopy. From line-broadening effects in ^{1}H NMR spectra dissociation (off) constants of neuraminic-acid binding to influenza viruses were determined.[71] In a recent study we demonstrated that the principles of STD NMR can also be successfully applied to native viruses. This result opens up new perspectives for the direct screening for entry inhibitors directed against human rhinoviruses. We succeeded in acquiring STD NMR spectra of a synthetic entry inhibitor, Repla 394 (**2**) in its binding to fully functional complete viruses.[71b] Nonbinding components showed no STD signals and showed that the binding was specific (Figure 7). In a competitive STD experiment another known entry inhibitor was added to a solution of HRV-2 and **2** causing the STD intensities of the signals from **2** to decrease. This competition experiment substantiates the assumption that it is possible to detect the binding of ligands to the canyon binding site of HRVs with STD NMR.

Using this method it will be possible to directly identify potential entry inhibitors for rhinoviruses and probably for other viruses as well.

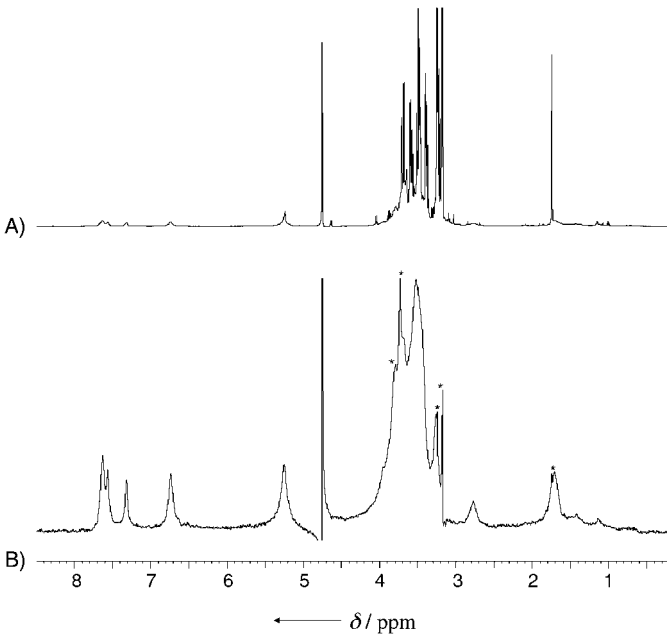

Figure 7. STD NMR spectrum (B) and ^{1}H NMR reference spectrum (A) of native HRV-2 (0.04 μM) in the presence of Repla 394 (**2**, 0.5 mM), methyl α-D-glucopyranoside (4.8 mM), and methanol (6.2 mM). The spectra were acquired at 500 MHz and 298 K with 4000 scans for the difference and 2000 scans for the reference spectrum. The signals in the difference spectrum are from Repla 394, an entry-inhibitor of HRV-2, unambiguously indicating binding of this ligand to the virus. Methyl α-D-glucopyranoside and methanol give no STD signals and no artifacts although they are present in large excess. This result is in accordance with the fact that both compounds do not bind to HRV-2.

2.1.4. *Epitope Mapping with STD NMR Spectroscopy*

STD NMR spectroscopy can easily be used to identify the building blocks of ligands in direct contact to the receptor because these components receive the highest degree of saturation. The interaction of a hexasaccharide with the lectin *Aleuria aurantia* agglutinin (AAA) shows unambiguously that only the fucosyl residues interact with the protein[54] (Figure 8).

In a recent example the binding epitope of the sialyl Lewis^X tetrasaccharide when bound to the L-fucose-recognizing lectin AAA was mapped by employing STD TOCSY experiments.[57] A normal TOCSY spectrum of sialyl Lewis^X and a STD TOCSY spectrum of sialyl Lewis^X in the presence of AAA are shown in Figure 9. The STD TOCSY spectrum only shows signals arising from the L-fucose residue of sialyl Lewis^X. This is a clear indication that the L-fucose residue is the main binding epitope of the tetrasaccharide.

STD-NMR-spectroscopy-based epitope mapping was also applied to study the recognition of bacterial lipopolysaccharide fragments by monoclonal antibodies. An interesting aspect of that study was that although the lipopolysaccharide fragments had a molecular weight of several kDa, it was possible to define the key functional groups that are recognized by different monoclonal antibodies. The experiments substantially helped in understanding the differential recognition of carbohydrate epitopes by the antibodies at an atomic level.[72]

2.1.5. *Group Epitope Mapping with STD NMR Spectroscopy*

Epitope mapping can be further refined to allow the so-called group epitope mapping (GEM).[58] For GEM it is important that the residence time of the ligand in the bound state is significantly shorter than the T_2 time of the ligand in the bound state. We have shown that the binding groups can

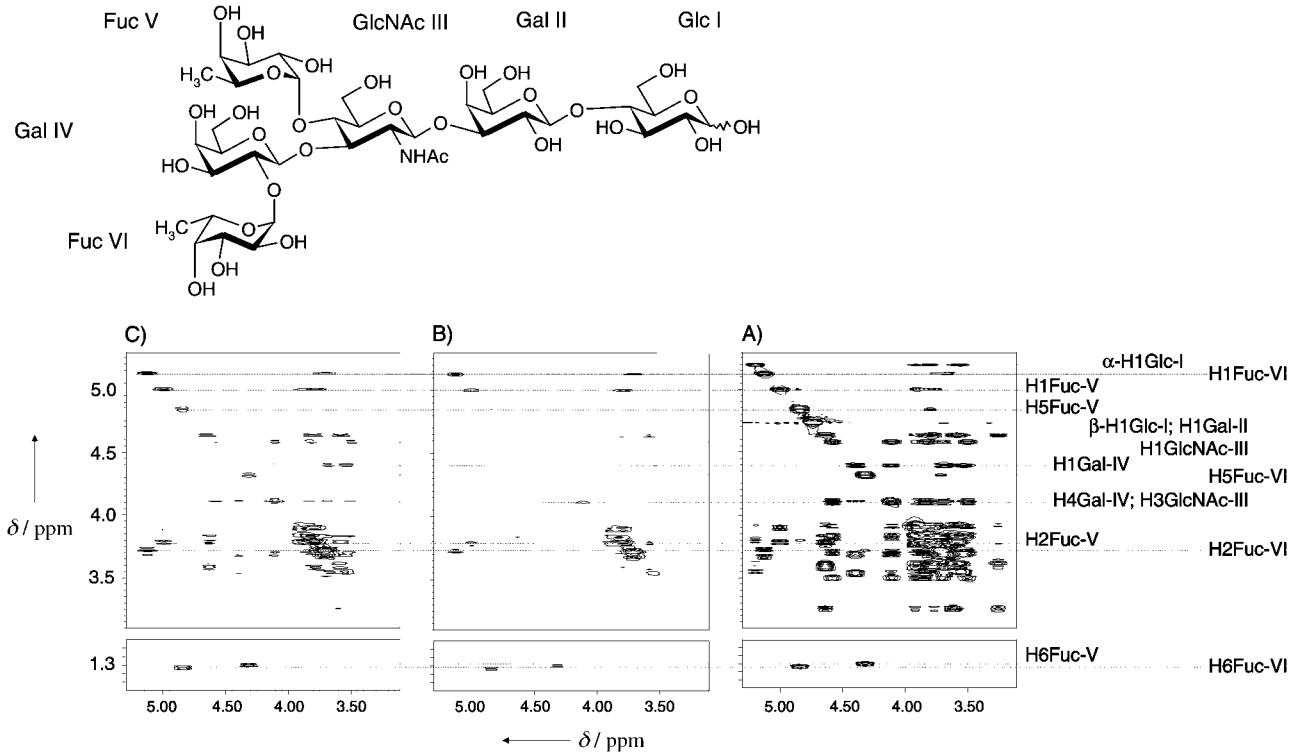

Figure 8. Epitope mapping for lacto-*N*-difucosylhexaose I bound to the protein AAA. A) TOCSY spectrum of ligand only (no protein); B) STD TOCSY spectrum in presence of the protein showing only the intensive signals of fucosyl residues V and VI; C) STD TOCSY spectrum at about 60% of the intensity level of that in (B) showing in addition to the fucosyl cross-peaks, cross-peaks originating from galactose IV and *N*-GlcNAc III. The full STD TOCSY exhibiting the even less-intense signals of galactose II and glucose I (at ≈30% of the intensity of cross-peaks in (B)) is not shown. The STD TOCSY spectrum was recorded at 300 K with on-resonance irradiation at 10 ppm and off-resonance irradiation at 30 ppm and the irradiation power set to 0.2 W.

be directly identified from STD NMR spectra[58] and that the identification of binding groups is not restricted to a particular residue that is separated from other groups in the molecule by the lack of spin–spin coupling. GEM can only be observed if the ligand has a relatively fast off-rate, which is normally the case at dissociation constants k_D of about 0.1 μM or higher. Stronger binding normally reduces the off rate so much that the residence time for the ligand on the receptor is too long. During this time spin diffusion erases the differences between protons within one residue. Thus, the distinction between protons in direct contact with the binding site from those that are not in direct contact with the protein is virtually made impossible. GEM is also possible with peptides, carbohydrates, and aromatic ligands. As an initial example, we studied carbohydrate recognition by lectins.

The functional groups involved in the binding of the ligand methyl β-D-galactoside (β-D-GalOMe) to the 120 kDa protein *Ricinus communis* agglutinin (RCA_{120}) could be determined by STD NMR spectroscopy. Only the H2, H3, H4, and H6 protons of the galactose were involved in direct binding to the protein (Figure 10). These data were in perfect agreement with earlier published results obtained from the chemical modification of these functional groups.[130]

The 1D spectra of the biantennary decasaccharide in an 11-fold excess over the RCA_{120} show clearly that the terminal residues galactose and GlcNAc are most distinctly involved in binding whereas signals of the sugars close to the reducing end are of very low intensity (Figure 11). The terminal β-D-galactose residue is involved in binding with its H2, H3, H4, and H6 protons. Furthermore, the H2, H3, and H4 protons of the penultimate β-D-GlcNAc residues are also close to the protein surface and contribute to binding. Because of signal overlap, the individual contributions of the β-D-GlcNAc protons H2, H3, and H4 to the binding could not be determined. The other protons of the GlcNAc residue make direct contact to the protein. This situation shows clearly that the GlcNAc residue carries a small portion of the binding specificity of the large carbohydrate ligand.

The same situation could be verified by using *N*-acetyllactosamine as the ligand. It was demonstrated earlier that elongation of a galactose residue by a GlcNAc residue increases the binding affinity for RCA_{120} by 20%.[131]

Another example illustrates the binding of the donor substrate UDP-Gal to a mammalian galactosyl-transferase, β-1,4-galactosyl-transferase (β4Gal-T1, EC 2.4.1.90/38). The enzyme is found membrane-bound in the Golgi apparatus and is responsible for the transfer of galactose from UDP-Gal to β-D-*N*-acetylglucosamine residues furnishing poly-*N*-acetyllactosamine chains found in glycoproteins and glycosphingolipids. STD NMR spectroscopy was applied to analyze the molecular details of the recognition reaction between β4Gal-T1 and UDP-Gal.[73] GEM clearly identified the protons of

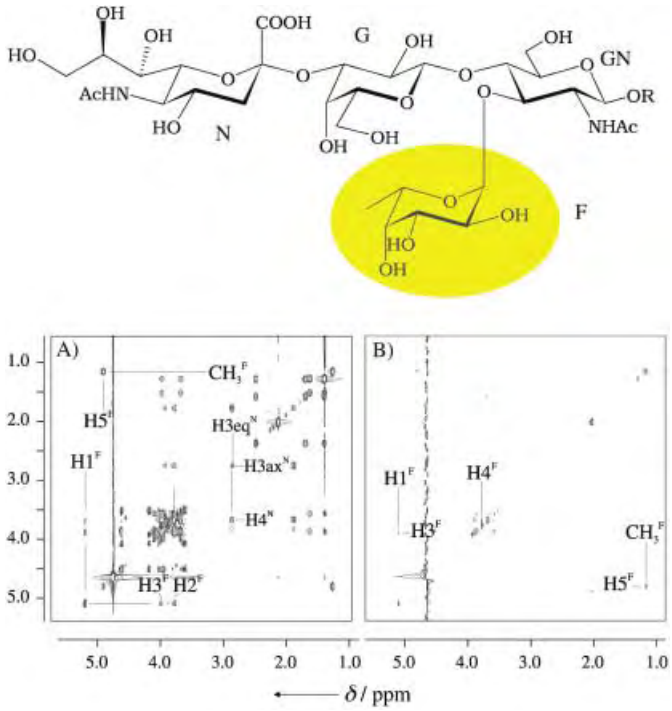

Figure 9. A) 500 MHz TOCSY spectrum of sialyl Lewis^X (see formula above the spectra): the complete spin systems of all the pyranose rings are clearly visible. B) STD TOCSY spectrum of sialyl Lewis^X in the presence of AAA (molar ratio of ligand to protein was 100:1): only the spin system of the L-fucose residue (F, yellow circle in the formula) is visible indicating that only this part of the tetrasaccharide makes contact with the protein. For the TOCSY spin-lock field a MLEV-17 sequence was used. The mixing time was 60 ms. For the saturation of the protein (on-resonance 8.8 ppm, off-resonance 40.0 ppm) a cascade of 40 selective Gaussian pulses (50 ms each) was applied resulting in a total saturation time of 2 s.

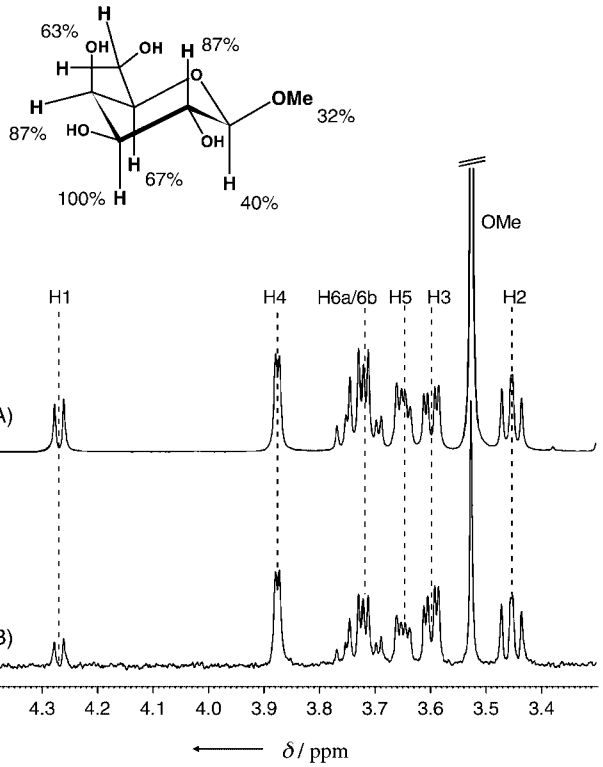

Figure 10. Top: Structure of β-D-GalOMe and the relative degrees of saturation of the individual protons normalized to that of the H3 proton as determined from 1D STD NMR spectra at a 100-fold excess: concentration of RCA_{120} was 40 μM and that of β-D-GalOMe 4 mM. Bottom: A) Reference WATERGATE NMR spectrum of a mixture of RCA_{120} (binding site concentration 40 μM) and β-D-GalOMe (1.2 mM) at a ratio of 1:30. B) WATERGATE STD NMR spectrum of the same sample. On-resonance irradiation was set to −0.4 ppm over a period of 2 s. Prior to acquisition a 30 ms $T_{1\rho}$ filter was applied to remove residual protein resonance signals. From the STD spectrum one can characterize the binding epitope by using relative integral intensities of the signals in spectrum (B).

the UDP part that are in close contact with the enzyme, whereas the galactose moiety received only very little saturation (Scheme 3).

Interestingly, the largest fraction of saturation in the galactose moiety is received by protons H2 and H4, which is in accordance with previous studies that indicated that the corresponding hydroxy functions are essential for catalytic activity of β4Gal-T1.[73,74] A recent X-ray crystallographic analysis of lactose synthase (β4Gal-T1 complexed with α-lactalbumin) complexed with UDP-Gal revealed a hydrogen bond between OH4 of galactose and Asp318 of the enzyme.[75] This orients H4 into the interior of the protein and explains the higher relative saturation transfer towards H4 of galactose. In another experiment the binding of UDP-glucose (UDP-Glc) to β4Gal-T1 was studied. UDP-Glc is a competitive inhibitor of β4Gal-T1 but it is a very poor donor substrate with less than 1% of the activity measured for UDP-Gal. The STD NMR spectra show that the UDP part of UDP-Glc binds to β4Gal-T1 whereas the glucose moiety does not receive any saturation. Clearly, upon binding to the enzyme the glucose part of UDP-Glc retains significant conformational freedom, and therefore transfer of glucose to an acceptor substrate is very inefficient.

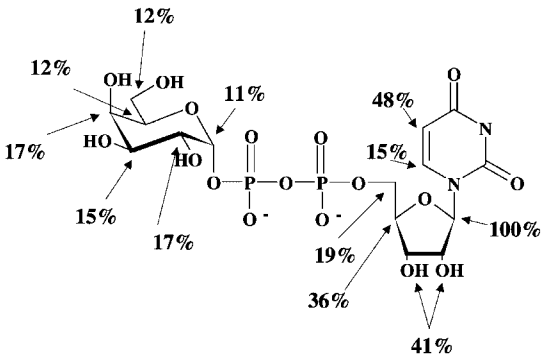

Scheme 3. Relative STD effects for UDP-Gal bound to β4Gal-T1. Values were calculated by determining individual signal intensities in the STD spectrum (I_{STD}), and in the reference 1D NMR spectrum (I_0).[73] The ratios of the intensities I_{STD}/I_0 were normalized using the largest STD effect (anomeric proton H1′ of the ribose unit, 100%) as a reference. Arrows indicate the position of the proton experiencing an STD effect. The value of 41% corresponds to the cumulative saturation transfer for H2′ and H3′. Likewise, 12% denotes the sum effect for both the H6 protons of the galactose residue. The values for protons H5 and H5′ are estimates because separate integration of the two signals was difficult.

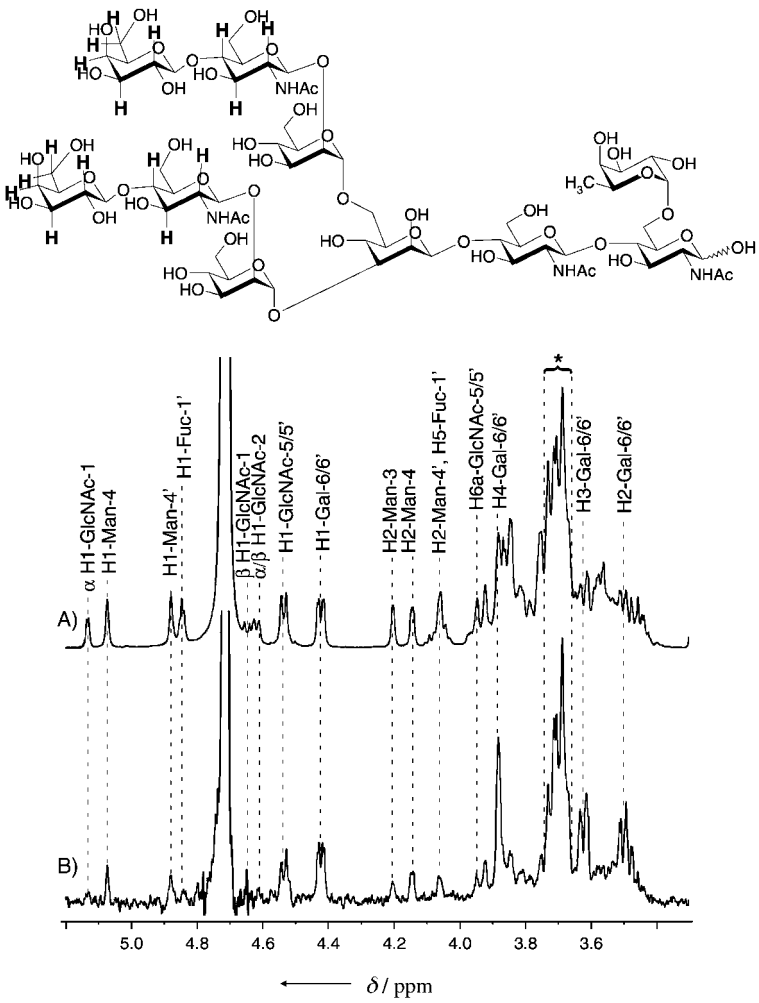

Figure 11. Top: Structure of the ligand: a biantennary complex type decasaccharide (NA_2). The groups highlighted in bold interact with RCA_{120} (as determined by STD NMR spectroscopy). Bottom: A) Section of a reference NMR spectrum of a mixture of the RCA_{120} tetramer (binding site concentration 50 μM) and NA_2 (0.55 mM) at a ratio of 1:11. B) STD NMR spectrum in which the strongest signals are from the directly interacting residues of NA_2. The resonances corresponding to the terminal galactoses Gal-6/6′ and the adjacent GlcNAc-5/5′ have the most intense STD signals. The spectral region from 3.65 to 3.75 ppm marked with the * shows strong STD signals which originate almost entirely from the H5 and H6a/6b of Gal-6/6′ and the H2, H3, and H4 of GlcNAc-5/5′ protons (see text). H1-Fuc-1′, and α-H1-GlcNAc-1 have almost no detectable STD signal intensity. This result shows that these protons are far away from the binding domain of the lectin.

2.1.6. *Binding Constants from STD NMR Experiments*

The binding constants of ligands can be obtained from STD NMR spectra. In the example described in Section 2.1.5, where the biantennary decasaccharide interacts with the receptor RCA_{120}, a competition titration can be performed with the weaker ligand β-D-GalOMe. The results of the titration give STD amplification factors as a function of the concentration of the ligand. The data shown in Figure 12 clearly show that the decasaccharide is replaced from the binding site upon adding the weaker ligand methyl galactoside. The absolute intensity of the β-D-GalOMe ligand signals increases with increasing concentration from 0 to 2.5 units (the STD amplification factor). The signal intensity of the decasaccharide protons is reduced from 1 to about 0.66 at the same time. This relatively small decrease in STD amplification factor for the decasaccharide compared to the strong increase of the signals for β-D-GalOMe shows clearly that the β-GalOMe is a weaker ligand whereas the decasaccharide binds stronger to the receptor protein. Using the decrease of the signal intensity of the decasaccharide and knowing the binding constant of the monosaccharide, one can easily obtain in a one-site competition model the dissociation constant of the decasaccharide to be $K_D = 27$ μM. The surface plasmon resonance experiment (Biacore) results in a comparable $K_D = 4.4$ μM.

2.1.7. *Boundary Conditions for STD NMR Spectroscopy*

The STD effect can best be viewed if the STD amplification factor[58] is being used for the quantification of the response of the ligand in interaction with the receptor protein. The STD amplification factor is obtained by multiplying the percent STD effect of a given proton at a given concentration with the excess of the ligand relative to the protein. Therefore, the STD amplification factor is effectively the intensity of the STD signal of the ligand proton relative to the intensity of a proton of the protein and is the best measure to assess the sensitivity of the method (Figure 13).

If the STD effect is determined as a function of saturation time for β-D methyl galactoside in its binding to RCA_{120}, it can clearly be seen that with a 12-fold excess of the ligand the STD amplification factor for the proton involved in direct binding (H3) and the amplification factor for the *O*-methyl protons, which are not involved in binding, varies by only a factor of about 1.5 (Figure 14A). Both saturation curves reach the maximum at about three seconds saturation time. Increasing the excess of the ligand (Figure 14B) to about 25-fold, increases the distinction between the proton involved in direct binding (H3 of galactose), and the *O*-methyl group that is not in close contact with the binding pocket by a factor of more than two. Now even at five seconds saturation time, the maximum STD amplification has not been reached. Increasing the excess of the ligand further to 100-fold, the absolute magnitude of the response from the ligand increases further (Figure 14C), and the discrimination between the protons of the *O*-methyl group and H3 is now better than a factor of three.

The complex type decasaccharide has a larger binding constant, and therefore a slower exchange rate. Here, lower maximum STD amplification factors are obtained than for the more weakly binding ligand β-D-Gal-OMe. The titration curve of the complex type decasaccharide in its binding to RCA_{120} gives a maximum STD amplification factor of 2 at a ligand concentration of 1.2 mM. The reason for the lower STD

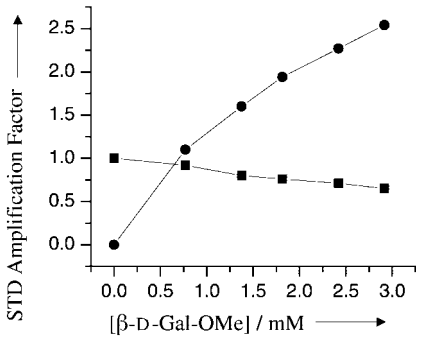

Figure 12. Diagram showing the STD amplification factors (● H1-β-GalOMe; ■ H1-Gal-6/6′ NA_2) determined from STD spectra on titration of β-GalOMe to a sample of RCA_{120} (binding site concentration 50 μM) and NA_2 (0.55 mM). The STD amplification factor of the signal corresponding to NA_2 decreases from 1 to 0.66 with increasing concentration of β-GalOMe. This competition experiment gives evidence to the specificity of the RCA_{120} towards galactose containing saccharides. The K_D of NA_2 can be calculated to 27 μM.

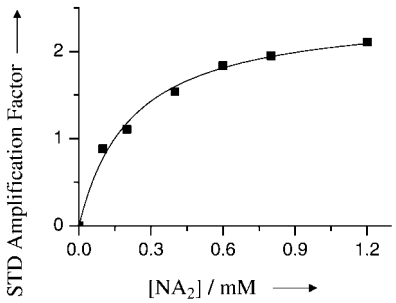

Figure 13. Titration plot of decasaccharide NA_2 to an RCA_{120} sample for NMR spectroscopy (binding site concentration 20 μM) monitoring the increase of the STD amplification factor of the H4-Gal proton versus the ligand concentration (t_{sat} = 2 s). STD amplification factor = $\frac{I_0 - I_{sat}}{I_0}$ ligand excess. I_0 = integral of one unsaturated proton, I_{sat} = integral of one proton after saturation.

amplification factor is the decreased off rate (k_{off}) of this ligand associated with the stronger binding.

The examples demonstrate that STD NMR spectroscopy is well suited to study the interactions of ligands with macromolecular receptors. As STD is a preparatory pulse sequence all types of NMR spectra can be recorded, for example, 1D NMR spectra, TOCSY, COSY, and HSQC. STD NMR spectroscopy can be used to identify from large complex mixtures of compounds those with bioactivity. The largest pool screened to date contained about 250 compounds. On the receptor side, there is no upper size limit of the protein. However, it should not be smaller than about 10 kDa because the protein has to be effectively saturated by

Box 4: The influence of competitive binding and allosteric effects

The binding of competitive inhibitors is readily monitored by any of the NMR spectroscopic techniques described in this review. As an example, here we explain how relative K_D values are obtained from STD NMR spectroscopy titrations.[58] Assuming simple bimolecular association reactions for the binding of a ligand L and a competitive inhibitor I to a receptor protein P yields the simultaneous equilibria Equation (10) and (11).

$$P + L \rightleftharpoons PL \text{ with } K_D = \frac{[P]\,[L]}{[PL]} \quad (10)$$

$$P + I \rightleftharpoons PI \text{ with } K_I = \frac{[P]\,[I]}{[PI]} \quad (11)$$

According to Cheng and Prusoff[123] under these conditions Equation (12) can be used for the determination of the K_D value of the

$$K_D = \frac{[L]\,K_I}{IC_{50} - K_I} \quad (12)$$

ligand L.The value of IC_{50} (i.e. when 50% of the protein is inhibited) is readily determined from a titration with the inhibitor I of a solution of the protein in the presence of ligand L at a fixed concentration [L].

More complicated situations arise from binding of ligands to secondary binding sites which may drastically influence the results of NMR spectroscopy binding assays. Three extreme cases A, B, and C are shown (top right).

A) The binding sites are independent: In this case two independent binding events would be detected with NMR experiments. Both binding sites may be characterized independently. A "classical example" is the binding of ligands to the FK 506 binding protein (FKBP).[103]

B) Binding of a ligand to a secondary site causes allosteric inhibition of the binding of a ligand to the primary site: as a consequence, the K_D value for the primary site is increased. With STD NMR (Section 2.1) titration experiments[58] in the presence of varying concentrations of the secondary-site ligand this allosteric inhibition can be detected because increasing apparent K_D values are expected and observed. With HSQC-based methods changes in the protein chemical-shift values occur upon the binding of a ligand to the secondary binding site, while the changes of the chemical shifts resulting from binding of the first ligand to the primary binding site are gradually lost.

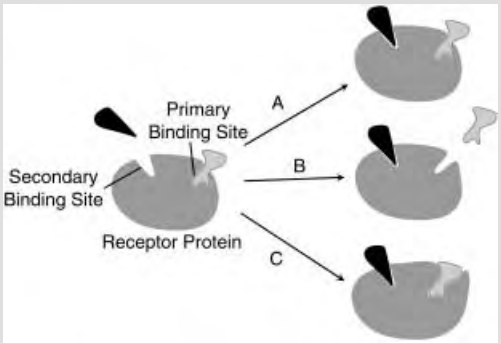

C) Binding of a secondary-site ligand leads to allosteric enhancement of ligand binding to the primary site: STD NMR spectroscopy titration experiments will identify the enhanced binding in the presence of a secondary site ligand. For HSQC-based experiments, an assignment of the spectra in the presence of saturating amounts of the second-site ligand is required, allowing the characterization of both binding pockets. Recent examples, where NMR spectroscopy experiments were involved in the analysis of allosteric effects, are studies on the tumor-suppressor protein p53[124] and the binding of the lymphocyte function-associated antigen 1 (LFA-1) to intercellular adhesion molecule ICAM-1.[125]

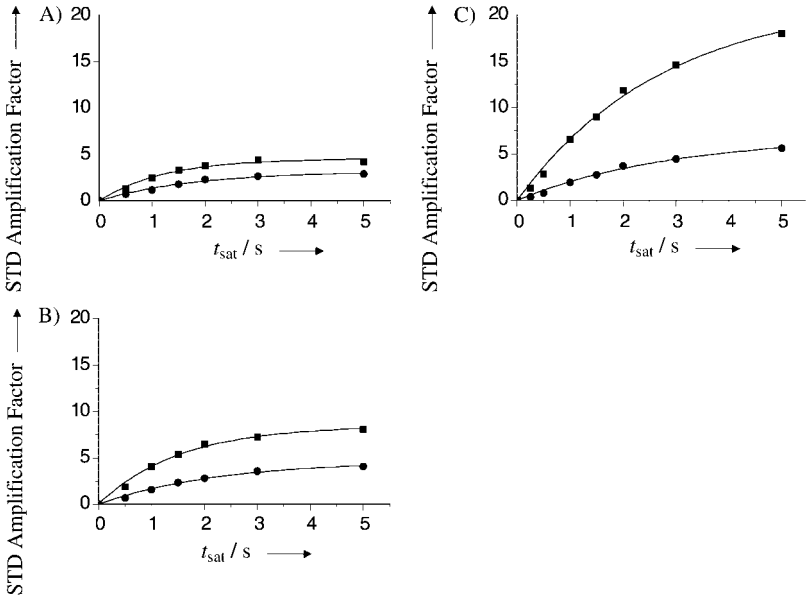

Figure 14. Observed STD amplification factors of two proton resonance signals of β-GalOMe plotted against the saturation time t_{sat} at three different ligand concentrations (■ H3 proton; ● OMe protons). A) STD amplification factor at a concentration of 0.5 mM, B) 1 mM, and C) 4 mM of β-GalOMe in the presence of RCA_{120} (binding site concentration 40 μM). A large ligand excess yields larger STD intensities and better discrimination between strongly and weakly binding groups.

spin diffusion. The receptor proteins can be coupled to a solid phase and proteins can also be integrated into liposomes giving access to screening of membrane-bound or membrane-integrated proteins. The ligands can be either carbohydrates, monosaccharides as well as oligosaccharides up to about 2 kDa, aromatic compounds, peptides, peptide mimetics, and other molecules. The only requirement being that a concentration of the ligand of about 50 μM can be prepared in a solvent system that is also compatible with the receptor protein.

2.2. Water-LOGSY

A variant of STD NMR spectroscopy utilizes the bound water at protein–ligand interfaces. It is well documented that NMR spectroscopy is well suited to study this bound water.[76–78] The observation of negative intermolecular water–ligand NOEs may be explained either by bound water squeezed in between ligand and protein or by a water shell surrounding the ligand.[79] Based on these observations experiments were developed that use the bulk water to detect the binding of ligands to proteins.[80] The experimental setup either utilizes the steady-state NOE experiment, where on-resonance saturation is applied to the water chemical shift, or an experimental scheme is applied where the water resonance signal is selectively inverted, such as in the NOE-ePHOGSY scheme.[81] Because of the chemical-shift equivalence of the water signal and the signals of the H^{α} protons a cumulative effect originating from both sources is observed. To generate the best sensitivity, the experiments are performed in H_2O containing only small amounts of D_2O. To eliminate artifacts from, for example, radiation damping, pulsed field gradients were employed for proper water suppression giving the method the name water-LOGSY (Water-Ligand Observation with Gradient Spectroscopy).

The technique has successfully been applied to study the binding of ten low-molecular-weight ligands (at a concentration of 100 μM each) to cyclin-dependent kinase 2 (cdk2, M_W ca. 34 kDa, concentration 10 μM). A clear discrimination between the binding ligand, an indole derivative, and the nonbinding ligands was straightforward and the resulting spectrum is shown in Figure 15. It appears that this approach is especially useful for complexes where either ligand or receptor are strongly hydrated, for example, for RNA-ligand interactions.

2.3. Cross Saturation

It was demonstrated recently that cross saturation is useful for mapping the sites of interaction in protein–protein complexes.[82] This cross-saturation mapping of protein–protein interfaces utilizes the steady-state NOE-difference experiment[14] where ^1H resonance signals of a nondeuterated component (target resonances) are saturated leading to the observation of magnetization of NH protons of a second, deuterated and fully ^{15}N-labeled protein (reporter resonances) as long as the two proteins bind to each other. The reason for deuteration is twofold: 1) a spectral window has to be

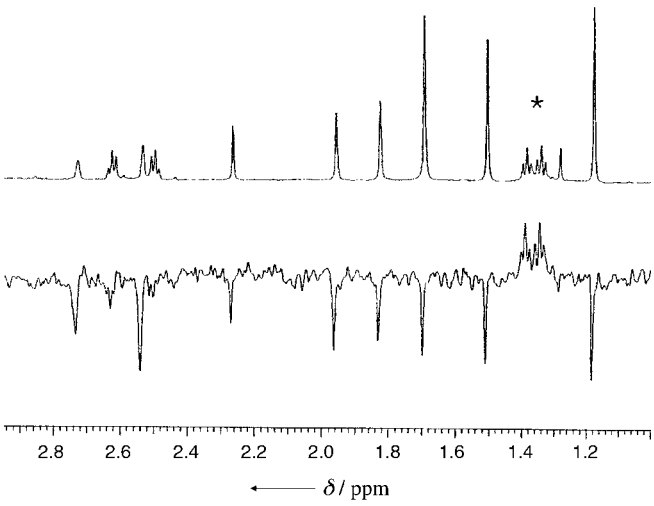

Figure 15. Water-LOGSY spectrum of a library of ten compounds in the presence of cdk2 (lower spectrum). Signals from the indole derivative with binding affinity for cdk2 are easily identified (positive signals). The upper spectrum displays the ^1H NMR reference spectrum. The signals belonging to the binding ligand are marked by *. Reproduced from ref. [80] with kind permission from Kluwer Academic Publishers.

present to selectively irradiate target resonances, and 2) spin-diffusion on the side of the reporter protein is reduced.

Since deuteration of a protein is costly and not always feasible, for RNA-protein complexes an elegant extension of this method was suggested.[83] By using the spectral window of the H1′ sugar resonances and H5 base resonances of the nucleic acid resonance signals centered at $\delta \sim 6$ ppm, or the imino protons with chemical shifts in excess of $\delta = 12$ ppm it was possible to carry out a saturation transfer for the protein that could be detected by difference $^{1}H/^{15}N$-HSQC spectra (with and without saturation of the corresponding resonances). For a complex of a multidomain RNA-binding protein, Nova1 KH3, cross-saturation $^{1}H/^{15}N$-HSQC experiments were performed in the presence of a 15-nucleotide RNA target. The binding site for the RNA on the protein was mapped, and the mapping was compared to the data obtained from the chemical-shift perturbation method and to X-ray data for the protein–RNA complex. The result from cross-saturation mapping is very similar to the that from the chemical-shift perturbation experiments with the latter giving a slightly too large binding site when compared to the X-ray data. This suggests that the combined use of chemical-shift perturbation and cross-saturation data allows the identification of interaction surfaces with greater confidence. The RNA-binding sites as identified by three different methods are depicted in Figure 16.

2.4. Transient Transferred NOE Experiments

In general, one distinguishes between steady-state and transient NOE experiments. Both experimental schemes are applicable to the observation of trNOEs. Steady-state techniques have been discussed above, and we will focus on transient NOE experiments in the following. In transient NOE experiments high-frequency pulses are utilized to generate a nonequilibrium state that during a mixing period returns to equilibrium by relaxation. NOEs are generated during this mixing time. Typically, the 2D NOESY experiment is used to detect transient NOEs.[14]

During the mixing time NOEs build up to a maximum value and then decrease to zero because of T_1 relaxation. In transient trNOE experiments intra- and intermolecular trNOEs build up during the mixing time. As mentioned above, intramolecular trNOEs are usually much larger than intermolecular effects. Both effects have been used for the detection of binding activity of ligands.[84–89]

2.4.1. Intramolecular Transferred NOEs

Small organic molecules show positive NOEs that build up during the mixing time of a NOESY experiment to reach a maximum value after a few seconds. Large molecules, such as proteins, show negative NOEs and reach the maximum value after a rather short time, often in less than 200 ms. In a trNOE experiment a small ligand in solution in the presence of a large receptor protein also shows negative NOEs, so-called transferred NOE (trNOEs). The motional characteristics about the bound state are carried into solution and detected using the signals of the free ligand.

Therefore, discrimination between ligands with binding activity from those without relies on the sign of the trNOEs being the opposite of that of the NOEs, and on the fact that the maximum enhancement of the NOEs is reached after a much shorter period of time. Figure 17 shows a comparison of typical NOE and trNOE curves.

From this it is clear that the mixing time is a critical parameter: it should be short enough so that the contribution of NOE signals of free ligands is negligible, but long enough that sufficient intensity in the NOE spectrum can be accumulated. The molar ratio of ligand molecules to receptor protein is another critical parameter. In a number of experimental and theoretical investigations it was shown, that depending on the kinetics and thermodynamics of the binding reaction different optimum values are possible. More

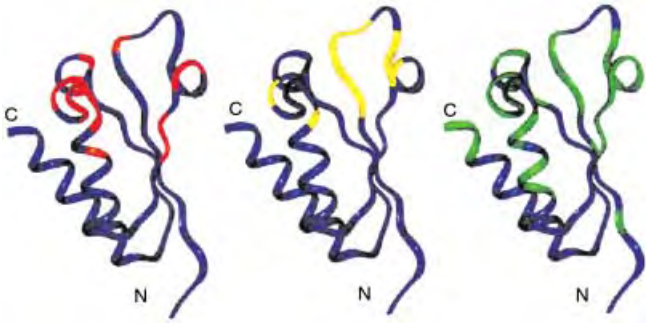

Figure 16. Structural homology model of Nova1 KH3 protein (SWISS-PROT) showing the protein backbone as a ribbon. Three different methods of identifying surface residues of the protein involved in binding are compared. Left: residues reported to make direct contact with the ligand in the crystal structure of a closely related complex (red). Center: residues identified using cross-saturation experiments (yellow). Right: residues identified from chemical-shift perturbation HSQC experiments (green). Reprinted with permission from ref. [83].

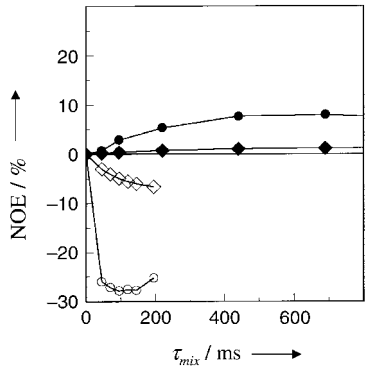

Figure 17. NOEs for free α-L-Fuc-(1→6)-β-D-GlcNac-OMe (filled symbols) and trNOEs for α-L-Fuc-(1→6)-β-D-GlcNac-OMe in the presence of AAA (open symbols), measured at 600 MHz as a function of the mixing times τ_{mix}. Circles and diamonds indicate the proton pairs H6proR^{GlcNAc}–H6proS^{GlcNAc} and H1^{Fuc}–H6proS^{GlcNAc}, respectively. Maximum NOEs for the free disaccharides are found around mixing times τ_{mix} of 1000 ms, whereas maximum trNOEs are reached at mixing times lower than 300 ms.

details can be found in, for example, ref. [30]. Since often neither dissociation constants K_D nor dissociation rates k_{off} are known, performing a titration and recording trNOE spectra at each individual step is recommended.

The first demonstration of the usefulness of the trNOESY experiment for screening libraries was for mixtures of carbohydrates that had potential binding affinity for a lectin, *Aleuria aurantia* agglutinin (AAA).[87,55] A clear distinction between binding and nonbinding components of the mixture was straightforward. The mixtures used are shown in Scheme 4 and the resulting trNOE spectra are depicted in Figure 18.

The trNOESY method was also successfully applied to identify binding activity in a mixture of potential E-selectin antagonists.[86] Here, conflicting results concerning the binding activity of ligands had been published before.[86] With trNOESY it was shown that in the library given in Scheme 5 only the sialyl Lewis^X derivative **5** and not the mimic **7** had binding affinity towards E-selectin. Figure 19 shows the NOESY spectrum and the trNOESY spectrum of the library. Clearly, only a small number of cross-peaks with negative sign (trNOEs) is observed in the trNOESY experiment. The cross-peak pattern was unambiguously assigned to derivative **5**. The NMR spectroscopic data were substantiated by separate ELISA measurements that gave the same relative binding affinities. It should be emphasized here that the trNOESY experiment in general works well for ligands that have K_D values in the range μM to mM. For tighter binding with dissociation constants in, for example, the nM range the applicability of trNOE experiments is limited.

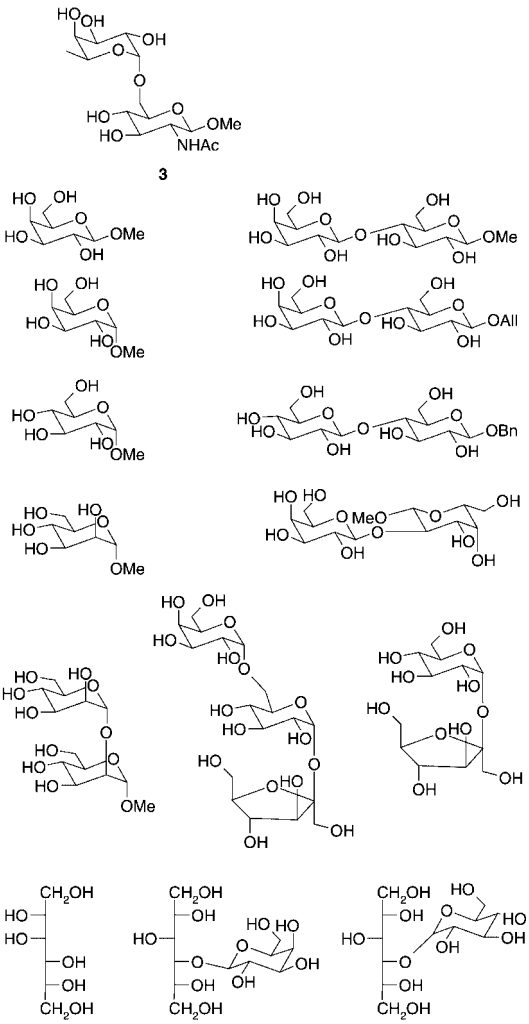

Scheme 4. Compound library tested for binding activity towards AAA.

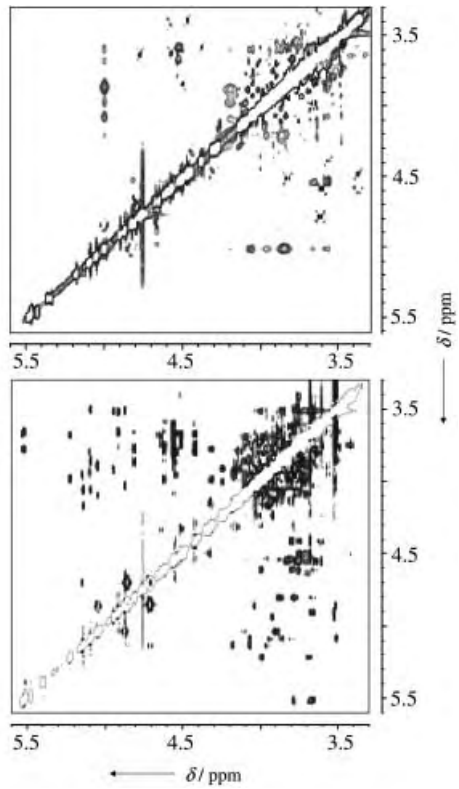

Figure 18. Bottom: 2D NOESY spectrum for the oligosaccharide library in Scheme 4. All components were in a concentration of approximately 10 mM in a binding-pocket:ligand ratio of 1:20. NOE cross-peaks are of opposite sign compared to the diagonal signals (positive NOEs). The diagonal is shown as one contour only. It is clear that an assignment of the library components is not straightforward. Top: 2D trNOESY spectrum for the oligosaccharide library in the presence of AAA displaying the trNOE pattern of α-L-Fuc-(1→6)-β-D-GlcNAc-OMe (**3** in scheme 4). The trNOE cross-peaks have the same sign as the diagonal signals (negative NOEs). The spectra were recorded in D_2O solution at 500 MHz and 306 K. A spin-lock filter after the first π/2-pulse was used to suppress the protein background.

Another application of the trNOE method to detect binding activity was the investigation of the binding of furanylacroyl (fa) amino acids and dipeptides to the angiotensin converting enzyme (ACE).[85] In this study the relative binding affinities of the ligands were estimated directly from the mixture by using trNOESY experiments. This was achieved by adding different components to the mixture whilst monitoring the trNOEs of one component. It was found that fa-Phe, fa-Trp, and fa-Gly-Leu are better binders than fa-Ala-Ala and fa-Phe-Phe. In addition, it was shown that these compounds did not interfere with the binding of captopril to

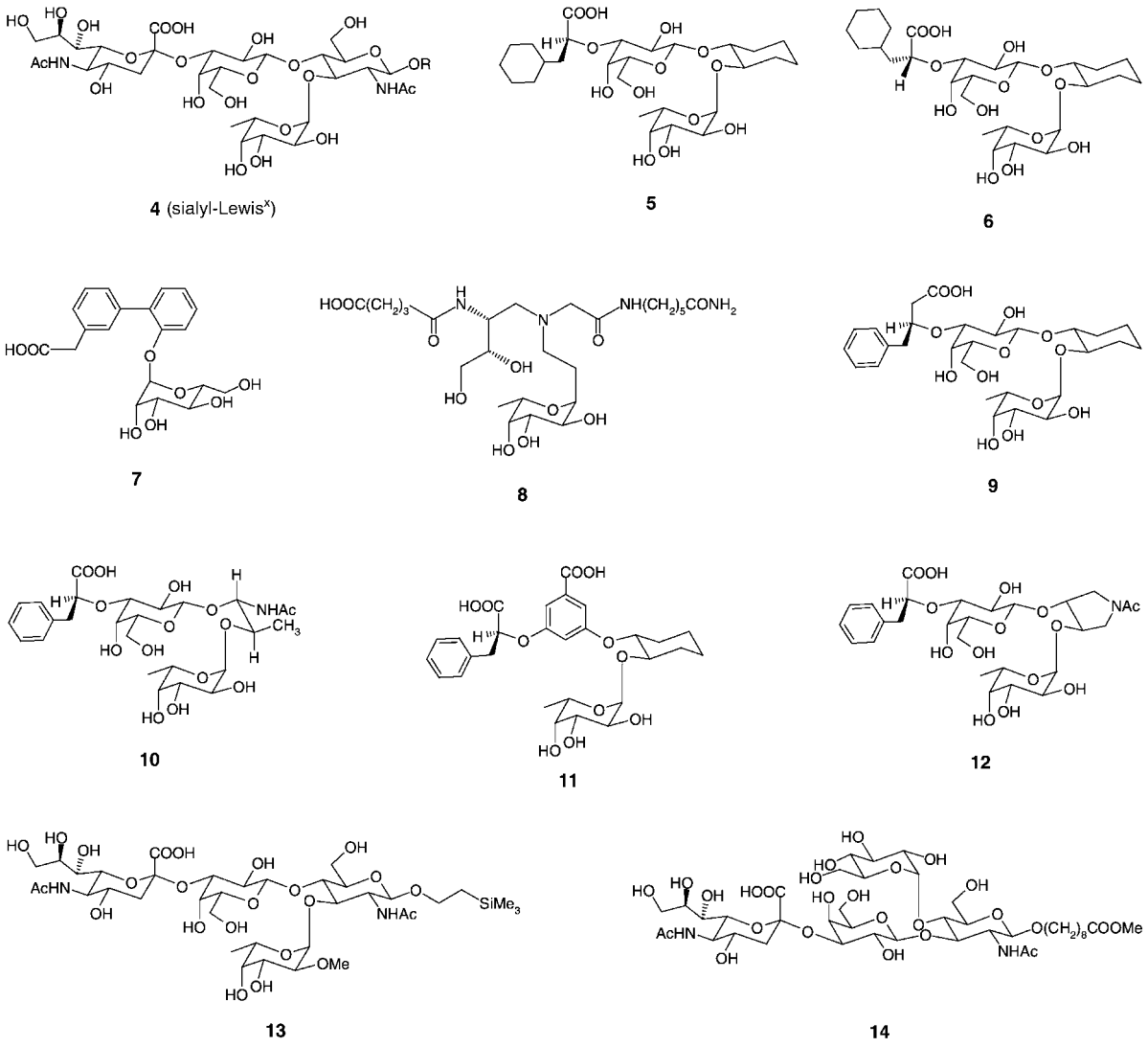

Scheme 5. Compound library of potential E-selectin antagonists. Sialyl Lewis^x is shown for comparison, it was not part of the library.

ACE. Captopril is known to be a ligand for the S1′ and S2′ binding site of ACE. No changes in the trNOE intensities arising from the fa amino acids were observed upon addition of captopril. It was concluded that the fa amino acids and fa-dipeptides preferably bind to the S1 and S2 pocket of the enzyme (Figure 20).

For the example of carbohydrate ligands in the presence of AAA shown above the ligand with binding activity was a disaccharide α-L-Fuc-(1-6)-β-D-GlcNAc-OMe. Comparison of typical chemical-shift values did not allow the unequivocally assignment of the type of glycosidic linkage. Therefore, a 3D TOCSY-trNOESY experiment was applied to assign the glycosidic linkage site of the active disaccharide directly from the mixture.[84] Indeed, this experiment allowed an unequivocal assignment. Because of the long experiment time this approach will certainly be of limited use for the analysis of compound mixtures.

2.4.2. *Intermolecular Transferred NOEs—NOE Pumping*

For the analysis of protein–ligand interactions not only intra- but also intermolecular transfer NOEs have been proven to be important. Especially, the orientation of a ligand in a binding pocket can be deduced from such data, given that the protein signals can be assigned.[90] This assignment certainly is impossible if the receptor protein is large (molecular weight above ca. 30 kDa) and not isotope enriched. On the other hand, if only information about ligand binding activity is sought, such an assignment is not necessary. In the analysis of bound conformations of low-molecular-weight compounds by using trNOE experiments it has been noted that two effects, spin diffusion and leakage of the magnetism to the protein can obscure the analysis of the bound conformation. Both effects are the result of intermolecular trNOEs between the protein and the ligand. In the case of spin diffusion false conformations may be deduced. In the case of leakage the magnetism to the protein, which

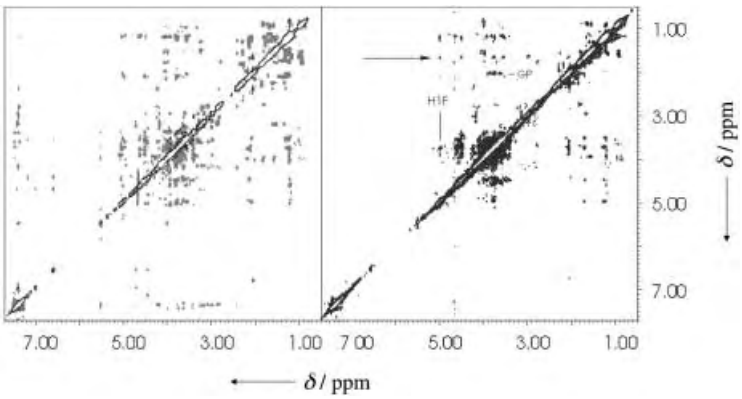

Figure 19. Left: 2D-NOESY spectrum of the compound mixture in Scheme 5 in D_2O at 310 K. The mixing time was 900 ms. Only positive NOEs were observed (red). Right: 2D-trNOESY spectrum of the compound mixture in the presence of E-selectin at a mixing time of 300 ms and a temperature of 310 K. A spin-lock filter of 15 ms duration was applied following the first $\pi/2$ pulse. The molar ratio of binding sites to ligand was 1:15. The cross-peaks shown are negative (trNOEs) and can be assigned to the bioactive component **5** (see Scheme 5). Only negative cross-peaks (black) are shown. Cross-peaks originating from spin diffusion are marked with an arrow. GP marks signals stemming from the glycan chains of E-selectin. H1F designates the anomeric proton of fucose of **5**.

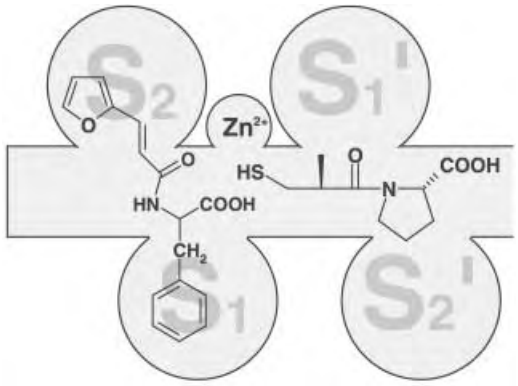

Figure 20. Proposed ACE binding site in presence of fa-Phe (left) and Captopril (right). The binding of fa-Phe is not influenced by the high-affinity inhibitor Captopril, and therefore it has the same binding affinity as in absence of the inhibitor.

usually occurs during longer mixing times, slightly expanded structures are obtained. Several experimental and computational schemes have been developed to alleviate such effects.[26] On the other hand these effects are very helpful if binding activity is to be detected. In recent years several experimental schemes have been developed for screening that relies upon intermolecular trNOEs and will be described below.

When binding to a protein a ligand not only alters its tumbling time but also changes its relaxation environment. Protons located in the binding pocket of the protein contribute to the relaxation of the ligand protons and vice versa. In the original NOE pumping experiment it was proposed that signals of nonbinding molecules could be suppressed by using a diffusion filter followed by a NOESY-type mixing time to make relaxation pathways from the protein to the ligand visible. This situation was achieved by subtraction of the spectrum from a suitable reference spectrum.[89] In an improved version the reverse experimental setup was chosen.[88] After excitation, a T_2 relaxation filter is applied to suppress protein signals, followed by a NOESY-type mixing period. As a consequence, intermolecular trNOEs between ligand protons and protein protons are suppressed. In a second reference experiment the T_2 filter is applied after the mixing period so that during the mixing time intermolecular trNOEs build up and lead to a decrease of the ligand signal intensities. The difference of the two experiments delivers signals stemming only from those compounds that were in contact with the protein binding site. An example for this reverse NOE pumping is shown in Figure 21 showing the binding of octanoic acid to human serum albumin (HSA). The method is especially useful for very small proteins (< 10 kDa) where selective irradiation of the protein is not possible.

3. Using Chemical-Shift Changes To Identify Ligand Binding and the Binding Pocket of the Receptor

Upon binding of a ligand to a receptor protein, the chemical shifts of both the ligand and protein proton resonance signals are affected. For the protein, nuclei located in the protein binding pocket usually show the largest effects. Protons are the most sensitive nuclei for NMR spectroscopy. Therefore, one can, for example, follow the binding of a ligand to a protein by observation of well separated signals of His residues in the protein binding pocket.[91–95] Theoretically, a complete ^{1}H MNR chemical-shift map can be obtained from a 2D homonuclear NMR experiment, such as TOCSY, and protein spectra with and without ligand present may be compared. In practice, an unambiguous assignment of corresponding chemical-shift changes of protein proton resonance signals upon addition of a ligand is very difficult because of severe signal overlap, and moreover, it is usually impossible to identify the amino acids involved in protein–ligand interactions. It follows, that to assign ^{1}H NMR chemical-shift changes of protein proton resonances that occur upon binding it is an advantage to employ heteronuclear correlation NMR spectroscopy experiments that lead to a deconvolution of the ^{1}H NMR signals.

For ligand protons the situation is different, because usually spectra of low-molecular-weight compounds are less complex, with less overlapping of signals. Therefore, several approaches utilize the changes of ligand proton resonance signals to characterize binding. One of the most common applications is the determination of dissociation constants from titration experiments. For the characterization of binding epitopes and for the determination of binding activity in compound mixtures the observation of ligand-proton resonance-signal chemical-shift changes is possible but difficult.

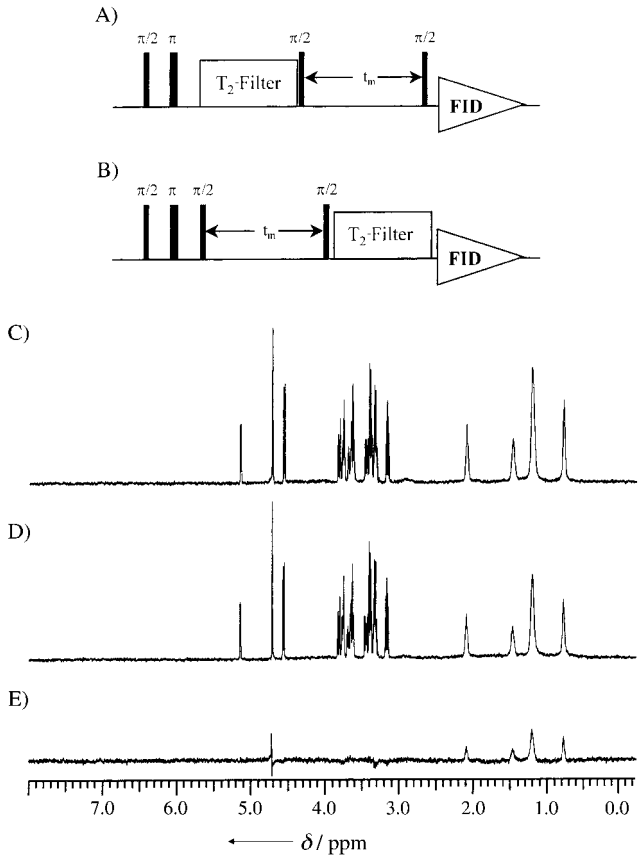

Figure 21. Example of a reverse NOE pumping experiment (RNP). Pulse sequence (A) generates RNP, whereas sequence (B) is used for referencing. The spectra (C)–(E) are obtained for a sample of 1 mM octanoic acid and 1 mM glucose in the presence of 20 μM HSA. (C) Reference spectrum, (D) RNP spectrum, (E) difference spectrum showing only the signals of octanoic acid nuclei that bind to HSA. Reprinted with permission from ref. [88].

On the other hand, the observation of chemical-shift changes of protein resonance signals by utilizing heteronuclear shift-correlation experiments has proven to be a very valuable tool in binding studies as this will become clear in the next section.

3.1. SAR by NMR Spectroscopy—The 1H/15N-HSQC Experiment

One experimental setup to detect binding of ligands to receptor proteins and to identify at the same time the amino acids in the binding pocket involves the acquisition of $^{1}H/^{15}N$ HSQC spectra of probes with and without ligands present. Spectra can be acquired in about 10 minutes and with very good separation of resonance signals. The technique requires that ^{15}N-labeled protein is available. The detection of ligand binding works as follows: One $^{15}N,^{1}H$ HSQC spectrum of the ^{15}N-labeled protein is acquired as a reference spectrum. Then, samples are prepared, that contain one or many potential ligands. If the resonance position of a cross-peak is significantly shifted compared to the reference spectrum this is an indication of binding (SAR by NMR).

If the sample contained only one sort of potential ligand molecules, the binding ligand is identified. If a mixture had been used, the active component has to be identified by separation. For mixtures of synthetic origin, such as combinatorial libraries, this usually is not a large problem because instead of separating the mixture smaller sub-libraries may be easily synthesized. Finally, single compounds have to be tested for binding activity. If plant extracts or the like had been used, deconvolution of the library may pose a serious problem, and the bioactive component may not be easily identified.

In principle, $^{1}H/^{15}N$-HSQC NMR experiments have been known for a while to be useful to study the binding of ligands to proteins. For instance, $^{1}H/^{15}N$-HSQC experiments were known to provide an effective method to investigate interactions of the guanidinium groups of arginine units with charged groups on the ligand.[96–102] However, the value of this chemical-shift perturbation technique for the screening of compound libraries was only discovered recently. The first application of $^{1}H/^{15}N$-HSQC experiments to screen ligands for binding activity was demonstrated for the FK506-binding protein FKBP.[103] Also, in the same study a linked-fragment approach was introduced which will be explained below. When complexed to FK506, FKBP binds tightly to calcineurin (Scheme 6) which plays a role in the regulation of a variety of transcription factors. As a result of the binding to calcineurin significant immuno suppression is observed. Therefore, FK506 is an important drug that, for instance, suppresses rejection reactions after organ transplants. Many current attempts are being made to develop drugs that maintain the FKBP binding activity but at the same time lack the high toxicity of FK506.

First, a compound library of approximately 1000 substances was screened for FK506-like binding activity. A solution containing uniformly $^{15}N,^{13}C$-labeled FKBP at a concentration of 2 mM was used for the HSQC binding experiments. From the library, a candidate, compound **15** (Scheme 6),with $K_D = 2$ μM was identified. To improve the binding activity, a linked-fragment approach was applied, in which, two ligands with moderate affinity are covalently bound to a ligand of higher affinity. In a second screen, a complex of FKBP and the pipecolinic acid derivative **15**, both components in a concentration of 2 mM, was used to screen for ligands that would bind to a second site near to the first binding site. By this method a benzanilide derivative **16** was identified that bound to FKBP with a $K_D = 100$ μM. The $^{1}H/^{15}N$-HSQC spectra of FKBP in the presence of saturating amounts of **15** and in the absence and presence of compound **16** are shown in Figure 22. The chemical-shift changes indicate that compound **16** binds to a second site and is not competing with the binding of **15** to the first site. To generate a higher-affinity ligand, the two fragments **15** and **16** were covalently joined together by a variety of linkers. Five different linked molecules were synthesized from which compound **23** had the highest binding affinity for FKBP ($K_D = 19$ nM). The complex of FKBP and **23** was then subjected to a detailed structural analysis using NMR spectroscopy.[103]

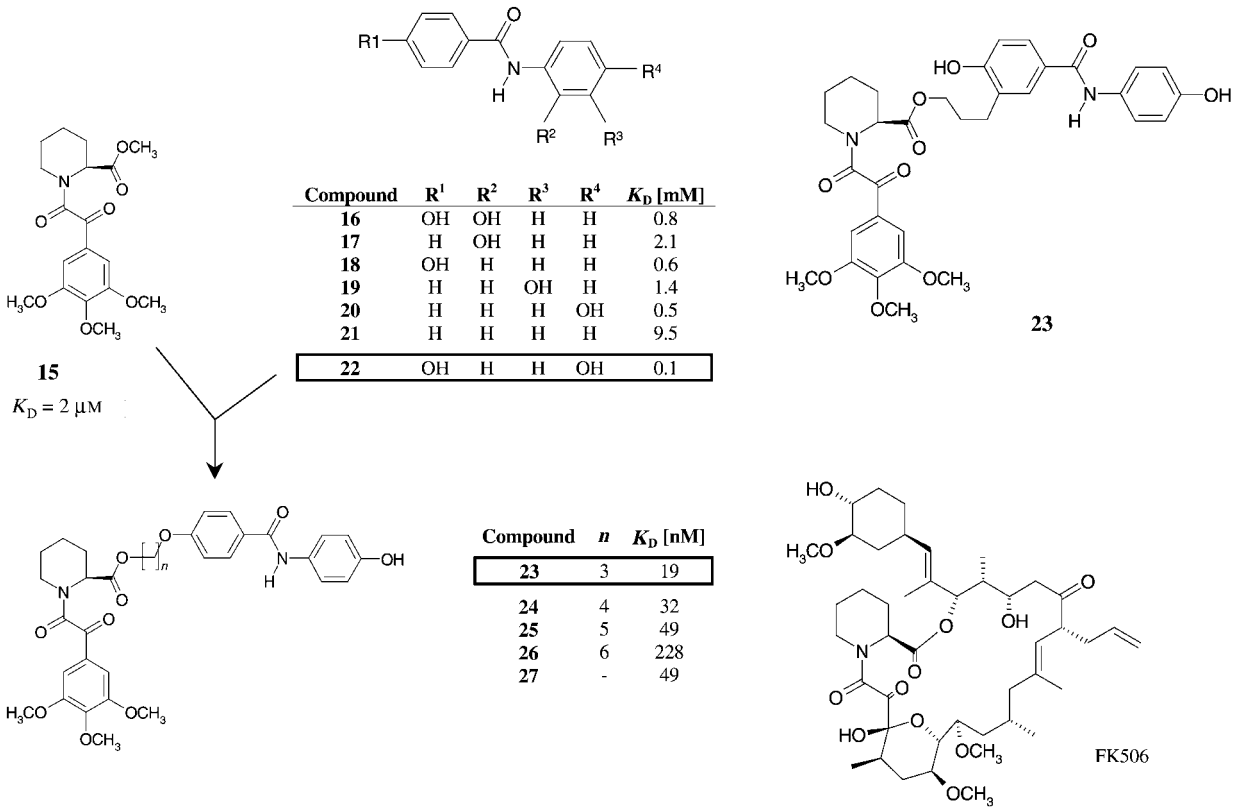

Scheme 6. Compounds tested in $^{1}H/^{15}N$-HSQC binding experiments for their binding affinity to FK506 analogues. Adapted with permission from ref. [103]. Copyright 1996 American Association for the Advancement of Science (http://www.sciencemag.org).

SAR by NMR spectroscopy is carried out in the five main steps shown in Scheme 7:

1. Identification of ligands with high binding affinity from a library of compounds by utilizing $^{1}H/^{15}N$-HSQC experiments.
2. Optimization of ligands by chemical modification.
3. Identification of ligands binding in the presence of saturating amounts of optimized ligands from step 2 by utilizing $^{1}H/^{15}N$-HSQC experiments.
4. Optimization of ligands for the second site.
5. Tethering the two ligands in various positions and checking again for binding.

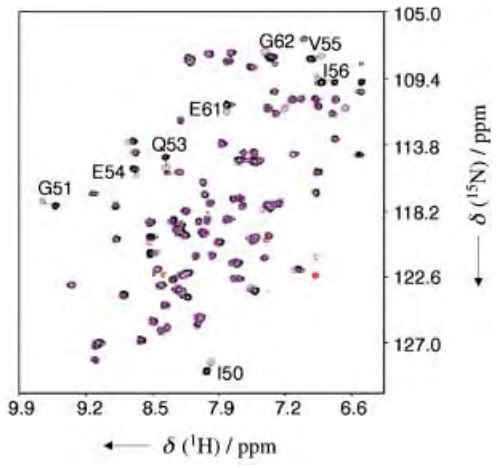

Figure 22. A superposition of $^{1}H/^{15}N$-HSQC spectra for FKBP in the absence (magenta contours) and presence (black contours) of compound **16**. Both spectra were acquired in the presence of saturating amounts of **15** (2.0 mM). Significant chemical-shift changes are observed for resonance signals of the residues indicated. Reprinted with permission from ref. [103] Copyright 1996 American Association for the Advancement of Science.

In general, SAR by NMR spectroscopy cannot uncover the identity of a compound with binding activity, if a mixture of compounds is present. Therefore, after having tested positive, a mixture has to be deconvoluted. If enough labeled protein is available $^{1}H/^{15}N$-HSQC spectra can be obtained in a few minutes. Therefore, for samples that contain receptor protein and, for example, ten different compounds, it is estimated that approximately 100 compounds could be screened per hour. It is important to be aware of the amounts of protein and respective ligands that are required for SAR by NMR spectroscopy. If, for example, a protein of molecular weight of 15 kDa is subjected to screening, 7.5 mg of protein will be necessary per probe (0.5 mL of a 1 mM sample for NMR spectroscopy). For 100 samples 750 mg of protein has to be available. Certainly, protein can be recovered by dialysis after having completed the measurement but to generate considerable throughput, or to get into the limits of high-throughput screening (HTS) with more than 5000 compounds tested per day it is necessary to have the ^{15}N-labeled protein available in gram quantities. As will be shown below, the

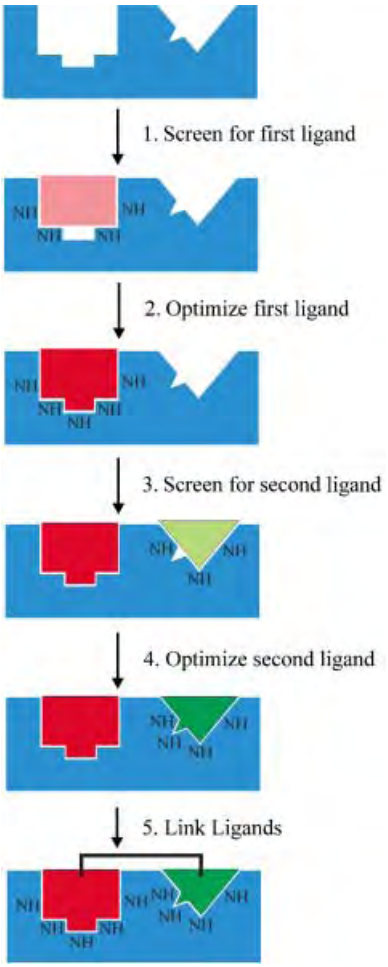

Scheme 7. Schematic overview of SAR by NMR spectroscopy for the identification of a high affinity binding ligand on the basis of two ligand fragments that bind to two neighboring binding sites. Reproduced with permission from ref. [103]. Copyright 1996 American Association for the Advancement of Science (http://www.sciencemag.org).

Box 5: The role of binding kinetics in HSQC-based NMR spectroscopy binding studies

The binding kinetics play a fundamental role for all NMR-spectroscopy-based binding experiments (see Box 1). HSQC-based experiments allow the detection of ligand binding even in the case of rather slow dissociation rates, usually associated with low K_D values. In fact there is no lower limit to K_D, and consequently there is also no lower limit to k_{off}.

To analyze the potential appearance of $^1H/^{15}N$-HSQC spectra upon binding of ligands requires Equations (3)–(5). An average weighted $^1H/^{15}N$ chemical-shift difference has been defined by Equation (13)

$$\delta(^1H/^{15}N) = \delta(^1H) + \delta(^{15}N)/5 \qquad (13)$$

where $\Delta\delta$ refers to the difference in chemical shifts of free and bound protein.[126]

A threshold value of $\Delta\delta(^1H/^{15}N) = 0.04$ ppm is considered to indicate that the corresponding amino acid is involved in binding to the ligand. Assuming equal contributions from the ^1H and ^{15}N chemical shifts, broad resonance signals with low intensity would be expected for a binding constant of 6 μM (see Box 1). For larger chemical-shift differences the coalescence point would shift to weaker binding and vice versa. For slower binding processes separate signals are observed for the bound and the free state, for faster processes an average signal is observed. For ligands with μM to mM K_D values the method requires an excess of ligand molecules so that the binding pocket is saturated with ligands.

According to Fesik et al., the limit for detecting changes in protein proton chemical shifts upon binding ligands that are in fast exchange is 20% occupation of the protein's binding sites.[108] From Equations (6) and (8) it is calculated that, assuming a K_D value of 1 mM and a total protein concentration $[P]_0$ of 0.5 mM, a ligand concentration $[L]_0$ of 0.5 mM results in approximately 27% saturation of binding sites. At a protein concentration $[P]_0$ of 0.05 mM a approximately fourfold excess of ligand is required to saturate about 16% of the binding sites. In HSQC-based screening, this condition is used to decrease the hit rate for mM-range binders by lowering the total protein concentration.[108] Usually HSQC-based screening is performed at equal concentrations of ligand and protein, and therefore a ligand with a K_D of 1 mM will not be detected at ligand and protein concentrations of 0.05 mM, because the fraction of occupied protein binding sites will be less than 5%.

sensitivity of SAR by NMR spectroscopy can be increased utilizing several improvements.

Since its first application to FKBP, SAR by NMR spectroscopy has been used to design many high-affinity ligands for several other proteins of therapeutic relevance. Several improvements of the method were made in the mean time. Before the introduction of TROSY (transverse relaxation optimized spectroscopy)[104] $^1H/^{15}N$-HSQC screening was limited to proteins with a molecular weight of less than 20–30 kDa in size. With TROSY much larger receptor proteins may be targeted,[105] although problems remain with the tremendous number of cross-peaks that have to be assigned. Strategies to achieve spectroscopic assignment as well as structural analysis of large proteins are known but require significantly more effort and time. One interesting approach to simplify TROSY spectra of large receptor proteins is the SEA-TROSY (solvent exposed amides by TROSY) experiment in which only exchangeable amino protons are detected. These protons belong mainly to amino acids at the periphery of the protein that contribute to ligand binding.[106,129] The SEA-TROSY experiment is performed by implementing a ^{15}N double filter in conjunction with a mixing time, during which magnetization is transferred from water to amino protons at the periphery of the protein. An example for the degree of simplification that may be achieved is shown in Figure 23 for a perdeuterated ^{15}N-labeled protein (71 kDa).

As a simple and practical alternative, individual ^{15}N-labeled amino acids can be incorporated into a protein.[107] By labeling, for example, Ala residues only, assignment problems are substantially reduced. To completely map a binding site on the protein surface this approach requires the preparation of several differently ^{15}N-labeled proteins.

A significant increase in sensitivity is achieved by applying cryo-probe technology. It has been shown that the concentration of the ^{15}N-labeled protein target can thus be reduced by a factor of four to 50 μM.[108] More importantly the stringency of the method is significantly enhanced by using

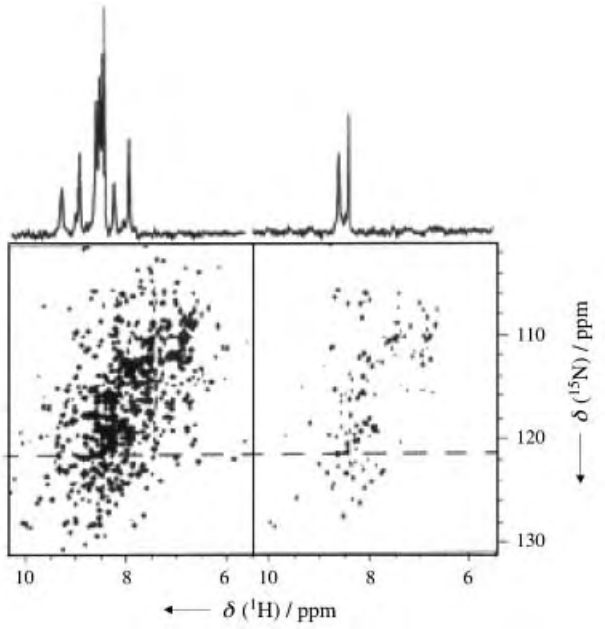

Figure 23. TROSY (left) and SEA-TROSY (right) $^{15}N/^{1}H$ correlation spectra of 0.5 mM $^{2}H,^{15}N$ labeled P450 reductase at 700 MHz and 303 K. Only solvent-exposed NH resonance signals are visible in the SEA-TROSY spectrum. Reprinted with permission from ref. [106].

lower concentrations. Using stromelysin as a target protein it was demonstrated that testing 100 compounds in one sample, in which the overall ligand concentration was only 5 mM, is possible without difficulties. Deconvolution of samples that display binding activity is achieved by first testing samples of ten compounds each, and then testing each individual component in the active sample of ten. With conventional-probe technology, approximately 10 compounds can be tested simultaneously. It follows, that a 10-fold increase in speed can be achieved by using cryo probes and it has been estimated that around 200000 compounds can be tested per month including deconvolution of active libraries.[108]

An interesting extension of the HSQC screening technique exploits differences in chemical shifts for closely related ligands.[109] It is not simple to deduce the ligand orientation from the chemical-shift perturbances observed in a $^{1}H/^{15}N$-HSQC spectrum. Although docking algorithms may be used to suggest a structure of the protein–ligand complex, a subsequent NMR spectroscopy structural analysis is necessary to unambiguously determine the orientation of the ligand. It is argued that if a variety of structurally similar ligands is available, it should be possible to define the orientation of the ligands in the binding pocket because differences in the HSQC chemical-shift maps can be directly related to the portion of the ligand that has been altered. Utilizing this principle it was possible to analyze the orientation of ascomycin, a FK506 analogue, when bound to FKBP.[109] Similarity between ligands is not only useful for the analysis of ligand orientations in protein binding pockets, for instance, a statistical analysis of binding data on 11 protein targets has identified molecular motifs that are preferred for protein binding.[110] This study showed that the biphenyl unit is one such structural building block that delivers binding activity whilst at the same time achieving significant binding specificity just for FKBP

3.2. The $^{1}H/^{13}C$-HSQC NMR Experiment—Selective ^{13}C Labeling

In general, labeling of proteins with ^{13}C is more expensive than with ^{15}N. Also, $^{1}H/^{13}C$-HSQC spectra are more complex than $^{1}H/^{15}N$-HSQC spectra. Therefore, $^{1}H/^{13}C$-HSQC experiments have not widely been employed to test for binding. To overcome the shortcomings of $^{1}H/^{13}C$-HSQC for screening, a labeling technique was suggested that allows the selective labeling of the protons of the methyl groups of valin, leucin, and isoleucin only.[105] This approach significantly reduces the complexity of the resulting HSQC spectra. At the same time the presence of three protons in methyl groups versus a single proton in an NH group increases the sensitivity, in addition the favorable relaxation properties of methyl groups also allows the application of HSQC-based screening to larger proteins. The labeling method was based on a previous labeling strategy where fully ^{13}C-labeled α-ketobutyrate and α-ketoisovalerate were used to incorporate protonated methyl groups of valin, leucin, and isoleucin into perdeuterated, completely ^{13}C- and ^{15}N-labeled proteins.[111–113] A synthetic route was devised to produce [3-^{13}C]-α-ketobutyrate and [3,3′-

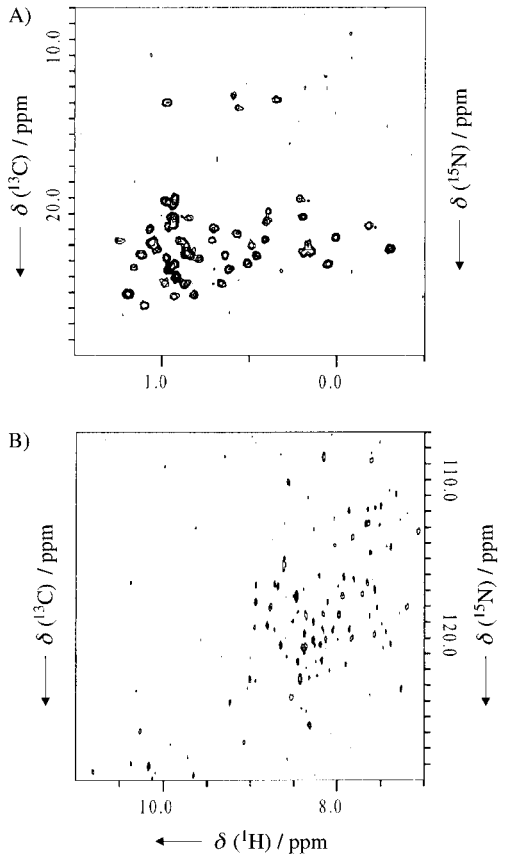

Figure 24. A) $^{1}H/^{13}C$-HSQC and B) $^{1}H/^{15}N$-HSQC spectra of ^{13}C(methyl)/[U-^{15}N]-labeled Bcl-xL (19 kDa) at 500 MHz. Reprinted with permission from ref. [108].

^{13}C]-α-ketoisovalerate utilizing ^{13}C-methyl iodide as the ^{13}C source.[105] Proteins with molecular weights ranging from 12–110 kDa were subjected to ^{1}H/^{13}C-HSQC screening.

For FKBP (12 kDa) and the apoptose inhibitor Bcl-xL (19 kDa) it was found that the ^{1}H/^{13}C-HSQC experiments give a nearly threefold higher sensitivity than ^{1}H/^{15}N-HSQC experiments. Therefore, throughput rates are possible that can only be achieved for ^{15}N-labeled samples by the use of cryo-probe technology.[108] In Figure 24 ^{1}H/^{15}N- and ^{1}H/^{13}C-HSQC spectra of a 50 μM sample of ^{13}C(methyl)/[U-^{15}N]-labeled Bcl-xL are compared. It is clear that the ^{1}H/^{13}C-HSQC spectrum is of superior quality.

For larger proteins ($M_W > 40$ kDa), maltose-binding protein (MBP; 42 kDa) and dihydroneopterin aldolase (DHNA; 110 kDa) served as examples. It was shown that acceptable throughput rates can only be achieved if the protein is perdeuterated.[105] The ^{13}C(methyl)-HSQC experiments turned out to be much more sensitive than the ^{1}H/^{15}N-TROSY (Figure 25).

The applicability of the ^{13}C(methyl)-labeling strategy clearly depends on the presence of valin, leucin, or isoleucin residues in the active site of the protein under investigation. A statistical analysis of 191 crystal structures of proteins bound to ligand molecules shows that 92% of the ligands were found to have a heavy atom within 6 Å of at least one methyl carbon of valin, leucin, or isoleucin where as 82% of the ligands have a heavy atom within 6 Å of at least one backbone nitrogen atom.

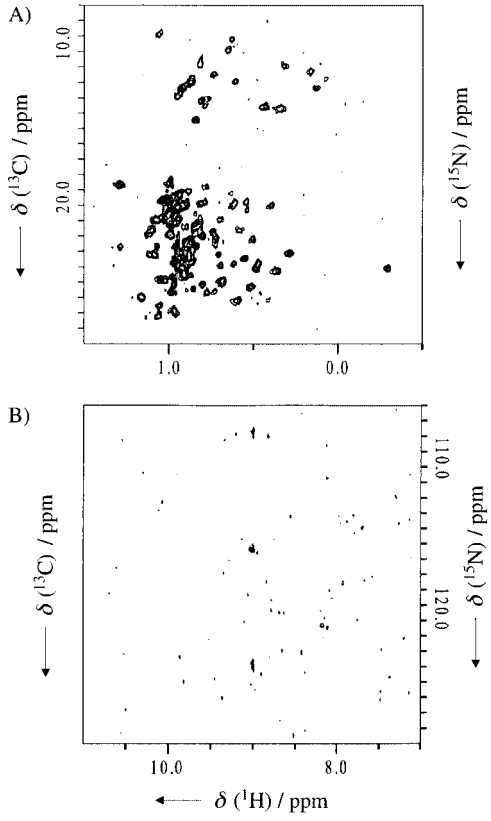

Figure 25. A) ^{1}H/^{13}C-HSQC and B) ^{1}H/^{15}N-TROSY spectra of ^{13}C(methyl)/[U-^{15}N]-labeled MBP (50 μM; 42 kDa) at 800 MHz. Reprinted with permission from ref. [105].

4. Use of Relaxation Times To Identify Ligand Binding

Line broadening which occurs upon binding has long been used to study the binding of ligands to proteins. Certainly, the observation and quantification of such effects requires well-separated signals, especially if compound mixtures are to be investigated.[8] Therefore, line-broadening effects then are of limited value for the detection of binding activity of one or more components of complex mixtures. Other experimental approaches rely on the separate acquisition of spectra of ligand molecules with and without protein receptor present.[114] Subsequent subtraction leads to spectra that only contain contributions from binding ligands. Unfortunately this approach requires a rather careful experimental setup rendering the technique somewhat time consuming. Moreover, it is difficult to eliminate artifacts from the resulting difference spectra.

Recently a spin-labeled first ligand was employed that binds to a main binding site of a protein, and subsequently to screen for binding of other ligands to so-called second binding sites.[115] The presence of a spin label causes a T_2 relaxation sink for ligands that bind to the second binding site of the protein, the effect depends greatly on the distance between the second site and the spin label. Therefore, in T_2-filtered NMR spectra resonance signals of ligands that bind to this second site are not visible because of fast T_2 relaxation. An example for this type of relaxation editing is shown in Figure 26.

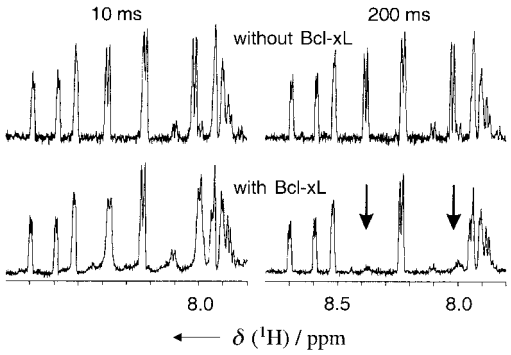

Figure 26. Spectra of a mixture of potential second-site ligands for Bcl-xL with and without Bcl-xL present top: ^{1}H NMR reference spectrum; bottom: compound mixture in the presence of Bcl-xL and saturating amounts of a spin-labeled first ligand. Reprinted with permission from ref. [115] The duration of the T_2 filter was 10 ms (left), and 200 ms (right).

The method has been extended to allow for the screening of primary binding sites by covalently attaching spin labels to the protein target.[116] The binding of low-affinity ligands to FKBP was investigated. Spin labels (2,2,6,6-tetramethylpiperidine-1-oxyl; TEMPO) were linked to the lysine side chains of FKBP. Since several lysine residues are in the proximity of the FK506 binding site, any ligand that binds to this site will experience significantly enhanced T_2 relaxation. For a mixture consisting of two weakly binding ligands and

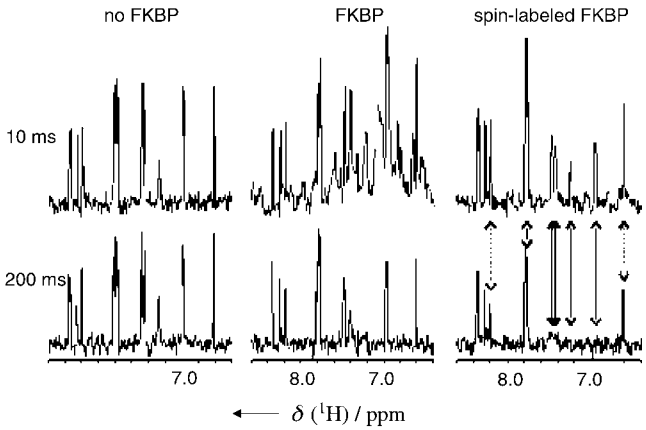

Figure 27. $T_{1\rho}$ relaxation experiments of two binding and four nonbinding compounds without FKBP (left, 60 μM) unlabeled FKBP (middle) and spin-labeled FKBP (right, 20 μM). The concentration of ligand each was 50 μM. Spin-lock times were 10 ms in the top and 200 ms in the bottom row. Arrows indicate the cancellation of signals originating from compounds with binding activity for FKBP. Reprinted with permission from ref. [116].

four nonbinding ligands it was demonstrated that the method works in principle (Figure 27). Because relaxation through electron spins is involved, the technique offers enhanced sensitivity. The method is limited by the requirement of covalent modification of the protein, which may also influence binding activity, and the fact that a lysine residue has to be close to the binding site to allow modification.

5. Use of Diffusion To Identify Ligand Binding

With the development of reliable gradient technology for high-resolution NMR spectroscopy the investigation of diffusion processes with NMR spectroscopy became possible. A variety of NMR pulse sequences has been developed that allow the investigation of diffusion constants in solution. On the basis of such experiments it is possible to discriminate compounds in mixtures according to their diffusion properties. This so-called diffusion editing has been successfully applied to deconvolute compound mixtures, and to detect molecular association processes.[114,117–121] For small- and intermediate-size molecules the approach works well, and in principle, diffusion editing is also applicable to the detection of binding of low-molecular-weight compounds to large protein receptors. In one approach, the preparation of different samples[114] (see also Section 3.5) of ligand mixtures with and without protein present was suggested and then the subtraction of the corresponding diffusion edited spectra should give information about the binding affinity. Using this approach it is difficult to avoid artifacts, as the preparation of two identical samples is required. The main difficulty is that for the detection of changes in the diffusion constant of a ligand that binds to a protein, it is necessary that a significant amount of the ligand is bound to the protein on the time average. The reason for this is that the observed averaged diffusion constant is a sum of the fraction of free ligand multiplied by the diffusion constant of the free state and the fraction of the ligand bound multiplied by the diffusion constant of the bound state. Therefore, an increasing excess of ligand molecules leads to small changes in the observed diffusion constant, which is the result of binding. It follows that low ligand-to-protein ratios are required to allow the detection of binding on the basis of averaged diffusion constants. The size of the protein target is limited because the averaging of the line widths of free and bound ligand results in ligand lines that are too broad when the ligand is bound to a very large protein is used. At low ligand-to-protein ratios no individual signals of the ligand can be identified because of severe line broadening. Diffusion editing has been proven to be a valuable tool where molecular interactions between small and intermediate size molecules is to be characterized.

Box 6: Diffusion editing as a tool to detect the binding of small-molecule ligands to receptor proteins

NMR spectroscopy experiments are well suited to determine diffusion coefficients of molecules, and are especially powerful for detecting the association of small molecules with other molecules not exceeding a few kDa in molecular weight as well as for determining K_D values. The association of small-molecule ligands with large receptor proteins often exceeding 100 kDa is not readily monitored by diffusion-edited NMR spectroscopy. Although the change in the diffusion speed of a small molecule is drastically altered upon binding to a large receptor protein, it is difficult to identify the resonance signals of the ligand at the low ligand-to-protein ratios required because of severe line broadening. One solution would be to apply a large excess of ligand but unfortunately this reduces the expected difference in the diffusion coefficient D considerably since it scales linearly with the mole fraction x of bound and free ligand, x_{bound} and x_{free}, respectively [Eq. (14)].

$$D_{observed} = x_{free}\, D_{free} + x_{bound}\, D_{bound} \qquad (14)$$

From this simple linear relationship it also follows that the best results would be obtained at high protein concentrations (in the mM range).

A simple example illustrates the point. A receptor protein of 100 kDa molecular weight has a diffusion coefficient of approximately 2×10^7. The corresponding ligand has a molecular weight of 1 kDa and a diffusion coefficient of about 20×10^7. Assuming a K_D value of 1 μM, and a protein concentration of 0.1 mM it follows that at a 0.1 mM ligand concentration approximately 90% of all binding sites are occupied. According to Equation (14) this would result in a significant change of the observed diffusion coefficient $D_{observed}$ [Eq. (15)].

$$D_{observed} = 0.1 \times 20 \times 10^7 + 0.9 \times 2 \times 10^7 = 3.8 \times 10^7 \qquad (15).$$

At an increased ligand concentration of 1 mM, around 99.9% of all binding sites are occupied. On the other hand, this tenfold excess of ligand over protein leads to a less then 10% lower value of D_{bound} compared to $D_{observed}$. Therefore, a value of around 18×10^7 is expected for $D_{observed}$ compared to a value of 20×10^7 for D_{free}. The situation gets even more unfavorable for increasing ligand concentrations. Therefore, relatively large amounts of protein are necessary for this technique.

Table 2: NMR spectroscopy techniques for the identification and characterization of binding of ligands to proteins

	SAR by NMR	STD NMR	Spin labeling	Diffusion editing	Inverse NOE Pumping	Water-LOGSY
Large protein (>30 kDa)	limited[a]	yes	yes	no	yes	yes
small protein (<10 kDa)	yes	no	yes	yes	no	no
Isotope-labeled protein required	yes	no	no	no	no	no
Binding epitope on protein	yes[c]	no	no	no	no	no
Binding epitope on ligand	no	yes	no	no	yes[d]	yes[e]
Amount of protein [nmol] at 500 MHz	25	0.1	~1	~100	~25	~25
K_D tight binding	no limit	100 pM	100 pM	~100 nM	1 nM	100 pM
K_D weak binding	~1 mM	~10 mM	~10 mM	~1 mM	~1 mM	~10 mM
Identification of ligand	no	yes	yes	yes	yes	yes
Comments	robust method	robust method	sensitive method, but results ambiguous if lysine positions unknown	relatively insensitive method	stable method, but ligand excess and mixing time need to be optimized	good for very hydrophilic targets and/or ligands

[a] TROSY necessary. [b] But chemical modification. [c] If protein is assigned. [d] Not realized. [e] But water contact surface.

6. Conditions for NMR Spectroscopy Screening and Characterization of Binding

A number of criteria have to be considered to choose the right method to identify and characterize binding by NMR spectroscopy. Table 2 is an attempt to provide a summary on some of the methods. Most data are from literature and some have been extrapolated by us.

This work was supported by the BMBF (FKZ 0311361), the DFG (sonderforschungsbereich 470; projects B2 and B3), the Graduiertenkolleg 464, and the Fonds der Chemischen Industrie. We also thank Dr. T. Keller and Dr. G. Wolff, Bruker BioSpin GmbH (Rheinstetten, Germany) for their support.

Received: February 14, 2002 [A518]

[1] T. Diercks, M. Coles, H. Kessler, *Curr. Opin. Chem. Biol.* **2001**, *5*, 285–291.
[2] M. Shapiro, *Farmaco* **2001**, *56*, 141–143.
[3] D. J. Craik, M. J. Scanlon, *Annu. Rep. NMR Spectrosc.* **2000**, *42*, 115–174.
[4] D. C. Fry, S. D. Emerson, *Drug Des. Discovery* **2000**, *17*, 13–33.
[5] G. C. Roberts, *Drug Discovery Today* **2000**, *5*, 230–240.
[6] A. K. Ghose, V. N. Viswanadhan, J. J. Wendoloski, *ACS Symp. Ser.* **1999**, *719*, 226–238.
[7] P. J. Hajduk, R. P. Meadows, S. W. Fesik, *Q. Rev. Biophys.* **1999**, *32*, 211–240.
[8] J. M. Moore, *Biopolymers* **1999**, *51*, 221–243.
[9] J. M. Moore, *Curr. Opin. Biotechnol.* **1999**, *10*, 54–58.
[10] M. J. Shapiro, J. S. Gounarides, *Prog. Nucl. Magn. Reson. Spectrosc.* **1999**, *35*, 153–200.
[11] M. J. Shapiro, J. R. Wareing, *Curr. Opin. Drug Discovery Dev.* **1999**, *2*, 396–400.
[12] D. C. Schriemer, O. Hindsgaul, *Comb. Chem. High Throughput Screening* **1998**, *1*, 155–170.
[13] P. J. Hajduk, R. P. Meadows, S. W. Fesik, *Science* **1997**, *278*, 497–499.
[14] D. Neuhaus, M. P. Williamson, *The Nuclear Overhauser Effect in Structural and Conformational Analysis*, Wiley-VCH, **2000**.
[15] K. Wüthrich, G. Wagner, R. Richarz, S. J. Perkins, *Biochemistry* **1978**, *17*, 2253–2263.
[16] N. R. Krishna, D. G. Agresti, J. D. Glickson, R. Walter, *Biophys. J.* **1978**, *24*, 791–814.
[17] A. Kumar, R. R. Ernst, K. Wüthrich, *Biochem. Biophys. Res. Commun.* **1980**, *95*, 1–6.
[18] W. Braun, C. Bosch, L. R. Brown, N. Go, K. Wüthrich, *Biochim. Biophys. Acta* **1981**, *667*, 377–396.
[19] G. Wagner, W. Braun, T. F. Havel, T. Schaumann, N. Go, K. Wüthrich, *J. Mol. Biol.* **1987**, *196*, 611–639.
[20] A. Bax, *Annu. Rev. Biochem.* **1989**, *58*, 223–256.
[21] P. Balaram, A. A. Bothner-By, E. Breslow, *J. Am. Chem. Soc.* **1972**, *94*, 4017–4018.
[22] P. Balaram, A. A. Bothner-By, J. Dadok, *J. Am. Chem. Soc.* **1972**, *94*, 4015–4017.
[23] J. P. Albrand, B. Birdsall, J. Feeney, G. C. K. Roberts, A. S. V. Burgen, *Int. J. Biol. Macromol.* **1979**, *1*, 37–41.
[24] G. M. Clore, A. Gronenborn, *J. Magn. Reson.* **1983**, *53*, 423–442.
[25] J. Feeney, B. Birdsall, G. C. Roberts, A. S. Burgen, *Biochemistry* **1983**, *22*, 628–633.
[26] N. R. Krishna, H. N. B. Moseley in *Structural Computation and Dynamics in Protein NMR, Vol. 17* (Eds.: N. R. Krishna, L. J. Berliner), Kluwer Academic, New York, **1999**, pp. 223–307.
[27] R. E. London, *J. Magn. Reson.* **1999**, *141*, 301–311.
[28] J. Jimenez-Barbero, J. L. Asensio, F. J. Canada, A. Poveda, *Curr. Opin. Struct. Biol.* **1999**, *9*, 549–555.

[29] T. Peters, B. M. Pinto, *Curr. Opin. Struct. Biol.* **1996**, *6*, 710 – 720.
[30] F. Ni, *Prog. Nucl. Magn. Reson. Spectrosc.* **1994**, *26*, 517 – 606.
[31] D. Li, L. A. Levy, S. A. Gabel, M. S. Lebetkin, E. F. DeRose, M. J. Wall, E. E. Howell, R. E. London, *Biochemistry* **2001**, *40*, 4242 – 4252.
[32] H. N. Moseley, W. Lee, C. H. Arrowsmith, N. R. Krishna, *Biochemistry* **1997**, *36*, 5293 – 5299.
[33] R. M. Keller, K. Wüthrich, *Biochim. Biophys. Acta* **1978**, *533*, 195 – 208.
[34] P. J. Cayley, J. P. Albrand, J. Feeney, G. C. Roberts, E. A. Piper, A. S. Burgen, *Biochemistry* **1979**, *18*, 3886 – 3895.
[35] R. M. Keller, D. Picot, K. Wüthrich, *Biochim. Biophys. Acta* **1979**, *580*, 259 – 265.
[36] G. M. Smith, *Biochemistry* **1979**, *18*, 1628 – 1634.
[37] B. Birdsall, J. Feeney, G. C. Roberts, A. S. Burgen, *FEBS Lett.* **1980**, *120*, 107 – 109.
[38] D. Cheshnovsky, G. Navon, *Biochemistry* **1980**, *19*, 1866 – 1873.
[39] E. I. Hyde, B. Birdsall, G. C. Roberts, J. Feeney, A. S. Burgen, *Biochemistry* **1980**, *19*, 3738 – 3746.
[40] J. R. Kalman, D. H. Williams, *J. Am. Chem. Soc.* **1980**, *102*, 906 – 912.
[41] R. M. Keller, K. Wüthrich, *Biochim. Biophys. Acta* **1980**, *621*, 204 – 217.
[42] J. Feeney, B. Birdsall, J. P. Albrand, G. C. Roberts, A. S. Burgen, P. A. Charlton, D. W. Young, *Biochemistry* **1981**, *20*, 1837 – 1842.
[43] D. G. Gorenstein, D. O. Shah, *Biochemistry* **1982**, *21*, 4679 – 4686.
[44] B. Birdsall, G. C. Roberts, J. Feeney, J. G. Dann, A. S. Burgen, *Biochemistry* **1983**, *22*, 5597 – 5604.
[45] D. G. Reid, S. A. Salisbury, D. H. Williams, *Biochemistry* **1983**, *22*, 1377 – 1385.
[46] H. Senn, K. Wüthrich, *Biochim. Biophys. Acta* **1983**, *743*, 69 – 81.
[47] R. E. Cohen, H. K. Schachman, *J. Biol. Chem.* **1986**, *261*, 2623 – 2631.
[48] M. Ikura, *Biochim. Biophys. Acta* **1986**, *872*, 195 – 200.
[49] L. B. Dugad, J. T. Gerig, *Biochemistry* **1988**, *27*, 4310 – 4316.
[50] A. M. Petros, V. Ramesh, M. Llinas, *Biochemistry* **1989**, *28*, 1368 – 1376.
[51] G. N. La Mar, G. Hernandez, J. S. de Ropp, *Biochemistry* **1992**, *31*, 9158 – 9168.
[52] K. Akasaka, *J. Magn. Reson.* **1979**, *36*, 135 – 140.
[53] L. Poppe, G. S. Brown, J. S. Philo, P. V. Nikrad, B. H. Shah, *J. Am. Chem. Soc.* **1997**, *119*, 1727 – 1736.
[54] M. Mayer, B. Meyer, *Angew. Chem.* **1999**, *111*, 1902 – 1906; *Angew. Chem. Int. Ed.* **1999**, *38*, 1784 – 1788.
[55] "*Method for Detecting Biologically Active Compounds from Compound Libraries*": T. Peters, B. Meyer, German Pat. No. 19649359, Swiss Pat. No. 690695, US Pat. No. 6214561, GB-Patent No. GB2321104 **1996**.
[56] M. Vogtherr, T. Peters, *J. Am. Chem. Soc.* **2000**, *122*, 6093 – 6099.
[57] T. Haselhorst, T. Weimar, T. Peters, *J. Am. Chem. Soc.* **2001**, *123*, 10705 – 10714.
[58] M. Mayer, B. Meyer, *J. Am. Chem. Soc.* **2001**, *123*, 6108 – 6117.
[59] H. Maaheimo, P. Kosma, L. Brade, H. Brade, T. Peters, *Biochemistry* **2000**, *39*, 12778 – 12788.
[60] J. Klein, R. Meinecke, M. Mayer, B. Meyer, *J. Am. Chem. Soc.* **1999**, *121*, 5336 – 5337.
[61] R. Meinecke, B. Meyer, *J. Med. Chem.* **2001**, *44*, 3059 – 3065.
[62] M. Pfaff, K. Tangemann, B. Muller, M. Gurrath, G. Muller, H. Kessler, R. Timpl, J. Engel, *J. Biol. Chem.* **1994**, *269*, 20233 – 20238.
[63] N. Verdaguer, D. Blaas, I. Fita, *J. Mol. Biol.* **2000**, *300*, 1179 – 1194.
[64] P. R. Kolatkar, J. Bella, N. H. Olson, C. M. Bator, T. S. Baker, M. G. Rossmann, *EMBO J.* **1999**, *18*, 6249 – 6259.
[65] J. M. Casasnovas, T. Stehle, J. H. Liu, J. H. Wang, T. A. Springer, *Proc. Natl. Acad. Sci. USA* **1998**, *95*, 4134 – 4139.
[66] Z. Che, N. H. Olson, D. Leippe, W. M. Lee, A. G. Mosser, R. R. Rueckert, T. S. Baker, T. J. Smith, *J. Virol.* **1998**, *72*, 4610 – 4622.
[67] E. A. Hewat, T. C. Marlovits, D. Blaas, *J. Virol.* **1998**, *72*, 4396 – 4402.
[68] R. Zhao, D. C. Pevear, M. J. Kremer, V. L. Giranda, J. A. Kofron, R. J. Kuhn, M. G. Rossmann, *Structure* **1996**, *4*, 1205 – 1220.
[69] J. M. Rogers, G. D. Diana, M. A. McKinlay, *Adv. Exp. Med. Biol.* **1999**, *458*, 69 – 76.
[70] A. Billich, *Curr. Opin. Invest. Drugs* **2000**, *1*, 303 – 307.
[71] a) J. E. Hanson, N. K. Sauter, J. J. Skehel, D. C. Wiley, *Virology* **1992**, *189*, 525 – 533; b) A. Benie, R. Moser, E. Bäuml, D. Blaas, T. Peters, *J. Am. Chem. Soc.* **2003**, *125*, 14 – 15.
[72] O. Kooistra, L. Herfurth, E. Lüneberg, M. Frosch, T. Peters, U. Zähringer, *Eur. J. Biochem.* **2002**, *269*, 573—582.
[73] a) M. M. Palcic, O. Hindsgaul, *Glycobiology* **1991**, *1*, 205 – 209; b) T. Biet, T. Peters, *Angew. Chem.* **2001**, *113*, 4320 – 4323; *Angew. Chem. Int. Ed.* **2001**, *40*, 4189 – 4192.
[74] G. Srivastava, O. Hindsgaul, M. M. Palcic, *Carbohydr. Res.* **1993**, *245*, 137 – 144.
[75] B. Ramakrishnan, P. K. Qasba, *J. Mol. Biol.* **2001**, *310*, 205 – 218.
[76] G. Otting, E. Liepinsh, B. T. Farmer, K. Wüthrich, *J. Biomol. NMR* **1991**, *1*, 209 – 215.
[77] G. Otting, E. Liepinsh, K. Wüthrich, *Science* **1991**, *254*, 974 – 980.
[78] G. Otting, *Prog. Nucl. Magn. Reson. Spectrosc.* **1997**, *31*, 259 – 285.
[79] C. Dalvit, S. Cottens, P. Ramage, U. Hommel, *J. Biomol. NMR* **1999**, *13*, 43 – 50.
[80] C. Dalvit, P. Pevarello, M. Tato, M. Veronesi, A. Vulpetti, M. Sundstrom, *J. Biomol. NMR* **2000**, *18*, 65 – 68.
[81] I. Bertini, C. Dalvit, J. G. Huber, C. Luchinat, M. Piccioli, *FEBS Lett.* **1997**, *415*, 45 – 48.
[82] H. Takahashi, T. Nakanishi, K. Kami, Y. Arata, I. Shimada, *Nat. Struct. Biol.* **2000**, *7*, 220 – 223.
[83] A. Ramos, G. Kelly, D. Hollingworth, A. Pastore, T. Frenkiel, *J. Am. Chem. Soc.* **2000**, *122*, 11311 – 11314.
[84] L. Herfurth, T. Weimar, T. Peters, *Angew. Chem.* **2000**, *112*, 2097 – 2099; *Angew. Chem. Int. Ed.* **2000**, *39*, 2097 – 2099.
[85] M. Mayer, B. Meyer, *J. Med. Chem.* **2000**, *43*, 2093 – 2099.
[86] D. Henrichsen, B. Ernst, J. L. Magnani, W. T. Wang, B. Meyer, T. Peters, *Angew. Chem.* **1999**, *111*, 98 – 102; *Angew. Chem. Int. Ed.* **1999**, *38*, 98 – 102.
[87] B. Meyer, T. Weimar, T. Peters, *Eur. J. Biochem.* **1997**, *246*, 705 – 709.
[88] A. Chen, M. J. Shapiro, *J. Am. Chem. Soc.* **2000**, *122*, 414 – 415.
[89] A. Chen, M. J. Shapiro, *J. Am. Chem. Soc.* **1998**, *120*, 10258 – 10259.
[90] M. J. Gradwell, J. Feeney, *J. Biomol. NMR* **1996**, *7*, 48 – 58.
[91] J. Feeney, G. Batchelor, J. P. Albrand, G. C. K. Roberts, *J. Magn. Reson.* **1979**, *33*, 519 – 529.
[92] J. Feeney, G. C. Roberts, J. W. Thomson, R. W. King, D. V. Griffiths, A. S. Burgen, *Biochemistry* **1980**, *19*, 2316 – 2321.
[93] B. Birdsall, J. Feeney, C. Pascual, G. C. Roberts, I. Kompis, R. L. Then, K. Muller, A. Kroehn, *J. Med. Chem.* **1984**, *27*, 1672 – 1676.
[94] L. Y. Lian, G. C. K. Roberts in *NMR of Macromolecules* (Ed.: G. C. K. Roberts), Oxford University Press, Oxford, **1993**, pp. 153 – 182.
[95] L. Y. Lian, I. L. Barsukov, M. J. Sutcliffe, K. H. Sze, G. C. Roberts, *Methods Enzymol.* **1994**, *239*, 657 – 700.

[96] S. M. Pascal, T. Yamazaki, A. U. Singer, L. E. Kay, J. D. Forman-Kay, *Biochemistry* **1995**, *34*, 11353 – 11362.
[97] T. Yamazaki, S. M. Pascal, A. U. Singer, J. Forman-Kay, L. E. Kay, *J. Am. Chem. Soc.* **1995**, *117*, 3556 – 3564.
[98] M.-H. Feng, M. Philippopoulos, A. D. McKerell, Jr., C. Lim, *J. Am. Chem. Soc.* **1996**, *118*, 11265 – 11277.
[99] A. R. Gargaro, T. A. Frenkiel, P. M. Nieto, B. Birdsall, V. I. Polshakov, W. D. Morgan, J. Feeney, *Eur. J. Biochem.* **1996**, *238*, 435 – 439.
[100] P. M. Nieto, B. Birdsall, W. D. Morgan, T. A. Frenkiel, A. R. Gargaro, J. Feeney, *FEBS Lett.* **1997**, *405*, 16 – 20.
[101] W. D. Morgan, B. Birdsall, P. M. Nieto, A. R. Gargaro, J. Feeney, *Biochemistry* **1999**, *38*, 2127 – 2134.
[102] V. I. Polshakov, W. D. Morgan, B. Birdsall, J. Feeney, *J. Biomol. NMR* **1999**, *14*, 115 – 122.
[103] S. B. Shuker, P. J. Hajduk, R. P. Meadows, S. W. Fesik, *Science* **1996**, *274*, 1531 – 1534.
[104] K. Pervushin, R. Riek, G. Wider, K. Wüthrich, *Proc. Natl. Acad. Sci. USA* **1997**, *94*, 12366 – 12371.
[105] P. J. Hajduk, D. J. Augeri, J. Mack, R. Mendoza, J. Yang, S. F. Betz, S. W. Fesik, *J. Am. Chem. Soc.* **2000**, *122*, 7898 – 7904.
[106] M. Pellecchia, D. Meininger, A. L. Shen, R. Jack, C. B. Kasper, D. S. Sem, *J. Am. Chem. Soc.* **2001**, *123*, 4633 – 4634.
[107] M. Kainosho, T. Tsuji, *Biochemistry* **1982**, *21*, 6273 – 6279.
[108] P. J. Hajduk, T. Gerfin, J. M. Boehlen, M. Haberli, D. Marek, S. W. Fesik, *J. Med. Chem.* **1999**, *42*, 2315 – 2317.
[109] A. Medek, P. J. Hajduk, J. Mack, S. W. Fesik, *J. Am. Chem. Soc.* **2000**, *122*, 1241 – 1242.
[110] P. J. Hajduk, M. Bures, J. Praestgaard, S. W. Fesik, *J. Med. Chem.* **2000**, *43*, 3443 – 3447.
[111] K. H. Gardner, L. E. Kay, *J. Am. Chem. Soc.* **1997**, *119*, 7599 – 7600.
[112] K. H. Gardner, X. C. Zhang, K. Gehring, L. E. Kay, *J. Am. Chem. Soc.* **1998**, *120*, 11738 – 11748.
[113] N. K. Goto, K. H. Gardner, G. A. Mueller, R. C. Willis, L. E. Kay, *J. Biomol. NMR* **1999**, *13*, 369 – 374.
[114] P. J. Hajduk, E. T. Olejniczak, S. W. Fesik, *J. Am. Chem. Soc.* **1997**, *119*, 12257 – 12261.
[115] W. Jahnke, L. B. Perez, C. G. Paris, A. Strauss, G. Fendrich, C. M. Nalin, *J. Am. Chem. Soc.* **2000**, *122*, 7394 – 7395.
[116] W. Jahnke, S. Ruedisser, M. Zurini, *J. Am. Chem. Soc.* **2001**, *123*, 3149 – 3150.
[117] M. Lin, M. J. Shapiro, *J. Org. Chem.* **1996**, *61*, 7617 – 7619.
[118] M. Lin, M. J. Shapiro, J. R. Wareing, *J. Org. Chem.* **1997**, *62*, 8930 – 8931.
[119] M. Lin, M. J. Shapiro, J. R. Wareing, *J. Am. Chem. Soc.* **1997**, *119*, 5249 – 5250.
[120] K. Bleicher, M. Lin, M. J. Shapiro, J. R. Wareing, *J. Org. Chem.* **1998**, *63*, 8486 – 8490.
[121] R. C. Anderson, M. Lin, M. J. Shapiro, *J. Comb. Chem.* **1999**, *1*, 69 – 72.
[122] M. Aumailley, M. Gurrath, G. Müller, J. Calvete, R. Timpl, H. Kessler, *FEBS Lett.* **1991**, *291*, 50 – 54.
[123] Y. Cheng, W. H. Prusoff, *Biochem. Pharmacol.* **1973**, *22*, 3099 – 3108.
[124] P. V. Nikolova, K.-B. Wong, B. DeDecker, J. Henckel, A. R. Fersht, *EMBO J.* **2000**, *19*, 370 – 378.
[125] J. R. Huth, E. T. Olejniczak, R. Mendoza, H. Liang, E. A. S. Harris, M. L. Lupher, Jr., A. E. Wilson, S. W. Fesik, D. E. Staunton, *Proc. Natl. Acad. Sci. USA* **2000**, *97*, 5231 – 5236.
[126] P. J. Hajduk, J. Dinges, G. F. Miknis, M. Merlock, T. Middleton, D. J. Kempf, D. A. Egan, K. A. Walter, T. S. Robins, S. B. Shuker, T. F. Holzman, S. W. Fesik, *J. Med. Chem.* **1997**, *40,* 3144 – 3150.
[127] R. Freeman, *Prog. Nucl. Magn. Reson. Spectrosc.* **1998**, *32,* 59 – 106.
[128] V. Jayalakshmi, N. R. Krishna, *J. Magn. Reson.* **2002**, *155*, 106 – 118.
[129] G. Gemmecker, W. Jahnke, H. Kessler, *J. Am. Chem. Soc.* **1993**, *115*, 11620 – 11621.
[130] L. Bhattacharyya, C. F. Brewer, *Eur. J. Biochem.* **1988**, *176*, 207 – 212.
[131] S. Sharma, S. Bharadwaj, A. Surolia, S. K. Podder, *Biochem. J.* **1998**, *333*, 539 – 542.

Communications

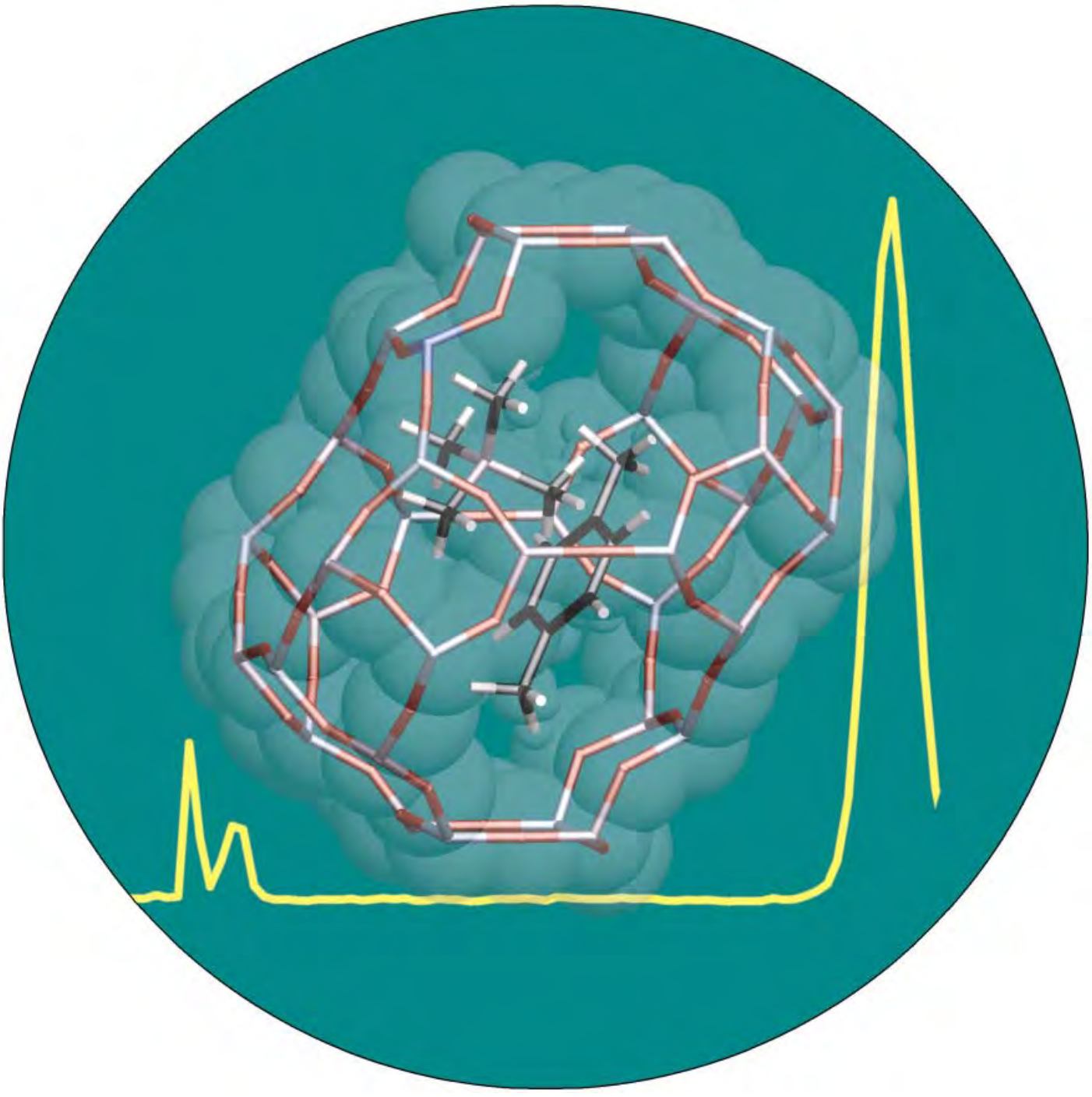

The synthesis of tetramethylphosphonium cations in the cages of HSAPO-34 (depicted) by using a ship-in-a-bottle approach, and the subsequent calcination of this material to form an active methanol-to-olefin catalyst, is described by J. F. Haw and W. Song on the following pages.

 © 2003 Wiley-VCH Verlag GmbH & Co. KGaA, Weinheim 1433-7851/03/4208-0891 $ 20.00+.50/0

Methanol-to-Olefin Catalyst

Improved Methanol-to-Olefin Catalyst with Nanocages Functionalized through Ship-in-a-Bottle Synthesis from PH_3**

*Weiguo Song and James F. Haw**

The catalytic conversion of methanol into olefins[1] is the remaining link in a chain of catalytic processes that convert natural gas into polyolefins. The most promising catalysts for commercial use are solid acids based on silico-aluminophosphates of the chabazite (CHA) structure, specifically HSAPO-34, which has one acid site per cage when prepared by our method.[2]. We recently demonstrated that the active site for methanol-to-olefin (MTO) chemistry on HSAPO-34 is a composite of an inorganic acid site and a methylbenzene molecule.[3] The latter self-assembles during a kinetic induction period and can not pass through the 0.38-nm windows interconnecting the 1.0 nm × 0.67 nm cages of the HSAPO-34 structure. The organic component is a scaffold on which carbon–carbon bonds can be formed and broken without recourse to high-energy intermediates and transition states. Herein, we build on this prior work to rationally design HSAPO-34 catalysts with improved selectivity, a very desirable property. Since we now know that MTO chemistry occurs in a nanometer-size cage already partially filled by a large hydrocarbon molecule, it is reasonable to say that olefin selectivity should be sensitive to further steric constraints.

For our first attempt at functionalization, we chose phosphorus chemistry, because phosphate species are hydrothermally stable modifiers of aluminosilicate zeolites,[4] and because we could use solid-state ^{31}P NMR spectroscopy to correlate structure with activity and selectivity. Few phosphorus reagents are adsorbed into HSAPO-34; $P(CH_3)_3$ is sterically excluded, and neither $PH(CH_3)_2$ nor PH_2CH_3 are commercially available. Thus, we chose PH_3, a toxic and pyrophoric gas that nevertheless proved to be easily handled by using lecture bottles and standard bench-top reactors assembled in a fume hood. Scheme 1 outlines our strategy for the modification of HSAPO-34 through ship-in-a-bottle routes starting with PH_3. In every case we held approximately 300 mg of HSAPO-34 in a flow reactor at 523 K and then introduced PH_3 gas into the He flow stream, while simultaneously delivering methanol by using a syringe pump. Each step in the scheme was achieved,[5] and representative ^{31}P spectra of thermally quenched catalyst beds are shown in Figure 1. In each spectrum, the ^{31}P resonance signal at $\delta = -28$ ppm arises from the phosphorus atoms in the framework. The initial products were protonated $P(CH_3)_3$ molecules ($\delta = -4$ ppm) and $P(CH_3)_4^+$ ions ($\delta = 23$ ppm).[6] The relative yields of these species are controlled by varying the ratio of PH_3 to CH_3OH. $P(CH_3)_3$ is commonly used as a spectroscopic probe for acidity.[7] The observation that all of the $P(CH_3)_3$ molecules in HSAPO-34 are protonated to $HP(CH_3)_3^+$ ions, and none is complexed to Lewis sites (Figure 1 a), is in itself an important finding. As Figure 1 c shows, we synthesized one

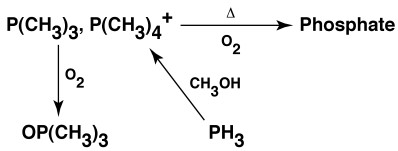

Scheme 1. Ship-in-a-bottle reactions of phosphane, methanol, and oxygen leading to a phosphate-modified HSAPO-34 catalyst with improved ethylene selectivity.

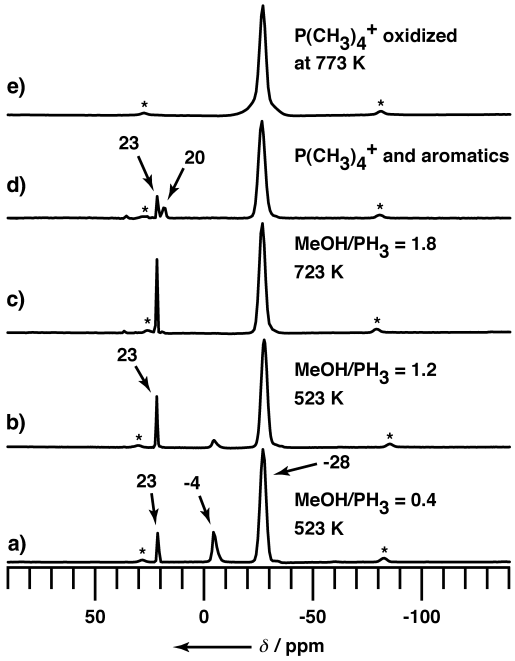

Figure 1. Examples of ^{31}P MAS-NMR spectra showing functionalization of the HSAPO-34 nanocages according to Scheme 1. The chemical shift arising from the phosphorus atoms in the HSAPO-34 framework is $\delta = -28$ ppm. In all cases PH_3 and methanol was passed over the catalyst bed for 10 min. The PH_3 flow rate was 14 sccm except for the sample in c) where 32 sccm was used. Methanol/PH_3 mole ratios are shown where important. a) With a limited amount of methanol, the major product in the nanocages was $P(CH_3)_3$, which was protonated by the Brønsted acid sites ($\delta = -4$ ppm). b) When methanol was in excess, $P(CH_3)_4^+$ (23 ppm) formed in most nanocages. c) With forcing conditions, $P(CH_3)_4^+$ formed in every cage. d) $P(CH_3)_4^+$ yields signals at both $\delta = 23$ ppm and 20 ppm when approximately half of the nanocages also contain aromatic compounds synthesized from methanol. e) If $P(CH_3)_4^+$ is formed in the nanocages and the catalyst is heated to high temperatures in air, a phosphate species forms, as indicated by the broad signal near that of the framework. ⋆ denotes spinning sidebands.

[*] Prof. J. F. Haw, W. Song
Loker Hydrocarbon Research Institute and
Department of Chemistry
University of Southern California
Los Angeles, CA 90089-1661 (USA)
Fax: (+1) 213-740-0930
E-mail: jhaw@usc.edu

[**] This work was supported by the National Science Foundation (CHE-0205939) and (CHE-9996109), and the U.S. Department of Energy (DOE) Office of Basic Energy Sciences (BES; Grant Nos. DE-FG03-93ER14354 and DE-FG03-99ER14956).

 © 2003 Wiley-VCH Verlag GmbH & Co. KGaA, Weinheim 1433-7851/03/4208-0892 $ 20.00+.50/0

$P(CH_3)_4^+$ ion in every nanocage by increasing the flow of PH_3 and methanol. Evidence for this includes the expected 5:1 ratio[8] for the integrals of the ^{31}P resonance signals of the phosphorus atoms of the framework to those of the cation. Figure 1d shows a ^{31}P NMR spectrum of SAPO-34 containing both $P(CH_3)_4^+$ ions and methylbenzene derivatives. Note that with aromatic species present there are two $P(CH_3)_4^+$ resonance signals, one as before at $\delta = 23$ ppm, and one at $\delta = 20$ ppm. We speculate that the signal at $\delta = 20$ ppm arises from $P(CH_3)_4^+$ ions situated in cages with an aromatic ring.

When $P(CH_3)_4^+$ in SAPO-34 was heated to 773 K, it decomposed to an inorganic phosphate species with a chemical shift similar to that of the framework phosphorus. Evidence for this species is visible as a broad feature at the base of the resonance signal at $\delta = -28$ ppm (Figure 1e). An identical ^{31}P signal was observed when we used the same chemistry to functionalize cages in aluminosilicate zeolites (results not shown).

The presence of this phosphate species in our functionalized HSAPO-34 catalyst improves the ethylene selectivity. Figure 2 shows the GC traces from the product streams of reactors converting methanol under steady-state conditions (weight-hourly space velocity, WHSV = 8 h^{-1} at 723 K) by using either standard HSAPO-34 or functionalized materials. For HSAPO-34 without PH_3 treatment, methanol conversion was 100% and ethylene selectivity was 37% (Figure 2a). Conversely, with one $P(CH_3)_4^+$ ion per cage and all acid sites consumed by phosphonium cation formation, conversion was near zero (Figure 2b). Calcination of this sample in the reactor to form a material with a phosphate species in every cage produced a catalyst with greatly improved ethylene selectivity (46%) but reduced activity (Figure 2c). When we prepared a material with a phosphate species in approximately a half of all cages, we achieved 95% conversion and retained an impressive ethylene selectivity of 44% (Figure 2d).

The results shown in Figure 1 and 2 are representative and reproducible. The functionalized catalysts deactivated at the same rate as standard catalysts. The ^{13}C NMR spectra showed, as before,[3] that deactivation occurred through the formation of aromatic species in nanocages well beyond the degree required for an active catalyst. The ^{31}P NMR spectrum of the deactivated catalyst showed that there was no loss of phosphate. Furthermore, we found that the catalyst containing the phosphate species could be reactivated by burning the sample to remove hydrocarbons in the cages. In this way the catalyst regained the activity and selectivity of a freshly prepared sample.

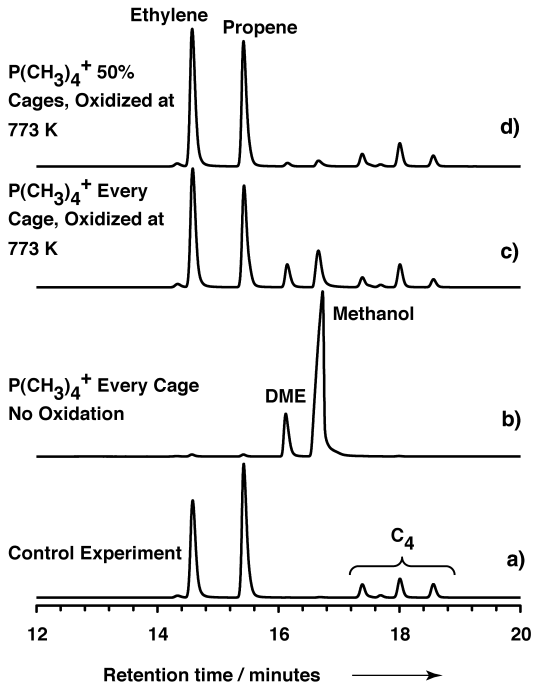

Figure 2. Examples of GC (flame ionization) analyses of the product gases in MTO conversion on catalysts functionalized by introducing phosphorus species into the nanocages. All experiments were performed at 723 K with a methanol WHSV of 8 h^{-1}. a) Control experiment on standard HSAPO-34, 100% conversion, ethylene selectivity 37%. b) Modified catalysts, $P(CH_3)_4^+$ ions in all nanocages, 0% conversion. c) Modified catalyst, phosphate species formed in every nanocage by aerial oxidation (773 K) of the $P(CH_3)_4^+$ ions, 50% conversion, ethylene selectivity 46%. d) Modified catalyst, phosphate formed in 50% of all nanocages by aerial oxidation (773 K) of the $P(CH_3)_4^+$ ions, 95% conversion, ethylene selectivity 44%. Note that the catalyst in this case has nearly the same activity as the standard catalyst, but significantly higher ethylene selectivity. DME = dimethyl ether.

Experimental Section

Functionalized catalyst samples were prepared for NMR studies by thermally quenching the reactor and then transferring the contents to MAS-NMR sample rotors as described previously.[9] The 121 MHz ^{31}P Bloch decay MAS-NMR spectra were acquired on a Chemagnetics CMX-300 spectrometer by using 400 scans, 90° flips, and 10 s delays. For product analysis, gas samples from MTO reactors were collected and introduced into a Hewlett-Packard Model 6890 gas chromatograph by means of a Valco valve. Standard response factors were used to correct the flame ionization response to percent composition.

Received: September 9, 2002 [Z50121]

[1] M. Stöcker, *Microporous Mesoporous Mater.* **1999**, *29*, 3–48.
[2] HSAPO-34 was prepared according to: B. M. Lok, C. A. Messina, R. L. Patton, R. T. Gajek, T. R. Cannan, E. M. Flanigen, US Patent 4,440,871 **1984**. XRD showed a pure crystalline phase with the CHA structure. The product was calcined at 873 K for 10 h to remove the template agent and pressed into 10–20 mesh pellets.
[3] a) W. Song, J. F. Haw, J. B. Nicholas, K. Heneghan, *J. Am. Chem. Soc.* **2000**, *122*, 10726–10727; b) W. Song, H. Fu, J. F. Haw, *J. Am. Chem. Soc.* **2001**, *123*, 4749–4754; other workers have come to similar conclusions, for example, see: c) B. Arstad, S. Kolboe, *J. Am. Chem. Soc.* **2001**, *123*, 8137–8138.
[4] a) W. W. Kaeding, S. A. Butter, US Patent 3,911,041 **1975**; b) H.-N. Sun, US Patent 5,925,586 **1999**.
[5] Air oxidation of catalysts containing $P(CH_3)_3$ gave partial conversion to $OP(CH_3)_3$, which had a ^{31}P chemical shift of $\delta =$ 39 ppm in SAPO-34 (spectra not shown).
[6] The $P(CH_3)_4^+$ ion has been synthesized on the surface of sulfated zirconia catalyst by the disproportionation of $P(CH_3)_3$. J. F. Haw, J. Zhang, K. Shimizu, T. N. Venkatraman, D.-P. Luigi, W. Song, D. H. Barich, J. B. Nicholas, *J. Am. Chem. Soc.* **2000**, *122*, 12561–12570.

 © 2003 Wiley-VCH Verlag GmbH & Co. KGaA, Weinheim 1433-7851/03/4208-0893 $ 20.00+.50/0

[7] W. P. Rothwell, W. Shen, J. H. Lunsford, *J. Am. Chem. Soc.* **1984**, *106*, 2452–2453.
[8] Each unit cell of CHA contains 36 T sites and three cages. The HSAPO-34 used has one Si, five P, and six Al atoms per cage.
[9] J. F. Haw, P. W. Goguen, T. Xu, T. W. Skloss, W. Song, Z. Wang, *Angew. Chem.* **1998**, *110*, 993–995; *Angew. Chem. Int. Ed.* **1998**, *37*, 948–949.

Surface Effects from Nanostructure

Structural Color and the Lotus Effect**

*Zhong-Ze Gu, Hiroshi Uetsuka, Kazuyuki Takahashi, Rie Nakajima, Hiroshi Onishi, Akira Fujishima, and Osamu Sato**

The study of biological microstructure is one of the most important research areas in biomimicry.[1–3] Microstructure plays many important roles in living things.[2,3] For example, the charming blue color of the *Morpho sulkowskyi* butterfly originates from light diffraction and scattering, which results from the ordered microstructure of its scales. This form of color is usually known as structural color, which is utilized by animals both for protection and as a warning. Today, the study of structural color has been extended from biology to optics.[4–6] As well as affecting coloration, microstructure also plays an important role in self-cleaning.[2,7] For the butterfly, the specific nanostructure enhances the hydrophobicity of its wings, which allows droplets of water to be dispersed more easily. During this process, dust particles on the surface of the wings are removed. This phenomenon is known as the "lotus effect", which is not only very useful for natural species, but also for materials applications, such as for decoration where a natural force might be used to clean a surface. It would be interesting to discover whether it is possible to design a material that incorporates both structural color and the lotus effect, thus mimicking the wings of a butterfly. Such a material should be of great biological and technological importance. In this paper, we will show one approach to fabricating such a biomimetic decorative material by taking advantage of a nanostructured inverse opal surface.

Inverse opal is a solid material that consists of a three-dimensional network.[6,8–10] Ordered monodisperse air spheres throughout the network contribute to an optical stop band, the position of which can be tuned by careful control of the periodicity of the air spheres. Colors can be observed by the naked eye when the stop band falls in the visible region. As a consequence of its unique optical properties, inverse opal has been regarded as a new-generation decorative material, in addition to its application as a photonic crystalline material.[6,11] Recently, we realized that inverse opal might also be incorporated into the design of a hydrophobic material. The solid material network of inverse opal contributes a rough surface composed of well-ordered meshes. According to the Cassie–Baxter law, the intrinsic wettability of the solid material can be greatly reduced.[12] Such a decorative material, which exhibits both structural color and the lotus effect, would be environmentally friendly and energy-efficient.

For practical applications, a convenient method of fabricating a uniform inverse opal film over a large area is required. In addition, the rough inverse opal surface needs to be further optimized to imbue the surface with superhydrophobic character. We describe here the development of a dipping method that can be used to meet these criteria, and which can derive uniform inverse opal films with a nanostructured surface. The procedure for the fabrication is as follows: First, submicron-sized monodisperse polystyrene spheres and nanosized particles were ultrasonically dispersed into deionised water. A glass substrate was then immersed into the solution and withdrawn at a constant speed. It is known that a mixture of spheres with different sizes cannot be used to fabricate colloidal crystals with long-range structural order by such a deposition method,[13–15] as phase separation occurs, or an amorphous structure is formed. In our experiment, we found that this conclusion is only partially correct. A structure with long-range order can be derived when the ratio of the diameters of the spheres falls into a particular regime. Figure 1a shows an image of a structure composed of monodisperse spheres, while Figure 1b–d displays three images of structures composed of spheres of two sizes, with diameter ratios of 0.94, 0.34, and 0.07, respectively. The structure formed by the spheres of varying size depends on the diameter ratio. A structure with long-range order can be observed in films composed of monodisperse spheres, however, such order is absent in films composed of spheres of two sizes, where the diameter ratio is larger than 0.15. Usually, the particles form a structure with discernible separation when the ratio between the two types of sphere is larger than 0.5 (Figure 1b), while the domains formed by different types of particles are separated when the ratio is smaller than this value (Figure 1c). When the diameter ratio between the

[*] Dr. O. Sato, Prof. Dr. Z.-Z. Gu, Dr. H. Uetsuka, K. Takahashi, R. Nakajima, Dr. H. Onishi
Kanagawa Academy of Science and Technology
KSP Bldg. East 412, 3-2-1 Sakado, Takatsu-ku, Kawasaki-shi, Kanagawa 213-0012 (Japan)
Fax: (+81) 44-819-2070
E-mail: sato@fchem.chem.t.u-tokyo.ac.jp
Prof. Dr. Z.-Z. Gu
National Laboratory of Molecular and Biomolecular Electronics
Southeast University
Nanjing 210096 (China)
Prof. Dr. A. Fujishima
Department of Applied Chemistry
School of Engineering, The University of Tokyo
7-3-1 Hongo Bunkyo-ku, Tokyo 113-8565 (Japan)

[**] This work was partially supported by a Grant-in-Aid for Scientific Research on Priority Areas (417) from the Ministry of Education, Culture, Sports, Science and Technology (MEXT) of the Japanese Government. Z.-Z.G. also thanks the Research Foundation (60228002) of the National Nature Science Foundation of China.

 © 2003 Wiley-VCH Verlag GmbH & Co. KGaA, Weinheim 1433-7851/03/4208-0894 $ 20.00+.50/0

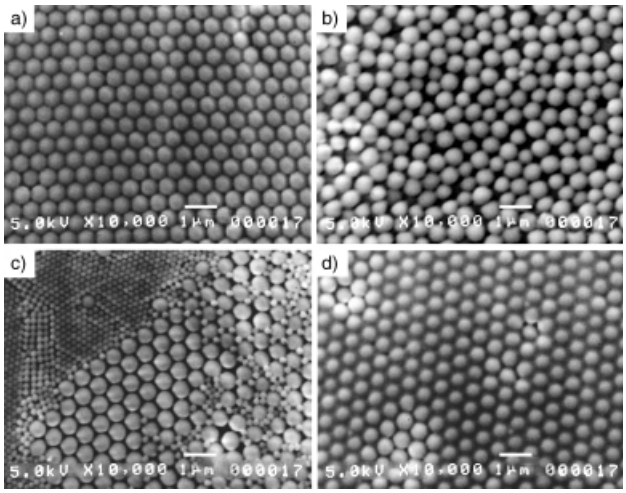

Figure 1. a) SEM image of a film composed of polystyrene spheres with a diameter of 680 nm; b–d) SEM image of a film composed of polystyrene spheres of two sizes. The diameter of the larger spheres is 680 nm in each case. The diameters of the smaller spheres are 580 (b), 230 (c), and 48 nm (d).

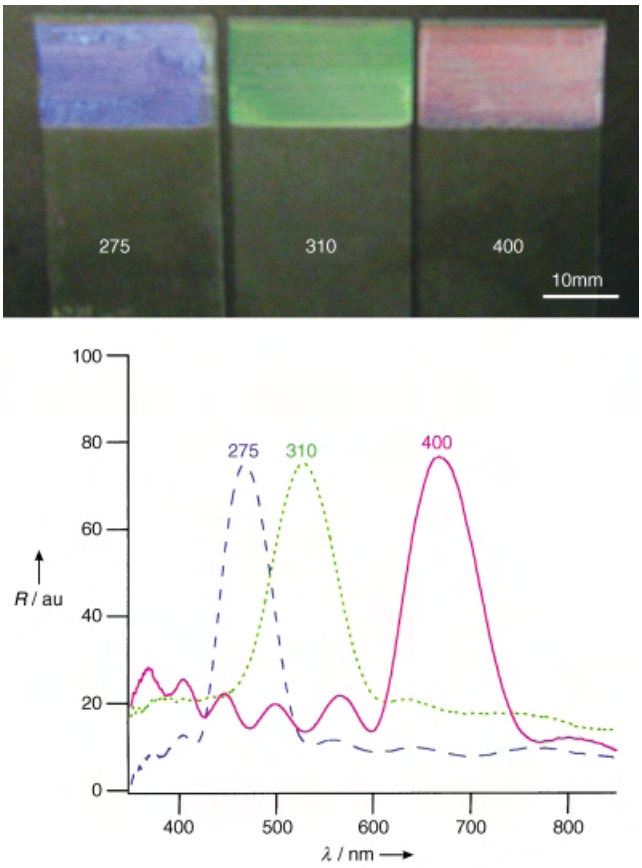

Figure 2. Pictures (top) and transmission spectra (bottom) of three types of inverse opal film with different structural periods. The center-to-center distances between two neighboring holes are 275, 310, and 400 nm, respectively.

spheres is smaller than 0.15, a close-packed cubic structure composed of large spheres is formed, with the small particles located within the voids formed between the large spheres (Figure 1 d). The mechanism for the formation of an ordered structure can be thought of as follows: During the formation of the film, large particles assemble first, followed by the smaller spheres. The face-centered cubic structure formed by the large spheres possesses interconnected voids. The diameter of the smallest voids is approximately 15 % of that of the spheres. Thus, when the diameter ratio of the small particles is less than 0.15, the small particles can enter the voids, rather than aggregating around the larger particles. As a result, there is no phase separation.

The inverse opal films were fabricated by taking advantage of the phenomena described above. The suspension used for the fabrication process contained polystyrene spheres and silica nanoparticles. The polystyrene spheres were several hundred micrometers in diameter, while the diameter of the silica nanoparticles was around 6 nm; the concentration of the polystyrene spheres and silica nanoparticles was 2 and 0.3 %, respectively. The speed of withdrawal of the glass substrate was 0.4 $\mu m\,s^{-1}$. After the film was formed, it was dried in air and then calcined at 450 °C to remove the polymer and to solidify the silica nanoparticles. Finally, the surface of the substrate was modified with a fluoroalkylsilane ($(CF_3(CF_2)_7CH_2CH_2Si(OCH_3)_3)$) by thermal chemical vapor deposition, to render the surface hydrophobic.

Figure 2 (top) displays the inverse opal films that were deposited onto glass substrates. Uniform colors extend over the whole substrates, which are over 2 cm wide. The color of the inverse opal film derives from microscopically ordered structures, which were observed by scanning electron microscopy (SEM) and which are exhibited in Figure 3. Figure 3 a shows the film as viewed from above. The hexagonal arrangement of the air spheres encircled by the silica networks can be clearly observed, through which the arrangement of the second layer can also be seen. The center-to-center distance between the neighboring air spheres is 275 nm, which is 5 % shorter than the distance before calcination. Information on the three-dimensional structure was derived from cross-sectional observations (Figure 3 b), which show that the ordered structure is continuous from the substrate to the top surface. Such a three-dimensionally ordered structure contributes to the stop band. Incident light whose wavelength is the same as the position of the stop band is reflected (Figure 2, bottom), and as a result, inverse opal films exhibit brilliant colors when their stop bands fall into the visible region. The color can be easily engineered to range from blue to red through a change in the size of the polystyrene spheres during the fabrication process.

The wettability of an inverse opal film was studied by measuring the angle of a water drop on the substrate. Figure 4 shows a picture of a water drop on an inverse opal film modified with the fluoroalkylsilane (top), where the contact angle was measured at 155°. This compares to a contact angle of only 100° for a glass substrate modified with the fluoroalkylsilane (Figure 4, bottom), and displays that the surface had been made superhydrophobic after coating it with the inverse opal. The reason for the great enhancement in the hydrophobicity depends on the surface morphology of the inverse opal film, which was studied by atomic force micros-

 © 2003 Wiley-VCH Verlag GmbH & Co. KGaA, Weinheim 1433-7851/03/4208-0895 $ 20.00+.50/0

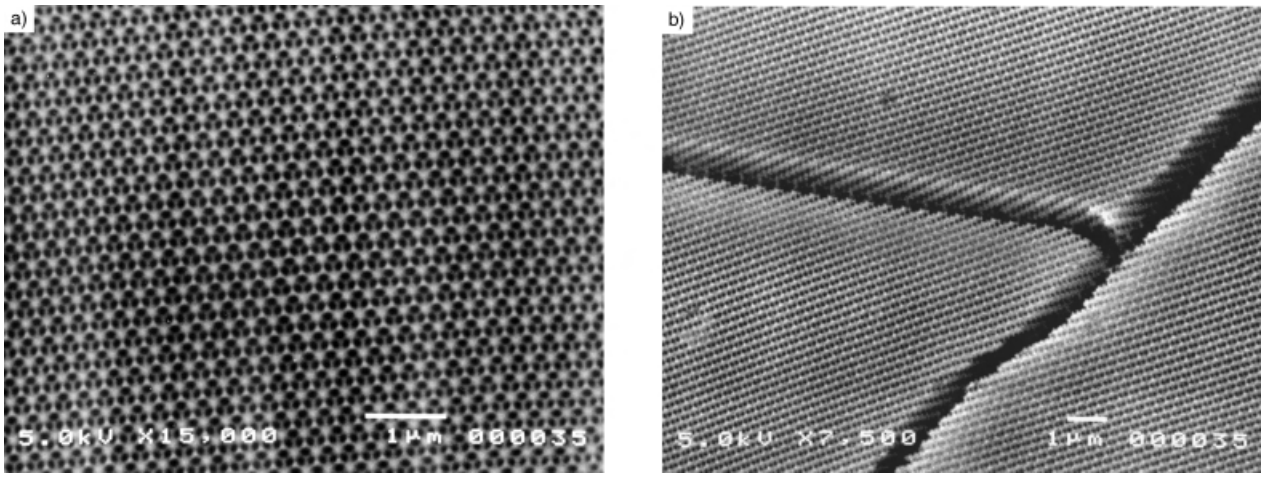

Figure 3. SEM image of an inverse opal film with a center-to-center distance between neighboring holes of 275 nm. a) Plan-view image; b) cross-sectional image.

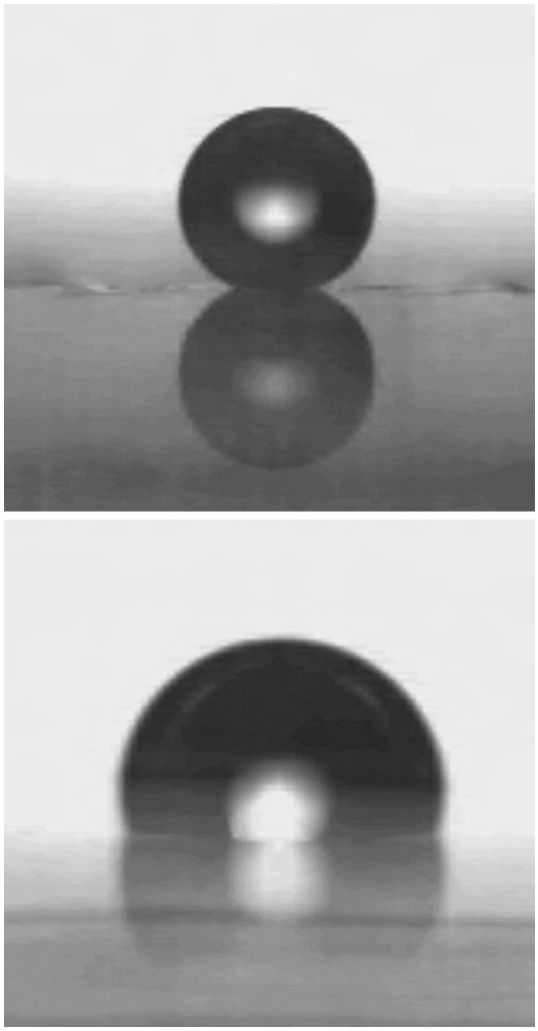

Figure 4. Water drops on a flat glass substrate (bottom) and an inverse-opal coated glass substrate (top) modified with a fluoroalkylsilane, which displays the enhanced hydrophobic character of the inverse opal film.

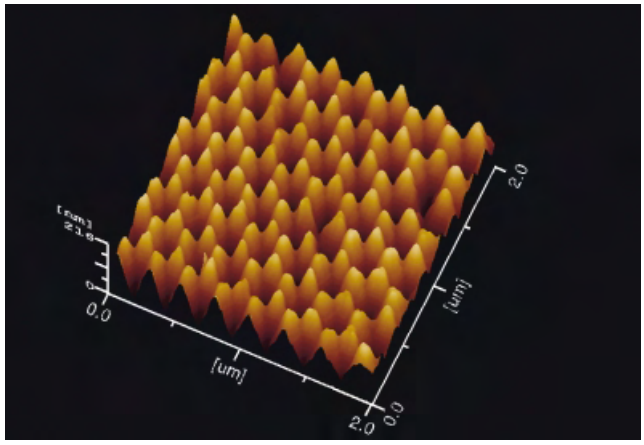

Figure 5. AFM image of the surface topography of an inverse opal film.

copy (AFM). Figure 5 is an AFM image of an inverse opal film with a center-to-center distance of 275 nm. From the AFM image it can be shown that the surface of the silica network encircling the air holes is not a flat surface but a collection of well-ordered bumps. Each air hole is surrounded by six distinct bumps, each with a diameter of approximately 100 nm, and which are located between three neighboring air holes. According to the Cassie–Baxter law, such a topography can greatly enhance the hydrophobicity, and even contribute to superhydrophobicity.[12,16]

In conclusion, we have demonstrated a convenient method of fabricating a uniform inverse opal film with a nanostructured surface. Both structural color and superhydrophobicity were derived simultaneously. Such films are anticipated to become a new generation of decorative materials. In addition, as the surface of the inverse opal fabricated by this method is composed of two dimensionally ordered nanosized dots, the fabrication method exhibited here might be a new approach for the preparation of a quantum dot array. Applications in the fields of nanomaterials, optical devices, and biology are anticipated.

Received: September 17, 2002 [Z50179]

 © 2003 Wiley-VCH Verlag GmbH & Co. KGaA, Weinheim 1433-7851/03/4208-0896 $ 20.00+.50/0

[1] J. Aizenberg, A. Tkachenko, S. Weiner, L. Addadi, G. Hendler, *Nature* **2001**, *412*, 819.
[2] W. Barthlott, C. Neinhuis, *Planta* **1997**, *202*, 1.
[3] H. Kasukawa, N. Oshima, R. Fujii, *Zool. Sci.* **1987**, *4*, 243.
[4] S. John, *Phys. Rev. Lett.* **1987**, *58*, 2486.
[5] E. Yablonovitch, *Phys. Rev. Lett.* **1987**, *58*, 2059.
[6] E. Yablonovitch, *Nature* **1999**, *401*, 539.
[7] V. Bergeron, D. Quere, *Phys. World* **2001**, *14*, 21.
[8] Z.-Z. Gu, S. Hayami, S. Kubo, Q.-B. Meng, Y. Einaga, D. A. Tryk, A. Fujishima, O. Sato, *J. Am. Chem. Soc.* **2001**, *123*, 175.
[9] P. Jiang, J. Cizeron, J. F. Bertone, V. L. Colvin, *J. Am. Chem. Soc.* **1999**, *121*, 7957.
[10] A. A. Zakhidov, R. H. Baughman, Z. Iqbal, C. X. Cui, I. Khayrullin, S. O. Dantas, J. Marti, V. G. Ralchenko, *Science* **1998**, *282*, 897.
[11] Z.-Z. Gu, A. Fujishima, O. Sato, *Angew. Chem.* **2002**, *114*, 2171; *Angew. Chem. Int. Ed.* **2002**, *41*, 2067.
[12] J. Bico, C. Marzolin, D. Quere, *Europhys. Lett.* **1999**, *47*, 220.
[13] M. Yamaki, J. Higo, K. Nagayama, *Langmuir* **1995**, *11*, 2975.
[14] P. Jiang, J. F. Bertone, K. S. Hwang, V. L. Colvin, *Chem. Mater.* **1999**, *11*, 2132.
[15] Z.-Z. Gu, O. Sato, A. Fujishima, *Chem. Mater.* **2002**, *14*, 760.
[16] S. Shibuichi, T. Yamamoto, T. Onda, K. Tsujii, *J. Colloid Interface Sci.* **1998**, *208*, 287.

Liquid-Crystal Molecular Design

Ionic Quaterrylenebis(dicarboximide): A Novel Mesogen and Long-Wavelength Polarizing Material**

Suk-Wah Tam-Chang, Wonewoo Seo, Isaac K. Iverson, and Sean M. Casey*

Within the broad scope of supramolecular chemistry,[1,2] the construction of materials and devices through self-assembly and self-organization processes is becoming one of the premier frontiers.[3–11] In the last decade, there has been extensive research on the interplay between molecular architecture, molecular order, and macroscopic properties.[12] In this paper, we report the aggregation and liquid-crystalline properties of a novel ionic quaterrylenebis(dicarboximide) **1** in aqueous solution. More importantly, by exploiting the self-organizing properties of **1**, unprecedented control of the molecular orientation of the quaterrylenebis(dicarboximide) in thin solid films was achieved, which produces a novel linear polarizer of light at long wavelengths.

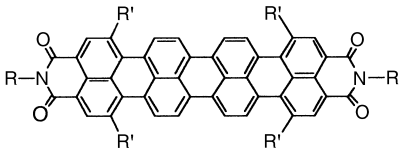

1, R' = H, R = $(CH_2)_2NEt_2H^+$ $HCOO^-$
2a, R' = H, R = $C_{12}H_{25}$,
2b, R' = H, R = C_6H_3-2,6-*i*Pr_2,
2c, R' = OC_6H_4-4-*t*Bu, R = C_6H_3-2,6-*i*Pr_2

Nonionic quaterrylenebis(dicarboximide)s **2a–c** are known to absorb light at long wavelengths. In chlorinated organic solvents, the absorption maxima of **2b** and **2c** are at 764 nm and 781 nm, respectively.[13,14] These thermally and photochemically stable dyes can potentially be used in optical applications in conjunction with commercially available GaAlAs lasers that emit at 780 nm. Near-infrared (NIR) absorbing and emitting dyes have potential use in high-technology applications such as optical recording, thermally written displays, laser printers, laser filters, infrared photography, and fiber-optic communications.[15,16] However, the solubility of **2a–c** in chlorinated solvents is only about 10^{-2} M.[13,14] The design and synthesis of more-soluble quaterrylenebis(dicarboximide) derivatives will allow greater convenience in the processing of such materials. In addition, because of the intrinsic anisotropy in the molecular optical properties of quaterrylenebis(dicarboximide)s, the development of techniques for controlling their orientation on a macroscopic scale in the solid state will lead to novel anisotropic materials and broaden their utility. For instance, NIR polarizers have applications as optical isolators that are used in conjunction with semiconductor lasers and fiber optics.[17]

In the structural design of **1**, we anticipated that the functionalization of the hydrophobic quaterrylenebis(dicarboximide) core with cationic pendant groups would impart amphiphilicity, which would render it soluble in aqueous solution. Aggregation of these molecules in an aqueous medium is expected because of π-stacking among the "plank-shaped" aromatic molecules and the entropy-driven hydrophobic interactions. Furthermore, it was expected that the introduction of flexible alkyl chains would enhance the formation of lyotropic (solvent-dependent) liquid-crystalline phases by hindering regular close-packing of the molecules into a crystalline phase. Although liquid-crystalline phases are only of short-range structural regularity, induced alignment of the self-organized ensembles under an external force can increase the degree of orientational order over a substantially longer range in thin liquid films.[18] By preserving this long-range anisotropic order during the transition from the liquid to the solid state, desirable structural regularity and aniso-

[*] Prof. S.-W. Tam-Chang, W. Seo, I. K. Iverson,[+] Prof. S. M. Casey
Department of Chemistry
University of Nevada
Reno, NV 89557 (USA)
Fax: (+1) 775-784-6804
E-mail: tchang@equinox.unr.edu
[+] Present address: Osmonics, Inc.
5951 Clearwater Drive, Minnetonka, MN 55343 (USA)

[**] S.-W.T.-C. is grateful for the Career Award (DMR-9876027) and the support of this work by the National Science Foundation. We appreciate the helpful suggestions of the reviewers.

Supporting information for this article is available on the WWW under http://www.angewandte.org or from the author.

 © 2003 Wiley-VCH Verlag GmbH & Co. KGaA, Weinheim 1433-7851/03/4208-0897 $ 20.00+.50/0

tropic properties persisting to the macroscopic scale can be obtained in thin solid films.[19,20]

The formate salt **1**[21] was only sparingly soluble in water (less than 10^{-7} M). However, it dissolved readily in 1.2 N $HCOOH_{(aq)}$ to give a 0.01 M solution, and its solubility increased at higher concentrations of formic acid. For instance, solutions with concentrations of **1** as high as 0.15 M could be prepared using 16.5 N $HCOOH_{(aq)}$ as the solvent.

Electronic absorption characteristics of **1** change significantly in different solvents (Figure 1). In concentrated sulfuric acid (98%) at 25 °C, the electronic absorption spectrum of **1** (1×10^{-5} M) showed an intense sharp band with an absorption maximum (λ_{max}) at 856 nm and two weaker peaks at 800 and 772 nm. An intense absorption peak at 907 nm was reported for **2b** in concentrated H_2SO_4, which was attributed to the protonation of the carboximide function of **2b**.[14] In concentrated formic acid (in water, 23.4 N), the position of λ_{max} for **1** (3×10^{-7} M) shifted to 740 nm and a shoulder at 830 nm was observed. At lower concentrations of HCOOH, the shoulder at 830 nm disappeared and further shifts in λ_{max} to lower wavelengths were observed. The λ_{max} wavelengths of **1** in 16.7 N and 1.2 N $HCOOH_{(aq)}$ were 694 and 675 nm, respectively.

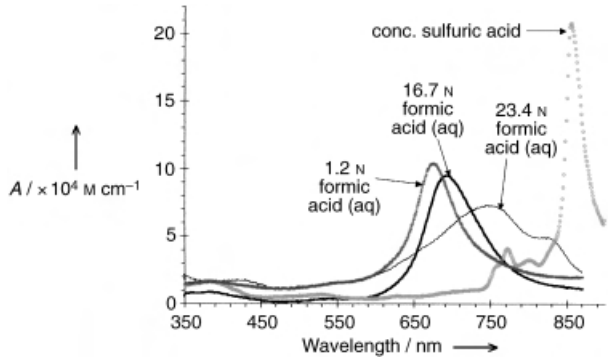

Figure 1. Effect of solvent on the electronic absorption of **1**. The concentration of **1** was approximately 3×10^{-7} M in the formic acid solutions, and 1×10^{-5} M in the concentrated sulfuric acid solution. *A* = molar absorptivity.

Furthermore, the absorption spectra of **1** in 23.4 N $HCOOH_{(aq)}$ varied with temperature (Figure 2) and the concentration of **1**. The absorption spectrum of **1** (5×10^{-7} M) in 23.4 N $HCOOH_{(aq)}$ showed a broad absorption band with λ_{max} at 740 nm and a shoulder at 830 nm at 25 °C. As the temperature of this solution was raised slowly to 85 °C, the λ_{max} wavelength shifted to 765 nm and the intensity of the shoulder at 830 nm increased gradually. At 85 °C, the peak at 830 nm became more prominent when lower concentrations of **1** were used.

These changes in the electronic absorption spectrum of **1** may be attributed to H-aggregate formation. Strong π stacking and hydrophobic interactions among the molecules of **1** in aqueous solution were expected because of the presence of the large conjugated ring structure. In a strongly acidic solution such as 23.4 N $HCOOH_{(aq)}$, and at high temperatures (85 °C), the extent of aggregation decreased,

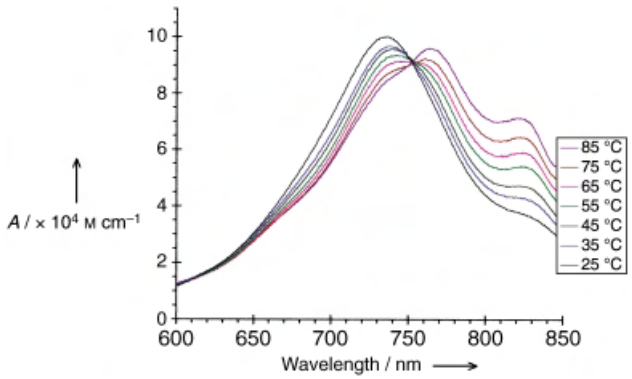

Figure 2. Effect of temperature (25 °C to 85 °C) on the absorption spectrum of **1** (5×10^{-7} M) in aqueous 23.4 N HCOOH. *A* = molar absorptivity.

which allows the absorption spectrum of the monomer at 830 nm to be observed. The extent of aggregation increased in dilute $HCOOH_{(aq)}$ (1.2 N), and only the broad absorption spectrum of the higher aggregates at 675 nm was observed at 25 °C. Since the wavelengths of the absorption maxima of the dimer and higher aggregates in $HCOOH_{(aq)}$ are blue-shifted from the monomer peaks, H-aggregates (in which the molecules are stacked in a ladder-like fashion)[22,23] are presumably formed.

When examined under a polarizing microscope, solutions of **1** (in 16.5 N $HCOOH_{(aq)}$) were birefringent at concentrations of 4 wt% and greater, which is indicative of the formation of a lyotropic liquid-crystalline phase.[18] The optical textures observed are consistent with a chromonic,[24] nematic liquid-crystalline phase (Figure 3).[25–27] In this type of phase, the mesogens typically stack to form columns (not necessarily simple one-molecule-wide columns), but there is no positional order among the columns. Similar optical textures were observed in 23.4 N $HCOOH_{(aq)}$ when the concentration of **1** was 15.7 wt% or greater.

Oriented thin solid films of **1** were prepared by simultaneously coating and aligning the solution of **1** (in the

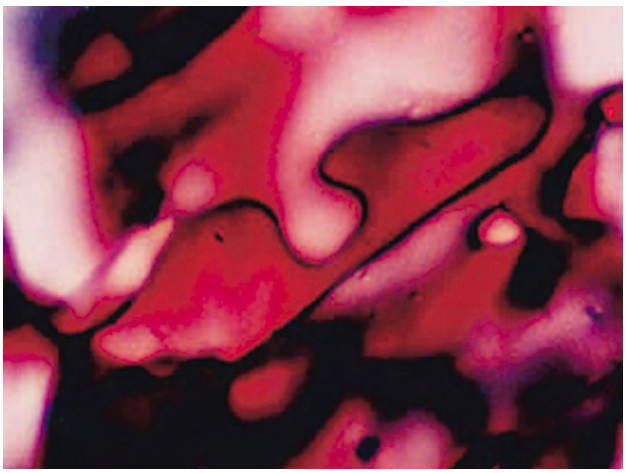

Figure 3. Optical photomicrograph of a solution of **1** (8.0 wt%) in aqueous 16.5 N HCOOH (200×, crossed polarizers).

 © 2003 Wiley-VCH Verlag GmbH & Co. KGaA, Weinheim 1433-7851/03/4208-0898 $ 20.00+.50/0

chromonic nematic phase) onto glass substrates using a mechanical shearing force. Solid films were obtained upon evaporation of solvent under ambient conditions. The anisotropic optical properties of the films were examined by polarized microscopy. The films were colorless and transparent (Figure 4, top) when the polarization axis of the incident light was parallel to the shearing direction. In contrast, only blue light was transmitted (green and red light was absorbed) when the polarization axis of the incident light was orthogonal to the shearing direction (Figure 4, bottom). When a liquid-crystalline solution of **1** was allowed to dry on a glass slide without alignment with the shearing force, no bulk anisotropic orientation or light polarization on a macroscopic scale was observed. In addition, no bulk orientation resulted if an isotropic solution of **1** was used. These results indicate that the self-organization of **1** into a liquid-crystalline phase and its induced orientation by shearing are both requirements for the fabrication of highly anisotropic films of **1**.

The optical properties of these films were quantified using polarized visible spectroscopy. As shown in Figure 5, the films exhibited very low transmittance (high absorbance) of green and red light when the shearing direction of the film was perpendicular to the polarization axis of the incident light. In contrast, when the film was rotated through 90°, such that the shearing direction was aligned with the polarization axis of the incident light, high transmittance was observed. The polarization efficiency of this film was greater than 98% in the range from 600 to 733 nm. These results suggest that the molecules on the glass substrate are oriented with their electronic transition moments preferentially aligned orthogonal to the shearing direction.

The absorbance at different wavelengths of light polarized perpendicular (A_{90}) and parallel (A_0) to the shearing direction of this film were used to calculate the dichroic ratios (A_{90}/A_0). The highest dichroic ratio (greater than 20) of this film occurred at approximately 611 nm, and significant polarization of light was still observed at wavelengths above 700 nm (Figure 6). For more accurate determination of the maximum

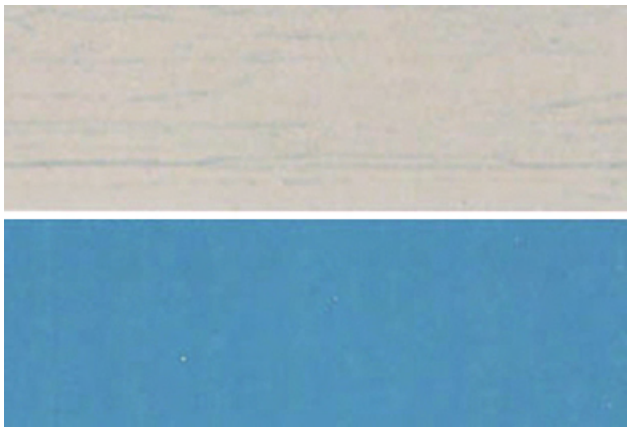

Figure 4. Optical photomicrograph of an air-dried oriented film prepared from a solution of **1** (11 wt%) in aqueous 16.5 N HCOOH: (top) polarization axis of incident light parallel to the shearing direction, and (bottom) polarization axis of incident light perpendicular to the shearing direction (200×, single polarizer).

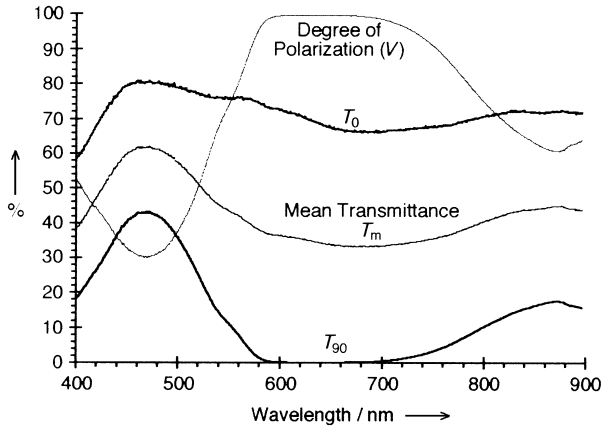

Figure 5. Optical properties of a solid film of **1** on glass prepared from a solution of **1** (11 wt%) in aqueous 16.5 N HCOOH. T_{90} is the transmittance when the shearing axis of the aligned film is perpendicular to the polarization of the incident light; T_0 is the transmittance when it is parallel. The mean transmittance (T_m) is calculated as $[T_0+T_{90}]/2$ and is a measure of the transmittance of unpolarized incident light. The degree of polarization (V) is calculated as $100\% \times [T_0-T_{90}]/[T_0+T_{90}]$.

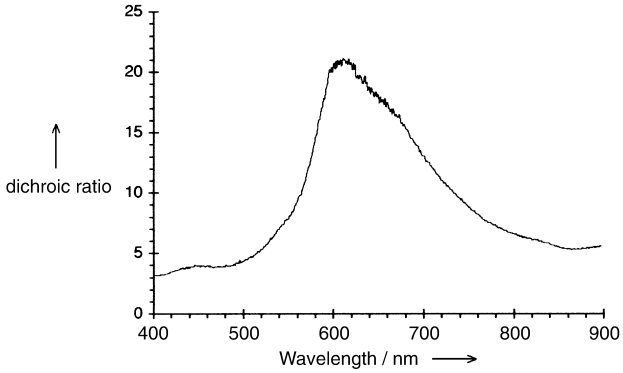

Figure 6. The change in the dichroic ratio of an oriented solid film of **1** with wavelength.

dichroic ratio of this film, the transmittance of the film as a function of the angle (θ) between the shearing direction and the polarization axis of the incident light (at 611 nm) was determined. The transmittance (T_θ) of the polarized incident light at an angle θ can be related to the transmittance at 90° (T_{90}) and 0° (T_0) by Equation (1)[28] as follows:

$$T_\theta = (T_0-T_{90})\cos^2\theta + T_{90} \quad (1)$$

Fitting the values of T_θ to Equation (1) allowed accurate determination of the values of T_{90} and T_0. These values were then converted to absorbance values (A_{90} and A_0) and their ratio yielded a dichroic ratio of 21.2 ± 0.2 at 611 nm. Since dichroic ratios are, in principle, independent of the thickness of the films, they serve as useful parameters for measuring anisotropic order in thin solid films.

This work has demonstrated, with quaterrylenebis(dicarboximide) **1** as an example, that large conjugated compounds can be imparted with lyotropic liquid-crystalline properties by molecular design. An important consequence of the self-

 © 2003 Wiley-VCH Verlag GmbH & Co. KGaA, Weinheim 1433-7851/03/4208-0899 $ 20.00+.50/0

organization of **1** into a liquid-crystalline phase is that it allows the unprecedented control of the molecular orientation of **1** in thin solid films. Induced orientation of the liquid-crystalline domains of **1** under a shearing force results in highly anisotropically ordered thin solid films that serve as dichroic polarizers of light at long wavelengths (greater than 600 nm). Future work will investigate the fluorescence, semiconducting, and photoconducting properties of **1**.

Received: September 19, 2002 [Z50199]

[1] M. C. Fyfe, J. F. Stoddart, *Acc. Chem. Res.* **1997**, *30*, 393 – 401.
[2] J.-M. Lehn, *Supramolecular Chemistry*, VCH, Weinheim, **1995**.
[3] D. L. Gin, W. Gu, B. A. Pindzola, W.-J. Zhou, *Acc. Chem. Res.* **2001**, *34*, 973 – 980.
[4] H. O. Jacobs, A. R. Tao, A. Schwartz, D. H. Gracias, G. M. Whitesides, *Science* **2002**, *296*, 323 – 325.
[5] S. M. Kauzlarich, P. K. Dorhout, J. M. Honig, *J. Solid State Chem.* **2000**, *149*, 3 – 8.
[6] G. Y. Liu, S. Xu, Y. Qian, *Acc. Chem. Res.* **2000**, *33*, 457 – 466.
[7] M. D. Ward, A. M. Pivovar, *Curr. Opin. Solid State Mater. Sci.* **1999**, *4*, 581 – 586.
[8] L. Schmidt-Mende, A. Fechtenkötter, K. Müllen, E. Moons, R. H. Friend, J. D. MacKenzie, *Science* **2001**, *293*, 1119 – 1122.
[9] A. B. Gregg, R. A. Cormier, *J. Am. Chem. Soc.* **2001**, *123*, 7959 – 7960.
[10] A. P. H. J. Schenning, J. V. Herrikhuyzen, P. Jonkheijm, Z. Chen, F. Würthner, E. W. Meijer, *J. Am. Chem. Soc.* **2002**, *124*, 10252 – 10253.
[11] F. Wurthner, C. Thalacker, S. Diele, C. Tschierske, *Chem. Eur. J.* **2001**, *7*, 2245 – 2253.
[12] J. S. Moore, *Curr. Opin. Solid State Mater. Sci.* **1996**, *1*, 777 – 788.
[13] H. Quante, K. Müllen, *Angew. Chem.* **1995**, *107*, 1487 – 1489; *Angew. Chem. Int. Ed. Engl.* **1995**, *34*, 1323 – 1325.
[14] Y. Geerts, H. Quante, H. Platz, R. Mahrt, M. Hopmeier, A. Bohm, K. Mullen, *J. Mater. Chem.* **1998**, *8*, 2357 – 2369.
[15] K. Y. Law, *Chem. Rev.* **1993**, *93*, 449 – 486.
[16] M. Emmelius, G. Pawlowski, H. W. Vollmann, *Angew. Chem.* **1989**, *101*, 1475 – 1502; *Angew. Chem. Int. Ed. Engl.* **1989**, *28*, 1445 – 1600.
[17] K. Shirai, M. Sumitani, N. Takeda, M. Arii, US patent 5,278,853 **1994**.
[18] P. J. Collings, J. S. Patel, *Handbook of Liquid Crystal Research*, Oxford University Press, New York, **1997**.
[19] I. K. Iverson, S. M. Casey, W. Seo, S.-W. Tam-Chang, B. A. Pindzola, *Langmuir* **2002**, *18*, 3510 – 3516.
[20] I. K. Iverson, S.-W. Tam-Chang, *J. Am. Chem. Soc.* **1999**, *121*, 5801 – 5802.
[21] A manuscript that describes the detailed procedure for the synthesis of **1** is in preparation.
[22] K. Saito, *J. Phys. Chem. B* **2001**, *105*, 4235 – 4238.
[23] P. M. Kamaier, R. A. Hoffmann, *J. Am. Chem. Soc.* **1994**, *116*, 9684 – 9691.
[24] Liquid crystals that result from the π-stacking interactions between aromatic molecules, in addition to hydrophobic interactions, are called lyotropic, chromonic liquid crystals as distinct from the lyotropic liquid crystals of aliphatic surfactants. See references [25] and [26].
[25] J. Lydon in *Handbook of Liquid Crystals, Vol. 2B* (Eds.: D. Demus, J. Goodby, G. W. Gray, H.-W. Spiess, V. Vill), Wiley-VCH, Weinheim, **1998**, pp. 981 – 1007.
[26] J. Lydon, *Curr. Opin. Colloid Interface Sci.* **1998**, *3*, 458 – 466.
[27] T. K. Attwood, J. E. Lydon, C. Hall, G. J. T. Tiddy, *Liq. Cryst.* **1990**, *7*, 657 – 668.
[28] C. D. West, R. C. Jones, *J. Opt. Soc. Am.* **1951**, *41*, 976 – 986.

Pentalene Bonding in Fullerenes

$Sc_3N@C_{68}$: Folded Pentalene Coordination in an Endohedral Fullerene that Does Not Obey the Isolated Pentagon Rule**

Marilyn M. Olmstead, Hon Man Lee, James C. Duchamp, Steven Stevenson, Daniela Marciu, Harry C. Dorn, and Alan L. Balch**

The new family of endohedral metallofullerenes, $Sc_3N@C_{80}$, $Sc_3N@C_{78}$, and $Sc_3N@C_{68}$, has been prepared by the Krätschmer–Huffman arc fullerene preparation with graphite rods doped with Sc_3O_2 in a dynamic atmosphere of helium and dinitrogen.[1–4] Crystallographic studies have shown that $Sc_3N@C_{80}$ contains a planar $\{Sc_3N\}$ unit within a C_{80} cage with I_h symmetry,[1] while $Sc_3N@C_{78}$ consists of a similar $\{Sc_3N\}$ unit contained within a fullerene cage of D_{3h} symmetry.[3] These endohedral structures, as well as most known empty-cage fullerenes, obey the isolated pentagon rule (IPR) which requires that each of the twelve pentagons in the carbon cage be surrounded by five hexagons. However, theoretical studies have suggested that some endohedral fullerenes (for example, $Ca@C_{72}$ and $La_2@C_{74}$) may not obey the IPR.[5] Additionally, two endohedral fullerenes, $Sc_3N@C_{68}$[4] and $Sc_2@C_{66}$,[6] and one empty-cage fullerene, C_{62},[7] have been recently reported, which cannot obey the IPR as no possible IPR cages exist for C_{62}, C_{64}, C_{66}, or C_{68}.[8]

Here we report the detailed structural characterization of $Sc_3N@C_{68}$. For a C_{68} cage whose surface consists solely of pentagons and hexagons, there are 6332 possible isomers, but the ^{13}C NMR spectrum of $Sc_3N@C_{68}$ restricts these possibilities to only 11 isomers that have either D_3 or S_6 symmetry.[4] On the basis of density functional calculations, two isomers (isomer 6140[4] and isomer 6275;[9] Figure 1) have emerged as the likely cage structures present in $Sc_3N@C_{68}$. As Figure 1 shows, these isomers have different shapes (6140 is rounded while 6275 is flattened), although both have D_3 symmetry.

Black crystals of $Sc_3N@C_{68}\cdot[Ni^{II}(OEP)]\cdot 2\,C_6H_6$ (OEP = 2,3,7,8,12,13,17,18-octaethylporphinate) were obtained by the gradual diffusion of a solution of $Sc_3N@C_{68}$ (prepared

[*] Prof. Dr. H. C. Dorn, Dr. J. C. Duchamp, Dr. S. Stevenson,[+]
Dr. D. Marciu[+]
Department of Chemistry
Virginia Polytechnic Institute and State University
Blacksburg, VA 24061 (USA)
Fax: (+1) 540-231-5953
E-mail: hdorn@chemserver.chem.vt.edu
Prof. Dr. A. L. Balch, Dr. M. M. Olmstead, Dr. H. M. Lee
Department of Chemistry
University of California, Davis
Davis, CA 95616 (USA)
Fax: (+1) 530-752-8995
E-mail: albalch@ucdavis.edu
[+] Current address: Luna Nanomaterials
2851 Commerce Street, Blacksburg, VA 24060 (USA)

[**] This work was supported by the U.S. National Science Foundation (CHE 0070291 to A.L.B.) and LUNA Innovations (to H.C.D.).

 © 2003 Wiley-VCH Verlag GmbH & Co. KGaA, Weinheim 1433-7851/03/4208-0900 $ 20.00+.50/0

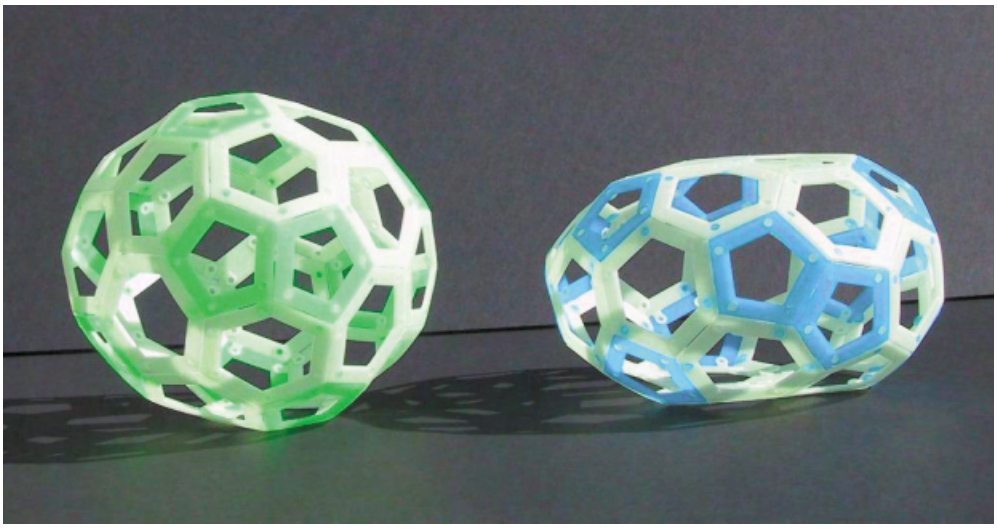

Figure 1. Idealized models of isomer 6140 (left, green pentagons) and isomer 6275 (right, blue pentagons) of C_{68}.

and purified as outlined previously[4]) in benzene into a solution of [Ni^{II}(OEP)] in benzene. This fullerene/porphyrin cocrystallization procedure has previously been demonstrated to form crystalline samples with sufficient order in the location of the fullerene cage to produce meaningful structural information.[10]

The structure was solved by direct methods which yielded the entire porphyrin, two benzene molecules, and the major {Sc_3N} unit (site **A**). Successive cycles of refinement, and the selection of atoms from difference maps produced one entire C_{68} molecule (site **A**) but with a fractional occupancy of only approximately 0.5, based on thermal parameters; at this stage the R1 value was 0.151. Refinement then took advantage of the D_3 symmetry to yield a set of 771 same-distance restraints that were used to preserve this symmetry. Further refinement resulted in the location of an additional 13 scandium sites with occupancies ranging from 0.25 to 0.04. By trial and error, a second orientation (site **B**) of the C_{68} cage was identified. This procedure used a rigid group constructed from the coordinates of the refined C_{68} cage (**A**) to fit peaks from the difference Fourier maps. This second orientation was the best fit when using the opposite enantiomer from that found in site **A**, and refined to a group occupancy of 0.29. Thus, another orientation of the cage needed to be located. Again, using the rigid group, and trial and error, the inclusion of a third cage (site **C**) with an occupancy of 0.21, which was also of the opposite hand to site **A**, brought the *R*1 value to 0.093.

Figure 2 shows a drawing of the orientations of the individual molecular components with only the major site **A** (with 0.50 site occupancy of the $Sc_3N@C_{68}$ molecule) shown. As usual in structures of this type, the $Sc_3N@C_{68}$ molecule is cupped in the cavity provided by the nickel porphyrin and its eight ethyl groups. There are no unusual aspects to the geometry of the nonfullerene components of this crystal.

Figure 3 shows diagrams of the major site **A**. The carbon cage is shown to be isomer 6140 with D_3 symmetry, as predicted by earlier theoretical work.[4] In this cage structure, there are three equivalent sites where pairs of pentagons share a side (pentalene units). The maximum degree of outward bulge in the cage occurs at these sites, and the principle scandium sites are located in these pockets. The {Sc_3N} portion is planar, and the N1–Sc bond lengths are

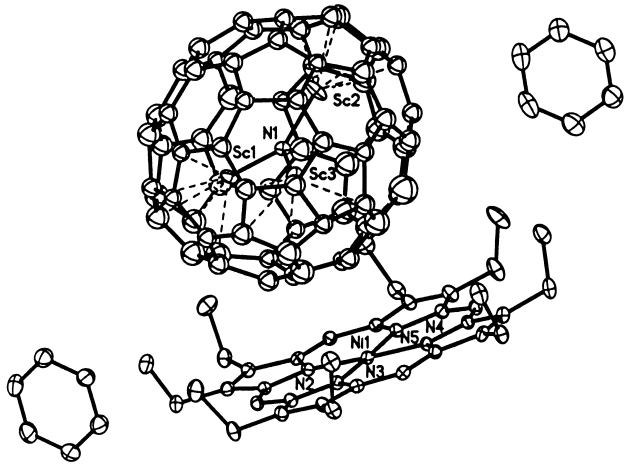

Figure 2. A drawing of the structure of $Sc_3N@C_{68}$·[Ni^{II}(OEP)]·2 C_6H_6 that shows the relative orientation of all components. Only the major orientation (0.50 site occupancy) of the $Sc_3N@C_{68}$ molecule is shown.

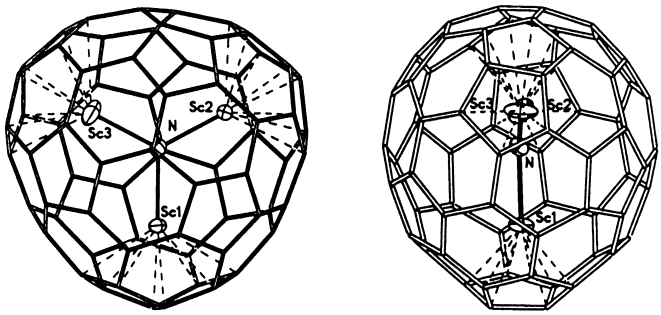

Figure 3. Two orthogonal views of the major form (0.50 site occupancy) of the $Sc_3N@C_{68}$ molecule in $Sc_3N@C_{68}$·[Ni^{II}(OEP)]·2 C_6H_6.

 © 2003 Wiley-VCH Verlag GmbH & Co. KGaA, Weinheim 1433-7851/03/4208-0901 $ 20.00+.50/0

2.022(3), 1.974(4), and 1.961(4) Å for Sc1, Sc2, and Sc3, respectively. These separations are just slightly shorter than their counterparts in $Sc_3N@C_{78}$ (1.983(15)–2.125(5) Å)[3] and in $Sc_3N@C_{80}$ (1.9931(14)–2.0526(14) Å).[1] The Sc-N-Sc angles are Sc1-N-Sc2 130.3(5), Sc1-N-Sc3 113.8(5), and Sc2-N-Sc3 115.9(5)°.

As was previously pointed out, the scandium atoms are situated over the centers of pentalene portions of the fullerene cage. There is an extensive literature on the organometallic chemistry of pentalene ligands, which frequently bridge two metals.[11] However, compounds containing a metal bonded at the center of a folded pentalene ligand have only recently been reported.[12,13] Figure 4 presents a comparison of the Sc–pentalene coordination geometry in $Sc_3N@C_{68}$ with the Ta–pentalene coordination in a conventional organometallic complex, $[\{\eta^8\text{-}C_8H_4(SiMe_3)_2\text{-}1,4\}TaCl_3]$.[12] The major differences all result from the fold angle of the pentalene unit, (45.6° in $Sc_3N@C_{68}$, 32.7° in $[\{\eta^8\text{-}C_8H_4(SiMe_3)_2\text{-}1,4\}TaCl_3]$) which is greater in the fullerene where the closed nature of the carbon cage more tightly constricts the geometry. As a consequence of this fold, the pyramidalization[14] of the carbon atoms at the 5:5-ring junction is significantly higher (16.5°) than it is for the other carbon atoms of the cage (which range from 8.8 to 12.2°). In $Sc_3N@C_{68}$, the Sc–C bond lengths fall in a narrower range (2.225(5)–2.450(5) Å) than they do in $[\{\eta^8\text{-}C_8H_4(SiMe_3)_2\text{-}1,4\}TaCl_3]$ (2.182(13)–2.582(12) Å). In both cases, the shortest metal-to-carbon separations involve the carbon atoms at the 5:5-ring junctions.

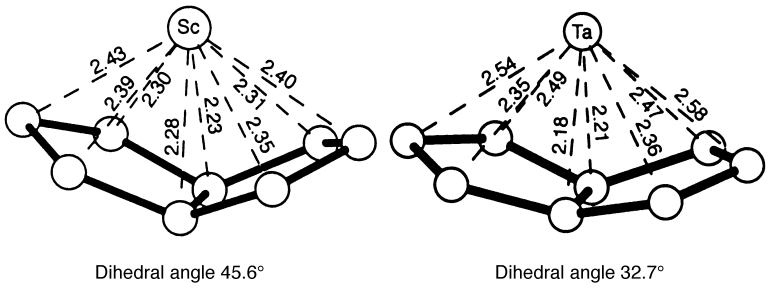

Figure 4. Comparison of the average pentalene coordination in $Sc_3N@C_{68}$ and in $[\{\eta^8\text{-}C_8H_4(SiMe_3)_2\text{-}1,4\}TaCl_3]$.

Disorder in the positioning of the fullerene has been resolved with a model that includes two other orientations (**B** and **C**) for the C_{68} cage. A central nitrogen atom is common to all three cage orientations. Three scandium atoms (Sc4, Sc5, and Sc6), each with an occupancy of 0.21, fit into the three pentalene units within the C_{68} cage at site **C** to create a molecule analogous to that in the major site. One additional scandium atom with an occupancy of 0.25 is situated within a pentalene unit of the cage occupying site **B**. Nine other scandium-atom positions with site occupancies ranging from 0.10 to 0.04 have been identified. These appear to be associated with the C_{68} cage in site **B** but they are situated in various locations within the cage. Highly correlated overlap of multiple $\{Sc_3N\}$ units precluded accurate identification of distinct entities except for one triangular array comprised of Sc7, Sc8, and Sc9, with an occupancy of 0.10. Thus, as is often the case with complex supramolecular structures, the model we have developed is the most plausible we could find, but is not without some ambiguities. Consequently, further structural work on non-IPR fullerene cages, particularly in endohedral complexes, is clearly warranted.

Coordination of the scandium atoms to the pentalene portion of a fullerene cage may provide a means of stabilizing this substructure. The computed non-IPR structures for $Ca@C_{72}$ and $Ca@C_{74}$ place the metals within the pentalene clefts.[5] A similar arrangement, with metal atoms over pentalene units, has been proposed for $Sc_2@C_{66}$.[6]

Experimental Section

Crystals of $Sc_3N@C_{68}\cdot[Ni^{II}(OEP)]\cdot 2\,C_6H_6$ were obtained by layering a purple solution of $Sc_3N@C_{68}$ (approximately 0.5 mg) in benzene (0.5 mL) of over a red solution of $[Ni^{II}(OEP)]$ (2.5 mg) in benzene (1.5 mL). The two solutions were allowed to diffuse together over five days, by which time, black crystals had formed.

Crystal data for $Sc_3N@C_{68}\cdot[\{Ni^{II}(OEP)\}\cdot 2\,C_6H_6$: black parallelepiped, $0.14\times0.10\times0.07$ mm, triclinic, space group $P\bar{1}$, $a=14.362(2)$, $b=14.3902(14)$, $c=18.986(2)$ Å, $\alpha=85.433(2)$, $\beta=88.606(23)$, $\gamma=61.786(3)°$, $V=3446.3(7)$ Å^3, $\lambda=0.71073$ Å, $Z=2$, $\rho_{calcd}=1.651$ Mg m^{-3}; $\mu(Mo_{K\alpha})=0.622$ mm^{-1}; $T=91(2)$ K; Bruker SMART 1000; ω scans, $2\Theta_{max}=60°$; 49366 reflections collected; 19925 independent ($R_{int}=0.079$) included in the refinement; min/max transmission = 0.92/0.96 (no absorption correction applied); Patterson and difference Fourier methods solution (SHELXS-97; Sheldrick, 1990); full-matrix least-squares based on F^2 (SHELXL-97; Sheldrick, 1998); $R=0.150$, $wR=0.302$ for all data; conventional $R1=0.093$ computed for 10967 observed data ($>2\sigma(I)$) with 771 restraints and 1015 parameters.

CCDC-190814 contains the supplementary crystallographic data for this paper. These data can be obtained free of charge via www.ccdc.cam.ac.uk/conts/retrieving.html (or from the Cambridge Crystallographic Data Centre, 12, Union Road, Cambridge CB21EZ, UK; fax: (+44) 1223-336-033; or deposit@ccdc.cam.ac.uk).

Received: July 31, 2002
Revised: November 18, 2002 [Z19864]

[1] S. Stevenson, G. Rice, T. Glass, K. Harich, F. Cromer, M. R. Jordan, J. Craft, E. Hadju, R. Bible, M. M. Olmstead, K. Maitra, A. J. Fisher, A. L. Balch, H. C. Dorn, *Nature* **1999**, *401*, 55.

[2] "Electronic Properties of Novel Materials and Molecular Nanostructures": H. C. Dorn, S. Stevenson, J. Craft, F. Cromer, J. Duchamp, G. Rice, T. Glass, K. Harich, P. W. Fowler, T. Heine, E. Hajdu, R. Bible, M. M. Olmstead, K. Maitra, A. J. Fisher, A. L. Balch, Proceedings of the IWEPNM2000 Conference, Kirchberg/Tyrol (Austria), **2000**, p. 135 (American Institute of Physics).

[3] M. M. Olmstead, A. de Bettencourt-Dias, J. C. Duchamp, S. Stevenson, D. Marciu, H. C. Dorn, A. L. Balch, *Angew. Chem.* **2001**, *113*, 1263; *Angew. Chem. Int. Ed.* **2001**, *40*, 1223.

[4] S. Stevenson, P. W. Fowler, T. Heine, J. Duchamp, G. Rice, T. Glass, K. Harich, E. Hajdu, R. Bible, H. C. Dorn, *Nature* **2000**, *408*, 427.

[5] K. Kobayashi, S. Nagase, M. Yoshida, E. Osawa, *J. Am. Chem. Soc.* **1997**, *119*, 12693.

[6] C.-R. Wang, T. Kai, T. Tomiyama, T. Yoshida, Y. Kobayashi, E. Nishibori, M. Takata, M. Sakata, H. Shinohara, *Nature* **2000**, *408*, 426.

 © 2003 Wiley-VCH Verlag GmbH & Co. KGaA, Weinheim 1433-7851/03/4208-0902 $ 20.00+.50/0

[7] W. Qian, M. D. Bartberger, S. J. Pastor, K. N. Houk, C. L. Wilkins, Y. Rubin, *J. Am. Chem. Soc.* **2000**, *122*, 8333.
[8] P. W. Fowler, D. E. Manoloupoulos, *An Atlas of Fullerenes*, Oxford Univeristy Press, Oxford, **1995**.
[9] J. Aihara, *Chem. Phys. Lett.* **2001**, *343*, 465.
[10] M. M. Olmstead, D. A. Costa, K. Maitra, B. C. Noll, S. L. Phillips, P. M. Van Calcar, A. L. Balch, *J. Am. Chem. Soc.* **1999**, *121*, 7090.
[11] H. Butenschön, *Angew. Chem.* **1997**, *109*, 1771; *Angew. Chem. Int. Ed. Engl.* **1997**, *36*, 1695.
[12] Q. A. Abbasali, F. G. N. Cloke, P. B. Hitchcock, S. C. P. Joseph, *Chem. Commun.* **1997**, 1541.
[13] K. Jonas, B. Gabor, R. Mynott, K. Angermund, O. Heinemann, C. Krüger, *Angew. Chem.* **1997**, *109*, 1790; *Angew. Chem. Int. Ed. Engl.* **1997**, *36*, 1712.
[14] R. C. Haddon, *Science* **1993**, *261*, 1545.

Multiparallel Organic Synthesis

A Three-Dimensional Array for Multiparallel Synthesis**

Sergey A. Kozmin and Ying Wang*

Multiparallel organic synthesis combined with high-content screening has emerged as a valuable approach for identification of new molecular function. Emulating basic principles of natural selection, this strategy has proven particularly successful for discovery and optimization of modulators of metabolic pathways,[1] identification of novel catalysts,[2] and development of unique functional materials.[3] Solid-phase synthesis[4] has provided a foundation for the development of several innovative methods for the synthesis of chemical libraries.[5–11] Among these formats, light-directed synthesis[8] and split synthesis are particularly noteworthy.[9] While the former provides complete positional encoding of individual library members,[8] the latter features high throughput and operational simplicity,[9] although it requires additional split–pool steps and encoding-decoding operations.[10,11]

We describe herein a conceptually novel format for the synthesis of chemical libraries based on three-dimensional arrays of interconnected reaction wells. This method is unique and differs significantly from the existing formats of generating chemical diversity,[5–11] combining the high efficiency of the split synthesis with a spatially addressable format.

The strategy entails layer-selective functionalization of a three-dimensional matrix, consisting of interconnected reaction wells. Each well is designed to encapsulate an individual library member by attachment to a physically localized solid support. Figure 1 provides a conceptual representation of the synthesis of an ABC library randomized with two building blocks at each position (A^1 and A^2, B^1 and B^2, C^1 and C^2). The first functionalization step entails simultaneous addition of building blocks A^1 and A^2 to two parallel layers of the array. Following a washing cycle and a 90° rotation, the synthesis process is repeated with building blocks B^1 and B^2. The third set of reactants—C^1 and C^2—is introduced in a similar fashion following the final 90° rotation. This process affords a library of spatially separated compounds. The identity of each compound is established by its physical location within the array.

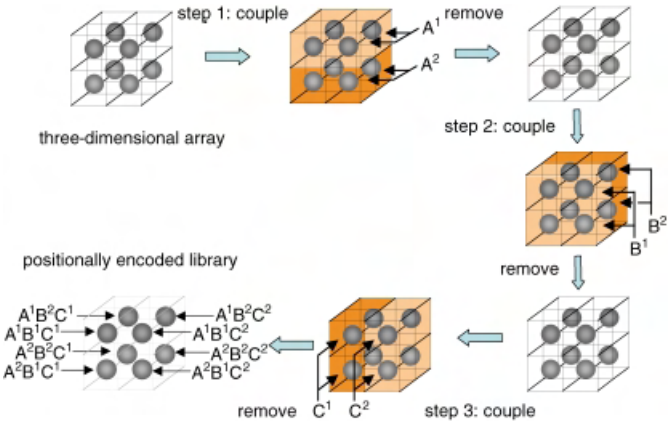

Figure 1. Conceptual representation of the synthesis of a chemical library in a three-dimensional array. The synthesis entails a layer-selective addition of reagents in each of the three dimensions. Three sets of building blocks (A^1 and A^2, B^1 and B^2, C^1 and C^2) are used sequentially. Each coupling step is followed by the appropriate washing and deprotection operations. The array is rotated by 90° prior to the addition of the next set of reagents. This process affords a positionally encoded library containing all the possible combinations.

The design of an individual reactor is depicted in Figure 2 A. Encapsulating a suitable polymeric support, each microwell is equipped with four openings, connecting it to four adjacent wells. Insertion of the appropriate sealing elements (i.e. taper pins) seals the walls of the reactors. Removal of pins allows addition and withdrawal of reagents. This simple concept provides a general method for layer-selective multiparallel chemical synthesis in each of the three dimensions without cross-contamination. The synthesis cycle begins with removal of all the pins from one side of the cube, while the perpendicular pins remain inserted (Figure 2 B). The first set of reagents (A^1 and A^2) is added, allowing all the coupling steps to be performed simultaneously. Following the washing cycle, and rotation by 90°, the second coupling step is performed with B^1 and B^2. The originally removed set of pins is reinserted, followed by withdrawal of the pins from the perpendicular side of the cube. The third coupling step is performed with C^1 and C^2, as shown. A noteworthy feature of

[*] Prof. Dr. S. A. Kozmin, Dr. Y. Wang
Department of Chemistry, University of Chicago
5735 South Ellis Avenue, Chicago, IL 60637 (USA)
Fax: (+1) 773-702-0805
E-mail: skozmin@uchicago.edu

[**] We thank David Plitt and Robert Metz for technical assistance. We also thank Professor Mrksich and Professor Ismagilov for helpful discussions. Financial support of this work was provided by the University of Chicago and the American Cancer Society Institutional Research Grant.

Supporting information for this article is available on the WWW under http://www.angewandte.org or from the author.

 © 2003 Wiley-VCH Verlag GmbH & Co. KGaA, Weinheim 1433-7851/03/4208-0903 $ 20.00+.50/0

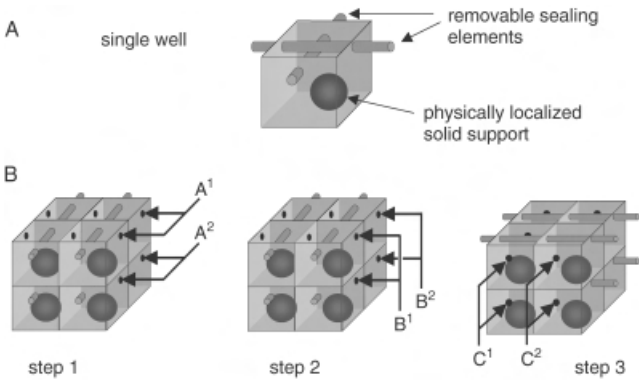

Figure 2. A) A single reaction well, equipped with four side openings, which allow insertion and removal of the sealing elements. B) Delivery of reagents in each of the three dimensions in a representative 2×2×2 array. Teflon gaskets are used to ensure solvent-tight seals between the layers (not shown). Each well is equipped with a single 12.5-mm SynPhase Lantern (18 mol/lantern loading). Stainless-steel 4-mm taper pins are used to achieve the desired sealing.

this design is that the bottom of each well remains impermeable, allowing direct cleavage of the compound from the solid support at the end of the synthesis cycle.

To validate the method described above, we conducted a synthesis of a model peptide library. The library was generated by randomization of the tripeptide at each position with five amino acids (Gly, Ala, Phe, Val, Leu) expected to produce 125 spatially addressed compounds (5^3). Three-dimensional arraying of the five amino acids in a $5\times5\times5$ array is schematically illustrated in Figure 3. We employed a conventional Fmoc solid-phase peptide synthesis by using a HOBt/DIC coupling protocol with commercially available SynPhase D-series PA lanterns[12,13] equipped with the Rink linker.[14] The synthesis was carried out within the expected 8-h period to afford 8–10 mg of target peptides (90–95% yield). Examination of 25 peptides, randomly selected from the final array, by means of ^{1}H NMR spectroscopy, HPLC, and APCI-MS confirmed the predicted identity of each product, as well as the high chemical purity (Figure 3). Importantly, no cross-contamination between neighboring library members was observed.

In conclusion, we have presented a novel format for multiparallel synthesis, featuring a three-dimensional delivery of reactants to an array of interconnected reaction wells. Generation of a model library of positionally encoded peptides validated this strategy, highlighting the high efficiency and throughput of our approach. Ideally suited for the preparation of trimeric libraries, this technology can be further adapted to the introduction of additional variables (i.e., by employing multiple copies of interconnected arrays). The noteworthy feature of this method is the ability to conduct *simultaneously* all the coupling, deprotection, and

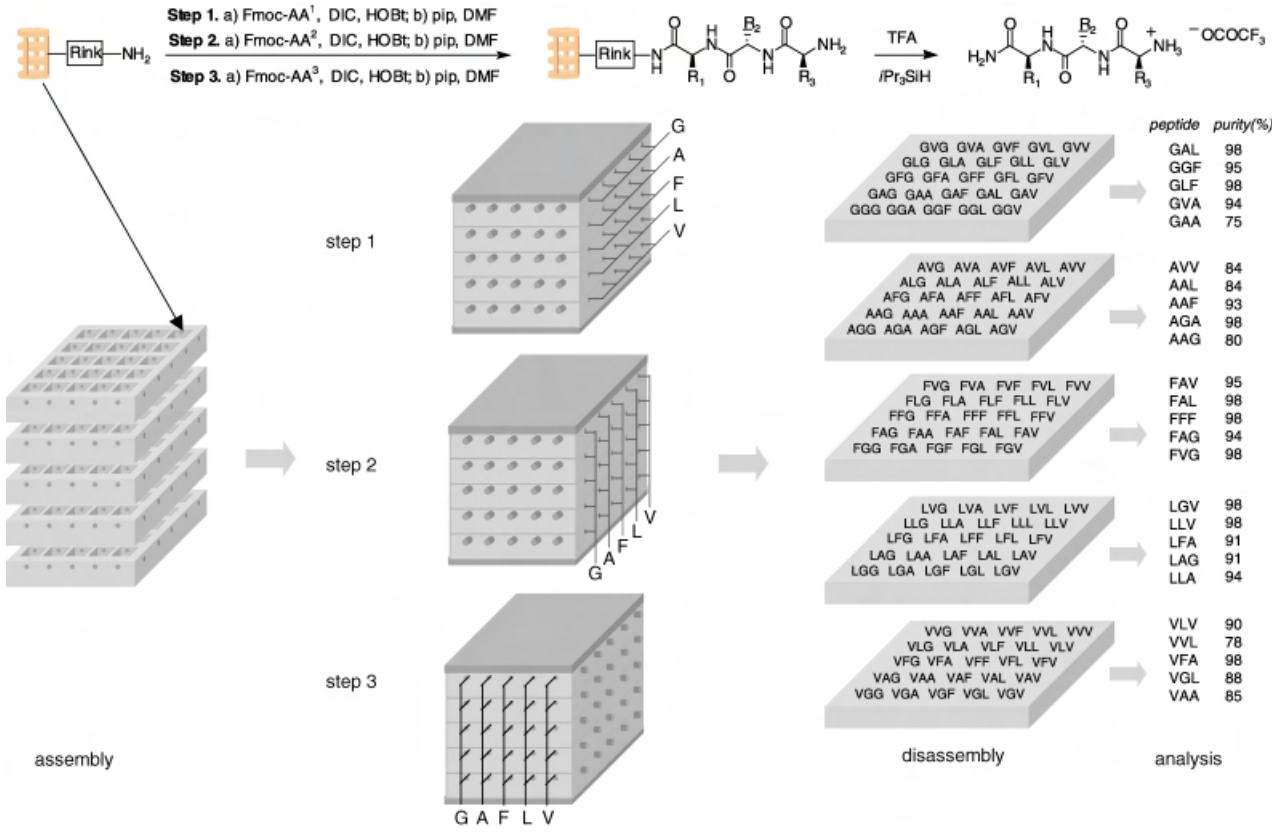

Figure 3. Generation of a 125-membered library of tripeptides in a 5×5×5 array. The system represents a set of five 25-well polypropylene plates stacked to form the desired 5×5×5 matrix. Each peptide coupling and Fmoc deprotection was followed by extensive washing (4×DMF). Following the completion of the synthesis process, the plates were disassembled, 25 representative peptides were removed, cleaved with TFA/H_2O/iPr_3SiH (95:2.5:2.5), and analyzed as described in the text and Supporting Information. Fmoc = 9-fluorenylmethoxycarbonyl, DIC = diisopropylcarbodiimide, HOBt = 1-hydroxy-1*H*-benzotriazole, pip = piperidine, DMF = *N*,*N*-dimethylformamide, TFA = trifluoroacetic acid.

 © 2003 Wiley-VCH Verlag GmbH & Co. KGaA, Weinheim 1433-7851/03/4208-0904 $ 20.00+.50/0

washing manipulations in the entire array. Significantly, the efficiency of the synthesis does not depend on the number of building blocks used along each axis. This feature provides a unique advantage of this method over the use of 2D arrays, representing a direct alternative to the split synthesis.[9] Although the operational simplicity of the split synthesis exceeds that of the present method, the ability to spatially resolve and positionally encode individual library members offered by the current approach compares favorably with the split synthesis, which requires additional encoding–decoding operations.[10,11] Extension of the work presented herein to the development of suitable systems for the synthesis of 1000–10000-membered small-molecule libraries is in progress and will be reported in due course.

Received: August 22, 2002 [Z50021]

[1] For selected reviews, see: a) E. M. Gordon, R. W. Barrett, W. J. Dower, S. P. A. Fodor, M. A. Gallop, *J. Med. Chem.* **1994**, *37*, 1385; b) L. A. Thompson, J. A. Ellman, *Chem. Rev.* **1996**, *96*, 555; c) D. G. Hall, *Nat. Biotechnol.* **2000**, *18*, 261.

[2] K. W. Kuntz, M. L. Snapper, A. H. Hoveyda, *Curr. Opin. Chem. Biol.* **1999**, *3*, 313.

[3] B. Jandeleit, D. J. Schaefer, T. S. Powers, H. W. Turner, W. H. Weinberg, *Angew. Chem.* **1999**, *111*, 2648; *Angew. Chem. Int. Ed.* **1999**, *38*, 2494.

[4] R. B. Merrifield, *J. Am. Chem. Soc.* **1963**, *85*, 2149.

[5] Multipin method: H. M. Geysen, R. H. Meloen, S. J. Barteling, *Proc. Natl. Acad. Sci. USA* **1984**, *81*, 3998.

[6] Simultaneous multiple-peptide synthesis: a) R. A. Houghten, *Proc. Natl. Acad. Sci. USA* **1985**, *82*, 5131; b) R. A. Houghten, C. Pinilla, S. E. Blondelle, J. R. Appel, C. T. Dooley, J. H. Cuervo, *Nature* **1991**, *354*, 84.

[7] Synthesis on cellulose disks: R. Frank, R. Doring, *Tetrahedron* **1988**, *44*, 6031.

[8] Light-directed synthesis: S. P. A. Fodor, J. L. Read, M. C. Pirrung, L. Stryer, A. T. Lu, D. Solas, *Science* **1991**, *251*, 767.

[9] Split synthesis: a) A. Furka, F. Sebestyen, M. Asgedom, G. Dibo, *Int. J. Pept. Protein Res.* **1991**, *37*, 487; b) K. S. Lam, S. E. Salmon, E. M. Hersh, V. J. Hruby, W. M. Kazmierski, R. J. Knapp, *Nature* **1991**, *354*, 82; for an automated protocol, see: c) M. Meldal, I. Svendsen, K. Breddam, F. Auzanneau, *Proc. Natl. Acad. Sci. USA* **1994**, *91*, 3314; for representative applications of split synthesis to small-molecule libraries, see: d) D. S. Tan, M. A. Foley, M. D. Shair, S. L. Schreiber, *J. Am. Chem. Soc.* **1999**, *121*, 9075; e) H. E. Pelish, N. J. Westwood, Y. Feng, T. Kirchhausen, M. D. Shair, *J. Am. Chem. Soc.* **2001**, *123*, 6740.

[10] Chemically encoded split synthesis: a) S. Brenner, R. A. Lerner, *Proc. Natl. Acad. Sci. USA* **1992**, *89*, 5381; b) M. C. Needels, D. G. Jones, E. H. Tate, G. L. Heinkel, L. M. Kochersperger, W. J. Dower, R. W. Barrett, M. A. Gallop, *Proc. Natl. Acad. Sci. USA* **1993**, *90*, 10700; c) M. H. J. Ohlmeyer, R. N. Swanson, L. W. Dillard, J. C. Reader, G. Asouline, R. Kobayashi, M. Wigler, W. C. Still, *Proc. Natl. Acad. Sci. USA* **1993**, *90*, 10922.

[11] RF-encoded split synthesis: a) E. J. Moran, S. Sarshar, J. F. Cargill, M. M. Shahbaz, A. Lio, A. M. M. Mjalli, R. W. Armstrong, *J. Am. Chem. Soc.* **1995**, *117*, 10787; b) K. C. Nicolaou, X. Y. Xiao, Z. Parandoosh, A. Senyei, M. P. Nova, *Angew. Chem.* **1995**, *107*, 2476; *Angew. Chem. Int. Ed. Engl.* **1995**, *34*, 2289.

[12] Mimotopes Pty. Ltd.

[13] We are currently developing a modification of this system with readily available 500–600-μm polystyrene beads.

[14] H. Rink, *Tetrahedron Lett.* **1987**, *28*, 3787.

DNA Structure

Hyperstranded DNA Architectures Observed by Cold-Spray Ionization Mass Spectrometry**

*Shigeru Sakamoto and Kentaro Yamaguchi**

Formation of duplex, triplex, and quadruplex DNA structures has been a subject of extensive investigation because of their fundamental functional roles in living organisms. The structures of these multistranded DNAs have been examined[1–3] by electrospray ionization[4] mass spectrometry (ESI-MS). However, noncovalent complexes of multiply stranded DNA are difficult to observe by conventional methods because of their low melting temperature (T_m). The heat from the desolvation chamber is thought to be necessary for ionization in the gas phase in conventional ESI. However, we recently developed a direct solution analysis method, cold-spray ionization (CSI)[5] mass spectrometry, a variant of ESI-MS operating at low temperature, and we have applied this method to study various labile solution structures.[6] Here we report the characterization of triple- and quadruple-stranded oligodeoxynucleotides by means of CSI-MS.

First, triple-stranded oligodeoxynucleotides $T_n{\cdot}A_n{\cdot}T_n$ derived from 2:1 mixtures of 5′-dT_n-3′ (T_n) and 5′-dA_n-3′ (A_n) ($n = 8$, 10, 15, 20, and 25) were analyzed. Negative CSI-MS measurements were performed with a two-sector (BE) mass spectrometer (JMS-700, JEOL) equipped with the CSI source.[7] In the case of the 8-mer (Figure 1a), comparable

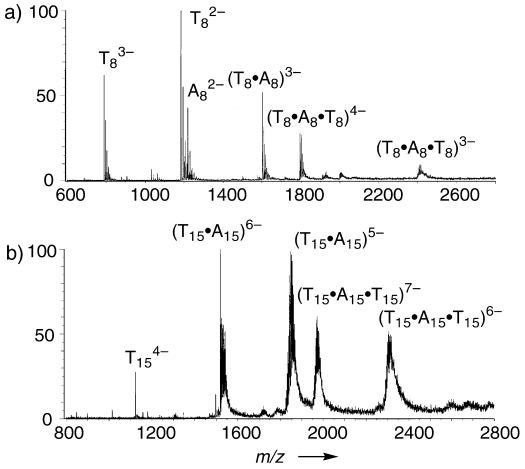

Figure 1. Negative CSI mass spectra of a) $T_8{\cdot}A_8{\cdot}T_8$ and b) $T_{15}{\cdot}A_{15}{\cdot}T_{15}$.

[*] Prof. Dr. K. Yamaguchi, Dr. S. Sakamoto
Chemical Analysis Center, Chiba University
Yayoicho, Inage-ku, Chiba, 263-8522 (Japan)

[**] This study was supported by a Grant-in-Aid for Scientific Research (No. 13557198) from the Ministry of Education, Culture, Sports, Science, and Technology. S.S. was recipient of a JSPS Research Fellowship for Young Scientists. K.Y. is responsible for the CREST project of the Japan Science and Technology Corporation (JST).

Supporting information for this article is available on the WWW under http://www.angewandte.org or from the author.

 © 2003 Wiley-VCH Verlag GmbH & Co. KGaA, Weinheim 1433-7851/03/4208-0905 $ 20.00+.50/0

ion peaks resulting from the duplex ($T_8{\cdot}A_8$) and a triplex ($T_8{\cdot}A_8{\cdot}T_8$) were observed, whereas the intensity of the ion peaks of the triplex became stronger when the number of base pairs increased. This might be explained by the higher stability of longer oligodeoxynucleotides with probably higher T_m values. The CSI mass spectrum of the 15-mer, exhibiting $(T_{15}{\cdot}A_{15}{\cdot}T_{15})^{x-}$ peaks ($x = 6,7$), is shown in Figure 1b. In the case of the 25-mer, ion peaks of the triplex were the major peaks, except for those of the single-stranded T_{25}^{5-}, and no ion peak of the duplex was observed (Figure 2a). The peaks of

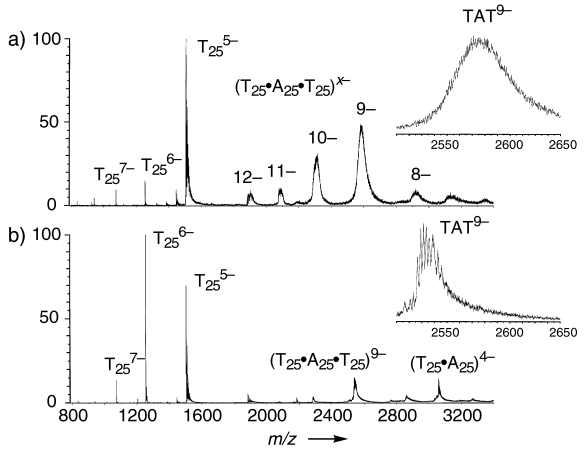

Figure 2. Negative a) CSI and b) ESI mass spectra of $T_{25}{\cdot}A_{25}{\cdot}T_{25}$.

the triplex ions $(T_{25}{\cdot}A_{25}{\cdot}T_{25})^{x-}$ ($x = 8$–12) are slightly broadened because of multiply attached NH_4^+ ions, which stabilize the triplex. From the broad $(T_{25}{\cdot}A_{25}{\cdot}T_{25})^{9-}$ peak follows that about 25 buffer molecules were attached to the triplex. The ions including buffer molecules can be interpreted as $[M-x\,H-y\,H+y\,(NH_4^+)]^{x-}$ (M: molecular weight of the multiply stranded DNA, x: charge state, y: number of buffer molecules attached). Only trace ion peaks resulting from the triplex and duplex, together with the major ion peaks of the single T_{25} strand, were observed by conventional ESI-MS in the case of the 25-mer (Figure 2b). The ESI-MS ion peaks were rather sharp compared to those of the CSI-MS, because NH_4^+ is dissociated by heat from the desolvation chamber in ESI-MS, and only two buffer molecules were left at the $(T_{25}{\cdot}A_{25}{\cdot}T_{25})^{9-}$ ion in the gas phase ($[M-9\,H-2\,H+2\,(NH_4^+)]^{9-}$). This destabilizes the triplex and promotes its dissociation. The triplex was thought to be formed by association of independently charged duplex and single-strand DNA in the presence of cationic buffer species. The complex $(T_{25}{\cdot}A_{25}{\cdot}T_{25})^{9-}$ might be formed from $(T_{25}{\cdot}A_{25})^{4-}$ and $(T_{25})^{5-}$, ions observed in the spectrum (Figure 2b). These experiments showed that CSI-MS is effective for characterizing unstable DNA complexes with low T_m values in solution.

Three main types of quadruplexes, composed of 1) one DNA strand folded intramolecularly,[8] 2) two DNA strands in various orientations,[9] and 3) four parallel DNA strands,[10] are known. We focused on the quadruplex type 3. Four DNA strands (8-mer) were prepared: 5′-d(AAAGGGAA)-3′ ($C_{80}H_{97}N_{40}O_{41}P_7$, $M_w = 2491.7$) (G3), 5′-d(AAGGGGAA)-3′ ($C_{80}H_{97}N_{40}O_{42}P_7$, $M_w = 2507.7$) (G4), 5′-d(AAGGGGGA)-3′ ($C_{80}H_{97}N_{40}O_{43}P_7$, $M_w = 2523.7$) (G5) and 5′-d(AGGGGGGA)-3′ ($C_{80}H_{97}N_{40}O_{44}P_7$, $M_w = 2539.7$) (G6). The negative CSI mass spectra of these oligomers at 7 °C are shown in Figure 3. In the case of G3 (37.5 % G), the ion peak of the

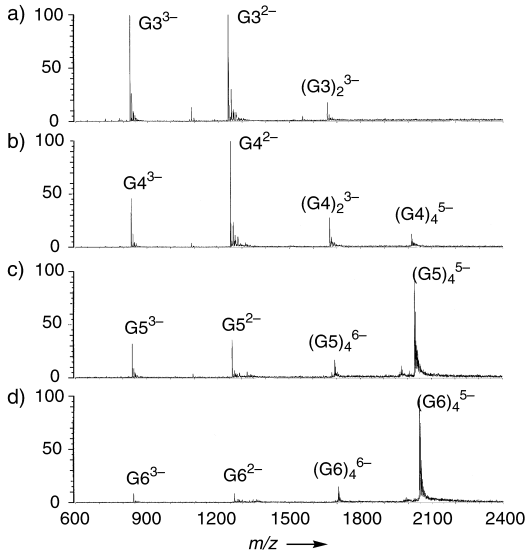

Figure 3. Negative CSI mass spectra of G3–G6.

quadruplex was not observed (Figure 3a). Trace ions of the quadruplex were observed for G4 (50 % G) together with major single- and minor double-stranded species (Figure 3b). Interestingly in the cases of G5 (62.5 % G; Figure 3c) and G6 (75 % G; Figure 3d), the ion peaks of the quadruplexes dramatically increased and became the major peaks. In addition, many NH_4^+ ions were attached to the quadruplexes, as observed in the case of the triplexes. We concluded that six bases G were necessary for stabilizing the telomeric G-quartet in 8-mer DNA.

Based on these results, several DNA molecules, which were expected to exhibit strong molecular recognition ability, were designed. Scheme 1 shows the schematic structures of the complexes identified in the CSI mass spectra of Figure 4. Figure 4a shows the forklike structure of a replicating DNA (Y-shaped duplex) consisting of a 1:1:2 mixture of 5′-d(CCCGGGCCAACGGCAA)-3′ ($C_{153}H_{193}N_{66}O_{90}P_{15}$, $M_w = 4861.2$) (**1**), 3′-d(GGGCCCGGAACGGCAA)-5′

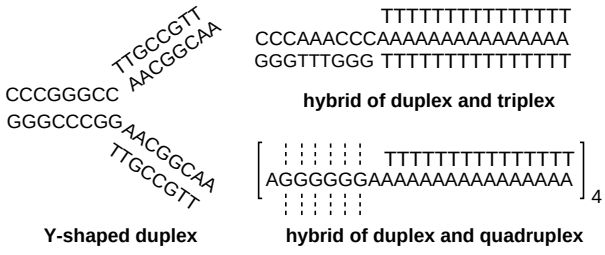

Scheme 1. Schematic structures of the DNA complexes discussed in Figure 4.

 © 2003 Wiley-VCH Verlag GmbH & Co. KGaA, Weinheim 1433-7851/03/4208-0906 $ 20.00+.50/0

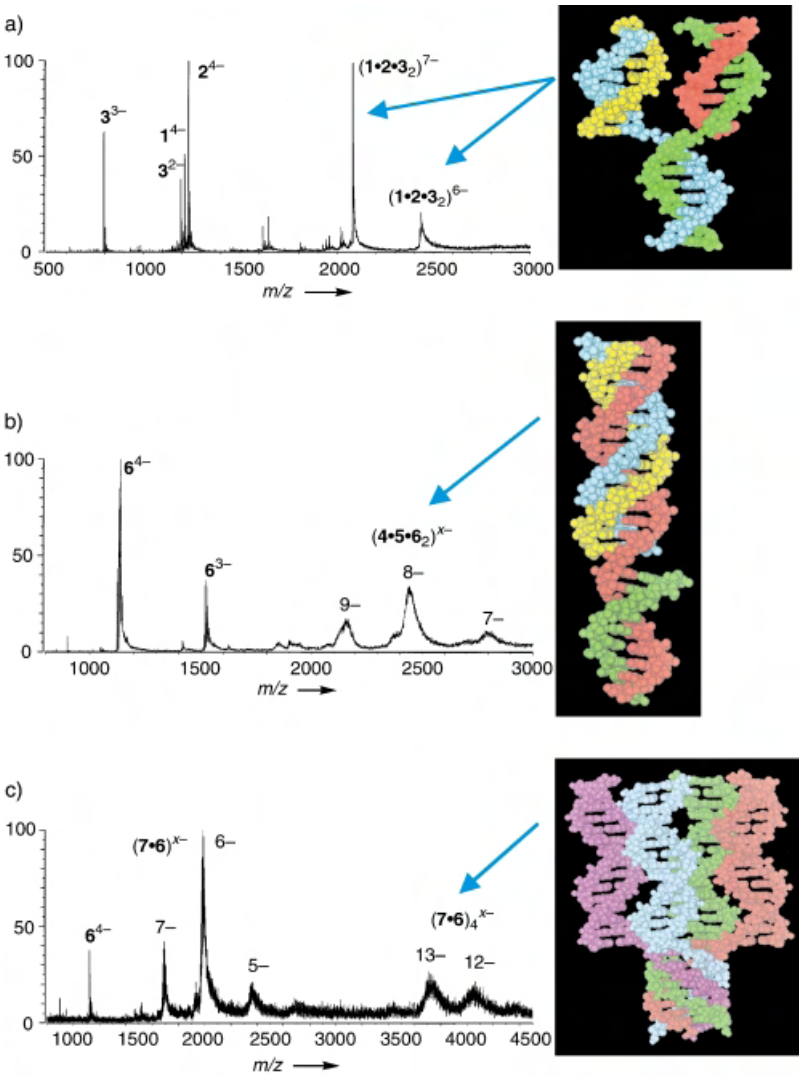

Figure 4. Negative CSI mass spectra of mixtures of a) **1, 2**, and **3**, b) **4, 5**, and **6** (1:1:2 ratios), and c) **7** and **6** (1:1 ratio) and the probable structures of the complexes.

($C_{155}H_{193}N_{70}O_{90}P_{15}$, $M_w = 4941.3$) (**2**), and 5′-d(TTGCCGTT)-3′ ($C_{78}H_{101}N_{24}O_{50}P_7$, $M_w = 2391.6$) (**3**). The expected negative ions (6− and 7−) of **1**·**2**·**3**$_2$ were clearly observed in the spectrum (Figure 4a).The complex **1**·**2**·**3**$_2$ consists of duplexes between **3** (8-mer) and the mismatched sites on **1** (16-mer) and **2** (16-mer), and between the sequences CCCGGGCC of **1** and GGGCCCGG of **2**.

When 5′-d(CCCAAACCCAAAAAAAAAAAAAAA)-3′ ($C_{234}H_{289}N_{108}O_{124}P_{23}$, $M_w = 7310.9$) (**4**), 5′-d(GGG-TTTGGG)-3′ ($C_{90}H_{112}N_{36}O_{55}P_8$, $M_w = 2825.9$) (**5**), and 5′-d(TTTTTTTTTTTTTTT)-3′ ($C_{150}H_{196}N_{30}O_{103}P_{14}$, $M_w = 4501.0$) (**6**) were mixed in 1:1:2 ratio, negative ions (7−, 8−, and 9−) of **4**·**5**·**6**$_2$ were observed. Duplex formation between the sequences CCCAAACCC of **4** and GGGTTTGGG of **5,** followed by double coordination of **6** (T_{15}) to the sequence A_{15} of **4** led to a duplex–triplex hybrid (Figure 4b).

Finally, a 1:1 mixture of 5′-d(AGGGGGGAA-AAAAAAAAAAAAAA)-3′ ($C_{230}H_{277}N_{115}O_{119}P_{22}$, $M_w = 7236.9$)(**7**) and **6** was analyzed. The negative ions (12− and 13−) of (**7**·**6**)$_4$, pointing to a duplex–quadruplex hybrid DNA structure, were clearly observed in the CSI mass spectrum of this DNA mixture (Figure 4c) together with the ions (7−, 8−, and 9−) of **7**·**6**. Various NH_4^+ attachments were also observed.

In summary, our results show that CSI-MS can be used to characterize triplex and quadruplex DNA as well as duplex DNA. This method is also applicable to unstable and complex species, hyperstranded DNAs, which are difficult to observe by other spectroscopic methods. The structure elucidation for a wide range of interesting biomolecules appears to be possible by using CSI-MS, including its negative mode.

Received: September 23, 2002 [Z50210]

[1] Duplex: a) D. C. Gale, D. R. Goodlett, K. J. Light-Wahl, R. D. Smith, *J. Am. Chem. Soc.* **1994**, *116*, 6027–6028; b) A. Kapur, J. L. Beck, M. M. Sheil, *Rapid Commun. Mass Spectrom.* **1999**, *13*, 2489–2497; c) V. Gabelica, E. D. Pauw, F. Rosu, *J. Mass Spectrom.* **1999**, *34*, 1328–1337; d) V. Gabelica, F. Rosu, C. Houssier, E. D. Pauw, *Rapid Commun. Mass Spectrom.* **2000**, *14*, 464–467; e) K. X. Wan, T. Shibue, M. L. Gross, *J. Am. Chem. Soc.* **2000**, *122*, 300–307.

[2] Triplex: F. Rose, V. Gabelica, C. Houssier, P. Colson, E. D. Pauw, *Rapid Commun. Mass Spectrom.* **2002**, *16*, 1729–1736.

[3] Quadruplex: W. M. David, J. Brodbelt, S. M. Kerwin, P. W. Thomas, *Anal. Chem.* **2002**, *74*, 2029–2033.

[4] a) J. B. Fenn, M. Mann, K. Meng, S. F. Wong, C. M. Whitehouse, *Science* **1989**, *246*, 64–70; b) P. Kebarle, L. Tang, *Anal. Chem.* **1993**, *65*, 972A–986A; c) A. P. Bruins, *J. Chromatogr. A* **1998**, *794*, 345–357.

[5] S. Sakamoto, M. Fujita, K. Kim, K. Yamaguchi, *Tetrahedron* **2000**, *56*, 955–964.

[6] a) Y. Yamanoi, Y. Sakamoto, T. Kusukawa, M. Fujita, S. Sakamoto, K. Yamaguchi, *J. Am. Chem. Soc.* **2001**, *123*, 980–981; b) Z. Zhong, A. Ikeda, M. Ayabe, S. Shinkai, S. Sakamoto, K. Yamaguchi, *J. Org. Chem.* **2001**, *66*, 1002–1008; c) S. Sakamoto, M. Yoshizawa, T. Kusukawa, M. Fujita, K. Yamaguchi, *Org. Lett.* **2001**, *3*, 1601–1604; d) S. Sakamoto, T. Imamoto, K. Yamaguchi, *Org. Lett.* **2001**, *3*, 1793–1795; e) C. Dietrich-Buchecker, N. Geum, A. Hori, M. Fujita, S. Sakamoto, K. Yamaguchi, J.-P. Sauvage, *Chem. Commun.* **2001**, 1182–1183; f) N. Fujita, K. Biradha, M. Fujita, S. Sakamoto, K. Yamaguchi, *Angew. Chem.* **2001**, *113*, 1768–1771; *Angew. Chem. Int. Ed.* **2001**, *40*, 1718–1721; g) T. Suzuki, N. Yamagiwa, Y. Matsuo, S. Sakamoto, K. Yamaguchi, M. Shibasaki, R. Noyori, *Tetrahedron Lett.* **2001**, *42*, 4669–4671; h) M. Kunimura, S. Sakamoto, K. Yamaguchi, *Org. Lett.* **2002**, *4*, 347–350; i) Y. Kubota, S. Sakamoto, K. Yamaguchi, M. Fujita, *Proc. Natl. Acad. Sci. USA* **2002**, *99*, 4854–4856; j) A. Tsuda, T. Nakamura, S. Sakamoto, K. Yamaguchi, A. Osuka, *Angew. Chem.* **2002**, *114*, 2941–2945; *Angew. Chem. Int. Ed.* **2002**, *41*, 2817–2821.

[7] An orthogonal cold-spray apparatus equipped with a spray- and ion-source temperature control system using liquid N_2 was used.

 © 2003 Wiley-VCH Verlag GmbH & Co. KGaA, Weinheim 1433-7851/03/4208-0907 $ 20.00+.50/0

Typical measurement conditions and sample preparation procedures are as follows: acceleration voltage −5.0 kV, needle voltage −1.7 kV, orifice voltage −100 to −60 V, ion source temperature 15 °C, spray temperature 7 °C, resolution (10% valley definition) 2000, sample flow rate 8 μL min^{-1}, DNA complex 20 μM DNA in aqueous 100 mM NH_4OAc annealed by heating to 90 °C for 10 min and slow cooling to room temperature (2 h), then diluted with MeOH. DNA concentration 10 μM, buffer (NH_4OAc) concentration 50 mM, solvent H_2O/MeOH 1:1.

[8] F. X. Han, R. T. Wheelhouse, L. H. Hurley, *J. Am. Chem. Soc.* **1999**, *121*, 3561 – 3570.

[9] a) C. Kang, X. Zhang, R. Ratliff, R. Moyzis, A. Rich, *Nature* **1992**, *356*, 126 – 131; b) N. V. Hud, P. Schultze, J. Feigon, *J. Am. Chem. Soc.* **1998**, *120*, 6403 – 6404.

[10] a) G. L. Laughlan, A. I. H. Murchie, D. G. Norman, M. H. Moore, P. C. E. Moody, D. M. J. Lilley, B. Luisi, *Science* **1994**, *265*, 520 – 524; b) E. Gavathiotis, R. A. Heald, M. F. Stevens, M. S. Searle, *Angew. Chem.* **2001**, *113*, 4885 – 4887; *Angew. Chem. Int. Ed.* **2001**, *40*, 4749 – 4751.

Magnetism: Molecules to Materials

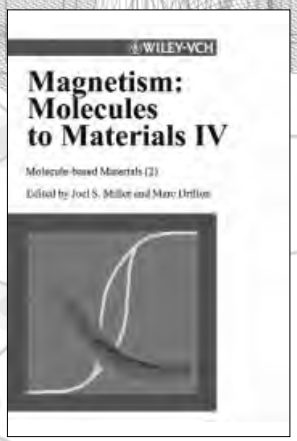

J.S. MILLER, University of Utah, Salt Lake City, USA; **M. DRILLON**, Inst. de Physique et Chimie des Materiaux de Strasbourg, France (Eds)

As a depository of contemporary knowledge on key topics related to magnetism, this open series of volumes provides a much-needed comprehensive overview of this growing interdisciplinary field. In topical reviews written by foremost scientists trends and recent advances focusing on the correlations between electronic structure and magnetic properties are explained in a clear and detailed way. The balance between theory and experiment within this series will guide advanced students and specialists alike to this research area. It will help evaluate own experimental observations and serve as a base for the design of new magnetic materials. A unique reference work, indispensable for everyone concerned with the phenomena of magnetism!

Reviews for Volume II:
"... presents a good ... current overview of an active and diverse research area."
Journal of the American Chemical Society

NEW: Magnetism: Molecules to Materials IV
Molecule-based Materials (2)
2002. XI, 492 pp. 300 fig. HC
€ 159.- /£ 95.- /US$ 125.-
3-527-30429-0

Magnetism: Molecules to Materials III
Nanosized Magnetic Materials
2001. XV, 388 pp. 209 fig. 14 tab. HC
€ 139.- /£ 80.- /US$ 125.-
3-527-30302-2

Magnetism: Molecules to Materials II
Molecule-Based Materials
2001. XIV, 489 pp. 323 fig. 43 tab. HC
€ 159.- /£ 95.- /US$ 125.-
3-527-30301-4

Magnetism: Molecules to Materials I
Models and Experiments
2001. XVI, 437 pp. 270 fig. 33 tab. HC
€ 139.- /£ 80.- /US$ 125.-
3-527-29772-3

John Wiley & Sons, Ltd.
Baffins Lane Chichester, West Sussex, PO 19 1UD, UK
Fax: +44 (0)1243-775878

WILEY-VCH · P.O. Box 10 11 61 · 69451 Weinheim, Germany · Fax: +49 (0) 62 01-60 61 84 · e-mail: service@wiley-vch.de · http://www.wiley-vch.de

WILEY

WILEY-VCH

 © 2003 Wiley-VCH Verlag GmbH & Co. KGaA, Weinheim 1433-7851/03/4208-0908 $ 20.00+.50/0

Reactions in Supercritical Water

Hydrogen from Methane and Supercritical Water**

Andrea Kruse and Eckhard Dinjus*

The production of hydrogen from methane is currently carried out industrially in a multistep process. The first stage is reforming [Eq. (1)], during which natural gas and steam are converted into a H_2-rich synthesis gas, which still contains a high percentage of CO, with the aid of a heterogeneous catalyst (Ni on an oxidic support) at temperatures of 700–900 °C and pressures of up to 50 MPa. As shown in Equation (2), the water–gas shift reaction, the CO is subsequently oxidized to CO_2 with the concomitant formation of hydrogen. The summation of both reaction equations gives Equation (3).

$$CH_4 + H_2O \rightleftharpoons CO + 3\,H_2 \quad (1)$$

$$CO + H_2O \rightleftharpoons CO_2 + H_2 \quad (2)$$

$$CH_4 + 2\,H_2O \rightleftharpoons CO_2 + 4\,H_2 \quad (3)$$

There are many technical variants of the shift reaction, which differ in the catalysts and the temperature ranges employed ($Cu/Zn/Al_2O_3$, 160–250 °C; Fe/Cr oxide, 350–450 °C). Given the diminishing oil reserves the production of synthesis gas from methane is of growing interest, since natural gas and also biogas can be used by way of this intermediate stage as a carbon source for the production of, for example, synthetic fuels.

Herein, we present the conversion of methane into hydrogen under supercritical conditions ($T > 374$ °C, $p >$ 22.1 MPa) and the effect of different catalysts on the above-mentioned partial steps. A review of the properties of supercritical water (SCW) and reactions in this medium is given in reference [1]. We also show that a one-step H_2 synthesis with a minor CO content of less than 0.2 vol % is achievable. Hereby, experiments were carried out in a laboratory autoclave (Figure 1) and catalysts were used which have led to higher gas yields in the conversion of more reactive biomass in SCW.[2]

Depending upon the desired gas composition nickel on oxidic support material,[3b] alkali metal salts (KOH, Na_2CO_3, K_2CO_3),[2] or coke[3b,c] have been used as "catalysts" in the production of gas from biomass in near- and supercritical water. Little is known about the mode of action of these additives or the nature of the catalytically active species.

[*] Dr. A. Kruse, Prof. Dr. E. Dinjus
Institut für Technische Chemie CPV
Forschungszentrum Karlsruhe
Postfach 3640, 76021 Karlsruhe (Germany)
Fax: (+49) 7247-82-2244
E-mail: andrea.kruse@itc-cpv.fzk.de

[**] We thank Mrs Hops and Mr. Kirschner for their experimental support.

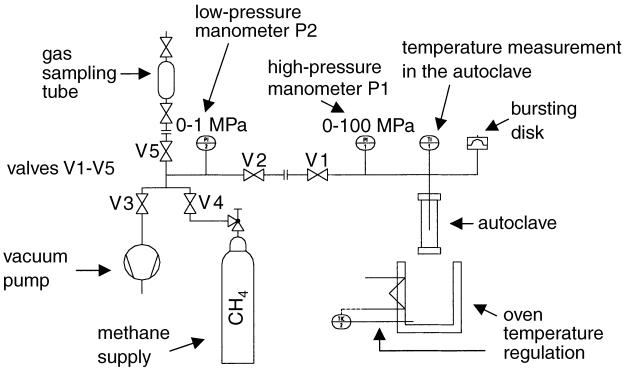

Figure 1. Schematic layout of the apparatus for charging the mini-autoclave.

Nickel catalysts are used predominantly in biomass gasification if methane is the target product and the conversion is carried out at temperatures below 400 °C. In the backreaction of Equation (1) the hydrogenation of CO is catalyzed and thus the otherwise kinetically highly inhibited formation of methane is possible.

If the temperature is so high that the equilibrium in Equation (1) lies on the side of hydrogen, nickel catalyzes the reforming of methane. The addition of alkali metal salts reduces (experimentally established) coke formation and catalyzes the water–gas shift reaction[2b,3a,3b] [Eq. (2)].

To determine the optimal reaction temperature thermodynamic calculations were carried out with the computer program equiTherm.[4] The components CH_4, H_2O, H_2, CO, CO_2, and soot as elemental carbon were considered. Figure 2

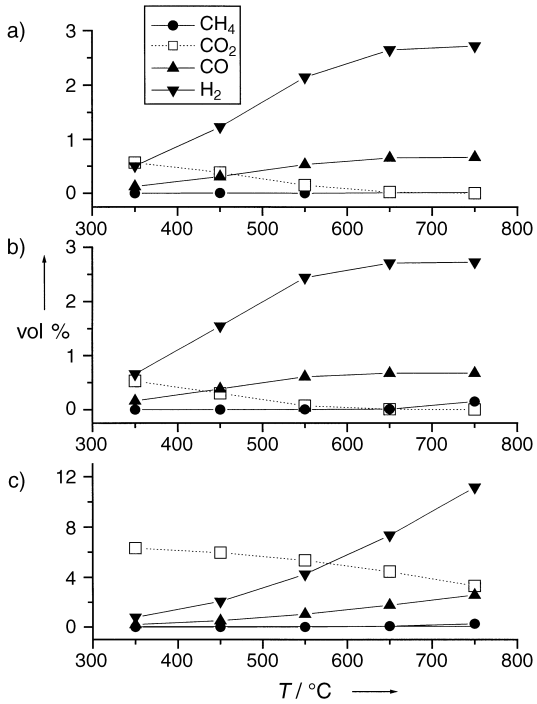

Figure 2. Thermodynamic calculations of the composition of the reaction mixture under the following reaction conditions (details of molar ratios): a) 60 MPa, $H_2O:CH_4 = 143:1$, b) 30 MPa, $H_2O:CH_4 = 143:1$, c) 60 MPa, $H_2O:CH_4 = 14.3:1$. (The main component, water, is not shown.)

 © 2003 Wiley-VCH Verlag GmbH & Co. KGaA, Weinheim 1433-7851/03/4208-0909 $ 20.00+.50/0

shows the calculated mole fractions of CH_4, H_2, CO, and CO_2 in relation to temperature under different reaction conditions. Water is present in excess and was not illustrated for reasons of clarity. The mole fraction of carbon is much smaller than that of the other components (0.0005–0.008) at a molar ratio of $H_2O:CH_4 = 143:1$; 0.03–0.065 at a molar ratio of $H_2O:CH_4 = 14.3:1$) and was therefore likewise omitted from the diagram. The calculations show that at a molar ratio of $H_2O:CH_4 = 143:1$ and 60 MPa a temperature of 650 °C is favorable for the reaction since in this case the CH_4 used should be converted mainly into CO_2 and H_2 (Figure 2a). When equilibrium is reached the reaction of CH_4 with water should lead to a gas mixture with the following composition: CO_2 20, H_2 79, CH_4 0.7, and CO 0.3 vol %. A further increase in temperature should lead to only a relatively small change in the composition. A lower pressure of 30 MPa has little effect upon the gas composition (Figure 2b). More methane remains in the reaction mixture at higher methane concentrations (Figure 2c).

Selected results of the investigation of the gas composition on using different catalysts/additives are shown in Figure 3. This selection serves to illustrate the principle effects. The volume percentage data are in each case corrected for the amount of methane in the dead space of the experimental apparatus (see Experimental Section). The experimental error in the determination of the gas composition is assumed to be ±15% relative to the given volume fraction. In these experiments CO_2 was detected in only small amounts in the gas phase since it was dissolved in the aqueous solution.

In Experiment 1 (Figure 3) methane and water were used without additives in an "aged" miniautoclave, that is one already used several times for the conversion of hydrocarbons in SCW, at 56 MPa and 650 °C. The measured H_2 yield was only very small since because of the "aging" of the reactor wall possible catalytic activity was greatly reduced by, for example, the carbon deposition at the wall, and the composition expected from the thermodynamic calculation was not achieved for kinetic reasons. Indications of changes in catalytic activity of a reactor wall with extended use of the reactor are available in the literature: Antal et al. reported a drop in methane formation in gas production from biomass because of reduced catalytic activity of the wall through "seasoning", that is extended use of the reactor.[3c] During the pyrolysis of *tert*-butylbenzene in SCW Kruse found a reduction in the concentration of leached out metals and the formation of a carbon film on the reactor surface with increasing duration of use of the reactor.[5]

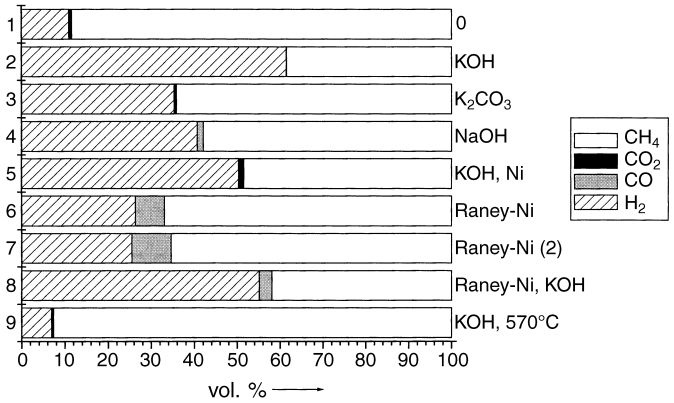

Figure 3. Selected experimentally determined gas compositions after reaction in the miniautoclave (reaction time 15 min, 650 °C).

In Experiment 2 (Figure 3) a KOH solution (1.1 wt % KOH, 650 °C, 64 MPa) was used instead of pure water which led to a considerable increase in the yield of H_2. The CO content was very low at 0.02 vol %. This low CO content with high H_2 yield demonstrates the catalytic activity of KOH in the shift reaction [Eq. (2)]. A mechanism for this catalysis by alkali metal carbonates below the critical point of water has been postulated in the literature[6] and is formulated for KOH in Equation (4) and (5).

$$KOH + CO \rightleftharpoons HCO_2K \quad (4)$$

$$HCO_2K + H_2O \rightleftharpoons KOH + CO_2 + H_2 \quad (5)$$

Formic acid has been analogously postulated as an intermediate in the shift reaction without salt addition.[7] Spectroscopic investigations, which confirm the high stability of formate in SCW, contradict the proposed mechanism for the addition of alkali metal salts.[8]

A very high yield of H_2 is comprehensible only if both the shift reaction [Eq. (2)] and the reforming step [Eq. (1)] are catalyzed. It is conceivable that KOH activates the autoclave wall, and hereby catalyzes the reforming step. The work of Antal et al.[3c] demonstrates that individual components of the autoclave material are leached out in supercritical water. This effect is reinforced by the added base because of the increased solubility of the oxides. Thus a detachment of the passivating layer and an activation of the surface by the increased leaching out of individual components by KOH addition is likely. Indications of a catalytic effect arising from a reactor wall consisting of a nickel alloy such as is present here on different reactions are given in references [3c, 7b]. Furthermore the leached-out components could themselves be catalytically active.

The use of K_2CO_3 and NaOH (Experiment 3 (Figure 3): 1.34 wt % K_2CO_3, 650 °C, 60 MPa; Experiment 4 (Figure 3): 0.2 M NaOH, 650 °C, 33 MPa) led to a lower yield of H_2. The addition of roughened and granulated nickel sheet with a KOH solution (Experiment 5 (Figure 3): 1.1 wt % KOH, 660 °C, 60 MPa) gave a similar gas composition.

The use of a suspension of Raney nickel (Experiment 6 (Figure 3): 650 °C, 53 MPa and Experiment 7 (Figure 3): 650 °C and 38 MPa) led to a totally different gas composition ($CO:H_2 \approx 1:3$) and a significantly lower CH_4 conversion. As expected the reforming reaction [Eq. (1)] was catalyzed by the addition of Raney nickel, but not the shift reaction [Eq. (2)]. It should be noted that nickel is converted into nickel oxide in supercritical water.[9] The catalytically active species on addition of nickel[2a,b], both here and in biomass gasification, is not known. The addition of KOH with concomitant use of Raney nickel (Experiment 8 (Figure 3): 650 °C, 33 MPa) led to a hydrogen yield similar to that obtained in the absence of Raney nickel (see Experiment 2), but with increased CO formation. A reduction in temperature from 650 to 570 °C (Experiment 9 (Figure 3): 1.1 wt % KOH,

 © 2003 Wiley-VCH Verlag GmbH & Co. KGaA, Weinheim 1433-7851/03/4208-0910 $ 20.00+.50/0

570¤C, 68 MPa) caused a more drastic reduction in H_2 yield than was expected on the basis of the thermodynamic calculations.

The presence of alkali metal salts leads to an increased CH_4 conversion and, in agreement with the thermodynamic calculations, to an almost exclusive formation of H_2 and CO_2. With regard to an industrial process this means that only one process step should be needed for H_2 formation from CH_4. Moreover, the solubility of CO_2 in water under pressure is significantly higher than that of H_2, which means that the two components can be readily separated. The use of the nickel catalyst alone leads only to reforming, that is to the formation of a CO/H_2 mixture which can be used for synthesis reactions. This means that under otherwise identical reaction conditions the gas composition can be varied by the choice of catalyst.

Regarding, the mode of action of the catalysts, the nature of the catalytically active species and the effect of the reactor wall, many questions remain open which cannot be answered with the experimental set up used here. The results presented here can be used for the development of a new process for hydrogen production. Detailed investigations in a continuous reactor are currently being undertaken by us to test shorter heating and cooling procedures and to guarantee a better mixing of the reaction mixture.

Experimental Section

Figure 1 illustrates the apparatus for charging the miniautoclave constructed of Hastelloy, a nickel alloy (ca. 4 mL internal volume). The autoclave was charged with the previously calculated amount of water, an aqueous solution (KOH, K_2CO_3, NaOH, each pa. Merck) or an aqueous Raney nickel suspension (Merck) under a constant flow of CH_4. The desired CH_4 pressure was set with the aid of manometer P2. The reactor was then released from the charging stand and heated in the oven.

Owing to the design of the autoclave a dead space which is filled with CH_4 and in which no reaction occurs is located between V1, the manometer, the bursting disk, and the heatable reaction space. The dead volume was determined by prior volume measurement and the amount of CH_4 measured after the reaction was corrected by the fraction contained within the dead space.

After the desired reaction time the autoclave was removed, attached again to the apparatus and a gas sampling tube was filled for analysis by gas chromatography. The resulting gas volume was calculated from the pressure indicated by manometer P2.

Received: July 12, 2002
Revised: October 11, 2002 [Z19724]

[1] a) D. Bröll, C. Kaul, A. Krämer, P. Krammer, T. Richter, M. Jung, H. Vogel, P. Zehner, *Angew. Chem.* **1999**, *111*, 3180 – 3196; *Angew. Chem. Int. Ed.* **1999**, *38*, 2998 – 3014; b) E. Dinjus, A. Kruse in *High Pressure Chemistry; Synthetic, Mechanistic, and Supercritical Applications* (Eds.: R. van Eldik, F.-G. Klärner), Wiley-VCH, Weinheim, **2002**, S. 422 – 446.

[2] a) H. Schmieder, J. Abeln, N. Boukis, E. Dinjus, A. Kruse, M. Kluth, G. Petrich, E. Sadri, M. Schacht, *J. Supercrit. Fluids* **2000**, *17*, 145 – 153; b) A. Kruse, D. Meier, P. Rimbrecht, M. Schacht, *Ind. Eng. Chem. Res.* **2000**, *39*, 4842 – 4848.

[3] a) D. C. Elliott, L. J. Sealock, Jr., E. G. Baker, R. S. Butner, *Ind. Eng. Chem. Res.* **1993**, *32*, 1535 – 1541; b) D. C. Elliott, L. J. Sealock, Jr., E. G. Baker, *Ind. Eng. Chem. Res.* **1993**, *32*, 1542 – 1548; c) M. J. Antal, Jr., S. G. Allen, D. Schulman, X. Xu, R. J. Divilio, *Ind. Eng. Chem. Res.* **2000**, *39*, 4040 – 4053; d) X. Xu, Y. Matsumura, J. Stenberg, M. J. Antal, Jr., *Ind. Eng. Chem. Res.* **1996**, *35*, 2522 – 2530.

[4] equiTherm Windows, Version 5.Y, Scienceware/VCH, **1997**.

[5] A. Kruse, *Kernforschungszent. Karlsruhe* **1994**, *5399*, 32.

[6] D. C. Elliott, R. T. Haller, L. J. Sealock, Jr., *Ind. Eng. Chem. Prod. Res. Dev.* **1983**, *22*, 426 – 431.

[7] a) C. F. Melius, N. E. Bergan, J. E. Shepherd, *Proc. 23th Symp. Combust.* **1990**, 217 – 223; b) J. Yu, P. E. Savage, *Ind. Eng. Chem. Res.* **1998**, *37*, 2 – 10.

[8] P. G. Maiella, T. B. Brill, *J. Phys. Chem. A* **1998**, *102*, 5886 – 5891.

[9] C. Kaul, H. Vogel, H. E. Exner, *Materialwiss. Werkstofftech.* **1999**, *30*, 326 – 331.

Clusters with Ge^0-Atoms

$[Ge_8\{N(SiMe_3)_2\}_6]$: A Ligand-Stabilized Ge Cluster Compound with Formally Zero-Valent Ge Atoms**

Andreas Schnepf and Ralf Köppe*

Polyhedral germanium compounds can be divided into two broad categories: Zintl anions, which can be made soluble through the use of chelating complexing agents such as [2.2.2]cryptands,[1] and ligand-stabilized complexes with the general formula Ge_nR_n ($n = 4$,[2] 6,[3] 8[4]), which are generated by the use of sterically demanding ligands in the reductive coupling of the appropriate halogen-containing precursors with alkali or alkaline earth metals.[5] As a result, only germanium clusters in which the average oxidation state of the Ge atoms is < 0 (Zintl anions) or $\geq +1$ (e.g. $[Ge_8tBu_8X_2]$; $X = Cl$,[6] Br[7]) exist to date. Germanium cluster compounds with an average Ge oxidation state between 0 and $+1$ are thus far unknown (in contrast to corresponding tin compounds).[8]

Here we describe an approach to such compounds by the disproportionation of subvalent germanium halides $(4/n(GeX_n) \rightarrow (4/n-1)Ge + GeX_4;\ n = 1,\ 2)$, during which germanium-rich intermediates, which are passed through on the way to elemental germanium, can be trapped by, for example, kinetic stabilization. The same concept was successfully used by Schnöckel et al. for the homologous aluminum and gallium compounds.[9] Germanium(II) halides are not suitable as starting materials because kinetic stabilization

[*] Dr. A. Schnepf, Dr. R. Köppe
Institut für Anorganische Chemie
Universität Karlsruhe (TH)
Engesserstrasse, Geb. 30.45, 76128 Karlsruhe (Germany)
Fax: (+49) 721-608-4854
E-mail: schnepf@aoc2.uni-karlsruhe.de

[**] We thank the DFG for financial support of this work through the "Semiconductor and Metal Clusters as Building Blocks for Organized Structures" program. We also thank Prof. H. Schnöckel for helpful discussions.

requires low temperatures and germanium(II) bromide, for example, only begins to disproportionate at 150 °C.[10] On the other hand, solid germanium(I) bromide disproportionates above 90 °C to produce germanium and germanium tetrabromide[11] and thus should make a reasonable starting material.

The $[Ge_8\{N(SiMe_3)_2\}_6]$ cluster **1** was isolated as dark red crystals from the reaction of germanium(I) bromide with $Na[N(SiMe_3)_2]$ in toluene. The molecular structure of **1** (Figure 1) consists of a cubane-like Ge_8 cluster, in which six of the eight Ge atoms in the core of the cluster are each bound to one ligand. There are thus two Ge atoms in **1** that are bound exclusively to other Ge atoms and which can therefore be assigned a formal oxidation state of 0. Compound **1** is thus the first polyhedral Ge compound in which the average oxidation state of all of the Ge atoms, at 0.75, lies between 0 and +1.

The cluster core of **1** differs from that in the analogous cluster $[Sn_8(SitBu_3)_6]$ (**2**), described by Wiberg et al.,[8b] in which the Sn–Sn distances are very similar, according to a preliminary crystal structure analysis. In **1** we find two distinctly different Ge–Ge distances (Ge(R)–Ge(R) 267 pm, Ge(R)–Ge 250 pm). According to quantum-chemical calculations (Table 1),[12] this structural difference between **1** and **2** results from the different ligands used for the two syntheses ($N(SiMe_3)_2$ or $SitBu_3$). For the model compound $[Ge_8(NH_2)_6]$ (**1′**), we thus calculate a distortion similar to that observed for the cluster core of **1** ($d(Ge(NH_2)–Ge(NH_2)) = 266.3$ pm, $d(Ge(NH_2)–Ge) = 254.8$ pm). In contrast, the model compounds $[E_8(SiMe_3)_6]$ (E = Ge (**1″**), Sn (**2″**)) are calculated to have nearly undistorted E_8 cubes ($d(Sn(SiMe_3)–Sn(SiMe_3)) = 294.3$ pm, $d(Sn(SiMe_3)–Sn) = 300.7$ pm). The distortion in **1′** can be traced to multicenter bonding (see below), which do not occur in **1″** and **2″**.

A further difference is that in the case of $R = NH_2$ (**1′**), the neutral compound is the energetically more stable form, whereas for $R = SiMe_3$ (**1″**, **2″**), the anion is favored. This demonstrates that the ligand employed not only provides kinetic stabilization, but also decidedly influences the electronic situation within the cluster.

A comparison of **1** with the fully substituted cube-shaped clusters $[Ge_8R'_8]$ (R′ = 2,6-diethylphenyl,[4a] 1,1,2-trimethylpropyl;[4b] Ge–Ge bond lengths 250 pm) shows that the extended Ge(R)–Ge(R) bonds result from the presence of the two "naked" Ge atoms. The lengths of the Ge(R)–Ge bonds to the "naked" Ge atoms are, in contrast, similar to those of the fully substituted cluster. The shared electron numbers (SENs) from an Ahlrichs–Heinzmann population analysis reproduce this trend (Table 1). Furthermore, there are three-centered bonding components in the three-membered (GeR-GeR-GeR) rings with an SEN of 0.13. This demonstrates that the two additional electrons[13] lead to delocalization of the bonding electrons within the cluster core; a bonding situation that has not previously been observed in ligand-stabilized Ge clusters.

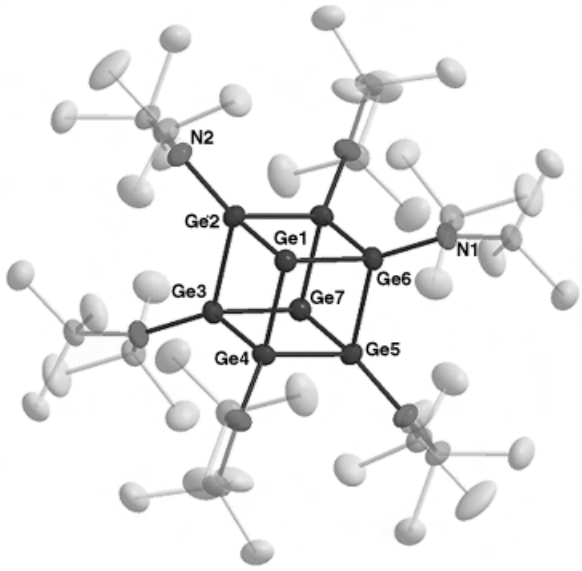

Figure 1. Molecular structure of $[Ge_8\{N(SiMe_3)_2\}_6]$ (**1**); the $SiMe_3$ groups are depicted transparently (thermal ellipsoids with 50% probability). Selected bond lengths [pm] and angles [°]: Ge1-Ge2 250.27(7), Ge1-Ge4 250.18(6), Ge1-Ge6 249.87(6), Ge1-Ge7 517.5(1), Ge2-Ge3 266.12(6), Ge3-Ge4 266.54(8), Ge4-Ge5 267.24(7), Ge6-N1 187.2(2), Ge2-N2 186.6(2); Ge2-Ge1-Ge6 81.50(3), Ge2-Ge1-Ge4 81.58(3), Ge3-Ge4-Ge5 75.41(3), Ge2-Ge3-Ge4 75.73(3), Ge5-Ge6-N1 125.30(6), Ge1-Ge6-N1 117.55(6).

Another interesting aspect of **1** is the arrangement of the Ge_8 cluster units in the crystal; between every two Ge clusters sit two toluene molecules parallel to each other, located above the "naked" Ge atoms. This arrangement of the clusters with "bridging" toluene molecules within the crystal strongly resembles the arrangement of the Ga_{84} units in $[Ga_{84}\{N(SiMe_3)_2\}_{20}][Li(thf)_4]_2[Li_2Br(thf)_6]_2 \cdot 2$ toluene (**4**).[14] As crystals of **4** demonstrate unusual physical properties (semiconducting and superconducting behavior),[15] we have begun to perform conductivity measurements on crystals of **1**. We hope that the results of these studies will provide fresh impetus to this area of research.

Table 1: Results of quantum-chemical RI-DFT calculations for **1′**, **1″**, and **2″**. The calculated values for the corresponding dianion are given in parenthesis.[a]

	$[Ge_8R_6]$ (**1′**)	$[Ge_8R^*_6]$ (**1″**)	$[Sn_8R^*_6]$ (**2″**)
$E_{tot.}$ [a.u.][b]	−16951.90439	−19071.060997	−2482.182402
	(−16951.878108)	(−19071.090935)	(−2482.230286)
$r_{M(R)–M}$ [pm]	254.8	256.6	300.7
	(258.4)	(262.5)	(307.71)
$r_{M(R)–M(R)}$ [pm]	266.3	252.6	294.3
	(254.3)	(253.1)	(296.7)
$SEN_{M(R)–M(R)}$	0.88	1.16	1.03
	(1.14)	(1.16)	(1.01)
$SEN_{M(R)–M}$	1.1	1.04	0.95
	(1.04)	(1.02)	(0.94)
$SEN_{M(R)_3}$	0.13	0.05	0
	(0.08)	(0.07)	(−0.01)

[a] $R = NH_2$, $R^* = Si(CH_3)_3$. [b] 1 a.u. = 2625.5 kJ mol^{-1}.

 © 2003 Wiley-VCH Verlag GmbH & Co. KGaA, Weinheim 1433-7851/03/4208-0912 $ 20.00+.50/0

Experimental Section

Liquid germanium was treated with HBr under high vacuum at 1550 °C, and the resulting gaseous products were condensed into a toluene/N*n*Pr$_3$ (5:1) mixture at −196 °C. After the cocondensate was allowed to warm up to −78 °C, a dark red emulsion, consisting of a dark red oil in a pale yellow solution, was obtained. The emulsion was then treated with Na[N-(SiMe$_3$)$_2$] in toluene at −78 °C and was slowly allowed to warm to room temperature, resulting in a nearly black reaction mixture. Removal of the solvent under vacuum yielded a black oil, which, when extracted with toluene, gave a black toluene extract and a white residue (NaBr). Over several weeks, dark red crystals of [Ge$_8${N-(SiMe$_3$)$_2$}$_6$] (50 mg, 0.032 mmol) formed in the black toluene extract.

Crystal structure data for **1**: $M_r = 1727.35\ g\,mol^{-1}$, crystal dimensions $0.5 \times 0.4 \times 0.2$ mm, triclinic, space group $P\bar{1}$, $a = 12.595(3)$, $b = 12.768(3)$, $c = 13.223(3)$ Å, $\alpha = 95.92(3)$, $\beta = 103.53(3)$, $\gamma = 91.53(3)°$, $V = 2053.4(7)$ Å^3, $Z = 1$, $\rho_{calcd} = 1.397\ g\,cm^{-3}$, $\mu_{Mo} = 3.094\ mm^{-1}$, $2\theta_{max} = 64.48°$, 51019 measured, 14354 independent reflections (R(int.) = 0.0366), absorption correction numerical (min./max. transmission 0.3683/0.5333), $R_1 = 0.0320$, $wR_2 = 0.0821$. Stoe-IPDS(II) diffractometer ($Mo_{K\alpha}$ radiation, $\lambda = 0.71073$ Å, 200 K). The structure was solved by direct methods and refined against F^2 for all observed reflections. Programs used: Shelxs and Shelxl (G. M. Sheldrick, Universität Göttingen). CCDC-192664 contains the supplementary crystallographic data for this paper. These data can be obtained online free of charge at www.ccdc.cam.ac.uk/conts/retrieving.html (or from the Cambridge Crystallographic Data Centre, 12 Union Road, Cambridge CB21EZ; Fax: (+44) 1223-336-033; or deposit@ccdc.cam.ac.uk).

Received: September 6, 2002 [Z50117]

[1] J. D. Corbett, *Angew. Chem.* **2000**, *112*, 682; *Angew. Chem. Int. Ed.* **2000**, *39*, 671.

[2] N. Wiberg, W. Hochmuth, H. Nöth, A. Appel, M. Schmidt-Amelunxen, *Angew. Chem.* **1996**, *108*, 1437; *Angew. Chem. Int. Ed. Engl.* **1996**, *35*, 1333.

[3] a) A. Sekigushi, C. Kabuto, H. Sakurai, *Angew. Chem.* **1989**, *101*, 97; *Angew. Chem. Int. Ed. Engl.* **1989**, *28*, 55; b) A. Sekigushi, T. Yatabe, S. Doi, H. Sakurai, *Phosphorus Sulfur Silicon Relat. Elem.* **1994**, *93*, 193.

[4] a) A. Sekigushi, T. Yatabe, H. Kamatani, C. Kabuto, H. Sakurai, *J. Am. Chem. Soc.* **1992**, *114*, 6260; b) M. Unno, K. Higuchi, K. Furuya, H. Shioyama, S. Kyushin, M. Goto, H. Matsumoto, *Bull. Chem. Soc. Jpn.* **2000**, *73*, 2093.

[5] A. Sekiguchi, H. Sakurai, *Adv. Organomet. Chem.* **1995**, *37*, 1.

[6] A. Sekiguchi, H. Naito, H. Nameki, K. Ebata, C. Kabuto, H. Sakurai, *J. Organomet. Chem.* **1989**, *368*, C1.

[7] M. Weidenbruch, F.-T. Grimm, S. Pohl, W. Saak, *Angew. Chem.* **1989**, *101*, 201; *Angew. Chem. Int. Ed. Engl.* **1989**, *28*, 198.

[8] a) L. R. Sita, R. D. Bickerstaff, *J. Am. Chem. Soc.* **1989**, *111*, 6454; b) N. Wiberg, H.-W. Lerner, S. Wagner, H. Nöth, T. Seifert, *Z. Naturforsch. B* **1999**, 877; c) B. E. Eichler, P. P. Power, *Angew. Chem.* **2001**, *113*, 818; *Angew. Chem. Int. Ed.* **2001**, *40*, 796; d) L. R. Sita, *Acc. Chem. Res.* **1994**, *27*, 191.

[9] C. Dohmeier, D. Loos, H. Schnöckel, *Angew. Chem.* **1996**, *108*, 141; *Angew. Chem. Int. Ed. Engl.* **1996**, *35*, 129; A. Schnepf, H. Schnöckel, *Angew. Chem.* **2002**, *114*, 3682; *Angew. Chem. Int. Ed.* **2002**, *41*, 3532.

[10] *CRC Handbook of Chemistry and Physics, 76th ed*, (Ed.: D. R. Lide), CRC, New York, **1995**, 4-95.

[11] A. Schnepf, R. Köppe, *Z. Anorg. Allg. Chem.* **2002**, *628*, 2914.

[12] Quantum-chemical calculations were carried out with the RI-DFT version of the Turbomole program package, by employing the Becke–Perdew 86-functional. The basis sets were of SVP quality. The electronic structure was analyzed with the Ahlrichs–Heinzmann population analysis based on occupation numbers. The SENs for bonds are a reliable measure of the covalent bonding strength. For example, the SEN for the Ge–Ge single bond in the model compound $R_3Ge–GeR_3$ ($R = NH_2$) is 1.04. Turbomole: O. Treutler, R. Ahlrichs, *J. Chem. Phys.* **1995**, *102*, 346; BP-86-functional: J. P. Perdew, *Phys. Rev. B* **1986**, *33*, 8822; A. D. Becke, *Phys. Rev. A* **1988**, *38*, 3098; RI-DFT: K. Eichkorn, O. Treutler, H. Öhm, M. Häser, R. Ahlrichs, *Chem. Phys. Lett.* **1995**, *240*, 283; SVP: A. Schäfer, H. Horn, R. Ahlrichs, *J. Chem. Phys.* **1992**, *97*, 2571; Ahlrichs–Heinzmann population analysis: E. R. Davidson, *J. Chem. Phys.* **1967**, *46*, 3320; K. R. Roby, *Mol. Phys.* **1974**, *27*, 81; R. Heinzmann, R. Ahlrichs, *Theor. Chim. Acta* **1976**, *42*, 33; C. Erhardt, R. Ahlrichs, *Theor. Chim. Acta* **1985**, *68*, 231.

[13] Compound **1** could thus be formally described as a triplet diradical; however, EPR measurements of **1** show no signal. This seems logical in light of the results of the quantum-chemical calculations, which calculate a singlet state as the ground state for all of the model compounds. Thus **1** can be formally described as a diradical in the singlet state, which invites comparison with the 1.1.1-propellanes[16] and diradicaloids.[17] While the distance between radical centers in the 1.1.1-propellanes is about 300 pm, the Ge–Ge distance in **1** of 518 pm is substantially larger, which makes a direct Ge–Ge interaction questionable. On the other hand, the energy difference of 96.5 kJ mol^{-1} between the singlet and triplet states is of the same order of magnitude as those of the 1.1.1-propellanes.

[14] A. Schnepf, H. Schnöckel, *Angew. Chem.* **2001**, *113*, 734; *Angew. Chem. Int. Ed.* **2001**, *40*, 711.

[15] J. Hagel, M. T. Kelemen, G. Fischer, B. Pilawa, J. Wosnitza, E. Dormann, H. von Löhneysen, A. Schnepf, H. Schnöckel, U. Neisel, J. Beck, *J. Low Temp. Phys.* **2002**, *129*, 133.

[16] M. S. Gordon, K. A. Nguyen, M. T. Carroll, *Polyhedron* **1991**, *10*, 1247.

[17] H. Grützmacher, F. Breher, *Angew. Chem.* **2002**, *114*, 4178; *Angew. Chem. Int. Ed.* **2002**, *41*, 4006.

Asymmetric Hydrogenation

Preparation and Asymmetric Hydrogenation of β-Aryl-Substituted β-Acylaminoacrylates**

*Jingsong You, Hans-Joachim Drexler, Songlin Zhang, Christine Fischer, and Detlef Heller**

The synthetic opportunities for the preparation of optically active β-amino acids are based mainly on stoichiometric reactions with chiral auxiliaries and to a significantly lesser

[*] Priv.-Doz. Dr. D. Heller, Dr. J. You, Dr. H.-J. Drexler, Dr. S. Zhang, Dr. C. Fischer
Institut für Organische Katalyseforschung
an der Universität Rostock e. V.
Buchbinderstrasse 5/6, 18055 Rostock (Germany)
Fax: (+49) 381-466-9383
E-mail: detlef.heller@ifok.uni-rostock.de

[**] We thank the Deutsche Forschungsgemeinschaft and the Fonds der Chemischen Industrie for the generous support of this work. We are grateful to Dr. R. McCague and Dr. A. Zanotti-Gerosa of ChiroTech for catalysts and ligands.

Supporting information for this article is available on the WWW under http://www.angewandte.de or from the author.

extent on stereoselective catalytic reactions.[1] Within this context the asymmetric hydrogenation of the respective β-dehydroamino acid precursors with chiral Rh or Ru catalysts is one of the most promising methods.[2] The required prochiral substrates are accessible by the reaction of β-ketocarboxylates with NH_4OAc and subsequent acylation.[2g,h] In this way *E/Z* mixtures are formed (Scheme 1), which in the case of β-alkyl-substituted β-acylaminoacrylates

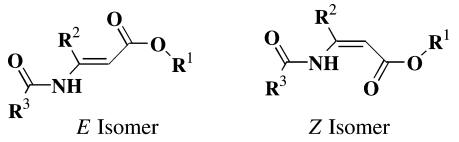

Scheme 1. Products of the reaction of β-ketocarboxylates with NH_4OAc and subsequent acylation.

(R^2 = alkyl) are readily separated and can be hydrogenated with high enantiomeric selectivity under mild conditions. The trend that in hydrogenation reactions the *E* isomers lead to higher—and also hydrogen pressure independent—enantioselectivities than the *Z* isomers appears characteristic,[2e,g] but see also reference [2b]. In contrast both isomer separation and asymmetric hydrogenation of the corresponding β-aryl-substituted β-acylaminoacrylates (R^2 = aryl) is problematic. Thus far the reduction of such substrates with sufficiently high enantioselectivities by Rh catalysis has not been successful.

Recently Zhang et al. successfully hydrogenated a broad spectrum of β-aryl-substituted β-acetylaminoacrylates[2c] with Ru catalysts with binapo derivatives[13] as ligands. At 50 °C and a hydrogen pressure of 5 bar enantiomeric excesses of up to 99 % could be achieved. However, the substrate/catalyst ratio is only 25:1, and the reaction time is 20 h. Since the *E/Z* mixtures clearly cannot be separated—*E/Z* ratios of 5:95 to 40:60 have been described for the different β-aryl substituted compounds—the possibility of hydrogenation of substrate mixtures is an advantage.

The aim of the present work was to investigate *E* isomers of β-aryl-substituted β-acylaminoacrylates in Rh-catalyzed asymmetric hydrogenation. During the preparation of methyl 3-acetylamino-3-phenylacrylate by the usual method a previously undescribed spot was found in the thin layer chromatogram in addition to the starting material, the C-acetylated compound, and the *Z* isomer together with the compound universally recognized in the literature[2c,g,h] as the "*E* isomer". After isolation by column chromatography its analysis showed surprisingly that this compound is the *E* isomer of methyl 3-acetylamino-3-phenylacrylate![3]

For its characterization the compound originally called the "*E* isomer" was next isolated.[4] Comprehensive analysis (see Supporting Information) shows unambiguously that the compound erroneously described in the literature as the "*E* isomer" is actually the N,N-diacetylated product. Figure 1 shows the crystal structure of this compound.[5]

The reason for the poor *E/Z* ratios in the usual synthesis of β-aryl-substituted β-acylaminoacrylates[2g,h] is evidently the heating under reflux during the acylation of the amine. As a result increased isomerization of the *E* to the thermodynamically more stable *Z* compound occurs.[6] If the acylation is

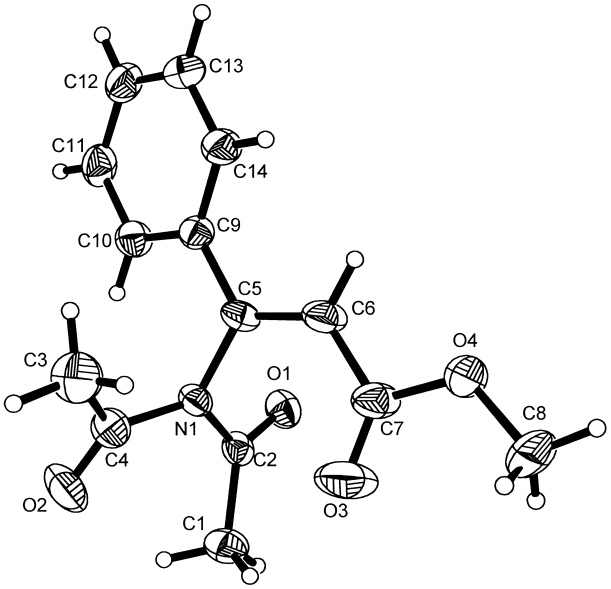

Figure 1. Crystal structure of methyl 3-diacetylamino-3-phenylacrylate (ellipsoids set at the 50 % probability level).

carried out at lower temperatures with less acylating agent (suppression of the formation of the N,N-diacylated product) the total amount of *E* isomer may be significantly increased. There is also the additional benefit that because of its poor solubility the *E* isomer usually crystallizes out on removal of the solvent (see Supporting Information).

Whereas classical ligands such as dipamp[13] or diop[13] induce only modest enantioselectivities, Rh catalysts of the DuPHOS type[13] lead to good *ee* values for the hydrogenation of β-alkyl-substituted substrates. Et-FerrroTANE[13] produces still further improvements for the *E* isomer substrates, with enantioselectivities of ≥ 99 % *ee* (Table 1). Thus the overall trend that *E* isomer substrates lead to higher enantioselectivities than the corresponding *Z*-isomers is confirmed. This difference is particularly large with the use of Et-FerroTANE as ligand, although the causes for this are not clear.

One advantage of the catalyst with Et-FerroTANE as ligand is that in contrast to DuPHOS derivatives the *E*

Table 1: Enantioselectivities of the hydrogenation of different *E* and *Z* isomers of β-alkyl-substituted β-acylaminoacrylates with [Rh(ligand)-$(MeOH)_2$]BF_4 as catalyst.[7] [a]

Ligand	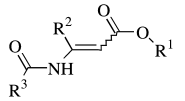			% *ee* for *Z* isomer	% *ee* for *E* isomer
	R^1	R^2	R^3		
diop[8a]	Me	Me	Me	17	71
dipamp[8b]	Me	Me	Me	68	90
Et-DuPHOS[8c,d]	Me	Me	Me	87	98
Me-DuPHOS[8c,d]	Me	Me	Ph	85	96
Et-FerroTANE[8e,f]	Me	Me	Me	28	99
Et-FerroTANE	Me	Me	Ph	32	> 99
Et-FerroTANE	Et	*i*Pr	Me	31	> 99

[a] Standard conditions: 0.005 mmol catalyst, 0.5 mmol substrate, 7.5 mL MeOH, 1.0 bar total pressure, 25 °C, in each case 100 % conversion.

 © 2003 Wiley-VCH Verlag GmbH & Co. KGaA, Weinheim 1433-7851/03/4208-0914 $ 20.00+.50/0

isomers are more rapidly hydrogenated than the *Z* isomers. The exceptional selectivity and activity of the Rh catalyst with the commercially available ligand Et-FerroTANE is also confirmed by the hydrogenation of β-aryl- substituted substrates (Table 2).[9]

Table 2: Enantioselectivities for the hydrogenation of β-aryl-substituted (*E*)-β-acetylaminoacrylates with [Rh{(*R,R*)-(Et-FerroTANE)}(MeOH)$_2$]BF$_4$ as catalyst.[a]

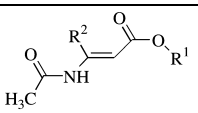

R^2	R^1	Enantiomeric excesses [% *ee*]
phenyl	Me	> 99 (*S*)[10]
phenyl	Et	99 (*S*)
p-methylphenyl	Me	> 99 (*S*)
p-methylphenyl	Et	99 (*S*)
p-methoxyphenyl	Me	98 (*S*)
p-chlorophenyl	Me	98 (*S*)
p-fluorophenyl	Me	> 99 (*S*)
p-fluorophenyl	Et	> 99 (*S*)
o-methoxyphenyl	Me	98 (*S*)
m-nitrophenyl	Et	99 (*S*)

[a] Standard conditions: 0.005 mmol catalyst, 0.5 mmol substrate, 7.5 mL MeOH, 1.0 bar total pressure, 25 °C, in each case 100% conversion.

With the exception of the *p*-methoxyphenyl-substituted substrate the enantioselectivities achieved are the same or better than those recently described by Zhang et al.[2c] It is noteworthy that in the case of Rh catalysis a higher enantiomeric excess is also obtained for the substrate with the *o*-methoxyphenyl moiety (Ru catalysis: 80% *ee* for the corresponding "*E*"/*Z* substrate mixture[2c]).

The high activity under the selected standard reaction conditions of 0.005 mol catalyst (0.666 mmol L^{-1}) and 0.5 mmol substrate must also to be stressed. All the substrates listed in Table 2 react in pseudo-first-order reactions, the half lifetimes lie between about 0.5 (aryl = phenyl) and about 1.8 min (aryl = *m*-nitrophenyl). Owing to the high activity the substrate/catalyst ratio can be increased to 1000 with complete conversion in the case of, for example, methyl (*E*)-3-acetylamino-3-phenylacrylate.

The reasons for the high activities and selectivities with the use of Et-FerroTANE as ligand are unclear, noticeable is however the large P-Rh-P angle (bite angle)[11] of 98.3° for the complex [Rh{(*R,R*)-(Et-FerroTANE)}(nbd)]BF$_4$[13] (Table 3 and Figure 2; further data on the X-ray structure analysis of this complex—to our knowledge the first structural confirmation for an Rh complex with a chelating *cis*-bonded ligand which contains phosphetanes—and the complex [Rh{(*S,S*)-(Me-DuPHOS)}(nbd)]BF$_4$ may be found in the Supporting Information).

In contrast, an average bite angle of 84.8 ± 0.5° is found for seven DuPHOS derivatives of known structure. This is clearly independent of the anion, different η^4-bonded diolefins or η^6-bonded arenes, and also independent of the substitution on the phospholane ring. In addition to the large bite angle it is also noteworthy that the phosphetane rings are highly tilted relative to each other at an angle of about 42°. In the case of phospholane rings the analogous angle is only about 8°. The example of Et-FerroTANE also shows that very high enantioselectivities and activities are achievable in asymmetric hydrogenation with ligands that have a very flexible backbone (ferrocene unit) and that lead to a large bite angle in the complex.

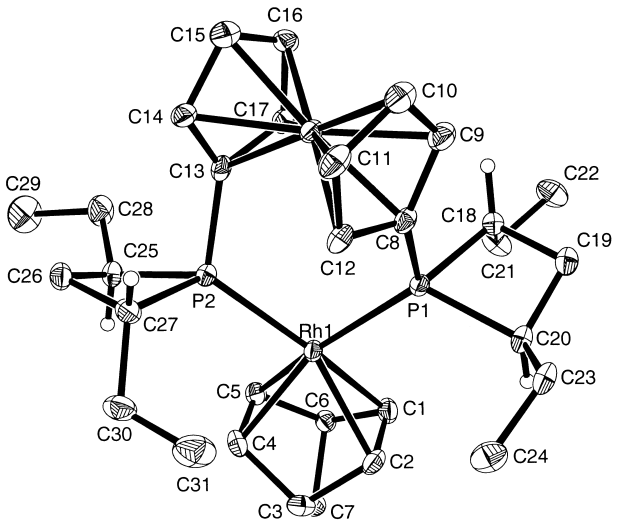

Figure 2. Crystal structure of the cation in [Rh{(*R,R*)-(Et-FerroTANE)}(nbd)]BF$_4$ (ellipsoids set at the 30% probability level, only the H atoms at the asymmetric C atoms are shown). Selected bond lengths [Å] and angle [°]: Rh1-P1 2.322(2), Rh1-P2 2.306(2); P1-Rh1-P2 98.27(5). The best planes for the four atoms of the two phosphetane rings intersect at an angle of 41.8° (mean deviation of the atoms 0.1328 and 0.1421 Å, respectively).

Table 3: P-Rh-P angles (bite angles) for different Rh^{I} complexes determined by X-ray structure analysis.

Complex	Bite angle [°]	Reference
[Rh(Me-DuPHOS)(cod)]SbF$_6$	84.7	[8d]
[Rh(Me-DuPHOS)(nbd)]BF$_4$	84.6	this work
[Rh(Me-DuPHOS)(toluene)]BF$_4$	84.9	[2d]
[Rh(Et-DuPHOS)(cod)]BARF	85.4	[12]
[Rh(Et-DuPHOS)(nbd)]BF$_4$	84.5/84.7	[7a]
[Rh(Et-DuPHOS)(cod)]BF$_4$	85.3	[7a]
[Rh(Et-DuPHOS)(benzene)]BF$_4$	84.5	[2d]
[Rh(Et-FerroTANE)(nbd)]BF$_4$	98.3	this work

Thus we have succeeded for the first time to prepare β-aryl-substituted (*E*)-β-acylaminoacrylates and to show that in the case of methyl 3-acetylamino-3-phenyl acrylate the compound originally considered erroneously to be the "*E* isomer" is the N,N-diacetylated product. By lowering the temperature during acylation and with smaller amounts of acylation agents the fraction of *E* isomer may be increased significantly. The Rh-catalyzed, asymmetric hydrogenation of further novel β-aryl-substituted (*E*)-β-acylaminoacrylates with the commercially available Et-FerroTANE as chiral ligand leads under very mild conditions (25 °C, normal

pressure) and high substrate/catalyst ratios to very good enantioselectivities.

Received: September 30, 2002 [Z50265]

[1] a) E. Juaristi, H. Lopez-Ruiz, *Curr. Med. Chem.* **1999**, *6*, 983 – 1004; b) *Enantioselective synthesis of β-amino acids* (Ed.: E. Juaristi), Wiley-VCH, Weinheim, **1997**; c) G. Cardillo, C. Tomasini, *Chem. Soc. Rev.* **1996**, *25*, 117 – 128; d) D. C. Cole, *Tetrahedron* **1994**, *50*, 9517 – 9582.

[2] a) D. Heller, H.-J. Drexler, J. You, W. Baumann, K. Drauz, H.-P. Krimmer, A. Börner, *Chem. Eur. J.* **2002**, *8*, 5196 – 5203; b) S. Lee, Y. J. Zhang, *Org. Lett.* **2002**, *4*, 2429 – 2431; c) Y. G. Zhou, W. Tang, W.-B. Wang, W. Li, X. Zhang, *J. Am. Chem. Soc.* **2002**, *124*, 4952 – 4953; d) D. Heller, H.-J. Drexler, A. Spannenberg, B. Heller, J. You, W. Baumann, *Angew. Chem.* **2002**, *114*, 814 – 817; *Angew. Chem. Int. Ed.* **2002**, *41*, 777 – 780; e) D. Heller, J. Holz, H.-J. Drexler, J. Lang, K. Drauz, H.-P. Krimmer, A. Börner, *J. Org. Chem.* **2001**, *66*, 6816 – 6817; f) M. Yasutake, I. D. Gridnev, N. Higashi, T. Imamoto, *Org. Lett.* **2001**, *3*, 1701 – 1704; g) G. Zhu, Z. Chen, X. Zhang, *J. Org. Chem.* **1999**, *64*, 6907 – 6910; h) W. D. Lubell, M. Kitamura, R. Noyori, *Tetrahedron: Asymmetry* **1991**, *2*, 543 – 554; i) K. Achiwa, T. Soga, *Tetrahedron Lett.* **1978**, 1119 – 1120; j) B. D. Vineyard, W. S. Knowles, M. J. Sabacky, G. L. Bachmann, D. J. Weinkauff, *J. Am. Chem. Soc.* **1977**, *99*, 5946 – 5952.

[3] Full characterization and X-ray structural analysis of this compound, which is reported for the first time, are found in the Supporting Information.

[4] The hydrogenation of an "*E*"/*Z* mixture under normal pressure at room temperature in MeOH with [Rh(Me-DuPHOS)(cod)]BF_4[13] leads to the hydrogenation of the *Z* isomer only, the "*E* isomer" remains unchanged. Unlike the starting materials, which are difficult to separate, the hydrogenation product is readily separated from the unchanged "*E* isomer" by column chromatography when the latter is obtained in a pure state.

[5] CCDC-194044 (methyl(*E*)-3-acetylamino-3-phenylacrylate), CCDC-194047 (methyl 3-diacetylamino-3-phenylacrylate), CCDC-194046 (methyl(*S*)-3-acetylamino-3-*p*-chlorophenylpropionate), CCDC-194045 ([Rh{(*R,R*)-(Et-FerroTANE)}(nbd)]BF_4), and CCDC-194043 ([Rh{(*S,S*)-(Me-DuPHOS)}(nbd)]BF_4) contain the supplementary crystallographic data for this paper. These data can be obtained free of charge via www.ccdc.cam.ac.uk/conts/retrieving.html (or from the Cambridge Crystallographic Data Centre, 12, Union Road, Cambridge CB21EZ, UK; fax: (+44) 1223-336-033; or deposit@ccdc.cam.ac.uk).

[6] Compare similar findings on the preparation of analogous but β-alkyl-substituted substrates: a) D. J. Aberhardt, H.-J. Lin, *J. Org. Chem.* **1981**, *46*, 3749 – 3751; b) P. deMayo, A. C. Weedon, R. W. Zabel, *Can. J. Chem.* **1981**, *59*, 2328 – 2333; c) C. A. Grob, *Helv. Chim. Acta* **1950**, *33*, 1787 – 1796.

[7] a) H.-J. Drexler, W. Baumann, A. Spannenberg, D. Heller, *J. Organomet. Chem.* **2001**, *621*, 89 – 102; b) A. Börner, D. Heller, *Tetrahedron Lett.* **2001**, *42*, 223 – 225; c) C. J. Cobley, I. C. Lennon, R. McCague, J. A. Ramsden, A. Zanotti-Gerosa, *Tetrahedron Lett.* **2001**, *42*, 7481 – 7483.

[8] a) H. B. Kagan, T.-P. Dang, *J. Am. Chem. Soc.* **1972**, *94*, 6429 – 6433; b) W. S. Knowles, M. J. Sabacky, B. D. Vineyard, D. J. Weinkauff, *J. Am. Chem. Soc.* **1975**, *97*, 2567 – 2568; c) M. J. Burk, *J. Am. Chem. Soc.* **1991**, *113*, 8518 – 8519; d) M. J. Burk, J. E. Feaster, W. A. Nugent, R. L. Harlow, *J. Am. Chem. Soc.* **1993**, *115*, 10125 – 10138; e) A. Marinetti, F. Labrue, J.-P. Genet, *Synlett* **1999**, *12*, 1975 – 1977; f) U. Berens, M. J. Burk, A. Gerlach, W. Hems, *Angew. Chem.* **2000**, *112*, 2057 – 2060; *Angew. Chem. Int. Ed.* **2000**, *39*, 1981 – 1984.

[9] The hydrogenation of the corresponding *Z* isomers with the Et-FerroTANE system leads, as expected, to enantioselectivities of only 25–80% *ee*. Orienting investigations with Me-DuPHOS with the *E* isomers as substrates gave throughout poorer enantioselectivities and activities.

[10] In the case of the *p*-chlorophenyl-substituted product the determination of the absolute *S* configuration was achieved by X-ray structure analysis (see Supporting Information). Since all other hydrogenation products also gave negative rotations they should equally be *S*-configurated, which is in agreement with literature data.

[11] P. Dierkes, P. W. N. M. van Leeuwen, *J. Chem. Soc. Dalton Trans.* **1999**, 1519 – 1529.

[12] B. Guzel, M. A. Omary, J. P. Fackler, A. Akgerman, *Inorg. Chim. Acta* **2001**, *325*, 45 – 50.

[13] Abreviations used: binapo = 2,2′-Bis(diphenylphosphanyl)-1,1′-binaphthyl, dipamp = 1,2-ethanediylbis[(2-methoxyphenyl)phenylphosphane], diop = 2,3-*O*-isopropylidene-2,3-dihydroxy-1,4-bis(diphenylphosphanyl)butane, Me-DuPHOS = 1,2-bis(2,5-dimethylphospholanyl)benzene, Et-FerroTANE = 1,1′-bis(2,4-diethylphosphetanyl)ferrocene, nbd = 3,5-norbornadiene, cod = 1,5-cyclooctadiene.

Synthesis of Lipoteichoic Acids

Synthesis of the First Fully Active Lipoteichoic Acid**

*Andreas Stadelmaier, Siegfried Morath, Thomas Hartung, and Richard R. Schmidt**

Dedicated to Professor Ewald Daltrozzo on the occasion of his 65th birthday

The inflammatory response to Gram-negative and Gram-positive bacteria can hardly be distinguished. However, while most of the responses to Gram-negative bacteria could be attributed to lipopolysaccharides (LPS) and their lipid anchor lipid A, as general principles,[1–3] no corresponding priniciple

[*] Prof. Dr. R. R. Schmidt, A. Stadelmaier
Fachbereich Chemie
Universität Konstanz, Fach M 725
78457 Konstanz (Germany)
Fax: (+49) 7531-883-135
E-mail: richard.schmidt@uni-konstanz.de
Dr. S. Morath, Dr. T. Hartung
Fachbereich Biologie
Universität Konstanz
78457 Konstanz (Germany)

[**] This work was supported by the Deutsche Forschungsgemeinschaft and the Fonds der Chemischen Industrie. We thank S. Deininger and J. Kley for technical assistance, L. Cobianchi for help in separating the final products by HI-chromatography, and Prof. Dr. A. Geyer and A. Friemel for help in the structural assignments of the final products by NMR experiments.

 © 2003 Wiley-VCH Verlag GmbH & Co. KGaA, Weinheim 1433-7851/03/4208-0916 $ 20.00+.50/0

for Gram-positive bacteria was identified unambiguously during the last few decades.[4,5] Lipoteichoic acids (LTAs) are found in most Gram-positive bacteria. Like LPS, they are amphiphilic, negatively charged glycoplipids.[5] Yet, studies with commercial LTA preparations exhibiting significant activities could be traced back to contaminations with LPS.[6–8] Furthermore, when carefully purified, phenol-extracted LTA from different sources turned out to be essentially inactive and cytokine release as a measure of immunostimulatory activity was not observed.[9–11] Only recently it was shown that these results are due to the preparation method employed for LTA:[12] a novel, less harsh preparation method led to pure, biologically active LTA.[6–8] By structural analysis a crucial role could be attributed to preserved D-alanine residues at the polyglycerophosphate backbone of LTA,[12–14] for instance from *Staphylococcus aureus*.

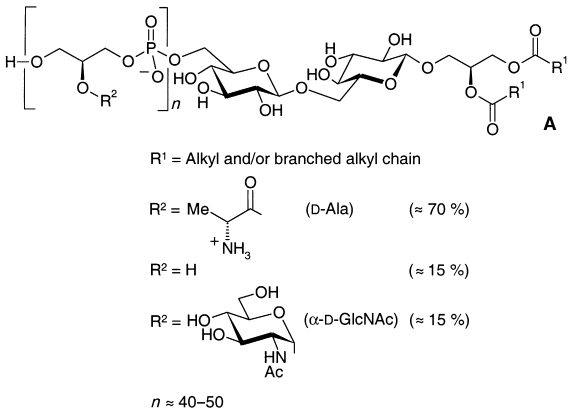

Scheme 1. General structure of lipoteichoic acid (LTA) from *Staphylococcus aureus*.

To prove the biological activity of D-alanine residues containing LTA and to allow structure–activity analysis, *S. aureus* LTA was synthesized (Scheme 1, **A**). In this case, the required combination of glycolipid synthesis with glycerophosphate diester formation having varying side chains is particularly demanding, because the D-alanine residues are readily cleaved already at pH 8.5. Herein, the first synthesis of this type of compounds (Scheme 1, with $n = 6$) is reported.[15] The versatility of this synthetic concept is further demonstrated by its application to structural variations. Previous syntheses of partial LTA structures lacked alanyl residues and thus did not lead to biologically active materials.[16–18]

The approximate ratio of the glycerophosphate 2-O-substituents in **A** (Scheme 1) of 70% D-alanyl, 15% α-D-GlcNAc, and 15% hydrogen[12] led us to design the synthesis of **1a** (Scheme 2) which with a 4:1:1 ratio of these residues has a composition closely related to that of the natural LTA. Disconnection of **1a** between the glycerophosphate backbone and gentiobiosyl diacylgycerol (see arrows in **1a**) leading to intermediates **2** and **3** and *N*-benzyloxycarbonyl(Z)-protected D-alanine should provide a viable approach to the synthesis of the target molecule. Thus, **2** should be accessible from glycerol derivatives **4**–**6** as building blocks, and **3** from the readily available gentiobiosyl diacylglycerol derivative **7**. The choice of permanent and temporary orthogonal protecting groups was clearly decisive for success: for chain extension of the glycerophosphate backbone and the final ligation between intermediates **2** and **3** the *tert*-butyldiphenylsilyl (TBDPS) group was selected, and for the execution of the

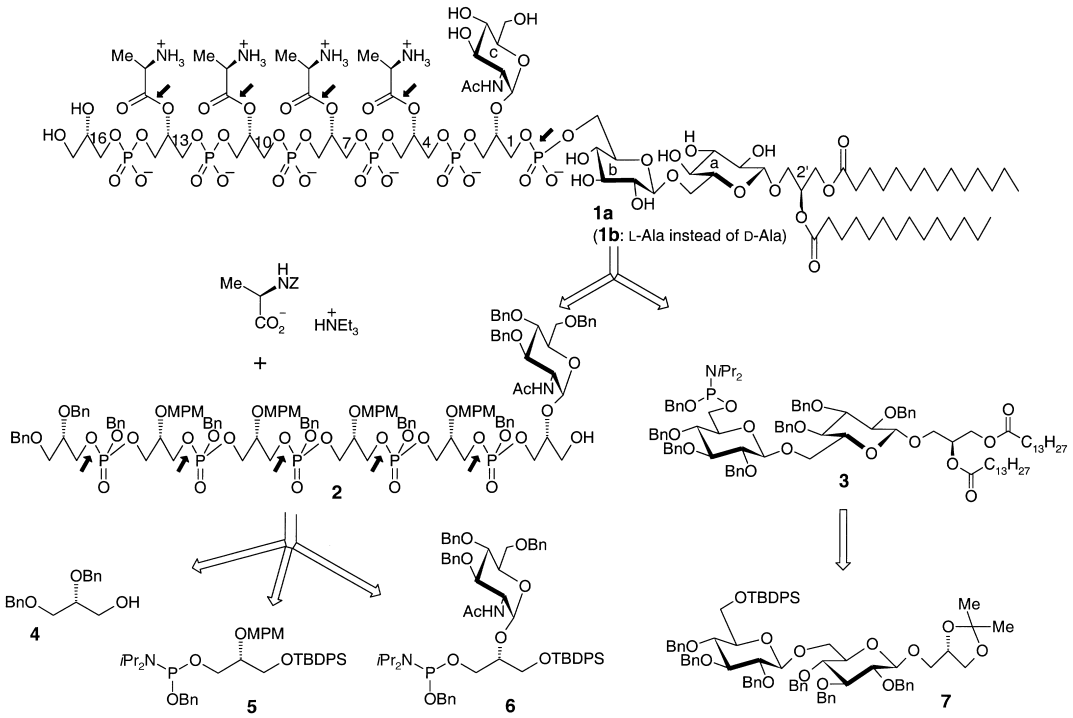

Scheme 2. Structure of target molecule **1a** and its retrosynthesis. Bn = benzyl.

 © 2003 Wiley-VCH Verlag GmbH & Co. KGaA, Weinheim 1433-7851/03/4208-0917 $ 20.00+.50/0

synthesis of **3** the isopropylidene group was chosen. The selective attachment of the alanyl residues was based on the mild oxidative removal of the methoxybenzyl (MPM) group, thus leading to the fully protected target molecule having only benzyl and Z-protecting groups which should finally be removable by hydrogenolysis. The variability of this concept in terms of different combinations of building blocks **4–6**, attachment of different amino acid residues, and variation of the diacylglycerol moiety led to several derivatives of **1a,**[19] for example **1b** with L-alanyl residues.

The required building block **4** was obtained from commercially available 1,2-*O*-isopropylidene-sn-glycerol.[20] Then O-allylation de-O-isopropylidenation[21] and regioselective introduction of the TBDPS group gave intermediate **8** (Scheme 3) which was used for the attachment of the MPM group. De-O-allylation of this MPM-protected intermediate, and then reaction with benzyloxybis(diisopropylamino)phosphane[22] in the presence of tetrazole afforded building block **5** (Scheme 2).

Glycosylation of intermediate **8** with known azidoglucosyl donor **9**[23] led under trimethylsilyl trifluoromethanesulfonate (TMSOTf) catalysis to α-connected glucoside **10** in excellent 75% yield (Scheme 3). Replacement of the O-acetyl groups by benzyl groups (→**11**) and then reduction of the azido group and N-acetylation under standard conditions[24] afforded **12**. De-O-allylation and then phosphitylation as described above furnished building block **6**.

With building blocks **4–6** in hand, intermediate **2** could be constructed (Scheme 4). Reaction of **4** with **5** in the presence of tetrazole and then addition of *tert*-butyl hydroperoxide as oxidizing agent afforded a phosphorus triester intermediate, which on successive treatment with tetrabutylammonium fluoride (TBAF) and reaction with **5** led to glycerophosphate intermediate **13**. Its reaction with TBAF, then reaction with **6** instead of **5**, and again treatment with TBAF furnished the desired compound **2** in very good overall yield.

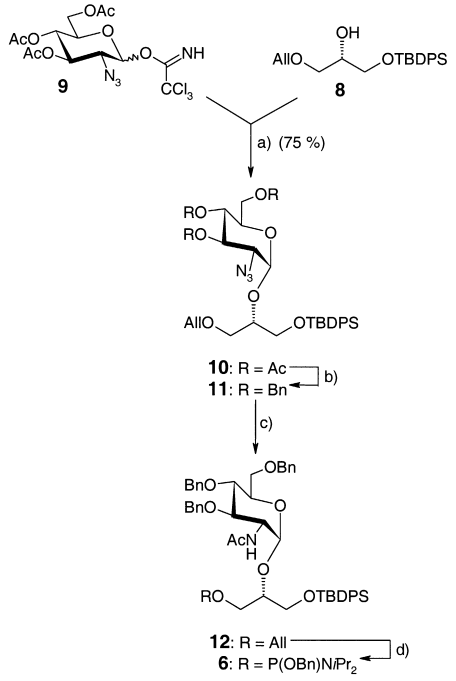

Scheme 3. Synthesis of building block **6**. a) TMSOTf, CH_2Cl_2, RT, 75%; b) 1. NaOMe, MeOH, 24 h; 2. BnBr, NaH, DMF, 24 h (74%); c) 1. 1,3-propanedithiol, pyridine, H_2O, RT, 24 h; 2. pyridine/Ac_2O, 2 h, 85%; d) 1. $[(PPh_3)_3RhCl]$, DBU, EtOH, 90°C; 2. 1 M HCl/actone (1:9), 77%; 3. benzyloxybis(diisopropylamino)phosphane, CH_2Cl_2, 85%. DBU = 1,8-diazabicyclo[5.4.0]undec-7-ene, All = allyl.

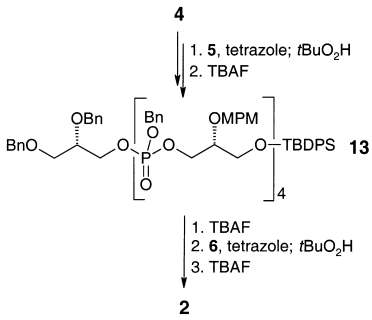

Scheme 4. Synthesis of intermediate **2**.

For the synthesis of **3**, gentiobiose was transformed under standard conditions (four steps) into glycoside **14** (Scheme 5). Removal of the O-benzoyl groups under Zemplén conditions, then regioselective silylation at the 6b oxygen atom and per-O-benzylation afforded building block **7**. Acid-catalyzed de-O-isopropylidenation, then acylation with myristoyl chloride in the presence of triethylamine followed by desilylation gave intermediate **15** which on phosphitylation as described above furnished the desired compound **3**; on hydrogenolytic de-O-benzylation gentiobiosyl diacylglycerol **16** was obtained. The latter compound was employed to study the biological effect of the lipid anchor having only the gentiobiose core.

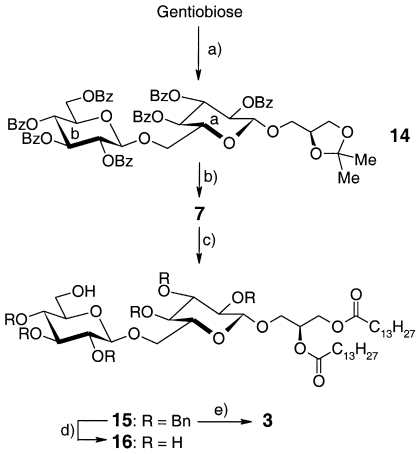

Scheme 5. Synthesis of intermediate **3** and of gentiobiosyl diacylglycerol **16**. a) 1. BzCl, pyridine, 40°C, 24 h, 98%; 2. N_2H_4·HOAc, DMF, 50°C, 3.5 h, 78%; CCl_3CN, DBU, CH_2Cl_2, 2 h, 97%; 3. BF_3·OEt_2 (0.2 equiv), 3-Å MS, −30°C, CH_2Cl_2, 1.2-*O*-isopropylidene-sn-glycerol, 80%; b) 1. NaOMe, MeOH, 24 h; TBDPS-Cl, pyridine, −15°C, two days, 91%; 2. BnBr, NaH, DMF, 66%; c) 1. HOAc (75%), 80°C, 1.5 h, 78%; 2. myristoyl chloride, NEt_3, THF, 50°C, 4 h, 81%; 3. TBAF, HOAc, THF, 40°C, three days, 76%; d) Pd/C, H_2, CH_2Cl_2/MeOH (2:5), 24 h, 71%; e) benzyloxybis(diisopropylamino)phosphane, CH_2Cl_2, 79%. Bz = benzoyl.

 © 2003 Wiley-VCH Verlag GmbH & Co. KGaA, Weinheim 1433-7851/03/4208-0918 $ 20.00+.50/0

The ligation of intermediate **2** and **3** could be performed with tetrazole as catalyst; oxidation with *tert*-butyl hydroperoxide furnished **17**, which contains the backbone of the target molecule (Scheme 6). Treatment with ceric(IV) ammonium nitrate (CAN) liberated four of the glycerol hydroxy groups, to which the Z-protected D-alanyl residues were immediately attached with (benzotriazol-1-yloxy)tripyrrolidinophosphonium hexafluorophosphate (PyBOP)/*N*-methylimidazole as condensing agent. Hydrogenolysis of this intermediate with Pearlman's catalyst[25] in a mixture of CH_2Cl_2/MeOH/H_2O (5:5:1) gave the desired final product **1a** after hydrophobic interaction (HI) chromatography on octylsepharose in 47% yield. The structural assignment was based on MS and NMR data[26] and comparison with naturally occuring material. Compound **17** was similarly transformed with Z-protected L-alanine into **1b**.

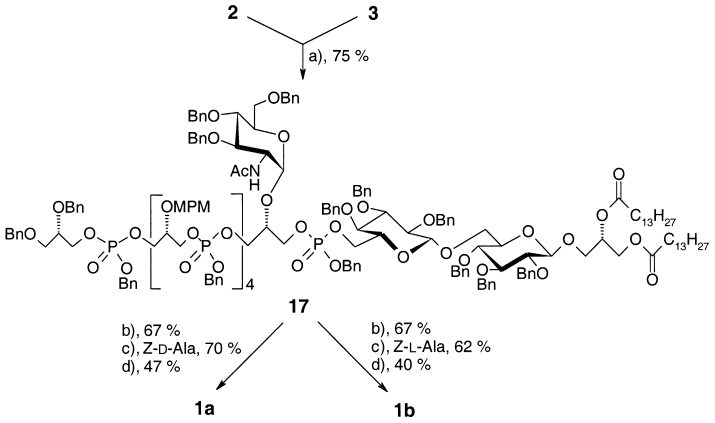

Scheme 6. Synthesis of target molecule **1a** and its diastereoisomer **1b**. a) Tetrazole, CH_2Cl_2; *t*BuO_2H, 75%; b) CAN, MeCN/toluene/H_2O (60:3:4), 45–60 min, 67%; c) 1. PyBOP (20 equiv), *N*-methylimidazole (40 equiv), Z-protected D/L-Ala ($HNEt_3^+$ salt) (20 equiv), CH_2Cl_2, 3 h; d) $Pd(OH)_2$/C, H_2, CH_2Cl_2/MeOH/H_2O = (5:5:1), 24 h; HI chromatography.

The evaluation of the biological activity of compounds **1a, 1b**, and **16** revealed that **1a** with D-alanyl residues (Figure 1) has practically the same activity in terms of initiation of cytokine release by human blood leukocytes as the natural LTA. Whereas the lipid anchor with the gentiobiose core alone (compound **16**) shows practically no activity, L-alanine-containing **1b** was about 10- to 100-fold less active than **1a.**[13,14]

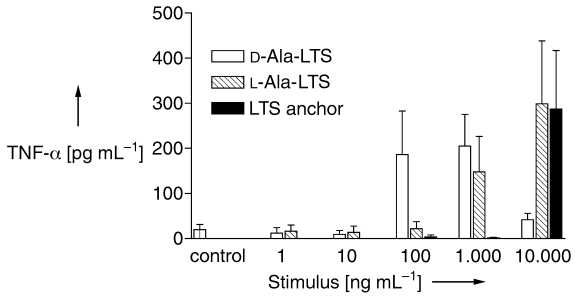

Figure 1. Concentration dependence of TNFα release of diluted human whole blood (20%) in response to **1a, 1b**, and **16**. TNFα was measured by ELISA. Data are means (± SEM) of twelve donors. SEM = standard error of the mean.

In conclusion, with the help of synthetic material the active principle of LTA stimulation of the immune system could be ascertained for the first time. The synthesis design presented considers the variable substitution pattern and the hydrolytic lability of the alanyl residues of the glycerophosphate backbone. It is also amenable to the combinatorial synthesis of a great variety of LTAs.

Received: September 20, 2002 [Z50223]

[1] J. B. Zivot, W. D. Hoffmann, *New Horiz.* **1995**, *3*, 267–275.
[2] E. T. Rietschel, H. Brade, O. Holst, L. Brade, S. Müller-Loennies, U. Mamat, U. Zähringer, F. Beckmann, U. Seydel, K. Brandenburg, A. Ulmer, T. Mattern, H. Heine, J. Schletter, S. Hauschildt, H. Loppnow, U. Schönbeck, H.-D. Flad, U. F. Schade, F. DiPadova, S. Kusumoto, R. R. Schumann, *Curr. Top. Microbiol. Immunol.* **1996**, *216*, 39–81.
[3] U. Seydel, M. Oikawa, K. Fukase, S. Kusumoto, K. Brandenburg, *Eur. J. Biochem.* **2000**, *267*, 3032–3039, and references therein.
[4] S. M. Opal, J. Cohen, *Crit. Care Med.* **1999**, *27*, 1608–1616.
[5] W. Fischer, *Med. Microbiol. Immunol.* **1994**, *183*, 61–76.
[6] J. J. Gao, Q. Xue, E. G. Zuvanich, K. R. Haghi, D. C. Morrison, *Infect. Immun.* **2001**, *69*, 751–757.
[7] N. Kawamura, N. Imanishi, H. Koike, H. Nakahara, L. Phillips, S. Morooka, *Biochem. Biophys. Res. Commun.* **1995**, *217*, 1208–1215.
[8] A. Sugiyama, R. Arakaki, T. Ohnishi, N. Arakaki, Y. Daikuhara, H. Takada, *Infect. Immun.* **1996**, *64*, 1426–1431.
[9] R. Keller, W. Fischer, R. Keist, S. Bassetti, *Infect. Immun.* **1992**, *60*, 3664–3672.
[10] T. Kusunoki, E. Hailman, T. S. Juan, H. S. Lichenstein, S. D. Wright, *J. Exp. Med.* **1995**, *182*, 1673–1682.
[11] Y. Suda, H. Tochio, K. Kawano, H. Takada, T. Yoshida, S. Kotani, S. Kusumoto, *FEMS Immunol. Med. Microbiol.* **1995**, *12*, 97–112.
[12] S. Morath, A. Geyer, T. Hartung, *J. Exp. Med.* **2001**, *193*, 393–397.
[13] S. Morath, A. Stadelmaier, A. Geyer, R. R. Schmidt, T. Hartung, *J. Exp. Med.* **2002**, *195*, 1635–1640.
[14] S. Deininger, A. Stadelmaier, S. von Aulock, S. Morath, R. R. Schmidt, T. Hartung, *J. Immunol.* submitted.
[15] Some biological data of these investigations have already been reported: see ref. [13].
[16] J. J. Oltvoort, C. A. A. van Boeckel, J. H. De Koning, J. H. van Boom, *Recl. Trav. Chim. Pays-Bas* **1982**, *101*, 87–91; J. J. Oltvoort, M. Kloosterman, C. A. A. van Boeckel, J. H. van-Boom, *Carbohydr. Res.* **1984**, *130*, 147–163.
[17] K. Fukase, T. Matsumoto, N. Ito, T. Yoshimura, S. Kotani, S. Kusumoto, *Bull. Chem. Soc. Jpn.* **1992**, *65*, 2643–2654; K. Fukase, T. Yoshimura, S. Kotani, S. Kusumoto, *Bull. Chem. Soc. Jpn.* **1994**, *67*, 473–482; S. Kusumoto, K. Fukase, Y. Suda, M. Oikawa, *J. Synth. Org. Chem. Jpn.* **1996**, *54*, 976–987.
[18] I. Jerić, L. Šimičić, M. Stipetić, Š. Horvat, *Glycoconjugate J.* **2000**, *17*, 273–282.
[19] A. Stadelmaier, Dissertation, University of Konstanz, submitted.
[20] B. Wickberg, *Acta Chem. Scand.* **1958**, *12*, 1187–1201.
[21] P. A. Gent, R. Gigg, *J. Chem. Soc. Perkin Trans. 1* **1975**, 364–370.
[22] W. Bannwarth, A. Trzeciak, *Helv. Chim. Acta* **1987**, *70*, 175–186.
[23] G. Grundler, R. R. Schmidt, *Liebigs Ann. Chem.* **1984**, 1826–1847.

 © 2003 Wiley-VCH Verlag GmbH & Co. KGaA, Weinheim 1433-7851/03/4208-0919 $ 20.00+.50/0

[24] H. Bayley, D. N. Standring, J. R. Knowles, *Tetrahedron Lett.* **1978**, 3633 – 3634.
[25] L. F. Fieser, M. Fieser, *Reagents for Organic Synthesis, Vol. 1*, Wiley, New York, **1967**, p. 782.
[26] NMR experiments were performed at 600 MHz and 300 K. The NMR spectra of the final compounds were related to 3-(trimethylsilyl) 3,3,2,2-tetradeuteropropionic acid Na salt ([D_4]TSPA). ^{13}C Assignments were based on heteronuclear multiple-quantum correlation (HMQC). The anomeric proton of *N*-acetylglucosamine in compound **10** showed a doublet with a vicinal coupling constant of 3.6 Hz as expected for an α-glycosidic bond. The protons of the anomeric center gentiobiose intermediate **14** resolved also to doublets with coupling constants of 7.9 Hz and 7.8 Hz as expected for β-glycoside bonds. **17**: TLC (toluene/acetone 1:1): $R_f = 0.4$; $[\alpha]_D^{20} = +12.1$ ($c = 1$, $CHCl_3$); ^1H NMR (600 MHz, $CDCl_3$, TMS): $\delta = 0.81$–0.92 (t, 6H; me), 1.11–1.35 (m, 40H; $CH_2(\gamma$-ω)), 1.44–1.61 (m, 4H; $CH_2(\beta)$), 1.84–1.98 (m, 3H; NHAc), 2.09–2.25 (m, 4H; $CH_2(\alpha)$), 3.32 (m, 1H; 5a/b-H), 3.33 (m, 1H; 2a-H), 3.35 (m, 1H; 1′-H), 3.37 (m, 1H; 5a/b-H), 3.38 (m, 1H; 2b-H), 3.43, 3.44 (m, 2H; 4a, 4b-H), 3.49 (m, 2H; 18-H), 3.57 (m, 2H; 3a, 3b-H), 3.58–3.60 (m, 3H; 6c, 6a-H), 3.63(m, 4H; 5, 8, 11, 14-H), 3.64 (m, 1H; 4c-H), 3.67 (m, 12H; OMe), 3.68 (m, 1H; 3c-H), 3.69 (m, 1H; 2-H), 3.72 (m, 1H; 17-H), 3.75 (m, 1H; 5c-H), 3.83 (m, 1H; 1′-H), 3.96, 4.04 (m, 18H; 3, 4, 6, 7, 9, 10, 12, 13, 15-H), 4.06, 4.15 (m, 2H; 3′-H), 4.08 (m, 1H; 6a-H, 4.07, 4.17(m, 4H; 16, 6b-H), 4.20 (m, 1H; 1a-H), 4.35 (m, 1H; 2c-H), 4.41 (m, 1H; 1b-H), 4.74 (m, 1H; 1c-H), 4.29–4.91 (m, 30H; CH_2Ph), 4.93 (m, 12H; POCH_2Ph), 5.06 (m, 1H; 2′-H), 6.69–6.80 (m, 8H; Ph_{MPM}), 7.03–7.34 ppm (m, 93H; Ph); ^{13}C NMR (150.8 MHz, $CDCl_3$, TMS): $\delta = 14.11$ (2C; me), 23.1 (1C; NHAc), 24.84 (2C; $CH_2(\beta)$), 22.68/29.14–31.91 (20C; $CH_2(\gamma$-ω)), 34.04, 34.22 (2C; $CH_2(\alpha)$), 52.8 (1C; 2c-C), 55.17 (4C; OMe), 63.2 (1C; 3′-C), 65.5–67.2 (12C; CH_2-Glyc., 6b-C), 68.1 (1C; 1′-C), 68.5 (1C; 6c-C), 68.6 (1C; 6a-C), 69.0 (1C; 18-C) 69.5 (6C; POCH_2Ph), 69.8 (1C; 2′-C), 72 (1C; 5c-C), 73.5 (1C; 5a/b-C), 75 (1C; 4a/b-C), 75.4 (4C; 5, 8, 11, 14-C), 72–77.0 (15C; CH_2Ph), 76.8 (1C; 17-C), 77.5 (1C; 4c-C), 78.2 (1C; 2-C), 81.2 (1C; 3c-C), 81.8 (2C; 2a, 2b-C), 84.6 (2C; 3a, 3b-C), 100.05 (1C; 1c-C), 103.1 (1C; 1a-C), 103.6 (1C; 1a-C), 103.6 ppm (1C; 1b-C); assignment according to **1a** in Scheme 2; MALDI-TOF MS (positive mode, matrix: *p*-nitroaniline + NaI, THF): [*M*+Na]$^+$, calcd: *m*/*z* 4002.3; found: *m*/*z* 4000.0; $C_{220}H_{271}NO_{54}P_6$ (3979.3): calcd: C 66.40, H 6.86, N 0.35; found: C 66.40, H 7.09, N 0.36. **1a**: $[\alpha]_D^{20} = +6.9$ ($c = 0.1$, H_2O); ^1H NMR (600 MHz, D_2O): $\delta = 0.82$–0.94 (m, 6H; Me), 1.16–1.43 (m, 40H; $CH_2(\gamma$-ω)), 1.55–1.69 (m, 16H; Ala-βH, $CH_2(\beta)$), 2.11 (s, 3H; NHAc), 2.29–2.47 (m, 4H; $CH_2(\alpha)$), 3.27–3.73, 3.75–4.34, 4.36–4.59 (m, 54H), 5.10 (bs, 1H; 1c-H), 5.31–5.43 ppm (m, 5H; 5, 8, 11, 14-H, 2′-H); ^{13}C NMR (150.8 MHz, D_2O): $\delta = 14.2$ (Me), 15.9 (Ala-Me), 22.6 (NHAc), 25.4 ($CH_2(\beta)$), 30.5 ($CH_2(\gamma$-ω)), 34.5 ($CH_2(\alpha)$), 49.2 ($CHNH_3^+$), 54.0 (2c-C), 60.9 (6c-C), 62.4 (18-C), 64.0 (CH_2-Glyc.-C, 3′-C), 65.5 (1, 3-C), 66.8 (16-C), 68.2 (1′-C), 70.3 (4c-C), 71.1 (17-C), 71.4 (3c-C), 72.4 (5c-C), 73.4 (2a, 2b-C), 74.4 (5, 8, 11, 14-C), 75.9 (3a, 3b-C), 76.2 (2-C), 97.2 ppm (1c-C); MALDI-TOF MS (negative mode, matrix: trihydroxyacetophenone/diammonium citrate 2:1): [*M*−H]$^-$, calcd: *m*/*z*: 2247.9, found: *m*/*z*: 2248.5; [(*M*-Ala]$^-$, calcd: *m*/*z*: 2176.9, found: *m*/*z*: 2177.6. **1b**: $[\alpha]_D^{20} = +5.1$ ($c = 0.2$, H_2O); NMR data are almost identical with those of diastereomer **1a**; MALDI-TOF MS (negative mode, matrix: trihydroxyacetophenone/diammonium citrate 2:1): [*M*−H]$^-$, calcd: *m*/*z*: 2247.9, found: *m*/*z*: 2245.5; [(*M*−Ala)]$^-$, calcd: *m*/*z*: 2176.9, found; *m*/*z*: 2174.8; (positive mode, matrix: DHB): [*M*+H]$^+$, calcd: *m*/*z*: 2249.9, found: *m*/*z*: 2249.9.
[27] Whole blood cytokine response: Differential blood cell counts were routinely performed with a Pentra 60 analyzer (ABX Diagnostics, Montpellier, France) to exclude acute infections of blood donors. Heparinized blood (200 μL) freshly taken from healthy volunteers was diluted fivefold with isotonic sodium chloride solution (0.9%, Boehringer Ingelheim, Germany). LTA was sonified before use to dissolve micelles. After addition of the LTA stimuli in a volume of 10 μL, incubations were carried out in polypropylene reaction tubes (Eppendorf, Hamburg, Germany) in the presence of 5% CO_2 at 37°C overnight. Cell-free supernatants were obtained by centrifugation at 400 × g for 2 min and stored at −70°C for cytokine determination. Cytokines were measured by sandwich ELISA (enzyme-linked immunosorbent assay) based on an antibody pair against human TNFα (Endogen, Eching, Germany). Recombinant human TNFα serving as the standard was a gift from Dr. S. Poole, National Institute for Biological Standards and Controls, London (UK). Binding of biotinylated antibody was quantified by using streptavidin peroxidase (Biosource, Camarillo, CA. USA) and the substrate TMB (3,3′,5,5′-tetramethylbenzidine, Sigma, Deisenhofen, Germany).

 © 2003 Wiley-VCH Verlag GmbH & Co. KGaA, Weinheim 1433-7851/03/4208-0920 $ 20.00+.50/0

Stable Spirobis(radical cation)

A Spiro-Fused Triarylaminium Radical Cation with a Triplet Ground State**

*Akihiro Ito, Masashi Urabe, and Kazuyoshi Tanaka**

The spiro structural motif has been occasionally revisited in the field of molecule-based materials science. For example, several spiro compounds were recently investigated for constructing metallic charge-transfer salts with unique three-dimensional structures[1,2] and molecular metals composed of a single molecular component.[3] With regard to molecule-based magnetism, Dougherty et al. elaborately examined the possibility of generating 1,4,6,9-spiro[4.4]nonatetrayl.[4,5] Recently, Frank et al. reported the synthesis of a spiro-fused bis(nitronyl nitroxide) biradical and the magnetic interaction between the two radical centers.[6] From the viewpoint of magnetic interaction, the spin preference in spirobiradicals is determined by the balance between two contributions: 1) the two perpendicular π systems, which favor ferromagnetic interaction resulting from the degeneracy of the magnetic orbital derived from the two ring systems, and 2) so-called spiroconjugation,[7] which can lift the degeneracy of the two magnetic orbitals and thus lead to a singlet spin state. In fact, the biradical reported in ref. [3] exhibited a weak antiferromagnetic interaction, probably because of the second contribution. Two nitronyl nitroxide radicals incorporated in the two subunits of a spiro compound can be regarded as localized spin centers. The further apart the nitroxide centers are in the molecule, the weaker their ferromagnetic interaction becomes. In contrast, triarylaminium cations have more delocalized spin distributions than the nitroxide radical,[8] and this ensures stronger exchange interaction between two radical centers. Furthermore, it is well known that all-*para*-substituted triarylamines often give thermally and chemically robust radical cations.[8] Here we report the synthesis of the novel spiro-fused triarylamine **1** and the magnetic properties of its bis(radical cation) $\mathbf{1}^{2+}$.

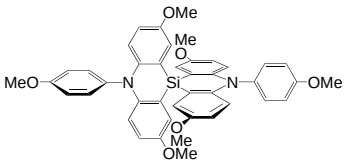

1

[*] Prof. K. Tanaka, Dr. A. Ito, M. Urabe
Department of Molecular Engineering
Graduate School of Engineering
Kyoto University
Sakyo-ku, Kyoto 606-8501 (Japan)
Fax: (+81) 75-771-0172
E-mail: a51053@sakura.kudpc.kyoto-u.ac.jp

[**] This work was supported by a Grant-in-Aid for Scientific Research (C) from Japan Society for the Promotion of Science (JSPS). Numerical calculations were partly carried out at the Supercomputer Laboratory of the Institute for Chemical Research of Kyoto University.

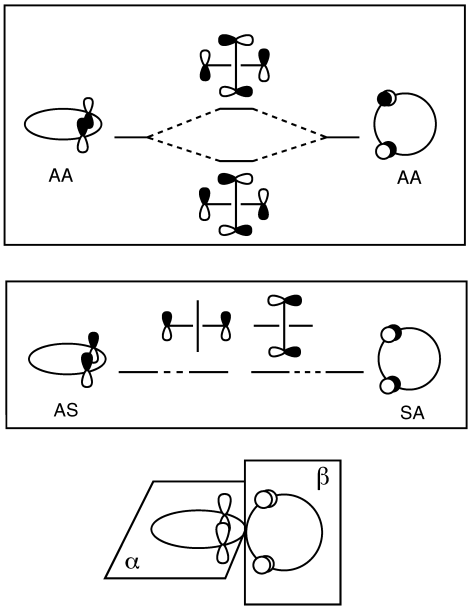

Figure 1. Schematic diagram of molecular interaction between two perpendicular subunits in a spiro compound. A and S denote antisymmetric and symmetric, respectively, with regard to the planes α and β.

In Figure 1, the fragment MOs of the mutually perpendicular π systems are classified by symmetry with respect to two planes α and β. By consideration of symmetry it can be deduced that the two fragment MOs can interact with each other only when they are antisymmetric (AA) to both planes.[7] The fragment MOs of a triarylamine such as **1** indeed have AA symmetry, as illustrated in Figure 2. Hence, the resulting HOMO for **1** is expected to be doubly degenerate. In fact, CAS(2,2)/6-31G* MO calculations[9] on the dication of the unsubstituted model compound of **1** revealed degeneracy of two singly occupied MOs (SOMOs).

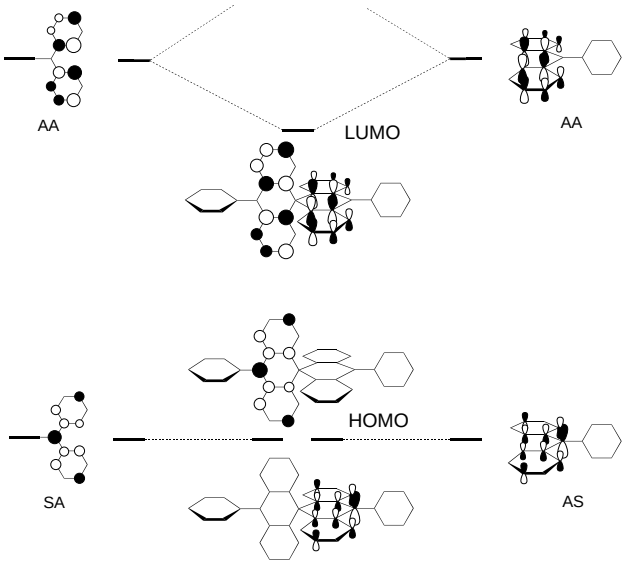

Figure 2. Schematic drawing of the frontier MOs for **1**. Methoxy groups are omitted for clarity.

 © 2003 Wiley-VCH Verlag GmbH & Co. KGaA, Weinheim 1433-7851/03/4208-0921 $ 20.00+.50/0

In addition, the singlet state is 167 J mol^{-1} higher in energy than the corresponding triplet state. Although the calculated Mulliken spin density is mainly concentrated on the two N atoms, it is delocalized over the benzene rings to some extent. The distance between the two N atoms was estimated to be 6.4 Å from the optimized structure.

The synthesis of **1** (Scheme 1) started with diarylamine **2**. As a facile method to construct a spiro structure, we selected the method of Gilmann et al.,[10] in which treatment of silicon tetrachloride with *N*-alkyl-2,2′-dilithiodiphenylamine gives a spirobis(dihydrophenazasiline) in high yield. In terms of retrosynthetic strategy, the route starting from 2,2′-dibromotrianisylamine **4** is more convenient. However, dilithiated **4** and $SiCl_4$ did not react, probably owing to the buttressing effect[11] of the bulky *N*-aryl group. However, when *N*-benzyl-2,2′-dibromodianisylamine (**5**) was employed, the corresponding spiro compound **6** was obtained in 60% yield. Finally, after removal of benzyl protecting groups, a Pd^0-catalyzed amination reaction[12] afforded the target molecule **1** in high yield.[13]

The redox behavior of **1**, in which two oxidizable subunits are connected by a spiro atom, is of interest, as it will give information on the spiroconjugation between the two subunits and hence the intramolecular magnetic interaction in $\mathbf{1}^{2+}$. The electrochemical properties of **1** were investigated by cyclic voltammetry (CV) at room temperature in acetonitrile (Figure 3). Compound **1** displayed two reversible one-electron oxidation waves at formal potentials of 0.30[14] and 0.46 V versus Fc/Fc^+, and this indicates that the first oxidation yields a monocation stabilized by spin delocalization over two trianisylamine units. The separation of the two oxidation potentials (160 mV) indicates that spiroconjugation between two subunits is weak but not negligible.

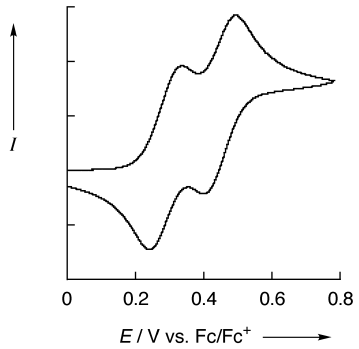

Figure 3. Cyclic voltammogram of **1** in MeCN at 25 °C (scan rate 100 mV s^{-1}).

The reversibility of the two oxidation processes encouraged us to prepare a salt of the dication of **1**. Taking into account the observed potentials, we oxidized **1** with antimony pentachloride in CH_2Cl_2. Dry diethyl ether was added to the resulting blue solution at −78 °C, and the hexachloroantimonate salt was isolated as a greenish blue powder.[15] In contrast to the comparatively high oxidation potentials of **1**, the isolated salt was quite stable in the solid state even at ambient temperature in air for days.[16] Although we have not yet obtained single crystals suitable for X-ray structural analysis, elemental analysis strongly suggested that the isolated salt has the composition $\mathbf{1}(SbCl_6)_2$.[15,17]

To gain information on whether $\mathbf{1}^{2+}$ has an open-shell electronic structure, we recorded the EPR spectrum of $\mathbf{1}(SbCl_6)_2$ in a frozen CH_2Cl_2 matrix (Figure 4). The distinct fine structure attributed to spin-triplet species was detected together with the forbidden resonance resulting from $\Delta m_S =$

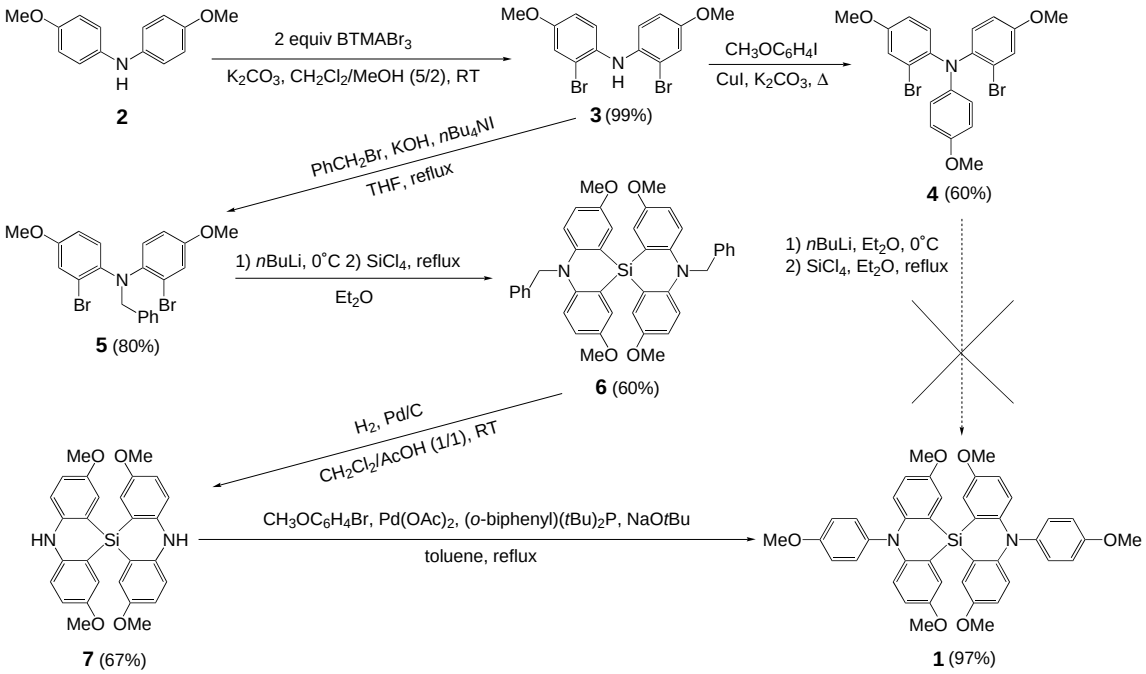

Scheme 1. Synthetic route for **1**. BTMA = Benzyltrimethylammonium.

 © 2003 Wiley-VCH Verlag GmbH & Co. KGaA, Weinheim 1433-7851/03/4208-0922 $ 20.00+.50/0

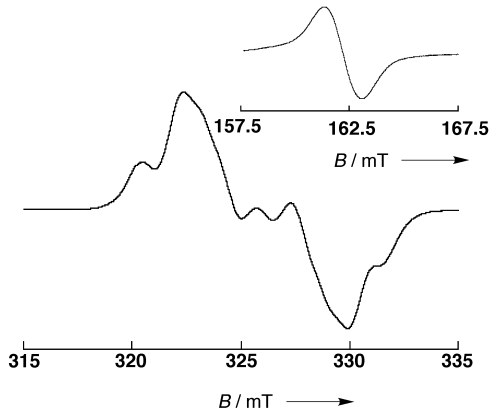

Figure 4. EPR spectra of $\mathbf{1}(SbCl_6)_2$ in CH_2Cl_2 at 123 K. Inset: The forbidden $\Delta M_S = \pm 2$ resonance at 123 K.

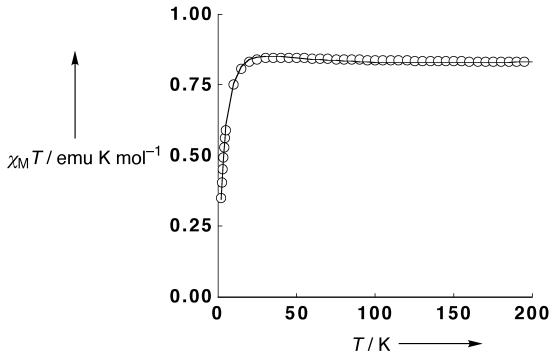

Figure 5. Plot of $\chi_M T$ versus T for $\mathbf{1}(SbCl_6)_2$ at 500 G. The solid line represents the best theoretical fit [Eq. (2)] to the data.

± 2. This clearly indicates that $\mathbf{1}^{2+}$ is a bis(radical cation). The zero-field splitting constants were determined from the $\Delta m_S = \pm 1$ transitions to be $D = 5.5$ mT and $E = 0.7$ mT by spectral simulation. The midpoints of three pairs of resonances did not coincide, and this indicates anisotropy of the g factor: $g_{xx} \approx g_{yy} = 2.0022$, $g_{zz} = 2.0034$ (the z axis is in the direction connecting the two nitrogen atoms). The average spin–spin distance was estimated to be 8.0 Å within the point-dipole approximation.[18] The discrepancy between the value of 8.0 Å and the distance between the two N atoms estimated from the aforementioned MO calculations on the unsubstituted model compound (6.4 Å) clearly shows deviation from the simple dipole approximation for $\mathbf{1}^{2+}$. For spin-delocalized diradical molecules, Equation (1) can be adopted[19] where r_{ij}

$$D = \frac{3}{4} g^2 \beta^2 \sum_{ij} \frac{r_{ij}^2 - 3 z_{ij}^2}{r_{ij}^5} \rho_i \rho_j \qquad (1)$$

is the distance between atoms i and j, r_i and r_j are the spin densities on atom i in one dianisylaminium moiety and on atom j on the other, and the z axis is in the direction connecting the two N atoms. On the basis of the B3LYP/6-31G* calculations on the dication of the unsubstituted model compound of **1**, the D value is estimated to be 6.0 mT. This indicates that the spin densities are to some extent delocalized over each dianisylaminium moiety. Furthermore, the temperature dependence of the signal intensity corresponding to the $\Delta m_S = \pm 2$ transition exhibited Curie-like behavior, which suggests that $\mathbf{1}^{2+}$ has a triplet ground state.

Corroboration for ferromagnetic interaction between two trianisylaminium radical cations was provided by magnetic susceptibility measurements in the range between 4 and 300 K (Figure 5). The $\chi_M T$ value was almost constant at 0.83 emu K mol^{-1} between room temperature and 100 K. This value is larger than that expected for two uncoupled spins of 1/2 (0.75 emu K mol^{-1}) and suggests high-spin correlation even at higher temperature. Furthermore, the $\chi_M T$ value increased gradually with decreasing temperature, reached a maximum value of 0.85 emu mol^{-1} K at 18 K, and finally decreased. The measured data best fit to Equation (2)

$$\chi_M = \frac{1}{k_B (T - \theta)} \frac{2 N g^2 \mu_B}{3 + \exp\left(-\frac{2J}{k_B T}\right)} \qquad (2)$$

corresponding to the modified Bleany–Bowers singlet–triplet model for a diradical[20] under a weak Weiss mean field (Weiss constant θ). The exchange coupling J is defined by a Heisenberg Hamiltonian for a diradical [Eq. (3)] where

$$\mathscr{H} = -2J \mathbf{S}_1 \mathbf{S}_2 \quad (S_1 = S_2 = 1/2) \qquad (3)$$

positive J indicates ferromagnetic interaction between two radical centers. The optimized values were estimated to be $J = 1.12$ cm^{-1} (1.6 K) and $\theta = -4.3$ K. The ferromagnetic J for $\mathbf{1}^{2+}$ is in contrast to the antiferromagnetic J (-4.00 cm^{-1} ($= -5.8$ K)) for the spirobis(nitronyl nitroxide) in ref. [3]

In summary, we have prepared a spiro compound with high-spin correlation. To the best of our knowledge, this is the first example of a stable organic spirobis(radical cation). It is of great interest to extend **1** to polymeric systems, and further work is in progress in this direction.

Received: June 14, 2002
Revised: November 4, 2002 [Z19531]

[1] P. Maslak, M. P. Augustine, J. D. Burkey, *J. Am. Chem. Soc.* **1990**, *112*, 5339 – 5360.
[2] K. Ueda, M. Yamanoha, T. Sugimoto, H. Fujita, A. Ugawa, K. Yakushi, K. Kano, *Chem. Lett.* **1997**, 461 – 462.
[3] X. Chi, M. E. Itkis, B. D. Patrick, T. M. Barclay, R. W. Reed, R. T. Oakley, A. W. Cordes, R. C. Haddon, *J. Am. Chem. Soc.* **1999**, *121*, 10395 – 10402.
[4] L. McElwee-White, W. A. Goddard III, D. A. Dougherty, *J. Am. Chem. Soc.* **1984**, *106*, 3461 – 3466.
[5] L. McElwee-White, D. A. Dougherty, *J. Am. Chem. Soc.* **1984**, *106*, 3466 – 3474.
[6] N. L. Frank, R. Clérac, J.-P. Sutter, N. Daro, O. Kahn, C. Coulon, M. T. Green, S. Golhen, L. Ouahab, *J. Am. Chem. Soc.* **2000**, *122*, 2053 – 2061.
[7] H. Dürr, R. Gleiter, *Angew. Chem.* **1978**, *90*, 591 – 601; *Angew. Chem. Int. Ed. Engl.* **1978**, *17*, 559 – 569.
[8] A. R. Forrester, J. M. Hay, R. H. Thomson, *Organic Chemistry of Stable Free Radicals*, Academic Press, New York, **1968**.
[9] Gaussian 98 (Revision A.7), M. J. Frisch, G. W. Trucks, H. B. Schlegel, G. E. Scuseria, M. A. Robb, J. R. Cheeseman, V. G. Zakrzewski, J. A. Montgomery, R. E. Stratmann, J. C. Burant, S.

 © 2003 Wiley-VCH Verlag GmbH & Co. KGaA, Weinheim 1433-7851/03/4208-0923 $ 20.00+.50/0

Dapprich, J. M. Millam, A. D. Daniels, K. N. Kudin, M. C. Strain, O. Farkas, J. Tomasi, V. Barone, M. Cossi, R. Cammi, B. Mennucci, C. Pomelli, C. Adamo, S. Clifford, J. Ochterski, G. A. Petersson, P. Y. Ayala, Q. Cui, K. Morokuma, D. K. Malick, A. D. Rabuck, K. Raghavachari, J. B. Foresman, J. Cioslowski, J. V. Ortiz, B. B. Stefanov, G. Liu, A. Liashenko, P. Piskorz, I. Komaromi, R. Gomperts, R. L. Martin, D. J. Fox, T. Keith, M. A. Al-Laham, C. Y. Peng, A. Nanayakkara, C. Gonzalez, M. Challacombe, P. M. W. Gill, B. G. Johnson, W. Chen, M. W. Wong, J. L. Andres, M. Head-Gordon, E. S. Replogle, J. A. Pople, Gaussian, Inc., Pittsburgh, PA, **1998**.

[10] D. Wittenberg, H. A. McNince, H. Gilman, *J. Am. Chem. Soc.* **1958**, *80*, 5418 – 5422.

[11] For examples, see M. S. Newman, *Effects in Organic Chemistry*, Wiley, New York, **1956**; L. N. Ferguson, *The Modern Structural Theory of Organic Chemistry*, Prentice-Hall, Englewood Cliffs, NJ, **1963**.

[12] a) M. Beller, *Angew. Chem.* **1995**, *107*, 1436 – 1437; *Angew. Chem. Int. Ed. Engl.* **1995**, *34*, 1316; b) J. F. Hartwig, *Synlett* **1997**, 329; c) J. F. Hartwig, *Angew. Chem.* **1998**, *110*, 2154 – 2177; *Angew. Chem. Int. Ed.* **1998**, *37*, 2046 – 2067; d) J. P. Wolfe, S. Wagaw, J.-F. Marcoux, S. L. Buchwald, *Acc. Chem. Res.* **1998**, *31*, 805; e) J. F. Hartwig, *Acc. Chem. Res.* **1998**, *31*, 852.

[13] Physical data for **1**: White solid; ^{1}H NMR (400 MHz, $CDCl_3$): $\delta = 7.30$ (d, 4H), 7.17 (d, 4H), 6.90 (d, 4H), 6.75 (dd, 4H), 6.47 (d, 4H), 3.94 (s, 6H), 3.64 ppm (s, 12H); ^{13}C NMR (75 MHz, $CDCl_3$): $\delta = 158.9$, 152.5, 145.2, 136.83, 132.30, 119.5, 118.0, 117.3, 116.8, 116.1, 55.5 ppm; ^{13}C NMR (75 MHz, C_6D_6): $\delta =$ 159.4, 153.7, 146.0, 137.5, 132.8, 119.3, 119.0, 118.7, 117.6, 116.4, 55.0, 54.9 ppm; elemental analysis (%): calcd for $C_{42}H_{38}N_2O_6Si$: C 72.60, H 5.51, N 4.03; found: C 72.41, H 5.44, N 3.97.

[14] The oxidation potential of trianisylamine was 0.16 V vs Fc/Fc^+ under the same conditions. This discrepancy of the first oxidation potential between **1** and trianisylamine probably results from a difference in conformation of the trianisylamine moieties. In **1**, the propellerlike conformation can be hardly adopted because of its spiro structure.

[15] Compound **1** (69 mg, 0.1 mmol) was dissolved in dry dichloromethane and stirred at −78 °C under argon. $SbCl_5$ (0.5 ml, 1M in CH_2Cl_2) was added to the solution. After 10 min, the resulting blue solution was poured into dry diethyl ether. The precipitate was washed with dry diethyl ether to provide **1**$(SbCl_6)_2$ (110 mg, 81%) as a greenish blue solid. **1**$(SbCl_6)_2$: elemental analysis (%): calcd for $C_{42}H_{38}Cl_{12}N_2O_6Sb_2Si$: C 36.99, H 2.81, N 2.05, Cl 31.19; found: C 36.99, H 2.71, N 2.05, Cl 29.61.

[16] The isolated solid sample was dissolved in CH_2Cl_2, and the ESR signal intensity was compared to that of a sample oxidized in situ at the same concentration. The two signals gave the same fine structure with almost the same intensity.

[17] Example of oxidation with $SbCl_5$ in CH_2Cl_2: H. Bock, A. Rauschenbach, K. Ruppert, Z. Havlas, *Angew. Chem.* **1991**, *103*, 706 – 708; *Angew. Chem. Int. Ed.* **1998**, *37*, 714 – 716.

[18] N. Hirota, *J. Am. Chem. Soc.* **1967**, *89*, 32 – 41.

[19] K. Mukai, A. Sogabe, *J. Chem. Phys.* **1980**, *72*, 598 – 601.

[20] B. Bleaney, K. D. Bowers, *Proc. R. Soc. London Ser. A* **1952**, *214*, 451 – 456.

Redox-Switchable Lithium Trap

[1.1]Diborataferrocenophane: A Highly Efficient Li^+ Scavenger**

*Matthias Scheibitz, Rainer F. Winter, Michael Bolte, Hans-Wolfram Lerner, and Matthias Wagner**

In various cases, electrophilic substitution reactions of ferrocene are known to proceed via precomplexation of the iron atom by the electrophile.[1] Moreover, direct iron-to-metal bonding appears to influence the complexation behavior of certain ferrocene-based redox-switchable cryptands,[2] as well as the properties of catalytically active 2-metalla[3]-ferrocenophanes (metal = Ti^{IV}, Pd^{II}, Pt^{II}).[3] The interaction of ferrocene with Li^+ was studied theoretically by Ugalde et al.,[4] who located two minima on the energy surface. In the lower energy structure, the lithium cation is η^5-coordinated on top of one of the cyclopentadienyl rings (**I**; Scheme 1). The second minimum structure **II** is 8 kcal mol^{-1} higher in energy and has the Li^+ ion bonded laterally to the iron atom. We recently reported the synthesis and structural characterization of a ferrocene/gallium(I) cation complex with essentially the same structural motif as **I**.[5] Here we report on the isolation of a ferrocene/lithium complex that provides experimental evidence for the existence of structure **II**.

When a slurry of 1,1′-dilithioferrocene (**1**)[6] in hexane is treated with a solution of 1,1′-bis(dimethylboryl)ferrocene (**2**) in THF,[7] the cyclic dinuclear aggregate $\mathbf{3}^{2-}$ is formed in good yield (Scheme 1). X-ray quality crystals of [**3**-Li]Li([12]crown-4)$_2$ were grown by gas-phase diffusion of diethyl ether into a solution of the crude material in THF after addition of [12]crown-4.

The ^{11}B NMR spectrum of [**3**-Li]Li([12]crown-4)$_2$ reveals one signal at $\delta(^{11}B, [D_8]THF) = -21.8$ ppm, which testifies to

[*] Prof. Dr. M. Wagner, Dipl.-Chem. M. Scheibitz, Dr. H.-W. Lerner
Institut für Anorganische Chemie
Johann Wolfgang Goethe-Universität Frankfurt
Marie-Curie-Strasse 11, 60439 Frankfurt/Main (Germany)
Fax: (+49) 69-798-29260
E-mail: matthias.wagner@chemie.uni-frankfurt.de
Dr. R. F. Winter
Institut für Anorganische Chemie
Universität Stuttgart
Pfaffenwaldring 55, 70569 Stuttgart (Germany)
Dr. M. Bolte[+]
Institut für Organische Chemie
Johann Wolfgang Goethe-Universität Frankfurt
Marie-Curie-Strasse 11, 60439 Frankfurt/Main (Germany)

[+] X-ray crystallography

[**] We wish to thank Prof. Dr. M. U. Schmidt (Universität Frankfurt) for helpful discussions. M.W. is grateful to the Deutsche Forschungsgemeinschaft (DFG) for financial support. M.S. wishes to thank the Fonds der Chemischen Industrie (FCI) and the Bundesministerium für Bildung und Forschung (BMBF) for a PhD grant. R.W. acknowledges support by the Stiftung Volkswagenwerk.

Supporting information for this article is available on the WWW under http://www.angewandte.org or from the author.

 © 2003 Wiley-VCH Verlag GmbH & Co. KGaA, Weinheim 1433-7851/03/4208-0924 $ 20.00+.50/0

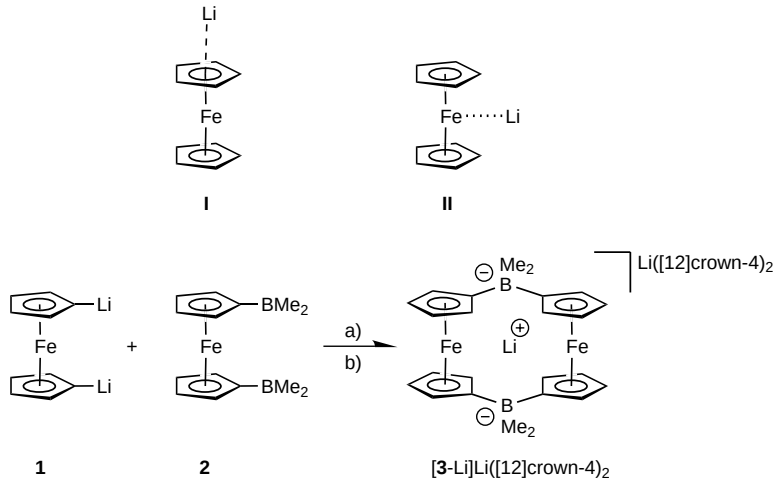

Scheme 1. a) THF/hexane, RT; b) excess [12]crown-4, RT.

the presence of tetracoordinate boron atoms.[8] In the ^{1}H NMR spectrum, only one signal is observed for all four methyl groups ($\delta(^1H, [D_8]THF) = -0.25$ ppm). The signal is broad and has a doublet line shape due to partially resolved ^2J(B,H) coupling. The cyclopentadienyl rings give rise to two well-resolved pseudotriplets at $\delta(^1H, [D_8]THF) = 3.86$ and 3.99 ppm; the corresponding carbon resonances appear at $\delta(^{13}C, [D_8]THF) = 69.8$ and 74.0 ppm. Both the ^{1}H and the ^{13}C NMR patterns indicate a high average symmetry of the molecule in solution. This observation can be explained by a degenerate *syn–syn* isomerization of the [1.1]ferrocenophane framework, which leads to fast exchange of the methyl groups in the *exo* and *endo* positions of the BMe_2 bridges (the *anti* conformation of [1.1]ferrocenophanes with small bridging atoms is disfavored for steric reasons).[9]

Most interestingly, the ^{7}Li NMR spectrum displays two signals at $\delta(^7Li, [D_8]THF) = -0.19$ and 4.29 ppm with an integral ratio of 1:1. Comparison with the spectra of LiCl ($\delta(^7Li, [D_8]THF) = 0.30$ ppm) and Li([12]crown-4)$_2$Cl ($\delta(^7Li, [D_8]THF) = -0.21$ ppm) clearly shows that the signal at higher field must be assigned to a [Li([12]crown-4)$_2$]$^+$ cation. The signal at 4.29 ppm obviously corresponds to the second lithium cation, which appears to be surrounded by a distinctly different ligand sphere. At ambient temperature, any exchange of Li$^+$ between the two coordination sites is clearly slow on the NMR timescale. The ^{7}Li NMR spectrum does not change when more [12]crown-4 is added to the NMR tube.

The structure of [**3**-Li]Li([12]crown-4)$_2$ in the solid state was finally established by X-ray crystallography (Figure 1).[10] The molecule contains a [1.1]ferrocenophane ring in a twisted *syn* conformation (dihedral angles: C1–C5//C31–C35 21.3°; C11–C15//C21–C25 23.1°).[11] In agreement with the NMR data, one of the lithium cations is coordinated by two crown ether molecules and forms the well-known complex [Li([12]-crown-4)$_2$]$^+$. The second lithium cation is located inside the ferrocenophane cavity, most likely trapped by the electrostatic field originating from the two anionic dimethylborate bridges (Li1···B1 2.314(6), Li1···B2 2.309(6) Å; B1···Li1···B2 179.2(3)°; Li1 is not located on a special position). The distances between the Li$^+$ ion and the iron centers are somewhat larger than the value calculated for structure **II** (**II**: Li···Fe 2.4 Å; [**3**-Li]$^-$: Li1···Fe1 2.720(6), Li1···Fe2 2.706(5) Å; Fe1···Li1···Fe2 128.2(2)°). As was predicted by Ugalde et al.,[4] the close vicinity of the Li$^+$ ion does not lead to a major distortion of the ferrocene structure (COG-Fe1-COG′ 175.6°, COG-Fe2-COG′ 174.9°; COG: center of gravity of a C_5H_4 ring). We observe only little bending of the boron centers out of the planes of the attached Cp rings (av COG-C(*ipso*)-B 167.3(3)°), and the distances between the carbon atoms C1, C11, C21, C31 and the Li$^+$ ion are rather large (av C(*ipso*)···Li1 2.361(5) Å). These findings suggest that there is no substantial degree of charge transfer from the Cp rings to the lithium cation. The question thus arises whether the function of the diborylated ferrocenophane is adequately described as merely providing an anionic macrocycle in which Li$^+$ is trapped. [**3**-Li]$^-$ containing a naked lithium cation in close proximity to a ferrocene moiety represents a reasonable approximation of **II**, as it was predicted to exist under gas-phase conditions. Ugalde et al. calculated the lithium cation basicity (LCB) of ferrocene at $T = 298$ K for structure **II** and obtained a value of 29.4 kcal mol^{-1},[4] which, in comparison with other LCB data determined both theoretically and experimentally by Burk et al.,[12] leads to the conclusion that ferrocene behaves as a moderately strong base toward the lithium cation. Since [**3**-Li]$^-$ has two ferrocene moieties which, in addition, are much more electron-rich than ferrocene itself (see below and also ref. [13]), a contribution from bonding Fe···Li interactions to the stability of the aggregate should be considered.

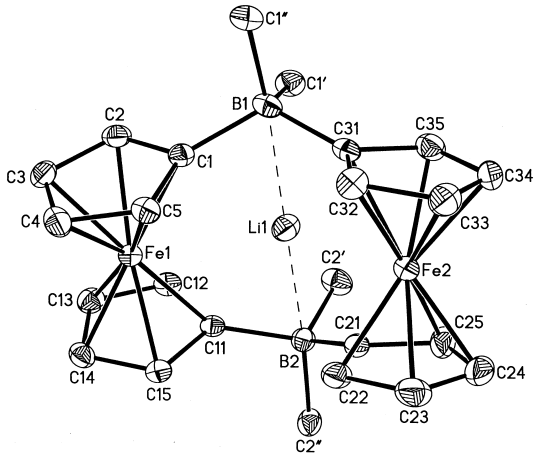

Figure 1. Molecular structure and numbering scheme of [**3**-Li]Li([12]-crown-4)$_2$ (thermal ellipsoids shown at the 50% probability level, Li([12]crown-4)$_2^+$ fragment and hydrogen atoms omitted for clarity). Selected atom–atom distances [Å], bond lengths [Å], angles [°], and torsion angles [°]: B1-C1 1.651(5), B1-C31 1.651(5), B2-C11 1.646(5), B2-C21 1.659(5), Li1···B1 2.314(6), Li1···B2 2.309(6), Li1···Fe1 2.720(6), Li1···Fe2 2.706(5); C1-B1-C31 115.7(3), C11-B2-C21 114.8(3), B1···Li1···B2 179.2(3), Fe1···Li1···Fe2 128.2(2); C2-C1-B1-C1′ −38.9(4), C2-C1-B1-C1″ 78.1(3), C25-C21-B2-C2′ −38.7(4), C25-C21-B2-C2″ 78.5(4).

In cyclic voltammetry experiments (CH_2Cl_2, 0.2 M NBu_4PF_6) [**3**-Li]Li([12]crown-4)$_2$ was irreversibly oxidized at a peak potential of -0.58 V (vs FcH/FcH$^+$, $\upsilon = 0.1$ V s^{-1}; Figure 2a).[14] This sizable cathodic shift with respect to ferrocene reflects the high electron density in the anionic [1.1]ferrocenophane.[15] When, after oxidation, the sweep is continued into the cathodic regime, two partially reversible waves emerge at even more negative half-wave potentials

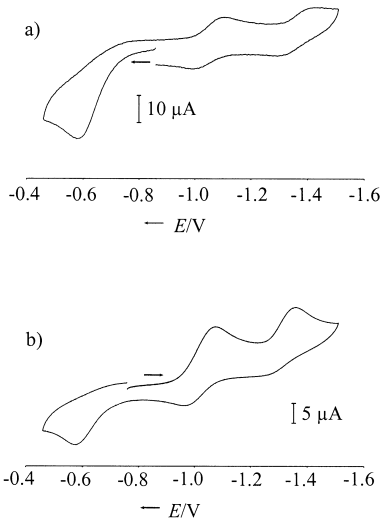

Figure 2. a) Cyclic voltammogram of [**3**-Li]Li([12]crown-4)$_2$ (CH_2Cl_2, 0.2 M NBu_4PF_6, $\upsilon = 0.1$ V s^{-1}, vs FcH/FcH$^+$); b) Cyclic voltammogram of [**3**-Li]Li([12]crown-4)$_2$ after exhaustive oxidation (CH_2Cl_2, 0.2 M NBu_4PF_6, $\upsilon = 0.1$ V s^{-1}, vs FcH/FcH$^+$).

($E_{1/2} = -1.02$, -1.33 V; $\Delta E_p = 84$ and 111 mV, respectively).[16] These waves are not observed if the cathodic scan is performed first and are thus assigned to electroactive product(s) arising from a chemical step following oxidation. On bulk electrolysis at -0.38 V the electroactive product(s) mentioned above were cleanly produced. Voltammetric scans after electrolysis reveal both cathodic waves to be only partially reversible, and this again indicates a chemical process following electron transfer. If after the cathodic scan the sweep is taken back into the more anodic regime, the oxidation wave of the parent [**3**-Li]Li([12]crown-4)$_2$ reappears (Figure 2b). In accordance with the voltammetric data, bulk reduction at -1.20 V gives back the starting material as the principal product. We conclude that the oxidation/reduction sequence constitutes an overall chemically reversible cycle connected by irreversible individual steps. Considering the pronounced cathodic shift of both reduction potentials relative to the oxidation potential of parent [**3**-Li]$^-$, a plausible scenario is that upon oxidation of [**3**-Li]$^-$ the encapsulated Li$^+$ ion is expelled from the macrocycle.

[**3**]$^{2-}$ is a novel type of redox-switchable lithium scavenger. Contrary to other functionally related complexes,[17] the lithium ion in [**3**-Li]$^-$ is not coordinated by main-group Lewis bases. We therefore suggest that [**3**-Li]Li([12]crown-4)$_2$ could be used as an easily accessible model system to study the interaction of ferrocene with the unperturbed naked lithium cation.

Experimental Section

[**3**-Li]Li([12]crown-4)$_2$: A solution of **2** (0.29 g, 1.09 mmol) in THF (5 mL) was added to a slurry of **1**·2 tmeda (0.47 g, 1.09 mmol; tmeda = *N,N,N′,N′*-tetramethylethylenediamine) in hexane (20 mL) with stirring at ambient temperature. The reaction mixture was stirred for 2 h. After filtration, the remaining solid was triturated in hexane (2 × 10 mL) and dried in vacuo. A solution of the crude product in THF was treated with [12]crown-4 (0.37 g, 2.20 mmol) and then slowly layered with diethyl ether by gas-phase diffusion to yield X-ray quality crystals of [**3**-Li]Li([12]crown-4)$_2$. Yield: 0.39 g (44 %).

^{11}B NMR (128.4 MHz, [D$_8$]THF): $\delta = -21.8$ ppm ($h_{1/2} = 20$ Hz); ^{7}Li NMR (155.5 MHz, [D$_8$]THF): $\delta = -0.19$ ([Li([12]crown-4)$_2$]$^+$), 4.29 ppm ([**3**-Li]$^-$); ^{1}H NMR (250.1 MHz, [D$_8$]THF): $\delta = -0.25$ (br, 12H; CH_3), 3.61 (s, 32H; CH_2), 3.86, 3.99 ppm (2 × t, 2 × 8H, $^3J(H,H) = {}^4J(H,H) = 1.7$ Hz; C_5H_4); ^{13}C NMR (62.9 MHz, [D$_8$]THF): δ = not observed (CH_3), 69.8 (C_5H_4), 72.0 (CH_2), 74.0 ppm (C_5H_4), not observed (C_5H_4-*ipso*). ^{11}B and ^{7}Li NMR spectra are reported relative to external $BF_3{\cdot}Et_2O$ and LiCl/D_2O, respectively. Elemental analysis (%) calcd for $C_{40}H_{60}B_2Fe_2Li_2O_8$ (816.08): C 58.87, H 7.41; found: C 58.55, H 7.51.

Received: July 17, 2002
Revised: November 20, 2002 [Z19759]

[1] M. J. Mayor-López, J. Weber, B. Mannfors, A. F. Cunningham, Jr., *Organometallics* **1998**, *17*, 4983 – 4991.
[2] J. C. Medina, T. T. Goodnow, M. T. Rojas, J. L. Atwood, B. C. Lynn, A. E. Kaifer, G. W. Gokel, *J. Am. Chem. Soc.* **1992**, *114*, 10583 – 10595.
[3] M. Herberhold, *Angew. Chem.* **2002**, *114*, 998 – 1000; *Angew. Chem. Int. Ed.* **2002**, *41*, 956 – 958.
[4] A. Irigoras, J. M. Mercero, I. Silanes, J. M. Ugalde, *J. Am. Chem. Soc.* **2001**, *123*, 5040 – 5043.
[5] S. Scholz, J. C. Green, H.-W. Lerner, M. Bolte, M. Wagner, *Chem. Commun.* **2002**, 36 – 37.
[6] M. D. Rausch, D. J. Ciappenelli, *J. Organomet. Chem.* **1967**, *10*, 127 – 136.
[7] W. Ruf, T. Renk, W. Siebert, *Z. Naturforsch. B* **1976**, *31*, 1028 – 1034.
[8] "Nuclear Magnetic Resonance Spectroscopy of Boron Compounds": H. Nöth, B. Wrackmeyer in *NMR Basic Principles and Progress, Vol. 14* (Eds.: P. Diehl, E. Fluck, R. Kosfeld), Springer, Berlin, **1978**.
[9] U. T. Mueller-Westerhoff, *Angew. Chem.* **1986**, *98*, 700 – 716; *Angew. Chem. Int. Ed. Engl.* **1986**, *25*, 702 – 717.
[10] X-ray crystal structure analysis of [**3**-Li]Li([12]crown-4)$_2$: STOE-IPDS-II two-circle diffractometer, $Mo_{K\alpha}$ radiation ($\lambda = 0.71073$ Å), ω scans, empirical absorption correction, the structure was solved by direct methods using SHELXS-97 and refined with SHELXL-97 (G. M. Sheldrick, Universität Göttingen, Germany, **1997**) by full-matrix least-squares methods against F^2. Hydrogen atoms were placed on ideal positions and refined with fixed isotropic displacement parameters using a riding model. In addition, the torsion angles about the B–CH_3 bonds were refined. $[C_{24}H_{28}B_2Fe_2Li]^-[(C_8O_4H_{16})_2Li]^+$, $M_r = 816.08$ g mol^{-1}, crystal dimensions $0.62 \times 0.16 \times 0.14$ mm, pale yellow needle, triclinic, space group $P\bar{1}$; $a = 10.519(1)$, $b = 13.643(1)$, $c = 14.986(2)$ Å, $\alpha = 69.208(8)$, $\beta = 88.794(8)$, $\gamma = 81.104(8)$°, $V = 1985.1(4)$ Å^3, $Z = 2$; $\rho_{calcd} = 1.365$ g cm^{-3}; $\mu = 0.781$ mm^{-1}, min./max. transmission 0.643/0.8985; $2\theta_{max} = 50.7$°; $T = 100(2)$ K; of 25706 measured reflections, 6953 were independent ($R_{int} = 0.0826$); 489 parameters refined; $R1 = 0.070$ (all data), $wR2 = 0.1048$ (all data); $S = 1.019$, min./max. residual electron density $-0.597/0.337$ e Å^{-3}. CCDC-189707 contains the supplementary crystallographic data for this paper. These data can be obtained free of charge via www.ccdc.cam.ac.uk/conts/

 © 2003 Wiley-VCH Verlag GmbH & Co. KGaA, Weinheim 1433-7851/03/4208-0926 $ 20.00+.50/0

retrieving.html (or from the Cambridge Crystallographic Data Centre, 12, Union Road, Cambridge CB21EZ, UK; fax: (+44) 1223-336-033; or deposit@ccdc.cam.ac.uk).
[11] For crystal structures of a) [1.1]disila-, b) [1.1]distanna-, c) [1.1]diplumba-, and d) [1.1]digallaferrocenophanes, see a) D. L. Zechel, D. A. Foucher, J. K. Pudelski, G. P. A. Yap, A. L. Rheingold, I. Manners, *J. Chem. Soc. Dalton Trans.* **1995**, 1893–1899; b) A. Clearfield, C. J. Simmons, H. P. Withers, Jr., D. Seyferth, *Inorg. Chim. Acta* **1983**, *75*, 139–144; c) G. Utri, K. E. Schwarzhans, G. M. Allmaier, *Z. Naturforsch. B* **1990**, *45*, 755–762; d) W. Uhl, I. Hahn, A. Jantschak, T. Spies, *J. Organomet. Chem.* **2001**, *637–639*, 300–303; P. Jutzi, N. Lenze, B. Neumann, H.-G. Stammler, *Angew. Chem.* **2001**, *113*, 1470–1473; *Angew. Chem. Int. Ed.* **2001**, *40*, 1424–1427.
[12] P. Burk, I. A. Koppel, I. Koppel, R. Kurg, J.-F. Gal, P.-C. Maria, M. Herreros, R. Notario, J.-L. M. Abboud, F. Anvia, R. W. Taft, *J. Phys. Chem. A* **2000**, *104*, 2824–2833.
[13] M. Fontani, F. Peters, W. Scherer, W. Wachter, M. Wagner, P. Zanello, *Eur. J. Inorg. Chem.* **1998**, 1453–1465; M. Fontani, F. Peters, W. Scherer, W. Wachter, M. Wagner, P. Zanello, *Eur. J. Inorg. Chem.* **1998**, 2087.
[14] a) The cell for voltammetric studies was designed as detailed in ref. [14b]. Voltammetric scans were referenced by addition of a small amount of ferrocene as internal standard at an appropriate time of the experiment. For referencing of the oxidized solution a small sample (ca. 3 mL) was transferred from the electrolysis cell to the voltammetric cell, the required amount of ferrocene added, and voltammetric traces were recorded. Higher electric currents could not be obtained in the CVs due to solubility and adsorption problems; b) R. F. Winter, F. M. Hornung, *Organometallics* **1999**, *18*, 4005–4014.
[15] For general information on the electrochemistry of ferrocenes, see a) P. Zanello in *Ferrocenes* (Eds.: A. Togni, T. Hayashi), VCH, Weinheim, **1995**; b) D. Astruc, *Electron Transfer and Radical Processes in Transition Metal Chemistry*, Wiley-VCH, Weinheim, **1995**.
[16] Values at $\upsilon = 0.2\ V s^{-1}$. For the internal ferrocene standard, a peak potential difference ΔE_p of 82 mV was obtained under these conditions.
[17] P. D. Beer, P. A. Gale, G. Z. Chen, *J. Chem. Soc. Dalton Trans.* **1999**, 1897–1909.

Li-Intercalated Oxometallocubanes

Intercalation of Alkali Metal Cations into Layered Organotitanium Oxides**

José Gracia, Avelino Martín, Miguel Mena, María del Carmen Morales-Varela, Josep-M. Poblet, and Cristina Santamaría*

Dedicated to Professor Pascual Royo on the occasion of his 65th birthday

Species with a metallocubane structure constitute an interesting building block in inorganic solids, and considerable effort has been invested in selecting the composition and geometry of the precursor complexes to obtain specific characteristics and properties.[1] Some examples of the wide variety of inorganic materials whose structures are based on molecular cubane-like motifs are the molybdenum[2] and aluminum phosphates,[3] $M_yMo_xP_yO_z$ (M = metal cation), or various hydroxometalates $[M_xO_y(OH)_z]L$ (M = Ge, Ln,…).[4]

We have reported the formation and structure of the oxoheterometallocubanes $[\{(CO)_3Mo\}(\mu_3\text{-}O)_3\{Ti_3(\eta^5\text{-}C_5Me_5)_3(\mu_3\text{-}CR)\}]$ (R = H, Me)[5], which were obtained from the preorganized organometallic oxides $[\{Ti(\eta^5\text{-}C_5Me_5)(\mu\text{-}O)\}_3(\mu_3\text{-}CR)]$ (R = H (**1**), Me (**2**)).[6] Once we observed that the latter might be involved directly as macrocyclic tridentate ligands in encapsulation processes of different metals, we became interested in incorporating diverse metal complex fragments at the free vertex of the μ_3-alkylidyne oxo derivatives to build up the corresponding oxoheterometallocubanes.

As part of these ongoing studies, here we present the intercalation of alkali metal ions into layered organometallic titanium oxides by treatment of the alkylidyne complex **1** with different alkali metal alkyl and amide reagents.

The one-pot reaction of the tripodal starting material **1** with MR (M = Li, R = CH_2SiMe_3, CH_2CMe_3, *n*Bu; M = Na, R = *n*Bu; M = K, R = *n*Bu, CH_2Ph) in toluene/hexane at room temperature leads to the oxoheterometallodicubanes **3**–**5** in good yields. These compounds can be also obtained by

[*] Dr. M. Mena, Dr. A. Martín, M. d. C. Morales-Varela, Dr. C. Santamaría
Departamento de Química Inorgánica
Universidad de Alcalá, Campus Universitario
28871 Alcalá de Henares-Madrid (Spain)
Fax: (+34) 91-885-4683
E-mail: miguel.mena@uah.es
J. Gracia, Prof. Dr. J.-M. Poblet
Departament de Química Física i Inorgánica
Universitat Rovira i Virgili
Imperial Tarraco 1, 43005 Tarragona (Spain)

[**] Financial support for this work was provided by the Ministerio de Ciencia y Tecnología (BQU2001-1499 and PB98-0916-C02-02), Universidad de Alcalá (2002/010), and Generalitat de Catalunya (SGR01–00315). M.C.M.-V. thanks the Comunidad de Madrid for a doctoral fellowship.

 © 2003 Wiley-VCH Verlag GmbH & Co. KGaA, Weinheim 1433-7851/03/4208-0927 $ 20.00+.50/0

using $M[N(SiMe_3)_2]$ ($M = Li$, Na, K) in toluene or hexane at 60 °C (Scheme 1).

Crystallization of **3** from a double layer toluene/hexane at room temperature gave dark green crystals suitable for an X-ray diffraction study.[7–9] A simplified view of the unit cell of **3** showing the intercalation of the lithium atoms into the

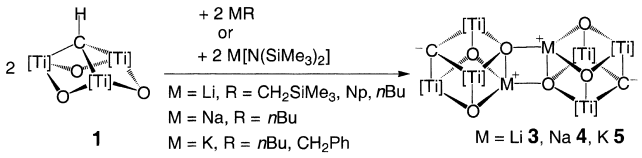

Scheme 1. Synthesis of the oxoheterometallodicubanes **3**–**5**. [Ti] = $Ti(\eta^5\text{-}C_5Me_5)$.

organometallic titanium oxide layers is given in Figure 1, and the molecular structure of **3** is shown in Figure 2. The structure reveals two LiO_3Ti_3C cubane cores directly linked through two Li–O bonds. The ensuing Li_2O_2 rhomb is planar and has the dimensions Li···Li 2.61(2) Å, (close to the value of 2.67 Å, reported for the diatomic species Li_2[10]), Li–O 2.386(13) and 1.891(12) Å, and O-Li-O 105.7(5)°, consistent with a trigonal-pyramidal LiO_4 coordination of its lithium atoms, analogous to that found for $[M(\mu_3\text{-}N)(\mu_3\text{-}NH)_2\{Ti_3(\eta^5\text{-}C_5Me_5)_3(\mu_3\text{-}N)\}]_2$ ($M = Li$, Na).[11]

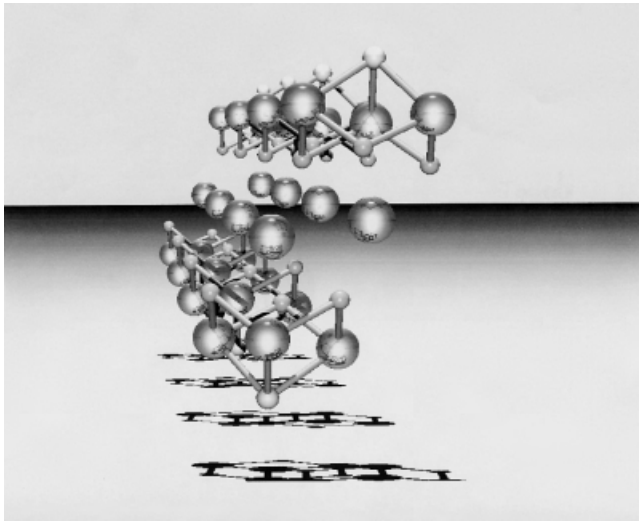

Figure 1. Simplified view of the unit cell of **3**, normal to the (100) plane.

The Ti_3O_3C subunits of **3** display several structural differences to that of the parent compounds **1** and **2**. The angles Ti-O-Ti (av 95.4°) and O-Ti-O (av 96.4°) in **3** are smaller than those in **1** and **2** (Ti-O-Ti av 100°, O-Ti-O av 104°).[6a,c] The Ti–C1 bond length (av 2.055 Å) lies between those in **1** (Ti–C1 2.10 Å),[6c] and **2** (Ti–C1 2.12 Å),[6a,c] and that in the zwitterionic derivative $[\{Ti(\eta^5\text{-}C_5Me_5)(\mu\text{-}O)\}_3\{\mu_3\text{-}\eta^2\text{-}C^-C(Me)N^+(2,6\text{-}Me_2C_6H_3)\}]$ (Ti–C$^-$ 2.017(5) Å).[12]

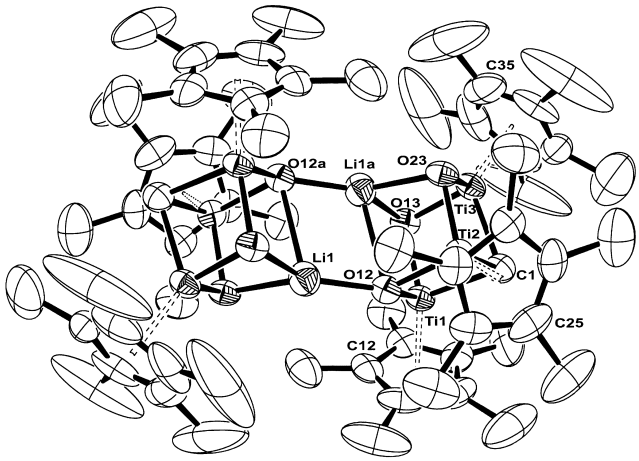

Figure 2. Structure of **3** (ORTEP drawing; 50% probability ellipsoids). The complex resides on an inversion center. Selected distances [Å] and angles [°]: Intercubane: Li···Li 2.61(2), Li-O 1.891(12); Li-(μ_4-O)-Li 74.3(5), (μ_4-O)-Li-(μ_4-O) 105.7(5), Ti-O(12)-Li(1) 130.2(4); intracubane: Ti···Ti 2.798(1) av, Li···Ti 2.885(11) av, (μ_4-O)-Li 2.386(13) av, (μ_3-O)-Li 2.057(12) av, Ti-O 1.891(4) av, Ti-C1 2.055(6) av; Ti-C1-Ti 85.8(2) av, C1-Ti-O 89.1(2) av, Ti-O-Ti 95.4(2) av, O-Ti-O 96.4(2) av, Ti-O12-Li1a 87.6(3) av, Ti3-O13-Li1a 86.1(4), Ti1-O13-Li1a 98.1(4), Ti3-O23-Li1a 87.5(4), Ti2-O23-Li1a 98.1(4).

DFT calculations reproduced quite well the X-ray geometry found for **3**.[13–17] However, for the central rhombic unit the optimization process yielded a structure with two short and two long Li–O bonds of 1.901 and 2.169 Å, respectively. Whereas the short bonds compare well with the experimental distance (1.891 Å), the discrepancy for the long bonds seems excessive (0.22 Å). In spite of this, we found that the energy difference between the complex optimized by keeping the central parallelepiped fixed at the experimental geometry and the fully optimized complex is only 12 kJ mol^{-1}.

The solid compounds **3**–**5** proved stable under argon at room temperature and practically insoluble in most common solvents (e.g. toluene, hexane, dichloromethane) with the exception of THF, which allowed the characterization of **4** and **5** by NMR spectroscopy. ^{1}H NMR spectra in [D$_8$]THF of **4** and **5** show only one signal at $\delta = 1.95$ and 1.94 ppm, respectively, which is assigned to the $\eta^5\text{-}C_5Me_5$ groups. The ^{13}C NMR spectra display signals with the appropriate multiplicity for the $\eta^5\text{-}C_5Me_5$ ligands, as well as a singlet for the apical μ_3-carbon atom ($\delta = 586.7$ (**4**) and 582.0 ppm (**5**)). These data indicate the removal of the proton of the μ_3-methylidyne fragment and are consistent with the formulation of these diamagnetic compounds as $[\{M(\mu_3\text{-}O)_3[Ti_3(\eta^5\text{-}C_5Me_5)_3(\mu_3\text{-}C)]\}_2]$ ($M = Li$, Na, K). Previously, Cummins et al. reported the formation of the carbidomolybdenum(VI) anions $[\{(Ar)RN\}_3Mo{\equiv}C]^-$ ($R = C(CD_3)_2CH_3$ or *t*Bu; $Ar = 3,5\text{-}Me_2C_6H_3$), which displayed a carbide chemical shift in the range $\delta = 474$–501 ppm.[18]

To clarify the magnitude of the chemical shifts found for the apical carbon atom in compounds **4** and **5**, we performed DFT-GIAO-based NMR calculations.[19] The computed δ value for the apical methylidyne-carbon atom in the precursor tridentate ligand model $[\{Ti(\eta^5\text{-}C_5H_5)(\mu\text{-}O)\}_3(\mu_3\text{-}CH)]$ (**1′**) was

 © 2003 Wiley-VCH Verlag GmbH & Co. KGaA, Weinheim 1433-7851/03/4208-0928 $ 20.00+.50/0

Table 1: Experimental and calculated ^{13}C chemical shifts (δ) for the apical carbon atom.

Molecule	δ	δ(DFT-GIAO)[b]	Shielding[a] σ_d[c]	σ_p[d]
$[\{TiCp^*(\mu\text{-}O)\}_3(\mu_3\text{-}CH)]$ (**1**)	383.2			
$[\{TiCp(\mu\text{-}O)\}_3(\mu_3\text{-}CH)]$ (**1′**)		385.3	241.2	−444.2
$[\{MeLi\}(\mu_3\text{-}O)_3\{Ti_3Cp_3(\mu_3\text{-}CH)\}]$		400.6	243.0	−461.3
$[Li(\mu_3\text{-}O)_3\{Ti_3Cp_3(\mu_3\text{-}C)\}]$		572.2	254.2	−644.1
$[\{Li(\mu_3\text{-}O)_3[Ti_3Cp_3(\mu_3\text{-}C)]\}_2]$(**3′**)		572.5	256.4	−646.6
$[\{Na(\mu_3\text{-}O)_3[Ti_3Cp^*_3(\mu_3\text{-}C)]\}_2]$ (**4**)	586.7			
$[\{K(\mu_3\text{-}O)_3[Ti_3Cp^*_3(\mu_3\text{-}C)\}_2]$ (**5**)	582.0			

[a] Shielding in ppm relative to TMS. [b] $\delta = \sigma(TMS) - (\sigma_d + \sigma_p)$ where the computed σ(TMS) is 182.3 ppm. For a detailed description of the implementation of the GIAO method in the ADF package as well as the calculation procedure of σ_d and σ_p see reference [19]. [c] Diamagnetic shielding. [d] Paramagnetic shielding.

385.3 ppm, a value that is almost identical to the experimental value found for **1** ($\delta = 383.2$ ppm). The formation of the carbido species induces an increase of the calculated δ value to 572.2 ppm, which is consistent with the experimental values measured for **4** ($\delta = 586.7$ ppm) and **5** ($\delta = 582.0$ ppm). These latter values can be explained in terms of a predominant paramagnetic contribution (Table 1), which could be attributed to the larger magnetic coupling between the σ carbon lone pair and the titanium orbitals. In the $[\{Ti(\eta^5\text{-}C_5H_5)(\mu\text{-}O)\}_3(\mu_3\text{-}C)]^-$ ionic fragment the HOMO orbital (−4.9 eV) is essentially the apical carbon lone pair, whereas in the corresponding nondeprotonated form $[\{Ti(\eta^5\text{-}C_5H_5)(\mu\text{-}O)\}_3(\mu_3\text{-}CH)]$ (**1′**), this orbital localizes very much lower in energy (at ~ −8 eV).

Because non-intermediates were detected during the course of this reaction, we used DFT calculations to propose the possible sequence leading to the formation of the oxometallodicubane model $[Li(\mu_3\text{-}O)_3\{Ti_3(\eta^5\text{-}C_5H_5)_3(\mu_3\text{-}C)\}]_2$ (**3′**; Figure 3). The initial step proceeds by coordination of the LiR unit to the oxomethylidyne ligand **1′** (Figure 3). The next step would consist in the CH_4 (or NH_3) elimination by deprotonation at the μ_3-methylidyne carbon atom, affording the monomer complex $[Li(\mu_3\text{-}O)_3\{Ti_3(\eta^5\text{-}C_5H_5)_3(\mu_3\text{-}C)\}]$. Finally, the assembly of two monomers leads to **3′**. All the processes are exothermic, especially those for the methane elimination.

The slow formation of the μ_3-ethylidyne complex $[Ti_3(\eta^5\text{-}C_5Me_5)_3(\mu_3\text{-}O)_3(\mu_3\text{-}CMe)]$ (**2**) from the reactions of **3–5** in $[D_6]$benzene with MeI confirmed unequivocally the existence of the μ_3-carbido group.

Herein we have focused on the reactions of the μ_3-methylidyne species **1** with alkali metal (Li, Na, K) alkyl or amide reagents. The process was analyzed by DFT calculations and the magnitude of the chemical shifts was determined for the apical μ_3-carbido groups in the products $[\{M(\mu_3\text{-}O)_3[Ti_3(\eta^5\text{-}C_5Me_5)_3(\mu_3\text{-}C)]\}_2]$ (M = Li, Na, K). As an extension of this work and to gain knowledge on the structural and electronic properties of this kind of compounds, we are currently investigating oxometallocubane-type systems containing the heaviest alkali metals as well as the incorporation of alkaline-earth metals into these sytems.

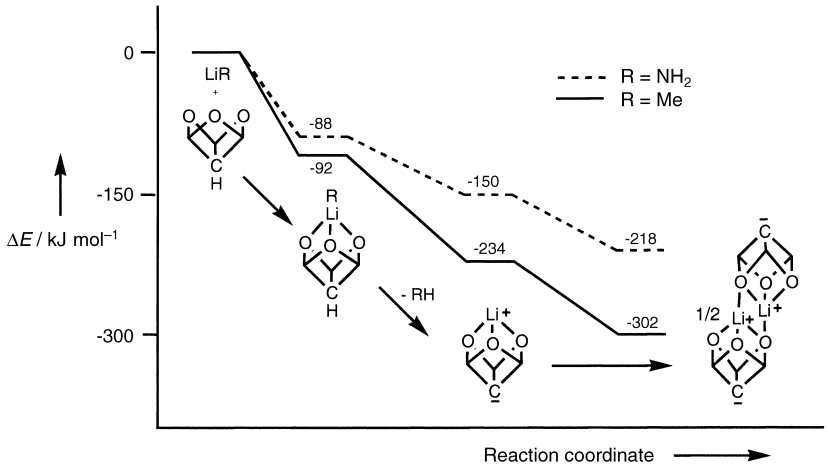

Figure 3. Computed ΔE (kJ mol^{-1}) values for the formation steps of the oxoheterometallodicubane model $[\{Li(\mu_3\text{-}O)_3[Ti_3(\eta^5\text{-}C_5H_5)_3(\mu_3\text{-}C)]\}_2]$ (**3′**).

Experimental Section

3: Treatment of **1** with $Li[N(SiMe_3)_2]$, NpLi, $Li[CH_2SiMe_3]$, or BuLi led to the formation of compound **3**. The reaction of **1** with BuLi is reported as an example. A solution of **1** (0.32 g, 0.52 mmol) in toluene (15 mL) and BuLi (0.3 mL, 0.52 mmol) in hexane (30 mL) was placed in a 100-mL Carious tube with a Young valve. The reaction mixture was left at room temperature overnight, after which a green microcrystalline solid was observed at the bottom of the flask. The solid was filtered and washed with hexane to yield **3** (0.30 g, 94%). This complex decomposed in THF precluding its characterization by NMR spectroscopy; IR (KBr): $\tilde{\nu} = 2907$ (vs), 2856 (vs), 1491 (w), 1437 (s), 1373 (s), 1023 (m), 801 (w), 681 (vs), 616 (vs), 464 (w), 416 cm^{-1} (s); elemental analysis calcd (%) for $Ti_6O_6C_{62}H_{90}Li_2$ (1232.50): C 60.41, H 7.36; found: C 60.40, H 7.34.

4: The treatment of **1** with BuNa or $Na[N(SiMe_3)_2]$ afforded compound **4**. The reaction of **1** with $Na[N(SiMe_3)_2]$ is reported as an example. A 100-mL Carious tube with a Young valve was charged with **1** (0.3 g, 0.49 mmol), $Na[N(SiMe_3)_2]$ (0.09 g. 0.49 mmol), and toluene (40 mL). The reaction mixture was heated at 60 °C overnight and the red solid formed was washed with hexane to give **4** (0.18 g, 58%); ^1H NMR (300 MHz, $[D_8]$THF, 25 °C, TMS): $\delta = 1.95$ ppm (s; C_5Me_5); ^{13}C NMR (300 MHz, $[D_8]$THF, 25 °C, TMS): $\delta =$ 11.7 ($C_5\mathit{Me}_5$), 115.4 (C_5Me_5), 586.7 ppm (μ_3-C); IR (KBr): $\tilde{\nu} = 2907$ (vs), 2850 (vs), 1493 (w), 1437 (s), 1372 (s), 1023 (m), 795 (w), 681 (vs), 621 (vs), 467 (w), 411 cm^{-1} (s); elemental analysis calcd (%) for $Ti_6O_6C_{62}H_{90}Na_2$ (1264.60): C 58.79, H 7.32; found: C 58.90, H 7.39.

5: Analogously to the preparation of **4, 1** (0.30 g, 0.49 mmol) and $K[N(SiMe_3)_2]$ (0.10 g, 0.49 mmol) were allowed to react in hexane (40 mL) to afford **5** as a red solid (0.21 g, 66%); ^1H NMR (500 MHz, $[D_8]$THF, 25 °C, TMS): $\delta =$

1.94 ppm (s, C_5Me_5); ^{13}C NMR (500 MHz, [D_8]THF, 25 °C, TMS): $\delta =$ 11.5 ($C_5\mathit{Me}_5$), 115.1 (C_5Me_5), 582.0 ppm (μ_3-C); IR (KBr): $\tilde{\nu} = 2910$ (vs), 2857 (vs), 1597 (w), 1495 (w), 1439 (s), 1375 (s), 1247 (w), 1067 (w), 916 (m), 899 (m), 852 (s), 784 (vs), 680 (s), 624 (m), 573 (m), 411 cm^{-1} (s); elemental analysis calcd (%) for $Ti_6O_6C_{62}H_{90}K_2$ (1296.82): C 57.42, H 6.99; found: C 56.99, H 7.10.

Received: July 24, 2002
Revised: October 16, 2002 [Z19810]

[1] A. P. Alivisatos, P. F. Barbara, A. W. Castleman, J. Chang, D. A. Dixon, M. L. Klein, G. L. McLendon, J. S. Miller, M. A. Ratner, P. J. Rossky, S. I. Stupp, M. E. Thompson, *Adv. Mater.* **1998**, *10*, 1297 – 1336.

[2] a) R. C. Haushalter, *J. Chem. Soc. Chem. Commun.* **1987**, 1566 – 1568; b) K. H. Lii, R. C. Haushalter, C. J. O'Connor, *Angew. Chem.* **1987**, *99*, 574 – 576; *Angew. Chem. Int. Ed. Engl.* **1987**, *26*, 549 – 551.

[3] P. Feng, X. Bu, G. D. Stucky, *Science* **1997**, *278*, 2080 – 2088.

[4] a) H. Li, M. Eddaoudi, O. M. Yaghi, *Angew. Chem.* **1999**, *111*, 682 – 685; *Angew. Chem. Int. Ed.* **1999**, *38*, 653 – 655; b) B.-Q. Ma, D.-S. Zhang, S. Gao, T.-Z. Jin, C.-H. Yan, G.-X. Xu, *Angew. Chem.* **1999**, *111*, 3790 – 3792; *Angew. Chem. Int. Ed.* **2000**, *39*, 3644 – 3646.

[5] A. Abarca, M. Galakhov, P. Gómez-Sal, A. Martín, M. Mena, J. M. Poblet, C. Santamaría, J. P. Sarasa, *Angew. Chem.* **2000**, *112*, 544 – 547; *Angew. Chem. Int. Ed.* **2000**, *39*, 534 – 537.

[6] a) R. Andrés, M. Galakhov, A. Martín, M. Mena, C. Santamaría, *Organometallics* **1994**, *13*, 2159 – 2163; b) R. Andrés, M. Galakhov, A. Martín, M. Mena, C. Santamaría, *J. Chem. Soc. Chem. Commun.* **1995**, 551 – 552; c) R. Andrés, PhD thesis, Universidad de Alcalá, Madrid, **1995**.

[7] X-ray crystal structure determination of **3**: All data were collected on an ENRAF NONIUS CAD4 diffractometer at room temperature, $Mo_{K\alpha} = 0.71073$ Å. The structure was solved, using the WINGX[8] package, by direct methods (SHELXS-97) and refined by least-squares against F^2 (SHELXL-97).[9] X-ray data for $C_{62}H_{90}Li_2O_6Ti_6$ (**3**): $0.45 \times 0.34 \times 0.30$ mm^3, triclinic, $P\bar{1}$, $a = 11.405(2)$, $b = 11.695(2)$, $c = 14.671(3)$ Å, $\alpha = 111.71(2)$, $\beta = 90.78(2)$, $\gamma = 116.39(3)$°, $V = 1590.9(5)$ Å^3, $\rho_{calcd} = 1.287$ Mg m^{-3}. Intensity measurements were performed by ω–2θ scans in the range $3° < \theta < 23°$, of the 4789 measured reflections, 4530 were independent; $R1 = 0.056$ and $wR2 = 0.138$ (for 2617 reflections with $F > 4\sigma(F)$). The values of $R1$ and $wR2$ are defined as follows: $R1 = \Sigma\,||F_o| - |F_c||/[\Sigma\,|F_o|]$; $wR2 = \{[\Sigma w(F_o^2 - F_c^2)^2]/[\Sigma w(F_o^2)^2]\}^{1/2}$. Largest difference peak and hole 0.380 and -0.318 e Å^{-3}. All non-hydrogen atoms were anisotropically refined. The hydrogen atoms were positioned geometrically and refined by using a riding model in the last cycles of refinement with a fixed value of $U(eq) = 0.08$. CCDC-190221 contains the supplementary crystallographic data for this paper. These data can be obtained free of charge via www.ccdc.cam.ac.uk/conts/retrieving.html (or from the Cambridge Crystallographic Data Centre, 12, Union Road, Cambridge CB2 1EZ, UK; fax: (+44) 1223-336-033; or deposit@ccdc.cam.ac.uk).

[8] WinGX:L. J. Farrugia, *J. Appl. Crystallogr.* **1999**, *32*, 837 – 838.

[9] G. M. Sheldrick, SHELX-97, *Program for Crystal Structure Analysis* (Release 97-2), University of Göttingen, Göttingen, Germany, **1998**.

[10] W. L. Jolly, *Modern Inorganic Chemistry*, 2nd ed., McGraw-Hill, New York, **1991**, p. 107.

[11] M. García-Castro, A. Martín, M. Mena, A. Pérez-Redondo, C. Yélamos, *Chem. Eur. J.* **2001**, *7*, 647 – 651.

[12] R. Andrés, M. Galakhov, M. P. Gómez-Sal, A. Martín, M. Mena, C. Santamaría, *Chem. Eur. J.* **1998**, *4*, 1206 – 1213.

[13] All DFT calculations were carried out with the ADF program[14] by using triple-ζ and polarization Slater basis sets to describe the valence electrons of C, O, and Li. For titanium, a frozen core composed of the 1s, 2s, and 2p orbitals was described by double-ζ Slater functions, the 3d and 4s orbitals by triple-ζ functions, and the 4p orbital by a single orbital. The geometries and binding energies were calculated with gradient corrections. We used the local spin density approximation, characterized by the electron gas exchange (Xα with $\alpha = 2/3$) together with Vosko–Wilk–Nusair parametrization[15] for correlation. Becke's nonlocal corrections[16] to the exchange energy and Perdew's nonlocal corrections[17] to the correlation energy were added.

[14] a) ADF 2000.01, Department of Theoretical Chemistry, Vrije Universiteit, Amsterdam; b) E. J. Baerens. D. E. Ellis, P. Ros, *Chem. Phys.* **1973**, *2*, 41 – 51; c) L. Versluis, T. Ziegler, *J. Chem. Phys.* **1988**, *88*, 322 – 328; d) G. Te Velde, E. J. Baerens, *J. Comput. Phys.* **1992**, *99*, 84 – 98; e) C. Fonseca Guerra, J. G. Snijders, G. Te Velde, E. J. Baerens, *Theor. Chem. Acc.* **1998**, *99*, 391 – 403.

[15] S. H. Vosko, L. Wilk, M. Nusair, *Can. J. Phys.* **1980**, *58*, 1200 – 1211.

[16] a) A. D. Becke, *J. Chem. Phys.* **1986**, *84*, 4524 – 4529; b) A. D. Becke, *Phys. Rev. A* **1988**, *38*, 3098 – 3100.

[17] a) J. P. Perdew, *Phys. Rev. B* **1986**, *33*, 8822 – 8824; b) J. P. Perdew, *Phys. Rev. B* **1986**, *34*, 7406 – 7406.

[18] a) J. C. Peters, A. L. Odom, C. C. Cummins, *Chem. Commun.* **1997**, 1995 – 1996; b) J. B. Greco, J. C. Peters, T. A. Baker, W. M. Davis, C. C. Cummins, G. Wu, *J. Am. Chem. Soc.* **2001**, *123*, 5003 – 5013.

[19] a) G. Schrekenbach, T. Ziegler, *J. Phys. Chem.* **1995**, *99*, 606 – 611; b) Y. Ruiz-Morales, G. Schrekenbach, T. Ziegler, *J. Phys. Chem.* **1996**, *100*, 3359 – 3367; c) Y. Ruiz-Morales, G. Schrekenbach, T. Ziegler, *Organometallics* **1996**, *15*, 3920 – 3923; d) G. Schrekenbach, T. Ziegler, *Int. J. Quantum Chem.* **1997**, 61, 899 – 918.

 © 2003 Wiley-VCH Verlag GmbH & Co. KGaA, Weinheim 1433-7851/03/4208-0930 $ 20.00+.50/0

Unselectivity as an Advantage

Unselective Phenolic Coupling of Methyl 2-Hydroxy-4-methoxy-6-methylbenzoate—A Valuable Tool for the Total Synthesis of Natural Product Families**

*Daniel Drochner, Wolfgang Hüttel, Martin Nieger, and Michael Müller**

The biaryl axis is a common feature of many herbal, fungal, and bacterial natural products.[1] For many of these biaryl compounds the biosynthesis contains an oxidative phenolic coupling step with a regio- and stereochemistry characteristic of the biological origin.[2] For this reason, families of closely related dimeric phenolic secondary metabolites are found in nature differing only in the linkage and spatial arrangement of their monomeric precursors. This kind of biodiversity is, for example, common to the naphthylisoquinoline alkaloids dioncophylline A, B, and C from *Triphyophyllum peltatum*,[3] to the dimeric dihydroanthracenones flavomannin (*Penicillium wortmannii, Cortinarius odoratus*), atrovirin (*Cortinarius atrovirens*), and phlegmacin (*Cortinarius sp., Cassia torosa*),[4] as well as to the dimeric coumarins kotanin (**1**) (*Aspergillus clavatus*), isokotanin A (**2**) (*Aspergillus alliaceus*), and desertorin C (**3**) (*Emericella desertorum*) (Scheme 1).[5]

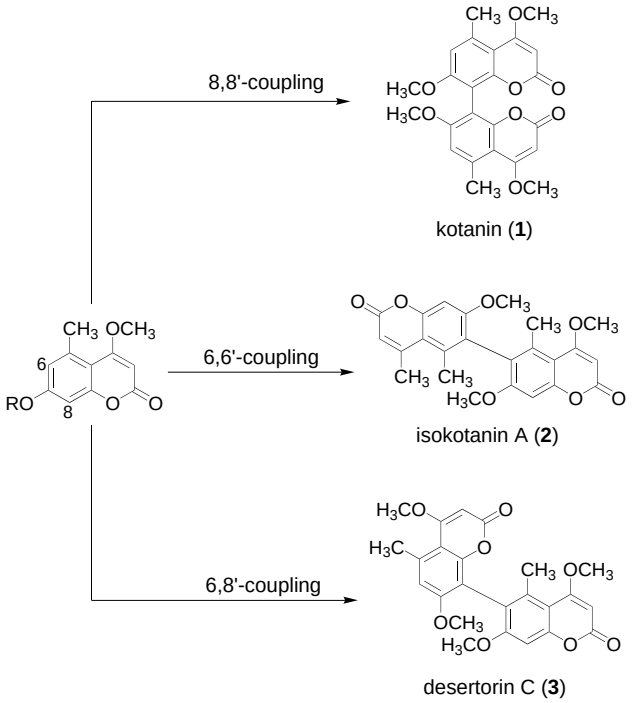

Scheme 1. Putative biosynthesis of dimeric coumarins.

In general, biaryl skeletons can be constructed by 1) the classical Ullmann reaction and other reductive processes[6] or 2) the oxidative (biomimetic) phenolic coupling reaction using heavy metal oxidants like thallium(III), vanadium(V), ruthenium(IV), and iron(III) salts.[7] Here we report on a new and highly efficient synthesis of the dimeric coumarins **1**–**3** by an unselective oxidative phenolic coupling reaction of a monomeric orsellinic acid derivative as the key step.

The synthesis of symmetric dimeric orsellinates starting from methyl 2-hydroxy-4-methoxy-6-methylbenzoate (**4**)[8] is well established. Ullmann reaction of the regioselectively iodinated and fully methylated derivatives of **4** followed by regioselective demethylation provided the 3,3′- and 5,5′-dimers **5** and **6**, respectively (see Scheme 2).[9] However, this multistep synthesis is limited to the methyl residue as the protecting group because the Ullmann reaction is sensitive to sterically more demanding substituents.[6] Moreover, the unsymmetrical 3,5′-dimer **7** is not accessible using this strategy.[10] Therefore, a more straightforward and flexible access to dimeric orsellinates would be desirable. In 1997, Harada et al. reported a highly selective oxidative phenolic coupling of 2,4-di-*O*-methylphloroacetophenone (phloroacetophenone = 2,4,6-trihydroxyacetophenone) in the solid state.[11] They heated a mixture of the substrate and iron(III) chloride adsorbed on silica gel at 45 °C for six days and obtained the symmetrical 5,5′-dimer in 81 % yield.

Because of its structural similarity to 2,4-di-*O*-methylphloroacetophenone, methyl 2-hydroxy-4-methoxy-6-methylbenzoate (**4**) seemed to be an appropriate substrate to extend this method to the phenolic coupling of orsellinates. The phenolic coupling was carried out by heating a mixture of **4** and ferric chloride adsorbed on silica gel at 60 °C for 20 h. Remarkably, this reaction required much shorter reaction times and was unselective with regard to the coupling position. After separation by a single flash chromatography on silica gel, the 3,3′-, 5,5′-, and 3,5′-dimers **5**–**7** were obtained in 17, 33, and 30 % yield, respectively (Scheme 2). This reaction was also performed on a 2 g scale with a total yield of 70 %. We assume that the modified reaction behavior (unselectivity and shorter reaction times) results from the electronic differences between 2,4-dimethylphloroacetophenone and **4**. Unselective oxidative phenolic couplings have been known for a long time,[12] however, only one attempt has been made to utilize this unselectivity in diversity-oriented natural product synthesis.[11c]

Starting from the three regioisomeric dimers of orsellinate **4** we designed the synthesis of **1**–**3**. The coumarin core was obtained by a new strategy—the nucleophilic addition of the acetonitrile anion to the carboxy carbon atoms of the dimeric

[*] Dr. M. Müller, Dipl.-Chem. D. Drochner, Dipl.-Chem. W. Hüttel
Institut für Biotechnologie 2
Forschungszentrum Jülich GmbH
52425 Jülich (Germany)
Fax: (+49) 2461-613870
E-mail: mi.mueller@fz-juelich.de
Dr. M. Nieger
Institut für Anorganische Chemie
Rheinische Friedrich-Wilhelms-Universität
53121 Bonn (Germany)

[**] D.D. was financially supported by the Fonds der Chemischen Industrie and DECHEMA. The skillful technical assistance of Petra Geilenkirchen is gratefully acknowledged. M.M. thanks Prof. W. Steglich for bringing the biosynthetic problem of regio- and stereoselective oxidative phenolic coupling to his attention.

 © 2003 Wiley-VCH Verlag GmbH & Co. KGaA, Weinheim 1433-7851/03/4208-0931 $ 20.00+.50/0

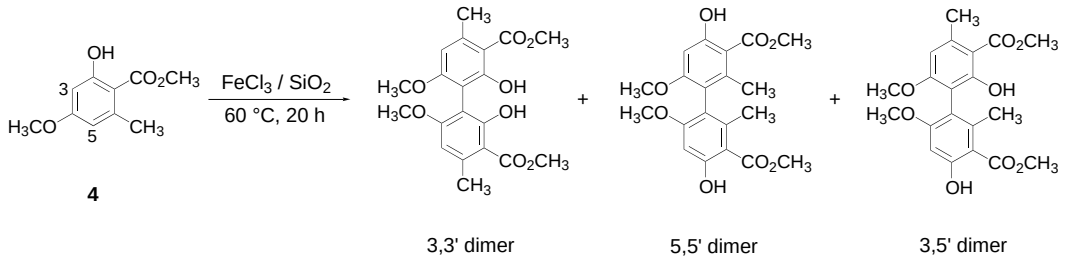

Scheme 2. Oxidative phenolic coupling of monomeric orsellinate **4**.

orsellinates.[13] After acidic hydrolysis followed by methylation of the free hydroxy groups with dimethylsulfate the dimeric coumarins were obtained in 30% yield for kotanin (**1**), 33% yield for isokotanin A (**2**), and 24% yield for desertorin C (**3**; Scheme 3).

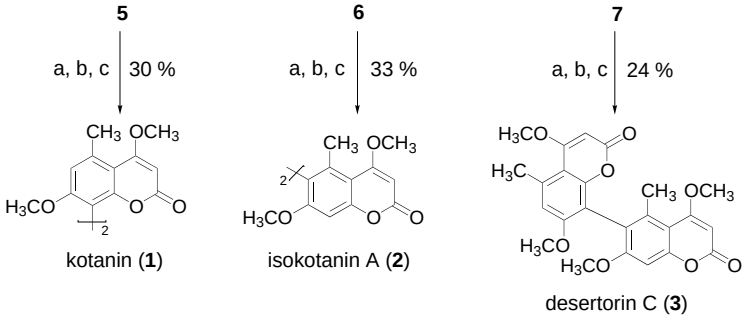

Scheme 3. a) MeCN, *n*BuLi, −78°C to RT; b) HCl, methanol, △; c) NaH, Me_2SO_4, HMPT (hexamethylphosphoric triamide).

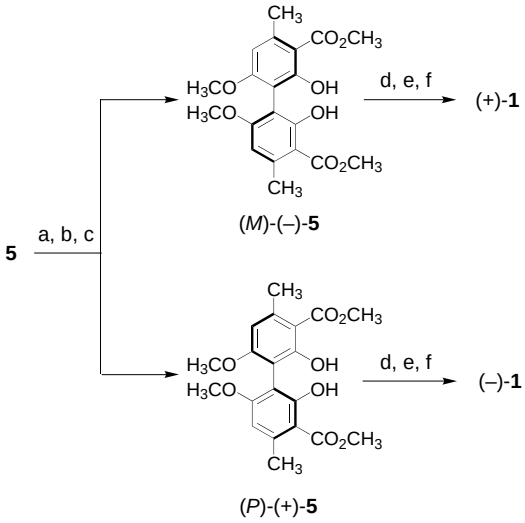

Scheme 4. a) (−)-camphanic acid chloride, DMAP (4-dimethylaminopyridine), pyridine, 84%; b) chromatographic separation on silica gel (isohexane/ethyl acetate, 1:1); c) NaOMe, methanol, 75%; d) MeCN, *n*BuLi, −78°C to RT, 75%; e) HCl, methanol, △, 67%; f) NaH, Me_2SO_4, HMPT, 59%.

As an example, the atropisomers of the racemic 3,3′-coupled orsellinate **5** were resolved as diastereomeric bis(camphanate) esters obtained with (−)-camphanic acid chloride as the chiral derivatizing agent.[11e] This reaction occurred with a yield of 84%, and the two diastereomers were formed in a ratio of 1:1. After separation (SiO_2), the absolute configuration of the biphenyl moiety of the first-eluting diastereomer was determined as *M* by X-ray structure analysis using the known absolute configuration of the camphanate ester residue.[14] Cleavage of the chiral moiety worked with sodium methanolate to give the atropisomeric 3,3′-coupled biaryls (*M*)-(−)-**5** and (*P*)-(+)-**5** in 75% yield. These two enantiomerically pure dimeric orellinates were used in the synthesis of (+)- and (−)-kotanin following the procedure described above (Scheme 4). Since the atropisomers of the two other dimeric orsellinates, **6** and **7**, should also be accessible by enantiomeric resolution or separation by HPLC on a chiral phase the synthesis of both enantiomers of isokotanin A (**2**) and desertorin C (**3**) seems possible.

In summary, a short and very efficient synthesis of the dimeric coumarins kotanin (**1**), isokotanin A (**2**), and desertorin C (**3**) has been presented. As a result of the unselective oxidative phenolic coupling of the monomeric orsellinate **4** all three regioisomeric biaryls are available starting from the same substrate. Thus the procedure mimics the biosynthesis of these natural products. Since the dimeric orsellinates are readily available and highly functionalized other classes of natural products should be similarly accessible.

Experimental Section

Phenolic coupling of **4**: Silica gel (7.24 g) was added to a solution of $FeCl_3 \cdot 6H_2O$ (3.52 g, 13.02 mmol) in diethyl ether (190 mL) and methanol (10 mL). The solvents were removed to give a yellow solid, which was dried at 50°C in vacuo (0.4 mbar) for 8 h to leave a yellow-green solid. This solid (1.40 g) was given to a solution of **4** (146 mg, 0.74 mmol) in dichloromethane (30 mL). After mixing well, the solvent was removed under reduced pressure to give a dark solid, which was heated at 60°C for 20 h. Methanol (50 mL) was added, and the mixture was filtered (celite). The solvent was removed in vacuo, and the dark residue was purified by column chromatography (gradient isohexane/ethyl acetate 5:1→2:1) to yield the biphenyldiols

 © 2003 Wiley-VCH Verlag GmbH & Co. KGaA, Weinheim 1433-7851/03/4208-0932 $ 20.00+.50/0

5 (22 mg, 17%), **6** (42 mg, 33%), and **7** (38 mg, 30%) as colorless solids.[15]

5: $R_f = 0.22$ (isohexane/ethyl acetate, 2:1); M.p. 246°C; ^{1}H NMR (300 MHz, $CDCl_3$): $\delta = 11.81$ (s, 2H, 2 × OH), 6.41 (s, 2H, 2 × Ar-H), 3.91 (s, 6H, 2 × OCH_3), 3.77 (s, 6H, 2 × OCH_3), 2.59 ppm (s, 6H, 2 × CH_3); ^{13}C NMR (75.5 MHz, $CDCl_3$): $\delta = 172.37$ (2 × C=O), 161.90 (2 × C_q), 161.50 (2 × C_q), 143.10 (2 × C_q), 107.84 (2 × C_q), 106.69 (2 × CH), 105.97 (2 × C_q), 55.82 (2 × OCH_3), 51.85 (2 × OCH_3), 24.96 ppm (2 × CH_3); MS: *m/z* (%): 390 (67) [M^+], 358 (70) [$C_{19}H_{18}O_7^+$], 327 (65) [$C_{18}H_{15}O_6^+$], 295 (100) [$C_{17}H_{11}O_5^+$]; HRMS: calcd for $C_{20}H_{22}O_8$ 390.1315; found 390.1311.

6: $R_f = 0.33$ (isohexane/ethyl acetate, 2:1); M.p. 183°C; ^{1}H NMR (300 MHz, $CDCl_3$): $\delta = 11.77$ (s, 2H, 2 × OH), 6.41 (s, 2H, 2 × Ar-H), 3.91 (s, 6H, 2 × OCH_3), 3.67 (s, 6H, 2 × OCH_3), 2.10 ppm (s, 6H, 2 × CH_3); ^{13}C NMR (75.5 MHz, $CDCl_3$): $\delta = 172.49$ (2 × C=O), 164.47 (2 × C_q), 162.25 (2 × C_q), 141.41 (2 × C_q), 119.15 (2 × C_q), 105.55 (2 × C_q), 97.29 (2 × CH), 55.69 (2 × OCH_3), 51.83 (2 × OCH_3), 19.36 ppm (2 × CH_3); MS: *m/z* (%): 390 (47) [M^+], 358 (31) [$C_{19}H_{18}O_7^+$], 327 (100) [$C_{18}H_{15}O_6^+$], 295 (100) [$C_{17}H_{11}O_5^+$]; HRMS: calcd for $C_{20}H_{22}O_8$ 390.1315; found 390.1314.

7: $R_f = 0.24$ (isohexane/ethyl acetate, 2:1); M.p. 190°C; ^{1}H NMR (300 MHz, $CDCl_3$): $\delta = 11.79$ (s, 1H, OH), 11.74 (s, 1H, OH), 6.44 (s, 1H, Ar-H), 6.38 (s, 1H, Ar-H), 3.92 (s, 3H, OCH_3), 3.90 (s, 3H, OCH_3), 3.75 (s, 3H, OCH_3), 3.70 (s, 3H, OCH_3), 2.60 (s, 3H, CH_3), 2.22 ppm (s, 3H, CH_3); ^{13}C NMR (75.5 MHz, $CDCl_3$): $\delta = 172.53$ (C=O), 172.41 (C=O), 164.74 (C_q), 162.34 (C_q), 161.90 (C_q), 161.35 (C_q), 142.80 (C_q), 141.64 (C_q), 115.71 (C_q), 111.16 (C_q), 106.45 (CH), 105.87 (C_q), 105.65 (C_q), 97.50 (CH), 55.81 (OCH_3), 55.69 (OCH_3), 51.91 (OCH_3), 51.78 (OCH_3), 24.94 (CH_3), 19.67 ppm (CH_3); MS: *m/z* (%): 390 (53) [M^+], 358 (66) [$C_{19}H_{18}O_7^+$], 326 (100) [$C_{18}H_{14}O_6^+$]; HRMS: calcd for $C_{20}H_{22}O_8$ 390.1315; found 390.1323.

Received: August 16, 2002 [Z19985]

[1] For leading references on both the synthesis and natural occurrence of biaryls, see a) G. Bringmann, R. Walter, R. Weirich, *Angew. Chem.* **1990**, *102*, 1006–1019; *Angew. Chem. Int. Ed. Engl.* **1990**, *29*, 977–990; b) D. A. Whiting in *Comprehensive Organic Synthesis, Vol. 3* (Eds.: B. M. Trost, I. Fleming, G. Pattenden), Pergamon, Oxford, **1991**, p. 659–701; c) G. Bringmann, C. Günther, M. Ochse, O. Schupp, S. Tasler, *Prog. Chem. Org. Nat. Prod.* **2001**, *82*, 1–249.

[2] a) D. H. R. Barton, T. Cohen, *Festschrift Prof. A. Stoll zum siebzigsten Geburtstag*, Birkhäuser, Basel, **1957**, p. 117; b) L. B. Davin, H. B. Wang, A. L. Crowell, D. L. Bedgar, D. M. Martin, S. Sarkanen, N. G. Lewis, *Science* **1997**, *275*, 362–366.

[3] G. Bringmann, C. Günther, E.-M. Peters, K. Peters, *Tetrahedron* **2001**, *57*, 1253–1259.

[4] M. Gill, W. Steglich, *Prog. Chem. Org. Nat. Prod.* **1987**, *51*, 1–317.

[5] a) G. Büchi, D. H. Klaubert, R. C. Shank, S. M. Weinreb, G. N. Wogan, *J. Org. Chem.* **1971**, *36*, 1143–1147; b) J. A. Laakso, E. D. Narske, J. B. Gloer, D. T. Wicklow, P. F. Dowd, *J. Nat. Prod.* **1994**, *57*, 128–133; c) K. Nozawa, H. Seyea, S. Nakajima, S.-I. Udagawa, K.-I. Kawai, *J. Chem. Soc. Perkin Trans. 1* **1987**, 1735–1738.

[6] a) F. Ullmann, J. Bielecki, *Ber. Dtsch. Chem. Ges.* **1901**, *34*, 2176–2184; b) R. C. Fuson, E. A. Cleveland, *Org. Synth. Coll. Vol. III* **1955**, 339; c) P. E. Fanta, *Synthesis* **1974**, 9–21.

[7] a) G. Bringmann, S. Tasler, *Tetrahedron* **2001**, *57*, 331–343; b) E. C. Taylor, J. G. Andrade, G. J. H. Rall, A. McKillop, *J. Am. Chem. Soc.* **1980**, *102*, 6513–6519; c) K. Tomioka, T. Ishiguro, Y. Itaka, K. Koga, *Tetrahedron* **1984**, *40*, 1303–1313; d) J. S. Buckleton, R. C. Cambie, G. R. Clark, P. A. Craw, C. E. F. Rickard, P. S. Rutledge, P. D. Woodgate, *Aust. J. Chem.* **1988**, *41*, 305–324; e) M. Tanaka, C. Mukaiyama, H. Mitsuhashi, M. Maruno, T. Wakamatsu, *J. Org. Chem.* **1995**, *60*, 4339–4352.

[8] a) J. Chiarello, M. M. Joullié, *Tetrahedron* **1988**, *44*, 41–48; b) T. Sala, M. V. Sargent, *J. Chem. Soc. Perkin Trans. 1* **1981**, 855–869.

[9] a) R. G. F. Giles, M. V. Sargent, *Aust. J. Chem.* **1986**, *39*, 2177–2181; b) G. Billen, U. Karl, T. Scholl, K. D. Stroech, W. Steglich in *Natural Products III* (Eds.: Atta-ur-Rahman, P. W. Le Quesne), Springer, Berlin, **1988**, p. 305–315; c) F. M. Hauser, P. J. F. Gauuan, *Org. Lett.* **1999**, *1*, 671–672.

[10] The tetramethoxy derivative of the unsymmetrical dimer **7** was obtained as a minor side product by Ullmann reaction of the 3,5-diiodo orsellinate: U. Karl, PhD thesis, Rheinische Friedrich-Wilhelms-Universität Bonn, **1988**.

[11] a) E. Keinan, Y. Mazur, *J. Org. Chem.* **1978**, *43*, 1020–1022; b) T. C. Jempty, L. L. Miller, Y. Mazur, *J. Org. Chem.* **1980**, *45*, 749–751; c) M. R. Parthasarathy, S. Gupta, *Indian J. Chem. Sect. B* **1984**, *23*, 227–230; d) F. Toda, K. Tanaka, S. Iwata, *J. Org. Chem.* **1989**, *54*, 3007–3009; e) H.-Y. Li, T. Nehira, M. Hagiwara, N. Harada, *J. Org. Chem.* **1997**, *62*, 7222–7227.

[12] a) R. Pummerer, H. Puttfarcken, P. Schopflocher, *Ber. Dtsch. Chem. Ges.* **1925**, *58*, 1808–1820; b) J. D. Edwards, J. L. Cashaw, *J. Chem. Soc.* **1954**, 6141–6143.

[13] a) A. K. Gupta, H. Ila, H. Junjappa, *Tetrahedron* **1990**, *46*, 2561–2572; b) W. Basinski, *Pol. J. Chem.* **1995**, *69*, 376–384; c) the resulting compounds presumably exist in an iminocoumarin- or iminochromenone-like structure since the proton NMR spectra reveal two vinyl protons but no methylene groups.

[14] X-ray structure analysis of dimethyl (*M*)-(−)-2,2′-bis(camphanate)-6,6′-dimethoxy-4,4′-dimethyl-1,1′-biphenyldicarboxylate ($C_{40}H_{46}O_{14}$): colorless crystals, crystal dimension 0.30 × 0.35 × 0.40 mm^3; $M = 750.77$; monoclinic, space group $P2_1$ (no. 4), $a = 10.5732(2)$, $b = 16.5829(3)$, $c = 11.0339(2)$ Å, $\beta = 105.317(1)°$, $V = 1865.90(6)$ nm^3, $Z = 2$, $\mu(Mo_{K\alpha}) = 0.101$ mm^{-1}, $T = 123(2)$ K, $F(000) = 796$. 20007 reflections up to $2\theta_{max} = 50.7°$ were measured on a Nonius Kappa-CCD diffractometer with $Mo_{K\alpha}$ radiation, 6614 of which were independent and used for all calculations ($R_{int} = 0.035$). The structure was solved by direct methods and refined to F^2 anisotropically, the H atoms were refined with a riding model. The final quality coefficient $wR2(F^2)$ was 0.113, with a conventional $R(F) = 0.043$ for 483 parameters and 165 restraints. One carboxylate group is disordered. The absolute structure cannot be determined reliably (Flack's *x* parameter 0.2(8)). CCDC-197800 contains the supplementary crystallographic data for this paper. These data can be obtained free of charge via www.ccdc.cam.ac.uk/conts/retrieving.html (or from the Cambridge Crystallographic Data Centre, 12, Union Road, Cambridge CB2 1EZ, UK; fax: (+44) 1223-336-033; or deposit@ccdc.cam.ac.uk).

[15] From fractions containing **5** and **7**, the symmetric compound crystallizes quantitatively to give after separation by centrifugation analytically pure (NMR) **5** and **7**.

3d-4f Metal Coordination Polymers

A Nanotubular 3D Coordination Polymer Based on a 3d–4f Heterometallic Assembly**

Bin Zhao, Peng Cheng, Yan Dai, Cai Cheng, Dai-Zheng Liao,* Shi-Ping Yan, Zong-Hui Jiang, and Geng-Lin Wang*

Interest in porous metal-coordination polymers that are constructed by self-assembly processes has mushroomed recently,[1] because of their use in, for example, redox catalysis, cathodic electrolysis, ion exchange, adsorption, separation, sensors, and molecular recognition.[2–5] However, much of the work has so far focused on coordination polymers containing transition metals,[2,6] while rare-earth metal compounds have received much less attention.[7] To date, no systematic investigation of zeolite-type structures containing metal atoms from the lanthanide series along with transition-metal atoms has been documented. Furthermore, the pores or channels reported were mainly formed through either hydrogen bonding,[2b] or π–π packing,[1b] and only in a few cases were they formed through metal–ligand bonding alone.[1c7f] On the other hand, the construction of mesoporous metal–organic polymers suffers from difficulties in the control of the polymer dimensionality. Although ligands can be designed to create a large hole, the resulting coordination polymers are often plagued by lattice interpenetration,[8] or framework breakdown on removal of a guest molecule.[9] In addition, the variable and versatile coordination behavior of 4f-metal ions limits their selective introduction into highly ordered structures.

Herein we report the syntheses and structures of three coordination polymers formed through hydrothermal synthesis: $[\{[Ln(dipic)_3Mn_{1.5}(H_2O)_3]\cdot n H_2O\}_\infty]$, H_2dipic = pyridine-2,6-dicarboxylic acid; Ln = Pr, $n = 2$ (**1**); Ln = Gd, $n = 3.5$ (**2**); Ln = Er, $n = 3$ (**3**). These compounds have the relatively large nanometer-sized tubes associated with self-assembly processes directed by metal–ligand coordination only, and the framework remains intact on removing water molecules trapped in the nanotube.

The three compounds are stable in air and are insoluble in common solvents. Single-crystal X-ray diffraction analyses were performed on selected crystal of these compounds. The crystal structures of the polymers are isomorphous, comprising a 3D framework containing nine-coordinate lanthanide-metal centers and six-coordinate transition-metal centers, which results in a nanotubelike structure (Figure 1). All three polymers crystallized in the hexagonal crystal system, space group *P6/mcc*. The crystal structure is built up of two distinct types of building blocks, $Ln(dipic)_3$ and $MnO_4(H_2O)_2$ (Figure 2). The Ln atom is located at the intersection of a threefold and a twofold axis and is coordinated by three tridentate (ONO) dipic anions; for which each carboxy group coordinates through one oxygen atom. Three N atoms and six O atoms complete the coordination sphere of the Ln^{3+} center, which conforms most closely to a tricapped trigonal prism. The coordination geometry around Mn^{2+} center is a slightly distorted octahedron, the equatorial plane of which comprises four O atoms from the carboxy groups of the dipic molecules that are chelated to four neighboring Ln^{3+} centers; two water molecules occupy the remaining apical coordinate sites. Each Mn atom is located at the intersection of a mirror plane and a twofold axis, namely the crystallographic 6*g* position of the *P6/mcc* space group, and its site symmetry is 2/*m*. There are three crystallographically independent dipic molecules in the structure, each has the same coordination mode, that is, chelated to one Ln atom, and linked to two Mn atoms. One

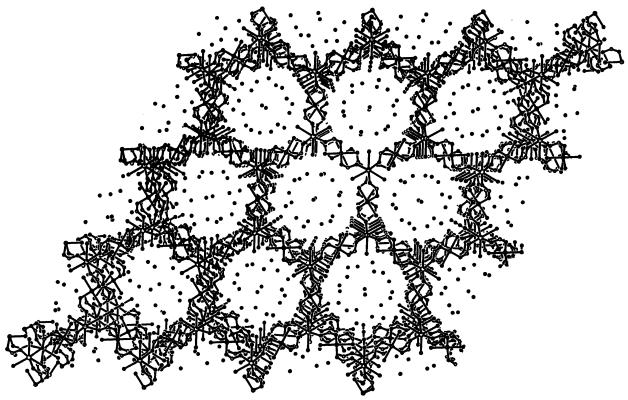

Figure 1. Projection of the 3D framework down the *c* axis in **1**; the C atoms of the pyridine rings and H atoms are omitted for clarity.

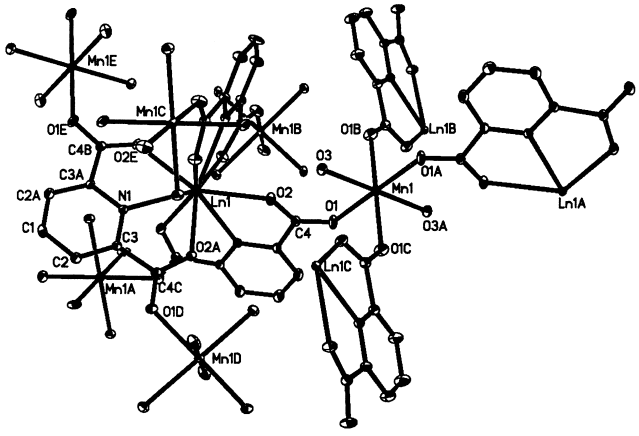

Figure 2. Diagram showing the two building units with atom labels of the Mn–Ln series; H atoms are omitted for clarity. Symmetry operations: A: 1+*y*, *x*, 0.5−*z*; B: *x*−*y*, −*y*, 0.5−*z*; C: 1−*x*+*y*, 1−*x*, *z*; D: 1−*y*, *x*−*y*, *z*; E: 1−*x*, 1−*x*+*y*, 0.5−*z*.

[*] Prof. Dr. P. Cheng, Prof. D.-Z. Liao, B. Zhao, Y. Dai, C. Cheng, S.-P. Yan, Z.-H. Jiang, G.-L. Wang
Department of Chemistry
Nankai University
Tianjin 300071 (P.R. China)
Fax: (+86) 22-2350-2458
E-mail: pcheng@nankai.edu.cn

[**] This work was supported by the National Natural Science Foundation of China (Nos. 90101028, 50173011), the NSF of Tianjin (No. 013801611) and the TRAPOYT of MOE, P.R. China

Supporting information for this article is available on the WWW under http://www.angewandte.org or from the author.

 © 2003 Wiley-VCH Verlag GmbH & Co. KGaA, Weinheim 1433-7851/03/4208-0934 $ 20.00+.50/0

oxygen atom from any carboxy group bonds to an Ln^{3+} center and the other oxygen atom bonds to an Mn^{2+} center; thus each Ln^{3+} center has six Mn^{2+} ions as the nearest metal center, while the Mn^{2+} center has four Ln^{3+} ions in its vicinity (Figure 2), as is consistent with the Mn:Ln molar ratio. Carboxy bridges exist between adjacent Ln and Mn atoms, and more importantly, each carboxy group also bridges each Mn–OCO–Ln unit, which creates a highly ordered 3D structure with tubular channels with a diameter of about 17.9 Å for **1** (defined by the separation between Pr1 and Pr1D, Figure 3a) along the [001] direction, as shown in Figure 1. Notably, many guest water molecules were trapped in the parallel tubes. A cross section of a nanotube (for Nn = Pr(**1**); Figure 3a) shows a 48-membered ring (48MR) comprising 6 Ln, 6 Mn, 12 C, and 24 O atoms, of which, the Ln and Mn atoms are arrayed alternately and connected by O–C–O bridges, thus leading to an overall C_6 symmetry. Six Ln atoms and six Mn atoms are rigidly coplanar and the distance between both planes is about 3.92 Å for **1** . The wall of the nanotube is made up of 16MRs (2 Ln, 2 Mn, 4 C, and 8 O atoms in each ring; ca. 5.91 × 5.91 Å for **1**). Compounds containing 18MRs,[10] 20MRs,[11] 24MRs,[12] and 30MRs[13] are well documented, however, to the best of our knowledge, 48MRs have not been previously reported. The Ln–O distance decreases with increasing lanthanide atomic number (Pr–O 2.501, Gd–O 2.442, and Er–O 2.411 Å) and the same trend is seen for Ln–N bond lengths and is interpreted as a result of the lanthanide contraction.

Thermal gravimetric analysis (TGA) reveals that these complexes can adsorb water molecules as a consequence of the large pores present. TGA was performed on crystalline samples of these compounds in the range of 14 to 620 °C. The weight loss of 9.43 % for **1** and 8.81 % for **3**, between 40 and 140 °C corresponds to the loss of all uncoordinated and adsorbed water molecules (calcd 8.52 % for **1**·2 H_2O and 8.27 % for **3**·H_2O). This is indicative of the adsorption of two water molecules per $PrMn_{1.5}$ unit of **1** and just one water molecule per $ErMn_{1.5}$ unit of **3**, and is consistent with the elemental analyses (EA) of **1**·2 H_2O and **3**·H_2O. For comparison, TGA and EA experiments for **2** were carried out after **2** had been dried, and the results show no adsorption of water into the pores; the weight loss of 7.1 % below 140 °C (calcd 7.4 %) corresponds to the loss of 3.5 uncoordinated water molecules per $Gd/Mn_{1.5}$ unit of **2**. Taking **1** as an example, we explored whether the framework would break down on removal of guest water molecules (uncoordinated and adsorbed water molecules). Water molecules were removed by heating **1** at 120 °C for 12 h. Powder X-ray diffraction patterns of hydrated and dehydrated samples of **1** are nearly identical, which supports the notion that the crystal lattice remains intact after the guest water molecules have been removed. TGA showed that samples of **1**–**3** lost coordinated water molecules between 140 and 280 °C, but did not decompose until 340 °C.

Magnetic measurements on the three coordination polymers show interesting behavior in a 10 kOe magnetic field. The plots of $\chi_M T$ versus temperature for polymers **1**–**3** are given in Figure 4. For **1**, $\chi_M T$ steadily decreases with decreasing temperature from 300 to 15.6 K, and dramatically drops to 5.14 $cm^3 K mol^{-1}$ at 2 K. For **3**, the plot of $\chi_M T$ versus temperature is similar in shape to that of **1**. The observed $\chi_M T$ values for **1** and **3** were 8.49 and 17.58 $cm^3 K mol^{-1}$ at 297 K, respectively, which are close to the theoretical values of 8.16 and 18.04 $cm^3 K mol^{-1}$, respectively, as expected for 1.5

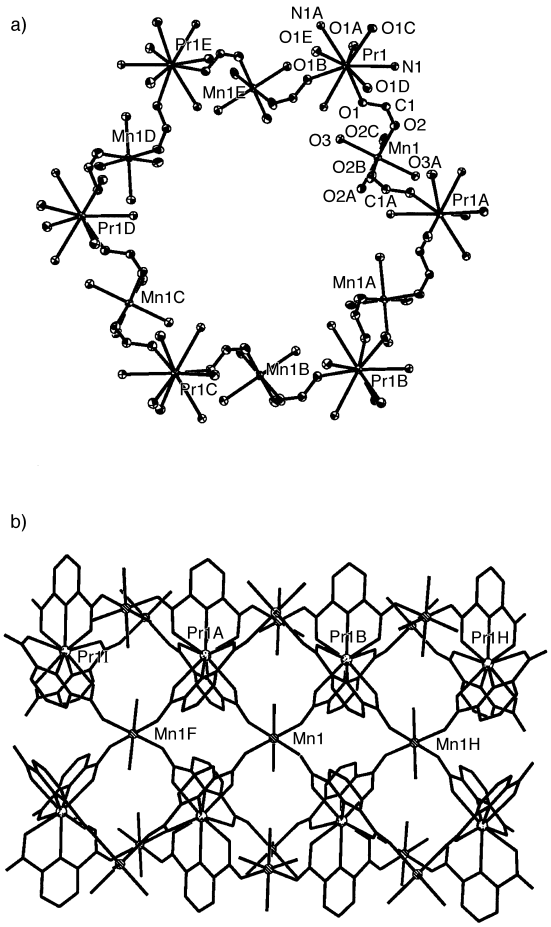

Figure 3. a) The cross section of the nanotube for **1**, which shows 48MRs and C_6 symmetry; the C atoms of the pyridine rings and H atoms are omitted for clarity. b) The 16MR structure of the tubular wall in **1**; H atoms are omitted for clarity.

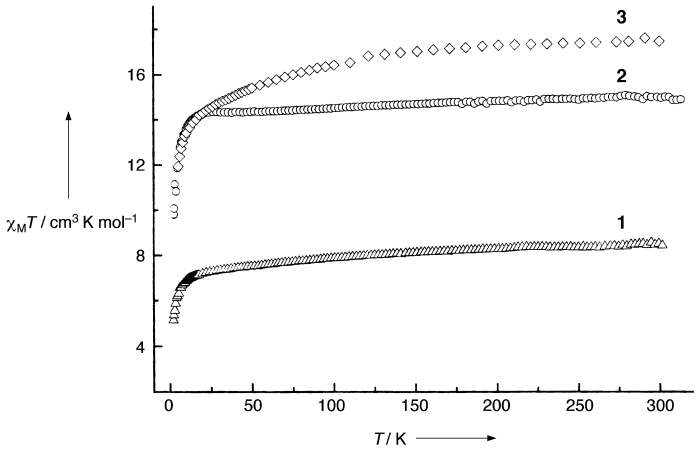

Figure 4. Plots of $\chi_M T$ versus T for **1** (△), **2** (○), and **3**(◇).

 © 2003 Wiley-VCH Verlag GmbH & Co. KGaA, Weinheim 1433-7851/03/4208-0935 $ 20.00+.50/0

Mn^{II} ions and one Pr^{III} (**1**) or Er^{III} (**3**) ion for the corresponding ground states $^3H_4$ ($g = 4/5$) and $^4I_{15/2}$ ($g = 6/5$), respectively. The coupling interactions between Pr and Mn, and between Er and Mn, are not explicitly characterized because of the strong spin–orbit coupling of the lanthanide atoms.[14] Attempts to explore in detail the magnetic interaction between Ln^{III} and Mn^{II} ions by synthesizing isomorphic coordination polymers to **1** and **3** containing diamagnetic transition metal ions have thus far failed.

The very slow decrease in the value of $\chi_M T$ for **2** with decreasing temperature from 14.95 $cm^3 K mol^{-1}$ at 313 K to 14.19 $cm^3 K mol^{-1}$ at 17.4 K, might be attributed to antiferromagnetic coupling between the Gd^{III} and Mn^{II} ions. Compared with the ferromagnetic coupling of the Gd^{III} and Cu^{II} ions,[14,15] the Mn^{II} ion with a $3d^5$ electronic configuration is very stable in energy, and unpaired electrons around Mn^{II} are very difficult to transfer to the 5d or 6s orbitals of the Gd^{III} ion. On the other hand, the nonzero overlapped integration between the Gd^{III} and Mn^{II} ions would result in an antiferromagnetic interaction between Gd^{III} and Mn^{II} ions within **2**.

In summary, we have synthesized three novel lanthanide–transitional-metal coordination polymers by hydrothermal reactions. They are the first 3d–4f zeolite-type structures containing nanotubes comprising 48MRs and have a previously unknown framework topology with the space group *P6/mcc*. The walls of the nanotubes include 16MR windows resulting in an unprecedented 3D 3d–4f heterometallic framework. Remarkably, the framework remains intact on removal of the guest water molecules. These results provide an opening into a promising new field of 3d–4f mixed-metal zeolite-type materials.

Experimental Section

Synthesis of **1**–**3**: A mixture of H_2dipic (0.8 mmol, 0.134 g), $Ln(ClO_4)_3 \cdot 6H_2O$ (Pr 0.109 g; Gd 0.113 g; Er 0.115 g), $MnCO_3$ (0.3 mmol, 0.034 g), and H_2O (10 mL) in the molar ratio of 4:1:1.5:2778 were put in a 20-mL acid digestion bomb and heated at 185 °C for three days. The products were collected after washing with H_2O (2 × 6 mL) and diethyl ether (2 × 6 mL).

Elemental analysis (%) calcd for **1**·2 H_2O: C 29.83, H 2.72, N 4.97; found: C 29.66, H 2.93, N 4.79. Crystal data of **1**: [{[$Pr(dipic)_3Mn_{1.5}(H_2O)_3]\cdot 2H_2O$}$_\infty$], $M_r = 808.71$, hexgonal, *P6/mcc*, $a = b = 15.512(2)$, $c = 15.645(3)$ Å, $\gamma = 120°$, $V = 3260.2(9)$ Å^3, $Z = 4$, $\rho = 1.648$ g cm^{-3}, $2\theta_{max} = 50.06$ ($-18 \le h \le 14$, $-17 \le k \le 18$, $-18 \le l \le 14$), $T = 293(2)$ K, 12182 measured reflections. $R1 = 0.0305$ for 626 reflections ($I > 2\sigma(I)$), $wR2 = 0.0723$ for 998 independent reflections (all data) and 76 parameters. $GOF = 1.032$.

Elemental analysis (%) calcd for **2**·3.5 H_2O: C 29.58, H 2.58, N 4.93; found: C 29.37, H 2.90, N 5.11. Crystal data of **2**: [{[$Gd(dipic)_3Mn_{1.5}(H_2O)_3]\cdot 3.5H_2O$}$_\infty$], $M_r = 852.03$, hexgonal, *P6/mcc*, $a = b = 15.307(3)$, $c = 15.695(4)$ Å, $\gamma = 120°$, $V = 3260.2(9)$ Å^3, $Z = 4$, $\rho = 1.664$ g cm^{-3}, $2\theta_{max} = 50.68$ ($-18 \le h \le 14$, $-17 \le k \le 18$, $-18 \le l \le 14$), $T = 293(2)$ K, 12182 measured reflections. $R1 = 0.0198$ for 655 reflections ($I > 2\sigma(I)$), $wR2 = 0.0475$ for 978 independent reflections (all data) and 76 parameters. $GOF = 0.995$.

Elemental analysis (%) calcd for **3**·H_2O: C 28.93, H 2.64, N 4.82; found: C 29.24, H 2.41, N 4.95. Crystal data of **3**: [{[$Er(dipic)_3Mn_{1.5}(H_2O)_3]\cdot 3H_2O$}$_\infty$], $M_r = 853.08$, hexgonal, *P6/mcc*, $a = b = 15.229(2)$, $c = 15.852(5)$ Å, $\gamma = 120°$, $V = 3183.6(11)$ Å^3, $Z = 4$, $\rho = 1.780$ g cm^{-3}, $2\theta_{max} = 47.60$ ($-18 \le h \le 13$, $-18 \le k \le 17$, $-15 \le l \le 18$), $T = 273(2)$ K, 11457 measured reflections. $R1 = 0.0216$ for 625 reflections ($I > 2\sigma(I)$), $wR2 = 0.0523$ for 937 independent reflections (all data) and 74 parameters. $GOF = 1.028$.

CCDC-191516–191518 (**1**–**3**) contain the supplementary crystallographic data for this paper. These data can be obtained free of charge via www.ccdc.cam.ac.uk/conts/retrieving.html (or from the Cambridge Crystallographic Data Centre, 12 Union Road, Cambridge CB2 1EZ, UK; fax: (+44) 1223-336-033; or deposit@ccdc.cam.ac.uk).

Received: August 23, 2002 [Z50032]

[1] a) M. Eddaoudi, J. Kim, N. Rosi, D. Vodak, J. Wachter, M. O'Keeffe, O. M. Yaghi, *Science* **2002**, *295*, 469; b) B. L. Chen, M. Eddaoudi, S. T. Hyde, M. O'Keeffe, O. M. Yaghi, *Science* **2001**, *291*, 1021; c) S. S.-Y. Chui, S. M.-F. Lo, J. P. H. Charmant, A. G. Orphen, I. D. Williams, *Science* **1999**, *283*, 1148; d) H. L. Li, M. Eddaoudi, M. O'Keeffe, O. M. Yaghi, *Nature* **1999**, *402*, 276; e) J. S. Seo, D. Whang, H. Lee, S. I. Jun, J. Oh, Y. J. Jeon, K. Kim, *Nature* **2000**, *404*, 982; f) M. Fujita, S. Y. Yu, T. Kusukawa, H. Funaki, K. Ogura, K. Yamaguchi, *Angew. Chem.* **1998**, *110*, 2192; *Angew. Chem. Int. Ed.* **1998**, *37*, 2082; g) M. Aoyagi, K. Biradha, M. Fujita, *J. Am. Chem. Soc.* **1999**, *121*, 7457.

[2] a) C. Janiak, *Angew. Chem.* **1997**, *109*, 1499; *Angew. Chem. Int. Ed. Engl.* **1997**, *36*, 1431; b) M. J. Zaworotko, *Chem. Soc. Rev.* **1994**, 283; c) S. R. Batten, R. Robson, *Angew. Chem.* 1998, *110*, 1558; *Angew. Chem. Int. Ed.* **1998**, *37*, 1460; d) M. Fujita, Y. J. Kwon, S. Washizu, K. Ogura, *J. Am. Chem. Soc.* **1994**, *116*, 1151; e) G. B. Gardner, D. Venkataraman, J. S. Moore, S. Lee, *Nature* **1995**, *374*, 792.

[3] M. Lwamoto, H. Furukawa, Y. Mine, F. Uemura, S. I. Mikuriya, S. Kagawa, *J. Chem. Soc. Chem. Commun.* **1986**, 1272.

[4] S. L. Brock, N. G. Duan, Z. R. Tian, O. Giraldo, H. Zhou, S. L. Suib, *Chem. Mater.* **1998**, *10*, 2619.

[5] A. K. Cheetham, G. Ferey, T. Loiseau, *Angew. Chem.* 1999, *111*, 3466; *Angew. Chem. Int. Ed.* **1999**, *38*, 3268.

[6] a) W. Lin, O. R. Evans, R. G. Xiong, Z. Wang, *J. Am. Chem. Soc.* **1998**, *120*, 13272; b) O. R. Evans, R. G. Xiong, Z. Wang, G. K. Wong, W. Lin, *Angew. Chem.* **1999**, *111*, 523; *Angew. Chem. Int. Ed.* **1999**, *38*, 536.

[7] a) L. Pan, X. Y. Huang, J. Li, Y. G. Wu, N. W. Zheng, *Angew. Chem.* **2000**, *112*, 537; *Angew. Chem. Int. Ed.* **2000**, *39*, 527; b) D. M. L. Goodgame, S. Menzer, A. T. Ross, D. J. Williams, *J. Chem. Soc. Chem. Commun.* **1994**, 2605; c) D. M. L. Goodgame, S. P. W. Hill, D. J. Williams, *Inorg. Chim. Acta* **1998**, *272*, 131; d) V. Kiritsis, A. Michaelides, S. Skoulika, S. Golhen, L. Ouahab, *Inorg. Chem.* **1998**, *37*, 3407; e) C. V. K. Sharma, R. D. Rogers, *Chem. Commun.* **1999**, 83; f) T. M. Reineke, M. Eddaoudi, M. Fehr, D. Kelley, O. M. Yaghi, *J. Am. Chem. Soc.* **1999**, *121*, 1651.

[8] a) T. Soma, H. Yuge, T. Lwanoto, *Angew. Chem.* **1994**, *106*, 1746; *Angew. Chem. Int. Ed. Engl.* **1994**, *33*, 1665; b) S. R. Batten, B. F. Hoskins, R. Robson, *J. Am. Chem. Soc.* **1995**, *117*, 5385.

[9] S. Subramanian, M. Zaworotko, *Angew. Chem.* **1995**, *107*, 2295; *Angew. Chem. Int. Ed. Engl.* **1995**, *34*, 2127.

[10] M. E. Davis, C. Saldarriaga, C. Montes, J. M. Garces, C. Crowder, *Nature* **1988**, *331*, 698.

[11] M. Esterman, L. B. Mccusker, C. Baerlocher, A. Merrouche, H. Kessler, *Nature* **1991**, *352*, 320.

[12] Y. M. Zhou, H. G. Zhu, Z. X. Chen, D. Zhao, *Angew. Chem.* **2001**, *113*, 2224; *Angew. Chem. Int. Ed.* **2001**, *40*, 2166.

[13] S. X. Liu, S. Lin, B. Z. Lin, C. C. Lin, J. Q. Huang, *Angew. Chem.* **2001**, *113*, 1118; *Angew. Chem. Int. Ed.* **2001**, *40*, 1084.

[14] C. Benelli, D. Gatteshi, *Chem. Rev.* **2002**, *102*, 2369.

[15] A. Bencini, C. Beneli, A. Caneschi, R. L. Carlin, A. Dei, D. Gatteshi, *J. Am. Chem. Soc.* **1985**, *107*, 8128.

 © 2003 Wiley-VCH Verlag GmbH & Co. KGaA, Weinheim 1433-7851/03/4208-0936 $ 20.00+.50/0

Capped Metal Polyhydride Clusters

Trinuclear Ruthenium Polyhydride Complexes with a Triply Bridging Ligand: $[\{(\eta^5\text{-}C_5Me_5)Ru\}_3(\mu_3\text{-}M)(\mu\text{-}H)_3(\mu_3\text{-}H)]$ (M = Li, Mg*i*Pr, and ZnEt) and $[\{(\eta^5\text{-}C_5Me_5)Ru\}_3(\mu_3\text{-}M)(\mu\text{-}H)_3]$ (M = AlEt and GaMe)**

*Masato Ohashi, Kouki Matsubara, Takashi Iizuka, and Hiroharu Suzuki**

We have shown that metal polyhydride clusters, especially those that have C_5Me_5 groups, have remarkable reactivity, such as an unprecedented mode of C–C bond cleavage, C=C double bond cleavage of terminal alkenes, and alkane C–H bond cleavage.[1] The reactivity of the cluster complex depends on the steric and electronic environment of the reaction site. Our effort has, therefore, been focused on developing a versatile method for changing the electron density at the metal center, and we reported the syntheses and reactions of di- and trinuclear clusters with μ-C=NHR, μ-PR_2, or μ_3-BR groups.[2] As an extension of this idea, we have investigated the synthesis of a series of trinuclear Ru clusters that have a variety of bridging ligands containing a metal atom. The introduction of a Lewis basic or acidic metal atom into the framework of the cluster would directly affect the electronic environment of the reaction site and, as a result, would give us control over the reactivity and selectivity of the cluster. Although there have been several studies on the reaction of a transition-metal hydride complex with metal alkyls such as RLi, R_2Mg, R_2Zn, R_3Al, and R_3Ga,[3] no attempts to control electron density at the metal center of the trimetallic cluster have been reported. Herein, we report the synthesis of a novel class of trinuclear polyhydride complexes of ruthenium that have a triply bridging metal alkyl ligand, and evaluate their influences on the reactivity of the clusters by means of cyclic voltammetry.

An equimolar amount of diethylzinc was added to a solution of **1** in THF at −78 °C, and this mixture was warmed to room temperature resulting in the clean formation the new cluster **2** (Scheme 1).[4] The introduction of the triply bridging ethylzinc ligand into the Ru_3 core was confirmed by ^{1}H NMR spectroscopy; a single resonance signal (45 H) arising from three C_5Me_5 groups, and a resonance signal at $\delta = -0.50$ ppm (2 H) arising from a methylene group bound to the zinc atom was observed in the ^{1}H NMR spectrum. The signals from the hydrides appear at $\delta = -26.97$ (1 H) and 2.56 ppm (3 H), and

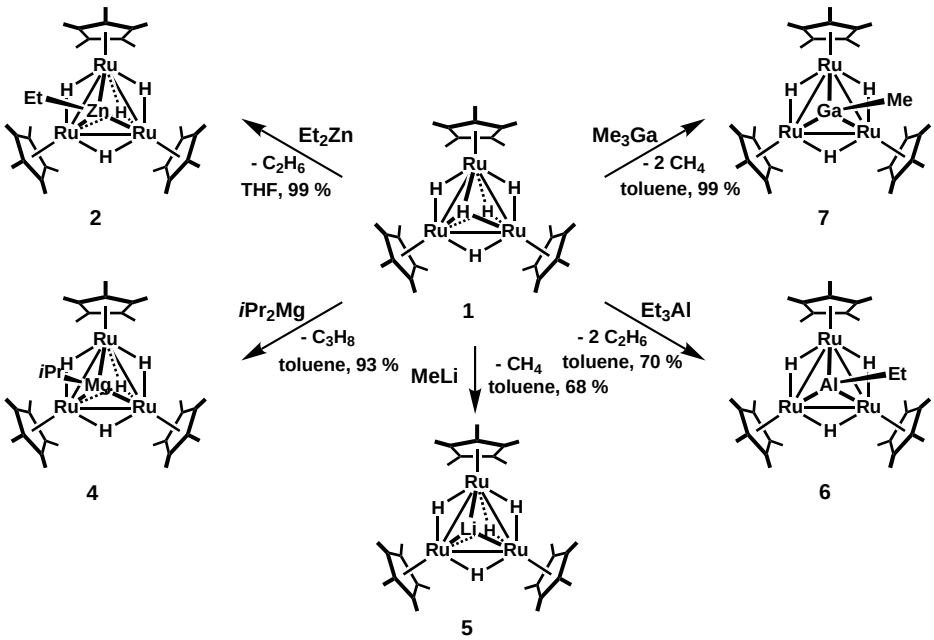

Scheme 1. Reactivity studies of **1** with metal alkyls.

[*] Prof. H. Suzuki, M. Ohashi, K. Matsubara, T. Iizuka
Department of Applied Chemistry,
Graduate School of Science and Engineering
Tokyo Institute of Technology and CREST
Japan Science and Technology Corporation (JST)
O-okayama, Meguro-ku, Tokyo 152-8552 (Japan)
Fax: (+81) 3-5734-3913
E-mail: hiroharu@n.cc.titech.ac.jp

[**] The authors are grateful to Kanto Chemical Co., Inc., for the generous gift of pentamethylcyclopentadiene.

Supporting information for this article is available on the WWW under http://www.angewandte.org or from the author.

assignment of these signals was confirmed with a labeling experiment by using $[\{(\eta^5\text{-}C_5Me_5)Ru\}_3(\mu\text{-}D)_3(\mu_3\text{-}D)_2]$ ($[D_5]$-**1**) and diethylzinc. The dramatic downfield shift of the signals from the three hydride ligands is consistent with a bonding interaction between the hydride and the zinc atom, which is observed in the structure determined by an X-ray study (see below).

$[\{(\eta^5\text{-}C_5Me_5)Ru\}_3(\mu\text{-}H)_3(\mu_3\text{-}H)_2]$ **1**

$[\{(\eta^5\text{-}C_5Me_5)Ru\}_3(\mu\text{-}H)_3(\mu_3\text{-}ZnEt)(\mu_3\text{-}H)]$ **2**

 © 2003 Wiley-VCH Verlag GmbH & Co. KGaA, Weinheim 1433-7851/03/4208-0937 $ 20.00+.50/0

It is important to introduce one bridging ligand onto only one side of the Ru_3 core. If both faces of the Ru_3 plane are each covered with a bridging ligand, then there is no space for substrate activation on the Ru_3 plane. Strict control of the stoichiometry of the reaction is, therefore, necessary to obtain selectively the monocapped ethylzinc complex **2**, otherwise, addition of excess diethylzinc causes a further reaction to yield a bicapped ethylzinc complex **3**.

$[\{(\eta^5\text{-}C_5Me_5)Ru\}_3(\mu\text{-}H)_3(\mu_3\text{-}ZnEt)_2]$ **3**

The reaction of **1** with a variety of metal-alkyl reagents such as iPr$_2$Mg, MeLi, Et$_3$Al, and Me$_3$Ga in toluene led to the formation of the corresponding mono-μ_3-metal complexes **4**–**7** (Scheme 1). All of these complexes dissolve in nonpolar solvents such as pentane, toluene, and benzene. Most of the complexes are air- and moisture-sensitive, even in the solid state, and should be handled in an inert-gas atmosphere. Interestingly, in the reactions of **1** with metal–alkyl reagents, except for $ZnEt_2$, the corresponding bicapped complexes were not formed. These products were unambiguously identified on the basis of NMR spectroscopy (Table 1).

The structure of each complex has an approximate threefold axis, and the resonance signals for the three C_5Me_5 groups are observed to be equivalent both in the ^{1}H and ^{13}C NMR spectra. In the ^{1}H NMR spectra of **2, 4**, and **5**, a signal assigned to a triply bonded hydride ligand capping the three Ru atoms was observed around $\delta = -25$ ppm. Noteworthy, the resonance signals of the rest of the hydrides shifted significantly downfield because of their bonding interaction with the triply bridging metal atom. Evidence for this interaction was obtained by NMR spectroscopy, and by an X-ray diffraction study. In the ^{1}H NMR spectrum of **5** recorded at −60 °C, two hydride signals appear at $\delta = -24.17$ (1H) and −10.88 ppm (3H; −10.01 at room temperature). The latter was coupled with the ^{7}Li nucleus ($S = 2/3$, $J_{Li,H} = 11.2$ Hz). Additionally, the ^{7}Li NMR spectrum of **5** exhibits a quartet at $\delta = -1.4$ ppm with the same coupling constant ($J_{Li,H} = 11.2$ Hz). Similar bonding interactions between the triply bridging metal and the Ru-bound hydride were also observed in **2**, and **4**, and confirmed by X-ray diffraction studies (see below). The shifts of $\delta = -3.37$ and −3.84 ppm for the hydrides in the μ_3-AlEt complex **6** and the μ_3-GaMe complex **7**, respectively, are more downfield than that reported[7] for a hydride that directly bridges Al and Ru atoms ($\delta = -13.55$ ppm), and are more upfield than the chemical shift of a terminal hydride directly bound to an Al atom ($\delta = 4.5$ ppm).[7] Although these NMR data suggest of a weak bonding interaction between the hydride and the bridging Al or Ga atom, this possibility was ruled out on the basis of the X-ray structure analysis.

The X-ray studies of **2, 4, 5** (not shown), and **7** show that a metal–alkyl ligand bridges three Ru atoms on one of the Ru_3 faces, and the opposite face of the Ru_3 core is available as a reaction site (Figure 1).[8] The Ru_3 core of these complexes consist of an approximately equilateral triangle with edges of about 2.75 Å, and this value is similar to that of the parent complex **1** (≈2.75 Å). Although the Ru−Ru distances in these complexes are very similar to those observed in the parent compound **1**, the Ru–CENT vectors tilt with respect to the Ru_3 plane (Figure 1; Table 1). Notably, the tilt angles are classified into two groups. The tilt angles in **7** are negative (see Table 1, footnote [c]) while those observed in **2, 4**, and **5** are positive. Consequently, the reaction site of **7** is more exposed than that of **1**, which is in contrast to the cases of **2, 4**, and **5**. Thus, the introduction of the triply bridging metal ligand

Table 1: Selected spectral data and structural parameters of trinuclear polyhydride complexes **1, 2**, and **4**–**7**.[6]

Complex	**2**[a]	**4**[a]	**5**[a]	**6**[a]	**7**[a] molecule 1	**7**[a] molecule 2	**1**[a]
^{1}H NMR (μ_3-H, 1H, δ, RT)	−26.97	−24.70	−24.02	–	–		–
^{1}H NMR (μ-H, 3H, δ, RT)	2.56	−5.25	−10.01	−3.37	−3.84		–
^{1}H NMR (hydride, δ, RT)	–	–	–	–	–		−7.23[b]
^{1}H NMR (μ_3-MR, δ, RT)	−0.50 (q)	−0.40 (sep)	–	−0.66(q)	−0.73 (s)		–
	1.11 (t)	1.34 (d)	–	0.81 (t)	–		–
^{13}C NMR (C_5Me_5, δ, RT)	85.4	84.4	79.9	87.1	84.4		85.7
^{13}C NMR ($C_5\mathit{Me}_5$, δ, RT)	13.0	13.1	13.8	13.2	12.9		13.1
Ru−Ru distance [Å]	2.7450(6)	2.7516(6)	2.735(5)	–	2.7309(13)	2.7311(11)	2.7503(8)
	2.7371(8)	2.7500(4)	2.737(4)	–	2.7348(12)	2.7353(13)	2.7534(8)
		2.7548(6)	2.723(5)	–	2.7381(13)	2.7336(12)	2.7453(6)
Ru−M distance [Å]	2.6747(10)	2.7487(13)	2.67(5)	–	2.480(2)	2.4934(18)	–
	2.6561(8)	2.8007(12)	2.84(9)	–	2.479(2)	2.4587(18)	–
		2.7715(13)	2.82(6)	–	2.458(2)	2.4780(18)	–
tilt angle [°][c]	4.6	8.1	9.7	–	−5.5	−5.2	0.0
	4.6	8.7	10.2	–	−6.2	−6.0	0.0
		7.8	12.7	–	−5.6	−5.3	0.0
first formal redox potential [mV]	−489	−1049	−1696	−521	−643		−510

[a] In C_6D_6. [b] A signal resonance signal was observed as a result of the site-exchange process between the μ-H and μ_3-H hydride ligands. [c] The angles between the Ru_3 plane and the Ru-CENT vector. When the Ru–CENT vector tilts away from the μ_3-M ligand with respect to the Ru_3 plane, the tilt angle is defined to be a positive value.

 © 2003 Wiley-VCH Verlag GmbH & Co. KGaA, Weinheim 1433-7851/03/4208-0938 $ 20.00+.50/0

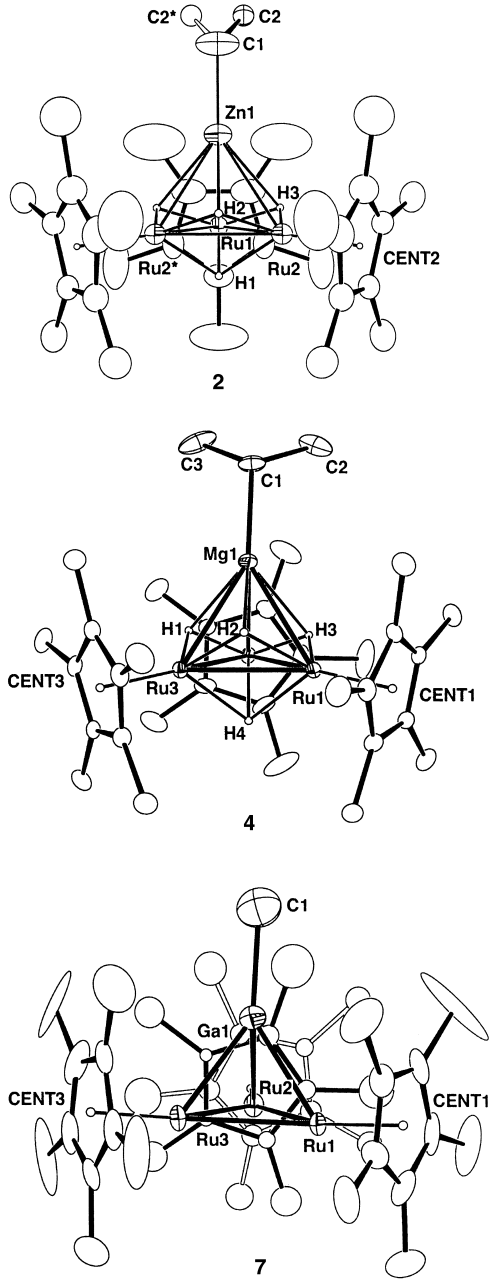

Figure 1. Molecular structures of **2, 4**, and **7** with thermal ellipsoids drawn at the 30% probability level. One of the two independent molecules in a unit cell of **7** is depicted. Selected bond lengths [Å] and angles [°] are shown in Table 1.

above the Ru_3 core affects the size of the reaction site. In the structures of **2** and **4**, the three hydride ligands triply bridge the two ruthenium atoms and the μ_3-metal, and the positive tilt angles observed arise from the steric repulsion between these hydride ligands and the C_5Me_5 group. The average tilt angle of 10.8° for **5** strongly indicates that the hydrides locate above the Ru_2Li plane as in **2** and **4**. In contrast, the negative tilt angle for **7** implies that the hydride ligands are likely to be positioned on the opposite side of the μ_3-GaMe group with respect to the Ru_3 plane and they have little bonding interaction with the Ga atom. The triply bridging metal atoms (Zn, Mg, and Ga) are located almost equidistant from the three Ru atoms, and the average Ru–Zn, Ru–Mg, and Ru–Ga bond lengths are about 2.66, 2.77, and 2.47 Å, respectively. While the Ru–Ga distance is very close to the sum of the covalent radii of Ru and Ga ($\approx$2.50 Å), the Ru–Zn and the Ru–Mg distances are significantly longer than the sum of the corresponding covalent radii, $\approx$2.50 and 2.61 Å, respectively.

A change in the electronic environment of the reaction site arising from the introduction of the μ_3-MR ligand to the Ru_3 core can be evaluated by cyclic voltammetry. The electron transfer between the Ru_3 core and the μ_3-MR ligand is certainly reflected in the redox potential, which is an important index of reactivity. In the cyclic voltammogram of the Ru_3Li cluster **5** recorded in THF, three one-electron oxidation waves are observed at −1696, −755 (E_{pa}), and −463 mV versus Ag/AgCl (Table 1, see also Supporting Information). The first and the third waves are reversible and the second wave is irreversible. The first anodic wave at −1696 mV corresponds to $\mathbf{5}^{0/+1}$. The oxidation potential of −1696 mV is much lower than that for the first oxidation wave of the parent triruthenium cluster **1** (−510 mV). This clearly shows an increase in electron density of the Ru_3 core of **5** because of polarization between the Ru atoms and the electropositive μ_3-Li ligand. The first oxidation wave for **4** was observed around −1050 mV. Therefore, the μ_3-MgR ligand similarly donates electrons to the Ru_3 core. As a result of the electron transfer from the μ_3-MR group to the Ru_3 core, the HOMO levels of **5** and **4** were significantly raised. In contrast, the first oxidation waves of the Ru_3M clusters containing Zn and Al appeared in the potential region similar to that of **1** but much higher than that of **4** and **5**. This is a consequence of the Lewis acidic character of these metals. Thus, the introduction of the triply bridging metal ligand is an effective method to change the redox potential, and therefore the reactivity of the trinuclear pentahydride cluster **1**.

In summary, we have synthesized and structurally characterized a series of trinuclear polyhydride clusters that contain triply bridging metal alkyls, and evaluated the change in the electronic environment of the reaction site by cyclic voltammetry.

Received: September 23, 2002
Revised: December 9, 2002 [Z50221]

[1] a) H. Suzuki, Y. Takaya, T. Takemori, M. Tanaka, *J. Am. Chem. Soc.* **1994**, *116*, 10779; b) K. Matsubara, R. Okamura, M. Tanaka, H. Suzuki, *J. Am. Chem. Soc.* **1998**, *120*, 1108; c) A. Inagaki, T. Takemori, M. Tanaka, H. Suzuki, *Angew. Chem.* **2000**, *112*, 411; *Angew. Chem. Int. Ed.* **2000**, *39*, 404; d) Y. Ohki, H. Suzuki, *Angew. Chem.* **2000**, *112*, 3605; *Angew. Chem. Int. Ed.* **2000**, *39*, 3463; e) T. Takemori, A. Inagaki, H. Suzuki, *J. Am. Chem. Soc.* **2001**, *123*, 1762.

[2] a) K. Tada, M. Oishi, H. Suzuki, M. Tanaka, *Organometallics* **1996**, *15*, 2422; b) R. Okamura, K. Tada, K. Matsubara, M. Oshima, H. Suzuki, *Organometallics* **2001**, *20*, 4772; c) Y. Ohki, H. Suzuki, *Angew. Chem.* **2002**, *114*, 3120; *Angew. Chem. Int. Ed.* **2002**, *41*, 2994.

[3] a) A. Storr, B. S. Thomas, *Can. J. Chem.* **1971**, *49*, 2506; b) R. A. Forder, M. L. H. Green, R. E. Mackenzie, J. S. Poland, K. Prout, *J.*

 © 2003 Wiley-VCH Verlag GmbH & Co. KGaA, Weinheim 1433-7851/03/4208-0939 $ 20.00+.50/0

Chem. Soc. Chem. Commun. **1973**, 426; c) F. W. S. Benfield, R. A. Forder, M. L. H. Green, G. A. Moser, K. Prout, *J. Chem. Soc. Chem. Commun.* **1973**, 759; d) F. N. Tebbe, *J. Am. Chem. Soc.* **1973**, *95*, 5412; e) M. L. H. Green, R. E. MacKenzie, J. S. Poland, *J. Chem. Soc. Dalton Trans.* **1976**, 1993; f) J. N. St. Denis, W. Butler, M. D. Glick, J. P. Oliver, *J. Organomet. Chem.* **1977**, *129*, 1; g) P. H. M. Budzelaaer, J. Boersma, G. J. M. van der Kerk, A. L. Spek, A. J. M. Duisenberg, *Inorg. Chem.* **1982**, *21,* 3777; h) P. H. M. Budzelaar, K. H. den Haan, J. Boersma, G. J. M. van der Kerk, A. L. Spek, *Organometallics* **1984**, *3*, 156; i) P. H. M. Budzelaar, A. A. H. van der Zeijden, J. Boersma, G. J. M. van der Kerk, A. L. Spek, A. J. M. Duisenberg, *Organometallics* **1984**, *3*, 159; j) J. W. Bruno, J. C. Huffman, K. G. Caulton, *J. Am. Chem. Soc.* **1984**, *106*, 444; k) W. A. Skupinski, J. C. Huffman, J. W. Bruno, K. G. Caulton, *J. Am. Chem. Soc.* **1984**, *106,* 8128; l) J. A. Bandy, A. Berry, M. L. H. Green, K. Prout, *J. Chem. Soc. Chem. Commun.* **1985**, 1462; m) M. D. Fryzuk, D. H. McConville, S. J. Rettig, *Organometallics* **1990**, *9*, 1359; n) R. A. Fischer, H. D. Kaesz, S. I. Khan, H.-J. Muller, *Inorg. Chem.* **1990**, *29*, 1601; o) M. D. Fryzuk, D. H. McConville, S. J. Rettig, *Organometallics* **1993**, *12*, 2152; p) M. D. Fryzuk, B. R. Lloyd, G. K. B. Clentsmith, S. J. Rettig, *J. Am. Chem. Soc.* **1994**, *116*, 3804; q) J. T. Golden, T. H. Peterson, P. L. Holland, R. G. Bergman, R. A. Andersen, *J. Am. Chem. Soc.* **1998**, *120*, 223; r) T. H. Peterson, J. T. Golden, R. G. Bergman, *Organometallics* **1999**, *18*, 2005; s) M. Stender, H. Oesen, S. Blaurock, E. Hey-Hawkins, *Z. Anorg. Allg. Chem.* **2001**, *627*, 980.

[4] A 50 mL Schlenk tube was charged with **1** (373 mg, 0.522 mmol) and THF (30 mL). After the solution had been cooled to −78 °C, diethylzinc (1.0 M solution in hexane: 520 μL, 0.520 mmol) was added dropwise while the solution was stirred vigorously. The cooling bath was removed, and the reaction mixture was warmed to room temperature to give a red-brown solution. Removal of solvent under reduced pressure gave **2** (420 mg, 0.520 mmol; 99 %) as a red-brown solid. **2**: ^{1}H NMR (300 MHz, [D$_6$]benzene, RT): $\delta = -26.97$ (br s, $w_{1/2} = 11.0$ Hz, 1H, RuH), −0.50 (q, $J_{H,H} = 7.8$ Hz, 2H, Zn*CH*$_2$CH$_3$), 1.11 (t, $J_{H,H} = 7.8$ Hz, 3H, ZnCH$_2$*CH*$_3$), 2.00 (s, 45H, C$_5$*Me*$_5$), 2.56 ppm (br s, $w_{1/2} = 6.0$ Hz, 3H, RuH); ^{13}C NMR (125 MHz, [D$_6$]benzene, RT): $\delta = 11.8$ (q, $J_{C,H} = 123.0$ Hz, ZnCH$_2$*CH*$_3$), 13.0 (q, $J_{C,H} = 125.4$ Hz, C$_5$*Me*$_5$), 20.3 (t, $J_{C,H} = 115.8$ Hz, Zn*CH*$_2$CH$_3$), 85.4 ppm (s, *C*$_5$Me$_5$); elemental analysis calcd (%) for $C_{32}H_{54}Ru_3Zn$: C, 47.61; H, 6.74; found: C, 47.42; H, 6.71.

[5] An X-ray study of [(Cp′Ru)$_3${μ$_3$-Li(thf)}(μ-H)$_3$(μ$_3$-H)] (**5**-thf) was carried out. The preliminary results ($R_1 = 0.200$) are shown in Table 1. The resulting data of this solution are insufficient to discuss in detail. However, it is sufficient to show the connectivity of the atoms of **5**-thf.

[6] a) H. Suzuki, *Eur. J. Inorg. Chem.* **2002**, 1009; b) H. Suzuki, T. Kakigano, K. Tada, M. Igarashi, K. Matsubara, A. Inagaki, M. Oshima, M. Tanaka, unpublished results.

[7] D.-H. Lee, H. Suzuki, Y. Moro-oka, *J. Organomet. Chem.* **1987**, *330*, C20.

[8] a) Crystal data for **2**: $C_{32}H_{54}Ru_3Zn$, $M_r = 807.33$; red prismatic (0.50 × 0.50 × 0.30 mm); monoclinic, space group *C*2/*m* (No.12), $a = 17.237(4)$, $b = 18.408(4)$, $c = 11.175(3)$ Å, $\beta = 104.903(14)°$, $V = 3426.5(14)$ Å^3, $Z = 4$, $\rho_{calcd} = 1.565$ g cm^{-3}, $T = 223(2)$ K, $\lambda(Mo_{K\alpha}) = 0.71070$ Å, $\mu(Mo_{K\alpha}) = 2.01$ mm^{-1}, $F(000) = 1632$, 11900 reflections collected, 4449 were unique reflections, 188 parameters, $R_1 = 0.0429$ for 4253 reflections ($I_o > 2\sigma(I_o)$), $wR_2 = 0.1200$ for all data, GOF = 1.076, min./max. residual electron density −0.793/0.728 e Å^{-3}. Crystal data for **4**: $C_{33}H_{56}Ru_3Mg$, $M_r = 780.30$; black block (0.30 × 0.30 × 0.20 mm); monoclinic, space group *C*2/*c* (No.15), $a = 24.826(10)$, $b = 18.174(2)$, $c = 17.383(3)$ Å, $\beta = 118.232(18)°$, $V = 6910(3)$ Å^3, $Z = 8$, $\rho_{calcd} = 1.500$ g cm^{-3}, $T = 123(2)$ K, $\lambda(Mo_{K\alpha}) = 0.71069$ Å, $\mu(Mo_{K\alpha}) = 1.331$ mm^{-1}, $F(000) = 3184$, 39681 reflections collected, 9571 were unique reflections ($R_{int} = 0.0682$), 372 parameters, $R_1 = 0.0388$ for 4133 reflections ($I_o > 2\sigma(I_o)$), $wR_2 = 0.0856$ for all data, GOF = 0.965, min./max. residual electron density −1.520/0.782 e Å^{-3}. Crystal data for **7**: $C_{31}H_{51}Ru_3Ga$, $M_r = 796.65$; red prismatic (0.50 × 0.50 × 0.30 mm); monoclinic, space group *Pn* (No.7), $a = 11.1306(3)$, $b = 18.8975(5)$, $c = 16.1142(5)$ Å, $\beta = 105.8670(10)°$, $V = 3260.33(16)$ Å^3, $Z = 4$, $\rho_{calcd} = 1.623$ g cm^{-3}, $T = 223(2)$ K, $\lambda(Mo_{K\alpha}) = 0.71069$ Å, $\mu(Mo_{K\alpha}) = 2.197$ mm^{-1}, $F(000) = 1600$, 27874 reflections collected, 7389 were unique reflections ($R_{int} = 0.0643$), 496 parameters, $R_1 = 0.0561$ for 6516 reflections ($I_o > 2\sigma(I_o)$), $wR_2 = 0.1335$ for all data, GOF = 1.045, min./max. residual electron density −1.011/1.692 e Å^{-3}. Instruments: All data were collected on a Rigaku RAXIS-CS imaging plate area detector to a maximum 2θ value of 60.1° (**2**), 60.0° (**4**), and 54.9° (**7**). A numerical absorption correction program NUMABS[8b] was applied to the reflection data for **7**. The structure for **2** and **7** were solved by the Patterson method (DIRDIF 94[8c] PATTY[8d]). The structure of **4** was solved by the Patterson method (SHELXS-97[8e]). Non-hydrogen atoms were refined on F^2 by using SHELXL-97.[8f] The methyl carbon atom of the ethylzinc group in **2** is disordered with thermal parameters with 50.0 %:50.0 % occupancy. The unit cell of **7** contains two molecules, and one of the C$_5$Me$_5$ groups in each molecule is disordered with thermal parameters with 65.7 %:34.3 % (illustrated in Figure 1) and 53.1 %:46.9 % occupancy, respectively. All non-hydrogen atoms except a disordered carbon atom in **2** and **7** were refined anisotropically. The metal-bound hydride ligands were located by sequential difference Fourier synthesis and refined with isotropic thermal parameters. The remaining hydrogen atoms were placed in ideal positions and refined with a riding model. b) T. HIGASHI, NUMABS, Rigaku Corporation, Japan, **1999**; c) P. T. Beurskens, G. Admiraal, G. Beurskens, W. P. Bosman, R. de Gelder, R. Israel, J. M. M. Smits, DIRDIF94, University of Nijmegen, The Netherlands, **1994**; d) P. T. Beurskens, G. Admiraal, G. Beurskens, W. P. Bosman, S. Garcia-Granda, R. O. Gould, J. M. M. Smits, C. Smykalla, PATTY, University of Nijmegen, The Netherlands, **1992**; e) G. M. Sheldrick, *Acta Crystallogr. Sect. D* **1993**, *49*, 18; f) G. M. Sheldrick, SHELXS-97, University of Göttingen, Göttingen (Germany), **1997**; g) CCDC-192701 (**2**), CCDC-192702 (**4**), and CCDC-192703 (**7**) contain the supplementary crystallographic data for this paper. These data can be obtained free of charge via www.ccdc.cam.ac.uk/conts/retrieving.html (or from the Cambridge Crystallographic Data Centre, 12 Union Road, Cambridge CB2 1EZ, UK; fax: (+44) 1223-336-033; or deposit@ccdc.cam.ac.uk).

Epoxidation

Asymmetric Epoxidation of Homoallylic Alcohols and Application in a Concise Total Synthesis of (−)-α-Bisabolol and (−)-8-*epi*-α-Bisabolol**

*Naoya Makita, Yujiro Hoshino, and Hisashi Yamamoto**

Catalytic asymmetric epoxidation is useful for the synthesis of chiral compounds in both academia and industry. A variety of carbon–carbon double bonds, for example those of allylic alcohols, α,β-unsaturated esters, and simple alkenes, can be catalytically epoxidized with several metal catalysts,[1] and catalytic asymmetric reactions have been developed.[2–4] Metal-catalyzed asymmetric epoxidation of homoallylic alcohols, however, is difficult with the catalysts reported previously.[5] It is well known that vanadium complexes effectively catalyze the epoxidation of allylic and homoallylic alcohols to the corresponding epoxy alcohols with good to high stereoselectivities.[6] In our research on the asymmetric epoxidation of allylic alcohols, we discovered that the chiral vanadium complex that was prepared from vanadium triisopropoxide oxide and an α-amino acid-based hydroxamic acid is an efficient catalyst for the epoxidation of disubstituted allylic alcohols with high enantioselectivities and in high yields (up to 96% *ee*, almost >95% yield).[7,8] Here we show that this catalytic system can also be used for the asymmetric epoxidation of homoallylic alcohols [Eq. (1)], and report the discriminating substitution pattern of the substrates. Concise total syntheses of (−)-α- and (−)-8-*epi*-α-bisabolol were achieved using this catalytic system.

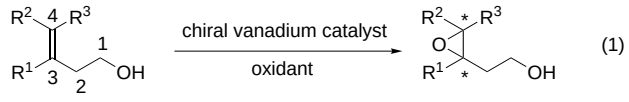

(1)

homoallylic alcohol

Our investigation into the vanadium-catalyzed asymmetric epoxidation of homoallylic alcohols commenced with the screening of hydroxamic acid ligands. Analogous to the method reported previously by our group,[8a] we first adjusted the α-amino acid part to the vanadium-catalyzed epoxidation

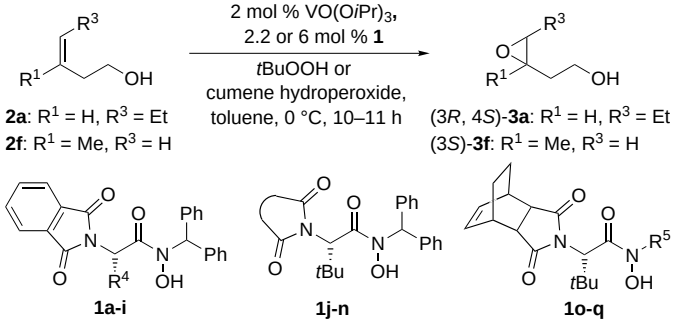

Scheme 1. Reagents and conditions for the reactions collected in Table 1.

of *cis*-3-hexen-1-ol (Scheme 1 and Table 1, entries 1–11).[9] The reactivity was relatively high compared to reports for other metal catalysts[5] (only 2 mol% vanadium catalyst at 0°C for 10 to 11 h gave the epoxy alcohol in around 45% yield). The enantioselectivities were low, and only when a hydroxamic acid derived from *tert*-leucine (trimethylalanine) was used as the ligand (**1g**), moderate enantioselectivity was obtained (entry 7, 23% *ee*). Next, the reaction conditions were optimized for **1g** as the ligand, and enantioselectivity went up to 52% *ee* with a slight loss of reactivity (entry 9). After a variety of homoallylic alcohols had been examined

Table 1: Ligand optimization for the asymmetric epoxidation of homoallylic alcohols **2a**[a] and **2f**[b] (see Scheme 1).

Entry	Homoallylic alcohol **2**	Hydroxamic acid **1**	*ee* [%][c]	Yield [%]
1	**2a**	**1a**: R^4 = Me	6	43
2	**2a**	**1b**: R^4 = *i*Pr	6	49
3	**2a**	**1c**: R^4 = *i*Bu	2	34
4	**2a**	**1d**: R^4 = *s*Bu	1	37
5	**2a**	**1e**: $R^4 = (CH_2)_2SMe$	–	trace
6	**2a**	**1f**: $R^4 = (CH_2)_4N$(phthaloyl)	7	41
7	**2a**	**1g**: R^4 = *t*Bu	23	24
8	**2a**[d]	**1g**: R^4 = *t*Bu[e]	44	48
9	**2a**[d]	**1g**: R^4 = *t*Bu[f]	52	41
10	**2a**	**1h**: $R^4 = CH_2$(3-indolyl)	8	35
11	**2a**	**1i**: $R^4 = CH_2(p\text{-}OMeC_6H_4)$	1	37
12	**2f**	**1e**: $R^4 = (CH_2)_2SMe$	84	58
13	**2f**	**1j** (1,8-naphthalenedicarbonyl)	85	69
14	**2f**	**1k** (2,3-naphthalenedicarbonyl)	85	45
15	**2f**	**1l** (2,3-dimethylmaloyl)	85	31
16	**2f**	**1m** (2,3-diphenylmaloyl)	82	23
17	**2f**	**1n** (bicyclo[2.2.1]hept-5-ene-2,3-dicarbonyl)	85	68
18	**2f**	**1o**: R^5 = diphenylmethyl	87	44
19	**2f**	**1p**: R^5 = cyclohexyl	70	4
20	**2f**	**1q**: R^5 = 9-fluorenyl	42	36

[a] Reaction conditions: $VO(OiPr)_3$ (2 mol%), **1** (2.2 mol%), *t*BuOOH (1.5 equiv), toluene, 10–11 h. [b] Reaction conditions: $VO(OiPr)_3$ (2 mol%), **1** (6 mol%), cumene hydroperoxide (1.5 equiv), toluene, 10 h. [c] The *ee* values of **3a** and **3f** were determined by chiral GLC (column, γ-TA) analysis, their absolute structures by comparison of the optical rotation with published data. [d] Cumene hydroperoxide was used as an oxidant. [e] 3 mol% of **1g** was used. [f] 6 mol% of **1g** was used.

[*] Prof. Dr. H. Yamamoto,[+] N. Makita, Dr. Y. Hoshino
Graduate School of Engineering
Nagoya University, SORST
Japan Science and Technology Corporation (JST)
Furo, Chikusa, Nagoya 464–8603 (Japan)
Fax: (+81) 52-789-3222
E-mail: yamamoto@cc.nagoya-u.ac.jp
[+] Present Address:
Department of Chemistry
The University of Chicago
5735 South Ellis Avenue, Chicago, IL 60637 (USA)
Fax: (+1) 773–702–0805
E-mail: yamamoto@uchicago.edu

[**] Support of the Japan Science and Technology Corporation (JST) is gratefully acknowledged.

and after we had determined the discriminating selection in the reaction, the imido and the hydroxylamine part of the hydroxamic acid ligand were changed as previously reported,[8a] however, in all cases nearly the same selectivities were obtained (entries 12–20).[10] Based on these results, it is likely that the asymmetric epoxidation of homoallylic alcohols is not parallel to that of allylic alcohols using these chiral vanadium catalysts.

We now turned our attention to the structure of the homoallylic alcohol **2** because asymmetric epoxidation of such alcohols has been rarely investigated. The epoxidation of 4-disubstituted alcohols **2** using ligand **1g** was faster than that of 4-monosubstituted ones (entries 3 and 4 vs. entries 1 and 2 in Table 2).[11,12] On the other hand, 3-monosubstituted alcohols **2** were effectively epoxidized with good to high enantioselectivities (see Experimental Section and entries 5–9). For example, the simple homoallylic alcohol 3-methyl-3-buten-1-ol **2f** was epoxidized to give (*S*)-3,4-epoxy-3-methyl-1-butanol with 84% *ee*, and the 3,4-disubstituted alcohol **2e** was epoxidized with moderate enantioselectivity (74% *ee*). It is likely that the 3-position of homoallylic alcohols is strongly recognized by catalysts with a positive effect on the selectivity, and that substituents in the 4-position provide a slightly negative effect.

To demonstrate that our method is useful for synthetic purposes, the total synthesis of (−)-α-bisabolol, which is known as a fragrance, was executed (Scheme 2).[13] Hydroxymethylation of (*S*)-limonene gave *S* alcohol **5**,[14] which was epoxidized diastereoselectively using hydroxamic acid D-**1g** as ligand to give epoxy alcohol **6** in 84% yield with 90% *de*. This optically active alcohol was reduced by lithium aluminum hydride to diol **7**, which was tosylated at the primary hydroxy group, and coupled with isopropenyl magnesium bromide to give (−)-(4*S*,8*S*)-α-bisabolol **9** ($[\alpha]_D^{25} = -51.0$ ($c =$ 1.22 in ethanol); total yield 21%).[15] With L-**1g**, *S* alcohol **5** was epoxidized to give epoxy alcohol (8*R*)-**6** (82% yield, 94% *de*), which was converted to (−)-(4*S*,8*R*)-*epi*-α-bisabolol in the same manner as described above.[16]

Table 2: Asymmetric epoxidation of homoallylic alcohols **2** using **1g** as ligand.

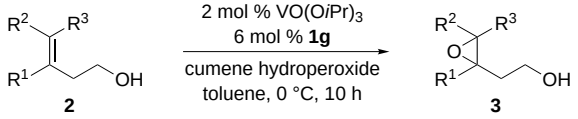

Entry	Homoallylic alcohol **2**	*ee* [%]	Yield [%]
1	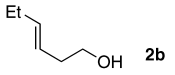 **2b**	40[a]	25
2	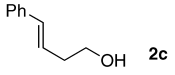 **2c**	46[c]	24
3	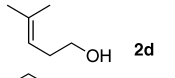 **2d**	36[a]	67
4	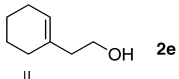 **2e**	74[b]	61
5	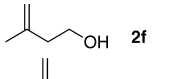 **2f**	84[a]	58
6	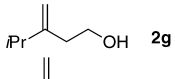 **2g**	90[a]	77
7	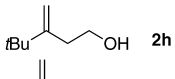 **2h**	90[b]	89
8	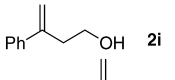 **2i**	89[c]	70
9	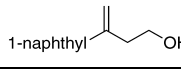 **2j**	91[d]	42

[a] Determined by chiral GLC (column, γ-TA). [b] Determined by chiral GLC (column, β-DM). [c] Determined by chiral HPLC (column, AD-H). [d] Determined by chiral HPLC (column, OD-H).

In summary, the asymmetric epoxidation of homoallylic alcohols using chiral vanadium catalysts was conducted under mild conditions, and a discriminating reactivity and selectivity for 3-monosubstituted homoallylic alcohols was determined (58–89% yield, 84–91% *ee*). To show its synthetic utility, the reaction was applied to the key step of the total synthesis of (−)-α- and (−)-8-*epi*-α-bisabolol.

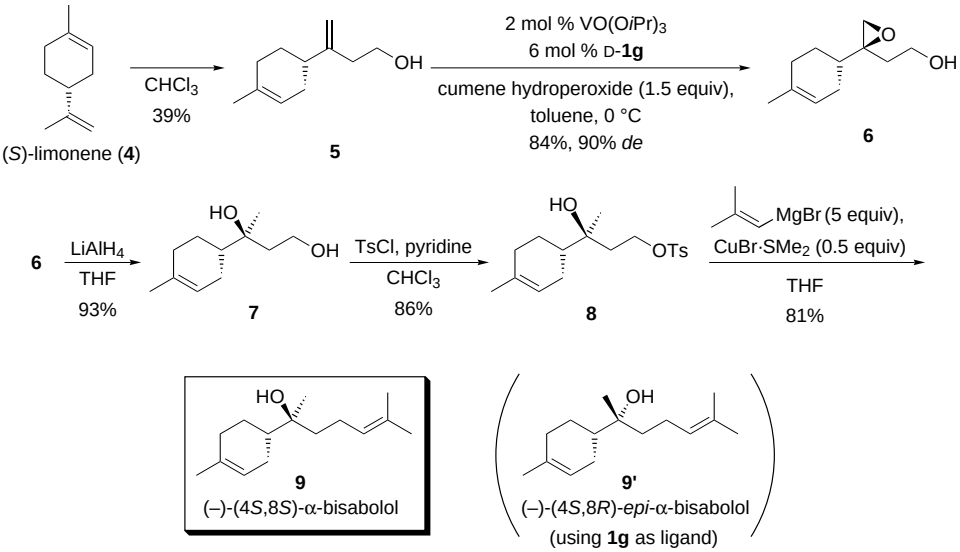

Scheme 2. A concise and stereoselective total synthesis of (−)-(4*S*,8*S*)-α- and (−)-(4*S*,8*R*)-*epi*-α-bisabolol.

 © 2003 Wiley-VCH Verlag GmbH & Co. KGaA, Weinheim 1433-7851/03/4208-0942 $ 20.00+.50/0

Experimental Section

Representative experimental procedure: $VO(OiPr)_3$ (5 μL, 20 μmol) and hydroxamic acid (26.6 mg, 60 μmol) were dissolved in toluene (1 mL), stirred for 1 hour, and cooled to 0 °C. Cumene hydroperoxide (275 μL, 1.5 mmol) and 3-(1-naphthyl)-3-buten-1-ol (**2j**) (198 mg, 1.0 mmol) were added at 0 °C. The reaction mixture was stirred for 10 h, then trimethylphosphite (177 μL, 1.5 mmol) was added at that temperature. The mixture was allowed to reach room temperature, then it was extracted with ethyl acetate, dried over sodium sulfate, and evaporated. The crude product was purified by column chromatography on a silica gel (eluent ethyl acetate/hexane, 1:1) to give 3,4-epoxy-3-(1-naphthyl)-1-butanol in 42% yield with 91% *ee*. ^{1}H NMR (300 MHz, $CDCl_3$, 25 °C, TMS): $\delta = 8.13$ (d, $J = 8.0$ Hz, 1H; Ar-H), 7.90 (d, $J = 8.0$ Hz, 1H; Ar-H), 7.83 (d, $J = 8.0$ Hz, 1H; Ar-H), 7.50 (m, 4H; Ar-H), 3.71 (m, 2H; CH_2OH), 3.35 (d, $J = 6.0$ Hz, 1H; OCH_2), 3.00 (d, $J = 6.0$ Hz, 1H; OCH_2), 2.45 (m, 1H; CCH_2CH_2), 2.29 (m, 1H; CCH_2CH_2), 1.69 ppm (br, 1H; OH). HPLC analysis (column: OD-H, Daisel): retention times 44.9 (main peak) and 68.1 min (minor peak) using hexane/2-propanol (40:1) as the eluent at a flow rate of 1.0 mL min^{-1}. For the epoxy alcohols **3a–e**, a saturated aqueous solution of sodium sulfite instead of trimethylphosphite was used for quenching the reaction.

Received: September 24, 2002 [Z50233]

[1] a) R. A. Sheldon, J. A. Kochi, *Metal-Catalyzed Oxidations of Organic Compounds*, Academic Press, New York, **1981**; b) *Organic Syntheses by Oxidation with Metal Compounds* (Eds.: W. J. Mijs, C. R. H. I. De Jonge), Plenum, New York, **1986**; c) M. Hudlický, *Oxidations in Organic Chemistry*, American Chemical Society, Washington, DC, **1990**; d) E. N. Jacobsen in *Comprehensive Organometallic Chemistry II, Vol. 12* (Eds.: E. W. Abel, F. G. A. Stone, G. Wilkinson), Elsevier Science, Oxford, **1995**, p. 1097.

[2] For selected recent reviews of the asymmetric epoxidation of functionalized alkenes, see: a) R. A. Johnson, K. B. Sharpless in *Catalytic Asymmetric Synthesis*, 2nd ed. (Ed.: I. Ojima), Wiley-VCH, New York, **2000**, p. 231; b) T. Katsuki in *Comprehensive Asymmetric Catalysis I–III, Vol. 2* (Eds.: E. N. Jacobsen, A. Pfaltz, H. Yamamoto), Springer, Berlin, **1999**, p. 621; c) T. Katsuki, V. S. Martin, *Org. React.* **1996**, *48*, 1.

[3] For selected recent reviews of the asymmetric epoxidation of α,β-unsaturated carbonyl compounds, see: a) V. K. Aggarwal in *Comprehensive Asymmetric Catalysis I–III, Vol. 2* (Eds.: E. N. Jacobsen, A. Pfaltz, H. Yamamoto), Springer, Berlin, **1999**, p. 679; b) M. J. Porter, J. Skidmore, *Chem. Commun.* **2000**, 1215.

[4] For selected reviews of the asymmetric epoxidation of unfunctionalized alkenes, see: a) V. Schurig, F. Betschinger, *Chem. Rev.* **1992**, *92*, 873; b) K. A. Jörgensen, *Chem. Rev.* **1989**, *89*, 431; c) T. Katsuki in *Catalytic Asymmetric Synthesis*, 2nd ed. (Ed.: I. Ojima), Wiley-VCH, New York, **2000**, p. 287; d) E. N. Jacobsen, M. H. Wu in *Comprehensive Asymmetric Catalysis I–III, Vol. 2* (Eds.: E. N. Jacobsen, A. Pfaltz, H. Yamamoto), Springer, Berlin, **1999**, p. 649.

[5] a) S. Ikegami, T. Katsuki, M. Yamaguchi, *Chem. Lett.* **1987**, 83; b) B. E. Rossiter, K. B. Sharpless, *J. Org. Chem.* **1984**, *49*, 3707; c) J. K. Karjalainen, O. E. Hormi, D. C. Sherrington, *Tetrahedron: Asymmetry* **1998**, *9*, 3895.

[6] F. Freeman in *Organic Syntheses by Oxidation with Metal Compounds* (Eds.: W. J. Mijs, C. R. H. I. De Jonge), Plenum, New York, **1986**, p. 1.

[7] The asymmetric epoxidation of allylic alcohols using vanadium and an optically active hydroxamic acid was first reported by K. B. Sharpless in 1977: R. C. Michaelson, R. E. Palermo, K. B. Sharpless, *J. Am. Chem. Soc.* **1977**, *99*, 1990.

[8] a) Y. Hoshino, H. Yamamoto, *J. Am. Chem. Soc.* **2000**, *122*, 10452; b) N. Murase, Y. Hoshino, M. Oishi, H. Yamamoto, *J. Org. Chem.* **1999**, *64*, 338; c) Y. Hoshino, N. Murase, M. Oishi, H. Yamamoto, *Bull. Chem. Soc. Jpn.* **2000**, *73*, 1653.

[9] The absolute configuration of **3a** (3*R*,4*S*) was determined by comparison of the optical rotation with published data.[5b]

[10] The absolute configuration of **3f** (*S*) was determined by comparison of the optical rotation of the derivative *O*-methoxymethyl-3,4-epoxy-3-methyl-1-butanol with published data, see: D. Behnke, L. Henning, M. Findeisen, P. Welzel, D. Müller, M. Thormann, H.-J. Hofmann, *Tetrahedron* **2000**, *56*, 1081.

[11] (*Z*)-4-Phenyl-3-buten-1-ol (**2c**) was obtained from *trans*-styrylacetic acid (*trans*-4-phenyl-3-butenoic acid) and lithium aluminum hydride. 3-Phenyl-3-buten-1-ol (**2i**) was prepared by Heck reaction according to ref. [12]. The homoallylic alcohols **2e, g, h,** and **j** were prepared by ene reaction using $BF_3{\cdot}OEt_2$ or Me_2AlCl and formaldehyde according to ref. [14a].

[12] W. Cabri, I. Candiani, A. Bedeschi, *J. Org. Chem.* **1992**, *57*, 3558.

[13] a) J.-D. Fourneron, M. Julia, *Bull. Soc. Chim. Fr.* **1981**, II-387; b) D. Babin, J.-D. Fourneron, M. Julia, *Tetrahedron* **1981**, *37*, 1; c) H. Nemoto, M. Shiraki, M. Nagamochi, K. Fukumoto, *Tetrahedron Lett.* **1993**, *34*, 4939; d) X.-J. Chen, A. Archelas, R. Furstoss, *J. Org. Chem.* **1993**, *58*, 5528.

[14] a) B. B. Snider, D. J. Rodini, T. C. Kirk, R. Cordova, *J. Am. Chem. Soc.* **1982**, *104*, 555; b) A. T. Blomquist, R. J. Himics, *J. Org. Chem.* **1968**, *33*, 1156; c) R. J. Crawford, W. F. Erman, C. D. Broaddus, *J. Am. Chem. Soc.* **1972**, *94*, 4298.

[15] **9**: $[\alpha]_D^{25} = -54.9$ ($c = 1.27$ in ethanol);[13d] ^{13}C NMR (300 MHz, $CDCl_3$, 25 °C, TMS): $\delta = 133.9$, 131.3, 124.6, 120.6, 74.1, 42.9, 40.1, 31.0, 26.9, 25.6, 23.3, 23.2, 23.0, 22.0, 17.6 ppm.

[16] **9′**: $[\alpha]_D^{25} = -61.4$ ($c = 1.70$ in ethanol), -69 ($c = 1.3$ in ethanol);[13d] ^{13}C NMR (300 MHz, $CDCl_3$, 25 °C, TMS): $\delta = 133.9$, 131.8, 124.7, 120.9, 74.4, 43.4, 39.4, 31.1, 26.2, 25.8, 24.1, 24.0, 23.5, 22.4, 17.8 ppm.

Catalytic Asymmetric Hydrogenation

Phospholane–Oxazoline Ligands for Ir-Catalyzed Asymmetric Hydrogenation**

*Wenjun Tang, Weimin Wang, and Xumu Zhang**

Although a lot of progress has been made in Rh- or Ru-catalyzed asymmetric hydrogenation, Ir-catalyzed asymmetric hydrogenation is relatively unexplored.[1] Pfaltz and co-workers first reported several Ir-phosphinooxazoline complexes as catalysts for asymmetric hydrogenation. With leading efforts by Pfaltz and co-workers,[2] and Burgess and

[*] Prof. X. Zhang, W. Tang, Dr. W. Wang
Department of Chemistry, The Pennsylvania State University
University Park, PA 16802 (USA)
Fax: (+1) 814-863-8403
E-mail: xumu@chem.psu.edu

[**] This work was supported by the National Institute of Health.

Supporting information for this article is available on the WWW under http://www.angewandte.org or from the author.

co-workers,[3] Ir-catalyzed asymmetric hydrogenation has been realized for some functionalized and nonfunctionalized olefins. However, since Ir-catalyzed asymmetric hydrogenation is still highly substrate dependent, the development of new efficient chiral ligands for Ir-catalyzed hydrogenation is a continuing challenge. Herein we report a new class of chiral N,P ligands, the phospholane–oxazolines **6** (Scheme 1), for Ir-catalyzed asymmetric hydrogenation. Excellent enantioselecitivities have been obtained in hydrogenation of methylstilbene derivatives and β-methylcinammic esters.

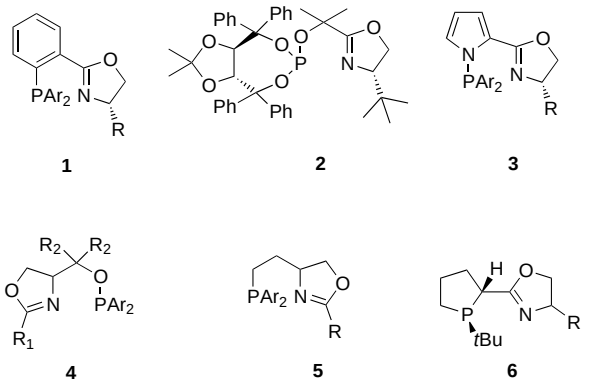

Scheme 1. N,P Ligands for enantioselective Ir-catalyzed hydrogenation.

After the development of phosphinooxazoline ligands (PHOX, **1**) for Ir-catalyzed asymmetric hydrogenation,[2a] Pfaltz and others have continued their efforts for the search of new efficient N,P ligands (Scheme 1). Various N,P ligands such as TADDOL-phosphite–oxazoline (**2**),[2b] PyrPHOX (**3**),[2d] and phosphinite-oxazoline (**4**),[2e,f,g] were subsequently developed by Pfalz and co-workers. Burgess and co-workers also reported JM-Phos (**5**)[3a,b] and imidazolylidene-oxazoline.[3c] These ligands expanded the reaction scope of Ir-catalyzed asymmetric hydrogenation. The closely related Crabtree's catalyst, $[Ir(cod)(Py)PCy_3]PF_6$ (cod = 1,5-cyclooctadiene, Py = pyridine, Cy = cyclohexyl), is an efficient achiral catalyst for the hydrogenation of tri- or tetrasubstituted olefins.[4] Since an electron-rich phosphane PCy_3 is used in this system, we aimed to develop a new class of chiral N,P ligands **6** with an electron-rich phosphorus center to match the electronic properties of Crabtree's catalyst. It is noteworthy that these phospholane–oxazoline ligands not only have a stereogenic center in the oxazoline ring but also at the phosphorus center.[5] The structure of **6** is modular since the oxazoline ring can vary with an array of R groups.

We reported the synthesis of an efficient chiral bisphospholane ligand, TangPhos, from 1-*tert*-butyl-phospholane 1-sulfide **8** in only three steps.[6] Phospholane–oxazolines **6** can also be synthesized easily from **8** in four steps (Scheme 2). Selective deprotonation of **8** by *n*-butyllithium in the presence of (−)-sparteine[7] followed by reaction with CO_2 provided acid **9** with 72% *ee*.[8,9] Recrystallization of the acid from ethanol yielded the enantiomerically pure **9** in 40% yield.[15] The absolute configuration of **9** was confirmed by its X-ray structure analysis.[10] The condensation of **9** with chiral amino

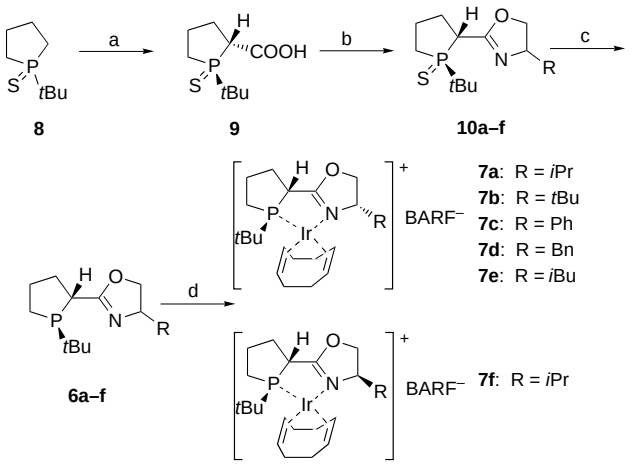

Scheme 2. Synthesis of phospholane–oxazoline ligands **6**. a) *n*BuLi, (−)-sparteine, CO_2, −78°C, recrystallization, 71% *ee* → 100% *ee*, 40%; b) 1. amino alcohol, EDC, HOBT, DMF, 70°C; 2. MsCl, CH_2Cl_2, 70–80%; c) Raney Ni, CH_3CN, 80–95%; d) $[\{Ir(cod)Cl\}_2]$, NaBARF, 50–70%. EDC = *N*-(3-dimethylaminopropyl)-*N*′-ethylcarbodiimide hydrochloride, HOBT = 1-hydroxybenzotriazole, cod = 1,5-cyclooctadiene, BARF = tetrakis[3,5-bis(trifluoromethyl)phenyl]borate, MsCl = methanesulfonyl chloride.

alcohols by using EDC/HOBT as the reagents proceeded smoothly to yield the coupling products, which were subsequently treated with MsCl to form the oxazoline compounds **10**. Desulfurization of **10** using Raney Ni[11] provided a set of phospholane–oxazoline ligands **6** in excellent yields. The corresponding iridium complexes **7a–f** were synthesized in good yields according to standard procedures.[2a] Although the iridium complexes **7a–f** are slightly air-sensitive, they can be stored under nitrogen for a long period of time without deterioration. To investigate the influence of the relative configuration of the chirality in the oxazoline ring, and the chiralities in the phospholane ring, two diastereomeric ligands **6a** and **6f** (R = *i*Pr) were synthesized. A series of ligands **6a–f** were also synthesized to study the influence of R in the oxazoline ring.

To test the effectiveness of the new chiral N,P ligands, iridium complexes **7a–f** were used as catalysts for asymmetric hydrogenation of methylstilbene derivatives.[12] The hydrogenations were carried out at room temperature under 50 bar of pressure using CH_2Cl_2 as the solvent. All the reactions proceeded to completion in the presence of 1 mol% of an iridium complex. The diastereomeric complexes **7a** and **7f** led to hydrogenation products with different configuration (Table 1), which indicated that the chirality in the oxazoline ring of the ligand determined the configuration of the product. Iridium complex **7a** was favored over **7b** for the reaction, as a higher *ee* value (91%) was obtained (Table 1, entries 1 and 6). Among the Ir complexes with different steric bulk (**7a–e**, Table 1, entries 1–5), the highest *ee* value (95%) was obtained with **7c**, which has a phenyl group on the oxazoline ring. The enantiomeric excess of the product is comparable to those reported by Pfalz et al[2a] with an Ir–PHOX system. With **7c** as the catalyst, another two substituted methylstilbene deriva-

 © 2003 Wiley-VCH Verlag GmbH & Co. KGaA, Weinheim 1433-7851/03/4208-0944 $ 20.00+.50/0

Table 1: Ir-catalyzed asymmetric hydrogenation of methylstilbene derivatives.

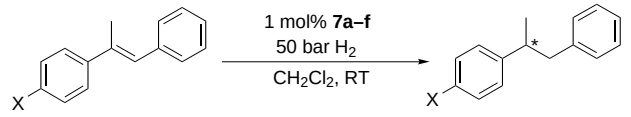

Entry[a]	Substrate	X	Catalyst	*ee* [%][b]	Config.[c]
1	**8**	H	**7a**	91	*R*
2	**8**	H	**7b**	81	*R*
3	**8**	H	**7c**	95	*R*
4	**8**	H	**7d**	89	*R*
5	**8**	H	**7e**	75	*R*
6	**8**	H	**7f**	77	*S*
7	**9**	OMe	**7c**	91	*R*
8	**10**	Cl	**7c**	90	*R*

[a] See Supporting Information for experimental details. [b] The enatiomeric excesses were determined by chiral HPLC (Chiralcel OJH). [c] The absolute configuration was assigned by comparison of the observed optical rotation with reported data.

tives were also subjected to hydrogenation and *ee* values over 90% were obtained (entry 7 and 8).

Asymmetric hydrogenation of β-methylcinnamic esters can directly form chiral 3-arylbutyric esters. The reduction products of 3-arylbutyric esters (i.e. chiral 3-arylbutanols) are important intermediates for the synthesis of aromatic sesquiterpenes of the bisabolane family.[13] Pfaltz and co-workers applied the iridium phosphinite–oxazoline system to the asymmetric hydrogenation of ethyl β-methylcinnamate ester and obtained the desired product in 94% *ee*.[2f] We used the iridium complexes **7a–f** for hydrogenation of (*E*)-β-methylcinnamic esters, which can be easily synthesized by using the Heck reaction from aryl halides and crotonic esters.[14] Methyl *(E)*-β-methylcinnamate was selected as the substrate to screen different iridium catalysts (Table 2, entries 1–6). The two diastereomeric catalysts **7a** and **7f** (R = *i*Pr) led to products with different configurations (Table 2, entries 1 and 6). The highest enantiomeric excess (98%) was obtained when **7c** was used as the catalyst (Table 2, entry 3). We therefore used **7c** as the catalyst for hydrogenation of a series of substituted *(E)*-β-methylcinnamic esters. A variety of chrial 3-arylbutyric esters were thus obtained in excellent enantiomeric excesses (95–99%) regardless of the substitution pattern on the phenyl ring (Table 2, entries 7–12). The electronic properties of the substrates did not have a significant influence on the enantioselectivities. Substrates with a 2-naphthyl group and a 1-naphthyl group also gave high *ee* values (Table 2, entries 13, 14). To our knowledge, these are highest enantioselectivities to date for asymmetric hydrogenation of β-methylcinnamic esters. Asymmetric hydrogenation of a (*Z*)-β-methylcinnamic ester led to a product with a different configuration, and a lower enantiomeric excess was obtained (entries 8 and 15).

In conclusion, we have developed a new class of phospholane–oxazoline ligands for Ir-catalyzed asymmetric hydrogenation. Excellent reactivities and enantioselectivities were obtained in the hydrogenation of methylstilbene derivatives and (*E*)-β-methylcinnamic esters. Since the phospholane–oxazoline ligands can be easily synthesized, these ligands are promising for the synthesis of chiral arenes and 3-arylbutyric esters.[15]

Received: October 2, 2002 [Z50283]

Table 2: Ir-catalyzed asymmetric hydrogenation of β-methylcinnamic esters.

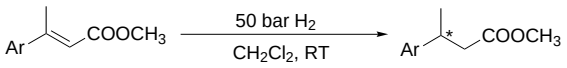

Entry[a]	Substrate	Ar	Catalyst	*ee* [%][b]	Config.[c]
1	**11**	Ph	**7a**	94	*R*
2	**11**	Ph	**7b**	91	*R*
3	**11**	Ph	**7c**	98	*R*
4	**11**	Ph	**7d**	92	*R*
5	**11**	Ph	**7e**	95	*R*
6	**11**	Ph	**7f**	93	*S*
7	**12**	*p*-F-C_6H_4	**7c**	95	*R*
8	**13**	*p*-Cl-C_6H_4	**7c**	98	*R*
9	**14**	*p*-CH_3-C_6H_4	**7c**	97	*R*
10	**15**	*p*-OCF_3-C_6H_4	**7c**	97	*R*
11	**16**	*p*-OCH_3-C_6H_4	**7c**	97	*R*
12	**17**	*m*-CH_3-C_6H_4	**7c**	99	*R*
13	**18**	1-naphthyl	**7c**	98	*R*
14	**19**	2-naphthyl	**7c**	95	*R*
15	(*Z*)-**13**	*p*-Cl-C_6H_4	**7c**	80	*S*

[a] See Supporting Information for experimental details. [b] The enantiomeric excesses were determined by chiral HPLC (Chiralcel OJH) or chiral GC (Chiralselect 1000). [c] The absolute configurations were assigned by comparison of the observed optical rotation with reported data or by analogy.

[1] For recent reviews, see: a) T. Ohkuma, M. Kitamura, R. Noyori in *Catalytic Asymmetric Synthesis* (Ed.: I. Ojima), Wiley-VCH, Weinheim, **2000**, p. 1; b) J. M. Brown in *Comprehensive Asymmetric Catalysis* (Eds.: E. N. Jacobsen, A. Pfaltz, H. Yamamoto), Springer, Berlin, **1999**, p. 121; c) R. L. Halterman in *Comprehensive Asymmetric Catalysis* (Eds.: E. N. Jacobsen, A. Pfaltz, H. Yamamoto), Springer, Berlin, **1999**, p. 183.

[2] a) A. Lightfoot, P. Schnider, A. Pfaltz, *Angew. Chem.* **1998**, *110*, 3047–3050; *Angew. Chem. Int. Ed.* **1998**, *37*, 2897–2899; b) R. Hilgraf, A. Pfaltz, *Synlett* **1999**, 1814–1816; c) D. G. Blackmond, A. Lightfoot, A. Pfaltz, T. Rosner, P. Schnider, N. Zimmermann, *Chirality* **2000**, *12*, 442–449; d) P. G. Cozzi, N. Zimmermann, R. Hilgraf, S. Schaffner, A. Pfaltz, *Adv. Synth. Catal.* **2001**, *343*, 450–454; e) J. Blankenstein, A. Pfaltz, *Angew. Chem.* **2001**, *113*, 4577–4579; *Angew. Chem. Int. Ed.* **2001**, *40*, 4445–4447; f) F. Menges, A. Pfaltz, *Adv. Synth. Catal.* **2002**, *344*, 40–44; g) Closely related ligands have been recently applied in Pd-catalyzed allylic alkylation: G. Jones, C. J. Richards, *Tetrahedron Lett.* **2001**, *42*, 5553–5555.

[3] a) D.-R. Hou, J. H. Reibenspies, K. Burgess, *J. Org. Chem.* **2001**, *66*, 206–215; b) D.-R. Hou, J. Reibenspies, T. J. Colacot, K. Burgess,

 © 2003 Wiley-VCH Verlag GmbH & Co. KGaA, Weinheim 1433-7851/03/4208-0945 $ 20.00+.50/0

Chem. Eur. J. **2001**, *7*, 5391 – 5400; c) M. T. Powell, D.-R. Hou, M. C. Perry, X. Cui, K. Burgess, *J. Am. Chem. Soc.* **2001**, *123*, 8878 – 8879.
[4] R. H. Crabtree, *Acc. Chem. Res.* **1979**, *12*, 331 – 338.
[5] Helmchen reported a P-chiral Phox ligand for Pd-catalyzed allylic alkylation, see: S. Kudis, G. Helmchen, *Angew. Chem.* **1998**, *110*, 3210 – 3212; *Angew. Chem. Int. Ed.* **1998**, *37*, 3047 – 3050.
[6] a) W. Tang, X. Zhang, *Angew. Chem.* **2002**, *114*, 1682 – 1684; *Angew. Chem. Int. Ed.* **2002**, *41*, 1612 – 1614; b) W. Tang, X. Zhang, *Org. Lett.* **2002**, *4*, 4159 – 4161.
[7] a) D. Hoppe, F. Hintze, P, Tebben, M. Paetow, H. Ahrens, J. Schwerdtfeger, P. Sommerfeld, J. Haller, W. Guarnieri, S. Kolczewski, T. Hense, I. Hoppe, *Pure Appl. Chem.* **1994**, *66*, 1479 – 1486, and references therein; b) P. Beak, S. T. Kerrick, S. Wu, J. Chu, *J. Am. Chem. Soc.* **1994**, *116*, 3231 – 3239, and references therein.
[8] Asymmetric deprotonation of phosphane sulfides or phosphane boranes have been reported, see: a) A. R. Muci, K. R. Campos, D. A. Evans, *J. Am. Chem. Soc.* **1995**, *117*, 9075 – 9076; b) T. Imamoto, J. Watanabe, W. Yoshiyuki, H. Masuda, H. Yamada, H. Tsuruta, S, Matsukawa, K. Yamaguchi, *J. Am. Chem. Soc.* **1998**, *120*, 1635 – 1636.
[9] Asymmetric deprotonation of a phospholane–borane complex was reported by Kobayashi, see: S. Kobayashi, N. Shiraishi, W. W.-L. Lam, K. Manabe, *Tetrahedron Lett.* **2001**, *42*, 7303 – 7306.
[10] CCDC-193670 contains the supplementary crystallographic data for this paper. These data can be obtained free of charge via www.ccdc.cam.ac.uk/conts/retrieving.html (or from the Cambridge Crystallographic Data Centre, 12 Union Road, Cambridge CB21EZ, UK; fax: (+44) 1223-336-033; or deposit@ccdc.cam.ac.uk). We thank Dr. H. Yennawar for solving the crystal structure.
[11] S. R. Gilbertson, Z. Fu, *Org. Lett.* **2001**, *3*, 161 – 164.
[12] For Ti-catalyzed asymmetric hydrogenation, see: R. D. Broene, S. L. Buchwald, *J. Am. Chem. Soc.* **1993**, *115*, 12569 – 12570.
[13] a) C. Fuganti, S. Serra, A. Dulio, *J. Chem. Soc. Perkin Trans. 1* **1999**, 279 – 282; b) C. Fuganti, S. Serra, *J. Chem. Soc. Perkin Trans. 1* **2000**, 3758 – 3764; c) A. I. Meyers, D. Stoianova, *J. Org. Chem.* **1997**, *62*, 5219 – 5221.
[14] A. F. Littke, G. C. Fu, *J. Am. Chem. Soc.* **2001**, *123*, 6989 – 7000.
[15] The Supporting Information contains the experimental details, and spectroscopic data of all the new ligands, their Ir complexes, new substrates, and new hydrogenation products.

Allylation of Aldehydes

A Highly Practical and Enantioselective Reagent for the Allylation of Aldehydes**

*Katsumi Kubota and James L. Leighton**

Owing mainly to the prevalence of secondary alcohols in bioactive natural products, chemists have developed many moderately to highly enantioselective chiral reagents[1] and catalytic systems[2] for the allylation of aldehydes. In terms of practical utility, an ideal reagent should 1. be readily prepared in both enantiomeric forms, 2. be a stable/storable solid that can be prepared in bulk and employed at will by using only trivial procedures, 3. possess a good safety profile both for the user and environmentally, and 4. be generally effective in terms of both efficiency and enantioselectivity. Herein we report a new reagent that almost completely satisfies all of these conditions.

Based on our discovery that silicon—constrained in a five-membered ring by 1,2-diols, 1,2-aminoalcohols and 1,2-diamines—possesses Lewis acidity sufficient for clean, uncatalyzed allylation of aldehydes, we recently described the pseudoephedrine-derived strained silacycle **1** as a reagent for the enantioselective allylation of aldehydes (Scheme 1).[3] Whereas this reagent is trivially prepared and employed, and the enantioselectivities for aliphatic aldehydes are good (87–89% *ee*, typically), they are unacceptably low for aromatic and conjugated aldehydes (60–81% *ee*, typically). This reagent thus falls short of ideal mainly in terms of condition 4 (see above). Also reported were preliminary data regarding reagent **2**, which was found to provide improved enantioselectivity, but also low reactivity. We therefore initiated a full investigation into the potential of the diamine-based system.

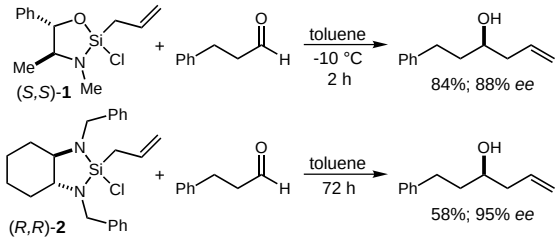

Scheme 1. Reagents for asymmetric allylation.

[*] Prof. J. L. Leighton, K. Kubota
Department of Chemistry
Columbia University
New York, NY 10027 (USA)
Fax: (+1) 212-932-1289
E-mail: leighton@chem.columbia.edu

[**] Financial support was provided by the Sumitomo Corp. (postdoctoral support of K.K.). We thank Merck Research Laboratories for generous financial support. J.L.L. is a recipient of a Pfizer Award for Creativity in Organic Chemistry.

Supporting information for this article is available on the WWW under http://www.angewandte.org or from the author.

 © 2003 Wiley-VCH Verlag GmbH & Co. KGaA, Weinheim 1433-7851/03/4208-0946 $ 20.00+.50/0

We began by optimizing the performance of reagent **2**, and were surprised to find that the use of CH_2Cl_2 as solvent led to a substantial increase in both efficiency and enantioselectivity (Table 1, entries 1 and 2), a result that did not hold for reagent **1**. With optimal conditions identified, the bis-(*p*-methoxybenzyl) and bis-(*p*-bromobenzyl) analogues of **2** were prepared[4] and screened for any effect on efficiency and selectivity. Interestingly, the latter sytem did provide a small but significant increase in efficiency and enantioselectivity with an aliphatic aldehyde (entry 1 versus entry 4) and with benzaldehyde (entry 2 versus entry 5). Perhaps more importantly, the bis-(*p*-bromobenzyl) substituted reagent is a moderately air-stable solid, and it was therefore selected for further study.

Table 1: Optimization of the diamine auxiliary.

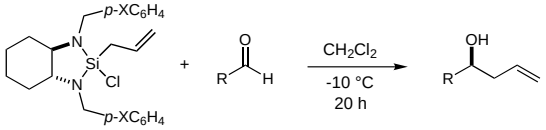

Entry[a]	X	R	Yield [%][b]	*ee* [%][c]
1	H	$PhCH_2CH_2$	79	96
2	H	Ph	61	94
3	OMe	$PhCH_2CH_2$	77	98
4	Br	$PhCH_2CH_2$	90	98
5	Br	Ph	69	98

[a] Reactions run with silane (1.0 equiv) and aldehyde (1.0 equiv) in CH_2Cl_2 at −10 °C for 20 h. [b] Yield of isolated product. [c] Determined by chiral HPLC analysis or by the Mosher ester method. See the Supporting Information.

With the bis-(*p*-bromobenzyl)–diamine system identified as the most effective and convenient system, we examined the scope of the reaction (Table 2). With respect to aliphatic aldehydes reagent **3** is generally effective and provides good to excellent yields and uniformly excellent enantioselectivities that are among the highest observed for this reaction. The conditions were carefully optimized to maximize yield and enantioselectivity. Reactions at room temperature are only slightly less selective, but the yields are significantly lower because of partial decomposition of the reagent.

Table 2: Enantioselective allylation of aliphatic aldehydes.

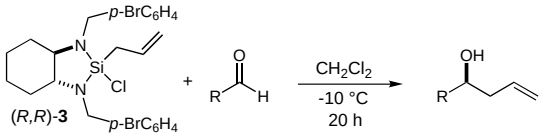

Entry[a]	R	Yield [%][b]	*ee* [%][c]
1	$PhCH_2CH_2$	90	98
2	$(CH_3)_2CHCH_2$	80[d]	96
3	*c*Hex	93	96
4	$PhCH_2OCH_2$	67	97
5	$PhCH_2OCH_2CH_2$	87	98
6	tBuMe$_2$SiOCH$_2$	61	98

[a] Reactions run with silane **3** (1.0 equiv) and aldehyde (1.0 equiv) in CH_2Cl_2 at −10 °C for 20 h. [b] Yield of isolated product. [c] Determined by chiral HPLC analysis or by the Mosher ester method. See the Supporting Information. [d] Because of product volatility, an alternative workup and purification was employed. See the Supporting Information.

We next turned to an investigation of the scope with respect to aromatic and conjugated aldehydes, a substrate class for which reagent **1** proved ineffective. A series of benzaldehydes were treated with reagent **3** and in every case moderate to good yields and excellent enantioselectivities could be obtained (Table 3, entries 1–3). Interestingly, *p*-anisaldehyde required 60 h to give a similar yield to that obtained with benzaldehyde and *p*-trifluoromethylbenzaldehyde after 20 h. Conjugated aldehydes proved less efficient still, but when the reaction was carried out at 8 °C for 72 h good yields and excellent enantioselectivities could be obtained (entries 4 and 5).

Table 3: Enantioselective allylation of aromatic and conjugated aldehydes.

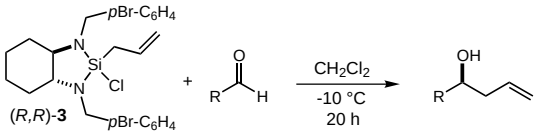

Entry[a]	R	Yield [%][b]	*ee* [%][c]
1	Ph	69	98
2[d]	*p*-$MeOC_6H_4$	62	96
3	*p*-$CF_3C_6H_4$	66	96
4[e]	(*E*)-PhCH=CH	75	96
5[e]	(*E*)-*n*PrCH=CH	71[f]	95

[a] Reactions run with silane **3** (1.0 equiv) and aldehyde (1.0 equiv) in CH_2Cl_2 at −10 °C for 20 h. [b] Yield of isolated product. [c] Determined by chiral HPLC analysis or by the Mosher ester method. See the Supporting Information. [d] Reaction run for 60 h. [e] Reaction run at 8 °C for 72 h. [f] Because of product volatility, an alternative workup and purification was employed. See the Supporting Information.

Especially in the context of applications in natural product synthesis, it was also of interest to investigate the use of reagent **3** with chiral aldehydes as the ability of this reagent to override any inherent substrate bias would add to its utility. Subjection of aldehyde **4** (98 % *ee*) to the standard allylation conditions with (*R,R*)-**3** gave protected *syn*-alcohol **5** in 86 % yield and 95:5 d.r. (Scheme 2). Subjection of aldehyde **4** (98 % *ee*) to the standard allylation conditions with the enantiomeric reagent (*S,S*)-**3** gave protected *anti*-alcohol **6** in 86 % yield and 98:2 d.r. Thus, although the expected substrate bias for 1,3-*anti* induction[5] was observed, excellent selectivity for either diastereomer may be achieved.

We have described a new reagent for the highly enantioselective allylation of a broad range of aldehydes. While the

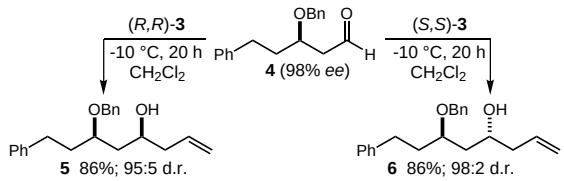

Scheme 2. Asymmetric allylation of chiral aldehydes.

reaction time (typically 20 h) would ideally be shorter, and aromatic and conjugated aldehydes tend to require even longer reaction times (Table 3), the four conditions for an ideal reagent outlined above have otherwise been met fully. In this context it is especially noteworthy, and bears repeating, that reagent **3** is a readily prepared stable solid that may be briefly handled in air with no apparent decomposition, and may be stored in a freezer under N_2 or Ar for long periods of time (> 1 month). Investigations into the mechanistic basis for the sluggish reactivity of some aromatic and conjugated aldehydes and a method to overcome this limitation have been initiated.

Experimental Section

Preparation of reagent (*R,R*)-**3**: To a cooled (0 °C) solution of allyltrichlorosilane (2.05 mL, 14.1 mmol) and 1,8-diazabicyclo[5.4.0]undec-7-ene (4.24 mL, 28.4 mmol) in dichloromethane (50 mL) was added (*R,R*)-*N,N′*-bis-(4-bromobenzyl)cyclohexane-1,2-diamine (5.37 g, 11.9 mmol) in dichloromethane (20 mL) over 50 min. After 2 h, the mixture was warmed to room temperature, and was stirred for 13 h. The reaction mixture was concentrated. After diethyl ether (60 mL) was added, the mixture was stirred for 1 h and filtered through a pad of celite, and the residue was washed with diethyl ether (2 × 10 mL). The filtrate was concentrated. Benzene (10 mL) was added, and the solution was concentrated. This procedure was repeated to give the product as an oil (5.37 g, 88 %). Upon standing (under Ar) in a freezer, the oil solidified to a white solid that may be stored in a freezer (under Ar) and used as needed. ^{1}H NMR (300 MHz, C_6D_6): $\delta = 7.43$ (d, $J = 8.4$ Hz, 2H; Ar-H), 7.42 (d, $J = 8.4$ Hz, 2H; Ar-H), 7.18 (d, $J = 8.5$ Hz, 2H; Ar-H), 7.17 (d, $J = 8.5$ Hz, 2H; Ar-H), 5.72 (m, 1H; C*H*=CH_2), 5.00–4.92 (m, 2H; CH=CH_2), 3.98 (d, $J = 16.2$ Hz, 1H; one of NCH_2Ar), 3.95 (d, $J = 15.1$ Hz, 1H; one of NCH_2Ar), 3.65 (d, $J = 15.1$ Hz, 1H; one of NCH_2Ar), 3.64 (d, $J = 16.2$ Hz, 1H; one of NCH_2Ar), 2.63–2.75 (m, 2H; two of C*H*N), 1.42–1.79 (m, 6H; four of Cy and SiCH_2CH=CH_2), 0.83–1.05 ppm (m, 4H; four of Cy); ^{13}C NMR (75 MHz, C_6D_6): $\delta = 141.7$, 140.7, 131.7, 131.4, 130.3, 129.5, 128.7, 121.2, 120.9, 116.6, 66.8, 65.8, 48.3, 47.5, 31.1, 30.7, 25.1, 25.0 ppm; ^{29}Si NMR (60 MHz, C_6D_6): $\delta = -4.4$ ppm.

General procedure for the reaction of (*R,R*)-**3** with aldehydes: To a cooled (−10 °C) solution of (*R,R*)-**3** in CH_2Cl_2 (0.2 M) was added the aldehyde (1.0 equiv). The reaction mixture was transferred to a freezer (−10 °C) and maintained at that temperature for 20 h. To this cooled solution was added 1N HCl and EtOAc, and the mixture was vigorously stirred at room temperature for 15 min. The layers were separated and the aqueous layer was extracted with EtOAc three times. The combined organic layers were diluted with hexane, dried ($MgSO_4$), filtered, and concentrated. The homoallylic alcohol products may be purified further by chromatography on silica gel. All yields listed in Tables 1–3 are for chromatographed, analytically pure material.

Received: October 24, 2002 [Z50425]

[1] a) S. E. Denmark, N. G. Almstead in *Modern Carbonyl Chemistry* (Ed.: J. Otera), Wiley-VCH, Weinheim, **2000**, chap. 10; b) S. R. Chemler, W. R. Roush in *Modern Carbonyl Chemistry* (Ed.: J. Otera), Wiley-VCH, Weinheim, **2000**, chap. 11; c) T. Herold, R. W. Hoffmann, *Angew. Chem.* **1978**, *90*, 822; *Angew. Chem. Int. Ed. Engl.* **1978**, *17*, 768; d) H. C. Brown, P. K. Jadhav, *J. Am. Chem. Soc.* **1983**, *105*, 2092; e) P. K. Jadhav, K. S. Bhat, P. T. Perumal, H. C. Brown, *J. Org. Chem.* **1986**, *51*, 432; f) U. S. Racherla, H. C. Brown, *J. Org. Chem.* **1991**, *56*, 401; g) W. R. Roush, A. E. Walts, L. K. Hoong, *J. Am. Chem. Soc.* **1985**, *107*, 8186; h) W. R. Roush, W. L. Banfi, *J. Am. Chem. Soc.* **1988**, *110*, 3979; i) M. T. Reetz, T. Zierke, *Chem. Ind.* **1988**, 663; j) R. P. Short, S. Masamune, *J. Am. Chem. Soc.* **1989**, *111*, 1892; k) E. J. Corey, C.-M. Yu, S. S. Kim, *J. Am. Chem. Soc.* **1989**, *111*, 5495; l) J. W. Faller, D. L. Linebarrier, *J. Am. Chem. Soc.* **1989**, *111*, 1937; m) A. Hafner, R. O. Duthaler, R. Marti, G. Rihs, Rothe-P. Streit, F. Schwarzenbach, *J. Am. Chem. Soc.* **1992**, *114*, 2321.

[2] For a recent review of enantioselective Lewis acid catalyzed allylmetal additions, see: a) A. Yanagisawa in *Comprehensive Asymmetric Catalysis, Vol. II* (Eds.: E. N. Jacobsen, A. Pfaltz, H. Yamamoto), Springer, Heidelberg, **1999**, chap. 27. Enantioselective Lewis base catalysis: b) S. E. Denmark, D. M. Coe, N. E. Pratt, B. D. Griedel, *J. Org. Chem.* **1994**, *59*, 6161; c) S. E. Denmark, J. Fu, *J. Am. Chem. Soc.* **2000**, *122*, 12021; d) S. E. Denmark, J. Fu, *J. Am. Chem. Soc.* **2001**, *123*, 9488; e) K. Iseki, Y. Kuroki, M. Takahashi, Y. Kobayashi, *Tetrahedron Lett.* **1996**, *37*, 5149; f) K. Iseki, Y. Kuroki, M. Takahashi, S. Kishimoto, Y. Kobayashi, *Tetrahedron* **1997**, *53*, 3513; g) K. Iseki, S. Mizuno, Y. Kuroki, Y. Kobayashi, *Tetrahedron Lett.* **1998**, *39*, 2767; h) K. Iseki, S. Mizuno, Y. Kuroki, Y. Kobayashi, *Tetrahedron* **1999**, *55*, 977; i) M. Nakajima, M. Saito, M. Shiro, S. Hashimoto, *J. Am. Chem. Soc.* **1998**, *120*, 6419; j) A. V. Malkov, M. Orsini, D. Pernazza, K. W. Muir, V. Langer, P. Meghani, P. Kocovsky, *Org. Lett.* **2002**, *4*, 1047.

[3] J. W. A. Kinnaird, P. Y. Ng, K. Kubota, X. Wang, J. L. Leighton, *J. Am. Chem. Soc.* **2002**, *124*, 7920.

[4] The cyclohexane diamine is treated with the appropriate substituted benzaldehyde to give the bis-Schiff base, which is reduced to the bis-(*p*-X-benzyl)diamine. The diamine is then treated with allyltrichlorosilane to give the active reagent. See the Supporting Information.

[5] a) M. T. Reetz, K. Kesseler, A. Jung, *Tetrahedron Lett.* **1984**, *25*, 729. For a comprehensive discussion regarding the tendency of β-alkoxyalkanals to favor the *anti* diastereomer in allylation and aldol reactions, see: b) D. A. Evans, M. J. Dart, J. L. Duffy, M. G. Yang, *J. Am. Chem. Soc.* **1996**, *118*, 4322.

One-Step Route to Tetrahydrofurans

A General Oxidative Cyclization of 1,5-Dienes Using Catalytic Osmium Tetroxide**

Timothy J. Donohoe and Sam Butterworth*

The oxidative cyclization of 1,5-dienes to produce tetrahydrofurans has been known for some time, and is a unique method for making these heterocycles. The reaction is

[*] Dr. T. J. Donohoe, S. Butterworth
Dyson Perrins Laboratory
South Parks Road, Oxford, OX1 3QY (UK)
Fax: (+44) 1865-275-674
E-mail: timothy.donohoe@chem.ox.ac.uk

[**] We thank the EPSRC and Merck, Sharp, and Dohme for funding this project. AstraZeneca, GlaxoSmithKline, Pfizer, and Novartis are thanked for unrestricted donations.

Supporting information for this article is available on the WWW under http://www.angewandte.org or from the author.

 © 2003 Wiley-VCH Verlag GmbH & Co. KGaA, Weinheim 1433-7851/03/4208-0948 $ 20.00+.50/0

particularly powerful because it involves the stereospecific suprafacial addition of two oxygen atoms across each of the two alkenes, coupled with the steroselective formation of a *cis*-substituted tetrahydrofuran ring (Scheme 1). Typically,

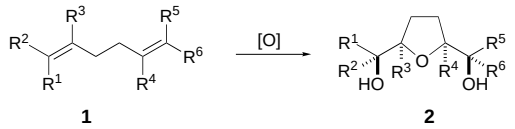

1 2

Scheme 1. Stereoselective formation of *cis*-tetrahydrofurans. [O] = $KMnO_4$, OsO_4, RuO_4.

this type of oxidation requires stoichiometric amounts of powerful oxidants such as $KMnO_4$[1] or CrO_3 derivatives,[2] which usually leads to low yields because of over-oxidation. Recently, conditions have been reported for accomplishing this reaction using catalytic osmium tetroxide[3] or ruthenium tetroxide[4] in conjunction with $NaIO_4$ reoxidant. However, while both of these processes are admirable, neither is particularly general or high yielding. For example, oxidation of geranyl acetate using Picialli's conditions (cat. OsO_4, $NaIO_4$, DMF[3]) gave 55% yield of a tetrahydrofuran, and a slightly lower yield with the isomeric neryl substrate (see entries 3 and 4, Table 1, see below); in our experience, these two substrates are often the ones that give the highest yields. In contrast, catalytic ruthenium tetroxide gave the same products as above from both geranyl and neryl acetates in 61 and 31% yield, respectively, but was not completely stereoselective for *cis*-tetrahydrofurans.

Our own work in this area had concentrated on the use of osmium tetroxide, which we believe is the oxidant with the most potential for the oxidative cyclizations of dienes. Initial results using the combination of OsO_4/tetramethylethylenediamine (TMEDA) with a diene had yielded an osmate ester **4**, which could be persuaded to cyclize (by adding the RO–Os=O unit across a distal alkene) under acidic conditions (Scheme 2).[5]

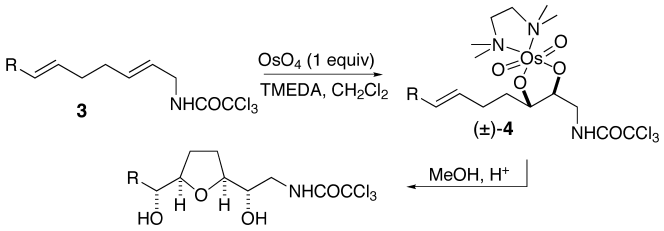

3 (±)-4

Scheme 2. Acid-promoted cyclization of osmate esters.

Although the yields of oxidative cyclization were good using this protocol (typically, 60–80%), the use of stoichiometric transition metals was unattractive and we sought out catalytic variants. Our early work had clearly shown that it was the acidic conditions that promoted cyclization of the osmate ester **4** to form the five-membered ring. Therefore, we examined the oxidative cyclization of a range of 1,5-dienes using catalytic OsO_4 (5%), Me_3NO (4 equiv), and either camphorsulfonic acid (CSA; 6 equiv) or trifluoroacetic acid (TFA; excess) to lower the pH. Remarkably, the dihydroxylation/oxidative cyclization sequence worked very well and provided several stereochemically defined tetrahydrofurans in good yield (Table 1), and as single stereoisomers. The conditions reported here are general for a range of 1,5-diene substrates and are a broad solution to the problems of yield and applicability, as outlined above. In fact, the lowest yield in Table 1 (60%) is a consequence of the volatility of the diene starting material (see entry 1). The stereoselective oxidation of both *cis* and *trans* isomers (compare entries 3 with 4 and 5 with 6, Table 1) is also noteworthy.[6]

In terms of mechanism, we suggest a similar scheme to that described above in Scheme 2. The initial reaction is dihydroxylation of the diene to yield an osmate ester (Scheme 3); this may then be cyclized to a tetrahydrofuan before the osmium is reoxidized back to

Table 1: Osmium-catalyzed cyclizations of 1,5-dienes.

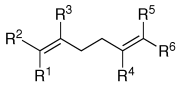

Entry	R^1	R^2	R^3	R^4	R^5	R^6	Product	Yield [%]
1	H	H	H	H	H	H	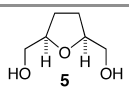 **5**	60[a]
2	H	H	Me	Me	H	H	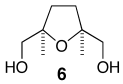 **6**	72[a]
3	Me	Me	H	Me	H	CH_2OBn	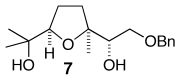 **7**	88[b]
4	Me	Me	H	Me	CH_2OBn	H	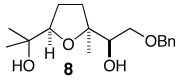 **8**	95[b]
5	H	Bu	H	H	H	Bu	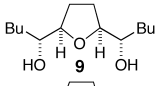 **9**	78[b]
6	Bu	H	H	H	Bu	H	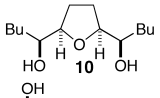 **10**	81[b]
7	H	$-(CH_2)_4-$	H	H	H	H	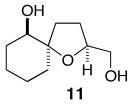 **11**	71[a]

[a] CSA conditions in CH_2Cl_2. [b] TFA conditions in acetone/water (9:1). Bn = benzyl.

 © 2003 Wiley-VCH Verlag GmbH & Co. KGaA, Weinheim 1433-7851/03/4208-0949 $ 20.00+.50/0

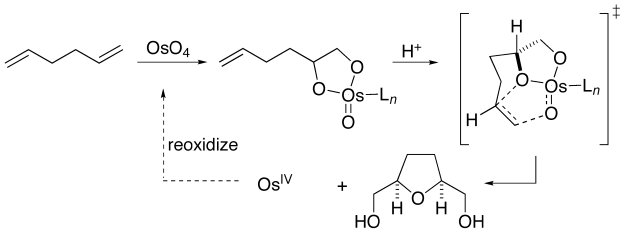

Scheme 3. Possible mechanism of oxidative cyclization.

Os^{VIII}.[7] The exact role of the acid in promoting cyclization is unknown, but we suggest that it protonates an oxo ligand on the osmium center, making it a more electron-deficient partner in the ensuing cycloaddition.

Our next objective was to search for methods of making these products enantiomerically pure.[8] We turned our attention to the role of stereodirecting groups on the diene backbone, between the two alkene groups: this is the first time that this possibility has been explored. The oxidation of substrate **12** is instructive for two reasons (Scheme 4). First, it

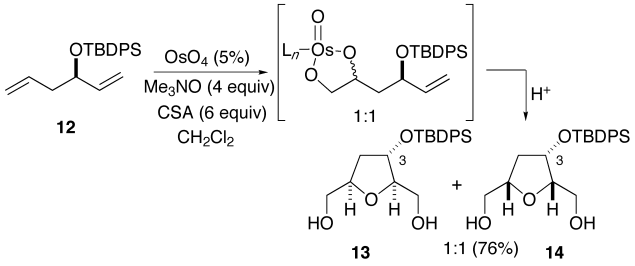

Scheme 4. Oxidation of substrate **12**. TBDPS = *tert*-butyldiphenylsilyl.

indicates that bulky silyl protecting groups are compatible with the oxidative regimen. Second, the lack of stereoselectivity with respect to the initial chiral center probably means that the reaction initiates through dihydroxylation of the unsubstituted alkene to give a mixture of osmate esters[9] (presumably, this reaction is nonstereoselective because the chiral center is too far removed). However, the presence of two *cis*-tetrahydrofuran products, **13** and **14,** means that the penchant for forming *cis* stereochemistry during cyclization clearly overrides any bias imposed by the substituent at C3. Hence, two *cis* isomers are formed in equal amounts, one from each isomer of the osmate ester.[10]

One consequence of this mechanism is that the readily available C_2-symmetric compound (+)-**15**[11] should be oxidized to give a single stereoisomer, whatever the outcome from the initial dihydroxylation (Scheme 5). This was indeed the case, and compound (+)-**16** was isolated pure in 84% yield from the oxidation reaction.

The utility of this substrate was illustrated when compound (+)-**16** was deprotected (H_2, Pd/C) to give (+)-anhydro-D-glucitol,[12] or then monoprotected with BnBr/Ag_2O to yield (+)-**17**. When compound **17** was oxidized to the carboxylic acid, and deprotected by hydrogenolysis, (+)-D-chitaric acid[13] was produced in a short sequence (Scheme 5).

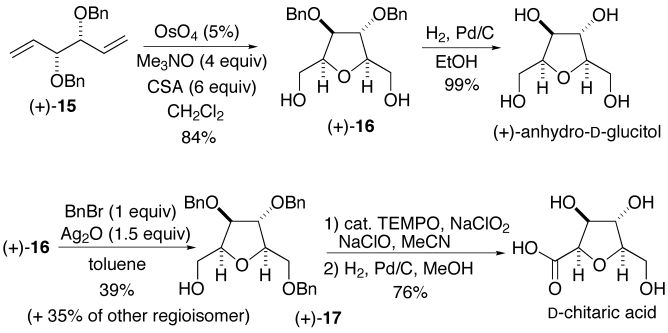

Scheme 5. Synthesis of anhydro-D-glucitol and D-chitaric acid. TEMPO = 2,2,6,6-tetramethyl-1-piperidinyloxyl.

To conclude, we report here for the first time a general and high-yielding oxidative cyclization of 1,5-dienes to *cis*-tetrahydrofurans. Our method is particularly attractive because it uses catalytic quantities of transition metal, in conjunction with an amine oxide as reoxidant and an acid to promote cyclization. Moreover, the potential of internal substituents on the diene backbone to act as stereodirecting groups has been explored and a short synthesis of highly functionalized enantiopure tetrahydrofuran natural products has been developed.

Received: November 12, 2002 [Z50535]

[1] E. Klein, W. Rojahn, *Tetrahedron* **1965**, *21*, 2353; J. E. Baldwin, M. J. Crossley, E.-M. M. Lehtonen, *J. Chem. Soc. Chem. Commun.* **1979**, 918; D. M. Walba, M. D. Wand, M. C. Wilkes, *J. Am. Chem. Soc.* **1979**, *101*, 4396.

[2] Chromium-promoted cyclization of diols derived from 1,5-diene give the same THF products, see: D. M. Walba, G. S. Stoudt, *Tetrahedron Lett.* **1982**, *23*, 727.

[3] V. Piccialli, *Tetrahedron Lett.* **2000**, *41*, 3731.

[4] P. H. J. Carlsen, T. Katsuli, V. S. Martin, K. B. Sharpless, *J. Org. Chem.* **1981**, *46*, 3936; V. Piccialli, N. Cavallo, *Tetrahedron Lett.* **2001**, *42*, 4695.

[5] T. J. Donohoe, J. J. G. Winter, M. Helliwell, G. Stemp, *Tetrahedron Lett.* **2001**, *42*, 971.

[6] Compound **5** is known, see: M. E. Jung, I. D. Trifunovich, A. W. Sledeski, *Heterocycles* **1993**, *35*, 273. Compound **6** was derivatized to a bis-Moshers ester that was no longer symmetrical; compounds **8, 10**, and **11** were characterized by X-ray crystallography. The structure of **7** is assigned by analogy to that of **8**, while compound **9** was converted into an authentic sample of **10** by a double Mitsunobu inversion/hydrolysis sequence.

[7] Preliminary experiments have shown that both first and second cycle osmium species are capable of undergoing the oxidative cyclization reaction and therefore we find it difficult to discriminate between the two.

[8] The pH of these oxidation reactions has been measured at <1; in this range we do not (nor would we expect to) observe asymmetric induction from a chiral cinchona alkaloid ligand. Previous attempts to make the cyclization products enantiopure have used acyl-derived auxiliaries, see: D. M. Walba, C. A. Przybyla, C. B. Walker, Jr., *J. Am. Chem. Soc.* **1990**, *112*, 5624; P. J. Kocienski, R. C. D. Brown, A. Pommier, M. Procter, B. Schmidt, *J. Chem. Soc. Perkin Trans. 1* **1998**, 9; A. R. L. Cecil, R. C. D. Brown, *Org. Lett.* **2002**, *4*, 3715; R. C. D. Brown, C. J. Bataille, R. M. Hughes, A. Kenney, T. J. Luker, *J. Org. Chem.*

 © 2003 Wiley-VCH Verlag GmbH & Co. KGaA, Weinheim 1433-7851/03/4208-0950 $ 20.00+.50/0

2002, *67*, 8079; or chiral phase-transfer catalysis, see: R. C. D. Brown, J. F. Keily, *Angew. Chem.* **2001**, *113*, 4628; *Angew. Chem. Int. Ed.* **2001**, *40*, 4496.

[9] Based on Sharpless' rate data, we estimate that the C1–C2 alkene unit is approximately ten times less reactive than the other towards dihydroxylation: H. C. Kolb, M. S. VanNieuwenhze, K. B. Sharpless, *Chem. Rev.* **1994**, *94*, 2483. Using OsO_4/TMEDA we have been able to isolate the two (inseparable) osmate ester diastereosiomers shown in Scheme 4 and show that they cyclize to a mixture of **13** and **14**.

[10] The structures of **13** and **14** were proven by protection of the primary hydroxy groups, desilylation, and oxidation to the C3 ketone. Both **13** and **14** gave the same ketone, which showed reciprocal NOE enhancements between H(C2) and H(C5).

[11] S. D. Burke, G. M. Sametz, *Org. Lett.* **1999**, *1*, 71.

[12] The spectroscopic data from our material matched exactly that in the literature, see: R. Persky, A. Albeck, *J. Org. Chem.* **2000**, *65*, 5632.

[13] E. Hardegger, F. Lohse, *Helv. Chim. Acta* **1957**, *40*, 2383; H. C. Cox, E. Hardegger, F. Kögl, P. Liechti, F. Lohse, C. A. Salemink, *Helv. Chim. Acta* **1958**, *41*, 229; E. Hardegger, H. Furter, J. Kiss, *Helv. Chim. Acta* **1958**, *41*, 2401.

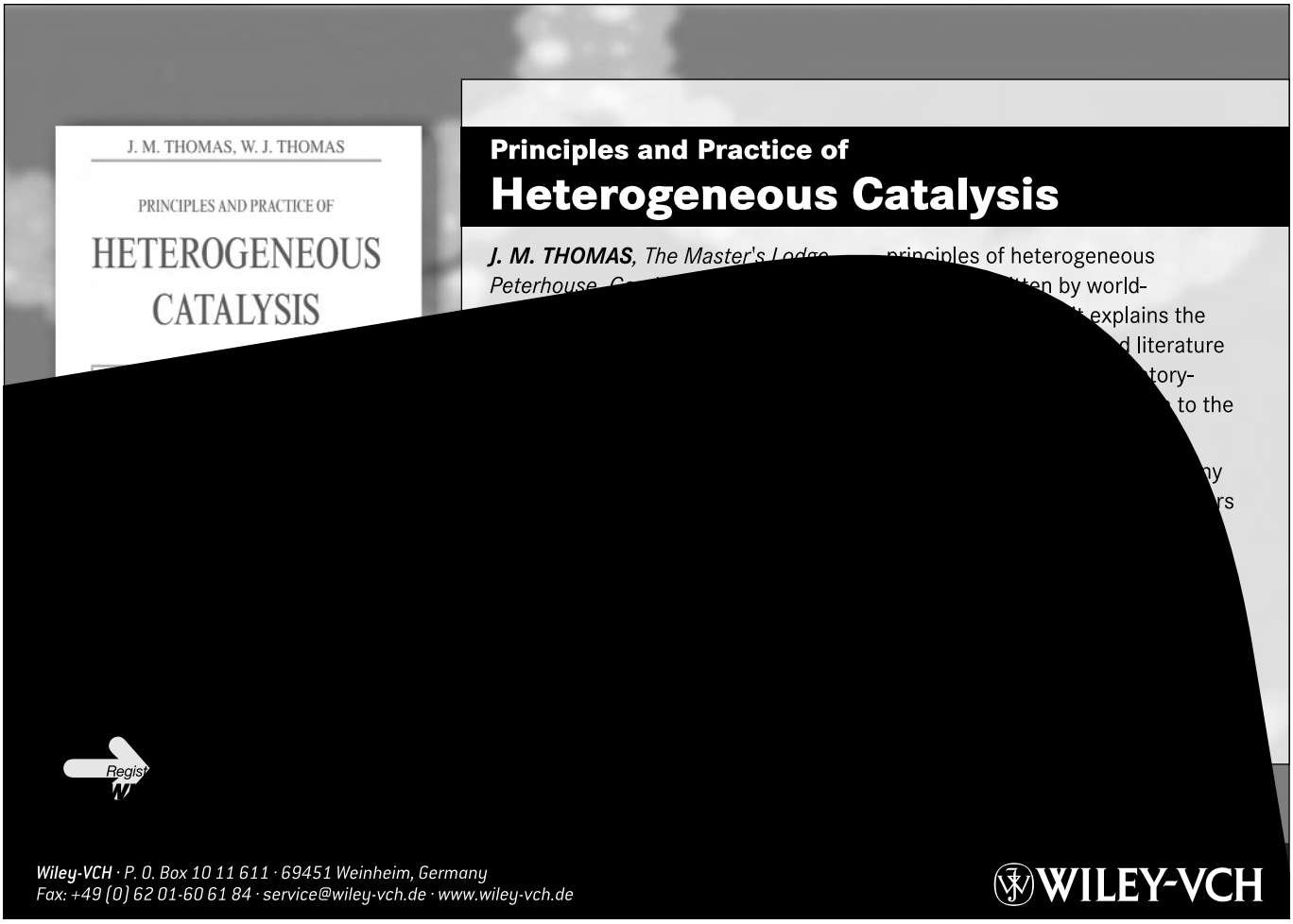

Cover Picture

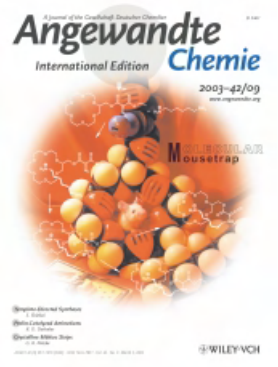

Wei Sun, Hongwang Wang, Chungu Xia,* Jingwei Li, and Peiqing Zhao

Molecular mousetraps are an unprecedented class of host–guest reagents. In the example shown in the cover picture, 18-crown-6 ether is utilized as the "bait" to attract target molecules with a protonated primary amine functional group. Appropriate activation of the noncovalent complex springs the diazo "trap", which leads to covalent attachment of the two molecules depicted in the reaction scheme. The research is detailed in the Communication by J. L. Beauchamp, B. M. Stoltz et al. on page 1012 ff.

Contents

Web Sites

The Vega Science Trust ——— **968** | Viewing La Vega | *P. K. Sharma, S. Shaik*

Books

Envisioning Science ——— **969** | Felice Frankel | *reviewed by E. Diemann*

Phosphorus-Carbon Heterocyclic Chemistry: The Rise of a New Domain ——— **970** | François Mathey | *reviewed by B. P. Johnson*

Nitrogen, Oxygen and Sulfur Ylide Chemistry ——— **971** | J. Stephen Clark | *reviewed by R. A. Aitken*

Highlights

Shape Control

G. R. Patzke* ——— **972 – 974**

Möbius Strips of $NbSe_3$: Morphology Design and Solid-State Chemistry

Keywords:
chemical vapor transport · crystal growth · niobium · selenium · synthesis design

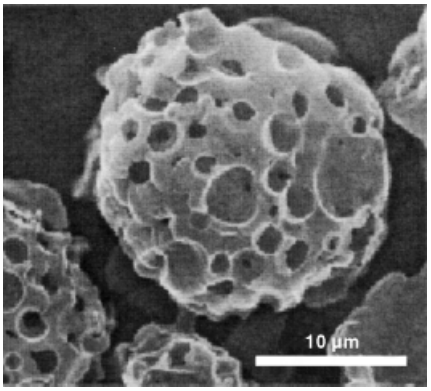

A preparative challenge in inorganic solid-state synthesis is to control the morphology of the arising products, for example, of vaterite microsponges (see picture). An important breakthrough in this area has now been achieved with the preparation of microcrystalline Möbius strips and rings from niobium selenide. The synthesis was achieved by a versatile combination of chemical transport reactions and templating techniques.

L-Proline-Catalyzed Amination

R. O. Duthaler* ——— **975 – 978**

Proline-Catalyzed Asymmetric α-Amination of Aldehydes and Ketones—An Astonishingly Simple Access to Optically Active α-Hydrazino Carbonyl Compounds

Keywords:
amination · azodicarboxylates · catalysis · enantioselectivity · proline

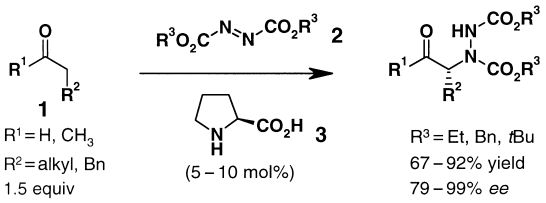

Simple, direct, and highly enantioselective α-amination of carbonyl compounds **1** with azodicarboxylates **2** no longer requires prior enolization of the substrate. The "magic" small-organic-molecule catalyst for this reaction in dichloromethane at room temperature is once again L-proline (**3**).

© 2003 Wiley-VCH Verlag GmbH & Co. KGaA, Weinheim

1433-7851/03/4209-0960 $ 20.00+.50/0

Reviews

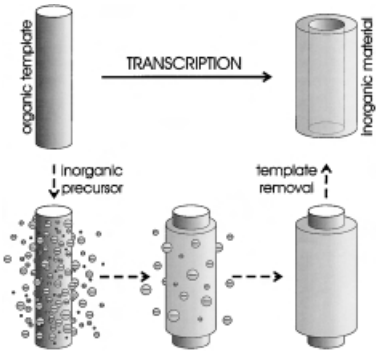

Shapely structured inorganic materials of diverse morphologies and compositions are nowadays obtainable through the transcription of organic templates (see picture). This review gives an overview of the various kinds of templates, precursors, and methods that have been employed for this purpose, as well as the diversity of inorganic materials that have been obtained.

Inorganic Microstructures

K. J. C. van Bommel, A. Friggeri, S. Shinkai* ——— **980 – 999**

Organic Templates for the Generation of Inorganic Materials

Keywords:
materials science · nanostructures · organic templates · sol–gel processes

Communications

A planar $C_{16}B_8$ octagonal macrocycle that incorporates four identical metallacarborane units, linked by four diethynyl chains, has been prepared from a monomeric cobaltacarborane through a designed multistep synthesis (see picture). The air-stable molecule undergoes stepwise electrochemical reduction in THF solution to generate mono-, di-, and tetraanions, with the cyclic and square-wave voltammetric data indicating significant electron delocalization in the ring system.

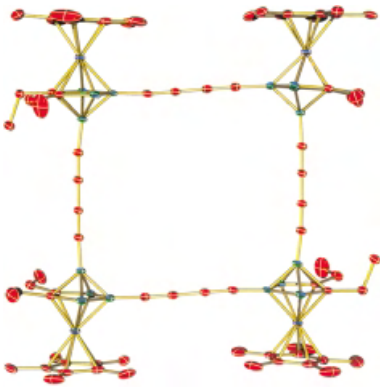

Cobaltacarborane Nanostructures

H. Yao, M. Sabat, R. N. Grimes,* F. Fabrizi de Biani, P. Zanello ——— **1002 – 1005**

Metallacarborane-Based Nanostructures: A Carbon-Wired Planar Octagon

Keywords:
alkynes · carboranes · cobalt · cyclic voltammetry · nanostructures

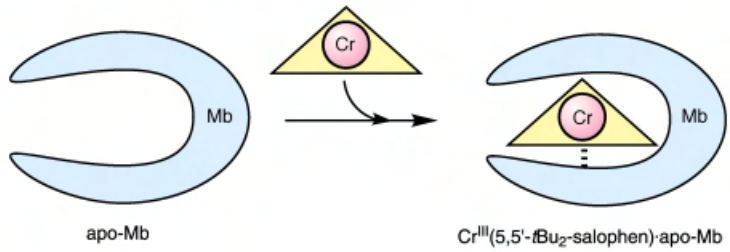

Insertion of a symmetric metal complex, $[Cr^{III}(5,5'\text{-}t\text{Bu-salophen})]^+$ (H_2salophen = *N*,*N*′-bis(salicylidene)-1,2-phenylenediamine), into the active site of apomyoglobin is demonstrated (see picture). The metal ion and the ligand structure are very important factors that influence the binding affinity of the metal complex with the myoglobin (Mb) cavity. Semisynthetic metalloenzymes can catalyze enantioselective sulfoxidation by using the chiral protein cavity.

Semisynthetic Metalloenzymes

M. Ohashi, T. Koshiyama, T. Ueno, M. Yanase, H. Fujii, Y. Watanabe* ——— **1005 – 1008**

Preparation of Artificial Metalloenzymes by Insertion of Chromium(III) Schiff Base Complexes into Apomyoglobin Mutants

Keywords:
asymmetric catalysis · chromium · myoglobin · oxidation · protein modifications · Schiff bases

For the USA and Canada:
ANGEWANDTE CHEMIE International Edition (ISSN 1433-7851) is published weekly by Wiley-VCH PO Box 191161, D 69451 Weinheim, Germany. Air freight and mailing in the USA by Publications Expediting Inc. 200 Meacham Ave., Elmont, NY 11003. Periodicals postage paid at Jamaica NY 11431. US POSTMASTER: send address changes to *Angewandte Chemie*, Wiley-VCH, 111 River Street, Hoboken, NJ 07030. Annual institutional subscription price for institutions: Europe € 2998.00/3148.00. Outside Europe US$ 3718.00/3904.00 (valid for print or electronic/print and electronic delivery); for individuals who are personal members of a national chemical society, or whose institution already subscribes, or who are retired or self-employed consultants, print only (including postage and handling charges): Europe € 248.00/Outside Europe US$ 348.00.

 © 2003 Wiley-VCH Verlag GmbH & Co. KGaA, Weinheim 1433-7851/03/4209-0961 $ 20.00+.50/0

Contents

Nucleotide Bolaamphiphiles

R. Iwaura, K. Yoshida, M. Masuda, M. Ohnishi-Kameyama, M. Yoshida, T. Shimizu* _____ **1009 – 1012**

Oligonucleotide-Templated Self-Assembly of Nucleotide Bolaamphiphiles: DNA-Like Nanofibers Edged by a Double-Helical Arrangement of A–T Base Pairs

A stack with a twist is formed when a thymidine bolaamphiphile (green rod with red ends in the scheme) is allowed to interact with strands of oligoadenylic acid (purple chain with yellow pentagons) in aqueous solution. Complementary A–T hydrogen bonding leads to nanofibers having a DNA-like double helix.

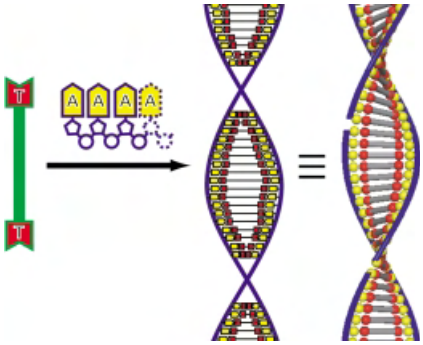

Keywords: amphiphiles · hydrogen bonds · nanostructures · oligonucleotides · supramolecular chemistry

Reactions in Host–Guest Complexes

R. R. Julian, J. A. May, B. M. Stoltz,* J. L. Beauchamp* _____ **1012 – 1015**

Molecular Mousetraps: Gas-Phase Studies of the Covalent Coupling of Noncovalent Complexes Initiated by Reactive Carbenes Formed by Controlled Activation of Diazo Precursors

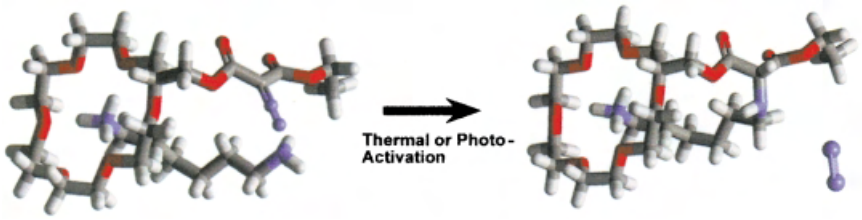

The covalent linking of noncovalently bound host–guest complexes in the gas phase is achieved by the formation of a highly reactive carbene from the host molecule, which is generated by collision-activated dissociation. Possible mechanisms for the resulting intermolecular reactions are explored by theory and experiment.

Keywords: amino acids · carbenes · electrospray ionization · host–guest systems · molecular recognition

Lanthanide–TCNQ Magnet

H. Zhao, M. J. Bazile, Jr., J. R. Galán-Mascarós, K. R. Dunbar* _____ **1015 – 1018**

A Rare-Earth Metal TCNQ Magnet: Synthesis, Structure, and Magnetic Properties of $\{[Gd_2(TCNQ)_5(H_2O)_9][Gd(TCNQ)_4(H_2O)_3]\}\cdot 4H_2O$

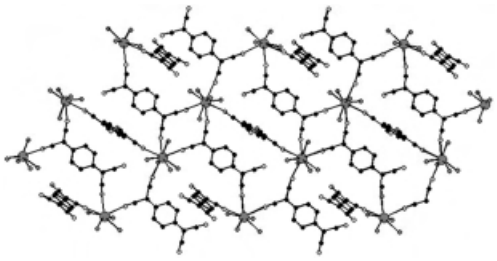

A lanthanide/organic radical based molecular magnet ($T_c = 3.5$ K) has been prepared from a reaction of $GdCl_3\cdot 6H_2O$ with Li[TCNQ] (TCNQ = 7,7,8,8-tetracyanoquinodimethane). The title compound was structurally characterized by single-crystal X-ray diffraction and contains distinct anionic and cationic (see picture) networks containing Gd, TCNQ, and H_2O in different ratios.

Keywords: lanthanides · magnetic properties · N ligands · radicals · tetracyanoethylene

 © 2003 Wiley-VCH Verlag GmbH & Co. KGaA, Weinheim 1433-7851/03/4209-0962 $ 20.00+.50/0

Sulfonation of Methane

S. Mukhopadhyay, A. T. Bell* ——— 1019 – 1021

Direct Liquid-Phase Sulfonation of Methane to Methanesulfonic Acid by SO_3 in the Presence of a Metal Peroxide

Activation of methane by metal peroxides: Calcium peroxide serves as an effective radical initiator in the liquid-phase sulfonation of methane to methansulfonic acid (MSA) by SO_3 [Eq. (1)]. Under the best reaction conditions a 91% conversion of SO_3 to MSA was achieved.

$$CH_4 + SO_3 \xrightarrow[\text{solvent sulfuric acid}]{\text{metal peroxide, } 65\,^\circ C,\ 5\,h} CH_3SO_3H \qquad (1)$$

Keywords: alkaline earth metals · C-H activation · methane activation · peroxides · sulfonation

Stereoselective Glycosidations

S. Tamura, H. Abe, A. Matsuda, S. Shuto* ——— 1021 – 1023

Control of α/β Stereoselectivity in Lewis Acid Promoted C-Glycosidations Using a Controlling Anomeric Effect Based on the Conformational Restriction Strategy

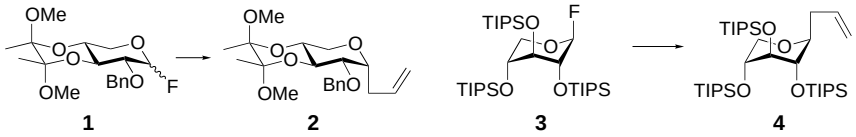

1 **2** **3** **4**

The kinetic anomeric effect has been used to control both α and β stereoselectivity in glycosidation reactions. Depending on the restricted conformation $^4C_1$ or $^1C_4$ of the substrate, the anomeric α (**1**→**2**) or β product (**3**→**4**) was obtained highly stereoselectively from the Lewis acid promoted anomeric allylation with allyltrimethylsilane (TIPS = triisopropylsilyl).

Keywords: anomeric effect · carbohydrates · glycosides · glycosylation · stereoselectivity

Pentacoordinate Silicon Complexes

D. Kost,* B. Gostevskii, N. Kocher, D. Stalke, I. Kalikhman* ——— 1023 – 1026

An Unexpected, Sterically Driven, Methyl Halide Elimination in Pentacoordinate Siliconium Halide Salts: Silicon Complexes with Equatorial Nitrogen Coordination

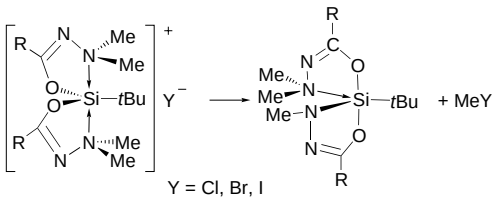

Sterically hindered pentacoordinate *tert*-butylsiliconium halide complexes undergo methyl halide elimination. The products have one covalent and one dative N–Si bond, *both* in the unprecedented equatorial position. A complete pseudorotation coordinate is demonstrated with suitable crystal structures.

Keywords: cations · elimination · hypervalent compounds · pseudorotation · silicon

Oxidation of Primary Amines

M. Largeron,* A. Neudorffer, M.-B. Fleury ——— 1026 – 1029

Oxidation of Unactivated Primary Aliphatic Amines Catalyzed by an Electrogenerated 3,4-Azaquinone Species: A Small-Molecule Mimic of Amine Oxidases

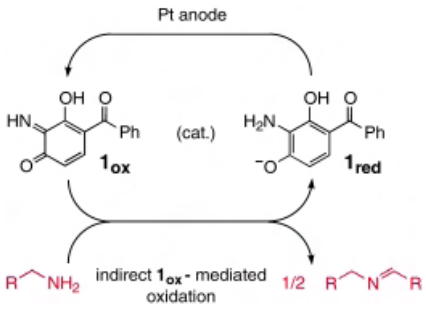

High catalytic performance of the electrogenerated amine oxidase mimic 3,4-iminoquinone $\mathbf{1}_{ox}$ is observed under metal-free conditions in the chemoselective oxidation reaction of unactivated primary aliphatic amines.

Keywords: amines · chemoselectivity · electrochemistry · enzyme models · oxidation

 © 2003 Wiley-VCH Verlag GmbH & Co. KGaA, Weinheim 1433-7851/03/4209-0963 $ 20.00+.50/0

Contents

Water Treatment

W. Ma, J. Li, X. Tao, J. He, Y. Xu, J. C. Yu, J. Zhao* ——— **1029 – 1032**

Efficient Degradation of Organic Pollutants by Using Dioxygen Activated by Resin-Exchanged Iron(II) Bipyridine under Visible Irradiation

Excellent response to visible light is shown by the $[Fe^{II}(bpy)_3]$–amberlite photocatalyst, which can effectively activate molecular oxygen in such a way as to put us one giant step nearer to our goal—the development of the ultimate green technology for decontamination [Eq. (1)].

organic pollutants $\xrightarrow[\geq 420\,nm\ visible\ light,\ dioxygen\ O_2]{[Fe(bpy)_3]^{2+}-amberlite}$ CO_2 + degraded products (1)

Keywords: iron · O–O activation · photochemistry · photodegradation

Highly Enantioselective Catalysts

A. Berkessel,* D. Menche, C. A. Sklorz, M. Schröder, I. Paterson ——— **1032 – 1035**

A Highly Enantioselective Catalyst for the Asymmetric Nozaki–Hiyama–Kishi Reaction of Allylic and Vinylic Halides

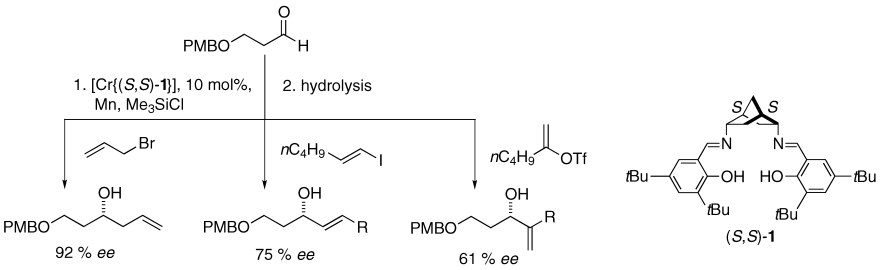

Catalytic asymmetric addition of vinylic halides and triflates to aldehydes, with useful levels of stereoinduction, has been achieved for the first time using the salen-type ligand (*S*,*S*)-**5** (see scheme; PMB = *para*-methoxybenzyl), which contains the novel *endo*,*endo*-2,5-diamino norbornane building block. This asymmetric Nozaki–Hiyama–Kishi reaction leads to the coupling of various halides and aldehydes with high yields and enantioselectivities (up to 92% *ee*).

Keywords: asymmetric catalysis · chromium · manganese · N,O ligands · Schiff bases

Catalytic C–P Ylide Reaction

Y. Du, X. Lu,* C. Zhang ——— **1035 – 1037**

A Catalytic Carbon–Phosphorus Ylide Reaction: Phosphane-Catalyzed Annulation of Allylic Compounds with Electron-Deficient Alkenes

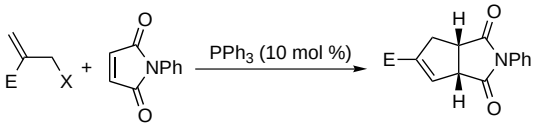

(1)

Readily available starting materials and high selectivity: These are two appealing features of the phosphane-catalyzed carbon–phosphorus ylide reaction described. Bromide, acetate, or *tert*-butyl carbonate derivatives of adducts formed by the Morita–Baylis–Hillman reaction react with PPh_3 to form an allylic ylide. Phosphane-catalyzed annulation of the ylides with electron-deficient alkenes results in the facile construction of cyclopentenes [Eq. (1)]. X = Br, OAc, OBoc; E = CO_2Et.

Keywords: alkenes · annulation · homogeneous catalysis · phosphanes · ylides

Subvalent Scandium Complexes

G. K. B. Clentsmith, F. G. N. Cloke,* J. C. Green,* J. Hanks, P. B. Hitchcock, J. F. Nixon* ——— **1038 – 1041**

Stabilization of Low-Oxidation-State Early Transition-Metal Complexes Bearing 1,2,4-Triphosphacyclopentadienyl Ligands: Structure of $[\{Sc(P_3C_2tBu_2)_2\}_2]$; Sc^{II} or Mixed Oxidation State?

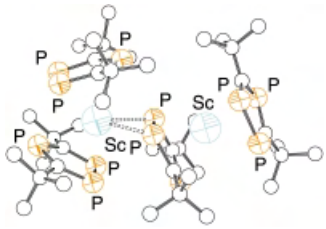

Sc^{II} or mixed oxidation state Sc^{III}/Sc^{I}? Reduction of the homoleptic Sc^{III} complex $[Sc(P_3C_2tBu_2)_3]$ allows access to the subvalent $[\{Sc(P_3C_2tBu_2)_2\}_2]$ complex (see picture), in which the metal centers are formally bivalent. DFT calculations support fomulation of the reduced species as a mixed oxidation state Sc^{III}/Sc^{I} complex.

Keywords: density functional calculations · lanthanides · scandium · subvalent compounds

© 2003 Wiley-VCH Verlag GmbH & Co. KGaA, Weinheim
1433-7851/03/4209-0964 $ 20.00+.50/0

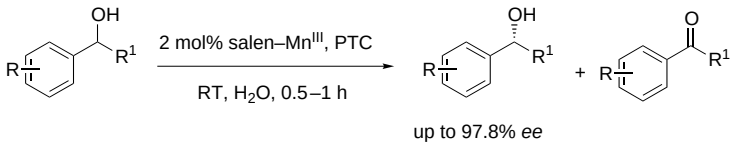

Asymmetric Catalysis in Water

W. Sun, H. Wang, C. Xia,* J. Li, P. Zhao ——— 1042 – 1044

Chiral-Mn(Salen)-Complex-Catalyzed Kinetic Resolution of Secondary Alcohols in Water

A mild, green method for enantioselective kinetic resolution of secondary alcohols has been developed using Mn(salen) complexes as catalysts in water. Up to 97.8% *ee* was attained. PTC = phase-transfer catalyst.

Keywords: alcohols · green chemistry · kinetic resolution · manganese complexes · salen ligands

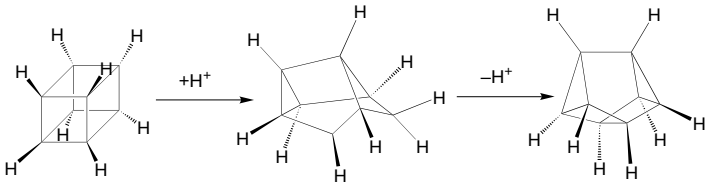

1 2 3

Structures of Protonated Cubane

J.-L. M. Abboud,* I. A. Koppel,* J. Z. Dávalos, P. Burk, I. Koppel, E. Quintanilla ——— 1044 – 1046

Protonation of Cubane in the Gas Phase: A High-Level Ab Initio and DFT Study

The tetracyclo[4.2.0.0^{2,4}.0^{3,8}] oct-7-ylium cation is the protonation product of cubane (**1**) in the gas phase according to ab initio and DFT calculations. At the G2(MP2) level, the calculated gas-phase basicity of **1** is about 60 kcal mol^{-1} larger than that determined experimentally. The experimental thermodynamics are consistent with fast deprotonation of **2** to give cuneane (**3**).

Keywords: ab initio calculations · basicity · cubanes · density functional calculations · gas-phase reactions

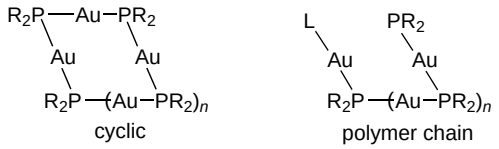

Gold–Phosphanyl Structures

D. M. Stefanescu, H. F. Yuen, D. S. Glueck,* J. A. Golen, A. L. Rheingold ——— 1046 – 1048

Synthesis and Structure of Cyclic Gold(I) Phosphanyl Complexes [{Au(PR$_2$)}$_n$]

Gold(I) Phosphanyl Complexes, such as [Au(PR$_2$)]$_n$, have been known for more than 25 years. However, the solid-state structure of such complexes, as well as their nature in solution, has remained somewhat of a mystery. The figure displays the cyclic and polymeric forms that are possible (L = endgroup). The structures of the complexes, and the occurrence of Au···Au interactions are discussed.

Keywords: aurophilic interactions · gold · P ligands · phosphanes · structure elucidation

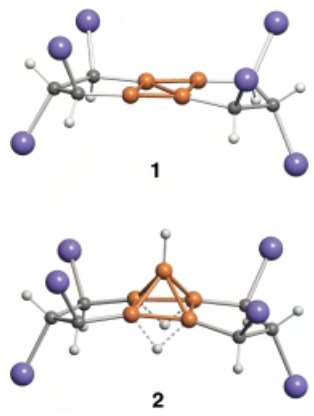

1 2

Isomerization of Boron Aromatics

C. Präsang, M. Hofmann, G. Geiseler, W. Massa, A. Berndt* ——— 1049 – 1052

Topomerization of a Distorted Diamond-Shaped Tetraborane(4) and Its Hydroboration to a *closo*-Pentaborane(7) with a *nido* Structure

The exchange of the short and long diagonal of the B$_4$ diamond of **1** is the simplest variant to date of the diamond–square–diamond rearrangement, which plays a central role in the isomerization of polyhedral boranes, carboranes, and metallaboranes. Compound **2**, which is readily accessible from **1**, is the first derivative of pentaborane(7).

Keywords: aromacity · boron · density functional calculations · isomerization · rearrangement

 © 2003 Wiley-VCH Verlag GmbH & Co. KGaA, Weinheim 1433-7851/03/4209-0965 $ 20.00+.50/0

Contents

Fluoroacylboron Complexes

M. Finze, E. Bernhardt, H. Willner,*
C. W. Lehmann* ——— **1052 – 1055**

The Fluoroacyltris(trifluoromethyl)borate Ion, $[(CF_3)_3BC(O)F]^-$, a Fluoroacylboron Complex

Keywords:
borates · density functional calculations · fluoroacyl ligands · NMR spectroscopy · vibrational spectroscopy

Nucleophilic addition of fluoride ions at the carbonyl carbon atom in $(CF_3)_3BCO$ in liquid sulfur dioxide leads to the formation of the boron acyl fluoride ion $[(CF_3)_3BC(O)F]^-$ (see structural formula), the first example of a compound with a BC(O)F group and an anionic acyl fluoride.

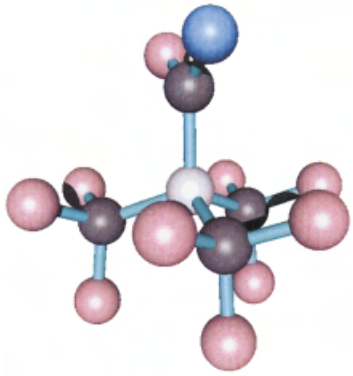

Pd-Catalyzed Cross-Coupling

A. Köllhofer, T. Pullmann,
H. Plenio* ——— **1056 – 1058**

A Versatile Catalyst for the Sonogashira Coupling of Aryl Chlorides

Keywords:
alkynes · aryl chlorides · cross-coupling · palladium · Sonogashira coupling

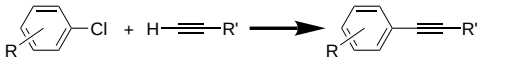

(a)

Aryl chlorides are suitable substrates for the Sonogashira coupling! By using the versatile catalyst system $Na_2[PdCl_4]/PR_3$/CuI ($PR_3 = (1\text{-Ad})_2PBn$, $PtBu_3$), the Sonogashira coupling [Eq. (a)] of aryl chlorides with alkynes generates excellent yields of the corresponding disubstituted aryl alkynes.

Hexacoordinate Silicates

K. Benner, P. Klüfers,*
M. Vogt ——— **1058 – 1062**

Hydrogen-Bonded Sugar-Alcohol Trimers as Hexadentate Silicon Chelators in Aqueous Solution

Keywords:
cooperative phenomena · O ligands · silicates · silicon transport

Building bridges: Fumed colloidal silica can be dissolved in alkaline aqueous solutions of the open-chain sugar alcohols mannitol, xylitol, and threitol. These polyols are able to form six-coordinate silicon complexes that are stabilized by intramolecular hydrogen bonds. The prototypical core is shown (yellow bars: the intramolecular H bonds).

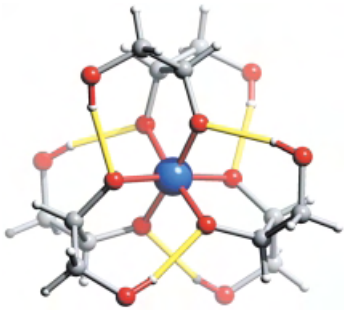

VIP Communications labeled with this symbol have been judged by two referees as being "very important papers".

The publication of Communications labeled with this symbol has been accelerated because of their topical or highly competitive nature.

Supporting information for articles labeled with this symbol can be found at www.angewandte.org or www.interscience.wiley.com.

The issues for February 2003 appeared online on the following dates:
Issue 5: January 30. · Issue 6: February 6. · Issue 7: February 17. · Issue 8: February 21.

© 2003 Wiley-VCH Verlag GmbH & Co. KGaA, Weinheim

1433-7851/03/4209-0966 $ 20.00+.50/0

Sources

Product and Company Directory

You can start the entry for your company in "Sources" in any issue of *Angewandte Chemie*.

If you would like more information, please do not hesitate to contact us.

Wiley-VCH Verlag – Advertising Department
Tel.: 0 62 01 - 60 65 65
Fax: 0 62 01 - 60 65 50
E-Mail: MSchulz@wiley-vch.de

Service

Keywords ____ *1064*

Authors ____ *1065*

Angewandte's Sister Journals ____ *1066 – 1067*

Vacancies ____ *1063*

Sources ____ *A17*

Preview ____ *1069*

40 Years of Chemistry History

★ The basis for a **journey of discovery** through all the important developments in chemistry and related disciplines

★ The **authors** and **keywords** of all the reviews that have appeared in ***Angewandte Chemie*** in the last 40 years

★ ***Now available at a special price of € 19.80*** (including postage)

Only available directly from:
Angewandte Chemie
Postfach 10 11 61
69451 Weinheim (Germany)
Telephone: (+49) 6201-606-265
Fax: (+49) 6201-606-331
E-mail: angewandte@wiley-vch.de

 © 2003 Wiley-VCH Verlag GmbH & Co. KGaA, Weinheim 1433-7851/03/4209-0967 $ 20.00+.50/0

Shape Control

Möbius Strips of $NbSe_3$: Morphology Design and Solid-State Chemistry

*Greta R. Patzke**

Keywords:
chemical vapor transport · crystal growth · niobium · selenium · synthesis design

The Interplay of Form and Structure in Chemistry

Chemists tend to interpret and design the "form" of a substance mainly with respect to its internal periodic order. This approach, however, is strictly focussed on the concept of 230 space groups—and it is therefore restricted to their symmetry limitations, which neglect the important phenomenon of complex external morphology. Consequently, rather universal "design" strategies in modern chemical synthesis are directed towards shaping the structure as well as the outer appearance of nano- and microscale materials. This Highlight illustrates how solid-state chemistry can benefit from an integral synthetic approach that has recently been utilized to generate $NbSe_3$ crystals with an unprecedented morphology.[1] The preparation of microcrystalline Möbius strips of $NbSe_3$ represents a breakthrough in classical solid-state synthesis with respect to shape design. The remarkable progress in the control of morphology in nanoscale or bio-inspired inorganic chemistry has been further developed successfully and is outlined below.

- Thorough investigations exploring the challenging area of "chemical topology" at the *molecular level* were driven by a desire to construct novel molecular architectures.[2] The well-known Möbius strip—a topological concept that fascinates both chemists and mathematicians—in particular, triggered considerable synthetic efforts until it was finally realized as an organic compound in 1982.[3] The Möbius strip represents a one-sided bounded surface and its unique properties can easily be demonstrated with a simple long rectangular strip of paper. Before putting the ends of the strip together, one end of the paper strip is twisted through an angle of 180° relative to the other so that a Möbius strip is obtained instead of a simple cylindrical two-sided bounded surface. Dissecting the Möbius strip twice along its axis delivers a set of catenanes.
- An elegant approach to the morphology design of *nanoparticles* has recently been reported by Stupp and co-workers: they produced CdS nanohelices in a synthetic approach that utilized the potential of supramolecular chemistry to build inorganic nanostructures.[4] The unique helical shape of the CdS particles is generated under the influence of organic supramolecular nanoribbons as templates.
- The intriguing vision of generating complex inorganic architectures on the laboratory scale is currently explored in *inorganic morphosynthesis*. Natural biomineralization processes provide a continuous source of inspiration for this innovative research area. Important developments—impressing with respect to both scientific impact and aesthetics—have been reported, such as spongelike vaterite spheroids, hollow shells of mesoporous aragonite, and mesoskeletal forms of calcium phosphate (Figure 1).[5]

Most of the above-mentioned synthetic routes depend on the presence of a structure-directing organic template that controls the course of an inorganic precipitation reaction. This pathway, however, has its limitations since the thermal instability of the organic component may give rise to decomposition processes and side reactions. Therefore, severe restrictions with respect to the fabrication of inorganic solids at elevated temperatures are imposed on the application of this synthetic principle in the solid state. So which parameters might exert efficient control over the morphology when applied at synthesis

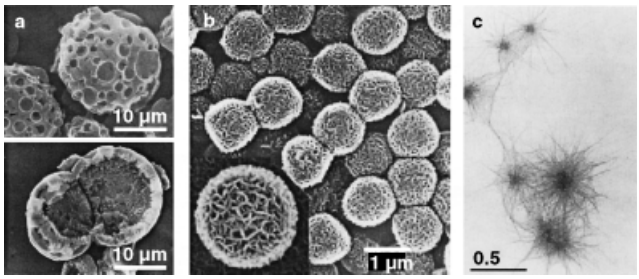

Figure 1. a) SEM images of spongelike vaterite spheroids.[12] b) SEM image of intact hollow shells of mesoporous aragonite.[13] c) TEM image of a calcium phosphate block copolymer.[14]

[*] Dr. G. R. Patzke
Laboratory of Inorganic Chemistry
ETH Hönggerberg—HCI
8093 Zürich (Switzerland)
Fax: (+41) 1-632-1149
E-mail: patzke@inorg.chem.ethz.ch

 © 2003 Wiley-VCH Verlag GmbH & Co. KGaA, Weinheim 1433-7851/03/4209-0972 $ 20.00+.50/0

temperatures far above the decomposition temperature of any organic additive? A convincing solution to this crucial problem has now been presented, and it has been successfully applied to $NbSe_3$, a compound attracting considerable interest in both structural and materials chemistry.

Morphology Design and Solid-State Chemistry

$NbSe_3$ has long been famous for its almost classical representation of a low-dimensional solid. The anisotropic properties arise from the high degree of anisotropy in the crystal structure. The latter consists essentially of three different types of [$NbSe_3$] chains comprised of face-sharing trigonal prisms that run parallel to the *b*-axis of the monoclinic unit cell. Consequently, $NbSe_3$ exhibits a distinct tendency to form crystals with a fibrous, ribbonlike morphology. Thus, it is a good candidate for synthetic attempts that focus on shape control. Indeed, remarkable variations in crystal growth that result in the formation of large circular microcrystals have already been reported for $NbSe_3$, but the origin and underlying growth mechanism of these $NbSe_3$ objects remains to be elucidated.[6] Tanda et al. have now established a synthetic breakthrough that provides controlled access to Möbius strips of $NbSe_3$ on the microscale.[1] Moreover, annular and figure-of-eight-shaped crystals of $NbSe_3$ have also been produced. The initial results with the tantalum-based analogues ($TaSe_3$, TaS_3) are also quite promising. The experimental approach chosen is of striking simplicity: a direct reaction of Se and Nb with no further additives involved. This leads to the question of how such an apparently simple reaction is capable of generating a geometry as rare and complex as the Möbius strip.

The reactants involved are indeed elementary, but they participate in an elaborate variation of the chemical transport reaction. A mixture of Se and Nb powder is treated in an evacuated quartz ampoule at 740 °C under special growth conditions and the reaction performed is in a furnace with a considerably extended temperature gradient. In this way, a nonequilibrium state is established that facilitates the coexistence and of selenium in the vapor, mist, and liquid (droplet) forms inside the quartz ampoule. The formation of microscale selenium droplets is essential, because they act as in situ templates during the next step of the reaction: ribbon-shaped $NbSe_3$ crystals are subsequently formed along the equator of the droplets and their interaction with the surface tension of the viscous selenium droplet determines the shape of the emerging crystals. There are several cyclization pathways for the whisker-shaped $NbSe_3$ crystals on the droplet surface which give rise to three different morphological variations (Figure 2):

⇒ Ring structures result when the ends of the crystal simply meet without any further twist (0π).

⇒ Möbius strips arise from twisting and subsequent connection of the ends (1π).

⇒ Figure-of-eight crystals are accessible either by double encircling or as the product of a double twisting (2π).

The design strategy presented here benefits from the bifunctional facilities of selenium which serves both as a reactant and as a templating agent. This means that template-directed inorganic syntheses can now be performed as "one-pot-procedures" without any extra or even thermally unstable additives involved.

No other previous process combines these advantages with such a broad applicability. Moreover, chemical transport reactions provide the unique combination of an effective synthetic approach with a particular rich fund of experimental experience that has continuously been systemized by theoretical considerations:[7]

⇒ Whole classes of inorganic substances (oxides, silicides, intermetallics, etc.) are easily accessible in single-crystalline form by means of chemical transport reactions and their morphology could potentially be adjusted by gas-phase deposition.

⇒ The systematic variation and optimization of the reaction parameters is possible, with the latter being monitored by tailor-made computational methods.

The preparation of $NbSe_3$ Möbius strips is not only of aesthetic interest, but offers a starting point for important applications in both theoretical and physical chemistry.

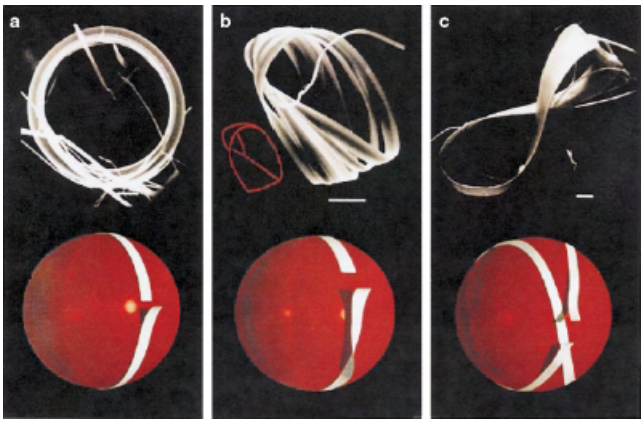

Figure 2. SEM images of the $NbSe_3$ crystal topology.[1] The scale bars correspond to 10 μm. a) Formation of a ring structure by direct linking of the ends (0π). b) Möbius strip arising from a simple twist (1π). c) Figure-of-eight crystal formed after a double twist (2π). Reprinted with permission from Nature (ref. [1], copyright 2002, Macmillan Publishers Ltd).

Möbius Strips of $NbSe_3$—Unique Topochemical Crystals

The outstanding low-dimensional properties of the chain structure of $NbSe_3$ give rise to a multitude of applications for the newly detected microcrystals:

- The chemical reactivity of low-dimensional solids can be considered to result from them lying at the interface between solid-state and molecular chemistry. They exhibit a rich chemical reactivity that encompasses redox, intercalation, and spe-

 © 2003 Wiley-VCH Verlag GmbH & Co. KGaA, Weinheim 1433-7851/03/4209-0973 $ 20.00+.50/0

cial acid–base reactions. Their structural chemistry can also be studied: the influence on both the chain structure of the host material and the resulting morphology of the ternary products can be elucidated by partial substitution of other atoms for niobium. This effect has been reported, for example, in $FeNb_3Se_{10}$, where a segregation of the characteristic trigonal-prismatic chains by iron-containing octahedral chains was found.[8] The variation in the physical properties reflects the degree of anisotropy in the chemical bonding, hence mixed selenides should exhibit modified characteristics.

- Charge density waves (CDWs) are displayed by $NbSe_3$ in an exemplary way so that it serves as a model substance for illustrating such phenomena. Thus, the impact of $NbSe_3$ Möbius strips goes far beyond the level of synthetic innovation and gives rise to fundamental theoretical studies. Although the appearance of charge density waves has been investigated in general, the effect of systems with closed-loop topologies on CDW still needs to be elucidated. The novel Möbius strips afford a unique insight since topological effects in quantum mechanics can now be studied in a real system. So what kind of CDW behavior will be observed in closed loops of $NbSe_3$? Maybe self-interference will appear, or even hitherto unknown processes might be found. Microring crystals of $NbSe_3$ are now readily available and have proven suitable for the experimental study of interference phenomena in the charge density waves.[9,10]
- A multitude of innovative practical applications of these novel microcrystals appears to be on the horizon. $NbSe_3$ is a promising cathode material for rechargeable lithium cells, since it is capable of intercalating three lithium ions per chalcogenide molecule.[11] Its unique combination of ribbonlike morphology and metallic conductivity gives rise to a whole set of technological benefits: the need for either additional binders or conducting additives is eliminated. Moreover, the large surface area of the fibers leads to enhanced electrochemical behavior. Now that a set of microcrystals with distinct shapes is accessible, further developments in the field of microbatteries will surely be possible.
- Möbius strips already imply the presence of catenanes that would result from their twofold longitudinal dissection. Thus, the $NbSe_3$ Möbius strips are promising precursors for the first inorganic catenane synthesis; they might enable the design of new components for microelectronics.

The development of a remarkably flexible gas-phase synthesis that could be elaborated into a general access to inorganic solids with a special morphology should provide entry to a new generation of compounds for modern materials chemistry.

[1] S. Tanda, T. Tsuneta, Y. Okajima, K. Inagaki, K. Yamaya, N. Hatakenaka, *Nature* **2002**, *417*, 397.
[2] H. L. Frisch, E. Wassermann, *J. Am. Chem. Soc.* **1961**, *83*, 3789.
[3] D. M. Walba, R. M. Richards, R. C. Haltiwanger, *J. Am. Chem. Soc.* **1982**, *104*, 3219.
[4] E. D. Sone, E. R. Zubarev, S. I. Stupp, *Angew. Chem.* **2002**, *114*, 1781; *Angew. Chem. Int. Ed.* **2002**, *41*, 1705.
[5] S. Mann, *Angew. Chem.* **2000**, *112*, 3532; *Angew. Chem. Int. Ed.* **2000**, *39*, 3392.
[6] F. A. Trumbore, L. W. ter Haar, *Chem. Mater.* **1989**, *1*, 490.
[7] R. Gruehn, R. Glaum, *Angew. Chem.* **2000**, *112*, 706; *Angew. Chem. Int. Ed.* **2000**, *39*, 692.
[8] J. Rouxel, *Acc. Chem. Res.* **1992**, *25*, 328.
[9] Y. Okajima, H. Kawamoto, M. Shiobara, K. Matsuda, S. Tanda, K. Yamaya, *Phys. B* **2000**, *284–288*, 1659.
[10] S. Tanda, H. Kawamoto, M. Shiobara, Y. Sakai, S. Yasuzuka, Y. Okajima, K. Yamaya, *Phys. B* **2000**, *284–288*, 1657.
[11] F. A. Trumbore, *J. Power Sources* **1989**, *26*, 65.
[12] D. Walsh, B. Lebeau, S. Mann, *Adv. Mater.* **1999**, *11*, 324.
[13] D. Walsh, S. Mann, *Nature* **1995**, *377*, 320; D. Walsh, S. Mann, *Adv. Mater.* **1997**, *9*, 658.
[14] M. Antonietti, M. Breulmann, C. G. Göltner, H. C. Cölfen, K. K. W. Wong, D. Walsh, S. Mann, *Chem. Eur. J.* **1998**, *4*, 2491.

L-Proline-Catalyzed Amination

Proline-Catalyzed Asymmetric α-Amination of Aldehydes and Ketones—An Astonishingly Simple Access to Optically Active α-Hydrazino Carbonyl Compounds

*Rudolf O. Duthaler**

Keywords:
amination · azodicarboxylates · catalysis · enantioselectivity · proline

The motivation to investigate enantioselective α-aminations of carbonyl compounds is provided by valuable synthetic targets such as α-amino acids and α-amino alcohols. The most prominent electrophilic amination reagents are azodicarboxylates, trisyl azide, and nitroso compounds, typically used in combination with chiral auxiliaries.[1] Recent developments include the catalytic use of a chiral base for the deprotonation of achiral *N*-acyl oxazolidinones[1b] and chiral Lewis acids that catalyze the addition of silyl enol ethers to azodicarboxylates.[1c,d] The osmium(VIII)-mediated asymmetric aminohydroxylation of styrenes offers a new strategy for the synthesis of the racemization-prone α-aryl glycines.[2]

Recently, Jørgensen and co-workers,[3a] as well as List[3b] almost simultaneously reported an intriguingly simple and efficient method for direct α-amination of aldehydes.[3] This amination was later extended to ketone substrates.[4] A solution of an aldehyde **1** or ketone **2** (1.5 equiv) and diethyl, dibenzyl, or di-*tert*-butyl azodicarboxylate (**3, 4, 5**, respectively) in dichloromethane or in another aprotic solvent was treated at room temperature with L-proline (**6**; 5–10 mol %), leading to the complete consumption of azodicarboxylate within 30 min to 96 h, as monitored by the fading of the yellow color. Simple aqueous workup and evaporation of the excess carbonyl substrate gives *R*-configured α-hydrazino aldehydes **7** or ketones **8**, respectively, in moderate to good yields and in many cases with impressive enantioselectivity (Scheme 1). Whereas the aldehydes **7** are prone to racemization, the ketone derivatives **8** can be purified by silica-gel chromatography without much loss of enantiomeric purity. In most cases, however, it is advantageous to reduce the primary products directly with $NaBH_4$ to form stable α-hydrazino alcohols **9**, which in turn can be cyclized to *N*-amino oxazolidinones **10** by treatment with dilute NaOH in a one-pot process. In the case of the ketone derivatives **8,** *syn*-α-hydrazino alcohols or 4,5-*trans*-oxazolidinones are formed with approximately 87 % diastereoselectivity. On the other hand, *anti* epimers or *cis*-oxazolidinones **11** are obtained by reduction with silane and cyclization (Scheme 1). After cleavage of the carbamate, the *N*-amino group can be cleaved reductively with Zn/acetone in AcOH, or with Raney nickel. α-Amino acid derivatives are also accessible by oxidation of aldehydes **7** to carboxylates (e.g. with $KMnO_4$), esterification, and reductive hydrazine cleavage.[3] Remarkably, in contrast to related aldol additions, unsymmetrical ketones **2** ($R^1 = CH_3$) react with good regioselectivity at the more substituted α carbon atom, and thus **8** is formed in preference to achiral **12** (Scheme 2).[4]

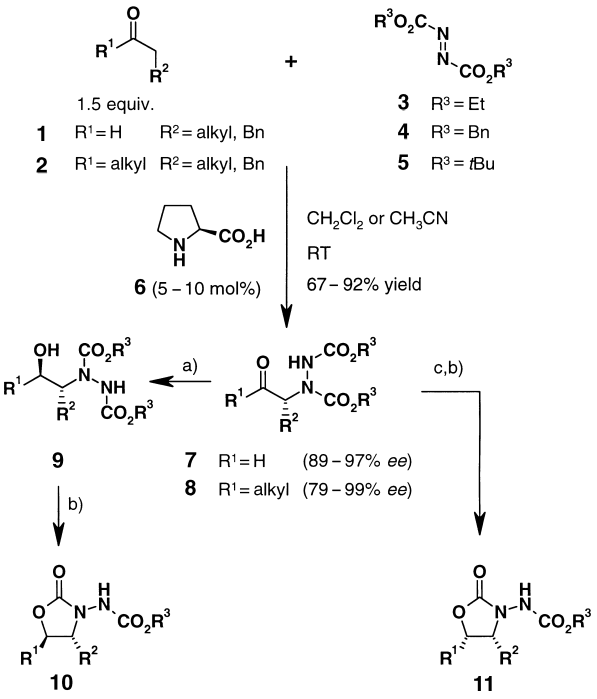

Scheme 1. Direct enantioselective amination of aldehydes and ketones: a) $NaBH_4$/MeOH; b) NaOH (0.5 N); c) $Et_3SiH/TiCl_4$.

Prior to these asymmetric aminations catalyzed by small or-

[*] Dr. R. O. Duthaler
Novartis Institutes for Biomedical Research
Postfach, 4002 Basel (Switzerland)
Fax: (+ 41) 61-324-9040
E-mail: rudolf.duthaler@pharma.novartis.com

 © 2003 Wiley-VCH Verlag GmbH & Co. KGaA, Weinheim 1433-7851/03/4201-0975 $ 17.50+.50/0

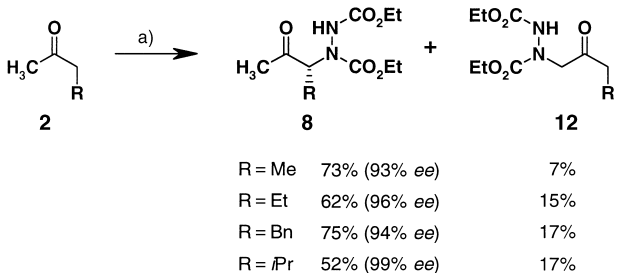

Scheme 2. Regioselective amination of methyl ketones: a) **3** (0.67 equiv), **6** (10 mol%), CH_3CN.

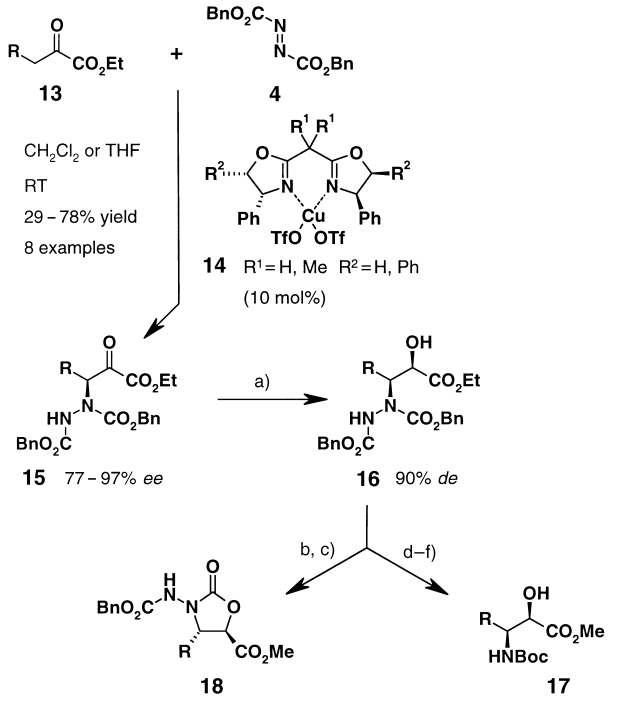

Scheme 3. Copper-catalyzed enantioselective amination of α-keto esters: a) L-selectride, −78 °C; b) NaOH (0.5 N); c) $TMSCHN_2$; d) H_2/Raney Ni, MeOH; e) Boc_2O/DMAP; f) NaOMe/MeOH. L-selectride = lithium tri-*sec*-butyl borohydride, TMS = trimethyl silyl, Boc = *tert*-butoxycarbonyl, DMAP = 4-dimethylaminopyridine, Tf = trifluoromethane sulfonyl.

ganic molecules (proline), a series of α-keto esters **13** had also been aminated directly, but under catalysis of chiral Lewis acidic copper complexes **14**, to give the configurationally labile products **15** (Scheme 3).[5] Reduction of **15** with L-selectride afforded the stable α-hydroxy-β-hydrazino acids **16**, which can be transformed into α-hydroxy-β-amino acid derivatives **17** or into oxazolidinones **18** (Scheme 3).

The historical roots of this elegant proline-mediated enantioselective process go back to the enantiotopically differentiating intramolecular aldol condensation pioneered by Hajos and Wiechert, and elaborated and reviewed by Agami.[6a] An improved protocol and screening for other catalysts has been reported recently.[6b] Researchers at The Scripps Research Institute have also successfully applied L-proline (**6**) in direct enantioselective aldol and Mannich reactions, processes that have recently been featured in special accounts,[7] and that are also treated in more general reviews on organocatalysts.[8] Because of the mechanistic relation with the proline-catalyzed aminations, these catalytic conversions are also discussed briefly.

When aromatic or aliphatic aldehydes **19** and excess acetone or another simple ketone **20** are treated with L-proline (**6**; 20 mol%) or (*R*)-5,5-dimethyl-thiazolidine-4-carboxylate (DMTC, **21**), aldol adducts **22** are formed in moderate yields and with moderate to good enantioselectivity (Scheme 4).[9] Notably, with the exception of hydroxyacetone,[9b] a methyl residue reacts in preference to a bulkier alkyl substituent R^1. Screens for catalysts other than proline (**6**) have so far only yielded closely related five-membered cyclic α-amino acids such as **21** and 4-substituted prolines. Aldehydes have a high tendency for self-condensations,[10] but enantioselective cross-aldol reactions between aldehydes were recently reported: simple acceptor aldehydes were added by means of a syringe pump to various donor aldehydes in *N,N*-dimethylformamide at 4 °C with **6** (10%) as catalyst.[10b] The method could also be applied to the addition of aldehydes to very reactive ketones such as keto malonates or trifluoropyruvate.[11]

L-Proline (**6**) also catalyzes the addition of ketones[12a] and aldehydes **23**[12b] to glyoxylimine **24** to give α-amino-γ-oxo esters **25** in moderate yields and enantioselectivities (Scheme 4). With the exception of fluoroacetone, the bulkier alkyl residue of unsymmetrical ketones reacts preferentially, analogous to the amination with azodicarboxylates **3** and **4** (Scheme 1),[4] but in contrast to the aldolization. Although large excesses of ketones are applied,[12a] 1.5–2 equivalents of the aldehyde **23** ($R^1 = H$) is sufficient.[12b] The aldehydes **25** are formed with higher *syn* selectivity, but undergo partial epimerization to the *anti* epimers upon chromatography on silica gel. Oxidation with chlorite and subsequent esterification

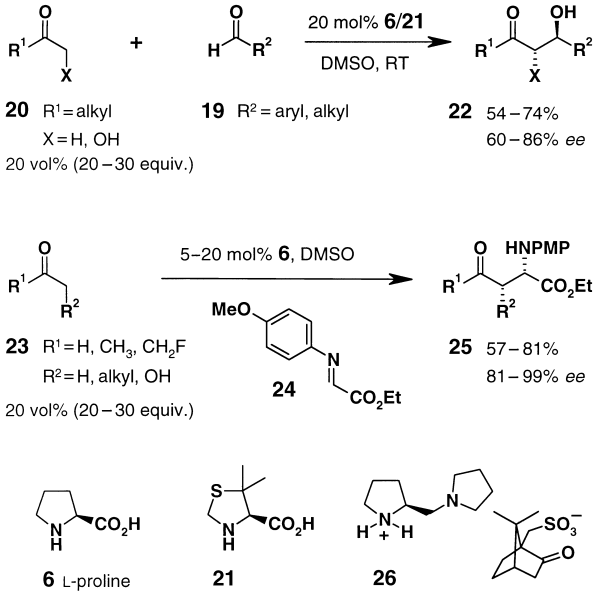

Scheme 4. Proline-catalyzed aldol and Mannich reactions. PMP = *p*-methoxyphenyl, DMSO = dimethyl sulfoxide.

 © 2003 Wiley-VCH Verlag GmbH & Co. KGaA, Weinheim 1433-7851/03/4201-0976 $ 17.50+.50/0

gives access to 3-substituted aspartic esters.[12b] Closely related are the Mannich-type reactions of simple ketones and aryl or alkyl aldimines of *para*- and *ortho*-anisidine, which can even be conducted as three-component condensation–addition reactions between the aldehyde, the anisidine, and the ketone.[13] Catalysts are again L-proline (**6**), DMTC (**21**), and (*S*)-1-(2-pyrrolidinomethyl)-pyrrolidine (**26**) as the camphorsulfonate salt. Interestingly, **26** gives rise to the antipode of the product obtained with **6** or **21** (Scheme 4).[13c] Other related processes are proline-catalyzed Michael additions of ketones and aldehydes to nitro olefins,[14] or the addition of ketones to alkylidene malonates mediated by **26** as a free diamine base.[15]

An attempt to explain these proline-catalyzed α-derivatizations of ketones and aldehydes mechanistically is given in Scheme 5. It is reasonable to assume that **6** forms enamine derivatives with aldehydes and ketones, probably via an iminium betaine **27**, which in turn might be in equilibrium with a bicyclic oxazolidinone, especially in the case of aldehydes.[16] To explain the opposite regioselectivity observed for Aldol reactions on the one hand and Mannich reactions or aminations on the other, one has to assume that an equilibrium of regioisomeric enamines **29** and **30** is established in case of unsymmetrical ketone substrates **28**. For the subsequent reactions with electrophiles of general formula **31**, a metal-free Zimmermann–Traxler-type transition state has been postulated. Crucial for the highly ordered transition state and the enantiofacial selectivity with respect to the enamine reactant is the triply bound proton, which is transferred from the carboxylate group of the proline to the electrophile. The opposite facial selectivity for the aldehydes and imines can be explained by the different conformations of the ring in the transition states. The chair conformation with equatorial R^1 and R^2 substituents (as in **32**) corresponds to the formation of *anti* diastereomers, as observed for the aldol additions.

The most interesting aspect, which however is still not sufficiently exploited, is the nature of the catalytic cycle with proline, which in general gives not only the best stereoselectivities, but also the best conversions. In fact, the whole cycle can be considered as a set of equilibria, at least for aldol processes, since proline was identified in a screening effort aimed at small molecules that mediate the retro-aldol reaction.[9a] It is therefore understandable, that for some conversions (but interestingly not for all), a large excess of substrate **28** is needed. The rather large amount of proline applied (5–20 mol%) might imply that the catalytic cycles of these conversions are inefficient. However, this is not necessarily true as under most reaction conditions a substantial amount of proline is not dissolved. When L-proline (10–20 mol%) is stirred with isovaleraldehyde (1.5 equiv) in dichloromethane at room temperature—the reaction conditions for the amination with azodicarboxylates[3]—most of the proline remains undissolved, and conversion into either bicyclic oxazolidinone, iminium adduct **27**, or enamine is not evident.[17] Many aprotic solvents ranging from intermediate (dichloromethane, THF, acetonitrile) to high polarity (DMSO) are suitable, and a small percentage of water is tolerated. Water is also involved in the catalytic cycle for the formation and cleavage of enamine intermediates. The primary products **33** are again iminium betaines, but with a bulkier α substituent than that of the starting reagent **27**. This might explain why these sterically more hindered analogues do not racemize through enamine tautomerization and are preferably cleaved to form product **34**, thus regenerating the catalyst **6**.

Proline in its isoelectric zwitterionic form is thus an efficient organocatalyst that reversibly forms reactive nucleophilic enamine derivatives from aldehydes and ketones under mild conditions. The reaction with a variety of electrophiles gives addition products under catalytic conditions. Conversions and yields are moderately high, and the products are often obtained with excellent enantiomeric purity. The optimization and scaling up of individual processes appear to be feasible. The mechanistic understanding of these catalytic cycles is, however, still in its infancy, and it is not even clear whether proline should be considered as a homogeneous or heterogeneous catalyst. The thermodynamic and kinetic profiles still need to be determined, and calculations have thus far been restricted to simple enamine derivatives of methyl- and dimethylamine.[18] These model compounds lack the salient features of proline: the five-membered ring, the carboxylate group responsible for proton transfer, and the enantiofacial differentiation in the transition state.

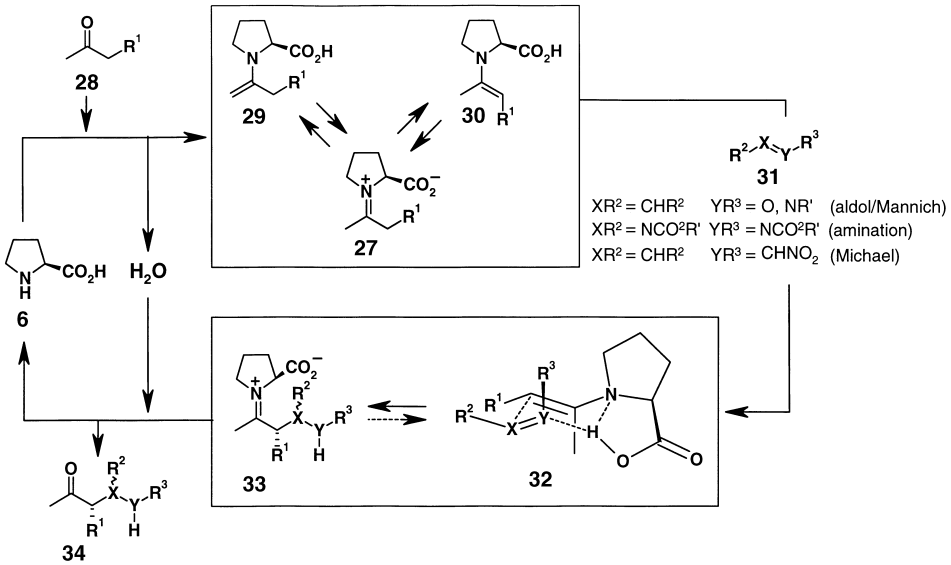

Scheme 5. Mechanistic considerations for L-proline-catalyzed reactions of ketones and aldehydes with electrophiles.

 © 2003 Wiley-VCH Verlag GmbH & Co. KGaA, Weinheim 1433-7851/03/4201-0977 $ 17.50+.50/0

[1] a) R. O. Duthaler, *Tetrahedron* **1994**, *50*, 1539 – 1650; b) D. A. Evans, S. G. Nelson, *J. Am. Chem. Soc.* **1997**, *119*, 6452 – 6453; c) D. A. Evans, D. S. Johnson, *Org. Lett.* **1999**, *1*, 595 – 598; d) Y. Yamashita, H. Ishitani, S. Kobayashi, *Can. J. Chem.* **2000**, *78*, 666 – 672.

[2] K. L. Reddy, K. B. Sharpless, *J. Am. Chem. Soc.* **1998**, *120*, 1207 – 1217.

[3] a) A. Bøgevig, K. Juhl, N. Kumaragurubaran, W. Zhuang, K. A. Jørgensen, *Angew. Chem.* **2002**, *114*, 1868 – 1871; *Angew. Chem. Int. Ed.* **2002**, *41*, 1790 – 1793; b) B. List, *J. Am. Chem. Soc.* **2002**, *124*, 5656 – 5657.

[4] N. Kumaragurubaran, K. Juhl, W. Zhuang, A. Bøgevig, K. A. Jørgensen, *J. Am. Chem. Soc.* **2002**, *124*, 6254 – 6255.

[5] K. Juhl, K. A. Jørgensen, *J. Am. Chem. Soc.* **2002**, *124*, 2420 – 2421.

[6] a) C. Agami, *Bull. Soc. Chim. Fr.* **1988**, 499 – 507; b) T. Bui, C. F. Barbas III, *Tetrahedron Lett.* **2000**, *41*, 6951 – 6954.

[7] a) H. Gröger, J. Wilken, *Angew. Chem.* **2001**, *113*, 545 – 548; *Angew. Chem. Int. Ed.* **2001**, *40*, 529 – 532; B. List, *Synlett* **2001**, 1675 – 1686; c) B. Alcaide, P. Almendros, *Eur. J. Org. Chem.* **2002**, 1595 – 1601.

[8] a) P. I. Dalko, L. Moisan, *Angew. Chem.* **2001**, *113*, 3840 – 3864; *Angew. Chem. Int. Ed.* **2001**, *40*, 3726 – 3748; b) E. R. Jarvo, S. J. Miller, *Tetrahedron* **2002**, *58*, 2481 – 2495.

[9] a) K. Sakthivel, W. Notz, T. Bui, C. F. Barbas III, *J. Am. Chem. Soc.* **2001**, *123*, 5260 – 5267; b) W. Notz, B. List, *J. Am. Chem. Soc.* **2000**, *122*, 7386 – 7387; c) B. List, P. Pojarliev, C. Castello, *Org. Lett.* **2001**, *3*, 573 – 575.

[10] a) A. Córdova, W. Notz, C. F. Barbas III, *J. Org. Chem.* **2002**, *67*, 301 – 303; b) A. B. Northrup, D. W. C. MacMillan, *J. Am. Chem. Soc.* **2002**, *124*, 6798 – 6799.

[11] A. Bøgewig, N. Kumaragurubaran, K. A. Jørgensen, *Chem. Commun.* **2002**, 620 – 621.

[12] a) A. Córdova, W. Notz, G. Zhong, J. M. Betancort, C. F. Barbas III, *J. Am. Chem. Soc.* **2002**, *124*, 1842 – 1843; b) A. Córdova, Sh.-i. Watanabe, F. Tanaka, W. Notz, C. F. Barbas III, *J. Am. Chem. Soc.* **2002**, *124*, 1866 – 1867.

[13] a) B. List, *J. Am. Chem. Soc.* **2000**, *122*, 9336 – 9337; b) B. List, P. Pojarliev, W. T. Biller, H. J. Martin, *J. Am. Chem. Soc.* **2002**, *124*, 827 – 833; c) W. Notz, K. Sakthivel, T. Bui, G. Zhong, C. F. Barbas III, *Tetrahedron Lett.* **2001**, *42*, 199 – 201.

[14] a) B. List, P. Pojarliev, H. J. Martin, *Org. Lett.* **2001**, *3*, 2423 – 2425; b) J. M. Betancort, C. F. Barbas III, *Org. Lett.* **2001**, *3*, 3737 – 3740; c) D. Enders, A. Seki, *Synlett* **2002**, 26 – 28.

[15] J. M. Betancort, K. Sakthivel, R. Thayumanavan, C. F. Barbas III, *Tetrahedron Lett.* **2001**, *42*, 4441 – 4444.

[16] F. Orsini, F. Pelizzoni, M. Forte, M. Sisti, G. Bombieri, F. Benetollo, *J. Heterocycl. Chem.* **1989**, *26*, 837 – 841.

[17] R. O. Duthaler, K. Martin, unpublished results.

[18] S. Bahmanyar, K. N. Houk, *J. Am. Chem. Soc.* **2001**, *123*, 11273 – 11283.

Inorganic Microstructures

Organic Templates for the Generation of Inorganic Materials**

*Kjeld J. C. van Bommel, Arianna Friggeri, and Seiji Shinkai**

Keywords:
materials science · nanostructures · organic templates · sol–gel processes

© 2003 Wiley-VCH Verlag GmbH & Co. KGaA, Weinheim

1433-7851/03/4209-0980 $ 20.00+.50/0

Mankind's fascination with shapes and patterns, many examples of which come from nature, has greatly influenced areas such as art and architecture. Science too has long since been interested in the origin of shapes and structures found in nature. Whereas organic chemistry in general, and supramolecular chemistry especially, has been very successful in creating large superstructures of often stunning morphology, inorganic chemistry has lagged behind. Over the last decade, however, researchers in various fields of chemistry have been studying novel methods through which the shape of inorganic materials can be controlled at the micro- or even nanoscopic level. A method that has proven very successful is the formation of inorganic structures under the influence of (bio)organic templates, which has resulted in the generation of a large variety of structured inorganic structures that are currently unattainable through any other method.

From the Contents

1. Introduction	981
2. Synthetic Polymers	982
3. Surfactants	984
4. Organogels	986
5. Carbon Nanotubes	992
6. Organic Crystals	993
7. Biomaterials	994
8. Summary and Outlook	996

1. Introduction

The use of organic compounds as templates for the generation of inorganic structures and materials has received increasing attention over the last decade.[1] Inorganic materials, although diverse in composition, generally lack the structural variety characteristic of supramolecular and other organic structures.[2] Although inorganic materials are easily molded on the macroscopic level, our ability to shape them on the microscopic level is, at best, deficient. However, the transfer of the structure from a variety of organic templates to the inorganic product allows for the formation of otherwise unattainable inorganic structures, examples of which will be discussed in this review. The formation of these inorganic structures is challenging not only from a pure scientific point of view, but these materials also have great potential for application in a large variety of fields. One can envision the use of hollow, inorganic spheres for the controlled release of a variety of substances, as well as their use as light, but strong filler material or as microreactors. Chiral inorganic materials might one day be applied in chiral catalysis, or ultrathin inorganic fibers used as nanowires in nanotechnological devices. The application of these materials in useful processes and devices is assured as soon as their production is accomplished in a precise, reproducible manner, and if possible at reasonable costs.

Many groups, including our own, have found new, creative methods and templates with which to transfer shape to inorganic materials. Although inorganic templates can also be used for the formation of inorganic materials,[3–6] in this review we focus on organic templates. Therefore, only examples of transcription will be discussed in which the structure of an organic template is transferred to an inorganic material. Furthermore, we will focus on the formation of discrete, inorganic structures such as fibers, tubules, or spheres; thus, the formation of mesoporous silicas consisting of continuous structures in which templated channels and cavities are present[7] will not be discussed.

The process of transcription can be divided into several steps: first of all an organic template which consists of either preformed or self-assembled entities is brought into contact with an inorganic precursor or small particles of the actual inorganic material that will be formed. This step usually takes place in solution, but can also occur in the gas phase. Deposition of the inorganic material on the inner or outer surface of the template will then result in the formation of an organic–inorganic hybrid material. The organic template material may then be removed (for example, through heat treatment,[8] microwave irradiation,[9] or washing with organic solvents[10]), thus resulting in the isolation of an inorganic material with a morphology directly related to the organic template. The heat treatment, which is often employed for the removal of the organic template, can simultaneously lead to calcination of the inorganic material, thus resulting in a harder, more stable inorganic product. The ease with which the original template structure can be removed is one of the advantages of using organic instead of inorganic templates. Naturally, template removal is optional, and the preceding organic–inorganic hybrid material may prove to be even more interesting than the inorganic structure itself from an applications point of view. Several examples of such interesting hybrid materials can be found in refs. [11, 12]

In many of the early examples of templated formation of inorganic materials, the product often consisted of SiO_2, TiO_2,

[*] Prof. S. Shinkai,[+] Dr. K. J. C. van Bommel,[++] Dr. A. Friggeri[++]
Chemotransfiguration Project
Japan Science and Technology Corporation (JST)
2432 Aikawa, Kurume, Fukuoka 839-0861 (Japan)
[+] Current address:
Department of Chemistry and Biochemistry
Graduate School of Engineering, Kyushu University
Fukuoka 812-8581 (Japan)
Fax: (+81) 92-642-3611
E-mail: seijitcm@mbox.nc.kyushu-u.ac.jp
[++] Current address:
BiOMaDe Technology Foundation
Nijenborgh 4, 9747 AG Groningen (Netherlands)
Both authors contributed equally to this paper.

[**] The pasta images in the frontispieceare reproduced with permission from "The Cooks Thesaurus" (http://www.foodsubs.com).

 © 2003 Wiley-VCH Verlag GmbH & Co. KGaA, Weinheim 1433-7851/03/4209-0981 $ 20.00+.50/0

or other common oxides, however, as can be seen in this review, there is a rapidly increasing number of materials (for example, GaN, CdS, NbS_2) that can nowadays be shaped into fascinating structures.

2. Synthetic Polymers

Numerous synthetic polymers have been employed as templates—mainly as colloidal particles—for the preparation of structured inorganic materials.[13] Many different methods have been used for the coating of these particles, whilst removal of the organic template is generally carried out by dissolution or calcination. The procedure of core/template removal by calcination was first introduced by Kawahashi and Matijeví during their search to produce hollow spheres of yttrium compounds.[8] As was subsequently observed also by other research groups, the rate of thermal decomposition of the polystyrene template cores affects the morphology of the particles obtained. In the case of $Y(OH)CO_3$-covered polystyrene particles, for example, exposure to very intense heat (up to 600 °C) causes decomposition of the template and formation of a Y_2O_3 shell. However, shell rupture can occur both at high heating rates, as a result of pressure build up from the evolution of CO_2 and H_2O vapor inside the spheres, and also at high cooling rates, because of thermal shrinkage of Y_2O_3.[8]

Hollow ZnS shells have been obtained through sonication of carboxy-modified polystyrene particles in the presence of zinc acetate and thioacetamide, followed by calcination of the polymer.[14] This is a rather simple method which could be extended to other materials (for example, PbS). Titania-coated particles are very useful as catalysts and pigments, but they can be particularly difficult to synthesize because of the high reactivity of titania precursors.[15] However, two research groups have recently presented simple coating methods involving the hydrolysis of titanium tetraisopropoxide[15] and titanium tetrabutoxide[16] in the presence of polystyrene microspheres as the template. Thermal decomposition of the polystyrene cores leads to the formation of hollow spheres. Increasing the calcination temperature results in these hollow spheres being of amorphous, anatase, or rutile types of TiO_2. Antonietti and co-workers recently prepared spherical capsules with very thin, practically impermeable walls.[17] Miniemulsions (consisting of small oil or water droplets 30–300 nm in diameter) containing styrene or other easily polymerizable monomers were chosen as templates to achieve this. After polymerization, the latexes formed were covered by clay sheets, which were then armored with tetramethylorthosilane by a polycondensation reaction to create nanocapsules with wall thicknesses of about 1.5 nm. Solid and hollow magnetic particles have, for example, also been produced by seeded polymerization of iron salts on polystyrene microspheres.[18] This process, however, yielded a noncontinuous coating of Fe_3O_4 on the polystyrene template, therefore an additional coating of silica nanoparticles was applied (by alkaline hydrolysis of tetraethylorthosilicate (TEOS)) to stabilize the spheres. These spheres are of particular interest in the field of biotechnology (for example, in bioseparations, immunoassays) and also for the formation of patterned surfaces by particle manipulation using magnetic fields.

Magnetic hollow spheres have been produced by Caruso et al. by using a much more convenient and versatile method, which is known as the layer-by-layer method (LbL).[19] In the LbL technique a multilayer film is formed by the alternate adsorption of oppositely charged species (Figure 1).[20] Magnetic hollow spheres have been obtained by depositing Fe_3O_4 nanoparticles and polyelectrolyte multilayers onto latex particles, followed by calcination to remove the template.[19] Inorganic silica spheres have been obtained in a similar fashion through the use of SiO_2 particles. After calcination, this procedure leads to silica shells with wall thicknesses in the nanometer range (20–200 nm), depending on the number of layer deposition cycles.[20,21] Hollow β zeolite and silicalite-1 spheres have also been produced by using the LbL method, with subsequent removal of the template by calcination.[22] Furthermore, titania and laponite nanoparticles have also been used to produce hollow spheres, which demonstrates the versatility and general nature of the LbL method.[23] Removal

Kjeld J. C. van Bommel was born in Rotterdam, The Netherlands, in 1971. He received his M.Sc. in Chemical Technology in 1995 from the University of Twente, and completed his PhD thesis "A Supramolecular Approach to Radiopharmaceuticals" in the laboratories of Prof. D. N. Reinhoudt. At the end of 2000 he moved to Kurume, Japan, where he worked as a Japan Science and Technology Agency Research Fellow within the Chemotransfiguration Project under the supervision of Prof. Seiji Shinkai. He is currently working as a researcher for the BiOMaDe Technology Foundation in Groningen, The Netherlands.

Arianna Friggeri was born in Montecchio Emilia, Italy, in 1971. She received her M.Sc. in Organic Chemistry in 1996 from the Università degli Studi di Parma, Italy. She then moved to the University of Twente, The Netherlands, where she worked on self-assembled monolayers on gold in the laboratories of Prof. D. N. Reinhoudt, and received her PhD in 2000. She then joined the Chemotransfiguration Project in Kurume, Japan, where she worked mainly on organogels and their transcription into inorganic materials under the supervision of Prof. Seiji Shinkai. She is currently working as a researcher for the BiOMaDe Technology Foundation in Groningen, The Netherlands.

Seiji Shinkai was born in 1944 in Fukuoka, Japan, and received his PhD in 1972 from Kyushu University. After postdoctoral work at the University of California, Santa Barbara, with T. C. Bruice, he joined Kyushu University in 1975 and became a full professor there in 1988. He acted as the director of the Chemotransfiguration Project (1997–2001) and is also acting as a leader of the Kyushu University COE Project entitled "Design and Control of Advanced Molecular Assembly Systems" (since 1998). His research interests include host–guest chemistry, molecular recognition, allosteric functions, organogels, sol–gel transcription, polysaccharide–polynucleotide interactions.

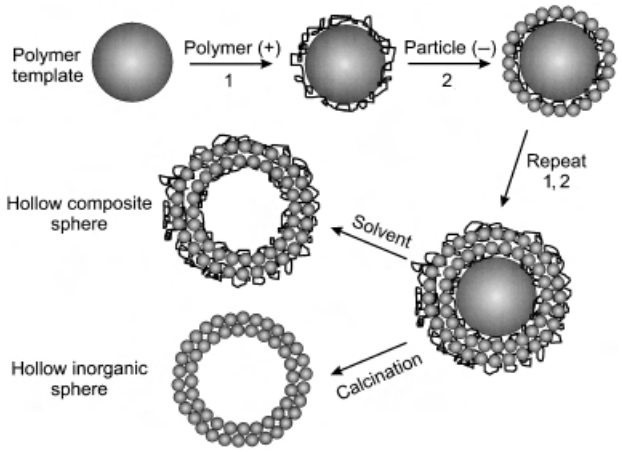

Figure 1. Schematic representation of the layer-by-layer method.

of the template can sometimes be achieved by simple dissolution of the core particles, as was reported for a weakly cross-linked melamine–formaldehyde template.[13b] This procedure gives rise to composite organic–inorganic hollow spheres instead of completely inorganic shells. In an interesting related experiment, composite hollow structures which mimicked the original shape of the template were obtained by coating echinocytes (red blood cells with many blunt spicules) with SiO_2/polymer multilayers and subsequent exposure to a deprotonizer to remove the template core (Figure 2).[13b]

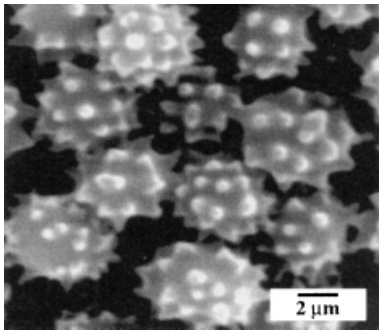

Figure 2. Scanning electron microscopy (SEM) image of glutaraldehyde-fixed echinocytes.

Xia and co-workers[10] have recently produced hollow, ellipsoids of titania by viscoelastic deformation of spherical polystyrene beads. The beads were dispersed in an elastic matrix and stretched at high temperature, thus causing the deformation of the polystyrene spheres into ellipsoids. After cooling, dissolution of the elastic matrix yielded the templates, which were subsequently exposed to a TiO_2 precursor. Finally, the titania shells were obtained by dissolving the polymer templates in toluene (Figure 3). Anion-exchange resin beads have been used by Tosheva and Sterte to prepare palladium-containing silica spheres.[24] This was accomplished by synthesizing resin–silica composites and then introducing $[PdCl_4]^{2-}$ into the spheres in a second step (this is very easy since the composites retain their anion-exchange capacity).

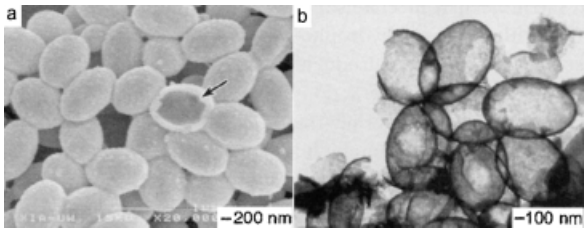

Figure 3. a) SEM image of titania shells generated by templating a sol–gel precursor solution (titanium(IV):isopropanol, 1:19) against a 3D array of polystyrene ellipsoids; b) transmission electron microscopy (TEM) image of titania shells; the wall thickness is approximately 40 nm.

After calcination, highly porous silica spheres containing a controllable amount of palladium oxide were obtained, which can be of interest for catalytic applications.

Latex nanoparticles have been used by Okuyama and co-workers[25] to create novel, spherical silica with templated mesopores. This was achieved by spraying a mixture of latex and silica nanoparticles (Figure 4, step a) into a vertical reactor with different temperature zones. During evaporation of the spraying solvent, the latex particles undergo a self-organization process (Figure 4, step b), which after drying at elevated temperature, leads to the formation of ordered mesopores into silica spheres (Figure 4, step c and Figure 5).

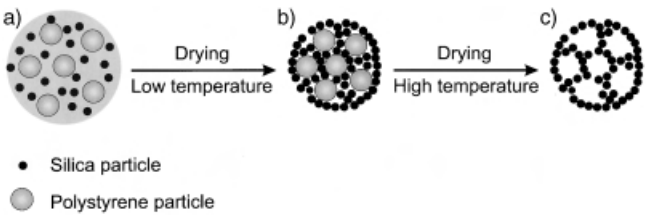

Figure 4. Formation of silica spheres with templated mesopores according to the method used by Okuyama and co-workers.[25] a) A mixture of latex and silica nanoparticles is sprayed into a vertical reactor. b) After evaporation of the spraying solvent the particles self-organize. c) Subsequent drying at elevated temperatures leads to the formation of ordered mesopores into the silica spheres.

Up until now, only a few non-polystyrene-based polymers have been employed as templates for the formation of morphologically interesting inorganic materials. A variation on the shape of polymer-templated materials has recently been proposed by Greiner and co-workers[26] Poly(L-lactide) fibers processed by electrospinning, coated with aluminum by physical vapor deposition, and subsequently subjected to thermal degradation of the polymer template gave rise to stiff single-walled aluminum tubes.[26] Our research group recently reported the use of poly(L-lysine)-amine aggregates as templates for the formation of hollow silica spheres by the sol–

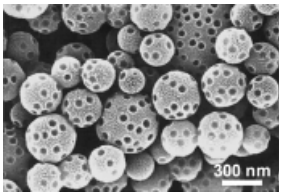

Figure 5. SEM image of a spherical silica powder produced by mixing 10 mL of silica colloids (0.05%) with 0.5 mL of latex particles (3.6×10^{13} particles per mL; 79 nm in size). Reproduced with permission from ref. [25].

gel transcription method (Figure 6).[27] The formation of the aggregate template has been shown to depend on the lipophilicity of the amine employed, while its successful transcription into silica is based on the hydrogen-bond-

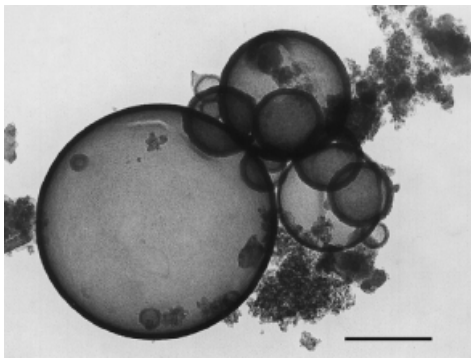

Figure 6. TEM image of silica obtained after transcription of benzyl amine–polylysine aggregates in water. The scale bar corresponds to 500 nm.

donating ability of the amine. This procedure demonstrates that not only dispersed particles but also dynamic aggregates can be employed as organic templates for inorganic structures. Poly(L-lysine) has also been used as a coating for gel beads based on alginic acid (a copolymer of guluronic and mannuronic acids) which have been employed as templates for the formation of hollow organic–inorganic silica spheres.[28] Interestingly, it was shown that silica spheres obtained from sodium silicate condensation led to much smoother, more robust coatings, whereas those formed through deposition of silica particles had more granular surfaces and lower mechanical stability. In an attempt to demonstrate the applicability of these spheres, the encapsulation of β-galactosidase was successfully performed, with 60–70% retention of enzymatic activity.[28]

Cysteine–lysine block copolypeptide aggregates (Scheme 1) have been used by Cha et al. as silicatein mimics to direct the formation of ordered silica morphologies.[29]

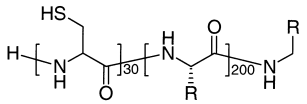

Scheme 1. Molecular structure of the cysteine–lysine block copolypeptide. $R = (CH_2)_4NH_3^+Br^-$.

Silicatein, a protein found in the sponge *Tethya aurantia*,[30] can hydrolyze and condense TEOS to form ordered silica structures at ambient conditions.[31] In a similar fashion, solutions containing a cysteine–lysine block copolypeptide and TEOS can give rise to either silica spheres or packed silica columns, depending on the degree of oxidation of the poly-L-cysteine domains of the polymer.[29] When the reaction was performed under a nitrogen atmosphere, and thus the copolypeptide was in its reduced form, spherical silica was obtained. However, ordered columnar silica was formed (Figure 7) when the reaction was performed in air and when the sulphydryl groups of the copolypeptide were partially converted into disulfides.

Although many different methods and inorganic precursors have been used for the coating of synthetic polymer templates, there has been very little variety in the morphologies obtained by using polymers as cores for inorganic materials; the spherical structure definitely dominates.

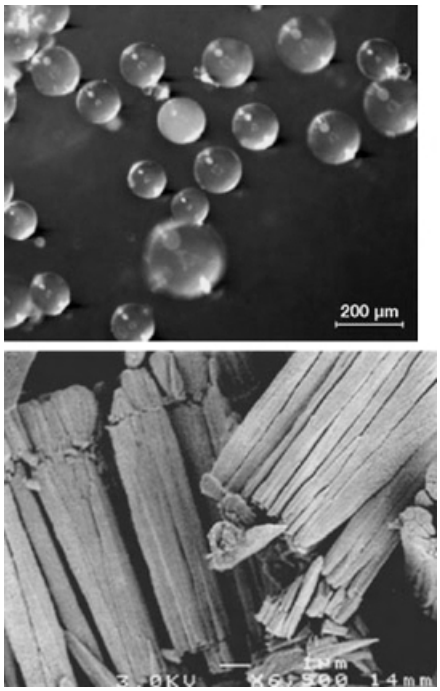

Figure 7. Different silica structures obtained using the block copolypeptide depicted in Scheme 1. Reproduced with permission from ref. [29].

3. Surfactants

Since the use of surfactant solutions for the synthesis of mesoporous silicates was proposed by Beck and co-workers[32] in 1992, surfactant-based aggregates have become more and more common as templates for the preparation of inorganic materials. Moreover, the rich variety of elaborate inorganic structures produced in nature, some of which derive from closed-packed arrays of large vesicles,[33] have also functioned as a great stimulus for the formation of complex, three-dimensional materials.[34] Walsh and Mann have synthesized networks of porous calcium carbonate from microemulsions of didodecyldimethyl ammonium bromide (DDAB), tetradec

ane, and aqueous calcium bicarbonate solution.[35] The addition of polystyrene spheres to this mixture resulted in the calcium carbonate networks growing around the spheres and giving rise to structures that resemble the coccospheres of certain marine algae (Figure 8).[35] Furthermore, crystalline

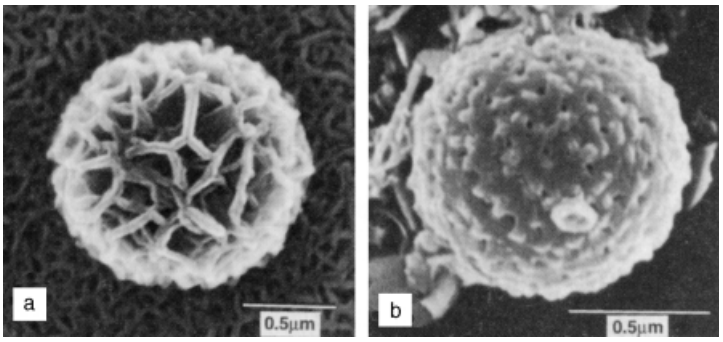

Figure 8. SEM images of a) a synthetic calcium carbonate shell; b) a coccosphere of the marine alga *Thoracosphaera* (courtesy of S. A. Davis). Reproduced with permission from ref. [35].

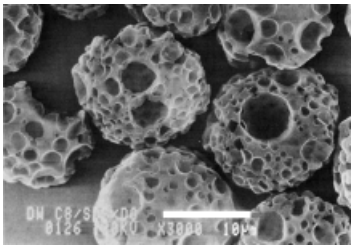

Figure 9. SEM picture of individual calcium carbonate spheroids with spongelike architecture.

calcium carbonate spheres have been synthesized from $CaHCO_3$ in a sodium dodecylsulfate/water microemulsion. Slow degassing of the CO_2 present in the solution induces crystallization of calcium carbonate at the interface of the emulsion droplets and leads to the formation of a material with a spongelike architecture (Figure 9).[36] In an attempt to mimic reticulated biominerals (for example, corals), crystalline calcium phosphate networks have been prepared by Mann and co-workers through mineralization of the water conduits found in DDAB microemulsions.[37] Hollow spherical silica has been readily obtained by Singh and Kosuge by the sol–gel method, using TEOS, octylamine, and aqueous HCl, followed by calcination of the sample.[38] The spherical shape of the octylamine aggregates in acidic solution is caused by Coulombic interactions between the protonated amines; the polycondensation of TEOS most probably occurs at the surface of the aggregate/solution interface.

Molecular sieves with vesicle-like morphologies are of particular interest as catalysts and sorbents, since the porous nature of vesicles can facilitate transport and exchange of guests to and from binding sites.[39] Pinnavaia and co-workers have used $RNH(CH_2)_2NH_2$ gemini-type surfactants[39] as well as $H_2N(CH_2)_nNH_2$ bolaamphiphiles[40] in combination with TEOS to obtain highly stable vesicular silica structures with very thin, but robust shells. Well-ordered, multilamellar vesicular structures have also been transcribed into silica by an aerosol-assisted self-assembly method, in which droplets of an ethanol/water acidic solution of TEOS and a non-ionic, ethylene oxide-based surfactant were dried and subsequently heated in a continuous, six-second process to yield well-defined vesicular mesostructures (Figure 10).[41]

The use of *uni*lamellar vesicles as templates for transcription into silica was described only recently by German and co-workers (Figure 11).[42] Vesicle-templated structures of more complex morphology have been obtained by other methodologies. Morphologically intriguing silica spheres containing pillarlike structures have been obtained (Figure 12) by controlling the rate of acidification of a solution of sodium silicate, butanol, and myristyltrimethylammonium bromide (C14TMAB).[43] Furthermore, spherical structures of aluminium phosphate with vesicle-templated surfaces were formed by using a vesicular aggregate of alkylammonium dihydrogen phosphate to which pseudoboehmite was added. Although this procedure requires some optimization, it shows strong similarity to the method used by radiolaria and diatoms for the formation of their skeletons, which are thought to be generated by the secretion of silica into a network of bubblelike alveoli (Figure 13).[44] In an interesting approach towards the synthesis of vesicle-templated materials, Kikuchi and co-workers have incorporated the inorganic precursor and the organic template into a single molecule (Scheme 2).[45] When the alkoxysilyl head group was subjected to hydrolysis, the organic–inorganic hybrid formed bilayer vesicles with a network of siloxane bonds on the membrane surface.

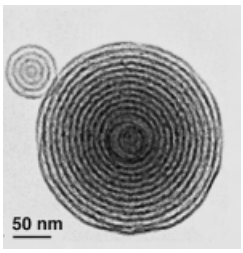

Figure 10. TEM image of calcined silica particles showing a vesicular mesophase. Reproduced with permission from ref. [41].

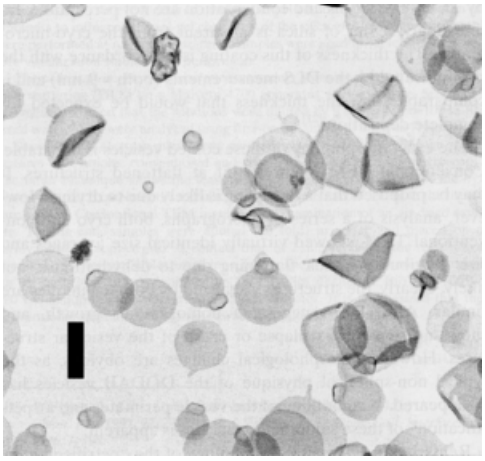

Figure 11. TEM image of a dried-out sample of silica-coated dioctadecyldimethyl ammonium bromide (DODAB) vesicles. The scale bar corresponds to 20 nm.

Figure 12. SEM image of pillarlike structures within a silica sphere (diameter about 11 μm) obtained from a mixture of sodium silicate, butanol, and C14TMAB. Reproduced with permission from ref. [43].

The control of shape and size is becoming increasingly important in regard to specific applications in materials science, and especially in the field of nanotechnology. Hence, the formation of tubular and wirelike structures

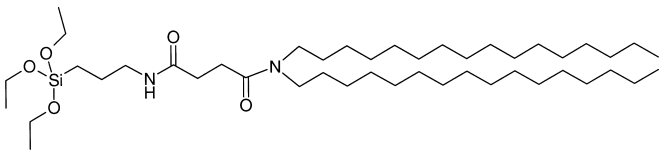

Scheme 2. Organic–inorganic hybrid used to form vesicles by Kikuchi and co-workers.[45]

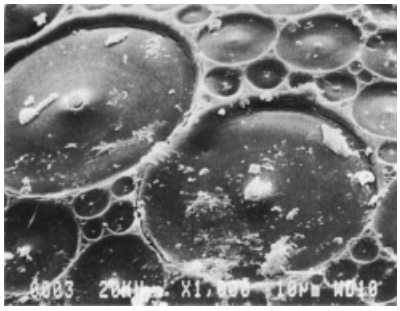

Figure 13. SEM image of the decylamine mesolamellar aluminophosphate product. The diameter of the bowls is 1–50 μm. Reproduced with permission from ref. [44].

has currently been receiving much attention. One of the first examples in which tubule formation was templated by a self-assembled amphiphile-based structure was presented by Baral and Schoen,[46] and consisted of coating phospholipid tubules with silica by the sol–gel procedure. Magnetic, as well as nonmagnetic iron oxide tubelike structures have also been synthesized by using the microstructures formed by mixtures of a sugar-based lipid and its anionic sulfated derivative as templates.[47] The anionic sites provide the starting points for mineralization, which leads to the formation of organic–inorganic composites. However, dense, uniform coatings of the templates did not form and at times intercalation of the inorganic material into the organic structure occurred, thus rendering any attempt to remove the template core futile. Single silica nanotubes, as well as bundles of tubes, have been prepared by Adachi et al. by using the sol–gel method with TEOS as the silica precursor and a template based on laurylamine hydrochloride (Figure 14).[48]

Figure 14. TEM image of the calcined silica templated with gellauryl amine hydrochloride. The scale bar corresponds to 100 nm. Reproduced with permission from ref. [48].

Other materials besides silica and iron oxide have been employed for coating surfactant-based, tubular templates. $VOCl_3$ and V_2O_5, for example, have been used as precursors for the formation of vanadium oxide nanotubes.[49] In the presence of long-chain primary amines the precursors form complexes that, after hydrolysis, give rise to lamellar-structured intermediates, which are subsequently subjected to a hydrothermal treatment to give vanadium oxide nanotubes. Jonas and co-workers have successfully applied coatings of Ni and Cu to bolaamphiphile nanotubes; however, removal of the template was not reported.[50] Single-crystal $BaCO_3$ nanowires have been constructed through the reaction of barium and carbonate ions in the cores of nonionic reverse micelles.[51] Wirelike crystal growth is assumed to occur because of the preferential orientation of surfactant molecules along the surface planes parallel to one crystal axis after $BaCO_3$ nucleation has started. Although this process is limited to crystals with morphologies compatible with the shape provided by the micelle, it provides a new methodology for the synthesis of nanowires.

4. Organogels

Organogels can be defined as thermally reversible viscoelastic liquidlike or solidlike materials comprised of an organic liquid and low concentrations (typically < 5 wt %) of relatively low molecular weight molecules (namely, gelators).[52] Organogels have been the topic of several extensive reviews[2a,b,52–54] and will only be introduced briefly here. An organogel is usually prepared by heating a mixture of a gelator and solvent until the solid dissolves; upon cooling, the solution (sol) then thickens to form a gel. The gel is usually characterized by several methods. The simplest one is the determination of the gelation transition temperature (T_{gel}), which may be done by simply heating the gel until it turns into a sol at $T = T_{gel}$. Electron microscopy techniques (SEM and TEM) are frequently used to observe the morphology of the gel (for example, fibrous or spherical). In the case of SEM, the freeze-dried gel (xerogel) is in general observed, rather than the "wet" gel. Other characterization methods, such as IR, UV, circular dichroism (CD), NMR spectroscopies, as well as rheological studies can be used to study these systems. As a consequence of their intriguing properties, gels have found applications in cosmetics,[55] plastic surgery,[56,57] contact lenses,[58,59] experimental solar cells,[60] electrochemical cells,[61] as well as many other products and areas.

The first successful employment of an organogel as a template for the formation of inorganic structures was published in 1998 by our research group.[62] Compound **1** (Scheme 3) was shown to gelate a number of organic solvents as well as the silanol compound TEOS.[63] However, since the silica that resulted after polycondensation of TEOS under acidic or basic conditions did not exhibit any characteristic structure,[64] a quaternary ammonium cation was introduced to mimic the character of conventional cationic surfactants that are generally used in sol–gel polymerization systems.[65] Compound **2** proved to be a less versatile gelator than **1**, however, it could still gelate a number of solvents. SEM

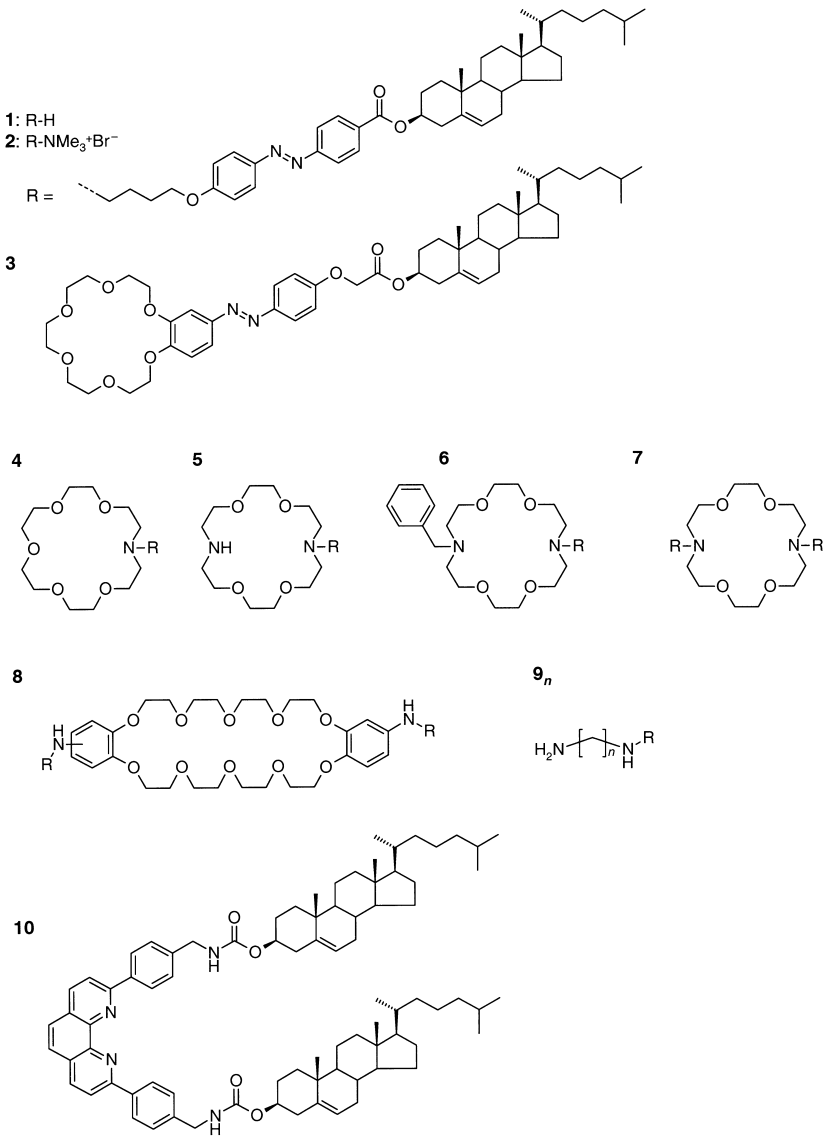

Scheme 3. Cholesterol-based gelators developed by our research group.

studies showed that the organogel of **2** existed of a network of fibers, with diameters ranging from 50 to 200 nm. A method was devised to obtain an acetic acid gel of **2** in the presence of TEOS and water, and after ten days the resultant silica was dried extensively at room temperature to remove the acetic acid and water. Subsequent drying and calcination steps resulted in silica without the presence of the original organic template.[66] TEM observations (Figure 15) proved it to consist of hollow, tubular silica with inner diameters comparable to those of the original gel fibers. Further experiments suggested that the presence of the cationic charge was indispensable for successful transcription. This observation can be rationalized by the fact that anionic silica species (≡Si-O$^-$) are present in moderately acidic solutions (pH 2–7).[67] These species are then adsorbed onto the cationic gelator fibrils and polymerization proceeds along these fibrils, which eventually results in fibrous, tubular silica structures.

Since the first example of the formation of inorganic materials by making use of organogel templates was reported, much progress has been made in the understanding, as well as in the successful exploitation, of such systems. After the discovery that cholesterol-based organogelators such as **1** and **2** form chirally oriented structures,[68] attempts were made to transfer this chirality into inorganic materials. Experiments using mixed organogels of **1** and **2** in various ratios showed that hollow, helical silica could only be obtained at certain ratios of the two organogelators. The "dilution" of the cationic charges present in the gel fibers clearly plays a decisive role in whether or not the chirality present in the template is transcribed into the silica material. A high concentration of cationic charges in the gel fibers simply results in a random adsorption of anionic silica precursors or particles, whereas a moderate concentration results in excellent transcription; a very low concentration on the other hand does not result in any transcription.[69] As was established later, the presence of extra cationic charges also proved to disrupt the transcription when present in high concentrations.[70] SEM analysis of the helical silica obtained through transcription of the organogel of **1** and **2**, clearly showed that all the silica structures possessed a right-handed helicity. This result was in accordance with CD measurements performed on organogels of **1** and **2**, which proved that the gelator molecules are arranged in a right-handed helical orientation.

Confirmation of the importance of cationic charges in the transcription process of organogels into silica came from Ono et al., who employed a cholesterol-based gelator functionalized with a crown ether moiety (Scheme 3, **3**) capable of binding potassium

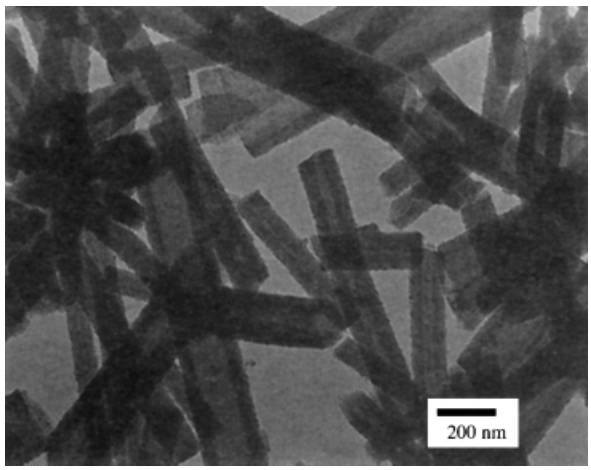

Figure 15. TEM image of tubular structures obtained after calcination of a gel of **2** and TEOS. Reproduced with permission from ref. [62].

cations.[71] It was found that the organogel of **3** could only be successfully transcribed into hollow silica fibers in the presence of substantial amounts of K^+ ions.[72] The addition of other cations (Li^+, Na^+, Rb^+, Cs^+) did not result in successful transcription and only granular silica was formed. The striking effect of the potassium cations could be ascribed to the high affinity of the benzo[18]crown-6 moiety for the K^+ ion.

Several other examples of organogelator systems based on the cholesterol/crown ether system have been reported.[73,74] An organogel consisting of curved lamellar structures was obtained using the aza[18]crown-6-functionalized gelator **4**.[73] The organogel of the diaza-analogue **5** on the other hand consists of fully formed tubular structures.[73] Transcription of these organogels in the presence of K^+ or Cs^+ ions resulted in the formation of "rolled paperlike" silica. Although, like gelator **3**, compounds **4** and **5** do not possess any positive charges, their organogels can be successfully transcribed into tubular silica even in the absence of added metal salts. The driving force for this transcription is the presence of cationic charges arising from protonation of the azacrown moieties. Transcription was also successfully carried out in the presence of added metal salts; however, in all cases the metal was never directly observed in the resultant silica. Silica containing nanosized metal particles (1–5 nm) was obtained for the first time by transcribing the organogel of **4** in THF after the addition of $AgNO_3$. As can be clearly seen in Figure 16, small silver particles are present in the interlayer space of the rolled paperlike silica.[73] Such metal-containing silica is thought to have interesting applications in catalysis.

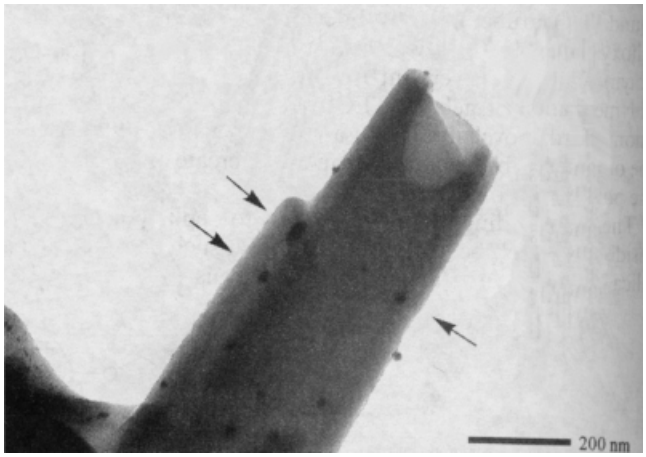

Figure 16. TEM image of the paper-roll-like silica obtained after transcription of the gel of **4** in THF, after addition of $AgNO_3$. The arrows indicate the large particles deposited between the layers. Reproduced with permission from ref. [73].

In all of the organogel examples discussed so far, positive charges present in the template enabled transcription of the organogel into the inorganic material. In a search to find an organogel system that would be able to act as a neutral template, Jung et al. synthesized compounds $\mathbf{9}_n$ (Scheme 3). They were designed to be gelator analogues of the diamine surfactants used by Pinnavaia and co-workers[39] to produce mesoporous silica (Section 3), with transcription occurring as a result of hydrogen bonding, rather than ionic interactions, between the template and the silica precursor. Similarly, transcription of organogels of compounds $\mathbf{9}_n$ was achieved under basic conditions, that is, without positive charges being present in the template.[75] The attractive forces between the negatively charged silica precursor species and the amide moieties of the gelator are large enough to result in a successful transcription of the template. Interestingly, different morphologies were observed for the organogels and the resultant silica products of gelators $\mathbf{9}_n$ for different values of n. In the cases of $n=1$ or 3, the organogels possessed a curved lamellar morphology, which resulted in silica with a structure like a paper roll (Figure 17). For even numbers of n (for example, 2 or 4), the morphology of the organogel was unmistakably fibrous in nature and resulted in hollow silica fibers (after transcription and calcination). These results clearly demonstrate that minor changes in the gelator structure can have a dramatic effect on the overall morphology of the inorganic material. Since the diamine moieties $\mathbf{9}_n$ (particularly for $n=2$ or 3) are known to be good ligands for transition metals, transcription was carried out in the presence of either $Ni(NO_3)_2$ or $Pd(NO_3)_2$. After calcination, small metal particles (Ni: <1 nm, Pd: 1–2 nm) could clearly be observed embedded within the resultant silica, thus making these systems interesting for many catalytic applications.[76]

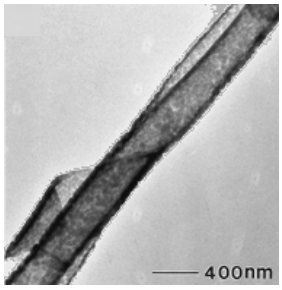

Figure 17. TEM image of the paper-roll-like silica obtained after transcription of the gel of $\mathbf{9}_n$ ($n=1$, 3). Reproduced with permission from ref. [76].

Not only did the original gelator system of **1** and **2**[62] function as the starting point for the investigation of the actual transcription mechanism, it also laid the foundation for the development of other cholesterol-based gelators which would lead to new, chiral inorganic materials. As mentioned earlier, our research group discovered that helical silica could be obtained by adjusting the charge density in the gel fibers.[69] Jung et al. subsequently reported that transcription of the organogel of **6** in the presence of Ag^+ or Cs^+ ions resulted in the formation of helical silica–metal hybrid materials.[77]

TEM analysis of the organogel of dibenzo[30]crown-10 derivative **8** (Scheme 3) in acetic acid proved it to consist of tubules, as well as linear and helical ribbon structures. Transcription was successfully carried out (gelator **8** possesses two amino moieties that become protonated under these acidic conditions) and resulted in the corresponding silica consisting of tubular and helical ribbon structures (Figure 18). Both organogel fibers and silica structures were right-handed (as shown by the CD spectra), which proved that the helicity present at the microscopic scale is reflected by the macroscopic helicity present in the inorganic material. Careful examination of the tubular silica after calcination showed that it consisted of two independent layers with an interlayer

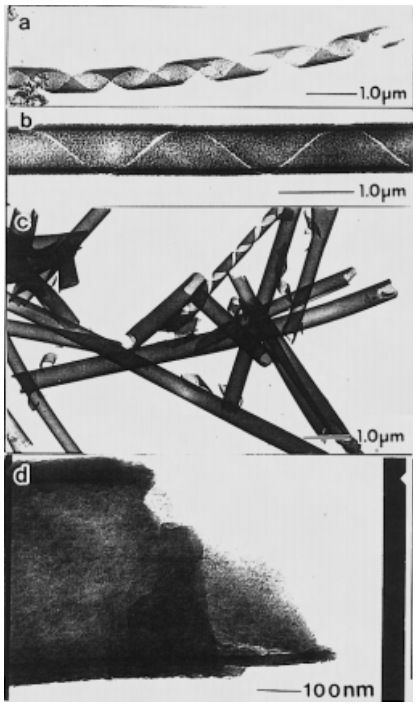

Figure 18. a–d) TEM images of tubular and ribbonlike silica structures obtained after transcription of the acetic acid gel of **8**. Reproduced with permission from ref. [78].

distance of 8–9 nm, which resulted from the removal of the organogel structure that was acting as the template during the transcription.[78] This example shows the exactness with which transcription of the template takes place to give well-defined inorganic structures with predetermined helicity.

In all of the examples based on cholesterol-based organogelators (often carrying crown ether moieties) discussed so far, helical and nonhelical fibrous, paper-roll-like, tubular, and helical ribbon silica structures were observed. However, compound **7** (Scheme 3), which consists of two cholesterol moieties linked to a diaza-crown (rather than a dibenzocrown as in **8**) was synthesized as a gelator analogue to a class of azacrown compounds capable of forming vesicular or lamellar structures.[79] Investigation of the acetic acid xero- and organogels of **7** by SEM and TEM, respectively, indeed proved them to consist of multilayered vesicles. Transcription of the organogel resulted in multiwalled silica spheres, with interlamellar distances of approximately 5 nm, again proving the accuracy of the transcription process. Interestingly, the organogel of **7**·$Pd(NO_3)_2$ in acetic acid displayed a structure strikingly different from the organogel lacking the metal. The fluffy, globular aggregates observed by SEM were also successfully transcribed into their silica analogues (Figure 19). Electron probe microanalysis (EPMA) studies clearly proved the uniform distribution of the palladium throughout the silica matrix.[80] Recently, ultrastabile, mesoporous, hollow silica fibers were produced using an organogel of **10** (Scheme 3) as the template for transcription. The phenanthroline moiety connecting the two

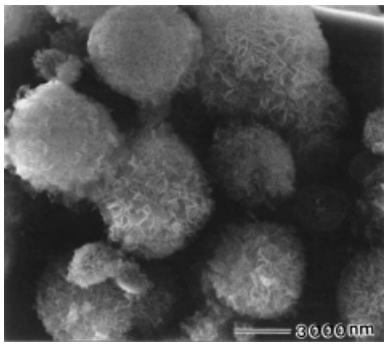

Figure 19. SEM image of silica obtained after transcription of the gel of **7**·$Pd(NO_3)_2$ in aniline. Reproduced with permission from ref. [80].

cholesterol units may be useful for the introduction of a variety of metal ions.[81] Now that the shape and (channel) dimensions of inorganic materials can be controlled, and metals of choice can be introduced, the application of these well-defined materials in the field of catalysis has been brought one step closer.

Although the use of cholesterol-based gelators can often result in chiral inorganic materials, the synthesis of the enantiomeric form of the gelator necessary to form the desired enantiomeric inorganic structure is not straightforward. Bis(ureido)cyclohexane-based compounds (similar to **13**/**13′**, Scheme 4), both enantiomers of which are easily synthesized, were reported by Hanabusa et al. in 1996 to act

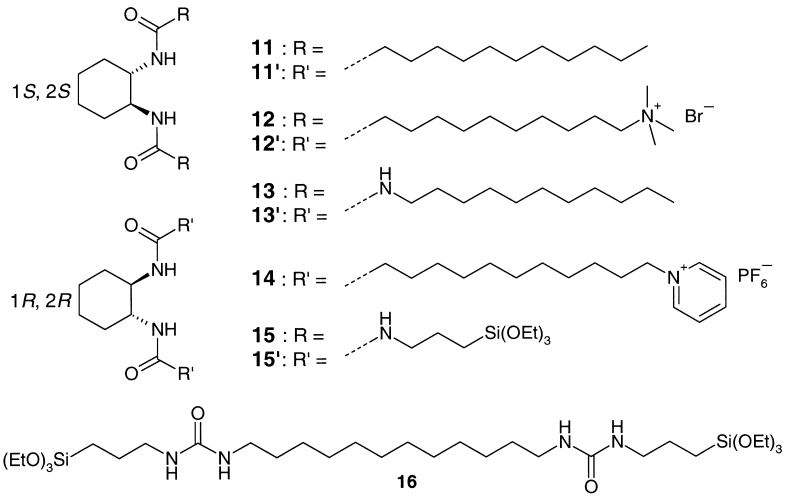

Scheme 4. Amide- and urea-containing gelators.

as gelators for different organic solvents.[82] TEM images had shown that these compounds gelate solvents through the formation of a fibrous network. Furthermore, CD experiments had proven that these compounds form chiral aggregates upon gelation and that the aggregates of the different enantiomers display opposite Cotton effects. Positive charges were introduced on the ends of the alkyl chains to enable these kinds of gel systems to be successfully transcribed.[83,84] A chiral organogel was formed from a mixture of the 1*S*/2*S*-diamides **11** (neutral) and **12** (charged). Transcription of this

organogel resulted in helical silica fibers, all of which right-handed (Figure 20b,d). Helical silica fibers of the opposite handedness were obtained using the enantiomeric mixture of 1*R*,2*R*-diamides **11′** and **12′** (Figure 20a,c). Transcription only proved successful when the ratio of noncharged gelator to

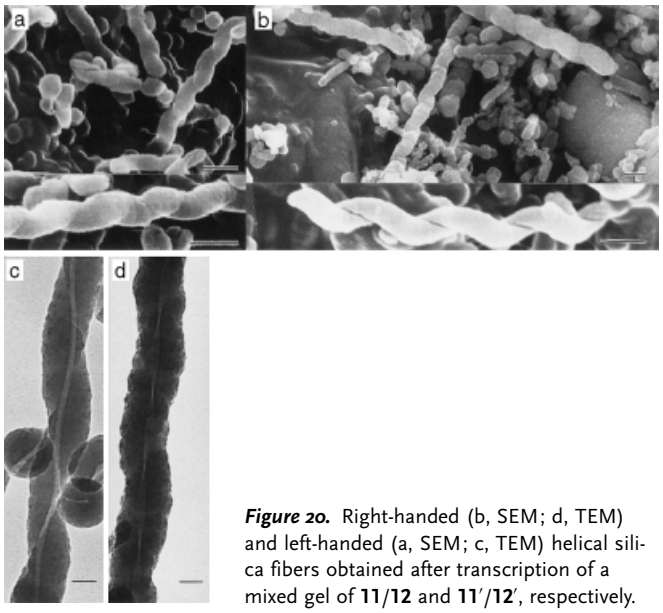

Figure 20. Right-handed (b, SEM; d, TEM) and left-handed (a, SEM; c, TEM) helical silica fibers obtained after transcription of a mixed gel of **11**/**12** and **11′**/**12′**, respectively.

charged gelator was lower than 70:30, a finding which, analogous to the results observed for the previously discussed mixed gel system of **1** and **2**,[62] indicates that a minimum amount of charge must be present to successfully transcribe the template structure.[85] Similar results were obtained using the combinations **12**/**13** and **12′**/**13′**.[84] After calcination of the silica fibers, inner channels possessing the same helicity as the fiber itself could be observed, thus proving that the organogel fibers had indeed been the template around which the silica structures had formed. Furthermore, it showed that the chirality present in the gelator molecules is transcribed consistently into the macroscopic silica material. This system is the most striking example of the strength of the organogel approach for the formation of inorganic materials.

To expand the organogel approach to other inorganic materials, gelator **14** (Scheme 4) was used in combination with $Ti(iOPr)_4$ to give, after calcination, hollow titania tubes with outer diameters of 150–600 nm and inner diameters of 50–300 nm, the latter corresponding to the diameters of the template fibers.[86] Recently, Moreau et al. reported an ingenious approach to form chiral, hybrid organic–inorganic solids by means of organogelators **15**/**15′** (Scheme 4).[87] These compounds, although similar in structure to those discussed before, differ in that the silica precursor had been covalently attached to the gelator structure, thus making the use of TEOS superfluous.[88] Peculiarly, however, the silica polycondensation was carried out in pure water, a solvent that cannot be gelatinized by these cyclohexane derivatives. Hence, the obtained materials did not display the well-defined morphologies observed for true organogel systems. Organogelator **16** was also used in the nongelating solvent water.[89] The compound is thought to self-organize in a lamellar fashion, as a result of hydrogen-bonding interactions between the urea moieties and chain–chain interactions. A lamellar organic–inorganic hybrid material with plates about 50–100 nm thick was obtained after reaction.

Another class of gelators that has been employed in the formation of well-defined inorganic materials is based on sugars (Scheme 5). Sugar-based organogels have been studied by several research groups, including our own;[90–92] however, most of these gels are not directly applicable as templates for sol–gel transcription because of the lack of either positive charges or amine moieties that are required for this process. A large library of sugar-based gelators has been synthesized by our research group.[93,94] This library includes a series of amine-bearing sugar-based gelators (**17′**–**20′**; Scheme 5) which are capable of gelating polar solvents.[95–97] Different combinations of gelators and solvent resulted in organogels with either fibrous or spherical morphologies. The amino moieties present in these organogels enabled transcription to be carried out successfully to give the corresponding hollow fibrous or hollow spherical silica after calcination. Transcription of the corresponding nitro analogues (**17**–**20**) was not successful, and only granular silica was obtained. Whereas the silica resulting from the ethanol gel of the amine-bearing α-glucose derivative **17′** has a fibrous structure with a single, central channel, the silica obtained from the ethanol gel of amine-bearing β-glucose derivative **18′** possesses several channels (Figure 21a) inside each silica fiber.[95] This structure bears a strong resemblance to the lotus root (Figure 21b), a

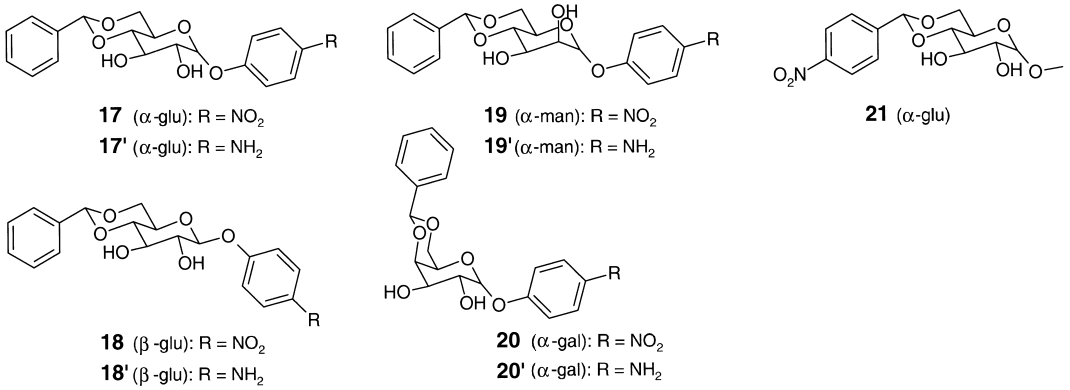

Scheme 5. Sugar-based gelators.

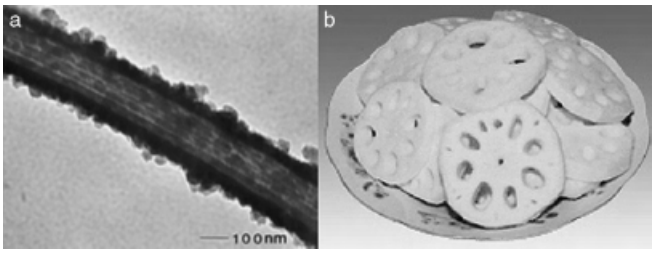

Figure 21. a) TEM image of a silica fiber with several channels obtained after transcription of the gel of **18′** in ethanol; b) sliced lotus root. Reproduced with permission from ref. [95, 96].

popular ingredient in Japanese cuisine. The variation in structure is thought to occur because the intermolecular hydrogen-bonding interactions of β-glucose derivatives are stronger than those of α-glucose derivatives.[98] This result means that the gel fibers of **17′** form no or only thin bundles, whereas the gel fibers of **18′** form large bundles.[99] After transcription, the separate channels resulting from the individual fibers of the bundles can still be observed in the silica obtained using **18′**.

The α-glucose-based gelator **21** was shown to gelate a range of organic solvents as well as water. Recently, our research group demonstrated that **21** can form fibers in two different ways.[100] In organic solvents, the polar sugar parts can form a chain of intermolecular hydrogen bonds upon stacking, which exposes the relatively apolar aromatic parts to the solvent. In water, the molecules are presumed to form fibers through π-π stacking, thus exposing the sugar parts to the solvent.[101] The stacking model indicated that other aromatic additives might also be incorporated into the fibers through stacking. The additive of choice was benzylamine, a catalyst frequently used in the silica-transcription process. Benzylamine can interact with the nitrobenzene moieties through π-π stacking or through hydrogen-bonding interactions. Formation of the hydrogel of **21** in the presence of one equivalent of benzylamine, followed by transcription and subsequent calcination, resulted in the isolation of hollow silica fibers, as observed by TEM. Clearly, the gel fibers acted as a template for silica transcription, even though they lacked the cationic charges or amine moieties hitherto deemed indispensable. Additional experiments indeed proved that part of the added benzylamine (about 20%) is incorporated into the gel fibers through π-π stacking and hydrogen-bonding interactions. This incorporation results in the template structure now possessing enough amine moieties to enable transcription. The major part (80%), which stays in solution, still acts as the traditional catalyst in the transcription process. Control experiments involving other catalysts unable to interact strongly with the gelator molecules did not result in transcription, thus proving the necessity of having good compatibility between the catalyst and gelator.[102] Since cationic charges and amine moieties are no longer prerequisites for gelator structures, these findings increase the variety of gelators that can be used for transcription into inorganic materials; compounds bearing a moiety that can interact strongly with a catalyst can now also be used.

As previously discussed, the gelator (or one of the gelators) used in an organogel system for transcription generally possesses either a positive charge or a hydrogen-bonding amine moiety.[103] The cationic charge or the amine group interacts with the negatively charged silica precursor species, while the catalyst is present in solution and promotes the TEOS hydrolysis and polycondensation reactions. One of the frequently used catalysts, benzylamine, is not only capable of catalysis, but can also interact with negatively charged silica precursors through hydrogen-bond formation (as can any other amine). Consequently, the idea arose to immobilize the benzylamine as part of the gelator structure to see whether it would be possible to transcribe an organogel without using a catalyst in solution. Cholesterol derivative **22** (Scheme 6),

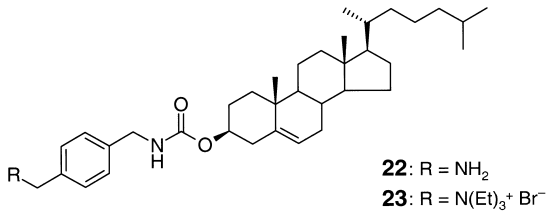

Scheme 6. Molecular structure of cholesterol derivatives **22** and **23**.

which bears a benzylamine moiety, was synthesized and proved capable of gelating a number of alcoholic solvents. Transcription in the absence of additional catalyst indeed resulted in silica consisting of hollow fibers after calcination, thus proving that the organogel fibers had indeed functioned both as a template and as a catalyst. Reference experiments using the cationic analogue **23** did not result in transcription, which proved that the transcription of the organogel of **22** did not just occur as a result of attractive forces between fibers and silica precursor species, but was indeed caused by the combined catalytic and attractive effect of the benzylamine moieties.[104]

The last two examples discussed in this section clearly show that the transcription of organogels has evolved very rapidly since the first publication in 1998.[62] The presence of either a positive charge or an amine group in the gelator structure and the use of a catalyst in solution, until recently deemed indispensable, have now been shown to be limitations that can be overcome by ingenious template design. One of the striking advantages of using organogels as templates for the formation of inorganic materials is the rich variety of organogel structures, and therefore of the resultant inorganic materials, available. Organogel morphologies, like the surfactant-based templates, are strongly based on noncovalent interactions, which is the main reason for the multitude of shapes that can be observed. To date, fibrous, (multilayer) spherical, lamellar, rolled-paper, tubular, as well as both enantiomeric forms of (hollow) helical silica have been obtained, and more shapes will undoubtedly follow.[105] Although the attention in this review is focused on the formation of pure inorganic materials, the organogel–inorganic hybrid materials (normally calcined to give the pure inorganic structures) also offer a wealth of interesting

properties. In the future, these hybrids may even prove to be more useful than either the organogel or the inorganic materials by themselves.

5. Carbon Nanotubes

Shortly after the successful laboratory synthesis of fullerenes,[106] carbon nanotubes (CNTs) were discovered.[107] They have since been the topic of a rapidly growing number of publications.[108] As a consequence of their shape, CNTs have been frequently used as organic templates for the formation of inorganic tubular or needlelike structures. In many cases the goal of the research is the generation of a hybrid CNT–inorganic material, which may have applications in fields such as nanotechnology[108] or energy storage.[109] Since transcription is often not the main focus of those applications, the final product frequently exists of CNTs with small metal particles deposited on either their in- or outsides.[109,110]

Not long after the discovery of CNTs it was predicted that they might be filled with liquid by capillary suction;[111] indeed, one year later this prediction was validated.[112] Heating a mixture of (opened) CNTs and lead nanoparticles above the melting point of the metal resulted in the filling of several tubes by the predicted capillary forces (Figure 22).

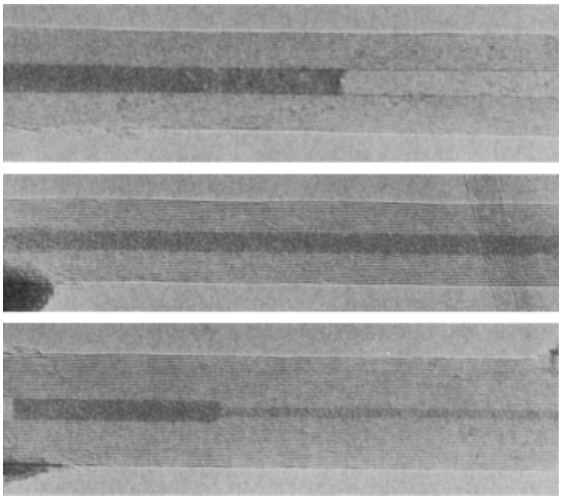

Figure 22. TEM image of carbon nanotubes filled to a length of tens of nanometers with solid (dark contrast). The distance between parallel fringes is 0.34 nm. Reproduced with permission from ref. [112].

The major drawback of this method, however, is that filling of the CNTs occurred only when the lead droplets were positioned on top of the open ends of the tubes.[112] By heating a mixture of ground V_2O_5 and CNTs, Ajayan et al. succeeded in filling the channels of the tubes with the metal oxide, again through capillary forces. Moreover, the capillary forces also resulted in the (thin) coating of the outer surfaces of some of the CNTs with V_2O_5.[113] Green and co-workers reported the chemical etching of the caps of CNTs in the presence of several metal salts. Capillary forces caused the nanotubes to fill with the metal salt solution upon opening the CNTs by this procedure. TEM investigation of the sample after drying and annealing proved the presence of short metal bars inside the CNTs. Around 50% of the CNTs were partially filled by using this method.[114] Filled CNTs have also been obtained by forming the CNTs in an arc discharge with metals present in situ.[115–118] However, since both the CNT and metal core are formed in a single process, this latter method cannot be classified as transcription, as the template was not present before the metal core was formed.

Several research groups used a two-step process to fabricate CNTs, a certain percentage of which became filled with metal rods (Figure 23). The first step involves the

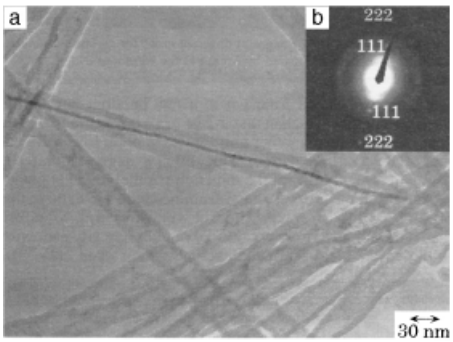

Figure 23. a) TEM image of a carbon nanotube in which a Ni wire is found; b) electron diffraction pattern. Reproduced with permission from ref. [122].

deposition of carbon on the inside walls of nanochannels present in a specially prepared oxide film[119] or membrane.[120] The second step involves the loading of the channels with the metal of choice through an evaporation process, followed by either reduction through heat treatment or chemical reduction. After this reduction, the CNT–metal composites can be liberated by dissolving the carrier material. Several inorganic materials have been incorporated into CNTs by this approach (for example, Pt, Ni, NiO).[121–123] In this method the deposited carbon on the inside of the channels functions as the template on which the metal structures grow. However, there are no direct interactions between the CNTs and the metal that bring about the actual transcription. The drawback of this method is that it is performed on a single oxide layer, and hence the amount of material that is formed is very small. Naturally, the drawback of all the methods mentioned in this section is that only one kind of structure can be produced, namely, the wire structure.

Unlike the examples mentioned so far, many papers describe the templated formation of inorganic structures around, rather than inside, the CNTs. Rao and co-workers reported a simple methodology to coat the outside of CNTs with SiO_2, Al_2O_3, and V_2O_5.[124] In their study CNTs (either pristine or acid-treated) were temporarily immersed in a solution containing the precursor of the inorganic material (namely, TEOS, aluminum isopropoxide, or V_2O_5 gel), followed in some cases by several washing steps, and finally heat treatment to polymerize the inorganic precursor. It

proved possible to produce SiO_2-coated CNTs doped with transition-metal oxides by adding metal salts to the solution containing TEOS. Burning off the CNTs by strongly heating the hybrid tubes resulted in the isolation of relatively well-preserved, inorganic, hollow tubes. Better results were obtained for the acid-treated CNTs[125] than for the pristine ones. The same authors later reported the use of acid-treated CNTs as templates for the formation of ZrO_2, V_2O_5, WO_3, MoO_3, Sb_2O_5, MoO_2, RuO_2, and IrO_2 nanorods or tubes.[126,127]

Recently, Kroto and co-workers also described a method to obtain SiO_2-coated CNTs. First multi-walled carbon nanotubes were coated with the polyelectrolyte polyethylimine (PEI), thus creating positive charges on the tube surface; the coated CNT solution was then mixed with a prehydrolyzed TEOS solution containing negatively charged silica precursor moieties. Silica particles are deposited onto the CNT surface, as a result of charge interactions, which leads to the formation of a relatively uniform SiO_2 coating.[128,129] No attempts were made to remove the CNT template. Kroto and co-workers also reported the formation of NbS_2-coated CNTs through exposure of CNTs to a solution of $NbCl_4$, followed by heat treatment under a H_2S atmosphere. The multilayered NbS_2 could be observed on 5–10% of the CNTs (Figure 24).[130]

As mentioned before, the final product in the formation of CNT–inorganic hybrid materials often consists of CNTs with small metal particles deposited either on the in- or outside of the tubes. In some cases, however, a high load of metal particles results in a semicontinuous metal coating and, therefore, actual transcription of the CNT into a metal fiber. Lin and co-workers reported the formation of CNTs coated with Cu by exposure of CNTs to a solution containing a mixture of Cu nanoparticles and a Cu salt. The spongy product that was obtained consisted of microsized Cu fibers with diameters ranging from 100 nm to 5 μm, and lengths up to hundreds of micrometers; however, removal of the templating CNTs was not attempted.[131] Similar results were obtained by Fitzmaurice and co-workers, who used gold nanocrystals (6 ± 1 nm) in combination with CNTs. Heating the coated CNTs to 300 °C for 120 s caused the gold nanocrystals to fuse to form a continuous Au nanowire around the CNT core.[132] Again, no removal of the template was attempted.

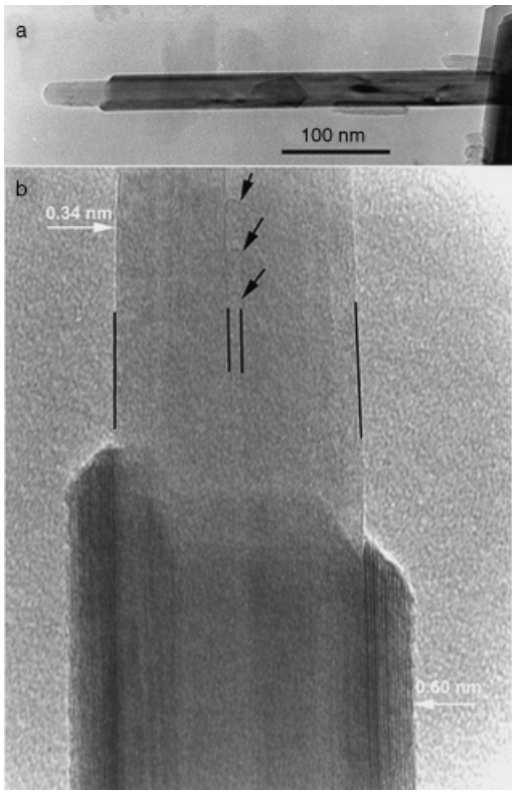

Figure 24. a) TEM image of a NbS_2-coated carbon nanotube; b) enlargement: the distance between the NbS_2 layers on the surface is ca. 0.6 nm, the distance between the carbon layers at the center is ca. 0.34 nm; the tube wall and the hollow core of the carbon template are marked by the vertical lines; and several closed inner layers of the carbon nanotube are marked by arrows. Reproduced with permission from ref. [130].

Besides the filling and coating of CNTs, a third transcription process has been described: In 1995, Lieber and co-workers reported the synthesis and characterization of carbide nanorods. CNTs were treated with volatile oxide and halide species and gave rise to the formation of solid carbide nanorods of TiC (Figure 25), NbC, Fe_3C, SiC, and BC_x in high yields. The rods, many of which show crystalline properties, have diameters between 2 and 30 nm and lengths of up to 20 μm.[133] A mechanistic study has shown that the reaction proceeds initially through the formation of a thin, uniform carbide coating and that further reaction proceeds by inward growth of this coating, thus consuming the CNT template until a solid nanotube is formed.[134] Many other papers employing this so-called "carbon nanotube confined" reaction have been published since this first example, thus widening the range of inorganic materials that can be obtained (for example, GaN,[135] α- and β-Si_3N_4, Si_2N_2O,[136] GeO_2[137]). It has to be noted, however, that since the template is consumed, this process cannot technically be classified as transcription using the definition applied in this article.

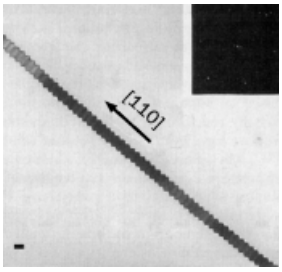

Figure 25. TEM image of a carbon nanorod with regular sawtooth morphology obtained after treatment of carbon nanotubes with volatile oxide and halide species. The scale bar corresponds to 20 nm. Reproduced with permission from ref. [133].

Clearly, the use of CNTs has led to many examples of successful transcription. Although it has shown excellent results for the formation of linear structures, the clear disadvantage of this approach is the lack of structural variety that can be obtained. Tubes and needles/rods are indeed the only two shapes that can be achieved.

6. Organic Crystals

Organic crystals are reproducible structures that are obtainable in relatively large quantities, and in several shapes and sizes, which makes them excellent candidates for transcription into inorganic materials. The first report of organic crystals being used as templates was published in 1995 by

Nakamura and Matsui.[138] They described the formation of hollow silica tubes with square-shaped cross-sections in an ethanolic TEOS solution containing DL-tartaric acid and ammonium hydroxide. It was postulated that formation of the silica tubes (with lengths of 200–300 μm, outer diameters of about 0.8–1.0 μm, and inner diameters of 0.02–0.8 μm) had been templated by chains of hydrogen-bonded DL-tartaric acid molecules. Mann and co-workers later showed that crystals of ammonium DL-tartrate that formed upon the addition of ammonium hydroxide solution to the TEOS/tartaric acid solution acted as the templates. The regularly spaced ammonium ions present in the side faces of the crystals can interact with silicate anions, thus initiating the transcription process (Figure 26). Similar silica structures could be

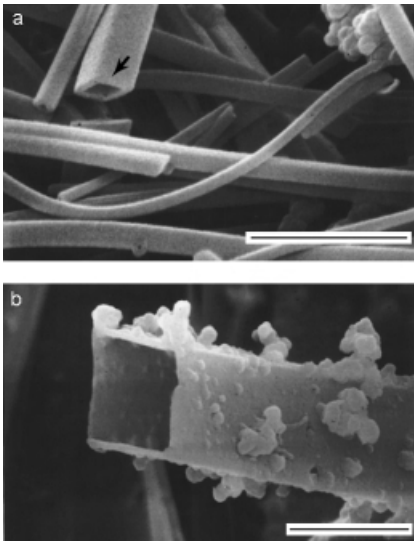

Figure 26. SEM images of a) silica tubes with rhomboidal central channels (scale bar corresponds to 2 μm); b) a silica tube with a large geometric channel and thin walls contaminated with aggregates of colloidal silica (the scale bar corresponds to 5 μm). Reproduced with permission from ref. [139].

obtained using the separate D and L enantiomers, as well as ammonium oxalate.[139] Miyaji et al. reported the formation of TiO_2, ZrO_2, Nb_2O_5, and Ta_2O_5 nanotubes in which they employed the same ammonium DL-tartrate crystal template.[140] Wark and co-workers made use of a similar system, in which crystals of a platinum salt containing ammonium groups $[Pt(NH_3)_4(HCO_3)_2]$ acted as the template for the formation of SiO_2 and TiO_2 nanotubes. The template could be removed through calcination, and resulted in hollow nanotubes possessing square-shaped cross-sections, and with encapsulated platinum clusters.[141]

The advantages of this method are that the template material can be cheap, thus allowing the large-scale formation of the inorganic materials. However, since the morphologies that can be obtained depend on the crystal template, only needles and polygons can be obtained, most of them having very similar shapes.

7. Biomaterials

Since nature is a great source of inspiration for the formation of well-defined, structured inorganic materials, it seems only logical to use (bio)organic templates taken from nature to fabricate inorganic materials; materials that may one day compete with those found in nature itself. Indeed several research groups (including our own) have employed natural templates for such a purpose. Since the presence of cationic charges in the template facilitates the transcription process (see Section 4),[62] natural proteins that also carry positive charges were investigated. Transcription of such species should result in the replication of the three-dimensional structure of the protein into the inorganic material. Collagen was found to satisfy the essential requirements in that it becomes positively charged at a pH value lower than 8 and it can form an interesting fibrous superstructure that possesses a periodic groove (every 67 nm of the fiber). Addition of TEOS to a buffered saline solution containing collagen fibers indeed resulted in the formation of silica fibers (Figure 27 a). The gnarled structure with a period of 60–80 nm was formed as a result of the periodicity present in the templating collagen fibers. TEM studies showed the silica fibers to possess an inner tube consisting of a bundle of individual channels (Figure 27 b); the latter correspond to the individual fibers which make up the collagen bundles, and thus demonstrate the accuracy with which the transcription takes place. These individual channels can still be observed in the pure inorganic material obtained after calcination of the hybrid.[142]

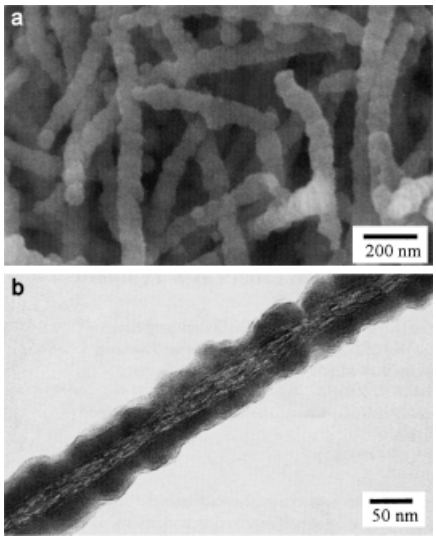

Figure 27. a) SEM image of silica fibers obtained after transcription of collagen; b) TEM image of one such fiber showing that the inner tube contains many individual channels. Reproduced with permission from ref. [142].

Transcription of a single biopolymer strand was accomplished by Braun et al. in 1998. They were able to bridge two gold electrodes with a single strand of derivatized DNA. Exchange of the DNA Na^+ counterions for Ag^+ ions followed

by reduction of the latter with hydroquinone resulted in the formation of small Ag particles on the DNA template. More silver was deposited on this DNA–Ag strand by standard photographic procedures, and resulted in the formation of a thin wire (length: 12 μm, diameter: ca. 100 nm) built up of small silver grains (30–50 nm). Thinner wires (25 nm) could also be produced by this method, but the silver coating was shown to be discontinuous, with some gaps between the silver grains.[143]

The well-known tobacco mosaic virus (TMV) is an extremely stabile virion, consisting of 2130 identical protein subunits, which self-assemble around a single strand of RNA to form a hollow protein tube with a length of 300 nm, an outer diameter of 18 nm, and an inner diameter of 4 nm.[144] The outer and inner surfaces of the tube are covered in charged amino acid residues,[145] which makes the TMV an excellent candidate for transcription into all sorts of inorganic materials. Indeed, the addition of a solution of TMV to an acidic ethanolic solution of TEOS gave rise to the formation of a silica layer around the TMV tubes. TEM pictures clearly showed the coated TMV particles, with silica walls of about 3 nm. Many of the TMV particles had self-assembled end-to-end to give rise to very long (>1 μm) silica–TMV tubes (Figure 28). Several other materials could be deposited onto the TMV surface (iron oxides, CdS, PbS), however, in none of these cases were the coated TMV particles calcined to give the pure inorganic product.[146]

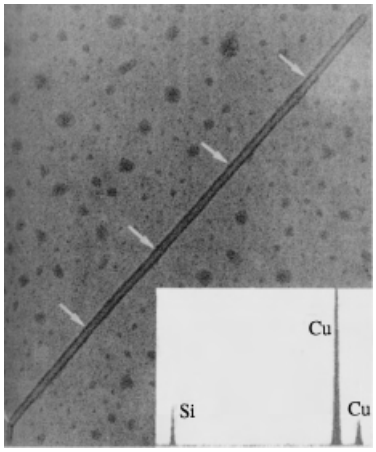

Figure 28. TEM image of a tubelike silica-coated tobacco mosaic virus (TMV). The arrows mark the ends of five individual TMV particles, each 300 nm in length. Inset: energy dispersive X-ray spectrum showing the Si peak (the Cu peaks are from the TEM grids).

In later work, the tendency of TMV to form nematic liquid crystals at high concentrations was used in the formation of mesostructured silica. The controlled hydrolysis of a mixture of a liquid crystalline gel of TMV particles and the silica precursors TEOS and aminopropyltriethoxysilane (APTES) gave a mineralized gel that, after having been crushed, was observed with TEM. The main part of the fragments were shown to consist of hexagonally ordered TMV fibers in a silica matrix. Reducing the amount of TEOS and APTES used in the transcription resulted in the formation of large numbers of spherical silica nanoparticles of peculiar morphology. The particles with diameters of 100–150 nm consisted of an array of 50-nm long, rod-shaped TMV fragments arranged radially around a silica core approximately 35 nm in diameter (Figure 29). Many of the nanoparticles were attached to a single silica tube arising from the

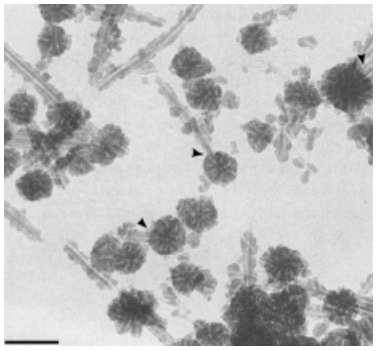

Figure 29. TEM image of silica–TMV nanoparticles with radially patterned interiors, together with threadlike mesostructures. The arrows denote nanoparticles with surface-attached threads. The scale bar corresponds to 200 nm.

more complete transcription of one of the TMV entities protruding from the silica core. Calcination of the hybrid material resulted in nanoparticles of similar size containing radially arranged channels. The origin for the formation of the spherical particles lies in the disruption of the liquid-crystalline phase as a result of the formation of small silica particles; however, the exact mechanism is not yet fully understood.[147]

Davis et al. described the use of a bacterial superstructure. By slowly drawing a macroscopic thread from a web culture of *B. subtillis*, individual multicellular filaments were coaligned in such a fashion that they resemble the hexagonal packing of surfactant cylinders in the surfactant–water phase. The fiber was air dried and then dipped into an aqueous sol of silica nanoparticles, which caused the fiber to swell to its original diameter. Upon drying, the silica particles, which are mainly located between the individual filaments, are compacted to give an extended organic framework. Removal of the organic template by controlled heating resulted in an inorganic fiber consisting of an organized array of uniform-sized 0.5-μm wide silica-walled channels parallel to the fiber axis.[148]

Instead of using relatively small biomaterials, Zink and co-workers employed arrays of yeast cells to pattern a surface by sol–gel transcription. A silicate sol mixed with a solution of yeast was used to dip-coat a microscope slide, which resulted in a silicate film with a pattern of yeast cells (Figure 30). A special treatment of the yeast cells guaranteed the presence of only small irregularities arising from different cell sizes. Arrays such as these are thought to have applications in screening genomic libraries.[149] Recently, recombinant bacteria, although being more sensitive to environmental conditions than their wild counterparts, have also been encapsulated in silicate films.[150] Undoubtedly these kinds of bio-inorganic combinations will continue to develop into interesting materials with fascinating applications.

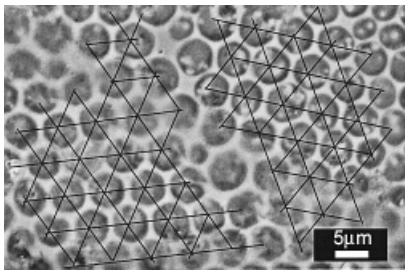

Figure 30. Photograph (at 1000x magnification) of a silicate film containing a monolayer of hexagonal close-packed yeast cells. The ordered regions are indicated by lines. Reproduced with permission from ref. [149].

Rather than using single cells, Mann and co-workers used a piece of cuttlebone, obtained from *Sepia officinalis* (commonly known as the cuttlefish), as a template for a novel inorganic structure. The cuttlebone is a macroporous structure consisting of aragonite ($CaCO_3$) and β-chitin. It can be demineralized to leave only the β-chitin framework, after which it can be remineralized by immersing it in a sodium silicate solution, followed by several immersions in ethanol/water and ethanol/ammonium hydroxide mixtures. Calcination of the hybrid material resulted in the isolation of the pure inorganic material possessing the chamberlike architecture of the cuttlebone.[151] Liu and co-workers reported the mineralization of wood tissue which resulted in the formation of a silica replica of the cellular structures present in poplar and pine. The template in this experiment was immersed in a solution containing prehydrolyzed TEOS and surfactant; subsequent calcination resulted in the isolation of the pure inorganic material (Figure 31). It was found that the presence of surfactant in the original TEOS solution was crucial for obtaining the intact inorganic replica. The continuous nanochannels found in the silica resulting from the presence of surfactant aggregates during the transcription process allowed the gaseous combustion products to exit the structure during calcination and leave it intact. Performing the transcription of the wood structure without using surfactants resulted in inorganic materials that collapsed after calcination.[152] Several more methods to convert wood into a variety of ceramic materials have been described by Greil et al.[153]

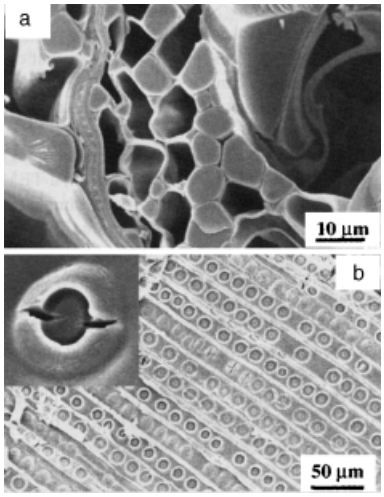

Figure 31. SEM images of surfactant-templated wood samples after calcination: a) poplar (cross-section); b) pine (longitudinal direction). Inset: pit structure.

Clearly, the use of biomaterials as templates can greatly facilitate the formation of all sorts of inorganic structures and materials—the materials found in nature are, after all, generally the result of millions of years of evolution and specialization. However, for the same reasons these materials can only be used as found, and therefore any desired alterations to these template structures can only be minor or not made at all (for example, changing the stereochemical configuration).

8. Summary and Outlook

In this review, a wide range of examples of organic templates and methods for the formation of morphologically interesting inorganic materials has been presented. In general, the variety of inorganic forms that can be obtained depends very strongly on whether the organic template is of a covalent or noncovalent nature. Synthetic polymers, for example, are practically unrivaled as templates for hollow spherical shapes, and carbon nanotubes are the ideal choice for the synthesis of many tubular structures. However, these two types of templates lack the shape versatility intrinsic to noncovalent, self-assembled systems. In this respect, surfactants can provide not only spherical and tubular transcribable cores, but can also self-organize in such a way as to promote the formation of wirelike structures or extended networks resembling some skeletal architectures found in nature. Organogels present an even wider variety of morphologies, such as fibrous, tubular, ribbonlike, lamellar, and hollow spherical, that have been transcribed so far. Moreover, helical forms of some organogel templates have been shown to induce chirality in the corresponding inorganic materials. Although organic molecules can crystallize in a wide range of forms, up until now only two examples of organic crystal-templated materials have been described, which leaves much room for development in this particular area of research. The structural complexity that can be achieved by using biomaterials as templates for transcription processes is the major advantage of these particular systems. However, suitable biotemplates are often difficult to obtain and modifications to their morphologies, if desired, are nearly impossible to implement.

Although the most frequently used material for template coating is silica, either deposited as nanoparticles or grown in situ by hydrolysis and polycondensation of TEOS, many other inorganic compounds are now also being employed for transcription processes, thus widening the scope of applications of the resultant materials. The choice of transcription procedures remains mostly limited to the sol–gel process and the layer-by-layer method. Both of these procedures have been extensively studied and can be utilized to produce finely tuned inorganic structures in a reproducible manner.

Prospects for the future include the development of novel transcription methodologies, as well as the creation of new transcribable templates which present a greater degree of structural complexity or can give rise to extended, patterned architectures. One of the principal challenges remaining consists of finding novel methodologies for obtaining transcribed structures with a high degree of order at the 2D or 3D level.

Received: April 19, 2002 [A532]

[1] For recent reviews, see a) N. K. Raman, M. T. Anderson, C. J. Brinker, *Chem. Mater.* **1996**, *8*, 1682 – 1701; b) S. Mann, S. L. Burkett, S. A. Davis, C. E. Fowler, N. H. Mendelson, S. D. Sims, D. Walsh, N. T. Whilton, *Chem. Mater.* **1997**, *9*, 2300 – 2310; c) L. A. Estroff, A. D. Hamilton, *Chem. Mater.* **2001**, *13*, 3227 – 3235; d) S. A. Davis, M. Breulmann, K. H. Rhodes, B. Zhang, S. Mann, *Chem. Mater.* **2001**, *13*, 3218 – 3226; e) R. A. Caruso, M. Antonietti, *Chem. Mater.* **2001**, *13*, 3272 – 3282.

[2] For recent reviews, see a) J. H. van Esch, B. L. Feringa, *Angew. Chem.* **2000**, *112*, 2351 – 2354; *Angew. Chem. Int. Ed.* **2000**, *39*, 2263 – 2265; b) D. J. Abdallah, R. G. Weiss, *Adv. Mater.* **2000**, *12*, 1237 – 1247; c) G. F. Swiegers, T. J. Malefetse, *Chem. Rev.* **2000**, *100*, 3483 – 3538; d) D. T. Bong, T. D. Clark, J. R. Granja, M. R. Ghadiri, *Angew. Chem.* **2001**, *113*, 1016 – 1041; *Angew. Chem. Int. Ed.* **2001**, *40*, 988 – 1011; e) L. J. Prins, D. N. Reinhoudt, P. Timmerman, *Angew. Chem.* **2001**, *113,* 2446 – 2492; *Angew. Chem. Int. Ed.* **2001**, *40*, 2382 – 2426; f) B. J. Holliday, C. A. Mirkin, *Angew. Chem.* **2001**, *113*, 2076 – 2097; *Angew. Chem. Int. Ed.* **2001**, *40*, 2022 – 2043.

[3] P. A. Buining, B. M. Humbel, A. P. Philipse, A. J. Verkleij, *Langmuir* **1997**, *13*, 3921 – 3926.

[4] M. Giersig, T. Ung, L. M. Liz-Márzan, P. Mulvaney, *Adv. Mater.* **1997**, *9*, 570 – 575.

[5] M. Kishida, T. Tago, T. Hatsuta, K. Wakabayashi, *Chem. Lett.* **2000**, 1108 – 1109.

[6] S. Santra, R. Tapec, N. Theodoropoulou, J. Dobson, A. Hebart, W. Tan, *Langmuir* **2001**, *17*, 2900 – 2906.

[7] For a review on the templated formation of porous silica, see ref. [1 a].

[8] N. Kawahashi, E. Matijević, *J. Colloid Interface Sci.* **1991**, *143*, 103 – 110.

[9] K. W. Gallis, C. C. Landry, *Adv. Mater.* **2001**, *13*, 23 – 26.

[10] Y. Lu, Y. Yin, Y. Xia, *Adv. Mater.* **2001**, *13*, 271 – 274.

[11] C. Sanchez, G. J. de A. A. Soler-Illia, F. Ribot, T. Lalot, C. R. Mayer, V. Cabuil, *Chem. Mater.* **2001**, *13*, 3061 – 3083, and references therein.

[12] P. Innocenzi, G. Brusatin, *Chem. Mater.* **2001**, *13*, 3126 – 3139, and references therein.

[13] a) F. Caruso, *Adv. Mater.* **2001**, *13*, 11 – 22; b) F. Caruso, *Chem. Eur. J.* **2000**, *6*, 413 – 419.

[14] M. L. Breen, A. D. Dinsmore, R. H. Pink, S. B. Qadri, B. R. Ratna, *Langmuir* **2001**, *17*, 903 – 907.

[15] A. Imhof, *Langmuir* **2001**, *17*, 3579 – 3585, and references therein.

[16] H. Shiho, N. Kawahashi, *Colloid Polym. Sci.* **2000**, *278*, 270 – 274.

[17] B. zu Putlitz, K. Landfester, H. Fischer, M. Antonietti, *Adv. Mater.* **2001**, *13*, 500 – 503.

[18] H. Bamnolker, B. Nitzan, S. Gura, S. Margel, *J. Mater. Sci. Lett.* **1997**, *16*, 1412 – 1415.

[19] F. Caruso, M. Spasova, A. Susha, M. Giersig, R. A. Caruso, *Chem. Mater.* **2001**, *13*, 109 – 116.

[20] F. Caruso, R. A. Caruso, H. Möhwald, *Science* **1998**, *282*, 1111 – 1114, and references therein.

[21] a) F. Caruso, R. A. Caruso, H. Möhwald, *Chem. Mater.* **1999**, *11*, 3309 – 3314; b) F. Caruso, H. Lichtenfeld, M. Giersig, H. Möhwald, *J. Am. Chem. Soc.* **1998**, *120*, 8523 – 8524; c) F. Caruso, H. Möhwald, *Langmuir* **1999**, *15*, 8276 – 8281.

[22] X. D. Wang, W. L. Yang, Y. Tang, Y. J. Wang, S. K. Fu, Z. Gao, *Chem. Commun.* **2000**, 2161 – 2162.

[23] R. A. Caruso, A. Susha, F. Caruso, *Chem. Mater.* **2001**, *13*, 400 – 409.

[24] L. Tosheva, J. Sterte, *Chem. Commun.* **2001**, 1112 – 1113.

[25] F. Iskandar, Mikrajuddin, K. Okuyama, *Nano Lett.* **2001**, *1*, 231 – 234.

[26] M. Bognitzki, H. Hou, M. Ishaque, T. Frese, M. Hellwig, C. Schwarte, A. Schaper, J. H. Wendorff, A. Greiner, *Adv. Mater.* **2000**, *12*, 637 – 640.

[27] K. J. C. van Bommel, J. H. Jung, S. Shinkai, *Adv. Mater.* **2001**, *13*, 1472 – 1476, and references therein.

[28] T. Coradin, E. Mercey, L. Linsnard, J. Livage, *Chem. Commun.* **2001**, 2496 – 2497.

[29] J. N. Cha, G. D. Stucky, D. E. Morse, T. J. Deming, *Nature* **2000**, *403*, 289 – 292.

[30] K. Shimizu, J. Cha, G. D. Stucky, D. E. Morse, *Proc. Natl. Acad. Sci. USA* **1998**, *95*, 6234 – 6238.

[31] Y. Zhou, K. Shimizu, J. N. Cha, G. D. Stucky, D. E. Morse, *Angew. Chem.* **1999**, *111,* 826 – 828; *Angew. Chem. Int. Ed.* **1999**, *38*, 780 – 782 and references therein.

[32] C. T. Kresge, M. E. Leonowicz, W. J. Roth, J. C. Vartuli, J. S. Beck, *Nature* **1992**, *359*, 710 – 712.

[33] O. R. Anderson in *Biomineralization in Lower Plants and Animals, Vol. 30* (Eds.: B. S. C. Leadbeater, R. Riding), Oxford University Press, Oxford, **1986**, pp. 375 – 391.

[34] S. Mann, G. A. Ozin, *Nature* **1996**, *382*, 313 – 318.

[35] D. Walsh, S. Mann, *Nature* **1995**, *377*, 320 – 323.

[36] D. Walsh, B. Lebeau, S. Mann, *Adv. Mater.* **1999**, *11*, 324 – 328.

[37] D. Walsh, J. D. Hopwood, S. Mann, *Science* **1994**, *264*, 1576 – 1578.

[38] P. S. Singh, K. Kosuge, *Chem. Lett.* **1998**, 101 – 102.

[39] S. S. Kim, W. Zhang, T. J. Pinnavaia, *Science* **1998**, *282*, 1302 – 1305.

[40] P. T. Tanev, Y. Liang, T. Pinnavaia, *J. Am. Chem. Soc.* **1997**, *119*, 8616 – 8624.

[41] Y. Lu, H. Fan, A. Stump, T. L. Ward, T. Rieker, C. J. Brinker, *Nature* **1999**, *398*, 223 – 226.

[42] a) D. H. W. Hubert, M. Jung, P. M. Frederik, P. H. H. Bomans, J. Meuldijk, A. L. German, *Adv. Mater.* **2000**, *12*, 1286 – 1290; b) D. H. W. Hubert, M. Jung, A. L. German, *Adv. Mater.* **2000**, *12*, 1291 – 1294.

[43] H.-P. Lin, Y.-R. Cheng, C.-Y. Mou, *Chem. Mater.* **1998**, *10*, 3772 – 3776.

[44] S. Oliver, A. Kuperman, N. Coombs, A. Lough, G. A. Ozin, *Nature* **1995**, *378*, 47 – 50, and references therein.

[45] K. Katagiri, K. Ariga, J.-i. Kikuchi, *Chem. Lett.* **1999**, 661 – 662.

[46] S. Baral, P. Schoen, *Chem. Mater.* **1993**, *5*, 145 – 147.

[47] D. D. Archibald, S. Mann, *Nature* **1993**, *364*, 430 – 433.

[48] a) M. Adachi, T. Harada, M. Harada, *Langmuir* **1999**, *15*, 7097 – 7100; b) M. Adachi, T. Harada, M. Harada, *Langmuir* **2000**, *16*, 2376 – 2384; c) M. Harada, M. Adachi, *Adv. Mater.* **2000**, *12*, 839 – 841.

[49] M. Niederberger, H.-J. Muhr, F. Krumeich, F. Bieri, D. Günther, R. Nesper, *Chem. Mater.* **2000**, *12*, 1995 – 2000.

[50] H. Matsui, S. Pan, B. Gologan, S. H. Jonas, *J. Phys. Chem. B* **2000**, *104*, 9576 – 9579.

[51] L. Qi, J. Ma, H. Cheng, Z. Zhao, *J. Phys. Chem. B* **1997**, *101*, 3460 – 3463.

[52] P. Terech, R. G. Weiss, *Chem. Rev.* **1997**, *97*, 3133 – 3159.

[53] S. Shinkai, K. Murata, *J. Mater. Chem.* **1998**, *8*, 485 – 495.

[54] O. Gronwald, S. Shinkai, *Chem. Eur. J.* **2001**, *7*, 4328 – 4334.

[55] V. Jenning, A. Gysler, M. Schafer-Korting, S. H. Gohla, *Eur. J. Pharm. Biopharm.* **2000**, *49*, 211 – 218.
[56] C. Bergeret-Galley, X. Latouche, Y. G. Illouz, *Aesthet. Plast. Surg.* **2001**, *25*, 249 – 255.
[57] D. Duke, J. M. Grevelink, *Dermatol. Surg.* **1998**, *24*, 201 – 206.
[58] S. H. Hyon, W. I. Cha, Y. Ikada, M. Kita, Y. Ogura, Y. Honda, *J. Biomater. Sci. Polym. Ed.* **1994**, *5*, 397 – 406.
[59] L. Alvord, J. Court, T. Davis, C. F. Morgan, K. Schindhelm, J. Vogt, L. Winterton, *Optometry Vision Sci.* **1998**, *75*, 30 – 36.
[60] W. Kubo, K. Murakoshi, T. Kitamura, Y. Wada, K. Hanabusa, H. Shirai, S. Yanagida, *Chem. Lett.* **1998**, 1241 – 1242.
[61] K. Hanabusa, K. Hiratsuka, M. Kimura, H. Shirai, *Chem. Mater.* **1999**, *11*, 649 – 655.
[62] Y. Ono, K. Nakashima, M. Sano, Y. Kanekiyo, K. Inoue, J. Hojo, S. Shinkai, *Chem. Commun.* **1998**, 1477 – 1478.
[63] For a review on the gelation of liquids by cholesterol derivatives, see ref. [53]. The aggregation structure of these gels has been studied by using small angle X-ray scattering: K. Sakurai, Y. Ono, J. H. Jung, S. Okamoto, S. Sakurai, S. Shinkai, *J. Chem. Soc. Perkin Trans. 2* **2001**, 108 – 112.
[64] K. Murata, Ph. D. Thesis, Graduate School of Engineering, Kyushu University, **1997**.
[65] A. Stein, B. J. Melde, R. Schroden, *Adv. Mater.* **2000**, *12*, 1403 – 1419, and references therein.
[66] Typical drying and calcination steps for organogel transcription systems consist of: 3–7 days under vacuum at RT (optional), 2 h at 100–200 °C (depending on the solvent) under N_2, 2 h at 500 °C under N_2, 4 h at 500 °C under aerobic conditions.
[67] C. J. Brinker, G. W. Scherer, *Sol-Gel Science*, Academic Press, San Diego, **1990**.
[68] Y.-C. Lin, R. G. Weiss, *Macromolecules* **1987**, *20*, 414 – 417.
[69] Y. Ono, K. Nakashima, M. Sano, J. Hojo, S. Shinkai, *Chem. Lett.* **1999**, 1119 – 1120.
[70] Y. Ono, K. Nakashima, M. Sano, J. Hojo, S. Shinkai, *J. Mater. Chem.* **2001**, *11*, 2412 – 2419.
[71] Y. Ono, Y. Kanekiyo, K. Inoue, J. Hojo, S. Shinkai, *Chem. Lett.* **1999**, 23 – 24.
[72] This experiment was carried out in BuOH, which necessitated the use of benzylamine as a catalyst for TEOS polycondensation. It also acted as the catalyst in all experiments where acetic acid was used as the solvent.
[73] J. H. Jung, Y. Ono, S. Shinkai, *J. Chem. Soc. Perkin Trans. 2* **1999**, 1289 – 1291.
[74] J. H. Jung, Y. Ono, S. Shinkai, *Langmuir* **2000**, *16*, 1643 – 1649.
[75] J. H. Jung, Y. Ono, S. Shinkai, *Chem. Lett.* **2000**, 636 – 637.
[76] J. H. Jung, S. Shinkai, *J. Chem. Soc. Perkin Trans. 2* **2000**, 2393 – 2398.
[77] J. H. Jung, Y. Ono, S. Shinkai, *Angew. Chem.* **2000**, *112,* 1931 – 1933; *Angew. Chem. Int. Ed.* **2000**, *39*, 1862 – 1865.
[78] J. H. Jung, H. Kobayashi, M. Masuda, T. Shimizu, S. Shinkai, *J. Am. Chem. Soc.* **2001**, *123*, 8785 – 8789.
[79] L. E. Echegoyen, J. Hernandez, A. E. Kaifer, G. W. Gokel, L. Echegoyen, *J. Chem. Soc. Chem. Commun.* **1988**, 836 – 837.
[80] J. H. Jung, Y. Ono, K. Sakurai, M. Sano, S. Shinkai *J. Am. Chem. Soc.* **2000**, *122*, 8648 – 8653.
[81] J. H. Jung, K. Nakashima, S. Shinkai, *Nano Lett.* **2001**, *1*, 145 – 148.
[82] K. Hanabusa, K. Shimura, K. Hirose, M. Kimura, H. Shirai, *Chem. Lett.* **1996**, 885 – 886.
[83] J. H. Jung, Y. Ono, K. Hanabusa, S. Shinkai, *J. Am. Chem. Soc.* **2000**, *122*, 5008 – 5009.
[84] J. H. Jung, Y. Ono, S. Shinkai, *Chem. Eur. J.* **2000**, *6*, 4552 – 4557.
[85] No gelation occurred at noncharged:charged ratios of $< 15{:}85$; only granular silica was obtained.
[86] S. Kobayashi, K. Hanabusa, N. Hamasaki, M. Kimura, H. Shirai, S. Shinkai, *Chem. Mater.* **2000**, *12*, 1523 – 1525.
[87] J. J. E. Moreau, L. Vellutini, M. Wong Chi Man, C. Bied, *J. Am. Chem. Soc.* **2001**, *123*, 1509 – 1510.
[88] In fact, this system no longer involves templation; it is based on a polymerization through which the superstructure is covalently captured.
[89] J. J. E. Moreau, L. Vellutini, M. Wong Chi Man, C. Bied, J.-L. Bantignies, P. Dieudonné, J.-L. Sauvajol, *J. Am. Chem. Soc.* **2001**, *123*, 7957 – 7958.
[90] U. Beginn, S. Keinath, M. Möller, *Macromol. Chem. Phys.* **1998**, *199*, 2379 – 2384.
[91] K. Yoza, Y. Ono, K. Yoshihara, T. Akao, H. Shinmori, M. Takeuchi, S. Shinkai, D. Reinhoudt, *Chem. Commun.* **1998**, 907 – 908.
[92] R. J. H. Hafkamp, M. C. Feiters, R. J. M. Nolte, *J. Org. Chem.* **1999**, *64*, 412 – 426.
[93] K. Yoza, Y. Ono, K. Yoshihara, T. Akao, H. Shinmori, M. Takeuchi, S. Shinkai, D. N. Reinhoudt, *Chem. Commun.* **1998**, 907 – 908.
[94] N. Amanokura, Y. Kanekiyo, S. Shinkai, D. N. Reinhoudt, *J. Chem. Soc. Perkin Trans. 2* **1999**, 1995 – 2000.
[95] J. H. Jung, M. Amaike, S. Shinkai, *Chem. Commun.* **2000**, 2343 – 2344.
[96] J. H. Jung, M. Amaike, K. Nakashima, S. Shinkai, *J. Chem. Soc. Perkin Trans. 2* **2001**, 1938 – 1943.
[97] J. H. Jung, M. Amaike, S. Shinkai, *Trans. Mater. Res. Soc. Jap.* **2001**, *26*, 527 – 530.
[98] N. Amanokura, Y. Kanekiyo, S. Shinkai, D. N. Reinhoudt, *J. Chem. Soc. Perkin Trans. 2* **1999**, 1995 – 2000.
[99] This was confirmed by TEM analysis of the original organogels, in which the α-glucose derivative formed a frizzled fibrous network with fiber diameters of about 5 to 20 nm. The β-glucose derivative on the other hand formed thick fibers with diameters ranging from 50 to 150 nm.
[100] K. Sakurai, A. Friggeri, O. Gronwald, S. Sakurai, S. Okamoto, K. Inoue, S. Shinkai, unpublished results.
[101] O. Gronwald, S. Shinkai, *J. Chem. Soc. Perkin Trans. 2* **2001**, 1933 – 1937.
[102] A. Friggeri, O. Gronwald, K. J. C. van Bommel, S. Shinkai, D. N. Reinhoudt, *Chem. Commun.* **2001**, 2434 – 2435.
[103] So far, transcription of gelators bearing *neutral* amine groups has only been performed in the case of a primary amine or a combination of a primary and secondary amine (see, for example, refs. [75, 95]).
[104] K. J. C. van Bommel, S. Shinkai, *Langmuir* **2002**, *18*, 4544 – 4548.
[105] In a very recent article Stupp and co-workers describe the innovative preparation of (racemic mixtures of) CdS helices under the influence of an organogel template: E. D. Sone, E. R. Zubarev, S. I. Stupp, *Angew. Chem.* **2002**, *114*, 1781 – 1785; *Angew. Chem. Int. Ed.* **2002**, *41*, 1705 – 1709.
[106] W. Kratschmer, L. D. Lamb, K. Fostiropoulos, R. D. Huffman, *Nature* **1990**, *347*, 354 – 358.
[107] S. Iijima, *Nature* **1991**, *354*, 56 – 58.
[108] For an overview on nanotubes, see C. N. R. Rao, B. C. Satishkumar, A. Govindaraj, M. Nath, *ChemPhysChem* **2001**, *2*, 78 – 105, and references therein.
[109] G. Che, B. B. Lakshmi, C. R. Martin, E. R. Fisher, *Langmuir* **1999**, *15*, 750 – 758.
[110] B. Xue, P. Chen, Q. Hong, J. Lin, K. L. Tan, *J. Mater. Chem.* **2001**, *11*, 2378 – 2381.
[111] M. R. Pederson, J. Q. Broughton, *Phys. Rev. Lett.* **1992**, *69*, 2689 – 2692.
[112] P. M. Ajayan, S. Iijima, *Nature* **1993**, *361*, 333 – 334.
[113] P. M. Ajayan, O. Stephan, P. Redlich, C. Colliex, *Nature* **1995**, *375*, 564 – 567.
[114] S. C. Tsang, Y. K. Chen, P. J. F. Harris, M. L. H. Green, *Nature* **1994**, *372*, 159 – 162.

[115] S. Seraphin, D. Zhou, J. Jiao, J. C. Withers, R. Loutfy, *Nature* **1993**, *362*, 503.
[116] C. N. R. Rao, R. Sen, B. C. Satishkumar, A. Govindaraj, *Chem. Commun.* **1998**, 1525 – 1526.
[117] R. Andrews, D. Jacques, A. M. Rao, F. Derbyshire, D. Qian, X. Fan, E. C. Dickey, J. Chen, *Chem. Phys. Lett.* **1999**, *303*, 467 – 474.
[118] C. N. R. Rao, A. Govindaraj, R. Sen, B. C. Satishkumar, *Mater. Res. Innovations* **1998**, *2*, 128 – 141.
[119] Frequently an aluminum oxide layer formed on an aluminum plate is employed.[120]
[120] J. C. Hulteen, C. R. Martin, *J. Mater. Chem.* **1997**, *7*, 1075 – 1087.
[121] T. Kyotani, L. Tsai, A. Tomita, *Chem. Commun.* **1997**, 701 – 702.
[122] B. K. Pradhan, T. Kyotani, A. Tomita, *Chem. Commun.* **1999**, 1317 – 1318.
[123] K. Matsui, B. K. Pradhan, T. Kyotani, A. Tomita, *J. Phys. Chem. B* **2001**, *105*, 5682 – 5688.
[124] B. C. Satishkumar, A. Govindaraj, E. M. Vogl, L. Basumallick, C. N. R. Rao, *J. Mater. Res.* **1997**, *12*, 604 – 606.
[125] The acid treatment results in the formation of acidic sites on the surface of the CNTs.[114]
[126] C. N. R. Rao, B. C. Satishkumar, A. Govindaraj, *Chem. Commun.* **1997**, 1581 – 1582.
[127] B. C. Satishkumar, A. Govindaraj, M. Nath, C. N. R. Rao, *J. Mater. Chem.* **2000**, *10*, 2115 – 2119.
[128] This deposition method is very similar to the one employed by Caruso.[13]
[129] T. Seeger, P. Redlich, N. Grobert, M. Terrones, D. R. M. Walton, H. W. Kroto, M. Rühle, *Chem. Phys. Lett.* **2001**, *339*, 41 – 46.
[130] Y. Q. Zhu, W. K. Hsu, H. W. Kroto, D. R. M. Walton, *Chem. Commun.* **2001**, 2184 – 2185.
[131] P. Chen, X. Wu, J. Lin, K. L. Tan, *J. Phys. Chem. B* **1999**, *103*, 4559 – 4561.
[132] S. Fullam, D. Cottell, H. Rensmo, D. Fitzmaurice, *Adv. Mater.* **2000**, *12*, 1430 – 1432.
[133] H. Dai, E. W. Wong, Y. Z. Lu, S. Fan, C. M. Lieber, *Nature* **1995**, *375*, 769 – 772.
[134] E. W. Wong, B. W. Maynor, L. D. Burns, C. M. Lieber, *Chem. Mater.* **1996**, *8*, 2041 – 2046.
[135] W. Han, S. Fan, Q. Li, Y. Hu, *Science* **1997**, *277*, 1287 – 1289.
[136] W. Han, S. Fan, Q. Li, B. Gu, X. Zhang, D. Yu, *Appl. Phys. Lett.* **1997**, *71*, 2271 – 2273.
[137] Y. Zhang, J. Zhu, Q. Zhang, Y. Yan, N. Wang, X. Zhang, *Chem. Phys. Lett.* **2000**, *317*, 504 – 509.
[138] H. Nakamura, Y. Matsui, *J. Am. Chem. Soc.* **1995**, *117*, 2651 – 2652.
[139] F. Miyaji, S. A. Davis, J. P. H. Charmant, S. Mann, *Chem. Mater.* **1999**, *11*, 3021 – 3024.
[140] F. Miyaji, Y. Tatematsu, Y. Suyama, *J. Ceram. Soc. Jpn.* **2001**, *109*, 924 – 928.
[141] C. Hippe, M. Wark, E. Lork, G. Schulz-Ekloff, *Microporous Mesoporous Mater.* **1999**, *31*, 235 – 239.
[142] Y. Ono, Y. Kanekiyo, K. Inoue, J. Hojo, M. Nango, S. Shinkai, *Chem. Lett.* **1999**, 475 – 476.
[143] E. Braun, Y. Eichen, U. Sivan, G. Ben-Yoseph, *Nature* **1998**, *391*, 775 – 778.
[144] G. Stubbs, *Semin. Virol.* **1990**, *1*, 450.
[145] K. Namba, G. Stubbs, *Acta Crystallogr. Sect. A* **1985**, *41*, 252 – 262.
[146] W. Shenton, T. Douglas, M. Young, G. Stubbs, S. Mann, *Adv. Mater.* **1999**, *11*, 253 – 256.
[147] C. E. Fowler, W. Shenton, G. Stubbs, S. Mann, *Adv. Mater.* **2001**, *13*, 1266 – 1269.
[148] S. A. Davis, S. L. Burkett, N. H. Mendelson, S. Mann, *Nature* **1997**, *385*, 420 – 423.
[149] S. Chia, J. Urano, F. Tamanoi, B. Dunn, J. I. Zink, *J. Am. Chem. Soc.* **2000**, *122*, 6488 – 6489.
[150] J. R. Premkumar, O. Lev, R. Rosen, S. Belkin, *Adv. Mater.* **2001**, *13*, 1773 – 1775.
[151] W. Ogasawara, W. Shenton, S. A. Davis, S. Mann, *Chem. Mater.* **2000**, *12*, 2835 – 2837.
[152] Y. Shin, J. Liu, J. H. Chang, Z. Nie, G. J. Exarhos, *Adv. Mater.* **2001**, *13*, 728 – 732.
[153] a) P. Greil, T. Lifka, A. Kaindl, *J. Eur. Ceram. Soc.* **1998**, *18*, 1961 – 1973; b) P. Greil, T. Lifka, A. Kaindl, *J. Eur. Ceram. Soc.* **1998**, *18*, 1975 – 1983; c) P. Greil, *J. Eur. Ceram. Soc.* **2001**, *21*, 105 – 118.

Communications

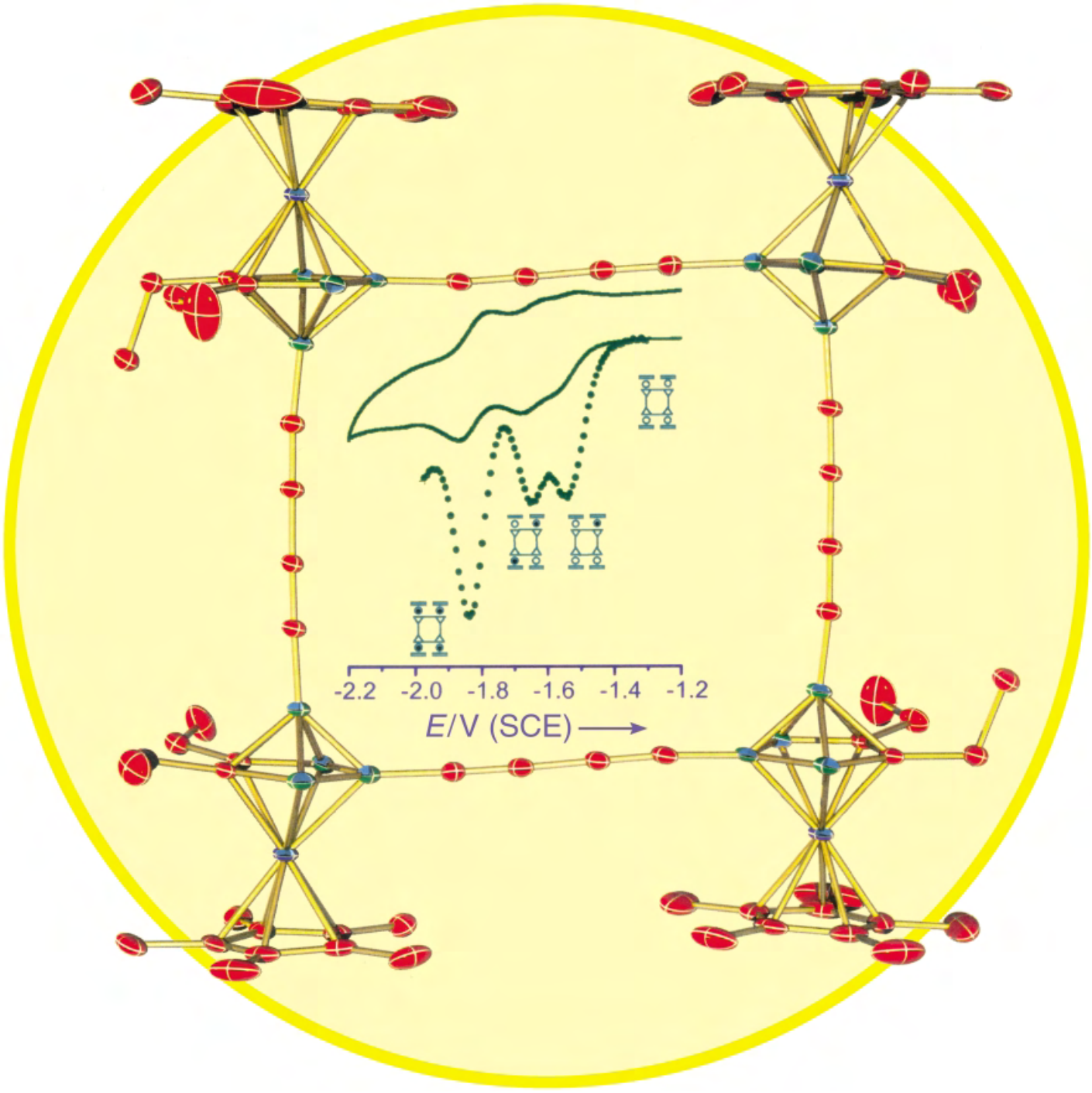

A planar octagonal cobaltacarborane macrocycle, which is air-stable and undergoes stepwise reduction, has been synthesized. Cyclic and square-wave voltammetric data indicate significant electron delocalization in the ring system. For more information see the Communication by R. N. Grimes et al. on the following pages.

 © 2003 Wiley-VCH Verlag GmbH & Co. KGaA, Weinheim 1433-7851/03/4209-1001 $ 20.00+.50/0

Cobaltacarborane Nanostructures

Metallacarborane-Based Nanostructures: A Carbon-Wired Planar Octagon**

Haijun Yao, Michal Sabat, Russell N. Grimes, Fabrizia Fabrizi de Biani, and Piero Zanello*

Stable, covalently bonded metallomacrocycles are currently of considerable interest, in part because of their role, actual and potential, in the development of new molecular materials having tailorable properties.[1] Among the types of target structures attracting attention are highly symmetrical, aesthetically appealing architectures such as molecular squares, rectangles, and boxes,[2] but controlled synthetic routes to metal-containing compounds of this class are relatively rare. Ideally, one looks for metal building-block units that remain intact in a range of environments, suitable organic or inorganic linkers, and efficient methods for assembling these parts into desired target molecules. Since the first of these often presents a challenge, metallacarboranes are obvious candidates for such application because of their synthetic versatility and well-developed derivative chemistry.[3] In recent publications from this laboratory, methods for the regiospecific functionalization of seven-vertex MC_2B_4 metallacarboranes and their linkage through alkynyl, arenyl, and other organic groups have been described.[4] This has allowed the construction of polymetallacarborane molecular architectures that take advantage of special attributes, such as orthogonal substitution at apex and equatorial boron vertices in seven-vertex pentagonal bipyramidal clusters.[4b] Here we report the stepwise assembly of a tetranuclear species that contains four identical cobaltacarborane clusters and features a planar octagonal (tetratruncated square) $\{C_{16}B_8\}$ macrocycle.

Scheme 1 shows the synthesis of the bifunctional 5-iodo-7-trimethylsilyl cobaltacarborane **4** in two steps from either the *closo*-cobaltacarboranes **1a** and **1b** or the *nido*-cobaltacarborane **2**. Desilylation of **4** gave the ethynyl derivative **5** which, in turn, was dimerized through either of two routes, as shown, to give the 5,5′-bis(trimethylsilyl) complex **8**. Treatment of **8** with fluoride ions yielded the 5,5′-diethynyl complex **9**, which was dimerized by treatment with copper acetate and copper(I) chloride to afford the target compound $[Cp^*Co(2,3\text{-}Et_2C_2B_4H_3\text{-}5\text{-}C{\equiv}C\text{-}7\text{-}C{\equiv}C)]_4$ (**10**, $Cp^* = \eta^5\text{-}C_5Me_5$) as a red crystalline air-stable solid (Scheme 2). Yields of isolated and chromatographically purified individual compounds in the sequence **1b**→**3**→**4**→**5**→**6**→**8**→**9**→**10** ranged between 78 and 99%.

The octagonal macrocyclic geometry of **10** in solution is supported by its extremely simple ^{11}B, ^{1}H, and ^{13}C NMR spectra, which reveal a 2:1:1 boron pattern, just two alkynyl carbon signals, and unique C–ethyl and CoCp* environments. An X-ray crystallographic study[5] of **10** (Figure 1) conducted on crystals grown from a pyridine solution established that the 24-atom ring formed by the four {–C≡C–C≡C–} and four carborane {–B–B–} linkages is essentially planar. The complex is centrosymmetric and crystallizes with two molecules of pyridine per molecule of **10**. Molecules in the crystal form discrete, well-separated layers (approximate interlayer distance of 10 Å), within each of which the $\{C_{16}B_8\}$ rings are nearly coplanar (Figure 2). The bond lengths and angles (Figure 1) are within normal ranges and the {B–C–C–C–C–B} edge lengths are 6.82 Å. The square defined by the centroids of the four $\{C_2B_3\}$ carborane rings is approximately 9.4 Å in length along each edge, and the diagonally measured distance across the molecule is approximately 24 Å.

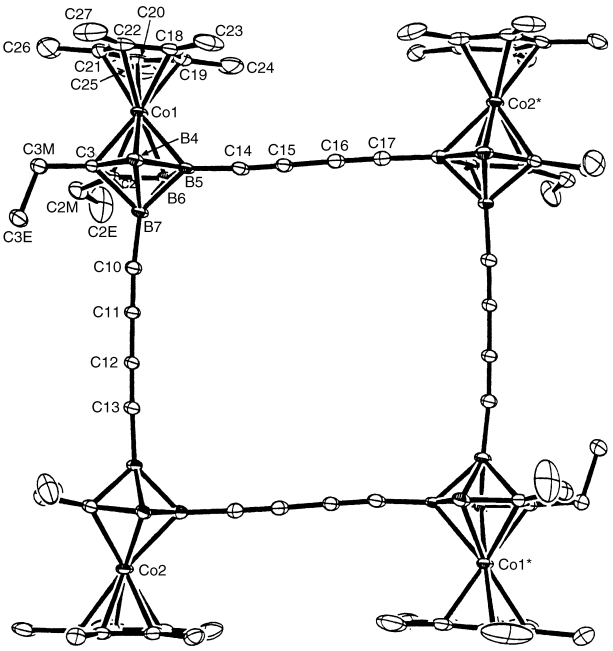

Figure 1. Molecular structure of **10**. Selected bond lengths [Å] and angles [°]: B5-B7 1.760(6), B5-C14 1.517(6), C14-C15 1.209(6), C15-C16 1.379(6), C16-C17, 1.216(6), B7-C10 1.516(5), C10-C11 1.217(5), C11-C12 1.372(5), C12-C13, 1.212(5); B7-B5-C14 137.3(3), B5-C14-C15 171.9(4), C14-C15-C16 177.6(4), C15-C16-C17 177.5(4), B5-B7-C10 136.9(3), B7-C10-C11 174.5(4), C10-C11-C12 178.2(5), C11-C12-C13 179.1(4).

The 24-atom $\{C_{16}B_8\}$ ring in **10** is one of the larger planar molecular macrocycles currently known, and it presents a variety of interesting avenues for exploration of its reactivity and electronic properties. Analysis of **10** by cyclic voltamme-

[*] Prof. Dr. R. N. Grimes, Dr. H. Yao, Dr. M. Sabat
Department of Chemistry
University of Virginia
Charlottesville, Virginia 22901 (USA)
Fax: (+1) 434-924-3710
E-mail: rng@virginia.edu
Dr. F. Fabrizi de Biani, Prof. Dr. P. Zanello
Dipartimento di Chimica dell'Università di Siena
Via Aldo Moro, 53100 Siena (Italy)

[**] Organotransition-Metal Metallacarboranes: Part 63. This work was supported in part by the National Science Foundation (Grant CHE 9980708). Part 62: J. M. Russell, M. Sabat, R. N. Grimes, *Organometallics* **2002**, *21*, 5613.

Supporting information for this article is available on the WWW under http://www.angewandte.org or from the author.

 © 2003 Wiley-VCH Verlag GmbH & Co. KGaA, Weinheim 1433-7851/03/4209-1002 $ 20.00+.50/0

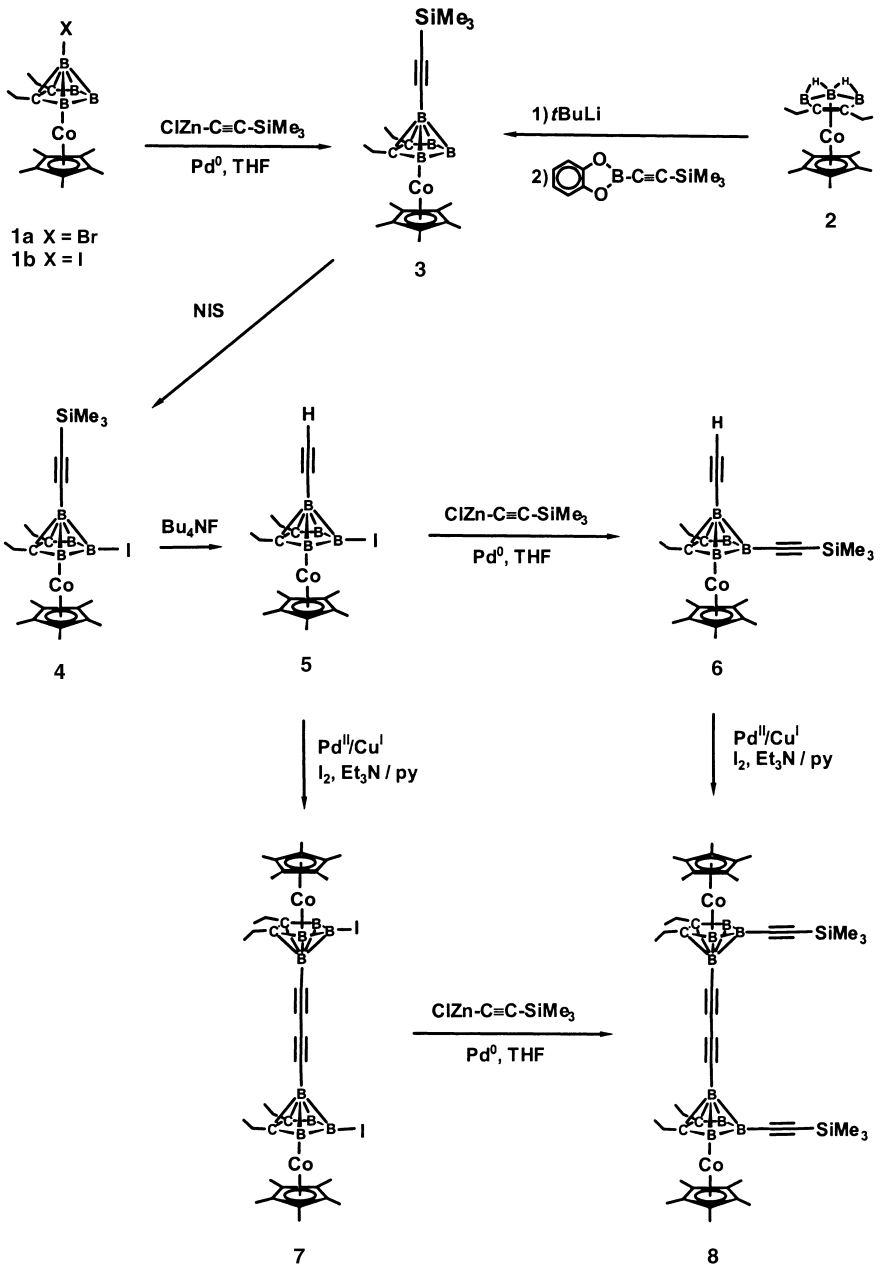

Scheme 1. B = B, BH

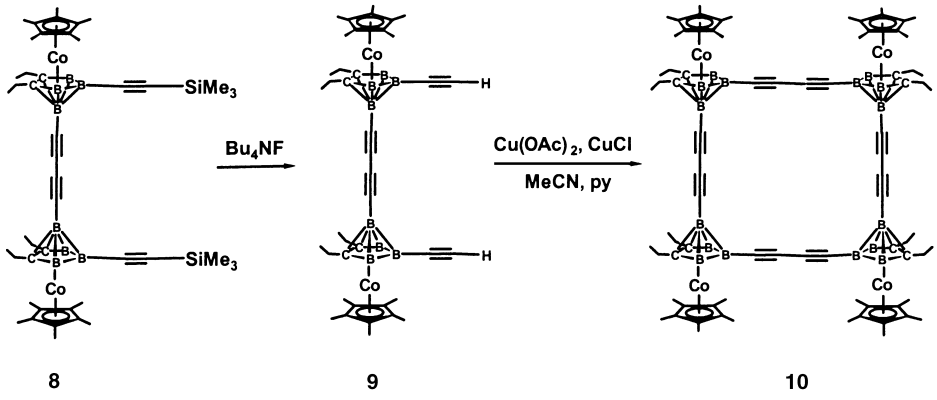

Scheme 2. B = B, BH

try[6] revealed two separate one-electron reductions followed by a single two-electron reduction (Figure 3), which indicates significant intramolecular electronic communication between the four cobalt centers. A possible pathway for the progressive four-electron addition is suggested in Figure 3. The concomitant entry of the last two electrons is likely because of the charge symmetry that exists following the addition of the first two electrons. Further studies of the electronic and other properties of this and related systems are in progress.

Experimental Section

Spectroscopic data for compounds **3**–**9** and details of the alternative preparations of **3** and **8** are available as Supporting Information.

3: $Me_3SiC{\equiv}CH$ (570 mg, 5.73 mmol) in THF (20 mL) was added to *n*BuLi (1.51 M in hexane, 3.8 mL, 5.73 mmol) at 0 °C. After stirring for 30 min, anhydrous $ZnCl_2$ (781 mg, 5.73 mmol) in THF (20 mL) was added at 0 °C, and the mixture was then stirred at room temperature for 2 h. [Cp*Co(2,3-$Et_2C_2B_4H_3$-7-I)] (**1b**, 860 mg, 1.91 mmol) and $[Pd(PPh_3)_4]$ (110 mg, 0.10 mmol) were then added. The mixture was refluxed for 4.5 days, after which time the solvent was removed in vacuo and the residue was purified by flash chromatography through 5 cm of silica gel in 1:1 hexane/CH_2Cl_2 to give one orange band. Removal of the solvent gave 755 mg (94 %) of an orange-red product. Compound **3** was also prepared in moderately lower yields by a similar procedure from [Cp*Co(2,3-$Et_2C_2B_4H_3$-7-Br)] (**1a**), or by the insertion of $C_6H_4O_2BC{\equiv}CSi(CH_3)_3$ into the *nido*-$[Cp^*Co(2,3\text{-}Et_2C_2B_3H_3)]^{2-}$ ion derived from **2**.

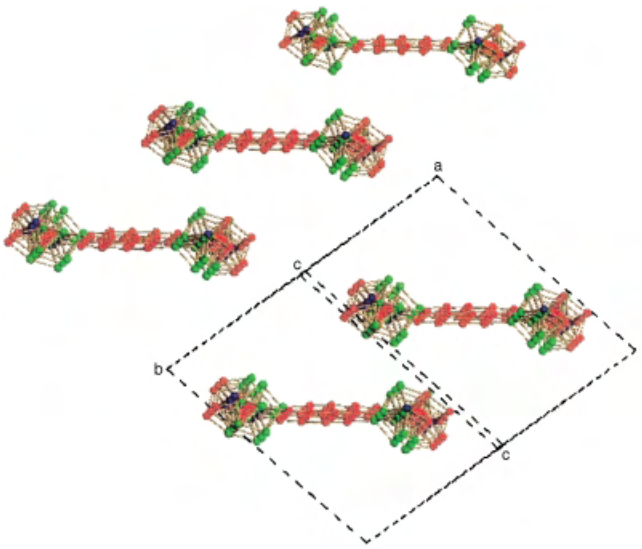

Figure 2. Unit cell packing diagram for **10** showing a view parallel to the *c* axis.

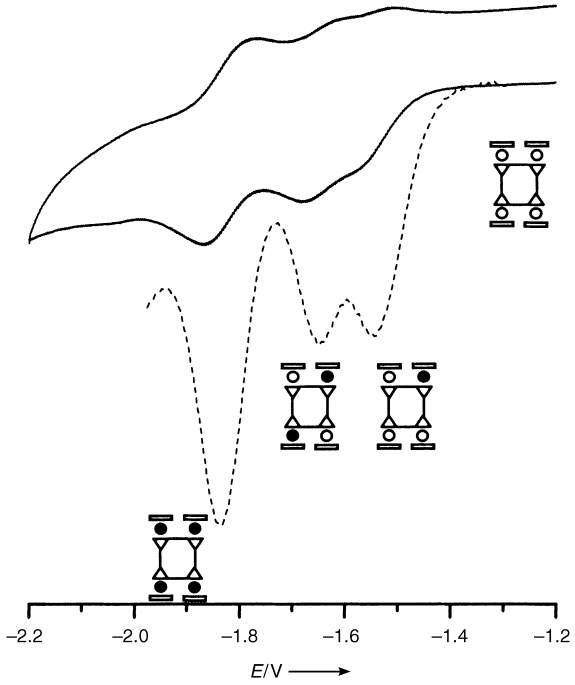

Figure 3. Cyclic (——) and Osteryoung square-wave (–•–•) voltammograms recorded at a gold electrode in a solution of **10** in THF (0.2×10^{-3} mol dm^{-3}) versus a saturated calomel electrode; Bu_4NPF_6 supporting electrolyte (0.2 mol dm^{-3}). Scan rates: (——) 0.2 V s^{-1}; (–•–•) 0.1 V s^{-1}.

4: *N*-iodosuccinimide (203 mg, 0.90 mmol) in CH_2Cl_2 (15 mL) was added dropwise to **3** (345 mg, 0.82 mmol) in dry CH_2Cl_2 (15 mL) at 0 °C. The mixture was stirred at that temperature for 1 h, followed by 1 h at room temperature, after which time the solvent was removed and the residue taken up in hexane. Purification by flash chromatography in hexane (to remove iodine) after washing with CH_2Cl_2 led to one orange band. Removal of the solvent gave orange-red **4** (445 mg, 99 %).

5: Compound **4** (445 mg, 0.816 mmol) was treated with a solution of Bu_4NF (1.0 M, 0.82 mL, 0.82 mmol) in dry THF (20 mL) for 40 min at 0 °C, after which the THF was removed and the residue was purified by flash chromatography in CH_2Cl_2 to give one orange band. Removal of the solvent gave red-orange solid **5** (370 mg, 96 %).

6: $Me_3SiC{\equiv}CH$ (157 mg, 1.6 mmol) was deprotonated in THF (8 mL) by the addition of *n*BuLi (1.51 mmol in hexane) at 0 °C. After stirring for 30 min, anhydrous $ZnCl_2$ (204.5 mg, 1.5 mmol) in THF (6 ml) was added at 0 °C, and the mixture was stirred at room temperature for 2 h, after which time compound **5** (237 mg, 0.5 mmol) and $[Pd(PPh_3)_4]$ (29 mg, 0.025 mmol) were added. The mixture was refluxed for 3.5 days, then the solvent was removed in vacuo and the residue purified by flash chromatography in 1:1 hexane/CH_2Cl_2 to give one orange band. Removal of the solvent gave orange-red **6** (185 mg, 83 %).

8: Compound **6** (166 mg, 0.374 mmol), $[Pd(PPh_3)_2Cl_2]$ (7 mg, 0.01 mmol), CuI (4 mg, 0.02 mmol), I_2 (50 mg, 0.2 mmol), pyridine (8 mL), and Et_3N (3 mL) were combined, and the mixture was stirred at room temperature for 12 h. The solvent was removed in vacuo and the residue was purified by flash chromatography through 5 cm of silica gel in 1:1 hexane/CH_2Cl_2 to give one orange band. Removal of solvent gave orange solid **8** (130 mg, 78 %).

9: Compound **8** (100 mg, 0.113 mmol) was desilylated with Bu_4NF (1.0 M, 0.23 mL, 0.23 mmol) in dry THF (15 mL). The mixture was stirred at 0 °C for 1 h, then the solvent was removed, and the residue purified by flash chromatography in CH_2Cl_2 to give one orange band. Removal of solvent gave orange solid **9** (71 mg, 85 %).

10: Compound **9** (22 mg, 0.03 mmol) in pyridine (10 ml) was added to a mixture of $Cu(OAc)_2$ (54 mg, 0.3 mmol) and CuCl (30 mg, 0.3 mmol) in CH_3CN (10 mL), and the mixture was stirred at 60 °C for 17 h. The mixture was allowed to cool down, and water (30 mL) was added. The resulting precipitate was filtered off, washed with water, and dried in vacuo. The residue was crystallized from pyridine, 1,2-dichloroethane, and ethanol at 0 °C to give red crystals (18 mg, 82 %). ^{1}H NMR (500 MHz, $CDCl_3$): $\delta = 1.26$ (t, 6 H, $J = 7.5$ Hz, ethyl CH_3), 1.77 (s, 15 H, C_5Me_5), 2.17 and 2.35 ppm (sextet, 4 H, $J = 7.5$ Hz, ethyl CH_2); ^{13}C NMR (75.5 MHz, pyridine-d_5): $\delta = 9.5$ (C_5Me_5), 14.9 (ethyl CH_3), 22.0 (ethyl CH_2), 75.6 (BC≡C–C≡CB), 91.9 (C_5Me_5), 95.2 (C_2B_4), 97.2 ppm (BC≡C–C≡CB); ^{11}B NMR (96.4 MHz, pyridine-d_5): $\delta = -4.5$ (s, 1 B), 4.5 (2 B, BH unresolved), 8.9 ppm (s, 1 B). IR (KBr pellet): $\tilde{\nu} = 2972.7$ (s), 2932.8 (m), 2913.0 (m), 2871.6 (w), 2545.2 (s, B–H), 2168.0 (w, C≡C), 2090.8 (m, C≡C), 1471.9 (m), 1456.7 (m), 1383.9 (vs), 1155.7 (w), 1114.9 (m), 1055.9 (m), 1028.6 (m), 804.9 (s), 633.7 (w) cm^{-1}. UV/Vis (CH_2Cl_2, nm (%)): 323 (100), 231 (67), 464 (4) $\varepsilon_{max} = 67\,170$ cm^{-1}M^{-1}. Positive-mode CI-MS: *m/z* (%) = 1479.9 ([M^+], 100).

Received: November 18, 2002 [Z50567]

[1] Recent reviews: a) M. Fujita, K. Umemoto, M. Yoshizawa, N. Fujita, T. Kusukawa, K. Biradha, *Chem. Commun.* **2001**, 509; b) F. A. Cotton, C. Lin, C. A. Murillo, *Acc. Chem. Res.* **2001**, *34*, 759; c) B. J. Holliday, C. A. Mirkin, *Angew. Chem.* **2001**, *113*, 2076; *Angew. Chem. Int. Ed.* **2001**, *40*, 2022; d) S. Leininger, B. Olenyuk, P. J. Stang, *Chem. Rev.* **2000**, *100*, 853; e) G. F. Swiegers, T. J. Malefetse, *Chem. Rev.* **2000**, *100*, 3483; f) R. V. Slone, K. D. Benkstein, S. Belanger, J. T. Hupp, I. A. Guzei, A. L. Rheingold, *Coord. Chem. Rev.* **1998**, *171*, 221; g) P. Siemsen, R. C. Livingston, F. Diederich, *Angew. Chem.* **2000**, *112*, 2740; *Angew. Chem. Int. Ed.* **2000**, *39*, 2632.

[2] Selected examples: a) M. I. Bruce, K. Costuas, J.-F. Halet, B. C. Hall, P. J. Low, B. K. Nicholson, B. W. Skelton, A. H. White, *J. Chem. Soc. Dalton Trans.* **2002**, 383; b) S. J. Lee, W. Lin, *J. Am. Chem. Soc.* **2002**, *124*, 4554; c) X. Liu, C. L. Stern, C. A. Mirkin, *Organometallics* **2002**, *21*, 1017; d) V. C. Lau, L. A. Berben, J. R. Long, *J. Am. Chem. Soc.* **2002**, *124*, 9042; e) H. Oshio, M. Yamamoto, T. Ito, *Inorg. Chem.* **2002**, *41*, 5817; f) R. Gheorghe, M. Andruh, A. Müller, M. Schmidtmann, *Inorg. Chem.* **2002**, *41*,

 © 2003 Wiley-VCH Verlag GmbH & Co. KGaA, Weinheim 1433-7851/03/4209-1004 $ 20.00+.50/0

5314; g) R. D. Adams, B. Qu, M. D. Smith, *Inorg. Chem.* **2001**, *40*, 2932; h) U. H. F. Bunz, G. Roidl, M. Altmann, V. Enkelmann, K. D. Shimizu, *J. Am. Chem. Soc.* **1999**, *121*, 10719.

[3] a) M. F. Hawthorne, G. B. Dunks, *Science* **1972**, *178*, 462; b) R. N. Grimes in *Comprehensive Organometallic Chemistry II, Vol. 1* (Eds.: E. W. Abel, F. G. A. Stone, G. Wilkinson), Pergamon, Oxford, **1995**, p. 373, and references therein; c) N. S. Hosmane in *Contemporary Boron Chemistry* (Eds.: M. Davidson, A. K. Hughes, T. B. Marder, K. Wade), Royal Society of Chemistry, London, **2000**, 299, and references therein.

[4] a) H. Yao, M. Sabat, R. N. Grimes, *Organometallics* **2002**, *21*, 2833; b) J. M. Russell, M. Sabat, R. N. Grimes, *Organometallics* **2002**, *21*, 4113; c) D. Malaba, M. Sabat, R. N. Grimes, *Eur. J. Inorg. Chem.* **2001**, 2557; d) M. Bluhm, H. Pritzkow, W. Siebert, R. N. Grimes, *Angew. Chem.* **2000**, *112*, 4736; *Angew. Chem. Int. Ed.* **2000**, *39*, 4562.

[5] Crystal structure determination of **10**: Data were collected on a Bruker SMART APEX CCD diffractometer ($Mo_{K\alpha}$ radiation, $\lambda = 0.71073$ Å, ω scans) at 153 K. 1800 frames were collected up to $2\theta = 65°$. Intensities were corrected for absorption applying the SADABS program.[7] The structure was solved by direct methods using the Bruker SHELXTL software.[8] Full-matrix least-squares refinement on F^2 was applied. All non-hydrogen atoms, except those on one of the pyridine solvent molecules, were refined with anisotropic thermal displacement parameters. The hydrogen atoms attached to boron were found in difference Fourier maps and were refined with isotropic thermal displacement parameters. All remaining hydrogen atoms of the complex molecule, as well as those of the pyridine ring C1S–N5S were fixed in calculated positions. Difference Fourier maps indicated the presence of three pyridine solvent molecules; since high values of the thermal displacement parameters for one pyridine suggested that the site was only partially occupied, its atoms were assigned population parameters of 0.5. A third pyridine was found disordered between two sites related by a center of symmetry. The atoms of this molecule were refined with isotropic thermal displacement parameters and occupancies of 0.5. The final difference map showed the presence of a residual peak with the height of 1.29 e Å^{-3}, located in the vicinity of a pyridine ring. $C_{90}H_{118}B_{16}Co_4N_2$, $M_W = 1636.54$, triclinic, space group $P\bar{1}$, $a = 11.8321(7)$, $b = 15.0873(8)$, $c = 15.2047(8)$ Å, $\alpha = 85.300(2)$, $\beta = 70.754(2)$, $\gamma = 89.068\ (1)°$, $V = 2553.8(2)$ Å^3, $Z = 1$, $\rho_{calcd} = 1.064$ g cm^{-3}. Of 35421 measured reflections, 18073 were independent ($R_{int} = 0.053$), 609 parameters, $R1 = 0.089$ (for reflections with $I > 2\sigma(I)$), $wR2 = 0.2506$ (for all reflections). CCDC-194783 contains the supplementary crystallographic data for this paper. These data can be obtained free of charge via www.ccdc.cam.ac.uk/conts/retrieving.html (or from the Cambridge Crystallographic Data Centre, 12, Union Road, Cambridge CB2 1EZ, UK; fax: (+44) 1223-336-033; or deposit@ccdc.cam.ac.uk).

[6] The electrochemical materials, apparatus, and procedures are described elsewhere: see F. Fabrizi de Biani, M. Fontani, E. Ruiz, P. Zanello, J. M. Russell, R. N. Grimes, *Organometallics* **2002**, *21*, 4129. THF was refluxed from metallic sodium under an inert atmosphere. All potential values are referred to the saturated calomel electrode (SCE). Under the experimental conditions used, the one-electron oxidation of ferrocene occurs at $E°' = +0.54$ V.

[7] G. M. Sheldrick, SADABS, Program for Empirical Absorption of Area Detector Data, University of Göttingen, Göttingen (Germany), **1996**.

[8] G. M. Sheldrick, SHELXTL Version 5.1 Reference Manual, Bruker AXS, Madison, WI, **1997**.

 © 2003 Wiley-VCH Verlag GmbH & Co. KGaA, Weinheim 1433-7851/03/4209-1005 $ 20.00+.50/0

Semisynthetic Metalloenzymes

Preparation of Artificial Metalloenzymes by Insertion of Chromium(III) Schiff Base Complexes into Apomyoglobin Mutants**

*Masataka Ohashi, Tomomi Koshiyama, Takafumi Ueno, Manabu Yanase, Hiroshi Fujii, and Yoshihito Watanabe**

Construction of artificial metalloenzymes is one of the most important subjects in bioinorganic chemistry, because metalloenzymes catalyze chemical transformations with high selectivity and reactivity under mild conditions.[1–4] There are several reports on protein design: introduction of metal binding sites,[1,3,5–8] design of substrate binding cavities,[9–12] chemical modification of prosthetic groups,[13–16] and covalent attachment of metal cofactors.[2,17–20] In particular, the covalent modification of proteins is a powerful tool for the generation of new metalloenzymes, while the efficiency of the modification is very much dependent on the position and reactivity of the cysteinyl thiol functional group.[2] Herein, we describe a novel strategy for the preparation of artificial metalloenzymes by noncovalent insertion of metal-complex catalysts into protein cavities. The resulting semisynthetic metalloenzymes, apo-myoglobin (apo-Mb) reconstituted with Cr^{III} Schiff base complexes, are able to catalyze enantioselective sulfoxidation.

Manganese(III) and chromium(III) Schiff base complexes are known to be catalysts for various oxidations in organic solvents.[21,22] Jacobsen,[23] and Katsuki[24] have already reported many examples of asymmetric oxidations catalyzed by chiral Mn Schiff base complexes. In our case, symmetric complexes, $[M^{III}(salophen)]^+$ (M·**1**; M = Mn, Cr; H_2 salophen

[*] Prof. Dr. Y. Watanabe, T. Koshiyama
Department of Chemistry
Graduate School of Science
Nagoya University
Nagoya 464-8602 (Japan)
Fax: (+81) 52-789-2953
E-mail: yoshi@nucc.cc.nagoya-u.ac.jp
M. Ohashi
Department of Structural Molecular Science
The Graduate University for Advanced Studies
Okazaki 444-8585 (Japan)
Dr. T. Ueno
Research Center for Materials Science
Nagoya University
Nagoya 464-8602 (Japan)
Dr. M. Yanase
Institute for Molecular Science
Okazaki 444-8585 (Japan)
Prof. Dr. H. Fujii
Center for Integrative Bioscience and Institute for Molecular Science
Okazaki 444-8585 (Japan)

[**] This work was supported by a Grant-in-Aid for Scientific Research 11490036 and 1122828 (to Y.W.), 13740384 (to T.U.). We also thank Prof. T. Yamane, Prof. A. Suzuki, and Mr. M. Kono at Nagoya University for valuable guidance and help with the X-ray crystallographic analysis.

 © 2003 Wiley-VCH Verlag GmbH & Co. KGaA, Weinheim 1433-7851/03/4209-1005 $ 20.00+.50/0

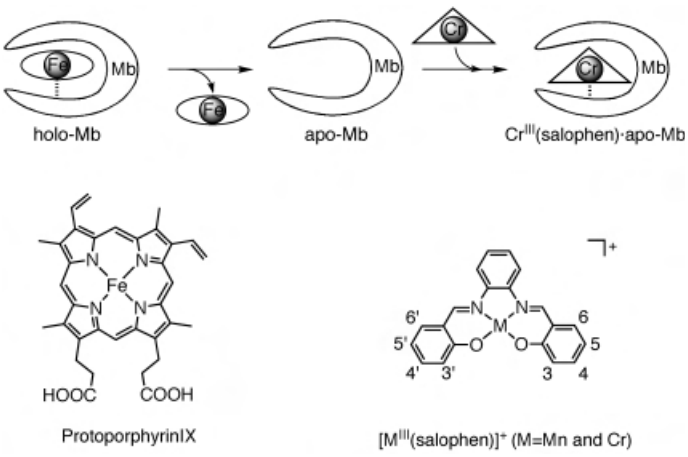

Figure 1. Insertion of a salophen complex into apo-Mb.

(**1**) = *N*,*N*′-bis(salicylidene)-1,2-phenylenediamine) are inserted into a chiral cavity of apo-Mb (Figure 1). In addition, the 5- and 5′- positions of salophen are substituted by a *tert*-butyl group, 5,5′-tBu$_2$-salophen (**2**) to improve the binding affinity to apo-Mb, that is, the binding affinity of heme in apo-Mb is provided by the hydrophobic interaction, and the ligand size.[25] We found that similar factors are important for metal complexes to be inserted into the Mb cavity.

For the creation of artificial metalloenzymes, apo-Mb is an excellent candidate, since reconstitution of apo-Mb with heme has been well studied.[13,26–28] We demonstrated that the catalytic selectivity and reactivity of Mb as a peroxygenase are controlled by appropriate site-directed mutagenesis in the active site.[10,11,29] On the basis of these results, we have designed a suitable apo-Mb mutant for the reconstitution with Schiff base complexes by using the Insight II/Discover 3 program. A designed protein structure, Cr·**2**·apo-H64D/A71GMb, is shown in Figure 2b. If we assume that Cr·**2** binds to His 93 as observed for heme, the replacement of His 64 with Asp (H64D) will provide increased access of substrates and oxidants to a vacant distal site above the Cr^{III} center.[11] At the same time, the alanyl side chain at the position 71 in Mb is expected to locate very close to the 4- and 5- positions of Cr·**2** (Figure 2). Thus, Ala 71 was replaced with Gly (A71G) to improve the binding affinity of Cr·**2** in the active site.

The reconstitution of apo-Mb with Cr·**2** was carried out by applying a method used for modified hemes;[28] [Cr·**2**·2H$_2$O]BF$_4$ dissolved in MeOH (0.9 equiv, 0.7 mM) was added dropwise to an apo-Mb solution in Tris/HCl (10 mM, pH 7.0). The mixture was dialyzed against Bis-Tris/HCl (10 mM pH 6.0) and then loaded on Sephadex G-25. The final purification was performed on a CM52 column with linear gradient Tris/HCl buffer (10–100 mM pH 7.0), which gave a 15% yield of isolated Cr·**2**·apo-Mb. The yield of isolated Cr·**2**·apo-H64D/A71GMb (4.3%) was about 15-fold larger than that of Cr·**1**·apo-H64D/A71GMb (0.3%) and almost twice as large as that of Cr·**2**·apo-H64DMb (2.4%). In contrast, all efforts made to prepare Mn·**1**·apo-H64D/A71GMb failed. These results imply that the type of metal ion and the ligand structure are important factors that influence the binding affinity of the metal complexes with the Mb mutants.

The deconvoluted ESI-TOF mass spectrum of purified Cr·**2**·apo-Mb in ammonium acetate (5 mM; Figure 3a) shows two peaks, which are readily assigned to Cr·**2**·apo-Mb (measured: 17808.3 ± 1.1 Da, calcd: 17808.6 Da) and a small portion of apo-Mb (measured: 17330.0 ± 0.1 Da, calcd: 17330.1 Da), respectively. The appearance of a small peak corresponding to apo-Mb is also observed for purified heme-bound Mb (holo-Mb) under the same conditions, which indicates that the binding affinity of Cr·**2** is comparable to that of heme. To confirm that Cr·**2** is incorporated into the heme position, the following experiments were performed. In the first experiment, a mixture of apo-Mb and two equivalents of hemin was analyzed by ESI-TOF mass spectrometry (MS) and holo-Mb was observed as the main peak of the resulting spectrum (measured: 17945.6 ± 0.1 Da, calcd: 17946.6 Da; Figure 3b). In the second experiment, a solution of hemin (two equiv) in DMF was added to purified Cr·**2**·apo-Mb in ammonium acetate (5 mM). The ESI-TOF mass spectrum of the resulting solution (Figure 3c) shows peaks assigned to holo-Mb and Cr·**2**·apo-Mb + heme (measured: 18421.6 ± 0.3 Da, calcd: 18424.7 Da), which are smaller than the peaks of Cr·**2**·apo-Mb. If the Cr^{III} complex binds to the surface of apo-Mb, we expect to observe Cr·**2**·apo-Mb + heme as the major peak, since the incorporation of heme into apo-Mb is very rapid and the mutation of His 64 and Ala 71 should not be effective for the reconstitution. In addition, the preliminary results of an X-ray crystallographic analysis of

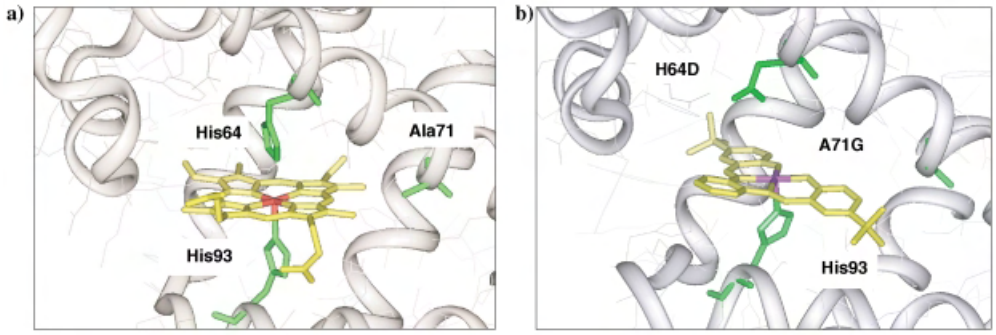

Figure 2. Comparison of a) the crystal structure of wild-type Mb (PDB code 2MBW) with b) a proposed structure of Cr·**2**·apo-H64D/A71GMb calculated by the Insight II/Discover 3 program (ESFF force field). The parts of apo-Mb that interact with Cr·**2** are shown in green, **2** is yellow, Cr is a) red or b) purple.

 © 2003 Wiley-VCH Verlag GmbH & Co. KGaA, Weinheim 1433-7851/03/4209-1006 $ 20.00+.50/0

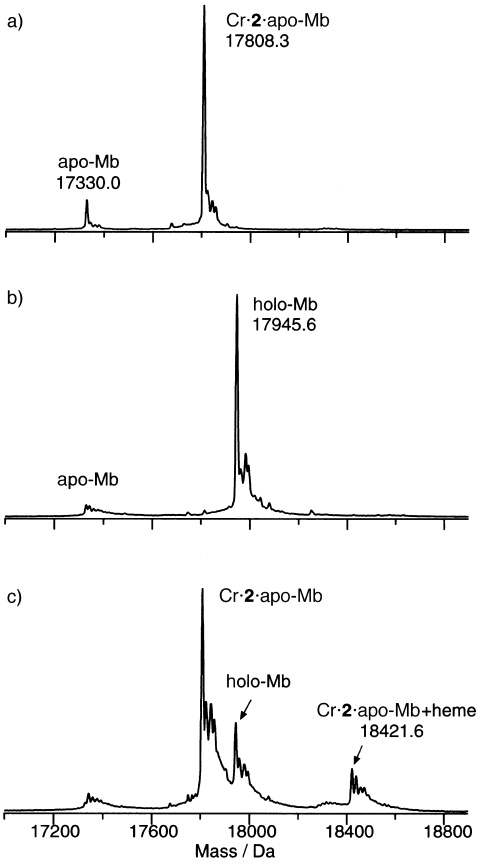

Figure 3. Deconvoluted ESI-TOF mass spectra of a) Cr·**2**·apo-Mb, b) apo-Mb with two equivalents of hemin, and c) Cr·**2**·apo-Mb with two equivalents of hemin in ammonium acetate (5 mM). Sample preparation for b) and c): two equivalents of hemin (1 mM, DMF solution) was added to purified Cr·**2**·apo-Mb (10 μM) and apo-Mb (10 μM), respectively. The mixtures were stirred for 10 min and then dialyzed against 5 mM ammonium acetate for 8 h at 4 °C.

Cr(3,3′-Me_2-salophen)·apo-A71GMb show that the Cr^{III} ion binds to the Nε atom of imidazole in His 93.[30] Thus, we concluded that the His 93 coordination is crucial for Cr·**2** to locate in the active site of Mb.

The H_2O_2-dependent sulfoxidation of thioanisole was examined at 35 °C and pH 5.0 (Table 1). The rate and enantiomeric excess of the sulfoxidation were determined by HPLC analysis (Daicel OD chiral-sensitive column).[9] Catalysts Cr·**1**·apo-H64D/A71GMb, and Cr·**2**·apo-H64D/A71GMb exhibit the highest sulfoxidation activities (entries 4 and 5), whereas Cr·**2**·apo-H64DMb has the lowest activity (entry 3). Catalysts Cr·**1**·apo-H64D/A71GMb and Cr·**2**·apo-H64D/A71GMb showed an approximately sixfold rate increase over Cr·**2** (entries 4,5 versus entry 7). Notably, Cr·**2**·apo-H64D/A71GMb gave (*S*)-methylphenyl sulfoxide with a 13 % *ee*, while the sulfoxidation catalyzed by Cr·**2** proceeded with no enantiomeric discrimination. The other mutants show lower enantioselectivity than that of Cr·**2**·apo-H64D/A71GMb. In a control experiment, the sulfoxidation by Cr·**2**·bovin serum albumin (BSA) was performed (Table 1, entry 6).[31] The enantioselectivity and rate were very low compared with those achieved with Cr·**2**·apo-H64D/A71GMb because of the nonspecific binding ability of Cr·**2** to BSA and the absence of histidine coordination to the Cr^{III} complex. This result indicates that the cavity of an apo-Mb mutant, and His 93 coordination to the Cr^{III} atom are important to improve the enantioselectivity and rate of the sulfoxidation. Furthermore, the EPR spectrum of Cr·**2**·apo-H64D/A71GMb oxidized by *m*-chloroperbenzoic acid at 5 K (pH 7.0) shows a signal at $g = 1.97$ assigned to an oxochromium(v) species.[32] Thus, the intermediate responsible for the catalytic sulfoxidation is expected to be the oxochromium(v) species formed in the Mb cavity. While the enantioselectivity is still low, the results clearly demonstrate that asymmetric reactions can be performed if we use protein cavities, even though symmetric metal complexes are employed.

In summary, we have demonstrated the insertion of symmetric metal complexes into the active site of apomyoglobin by binding to His 93, and that semisynthetic metalloenzymes catalyze enantioselective sulfoxidation by using the chiral protein cavity. Although the semisynthetic metalloenzymes still exhibit low reactivity and enantioselectivity, our experiments suggest the possible use of this method for the design of artificial metalloenzymes. Refinement of the crystal structure and further design to improve the reactivity and selectivity of the metalloenzymes are currently in progress.

Table 1: The different rates and enantiomeric excesses obtained in the sulfoxidation of thioanisole by using a range of catalysts based on chromium Schiff base complexes in a range of proteins.[a]

Entry	Catalyst	Rate[b]	*ee* [%]
1	Cr·**2**·apo-Mb	46	4.3 (*R*)
2	Cr·**2**·apo-A71GMb	54	6 (*S*)
3	Cr·**2**·apo-H64DMb	27	0.3 (*S*)
4	Cr·**1**·apo-H64D/A71GMb	83	8.3 (*S*)
5	Cr·**2**·apo-H64D/A71GMb	78	13 (*S*)
6	Cr·**2**·BSA	12	0.5 (S)
7	Cr·**2** in buffer	13	0

[a] Sulfoxidations were carried out in sodium acetate buffer (50 mM, pH 5.0) at 35 °C in the presence of a Mb complex (10 μM), thioanisole (1 mM), and H_2O_2 (1 mM). [b] The unit of the rate is 10^{-3} turnover min^{-1}.

Experimental Section

The mutants were constructed by cassette mutagenesis. Expression and purification of the mutants were performed as reported previously.[33] Ligands **1** and **2**, and their Cr^{III} complexes were synthesized by methods described in the references [34, 35].

[Cr·**2**·$2H_2O$]BF_4: ESI-TOF MS: Cr·**2**·$2CH_3CN$ 560 (calcd 560); UV/Vis: λmax (ε $M^{-1}cm^{-1}$) 480 (0.93×10^4), 337 nm (2.35×10^4).

[Cr·**1**·$2H_2O$]BF_4: ESI-TOF MS: Cr·**1**·$(CH_3CN)_2$ 448 (calcd 449); UV/Vis: λmax (ε $M^{-1}cm^{-1}$) 469 (1.04×10^4), 334 nm (2.54×10^4).

Cr·**2**·apo-Mb: ESI-TOF MS: 17808.3 ± 1.1 (calcd 17808.3);UV/Vis: λmax (ε $M^{-1}cm^{-1}$) 485 (1.02×10^4), 341 (2.45×10^4), 270 nm (3.75×10^4).

Cr·**2**·apo-A71GMb: ESI-TOF MS:17793.9 ± 0.9 (calcd 17794.3); UV/Vis: λmax (ε $M^{-1}cm^{-1}$) 483 (1.02×10^4), 341 (2.88×10^4), 281 nm (4.38×10^4).

Cr·**2**·apo-H64DMb: ESI-TOF MS: 17786.0 ± 0.6 (calcd 17786.2); UV/Vis: λmax (ε $M^{-1}cm^{-1}$) 474 (0.95×10^4), 338 (2.39×10^4), 321 (2.41×10^4), 282 nm (3.52×10^4).

 © 2003 Wiley-VCH Verlag GmbH & Co. KGaA, Weinheim 1433-7851/03/4209-1007 $ 20.00+.50/0

Cr·**2**·apo-H64D/A71GMb: ESI-TOF MS: 17772.1 ± 0.3 (calcd 17772.2); UV-Vis: λmax (ε $M^{-1}cm^{-1}$) 471 (1.02×10^4), 339 (2.61×10^4), 280 nm (4.18×10^4).

Cr·**1**·apo-H64D/A71GMb: ESI-TOF MS: 17658.2 ± 0.7 (calcd 17660.1); UV/Vis: λmax (ε $M^{-1}cm^{-1}$) 460 (1.18×10^4), 320 (1.2×10^3), 282 nm (2.3×10^3).

The concentration of Cr ion in the purified enzymes was determined by inductively coupled plasma atom emission spectrometry (ICPAES). The spectra were recorded on a SEIKO SPS 7000 that was calibrated with $K_2Cr_2O_7$ in 0.1 mol L^{-1} HNO_3 (100.3 mg L^{-1}, Wako).

ESI-TOF MS were measured on a LCT (Micromass, UK). Typical parameters: capillary, 3 kV; cone, 60 V; source temperature, 60 °C; flow-rate, 5 μL min^{-1}; mass scale calibration, CsI (1 mg mL^{-1}) in 50 % H_2O/CH_3CN. All samples were dialyzed against 5 mM ammonium acetate for 8–10 h at 4 °C.

EPR spectra were recorded at 5 K on a Bruker E500 (X band) with an Oxford helium cryostat. Samples were prepared by addition of 100 equivalents of *m*-chloroperbenzoic acid (1M in MeOH) to purified Cr·**2**·apo-H64D/A71GMb (1 mM in 10 mM Tris/HCl at pH 7.0). The reaction mixtures were then frozen in liquid nitrogen.

Received: July 15, 2002
Revised: November 19, 2002 [Z19733]

[1] Y. Lu, S. M. Berry, T. D. Pfister, *Chem. Rev.* **2001**, *101*, 3047 – 3080, and references therein.
[2] D. Qi, C.-M. Tann, D. Haring, M. D. Distefano, *Chem. Rev.* **2001**, *101*, 3081 – 3111, and references therein.
[3] D. E. Benson, M. S. Wisz, H. W. Hellinga, *Curr. Opin. Biotechnol.* **1998**, *9*, 370 – 376.
[4] F. v. d. Velde, F. v. Rantwijk, R. A. Sheldon, *Trends Biotechnol.* **2001**, *19*, 73 – 80.
[5] J. A. Sigman, B. C. Kwok, Y. Lu, *J. Am. Chem. Soc.* **2000**, *122*, 8192 – 8196.
[6] O. Braha, B. Walker, S. Cheley, J. J. Kasianowicz, L. Song, J. E. Gouaux, H. Bayley, *Chem. Biol.* **1997**, *4*, 497 – 505.
[7] A. Miyawaki, J. Llopis, R. Heim, J. M. McCaffery, J. A. Adams, M. Ikura, R. Y. Tsien, *Nature* **1997**, *388*, 882 – 887.
[8] A. L. Pinto, H. W. Hellinga, J. P. Caradonna, *Proc. Natl. Acad. Sci. USA* **1997**, *94*, 5562 – 5567.
[9] S. Ozaki, H.-J. Yang, T. Matsui, Y. Goto, Y. Watanabe, *Tetrahedron: Asymmetry* **1999**, *10*, 183 – 192.
[10] I. Hara, T. Ueno, S. Ozaki, S. Itoh, K. Lee, N. Ueyama, Y. Watanabe, *J. Biol. Chem.* **2001**, *276*, 36067 – 36070.
[11] S. Kato, H.-J. Yang, T. Ueno, S. Ozaki, J. George N. Phillips, S. Fukuzumi, Y. Watanabe, *J. Am. Chem. Soc.* **2002**, *124*, 8506 – 8507.
[12] S. Ozaki, P. R. Ortiz de Montellano, *J. Am. Chem. Soc.* **1995**, *117*, 7056 – 7064.
[13] S. Neya, N. Funasaki, *J. Biol. Chem.* **1988**, *263*, 8810 – 8815.
[14] T. Hayashi, Y. Hitomi, T. Ando, T. Mizutani, Y. Hisaeda, S. Kitagawa, H. Ogoshi, *J. Am. Chem. Soc.* **1999**, *121*, 7747 – 7750.
[15] Y.-Z. Hu, S. Tsukiji, S. Shinkai, S. Oishi, I. Hamachi, *J. Am. Chem. Soc.* **2000**, *122*, 241 – 253.
[16] E. Monzani, G. Alzuet, L. Casella, C. Redaelli, C. Bassani, A. M. Sanangelantoni, M. Gullotti, L. D. Gioia, L. Santagostin, F. Chillemi, *Biochemistry* **2000**, *39*, 9571 – 9582.
[17] R. R. Davies, M. D. Distefano, *J. Am. Chem. Soc.* **1997**, *119*, 11643 – 11652.
[18] S. K. Ma, Y. Lu, *J. Inorg. Biochem.* **1999**, *74*, 217.
[19] M. R. Ermacora, J. M. Delfino, B. Cuenoud, A. Schepartz, *Proc. Natl. Acad. Sci. USA* **1992**, *89*, 6383 – 6387.
[20] D. S. Sigman, T. W. Bruice, A. Mazumder, C. L. Sutton, *Acc. Chem. Res.* **1993**, *26*, 98 – 104.
[21] E. G. Samsel, K. Srinivasan, J. K. Kochi, *J. Am. Chem. Soc.* **1985**, *107*, 7606 – 7617.
[22] K. Srinivasan, P. Michaud, J. K. Kochi, *J. Am. Chem. Soc.* **1986**, *108*, 2309 – 2320.
[23] E. N. Jacobsen in *Comprehensive organometallic chemistry II, Vol. 12* (Eds.: E. W. Abel, F. G. A. Stone, G. Wilkinson), Pergamon, New York, **1995**, pp. 1097 – 1135.
[24] T. Katsuki, *Coord. Chem. Rev.* **1995**, *140*, 189 – 214.
[25] C. L. Hunter, E. Lloyd, L. D. Eltis, S. P. Rafferty, H. Lee, M. Smith, A. G. Mauk, *Biochemistry* **1997**, *36*, 1010 – 1017.
[26] T. Hayashi, Y. Hisaeda, *Acc. Chem. Res.* **2002**, *35*, 35 – 43.
[27] I. Hamachi, S. Shinkai, *Eur. J. Org. Chem.* **1999**, 539 – 549.
[28] M. Tamura, T. Asakura, T. Yonetani, *Biochim. Biophys. Acta* **1973**, *295*, 467 – 479.
[29] S. Ozaki, M. Roach, T. Matsui, Y. Watanabe, *Acc. Chem. Res.* **2001**, *34*, 818 – 825.
[30] A crystal structure of Cr(3,3′-Me_2-salophen)·apo-A71GMb with a resolution of 1.8 Å shows a distance of 2.12 Å between the Cr^{III} ion and the Nε atom of imidazole in His 93. While we do not have the crystal structure of Cr·**2**·apo-Mb, we believe that it has the same coordination structure. The final refinement of the X-ray crystal structure of Cr(3,3′-Me_2-salophen)·apo-A71GMb is being completed by our group.
[31] Cr·**2**·BSA was synthesized by using a reported procedure.[36] The Cr atom content was determined by ICPAES, and protein concentration was determined by the bicinchoninic acid (BCA) method,[37] the protein/chromium ratio was determined to be 1:0.3. Catalytic reactions were carried out under the conditions described in Table 1 except for the concentration ([Cr] = 10 μM).
[32] K. Srinivasan, J. K. Kochi, *Inorg. Chem.* **1985**, *24*, 4671 – 4679.
[33] B. A. Springer, K. D. Egeberg, S. G. Sligar, R. J. Rohlfs, A. J. Mathews, J. S. Olson, *J. Biol. Chem.* **1989**, *264*.
[34] H. Chen, J. A. Cronin, R. D. Archer, *Macromolecules* **1994**, *27*, 2174 – 2180.
[35] P. Coggon, A. T. Mcphail, P. E. Mabbs, A. Richards, A. S. Thornley, *J. Chem. Soc. A* **1970**, 3296 – 3303.
[36] H. Y. Shrivastava, B. U. Nair, *Biochem. Biophys. Res. Commun.* **2000**, *270*, 749 – 754.
[37] P. K. Smith, R. I. Krohn, G. T. Hermanson, A. K. Mallia, F. H. Gartner, M. D. Provenzano, E. K. Fujimoto, N. M. Goeke, B. J. Olson, D. C. Klenk, *Anal. Biochem.* **1985**, *150*, 76 – 85.

 © 2003 Wiley-VCH Verlag GmbH & Co. KGaA, Weinheim 1433-7851/03/4209-1008 $ 20.00+.50/0

Nucleotide Bolaamphiphiles

Oligonucleotide-Templated Self-Assembly of Nucleotide Bolaamphiphiles: DNA-Like Nanofibers Edged by a Double-Helical Arrangement of A–T Base Pairs

*Rika Iwaura, Kaname Yoshida, Mitsutoshi Masuda, Mayumi Ohnishi-Kameyama, Mitsuru Yoshida, and Toshimi Shimizu**

In nanotechnology the "bottom-up" approach, the fabrication of nanostructures from molecular building blocks, is of great interest owing to its ease in preparation, low energy consumption, and potential to produce a great number of molecular nanostructures with well-defined three-dimensional morphologies.[1,2] In particular, self-assembly driven by molecular recognition has been recognized as a powerful strategy to give well-controlled hierarchical supramolecular assemblies[3] as well as hetero-assembled liquid crystals.[4] Recently, the combination of template effects with molecular recognition resulted in the hierarchical generation of supramolecular fibers, in which oligoisophthalamide and cyanuric acid served as the template.[5] The most sophisticated and advanced system based on template-induced and multiple-recognition-controlled fabrication is exemplified by natural DNA. It is, therefore, reasonable to use DNA as a template for making novel structures and highly functionalized materials. Most DNA-templated molecular assembly is, however, based on either the use of complementary DNAs[6] or the use of multiple electrostatic interactions along the DNA backbone.[7] Some researchers have also described DNA-ordered assembly in between lipid membranes by using a cationic lipid and anionic DNA.[8] We report here on the formation of DNA-like nanofibers, which are edged by a double-helical arrangement of A–T base pairs. These nanofibers result from the complementary oligonucleotide-templated self-assembly of the thymidine-appended bolaamphiphile **dTp-20-dTp** with a series of oligoadenylic acids $\mathbf{d(A)}_n$ ($n = 2$, 4, 6, 8, 10, 20, 40) .

The binary self-assembly of **dTp-20-dTp**/$\mathbf{d(A)}_n$ ($n = 2$, 4, 6, 8, 10, 20, 40) having the same number of adenine and thymine residues was found to gelatinize water after incubation for several days. These hydrogels have very different appearances. With increasing chain length of the template oligoadenylic acid, the color of the hydrogel changes gradually from white to transparent, and also the gel stiffness changes from rigid to loose. The morphology of the self-assembled nanofibers of the thymidine bolaamphiphiles proved to be strongly dependent on the chain length of the complementary oligoadenylic acid template. We recently reported on a TEM study of the hydrogel formed from **dTp-20-dTp** alone, in which we found three-dimensionally intertwined nanofibers 10–30 nm wide and several micrometers long,[9] dimensions typically seen in the gel structures of low-molecular-weight gelators.[10] Now we find that the nanofiber networks arising from the self-assembly of **dTp-20-dTp** in the presence of the relatively short templates $\mathbf{d(A)}_n$ ($n = 2$, 4, 6, 8) are similar to those formed from the single component alone (Figure 1a–d). When the chain length of the template is increased ($n = 10$, 20, 40), discrete helical nanofibers become evident, which have a width of 7–8 nm and length of several hundred nm (Figure 1e, 1f, and 1h). From the high-magnification image we estimate a helical pitch of approximately 20 nm (Figure 1g). Interestingly, the fiber lengths of the binary **dTp-20-dTp**/$\mathbf{d(A)}_{40}$ self-assembly extend to > 1 μm—much longer than that of the **dTp-20-dTp**/$\mathbf{d(A)}_{20}$ assembly (150–700 nm). Thus, for the nanostructures obtained with the range of templates from $\mathbf{d(A)}_2$ to $\mathbf{d(A)}_{40}$ we clearly observe both the increasing length of the nanofiber and, for templates with $n \geq 10$, the manifestation of helical structure.

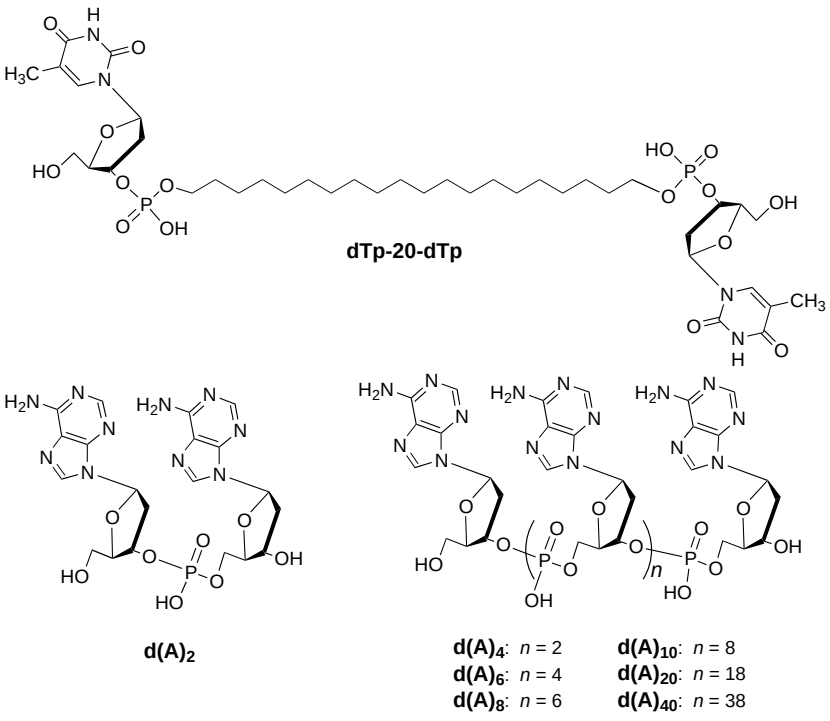

[*] Dr. T. Shimizu, Dr. K. Yoshida, Dr. M. Masuda
Nanoarchitectonics Research Center (NARC)
National Institute of Advanced Industrial Science and Technology (AIST)
CREST, Japan Science and Technology Corporation (JST)
Tsukuba Central 5, 1-1-1 Higashi, Tsukuba, Ibaraki 305-8565 (Japan)
Fax: (+81) 29-861-4545
E-mail: tshmz-shimizu@aist.go.jp
R. Iwaura
Graduate School of Chemistry, University of Tsukuba
1-1-1 Tennodai, Tsukuba, Ibaraki 305-8571 (Japan)
Dr. M. Ohnishi-Kameyama, Dr. M. Yoshida
National Food Research Institute
2-1-2 Kannondai, Tsukuba, Ibaraki 305-8642 (Japan)

 © 2003 Wiley-VCH Verlag GmbH & Co. KGaA, Weinheim 1433-7851/03/4209-1009 $ 20.00+.50/0

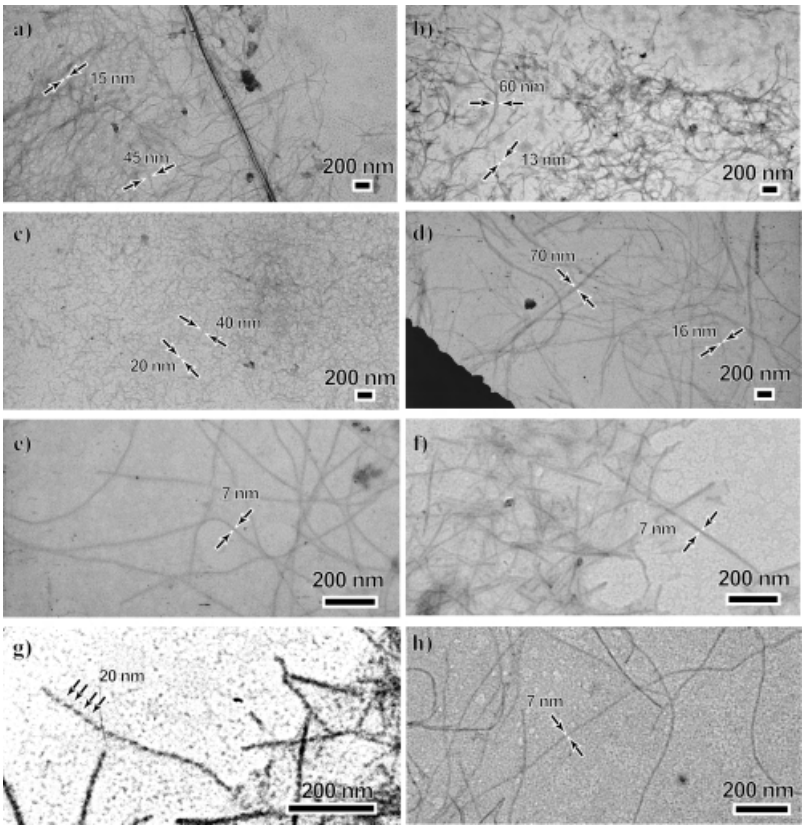

Figure 1. TEM image of nanofibers self-assembled from **dTp-20-dTp** in the presence of a) $\mathbf{d(A)_2}$, b) $\mathbf{d(A)_4}$, c) $\mathbf{d(A)_6}$, d) $\mathbf{d(A)_8}$, and e) $\mathbf{d(A)_{10}}$. TEM image of discrete, relatively long nanofibers self-assembled from **dTp-20-dTp** in the presence of f) $\mathbf{d(A)_{20}}$ and h) $\mathbf{d(A)_{40}}$. g) High-magnification TEM image of discrete supramolecular DNA-like nanofibers in f). The arrows note the helical pitch of 20 nm.

To verify that **dTp-20-dTp** actually complexes with each adenine unit of the oligoadenylic acid in water, we carried out electrospray-ionization Fourier-transform ion cyclotron resonance mass spectrometry (ESI-FTICR-MS), which has proved to be a powerful tool for the analysis of weakly bound species.[11] The soft ionization, high resolution, and high sensitivity of ESI-FTICR MS allow us to detect three peaks for **dTp-20-dTp** and $\mathbf{d(A)_2}$ in aqueous solutions, which are attributable to the 1:1 and 2:1 complexes.[12] These findings strongly support the view that **dTp-20-dTp** first complexes with a complementary oligoadenylic acid and then assembles to form nanofibers.

Attenuated total reflectance (ATR)-FTIR spectroscopic studies of each binary self-assembly in D_2O dispersion are quite compatible with this observation. In the case of the single-component **dTp-20-dTp** hydrogel, the thymine carbonyl stretching vibration appears at 1712 cm^{-1}, indicating that the thymine carbonyl groups take part in hydrogen bonding through either the T–T base pair or thymine–water interaction. In contrast, this band completely disappears for the $\mathbf{dTp\text{-}20\text{-}dTp/d(A)_{10}}$ hydrogel, indicating the liberation of the thymine carbonyl groups from hydrogen bonding (Figure 2). It should be noted here that the thymine carbonyl groups are free in Watson–Crick and Hoogsteen base-pairing.[13] Thus, this observation can support the fact that the thymidine bolaamphiphile **dTp-20-dTp** forms a complementary complex with $\mathbf{d(A)_{10}}$ at both ends through hydrogen-bonded A–T base pairs. The $\mathbf{dTp\text{-}20\text{-}dTp/d(A)_n}$ ($n = 20, 40$) binary self-assemblies also did not display this carbonyl vibration band. These ESI-FTICR and ATR-FTIR results also exclude the possibility of T-A-T base alignment upon complexation of **dTp-20-dTp** with the comparably longer $\mathbf{d(A)_n}$ ($n = 10, 20, 40$). Eventually the binary assemblies organize to form discrete nanofibers 7 nm wide. On the other hand, the observed nanofiber bundles and branches for $\mathbf{dTp\text{-}20\text{-}dTp/d(A)_n}$ ($n = 2, 4, 6, 8$) may arise from the cross-linking of the shorter oligoadenylic acids with **dTp-20-dTp** through A–T base pairs since the shorter $\mathbf{d(A)_n}$ ($n = 2, 4, 6, 8$) oligonucleotides are too short to act as templates for the formation of single nanofibers.

Variable-temperature circular dichroism (VT-CD) spectroscopy was very useful to get insight into both the enhancement of the helical profile and the melting behavior of the obtained nanofibers depending on the template lengths. Figure 3 displays VT-CD spectra for the binary self-assemblies in aqueous solutions. The CD spectrum of the $\mathbf{dTp\text{-}20\text{-}dTp/d(A)_2}$ assembly looks much different from those of the $\mathbf{dTp\text{-}20\text{-}dTp/d(A)_n}$ ($n = 10, 20, 40$) assemblies and also displays little change upon heating from 25 °C to 90 °C (Figure 3a). In contrast, the CD spectra of the $\mathbf{dTp\text{-}20\text{-}dTp/d(A)_{20}}$ and $\mathbf{dTp\text{-}20\text{-}dTp/d(A)_{40}}$ assemblies are temperature dependent (Figures 3b and 3c). The CD spectral profiles for the series of binary self-assemblies $\mathbf{dTp\text{-}20\text{-}dTp/d(A)_{20}}$ ($n = 10, 20, 40$) quite resemble that of **poly(dA)-poly(dT)** B-DNA,[14] in which the two strands of the sugar–phosphate backbone are stabilized by A–T base pairs. Furthermore, the temperature dependence of the CD intensities evaluated at $\lambda = 250$ nm shows a drastic increase at approximately 50 °C for $\mathbf{dTp\text{-}20\text{-}dTp/d(A)_{20}}$ and at 60 °C for $\mathbf{dTp\text{-}20\text{-}dTp/d(A)_{40}}$ (Figure 3b and 3c, inset). These observed T_m values are comparable to the previously measured T_m ($T_m = 53$ °C under the condition of $[Na^+] = 0.02$ M)[15] of the **poly(dA)-poly(dT)** B-DNA, which

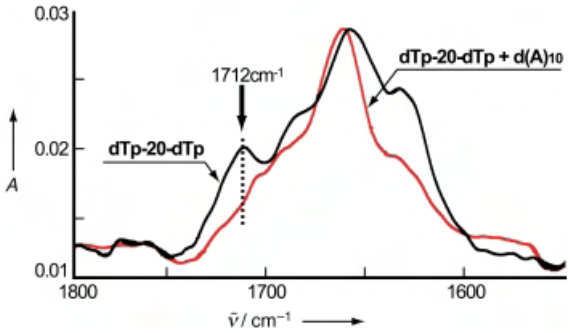

Figure 2. ATR-FTIR spectra of the **dTp-20-dTp** monoassembly and the $\mathbf{dTp\text{-}20\text{-}dTp/d(A)_{10}}$ binary assembly in D_2O. A = absorbance.

 © 2003 Wiley-VCH Verlag GmbH & Co. KGaA, Weinheim 1433-7851/03/4209-1010 $ 20.00+.50/0

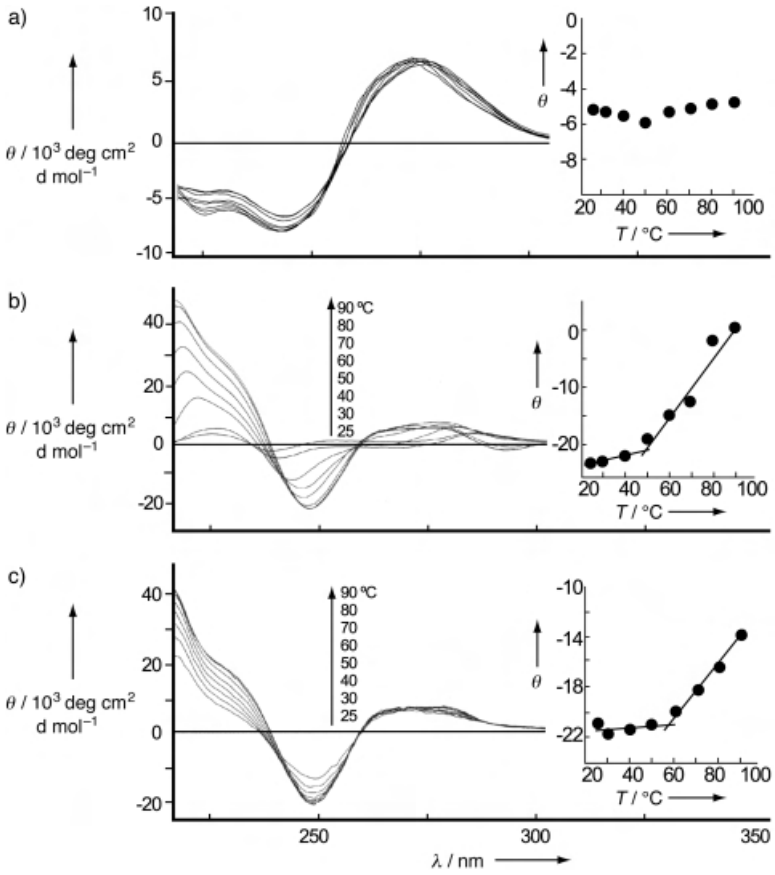

Figure 3. CD spectra of highly dilute aqueous solutions of the binary assemblies a) **dTp-20-dTp/d(A)$_2$**, b) **dTp-20-dTp/d(A)$_{20}$**, and c) **dTp-20-dTp/d(A)$_{40}$**, which were recorded with a 0.01-cm quartz cell ($c = 4 \times 10^{-3}$ M). Each inset shows the temperature dependence of the CD intensities at $\lambda = 250$ nm. θ = molar ellipticity.

proves directly the dissociation of the A–T base pairing. At this time, the possibility of the T-A-T base pair alignment can also be excluded since the concentration of divalent cations is very low and the pH is close to neutral in this system. One may notice here the relatively high thermal stability for the **dTp-20-dTp/d(A)$_{40}$** assembly. Thus, the template effect of the oligoadenylic acids on the self-assembled morphologies becomes evident with increasing chain length. In addition, longer templates **d(A)$_n$** ($n = 10$, 20, 40) are able to induce helical morphologies in single nanofibers, which are absent in the homo-assembled nanofibers.

Considering all of data and evidence presented here, one may envisage that the complementary A–T base pairs are aligned helically, edging both ends of the bolaamphiphile. Double strands of the oligonucleotide wind around the vertically stacked rods of the bolaamphiphiles around the same axis to give helical nanofibers (Figure 4). The CH_2 symmetric and antisymmetric stretching bands appear at 2918 and 2845 cm^{-1}, respectively, indicating a highly populated all-*trans* conformation on the oligomethylene chain. The center-to-center distance between two neighboring phosphate moieties of poly(adenylic acid)s is known to be approximately 0.7 nm in B-DNA, which fixes the spatial arrangement of two neighboring thymine residues of the stacked bolaamphiphiles at rotation angles of 8–10°. Thus, 36–45 of the thymidine bolaamphiphiles will be maximized at helical pitches of about 20 nm. This situation allows the base pair to be in the hydrophobic environment. Thus, the hydrophilic moieties of deoxyribose and phosphodiester of **dTp-20-dTp** are successfully exposed to external aqueous dispersion. The top view of the schematic illustration of molecular packing clearly shows this convenient circumstance for nanofiber formation (Figure 4). On the basis of the similarity of the CD spectra to that of B-DNA, the A–T base stacking is considered to form right-handed helical structures.

The diameter of the nanofiber obtained (7–8 nm) is slightly greater than the length of extended **dTp-20-dTp** molecules (3.5 nm). The double-helical strands of the sugar–phosphodiester backbone chains (two species, each 1.8–2.0 nm wide) of oligoadenylic acid are edging each end of the bolaamphiphile. Therefore, the measured widths of the nanofibers are well compatible the proposed structure.

In summary, we have demonstrated the formation of DNA-like nanofibers that can be seen in TEM through complementary oligonucleotide-templated self-assembly. This methodology should aid in accurately tuning the dimensions of high-axial-ratio nanostructures.

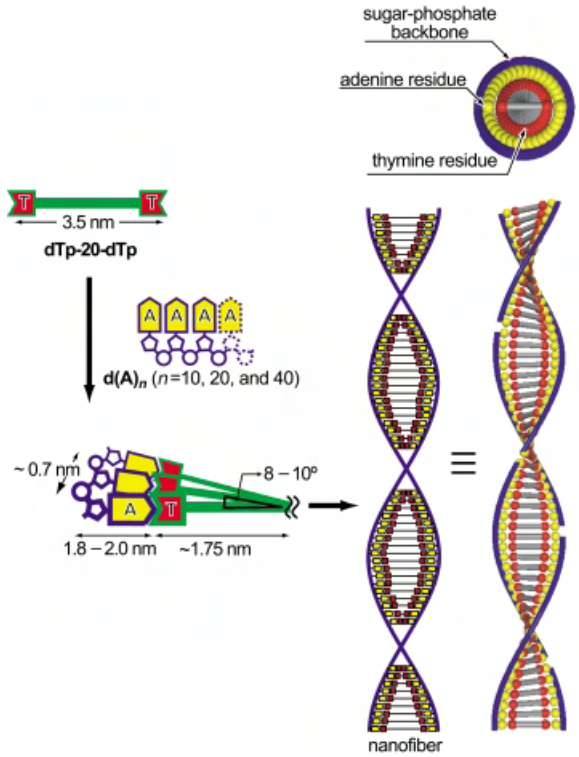

Figure 4. Illustration of the proposed mechanism of formation of the oligoadenylic acid templated self-assembly of the thymidine bolaamphiphiles. Red and yellow units represent the thymine and adenine residues, respectively.

 © 2003 Wiley-VCH Verlag GmbH & Co. KGaA, Weinheim 1433-7851/03/4209-1011 $ 20.00+.50/0

Experimental Section

The thymidine bolaamphiphile **dTp-20-dTp** was synthesized by using the phosphoramidite technique as described in reference [9]. Bolaamphiphile **dTp-20-dTp** was dispersed in water and completely dissolved by heating at 60 °C and sonication. To this aqueous solution was added an aqueous solution of $\mathbf{d(A)_n}$ ($n = 2, 4, 6, 8, 10, 20, 40$). For all the thymine residues to complex with adenine residues in a 1:1 ratio, the concentrations of **dTp-20-dTp** and $\mathbf{d(A)_{40}}$ were, for example, adjusted to 2.2×10^{-2}, 4.4×10^{-2}, 2.2×10^{-3}, and 1.1×10^{-3} M, respectively. TEM was carried out with a LEO 912 instrument (acceleration voltage 120 kV, Carl Zeiss). CD studies were performed on a JASCO J-800 spectropolarimeter operating between 220 and 400 nm.

Received: August 12, 2002
Revised: December 5, 2002 [Z19949]

[1] a) J.-M. Lehn, *Makromol. Chem. Macromol. Symp.* **1993**, *69*, 1; b) J.-H. Fuhrhop, J. Koening, *Membranes and Molecular Assemblies: The Synkinetic Approach*, The Royal Society of Chemistry, Cambridge, **1994**; c) G. M. Whitesides, E. E. Simanek, J. P. Mathias, C. T. Seto, D. N. Chin, M. Mammen, D. N. Gordon, *Acc. Chem. Res.* **1995**, *28*, 37; d) D. Philp, J. F. Stoddart, *Angew. Chem.* **1996**, *108*, 1242; *Angew. Chem. Int. Ed. Engl.* **1996**, *35*, 1154; e) S. C. Zimmerman, F. Zeng, D. E. C. Reichert, S. V. Kolotuchin, *Science* **1996**, *271*, 1095; f) T. Shimizu, M. Masuda, *J. Am. Chem. Soc.* **1997**, *119*, 2812; g) T. Kawasaki, M. Tokuhiro, N. Kimizuka, T. Kunitake, *J. Am. Chem. Soc.* **2001**, *123*, 6792; h) W. D. Jang, D. L. Jiang, T. Aida, *J. Am. Chem. Soc.* **2000**, *122*, 3232; i) M. Fujita, *Chem. Commun.* **2001**, 509, and references therein; j) M. Enomoto, A. Kishimura, T. Aida, *J. Am. Chem. Soc.* **2001**, *123*, 5608; k) T. Shimizu, *Macromol. Rapid Commun.* **2002**, *23*, 311; l) T. Kato, *Science* **2002**, *295*, 2414.

[2] a) J. H. Georger, A. Singh, R. R. Price, J. M. Schnur, P. Yager, P. E. Schoen, *J. Am. Chem. Soc.* **1987**, *109*, 6169; b) T. Shimizu, M. Mori, H. Minamikawa, M. Hato, *J. Chem. Soc. Chem. Commun.* **1990**, 183; c) B. N. Thomas, C. R. Safinya, R. J. Plano, N. A. Clark, *Science* **1995**, *267*, 1635; d) M. S. Spector, J. V. Selinger, A. Singh, J. M. Rodriguez, R. R. Price, J. M. Schnur, *Langmuir* **1998**, *14*, 3493; e) R. Oda, I. Huc, M. Schmutz, S. J. Candau, F. C. Mackintosh, *Nature* **1999**, *399*, 566.

[3] a) T. Gulik-Krzywicki, C. Fouquey, J.-M. Lehn, *Proc. Natl. Acad. Sci. USA* **1993**, *90*, 163; b) R. P. Sijbesma, F. H. Beijer, L. Brunsveld, B. J. B. Folmer, J. H. K. K. Hirschberg, R. F. M. Lange, J. K. L. Lowe, E. W. Meijer, *Science* **1997**, *278*, 1601; c) N. Kimizuka, T. Kawasaki, K. Hirata, T. Kunitake, *J. Am. Chem. Soc.* **1998**, *120*, 4094; d) T. Shimizu, R. Iwaura, M. Masuda, T. Hanada, K. Yase, *J. Am. Chem. Soc.* **2001**, *123*, 5947; e) T. Kawasaki, M. Tokuhiro, N. Kimizuka, T. Kunitake, *J. Am. Chem. Soc.* **2001**, *123*, 6792.

[4] a) T. Kato, M. Nakano, T. Moteki, T. Uryu, S. Ujiie, *Macromolecules* **1995**, *28*, 8875; b) T. Kawakami, T. Kato, T. *Macromolecules* **1998**, *31*, 4475.

[5] V. Berl, M. J. Krische, I. Huc, J.-M. Lehn, M. Schmutz, *Chem. Eur. J.* **2000**, *6*, 1938.

[6] a) N. C. Seeman, *Angew. Chem.* **1998**, *110*, 3408; *Angew. Chem. Int. Ed.* **1998**, *37*, 3220; b) J. J. Storhoff, C. A. Mirkin, *Chem. Rev.* **1999**, *99*, 1849; c) M. Scheffler, A. Dorenbeck, S. Jordan, M. Wustefeld, G. V. Kiedrowski, *Angew. Chem.* **1999**, *111,* 3514; *Angew. Chem. Int. Ed.* **1999**, *38*, 3312; d) B. Yurke, A. J. Turberfield, A. P. Mills, Jr, F. C. Simmel, J. L. Neumann, *Nature* **2000**, *406*, 605.

[7] C. M. Niemeyer, *Angew. Chem.* **2001**, *113*, 4254; *Angew. Chem. Int. Ed.* **2001**, *40*, 4128, and references therein.

[8] a) P. L. Felgner, G. Rhodes, *Nature* **1991**, *349*, 351; b) J. O. Raedler, I. Koltover, T. Salditt, C. R. Safinya, *Science* **1997**, *275*, 810.

[9] R. Iwaura, K. Yoshida, M. Masuda, K. Yase, T. Shimizu, *Chem. Mater.* **2002**, *14*, 3047.

[10] a) J.-H. Fuhrhop, C. Boettcher, *J. Am. Chem. Soc.* **1990**, *112*, 1768; b) G. R. Newkome, G. R. Baker, S. Arai, M. J. Saunders, P. S. Russo, K. J. Theriot, C. N. Moorefield, L. E. Rogers, J. E. Miller, T. R. Lieux, M. E. Murray, B. Phillips, L. Pascal, *J. Am. Chem. Soc.* **1990**, *112*, 8458; c) K. Hanabusa, M. Yamada, M. Kimura, H. Shirai, *Angew. Chem.* **1996**, *108*, 2086; *Angew. Chem. Int. Ed. Engl.* **1996**, *35*, 1949.

[11] a) J. E. Bruce, S. L. van Ordern, G. A. Anderson, S. A. Hofstadler, M. G. Sherman, A. L. Rockwood, R. D. Smith, *J. Mass Spectrom.* **1995**, *30*, 124; b) R. H. Griffey, K. A. Sannes-Lowery, J. J. Drader, V. Mohan, E. E. Swayze, S. A. Hofstadler, *J. Am. Chem. Soc.* **2000**, *122*, 9933; c) A. Sautter, D. G. Shmidt, G. Jung, F. Wuerthner, *J. Am. Chem. Soc.* **2001**, *123*, 5424.

[12] R. Iwaura, M. O. Kameyama, M. Yoshida, T. Shimizu, *Chem. Commun.* **2002**, 2658.

[13] H. H. Mantsch, D. Chapman, *Infrared Spectroscopy of Biomolecules*, Wiley-Liss, New York, **1996**.

[14] D. M. Gray, K. H. Johnson, M. R. Vaughan, P. A. Morris, J. C. Sutherland, R. L. Ratliff, *Biopolymers* **1990**, *29*, 317.

[15] O. Gotoh, Y. Tagashira, *Biopolymers* **1981**, *20*, 1033.

 © 2003 Wiley-VCH Verlag GmbH & Co. KGaA, Weinheim 1433-7851/03/4209-1012 $ 20.00+.50/0

Reactions in Host–Guest Complexes

Molecular Mousetraps: Gas-Phase Studies of the Covalent Coupling of Noncovalent Complexes Initiated by Reactive Carbenes Formed by Controlled Activation of Diazo Precursors**

Ryan R. Julian, Jeremy A. May, Brian M. Stoltz, and J. L. Beauchamp**

Molecular recognition is a powerful technique that can be used to generate noncovalently bound host–guest complexes for a variety of purposes.[1,2] These noncovalent complexes are easily transferred to the gas phase by electrospray ionization

[*] Prof. J. L. Beauchamp, R. R. Julian
Beckman Institute
California Institute of Technology
Pasadena, CA 91125 (USA)
Fax: (+1) 626-568-8641
E-mail: jlbchamp@its.caltech.edu
Prof. B. M. Stoltz, J. A. May
The Arnold and Mabel Beckman Laboratories of Chemical Synthesis, Division of Chemistry and Chemical Engineering
California Institute of Technology
Pasadena, CA 91125 (USA)
Fax: (+1) 626-564-9297
E-mail: stoltz@caltech.edu

[**] The authors gratefully acknowledge funding provided by NSF (Grant CHE-9727566), the Beckman Institute Foundation, the California Institute of Technology, the Camille and Henry Dreyfus Foundation (New Faculty Award to B.M.S.), and Abbott Labs (graduate fellowship to J.A.M.). Special thanks to the Peter Dervan group for aid in the use of their HPLC apparatus.

Supporting information for this article is available on the WWW under http://www.angewandte.org or from the author.

 © 2003 Wiley-VCH Verlag GmbH & Co. KGaA, Weinheim 1433-7851/03/4209-1012 $ 20.00+.50/0

(ESI).[3] Attempts to effect intermolecular reactions between the cluster components are often frustrated by the lability of noncovalent complexes, which results from the relatively weak interactions that hold them together. In the present work, we have successfully initiated intermolecular reactions in noncovalent clusters. First, a strongly bound host–guest complex is formed in solution and transferred to the gas phase by ESI. Second, a diazo group that has been incorporated into the host is efficiently and easily converted into a highly reactive carbene[4] by low-energy collision-activated dissociation (CAD).[5] This carbene[6,7] then reacts in an intermolecular fashion, covalently binding the host–guest complex. These reagents are herein referred to as "molecular mousetraps".

We have synthesized and examined the chemistry of the prototypical molecular mousetraps **1** and **2**. 18-Crown-6 (18C6) is a well-known host for protonated primary amines, both in solution and in the gas phase.[8] For example, we have recently shown that 18C6 selectively binds to lysine residues in small peptides.[3a] Mousetrap **1** is designed to bind molecules with either one or, preferentially, two protonated primary amines. Mousetrap **2**, with a single 18C6 unit, binds to a single protonated primary amine. Structure **3** was used as a model compound in computations.

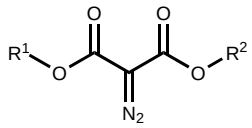

1 $R^1 = R^2 = CH_2$–18C6
2 R^1 = Et, $R^2 = CH_2$–18C6
3 $R^1 = R^2$ = Me

A possible interaction between **1** and doubly protonated 1,6-diaminohexane (DAH) is shown in Figure 1. This complex forms in solution, and can be transferred intact to the gas phase by ESI, as seen in Figure 2a. The complex can be isolated and subjected to CAD, as shown in Figure 2b. The sole product results from a neutral loss of 28 Da, which is interpreted to be the loss of N_2 from the diazo group. Significantly, the result shown in Figure 2b provides evidence for covalent-bond cleavage in preference to dissociation of the complex. The loss of N_2 from the diazo group should yield the corresponding carbene (**:1**) as a highly reactive, short-lived intermediate. This carbene can then undergo either intermolecular or intramolecular reaction.

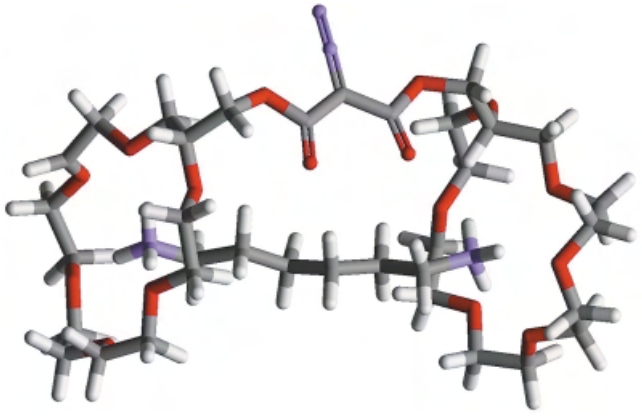

Figure 1. One possible structure for the noncovalent adduct of **1** and doubly protonated 1,6-diaminohexane (DAH) in the gas phase, as determined by PM3 semiempirical calculations.

The product described in Figure 2b is subjected to further collisional activation, as shown in Figure 2c. The majority of the product-ion intensity results from covalent-bond cleavage with loss of a crown, or part of a crown and retention of DAH. The fragmentation of the host without the accompanying loss of the guest provides evidence that an intermolecular reaction involving covalent coupling between the host and guest occurs by C–H insertion of the carbene. For the doubly protonated DAH, the complexation of the protonated primary amines by the crown ethers reduces the likelihood of an N–H insertion reaction by the carbene.[9] It is also observed in Figure 2c that some of the DAH appears to dissociate from the complex, which suggests that an intramolecular process[10] is competitive in this case.

Singly charged DAH has a lower binding energy to **1** than the doubly charged species, yet Figure 2d illustrates that $[\mathbf{:1} + \mathrm{DAH} + \mathrm{H}]^+$ is generated with high efficiency from the $[\mathbf{1} + \mathrm{DAH} + \mathrm{H}]^+$ complex. The loss of nitrogen is accompanied by an additional loss of 294 Da, which can be accounted for by the loss of 18-crown-6 methanol. This additional loss is observed for all complexes of both **1** and **2** in which there is an unprotonated primary amine or alcohol available (in experiments with **2**, the loss of ethanol is also observed). DFT calculations at the B3LYP/CCPVTZ(-F)$^+$ level on **:3** describe a singlet ground state, with a singlet/triplet splitting of 3 ± 1 kcal mol^{-1}. This result suggests that the singlet state is certainly accessible and perhaps favorable, which is in agreement with experimental results.[11] DFT calculations at the B3LYP/6-31G** level on **:3** and methylamine lead to the formation of an ammonium ylide without a barrier. The ammonium ylide is a local minimum on the potential energy surface, and previous reports have suggested that all carbenes will initially react with amines by the formation of an intermediate ylide.[12] From this ammonium ylide two reaction pathways with minimal barriers are possible, as shown in Scheme 1, and it should be pointed out that both pathways lead to covalent attachment of the host–guest complex through intermolecular reactions; one route leads to formal N–H insertion, and the other leads to the loss of an alcohol group and the generation of a ketene.

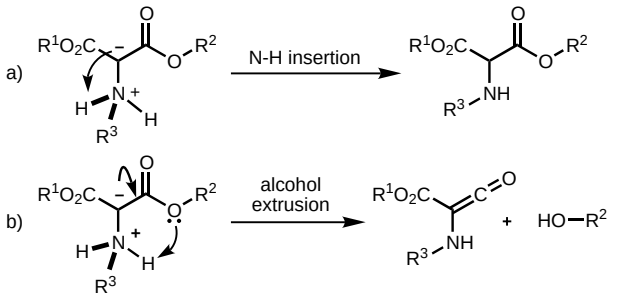

Scheme 1.

 © 2003 Wiley-VCH Verlag GmbH & Co. KGaA, Weinheim 1433-7851/03/4209-1013 $ 20.00+.50/0

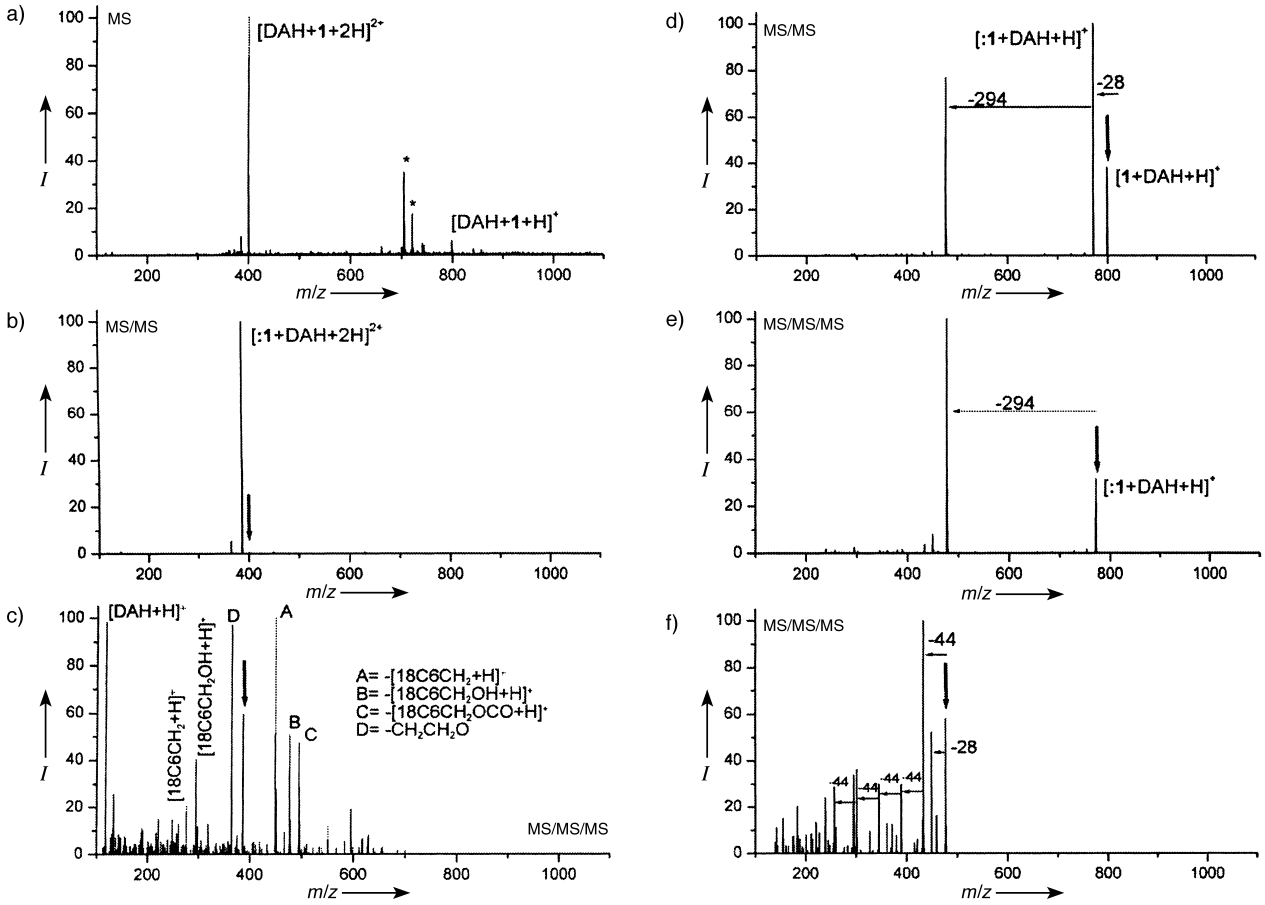

Figure 2. a) Mass spectrum of **1** with DAH; b) CAD spectrum of $[\mathbf{1}+\mathrm{DAH}+2\mathrm{H}]^{2+}$ which shows the almost exclusive loss of 28 Da and indicates the generation of carbene **:1**; c) MS/MS/MS analysis of the $[\mathbf{:1}+\mathrm{DAH}+2\mathrm{H}]^{2+}$ peak. Dissociation is accompanied by covalent bond cleavage, which suggests C–H insertion by **:1** and the formation of a new molecule; d) CAD of $[\mathbf{1}+\mathrm{DAH}+\mathrm{H}]^{+}$, which leads entirely to intermolecular reaction products; e) MS/MS/MS analysis of $[\mathbf{:1}+\mathrm{DAH}+\mathrm{H}]^{+}$, which only results in the loss of 294 Da. The absence of complex dissociation suggests covalent attachment; f) MS/MS/MS analysis of $[\mathbf{:1}+\mathrm{DAH}+\mathrm{H\text{-}294}]^{+}$. In the absence of both crowns DAH is retained, which confirms the covalent coupling of the complex. A bold downward arrow indicates the peak being subjected to CAD. *I* = relative intensity, * = 1 + alkali-metal adduct peaks.

Further excitation of the isolated $[\mathbf{:1}+\mathrm{DAH}+\mathrm{H}]^{+}$ species, after the loss of nitrogen, exclusively leads to the loss of 294 Da, as shown in Figure 2e. The N–H insertion product shown in Scheme 1a is protonated at the secondary amine. Transfer of this proton to the ester can lead to the loss observed in Figure 2e by alcohol extrusion. It is also possible, though unlikely, that the ammonium ylide, represented by the data in Figure 2d, could be sufficiently long-lived to yield this product directly.

Figure 2f offers several critical results. First, the loss of 28 Da is probably a result of the loss of CO from the ketene product shown in Scheme 1b. Second, the fragment being subjected to further collisional activation in Figure 2f contains only a single remaining crown. The primary losses are multiple $\{CH_2CH_2O\}$ fragments from this remaining crown. The data reveals the sequential removal of almost the entire remaining crown ether without the loss of the guest molecule. In the absence of both crowns, retention of the guest can only be explained by a newly formed covalent bond.

These studies demonstrate that reagents that bind to specific functional groups in complex molecules can be derivatized to introduce the means to covalently couple them to target molecules with appropriate methods of activation. We have combined 18C6, which binds strongly to protonated primary amines,[3a] with a diazo precursor to a reactive carbene to form a potent "molecular mousetrap" that can be used to target lysines in peptides or proteins. Full details of the chemistry and applications of these and related molecular mousetraps will be described in further publications.

Experimental Section

All spectra were obtained using a Finnigan LCQ ion-trap quadrupole mass spectrometer without modification. Sample concentrations were typically kept in the 10 to 100 μM range for all species of interest. All samples were electrosprayed in an 80:20 mixture of methanol/water. The appropriate host was added to the sample and electrosprayed with the guest in order to observe adduct formation. Full characterization and synthetic details for hosts **1** and **2** are available in the Supporting Information. Semiempirical calculations for Figure 1 were performed on HyperChem 5.1 Professional Suite using the PM3 parameter set.

 © 2003 Wiley-VCH Verlag GmbH & Co. KGaA, Weinheim 1433-7851/03/4209-1014 $ 20.00+.50/0

Calculations to determine the singlet/triplet splittings were performed on structures fully optimized at the B3LYP/CCPV-TZ(-F)+ level of theory. Comparison of this methodology with previous computational and experimental results for the following carbenes: CH_2, HCCl, HCF, CCl_2, CF_2, and HCCHO yielded results within (on average) ± 0.6 kcal mol^{-1} of the best experimental or theoretical value.[13] Zero-point energy corrections were not included. Reactions were modeled at the B3LYP/6-31G** level of theory by minimizing structures containing both reactants, with several different starting geometries. Initial geometries included likely starting points for the most probable reaction mechanisms, that is, hydrogen abstraction, concerted insertion, and ylide formation. The DFT calculations were carried out using Jaguar 4.1 (Schrödinger, Inc., Portland, Oregon).

Received: October 23, 2002 [Z50415]

[1] M. W. Peczuh, A. D. Hamilton, *Chem. Rev.* **2000**, *100*, 2479 – 2494.

[2] P. D. Beer, P. A. Gale, D. K. Smith, *Supramolecular Chemistry*, Oxford University Press, New York, **1999**.

[3] a) R. R. Julian, J. L. Beauchamp, *Int. J. Mass Spectrom.* **2001**, *210*, 613 – 623; b) R. D. Smith, J. E. Bruce, Q. Y. Wu, Q. P. Lei, *Chem. Soc. Rev.* **1997**, *26*, 191 – 202; c) T. D. Veenstra, *Biophys. Chem.* **1999**, *79*, 63 – 79; d) J. A. Loo, *Int. J. Mass Spectrom.* **2000**, *200*, 175 – 186.

[4] A neutral, two-electron carbene is formed. Other studies have focused on carbene radical cations such as $[CH_2]^+$, see for example: R. Flammang, M. T. Nguyen, G. Bouschoux, P. Gerbaux, *Int. J. Mass Spectrom.* **2002**, *202*, A8 – A25.

[5] a) E. M. Marzluff, J. L. Beauchamp in *Large Ions: Their Vaporization, Detection, and Structural Analysis*; (Eds.: T. Baer, C. Y. Ng, I. Powis), Wiley, New York, **1996**, pp. 115 – 143; b) S. A. McLuckey, *J. Am. Soc. Mass Spectrom.* **1992**, *3*, 599 – 614; c) R. N. Hayes, M. L. Gross, *Methods Enzymol.* **1990**, *193*, 237 – 263.

[6] a) F. O. Rice, A. L. Glasebrook, *J. Am. Chem. Soc.* **1934**, *56*, 2381 – 2383; b) G. Herzberg, *Proc. R. Soc. London Ser. A* **1961**, *262*, 291 – 317; c) *Carbenes, Vols. 1 and 2* (Eds.: R. A. Moss, M. Jones, Jr.), Wiley, New York, **1973**, 1975; d) J. D. Rynbrandt, B. S. Rabinovitch, *J. Phys. Chem.* **1970**, *74*, 4175 – 4176; e) J. D. Rynbrandt, B. S. Rabinovitch, *J. Chem. Phys.* **1971**, *54*, 2275 – 2276; f) J. C. Poutsma, J. J. Nash, J. A. Paulino, R. R. Squires, *J. Am. Chem. Soc.* **1997**, *119*, 4686 – 4697; g) J. A. Paulino, R. R. Squires, *J. Am. Chem. Soc.* **1991**, *113*, 5573 – 5580; h) D. G. Leopold, K. K. Murray, A. E. S. Miller, W. C. Lineberger, *J. Chem. Phys.* **1985**, *83*, 4849 – 4865, and references therein; i) R. Bertani, R. A. Michelin, M. Mozzon, P. Traldi, R. Seraglia, L. Busetto, M. C. Cassani, P. Tagleatesta, G. D'Arcangelo, *Organometallics* **1997**, *16*, 3229 – 3233.

[7] a) M. P. Doyle, M. A. McKervey, T. Ye, *Modern Catalytic Methods for Organic Synthesis with Diazo Compounds*, Wiley-Interscience, New York, **1998**; b) C. J. Moody, Whitham, G. H. *Reactive Intermediates*, Oxford University Press, New York, **1992**, pp. 26 – 50.

[8] a) J. S. Bradshaw, R. M. Izatt, A. V. Borkunov, C. Y. Zhu, J. K. Hathaway, *Comprehensive Supramolecular Chemistry, Vol. 1* (Ed.: G. W. Gokel), Pergamon/Elsevier, Oxford, **1996**, pp. 35 – 95; b) S. Maleknia, J. Brodbelt, *J. Am. Chem. Soc.* **1993**, *115*, 2837 – 2843; c) D. V. Dearden, C. Dejsupa, Y. Liang, J. S. Bradshaw, R. M. Izatt, *J. Am. Chem. Soc.* **1997**, *119*, 353 – 359; d) C. A. Schalley, *Mass Spectrom. Rev.* **2001**, *20*, 253 – 309; e) J. A. Loo, *Int. J. Mass Spectrom.* **2000**, *200*, 175 – 186.

[9] 18C6 locks protons onto primary amines, see ref. [3a] and: S.-W. Lee, H.-N. Lee, H. S. Kim, J. L. Beauchamp, *J. Am. Chem. Soc.* **1998**, *120*, 5800 – 5805.

[10] A Wolff rearrangement is a likely competing reaction for the carbene. See, for example, a) I. Likhotvorik, Z. Zhendong, E. L. Tae, E. Tippmann, B. T. Hill, M. S. Platz, *J. Am. Chem. Soc.* **2001**, *123*, 6061 – 6068; b) ref. [13].

[11] Both results obtained in the current work and in: D. C. Richardson, M. E. Hendrick, M. Jones, *J. Am. Chem. Soc.* **1971**, *93*, 3790 – 3791, where Wolff rearrangement is observed, must proceed through the singlet state.

[12] J. R. Pliego, W. B. Almeida, *J. Phys. Chem. A* **1999**, *103*, 3904 – 3909.

[13] A. P. Scott, M. S. Platz, L. Radom, *J. Am. Chem. Soc.* **2001**, *123*, 6069 – 6076.

 © 2003 Wiley-VCH Verlag GmbH & Co. KGaA, Weinheim 1433-7851/03/4209-1015 $ 20.00+.50/0

Lanthanide–TCNQ Magnet

A Rare-Earth Metal TCNQ Magnet: Synthesis, Structure, and Magnetic Properties of $\{[Gd_2(TCNQ)_5(H_2O)_9][Gd(TCNQ)_4(H_2O)_3]\}\cdot 4H_2O$**

*Hanhua Zhao, Mervin J. Bazile, Jr., José R. Galán-Mascarós, and Kim R. Dunbar**

One of the most rapidly expanding areas of coordination chemistry research is the design of magnetic materials based on molecular building blocks.[1] A perusal of the literature reveals that a successful design strategy for preparing molecular magnets is the coordination of organic radicals such as nitronyl nitroxides[2] and organocyanides such as $TCNE^{-\cdot}$ (tetracyanoethylene)[3] and $TCNQ^{-\cdot}$ (7,7,8,8-tetracyanoquinodimethane)[4] to paramagnetic transition metal ions. The presence of both metal spins (typically $S > 1/2$) and organic spin carriers ($S = 1/2$) leads to strong local super-

[*] Prof. K. R. Dunbar, H. Zhao, M. J. Bazile, Jr.
Department of Chemistry
Texas A&M University
College Station, TX 77842–3012 (USA)
Fax: (+1) 979-845-7177
E-mail: dunbar@mail.chem.tamu.edu
Dr. J. R. Galán-Mascarós
Instituto de Ciencia Molecular
Universidad de Valencia
Dr. Moliner, 50, 46100 Burjasot (Spain)

[**] K.R.D. gratefully acknowledges the National Science Foundation for a Nanoscale Science and Engineering NIRT Grant (DMR-0103455) and a PI Grant (CHE-9906583) and for equipment grants to purchase the CCD X-ray equipment (CHE-9807975) and the SQUID magnetometer (NSF-9974899). H.Z. acknowledges the Science and Technology Committee of Jiangsu Province of China for the donation of f-block starting materials. M.J.B. thanks the Welch Foundation (A1449) and NSF (CHE-9906583) for support and Professor T. R. Hughbanks for his helpful advice and discussion. TCNQ = 7,7,8,8-tetracyanoquinodimethane.

Supporting information for this article is available on the WWW under http://www.angewandte.org or from the author.

 © 2003 Wiley-VCH Verlag GmbH & Co. KGaA, Weinheim 1433-7851/03/4209-1015 $ 20.00+.50/0

exchange interactions, the ultimate result of which is typically ferro- or ferrimagnetic ordering.

Although molecular magnetic materials based on 3d metals are quite common, analogous 4f element compounds are relatively rare. A few research groups have explored the magnetic-exchange interactions in mixed 3d–4f compounds[5] and 4f–organic radical materials. A notable example is the recently reported compound $[\{CuL\}_2Gd(TCNQ)_2]\cdot TCNQ\cdot CH_3OH\cdot 2\,CH_3CN$ (L = *N,N′*-propylenebis(3-methoxysalicylideneiminato) containing three different types of spin carriers (3d–4f–organic radical).[6] The magnetic properties of this mixed salt are indicative of ferromagnetic coupling between Cu^{II} and Gd^{III} ions with no contribution from the TCNQ radicals, presumably due the presence of $[TCNQ_2]^{2-}$ dimers.

Until recently, the issue of whether magnetic ordering is possible in 4f coordination polymers was an open question,[7] but recent work by Miller and co-workers have provided the first examples in which 4f elements coordinated to $TCNE^{-\bullet}$ yield products that undergo spontaneous magnetization after thermal annealing.[8] Unfortunately, no structural information is yet available for these phases. Herein we report a crystalline rare-earth TCNQ magnet that magnetically orders at 3.5 K.

Slow diffusion of deoxygenated water solutions of $GdCl_3\cdot 6H_2O$ and Li[TCNQ] (1:1 ratio) yields crystals of the title compound, $\{[Gd_2(TCNQ)_5(H_2O)_9][Gd(TCNQ)_4(H_2O)_3]\}\cdot 4H_2O$ (**1**). The unusual structure of the material consists of alternating anionic and cationic layers perpendicular to the *c* axis, both of which are based on a 2D network of Gd^{III} ions coordinated to TCNQ radical anions. The different ratios of Gd^{III} and $TCNQ^{-\bullet}$ in the two independent layers leads to the unusual situation of having both cationic and anionic networks. Thermal ellipsoid plots of both networks for the crystal are depicted in Figure 1.[9]

The cationic network, $[Gd_2(TCNQ)_5(H_2O)_9]^+$ contains two crystallographically independent Gd^{III} (Gd1 and Gd3) ions and five $TCNQ^-$ molecules. Both Gd^{III} ions are nine-coordinate, but Gd1 is coordinated to five $TCNQ^-$ radicals and four water molecules, whereas Gd3 is bound to four TCNQ and five water molecules. The $TCNQ^-$ ligands exhibit three different binding modes, namely μ_3-$TCNQ^-$ (bridging between two Gd3 and one Gd1 ions), μ_2-$TCNQ^-$ (bridging between Gd1 and Gd3) and terminal $TCNQ^-$. The result of this complicated connectivity pattern is the 2D network depicted in Figure 2a which consists of "$(Gd3)_2TCNQ_2$ dimers" connected to a third Gd atom (Gd1) by another $TCNQ^-$ bridging ligand to yield "chains" which are further stitched together by Gd1 ions to form the 2D network in the *ab* plane.

The anionic network, $[Gd(TCNQ)_4(H_2O)_3]^-$ contains one unique Gd^{III} ion (Gd2) and four $TCNQ^-$ molecules (Figure 1b). The nine-coordinate Gd2 ion is surrounded by six N atoms from $TCNQ^-$ ligands acting as nitriles and three H_2O molecules. Three of the four unique $TCNQ^-$ ligands act as μ_2-bridges and one is a terminal ligand. The result of these binding modes is a network formed by $[Gd_2TCNQ_2]$ "dimers" which are connected through perpendicularly oriented $TCNQ^-$ ligands to yield a pseudo-hexagonal motif (Figure 2b), in which each "dimer" is connected to four near neighboring dimers.

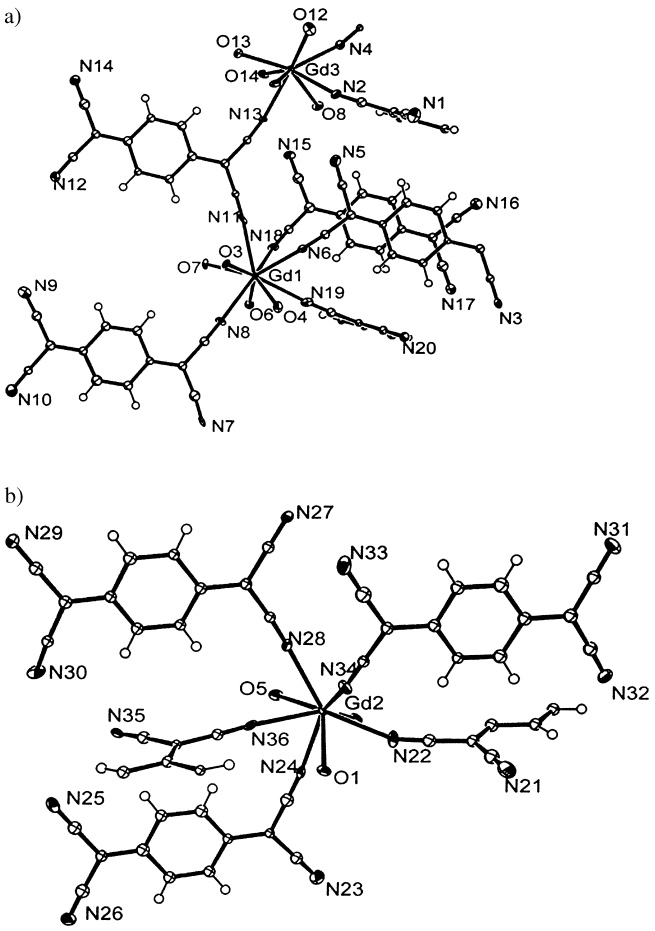

Figure 1. Structure of $\{[Gd_2(TCNQ)_5(H_2O)_9][Gd(TCNQ)_4(H_2O)_3]\}\cdot 4H_2O$; thermal ellipsoid representations of the cationic (a) and anionic (b) networks.

Two important supramolecular features regarding the structure of $\{[Gd_2(TCNQ)_5(H_2O)_9][Gd(TCNQ)_4(H_2O)_3]\}\cdot 4H_2O$ are worthy of note. The dangling nitrile substituents of the $TCNQ^-$ ligands are involved in hydrogen bonding to coordinated H_2O molecules, which affords extra stabilization to the 2D networks, and, most importantly, the anionic and cationic frameworks are involved in 1D π-stacking interactions between $TCNQ^-$ radicals. The stacking distances are uniform, (~3.2 Å) with no apparent dimerization being evident. There are also TCNQ ligands that do not participate in the stacking interactions, which lie perpendicular to these chains. Overall, it is evident that the packing is very efficient and there is little available free space.

The title compound **1** can also be prepared in bulk as a polycrystalline material from $GdCl_3\cdot 6H_2O$ and LiTCNQ. Elemental and thermal gravimetric analyses as well as powder X-ray diffraction analysis support the conclusion that this polycrystalline material is structurally very similar to the crystals obtained by slow diffusion (see Supporting Information). The IR spectrum exhibits a similar stretching frequency for the bulk material, ν(C≡N) 2177 cm^{-1}. That value is similar to that of the crystals, ν(C≡N) 2180 cm^{-1}. These values are typical for mono-reduced TCNQ. Notably, the number of

 © 2003 Wiley-VCH Verlag GmbH & Co. KGaA, Weinheim 1433-7851/03/4209-1016 $ 20.00+.50/0

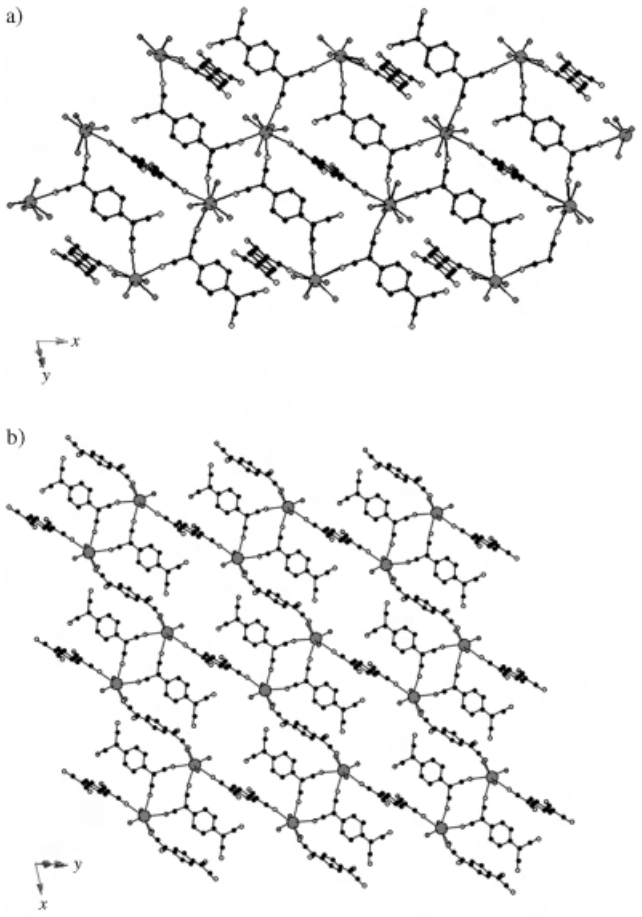

Figure 2. a) Top view of the tetrameric chains (terminal TCNQ ligands have been omitted for clarity) in the cationic network of **1**. b) Top view of the 2D anionic network (terminal TCNQ ligands have been omitted for clarity) in **1**.

water molecules present in the bulk material varies with the extent of drying as supported by TGA analysis.

The magnetic properties of **1** were investigated over the temperature range 2–300 K at 1000 G. The $\chi_m T$ product shows a slight decrease from a room-temperature value of 27.3 emu K mol^{-1}, down to 25.6 emu K mol^{-1} at 50 K. The high-temperature data were fit to a Curie–Weiss law, with a Curie constant of 27.1 emu K mol^{-1}, which is in good agreement with the expected value for three isolated Gd^{III} ions ($S = 7/2$) and nine $TCNQ^-$ radical anions ($S = 1/2$) in a magnetically dilute sample (27 emu K mol^{-1} for $g = 2$). The Weiss constant ($\theta = -5.07$ K) is small and negative, indicative of antiferromagnetic interactions between spin carriers. At temperatures near 10 K, the value of $\chi_m T$ begins to increase, and at 2 K the value abruptly increases, which is an indication of the onset of spontaneous magnetization. In accord with the conclusion that magnetic ordering is occurring, AC magnetic susceptibility measurements were performed. The results are plotted in Figure 3 where it can be clearly seen that the material exhibits an out-of-phase signal (χ''_m) at T_c ~3.5 K. No AC frequency dependence of the AC signal was observed up to 1000 Hz.

The presence of antiferromagnetic interactions, as hinted by the thermal dependence of the DC susceptibility, was confirmed by the field dependence of the magnetization at 1.8 K. The magnetization increases rapidly at low fields, and at $H > \sim 4$ T, the signal reaches saturation at a magnetization value of 18.1 μB, or 18 spins, which represents an intermediate value from the total 30 spins present. This result supports the conclusion that the nature of the magnetic ordering is, indeed, ferrimagnetic, and arises from the non-compensated spins in an antiparallel spin alignment. Notably, magnetically, this material is actually three-dimensional with multiple interactions. The structure renders it very difficult to provide a simple rationalization of the magnetic data. In addition to the intra-layer interactions, including direct exchange (Gd-TCNQ) and superexchange (between TCNQ groups through the Gd bridges, and vice versa); there are also strong magnetic interactions between layers through the short π–π contacts between TCNQ units in adjacent layers. It is well known that the latter type of interaction is antiferromagnetic. Unfortunately, the complexity of the system does not allow further magnetic analysis at this point, including the sign and strength of every single magnetic interaction present in the compound. But the magnetic data clearly indicate that some of the magnetic interactions are antiferromagnetic, a situation that leads us to define the material as a ferrimagnet. The preparation of molecular model compounds (dimers) is needed to reach a better understanding of this material. The material behaves as a soft magnet and does not show hysteretic behavior at 1.8 K.

In conclusion, the polymeric salt $\{[Gd_2(TCNQ)_5(H_2O)_9][Gd(TCNQ)_4(H_2O)_3]\}\cdot 4H_2O$ has been crystallized and shown to consist of both cationic and anionic layers that exhibit different ratios of Gd^{III} and $TCNQ^-$ radicals. This material is only the third example of a lanthanide/organic radical based magnet to our knowledge and the first lanthanide–TCNQ magnet. Efforts to incorporate more anisotropic lanthanide ions such as Eu^{3+} and Dy^{3+} into polymeric materials with $TCNQ^{-\bullet}$ are currently in progress.

Experimental Section

All reactions were performed under nitrogen using standard Schlenk techniques. Single crystals were obtained by layering a solution of

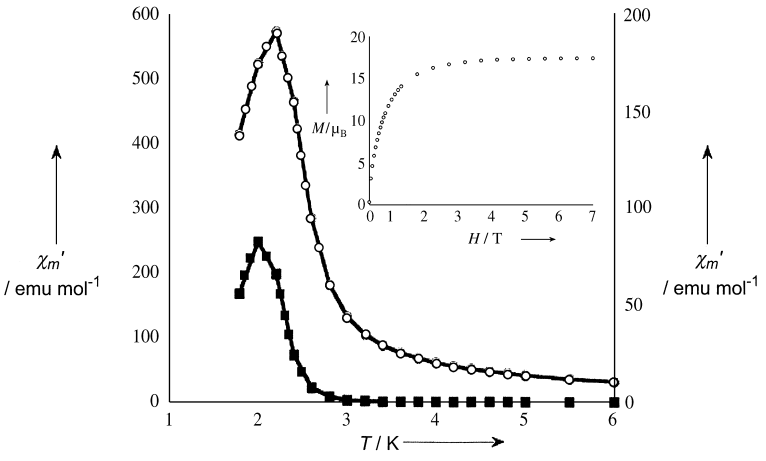

Figure 3. AC susceptibility data for **1**: (○) in-phase response (χ'_m); (■) out-of-phase response (χ''_m). The inset is the plot of magnetization versus field performed at 1.8 K.

 © 2003 Wiley-VCH Verlag GmbH & Co. KGaA, Weinheim 1433-7851/03/4209-1017 $ 20.00+.50/0

$GdCl_3 \cdot 6H_2O$ (150 mg in 20 mL of degassed H_2O) with Li[TCNQ] (84 mg in 20 mL of degassed H_2O) in a Schlenk tube. The bulk reaction product was obtained in the form of a dark purple precipitate by adding degassed H_2O (20 mL) to a solid mixture of $GdCl_3 \cdot 6H_2O$ (220 mg, 0.59 mmol) and Li[TCNQ] (125 mg, 0.59 mmol) in a Schlenk flask. The solution was stirred for 30 min and then left undisturbed overnight. The powder was collected by vacuum filtration, washed with copious amounts of H_2O, and dried under vacuum; yield 162 mg (31 %).

DC magnetic susceptibility measurements were preformed on crushed single crystals of **1** (2.89 mg) with a Quantum Design MPMS-2 SQUID magnetometer operating in the temperature range of 1.8–300 K at 1000 G. AC magnetic susceptibility measurements were performed on the same sample with an oscillating frequency of 125 Hz.

Received: July 22, 2002
Revised: December 16, 2002 [Z19800]

[1] a) O. Kahn, *Molecular Magnetism*, VCH, New York, **1993**; b) O. Kahn, *Angew. Chem.* **1985**, *97*, 837; *Angew. Chem. Int. Ed. Engl.* **1985**, *24*, 834; c) *Molecular Magnetism: From Molecular Assemblies to the Devices* (Eds.: E. Coronado, P. Delhaès, D. Gatteschi, J. S. Miller), Kluwer Academic, Netherlands, **1996**; d) Y. Pei, O. Kahn, K. Nakatani, E. Codjovi, C. Mathoniere, J. Sletten, *J. Am. Chem. Soc.* **1991**, *113*, 6558; e) H. O. Stumpf, Y. Pei, C. Michaut, O. Kahn, J. R. Renard, L. Ouahab, *Chem. Mater.* **1994**, *6*, 257; f) J. R. Galán-Mascarós, C Giménez-Saiz, S. Triki, C. J. Gómez-García, E. Coronado, L. Ouahab, *Agnew. Chem.* **1995**, *107*, 1601–1603; *Agnew. Chem. Int. Ed. Engl.* **1995**, *34*, 1460–1462; g) L. Thomas, F. Lionti, R. Ballou, D. Gatteschi, R. Sessoli, B. Barbara, *Nature* **1996**, *383*, 145; h) M. Verdaguer, A. Bleuzen, V. Marvaud, J. Vaissermann, M. Seuleiman, C. Desplanches, A. Scuiller, C. Train, R. Garde, G. Gelly, C. Lomenech, I. Rosenman, P. Veillet, C. Cartier, F. Villain, *Coord. Chem. Rev.* **1999**, *190–192*, 1023; i) S. M. Holmes, G. Girolami, *J. Am. Chem. Soc.* **1999**, *121*, 5593; j) O. Hatlevik, W. E. Buschmann, J. Zhang, J. L. Manson, J. S. Miller, *Adv. Mater.* **1999**, *11*, 914.

[2] a) A. Caneschi, D. Gatteschi, R. Sessoli, *Inorg. Chem.* **1993**, *32*, 4612; b) A. Caneschi, D. Gatteschi, A. Lelirzin, *J. Mater. Chem.* **1994**, *4*, 319; c) D. Luneau, P. Rey, *Mol. Cryst. Liq. Cryst. Sci. Technol. Sect. A* **1995**, *273*, 81; d) A. Caneschi, D. Gatteschi, R. Sessoli, *Mol. Cryst. Liq. Cryst. Sci. Technol. Sect. A* **1996**, *278*, A177.

[3] a) J. M. Manriquez, G. T. Yee, R. S. McClean, A. J. Epstein, J. S. Miller, *Science* **1991**, *252*, 1415; b) J. Zhang, J. Ensling, V. Ksenofontov, P. Gütlich, A. J. Epstein, J. S. Miller, *Angew. Chem.* **1998**, *110*, 676; *Angew. Chem. Int. Ed.* **1998**, *37*, 657; c) D. K. Rittenberg, A. M. Arif, J. S. Miller, *J. Chem. Soc. Dalton Trans.* **2000**, 3939; d) J. S. Miller, A. J. Epstein, *Chem. Commun.* **1998**, 1319; e) J. S. Miller, J. C. Calabrese, H. Rommelmann, S. R. Chittipeddi, J. H. Zhang, W. M. Reiff, A. J. Epstein, *J. Am. Chem. Soc.* **1987**, *109*, 769.

[4] a) R. C. Thompson, V. K. Gujral, H. J. Wagner, C. F. Schwerdtfeger, *Phys. Status Solidi A* **1979**, *53*, 181; b) R. C. Thompson, Y. Hoyano, C. F. Schwerdtfeger, *Solid State Commun.* **1977**, *23*, 633; c) K. R. Dunbar, *Angew Chem.* **1996**, *108*, 1769; *Angew. Chem. Int. Ed. Engl.* **1996**, *35*, 1659; d) H. Zhao, R. A. Heintz, R. D. Rogers, K. R. Dunbar, *J. Am. Chem. Soc.* **1996**, *118*, 12844; e) H. Zhao, R. A. Heintz, X. Ouyang, K. R. Dunbar, C. F. Campana, R. D. Rogers, *Chem. Mater.* **1999**, *11*, 736; f) K. I. Pokhodnya, N. Petersen, J. S. Miller, *Inorg. Chem.* **2002**, *41*, 1996.

[5] a) M. L. Kahn, C. Mathonière, O. Kahn, *Inorg. Chem.* **1999**, *38*, 3692; b) T. Kido, S. Nagasato, Y. Sunatsuki, N. Matsumoto, *Chem. Commun.* **2000**, 2113; c) Y. Liang, M. Hong, W. Su, R. Cao, W. Zhang, *Inorg. Chem.* **2001**, *40*, 4574; d) E. K. Brechin, S. G. Harris, S. Parsons, R. E. P. Winpenny, *J. Chem. Soc. Dalton Trans.* **1997**, 1665; e) X. Chen, Y. Wu, Y. Yang, S. M. J. Aubin, D. N. Hendrickson, *Inorg. Chem.* **1998**, *37*, 6186; f) S. Decurtins, M. Gross, H. W. Schmalle, S. Ferlay, *Inorg. Chem.* **1998**, *37*, 2443.

[6] A. M. Madalan, H. W. Roesky, M. Andruh, M. Noltemeyer, N. Stanica, *Chem. Commun.* **2002**, 1638.

[7] a) C. Benelli, A. Caneschi, D. Gatteschi, R. Sessoli, *Inorg. Chem.* **1993**, *32*, 4797; b) C. Benelli, A. Caneschi, D. Gatteschi, L. Pardi, *Inorg. Chem.* **1992**, *31*, 741; c) J. Sutter, M. L. Kahn, S. Golhen, L. Ouahab, O. Kahn, *Chem. Eur. J.* **1998**, *4*, 571; d) C. Benelli, A. Caneschi, D. Gatteschi, L. Pardi, P. Rey, *Inorg. Chem.* **1990**, *29*, 4223; e) D. K. Rittenberg, K. Sugiura, Y. Sakata, A. M. Arif, J. S. Miller, *Inorg. Chem.* **2001**, *40*, 3654; f) M. Tamura, K. Yamanaka, Y. Mori, Y. Nishio, K. Kajita, H. Mori, S. Tanaka, J. Yamaura, Y. Imakubo, R. Kato, Y. Misaki, K. Tanaka, *Synth. Met.* **2001**, *120*, 1041.

[8] J. W. Raebiger, J. S. Miller, *Inorg. Chem.* **2002**, *41*, 3308.

[9] Crystal data for $\{[Gd_2(TCNQ)_5(H_2O)_9][Gd(TCNQ)_4(H_2O)_3]\} \cdot 4H_2O$ (**1**) at 110(2) K: $C_{108}H_{68}N_{36}O_{16}Gd_3$, $M_r = 2597.73$, dark purple blocks, $0.067 \times 0.058 \times 0.030$ mm, triclinic, space group $P\bar{1}$, $a = 15.767(3)$, $b = 17.806(4)$, $c = 19.406(4)$ Å, $\alpha = 74.59(3)$, $\beta = 81.61(3)$, $\gamma = 76.64(3)°$, $V = 5089(2)$ Å^3, $Z = 2$, $\rho_{calcd} = 1.695$ g cm^{-3}; $2\theta_{max} = 46.54°$; $Mo_{K\alpha}$ radiation, $\lambda = 0.71073$ Å; $T = 293(2)$ K; 20045 reflections, of which 14276 are unique, and of which 9001 were included in the refinement ($I > 2\sigma$); solution by direct methods (G. M. Sheldrick, SHELXS-97, University of Göttingen, Göttingen (Germany), **1997**) and refinement on F^2 by full-matrix least-squares procedure (G. M. Sheldrick, SHELXL-97, University of Göttingen, Göttingen (Germany), **1997**); 918 parameters; isotropic refinement of all C atoms, O6 and N4, the remaining non-hydrogen atoms were refined anisotropically; H atoms were included in their calculated positions, except in solvent water molecules; final values $R(F) = 0.0603$, $R_w(F^2) = 0.1136$. CCDC-199356 contains the supplementary crystallographic data for this paper. These data can be obtained free of charge via www.ccdc.cam.ac.uk/conts/retrieving.html (or from the Cambridge Crystallographic Data Centre, 12, Union Road, Cambridge CB21EZ, UK; fax: (+44) 1223-336-033; or deposit@ccdc.cam.ac.uk).

 © 2003 Wiley-VCH Verlag GmbH & Co. KGaA, Weinheim 1433-7851/03/4209-1018 $ 20.00+.50/0

Sulfonation of Methane

Direct Liquid-Phase Sulfonation of Methane to Methanesulfonic Acid by SO_3 in the Presence of a Metal Peroxide**

*Sudip Mukhopadhyay and Alexis T. Bell**

Selective functionalization of methane to value-added products is a significant contemporary challenge.[1] Methane is a very unreactive molecule, as demonstrated by its high C–H bond strength (438.8 kJ mol^{-1}), high ionization potential (12.5 eV), low proton affinity (4.4 eV), and low acidity ($pK_a = 48$). Because of favorable thermodynamics, considerable effort has been devoted to the oxidation and oxidative carbonylation of methane.[2] By contrast, the sulfonation of methane has not received as much attention despite its commercial importance.[3] Sen and co-workers,[4] and more recently we,[5] have shown that $K_2S_2O_8$ can be used as a free-radical initiator to sulfonate methane with SO_3 in fuming sulfuric acid.[6] However, even with a methane pressure of 1000 psig (6.89 MPa), methane conversions to methanesulfonic acid (MSA) of only 3 to 6% could be achieved.[4,5] This together with difficulties associated with the separation of the highly soluble potassium salts from the reaction mixture have motivated the search for a more efficient process. While Ishii and co-workers have reported success in the vanadium-catalyzed sulfonation of adamantane to the corresponding sulfonic acids using SO_2 and O_2, methane did not undergo sulfonation to MSA.[7] The question therefore arises as how to sulfonate methane under low to moderate methane pressure. Herein, we show that methane will undergo liquid-phase sulfonation with 30 wt% SO_3 in sulfuric acid to form MSA, using metal peroxides as free-radical initiators. To the best of our knowledge, this is the first example of using metal peroxides in the liquid-phase at slightly above atmospheric pressure and room temperature to activate methane.

In a typical reaction CH_4 and SO_3 were allowed to react in fuming sulfuric acid in a high-pressure, glass-lined autoclave.[8] A small amount of metal peroxide was added to the liquid phase. Reactions were carried out for 5 h, and the resulting MSA was identified and quantified by ^{1}H NMR spectroscopy.[5]

Calcium peroxide is the best initiator for the reaction conditions used (Table 1, entry 7). The peroxides of strontium and lead are only minimally effective in promoting the sulfonation of methane (Table 1, entries 1 and 2), as compared to calcium peroxide. On the other hand, peroxides of Na, Li, Ba, and Mg are moderately effective (entries 3–6).

[*] Prof. A. T. Bell, Dr. S. Mukhopadhyay
Department of Chemical Engineering
University of California
Berkeley, CA 94720-1462 (USA)
Fax: (+1) 510-642-4778
E-mail: bell@cchem.berkeley.edu

[**] This work was supported by a grant from ATOFINA Chemicals, Inc.

Table 1: Effect of different metal peroxides on the conversion of SO_3 to MSA.[a]

Entry	Metal peroxide	Amount [mmol]	% Conv. of SO_3 to MSA
1	strontium peroxide	0.212	8
2	lead peroxide	0.212	16
3	sodium peroxide	0.212	24
4	lithium peroxide	0.212	29
5	barium peroxide	0.212	30
6	magnesium peroxide	0.25	34
7	calcium peroxide	0.2	43

[a] Reaction conditions unless otherwise stated: methane: 650 psig; SO_3: 30 wt%, 1.7 g; molar ratio of methane to SO_3: 8.4:1; fuming sulfuric acid: 5.67 g; time: 5 h; temperature: 65 °C.

Table 2 shows the effects of varying the reaction conditions on the conversion of SO_3 to MSA. By using BaO_2 as the initiator, the conversion of SO_3 to MSA increased from 2 to 48% when the methane pressure was increased from 50 to 1000 psig (Table 2, entries 1–5). The reaction rate also depends on the initial SO_3 concentration. With an increase in SO_3 concentration the MSA conversion increased initially; however, above an initial concentration of 42%, the conversion of SO_3 to MSA decreased due to the formation of methanedisulfonic acid and methane bisulfate (Table 2, entries 6–8). The conversion increased when the amount of barium peroxides in the reaction mixture was raised from 0 to 0.6 mmol. However, a further increase in the amount of metal peroxide resulted in a decrease in the SO_3 conversion (Table 2, entries 9–13).

The conversion of SO_3 to MSA observed after 5 h increased with increasing temperature up to 70 °C. However, a decrease in the conversion to MSA was observed for temperatures greater than 70 °C (Table 2, entries 14–18).

Table 2: Effect of reaction conditions on the conversion of SO_3 to MSA.[a]

Entry	CH_4 [psig]	SO_3 [wt %]	Metal peroxide M	Metal peroxide amount [mmol]	t [h]	T [°C]	Conv. of SO_3 to MSA [%]
1	50	30	Ba	0.212	5	65	2
2	200	30	Ba	0.212	5	65	11
3	300	30	Ba	0.212	5	65	24
4	650	30	Ba	0.212	5	65	30
5	1000	30	Ba	0.212	5	65	48
6	650	21	Ba	0.212	5	65	40
7	650	42	Ba	0.212	5	65	42
8	650	56	Ba	0.212	5	65	22
9	650	30	Ba	0.0	5	65	0
10	650	30	Ba	0.118	5	65	25
11	650	30	Ba	0.414	5	65	70
12	650	30	Ba	0.6	5	65	74
13	650	30	Ba	0.8	5	65	61
14	650	30	Ba	0.212	5	35	2
15	650	30	Ba	0.212	5	45	12
16	650	30	Ba	0.212	5	70	34
17	650	30	Ba	0.212	5	85	29
18	650	30	Ba	0.212	5	100	14
19	650	30	Ca	0.41	5	65	89
20	650	30	Ca	0.6	5	65	91
21	30	46	Ca	0.42	36	70	10

[a] Reaction conditions unless otherwise stated: time: 5 h; solvent: fuming sulfuric acid (30 wt% SO_3), 5.67 g.

 © 2003 Wiley-VCH Verlag GmbH & Co. KGaA, Weinheim 1433-7851/03/4209-1019 $ 20.00+.50/0

Under the best reaction conditions with 650 psig methane and using 0.41 to 0.6 mmol of CaO_2 as the radical initiator, a 89 to 91% conversion of SO_3 to MSA was observed (Table 2, entries 19 and 20). The methane conversion to MSA under these conditions was 11%. Remarkably, 18% of the methane, and correspondingly 10% of the SO_3, was converted to MSA at 70°C with a methane pressure of only 30 psig using CaO_2 as the initiator (Table 2, entry 21).

The acidity of the solvent media has a marked influence on the rate of MSA formation (Table 3). Thus, in trifluoroacetic acid, a 19% conversion of SO_3 to MSA was attained,

Table 3: Effect of solvent media on the conversion of SO_3 to MSA[a]

Solvent	*t* [h]	Conv. of SO_3 to MSA [%]
CF_3COOH	10	19
H_2SO_4	5	89
CF_3SO_3H	5	53

[a] Reaction conditions unless otherwise stated: methane: 650 psig; CaO_2: 0.4 mmol; SO_3: 1.7 g; molar ratio of methane to SO_3: 8.4:1; fuming sulfuric acid: 5.67 g; time: 5 h; temperature: 65°C.

whereas in sulfuric acid the conversion rose to 89%. Triflic acid was not as effective as sulfuric acid due possibly to the consumption of SO_3 to form polysulfonic acids of the general formula $CF_3(SO_3)_nH$ by the reaction of triflic acid and SO_3.

The mechanism by which CH_4 reacts with SO_3 to form MSA is not understood; however, it is reasonable to suggest that the reaction proceeds by a mechanism inovolving free radicals, since the presence of molecular oxygen inhibits the formation of MSA. It is conceivable that methane activation involves Ca^{+2} ions and H_2O_2 generated by the reaction of CaO_2 and H_2SO_4. Once $CH_3^{\bullet}$ radicals are generated they can react with SO_3 to form $CH_3SO_3^{\bullet}$ radicals, which can in turn, abstract hydrogen from methane to form MSA.[5] To assess whether H_2O_2 generated by the reaction of CaO_2 and H_2SO_4 might be solely responsible for the activation of CH_4, an experiment was conducted in which 0.6 mmol of H_2O_2 was used as the initiator.[9] A SO_3 conversion to MSA of 9% was obtained in this experiment. If $CaCl_2$ (0.6 mmol) was added to the synthesis mixture containing H_2O_2, while keeping the amount of free SO_3 the same, the conversion of SO_3 to MSA rose to 16%. This is considerably lower than the 72% conversion of SO_3 to MSA observed when 0.6 mmol of CaO_2 was used in place of $CaCl_2$ and H_2O_2, which suggests that CaO_2 has a unique role in the activation of methane.

The observed lowering in the conversion of SO_3 to MSA (Table 2, entries 13 and 14) when more than 0.6 mmol of metal peroxide was used in the synthesis mixture can be attributed to the high rate of decomposition of H_2O_2 to O_2, which can act as a free radical scavenger,[4] thereby inhibiting the formation of MSA. This interpretation is consistent with the failure to observe any MSA when the reaction was carried out in the presence of 30 psig of O_2.

The observation of a maximum in the conversion of SO_3 to MSA with increasing temperature, such as that seen in entries 15–18 in Table 2, can be interpreted as follows: For temperatures lower than that for the best conversion, increasing the temperature accelerates the kinetics of MSA formation. When temperature is raised above that for the maximum conversion of SO_3 to MSA, a rapid decomposition of CaO_2 or H_2O_2 generated in situ occurs and the O_2 thus released inhibits the free-radical processes leading to MSA.

In conclusion, we have demonstrated a synthetic approach for the direct, liquid-phase sulfonation of methane with 30 wt% SO_3 in sulfuric acid. Under the best reaction conditions, 91% conversion of SO_3 to MSA was achieved. The respective methane conversion to MSA was 11–18%. CaO_2 is an effective radical initiator even at low reaction temperatures and CH_4 pressures.

Received: August 8, 2002
Revised: December 3, 2002 [Z19922]

[1] a) C. L. Hill, *Activation and Functionalization of Alkanes*, Wiley, New York, **1989**; b) M. G. Axelrod, A. M. Gaffney, R. Pitchai, J. A. Sofranko, *Natural Gas Conversion II*, Elsevier, Amsterdam, **1994**, p. 93; c) C. Starr, M. F. Searl, S. Alpert, *Science* **1992**, *256*, 981; d) A. E. Shilov, *Activation of Saturated Hydrocarbons by Transition Metal Complexes* (Ed.: D. Reidel), Dordrecht, **1984**; e) G. A. Olah, A. Molnar, *Hydrocarbon Chemistry*, Wiley, New York, **1995**; f) M. Lin, A. Sen, *Nature* **1994**, *368*, 613; g) A. Sen, *Acc. Chem. Res.* **1998**, *31*, 550; h) J. A. Labinger, *Fuel Process. Technol.* **1995**, *42*, 325; i) R. H. Crabtree, *Chem. Rev.* **1995**, *95*, 987; j) A. E. Shilov, G. B. Shul'pin, *Chem. Rev.* **1997**, *97,* 2879; k) G. Dyker, *Angew. Chem.* **1999**, *111*, 1808; *Angew. Chem. Int. Ed.* **1999**, *38,* 1698; l) H. D. Gesser, N. R. Hunter, *Catal. Today* **1998**, *42*, 183; m) J. A. Labinger, J. E. Bercaw, *Nature* **2002**, *417*, 507.

[2] a) M. Asadullah, T. Kitamura, Y. Fujiwara, *Angew. Chem.* **2000**, *112*, 2609; *Angew. Chem. Int. Ed.* **2000**, *39*, 2475; b) E. G. Chepaikin, A. P. Bezruchenko, A. A. Leshcheva, G. N. Boyko, I. V. Kuzmenkov, E. H. Grigoryan, A. E. Shilov, *J. Mol. Catal. A* **2001**, *169*, 89; c) R. A. Periana, D. J. Taube, E. R. Evitt, D. G. Loffer, P. R. Wentrcek, G. Voss, T. Masuda, *Science* **1993**, *259*, 340; d) R. A. Periana, D. J. Taube, S. Gamble, H. Taube, T. Satoh, H. Fujii, *Science* **1998**, *280*, 560; e) R. A. Periana, O. Mirinov, D. J. Taube, S. Gamble, *Chem. Commun.* **2002**, 2376.

[3] a) *Ullmann's Encyclopedia of Industrial Chemistry, Vol. A25*, VCH, Weinheim, **1994**, pp. 503–506; b) F. M. Beringer, R. A. Falk, *J. Am. Chem. Soc.* **1959**, *81*, 2997; c) H. A. Young, *J. Am. Chem. Soc.* **1937**, *59*, 811; d) R. C. Murray, *J. Chem. Soc.* **1933**, 739.

[4] N. Basickes, T. E. Hogan, A. Sen, *J. Am. Chem. Soc.* **1996**, *118*, 13111.

[5] a) L. J. Lobree, A. T. Bell, *Ind. Eng. Chem. Res.* **2001**, *40*, 736; b) S. Mukhopadhyay, A. T. Bell, *Ind. Eng. Chem. Res.* **2002**, *41*, 5901.

[6] *Sulfur Trioxide and Oleum: Storage and Handling*, Dupont Corporation, Wilmington, DE.

[7] Y. Ishii, K. Matsunaka, S. Sakaguchi, *J. Am. Chem. Soc.* **2000**, *122*, 7390.

[8] In a 100-mL glass-lined Parr autoclave, CaO_2 (0.6 mmol), and SO_3 (1.7 g) and H_2SO_4 (3.99 g) were charged, together with a small teflon-coated magnetic stirring bar. The reactor was purged with N_2 to expel the air out of the system and sealed. The autoclave was then pressurized with 650 psig methane and heated to 70°C for 5 h while stirred. After the stipulated period of time, the reactor was quenched with ice and opened to collect the reaction mixture. The reaction mixture was then added slowly to water (0.5 g) and analyzed by ^1H NMR spectroscopy. D_2O and methanol, contained in a capillary placed adjacent to the NMR tube containing the sample, were used as the lock and references. The corresponding

 © 2003 Wiley-VCH Verlag GmbH & Co. KGaA, Weinheim 1433-7851/03/4209-1020 $ 20.00+.50/0

chemical shift for MSA was $\delta = 2.82$ ppm to 3.02 ppm, depending on the concentration of MSA in the mixture.

[9] For the H_2O_2 (0.6 mmol) initiated reaction, 50% H_2O_2 (0.04 g; Aldrich) and liquid SO_3 (0.1 g; Aldrich) were added to fuming sulfuric acid (5.67 g, 30% SO_3). For the $CaCl_2$ (0.6 mmol) and H_2O_2 (0.6 mmol) initiated reaction, $CaCl_2$ (0.067 g), 50% H_2O_2 (0.04 g; Aldrich), and liquid SO_3 (0.1 g; Aldrich) were used with fuming sulfuric acid (5.67 g). For an accurate comparison, in the CaO_2 (0.6 mmol) initiated reaction mixture, water (0.02 g) and SO_3 (0.1 g) were also added to fuming sulfuric acid (5.67 g).

 © 2003 Wiley-VCH Verlag GmbH & Co. KGaA, Weinheim 1433-7851/03/4209-1021 $ 20.00+.50/0

Contents

anti-Bredt Bridgehead Olefin

P. Roach, R. Warmuth* ____ **3039 – 3042**

The Room-Temperature Stabilization of Bicyclo[2.2.2]oct-1-ene and Bicyclo[3.2.1]oct-1-ene

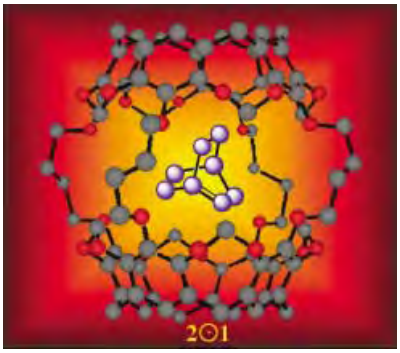

Retardation through incarceration: The highly strained anti-Bredt bridgehead olefin bicyclo[2.2.2]oct-1-ene (**1**) is remarkably stable at 60 °C, if generated photochemically inside the hemicarcerand **2** (see picture). The surrounding host not only prevents the dimerization of **1**, but also retards strongly its intramolecular retro-Diels–Alder reaction by several orders of magnitude.

Catalytic Indol Synthesis

H. Siebeneicher, I. Bytschkov, S. Doye* ____ **3042 – 3044**

A Flexible and Catalytic One-Pot Procedure for the Synthesis of Indoles

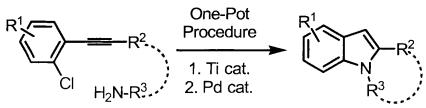

One pot, two bonds, three rings: A clever combination of a [Cp_2TiMe_2]-catalyzed hydroamination of alkynes with a Pd-catalyzed N-arylation of imines results in a new and general method for the synthesis of indoles. Impressively, two new C–N bonds are formed during the one-pot procedure (see scheme).

Communications labeled with this symbol have been judged by two referees as being "very important papers".

The publication of Communications labeled with this symbol has been accelerated because of their topical or highly competitive nature.

Sources

Product and Company Directory

You can start the entry for your company in "Sources" in any issue of *Angewandte Chemie*.

If you would like more information, please do not hesitate to contact us.

Wiley-VCH Verlag – Advertising Department
Tel.: 0 62 01 - 60 65 65
Fax: 0 62 01 - 60 65 50
E-Mail: MSchulz@wiley-vch.de

Service

Keywords ____ *3046*

Authors ____ *3047*

Angewandte's Sister Journals ____ *3048 – 3049*

Vacancies ____ *3045*

Preview ____ *3051*

Apology

In the Communication "Direct Liquid-Phase Sulfonation of Methane to Methanesulfonic Acid by SO_3 in the Presence of a Metal Peroxide" by S. Mukhopadhyay and A. T. Bell (*Angew. Chem.* **2003**, *115*, 1049 – 1051; *Angew. Chem. Int. Ed.* **2003**, *42*, 1019 – 1021), the authors missed a cross-reference to their thematically related but independent Communication "Direct Sulfonation of Methane to Methanesulfonic Acid with SO_2 Using Ca Salts as Promoters" (S. Mukhopadhyay und A. T. Bell, *J. Am. Chem. Soc.* **2003**, *125*, 4406 – 4407), and vice versa. The authors apologize for the oversight.

Stereoselective Glycosidations

Control of α/β Stereoselectivity in Lewis Acid Promoted C-Glycosidations Using a Controlling Anomeric Effect Based on the Conformational Restriction Strategy**

*Satoru Tamura, Hiroshi Abe, Akira Matsuda, and Satoshi Shuto**

The synthesis of C-glycosides has been extensively studied because of their importance as stable mimics for natural O-glycosides.[1] Lewis acid promoted C-glycosidation is effective in providing a wide variety of C-glycosidic compounds. However, control of the stereochemistry is often problematic.[1] For example, although allyltrimethylsilanes can be used as nucleophiles in reactions with pyranosyl donors to provide the α products stereoselectively, it is difficult to carry out β-selective C-glycosidations by this method.[2–5] We report herein an anomeric-effect-dependent, highly α- and β-selective, Lewis acid promoted C-glycosidation based on the conformational restriction of the pyranose ring.[6–9]

Experimental and theoretical studies have shown that conformational features and the reactivity of the anomeric position of sugars are affected by the anomeric effect,[10] which is a stereoelectronic effect resulting from n→σ* hyperconjugation between the nonbonding orbital of the oxygen atom in the ring and the antibonding orbital of the anomeric carbon–heteroatom bond in their planar arrangement.[10–14] This kind of orbital interaction gives rise to a phenomenon known as the kinetic anomeric effect, which stabilizes the transition state during bond-forming (or bond-cleavage) processes at the anomeric center, where nucleophilic attack occurs through an axial trajectory.[10–14] We recently developed a highly stereoselective radical C-glycosidation reaction in which the stereochemistry is controlled by the kinetic anomeric effect, depending on the conformation of the substrate.[9]

Although the kinetic anomeric effect for α-axial attack at the oxocarbenium ion in C-glycosidations is considered to be very weak,[5] we speculated that the stereoselectivity of S_N1-type C-glycosidations of pyranoses may be controlled effectively by the kinetic anomeric effect when conformationally restricted substrates are employed. Our working hypothesis, summarized in Scheme 1, is based on the principle that the conformation of the transition state and that of the reactive intermediate are strongly influenced by the conformational effects that stabilize the ground-state conformation.[8,9,11] In the S_N1-type C-glycosidation reaction of substrate **A**, which is conformationally restricted in a $^4C_1$-chair form, the transition state would assume the $^4C_1$-chairlike form **C** as a result of conformational restriction of the pyranose backbone, in which conformation the anomeric center would be pyramidal. Thus, the α-product **E** can be formed highly selectively as a consequence of the kinetic anomeric effect. Similarly, when the conformation of the substrate is restricted to the unusual $^1C_4$-chair form **B**, the kinetic anomeric effect promotes selective formation of the β-product **F** via the $^1C_4$-chairlike transition state **D**. Both axial-attack transition states $^4C_1$-restricted **C** and $^1C_4$-restricted **D** should be significantly stabilized by the interaction between the antibonding $\sigma^{*\mp}$ of the anomeric C–C bond being formed and the orbital of a nonbonded electron pair (n_O) on the oxygen atom in the ring because of their planar arrangement,[9,13] while both the axial-attack transition states would be accompanied by significant 1,3- and 1,5-diaxial steric repulsion caused by the conformational restriction.

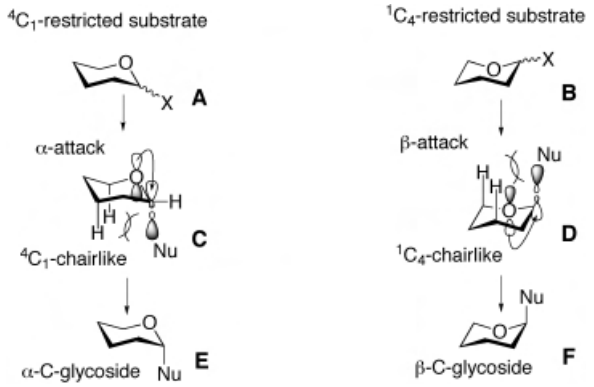

Scheme 1. The working hypothesis for the kinetic-anomeric-effect-dependent α- and β-selective C-glycosidation reaction.

We selected allyltrimethylsilane as the model nucleophile, because its Lewis acid promoted anomeric attack seems to proceed via an oxocarbenium intermediate, at least in a nonpolar solvent such as CH_2Cl_2,[5,8,15] which would make the experimental results easier to interpret. Furthermore, anome-

[*] Prof. S. Shuto, S. Tamura, Dr. H. Abe, Prof. A. Matsuda
Graduate School of Pharmaceutical Sciences
Hokkaido University
Kita-12, Nishi-6, Kita-ku, Sapporo 060-0812 (Japan)
Fax: (+81) 11-706-4980
E-mail: shu@pharm.hokudai.ac.jp

[**] This work was supported by a Grant-in-Aid for Creative Scientific Research (13NP0401) and a Research Fellowship for Young Scientists (to H.A.) from the Japan Society for the Promotion of Science.

Supporting information for this article is available on the WWW under http://www.angewandte.org or from the author.

 © 2003 Wiley-VCH Verlag GmbH & Co. KGaA, Weinheim 1433-7851/03/4209-1021 $ 20.00+.50/0

ric allylation reactions are very useful in synthetic organic chemistry.[1] Thus, we planned anomeric allylation reactions of the 1-fluoro-D-xylose substrates **2** (restricted in the $^4C_1$

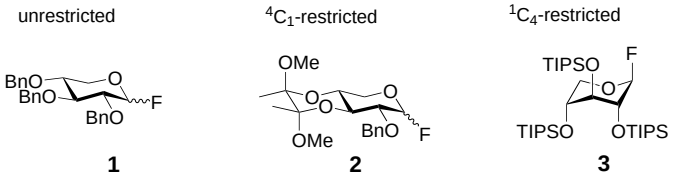

conformation by the cyclic 3,4-diketal)[16] and **3** (restricted in the $^1C_4$ conformation by bulky *O*-silyl groups),[17] and of the unrestricted tri-*O*-benzylated 1-fluoro-D-xylose **1**.[18]

Glycosyl fluorides are relatively stable and readily prepared, and are also very effective glycosyl donors.[19] The substrates **2** and **3** were prepared from tetra-*O*-acetyl-D-xylose (**4**) (Scheme 2). ^{1}H NMR and ^{19}F NMR spectroscopic

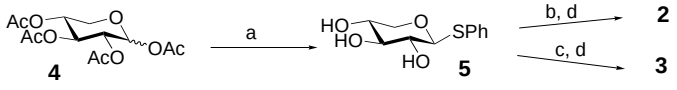

Scheme 2. Synthesis of the substrates **2** and **3**: a) 1) HBr/AcOH, CH_2Cl_2; 2) PhSH, Et_3N, CH_3CN; 3) NaOMe, MeOH, 84%; b) 1) $[Me(MeO)_2C]_2$, $(MeO)_3CH$, CSA, MeOH; 2) BnBr, NaH, THF, 60%; c) TIPSOTf, NaH, THF, 85%; d) DAST, NBS, CH_2Cl_2, 84% (**2**), 60% (**3**). CSA = camphorsulfonic acid, Bn = benzyl, TIPSOTf = triisopropylsilyl trifluoromethanesulfonate, DAST = (diethylamino)sulfur trifluoride, NBS = *N*-bromosuccinimide.

analysis showed that they are conformationally restricted in the $^4C_1$ and the $^1C_4$ conformations, respectively.[20]

C-glycosidation of **1, 2**, and **3** was performed with allyltrimethylsilane (2.0 equiv) and $BF_3{\cdot}OEt_2$ (0.05 equiv) in CH_2Cl_2 at room temperature (Table 1).[21] The products were converted into the corresponding tri-*O*-benzoates **9** and **10** (Scheme 3), the structures of which were confirmed by ^{1}H NMR spectroscopic analysis.[22,23] The reaction of the unrestricted substrate **1** ($\alpha/\beta = 1{:}3.3$) showed moderate α selectivity to give **6** (Table 1, entry 1, $\alpha/\beta = 2.2{:}1$), which was in accord with previous results.[2b,c,5] The reaction of the $^4C_1$-restricted substrate **2** ($\alpha/\beta = 1.7{:}1$) proceeded with high α-selectivity to give **7** (Table 1, entry 2, $\alpha/\beta > 50{:}1$), which is the first highly α-selective example of this kind of Lewis acid promoted anomeric allylation in the absence of acetonitrile as solvent.[5] Thus, the conformational restriction in the $^4C_1$ form significantly increased α selectivity. When the $^1C_4$-restricted β-fluoro substrate **3** was used, the stereoselectivity was completely reversed to give the product of retention of configuration, the β-*C*-allyl glycoside **8**, as the sole product (Table 1, entry 3).

Table 1: The C-glycosidation reaction of substrates **1, 2**, and **3** with allyltrimethylsilane.[a]

Entry	Substrate	Conformation	Product	Yield [%][b]	α/β[c]
1	**1**	unrestricted	**6**	70	2.2:1
2	**2**	$^4C_1$	**7**	85	>50:1
3	**3**	$^1C_4$	**8**	73	only β

[a] The substrate was treated with allyltrimethylsilane (2.0 equiv) and $BF_3{\cdot}OEt_2$ (0.05 equiv) in CH_2Cl_2 at room temperature in the presence of 4-Å molecular sieves. [b] Yield of isolated product. [c] Determined by ^{1}H NMR spectroscopy.

The stereochemical results suggest that the allylation proceeds through an S_N1-type mechanism.[24] These results clearly demonstrate that conformational restriction increases and can also invert the stereoselectivity in C-glycosidations, as we had hypothesized. It should be noted that highly selective α-and β-axial nucleophilic attack occurred in the reactions with **2** and **3**, even though the transition states for the reactions would have been accompanied by significant 1,3- and 1,5-diaxial steric repulsion because of the conformational restriction to the $^4C_1$- or the $^1C_4$-chair conformation.

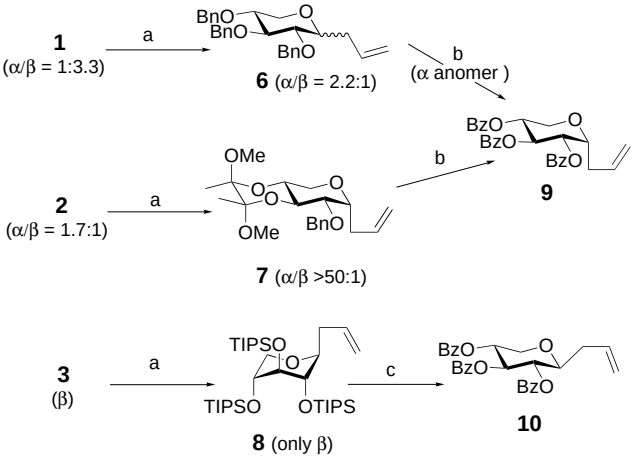

Scheme 3. Anomeric allylation of the xylosyl fluorides **1, 2**, and **3**: a) see Table 1; b) 1) BCl_3, CH_2Cl_2; 2) BzCl, DMAP, pyridine, 38% from the α anomer of **6**, 75% from **7**; c) 1) TBAF, THF; 2) BzCl, Et_3N, DMAP, MeCN, 72%. Bz = benzoyl, DMAP = 4-(dimethylamino)pyridine, TBAF = tetrabutylammonium fluoride.

In summary, depending on the restricted conformation of the substrate ($^4C_1$ or $^1C_4$), either the α or the β product was formed highly stereoselectively in our C-glycosidation reaction. This study has shown that the kinetic anomeric effect can be used effectively for controlling both α and β stereoselectivity in glycosidation reactions.

Received: August 8, 2002
Revised: December 9, 2002 [Z19925]

[1] a) D. E. Leavy, C. Tang, *The Chemistry of C-Glycosides*, Pergamon, Oxford, **1995**; b) M. H. D. Postema, *C-Glycoside Synthesis*, CRC, Boca Raton, **1995**; c) Y. Du, R. J. Linhardt, *Tetrahedron* **1998**, *54*, 9913–9959.

[2] For examples, see: a) M. D. Lewis, J. K. Cha, Y. Kishi, *J. Am. Chem. Soc.* **1982**, *104*, 4976–4978; b) A. Hosomi, Y. Sakata, H. Sakurai, *Tetrahedron Lett.* **1984**, *25*, 2383–2386; c) A. Giannis, K. Sandhoff, *Tetrahedron Lett.* **1985**, *26*, 1479–1482.

 © 2003 Wiley-VCH Verlag GmbH & Co. KGaA, Weinheim 1433-7851/03/4209-1022 $ 20.00+.50/0

[3] For a β-selective C-glycosidation (α/β = 1:1.1–< 1:10) with hindered and highly nucleophilic silyl ketene acetals, which probably occurs by a neighboring-group participation mechanism, see: T. G. Minehan, Y. Kishi, *Tetrahedron Lett.* **1997**, *38*, 6815–6818; see also reference [1c].
[4] For a stereoselective route for the preparation of β-C-glycosides through anomeric deoxygenation, see reference [2a].
[5] R. W. Frank reported that in the Lewis acid promoted anomeric allylation, the kinetic anomeric effect should not be considered responsible for the α selectivity observed, as acetonitrile is essential as the reaction solvent for α selectivity. Therefore, the α product is thought to be formed through a back-side displacement of the β-equatorial nitrilium species: R. W. Frank in *Conformational Behavior of Six-Membered Rings* (Ed.: E. Juaristi), VCH, New York, **1995**, pp. 159–200.
[6] For a highly β-stereoselective O-glycosylation using conformationally restricted 4,6-*O*-benzylidenemannose donors, see: D. Crich, W. Cai, Z. Dai, *J. Org. Chem.* **2000**, *65*, 1291–1297.
[7] For a stereoselective synthesis of β-D-mannopyranosides with reactive mannosyl donors possessing an electron-withdrawing group at the 2-position, see: A. A.-H. Abdel-Rahman, S. Jonke, E. S. H. E. Ashry, R. R. Schmidt, *Angew. Chem.* **2002**, *114*, 3100–3103; *Angew. Chem. Int. Ed.* **2002**, *41*, 2972–2974.
[8] For a stereoelectronic model explaining stereoselective nucleophilic reactions that occur via six-membered-ring oxocarbenium ions, see: J. A. C. Romero, S. A. Tabacco, K. A. Woerpel, *J. Am. Chem. Soc.* **2000**, *122*, 168–189.
[9] H. Abe, S. Shuto, A. Matsuda, *J. Am. Chem. Soc.* **2001**, *123*, 11870–11882.
[10] a) E. Juaristi, G. Cuevas, *Tetrahedron* **1992**, *48*, 5019–5087; b) "The Anomeric Effect and Associated Stereoelectronic Effects": *ACS Symp. Ser.* **1993**, *539*; c) E. Juaristi, G. Cuevas, *The Anomeric Effect*, CRC, Boca Raton, **1995**; d) C. Thibaudeau, J. Chattopadhyaya, *Stereoelectronic Effects in Nucleosides and Nucleotides and their Structural Implications*, Uppsala University Press, Uppsala, **1999**.
[11] N. Pothier, S. Goldstein, P. Deslongchamps, *Helv. Chim. Acta* **1992**, *75*, 604–620.
[12] P. Deslongchamps, *Stereoelectronic Effects in Organic Chemistry*, Pergamon, New York, **1983**, pp. 209–221.
[13] It has been recognized that from the viewpoint of stereoelectronic effects, the axial attack of nucleophiles at an electrophilic carbon center in six-membered-ring systems such as cyclohexanones, cyclohexenones, or piperidyl iminium ions is favored over the corresponding equatorial attack; see reference [12].
[14] The theory that the transition-state energy can be lowered by the orbital interaction involving σ^{*+} of the bond being formed was originally put forward by Cieplak to expound the stereoselectivity of nucleophilic additions: A. S. Cieplak, *J. Am. Chem. Soc.* **1981**, *103*, 4540–4552.
[15] T. Sammakia, R. S. Smith, *J. Am. Chem. Soc.* **1994**, *116*, 7915–7916.
[16] J. L. Montchamp, F. Tian, M. E. Hart, J. W. Frost, *J. Org. Chem.* **1996**, *61*, 3897–3899.
[17] Bulky silyl protecting groups on the 3,4-*trans*-hydroxy groups of pyranoses cause a conformation "flip", leading to a $^1C_4$ form: a) T. Hosoya, Y. Ohashi, T. Matsumoto, K. Suzuki, *Tetrahedron Lett.* **1996**, *37*, 636–666; b) S. Ichikawa, S. Shuto, A. Matsuda, *J. Am. Chem. Soc.* **1999**, *121*, 10270–10280; c) H. Abe, S. Shuto, S. Tamura, A. Matsuda, *Tetrahedron Lett.* **2001**, *42*, 6159–6161.
[18] In hexopyranoses, the steric effect of the 5-hydroxymethyl moiety would significantly affect the course of their glycosidation reactions, especially in the case of β-axial attack at the $^1C_4$-restricted substrate because of 1,5-diaxial repulsion, and this would disturb the exact estimation of the anomeric effect on the stereoselectivity. Thus, xylose derivatives that lack a carbon substituent at the 5-position were selected as model substrates.
[19] a) T. Mukaiyama, Y. Murai, S. Shoda, *Chem. Lett.* **1981**, 431–432; b) K. C. Nicolaou, R. E. Dolle, D. P. Panahatjis, J. L. Randall, *J. Am. Chem. Soc.* **1984**, *106*, 4189–4192.
[20] Typical ^{1}H NMR coupling constants for the conformationally restricted substrates in $CDCl_3$: **2** (α-anomer), $J_{1,2} = 2.8$, $J_{2,3} = 9.4$, $J_{4,5b} = 9.7$ Hz; **3**, $J_{1,2}$, $J_{2,3}$, $J_{3,4}$, $J_{4,5b}$, $J_{2,3} \approx 0$ Hz. The $^1C_4$-restricted 1-β-fluoro structure of **3** was also confirmed by ^{19}F NMR spectroscopy in $CDCl_3$: $J_{F,1} = 49.9$, $J_{F,2} = 5.1$ Hz (conformational analysis of pyranoses by ^{19}F NMR: M. Michalik, M. Hein, M. Frank, *Carbohydr. Res.* **2000**, *327*, 185–218).
[21] For experimental details, see Supporting Information.
[22] The ^{1}H NMR spectral data of the tri-*O*-benzoates **9** and **10** were in accord with those of authentic samples synthesized previously by another method.[9]
[23] The α/β ratio was determined based on the anomeric proton signals in the ^{1}H NMR spectrum.
[24] It may be possible that the β-product **7** was produced in part through the S_N2 reaction of the α anomer of the donor **2**.

 © 2003 Wiley-VCH Verlag GmbH & Co. KGaA, Weinheim 1433-7851/03/4209-1023 $ 20.00+.50/0

Pentacoordinate Silicon Complexes

An Unexpected, Sterically Driven, Methyl Halide Elimination in Pentacoordinate Siliconium Halide Salts: Silicon Complexes with Equatorial Nitrogen Coordination**

Daniel Kost, Boris Gostevskii, Nikolaus Kocher, Dietmar Stalke, and Inna Kalikhman**

Donor-stabilized silyl cation salts have recently drawn considerable attention.[1–6] Several reactions leading to such complexes[2–6] and the utility of these complexes as catalysts have been reported.[7] While dozens of previously reported pentacoordinate (as well as hexacoordinate) silicon complexes with a dimethylamino donor group (**1, 2**) are thermally stable,[8] we now report that certain pentacoordinate siliconium halide salts undergo a facile and quantitative elimination of a methyl halide to produce neutral pentacoordinate silicon complexes with unprecedented equatorial nitrogen coordination (Scheme 1).

[*] Prof. D. Kost, Dr. I. Kalikhman
Department of Chemistry, Ben-Gurion University
Beer-Sheva 84105 (Israel)
Fax: (+972) 8-647-2943
E-mail: kostd@bgumail.bgu.ac.il
innakal@bgumail.bgu.ac.il

Dr. B. Gostevskii
Ben-Gurion University and
A. E. Favorsky Irkutsk Institute of Chemistry
Russian Academy of Sciences (Russia)

N. Kocher, Prof. Dr. D. Stalke
Institut für Anorganische Chemie der Universität Würzburg
(Germany)

[**] Donor-stabilized silyl cations, part 6. For parts 1–5 see reference [6]. This work was supported by the German Israeli Scientific R&D Foundation (GIF), grant I-628-58.5/1999.

 © 2003 Wiley-VCH Verlag GmbH & Co. KGaA, Weinheim 1433-7851/03/4209-1023 $ 20.00+.50/0

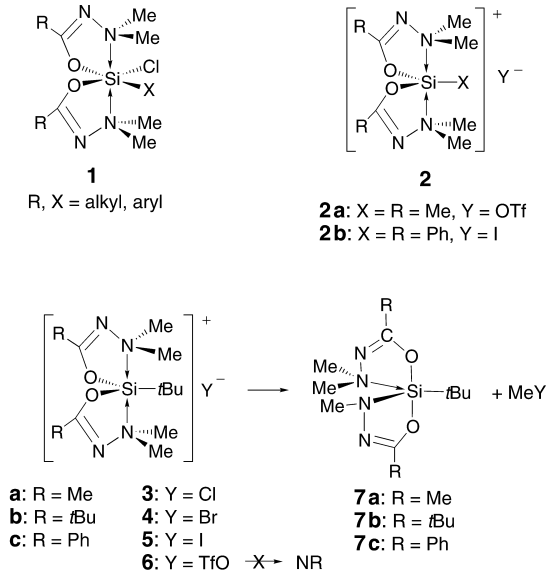

Scheme 1. Elimination of a methyl halide from bis-(N→Si)-coordinated siliconium salts **3**–**5** to give neutral, singly (N→Si)-coordinated complexes **7**.

tert-Butylsiliconium chlorides **3a**–**c** were obtained by transsilylation of tBuSiCl$_3$ with the corresponding *N*-dimethylamino-*O*-trimethylsilylimidates [Me$_3$SiOC(R)=NNMe$_2$] and readily converted into the siliconium halides or triflates **4**–**6** by treatment with Me$_3$SiY.[6c]

A unique feature of the tBu-substituted compounds **3**–**5** is that under mild heating (65 °C) they quantitatively undergo methyl halide elimination to form novel, neutral pentacoordinate complexes **7** (Scheme 1).[9] In this reaction, one of the two initially equivalent Me$_2$N groups loses a methyl substituent to produce a complex with one covalent and one dative N–Si bond. The products of elimination were isolated and characterized by X-ray crystal-structure analysis (Figure 1 a)[10] and by standard methods.

The progress of the elimination reaction (at 65 °C, in CDCl$_3$, in a flask sealed under vacuum) was monitored by ^{1}H and ^{29}Si NMR spectroscopy, and was found to depend on the counterion: With respect to the halide the order of reactivity is I > Br > Cl (50 % elimination after 85, 130, and 175 min, respectively, from **5c, 4c**, and **3c**), whereas the siliconium triflates **6a**–**6c** did not react. It is thus evident that nucleophilic attack of the anion at one of the *N*-methyl groups is involved in the rate-determining step of the elimination.

The special observations made regarding the tBu complexes **3**–**6** can be rationalized in terms of steric bulk: a) the direct formation of **3** by transsilylation (in contrast with analogues **2**, which contain X = Me, Ph, or PhCH$_2$ in place of the tBu group and are formed via the neutral hexacoordinate species **1**) results from the difficulty in accommodating both the tBu and the halide ligands next to each other; b) likewise, steric repulsion between the adjacent tBu and Me$_2$N groups in **3**–**5**, which is at least partly released by elimination, may account for the facile loss of the methyl halide. These arguments are strengthened by comparison of the crystal structures of the relevant complexes (**6a, 7b**, Figure 1, Table 1).[10]

Table 1: Selected bond lengths and angles for **6a** and **7b**.

	Si–O [Å]	Si–N [Å]	Si–C [Å]	O-Si-O [°]	N-Si-N [°]
6a	1.7240(8)	1.9397(10)	1.8964(11)	152.22(4)	133.54(4)
	1.7266(8)	1.9470(10)			
7b	1.7844(7)	1.7265(9)	1.9115(10)	165.74(4)	121.51(4)
	1.7591(7)	1.9496(9)			

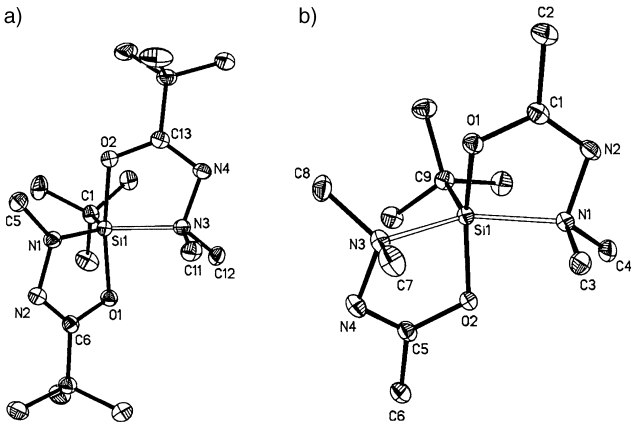

Figure 1. Crystallographic molecular structures of **7b** (a) and **6a** (b) at the 50 % probability level. Hydrogen atoms omitted for clarity. For **6a** only the cation is shown; the separate triflate anion has been omitted.

The striking feature of the structure of the elimination product **7b** is that the Me$_2$N donor ligand, as well as the covalent Si–N bond, occupy *equatorial* positions in the slightly distorted trigonal bipyramidal (TBP) complex. To the best of our knowledge, no equatorial coordination by a nitrogen ligand has been reported in pentacoordinate silicon complexes.[8]

The molecular structure of **6a**, the triflate analogue of the elimination precursors **3a**–**5a**,[11] was also unexpected: Even in the elimination precursor the nitrogen ligands occupy the equatorial-like and the oxygen ligands the axiallike positions, as judged from the corresponding N-Si-N (133.54°) and O-Si-O (152.22°) bond angles. This is in sharp contrast to all previously reported crystal structures for analogous siliconium salts **2** with different X ligands, in all of which the nitrogen ligands occupy essentially axial positions.[6c]

Like the elimination itself, the uncommon N,N-diequatorial geometry in **7b** and **6a** must also be imposed by steric requirements: The bulky tBu ligand prefers to have the smaller oxygen ligands in its vicinity (~90° bond angle) over the relatively large *N*-methylamino and *N,N*-dimethylamino groups. The latter are therefore placed at greater distances from the tBu group by opening up the bond angles (~120°). These substantial modifications of the crystal structures of tBu-substituted complexes are in line with the observation that only *tert*-butylsiliconium halide complexes undergo facile methyl halide elimination, whereas methyl- and benzylsiliconium complexes **2** resist this reaction, and the bulkier **2b**

 © 2003 Wiley-VCH Verlag GmbH & Co. KGaA, Weinheim 1433-7851/03/4209-1024 $ 20.00+.50/0

undergoes a much slower elimination (50% MeI elimination after 90 h at 65 °C).

The uncommon molecular geometries found in the crystal structures of **7b** and **6a** can be viewed within a larger framework as points along a hypothetical Berry pseudorotation reaction coordinate.[12] A single pseudorotation process is depicted schematically in Figure 2. Each point along the

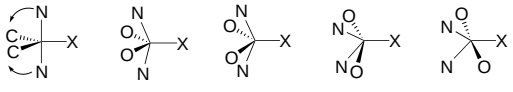

	TBP1	35% TBP1	SP	31% TBP2	TBP2
NSiN	171.2	155.6	146.9	133.5	121.5
OSiO (CSiC)	119.8	134.3	146.0	152.2	165.7
Compound	**9**	**2a**	**8**	**6a**	**7b**

Figure 2. Schematic progress along a Berry pseudorotation coordinate, with corresponding molecular structures and N-Si-N and O-Si-O angles (°). For references, see text. TBP = trigonal bipyramidal, SP = square planar.

pseudorotation coordinate has a corresponding crystal structure, and thus the entire process can be followed crystallographically, in a Burgi–Dunitz sense.[13]

The progress along the reaction coordinate is evident from the variation in the N-Si-N and O-Si-O (or C-Si-C) angles, which determine the overall geometry. Initially the geometry corresponds to TBP1, with two *trans*-diaxial nitrogen ligands (**9**).[2a] This is the common geometry for pentacoordinate

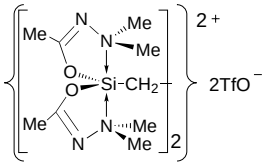

8

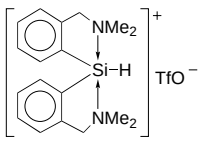

9

bischelates with two nitrogen donor ligands.[8] The N-Si-N angle gradually decreases along the series, while the O-Si-O angle increases, via a distorted TBP (**2a**, ~65% TBP1→SP),[6c] through pure square planar (SP) geometry (**8**; evidenced by the N-Si-N ≃ O-Si-O angles),[6e] then through another distorted TBP with axiallike oxygen ligands (**6a**), and finally to the TBP2 geometry of **7b**, which is essentially an inverted TBP in which axial and equatorial groups have exchanged their positions. Throughout this process the *t*Bu group acts as a "pivot" for the pseudorotation.

As mentioned above, most pentacoordinate bischelates of silicon with two N→Si dative bonds have TBP1 geometry. Clearly this geometry is preferred. It is only the steric strain introduced by the *t*Bu group in **3**–**5** and **7**, or in the binuclear **8**, that pushes the geometry towards the other end of the reaction coordinate and enables the demonstration of stable points along the entire pseudorotation coordinate. The methyl halide elimination described herein may provide a new synthetic route to MeN-Si compounds.

Experimental Section

4a–c–6a–c were obtained from **3a–c**[6c] by reaction with excess Me_3SiY in 80–97% yield. **6a**: $Me_3SiOSO_2CF_3$ (0.777 g, 3.5 mM) was added as a solution in hexane to **3a**[6c] (0.977 g, 3.4 mM), and the mixture was stirred for 2 h at room temperature. The volatile components were removed at 0.02 mmHg, leaving **6a** (1.205 g, 88%) as a white precipitate, m.p. 197–198 °C, which was recrystallized for X-ray analysis from CH_2Cl_2. ^{1}H NMR (500 MHz, $CDCl_3$, 300 K): $\delta = 1.07$ (s, 9H, *t*Bu), 2.08 (s, 6H, CMe), 3.05, 3.12 ppm (2 s, 6H, NMe_2); ^{13}C NMR (125.8 MHz, $CDCl_3$, 300 K): $\delta = 16.9$ (CCH_3), 23.0 (Me_3C), 29.7 ($CH_3)_3C$), 49.7, 51.8 (NMe_2), 120.6 (q, $^1J = 321$ Hz, CF_3), 169.0 ppm (C=N); ^{29}Si NMR (99.4 MHz, $CDCl_3$, 300 K): $\delta = -61.2$ ppm. **7b**: A solution of **3b** (0.804 g, 1.97 mM) in $CHCl_3$ (5 mL) was kept in a preevacuated flask immersed in a 90 °C bath for 6 days. The volatiles were removed at 0.02 mmHg, and the residue was recrystallized from hexane, to give **7b** (0.386 g, 55%), m.p. 77–78 °C. ^{1}H NMR (500 MHz, $CDCl_3$, 300 K): $\delta = 0.86$ (s, 9H, *t*Bu-Si), 1.09 (s, 18H, *t*Bu-C), 2.40 (s, 3H, NMe), 2.88, 3.01 ppm (2 s, 6H, NMe_2); ^{13}C NMR (125.8 MHz, $CDCl_3$, 300 K): $\delta = 25.0$ (Me_3CSi), 27.3, 27.7, 29.3 (($CH_3)_3C$), 33.9, 35.1 (Me_3CC), 36.8 (NMe), 47.8, 49.0 (NMe_2), 160.9, 176.8 ppm (C=N); ^{29}Si NMR (99.4 MHz, $CDCl_3$, 300 K): $\delta = -73.1$ ppm; elemental analysis: calcd for $C_{17}H_{36}N_4O_2Si$: C 57.26, H 10.18, N 15.71. Found: C, 57.21; H, 10.29; N, 15.59. **7a** and **7c** were prepared in the same way as **7b** and were characterized by analogy based on their NMR spectra. **7a**: ^{1}H NMR (500 MHz, $CDCl_3$, 300 K): $\delta = 0.85$ (s, 9H, *t*BuSi), 1.85, 1.93 (2 s, 6H, MeC), 2.56 (s, 3H, NMe), 3.00, 3.90 ppm (2 s, 6H, NMe_2); ^{13}C NMR (125.8 MHz, $CDCl_3$, 300 K): $\delta = 16.0$, 17.0 (CCH_3), 24.1 (Me_3CSi), 28.7 (($CH_3)_3C$), 36.0 (NMe), 49.7, 56.9 (NMe_2), 169.1, 170.2 ppm (C=N); ^{29}Si NMR (99.4 MHz, $CDCl_3$, 300 K): $\delta = -71.8$ ppm. **7c**: ^{1}H NMR (500 MHz, $CDCl_3$, 300 K): $\delta = 1.03$ (s, 9H, *t*BuSi), 2.79, 3.32 (2 s, 6H, NMe_2), 3.47 (s, 3H, NMe), 7.30–8.10 ppm (m, 10H, Ph); ^{13}C NMR (125.8 MHz, $CDCl_3$, 300 K): $\delta = 24.6$ (Me_3CSi), 28.8 (($CH_3)_3C$), 36.8 (NMe), 48.4, 50.0 (NMe_2), 124.9–132.4 (Ph), 152.8, 166.1 ppm (C=N); ^{29}Si NMR (99.4 MHz, $CDCl_3$, 300 K): $\delta = -71.7$ ppm.

Received: October 11, 2002 [Z50346]

[1] For reviews, see: a) P. Lickiss in *The Chemistry of Organic Silicon Compounds, Vol. 2, Part 1* (Eds.: Z. Rappoport, Y. Apeloig), Wiley, Chichester, UK, **1998**, pp. 557–594; b) J. B. Lambert, L. Kania, S. Zhang, *Chem. Rev.* **1995**, *95,* 1191.

[2] a) J. Belzner, D. Schär, B. O. Kneisel, R. Herbst-Irmer, *Organometallics* **1995**, *14*, 1840; b) D. Schär, J. Belzner in *Organosilicon Chemistry III* (Eds.: N. Auner, J. Weis), VCH, Weinheim, **1997**, p. 429.

[3] U.-H. Berlekamp, P. Jutzi, A. Mix, B. Neumann, H.-G. Stammler, W. W. Schoeller, *Angew. Chem.* **1999**, *111*, 2071; *Angew. Chem. Int. Ed.* **1999**, *38*, 2048.

[4] a) C. Chuit, R. J. P. Corriu, A. Mehdi, C. Reyé, *Angew. Chem.* **1993**, *105*, 1370; *Angew. Chem. Int. Ed. Engl.* **1993**, *32,* 1311; b) M. Chauhan, C. Chuit, R. J. P. Corriu, C. Reyé, *Tetrahedron Lett.* **1996**, *37*, 845; c) M. Chauhan, C. Chuit, R. J. P. Corriu, A. Mehdi, C. Reyé, *Organometallics* **1996**, *15*, 4326.

[5] Yu. E. Ovchinnikov, S. A. Pogozhikh, I. V. Razumovskaya, A. G. Shipov, E. P. Kramarova, S. Yu. Bylikin, V. V. Negrebetsky, Yu. I. Baukov, *Russ. Chem. Bull.* **1998**, *47*, 967.

[6] a) I. Kalikhman, S. Krivonos, L. Lameyer, D. Stalke, D. Kost, *Organometallics* **2001**, *20*, 1053; b) V. Kingston, B. Gostevskii, I. Kalikhman, D. Kost, *Chem. Commun.* **2001**, 1272; c) D. Kost, V. Kingston, B. Gostevskii, A. Ellern, D. Stalke, B. Walfort, I. Kalikhman, *Organometallics* **2002**, *21*, 2293; d) I. Kalikhman, B. Gostevskii, O. Girshberg, S. Krivonos, D. Kost, *Organometallics* **2002**, *21*, 2551; e) I. Kalikhman, V. Kingston, B. Gostevskii, V. Pestunovich, D. Stalke, B. Walfort, D. Kost, *Organometallics* **2002**, *21*, 4468.

[7] M. Tanaka, Y. Hatanaka, 35th Organosilicon Symposium, Guanajuato, Mexico, **2002**, Abstract C-06/IL, p. 28.
[8] For recent reviews on hypervalent silicon complexes, see: a) D. Kost, I. Kalikhman in *The Chemistry of Organic Silicon Compounds, Vol. 2, Part 2* (Eds.: Z. Rappoport, Y. Apeloig), Wiley, New York, **1998**, p. 1339; b) C. Chuit, R. J. P. Corriu, C. Reyé in *The Chemistry of Hypervalent Compounds* (Ed.: Kin-ya Akiba), Wiley-VCH, Weinheim, **1999**, p. 81; c) Brook, M. A. *Silicon in Organometallic and Polymer Chemistry*, Wiley, New York, **2000**, p. 97.
[9] Elimination of methyl chloride from quaternary hydrazonium chloride compounds (in the absence of silicon coordination) has been reported, and was observed at substantially higher temperature (220 °C): W. Sucrow, M. Slopianka, *Chem. Ber.* **1978**, *111*, 780.
[10] **6a**: $T = 100(2)$ K, triclinic, space group: $P\bar{1}$; $a = 8.0805(4)$, $b = 11.0395(6)$; $c = 11.6194(6)$ Å; $\alpha = 83.063(1)$; $\beta = 75.121(1)$; $\gamma = 81.860(1)°$, $Z = 2$, $V = 987.79(9)$ Å^3. $R_F = 0.0269$ ($wR_F = 0.0737$) for $I > 2\sigma$. **7b**: $T = 100(2)$ K, triclinic, space group: $P\bar{1}$; $a = 7.5031(5)$, $b = 11.7898(8)$; $c = 12.0470(8)$ Å; $\alpha = 82.708(1)$; $\beta = 87.980(1)$; $\gamma = 84.512(1)°$, $Z = 2$, $V = 1051.93(12)$ Å^3. $R_F = 0.0345$ ($wR_F = 0.0906$) for $I > 2\sigma$. CCDC-195084 (**6a**) and CCDC-195085 (**7b**) contain the supplementary crystallographic data for this paper. These data can be obtained free of charge via www.ccdc.cam.ac.uk/conts/retrieving.html (or from the Cambridge Crystallographic Data Centre, 12, Union Road, Cambridge CB2 1EZ, UK; fax: (+44) 1223-336-033; or deposit@ccdc.cam.ac.uk).
[11] The exact precursors to **7b** (**3b**–**5b**) did not yield suitable crystals for X-ray crystal-structure analysis. However, the identical ^{1}H, ^{13}C, and ^{29}Si NMR spectra of **3b** and **6b**, as well as previous experience with siliconium salts with different counterions,[6c] indicate that the siliconium ion portions of **3b** and **6b** are equivalent. The replacement of the remote substituent R = *t*Bu in **6b** by R = Me in **6a** is not expected to have a substantial effect on the geometry about the silicon atom.
[12] R. S. Berry, *J. Chem. Phys.* **1960**, *32*, 933; R. R. Holmes, J. A. Deiters, *J. Am. Chem. Soc.* **1977**, *99*, 3318.
[13] H. B. Bürgi, J. Dunitz, *Acc. Chem. Res.* **1983**, *16*, 153.

 © 2003 Wiley-VCH Verlag GmbH & Co. KGaA, Weinheim 1433-7851/03/4209-1026 $ 20.00+.50/0

Oxidation of Primary Amines

Oxidation of Unactivated Primary Aliphatic Amines Catalyzed by an Electrogenerated 3,4-Azaquinone Species: A Small-Molecule Mimic of Amine Oxidases

Martine Largeron, Anne Neudorffer, and Maurice-Bernard Fleury*

The copper amine oxidases are ubiquitous enzymes that occur in bacteria, yeast, plants, and mammals. These enzymes catalyze the two-electron oxidative deamination of a primary amine to produce the corresponding aldehyde and ammonia, with subsequent two-electron reduction of dioxygen to hydrogen peroxide. To carry out this reaction, copper amine oxidases, which belong to the new class of proteins designated quinoproteins, contain two cofactors: an organic cofactor, 2,4,5-trihydroxyphenylalanine quinone (TPQ, Scheme 1), and a cupric ion.[1] This class also includes bacterial methylamine oxidases, which use a peptide-bound tryptophan tryptophylquinone (TTQ)[2] and lysyl oxidase, a mammalian copper amine oxidase whose active site has been identified as lysine tyrosylquinone (LTQ).[3]

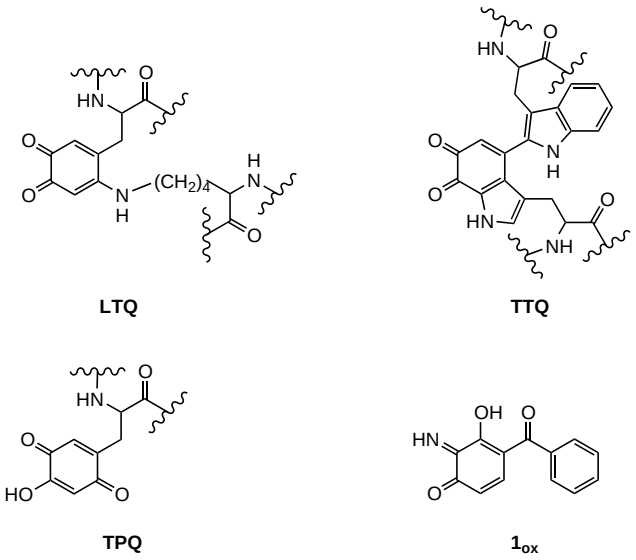

Scheme 1. Quino cofactors derived from protein-bound tyrosine (TPQ, LTQ), tryptophan (TTQ), together with 3,4-iminoquinone model cofactor $\mathbf{1}_{ox}$.

It is well established that TPQ catalyzes the conversion of an amine substrate into an aldehyde through a pyridoxal-like transamination mechanism, which results in the reduction of TPQ to an aminoquinol form.[4] Although there is no question regarding the crucial role of copper in the biogenesis of TPQ from its tyrosine precursor, the role of the copper cofactor during amine oxidation is, however, less well understood. Recent intensive studies have shown that an electron transfer from the cofactor to the metal is not required during the catalytic turnover, so that the metal essentially stabilizes a reduced oxygen intermediate.[5] These results are supported by the fact that the mature form of bovine lysyl oxidase retains its catalytic function in the absence of copper.[6]

Substantial mechanistic information has been obtained through catalytic aerobic deamination of benzylamine mediated by synthetic models of natural quinones which confirm the occurrence of the transamination mechanism.[7] However, these models failed to oxidize unactivated primary aliphatic amines under the same experimental conditions, with the exception of a recent study showing that the metal ion complex of the TTQ model compound was able to oxidize aliphatic amines in anhydrous organic media, whereas no reaction took place in the absence of the metal ion.[8]

[*] Dr. M. Largeron, Dr. A. Neudorffer, Prof. M.-B. Fleury
Laboratoire de Chimie Analytique et Electrochimie, UMR 8638
CNRS-Université René Descartes
Faculté des Sciences Pharmaceutiques et Biologiques
4 Avenue de L'Observatoire, 75270 Paris Cedex 06 (France)
Fax: (+33) 1-4407-3588
E-mail: largeron@pharmacie.univ-paris5.fr

 © 2003 Wiley-VCH Verlag GmbH & Co. KGaA, Weinheim 1433-7851/03/4209-1026 $ 20.00+.50/0

We recently showed that electrogenerated 3,4-iminoquinone $\mathbf{1}_{ox}$ (Scheme 1) acts as an efficient catalyst for the autorecycling oxidation of benzylamine through the transamination process reported for amine oxidase cofactors. The catalytic cycle produced the reduced catalyst $\mathbf{1}_{red}$ and *N*-benzylidenebenzylamine as the product of benzylamine oxidation in 3200% yield (based on the initial concentration of $\mathbf{1}_{red}$).[9] In contrast to other existing amine oxidase model cofactors, $\mathbf{1}_{ox}$ was also very active toward aliphatic amines. Herein, we report for the first time the catalytic oxidation of unactivated primary aliphatic amines by a small-molecule enzyme mimic in the absence of a metal ion.

Unstable 3,4-iminoquinone $\mathbf{1}_{ox}$ was electrogenerated from $\mathbf{1}_{red}$ by using anodic-controlled potential electrolysis, at a platinum electrode in deaerated methanol that contained an excess of primary aliphatic amine. At a potential at which $\mathbf{1}_{red}$ could be oxidized to the iminoquinone form $\mathbf{1}_{ox}$ (see Experimental Section),[10] the anodic current remained unchanged for a long time, consistent with steady-state catalytic behavior. Accordingly, a high value was found for the total number of electrons (n) transferred per molecule of $\mathbf{1}_{red}$ in the catalytic process. These results indicated that the $\mathbf{1}_{red}/\mathbf{1}_{ox}$ system behaved as a redox mediator for the indirect electrochemical oxidation of unactivated primary aliphatic amines to the corresponding alkylimines, according to the transamination mechanism reported in Scheme 2.[9] After exhaustive electrolysis, the catalyst $\mathbf{1}_{ox}$ was lost irreversibly, as corroborated by the anodic current, which remained negligible upon further addition of amine substrate. Unstable alkylimine was isolated in terms of the corresponding aldehyde 2,4-dinitrophenylhydrazone (DNPH) obtained upon workup of the oxidized solution with 2,4-dinitrophenylhydrazine. Table 1 shows the effects of varying the structure of the amine substrate.[11] The most efficient substrates for $\mathbf{1}_{ox}$ were primary alkyl amines (Table 1, entries 1–6), with high yields of isolated DNPH ranging from 1000 to 2300% (relative to the mediator). With *n*-hexylamine (Table 1, entry 7), although a high value of 48 was found for n, the catalytic oxidation of more hydrophobic longer-chain amine produced DNPH in only 305% yield (based on $\mathbf{1}_{red}$), along with 255% of a second product identified as the osazone (1,2-bis-DNPH). Interestingly, as for the enzymes themselves, α-branched amines such as cyclohexylamine (Table 1, entry 8) were found to be poor substrates for the model catalyst $\mathbf{1}_{ox}$, whereas secondary amines (Table 1, entries 9 and 10) were not reactive at all.

Primary amines bearing aromatic substituents also underwent deamination, though the turnover was much lower on account of a more rapid deterioration of the catalyst. With phenylpropylamine (Table 1, entry 11), a value of 38 was found for n. Similarly to *n*-hexylamine (Table 1, entry 7), both DNPH (650%) and 1,2-bis-DNPH (100%) could be isolated at the end of the catalytic process. Further investigations would be necessary to justify the formation of the osazone,

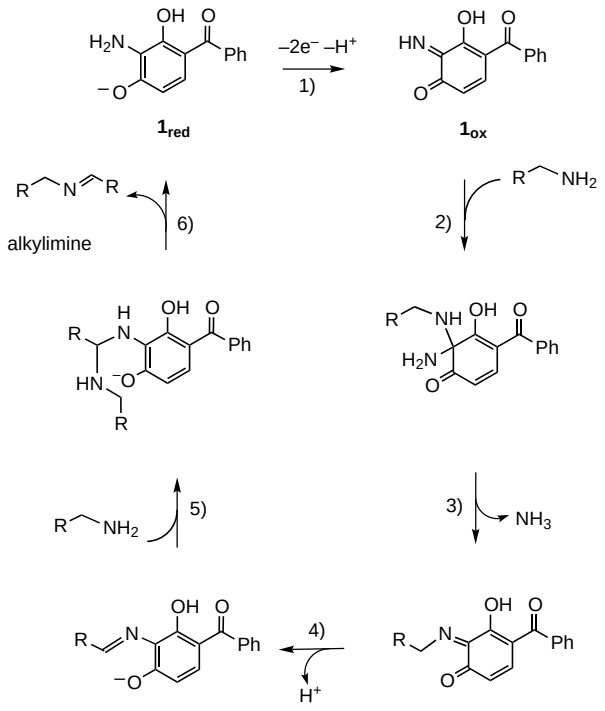

Scheme 2. Mechanism of catalytic oxidation of primary aliphatic amines mediated by electrogenerated 3,4-iminoquinone model cofactor $\mathbf{1}_{ox}$.

Table 1: Catalytic oxidation of primary aliphatic amines mediated by the electrogenerated 3,4-iminoquinone $\mathbf{1}_{ox}$ model cofactor.

Entry	Amine	n[a]	Turnover	Yields[%][b] (A)	(B)
1	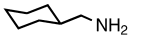	54	20.0	2000	40.0
2	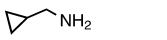	52	17.5	1750	35.0
3	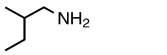	55	19.5	1950	39.0
4	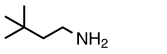	56	23.0	2300	46.0
5	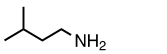	48	10.0	1000	20.0
6	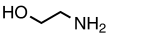	46	10.0	1000	20.0
7	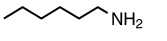	48	3.0[c]	305	6.1
8	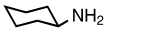	8	1.1	110	2.2
9	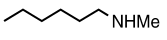	4	–	–	–
10		3	–	–	–
11	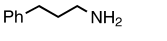	38	6.5[c]	650	13.0
12	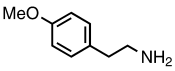	10	2.1	210	4.2
13	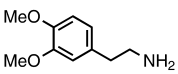	9	1.3	130	2.6

[a] Total number of electrons transferred per molecule of mediator. [b] Determined by weight of the aldehyde derivative DNPH, relative to the mediator (A) and to the amine substrate (B), respectively. [c] The 1,2-bis-DNPH derivative was also formed; turnover: 2.5 (entry 7); 1.0 (entry 11).

 © 2003 Wiley-VCH Verlag GmbH & Co. KGaA, Weinheim 1433-7851/03/4209-1027 $ 20.00+.50/0

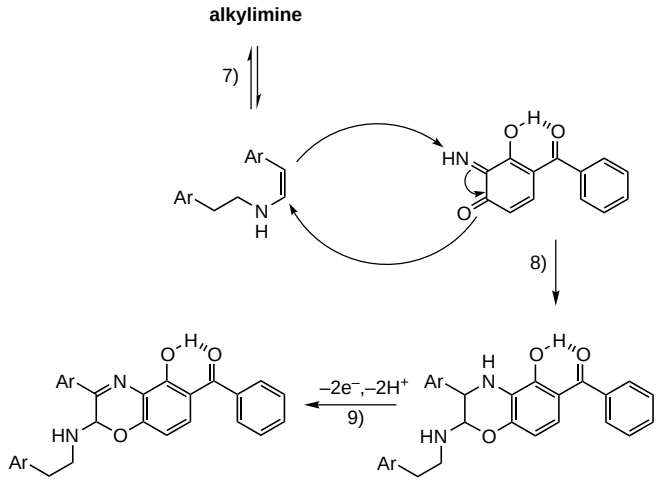

2: Ar = 4-MeO-C_6H_4

3: Ar = 3,4-MeO-C_6H_3

Scheme 3. Inactivation of model cofactor $\mathbf{1_{ox}}$ by ring-substituted phenylethylamine substrates, leading to 1,4-benzoxazine derivatives **2** and **3**.

which seems favored when starting amines are not sterically encumbered by β and γ branching.

With ring-substituted phenylethylamines, the catalytic process ceased after roughly 2 turnovers (Table 1, entries 12 and 13). Close inspection of the exhaustively oxidized solution revealed that electrogenerated 3,4-iminoquinone $\mathbf{1_{ox}}$ was trapped with the tautomeric enamine form of the alkylimine extruded during the catalytic process (Scheme 3, step 7) through an inverse-electron-demand Diels–Alder reaction,[12] affording unstable 1,4-benzoxazine derivatives (Scheme 3, step 8). However, these compounds could be isolated as stable products **2** and **3** in 50 and 65% yields, respectively, after a subsequent two-electron oxidation reaction (Scheme 3, step 9). Interestingly, this multistep one-pot electrochemical procedure could lead to novel neuroprotective agents as a consequence of the structural similarity of **2** and **3** with earlier reported 1,4-benzoxazine derivatives.[13]

In summary, we have demonstrated for the first time that unactivated primary aliphatic amines can be efficiently oxidized by a synthetic model cofactor of amine oxidases in the absence of a metal ion. The catalyst $\mathbf{1_{ox}}$ exhibits the same substrate specificity as the copper amine oxidases themselves, that is, poor reactivity with α-branched primary amines and no reactivity toward secondary amines. The reaction displays two features that are most often associated with enzymatic systems: a) the reaction is likely enhanced through the participation of neighboring substituents, as they prevented the competing formation of Michael adducts (in this case, the benzoyl and 2-hydroxy groups); b) the presence of an active hydroxy proton very probably constitutes an essential component of the catalytic activity (in this case, the 2-hydroxy proton, analogous to that of TPQ).[14] We are currently developing further analogues to confirm the substantial role of the 2-hydroxy group to convert a catalytic inert species into a highly effective enzymatic prosthetic group.

Experimental Section

General procedure: Controlled-potential electrolysis was carried out in a cylindrical, three-electrode, divided cell (9 cm diameter), using an electronic potentiostat. In the main compartment, a platinum grid (area = 60 cm^2) served as the anode (working electrode). A platinum sheet was placed in the concentric cathodic compartment (counter-electrode), which was separated from the main compartment with a glass frit. The reference electrode was an aqueous saturated calomel electrode (SCE), which was isolated from the bulk solution in a glass tube with a fine-porosity frit. The electrolyte solution (0.04 mol L^{-1} lithium perchlorate or tetraethylammonium perchlorate in methanol) was poured into the anodic and the cathodic compartments, as well as into the glass tube that contained the SCE electrode. 3,4-Aminophenol[15] $\mathbf{1_{red}}$ (0.1 mmol) and an excess of primary aliphatic amine (5 mmol) were added to the solution in the main compartment (250 mL), and the resulting solution was then oxidized under nitrogen at room temperature at +600 mV vs. SCE (initial current 30–40 mA), that is, at a potential following the anodic peak observed in cyclic voltammetry, characteristic of the two-electron oxidation of $\mathbf{1_{red}}$ to $\mathbf{1_{ox}}$. After exhaustive electrolysis (6–10 h, n = 8–56), that is, when a negligible value of the current was recorded (0.5–1.0 mA), the solution was worked up by addition of 2.5 mmol of 2,4-dinitrophenylhydrazine reagent (in 5 mL of H_2SO_4, 15 mL of EtOH and 5 mL of water) because 5 mmol of primary amine gave 2.5 mmol of alkylimine (Scheme 2). After 1 h, the resulting solution was concentrated to 40 mL. The solid was collected by filtration, washed with water, and dried in a vacuum desiccator. The identity and purity of DNPH was confirmed by thin-layer chromatography (TLC) and ^{1}H NMR spectroscopy, after comparison with an authentic sample. In the case of *n*-hexylamine or phenylpropylamine, the solid was purified by chromatography on silica gel to separate DNPH from 1,2-bis-DNPH. Control studies indicated that the amount of aldehyde produced either from simple autoxidation or from electrochemical oxidation of the starting amine in the absence of catalyst was negligible.

Isolation of **2** and **3**: After exhaustive electrolysis (6 h, n = 9 or 10), the electrolysis solution was poured into an acetic acid buffered aqueous solution of pH 4.8 (1 mol L^{-1}, 50 mL). The resulting hydroalcoholic solution was concentrated to remove methanol. The yellow solid, identified as the 1,4-benzoxazine derivative, was collected by filtration, washed with water, and dried in a vacuum desiccator.

2: M.p. 162 °C; ^{1}H NMR (300 MHz, $CDCl_3$): δ = 2.25 (m, 1H), 2.75 (t, J = 6 Hz, 2H), 3.15(m, 2H), 3.75 (s, 3H), 3.90 (s, 3H), 5.90 (d, J = 8 Hz, 1H), 6.55 (d, J = 9 Hz, 1H), 6.75 (d, J = 8 Hz, 2H), 6.95 (d, J = 8 Hz, 2H), 7.05 (d, J = 8 Hz, 2H), 7.45 (d, J = 9 Hz, 1H), 7.55 (m, 3H), 7.70 (d, J = 8 Hz, 2H), 8.00 (d, J = 8 Hz, 2H), 13.10 ppm (s, 1H); ^{13}C NMR (75 MHz, $CDCl_3$): δ = 35.7, 46.2, 55.2, 55.3, 81.2, 108.3, 113.9, 114.2, 122.7, 127.9, 128.3, 128.9, 129.2, 129.6, 131.2, 131.6, 133.2, 138.2, 150.7, 154.5, 158.1, 160.3, 161.9, 202.2 ppm; DCI (desorption chemical ionization) MS: m/z: 509 [MH$^+$].

Received: October 14, 2002 [Z50356]

[1] a) J. P. Klinman, *Chem. Rev.* **1996**, *96*, 2541–2561; b) J. P. Klinman, *J. Biol. Chem.* **1996**, *271*, 27189–27192; c) J. A. Stubbe, W. A. Van der Donk, *Chem. Rev.* **1998**, *98*, 705–776; d) J. P. Klinman, *Proc. Natl. Acad. Sci. USA* **2001**, *98*, 14766–14768; e) M. A. Halcrow, *Angew. Chem.* **2001**, *113*, 358–362; *Angew. Chem. Int. Ed.* **2001**, *40*, 346–349.

[2] Y.-L. Hyun, V. L. Davidson, *Biochemistry* **1995**, *34*, 816–823, and references therein.

[3] S. X. Wang, N. Nakamura, M. Mure, J. P. Klinman, J. Sanders-Loehr, *J. Biol. Chem.* **1997**, *272*, 28841–28844.

[4] M. Mure, S. A. Mills, J. P. Klinman, *Biochemistry* **2002**, *41*, 9269–9278.

[5] a) S. A. Mills, J. P. Klinman, *J. Am. Chem. Soc.* **2000**, *122*, 9897–9904; b) B. Schwartz, A. K. Olgin, J. P. Klinman, *Biochemistry*

 © 2003 Wiley-VCH Verlag GmbH & Co. KGaA, Weinheim 1433-7851/03/4209-1028 $ 20.00+.50/0

2001, *40*, 2954 – 2963; c) S. A. Mills, Y. Goto, Q. Su, J. Plastino, J. P. Klinman, *Biochemistry* **2002**, *41*, 10577 – 10584; d) E. I. Solomon, P. Chen, M. Metz, S.-K. Lee, A. E. Palmer, *Angew. Chem.* **2001**, *113*, 4702 – 4724; *Angew. Chem. Int. Ed.* **2001**, *40*, 4570 – 4590.

[6] C. Tang, J. P. Klinman, *J. Biol. Chem.* **2001**, *276*, 30575 – 30578.

[7] a) E. J. Rodriguez, T. C. Bruice, *J. Am. Chem. Soc.* **1989**, *111*, 7947 – 7956; b) S. Itoh, M. Mure, M. Ogino, Y. Ohshiro, *J. Org. Chem.* **1991**, *56*, 6857 – 6865; c) M. Mure, J. P. Klinman, *J. Am. Chem. Soc.* **1995**, *117*, 8707 – 8718; d) Y. Lee, L. M. Sayre, *J. Am. Chem. Soc.* **1995**, *117*, 11823 – 11828, and references therein; e) S. Itoh, N. Takada, S. Haranou, T. Ando, M. Komatsu, Y. Ohshiro, S. Fukuzumi, *J. Org. Chem.* **1996**, *61*, 8967 – 8974, and references therein; f) K. Q. Ling, J. Kim, L. M. Sayre, *J. Am. Chem. Soc.* **2001**, *123*, 9606 – 9611.

[8] S. Itoh, M. Tanaguchi, N. Takada, S. Nagatomo, T. Kitagawa, S. Fukuzumi, *J. Am. Chem. Soc.* **2000**, *122*, 12087 – 12097.

[9] M. Largeron, M.-B. Fleury, *J. Org. Chem.* **2000**, *65*, 8874 – 8881.

[10] The cyclic voltammogram of $\mathbf{1}_{red}$ (0.1 mmol), recorded under our experimental conditions (see Experimental Section), showed an oxidation peak Pa at +500 mV vs. SCE, the sweep rate being 0.5 $V s^{-1}$. The addition of 5 mmol of primary amine had two effects: 1) a shift of the peak Pa to 0.0 mV vs. SCE as a result of the ionization of the 4-hydroxy group; 2) an increase in the anodic peak intensity which suggests that 3,4-iminoquinone $\mathbf{1}_{ox}$ can act competitively as a catalyst (even on the time scale of cyclic voltammetry) with the succeeding oligomerization. For similar behavior of quinonoid species, see: K. Kano, M. Nakagawa, K. Takagi, T. Ikeda, *J. Chem. Soc. Perkin Trans. 2* **1997**, 1111 – 1119, and references therein.

[11] In some cases, the yield of DNPH was lower than that expected from the value of *n* as a result of the partial conversion of unstable alkylimine into volatile aldehyde on the time scale of anodic electrolysis.

[12] We recently showed similar inverse-electron-demand Diels–Alder reactions of $\mathbf{1}_{ox}$ with $R^1R^2CHCH_2NH_2$ amines, but under different experimental conditions, which have been defined as optimal for the synthesis of 1,4-benzoxazine derivatives; see: M. Largeron, A. Neudorffer, M. Vuilhorgne, E. Blattes, M.-B. Fleury, *Angew. Chem.* **2002**, *114*, 852 – 855; *Angew. Chem. Int. Ed.* **2002**, *41*, 824 – 827.

[13] M. Largeron, B. Lockhart, B. Pfeiffer, M.-B. Fleury, *J. Med. Chem.* **1999**, *42*, 5043 – 5052.

[14] M. Mure, J. P. Klinman, *J. Am. Chem. Soc.* **1993**, *115*, 7117 – 7127.

[15] Reduced catalyst $\mathbf{1}_{red}$ was synthesized from commercially available 2-nitroresorcinol through a four-step sequence previously reported; see: R. Larget, B. Lockhart, B. Pfeiffer, A. Neudorffer, M.-B. Fleury, M. Largeron, *Bioorg. Med. Chem. Lett.* **1999**, *9*, 2929 – 2934.

 © 2003 Wiley-VCH Verlag GmbH & Co. KGaA, Weinheim 1433-7851/03/4209-1029 $ 20.00+.50/0

Water Treatment

Efficient Degradation of Organic Pollutants by Using Dioxygen Activated by Resin-Exchanged Iron(II) Bipyridine under Visible Irradiation**

*Wanhong Ma, Jing Li, Xia Tao, Ju He, Yiming Xu, Jimmy C. Yu, and Jincai Zhao**

The treatment of persistent organic pollutants in water by green chemical processes has been a very active research topic in recent years.[1] To mimic the oxidative characteristics of iron-containing oxygenase enzymes such as cytochrome P450 and non-heme methane monooxygenase (MMO), several synthetic analogues that allow the use of environmentally friendly oxidants (O_2 or H_2O_2) in pollution treatment have been developed.[2–8] For example, Meunier and coworkers reported that 2,4,6-trichlorophenol (TCP) in a CH_3CN/water solvent mixture could be efficiently degraded in the presence of H_2O_2 and iron phthalocyaninesufonate (FePcS), resulting in a 14% mineralization of TCP.[3,4] However, when water was used as the only solvent, the conversion rate was greatly decreased. Taking advantage of the strong absorption of FePcS in the visible range, we showed recently that visible-light irradiation can accelerate the degradation of salicylic acid, orange II, and rhodamine B in the presence of FePcS and H_2O_2 without the addition of CH_3CN.[7,8] In some organic synthetic processes, dioxygen can be used as an oxidant.[9,10] However, an additional reducing reagent such as zinc metal, ferrocene, ascorbate, or hydrogen/colloidal platinum is required in these systems to reduce the second oxygen atom of O_2 to H_2O (the Gif system).[11–13] The requirement of sacrificial reagents causes problems in separation and may even be considered as secondary contamination if these methods are used for the treatment of water.

Elimination of organic pollutants in water by oxidation with molecular oxygen and sunlight is the most environmentally friendly pollution-treatment method. Herein we show that FeBR, an iron(II) complex of 2,2′-bipyridine ($[Fe^{II}(bpy)_3]^{2+}$) supported on a commercial cationic ion-exchange resin (amberlite IRA 200), is an efficient catalyst for the activation of O_2 at room temperature to degrade organic pollutants including rhodamine B (RhB), malachite

[*] Prof. J. Zhao, Dr. W. Ma, Dr. J. Li, Dr. X. Tao, Dr. J. He, Dr. Y. Xu
Center for Molecular Sciences, Institute of Chemistry
Chinese Academy of Science
Beijing 100080 (China)
Fax: (+86) 10-6255-9373
E-mail: jczhao@infoc3.icas.ac.cn
Dr. J. C. Yu
Department of Chemistry and Environmental Science Programme
The Chinese University of Hong Kong
Shatin, N.T., Hong Kong (China)

[**] This work was supported by NSFC (Nos. 20133010, 20077027, 20277038, and 4001161947), CAS, and the China National Ministry for Science and Technology.

Supporting information for this article is available on the WWW under http://www.angewandte.org or from the author.

 © 2003 Wiley-VCH Verlag GmbH & Co. KGaA, Weinheim 1433-7851/03/4209-1029 $ 20.00+.50/0

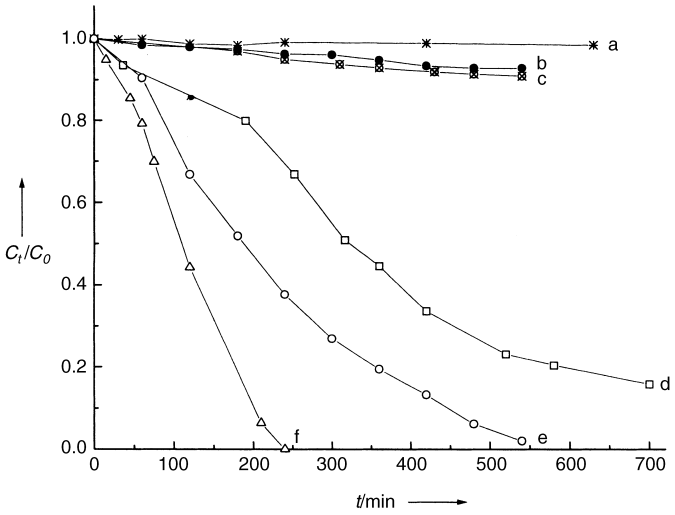

Figure 1. Concentration changes of substrates (50 mL) as a function of irradiation time under different conditions. a) Homogenous solution of RhB (20 μM) and $[Fe^{II}(bpy)_3]^{2+}$ (10 μM) at pH 2.6 under visible-light irradiation; b) heterogeneous dispersion of RhB (20 μM) and FeBR (5 mg) at pH 2.6 in the dark; c) deaerated heterogeneous dispersion of RhB (20 μM) and FeBR (5 mg) at pH 2.6 under visible-light irradiation; d) heterogeneous dispersion of DMA (100 μM) and FeBR (5 mg) at pH 4.6 under visible-light irradiation; e) heterogeneous dispersion of RhB (20 μM) and FeBR (5 mg) at pH 2.6 under visible-light irradiation; f) heterogeneous dispersion of MG (100 μM) and FeBR (5 mg) at pH 5.0 under visible-light irradiation.

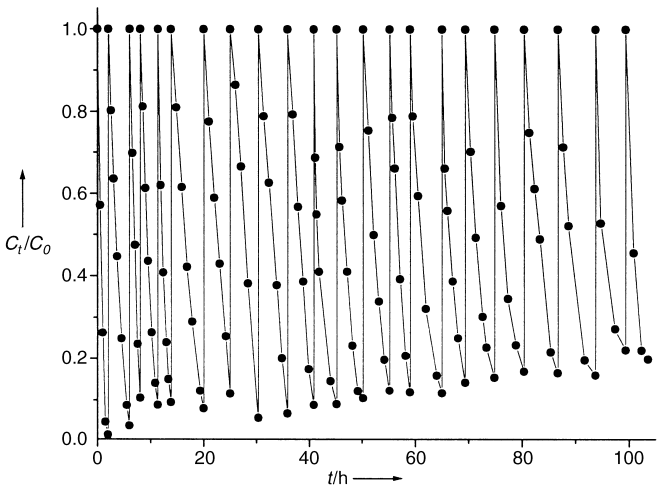

Figure 2. Cycling runs in the photodegradation of RhB in the presence of FeBR under visible-light irradiation. FeBR (10 mg/100 mL); addition of RhB (5 μmol/run).

green (MG), and *N,N*-dimethylaniline (DMA) in aerated aqueous solutions under visible-light irradiation ($\lambda > 420$ nm) (Figure 1). The catalytic reaction with FeBR proceeded efficiently without addition of any sacrificial reagents. The total organic carbon (TOC) removal yield reached 60% for RhB (20 μM, pH 2.6), 58% for MG (400 μM, pH 5.0), and 75% for DMA (100 μM, pH 4.6). The catalytic activity of the FeBR catalyst in the degradation of RhB was maintained effectively even after 22 repeated experiments (~100 h) (Figure 2). Another advantage of the proposed system is that the FeBR catalyst can be separated from the solution simply by filtration. Control experiments 1) with the catalyst in the dark, 2) in the absence of the catalyst, under irradiation, 3) with the resin itself, under irradiation, 4) with the iron(II)/resin (or iron(III)/resin), under irradiation, and 5) with a homogeneous, aqueous $[Fe^{II}(bpy)_3]^{2+}$ solution under visible-light irradiation all showed no significant degradation of the organic species. In aqueous solutions purged with nitrogen or helium gas the photodegradation rate of RhB was greatly decreased. These results demonstrated that both molecular oxygen and visible-light irradiation are necessary for the degradation of organic compounds.

The catalyst displays a broad absorption band in the region of 240–700 nm with a maximum located at 522 nm. Such extended coverage in the visible spectrum makes it possible to utilize most of the energy from sunlight. The quantum yield was 2.1×10^{-2} at 500 ± 5 nm for the degradation of MG.[14] Notably, Figure 1 shows substantial degradation of DMA (which does not absorb at wavelengths longer than 310 nm) under visible-light irradiation in the presence of the FeBR catalyst. This rapid degradation of DMA illustrates that the photoexcitation of FeBR initiates the photocatalytic degradation process and that the photosensitization process induced by the photoexcitation of substrates does not play a major role.

In the RhB photodegradation process, infrared spectroscopy (IR) and GC–MS were used to monitor the reaction and to identify the products. The IR study revealed ring opening as shown by the decrease and final disappearance of the vibration peaks of the aromatic ring at 1648, 1589, 1548, and 1527 cm^{-1}. The main degradation by-products identified by GC–MS (see Supporting Information) are shown in Scheme 1. About 60% of the organic carbon was mineralized into CO_2; the remaining by-products were mainly small molecular compounds such as *N,N*-diethylamine and *N,N*-diethylformamide, which are known to be biologically degradable. As expected, no hydroxylated or degraded species resulting from the photooxidation of the bipyridine ligands in FeBR were detected by GC–MS.

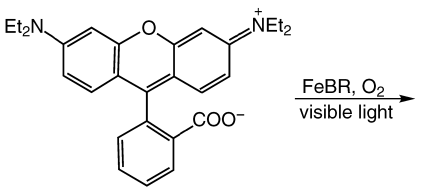

CO_2	60.0%
$NH(CH_2CH_3)_2$	19.9%
$HCN(CH_3)_2$	1.4%
$(CH_3CH_2)_2NN{=}O$	3.3%
$HCN(CH_2CH_3)_2$	7.6%
$H_3CCN(CH_2CH_3)_2$	1.8%
$CH_3CH_2NHCNHCH_2CH_3$	1.5%
$(CH_3CH_2)_2NCCH_2CH_3$	0.7%
Total C%	96.2%

Scheme 1. Products remaining after photodegradation of RhB catalyzed by FeBR.

 © 2003 Wiley-VCH Verlag GmbH & Co. KGaA, Weinheim 1433-7851/03/4209-1030 $ 20.00+.50/0

The X-ray photoemission spectra (XPS) of the FeBR catalyst before and after photoreaction are virtually identical. They all show the presence of only the iron(II) species (2p3 BE 708.85 eV). Unlike $[Ru^{II}(bpy)_3]^{2+}$ and $[Os^{II}(bpy)_3]^{2+}$, $[Fe^{II}(bpy)_3]^{2+}$ in solution did not exhibit the ability to activate dioxygen because of the extremely rapid deactivation of the excited states of the iron(II) bipyridine complex.[15,16] However, $[Fe^{II}(bpy)_3]^{2+}$ supported on amberlite could activate molecular oxygen efficiently to oxidize substrates under visible-light irradiation. This suggests that the resin not only acts as a support for the $[Fe^{II}(bpy)_3]^{2+}$ exchange, but also provides a unique framework that significantly alters the photochemical properties of $[Fe^{II}(bpy)_3]^{2+}$. Just as hydrogen bonds are instrumental in regulating chemical processes, including those observed in respiratory proteins and metal-containing hydrolases,[17] the interaction between the resin and $[Fe^{II}(bpy)_3]^{2+}$ may play an important role in prolonging the lifetime of the FeBR excited state and thus enhancing the probability of its transferring electrons to O_2. The fluorescence measurements provided direct evidence for the interaction between $[Fe^{II}(bpy)_3]^{2+}$ and the resin. FeBR clearly exhibited fluorescence at $\lambda_{max}^{ex} = 522$ nm and $\lambda_{max}^{em} = 588$ nm, while both $[Fe^{II}(bpy)_3]^{2+}$ in solution and the resin itself were nonluminescent.

The reactive oxygen species formed in the photoreaction process were examined by spin-trapping ESR spectroscopy. Experiments were carried out for the degradation of RhB (20 μM) both in water and in methanol. The formation of $^{\bullet}OH$ radicals would be expected in the aqueous system, whereas $^{\bullet}OOH/O_2^{\bullet-}$ radicals that are unstable in water at room temperature should appear in methanol.[18] Upon visible-light irradiation, the ESR signals of DMPO–$^{\bullet}OOH/O_2^{\bullet-}$ adducts with the characteristic six peaks were observed in the methanol system, and the intensity increased slightly with irradiation time. These results confirm that $^{\bullet}OOH/O_2^{\bullet-}$ radicals are formed through the activation of molecular oxygen in the photocatalytic process. However, $^{\bullet}OH$ radicals were not found during photoreactions in either aqueous or methanolic solutions. In another experiment, it was found that addition of 2-propanol, a known scavenger of $^{\bullet}OH$ radicals,[19] to the photoreaction system did not cause any apparent changes in the degradation rate of RhB. This indicates that $^{\bullet}OH$ radicals are not the main active oxygen species involved in the photoreaction catalyzed by FeBR. The formation of H_2O_2 was also observed during the photodegradation of both RhB and MG. However, when we directly introduced H_2O_2 (100 μM) into the RhB degradation system we did not find any acceleration in the degradation of RhB. It may be concluded that H_2O_2 is formed in a side reaction and is not the main active oxygen species involved in the photodegradation of RhB in the presence of FeBR. Therefore the photodegradation of organic pollutants catalyzed by FeBR must mainly involve the superoxide (resin–$[Fe^{III}(bpy)_3O_2^{\bullet-}]$ and the oxoiron (resin–$[Fe^{IV}(bpy)_3{=}O]$) as the active oxygen species, rather than $^{\bullet}OH$ radicals (Fenton mechanism[20]). Mechanisms involving similar intermediates have been proposed by other groups for the oxidation of organic species, catalyzed by iron complexes in organic solvents.[21–23]

This work introduces a simple and green heterogeneous photocatalytic approach for the degradation of organic pollutants. It may also provide useful insight for the development of new routes in synthetic chemistry.

Experimental Section

The FeBR catalyst was prepared by an ion-exchange method. Amberlite IRA 200 resin (Alfa Aesar Co. ~1.0 mmol g^{-1} saturated loading) was ground and then sieved to a size of ~200 mesh. These resin particles were washed with alcohol, HCl, and NaOH to remove any possible contaminants. An appropriate amount of the resin was added to a $[Fe^{II}(bpy)_3]^{2+}$ solution at a suitable concentration at pH 4 and was stirred until all $[Fe^{II}(bpy)_3]^{2+}$ ions were exchanged. Different loadings of $[Fe^{II}(bpy)_3]^{2+}$ catalysts (20%, 50%, 75%, and 100% of the saturated exchange amount) were prepared. The FeBR catalyst of 50% loading (i.e. $[Fe^{II}(bpy)_3]^{2+} = 0.5$ mmol g^{-1} resin) exhibited the highest activity (with relative rates for the degradation of RhB of 0.61 for 20%, 1.0 for 50%, 0.50 for 75%, and 0.03 for 100% of saturated loading), and therefore was used for all experiments.

The reaction system containing the catalyst and the substrate was magnetically stirred in a pyrex glass vessel and irradiated with a 500 W halogen lamp. A pyrex jacket with water circulation was used to cool the lamp. A light filter was placed outside the pyrex jacket to completely cut out light below 420 nm and guarantee irradiation with visible light. ESR spectroscopic experiments were carried out at ambient temperature (298 K) with a Bruker ESP 300E spectrometer. XPS was performed on a 220I-XL multifunctional spectrometer (VG Scientific England) using $Al_{K\alpha}$ radiation. GC–MS analysis was carried out on a Trio 2000 (Micromass UK Ltd).

Received: October 16, 2002 [Z50381]

[1] B. Meunier, *Science* **2002**, *296*, 270–271.
[2] B. Meunier, *Chem. Rev.* **1992**, *92*, 1411–1456.
[3] A. Sorokin, J. L. Séris, B. Meunier, *Science* **1995**, *268*, 1163–1166.
[4] A. Sorokin, B. Meunier, *J. Chem. Soc. Chem. Commun.* **1994**,1799–1800.
[5] C. P. Horwitz, D. R. Fooksman, L. D. Vucolo, S. W. Gordon-Wylie, N. J. Cox, T. J. Collins, *J. Am. Chem. Soc.* **1998**, *120*, 4867–4868.
[6] S. S. Gupta, M. Stadler, C. A. Noser, A. Ghosh, B. Steinhoff, D. Lenoir, C. P. Horwitz, K. W. Schramm, T. J. Collins, *Science* **2002**, *296*, 326–328.
[7] X. Tao, W. Ma, T. Zhang, J. Zhao, *Angew. Chem.* **2001**, *113*, 3103–3105; *Angew. Chem. Int. Ed.* **2001**, *40*, 3014–3016.
[8] X. Tao, W. Ma, T. Zhang, J. Zhao, *Chem. Eur. J.* **2002**, *8*, 1321–1326.
[9] R. A. Sheldon, I. W. C. E. Arends, G. J. ten Brink, A. R. Dijksman, *Acc. Chem. Res.* **2002**, *35*, 774–781.
[10] G-J. ten Brink, I. W. C. E. Arends, R. A. Sheldon, *Science* **2000**, *287*, 1636–1639.
[11] D. H. R. Barton, D. Doller, *Acc. Chem. Res.* **1992**, *25*, 504–512.
[12] P. Stavropoulos, R. Celenligil-Cetin, A. E. Tapper, *Acc. Chem. Res.* **2001**, *34*, 745–752.
[13] B. Singh, J. R. Long, F. Fabrizi de Biani, D. Gatteschi, P. Stavropoulos, *J. Am. Chem. Soc.* **1997**, *119*, 7030–7047.
[14] E. E. Wegner, A. W. Adamson, *J. Am. Chem. Soc.* **1966**, *88*, 394–404.
[15] S. Ferrere, *Chem. Mater.* **2000**, *12*, 1083–1089.
[16] J. Phillips, J. A. Koningstein, C. H. Langford, R. Sasseville, *J. Phys. Chem.* **1978**, *82*, 622–623.
[17] W. N. Lipscomb, N. Sträter, *Chem. Rev.* **1996**, *96*, 2375–2433.
[18] D. T. Sawyer, J. S. Valentine, *Acc. Chem. Res.* **1981**, *14*, 393–400.

 © 2003 Wiley-VCH Verlag GmbH & Co. KGaA, Weinheim 1433-7851/03/4209-1031 $ 20.00+.50/0

[19] C. Kormann, D. W. Bahnemann, M. Hoffmann, *Environ. Sci. Technol.* **1988**, *22*, 998 – 1004.
[20] C. Walling, *Acc. Chem. Res.* **1975**, *8*, 125 – 131.
[21] L. Weber, R. Hommel, J. Behling, G. Haufe, H. Hennig, *J. Am. Chem. Soc.* **1994**, *116*, 2400 – 2408.
[22] C. E. MacBeth, A. P. Golombek, V. G. Young, Jr., C. Yang, K. Kuczera, M. P. Hendrich, A. S. Borovik, *Science* **2000**, *289*, 938 – 941.
[23] T. J. Collins, *Acc. Chem. Res.* **2002**, *35*, 782 – 790.

 © 2003 Wiley-VCH Verlag GmbH & Co. KGaA, Weinheim 1433-7851/03/4209-1032 $ 20.00+.50/0

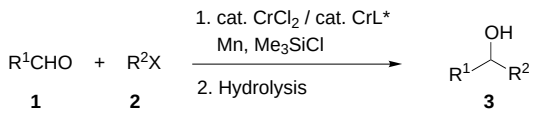

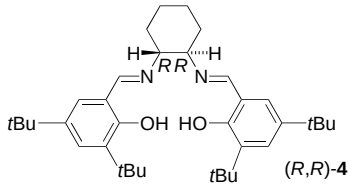

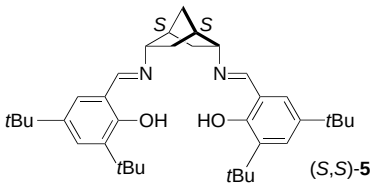

Scheme 1. Ligands for the catalytic asymmetric Nozaki–Hiyama–Kishi reaction; diaminocyclohexane-derived salen **4** and the novel ligand **5**, based on *endo,endo*-2,5-diaminonorbornane (DIANANE).

Highly Enantioselective Catalysts

A Highly Enantioselective Catalyst for the Asymmetric Nozaki–Hiyama–Kishi Reaction of Allylic and Vinylic Halides**

Albrecht Berkessel, Dirk Menche, Christoph A. Sklorz, Michael Schröder, and Ian Paterson*

Dedicated to Professor Emanuel Vogel on the occasion of his 75th birthday

The nucleophilic addition of organochromium reagents to aldehydes (Scheme 1) is a versatile carbon–carbon bond-forming reaction that is compatible with a wide range of functionality in both components.[1] A large number of applications, particularly in the synthesis of structurally diverse natural products, have resulted. The organochromium reagents are easily prepared in situ by the oxidative addition of chromium(II) species to allyl, propargyl, aryl, and vinyl halides or triflates **2** (requiring catalytic amounts of a Ni^{II} salt for sp^2 carbon centers), and efficiently add to aldehydes **1** to give the corresponding alcohols **3** in good yields (Scheme 1).[1] While the original procedure for the Nozaki–Hiyama–Kishi (NHK) reaction relies on the use of stoichiometric quantities of chromium(II) chloride, Fürstner et al. have developed a method requiring only catalytic amounts of the active Cr^{II} species; cheap and toxicologically benign manganese is used as the reducing agent, and a trialkylchlorosilane effects the perpetuation of the catalytic cycle.[2] This important finding triggered numerous efforts to develop a catalytic and enantioselective version of this reaction.[2–5] Nevertheless, only one such example appears to have been reported, namely by the research group of Umani-Ronchi, which uses the salen ligand **4**, derived from *trans*-1,2-diaminocyclohexane (Scheme 1).[5] Whereas the enantioselectivities observed for allyl chorides were high (for example, up to 84% *ee* in the addition to benzaldehyde), the use of the ligand **4** does not yet provide a broadly applicable synthetic method. In particular, the substrate spectrum is still fairly narrow; other halides such as allyl bromide and iodide were found to add with only moderate (52% *ee*) or no selectivity to benzaldehyde. As an asymmetric NHK process for generating enantiomerically enriched allylic alcohols would be extremely valuable, the omission of vinyl halides as substrates for this reaction is significant.[5a–e] We now report our preliminary results using the novel salen ligand (*S,S*)-**5** in NHK reactions, which surpasses the current limitations of **4** by promoting the catalytic addition of allylic and vinylic halides (and triflates) to aromatic and aliphatic aldehydes with synthetically useful levels of asymmetric induction.

Salen ligands used in asymmetric catalysis are mainly based on commercially available chiral 1,2-diamines and various salicylic aldehyde components. Comparatively little attention has been paid to significantly modifying the diamine backbone, for example, by attenuating the separation of the nitrogen atoms. We imagined that this parameter might play a particularly important role in further improving the catalytic properties and, thus, we devised a novel chiral diamine that exhibits a larger nitrogen-atom separation.[6,7] We envisaged *endo,endo*-2,5-diamino-norbornane (**9**, DIANANE, Scheme 2) to be a promising candidate. This novel building block has the advantages of possessing C_2 symmetry and having a rigid hydrocarbon backbone. In our synthesis of **9**, the diketone **6** is converted to a bis(*endo* diamine) by

[*] Prof. Dr. A. Berkessel, Dr. D. Menche, Dr. C. A. Sklorz, Dipl.-Chem. M. Schröder
Institut für Organische Chemie
Universität zu Köln
Greinstrasse 4, 50939 Köln (Germany)
Fax: (+49) 221-470-5102
E-mail: berkessel@uni-koeln.de
Prof. Dr. I. Paterson
University Chemical Laboratory
Lensfield Road, Cambridge CB2 1EW (United Kingdom)

[**] This work was supported by the European Community (Research Training Network "Combinatorial Catalysis") and by the Fonds der Chemischen Industrie. We thank Dr. Ira Fiolia for technical support.

 © 2003 Wiley-VCH Verlag GmbH & Co. KGaA, Weinheim 1433-7851/03/4209-1032 $ 20.00+.50/0

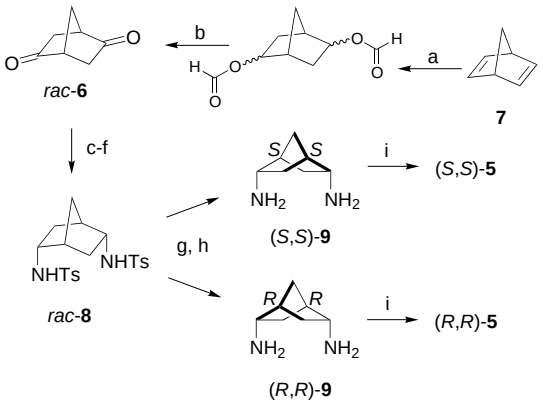

Scheme 2. Enantiodivergent synthesis of (*S,S*)-**5** and (*R,R*)-**5**. a) HCO_2H, reflux, 84%;[9] b) Jones reagent, 44%;[9] c) $NH_2OH{\cdot}HCl$, EtOH, reflux, 1 h; d) $NiCl_2$, $NaBH_4$, MeOH, −35 °C to −20 °C, 1 h, 70–75% (over two steps); e) TsCl, NEt_3, CH_2Cl_2, −78 °C to RT; f) crystallization from MeOH, 35% (over two steps); g) preparative HPLC, Chiralpak AD, 50 cm, 5 cm diameter, flow: 80 mL min^{-1}, eluent: hexane/isopropanol 60:40, retention times: 24–33 min for (*R,R*)-**8** and 46.5–62.5 min for (*S,S*)-**8**; h) Li, NH_3, −33 °C, 80 min, 85%; i) 3,5-di-*tert*-butyl salicylic aldehyde, MeOH, RT, 30 min, 76–81%.

treatment of the corresponding dioxime with $NaBH_4/NiCl_2$ (Scheme 2). Consequently, the pure enantiomers of DIANANE **9** (that is, (*S,S*)-**9** and (*R,R*)-**9**) can be prepared from the enantiomerically pure diketone **6** and *ent*-**6**, respectively. However, instead of relying on the known enantioselective, but multistep approach to **6**/*ent*-**6** from norbornadiene (**7**),[8] we employed the readily available racemic form of the diketone (*rac*-**6**),[9] and resolved the racemic mixture of DIANANE at a later stage. As summarized in Scheme 2, the *N,N′*-bistosylates of DIANANE (**8** and *ent*-**8**) were efficiently separated by preparative HPLC on a chiral stationary phase. Absolute configurations of the crystalline sulfonamides **8** and *ent*-**8** were determined by X-ray crystallography.[10] Reductive *N*-detosylation followed by condensation with 3,5-di-*tert*-butyl salicylic aldehyde afforded the desired salen ligands (*S,S*)-**5** and (*R,R*)-**5**, respectively.

An evaluation of the catalytic performance of the (*S,S*)-**5** and (*R,R*)-**5** ligands was performed. Typical reaction conditions[2,5] comprised 10 mol% of $CrCl_3$, an excess of Mn and Me_3SiCl, and in situ preparation of the Cr^{II} complex, in the presence of NEt_3 and MeCN as solvent (Table 1). The addition of allyl bromide to benzaldehyde proceeded asymmetrically (46% *ee*, room temperature). After optimization of the reaction parameters (solvent, concentration, and temperature), the corresponding homoallylic alcohol was obtained with high enantioselelectivity (90% *ee*) and good yield (72%; Table 1, entry 1). THF proved to be the best solvent among those tested (DMF, DME, CH_3CN), while a catalyst concentration of 0.025 M gave the best results. Optimal enantioselectivity was observed for the allyl bromide/benzaldehyde system at 5 °C (90% *ee*). A variety of different substrates was screened under these conditions. In

Table 1: Catalytic, enantioselective Nozaki–Hiyama–Kishi-type additions in the presence of ligand (*S,S*)-**5**.

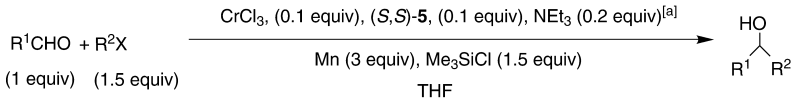

Entry	Aldehyde	Halide	Product	*ee* [%]	Yield [%][b]	Reaction temperature[c]
1			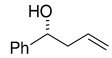	90[d,e]	72	5 °C
2			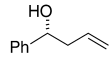	31[d,f]	[g]	RT
3			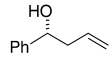	79[d,e]	76	RT
4			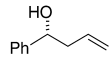	54[e,h]	78	RT
5			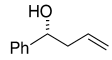	64[f,h]	[g]	RT
6	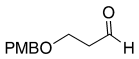		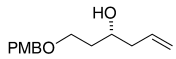	92[e,h]	69[i]	10 °C
7	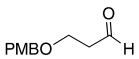	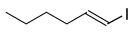	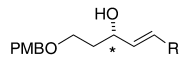	75[h,j]	59[i]	15 °C
8	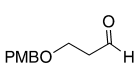	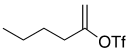	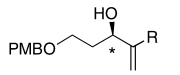	61[h,k,l]	54[i]	20 °C

[a] For entries 7 and 8, the reaction was run in the presence of 0.02 equiv of $NiCl_2$. [b] Yield after flash chromatography. [c] Reaction temperature was optimized for entries 1, 2, 5, 6, 7, and 8. [d] Enantiomeric excess was determined by gas chromatography (GC) of the corresponding TMS ethers on a chiral stationary phase (Macherey–Nagel: Lipodex A, 95 °C). [e] Absolute configurations were assigned by comparison of optical rotations with literature data.[5d,11,12] [f] Absolute configuration based on GC/HPLC data (that is, comparison of the products of entries 2 and 1 and of the products of entries 3 and 5 on an analytical scale). [g] Not determined. [h] Enantiomeric excess determined by HPLC on a chiral phase (Daicel: Chiralcel OD-H). [i] Some debenzylation occured as a side reaction. [j] Absolute configuration determined by 1) oxidative cleavage (ozonolysis), 2) reduction to 1,2,4-butanetriol, 3) GC co-injection with a sample of known absolute configuration.[13] [k] Reaction was performed with (*R,R*)-**5**. [l] Assignment of absolute configuration in analogy to entry 7.

 © 2003 Wiley-VCH Verlag GmbH & Co. KGaA, Weinheim 1433-7851/03/4209-1033 $ 20.00+.50/0

contrast to the salen ligand **4**, ligand **5** was also able to effect, for the first time, an enantioselective addition of allyl iodide (Table 1, entry 2). Allyl chloride added with similar selectivity (84% *ee* using **4**,[5] versus 79% *ee* using DIANANE-based **5**; Table 1, entry 3). Of the three allyl halides tested, the bromide thus afforded the best enantioselectivity. The related β-methylallyl halides (Table 1, entries 4 and 5) reacted just as smoothly as the allyl halides. However, the observed enantioselectivities for these compounds (54% and 64% *ee* for the chloride and bromide, respectively) were not as high as for allyl bromide (90% *ee*). As a model for projected applications in polyketide natural-product synthesis, we tested PMB-protected 3-hydroxypropanal (PMB = *para*-methoxybenzyl), shown in entry 6 of Table 1.[12,14,15] Again, after optimizing the reaction temperature, coupling with allyl bromide occurred with high enantioselectivity (92% *ee*).[16]

The encouraging results achieved with allylic halides prompted us to examine the use of our catalytic NHK process with vinyl iodides and triflates for the enantioselective synthesis of allylic alcohols. As expected, 2 mol% of Ni^{II} (in the form of $NiCl_2$) was required for the coupling reaction to occur efficiently.[2] Under these reaction conditions, the addition of *E*-1-iodohex-1-ene[17] to the PMB-protected 3-hydroxypropanal test system afforded the corresponding *E*-allylic alcohol adduct in an unoptimized 59% yield with 75% *ee* (Table 1, entry 7). Likewise, the vinyl triflate[18] (entry 8, Table 1) added to this same aldehyde to produce the isomeric allylic alcohol with 61% *ee*. Notably, these last two addition reactions represent the first examples of synthetically useful levels of asymmetric induction being realized for catalytic, enantioselective NHK reactions of vinylic halide and triflate substrates.

In summary, we have demonstrated that our DIANANE-based salen ligands, (*S,S*)-**5** and (*R,R*)-**5**, promote efficient and highly enantioselective catalytic Nozaki–Hiyama–Kishi reactions. With this novel ligand modification, the addition of various organochromium intermediates to aromatic and aliphatic aldehydes proceeded under catalytic conditions with good levels of stereoinduction (up to 92% *ee*). Notably, the asymmetric additions of allyl iodide and, in particular, vinyl halides and triflates to aldehydes were achieved with useful levels of enantioselectivity. We are currently exploring the generality and functional-group compatibility of this catalytic carbon–carbon bond-forming process, together with examining its utility with chiral substrates, in the context of projected applications to the stereocontrolled synthesis of more complex structures, such as those that occur in polyketide natural products.

Experimental Section

Typical Procedure: Anhydrous THF (1 mL) was added to $CrCl_3$ (4.0 mg, 25.0 μmol) and Mn (42 mg, 750 μmol) in a dried Schlenk tube under argon, and the mixture was stirred for 1 h at room temperature. After addition of the ligand (*S,S*)-**5** (14.0 mg, 25.0 μmol) and anhydrous NEt_3 (7 μL, 5.0 mg, 50 μmol), the suspension was stirred for another hour at room temperature.[19] Finally, allyl bromide was added (32 μL, 45.4 mg, 375 μmol). After 1 h, the mixture was cooled to 5 °C, PhCHO (25 μL, 26.2 mg, 250 μmol) and Me_3SiCl (48 μL, 41.2 mg, 380 μmol) were added, and the suspension was stirred at that temperature. When the aldehyde was completely consumed (as confirmed by thin-layer chromatography (TLC)), saturated aqueous $NaHCO_3$ was added. After filtration and evaporation, the aqueous phase was extracted with Et_2O. After evaporation of the combined organic phases, the residue was dissolved in THF (1 mL). Aqueous 1M HCl (0.5 mL) was added and the mixture was stirred until desilylation was complete (confirmed by TLC). The solvent was removed, the residue extracted with Et_2O, and the combined organic phases were dried over $MgSO_4$. Evaporation of the solvent and flash chromatography (hexane/Et_2O 4:1) gave (*R*)-1-phenyl-3-buten-1-ol as a pale-yellow oil (26.7 mg, 180 μmol, 72% yield, 90% *ee*).

Received: October 21, 2002 [Z50397]

[1] For reviews, see: a) A. S. K. Hashmi, *J. Prakt. Chem.* **1996**, *338*, 491–495; b) L. A. Wessjohann, G. Scheid, *Synthesis* **1999**, 1—36; c) A. Fürstner, *Chem. Rev.* **1999**, *99*, 991–1045; d) A. Fürstner, *Chem. Eur. J.* **1998**, *4*, 567–570.

[2] A. Fürstner, N. Shi, *J. Am. Chem. Soc.* **1996**, *118*, 12349–12357.

[3] a) C. Chen, K. Tagami, Y. Kishi, *J. Org. Chem.* **1995**, *60*, 5386–5387; b) Y. Kishi, *Tetrahedron* **2002**, *58*, 6239–6258; c) H. S. Schrekker, M. W. G. de Bolster, R. V. A. Orru, L. A. Wessjohann, *J. Org. Chem.* **2002**, *67*, 1975–1981.

[4] For asymmetric versions of the NHK reaction using stoichiometric amounts of chiral organochromium agents, see: a) B. Cazes, C. Verniere, J. Goré, *Synth. Commun.* **1983**, *13*, 73–79; b) K. Sugimoto, S. Aoyagi, C. Kibayashi, *J. Org. Chem.* **1997**, *62*, 2322–2323; and ref. [3a].

[5] a) M. Bandini, P. G. Cozzi, P. Melchiorre, A. Umani-Ronchi, *Angew. Chem.* **1999**, *111*, 3558–3561; *Angew. Chem. Int. Ed.* **1999**, *38*, 3357–3359; b) M. Bandini, P. G. Cozzi, A. Umani-Ronchi, *Polyhedron* **2000**, *19*, 537–539; c) M. Bandini, P. G. Cozzi, A. Umani-Ronchi, *Angew. Chem.* **2000**, *112*, 2417–2420; *Angew. Chem. Int. Ed.* **2000**, *39*, 2327–2330; d) M. Bandini, P. G. Cozzi, A. Umani-Ronchi, *Tetrahedron* **2001**, *57*, 835–843; e) M. Bandini, P. G. Cozzi, P. Melchiorre, S. Morganti, A. Umani-Ronchi, *Org. Lett.* **2001**, *3*, 1153–1155; f) After submission of this manuscript, a report by Kishi et al. on a catalytic enantioselective process using an oxazoline sulfonamide ligand appeared: H.-W. Choi, K. Nakajima, D. Demeke, F.-A. Kang, H.-S. Jun, Z.-K. Wan, Y. Kishi, *Org. Lett.* **2002**, *4*, 4435–4438. However, the enantioselectivities reported are not as high as our best examples.

[6] For a review of applications of Cr–salen complexes in asymmetric catalysis, see: M. Bandini, P. G. Cozzi, A. Umani-Ronchi, *Chem. Commun.* **2002**, 919–927.

[7] For two examples, see: a) X.-G. Zhou, J.-S. Huang, X.-Q. Yu, Z.-Y. Zhou, C.-M. Che, *J. Chem. Soc. Dalton Trans.* **2000**, 1075–1080; b) D. Seebach, A. K. Beck, A. Heckel, *Angew. Chem.* **2001**, *113*, 96–142; *Angew. Chem. Int. Ed.* **2001**, *40*, 92–138.

[8] a) T. Hayashi, *Acta Chem. Scand.* **1996**, *50*, 259–266; b) A. Weissfloch, R. Azerad, *Bioorg. Med. Chem.* **1994**, *2*, 493–500.

[9] R. T. Hawkins, R. S. Hsu, S. G. Wood, *J. Org. Chem.* **1978**, *43*, 4648–4650.

[10] A full account of the synthesis and configurational assignment of (+)- and (−)-DIANANE (**9**) will be published elsewhere.

[11] K. Ishihara, M. Mouri, Q. Gao, T. Maruyama, K. Furuta, H. Yamamoto, *J. Am. Chem. Soc.* **1993**, *115*, 11490–11495.

[12] A. B. Smith III, K. P. Minibiole, P. R. Verhoest, M. Schelhaas, *J. Am. Chem. Soc.* **2001**, *123*, 10942–10953.

[13] V. K. Tandon, A. M. van Leusen, H. Wynberg, *J. Org. Chem.* **1983**, *48*, 2767–2769.

[14] Y. Wu, L. Esser, J. K. De Brabander, *Angew. Chem.* **2000**, *112*, 4478–4480; *Angew. Chem. Int. Ed.* **2000**, *39*, 4308–4310.

 © 2003 Wiley-VCH Verlag GmbH & Co. KGaA, Weinheim 1433-7851/03/4209-1034 $ 20.00+.50/0

[15] The synthesis of the aldehyde was performed according to: a) M. J. Martinelli, *J. Org. Chem.* **1990**, *55*, 5065 – 5073; b) T. Oka, A. Murai, *Tetrahedron* **1998**, *54*, 1 – 20.
[16] The possibility to recover the valuable ligand by column chromatography after aqueous work-up further adds to the efficiency of our process. Usually, at least 80 % of ligand could be recovered in pure form.
[17] J. K. Stille, J. H. Simpson, *J. Am. Chem. Soc.* **1987**, *109*, 2138 – 2152.
[18] K. Takai, K. Sakogawa, Y. Kataoka, K. Oshima, K. Utimoto, *Org. Synth.* **1995**, *72*, 180 – 188.
[19] For entries 7 and 8, 0.02 equiv of $NiCl_2$ were added prior to the halide.

 © 2003 Wiley-VCH Verlag GmbH & Co. KGaA, Weinheim 1433-7851/03/4209-1035 $ 20.00+.50/0

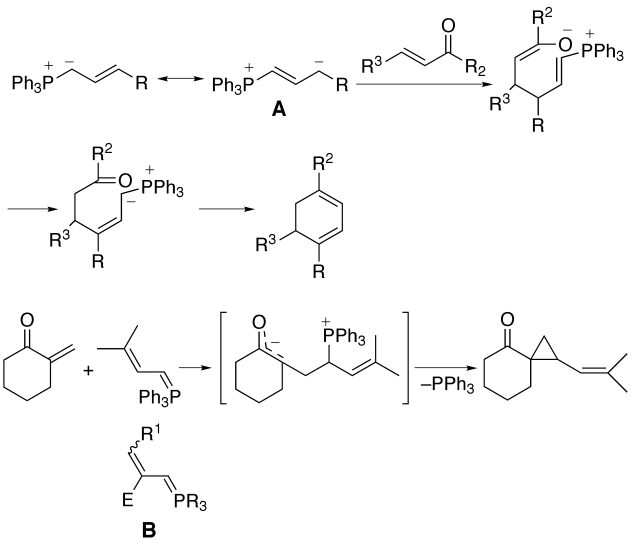

Scheme 1. Two types of reactions of allylic phosphorus ylides.

Catalytic C–P Ylide Reaction

A Catalytic Carbon–Phosphorus Ylide Reaction: Phosphane-Catalyzed Annulation of Allylic Compounds with Electron-Deficient Alkenes**

Yishu Du, Xiyan Lu, and Chunming Zhang*

To ensure high efficiency, turning a stoichiometric reaction into a catalytic one, and developing new catalytic reactions have been long-standing goals in modern synthesis. Ylide reactions are among the most powerful tools for constructing olefins[1] and small rings,[2] but few are catalytic, in particular those involving phosphorus ylides.[3] The first example of a catalytic Wittig-type reaction of arsenic ylides, in which a stoichiometric amount of reducing agent was used to regenerate the arsane, was described by Huang's group in 1989.[4] Afterwards, catalytic olefinations, epoxidations, aziridinations, and cyclopropanations of tellurium or sulfur ylides were accomplished.[2,5] Aggarwal's group developed catalytic, asymmetric ylide reactions that afforded three-membered rings by a carbene approach, in which the ylide was formed directly from aryl diazomethane in the presence of a catalytic amount of a chiral sulfide and a transition-metal complex.[6] To our knowledge, there are no phosphane-catalyzed versions of the carbon–phosphorus ylide reaction.[7] This might be due to the fact that, compared to other elemento-organic compounds of Groups 15 and 16, phosphanes exhibit higher oxyphilicity and the phosphorus–oxygen bond in phosphine oxides have a higher bond energy. To develop a catalytic reaction with carbon–phosphorus ylides, it was thus necessary to explore a new type of reaction.

Two types of reactions of allylic phosphorus ylides **A** with electron-deficient alkenes have been reported (Scheme 1). The initial nucleophilic addition of the ylide to the olefin is followed by an intramolecular Wittig reaction to afford 1,3-cycloalkadienes[8a–f] or by intramolecular nucleophilic substitution to give cyclopropanes.[8f,g] However, both reactions are stoichiometric with regard to the phosphane and the products are obtained in low yields.

The success of the phosphane-catalyzed isomerizations, α- and γ-additions, and [3+2] cycloadditions of electron-deficient allenes or alkynes was ascribed to the presence of electron-withdrawing groups, which facilitated the nucleophilic additions and the elimination of phosphanes to complete the catalytic cycles.[9] With this in mind, we thought that phosphane-catalyzed reactions might be realized with a modified allylic phosphorus ylide **B** (see Scheme 1). Here we report a novel phosphane-catalyzed annulation reaction of modified allylic compounds with electron-deficient alkenes.

To initiate our study, phosphonium salt **1**, compound **2**, and potassium carbonate were stirred in toluene at 90 °C to afford the adduct **3a** and triphenylphosphane [Eq. (1); E = CO_2Et]. Since **1** was prepared from ethyl 2-bromomethyl-2-propenoate (**4a**) and PPh_3, it was expected that this reaction might take place starting from **4a** by utilizing a catalytic amount of PPh_3. Indeed, the phosphane-catalyzed annulation

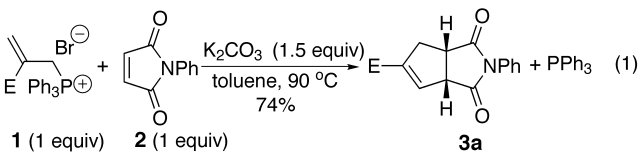

[*] Prof. X. Lu, Dr. Y. Du, Dr. C. Zhang
State Key Laboratory of Organometallic Chemistry
Shanghai Institute of Organic Chemistry
Chinese Academy of Sciences
354 Fenglin Lu, Shanghai 200032 (China)
Fax: (+86) 21-6416-6128
E-mail: xylu@pub.sioc.ac.cn

[**] This work was funded by the Major State Basic Research Program (grant G2000077502-A). We also thank the National Natural Science Foundation of China and the Chinese Academy of Sciences for financial support.

Supporting information for this article is available on the WWW under http://www.angewandte.org or from the author.

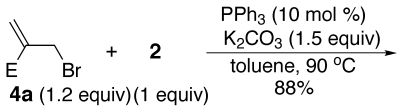

(2)

of ylides did proceed [Eq. (2); E = CO_2Et], implying that a catalytic ylide reaction is possible.

We then turned our attention to studying the scope of this reaction with respect to the C_3 component. Under similar conditions, the reaction of **4b** and **2** proceeded smoothly upon reflux, albeit in lower yields (50%; Table 1, entry 2). The yield was improved to 68% by the slow addition of the reactants to maintain low concentrations of **2** and **4b** in the reaction system (entry 3). Under these conditions, good yields of adducts were obtained for C_3 components containing aromatic as well as aliphatic substituents (Table 1, entries 3–7). The stereochemistry of the products was assigned on the basis of the NOESY spectra of **3c**.[10] It is worth noting that, in only a single step, cyclopentenes with two or three stereogenic centers were constructed stereoselectively.

The scope of this novel ylide reaction with respect to the C_2 component was also investigated, focusing on reactions of compound **4a** with various compounds in place of **2**. Terminal olefins or unsymmetrical C_2 components reacted smoothly with **4a** to give annulation products with high selectivities (Table 1, entries 8, 9, 11, and 12).[10] While the reaction of **7** with **4a** provided the expected product with lower yield (61%), it still showed a high regioselectivity (**8a**/**9a**: 90/10, entry 9).[10,11]

Further investigation revealed that the key intermediate (ylide **B**; see Scheme 1) of this catalytic annulation reaction could be generated not only from the corresponding bromides **4a–f** but also from the acetates **12a–c** (Table 1, entries 13–15).[12,13] We also found that the reaction could be modified from heterogeneous conditions to homogeneous conditions by using the *tert*-butyl carbonate **14,** from which the *tert*-butoxide anion was generated as a base in situ (entry 16).

Although detailed mechanistic studies have not been undertaken, a plausible mechanism for the phosphane-catalyzed annulation reaction of ylides is proposed (Scheme 2). The reaction might be initiated by the formation of the phosphonium salt from **4** by an S_N2 or addition–elimination step.[11] This salt can be deprotonated by a base such as potassium carbonate or the in situ generated *tert*-butoxide anion to afford ylide **B**. As exemplified by the annulation reaction of **7** and **4a**, subsequent nucleophilic addition of **B** to the electron-deficient olefin yields zwitterionic intermediates. Subsequent cyclization upon intramolecular conjugate addition provides betaine-like intermediates. Finally, elimination of the phosphane completes the catalytic cycle. As shown in the bottom part of Scheme 2, the formation of the two isomers **8a** and **9a** can be explained by α- or γ-attack of ylide **4a** to **7**. Of course, the possibility of migration of the double bond in cyclopentene products under the reaction conditions cannot be excluded.

In conclusion, the first phosphane-catalyzed allylic ylide reaction was developed. The appealing features of this process involve the

Table 1: Phosphane-catalyzed annulation reaction of ylides.[a]

Entry	C_3 component	C_2 component	T [°C]	t [h]	Product	Yield [%][b]
	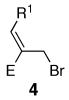 **4**	**2**			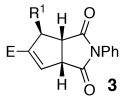 **3**	
1[c]	**4a**: R^1 = H	**2**	90	12	**3a**: R^1 = H	88
2[c]	**4b**: R^1 = Ph	**2**	110	4	**3b**: R^1 = Ph	50[d]
3	**4b**	**2**	110	4	**3b**	68[d]
4	**4c**: R^1 = *p*-MeC_6H_4	**2**	110	4	**3c**: R^1 = *p*-MeC_6H_4	66[d]
5	**4d**: R^1 = *p*-$O_2NC_6H_4$	**2**	110	4	**3d**: R^1 = *p*-$O_2NC_6H_4$	71[d]
6	**4e**: R^1 = *p*-$MeOC_6H_4$	**2**	110	4	**4e**: R^1 = *p*-$MeOC_6H_4$	74[d]
7	**4f**: R^1 = *n*Pr	**2**	110	4	**4f**: R^1 = *n*Pr	60[d]
8	**4a**	**5**	110	20	**6**	70[e]
		7			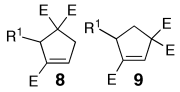 **8** **9**	
9	**4a**	**7**	110	20	**8a**: R^1 = H; **9a**: R^1 = H	61[f]
10	**4d**	**7**	110	6	**8d**: R^1 = *p*-$O_2NC_6H_4$	66
		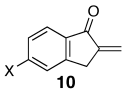 **10**			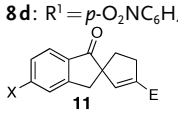 **11**	
11	**4a**	**10a**: X = H	110	20	**11a**: X = H	72[g]
12	**4a**	**10b**: X = MeO	110	20	**11b**: X = MeO	65
	12					
13	**12a**: R^1 = H	**2**	70	4	**3a**	76
14	**12b**: R^1 = Ph	**2**	110	4	**3b**	62[d]
15	**12c**	**2**	30	2	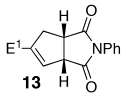 **13**	64
16[h]	**14**	**2**	110	2	**3a**	74

[a] For the typical reaction conditions, see the Experimental Section. E = CO_2Et, E^1 = COPh. [b] Yield of isolated product. [c] The reaction conditions were similar to those in [a], except without slow addition. [d] *trans*:*cis* > 97:3 (relative stereochemistry of the R^1 group and the other substituents). [e] A minor by-product was also isolated which was not fully characterized. [f] **8a**:**9a** = 90:10. [g] The regioselectivity of the reaction was higher than 97:3. [h] The reaction conditions were similar to those in [a], except without the addition of K_2CO_3. Boc = *tert*-butyloxycarbonyl.

 © 2003 Wiley-VCH Verlag GmbH & Co. KGaA, Weinheim 1433-7851/03/4209-1036 $ 20.00+.50/0

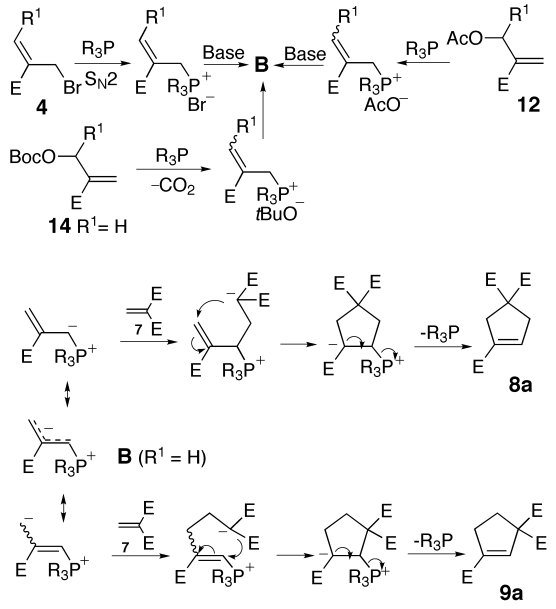

Scheme 2. Proposed mechanism of the phosphane-catalyzed annulation reaction of ylides.

ready availability of the starting materials—for example, the C_3 components including bromides, acetates, or *tert*-butyl carbonates could be easily obtained by further transformation of the adduct of Morita–Baylis–Hillman reactions—and its high selectivity. The synthetic utility of the active intermediate was exemplified by the facile construction of different cyclopentenes.

Experimental Section

Typical reaction conditions: Under argon a mixture of **4a** (116 mg, 0.60 mmol) and **2** (87 mg, 0.50 mmol) in toluene (2.0 mL) was added over the indicated time (see Table 1) with a syringe pump to a mixture of PPh_3 (13 mg, 0.05 mmol) and K_2CO_3 (104 mg, 0.75 mmol) in toluene (0.5 mL) at the temperature indicated (K_2CO_3 was not added for the reaction of **14**). The reaction mixture was stirred for a further 1 h. The reaction mixture was directly subjected to column chromatography (ethyl acetate/petroleum ether) on silica gel to give **3a** (125 mg, 88 %).

Received: October 28, 2002 [Z50449]

[1] a) O. I. Kolodiazhnyi, *Phosphorus Ylides: Chemistry and Application in Organic Synthesis*, Wiley-VCH, New York, **1999**; b) B. E. Maryanoff, A. B. Reitz, *Chem. Rev.* **1989**, *89,* 863, and references therein.

[2] A.-H. Li, L.-X. Dai, V. K. Aggarwal, *Chem. Rev.* **1997**, *97,* 2341.

[3] For a catalytic P–Te ylide reaction, see: L.-B. Han, F. Mirzaei, M. Tanaka, *Organometallics* **2000**, *19,* 722.

[4] L. Shi, W. Wang, Y. Wang, Y.-Z. Huang, *J. Org. Chem.* **1989**, *54,* 2028.

[5] a) Z.-L. Zhou, L.-L. Shi, Y.-Z. Huang, *Tetrahedron Lett.* **1990**, *31,* 7657; b) Y.-Z. Huang, Y. Tang, Z.-L. Zhou, W. Xia, L.-P. Shi, *J. Chem. Soc. Perkin Trans. 1* **1994**, 893; c) V. K. Aggarwal, E. Alonso, G. Hynd, K. M. Lydon, M. J. Palmer, M. Porcelloni, J. R. Studley, *Angew. Chem.* **2001**, *113*, 1479; *Angew. Chem. Int. Ed.* **2001**, *40*, 1430; d) V. K. Aggarwal, E. Alonso, G. Fang, M. Ferrara, G. Hynd, M. Porcelloni, *Angew. Chem.* **2001**, *113*, 1482; *Angew. Chem. Int. Ed.* **2001**, *40*, 1433; e) Z.-Z. Huang, S. Ye, W. Xia, Y.-H. Yu, Y. Tang, *J. Org. Chem.* **2002**, *67,* 3096.

[6] V. K. Aggarwal, *Synlett* **1998**, 329.

[7] For recent reports on phosphane-catalyzed reactions, see: a) M. Wende, R. Meier, J. A. Gladysz, *J. Am. Chem. Soc.* **2001**, *123*, 11490; b) S. A. Frank, D. J. Mergott, W. R. Roush, *J. Am. Chem. Soc.* **2002**, *124*, 2404; c) L.-C. Wang, A. L. Luis, K. Agapiou, H.-Y. Jang, M. J. Krische, *J. Am. Chem. Soc.* **2002**, *124*, 2402; d) M. Lumbierres, M. Moreno-Mañas, A. Vallribera, *Tetrahedron* **2002**, *58*, 4061.

[8] a) G. Büchi, H. Wüest, *Helv. Chim. Acta* **1971**, *54*, 1767; b) F. Bohlmann, C. Zdero, *Chem. Ber.* **1973**, *106*, 3779; c) W. G. Dauben, J. Ipaktschi, *J. Am. Chem. Soc.* **1973**, *95*, 5088; d) A. Padwa, L. Brodsky, *J. Org. Chem.* **1974**, *39*, 1318; e) D. F. Schneider, A. C. Venter, *Synth. Commun.* **1999**, *29*, 1303; f) W. G. Dauben, D. J. Hart, J. Ipaktschi, A. P. Kozikowski, *Tetrahedron Lett.* **1973**, 4425; g) W. G. Dauben, A. P. Kozikowski, *Tetrahedron Lett.* **1973**, 3711;

[9] a) X. Lu, C. Zhang, Z. Xu, *Acc. Chem. Res.* **2001**, *34*, 535; b) B. M. Trost, U. Kazmaier, *J. Am. Chem. Soc.* **1992**, *114*, 7933; c) C. Guo, X. Lu, *J. Chem. Soc. Perkin Trans. 1* **1993**, 1921; d) J. Inanaga, Y. Baba, T. Hanamoto, *Chem. Lett.* **1993**, 241; e) B. M. Trost, C.-J. Li, *J. Am. Chem. Soc.* **1994**, *116*, 3167; f) B. M. Trost, C.-J. Li, *J. Am. Chem. Soc.* **1994**, *116*, 10819; g) C. Zhang, X. Lu, *J. Org. Chem.* **1995**, *60*, 2906; h) B. M. Trost, G. R. Dake, *J. Am. Chem. Soc.* **1997**, *119*, 7595; i) B. M. Trost, G. R. Dake, *J. Org. Chem.* **1997**, *62,* 5670; j) Z. Xu, X. Lu, *J. Org. Chem.* **1998**, *63*, 5031.

[10] Experimental procedures and characterization data of new compounds as well as NOESY spectra of compound **3c** and ^{1}H–^{1}H COSY spectra of compounds **6, 8a, 9a**, and **11a** are available in the Supporting Information.

[11] The high regioselectivity of the reaction might be explained by steric factors. A similarly high regioselectivity was reported in a phosphane-catalyzed cycloaddition reaction: G. Zhu, Z. Chen, Q. Jiang, D. Xiao, P. Cao, X. Zhang, *J. Am. Chem. Soc.* **1997**, *119*, 3836.

[12] The isolation of the same product **3b** starting from **4b** and **12b** implies that the reaction of **12b** was initiated by the nucleophilic addition of PPh_3 to the electron-deficient double bond of **12b** followed by elimination of the acetate ion (compare entries 3 and 13 of Table 1). The ylide formed from the resulting phosphonium salt is the same as that generated from the reaction of **4b** with PPh_3. For a similar addition–elimination reaction, see: M. Harre, P. Raddatz, R. Walenta, E. Winterfeldt, *Angew. Chem.* **1982**, *94*, 496; *Angew. Chem. Int. Ed. Engl.* **1982**, *21*, 480; D. Seebach, M. Missbach, G. Calderari, M. Eberle, *J. Am. Chem. Soc.* **1990**, *112*, 7625.

[13] In general, it is very difficult to generate the ylide directly from allylic acetate without the assistance of a transition metal. For an example of the transition-metal-assisted formation of ylide from allylic acetate, see: R. Tamura, M. Kato, K. Saegusa, M. Kakihana, D. Oda, *J. Org. Chem.* **1987**, *52*, 4121.

 © 2003 Wiley-VCH Verlag GmbH & Co. KGaA, Weinheim 1433-7851/03/4209-1037 $ 20.00+.50/0

Subvalent Scandium Complexes

Stabilization of Low-Oxidation-State Early Transition-Metal Complexes Bearing 1,2,4-Triphosphacyclopentadienyl Ligands: Structure of $[\{Sc(P_3C_2tBu_2)_2\}_2]$; Sc^{II} or Mixed Oxidation State?

Guy K. B. Clentsmith, F. Geoffrey N. Cloke, Jennifer C. Green,* John Hanks, Peter B. Hitchcock, and John F. Nixon**

The prevalence of the tervalent oxidation state for complexes of the rare-earth elements is both well understood and amply documented.[1] Traditionally, bivalent lanthanide chemistry has been limited to just Eu^{II}, Yb^{II}, and Sm^{II},[2,3] however, quite recent work has detailed the syntheses of well-characterized Tm^{II},[4–6] Nd^{II},[5] and Dy^{II}[7] complexes and has reported their impressive and unprecedented reactivity towards otherwise unreactive small molecules.[4,7,8] Parallel development of bivalent chemistry for the earlier, larger lanthanides might seem an impossible task by comparison. The Ln^{III}/Ln^{II} couple, already high for the late series lanthanides (≥ -2.5 V versus NHE),[3] might prove to be of prohibitively high magnitude for the larger, earlier members. Nevertheless, under special conditions, for instance those operating in metal vapor synthesis (MVS) experiments,[9] zero-, uni-,[10] and bivalent[11] metal centers can be accessed even for the electropositive Group 3 metals. The volatile and reactive phosphaalkyne, tBuC≡P, has proved to be an important feedstock in such MVS reactions, as it is able to undergo cyclization reactions in the MVS reactor to give a variety of heterocyclic ligands capable of supporting oxidation states that were hitherto unknown for these highly Lewis-acidic metals.[12] The presence of phosphorus atoms in the ring lowers the energy of the unoccupied orbitals and promotes δ back-bonding from the metal, thus stabilizing the d electrons of reduced oxidation states.[13] The work reported here describes the application of the aromatic triphospholyl ring $P_3C_2tBu_2$ to the chemistry of the smallest Group 3 metal, namely scandium, but without resort to the MVS technique. Treatment of ScI_3 with the 1,3-$P_3C_2tBu_2$ anion, as its base-free potassium salt,[14] gives the homoleptic, tervalent complex $[Sc(P_3C_2tBu_2)_3]$. This proves to be a convenient entry point for subvalent scandium chemistry, as the $P_3C_2tBu_2$ ring is a much poorer electron donor than either Cp* or Cp″ (Cp* = $C_5Me_5^-$, Cp″ = 1,3-$C_5H_3(SiMe_3)_2^-$), and is capable of acting as a leaving group. Here the solid-state and solution structures of a reduced, formally bivalent Sc complex stabilized by the 1,2,4-triphosphacyclopentadienyl ring are presented, along with details of its parent Sc^{III} complex. In addition, we describe the results of DFT calculations on both new Sc complexes, which are in excellent agreement with the experimental findings.

Prolonged heating of base-free $K[P_3C_2tBu_2]$ and ScI_3 in toluene or mesitylene at reflux gives rise to a deep red solution from which red crystals may be isolated upon workup. The mass spectrum of the red product (*m*/*z* 738)

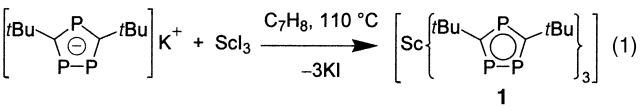

(1)

1

suggests its formulation as $[Sc(P_3C_2tBu_2)_3]$ (**1**) [Eq. (1)].

Crystals suitable for an X-ray diffraction experiment were grown from heptane and the structure of **1** is presented in Figure 1. The scandium atom of compound **1** is η^5-bound to two of the $P_3C_2tBu_2$ rings and coordination is completed by a third $P_3C_2tBu_2$ ring bound in an η^2 fashion to two adjacent phosphorus centers. The Sc–M distances (M = ring centroid) are 2.326(9) and 2.371(9) Å, respectively, and the η^2-bound phosphorus atoms are coordinated symmetrically (Sc–P4 2.762(3), Sc–P5 2.792(3) Å). Although there are no other examples of $[M(P_3C_2tBu_2)_3]$ compounds in the literature, we have in unpublished work synthesized and structurally characterized the homologous Y^{III}, Tm^{III}, and U^{III} derivatives that are all isostructural, but have longer Ln/Ac–M and Ln/Ac–(η^2-P_2) bond lengths.[15] The corresponding Ce, Sm, and

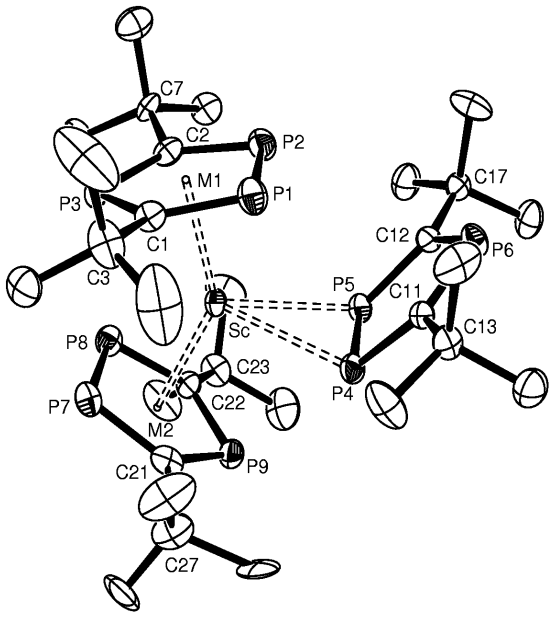

Figure 1. Structure of $[Sc(\eta^5\text{-}P_3C_2tBu_2)(\eta^2\text{-}P_3C_2tBu_2)]$ (**1**) (ORTEP view). Selected bond lengths [Å] and angles [°]: Sc-M1 2.326(9), Sc-M2 2.371(9), P1-P2 2.117(4), Sc-P4 2.762(3), Sc-P5 2.796(3); M1-Sc-M2 140.2(2), M2-Sc-P4 102.70(8), M2-Sc-P5 103.85(7), M1-Sc-P4 114.10(8), M1-Sc-P5 112.75(7).[23]

[*] Prof. Dr. F. G. N. Cloke, Prof. Dr. J. F. Nixon, Dr. G. K. B. Clentsmith, Dr. J. Hanks, Dr. P. B. Hitchcock
The Chemistry Laboratory, CPES
University of Sussex
Falmer Brighton Sussex BN1 9QJ (UK)
Fax: (+44) 1273-677-196
E-mail: f.g.cloke@sussex.ac.uk
j.nixon@sussex.ac.uk
Prof. Dr. J. C. Green
Inorganic Chemistry Laboratory
South Parks Road Oxford OX1 3QR (UK)
E-mail: jennifer.green@chemistry.oxford.ac.uk

 © 2003 Wiley-VCH Verlag GmbH & Co. KGaA, Weinheim 1433-7851/03/4209-1038 $ 20.00+.50/0

Th derivatives of the cyclopentadienyl ring $C_5H_3(SiMe_3)_2$, which is arguably similar in steric properties to $P_3C_2tBu_2$, each show η^5-bound rings exclusively, and it seems likely therefore that the η^5/η^2 bonding motif observed for the Sc–U series above is electronic rather than steric in origin. The presence of phosphorus centers on the ring demonstrably allows more versatile binding modes than its carbocyclic equivalent.[16]

Density functional calculations on $[Sc(P_3C_2H_2)_3]$ as a model for **1** gave an optimized geometry in good agreement with the crystal structure of **1**. Sc–M ring distances were calculated as 2.20 and 2.21 Å and the Sc–P distances to the η^2 ring as 2.76 and 2.74 Å. The model calculation thus results in smaller distances for the metal to ring centroid distances.

The alternative C_{3h} structure, in which all three rings are bound in an η^5 fashion, allows a formal symmetry match between the metal and all possible combinations of π-donor orbitals. However, the a′ combination formed by the π_3 orbitals would have three angular nodes and thus have effectively no overlap with the metal d orbitals. Distortion of one ligand to an η^2-coordination mode should enhance the electron donation to the electrophilic Sc center.

Interestingly, although the solid-state structure of **1** shows the $P_3C_2tBu_2$ rings to be coordinated in two different modes, the compound exhibits fluxional behavior in solution and all three rings are equivalent in the solution ^1H and $^{31}P\{^1H\}$ NMR spectra. The ^1H NMR spectrum displays only a singlet at $\delta = 1.67$ ppm, and the $^{31}P\{^1H\}$ NMR spectrum comprises a symmetric $[AX_2]_3$ coupling pattern ($\delta_{A,X} = 296.5$, 265.0 ppm; Figure 2). Fluxional equilibrium between η^5 and η^2 modes of coordination in solution must therefore be rapid and the variable-temperature $^{31}P\{^1H\}$ NMR spectrum of **1** in $[D_8]$toluene loses resolution before the limiting spectrum is reached.

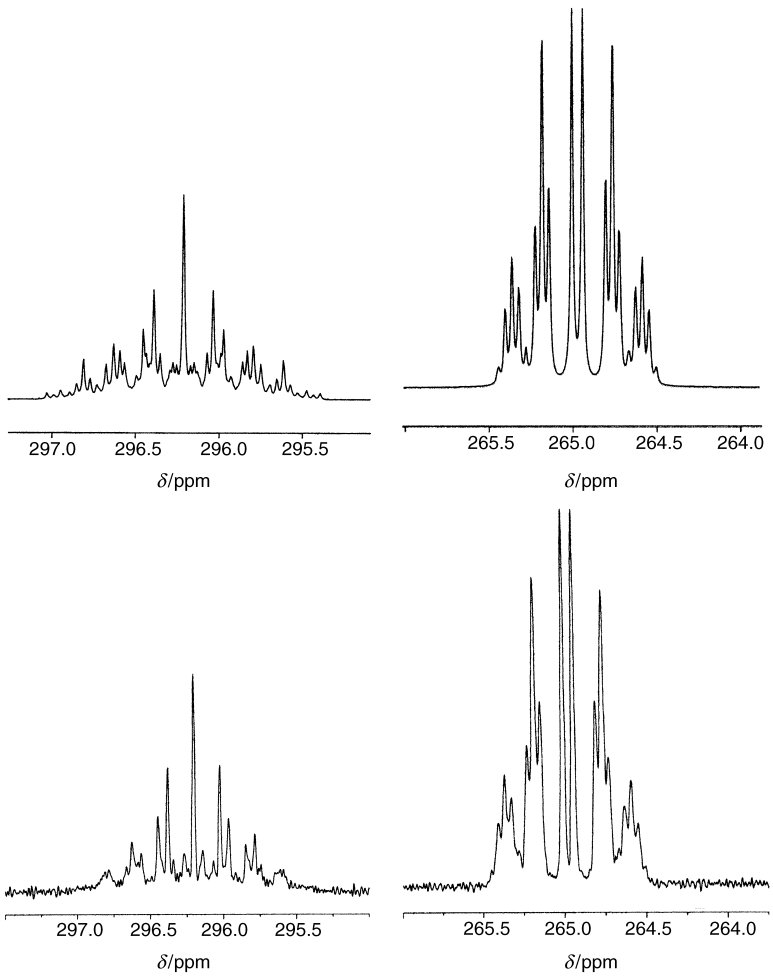

Figure 2. Simulated (top) and experimental (bottom) $^{31}P\{^1H\}$ NMR spectrum of **1**.

Although the metal center of **1** is sterically congested, one way of promoting reactivity is to designate one of the heterocyclic rings as a leaving group.[17] Such an approach has been used in the synthesis of bivalent lanthanides from coordinatively saturated triscyclopentadienyllanthanide(III) species such as $[Ln(\eta^5\text{-}Cp'')_3]$ (Ln = Ce, Yb; Cp″ = 1,3-$C_5H_3(SiMe_3)_2$).[18] In the case of **1** the $P_3C_2tBu_2$ rings are much poorer electron donors than a corresponding carbocyclic ring and should therefore in principle be much better leaving groups. Furthermore the presence of three phosphorus atoms in the ring makes the unsaturated rings better acceptors for the d electrons of any reduced species. Accordingly, treatment of **1** with one equivalent of KC_8 in toluene at low temperature (−78 °C) produces a very deep blue solution whose color persists upon warming to room temperature. Sublimation (170–180 °C, 1×10^{-5} bar) of the residue after removal of the volatiles, and recrystallization from hexane gives very dark blue crystals of **2**, whose mass spectrum (*m*/*z* 550) indicates a formulation of $[Sc(P_3C_2tBu_2)_2]$ [Eq. (2)].

$$[Sc(\eta^5\text{-}P_3C_2tBu_2)_2(\eta^2\text{-}P_3C_2tBu_2)] + KC_8 \xrightarrow{C_7H_8,\ -78^\circ C} [Sc(P_3C_2tBu_2)_2]_n + K[P_3C_2tBu_2] \quad (2)$$

The single-crystal X-ray structure of **2** (Figure 3) reveals an unusual dimer containing two Sc centers bridged by a $(\mu\text{-}\eta^2{:}\eta^5)\text{-}P_3C_2tBu_2$ ring.

Remarkably, the Sc1 atom lies in a coordination environment whose metrical parameters are virtually indistinguishable from those of the parent molecule **1**. On the other hand, the Sc2 metal center is sandwiched between two η^5-bound heterocycles with two quite distinct Sc2–M distances (Sc2–M1 2.046(4), Sc2–M(4) 2.253(4) Å). The $\mu\text{-}\eta^2{:}\eta^5$ ring shows slight deviation from the geometry of the η^5 rings, with longer P–C distances observed (P1–C1 1.832(4), P2–C2 1.831(4) Å) and a longer P1–P2 distance of 2.21 Å. The M1-Sc1-M4 angle is slightly bent at 168.27(16)°.

DFT geometry optimizations were carried out on the dimer $[Sc_2(P_3C_2H_2)_4]$ in two different spin states, that is, with $S = 0$ and $S = 1$. The crystal structure data were used for the initial calculations and the $S = 0$ structure was found to be 0.47 eV lower in energy. Both calculations gave an optimized geometry in good general agreement with that found for **2,** however the distances for the bridging ring were in better accord with the $S = 0$ structure (Table 1). The calculations therefore support a diamagnetic ground state in the solid state.

 © 2003 Wiley-VCH Verlag GmbH & Co. KGaA, Weinheim 1433-7851/03/4209-1039 $ 20.00+.50/0

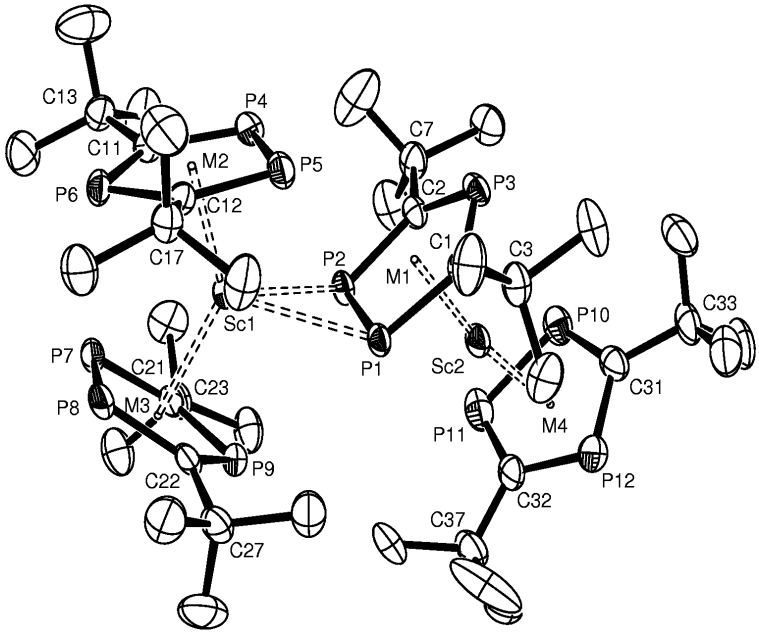

Figure 3. Structure of $[Sc(\eta^5\text{-}P_3C_2tBu_2)(\mu\text{-}\eta^2\text{:}\eta^5\text{-}P_3C_2tBu_2)Sc(\eta^5\text{-}P_3C_2tBu_2)]$ (**2**) (ORTEP view). Selected bond lengths [Å] and angles [°]: Sc1-M2 2.322(4), Sc1-M3 2.360(4), P1-P2 2.2146(16), Sc1-P1 2.7646(13), Sc1-P2 2.7904(13), Sc2-M1 2.046(4), Sc2-M4 2.253(4); M2-Sc-M3 136.62(13), M1-Sc2-M4 168.27(16).[23]

Table 1: Calculated distances for $Sc_2(P_3C_2H_2)_4$ with $S=0$ and $S=1$. Experimental distances are given for comparison.

	$[Sc_2(P_3C_2H_2)_4]$ $S=0$	$[Sc_2(P_3C_2H_2)_4]$ $S=1$	**2**
Sc1–M1	3.31	3.36	
Sc1–M2	2.16	2.17	2.32
Sc1–M3	2.18	2.19	2.36
Sc2–M1	1.99	2.06	2.04
Sc2–M4	2.16	2.11	2.25
P–P ring 2	2.12	2.18	2.12
P–P ring 2	2.18	2.18	2.12
P–P ring 3	2.16	2.16	2.12
P–P ring 1	2.25	2.19	2.21
ring1			
P1–C1	1.82	1.78	1.832
P2–C2	1.82	1.79	1.831
Sc1–P1	2.75	2.81	2.76
Sc1–P2	2.75	2.75	2.79

The orbitals occupied by the two d electrons in both magnetic states are of interest (Figure 4). With $S=0$, both electrons occupy orbital A61, which is back-bonding from Sc2 to the bridging ring and can be seen to be responsible for the lengthening of the P–P, P1–C1, and P2–C2 bonds. On the other hand with $S=1$, one of the unpaired electrons occupies a similar orbital, while the other, A62, is back-bonding from Sc2 to both rings. In both cases, the description of **2** as a mixed oxidation state Sc^{I}/Sc^{III} complex is more appropriate than two Sc^{II} centers.

The X-ray crystal structure and theoretical calculations thus both support the formulation of **2** as a mixed-valence Sc^{I}/Sc^{III} complex. Indeed, SQUID magnetometry performed upon a solid sample of **2** indicates diamagnetic material. In solution in benzene or toluene, however, **2** exhibits a magnetic moment as measured by Evans' method ($\mu_{eff}=1.7\ \mu_B$ per Sc atom), which is fully consistent with a d^1 metal center. This suggests that in solution a monomer/dimer equilibrium may operate, in which the hypothetical monomer $[Sc(P_3C_2tBu_2)_2]$ is responsible for the observed magnetic moment. In cyclohexane solution, a molecular weight determination by cryoscopy gave a value consistent with the dimer (900 $g\,mol^{-1}$); the corresponding experiment in benzene was inconclusive. On the basis of these experiments, it would appear that the aromatic solvent facilitates dissociation of the dimer and a concomitant change in spin state. The ESR spectrum of **2** in toluene did not reveal a signal attributable to $[Sc(P_3C_2tBu_2)_2]$; presumably, association of the monomer occurs to give the diamagnetic system before the ESR spectrum of monomeric **2** is resolved. By contrast, $[Sc(P_2C_3tBu_3)_2]$ exhibits a septet of binomial quintets in its ESR spectrum, attributable to a monomeric complex, in frozen toluene.[11] The difference in molecularity between **2** and $[Sc(P_2C_3tBu_3)_2]$ is likely to be a result of the greater steric demand of the $P_2C_3tBu_3$ ring.

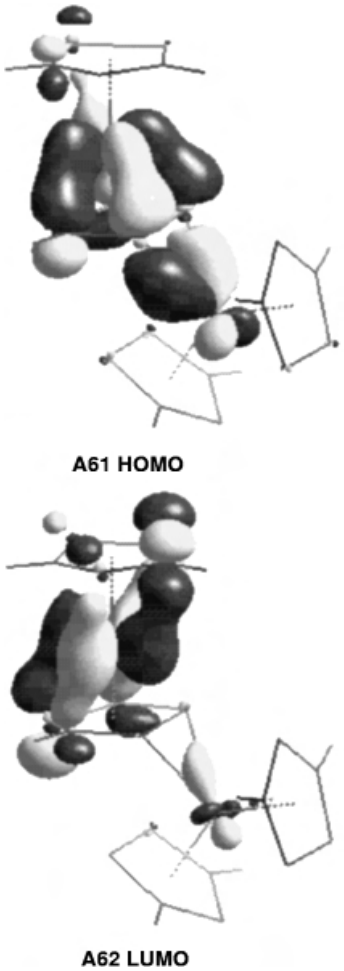

Figure 4. Isosurfaces of orbitals A61 (HOMO) and A62 (LUMO) calculated for $[\{Sc(P_3C_2H_2)_2\}_2]$.

 © 2003 Wiley-VCH Verlag GmbH & Co. KGaA, Weinheim 1433-7851/03/4209-1040 $ 20.00+.50/0

In summary, isolation of a homoleptic complex of tervalent scandium bearing 1,2,4-triphosphacyclopentadienyl ligands has allowed access to a subvalent or nonclassical Sc complex.[17] Although formally bivalent with respect to scandium, **2** is best described as a mixed oxidation state complex containing both Sc^{I} and Sc^{III} centers. DFT calculations show that the d electrons retained by the Sc^{I} center are stabilized by δ bond formation with the heterocyclic rings. Evidence for the solution-state structure of **2** is ambiguous, the choice of saturated or aromatic solvent apparently influencing its molecularity. Details of the solid-state structure are unequivocal and represent only the second unambiguously subvalent Sc complex and the first such complex to be isolated by conventional means.

Experimental Section

1: Under argon, $K[P_3C_2tBu_2]$ (500 mg, 1.85 mmol) and ScI_3 (254 mg, 0.597 mmol) were placed in an ampoule and slurried in toluene (50 mL). The ampoule was evacuated and then heated at 110 °C for 48 h during which time a dark red color developed. The reaction mixture was filtered and the toluene was removed by suction to leave a red solid. Recrystallization from heptane (20 mL) at −40 °C gave dark red crystals (254 mg, 54 %). ^{1}H NMR (300 MHz, [D$_6$]benzene, 20 °C): $\delta = 1.67$ ppm (s, *t*Bu); ^{31}P{^{1}H} NMR (121.5 MHz, [D$_6$]benzene, 20 °C): $\delta_{A,X} = 296.5$, 265.0 ppm ($[AX_2]_3$, $J(A,X) = -50.7$ Hz; $J(A',X) = 21.5$ Hz; $J(X,X') = 5.0$ Hz; $J(A,A') = 0$ Hz); MS (70 eV): *m*/*z* (%): 738 (35) [*M*$^+$], 681 (21) [*M*$^+$−*t*Bu], 57 (100) [*t*Bu$^+$]; elemental analysis (%) calcd for $C_{30}H_{54}P_9Sc$ (738.48): C 48.79, H 7.37; found: C 48.54, H 7.21.

2: Under 99.999 % argon, **1** (100 mg, 0.14 mmol) and KC_8 (25 mg, 0.18 mmol) were placed in a sublimation tube and slurried in cold (−78 °C) toluene (10 mL). An intense blue color rapidly developed and the mixture was warmed to room temperature. The volatiles were removed by suction and the crude product was sublimed (170 °C, 1×10^{-5} mbar). Recrystallization of the sublimate from pentane (2.5 mL) at 4 °C yielded dark blue crystals (50 mg, 65 %). μ_{eff} (25 °C) = 1.7 μ_B; MS (70 eV): *m*/*z* (%): 507 (65) [*M*$^+$], 450 (26) [*M*$^+$−*t*Bu], 57 (100) [*t*Bu$^+$]; UV/Vis (*n*-heptane): λ_{max} (ε) = 613 (15 000); molecular weight in solution (C_6H_{12}): 900 g mol^{-1}; elemental analysis (%) calcd for $C_{20}H_{36}P_6Sc$ (507.30): C 47.35, H 7.15; found: C 47.34, H 7.41.

DFT calculations were carried out using the Amsterdam Density functional code version 2002.2.[19] Type IV basis sets were used with triple ζ accuracy sets of Slater type orbitals, with a single polarization function added to the main-group atoms. The cores of the atoms were frozen up to 2p for Sc, 1s for C, and 2p for P. The local density approximation of Vosko,[20] Wilk and Nusair was used with the nonlocal exchange corrections of Becke,[21] and nonlocal correlation corrections by Perdew.[22]

Received: October 28, 2002 [Z50450]

[1] a) F. T. Edelmann, in *Synthetic Methods of Organometallic and Inorganic Chemistry, Vol. 6* (Eds.: G. Brauer, W. A. Herrmann), Thieme, Stuttgart, **1997**; b) C. J. Schaverien, *Adv. Organomet. Chem.* **1994**, *36*, 283 – 362.

[2] W. J. Evans, *J. Organomet. Chem.* **2002**, *647*, 2 – 11.

[3] W. J. Evans, *Coord. Chem. Rev.* **2000**, *206*, 263 – 283.

[4] W. J. Evans, N. T. Allen, J. W. Ziller, *Angew. Chem.* **2002**, *114*, 369 – 371; *Angew. Chem. Int. Ed.* **2002**, *41*, 359 – 361.

[5] M. N. Bochkarev, I. L. Fedushkin, S. Dechert, A. A. Fagin, H. Schumann, *Angew. Chem.* **2001**, *113*, 3268 – 3270; *Angew. Chem. Int. Ed.* **2001**, *40*, 3176 – 3178.

[6] M. N. Bochkarev, I. L. Fedushkin, A. A. Fagin, T. V. Petrovskaya, J. W. Ziller, R. N. R. Broomhall-Dillard, W. J. Evans, *Angew. Chem.* **1997**, *109*, 123 – 124; *Angew. Chem. Int. Ed. Engl.* **1997**, *36*, 133 – 135.

[7] W. J. Evans, N. T. Allen, J. W. Ziller, *J. Am. Chem. Soc.* **2000**, *122*, 11 749 – 11 750.

[8] a) K. Izod, *Angew. Chem.* **2002**, *114*, 769 – 770; *Angew. Chem. Int. Ed.* **2002**, *41*, 743 – 745; b) W. J. Evans, N. T. Allen, J. W. Ziller, *J. Am. Chem. Soc.* **2001**, *123*, 7927 – 7928; c) I. L. Fedushkin, M. N. Bochkarev, S. Dechert, H. Schumann, *Chem. Eur. J.* **2001**, *7*, 3558 – 3563.

[9] F. G. N. Cloke, *Chem. Soc. Rev.* **1993**, *22*, 17 – 24.

[10] P. L. Arnold, F. G. N. Cloke, P. B. Hitchcock, J. F. Nixon, *J. Am. Chem. Soc.* **1996**, *118*, 7630 – 7631.

[11] P. L. Arnold, F. G. N. Cloke, J. F. Nixon, *Chem. Commun.* **1998**, 797 – 798.

[12] K. B. Dillon, F. Mathey, J. F. Nixon, *Phosphorus: The Carbon Copy*, Wiley, Chichester, **1998**.

[13] a) F. G. N. Cloke, J. C. Green, J. R. Hanks, J. F. Nixon, J. L. Suter, *J. Chem. Soc. Dalton Trans.* **2000**, 3534 – 3536; b) G. K. B. Clentsmith, F. G. N. Cloke, M. D. Francis, J. C. Green, P. B. Hitchcock, J. F. Nixon, J. L. Suter, D. M. Vickers, *J. Chem. Soc. Dalton Trans.* **2000**, *11*, 1715 – 1721.

[14] C. Callaghan, G. K. B. Clentsmith, F. G. N. Cloke, P. B. Hitchcock, J. F. Nixon, D. M. Vickers, *Organometallics* **1999**, *18*, 793 – 795.

[15] G. K. B. Clentsmith, F. G. N. Cloke, M. D. Francis, J. Hanks, P. B. Hitchcock, J. F. Nixon, unpublished results.

[16] G. B. Deacon, E. E. Delbridge, G. D. Fallon, C. Jones, D. E. Hibbs, M. B. Hursthouse, B. W. Skelton, A. H. White, *Organometallics* **2000**, *19*, 1713 – 1721.

[17] M. C. Cassani, Y. K. Gun'ko, P. B. Hitchcock, A. G. Hulkes, A. V. Khvostov, M. F. Lappert, A. V. Protchenko, *J. Organomet. Chem.* **2002**, *647*, 71 – 83.

[18] a) M. C. Cassani, Y. K. Gun'ko, P. B. Hitchcock, M. F. Lappert, F. Laschi, *Organometallics* **1999**, *18*, 5539 – 5547; b) M. C. Cassani, D. J. Duncalf, M. F. Lappert, *J. Am. Chem. Soc.* **1998**, *120*, 12 958 – 12 959.

[19] a) E. J. Baerends, E. G. Ellis, P. Ros, *J. Chem. Phys.* **1973**, *2*, 41 – 50; b) B. te Velde, E. J. Baerends, *J. Comput. Phys.* **1992**, *99*, 84 – 93.

[20] S. H. Vosko, L. Wilk, M. Nusair, *Can. J. Phys.* **1980**, *58*, 1200 – 1211.

[21] A. D. Becke, *Phys. Rev. A* **1988**, *38*, 3098 – 3100.

[22] J. Perdew, *Phys. Rev. B* **1986**, *33*, 8822 – 8824.

[23] CCDC-196035 (**1**) and CCDC-196036 (**2**) contain the supplementary crystallographic data for this paper. These data can be obtained free of charge via www.ccdc.cam.ac.uk/conts/retrieving.html (or from the Cambridge Crystallographic Data Centre, 12, Union Road, Cambridge CB2 1EZ, UK; fax: (+44) 1223-336-033; or deposit@ccdc.cam.ac.uk).

Asymmetric Catalysis in Water

Chiral-Mn(Salen)-Complex-Catalyzed Kinetic Resolution of Secondary Alcohols in Water**

Wei Sun, Hongwang Wang, Chungu Xia, Jingwei Li, and Peiqing Zhao*

The development of efficient catalytic asymmetric reactions is currently one of the most challenging tasks in synthetic chemistry. Many efforts have been devoted to the creation of chiral metal complexes for use in advanced asymmetric catalysis.[1] Salen ligands are now recognized as efficient auxiliaries and many metallosalen complexes have been found to serve as excellent catalysts for various asymmetric reactions, such as epoxidation, aziridination, cyclopropanation, and Diels–Alder reactions, for kinetic resolution of racemic epoxides, and for asymmetric ring opening of meso epoxides.[2,3] In particular, the pioneering studies of Jacobsen and co-workers and Katsuki and co-workers have led to the development of a variety of chiral Mn(salen) catalysts that epoxidize alkenes with high enantioselectivity.[2d]

Recently, we found that Mn(salen) complexes were effective catalysts for the oxidation of secondary alcohols to ketones in the presence of the cooxidant diacetoxyiodobenzene ($PhI(OAc)_2$).[4] We became interested in extending the scope of this potentially useful reaction to asymmetric catalysis and envisaged applying it to the oxidative kinetic resolution of secondary alcohols, the kinetic resolution of which has previously been accomplished through acylation[5,6] and oxidation.[7] Katsuki and co-workers have reported the use of binol-derived Ru(salen) complexes as catalysts in the photoinduced aerobic oxidation of racemic secondary alcohols. In spite of the high enantioselectivities reported, the reaction times for Katsuki's catalyst under photolytic conditions are generally long.[7a] Asymmetric oxidation of alcohols in the presence of catalytic binol-derived Mn(salen) complexes with PhIO as the cooxidant were also reported by Katsuki and co-workers; however only low yields and moderate enantioselectivities were observed.[7b] Herein we report a convenient, mild, enantioselective oxidation of alcohols catalyzed by chiral Mn(salen) complexes in water, with $PhI(OAc)_2$ as the cooxidant.

Water is the basis and bearer of life in Nature. Numerous biochemical organic reactions (and inorganic reactions) within living systems inevitably occur in aqueous media. On the other hand, most laboratory and industrial organic reactions are carried out in organic solvents. In recent decades, chemists have begun to investigate the possibility of using water as a solvent for organic reactions, with sometimes surprising and unforeseen results.[8] In initial investigations, we studied the oxidative kinetic resolution of α-methylbenzyl alcohol catalyzed by the Mn(salen) complex **1b**, with $PhI(OAc)_2$ as the cooxidant (Table 1). When the reaction was carried out in CH_2Cl_2 only 2% *ee* was attained (Table 1, entry 1). When water was used instead of CH_2Cl_2, 8.9% *ee* was observed (Table 1, entry 2). As the substrate and catalyst were insoluble in water, the phase-transfer catalyst (PTC) tetraethylammonium bromide was then included in the aqueous system, and the product was formed with an unexpected 84.1% *ee* (Table 1, entry 3). Further optimization of the reaction conditions resulted in 51.7% conversion and 85.2% *ee* (Table 1, entry 4). This excellent result led us to believe that water is important for the reaction. The use of water as the solvent is also advantageous in other respects, for example in terms of environmental considerations.

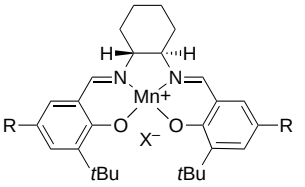

1a: R=*t*Bu, X=Cl; **1b**: R=*t*Bu, X=PF_6
2: R=Me, X=PF_6

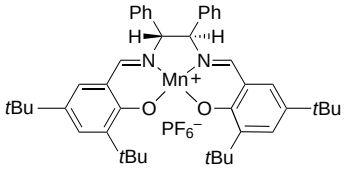

3

Effective stereochemical communication between substrate and catalyst is essential for attaining high enantioselectivities in reactions involving an asymmetric catalyst.[9] Thus, we examined a selection of catalysts for the oxidative kinetic resolution of alcohols. When the *tert*-butyl groups at the 5,5′-positions in complex **1a** were replaced by methyl

Table 1: Initial experiments.[a]

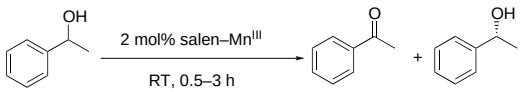

Entry	Cat.	Additive	*t* [h]	Conv. [%][b]	*ee* [%][c]	k_{rel}
1[d]	**1b**	–	3	55.5	2.0	<1.1
2	**1b**	–	2	25.0	8.9	1.9
3	**1b**	$N(C_2H_5)_4Br$	2	63.4	84.1	7.2
4	**1b**	$N(C_2H_5)_4Br$	1	51.7	85.2	23.7
5	**1b**	$N(C_2H_5)_4Br$	0.5	48.1	71.9	16.8
6	**1a**	$N(C_2H_5)_4Br$	1	51.5	80.1	17.3
7	**2**	$N(C_2H_5)_4Br$	1	42.5	19.1	<1.1
8	**3**	$N(C_2H_5)_4Br$	0.5	62.5	88.1	8.9

[a] Reaction was carried out at room temperature (20°C) with catalyst (2 mol%), $N(C_2H_5)_4Br$ (8 mol%), α-methylbenzyl alcohol (0.25 mmol), $PhI(OAc)_2$ (0.175 mmol), and H_2O (1 mL). [b] Conversion determined by GC using an internal standard. [c] Determined by GC on a CP-Chirasil-Dex CB capillary column. [d] Reaction was carried out in CH_2Cl_2.

[*] Prof. Dr. C. Xia, Dr. W. Sun, H. Wang, J. Li, P. Zhao
State Key Laboratory for Oxo Synthesis and Selective Oxidation
Lanzhou Institute of Chemical Physics
Chinese Academy of Sciences
Lanzhou, 730000 (P. R. China)
Fax: (+86) 931-827-7088
E-mail: cgxia@ns.lzb.ac.cn

[**] This work was supported financially by the National Natural Science Foundation of China (29933050)

Supporting information for this article is available on the WWW under http://www.angewandte.org or from the author.

 © 2003 Wiley-VCH Verlag GmbH & Co. KGaA, Weinheim 1433-7851/03/4209-1042 $ 20.00+.50/0

substituents (complex **2**), low enantioselectivity in the kinetic resolution of α-methylbenzyl alcohol was observed (Table 1, entry 7). Hence, it appeared that the steric hindrance at the 5,5′-positions was favorable for the enantioselectivity of the reaction. The Mn(salen) complex **3,** derived from (*R,R*)-diphenylethylenediamine, was more efficient than the Mn(salen) complex **1b**. Jacobsen's catalyst **1a** (a good catalyst for epoxidation reactions) also gave good results (Table 1).

Next, the substrate scope of the oxidative kinetic resolution was evaluated (Table 2). It can be seen that α-methylbenzyl alcohols with a substituent at the 4-position are generally good substrates for oxidative kinetic resolution with high k_{rel} values.[10] However, when the R^1 group of the substrate was changed from methyl to ethyl, or to even bulkier substituents, the enantioselectivity of the reaction decreased sharply (Table 2, entries 12 and 13). In the case of α-methylbenzyl alcohol (Table 2, entries 1 and 2) and 1-phenyl-2-propanol (Table 2, entries 10 and 11), the Mn(salen) complex **3** was more effective in distinguishing between the enantiomers of the substrate than complex **1b**. However, for the other substrates with substituents on the aromatic ring, use of the complex **1b** gave rise to higher enantioselectivities. The results showed that electronic cooperation between the catalyst and the substrate had a strong influence on the enantioselectivity of the reaction.

In conclusion, a mild, convenient method for the enantioselective kinetic resolution of secondary alcohols in the presence of Mn(salen) catalysts has been discovered. Water can be used successfully as a benign solvent in this reaction system. The use of water makes the reaction more significant in terms of potential industrial applications. Further studies into the mechanism and other potential catalysts are now underway in our laboratory.

Experimental Section

General procedure for the Mn(salen)-complex-catalyzed kinetic resolution of secondary alcohols in water.

A mixture of the substrate (0.25 mmol), catalyst (0.005 mmol), tetraethylammonium bromide (0.02 mmol) and water (1 mL) was stirred in a 5-mL tube for a few minutes at room temperature. The cooxidant, $PhI(OAc)_2$ (0.175 mmol), was then added and the reaction system was stirred for a further 0.5–1 h. The products were extracted with diethyl ether when the reaction was complete. The conversion and *ee* values were determined by GC.

Received: October 31, 2002 [Z50464]

Table 2: Asymmetric kinetic resolution of secondary alcohols.[a]

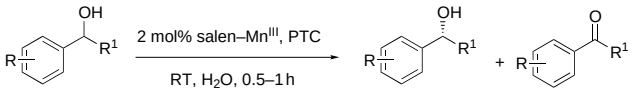

Entry	Substrate	Cat.	*t* [h]	Conv. [%][b]	*ee* [%][c]	k_{rel}
1		**1b**	1	51.7	85.2	23.7
2		**3**	0.5	62.5	88.1	8.9
3	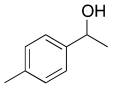	**1b**	1	67.7	90.0	7.0
4		**3**	0.5	61.9	55.4	3.4
5	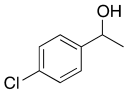	**1b**	1	61.1	97.8	18.2
6		**3**	0.5	56.7	90.5	16.6
7		**1b**	1	12.3	3.0	1.6
8	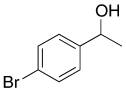	**1b**	1	65.9	96.8	11.3
9		**3**	0.5	60.4	79.5	7.4
10	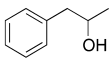	**1b**	1	56.3	73.0	7.6
11		**3**	0.5	60.0	80.1	7.7
12	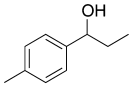	**1b**	1	64.8	5.4	1.1
13		**1b**	1	67.7	23.9	1.5

[a] Reaction carried out at room temperature (20 °C) with catalyst (2 mol%), $N(C_2H_5)_4Br$ (8 mol%), substrate (0.25 mmol), $PhI(OAc)_2$ (0.175 mmol), and H_2O (1 mL). [b] Conversion determined by GC using an internal standard. [c] Determined by GC on a CP-Chirasil-Dex CB capillary column.

[1] R. Noyori, *Asymmetric Catalysis in Organic Synthesis*, Wiley, New York, **1993**.

[2] For a review, see: a) T. Katsuki, *Coord. Chem. Rev.* **1995**, *140*, 189; b) T. Katsuki, *J. Mol. Catal. A* **1996**, *113*, 87; c) Y. N. Ito, T. Katsuki, *Bull. Chem. Soc. Jpn.* **1999**, *72*, 603; d) E. N. Jacobsen, M. H. Hu in *Comprehensive Asymmetric Catalysis, Vol. 2* (Eds.: E. N. Jacobsen, A. Pfaltz, H. Yamamoto), Springer, Berlin, **1999**, p. 649; e) T. Katsuki in *Comprehensive Asymmetric Catalysis, Vol. 2* (Eds.: E. N. Jacobsen, A. Pfaltz, H. Yamamoto), Springer, Berlin, **1999**, p. 791; f) J. M. Keith, J. F. Larrow, E. N. Jacobsen, *Adv. Synth. Catal.* **2001**, *343*, 5.

[3] a) M. Tokunaga, J. F. Larrow, F. Kakiuchi, E. N. Jacobsen, *Science* **1997**, *277*, 936; b) D. A. Annis, E. N. Jacobsen, *J. Am. Chem. Soc.* **1999**, *121*, 4147; c) L. E. Martinez, J. L. Leighton, D. H. Carsten, E. N. Jacobsen, *J. Am. Chem. Soc.* **1995**, *117*, 5897; d) S. E. Schaus, J. F. Larrow, E. N. Jacobsen, *J. Org. Chem.* **1997**, *62*, 4197; e) J. F. Larrow, E. N. Jacobsen, *J. Am. Chem. Soc.* **1996**, *118*, 7420; f) E. N. Jacobsen, F. Kakiuchi, R. G. Konsler, J. F. Larrow, M. Tokunaga, *Tetrahedron Lett.* **1997**, *38*, 773; g) M. Wu, E. N. Jacobsen, *J. Org. Chem.* **1998**, *63*, 5252; h) J. A. Miller, W. Jin, S. T. Nguyen, *Angew. Chem.* **2002**, *114*, 3077; *Angew. Chem. Int. Ed.* **2002**, *41*, 2953.

[4] W. Sun, H. W. Wang, C. G. Xia, P. Q. Zhao, unpublished results.

[5] Catalytic acylation: a) E. Vedejs, J. A. MacKay, *Org. Lett.* **2001**, *3*, 535; b) E. Vedejs, O. Daugulis, *J. Am. Chem. Soc.* **1999**, *121*, 5813; c) E. Vedejs, O. Daugulis, S. T. Diver, *J. Org. Chem.* **1996**, *61*, 430; d) S. J. Miller, G. T. Copeland, N. Papaionnou, T. E. Horstmann, E. M. Ruel, *J. Am. Chem. Soc.* **1998**, *120*, 1629; e) J. C. Ruble, H. A. Latham, G. C. Fu, *J. Am. Chem. Soc.* **1997**, *119*, 1492; f) J. C. Ruble, J. Tweddell, G. C. Fu, *J. Org. Chem.* **1998**, *63*, 2794; g) C. E. Garrett, M. M.-C. Lo, G. C. Fu, *J. Am. Chem. Soc.* **1998**, *120*, 7479; h) B. Tao, J. C. Ruble, D. A. Hoic, G. C. Fu, *J. Am. Chem. Soc.* **1999**, *121*, 5091; i) T. Kawabata, M. Nagato, K. Takasu, K. Fuji, *J. Am. Chem. Soc.* **1997**, *119*, 3169; j) T. Oriyama, Y. Hori, K. Imai, R. Sasaki, *Tetrahedron Lett.* **1996**, *37*, 8543; k) T. Sano, K. Imai, K. Ohashi, T. Oriyama, *Chem. Lett.* **1999**, 265.

[6] Enzymatic acylation: a) J. H. Choi, Y. H. Kim, S. H. Nam, S. T. Shin, M.-J. Kim, J. Park, *Angew. Chem.* **2002**, *114*, 2479; *Angew.*

Chem. Int. Ed. **2002**, *41*, 2373; b) A. L. E. Larsson, B. A. Persson, J.-E. Bäckvall, *Angew. Chem.* **1997**, *109*, 1256; *Angew. Chem. Int. Ed. Engl.* **1997**, *36*, 1211; c) B. A. Persson, A. L. E. Larsson, M. L. Ray, J.-E. Bäckvall, *J. Am. Chem. Soc.* **1999**, *121*, 1645; d) B. A. Persson, F. F. Huerta, J.-E. Bäckvall, *J. Org. Chem.* **1999**, *64*, 5237; e) F. F. Huerta, J.-E. Bäckvall, *Org. Lett.* **2001**, *3*, 1209; f) P. C. D. Jesus, M. C. Rezende, M. D. G. Nascimento, *Tetrahedron: Asymmetry* **1995**, *6*, 63.

[7] For the oxidative kinetic resolution of secondary alcohols, see: a) K. Masutani, T. Uchida, R. Irie, T. Katsuki, *Tetrahedron Lett.* **2000**, *41*, 5119; b) T. Hamada, R. Irie, J. Mihara, K. Hamachi, T. Katsuki, *Tetrahedron* **1998**, *54*, 10017; c) I. Nishibayashi, I. Takei, S. Uemura, M. Hidai, *Organometallics* **1999**, *18*, 2291; d) S. Hashiguchi, A. Fujii, K. J. Haack, K. Matsumura, T. Ikariya, R. Noyori, *Angew. Chem.* **1997**, *109*, 300; *Angew. Chem. Int. Ed. Engl.* **1997**, *36*, 288; e) E. M. Ferreira, B. M. Stoltz, *J. Am. Chem. Soc.* **2001**, *123*, 7725; f) D. R. Jensen, J. S. Pugsley, M. S. Sigman, *J. Am. Chem. Soc.* **2001**, *123*, 7475; g) J. A. Mueller, D. R. Jensen, M. S. Sigman, *J. Am. Chem. Soc.* **2002**, *124*, 8202.

[8] For a recent review, see: a) U. M. Lindström, *Chem. Rev.* **2002**, *102*, 2751; b) C. J. Li in *Green Chemistry: Frontiers in Benign Chemical Syntheses and Processes*, (Eds.: P. T. Anastas, T. C. Williamson), Oxford, New York, **1998**, chap. 14, p. 234.

[9] M. Palucki, N. S. Finney, P. J. Pospisil, M. L. Güler, T. Ishida, E. N. Jacobsen, *J. Am. Chem. Soc.* **1998**, *120*, 948.

[10] $k_{rel} = \ln[(1-C)(1-ee)]/\ln[(1-C)(1+ee)]$, where C is the conversion and *ee* is the enantiomeric excess; for an excellent discussion of kinetic resolution, see: H. B. Kagan, J. C. Fiaud, Kinetic Resolution, *Top. Stereochem.* **1988**, *18*, 249.

 © 2003 Wiley-VCH Verlag GmbH & Co. KGaA, Weinheim 1433-7851/03/4209-1044 $ 20.00+.50/0

Structures of Protonated Cubane

Protonation of Cubane in the Gas Phase: A High-Level Ab Initio and DFT Study**

José-Luis M. Abboud, Ilmar A. Koppel,* Juan Z. Dávalos, Peeter Burk, Ivar Koppel, and Esther Quintanilla*

We are presently studying ion–molecule reactions of some cubane[1] derivatives. This prompted us to examine the protonation of the parent compound **1**, for which Fourier transform ion cyclotron resonance (FT-ICR) spectroscopy studies[2] led to experimental gas-phase basicities GB(**1**) of 200.7 ± 3.0[2] and 199.2 ± 3.0 kcal mol^{-1}.[3] Here we report the main results of ab initio and DFT calculations on this reaction.[4]

Cubane has three potential basic sites: face, edge, and corner.[5] On protonation, they lead to $\mathbf{1}H_f^+$ (C_{4v}), $\mathbf{1}H_e^+$ (C_{2v}), and $\mathbf{1}H_c^+$ (C_s; Scheme 1), respectively. The first two sites are expected to be favored by the buildup of negative charge in highly strained C–C bonds,[6] while bending of a C–H bond shifts the negative charge towards the carbon atom.[6]

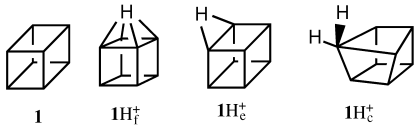

Scheme 1. Cubane and its different protonated forms.

At the B3LYP/6-311+G(d,p)[7] and MP2/6-311+G(d,p) levels,[8] we find that $\mathbf{1}H_c^+$ is more stable than $\mathbf{1}H_f^+$ and $\mathbf{1}H_e^+$ by 108.7 (104.5) and 54.1 (56.7) kcal mol^{-1}, respectively (in terms of total energies; for full details, see Supporting Information). None of the three structures appears as a minimum on the potential energy surface of protonated cubane ($\mathbf{1}H^+$). The imaginary vibrational frequencies[9] in structures $\mathbf{1}H_e^+$ and $\mathbf{1}H_f^+$ are associated with the motion of the proton towards a carbon atom. Relaxation of symmetry constraints on structures $\mathbf{1}H_c^+$, $\mathbf{1}H_e^+$, and $\mathbf{1}H_f^+$ leads to the same open structure, $\mathbf{1}H_o^+$ (C_1 symmetry), corresponding to tetracyclo[4.2.0.0^{2,4}.0^{3,8}]oct-7-ylium cation (Scheme 2). This opening of the rigid framework of **1** on protonation is quite consistent with the smooth, essentially barrierless evolution of a corner-protonated structure through an electrocyclic process.[10]

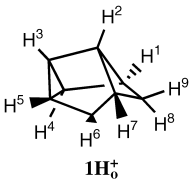

Scheme 2. Tetracyclo-[4.2.0.0^{2,4}.0^{3,8}]oct-7-ylium cation.

The above results encouraged us to perform modified G2(MP2)[11] (geometries optimized and frequencies calculated at the MP2/6-311+G(d,p) level) calculations on **1** and $\mathbf{1}H_o^+$, since we considered $\mathbf{1}H_o^+$ to be the most likely structure for $\mathbf{1}H^+$ (Table 1 and Supporting Information). The standard enthalpy and Gibbs energy changes for reaction (1), $\Delta_r H_m^\circ(1)$ and $\Delta_r G_m^\circ(1)$ thus calculated are −265.1 and −258.8 kcal mol^{-1}, respectively (Table 1).

$$\mathbf{1}(g) + H^+(g) \rightarrow \mathbf{1}H_o^+(g) \quad \Delta_r H_m^\circ(1),\ \Delta_r G_m^\circ(1) \qquad (1)$$

By definition,[3] the experimental gas-phase basicity of **1**, GB(**1**), is the negative of $\Delta_r G_m^\circ(1)$. The difference between the experimental and calculated GB values thus amounts to about 60 kcal mol^{-1}. This strongly suggests that the experimental GB determined by FT-ICR spectroscopy does not correspond to the reversible protonation of **1**(g). Furthermore, the large absolute value of $\Delta_r G_m^\circ(1)$ is most consistent with the expected relief of strain attending opening of **1**(g).[2,12]

[*] Prof. Dr. J.-L. M. Abboud, Dr. J. Z. Dávalos, Eng. E. Quintanilla
Instituto de Química Física "Rocasolano", CSIC
C/Serrano, 119, 28006 Madrid (Spain)
Fax: (+34) 91-585-5184
E-mail: jlabboud@iqfr.csic.es

Prof. Dr. I. A. Koppel, Prof. Dr. P. Burk, Dr. I. Koppel
Institute of Chemical Physics, University of Tartu
2 Jakobi St. 51014 Tartu (Estonia)
Fax: (+372) 7-375-264
E-mail: ilmar@chem.ut.ee

[**] This work was supported by grants BQU2000-1497 (Spanish DGES) and 5226 (Estonian Science Foundation) and by a Joint Project CSIC–Estonian Academy of Sciences "The Reactivity of the Strained Cage Molecules".

Supporting information for this article is available on the WWW under http://www.angewandte.org or from the author.

 © 2003 Wiley-VCH Verlag GmbH & Co. KGaA, Weinheim 1433-7851/03/4209-1044 $ 20.00+.50/0

Table 1: Absolute G2(MP2) enthalpies (H_{298}, in a.u.), Gibbs energies (G_{298}, in a.u.), and corresponding relative values (ΔH_{298} and ΔG_{298}, relative to **1**, in kcal mol^{-1}) for relevant species.[a]

Species	H_{298}	ΔH_{298}	G_{298}	ΔG_{298}
1	−308.84989	0.0	−308.88062	0.0
$\mathbf{1}H_o^+$	−309.26858	−262.7	−309.30249	−264.7
2	−308.94420	−59.2	−308.97874	−61.6
3	−308.91972	−43.8	−308.95515	−46.8
4	−308.86704	−10.8	−308.90247	−13.7

[a] Structures fully optimized at the MP2/6-311+G(d,p) level. Numbering of species as in the text.

Reaction (2) corresponds to the protonation of **1**(g) by the acidic species BH^+(g) in the process taking place in the FT-ICR experiments.[2]

$$\mathbf{1}(g) + BH^+(g) \rightarrow \mathbf{1}H^+(g) + B(g)\ \ \Delta_r H_m^\circ(2),\ \Delta_r G_m^\circ(2) \qquad (2)$$

Since the experimental GB(B) is ca. 200 kcal mol^{-1} and the computed GB(**1**), $\Delta_r G_m^\circ(3)$, is close to 260 kcal mol^{-1} (assuming again that $\mathbf{1}H^+$(g) has the structure $\mathbf{1}H_o^+$), it follows that the observed reaction (2) is substantially exergonic and exothermic, and isomerization of $\mathbf{1}H_o^+$ to yield some other ion of the $C_8H_9^+$ manifold cannot be entirely ruled out. We consider, however, that no isomerization of this ion occurs and explored the outcome of its deprotonation by the reference bases used in the experiments. At the B3LYP/6-311+G(d,p) and MP2/6-311+G(d,p) levels, the less endergonic processes are those corresponding to the abstraction of H^8 (or H^9), H^3, and H^1. Proton abstraction from other positions are less favored by at least 33 kcal mol^{-1} (Supporting Information). The G2(MP2) calculations were performed on the most stable deprotonated species. The results, summarized in Table 1, show that the most stable product is the hydrocarbon cuneane[13] (**2**; Scheme 3). It originates from removal of protons H^8 or H^9 [reaction (2)]. Removal of H^1 and H^3 leads to the highly strained species **3** and **4**, respectively (Scheme 3) and is less favorable.

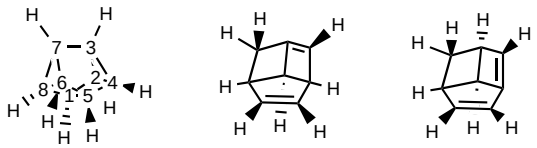

2 **3** **4**

Scheme 3. Deprotonation products of $\mathbf{1}H_o^+$.

Importantly, the G2(MP2)-calculated standard Gibbs energy change for reaction (3), $\Delta_r G_m^\circ(3)$, amounts to 198.0 kcal mol^{-1}, a value that agrees (within the usual limits)[9,11,14] with the reported experimental gas-phase basicity of **1**. This and the clean results of ion-selection experiments described in ref. [2] are consistent with the observation in the FT-ICR studies of the protonation process (2) with $\mathbf{1}H^+$ having the structure $\mathbf{1}H_o^+$, followed by reaction (4).

$$\mathbf{1}H_o^+(g) \rightarrow \mathbf{2}(g) + H^+\ \ \Delta_r H_m^\circ(3),\ \Delta_r G_m^\circ(3) \qquad (3)$$

$$\mathbf{1}H_o^+(g) + B(g) \rightarrow \mathbf{2}(g) + BH^+\ \ \Delta_r H_m^\circ(4),\ \Delta_r G_m^\circ(4) \qquad (4)$$

Thus, even though **1**(g) is able to deprotonate bases with GB ≈ 260 kcal mol^{-1}, $\mathbf{1}H_o^+$(g) can be deprotonated by bases with GB ≈ 198 kcal mol^{-1}, and, under the experimental working conditions, $\mathbf{1}H^+$(g) is not observed in the presence of bases with GB values significantly larger than the latter value. The possibility of gas-phase isomerization through protonation/deprotonation processes is well documented.[15] It is also known that, in solution, **1** readily isomerizes to **2** in the presence of Ag^I,[13] Pd^{II},[13] or Li^I.[16] These facts support the likelihod of the suggested mechanism.

Our results strongly suggest that the gas-phase protonation of cubane is an irreversible process leading to the formation of tetracyclo[4.2.0.0^{2,4}.0^{3,8}]oct-7-ylium cation ($\mathbf{1}H_o^+$). It is likely that under the experimental FT-ICR conditions, this process is followed by the deprotonation of this ion to yield cuneane. These conclusions are perfectly consistent with the experimental information available. At this point we are conducting experimental studies on the gas-phase protonation of cuneane.

Received: November 7, 2002 [Z50501]

[1] a) Pentacyclo[4.2.0.0^{2,5}.0^{3,8}.0^{4,7}]octane. b) P. E. Eaton, T. W. Cole, Jr., *J. Am. Chem. Soc.* **1964**, *86*, 962–964; c) P. E. Eaton, *Angew. Chem.* **1992**, *104*, 1447–1462; *Angew. Chem. Int. Ed. Engl.* **1992**, *31*, 1421–1436; d) T. Yildirim, P. M. Gehring, D. A. Neumann, P. E. Eaton, T. Emrick, *Carbon* **1998**, *36*, 809–815.

[2] I. Santos, D. W. Balogh, C. W. Doecke, A. G. Marshall, L. A. Paquette, *J. Am. Chem. Soc.* **1986**, *108*, 8183–8185.

[3] E. P. L. Hunter, S. G. Lias, *J. Phys. Chem. Ref. Data* **1998**, *27*, 413–656.

[4] Full computational details are given in the Supporting Information.

[5] There is also an isomer in which the proton is located at the center of the cube (O_h symmetry). At the B3LYP/6-311+G(d,p) level, this endohedral structure, $\mathbf{1}H_{endo}^+$, is 199.7 kcal mol^{-1} less stable than $\mathbf{1}H_c^+$ and is not a minimum on the potential energy surface of $\mathbf{1}H^+$ (see Supporting Information).

[6] P. Politzer, L. N. Domelsmith, L. Abrahmsen, *J. Phys. Chem. A* **1984**, *88*, 1752–1758.

[7] a) A. D. Becke, *J. Chem. Phys.* **1993**, *98*, 5648–5652; b) C. Lee, W. Yang, R. G. Parr, *Phys. Rev. B* **1988**, *37*, 785–789; c) S. H. Vosko, L. Wilk, M. Nusair, *Can. J. Phys.* **1980**, *58*, 1200–1211; d) P. J. Stephens, F. J. Devlin, C. F. Chabalowski, M. J. Frisch, *J. Phys. Chem.* **1994**, *98*, 11623–11627.

[8] W. J. Hehre, L. Radom, P. von R. Schleyer, J. A. Pople, *Ab Initio Molecular Orbital Theory*, Wiley, New York, **1986**.

[9] J. B. Foresman, Æ. Frisch, *Exploring Chemistry with Electronic Structure Methods*, 2nd ed., Gaussian Inc., Pittsburgh, **1996**.

[10] H. Jiao, P. von R. Schleyer, *J. Am. Chem. Soc.* **1995**, *117*, 11529–11535.

[11] L. A. Curtiss, K. Raghavachari, J. A. Pople, *J. Chem. Phys.* **1993**, *98*, 1293–1298.

[12] For example, see D. W. Rogers, *J. Mol. Struct.* **2000**, *556*, 207–215, and references therein.

[13] a) Pentacyclo[3.3.0.0^{2,4}.0^{3,7}.0^{6,8}]octane. b) L. Cassar, P. E. Eaton, J. Halpern, *J. Am. Chem. Soc.* **1970**, *92*, 6366–6368.

[14] a) J.-L. M. Abboud, O. Castaño, J. Z. Dávalos, P. Jiménez, R. Gomperts, P. Müller, M. V. Roux, *J. Org. Chem.* **2002**, *67*, 1057–

 © 2003 Wiley-VCH Verlag GmbH & Co. KGaA, Weinheim 1433-7851/03/4209-1045 $ 20.00+.50/0

1060; b) J.-L. M. Abboud, O. Castaño, J. Z. Dávalos, R. Gomperts, *Chem. Phys. Lett.* **2001**, *337*, 327 – 330.
[15] R. Wolfshütz, H. Schwarz, *Int. J. Mass Spectrom. Ion Phys.* **1980**, *33*, 291 – 297.
[16] S. Moss, B. T. King, A. de Meijere, S. I. Kozhushkov, P. E. Eaton, J. Michl, *Org. Lett.* **2001**, *3*, 2375 – 2377.

 © 2003 Wiley-VCH Verlag GmbH & Co. KGaA, Weinheim 1433-7851/03/4209-1046 $ 20.00+.50/0

Gold–Phosphanyl Structures

Synthesis and Structure of Cyclic Gold(I) Phosphanyl Complexes $[\{Au(PR_2)\}_n]$**

Diana M. Stefanescu, Holming F. Yuen, David S. Glueck, James A. Golen, and Arnold L. Rheingold*

Since their discovery in 1976, homoleptic gold(I) phosphanyl complexes of the form $[\{Au(PR_2)\}_n]$ have remained a mysterious class of compounds.[1] The parent, and most investigated of the family, $[\{Au(PPh_2)\}_n]$, is insoluble; its color was reported to depend on the base used in its preparation from $[Au(PHPh_2)(Cl)]$ or related precursors.[2] Parish and co-workers prepared several related $[\{Au(PR_2)\}_n]$ complexes (R = Et, *n*-octyl, *p*-MeC_6H_4, *p*-(*t*Bu)C_6H_4), which could be obtained in soluble and insoluble forms, that were proposed to be either cyclic or linear chain polymers.[2d] NMR studies of these materials, although made difficult by precipitate formation, suggested that several species were present in solution. Mössbauer spectra indicated the expected linear coordination with two phosphanyl ligands binding to a gold center, but structural details were not available.[2d,f] We report here that using bulkier R groups enables the synthesis of soluble gold phosphanyl complexes of the form $[\{Au(PR_2)\}_n]$ ($PR_2 = PCy_2$ (**1**, Cy = c-C_6H_{11}), $P(tBu)_2$ (**2**), $PMes_2$ (**3**, Mes = 2,4,6-$Me_3C_6H_2$), and PIs_2 (**4**, Is = 2,4,6-$(iPr)_3C_6H_2$)), whose novel cyclic structures were determined by X-ray crystallography.[3]

Treatment of the known compounds $[Au(PHR_2)(Cl)]$[4] and the novel $[Au(PHIs_2)(Cl)]$ (**5**) with aqueous ammonia in THF or CH_2Cl_2 caused precipitation of the white, toluene-soluble and air-stable $[\{Au(PR_2)\}_n]$ complexes **1**–**4** (Scheme 1). ^{31}P NMR spectra of these crude products showed the presence of several species (for **1** and **3**: four species; for **2**: five or ten species depending on reaction time; for **4**: only one form). Recrystallization of **1** from toluene gave a mixture of two compounds which could not be separated, but on one occasion crystals of one of these forms were isolated. Recrystallization of **2** from toluene yielded a mixture of two compounds; the less soluble one was isolated after further recrystallization. Heating **3** in toluene caused partial conversion to a major product, which then crystallized preferentially. After isolation, these materials were characterized by elemental analyses, multinuclear NMR and IR spectroscopies, and MALDI mass spectrometry (molecular ions were observed).

$$[Au(PHR_2)Cl] \xrightarrow{NH_4OH} [\{Au(PR_2)\}_n]$$

$PR_2 = PCy_2$ (**1**), $P(tBu)_2$ (**2**), $PMes_2$ (**3**), PIs_2 (**4**)

Scheme 1. Synthesis of Au^I–Phosphanyl Complexes.

The crystal structures of cyclic $[\{Au(PCy_2)\}_6]\cdot 2\,C_7H_8$ (**1**·2 C_7H_8), $[\{Au(P(tBu)_2)\}_6]\cdot C_7H_8$ (**2**·C_7H_8), $[\{Au(PMes_2)\}_4]$ (**3**), and $[\{Au(PIs_2)\}_3]$(**4**) are shown in Figures 1–4.[5] Toluene molecules are not illustrated in these figures, but in both **1**·2 C_7H_8 and **2**·C_7H_8, they are present in the channels between the rings, which stack to yield an extended structure. Not surprisingly, an increase in the size of the P substituents leads

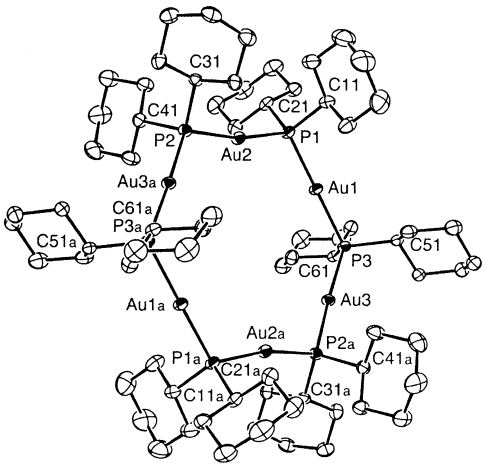

Figure 1. ORTEP diagram of $[Au(PCy_2)]_6\cdot 2\,C_7H_8$ (**1**·2 C_7H_8). The hydrogen atoms and solvent molecules are not shown. Selected bond lengths [Å] and angles [°]: Au1-P1 2.3116(12), Au1-P3 2.3150(12), Au2-P2 2.3132(12), Au2-P1 2.3166(13), Au3-P2a 2.3145(12), Au3-P3 2.3223(12); P1-Au1-P3 174.09(4), P2-Au2-P1 168.83(4), P2a-Au3-P3 174.39(4).

[*] Prof. D. S. Glueck, D. M. Stefanescu, H. F. Yuen
Department of Chemistry and Dartmouth Molecular Materials Group
6128 Burke Laboratory
Dartmouth College, Hanover, New Hampshire, 03755 (USA)
Fax: (+1) 603-646-3946
E-mail: Glueck@Dartmouth.edu
Prof. J. A. Golen, Prof. A. L. Rheingold
Department of Chemistry
University of Delaware
Newark, Delaware, 19716 (USA)
[+] Permanent address:
Department of Chemistry and Biochemistry
University of Massachusetts Dartmouth
North Dartmouth, Massachusetts, 02747 (USA)

[**] We thank the NSF for support, including an REU fellowship for H.F.Y.

Supporting information for this article is available on the WWW under http://www.angewandte.org or from the author.

 © 2003 Wiley-VCH Verlag GmbH & Co. KGaA, Weinheim 1433-7851/03/4209-1046 $ 20.00+.50/0

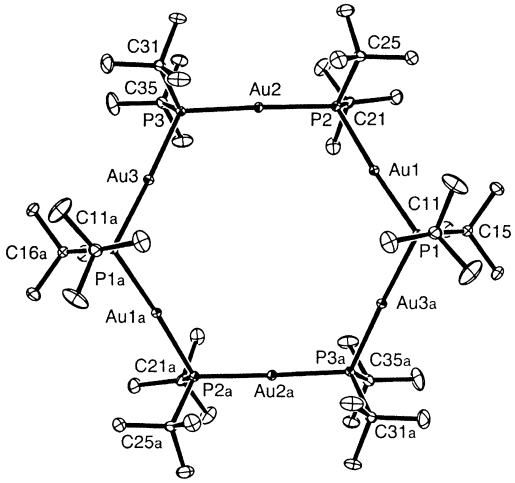

Figure 2. ORTEP diagram of $[\{Au(P(tBu)_2)\}_6]\cdot C_7H_8$ ($\mathbf{2}\cdot C_7H_8$). The hydrogen atoms and solvent molecule are not shown. Selected bond lengths [Å] and angles [°]: Au1-P1 2.3287(12), Au1-P2 2.3306(12), Au2-P2 2.3324(12), Au2-P3 2.3363(12), Au3-P1a 2.3280(12), Au3-P3 2.3295(12); P1-Au1-P2 174.85(4), P2-Au2-P3 178.12(4), P1a-Au3-P3 176.86(4).

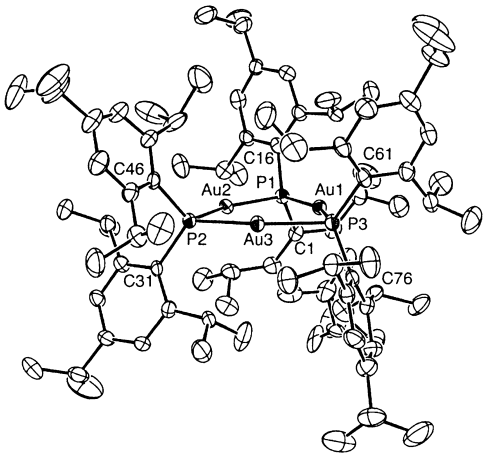

Figure 4. ORTEP diagram of $[\{Au(PIs_2)\}_3]$ (**4**). The hydrogen atoms and disorder in the isopropyl groups are not shown. Selected bond lengths [Å] and angles [°]: Au1-P3 2.332(2), Au1-P1 2.335(2), Au1···Au3 3.0661(4), Au1···Au2 3.0821(4), Au2-P1 2.314(2), Au2-P2 2.319(2), Au2···Au3 3.0970(5), Au3-P3 2.321(2), Au3-P2 2.323(2); P3-Au1-P1 157.30(7), P1-Au2-P2 156.47(8), P3-Au3-P2 157.02(8).

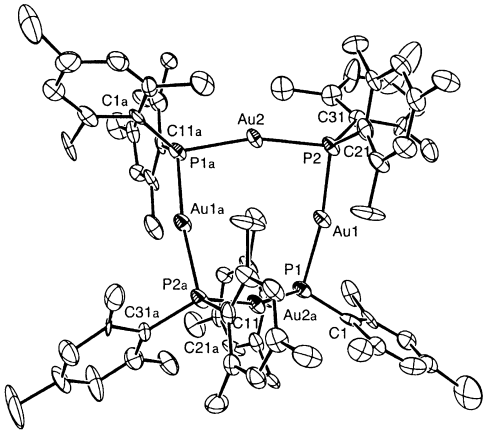

Figure 3. ORTEP diagram of $[\{Au(PMes_2)\}_4]$ (**3**). The hydrogen atoms are not shown. Selected bond lengths [Å] and angles [°]: Au1-P1 2.311(6), Au1-P2 2.318(6), Au1···Au2 3.3414(14), Au2-P1a 2.312(6), Au2-P2 2.320(6); P1-Au1-P2 170.3(2), P1a-Au2-P2 163.8(2).

to a decreased ring size, presumably to reduce unfavorable steric interactions.

As expected, the P-Au-P angles are close to linear, and the phosphorus atoms are approximately tetrahedral (Table 1). The Au–P bond lengths are similar in all four complexes, and the average Au–P bond length in $\mathbf{2}\cdot C_7H_8$ (2.3309(12) Å) is slightly longer than that in the precursor $[Au(PH(tBu)_2)(Cl)]$ (2.230(2) Å).[4] Aurophilic interactions[6] are clearly present in the $\{Au_3\}$ triangle of **4**, with Au···Au separations ranging from 3.0661(4) to 3.0970(5) Å, and may also be important in **3**, with Au···Au separations of 3.3414(14) and 3.4448(12) Å observed. In contrast, the shortest Au···Au separations in $\mathbf{1}\cdot 2\,C_7H_8$ and $\mathbf{2}\cdot C_7H_8$ are 3.8992(3) and 3.9183(3) Å, respectively.

Although the ring in $\mathbf{1}\cdot 2\,C_7H_8$ is almost planar (mean deviation from the plane is 0.1116 Å) and that in **4** is planar (mean deviation 0.0075 Å), $\mathbf{2}\cdot C_7H_8$ and **3** adopt puckered structures (Figure 5). The structure of **3** may be described as "butterfly-like", with an angle between the planes of 125.24(9)°, or as a plane of Au atoms with P atoms alternating above and below the plane. In the twisted $\mathbf{2}\cdot C_7H_8$, two planes of P atoms (P1, P2, P3, P1a and P1, P2a, P3a, P1a) intersect at an angle of 34.15(2)°.

Hexameric $\mathbf{1}\cdot 2\,C_7H_8$ and $\mathbf{2}\cdot C_7H_8$ have the same nuclearity as $[\{Au(S(2,4,6\text{-}(iPr)_3C_6H_2)\}_6]$, in which the $\{Au_6S_6\}$ ring adopts a chair conformation.[3a,e] However, $\mathbf{1}\cdot 2\,C_7H_8$ is almost planar and the twisted ring in $\mathbf{2}\cdot C_7H_8$ is closer to a boat conformation. The structure of the cyclic tetramer **3** may be compared to that of $[\{Au(N(SiMe_3)_2)\}_4]$, which contains a planar $\{Au_4N_4\}$ core. The shorter Au–N bond length (2.082(3) Å) is accompanied by reduced Au···Au distances (3.0100(3) and 3.0355(3) Å).[3f] In contrast, the $\{Au_4S_4\}$ core in $[\{Au(S\{SiO(tBu)_3\})\}_4]$ is folded as in **3** with an angle of 157.3° with respect to the S–S diagonal,[3c] but $[\{Au(SC(SiMe_3)_3)\}_4]$ is planar and $[\{Au(TeC(SiMe_3)_3)\}_4]$ adopts a butterfly structure with a dihedral angle of 144.98(6)°.[3b]

Several planar complexes with a $\{Au_3\}$ triangle supported by bridging ligands are known, but these include two-atom bridges and nine-membered rings.[7] In contrast,

Table 1: Selected bond lengths [Å] and angles [°] in the gold(I) phosphanyl complexes $\mathbf{1}\cdot 2\,C_7H_8$, $\mathbf{2}\cdot C_7H_8$, **3**, and **4**.

Complex	$\mathbf{1}\cdot 2\,C_7H_8$	$\mathbf{2}\cdot C_7H_8$	**3**	**4**
Au–P (av)	2.3155(13)	2.3309(12)	2.315(6)	2.324(2)
P-Au-P (av)	172.44(4)	176.61(4)	167.0(2)	156.93(8)
Au-P-C (av)	108.18(18)	106.93(17)	114.6(7)	115.2(3)
Au-P-Au (av)	117.51(5)	115.76(5)	94.2(2)	83.06(7)
C-P-C (av)	105.8(2)	113.5(2)	105.4(9)	110.9(4)

 © 2003 Wiley-VCH Verlag GmbH & Co. KGaA, Weinheim 1433-7851/03/4209-1047 $ 20.00+.50/0

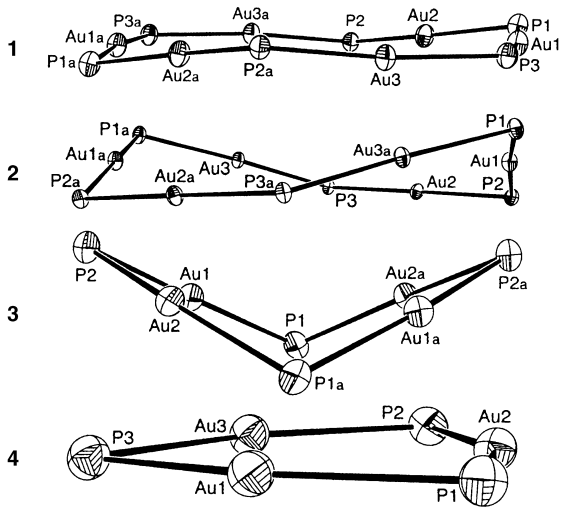

Figure 5. The Au–P rings have different shapes: almost planar in **1**·2 C_7H_8, twisted in **2**·C_7H_8, butterfly in **3**, and planar in **4**.

the shorter bridges in **4** lead to unusually bent P-Au-P angles (average 156.93(8)°). We are not aware of other simple [{AuX}$_n$] complexes with trinuclear structures; the closest precedent is the Au–Nb raft cluster [{Au(Cp′$_2$NbH$_2$)}$_3$] (Cp′ = η^5-$C_5H_4SiMe_3$), which also features bridging hydrides.[8] These comparisons suggest that ring size and conformation in these classes of homoleptic compounds depend strongly on the substituents and the possibility of Au···Au interactions.

In conclusion, X-ray crystallographic studies of gold(I) phosphanyl complexes have for the first time established the structures of this class of compounds as cyclic oligomers. ^{31}P NMR spectroscopy showed that several species, presumably rings of different sizes, exist in solution, and that they can interconvert in some cases. These advances pave the way for further investigation of the structure and reactivity of Au^{I} phosphanyl complexes and their potential applications.[9]

Experimental Section

A representative synthesis is described. Full details of the synthesis and characterization of the other complexes are in the Supporting Information.

3: Aqueous ammonia (approximately 5 mL, 29.6%, 78 mmol) was added to a solution of [Au(PHMes$_2$)(Cl)] (340 mg, 0.68 mmol) in THF (10 mL); a white precipitate was formed. After stirring for 30 min, the solvent was pumped off, and the resulting white solid was washed with water (30 mL) to give **3** (220 mg, 69%). ^{31}P{^{1}H} NMR ([D$_8$]toluene, 121.4 MHz): $\delta = -17.0$ (major), -18.8 (minor), -23.4 (minor), -36.1 ppm (minor). This material could be dissolved in heated toluene (70°C). Slow evaporation of toluene at room temperature yielded a single product, shown to be a cyclic tetramer by X-ray crystallography (Yield 42%).

Elemental analysis (%) calcd for $C_{72}H_{88}Au_4P_4$: C 46.36, H 4.76. Found: C 46.20, H 4.58. ^{31}P{^{1}H} NMR (C_6D_6, 121.4 MHz): $\delta = -36.1$ ppm; ^{1}H NMR (C_6D_6, 300 MHz): $\delta = 6.70$ (16H), 2.65 (48H), 2.07 ppm (24H). IR (KBr): $\tilde{\nu} = 3015$, 2954, 2915, 1715, 1592, 1546, 1454, 1392, 1292, 1246, 1015, 838, 700, 615, 554, 423 cm^{-1}. MALDI-TOF-MS (Cyano-4-hydroxycinnamic acid): m/z 2799.65 ((AuPMes$_2$)$_6$), 2529.86 (Au$_6$(PMes$_2$)$_5$), 2333.22 ((AuPMes$_2$)$_5$), 2202.19, 2153.50, 2108.03, 2063.85 (Au$_5$(PMes$_2$)$_4$), 1883.82, 1867.24 ((AuPMes$_2$)$_4$), 1783.39, 1717.12, 1641.44, 1597.32 (Au$_4$(PMes$_2$)$_3$), 1417.18, 1317.02, 1236.70, 1174.88, 951.23.

Received: November 8, 2002 [Z50508]

[1] R. J. Puddephatt, P. J. Thompson, *J. Organomet. Chem.* **1976**, *117*, 395–403.

[2] a) J. Vicente, M. T. Chicote, P. G. Jones, *Inorg. Chem.* **1993**, *32*, 4960–4964; b) J. Vicente, M. T. Chicote, I. Saura-Llamas, M.-C. Lagunas, *J. Chem. Soc. Chem. Commun.* **1992**, 915–916; c) T. A. Annan, R. Kumar, D. G. Tuck, *J. Chem. Soc. Dalton Trans.* **1991**, 11–18; d) D. B. Dyson, R. V. Parish, C. A. McAuliffe, R. G. Pritchard, R. Fields, B. Beagley, *J. Chem. Soc. Dalton Trans.* **1989**, 907–914; e) T. A. Annan, R. Kumar, D. G. Tuck, *J. Chem. Soc. Chem. Commun.* **1988**, 446–448; f) D. B. Dyson, R. V. Parish, C. A. McAuliffe, R. Fields, *Hyperfine Interact.* **1988**, *40*, 327–330.

[3] For related structures of Au^{I} chalcogenolates and of an amide, see: a) I. Schroter, J. Strahle, *Chem. Ber.* **1991**, *124*, 2161–2164; b) P. J. Bonasia, D. E. Gindelberger, J. Arnold, *Inorg. Chem.* **1993**, *32*, 5126–5131; c) W. Wojnowski, B. Becker, J. Sassmanhausen, E.-M. Peters, K. Peters, H. G. von Schnering, *Z. Anorg. Allg. Chem.* **1994**, *620*, 1417–1421; d) M. R. Wiseman, P. A. Marsh, P. T. Bishop, B. J. Brisdon, M. F. Mahon, *J. Am. Chem. Soc.* **2000**, *122*, 12598–12599; e) D. J. LeBlanc, C. J. L. Lock, *Acta Crystallogr. Sect. C* **1997**, *53*, 1765–1768; f) S. D. Bunge, O. Just, W. S. Rees, Jr., *Angew. Chem.* **2000**, *112*, 3199–3200; *Angew. Chem. Int. Ed.* **2000**, *37*, 3082–3084.

[4] a) H. Schmidbaur, G. Weidenhiller, A. A. M. Aly, O. Steigelmann, G. Muller, *Z. Naturforsch. B* **1989**, *44*, 1503–1508; b) H. Schmidbaur, A. A. M. Aly, *Z. Naturforsch. B* **1979**, *34*, 23–26.

[5] Crystallographic data for **1**–**4**: recorded at 223(2) K (**1**·2 C_7H_8 and **3**), 150(2) K (**2**·C_7H_8), and 218(2) K (**4**) with Mo$_{K\alpha}$ (0.71073 Å) radiation: **1**·2 C_7H_8: triclinic, space group $P\bar{1}$, $a = 11.7057(7)$, $b = 15.2817(9)$, $c = 15.3080(9)$ Å, $\alpha = 63.2510(10)$, $\beta = 73.1750(10)$, $\gamma = 88.0730(10)$°, $Z = 2$, $R1 = 0.0313$ for 10891 ($I > 2\sigma(I)$) data; **2**·C_7H_8: monoclinic, space group $C2/c$, $a = 30.0553(16)$, $b = 8.8627(5)$, $c = 29.4648(16)$ Å, $\beta = 115.4920(10)$°, $Z = 4$, $R1 = 0.0278$ for 8504 ($I > 2\sigma(I)$) data; **3**: monoclinic, space group $C2/c$, $a = 23.830(5)$, $b = 12.160(2)$, $c = 27.254(6)$ Å, $\beta = 108.322(4)$°, $Z = 8$, $R1 = 0.0728$ for 5526 ($I > 2\sigma(I)$) data; **4**: orthorhombic, space group $Pna2_1$, $a = 24.6277(14)$, $b = 15.3421(9)$, $c = 23.5866(14)$ Å, $Z = 4$, $R1 = 0.0474$ for 19538 ($I > 2\sigma(I)$) data; CCDC 196576–196579 (complexes **1**·2 C_7H_8, **2**·C_7H_8, **3**, and **4**, respectively) contains the supplementary crystallographic data for this paper. These data can be obtained free of charge via www.ccdc.cam.ac.uk/conts/retrieving.html (or from the Cambridge Crystallographic Data Centre, 12, Union Road, Cambridge CB2 1EZ, UK; fax: (+44) 1223-336-033; or deposit@ccdc.cam.ac.uk).

[6] a) H. Schmidbaur, *Gold Bull.* **2000**, *33*, 3–10; b) H. Schmidbaur, *Chem. Soc. Rev.* **1995**, *24*, 391–400.

[7] A. L. Balch, M. M. Olmstead, J. C. Vickery, *Inorg. Chem.* **1999**, *38*, 3494–3499, and references therein.

[8] A. Antinolo, J. K. Burdett, B. Chaudret, O. Eisenstein, M. Fajardo, F. Jalon, F. Lahoz, J. A. Lopez, A. Otero, *J. Chem. Soc. Chem. Commun.* **1990**, 17–19.

[9] a) G. Landgraf in *Gold. Progress in Chemistry, Biochemistry and Technology* (Ed.: H. Schmidbaur), Wiley, Chichester **1999**, pp. 143–171; b) C. F. Shaw III in *Gold. Progress in Chemistry, Biochemistry and Technology* (Ed.: H. Schmidbaur), Wiley, Chichester, **1999**, pp. 259–308.

 © 2003 Wiley-VCH Verlag GmbH & Co. KGaA, Weinheim 1433-7851/03/4209-1048 $ 20.00+.50/0

Isomerization of Boron Aromatics

Topomerization of a Distorted Diamond-Shaped Tetraborane(4) and Its Hydroboration to a *closo*-Pentaborane(7) with a *nido* Structure**

*Carsten Präsang, Matthias Hofmann, Gertraud Geiseler, Werner Massa, and Armin Berndt**

Known tetraorganyltetraboranes(4) **1a** and **1b** have a tetrahedral structure,[1,2] the recently described planar 1,3-diamino-2,4-diboryltetraborane(4) **2a**[3] is diamond-shaped with edges of about equal length (Scheme 1). We present here

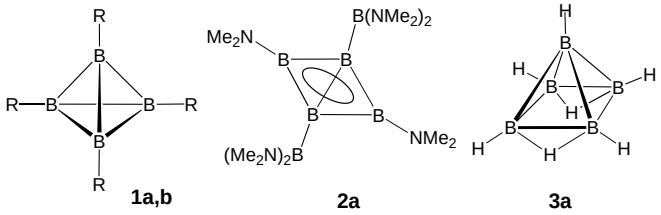

Scheme 1. Known tetrahedral tetraorganyltetraboranes(4) **1a** (R = *t*Bu)[1] and **1b** (R = 2,4,6-trimethylphenyl),[2] the planar tetraborane(4) **2a**,[3] as well as the unknown pentaborane(7) **3a**. The ellipse denotes two cyclically delocalized π electrons.

compound **2b**, a tetraalkyltetraborane(4) with a distorted diamond-shaped structure (Scheme 2). Density functional computations[4] for the tetramethyltetraborane(4) **2c** (Scheme 3) show that this distortion is a characteristic property of planar tetraalkyltetraboranes(4). The exchange of the short and long diagonal of a diamond, which, as the diamond–square–diamond (dsd) rearrangement,[5] plays a central role in isomerizations of boranes, carboranes, and metallaboranes (Scheme 4), is investigated for the first time, by way of the topomerization of **2b**, in a diamond that is not part of a polyhedron. Furthermore, **2b** provides access to the first derivative **3b** of the hitherto unknown pentaborane(7) (**3a**).

The tetraalkyltetraborane(4) **2b** is obtained by reaction of a solution of **4**[6] in diethyl ether at −100 °C with two equivalents of lithium naphthalenide in tetrahydrofuran (Scheme 2). Since **2b** is thermally stable (m.p.: 140 °C without decomposition), the naphthalene formed can be removed

[*] Prof. Dr. A. Berndt, Dr. C. Präsang, G. Geiseler, Prof. Dr. W. Massa
Fachbereich Chemie
Universität Marburg
35032 Marburg (Germany)
Fax: (+49) 6421-282-8917
E-mail: berndt@chemie.uni-marburg.de
Dr. M. Hofmann
Anorganisch-Chemisches Institut
Universität Heidelberg
Im Neuenheimer Feld 270, 69120 Heidelberg (Germany)

[**] This work was supported by the Deutsche Forschungsgemeinschaft and the Fonds der Chemischen Industrie.

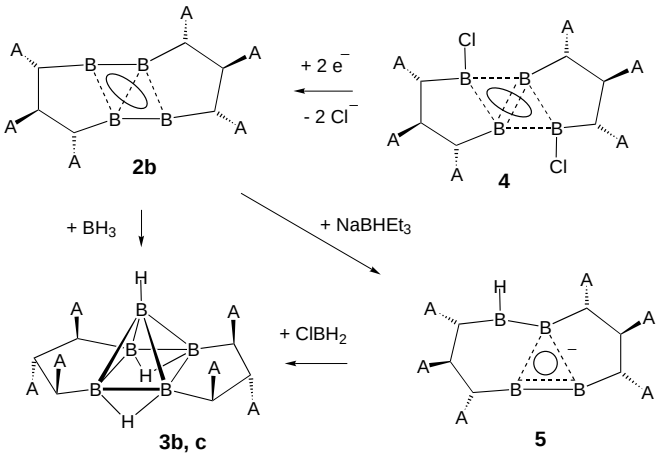

Scheme 2. Synthesis of the tetraalkyltetraborane(4) **2b** from the tetraborane(6) **4** with retention of the two-electron aromaticity, as well as conversion of **2b** into the pentaborane(7) **3b** or into the aromatic triboracyclopropanate **5**. The ellipses and the circle denote two cyclically delocalized π electrons, three dashed lines two σ electrons, which are delocalized over more than two centers. (A = $SiMe_3$, **3c**: A = H).

easily at 55 °C under vacuum. Compound **2b** reacts with $BH_3{\cdot}SMe_2$ to form **3b** (ca. 11 % yield), which is obtained in 85 % yield if **2b** is allowed to react initially with $NaBHEt_3$ and then with $H_2BCl{\cdot}SMe_2$. The triboracyclopropanate **5** is the intermediate in this reaction.[7] The constitutions of the new compounds are established by NMR data (Table 1) and X-ray structure analyses.[8] Figure 1 shows the structures of **2b** and **3b** in the crystal. Selected structural data of **2b** and **3b** are compared with those computed for the model molecules **2c,d** (Scheme 3) and **3a,c** (Scheme 1 and 2) in Table 2.

Table 1: Selected physical and spectroscopic properties of **2b, 3b,** and **5**·$Na(THF)_2$.

2b: yellow solid, m.p. 140 °C, yield 95 %; ^{1}H NMR (300 MHz, C_6D_6, 27 °C): δ = 2.60 (m, 4H, C_2CHSi and B_3BCHSi), 2.30 (m, 2H, B_2BCHSi), 0.28, 0.26, 0.12 ppm (each s, each 18H, $SiMe_3$); ^{13}C NMR (75 MHz, C_6D_6, 27 °C): δ = 39.9 (d, ^1J(C,H) = 122 Hz, C_2CHSi), 31.8 (br. d, ^1J(C,H) = 110 Hz, B_2BCHSi), 23.1 (br. d, ^1J(C,H) = 109 Hz, B_3BCHSi), 0.5, 0.1, −3.7 ppm (each q, $SiMe_3$); ^{11}B NMR (96 MHz, C_6D_6, 27 °C): δ = 125, 33 ppm.

3b: colorless solid, m.p. 113 °C (decomp), yield: 90 % (from **5**) or 11 % (NMR spectrocopy, from **2b**); ^{1}H NMR (300 MHz, $CDCl_3$, 27 °C): δ = 2.51 (br. q, 1H, ^1J(H,B) = 158 Hz, BH), 2.34 (br. s, 2H, BHB), 1.97 (t, 2H, C_2CHSi), 0.91 (s, 4H, $BCHSi$), 0.06, −0.09 ppm (each s, in total 54H, $SiMe_3$); ^{13}C NMR (75 MHz, $CDCl_3$, 27 °C): δ = 38.3 (d, ^1J(C,H) = 125 Hz, C_2CHSi), 18.2 (br. d, ^1J(C,H) = 115 Hz, $BCHSi$), 0.3, −3.2 ppm (each q, $SiMe_3$); ^{11}B NMR (96 MHz, $CDCl_3$, 27 °C): δ = 8 (s, 4B), −14 ppm (d, 1B, ^1J(B,H) = 158 Hz).

5·$Na(THF)_2$: orange solid, m.p. 103 °C (decomp), yield: 83 %; ^{1}H NMR (300 MHz, C_6D_6, 27 °C): δ = 5.82 (br. s, 1H, BH), 3.44, 1.38 (THF), 2.96 (pseudo t, 1H, C_2CHSi), 2.33 (d, 1H, $BCHSi$), 2.22 (pseudo t, 1H, $BCHSi$), 2.06 (pseudo t, 1H, C_2CHSi), 1.58, 1.45 (each d, each 1H, $BCHSi$), 0.49, 0.46, 0.41, 0.39, 0.18, 0.16 ppm (each s, each 9H, $SiMe_3$); ^{13}C NMR (75 MHz, C_6D_6, 27 °C): δ = 68.7, 25.4 (THF), 44.3 (C_2CHSi), 38.0, 36.2, 30.2 (each br., $BCHSi$), 30.1 (C_2CHSi), 26.1 (br., $BCHSi$), 1.8, 1.6, 1.1, 0.9, −2.0, −2.6 ppm ($SiMe_3$); ^{11}B NMR (96 MHz, C_6D_6, 27 °C): δ = 74, 54 (2B), 26 ppm.

 © 2003 Wiley-VCH Verlag GmbH & Co. KGaA, Weinheim 1433-7851/03/4209-1049 $ 20.00+.50/0

Table 2: Selected structural data [pm] of **2a, 2b**, and **3b** (exp.), **2c, 2d**, and **3a, 3c** (computed at the B3LYP/6-31G* level).

	2a	2b	2c	2d	3a	3b	3c
B1–B2′	160.5(2)	153.6(3)	154.0	153.0	165.9	167.9(3)	165.5
B1–B2	163.2(2)	179.1(3)	175.6	182.3	192.1	187.3(3)	192.8
B1–B1′	163.3(2)	169.3(5)	165.8	168.9	168.6	246.3(3)[a]	168.7

[a] B1–B3 168.8(3); B2–B3 168.2(3).

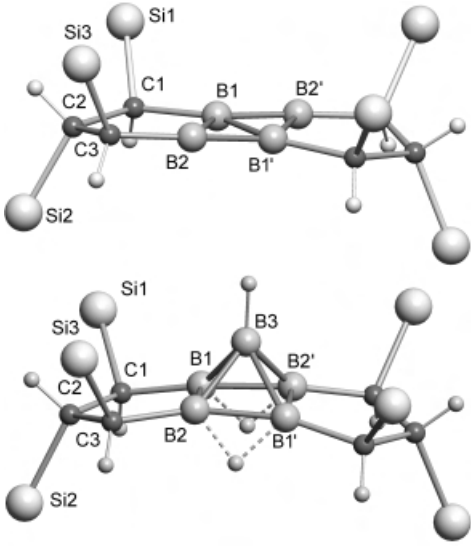

Figure 1. Structures of **2b** (top) and **3b** (bottom) in the crystal. The methyl groups at the Si atoms are omitted for clarity. Selected bond lengths [pm] and angles [°] (see also Table 2). **2b**: B1-C1 161.1(3), B2-C3 152.9(3), C1-C2 158.1(3), C2-C3 156.9(3); B1′-B2-C3 174.6(2), B2′-B1-C1 145.9(2), C1-B1-B2 94.8(2), B1-B2-C3 114.1(1); B2′-B1-B1′-B2 −177.1(2). **3b**: B1-C1 157.3(3), B2-C3 156.6(3) C1-C2 159.3(3), C2-C3 159.3(2); B1-B2-B1′ 87.6(1), B2-B1-B2′ 92.3(1), C1-B1-B3 137.5(2), C3-B2-B3 135.8(2); B1′-B2-B1-B2′ −4.5(2).

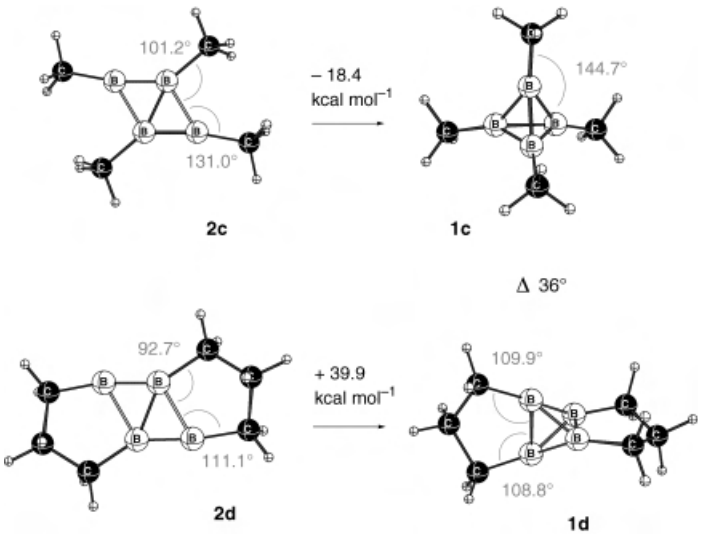

Scheme 3. Computed[4] structures of planar and tetrahedral tetraalkyltetraboranes(4), relevant angles, and energy differences.

The pentaborane(7) derivative **3b** is the first structurally characterized neutral *closo*-borane.[9,10] With six skeletal electron pairs for five centers, **3b** is to be classified as a *closo* compound. As a tetragonal pyramid, it has, however, a *nido* structure.[11,12] The distances between the boron atoms in the base (167.9 (H-bridged) and 187.3 pm) are considerably different from the value of 181.1 pm in *nido*-B_5H_9.[13] Furthermore, remarkable NMR shifts are observed for **3b**: The apical boron atom ($\delta = -13.6$ ppm) is strongly deshielded (compared to $\delta = -48.3$ ppm for *nido*-B_5H_9, $\delta = -53.1$ ppm for 2,3,4-trimethylpentaborane(9)),[14] as are the bridging hydrogen atoms ($\delta = +2.34$ compared to $\delta = -2.28$ ppm in *nido*-B_5H_9). The unusual values are in agreement with the results of computations for **3a** and **3c**[4] which gave ^{11}B NMR shifts of $\delta = 1.0$ (1B) and 7.0 (4B), and −16.9 (1B) and 3.9 (4B) ppm, respectively, as well as NMR shifts of the bridging hydrogen atoms of $\delta = 0.1$ and 2.1 ppm, respectively. At the same level of theory, shifts computed for B_5H_9 were close to those determined experimentally (^{11}B NMR: $\delta = -60.8$ (1B), −18.1 ppm (4B), ^{1}H NMR: $\delta = -2.5$ ppm).

The molecule **2b** has a C_2 axis perpendicular to the B_4 plane. Its boron atoms form an almost planar (B2,B1,B1′,B2′ = 177°) diamond with two short (153.6 pm) and two long (179.1 pm) edges and a short diagonal (B1–B1′) of 169.3 pm (**2a**: 160.5 and 163.2 as well as 163.3 pm, respectively). The orientations of the bonds to the substituents at the tips of the B_4 ring deviate strongly (by 37.6°) from the extended long diagonal in **2b**. In contrast the deviation in **2a** is much smaller (2.4°). These distortions, however, are not the result of the five-membered rings fused to the B_4 ring of **2b**: Computations[4] for tetramethyltetraborane(4) **2c** (Scheme 3) give a similar distorted structure (154.0 and 175.6, as well as 165.9 pm).[15] Also in **2c**, the bonds to the boron-bound carbon atoms at the tips of the B_4 diamond do not lie along an extended long diagonal ($\Delta = 21.2°$).

Computations[4] also show that tetrahedral **1c** (Scheme 3) is 18.4 kcal mol^{-1} lower in energy than planar **2c**, in contrast, tetrahedral **1d** is 40 kcal mol^{-1} higher in energy than planar **2d**. This can be explained by the strong distortion (by ca. 36°) of four B-B-C angles in **1d** (108.8 or 109.9°) compared to the angle of 145° in undistorted **1c**.

Compound **2b** provides the first opportunity to study the exchange of tri- and tetracoordinate boron atoms, that is the long and short diagonal of a diamond, which is not part of a polyhedron.[5] Upon raising the temperature, two of the three signals for trimethylsilyl groups broaden in the ^{1}H NMR spectra of **2b**. By line shape analyses we have determined a barrier of 22 kcal mol^{-1} for the exchange of these silyl groups, which are adjacent to the tri- and tetracoordinate boron atoms. Computations[4] for the models **2c** and **2d** give barriers

 © 2003 Wiley-VCH Verlag GmbH & Co. KGaA, Weinheim 1433-7851/03/4209-1050 $ 20.00+.50/0

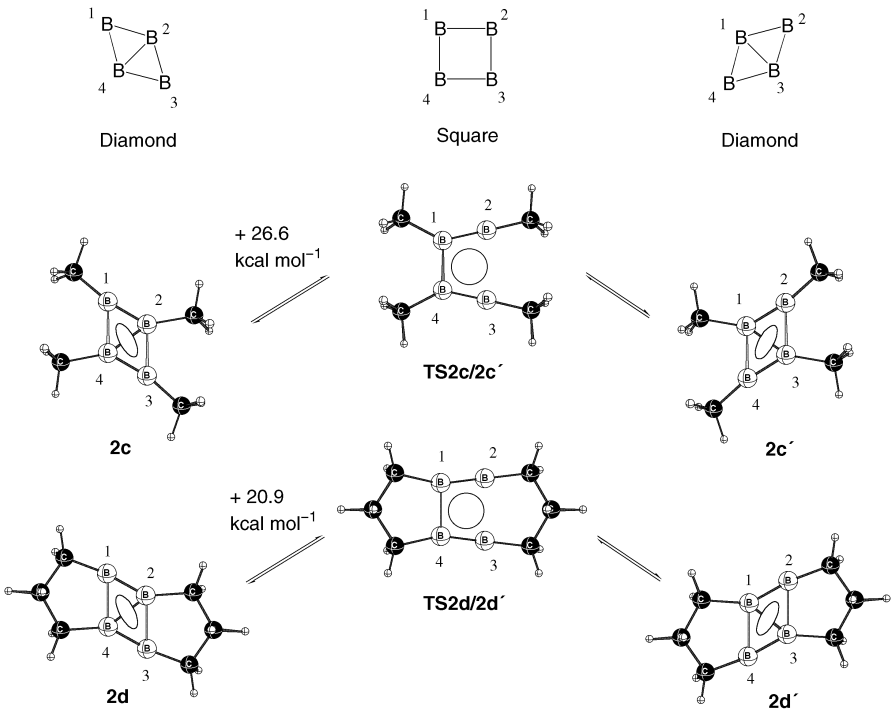

Scheme 4. Exchange of the short and long diagonal of diamonds. Top: By way of the diamond–square–diamond rearrangement in polyhedral boranes, carboranes, and metallaboranes.[5] Bottom: In the tetraboranes(4) **2c** and **2d**.

of 26.6 and 20.9 kcal mol^{-1}, respectively, and transition states **TS2c/2c′** and **TS2d/2d′** (Scheme 4), whose B_4 skeletons are strongly distorted as compared to the square of the dsd rearrangement.

According to natural bond orbital (NBO) analyses the transition states **TS2c/2c′** and **TS2d/2d′**, as well as the ground states **2c** and **2d**, are each characterized by six electrons for the σ skeleton and two cyclically delocalized π electrons. The topomerizations of **2c** and **2d**—and thus also that of **2b**—therefore occur with retention of the aromaticity. A square transition state is prohibited due to the crossing of π and σ molecular orbitals.

Received: September 2, 2002 [Z50092]

[1] T. Davan, J. A. Morrison, *J. Chem. Soc. Chem. Commun.* **1981**, 250; T. Mennekes, P. Paetzold, R. Boese, D. Bläser, *Angew. Chem.* **1991**, *103*, 199; *Angew. Chem. Int. Ed. Engl.* **1991**, *30*, 173; D. Hnyk, *Polyhedron* **1997**, *16*, 603; A. Neu, T. Mennekes, P. Paetzold, U. Englert, M. Hofmann, P. von R. Schleyer, *Inorg. Chim. Acta* **1999**, *289*, 58.

[2] Tetramesityltetraborane(4): H. Nöth, personal communication; W. Ponikwar, Dissertation, Universität München, **2000**.

[3] A. Maier, M. Hofmann, H. Pritzkow, W. Siebert, *Angew. Chem.* **2002**, *114*, 1600; *Angew. Chem. Int. Ed.* **2002**, *41*, 1529.

[4] All geometries were optimized by employing the B3LYP hybrid functional together with the 6-31G(d) basis set. Relative energies are based on energy computations with 6-311+G(d,p) and are corrected for zero-point energies. a) M. J. Frisch, G. W. Trucks, H. B. Schlegel, G. E. Scuseria, M. A. Robb, J. R. Cheeseman, V. G. Zakrzewski, J. A. Montgomery, R. E. Stratmann, J. C. Burant, S. Dapprich, J. M. Millam, A. D. Daniels, K. N. Kudin, M. C. Strain, O. Farkas, J. Tomasi, V. Barone, M. Cossi, R. Cammi, B. Mennucci, C. Pomelli, C. Adamo, S. Clifford, J. Ochterski, G. A. Petersson, P. Y. Ayala, Q. Cui, K. Morokuma, D. K. Malick, A. D. Rabuck, K. Raghavachari, J. B. Foresman, J. Cioslowski, J. V. Ortiz, B. B. Stefanov, G. Liu, A. Liashenko, P. Piskorz, I. Komaromi, R. Gomperts, R. L. Martin, D. J. Fox, T. Keith, M. A. Al-Laham, C. Y. Peng, A. Nanayakkara, C. Gonzalez, M. Challacombe, P. M. W. Gill, B. G. Johnson, W. Chen, M. W. Wong, J. L. Andres, M. Head-Gordon, E. S. Replogle, J. A. Pople, Gaussian 98 (Revision A.7), Gaussian Inc., Pittsburgh, PA, **1998**; b) A. D. Becke, *J. Chem. Phys.* **1993**, *98*, 1372; A. D. Becke, *J. Chem. Phys.* **1993**, *98*, 5648; c) C. Lee, W. Yang, R. G. Parr, *Phys. Rev. B* **1988**, *37*, 785.

[5] W. N. Lipscomb, *Science* **1966**, *153*, 373; S. Wu, M. Jones, Jr., *J. Am. Chem. Soc.* **1989**, *111*, 5373, and references therein; A. J. Welch, A. S. Weller, *J. Chem. Soc. Dalton Trans.* **1997**, 1205, and references therein; R. B. King, *Inorg. Chem.* **1999**, *38*, 5151, and references therein.

[6] C. Präsang, M. Hofmann, G. Geiseler, W. Massa, A. Berndt, *Angew. Chem.* **2002**, *114*, 1597; *Angew. Chem. Int. Ed.* **2002**, *41*, 1526.

[7] C. Präsang, A. Mlodzianowska, Y. Sahin, M. Hofmann, G. Geiseler, W. Massa, A. Berndt, *Angew. Chem.* **2002**, *114*, 3529; *Angew. Chem. Int. Ed.* **2002**, *41*, 3380.

[8] Crystal structure analyses: **2b**: A pale yellow crystal ($0.50\times0.05\times0.05$ mm) was measured at 193 K on an IPDS area detector system (Stoe) with $Mo_{K\alpha}$ radiation. $C_{24}H_{60}B_4Si_6$, orthorhombic, space group *Pbcn*, $Z=4$, $a=1914.3(1)$, $b=1451.0(1)$, $c=1335.7(1)$ pm, $V=3710.1(4)\times10^{-30}$ m^3, $\rho_{calcd}=1.003$ Mg m^{-3}, 20960 reflections up to $\theta=25.94°$, 3613 independent ($R_{int}=0.1105$), 2206 with $I>2\sigma(I)$. The structure was solved by direct methods and refined against F^2 with full matrix. The hydrogen atoms of the $SiMe_3$ groups were refined according to a riding model, the remainder were refined free with isotropic displacement factors; $wR_2=0.0825$ for all reflections, $R=0.0383$ for the observed. **3b**: Under similar conditions a colorless crystal ($0.40\times0.15\times0.15$ mm) was measured. $C_{24}H_{63}B_5Si_6$, orthorhombic, space group *Pbcn*, $Z=4$, $a=1993.1(1)$, $b=1425.2(1)$, $c=1336.8(1)$ pm, $V=3797.3(4)\times10^{-30}$ m^3, $\rho_{calcd}=1.005$ Mg m^{-3}, 20957 reflections up to $\theta=25.96°$, 3675 independent ($R_{int}=0.0801$), 2258 with $I>2\sigma(I)$. The structure was treated analogously to that of **2b**. The hydrogen atoms H1–H6 were refined freely; $wR_2=0.0680$ for all reflections and $R=0.0341$ for the observed. CCDC-192460 (**2b**) and CCDC-192459 (**3b**) contain the supplementary crystallographic data for this paper. These data can be obtained free of charge via www.ccdc.can.ac.uk/conts/retrieving.html (or from the Cambridge Crystallographic Center, 12 Union Road, Cambridge CB21EZ, UK; Fax: (+44) 1223-336033; or deposit@ccdc.cam.ac.uk).

[9] The neutral *closo*-borane $B_4tBu_4H_2$ has been characterized unambiguously by spectroscopy and by computations on model compounds, in addition, its deprotonated form has been structurally characterized.[10]

[10] A. Neu, T. Mennekes, U. Englert, P. Paetzold, M. Hofmann, P. von R. Schleyer, *Angew. Chem.* **1997**, *109*, 2211; *Angew. Chem. Int. Ed. Engl.* **1997**, *36*, 2117.
[11] The *closo* structure of a trigonal bipyramid was computed for $B_5H_5^{2-}$, the doubly deprotonated form of B_5H_7.[12] Our calculations for $B_5H_6^-$ give a distorted trigonal bipyramid. Evidently, the presence of two additional protons is the reason for the opening of the *closo* form, which is expected according to the rules, to the *nido* form. For singly or doubly deprotonated **3c**, relative energies of $+7.7$ and $+19.0$ kcal mol^{-1}, respectively, were computed for the *nido* structure in comparison with the *closo* structure.
[12] M. McKee, Z.-X. Wang, P. von R. Schleyer, *J. Am. Chem. Soc.* **2000**, *122*, 4781, and references therein; S. Kalvoda, B. Paulus, M. Dolg, H. Stoll, H.-J. Werner, *Phys. Chem. Chem. Phys.* **2001**, *3*, 514.
[13] R. Greatrex, N. N. Greenwood, D. H. Rankin, H. E. Robertson, *Polyhedron* **1987**, *6*, 1849, and references therein.
[14] P. M. Tucker, T. Onak, J. B. Leach, *Inorg. Chem.* **1970**, *9*, 1430.
[15] Computations[4] reveal that tetramethyltetraborane(4) in the distorted form **2c** is only about 3.7 kcal mol^{-1} lower in energy than a regular form with C_{2v} symmetry, which, however, corresponds to a fifth-order saddle point.

 © 2003 Wiley-VCH Verlag GmbH & Co. KGaA, Weinheim 1433-7851/03/4209-1052 $ 20.00+.50/0

Fluoroacylboron Complexes

The Fluoroacyltris(trifluoromethyl)borate Ion, $[(CF_3)_3BC(O)F]^-$, a Fluoroacylboron Complex**

Maik Finze, Eduard Bernhardt, Helge Willner, and Christian W. Lehmann**

Although numerous acyl fluorides are known in organic chemistry[1] no analogous isoelectronic boron compounds have been described to date. This is surprising since acyl fluorides of many nonmetals, such as hydrogen,[2] nitrogen,[3] sulfur,[4], oxygen,[4,5] and halogens[6] exist. Whereas there are no examples of fluoroacyl complexes of main-group metals, a number of analogous coordination compounds of transition metals are known: $[Ir(CO)_2F\{C(O)F\}(PEt_3)]^+$,[7] $[Ir(CO)_5\{C(O)F\}]^{2+}$,[8] $[MF\{C(O)F\}(CO)_2(PPh_3)_2]$ (M = Ru, Os).[9]

Recently we reported on carbonyltris(trifluoromethyl)borane, $(CF_3)_3BCO$.[10,11] This reactive carbonyl compound is an ideal building block for the insertion of the $(CF_3)_3B$ group into a number of different molecules. Thus, this enables the generation of weakly coordinating anions in which in comparison to the tetrakis(trifluoromethyl)borate ion, $[B(CF_3)_4]^-$,[12] a trifluoromethyl ligand is replaced by another ligand. The fluoroacyltris(trifluoromethyl)borate ion, $[(CF_3)_3BC(O)F]^-$, described herein is the first example of a boron acyl fluoride; moreover, it is a better substrate than $(CF_3)_3BCO$ in a number of different chemical reactions since it is more stable and easier to handle.

$K[(CF_3)_3BC(O)F]$ and $Cs[(CF_3)_3BC(O)F]$ are obtained by the reaction of $(CF_3)_3BCO$ with KF and CsF, respectively, in liquid SO_2 [Eq. (1)] as white solids, which in the absence of

$$(CF_3)_3BCO + MF \xrightarrow{SO_{2(l)}} M[(CF_3)_3BC(O)F] \quad (1)$$

moisture are stable up to 130 °C and 140 °C, respectively (differential scanning calorimetry).

The fluoroacyltris(trifluoromethyl)borate ion is one of the possible intermediates in the acid hydrolysis of $[B(CF_3)_4]^-$ to $(CF_3)_3BCO$ [Eq. (2)].

$$[B(CF_3)_4]^-_{(solv)} + H_3O^+ \xrightarrow{25\,^\circ C,\ conc.\ H_2SO_4} (CF_3)_3BCO_{(g)} + 3\,HF_{(solv)} \quad (2)$$

The synthesis described here is the first step of the reverse reaction, the fluorination of $(CF_3)_3BCO$ to $[B(CF_3)_4]^-$.

Except for the oxygen atom all atoms in $[(CF_3)_3BC(O)F]^-$ may be investigated by NMR spectroscopy. Since both ^{11}B and ^{10}B exhibit a quadrupole moment, broad signals are usually observed in ^{11}B NMR spectra.[13,14] In the case of $[(CF_3)_3BC(O)F]^-$, however, the observed spectra display unusual sharp signals (see Table S1 in the Supporting Information), which can be explained by a relatively small electric field gradient at the central B atom.[15]

The ^{19}F NMR spectrum of the $[(CF_3)_3BC(O)F]^-$ ion (Figure 1) shows two signals at $\delta = 78.3$ and -61.2 ppm with an intensity ratio of 1:9. The signal at the lower frequency is in

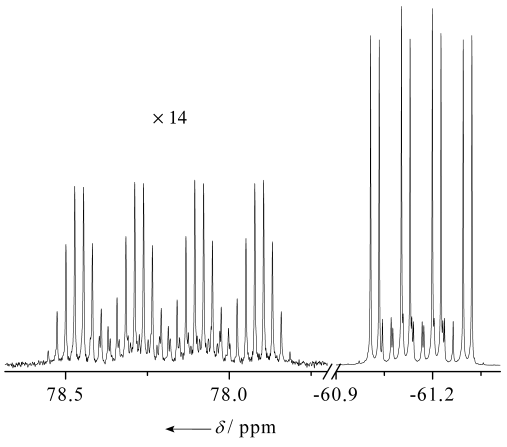

Figure 1. ^{19}F NMR spectrum of $[(CF_3)_3BC(O)F]^-$ in CD_3CN (the signal set at $\delta = 78.2$ ppm is amplified by a factor of 14).

[*] Prof. Dr. H. Willner, Dipl.-Chem. M. Finze, Dr. E. Bernhardt
Fakultät 4, Anorganische Chemie
Gerhard-Mercator-Universität Duisburg
Lotharstrasse 1, 47048 Duisburg (Germany)
Fax: (+49) 203-379-2231
E-mail: willner@uni-duisburg.de
Dr. C. W. Lehmann
Max-Planck-Institut für Kohlenforschung
Kaiser-Wilhelm-Platz 1, 45470 Mülheim an der Ruhr (Germany)
Fax: (+49) 208-306-2989
E-mail: lehmann@mpi-muelheim.mpg.de

[**] This work was supported by the Deutsche Forschungsgemeinschaft, the Fonds der Chemischen Industrie, and Merck KGaA, Darmstadt.

Supporting information for this article is available on the WWW under http://www.angewandte.org or from the author.

 © 2003 Wiley-VCH Verlag GmbH & Co. KGaA, Weinheim 1433-7851/03/4209-1052 $ 20.00+.50/0

the region typical for CF_3 groups (Table 1). The ^{19}F NMR shift of acyl fluorides, RC(O)F, is highly dependent upon the substituent. Thus, values between $\delta = -50$ and $+50$ ppm for FC(O) groups attached to nonmetal atoms[17] and values greater than $\delta = +100$ ppm for transition-metal–FC(O) complexes are typical (Table 2). The measured chemical shifts of the boron complex lie between those of fluoroacyl transition-metal complexes and nonmetal acyl fluorides. The assignment of the signals is confirmed by the observed coupling patterns. The ^{19}F nuclei couple with the ^{11}B nucleus (quartets with the same relative intensities for the four components), whereby the respective coupling constants are derived from the ^{11}B NMR spectrum in Figure 2. The ^4J coupling of the F atom of the acyl ligand with the F atoms of the CF_3 groups is 7.6 Hz and is thus of the same order of magnitude as that in $[B(CF_3)_3(^{13}CF_3)]^-$ (Table 1).[12]

The ^{11}B NMR signal of $[(CF_3)_3BC(O)F]^-$ (Figure 2) is split into a doublet of decets through the coupling of the F atom of the acyl ligand and the CF_3 groups. The ^{11}B NMR shift is similar to those of other borate complexes with three CF_3 ligands (Table 1).[10,12]

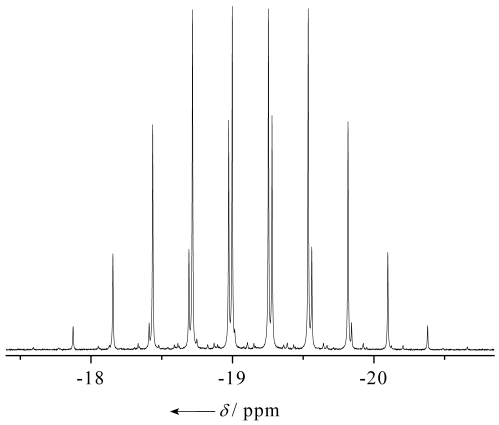

Figure 2. ^{11}B NMR spectrum of $[(CF_3)_3BC(O)F]^-$ in CD_3CN.

The ^{13}C NMR spectrum of $[(CF_3)_3BC(O)F]^-$ in Figure 3 shows two signals at $\delta = 173.7$ and 132.8 ppm with a relative intensity ratio of 1:3. The chemical shift of the signal at higher frequency is similar to those of carbonyl ligands in tris(trifluoromethyl)boron derivatives and to those of other fluoroacyl groups (Tables 1 and 2).[7,9,10,17] The coupling pattern shows the interaction of the acyl C atom with the directly bonded F atom and the central B atom as well as the ^3J coupling with the F atoms of the CF_3 groups. The position and the coupling pattern of the ^{13}C NMR signal of the CF_3 groups is comparable to those of similar compounds (Table 1).[10,12] However, in contrast to the ^{13}C signal of the fluoroacyl ligand the $^3J(^{13}C,^{19}F)$ coupling is not resolved.

The IR and Raman spectra of $K[(CF_3)_3BC(O)F]$ shown in Figure 4 confirm the formation of the fluoracyl complex as shown in Equation (1). The band at 1829 cm^{-1} lies in a region that is typical of CO vibrations of fluoracyl

Table 1: NMR data of $[(CF_3)_3BC(O)F]^-$ and similar compounds.[a,b]

Parameter	$[(CF_3)_3BC(O)F]^-$	$(CF_3)_3BCO$[c]	$[(CF_3)_3BC(O)OH]^-$	$[B(CF_3)_4]^-$	$[(CF_3)_3BF]^-$
$\delta(^{11}B)$	−19.1	−17.9	−18.9	−18.9	−7.1
$\delta(^{13}C)$ (CF_3)	132.8	126.2	133.9	132.9	132.6
$\delta(^{13}C)$ (C(O))	173.7	159.8	186.4	–	–
$\delta(^{19}F)$ (CF_3)	−61.2	−58.7	−60.3	−61.6	−68.8
$\delta(^{19}F)$ (C(O)F)	78.3	–	–	–	–
$^1J(^{11}B,^{13}CF_3)$	74.6	80 ± 5	72.8	73.4	80.0
$^1J(^{11}B,^{13}C(O))$	73.1	30 ± 5	68.2	–	–
$^1J(^{13}CF_3,C^{19}F_3)$	303.9	298 ± 3	305.5	304.3	309.4
$^1J(^{13}C(O)F,C(O)^{19}F)$	398.0	–	–	–	–
$^2J(^{11}B,C^{19}F_3)$	27.1	36 ± 2	25.8	25.9	28.3
$^2J(^{11}B,C(O)^{19}F)$	51.7	–	–	–	–
$^3J(^{13}CF_3,^{12}C^{19}F_3)$	4.0	n.o.	4.0	3.9	n.o.
$^3J(^{13}CF_3,^{12}C(O)^{19}F)$	n.o.	–	–	–	–
$^3J(^{13}C(O),^{12}C^{19}F_3)$	4.0	n.o.	3.5	–	–
$^4J(^{12}C^{19}F_3,^{13}C^{19}F_3)$	6.3	n.o.	n.o.	5.8	n.o.
$^4J(^{12}C^{19}F_3,^{12}C(O)^{19}F)$	7.6	–	–	–	–
ref.	this work	[10,11]	[10]	[12]	[12,16]

[a] J in Hz, δ in ppm. [b] Unless otherwise stated the NMR spectra were measured in CD_3CN. [c] Measured in CD_2Cl_2. [d] n.o. = not observed.

Table 2: Characteristic data of selected fluoroacyl compounds.

Compound	$\tilde{\nu}$ [cm^{-1}] $\nu_{(CO)}$	$\tilde{\nu}$ [cm^{-1}] $\nu_{(CF)}$	$\tilde{\nu}$ [cm^{-1}] $\delta_{(COF)}$	$\delta(^{19}F)$ [ppm] (FCO)	$\delta(^{19}F)$ [ppm] (CF_3)	$^4J(^{19}F,^{19}F)$ [Hz] (CF_3/FCO)	$\delta(^{13}C)$ [ppm] (FCO)	Ref.
$[(CF_3)_3B\text{-}C(O)F]^-$[a]	1829	1077	667	78.3	−61.2	7.6	173.7	this work
$(CF_3)_3C\text{-}C(O)F$	1880	990	660	42.3	−67.1	11.4	n.o.[b]	[18]
$(CF_3)_2N\text{-}C(O)F$	1883	996	n.o.	5.4	−56.5	17.0	n.o.	[19,20]
$CF_3O\text{-}C(O)F$	1900	1020	608	−13.6	−71.9	9.8	136.9	[5,21]
F-C(O)F	1943	1107[c]	626	−23.0	–	–	133.6	[17,22]
H-C(O)F	1837	1065	663	42.0	–	–	n.o.	[2,17]
$[Ir(CO)_5\{C(O)F\}]^{2+}$	1849	1049	n.o.	n.o.	–	–	n.o.	[7]
$[IrF(CO)_2\{C(O)F\}(PEt_3)_2]^+$	1815	n.o.	n.o.	132.4	–	–	154.5	[8]
$[RuF(CO)_2\{C(O)F\}(PPh_3)_2]$	n.o.	n.o.	n.o.	156	–	–	n.o.	[9]
$[OsF(CO)_2\{C(O)F\}(PPh_3)_2]$	1651	n.o.	n.o.	146	–	–	n.o.	[9]

[a] K^+ salt. [b] n.o. = not observed. [c] Mean value from $\tilde{\nu} = 1249$ cm^{-1} ($\nu_{as}(CF)$) and $\tilde{\nu} = 965$ cm^{-1} ($\nu_s(CF)$).

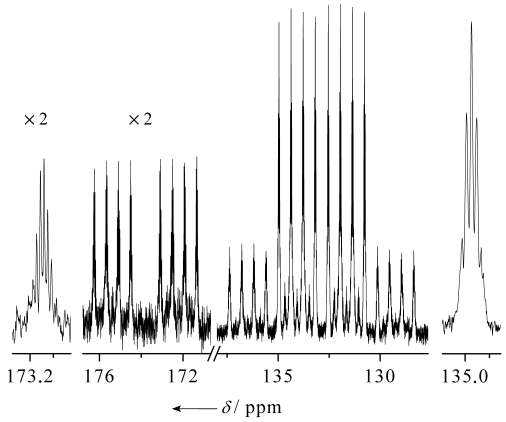

Figure 3. ^{13}C NMR spectrum of $[(CF_3)_3BC(O)F]^-$ in CD_3CN. The signal at $\delta = 173.7$ ppm is amplified by a factor of 2; the enlarged sections left and right illustrate more clearly the $^3J(^{13}C,^{19}F)$ couplings.

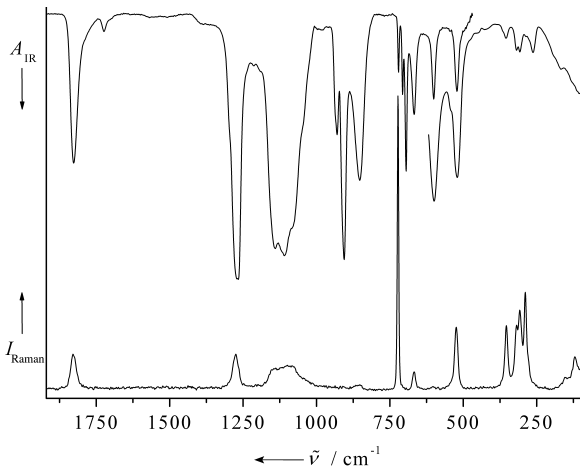

Figure 4. FT-IR and Raman spectrum of $[(CF_3)_3BC(O)F]^-$.

derivatives (Table 2).[23] The characteristic band pattern of the $B(CF_3)_3$ group lies between 1300 and 400 cm^{-1},[11,12] an additional IR band at 600 cm^{-1} can be assigned to FCO deformation. The wavenumber of the CF vibration of the fluoroacyl ligand in the potassium salt is 1077 cm^{-1} and thus is within the range (1020–1145 cm^{-1}) which is dominated by the absorption of the $\nu_{as}(CF_3)$ vibrations.

Gaussian 98 geometry and vibrational frequency calculations[24] performed for $[(CF_3)_3BC(O)F]^-$ with the B3LYP/6-311G* basis set give wavenumbers for the normal vibrations which are in good agreement with those observed (see Table S2 in the Supporting Information). At the energy minimum the anion exhibits C_1 symmetry (see Figure S1 in the Supporting Information) in which the CF_3 groups are present in a staggered conformation. Since the energy difference between the C_1 and the C_s symmetry conformations (see Figure S2 in the supporting information) is only 0.3 kJ mol^{-1} and the fluoroacyl ligand in C_1 symmetry is twisted by only 8.5° from the plane of symmetry it is understandable why a conformation with C_s symmetry is present in the crystal.

As the crystal structure shows, the O atom of the FCO group is adjacent to the CF_3 group in the plane of symmetry,

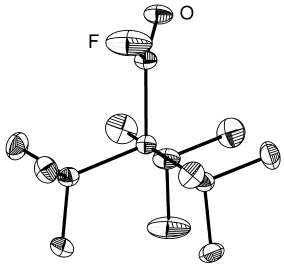

Figure 5. Structure of the $[(CF_3)_3BC(O)F]^-$ ion in $K[(CF_3)_3BC(O)F]$ (50% probability ellipsoids).

whereas the F atom of the fluoracyl ligand protrudes into the gap between the two remaining CF_3 groups (Figure 5).[25] The structural parameters agree well with the calculated values of the $[(CF_3)_3BC(O)F]^-$ ion and with the values of similar fluoracyl compounds, for example $CF_3C(O)F$,[26] $(CF_3)_2NC(O)F$,[27] F_2CO,[28] $CF_3OC(O)F$,[5] and $[IrF(CO)_2\{C(O)F\}(PEt_3)_2]^+$[7] (Table 3). The distance between the O atom and the nearest K^+ ion is 2.748(2) Å. A K^+ ion in the solid is surrounded by ten F atoms at distances of 2.694(2) to 3.196(2) Å. The distance between the F atom and the fluoracyl ligand to the K^+ ion is 2.729(3) Å. All distances indicate weak interionic interactions.[29]

The synthesis of $K[(CF_3)_3BC(O)F]$ provides one of the few examples of a nucleophilic attack of an F^- ion at a CO ligand with the formation of a fluoracyl complex. Notably, $[(CF_3)_3BF]^-$[12,16] is not formed by exchange of the CO ligand in $(CF_3)_3BCO$ by an F^- ion. The observed reaction course is attributed to two reasons: 1) the attacking F^- ion forms a relatively stable bond with the C atom of the carbonyl ligand, and 2) the B–CO bond is stabilized by association with SO_2 molecules.[10] The synthesis, and spectroscopic and thermal properties of the homologous halogen acyl complexes $[(CF_3)_3BC(O)X]^-$ (X = Cl, Br, I) will be reported elsewhere.

Table 3: Selected bond parameters of the $[(CF_3)_3BC(O)F]^-$ ion from the structure of the potassium salt and DFT calculations.

	Solid	B3LYP/6-311+G*
bond lengths [Å]		
B–C(O)F	1.621(5)	1.6291
C–O	1.208(4)	1.1862
C(O)–F	1.351(4)	1.4033
B–CF_3	1.622[a]	1.6377[a]
C–F	1.387[a]	1.3678[a]
bond angles [°]		
O-C-F	120.5(3)	116.604
C(O)-B-CF_3	109.50[a]	108.788[a]

[a] Mean values of different bond lengths and angles.

Experimental Section

Preparation of $K[(CF_3)_3BC(O)F]$: In a dry box, KF (1.50 g, 25.8 mmol) was weighed into a 50-mL round bottom flask equipped with a valve with PTFE piston (Young, London) and a magnetic stirring bar. Then in vacuo $(CF_3)_3BCO$ (4.86 g, 19.8 mmol) and dry SO_2 (30 mL) were condensed into the flask. The reaction mixture was warmed to room temperature and stirred for about 1 h. All volatile

 © 2003 Wiley-VCH Verlag GmbH & Co. KGaA, Weinheim 1433-7851/03/4209-1054 $ 20.00+.50/0

components were removed under vacuum and a white residue remained in the flask. This residue was extracted with diethyl ether (2×40 mL) and filtered under nitrogen through a Schlenk frit packed with celite. After removal of the diethyl ether under vacuum white $K[(CF_3)_3BC(O)F]$ remained. Yield: 5.33 g (17.5 mmol, 88%). Elemental analysis calcd (%) for $C_4BF_{10}KO$: C 15.87; found: C 15.81.

Preparation of $Cs[(CF_3)_3BC(O)F]$: CsF (1.08 g, 7.1 mmol) was allowed to react with $(CF_3)_3BCO$ (1.34 g, 5.5 mmol) under the same conditions as for the preparation of $K[(CF_3)_3BC(O)F]$. Yield: 1.89 g (4.8 mmol, 87%). Elemental analysis calcd (%) for $C_4BF_{10}CsO$: C 12.08; found: C 12.49.

Received: October 4, 2002 [Z50303]

[1] M. H. Rock in *Methods of Organic Chemistry (Houben-Weyl) 4th ed. 1952–, vol. E10b/Part 1* **1999**.

[2] R. F. Stratton, A. H. Nielsen, *J. Mol. Spectrosc.* **1960**, *4*, 373.

[3] D. Koschel, U. Niemann, *Gmelin Handbook of Inorganic and Organometallic Chemistry: Perfluorohalogenoorgano Compounds of Main Group Elements—Aliphatic and Aromatic Compounds of Nitrogen, vol. 8 (Supplement Vol. 5)*, Springer, Berlin, **1991**.

[4] A. Haas, *Gmelins Handbuch der anorganischen Chemie: Perfluorhalogenorgano-Verbindungen der Hauptgruppenelemente, vol. 8 (Supplement Vol. 9)*, VCH, Weinheim, **1973**.

[5] A. Hermann, F. Trautner, K. Gholivand, S. von Ahsen, E. L. Varetti, C. O. Della, H. Willner, H. Oberhammer, *Inorg. Chem.* **2001**, *40*, 3979.

[6] J. Overend, J. C. Evans, *J. Chem. Soc. Faraday Trans.* **1959**, *55*, 1817.

[7] A. J. Blake, R. W. Cockman, E. A. V. Ebsworth, J. H. Holloway, *J. Chem. Soc. Chem. Commun.* **1988**, 529.

[8] B. von Ahsen, M. Berkei, G. Henkel, H. Willner, F. Aubke, *J. Am. Chem. Soc.* **2002**, *124*, 8371.

[9] S. A. Brewer, K. S. Coleman, J. Fawcett, J. H. Holloway, E. G. Hope, D. R. Russel, P. G. Watson, *J. Chem. Soc. Dalton Trans.* **1995**, 1073.

[10] M. Finze, E. Bernhardt, A. Terheiden, M. Berkei, H. Willner, D. Christen, H. Oberhammer, F. Aubke, *J. Am. Chem. Soc.* **2002**, *124*, 15385.

[11] A. Terheiden, E. Bernhardt, H. Willner, F. Aubke, *Angew. Chem.* **2002**, *114*, 823; *Angew. Chem. Int. Ed.* **2002**, *41*, 799.

[12] E. Bernhardt, G. Henkel, H. Willner, G. Pawelke, H. Bürger, *Chem. Eur. J.* **2001**, *7*, 4696.

[13] P. S. Hubbard, *J. Chem. Phys.* **1970**, *53*, 985.

[14] T. K. Halstead, P. A. Osment, B. C. Sanctuary, J. Tagenfeldt, I. J. Lowe, *J. Magn. Reson.* **1986**, *67*, 267.

[15] A. Abragam, *Principles of Nuclear Magnetism*, Clarendon, Oxford, **1986**.

[16] D. J. Brauer, H. Bürger, Y. Chebude, G. Pawelke, *Inorg. Chem.* **1999**, *38*, 3972.

[17] S. Berger, S. Braun, H.-O. Kalinowski, *NMR-Spektroskopie von Nichtmetallen, vol. 4*, Thieme, Stuttgart, **1994**.

[18] J. L. Adcock, R. J. Lagow, *J. Am. Chem. Soc.* **1974**, *96*, 7588.

[19] H. Schachner, W. Sundermeyer, *J. Fluorine Chem.* **1981**, *18*, 259.

[20] N. V. Ignat'ev, M. Schmidt, U. Heider, A. Kucherina, P. Sartori, F. M. Helmy, *J. Fluorine Chem.* **2002**, *113*, 201.

[21] G. A. Argüello, H. Willner, F. E. Malanca, *Inorg. Chem.* **2000**, *39*, 1195.

[22] A. H. Nielsen, T. G. Burke, P. J. H. Woltz, E. A. Jones, *J. Chem. Phys.* **1952**, *20*, 596.

[23] J. Weidlein, *Schwingungsspektroskopie*, 2. ed., Thieme, Stuttgart, **1988**.

[24] Gaussian 98 (Revision A.6), M. J. Frisch, G. W. Trucks, H. B. Schlegel, G. E. Scuseria, M. A. Robb, J. R. Cheeseman, V. G. Zakrzewski, J. A. Montgomery, R. E. Stratmann, J. C. Burant, S. Dapprich, J. M. Millam, A. D. Daniels, K. N. Kudin, M. C. Strain, O. Farkas, J. Tomasi, V. Barone, M. Cossi, R. Cammi, B. Mennucci, C. Pomelli, C. Adamo, S. Clifford, J. Ochterski, G. A. Petersson, P. Y. Ayala, Q. Cui, K. Morokuma, D. K. Malick, A. D. Rabuck, K. Raghavachari, J. B. Foresman, J. Cioslowski, J. V. Ortiz, A. G. Baboul, B. B. Stefanov, G. Liu, A. Liashenko, P. Piskorz, I. Komaromi, R. Gomperts, R. L. Martin, D. J. Fox, T. Keith, M. A. Al-Laham, C. Y. Peng, A. Nanayakkara, C. Gonzalez, M. Challacombe, P. M. W. Gill, B. G. Johnson, W. Chen, M. W. Wong, J. L. Andres, M. Head-Gordon, E. S. Replogle, J. A. Pople, Gaussian, Inc., Pittsburgh, PA, **1998**.

[25] a) Crystal structure analysis of $K[(CF_3)_3BC(O)F]$: $C_4BF_{10}KO$, KappaCCD diffractometer (Bruker AXS), $Mo_{K\alpha}$ radiation ($\lambda = 0.71073$ Å, graphite monochromator), measurement temperature 100 K. Colorless crystals ($0.11 \times 0.04 \times 0.04$ mm^3), obtained from Et_2O/CH_2Cl_2, orthorhombic, space group *Pnma* (no. 62), $a = 9.1895(3)$, $b = 10.2046(5)$, $c = 9.7013(3)$ Å, $V = 909.74(6)$ Å^3, $Z = 4$, $\rho_{cald} = 2.219$ Mg m^{-3}, $\mu(Mo_{K\alpha}) = 0.726$ mm^{-1}, $F(000) = 584$, 10992 measured reflections ($3.65 < \Theta < 30.98°$). Integration and empirical absorption corrections (DENZO scalepack)[30] are applied to obtain a structure solution by direct methods and crystal structure refinement against F^2 with 1519 independent reflections (1199 independent reflections with $I > 2\sigma(I)$) and 88 variables (SHELXS-97).[31] All atoms were refined anistropically. $R_1 = 0.0514$ ($I > 2\sigma(I)$). b) CCDC-197603 ($K[(CF_3)_3BC(O)F]$) contains the supplementary crystallographic data for this paper. These data can be obtained free of charge via www.ccdc.cam.ac.uk/conts/retrieving.html (or from the Cambridge Crystallographic Data Centre, 12, Union Road, Cambridge CB2 1EZ, UK; fax: (+44) 1223-336-033; or deposit@ccdc.cam.ac.uk).

[26] J. H. M. Brake, R. A. J. Driessen, F. C. Mijlhoff, G. H. Renes, A. H. Lowrey, *J. Mol. Struct.* **1982**, *81*, 277.

[27] F. Trautner, S. Reinemann, R. Minkwitz, H. Oberhammer, *J. Am. Chem. Soc.* **2000**, *122*, 4193.

[28] J. H. Carpenter, *J. Mol. Struct.* **1974**, *50*, 182.

[29] R. D. Shannon, *Acta Crystallogr. Sect. A* **1976**, *32*, 751.

[30] Z. Otwinowski, W. Minor, *Methods Enzymol.* **1997**, *276*, 307.

[31] G. M. Sheldrick, SHELXS-97 and SHELXL-97, Program System for the Determination and Refinement of Crystal Structures, University of Göttingen, **1997**.

Pd-Catalyzed Cross-Coupling

A Versatile Catalyst for the Sonogashira Coupling of Aryl Chlorides**

*Axel Köllhofer, Thomas Pullmann, and Herbert Plenio**

Palladium-catalyzed cross-coupling reactions are extremely useful synthetic tools.[1,2] The Sonogashira reaction[3] is applied for the coupling of terminal alkynes and aryl or vinyl halides to produce antimycotics,[4] antibiotics,[5] liquid crystals, polymers, and optical or electronic materials.[6] Whereas aryl bromides and aryl iodides are well known to undergo this reaction in the presence of suitable catalysts, there is no efficient protocol for the Sonogashira coupling of alkynes with aryl chlorides, which would be the most attractive starting materials because of the wide variety of cheaply available derivatives. There are a few examples of Sonogashira reactions with alkynes and activated aryl chlorides,[7,8] but even under microwave irradiation only poor yields are observed.[9] Alternatively, there is a less frequently used variation of a Negishi-type coupling, which requires the synthesis of zinc(II) acetylides[10] or a Suzuki-type coupling that utilizes alkynyltrifluoroborates.[11] A significant step forward in the development of the Sonogashira reaction was achieved by Eberhard et al. who treated various aryl chlorides with phenylacetylene in the presence of a palladium phosphonito pincer catalyst (5 mol%) and $ZnCl_2$ (10–100 mol%) over 24 h at 160 °C to produce the coupling product in good yields in the case of activated chloroarenes.[12] Apart from this work the state-of-the-art catalysts are based on the system $(PhCN)_2PdCl_2$/P*t*Bu_3/CuI, which was described by Buchwald, Fu et al.[13] as well as by Herrmann and Böhm,[14] which only allows room-temperature coupling of aryl bromides with acetylenes.

The catalytically active species in various coupling reactions appears to be a $(PR_3)Pd$ complex.[15] Consequently, the most active catalyst should be the one that generates the highest concentration of this species during catalysis. Pd^{II} salts or Pd^0 complexes, such as $[Pd_2(dba)_3]$ (dba = dibenzylideneacetone), serve as the source of palladium. A disadvantage of Pd^0 complexes is that the ligands needed to stabilize Pd^0 invariably have coordinating properties, which hinders the formation of the $(PR_3)Pd$ species. A diminished catalytic activity in Suzuki coupling reactions by using ligands such as dba has been observed by Beller et al.[16] Using a Pd^{II} salt is a feasible alternative, even though this requires an additional preactivation step to generate the active Pd^0 species. $(PhCN)_2PdCl_2$, $Pd(OAc)_2$, and $(MeCN)_2PdCl_2$ are commonly used as Pd^{II} sources, while reagents such as amines, phosphanes, and acetates serve as reducing agents.[3b] However, it should be noted that all of the aforementioned Pd^{II} salts still have coordinating ligands that might interfere with the formation of the active species. We reasoned that a more active catalyst should be formed when Pd^{II} sources were used that contained ligands suitable primarily for the stabilization of Pd^{II} and not of Pd^0. Ideal compounds in this respect appear to be $Na_2[PdCl_4]$ or $PdCl_2$, since the hard Cl^- ion is not expected to show high affinity towards the soft Pd^0 center. Furthermore, the solvent for the coupling reaction should not possess donor groups other than hard oxygen atoms, to avoid blocking the active Pd^0 species.

We describe here a high-yielding catalyst based on $Na_2[PdCl_4]/PR_3$/CuI ($PR_3 = (1\text{-Ad})_2PBn$, P*t*$Bu_3$) for the Sonogashira coupling of various aryl chlorides and alkynes. An important component of such a catalyst is a sterically demanding and electron-rich phosphane ligand at the palladium center. After screening different phosphanes (Table 1), we selected $(1\text{-Ad})_2PBn$ (1-Ad = 1-adamantyl, Bn = benzyl) and P*t*Bu_3 for more detailed studies.

Table 1: Screening of phosphane ligands.[a]

Phosphane	Yield (3 h) [%][b]	Yield (16 h) [%][b]
$(1\text{-Ad})_2PBn$[c]	>95	quantitative
P*t*Bu_3[c]	>95	quantitative
$(1\text{-Ad})_2P$*t*Bu[c]	25	80
$(1\text{-Ad})_2PPh$[c]	<5	<5
tBu_2PBn[c]	20	65
$(1\text{-Ad})_2P$*n*Bu[c]	25	75
$(1\text{-Ad})_2PCH_2Fc$[c]	<5	<5
$(1\text{-Ad})_2PBn$[d]	–	80
P*t*Bu_3[d]	–	85

[a] Reaction conditions: 2 mol% $Na_2[PdCl_4]$, 4 mol% PR_3, 1.5 mol% CuI, DMSO, Na_2CO_3, 100 °C. [b] Yields determined by GC. [c] Coupling of 4-chloroacetophenone and PhCCH. [d] Coupling of 4-chloroanisole and PhCCH.

Adamantyl-substituted phosphane ligands have been used successfully by Beller et al.[17] and Hartwig et al.[18] for various coupling reactions. The respective phosphonium salts $(1\text{-Ad})_2PBn{\cdot}HBr$ and P*t*$Bu_3{\cdot}HBF_4$ are ideal ligand precursors since they are insensitive towards oxidation and are deprotonated at the beginning of the coupling reactions.[19] One equivalent of $Na_2[PdCl_4]$ and two equivalents of phosphane are used for the coupling reaction (Scheme 1). The choice of the base is decisive for the success of the reactions described here. Whereas amines such as $HNiPr_2$ work well for the coupling of alkynes and aryl bromides at room temperature,[13] they do not function in corresponding reactions with

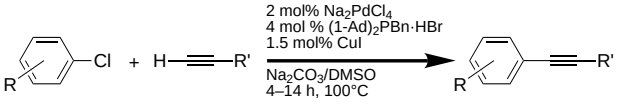

Scheme 1. Sonogashira coupling of aryl chlorides with alkynes.

[*] Prof. Dr. H. Plenio, Dipl.-Chem. A. Köllhofer, T. Pullmann
Institut für Anorganische und Physikalische Chemie
Technische Universität Darmstadt
Petersenstrasse 18, 64287 Darmstadt (Germany)
Fax: (+49) 6151-16-6040
E-mail: plenio@tu-darmstadt.de

[**] This work was supported by the Deutsche Forschungsgemeinschaft and the TU Darmstadt.

 © 2003 Wiley-VCH Verlag GmbH & Co. KGaA, Weinheim 1433-7851/03/4209-1056 $ 20.00+.50/0

aryl chlorides. In our experiments, Na_2CO_3 appears to be the best base, while Cs_2CO_3 is less efficient. Furthermore, the nature of the Pd source is critical for the success of the coupling reaction. The best results were achieved with $Na_2[PdCl_4]$, whereas $(PhCN)_2PdCl_2$ or $Pd(OAc)_2$ are unsuitable. Although, the Pd/Cu ratio is not critical, the reaction slows considerably without a certain amount of CuI. Temperatures of 100 °C are sufficient for the coupling of activated aryl chlorides (Table 2, entries 1–9). The best solvents are DMSO and toluene; the latter is preferable due to its lower boiling point and easier workup. Efficient reactions of deactivated substrates (Table 2, entries 10–21) in DMSO or in xylene require a reaction temperature of 120 °C. Remarkably, sterically hindered aryl chlorides such as 1-chloro-2-methylbenzene (entry 19) yield the coupling product in excellent yields, while even 2-chloro-1,3-dimethylbenzene can be synthesized in 62 % yield. Interestingly, all coupling reactions are characterized by an induction period of between 5–20 min after which the reaction mixture changes from colorless to dark red. In conclusion, we have demonstrated an efficient catalyst system, $Na_2[PdCl_4]/PR_3$/CuI (1:2:0.75; PR_3 = (1-Ad)$_2$PBn, P*t*Bu$_3$), for the Sonogashira coupling of aryl chlorides in excellent yields, which is almost one order of magnitude more active than the previous best system.[12] It is worth noting that all reagents, except for the solvents, were used as received without any purification.

Table 2: Sonogashira coupling of aryl chlorides RC_6H_4Cl with alkynes R′C≡CH (see Scheme 1).[a]

Entry	R	R′	*T* [°C]	*t* [h]	Yield [%][b]
1	4-CH_3CO	Ph	100	4	90
2	4-CH_3CO	*n*-C_6H_{13}	100	10	92
3	4-CH_3CO	*i*Pr$_3$Si	100	4	91
4	4-NO_2	Ph	100	4	96
5	4-NO_2	*n*-C_6H_{13}	100	10	93
6	4-NO_2	*i*Pr$_3$Si	100	4	89
7	4-CF_3	Ph	100	6	93
8	4-CF_3	*n*-C_6H_{13}	100	10	93
9	4-CF_3	*i*Pr$_3$Si	100	6	89
10	H	Ph	120	14	76 (83)
11	H	*n*-C_6H_{13}	120	14	85 (84)
12	H	*i*Pr$_3$Si	120	14	75 (77)
13	4-MeO	Ph	120	14	75 (81)
14	4-MeO	*n*-C_6H_{13}	120	14	54 (78)
15	4-MeO	*i*Pr$_3$Si	120	14	56 (84)
16	4-Me	*n*-C_6H_{13}	120	14	79 (83)
17	4-Me	Ph	120	14	70 (78)
18	4-Me	*i*Pr$_3$Si	120	14	71 (79)
19	2-Me	Ph	120	14	(80)
20	1,3-Me_2	Ph	120	14	(62)

[a] Reaction conditions: 2 mol % $Na_2[PdCl_4]$, 4 mol % PR_3, 1.5 mol % CuI, toluene or xylene, Na_2CO_3. [b] Yields of isolated product after chromatographic purification (for PR_3 = (1-Ad)$_2$PBn); values in parentheses correspond to yields for reactions with PR_3 = P*t*Bu$_3$.

Experimental Section

General procedure for the Sonogashira coupling of alkynes and aryl chlorides: To a thoroughly degassed slurry of Na_2CO_3 (230 mg, 2.1 mmol) in toluene (or DMSO or xylene) (3 mL) were added $Na_2[PdCl_4]$ (8.8 mg, 30 μmol, 2 mol %), (1-Ad)$_2$PBn·HBr (28 mg, 60 μmol), CuI (4.4 mg, 23 μmol, 1.5 mol %), the chloroarene (1.5 mmol), and the alkyne (2 mmol). The mixture was heated to the respective reaction temperature under vigorous stirring. After completion of the reaction (GC control) and cooling to room temperature, the volatiles (toluene or 1,3-xylene) were removed in vacuo. When DMSO was used as the solvent, the reaction mixture was poured into a separating funnel containing water (20 mL) and diethyl ether (30 mL). The organic layer was washed with water (20 mL), dried over $MgSO_4$, and evaporated to dryness. The crude products were purified by chromatography on silica to give the yields in Table 2. NMR spectroscopic data of the coupling products are identical to those reported in the literature.

Received: November 8, 2002 [Z50513]

[1] *Metal-catalyzed Cross-Coupling Reactions* (Eds.: F. Diederich, P. J. Stang), Wiley-VCH, Weinheim, **1998**.

[2] a) N. J. Whitcombe, K. K. Hii, S. E. Gibson, *Tetrahedron* **2001**, *57*, 7449; b) H. Gröger, *J. Prakt. Chem.* **2000**, *342*, 334; c) M. Jørgensen, S. Lee, X. Liu, J. P. Wolkowski, J. F. Hartwig, *J. Am. Chem. Soc.* **2002**, *124*, 12557; d) N. Kataoka, Q. Shelby, J. P. Stambuli, J. F. Hartwig, *J. Org. Chem.* **2002**, *67*, 5553; e) W. Mägerlein, A. F. Indolese, M. Beller, *Angew. Chem.* **2001**, *113*, 2940; *Angew. Chem. Int. Ed.* **2001**, *40*, 2856; f) A. Krotz, F. Vollmüller, G. Stark, M. Beller, *Chem. Commun.* **2001**, 195; g) J. Yin, M. P. Rainka, X.-X. Zhang, S. L. Buchwald, *J. Am. Chem. Soc.* **2001**, *123*, 1162; h) A. Schnyder, A. F. Indolese, M. Studer, H.-U. Blaser, *Angew. Chem.* **2002**, *114*, 3820; *Angew. Chem. Int. Ed.* **2002**, *41*, 3668; i) L. Botella, C. Nájera, *Angew. Chem.* **2002**, *114*, 187; *Angew. Chem. Int. Ed.* **2002**, *41*, 179; j) A. C. Hillier, G. A. Grassa, M. S. Viciu, H. M. Lee, C. Yang, S. P. Nolan, *J. Organomet. Chem.* **2002**, *653*, 69; k) A. Zapf, M. Beller, *Top. Catal.* **2002**, *19*, 101; l) J. Dupont, M. Pfeffer, J. Spencer, *Eur. J. Inorg. Chem.* **2001**, 1917.

[3] a) K. Sonogashira, Y. Tohda, N. Hagihara, *Tetrahedron Lett.* **1975**, 4467; b) I. B. Champbell in *Organocopper Reagents*, (Ed.: R. J. K Taylor), Oxford University Press, Oxford, **1994,** pp. 217..

[4] U. Beutler, J. Mazacek, G. Penn, B. Schenkel, D. Wasmuth, *Chimia* **1996**, *50*, 154.

[5] J. W. Grissom, G. U. Gunawardena, D. Klingenberg, D. Huang, *Tetrahedron* **1996**, *52*, 6453.

[6] a) L. Anastasia, E. Negishi, *Org. Lett.* **2001**, *3*, 3111; b) C. Yang, S. P. Nolan, *Organometallics* **2002**, *21*, 1020; c) H. Plenio, J. Hermann, A. Sehring, *Chem. Eur. J.* **2000**, *6*, 1820; d) M. Alami, B. Crousse, F. Ferri, *J. Organomet. Chem.* **2001**, *624*, 114; e) R. A. Batey, M. Shen, A. J. Lough, *Org. Lett.* **2002**, *4*, 1411.

[7] G. C. Fu, A. Littke, *Angew. Chem.* **2002**, *114*, 4350; *Angew. Chem. Int. Ed.* **2002**, *41*, 4176.

[8] a) M. Ansorge, T. J. J. Müller, *J. Organomet. Chem.* **1999**, *585*, 174; b) Y. Nishihara, K. Ikegashira, K. Hirabayashi, J. Ando, A. Mori, T. Hiyama, *J. Org. Chem.* **2000**, *65*, 1780; c) M. R. Buchmeiser, T. Schareina, R. Kempe, K. Wurst, *J. Organomet. Chem.* **2001**, *634*, 39.

[9] M. Erdélyi, A. Gogoll, *J. Org. Chem.* **2001**, *66*, 4165.
[10] M. Sonoda, A. Inaba, K. Itahashi, Y. Tobe, *Org. Lett.* **2001**, *3*, 2419.
[11] G. A. Molander, B. W. Katona, F. Machrouchi, *J. Org. Chem.* **2002**, *67*, 8416.
[12] M. R. Eberhard, Z. Wang, C. M. Jensen, *Chem. Commun.* **2002**, 818.
[13] T. Hundertmark, A. F. Littke, S. L. Buchwald, G. C. Fu, *Org. Lett.* **2000**, *2*, 1729.
[14] V. P. W. Böhm, W. A. Herrmann, *Eur. J. Org. Chem.* **2000**, 3679.
[15] J. P. Stambuli, M. Bühl, J. F. Hartwig, *J. Am. Chem. Soc.* **2002**, *124*, 9346.
[16] M. G. Andreu, A. Zapf, M. Beller, *Chem. Commun.* **2000**, 2475.
[17] A. Zapf, A. Ehrentraut, M. Beller, *Angew. Chem.* **2000**, *112*, 4315; *Angew. Chem. Int. Ed.* **2000**, *39*, 4153.
[18] J. P. Stambuli, S. R. Stauffer, K. H. Shaugnessy, J. Hartwig, *J. Am. Chem. Soc.* **2001**, *123*, 2677.
[19] M. R. Netherton, G. C. Fu, *Org. Lett.* **2001**, *3*, 4295.

 © 2003 Wiley-VCH Verlag GmbH & Co. KGaA, Weinheim 1433-7851/03/4209-1058 $ 20.00+.50/0

Hexacoordinate Silicates

Hydrogen-Bonded Sugar-Alcohol Trimers as Hexadentate Silicon Chelators in Aqueous Solution**

Klaus Benner, Peter Klüfers, and Martin Vogt*

Dedicated to Professor Hartmut Bärnighausen on the occasion of his 70th birthday

The transport form of silicon in silica-depositing organisms is unknown. Although Birchall has argued against any significant role for silicic acid esters derived from the carbohydrates because of their hydrolytic sensitivity in aqueous media,[1] the stability of Si-O-C linkages towards hydrolysis has been demonstrated recently for hypervalent derivatives of polyol esters.[2] Presently, two structural motifs common to carbohydrates have been recognized to support the formation of hydrolytically stable silicate ions, namely the diol function attached to a *cis*-furanoidic ring,[2a] and the *threo*-configured 1,2,3,4-tetraol moiety that is present in various sugar alcohols.[2b–d] The silica-dissolving properties of the latter have been demonstrated by means of ^{29}Si NMR spectroscopy. In the solution state, silicon is present as penta- and hexacoordinate silicate in high amounts when the aqueous solutions are highly concentrated with respect to the polyol. The *threo* specificity led Kinrade et al. to suggest that in these cases 1,4-diol functions should form seven-membered chelate rings with a central silicon atom,[2b–d] which would, however, be a rather unusual structural motif for a polyolato complex with a small central atom.

To achieve reliable information on the alditol–silicon bonding by means of crystal-structure analysis, we tried to adopt a similar crystallization technique to that which recently led to the formation of crystals of diolato silicates of the furanose type from aqueous solutions.[2a] Eventually, crystallization succeeded from strongly alkaline aqueous alditolato–silicate solutions, typically over several weeks. The main difficulty to be mastered was a marked delay in nucleation, hence often glassy material was obtained instead of crystals when evaporation proceeded too quickly in the oversaturation range. We now report the first crystal-structure determinations of alditolato silicates of D-mannitol, xylitol, and D-threitol, all of which bear a *threo*-configured C_4 chain (Scheme 1). In addition to structural work, ^{29}Si NMR spectroscopy was used to compare the stability of the various structural motifs in aqueous solution.

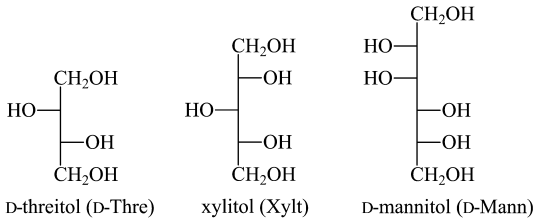

Scheme 1. Fischer projections of D-threitol, xylitol, and D-mannitol.

Of the polyols investigated, D-mannitol (coded as D-Mann in the formulae) supports silica dissolution most efficiently. Typically, fumed colloidal silica dissolves in aqueous sodium hydroxide solutions containing D-mannitol in one hour (room temperature, ultrasonic bath; molar Si:D-Mann:NaOH ratio of 1:3:3; total final silicon concentration 1.5 M). As expected, silica may be replaced by tetramethoxysilane to obtain clear solutions more rapidly. Colorless crystalline aggregates of $Na_3[\Lambda\text{-Si(D-Mann3,4H}_{-2})_3H_{-1}]\cdot 12\,H_2O$ (**1**) formed upon evaporation of these concentrated, highly alkaline solutions. Crystals of **1** have a pseudo-hexagonal habit. Attempts were made to solve the structure in hexagonal or trigonal space groups, and the inner core of the anion shown in Figure 1 could be resolved. However, the terminal hydroxymethyl functions of the mannitolato ligands, the sodium counterions, and some of the water molecules are heavily disordered (see legend to Figure 2). In contradiction to the threefold symmetry of the mannitolato-silicate, the solid-state ^{13}C magic-angle spinning (MAS) NMR spectra show 18 signals as expected for a C_1-symmetric anion with three independent mannitol ligands. The diffraction pattern of a fragment cleaved off from a larger crystal clearly showed that the hexagonal

[*] Prof. Dr. P. Klüfers, Dr. K. Benner, Dipl.-Chem. M. Vogt
Department Chemie
Ludwig-Maximilians-Universität München
Butenandtstrasse 5–13, 81377 München (Germany)
Fax: (+49) 89-2180-77407
E-mail: kluef@cup.uni-muenchen.de

[**] Polyol metal complexes, Part 41. This work was supported by the Deutsche Forschungsgemeinschaft within the framework of the program "Principles of Biomineralization" (grant Kl 624/7-1). We are indebted to Dipl.-Chem. M. Bootz (LMU Munich) for DFT calculations, and Dr. J. Senker (LMU Munich) for the ^{29}Si and ^{13}C solid-state NMR experiments.—Part 40: P. Klüfers, O. Krotz, M. Oßberger, *Eur. J. Inorg. Chem.* **2002**, *6*, 1919–1923.

 © 2003 Wiley-VCH Verlag GmbH & Co. KGaA, Weinheim 1433-7851/03/4209-1058 $ 20.00+.50/0

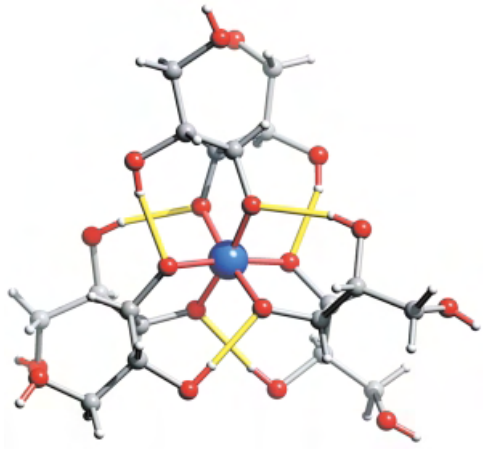

Figure 1. The Λ-configured trianion in **1**. Mean Si–O separation 1.784(2) ± 0.006 Å; mean O-C-C-O torsion angle of chelating diolato function: 26.6(3) ± 0.4°; mean O···O distance in intramolecular hydrogen bonds: 2.689(3) ± 0.027 Å.

symmetry was broken. The correct crystal system was determined as orthorhombic despite the pseudohexagonal cell parameters ($b/a = 1.726$; compared to $\sqrt{3} = 1.732$), and the structure was solved and refined considering a partial pseudomerohedral trilling with two major and one minor component.[3]

The structure of the silicate anion is shown in Figure 1. Three mannitolato ligands coordinate a central silicon atom through the oxygen atoms in the middle of the C_6 chain (O3 and O4), thus, the normal five-membered chelate rings are formed. Although the hydroxy functions of O2 and O5 do not bind to the central atom, their spatial distribution plays a crucial role. Owing to the *threo* pattern, these hydroxy groups are arranged properly to establish strong hydrogen bonds of the O–H···O$^-$ type towards ligating alkoxo functions. The enhanced coordination ability of *threo*-configured tetraol moieties stems from the formation of a hydrogen-bonded, hexadentate ligand trimer. The *threo*-configured C_4 zigzag chain made up by the atoms C2 to C5 is parallel to the C_3 axis of the anion core; in the following, this bonding mode is termed "vertical". The structure of **3** (see below) shows that the vertical mode is not the only one possible for a *threo* chain but also a "horizontal" mode with the *threo*-C_4 chain perpendicular to the pseudo-C_3 axis assures intramolecular hydrogen bonding. The stereochemistry around the central atom depends both on the vertical/horizontal orientation of the carbon chain and the chirality of the C_4 chain. D-mannitol, with its carbon atoms 2–5, provides a D-*threo* chain, which, in vertical mode, causes Λ configuration of the tris(diolato)-silicate core. In addition to intramolecular hydrogen bonding, counterion binding is another secondary interaction that supports the complex structure. Remarkably, the counterion binding is the same in all the structures reported here. Typically, two counterions are found along the (pseudo-) C_3 axis of the silicate anion, thus forming electroneutral assemblies. The dianionic silicate octahedra (SiO_6) and the coordination polyhedra of the alkali-metal counterions are linked in a face-sharing mode (Na1 and Na2 in Figure 2; further details are given in the legend). There seem to be no further stabilizing factors in the structure of **1**. In particular, the hydroxymethyl substituents with C1 and C6 support neither the ligand trimer nor counterion binding. Hence, despite a little loss in acidity, the C_2-symmetric C_4 sugar alcohol threitol appears as the prototypic ligand to provide the observed bonding pattern for the central silicon atom in **1**.

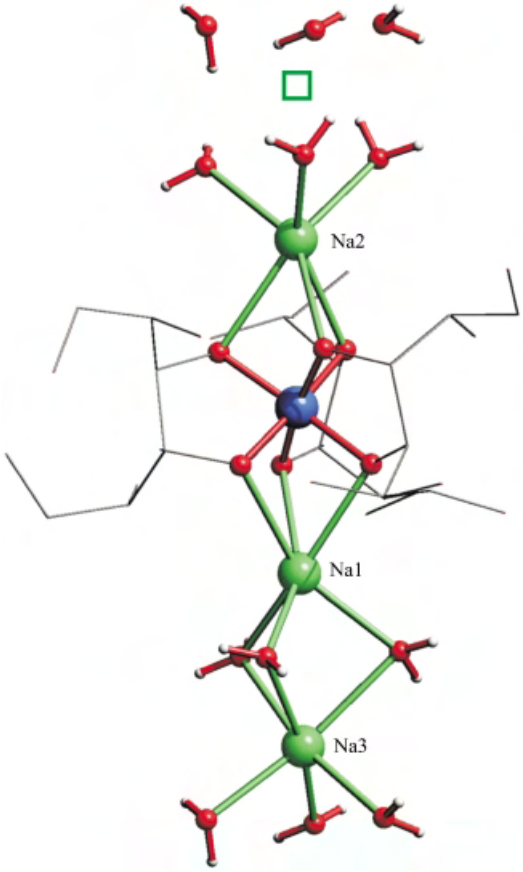

Figure 2. Electroneutral $Na_3[\Lambda\text{-Si}(\text{D-Mann3,4H}_{-2})_3\text{H}_{-1}]\cdot 9\,H_2O$ aggregates in **1**; crystallization at a high pH value results in deprotonation of one of the terminal hydroxymethyl residues of the mannitolato ligands (top right O atom in Figure 1). In the crystal, this O$^-$ group is stabilized by three hydrogen bonds, one of these being a short but asymmetric bond towards a hydroxymethyl donor (O···O distance: 2.468(2) Å). Disorder models without taking into account trilling formation show statistical occupation of the Na3 position and the unoccupied $\square(H_2O)_6$ octahedron by one sodium ion ($R_w(F^2) > 0.3$; additionally there is disorder of the terminal mannitol O atoms and no H-atom location possible). The depicted motif generates the crystal by stacking pseudo-hexagonally. An idealized stacking with statistical Na/□ distribution may be realized in the hexagonal space group $P6_322$; the actual space group can be derived according to the path $P6_322$ [*t*3]→$P2_122$ ($C222_1$) [*k*2,($^1/_2$,$^1/_2$,0)]→$P2_12_12_1$, that is, the crystals should be affected by antiphase domains (*k*2), but in particular, the massive disruption by trilling formation (*t*3) is to be expected.

To synthesize the basic structural motif of a threitolato-coordinated silicon atom, fumed silica was dissolved in aqueous alkali-metal hydroxide solution containing D-threitol (D-Thre). Crystals were obtained with cesium counterions. However, our crystallization technique did not yield a single substance. Instead, mixtures of crystalline cesium threitolato

 © 2003 Wiley-VCH Verlag GmbH & Co. KGaA, Weinheim 1433-7851/03/4209-1059 $ 20.00+.50/0

silicates were obtained on concentrating the solutions. All the crystals were hexagonal, and at least two components have been identified. Structural analysis on small, hexagonal crystals of solvent-free $Cs_2[\Lambda\text{-Si}(\text{D-Thre2,3H}_{-2})_3]$ (**2a**) revealed the threitolato silicate ions with the desired structural motif (Figure 3).[3] The Λ-configured anions occupy sites

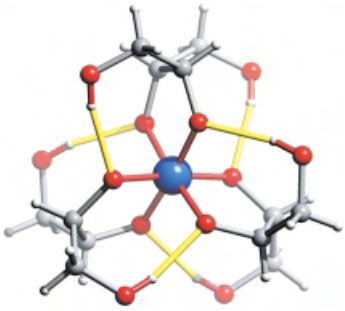

Figure 3. The D_3-symmetric dianion in **2a**. Si-O separation: 1.779(4) Å; O-C-C-O torsion angle of chelating diolato function: 17.2(6)°; intramolecular hydrogen bond: O···O 2.714(7) Å; H···O 1.91(2) Å, O···H–O 166(6)° for H–O fixed to 0.83 Å. Counterion binding resembles that of Na1 and Na2 Figure 2,.

of D_3 symmetry in space group $P6_322$. Two cesium atoms (site-symmetry C_3) support the anion structure in the same way as has been found for the Na1 and Na2 counterions in **1** (Figure 2). Compound **2a** not only is prototypical with respect to the anion structure, but also the packing of the ionic assemblies in the crystal defines the aristo type for all the structures reported here. Regarding the $Cs_2[\Lambda\text{-Si}(\text{D-Thre2,3H}_{-2})_3]$ moieties as very large spheres, hexagonal close packing (hcp) of these building blocks is found in the solid state (note that because of the chiral motif D-threitol, the space group of **2a**, $P6_322$, is a maximal subgroup of the hcp space group $P6_3/mmc$). The crystal structures of the silicates described here are not only derived from the archetypal structure of **2a**, but in particular, the crystal pathology of **1** has its origin in nature's striving to conserve the symmetry of the hexagonal close-packing in the macroscopic symmetry of the trilling.

The stability of highly symmetrical structural motifs, such as that in **1** and **2a**, may be overestimated particularly when many binding interactions, including counterion binding, can be drawn in the corresponding figures. This problem is suggested when a hydrated analogue of **2a** is inspected. The analogue was isolated as a second compound from the crystalline mixture. X-ray investigations revealed the very low quality crystals to be of a trihydrate of **2a**. Fortunately, good crystals of the isotypic rubidium homologue could be isolated. This compound $Rb_2[\Lambda\text{-Si}(\text{D-Thre2,3H}_{-2})_3]\cdot 3\,H_2O$ (**2b**) is built up from approximately C_2-symmetric threitolato silicate ions (Figure 4) that share basic structural principles with the "ideal" D_3-symmetrical motif of **2a** but with marked deviations. As with **2a**, three D-threitolato ligands in vertical mode coordinate silicon in a Λ-configured silicate. However, of the six hydrogen bonds found in the ideal pattern, only four start from threitol hydroxy groups, the remaining two are

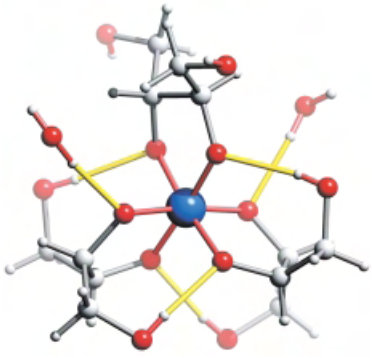

Figure 4. The dianion in **2b**. Mean separations and angles: Si-O 1.783(2) ± 0.004 Å; O-C-C-O torsion of chelating diolato functions: 21.7(3) ± 1.6°; intramolecular hydrogen bonds: O···O 2.673(3) ± 0.043 Å; hydrogen bonds from water donors to alkoxide acceptors: O···O 2.763(3) ± 0.029 Å. Counterion binding resembles that of **2a**. Crystal packing can be derived from the **2a** structure in only two steps ($P6_322 \rightarrow P6_3 \rightarrow P2_1$); note the similarity of the lattice constants of **2a** and **2b**.

from water donors. Hence, at least in highly concentrated solutions, neither the high symmetry of the silicates nor intramolecular hydrogen bonding appear to be decisive for complexation. Instead, it is the number of hydrogen bonds that is important. This finding is corroborated by investigating a third alditol: On replacement of only one of the terminal hydroxymethyl groups of D-mannitol by a hydrogen atom the achiral sugar alcohol xylitol (Xylt) is obtained, which provides either a D- or an L-*threo* chain of four adjacent C atoms (Scheme 1). At high concentrations of alkali hydroxide, fumed silica, and the pentitol, aqueous solutions are obtained. With cesium as the counterion, $Cs_2[Si(XyltH_{-2})_3]\cdot 2\,H_2O$ (**3**) crystallizes in the form of colorless racemic twins. Structural analysis reveals another variant of a hexacoordinate silicate that is supported by a total of six hydrogen bonds (Figure 5).[3]

Contrary to **1** and **2**, compound **3** is not homochiral with respect to the binding threitol moieties of the xylitol chain. Instead, the Λ-configured silicate, which is the enantiomer depicted in Figure 5, is made up from one L- and two D-threitol fragments. The latter are in vertical mode as in **1**

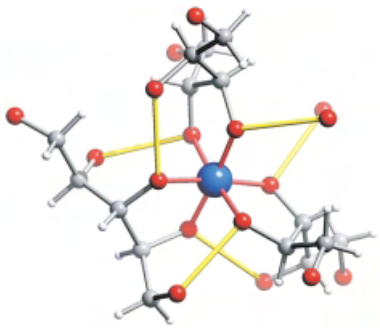

Figure 5. The dianion in **3**. The pendent hydroxymethyl group of the horizontal ligand is disordered; only one of the two forms is shown. The positions of O-bonded hydrogen atoms have not been determined. Mean Si-O distance 1.779(5) ± 0.012 Å; mean O-C-C-O torsion angle of the vertical chelating diolato functions: 4.6(8) ± 2.6°, of the horizontal function: 26.0(4)°.

 © 2003 Wiley-VCH Verlag GmbH & Co. KGaA, Weinheim 1433-7851/03/4209-1060 $ 20.00+.50/0

and **2**, the L-threitol is in the alternative horizontal bonding mode with its C_4 chain, which exhibits essentially the same zigzag conformation in both bonding modes, at right angles with respect to the pseudo C_3 axis of the anion. In contrast, the Δ-configured silicate ions in the racemic twins contain two L-(vertical) and one D-threitol (horizontal) units. The horizontal mode as the only ligand orientation is observed with larger central atoms such as chromium(III).[4] Again, in **3**, a total of six hydrogen bonds towards the six alkoxo acceptors appears to be decisive for silicon complexation whereas the presence of the ideal D_3 symmetric core is not.

In solution, the hexacoordinate species can be detected by ^{29}Si NMR spectroscopy ($\delta = -144.8, -141.0, -142.9, -143.7$ for D-mannitol, Cs-D-threitol, Rb-D-threitol, and xylitol, respectively); compare to the respective solid-state data for **1, 2a, 2b, 3**: $\delta = -141.4, -142.9, -142.0, -141.0$) and ^{13}C NMR spectroscopy at high total concentrations.[5] There are two ways to make hexacoordinate silicate the main solution species: in the method used by Kinrade et al.,[2b] the polyol concentration is made high compared to that of silicon and base; alternatively, polyol and silicon are combined approximately stoichiometrically but base is used in excess. The latter strategy lead to the formation of the crystals described herein. Starting with solutions of both kinds, dilution with water largely increases the amount of simple oxo-silicate at the expense of hypervalent species. In such experiments, a marked dependence of complex stability in the series mannitol > xylitol > threitol is observed. In fact, under the conditions described here, with D-threitol, only small amounts of hypervalent species are detected in the solution equilibria, whereas D-mannitol converts most of the silicon into the hexacoordinate silicate.[6] Under the conditions chosen by the Kinrade group, the same situation was observed.[2b] Because the same underlying structural principles apply, the small variation in the acidity constants of the sugar alcohols appear to be the reason for this observation. For a particular polyol, the concentrations of silicate, polyol, and hydroxide seem to be the only significant factors for complex formation. The ^{29}Si NMR solution spectra do not show any dependence on the type of counterion, which has been tested for sodium, potassium, and cesium (lithium experiments are disrupted by lithium silicate precipitation). In view of the structures this is a plausible finding. The two accessible binding sites for the counterions require face-sharing of the silicon-centered octahedron and the counterion-centered coordination polyhedron. Face-sharing is electrostatically unfavorable: For a small counterion, which would be expected to stabilize the silicate more efficiently, the increased attraction between the counterion and the tridentate alkoxo pattern of the binding site is counteracted by an increased repulsion between silicon atoms.

When glycosides, which are as base stable as alditols, are included into the solution studies, an astonishing result is obtained. Under the reaction conditions given above, furanosides—which include anhydroerythritol (*meso*-oxolane-3,4-diol), the basic structural fragment of furanoidic compounds—enriches the solutions with about the same amount of pentacoordinate species as D-mannitol does with hexacoordinate ones.[6] The unexpected aspect of this finding is that with this simple diol there is no support of silicon complexation by secondary interactions, such as intramolecular hydrogen bonding. Contrary to the furanosides, pyranosides fail to form hypervalent silicon complexes in amounts detectable by ^{29}Si NMR spectroscopy. This latter finding, together with the structural information available now, indicate the significance of the silicon–diolate chelate ring. Because of the relatively small central atom, the O-C-C-O torsion angle should be near to 0°, which is increasingly unfavorable for the diols in the sequence furanoses < open-chain diols < pyranoses: Not much energy is gained by a flexible furanose ring adopting the required torsion angle; open-chain diols, on the other hand, exhibit Pitzer strain at zero torsion angle, which is a destabilizing contribution and in the title compounds may be counterbalanced by hydrogen bonding (note in this context the still larger strain of *erythro*-configured bidentate ligands at 0° torsion). For pyranoses at least, 0° torsion is not realistic as a result of the massive strain for this conformation. It should be noted that structural drawings, such as the figures herein, get the viewer to believe in particularly stable moieties, because they do not emphasize repulsive interactions such as Pitzer strain. Repulsive interactions of this kind, however, are counterbalanced in the less spectacular furanose-derived structures.

Having demonstrated that the Si-O-C linkage is stable towards hydrolysis in special diolato and alditolato ligands, this work shows the significance of specific patterns of stabilizing secondary interactions which have their origin in the unique polyfunctionality of the carbohydrates. The hydrogen bonds described counterbalance other destabilizing factors. Whether or not silicon complexation by carbohydrates is a potential transport mechanism of silica in organisms depends on the discovery of ligands that combine the principles outlined here: the stability range of complexes around neutral pH may be broadened by using ligands that are free of strain, that give complexes that can be further stabilized by secondary interactions.

Experimental Section

Reagent-grade chemicals were purchased from Fluka and used as supplied; fumed colloidal silica (0.4 μm aerosil) was purchased from ABCR; bidestilled water was deoxygenated by bubbling nitrogen through it.

Preparation of Crystals: **1**: D-mannitol (0.55 g, 3.0 mmol) and sodium hydroxide (0.12 g, 3.0 mmol) were dissolved in water (2.0 mL). Tetramethoxysilane (0.23 g, 1.5 mmol) was added slowly. The mixture was heated briefly. On slow evaporation colorless crystals formed over several weeks. **2a**: fumed silica (0.060 g 1.0 mmol) and D-threitol (0.37 g, 3.0 mmol) were added to 2 M cesium hydroxide (1.0 mL). The suspension was treated at room temperature in an ultrasonic bath for 30 min. The resulting clear solution was slowly concentrated at 4 °C. Crystalline mixtures of threitolato silicates formed within three months. The anhydrous form **2a** preferentially precipitated at low water content in the final stage of preparation. **2b**: Same procedure as for **2a** but with 1.74 M rubidium hydroxide solution (1.15 mL) instead cesium hydroxide. Crystals of **2b** formed within six months. **3**: The same procedure using xylitol (0.46 g 3.0 mmol) yielded crystals of **3** within three weeks to three months.

 © 2003 Wiley-VCH Verlag GmbH & Co. KGaA, Weinheim 1433-7851/03/4209-1061 $ 20.00+.50/0

NMR spectroscopy: NMR spectra of solutions of **1**–**3** were recorded using Jeol Eclipse 270 and EX 400 spectrometers. The ^{29}Si chemical-shift values are relative to tetramethylsilane as an external standard. ^{13}C NMR resonance signals were assigned by means of DEPT, COSY, HETCOR, and HMQC experiments. All measurements were carried out using aqueous solutions with an internal concentric tube containing C_6D_6 for the lock signal. Solid state ^{29}Si cross polarization (CP) and ^{13}C MAS NMR spectra were recorded using a Bruker DSX Avance 500 FT spectrometer (11.2 T) at a resonance frequency of 99.37 MHz (**1**/**2a**/**2b**/**3**: 1000/3000/5000/3000 Hz spinning rate, 1/3/2/3 ms contact time, 2.8/3.0/2.6/3.0 μs ^{1}H transmitter pulse length, 0.164/0.082/0.205/0.123 s acquisition time, 128/440/256/816 scans). Chemical shifts are relative to tetramethylsilane. For the ^{13}C MAS NMR spectra of **1** at a resonance frequency of 125.79 MHz an antiring pulse sequence was used (5000 Hz spinning rate, 3.0 μs 90° pulse length, 0.123 s acquisition time, 1164 scans).[7] Overlapping signals were deconvoluted by using a Lorentz profile. Prior to measurement, the crystals were dried between filter papers and packed into a rotor of 4 mm outer diameter.

Received: April 25, 2002
Revised: December 3, 2002 [Z19177]

[1] J. D. Birchall, *Chem. Soc. Rev.* **1995**, *24*, 351–357; silica mobilization in marine sponges by ascorbate is discussed in: G. Bavestrello, A. Arillo, U. Benatti, C. Cerrano, R. Cattaneo-Vietti, L. Cortesogno, L. Gaggero, M. Giovine, M. Tonetti, M. Sarà, *Nature* **1995**, *378*, 374–376,.

[2] a) K. Benner, P. Klüfers, J. Schuhmacher, *Z. Anorg. Allg. Chem.* **1999**, *625*, 541–543; b) S. D. Kinrade, J. W. Del Nin, A. S. Schach, T. A. Sloan, K. L. Wilson, C. T. G. Knight, *Science* **1999**, *285*, 1542–1545; c) S. D. Kinrade, R. J. Hamilton, A. S. Schach, C. T. G. Knight, *J. Chem. Soc. Dalton Trans.* **2001**, 961–963; d) S. D. Kinrade, A. S. Schach, R. J. Hamilton, C. T. G. Knight, *Chem. Commun.* **2001**, 1564–1565.

[3] **1**: $C_{18}H_{35}Na_3O_{18}Si\cdot 12H_2O$, $M_r = 852.70$, $\rho_{calcd} = 1.6007(1)$ g cm^{-1}, pseudo-hexagonal trilling of $0.36 \times 0.28 \times 0.19$ mm size, orthorhombic, $P2_12_12_1$, $a = 11.824(2)$, $b = 20.410(2)$, $c = 14.662(3)$ Å, $V = 3538.3(10)$ Å^3, $Z = 4$, $T = 200$ K, Stoe IPDS area detector, $Mo_{K\alpha}$ (graphite monochromator, $\lambda = 0.71069$ Å), $\mu = 0.21$ mm^{-1}, 44133 *hkl* measured, $2\theta_{max} = 56°$, Lp correction, no absorption correction, 28282 *hkl* with $I \geq \sigma(I)$ used in trilling refinement, 17229 of these free of covering by reflexions of other two trilling components, the remaining 11053 dominant *hkl* belonged to the common hexagonal subcell (see Figure 3), and are affected by contributions of all the three crystalline individua; mean $\sigma(I)/I = 0.0817$, 21979 *hkl* with $I \geq 2\sigma(I)$, direct methods (SHELXS), full-matrix refinement against F^2 (SHELXL), $w^{-1} = \sigma^2(F_o) + (0.0500P)^2$, absolute structure parameter according to H. D. Flack, *Acta Crystallogr. Sect. A* **1983**, *39*, 876–881: −0.06(12), 578 parameters, 47 restraints, H(C) positions calculated, H(O) with one common O-H separation, in water molecules additionally $d(H\cdots H) = 1.57\,d(O\text{-}H)$, one common U_{iso} for all H atoms, $R(F)_{2\sigma} = 0.0474$, $R_w(F^2) = 0.1166$, $S = 0.964$, maximum shift: 0.001 σ, maximum residual electron density: 1.155 e Å^{-3} close to Si. Geometrical analysis and graphics with Platon, ORTEP, and Schakal. **2a**: $C_{12}H_{24}Cs_2O_{12}Si$, $M_r = 654.208$, $\rho_{calcd} = 2.0422(4)$ g cm^{-1}, colorless needle, $0.27 \times 0.09 \times 0.05$ mm, hexagonal, $P6_322$, $a = 9.4590(10)$, $c = 13.7305(16)$ Å, $V = 1063.9(2)$ Å^3, $Z = 2$, $T = 298$ K, Stoe IPDS area detector, $\mu(Mo_{K\alpha}) = 3.54$ mm^{-1}, 5972 *hkl* measured, $2\theta_{max} = 48°$, numerical absorption correction (8 faces), transmission factor range 0.628 to 0.821, mean $\sigma(I)/I = 0.0507$, 558 independent *hkl*, $R_{int} = 0.088$, 380 *hkl* with $I \geq 2\sigma(I)$, $w^{-1} = \sigma^2(F_o) + (0.0275P)^2$, absolute structure parameter: 0.03(7), 46 parameters, 1 restraint, H(C) positions calculated, H-O fixed to 0.82 Å, $R(F)_{2\sigma} = 0.0272$, $R_w(F^2) = 0.0520$, $S = 0.860$, maximum shift: 0.001 σ, maximum residual electron density: 0.459 e Å^{-3}. **2b**: $C_{12}H_{24}O_{12}Rb_2Si\cdot 3H_2O$, $M_r = 613.379$, $\rho_{calcd} = 1.87050(3)$ g cm^{-3}, colorless prism, $0.34 \times 0.32 \times 0.22$ mm, monoclinic, $P2_1$, $a = 9.03740(10)$, $b = 13.4190(2)$, $c = 9.61360(10)$ Å, $\beta = 110.9119(7)°$, $V = 1089.07(2)$ Å^3, $Z = 2$, $T = 200(2)$ K, Enraf-Nonius Kappa CCD area detector, $\mu(Mo_{K\alpha}) = 4.619$ mm^{-1}, 15010 *hkl* measured, $2\theta_{max} = 48°$, numerical absorption correction (9 faces), transmission factor range 0.384 to 0.468, mean $\sigma(I)/I = 0.0240$, 3370 independent *hkl*, $R_{int} = 0.0337$, 3335 with $I = 2\sigma(I)$, $w^{-1} = \sigma^2(F_o) + (0.0250P)^2 + 0.2426P$, abs. structure parameter: −0.003(4), 319 parameters, H(C) positions calculated, H(O) freely refined, $R(F)_{2\sigma} = 0.0180$, $R_w(F^2) = 0.0455$, $S = 1.141$, maximum shift: 0.001 σ, minimum and maximum residual electron density: −0.559, 0.237 e Å^{-3}. **3**: $C_{15}H_{30}Cs_2O_{15}Si\cdot 2H_2O$, $M_r = 780.317$, $\rho_{calcd} = 2.06793(17)$ g cm^{-1}, colorless block, $0.35 \times 0.22 \times 0.13$ mm, orthorhombic, $Pna2_1$, $a = 14.1338(7)$, $b = 17.5487(7)$, $c = 10.1054(5)$ Å, $V = 2506.4(2)$ Å^3, $Z = 4$, $T = 298$ K, Stoe IPDS area detector, $\mu = 3.035$ mm^{-1}, 13929 *hkl* measured, $2\theta_{max} = 48°$, numerical absorption correction (10 faces), transmission factor range 0.5083 to 0.6883, mean $\sigma(I)/I = 0.0253$, 3893 independent *hkl*, $R_{int} = 0.0381$, 3381 *hkl* with $I \geq 2\sigma(I)$, $w^{-1} = \sigma^2(F_o) + (0.0564P)^2 + 0.7978P$, racemic twin, 337 parameters, 1 restraint, H(C) positions calculated, H(O) riding with fixed distance (xylitol H(O)s only), $R(F)_{2\sigma} = 0.0319$, $R_w(F^2) = 0.0842$, $S = 1.048$, maximum shift: 0.001 σ, maximum residual electron density: 1.079 e Å^{-3}. Further details on the crystal structure investigation may be obtained from the Fachinformationszentrum Karlsruhe, 76344 Eggenstein-Leopoldshafen, Germany (fax: (+49) 7247-808-666; e-mail: crysdata@fiz-karlsruhe.de), on quoting the depository number CSD-407931 (**1**). Preliminary data on the cesium homologue of **2b**: CCDC-183177; CCDC-183176 (**2a**), CCDC-194195 (**2b**), and CCDC-183175 (**3**) contains the supplementary crystallographic data for this paper. These data can be obtained free of charge via www.ccdc.cam.ac.uk/conts/retrieving.html (or from the Cambridge Crystallographic Data Centre, 12 Union Road, Cambridge CB21EZ, UK; fax: (+44) 1223-336-033; or deposit@ccdc.cam.ac.uk).

[4] K. Isele, P. Klüfers, unpublished results.

[5] Crystals of **1** are redissolved in water to give a concentration of about 1.5 M. Because of hydrolysis, the main mannitol species is free mannitol itself under these conditions, but about one quarter of the manitol remains in not-hydrolyzed silicate which gives rise to another set of three NMR resonance signals; signal assignment succeeds with ^{13}C-enriched mannitol (in parentheses: $\delta_{Si\text{-}bound}$-δ_{free}): C1/6 ($\delta = 62.8$, −0.5 ppm); assignment of the C2/5 ($\delta = 75.7$, 4.1 ppm) and C3/4 signals ($\delta = 69.9$, −0.4 ppm); see the interpretation of ^{13}C NMR data in ref. [2b]. Note that the high $\Delta\delta$ of 4.1 for C2/5 is not an (unexpectedly large) CIS but clearly is caused by a significant difference between the conformations of Si-bound and free mannitol. Accordingly, DFT calculations [B3LYP/6-311 + G(2d,p)//B3LYP/6-31G(d) basis set] result in $\Delta\delta$ values of: C1/6 3.1, C2/5 4.7, C3/4 −1.1; note that the largest deviation between calculation and experiment is to be expected for C1/6 b result of an intramolecular hydrogen bond in the calculation, which is not observed in the crystal structure. In the same calculation, an Si chemical shift of −145.0 was obtained (exp. −144.8).

[6] 1 M solutions with respect to Si, molar ratio OH^-:SiO_2:polyol = 2:1:2, SiO_2 added as fumed silica, OH^- as NaOH or KOH (Cytidine). The following total percentage values for the sum of five- and six-coordinate species are obtained by ^{29}Si NMR spectroscopy: D-Mann 75%, Xyl 70%, D-Thre 10%, anhydroerythritol 60%, Cytidine 75%.

[7] S. Zhang, X. Wu, M. Mehring, *Chem. Phys. Lett.* **1990**, *173*, 481–484.

 © 2003 Wiley-VCH Verlag GmbH & Co. KGaA, Weinheim 1433-7851/03/4209-1062 $ 20.00+.50/0

Cover Picture

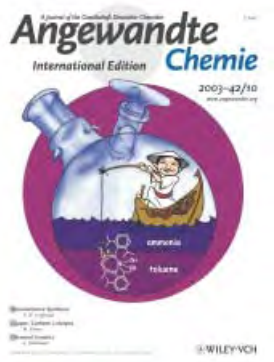

Guangcai Bai, Ying Peng, Herbert W. Roesky,* Jiyang Li, Hans-Georg Schmidt, and Mathias Noltemeyer

This week's catch is an unprecedented aluminum compound of the form $[LAl(OH)_2]$, prepared via the hydrolysis of $[LAlI_2]$ in a two-phase toluene/liquid ammonia system. The solid-state structure reveals a weakly hydrogen-bonded dimer; electrostatic potential analysis indicates that electrophilic attack at the oxygen sites is preferred, and that π-electron density is increased upon formation of the dimer. More details of this congener of $RB(OH)_2$ are given in the Communication by H. W. Roesky and co-workers on page 1132 ff.

Contents

News

Inorganic Chemistry: G. Schmid Recognized ____ 1082

Chirality: A. Pfaltz Receives Prize ____ 1082

Biochemistry: H. Bayley Back to Britain ____ 1082

Organic Chemistry: Duisberg Award to B. List ____ 1082

Books

Antisense Drug Technology ____ 1083 — Stanley T. Crooke — *reviewed by C. Giovannangeli*

Surface and Thin Film Analysis ____ 1083 — Henning Bubert, Holger Jenett — *reviewed by A. Terfort, M. Brunnbauer*

Highlights

Phenotype Assays in Screening

R. Breinbauer* ____ 1086 – 1087

Chemical Genetics Goes (Zebra) Fishing

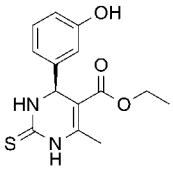

(*S*)-monastrol (**1**)

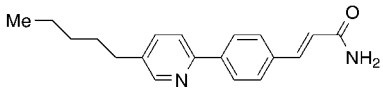

concentramide (**2**)

Parallel to screening combinatorial libraries against preselected biological targets, a new assay type has developed. The effect of small molecules on whole cells or organisms (e.g. the zebra fish) is investigated in phenotypic screens. Monastrol (**1**) and concentramide (**2**) were identified in such screens and allow the study of new biological pathways.

Minireviews

Copper-Carbene Catalysts

W. Kirmse* ____ 1088 – 1093

Copper Carbene Complexes: Advanced Catalysts, New Insights

Cycles of cycloaddition. Speculation on the course of the copper-mediated cyclopropanation of alkenes has come to an end: the elusive copper carbenoids **1** have been characterized for the first time. Insight into details of the catalytic cycle (see scheme) has been provided by experiment and computation. The construction of new ligands has led to catalysts that show extraordinary levels of both diastereoselectivity and asymmetric induction.

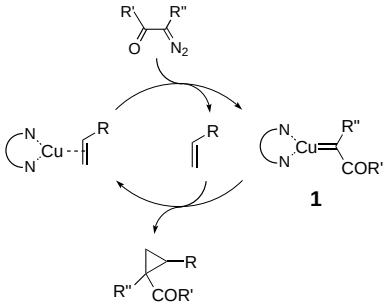

1

Reviews

Stereoselective Syntheses

R. W. Hoffmann* ____ 1096 – 1109

meso Compounds: Stepchildren or Favored Children of Stereoselective Synthesis?

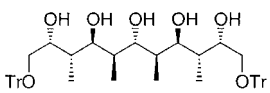

1

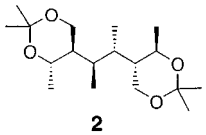

2

On first thought, symmetrical molecules should be easier to synthesize than asymmetrical compounds. This does not, however, hold for *meso* compounds, that is, molecules with a mirror plane (**1**; σ-symmetry Tr = triphenylmethyl) or a center of inversion (**2**; i-symmetry) and with multiple stereogenic centers. The principal strategies available for the synthesis of such compounds are delineated and illustrated in this review.

Communications

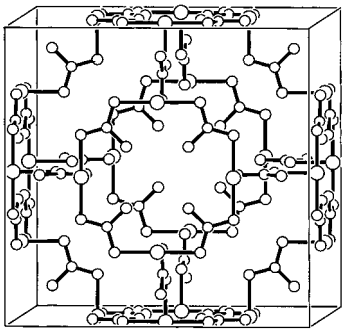

Cupric ions and carbonate ions, under the templating influence of pairs of hydrogen-bonding guanidinium ions, associate to form an infinite network with the topology of the $4^2 6^4$ sodalite net. This cage structure (see picture; for clarity, only copper centers and carbonate ions are shown) offers great scope for crystal engineering.

Crystal Engineering

B. F. Abrahams, M. G. Haywood, R. Robson,* D. A. Slizys ____ **1112 – 1115**

New Tricks for an Old Dog: The Carbonate Ion as a Building Block for Networks Including Examples of Composition $[Cu_6(CO_3)_{12}\{C(NH_2)_3\}_8]^{4-}$ with the Sodalite Topology

Degrading films: Surface-component-dependent and time-controlled degradation of a layer-by-layer (LbL) assembly comprising DNA and a cationic synthetic polymer is demonstrated through enzymatic hydrolysis by DNase I (see picture). The negatively charged enzyme is preserved on the cationic polymer surface in an inactive state, and changes in the concentrations of the essential Mg^{2+} and Ca^{2+} ions are used to control the activity of the enzyme, and thus control the desorption of the assembly.

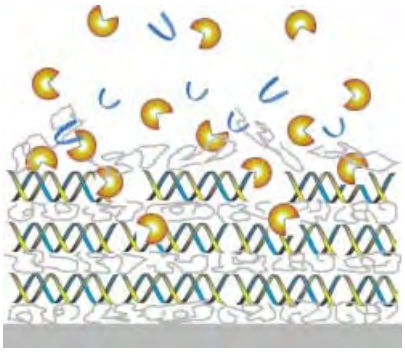

Contolled Desorption of Films

T. Serizawa, M. Yamaguchi, M. Akashi* _____ **1115 – 1118**

Time-Controlled Desorption of Ultrathin Polymer Films Triggered by Enzymatic Degradation

Incorporating films: An ultrathin polymer film that is molecularly porous and conformationally regular is prepared by the selective solvent extraction of one component from a layer-by-layer stereocomplex assembly. The resulting host film can reincorporate the extracted polymer (see picture; PMMA: poly(methyl methacrylate), it: isotactic, st: syndiotactic). The film also recognizes the length of the alkyl side-chain of an interactive polymer in the incorporation.

Porous Ultrathin Polymer Films

T. Serizawa, K.-i. Hamada, T. Kitayama, M. Akashi* _____ **1118 – 1121**

Recognition of Stereoregular Polymers by Using Structurally Regulated Ultrathin Polymer Films

For the USA and Canada:
ANGEWANDTE CHEMIE International Edition (ISSN 1433-7851) is published weekly by Wiley-VCH PO Box 191161, D 69451 Weinheim, Germany. Air freight and mailing in the USA by Publications Expediting Inc. 200 Meacham Ave., Elmont, NY 11003. Periodicals postage paid at Jamaica NY 11431. US POSTMASTER: send address changes to *Angewandte Chemie*, Wiley-VCH, 111 River Street, Hoboken, NJ 07030. Annual institutional subscription price for institutions: Europe € 2998.00/3148.00. Outside Europe US$ 3718.00/3904.00 (valid for print or electronic/print and electronic delivery); for individuals who are personal members of a national chemical society, or whose institution already subscribes, or who are retired or self-employed consultants, print only (including postage and handling charges): Europe € 248.00/Outside Europe US$ 348.00.

 © 2003 Wiley-VCH Verlag GmbH & Co. KGaA, Weinheim 1433-7851/03/4210-1075 $ 20.00+.50/0

Contents

Organic Nanotubes

Y. Kim, M. F. Mayer, S. C. Zimmerman* ——— 1121 – 1126

A New Route to Organic Nanotubes from Porphyrin Dendrimers

By chemically cleaving out the core of a dendritic metalloporphyrin coordination polymer, organic nanotubes can be created (see schematic representation). This is made possible by intramolecularly cross-linking the periphery of the oligomer with a ring-closing metathesis reaction prior to coring.

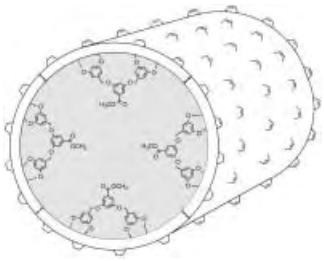

Supramolecular Photodimerization

D. G. Amirsakis, A. M. Elizarov, M. A. Garcia-Garibay,* P. T. Glink, J. F. Stoddart,* A. J. P. White, D. J. Williams* ——— 1126 – 1132

Diastereospecific Photochemical Dimerization of a Stilbene-Containing Daisy Chain Monomer in Solution as well as in the Solid State

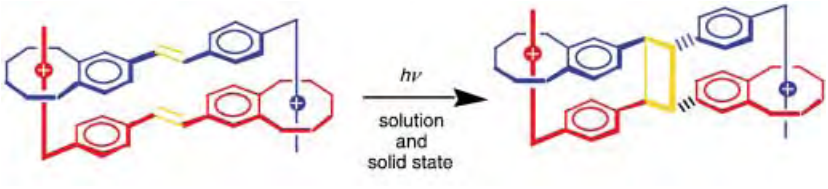

A crown ether/dialkylammonium ion hybrid containing a stilbene group self-assembles into a [c2]daisy chain-like pseudorotaxane, the solid-state superstructure of which was confirmed by X-ray crystallography. Upon irradiation, the pseudorotaxane undergoes an efficient photochemical [2+2] dimerization, both in solution as well as in the solid state, to yield one cyclobutane diastereoisomer with *syn-anti-syn* stereochemistry and head-to-tail regiochemistry (see scheme).

Dimeric Aluminum Dihydroxides

G. Bai, Y. Peng, H. W. Roesky,* J. Li, H.-G. Schmidt, M. Noltemeyer ——— 1132 – 1135

Aluminum Dihydroxide with Terminal OH Groups: An Unprecedented Congener of Boronic Acid

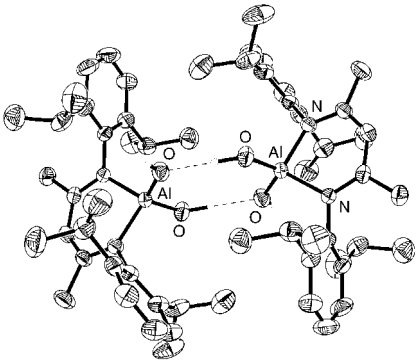

A synthetic approach to $[LAl(OH)_2]$ ($L = HC\{(CMe)(2,6\text{-}iPr_2C_6H_3N)\}_2$) is described. A novel congener of boronic acid, the single-crystal X-ray structure of the complex is shown to be a dimer (see picture) displaying short Al–OH bonds, and exhibiting interdimer hydrogen bonding, the origin of which has been discerned by theoretical and spectroscopic analysis.

Synthetic Protein Arrays

F. Toepert, T. Knaute, S. Guffler, J. R. Pirés, T. Matzdorf, H. Oschkinat, J. Schneider-Mergener* ——— 1136 – 1140

Combining SPOT Synthesis and Native Peptide Ligation to Create Large Arrays of WW Protein Domains

More than 10000 variants of a 38 mer WW protein domain were prepared and screened successively with 22 different dye-labeled peptide ligands (see picture). This approach has enabled more than 250000 binding experiments to be performed and has revealed comprehensive information regarding the sequence requirements for binding. Thus, WW variants with novel binding specificities were identified.

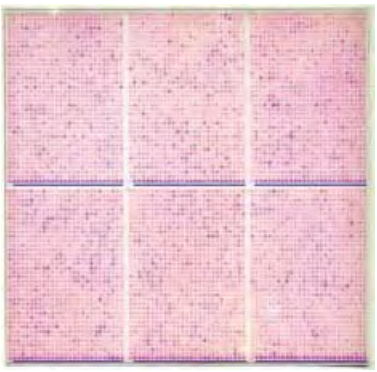

© 2003 Wiley-VCH Verlag GmbH & Co. KGaA, Weinheim
1433-7851/03/4210-1076 $ 20.00+.50/0

The oxidant H_2O_2 is generated in situ in this clean, one-step conversion of propylene into propylene oxide. Contrary to expectations, the catalyst—palladium on titanium silicalite—does not require methanol for activity, and solvent-based side reactions are avoided by conducting the reaction in CO_2.

Oxidation of Propylene

T. Danciu, E. J. Beckman,* D. Hancu, R. N. Cochran, R. Grey, D. M. Hajnik, J. Jewson ——— 1140 – 1142

Direct Synthesis of Propylene Oxide with CO_2 as the Solvent

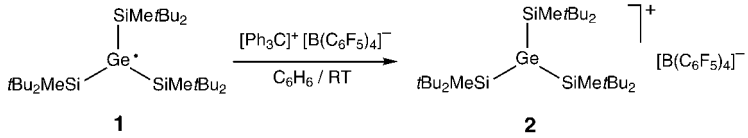

1 **2**

Born free: The germanium compound $[(tBu_2MeSi)_3Ge]^+[B(C_6F_5)_4]^-$ (**2**), is obtained as extremely moisture-sensitive dark red crystals by the treatment of the germyl radical **1** with $[Ph_3C]^+[B(C_6F_5)_4]^-$ in benzene. The molecular structure of **2**, determined by X-ray crystallography, suggests that **2** is a free germyl cation without π-bond conjugation, with no interaction with either solvent molecules or counteranion.

Germyl Cation

A. Sekiguchi,* T. Fukawa, V. Ya. Lee, M. Nakamoto, M. Ichinohe ——— 1143 – 1145

$[(tBu_2MeSi)_3Ge]^+$: An Isolable Free Germyl Cation Lacking Conjugation to π Bonds

Liquid crystals to the rescue: A remarkably increased selectivity for the separation of a binary gas pair (O_2/N_2) by a composite polymer film is reported. The composite film is made of a thermotropic liquid-crystalline polymer dispersed in a poly(ether imide) and a compatibilizer (poly(ester imide)). The limit imposed by what was previously considered to be an upper bound is overcome (see graph; ◇ the new composite film; the other symbols are values that were obtained for other films; α = selectivity).

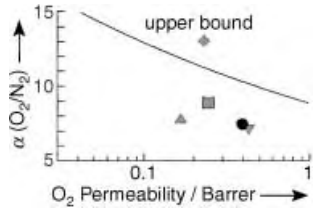

Gas Separation

Y. Seo,* S. U. Hong,* B.-S. Lee ——— 1145 – 1149

Overcoming the "Upper Bound" in Polymeric Gas-Separation Membranes

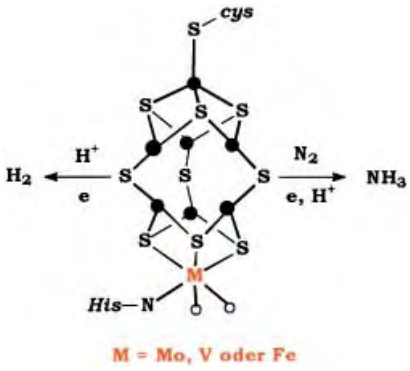

The core issue: Cofactors in nitrogenases transform dinitrogen into ammonia, and protons into dihydrogen (see scheme). Studies on cuboidal $\{Fe_4S_4\}^{2+}$ and $\{MoFe_3S_4\}^{3+}$ clusters show that Mo clusters are protonated more slowly, but have a higher affinity for binding substrates, than Mo-free clusters. These reactivities explain why the Mo-based nitrogenase is the most efficient at fixing dinitrogen rather than producing dihydrogen.

Nitrogen Fixation by Mo Clusters

J. Bell, A. J. Dunford, E. Hollis, R. A. Henderson* ——— 1149 – 1152

The Role of Mo Atoms in Nitrogen Fixation: Balancing Substrate Reduction and Dihydrogen Production

 © 2003 Wiley-VCH Verlag GmbH & Co. KGaA, Weinheim 1433-7851/03/4210-1077 $ 20.00+.50/0

Contents

Analysis of Catalytic Reactions

R. J. Hendershot, P. T. Fanson, C. M. Snively, J. A. Lauterbach* ——— **1152 – 1155**

High-Throughput Catalytic Science: Parallel Analysis of Transients in Catalytic Reactions

The simultaneous study of multiple catalyst samples can now be performed with Fourier transform infrared imaging. This technique is not only capable of allowing the comparison of catalysts, but also provides insight into the elementary steps since it is possible to follow transients in the concentration of effluent species in real time (e.g. see picture).

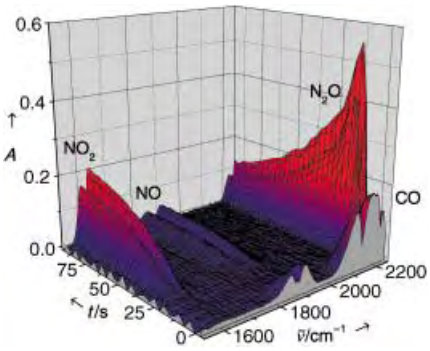

Zeolite Structure

A. Corma,* M. Puche, F. Rey, G. Sankar, S. J. Teat ——— **1156 – 1159**

A Zeolite Structure (ITQ-13) with Three Sets of Medium-Pore Crossing Channels Formed by 9- and 10-Rings

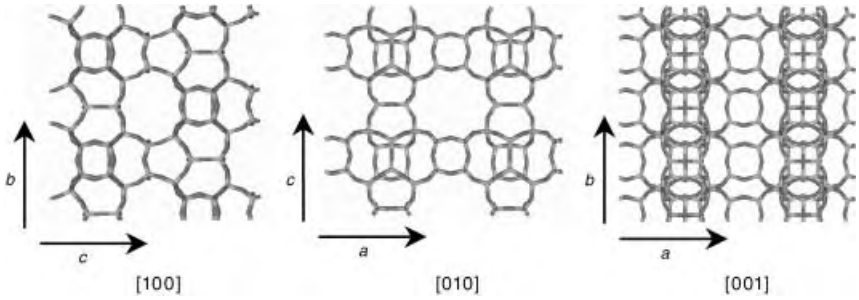

The unique structure of the ITQ-13 zeolite has been determined, which consists of an intercrossed system of medium-pore channels, made up of 9- and 10-ring pore apertures that run parallel to the crystallographic axes (see picture). Moreover, it has been possible to introduce acid sites into this structure, which opens the possibility for its use in acid catalysis.

Organic Field-Effect Transistors

K. Ito, T. Suzuki,* Y. Sakamoto, D. Kubota, Y. Inoue, F. Sato, S. Tokito ——— **1159 – 1162**

Oligo(2,6-anthrylene)s: Acene–Oligomer Approach for Organic Field-Effect Transistors

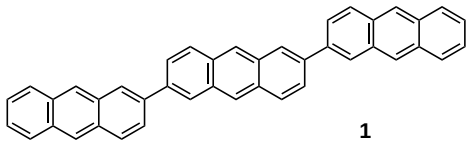

1

Oligo(2,6-anthrylene)s 1 and their dihexyl derivatives have been synthesized by Suzuki coupling using palladium catalysts. Organic field-effect transistors (OFETs) of these anthracene oligomers exhibited FET activity, and high hole mobilities up to 0.18 $cm^2V^{-1}s^{-1}$ were observed.

Mixed-Valent Cluster Compounds

J. Spandl, C. Daniel, I. Brüdgam, H. Hartl* ——— **1163 – 1166**

Synthesis and Structural Characterization of Redox-Active Dodecamethoxo-heptaoxohexavanadium Clusters

By means of suitable reduction and oxidation reactions, $[V_4^{IV}V_2^{V}O_7(OCH_3)_{12}]$ (see picture) can be converted into three further representatives of this cluster with varying V^{IV}/V^{V} ratios $([V_n^{IV}V_{6-n}^{V}O_7(OCH_3)_{12}]^{(4-n)}$ with $n = 3, 5, 6)$, even in the cationic form which is unusual for the classic polyoxometalate-forming metals V, Nb, Ta, Mo, and W ($n = 3$).

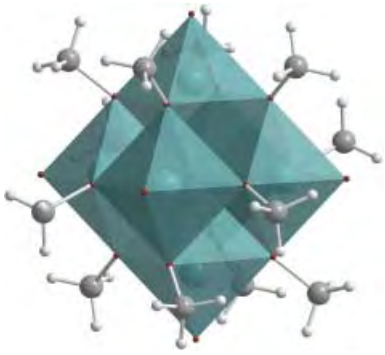

© 2003 Wiley-VCH Verlag GmbH & Co. KGaA, Weinheim
1433-7851/03/4210-1078 $ 20.00+.50/0

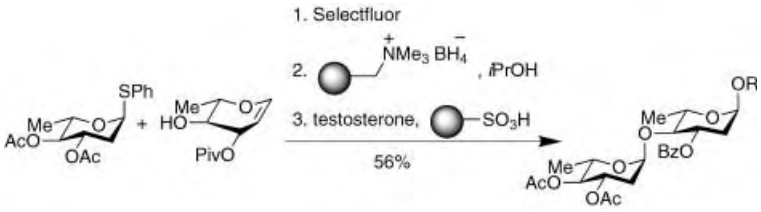

Minimum effort—maximum effect: Deoxygenated oligosaccharides and glycoconjugates are prepared in high yields with minimum purification from thioglycosides (see scheme) by exclusively employing reagents that are removed by simple filtration. New solid-phase-assisted synthetic protocols for removal of thiophenol and diphenyl disulfide are disclosed that make use of functionalized polymers. RO = testosteryl.

Synthesis of Glycoconjugates

J. Jaunzems, E. Hofer, M. Jesberger, G. Sourkouni-Argirusi, A. Kirschning* ——— **1166 – 1170**

Solid-Phase-Assisted Solution-Phase Synthesis with Minimum Purification—Preparation of 2-Deoxyglycoconjugates from Thioglycosides

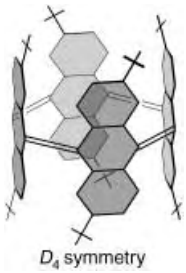

"Picotubes": A chiral tube is formed in the surprisingly clean Friedel–Crafts alkylation of a fully conjugated tubelike structure. Unlike helical carbon nanotubes synthesized at high temperatures, this chemically modified picotube is chiral by substitution. The two enantiomers were separated by chromatography on a chiral stationary phase.

Chiral Picotube Derivatives

R. Herges,* M. Deichmann, T. Wakita, Y. Okamoto* ——— **1170 – 1172**

Synthesis of a Chiral Tube

Significant charge alternation encircles the central carbon belt of a conjugated tubelike system, which forms a stable tetraanion upon reduction with lithium. Density functional theory calculations strongly suggest that the tube host two Li cations within its inner domain (Li purple). The dynamic topomerization barrier of the neutral compound is increased considerably in the tetraanion, which reduces the symmetry of the system.

Stable Tetraanionic Carbon Tubes

N. Treitel, M. Deichmann, T. Sternfeld, T. Sheradsky, R. Herges,* M. Rabinovitz* ——— **1172 – 1176**

Picotube Tetraanion: A Novel Lithiated Tubular System

VIP Communications labeled with this symbol have been judged by two referees as being "very important papers".

The publication of Communications labeled with this symbol has been accelerated because of their topical or highly competitive nature.

Supporting information for articles labeled with this symbol can be found at www.angewandte.org or www.interscience.wiley.com.

Sources

Product and Company Directory

You can start the entry for your company in "Sources" in any issue of *Angewandte Chemie*.

If you would like more information, please do not hesitate to contact us.

Wiley-VCH Verlag – Advertising Department
Tel.: 0 62 01 - 60 65 65
Fax: 0 62 01 - 60 65 50
E-Mail: MSchulz@wiley-vch.de

Service

Keywords ——— *1178*

Authors ——— *1179*

Vacancies ——— *1080, 1081*

Preview ——— *1182*

 © 2003 Wiley-VCH Verlag GmbH & Co. KGaA, Weinheim 1433-7851/03/4210-1079 $ 20.00+.50/0

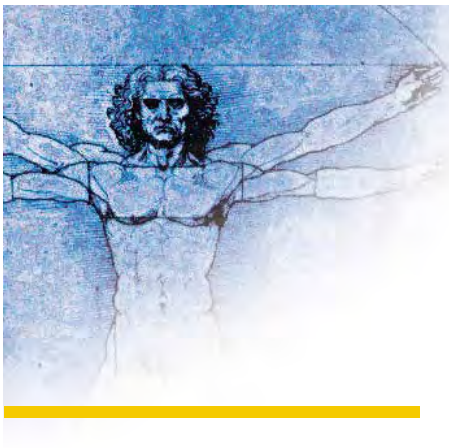

The annual "Chemiedozententagung" (CDT) is Germany's most important event for young researchers at the beginning of an independent academic career to present their work to a wide audience. In March this year, the conference is hosted by the Technical University in Chemnitz. Prestigious awards of the German Chemical Society (GDCh) are presented during the opening session. The prizes are financed from an important donation of BASF, Bayer, Degussa, Henkel, Hoechst, and Hüls.

Wilhelm Klemm Prize to G. Schmid

Günter Schmid

The Wilhelm Klemm Prize 2003 is awarded to Günter Schmid (Essen, Germany) for his achievements in inorganic chemistry. Schmid received his doctorate in 1965 from the University of Munich under the guidance of H. Nöth and his habilitation from the University of Marburg (Germany). He has been a professor at the University of Essen since 1970. The interests of his research group are devoted to clusters and colloids of main group and transition metals in heterogeneous catalysis and their stabilization by ligands. Furthermore, they work on photo- and electroluminescent inorganic systems as well as the one-, two- and three-dimensional organization of clusters and colloids. An example of this research is described in a recent Communication on "The Diode Behavior of Asymmetrically Ordered Au_{55} Clusters."[1]

The prize is devoted to the memory of Wilhelm Klemm (1896–1985), professor of inorganic chemistry at the University of Münster (Germany) and long-time member of the Editorial Board of *Angewandte Chemie*, and has been given every one or two years since 1985. It was originally donated by Degussa.

Horst Pracejus Prize to A. Pfaltz

Andreas Pfaltz

Andreas Pfaltz (Basel, Switzerland) is recognized for his outstanding research on chirality. Pfaltz earned his doctorate under the guidance of A. Eschenmoser from ETH Zurich in 1978. He was a director at the Max Planck Institute for Coal Research in Mülheim (Germany) from 1995 to 1998 and accepted an appointment at the University of Basel in 1999. Enantioselective catalysis through transition metal complexes with chiral ligands, such as semicorrin, bisoxazoline, and phosphinooxazoline derivatives, as well as heterogeneous catalysis with chirally modified metal surfaces are the main topics of his group's research. His Review on "Iridium-Catalyzed Enantioselective Hydrogenation of Olefins"[2] just appeared in a thematic issue on catalytic hydrogenation of *Advanced Synthesis & Catalysis*. Pfaltz is a member of its Editorial Board.

The prize is awarded every two years for outstanding achievements in the field of chirality. It was donated in memory of Horst Pracejus (1927–1987), a director of the Institute of Catalysis Research (former Academy of Sciences of the GDR) in Rostock.

B. List Receives Carl Duisberg Memorial Award

The Carl Duisberg Memorial Award is given to young researchers for excellent creative research. This year, Benjamin List (La Jolla, CA, USA) is to receive the price. List obtained his doctorate from the University of Frankfurt (Germany) for the synthesis of a Vitamin B_{12} A–B semicorrin (supervisor: J. Mulzer). He then moved to the Scripps Research Institute in La Jolla. His research activities are centered around asymmetric organic and bioorganic catalysis by means of amines and antibodies. The prize lecture will detail latest results on asymmetric aminocatalysis. It is complemented by a Concept article on "Catalytic Antibodies as Magic Bullets"[3] to give a more comprehensive overview of List's work.

Benjamin List

The Carl Duisberg Memorial Award is presented at the CDT every year.

H. Bayley Back to Britain

Hagan Bayley, currently head of the medical biochemistry and genetics department at Texas A&M University near Austin, TX, will assume a chair of chemical biology at the University of Oxford (UK) in October. By that time, the University's new 100 M€ chemistry research laboratory will be completed. His research is devoted to modified proteins that can be actuated through chemical, biochemical, and physical stimuli as described in a recent Communication on the "Kinetics of a Reversible Covalent-Bond-Forming Reaction Observed at the Single-Molecule Level."[4] Another one is to be published in this journal soon.

[1] V. Torma, T. Reuter, O. Vidoni, M. Schumann, C. Radehaus, G. Schmid, *ChemPhysChem* **2001**, *2*, 546.

[2] A. Pfaltz, J. Blankenstein, R. Hilgraf, E. Hörmann, S. McIntyre, F. Menges, M. Schönleber, S. P. Smidt, B. Wüstenberg, N. Zimmermann, *Adv. Synth. Catal.* **2002**, *345*, 33.

[3] C. Rader, B. List, *Chem. Eur. J.* **2000**, *6*, 2091.

[4] S.-H. Shin, T. Luchian, S. Cheley, O. Braha, H. Bayley, *Angew. Chem.* **2002**, *114*, 3859, *Angew. Chem. Int. Ed.* **2002**, *41*, 3707.

 © 2003 Wiley-VCH Verlag GmbH & Co. KGaA, Weinheim 1433-7851/03/4210-1082 $ 20.00+.50/0

Phenotype Assays in Screening

Chemical Genetics Goes (Zebra) Fishing

*Rolf Breinbauer**

Keywords:
assays · biological chemistry · combinatorial chemistry · high-throughput screening

Over the last two decades biochemists, molecular biologists, and geneticists have been tremendously successful in identifying new biological targets potentially useful for the treatment of diseases. At the beginning it seemed that the only missing part to exploit this wealth of opportunities was the identification of chemical compounds that address these targets. Combinatorial methods gave organic synthesis an extra push to be able to deliver the desired quantity of compounds needed to feed high-throughput-screening systems for a particular target protein. This approach has produced some very exciting success stories, culminating recently with the introduction of Gleevec, a Brc-Abl kinase inhibitor for the treatment of chronic myelogenous leukemia.[1] Nevertheless, this approach, which is focused on preselected mechanisms/targets, has often not been rewarded with success, although compounds have been identified that exhibited excellent binding properties to the target in question. As it turned out, complications arose when the investigations were carried out at the more complex organization level of a cell or a whole organism. Unspecific binding, poor bioavailability, and insufficient target validation should be named here as a few of the reasons why the compounds failed. A growing number of scientists have proposed that chemical biology should reconsider its roots and return to phenotypic screens instead of focusing on preidentified and isolated targets alone. The approach of phenotypic screening has been successful for many decades, especially in those areas of science that are poorly understood as a result of their intrinsic complexity (e.g. developmental biology or heterogeneous catalysis). Often further investigations then revealed some surprising and unanticipated mechanisms. Libraries of chemical compounds will play an important role for this undertaking in chemical biology.

Schreiber and Mitchison were the first to formulate the elements of a program named "chemical genetics",[2] whose goal is the investigation of cellular biology and the understanding of signaling pathways for particular gene products by using small molecules as modulating ligands.[3] Chemical genetics differs in several fundamental aspects from conventional genetic methods, such as mutations genetics or knockout organisms and offers several advantages over the latter:

- The effect of small molecules is rapid.
- In most cases the effect is reversible (as a result of metabolism and clearing), allowing temporal control of protein function.
- The effect is tunable, enabling grades of phenotypes by varying concentration.
- The effect is conditional, because they can be introduced at any point in development. A knockout, which is lethal for the embryonic development of an organism, cannot be studied for an adult organism.
- Knockout studies cannot dissect the role of different protein forms derived from the same gene, whereas a small molecule should, in principle, be able to differentiate among these functions.

The success of chemical genetics depends on the identification of compounds that bind with high affinity specifically to a single protein out of probably 100000.[3] The strategy of phenotypic screening of compound libraries will be discussed in this highlight as a successful way of tackling this task.

The groups of Schreiber and Mitchison used two phenotypic assays to screen a library of 16320 small molecules for their influence on the cell cycle.[4] In the first round of screening they used a whole-cell immunodetection (cytoblot) assay, in which cells were first incubated with small molecules. Then a labeled antibody targeted against phosphonuclein was added to report changes in the amount of this particular protein. The phenotype of increased amounts of phosphonuclein can be correlated with cells in mitotic arrest. Only 139 compounds of the original library exhibited this effect. After elimination of compounds that target the protein tubulin, which is known to be involved in this process, the remaining 86 compounds were investigated in a phenotypic screen in which in vivo staining for chromosomes and tubulin was studied by fluorescence microscopy. One compound exhibited previously unknown phenotype of monastral spindles in mitotic cells in which the chromosomes are located at the corona of the starburstlike spindle apparatus. The compound, monastrol (**1**), provided the desired molecular probe required for further studies. The kinesin protein Eg5 was identified as its molecular target. (*S*)-Monastrol (**1**) binds to a novel allosteric site in the motor domain of Eg5, thus

[*] Dr. R. Breinbauer
Department of Chemical Biology
Max-Planck-Institut für molekulare Physiologie, Otto-Hahn-Strasse 11
44227 Dortmund (Germany)
and
Fachbereich 3, Organische Chemie
Universität Dortmund
44221 Dortmund (Germany)
Fax: (+49) 231-133-2499
E-mail: rolf-peter.breinbauer@mpi-dortmund.mpg.de

 © 2003 Wiley-VCH Verlag GmbH & Co. KGaA, Weinheim 1433-7851/03/4210-1086 $ 20.00+.50/0

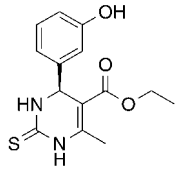

(*S*)-monastrol (**1**)

inhibiting its ATPase activity. In this way, a new target for high-throughput screening of chemical libraries has been identified.[5]

Recently, a new level of phenotypic screening has been reached by expanding the screening to whole vertebrates.[6,7] The zebra fish (*Danio rerio*) proved to be a particularly rewarding test object and had already been the subject of large-scale mutational screens carried out by the group of Nüsslein-Volhard and in the laboratories of Fishman and Driever.[8] Some characteristics of the zebra fish have made it a useful model organism: 1) its generation time is short; 2) large numbers of eggs are produced by each mating; and 3) fertilization is external, thus allowing all stages of embryonic development to be accessible; 4) crucial for small-molecule screening is the good permeability of the zebra fish for small molecules; 5) approximately 48 h after fertilization, the zebra fish embryo hatches and becomes a free-swimming larva, which shows a wide range of behavior such as swimming and touch sensitivity; 6) the development of the zebra fish can be conveniently studied by a wide range of optical methods as it is transparent for the first 5 days; 7) finally, it has been shown that there is a strong homology between the genes of mammalians and those of the zebra fish.

Peterson, Schreiber and co-workers screened a library of 1100 compounds against zebra fish eggs arrayed in 96-well plates.[6] Visual screening with a dissecting microscope allowed the selection of changes in the central nervous system, the cardiovascular system, pigmentation, and the ear. Approximately 1% of the small molecules affected a specific aspect of one of the systems screened and stimulated further investigations. One of the compounds, concentramide (**2**), alters the global organization of the zebra fish heart with an

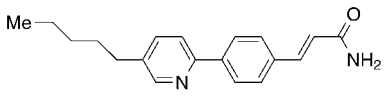

concentramide (**2**)

effective dosage (ED_{50}) of about 2 nM. After exposure to concentramide, both atrial and ventricular cells are generated, and both heart chambers form, but the ventricle itself is generated within the atrium. The group of Fishman analyzed this morphological effect generated by the exposure to concentramide with respect to the heart-and-soul (*has*) mutation.[9] This mutation was previously found in a genetic screen and exhibits a nearly identical phenotype. Whereas the *has* mutation effects a point mutation in the kinase PKCλ, additionally leading to defects in many tissues, including the retina, kidney, gut, and brain, the concentramide-treated embryos appear to have fewer developmental defects elsewhere. Taking advantage from the complementary type of information gained from chemical and genetic dissection, Fishman and co-workers showed that the polarity of cardiac tube assembly is controlled by at least two distinct molecular pathways. Although the molecular target of concentramide has not been identified yet, there is strong evidence that it disrupts anterior–posterior patterning in the heart.

The examples outlined above suggest that phenotype-oriented screening of combinatorial libraries against cells or whole organisms will provide a rich source of interesting and sometimes unanticipated biological phenomena. It seems that another lesson also can be learned from these examples: Discovering a treasure might have become easier, but recovering the treasure (that is, identifying the biological target of the small molecule) still appears to be very difficult.[10]

[1] R. Capdeville, E. Buchdunger, J. Zimmermann, A. Matter, *Nat. Rev. Drug Discovery* **2002**, *1*, 493–502.

[2] a) T. J. Mitchison, *Chem. Biol.* **1994**, *1*, 3–6; b) S. L. Schreiber, *Bioorg. Med. Chem.* **1998**, *6*, 1127–1152; c) C. M. Crews, U. Splittgerber, *Trends Biochem. Sci.* **1999**, *24*, 317–320; d) B. R. Stockwell, *Trends Biotechnol.* **2000**, *18*, 449–455; e) B. R. Stockwell, *Nat. Rev. Genet.* **2000**, *1*, 116–125.

[3] For excellent reviews of chemical approaches to study biological systems, see: a) P. J. Alaimo, M. A. Shogren-Knaak, K. M. Shokat, *Curr. Opin. Chem. Biol.* **2001**, *5*, 360–367; b) M. A. Shogren-Knaak, P. J. Alaimo, K. M. Shokat, *Annu. Rev. Cell Dev. Biol.* **2001**, *17*, 405–433; c) K. M. Shokat, M. Vellaca, *Drug Discovery Today* **2002**, *7*, 872–879; d) G. E. Ward, K. L. Carey, N. J. Westwood, *Cell. Microbiol.* **2002**, *4*, 471–482.

[4] T. U. Mayer, T. M. Kapoor, S. J. Haggarty, R. W. King, S. L. Schreiber, T. J. Mitchison, *Science* **1999**, *286*, 971–974.

[5] Z. Maliga, T. M. Kapoor, T. J. Mitchison, *Chem. Biol.* **2002**, *9*, 989–996.

[6] R. T. Peterson, B. A. Link, J. E. Dowling, S. L. Schreiber, *Proc. Natl. Acad. Sci. USA* **2000**, *97*, 12965–12969.

[7] H.-S. Moon, E. M. Jacobson, S. M. Kheronsky, M. R. Luzung, D. P. Walsh, W. Xiong, J. W. Lee, P. B. Parikh, J. C. Lam, T.-W. Kang, G. R. Rosania, A. F. Schier, Y.-T. Chang, *J. Am. Chem. Soc.* **2002**, *124*, 11608–11609.

[8] a) J. P. Briggs, *Am. J. Physiol. Regul. Integr. Comp. Physiol.* **2002**, *282*, R3–R9; b) R. S. Hauptschein, B. K. Eustace, D. G. Jay, *Exp. Hematol.* **2002**, *30*, 381–387; c) E. E. Patton, L. I. Zon, *Nat. Genet.* **2001**, *2*, 956–966; d) C. Nüsslein-Volhard, *Angew. Chem.* **1996**, *108*, 2316–2328; *Angew. Chem. Int. Ed. Engl.* **1996**, *35*, 2176–2187.

[9] R. T. Peterson, J. D. Mably, J.-N. Chen, M. C. Fishman, *Chem. Biol.* **2001**, *11*, 1481–1491.

[10] For a review of new tools for the identification of biological targets of small molecules, see: R. W. King, *Chem. Biol.* **1999**, *6*, R327–R333.

 © 2003 Wiley-VCH Verlag GmbH & Co. KGaA, Weinheim 1433-7851/03/4210-1087 $ 20.00+.50/0

Copper-Carbene Catalysts

Copper Carbene Complexes: Advanced Catalysts, New Insights

*Wolfgang Kirmse**

Keywords:
asymmetric catalysis · carbenoids · cyclopropanation · diastereoselectivity · transition-metal complexes

Controlling the selectivity of reactive intermediates is a major goal of organic chemists. Carbenes generated by thermal or photochemical extrusion of nitrogen from diazo compounds defy external control and tend to give complex product mixtures. However, the catalyzed decomposition of diazo compounds gives rise to highly selective "carbenoids" which have found extensive application in synthesis although little is known of their precise nature. On the other hand, a large variety of carbene metal complexes have been prepared and characterized which more or less lack carbenoid reactivity. Structural evidence for the transients of catalyzed diazo decomposition is becoming available through experiment and computation. Although the present report focuses on copper complexes, outstanding results with other metals are also covered.

1. Introduction

Carbenes are useful reactants in organic synthesis. Two bonds to the divalent carbon atom are formed in reactions such as C–H insertion or cyclopropanation—transformations that are difficult to achieve otherwise. Weak complexation to transition-metal atoms is an elegant way of controlling the reactivity and stereoselectivity of carbenes. The interaction of diazo compounds **1** with transition-metal complexes **2** is thought to generate metal-stabilized carbene compounds **5** by way of diazo complexes **4**. With an appropriate choice of metal (M) and ligand(s) (L), carbene transfer from the "carbenoids" **5** to π systems (such as, alkenes, alkynes, arenes, imines) leads to three-membered rings **3**. X–H bonds (for example, C–H, O–H, N–H) react with formal insertion (→**6**) while nucleophiles X**:** give rise to ylides **7** and their subsequent transformation products (Scheme 1). Extraordinary levels of enantioselectivity have been achieved in carbenoid reactions through the design of chiral catalysts. These developments have been summarized in an authoritative book[1] and in several more specialized reviews.[2] The present report focuses on progress that has been made very recently, particularly in the field of copper carbene complexes.

Coordinative unsaturation at the metal center allows transition-metal complexes to react as electrophiles (Lewis acids) with diazo groups. Numerous diazoalkane complexes of transition metals have been prepared in which the metal center is coordinated to the terminal nitrogen group (end-on) or to the N=N bond (side-on).[3] Many of these complexes are amazingly stable. Therefore, their participation in the catalytic process is unlikely. In contrast, coordination of the metal center to the carbon atom of the diazo (CN_2) group is conducive to nitrogen elimination. Upon addition of ethyl diazoacetate (EDA) to a CD_2Cl_2 solution of iodorhodium tetra(*p*-tolyl)porhyrin, [Rh(ttp)I], at −40 °C, Kodadek et al. observed complexation at the α carbon atom.[4] The structure of **9** was supported by IR ($\tilde{\nu}_{N=N} = 2338\ cm^{-1}$) and NMR spectroscopic data ($J_{Rh\text{-}H} = 2.4$ Hz). Above −20 °C, nitrogen

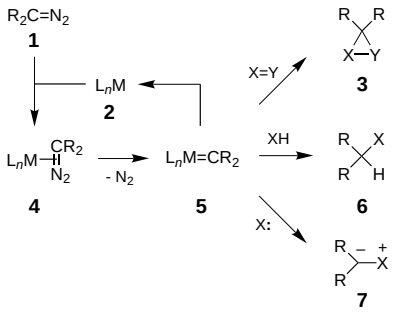

Scheme 1. Catalyzed decomposition of diazo compounds.

[*] Prof. Dr. W. Kirmse
Fakultät für Chemie
Ruhr-Universität Bochum
Universitätsstrasse 150, 44780 Bochum (Germany)
Fax: (+49) 234-321-4353
E-mail: kirmse@xenon.orch.ruhr-uni-bochum.de

 © 2003 Wiley-VCH Verlag GmbH & Co. KGaA, Weinheim 1433-7851/03/4210-1088 $ 20.00+.50/0

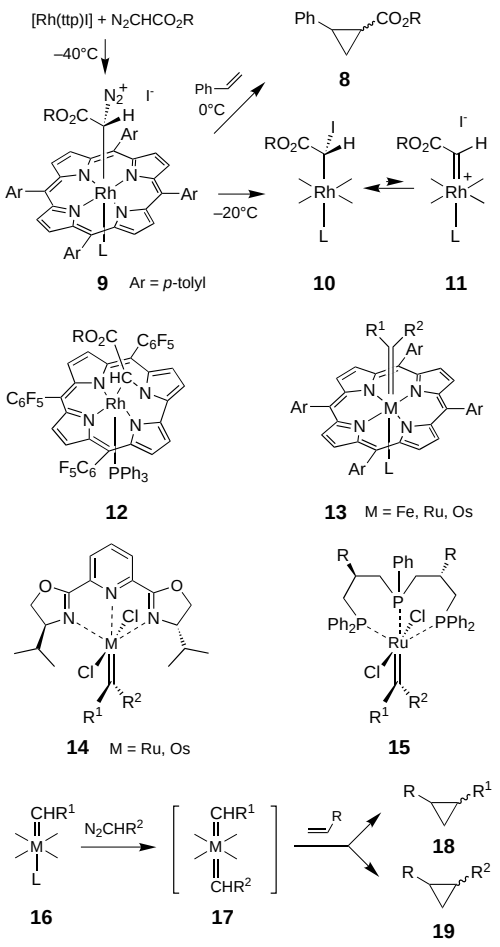

Scheme 2. Catalytically active carbene complexes of transition metals. (L is not specified in the original paper, **9** is only detected by NMR spectroscopy.)

was evolved with concomitant carbene transfer to alkenes (→**8**).[5] In the absence of a carbene acceptor, the iodoalkyl complex **10** was formed, which appears to be more stable than the ionic carbene complex **11** (Scheme 2).

In contrast to **11**, the rhodium corrole complex **12** was stable enough for spectroscopic investigation.[6] However, the carbene fragment of **12** is bonded to one of the corrole nitrogen atoms as well as to the rhodium center. Numerous carbene complexes **13** of metal porphyrins have been obtained, with M = Fe,[7] Ru,[8] and Os,[9] in which the carbene moiety is bound exclusively to the metal center. Tridentate amine and phosphane ligands were employed to prepare the carbene complexes **14**[10] and **15,**[11] respectively. Some of the structures have been confirmed by X-ray crystallography.[8b,c,10b] The carbene complexes shown in Scheme 2 undergo carbene transfer with alkenes,[12] and they are active catalysts of diazoalkane decomposition. In some cases, the stoichiometric reaction is too slow to be part of the catalytic process. Woo et al. have suggested that bis(carbene) species **17** are the active catalysts.[9c] The reaction of **16** with R^2CHN_2 was found to produce both **18** and **19**, thus supporting the formation of the intermediate **17** (scheme 2). Moreover, the bis(carbene) complex [Ph_2C=Os(tpfpp)=CPh_2] has been isolated (tpfpp = tetra(pentafluorophenyl)porphyrin).[13]

2. Mechanism of Copper Catalysis

Copper bronze,[14] copper(II) sulfate,[15] and copper(II) oxide[16] are the oldest catalysts employed for diazo decomposition. In the 1960s, copper(II) chelates **20**[17] and phosphite complexes of copper(I) chloride, [{$(RO)_3P$}CuCl],[18] were developed for homogeneous catalysis in organic solvents (Scheme 3). In their seminal papers, Nozaki, Noyori, et al. reported asymmetric induction for cyclopropanation reactions effected by the chiral copper salicylaldimine complex **21**.[17,19] Participation of the catalyst in the product-determining step was thus conclusively demonstrated.

It was originally believed that both Cu^I and Cu^{II} species were catalytically active.[20] Kochi et al. demonstrated that CuOTf (OTf = trifluoromethanesulfonate) is highly efficient in promoting the decomposition of diazo compounds, and that Cu^{II} complexes are reduced to Cu^I derivatives by the diazo compounds.[21] Cu^{II} complexes have also been "activated" by reduction with substituted hydrazines[22] or diisobutylaluminum hydride.[23] Although in situ preparation of catalysts is convenient, little is known about the species thus generated. Well-defined Cu^I complexes are clearly preferable for mechanistic studies.

Anionic ligands form neutral Cu^I complexes, as exemplified by semicorrins (→**22**),[22a,24] polypyrazolylborates (→**24**),[25,26] and iminophosphanamidates (→**25**).[27] With bipyridines (→**27**),[28–32] phenanthrolines,[30,33] and terpyridines,[30,34,35] cationic complexes are obtained. The widely used bisoxazolines afford either neutral complexes **23**[22b,36] or cationic complexes **26**,[37] depending on the nature of the 2,2′

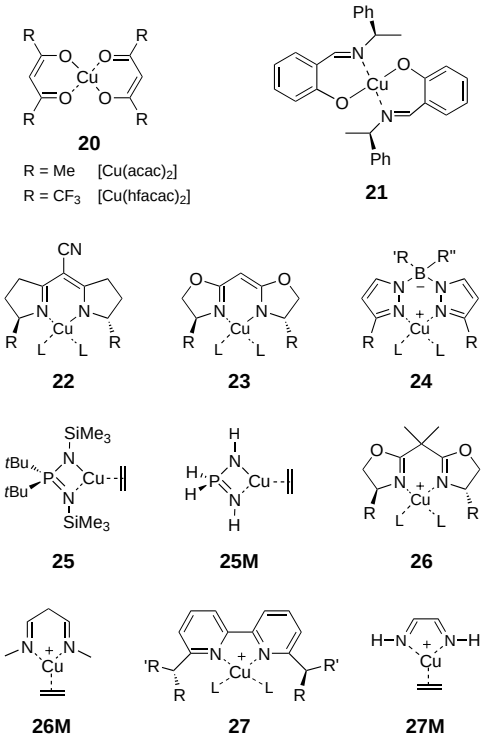

Scheme 3. Copper catalysts and models (M) employed for computation.

 © 2003 Wiley-VCH Verlag GmbH & Co. KGaA, Weinheim 1433-7851/03/4210-1089 $ 20.00+.50/0

link. The reactivity of cationic complexes is strongly influenced by the counterion. Triflates (TfO^-)[37] and hexafluorophosphates (PF_6^-)[38] were found to be highly effective catalysts whereas halides, cyanides, acetates, and perchlorates show little or no catalytic activity.

Several research groups have studied the mechanism of copper(I) catalysis by computation at the DFT (mostly B3LYP) level of theory. Simplified model compounds have been employed, such as **25M**,[39] **26M**,[40] and **27M**.[41] Chiral analogues of **26** (**26M**) have also been explored, although less extensively.[42] The first step is complexation of the diazo compound, through displacement of ligand(s) L (ethene in **25M**–**27M**). This step is rate-determining. Kinetic studies reveal that the rate of reaction decreases in the presence of excess olefin or excess ligand(s) L.[43] The kinetic data have been interpreted in terms of a dissociative ligand exchange whereas computation indicates that an associative mechanism is energetically more favorable.[39,40] (The absence of solvent molecules in calculations limits the utility of comparing the energies of associative and dissociative pathways.) In the case of α-diazocarbonyl compounds (N_2CHCHO,[39] EDA[40]), the most stable form of the diazo complex is **29** (Scheme 4). This assignment has been supported by the X-ray structure of **36**, which is formed reversibly from **25** and diazophenanthrone.[44] Intermediates with a η^2-carbonyl-bound diazoketone and with bonding to both carbon atoms of the OC-CN_2 moiety are higher in energy.[39] The transition state of nitrogen extrusion, **30,** is 80–90 kJ mol^{-1} above **29**.[39,40] Owing to steric effects, an analogous transition state (TS) is difficult to attain from **36**.

All theoretical studies attribute a central role to the carbene complex **34**. The first observation of a copper(I) carbenoid has recently been accomplished by Straub and Hofmann,[27] who designed a highly basic, sterically demanding, iminophosphanamide ligand for that purpose. The reaction of **25** with 2-aryl-2-diazoacetates generated **37** in steady-state concentrations ranging from 16% (Ar = Ph, R′ = Me) to 32% (Ar = 9-phenanthryl, R′ = 2-Pr).[27,39] The main evidence for the structure of **37** is derived from the resonance signals of the carbene carbon atom in the ^{13}C NMR spectrum ($\delta = 229.9$ for Ar = Ph, R′ = Me and $\delta = 226.0$ for Ar = Ph, R′ = $CH(4\text{-}C_6H_4Cl)_2$). The resonance signals arising from the diastereotopic *tert*-butyl groups indicate that the carbene plane is orthogonal to that of the PN_2Cu chelate. Addition of styrene to **37** led to rapid cyclopropanation. In the absence of a carbene acceptor, **37** decomposed slowly to give the "carbene dimer" $(RO_2C)ArC{=}CAr(CO_2R)$.

Two different mechanisms for the reaction of **34** with alkenes have been proposed: a) a concerted pathway resembling the addition of free carbenes to C=C bonds (TS **33**) and b) a two-step process involving a metallacyclobutane intermediate **35**. The computational results are in favor of the concerted mechanism.[40,42] Deuterated and *p*-substituted styrenes have been employed to investigate the product-forming step experimentally. Small ρ values ($\rho = -0.85$ for **24**,[45] $\rho^+ = -0.51$ for **26**[42]) and isotope effects ($PhCD{=}CH_2$/$PhCH{=}CH_2 = 1.02$, $PhCH{=}CD_2/PhCH{=}CH_2 = 0.95$[42]) are consistent with a concerted but asynchronous mechanism. The displacement of cyclopropane **31** from the catalyst–product complex **32**, presumably by an associative mechanism,[40] regenerates **28**, the resting state of the catalyst.

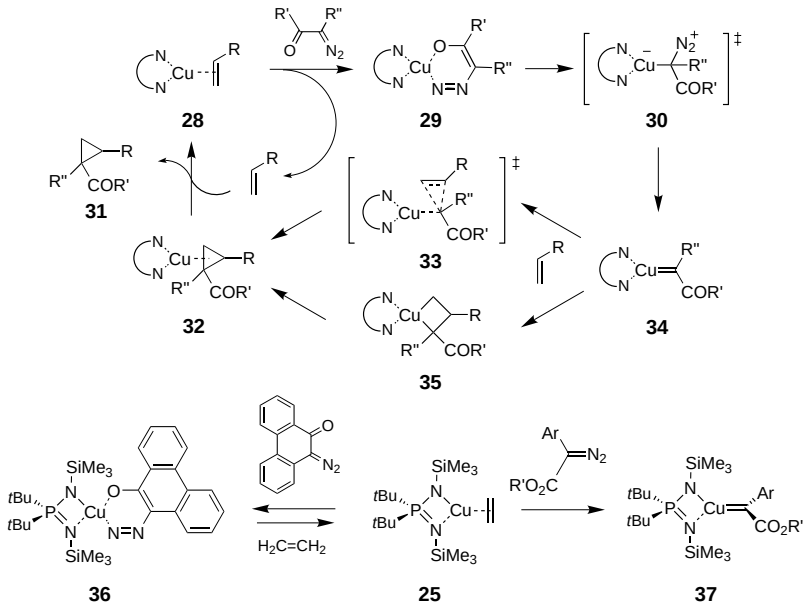

Scheme 4. Mechanism of copper(I)-catalyzed cyclopropanation reactions.

3. Stereoselectivity

In the prototypical cyclopropanation of styrene (**38**), copper complexes of the semicorrin **40**[22] and the azasemicorrin **41**,[46] as well as the bis(oxazoline) **42**[37] provide cyclopropanes **39** with a high level of enantioselectivity (Scheme 5 and Table 1). If EDA is employed, the reactions are only moderately diastereoselective. Bulkier groups R enhance the *trans*:*cis* ratio without affecting the enantiomeric excess (*ee*). Various 1-, 1,1-, and 1,2-substituted alkenes gave similar results to styrene. The selectivity reported for bipyridine ligands **43**[28] and **44**[29] is only slightly inferior to that obtained with ligands **40**–**42**. Recently developed di- and tripyridine ligands[30–35,47] do not significantly improve on **40**–**44**, nor do new diimine,[48] diamine,[49] and phosphoramidite[50] ligands.

The goal of high *trans* selectivity was pursued with remarkable success. The iminodiazaphospholidine catalyst **45**–CuOTf afforded *trans*:*cis* ratios ≥ 9 with various alkenes.[51] However, the *ee* value was only high with styrene. The planar-chiral bisazaferrocene ligand **46** induced excellent diastereoselectivity (*trans*:*cis* = 13–100) and enantioselectivity (*ee* = 90–95%), provided that the 4-methyl-2,6-*tert*-butylphenyl (BHT) ester of diazoacetic acid was employed.[52] The racemic ferrocene catalyst **47**–CuOTf was reported to give *trans*-**39** (R = Et) quantitatively.[53] A very favorable combination of *trans* selectivity and *ee* value has been accomplished by

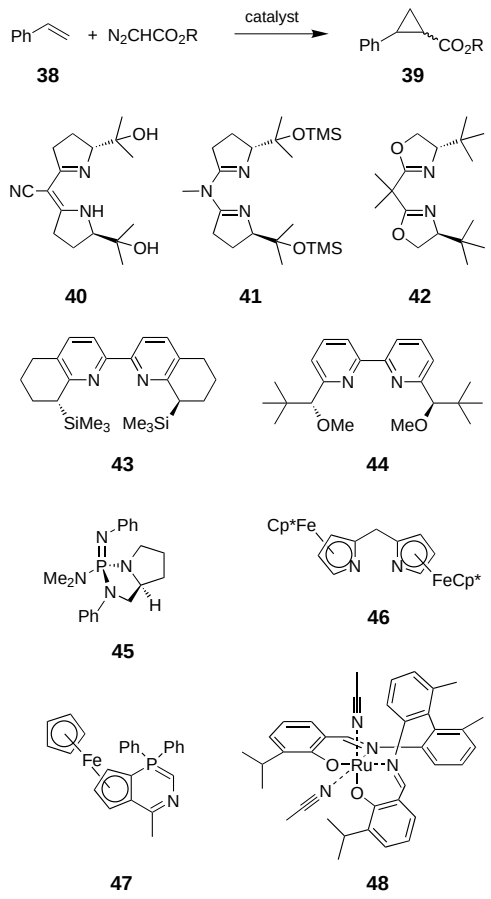

Scheme 5. Ligands and catalysts for stereoselective cyclopropanation. TMS = trimethylsilyl, Cp* = C_5Me_5.

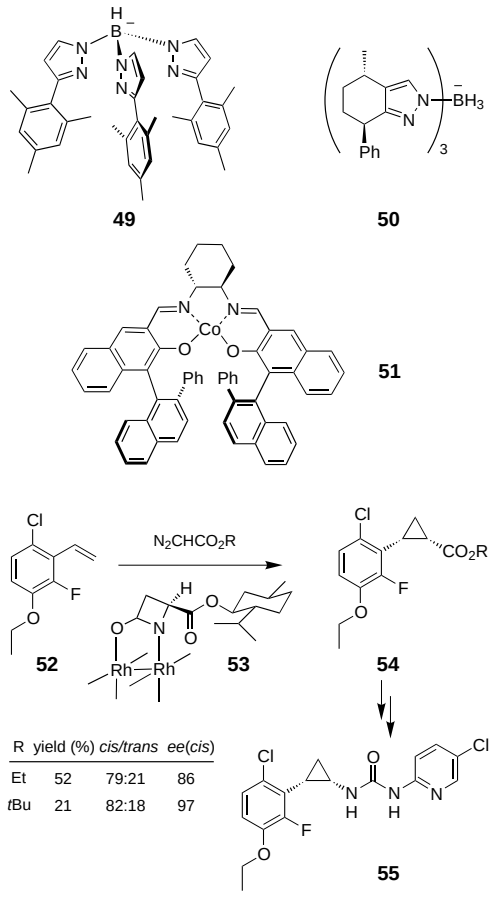

Scheme 6. Ligands and catalysts for *cis*-selective cyclopropanation.

use of the ruthenium catalysts **14** (Scheme 2, only with bulky substrate R groups)[10a] and **48** (with R = Et, where R refers to the diazoester N_2CHCO_2R, Scheme 5).[54]

Diastereoselectivity toward the *cis* isomer has been effected but recently with the tris(pyrazolyl)borate (homoscorpionate) complex **49**–Cu^+ (Scheme 6).[55] Such Cu^I-tris-(pyrazolyl)borate complexes also catalyze the cyclopropenation of alkynes[56] and insertion into C–H bonds of alkanes.[57] The design of efficient chiral analogues remains a challenge,[26] as is demonstrated by the results obtained with **50**–Cu^+.[58] However, the Co^{II}-salen complex **51** has been reported to induce high *cis* selectivity and enantioselectivity concurrently.[59] Related ruthenium complexes are somewhat inferior to **51** with regard to yield and *ee* value.[60]

The need for highly *cis*-selective and enantioselective cyclopropanation reactions is illustrated by the recent synthesis of **55**, a potent HIV-1 reverse transcriptase inhibitor.[61] For the key step, **52**→**54**, Doyle chose the dirhodium catalyst **53**, the use of which necessitated a compromise on yield and selectivity.

Models of the cyclopropanation transition state **33** (Scheme 4) have been proposed that explain the stereochemical preferences.[1,2] However, the predictive power of such models is limited. Seemingly

Table 1: Stereoselective cyclopropanations of styrene with alkyl diazoacetates (**38**→**39**).

Catalyst	Ester R group	Yield [%]	*trans*:*cis*	*ee* (*trans*)	*ee* (*cis*)	Ref.
[(**40**)$_2$Cu]	Et	65	78:22	92	80	[22a]
	*t*Bu	60	84:16	93	92	
41–CuOTf	Et	80	75:25	94	68	[46]
	*t*Bu	87	86:14	96	90	
42–CuOTf	Et	77	73:27	99	97	[37]
	BHT[a]	85	94:6	99		
43–CuOTf	*t*Bu	75	86:14	92	98	[28c]
44–CuOTf	*t*Bu	75	90:10	92	71	[29a]
45–CuOTf	Et	80	98:2	94	90	[51]
46–CuOTf	BHT[a]	79	96:4	94	79	[52]
47–CuOTf	Et	99	100:0			[53]
14(M = Ru)	mesityl	95	98:2	93	98	[10a]
48	Et	94	98:2	95		[54]
49–Cu^+	Et	98	2:98			[55]
50–Cu^+	Et	46	40:60	85	81	[58]
51	Et	quant.	1:99		96	[59]

[a] BHT = 4-methyl-2,6-di-*tert*-butylphenyl.

small alterations of the ligand structure can have a big impact on the stereoselectivity. For instance, if the Ph residues in **51** are replaced with Me groups, then *trans*-cyclopropane is formed preferentially.[59] Computations on "real" catalysts are not accurate enough to predict reliably the small differences in energy of diastereomeric transition states.[41,42] Therefore, progress in the field of stereoselective carbenoids continues to be guided by experience and intuition.

Received: August 20, 2002 [M1593]

[1] M. P. Doyle, M. A. McKervey, T. Ye, *Modern Catalytic Methods for Organic Synthesis with Diazo Compounds*, Wiley, New York, **1998**.

[2] a) M. P. Doyle, D. C. Forbes, *Chem. Rev.* **1998**, *98*, 911–935; b) M. P. Doyle, M. N. Protopopova, *Tetrahedron* **1998**, *54*, 7919–7946; c) *Comprehensive Asymmetric Catalysis* (Eds.: E. N. Jacobsen, A. Pfaltz, H. Yamamoto), Springer, Berlin, **1999**, pp. 513–603; d) H. M. L. Davies, E. G. Antoulinakis, *J. Organomet. Chem.* **2001**, *617*, 47–55; e) D. J. Timmons, M. P. Doyle, *J. Organomet. Chem.* **2001**, *617*, 98–104; f) M. P. Doyle, T. Ren, *Prog. Inorg. Chem.* **2001**, *49*, 113–168; g) T. Rovis, D. A. Evans, *Prog. Inorg. Chem.* **2001**, *50*, 1–150.

[3] Review: a) M. Dartiguenave, M. J. Menu, E. Deydier, Y. Dartiguenave, H. Siebald, *Coord. Chem. Rev.* **1998**, *180*, 623–663; b) Y. Mizobe, Y. Ishii, M. Hidai, *Coord. Chem. Rev.* **1995**, *139*, 281–311; c) W. A. Herrmann, *Angew. Chem.* **1978**, *90*, 855–868; *Angew. Chem. Int. Ed. Engl.* **1978**, *17*, 800–813.

[4] J. L. Maxwell, K. C. Brown, D. W. Bartley, T. Kodadek, *Science* **1992**, *256*, 1544–1547.

[5] D. W. Bartley, T. Kodadek, *J. Am. Chem. Soc.* **1993**, *115*, 1656–1660.

[6] L. Simkhovich, A. Mahammed, I. Goldberg, Z. Gross, *Chem. Eur. J.* **2001**, *7*, 1041–1055.

[7] C. G. Hamaker, G. A. Mirafzal, L. K. Woo, *Organometallics* **2001**, *20*, 5171–5176.

[8] a) J. P. Collman, E. Rose, G. D. Venburg, *J. Chem. Soc. Chem. Commun.* **1993**, 934–935; b) E. Galardon, P. Le Maux, L. Toupet, G. Simmoneaux, *Organometallics* **1998**, *17*, 565–569; c) C.-M. Che, J.-S. Huang, F.-W. Lee, Y. Li, T.-S. Lai, H.-L. Kwong, P.-F. Teng, W.-S. Lee, W.-C. Lo, S.-M. Peng, Z.-Y. Zhou, *J. Am. Chem. Soc.* **2001**, *123*, 4119–4129.

[9] a) L. K. Woo, D. A. Smith, *Organometallics* **1992**, *11*, 2344–2346; b) D. A. Smith, D. N. Reynolds, L. K. Woo, *J. Am. Chem. Soc.* **1993**, *115*, 2511–2513; c) C. G. Hamaker, J.-P. Djukic, D. A. Smith, L. K. Woo, *Organometallics* **2001**, *20*, 5189–5199.

[10] a) S.-B. Park, N. Sakata, H. Nishiyama, *Chem. Eur. J.* **1996**, *2*, 303–306; b) H. Nishiyama, K. Aoki, H. Itoh, T. Iwamura, N. Sakata, O. Kurihara, Y. Motoyama, *Chem. Lett.* **1996**, 1071–1072; c) H. Nishiyama, Y. Itoh, Y. Sugawara, H. Matsumoto, K. Aoki, K. Itoh, *Bull. Chem. Soc. Jpn.* **1995**, *68*, 1247–1262; d) S. B. Park, K. Murata, H. Matsumoto, H. Nishiyama, *Tetrahedron: Asymmetry* **1995**, *6*, 2487–2494; e) H. Nishiyama, N. Soeda, T. Naito, Y. Motoyama, *Tetrahedron: Asymmetry* **1998**, *9*, 2865–2869; f) S. Isawa, F. Takezawa, Y. Tuchiya, H. Nishiyama, *Chem. Commun.* **2001**, 59–60.

[11] H. M. Lee, C. Bianchini, G. Jia, P. Barbaro, *Organometallics* **1999**, *18*, 1961–1966.

[12] Review: a) J. W. Herndon, *Coord. Chem. Rev.* **2000**, *206–207*, 237–262; b) L. S. Hegedus, *Transition Metals in the Synthesis of Complex Organic Molecules*, 2nd Ed., University Science Books, Mill Valley, CA, **1999**, chap. 6; c) K. H. Dötz, *Angew. Chem.* **1984**, *96*, 573–594; *Angew. Chem. Int. Ed. Engl.* **1984**, *23*, 587–608; d) K. H. Dötz, H. Fischer, P. Hofmann, F. R. Kreißl, U. Schubert, K. Weiß, *Transition Metal Carbene Complexes*, Verlag Chemie, Weinheim, **1983**.

[13] Y. Li, J.-S. Huang, Z.-Y. Zhou, C.-M. Che, *J. Am. Chem. Soc.* **2001**, *123*, 4843–4844.

[14] a) O. Silberrad, C. S. Roy, *J. Chem. Soc.* **1906**, *89*, 179–182; b) A. Loose, *J. Prakt. Chem.* **1909**, *79*, 505–510; c) L. Wolff, *Justus Liebigs Ann. Chem.* **1912**, *394*, 23–59.

[15] K. Lorey, *J. Prakt. Chem.* **1930**, *124*, 185–190.

[16] C. Grundmann, *Justus Liebigs Ann. Chem.* **1938**, *536*, 29–36.

[17] a) H. Nozaki, S. Moriuti, M. Yamabe, R. Noyori, *Tetrahedron Lett.* **1966**, 59–63; b) H. Nozaki, S. Moriuti, H. Takaya, R. Noyori, *Tetrahedron Lett.* **1966**, 5239–5244; c) H. Nozaki, H. Takaya, S. Moriuti, R. Noyori, *Tetrahedron* **1968**, *24*, 3655–3669.

[18] W. R. Moser, *J. Am. Chem. Soc.* **1969**, *91*, 1135–1140; W. R. Moser, *J. Am. Chem. Soc.* **1969**, *91*, 1141–1146.

[19] R. Noyori, H. Takaya, Y. Nakanisi, H. Nozaki, *Can. J. Chem.* **1969**, *47*, 1242–1245.

[20] Review: D. S. Wulfman, G. Linstrumelle, C. F. Cooper in *The Chemistry of Diazonium and Diazo Groups*, Part 2 (Ed.: S. Patai), Wiley, New York, **1978**, chap. 18.

[21] R. G. Salomon, J. K. Kochi, *J. Am. Chem. Soc.* **1973**, *95*, 3300–3310.

[22] a) H. Fritschi, U. Leutenegger, A. Pfaltz, *Helv. Chim. Acta* **1988**, *71*, 1553–1565; b) R. E. Lowenthal, A. Abiko, S. Masamune, *Tetrahedron Lett.* **1990**, *31*, 6005–6008.

[23] W. G. Dauben, R. T. Hendricks, M. J. Luzzio, H. P. Ng, *Tetrahedron Lett.* **1990**, *31*, 6969–6972.

[24] Review: A. Pfaltz, *Acc. Chem. Res.* **1993**, *26*, 339–345.

[25] a) P. J. Pérez, M. Brookhart, J. L. Templeton, *Organometallics* **1993**, *12*, 261–262; b) Review: M. M. Diaz-Requejo, P. J. Pérez, *J. Organomet. Chem.* **2001**, *617–618*, 110–118.

[26] a) H. Brunner, U. P. Singh, T. Boeck, S. Altmann, T. Scheck, B. Wrackmeyer, *J. Organomet. Chem.* **1993**, *443*, C16–C18; b) P. Babbar, H. Brunner, U. P. Singh, *Indian J. Chem. Sect. A* **2001**, *40*, 225–227; c) U. P. Singh, P. Babbar, B. Hassler, H. Nishiyama, H. Brunner, *J. Mol. Catal. A* **2002**, *185*, 33–39.

[27] B. F. Straub, P. Hofmann, *Angew. Chem.* **2001**, *113*, 1328–1330; *Angew. Chem. Int. Ed.* **2001**, *40*, 1288–1290.

[28] a) K. Ito, S. Tabuchi, T. Katsuki, *Synlett* **1992**, 575–576; b) K. Ito, T. Katsuki, *Synlett* **1993**, 638–640; c) K. Ito, T. Katsuki, *Tetrahedron Lett.* **1993**, *34*, 2661–2664.

[29] a) H.-L. Kwong, W.-S. Lee, H, -F. Ng, W.-H. Chiu, W.-T. Wong, *J. Chem. Soc. Dalton Trans.* **1998**, 1043–1046; b) H.-L. Kwong, L.-S. Cheng, W.-S. Lee, W.-L. Wong, W.-T. Wong, *Eur. J. Inorg. Chem.* **2000**, 1997–2002.

[30] G. Chelucci, S. Gladiali, M. G. Sanna, H. Brunner, *Tetrahedron: Asymmetry* **2000**, *11*, 3419–3426.

[31] D. Lotscher, S. Rupprecht, H. Stoeckli-Evans, A. von Zelewsky, *Tetrahedron: Asymmetry* **2000**, *11*, 4341–4357.

[32] A. V. Malkov, I. R. Baxendale, M. Bella, V. Langer, J. Fawcett, D. R. Russell, D. J. Mansfield, M. Valko, P. Kocovsky, *Organometallics* **2001**, *20*, 673–690.

[33] F. Löffler, M. Hagen, U. Lüning, *Synlett* **1999**, 1826–1828.

[34] a) H.-L. Kwong, W.-S. Lee, *Tetrahedron: Asymmetry* **2000**, *11*, 2299–2308; b) H.-L. Kwong, W.-L. Wong, W.-S. Lee, L.-S. Cheng, W.-T. Wong, *Tetrahedron: Asymmetry* **2001**, *12*, 2683–2694.

[35] a) G. Chelucci, A. Saba, D. Vignola, C. Solinas, *Tetrahedron* **2001**, *57*, 1099–1104; b) G. Chelucci, A. Saba, F. Soccolini, D. Vignola, *J. Mol. Catal. A* **2002**, *178*, 27–33.

[36] D. Müller, G. Umbricht, B. Weber, A. Pfaltz, *Helv. Chim. Acta* **1991**, *74*, 232–240.

[37] a) D. A. Evans, K. A. Woerpel, M. M. Hinman, M. M. Faul, *J. Am. Chem. Soc.* **1991**, *113*, 726–728; b) D. A. Evans, K. A. Woerpel, M. J. Scott, *Angew. Chem.* **1992**, *104*, 439–441; *Angew. Chem. Int. Ed. Engl.* **1992**, *31*, 430–432.

[38] a) M. P. Doyle, C. S. Peterson, D. L. Parker, Jr., *Angew. Chem.* **1996**, *108*, 1439 – 1440; *Angew. Chem. Int. Ed. Engl.* **1996**, *35*, 1334 – 1336.
[39] a) B. F. Straub, Dissertation, Universität Heidelberg, **2000**; b) B. F. Straub, P. Hofmann, unpublished results.
[40] J. M. Fraile, J. I. García, V. Martínez-Merino, J. A. Mayoral, L. Salvatella, *J. Am. Chem. Soc.* **2001**, *123*, 7616 – 7625.
[41] M. Bühl, F. Terstegen, F. Löffler, B. Meynhardt, S. Kierse, M. Müller, C. Näther, U. Lüning, *Eur. J. Org. Chem.* **2001**, 2151 – 2160.
[42] T. Rasmussen, J. F. Jensen, N. Østergaard, D. Tanner, T. Ziegler, O.-O. Norrby, *Chem. Eur. J.* **2002**, *8*, 177 – 184.
[43] a) M. M. Díaz-Requejo, T. R. Balderrain, M. C. Nicasio, F. Prieto, P. J. Pérez, *Organometallics* **1999**, *18*, 2601 – 2609; b) M. M. Díaz-Requejo, M. C. Nicasio, P. J. Pérez, *Organometallics* **1998**, *17*, 3051 – 3057.
[44] B. F. Straub, F. Rominger, P. Hofmann, *Organometallics* **2000**, *19*, 4305 – 4309.
[45] M. M. Díaz-Requejo, P. J. Pérez, M. Brookhart, J. L. Templeton, *Organometallics* **1997**, *16*, 4399 – 4402.
[46] U. Leutenegger, G. Umbricht, C. Fahrni, P. von Matt, A. Pfaltz, *Tetrahedron* **1992**, *48*, 2143 – 2156.
[47] a) F. Pezet, I. Sasaki, J.-C. Daran, J. Hydrio, H. Ait-Haddou, G. Balavoine, *Eur. J. Inorg. Chem.* **2001**, 2669 – 2674; b) Y.-Z. Zhu, Z.-P. Li, J.-A. Ma, F.-Y. Tang, L. Kang, Q.-L. Zhou, A. S. C. Chan, *Tetrahedron: Asymmetry* **2002**, *13*, 161 – 165.
[48] a) Y. Imai, W. Zhang, T. Kida, Y. Nakatsui, I. Ikeda, *J. Org. Chem.* **2000**, *65*, 3326 – 3333; b) C. Borriello, M. E. Cucciolito, A. Panunzi, F. Ruffo, *Tetrahedron: Asymmetry* **2001**, *12*, 2467 – 2471.
[49] a) J.-A. Ma, L.-X. Wang, Q.-L. Zhou, *Tetrahedron: Asymmetry* **2001**, *12*, 2801 – 2804; b) M. Shi, J.-K. Jiang, Y.-M. Shen, Y.-S. Feng, *J. Chem. Res. Synop.* **2001**, 375 – 377.
[50] P. Müller, P. Nury, G. Bernardinelli, *Helv. Chim. Acta* **2000**, *83*, 843 – 854.
[51] J. M. Brunel, O. Legrand, S. Reymond, G. Buono, *J. Am. Chem. Soc.* **1999**, *121*, 5807 – 5808.
[52] M. M.-C. Lo, G. C. Fu, *J. Am. Chem. Soc.* **1998**, *120*, 10270 – 10271.
[53] G.-H. Hwang, E.-S. Ryu, D.-K. Park, S. C. Shim, C. S. Cho, T.-J. Kim, J. H. Jeong, M. Cheong, *Organometallics* **2001**, *20*, 5784 – 5787.
[54] I. J. Munslow, K. M. Gillespie, R. J. Deeth, P. Scott, *Chem. Commun.* **2001**, 1638 – 1639; W. Tang, X. Hu, X. Zhang, *Tetrahedron Lett.* **2002**, *43*, 3075 – 3078; J. A. Miller, W. Jin, S. T. Nguyen, *Angew. Chem.* **2002**, *114*, 3077 – 3080; *Angew. Chem. Int. Ed.* **2002**, *41*, 2953 – 2956.
[55] a) M. M. Díaz-Requejo, T. R. Belderraín, S. Trofimenko, P. J. Pérez, *J. Am. Chem. Soc.* **2001**, *123*, 3167 – 3168; b) M. M. Díaz-Requejo, A. Caballero, M. C. Nicasio, T. R. Belderraín, S. Trofimenko, P. J. Pérez, *J. Am. Chem. Soc.* **2002**, *124*, 978 – 983.
[56] M. M. Díaz-Requejo, M. A. Mairena, T. R. Belderraín, M. C. Nicasio, S. Trofimenko, P. J. Pérez, *Chem. Commun.* **2001**, 1804 – 1805.
[57] M. M. Díaz-Requejo, T. R. Belderraín, M. C. Nicasio, S. Trofimenko, P. J. Pérez, *J. Am. Chem. Soc.* **2002**, *124*, 896 – 897.
[58] M. C. Keyes, B. M. Chamberlain, S. A. Caltagirone, J. A. Halfen, W. B. Tolman, *Organometallics* **1998**, *17*, 1984 – 1992.
[59] a) T. Niimi, T. Uchida, R. Irie, T. Katsuki, *Tetrahedron Lett.* **2000**, *41*, 3647 – 3651; b) T. Niimi, T. Uchida, R. Irie, T. Katsuki, *Adv. Synth. Catal.* **2001**, *343*, 79 – 88.
[60] a) T. Uchida, R. Irie, T. Katsuki, *Tetrahedron* **2000**, *56*, 3501 – 3508; b) S. Bachmann, M. Furler, A. Mezzetti, *Organometallics* **2001**, *20*, 2102 – 2108; c) T. Katsuki, *Adv. Synth. Catal.* **2002**, *344*, 131 – 147.
[61] W. Hu, D. J. Timmons, M. P. Doyle, *Org. Lett.* **2002**, *4*, 901 – 904.

Stereoselective Syntheses

meso Compounds: Stepchildren or Favored Children of Stereoselective Synthesis?

*Reinhard W. Hoffmann**

Keywords:
asymmetric induction · *meso* compounds · stereoselective synthesis · synthetic methods

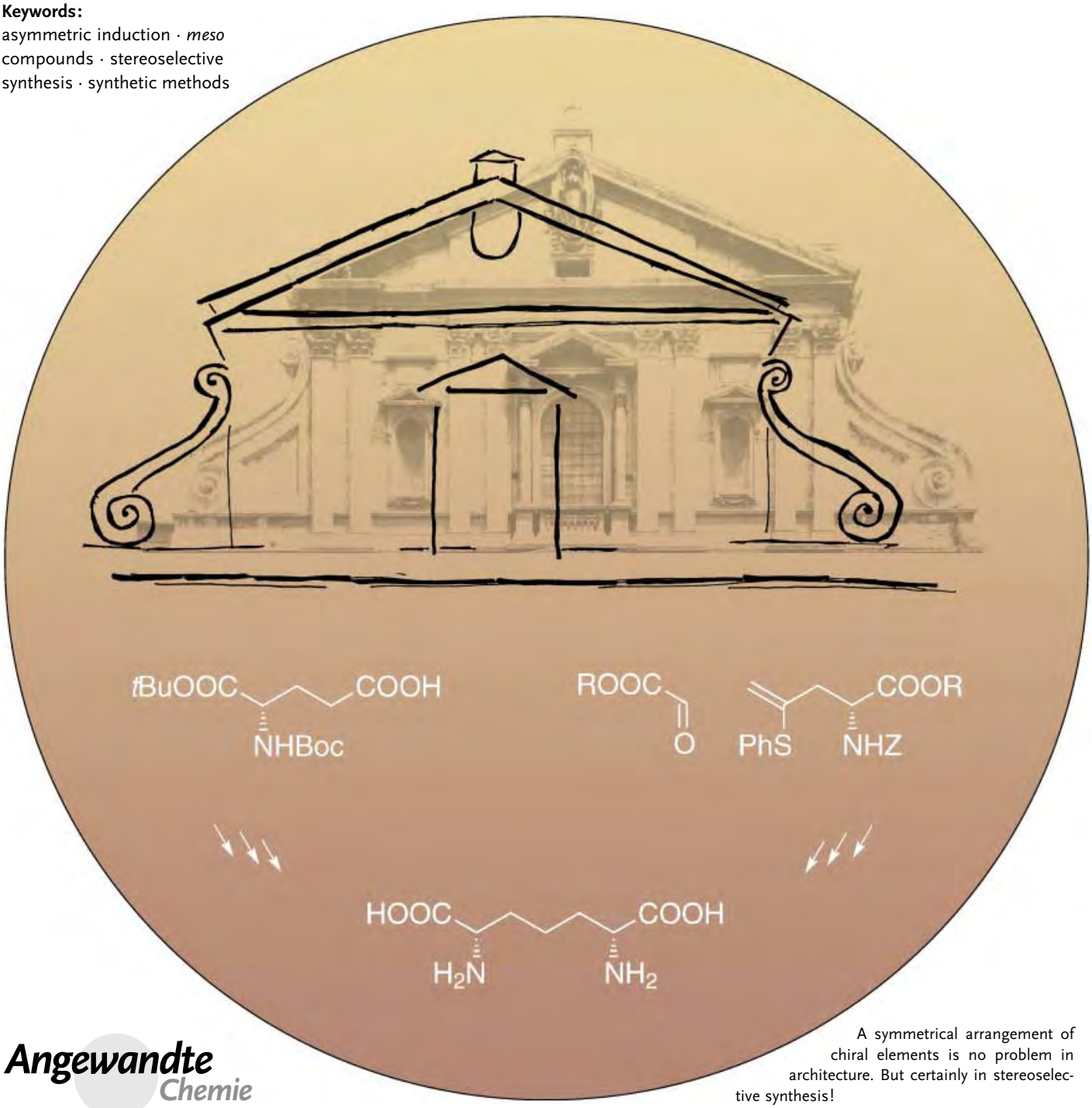

A symmetrical arrangement of chiral elements is no problem in architecture. But certainly in stereoselective synthesis!

© 2003 Wiley-VCH Verlag GmbH & Co. KGaA, Weinheim
1433-7851/03/4210-1096 $ 20.00+.50/0

After more than a quarter of a century of development, the methodology of stereoselective synthesis appears to be fully matured. In line with this, the potential that* meso *compounds offer in stereoselective synthesis is clearly recognized. The use of* meso *compounds in synthesis is, however, in no way commensurate with this potential, because, ironically, the synthesis of* meso *compounds in the first place is a problem of stereoselective synthesis. Present-day methodology does not provide many useful solutions to this problem. This Review therefore addresses the strategies available for the synthesis of more elaborate* meso *compounds whose stereogenic centers have a distance > 1,4 between them.* meso *Compounds with more than four stereogenic centers are also considered. The criteria used in choosing from several strategies in the synthesis of such compounds are discussed.

From the Contents

1. Introduction 1097

2. The Classical Synthesis of meso Compounds 1098

3. Principal Approaches to meso Compounds 1099

4. The Bidirectional Approach 1100

5. The Convergent Approach 1103

6. The Linear Approach 1106

1. Introduction

meso Compounds? The name brings back memories of introductory organic chemistry, when tartaric acid was the subject of the lecture. *meso*-Tartaric acid (**1**) is one of the four different substances that have the constitution of tartaric acid (Scheme 1).

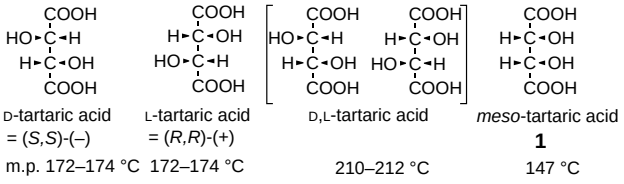

Scheme 1. Overview of the various tartaric acids.

meso Compounds can reach a conformation with a plane of symmetry in conformation **1a** or a center of inversion in conformation **1b** among the continuum of freely accessible conformations (Scheme 2). The symmetrical nature of *meso*-tartaric acid derives from the fact that it has two stereogenic centers with identical substitution but opposite configuration. *meso*-Tartaric acid (**1**) is therefore optically inactive, as the contributions of the two stereogenic centers to the Cotton effect compensate each other.

Is this property more than a superfluous curiosity that one has to memorize? Some may remember that 100 years ago the properties of *meso* compounds were the key feature in the argumentation that led Emil Fischer to the assignment of the configuration of the carbohydrates (Scheme 3), one of the true momentous achievements of chemical science.[1]

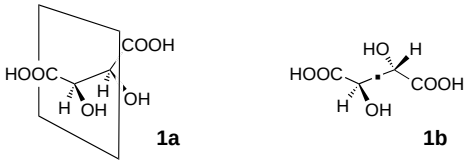

Scheme 2. Symmetric conformations of *meso*-tartaric acid.

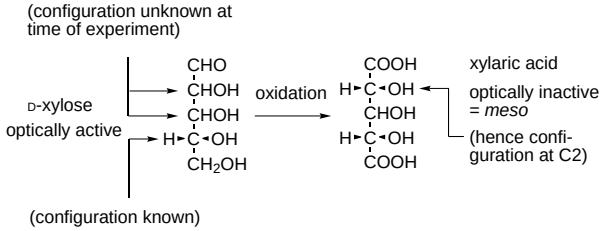

Scheme 3. Configuration assignment at C2 of xylose based on the symmetry of xylaric acid.

Furthermore, *meso* compounds fell into and rested in oblivion for a long time until enantioselective synthesis emerged as a topic of general interest. We therefore take a brief look at the stereochemical aspects of reactions of *meso* compounds. What happens if a *meso* compound, for example, anhydride **2** reacts with an *achiral* reagent at only one of the two mirror-image-related (i.e. enantiotopic) carbonyl groups (Scheme 4)? This reaction breaks the symmetry and therefore generates a chiral product **3**. For reasons of symmetry the rate of reaction is equal at either carbonyl group of **2**. The product **3** is therefore obtained as a racemate.

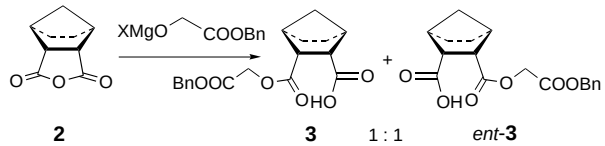

Scheme 4. Reaction of a *meso* anhydride with an achiral alkoxide.

[*] Prof. Dr. R. W. Hoffmann
Fachbereich Chemie, Philipps-Universität Marburg
Hans-Meerwein-Strasse, 35032 Marburg (Germany)
Fax: (+49) 6421-282-5677
E-mail: rwho@chemie.uni-marburg.de

 © 2003 Wiley-VCH Verlag GmbH & Co. KGaA, Weinheim 1433-7851/03/4210-1097 $ 20.00+.50/0

When a *meso* compound reacts in the same fashion with an enantiomerically pure *chiral* reagent, diastereomeric products are generated. An example is given in Scheme 5 by the reaction of the *meso* anhydride **2** with the chiral alkoxide **4**.[2] The resulting products **5** and **6** are enantiomerically pure and are formed in a ratio determined by kinetic

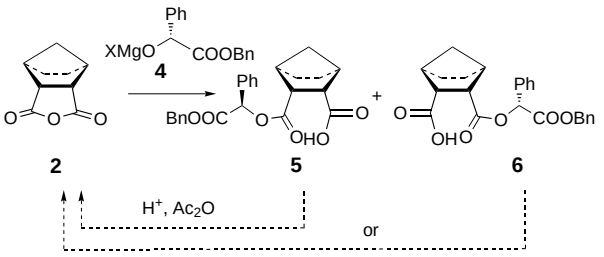

Scheme 5. Reaction of a *meso* anhydride with a chiral alkoxide.

resolution (1:1 for the magnesium alkoxide; 6:1 for the lithium alkoxide). Being diastereomeric, the products **5** and **6** may be separated by simple means.

This process is in all respects identical to the classical resolution of racemates. In both cases, one is generally interested in only one of the diastereomeric products. Thus, at most 50% of the starting material can be converted into the desired product. Fischli et al. pointed out that *meso* compounds may have an advantage in such situations, the so-called "*meso* trick".[3] This advantage is a consequence of the fact that when starting from a *meso* compound it is in many cases possible to convert the undesired diastereomer back into the precursor *meso* compound. On account of this recycling step technically all of a *meso* compound can be converted into the desired enantiomer of the product.

Of course, not only classical resolution using an enantiomerically pure "resolving agent" can be applied to *meso* compounds. Much more attractive is kinetic resolution,[4] which allows the effective differentiation between two enantiotopic functional groups of a *meso* compound. This provides directly high yields of a single product with high enantiomeric enrichment. An example is given in Scheme 6.[5]

These advantageous techniques were developed rapidly over the last years and have been reviewed frequently.[6] In turn, the bottleneck of a more general application lies more

Reinhard W Hoffmann studied at the Universität Bonn (1951–1958) and completed his PhD under B. Helferich. Two years of postdoctoral studies at the Pennsylvania State University were followed by a second postdoctoral stay with G. Wittig at the Universität Heidelberg. He completed his habilitation at the Universität Heidelberg in 1964. In 1967 he was appointed lecturer at the TH Darmstadt. Since 1970 he has been professor of organic chemistry at the Universität Marburg (emeritus status since 2001). He has been visiting professor at several universities worldwide.

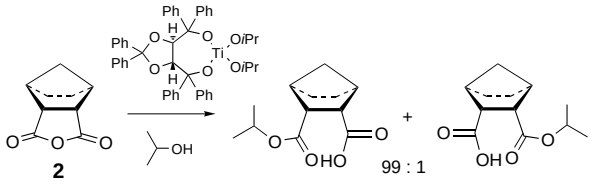

Scheme 6. Kinetic resolution applied to the desymmetrization of a *meso* compound.

and more in our ability to generate *meso* compounds in the first place. A short overview (Scheme 7) shows that the *meso* compounds typically used in synthesis are small molecules such as **7**–**13** with two to four—frequently adjacent—stereogenic centers.

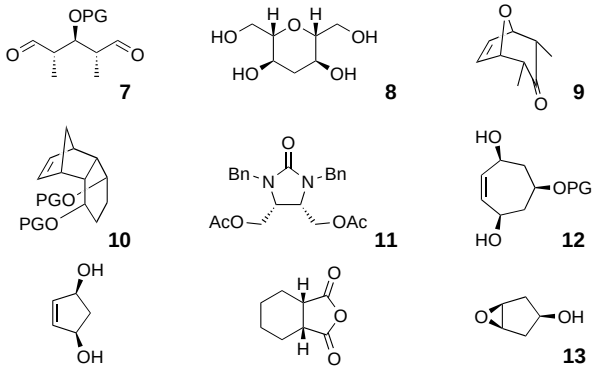

Scheme 7. Examples of common *meso* compounds used in synthesis: **7**,[7] **8**,[8] **9**,[9] **10**,[10] **11**,[11] **12**,[12] and **13**.[13]

meso Compounds with more than four stereogenic centers, or *meso* compounds with nonadjacent stereocenters find current interest because of their physical properties, for example, their conformational behavior.[14] Their main importance, however, relates to subsequent enantiotope-selective desymmetrization, which gives rapid access to enantiomerically pure intermediates with long sequences of stereocenters. The methods to synthesize such *meso* compounds are, however, underdeveloped and in clear disproportion to their importance. We therefore review herein strategies and problems related to the synthesis of *meso* compounds with a $>1,4$ distance between stereogenic centers, including those with more than four stereogenic centers. This review is not intended to be comprehensive, but illustrates the principles with examples, among others, from the research of our own group. We hope to elaborate in this review the criteria by which a judgement between the alternative strategies and any combination thereof in the synthesis of complex *meso* compounds can be made.

2. The Classical Synthesis of meso Compounds

meso Compounds are symmetrical and therefore their synthesis may be based on pairwise symmetrical bond formation, (Scheme 8, [Eq. (1)]), or on the reaction at one

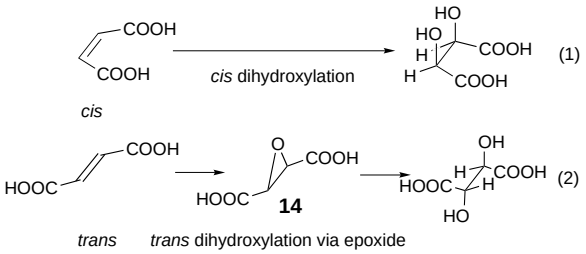

Scheme 8. Classical approach to *meso* compounds by addition to prochiral alkenes.

of two symmetry-related homotopic groups, (Scheme 8, [Eq. (2)]). In the latter approach, the intermediate **14** can be used as a racemate.

The classical approach of *syn* addition to a π system can readily be extended to the Diels–Alder addition and all related cycloaddition reactions (e.g. photo [2+2] cycloadditions, oxy–allyl cycloadditions) in which each of the reaction partners has (or is able to reach a conformation which has) C_{2v} symmetry. In the generalized cycloaddition shown in Scheme 9, the formation of two products, the *exo*-**15** and the *endo* cycloadduct (**17**) is possible. *exo*/*endo*-Selectivity[15] is an important issue in synthesis, but this topic is not addressed in this Review, as both the *endo* and *exo* products are *meso* compounds (Scheme 9). Although the *meso* compounds **15** and **17** obtained in this manner are cyclic, opening of a ring bond that is bisected by the plane of symmetry allows access to open-chain *meso* compounds, for example, **16** and **18**.

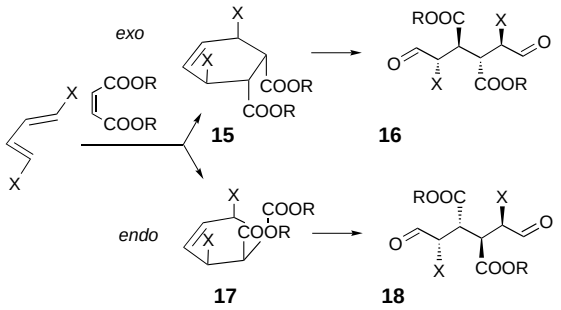

Scheme 9. Classical approach to *meso* compounds through Diels–Alder addition.

A further discussion of this classical chemistry is not intended. But if one recognizes that cyclic or open-chain *meso* compounds with a distance of $>1,4$ between stereocenters or *meso* compounds with ≥ 4 adjacent stereocenters may not generally be approached by this classical technique, one appreciates exceptions from this generalization as spectacular (Scheme 10).[16]

3. Principal Approaches to meso Compounds

Other routes are required if the synthesis of more elaborate *meso* compounds is to be advanced. Principally

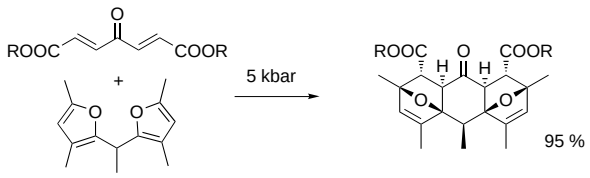

Scheme 10. Double Diels–Alder addition to give a *meso* compound with nine stereogenic centers.

the following three strategies can be used to prepare complex *meso* compounds such as **19** (Scheme 11):

1) One could start from a small *meso* compound, the core structure, and extend it *bidirectionally* (from both termini), thus creating the additional stereogenic centers in a symmetrical fashion. The problem with this approach is that in a single operation, stereogenic centers of opposite configuration are to be generated. This precludes the use of any chiral

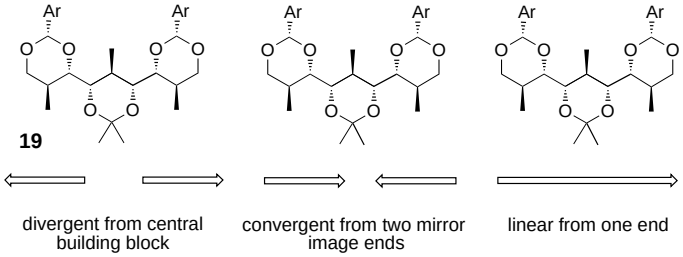

Scheme 11. Principal synthetic approaches to *meso* compounds.

reagents, catalysts, or auxiliaries and leaves one to deal with substrate-based asymmetric induction as the only tool to be used.

2) A second option involves the construction of the desired *meso* compound in a *convergent* fashion. This requires access to two constitutionally identical, but enantiomeric building blocks, each with high enantiomeric purity, and to combine these building blocks. This approach can be successful if the linkage region is devoid of stereogenic centers. If the linkage region includes several stereogenic centers, as is the case in **19**, this approach becomes problematic: in setting up these stereocenters there is a potentially opposing asymmetric induction from each of the two enantiomorphous ends of the molecule.

3) Clearly, there is always the possibility of a *linear* approach starting from one end of the target molecule. In such an approach, it is normally advantageous to have the starting building block enantiomerically pure. This then allows all the additional stereogenic centers to be created step by step, using the currently available tools of stereoselective synthesis. Evidently, the stereogenic centers have to be created in such a fashion, that in the end a symmetrical molecule, the *meso* compound, is obtained.

In practice, the synthesis of *meso* compounds may combine elements of all three strategies. It is the aim of this Review, to illustrate the three different approaches and to discuss the advantages and disadvantages associated with these approaches.

4. The Bidirectional Approach

Bidirectional chain extension of a symmetrical molecule allows rapid evolution of a synthesis, as two skeletal bonds are formed in a single operation. This has been highlighted in reviews by Poss and Schreiber[17] and by Magnuson,[18] in which examples are give for the bidirectional elaboration of both C_2-symmetric and σ-symmetric precursor molecules. Although the former is easy, only the latter gives rise to *meso* compounds. The starting compounds may be a small *meso* compound, being itself generated by one of the classical approaches or in a nonstereoselective manner. The latter holds in an early example of a bidirectional approach to a *meso* compound from Schreiber and Goulet (Scheme 12).[19]

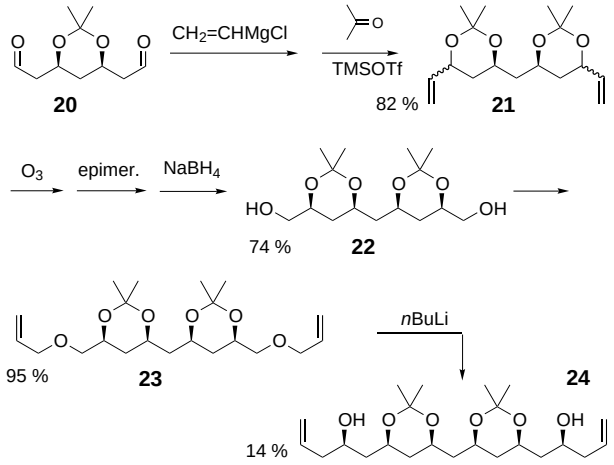

Scheme 12. Bidirectional synthesis of a *meso* polyol derivative.

The starting material *meso* dialdehyde **20** was obtained from a nonstereospecific reaction followed by diastereomer separation. The addition of vinylmagnesium chloride to **20** in the next step was also nonstereospecific. However, thermodynamic control was enlisted to give a stereochemically homogeneous *meso* product **22** after epimerization of the dialdehyde derived from **21**. Further bidirectional elaboration was effected via the bisallyl ether **23**, Wittig rearrangement of which proceeded under substrate-based asymmetric induction to give the *meso* polyol derivative **24**.

The starting point for a bidirectional approach does not necessarily have to be a *meso* compound such as **20**. It is sufficient when the starting compound has σ symmetry, as is the case with the alcohol **25**. Its elaboration into tolytoxin (**30**; Scheme 13) was a landmark achievement in synthetic development,[20] and demonstrated a focused access to a complex *meso* compound **28** with multiple stereogenic centers and its ultimate conversion into an enantiomerically pure product.

The sequence started with the bishomoallylic alcohol **25**. The hydroxy group served to direct[21] the epoxidation to give the *meso* bisepoxide **26** with 15:1 selectivity. Next, the aromatic rings were elaborated into β-ketoester functions. 1,3-*syn*-Selective reductions furnished the tetraol **27** with 12:1 diastereoselectivity. Finally, the product was refunctionalized

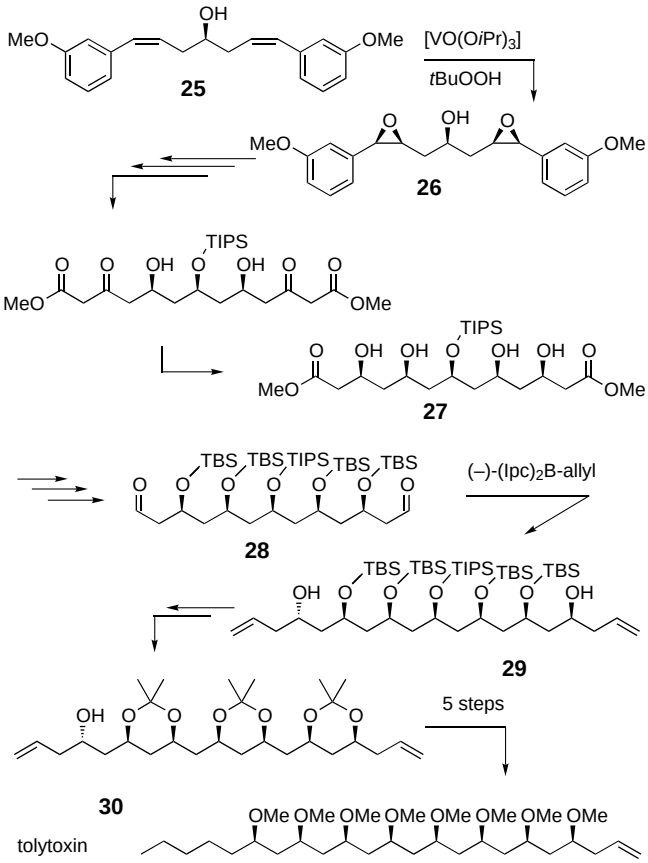

Scheme 13. Bidirectional synthesis of tolytoxin via a *meso* polyol derivative.

to give the *meso* dialdehyde **28**, which marked the end of the bidirectional elaboration. The symmetry-breaking step was the reaction with (−)-$(Ipc)_2$B-allyl, which produced the diol **29** with $>98\,\%$ *ee* under reagent control of diastereoselectivity. Chemodifferentiation of the end groups was then achieved by acetonide formation under thermodynamic control, favoring the *all-syn* acetonide. The rest of the synthesis of tolytoxin (**30**) was unexceptional.

Instructive examples in the synthesis of complex molecules with (latent) σ symmetry come from the synthetic efforts towards rifamycin S. The ansa chain between C19 and C27 (see **31**) has a plane of symmetry (cf. Scheme 14). Hence, an effective synthesis of rifamycin could be based on a *meso* compound of type **31** and ultimate end-group differentiation.

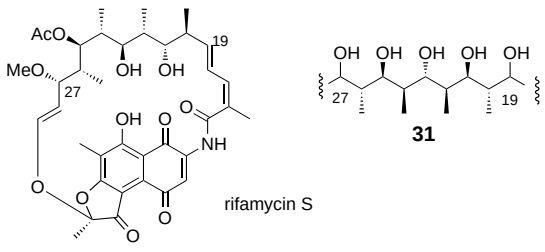

Scheme 14. Symmetry in the ansa chain of rifamycin S.

This was demonstrated in a bidirectional strategy by Still and Barrish (Scheme 15).[22] Hydroboration of the symmetrical bisallylic alcohol **32** set up four new stereogenic centers under

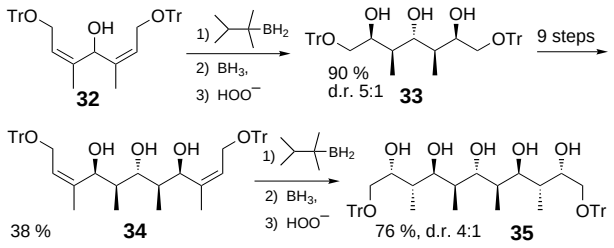

Scheme 15. Double hydroboration for bidirectional synthesis of the rifamycin ansa chain.

substrate-based asymmetric induction (*meso*/*rac* = 5:1). The triol **33** was then elaborated into the substrate **34** for the next bidirectional hydroboration, which furnished the pentaol **35** with a 4:1 *meso*/*rac* selectivity.

Another landmark paper in the synthetic efforts towards rifamycin S describes the synthesis by Harada et al.[23] of the building block **42** (Scheme 16). The starting point was the σ-symmetric TBS-protected bisallylic alcohol **36**. Diastereose-

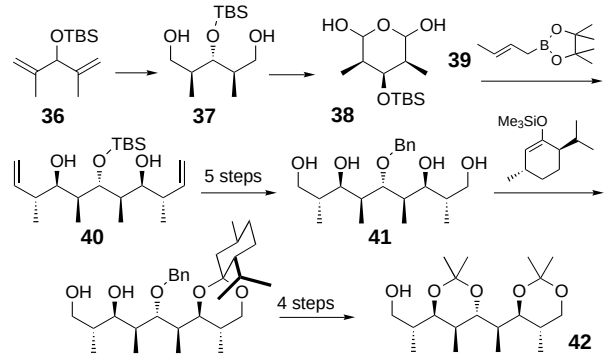

Scheme 16. Bidirectional synthesis of the ansa chain of rifamycin using a double crotylboration reaction.

lective bidirectional hydroboration provided the *meso* diol **37** with 13:1 selectivity. Oxidation of **37** gave the latent dialdehyde **38**. The next chain extension is a bidirectional crotylation with the crotylboronate (*E*)-**39**, which proceeded with high asymmetric induction from the stereocenters α to the aldehyde function.[24] The resulting *meso* compound **40** with seven contiguous stereogenic centers was then subjected to a laborious protecting-group exchange to give **41** in preparation for the desymmetrization step. The latter was effected by kinetic resolution of the enantiotopic diol units in **41** with a menthone derivative; a selectivity of 4.5:1 was attained. Up to this symmetry-breaking step, all new stereocenters had to be created by substrate-based asymmetric induction while proceeding in a bidirectional manner.

The elegance of this approach becomes apparent when comparing the route of Harada and co-workers (Scheme 16) with an earlier synthesis of a rifamycin building block **50** published by Born and Tamm, (Scheme 17) who also noted the latent σ symmetry of the target structure **31**.[25] They therefore started from the *meso* diester **43**, but broke the symmetry in the first step by a PLE-catalyzed enantiotopi-

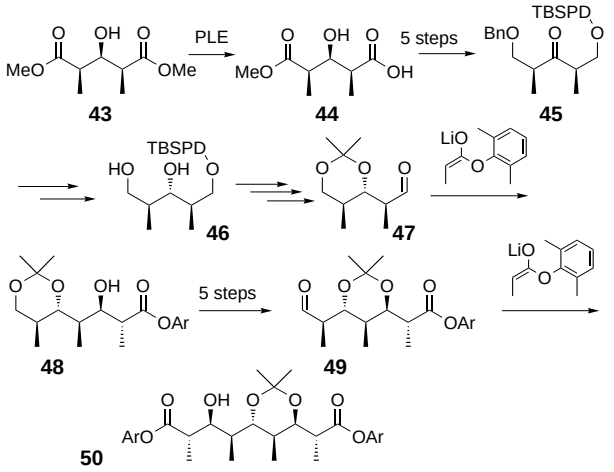

Scheme 17. Sequential bidirectional elaboration of the ansa chain of rifamycin.

cally selective ester hydrolysis. The resulting half-ester **44** was converted into the ketone **45**, reduction of which set the central pseudostereogenic center in **46** by substrate-based asymmetric induction. The product **46** was converted into the aldehyde **47**. Chain extension was then effected by an aldol addition with high asymmetric induction from the stereocenters resident in the aldehyde **47**.[26] The resulting β-hydroxyester **48** was then subjected to another round of protecting-group- and functional-group-interconversion steps to give the aldehyde **49**. The same aldol chain extension was then carried out a second time to give the target molecule **50**.

In essence, Born and Tamm used a bidirectional strategy, but executed the chain extension sequentially, thus requiring numerous protecting-group manipulations. Harada and co-workers carried out the synthesis via the *meso* compound **38** and attained a simultaneous chain extension at both ends. One can speculate that a lithium enolate addition to **38** or an equivalent dialdehyde may not have succeeded on both aldehyde functions concomitantly, because the first aldol formed would have led to an unreactive hemiacetal with the second aldehyde moiety. In this vein, the crotylboration reaction used by Harada and co-workers was the right choice, because hemiacetals also react with crotylboronates, albeit quite sluggishly.

The lesson from these two syntheses is that a bidirectional approach to *meso* compounds works, if the two reacting ends of the molecule do not interfere with one another. Such noninterference holds clearly for the two aldehyde functions in the *meso* dialdehyde **51** used in our synthesis of **56** by a bidirectional approach (Scheme 18).[27] Bidirectional Mukaiyama aldol addition to the dialdehyde **51** proceeded with a 6:1 selectivity favoring the *meso* dialdol **52**. After protection of the hydroxy groups as pMB ethers, the derived dicyclohex-

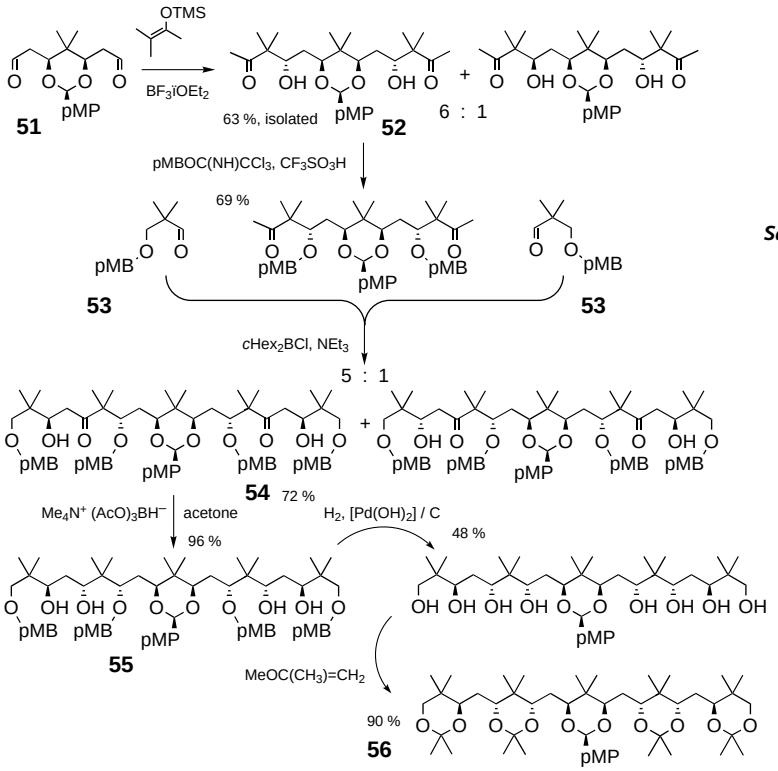

Scheme 18. Bidirectional synthesis of oligodioxanylmethanes with σ-symmetry.

ylboron enolate could be added in a bidirectional manner to the aldehyde **53** to give the bisaldol with a 5:1 selectivity favoring the *meso* compound **54**. Subsequent 1,3-*anti*-selective reduction with triacetoxyborohydride furnished the *meso* tetraol **55**, again in a twofold manner. The tetraol **55** was than readily converted into *meso*-**56**. The rapid evolution of this synthesis demonstrates the power of the bidirectional approach to *meso* compounds with multiple stereocenters.

It is worth repeating that this bidirectional-synthesis strategy is successful if the reactive end groups do not interfere with one another. This situation was not the case when we targeted the *meso* compound **57** in a bidirectional approach (Scheme 19).[28] We planned to elaborate the *meso* diester **59** into the *meso* diiodo compound **58** and onward to the target molecule **57**, all in a bidirectional manner. The *meso* diester was readily derived by a Claisen rearrangement of crotyl propionate **60**. Bidirectional reduction to the *meso* diol **61** was no problem, but after oxidation of **61** to the dialdehyde **62,** a bidirectional Wittig reaction was not possible (Scheme 20).

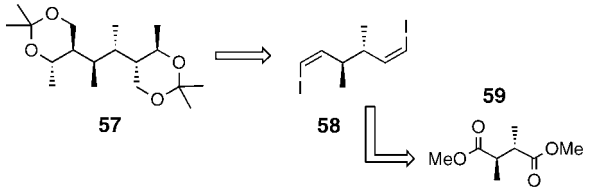

Scheme 19. Retrosynthetic analysis of open-chain *meso* compound **57**.

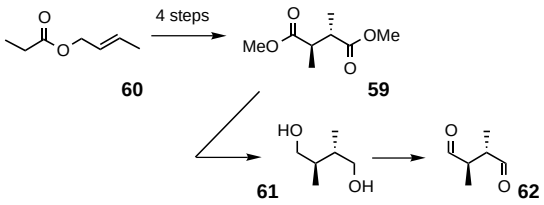

Scheme 20. Synthesis of *meso*-dimethylsuccindialdehyde.

Apparently the reactive end groups in **62** interacted with each another. We were therefore forced to take the same detour as Born and Tamm and turned to a sequential chain extension at each end of the molecule (Scheme 21), certainly not an efficient synthetic sequence. However, once we had reached the diiodo compound **58**, the reacting ends of the molecule were separated from each other far enough to allow a bidirectional continuation of the synthesis up to the end. This allowed the conversion of the diiodo compound **58** into the bisallylboronate **63**. Its bidirectional reaction with formaldehyde proceeded under unprecedented substrate-based asymmetric induction ($A^{1,3}$-strain control)[29] to give the diol **64**. The latter was protected and converted into the dialdehyde **65**, in which the carbonyl groups are in the 1,6-positions. These functional groups were apparently remote enough from one another to allow a bidirectional cuprate addition, which furnished the diol **66** under Felkin–Anh control. The diol **66** was then readily converted into the target *meso* compound **57** (Scheme 22). For a related approach to another *meso* compound with six adjacent stereocenters, see reference [30].

When dealing with cyclic systems with σ symmetry one usually does not consider them as *meso* compounds, but there is really no difference regarding the strategies of synthesis. A bidirectional synthesis starting from a σ-symmetric building block is the method of choice. Two recent examples may illustrate this idea. First, Spivey et al.[31] converted the epoxide **67** into the β-cyanoalcohol **68**. Epoxidation of the two symmetry-related double bonds could be effected under the direction of the tertiary hydroxy group to give the *meso* bisepoxide **69**. Reaction of the latter with $AlMe_3$ furnished the *meso* triol **70** (Scheme 23).

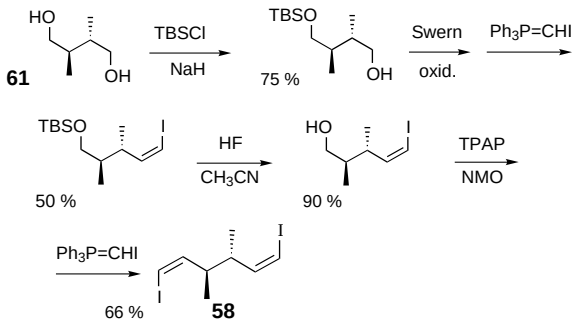

Scheme 21. Sequential bidirectional synthesis of *meso* bisiodoalkene **58**.

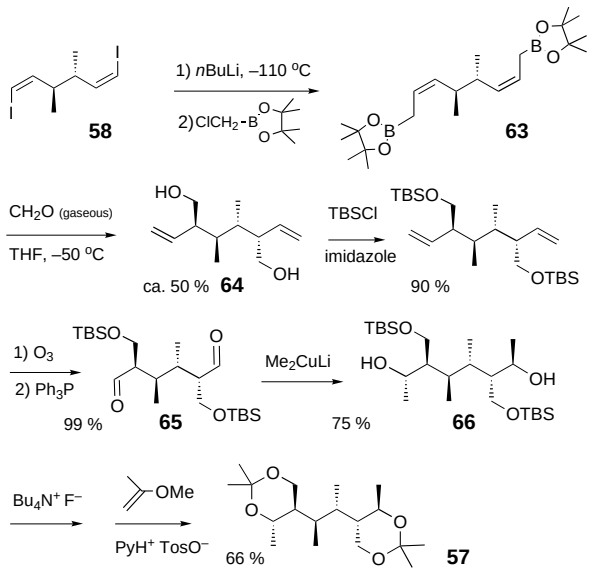

Scheme 22. Bidirectional synthesis of a *meso* bisdioxanylethane.

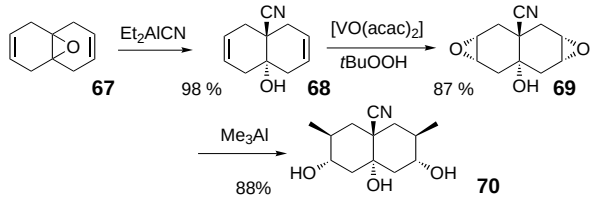

Scheme 23. Symmetrical synthesis of a *meso* triol.

The second example involves the synthesis of **76**, a precursor for polyether antibiotics (Scheme 24). Nelson and co-workers[32] converted the racemic epoxide **71** in one step into the centrosymmetric and hence achiral bisacetal **72**. This first step corresponds to the classical route to *meso* compounds delineated in Scheme 8, as the epoxide is opened with inversion of configuration. The concomitant acetal formation proceeded under thermodynamic control to place both methoxy groups in **72** in axial positions. The bisacetal **72** was then elaborated further in a bidirectional manner:

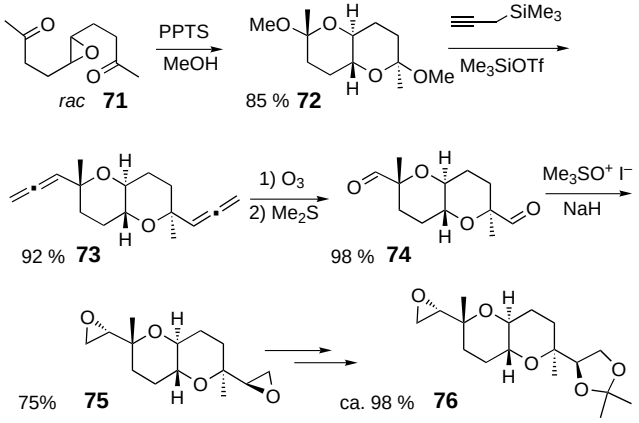

Scheme 24. Synthesis of a centrosymmetric brevetoxin building block.

Reaction with 3-trimethylsilylpropyne provided the bisallene **73** with axial entry of the allene moieties. Oxidative degradation furnished the dialdehyde **74**, which on reaction with dimethylsulfoxonium ylide furnished the diepoxide **75** with 20:1 asymmetric induction from the resident stereocenters. The symmetry of this centrosymmetric diepoxide was then broken by an enantioselective epoxide hydrolysis,[33] that is, by kinetic resolution of the two enantiotopic ends of the molecule to give the desired building block **76**. This approach to **76** is much shorter than a reaction sequence reported earlier, which did not capitalize on the latent symmetry of the target structure.[34]

5. The Convergent Approach

As a prelude to a synthesis of a conformationally preorganized flexible β-turn mimetic,[35] we targeted the *meso* diol **77** to study its conformational properties.[36] The stereogenic centers in **77** are not adjacent and span a distance of > 1,4. Especially as the bond that is the locus of the center of inversion (or that is bisected by a plane of symmetry) is not attached to stereogenic centers, a convergent approach was envisaged (Scheme 25), by which two formally enantiomeric

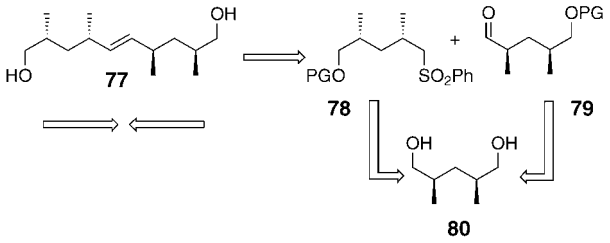

Scheme 25. Retrosynthetic analysis of extended σ-symmetric diol **77**.

building blocks **78** and **79** were to be linked to one another.

The task of having to prepare two essentially enantiomeric building blocks can be lessened in this case, as **78** and **79** have a latent plane of symmetry themselves. They could therefore both be derived by enantiotope-selective desymmetrization of a *meso* compound such as **80**. Compound **80** is readily available by reduction of *meso*-2,4-dimethylglutaric anhydride (**81**; Scheme 26).

Desymmetrization of **80** was effected by lipase-catalyzed acetylation to give **82** in 62% yield and 87% *ee*. Although

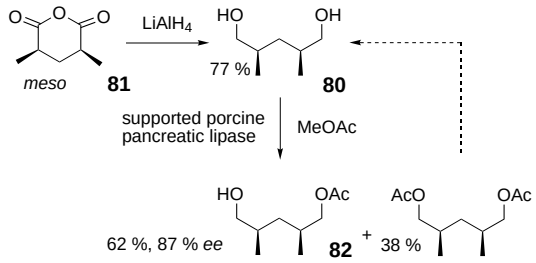

Scheme 26. Enzymatic desymmetrization of a *meso* diol.

longer reaction times could have led to **82** with higher *ee* values at the expense of the yield,[37] the use of this option was not deemed necessary because the *ee* value would be increased upon combination of the two building blocks **78** and **79** based on Horeau's principle.[38] The monoacetate **82** with 87% *ee* was therefore used as the starting point for the generation of the building blocks **83** (corresponding to **79**) and **85** (corresponding to **78**) as shown in Scheme 27.

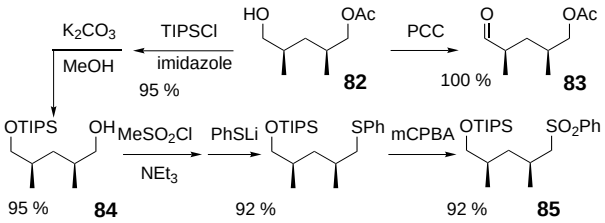

Scheme 27. Synthesis of two enantio-complementary building blocks from a single precursor.

The monoacetate **82** was directly oxidized to the required aldehyde **83**. Entry into the quasienantiomeric series was gained by interchange of the end-group protecting groups of **82** to give **84**, a possibility opened by the latent symmetry of the compounds. The elaboration of **84** into the building block **85** was then straightforward. The two quasienantiomeric building blocks were then joined in an *E*-selective Julia–Lythgoe olefination to give the target molecule **77** (Scheme 28).

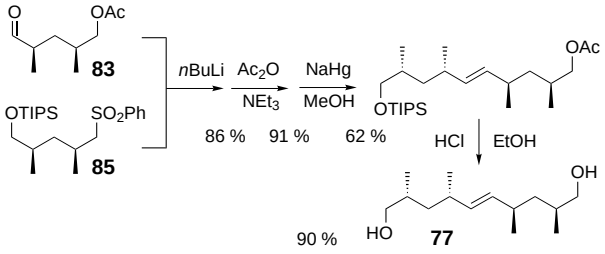

Scheme 28. Convergent synthesis of an extended open-chain *meso* diol.

Thus, in the case of **77** the convergent approach proved to be quite effective as both quasienantiomeric building blocks **83** and **85** could be derived easily in an enantiodivergent fashion from a simple *meso* diol **80** and because the linkage region in the target structure did not contain any stereogenic centers. If the latter condition does not hold, as in the target structure **86**, the convergent approach becomes unpredictable. Nevertheless, compound **86** suggested a convergent synthesis from **87** and *ent*-**87** as end groups to be linked by construction of the central dioxane ring (Scheme 29).[39]

A disadvantage of this approach is the inconvenience of having to synthesize both **87** and *ent*-**87** in separate, however identical, reaction sequences from (*S*)- and (*R*)-dimethyl malate through Frater alkylation, borane reduction, regioselective acetalization, and oxidation (Scheme 30). For the linkage of these two building blocks and the construction of

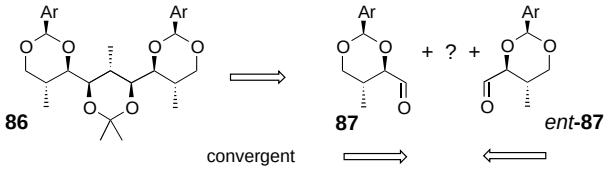

Scheme 29. Retrosynthesis of a *meso* terdioxane.

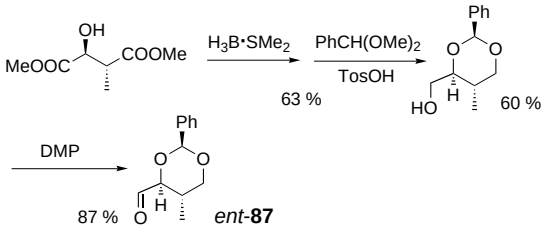

Scheme 30. Synthesis of the enantiomerically pure building blocks.

the central ring we envisaged an aldol addition of ketone **88** and the aldehyde **87**. This amounts to the creation of two (ultimately three) stereogenic centers in the linkage region, and that is where the problem resides.

Both the aldehyde **87** and the ketone **88** have stereogenic centers from which substrate-based asymmetric induction in the formation of the new stereogenic centers may originate. The configuration of the resident stereocenters in **88** and **87** is opposite, although this fact is not necessarily relevant. It is thus not known whether the asymmetric induction from the two components is matched or mismatched.[40] If the latter situation prevails, low diastereoselectivity is to be expected. Even, in matched situations the desired stereoisomer is not necessarily favored. Hence the convergent approach to **86** is a gamble. All one can hope for is that the odds could somehow be turned in our favor by recourse to the multitude of variants of stereoselective aldol additions.[41]

The synthesis began with the conversion of the aldehyde *ent*-**87** into the ketone **88** (Scheme 31).[39] As the relative configuration of the stereogenic centers of the central ring in **86** required an *anti* aldol **89** as precursor, ketone **88** was

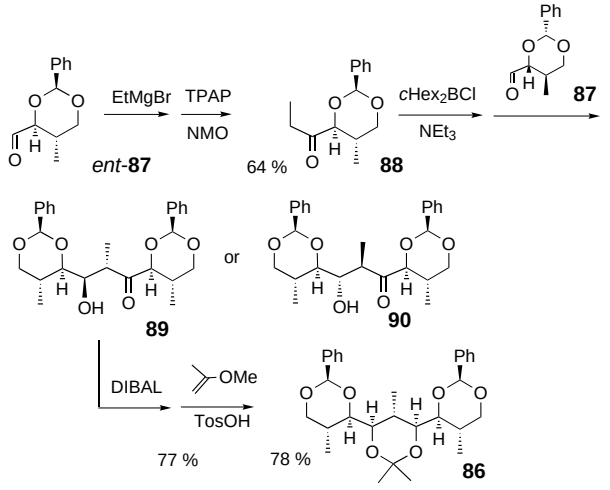

Scheme 31. Convergent synthesis of a *meso* terdioxane.

converted into an *E*-enolborinate, which upon addition to the aldehyde **87** furnished a single product in 89% yield. The obtained product was an *anti* aldol product, but we had no means to establish whether it is the desired **89** or the undesired **90**. Nevertheless, we converted the aldol into the terdioxane by 1,3-*syn* reduction followed by acetalization. At this stage, a comparison of experimental and calculated $^3J_{H,H}$ coupling constants suggested that we had indeed obtained the desired compound **86**.

With hindsight, the convergent approach proved to be viable in the case of **86**; this was rather fortunate as the stereochemical outcome of the aldol addition was not predictable. In a way, this situation resembles that in convergent natural product syntheses, in which stereogenic centers have to be formed during the linkage of the components, each of which have several stereogenic centers. This is a problematic situation, which one normally tends to avoid.[24,42]

As *meso* compounds are achiral, it is tempting to ask why a convergent synthesis of a *meso* compounds starting with a *racemate* of the end groups is not feasible? The answer lies in the fact that the techniques of stereoselective synthesis have not been developed to the point at which it is possible to handle *meso*/D,L selectivity to an acceptable level. This can be illustrated with *meso* compounds **93** and **94** (Scheme 32).

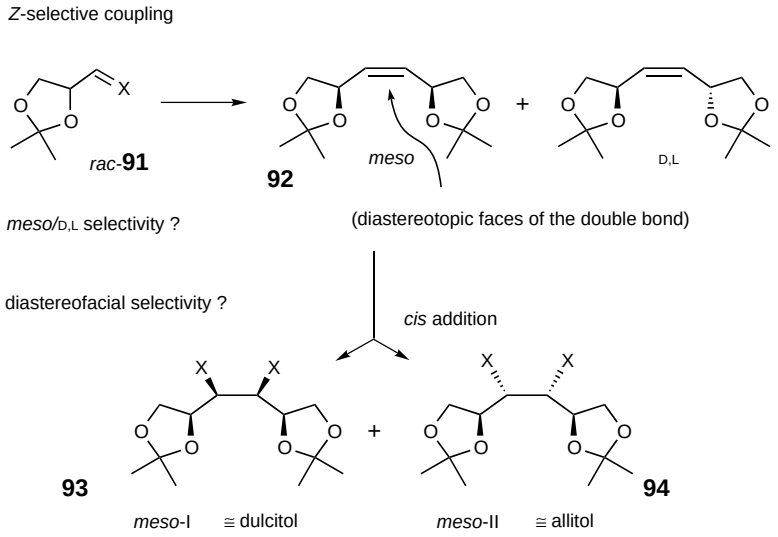

Scheme 32. Hypothetical access to *meso* compounds through *Z*-selective coupling of a racemate.

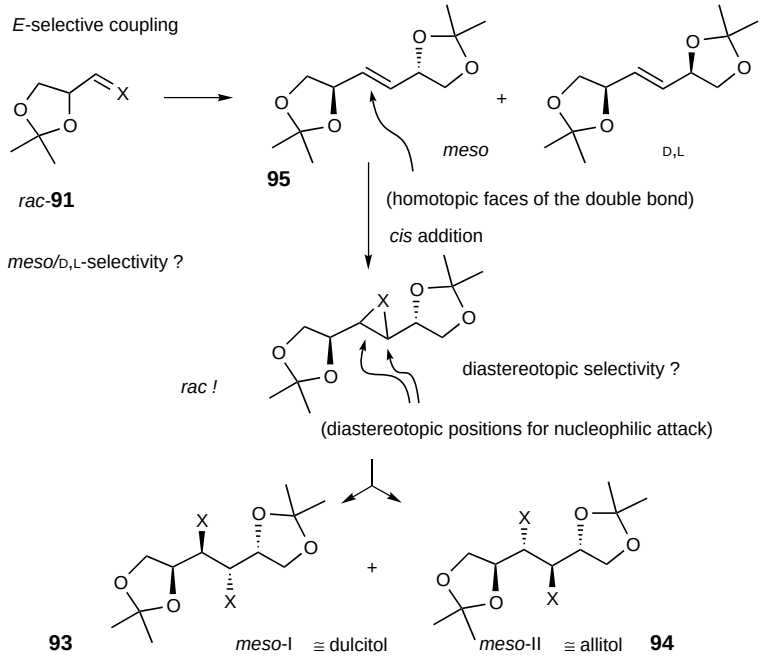

Scheme 33. Hypothetical access to *meso* compounds through *E*-selective coupling of a racemate.

To reach the *meso* compounds in such a coupling reaction, several selectivities have to be mastered simultaneously. The coupling of the two end groups **91** could be envisioned, for example, by a McMurry reaction (X = O), olefin metathesis (X = CH_2), or oxidation (X = PPh_3) to form an alkene in the linkage region. This coupling involves, first, *meso*/D,L selectivity. Moreover, the *E* or *Z* geometry of the double bond has to be controlled. If we were in a position to perform this coupling *Z* selectively, once compound **92** was obtained with sufficient selectivity, its further conversion into either compound **93** (*meso*-I) or **94** (*meso*-II) would involve diastereofacially selective functionalization of a double bond, a task that appears to be manageable.[43,44]

It is quite clear that the key problem in the conversion of *rac*-**91** into either **93** or **94** is the mastering of *meso*/D,L selectivity. Unfortunately, such selectivity is generally not observed in the doubling up of a racemate such as **91** by a coupling reaction. Indeed, this fact forms the basis of Horeau's test to determine enantiomeric enrichment.[38] Admittedly, there had been no efforts to optimize *meso*/D,L selectivity for application in synthesis.

In a related approach, if we were in a position to perform the coupling of the end groups **91** in an *E*-selective manner to give **95**, *meso*/D,L selectivity would once again be the main problem (Scheme 33). Once compound **95** were in hand, the next step, for example, epoxidation of the homotopic face of the double bond to give a racemate of the epoxide,[45] would not present problems of stereochemistry. However, the subsequent opening of the epoxide would require a diastereotopically selective nucleophilic attack to reach either compound **93** (*meso*-I) or **94** (*meso*-II) in a controlled manner. The latter selectivity is also an uncharted area of stereoselective synthesis.

In the approaches just discussed, the hopefully *meso*-selective coupling of the end groups and the establishment of the stereogenic centers in the linkage region were assigned to two different chemical operations. A pinacol coupling of **91** would combine both operations in one step (Scheme 34). The pinacol coupling could, however, give rise to a total of six isomeric coupling products. The development of methods in stereoselective synthesis has not reached the stage at which

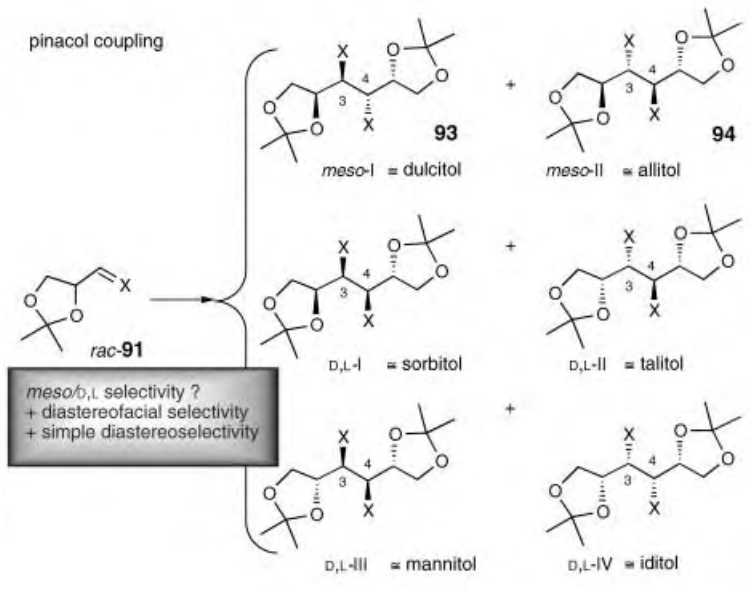

Scheme 34. Hypothetical access to *meso* compounds through reductive pinacol coupling of a racemic aldehyde.

the three types of selectivities involved in this reaction can be controlled simultaneously. One such type is simple diastereoselectivity (3,4-*syn* versus 3,4-*anti*). The formation of compounds **93** (*meso*-I) and **94** (*meso*-II) requires a 3,4-*anti* arrangement, which is disfavored in most reported pinacol coupling reactions.[46,47]

The current lack of *meso*-selective coupling reactions of racemates is reflected in the otherwise spectacular synthesis of an expanded cubane, which is hampered by separation problems and substantial losses of material.[58] These deficiencies in stereoselective synthesis demonstrate why convergent synthesis of *meso* compounds still relies on a pair of enantiomerically pure starting materials of opposite configuration.

6. The Linear Approach

The linear approach to stereochemically complex *meso* compounds is unattractive, as is the case in any linear synthesis, because it generally requires more steps than a convergent approach. On the other hand, a linear synthesis has the advantage of higher predictability and—in the case of *meso* compounds—of not having any restrictions in the methods to be used. In fact, it is preferable to use enantiomerically pure starting materials, because the total arsenal of stereoselective synthesis, including chiral reagents, chiral catalysts, and chiral auxiliaries, may be applied to set up the stereogenic centers in the target structures. It is therefore not surprising that the majority of approaches in the synthesis of the ansa chain **31** of rifamycin S are linear.[42]

Both the advantages and disadvantages of a linear synthesis can be illustrated in a synthesis of **96**,[48] which is related to **86**. As pointed out above, the stereochemical outcome of the synthesis of **86** was unpredictable and concrete proof of the relative configuration of the product was not available. We therefore embarked on a linear synthesis of **96** that would also allow the stereochemical assignment of **86**. This overall linear approach contains some bidirectional and convergent elements (Scheme 35).

The plan was to use enantiomerically pure building blocks **97** and **98** of defined absolute configuration, despite the fact that the target structure **96** is achiral. The synthesis started from (*R,R*)-dimethyl tartrate (**99**), which was converted into the known bisisopropenyl dioxane **100** (Scheme 36).[49] The two additional stereogenic centers were created subsequently in a bidirectional hydroboration to give the diol **101**. Since this is a C_2-symmetric compound, the ends of the molecule are homotopic. Therefore, monoprotection of one hydroxy group to give **102** proceeded without a problem of stereochemistry.

The linear part of the synthesis begins at this point (Scheme 37): The free hydroxy group in **102** was converted into a sulfone function to set the

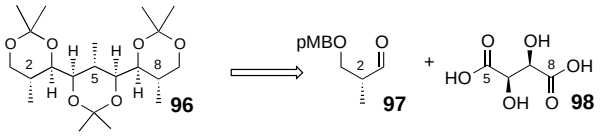

Scheme 35. Retrosynthesis for a linear approach to a *meso*-terdioxane.

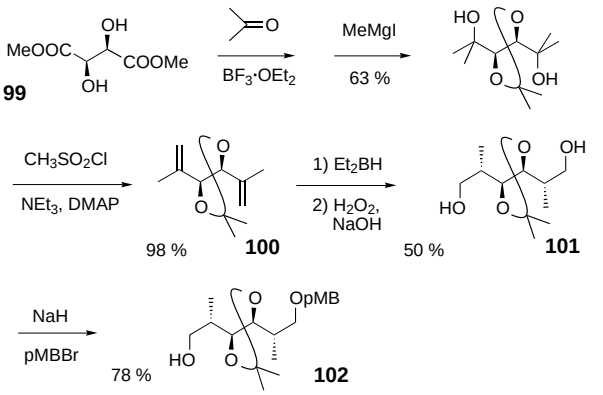

Scheme 36. Linear synthesis via C_2-symmetric intermediates.

stage for a Julia–Lythgoe olefination. Combination of the sulfone **103** with the aldehyde **97** furnished the olefin (*E*)-**104**, which contained minor amounts of the *Z* counterpart; however, the latter were unreactive in the next step, the dihydroxylation reaction, and were therefore not removed. Simple dihydroxylation of **104,** which relies on substrate-based asymmetric induction, met with low diastereoselectivity. Here, the advantage of a synthesis in the enantiomerically pure series becomes clear, as asymmetric dihydroxylation, that is, reagent control of diastereoselectivity, may be applied. This allowed the dihydroxylation to proceed with 10:1

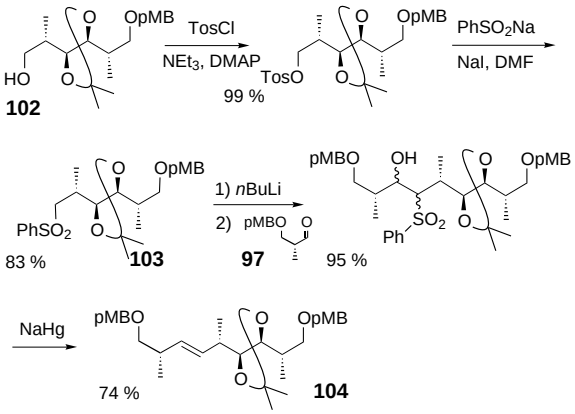

Scheme 37. Elaboration of intermediates for a linear synthesis of a *meso* terdioxane.

selectivity in favor of **105**. That the major diastereomer is the correct one, followed from its ultimate conversion into the symmetrical *meso* hexaol **106**, which in turn was converted into the terdioxane **96** (Scheme 38).[48]

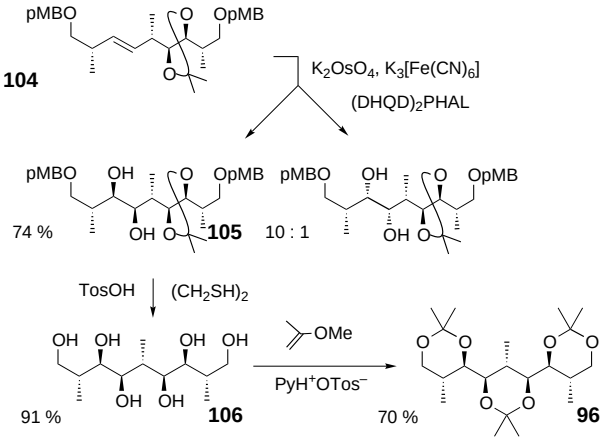

Scheme 38. Final steps in a linear synthesis of a *meso* terdioxane.

The synthesis of **96** demonstrated that the linear approach in the enantiomerically pure series is reliable and lacks any stereochemical ambiguity, albeit more laborious. The hallmark of the linear approach is that every stereogenic center in the target molecule is introduced with defined absolute configuration to afford a symmetrical molecule in the end.

Such an approach is attractive if the number of (remote) stereogenic centers in the desired *meso* compound is low. This is illustrated in Scheme 39 with respect to *meso*-diaminopimelic acid (**110**), a compound of continuing interest.[50] Two syntheses,[51] which feature the independent generation of stereocenters, are depicted below (for further syntheses, see reference [52])

In one of the syntheses, the first stereogenic center stems from natural glutamic acid. This starting compound **107** was elaborated into the α,β-unsaturated amino ester **108**. Subsequently, the second stereogenic center was introduced by

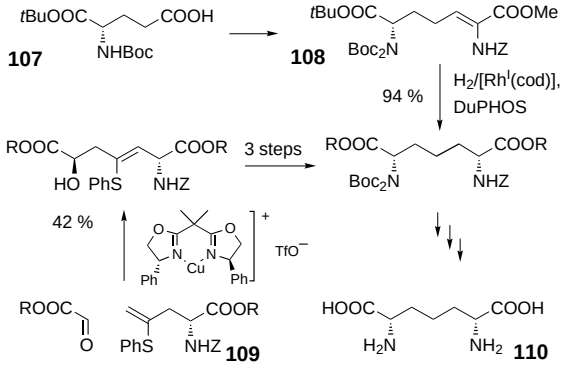

Scheme 39. Synthetic approaches to *meso*-diaminopimelic acid.

reagent control of diastereoselectivity, that is, by asymmetric hydrogenation with a chiral catalyst. In the second synthesis, the modified amino acid derivative **109** was generated from the chiral pool. Chiral catalysis of an ene reaction was then used to set up the second stereocenter. These are typical examples in which the creation of the second stereocenter does not depend on the configuration of the (remote) resident stereocenter.

If, however, long-range (i.e. $\geq$1,5) asymmetric induction can be applied, external asymmetric induction is not necessary (reagent control of the diastereoselectivity) and a linear synthesis of a *meso* compound is also possible from a racemate. This is illustrated in Scheme 40 in the conversion of the hemiacetal **111** into the diol *meso*-**112**.[53]

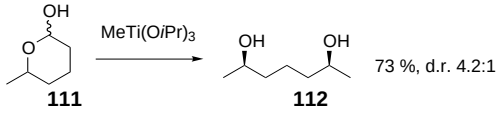

Scheme 40. Linear synthesis of a *meso* 1,5-diol with 1,5-asymmetric induction.

Abbreviations

Bn	benzyl
Boc	*tert*-butyloxycarbonyl
cod	1,4-cyclooctadiene
$(DHQD)_2PHAL$	dihydroquinidine-(1,4-phthalazinediyl diether) (chiral ligand for asymmetric dihydroxylation)[55]
DIBAL	diisobutylaluminum hydride
DMAP	4-dimethylaminopyridine
DMF	*N,N*-dimethylformamide
DMP	Dess–Martin periodinane[54]
DPTBS	*tert*-butyldiphenylsilyl
DuPHOS	chiral ligand for hydrogenation[56]
Ipc	isopinocampheyl
MCPBA	*m*-chloroperbenzoic acid
NMO	*N*-methylmorpholine *N*-oxide
PCC	pyridinium chlorochromate
PG	protecting group

PLE	porcine liver esterase
pMB	*p*-methoxybenzyl
pMP	*p*-methoxyphenyl
PPTS	pyridinium *p*-toluenesulfonate
py	pyridine
Swern	Swern oxidation[57]
TBS	*tert*-butyldimethylsilyl
TIPS	triisopropylsilyl
Tf	trifluoromethanesulfonyl
TMS	trimethylsilyl
Tos	*p*-toluenesulfonyl
TPAP	tetrapropylammonium perruthenate
Tr	triphenylmethyl
Z	benzyloxycarbonyl

The results from the research of our own group described in this review could not have been obtained without the continued support from the Fonds der Chemischen Industrie, the Deutsche Forschungsgemeinschaft, and the Volkswagen Stiftung.

Received: June 14, 2002 [A542]

[1] F. W. Lichtenthaler, *Angew. Chem.* **1992**, *104*, 1577 – 1593; *Angew. Chem. Int. Ed. Engl.* **1992**, *31*, 1541 – 1556.
[2] M. Ohtani, T. Matsuura, F. Watanabe, M. Narisada, *J. Org. Chem.* **1991**, *56*, 4120 – 4123.
[3] a) A. Fischli, M. Klaus, H. Mayer, P. Schönholzer, R. Rüegg, *Helv. Chim. Acta* **1975**, *58*, 564 – 584; b) A. Fischli, *Nachr. Chem. Tech. Lab.* **1977**, *25*, 390 – 394.
[4] H. B. Kagan, J. C. Fiaud, *Top. Stereochem.* **1988**, *18*, 249 – 330.
[5] D. Seebach, G. Jaeschke, *J. Org. Chem.* **1998**, *63*, 1190 – 1197.
[6] a) R. S. Ward, *Chem. Soc. Rev.* **1990**, *19*, 1 – 19; b) M. Ohno, M. Otsuka, *Org. React.* **1989**, *37*, 1 – 55; c) H.-J. Gais, *Methods Org. Synth. (Houben-Weyl) 4th ed. 1952–, Vol. E21a*, **1995**, pp. 589 – 643; d) E. Schoffers, A. Golebiowski, C. R. Johnson, *Tetrahedron* **1996**, *52*, 3769 – 3826; e) D. M. Hodgeson, A. R. Gibbs, G. P. Lee, *Tetrahedron* **1996**, *52*, 14361 – 14384; f) P. Chiu, M. Lautens, *Top. Curr. Chem.* **1997**, *190*, 1 – 85; g) M. C. Willis, *J. Chem. Soc. Perkin Trans. 1* **1999**, 1765 – 1784; h) E. N. Jacobsen, *Acc. Chem. Res.* **2000**, *33*, 421 – 423; i) M. Lautens, C. Dockendorff, K. Fagnou, A. Malicki, *Org. Lett.* **2002**, *4*, 1311 – 1314.
[7] a) S. BouzBas, J. Cossy, *Org. Lett.* **2001**, *3*, 3995 – 3998; b) J. Tullis, L. Vares, N. Kann, P.-O. Norrby, T. Rein, *J. Org. Chem.* **1998**, *63*, 8284 – 8294.
[8] a) Y. Mori, H. Hayashi, *J. Org. Chem.* **2001**, *66*, 8666 – 8668; b) vgl. auch: H. M. R. Hoffmann, R. Dunkel, M. Mentzel, H. Reuter, C. B. W. Stark, *Chem. Eur. J.* **2001**, *7*, 4772 – 4789.
[9] a) A. M. Miske, H. M. R. Hoffmann, *Chem. Eur. J.* **2000**, *6*, 3313 – 3320; b) G. W. Hunt, P. A. Grieco, *Org. Lett.* **2002**, *4*, 245 – 248; c) S. Woo, B. A. Keay, *Synthesis* **1996**, 669 – 686; d) M. Lautens, J. T. Colucci, S. Hiebert, N. D. Smith, G. Bouchain, *Org. Lett.* **2002**, *4*, 1879 – 1882.
[10] K. Hiroya, Y. Kurihara, K. Ogasawara, *Angew. Chem.* **1995**, *107*, 2245 – 2248; *Angew. Chem. Int. Ed. Engl.* **1995**, *34*, 2287 – 2289.
[11] Y.-F. Wang, C. J. Sih, *Tetrahedron Lett.* **1984**, *25*, 4999 – 5002.
[12] C. R. Johnson, A. Golebiowski, D. H. Steensma, *J. Am. Chem. Soc.* **1992**, *114*, 9414 – 9418.
[13] a) M. Asami, *Tetrahedron Lett.* **1985**, *26*, 5803 – 5806; b) D. Milne, P. J. Murphey, *J. Chem. Soc. Chem. Commun.* **1993**, 884 – 886.
[14] R. W. Hoffmann, *Angew. Chem.* **2000**, *112*, 2134 – 2150; *Angew. Chem. Int. Ed.* **2000**, *39*, 2054 – 2070.
[15] J. Sauer, R. Sustmann, *Angew. Chem.* **1980**, *92*, 773 – 801; *Angew. Chem. Int. Ed. Engl.* **1980**, *19*, 779 – 807.
[16] C. Marchionni, P. Vogel, P. Roversi, *Tetrahedron Lett.* **1996**, *37*, 4149 – 4152.
[17] C. S. Poss, S. L. Schreiber, *Acc. Chem. Res.* **1994**, *27*, 9 – 17.
[18] S. R. Magnuson, *Tetrahedron* **1995**, *51*, 2167 – 2213.
[19] S. L. Schreiber, M. T. Goulet, *J. Am. Chem. Soc.* **1987**, *109*, 4718 – 4720.
[20] Z. Wang, D. Deschenes, *J. Am. Chem. Soc.* **1992**, *114*, 1090 – 1091.
[21] A. H. Hoveyda, D. A. Evans, S. C. Fu, *Chem. Rev.* **1993**, *93*, 1307 – 1370.
[22] W. C. Still, J. C. Barrish, *J. Am. Chem. Soc.* **1983**, *105*, 2487 – 2489.
[23] a) T. Harada, Y. Kagamihara, S. Tanaka, K. Sakamoto, A. Oku, *J. Org. Chem.* **1992**, *57*, 1637 – 1639; b) T. Harada, T. Egusa, Y. Igarashi, M. Kinugawa, A. Oku, *J. Org. Chem.* **2002**, *67*, 7080 – 7090.
[24] R. W. Hoffmann, *Angew. Chem.* **1987**, *99*, 503 – 517; *Angew. Chem. Int. Ed. Engl.* **1987**, *26*, 489 – 503.
[25] M. Born, C. Tamm, *Helv. Chim. Acta* **1990**, *73*, 2242 – 2250.
[26] H. Nagaoka, Y. Kishi, *Tetrahedron* **1981**, *37*, 3873 – 3888.
[27] T. Trieselmann, R. W. Hoffmann, K. Menzel, *Eur. J. Org. Chem.* **2002**, 1292 – 1304.
[28] R. W. Hoffmann, K. Menzel, K. Harms, *Eur. J. Org. Chem.* **2002**, 2603 – 2612.
[29] a) F. Johnson, *Chem. Rev.* **1968**, *68*, 375 – 413; b) R. W. Hoffmann, *Chem. Rev.* **1989**, *89*, 1841 – 1860.
[30] R. W. Hoffmann, K. Menzel, *Eur. J. Org. Chem.* **2001**, 2749 – 2755.
[31] A. C. Spivey, S. J. Woodhead, M. Weston, B. I. Andrews, *Angew. Chem.* **2001**, *113*, 791 – 793; *Angew. Chem. Int. Ed.* **2001**, *40*, 769 – 771.
[32] J. M. Holland, M. Lewis, A. Nelson, *Angew. Chem.* **2001**, *113*, 4206 – 4208; *Angew. Chem. Int. Ed.* **2001**, *40*, 4082 – 4084.
[33] D. M. Tokunaga, J. F. Larrow, F. Kakiuchi, E. N. Jacobsen, *Science* **1997**, *277*, 936 – 938.
[34] T. Nakata, *J. Synth. Org. Chem., Jpn.* **1998**, *56*, 940 – 951.
[35] U. Schopfer, M. Stahl, T. Brandl, R. W. Hoffmann, *Angew. Chem.* **1997**, *109*, 1805 – 1807; *Angew. Chem. Int. Ed. Engl.* **1997**, *36*, 1745 – 1747.
[36] R. W. Hoffmann, U. Schopfer, M. Stahl, *Tetrahedron Lett.* **1997**, *38*, 4055 – 4058.
[37] a) Y.-F. Wang, C.-S. Chen, G. Girdaukas, C. J. Sih, *J. Am. Chem. Soc.* **1984**, *106*, 3695 – 3696; b) C. J. Sih, S.-H. Wu, *Top. Stereochem.* **1989**, *19*, 63 – 125.
[38] a) V. Rautenstrauch, *Bull. Soc. Chim. Fr.* **1994**, *131*, 515 – 524; b) I. Fleming, S. K. Ghosh, *J. Chem. Soc. Chem. Commun.* **1994**, 99 – 100.
[39] R. W. Hoffmann, G. Mas, T. Brandl, *Eur. J. Org. Chem.* **2002**, 3455 – 3464.
[40] S. Masamune, W. Choy, J. S. Petersen, L. R. Sita, *Angew. Chem.* **1985**, *97*, 1 – 31; *Angew. Chem. Int. Ed. Engl.* **1985**, *24*, 1 – 30.
[41] C. J. Cowden, I. Paterson, *Org. React.* **1997**, *51*, 1 – 200.
[42] I. Paterson, M. M. Mansuri, *Tetrahedron* **1985**, *41*, 3569 – 3624.
[43] cf.: T. K. M. Shing, E. K. W. Tam, V. W-F. Tai, I. H. F. Chung, Q. Jiang, *Chem. Eur. J.* **1996**, *2*, 50 – 57.
[44] Such a coupling of racemic building block I was considered as a route to *meso* compound IV (A. Pletsch, Diplomarbeit Universität Marburg 2001). An identification of the individual coupling products II and III would have been possible by coupling of enantiomerically pure building block I, which gives rise to II only. The approach to IV shown in Scheme 41 was eventually abandoned on account of our inability to effect the *Z*-selective coupling of the building blocks.
[45] P. Köll, J. Kopf, J. O. Metzger, W. Schwarting, M. Oelting, *Liebigs Ann. Chem.* **1987**, 199 – 204.

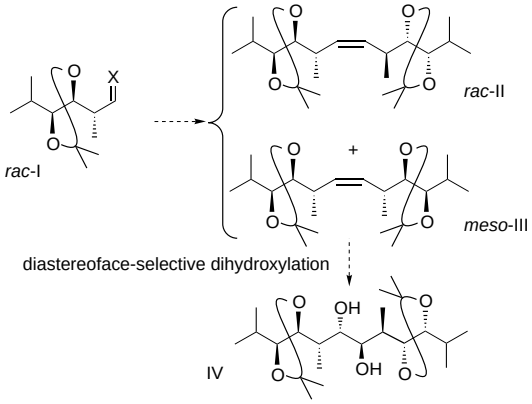

Scheme 41. Coupling of a racemate as a potential convergent route to a *meso* compound.

[46] For an example, see: B. K. Banik, *Eur. J. Org. Chem.* **2002**, 2431 – 2444.
[47] For an exception, see: R. Yanada, N. Negero, K. Yanada, T. Fujita, *Tetrahedron Lett.* **1997**, *38*, 3271 – 3274.
[48] T. Brandl, R. W. Hoffmann, *Eur. J. Org. Chem.* **2002**, 2613 – 2623.
[49] D. S. Matteson, E. C. Beedle, A. A. Kandil, *J. Org. Chem.* **1987**, *52*, 5034 – 5036.
[50] R. J. Cox, J. Durston, D. I. Roper, *J. Chem. Soc. Perkin Trans. 1* **2002**, 1029 – 1035, and references therein.
[51] a) W. Wang, C. Xiong, J. Yang, V. Hruby, *Synthesis* **2002**, 94 – 98; b) Y. Gao, P. Lane-Bell, J. C. Vederas, *J. Org. Chem.* **1998**, *63*, 2133 – 2143.
[52] a) R. M. Williams, C. Yun, *J. Org. Chem.* **1992**, *57*, 6519 – 6527; b) F. A. Davis, V. Sirirajan, *J. Org. Chem.* **2000**, *65*, 3248 – 3251; c) J. L. Roberts, C. Chan, *Tetrahedron Lett.* **2002**, *43*, 7679 – 7682.
[53] a) K. Tomooka, T. Okinaga, K. Suzuki, G. I. Tsuchihashi, *Tetrahedron Lett.* **1987**, *28*, 6335 – 6338; b) E. M. Flamme, W. R. Roush, *J. Am. Chem. Soc.* **2002**, *124*, 13644 – 13645.
[54] D. B. Dess, J. C. Martin, *J. Am. Chem. Soc.* **1991**, *113*, 7277 – 7287.
[55] H. C. Kolb, M. S. VanNieuwenhze, K. B. Sharpless, *Chem. Rev.* **1994**, *94*, 2483 – 2547.
[56] M. J. Burk, J. E. Feaster, W. A. Nugent, R. L. Harlow, *J. Am. Chem. Soc.* **1993**, *115*, 10125 – 10138.
[57] A. J. Manusco, S.-L. Huang, D. Swern, *J. Org. Chem.* **1978**, *43*, 2480 – 2484.
[58] P. Manini, W. Amrein, V. Gramlich, F. Diederich, *Angew. Chem.* **2002**, *114*, 4515 – 4519; *Angew. Chem. Int. Ed.* **2002**, *41*, 4339 – 4343.

Communications

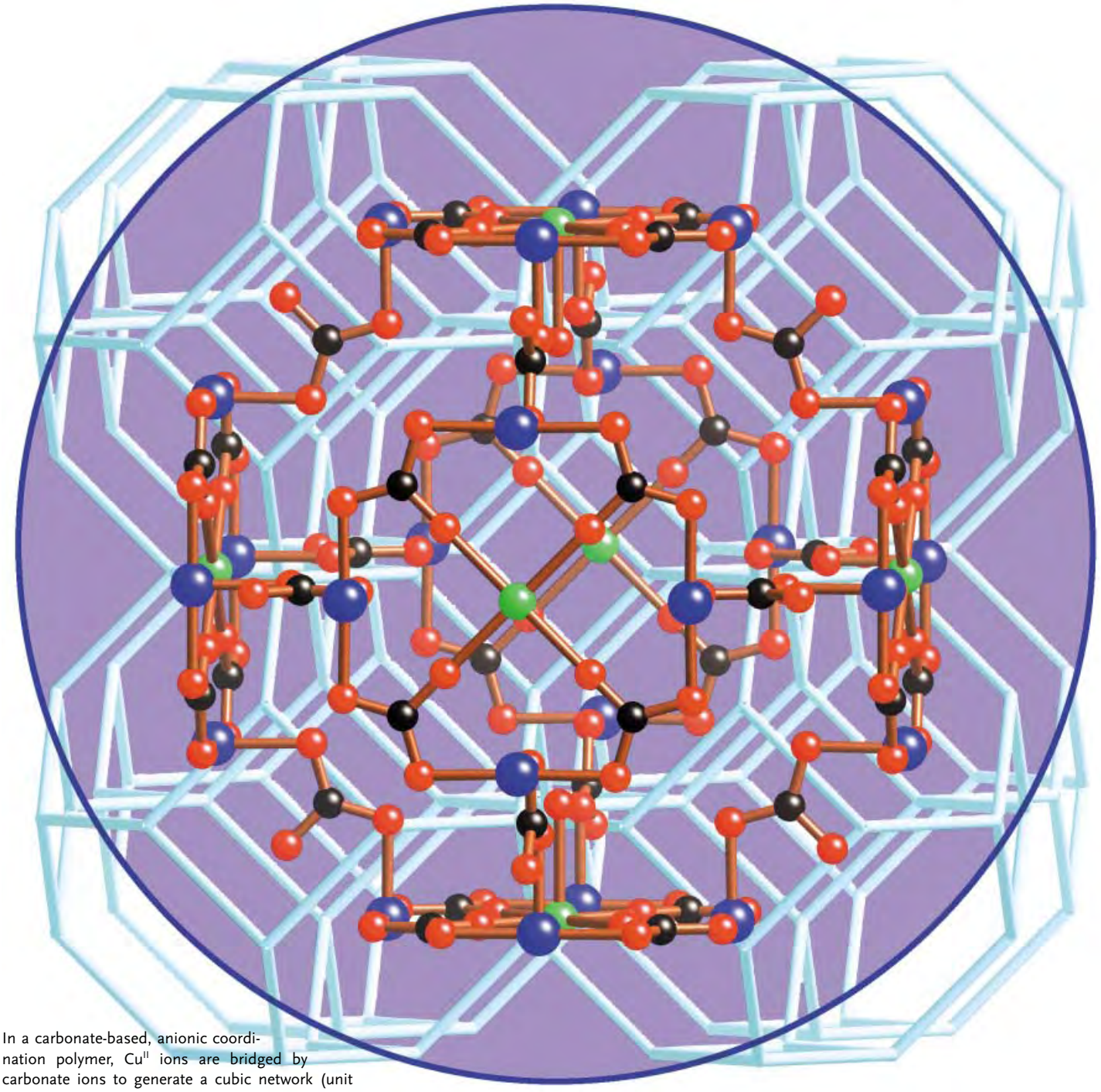

In a carbonate-based, anionic coordination polymer, Cu^{II} ions are bridged by carbonate ions to generate a cubic network (unit cell shown) with the same topology as the sodalite net depicted in the background. Pairs of guanidinium ions (not shown) serve as H-bonding templates located in the hexagonal windows of the sodalite cage, whilst alkali-metal ions (green) fit neatly into the square windows. For more information see the article by Robson and co-workers on the following pages.

 © 2003 Wiley-VCH Verlag GmbH & Co. KGaA, Weinheim 1433-7851/03/4210-1111 $ 20.00+.50/0

Crystal Engineering

New Tricks for an Old Dog: The Carbonate Ion as a Building Block for Networks Including Examples of Composition $[Cu_6(CO_3)_{12}\{C(NH_2)_3\}_8]^{4-}$ with the Sodalite Topology**

Brendan F. Abrahams, Marissa G. Haywood, Richard Robson, and Damian A. Slizys*

In memory of Bernard Hoskins

Metal carbonates have been extensively studied and the carbonate ion has been widely used as a ligand in coordination chemistry since Werner's day.[1] Despite this, we are convinced that large tracts of unexplored carbonate-based chemistry still lay open for exploration. Here we describe some new, highly symmetrical metal–carbonate networks that have the topology of the 4^26^4 sodalite net.[2] Structural studies of one-,[3] two-,[4] and three-dimensional[5] metal–carbonate polymers have been reported. In 1996 a beautiful network with cubic symmetry was described by Stucky et al. for the compound $Na_2Zn_3(CO_3)_4\cdot 3H_2O$.[6] We recently reported metal derivatives of a nitrogen-containing close analog of carbonate in a triply chelating connecting unit constructed around a dianionic, guanidine-based CN_3 core.[7] Because of its potential threefold axial symmetry, the CN_3 moiety is an attractive unit for network building, and the guanidinium ion, $[C(NH_2)_3]^+$, is an essential component of all the structures described below. The structures of the guanidinium-containing carbonate compounds $(CH_6N_3)_2[Zn(CO_3)_2]$[8] and $(CH_6N_3)_6[M(CO_3)_5]\cdot 4H_2O$, M = Ce,[9] Th,[10] have been reported previously.

$Cu(NO_3)_2$ dissolves readily in aqueous solutions containing $KHCO_3$ and K_2CO_3 in excess to give deep blue solutions. Upon treatment with a guanidinium salt in excess such solutions deposit crystals of royal blue **1**, which has according to X-ray diffraction studies[11] a diamond-like topology (Figure 1). It is interesting to note that the tetrahedral nodes required for the diamond net are here provided by seemingly incompatible square-planar O_4-coordinated copper centers: the pronounced bends in the carbonate connections between copper nodes make this possible. The guanidinium ion is secured within every cyclohexane-like $Cu_6(CO_3)_6$ "window" by multiple hydrogen bonds to carbonate oxygen atoms (Figure 1). This structure is surprisingly similar to that of $(CH_6N_3)_2[Zn(CO_3)_2]$,[8] which also has the diamond topology—surprising in our view because the zinc centers have

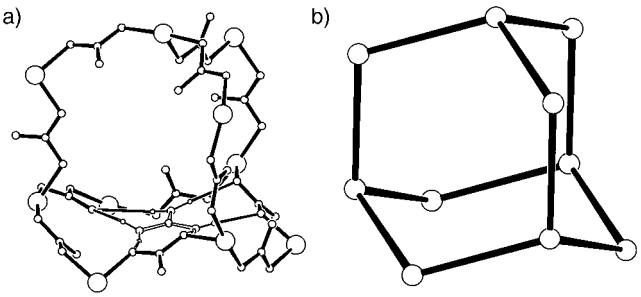

Figure 1. An adamantane unit in the diamond-like structure of **1**. a) Circles in order of decreasing radius represent Cu, O, N, C, and H. The Cu/CO_3 framework is indicated by heavy lines. For clarity, only the details of the hydrogen-bonded incorporation of the guanidinium ion into one of the cyclohexane-like windows is shown, represented by "open" connections. b) Only the Cu centers seen from the same angle as in (a).

an essentially tetrahedral O_4 environment in contrast to the square-planar O_4 environment of copper in **1**.

$(CH_6N_3)_2[Cu(CO_3)_2]$ **1**

In some reactions in which reduced proportions of guanidinium salt were added to the $Cu^{II}/KHCO_3/K_2CO_3$ solutions, we noticed that small quantities of a paler blue crystalline by-product, **2**, accompanied the predominant royal blue **1**. X-ray diffraction studies of **2**[11] revealed cubic symmetry and the topology of the 4^26^4 net. A representation of the parent 4^26^4 net, referred to here as the sodalite net is given in Figure 2; it can be visualized in terms of truncated

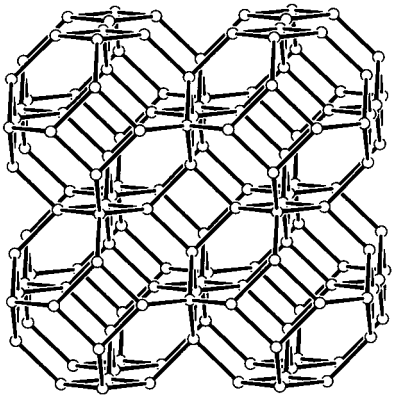

Figure 2. The 4^26^4 sodalite net showing a central sodalite cage surrounded by eight others.

octahedral sodalite cages sharing faces, both square and hexagonal. A representation of the copper and carbonate components of one such cage of **2** is shown in Figure 3a, and Figure 3b shows the truncated octahedron defined by the 24 copper centers associated with each cage. Again, as in the diamond-like structure of **1**, the essentially tetrahedral nodes of the sodalite net are provided by seemingly incompatible square-planar coordinated copper centers. Every $Cu_6(CO_3)_6$ hexagonal ring in the structure is occupied by a pair of

[*] Prof. R. Robson, Dr. B. F. Abrahams, M. G. Haywood, Dr. D. A. Slizys
School of Chemistry
University of Melbourne
Parkville, Victoria 3010 (Australia)
Fax: (+61) 3-9347-5180
E-mail: r.robson@unimelb.edu.au

[**] The authors gratefully acknowledge support from the Australian Research Council.

 © 2003 Wiley-VCH Verlag GmbH & Co. KGaA, Weinheim 1433-7851/03/4210-1112 $ 20.00+.50/0

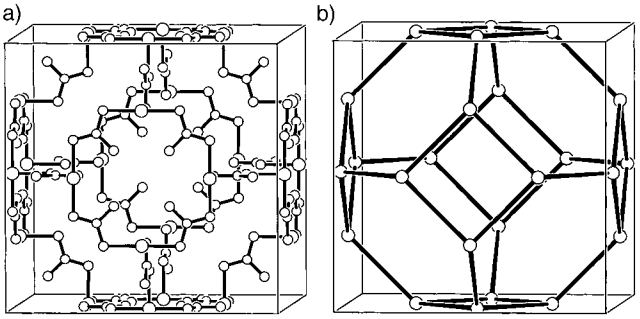

Figure 3. a) A single sodalite cage in the structure of **2**. For clarity, only copper and carbonate are shown. b) The truncated octahedron defined by the 24 copper centers associated with each cage seen from the same angle as in (a).

guanidinium ions arranged around a $\bar{3}m$ site (Figure 4). The separation between the guanidinium ions (C···C 3.19 Å) is remarkably close for two like-charged species. The pair is held in place by a symmetrical array of twelve equivalent hydrogen bonds to the coordinated carbonate oxygen atoms of the surrounding $Cu_6(CO_3)_6$ ring.

$[Cu_6(CO_3)_{12}(CH_6N_3)_8] \cdot 4\,K \cdot 8\,H_2O$ **2**

All atoms within the $Cu_4(CO_3)_4$ units of **2** representing the square faces of the truncated octahedral cages are internally coplanar and the carbonate ions are so oriented that the four noncoordinated C=O groups point directly at the center of the square (see Figure 3a). We refer to the spaces at the centers of such quartets of noncoordinated oxygen atoms below as "the O_4 holes". The sodalite cages in **2** are larger than those in the aluminosilicate compounds sodalite and ultramarine and contain four K^+ ions and eight H_2O molecules which are disordered, as are the contents of the cages in the other sodalite analogs we report below and as are the contents of the cages in many of the aluminosilicate analogs. The K^+ ions are located equidistant from the four oxygen atoms of an O_4 hole (K-O 2.7 Å, Figure 5). The four K^+ ions are disordered over all six such sites in the cage. The two sites of this type not occupied by K^+ are occupied by two of the water molecules which have not exactly the same

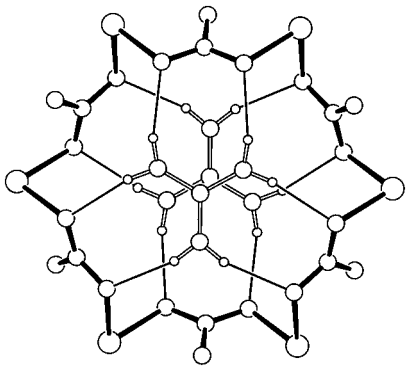

Figure 4. Representation of the pair of guanidinium ions hydrogen-bonded (thin lines) inside a $Cu_6(CO_3)_6$ hexagonal face in the structure of **2**.

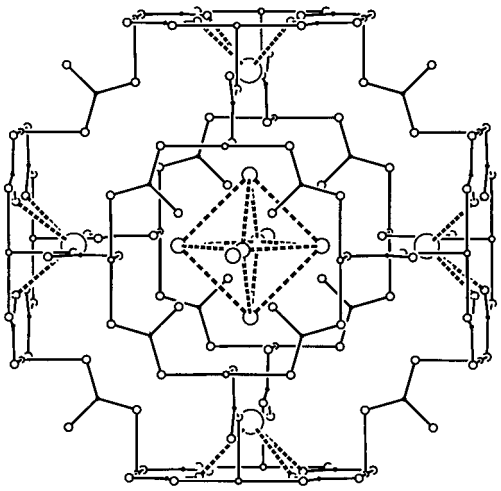

Figure 5. Representation of one possible arrangement of the disordered four K^+ ions and eight H_2O molecules within a sodalite cage of **2**. Circles in order of decreasing radius represent K, O_{H_2O}, $O_{CO_3^{2-}}$, and Cu.

distance from the O_4 set as have the K^+ ions. The remaining six water molecules form an inner shell located roughly at the corners of an octahedron (see Figure 5).

We noticed that the O_4 square holes, with an O···O diagonal of 4.16 Å, although far too small to accomodate K^+ within the O_4 plane (as we saw above), might possibly accomodate an in-plane Li^+ ion very satisfactorily. If it were possible to incorporate Li^+ into every O_4 hole the composition and charge per cage would be $[\{Cu_6(CO_3)_{12}(CH_6N_3)_8\}Li_3]^-$ and we wondered if a tetramethylammonium ion might then be nicely accomodated inside the mononegative cage so formed. We discovered that crystals of **3**[11] with the intended composition and with the intended sodalite structure were indeed formed when aqueous solutions of NMe_4HCO_3 and $(NMe_4)_2CO_3$ in excess, $Cu(NO_3)_2$, $LiNO_3$, and guanidinium nitrate were brought together at room temperature. This constitutes the assembly of five components under extremely simple conditions into a deliberately intended extended three-dimensional structure—true crystal engineering.

$[Cu_6(CO_3)_{12}(CH_6N_3)_8] \cdot 3\,Li \cdot NMe_4 \cdot 5\,H_2O$ **3**

Subsequently we discovered that **3** could also be obtained by adding $LiNO_3$, guanidinium nitrate, and NMe_4Cl to the Cu/$KHCO_3$/K_2CO_3 solutions referred to above; it is significant in this procedure that the crystallizing system incorporates Li^+ in preference to K^+ that is available in large excess. X-ray diffraction analysis[11] indicates that the $[Cu_6(CO_3)_{12}(CH_6N_3)_8]^{4-}$ components adopt a sodalite-like topology essentially identical to that seen in **2**, with Li^+ located at the center of every O_4 hole. The $(NMe_4^+)(H_2O)_5$ contents of the cages are disordered. The five water molecules are located 2.01 Å from Li^+ on the normal to the O_4 plane and are disordered over the six available sites of this type. The NMe_4^+ ions are orientationally disordered in compliance with the particular distribution of the five water molecules.

 © 2003 Wiley-VCH Verlag GmbH & Co. KGaA, Weinheim 1433-7851/03/4210-1113 $ 20.00+.50/0

It was clear from the structure of **2** that the K^+ ion, constrained by its size to a location well out of the plane of the O_4 hole, together with its associated water molecule, would occupy too much space to allow the simultaneous incorporation of NMe_4^+ in the cage, and not surprisingly, all attempts to generate a K^+/NMe_4^+ sodalite structure have failed. However it was of interest to explore the combination of NMe_4^+ with Na^+ the size of which is intermediate between those of K^+ and Li^+. Crystals of **4**[11] were obtained by the addition of $NaNO_3$ and guanidinium nitrate to solutions of copper nitrate and NMe_4HCO_3 and $(NMe_4)_2CO_3$ in excess. The sodalite structure is again observed.[11]

$[Cu_6(CO_3)_{12}(CH_6N_3)_8] \cdot 3\,Na \cdot NMe_4 \cdot H_2O$ **4**

Subsequently we discovered that **4** could also be obtained by adding $NaNO_3$ and guanidinium nitrate to the $Cu/KHCO_3/K_2CO_3$ solution—again, the K^+ ions present in large excess are not incorporated. It is significant that whilst the Li^+ ions in **3** allow the incorporation of five water molecules the larger Na^+ ions allow only one water molecule per cage. The cage contents are again disordered. The nitrogen atom of NMe_4^+ lies on a $m\bar{3}m$ position and the methyl groups are disordered over a number of positions. It appears that, as a consequence of the fact that the single "coordinated" water molecule per cage projects further into the cage towards the NMe_4^+ ion than in the Li^+ case, the water molecule can be accomodated only when a methyl group is pointing directly away from it.

The presence of Gd^{3+} has a profound effect on the course of reactions between Cu^{2+}, CO_3^{2-}, and $CH_6N_3^+$ that would otherwise have given **1**. Two side-by-side aqueous reaction mixtures containing the same reactants in the same concentrations (i.e. $KHCO_3$ and K_2CO_3 in excess, $Cu(NO_3)_2$, and guanidinium nitrate), differing only in that $Gd(NO_3)_3$ is present in one, follow visibly very different courses: royal blue crystals of **1** are formed in the Gd-free mixture and pale blue crystals of **5** separate from the other. Somehow Gd^{3+} redirects the assembly of the components away from diamond-like **1** towards **5** which according to diffraction studies has the sodalite structure.[11] The contents of the cages are highly disordered.

$[Cu_6(CO_3)_{12}(CH_6N_3)_8] \cdot 2\,Gd \cdot 2\,K \cdot 4\,OH \cdot H_2O$ **5**

Preliminary experiments indicate that it is possible to incorporate divalent cations such as Mg^{2+} into the O_4 holes and that sodalite networks can be generated with cobalt(II) or zinc(II) in place of copper(II). The results presented here point to rich opportunities for truly deliberate crystal engineering of a wide range of related networks in which a variety of paramagnetic and/or redox-active metal centers could conceivably be organized in close proximity, the properties of which could be unusual and useful. The prospects for future developments in this area are enhanced by the extreme simplicity of the preparative procedures and the ready availability and cheapness of the components.

Experimental Section

1 and **2**: A solution of CH_6N_3Cl (595 mg, 4.9 mmol) in water (1 mL) was added to a solution of $K_2(CO_3)_2$ and $KHCO_3$ (2.4 and 1.25 M, respectively, 2 mL) in which $Cu(NO_3)_2 \cdot 3\,H_2O$ (196 mg, 0.81 mmol) had been dissolved. Royal blue crystals of **1** were collected after four days, washed with water, and dried in air. Yield: 235 mg, 95%. Elemental analysis: found: C 16.0, H 4.1, N 27.6, Cu 20.6; calc.: C 15.8, H 4.0, N 27.7, Cu 20.9. A reaction conducted as above, except that a smaller amount of CH_6N_3Cl (303 mg, 2.45 mmol) was used, yielded pale blue crystals of **2** together with the predominant deeper blue crystals of **1**. Crystals of **1** were separated from crystals of **2** by hand under the microscope for elemental analysis. Found (%): C 12.7, H 3.2, N 17.0, Cu 20.3, K 8.3; calcd: C 12.8, H 3.4, N 17.9, Cu 20.3, K 8.3. The crystals of **2** were insoluble in water.

3: A mixture of $LiNO_3$ (51 mg, 0.74 mmol), Me_4NCl (182 mg, 1.65 mmol), and $(CH_6N_3)_2CO_3$ (74 mg, 0.41 mmol) in water (1 mL) was added to a solution containing K_2CO_3, $KHCO_3$, and $Cu(NO_3)_2$ (2.41, 1.25, and 0.34 M, respectively, 2 mL). The pale blue-green crystals of **3** which separated were collected after 5 h, washed with water, and dried in air. Yield: 35 mg, 38%. Elemental analysis: found (%): C 16.8, H 3.7, N 19.8, Cu 22.4, Li 1.3; calcd: C 16.3, H 4.0, N 19.8, Cu 21.6, Li 1.2. The crystals were insoluble in water.

4: A solution containing $NaNO_3$ (316 mg, 3.72 mmol), $(CH_6N_3)_2CO_3$ (330 mg, 1.86 mmol), and Me_4Cl (680 mg, 6.2 mmol) in water (2 mL) was added to a solution containing K_2CO_3, $KHCO_3$, and $Cu(NO_3)_2$ (2.4, 1.25, and 0.34 M, respectively, 3 mL). The pale blue crystals of **4** that formed were collected after 15 min, washed with water, and dried in air. Yield: 186 mg, 45%. Elemental analysis: found (%): C 16.3, H 3.5, N 19.8, Cu 22.0, Na 4.5; calcd: C 16.5, H 3.6, N 20.1, Cu 21.9, Na 4.0. The crystals were insoluble in water.

5: A solution containing CH_6N_3Cl (119 mg, 1.25 mmol) in water (0.5 mL) was added to a solution (1 mL) containing K_2CO_3 (2.4 M), $KHCO_3$ (1.25 M), $Cu(NO_3)_2$ (0.17 M), and $Gd(NO_3)_3$ (0.092 M). Blue crystals began to form after 1 h and were collected after 1 day, washed with water, and dried in air. Yield: 60 mg, 63%. Elemental analysis: found (%): C 11.8, H 3.2, N 16.3, Cu 17.8, K 4.8, Gd 15.0; calcd: C 11.7, H 2.6, N 16.3, Cu 18.5, K 3.8, Gd 15.3. The crystals were insoluble in water.

Received: October 14, 2002 [Z50362]

Keywords: cage compounds · carbonates · coordination polymers · guanidinium ion · sodalite

[1] D. A. Palmer, R. van Eldik, *Chem. Rev.* **1983**, *83*, 651.
[2] A. F. Wells, *Three-Dimensional Nets and Polyhedra*, Wiley, New York, **1977**, p. 129.
[3] P. D. Brotherton, A. H. White, *J. Chem. Soc. Dalton Trans.* **1973**, 2338.
[4] P. C. Healy, A. H. White, *J. Chem. Soc. Dalton Trans.* **1972**, 1913.
[5] V. H. Seidel, K. Viswanathan, W. Johannes, H. Ehrhardt, *Z. Anorg. Allg. Chem.* **1974**, *410*, 138.
[6] T. E. Gier, X. Bu, S.-L. Wang, G. D. Stucky, *J. Am. Chem. Soc.* **1996**, *118*, 3039.
[7] I. M. Mueller, R. Robson, *Angew. Chem.* **2000**, *112*, 4327; *Angew. Chem. Int. Ed.* **2000**, *39*, 4357.
[8] W. T. A. Harrison, M. L. F. Phillips, T. M. Nenoff, E. J. MacLean, S. J. Teat, R. S. Maxwell, *J. Chem. Soc. Dalton Trans.* **2001**, 546.
[9] P. S. Voliotis, A. Rimsky, J. Faucherre, *Acta Crystallogr. Sect. B* **1975**, *31*, 2607.
[10] P. S. Voliotis, A. Rimsky, *Acta Crystallogr. Sect. B* **1975**, *31*, 2612.
[11] Crystal data for compounds **1**–**5**: **1**: Tetragonal, $P\bar{4}n2$, $a = 9.0368(6)$, $c = 12.5364(16)$ Å, $V = 1023.77(16)$ Å^3, $\rho_{calcd} = 1.971$ g cm^{-3}. 1187 unique reflections out of 6089 reflections measured, $R_1 = 0.0206$, $wR_2 = 0.0582$. Compounds **2**–**5** are all

 © 2003 Wiley-VCH Verlag GmbH & Co. KGaA, Weinheim 1433-7851/03/4210-1114 $ 20.00+.50/0

cubic, space group $Im\bar{3}m$. **2**: $a = 14.3828(4)$ Å, $V = 2975.30(14)$ Å^3, $\rho_{calcd} = 2.101$ g cm^{-3}, 374 unique reflections out of 9423 reflections measured, $R_1 = 0.0482$, $wR_2 = 0.1425$. **3**: $a = 14.3228(5)$ Å, $V = 2938.22(18)$ Å^3, $\rho_{calcd} = 1.997$ g cm^{-3}, 374 unique reflections out of 9328 reflections measured, $R_1 = 0.0552$, $wR_2 = 0.1503$. **4**: $a = 14.4113(18)$ Å, $V = 2993.0(6)$ Å^3, $\rho_{calcd} = 1.934$ g cm^{-3}, 378 unique reflections out of 9427 reflections measured, $R_1 = 0.0362$, $wR_2 = 0.0991$. **5**: $a = 14.5275(6)$ Å, $V = 3066.0(2)$ Å^3, $\rho_{calcd} = 2.232$ g cm^{-3}, 389 unique reflections out of 9770 reflections measured, $R_1 = 0.0776$, $wR_2 = 0.2123$. The data for **1**–**5** were measured on a Siemens SMART/CCD diffractometer fitted with $Mo_{K\alpha}$ radiation. For all structures data were measured in the range $2° < \theta < 27.5°$ at 293 K. Empirical absorption corrections were applied using the SADABS program. Structures were solved using direct methods (SHELXTL[12]) and refined using a full-matrix least squares procedure based on F^2 (SHELX97[13]). CCDC194983–CCDC194987 (**1**–**5**) contain the supplementary crystallographic data for this paper. These data can be obtained free of charge via www.ccdc.cam.ac.uk/conts/retrieving.html (or from the Cambridge Crystallographic Data Centre, 12 Union Road, Cambridge CB21EZ, UK; fax: (+44) 1223-336-033; or deposit@ccdc.cam.ac.uk).

[12] G. M. Sheldrick, SHELXTL V5.1 Software Reference Manual, Bruker AXS, Inc., Madison, Wisconsin, USA, **1997**.

[13] G. M. Sheldrick, SHELX97, Program for Crystal Structure Analysis, Universität Göttingen, **1997**.

 © 2003 Wiley-VCH Verlag GmbH & Co. KGaA, Weinheim 1433-7851/03/4210-1115 $ 20.00+.50/0

Controlled Desorption of Films

Time-Controlled Desorption of Ultrathin Polymer Films Triggered by Enzymatic Degradation**

*Takeshi Serizawa, Miyuki Yamaguchi, and Mitsuru Akashi**

The fabrication of ultrathin polymer films on materials modifies the intact surface characteristics without changing the bulk properties. Time-controlled desorption of polymers from ultrathin films deposited on materials is an essential requirement for the time control of the surface characteristics and for the controlled release of substances from materials.

[*] Prof. M. Akashi, Prof. T. Serizawa, M. Yamaguchi
Department of Nanostructured and Advanced Materials
Graduate School of Science and Engineering
Kagoshima University
1-21-40 Korimoto, Kagoshima 890-0065 (Japan)
Fax: (+81) 99-255-1229
E-mail: akashi@apc.kagoshima-u.ac.jp

[**] This work was financially supported in part by a Grant-in-Aid for Scientific Research in the Priority Area of "Molecular Synchronization for Design of New Materials System" (No. 404/11167270, 13022258) from the Ministry of Education, Culture, Sports, Science and Technology, Japan.

Supporting information for this article is available on the WWW under http://www.angewandte.org or from the author.

These properties are especially important for applications in biomedical devices. The regulation of assembled polymer structures at the molecular level, as well as the suitable selection of polymer constituents, enables the systematic design and construction of tailored polymer architecture. It is, however, difficult to achieve these requirements by conventional methodologies.

The most attractive method for the fabrication of multilayered ultrathin polymer films is layer-by-layer (LbL) assembly, which is simply performed by repetitive alternate immersion of materials into interactive polymer solutions.[1] This method does not restrict the material shapes in the LbL assembly. The number of steps in the LbL assembly permits easy control of the thickness of the polymer to a molecular level. LbL assembly is applicable to all interactive polymer combinations, including synthetic and biopolymers. Not only electrostatic interactions but also other interactions between polymers have been utilized for the LbL assembly of functional polymers.[2] The LbL assembly method potentially could be used in applications involving time-controlled desorption of polymer constituents. Several reports have already demonstrated deconstruction (or simple desorption) of LbL assemblies that depend on the preparation conditions and/or the immersion media.[3]

Suitable combinations of biopolymers and enzymes, which hydrolyze the corresponding biopolymers in the LbL assembly, permit development of a model system that demonstrates controlled desorption of ultrathin polymer films. We previously reported desorption of the LbL assembly between cationic chitosan and anionic dextran sulfate through the hydrolysis of chitosan by chitosanase.[4] When the solution temperature was raised to a temperature at which the enzyme was active (40 °C), after electrostatic condensation of the cationic enzyme on the outermost surface of dextran sulfate at 4 °C, the multilayered film was immediately hydrolyzed. Conversely, the film with an outermost surface composed of chitosan was not hydrolyzed. While the bioactivity of each alternating layer of the LbL assembly has been demonstrated, time-controlled desorption has not. The results from using the system also suggested that it is not necessary for all the polymers to be hydrolyzed by enzymes for desorption of the LbL assembly to occur.

To generate the present model system, we have carried out the LbL assembly by using a combination of an anionic biopolymer DNA, a cationic synthetic polymer poly(diallyldimethylammonium chloride) (PDDA), and the endonuclease deoxyribonuclease I (DNase I) as a single-component-specific enzyme, which can be electrostatically adsorbed onto the PDDA surface. Not only differences in the activity of the alternating layers of the enzymatic hydrolysis of the LbL assembly but also time-controlled desorption on the basis of enzymatic hydrolysis are expected, since the activity of DNase I is strongly dependent on the concentration of essential metal ions, Mg^{2+} and Ca^{2+}.[5] Both cations activate the phosphodiester of DNA, and Ca^{2+} ions coordinate to DNase I to stabilize the structure. Accordingly, it is worthwhile to analyze whether enzymes already adsorbed onto the surface of the LbL assembly that are not denatured can hydrolyze DNA in the LbL assembly in response to changes

 © 2003 Wiley-VCH Verlag GmbH & Co. KGaA, Weinheim 1433-7851/03/4210-1115 $ 20.00+.50/0

in the ionic environment. The necessity for another polymer component corresponding to PDDA, which is not hydrolyzed by the enzyme, is also clearly demonstrated by the present system. Herein, we report the time-controlled desorption of an LbL assembly of DNA and PDDA on the basis of the enzymatic hydrolysis by DNase I (Figure 1), which is condensed on the PDDA surface and activated by metal ions in the media.

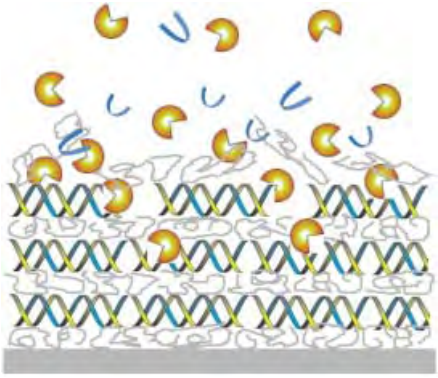

Figure 1. Schematic representation of the enzymatic hydrolysis of a DNA–PDDA assembly.

Researchers have already demonstrated that enzymes incorporated into the LbL assemblies on a porous filter membrane are active against small-molecule substrates that were applied across the membrane.[6] In the present case, the anionic charges of the DNA phosphodiester, which bind two metal ions, were used to provide electrostatic interactions with the quaternary amines of PDDA. Thus, for the coordinated interaction of PDDA with the phosphodiester, the metal ions would have to dissociate these ionic pairs. In other words, the dissociation could potentially be controlled by means of ion concentration. Furthermore, it is interesting to consider whether DNase I adsorbed onto the outermost surface can hydrolyze the DNA assembled inside the LbL structure. To achieve this, DNase I would have to progress to the inner layer by performing repetitive hydrolysis.

Before the demonstration of time-controlled desorption of the LbL assembly, differences in the activity of DNase I condensed onto the assembly were analyzed by using the 16- and 17-step assemblies with the respective surfaces of DNA and PDDA. Quantitative analysis by using a quartz crystal microbalance (QCM) as the assembly substrate revealed a clear difference in activity between the two assemblies (Figure 2). DNase I did not adsorb onto the DNA surface by substrate affinity, and desorption was not observed even after immersion into a buffer solution containing the essential ions. On the other hand, DNase I was electrostatically adsorbed onto the PDDA surface, since the enzyme was anionically charged in Tris buffer at pH 7.8 (the isoelectric point of the enzyme was 5.0). Subsequently, the assembly was clearly desorbed in the presence of Mg^{2+} and Ca^{2+} ions at concentrations of 50 mM for each ion. These observations suggest that DNase I electrostatically condensed on the PDDA surface became active through the binding of the

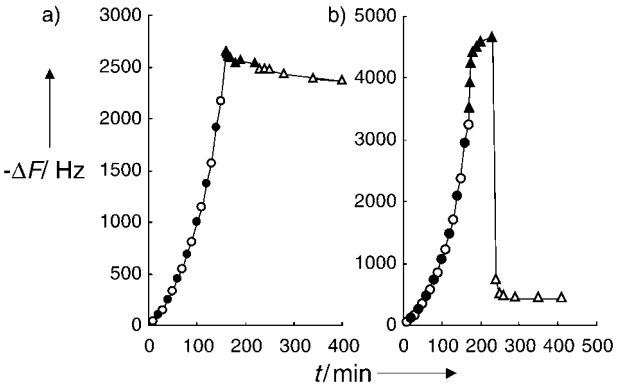

Figure 2. LbL assemblies of DNA and PDDA with outermost surfaces of a) DNA (16 steps) and b) PDDA (17 steps) and their hydrolyses by DNase I. Open and closed circles show the assembly steps of PDDA and DNA, respectively. The closed triangle shows the adsorption of DNase I at 4 °C. The subsequent open triangle shows desorption triggered by enzymatic degradation of the DNA in the assembly at 25 °C. $-\Delta F$ = Frequency shift.

ions to suitable sites. After fragmentation of the DNA, the assembly was desorbed by the formation of soluble polyion complexes with PDDA[7] or by dissociation of polyion complexes, which indicates that more than one component is required in the assembly to form a degradable polymer that desorbs by enzymatic hydrolysis. Note that the temperature required for condensation of the enzyme did not affect subsequent enzymatic activity.

The fragmentation of DNA solubilized in the reaction media was confirmed by the addition of the stain ethidium bromide, which inserts itself between double-stranded DNA base pairs at 590 nm and at ambient temperature, and is revealed by excitation at 260 nm. At 25 °C fluorescence was observed from the native DNA solution, and from the mixed solution containing DNA and PDDA, the concentrations of which were set at the same as those ideally desorbed based on the results of quantitative QCM analysis. However, at this temperature fluorescence was barely visible from the reaction media. This observation strongly suggests that DNase I fragmented the DNA in the assembly, which was followed by a decrease in the melting temperature (T_m) of the DNA. The T_m of the DNA desorbed was estimated to be between 4 °C and ambient temperature, since the fluorescence was observed from the reaction media at 4 °C (see Supporting Information). This observation indicates that the single-stranded DNA was desorbed from the assembly at a reaction temperature of 25 °C.

It is interesting to discuss whether DNase I was adsorbed on the PDDA surface of the 17-step assembly, or incorporated into the assembly. Atomic force microscopic (AFM) observation revealed that the mean roughness (Ra) of the assembly deposited on a mica substrate, the protein-adsorbed assembly, and the desorbed assembly were 3.0, 3.0, and 0.33 nm, respectively. The surface topology of the first two surfaces was clearly different, indicating the adsorption of enzymes (see Supporting Information). As suggested in previous reports, the charges that exist inside the LbL assemblies are compensated by electrostatic interactions.[8] Accordingly, the

 © 2003 Wiley-VCH Verlag GmbH & Co. KGaA, Weinheim 1433-7851/03/4210-1116 $ 20.00+.50/0

enzyme adsorbed on the surface seemed to hydrolyze the DNA in a stepwise fashion, thus progressing to the inner layer. Small amounts of the assembly as well as the enzyme remained even after sufficient reaction time, possibly because of difficulties associated with desorption (Figure 2b).

To demonstrate the time-controlled desorption, the 17-step assembly with PDDA on the outermost surface was hydrolyzed by the condensed DNase I under different concentrations of essential metal ions, based on the results of quantitative QCM analysis (Figure 3). While only the enzyme

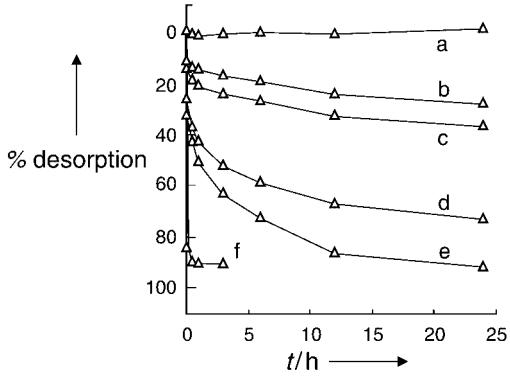

Figure 3. Desorption (%) of the 17-step LbL assembly with an outer surface composed of PDDA triggered by the enzymatic degradation of DNA in the assembly at 25 °C at concentrations of both Mg^{2+} and Ca^{2+} of a) 0, b) 0.5, c) 1, d) 3, e) 5, f) 50 mM after electrostatic condensation of the enzyme at 4 °C.

that was condensed on the polymer surface was desorbed in buffer solution, the degree of desorption increased with increasing ion concentrations. Mg^{2+} and Ca^{2+} ions clearly accelerated the hydrolysis of DNA, and the desorption could be controlled by altering the ion concentration. The presence of both types of ions was essential for desorption of the assembly; the assembly was not desorbed in the presence of only a single type of ion. Even in the presence of 100 mM NaCl there was no desorption of the LbL assembly, thus the specificity of the metal ions is demonstrated. Desorption was not complete even after sufficient reaction time had passed, and the amount that remained increased with decreased ion concentration. Since the charges of the DNA and the enzyme were already used for the LbL assembly process and electrostatic condensation onto the PDDA surface, respectively, replacement by ions, which is directly related to enzymatic activity, seemed to be dependent on ion concentration. The degree of desorption was also controllable by the adsorption time of the enzyme as well as enzyme concentration. In fact, an immersion of the assembly for 5 s in an enzyme solution of 0.05 mg mL^{-1}, a concentration which was a tenth of that used in the above measurements, resulted in approximately half the desorption at concentrations of both cations of 50 mM, and a netlike surface topology was observed by using AFM analysis (see Supporting Information). This result suggests that the present methodology enables three-dimensional regulation of the surfaces of the nanostructure of ultrathin polymer films. Notably, the enzyme incorporated inside the film composed of $(PDDA\text{-}DNA)_8$-PDDA-DNase I-PDDA-$(PDDA\text{-}DNA)_8$ and prepared by stepwise assembly did not degrade the DNA at concentrations of both cations of 5 mM, indicating that the ions did not diffuse into the film to allow enzymatic activity.

Time-controlled desorption of the LbL assembly was demonstrated by the electrostatic condensation of the enzyme that is specific for a single component of the assembly, and subsequent hydrolysis under suitable concentrations of ions essential for the enzyme. The enzyme was preserved on the surface of the LbL assemblies without being denatured, and was activated by external ionic stimuli. It would be interesting to imbed the enzymes into the LbL assemblies for further controlled desorption of the assembly. We are also currently investigating the application of the present desorption feature for the controlled release of substances from bulk materials.

Experimental Section

Materials: Salmon testis DNA (Wako, $\bar{M}_w$ 2–3 × 10^4 Da) and PDDA (Aldrich, $\bar{M}_w$ of 1–2 × 10^5) were used without further purification. DNase I (Nacalai, $\bar{M}_w$ 31 000) was dissolved in 10 mM Tris buffer at pH 7.8 before use.

LbL assembly: A 9 MHz QCM plate (USI System, Japan) with polished gold electrodes, and a diameter of 4.5 mm was used as the assembly substrate. The frequency shift (ΔF) was related to the amount of assembly (Δm) in accordance with the Sauerbrey's equation[9]: $-\Delta F\,[\mathrm{Hz}] = 1.15\,\Delta m\,[\mathrm{ng}]$. The QCM was alternately immersed into aqueous solutions of PDDA (1 mg mL^{-1}) and DNA (1 mg mL^{-1}) for 10 min each immersion at 25 °C. A sample was taken, which was rinsed with pure water, dried with nitrogen gas, and then the frequency of the sample was measured. NaCl was added into both solutions at 0.1M, to increase amounts of the assembly.

Enzymatic degradation: The LbL assembly deposited on the QCM was immersed in DNase I Tris buffer solution with a concentration of 0.5 mg mL^{-1} in the presence of a suitable concentration of $MgCl_2$ and/or $CaCl_2$. After adequate reaction time, the QCM was rinsed with pure water, dried with nitrogen gas, and then the frequency was measured as above.

AFM: Images were obtained with a Digital Instruments Nano-Scope III operating in a tapping mode in air at ambient temperature. We did not perform any image processing other than flat leveling.

Received: October 7, 2002 [Z50313]

Keywords: DNA · enzyme catalysis · layered compounds · polymers · ultrathin films

[1] G. Decher, *Science* **1997**, *277*, 1232–1237; P. Bertrand, A. Jonas, A. Laschewsky, R. Legras, *Macromol. Rapid Commun.* **2000**, *21*, 319–348; *Handbook of Polyelectrolytes and Their Applications, Vol. 1* (Eds.: S. Tripathy, J. Kumar, H. S. Nalwa), American Scientific Publishers, Los Angeles, **2002**.

[2] W. B. Stockton, M. F. Rubner, *Macromolecules* **1997**, *30*, 2717–2725; S. A. Sukhishvili, S. Granick, *J. Am. Chem. Soc.* **2000**, *122*, 9550–9551; L. Wang, S. Cui, Z. Wang, X. Zhang, *Langmuir* **2000**, *16*, 10490–10494; E. Hao, T. Lian, *Chem. Mater.* **2000**, *12*, 3392–3396; D. E. Bergbreiter, G. Tao, J. G. Franchina, L. Sussman, *Macromolecules* **2001**, *34*, 3018–3023; Y. Shimazaki, M. Mitsuishi, S. Ito, M. Yamamoto, *Macromolecules* **1999**, *32*, 8220–8223; Y. Zhang, W. Cao, *Langmuir* **2001**, *17*, 5021–5024; T. Serizawa, K.-I. Hamada, T. Kitayama, N. Fujimoto, K. Hatada, M.

 © 2003 Wiley-VCH Verlag GmbH & Co. KGaA, Weinheim 1433-7851/03/4210-1117 $ 20.00+.50/0

Akashi, *J. Am. Chem. Soc.* **2000**, *122*, 1891 – 1899; T. Serizawa, S. Hashiguchi, M. Akashi, *Langmuir* **1999**, *15*, 5363 – 5368.
[3] S. A. Sukhishvili, S. Granick, *J. Am. Chem. Soc.* **2000**, *122*, 9550 – 9551; S. Y. Yang, M. F. Rubner, *J. Am. Chem. Soc.* **2002**, *124*, 2100 – 2101; S. Dubas, T. R. Farhat, J. B. Schlenoff, *J. Am. Chem. Soc.* **2001**, *123*, 5368 – 5369; S. T. Dubas, J. B. Schlenoff, *Macromolecules* **2001**, *34*, 3736 – 3740; C. Schuler, F. Caruso, *Biomacromolecules* **2001**, *2*, 921 – 926.
[4] T. Serizawa, M. Yamaguchi, M. Akashi, *Macromolecules* **2002**, *35*, 8656 – 8658.
[5] L. Perlgut, V. Hernandez, *Biochim. Biophys. Acta* **1972**, *289*, 169 – 173; P. Price, *J. Biol. Chem.* **1972**, *247*, 2895 – 2899; D. Suck, C. Oefner, *Nature* **1986**, *321*, 620 – 625.
[6] M. Sano, Y. Lvov, T. Kunitake, *Annu. Rev. Mater. Sci.* **1996**, *26*, 153 – 187; Y. Lvov, H. Möhwald, *Protein Architecture: Interfacing Molecular Assemblies and Immobilization Biotechnology*, Dekker, New York, **2000**.
[7] H. Dautzenberg, W. Jaeger, J. Kötz, B. Philipp, C. Seidel, D. Stscherbina, *Polyelectrolytes: Formation, Characterization and Application*, Hanser, Munich, **1994**, chap. 6.
[8] J. B. Schlenoff, H. Ly, M. Li, *J. Am. Chem. Soc.* **1998**, *120*, 7626 – 7634; T. Farhat, G. Yassin, S. T. Dubas, J. B. Schlenoff, *Langmuir* **1999**, *15*, 6621 – 6623; S. T. Dubas, J. B. Schlenoff, *Macromolecules* **1999**, *32*, 8153 – 8160.
[9] G. Sauerbrey, *Z. Phys.* **1959**, *155*, 206 – 222.

 © 2003 Wiley-VCH Verlag GmbH & Co. KGaA, Weinheim 1433-7851/03/4210-1118 $ 20.00+.50/0

Porous Ultrathin Polymer Films

Recognition of Stereoregular Polymers by Using Structurally Regulated Ultrathin Polymer Films**

*Takeshi Serizawa, Ken-ichi Hamada, Tatsuki Kitayama, and Mitsuru Akashi**

The creation of molecular recognition systems with suitably designed molecular assemblies is of great interest.[1–6] Most of the recognition systems target small molecules except for those that use combinations of biomacromolecules. Recently, chain length recognition of synthetic polymers was reported on the basis of the electrostatic interaction between oppositely charged polymers in polyion complex micelles.[7] The recognition of synthetic linear polymers using certain assemblies is relatively difficult because of their lack of regulated conformations with spatially oriented functional groups.

The layer-by-layer (LbL) assembly of interactive polymers on surfaces results in constructions of multilayered ultrathin polymer films and is performed by simple alternate immersion of substrates into various solutions.[8] Electrostatic interactions between water-soluble polyelectrolytes are normally used for LbL assembly. Most of the assembled polymers seem to have random-coiled conformations in the films, although biomacromolecules, such as proteins and DNA, have also been applied in LbL assemblies. Recently, we studied LbL assembly by using stereocomplexes between isotactic (it) and syndiotactic (st) poly(methyl methacrylate)s (PMMAs).[9] The PMMAs in the assembly showed a double-stranded helical structure, in which it-PMMA was surrounded by twice the molar amount of st-PMMA, and these polymers had a molecularly regulated conformation. Stereocomplex formation was also applied in LbL assembly between it-PMMA and st-poly(methacrylic acid) (PMAA) with different solvent solubilities,[10] and between it-PMMA and st-poly(-alkyl methacrylate)s[11]. Herein, we report a macromolecular recognition system resulting from the incorporation of st-polymers of methacrylic acid or methacrylates into an ultrathin it-PMMA film designed by LbL assembly on the basis of stereocomplex formation (Figure 1).

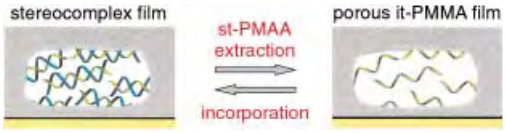

Figure 1. A schematic representation of the selective extraction of st-PMAA from the LbL assembly of it-PMMA and st-PMAA on the basis of stereocomplex formation, and the subsequent incorporation of st-polymers of methacrylic acid or methacrylates.

The first step in the preparation of the designed ultrathin it-PMMA film is the LbL assembly between it-PMMA and st-PMAA by stereocomplex formation. The alternate immersion of a quartz crystal microbalance (QCM) substrate into both solutions resulted in a stepwise decrease of the frequency (Figure 2). The molar ratio of the unit assembled from st-PMAA and it-PMMA calculated from the QCM analysis was 2.1(±0.2):1 (st-PMAA/it-PMMA), which is consistent with that of an ideal complex stoichiometry with a double-stranded helical structure.[12] The mean thickness of the LbL assembly after 12-steps was calculated to be 48 nm, after the density was assumed to be the same as that of the glass state solid PMMA (1.118 g cm^{-3}). The subsequent immersion of the assembly in an aqueous solution of sodium hydroxide (10 mM) for 5 min resulted in a drastic increase in frequency, which indicates a desorption of some of the polymers from the assembly (Figure 2). There was no frequency change with long-term immersion even after several hours had elapsed. This observation indicates selective extraction of st-PMAA, which can be readily dissolved in

[*] Prof. M. Akashi, Prof. T. Serizawa, K.-i. Hamada
Department of Nanostructured and Advanced Materials
Graduate School of Science and Engineering
Kagoshima University
1-21-40 Korimoto, Kagoshima 890-0065 (Japan)
Fax: (+81) 99-255-1229
E-mail: akashi@apc.kagoshima-u.ac.jp
Prof. T. Kitayama
Graduate School of Engineering Science
Osaka University
1-16 Machikaneyama-cho, Toyonaka 560-0043 (Japan)

[**] This work was financially supported in part by a Grant-in-Aid for Scientific Research in the Priority Area of "Molecular Synchronization for Design of New Materials System" (No. 404/11167270, 13022258) from the Ministry of Education, Culture, Sports, Science and Technology, Japan.

 © 2003 Wiley-VCH Verlag GmbH & Co. KGaA, Weinheim 1433-7851/03/4210-1118 $ 20.00+.50/0

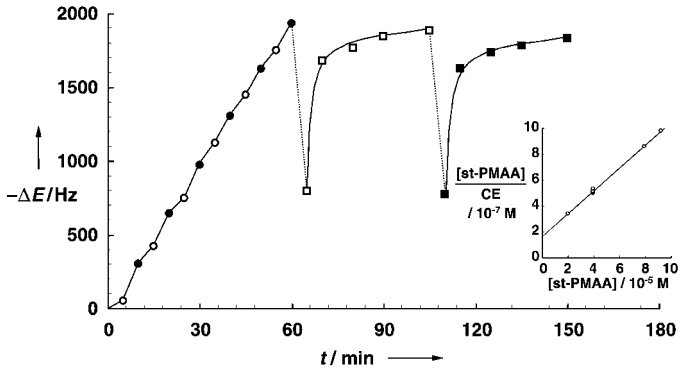

Figure 2. QCM analysis of the LbL assembly, selective extraction, and subsequent st-PMAA incorporation. The it-PMMA (○) in acetonitrile and st-PMAA (●) in an acetonitrile/water (4/6, v/v) were alternately assembled on a QCM substrate for a 12-step assembly at the concentration of 0.017 unitM at 25 °C, in accordance with our previous study.[10] •••••: The selective extraction process of st-PMAA in a 10 mM NaOH aqueous solution for 5 min, to obtain the designed host, the it-PMMA film. □: The subsequent incorporation of st-PMAA in the it-PMMA film from the acetonitrile/water (4/6, v/v) solution at the concentration of 0.017 unitM at 25 °C. ■: The extraction and incorporation was repeated again . The inset shows the apparent Langmuir plot, which is explained in reference [13], to obtain the maximum CE and the apparent incorporation constant. $-\Delta F=$ frequency shift.

an aqueous alkaline solution (see reflection absorption spectra (RAS)). The amount extracted was also consistent with the amount of st-PMAA assembled on the QCM substrate, thus indicating a 100% extraction of st-PMAA. Since an aqueous alkaline solution was used for extracting st-PMAA, the remaining it-PMMA should not swell with water molecules. However, st-PMMA was successfully extracted from the assembly to give an ultrathin it-PMMA film.

The polymer st-PMAA was incorporated into the ultrathin it-PMMA film by immersing the film in a solution of st-PMAA (0.017 unitM), with a complexing efficiency of around 80% (Figure 2). The efficiency was calculated as the percentage of the incorporated st-PMAA against the host it-PMMA under the assumption that the complex was formed with ideal stoichiometry (2:1 unit ratio st-PMAA/it-PMMA), and incorporation became saturated over time. The extraction was repeated again, and subsequent incorporation of st-PMAA was also observed with the same complexing efficiency (CE). This extraction–incorporation cycle could be repeated several times. Incorporation with the same efficiency indicated that the process was governed by the apparent incorporation constant. The Langmuir plot showed a linear relationship (coefficient of variation; $R^2 = 0.998$; inset in Figure 2).[13] The apparent incorporation constant was estimated to be $5.4 \times 10^4\,\text{M}^{-1}$. This is the first case of an estimation of an affinity constant for the present stereocomplex, which was obtained by a structural fitting with van der Waals interactions. The maximum value of the complexing efficiency was estimated to be 113%, assuming 2:1 st-PMAA/it-PMAA stoichiometry. Although the maximum efficiency was more than 100%, the st-PMAA partially incorporated into the host might also be present on the film surface. In fact, the complexing efficiency was maintained even after thermal treatment of the it-PMMA film until a temperature of 110 °C was reached, although the glass transition temperature of it-PMMA films on surfaces was approximately 90 °C.[14] This result suggests that a structurally stable film was prepared by using the present process. Furthermore, the incorporation constants for the st-PMAA with smaller $\bar{M}_n$ values of 14400, and 4650 were $1.5 \times 10^4\,\text{M}^{-1}$ and $7.0 \times 10^3\,\text{M}^{-1}$, respectively, which indicates that the incorporation constant increases with increased molecular weight. On the other hand, the fact that atactic PMAA was not incorporated into the it-PMMA film suggests that the above incorporation occurred by stereocomplex formation.

The RAS in the carbonyl vibration region were used to detect complex formation, and obtain conformational information, as described in our previous studies (Figure 3).[9–11] There are two peaks in this region of the spectrum arising from the LbL assembly at 1737 and 1725 cm^{-1}, which are assigned to it-PMMA and st-PMAA, respectively (Figure 3a). The peak intensity at the lower wavenumber was larger than that at the higher wavenumber. This suggests that the designation of these peaks is reasonable because the larger molar amount of st-PMAA was assembled for stereocomplex formation as shown in the QCM analysis. The RAS peaks shifted to a higher wavenumber compared to those for their individual cast films, which also indicates stereocomplex formation (Figure 3d and e). After the film was immersed in an alkaline solution, only one peak was observed at 1739 cm^{-1} in the reflection absorption spectrum (Figure 3b), thus, one component was completely extracted from the LbL assembly. The position of the peak in the spectrum in Figure 3b was almost the same as that at the higher wavenumber in the spectrum of the LbL assembly (Figure 3a). These observations suggest that st-PMAA was extracted from the LbL assembly with an alkaline solution, and that the conformation (or microenvironment) of it-PMMA was maintained after the extraction.

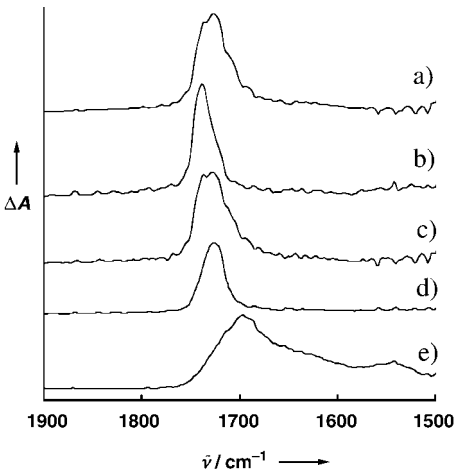

Figure 3. RAS of a) the LbL assembly of it-PMMA and st-PMAA for a 12-step assembly, b) the extracted film, c) the st-PMAA incorporated film, d) a cast film of it-PMMA, e) a cast film of st-PMAA. The films were similarly prepared on a gold-sputtered poly(ethylene terephthalate) film.

 © 2003 Wiley-VCH Verlag GmbH & Co. KGaA, Weinheim 1433-7851/03/4210-1119 $ 20.00+.50/0

The two peaks were observed again after the film was immersed in a solution of st-PMAA (Figure 3c), thus indicating the reformation of the two-component complex. However, the peak intensity corresponding to st-PMAA was smaller than that for the LbL assembly, which is reasonable because the complexing efficiency was smaller and around 80% at the st-PMAA concentration as shown in the QCM analysis.

The surface topology and the thickness of the above assemblies on the QCM were directly analyzed by atomic force microscopy (AFM). The mean roughness (Ra) of the surface of the LbL assembly was 2.6 nm (1.8 nm for QCM). The thickness estimated by scratching the film with a cantilever was 43.6 ± 4.3 nm, which is consistent with that calculated from the QCM analysis (48 nm). This result means that the LbL assembly in the present study has a similar density to that of solid PMMA. The roughness of the surface of the film after the extraction of st-PMAA was 3.2 nm, rougher than before the extraction, which indicates that a molecular-level extraction occurred even at the surface. However, the thickness (44.1 ± 3.8 nm) was not significantly altered by the extraction. This finding strongly suggests that an ultrathin it-PMMA film with a macromolecular porous structure was obtained. It is difficult to explain why the porous it-PMMA film was not squashed. The terminals of it-PMMA, which do not form the stereocomplex, might support the film structure even after the extraction of st-PMAA. The roughness reoccurred with the incorporation of st-PMAA (2.6 nm), and the thickness was the same (42.9 ± 4.6 nm), thus indicating a reversible change in only the surface topography.

The structurally regulated ultrathin it-PMMA film, prepared by the selective extraction of st-PMAA from the LbL assembly between it-PMMA and st-PMAA, was used as a host for the incorporation of other st-poly(alkyl methacrylate)s (Figure 4). St-poly(alkyl methacrylate)s also form stereocomplexes with it-PMMA. If the complex is rapidly formed in the film, the host it-PMMA film should not dissolve in an acetonitrile phase. When a normally spin-coated it-PMMA film on QCM was immersed in solutions of polymer in acetonitrile, which is a polar solvent that accelerates complex formation, rapid desorption of it-PMMA was observed. Since it-PMMA can readily dissolve in acetonitrile, the stereocomplex was not formed on/in the film. On the other hand, incorporation of st-poly(alkyl methacrylate)s into the designed it-PMMA film was dependent on the chain length of the lateral group. The complexing efficiencies for st-PMMA, st-poly(ethyl methacrylate) (PEMA), and st-poly(propyl methacrylate) (PPMA) at the same concentration as used in the st-PMAA incorporation system were 43, 8, and 6%, respectively. These values were significantly decreased with increased alkyl chain length. Since the it-PMMA film was designed using st-PMAA as a template, a porous structure fitting to st-PMAA should be conserved in the film. There must be steric hindrance associated with the incorporation of st-poly(alkyl methacrylate)s. Although st-PMMA was incorporated into the host with moderate efficiency, there may be a small difference between the proton and methyl groups as side chains for st-PMAA and st-PMMA, respectively. The apparent incorporation constant and the maximum complexing efficiency of st-PMMA similarly estimated by the Langmuir plot were $4.0 \times 10^3\,\text{M}^{-1}$ and 47%, respectively, which indicates weaker and smaller incorporation of st-PMMA compared to st-PMAA. Notably, the it-PMMA film did not dissolve, even though the complexing efficiency was small for st-PEMA and st-PPMA. This observation suggests that the slight incorporation of the st-polymers onto the film surface suppressed dissolution in the acetonitrile phase.

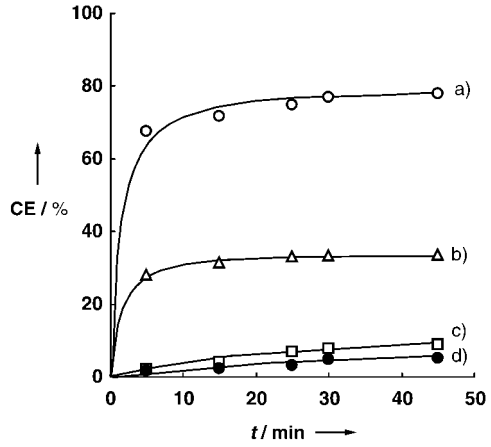

Figure 4. The time dependence of CE for the incorporation of a) st-PMAA, b) st-PMMA, c) st-PEMA, d) st-PPMA in the designed it-PMMA film at the concentration of 0.017 unitM at 25 °C. The LbL assembly and the selective extraction were similarly demonstrated in Figure 2.

Preliminary experiments revealed reversible incorporation and extraction of st-PMAA using spin-coated it-PMMA. However, an it-PMMA film prepared by a similar st-PMAA extraction did not show any alkyl-chain recognition, and in the corresponding reflection absorption spectrum, the peak representing the carbonyl vibration band was also reversibly shifted after the incorporation and extraction processes, thus indicating a reversible conformational change (i.e. no conservation of conformation). The present system is based on the characteristic property of LbL assemblies, which permits tight deposition of interactive polymers at the molecular level.

In summary, we have demonstrated that st-PMAA is selectively extracted in an aqueous alkaline solution from an LbL assembly of it-PMMA and st-PMAA with stereocomplex formation. The resulting ultrathin it-PMMA film is molecularly porous and has a regulated conformation. The extraction and the subsequent incorporation of st-PMAA were reversible. The designed host it-PMMA film incorporated st-poly(alkyl methacrylate)s with shorter alkyl side chains. This is the first report of selective extraction of one component in an LbL assembly giving rise to macromolecular recognition. The present concept may be applied to various systems of interactive polymers, not only synthetic polymers but also biomacromolecules, with differential solubility, or different properties of degradation. Detailed parameters for demonstrating the present macromolecular recognition such as pH for extraction film thickness, stability of porous films, solvent incorporation, incorporation of other polymers will appear in

 © 2003 Wiley-VCH Verlag GmbH & Co. KGaA, Weinheim 1433-7851/03/4210-1120 $ 20.00+.50/0

the near future. The present host film might be applied to template polymerization for the preparation of stereoregular polymers. This method also facilitates easy preparation of a molecularly porous ultrathin film by using selective extraction of one component from LbL assemblies.

Experimental Section

Materials: it-PMMA, st-PMAA, and other st-poly(alkyl methacrylate)s were synthesized by conventional anionic polymerization using suitable monomers and initiators. The $\bar{M}_n$ values, molecular weight distributions ($\bar{M}_w/\bar{M}_n$), tacticities (*mm:mr:rr*) were as follows: it-PMMA 20750, 1.26, 97:2:1; st-PMAA 37940, 1.26, 1:2:97 (mainly used); 14400, 1.25, 1:3:96; 4650, 1.21, 0:4:96; st-PMMA 22700, ,1.26, 0:11:89; st-PEMA 21340, 1.11, 1:8:91; st-PPMA 23800, 1.09, 2:7:91.

LbL assembly: The assembly was carried out in accordance with our previous studies.[9–11] For details, see Experimental Section of the preceding communication.[15] The it-PMMA film was prepared by the selective extraction of st-PMAA in an aqueous alkaline solution from the LbL assembly between it-PMMA and st-PMAA. Frequency shifts were measured after drying a QCM substrate by using nitrogen gas in all experiments.

Characterization: RAS were measured with a Herschel FT/IR-610, Jasco (Japan) in nitrogen atmosphere at ambient temperature. The interferograms were superimposed 50 times and Fourier transformed at a resolution of 4 cm^{-1}. AFM images were obtained by a Digital Instruments NanoScope III that was operated with a tapping or a contact mode in the air at ambient temperature. We have not performed any image processing other than flat leveling. The Ra in given observed areas was estimated from the following Equation (1)

$$\mathrm{Ra} = \frac{1}{Lx\,Ly}\int_0^{Lx}\int_0^{Ly}|F(x,y)|\,\mathrm{d}x\,\mathrm{d}y \qquad (1)$$

in which $F(x,y)$ is the surface relative to the center plane that is a flat plane parallel to the mean plane, and Lx and Ly are the dimensions of the surface.

Received: October 16, 2002 [Z50380]

Keywords: layered compounds · molecular recognition · polymers · ultrathin films

[1] J.-M. Lehn, *Angew. Chem.* **1990**, *102*, 1347; *Angew. Chem. Int. Ed. Engl.* **1990**, *29*, 1304 – 1319.
[2] M. Ahlers, W. Müller, A. Reichert, H. Ringsdorf, J. Venzmer, *Angew. Chem.* **1990**, *102*, 1328; *Angew. Chem. Int. Ed. Engl.* **1990**, *29*, 1269 – 1285.
[3] M. Mammen, S.-K. Chio, G. M. Whitesides, *Angew. Chem.* **1998**, *110*, 2908 – 2953; *Angew. Chem. Int. Ed.* **1998**, *37*, 2755 – 2794.
[4] T. Martin, U. Obst, J. J. Rebek, *Science* **1998**, *281*, 1842 – 1845.
[5] L. J. Prins, J. Huslens, F. De Jong, P. Timmerman, D. N. Reinhoudt, *Nature* **1999**, *398*, 498 – 502.
[6] M. Fujita, N. Fujita, K. Ogura, K. Yamaguchi, *Nature* **1999**, *400*, 52 – 55.
[7] A. Harada, K. Kataoka, *Science* **1999**, *283*, 65 – 67.
[8] G. Decher, *Science* **1997**, *277*, 1232 – 1237.
[9] T. Serizawa, K.-I. Hamada, T. Kitayama, N. Fujimoto, K. Hatada, M. Akashi, *J. Am. Chem. Soc.* **2000**, *122*, 1891 – 1899.
[10] T. Serizawa, K.-I. Hamada, T. Kitayama, K.-I. Katsukawa, K. Hatada, M. Akashi, *Langmuir* **2000**, *16*, 7112 – 7115.
[11] K.-I. Hamada, T. Serizawa, T. Kitayama, N. Fujimoto, K. Hatada, M. Akashi, *Langmuir* **2001**, *17*, 5513 – 5519.
[12] E. Schomaker, G. Challa, *Macromolecules* **1989**, *22*, 3337 – 3341.
[13] We assumed the presence of a Langmuirian type adsorption and fitted the data to Equation (2) in which CE is the complexing

$$\frac{[\mathrm{st{-}PMAA}]}{\mathrm{CE}} = \frac{1}{\mathrm{CE}_{max}}\,[\mathrm{st{-}PMAA}] + \frac{1}{\mathrm{CE}_{max}\,K_{app}} \qquad (2)$$

efficiency, CE_{max} is the maximum complexing efficiency, and K_{app} is the apparent affinity constant.
[14] Y. Grohens, M. Brogly, C. Labbe, J. Schultz, *Polymer* **1997**, *38*, 5913 – 5920.
[15] T. Serizawa, M. Yamaguchi, M. Akashi, *Angew. Chem.* **2003**, *115*, 1147 – 1150; *Angew. Chem. Int. Ed.* **2003**, *42*, 1115 – 1118.

 © 2003 Wiley-VCH Verlag GmbH & Co. KGaA, Weinheim 1433-7851/03/4210-1121 $ 20.00+.50/0

Organic Nanotubes

A New Route to Organic Nanotubes from Porphyrin Dendrimers**

*Yoonkyung Kim, Michael F. Mayer, and Steven C. Zimmerman**

The controlled synthesis of discrete nanostructures is an exciting challenge that remains the cornerstone of the bottom-up approach. In this regard, considerable effort has been directed toward nanotubes. Within the last decade, numerous reports have described the synthesis and properties of carbon (single-walled and multi-walled nanotubes (SWNTs and MWNTs, respectively)),[1] inorganic,[2] and non-fullerene organic nanotubes.[3] In particular, organic nanotubes have been synthesized from oligopeptides,[4] oligosaccharides,[5] block copolymers,[6] and a variety of other organic building blocks.[7] Many of these nanotubes, however, are formed as noncovalent assemblies and are, thus, stable only under specific conditions. Herein we report a core–shell approach[8] to covalent organic nanotubes by molding dendritic building blocks around an oligoporphyrin core.

[*] Prof. S. C. Zimmerman, Y. Kim, Dr. M. F. Mayer
Department of Chemistry
University of Illinois at Urbana-Champaign
600 S. Mathews Avenue, Urbana, IL 61801 (USA)
Fax: (+1) 217-244-9919
E-mail: sczimmer@uiuc.edu

[**] Taken in part from the Ph.D. Thesis of Y.K., University of Illinois at Urbana-Champaign, 2001. Funding by the NIH (GM39782-11) and ARO-MURI-2778 is gratefully acknowledged. M.F.M. thanks the NIH for a postdoctoral research fellowship (GM-065707-01). We thank Mr. Larry Markoski for running the size-exclusion chromatographic analyses in 1-methyl-2-pyrrolidinone. Transmission electron microscopy was carried out at the Center for Microanalysis of Materials, University of Illinois, which is partially supported by the US Department of Energy under grant DEFG02-96-ER45439.

Supporting information for this article is available on the WWW under http://www.angewandte.org or from the author.

 © 2003 Wiley-VCH Verlag GmbH & Co. KGaA, Weinheim 1433-7851/03/4210-1121 $ 20.00+.50/0

The specific method involves three key steps: 1) formation of a coordination polymer from a dendritic metalloporphyrin containing multiple alkene end groups,[9] 2) extensive cross-linking of the dendrons by a ring-closing metathesis (RCM) reaction,[10] and 3) cleavage of the focal point linkages (dendron-to-porphyrin) to remove the oligomerized core.[11] The synthesis began with porphyrin dendrimer **1**,[12,13] which was treated with tin(II) chloride (by using the DMF method[14]) to produce tin(IV) porphyrin complex **2** (Scheme 1). The metalation was quantitative, but was accompanied by a small amount of cleavage of the porphyrin dendron ester, thus resulting in a 95% yield. Analytically pure **2** was obtained after size-exclusion chromatography (SEC). The oligomerization of **2** was carried out in a concentrated THF solution with excess Ag_2O and using one equivalent of succinic acid as the bridging bidentate ligand. The reaction was monitored by analytical SEC and UV/Vis spectroscopy. As the reaction progressed, the Soret band of the tin porphyrin shifted from 430 to 420 nm and the SEC analysis showed significant peak broadening along with a shift to shorter retention time; the leading edge of the broadened peak corresponded to the size exclusion limit of the column (Figure 1). Key to the success of this oligomerization was the gradual concentration of the reaction mixture by slow evaporation of the solvent over the course of the reaction. After filtration, the crude product **3** was characterized and used directly in the next step.

The oligomerized product **3** was sufficiently soluble and stable in common organic solvents to allow characterization by ^{1}H NMR spectroscopy and SEC. The ^{1}H NMR spectrum of **3** showed significant peak broadening relative to that of **2**.[12] A broad peak at $\delta = -3.3$ ppm was observed and assigned to the methylene groups of the axially bridging succinate ligand. Analysis of **3** by SEC was carried out in toluene with molecular-weight (M_W) calibration performed both with conventional polystyrene (PS) and dendrimer standards.[16] Although dendrimers are considered more appropriate size standards, the current calibration used just three compounds and considerable extrapolation was required for the high-molecular-weight oligomeric porphyrins. The two sets of standards, PS and dendrimers, gave average M_W values of 23000 and 72600 Da for **3**, roughly corresponding to a

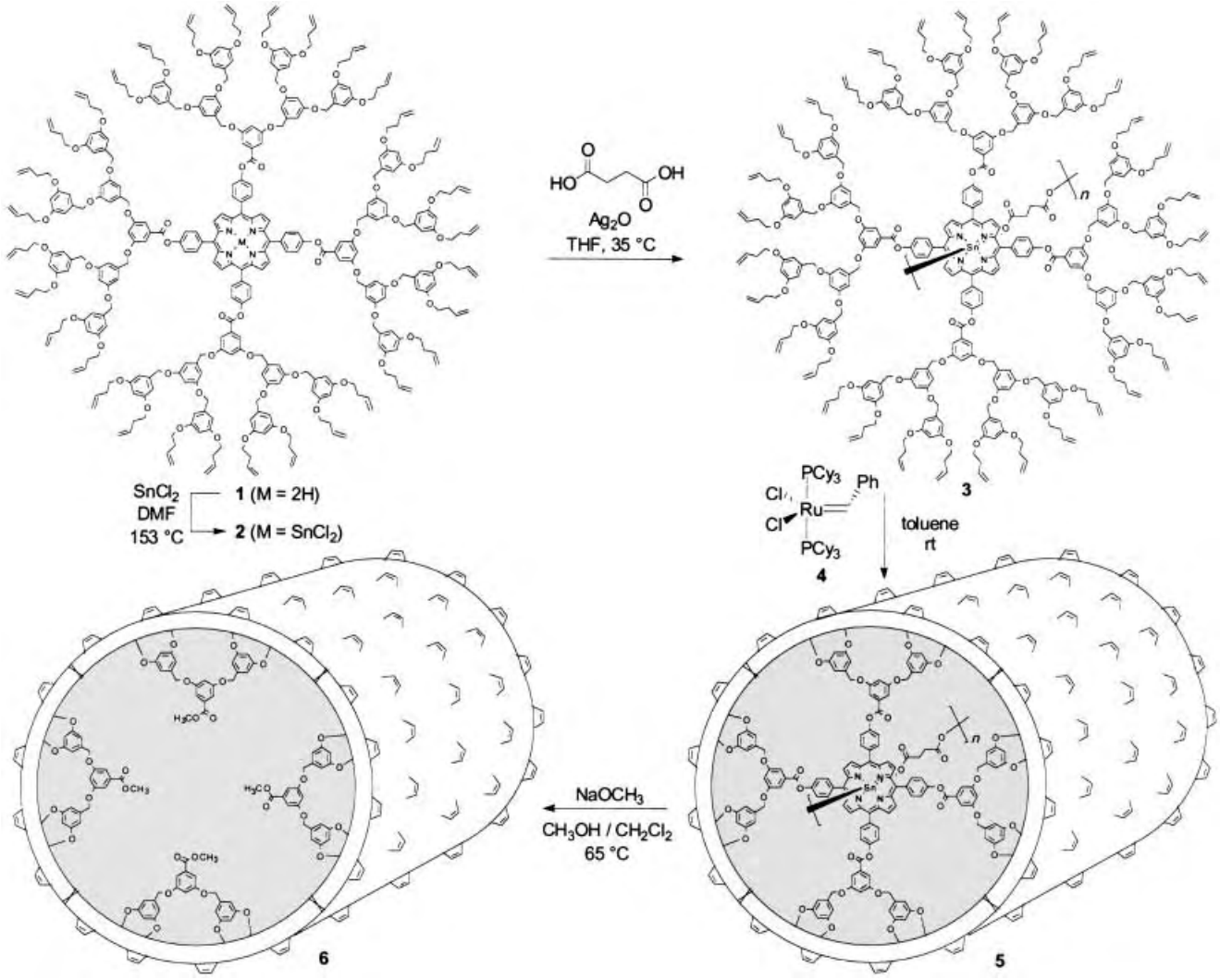

Scheme 1. The synthetic route to organic nanotubes.[15]

 © 2003 Wiley-VCH Verlag GmbH & Co. KGaA, Weinheim 1433-7851/03/4210-1122 $ 20.00+.50/0

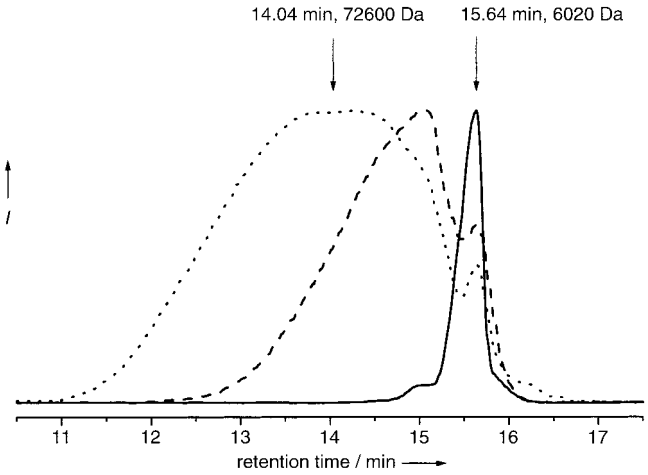

Figure 1. SEC traces (toluene, UV detector at 289 nm) obtained on a double Waters Styragel HR 4E column (M_w range is 50–100000 Da) from an oligomerization to form **3,** reaction time: 4 h: ——, 29 h: -----, and 45 h: •••••. Each plot was normalized according to the peak maximum. Peak picking was done at the maximum and the center of the bandwidth at the half-height for traces —— and •••••, respectively. Molecular weights were estimated by calibration with dendrimer standards.

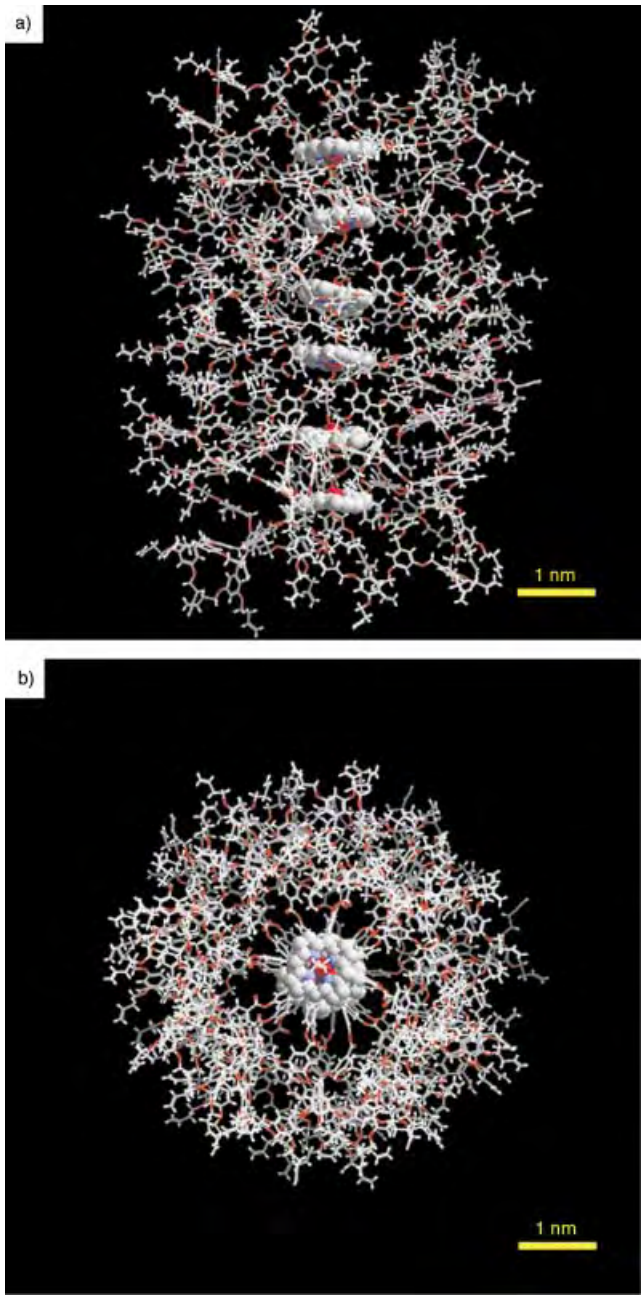

Figure 2. Computer-generated structure of **3** (a hexameric tin–porphyrin dendrimer bridged by succinate ligands). Energy minimization of the hexamer was performed by using the modeling program Cerius² (MSI, Inc.) and its Dreiding force field. a) Side view; b) top view.

tetramer and dodecamer, respectively (Figure 1 and Table 1). These values likely set the limits on the size of **3**. Peaks corresponding to oligomer **3** were not observed by MALDI-TOF-MS, instead peaks for the monomer (**3**, $n=1$) and a tin porphyrin dendrimer adduct of the matrix, 2-([4-hydroxyphenyl)azo]benzoic acid (HABA) were present.[12]

Computer modeling studies on hexameric **3** were performed to show the approximate dimensions of a small oligomer and the possibility of cross-linking the alkene groups between monomers (Figure 2). The model suggests a Sn to Sn distance (terminal units) of about 4.5 nm and a dendron focal point to focal point (*trans*) distance of about 1.5 nm. The alkene moieties of dendrons attached to the same and adjacent porphyrin units are proximate, which suggests that extensive interdendron cross-linking would be feasible along porphyrin oligomer **3**. The potential for interoligomer cross-linking was estimated by performing RCM reactions of **2** at 10^{-5} and 10^{-4} M with 15 mol% of the Grubbs ruthenium catalyst **4**[10] per alkene group. Analysis of the cross-linked products by SEC showed that the intramolecularly cross-linked product (**7**) was the major product and that the amount of dimer formed from **2** was 11% at 10^{-5} M and 37% at 10^{-4} M, which is consistent with previous studies.[17]

Oligomer **3** was cross-linked immediately after work-up because the molecular weight of **3**, as determined by SEC, was found to decrease over time.[12] The homoallyl groups of oligomer **3** were metathesized by using the same procedure as described for **2** at a concentration of 10^{-5} M in the monomeric unit. With a degree of polymerization (DP) between four and twelve, the actual molar concentration of oligomer **3** should be well below 10^{-5} M, thus ensuring much less than 10% interoligomer cross-linking.

The RCM reaction was monitored by MALDI-TOF-MS and conducted until the highest peak for the monomer (namely, **5**, $n=1$) corresponded to a product with 15 out of 16 possible cross-links. In addition to monomer, the MALDI-MS of **5** contained a distribution of broad peaks (Figure 3a) roughly separated by the mass of the monomeric unit. The detection of oligomers with molecular weights over 100000 Da (DP $\geq$ 18) was not possible as these peaks were too broad. Peak broadening was also observed in the ^{1}H NMR spectrum of **5**.[12] An upfield shift for the methine peak of the alkene moieties from 5.74 to 5.49 ppm was observed, which is diagnostic of conversion of a terminal alkene into an internal alkene.[17c]

 © 2003 Wiley-VCH Verlag GmbH & Co. KGaA, Weinheim 1433-7851/03/4210-1123 $ 20.00+.50/0

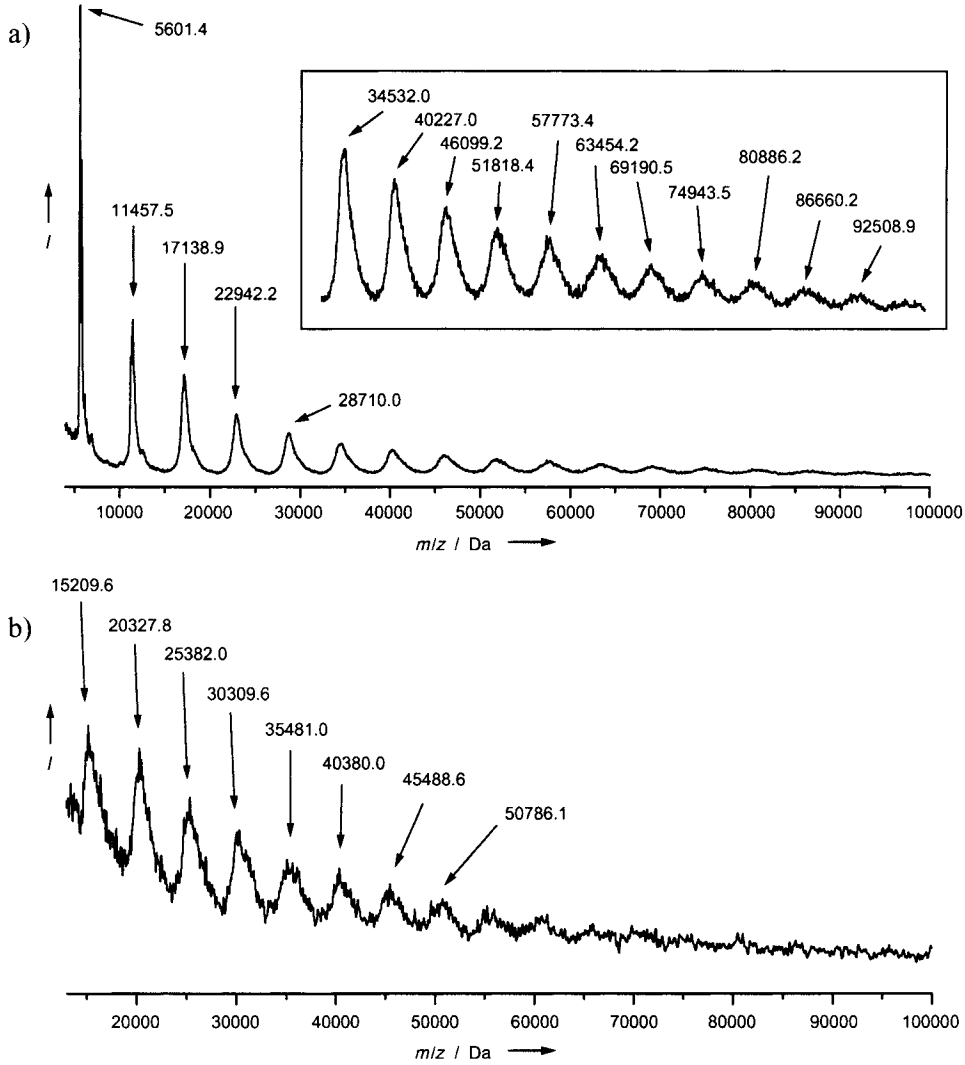

Figure 3. MALDI-MS spectra of a) **5** (the inset shows the expanded region for *m/z* 32000–100000 Da) and b) **6**. The *m/z* values were assigned at the center of the bandwidth at the half-height for each broad peak. The spectrum of **6** was obtained using a column fraction from preparative SEC containing oligomers of trimer and higher.

Table 1: Comparison of molecular weights calculated by SEC in toluene or NMP, using PS and dendrimer standards (DS).

Cmpd	Theoretical	Toluene[b]		NMP[c]			
	M_W[a]	PS[d,e]	DS[d]	PS[d,e]			DS[d]
				M_n[f]	M_w[g]	PDI[h]	
2	6073	6020	5840	14200	15900	1.12	6130
3	*n*(6118)	23000	72600	N/A	N/A	N/A	N/A
5	*n*(5669)	N/A	N/A	35000	83800	2.40	30500
6[i]	*n*(4886)	N/A	N/A	32000	124000	3.88	39700
7[j]	5624	4260	3040	12500	13600	1.09	3950

[a] The theoretical molecular weights for oligomers **3, 5**, and **6** are shown in terms of the monomeric unit (*n* = integer). The theoretical molecular weights for **5, 6**, and **7** correspond to fully cross-linked compounds. [b] UV detector at 289 nm. [c] Refractive index detector. [d] Calculated on the basis of the center of the bandwidth at the half-height of the broad peak for **3, 5**, and **6**. For details see ref. [12]. [e] Estimated with a conventional PS calibration. [f] Number-average molar mass. [g] Weight-average molar mass. [h] Polydispersity index. [i] SEC data for **6** were obtained by using combined preparative SEC column fractions composed of trimer and higher oligomers. [j] Compound **7** is the intramolecular cross-linked product of the RCM reaction of **2**.

Compound **5** was not fully soluble in either toluene or THF so its SEC analysis (Figure 4) was performed in 1-methyl-2-pyrrolidinone (NMP). The molecular weights determined with PS standards (35000 Da) and dendrimer standards (30500 Da) agreed well in this solvent, and suggested that oligomer **5** corresponded, on average, to a pentamer. However, similarly cross-linked dendrimers are significantly more compact than their precursors and, thus, their molecular weights determined by SEC are typically underestimated by 20–30% (for example, see **7** versus **2** in Table 1 and ref. [17]). As such, **5** may be somewhat longer than a pentamer.

In the final step of the synthetic route, the internal oligoporphyrin core of **5** was removed through a transesterification reac-

 © 2003 Wiley-VCH Verlag GmbH & Co. KGaA, Weinheim 1433-7851/03/4210-1124 $ 20.00+.50/0

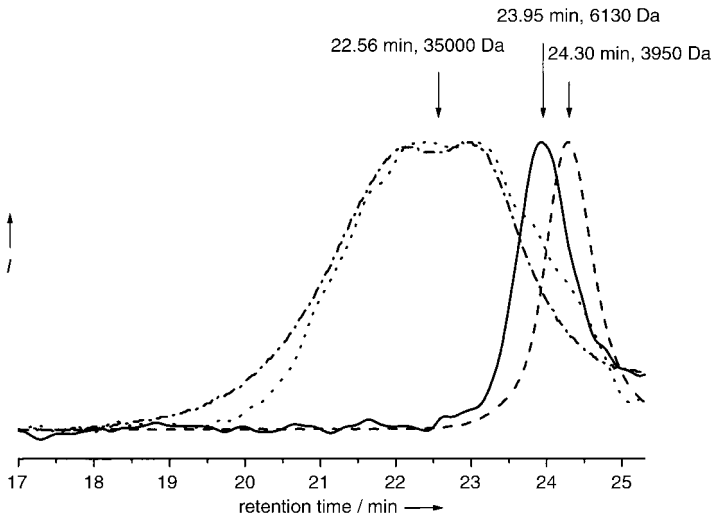

Figure 4. SEC traces (NMP, RI detector) of **2** (——), **7** (----), **5** (••••), and **6** (–•–•). SEC was performed on a triple PLgel 10 μm MIXED-B LS column (M_W range 500–10000000 Da) from Polymer Laboratories. Each plot was normalized according to the peak maximum. Peaks were picked at the maxima for **2** and **7**, and at an arbitrary value at the approximate center of the broad regions for **5** and **6**. Molecular weights were estimated by calibration with dendrimer standards. The trace of **6** was obtained using a column fraction from preparative SEC containing oligomers of trimer and higher.

tion. The resultant cored compound **6** was relatively soluble in organic solvents, thus enabling purification and partial fractionation by SEC. A portion of reaction mixture was eluted with THF through a preparative SEC column and two widely separated major bands were observed. A first light-green band was collected in several fractions. Analytical SEC of these fractions showed that **6** was not only separated from the core but also partially fractionated by length. Each column fraction was analyzed by MALDI-TOF-MS and only the fractions containing trimer and higher were combined for further analysis. The mass spectra show a straightforward relationship in the M_W differences between **5** and **6** for each oligomer (Figure 3), with an average loss of 734 Da per monomeric unit after removal of the core.[12] This value is in reasonable agreement with the calculated effective loss of mass of a core per monomer (783 Da). Mass balance of the combined fractions (trimer and higher) was 56% of all the fractions containing cross-linked dendritic structures.

The second preparative SEC band was dark turquoise and showed an intense Soret band at 435 nm, which is consistent with a monomeric Sn(IV) porphyrin. Interestingly, **6** had a similar UV/Vis spectrum to that of the cleaved porphyrin core (**8**), but the absorbance intensity of **6** was much lower at 425 nm (Soret band) than at 289 nm (aromatic absorption). This observation indicated that a minor amount of porphyrin remained—probably the result of incomplete transesterification or a small amount of encapsulation by either noncovalent or mechanical means. Oligomeric **6** (trimer and higher) was analyzed by SEC in NMP (Table 1). An M_n value of 35 kDa was obtained, which corresponds to a heptamer. However, as described above for **5** the actual oligomer length may be somewhat longer.[18]

Additional structural information is needed to determine whether the hollow channel collapses or remains open. Nonetheless, the route to non-fullerene organic nanotubes described herein features significant potential versatility. For example, the thickness of the tube wall may be modulated by choice of the generation of the dendron while the diameter of the inner tube may be controlled by adoption of suitably sized cores. Additionally, the functionality on the outer tube can be selected by use of appropriate dendron precursors. In a similar way, the functionality on the inner tube can be controlled by both the linking functionality and type of cleavage reaction employed. Although this route does not feature significant control over the length of the nanotube, fractionation of the product by SEC does allow particular distributions to be isolated. In closing, we have demonstrated a new application for our recently disclosed method of dendrimer coring.[17]

Received: August 9, 2002
Revised: November 27, 2002 [Z19931]

Keywords: coordination polymers · dendrimers · metathesis · nanotubes · porphyrinoids

[1] a) C. N. R. Rao, B. C. Satishkumar, A. Govindaraj, M. Nath, *ChemPhysChem* **2001**, *2*, 78; b) M. Terrones, W. K. Hsu, H. W. Kroto, D. R. M. Walton, *Top. Curr. Chem.* **1999**, *199*, 189; c) P. M. Ajayan, *Chem. Rev.* **1999**, *99*, 1787.

[2] a) R. Tenne, *Prog. Inorg. Chem.* **2001**, *50*, 269; b) W. Tremel, *Angew. Chem.* **1999**, *111*, 2311; *Angew. Chem. Int. Ed.* **1999**, *38*, 2175.

[3] a) D. T. Bong, T. D. Clark, J. R. Granja, M. R. Ghadiri, *Angew. Chem.* **2001**, *113*, 1016; *Angew. Chem. Int. Ed.* **2001**, *40*, 988; b) B. Gong, *Chem. Eur. J.* **2001**, *7*, 4336; c) S. Matile, *Chem. Soc. Rev.* **2001**, *30*, 158; d) B. König, *Angew. Chem.* **1997**, *109*, 1919; *Angew. Chem. Int. Ed. Engl.* **1997**, *36*, 1833.

[4] a) H. Matsui, R. MacCuspie, *Nano Lett.* **2001**, *1*, 671; b) D. Ranganathan, *Acc. Chem. Res.* **2001**, *34*, 919; c) T. D. Clark, K. Kobayashi, M. R. Ghadiri, *Chem. Eur. J.* **1999**, *5*, 782; d) D. Seebach, J. L. Matthews, A. Meden, T. Wessels, C. Baerlocher, L. B. McCusker, *Helv. Chim. Acta* **1997**, *80*, 173; e) J.-H. Fuhrhop, D. Spiroski, C. Boettcher, *J. Am. Chem. Soc.* **1993**, *115*, 1600.

[5] a) T. Kraus, M. Buděšínský, I. Císařová, J. Závada, *Angew. Chem.* **2002**, *114*, 1791; *Angew. Chem. Int. Ed.* **2002**, *41*, 1715; b) Y. Liu, C.-C. You, H.-Y. Zhang, S.-Z. Kang, C.-F. Zhu, C. Wang, *Nano Lett.* **2001**, *1*, 613; c) G. Gattuso, S. Menzer, S. A. Nepogodiev, J. F. Stoddart, D. J. Williams, *Angew. Chem.* **1997**, *109*, 1615; *Angew. Chem. Int. Ed. Engl.* **1997**, *36*, 1451; d) A. Harada, J. Li, M. Kamachi, *Nature* **1993**, *364*, 516.

[6] a) R. Saito, *Macromolecules* **2001**, *34*, 4299; b) R. Mäki-Ontto, K. de Moel, W. de Odorico, J. Ruokolainen, M. Stamm, G. ten Brinke, O. Ikkala, *Adv. Mater.* **2001**, *13*, 117; c) S. Stewart, G. Liu, *Angew. Chem.* **2000**, *112*, 348; *Angew. Chem. Int. Ed.* **2000**, *39*, 340; d) J. Raez, R. Barjovanu, J. A. Massey, M. A. Winnik, I. Manners, *Angew. Chem.* **2000**, *112*, 4020; *Angew. Chem. Int. Ed.* **2000**, *39*, 3862; e) K. Yu, A. Eisenberg, *Macromolecules* **1998**, *31*, 3509.

[7] Selected examples: a) H. Fenniri, B.-L. Deng, A. E. Ribbe, K. Hallenga, J. Jacob, P. Thiyagarajan, *Proc. Natl. Acad. Sci. USA* **2002**, *99*, 6487 (Suppl. 2); b) B. H. Hong, J. Y. Lee, C.-W. Lee, J. C. Kim, S. C. Bae, K. S. Kim, *J. Am. Chem. Soc.* **2001**, *123*,

 © 2003 Wiley-VCH Verlag GmbH & Co. KGaA, Weinheim 1433-7851/03/4210-1125 $ 20.00+.50/0

10748; c) G. John, M. Masuda, Y. Okada, K. Yase, T. Shimizu, *Adv. Mater.* **2001**, *13*, 715; d) G. W. Orr, L. J. Barbour, J. L. Atwood, *Science* **1999**, *285*, 1049; e) N. Kimizuka, T. Kawasaki, K. Hirata, T. Kunitake, *J. Am. Chem. Soc.* **1995**, *117*, 6360; f) J. M. Schnur, *Science* **1993**, *262*, 1669.

[8] Reviews: a) K. L. Wooley, *J. Polym. Sci. Part A* **2000**, *38*, 1397; b) W. Meier, *Chem. Soc. Rev.* **2000**, *29*, 295.

[9] Lead references to nondendritic metalloporphyrin coordination polymers: a) J. E. Redman, N. Feeder, S. J. Teat, J. K. M. Sanders, *Inorg. Chem.* **2001**, *40*, 2486; b) A. K. Burrell, D. L. Officer, P. G. Plieger, D. C. W. Reid, *Chem. Rev.* **2001**, *101*, 2751; c) J. Wojaczyński, L. Latos-Grażyński, *Coord. Chem. Rev.* **2000**, *204*, 113. Dendronized polymers: d) A. D. Schlüter, J. P. Rabe, *Angew. Chem.* **2000**, *112*, 860; *Angew. Chem. Int. Ed.* **2000**, *39*, 864, and references therein.

[10] T. M. Trnka, R. H. Grubbs, *Acc. Chem. Res.* **2001**, *34*, 18.

[11] For examples of related efforts toward synthetic nanostructures: a) S. Tamaru, M. Takeuchi, M. Sano, S. Shinkai, *Angew. Chem.* **2002**, *114*, 881; *Angew. Chem. Int. Ed.* **2002**, *41*, 853; and a review: b) J.-H. Fuhrhop in *Comprehensive Supramolecular Chemistry, Vol. 9* (Eds.: J.-P. Sauvage, M. W. Hosseini), Pergamon, Oxford, **1996**, chap. 11.

[12] See Supporting Information.

[13] A review of porphyrin dendrimers: T. Aida, D.-L. Jiang in *The Porphyrin Handbook, Vol. 3* (Eds.: K. M. Kadish, K. M. Smith, R. Guilard), Academic Press, San Diego, **2000**, chap. 23.

[14] J. W. Buchler in *The Porphyrins: Structure and Synthesis, Part A, Vol. 1* (Ed.: D. Dolphin), Academic Press, New York, **1978**, chap. 10.

[15] The illustrations of **5** and **6** represent mixtures of the oligomers where many combinations of intramolecular cross-links are possible; they are not meant to suggest a single product.

[16] PS-derived M_W values typically underestimate the molecular weight of highly branched dendrimers, see a) E. M. Harth, S. Hecht, B. Helms, E. E. Malmstrom, J. M. J. Fréchet, C. J. Hawker, *J. Am. Chem. Soc.* **2002**, *124*, 3926; b) L. Shu, A. D. Schlüter, C. Ecker, N. Severin, J. P. Rabe, *Angew. Chem.* **2001**, *113*, 4802; *Angew. Chem. Int. Ed.* **2001**, *40*, 4666.

[17] a) S. C. Zimmerman, M. S. Wendland, N. A. Rakow, I. Zharov, K. S. Suslick, *Nature* **2002**, *418*, 399; b) L. G. Schultz, Y. Zhao, S. C. Zimmerman, *Angew. Chem.* **2001**, *113*, 2016; *Angew. Chem. Int. Ed.* **2001**, *40*, 1962; c) M. S. Wendland, S. C. Zimmerman, *J. Am. Chem. Soc.* **1999**, *121*, 1389.

[18] Transmission electron microscopy was performed on **5** and **6** but mainly resulted in images of aggregates with sizes that were dependent on the method of sample preparation.[12]

 © 2003 Wiley-VCH Verlag GmbH & Co. KGaA, Weinheim 1433-7851/03/4210-1126 $ 20.00+.50/0

Supramolecular Photodimerization

Diastereospecific Photochemical Dimerization of a Stilbene-Containing Daisy Chain Monomer in Solution as well as in the Solid State**

Dafni G. Amirsakis, Arkadij M. Elizarov, Miguel A. Garcia-Garibay, Peter T. Glink, J. Fraser Stoddart,* Andrew J. P. White, and David J. Williams**

The solid-state [2+2] photochemical dimerization[1] of olefins such as stilbenes is a highly efficient method for the stereospecific synthesis of cyclobutanes. In solution, however, the photochemical reactions of such olefins generally result in mixtures of products. For example, irradiation of *trans*-stilbene in solution leads to several products: *trans*-to-*cis* isomerization yields *cis*-stilbene, which then can undergo electrocyclic ring closure to form dihydrophenanthrene, which, in the presence of oxygen, is oxidized to phenanthrene[2] while [2+2] cycloaddition of *trans*-stilbene yields[3] cyclobutane products with both *syn-anti-syn* and *all-anti* stereochemistries. The reaction rates, yields, and the distribution of products from photochemical reactions are dependent on the choice of solvent.[4] For example, in nonpolar solvents, such as benzene, *trans*-to-*cis* isomerization of stilbenes is favored over a very slow dimerization process.[3] In more polar solvents, such as methanol or water, hydrophobic interactions and possibly aromatic π-π stacking interactions lead to relatively rapid formation of a cyclobutane ring as the major, albeit low-yielding, reaction pathway, but with very little stereo- or regiocontrol.[4] Supramolecular assistance has provided solutions to the problem of preorganizing pairs of olefins in solution, such that efficient photochemical [2+2] dimerizations may occur. Examples of such supramolecular assistance in solution include 1) the dimerization of stilbenes within the cavities of γ-cyclodextrins[5] and cucurbit[8]uril,[6] 2) the use of hydrogen bonding to orchestrate a reaction[7] between a bisammonium-substituted dipyridylethylene and a bis([18]crown-6)-substituted stilbene derivative, 3) using metal cations, such as K^+ and Mg^{2+}, to template the reaction between the olefinic components of

[*] Prof. M. A. Garcia-Garibay, Prof. J. F. Stoddart, Dr. D. G. Amirsakis, Dr. A. M. Elizarov, Dr. P. T. Glink
Department of Chemistry and Biochemistry
University of California, Los Angeles
405 Hilgard Avenue, Los Angeles, CA 90095-1569 (USA)
Fax: (+1) 310-206-1843
E-mail: mgg@chem.ucla.edu
stoddart@chem.ucla.edu

Prof. D. J. Williams, Dr. A. J. P. White
Chemical Crystallography Laboratory
Department of Chemistry, Imperial College
South Kensington, London, SW7 2AY (UK)
Fax: (+44) 207-594-5835

[**] We thank the National Science Foundation for funding this research (CHE 9910199) which was also supported in part by an equipment grant (CHE 9974928).

 © 2003 Wiley-VCH Verlag GmbH & Co. KGaA, Weinheim 1433-7851/03/4210-1126 $ 20.00+.50/0

derivatized crown ether molecules,[8] and 4) the encapsulation and reaction[9] of acenaphthylenes and naphthoquinones within self-assembled coordination cages.

For successful dimerizations to occur in the solid state, the olefinic units must be aligned in a parallel manner with centroid···centroid separations[10] of about 3.5–4.2 Å. Supramolecular approaches have been used successfully to align stilbenes in the solid state, and their corresponding cyclobutane products have been obtained stereospecifically after photoirradiation.[11] Recently, we reported[12] a highly stereospecific, solid-state, [2+2] photocycloaddition between two bis(dialkylammonium ion)-substituted stilbene dications in a crystalline, doubly encircled and double-stranded, 2:2 host–guest complex with bisparaphenylene[34]crown-10. Although this and other examples of supramolecular preorganization in the solid state are highly efficient methods for the diastereospecific preparation of *syn-anti-syn*-substituted cyclobutanes, solid-state reactions do have their drawbacks, such as the need to obtain crystalline substrates, their relatively slow rates of reaction, and the difficulty in scaling reactions up to preparatively useful levels. As a result, it is important to find equally efficient methods for the dimerization of olefins—with both high stereo- and regiospecificity—in solution. Herein we describe a stilbene-containing crown ether/dialkylammonium ion hybrid that self-assembles into a [c2]daisy-chain-like pseudorotaxane both in solution as well as in the solid state. In this complex, the stilbene units are aligned in a head-to-tail manner with their olefinic groups positioned for efficient diastereospecific photochemical dimerizations.

Supramolecular and molecular daisy-chain-like entities[13] are becoming increasingly more appealing targets in synthesis. Previously, we demonstrated that **1**-H·O_2CCF_3—a self-complementary dialkylammonium salt incorporating a dibenzo[24]crown-8 (DB24C8) unit—forms dimers in a head-to-tail manner, in relatively nonpolar solvents and in the solid state, in which the NH_2^+ unit of one monomer is positioned inside the DB24C8 unit of another, and vice versa.[14] As a consequence of the asymmetric nature of the substitution of one of the catechol units of **1**-H·O_2CCF_3, two diastereoisomeric [c2]daisy-chain-like complexes (Scheme 1a) are observed to interconvert slowly on the ^{1}H NMR time-scale at room temperature. In the solid state, pairs of the trisubstituted catechol rings of **1**-H·O_2CCF_3 are aligned in a parallel manner with a centroid···centroid separation of 3.55 Å. This observation prompted us to consider replacing the central benzene unit of $\mathbf{1}^+$ with a *trans*-stilbenoid unit (namely, to prepare *E*-**2**-H·O_2CCF_3) with the anticipation that diastereoisomeric cyclic dimer complexes (*E*-**2**-H)$_2$·(O_2CCF_3)$_2$ (Scheme 1b) would form in which adjacent *trans*-stilbene olefinic groups are aligned in a head-to-tail manner at a distance suitable for a photochemical [2+2] cycloaddition.

The stilbene-containing daisy-chain monomer *E*-**2**-H·O_2CCF_3 was prepared according to the reaction sequence summarized in Scheme 2. The benzylic alcohol[15] **4** was converted using triphenylphosphane and *N*-chlorosuccinimide (NCS) into the chloride **5**, which in turn was converted by a Finkelstein reaction[16] into the iodide **6**, which underwent nucleophilic substitution to give the triphenylphosphonium iodide **7**-I. A Wittig reaction[17] between **7**-I and (2-formyl)dibenzo[24]crown-8[14b] **8** gave the corresponding stilbene derivative *E*-**9**. The Boc protecting groups were removed using trifluoroacetic acid to give *E*-**2**-H·O_2CCF_3.

Single crystals were obtained by layer diffusion of hexanes into a solution of *E*-**2**-H·O_2CCF_3 in CH_2Cl_2. The X-ray structure[18] of *E*-**2**-H·O_2CCF_3 reveals the formation (Figure 1) of a centrosymmetric [c2]daisy chain wherein the dibenzylammonium component of one molecule is threaded through the polyether ring of the other and vice versa (Figure 1). This mutual threading is accompanied by an essentially parallel stacking of the *trans*-stilbene units of the two component molecules such that the centers of the two *trans* olefinic bonds are held at 3.94 Å from each other (see Figure 2)—a geometry that should facilitate subsequent photodimerization. The co-conformation of the [c2]daisy chain is stabilized by a combination of N^+–H···O, C–H···O, C–H···π, and π···π interactions (interactions **a–c, d, e**, and **f,** respectively, in Figure 1). The dimers form stepped stacks, with the catechol ring in one dimer entering into a parallel π-π stacking interaction with its symmetry-related counterpart in the next; the centroid···centroid and mean interplanar separations are 3.70 and 3.61 Å, respectively. These stacks and their lattice-translated counterparts are arranged to form sheets with the $CF_3CO_2^-$ ions and the CH_2Cl_2 solvent molecules (both of which are disordered) intercalated

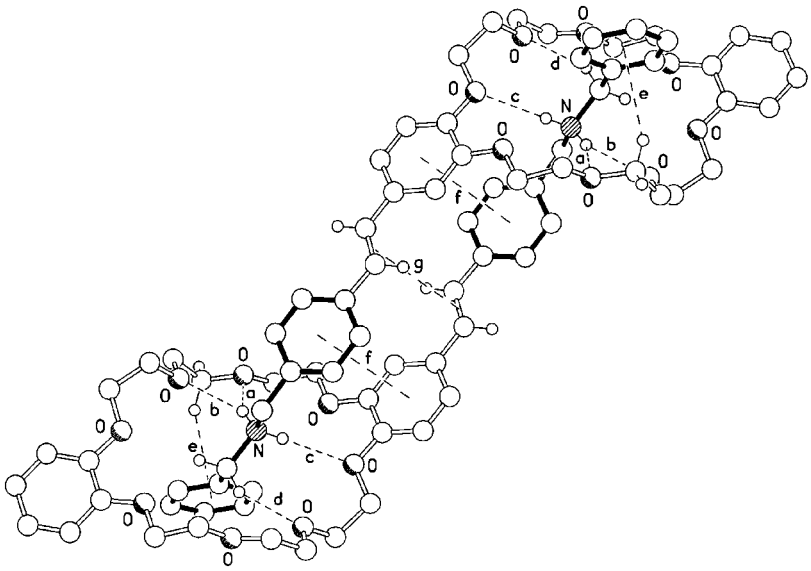

Figure 1. Ball-and-stick representation of the [c2]daisy chain formed by a pair of [*E*-**2**-H]$^+$ ions. Hydrogen-bonding interactions X···O, H···O [Å], X–H···O [°]: **a**: 2.96, 2,17, 147; **b**: 2.98, 2.25, 138; **c**: 3.25, 2.37, 165; **d**: 3.21, 2.35, 146; the C–H···π interaction **e** has H···π 2.86 Å and C–H···π 153°; the π···π interaction **f** has centroid···centroid and mean interplanar separations of 3.96 and 3.38 Å, respectively, the rings are inclined by approximately 8°; the centroid···centroid distance **g** is 3.94 Å and the planes of the olefinic groups are separated by about 3.29 Å.

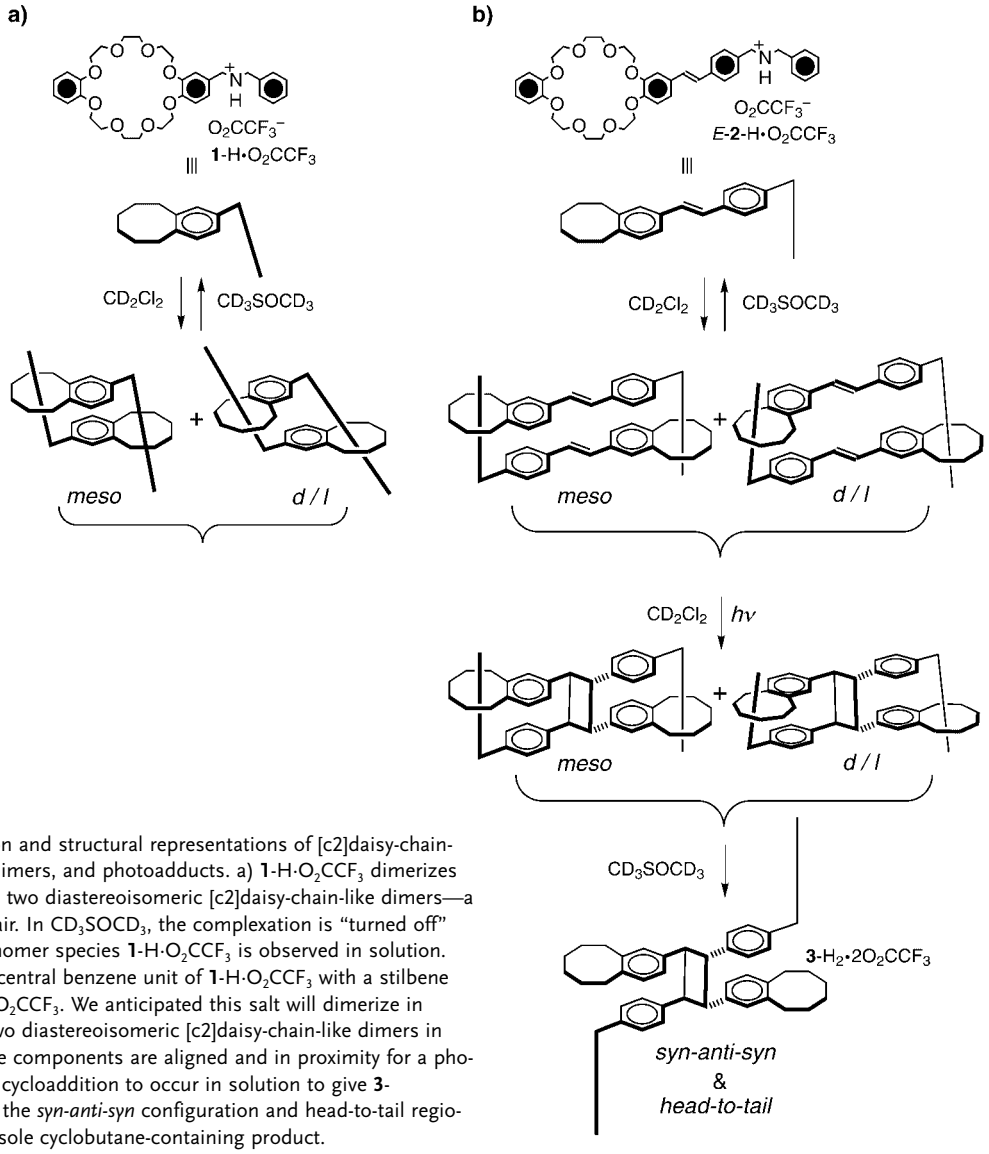

Scheme 1. Cartoon and structural representations of [c2]daisy-chain-like monomers, dimers, and photoadducts. a) **1**-H·O_2CCF_3 dimerizes in CD_2Cl_2 to form two diastereoisomeric [c2]daisy-chain-like dimers—a *meso* and a *d*/*l* pair. In CD_3SOCD_3, the complexation is "turned off" and only the monomer species **1**-H·O_2CCF_3 is observed in solution. b) Replacing the central benzene unit of **1**-H·O_2CCF_3 with a stilbene unit gives *E*-**2**-H·O_2CCF_3. We anticipated this salt will dimerize in CD_2Cl_2 to form two diastereoisomeric [c2]daisy-chain-like dimers in which the stilbene components are aligned and in proximity for a photochemical [2+2] cycloaddition to occur in solution to give **3**-H_2·2O_2CCF_3 with the *syn-anti-syn* configuration and head-to-tail regiochemistry as the sole cyclobutane-containing product.

between adjacent sheets, there being no immediately evident electrostatic cation···anion interactions.

A powdered crystalline sample of *E*-**2**-H·O_2CCF_3 was placed between two pyrex microscope slides and irradiated for 3 h, after which, an ^{1}H NMR (500 MHz, CD_3SOCD_3) spectrum (Figure 3c) of the product displayed a resonance at $\delta = 4.41$ ppm. The chemical shift of this signal is characteristic of the methine protons of a cyclobutane derivative—presumably **3**-H_2·2O_2CCF_3—possessing a *syn-anti-syn* arrangement of its tetraaryl substituents.[19] Additionally, the appearance of only one cyclobutane signal in the ^{1}H NMR spectrum suggested that only one cyclobutane diastereoisomer had been formed in quantitative yield. This observation confirmed that the pairs of **3**-H^{2+} dications exist in the crystal as [c2]daisy chain dimers with eclipsed stilbene units, as illustrated in the X-ray crystal structure (Figure 1).

A solution (3.8 μM) of the daisy chain monomer *E*-**2**-H·O_2CCF_3 in CD_2Cl_2 was studied by ^{1}H NMR spectroscopy. The ^{1}H NMR spectrum is very complex (Figure 3a) as a result of the slow kinetics[20] of association and dissociation of the subunits and the existence of diastereoisomeric [c2]daisy-chain-like complexes; for example, two doublets at $\delta = 6.28$ and 6.43 ppm ($J = 1.5$ Hz) are observed for the aromatic H_1 proton, which suggests[21] that two diastereoisomeric dimers of *E*-**2**-H·O_2CCF_3—presumably a *meso* one and a *d*/*l* pair—exist in solution. Additionally, three of the four expected doublets, with coupling constants of 16 Hz, appear between $\delta = 6.48$ and 6.63 ppm; two of these signals correspond to the olefinic protons of the major diasteroisomer of (*E*-**2**-H)$_2$·(O_2CCF_3)$_2$ and one to the olefinic protons of the minor one.[22] The upfield positioning of these signals suggests that their protons experience a shielding environment, which is expected in the [c2]daisy-chain-like complexes. The ^{1}H NMR spectrum of *E*-**2**-H·O_2CCF_3 in CD_3SOCD_3 is much less complicated (Figure 3b) since only the monomer species *E*-**2**-H·O_2CCF_3 is expected[23] to exist in this highly polar solvent.

 © 2003 Wiley-VCH Verlag GmbH & Co. KGaA, Weinheim 1433-7851/03/4210-1128 $ 20.00+.50/0

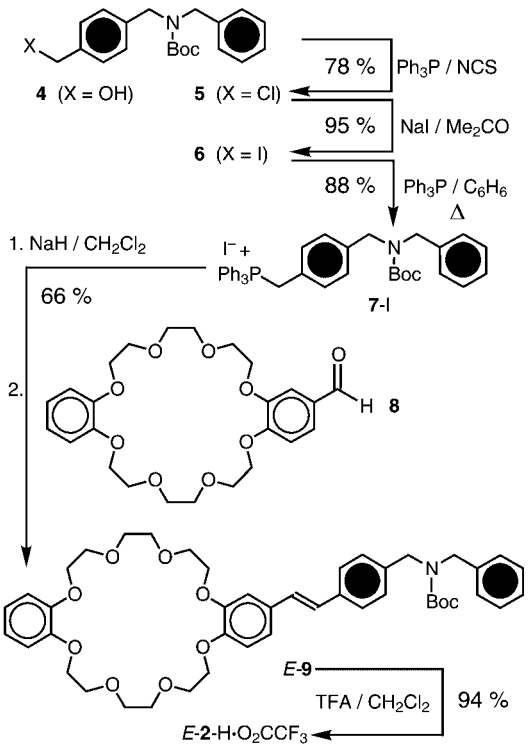

Scheme 2. Synthesis of *E*-**2**-H·O_2CCF_3. Boc = *tert*-butoxycarbonyl. TFA = trifluoroacetic acid.

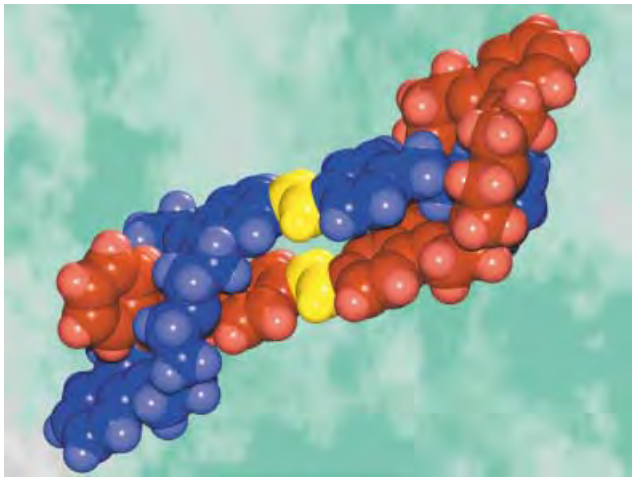

Figure 2. Space-filling representation of the [c2]daisy chain formed by a pair of [*E*-**2**-H]$^+$ ions. One monomer unit is red and the other blue; the stilbenoid carbon–carbon double bond is yellow.

We investigated the [2+2] photoaddition of *E*-**2**-H·O_2CCF_3 in CD_2Cl_2 because of its strong tendency to aggregate to afford cyclic noncovalent dimers in this solvent. Thus, a solution of *E*-**2**-H·O_2CCF_3 in CD_2Cl_2 was placed in a pyrex NMR tube, degassed by sonication, and then irradiated through a cut-off filter ($\lambda > 350$ nm) for about 20 min. Since the ^{1}H NMR spectrum of the reaction mixture in CD_2Cl_2 was extremely complex, the solvent was evaporated and the spectrum (Figure 1d) of the product was recorded in CD_3SOCD_3.[24] It reveals that a significant change has occurred upon irradiation. Most diagnostically, the signals for the olefinic protons have disappeared and a broad singlet, which represents the *syn-anti-syn* cyclobutane derivative **3**-H_2·2 O_2CCF_3, has once again appeared at $\delta = 4.41$ ppm. This solution-state photodimerization appears to give rise to only one diastereoisomer of the cyclobutane derivative **3**-H_2·2 O_2CCF_3 with greater than 95% conversion.[25,26]

Moreover, the ^{1}H NMR spectrum (Figure 3d), obtained after photoirradiation of *E*-**2**-H·O_2CCF_3 in a CD_2Cl_2 solution is virtually identical to that (Figure 3c) obtained following the solid-state photoirradiation of *E*-**2**-H·O_2CCF_3. Hence, not only can it be inferred that [c2]daisy-chain-like pseudorotaxanes are formed in solution as well as in the solid state, it can also be concluded that the relative alignment of the stilbenoid double bonds is roughly the same in the reactive solution-state complex—namely, they are eclipsed[27]—as it is in the solid-state dimer.

This fundamental investigation has established that supramolecular assistance to the [2+2] photodimerization can be carried out in solution as well as in the solid state, and that the photoreaction occurs with exactly the same stereospecificity in solution as it does in the solid state. This observation is important in designing supramolecular systems with multiple matching reaction centers for the construction of large cluster-like and ribbon-like compounds incorporating functionality.

Experimental Section

5: Addition of a solution of PPh_3 (1.67 g, 6.40 mmol) in dry THF (32 mL) to a solution of *N*-chlorosuccinimide (NCS) (980 mg, 7.3 mmol) in dry THF (37 mL) resulted in the formation of a white precipitate. A solution of **4**[15] (1.0 g, 3.20 mmol) in dry THF (10 mL) was added to the suspension, and the mixture was stirred overnight at room temperature. The THF was evaporated and the residue was subjected to column chromatography (SiO_2; EtOAc/hexanes, 1:10), to afford **5** (890 mg, 78%) as a clear oil. ^{1}H NMR ($CDCl_3$, 500 MHz, 298 K): $\delta = 1.54$ (s, 9H), 4.38 (brs, 2H), 4.46 (brs, 2H), 4.63 (s, 2H), 7.24 (brs, 2H), 7.27 (brs, 2H), 7.32 (brs, 1H), 7.33 (brs, 1H), 7.36–7.30 ppm (m, 4H); ^{13}C NMR ($CDCl_3$, 125 MHz, 298 K): $\delta = 28.5$, 31.5, 45.6, 49.0, 79.9, 127.2, 127.4, 127.7, 127.9, 128.3, 128.5, 128.6, 128.8, 129.0, 129.1, 136.4, 155.9 ppm; HR-EIMS calcd for $C_{20}H_{25}ClNO_2$ $[M+H]^+$: m/z 346.1496, found: 346.1566.

6: A solution of **5** (371 mg, 1.07 mmol) in Me_2CO (10 mL) was added dropwise to a suspension of NaI (176 mg, 1.17 mmol) in Me_2CO (30 mL), and then stirred overnight at room temperature. The salts were filtered off and the solvent was evaporated to give **6** (465 mg, 95%) as a light-brown oil, which was used without further purification. ^{1}H NMR ($CDCl_3$, 500 MHz, 298 K): $\delta = 1.32$ (s, 9H), 4.12–4.21 (brm, 4H), 4.26 (s, 2H), 6.95–7.08 (brm, 4H), 7.12–7.16 ppm (m, 5H); ^{13}C NMR ($CDCl_3$, 125 MHz, 298 K): $\delta = 5.4$, 28.1, 29.5, 49.4, 53.5, 127.0, 127.2, 127.6, 128.0, 128.3, 128.6, 128.7, 129.0, 129.1, 138.1, 155.6 ppm; HR-EIMS calcd for $C_{20}H_{25}INO_2$ $[M+H]^+$: m/z 448.0852, found: 448.0921.

7-I: A solution of **6** (262 mg, 0.60 mmol) and PPh_3 (173 mg, 0.66 mmol) in benzene (50 mL) was heated under reflux for 2 h. After cooling the reaction mixture down to room temperature, the precipitate was filtered off to give **7**-I (371 mg, 88%) as a white solid. ^{1}H NMR ($CDCl_3$, 500 MHz, 298 K): $\delta = 1.45$ (s, 9H), 4.21–4.31 (brm, 4H), 5.24 (d, 2H, $J = 13.1$ Hz), 6.97–7.26 (brm, 4H), 7.26–7.34 (m, 5H), 7.61–7.69 ppm (m, 15H); ^{13}C NMR ($CDCl_3$, 125 MHz, 298 K): $\delta = 28.3$, 30.6 ($J_{PC} = 45.8$ Hz), 48.4, 49.5, 117.5 ($J_{PC} = 85.3$ Hz),

 © 2003 Wiley-VCH Verlag GmbH & Co. KGaA, Weinheim 1433-7851/03/4210-1129 $ 20.00+.50/0

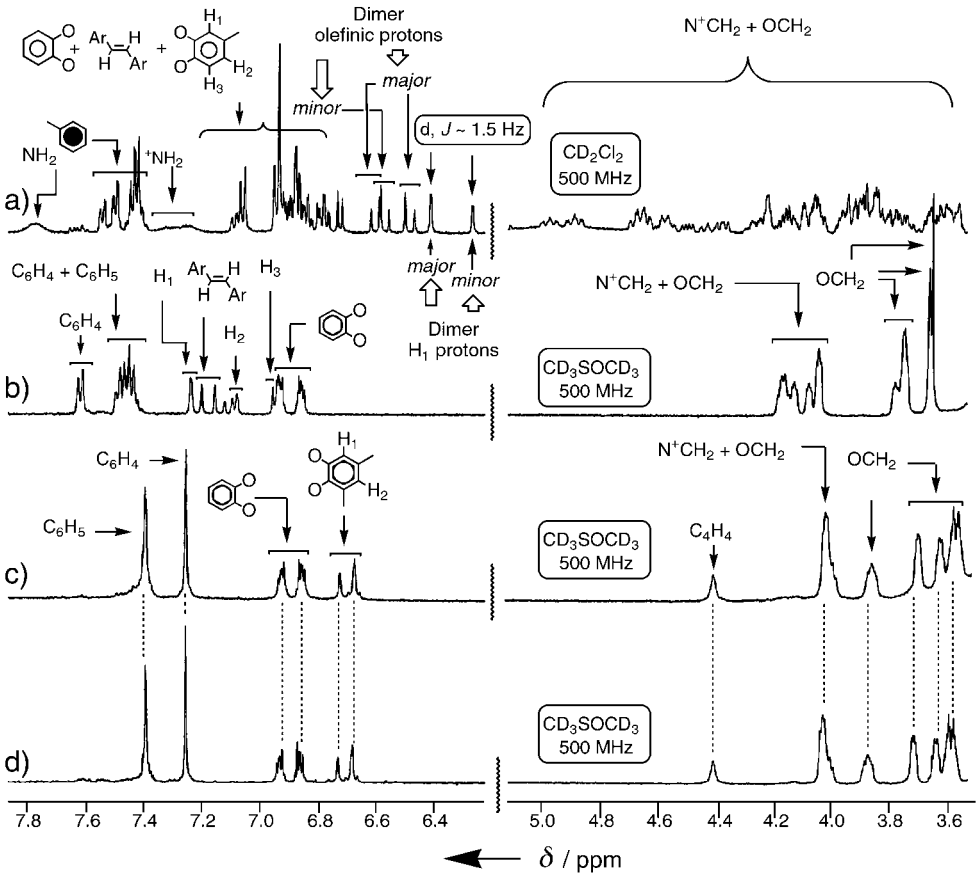

Figure 3. a) The ^{1}H NMR spectrum of *E*-**2**-H·O_2CCF_3 in CD_2Cl_2 shows two major diastereoisomeric [c2]daisy-chain-like complexes in solution, presumably the *meso* and *d*/*l* pairs. b) A much simpler ^{1}H NMR spectrum of *E*-**2**-H·O_2CCF_3 in CD_3SOCD_3 where complexation is "turned off". This spectrum reveals how *E*-**2**-H·O_2CCF_3 looks in CD_3SOCD_3 before photochemical irradiation. c) ^{1}H NMR spectrum of **3**-H_2·2O_2CCF_3 after solid-state irradiation of crystalline *E*-**2**-H·O_2CCF_3. d) After irradiation of *E*-**2**-H·O_2CCF_3 in CD_2Cl_2, a ^{1}H NMR spectrum of the photoproduct taken in CD_3SOCD_3 reveals **3**-H_2·2O_2CCF_3 as the major product. A singlet centered on $\delta = 4.41$ ppm corresponds to the methine protons present in a cyclobutane ring with *syn-anti-syn* stereochemistry.

125.6, 127.2, 128.0, 128.2, 128.4, 130.1 ($J_{PC} = 12.5$ Hz), 131.6 ($J_{PC} = 5.3$ Hz), 134.3 ($J_{PC} = 9.8$ Hz), 135.0 ($J_{PC} = 2.8$ Hz), 137.6, 138.4, 155.7 ppm; HR-FABMS calcd for $C_{38}H_{39}NO_2P^+$ $[M]^+$: *m*/*z* 572.2718, found: 572.2713.

E-**2**-H·O_2CCF_3: A mixture of **7**-I (371 mg, 0.53 mmol) and NaH (51 mg, 2.1 mmol) in CH_2Cl_2 (25 mL) was stirred at ambient temperature for 30 min and then a solution of **8** (253 mg, 0.53 mmol) in CH_2Cl_2 (5 mL) was added slowly. The mixture was stirred for 20 h, before 1N HCl (2 mL) was added to quench the reaction. The mixture was partitioned between CH_2Cl_2 (25 mL) and H_2O (20 mL). The organic layer was washed with 1N HCl (2 × 20 mL), dried ($MgSO_4$), and then evaporated to dryness. The residue was subjected to column chromatography (SiO_2; EtOAc/hexanes, 3:7) to afford *E*-**9** as a clear oil (269 mg, 66%). ^{1}H NMR ($CDCl_3$, 500 MHz, 298 K): $\delta = 1.50$ (s, 9H), 3.83–3.85 (m, 8H), 3.91–3.96 (m, 8H), 4.13–4.18 (m, 6H), 4.21–4.23 (m, 2H), 4.34 (brs, 2H), 4.44 (brs, 2H), 6.84 (d, $J = 8$ Hz, 1H), 6.86–6.92 (m, 4H), 6.93 (d, $J = 16$ Hz, 1H), 6.99 (d, $J = 16$ Hz), 7.02–7.04 (m, 1H), 7.06 (d, $J = 1.8$ Hz, 1H), 7.12–7.29 (m, 7H), 7.44 ppm (d, $J = 8$ Hz, 2H); ^{13}C NMR ($CDCl_3$, 125 MHz, 298 K): $\delta = 28.3$, 31.5, 69.2, 69.3, 69.4, 69.7, 69.8, 80.0, 111.6, 113.7, 113.9, 120.3, 121.3, 126.3, 127.1, 128.2, 128.4, 130.8, 148.7, 148.8, 148.9, 155.9 ppm; HR-FABMS calcd for $C_{45}H_{55}NO_{10}Na^+$ $[M+Na]^+$: *m*/*z* 792.3749, found: 792.3718. TFA (1 mL, 13 mmol) was added to a solution of *E*-**9** (269 mg, 0.35 mmol) in CH_2Cl_2 (20 mL) and the mixture was stirred for 1 h before being evaporated to dryness to yield *E*-**2**-H·O_2CCF_3 as a white solid (207 mg, 94%). ^{1}H NMR (CD_3SOCD_3, 500 MHz, 298 K): $\delta =$ 3.65–3.66 (m, 8H), 3.74–3.79 (m, 8H), 4.04–4.12 (m, 8H), 4.13–4.19 (m, 4H), 6.85–6.87 (m, 2H), 6.93–6.95 (m, 3H), 7.08 (dd, $J = 8.3$, 1.5 Hz, 1H), 7.14 (d, $J = 16.3$ Hz, 1H), 7.22 (d, $J = 16.3$ Hz, 1H), 7.24 (d, $J = 1.5$ Hz, 1H), 7.42–7.49 (m, 7H), 7.62 (d, $J = 8$ Hz, 2H), 9.18 ppm (brs, 2H); ^{13}C NMR (CD_3SOCD_3, 125 MHz, 298 K): $\delta =$ 50.4, 50.5, 69.0, 69.1, 69.4, 69.5, 70.7, 111.7, 114.0, 114.4, 120.9, 121.5, 125.9, 126.6, 129.0, 129.1, 129,4, 129.7, 130.2. 130.3, 130.4, 130.7, 132.1, 132.2, 138.4, 148.9, 158.3 ppm; HR-FABMS calcd for $C_{40}H_{48}NO_8$ [*E*-**2**]$^+$: *m*/*z* 670.3408, found: 670.3374.

3-H_2·2O_2CCF_3: Irradiation in solution: A solution of *E*-**2**-H·O_2CCF_3 (2.6 mg, 3.8 μmol) in CD_2Cl_2 (1 mL) was degassed by sonication in a pyrex NMR tube for about 20 min. The reaction mixture was then irradiated for 20 min with UV light from a Hanovia lamp in the presence of a filter ($\lambda > 350$ nm). The solvent was evaporated to give **3**-2H_2·2O_2CCF_3 as a white solid (2.6 mg, 95%). ^{1}H NMR (CD_3SOCD_3, 500 MHz, 298 K): $\delta = 3.45$–3.49 (m, 8H), 3.58–3.59 (m, 8H), 3.64–3.65 (brs, 8H), 3.72 (brs, 8H), 3.88–3.89 (brs, 8H), 3.99–4.03 (brs, 16H), 4.41 (brs, 4H), 6.69 (brs, 4H), 6.74 (brs, 2H), 6.86–6.88 (m, 4H), 6.93–6.95 (m, 4H), 7.27 (s, 8H), 7.40 (s, 10H), 9.09 ppm (brs, 4H); ^{13}C NMR (CD_3SOCD_3, 125 MHz, 298 K): $\delta =$

 © 2003 Wiley-VCH Verlag GmbH & Co. KGaA, Weinheim 1433-7851/03/4210-1130 $ 20.00+.50/0

46.5, 47.0, 49.9, 50.0, 68.8, 68.9, 69.5, 70.2, 114.4, 121.5, 128.8, 128.9, 129.3, 129.8, 130.2, 132.0, 133.7, 142.3, 146.9, 147.9, 148.8 ppm; HR-FABMS calcd for $C_{80}H_{95}N_2O_{16}\cdot 2\,TFA$ $[\mathbf{3}\text{-}H]^+$: m/z 1339.6603, found: 1339.6719. Irradiation in the solid state: Crystals were grown by layering hexanes over a solution of E-**2**-H·O_2CCF_3 (5 mg) in CH_2Cl_2 (0.5 mL). The crystals were filtered, air-dried, placed between two pyrex microscope slides, and then irradiated for about 3 h to give **3**-$2\,H_2\cdot O_2CCF_3$ (5 mg, 100%) as a white solid.

Received: September 30, 2002 [Z50266]

Keywords: dimerization · photochemistry · pseudorotaxane · solid-state reactions · structure-directed synthesis

[1] For reviews on solid-state photochemistry, see a) M. Hasegawa, *Chem. Rev.* **1983**, *83*, 507–518; b) V. Ramamurthy, K. Venkatesan, *Chem. Rev.* **1987**, *87*, 433–481; c) F. Toda, *Acc. Chem. Res.* **1995**, *28*, 480–486; d) J. N. Gamlin, R. Jones, M. Leibovitch, B. Patrick, J. R. Scheffer, J. Trotter, *Acc. Chem. Res.* **1996**, *29*, 203–209; e) Y. Ito, *Synthesis* **1998**, 1–32; f) A. E. Keating, M. A. Garcia-Garibay in *Organic and Inorganic Photochemistry* (Eds.: V. Ramamurthy, K. S. Schanze), Marcel Dekker, New York, **1998**, pp. 195–248; g) K. Tanaka, F. Toda, *Chem. Rev.* **2000**, *100*, 1025–1074; h) L. R. MacGillivray, *CrystEngComm* **2002**, *4*, 37–41.

[2] a) F. B. Mallory, C. S. Wood, J. Gordon, L. C. Lindquist, M. L. Saviz, *J. Am. Chem. Soc.* **1962**, *84*, 4361–4362; b) H. Meier, *Angew. Chem.* **1992**, *104*, 1425–1576; *Angew. Chem. Int. Ed. Engl.* **1992**, *31*, 1399–1420.

[3] a) H. Shechter, W. J. Link, G. V. D. Tiers, *J. Am. Chem. Soc.* **1963**, *85*, 1601–1605; b) H. Ulrich, D. V. Rao, F. A. Stuber, A. A. R. Sayigh, *J. Org. Chem.* **1970**, *35*, 1121–1125; c) B. S. Green, J. Heller, *J. Org. Chem.* **1974**, *39*, 196–201.

[4] a) M. S. Syamala, V. Ramamuthy, *J. Org. Chem.* **1986**, *51*, 3712–3715; b) Y. Ito, T. Kajita, K. Kunimoto, T. Matsuura, *J. Org. Chem.* **1989**, *54*, 587–591.

[5] a) W. Herrmann, M. Schneider, G. Wenz, *Angew. Chem.* **1997**, *109*, 2621–2624; *Angew. Chem. Int. Ed. Engl.* **1997**, *36*, 2511–2514; b) W. Herrmann, S. Wehrle, G. Wenz, *Chem. Commun.* **1997**, 1709–1710.

[6] S. Y. Jon, Y. H. Ko, S. H. Park, H.-J. Kim, K. Kim, *Chem. Commun.* **2001**, 1938–1939.

[7] a) S. P. Gromov, E. N. Ushakov, A. I. Vedernikov, N. A. Lobova, M. V. Alfimov, Y. A. Strelenko, J. K. Whitesell, M. A. Fox, *Org. Lett.* **1999**, *1*, 1697–1699; b) D. M. Bassani, V. Darcos, S. Mahony, J.-P. Desvergne, *J. Am. Chem. Soc.* **2000**, *122*, 8795–8796; c) D. M. Bassani, X. Sallenave, V. Darcos, J.-P. Desvergne, *Chem. Commun.* **2001**, 1446–1447.

[8] a) S. Inokuma, T. Yamamoto, J. Nishimura, *Tetrahedron Lett.* **1990**, *31*, 97–100; b) S. P. Gromov, O. A. Fedorova, E. N. Ushakov, A. V. Buevich, I. I. Baskin, Y. V. Pershina, B. Eliasson, U. Edlund, M. V. Alfimov, *J. Chem. Soc. Perkin Trans. 2* **1999**, 1323–1329; c) O. A. Fedorova, S. P. Gromov, M. V. Alfimov, *Russ. Chem. Bull.* **2001**, *50*, 1970–1983.

[9] M. Yoshizawa, Y. Takeyama, T. Kusukawa, M. Fujita, *Angew. Chem.* **2002**, *114*, 1403–1405; *Angew. Chem. Int. Ed.* **2002**, *41*, 1347–1349.

[10] a) M. D. Cohen, G. M. J. Schmidt, F. I. Sonntag, *J. Chem. Soc.* **1964**, 2000–2013; b) G. M. J. Schmidt, *J. Chem. Soc.* **1964**, 2014–2021; c) G. M. J. Schmidt, *Pure Appl. Chem.* **1971**, *27*, 647–678.

[11] a) K. S. Feldman, R. F. Campbell, *J. Org. Chem.* **1995**, *60*, 1924–1925; b) Y. Ito, B. Borecka, J. Trotter, J. R. Scheffer, *Tetrahedron Lett.* **1995**, *36*, 6083–6086; c) Y. Ito, B. Borecka, G. Olovsson, J. Trotter, J. R. Scheffer, *Tetrahedron Lett.* **1995**, *36*, 6087–6090; d) A. J. Blake, N. R. Champness, S. S. M. Chung, W.-S. Li, M. Schröder, *Chem. Commun.* **1997**, 1675–1676; e) G. W. Coates, A. R. Dunn, L. M. Henling, J. W. Ziller, E. B. Lobkovsky, R. H. Grubbs, *J. Am. Chem. Soc.* **1998**, *120*, 3641–3649; f) K. S. S. P. Rao, S. M. Hubig, J. N. Moorthy, J. K. Kochi, *J. Org. Chem.* **1999**, *64*, 8098–8104; g) K. Tanaka, F. Toda, E. Mochizuki, N. Yasui, Y. Kai, I. Miyahara, K. Hirotsu, *Angew. Chem.* **1999**, *111*, 3733–3736; *Angew. Chem. Int. Ed.* **1999**, *38*, 3523–3525; h) L. R. MacGillivray, J. L. Reid, J. A. Ripmeester, *J. Am. Chem. Soc.* **2000**, *122*, 7817–7818; i) G. S. Papaefstathiou, A. J. Kipp, L. R. MacGillivray, *Chem. Commun.* **2001**, 2462–2463; j) L. R. MacGillivray, J. L. Reid, J. A. Ripmeester, G. S. Papaefstathiou, *Ind. Eng. Chem. Res.* **2002**, *41*, 4494–4497; k) T. D. Hamilton, G. S. Papaefstathiou, L. R. MacGillivray, *CrystEngComm* **2002**, *4*, 223–226; l) T. D. Hamilton, G. S. Papaefstathiou, L. R. MacGillivray, *J. Am. Chem. Soc.* **2002**, *124*, 11606–11607.

[12] D. G. Amirsakis, M. A. Garcia-Garibay, S. J. Rowan, J. F. Stoddart, A. J. P. White, D. J. Williams, *Angew. Chem.* **2001**, *113*, 4386–4391; *Angew. Chem. Int. Ed.* **2001**, *40*, 4256–4261.

[13] a) S. J. Rowan, S. J. Cantrill, J. F. Stoddart, A. J. P. White, D. J. Williams, *Org. Lett.* **2000**, *2*, 759–763; b) M. C. Jiménez, C. Dietrich-Buchecker, J.-P. Sauvage, A. De Cian, *Angew. Chem.* **2000**, *112*, 1351–1354; *Angew. Chem. Int. Ed.* **2000**, *39*, 1295–1298; c) M. C. Jiménez, C. Dietrich-Buchecker, J.-P. Sauvage, *Angew. Chem.* **2000**, *112*, 3422–3425; *Angew. Chem. Int. Ed.* **2000**, *39*, 3284–3287; d) S.-H. Chiu, S. J. Rowan, S. J. Cantrill, J. F. Stoddart, A. J. P. White, D. J. Williams, *Chem. Commun.* **2002**, 2948–2949.

[14] a) P. R. Ashton, I. Baxter, S. J. Cantrill, M. C. T. Fyfe, P. T. Glink, J. F. Stoddart, A. J. P. White, D. J. Williams, *Angew. Chem.* **1998**, *110*, 1344–1347; *Angew. Chem. Int. Ed.* **1998**, *37*, 1294–1297; b) S. J. Cantrill, G. J. Youn, J. F. Stoddart, *J. Org. Chem.* **2001**, *66*, 6857–6872.

[15] P. R. Ashton, J. Becher, M. C. T. Fyfe, M. B. Nielsen, J. F. Stoddart, A. J. P. White, D. J. Williams, *Tetrahedron* **2001**, *57*, 947–956.

[16] L. F. Tietze, T. Eicher in *Reactions and Synthesis in the Organic Chemistry Laboratory* (Trans.: D. Ringe), University Science Books, Mill Valley, CA, **1989**, p. 48–49.

[17] S.-H. Chiu, S. J. Rowan, S. J. Cantrill, J. F. Stoddart, A. J. P. White, D. J. Williams, *Chem. Eur. J.* **2002**, *8*, 5170–5183.

[18] Crystal data for **2**-H·O_2CCF_3·HO_2CCF_3·$1.5\,CH_2Cl_2$: $[C_{40}H_{48}NO_8](O_2CCF_3)\cdot HO_2CCF_3\cdot 1.5\,CH_2Cl_2$, $M_r = 1025.2$, triclinic, space group $P\bar{1}$ (no. 2), $a = 10.195(1)$, $b = 11.740(1)$, $c = 21.690(2)$ Å, $\alpha = 95.39(1)$, $\beta = 102.89(1)$, $\gamma = 100.59(1)°$, $V = 2462.5(4)$ Å^3, $Z = 2$, $\rho_{calcd} = 1.383\,g\,cm^{-3}$, $\mu(Cu_{K\alpha}) = 2.41\,mm^{-1}$, $T = 203$ K, colorless prisms; 7292 independent measured reflections, F^2 refinement, $R_1 = 0.105$, $wR_2 = 0.277$, 3751 independent observed reflections ($|F_o| > 4\sigma|$ $2\theta \le 120°$), 675 parameters. CCDC-191314 contains the supplementary crystallographic data for this paper. These data can be obtained free of charge via www.ccdc.cam.ac.uk/conts/retrieving.html (or from the Cambridge Crystallographic Data Centre, 12 Union Road, Cambridge CB2 1EZ, UK; fax: (+44) 1223-336-033; or deposit@ccdc.cam.ac.uk).

[19] The chemical shift of this signal at $\delta = 4.41$ ppm is consistent with the *syn-anti-syn* isomer **3**-$H_2\cdot 2\,O_2CCF_3$, since other *syn-anti-syn* tetraaryl-substituted cyclobutane derivatives have been reported (see refs. [3], [6], [11f], and [12]) to exhibit resonance of the corresponding ring proton in the range $\delta = 4.10$ to 5.00 ppm. In contrast, the *all-anti* tetraaryl-substituted isomer is expected to contain cyclobutane ring protons resonating between $\delta = 3.50$ and 3.80 ppm.

[20] P. R. Ashton, E. J. T. Chrystal, P. T. Glink, S. Menzer, C. Schiavo, N. Spencer, J. F. Stoddart, P. A. Tasker, A. J. P. White, D. J. Williams, *Chem. Eur. J.* **1996**, *2*, 709–728.

[21] Although we have depicted (Scheme 1) the major and minor co-conformations of (E-**2**-H)$_2$·$(O_2CCF_3)_2$ to be those in which the olefinic units of each monomer are eclipsed, there exists the

possibility of other co-conformations being populated in which the olefinic units are oriented in staggered arrangements. Since these staggered co-conformations are diastereoisomeric with respect to the eclipsed ones, the well-resolved signals observed for the olefinic protons suggest that if these co-conformations are populated, then they are interconverting rapidly with the eclipsed co-conformations on the ^{1}H NMR time-scale at 500 MHz at 300 K.

[22] We reached this conclusion by analogy to the similar set of two signals for the corresponding H_1 proton of **1**-H·O_2CCF_3 observed in its ^{1}H NMR spectrum in CD_3CN. See ref. [14].

[23] The FAB mass spectrum of *E*-**2**-H·O_2CCF_3 in Me_2SO reveals peaks at *m*/*z* 692.52 (100%) and 1339.98 (10%), which correspond to monomeric [*E*-**2**+Na]$^+$ and a small amount of the dimeric [(*E*-**2**)$_2$-H]$^+$, respectively. By contrast, the FAB mass spectrum of *E*-**2**-H·O_2CCF_3 in CH_2Cl_2 reveals peaks at *m*/*z* 670.34 (60%) and 692.33 (20%) which correspond to the doubly charged [c2]daisy-chain-like pseudorotaxane [(*E*-**2**)$_2$+H+Na]$^{2+}$ and a small amount of the monomer [*E*-**2**+Na]$^+$, respectively.

[24] When a solution of *E*-**2**-H·O_2CCF_3 (3.8 μmol) was irradiated in CD_3SOCD_3 (1 mL) for 20 min, *trans*-to-*cis* isomerization occurred to yield *E*-**2**-H·O_2CCF_3 and *Z*-**2**-H·O_2CCF_3 as the only two species present in solution. No cyclobutane derivative was observed in the ^{1}H NMR spectrum. This result is not surprising since no dimerization is expected to occur in CD_3SOCD_3. See ref. [20].

[25] A slight impurity is suggested by the presence of a small signal at $\delta = 7.6$ ppm in the ^{1}H NMR spectrum, but this contaminant also appears to be present in the initial sample of *E*-**2**-H·O_2CCF_3.

[26] It is worth noting that both the *meso* and *d*/*l* pair of diastereoisomers of (*E*-**2**-H)$_2$·(O_2CCF_3)$_2$ yield the same head-to-head and *syn-anti-syn* diastereoisomer of **3**-H_2·2 O_2CCF_3. The *meso* and *d*/*l* diastereoisomeric self-complexes of **3**-H_2·2 O_2CCF_3 are not observed in CD_3SOCD_3 because intramolecular hydrogen-bonding interactions are eradicated. These two self-complexes exist in less polar solvents, a feature that explains the complicated nature of the ^{1}H NMR spectrum of **3**-H_2·2 O_2CCF_3 in CD_2Cl_2.

[27] If the staggered co-conformations of (*E*-**2**-H)$_2$·(O_2CCF_3)$_2$ (see ref. [22]) were capable of undergoing [2+2] cycloaddition in solution, we would expect to observe also the formation of the *all-anti* cyclobutane diastereoisomer as a product.

 © 2003 Wiley-VCH Verlag GmbH & Co. KGaA, Weinheim 1433-7851/03/4210-1132 $ 20.00+.50/0

Dimeric Aluminum Dihydroxides

Aluminum Dihydroxide with Terminal OH Groups: An Unprecedented Congener of Boronic Acid**

Guangcai Bai, Ying Peng, Herbert W. Roesky, Jiyang Li, Hans-Georg Schmidt, and Mathias Noltemeyer*

Dedicated to Professor Marc Julia on the occasion of his 80th birthday

Alumoxanes as highly active catalysts and cocatalysts are of tremendous importance for the polymerization of a wide range of organic monomers.[1] Compounds of the general formula $[RAlO]_n$ or $[R_2AlOAlR_2]_n$ can be regarded as intermediates in the hydrolysis of aluminum compounds to aluminum hydroxide, which are prepared by the controlled reaction of aluminum compounds with water[2] or reactive oxygen-containing species.[3] In the course of numerous investigations of the controlled hydrolysis of aluminum compounds, some alumoxanes with bridged or capped OH groups have been isolated and structurally characterized.[4] Although the organic or organically modified terminal aluminum hydroxides are very rare, the hydrolysis of trimesitylaluminum was accomplished in a controlled reaction involving THF as a coordinating solvent.[5] Nonetheless, alkyl alumoxanes with the general formula $[R_2AlOLi]_n$ ($n =$ 2, 3, 4) have been obtained by using anhydrous lithium hydroxide instead of water, or by deprotonation of the hydroxide $[R_2AlOH]_n$ with *t*BuLi or MeLi.[6] Our recent demonstration that the liquid ammonia/toluene two-phase system is highly effective for the hydrolysis and ammonolysis of transition-metal compounds has led to the preparation of the organozirconium oxide and hydroxide clusters $[\{(EtMe_4C_5)Zr\}_6(\mu_6\text{-}O)(\mu_3\text{-}O)_8]\cdot C_7H_8$, $[\{(EtMe_4C_5)Zr\}_6(\mu_6\text{-}O)(\mu_3\text{-}O)_8]\cdot C_9H_{12}$,[7] $[\{(Me_5C_5)Zr\}_6(\mu_4\text{-}O)(\mu\text{-}O)_4(\mu\text{-}OH)_8]\cdot 2\,C_7H_8$,[8] and related systems.[9] Herein we report the first hydrolysis of a main-group-metal halide using an aluminum compound supported by a β-diketiminato ligand in a two-phase system.

Treatment of $[LAlI_2]$ (**1**; $L = HC\{(CMe)(2,6\text{-}iPr_2C_6H_3N)\}_2$) with KOH containing 10–15% H_2O (1:1.3 molar ratio of pure KOH) and KH (1:0.7 molar ratio) in liquid ammonia and toluene at −78 °C results in the complete removal of iodide and the formation of the aluminum dihydroxide $[LAl(OH)_2]$ (**2**; Scheme 1). A pro-

[*] Prof. Dr. H. W. Roesky, Dr. G. Bai, Y. Peng, Dr. J. Li, H.-G. Schmidt, Dr. M. Noltemeyer
Institut für Anorganische Chemie der Universität
Tammannstrasse 4, 37077 Göttingen (Germany)
Fax: (+49) 551-39-3373
E-mail: hroesky@gwdg.de

[**] This work was supported by the Deutsche Forschungsgemeinschaft and the Fonds der Chemischen Industrie. We are thankful to Vojtech Jancik and Lukas Richtera for their artwork.

 © 2003 Wiley-VCH Verlag GmbH & Co. KGaA, Weinheim 1433-7851/03/4210-1132 $ 20.00+.50/0

posed mechanism for the formation of **2** is given in Equations (1)–(7) in Scheme 2 . The rapid initial reactions are the coordination of water [Eq. (1)] and the formation of NH_4I [Eq. (2)]; the latter species was converted to KI

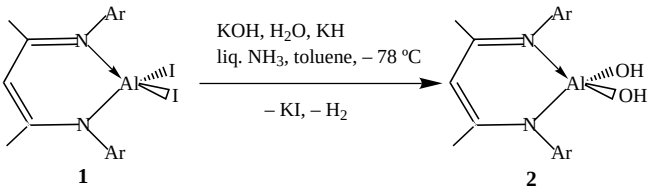

1 **2**

Scheme 1. Ar = 2,6-$iPr_2C_6H_3$

$$LAlI_2(NH_3)_n + H_2O \rightleftharpoons LAlI_2(H_2O)(NH_3)_{n-1} + NH_3 \quad (1)$$

3

$$\mathbf{3} + 2\,NH_3 \rightleftharpoons LAlI(OH)(NH_3)_n + NH_4I \quad (2)$$

4

$$KH + NH_3 \longrightarrow KNH_2 + H_2 \quad (3)$$

$$NH_4I + KOH/KNH_2 \longrightarrow H_2O/NH_3 + KI \quad (4)$$

$$\mathbf{4} + H_2O \rightleftharpoons LAlI(OH)(H_2O)(NH_3)_{n-1} + NH_3 \quad (5)$$

5

$$\mathbf{5} + 2\,NH_3 \rightleftharpoons LAl(OH)_2(NH_3)_n + NH_4I \quad (6)$$

6

$$\mathbf{6} \rightleftharpoons \mathbf{2} + n\,(NH_3) \quad (7)$$

L = HC[(CMe)(2, 6-$iPr_2C_6H_3N$)]$_2$

Scheme 2.

[Eq. (4)]. Further hydrolysis of **4** led to the intermediates **5** and **6** [Eqs. (5) and (6)], which yields **2** after the complete release of the coordinated ammonia molecules [Eq. (7)]. It has been well documented that the hydrolysis of alkyl aluminum compounds generates aluminum–water adducts $[R_3Al{\cdot}OH_2]$.[5] A similar mechanism was reported for the ammonolysis of aluminum triiodide in the presence of K or KNH_2 in liquid ammonia, which results in the formation of aluminum amides.[10] In contrast, the reaction of $[LAlH_2]$ with H_2O in THF or toluene does not isolate **2**, but instead leads to complete hydrolysis, which yielded an insoluble aluminum oxide or hydroxide, and the LH ligand. The Lewis acidity of the intermediates **3**–**6** is considerably decreased because of presence of coordinatively saturated aluminum centers in proximity with the donor ammonia molecules. Consequently, the aluminum compounds undergo hydrolysis to form the Brønsted-acidic aluminum hydroxide in liquid ammonia. In addition, the reaction occurring preferentially at the interface can be rationalized as the two-phase system (ammonia/toluene) increases the solubility of the organic and inorganic components. Therefore, we believe that the liquid ammonia/toluene two-phase system is essential for the formation of **2**, and the bulky L ligand on the aluminum center serves to stabilize the dihydroxide complex.

Compound **2** is a colorless crystalline solid that decomposes above 140 °C. However, no decomposition or polymerization was observed when **2** was kept in toluene solution, or in the solid state in a dry-box. The most intense peak in the EI mass spectrum of **2** appeared at m/z 403 [M^+–Me–iPr–OH], and the signal at m/z 478 (14 %) was assigned to the molecular ion [M^+].

Single crystals of **2**[11] suitable for X-ray structural analysis were obtained by maintaining the reaction mixture in toluene/hexane at −20 °C for one week. Compound **2** crystallizes in the monoclinic space group $C2/c$. Hydrogen bonding between the hydroxyl H atom of one molecule and the hydroxyl O atom of another molecule results in a dimeric structure for **2** with a centrosymmetric planar eight-membered $\{OAlOH\}_2$ ring (Figure 1). The hydrogen-bonded donor–acceptor separations (O···O 2.781 and 2.780 Å) are within the range of other similar interactions (O···O 2.7 to 3.0 Å).[12] The Al center exhibits a distorted tetrahedral geometry with two nitrogen atoms of the L ligand and two OH groups. The most acute N-Al-N angle (96.97(7)°) is the result of forming the β-diketiminato-Al six-membered ring. The C(1) and C(3) atoms of the ligand are both slightly bent out of the N(1)-C(2)-N(2) plane toward the same side (by 5.74 and 5.59°, repsectively), while the Al atom is tilted toward the opposite side of the same plane (23.98°).

The Al–OH bond lengths (1.6947(15) and 1.7107(16) Å) are significantly shorter than those of the Al–(μ-OH) and Al–(μ_3-OH) bonds in $[\{(Ph_2Si)_2O_3\}_4Al_4(\mu\text{-}OH)_4]$ (1.787(3) to 1.814(3) Å, av 1.800 Å),[13] $[Mes_2Al(\mu\text{-}OH)]_2{\cdot}2\,THF$ (1.822 Å; Mes = mesityl),[5] and $[Al_5(t\text{Bu})_5(\mu_3\text{-}O)_2(\mu_3\text{-}OH)_2(\mu\text{-}OH)_2(\mu\text{-}O_2CPh)_2]$ (Al–(μ_3-OH) 1.914(5) to 2.086(4) Å; Al–(μ-OH) 1.820(3) to 1.828(3) Å).[14] However, The Al–OH bond lengths of **2** are comparable to those of the Al–(μ-O) bonds in $[(HC\{(CMe)(NMe)\}_2AlCl)_2(\mu\text{-}O)]$ (1.6770(6) Å)[15] and $[\{(t\text{Bu})_2Al(NH(Me)CH_2CH_2NMe_2)\}_2(\mu\text{-}O)]$ (1.690(7) and 1.714(7) Å),[16] in which the linear or almost linear $\{Al_2(\mu\text{-}O)\}$ cores lead to the significant double-bond

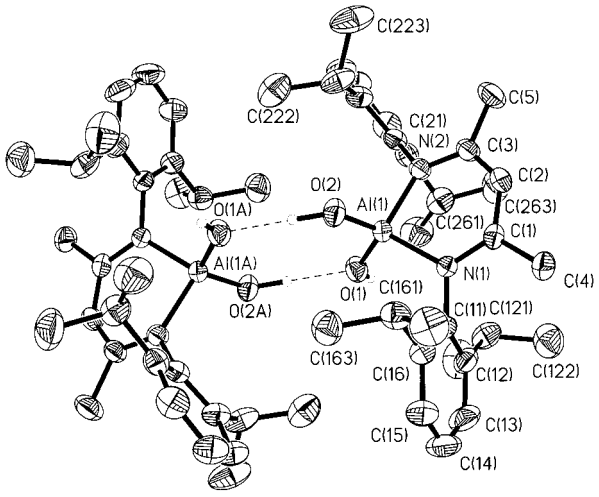

Figure 1. The crystal structure of **2**. The hydrogen atoms of the C–H bonds are omitted for clarity. Selected bond lengths [Å] and angles [°]: Al(1)-O(1) 1.7107(16), Al(1)-O(2) 1.6947(15), Al(1)-N(1) 1.8903(16), Al(1)-N(2) 1.8881(17); O(1)-Al(1)-O(2) 115.38(8), O(1)-Al(1)-N(1) 111.61(8), N(1)-Al(1)-N(2) 96.97(7).

 © 2003 Wiley-VCH Verlag GmbH & Co. KGaA, Weinheim 1433-7851/03/4210-1133 $ 20.00+.50/0

character of the Al–O bonds. The Al–N bond lengths (1.8881(17) and 1.8903(16) Å) are longer than those observed in $[(HC\{(CMe)(NMe)\}_2AlCl)_2(\mu\text{-}O)]$ (1.8611(16) and 1.8617(16) Å),[15] and similar to those in $[LAl(SeH)_2]$ (1.8996(6) Å).[17]

Ab initio[18] calculations were carried out to investigate the intermolecular hydrogen bonding and the electronic structure of **2**. The computed interaction energy of the two monomers of **2** ($-12.38\ kcal\,mol^{-1}$) shows the presence of weak intermolecular hydrogen bonding that is in agreement with the observed O···O distances in the X-ray structural analysis. If the protons are placed between donor–acceptor oxygen atoms at two positions (O–H = 0.96 Å for the free OH group,[19] and O–H = 1.00 Å for the coordinated O–H···O moiety[20]), the difference of the energies between these two positions would be very small (less than $1\ kcal\,mol^{-1}$) and the protons should vibrate between the O(1) and O(2A) or the O(2) and O(1A) atoms. These results should explain why there are no resonances observed for the coordinated protons in the ^1H NMR spectrum of **2**.

The calculated molecular electrostatic potential (MESP) isosurfaces of the dimer, in comparison with the monomer, are presented in Figure 2. Two negative potential regions (less than $-20\ kcal\,mol^{-1}$) of the lone pairs of the oxygen atoms are arranged *exo* to two oxygen atoms in the monomer (Figure 2a). This would support the reactivity of the oxygen atoms and favor electrophilic attack. The negative regions of MESP on the oxygen atoms in the dimer (Figure 2b) become larger and overlap for the hydrogen-bond interaction. Furthermore, the π electrons on the aromatic rings, as shown in the MESP map, become stronger and interact with the lone pairs of the oxygen atoms. The argument that the lone-pair electron density of the oxygen atoms is partially transferred to the aromatic rings supports the partial double-bond character of the Al–O bonds. A comparable interaction between the aryl oxide lone pairs and the benzophenone Al–O σ^* orbital was observed in $[AlMe(BHT)_2]$ (HBHT = 2,6-di-*tert*-4-methylphenol),[21] which results in short Al–O bond lengths (1.733(5) and 1.721(6) Å).

As a result of proximity to the Lewis acidic Al^{III} center, the protons of **2** are expected to be Brønsted acidic. The solid-state IR spectrum (Nujol) of **2** exhibits a sharp band ($\tilde{\nu} = 3727\ cm^{-1}$) for the free OH groups and a broad band ($\tilde{\nu} = 3450\ cm^{-1}$) for the coordinated OH groups which is in agreement with the dimeric structure of **2** in the solid state. It has been demonstrated that the gradient of the electrostatic potential at the proton correlates with the O–H stretching frequency.[22] However, the stretching mode of the O–H group is a qualitative indicator for the acidity of the proton. The absorption of the free OH groups of **2** is higher than those found in the Brønsted acids SAPO-34 ($\tilde{\nu} = 3600$–$3625\ cm^{-1}$)[23] and the zeolite Chabazite ($\tilde{\nu} = 3603\ cm^{-1}$)[24] and, therefore, **2** is a strong Brønsted acid, which is also in agreement with the resonance observed at very low field ($\delta = 12.47$ ppm) in the ^1H NMR spectrum for the free OH groups.

The IR spectra of the filtrate and the THF solution of **2** exhibit broad absorptions at $\tilde{\nu} = 3434$ and $3496\ cm^{-1}$ which result from hydrogen bridges, while a sharp ($\tilde{\nu} = 3703\ cm^{-1}$) and a broad ($\tilde{\nu} = 3438\ cm^{-1}$) absorption is observed for the toluene solution of **2**. This indicates that the monomeric species exists in both the filtrate and in THF solution, in which the NH_3 and THF molecules were coordinated to these OH groups. In contrast, the species in toluene is a hydrogen-bonded dimer of **2**.

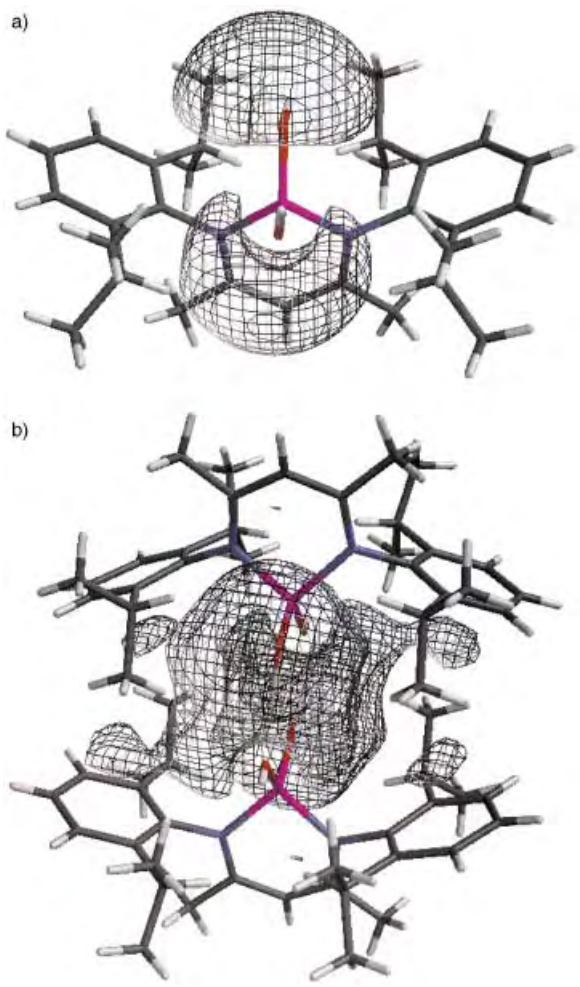

Figure 2. Calculated molecular potential isosurfaces ($-20\ kcal\,mol^{-1}$) for a) monomer $[LAl(OH)_2]$ (area: 74.82 Å^2, volume: 34.25 Å^3) and b) dimer $[LAl(OH)_2]_2$ (area: 181.77 Å^2, volume: 87.93 Å^3) at the HF/STO-3G level, show the locations of the lone pairs of the oxygen atoms and the π electrons of the aromatic rings.

Thus, a new synthetic approach is presented here for the hydrolysis of aluminum compounds, which involves a liquid NH_3/toluene two-phase system, to yield hitherto unknown $[LAl(OH)_2]$ species. To the best of our knowledge, compound **2** represents an unprecedented congener of the widely explored boronic acid derivative $RB(OH)_2$, and may find new and unusual applications in the near future. Such an investigation is currently in progress in our laboratories.

Experimental Section

2: Ammonia (40 mL) was condensed onto a stirred suspension of **1** (2.64 g, 3.8 mmol), KOH (KOH >85%, H_2O 10–15%; 0.32 g, 4.9 mmol) and KH (0.11 g, 2.8 mmol) in toluene (80 mL) at −78 °C. The mixture was then stirred for 1 h at this temperature, then the

 © 2003 Wiley-VCH Verlag GmbH & Co. KGaA, Weinheim 1433-7851/03/4210-1134 $ 20.00+.50/0

excess ammonia was allowed to evaporate from the reaction mixture over a period of 4 h. During this time, the mixture was warmed slowly to room temperature. After filtration and subsequent concentration (to 5 mL) in vacuo, hexane (5 mL) was added to the above filtrate. The resulting colorless solution was kept at −20 °C for one week to isolate colorless crystals of **2** (0.48 g). After isolating the crystals, and the subsequent removal of the solvents from the mother liquor, the hexane (8 mL) was added and the resulting colorless solution was maintained at −20 °C for two days, from which, additional crystals of **2** (0.39 g) were obtained. Total yield 0.87 g (48 %); m.p. 140 °C (decomp); IR (Nujol): $\tilde{\nu}$ = 3727, 3450, 1319, 1253, 1178, 1101, 1019, 844, 780, 760 cm^{-1}; IR (filtrate): $\tilde{\nu}$ = 3434, 1604, 1494, 1458, 1080, 1030, 729, 694, 463 cm^{-1}; IR (toluene): $\tilde{\nu}$ = 3703, 3438, 1621, 1604, 1493, 1459, 1080, 1030, 727, 694, 463 cm^{-1}; IR (THF): $\tilde{\nu}$ = 3496, 1458, 1179, 1075, 916, 659 cm^{-1}; ^1H NMR (200 MHz, C_6D_6): δ = 12.47 (bs, 1H, OH), 4.88 (s, 1H, γ-CH), 3.31 (sept, $^3J_{HH}$ = 6.9 Hz, 1H, C*H*Me_2), 1.66 (s, 6H, CMe), 1.25, 1.10 (dd, $^3J_{HH}$ = 6.9 Hz, 24H, $CHMe_2$); EI-MS: *m*/*z* (%): 478 (14) [M^+], 403 (100) [M^+−Me−*i*Pr−OH]; elemental analysis (%) calcd for $C_{29}H_{43}AlN_2O_2$ (478.63): C 72.8, H 9.1, N 5.9; found: C 72.9, H 9.0, N 5.8.

Received: October 21, 2002 [Z50396]

Keywords: aluminum · ammonia · hydrolysis · hydroxides · two-phase systems

[1] a) H. Sinn, W. Haminsky, *Adv. Organomet. Chem.* **1980**, *18*, 99–149; b) R. O. Colclough, G. Gee, A. H. Jagger, *J. Polym. Sci.* **1960**, *48*, 273–278; c) E. J. Vandenberg, *J. Polym. Sci.* **1960**, *47*, 486–489; d) C. Sishta, R. M. Hathorn, T. J. Marks, *J. Am. Chem. Soc.* **1992**, *114*, 1112–1114; e) Y. Koide, S. G. Bott, A. R. Barron, *Organometallics* **1996**, *15*, 2213–2226; f) H.-H. Brintzinger, D. Fischer, R. Mülhaupt, B. Rieger, R. Waymouth, *Angew. Chem.* **1995**, *107*, 1255–1283; *Angew. Chem. Int. Ed. Engl.* **1995**, *34*, 1143–1170; g) S.-I. Ishida, *J. Polym. Sci.* **1962**, *62*, 1–14.

[2] a) A. Storr, K. Jones, A. W. Laubengayer, *J. Am. Chem. Soc.* **1968**, *90*, 3173–3177; b) K. Ziegler, *Angew. Chem.* **1956**, *68*, 721–729; c) M. Boleslawski, S. Pasynkiewicz, A. Minorska, W. Hryniów, *J. Organomet. Chem.* **1974**, *65*, 165–167.

[3] a) W. Kosinska, A. Kunicki, M. Boleslawski, S. Pasynkiewicz, *J. Organomet. Chem.* **1978**, *161*, 289–297; b) N. Ueyama, T. Araki, H. Tani, *Inorg. Chem.* **1973**, *12*, 2218–2225; c) J. L. Atwood, D. C. Hrncir, R. D. Priester, R. D. Rogers, *Organometallics* **1983**, *2*, 985–989.

[4] a) T. L. Feng, P. L. Gurian, M. D. Healy, A. R. Barron, *Inorg. Chem.* **1990**, *29*, 408–411; b) C. J. Harlan, M. R. Mason, A. R. Barron, *Organometallics* **1994**, *13*, 2957–2969; c) M. R. Mason, J. M. Smith, S. G. Bott, A. R. Barron, *J. Am. Chem. Soc.* **1993**, *115*, 4971–4984; d) R. J. Wehmschulte, W. J. Grigsby, B. Schiemenz, R. A. Bartlett, P. P. Power, *Inorg. Chem.* **1996**, *35*, 6694–6702.

[5] J. Storre, A. Klemp, H. W. Roesky, H.-G. Schmidt, M. Noltemeyer, R. Fleischer, D. Stalke, *J. Am. Chem. Soc.* **1996**, *118*, 1380–1386.

[6] J. Storre, C. Schnitter, H. W. Roesky, H.-G. Schmidt, M. Noltemeyer, R. Fleischer, D. Stalke, *J. Am. Chem. Soc.* **1997**, *119*, 7505–7513.

[7] G. Bai, H. W. Roesky, P. Lobinger, M. Noltemeyer, H.-G. Schmidt, *Angew. Chem.* **2001**, *113*, 2214–2217; *Angew. Chem. Int. Ed.* **2001**, *40*, 2156–2159.

[8] G. Bai, H. W. Roesky, J. Li, T. Labahn, F. Cimpoesu, J. Magull, *Eur. J. Inorg. Chem.*, submitted.

[9] a) G. Bai, H. W. Roesky, P. Müller, *Bull. Pol. Acad. Sc. Chem.* **2002**, *50(1)*, 1–10; b) G. Bai, H. W. Roesky, M. Noltemeyer, H. Hao, H.-G. Schmidt, *Organometallics* **2000**, *19*, 2823–2825; c) G. Bai, P. Müller, H. W. Roesky, I. Usón, *Organometallics* **2000**, *19*, 4675–4677; d) G. Bai, H. W. Roesky, H.-G. Schmidt, M. Noltemeyer, *Organometallics* **2001**, *20*, 2962–2965.

[10] a) W. L. Taylor, E. Griswold, J. Kleinberg, *J. Am. Chem. Soc.* **1955**, *77*, 294–298; b) G. W. Watt, J. L. Hall, G. R. Choppin, *J. Phys. Chem.* **1953**, *57*, 567–570.

[11] a) Crystal data for **2**: $C_{29}H_{43}AlN_2O_2$, M_W = 478.63, monoclinic, space group *C*2/*c*, *a* = 25.542(7), *b* = 15.046(2), *c* = 14.7241(18) Å, β = 93.35(2)°, *V* = 5648.7(18) $Å^3$, *Z* = 8, ρ_{calcd} = 1.126 $Mg\,m^{-3}$, *F*(000) = 2080, λ = 0.71073 Å, *T* = 203(2) K, $\mu(Mo_{K\alpha})$ = 0.098 mm^{-1}. Data for the structure were collected on a Stoe-Siemens-AED2 four-circle diffractometer. Intensity measurements were performed on a rapidly cooled crystal (dimensions 0.8 × 0.7 × 0.5 mm) in the range $7.62 \le 2\theta \le 50.00°$. Of the 6043 measured reflections, 4959 were independent (R_{int} = 0.0320). The structure was solved by direct methods (SHELXS-97)[25] and refined with all data by full-matrix least-squares on F^2. The hydrogen atoms of C–H bonds were placed in idealized positions. The final refinements converged at $R1 = 0.0464$ for $I > 2\sigma(I)$, $wR2 = 0.1284$ for all data. The final difference Fourier synthesis gave a min/max residual electron density −0.307/+0.198 e $Å^{-3}$. CCDC-193832 (**2**) contains the supplementary crystallographic data for this paper. These data can be obtained free of charge via www.ccdc.cam.ac.uk/conts/retrieving.html (or from the Cambridge Crystallographic Data Centre, 12, Union Road, Cambridge CB2 1EZ, UK; fax: (+44) 1223-336-033; or deposit@ccdc.cam.ac.uk).

[12] T. K. Harris, Q. Zhao, A. S. Mildvan, *J. Mol. Struct.* **2000**, *552*, 97–109.

[13] M. Veith, M. Jarczyk, V. Huch, *Angew. Chem.* **1997**, *109*, 140–142; *Angew. Chem. Int. Ed. Engl.* **1997**, *36*, 117–119.

[14] Y. Koide, A. R. Barron, *Organometallics* **1995**, *14*, 4026–4029.

[15] N. Kuhn, S. Fuchs, E. Niquet, M. Richter, M. Steimann, *Z. Anorg. Allg. Chem.* **2002**, *628*, 717–718.

[16] C. N. McMahon, A. R. Barron, *J. Chem. Soc. Dalton Trans.* **1998**, 3703–3704.

[17] C. Cui, H. W. Roesky, H. Hao, H.-G. Schmidt, M. Noltmeyer, *Angew. Chem.* **2000**, *112*, 1885–1887; *Angew. Chem. Int. Ed.* **2000**, *39*, 2156–2159.

[18] a) The RHF (Restricted Hartree–Fock) calculations with STO-3G basis set were performed with the Spartan'02 software: W. J. Hehre, R. F. Stewart, J. A. Pople, *J. Chem. Phys.* **1969**, *51*, 2657–2664; b) All calculations are based on the experimental structure of **2**. The single-point energies of **2** were calculated by fixing all atoms, and by changing the OH bond length from 0.96 to 1.00 Å.

[19] D. Michalska, D. C. Bieńko, A. J. Abkowicz-Bieńko, Z. Latajka, *J. Phys. Chem.* **1996**, *100*, 17786–17790.

[20] M. Ichikawa, *J. Mol. Struct.* **2000**, *552*, 63–70.

[21] M. B. Power, S. G. Bott, J. L. Atwood, A. R. Barron, *J. Am. Chem. Soc.* **1990**, *112*, 3446–3451.

[22] G. Sastre, D. W. Lewis, *J. Chem. Soc. Faraday Trans.* **1998**, *94*, 3049–3058.

[23] R. Shah, J. D. Gale, M. C. Payne, *Chem. Commun.* **1997**, 131–132.

[24] P. Ugliengo, B. Civalleri, C. M. Zicovich-Wilson, R. Dovesi, *Chem. Phys. Lett.* **2000**, *318*, 247–255.

[25] G. M. Sheldrick, SHELXS-97, *Program for Crystal Structure Refinement*, University of Göttingen, Göttingen (Germany), **1997**

 © 2003 Wiley-VCH Verlag GmbH & Co. KGaA, Weinheim 1433-7851/03/4210-1135 $ 20.00+.50/0

Synthetic Protein Arrays

Combining SPOT Synthesis and Native Peptide Ligation to Create Large Arrays of WW Protein Domains**

*Florian Toepert, Tobias Knaute, Stefan Guffler, José R. Pirés, Thorsten Matzdorf, Hartmut Oschkinat, and Jens Schneider-Mergener**

Screening libraries of recombinantly expressed proteins and peptides is a common method to identify ligands with desired binding properties. Recent advances in protein synthesis, however, provide a basis for the chemical generation of large arrays of synthetic proteins that represent an alternative to recombinant technology. Novel synthetic procedures allow the chemoselective coupling of unprotected protein fragments, which can be produced synthetically or by recombinant expression (semi-synthesis).[1–8] The chemical synthesis of proteins allows the direct introduction of several post-translational modifications and a number of nonproteinogenic residues. Here we report on the identification of variants of the human Yes-kinase associated protein (hYAP) WW protein domain with novel binding specificities within an array of 11859 synthetic variants of the WW domain.

WW domains have a length of about 40 amino acids. They mediate protein–protein interactions in the cell and were shown to be important in numerous diseases, such as Liddle's syndrome, muscular dystrophy, Alzheimer's disease, chorea Huntington, and cancer.[9,10] WW domains are also important model proteins for studying β-sheet motifs.[11] The hYAP WW domain binds to proline-rich sequence motifs PPxY (x = L-amino acid).[10] Substituting or phosphorylating tyrosine (Y) in the PPxY motif disrupts binding to the hYAP WW domain. The three-dimensional structure of the complex formed between the hYAP WW domain and the ligand shows the amino acids located at the binding interface (Figure 1a).[12] The essential tyrosine residue from the peptide ligand points into a binding groove composed of L30, H32, and Q35, which suggests that these three residues are key determinants for tyrosine recognition (the residues are numbered according to ref. [13]). These positions were selected for substitution to alter the binding specificity of the hYAP WW domain.

[*] Prof. Dr. J. Schneider-Mergener, Dr. F. Toepert, Dipl.-Chem. T. Knaute
Institut für Medizinische Immunologie
Charité, Humboldt-Universität Berlin
Hessische Strasse 3-4, 10115 Berlin (Germany)
Fax: (+49) 030-450-524-942
E-mail: jsm@charite.de

Dr. J. R. Pirés, T. Matzdorf, Prof. Dr. H. Oschkinat
Forschungsinstitut für Molekulare Pharmakologie
Robert-Rössle-Strasse 10, 13125 Berlin (Germany)

Prof. Dr. J. Schneider-Mergener, S. Guffler
Jerini AG
Invalidenstrasse 130, 10115 Berlin (Germany)

[**] This work was supported by the DFG, Universitätsklinikum Charité Berlin, and the Fonds der Chemischen Industrie.

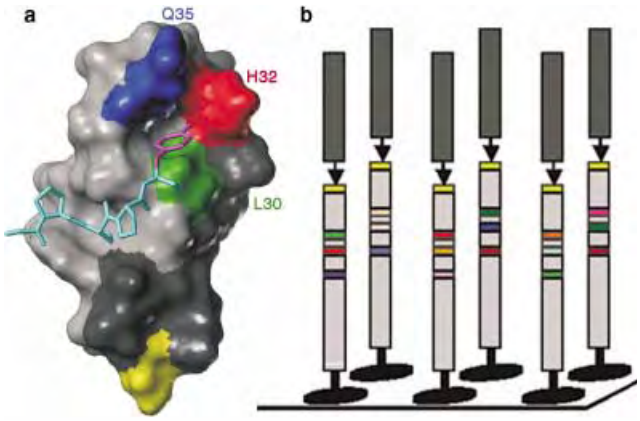

Figure 1. a) Model of the hYAP WW domain complexed with peptide ligand GPPPY:[12] The tyrosine residue (magenta) of the peptide ligand (light blue) interacts with residues L30 (green), H32 (red), and Q35 (dark blue) of the WW domain. The ligation site at position 24[17] is yellow. b) Synthesis strategy: Variants of the C-terminal fragment (residues 24–47, light gray) carrying an N-terminal cysteine for ligation (yellow) were prepared by stepwise SPOT synthesis[14–16] in an array format on a cellulose membrane (NH_2-C^{24}GQRY(X^{14})RKAML^{47}-membrane). Positions 30, 32, and 35 were varied systematically (colored). The N-terminal fragment (residues 10–23, NH_2-D^{10}VPLPAGWEMAKTS^{23}-COSR), dark gray) was coupled to the C-terminal fragments by native chemical ligation[1,3,7] to yield full-length membrane-bound WW domains.

The combination of SPOT synthesis[14–16] and native chemical peptide ligation[1,3,7] (Figure 1b) enabled us to synthesize large arrays of hYAP WW domain variants (38 mers) comprising the complete set of simultaneous substitutions of positions 30, 32, and 35 against any of the 19 proteinogenic L-amino acids, excluding cysteine. This process resulted in $19^3 = 6859$ different variants (array 1). A further 5000 variants were synthesized bearing combinations of amino acids from an expanded set of residues (19 L-amino acids and 20 nonproteinogenic and phosphorylated amino acids) in positions 30, 32, and 35 (array 2). Position 24 had been identified as a suitable ligation site in a previous study.[17] The identity of the wild-type WW domain synthesized on the cellulose membrane was confirmed by mass spectrometry (not shown).

Incubating arrays 1 and 2 with dye-labeled peptide ligand GTPPPPYTVG (Y-pep) resulted in strong signals from the 26 wild-type-containing spots at the bottom of each spot block, thus demonstrating the presence of functional WW domains on the cellulose membrane (Figure 2, underlined). The other spots resulted in signals with a wide range of intensities. To facilitate interpretation of these data the signal intensities obtained from array 1 were represented in a compact three-dimensional diagram (cube plot; Figure 3a).

Cubes in the diagram represent WW variants that yield signal intensities that are significantly higher than the average of all the signals (see methods). The red cube in the foreground of Figure 3a represents WW variant I30, H32, M35 (IHM), which is a strong binder to peptide ligand GTPPPPYTVG (Table 1). The cube marked by a white circle represents the hYAP WW wild-type (L30, H32, Q35; average

 © 2003 Wiley-VCH Verlag GmbH & Co. KGaA, Weinheim 1433-7851/03/4210-1136 $ 20.00+.50/0

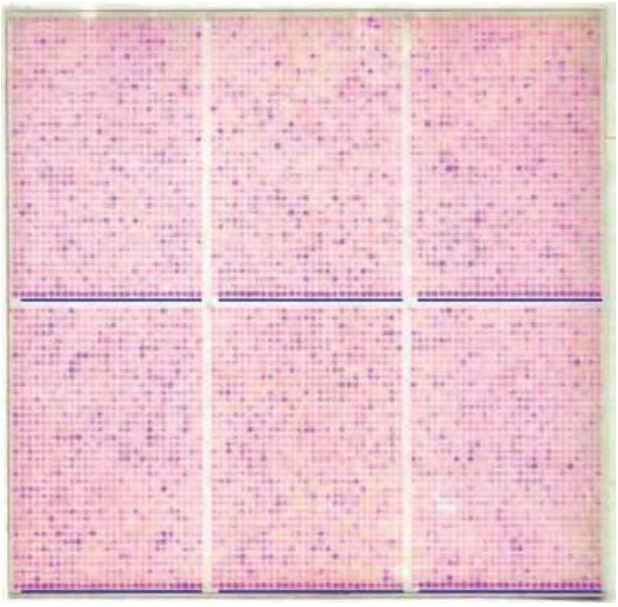

Figure 2. Interaction of peptide ligand TMR-GTPPPPYTVG with an array of WW domain variants (TMR = tetramethylrhodamine). Each spot comprises a WW variant with positions 30, 32, and 35 substituted by one of 19 L-amino acids (cysteine excluded). All possible $19^3 = 6859$ variants containing L-amino acids were synthesized (6000 shown). 26 spots at the bottom of each spot block contain the WW wild-type domain as a positive control (underlined).

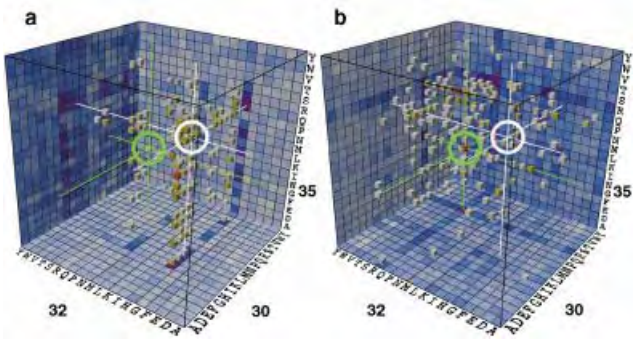

Figure 3. Cube plots displaying the binding data obtained from the interaction of peptide ligands GTPPPPYTVG (a) and GTPPPPpYTVG (b) with the array of WW domains. Cubes in the diagram represent WW variants of the array that yield signal intensities that are significantly higher than the average of all signal intensities (red = highest values). The position of a cube in the diagram reflects the amino acid substitutions at positions 30, 32, and 35. The background tiles mirror the average signal intensity of the spots corresponding to the 19 cubes perpendicular to the tile (red = highest values).

of the signals from the wild-type-containing spots). The clustering of cubes in Figure 3a reveals there are similarities in the sequences of WW variants that bind Y-pep. A distinct cluster of cubes represents WW variants that contain histidine at position 32. Less prominent accumulations of cubes can be identified that represent WW variants containing N32, I30, K30, L30, M30, V30, G35, K35, M35, Q35, and R35. Previous binding studies with single-substitution variants of the hYAP WW domain corroborate the requirement for histidine or asparagine in position 32 and the less stringent prerequisites for positions 30 (I, L, M, V) and 35 (A, G, H, K, M, Q, R).[17]

Having identified WW variants that bind Y-pep we searched for WW variants that bind other peptide ligands. Twenty-one dye-labeled peptide ligands GTPPPPxTVG (x-pep; x = L-amino acid excluding cysteine and tyrosine but including phosphoserine (pS), phosphothreonine (pT), and phosphotyrosine (pY)) were incubated with both arrays successively and the signal intensities obtained from array 1 were represented in cube plots. Figure 3b shows the cube plot obtained for peptide ligand GTPPPPpYTVG (pY-pep). The different clustering of cubes in the two plots (Figure 3) reflects a fundamental change of amino acid requirements at positions 30, 32, and 35 of the WW domain upon phosphorylation of the tyrosine residue in the peptide ligand. As expected, the wild-type domain does not bind pY-pep (white circle in Figure 3b—no cube). There are, however, several WW variants that interact significantly with pY-pep, as represented by the cubes in Figure 3b. The variant showing the highest signal intensity for pY-pep interaction has amino acids R, R, and K in positions 30, 32, and 35, respectively (RRK; green circle in Figure 3b—red cube). However, this RRK variant does not bind to wild-type ligand Y-pep, thus indicating that the wild-type WW domain and WW variant RRK have distinct binding specificities (green circle in Figure 3a—no cube).

Selected WW variants were synthesized by standard methods and their affinities towards different peptide ligands were measured by surface plasmon resonance spectroscopy (SPR; Table 1). The affinities that were detected are in the same range as the wild-type interaction (hYAP WW wild-type for Y-pep, $K_D = 94\ \mu M$) and, in accordance with previous studies, we find a good correlation between binding affinities and the signal intensities obtained in array-based binding experiments (Table 1).[17]

As in WW variant RRK, a cluster of basic residues is frequently found in proteins that bind phosphate groups,[18] which suggests that polar interactions contribute significantly to the binding affinity. WW variant RRK, however, has a much higher affinity towards pY-pep as compared to variant

Table 1: Binding constants and signal intensities of complexes formed between the WW domain and the ligand.

WW variant[a]	Peptide ligand[b]	K_D [μM][c]	Signal intensity
LHQ (wt)	Y-pep (wt)	94 ± 18	100
IHM	Y-pep (wt)	68 ± 13	147
RRK	Y-pep (wt)	nb	< 1
RRR	Y-pep (wt)	nb	3
LHQ (wt)	pY-pep	nb	3
IHM	pY-pep	nb	< 1
RRK	pY-pep	40 ± 8	141
RRR	pY-pep	174 ± 33	75

[a] WW variants (left column) are denoted according to their substitutions at positions 30, 32, and 35 (LHQ = wt). Peptide ligands x-pep (central column) are denoted according to the amino acid (x) in the 7′-position (GTPPPPxTVG). None of the WW variants examined binds peptide ligands pS-pep or pT-pep. [b] wt = wild-type. [c] Binding constants (K_D) were determined by SPR. nb = no binding detected.

 © 2003 Wiley-VCH Verlag GmbH & Co. KGaA, Weinheim 1433-7851/03/4210-1137 $ 20.00+.50/0

RRR (Table 1). Moreover WW variant RRK does not bind pS-pep (GTPPPPpSTVG) or pT-pep (GTPPPPpTTVG), which indicates that the phosphate moiety has to be presented in a specific structural context to permit binding of the ligand.

The three-dimensional structure of WW variant RRK complexed with pY-pep was determined by NMR spectroscopy (Figure 4a) and compared to the structure of the wild-type hYAP WW domain complexed with the unphosphorylated peptide ligand GPPPPY[12] (Figure 4b). Both structures are superimposed in Figure 4c. The configuration of the peptide ligands is slightly different in these complexes but a number of hydrophobic contacts (seven intermolecular NOE interactions) and two intermolecular hydrogen bonds present in both complexes demonstrate that the overall orientation of the ligands is the same. The altered configuration of the peptide ligand in the RRK complex enhances electrostatic and possibly H-bonding interactions of the phosphotyrosine moiety with R30 and R32 (supported by five intermolecular NOE interactions).

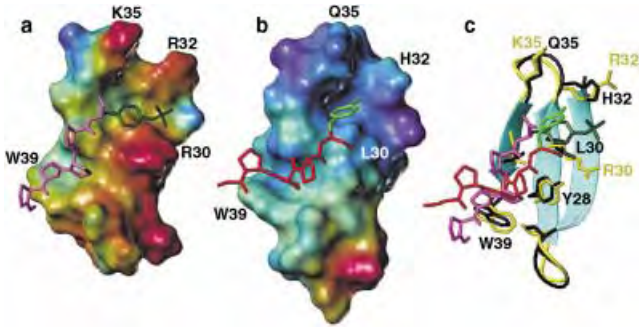

Figure 4. Comparison of three-dimensional structures of hYAP WW wild-type and variant RRK in complex with peptide ligands. Protein surfaces are colored by electrostatic potential; red indicates a positive and blue a negative potential. Peptide ligands are truncated for visual clarity. a) Three-dimensional structure of hYAP WW variant R30, R32, K35 (RRK) in the complex with peptide ligand GTPPPPpYTVG determined by NMR spectroscopy. b) Three-dimensional structure of hYAP WW wild-type complexed with peptide ligand GPPPY.[12] c) Ribbon representation of both complexes superimposed by matching the α-carbon atoms of residues 28, 30, 32, 35, 37, and 39.

Until now no naturally occurring phosphotyrosine-specific WW domains have been reported. Furthermore, searching a database of WW domains identified by sequence homology did not reveal any naturally occurring WW domains carrying amino acid substitutions R, R, and K in the sequence positions equivalent to positions 30, 32, and 35 of the hYAP WW domain. Thus, this result suggests that if phosphotyrosine-specific WW domains are present in the cell, then amino acids different from the positions that were varied in this study contribute essential contacts to the phosphotyrosine residue of the ligand.

Incubation of F-pep (GTPPPPFTVG) with array 1 resulted in a cube-plot profile (not shown) that was significantly different from that for the structurally similar Y-pep (Figure 3a). This result indicates the high sensitivity of the interaction between the WW domain and the ligand towards small structural changes. Maximum signal intensities were lower in this experiment though, and we did not identify a specific binder to F-pep in subsequent conventional binding studies using SPR.

Cube plots obtained from incubations with Y-pep, pY-pep, F-pep, W-pep, L-pep, K-pep, and R-pep were found to display distinct clusters of cubes that indicated the presence of specific interactions. We did not identify specific binders to W-pep, L-pep, K-pep, or R-pep in subsequent conventional binding studies using SPR, however.

Cube plots obtained from incubations with the remaining peptide ligands (GTPPPPxTVG) displayed either no strong interactions at all or strong interactions between peptide ligands and WW variants containing at least two aromatic amino acids in the variable positions. These interactions can propably be attributed to nonspecific interactions of aromatic amino acids with the proline residues that are present in all of the ligands. However, the library versus library approach presented in this study provided us with the opportunity to compare the results from binding experiments with different peptide ligands, thus enabling us to distinguish specific and nonspecific interactions in a straightforward manner.

The study presented here shows that a combination of SPOT synthesis and native chemical peptide ligation can be used to generate large arrays of variants of a protein domain. The novel approach significantly expands the size-range of polypeptides that is accessible in an array format. Synthesis of an array of more than 10000 variants of the WW protein domain and screening with 22 different peptide ligands successively facilitated the observation and documentation of more than 250000 binding experiments, and revealed comprehensive information regarding the sequence requirements for binding (cube plots). Furthermore, the library versus library approach presented here allows a facile distinction between specific and nonspecific interactions. The discovery of a WW domain variant with novel binding specificity presented in this study makes synthetic protein arrays a promising new tool for the identification of tailor-made specific binders. Advances in automation and protein chemistry will promote the development of even larger arrays of synthetic proteins with an extended range of applications. Since the synthetic generation of proteins allows the facile and defined introduction of posttranslational modifications frequently involved in the regulation of protein interactions,[19–22] arrays of synthetic protein domains may also become a valuable complement to existing methods for examining the network of cellular protein interactions.

Experimental Section

Synthesis of peptide ligands and soluble WW variants for binding studies: Syntheses were carried out according to standard protocols by using 9-fluorenylmethoxycarbonyl (Fmoc) chemistry with an automated peptide synthesizer (Intavis Bioanalytical Instruments AG, Bergisch Gladbach, Germany). Products were purified using HPLC and analyzed by MALDI-TOF mass spectrometry.

Synthesis of WW domain arrays: A library of different WW C-termini containing an N-terminal cysteine for ligation was produced by semi-automatic SPOT synthesis (Intavis Bioanalytical Instru-

 © 2003 Wiley-VCH Verlag GmbH & Co. KGaA, Weinheim 1433-7851/03/4210-1138 $ 20.00+.50/0

ments AG, Bergisch Gladbach, Germany; software LISA (Jerini AG, Berlin, Germany)) on Whatman 50 cellulose membranes.[14–16] Nonproteinogenic amino acids were coupled with one equivalent of 1-ethoxycarbonyl-2-ethoxy-1,2-dihydroquinoline (EEDQ) in DMF (0.3 M). The following nonproteinogenic residues were used: L-biphenylalanine, L-(2-naphthyl)alanine, L-phenylglycine, aminocyclopropionic acid, L-(2-thienyl)alanine, L-(3-pyridyl)alanine, L-citrulline, L-homoserine, L-homophenylalanine, L-(4-nitrophenyl)alanine, L-(4-guanidino)phenylalanine, L-(3,3-diphenyl)alanine, L-(2,3-diamino)-propionic acid, L-(2,4-diamino)butanoic acid, L-ornithine, L-cyclohexylglycine, L-phosphoserine, L-phosphothreonine, L-phosphotyrosine, *N*-[3,4,6-tri-*O*-acetyl-2-(acetylamino)-deoxy-2-β-glucopyranosyl]-L-asparagine. The N-terminal fragment (uniform for all WW variants) containing a C-terminal thioester for ligation was synthesized as described.[3] Ligation was achieved by dissolving the N-terminal fragment (15 mM) in ligation buffer (0.4 M sodium phosphate, pH 7.5, saturated with *p*-acetamidothiophenol) followed by incubation with the array of C-terminal fragments for 24 h. Ligation of the N-terminal WW fragment to a cellulose-bound peptide was found to proceed in 2 h with good yield. No starting material could be detected after 16 h.

Analysis of cellulose-bound wild-type hYAP WW domains: Ten spots (ca. 3 nmol peptide per spot) were punched out of the cellulose membrane. The peptides bound to the solid phase through an ester linkage were cleaved off by treatment with gaseous NH_3 for 16 h. The peptide was then eluted from the membrane with H_2O/trifluoroacetic acid (0.5%) and analyzed by HPLC-MS (system: Hewlett Packard series 1100 coupled with a Finnigan LCQ Ion Trap ESI mass spectrometer; column: Vydac C18, 150 × 2.1 mm, 300 Å, 5 μm; flow rate: 0.3 mL min^{-1}; gradient: 5–95% (acetonitrile in 0.05% aqueous TFA) in 17 min). The desired product had a retention time of 10.1 min.

Labeling of peptide ligands: Peptide ligands CββGTPPPPxTVG (x = L-amino acid, including pS, pT, pY; β = β-alanine) were linked to maleimide-activated tetramethylrhodamine (TMR, Molecular Probes, Eugene, OR, USA) through the cysteine residue according to the supplier's instructions. Remaining maleimido groups were deactivated with a tenfold excess of ethanethiol (1 h, RT), followed by purification by HPLC.

Incubation of the membrane and data acquisition: WW arrays were incubated in blocking Tris-buffered saline (TBS; 10% blocking reagent (CRB, Norwich, UK), 1% sucrose in TBS; TBS: 50 mM tris(hydroxymethyl)aminoethane (Tris), 100 mM NaCl, pH 8.0) for 1 h. Labeled peptide ligand (5 μM) was then incubated with the membrane in the same buffer at 4 °C for 2 h then washed three times with TBS. The resulting spot patterns were recorded with a flatbed scanner (Snapscan e40, Agfa, Mortsel, Belgium). WW arrays were regenerated by washing with DMF (4 × 20 min) followed by washing with ethanol (3 × 3 min) and drying.

Representation of the array-based binding data in cube plots: Spot patterns obtained from the incubation of peptide ligands with array 1 were analyzed densitometrically to yield primary intensity data (software: Lumi Analysis, Roche, Mannheim, Germany). Since we wanted to focus on the effect of the variable position x of the peptide ligands (GTPPPPxTVG) upon the interaction with WW variants we compensated for possible interactions with invariable parts of the peptide ligand by subtracting, for each spot, the average primary intensity obtained by the successive interaction with all 22 peptide ligands from the primary intensity obtained with a particular ligand. The resulting signal intensities were represented in cube plots. A spot in the array was represented in the cube plot when its signal intensity was larger than the lower cut-off value, which is defined as: lower cut-off = $\varnothing + 2.58\sigma$; with $\varnothing$ being the average and σ the standard deviation of all calculated signal intensities obtained for a particular peptide ligand. Background tiles represent the average signal intensity of the 19 variants of the WW domain that are identical in the sequence positions defined by the tile. Cube plots were generated with the software ICM (Molsoft, California, USA).

Measuring binding affinities of WW variants to peptide ligands: Measurements were made with a BIAcoreX system in TBS buffer. Peptide ligands were immobilized on a CM5-sensorchip through the cysteine residue with the ligand–thiol method according to the supplier's instructions. The amount of immobilized ligand corresponded to a signal increase of about 400 resonance units (RU). An equivalent amount of nonbinding peptide CββGTPPPPATVG was immobilized in the reference cell by using the same procedure. Binding experiments were performed with WW variant concentrations ranging from 1 to 500 mM (8 different concentrations were applied for each experiment). Binding experiments were performed at 25 °C with a flow rate of 15 μL min^{-1}. Data were evaluated with the software BIAevaluation 3.0 according to the steady-state procedure. Error bars were estimated from a set of seven measurements of WW wild-type versus peptide ligand CββGTPPPPYTVG (reference cell: CββGTPPPPATVG) using three independently prepared sensor chips.

Determining the three-dimensional structure of WW variant RRK in the complex with peptide ligand GTPPPPpYTVG: 2D-NOESY[23] with 150 ms mixing time and 2D-TOCSY[24] experiments with 20, 35, and 70 ms spinlock were recorded for the complex formed between the WW domain and the ligand (1.0 mM domain and twofold molar excess of ligand) and for the WW domain alone on 600 MHz DRX or 750 MHz DMX Bruker spectrometers, respectively. Experiments were carried out in 10 mM potassium phosphate buffer, pH 6, 100 mM NaCl, 0.1 mM 1,4-dithiothreitol (DTT), 0.1 mM ethylenediamine tetraacetate (EDTA), in 90% H_2O/10% D_2O, and in 100% D_2O at 15 °C. Spectra were processed with XWINNMR (Bruker) and analyzed with SPARKY (T. D. Goddard, D. G. Kneller, Sparky 3, University of California, San Francisco). 139 inter-residue NOE restraints, 12 of them intermolecular were derived from the NOESY experiment and assigned to four classes of distances (2.5 Å −0.7/+0.7; 3.5 Å −1.7/+0.7; 4.5 Å −2.7/+1.0; 5.5 Å −3.7/+1.0). Ten hydrogen bonds between the strands and two intermolecular ones were included. Eight dihedral angle restraints were added to force the ligand into a PPII helix conformation ($\phi = -78°$; $\psi = +149°$). Structures were calculated by simulated annealing[25] at 2000 K by using X-PLOR 3.1 (A.T. Brünger, *X-Plor 3.1: A system for X-ray crystallography and NMR*, Yale University Press, New Haven, CT, **1993**) and a floating stereospecific assignment. Force constants for NOE, bond lengths, bond angles, and improper angles were 50 kcal mol^{-1} Å^{-2}, 1000 kcal mol^{-1} Å^{-2}, 500 kcal mol^{-1} rad^{-2}, and 500 kcal mol^{-1} rad^{-2}, respectively.

Received: November 6, 2002 [Z50483]

Keywords: peptides · protein arrays · protein design · protein modifications

[1] P. E. Dawson, T. W. Muir, I. Clark-Lewis, S. B. H. Kent, *Science* **1994**, *266*, 776.
[2] L. E. Canne, S. J. Bark, S. B. H. Kent, *J. Am. Chem. Soc.* **1996**, *118*, 5891.
[3] T. M. Hackeng, J. H. Griffin, P. E. Dawson, *Proc. Natl. Acad. Sci. USA* **1999**, *96*, 10068.
[4] P. Botti, M. R. Carrasco, S. B. H. Kent, *Tetrahedron Lett.* **2001**, *42*, 1831.
[5] T. Kawakami, K. Akaji, S. Aimoto, *Org. Lett.* **2001**, *3*, 1403.
[6] J. Offer, C. N. Boddy, P. E. Dawson, *J. Am. Chem. Soc.* **2002**, *124*, 4642.
[7] P. E. Dawson, S. B. H. Kent, *Annu. Rev. Biochem.* **2000**, *69*, 923.
[8] M. Q. Xu, T. C. Evans, Jr., *Methods Enzymol.* **2001**, *24*, 257.
[9] P. Bork, M. Sudol, *Trends Biochem. Sci.* **1994**, *19*, 531.
[10] M. Sudol, T. Hunter, *Cell* **2000**, *103*, 1001.
[11] M. Jager, H. Nguyen, J. C. Crane, J. W. Kelly, M. Gruebele, *J. Mol. Biol.* **2001**, *311*, 373.

 © 2003 Wiley-VCH Verlag GmbH & Co. KGaA, Weinheim 1433-7851/03/4210-1139 $ 20.00+.50/0

[12] J. R. Pires, F. Taha-Nejad, F. Toepert, T. Ast, U. Hoffmüller, J. Schneider-Mergener, R. Kuhne, M. J. Macias, H. Oschkinat, *J. Mol. Biol.* **2001**, *314*, 1147.
[13] M. J. Macias, M. Hyvonen, E. Baraldi, J. Schultz, M. Sudol, M. Saraste, H. Oschkinat, *Nature* **1996**, *382*, 646.
[14] R. Frank, *Tetrahedron* **1992**, *48*, 9217.
[15] A. Kramer, U. Reineke, L. Dong, B. Hoffmann, U. Hoffmuller, D. Winkler, R. Volkmer-Engert, J. Schneider-Mergener, *J. Pept. Res.* **1999**, *54*, 319.
[16] U. Reineke, R. Volkmer-Engert, J. Schneider-Mergener, *Curr. Opin. Biotechnol.* **2001**, *12*, 59.
[17] F. Toepert, J. R. Pires, C. Landgraf, H. Oschkinat, J. Schneider-Mergener, *Angew. Chem.* **2001**, *113*, 922; *Angew. Chem. Int. Ed.* **2001**, *40*, 897.
[18] J. Kuriyan, D. Cowburn, *Annu. Rev. Biophys. Biomol. Struct.* **1997**, *26*, 259.
[19] P. J. Lu, X. Z. Zhou, Y. C. Liou, J. P. Noel, K. P. Lu, *J. Biol. Chem.* **2002**, *277*, 2381.
[20] D. R. Stover, P. Furet, N. B. Lydon, *J. Biol. Chem.* **1996**, *271*, 12481.
[21] M. A. Broome, T. Hunter, *Oncogene* **1997**, *14*, 17.
[22] H. Park, M. I. Wahl, D. E. Afar, C. W. Turck, D. J. Rawlings, C. Tam, A. M. Scharenberg, J. P. Kinet, O. N. Witte, *Immunity* **1996**, *4*, 515.
[23] J. Jeener, B. H. Meier, P. Bachmann, R. R. Ernst, *J. Chem. Phys.* **1979**, *71*, 4546.
[24] L. Braunschweiler, R. R. Ernst, *J. Magn. Reson.* **1983**, *53*, 521.
[25] J. Kuszewski, M. Nilges, A. T. Brunger, *J. Biomol. NMR* **1992**, *2*, 33.

 © 2003 Wiley-VCH Verlag GmbH & Co. KGaA, Weinheim 1433-7851/03/4210-1140 $ 20.00+.50/0

Oxidation of Propylene

Direct Synthesis of Propylene Oxide with CO_2 as the Solvent

Tiberiu Danciu, Eric J. Beckman, Dan Hancu, Robert N. Cochran, Roger Grey, Dennis M. Hajnik, and Jennifer Jewson*

Over four million tons of propylene oxide (PO) are produced worldwide each year by either chlorohydrin or coproduct processes.[1] While these are well-established processes, they produce PO by indirect routes and therefore require substantial amounts of raw materials and energy as well as high capital investment. In the chlorohydrin route to PO, propylene is treated with chlorine to produce 1-chloro-2-propanol (and HCl), which is then treated with base to generate PO and salt. In this process approximately two pounds of salt waste are produced per pound of product, which leads to production of wastewater at volumes roughly 40 times that of the PO produced.

Hydroperoxide-based processes generate PO and a coproduct, either styrene or isobutylene. The process with styrene as the coproduct (Scheme 1) now predominates, although this route requires five major reaction steps to produce PO and recover the styrene coproduct. The high capital requirement of this process for producing PO is partially offset by the production of styrene, yet current PO producers have been searching for some time for alternatives.

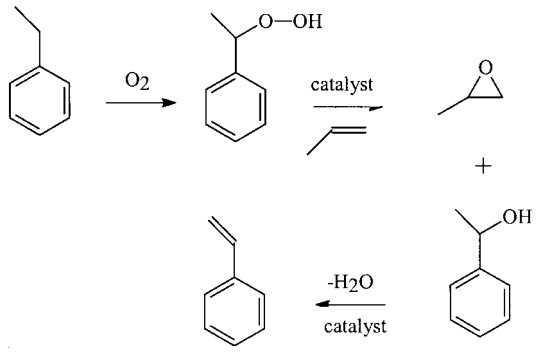

Scheme 1. Hydroperoxide process for generation of PO with styrene as the coproduct.

Direct oxidation of propylene to PO with O_2 would be highly desirable,[2] but as propylene with its allylic hydrogen atoms is highly combustible, this is quite difficult.[3,4] Researchers have shown[5] that a titanium silicalite (TS-1) catalyst promotes the formation of PO from propylene and H_2O_2 at selectivities approaching 100%. Because H_2O_2 is an environmentally benign oxidant, this route would seem to combine both green and economic advantages. Unfortunately, premanufactured H_2O_2 is currently too expensive to allow an economically viable process.[6] What if H_2O_2 could be generated in situ from hydrogen and oxygen? Holderich and colleagues[7] have examined the liquid-phase generation of PO from hydrogen, oxygen, and propylene in methanol/water over Pd (alone and with Pt) on TS-1. Inclusion of promoters (such as NaBr) resulted in conversion and selectivity of 40% in batch experiments. Semicontinuous runs increased the selectivity to over 60% while the conversion dropped substantially.

The use of TS-1 to generate propylene oxide from propylene and hydrogen peroxide (either premanufactured or generated in situ) has been investigated extensively over the past decade. In general researchers have concluded that an alcohol (preferably methanol) is needed as part of the solvent mixture to perform the reaction efficiently. Clerici and colleagues, for example, propose that methanol interacts with the catalyst surface at the active site.[8] Other researchers[5b,7a,9] confirm Clerici's contention that the highest activities in traditional solvent systems are obtained with methanol as the sole solvent or as the cosolvent with water.

[*] Prof. E. J. Beckman, Dr. T. Danciu
Chemical Engineering Department
University of Pittsburgh
Pittsburgh, PA 15261 (USA)
Fax: (+1) 412-624-9639
E-mail: beckman@engr.pitt.edu
Dr. D. Hancu, Dr. R. N. Cochran, Dr. R. Grey, D. M. Hajnik, Dr. J. Jewson
Lyondell Corporation
3801 West Chester Pike
Newtown Square, PA 19073-2387 (USA)

 © 2003 Wiley-VCH Verlag GmbH & Co. KGaA, Weinheim 1433-7851/03/4210-1140 $ 20.00+.50/0

Jenzer et al. have recently investigated the generation of PO from H_2, O_2, and propylene over a Pt/Pd/TS-1 catalyst in a continuous fixed-bed reactor[10] with a mixture of methanol and water as the solvent. Byproduct generation was extensive, where the primary byproduct was methyl formate (acetone, acrolein, acrylic acid, and PO ring-opening products were also observed). The formates were formed by the oxidation of methanol, a known reaction that takes place under mild conditions. Hydrolysis followed by further oxidation creates formic acid, which then reacts with methanol to generate the formate.

In summary, the literature suggests that methanol is needed for efficient epoxidation, yet the methanol/water solvent is also the major source of the byproducts. The presence of the liquid solvent also creates certain process problems. The rate of the reaction is most likely limited by the diffusion of the gaseous reactants across the vapor–liquid interface. Water is a benign and safe solvent, yet the solubility of the gases (H_2, O_2, and propylene) in water is low, which creates a potential mass transfer problem. The addition of methanol improves the solubility of the gases in the liquid phase, yet reactions with methanol are a prime source for byproducts.

Given this background, we have investigated the use of carbon dioxide as the sole solvent for the generation of PO from hydrogen, oxygen, and propylene over a Pd/TS-1 catalyst. We wished to determine whether we could reap the benefits of CO_2 use (vide infra) while avoiding the problems of by-products arising from methanol. Given the results of Clerici et al.[8] and of others,[5b,7a,8,9] a key question was whether the reaction would proceed effectively in the absence of methanol. We have previously shown that one can generate H_2O_2 in CO_2 from O_2 and H_2 and that liquid CO_2 is a safe solvent that will not form oxidation byproducts.[11] Further, the chemistry could proceed without the transport limitations across liquid and gas phases. CO_2 provides a unique combination of advantages to this process: it can solubilize large quantities of gases, is immune to oxidative degradation, provides a nonflammable environment in which to mix H_2 and O_2, and is miscible with both propylene and PO. The use of CO_2 as a safe, benign solvent in oxidations has gained increasing interest in the research community over the past five years.[12]

The effect of the solvent system (CO_2 versus water/MeOH) was compared in three sets of experiments, in which a) CO_2 served as the sole solvent, b) a methanol/water solvent system was employed with nitrogen at the same operating pressure as in a), and c) a methanol/water solvent system was used with CO_2 at the same operating pressure as in a). The results are reported as the conversion of propylene and selectivity of the oxidation to PO (total PO divided by total amount of propylene in the products detected) at the conclusion of the 4.5-h runs.

As shown in Table 1, the use of CO_2 as the sole solvent in the reaction allows high selectivity to PO at reasonable conversions, whereas selectivity drops when methanol/water is added. The latter results are consistent with Jenzer's observations that methanol is a major contributor to byproduct formation (both through reaction with PO and oxidation), and that use of CO_2 in place of nitrogen leads to improvements. Additional byproducts observed when methanol was present include methyl formate, 1-methoxypropan-2-ol, and 2-methoxypropan-1-ol. Typically, the molar ratio of these three was 12:1.7:1, in agreement with previous observations that methyl formate is the major byproduct when methanol is present.

Table 1: Results for batch epoxidation of propylene in three different systems.[a]

Solvent system	Catalyst mass [g]	Propylene conversion [%]	Propylene selectivity to PO [%]	C_3H_8 [%]	ring-opened byproducts [%]
CO_2	0.1502	9.5	77.1	22.9	–[b]
CO_2	0.1952	6.5	91.2	8.8	–[b]
CO_2	0.2998	7.5	94.3	5.7	–[b]
MeOH + H_2O + CO_2	0.1565	3.5	17.4	75.0	7.6
MeOH + H_2O + CO_2	0.2063	4.7	41.1	46.5	12.4
MeOH + H_2O + N_2	0.1993	16	3.5	95.2	1.4

[a] Total pressure = 13.1 MPa, T = 318 K, 4.5 h reaction time. In all cases the absolute concentrations were 4 mM for propylene, 1.26 mM for H_2, and 8.3 mM for O_2, in 3.84×10^{-5} m^3 CO_2. Conversion continued to change up to 4.5 h, so we believe that the hydrogen had not yet been completely consumed at that point. [b] No PO ring-opened byproducts (propylene glycols, methoxypropanols, or propylene carbonate) were detected by online GC analysis.

From entries 1–3 in Table 1, it would appear that simply increasing the amount of catalyst in the reactor increases the selectivity of the reaction, but this is somewhat deceiving. We strongly suspect that, although the catalyst was pretreated with hydrogen before the experiment, the first step in the process in the reactor is additional reduction of the catalyst by available hydrogen, which then changes the hydrogen:oxygen ratio (from a molar perspective, the amounts of palladium and hydrogen are indeed comparable at higher levels of catalyst). It is known that lowering the hydrogen:oxygen ratio favors the formation of H_2O_2 rather than H_2O over palladium. Further, the reduction in the amount of available hydrogen lessens the chances for simple hydrogenation of propylene to propane.

The presence of the gas–liquid interface (entries 3—6, Table 1) also contributes to decreasing selectivity, as any splashing of the powder catalyst onto the walls of the reactor would lead to the gas-phase hydrogenation of propylene. The last two entries in Table 1 show that use of nitrogen as the pressure-transmitting medium leads to enhanced conversion but low selectivity as the significant gas–liquid interface promotes propane formation. (It is also possible that methanol can further reduce the palladium to the point where hydrogenation of propylene is favored over production of hydrogen peroxide.) The fact that the conversion and selectivity were better with CO_2 and MeOH/water than with N_2 and MeOH/water can be explained by phase-behavior effects. CO_2 will swell a mixture of methanol/water (3/1), and hence improvements owing to the replacement of nitrogen by CO_2 may arise from increased solubility of the gaseous reactants (O_2, H_2 and propylene) in the liquid phase due to the presence of CO_2. Also, a mixture of N_2, propylene, O_2, H_2 and MeOH/water will likely create a three-phase mixture,

 © 2003 Wiley-VCH Verlag GmbH & Co. KGaA, Weinheim 1433-7851/03/4210-1141 $ 20.00+.50/0

while use of CO_2 (in place of N_2) will likely create a two-phase mixture, which thus reduces the number of interfaces and enhances transport. When CO_2 is employed as the sole solvent, the gas–liquid interface is eliminated entirely, further enhancing selectivity.

Since we conducted our experiments in batch mode with relatively small amounts of H_2 and O_2, we were not fully able to gauge the effect of the MeOH/water solvent vs. CO_2 on the formation of PO ring-opened products. Consequently, control experiments were conducted in which catalyst, PO, water (only the relatively small amount of water that would be expected to be produced with the PO), and CO_2 (13.1 MPa, 318 K) were added to the reactor. After 4.5 h only 4.5 % of the PO was converted to ring-opening products (i.e. propylene glycol). The analogous experiment conducted with the MeOH/water solvent system and N_2 resulted in 60 % conversion of PO to methoxypropanols. These results can be accounted for in large part by the fact that with CO_2 as the sole solvent there is a much lower concentration of hydroxy-containing compounds that can react with PO.

In summary, we have found that carbon dioxide is an excellent solvent for the epoxidation of propylene, where the in situ reaction of H_2 and O_2 creates the oxidant. Unlike organic solvents, CO_2 can solubilize large quantities of gases, is immune to oxidative degradation, provides a nonflammable environment in which to mix H_2 and O_2, is miscible with both propylene and PO, and is chemically inert to the PO product. Significantly, we have found that methanol is not required for the efficient production of PO from propylene and H_2O_2 produced in situ, contrary to suggestions from previous reports.

Experimental Section

The catalyst was prepared by suspending TS-1 (1.6 % Ti, 20 g) in deionized water (8.0×10^{-5} m^3) in the presence of tetraamine palladium nitrate (5 % Pd, 2.542 g) at 353 K for 24 h. The solid was recovered by filtration under pressurized N_2, washed with deionized water, dried under vacuum at 323 K, and then calcined at 423 K for 4 h in 5 % O_2/95 % N_2. The resulting catalyst has 0.47 % Pd by weight. Pd/TS-1 catalyst prepared in this way was then suspended in methanol/water (3/1; 2 g catalyst in 100 mL solvent) and preactivated in a 1×10^{-4} m^3 min^{-1} gas flow (10 % propylene, 4 % O_2, and 4 % H_2) at 318 K and 0.02 MPa for 22 h.

Reactions were carried out in a 4×10^{-5} m^3 stainless steel batch reactor capable of operating pressures to 40.0 MPa at temperatures up to 373 K. The contents were mixed with a multiblade stirrer (Parr Instrument Co) that had been mated to the reactor lid. Gases were introduced with a calibrated high-pressure syringe pump (High Pressure Equipment Co, Erie, PA). The temperature of the reactor was monitored with a thermocouple fitted through one of the five reactor ports, while the pressure was monitored with a transducer and readout. Samples could be withdrawn from either liquid or gas phases through an additional pair of ports, each fitted with a frit filter to retain catalyst. Material was injected through the final two ports. Samples were analyzed by GC (Hewlett Packard 5890 Series 2, with either a TCD or FID detector). Where CO_2 alone was the solvent, the reactor was charged with a known amount of catalyst, and then evacuated. The reactor was heated to 318 K and known amounts of CO_2, hydrogen, O_2/N_2, and propylene were added in that order. Additional CO_2 was added by using the compressor (Haskell Equipment Co, Houston) to achieve a final pressure of 13.1 MPa. The mixture was mixed vigorously, sampled at intervals for GC analysis, and then slowly depressurized to 1 atm. Any side products that precipitated on the catalyst were extracted in methanol and analyzed separately by GC. When methanol/water was employed as the solvent, methanol/water (3/1; 1.0×10^{-5} m^3) was added to the reactor with the catalyst before the experiment. Both the gas and liquid phases were sampled and analyzed for PO and other products. For some of the two-phase (gas–liquid) experiments, N_2 was substituted for CO_2.

Received: July 9, 2002
Revised: December 5, 2002 [Z19692]

Keywords: carbon dioxide · green chemistry · heterogeneous catalysis · oxidation · supercritical fluids

[1] "Propylene Oxide": D. L. Trent in *Kirk-Othmer Encyclopedia of Chemical Technology, Vol. 20*, Wiley, New York, **1996**.
[2] J. R. Monnier, *Appl. Catal. A* **2001**, *221*, 73.
[3] G. Lu, X. Zuo, *Catal. Lett.* **1999**, *58*, 67.
[4] K. Murata, Y. Kiyozumi, *Chem. Commun.* **2001**, 1356.
[5] a) W. Laufer, R. Meiers, W. Holderich, *J. Mol. Catal. A* **1999**, *141*, 215; b) G. F. Thiele, E. Roland, *J. Mol. Catal. A* **1997**, *117*, 351; c) M. A. Mantegazza, G. Petrini, G. Spano, R. Bagatin, F. Rivetti, *J. Mol. Catal. A* **1999**, *146*, 223; d) L. Y. Chen, G. K. Chuah, S. Jaenicke, *J. Mol. Catal. A* **1998**, *132*, 281; e) G. Li, X. Wang, H. Yan, Y. Chen, Q. Su, *Appl. Catal. A* **2001**, *218*, 31.
[6] M. McCoy, *Chem. Eng. News* **2001**, *79*(43), 19.
[7] a) W. Laufer, W. F. Holderich, *Appl. Catal. A* **2001**, *213*, 163; b) F. Kollmer, W. F. Holderich, *Pure Appl. Chem.* **2000**, *72*, 1273; c) R. Meiers, W. F. Holderich, *Catal. Lett.* **1999**, *59*, 161.
[8] a) M. G. Clerici, G. Bellussi, U. Romano, *J. Catal.* **1991**, *129*, 159; b) G. Bellussi, A. Carati, M. G. Clerici, G. Maddinelli, M. R. Giuseppe, *J. Catal.* **1992**, *133*, 220; c) M. G. Clerici, P. Ingallina, *J. Catal.* **1993**, *140*, 71.
[9] B. Notari, *Adv. Catal.* **1996**, *41*, 253.
[10] G. Jenzer, T. Mallat, M. Maciejewski, F. Eigenmann, A. Baiker, *Appl. Catal. A* **2001**, *208*, 125.
[11] D. Hancu, E. J. Beckman, *Green Chem.* **2001**, *3*, 80.
[12] See, for example, a) A. Baiker, *Chem. Rev.* **1999**, *99*, 453; b) P. G. Jessop, T. Ikariya, R. Noyori, *Chem. Rev.* **1999**, *99*, 475; c) G. Musie, M. Wei, B. Subramaniam, D. H. Busch, *Coord. Chem. Rev.* **2001**, 219–221, 789; d) F. Loeker, W. Leitner, *DGMK Tagungsber.* **1998**, *9803*, 209.

 © 2003 Wiley-VCH Verlag GmbH & Co. KGaA, Weinheim 1433-7851/03/4210-1142 $ 20.00+.50/0

Germyl Cation

$[(t\mathrm{Bu_2MeSi})_3\mathrm{Ge}]^+$: An Isolable Free Germyl Cation Lacking Conjugation to π Bonds**

Akira Sekiguchi, Tomohide Fukawa, Vladimir Ya. Lee, Masaaki Nakamoto, and Masaaki Ichinohe*

Carbocations, together with carbanions, free radicals, and carbenes, are the most fundamental species in organic chemistry.[1] In contrast to the well-established chemistry of carbocations, we still do not know much about the chemistry of their heavier Group 14 element congeners. The crystal-structure data of the two isolable silyl "cation-like" species, $[\mathrm{Et_3Si(toluene)}]^+[\mathrm{B(C_6F_5)_4}]^-$[2] and $[i\mathrm{Pr_3Si}]^{\delta+}[\mathrm{CB_{11}H_6Br_6}]^{\delta-}$,[3] were reported by groups of Lambert and Reed, respectively. Such silyl cations were not "free", they were coordinated by either solvent molecules or counteranions. Later, $[\mathrm{Mes_3Si}]^+[\mathrm{B(C_6F_5)_4}]^-$[4] was reported by Lambert and co-workers as a free silyl cation in solution, and just recently crystallographic evidence for the free $[\mathrm{Mes_3Si}]^+$ ion was given by Reed and Lambert and co-workers.[5] Examples of Ge-centered three-coordinate cations are still very rare, and include the germanium poly(pyrazolyl)borate complex $[\mathrm{HB(3,5\text{-}Me_2pz)_3Ge}]^+\mathrm{I}^-$, which synthesis and crystal structure were reported in 1996 by Reger and Coan.[6] In 1997 we synthesized an isolable free germyl cation, $[(t\mathrm{Bu_3E})_3\mathrm{Ge_3}]^+[\mathrm{B(C_6H_5)_4}]^-$ (E = Si, Ge) as a 2π-electron aromatic system[7] and then prepared the stable free silyl cation, $[(t\mathrm{Bu_2MeSiSi})_3\mathrm{Si}t\mathrm{Bu_2}]^+[\mathrm{TPFPB}]^-$ ($\mathrm{TPFPB^-}$ = tetrakis(pentafluorophenyl)borate) which has a homoaromatic character.[8,9] However, in both cases these free germyl and silyl cations were stabilized by conjugation with Ge=Ge or Si=Si double bonds. Recently, we reported the synthesis of the isolable Ge-centered radical $(t\mathrm{Bu_2MeSi})_3\mathrm{Ge}^\bullet$ (**1**), which lacks stabilization by π-conjugation effects.[10] This compound seemed to be an ideal starting point for a one-electron oxidation reaction to form the corresponding germyl cation species. Herein we report our successful oxidation of Ge radical **1** with $[\mathrm{Ph_3C}]^+[\mathrm{TPFPB}]^-$ to produce the corresponding free germyl cation that can be isolated as a stable compound, the crystal structure and reactivity of which are also given.

Reaction of the free radical $(t\mathrm{Bu_2MeSi})_3\mathrm{Ge}^\bullet$ (**1**) with the stoichiometric amount of $[\mathrm{Ph_3C}]^+[\mathrm{TPFPB}]^-$ was complete in five minutes, which results in the formation of a dark red reaction mixture, from which tris[di-*tert*-butyl(methyl)silyl]-germanylium tetrakis(pentafluorophenyl)borate $[(t\mathrm{Bu_2MeSi})_3\mathrm{Ge}]^+[\mathrm{TPFPB}]^-$ (**2**), was isolated as extremely moisture-sensitive dark red crystals in 75% yield (Scheme 1).

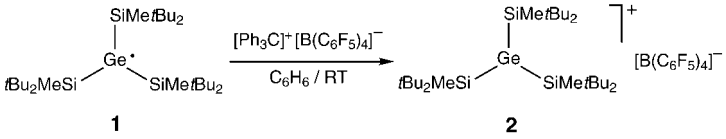

1 **2**

Scheme 1. Synthesis of the germyl cation **2**.

The NMR spectra of **2** are very simple, in accordance with its highly symmetrical structure. It is interesting that the Me groups on the Si substituents are greatly deshielded (δ = 1.17 ppm), appearing in the region of *t*Bu groups (δ = 1.19 ppm). The ^{29}Si NMR resonance signal of the silyl substituents is also greatly shifted downfield (δ = + 49.9 ppm) compared with the related compounds $(t\mathrm{Bu_2MeSi})_3\mathrm{GeX}$ (δ = 25.6 ppm for X = H, δ = 29.9 ppm for X = Cl).[10] This effect can be explained by the positive charge not being localized on the central germanium atom, but being transferred to the electropositive silicon atoms, similar to the case of the cyclotrigermenylium ion $[\{(t\mathrm{Bu_3Si})_3\mathrm{Ge}\}_3]^+$.[7,11] Indeed, DFT calculations at the B3LYP/6-31G(d) level on the model compound $[(\mathrm{H_3Si})_3\mathrm{Ge}]^+$ have demonstrated the distribution of the positive charge over the three Si atoms: Ge −0.12, Si + 0.37.

The crystal structure of **2** was determined by X-ray analysis to have a completely planar geometry around the Ge center (Figure 1).[12] Similar to the precursor Ge radical **1**,[10] the methyl substituents on the Si atoms all lie in the Ge(1)-Si(1)-Si(2)-Si(3) plane, apparently to minimize steric hindrance. The Si–Ge bond lengths in **2** are very long, ranging from 2.5036(10) to 2.5379(10) Å (av. 2.5195(10) Å), which greatly exceeds the normal values of Si–Ge bond lengths (2.384–2.462 Å),[13] and the corresponding Si–Ge bond lengths in radical **1** (2.4514(4)–2.4553(4) Å (av. 2.4535(4) Å).[10] We can explain the elongation of the Si–Ge bonds in **2** by the different extent of hyperconjugation between the cationic Ge center ($4p_z$) and σ* orbitals of the Si–C(*t*Bu) bonds. The degree of such interaction depends on the $4p_z$ orbital occupancy: 0 for the cation **2** (2.5195(10) Å), 1 for the radical **1** (2.4535(4) Å), 2 for the anion $(t\mathrm{Bu_2MeSi})_3\mathrm{Ge}^-$ (2.4332(10) Å).

The closest distance between the Ge center of the cation and the F atoms of the aromatic rings of the anion is greater than 5.4 Å, which shows the absence of any interaction between the cation and anion. Thus, **2** represents a free Ge cation in the solid state, it lacks any interaction with either solvent molecules or counteranion. This independence of **2** is retained in solution. The ^{29}Si NMR resonance signal of **2** is nearly the same in different solvents, that is, at 49.9 ppm in $[\mathrm{D_2}]$dichoromethane, 49.9 ppm in $\mathrm{CDCl_3}$, and 50.3 ppm in $[\mathrm{D_6}]$benzene, which indicates that **2** is indeed a free cation in solution. Compound **2** possesses a much higher electrophilicity towards nucleophilic solvents than the $[(t\mathrm{Bu_3Si})_3\mathrm{Ge_3}]^+$ ion. For example, decomposition of **2** in $[\mathrm{D_8}]$THF

[*] Prof. Dr. A. Sekiguchi, Dipl.-Chem. T. Fukawa, Dr. V. Ya. Lee, Dr. M. Nakamoto, Dr. M. Ichinohe
Department of Chemistry
University of Tsukuba
Tsukuba, Ibaraki 305-8571 (Japan)
Fax: (+81) 298-53-4314
E-mail: sekiguch@staff.chem.tsukuba.ac.jp

[**] This work was supported by a Grant-in-Aid for Scientific Research (Nos. 13440185, 14044015, 14078204) from the Ministry of Education, Science and Culture of Japan, TARA (Tsukuba Advanced Research Alliance), and the COE (Center of Excellence) program.

 © 2003 Wiley-VCH Verlag GmbH & Co. KGaA, Weinheim 1433-7851/03/4210-1143 $ 20.00+.50/0

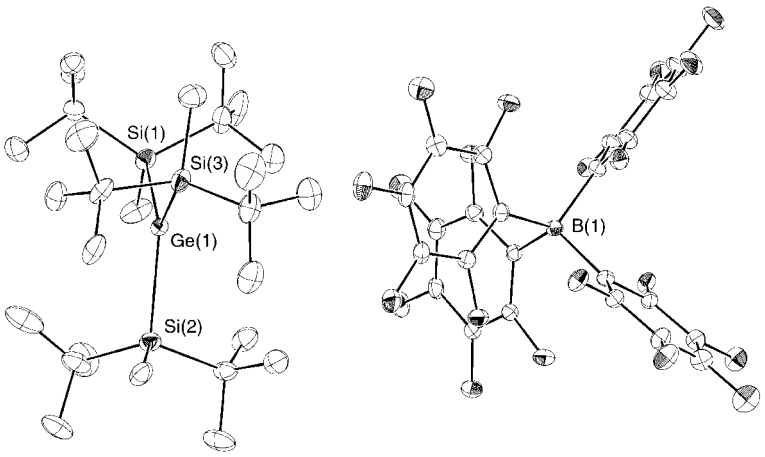

Figure 1. Molecular structure of **2** (ORTEP plot, thermal ellipsoids set at 30% probability; hydrogen atoms omitted for clarity). Selected bond lengths [Å] and angles [°]: Ge(1)-Si(1) 2.5170(9), Ge(1)-Si(2) 2.5379(10), Ge(1)-Si(3) 2.5036(10); Si(3)-Ge(1)-Si(1) 119.79(4), Si(3)-Ge(1)-Si(2) 119.11(4), Si(1)-Ge(1)-Si(2) 121.09(4).

proceeds very quickly, and results in an immediate color change from dark red to yellow and formation of a polymeric material, probably through the ring opening of THF. This enhanced electrophilicity of **2** over the $[(t\mathrm{Bu_3Si})_3\mathrm{Ge_3}]^+$ ion is to be expected, since **2** lacks the highly stabilizing π-bond conjugation effects.[7,11]

The cation **2** quickly reacts with acetonitrile to produce the corresponding nitrile complex **3** (Scheme 2), which was isolated quantitatively as colorless crystals. The crystal structure of **3** was determined by X-ray crystallography (Figure 2).[12] The geometry of the cation of **3** differs from that of **2**, being slightly pyramidalized; the sum of the bond angles around the Ge atom is 358.4°. The arrangement of the Me groups is also different, two of them (C(1) and C(10)) are directed towards the nitrile unit, whereas one (C(19)) points in the opposite direction. The acetonitrile molecule coordinates to the Ge center by the nitrogen lone-pair electrons in a linear fashion, although not quite perpendicular to the mean plane of the cation (Ge(1)-Si(1)-Si(2)-Si(3)). The Ge–N interatomic distance is 2.0119(17) Å, similar to that of $[t\mathrm{Bu_3Ge(NC}t\mathrm{Bu)}]^+[\mathrm{TFPB}]^-$ (Ge–N: 1.975(7) Å, $\mathrm{TFPB^-}$ = tetrakis[3,5-bis(trifluoromethyl)phenyl]borate).[14]

As expected, the germyl cation **2** is very reactive. For example, reaction with $\mathrm{LiAlH_4}$ quantitatively produces the corresponding hydride **4**, whereas with the bulky *t*BuLi a one-electron-transfer reaction occurred instead of alkylation to form the starting germyl radical **1** (Scheme 2).

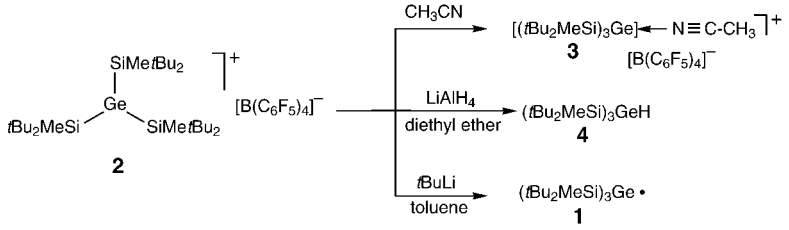

Scheme 2. Reactivity of the germyl cation **2**.

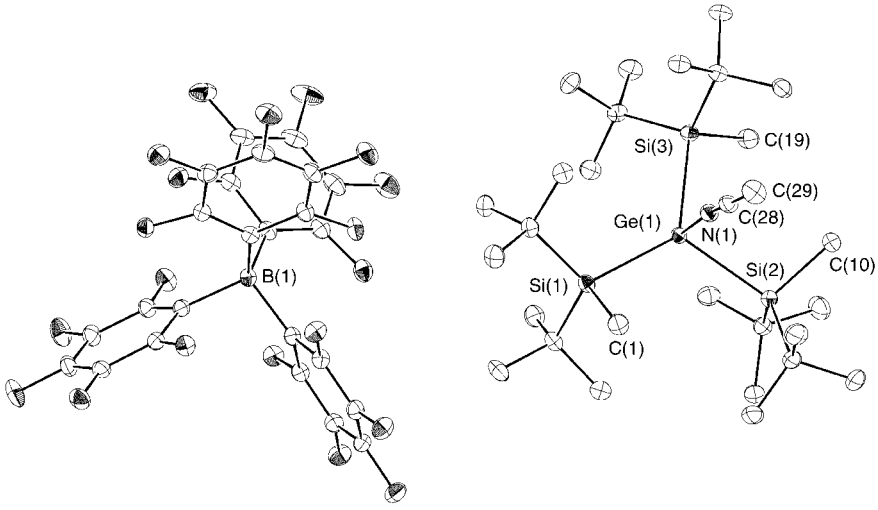

Figure 2. Molecular structure of **3** (ORTEP plot, thermal ellipsoids set at 30% probability; hydrogen atoms omitted for clarity). Selected bond lengths [Å] and angles [°]: Ge(1)-Si(1) 2.5270(6), Ge(1)-Si(2) 2.5210(6), Ge(1)-Si(3) 2.5614(6), Ge(1)-N(1) 2.0199(17), C(28)-C(29) 1.447(3); Si(3)-Ge(1)-Si(1) 128.682(19), Si(3)-Ge(1)-Si(2) 110.562(19), Si(1)-Ge(1)-Si(2) 119.11(2), N(1)-Ge(1)-Si(1) 92.14(5), N(1)-Ge(1)-Si(2) 92.20(5), N(1)-Ge(1)-Si(3) 98.27(5).

Experimental Section

Compound **2**: To a mixture of tris[di-*tert*-butyl(methyl)silyl]germyl radical **1** (80 mg, 0.15 mmol) and $[\mathrm{Ph_3C}]^+[\mathrm{TPFPB}]^-$ (135 mg, 0.15 mmol) dry oxygen-free benzene (3 mL) was introduced by vacuum transfer, and then the mixture was stirred at room temperature for 5 min. After evaporation of solvent, the residue was recrystallized from benzene to give **2** as dark red crystals (134 mg, 75%). ^{1}H NMR ($\mathrm{CD_2Cl_2}$, TMS): $\delta = 1.17$ (s, 9H; Me), 1.19 ppm (s, 54H; *t*Bu); ^{13}C{^{1}H} NMR ($\mathrm{CD_2Cl_2}$, TMS): $\delta = -0.9$, 26.5, 29.5, 123.7 (m, *ipso* C), 136.0 (d, $^1J_{\mathrm{C\text{-}F}} = 247$ Hz), 137.9 (d, $^1J_{\mathrm{C\text{-}F}} = 245$ Hz), 147.8 ppm (d, $^1J_{\mathrm{C\text{-}F}} = 240$ Hz); ^{29}Si{^{1}H} NMR ($\mathrm{CD_2Cl_2}$, TMS): $\delta = 49.9$ ppm.

Compound **3**: Dry and degassed acetonitrile (0.5 mL) was transferred through the vacuum line to the germyl cation **2** (30 mg, 0.02 mmol). The dark red color of **2** immediately vanished, and NMR spectroscopy indicated clean formation of the nitrile complex **3**, which was quantitatively isolated upon cooling as colorless crystals. ^{1}H NMR ($\mathrm{CD_2Cl_2}$, TMS): $\delta = 0.70$ (s, 9H; Me), 1.21 (s, 54H; *t*Bu), 2.62 ppm (s, 3H; $\mathrm{CH_3CN}$); ^{13}C{^{1}H} NMR ($\mathrm{CD_2Cl_2}$, TMS): $\delta = -1.2$, 4.1 (*Me*CN), 24.3, 29.8, 123.6 (m, *ipso* C),

 © 2003 Wiley-VCH Verlag GmbH & Co. KGaA, Weinheim 1433-7851/03/4210-1144 $ 20.00+.50/0

127.9 (Me*C*N), 135.9 (d, $^1J_{C\text{-}F} = 244$ Hz), 137.9 (d, $^1J_{C\text{-}F} = 246$ Hz), 147.8 ppm (d, $^1J_{C\text{-}F} = 241$ Hz); $^{29}Si\{^1H\}$ NMR (CD_2Cl_2, TMS): $\delta = 37.8$ ppm.

Received: August 14, 2002 [Z19964]

Keywords: cations · germanium · oxidations · radicals · solid-state structures

[1] F. A. Carey, R. J. Sundberg, *Advanced Organic Chemistry, Part A: Structure and Mechanisms*, 4th ed., Kluwer Academic/Plenum Publishers, New York, **2000**.
[2] J. B. Lambert, S. Zhang, C. L. Stern, J. C. Huffman, *Science* **1993**, *260*, 1917.
[3] C. A. Reed, Z. Xie, R. Bau, A. Benesi, *Science* **1993**, *263*, 402.
[4] a) J. B. Lambert, Y. Zhao, *Angew. Chem.* **1997**, *109*, 389; *Angew. Chem. Int. Ed. Engl.* **1997**, *36*, 400; b) T. Müller, Y. Zhao, J. B. Lambert, *Organometallics* **1998**, *17*, 278; c) J. B. Lambert, Y. Zhao, H. Wu, W. C. Tse, B. Kuhimann, *J. Am. Chem. Soc.* **1999**, *121*, 5001.
[5] K.-C. Kim, C. A. Reed, D. W. Elliott, L. J. Mueller, F. Tham, L. Lin, J. B. Lambert, *Science* **2002**, *297*, 825.
[6] D. L. Reger, P. S. Coan, *Inorg. Chem.* **1996**, *35*, 258.
[7] A. Sekiguchi, M. Tsukamoto, M. Ichinohe, *Science* **1997**, *275*, 60.
[8] A. Sekiguchi, T. Matsuno, M. Ichinohe, *J. Am. Chem. Soc.* **2000**, *122*, 11250.
[9] For the germanium-cation cluster with trishomoaromaticity, see: A. Sekiguchi, Y. Ishida, Y. Kabe, M. Ichinohe, *J. Am. Chem. Soc.* **2002**, *124*, 8776.
[10] A. Sekiguchi, T. Fukawa, M. Nakamoto, V. Ya. Lee, M. Ichinohe, *J. Am. Chem. Soc.* **2002**, *124*, 9865.
[11] a) M. Ichinohe, N. Fukaya, A. Sekiguchi, *Chem. Lett.* **1998**, 1045; b) A. Sekiguchi, N. Fukaya, M. Ichinohe, Y. Ishida, *Eur. J. Inorg. Chem.* **2000**, 1155.
[12] Crystal structure analyses of **2** and **3**: The single crystals for X-ray analysis were grown from the benzene solution for **2** and acetonitrile solution for **3**. Diffraction data were collected at 120 K on a MacScience DIP2030K Image-Plate Diffractometer employing graphite-monochromated $Mo_{K\alpha}$ radiation ($\lambda = 0.71070$ Å). Crystal data for **2**: $[(t\mathrm{Bu_2MeSi})_3\mathrm{Ge}]^+$ $[\mathrm{B(C_6F_5)_4}]^-$, $C_{51}H_{63}BF_{20}GeSi_3$, $M_r = 1223.68$, monoclinic, space group = $P2_1/n$, $a = 14.9940(3)$, $b = 21.0240(6)$, $c = 18.1160(5)$ Å, $\beta = 101.803(2)°$, $V = 5590.0(2)$ Å^3, $Z = 4$, $\rho_{calcd} = 1.454$ g cm^{-3}, GOF = 0.999. The final R factor was 0.0604 ($R_w = 0.1680$ for all data) for 10781 reflections with $I_o > 2\sigma(I_o)$. Crystal data for **3**: $[(t\mathrm{Bu_2MeSi})_3\mathrm{Ge(NCMe)}]^+$ $[\mathrm{B(C_6F_5)_4}]^-\cdot(\mathrm{MeCN})$, $C_{55}H_{69}BF_{20}GeN_2Si_3$, $M_r = 1305.79$, triclinic, space group = $P\bar{1}$, $a = 13.2440(6)$, $b = 15.2880(8)$, $c = 16.0780(7)$ Å, $\alpha = 91.241(3)$, $\beta = 90.848(3)$, $\gamma = 108.983(3)°$, $V = 3076.8(3)$ Å^3, $Z = 2$, $\rho_{calcd} = 1.409$ g cm^{-3}, GOF = 1.030. The final R factor was 0.0432 ($R_w = 0.1216$ for all data) for 11598 reflections with $I_o > 2\sigma(I_o)$. The structures were solved by the direct method and refined by the full-matrix least-squares method using SHELXL-97 program. CCDC-191270 (**2**) and CCDC-191271 (**3**) contain the supplementary crystallographic data for this paper. These data can be obtained free of charge via www.ccdc.cam.ac.uk/conts/retrieving.html (or from the Cambridge Crystallographic Data Centre, 12 Union Road, Cambridge CB21EZ, UK; fax: (+44) 1223-336-033; or deposit@ccdc.cam.ac.uk).
[13] K. M. Baines, W. G. Stibbs, *Coord. Chem. Rev.* **1995**, *145*, 157.
[14] For the nitrile complexes of $[t\mathrm{Bu_3Ge}]^+$ and $[t\mathrm{Bu_3Si}]^+$, see: M. Ichinohe, H. Fukui, A. Sekiguchi, *Chem. Lett.* **2000**, 600.

Gas Separation

Overcoming the "Upper Bound" in Polymeric Gas-Separation Membranes**

Yongsok Seo, Seong Uk Hong,* and Bon-Soo Lee*

Polymer membranes are used commercially to separate air, to remove carbon dioxide from natural gas, and to remove hydrogen from mixtures with nitrogen or hydrocarbons in petrochemical processing applications.[1–8] For a given pair of gases (e.g., O_2/N_2, CO_2/CH_4, H_2/N_2), the fundamental parameters characterizing membrane separation performance are the permeability coefficient, P_A, and the selectivity, $\alpha_{A/B}$. The permeability coefficient is the product of the gas flux and the membrane thickness, divided by the pressure difference across the membrane. The gas selectivity is the ratio of the permeability coefficients of the two gases ($\alpha_{A/B} = P_A/P_B$), where P_A is the permeability of the more permeable gas and P_B is the permeability of the less permeable gas. For high-performance polymer membranes, both high permeability and selectivity are desirable because higher permeability decreases the size of the membrane area required to treat a given amount of gas, thereby decreasing the capital cost of membrane units, and because higher selectivity results in a higher purity product gas. However, it is well known that polymers which are more permeable are generally less selective and vice versa. A rather general trade-off has always existed between permeability and selectivity. Robeson[1] has quantified this notion on the basis of an exhaustive literature survey by plotting the available data. According to Robeson,[1,2] the upper bound performance characteristics can be described by an empirical equation; $\alpha_{A/B} = \beta_{A/B} P_A^{\lambda A/B}$, where $\lambda_{A/B} < 0$ which indicates that, as the permeability of an upper bound polymer to gas A, P_A, increases, the selectivity of the polymer for gas A over gas B, $\alpha_{A/B}$, decreases. This is the so-called trade-off. In a recent work, Freeman[3] theoretically justified the reason for this trade-off. His model suggests that

[*] Dr. Y. Seo
Supercomputational Modeling and Simulation Laboratory
Future Technology Research Division
Korea Institute of Science and Technology (KIST)
P.O.Box 131, Cheongryang, Seoul (Korea)
Fax: (+82) 2-958-7034
E-mail: ysseo@kist.re.kr

Prof. S. U. Hong
Department of Chemical Engineering
Hanbat National University
San 16-1, Deokmyeongdong, Yuseong-ku, Daejon (Korea)
Fax: (+82) 42-821-1536
E-mail: suhong@hanbat.ac.kr

Prof. B.-S. Lee
Department of Chemistry, Inha University
Yonghyun-dong 253, Nam-ku, Inchon (Korea)

[**] We thank Drs. G. Maier (Technischen Universität München), W. J. Koros (Georgia Institute of Technology), I. Lee, S. M. Lee, J. M. Hong, and Y. S.Kang (KIST) for discussion and experimental help. This work was supported by KIST and BIONAST (Y.S.), KOSEF through AMAREN (S.U.H.).

 © 2003 Wiley-VCH Verlag GmbH & Co. KGaA, Weinheim 1433-7851/03/4210-1145 $ 20.00+.50/0

the slope of the upper bound is a natural consequence of the strong size-sieving nature of stiff-chain glassy polymeric materials. Interestingly, the polymers that define the "upper bound" relation are stiff-chain amorphous glassy polymers. The Freeman model implies that polymer structure has no influence on the slope of the upper-bound or trade-off curves since the parameter $\lambda_{A/B}$ depends only on penetrant size ratio.[3] He concludes that the slopes of the upper-bound lines are unlikely to change with further polymer development efforts. Over the past 30 years, a substantial research effort has been directed to overcoming the limit imposed by the upper bound; chemically different polymers and various techniques, such as surface modification[1,2] have been used, but without much success.[5,6] Though some inorganic membranes, such as purely molecular sieving zeolites or carbon membranes show superior performance, it is not yet clear if these materials will become economically viable for large-scale applications.[4] Besides they are quite fragile and not easily processable. Herein, we focus on polymer membranes that are widely used; we present a novel approach based on preparing hybrid polymeric films that included a thermotropic liquid-crystalline polymer(TLCP) and a compatibilizer in the polymer matrix. Although some studies have been carried out on TLCP membranes,[7–11] to date TLCP composite membranes have not received much attention.

We designed and prepared composite films by using a TLCP (poly(ester amide)), a thermoplastic matrix (poly(ether imide), PEI), and an amorphous compatibilizer (a poly(ester imide), PEsI). Chemical structures of these polymers are shown in Scheme 1. The TLCP content was kept at 10 wt% while the amount of PEsI was varied. TEM photographs in Figure 1 show that addition of the compatibilizer leads to improved adhesion, better stress transmission, reduced interfacial tension, hence, finer dispersion of the TLCP phase as well as easier deformation.[12,13] It is also

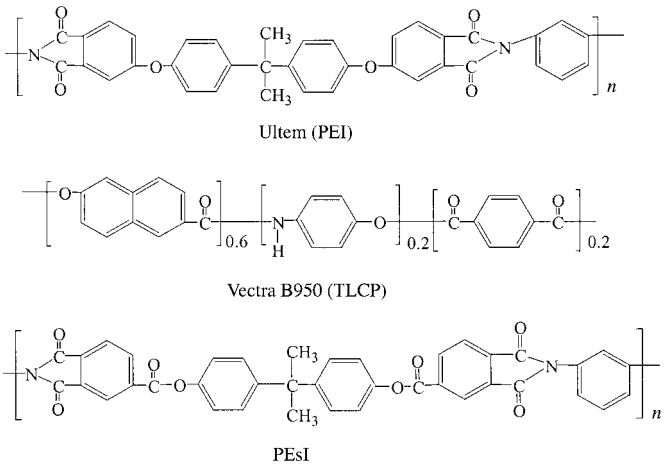

Scheme 1. Chemical structures of the polymers Ultem (matrix), Vectra B950 (TLCP, barrier), PEsI (compatibilizer)).

evident that the amount of compatibilizer plays an important role in the dispersion and the deformation of the TLCP phase. Adding a certain amount of compatibilizer induces a finer dispersion of the TLCP phase. It was found that 0.6 wt% of the compatibilizer was the optimum amount when 10 wt% TLCP was included.[12,13] Coalescence of the TLCP phase was observed when excessive amount of the compatibilizer was used (Figure 1 A c and B c), which results in a larger dispersed-phase size. The SEM images show films containing stripes resulting from the biaxial orientations.

The performance test was done for oxygen–nitrogen separation, which presents the greatest challenge for membrane systems because the kinetic diameters of these two gases differ only by a few tenths of an angstrom (3.46 Å for O_2 versus 3.64 Å for N_2).[7] The pure gas permeabilities of O_2 and N_2 were measured for all of the films at 1 atm (upstream

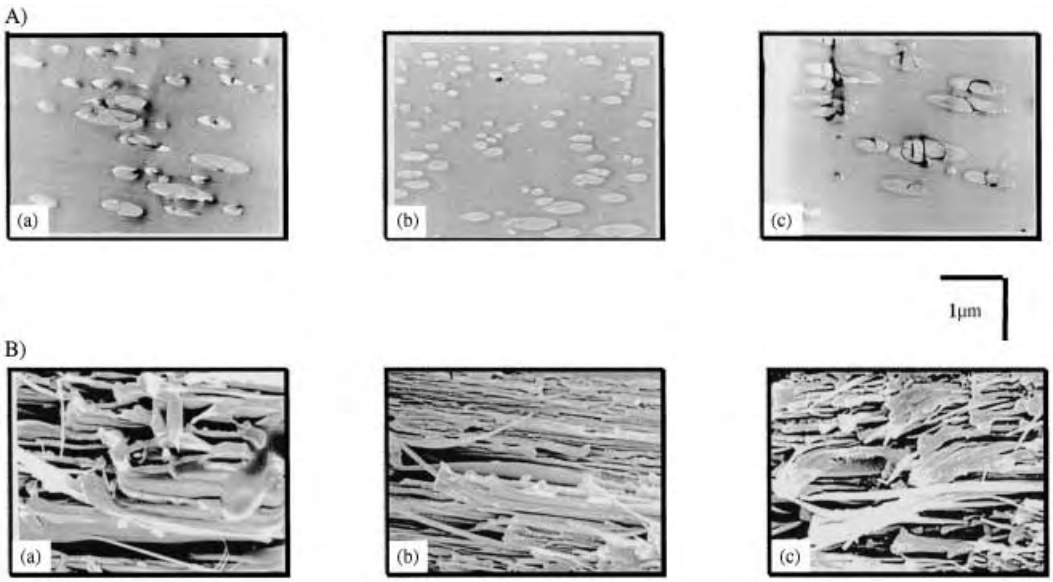

Figure 1. Transmission electron micrographs of microtomed surfaces normal to flow direction (A) and scanning electron micrographs of fractured surface parallel to flow direction (B) in each case: a) a binary blend of TLCP and PEI, b) a ternary blend including 0.6 wt% PEsI, and c) a ternary blend including 1.3 wt% PEsI, this film which contains an excessive amount of PEsI shows a coalescence of the TLCP phase.

 © 2003 Wiley-VCH Verlag GmbH & Co. KGaA, Weinheim 1433-7851/03/4210-1146 $ 20.00+.50/0

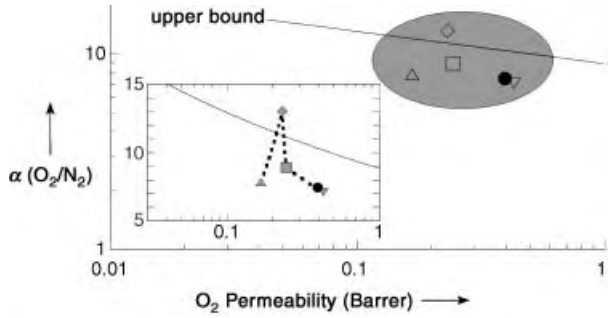

Figure 2. The relationship between the oxygen permeability and the O_2/N_2 selectivity for PEI and TLCP blended films. (▽) PEI, (●) PEI literature value,[14] (□) a binary blend, (◇) a ternary blend with 0.6 wt% PEsI, and (△) a ternary blend with 1.3 wt% PEsI. The solid line is an empirical upper bound.[1–3] Numerical values are provided in the Table 1. The inset shows the shaded region with a linear *y*-axis scale. The dashed line is a guide for the eyes.

pressure) and 35 °C, and Figure 2 shows the performance of the composite films. The O_2 permeability and selectivity for PEI, which were measured in this study, are in good agreement with the values reported in the literature.[14] The addition of the almost impermeable TLCP phase to PEI slightly, but not greatly, decreases the O_2 permeability compared to that of PEI film. This is ascribed to a reduction in the surface area for the glassy polymer (PEI) caused by migration of the TLCP phase to the surface[12] and thus to a slight decrease in the free volume of the composite film. On the other hand, the selectivity of the binary film increases significantly. The selectivity of the ternary blend film containing 0.6 wt% PEsI exceeds the upper bound, which has never happened before for this O_2 permeability range. In addition, the permeability of this film was not noticeably different from that of the binary-blend film. This is the first time that a dramatic increase has been observed in the selectivity of the O_2/N_2 pair without the permeability being significantly sacrificed (Table 1). Because the compatibilizer acts at the interface to reduce the interfacial tension between the TLCP phase and the matrix, it induces a fine dispersion of the TLCP phase (see Figure 1) and the number of the dispersed phase in the matrix for the compatibilized ternary system is much more than that for the binary (uncompatibilized) blend system.[12,13]

We consider two roles of the TLCP phase dispersed in the matrix polymer; an almost impermeable barrier and a very low-permeable, but highly selective, layer. Both of which are possible.[7] First, we consider the TLCP phase as an impermeable barrier. In both actual and idealized membranes which contain impermeable flakes, diffusion is retarded because diffusing gases must take tortuous paths around the impermeable flakes.[15,16] Most diffusion occurs around the nearest boundary. The solute diffuses around this boundary and across the membrane until it meets the next random flake. In our work, we used a compatibilizer for the uniform dispersion of the TLCP phase. The boundaries of the impermeable flakes are surrounded by a compatibilizer, which should exist there as a result of free-energy restrictions.[12] If the compatibilizer is amorphous, the diffusing gas molecules will pass through it, thus making it a channel that the diffusing gas must use.[13] Since diffusion of different permeants are different in all known polymers, one that diffuses slowly takes a longer time to pass through while another passes through faster (Figure 3). The concentration of the fast-diffusing molecules through the compatibilizer goes up after each passage around a dispersed TLCP phase. It is like a chromatography having many separation steps. As shown in Figure 1, a ternary-blend film containing 0.6 wt% PEsI has a small and uniformly distributed TLCP phase because of the compatibilizer, which is located at the boundary of the TLCP phase. Since almost none of the gas molecules diffuse through TLCP phase, most diffusion occurs around the nearest boundary, where the amorphous compa-

Table 1: O_2 permeability, N_2 permeability, and selectivity of PEI and blended films.

Film	$P(O_2)$ [Barrer]	$P(N_2)$ [Barrer]	$\alpha(O_2/N_2)$
PEI (ultem)[a]	0.400	0.053	7.6
PEI (ultem)[b]	0.432	0.060	7.2
binary	0.246	0.027	9.2
ternary (0.6% PEsI)	0.234	0.018	13.0
ternary (1.3% PEsI)	0.170	0.021	8.0

[a] The values reported in the literature.[14] [b] Values obtained in this work.

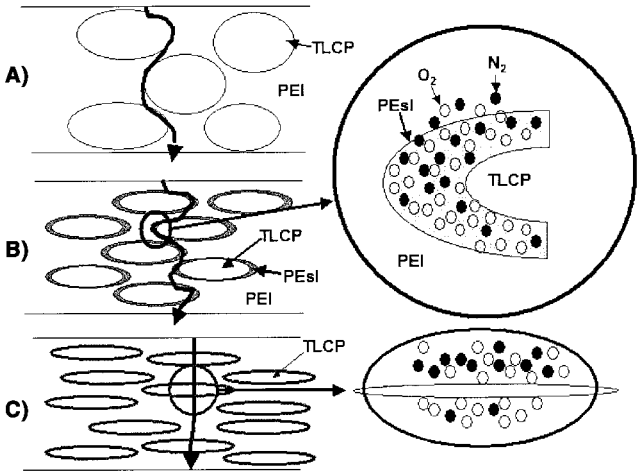

Figure 3. Solute-molecule diffusion through the composite films. The total volume of the TLCP phase is the same in all cases. A) The binary-blend film has a large TLCP phase because TLCP is immiscible with the matrix. Permeant molecules pass around the impermeable TLCP phase. B) A ternary-blend film has a small and uniformly distributed impermeable TLCP phase because of the compatibilizer. In the ternary composite films, the gas molecules must pass around the dispersed TLCP phase and pass through the PEsI phase which lies at the interface between the matrix and the dispersed phase. The inset shows a representation of gas molecules diffusing in the PEsI phase which is exaggerated for clarity. The gas molecules of larger size diffuse more slowly while those of smaller size diffuse more rapidly.[2,3]. Thus, the selectivity becomes larger than the value for the corresponding binary blend film. C) The thin TLCP phase acts as a very low-permeable highly selective phase. The inset shows a representation of gas molecules diffusing through very thin TLCP phase.

 © 2003 Wiley-VCH Verlag GmbH & Co. KGaA, Weinheim 1433-7851/03/4210-1147 $ 20.00+.50/0

tibilizer, PEsI, is mostly located.[13] Based on the free-volume calculation, PEsI is expected to have a higher selectivity than PEI.[17] With increasing number of passes around TLCP flakes, the difference between the diffused amounts of the different gas molecules becomes larger and larger (Figure 3); hence, the selectivity is increased. When 1.3 wt% PEsI was added, both the selectivity and the permeability dropped because the dispersed TLCP phase has poor morphology as a result of coalescence or coagulation (Figure 1). The selectivity of morphologically optimized composite films having a compatibilizer, in which different gas molecules diffuse with different rate, can be theoretically much higher than the value previously considered to be the upper bound.

Second, we consider the thin TLCP phase to be very low-permeable phase but highly selective one. The concentration of more permeable gas molecules increases while it is passing through each TLCP phase. Even though the amount of the permeant going through each TLCP phase is small, the total amount will increase; thus, the selectivity will also increase. Paul and co-workers reported that a Vectra-type membrane shows a high O_2/N_2 selectivity with very low O_2 permeability (16 at 4.7×10^{-4} Barrer; $1\,\text{Barrer}=10^{-10}\,\text{cm(STP)cm/(cm}^2\,\text{sec cmHg)}$).[7] After each passage the relative concentration of O_2 increases (Figure 3). The amount of diffused gas molecules is very small but the diffused gas contains more O_2 than N_2 because of the high selectivity of TLCP. The selectivity increase in the binary film can be also ascribable to this mechanism. Thus, the resulting composite films containing 0.6 wt% PEsI, which has a lot of small and uniformly distributed TLCP phase because of the compatibilizer, exhibited unusually high selectivity, overcoming the upper-bound limit without any significant sacrificing of the permeability. When excessive PEsI (1.3 wt%) was added, both the selectivity and the permeability dropped because of the poor morphology. We emphasize that the important factor is not the film thickness but the number of dispersed TLCP phases. A similar idea was suggested by Robeson and co-workers a few years ago.[2] They suggested that the upper bound could be overcome if a highly permeable polymer were to be surface modified such that the surface modification created a highly selective layer. Similar in construction, a mixed-material composite (MMC) membrane with tightly packed submicron molecular sieve was reported to improve the selectivity for the oxygen/nitrogen separation,[4] but there are problems with MMC membranes such as, poor adhesion between the polymeric phase and the molecular-sieve phase.

Currently we are not sure which mechanism is more feasible, both are possible. To clarify this issue, the performance of PEsI and VB membranes should be investigated. Though difficult because both membranes are hard to make (PEsI is easily broken and VB is hard to process), we are currently investigating this. The results will be reported in the future.

The combination of the compatibilizer's role of controlling the morphology and selecting different gas molecules and the TLCP's role as a barrier and/or in allowing the diffusion of various gas molecules at different rates allowed us to experimentally show that the limit imposed by what was considered to be an upper bound could be overcome. This strategy can be easily used to make extraordinary polymeric membranes. The result should stimulate researchers to use this method for practical applications in gas-separation processes.

Experimental Section

The TLCP used in our experiments was a copolyester amide of 6-hydroxy-2-naphthoic acid (60%), terephthalic acid (20%), and 4-amino phenol (20%), commercially known as Vectra B950 (VB), manufactured by Celanese Hoechst. Poly(ether imide) (PEI), commercially known as Ultem 1000, an amorphous polymer having a high glass-transition temperature and made by General Electric, was used as the matrix. A poly(ester imide) (PEsI) synthesized in our laboratory was used as a compatibilizer. Details of its synthesis and miscibility with VB and PEI, as well as its activity as a compatibilizer were fully described elsewhere.[12,13] The TLCP content was kept at 10 wt% while the amount of PEsI was varied. After the polymers were blended in a twin-screw extruder, the blended melt was blown into a parison. Films having thicknesses of 0.04 mm were taken for the gas-permeability test. The film samples were mounted in the test cell and thoroughly degassed under very high vacuum before they were used in the permeability tests. An established constant-volume method[4,6,7] was used in the test system to measure the gas flux on the low-pressure side of the membrane.

Received: August 19, 2002
Revised: January 3, 2003 [Z19995]

Keywords: gas separation · liquid crystals · membranes · polymers · thin films

[1] L. M. Robeson, *J. Membr. Sci.* **1991**, *62*, 165–185.
[2] L. M. Robeson, W. F. Burgoyne, M. Langsam, A. C. Savoca, C. F. Tien, *Polymer* **1994**, *35*, 4970–4978.
[3] B. D. Freeman, *Macromolecules* **1999**, *32*, 375–380.
[4] a) W. J. Koros, R. Mahajan, *J. Membr. Sci.* **2000**, *175*, 181–196; b) "Polymer Membranes for Gas and Vapor Separation": R. Mahajan, C. M. Zimmerman, W. J. Koros, *ACS Symp. Ser.* **1999**, *733*, 277–286; c) C. M. Zimmerman, W. J. Koros, *Macromolecules*, **1999**, *32*, 3341–3346.
[5] P. H. Abelson, *Science* **1989**, *244*, 1421.
[6] C. Liu, C. R. Martin, *Nature* **1991**, *352*, 50–52.
[7] a) D. H. Weinkauf, H. D. Kim, D. R. Paul, *Macromolecules* **1992**, *25*, 788–796; b) "Barrier Polymers and Structures": D. H. Weinkauf, D. R. Paul, *ACS Symp. Ser.* **1990**, *423*, 60–91; c) D. H. Weinkauf, D. R. Paul, *J. Polym. Sci. Part B* **1992**, *30*, 817–835 and D. H. Weinkauf, D. R. Paul, *J. Polym. Sci. Part B* **1992**, *30*, 837–849; d) D. H. Weinkauf, D. R. Paul, *J. Polym. Sci. Part B* **1991**, *29*, 329–340.
[8] G. Maier, *Angew. Chem.* **1998**, *110*, 3128–3143; *Angew. Chem. Int. Ed.* **1998**, *37*, 2960–2974.
[9] Y. Ly, Y. L. Cheng, *J. Membr. Sci.* **1993**, *77*, 99–112.
[10] N. R. Miranda, J. T. Willitis, B. D. Freeman, H. B. Hopfenberg, *J. Membr. Sci.* **1994**, *94*, 67–83.
[11] a) T. Kajiyama, H. Kikuchi, *J. Membr. Sci.* **1988**, *36*, 243–255; b) T. Kajiyama, S. Washizu, Y. Obomori, *J. Membr. Sci.* **1985**, *24*, 73–81; c) T. Kajiyama, *Polymers for Gas Separation* (Ed.: N. Toshima), VCH, New York, **1992**, chap. 3.
[12] Y. Seo, S. M Hong, S. S. Hwang, T. S. Park, K. U. Kim, S. Lee, J. W. Lee, *Polymer* **1995**, *36*, 515–523.
[13] Y. Seo, S. M Hong, S. S. Hwang, T. S. Park, K. U. Kim, S. Lee, J. W. Lee, *Polymer* **1995**, *36*, 525–534.
[14] T. A. Barbari, W. J. Koros, D. R. Paul, *J. Membr. Sci.* **1989**, *42*, 69–86.

 © 2003 Wiley-VCH Verlag GmbH & Co. KGaA, Weinheim 1433-7851/03/4210-1148 $ 20.00+.50/0

[15] B. D. Freeman, *Polym. Prepr. Am. Chem. Soc. Div. Polym. Chem.* **1999**, *40*, 478 – 479.
[16] E. L. Cussler, S. E. Hughes, W. J. Ward III, R. Aris, *J. Membr. Sci.* **1988**, *38*, 161 – 174.
[17] J. Y. Park, D. R. Paul, *J. Membr. Sci.* **1997**, *125*, 23 – 39.

 © 2003 Wiley-VCH Verlag GmbH & Co. KGaA, Weinheim 1433-7851/03/4210-1149 $ 20.00+.50/0

Nitrogen Fixation by Mo Clusters

The Role of Mo Atoms in Nitrogen Fixation: Balancing Substrate Reduction and Dihydrogen Production**

*Jon Bell, Adrian J. Dunford, Emmalina Hollis, and Richard A. Henderson**

Nitrogenases are metalloenzymes that catalyze the conversion of dinitrogen into ammonia by coupled electron- and proton-transfer reactions.[1,2] Three types of nitrogenases have been characterized[3] and are distinguished by their metal content: molybdenum nitrogenase contains Mo and Fe atoms; vanadium nitrogenase contains V and Fe atoms; and iron-only nitrogenase contains Fe centers and no other transition-metal atoms. The difference in metal-atom content is associated with the Fe–S-based clusters called cofactors, which are the active sites of these enzymes.[4,5] In molybdenum nitrogenase the FeMo cofactor comprises one molybdenum, seven iron, and nine sulfur atoms (Figure 1). The structure of FeMo cofactor has been established by X-ray analysis,[2] but the structures of the other nitrogenases have yet to be determined. Nevertheless, the close homology between the enzymes[3] strongly indicates that the FeV and FeFe cofactors are structurally analogous to the FeMo cofactor, with V or Fe atoms in place of the Mo atom, respectively. Thus, Mo atoms are not essential for nitrogen fixation, but studies on these three types of nitrogenases have shown that the Mo nitrogenase is the most efficient.[3,6]

The different cofactors impart distinct reactivity characteristics to the nitrogenases. Most notably there are subtle differences in the product specificities formed with ethyne, and dinitrogen.[3] In the absence of substrates all nitrogenases reduce protons to dihydrogen, but in the presence of dinitrogen the electron flux is divided between reduction of dinitrogen (to form ammonia) and protons (to form dihydrogen). Since the formation and evolution of every dihydrogen molecule consumes two electrons (and hence four ATP molecules), dihydrogen production wastes energy.[2–4] The molybdenum nitrogenase is the most efficient, but it still produces at least one molecule of dihydrogen for every dinitrogen molecule converted into ammonia. The vanadium and iron-only nitrogenases are markedly less efficient (Figure 1). There is still much debate about the role of the Mo atoms in the cofactor. Herein, we present work that indicates that, irrespective of where dinitrogen binds to the cofactor, the Mo atoms affect the reactivity of the cofactor in a way that facilitates efficient nitrogen fixation. The Mo atoms slow the protonation of the cluster, which, in turn, suppresses dihydrogen production.

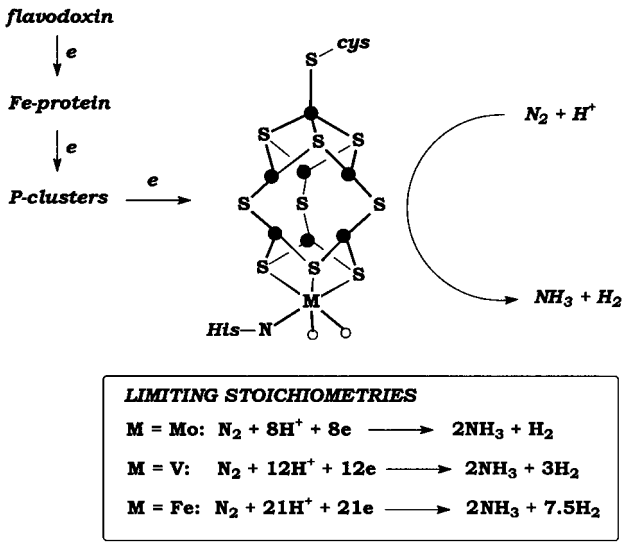

Figure 1. Electron-transfer pathway for the nitrogenases, which culminates in the reduction of dinitrogen to ammonia, and protons to dihydrogen. The limiting stoichiometries of the three types of nitrogenase are shown.

The cuboidal clusters $[Fe_4S_4X_4]^{2-}$ and $[\{MoFe_3S_4X_3\}_2(\mu\text{-}SR)_3]^{3-}$ (X = Cl or RS; R = Ph or Et) are structurally simpler than cofactors. Although they contain many of the structural features of cofactors, the coordination environments of the central Fe atoms in cofactors have yet to be observed in synthetic systems.[7] Herein, we report the rates of proton transfer to both types of synthetic cluster (X = Cl) and show how the rates are affected by: 1) prior binding of the nucleophile to the cluster, and 2) the composition of the cluster core (i.e. $\{Fe_4S_4\}^{2+}$ or $\{MoFe_3S_4\}^{3+}$ ions).

Earlier work has shown that for all synthetic Fe–S-based clusters, protonation of the cluster core (presumably at the S atoms) is a common reaction.[8–10] Recently,[11,12] we studied the substitution reactions of $[Fe_4S_4Cl_4]^{2-}$ clusters with PhS^- ions to form $[Fe_4S_4(SPh)_4]^{2-}$ clusters, in the presence of $[H_2N(CH_2)_3CH_2]^+$ ions, in MeCN. Because the chloro ligands in the $[Fe_4S_4Cl_4]^{2-}$ cluster are labile, and the $[H_2N(CH_2)_3CH_2]^+$ ion is a weak acid ($pK_a = 21.5$ in MeCN), the protonation of the cluster core is the rate-limiting step in the reaction.[11] Stopped-flow spectrophotometric studies of

[*] Prof. Dr. R. A. Henderson, J. Bell, A. J. Dunford, E. Hollis
Department of Chemistry, Bedson Building
University of Newcastle
Newcastle-upon-Tyne, NE1 7RU (UK)
Fax: (+44) 191-222-6929
E-mail: r.a.henderson@ncl.ac.uk

[**] We thank the University of Newcastle for a studentship (A.J.D) and financial support (J.B.).

Supporting information for this article is available on the WWW under http://www.angewandte.org or from the author.

 © 2003 Wiley-VCH Verlag GmbH & Co. KGaA, Weinheim 1433-7851/03/4210-1149 $ 20.00+.50/0

the reactions between the $[\{MoFe_3S_4Cl_3\}_2(\mu\text{-}SR)_3]^{3-}$ clusters (R = Et or Ph) and PhS^- ions in the presence of $[H_2N\overbrace{(CH_2)_3CH_2}]^+$ ions show that these reactions have kinetic behavior analogous to that of the reaction between the $[Fe_4S_4Cl_4]^{2-}$ cluster and PhS^- ions. The reaction of the $[\{MoFe_3S_4Cl_3\}_2(\mu\text{-}SEt)_3]^{3-}$ cluster exhibits a first-order dependence on the concentration of the PhS^- ions (Figure 2) and a nonlinear dependence on the concentration of acid as described by Equation (1).

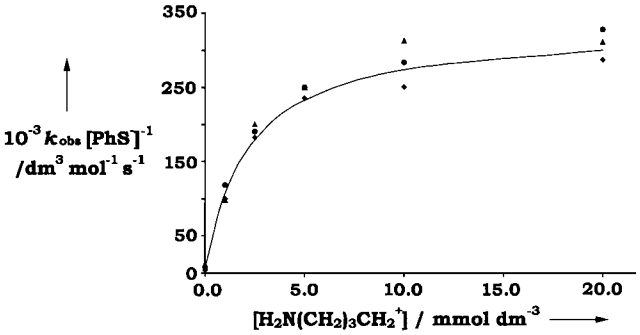

Figure 2. Kinetic data for the reaction of the $[\{MoFe_3S_4Cl_3\}_2(\mu\text{-}SEt)_3]^{3-}$ cluster with PhS^- ions in the presence of $[H_2N\overbrace{(CH_2)_3CH_2}]^+$ ions in (MeCN, 25.0 °C). The data points correspond to: ■ $[PhS^-] = 0.50$; ▲ $[PhS^-] = 1.25$; ◆ $[PhS^-] = 2.50$ mmol dm^{-3}. The curve is that defined by Equation (1) and the corresponding values are shown in Table 1.

$$\frac{-d[\text{cluster}]}{dt} = \frac{k_1^{PhS}(k_2^{PhS} + k_5^{PhS}[H_2N\overbrace{(CH_2)_3CH_2^+}])\,[PhS^-]\,[\text{cluster}]}{k_{-1}^{PhS} + k_2^{PhS} + k_5^{PhS}[H_2N\overbrace{(CH_2)_3CH_2^+}]} \quad (1)$$

This rate law is consistent with the mechanism of path a in Figure 3, in which the initial binding of the PhS^- ion to the cluster is followed by the protonation or dissociation of a chloride ion. A comparison of the rate constants (Table 1), which were obtained from an analysis of the data,[13] indicates the following features: 1) The $\{MoFe_3S_4\}^{3+}$ clusters have a higher affinity than the $\{Fe_4S_4\}^{2+}$ clusters for binding PhS^- ($K_1^{PhS} = k_1^{PhS}/k_{-1}^{PhS}$). Such behavior is entirely general and has been observed before for a variety of molecules and ions (halides, PhS^- ions, CO, and N_2O).[14] The increased affinity is the result of a combination of an increase in the rate of binding (k_1^{PhS}), and a decrease in the rate of dissociation (k_{-1}^{PhS}). 2) When the PhS^- ion is bound, the rate of protonation of the $\{MoFe_3S_4\}^{3+}$ cluster is little different to that of the $\{Fe_4S_4\}^{2+}$ cluster, and corresponds to the maximum rate of protonation of Fe–S-based clusters ($k \sim 10^6$ dm^3 mol^{-1} s^{-1}).[11] It seems likely that the binding of thiolate to the cluster increases the basicity of the cluster, and the presence of the bound thiolate is the major factor influencing the rate of proton transfer.[15]

The rate of proton transfer to the clusters prior to the binding of the nucleophile (i.e. path b of Figure 3) can be measured in the substitution reactions of the clusters with Br^- ions in the presence of $[H_2N\overbrace{(CH_2)_3CH_2}]^+$ ions. Bromide is a poor nucleophile for $[Fe_4S_4Cl_4]^{2-}$ and $[\{MoFe_3S_4Cl_3\}_2(\mu\text{-}SR)_3]^{3-}$ clusters, consequently proton transfer from the $[H_2N\overbrace{(CH_2)_3CH_2}]^+$ acid is faster than the binding of the bromide ion.[18] Hence, by measuring the kinetics of the reaction of the clusters with Br^- ions in the presence of $[H_2N\overbrace{(CH_2)_3CH_2}]^+$ ions, the rate constants for the protonation of the clusters before the binding of the nucleophile can be determined. At low concentrations of acid the reaction with

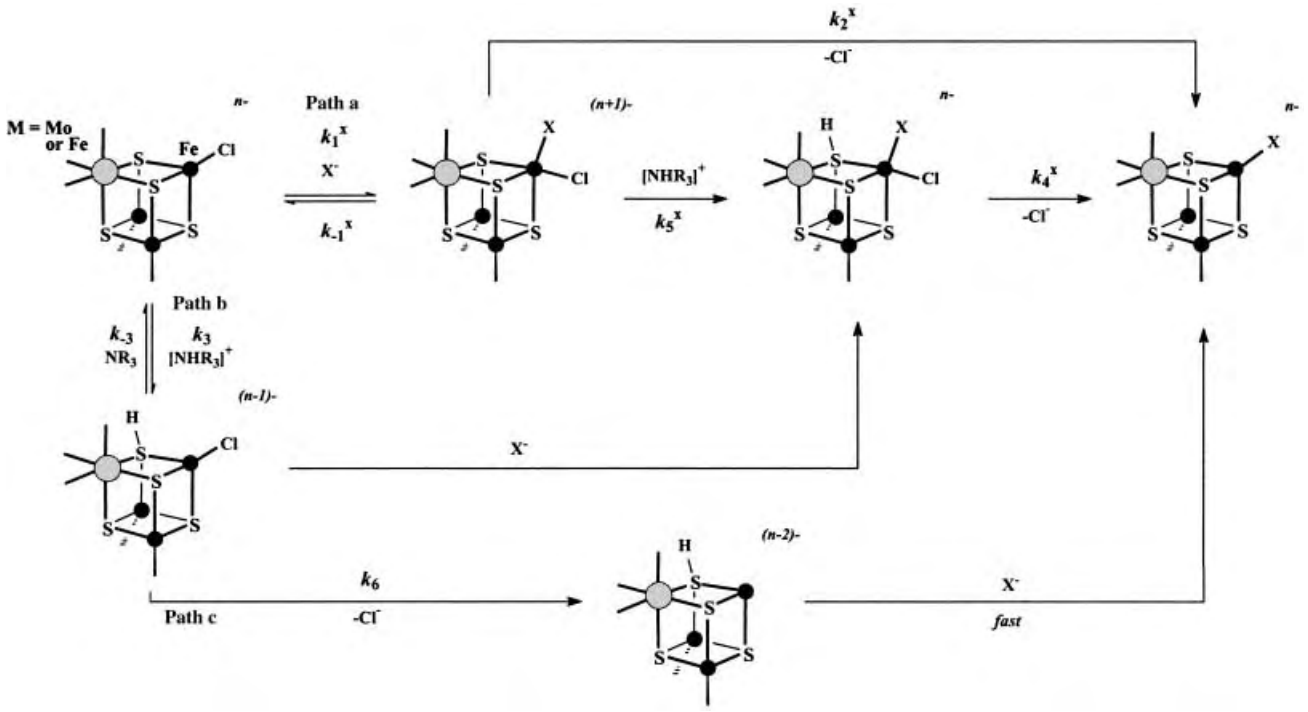

Figure 3. Summary of the pathways for the substitution reactions of synthetic Fe–S clusters in the presence of acids, where $[NHR_3]^+ = [H_2N\overbrace{(CH_2)_3CH_2}]^+$ ion. Path C is not discussed herein but is included for completeness since this is the acid-catalyzed dissociative pathway observed in the reactions of many clusters ($X^- = PhS^-$, Ph^-).[8,9,13]

 © 2003 Wiley-VCH Verlag GmbH & Co. KGaA, Weinheim 1433-7851/03/4210-1150 $ 20.00+.50/0

Table 1: Summary of rate constants for the elementary reactions of $[Fe_4S_4Cl_4]^{2-}$ and $[\{MoFe_3S_4Cl_3\}_2(\mu\text{-}SR)_3]^{3-}$ clusters with PhS^- or Br^- ions in the Presence of $[H_2N(CH_2)_3CH_2]^+$ in MeCN at 25.0°C

Cluster	Nucleophile	$10^{-5}\ k_1^{PhS}$ [$dm^3\,mol^{-1}\,s^{-1}$]	$10^{-5}\ k_{-1}^{PhS}$ [s^{-1}]	k_2^{PhS}	$10^{-6} k_5^{PhS}$ [$dm^3\,mol^{-1}\,s^{-1}$]	$10^{-2}\ k_3$ [$dm^3\,mol^{-1}\,s^{-1}$]	k_6 [s^{-1}]
$[Fe_4S_4Cl_4]^{2-}$	PhS^-	1.4 ± 0.03	2.20 ± 0.24	300 ± 20	1.80 ± 0.27		
	Br^-					240 ± 40[a]	156 ± 12
$[\{MoFe_3S_4Cl_3\}_2(\mu\text{-}SEt)_3]^{3-}$	PhS^-	3.3 ± 0.3	1.3 ± 0.04	260 ± 15	6.0 ± 0.4		
	Br^-					2.5 ± 0.4[b]	
$[\{MoFe_3S_4Cl_3\}_2(\mu\text{-}SPh)_3]^{3-}$	PhS^-	3.8 ± 0.4	1.3 ± 0.1	230 ± 20	1.6 ± 0.3		
	Br^-					5.0 ± 0.8	

[a] $\Delta H^{\neq} = 0.45 \pm 0.2$ kcal mol^{-1}; $\Delta S^{\neq} = -47 \pm 5$ cal deg^{-1} mol^{-1}. [b] $\Delta H^{\neq} = 0.0 \pm 0.2$ kcal mol^{-1}; $\Delta S^{\neq} = -65 \pm 27$ cal deg^{-1} mol^{-1}.

the $[Fe_4S_4Cl_4]^{2-}$ clusters exhibits a first-order dependence on the concentration of $[H_2N(CH_2)_3CH_2]^+$ ions, and is independent of the concentration of Br^- ions (Figure 4). The rate constants are summarized in Table 1. At high concentrations of the acid, the protonation of the $[Fe_4S_4Cl_4]^{2-}$ cluster is sufficiently fast that a unimolecular reaction becomes rate-limiting. It seems likely that this observation corresponds to the rate-limiting dissociation of the chloro group (k_4).

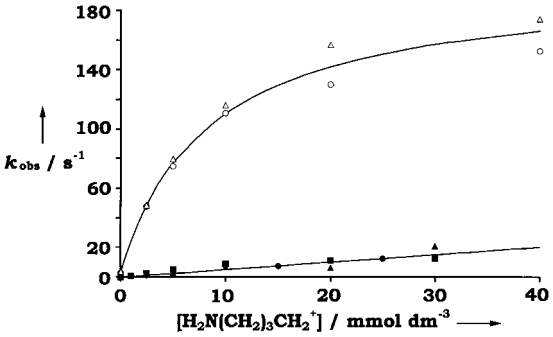

Figure 4. Kinetic data for the reactions of $[Fe_4S_4Cl_4]^{2-}$ (curve) and $[\{MoFe_3S_4Cl_3\}_2(\mu\text{-}SEt)_3]^{3-}$ (line) clusters with Br^- ions in the presence of $[H_2N(CH_2)_3CH_2]^+$ ions (MeCN, 25.0°C). The data points correspond to the $[Fe_4S_4Cl_4]^{2-}$ cluster: ○ $[Br^-] = 5.00$; $[Br^-] = 5.00$ mmol dm^{-3} in the presence of $[D_2N(CH_2)_3CH_2]^+$ (△) and $[\{MoFe_3S_4Cl_3\}_2(\mu\text{-}SPh)_3]^{3-}$: ■ $[Br^-] = 2.50$; ▲ $[Br^-] = 5.0$; ● $[Br^-] = 10.0$ mmol dm^{-3}. The curve and linear fits to the data are those defined by the rate constants shown in the Table 1.

The kinetics of the reactions of $[\{MoFe_3S_4Cl_3\}_2(\mu\text{-}SR)_3]^{3-}$ clusters with Br^- ions in the presence of $[H_2N(CH_2)_3CH_2]^+$ ions are similar to those of the $[Fe_4S_4Cl_4]^{2-}$ cluster with Br^- ions; the rate exhibits a first-order dependence on the acid concentration and is independent of the concentration of Br^- ions (Figure 4). A comparison of the k_3 values shows that: 1) proton-transfer to Fe–S clusters is appreciably slower before a nucleophile is bound, and 2) proton transfer to $[\{MoFe_3S_4Cl_3\}_2(\mu\text{-}SR)_3]^{3-}$ clusters is approximately 50–100 times slower than proton transfer to the $[Fe_4S_4Cl_4]^{2-}$ cluster.

Why the Mo atoms within Fe–S clusters lower the rate of proton transfer could be simplistically attributed to the Mo atoms exerting a general electron-withdrawing effect from the cluster, and this same effect could lead to the increased affinity of the cluster for binding substrates. However, earlier studies[9] established that the pK_a values of protonated Fe–S clusters fall in the narrow range, $18.9 > pK_a > 17.9$ (in MeCN), irrespective of the nature of the terminal ligands, the topology, the nuclearity, the coordination of the S atom (μ_2-S or μ_3-S), or the composition of the core; specifically, for the clusters studied here, $[Fe_4S_4Cl_4]^{2-}$ $pK_a = 18.8$, and $[\{MoFe_3S_4Cl_3\}_2(\mu\text{-}SEt)_3]^{3-}$ $pK_a = 18.6$. The fact that the presence of the Mo atom has little effect on the basicity of the cluster is evidence against there being a general electron-withdrawing effect exerted by the Mo atom. Previously, we showed that the rates of protonation of Fe–S clusters are affected by bond-length changes of the ligands during proton transfer.[11,12] It may be that bond-length changes are energetically more demanding in Mo–Fe–S clusters.

Proton transfer, coupled with electron transfer, is central to the action of cofactors in nitrogenases: to transform dinitrogen into ammonia, and to act as a prequel to dihydrogen production by coupling hydrogen atoms, either on the sulfur atom, or after the hydrogen atoms have migrated from the sulfur atom to a metal center. The presence of the Mo atom in synthetic Fe–S-based clusters makes proton transfer to the clusters slow, and consequently is advantageous to a site that fixes dinitrogen, especially in the binding of the substrate. The bonding between a transition-metal center and dinitrogen consists of nitrogen-to-metal σ-donation and metal-to-nitrogen π-donation.[19] Consequently, a binding site[20] that activates dinitrogen towards protonation (ammonia formation) must be electron rich and thus is inherently susceptible to being protonated.[21] Therefore, any nitrogen-fixing site must maximize the binding and protonation of dinitrogen, but minimize the protonation of the binding site. As noted above, the protonation of core sulfur atoms is a persistent characteristic of Fe–S clusters,[22] including the FeMo cofactor.[9,23] The protonation of sulfur in the FeMo cofactor would make bound dinitrogen labile. This effect could be annulled if protonation is followed by electron transfer. However, the reduction of protonated cofactor could also facilitate dihydrogen production. The simplest way to maximize dinitrogen binding to a site that is also capable of being protonated is to ensure that protonation of the binding site is slow. Proton transfer to all Fe–S cluster cores is slow (at least 10^4 times slower than the diffusion-

 © 2003 Wiley-VCH Verlag GmbH & Co. KGaA, Weinheim 1433-7851/03/4210-1151 $ 20.00+.50/0

controlled limit) and, most importantly, Mo–Fe–S clusters protonate appreciably slower than Fe–S-only clusters. The presence of Mo in FeMo cofactor may facilitate nitrogen fixation in the following ways: 1) By slowing protonation of the active site and maximizing the opportunity for dinitrogen to bind. Irrespective of the intimate mechanism of dihydrogen production, when the protonation process is slowed the rate of dihydrogen production is suppressed. 2) Earlier work[14] has shown that Mo-containing Fe–S-based clusters have an increased affinity to bind substrates compared to Fe–S-only clusters. Our results indicate a previously unidentified possible role for Mo in nitrogenase: to make the enzyme a good nitrogenase but a poor hydrogenase.

Received: September 2, 2002 [Z50090]

Keywords: cluster compounds · iron · kinetics · molybdenum · nitrogen fixation

[1] D. J. Evans, R. A. Henderson, B. E. Smith, *Bioinorganic Catalysis* (Eds.: E. Bouwmann, J. Reedijk), Marcel Dekker, New York, **1999**, chap. 7, and refrences therein.
[2] J. B. Howard, D. C. Rees, *Chem. Rev.* **1996**, *96*, 2965, and refrences therein.
[3] R. R. Eady, *Chem. Rev.* **1996**, *96*, 3013, and refrences therein.
[4] B. K. Burgess, D. J. Lowe, *Chem. Rev.* **1996**, *96*, 2983, and refrences therein.
[5] B. K. Burgess, *Chem. Rev.* **1990**, *90*, 377.
[6] R. A. Henderson, *Recent Advances in Hydride Chemistry* (Eds.: M. Peruzzini, R. Poli), Elsevier, Amsterdam, **2001**, chap. 16, and refrences therein.
[7] R. H. Holm, *Chem. Soc. Rev.* **1981**, *10*, 455, and refrences therein.
[8] R. A. Henderson, K. E. Oglieve, *J. Chem. Soc. Chem. Commun.* **1994**, 377.
[9] V. R. Almeida, C. A. Gormal, K. L. C. Grönberg, R. A. Henderson, K. E. Oglieve, B. E. Smith, *Inorg. Chim. Acta* **1999**, *291*, 212, and refrences therein.
[10] R. A. Henderson, K. E. Oglieve, *J. Chem. Soc. Dalton Trans.* **1998**, 1731.
[11] R. A. Henderson, K. E. Oglieve, *J. Chem. Soc. Dalton Trans.* **1999**, 3927.
[12] A. J. Dunford, R. A. Henderson, *Chem. Commun.* **2002**, 360.
[13] The calculation of the elementary rate constants for each cluster involves the use of the kinetics of the reaction between each cluster and the PhS^- ions in the absence of acid as described before.[11,12] In the absence of acid $k_{obs} = K_1^{PhS} k_2^{PhS}[PhS^-]/(1 + K_1^{PhS}[PhS^-])$.
[14] R. A. Henderson, K. E. Oglieve, *J. Chem. Soc. Dalton Trans.* **1993**, 1473.
[15] Studies with solutions containing $[D_2\overline{N(CH_2)_3CH_2}]^+$ ions show that the protonation reaction does not exhibit a discernable isotope effect. This observation is in line with other protonation reactions of Fe–S clusters.[16] However, studies in the temperature range 5–40 °C shows that these reactions are associated with small ΔH^+ values, which is consistent with proton transfer reactions,[17] and negative ΔS^+ values (Table 1), which is consistent with an ordered transition state involving the acid and cluster.
[16] A. J. Dunford, R. A. Henderson, *J. Chem. Soc. Dalton Trans.* **2002**, 2837.
[17] a) W. J. Albery, *Annu. Rev. Phys. Chem.* **1980**, *31*, 227; b) W. J. Albery, *Faraday Discuss. Chem. Soc.* **1982**, *74*, 245.
[18] A comparison of the rates of the reactions of the clusters with PhS^- (k^{PhS}) or Br^- ions (k^{Br}), in the absence of acid[14] shows that the Br^- ion is at least 50 times a weaker nucleophile than PhS^-: $[Fe_4S_4Cl_4]^{2-}$ $k^{PhS} = 1.9 \times 10^4$,[12] $k^{Br} = 5.1 \times 10^2\ dm^3\,mol^{-1}\,s^{-1}$;[16] $[\{MoFe_3S_4\}_2(\mu\text{-}SEt)_3]^{3-}$ $k^{PhS} = 6.6 \times 10^4$, $k^{Br} = 5.0$; $[\{MoFe_3S_4\}_2(\mu\text{-}SPh)_3]^{3-}$ $k^{PhS} = 6.7 \times 10^4$, $k^{Br} = 25\ dm^3\,mol^{-1}\,s^{-1}$.
[19] G. J. Leigh, *Acc. Chem. Res.* **1992**, *25*, 177, and refrences therein.
[20] By binding site we mean the atom that dinitrogen is attached to and all the coligands. Therefore, in the enzyme the binding site is the entire FeMo cofactor cluster.
[21] Studies on simple mononuclear complexes such as *trans*-$[Mo(N_2)_2(Ph_2PCH_2CH_2PPh_2)_2]$ have shown that protonation of the binding site deactivates dinitrogen.[1]
[22] Studies on the clusters reported herein were performed in MeCN. We have shown that analogous protonation chemistry operates in protic solvents (S. C. Davies, D. J. Evans, R. A. Henderson, D. L. Hughes, S. Longhurst, *J. Chem. Soc. Dalton Trans.* **2001**, 3470).
[23] K. L. C. Grönberg, C. A. Gormal, M. C. Durrant, B. E. Smith, R. A. Henderson, *J. Am. Chem. Soc.* **1998**, *120*, 10613, and refrences therein.

 © 2003 Wiley-VCH Verlag GmbH & Co. KGaA, Weinheim 1433-7851/03/4210-1152 $ 20.00+.50/0

Analysis of Catalytic Reactions

High-Throughput Catalytic Science: Parallel Analysis of Transients in Catalytic Reactions**

*Reed J. Hendershot, Paul T. Fanson, Christopher M. Snively, and Jochen A. Lauterbach**

In the field of heterogeneous catalysis, variations in temperature, pressure, or reactant concentration are commonly encountered under real operating conditions. Experiments to identify transients, such as the titration of adsorbed species, exchange of isotopically labeled reactants, and step changes in the reaction conditions are invaluable tools in understanding the synergy between the catalyst nanostructure and the kinetics of a catalytic reaction.[1] When deciding between competing kinetic models, often the key distinguishing feature is their ability to model transient as well as steady-state behavior. Furthermore, the analysis of oscillations in kinetics and spatio-temporal pattern formation on catalysts can greatly increase our understanding of dynamic processes and interactions on catalyst particles.[2]

[*] Prof. Dr. J. A. Lauterbach, R. J. Hendershot, Dr. P. T. Fanson, Dr. C. M. Snively
Department of Chemical Engineering, University of Delaware
Newark, DE 19716 (USA)
Fax: (+1) 302-831-1048
E-mail: lauterba@che.udel.edu

[**] We are grateful to the National Science Foundation (grant CTS-0071730) for the support of this research. We also thank Margaret Horton for preparing and characterizing the catalyst samples.

 © 2003 Wiley-VCH Verlag GmbH & Co. KGaA, Weinheim 1433-7851/03/4210-1152 $ 20.00+.50/0

Historically, catalysis studies have been performed by testing a single catalyst formulation at a time. However, catalysts are very complex systems with compositional heterogeneity on both the nano- and mesoscales. Using a single reactor to study hundreds or even thousands of catalyst formulations systematically in order to understand reaction behavior as a function of composition would entail a prohibitive amount of time. Combinatorial catalysis, or high-throughput screening, has created significant excitement in the past few years, opening new possibilities for catalyst discovery and optimization.[3] Several analytical approaches to high-throughput experimentation (HTE) have emerged for the rapid screening of catalyst activity. The true power of the combinatorial approach, however, can only be realized with the ability to perform quantitative studies in parallel. This methodology, in combination with microkinetic modeling of the quantitative data, can take our understanding of heterogeneously catalyzed reactions to a higher level, accelerate discovery of novel catalyst formulations, and ultimately lead to rational catalyst design.[4] Novel high-throughput approaches are therefore needed to study catalytic reactions quantitatively, in parallel, and under both transient and steady-state conditions. To answer this need, we have developed Fourier transform infrared (FTIR) imaging for the study of multiple catalytic reactors simultaneously with a time resolution below 2 s.[3i,j,5]

Table 1: The catalysts tested with Fourier transform infrared (FTIR) imaging.

Catalyst	Loading [wt%]			Preparation method
	Ba	Pt	Fe	
1	26.3	1.5	0	four-step sequential impregnation: Ba (3×) then Pt
2[a]	30	1.5	0	one-step wet impregnation
3	30	1.3	9	four-step coimpregnation
4[a]	15	0	10	three-step sequential impregnation: Ba (2×) then Fe
5	28	1.5	11	five-step sequential impregnation: Ba (3×), Fe then Pt
6	14.2	0	0	two-step impregnation
7[a]	5	1	3	one-step coimpregnation
8	0	1.7	0	one-step impregnation
9[a]	15	1.5	10	four-step sequential impregnation: Ba (2×), Fe then Pt
10[a]	30	1.5	0	one-step slurry impregnation
11	0	0	0	
12[a]	30	1.5	10	one-step slurry impregnation
13[a,b]	0	1.5	0	one-step impregnation
14[a]	30	1.5	10	one-step slurry impregnation
15	25.7	0	0	three-step impregnation
16	–	–	–	no catalyst

[a] Nominal weight loading. [b] Titania support was used instead of alumina.

To demonstrate the power of parallel transient studies, we present results on a library of NO_x storage and reduction (NSR) catalysts supported on γ-alumina (Table 1). As government and consumer demands for automotive fuel economy and emission controls become more stringent, new catalysts are needed for exhaust aftertreatment.[6] These emission regulations include controls on pollutants such as nitrogen oxides (NO_x), carbon monoxide (CO), hydrocarbons (HC), and carbon dioxide (CO_2). To increase fuel economy, automobile manufacturers are introducing lean-burn engines in which combustion occurs in an excess of air, as opposed to a stoichiometric mixture of fuel to air. Current three-way catalytic converters cannot reduce NO_x emissions to acceptable levels under these conditions. The NSR catalysts are designed to reduce NO_x from automotive exhaust in the presence of excess oxygen by cycling the automobile engine between a fuel-lean phase (FLP), in which NO_x is stored on the catalyst surface, and a fuel-rich phase (FRP), in which the NO_x is released and reduced to N_2.[7] The complexity of the formulation of these catalysts—which typically contain noble metals (for oxidation and reduction), alkaline earth metals (for NO_x storage), and transition metals or other additives (for improved sulfur tolerance)[8]—clearly displays the necessity of a combinatorial approach for the successful discovery of optimum formulations. Since these catalysts are designed to operate under transient conditions, a HTE system that can monitor effluent compositions rapidly and in parallel is essential for a systematic study of NSR catalysts.

The transient responses of a library of NSR catalysts were monitored during step changes between the FRP and the FLP at six different temperatures.[9] During the transition, spectral images were collected every three seconds of the effluents from 16 reactors simultaneously. Figure 1 presents representative IR spectra of the effluent stream from one of the 16 reactors during a portion of the switch from the FRP to the FLP. The concentrations of NO, NO_2, NO_x, and N_2O calculated from the IR spectra during this switch are shown in Figure 2.

A key characteristic of NSR catalysts is their ability to store NO_x during the FLP. A steady concentration of NO_x after switching from the FRP to the FLP signifies that the

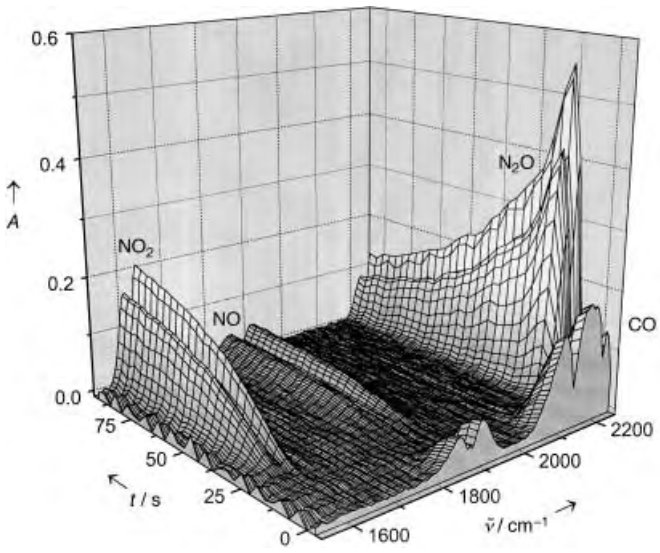

Figure 1. Transient IR spectra after the switch from the FRP to the FLP at 300°C for catalyst 1. During the FRP the CO and NO are not fully oxidized or reduced at this temperature. When the reaction conditions were switched to the FLP at $t = 0$ s, the CO was completely oxidized to CO_2, the N_2O band grows and decays, and later ($t \approx 25$ s) the NO_2 and NO bands appear. A = absorption.

 © 2003 Wiley-VCH Verlag GmbH & Co. KGaA, Weinheim 1433-7851/03/4210-1153 $ 20.00+.50/0

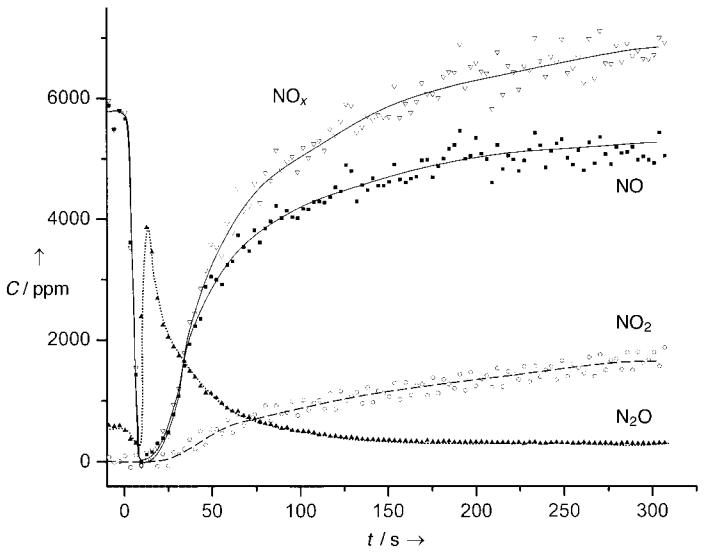

Figure 2. Concentration C for NO, NO_2, NO_x, and N_2O for the same catalyst and conditions as in Figure 1.

NO_x storage sites on a catalyst are saturated. Figure 3 is a plot of the NO_x concentration for five selected catalysts as a function of moles of NO_x introduced into each reactor. The difference in the number of moles of NO_x necessary to observe saturation is a consequence of differing NO_x storage capacities. The storage capacity of all 16 reactors under these conditions as a function of temperature are given in Table 2.

The results corroborate previously published data for storage capacities determined in single reactors and show the maximum in NO_x storage capacity between 350 and 400 °C.[10] The differences in the reported NO_x storage capacities can be attributed to different operating conditions and catalyst amount, type, and preparation. Our findings are also consistent with other results indicating that increasing the amount of alkaline earth metal increases the NO_x storage capacity (compare catalysts 5 and 9).[10b] In addition, these results indicate that the catalyst preparation technique affects the performance of the catalysts (compare catalysts 1 and 2 and catalysts 3 and 5).

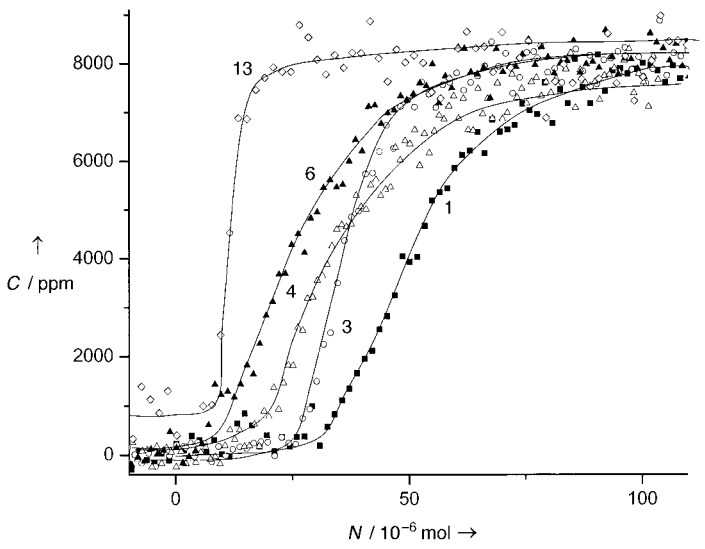

Figure 3. Concentration C of NO_x for catalysts 1, 3, 4, 6, and 13 as a function of moles N of NO_x passed through the catalyst at 400 °C during the switch from the FRP to the FLP.

Table 2: Amount of NO_x stored during the FLP until saturation.

Catalyst[a]	Amount of NO_x stored [$\times 10^{-6}$ mol]					
	250 °C	300 °C	350 °C	400 °C	450 °C	500 °C
1	8	29	48	47	44	38
2	9	25	38	41	39	24
3	4	28	38	37	29	17
4	20	19	24	33	29	24
5	25	15	13	30	41	34
6	5	15	24	27	20	17
7	1	8	20	26	27	25
8	1	22	24	25	22	16
9	3	14	21	25	19	16
10	7	15	20	22	22	20
11	23	28	28	22	12	12
12	0	10	12	13	10	9
13	9	7	10	8	4	6
14	6	1	1	3	4	10
15	12	16	0	1	6	18
16	2	1	2	1	0	1

[a] See Table 1.

Our technique is not only capable of comparing catalysts, but also provides insight into the elementary reaction steps. For example, the rate at which the NO_x concentration increases varies (Figure 3), thus indicating differences in the kinetics of the underlying elementary reactions. Likewise, the concentration of NO increases before NO_2 (Figure 2), which indicates the oxidation of surface nitrite species to surface nitrate as the stored NO_x first exists on the BaO surface as nitrite. Nitrogen dioxide is able to adsorb onto the surface and oxidize nitrite to nitrate, resulting in the release of NO to the gas phase.[10a,11] As the BaO surface becomes saturated with nitrate, NO_2 begins to appear in the gas phase. At complete saturation, the concentrations of NO and NO_2 reach a steady-state value determined by the rate of NO oxidation over the catalyst.

By comparing transient responses, we also noticed a maximum in the N_2O concentration before saturation of the NO_x storage sites for some of the catalysts. This effect is most prominent at temperatures below 400 °C. This magnitude in the N_2O concentration has not been previously reported, even in single-reactor experiments.[10,12] The difference can be attributed to several factors, including enhanced time resolution and chemical sensitivity of our analytical technique and slight differences in reaction conditions or catalyst preparation methods between the two studies. In a previous investigation, the time resolution of approximately 40 s between data points was not fine enough to resolve the brief N_2O maxima clearly observed in our experiments.[12] In another study by mass spectrometry, a similar response was reported for an unspecified mass to charge ratio (m/e) assigned to be CO_2 by the authors.[11b] It is unclear what m/e was used, but the species could be N_2O since the resolution of the mass spectrometers employed in these studies is most likely

 © 2003 Wiley-VCH Verlag GmbH & Co. KGaA, Weinheim 1433-7851/03/4210-1154 $ 20.00+.50/0

sufficiently low such that both N_2O and CO_2 would appear at an *m*/*e* of 44.

This work provides the first example of an analytical approach capable of truly parallel, quantitative analysis with a temporal resolution applicable to transient experiments. FTIR imaging is a flexible technique capable of studying a large number of catalytic reactions and unambiguously identifying various components. The speed of data acquisition and the quantitative capability of this new technique marks the dawn of a new field of scientific endeavor: high-throughput catalytic science. We now have the ability to study rapidly many formulations of catalytic materials at a level that allows successful kinetic modeling. This enables us to rise above simple screening to the level of fundamental understanding of reaction mechanisms, which will lead us to rational catalyst design.

Experimental Section

The catalysts were tested simultaneously in a 16-channel vertical microreactor developed in-house.[13] The effluents from the 16 channels were analyzed simultaneously using an FTIR imaging system slightly modified from the one described in references [3i] and [5]. The optical setup consists of a Bruker Equinox 55 FTIR spectrometer, barium fluoride optics, a long pass optical filter (3750 nm), and a 64×64 mercury cadmium telluride focal plane array detector (Santa Barbara Focalplane) collecting at a frame rate of 315 Hz. Data processing is automated by software written in-house and run on a standard Pentium 4 2.4 GHz desktop computer. The raw data files, consisting of 4096 interferograms for each spectral image, serve as input to our program and a series of data-processing steps (Fourier Transform, absorbance calculation, baseline correction, peak integration, and conversion to concentration from previously performed calibrations) are then performed in a batch mode. The program produces a text file consisting of concentrations as a function of time combined from the different data spectral images. For example, a data set consisting of 672 MB and 140 spectral images (or 573 440 interferograms and a collection time of about 7 min) can be processed and the concentration evolution for five different species for all 16 reactors written to a 285 kB text file in less than 10 min. The entire process is automated and requires less than 20 s of input from the user before starting the analysis. A graph can be generated from the data with Microsoft Excel by using a macro written with Microsoft Visual Basic for Applications.

Each channel in the microreactor holds 150 mg of catalyst. The catalysts were pretreated before testing with two successive cycles of 15 min of 17 % O_2 in He followed by 15 min of 9 % H_2 in He at 773 K. The catalysts were then exposed to five cycles of switching between the FLP followed by the FRP at 250 °C to age the catalysts before testing. At subsequent temperatures, two cycles of switching between the FLP followed by the FRP were completed before testing.

Received: September 12, 2002 [Z50145]

Keywords: combinatorial chemistry · heterogeneous catalysis · IR spectroscopy · nitrogen oxides · transient analysis

[1] a) C. O. Bennett in *Advances in Catalysis, Vol. 44* (Eds.: W. O. Haag, B. Gates, H. Knözinger), Elsevier Sciences, Dordrecht, **2000**, p. 329; b) C. Mirodatos, *Catal. Today* **1991**, *9*, 83.

[2] a) G. Ertl, *Appl. Surf. Sci.* **1997**, *121*, 20; b) C. Sachs, M. Hildebrand, S. Volkening, J. Wintterlin, G. Ertl, *Science* **2001**, *293*, 1635; c) P. T. Fanson, W. N. Delgass, J. Lauterbach, *J. Catal.* **2001**, *204*, 35.

[3] a) S. Senkan, *Angew. Chem.* **2001**, *113*, 322; *Angew. Chem. Int. Ed.* **2001**, *40*, 312; b) W. F. Maier, G. Kirsten, M. Orschel, P. A. Weiss, *Chim. Oggi* **2000**, *18*, 15; c) W. F. Maier, *Angew. Chem.* **1999**, *111*, 1294; *Angew. Chem. Int. Ed.* **1999**, *38*, 1216; d) P. Cong, R. Doolen, Q. Fan, D. M. Giaquinta, S. Guan, E. W. McFarland, D. M. Poojary, K. Self, H. W. Turner, W. H. Weinberg, *Angew. Chem.* **1999**, *111*, 507; *Angew. Chem. Int. Ed.* **1999**, *38*, 483; e) B. Jandeleit, H. W. Turner, T. Uno, J. A. M. van Beek, W. H. Weinberg, *CATTECH* **1998**, *2*, 101; f) B. Jandeleit, D. J. Schaefer, T. S. Powers, H. W. Turner, W. H. Weinberg, *Angew. Chem.* **1999**, *111*, 2648; *Angew. Chem. Int. Ed.* **1999**, *38*, 2494; g) W. H. Weinberg, E. W. McFarland, *Trends Biotechnol.* **1999**, *17*, 107; h) A. Hagemeyer, B. Jandeleit, Y. M. Liu, D. M. Poojary, H. W. Turner, A. F. Volpe, W. H. Weinberg, *Appl. Catal. A* **2001**, *221*, 23; i) C. M. Snively, G. Oskarsdottir, J. Lauterbach, *Catal. Today* **2001**, *67*, 357; j) C. M. Snively, G. Oskarsdottir, J. Lauterbach, *Angew. Chem.* **2001**, *113*, 3117; *Angew. Chem. Int. Ed.* **2001**, *40*, 3028; k) J. M. Newsam, F. Schuth, *Biotechnol. Bioeng.* **1999**, *61*, 203.

[4] J. M. Caruthers, J. A. Lauterbach, K. T. Thomson, V. Venkatasubramanian, C. M. Snively, A. Bhan, S. Katare, G. Oskarsdottir, *J. Catal.* **2003**, in press.

[5] C. M. Snively, J. Lauterbach, *Spectroscopy* **2002**, *17*, 26.

[6] C. T. Goralski, W. F. Schneider, *Appl. Catal. B* **2002**, *37*, 263.

[7] N. Takahashi, H. Shinjoh, T. IIjima, T. Suzuki, K. Yamazaki, K. Yokota, H. Suzuki, N. Miyoshi, S.-i. Matsumoto, T. Tanizawa, T. Tanaka, S.-s. Tateishi, K. Kasahara, *Catal. Today* **1996**, *27*, 63.

[8] K. Yamazaki, T. Suzuki, N. Takahashi, K. Yokota, M. Suguira, *Appl. Catal. B* **2001**, *30*, 459.

[9] The FLP consisted of 8.0 % O_2, 4.0 % CO, 0.87 % NO in He while the FRP consisted of 4.0 % CO, 0.87 % NO in He.

[10] a) E. Fridell, M. Skoglundh, B. Westerberg, S. Johansson, G. Smedler, *J. Catal.* **1999**, *183*, 196; b) H. Mahzoul, J. F. Brilhac, P. Gilot, *Appl. Catal. B* **1999**, *20*, 47.

[11] a) S. Erkfeldt, E. Jobson, M. Larsson, *Top. Catal.* **2001**, *16*/17, 127; b) I. Nova, L. Castoldi, L. Lietti, E. Tronconi, P. Forzatti, *Catal. Today* **2002**, *75*, 431.

[12] E. Fridell, H. Persson, L. Olsson, B. Westerberg, A. Ambderntsson, M. Skoglundh, *Top. Catal.* **2001**, *16*/17, 133.

[13] R. J. Hendershot, S. S. Lasko, M. F. Fellmann, G. Oskarsdottir, W. N. Delgass, C. M. Snively, J. Lauterbach, *Appl. Catal. A* **2003**, in press.

 © 2003 Wiley-VCH Verlag GmbH & Co. KGaA, Weinheim 1433-7851/03/4210-1155 $ 20.00+.50/0

Zeolite Structure

A Zeolite Structure (ITQ-13) with Three Sets of Medium-Pore Crossing Channels Formed by 9- and 10-Rings**

Avelino Corma, Marta Puche, Fernando Rey, Gopinathan Sankar, and Simon J. Teat*

ZSM-5 (MFI code)[1] is a medium-pore zeolite that has 10-ring channels with pore diameters of 5.1×5.5 and 5.3×5.6 Å, and has been a very successful zeolite for shape-selective catalysis[2–4] that has found many industrial applications.

By considering the structure of ZSM-5 and the catalytic results obtained in the fields of oil refining and petrochemistry,[2–4] one could intuitively predict that a medium-pore zeolite with intersecting channels and pore dimensions that are slightly smaller than those of ZSM-5 should enhance the possibilities for shape-selective catalysis in the fields of fluid catalytic cracking (FCC) additives, catalytic dewaxing, toluene disproportionation, alkylation of aromatics, isomerization of alkylaromatics, and so forth.

Herein, we will describe such a zeolite structure (ITQ-13), which exhibits three sets of intercrossed medium-pore channels; a 9-ring channel, with a pore aperture of 4.0×4.9 Å, runs parallel to the crystallographic *a* axis, a 10-ring channel system (4.8×5.7 Å) runs parallel to the *c* axis, and another 10-ring set of channels (4.7×5.1 Å) runs parallel to the *b* axis.

Although it was not possible to determine the structure from powder diffraction alone, a preliminary powder diffraction study revealed the unit cell to be orthorhombic, with cell parameters of $a = 12.5$, $b = 11.3$ and $c = 21.9$ Å, which indicated that ITQ-13 is a unique microporous zeolitic material. With the advent of microdiffraction, we are now able to collect good-quality single-crystal data using a crystal with dimensions of $40 \times 30 \times 20$ μm, to successfully solve the structure by direct methods. The Amm2 space group was confirmed by comparing the simulated powder X-ray diffraction (XRD) pattern using the single-crystal data, and the high-resolution XRD pattern recorded from the same powdered sample. Both analyses suggest a single-phase material with a unique structure. By using the coordinates of the tetrahedral cations (T-atoms), we calculated the coordination sequence and the vertex indexes (see Supporting Information),[5] which prove without doubt that the structure of ITQ-13 corresponds to a new zeolite topology.

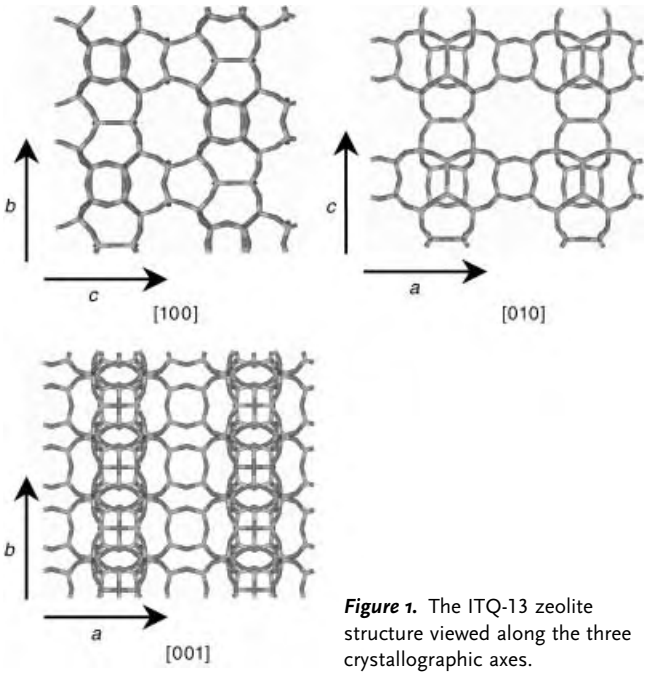

Figure 1. The ITQ-13 zeolite structure viewed along the three crystallographic axes.

The framework structure of the ITQ-13 zeolite along the three crystallographic axes is presented in Figure 1, and provides an illustration of the pore channels. The most striking feature is the three-dimensional connectivity of this medium-pore system, with three channels running parallel to the *a, b*, and *c* crystallographic axes. One set of channels consists of an unusual 9-ring pore, which runs parallel to the *a* axis and has dimensions of approximately 4.0×4.9 Å (assuming that the van der Waals diameter of the oxygen atom is 2.7 Å); these dimensions are similar to those of some 10-ring-pore zeolites. The other sets of channels run parallel to the *b* and *c* axes, and have pore apertures of approximately 4.8×5.1 and 4.8×5.7 Å, respectively. They consist of 10-ring systems that are similar to those seen in ZSM-5-type materials. The 9- and 10-ring channels are intercrossed

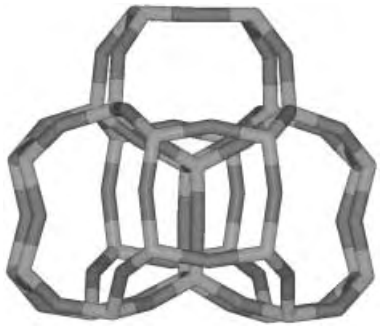

Figure 2. Characteristic building block of the ITQ-13 structure.

[*] Prof. A. Corma, M. Puche, Dr. F. Rey
Instituto de Tecnología Química (UPV-CSIC)
Universidad Politécnica de Valencia
Avenida Los Naranjos s/n, 46022 Valencia (Spain)
Fax: (+34) 96-3877809
E-mail: acorma@itq.upv.es
Dr. G. Sankar
Davy-Faraday Research Laboratory
The Royal Institution of Great Britain
21 Albemarle Street, London W1X 4BS (UK)
Dr. S. J. Teat
CLRL, Daresbury Laboratory
Daresbury, Warrington, Cheshire, WA4 4AD (UK)

[**] We thank Spanish CICYT (projects MAT 2000–1392 and MAT 2000-1167-C02-01) for financial support. A.C., M.P., and F.R acknowledge EXXON-Mobil for valuable support. G.S. and S.J.T thank the EPSRC for financial support. Also, the CRLC Daresbury Laboratory is gratefully acknowledged for their beam-time allocation.

Supporting information for this article is available on the WWW under http://www.angewandte.org or from the author.

 © 2003 Wiley-VCH Verlag GmbH & Co. KGaA, Weinheim 1433-7851/03/4210-1156 $ 20.00+.50/0

throughout the material; this is the only zeolite reported to date that possesses 9- and 10-ring channels.

The unique aspects of the structure may be described more conveniently by considering the tertiary building block shown in Figure 2. It is interesting to note this subunit is related to the characteristic tertiary building block of the ITQ-21 zeolite,[6] which consists of a [$4^6 6^{12}$] cage with a 4-ring in its interior. In ITQ-13, however, one of the external 4-rings is absent, as illustrated in Figure 3.

The ITQ-13 subunits stack in the *a* direction through the connection of adjacent 4-rings of neighboring tertiary building blocks. The linkage yields a double 4-ring (D4R), which also appear in ITQ-21. The two neighboring tertiary building blocks in ITQ-13 also share a common 4-ring in the *b* direction. The presence of these fused 4-rings effectively results in a reduction in the pore opening from the 12-ring in ITQ-21 to a 9-ring in ITQ-13, and also decreases the symmetry within the *bc* plane. The topological analogies between zeolites ITQ-13 and ITQ-21 are more clearly shown in Figure 4.

The stacking sequence of the layers in the ITQ-13 structure, viewed along the *c* axis, is depicted in Figure 5. The framework is formed by an ABAB stacking sequence, which occurs through shifting the second layer by $\pm b/2$, with respect to its neighboring layer. This particular connectivity gives rise to 9-ring channels that intersect the 10-ring pores aligned parallel to the *a* and *b* axes. In addition, the $\pm b/2$ shift of the second layer produces the observed sinuosity of the channel running along the *c* axis. The staggered arrangements of D4Rs blocks the otherwise uninterrupted 10-ring channels parallel to the *c* axis. As a result, cylindrical cavities are formed with an approximate length and width of 15.5 and 5.3 Å, respectively. It is in these cavities where the hexamethonium structure-directing agent (SDA) is located, as illustrated in Figure 6. The long axes of the hexamethonium ions lie parallel to the *c* axis, but in a zigzag fashion that forms the sinusoidal 10-ring channels located along that crystallographic axis. Meanwhile, interactions between the charged alkyltrimethylammonium groups open the perpendicular 10-ring channel along the *b* axis.

Fluoride ions were located in two different crystallographic positions. One set are located in the center of the small D4R cages (two D4Rs per unit cell). However, since the two occluded hexamethonium dications give four positive charges per unit cell, only half of this charge is compensated by the fluoride ions in the D4R cages. The remaining fluoride

Table 1: Chemical composition of ITQ-13.

	Content [wt%]		X/N ratio	
	Experimental	Calculated[a]	Experimental	Calculated[a]
C	7.9	7.3	5.8	6.0
N	1.6	1.4	1.0	1.0
H	1.7	1.9	15.2	15.0
F	2.1	1.9	1.0	1.0
SiO_2	83.5[b]	85.9	12.2	14

[a] Values calculated for the following unit cell composition $[\{SiO_2\}_{56}\{[(CH_3)_3N(CH_2)_6N(CH_3)_3]^{2+}[F^-]_2\}_2]\cdot 4H_2O$. [b] Determined from thermogravimetic analysis.

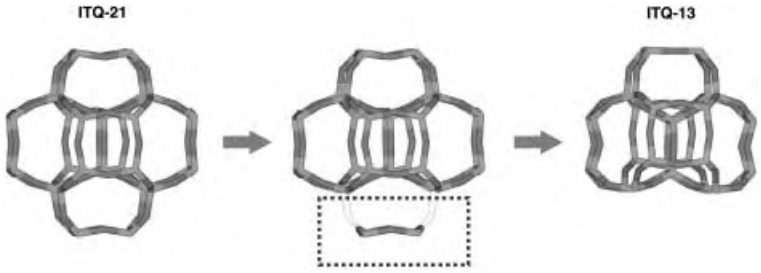

Figure 3. Relationship between the characteristic building blocks of the ITQ-13 and ITQ-21 zeolites.

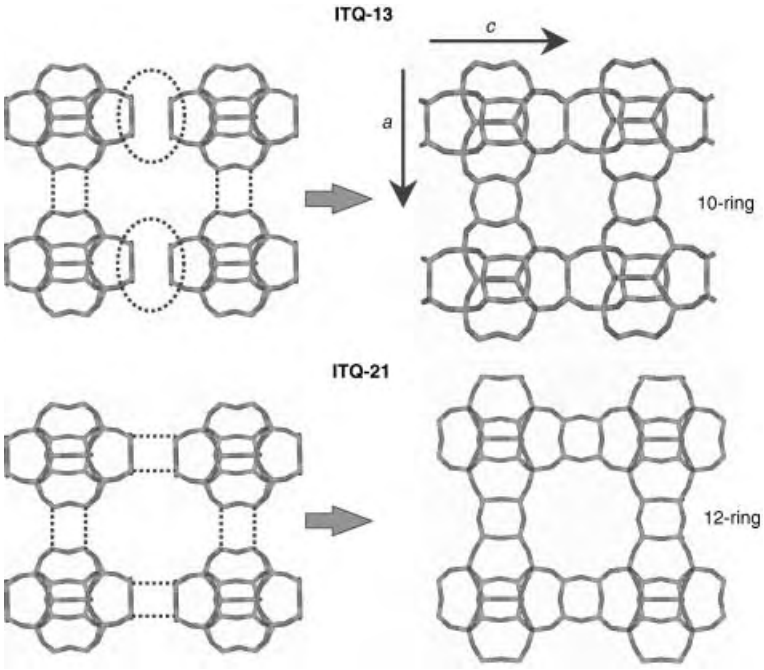

Figure 4. The building-block packing in the ITQ-13 structure normal to the *c* axis, compared to that of ITQ-21.

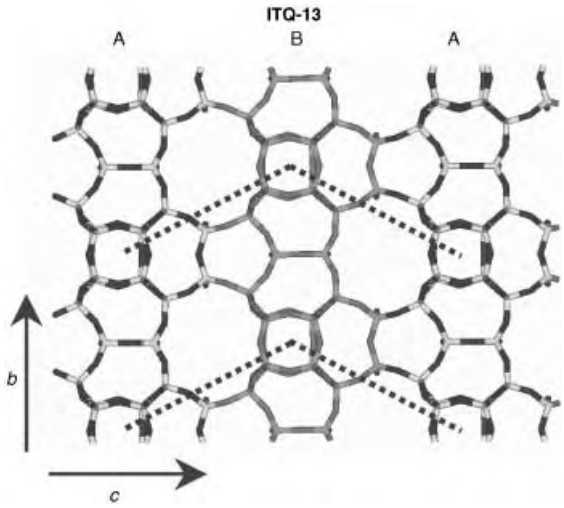

Figure 5. Stacking sequence of the characteristic layers of ITQ-13 along the *c* axis.

 © 2003 Wiley-VCH Verlag GmbH & Co. KGaA, Weinheim 1433-7851/03/4210-1157 $ 20.00+.50/0

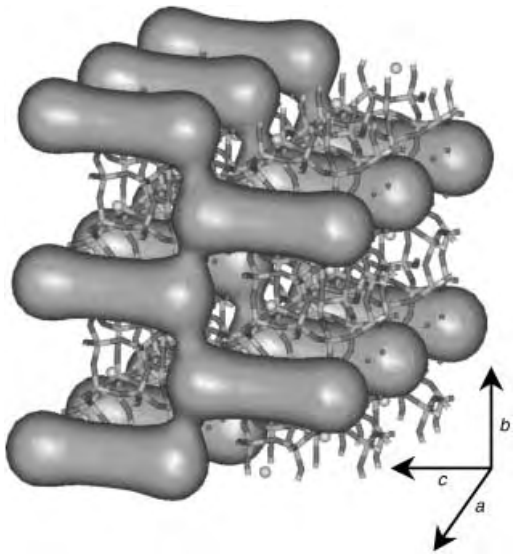

Figure 6. Idealised view of the location of the occluded hexamethonium cations that fill the pores of the ITQ-13 zeolite.

ions are located inside the $[4^15^26^2]$ cages; the smallest remaining cages within the ITQ-13 structure. The fluoride ions positioned at the center of the D4R cages are responsible for the observed ^{19}F MAS NMR signal at $\delta = -38$ ppm,[7] while the other resonance at $\delta = -66$ ppm can be attributed to those within the small $[4^15^26^2]$ cages,[8] with approximately the expected intensity ratio observed between the two signals.

The extra fluoride ions compensate for the charge of the organic dications located between the D4R units, and yields a final unit-cell composition of $[\{SiO_2\}_{56}\{[(CH_3)_3N(CH_2)_6N(CH_3)_3]^{2+}[F^-]_2\}_2]\cdot 4H_2O$, which is in good agreement with the experimental chemical analysis reported in Table 1.

We have previously reported other zeolites that contain D4R units as secondary building blocks.[6,9,10] The presence of D4R cages in the structure of ITQ-13 suggested that adding Ge to the synthesis gel should facilitate the formation of such D4R cages by aiding the nucleation process and, therefore, accelerating the crystallization rate of the zeolite. This phenomenon has been observed for ITQ-13; the synthesis time decreases when Ge was introduced to the synthesis gel. It should be noted, however, that for synthesis gels having a Si/Ge ratio lower than 5, ITQ-17, with the BEC structure,[10,11] starts to compete.

More importantly, we have succeeded in incorporating trivalent cations (B and Al) at framework positions. The ^{27}Al MAS NMR spectrum of an Al-containing ITQ-13 zeolite indicates the presence of tetrahedrally coordinated Al ions, which produce a resonance at $\delta = -52$ ppm. The IR spectrum of a calcined Al-ITQ-13 sample shows bands at 3614 and 3573 cm^{-1} that indicate the presence of hydroxyl groups; these bands disappear upon the adsorption of pyridine. Another distinct band at 1545 cm^{-1}, which results from protonated pyridine, indicates the presence of acid sites in this material.

In conclusion, the structure of ITQ-13 has been determined. The pore topology of this zeolite is unique, with a 9-ring channel system along the *a* axis, and 10-ring channel systems parallel to the *b* and *c* axes. Acid sites can be introduced into the structure, which opens the possibility for use in acid catalysis. Additionally, X-ray microdiffraction techniques have been used to solve the structure of ITQ-13 materials, and precisely locate the organic SDA and the corresponding fluoride ions.

Experimental Section

Synthesis: The synthesis protocol reported in example 1 of reference [13] was modified to maximize the average crystal size of ITQ-13, so that crystals large enough for single-crystal X-ray diffraction techniques were available.

The synthesis gel was prepared by hydrolyzing tetraethyl orthosilicate (31.20 g, 150 mmol) in an ethanolic solution (0.527 M) of hexamethonium dihydroxide ($HM(OH)_2$, 79.63 g, 42 mmol) with continuous stirring until all the ethanol had completely evaporated. Then, a 49 wt % aqueous solution of HF (3.495 g, 84 mmol) was introduced and water was added to give a water/silica ratio of 7. The final gel composition had the following molar composition:

$$SiO_2 : 0.28\,HM(OH)_2 : 0.56\,HF : 7\,H_2O.$$

Finally, the gel was autoclaved at 135 °C for 24 days. The solid was recovered by filtration, washed repeatedly with distilled water and acetone, then dried overnight at 80 °C. The occluded organic species were isolated by calcination in air at 550 °C.

The chemical composition of the as-prepared ITQ-13 zeolite is given in Table 1; the occluded organic cation remains intact after hydrothermal treatment and fully compensates the charge of the fluoride ions.

Synthesis of the Al-containing ITQ-13 was achieved by exchange of the boron ions[12] in B-ITQ-13, which was prepared by introducing the appropriate amount of boric acid to reach the following molar composition of the gel:

$$SiO_2 : 0.01\,B_2O_3 : 0.29\,R(OH)_2 : 0.64\,HF : 7\,H_2O$$

4 wt % SiO_2 was added to purely siliceous ITQ-13 as seeds for the acceleration of crystallization. The resulting gel was autoclaved at 135 °C for 24 days, and the as-prepared B-ITQ-13 was recovered by filtration, repeatedly washed with distilled water, and dried at 80 °C for 12 h.

As-prepared B-ITQ-13 was calcined at 550 °C for 6 h in air. The sample was then treated with an aqueous solution of aluminum nitrate (8 wt %) at 140 °C for 72 h under hydrothermal conditions, and Al-ITQ-13 was recovered by filtration, repeatedly washed with distilled water, and dried at 80 °C for 12 h.

X-ray diffraction: Powder diffraction data were collected on an X'Pert diffractometer with Bragg–Brentano geometry provided with a secondary graphite monochromator. Intensity data were obtained with a variable-divergence slit using $Cu_{K\alpha 1,2}$ radiation ($\lambda = 1.5406$, 1.5444 Å). The tube settings were 45 kV and 40 mA and the step scan size and time were 0.02° and 10 s, respectively.

Microcrystal X-ray diffraction data were obtained at Station 9.8 of the CLRC Daresbury Laboratory Synchrotron Radiation Source equipped with a Bruker AXS diffractometer with a CCD detector. X-ray radiation was selected at $\lambda = 0.6942$ Å by using a Si(111) monochromator and vertically focused by a cylindrically bent Pd-coated zerodur mirror. The single-crystal data were collected at low temperature ($T = 150$ K). The structure was solved and refined on F^2 using published programs and techniques[14] to converge at R1 = 0.0800 (for reflections with $I > 2\sigma(I)$), $wR2 = 0.2081$, and $S = 1.014$ for 280 parameters. Maximum residual electron density = 2.87 e $Å^{-3}$. The template molecule was modeled isotropically with geometrical and displacement parameter restraints; hydrogen atoms were placed in calculated positions and refined using a riding model. The framework atoms were modeled anisotropically with displacement

 © 2003 Wiley-VCH Verlag GmbH & Co. KGaA, Weinheim 1433-7851/03/4210-1158 $ 20.00+.50/0

parameter restraints. The Si7–F2 bond length was constrained to be that obtained from NMR data.[15]

CCDC-196854 contains the supplementary crystallographic data for this paper. These data can be obtained free of charge via www.ccdc.cam.ac.uk/conts/retrieving.html (or from the Cambridge Crystallographic Data Centre, 12 Union Road, Cambridge CB2 1EZ, UK; fax: (+44) 1223-336-033; or deposit@ccdc.cam.ac.uk).

Solid-state NMR: Spectra were recorded using magic-angle spinning (MAS) techniques at room temperature. ^{19}F spectra were measured in a Bruker Av-400 spectrometer at 376.8 MHz in 2.5 mm diameter zirconia rotors at a spinning rate of 30 kHz. The spectra were collected using 3 μs pulses, which correspond to a magnetization flip angle of $\pi/2$ rad and a recycle delay of 100 s, to ensure the complete recovery of the magnetization; the spectra were referenced to $CFCl_3$. Solid-state ^{27}Al MAS NMR spectra were recorded on a Varian Unity VXR-400 WB spectrometer at 104.2 MHz, with a $\pi/18$ rad pulse length, a recycle delay of 0.5 s, and spinning rate of 7 kHz.

Received: November 11, 2002 [Z50514]

Keywords: heterogeneous catalysis · microporous materials · structure elucidation · X-ray diffraction · zeolites

[1] C. Baerlocher, W. M. Meier, D. H. Olson, *Atlas of zeolite framework types*, 5th rev. ed., Elsevier, Amsterdam, **2001**. Also in http://www.iza-structure.org/.
[2] A. Corma, *Chem. Rev.* **1995**, *95*, 559.
[3] a) P. B. Venuto, *Microporous Mater.* **1994**, *2*, 297; b) P. B. Venuto, *Stud. Surf. Sci. Catal.* **1997**, *105*, 811.
[4] N. Y. Chen, W. E. Garwood, F. G. Dwyer, *Shape Selective Catalysts in Industrial Applications*, 2nd rev. ed., Marcel Dekker, New York, **1996**.
[5] G. Sastre, J. D. Gale, *Microporous Mesoporous Mater.* **2001**, *43*, 27.
[6] A. Corma, M. J. Díaz-Cabañas, J. Martínez-Triguero, F. Rey, J. Rius, *Nature* **2002**, *418*, 514.
[7] a) P. Caullet, J. L. Guth, J. Hazm, J. M. Lamblin, *Eur. J. Solid State Inorg. Chem.* **1991**, *28*, 359; b) J. L. Guth, H. Kessler, P. Caullet, J. Hazm, A. Merrouche, J. Patarin in *Proc. 9th Inter. Zeolite Conf., Vol. I* (Eds.: R. Von Ballmoos, J. B. Higgins, M. M. J. Treacy) Butterworth-Heinemann, London, **1993**, p. 215.
[8] C. A. Fyfe, D. H. Brouwer, A. R. Lewis, J. M. Chézeau, *J. Am. Chem. Soc.* **2001**, *123*, 6882.
[9] a) A. Corma, M. J. Díaz-Cabañas, V. Fornés, *Angew. Chem.* **2000**, *112*, 2436; *Angew. Chem. Int. Ed.* **2000**, *39*, 2346; b) T. Blasco, A. Corma, M. J. Diaz-Cabañas, F. Rey, J. A. Vidal-Moya, C. M. Zicovich-Wilson, *J. Phys. Chem. B* **2002**, *106*, 2637.
[10] a) A. Corma, M. T. Navarro, F. Rey, J. Rius, S. Valencia, *Angew. Chem.* **2001**, *113*, 2337; *Angew. Chem. Int. Ed.* **2001**, *40*, 2277; b) A. Corma, M. T. Navarro, F. Rey, S. Valencia, *Chem. Commun.* **2001**, 1486.
[11] a) C. Baerlocher, W. M. Meier, D. H. Olson, *Atlas of zeolite framework types*, 5th rev. ed., Elsevier, Amsterdam, **2001**). Also in http://www.iza-structure.org/. b) T. Conradsson, M. S. Dadachov, X. D. Zou, *Microporous Mesoporous Mater.* **2000**, *41*, 183.
[12] T. Boix, M. Pucha, M. A. Camblor, A. Corma, U.S. Pat. 6,471,941 B1 **2000**.
[13] C. Y. Chen, S. I. Zones, *Stud. Surf. Sci. Catal.* **2001**, *135*, 1710.
[14] a) G. M. Shelrick, SHELXS and SHELXL programs. University of Göttingen, Germany, **1997**; b) W. Clegg, M. R. J. Elsegood, S. J. Teat, C. Redshaw, V. C. Gibson, *J. Chem. Soc. Dalton Trans.* **1998**, 3037.
[15] I. Bull, L. A. Villaescusa, S. J. Teat, M. A. Camblor, P. A. Wright, P. Lightfoot, R. E. Morris, *J. Am. Chem. Soc.* **2000**, *122*, 7128.

 © 2003 Wiley-VCH Verlag GmbH & Co. KGaA, Weinheim 1433-7851/03/4210-1159 $ 20.00+.50/0

Corrigenda

In the Communication "A Zeolite Structure (ITQ-13) with Three Sets of Medium-Pore Crossing Channels Formed by 9- and 10-Rings" by **A. Corma et al.** in *Angew. Chem.* **2003**, *115*, 1188–1191; *Angew. Chem. Int. Ed.* **2003**, *42*, 1156–1159, it should have been made clear early on in the manuscript that the synthesis of the ITQ-13 material was first reported in a patent published in 2002 (T. Boix, M. Puche, M. A. Camblor, A. Corma, US Patent 6 471 941 B1, **2002**; reference [12] in the manuscript). Furthermore, owing to an editorial error the reference to this patent was wrongly introduced into the *Experimental Section*, where reference [13] should read reference [12] and vice versa.

We apologize to our readers and to the authors of the above mentioned patent if this mistake has resulted in any misunderstanding.

Avelino Corma
Corresponding Author

Peter Gölitz
Editor

In the Communication by **S. Shimada, M. Tanaka et al.** published in *Angew. Chem. Int. Ed.* **2003**, *42*, 1845–1848, the incorrect formula was printed on p. 1845. The correct formula is that shown below. Furthermore, the e-mail address for Professor Tanaka should be m.tanaka@res.titech.ac.jp.

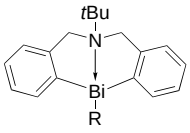

3a – 3g

3a: R = Ph
3b: R = 3,5-$(CF_3)_2C_6H_3$-
3c: R = 3,4-$(CH_2O_2)C_6H_3$-
3d: R = 2,4,6-$(MeO)_3C_6H_2$-
3e: R = CH_2=C(Me)-
3f: R = Br
3g: R = Cl

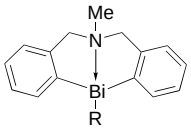

4

 © 2003 Wiley-VCH Verlag GmbH & Co. KGaA, Weinheim

Organic Field-Effect Transistors

Oligo(2,6-anthrylene)s: Acene–Oligomer Approach for Organic Field-Effect Transistors**

Kaname Ito, Toshiyasu Suzuki, Youichi Sakamoto, Daisuke Kubota, Youji Inoue, Fumio Sato, and Shizuo Tokito*

Anthracene has been widely studied as an organic photoconductor during the past five decades.[1] Hole mobilities in anthracene single crystals were measured by the time-of-flight photocurrent technique and were found to reach up to 3 $cm^2 V^{-1} s^{-1}$ at 300 K.[2] Although anthracene may be a good candidate for a p-type semiconductor for organic field-effect transistors (OFETs),[3] FET activity has not yet been observed. Recently, OFETs with tetracene were realized and showed a hole mobility of 0.01 $cm^2 V^{-1} s^{-1}$ on SiO_2/Si.[4] Of all the OFET materials reported so far, the highest field-effect mobility has been recorded in pentacene (0.3–0.7 $cm^2 V^{-1} s^{-1}$ on SiO_2/Si and 1.5 $cm^2 V^{-1} s^{-1}$ on chemically modified SiO_2/Si).[5] The HOMO energy level in linear [*n*]acenes ($n = 2$: naphthalene, 3: anthracene, 4: tetracene, 5: pentacene) significantly increases with increasing *n*, which facilitates the formation of radical cations (holes) at the interface between a dielectric and a semiconducting layer. Furthermore, the extended π system of a higher acene enhances the intermolecular overlap of π–π systems in the solid state and leads to high mobility. However, a problem of the linear acene approach is the chemical instability of higher acenes. We thought that the oligomerization of a small acene could also be an effective way to extend a π system.[6,7] Oligo(2,6-anthrylene)s would be interesting because the anthracene monomer itself has high time-of-flight mobility (Scheme 1), and 2,6-substitution is expected to give the most extended π conjugation[8] and the highest planarity.[9] We report herein the synthesis and characterization of 2,2′-bianthryl (**2A**), 2,6-trianthrylene (**3A**), and their dihexyl derivatives (**DH-2A** and **DH-3A**). OFETs with these oligomers have been constructed, and their performances as p-type semiconductors are also presented.

Anthracene oligomers have been synthesized by the Suzuki coupling using palladium catalysts.[10] As shown in Scheme 2, 2-bromoanthracene (**1**) was treated with bis(pina-

[*] Prof. T. Suzuki, K. Ito, Dr. Y. Sakamoto
Institute for Molecular Science and
Department of Structural Molecular Science
The Graduate University for Advanced Studies
Myodaiji, Okazaki 444-8585 (Japan)
Fax: (+81) 564-54-2254
E-mail: toshy@ims.ac.jp
D. Kubota, Dr. Y. Inoue, Dr. F. Sato, Dr. S. Tokito
NHK Science and Technical Research Laboratories
Kinuta, Setagaya-ku, Tokyo 157-8510 (Japan)

[**] This work was supported by the Japan Society for the Promotion of Science (Grant-in-Aid for Scientific Research B 14340226).

Supporting information for this article is available on the WWW under http://www.angewandte.org or from the author.

 © 2003 Wiley-VCH Verlag GmbH & Co. KGaA, Weinheim 1433-7851/03/4210-1159 $ 20.00+.50/0

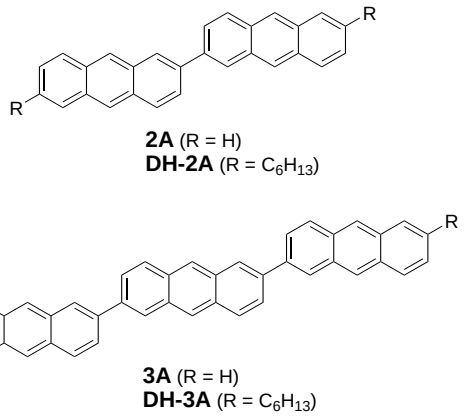

Scheme 1. Structures of anthracene oligomers.

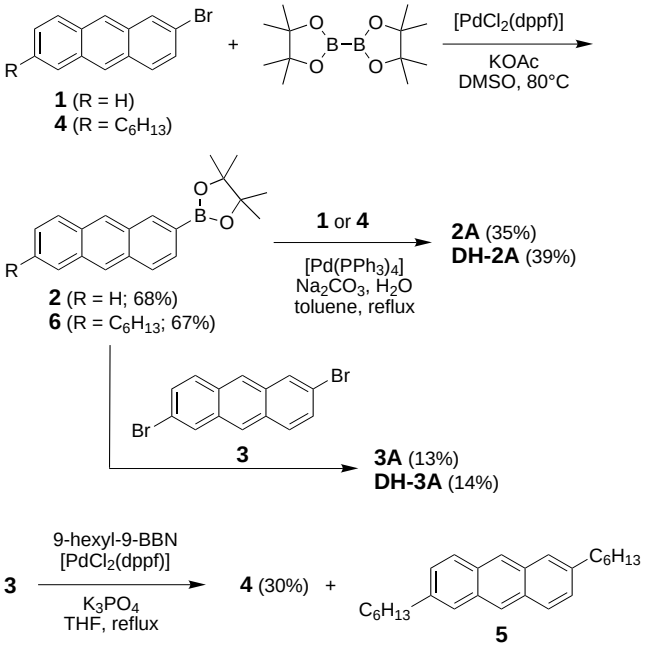

Scheme 2. Synthesis of oligo(2,6-anthrylene)s by Suzuki coupling.

colato)diboron in the presence of [$PdCl_2$(dppf)] (dppf = 1,1′-bis(diphenylphosphanyl)ferrocene) to give boronic ester **2** in 68% yield. The Suzuki coupling of **1** with **2** in the presence of [$Pd(PPh_3)_4$] afforded **2A** in 35% yield. Similarly, the cross-coupling of 2,6-dibromoanthracene (**3**) with two equivalents of **2** provided **3A** in 13% yield.[11] An equivalent of 9-hexyl-9-BBN (9-BBN = 9-borabicyclo[3.3.1]nonane), which was prepared from 1-hexene and 9-BBN, was allowed to react with **3** in the presence of [$PdCl_2$(dppf)] to give a mixture of 2-bromo-6-hexylanthracene (**4**, 30%), 2,6-dihexylanthracene (**5**), and **3**. This mixture was converted into boronic esters, and **6** was isolated in pure form (67%). The Suzuki coupling of **4** with **6** afforded **DH-2A** in 39% yield. The cross-coupling of **3** with two equivalents of **6** yielded **DH-3A** in 14% yield.

Anthracene oligomers purified by train sublimation are bright-yellow crystalline solids. Although **2A** and **DH-2A** are slightly soluble in aromatic solvents such as 1,2-dichlorobenzene, **3A** and **DH-3A** are almost insoluble in organic solvents. The structures were determined by mass spectrometry and elemental analyses. Differential scanning calorimetry (DSC) measurements on **2A** and **3A** showed sharp melting endotherms at 374 and 490 °C, respectively.[10] **DH-2A** and **DH-3A** are thermally less stable than the parent compounds and decompose before melting. The dimers (**2A** and **DH-2A**) and the trimers (**3A** and **DH-3A**) exhibit strong blue-green and green photoluminescence, respectively, in the solid state. The emission maxima in chloroform shift to lower energies in the order **2A** > **DH-2A** > **3A** > **DH-3A** (431, 436, 447, and 454 nm, respectively).[12] The electrochemical measurement on **DH-2A** was performed in 1,2-dichlorobenzene. The cyclic voltammogram (CV) showed a quasireversible oxidation at 0.69 V, and the differential pulse voltammogram (DPV) exhibited two oxidation peaks at 0.69 and 0.99 V and a reduction peak at −2.40 V (versus the ferrocene/ferrocenium couple (Fc/Fc^+)).

OFETs of anthracene oligomers were constructed on SiO_2/Si substrates by high-vacuum evaporation at different substrate temperatures using top-contact geometry. The electrical measurements were performed at room temperature. Figure 1 shows the drain current (I_D) versus drain voltage (V_D) characteristics for OFETs with **2A, 3A, DH-2A**, and **DH-3A** at various gate voltages (V_G). FET activity was observed at the substrate temperatures (T_{sub}) between 50 and 70 °C in OFETs with **2A** (Table 1). The hole mobilities

Table 1: FET characteristics of anthracene oligomers fabricated at different substrate temperatures.

Compd	T [°C]	Mobility [$cm^2V^{-1}s^{-1}$]	On/off ratio
2A	50	0.0031	10^3–10^4
	60	0.0088	10^3–10^4
	70	0.013	10^3–10^4
3A	100	0.064	10^5
	125	0.069	10^4
	150	0.072	10^4–10^5
	175	0.031	10^4
DH-2A	70	0.11, 0.13	10^4
	90	0.040	10^4
DH-3A	100	0.027	10^4
	150	0.044	10^4
	175	0.14, 0.18	10^4

calculated in the saturation regime ranged from 0.0031 to 0.013 $cm^2V^{-1}s^{-1}$, and the on/off ratios were 10^3–10^4.[13] The oligomer **3A** showed even higher mobil

ities (0.031–0.072 $cm^2V^{-1}s^{-1}$) and on/off ratios (10^4–10^5) at T_{sub} = 100–175 °C. The FET performances were dramatically improved when **2A** and **3A** were modified with two hexyl groups:[14] OFETs with **DH-2A** have shown field-effect mobilities greater than 0.1 $cm^2V^{-1}s^{-1}$ at T_{sub} = 70 °C. Although mobilities of **DH-3A** OFETs were lower than those of **3A** OFETs at T_{sub} = 100–150 °C, the highest mo

bilities (0.14–0.18 $cm^2V^{-1}s^{-1}$) were observed at T_{sub} = 175 °C. These mobilities are still lower than that of pentacene but higher than those of oligothiophenes.[6]

Films deposited on Si/SiO_2 substrates were studied by X-ray diffraction in reflection mode at room temperature. Sharp

 © 2003 Wiley-VCH Verlag GmbH & Co. KGaA, Weinheim 1433-7851/03/4210-1160 $ 20.00+.50/0

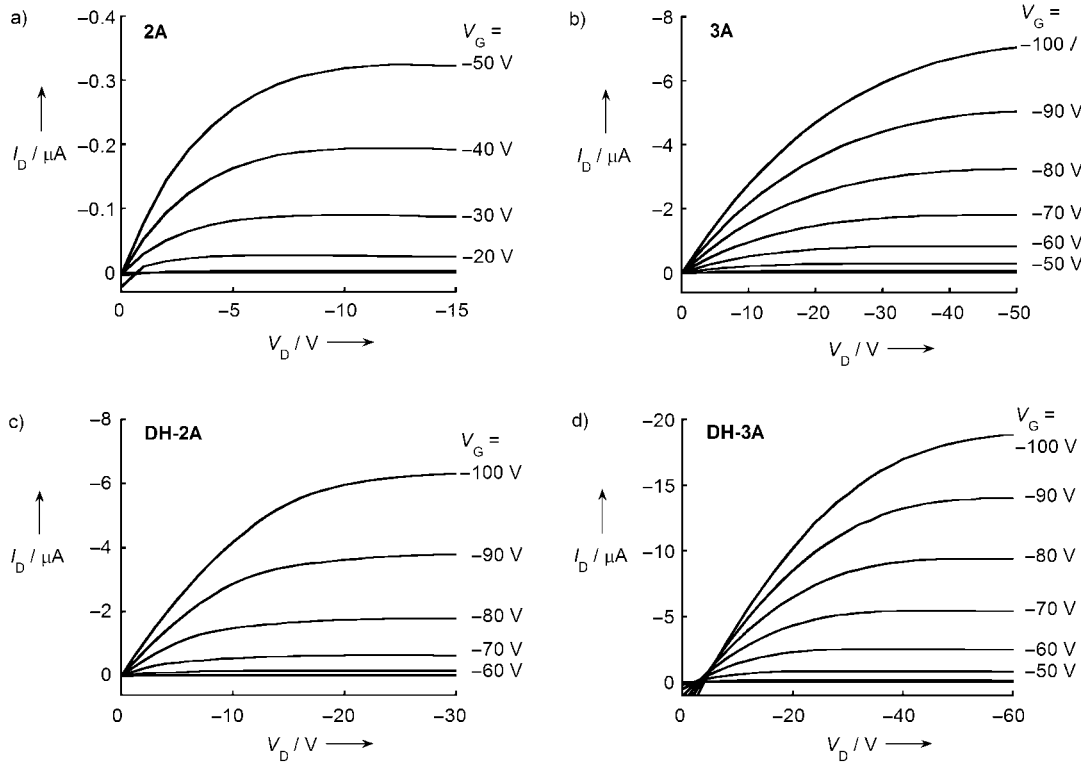

Figure 1. Drain current (I_D) versus drain voltage (V_D) as a function of gate voltage (V_G) for OFETs with anthracene oligomers. a) **2A** (T_{sub} = 70 °C); b) **3A** (T_{sub} = 150 °C); c) **DH-2A** (T_{sub} = 70 °C); d) **DH-3A** (T_{sub} = 175 °C). Channel length L: 100 μm; channel width W: 1 mm (W/L = 10).

and strong reflections up to the sixth order indicated a high degree of lamellar ordering and crystallinity. In the cases of **2A, 3A**, and **DH-2A**, the layer spacings obtained from the first reflection peaks (1.94, 2.84, and 3.20 nm, respectively) correspond to the extended molecular lengths calculated by PM3 (1.83, 2.71, and 3.16 nm, respectively).[15] This result suggests the molecules have a perpendicular orientation on the substrates. Interestingly, the layer spacings of **DH-3A** increase with increasing substrate temperatures during fabrication (T_{sub} = 100 °C: 3.52; 150 °C: 3.64; 175 °C: 3.73 nm) and are shorter than the calculated molecular length (3.94 nm). This observation indicates that the molecules are inclined relative to the substrate or there is interdigitation of the hexyl chains.

The field-effect mobilities of anthracene oligomers increased in the order **2A** < **3A** < **DH-2A** < **DH-3A** (0.01, 0.07, 0.13, and 0.18 $cm^2 V^{-1} s^{-1}$, respectively). The addition of alkyl groups (from **2A** to **DH-2A**) is more effective than the extension of π conjugation (from **2A** to **3A**).[16] Although the oxidation potential of **DH-2A** (0.69 V) is more positive than that of tetracene (0.52 V versus Fc/Fc^+ in 1,2-dichlorobenzene), the field-effect mobility of **DH-2A** (0.13 $cm^2 V^- s^{-1}$) is much higher than that of tetracene (0.01 $cm^2 V^{-1} s^{-1}$).[4] These results may indicate that the quality of a thin film is more important than the ionization potential of a semiconductor.

In summary, we have shown that the acene–oligomer approach is useful for producing stable p-type organic semiconductors with high field-effect mobilities. The fabrication of OFETs from a solution of **DH-2A** and the synthesis of soluble oligomers based on 9,10-dialkylanthracenes are currently in progress and will be reported elsewhere.

Received: November 12, 2002 [Z50527]

Keywords: biaryls · cross-coupling · oligomerization · semiconductors · thin films

[1] P. M. Borsenberger, D. S. Weiss, *Organic Photoreceptors for Xerography*, Marcel Dekker, New York, **1998**, pp. 234–242.
[2] a) M. Pope, C. E. Swenberg, *Electronic Processes in Organic Crystals and Polymers*, Oxford University Press, New York, **1999**; b) N. Karl, J. Marktanner, *Mol. Cryst. Liq. Cryst.* **2001**, *355*, 149–173, and references therein.
[3] For a recent review, see C. D. Dimitrakopoulos, P. R. L. Malenfant, *Adv. Mater.* **2002**, *14*, 99–117.
[4] D. J. Gundlach, J. A. Nichols, L. Zhou, T. N. Jackson, *Appl. Phys. Lett.* **2002**, *80*, 2925–2927.
[5] a) D. J. Gundlach, Y.-Y. Lin, T. N. Jackson, S. F. Nelson, D. G. Schlom, *IEEE Electron Device Lett.* **1997**, *18*, 87–89; b) Y.-Y. Lin, D. J. Gundlach, S. F. Nelson, T. N. Jackson, *IEEE Electron Device Lett.* **1997**, *18*, 606–608.
[6] The oligomer approach for OFETs is the most successful in oligothiophene semiconductors, see a) H. E. Katz, Z. Bao, S. L. Gilat, *Acc. Chem. Res.* **2001**, *34*, 359–369; b) F. Garnier, A. Yassar, R. Hajlaoui, G. Horowitz, F. Deloffre, B. Servet, S. Ries, P. Alnot, *J. Am. Chem. Soc.* **1993**, *115*, 8716–8721.
[7] Oligo(*p*-phenylene)s for OFETs: D. J. Gundlach, Y.-Y. Lin, T. N. Jackson, D. G. Schlom, *Appl. Phys. Lett.* **1997**, *71*, 3853–3855.

 © 2003 Wiley-VCH Verlag GmbH & Co. KGaA, Weinheim 1433-7851/03/4210-1161 $ 20.00+.50/0

[8] Poly(2,6-anthrylene) as a conducting polymer and a potential electroluminescent material: P. Hodge, G. A. Power, M. A. Rabjohns, *Chem. Commun.* **1997**, 73 – 74.
[9] In crystalline oligo(9,10-anthrylene)s, the dihedral angles between anthracene moieties were more than 75° as a consequence of steric hindrance: a) U. Müller, M. Adam, K. Müllen, *Chem. Ber.* **1994**, *127*, 437 – 444; b) H.-D. Becker, V. Langer, J. Sieler, H.-C. Becker, *J. Org. Chem.* **1992**, *57*, 1883 – 1887.
[10] See Supporting Information for the experimental details.
[11] Dehalogenation is a side reaction of the Suzuki coupling and responsible for the low yields of the anthracene oligomers: N. Miyaura, *Top. Curr. Chem.* **2002**, *219*, 11 – 59.
[12] This is in agreement with the result of PM3 calculations: The HOMO–LUMO energy gaps decrease in the order **2A** (6.94 eV) > **DH-2A** (6.91 eV) > **3A** (6.86 eV) > **DH-3A** (6.82 eV).
[13] Interestingly, **2A** is isoelectronic ($14\pi \times 2$) with p-type OFET materials such as bis(benzodithiophene) and bis(dithienothiophene): a) J. G. Laquindanum, H. E. Katz, A. J. Lovinger, A. Dodabalapur, *Adv. Mater.* **1997**, *9*, 36 – 39; b) X.-C. Li, H. Sirringhaus, F. Garnier, A. B. Holmes, S. C. Moratti, N. Feeder, W. Clegg, S. J. Teat, R. H. Friend, *J. Am. Chem. Soc.* **1998**, *120*, 2206 – 2207.
[14] OFET materials with self-assembly properties by alkyl groups: H. Meng, Z. Bao, A. J. Lovinger, B.-C. Wang, A. M. Mujsce, *J. Am. Chem. Soc.* **2001**, *123*, 9214 – 9215. Also, see references [6a] and [6b].
[15] Atomic force microscopy (AFM) images of **2A** films prepared at 50–70 °C showed a series of terraces with the step height of 2.0 nm. See Supporting Information.
[16] A similar effect was observed in oligothiophenes: The field-effect mobilities increased in the order **4T** < **6T** < **DH-4T** < **DH-6T** (0.003, 0.02, 0.03, and 0.08 $cm^2 V^{-1} s^{-1}$, respectively): F. Garnier, R. Hajlaoui, A. E. Kassmi, G. Horowitz, L. Laigre, W. Porzio, M. Armanini, F. Provasoli, *Chem. Mater.* **1998**, *10*, 3334 – 3339.

 © 2003 Wiley-VCH Verlag GmbH & Co. KGaA, Weinheim 1433-7851/03/4210-1162 $ 20.00+.50/0

Mixed-Valent Cluster Compounds

Synthesis and Structural Characterization of Redox-Active Dodecamethoxoheptaoxohexavanadium Clusters

*Johann Spandl, Charles Daniel, Irene Brüdgam, and Hans Hartl**

The chemical behavior of alkoxo-oxovanadium clusters lies between that of metal oxides and metal alkoxides.[1,2] These compounds are important as precursors for the synthesis of new polyoxometalates and as reagents for sol–gel processes and chemical vapor deposition (CVD) methods for the generation of metal oxides.[3] The interest in this substance class for basic research as well as for technical applications is attributed to vanadium's facile and often reversible change in its oxidation state.[4] By varying the alkoxo ligands and the V^{IV}/V^{V} ratio in such clusters, it is possible to control the properties and the composition of the metal oxides obtained by their thermal decomposition, which is of particular importance, for example, for the development of heterogeneous catalysts based on vanadium oxides.

It is remarkable that up to now, $[NnBu_4][V_6O_{12}(OCH_3)_7]$[5] and $[V_6O_7(OC_2H_5)_{12}]$[6] were the only two examples of structurally characterized alkoxo-oxovandium clusters that contain no further substituents other than monodentate alkoxo ligands. In all other cases, stabilization is achieved either by multidentate alkoxo ligands[2b] or by complementary ligands such as squarate,[7] oxalate, acetylacetonate, or phenylphosphonate[2b] as well as metal[8] and organometallic[9] complexes.

Recently we synthesized a series of dodecamethoxoheptaoxohexavanadium compounds $[V^{IV}_nV^{V}_{6-n}O_7(OCH_3)_{12}]^{(4-n)}$ which, while differing in their V^{IV}/V^{V} ratios ($n=3$, 4, 5, 6), remain identical in their structural composition. Noteworthy is the fact that these compounds were not only observed as intermediates by electrochemical and spectroscopical methods, but have also been isolated and characterized by X-ray structural analysis.

Besides vanadium oxides and vanadates,[1] polyoxovanadates containing large organic cations,[10] and thus soluble in organic solvents, as well as orthovanadic acid esters $VO(OR)_3$ of primary alcohols have also proven to be suitable precursors for the synthesis of alkoxo-oxovanadium compounds.[7,11] The uncharged coumpound of mixed valency $[V^{IV}_4V^{V}_2O_7(OCH_3)_{12}]$ (**1**; Figure 1) for example, is formed under solvothermal conditions by reaction of *tert*-butyl orthovanadate $[VO(OtBu)_3]$ with methanol. The structure of **1** can be

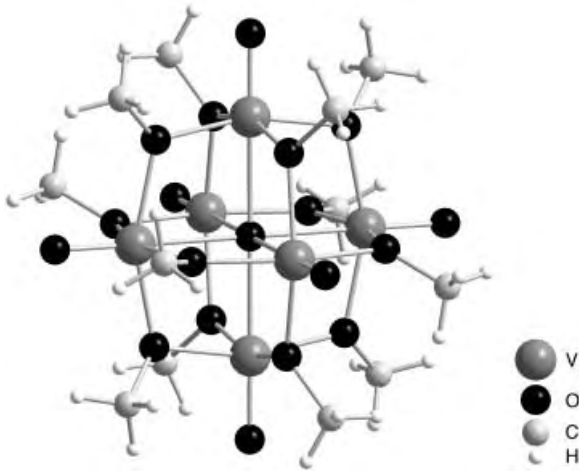

Figure 1. Ball-and-stick model of the uncharged cluster **1**. Bond lengths [Å]: V-O_t 1.585(2)–1.592(2), V-O_b 1.896(2)–2.009(2), V-O_c 2.266(1)–2.296(1); O_t: terminal oxo groups, O_b: bridging O-CH_3 groups, O_c: central oxygen atom).

derived from the hexametalate(v) anion $[M_6O_{19}]^{8-}$ (M = Nb, Ta),[12] yet unknown for vanadium, by replacing the 12 μ_2-bridging oxygen atoms with methoxo groups. In this cluster, four vanadium atoms are present in the oxidation state +IV and the remaining two in the oxidation state +V. As could be expected from the strong molar mass peak in the mass spectrum (see Experimental Section), **1** can be sublimed under reduced pressure without noticeable decomposition. This makes **1** an interesting candidate for CVD experiments. During the thermal decomposition of the compound in the absence of oxygen, continuous mass loss occurs beginning at 200 °C and ending with the formation of V_2O_3 at approximately 380 °C (mass loss (%): found: 43.0; calcd: 43.1).

The cyclic voltammogram[13] of **1** (Figure 2) turns out to be a challenge for synthetic chemists because it reveals a series of electronic transitions assigned to hexametalate clusters

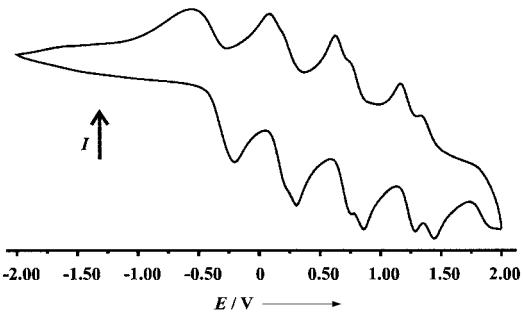

Figure 2. Cyclic voltammogram of **1** (10^{-3} M, acetonitrile; supporting electrolyte $[NnBu_4]PF_6$ (0.1 M), sweep rate = 200 mV s^{-1}).

$[V^{IV}_nV^{V}_{6-n}O_7(OCH_3)_{12}]^{(4-n)}$ of identical composition and structure, yet having different V^{IV}/V^{V} ratios.

Starting from **1** ($n=4$) and using suitable reducing and oxidizing agents, it was indeed possible to synthesize the singly ($n=5$) and doubly ($n=6$) reduced clusters in compounds **3b**, **3a**, **2a**, and **2b** respectively, as well as the singly

[*] Prof. Dr. H. Hartl, Dr. J. Spandl, Dipl.-Chem. C. Daniel, I. Brüdgam
Institut für Chemie/Anorganische und Analytische Chemie
Freie Universität Berlin
Fabeckstrasse 34–36, 14195 Berlin (Germany)
Fax: (+49) 30-8385-4003
E-mail: hartl@chemie.fu-berlin.de

Supporting information for this article is available on the WWW under http://www.angewandte.org or from the author.

 © 2003 Wiley-VCH Verlag GmbH & Co. KGaA, Weinheim 1433-7851/03/4210-1163 $ 20.00+.50/0

oxidized form ($n=3$) in **4a**, **4b**, $[V_3^{IV}V_3^{V}O_7(OCH_3)_{12}]Br_3$ (**4c**), and **4d** (Scheme 1).[14]

For the preparation of the singly reduced cluster in **3b** tetrabutylammonium tetrabutylborate was used, which acts as a mild reducing agent[15] and furthermore provides the desired

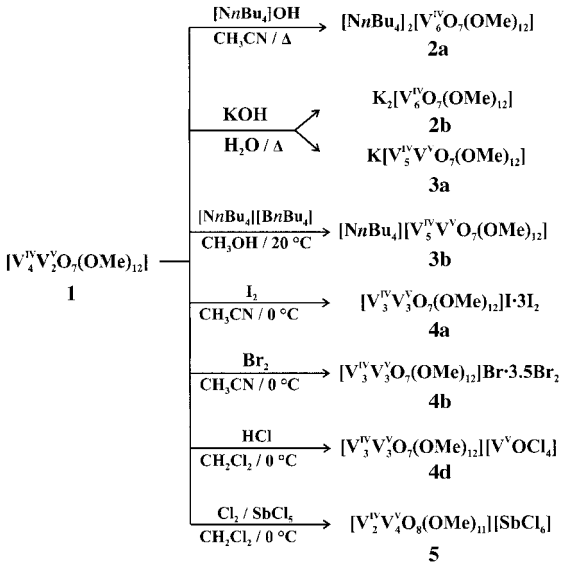

Scheme 1. Synthesis of the reduced (**2a–3b**) and oxidized (**4a–5**) cluster compounds starting from **1**.

tetrabutylammonium ion. Surprisingly, the reaction of a solution of **1** in acetonitrile with an excess of tetrabutylammonium hydroxide leads upon heating to the tetrabutylammonium salt of the dinegative species **2a**; the hydroxide ion presumably acts as the reducing agent. When **1** is treated with a potassium hydroxide solution of varying concentration, both forms can be isolated as their potassium salts (**2b** and **3a**, respectively) depending on the amount of KOH used. In these reactions the astonishingly high stability of the $[V_6O_7(OCH_3)_{12}]$ framework towards hydroxide ions is apparent.

The synthesis of the singly oxidized species ($n=3$) by the oxidation of **1** succeeded with bromine as well as with iodine. In both cases, the resulting cation $[V_3^{IV}V_3^{V}O_7(OCH_3)_{12}]^+$ is embedded in a polyhalide matrix (**4a** or **4b**). Under reduced pressure, the bromine incorporated in compound **4b** partially escapes resulting in the formation of the corresponding tribromide salt **4c**.

If the reduction of **1** by tetrabutylammonium hydroxide in acetonitrile and by KOH in aqueous solution was unexpected, the conversion of **1** to the singly oxidized cluster **4d** by bubbling hydrogen chloride through a solution of **1** in dichloromethane was even more surprising. The unusual redox behavior of **1** in water as well as in aprotic solvents reveals a reaction potential that could lead to the use of these substances as renewable reduction and oxidation reagents or even as homogeneous redox catalysts. The differing solubility of the uncharged cluster **1** in aqueous solution and organic solvents considerably extends the field of potential applications by also allowing the investigation of its catalytic activity in two-phase systems. The solubility behavior of the ionic clusters $[V_n^{IV}V_{6-n}^{V}O_7(OCH_3)_{12}]^{(4-n)}$ is determined by their respective counterions (e.g. K^+ or $[NnBu_4]^+$ in the anionic and polyhalides or $V^{V}OCl_4^-$ in the cationic varieties). Accordingly, diverse solvents ranging from water to organic solvents such as acetonitrile, acetone, alcohols, diethyl ether, or dichloromethane can be used.

Compounds **4a–4d** are among the first examples of structurally characterized, positively charged polynuclear oxometalate clusters belonging to the classic "polyoxo metals" vanadium, niobium, tantalum, molybdenum, and tungsten.[16] Attempts to synthesize the dipositive hexavanadium cluster $[V_2^{IV}V_4^{V}O_7(OCH_3)_{12}]^{2+}$ ($n=2$) by means of oxidation of **1** with chlorine have yet been unsuccessful. To increase the oxidation potential of chlorine, it was used in the presence of the Lewis acid $SbCl_5$. The X-ray structural analysis of the reaction product revealed that **1** had indeed been oxidized twice, yet an oxo ligand had taken the place of a methoxo group to reduce the cluster's net positive charge, resulting in the formation of **5** (Scheme 1). This substitution can take place by nucleophilic attack of a chloride ion, leading to the elimination of CH_3Cl.

Compound **5** indicates that it is possible to replace the methoxo ligands in the $[V_n^{IV}V_{6-n}^{V}O_7(OCH_3)_{12}]^{(4-n)}$ clusters by other groups. This opens up a new way for synthesizing novel compounds in which the ligand system or supporting materials can vary, while the $\{V_6O_{19}\}$ framework is maintained. This modification capacity "offers a way to fine-tune potential catalytic properties of the polyoxovanadate unit," as was recently discussed using the crystal structure of $[\{VO(bmimpm)(acac)\}_2\{V_6O_{13}(OCH_3)_6\}]$ (bmimpm = bis(1-methylimidazol-2-yl)-4-methoxyphen-1-ylmethanol, acac = acetylacetonate) as an example.[8] A major advantage of the present system is not only the fact that vanadium's oxidation states in the polyoxovanadate framework can be modified, but also that vibrational spectroscopy provides a powerful analytical tool for the investigation of the hexavanadium clusters and their redox reactions. The differently charged clusters in compounds **1–4** can be distinguished simultaneously in both solid state and solution infrared spectra by the frequencies of their respective $V–O_t$ stretching and $V\text{-}O_b\text{-}V$ bending vibrations. Thus it is possible to monitor and analyze in situ the course of a redox reaction during its process. A comparison of the characteristic frequencies shows that in the $[V_n^{IV}V_{6-n}^{V}O_7(OCH_3)_{12}]^{(4-n)}$ series ($n=3$–6), the $V–O_t$ stretching as well as the $V\text{-}O_b\text{-}V$ bending vibrations are shifted to lower wavenumbers with increasing n, that is, with rising V^{IV} content. This is accompanied by an increase in the respective $V–O_t$ and $V–O_b$ average bond lengths (Table 1).

The fact that clusters **1–4** are isostructural and only differ in the oxidation states of their vanadium centers makes these compounds interesting for the investigation of the principles that direct the organization of metal centers of different valency. For yet unknown reasons, short regions of antiferromagnetic spin–spin coupling only seem to occur in oxygen compounds of vanadium(IV).[17]

As bond-valence calculations for the vanadium atoms show, the V^{IV} and V^{V} centers are not statistically distributed in the presented compounds. Bond-valence sums for several of

 © 2003 Wiley-VCH Verlag GmbH & Co. KGaA, Weinheim 1433-7851/03/4210-1164 $ 20.00+.50/0

Table 1: Characteristic IR frequencies and associated average bond lengths in **1** and its derivatives.

Compound	V^{IV}	V^{V}	ν(V-O_b-V) [cm^{-1}] (V—O_b distance [Å])	ν(V-O_t) [cm^{-1}] (V—O_t distance [Å])
4c	3	3	600 (1.945)	988 (1.570)
1	4	2	587 (1.963)	975 (1.589)
3b	5	1	584 (1.990)	957 (1.601)
3a			580 (1.983)	958 (1.591)
2a	6	0	578 (1.999)	941 (1.606)
2b			574 (2.000)	946 (1.612)

these compounds are listed in Table 2. The calculations were performed twice for each individual vanadium atom using bond-valence parameters presented by Brese and O'Keeffe[18]

Table 2: Bond-valence sums for vanadium atoms of selected methoxo-oxohexavanadium clusters.

Compound (counterion)	V^{IV}	V^{V}		Bond-valence sums V_1	V_2	V_3	V_4	V_5	V_6
5	2	4	V^{IV}	4.80	4.75	4.74	4.73	*4.25*	*4.24*
($[SbCl_6]^-$)			V^{V}	*5.06*	*5.00*	*4.99*	*4.98*	4.47	4.47
4d	3	3	V^{IV}	*4.39*	*4.29*	4.74	4.70	*4.27*	4.61
($[V^{V}OCl_4]^-$)			V^{V}	4.62	4.51	*4.99*	*4.95*	4.50	*4.86*
4c	3	3	V^{IV}	4.60	4.45	4.50	4.62	–	–
($[Br_3]^-$)			V^{V}	4.84	4.68	4.73	4.86	–	–
1	4	2	V^{IV}	*4.19*	4.71	4.41	–	–	–
			V^{V}	4.41	*4.96*	4.64	–	–	–
3a	5	1	V^{IV}	*4.13*	*4.27*	4.87	*4.15*	*4.12*	*4.14*
(K^+)			V^{V}	4.35	4.46	*5.12*	4.37	4.33	4.36
2b	6	0	V^{IV}	*4.04*	*4.07*	*4.09*	*4.02*	*4.06*	*4.06*
(K^+)			V^{V}	4.26	4.28	4.30	4.23	4.27	4.28

for V^{IV} and V^{V}. The calculated bond-valence sums for identical vanadium atoms vary only by approximately 0.25. In compounds with harder counterions (K^+, $V^{V}OCl_4^-$, $SbCl_6^-$), the assignment of the oxidation states of the vanadium atoms is more reliable than in those containing softer counterions ($[NnBu_4]^+$, polyhalide). The reason for this may be the increasing tendency to rotational disorder of the hexavanadium clusters in the solid phase of the latter compounds. In their octahedral coordination around the central oxygen atom, an even number of V^{IV} and V^{V} centers causes the vanadium atoms of equal valency to adopt a *trans* arrangement. Compounds with a V^{IV}/V^{V} ratio of 3:3 display a *mer*-configuration of these centers. Both EPR-spectroscopic studies of these compounds and the investigation of their magnetic properties should provide a better understanding of the exchange interactions between V^{IV} and V^{V} centers in oxovanadium clusters of mixed valency.

Experimental Section

1: $[VO(OtBu)_3]$ (1.43 g, 5 mmol) in methanol (25 mL) was heated for 24 h at 125 °C in a 50-mL Teflon-lined autoclave (Berghof). The resulting solution of the solvothermal reaction was evaporated to dryness under reduced pressure. The black residue was extracted with hexane (ca. 50 mL) in a Soxhlet apparatus until the extracting solvent remained nearly colorless. The dark green solution was concentrated to half of its volume and subsequently cooled to −30 °C. The resultant crystals were filtered and washed with a small amount of cold hexane. Yield: 0.41 g (0.51 mmol), 62 %. Elemental analysis calcd (%) for $H_{36}C_{12}O_{19}V_6$ ($M = 790.04\ g\,mol^{-1}$): C 18.24, H 4.59; found: C 18.07, H 4.51; IR (KBr, 400–1100 cm^{-1}): $\tilde{\nu} = 411$ (s), 436 (s), 587 (vs), 714 (m), 975 (vs), 1031 cm^{-1} (vs); MS (EI, 80 eV): *m*/*z* (%): 790 (60) $[M]^+$, 630 (32) $[M-VO(OCH_3)_3]^+$, 470 (100) $[M-V_2O_2(OCH_3)_6]^+$.

The syntheses and experimental values of compounds **2a**–**5** are given in the Supporting Information.

Received: June 20, 2002
Revised: November 26, 2002 [Z19599]

Keywords: cluster compounds · cyclic voltammetry · redox chemistry · solvothermal synthesis · vanadium

[1] D. C. Bradley, R. C. Mehrotra, I. P. Rothwell, A. Singh *Alkoxo and Aryloxo Derivatives of Metals*, Academic Press, San Diego, **2001**.
[2] a) P. Gouzerh, A. Proust, *Chem. Rev.* **1998**, *98*, 77–111; b) M. I. Khan, J. Zubieta, *Prog. Inorg. Chem.* **1995**, *43*, 1–149.
[3] a) D. E. Katsoulis, *Chem. Rev.* **1998**, *98*, 359–388; b) W. A. Hermann, N. W. Huber, O. Runte, *Angew. Chem.* **1995**, *107*, 2371–2390; *Angew. Chem. Int. Ed. Engl.* **1995**, *34*, 2187.
[4] *Polyoxometalate Chemistry* (Eds.: M. T. Pope, A. Müller), Kluwer, Dordrecht, **2001**.
[5] D. Hou, Gyu-Shik Kim, K. S. Hagen, C. L. Hill, *Inorg. Chim. Acta* **1993**, *211*, 127–130.
[6] V. G. Kessler, G. A. Seisenbaeva, *Inorg. Chem. Commun.* **2000**, *3*, 203–204. Note: According to the author's declarations, crystals of this compound were found in an inadequately sealed flask of $[VO(OEt)_3]$ (Aldrich); there is no information on the synthesis of this compound.
[7] J. Spandl, I. Brüdgam, H. Hartl, *Angew. Chem.* **2001**, *113*, 4141–4143; *Angew. Chem. Int. Ed.* **2001**, *40*, 4018–4019.
[8] M. Piepenbrink, M. U. Triller, N. H. J. Gormann, B. Krebs, *Angew. Chem.* **2002**, *114*, 2633–2635; *Angew. Chem. Int. Ed.* **2002**, *41*, 2523–2525.
[9] H. K. Chae, W. G. Klemperer, V. W. Day, *Inorg. Chem.* **1989**, *28*, 1423–1424.
[10] V. W. Day, W. G. Klemperer, D. J. Maltbie, *J. Am. Chem. Soc.* **1987**, *109*, 2991–3002.
[11] J. Spandl, I. Brüdgam, H. Hartl, *Z. Anorg. Allg. Chem.* **2000**, *626*, 2125–2132.
[12] a) F. Pickhard, H. Hartl, *Z. Anorg. Allg. Chem.* **1997**, *623*, 1311–1316; b) H. Hartl, F. Pickhard, F. Emmerling, C. Röhr, *Z. Anorg. Allg. Chem.* **2001**, *627*, 2630–2638.
[13] Cyclic voltammetry was conducted by using a potentiostat/galvanostat PGSTAT 12 from Metrohm/Autolab. The results were analyzed with the supplied software. Measurements were conducted in anhydrous acetonitrile with tetrabutylammonium hexafluorophosphate as supporting electrolyte (0.1 M) and a 10^{-3} M concentration of **1** (reference electrode: Ag/AgCl double-chamber electrode, inner chamber: 3 M KCl solution, outer chamber: 0.1 M $[NnBu_4]PF_6$ solution; working electrode: platinum).
[14] Crystal structure determination of compounds **1**–**5**: Bruker XPS diffractometer (CCD area detector, $Mo_{K\alpha}$ radiation, $\lambda =$

 © 2003 Wiley-VCH Verlag GmbH & Co. KGaA, Weinheim 1433-7851/03/4210-1165 $ 20.00+.50/0

0.71073 Å, graphite monochromator), empirical absorption correction using symmetry-equivalent reflections (SADABS), direct methods, difference Fourier syntheses. The initial structures were refined against F^2 (Bruker-SHELXTL, version 5.1, **1998**). The hydrogen atoms were calculated in geometrically idealized positions. The crystals were picked directly out of the mother liquor under a cold nitrogen stream. **1**: Crystal size: $0.33 \times 0.32 \times 0.31$ mm, $T = 193$ K, monoclinic $P2_1/n$, $a = 10.140(2)$, $b = 13.081(2)$, $c = 10.438(2)$ Å, $\beta = 97.050(2)$ Å, $V = 1373.9(2)$ Å^3, $Z = 2$, $\rho_{calcd} = 1.910$ g cm^{-3}, $2\theta_{max} = 60.02°$, 16192 collected reflections, 4009 unique reflections, 176 parameters, $\mu = 2.034$ mm^{-1}, absorption correction, effective transmission max./min. = 0.64/0.53, R_1 $[I > 2\sigma(I)] = 0.0422$, wR_2 $[I > 2\sigma(I)] = 0.1243$, R_1 (all data) = 0.0541, wR_2 (all data) = 0.1331, largest difference peaks 0.837/−0.691 e Å^{-3}. Abridged versions of the crystallographic data of compounds **2a**–**5** are given in the Supporting Information. CCDC-186491 (**1**), CCDC-186494 (**2a**), CCDC-186495 (**2b**), CCDC-186493 (**3a**), CCDC-186492 (**3b**), CCDC-186496 (**4a**), CCDC-186497 (**4b**), CCDC-186498 (**4c**), CCDC-186499 (**4d**), and CCDC-186500 (**5**) contain the supplementary crystallographic data for this paper. These data can be obtained free of charge via www.ccdc.cam.ac.uk/conts/retrieving.html (or from the Cambridge Crystallographic Data Centre, 12 Union Road, Cambridge CB2 1EZ, UK; fax: (+44) 1223-336-033; or deposit@ccdc.cam.ac.uk).

[15] R. Damico, *J. Org. Chem.* **1964**, *29*, 1971 – 1976.

[16] C. H. Ng, C. W. Lim, S. G. Teoh, H.-K. Fun, A. Usman, S. W. Ng, *Inorg. Chem.* **2002**, *41*, 2 – 3.

[17] A. Müller, F. Peters, M. T. Pope, D. Gatteschi, *Chem. Rev.* **1998**, *98*, 239 – 271.

[18] N. E. Brese, M. O'Keeffe, *Acta Crystallogr. Sect. B* **1991**, *47*, 192 – 197. The oxidation state of atom i is given by $\sum_j v_{ij} = V$ with $v_{ij} = \exp[(R_{ij} - d_{ij})/b]$. Here b is taken to be a 'universal' constant equal to 0.37 Å, v_{ij} is the valence of a bond between two atoms i and j, R_{ij} is the empirical parameter, and d_{ij} is the observed bond length.

 © 2003 Wiley-VCH Verlag GmbH & Co. KGaA, Weinheim 1433-7851/03/4210-1166 $ 20.00+.50/0

0.71073 Å, graphite monochromator), empirical absorption correction using symmetry-equivalent reflections (SADABS), direct methods, difference Fourier syntheses. The initial structures were refined against F^2 (Bruker-SHELXTL, version 5.1, **1998**). The hydrogen atoms were calculated in geometrically idealized positions. The crystals were picked directly out of the mother liquor under a cold nitrogen stream. **1**: Crystal size: $0.33 \times 0.32 \times 0.31$ mm, $T = 193$ K, monoclinic $P2_1/n$, $a = 10.140(2)$, $b = 13.081(2)$, $c = 10.438(2)$ Å, $\beta = 97.050(2)$ Å, $V = 1373.9(2)$ Å^3, $Z = 2$, $\rho_{calcd} = 1.910$ g cm^{-3}, $2\theta_{max} = 60.02°$, 16192 collected reflections, 4009 unique reflections, 176 parameters, $\mu = 2.034$ mm^{-1}, absorption correction, effective transmission max./min. = 0.64/0.53, R_1 $[I > 2\sigma(I)] = 0.0422$, wR_2 $[I > 2\sigma(I)] = 0.1243$, R_1 (all data) = 0.0541, wR_2 (all data) = 0.1331, largest difference peaks 0.837/−0.691 e Å^{-3}. Abridged versions of the crystallographic data of compounds **2a**–**5** are given in the Supporting Information. CCDC-186491 (**1**), CCDC-186494 (**2a**), CCDC-186495 (**2b**), CCDC-186493 (**3a**), CCDC-186492 (**3b**), CCDC-186496 (**4a**), CCDC-186497 (**4b**), CCDC-186498 (**4c**), CCDC-186499 (**4d**), and CCDC-186500 (**5**) contain the supplementary crystallographic data for this paper. These data can be obtained free of charge via www.ccdc.cam.ac.uk/conts/retrieving.html (or from the Cambridge Crystallographic Data Centre, 12 Union Road, Cambridge CB2 1EZ, UK; fax: (+44) 1223-336-033; or deposit@ccdc.cam.ac.uk).

[15] R. Damico, *J. Org. Chem.* **1964**, *29*, 1971–1976.

[16] C. H. Ng, C. W. Lim, S. G. Teoh, H.-K. Fun, A. Usman, S. W. Ng, *Inorg. Chem.* **2002**, *41*, 2–3.

[17] A. Müller, F. Peters, M. T. Pope, D. Gatteschi, *Chem. Rev.* **1998**, *98*, 239–271.

[18] N. E. Brese, M. O'Keeffe, *Acta Crystallogr. Sect. B* **1991**, *47*, 192–197. The oxidation state of atom i is given by $\sum_j v_{ij} = V$ with $v_{ij} = \exp[(R_{ij} - d_{ij})/b]$. Here b is taken to be a 'universal' constant equal to 0.37 Å, v_{ij} is the valence of a bond between two atoms i and j, R_{ij} is the empirical parameter, and d_{ij} is the observed bond length.

Synthesis of Glycoconjugates

Solid-Phase-Assisted Solution-Phase Synthesis with Minimum Purification—Preparation of 2-Deoxyglycoconjugates from Thioglycosides**

*Janis Jaunzems, Edgar Hofer, Martin Jesberger, Georgia Sourkouni-Argirusi, and Andreas Kirschning**

Dedicated to Professor Lutz F. Tietze on the occasion of his 60th birthday

High-throughput synthesis is one of the major challenges for organic chemistry today and solid supports have played a dominant role in this field.[1] However, disadvantages of solid-phase synthesis are a) the necessity for robust linkers that are stable under various reaction conditions, b) difficulties in the structural analysis of the supported species, as well as c) the requirement that every functional site on the support needs to react. These problems are also found in solid-phase synthesis of oligosaccharides and glycoconjugates. Therefore, various techniques that are capable for performing high-throughput solution-phase synthesis have seen a renaissance lately or have been developed recently. In the context of carbohydrates, important examples of solution-phase synthesis include the use of fluorous phases,[2] functionalized polymers,[3] scavenging protocols based on "capping and tagging" protecting groups,[4] multienzyme loaded beads for sugar nucleotide regeneration,[5] and computer-assisted planning of syntheses in solution.[6]

In the context of general applicability, the development and use of solid-phase-attached reagents is particularly appealing[7] because workup is minimized and the reagent can be employed in excess. The activation of glycosyl bromides with silver ions that are immobilized on a solid phase was first studied by Paulsen and Lockhoff[8] and later by Capillon et al.[9] In conjunction with our research activities in this field, we recently initiated a program that is dedicated to the polymer-assisted solution-phase synthesis of deoxysugar-based glycoconjugates. We demonstrated that glycosyl acetates can be activated by polymer-bound Lewis acids.[3] Here, we describe the high-yielding preparation of oligodeoxysac-

[*] Prof. Dr. A. Kirschning, J. Jaunzems, Dr. E. Hofer
Institut für Organische Chemie
Universität Hannover
Schneiderberg 1b, 30167 Hannover (Germany)
Fax: (+49) 511-726-3011
E-mail: andreas.kirschning@oci.uni-hannover.de
Dr. M. Jesberger, Dr. G. Sourkouni-Argirusi
Institut für Organische Chemie
Technische Universität Clausthal
Leibnizstrasse 6, 38678 Clausthal (Germany)

[**] This work was supported by the Deutsche Forschungsgemeinschaft (SFB 416) and the Fonds der Chemischen Industrie. This project is part of the joint initiative "Biologisch aktive Naturstoffe—Chemische Diversität" at the University of Hannover.

Supporting information for this article is available on the WWW under http://www.angewandte.org or from the author.

 © 2003 Wiley-VCH Verlag GmbH & Co. KGaA, Weinheim 1433-7851/03/4210-1166 $ 20.00+.50/0

charides and glycoconjugates derived therefrom by using thioglycosides as glycosyl donors.[10] Main features of this work are simple workup protocols that for the first time solely rely on the removal of by-products by simple filtration.

Problematic by-products that always result when employing phenylthioglycosides are thiophenol and diphenyl disulfide (**1**). Therefore, it first became necessary to develop scavenging protocols that allow quantitative removal of these two by-products from the reaction mixture (Scheme 1). Both

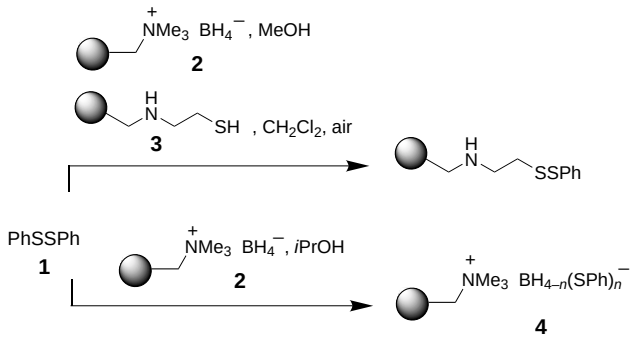

Scheme 1. Polymer-assisted removal of diphenyl disulfide (**1**) and thiophenol from solutions.

of our purification methods rely on borohydride exchange resin (BER) **2**.[11] Thus, treatment of **1** with **2** in methanol yields thiophenol (Scheme 1), which, after filtration, is quantitatively scavenged by adding polymer-bound thiol **3** to the reaction mixture under air. However, this reagent requires covalent attachment of 2-sulfanylethylamine to polystyrene.[12] Therefore, we searched for a simpler scavenging protocol. We found that 2-propanol is a solvent that reacts only very sluggishly with **2**. This observation allowed us to make double use of it: First, **2** acts as a reducing agent for **1** and second, it promotes the scavenging of the nucleophilic thiophenol in the presence of 2-propanol to furnish resin **4**. Both methods quantitatively remove thiophenol and **1** from reaction mixtures by simple filtration. Consequently, both protocols are truly of general importance.

In the next phase of the project a glycosidation protocol was envisaged that relies on our newly developed thiophilic polymer-bound reagent **5**[13,14] and alternatively on the fluorinating agent Selectfluor (**6**),[15] which also shows electrophilic and thiophilic properties. Advantageously, the resulting salt is insoluble in most organic solvents including acetonitrile and can be removed by simple filtration. Both reagents are able to activate the phenylthio group in glycosides **7**–**9** (Scheme 2).[16]

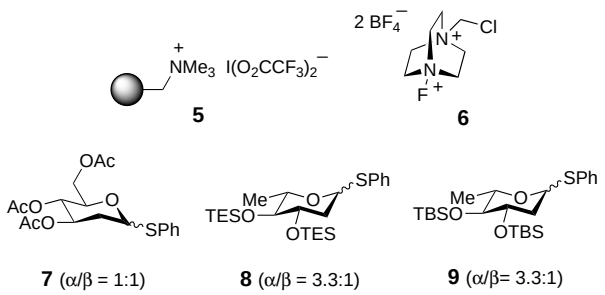

7 (α/β = 1:1) **8** (α/β = 3.3:1) **9** (α/β= 3.3:1)

The glycosidation commonly proceeds in high yields. Consumption of thioglycosides is observed for both reagents within 5 to 10 min. The best solvent for activation of thioglycosides promoted by reagent **5** is THF/CH_3CN in the ratio 1:2 at −50 °C. In CH_2Cl_2, the thioglycosides react at room temperature, but the glycosidation products are formed with reduced purity. The glycosidation is terminated after 2 to 3 h by addition of Amberlyst A-21 (**10**), which scavenges trifluoroacetic acid. In contrast to polymer-bound reagent **5**, acetonitrile is the solvent of choice when employing reagent **6**, and the reaction time is only 10 to 20 min. The workup is identical for both reagents. After filtration and concentration, **1** was sequestered as described in Scheme 1 so that the target glycosides **11**–**29** were isolated with preference for α anomers and free of thiophenol or **1** (Scheme 2). The stereoselectivities[17] observed are in accordance with those obtained for conventional solution-phase glycosidations of 2-deoxythioglycosides when no stereodirecting group is present at C2.[18] In general, the reaction conditions are very mild as is demonstrated for the preparation of highly reactive glycal **14**,[19] acid- and base-labile glycosylated digitoxigenin derivatives **18** and **29,** or the glycosylated decanolide decarestrictine D **19**.[20] Importantly, also the reductive removal of thiophenol and **1** kept the carbonyl groups in glycosides **16**–**19**, **23**, **24**, and **26**–**29** intact.[21]An important demonstration of the efficiency of the scavenging protocol is depicted in Scheme 3. Di-O-benzylated thioglycoside **30** was subjected to the usual glycosidation conditions, and after thorough removal of thio-containing impurities by using our scavenging protocol, the crude product was de-O-benzylated under catalytic hydrogenation conditions (RT, 2 h, 20 bar) to yield glycoside **31**. After one scavenging step the reaction mixture was basically free of any sulfur-containing impurities as judged from the crude ^{1}H NMR spectrum. As the catalytic hydrogenation proceeded only very sluggishly, we repeated the scavenging protocol. Based on the results described here we developed a multistep glycosidation strategy for the synthesis of oligodeoxysaccharides that is solely based on reagents that are removed by simple filtration after use (see Scheme 3).

Under the glycosidation conditions and purification protocols 2,6-dideoxythioglycoside **32** and glycals **33** and **34** exclusively furnished α-linked disaccharides **35** and **36**, respectively, in high purity (see Scheme 4). After filtration and proton-induced activation of the enol ether double bond in **35** in the presence of testosterone using polymer-bound sulfonic acid **37**, we obtained glycoconjugate **38**. Likewise, polymer-assisted deprotection of disaccharide **36** followed by activation using β-configured thioglycoside **32** afforded trisaccharide **40** (α/β = 4.3:1), again after the polymer-assisted scavenging of **1**.

In conclusion, we developed a multistep solution-phase approach to 2-deoxyoligosaccharides and glycoconjugates in which workup of each transformation is achieved by simple

 © 2003 Wiley-VCH Verlag GmbH & Co. KGaA, Weinheim 1433-7851/03/4210-1167 $ 20.00+.50/0

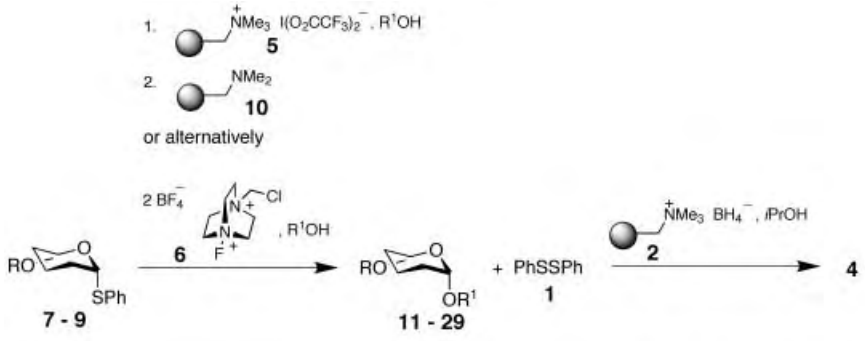

Glycosidation[a] products with R^1 (R^1 refers to glycosyl acceptor R^1OH)

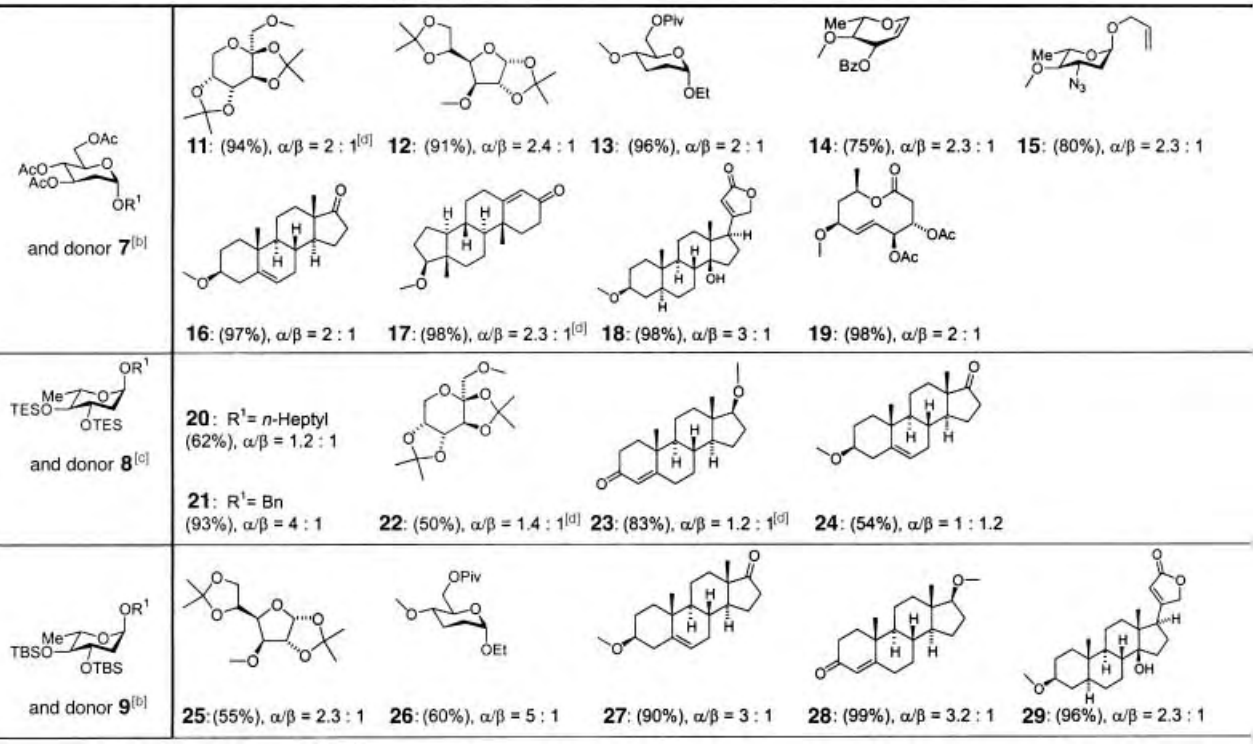

Scheme 2. Glycosidations with minimum purification using thioglycosides **7**–**9**. [a] Only α isomers are depicted; product ratios were determined from the ^{1}H NMR spectra of the crude products; yields refer to isolated pure products. If not otherwise stated, thioglycosides are employed as anomeric mixtures. [b] Typical reaction conditions for Selectfluor (**6**)-mediated glycosidations: CH_3CN, 0 °C, 10–20 min. [c] Typical reaction conditions when reagent **5** is employed: THF/CH_3CN (1:2), −50 °C, 2–3 h (TES = triethylsilyl, TBS = *tert*-butyldimethylsilyl). [d] The scavenging protocol using reagent **3** was employed (see Scheme 1).

filtration. These steps include removal of thiophenol and diphenyl disulfide (**1**) from solution and activation of thioglycosides and a glycal. Studies towards automated solution-phase glycosidation are in progress in our laboratories.

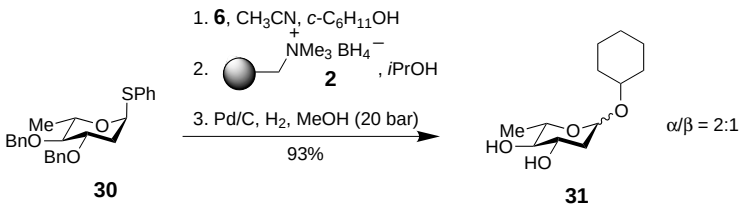

Scheme 3. Multistep polymer-assisted glycosidations. Bn = benzyl.

Experimental Section

Activation of thioglycosides with **5** followed by sequestration of **1**: To a solution of thioglycoside (1 equiv) in absolute THF/CH_3CN (1:2; 50 mL mmol^{-1}) at −50 °C were added the glycosyl acceptor (1.0 equiv) and resin **5** (1 equiv; 2.5 mmol g^{-1} based on the original loading of the commercial resin). The reaction mixture was shaken at −50 °C for 2–3 h at 300 rpm under exclusion of light. The reaction was monitored by TLC and was terminated by addition of Amberlyst A-21 (3 equiv; 0.11 equiv g^{-1} for the

 © 2003 Wiley-VCH Verlag GmbH & Co. KGaA, Weinheim 1433-7851/03/4210-1168 $ 20.00+.50/0

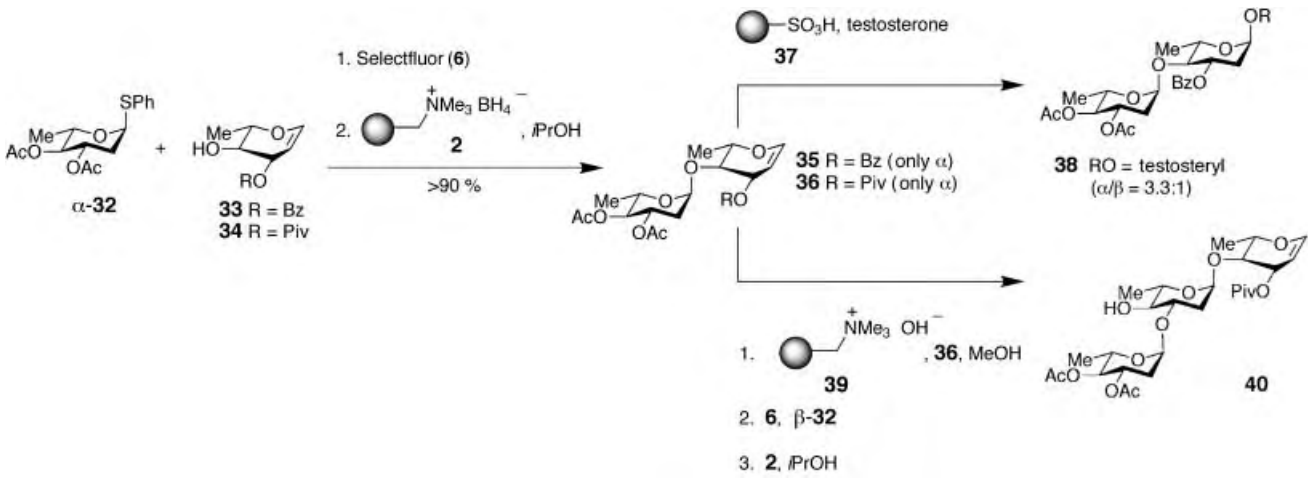

Scheme 4. Preparation of α-linked disaccharides **35** and **36** and their subsequent conversion to glycoconjugate **38** and trisaccharide **40**, respectively. Bz = benzoyl, Piv = pivaloyl.

dry resin). Shaking was continued for 30 min. After filtration, the resin was washed with CH_2Cl_2 and the combined filtrates were concentrated under reduced pressure to yield the desired glycoside along with impurities of **1**. The crude material was taken up in *i*PrOH (50 mL mmol^{-1}) and **2** (100 mg mmol^{-1}; 3 mmol g^{-1} loading) was added. The reaction mixture was shaken overnight at room temperature, filtered, and concentrated under reduced pressure to yield the desired glycoside. Isolation of each anomeric isomer required column chromatography on silica gel.

Activation of thioglycosides with **6** and hydrogenolytic deprotection of benzyl ethers: To an icecold suspension of thioglycoside (1 equiv), glycosyl acceptor (1 equiv), and powdered molecular sieves (1 g mmol^{-1}; 4 Å) in absolute acetonitrile (100 mL mmol^{-1}) was added **6** (1.05 equiv) and stirring was continued for 10–20 min. The reaction was terminated by addition of dry Amberlyst A-21. After filtration through a pad of basic Al_2O_3 the solid material was washed with acetonitrile and the combined filtrates were concentrated under reduced pressure. Again, sequestration of **1** was achieved as described above. In the case of 3,4-di-*O*-benzyl-2,6-dideoxy-1-phenylthio-*arabino*-pyranoside (**30**) sequestration of sulfur-containing impurities was achieved by repeating the scavenging procedure a second time (12 h) followed by filtration and removal of the solvent in vacuo. To the resulting material in methanol (20 mL 0.1 mmol^{-1}) was added a catalytic amount (5 mol %) of Pd/C (10 %). Deprotection was achieved within 2 h under a hydrogen atmosphere at 20 bar. After filtration and removal of the solvent under reduced pressure the deprotected glycoside **31** was isolated as pure material (α/β = 2:1; 93 %).

Received: August 26, 2002
Revised: November 12, 2002 [Z50042]

Keywords: functionalized polymers · glycosidation · separation techniques · solid-phase synthesis · thioglycosides

[1] a) D. E. Bergbreiter, *Med. Res. Rev.* **1999**, *19*, 439–450; b) J. S. Früchtel, G. Jung, *Angew. Chem.* **1996**, *108*, 19–46; *Angew. Chem. Int. Ed. Engl.* **1996**, *35*, 17–42; c) F. Balkenhohl, C. von Bussche-Hünnefeld, A. Lansky, C. Zechel, *Angew. Chem.* **1996**, *108*, 2436–2488; *Angew. Chem. Int. Ed. Engl.* **1996**, *35*, 2288–2337.

[2] D. P. Curran, R. Ferritto, Y. Hua, *Tetrahedron Lett.* **1998**, *39*, 4937–4940.

[3] A. Kirschning, M. Jesberger, A. Schönberger, *Org. Lett.* **2001**, *3*, 3623–3626.

[4] a) E. R. Palmacci, M. C. Hewitt, P. H. Seeberger, *Angew. Chem.* **2001**, *113*, 4565–4568; *Angew. Chem. Int. Ed.* **2001**, *40*, 4433–4437; b) V. Pozgay, *Org. Lett.* **1999**, *1*, 477–479.

[5] X. Chen, J. Fang, J. Zhang, Z. Liu, J. Shao, P. Kowal, P. Andreana, P. G. Wang, *J. Am. Chem. Soc.* **2001**, *123*, 2081–2082.

[6] a) Z. Zhang, I. R. Ollmann, X.-S. Ye, R. Wischnat, T. Baasov, C.-H. Wong, *J. Am. Chem. Soc.* **1999**, *121*, 734–753; b) F. Burkhart, Z. Zhang, S. Wacowich-Sgarbi, C.-H. Wong, *Angew. Chem.* **2001**, *113*, 1314–1317; *Angew. Chem. Int. Ed.* **2001**, *40*, 1274–1277.

[7] Recent reviews on polymer-supported reagents: a) A. Kirschning, H. Monenschein, R. Wittenberg, *Angew. Chem.* **2001**, *113*, 670–701; *Angew. Chem. Int. Ed.* **2001**, *40*, 650–679; b) S. V. Ley, I. R. Baxendale, R. N. Bream, P. S. Jackson, A. G. Leach, D. A. Longbottom, M. Nesi, J. S. Scott, R. I. Storer, S. J. Taylor, *J. Chem. Soc. Perkin Trans. 1* **2000**, 3815–4195; c) D. H. Drewry, D. M. Coe, S. Poon, *Med. Res. Rev.* **1999**, *19*, 97–148.

[8] H. Paulsen, O. Lockhoff, *Chem. Ber.* **1981**, *114*, 3102–3114.

[9] J. Capillon, A. Richard, R. Audebert, C. Quivoron, *Polym. Bull.* **1985**, *13*, 185–192.

[10] Thioglycosides have proven to be excellent glycosyl donors for the synthesis of deoxyglycoconjugates such as cyclamycin 0: S. Rhagavan, D. Khane, *J. Am. Chem. Soc.* **1993**, *115*, 1580–1581.

[11] A. Kirschning, *J. Prakt. Chem.* **2000**, *342*, 508–511.

[12] S. E. Ault-Justus, J. C. Hodges, M. W. Wilson, *Biotechnol. Bioeng.* **1998**, *61*, 17–22.

[13] In analogy to our earlier work we prepared reagent **5** by oxidative ligand transfer of the mobile ligands in [bis(trifluoroacetoxy)iodo]benzene onto polymer-bound iodide. After washing with dry dichloromethane, this new functionalized polymer is obtained, which can be stored at −20 °C for weeks: a) G. Sourkouni-Argirusi, A. Kirschning, *Org. Lett.* **2000**, *2*, 3781–3784; b) H. Monenschein, G. Sourkouni-Argirusi, K. M. Schubothe, T. O'Hare, A. Kirschning, *Org. Lett.* **1999**, *1*, 2101–2104; c) A. Kirschning, H. Monenschein, C. Schmeck, *Angew. Chem.* **1999**, *111*, 2720–2722; *Angew. Chem. Int. Ed.* **1999**, *38*, 2594–2596.

[14] Proposed structure is depicted based on observations described in ref. [13].

[15] V. Gouverneur, B. Greedy, *Chem. Eur. J.* **2002**, *8*, 766–771.

[16] We screened for thiophilicity among a wide range of polymer-bound halogenate(I) complexes such as $I(OAc)_2^-$, $Br(OAc)_2^-$, $Br(O_2CCF_3)_2^-$, as well reagent mixtures like $Br(OAc)_2^-$/

 © 2003 Wiley-VCH Verlag GmbH & Co. KGaA, Weinheim 1433-7851/03/4210-1169 $ 20.00+.50/0

TMSOTf, $I(OAc)_2^-$/TMSOTf which all failed to efficiently promote glycosidation.
[17] Pure α-configured thioglycoside **31** was glycosidated with testosterone in the presence of reagent **6**. It gave an α/β mixture of anomers in a 2.3:1 ratio, which was exactly the same ratio found when the β-configured thioglycoside **31** was employed.
[18] a) K. C. Nicolaou, S. P. Seitz, D. P. Papahatjis, *J. Am. Chem. Soc.* **1983**, *105*, 2430–2434; b) W. R. Roush, X. Lin, J. A. Straub, *J. Org. Chem.* **1991**, *56*, 1649–1655; c) K. Fukase, A. Hasuoka, S. Kusumoto, *Tetrahedron Lett.* **1993**, *34*, 2187–2190.
[19] Selectfluor (**6**) is capable of performing facile nucleophilic addition reactions to glycals: a) M. D. Burkhart, Z. Zhang, S.-C. Hung, C.-H. Wong, *J. Am. Chem. Soc.* **1997**, *119*, 11743–11746; b) S. P. Vincent, M. D. Burkart, C.-Y. Tsai, Z. Zhang, C.-H. Wong, *J. Org. Chem.* **1999**, *64*, 5264–5279; c) M. Albert, K. Dax, J. Ortner, *Tetrahedron* **1998**, *54*, 4839–4848; d) M. Albert, B. J. Paul, K. Dax, *Synlett* **1999**, 1483–1485; e) J. Ortner, M. Albert, H. Weber, K. Dax, *J. Carbohydr. Chem.* **1999**, *18*, 297–316.
[20] a) S. Grabley, E. Granzer, K. Hütter, D. Ludwig, M. Mayer, R. Thiericke, G. Till, J. Wink, S. Phillips, A. Zeeck, *J. Antibiot.* **1992**, *45*, 56–65; b) A. Göhrt, A. Zeeck, K. Hütter, R. Hirsch, H. Kluge, R. Thiericke, *J. Antibiot.* **1992**, *45*, 66–73.

Chiral Picotube Derivatives

Synthesis of a Chiral Tube**

Rainer Herges, Markus Deichmann, Tsuneki Wakita, and Yoshio Okamoto**

The conventional synthesis of belt- and tubelike conjugated compounds[1] and the derivatization of carbon nanotubes[2] at either the sidewalls[3] or at the tip[4] are subjects of recent research because of their potential in supramolecular chemistry[5] and applications in nanotechnology.[4b,d,e] Covalently modified nanotube tips, for example, enable the mapping of chemical and biological functions in atomic probe microscopes. Herein, we report on a combination of both fields, in which the exhaustive alkylation of the rim of a synthetic tubelike structure leads to the formation of a chiral tube.

Compound **1** [Eq. (1)] was synthesized by the dimerizing metathesis of tetradehydrodianthracene.[1c] Since **1** is a small substructure of an armchair carbon nanotube, we named it "picotube". The fully conjugated structure is 8.2 Å in length and 5.4 Å in diameter, and it is the first conventionally synthesized compound that exhibits tubular aromaticity.

[*] Prof. Dr. R. Herges, M. Deichmann
Institut für Organische Chemie
Universität Kiel
Otto-Hahn-Platz 4, 24098 Kiel (Germany)
Fax: (+49) 431-880-1558
E-mail: rherges@uni-kiel.de
Prof. Dr. Y. Okamoto, T. Wakita
Department of Applied Chemistry
Graduate School of Engineering, Nagoya University
Furo-Cho, Chikusa-Ku, Nagoya 464-01 (Japan)
Fax: (+81) 52-789-3188
E-mail: okamoto@apchem.nagoya-u.ac.jp

[**] This work was funded by the Deutsche Forschungsgemeinschaft. We thank Dr. C. Näther for the X-ray analysis.

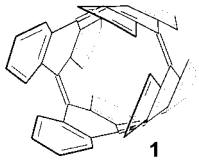

(1)

Although unreactive towards oxidation (stable in air up to 450 °C; no reaction with peracids at room temperature) it smoothly reacts under Friedel–Crafts conditions. Alkylation with $CH_3Cl/AlCl_3$ leads to a number of isomers. Treatment with a large excess of *t*BuCl and catalytic amounts of $AlCl_3$, however, only gives two major products (**2** and **3**), in 15 and 14 % yield, which could be separated and isolated by HPLC [Eq. (1)].

The ^{13}C NMR spectra of the two products, which display seven and eight signals, respectively, point to a high symmetry in both isomers. X-ray structural analysis confirms this assumption, with **2** shown to be an octasubstituted picotube with D_4 symmetry (Figure 1).[6] Despite its high symmetry, **2** is chiral because it does not contain any symmetry element other than C_4 and C_2 symmetry axes. The structure of **3** has C_{4h} symmetry and is not chiral. The space-filling model based on an optimized structure derived from density functional theory (DFT) calculations (B3LYP/3-21G, Figure 2) reveals

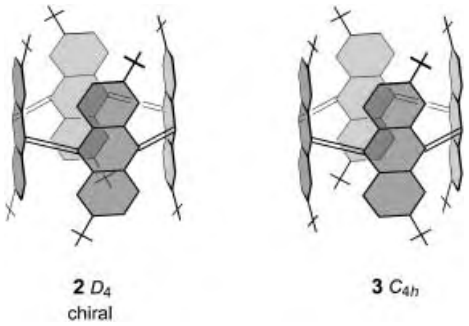

Figure 1. Structures of picotubes **2** and **3**.

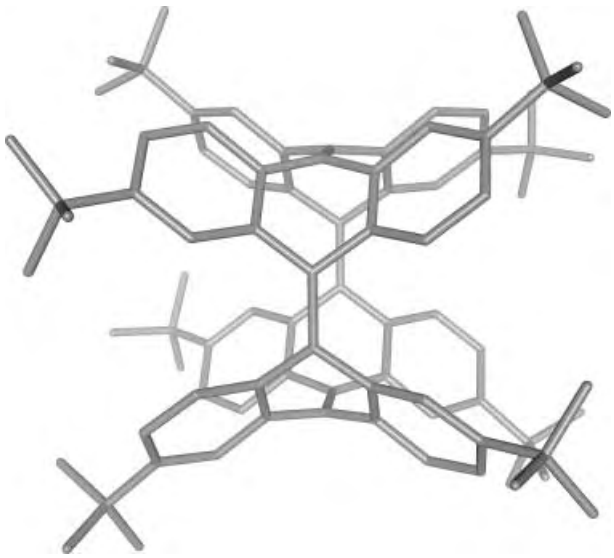

Figure 2. Structure of the chiral tube **2,** as derived by DFT calculations (H atoms are omitted).

 © 2003 Wiley-VCH Verlag GmbH & Co. KGaA, Weinheim 1433-7851/03/4210-1170 $ 20.00+.50/0

that both ends of the picotube are blocked by the bulky *t*Bu groups.

The enantiomers of **2** were separated under reverse-phase conditions using a mixture of ethanol and water (9:1) on amylose tris(3,5-dimenthylphenylcarbamate) (CHIRALPAK AD). Circular dichroism (CD) spectra for both enantiomers could be recorded separately (Figure 3).

Isomers of lower symmetry were also formed, but in much lower yields. Steric hindrance directs the electrophilic substitution in such a way that the *t*Bu groups are placed as far away from each other as possible. Our results may have an impact on the derivatization of larger carbon nanotubes. Friedel–Crafts alkylation of open tubes with *t*BuCl should lead to well-defined products with increased solubility, stability to further oxidation, and a reduction in the diameter of the opening of the tube.

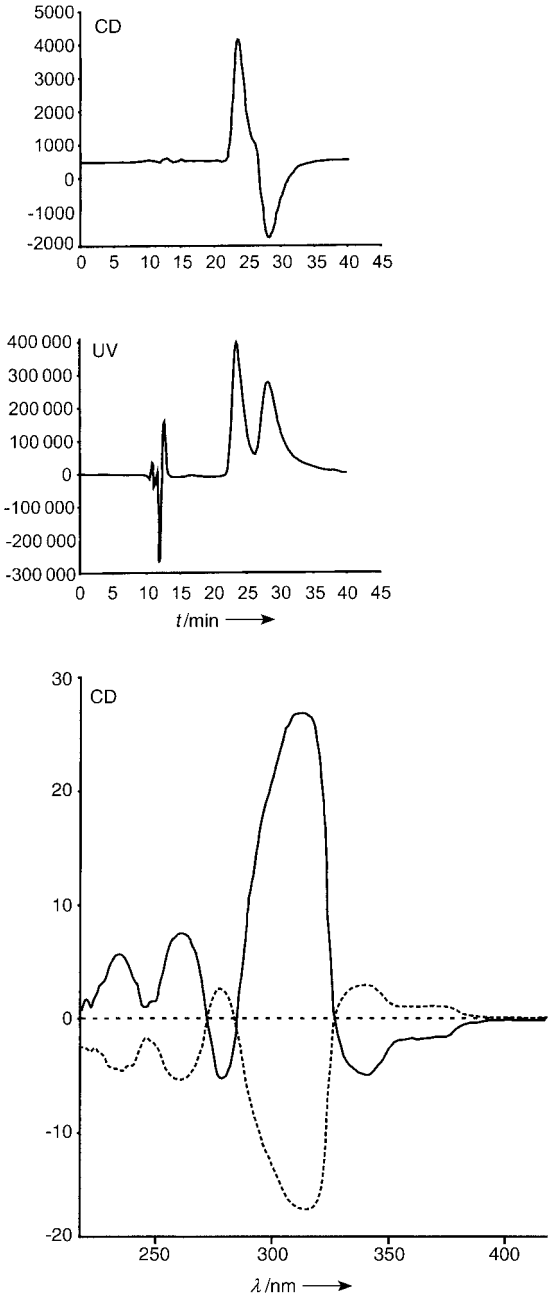

Figure 3. Enantioseparation of the chiral tube **2**. Top, center: CD and UV spectra are plotted as a function of the elution time *t* on the chiral HPLC phase at 254 nm. Bottom: The CD spectrum of the first eluted enantiomer is plotted as a solid line, and that of the second enantiomer as a dashed line.

Experimental Section

2 and **3**: Picotube **1** (100 mg, 142 μmol) was dissolved in dichloromethane (200 mL) and *tert*-butyl chloride (3 mL, 28 mmol), to which anhydrous aluminum chloride (100 mg, 0.75 mmol) was added. After stirring the green solution for 5 h at room temperature, water (50 mL) was added. The organic phase was separated and dried over magnesium sulfate. The remaining solution was filtered over silica gel using additional dichloromethane (400 mL). After the solvent had been removed, 160 mg of the isomeric mixture (139 μmol; 98 % yield) was separated by HPLC (Rainin Dynamax Si 8 μ, 60 Å, 41.4 × 250 mm, hexane/dichloromethane (95:5)). Pure fractions of isomers **2** and **3** were obtained.

2: Yield 24 mg (15 %); m.p. >280 °C; ^{1}H NMR (400 MHz, $CDCl_3$): $\delta = 7.89$ (d, 8H, $^4J_{H,H} = 1.9$ Hz), 7.86 (d, 8H, $^3J_{H,H} = 8.1$ Hz), 6.99 (dd, 8H, $^3J_{H,H} = 8.1$ Hz, $^4J_{H,H} = 1.9$ Hz), 1.31 ppm (s, 72H, $C(CH_3)_3$); ^{13}C NMR (100.6 MHz, $CDCl_3$): $\delta = 146.68$ (C_{quat}, arom.), 139.76 (C_{quat}, arom.), 137.05 (C_{quat}, arom.), 134.98 (C_{quat}, arom.), 129.01 (CH, arom.), 127.04 (CH, arom.), 121.39 (CH, arom.), 34.44 (C_{quat}), 31.35 (CH_3). MS (70 eV): *m*/*z* (%): 1152.6 (100) [M^+], 576 (22) [M^{2+}], 57 (60) [*t*Bu]; IR (KBr): $\tilde{\nu} = 2963, 2905, 2869, 1479, 1463, 1363, 1258, 815\ cm^{-1}$. UV/Vis ($CH_2Cl_2$): λ_{max} (ε) = 250 (59601, sh), 304 (71321), 340 (10007, sh).

3: Yield 23 mg (14 %); m.p. >280 °C; ^{1}H NMR (400 MHz, $CD_2Cl_2/AsCl_3$)[7]: $\delta = 7.98$ (d, 8H, $^4J_{H,H} = 1.8$ Hz), 7.93 (d, 8H, $^3J_{H,H} = 8.1$ Hz), 7.12 (dd, 8H, $^3J_{H,H} = 8.1$ Hz, $^4J_{H,H} = 1.8$ Hz), 1.35 ppm (s, 72H, $C(CH_3)_3$); ^{13}C NMR (100.6 MHz, $CD_2Cl_2/AsCl_3$): $\delta = 147.12$ (C_{quat}, arom.), 138.33 (C_{quat}, arom.), 135.66 (C_{quat}, arom.), 134.96 (C_{quat}, arom.), 133.12 (C_{quat}, arom.), 128.29 (CH, arom.), 126.50 (CH, arom.), 121.67 (CH, arom.), 33.98 ($C(CH_3)_3$), 30.85 ppm ($C(CH_3)_3$). MS, IR, and UV/Vis: see above.

Received: September 5, 2002 [Z50106]

Keywords: alkylation · aromatic substitution · chiral resolution · circular dichroism · nanotubes

[1] a) T. Kawase, H. R. Darabi, M. Oda, *Angew. Chem. Int. Ed. Engl.* **1996**, *108*, 2803–2805; *Angew. Chem. Int. Ed. Engl.* **1996**, *35*, 2664–2666; b) S. Kammermeier, R. Herges, *Angew. Chem.* **1996**, *108*, 470–472; *Angew. Chem. Int. Ed. Engl.* **1996**, *35*, 417–419; c) S. Kammermeier, P. G. Jones, R. Herges, *Angew. Chem.* **1996**, *108*, 2834–2836; *Angew. Chem. Int. Ed. Engl.* **1996**, *35*, 2669–2671; d) S. Kammermeier, P. G. Jones, R. Herges, *Angew. Chem.* **1997**, *109*, 2317; *Angew. Chem. Int. Ed. Engl.* **1997**, *36*, 2200–2202; e) S. Kammermeier, P. G. Jones, I. Dix, R. Herges, *Acta Crystallogr. Sect. C* **1998**, *54*, 1078–1081; f) R. Herges, M. Deichmann, J. Grunenberg, G. Bucher, *Chem. Phys. Lett.* **2000**, *327*, 149–152; g) F. Diederich, Y. Rubin, C. B. Knobler, R. L. Whetten, K. E. Schriver, K. N. Houk, *Science* **1989**, *245*, 1088–1090; h) Y. Rubin, C. B. Knobler, F. Diederich, *J. Am. Chem. Soc.* **1990**, *112*, 1607–1617; i) Y. Tobe, T. Fujii, H. Matsumoto, K. Naemura, Y. Achiba, T. Wakabayashi, *J. Am. Chem. Soc.* **1996**, *118*, 2758–2759.

[2] For review see: A. Hirsch, *Angew. Chem.* **2002**, *114*, 1933–1939; *Angew. Chem. Int. Ed.* **2002**, *41*, 1853–1859.

 © 2003 Wiley-VCH Verlag GmbH & Co. KGaA, Weinheim 1433-7851/03/4210-1171 $ 20.00+.50/0

[3] a) C. W. Bauschlicher, *Chem. Phys. Lett.* **2000**, *322*, 237–241; b) K. F. Kelly, I. W. Chiang, E. T. Mickelson, R. H. Hauge, J. L. Margrave, X. Wang, G. E. Scuseria, C. Radloff, N. J. Halas, *Chem. Phys. Lett.* **1999**, *313*, 445–450; c) P. J. Boul, J. Liu, E. T. Mickelson, C. B. Huffman, L. M. Ericson, I. W. Chiang, K. A. Smith, D. T. Colbert, R. H. Hauge, J. L. Margrave, R. E. Smalley, *Chem. Phys. Lett.* **1999**, *310*, 367–372; d) E. T. Mickelson, C. B. Huffman, A. G. Rinzler, R. E. Smalley, R. H. Hauge, J. L. Margrave, *Chem. Phys. Lett.* **1998**, *296*, 188–194; e) Y. Chen, R. C. Haddon, S. Fang, A. M. Rao, P. C. Eklund, W. H. Lee, E. C. Dickey, E. A. Grulke, J. C. Pendergrass, A. Chavan, B. E. Haley, R. E. Smalley, *J. Mater. Res.* **1998**, *13*, 2423–2431; f) S. Banerjee, S. Wong, *J. Am. Chem. Soc.* **2002**, *124*, 8940–8948.

[4] a) D. B. Mawhinney, V. Naumenko, A. Kuznetsova, J. T. Yates, Jr., J. Liu, R. E. Smalley, *J. Am. Chem. Soc.* **2000**, *122*, 2383–2384; b) S. S. Wong, A. T. Wooley, E. Joselevich, C. M. Lieber, *Chem. Phys. Lett.* **1999**, *306*, 219–225; c) J. E. Riggs, D. B. Walker, D. L. Carroll, Y.-P. Sun, *J. Phys. Chem. B* **2000**, *104*, 7071–7076; d) S. S. Wong, E. Joselevich, A. T. Wooley, C. L. Cheung, C. M. Lieber, *Nature* **1998**, *394*, 52–55; e) S. S. Wong, A. T. Wooley, E. Joselevich, C. L. Cheung, C. M. Lieber, *J. Am. Chem. Soc.* **1998**, *120*, 8557–8558; f) J. Chen, H. H. Hamon, Y. Chen, A. M. Rao, P. C. Eklund, R. C. Haddon, *Science* **1998**, *282*, 95–98.

[5] a) M. Oda, H. R. Darabi, private comunication; b) A. Kuznetsova, J. T. Yates, Jr., J. Liu, R. E. Smalley, *J. Chem. Phys.* **2000**, *112*, 9590–9598; c) B. W. Smith, D. E. Luzzi, *Chem. Phys. Lett.* **2000**, *321*, 169–174; d) S. M. Lee, K. S. Park, Y. C. Choi, Y. S. Park, J. M. Bok, D. J. Bae, K. S. Nahm, Y. G. Choi, S. C. Yu, N.-G. Kim, T. Frauenheim, Y. H. Lee, *Synth. Met.* **2000**, *113*, 209–216; e) X. Fan, E. C. Dickey, P. C. Eklund, K. A. Williams, L. Grigorian, R. Buczko, S. T. Pantelides, S. Pennycook, *Phys. Rev. Lett.* **2000**, *84*, 4621–4624.

[6] However, because of solvent disorder, the refinement was not sufficiently accurate to obtain reliable geometry parameters.

[7] In accordance with H. A. Szymanski, J. J. Antkowiak, L. A. Baumann, Jr., *Anal. Chem.* **1968**, *40*, 243 and A. K. Bose, M. Sugiura, P. R. Srinivasan, *Tetrahedron Lett.* **1975**, 1251–1254, we found that $AsCl_3$ is a very good solvent for large polycyclic aromatic compounds. The solubility of **1**–**3** is an order of magnitude higher in this solvent than in CS_2 and chlorotoluene.

 © 2003 Wiley-VCH Verlag GmbH & Co. KGaA, Weinheim 1433-7851/03/4210-1172 $ 20.00+.50/0

Stable Tetraanionic Carbon Tubes

Picotube Tetraanion: A Novel Lithiated Tubular System**

Noach Treitel, Markus Deichmann, Tamar Sternfeld, Tuvia Sheradsky, Rainer Herges, and Mordecai Rabinovitz**

Carbon nanotubes have attracted considerable attention since their discovery,[1] and have recently been the focus of intensive investigations. Studies have revealed that nanotubes exhibit extraordinary electronic properties.[2,3] Nanotubes have been shown to ignite upon exposure to short-range flashes of light,[2] and recently ultrafast carbon-nanotube-based transistors have been shown to outperform their silicon counterparts.[3]

The electronic and magnetic properties of such tubes might be studied with guest atoms present inside the tube, such as in fullerenes.[4] However, standard nanotubes, as well as fullerenes, are highly insoluble in most solvents, which makes such studies rather intricate. Additionally, nanotubes are end-capped, and the insertion of atoms or cations into the tube is very difficult. The conjugated tubelike polycyclic aromatic hydrocarbon (PAH) 5,24:6,11:12,17:18,23-tetra[1,2]-benzenotetrabenzo[*a,e,i,m*]cyclohexadecene (**1**), dubbed "picotube",[5] has successfully been synthesized in gram amounts through the dimerization metathesis of tetradihydrodianthracene.[6a]

Picotube **1** possesses open ends and is more soluble than standard nanotubes. In addition, its nanotube-like structure and fullerene-like ability to include endohedral atoms makes it an ideal candidate for further study. The picotube could play a role as a host molecule, by encapsulating one or more counterions upon charging, while possibly coordinating with others on the exterior. The specific orientation of such cations could also reveal information regarding the charge distribution within the molecule.

[*] Prof. Dr. R. Herges, M. Deichmann
Institut für Organische Chemie
Universität Kiel
Otto-Hahn Platz 4, 24098 Kiel (Germany)
Fax: (+49) 431-8801-558
E-mail: rherges@oc.uni-kiel.de

Prof. M. Rabinovitz, N. Treitel, T. Sternfeld, Prof. T. Sheradsky
Department of Organic Chemistry and
The Lise Meitner Minerva Center for Computational Chemistry
Safra Campus, The Hebrew University of Jerusalem
Givat Ram, Jerusalem 91904 (Israel)
Fax: (+972) 2-652-7547
E-mail: mordecai@vms.huji.ac.il

[**] Financial support from the US-Israel Binational Science Foundation (BSF) and from the Lise Meitner-Minerva Center for Computational Quantum Chemistry is gratefully acknowledged. We thank Prof. Silvio Biali for insight and fruitful discussions.

Supporting information for this article is available on the WWW under http://www.angewandte.org or from the author.

 © 2003 Wiley-VCH Verlag GmbH & Co. KGaA, Weinheim 1433-7851/03/4210-1172 $ 20.00+.50/0

Picotube **1** has been fully characterized by NMR spectroscopy, mass spectrometry, density functional theory (DFT) calculations, matrix IR spectroscopy and crystal structure analysis.[6a–c] The latter reveals that the picotube, which consists of four anthracene units, has a diameter of 5.4 Å and a length of 8.2 Å, and shows D_{4h} symmetry for the neutral species **1**.[6c] However, DFT calculations and low-temperature IR studies indicate that the D_{4h} symmetry is only a time-averaged structure of two rapidly interconverting D_{2d} isomers (Figure 1), obtained by twisting of the quinoid double

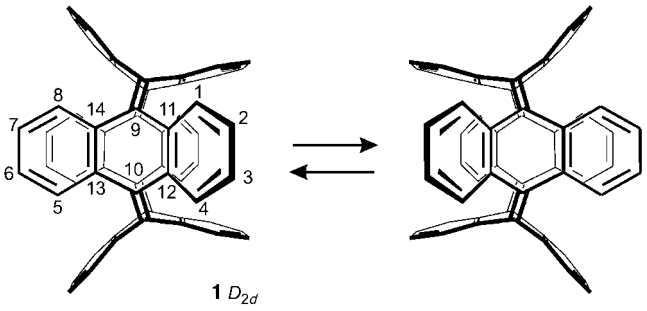

Figure 1. Rapid interconversion of neutral **1** (D_{2d}), to yield a D_{4h} time-averaged structure.

bonds.[7] This lowering of symmetry has been calculated to provide an energy gain of about 4.5 kcal mol^{-1}, relative to D_{4h} symmetry.

^{1}H and ^{13}C NMR spectroscopy[6a] show that picotube **1** indeed possesses D_{4h} symmetry on the NMR timescale, with only one AA′BB′ pattern in the proton spectrum and four resonances in the carbon spectrum (Figure 2a). Previously,[6a] the freezing of conformational movement could not be observed down to 203 K, and in the present study, no splitting of the signals was seen, even at 150 K, which indicates that the barrier for topomerization of the neutral molecule is lower than 7.8 kcal mol^{-1},[8] in good agreement with calculated values.[6b]

In view of the interest in introducing alkali metals into nanotubes, we report that the picotube undergoes slow chemical reduction by lithium metal to form an unusually stable charged species.[9] The ^{1}H NMR spectrum of the light-yellow neutral species tends to broaden as the solution becomes olive green. The spectrum loses its form as the solution further changes color, first to dark green, and then to dark blue, most likely as a result of the formation of paramagnetic species. Finally a dark-brown solution is obtained which gives a different ^{1}H NMR spectrum (Figure 2b) to that of the neutral species. Since the olive-green solution must contain a species that has, at least, been reduced to a radical anion, and the dark-blue solution contains a dianionic species, then the diamagnetic dark-brown solution must contain a species which can be no less reduced than a tetraanion. Charge-density calculations from ^{13}C NMR spectroscopy show a value for K_c[10] of approximately 131 ppm per electron, in accordance with the formation of a quadruply charged species.[11] DFT calculations using gauge-including atomic orbitals (GIAO) [12] also reinforce the assessment that the reduced species is a tetraanion (see below).

No diamagnetic species were observed until the formation of the tetraanion, and further attempts at reduction failed to yield new products. The dianion is, therefore, likely to be an easily reduced triplet diradical or unstable singlet. The tetraanion was fully characterized by NMR spectroscopy, and charge-density calculations support its nature. According to the ^{1}H NMR spectrum, quenching of the tetraanion with oxygen leads to the near quantitative and immediate recovery

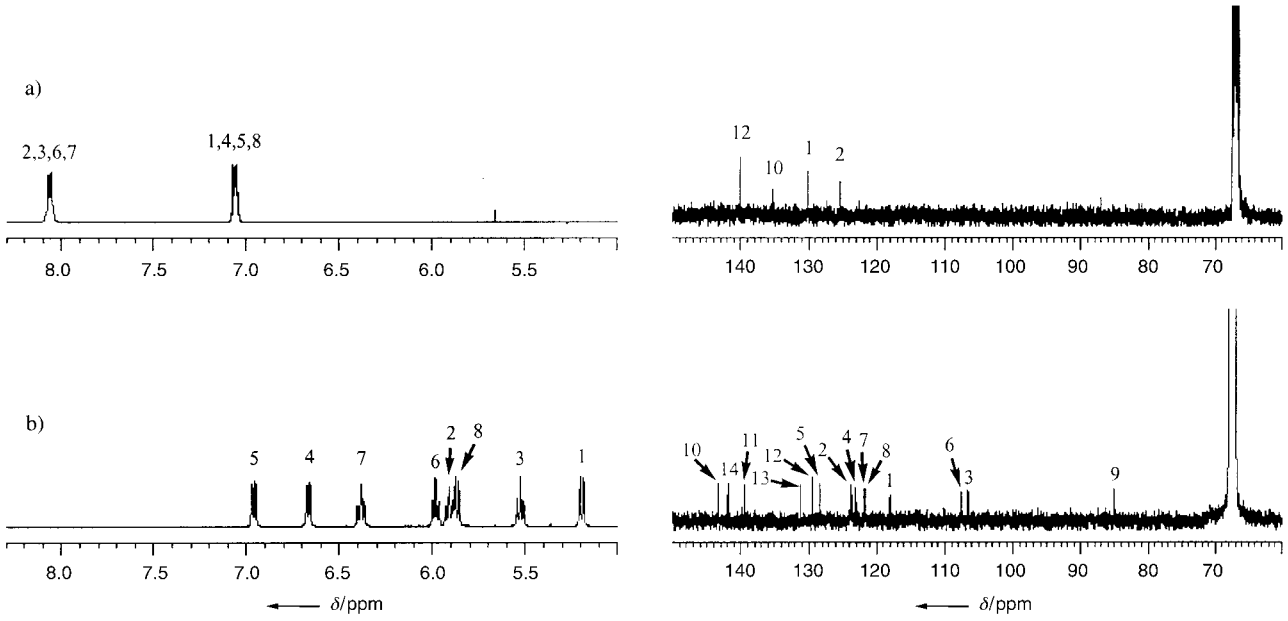

Figure 2. ^{1}H and ^{13}C NMR (400 and 100 MHz, respectively, [D$_8$]THF, 298 and 220 K for the neutral and charged species, respectively) of a) the neutral picotube and b) the charged species.

 © 2003 Wiley-VCH Verlag GmbH & Co. KGaA, Weinheim 1433-7851/03/4210-1173 $ 20.00+.50/0

of the neutral compound, which indicates that no bonds are formed or cleaved during the reduction process.

In contrast to the neutral compound, the tetraanion gives more complex spectra, with eight proton signals and fourteen carbon lines observed (Figure 2b). The picotube is thus reduced to a species with lower symmetry (C_2, C_4, or D_2). The proton signals are found in two groups, and can be shown[13a] to be representative of one system, the anthracenic unit. Each hydrogen and carbon atom of any given anthracene unit is different, and gives a characteristic resonance; bond cleavage would result in a different number of proton and carbon signals. The very fast dynamic motion, which is only detectable by matrix IR spectroscopy in the neutral compound, slows down dramatically in the charged species. The tetraanion shows no coalescence of signals, even at 325 K. This result means that the barrier of the "$D_{2d} \rightleftarrows [D_{4h}]^{\pm} \rightleftarrows D_{2d}$"[14] dynamic process (Figure 1) increases considerably to give a lower limit for $\Delta G^{\pm}_{325}$ of approximately 19.3 kcal mol^{-1} for the tetraanion.[15]

No decomposition of the tetraanion is seen, even after standing at room temperature for one week. Furthermore, after heating the tetraanion to 325 K, the NMR signals only become slightly broadened, and only disappear when the temperature is further raised to that of boiling THF; upon cooling the solution, the signals return to their original intensity. Only a few PAH tetraanions without stabilizing substituents that are stable in boiling THF are currently known.

The tetraanion exhibits a significant charge alternation[16] encircling the 9,10 positions of the anthracenylidene units. While the carbon atom in the 9 position shows a ^{13}C NMR resonance at $\delta = 85.0$ ppm, position 10 gives rise to a signal at $\delta = 143.3$ ppm. This difference between the two carbon atoms, which have identical chemical shifts in the neutral compound, is significant and indicates a highly irregular charge distribution within the anthracenylidene units (Figure 3a), which is contrary to the behavior of anthracene upon reduction[17] (Figure 3b). The carbon atom in the 9 position bears a partial negative charge (ca. -0.4), while that in the 10 position carries a positive charge of $+0.06$. The question as to whether the anthracene units arrange the charge alternation in a neutral-neutral-negative-negative or a neutral-negative-neutral-negative fashion was answered by 2D NMR methods;[13b] the preferred pattern is charge alternation (Figure 4).

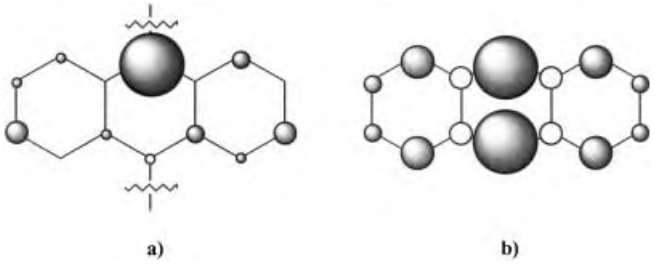

Figure 3. Charge distribution within a) the anthracenylidene units of **1** and b) the anthracene dianion[17], as calculated from ^{13}C NMR chemical shifts. Filled circles represent negative charge; hollow circles represent positive charge.

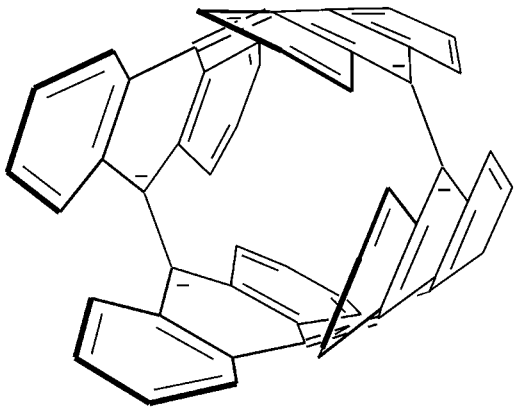

Figure 4. Charge alternation throughout the tetraanion.

In agreement with similar structures investigated by Schleyer and Pople,[18a] the NMR data strongly suggest that two of the Li atoms are coordinated to two of the quinoid "double bonds"[19] and bridge the sp^2 carbon atoms. The remaining two olefin units are uncoordinated according to the experimental data (charge alternation). Because of the small size of the cavity, coordination is only possible from outside the tube. The remaining two Li atoms are located so as to interact with the aromatic systems, either outside or inside the tube. A systematic DFT study[12] of numerous conceivable geometries was performed to find the optimum location of the other two Li atoms, which led to a global minimum of C_2 symmetry, with two Li atoms positioned inside the tube, separated by 2.61 Å. The endohedral Li atoms coordinate to the double bonds that are already coordinated by Li$^+$ ions from outside the tube, to form doubly bridged ethylene units that are analogous to the 1,2-dilithioethane structure investigated by Schleyer, Pople, et al.[18a] A similar structure has been observed in a stilbene–dilithium complex.[18c] An even stronger interaction (C–Li 2.14 Å) was found with the *ipso* carbon atom of a neighboring benzene ring. Our theoretical finding that two of the Li atoms are bound inside the tube is further supported by an X-ray structural analysis of the picotube–Ag$^+$ complex (1:2 stoichiometry), in which two Ag$^+$ ions occupy similar positions inside the tube[6c] as were found for Li$^+$ ions in our calculations. Structures investigated with four Li atoms either all outside or inside the tube were all found to be considerably less stable than the above C_2 structure. According to the calculations, the C_2 structure undergoes a fast racemization to give a time-averaged D_2 structure.

The proposed structure is corroborated by a comparison of the theoretically calculated and experimental ^{13}C NMR spectra of the time-averaged D_2 structure (Figure 5). The calculations[12] confirm the large variance between the carbon atoms in the 9 and 10 positions, and predict an even larger difference in $\Delta\delta$ than found by experimentation. All other shifts agree within the error limit of the method (Table 1). The large deviation between theory and experiment of almost 25 ppm for the anionic centers (position 9) can be accounted for by solvation of the coordinated Li ions. While the Li atoms inside the tube are shielded from the solvent, the

 © 2003 Wiley-VCH Verlag GmbH & Co. KGaA, Weinheim 1433-7851/03/4210-1174 $ 20.00+.50/0

Table 1: Calculated (B3LYP/6-31G*, GIAO) and experimental ^{13}C NMR shifts of the tetraanion.

Carbon No.	1	2	3	4	5	6	7	8	9	10	11	12	13	14
Experimental[a,b] (Rank)[c]	118.1(11)	123.7(7)	106.6(13)	123.0(8)	128.4(6)	107.7(12)	121.8(9)	121.6(10)	85.0(14)	143.3(1)	139.4(3)	129.4(5)	131.1(4)	141.9(2)
Calculated[a,d,e] (Rank)[c]	111.3(12)	120.9(9)	110.6(13)	125.8(6)	121.3(7)	112.5(11)	121.1(8)	119.4(10)	60.3(14)	140.2(1)	133.0(2)	126.8(5)	129.5(4)	131.0(3)
Deviation [%][f]	5.8	2.3	3.7	2.2	5.5	4.3	0.6	1.8	29.1	2.2	4.6	2.0	1.2	7.7
Rank Deviation[g]	1	2	0	2	1	1	1	0	0	0	1	0	0	1

[a] In ppm, relative to TMS. [b] In [D_8]THF, at 220 K. [c] Rank order for experimental and calculated values: 1–14 = lowest-to-highest field. [d] B3LYP/6-31G* optimized GIAO single-point calculation. [e] Averaged values for two independent anthracene units (see Supporting Information). [f] Deviation between experimental and calculated values. [g] Difference in experimental and calculated ranks.

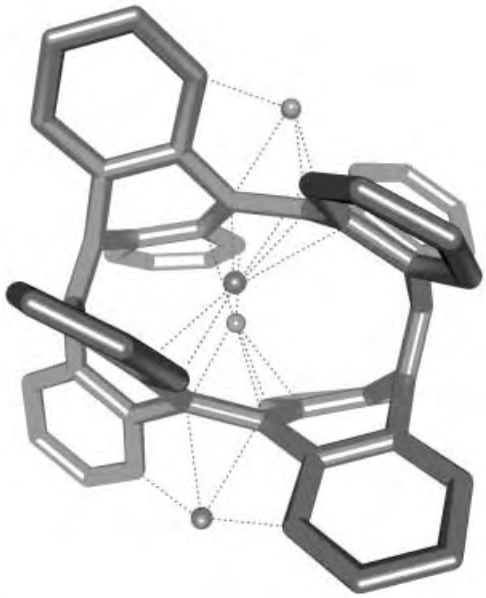

Figure 5. Computer-generated optimized structure of the picotube^{4-}/4 Li^+ complex at the B3LYP/6-31G* level, with black spheres representing the Li^+ cations. All Li–C distances shorter than 2.4 Å are indicated as dashed lines.

external Li atoms are strongly coordinated to THF. To estimate the solvent effect on the ^{13}C shifts of these carbon atoms, we performed calculations on the water-solvated (as a model for THF) system (fully optimized within C_2 symmetry). With one solvent molecule at each Li atom, the deviation is reduced to 21 ppm. Further solvation, or even formation of a solvent-separated ion pair thus accounts for the variation between theory and experiment.[20]

Consequently, it is most probable that a D_2 time-averaged structure is observed,[21] with a fast $C_2 \rightleftarrows [D_2]^{\ddagger} \rightleftarrows C_2$ equilibrium existing in solution. However, this process was not observed by NMR spectroscopy as the motion was apparently too rapid; no splitting of the signals was observed, even at 170 K. The conformational change could arise by small movements of two opposing anthracene units with respect to each other, rather than a concerted movement of all four units in the "$D_{2d} \rightleftarrows [D_{4h}]^{\ddagger} \rightleftarrows D_{2d}$" equilibrium.

The reduction in symmetry during the charging process is most probably a result of charge localization by the Li^+ counterions. Carbanions with Li^+ counterions are anything but free anions.[22] The C–Li bond may have a partial covalent character. ^7Li NMR indicates two different lithium cations, with a sharp signal at $\delta = -3.6$ ppm and a broader signal at $\delta = 0.2$ ppm (at 220 K). The latter signal may be attributed to a lithium cation that is externally coordinated to the picotube, while the former attests to another type, located within the tube;[23] support for this type of structure can be gained from calculations.[12]

To summarize, a host molecule in a stable tetraanionic state has been prepared that can host two Li^+ cations within the inner domain of a "tube-like" system resembling the edges of an open nanotube; this anion exhibits a lower symmetry than the neutral molecule. The change from a $D_{2d} \rightleftarrows [D_{4h}]^{\ddagger} \rightleftarrows D_{2d}$ dynamic process in the neutral system to a $C_2 \rightleftarrows [D_2]^{\ddagger} \rightleftarrows C_2$ equilibrium in the tetraanion is mainly caused by coordination of Li atoms[24] to the inner "walls" of the tube.

Received: October 1, 2002 [Z50277]

Keywords: carbon · density functional calculations · lithium · nanotubes · reduction

[1] S. Ijima, *Nature* **1991**, *354*, 56.
[2] P. M. Ajayan, M. Terrones, A. de la Guardia, V. Huc, N. Grobert, B. Q. Wei, H. Lezec, G. Ramanath, T. W. Ebbesen, *Science* **2002**, *296*, 705.
[3] S. J. Wind, J. Appenzeller, R. Martel, V. Derycke, P. Avouris, *Appl. Phys. Lett.* **2002**, *80*, 3817.
[4] a) M. Saunders, H. A. Jimenez-Vazquez, R. J. Cross, S. Mroczkowski, D. I. Freedberg, F. A. L. Anet, *Nature* **1994**, *367*, 256; b) E. Shabtai, A. Weitz, R. C. Haddon, R. E. Hoffman, M. Rabinovitz, A. Khong, R. J. Cross, M. Saunders, P.-C. Cheng, L. T. Scott, *J. Am. Chem. Soc.* **1998**, *120*, 6389.
[5] In analogy to the larger and fully conjugated nanotubes, and for simplicity.
[6] a) S. Kammermeier, P. G. Jones, R. Herges, *Angew. Chem.* **1996**, *108*, 2834; *Angew. Chem. Int. Ed. Engl.* **1996**, *35*, 2669; b) R. Herges, M. Deichmann, J. Grunenberg, G. Bucher, *Chem. Phys. Lett.* **2000**, *327*, 149; c) S. Kammermeier, P. G. Jones, I. Dix, R. Herges, *Acta Crystallogr. Sect. C* **1998**, *54*, 1078.
[7] Despite torsion of the double bonds in the neutral compound, the electronic structure is mainly quinoid, rather than benzoid, and is slightly antiaromatic with 16 π electrons in the periphery. This is confirmed by the ACID method: R. Herges, A. Papafilippopoulos, *Angew. Chem.* **2001**, *113*, 4809; *Angew. Chem. Int. Ed.* **2001**, *40*, 4671; R. Herges, D. Geuenich, *J. Phys. Chem. A* **2001**, *105*, 3214.

 © 2003 Wiley-VCH Verlag GmbH & Co. KGaA, Weinheim 1433-7851/03/4210-1175 $ 20.00+.50/0

[8] Estimated with $\Delta G^{\ddagger} = 4.57\,T[10.32 - \log(k/T)]$, where $k = (\pi\Delta\upsilon)/\sqrt{2}$, and using a reasonable minimum proton resonance difference, $\Delta\upsilon_{min} = 5$ Hz, in the neutral state.

[9] The anions were prepared in the following manner: Lithium was directly inserted as a freshly produced wire into the upper part of an extended NMR tube containing the PAH (2–4 mg). The tube was first filled with argon, attached to a vacuum line, and flame-dried under vacuum. Approximately 0.5 mL of [D_8]THF (yielding 6–11 mM solutions), dried over a sodium/potassium alloy under high vacuum, was vacuum transferred from a reservoir into the tube. The sample was degassed under vacuum using the freeze-pump-thaw technique and flame sealed. The solution was brought into contact with the lithium wire by turning the tube upside down and the tube was repeatedly inverted at −78 °C. ^{1}H NMR spectroscopy detected the formation of the anions.

[10] This parameter has been empirically shown to correlate between the total change in chemical shift of the ^{13}C NMR spectrum upon charging, $\Sigma\Delta\delta$, and the total extra charge added to the π system of the molecule upon charging, $\Sigma\Delta q_\pi$, as expressed in the equation: $\Sigma\Delta\delta = K_c\Sigma\Delta q_\pi$. In our case, $\Sigma\Delta\delta = 524$ ppm. For a review, see: a) S. Braun, H.-O. Kalinowski, S. Berger, *150 and More Basic NMR Experiments: A Practical Course*, VCH-Wiley, Weinheim, **1998**; b) R. Schaefer, W. G. Schneider, *Can. J. Chem.* **1963**, *41*, 966; c) H. Spiesecke, W. G. Schneider, *Tetrahedron Lett.* **1961**, 468; d) P. C. Lauterbur, *J. Am. Chem. Soc.* **1961**, *83*, 1838; e) P. C. Lauterbur, *Tetrahedron Lett.* **1961**, 274.

[11] a) A. Ayalon, M. Rabinovitz, P.-C. Cheng, L. T. Scott, *Angew. Chem.* **1992**, *104*, 1691; *Angew. Chem. Int. Ed. Engl.* **1992**, *31*, 1636; b) B. Eliasson, U. Edlund, K. Müllen, *J. Chem. Soc. Perkin Trans. 2* **1986**, 937.

[12] All structures were optimized at the B3LYP/6-31G* level of DFT theory within the corresponding point group, and confirmed by harmonic frequency analysis to be either minima or transition states. NMR shifts were calculated using the GIAO method. An extensive investigation of the energy hypersurface using the semiempirical PM3 method preceded the DFT calculations.

[13] a) Using standard 2D NMR techniques, that is, COSY, NOESY, HSQCSI, and HMBC. b) Clear nOe signals pertaining to carbon pairs 4 and 5, as well as 1 and 8, dismissed the possibility that the alternation is in a neutral-negative-neutral-negative fashion. A structure of two neutral anthracene units alternating with two anthracene dianion units is also possible, which gives the same symmetry. However, DFT calculations confirm the proposed structure, rather than this possibility.

[14] Quotation marks indicate that the dynamic process still exists in the tetraanion, although it is too slow to observe.

[15] Deduced from the Eyring equation, $\Delta G^{\ddagger} = 4.57\,T[10.32 - \log(k/T)]$; $k = 0.7$ s (from T_1), from NOESY spectrum at 325 K (maximum working temperature for THF). See, for example: J. Sandström, *Dynamic NMR Spectroscopy*, Academic Press, London, **1982**, p. 96.

[16] a) J. Klein, *Tetrahedron* **1983**, *39*, 2733; b) Y. Cohen, J. Klein, M. Rabinovitz, *J. Am. Chem. Soc.* **1988**, *110*, 4634.

[17] R. E. Hoffman, N. Treitel, E. Shabtai, R. Benshafrut, M. Rabinovitz, *J. Chem. Soc. Perkin Trans. 2* **2000**, 1007.

[18] a) A. J. Kos, E. D. Jemmis, P. von R. Schleyer, R. Gleiter, U. Fischbach, J. A. Pople, *J. Am. Chem. Soc.* **1981**, *103*, 4996; For further olefinic and aromatic lithium complexes, see for example: b) D. Scheschkewitz, M. Menzel, M. Hofmann, P. von R. Schleyer, G. Geiseler, W. Massa, K. Harms, A. Berndt, *Angew. Chem.* **1999**, *111*, 3116; *Angew. Chem. Int. Ed.* **1999**, *38*, 2936; c) R. Benken, W. Andres, H. Günther, *Angew. Chem.* **1988**, *100*, 1212; *Angew. Chem. Int. Ed. Engl.* **1988**, *27*, 1182; d) M. Walczak, G. Stucky, *J. Am. Chem. Soc.* **1976**, *98*, 5531; e) *Ab Initio Molecular Orbital Theory*, (Eds.: W. J. Hehre, L. Radom, P. von R. Schleyer, J. A. Pople), Wiley-Interscience, New York, **1986**, p. 450.

[19] In reference to the original double bonds in the neutral compound.

[20] Model calculations of the D_{2h} symmetric dilithio ethylene group at the same level of theory for both the unsolvated and solvated forms (with 4 H_2O ligands, D_{2h}) revealed an upfield shift of the sp^2 carbon atoms of as much as 45.6 ppm.

[21] C_2 symmetry would give rise to 16 proton and 28 carbon resonances.

[22] M. Szwarc, *Carbanions, living polymers, and electron transfer processes*, Wiley, New York, **1968**.

[23] An extreme case in which two types of Li^+ cations appear is reported in: A. Ayalon, A. Sygula, P.-C. Cheng, M. Rabinovitz, P. W. Rabideau, L. T. Scott, *Science* **1994**, *265*, 1065.

[24] The picotube also undergoes reduction with a potassium metal mirror. However, preliminary results show that potassium apparently leads to bond cleavage, to yield a species with different symmetry than that of the [picotube]$^{4-}$/4 Li^+ complex.

 © 2003 Wiley-VCH Verlag GmbH & Co. KGaA, Weinheim 1433-7851/03/4210-1176 $ 20.00+.50/0

Cover Picture

Peter Schwerdtfeger,* Johannes Gierlich, and Tobias Bollwein

What you see is not always what you get. The cover picture shows Lake Matheson in New Zealand, famous for its reflections of Mt. Cook and Mt. Tasman, where the still waters can make it difficult to tell the mountains from their reflection. Mirror-image symmetry can break down in the microscopic world (parity violation), and high-resolution spectroscopy cannot distinguish between molecular enantiomers. The $[(C_5H_5)Re(CO)(NO)I]$ molecule gives very large parity-violation energy differences that bring us closer to detecting such tiny effects. More details of this study are given in the Communication by P. Schwerdtfeger et al. on page 1293ff.

Contents

Web Sites

Proteins: Consurf ——— 1193 | Never Change a Winning Horse | *C. Weise*

Books

The Politics of Excellence: Behind the Nobel Prize in Science ——— 1194 | Robert Marc Friedman | *reviewed by George B. Kauffman*

Robert Burns Woodward ——— 1196 | Otto T. Benfey, Peter J. T. Morris | *reviewed by Kyriacos C. Nicolaou*

Highlights

Beyond the Icosahedral Carborane

R. N. Grimes* ——— 1198 – 1200

Supercarboranes

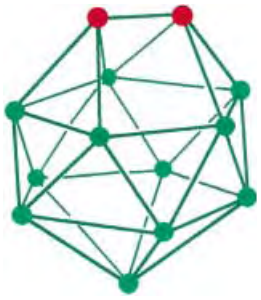

The "icosahedral barrier" in carborane chemistry has remained intact until now. Welch and co-workers have employed a carefully designed synthetic strategy to prepare and structurally characterize the first supra-icosahedral carborane having only boron and carbon in the framework (see picture), thereby ushering in a new and potentially exciting era in the so-called "mature" field of carborane chemistry.

Essays

Early Days of Structure Determination

L. Birladeanu* ——— 1202 – 1208

The Stories of Santonin and Santonic Acid

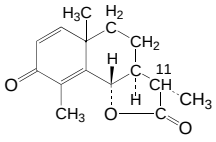

(–)-α-Santonin

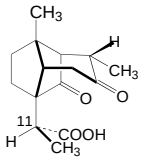

Santonic Acid

A juicy tale based on many fruitless efforts: The determination of the structure of the natural product santonin and its transformation product, santonic acid (see formulas), occupied organic chemists for nearly 80 years. The story of these efforts captures the early days in the practice of structure determination, and shows how difficult this exercise was before the availability of the powerful tools of IR and NMR spectroscopy, mass spectrometry, and the ultimate weapon, X-ray crystallography.

Reviews

Interactions with Arenes

E. A. Meyer, R. K. Castellano,*
F. Diederich* ——— 1210 – 1250

Interactions with Aromatic Rings in Chemical and Biological Recognition

The geometries and energetics of noncovalent interactions in chemistry and biology involving aromatic rings—such as π–π stacking and edge-to-face contacts, cation–π, arene–perfluoroarene, and sulfur–arene interactions, as well as H bonding to π surfaces—are analyzed taking into account the results from molecular recognition studies with artificial receptors, biostructural work, crystallographic database mining, gas-phase studies, and theoretical calculations. Shown here is a portion of the structure of

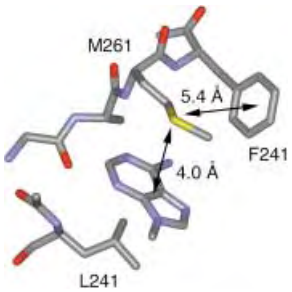

the chalcone *O*-methyltransferase with sulfur–adenosine interactions.

© 2003 Wiley-VCH Verlag GmbH & Co. KGaA, Weinheim

1433-7851/03/4211-1186 $ 20.00+.50/0

Communications

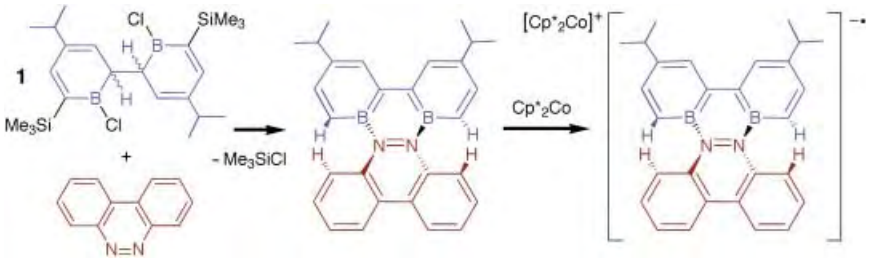

Lewis Acid Analogues of Bipyridines

D. J. H. Emslie, W. E. Piers,*
M. Parvez ——— 1252 – 1255

2,2′-Diborabiphenyl: A Lewis Acid Analogue of 2,2′-Bipyridine

A chelating Lewis acid analogue of the ubiquitous "bipy" ligand system has been prepared from the dichlorodiborane **1** (see scheme). Treatment of **1** with a variety of Lewis bases, such as the bifunctional benzo[*c*]cinnoline shown, leads to loss of two equivalents of Me_3SiCl and formation of the Lewis base adducts of 2,2′-diborabiphenyl. Some of these compounds are isoelectronic with polycyclic aromatic hydrocarbons and exhibit interesting optical and redox properties.

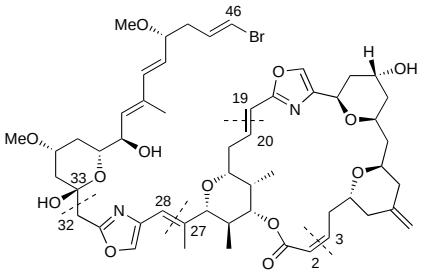

Macrolide Synthesis

M. A. González,
G. Pattenden* ——— 1255 – 1258

A Convergent Total Synthesis of Phorboxazole A

The potent cytostatic marine metabolite phorboxazole A (see structure) was prepared from three key fragments. Following attachment of a major portion of the side chain through C32–C33 and an intermolecular *E*-selective olefination reaction to form the C19–C20 double bond, the C2–C3 double bond was put in place through an intramolecular *Z*-selective olefination reaction, with formation of the macrolide.

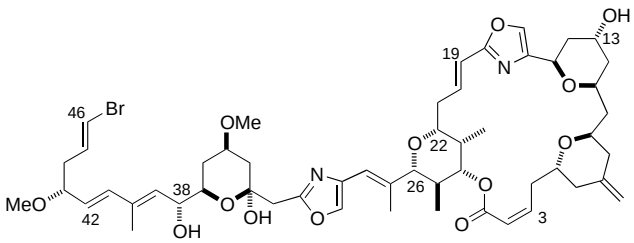

Macrolide Synthesis

D. R. Williams,* A. A. Kiryanov, U. Emde, M. P. Clark, M. A. Berliner, J. T. Reeves ——— 1258 – 1262

Total Synthesis of Phorboxazole A

Asymmetric allylation reactions of stannyl-derived allyldiazaborolanes, a stereoselective cationic cyclization reaction for the formation of the fully substituted C22–C26 tetrahydropyran, and the use of a Julia olefination for the incorporation of the sensitive C37–C46 dienyl system are key features of a highly convergent, stereocontrolled total synthesis of phorboxazole A (see structure).

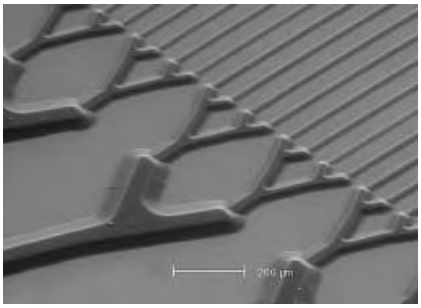

Microfabrication of 3D Structures

D. A. LaVan, P. M. George, R. Langer* ——— 1262 – 1265

Simple, Three-Dimensional Microfabrication of Electrodeposited Structures

A simplified preparation of three-dimensional microfabricated structures requires only a small number of experimental steps and a single photolithographic mask. The process has been used to mimic microfluidic vascular networks (see picture) and can be achieved with such diverse materials as pure nickel and polypyrrole, thus allowing for great diversity in the as-prepared devices.

 © 2003 Wiley-VCH Verlag GmbH & Co. KGaA, Weinheim 1433-7851/03/4211-1187 $ 20.00+.50/0

Contents

Aerobic Oxidation of Amines

S. L. Jain, B. Sain* ——— **1265 – 1267**

An Unconventional Cobalt-Catalyzed Aerobic Oxidation of Tertiary Nitrogen Compounds to *N*-Oxides

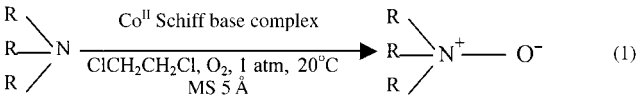

A simple system, simple workup, and excellent yields make the new method for the oxidation of tertiary nitrogen compounds described in Equation (1) an attractive, environmentally acceptable synthetic tool. Molecular oxygen serves as the oxygen source and no sacrificial agents are required.

Diterpene Anti-tuberculosis Agents

A. I. Kim, S. D. Rychnovsky* **1267 – 1270**

Unified Strategy for the Synthesis of (−)-Elisapterosin B and (−)-Colombiasin A

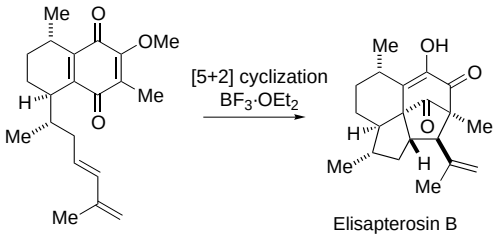

1

A biomimetic [5+2] cyclization of a serrulatane diene (**1**) forms the basis of a concise synthesis of (−)-elisapterosin B. The diene **1** was prepared in 15 steps by using a Diels–Alder reaction between an oxygenated diene and a quinone, followed by the introduction of the methyl group at C3. The same diene **1** was used to prepare the natural product (−)-colombiasin A by a thermal [4+2] cycloaddition and demethylation.

Dynamic Combinatorial Libraries

B. Brisig, J. K. M. Sanders, S. Otto* ——— **1270 – 1273**

Selection and Amplification of a Catalyst from a Dynamic Combinatorial Library

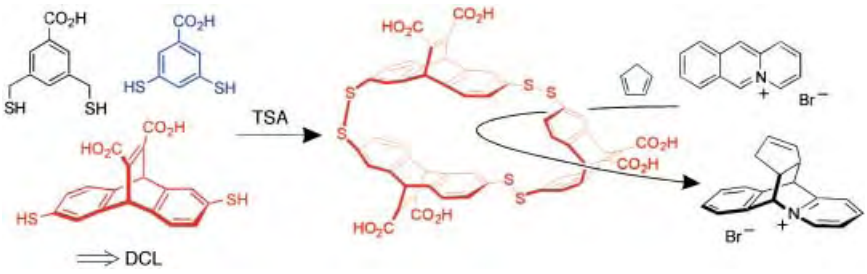

Amplification of the fittest: A dynamic combinatorial library (DCL) of macrocyclic disulfides in water was exposed to a transition-state analogue (TSA) for a Diels–Alder reaction. Two receptors were selected and amplified, of which one binds to the TSA more strongly than to the starting material and catalyzes the Diels–Alder reaction (see scheme).

Allyl-Transfer Reactions

J. Nokami,* K. Nomiyama, S. Matsuda, N. Imai, K. Kataoka ——— **1273 – 1276**

Highly Enantioselective Alk-2-enylation of Aldehydes through an Allyl-Transfer Reaction

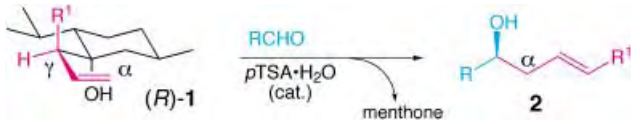

Enantiopure homoallylic alcohols such as **1** (conveniently prepared from alk-2-enyl metal reagents with (−)- or (+)-menthone) serve as alk-2-enyl donors to aldehydes. The allyl-transfer reaction, which proceeds via a chairlike six-membered-ring transition state, gives the corresponding α adduct of the homoallylic alcohols, **2**, in good yields with >99% *ee*. *p*TSA = *p*-toluenesulfonic acid.

© 2003 Wiley-VCH Verlag GmbH & Co. KGaA, Weinheim
1433-7851/03/4211-1188 $ 20.00+.50/0

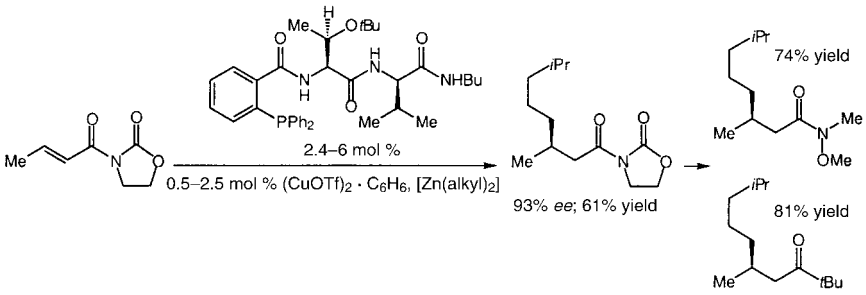

Asymmetric Conjugate Addition

A. W. Hird, A. H. Hoveyda* — 1276 – 1279

Cu-Catalyzed Enantioselective Conjugate Additions of Alkyl Zinc Reagents to Unsaturated *N*-Acyloxazolidinones Promoted by a Chiral Triamide Phosphane

A chiral triamide phosphane promotes highly efficient and enantioselective Cu-catalyzed conjugate additions of alkyl zinc compounds to unsaturated oxazolidinones (see scheme). The resulting β-alkyl chiral oxazolidinones are readily converted into synthetically useful carbonyl compounds not accessible by alternative catalytic methods.

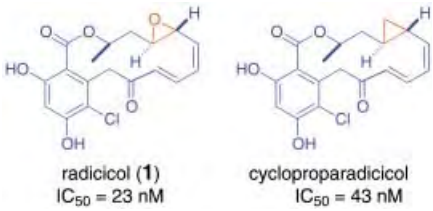

Synthesis of Antitumor Agents

K. Yamamoto, R. M. Garbaccio, S. J. Stachel, D. B. Solit, G. Chiosis, N. Rosen, S. J. Danishefsky* — 1280 – 1284

Total Synthesis as a Resource in the Discovery of Potentially Valuable Antitumor Agents: Cycloproparadicicol

A highly convergent synthesis was used to prepare a series of epimers and analogues of radicicol (**1**). Biological assessment revealed a previously unrecognized correlation between stereochemistry and antitumor potential in these compounds. Significantly, cycloproparadicicol (**2**) showed promising therapeutic properties based on inhibition of chaperones.

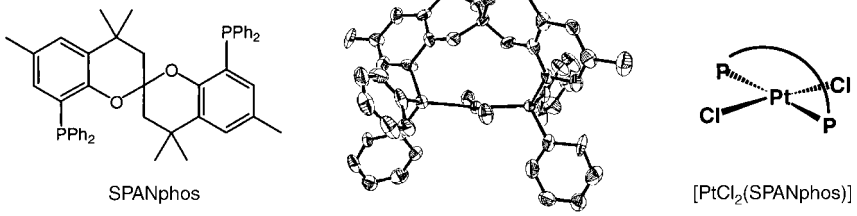

trans-Coordinating Diphosphane

Z. Freixa, M. S. Beentjes, G. D. Batema, C. B. Dieleman, G. P. F. van Strijdonck, J. N. H. Reek, P. C. J. Kamer, J. Fraanje, K. Goubitz, P. W. N. M. van Leeuwen* — 1284 – 1287

SPANphos: A C_2-Symmetric *trans*-Coordinating Diphosphane Ligand

Exclusively *trans* coordination is exhibited by SPANphos, a C_2-symmetric diphosphane ligand containing a spiro center, which can be easily synthesized in three steps from cheap reagents. The crystal structures of the ligand and of the complex [$PtCl_2$(SPANphos)] show large P···P distances, and reflect the C_2 symmetry of the ligand.

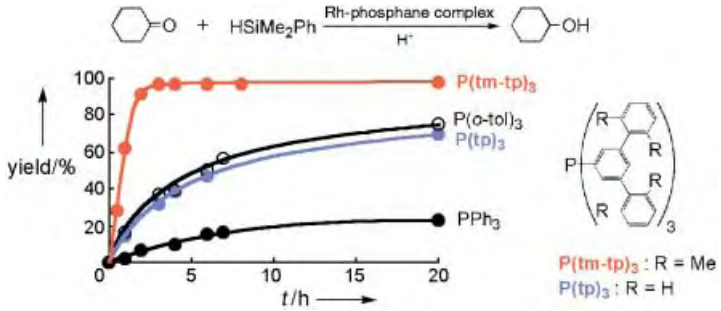

High-Speed Hydrosilylation

O. Niyomura, M. Tokunaga, Y. Obora, T. Iwasawa, Y. Tsuji* — 1287 – 1289

Rate Enhancement with a Bowl-Shaped Phosphane in the Rhodium-Catalyzed Hydrosilylation of Ketones

Up to 154-fold rate enhancement (see picture) and higher yields are achieved with the bowl-shaped triarylphosphane ligand P(tm-tp)$_3$ compared with common phosphane ligands in Rh-catalyzed hydrosilylation of ketones. The superior performance of P(tm-tp)$_3$ over the similar P(tp)$_3$ is apparently related to the deeper bowl formed by the methyl-bearing terphenyl substituents in the former.

 © 2003 Wiley-VCH Verlag GmbH & Co. KGaA, Weinheim 1433-7851/03/4211-1189 $ 20.00+.50/0

Contents

Radioactive Isotope Complexation

M. Desage-El Murr, S. Nowaczyk, T. Le Gall,* C. Mioskowski,* B. Amekraz,* C. Moulin _____ **1289 – 1293**

Norbadione A: Synthetic Approach to the Bis(pulvinic acid) Moiety and Cesium-Complexation Studies

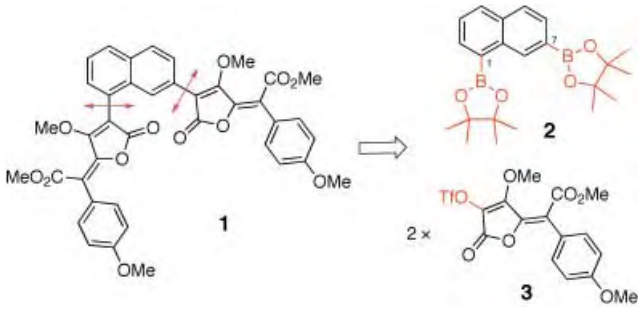

A permethylated analogue 1 of the mushroom pigment norbadione A was synthesized through a double Suzuki–Miyaura coupling of 1,7-diboronated naphthalene **2** and triflate **3**. ESI-MS studies showed similar constants for the formation of the complexes of the norbadione A dipotassium salt and of **1** with a cesium ion, thus suggesting that cesium complexation involves the two pulvinic acid parts of these molecules. T_f = trifluoromethanesulfonyl.

Parity-Violation Effects

P. Schwerdtfeger,* J. Gierlich, T. Bollwein _____ **1293 – 1296**

Large Parity-Violation Effects in Heavy-Metal-Containing Chiral Compounds

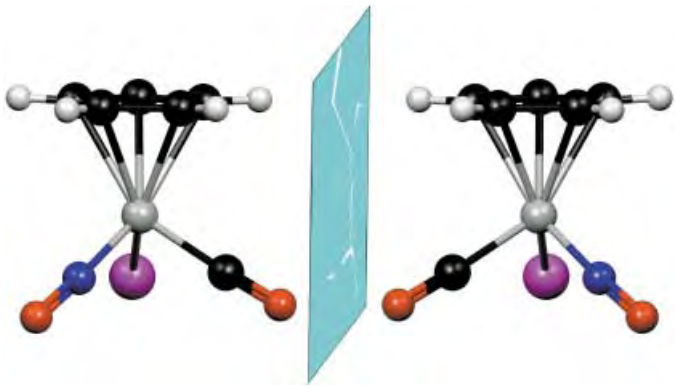

Mirror, mirror on the wall, which is the most stable of them all? Large parity-violation energy differences of up to 300 Hz are predicted for a number of chiral transition-metal compounds containing heavy elements. These molecules are ideal candidates for high-resolution spectroscopy experiments to detect the breakdown of mirror-image symmetry in molecules for the first time.

Cluster-Dependent Catalysis

H. Häkkinen,* S. Abbet, A. Sanchez, U. Heiz,* U. Landman _____ **1297 – 1300**

Structural, Electronic, and Impurity-Doping Effects in Nanoscale Chemistry: Supported Gold Nanoclusters

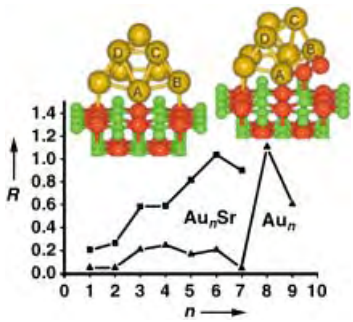

A nano gold rush: Nanoscale gold clusters on oxide surfaces exhibit unique catalytic activity (▲; R = chemical reactivity). The factors for these remarkable nanocatalytic properties are 1) structural dynamical fluxionality, 2) quantum size effects, 3) charge transfer from the support to the clusters, and 4) impurity doping effects (■) that allow control of the electronic structure of small clusters.

© 2003 Wiley-VCH Verlag GmbH & Co. KGaA, Weinheim
1433-7851/03/4211-1190 $ 20.00+.50/0

Differentiating the identical: The measurement of homonuclear coupling constants of spins with identical chemical shifts (as observed in 1,2-disubstituted ethenes) provides important structural information, but its experimental realization is not trivial. A new method results in high sensitivity and simple spectra (see picture) that are easy to interpret. The underlying principle of this method is not limited to symmetric molecules with equivalent spins, but can also be applied to olefinic protons that have similar resonance frequencies.

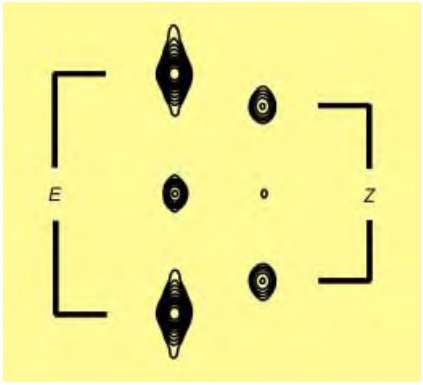

NMR Techniques

B. Luy, G. Hauser, A. Kirschning, S. J. Glaser* ——— **1300 – 1302**

Optimized NMR Spectroscopic Method for the Configurational Analysis of Chemically Equivalent Vicinal Protons

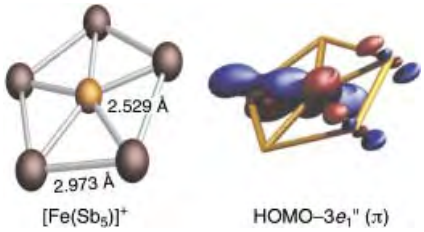

Iron enters the pentagon: Quantum chemical calculations using gradient-corrected DFT predict that the cations $[Fe(Sb_5)]^+$ and $[Fe(Bi_5)]^+$ in the electronic singlet state have planar (D_{5h}) equilibrium geometries (see scheme). Analysis of the electronic structure shows that the molecules are metal-centered six-π-electron aromatic species with strong iron–ligand π bonds which involve the d(π) atomic orbitals of the Fe center and the degenerate π orbital of the ring. The calculated ^{57}Fe NMR chemical shifts indicate extremely high deshielding of the metal nucleus.

Inorganic Cp Analogues

M. Lein, J. Frunzke, G. Frenking* ——— **1303 – 1306**

A Novel Class of Aromatic Compounds: Metal-Centered Planar Cations $[Fe(Sb_5)]^+$ and $[Fe(Bi_5)]^+$

The end of the Ice Age? Polyisobutenes with a high content of olefinic terminal groups can be synthesized by the use of manganese(II) initiators in homogeneous solution. These easily accessible complexes (see structure) initiate at room temperature, rather than at the sub-zero temperatures usually required, and allow the formation of highly reactive, gel-free polyisobutenes with a high viscosity. Furthermore, the initiators were successfully used for the copolymerization of isobutene with isoprene.

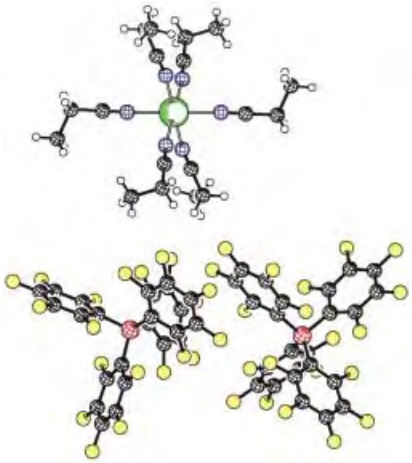

Manganese-Based Initiators

M. Vierle, Y. Zhang, E. Herdtweck, M. Bohnenpoll, O. Nuyken,* F. E. Kühn* ——— **1307 – 1310**

Highly Reactive Polyisobutenes Prepared with Manganese(II) Complexes as Initiators

VIP Communications labeled with this symbol have been judged by two referees as being "very important papers".

The publication of Communications labeled with this symbol has been accelerated because of their topical or highly competitive nature.

Supporting information for articles labeled with this symbol can be found at www.angewandte.org or www.interscience.wiley.com.

 © 2003 Wiley-VCH Verlag GmbH & Co. KGaA, Weinheim 1433-7851/03/4211-1191 $ 20.00+.50/0

Looking for outstanding employees?

Do you need another expert for your excellent team?
...Chemists, PhD Students, Managers, Professors, Sales Representatives...

Place an advert in the printed version and have it made available online for 1 month, free of charge!

Angewandte Chemie International Edition
Advertising Sales Department: Marion Schulz
Phone: 0 62 01 - 60 65 65
Fax: 0 62 01 - 60 65 50
E-Mail: MSchulz@wiley-vch.de

Service

Keywords ____ *1312*

Authors ____ *1313*

Angewandte's Sister Journals ____ *1314*

Preview ____ *1317*

40 Years of Chemistry History

★ The basis for a **journey of discovery** through all the important developments in chemistry and related disciplines

★ The **authors** and **keywords** of all the reviews that have appeared in ***Angewandte Chemie*** in the last 40 years

★ ***Now available at a special price of € 19.80*** (including postage)

Only available directly from:
Angewandte Chemie
Postfach 10 11 61
69451 Weinheim (Germany)
Telephone: (+49) 6201-606-265
Fax: (+49) 6201-606-331
E-mail: angewandte@wiley-vch.de

 © 2003 Wiley-VCH Verlag GmbH & Co. KGaA, Weinheim 1433-7851/03/4211-1192 $ 20.00+.50/0

Beyond the Icosahedral Carborane

Supercarboranes

*Russell N. Grimes**

Keywords:
boron · carboranes · cluster compounds · supercarboranes

The icosahedron is to boron what the hexagon is to carbon. The familiar layered structure of graphite, the thermodynamically preferred form of elemental carbon, is paralleled in boron chemistry by the B_{12} icosahedral unit, which is a feature of all known allotropes of the pure element.[1] The icosahedral $[B_{12}H_{12}]^{2-}$ dianion is the most stable covalently bonded molecule in all of chemistry (it is unaffected by 3 M aqueous HCl or concentrated NaOH, and its dicesium salt is unchanged at 810 °C);[2] it is, in fact, a three-dimensional "superaromatic" counterpart of benzene that has 26 delocalized valence electrons in its σ-bonded skeletal framework.[3] An icosahedral architecture is also found in the isoelectronic carborane analogues of $[B_{12}H_{12}]^{2-}$, which include the $[CB_{11}H_{12}]^-$ monoanion and the neutral dicarbon carboranes 1,2-, 1,7-, and 1,12-$C_2B_{10}H_{12}$, all of which exhibit extremely high oxidative and thermal stability and have given rise to thousands of characterized derivatives.[1,4] Additionally, there are many types of heterocarboranes—clusters having main-group atoms such as P, As, S, Se, Ge, Sn, or Pb as well as carbon in the cage framework—and metallacarboranes, in which transition-metal atoms are incorporated into the cluster skeleton.[1,4]

The carboranes and their cousins vary not only in composition, but in cluster size as well. For example, the *n*-vertex closed polyhedral (*closo*) carboranes of the general formula $C_2B_{n-2}H_n$ are known for all values of *n* from 5 to 12 (in some cases as more than one isomer), and a similar size range is found in the hetero- and metallacarboranes. Boron clusters with more than 12 vertices are confined to the 13- or 14-vertex $M_xC_2B_{10}$ or $M_xC_4B_8$ metallacarboranes where M is a transition metal and *x* is 1 or 2;[4a,5] the first clear example of a p-block 13-vertex cluster, $SnC_2B_{10}H_{12}$, was reported very recently.[6] Until now, the "icosahedral barrier" has remained intact for binary boron hydrides and for carboranes lacking cage heteroatoms, despite many theoretical predictions of the viability of supra-icosahedral boron hydride clusters.[7] Because of the extraordinary stability of the B_{12} icosahedron, cage-expansion methods that work with smaller clusters have, to date, been unsuccessful when applied to C_2B_{10}, CB_{11}, or B_{12} polyhedra; although attempted insertions of heteroatoms may in some cases form 13-vertex species, they are not isolable and revert to icosahedral products. So-called macropolyhedral boranes, which are covalently linked or fused assemblies of borane, carborane, or metallaborane cage units, have long been known,[1] but while their architectures are often interesting[8] these molecules contain no individual cluster modules larger than 12 vertices.

In light of this history, the achievement of Welch and his co-workers in breaching this formidable barrier, as described recently,[9] is impressive. More importantly, their approach is an eminently rational one that may well open the way to the controlled synthesis of even larger carborane polyhedra—a truly fascinating prospect that could lead to unprecedented new carborane-based chemistry. Their synthetic strategy employs a long-known technique in polyhedral borane chemistry, but with a novel twist.

Polyhedral expansion, a reaction type originated by Hawthorne and his students in the 1960s[10] and subsequently exploited greatly in metallacarborane chemistry,[1,4] is normally a two-stage process: a *closo* *n*-vertex cage system undergoes a cage-opening reduction that is followed by insertion of a new vertex into the "hole" to create an $(n+1)$-vertex *closo* polyhedron. The reverse process, oxidative cage-closure or polyhedral contraction,[10] entails the extraction of a boron vertex from an *n*-vertex cluster and the oxidation of the resulting anionic species to afford a neutral $(n-1)$-vertex product.[11] As applied to an icosahedral cage (structure **A**, Scheme 1), the addition of two electrons generates an open 12-vertex dianion, for example **B**, into which one can, in principle, insert $[BR]^{2+}$ (where R is H or a substituent group) to complete a neutral 13-vertex cluster such as **C**. Early carborane investigators found that the first step works easily with the $C_2B_{10}H_{12}$ isomers, and isomeric *nido*-$[C_2B_{10}H_{12}]^{2-}$ ions are well known.[4c] However, attempted insertions of nonmetal atoms into these ions have never produced the desired 13-vertex target species. Nonetheless, there have been some intriguing hints. For example, when the Welch group treated the *nido*-$[C_2B_{10}H_{12}]^{2-}$ dianion with BI_3, the isolated product was the boron–iodo derivative, 1,2-$C_2B_{10}H_{11}$-3-I, which suggests that a B–I unit may have been initially incorporated to generate a 13-vertex cage that subsequently loses BH.[9]

Since it is well established that the carbon atoms become separated when the neutral carborane is reduced to *nido*-$[C_2B_{10}H_{12}]^{2-}$, these workers reasoned that if the carbon separation could be prevented, one might then

[*] Prof. Dr. R. N. Grimes
Department of Chemistry
University of Virginia
Charlottesville, VA 22901 (USA)
Fax: (+1) 434-924-3710
E-mail: rng@virginia.edu

 © 2003 Wiley-VCH Verlag GmbH & Co. KGaA, Weinheim 1433-7851/03/4211-1198 $ 20.00+.50/0

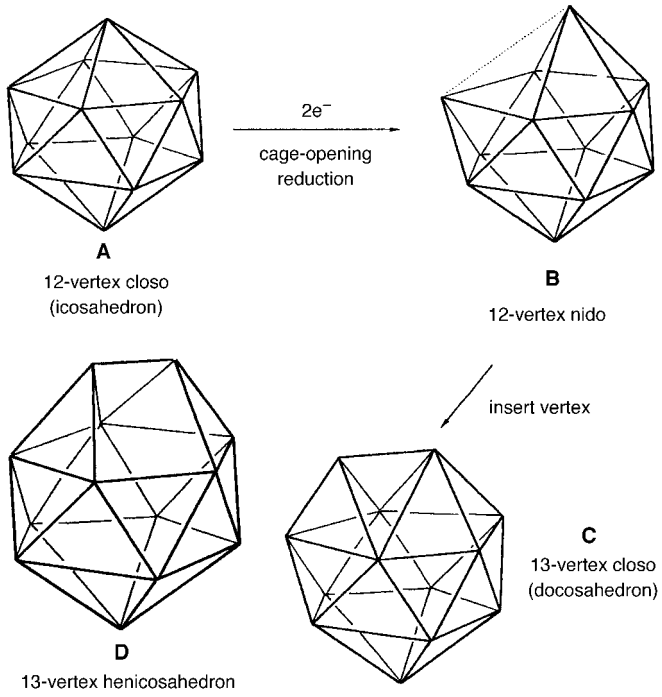

Scheme 1.

successfully achieve insertion, and thus complete the expansion to a 13-vertex carborane. A way to accomplish this, they conjectured, would be to prepare a derivative of 1,2-$C_2B_{10}H_{12}$ in which the cage carbon atoms are firmly tethered together by a suitable linking group. Accordingly, they prepared 1,2-μ-{$C_6H_4(CH_2)_2$}-1,2-$C_2B_{10}H_{10}$, a carborane that has an α,α-*o*-xylene bridge, and reduced it to the *nido*-[7,8-μ-{$C_6H_4(CH_2)_2$}-7,8-$C_2B_{10}H_{11}]^-$ monoanion. X-ray crystallographic data on this ion proved that its carborane carbon atoms remain adjacent and constitute one edge of a six-vertex C_2B_4 open face. To facilitate insertion into this face, its bridging proton had to be removed, and this was accomplished by treatment with butyllithium to generate the *nido*-[7,8-μ-{$C_6H_4(CH_2)_2$}-7,8-$C_2B_{10}H_{10}]^{2-}$ dianion (the same species can also be obtained directly from the neutral 1,2-μ-{$C_6H_4(CH_2)_2$}-1,2-$C_2B_{10}H_{10}$ through two-electron reduction with Na metal). Reaction of the dianion with phenylboron dichloride gave the desired 13-vertex target species 1,2-μ-{$C_6H_4(CH_2)_2$}-1,2-$C_2B_{11}H_{10}$-3-Ph, the first example of a supra-icosahedral boron cluster having no metal atoms.

This compound is unprecedented not only as the first 13-vertex carborane, but also in light of its surprising cage geometry; instead of the docosahedron **C** that has been predicted[7d] for the as-yet unknown $[B_{13}H_{13}]^{2-}$ anion (and is well established in structurally characterized 13-vertex MC_2B_{10} metallacarboranes[1a,4a]), the C_2B_{11} cluster adopts a henicosahedral structure **D** which features a four-sided trapezoidal face. As the authors note, these two geometries **D** and **C** are, in fact, in principle easily interconverted by a diamond-square operation (based on the diamond-square-diamond or dsd process proposed by Lipscomb)[12] in which two diagonal corners of the four-sided face of **D** are moved closer to form a new edge, generating the all-triangulated polyhedron **C**. To my knowledge, the henicosahedron has not previously been observed in a boron cluster.

The synthetic approach that allowed this breakthrough should enable further advances, since theory suggests that the energy barrier of 12-to-13 vertex conversion is higher than those involving further expansion to larger polyhedra having 14, 15, or more vertices.[7d] Hence, as Welch and co-workers propose, it may be feasible to expand the C_2B_{11} polyhedron through cage-opening and boron insertion to afford successively larger C_2B_n clusters. For those having more than 13 vertices, they calculate that it might be possible to eliminate the external group tethering the cage carbons together, thus enlarging the scope of synthetic possibilities even further.

To those of us who have labored in the carborane vineyards for years, this work potentially opens new possibilities that may well have ramifications extending far beyond boron chemistry; thus empty (no internal atoms) metal-containing polyhedral clusters of extraordinary size may now be within reach. For example, the expansion of carboranes by the insertion of metal–ligand units such as {(η^5-C_5Me_5)M} is well established and has produced, among other things, the previously mentioned 13-and 14-vertex metallacarboranes. Extension of this approach by metal insertion into supra-icosahedral carborane frameworks to generate new, structurally unprecedented macrometallacarboranes appears feasible. It does not seem excessively speculative to think in terms of novel metal-containing nanostructured materials constructed from such molecules. Now that the icosahedral barrier has been surmounted, it will be fascinating indeed to discover what lies beyond.

[1] a) F. A. Cotton, G. Wilkinson, C. A. Murillo, M. Bochmann, *Advanced Inorganic Chemistry*, 6th ed., Wiley-Interscience, New York, **1999**, chap. 5; b) N. N. Greenwood, *The Chemistry of Boron*, Pergamon, Oxford, **1973**.

[2] For a recent review, see I. B. Sivaev, V. I. Bregadze, S. Sjöberg, *Collect. Czech. Chem. Commun.* **2002**, *67*, 679.

[3] a) R. B. King, *Chem. Rev.* **2001**, *101*, 1119; b) J.-i. Aihara, *Inorg. Chem.* **2001**, *40*, 5042; c) M. L. McKee, *Inorg. Chem.* **2002**, *41*, 1299.

[4] a) *Comprehensive Organometallic Chemistry II, Vol. 1* (Eds.: E. W. Abel, F. G. A. Stone, G. Wilkinson), Pergamon, Oxford, UK, **1995**; b) *Contemporary Boron Chemistry* (Eds.: M. Davidson, A. K. Hughes, T. B. Marder, K. Wade), Royal Society of Chemistry, Cambridge, UK, **2000**; c) R. N. Grimes, *Carboranes*, Academic Press, New York, **1970**.

[5] a) W. J. Evans, M. F. Hawthorne, *J. Chem. Soc. Chem. Commun.* **1974**, 38; b) W. M. Maxwell, R. F. Bryan, E. Sinn, R. N. Grimes, *J. Am. Chem. Soc.* **1977**,

 © 2003 Wiley-VCH Verlag GmbH & Co. KGaA, Weinheim 1433-7851/03/4211-1199 $ 20.00+.50/0

99, 4016; c) J. R. Pipal, R. N. Grimes, *Inorg. Chem.* **1978**, *17*, 6.
[6] N. M. M. Wilson, D. Ellis, A. S. F. Boyd, B. T. Giles, S. A. Macgregor, G. M. Rosair, A. J. Welch, *Chem. Commun.* **2002**, 464.
[7] a) L. D. Brown, W. N. Lipscomb, *Inorg. Chem.* **1977**, *16*, 2989; b) J. Bicerano, D. S. Marynick, W. N. Lipscomb, *Inorg. Chem.* **1978**, *17*, 2041; c) J. Bicerano, D. S. Marynick, W. N. Lipscomb, *Inorg. Chem.* **1978**, *17*, 3443; d) P. von R. Schleyer, K. Najafian, A. M. Mebel, *Inorg. Chem.* **1998**, *37*, 6765.
[8] J. Bould, M. G. S. Londesborough, D. L. Ormsby, J. A. H. MacBride, K. Wade, C. A. Kilner, W. Clegg, S. J. Teat, M. Thornton-Pett, R. Greatrex, J. D. Kennedy, *J. Organomet. Chem.* **2002**, *657*, 256.
[9] A. Burke, D. Ellis, B. T. Giles, B. E. Hodson, S. A. Macgregor, G. M. Rosair, A. J. Welch, *Angew. Chem.* **2003**, *115*, 235; *Angew. Chem. Int. Ed.* **2003**, *42*, 225.
[10] M. F. Hawthorne, G. B. Dunks, *Science* **1972**, *178*, 462.
[11] Both processes have recently been exploited in the synthesis and interconversion of small six- and seven-vertex metallacarboranes: See H.-J. Schanz, M. Sabat, R. N. Grimes, *Angew. Chem.* **2001**, *113*, 2777; *Angew. Chem. Int. Ed.* **2001**, *40*, 2705.
[12] W. N. Lipscomb, *Science* **1966**, *153*, 373.

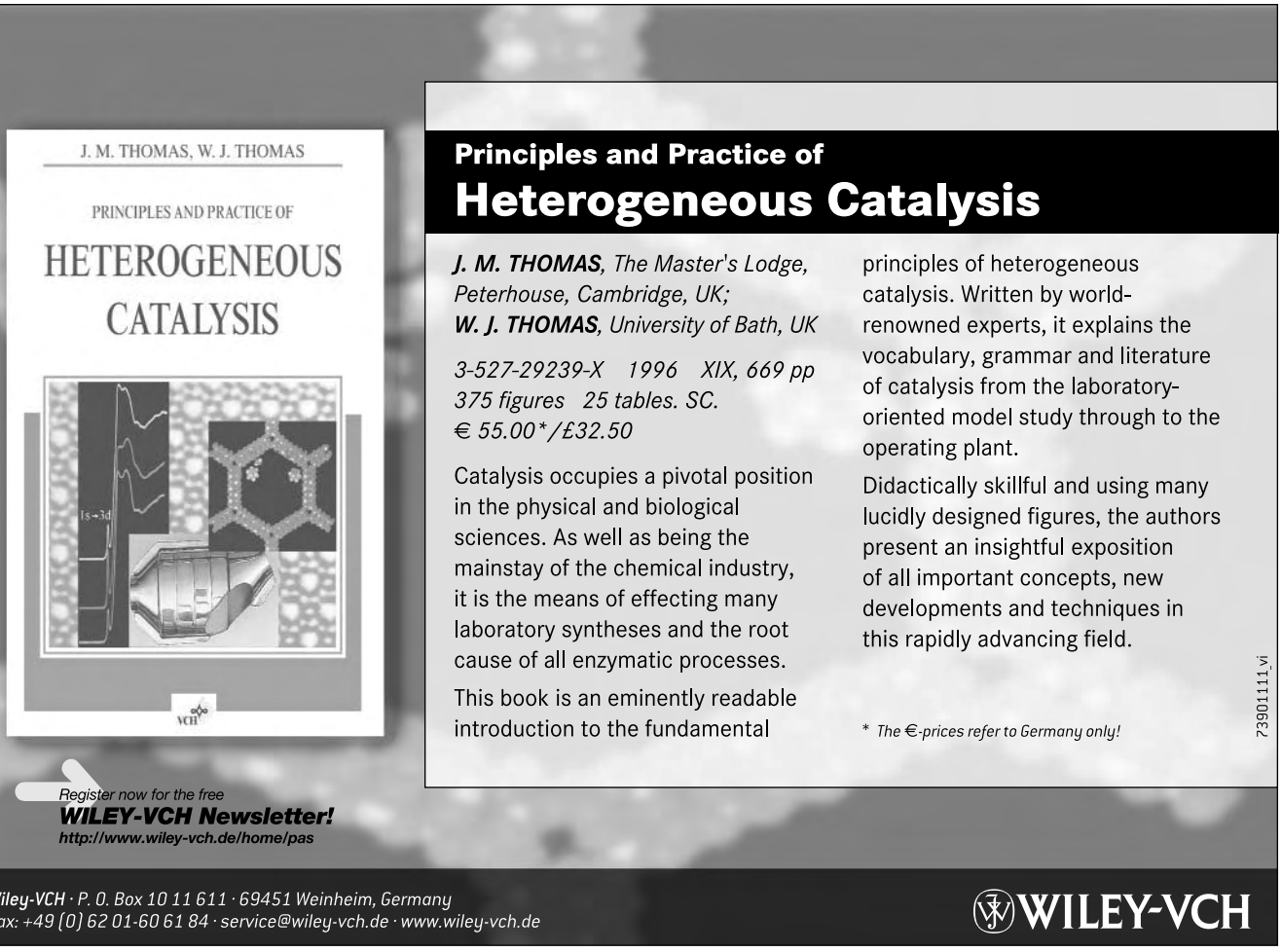

Early Days of Structure Determination

The Stories of Santonin and Santonic Acid**

*Ludmila Birladeanu**

Keywords:
history of chemistry · natural products · reaction mechanisms · santonin · structure elucidation

Since the middle of the 19th century, a major goal of organic chemistry has been the determination of the structure of natural products. Fascination with naturally occurring products dates back to time immemorial, stimulated by exquisite colors, seductive smells, and often very remarkable physiological effects.

Before 1859 the concept of structure did not exist. Only with the invention of the structural theory by Butlerov, Couper, Kekulé, and van't Hoff could structure determination become a conceivable goal. The late Robert Burns Woodward extolled the creation of structural theory in these words, "The discovery that the structure and form of molecules provide the fundamental basis for the differentiation of all forms of matter was one of man's greatest discoveries".[1]

Today's chemists can scarcely imagine how structures of great complexity were determined before the availability of the powerful physical tools of IR and NMR spectroscopy, mass spectrometry, and the ultimate weapon, X-ray crystallography. But two earlier stages in the practice of structure determination can be distinguished, and are exemplified in this history of santonin and its provocative derivative, santonic acid.

In the first period, between around 1870 to 1900, characterization depended on melting points, boiling points, densities, refractive indices, and optical activity. Elemental analysis provided empirical formulas. Depression of freezing point, elevation of boiling point provided molecular weights. Major structural insights came exclusively from chemical transformations and degradations into more simple, already recognized structures. Inferences from such transformations were based on analogy, empirical approaches, and intuition. Chance—according to Pasteur, an important ingredient in scientific advances when its significance is correctly perceived—played its role.

In the second period, as theories of the mechanisms of reactions were rapidly developing, inferences about structure derived from chemical transformations could be subjected to a new type of critical evaluation. At the turn of the last century, organic chemistry began its rapid change from an empirical, essentially taxonomic science into one dramatically enhanced by theories of the mechanism by which reactions occurred. True pioneers, Arthur Lapworth and Sir Robert Robinson, mark the beginning, but many years would pass before the powers of these new insights would be widely incorporated into the thinking of natural-product chemists. During both periods, structural hypotheses received their final verification through rational synthesis, and the establishment of the identity of the synthetic and the natural product.

The story of santonin and its transformation product, santonic acid, captures the working of these earlier periods. It not only reveals how the limitations of the thinking in the first period could totally block a successful resolution of structure, but how the new concepts of mechanism could bring light into an otherwise impenetrable darkness.

Space limitation precludes a comprehensive discussion of both stories, but since a brief history of the structure determination of santonin has been mentioned before,[2] whereas that of santonic acid has never been reviewed, the former is limited to its essentials, while the latter constitutes the main focus of this essay.

Santonin

Santonin was first isolated by Kahler in 1830 from *Artemisia Santonica*, a member of a family of plants known for centuries as "wormseed".[3] The very name attests to their remarkable efficacy in ridding both human beings and animals of debilitating round worms (Nematodes).

Early knowledge of its chemistry came almost entirely from the investigations the Italian chemist Cannizzaro and his school carried out in the decades between 1870 and 1920. Elemental analysis for carbon and hydrogen (oxygen by difference) established the empirical formula $C_{15}H_{18}O_3$. The difference of 14 between its 18 hydrogen atoms and the 32 hydrogen atoms required by a saturated hydrocarbon $C_{15}H_{32}$ divided by two, implied seven degrees of unsaturation.

The behavior of santonin on treatment with dilute base or acid, as well as towards reagents regarded as being able to indicate the presence of a carbonyl group led the Italian researchers to the conclusion that santonin is a γ-ketolactone. This inference accounted for all three oxygen atoms and three degrees of unsaturation (two carbonyl groups and the ring of the lactone). Reduction with hydrogen iodide and red phosphorus gave a monobasic acid, santonous acid,

[*] Dr. L. Birladeanu
Department of Chemistry and Chemical Biology
Harvard University
Cambridge, MA 02138 (USA)
Fax: (+1) 617-495-1792
E-mail: lily@chemistry.harvard.edu

[**] I thank Professor W. von E. Doering for his suggestions and corrections and Dr. Edmund Keliher for his assistance in preparing the manuscript.

 © 2003 Wiley-VCH Verlag GmbH & Co. KGaA, Weinheim 1433-7851/03/4211-1202 $ 20.00+.50/0

which on distillation with barium hydroxide at 300 °C gave a phenol, $C_{12}H_{12}O$, recognized as 1,4-dimethyl-2-naphthol. Heating at still higher temperature led to the identification of propene and propionic acid. A three-carbon fragment, two methyl groups, and the C_{10} naphthalene now accounted for all 15 carbon atoms in santonin. Two fused six-membered rings accounted for two more elements of unsaturation, bringing the total to five. The two remaining of the seven degrees of unsaturation required by the empirical formula were assigned by default to two carbon–carbon double bonds.

From the recognition of the 1,4-dimethyl-2-naphthol and the easy transformation of santonin on treatment with acid into the isomeric phenol, desmotroposantonin, it was concluded that the two methyl groups and the keto group were located in the same ring. The isolation of propene and propionic acid placed a methyl group in the ring of the lactone. These facts led to the proposal of formulas **1** or **1a** for santonin, with

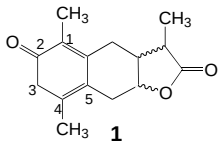

1

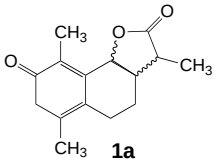

1a

the correct location of the lactone oxygen atom and of the isopropyl side chain remaining to be determined.[4] Formula **1** was given preference over **1a**, but quite arbitrarily. Desmotroposantonin and santonous acid were assigned structures **2** and **3**, respectively.

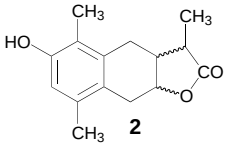

2

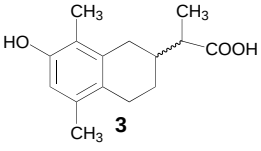

3

The acceptance of structure **1** was far from universal. Particularly questionable was the grouping $-CH_2-CO-$, since the santonin molecule could not be made to participate in such characteristic reactions as, for example, aldol condensation with an aldehyde. The problem remained unsolved. Today it is hard to understand how structure **1** could have been thought to represent a stable compound like santonin, without realizing that it was the keto form of a phenol, desmotroposantonin, which they had in their hands, and that the existence of such keto forms in equilibrium with phenols had never been observed. But then, tautomerism, although discovered decades earlier, was still not a familiar concept. What we now take for granted took decades to become universally accepted.

An even bigger blow to formula **1** came several years later. when Angeli and Marino isolated a heptanetetracarboxylic acid, $C_{11}H_{16}O_8$, from the mixture obtained on oxidation of santonin with permanganate.[5] This acid behaved like a disubstituted malonic acid and thus contained a quaternary carbon. But formulas **1** or **1a** did not contain such a carbon atom! Unfortunately, the numerous structures subsequently proposed to accommodate the quaternary carbon were no better and so **1** continued to be accepted by default.

In a 1924 review Angeli stressed again the significance of the existence of a quaternary carbon in the isolated heptanetetracarboxylic acid.[6] The chemists who had been involved for decades in work on the structure of santonin were fully aware that they had not succeeded in solving the problem.[7]

The problem lay dormant for many years until a solution was finally provided by Clemo and his co-workers in 1929.[8] Armed with a greatly increased awareness and understanding of the keto–enol equilibrium,[9] and rearrangements of carbon skeletons, often induced by acidic conditions,[10] Clemo was able to state that "on general theoretical grounds, structure **1** should be an unstable form of the stable phenolic isomeride desmotroposantonin" and to propose for santonin a new structure, **4**, based on the assumption that the two methyl groups in santonin were *not* situated in the same ring. By shifting the methyl group from position 4 to position 5 he obtained a structure containing a quaternary carbon, which on treatment with acid could undergo a

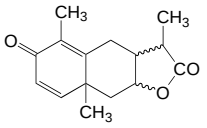

4

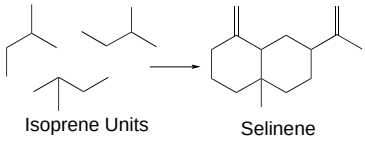

dienone–phenol rearrangement to the phenol desmotroposantonin. In addition, structure **4** could be constructed on the principle of Ruzicka's isoprene rule, showing a close relationship to the terpene selinene.

The correctness of the assumptions made by Clemo et al. were proven by the synthesis of racemic santonous acid,[11] and racemic desmotroposantonin,[12] both readily obtainable from natural santonin. Santonous acid, obtained by a six-step synthesis, was identical in all respects with the natural one. In addition, by this synthesis the β position for the acidic side chain was now firmly established.

Based on the structure of santonous acid, two formulas could now be suggested for desmotroposantonin, depending on whether the lactonic oxygen was assigned to position 7 (**I** = **2**) or 9 (**II**). Clemo et al. resolved the problem

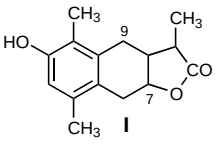

I

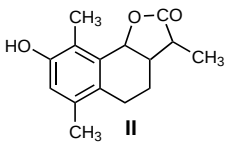

II

by synthesizing a compound of structure **II** which turned out to be identical to a sample of natural racemic desmotroposantonin.

Consistent with structure **II** for desmotroposantonin, the structure of santonin had to be rewritten as **4a**. This structure became now universally accepted.

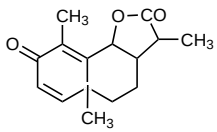

Santonin (**4a**)

 © 2003 Wiley-VCH Verlag GmbH & Co. KGaA, Weinheim 1433-7851/03/4211-1203 $ 20.00+.50/0

But there still remained a dark shadow lingering over the santonin problem. Although Clemo's formulation permitted a decisive clarification of the results obtained both on oxidative degradation and on treatment with acid, it was unable to account for the behavior of santonin on treatment with strong base. Whereas in dilute sodium hydroxide santonin gave the isolable salt of santoninic acid, from which it was easily regenerated on acidification, treatment with more concentrated sodium hydroxide gave an isomeric acid, santonic acid, with totally different properties. "While there was no longer any question of the validity of formula **4a**, the situation remained somewhat unsatisfactory in so far as all attempts at a rational formulation of santonic acid and the extensive series of substances derived from it by degradation have failed".[21] Not surprisingly, the elucidation of the structure of santonic acid became the most intriguing aspect of the chemistry of santonin.

The Structure of Santonic Acid

One of the first transformation products of santonin was discovered by Hvoslev in 1863,[13] and rediscovered some ten years later by Cannizzaro and Sestini[14] in apparent unawareness of the previous work (means for searching the "literature" did not become available until many years later). As shown above, Hvoslev had found that the action of concentrated sodium hydroxide on santonin gave rise to an acid, isomeric with santoninic acid, named santonic acid. The ease and simplicity of its formation from santonin prompted many to investigate its chemistry in the hope of arriving at a structure of santonin. The Cannizzaro school, mainly at the hands of Francesconi, devoted almost fifty years to the effort.

So fruitless were these efforts that santonic acid played no role whatsoever in the elucidation of santonin, but instead became itself an even thornier problem. One might have expected the structure of santonic acid to become clear once the correct structure of santonin had been elucidated by Clemo et al. But, "No"! The problem remained as intractable as ever. The state of affairs in 1934 was reviewed in detail by Wedekind and Engel.[15] Here only the few well established facts relating to santonic acid are presented.

From the empirical formula, $C_{15}H_{20}O_4$, santonic acid was seen to contain six elements of unsaturation and to be isomeric with santoninic acid, the product of the mild alkaline hydrolysis of santonin. Titration and analysis of its salts established santonic acid as monobasic, and thereby accounted for two oxygen atoms and one degree of unsaturation. Unlike santoninic acid, which rapidly lactonized to santonin, santonic acid did not revert to santonin on acidification but remained unchanged.[16] Treatment with hydroxylamine gave a monoxime under normal conditions and a dioxime under more drastic conditions.[17] The remaining two oxygen atoms, therefore, were present as ketones of differing reactivity, and accounted for two more degrees of unsaturation. Unlike santonin and santoninic acid, santonic acid did not add bromine or undergo catalytic hydrogenation. It was oxidized only very slowly by permanganate, and was not reduced by hydrogen iodide and phosphorus, a treatment which had converted santoninic acid into santonous acid. It was concluded that santonic acid did not contain carbon–carbon double bonds, and must therefore be saturated and *tricyclic*, if the final three degrees of unsaturation were to be accommodated.

The relation of the more reactive, less hindered carbonyl group and the carboxylic acid was revealed by the behavior of a reduction product, a secondary alcohol, dihydrosantonic acid. Among the products formed on treatment with acetic anhydride was an acetyl lactone, which could be hydrolyzed to a hydroxy acid and reclosed to the lactone with the ease normally associated with a γ-lactone.[18] This behavior placed the carbonyl group of santonic acid no further than two carbon atoms away from the carboxylic acid group.

Vigorous oxidation by potassium permanganate transformed santonic acid into santoric acid, $C_{13}H_{18}O_8$, a saturated, monocyclic tetrabasic acid. This compound reacted with acetic anhydride to afford a monoanhydride and two isomeric dianhydrides. Fusion of santoric acid with sodium hydroxide at 300 °C gave (along with acetic acid, carbon dioxide, and hydrogen) santoronic acid, $C_{10}H_{16}O_6$, a saturated, consequently acyclic tricarboxylic acid. On further heating with potassium hydroxide at still higher temperature santoronic acid was transformed into a ketone, santorone, $C_8H_{14}O$, by loss of two more carbon atoms.[19] These products were of unknown structure at the time and made no contribution to the proposed skeleton of santonic acid. Only the barest partial structure could be written (Scheme 1). More detailed structures

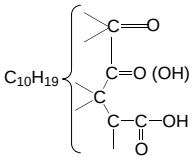

Scheme 1. Imprecise partial structure of santonic acid.

were proposed, but, being based on erroneous structures for santonin, were themselves of no value.

After the establishment of the structure of santonin by Clemo et al., Wedekind (and others) attempted further degradations of santonic acid, but the reaction products remained obstinately unidentifiable.[20] The structure of santonic acid continued to remain elusive. The classical approach of the first period which involved reassembling a structural hypothesis from various bits of information gleaned from smaller components produced by degradation, and from studies of the response to chemical reagents, was not working in the case of santonic acid. As we saw, even in the case of santonin, Clemo had to place critical reliance on the knowledge of the mechanisms of the Wagner–Meerwein rearrangement and of base-catalyzed tautomerization, thus providing an early example of the impact of the emerging mechanistic way of thinking about chemical transformations on structure determination.

In the case of santonic acid, the time had not yet come when mechanistic analysis alone would lead to the complete elucidation of structure. The problem lay dormant for more than a decade until R. B. Woodward took up the

challenge in the early 1940s.[21] In contemplating the changes that had been brought about by hydroxide ion in the transformation of santonin to santonic acid, he was struck by several observations that seemed particularly in need of rationalization. In the overall change, the two carbon–carbon double bonds of santonin had disappeared, one to reappear as a carbon–oxygen double bond at the cost of the incipient hydroxy group of the lactone ring, the second to appear as a third ring. He was further impressed that the heptanetetracarboxylic acid isolated by Angeli and Marino from the alkaline permanganate oxidation of santonin still contained a quaternary carbon. This observation implied that the methyl group at the 5-position in santonin had not rearranged to the 4-position as it had under the influence of acids. Woodward was convinced that the transformation by alkali was unique to santonin, unlikely to be the result of a simple process, and could be resolved "by a rational consideration of the effects to be anticipated in the action of strong bases on the santonin molecule". His approach was based on his life-long faith that chemical transformations could be understood through insight into their mechanism.

By the time Woodward tackled the santonic acid problem, giving it his almost undivided attention in the early months of 1943,[22] the mechanisms of a large number of base-catalyzed reactions had been elucidated, most notably through the ground-breaking achievements of Arthur Lapworth.[23] Systematically and exhaustively, Woodward analyzed the consequences of addition of hydroxide ion to each of the several electrophilic carbon atoms in santonin and the consequences of removal of acidic hydrogen atoms, no matter how weakly they might appear to be activated.

The first response of santonin to hydroxide ions had been the addition to the carbonyl group of the lactone ring to give the sodium salt of santoninic acid. The problem then was to predict the further changes that a hydroxide ion might initiate in this acid. For example, a Michael-type addition to the electrophilic β carbon atom of either of the α,β unsaturated carbonyl systems could be followed by a retroaldol cleavage to an aldehyde and methyl ketone, and these in turn could lead to further transformations. But such journeys ended only in blind alleyways and certainly not in a tricyclic system.

Turning to the consequences of abstraction of acidic hydrogen atoms, Woodward focused his attention on the hydrogen atom attached to the C-9 carbon atom bearing the hydroxy group. At first glance, this hydrogen atom might not have appeared to be particularly acidic—unless one were familiar with Lapworth's demonstration that a γ hydrogen atom in an α,β-unsaturated carbonyl system is as acidic and easily removable by base as the α hydrogen atom of a carbonyl compound. An appropriate example, known to Woodward, had been discovered independently by Butenandt and Schramm,[24a] and Heilbron et al.[24b] It involved conversion of 3-hydroxy-6-ketocholestene-4 with hydroxide ions into 3,6-diketocholestane (Scheme 2).

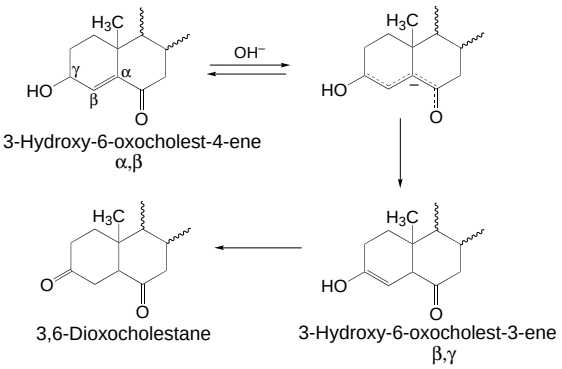

Scheme 2. Rearrangement of 3-hydroxy-6-oxocholest-4-ene induced by the abstraction of a proton.

In this instance the β,γ isomer is also the enol of a γ diketone and, consequently, is transformed essentially irreversibly into 3,6-diketocholestane. Woodward recognized that the relative positions of the double bond, keto, and hydroxy groups in santoninic acid were identical to those in 3-hydroxy-6-ketocholestene. He assumed that the same sequence of events could take place in santoninic acid and would lead to the diketone **III** [Eq. (1)]. The attractiveness of this hypothesis was irresistible:

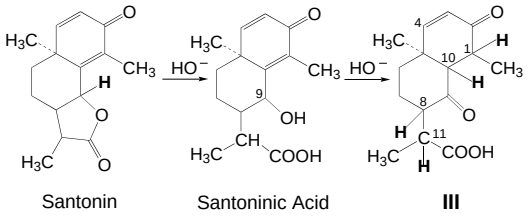

(1)

the unsaturation in one carbon–carbon double bond transformed the hydroxy group of santoninic acid into the obligatory second carbonyl group, and thereby provided an intermediate containing four acidic hydrogen atoms, three of them α to carbonyl groups, the fourth only weakly activated by a carboxylate anion (see **III**).

The task then was to discover how the carbon–carbon double bond remaining in **III** might give rise to the tricyclic system present in santonic acid. Any of the four carbanions hypothetically derivable from **III** by extraction of hydrogen atoms, C-1, C-10, C-8, and C-11, could in principle engage the α,β unsaturated ketone in an intramolecular Michael condensation at the β C-4 atom to generate a third ring by formation of a new carbon–carbon bond. Intramolecular additions to carbonyl groups were not considered on the grounds that they would destroy a carbonyl group and leave the carbon–carbon double bond intact.

The results of the four possible intramolecular Michael condensations are the structures **a**–**d**. Two of the hypothetical structures, **a** and **b**, would contain strained four-and three-membered rings (~26 kcal mol^{-1}), respectively, and thus would not be favored at equilibrium in a reversible Michael reaction. Woodward recognized that the carbanion at C-8 leading to **c** was five

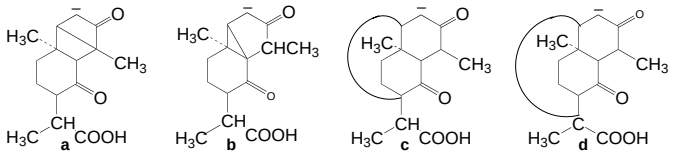

carbon atoms removed from the C-4 of the double bond, a potentially ideal relation for an intramolecular Michael reaction. However, it was not clear if these two carbon atoms were close enough in space to allow the reaction to occur. The same doubt applied to the fourth possibility, **d**. Unlike the previous examples of intramolecular Michael additions, first observed by Guthzeit,[25] that could be easily visualized in two dimensions, a planar representation of **c** obscured its viability. Only when Woodward had rethought the required bond making in three dimensions did the difficulty disappear. In the three-dimensional model, the distance between C-8 and C-4 was no longer prohibitive, but ideal for generation of the new bond. The resulting structure **IV** (or **c** in two dimensions) became a credible and attractive structure for santonic acid. The structure **IV** contained the same, only slightly strained bicyclo[2.2.1]heptane system found in camphor. It was not expected to suffer further changes in alkali, and could be reasonably considered to be the mechanistically logical end product of the treatment of santonin with strong base.

But did the mechanistically attractive, hypothetical structure **IV** actually represent santonic acid? The experimental facts presented above were certainly satisfied by structure **IV**: It represented a saturated, tricyclic, monobasic acid having a more sterically hindered ketone group (at C-2) and a less hindered ketone group (at C-9). More convincing evidence for structure **IV** came from one of the degradation experiments carried out by Francesconi. Permanganate oxidation of santonic acid had given α-santoric acid, a saturated, monocyclic tetrabasic acid, $C_{13}O_{18}O_8$. In terms of **IV**, this degradation would have occurred by oxidative cleavage along the indicated dotted lines in Scheme 3 by way of the enol tautomers of the ketones, and would be expected to give a compound of structure **V**.

On treatment with acetic anhydride, α-santoric acid gave, among other products, a monoanhydride from which it was regenerated by hydrolysis. This anhydride was converted into an isomeric, thermally stable anhydride on further heating. Hydrolysis of this second anhydride gave β-santoric acid, an isomer of α-santoric acid. This complicated behavior was also explicable in terms of structure **V** by hypothesizing epimerization of the hydrogen atom in bold face in Scheme 3 during the transformation to β-santoric acid.

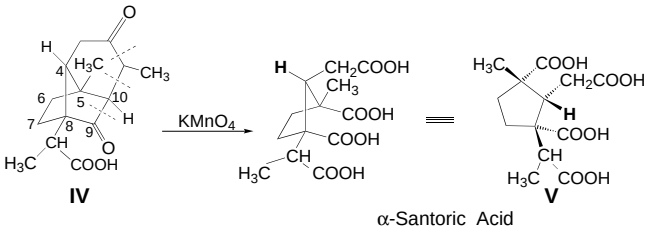

Scheme 3. Suggestions for the formation of α-santoric acid from the hypothetical structure of santonic acid **IV**.

A more critical test was provided by Francesconi's finding that fusion of either α- or β-santoric acids with alkali generated acetic acid, carbon dioxide, and santoronic acid, a tribasic, saturated, optically inactive acid of empirical formula $C_{10}H_{16}O_3$, m.p. 127 °C. Was the structure **V** proposed for santoric acid compatible with this degradation product? At the time no experience was available in the literature on the basis of which the course of the high-temperature alkali fusion of saturated, cyclic polyacids could be predicted. Woodward hypothesized that at the high temperature of alkali fusion, loss of a very weakly acidic hydrogen α to a carboxylate ion could generate a dicarbanion, that would behave similarly to conventional better-stabilized carbanions. With this mechanistic hypothesis in mind, he envisioned the following sequence of events (Scheme 4): during alkali fusion loss of a proton from the carbon atom α to a carboxylate anion would give **VI;** breaking of a carbon–carbon bond by a reverse Michael reaction[26] indicated by either arrow a or b, both giving the same end result; cleaving the resulting α,β unsaturated compound **VII** by the two-step sequence of addition of a hydroxide ion and retro-aldol-like condensation of the β hydroxycarboxylate anion to generate **VIII** and

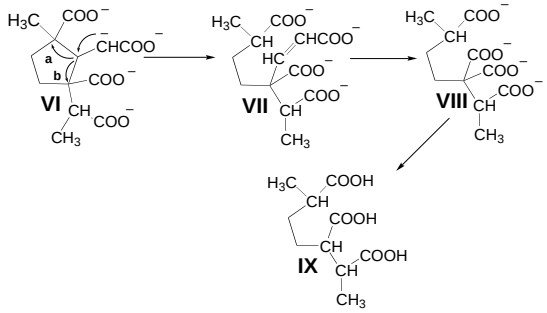

Scheme 4. Woodwards explanation for the conversion of santoric acid into santoronic acid.

an acetate ion; (a precedent for such a change was known in the conversion, on alkali fusion, of oleic acid to palmitic acid).[27] As the dicarboxylate of a malonic acid, **VIII** could reasonably be expected to undergo decarboxylation at the high temperature of the fusion to give, after neutralization, the saturated, acyclic tribasic heptane-2,3,6-tricarboxylic acid, $C_{10}H_{16}O_6$, of structure **IX**. According to Woodward's mechanistic analysis, this should be the correct expression for Francesconi's santoronic acid. But it could also be the structure of the heptane tricarboxylic acid of m.p. 88 °C that Angeli and Marino had ob-

tained by permanganate oxidation of santonin, or of the acid of m.p. 137 °C that had been synthesized by Ruzicka to establish the position of the angular methyl group in santonin.[28] On the resolution of this dilemma depended the credibility of the edifice of Woodward's analysis.

Woodward, Brutschy, and Baer resolved the dilemma by repeating Ruzicka's synthesis of the racemic acid of m.p. 137 °C and finding that on fusion with alkali, it was indeed isomerized to the same acid of m.p. 127 °C that Francesconi had obtained from the fusion of santoric acid, that Angeli and Marino had obtained on fusion of the acid of m.p. 88 °C, and that Ruzicka also had obtained from the fusion of his synthetic acid.[28] On repeating the work of Angeli and Marino, Woodward et al. confirmed that the optically active acid of m.p. 88 °C gave the racemic acid of m.p. 127 °C on alkali fusion. With this last obstacle removed, structure **IV** for santonic acid turned out to be, in Woodward's words, "the most satisfactory vehicle for the rationalization of the hitherto baffling chemistry of santonic acid".

It is impossible to overestimate the beauty, elegance, and impact of Woodward's mechanistic scheme. Not only did it solve the elusive structure of santonic acid, but it illustrated the power of the mechanistic approach, and the importance of thinking in terms of three-dimensional models. The market for Dreiding models and later 3-D computer models was assured!

Incidentally, this achievement served as a basis for a new approach to the construction of a complicated ring system. An example is the historically important synthesis of longifolene by Corey et al.[29] Corey had conceived a homodecalin system, to serve as the precursor of an intramolecular Michael addition (Scheme 5). "Although this change would seem unusual and perhaps unreasonable, some confidence in its validity seemed indicated from the remarkably smooth transformation of santonin to santonic acid under the influence of alkali".

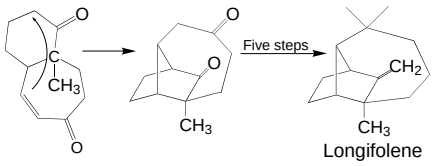

Scheme 5. Corey's proposal for the synthesis of Longifolene under following the conversion of santonin into santonic acid.

In the third and current phase of structure determination, physical methods have displaced both the first, classical phase, and the second phase in which the power of careful mechanistic analysis of chemical transformations played such an important role. NMR spectroscopy and X-ray single-crystal analysis as the ultimate weapon have made structure determination a routine process requiring little or no "chemical intuition". One may well ask whether there will be stories like that of santonin and santonic acid to tell in the future. Probably not.

Santonin is an easily accessible, crystalline natural product, the structure of which can (and has been) determined by X-ray analysis in a matter of days, rather than the decades of chemical investigation. Santonic acid is not a natural product, but rather the product of the chemical transformation of santonin on vigorous boiling with concentrated alkali, one of the many reactions carried out in the course of the classical search for transformations leading to useful structural information. Would this experiment be done today? Probably not. One could argue, that the more rapid progress resulting from the availability of modern tools is infinitely more important than a missed chemically provocative experiment. I will let Sir Robert Robinson give the answer: "….there is a price to pay and that is the short-circuiting of chemical investigation, because it resulted in the loss of general and important chemical information, and substitution by rather mechanical means of the complex intuitive puzzle-solving processes".[30] No better testimony to the validity of this prognosis is needed than Woodward's santonic acid paper.[31]

[1] "Art and Science in the Synthesis of Organic Compounds: Retrospect and Prospect": R. B. Woodward in *Pointers and Pathways in Research*, CIBA of India, Bombay, **1954**.

[2] J. B. Hendrickson, *The Molecules of Nature* (Ed.: R. Breslow), Benjamin Reading, Massachusetts, **1973**, pp. 111–112.

[3] M. Kahler, *Arch. Pharm.* **1830**, *34*, 318.

[4] S. Cannizzaro, P. Gucci, *Rend. Accad. Naz. Lincei Ser. 5* **1892**, *1*, 149.

[5] A. Angeli, L. Marino, *Rend. Accad. Naz. Lincei Ser. 5* **1907**, *16*, 385.

[6] A. Angeli, *Rend. Accad. Naz. Lincei Ser. 6* **1924**, *33*, 10.

[7] The essential papers pertinent to this work can be found in the bibliography to ref. [21].

[8] G. R. Clemo, R. D. Haworth, E. J. Walton, *J. Chem. Soc.* **1929**, 2368–2387; G. R. Clemo, R. D. Haworth, E. J. Walton, *J. Chem. Soc.* **1930**, 1110–1115.

[9] C. K. Ingold, *Structure and Mechanism in Organic Chemistry*, Cornell University Press, Ithaca, **1953**, pp. 794–802.

[10] L. Birladeanu, *J. Chem. Educ.* **2000**, *77*, 858–863.

[11] S. Cannizzaro, J. Carnelutti, *Ber. Dtsch. Chem. Ges.* **1880**, *13*, 1516–1517.

[12] A. Andreocci, P. Bertolo, *Ber. Dtsch. Chem. Ges.* **1898**, *31*, 3131–3133.

[13] H. Hvoslev, *Förhandlingar vod Skandinaviska Naturforsharemötat* **1863**, 304.

[14] S. Cannizzaro, F. Sestini, *Gazz. Chim. Ital.* **1873**, *3*, 241–251.

[15] E. Wedekind, O. Engel, *J. Prakt. Chem.* **1934**, *139*, 115–140.

[16] S. Cannizzaro, *Gazz. Chim. Ital.* **1876**, *6*, 355; F. Sestini, *Gazz. Chim. Ital.* **1876**, *6*, 148.

[17] L. Francesconi, *Gazz. Chim. Ital.* **1899**, *29ii*, 181.

[18] S. Cannizzaro, F. Sestini, *Gazz. Chim. Ital.* **1876**, *6*, 345.

[19] L. Francesconi, *Gazz. Chim. Ital.* **1892**, *22i*, 181; L. Francesconi, *Gazz. Chim. Ital.* **1893**, *23ii*, 452; L. Francesconi, *Gazz. Chim. Ital.* **1899**, *29ii*, 224; L. Francesconi, *Rend. Accad. Naz. Lincei Ser. 5* **1896**, 5ii, 214.

[20] K. Tettweiler, O. Engel, E. Wedekind, *Liebigs Ann. Chem.* **1932**,*492*, 105.

[21] R. B. Woodward, F. G. Brutschy, H. Baer, *J. Am. Chem. Soc.* **1948**, *70*, 4216–4221.

[22] W. von E. Doering, private communication.

[23] M. Saltzman, *J. Chem. Educ.* **1972**, *49*, 750–753.

[24] a) A. Butenandt, G. Schramm, *Ber. Dtsch. Chem. Ges.* **1936**, *69*, 2289–2299; b) I. M. Heilbron, E. R. H. Jones, F. S. Spring, *J. Chem. Soc.* **1937**, 801–805.

[25] M. Guthzeit, *Ber. Dtsch. Chem. Ges.* **1898**, *31*, 2753–2758; M. Guthzeit, *Ber. Dtsch. Chem. Ges.* **1901**, *34*, 675–680.

[26] C. K. Ingold, W. J. Powell, *J. Chem. Soc.* **1921**, *119*, 1976–1982.

[27] F. G. Edmed, *J. Chem. Soc.* **1898**, 627–634.

[28] L. Ruzicka, L. Steiner, *Helv. Chim. Acta* **1934**, *17*, 614–621.

[29] E. J. Corey, M. Ohno, R. B. Mitra, P. A. Vatakencherry, *J. Am. Chem. Soc.* **1964**, *86*, 478 – 485.
[30] Robert Robinson, as quoted by in "Sir Robert Robinson: A Contemporary Historical Assessment and a Personal Memoir", A. J. Birch, *J. Proc. R. Soc. N. S. W.* **1976**, *109*, 151 – 160.
[31] It must be mentioned that Clemo's work resulted in the determination of the gross structure of santonin, but had nothing to say about its detailed stereochemistry. It took quite a few years to establish the absolute configuration of the natural (–)-α-santonin, one of the 16 theoretically possible stereoisomers. This topic is not pursued here. The interested reader may find a complete list of references in J. W. Huffman, W. T. Pennington, D. W. Bearden, *J. Nat. Prod.* **1992**, *55*, 1087 – 1092). The absolute configuration of santonic acid was firmly established in 1999 by single crystal X-ray analysis; A. P. J. Brunskill, H. W. Thompson, R. A. Lalancette, *Acta Crystallogr. Sect. C* **1999**, *55*, 566 – 568. The two configurations are:

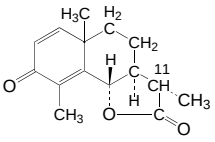

(–)-α-Santonin

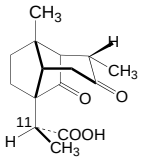

Santonic Acid

HOT TOPICS BY WILEY-VCH

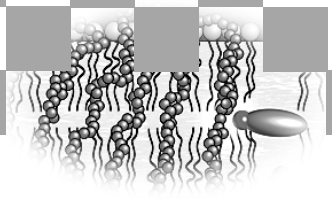

Directed Molecular Evolution of Proteins

or How to Improve Enzymes for Biocatalysis

S. Brakmann, University of Leipzig, Germany; K. Johnsson, Dept. of Chemistry, Inst. of Organic Chemistry, EPFL - BCH, Switzerland

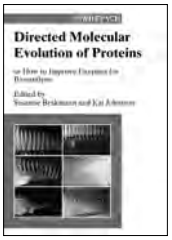

The book presented here focuses on the directed evolution of proteins, which has established itself as a powerful method for designing enzymes showing new substrate specificities. It includes a comprehensive repertoire of techniques for producing combinatorial enzyme libraries, while the functional gene expression in a suitable host helps in selecting the appropriate structure, making fast screening a necessity. It illustrates both the theoretical background as well as the potential of this interesting method in practice - which is becoming ever more important even in classical organic synthesis!

The contributing authors are internationally most renowned experts in their field.

3527 30423 1, 2002, XI, 357 pp with 121 fig, 13 in color, 15 tab, HC € 129.00/£ 75.00/US$ 115.00

Drug-Membrane Interactions

Analysis, Drug Distribution, Modeling

J.K. Seydel, Research Center Borstel, Germany; M. Wiese, University of Bonn, Germany
Series: Methods and Principles in Medicinal Chemistry (Volume 15)

Barrier, reservoir, target site - those are but some of the possible functions of biological lipid membranes in the complex interplay of drugs with the organism. A profound knowledge of membrane properties and of the various modes of drug-membrane interaction is therefore the prerequisite for a better understanding of drug action.

This unique reference volume builds on the authors' long experience in the study of drug-membrane interaction. Recommended reading for everyone involved in pharmaceutical research.

3527 30427 4, 2002, XVIII, 349 pp with 125 fig, 99 tab, HC € 139.00/£ 80.00/US$ 128.00

Wiley-VCH, P.O. Box 10 11 61, 69451 Weinheim, Germany, Fax: +49 (0) 62 01- 606 184, e-mail: service@wiley-vch.de, http://www.wiley-vch.de

WILEY-VCH

92502034_gu

Interactions with Arenes

Interactions with Aromatic Rings in Chemical and Biological Recognition

Emmanuel A. Meyer, Ronald K. Castellano, and François Diederich**

Keywords:
arenes · hydrogen bonds · molecular recognition · noncovalent interactions · receptors

Dedicated to Professor Dieter Seebach

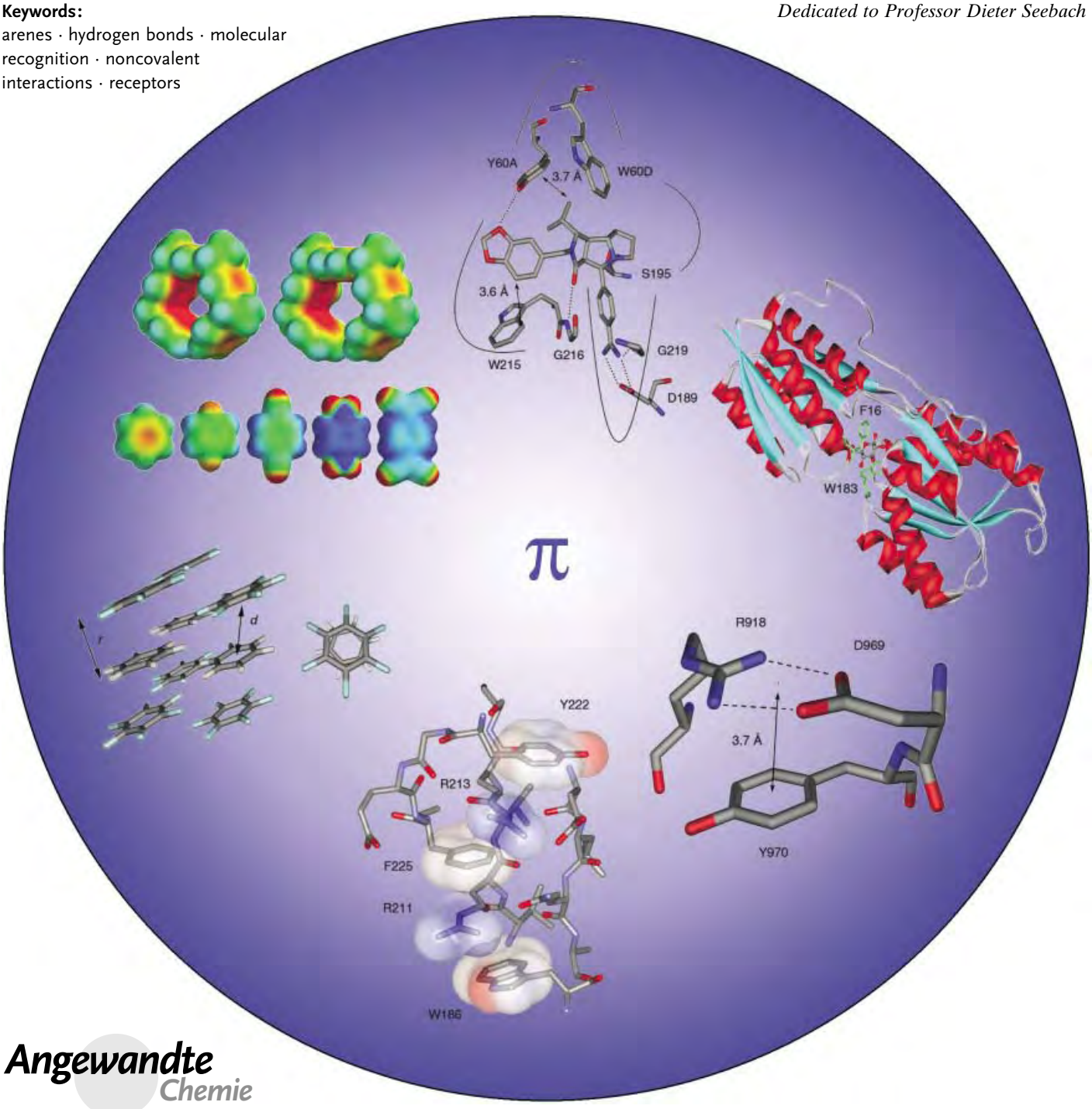

 © 2003 Wiley-VCH Verlag GmbH & Co. KGaA, Weinheim 1433-7851/03/4211-1210 $ 20.00+.50/0

Intermolecular interactions involving aromatic rings are key processes in both chemical and biological recognition. Their understanding is essential for rational drug design and lead optimization in medicinal chemistry. Different approaches—biological studies, molecular recognition studies with artificial receptors, crystallographic database mining, gas-phase studies, and theoretical calculations—are pursued to generate a profound understanding of the structural and energetic parameters of individual recognition modes involving aromatic rings. This review attempts to combine and summarize the knowledge gained from these investigations. The review focuses mainly on examples with biological relevance since one of its aims it to enhance the knowledge of molecular recognition forces that is essential for drug development.

From the Contents

1. Introduction 1211
2. Thermodynamics of Arene Complexation 1212
3. What Do We Learn from Crystals? 1216
4. Arene–Arene Interactions 1218
5. Hydrogen Bonding to Aromatic π Systems 1225
6. Cation–π Interactions 1227
7. Interactions between Aromatic and Perfluoroaromatic Compounds 1232
8. Sulfur–Arene Interactions 1235
9. Summary 1239

1. Introduction

Noncovalent interactions involving aromatic rings are pivotal to protein–ligand recognition and concomitantly to drug design. Indeed, the vast majority of X-ray crystal structures of protein complexes with small molecules reveals bonding interactions involving aromatic amino acid side chains of the receptor and/or aromatic and heteroaromatic rings of the ligand. The complex of the enzyme acetylcholinesterase (AChE) with the drug E2020 (Aricept), which was developed to treat symptoms of Alzheimer's disease, is one example of the diversity of these interactions (Figure 1).[1] The X-ray crystal structure analysis reveals π–π stacking, O–H/π, and cation–π interactions as major forces that stabilize the association. Accordingly, investigations aimed at an energetic quantification of individual interactions with aromatic rings in biological complexes are of paramount importance for improved drug design and lead optimization. Three main research approaches are pursued in order to reach this objective: 1) the biological recognition processes are analyzed in quantitative structure–activity relationships; 2) individual aromatic interactions are investigated in molecular recognition studies with designed synthetic receptors;[2] and increasingly 3) the magnitude of individual nonbonded interactions is addressed by high-level computational studies. This review attempts to present a unified picture of the understanding of the recognition of aromatic rings as it has emerged from all three approaches. Given the enormity of the topic, this task can only be approached in an incomplete way, with a relatively small number of studies—preferentially those providing novel structural and thermodynamic insight—being addressed in detail. Nevertheless, this is a worthwhile, timely endeavor in light of the huge number of potential new therapeutic targets for drug design and development emerging from genomics and proteomics.[3]

The review begins with a discussion of the solvent dependency of the complexation of aromatic substrates in chemical and biological systems (Section 2). This topic has witnessed major extensions from the classical concepts of hydrophobically driven apolar complexation over the past 15 years. Section 3 highlights the crystal structures of small aromatic molecules and how analysis of their crystal-packing patterns provides a source of inspiration for the discovery of new intermolecular forces. For example, the crystal packing of a precursor to an inhibitor of thrombin,[4] a serine protease in the blood coagulation cascade targeted in the fight against thrombotic disorders, not only shows aromatic rings in classic

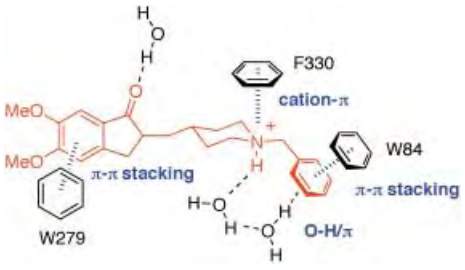

Figure 1. Binding mode of the anti-Alzheimer drug E2020 within the active site of acetylcholinesterase from *Torpedo californica* (PDB code: 1EVE).[1]

[*] Prof. Dr. R. K. Castellano
Department of Chemistry
University of Florida
P.O. Box 117200
Gainesville, Florida 32611-7200 (USA)
Fax: (+1) 352-846-0296
E-mail: castellano@chem.ufl.edu
Prof. Dr. F. Diederich, Dipl.-Chem. E. A. Meyer
Laboratorium für Organische Chemie
Departement für Chemie und Angewandte Biowissenschaften
ETH-Hönggerberg, HCI, 8093 Zürich (Switzerland)
Fax: (+41) 1-632-1109
E-mail: diederich@org.chem.ethz.ch

 © 2003 Wiley-VCH Verlag GmbH & Co. KGaA, Weinheim 1433-7851/03/4211-1211 $ 20.00+.50/0

edge-to-face (T-shaped) and parallel-displaced (stacking) arrangements, but also shows a notably short C(aromatic)–N(nitrile) distance (3.47 Å) that represents a type of weak H bond to the π system of the cyano group (Figure 2). Figure 3 shows the crystal structure of the complex of thrombin with a highly active inhibitor (inhibition constant $K_i = 7$ nM), developed by structure-based de novo design.[5] The intermolecular contacts in this complex, such as the edge-to-face interaction in the distal D pocket, the C–H/π interactions in the proximal P pocket, and the contacts between the amidinium-substituted phenyl ring and the surrounding protein in the specificity pocket S1 are discussed in detail in Section 4.

Since the seminal work of Burley and Petsko on aromatic–aromatic interactions in proteins,[6] database mining of the Cambridge Structural Database (CSD) and the Brookhaven Protein Data Bank (PDB) have increasingly been applied to identify and characterize weak intermolecular interactions in chemical and biological systems. H bonds to π systems provide examples for such weak bonding contacts and are discussed in Section 5. The importance of cation–π interactions was first recognized by Ma and Dougherty, who reviewed this field comprehensively in 1997.[7] Section 6 will thus only survey the most recent investigations of this interaction in chemistry and biology. A beautiful example is the strong complexation of 7-methylated GTP (association constant $K_a \approx 1.1 \times 10^8\,\text{M}^{-1}$, $\Delta G^\circ = -11.0$ kcal mol^{-1}) by a messenger RNA 5′-cap-binding protein, the eukaryotic translation initiation factor eIF4E. The cationic nucleobase in this complex is sandwiched at van der Waals distance (ca. 3.5 Å) between two Trp side chains (Figure 4).[8]

The last two sections address two emerging areas of research which have only been sparsely reviewed up to this point, namely fluoroaromatic interactions (Section 7) and those involving divalent sulfur (Section 8).

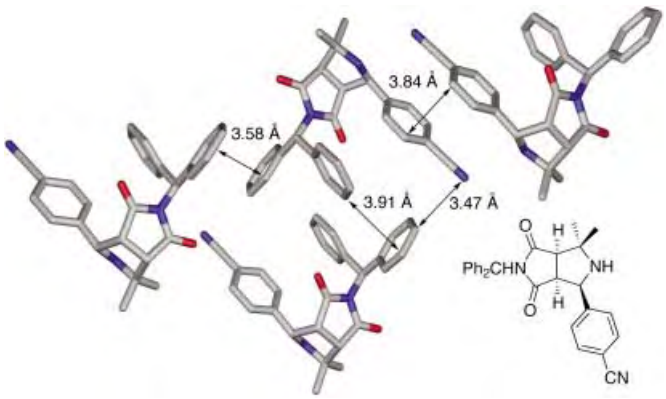

Figure 2. Edge-to-face and π-stacking interactions operative in the crystal packing of a precursor to an inhibitor of thrombin (CCDC-177644).[4] Color code: C: gray, N: blue, O: red, S: yellow, F: cyan. Unless noted otherwise, this color code is applied systematically in all subsequent figures.

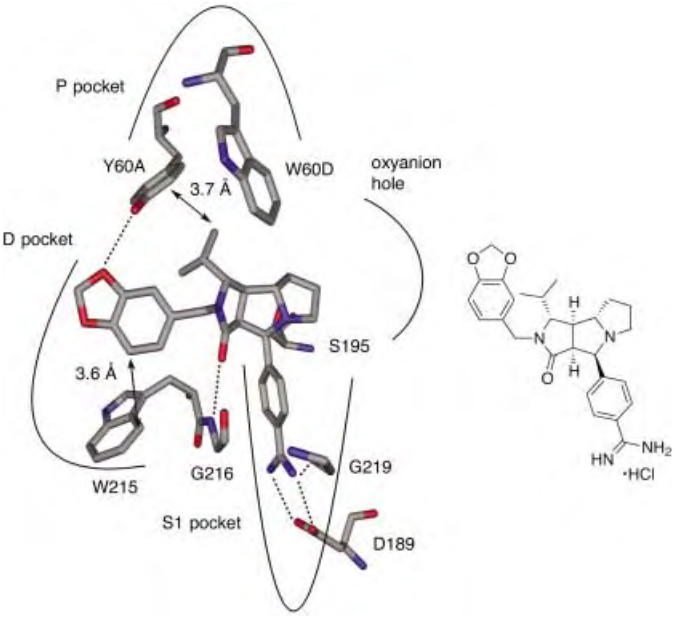

Figure 3. The active site in the X-ray crystal structure of the complex formed between thrombin and a designed inhibitor; edge-to-face and C–H/π contact distances are given; hydrogen bonds are represented as dashed lines.[5]

2. Thermodynamics of Arene Complexation

2.1. Complexation of Arenes with Chemical and Biological Receptors in Water

Inclusion complexation of aromatic solutes by cyclophanes in water has been intensively investigated over the past two decades, and these studies have been extensively

François Diederich, born in 1952 in the Grand Duchy of Luxembourg, received his Ph.D. in 1979 from the University of Heidelberg. After postdoctoral studies at the University of California at Los Angeles (UCLA) from 1979–1981, he was a research associate at the Max-Planck-Institut für medizinische Forschung in Heidelberg. After his Habilitation in 1985, he joined the faculty of the Department of Chemistry and Biochemistry at UCLA where he became full professor in 1989. Since April 1992, he has been a professor of organic chemistry at ETH Zürich.

Ronald K. Castellano was born in Toms River, New Jersey in 1973 and received his B.S. in chemistry from Gettysburg College in 1995. He received his Ph.D. in 2000 under the tutelage of Professor Julius Rebek, Jr., both at MIT and The Scripps Research Institute. His studies continued at the ETH Zürich as an NSF postdoctoral fellow with Prof. François Diederich. Since August 2002, he has been an Assistant Professor of Chemistry at the University of Florida.

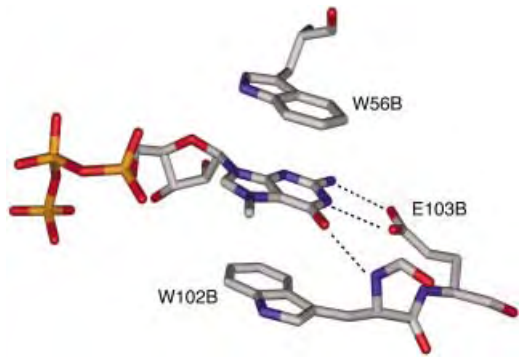

Figure 4. Partial view of the X-ray crystal structure (PDB code: 1L8B) of the messenger RNA 5′-cap-binding protein eIF4E bound to 7-methyl-GTP, which shows the sandwiching of the cationic nucleobase between the side chains of Trp102B and Trp56B.[8]

reviewed.[2d,9,10] Efficient apolar binding sites have not only been shaped by the covalent construction of large macrocycles with aromatic cavity walls, but also by metal-ion-mediated self-assembly.[11]

We conducted calorimetric studies with cyclophanes, such as **1**, to investigate the nature of the driving force for inclusion complexation of *para*-disubstituted benzene derivatives, such as **2a**–**e**, in water.[12–15] These cyclophanes form stable inclusion complexes in which the aromatic substrates undergo both aromatic π–π stacking and edge-to-face interactions (see Section 4) with the cavity walls of the host.[16] We expected to

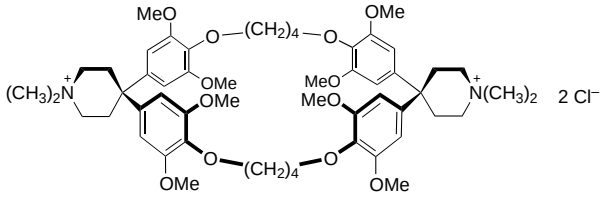

1

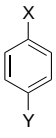

	X	Y
2a	COOMe	COOMe
2b	Me	NO_2
2c	HO	NO_2
2d	MeO	MeO
2e	Me	Me

Emmanuel A. Meyer was born in 1975 in Zürich, Switzerland. From 1994 to 1999 he studied Chemistry at the ETH Zürich and Imperial College, London. He is currently a graduate student in the group of Prof. François Diederich, and his research is concerned with the design and synthesis of inhibitors for prokaryotic tRNA-guanine transglycosylase (TGT).

measure thermodynamic quantities characteristic for binding driven by the classical hydrophobic effect, namely, 1) a large favorable complexation entropy $T\Delta S^{o}$, 2) a small complexation enthalpy ΔH^{o}, and 3) an increasingly favorable enthalpic term upon raising the temperature, as expressed by a large negative change in heat capacity $\Delta C_p{}^{o}$.[17,18] The classical hydrophobic effect had originally been defined to account for the thermodynamic characteristics measured for the transfer of small apolar solutes from the gas phase into water.[17,18]

We were at first rather surprised to obtain very different thermodynamic quantities, namely, a large enthalpic driving force for complexation, which was partially compensated by an unfavorable entropic term (Table 1). Only the measured negative changes in heat capacity were in agreement with our

Table 1: Thermodynamic parameters describing the complexation between cyclophane **1** and 1,4-disubstituted benzene guests in water and methanol.[a]

Guest	ΔG^{o}_{293K} [kcal mol^{-1}]	ΔH^{o}_{293K} [kcal mol^{-1}]	$\Delta C_p{}^{\circ}$ [cal mol^{-1} K^{-1}]	$T\Delta S^{o}_{293K}$ [kcal mol^{-1}]
Complexes in water				
2a	−6.81	−11.8	−60	−5.0
2b	−6.01	−8.1	−50	−2.1
2c	−5.86	−10.5	−130	−4.6
2d	−5.38	−10.0	−20	−4.6
2e	−5.33	−7.2	−20	−1.9
Complex in methanol				
2d	−1.20	−3.7	–	−2.5

[a] The enthalpic terms have an uncertainty of ±0.2 kcal mol^{-1}; the binding free energies have an uncertainty of ±0.07 kcal mol^{-1} (in water) and ±0.17 kcal mol^{-1} (in methanol); for further details, see ref. [13].

initial expectations. On the other hand, negative changes in heat capacity had already been reported for cyclophane–arene inclusion complexation in organic solvents, such as methanol or chloroform, and therefore are not characteristic of complexation processes in water.[13,19] It, therefore, seemed unlikely that our inclusion complexation processes were promoted to a large extent by the classical hydrophobic effect.

Similar thermodynamic quantities—a large enthalpic driving force partially compensated by an unfavorable complexation entropy—have more recently been reported for the complexation of benzene derivatives and other substrates by the closed-shell hemicarcerand host **3** in an aqueous borate buffer at pH 9 (Table 2).[20,21] The complete and tight guest encapsulation by the spherical receptor results in the complexes being much more stable than those formed by the more open cyclophane **1**.

A literature search following our initial experimental work[15] readily showed that these complexation thermodynamics (that is, $\Delta H^{o} \ll 0$; $T\Delta S \ll 0$), which in the meantime had been named the "nonclassical hydrophobic effect" and which we also observed in the complexation of a steroid by a cyclophane receptor in water/methanol (1:1),[22] had been encountered in many arene binding studies with other synthetic and biological receptors. Thus, the inclusion com-

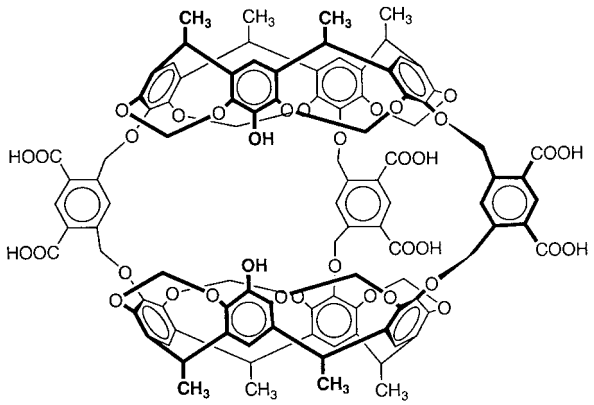

3

Table 2: Thermodynamic parameters describing the complexation between the spherical hemicarcerand host **3** and 1,4-disubstituted benzene guests in aqueous borate buffer (pH 9).[a]

Guest	ΔG°_{293K} [kcal mol^{-1}]	ΔH°_{293K} [kcal mol^{-1}]	$T\Delta S^{\circ}_{293K}$ [kcal mol^{-1}]
2d	−7.9	−10.9	−3.0
2e	−9.6	−12.3	−2.6

[a] Thermodynamic data for more complexation processes are reported in ref. [20].

plexation of benzene and naphthalene derivatives by natural and modified cyclodextrins is enthalpy driven, as demonstrated in a variety of calorimetric and other investigations.[23–27] The negative changes in the heat capacity recorded for these recognition processes are of similar magnitude to those reported in Table 1.[24,26] These and related thermodynamic data for cyclodextrin complexation have been compiled by Rekharsky and Inoue in a comprehensive review.[28]

Although calorimetric data on biological recognition processes remain disappointingly scarce,[29] the first examples reporting thermodynamic driving forces for apolar complexation different from those expected by the hydrophobic effect were reported as early as 1969 by Shiao and Sturtevant.[30] The authors measured the thermodynamic quantities for the complexation of small aromatic substrates in the arene binding pocket at the active site of the digestive serine protease α-chymotrypsin by flow calorimetry. They determined that the complexation of indole ($\Delta H^{\circ} = -15.2$ kcal mol^{-1}), *N*-acetyl-D-tryptophan ($\Delta H^{\circ} = -19.0$ kcal mol^{-1}), and proflavin ($\Delta H^{\circ} = -11.3$ kcal mol^{-1}) at 298 K in aqueous buffer (pH 7.8) was strongly enthalpy driven. The authors noted that these data were not consistent with those expected for classical hydrophobic interactions. They rationalized their observations by invoking Coulombic enzyme–substrate interactions as well as large conformational changes of the enzyme upon complexation of the inhibitors—the nonclassical hydrophobic effect had yet to be recognized. A large variety of complexation processes between enzymes and aromatic substrates have subsequently been described that feature a strong enthalpic driving force at ambient temperature, with a compensating unfavorable entropic term and negative change in the heat capacity between 100 and 500 cal mol^{-1} K^{-1}.[31]

A favorable enthalpy and entropy of complexation have both been recorded for the complexation of aromatic substrates that also undergo ion pairing, which is well known to be entropically favored.[32] This is the case at ambient temperature for the complexation of *para*-substituted benzamidinium substrates in the selectivity pocket of the serine protease trypsin (similar to thrombin, Figure 3) containing an Asp carboxylate group at its bottom.[33] Complexation at elevated temperatures is only enthalpy driven as a result of a large negative change in the heat capacity and a significant enthalpy–entropy compensation (see below).

The examples of biological complexation processes featuring the thermodynamic characteristics of the nonclassical hydrophobic effect are not limited to enzyme–aromatic substrate binding, but also include: 1) DNA intercalation by arenes such as ethidium bromide,[34–36] 2) DNA association with intercalator/minor groove binders such as the antitumor drug daunomycin,[36] and 3) DNA minor groove intercalation of antitumor drugs such as netropsin and distamycin as well as hairpin polyamides.[37–39] An increasing number of studies also report enthalpic driving forces for protein–protein,[40,41] protein–DNA,[42] and protein–lipid interactions.[43] The stacking interaction between the antimalarial drug chloroquine and hematin provides another example of enthalpy-driven association of aromatic rings in water.[44,45]

In view of this increasing amount of data, it is surprising that the nonclassical hydrophobic effect, with a strong enthalpic driving force for biological recognition, is almost entirely ignored in modern biochemistry textbooks. Instead, biological complexation processes are still mainly described as being driven by the classical hydrophobic effect.

It should be noted that many of the complexation studies cited in this section report strong enthalpy–entropy compensations upon variation of the host and/or guest: an increasingly favorable enthalpic driving force for complexation is compensated by an increasingly unfavorable entropic term.[26,35,38,41,42,44,46] The reader is referred to various theoretical models that have been proposed to explain the linear enthalpy–entropy compensation that is nearly universally observed in chemical and biological recognition processes.[47]

2.2. Solvent Dependency of the Inclusion Complexation of Aromatic Substrates

A very strong solvent dependence has been observed for the stability of pyrene complex **4**.[13,14,48] Upon changing from water, the most polar, to carbon disulfide, the least polar of the considered solvents, the complexation free enthalpy decreases from $\Delta G^{\circ} = -9.4$ kcal mol^{-1} to $\Delta G^{\circ} =$

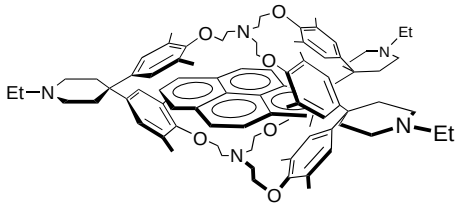

4

Table 3: Thermodynamic characteristics for the formation of complex **4** in solvents of differing polarity.[14]

Solvent	ΔG°_{303K} [kcal mol^{-1}]	ΔH°_{303K} [kcal mol^{-1}]	$T\Delta S^{\circ}_{303K}$ [kcal mol^{-1}]
water	−9.4	–	–
2,2,2-trifluoroethanol	−7.8	−20.0	−12.2
ethylene glycol	−7.3	–	–
methanol	−6.4	−12.0	−5.6
formamide	−6.2	–	–
ethanol	−6.1	−11.0	−4.9
N-methylacetamide	−5.8	−9.0	−3.2
N-methylformamide	−5.1	−5.6	−0.5
N,N-dimethylacetamide	−4.4	−2.0	+2.4
acetone	−4.3	−6.6	−2.3
dimethyl sulfoxide	−3.9	−6.4	−2.5
N,N-dimethylformamide	−2.9	−3.7	−0.8
dichloromethane	−2.9	–	–
tetrahydrofuran	−2.7	−3.0	−0.3
chloroform	−2.3	−3.1	−0.8
benzene	−1.5	−0.8	+0.7
carbon disulfide	−1.3	–	–

−1.3 kcal mol^{-1} (303 K, Table 3). Thus, the apolar binding strength increases consistently from apolar to dipolar aprotic solvents, to protic solvents, and to water. Since complex **4** has nearly the same geometry in all solvents, the measured modulation of association strength is mostly solvent-controlled.[49]

A strong linear free-energy relationship was found to exist between the free enthalpy of formation of complex **4** and the solvent polarity parameter $E_T(30)$[50] of the various solvents investigated, including water.[48] Thus, the apolar complexation-promoting characteristics of water can be correlated with such characteristics of other solvents (as expressed by $E_T(30)$) and are predictable solely on the basis of physical constants and properties. Linear free-energy relationships with $E_T(30)$ or related empirical solvent parameters have also been useful in describing the solvent dependencies of other host–guest complexation processes,[12,48,51] conformational reorganizations,[52] and chemical transformations.[53]

A calorimetric study (Table 3) revealed that the formation of complex **4** is enthalpy driven in all solvents.[13,14] The complexation in alcohols are the most exothermic and, in general, the enthalpic driving force decreases from polar protic solvents, to dipolar aprotic solvents, and to apolar solvents. Correspondingly, the complexation entropy becomes increasingly less favorable as the exothermicity increases, which results in a strong enthalpy–entropy compensation. This calorimetric investigation, which revealed the thermodynamic signatures for arene complexation in solvents of all polarities, provided substantial support for our explanation of the nonclassical hydrophobic effect.

2.3. The Nonclassical Hydrophobic Effect

We identified favorable changes in solvent cohesive interactions and a gain in dispersion interactions as the main components of the enthalpic driving force for apolar complexation in aqueous solution, that is, the nonclassical hydrophobic effect.[12–15] Thus, the stability of complex **4** (Table 3) is highest and the complexation enthalpy the most favorable in solvents characterized by high cohesive interactions and low molecular polarizability.

Solvents with high cohesive interactions prefer to interact with bulk solvent molecules rather than to solvate the complementary apolar surfaces of host and guest molecules. We proposed that "water molecules around apolar surfaces participate in fewer strong hydrogen bonds than bulk solvent molecules".[54] Therefore, enthalpy is gained upon release of surface-solvating molecules to the bulk during the complexation step. Water has the highest cohesive interactions and, therefore, the enthalpic driving force in this solvent is particularly favorable. Saenger, in his seminal review on cyclodextrin complexation in 1980, already stated correctly that water molecules solvating the cavities of the receptors are higher in energy than water molecules in the bulk solvent.[55]

A similar explanation for the role of internal solvent-cohesive interactions in promoting apolar binding processes in water had already been proposed by Sinanoglu as early as in 1968.[56] As a result of the strong cohesive forces in water, energy is required to create a cavity in the bulk liquid to accommodate an apolar guest molecule. Such cavities are also created when water molecules enter the binding site of the free host for solvation. Other authors have also pointed to the unfavorable energetics for cavitation in pure solvent.[18,57] Free-enthalpy calculations on the pyrene complex **4** in water and chloroform indeed provided impressive support for the major role of internal solvent-cohesive interactions.[49] This computational study revealed that the key process which determines the difference in binding in the two solvents ($\Delta\Delta G^{\circ} = 7.1$ kcal mol^{-1}; Table 3) is the elimination of pyrene molecules from the solvent and not directly the cyclophane–pyrene interactions, which are of similar magnitude in both solvents. From the calculated difference in the free enthalpy of complexation between water and chloroform ($\Delta\Delta G =$ 10.2 kcal mol^{-1}), 8.6 kcal mol^{-1}, that is, about 84%, is caused by the differences in the free enthalpy of solvation of the pyrene molecule in the two solvents!

Recent computational studies provide further evidence for the importance of the proposed large contribution of solvent-cohesive interactions to enthalpy-controlled apolar binding processes. Rossky and co-workers[58] carried out simulations of the hydration structure of the aromatic binding pocket at the active site of the digestive serine protease α-chymotrypsin. They found that the highly constrained concave geometry of the pocket prevents the formation of a hydrogen-bonding network between the solvating molecules. Correspondingly, solvent displacement by the incoming substrate is associated with a large enthalpic driving force.

Southall and Dill[59] observed in Monte Carlo simulations a large dependence of the hydration efficiency on the shape and curvature of the solute. Small solutes, for which the classical hydrophobic effect was derived, undergo an ordered "iceberg"-like solvation (characterized by $\Delta S \ll 0$) to avoid breaking H bonds. In contrast, the geometry of larger nonpolar solutes, in particular planar ones such as arenes, force

first-shell water molecules to break their H bonds ($\Delta H^o \gg 0$). This study also analyzes in greater detail the origin of the negative changes in heat capacity accompanying apolar binding processes in water. Similar conclusions with respect to topography-dependent H-bonding sacrifices upon the hydration of apolar surfaces have also been drawn by other authors.[60]

A second major contribution to the favorable enthalpic driving force in water results from the substitution of less favorable dispersion interactions between water molecules and the complementary surfaces of the host and guest molecules by more favorable dispersion interactions between the hydrocarbon surfaces in the complex.[12–15,48,61] The attractive B term in the Lennard–Jones potential [Eq. (1); U: potential energy] that describes the London dispersion interactions is directly proportional to the polarizability α [Å^3] of the interacting atoms and groups [Slater–Kirkwood equation (2); α: polarizability, e: charge on an electron, m: mass of an electron, $\hbar$: Dirac's constant, N: effective number of electrons in the outer shell].[62]

$$U = \frac{A}{r^{12}} - \frac{B}{r^6} \quad (1)$$

$$B = \frac{^3/_2 e(\hbar/m^{1/2})\alpha_i\alpha_j}{(\alpha_i/N_i)^{1/2} + (\alpha_j/N_j)^{1/2}} \quad (2)$$

At constant distances between interacting atoms, attractive dispersion interactions increase with increasing atom polarizability. The constituents of water (O: $\alpha = 0.84$ Å^3; HO: $\alpha = 1.20$ Å^3) have much lower polarizabilities than hydrocarbon groups (CH_2: $\alpha = 1.77$ Å^3; CH_3: $\alpha = 2.17$ Å^3; aromatic CH: $\alpha = 2.07$ Å^3).[62] Therefore, the dispersion forces between water molecules and a hydrocarbon surface are weaker than those between two hydrocarbon surfaces. Thus, upon apolar complexation, less favorable water–solute contacts are replaced by more favorable contacts between the surfaces of the binding partners. The importance of molecular polarizability for apolar binding in water has also been recognized in other investigations.[26,27,63]

The tightness of the fit between the associating molecules affects the thermodynamic characteristics of host–guest binding.[24,25,27,64,65] Efting and co-workers showed in calorimetric studies that tight inclusion of apolar aromatic and aliphatic guests in the smaller cavity of α-cyclodextrin at 298 K is characterized by a much larger enthalpic driving force than the inclusion of the same guest in the wider cavity of β-cyclodextrin.[24,25,64] In some cases involving aliphatic guests, changing from the smaller to the larger binding site was associated with a change from an enthalpy- to an entropy-driven process. The strongly distance-dependent (ca. $1/r^6$) attractive van der Waals interactions between the host and guest in a tight complex[66] are much more effective than in a loose complex, whereas translational and rotational degrees of freedom of the interacting partners become substantially reduced. A loose association, on the other hand, is predominately driven by the desolvation entropy.

In view of the lack of calorimetric data for apolar complexation processes of biological and chemical systems in water, we suggested around 1990[10,12–15] that characterizing apolar binding processes in water as hydrophobically driven should not imply a predominant enthalpic or entropic driving force. However, it is also becoming increasingly clear that tight complexation in deep apolar pockets of biological and synthetic receptors is mostly enthalpy driven, that is, obeys the nonclassical hydrophobic effect.

3. What Do We Learn from Crystals?

A crystal is an ordered supramolecular system, and according to Dunitz "a supermolecule par excellence".[67] X-ray crystallography provides accurate information on the structures of molecular complexes and the nature of the nonbonded interactions between the binding partners in the solid state. This technique has become a central one in molecular recognition studies.

Rational drug design, as a biological extension of the supramolecular sciences, is increasingly dependent on available protein crystal structures taken from the Protein Data Bank (PDB) or in-house databases.[68] In addition, new programs, such as Isostar,[69a] SuperStar,[69b] and the impressive Relibase,[69c] permit the systematic investigation of protein–protein or protein–ligand interactions. The use of the Cambridge Structural Database (CSD) is also important for the life sciences.[70] Both sets of databases are growing at an exponential rate,[71] and have been vaults for finding information on chemical interactions: they have been the basis for extensive investigations of classical H bonds in the past,[72,73] and more recently have been used to explore weaker H bonds, such as C–H···O, C–H···N, and C–H···Cl.[74] Directionality, energetics, distance relative to van der Waals radii, and bond length are useful criteria for classifying H bonds. In this context, the C–H/π interaction between aromatic rings has been defined as an H bond (see Section 5). Moreover, although of controversial importance, the C–H···O hydrogen bond remains a prominent example because of its wide occurrence in crystal structures and its postulated structural role in biology.[75] We shall conclude these introductory remarks with the statement that "atoms have to go somewhere", a perhaps discouraging view of a crystallization process, but one that reminds us of the maximization of dispersive and minimization of repulsive interactions in crystals—"real" and measurable structure-determining processes—that need to be considered when describing weak intermolecular forces.[76]

Parallels can be drawn between molecular recognition events that occur within model systems in the liquid phase and those that define the supramolecular nature of a molecular network in the solid state. The crystal structure of benzene laid the structural basis for recognizing attractive interactions between aromatic rings (Section 4).[77] Benzene crystallizes in the space group *Pbca*, with four molecules in the unit cell, and each molecule being surrounded by twelve neighbors. Three types of next-neighbor interactions are observed (Figure 5): The most favorable interaction is the edge-to-face arrangement with a distance of 5.025 Å between the ring centers. However, as pointed out by Williams and Xiao,[78] none of the

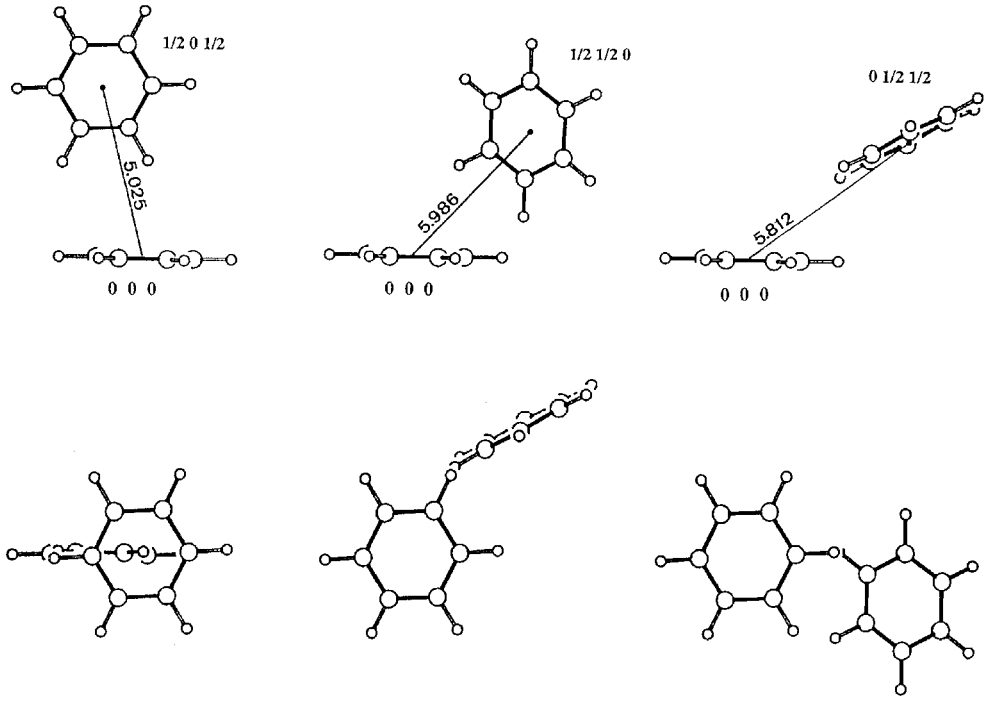

Figure 5. Two orthogonal views (upper and lower rows) of the basic next-neighbor motifs in crystalline benzene (*Pbca*). Left: most favorable edge-to-face orientation with a center-to-center distance of 5.025 Å; rings located at (0,0,0) and ($^1/_2$,0,$^1/_2$) in the unit cell. Middle: dimer with perpendicular arrangement but a larger offset (5.986 Å, rings at (0,0,0) and ($^1/_2$,$^1/_2$,0)). Right: pairing with inclined ring moieties (5.812 Å, rings at (0,0,0) and (0,$^1/_2$,$^1/_2$)); Reprinted with permission from The Royal Society (London).[80]

pairs in the benzene crystal corresponds to the lowest energy arrangements observed in the gas-phase dimer. This discrepancy arises from the presence of *several* nearest neighbor molecules in the vicinity of an individual benzene molecule and of long-range intermolecular interactions in the solid state. Modifications to the benzene lattice structure have been realized experimentally by using different pressures, with many of the attempts being made with the aim of predicting the resulting crystal structure.[79] The search for polymorphic structures facilitates a deeper understanding of the thermodynamics of crystallization and comparisons with predicted models. The smaller polycyclic aromatic hydrocarbons (PAHs), such as naphthalene or pyrene, prefer T-shaped interaction geometries, similar to benzene. The larger aromatic molecules (such as coronene, kekulene, or hexabenzocoronene) show offset π–π stacking, since for these molecules there is a substantial gain in dispersion interactions that results from the contact of such large polarizable surfaces. In each of these crystals, however, there also exist edge-to-face interactions between molecules of neighboring stacks in the so-called "herringbone pattern".

The crystal structure of benzene, in a least-squares superimposition, was matched geometrically with the structure of an inclusion complex of cyclophane **5** with benzene (Figure 6).[80] This study revealed that the interactions of the benzene rings in the host with the included benzene ring are similar to those seen between nearest neighbors in crystalline benzene. Klebe and Diederich concluded that the self-recognition of molecules in the solid state provides a guide for the design of hosts that are specific receptors for the molecule in question. This analysis has been useful for modeling a pseudoreceptor during drug design.[81] The analysis of the benzene crystal has been extended to other systems displaying similar packing modes, such as the self-assembling cyclic peptide nanocylinders of Bong and Ghadiri.[82]

The Holy Grail of crystallography remains the prediction of crystal structures from molecular structures.[83] The last workshop held on this subject produced only a few correct predictions, which emphasizes how limited our knowledge is in this area.[84] The problem of crystal-structure prediction has been recognized as more complex than originally thought, but steady progress has been made. By considering molecular size, shape, stoichiometry, and topology; Desiraju and Gavezotti were able to assign a set of 32 PAHs into four different crystal packings.[85] Correlations between molecular size, packing energy, and other crystal properties made it possible to predict physical properties, such as sublimation enthalpy and density of unknown aromatic hydrocarbons.[76]

Crystal engineering has enabled connections between molecular and supramolecular structure to be established on the basis of intermolecular interactions.[86] In this context, supramolecular synthons have been defined as structural units within supermolecules that can be formed and/or assembled by known or conceivable synthetic operations involving intermolecular interactions. The aryl–aryl synthons, for example, are based on edge-to-face and stacking arrangements of two aromatic rings. An example of an application of the latter lies in the topochemical solid-state synthesis of 3,4-diphenyl-substituted cyclobutane-1,2-dicarboxylic acids using the attractive interactions between aromatic donor and acceptor moieties.[87]

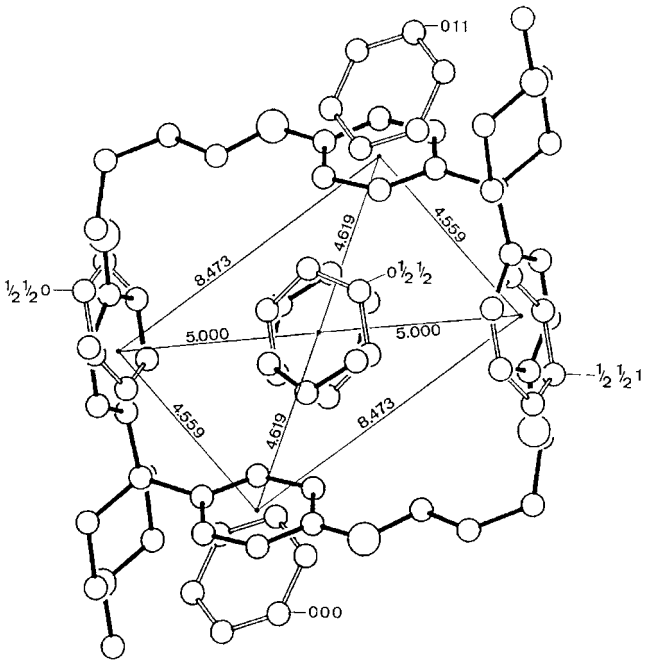

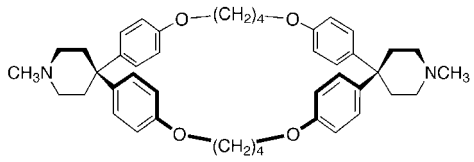

5

Figure 6. Superimposition of a subset from the packing of crystalline benzene (empty bonds, classified by their centering in the crystal packing) with the molecular structure of the benzene·**5** complex in the crystal (solid bond). Mutual center-to-center distances between the aromatic rings in the cyclophane complex are given.[80]

4. Arene–Arene Interactions

4.1. Biological Relevance

Arene–arene interactions play an essential role in the structure of biological macromolecules such as DNA and proteins, as well as in their interaction with small molecules.[88] However, their weak and poorly directional character hindered for some time the development of a general, structural, and energetic model for their description.[89]

Interactions between aromatic amino acid side chains are abundant in proteins, as shown by the pioneering work of Burley and Petsko.[6,90] They demonstrated in a study involving 34 proteins that on average 60% of aromatic side chains (Phe, Trp, Tyr) are involved in π–π interactions, where the predominant arrangement was found to be the T-shaped edge-to-face structure **6** (Figure 7). McGaughey, et al. extended the analysis to a larger sample of proteins and suggested that the parallel-displaced geometry **7** was a preferred orientation.[91] Remarkably, none of these studies described the face-to-face geometry **8**.

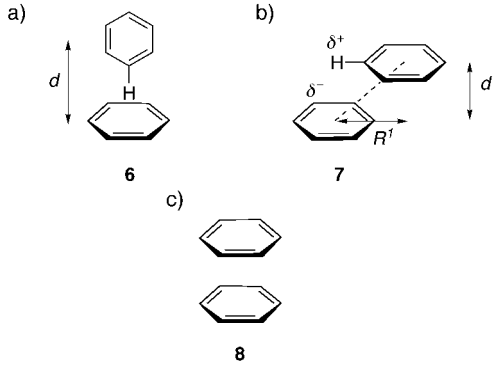

Figure 7. Proposed lowest energy structures of the benzene dimer. *d*: distance between planes, R^1: lateral offset.

Several other statistical analyses of PDB structures have elucidated the preferential arrangement of specific aromatic amino acid pairs in proteins or α-helices.[92,93] When these results are combined with computational work, the general view is a competition between stacked and T-shaped complexes; however, an uneven distribution can be seen depending on the aromatic amino acid pair analyzed, the distance of the two aromatic rings, their location in the protein (in the core or on the surface), and whether clustering of the aromatic amino acids is involved.[94]

Although π–π interactions are accepted as weak, they have been recognized to play an important role in the folding[93] and the thermal stability of proteins.[95] Other biological contributions are noteworthy. The recent literature provides several illustrative examples: Edge-to-face interactions are implicated in the decrease of the pK_a value of Tyr9, which is located in the vicinity of Phe10 in the active site of glutathione *S*-transferase A1-1. This enzyme catalyzes the conjugation of glutathione to electrophilic substrates (drugs, toxins, endogenous compounds).[96] Stacking interactions play an essential role in mRNA-cap recognition by proteins (in combination with cation–π interactions, see Figure 4 and Section 6),[97] in the arrangement of porphyrin units in water or inside proteins,[98] in the binding of carotenoids in a light-harvesting complex,[99] and have been suggested to govern the self-assembly of amyloid fibrils.[100] Introduction of aromatic side chains in a hairpin motif of a de novo designed β sheet produces an enthalpy-driven interaction between β strands.[101] The self-association of a 12-residue β hairpin through aromatic side chains was investigated, and the Phe–Phe pair that are found in an edge-to-face geometry gave an increment in the interaction free enthalpy of $-0.55\ kcal\,mol^{-1}$.[102] This value is similar in magnitude to that found by double mutant cycles in the cold-shock protein CspA (Phe→Leu),[103] but lower than what has been previously observed in barnase by Fersht and co-workers (Tyr→Ala, $-1.3\ kcal\,mol^{-1}$).[104] Moreover, the Phe–Phe interaction can stabilize monomeric α helices by up to $\Delta G = -0.8\ kcal\,mol^{-1}$, as determined recently by circular dichroism studies.[105]

4.2. Geometrical and Energetic Aspects

The benzene dimer has often been chosen as a model system for the investigation of π–π interactions. The earliest gas-phase studies began with the work of the Klemperer research group who deduced, by using molecular beam spectroscopy, there was an edge-to-face arrangement between neighboring molecules.[106] This T-shaped arrangement has been confirmed in a large number of experimental studies. Although the observed intermolecular arrangements have been shown to be often dependent upon the experimental technique used,[107] the T-shaped motif also appears as the preferred one for both liquid benzene (as revealed by ^{1}H NMR investigations)[108] and, as seen in Section 3, for benzene in the crystal.

Molecular mechanics, ab initio, and density functional calculations at several levels of theory have been employed to describe and predict the structure of the benzene dimer.[109] Different minima have been proposed, where the interaction energy is often dependent on the method used.[110] Very recent calculations gave two nearly isoenergetic minima for the edge-to-face and parallel-displaced arrangements with values for the CCSD(T) (coupled cluster calculation with single and double substitutions with noniterative triple excitations) interaction energy of $D_e = -2.48$ and -2.46 kcal mol^{-1}, respectively.[111] This low calculated difference in binding energy is in good qualitative agreement with the observation that no strong preference for either arrangement has been found for Phe, Tyr, and Trp side chains in proteins. Experimental measurements in the gas phase have shown the stabilization enthalpy of the benzene dimer to range from $D_0 = -1.6 \pm 0.2$ kcal[112] to -2.4 ± 0.4 kcal.[113] Finally, the sandwich structure **8** (Figure 7) is more unfavorable ($D_e = -1.48$ kcal mol^{-1}) than the other two, even though it is an energy minimum and still attractive in nature. The energy barriers for interconversion of the three most stable minima geometries are very low, and hence they are in dynamic equilibrium.[114] We should mention the geometric values that describe the most stable arrangements **6** and **7**. Structure **6** has an experimentally determined ring-center separation of 4.96 Å, with the partially positively charged H atom pointing perpendicular into the partially negatively charged center of the second ring (Figure 7). The parallel-displaced stacking dimer **7** has an interplanar distance d of 3.4–3.6 Å with a displacement $R^1 = 1.6$–1.8 Å. The application of ab initio techniques to even larger polycyclic aromatic hydrocarbon dimers has upheld the arrangement seen in the corresponding crystal structures (Section 3).[115]

It is nowadays recognized that London dispersion interactions are the major source of stabilization energy between two aromatic molecules; however, the electrostatic component associated with the large quadrupole moment[116] of benzene (-28.3×10^{-40} C m^2)[117] is an influential factor in determining the geometry of the interaction. For example, the parallel-displaced arrangement is a compromise between optimal surface overlap that maximizes the dispersive attraction (distance dependency r^{-6}) and quadrupole moment positioning (r^{-5}). Short-range repulsive interactions (Pauli-exchange/repulsion forces) also influence the interplanar distance.[118] Assessment of these binding interactions in aqueous solution is complicated by additional hydrophobic effects; these of course lead to apolar complexation or to intramolecular hydrophobic collapse (Section 2).[119] A deeper view of the solvent-dependency of the interaction energy in the benzene dimer is available from computational studies. The calculated Gibbs free energy minimum (ΔG) for the benzene dimer in liquid benzene, chloroform, and water is -0.4, -1.0, and -1.5 kcal mol^{-1}, respectively.[120] Thus, there appears to be a solvophobic enhancement of the binding on progression to more polar solvents. The more favorable gas-phase interaction is considerably dampened by solvent competition and entropic effects.[120] Finally, it is interesting to note that the T-shaped structure has been confirmed through computational investigations to be an energetic minimum in aqueous solutions.[121,122]

The parallel-stacked arrangement **8** that would permit a HOMO–LUMO charge-transfer interaction is estimated to be 0.7–1.5 kcal mol^{-1} (gas phase or aqueous solution) less stable than the T form.[122] This geometry is unfavorable because of repulsive interactions between the negatively charged electron clouds or quadrupole moments of equal sign.

The benzene dimer is not necessarily a good model for the π–π interaction since polarization or enlargement of the π system changes the preferred intermolecular arrangement dramatically. To this end, the toluene dimer has been shown to have stacked arrangements as global minima as a result of a small dipole originating from the methyl group. Toluene has, therefore, been proposed as an improved model for phenylalanine for the study of π–π interactions in proteins.[122,123]

4.3. Experimental Study of π–π Interactions

4.3.1. Background Information

We have shown that one of our cyclophane receptors (similar to **1** (Section 2) but with the eight MeO groups exchanged for Me groups) is able to complex 2,6-disubstituted naphthalene derivatives in CD_3OD, with the cavity-bound guests undergoing both edge-to-face and π-stacking interactions with the receptor.[124] Complementarity between the electron-rich host and electron-poor guests led to particularly stable association (for example, $K_a = 280\,\text{M}^{-1}$, $-\Delta G = 3.4$ kcal mol^{-1} for the complex of 2,7-dicyanonaphthalene as compared to $K_a = 50\,\text{M}^{-1}$, $-\Delta G = 2.3$ kcal mol^{-1} for the complex of 2,7-dimethoxynaphthalene; $T = 303$ K), which stresses the importance of polar contributions in π–π interactions.[125]

Klärner and co-workers have shown that the convex-concave topology of aromatic surfaces influences the binding properties of tweezer-shaped receptors.[126a] Computational methods at different levels of theory have been used to generate electrostatic potential surfaces for both the convex and concave faces (Figure 8). The results are striking: the concave surface features convergent π-electron systems (Figure 8c) that lead to a considerably larger negative potential within the tweezer's interior than at the exterior. This observation explains the experimentally observed high preference of receptor **9** (Figure 8b) for complexing electron-

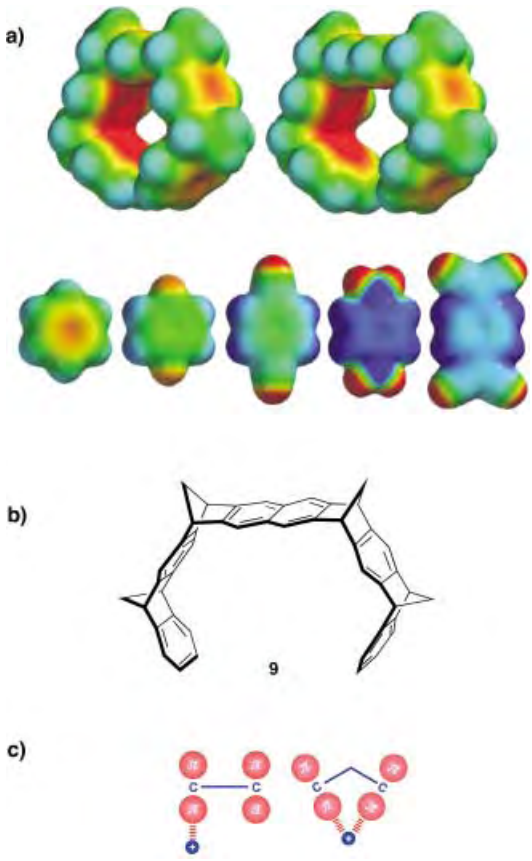

Figure 8. a) Electrostatic potential surfaces of molecular tweezers with benzene (left) and naphthalene (right) spacers developed by Klärner and co-workers (top) and aromatic guests (bottom, from left to right: benzene, *p*-difluorobenzene, *p*-dicyanobenzene, *p*-dinitrobenzene, and 7,7,8,8-tetracyanoquinodimethane) calculated by semiempirical methods. The color code spans from −25 (red) to +25 kcal mol^{-1} (blue). b) Receptor **9** for which the electrostatic potential surface is shown in (a). c) Schematic representation of the interaction of a positive test charge with nonconjugated "idealized" sp^2 C atoms with linear (left) and concave geometry (right).[126a]

deficient guests in its interior in a position parallel to the central naphthalene spacer.[126b] This result demonstrates the importance of molecular receptor topology: evaluation of host–guest complexation processes needs to take into account the complementarity of both the shape and molecular electrostatic potential (MEP). This principle has been employed to rationalize the complexation behavior of various curved aromatic hosts and even cyclic peptides.[127,128]

In 1990 Hunter and Sanders developed a simple electrostatic model where a set of point charges is used to represent the electrostatic charge distribution in a π system. Useful general rules have been derived from this work for a qualitative understanding of π–π interactions.[129] The key feature of the model is that it considers π electrons and the σ-bonding system separately, and reveals π–π repulsions and π–σ attractions to be the governing factors in the interaction between two aromatic molecules. This model has been challenged recently by ab initio studies, which contend it should be sufficient to recognize solely the role of molecular quadrupoles when describing aromatic interactions.[130]

4.3.2. ***Edge-to-Face Interactions***

Many chemical model systems have been designed to investigate both edge-to-face and π-stacking geometries of interacting aromatic rings, and a plethora of receptors, in particular cyclophanes, have demonstrated these arrangements during complexation.[2,9–16,126,131] The intermolecular edge-to-face aromatic interactions have been analyzed by Hunter and co-workers using chemical double-mutant cycles.[132] This elegant method allows individual assignment of the contribution from T-shaped interactions between differently substituted terminal phenyl rings in the host (substituent X) and guest (substituent Y) to the overall binding free enthalpy in the molecular zipper complexes **10** (Figure 9). The obtained increment in free enthalpy for the edge-to-face interaction, $\Delta\Delta G$, is on average −0.3 kcal mol^{-1} (for X = Y = H) and is sensitive to the nature of the substituents on the aromatic rings, and varies from unfavorable ($\Delta\Delta G = +0.29$ kcal mol^{-1} when X = NO_2 and Y = NO_2) to favorable (−1.1 kcal mol^{-1} when X = NO_2 and Y = NMe_2).[133] Thus, the highest edge-to-face attraction is found when an electron-attracting substituent renders the interacting H atom more acidic (higher positive partial charge) and an electron-donating substituent increases the basicity (π-electron density) of the interacting π system. Equation (3) in Figure 9 gives the relationship between the Hammett substituent constants σ and the observed interaction energies for this system: In addition to the attraction between the partially positively charged edge H atoms (of the host) with the terminal aromatic ring (of the guest), the crucial influence of the global dipoles can be seen (cross-term $5.2\cos(\phi)\sigma_X\sigma_Y$). However, the incremental free enthalpy values $\Delta\Delta G$ are not likely to be universal values for edge-to-face interactions between aromatic rings as a result of the lack of rigidity in the zipper complex, as pointed out by Martínez et al.[134]

Wilcox and co-workers developed the molecular torsion balance **11** based on rotational isomerism (Figure 10) to quantify edge-to-face interactions.[135] The following findings were made in this study that was recently reviewed:[136] 1) The folded conformation in a series of phenyl esters (X in **11**: Me) is preferred by $-\Delta G° = 0.4$ to 0.65 kcal mol^{-1} (298 K), with the variation depending on the nature of substitution on the phenyl ring (0.24 kcal mol^{-1} for the *p*-methoxyphenyl ester, and 0.65 kcal mol^{-1} for the *p*-nitrophenyl ester). 2) The folded conformation of the corresponding cyclohexyl ester was also stabilized to a similar extent (0.37 kcal mol^{-1}). 3) Variation of the substituent X in **11** from donor (NH_2) to acceptor (CN) did not affect the magnitude of the energetic preference for the folded conformation ($\Delta G = -0.18$ to -0.30 kcal mol^{-1}). 4) The folding of isopropyl ester **12** (Figure 10b) was more exergonic ($\Delta G = -0.34$ to -0.64 kcal mol^{-1}, depending on substituent X) than the folding of the phenyl ester. These results support the notion that dispersion, and not electrostatic forces, are largely responsible for the attractive edge-to-face interaction. However, computational investigations suggested that the preference for the folded state arising from the aromatic interactions could have been underestimated.[137a,b] The calculations showed that differences in the solvent-accessible surfaces of the two conformations in **11** may push

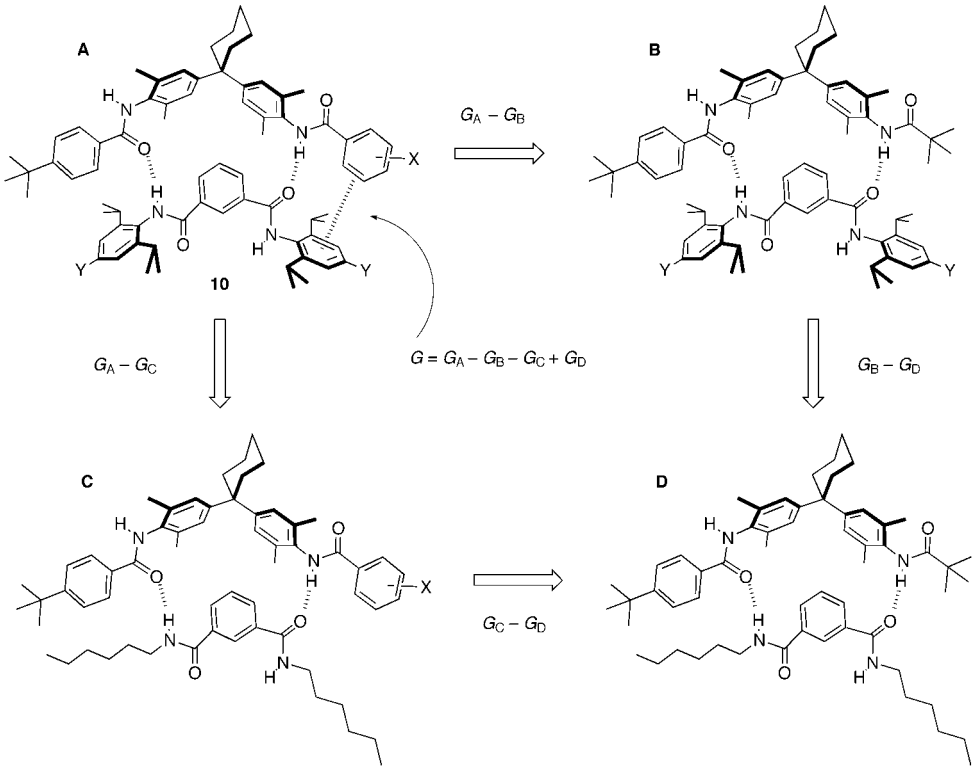

Figure 9. Chemical double-mutant cycle by Hunter and co-workers for probing the magnitude ($\Delta\Delta G$) of the edge-to-face aromatic interaction between the terminal phenyl rings of molecular zipper **10** and isophthalic acid diamide guests.[132,133]

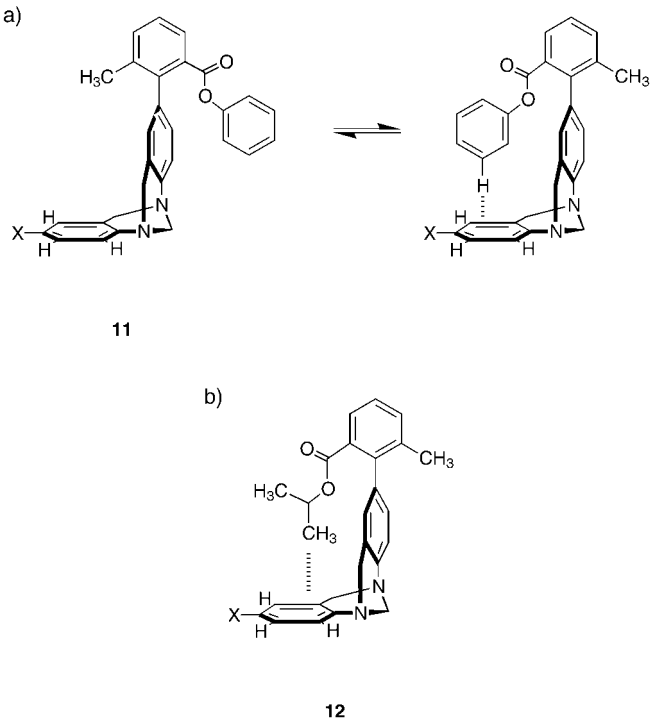

Figure 10. a) Molecular torsional balance **11** described by Wilcox and co-workers to quantify aromatic edge-to-face interactions. T-shaped aromatic interactions are effective only in the folded conformation.[135] b) Preferred folded state of isopropyl ester **12**. X = NO_2, CN, I, Br, Me, OH, NH_2.

the equilibrium toward the unfolded state; thus, a more favorable free enthalpy of interaction might be expected when solvent effects are fully considered.[137c]

Clearly, solvent effects greatly increase the challenge—not only in computational work but also in studies of elegantly designed supramolecular model systems—to quantify a single individual intermolecular bonding interaction, such as an edge-to-face aromatic contact. Over the past few years we have recognized this challenge with model systems, and have complemented our molecular-recognition studies on synthetic receptors with the analysis of intermolecular interactions in structurally well-defined enzyme–inhibitor complexes. In this approach, we introduce defined mutations in substrates that form complexes of similar geometry with the biological receptor (which we prove by X-ray crystallography) and evaluate the differences in binding free enthalpy, thereby obtaining valuable information on the magnitude of individual intermolecular interactions.

We found for a series of inhibitors of thrombin (such as the one shown in Figure 3, Section 1) that measured changes in binding free enthalpy can be directly correlated with the bonding contributions of individual substituents of the inhibitors.[5] Thus, similar binding affinities were obtained for the benzyl- and cyclohexylmethyl-substituted inhibitors **13** (inhibition constant $K_i = 220$ nM) and **14** ($K_i = 350$ nM) that adopt an edge-to-face geometry with respect to Trp215 in the D pocket of the enzyme active site (Figure 3).[138] This result suggests, in agreement with the studies of Wilcox and co-workers, that specific electrostatic C–H/π interactions need

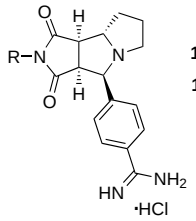

13 R = $PhCH_2$
14 R = Cyclohexylmethyl

not be invoked. Model investigations by Turk and Smithrud also came to the conclusion that aliphatic–aromatic and aromatic–aromatic edge-to-face contacts provide similar energetic stabilization.[139]

Clearly, there remains some controversy with respect to the directional, electrostatic component of the edge-to-face interactions, which have been identified in a variety of X-ray crystal structures of other protein–inhibitor complexes.[140] We presume that a substantial electrostatic component of the interaction, in addition to the dominating dispersion term, only exists if the partial positive charge on the interacting edge H atoms is substantially enhanced by strong electron-withdrawing *ortho*- and/or *para* substituents, which the aromatic amino acid side chains are lacking.

4.3.3. The C–H/π Interaction

Although the attraction between arenes, alkenes, or alkynes with hydrocarbons (the C–H/π interaction) is not an interaction between aromatic rings, it should be briefly discussed here, in view of its similarity to the edge-to-face aromatic interaction. The C–H/π interaction, while considerably weaker than classical H bonding, also plays notable structure-determining and structure-stabilizing roles throughout chemistry and biology.[141,142] High-level ab initio calculations of benzene–hydrocarbon complexes give interaction energies (D_e) of −1.82, −2.06, and −2.83 kcal mol^{-1} for the ethane, ethylene, and acetylene complexes, respectively, with benzene.[143] An increase in the electrostatic contribution upon changing from ethane (−0.17 kcal mol^{-1}) to acetylene (−2.01 kcal mol^{-1}) clearly reflects the differences in the hybridization state and the acidity of the C–H residue participating in the binding.[143] Even for alkanes, the orientation of the C–H bond toward the ring center is controlled to some extent by the relatively weak, but directional electrostatic interaction; however, the dispersion term provides the major source of attraction in all the complexes.

We limit our discussion of C–H/π interactions to a few examples since the field is comprehensively and continuously overviewed by Nishio et al., who published a pertinent monograph on the subject and provide a constantly updated reference list on the internet.[144,145] The C–H residues of sugars have been shown in many X-ray crystal structures of protein complexes to undergo interactions with aromatic amino acid side chains. A beautiful example of C–H/π interactions in biology is provided by the complex of the D-galactose/D-glucose binding protein with β-D-glucose, in which the aromatic side chains of Trp 183 (on the β face) and Phe 16 (on the α face) sandwich the hexose ring at van der Waals distance (Figure 11).[146] The sugar C–H residues have a

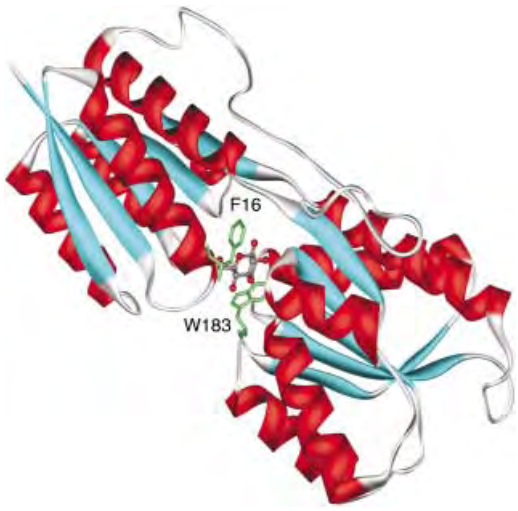

Figure 11. Complexation of β-D-glucose by the D-galactose/D-glucose binding protein (PDB code: 2GBP).[146]

significant partial positive charge on their H atoms as a consequence of an inductive effect provided by the neighboring O and OH groups which should enhance their interactions with the aromatic rings.

As a second example for the ubiquitous C–H/π interactions, we refer to the close contacts (3.3–4.1 Å) established by the isopropyl group of our thrombin inhibitor with the aromatic rings of Tyr 60A and Trp 60D in the narrow P pocket of the enzyme (Figure 3).[5]

4.3.4. Stacking Interactions

The other important arrangement of aromatic rings, besides the edge-to-face contact, is the parallel alignment. It is well known that two aromatic partners, one bearing strong electron-donor and the other strong electron-acceptor groups, form parallel stacking complexes in solution and often in the solid state, with the geometry largely determined by molecular orbital interactions (charge-transfer complexes). On the other hand, few chemical model systems have been designed to evaluate the optimum orientation, the role of substitution, and the underlying forces in the attraction of aromatic rings which do not differ greatly in their ionization potential (and electron affinity).

The forced face-to-face arrangement in 1,8-diarylnaphthalenes has offered the possibility to investigate the stacking interactions of substituted aromatic rings (Figure 12a). ^{1}H NMR measurements by Cozzi and Siegel of the barrier to rotation about the aryl–naphthyl bond in $(CD_3)_2SO$ demonstrated there was a linear relationship between the barrier of rotation $\Delta G^{\neq}$ and the Hammett parameter σ_{para}.[147] The barrier to rotation depends on the strength of the parallel-stacked interaction in the ground state, which is much larger when the substituent X is electron withdrawing (X = NO_2: $\Delta G^{\neq} = 17.3$ kcal mol^{-1}) than if X is electron donating (X = MeO: $\Delta G^{\neq} = 13.9$ kcal mol^{-1}). This finding that electron-deficient rings prefer stacking interactions over electron-rich ones is in agreement with the electrostatic model by

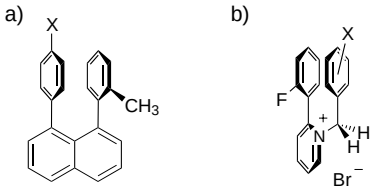

15

Figure 12. Dynamic ^{1}H NMR investigations of 1,8-diarylnaphthalenes (a)[147] and pyridinium bromide **15** (b)[149] have provided evidence for polar effects in aromatic stacking interactions.

Hunter and Sanders.[129] The term "polar/π" interaction was introduced to emphasize the importance of the electrostatic term in π stacking and the fact that the aromatic ring with the substituent X possesses a distinctly polar character. This support for the relevance of polar, electrostatic effects in π–π stacking is in good agreement with the semiempirical AM1 study of the conformational equilibria performed on *cis*-1,3-diphenylcyclohexanes.[148]

^{1}H NMR spectroscopic measurements in water were carried out by Rashkin and Waters to determine the barriers to rotation about the biaryl bond in pyridinium bromides **15** (Figure 12 b) which, according to ab initio geometry optimization studies, features an offset stacking arrangement between the fluorinated phenyl and the benzyl ring.[149] In agreement with the results obtained by Siegel and co-workers, they found a rise in the barrier of rotation when the *para* substituent X in the benzyl ring was changed from electron donating (Me) to electron accepting (NO_2). This effect was even more pronounced when the nitro group was in the *meta* position; the authors explained this effect by interannular electrostatic attraction between the nitro group and H atoms of the fluorinated phenyl ring.

It is often possible to rationalize stacking interactions by considering the quadrupole moments of the aromatic partners, or alternatively through visualization of the molecular electrostatic potentials (MEPs). Examples are anthracene–dinitrobenzene conjugates with flexible spacers (which prefer to adopt U-shaped conformations),[150] stacks formed by fluoroaromatic compounds (Section 7), and multichromophoric oligomers which fold into a pleated structure in water as a result of interactions between alternating electron-rich (1,5-dialkoxynaphthalene) and electron-poor (1,4,5,8-naphthalenetetracarboxylic diimide) moieties.[151] Although the latter system exhibits a strong charge-transfer band, the driving forces for formation of such "charge-transfer complexes" are mainly dispersion and dipolar interactions as well as—in water—hydrophobic effects. Charge transfer contributes very little to ground-state stabilization, but is very effective in the excited state.

4.3.5. *Aromatic Interactions Involving Heteroaromatic Compounds*

The tetracationic cyclophane **16** is one of the most versatile hosts known for the inclusion complexation of electron-rich aromatic rings (such as dialkoxy-substituted benzene and naphthalene derivatives or tetrathiafulvalene (TTF))[152] and has been used by Stoddart and co-workers as a fundamental component in the construction of a large diversity of catenanes and rotaxanes. This work has already been comprehensively reviewed.[153] The encapsulated π donors undergo both π–π stacking with the two sandwiching bipyridinium rings in **16**—which includes a cation–π interaction component (Section 6)—as well as edge-to-face interactions with the *p*-xylylene bridges.[154]

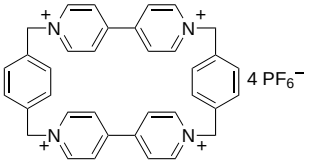

16

The introduction of heteroatoms into aromatic rings has a significant influence on the π–π interaction. Electrostatic attraction between atoms with positive or negative partial charges[155] and the alignment of molecular dipoles become important in determining how two or more heterocyclic π systems interact. This has been nicely illustrated in molecular-recognition studies with the 1-butylthymine receptors **17** and **18** by Hamilton and co-workers.[156] Whereas **17** forms a solid-state complex in which thymine undergoes π stacking with the naphthalene ring of the host, an edge-to-face orientation is found in the complex of **18**, with the naphthalene ring adopting an orthogonal orientation with respect to the host–guest H-bonding array (Figure 13). The geometrical preferences are best explained by considering the distribution of the electronic charge on the atoms of the thymine guest and the naphthalene moiety of the host. In the stacking geometry seen with **17**, atom centers of opposite partial charges face each other, which provides a favorable electrostatic stabilization of the complex. On the other hand, a stacking complex of **18** would place centers of the same (+ or −) charge opposite each other, which would destabilize the association. The edge-to-face geometry is, therefore, adopted in the complex to avoid this electrostatic repulsion.

Since attractive electrostatic interactions between atoms of opposite partial charges often overcome the repulsion between closed-shell π clouds, π–π-stacking interactions are abundant between heterocyclic π systems. In addition, the orientations of the molecular dipoles between the interacting chromophores may play a prominent role in determining the orientation of stacking heterocycles, as shown by Rotello and co-workers for flavin–substrate recognition in chemical model systems.[157] A nice example of heterocyclic π stacking is provided by the ternary complex of the anticancer drug 1843U89 and dUMP formed at the active site of thymidylate synthase (Figure 14).[158]

Many other receptors have been designed for complexation by π–π stacking of nucleobases and related heteroaromatic systems.[159] Moreover, supramolecular architectures, such as helices, have been constructed through stacking interactions; the reader is referred to the pertinent literature references.[160]

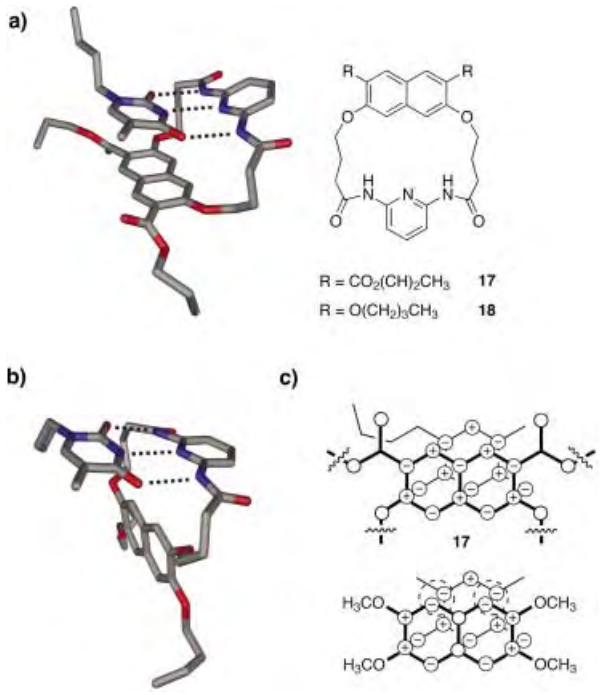

Figure 13. X-ray crystal structures of the complexes formed by receptors **17** (CSD code: VABVID; a) and **18** (CSD code: VABVOJ; b) with 1-butylthymine.[156] c) Consideration of atomic partial charge interactions in the complexes explains the preference for the face-to-face orientation in the complex of **17** as well as why **18** (2,3,6,7-tetramethoxynaphthalene as model for **18** interacting with 1-butylthymine)[156c] avoids the stacking geometry.

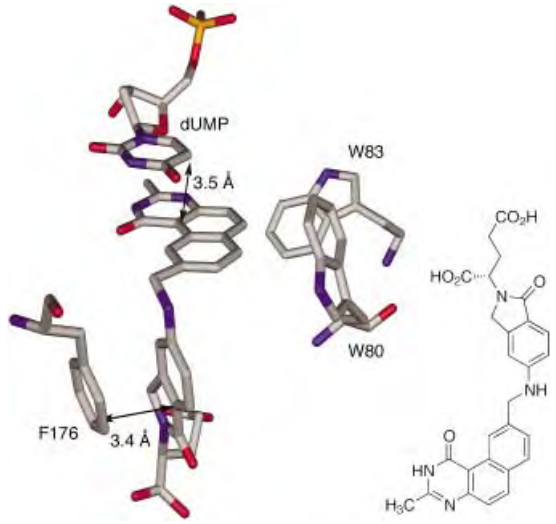

Figure 14. Heterocyclic π stacking between dUMP and the anticancer drug 1843U89 bound at the active site of thymidylate synthase (PDB code: 1TSD).[158]

The geometries of DNA duplexes are largely determined by H-bonded nucleobase pairing,[161a] offset base stacking at a vertical base distance of 3.4 Å, the conformation of the sugar backbone,[161b] the base sequence, the hydrophobic effect, and presumably specific solvation patterns in the minor and major grooves.[161c] The geometries of DNA duplexes have increasingly been subjected to high-level theoretical calculations, and the results have been summarized in a recent review.[162] According to these studies, the stacking of nucleic acids in the gas phase is dominated by dispersion forces. A terminal (dangling) base has been reported to contribute up to 1 kcal mol^{-1} in stacking energy to the total stability of the DNA duplex in water.[163] The main driving force for base stacking in water, be it the hydrophobic effect, polar and dipolar interactions, or dispersion forces, remains a matter of some debate.[164]

Natural bases in the DNA duplex can be substituted by apolar artificial ones (nucleobase isosteres) that do not undergo Watson–Crick H bonding but fit geometrically and electronically into the stacking base-pair array.[165] Furthermore, stacking is the dominant feature of DNA-intercalating agents, such as nogalamycin, 9-aminoacridine, and ethidium bromide.[166]

As was already shown in Figure 13 for the complex of 1-butylthymine with the artificial receptor **18**, π–π stacking and edge-to-face interactions may also occur between H-bonding arrays and aromatic or heteroaromatic rings.[156,167,168] H-bonding arrays such as those between the guanidinium residue of Arg and the carboxylate of Glu or Asp are planar and only require additional solvation within the plane. Perpendicular to this plane they are rather apolar, and their highly polarizable bonds enables them to undergo efficient interactions with aromatic rings. To this end, Castellano et al. provided X-ray structural evidence for π stacking (3.4 Å) between a 9-ethyladenine molecule and the Hoogsteen H-bonding array formed from an imide-type receptor designed by Rebek and co-workers and a second adenine molecule (Figure 15).[167]

However, attractive examples can also be found in the crystal structures of proteins. Thus, Figure 16 shows the stacking of Tyr 970A parallel to the hydrogen-bonding network formed between the side chains of Arg 918A and Asp 969A in the furoloyl esterase module of xylanase 10B.[169] Related to this topic is the flanking of aromatic rings by carboxylate groups, a positioning that can dramatically influence their pK_a values,[170] facilitate desolvation, and promote the formation of salt bridges (see Section 6).[171]

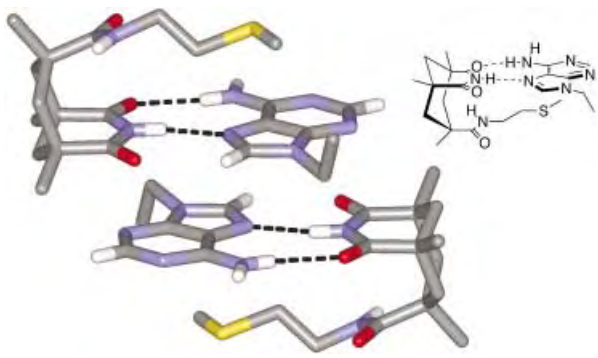

Figure 15. π Stacking over a H-bonding network in the solid-state structure of the complex formed by H bonding between a Rebek imide-type receptor and 9-ethyladenine (CCDC-167543).[167]

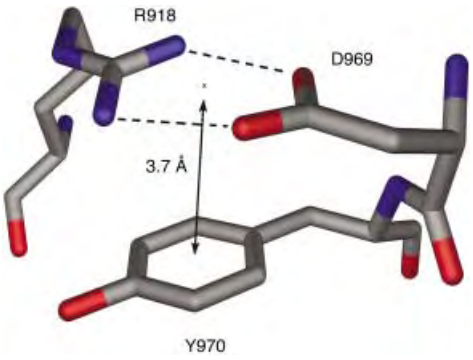

Figure 16. Parallel-stacking interaction between Tyr 970A and the H-bonding network between the side chains of Arg 918A and Asp 969A in the feruloyl esterase module of xylanase 10B (PDB code: 1GKK).[169]

The implications of π–π interactions in chemistry and biology are broad, and we conclude this section by listing a few additional examples. Aromatic–aromatic interactions can play a key role in synthesis (for example, in asymmetric induction),[172] in separation science (for example, in chiral chromatography),[173] and transition-metal complexation.[174] π–π Stacking has also recently been shown to be influential in stereoselective epoxidations with *m*-chloroperbenzoic acid;[175] in this study, polar/π effects similar to those reported by Siegel and co-workers were observed.

5. Hydrogen Bonding to Aromatic π Systems

5.1. Introductory Remarks

Traditionally, hydrogen bonds have been defined as A–H···B, wherein both the donor A and acceptor B are electronegative atoms, such as N, O, or F. Since there is no strictly defined cut-off for an atom's ability to participate in hydrogen bonding, this concept has been extended to weaker donor atoms such as carbon (in all three hybridization states) or unusual acceptors such as π systems.[74,176] Commonly encountered hydrogen-bond energies calculated for gas-phase complexes −0.5–1.5 kcal mol^{-1} for neutral C–H/π interactions to greater than −10 kcal mol^{-1} for the strongest ionic H bonds such as O–H···O$^-$ (−23 kcal mol^{-1}) or F–H···F$^-$ (−39 kcal mol^{-1}).[74] As a comparison, the widely occurring N–H···O (for example, in proteins) and O–H···O hydrogen bonds (for example, in the water dimer) are considered to be of intermediate strength, that is, about −5–7 kcal mol^{-1}.[177,178] The contribution of a hydrogen bond can be reduced dramatically in solution or the solid state because of entropic effects, solvation, or dielectric conditions imposed by the environment.[179]

The energetically attractive contacts involving hydrogen-bond donors and aromatic rings are called π-hydrogen bonds; they are several kcal mol^{-1} weaker than classical H bonds. The often observed contraction of the A–H bond in these arrangements is opposite to what is observed for classical H bonds, where the H-bond strength is proportional to the elongation of the A–H bond. This contraction leads to a shift of the A–H stretch to higher frequency in the IR spectrum, and the bonds displaying this feature have been described as anti-hydrogen bonds, and more recently, blue-shifting hydrogen bonds.[180]

5.2. Biological Aspects

Each amino acid has a potential N–H hydrogen-bond donor in its backbone, and several possess additional donor centers in their side chains (for example, Lys, Arg, Asn, Gln, His), thus making N–H/π contacts statistically probable. One of the earliest examples of an N–H/π interaction was seen by Perutz et al. in the X-ray crystallographic study of the interaction of hemoglobin with the drug bezafibrate. In this association an asparagine side chain N–H residue points into the center of the *p*-chlorobenzamide ring of the drug.[181] Many other examples of X–H/π contacts (X = N, O, S) occurring at a mean distance of X to centroid of the aromatic ring of 3.2–3.8 Å can be found in proteins.[182] Peptides have also been used as model systems to investigate the effect of N–H/π interactions on the secondary structure of proteins.[183] In this context, the crystal structure of bovine pancreatic trypsin inhibitor (BPTI) has been solved and shown to display a backbone N–H/π interaction between Gly 37 and Tyr 35 with an N···ring centroid distance of 3.5 Å. The other face of the tyrosine ring interacts with the side chain NH_2 group of Asn 44 at a distance of 3.5 Å (Figure 17 a).[184]

A rare example of O–H/π hydrogen bonding in proteins is provided by the complex of the enzyme glutathione transferase with glutathione (GSH), in which the side chain of Thr 13 is arranged face-on to the aromatic face of Tyr 6 (Figure 17 b).[185] This interaction decreases the pK_a value of the Tyr HO group and strengthens its hydrogen-bonding capacity to the HS group of GSH, thereby influencing the reactivity of the latter.[186] The occurrence of O–H/π and N–H/π interactions in proteins has been investigated in detail through several PDB searches.[187–191] Mitchell et al. showed that there is a preference for sp^2-hybridized nitrogen atoms to be located above aromatic rings.[188] In this case, parallel

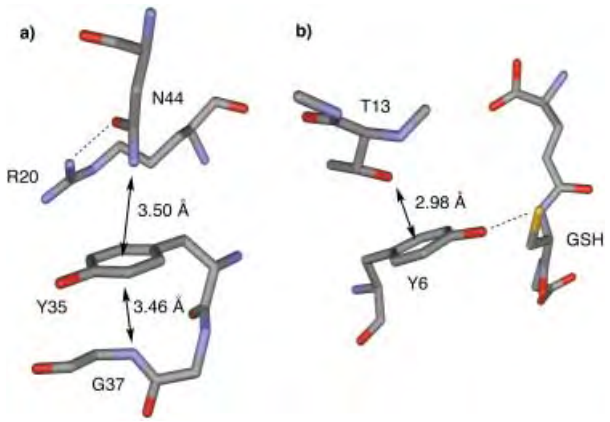

Figure 17. a) N–H/π interaction in the bovine pancreatic trypsin inhibitor (PDB code: 4PTI)[184] and b) O–H/π interaction in the complex of glutathione transferase with glutathione (GSH; PDB code: 6GST).[185]

stacking of N–H bonds is favored relative to the T-shaped arrangement. Recently, Steiner and Koellner performed a comprehensive structural analysis of X–H/π hydrogen bonding in a set of 592 high-resolution protein crystal structures:[182] They found that about 1 out of 11 aromatic amino acids acts as a π acceptor for H bonding with O–H, N–H, and S–H donors, with the best aromatic acceptor being Trp. This relatively high frequency, although small compared to classical hydrogen bonds, supports the postulated role that these contacts play in stabilizing the secondary structures of proteins.[192]

O–H/π contacts are observed in protein–water interactions and, if attractive, they contribute to the hydration energy.[193] Furthermore, water molecules interacting with the aromatic rings of Phe, Trp, and Tyr inside hydrophobic cavities may make significant contributions to stabilizing the local protein structure.[194] In this context, water molecules have been shown to fill and be conducted through carbon nanotubes (CNTs).[195] On the other hand, statistical analyses of protein structures show that water molecules are generally found at the edges of aromatic rings when a C–H···O interaction with the δ^+ polarized hydrogen atoms occurs.[196] This arrangement is also preferentially found for all types of oxygen atoms in amino acids.[189]

5.3. Physical and Theoretical Aspects

Complexes between benzene and H-bonding partners have been the subject of numerous theoretical and experimental investigations.[178] In particular, the solvation of benzene has attracted considerable attention.[197] We refer here to recent ab initio studies from Tsuzuki et al.,[198] although we are well aware that other notable contributions have been published on this subject. The stabilization enthalpy for monodentate H bonding of water to the π system of benzene (Figure 18a) has been calculated by high-level CCSD(T) calculations to give $D_0 = -2.0$ kcal mol^{-1} (O···centroid distance = 3.4 Å),[198] which agrees nicely with the experimental value ($D_0 = -2.44 \pm 0.09$ kcal mol^{-1}).[199]

The calculated potential well is extremely flat over the aromatic surface, which makes benzene an excellent target as a hydrogen-bond acceptor.[200] The attractive character of the water–benzene interaction could explain the higher solubility of aromatic hydrocarbons in water relative to alkanes,[201] as reflected by the lg(P_{ow}) values (the partition coefficients P between octanol and water) for benzene and cyclohexane (2.13 and 3.44, respectively).[202]

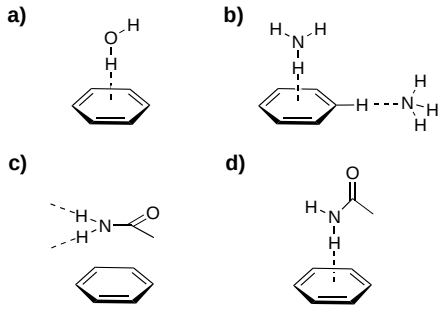

Figure 18. a) Preferred interactions of benzene with water (a), ammonia (b), and amides (c, d).

Another model system of H bonding to aromatic rings in proteins is the complex formed between benzene and ammonia.[203] This H-bond donor interacts more weakly with aromatic rings, a fact rationalized by the lower electronegativity of nitrogen relative to oxygen.[203] The stabilization enthalpy for H bonding to the π system of benzene (Figure 18b) was determined experimentally in the gas phase to be $D_0 = -1.84 \pm 0.12$ kcal mol^{-1},[204] which is similar to the value derived from CCSD(T) calculations ($D_0 = -1.61$ kcal mol^{-1}, d(N···centroid) = 3.6 Å).[198,205] Only slightly lower D_0 values, however, were calculated for the edge binding through a C–H···N contact (Figure 18b). Of course, ammonia is only a limited model for the side chain of Lys, which under physiological conditions is mostly protonated and, therefore, participates more frequently in cation–π interactions (Section 6). Hydrogen bonding between the π systems of aromatic compounds and thiols has been very recently probed by ab initio calculations and protein database analyses (interactions between divalent sulfur and aromatic rings are described in Section 8).[206] High-level ab initio calculations have shown this contact can achieve a stabilization enthalpy of −2.6 kcal mol^{-1}, and is thus stronger than the corresponding hydrogen bonds formed by amino or hydroxy groups. It should be noted, however, that out of 609 studied X-ray crystal structures of proteins, only 4 Cys residues (among the 2542 Cys residues, 1860 form disulfide bonds) were found in hydrogen-bonding arrangements with Phe.

H bonds are composed of electrostatic (ES), dispersive, charge-transfer, exchange-repulsion (EX), and polarization terms. The ES and EX terms account for more than 80% of the interaction energy in classical, moderate H bonds.[72] Separation of the binding energies into individual terms for the X–H/π contacts gives insight into the observed differences in interaction when X is varied. Thus, there is an increase in the electrostatic term from X = C, to N, and to O, as expected from atom electronegativity, while the dispersive and repulsive terms remain essentially constant across the series.[198]

Searches for X–H/π(phenyl) contacts in the CSD have revealed that the optimum T-shaped geometry, where the H atom points into the centroid of the aromatic ring, is rarely adopted and that the preferred geometry instead involves direct interaction of the X–H group with the carbon atoms of the ring.[207] In general, X–H/π hydrogen bonds are rather uncommon in biology, although they have been recognized for many years.[208]

MP2 calculations of the benzene–formamide complex have been performed to better model the aromatic–amide-(backbone) interaction found in proteins. They revealed a significant stabilization energy (−4.0 kcal mol^{-1}),[209] with two energetically similar conformations of the complex—the parallel stacking (Figure 18c) and the perpendicular, T-shaped geometry with the N–H/π contact (Figure 18d).[210] The pyrrole dimer displays, similar to its benzene counterpart, a T-shaped structure wherein the N–H bond is directed into the π system of a neighboring ring.[211]

The origin of the chaotropic effect of the urea and guanidinium ions has been studied by Monte Carlo simulations in water and in the gas phase by Jorgensen and coworkers. Their results indicate that the interaction of these species with aromatic rings, which may involve both π stacking and T-shaped geometries, likely promotes protein denaturation.[212]

5.4. Studies with Synthetic Receptors

In contrast to aromatic π–π interactions, hydrogen bonding to π systems has not been extensively investigated in supramolecular chemistry. Hunter and co-workers investigated the inclusion complexation of six-membered ring dicarbonyl compounds by cyclophane **19** (Figure 19).[213] ^{1}H NMR titrations in $CDCl_3$ provided the association constants K_a for the 1:1 complexes of **19** with **20** ($2.3 \pm 0.4 \times 10^2\,M^{-1}$), **21** ($3.4 \pm 0.6 \times 10^2\,M^{-1}$), and **22** ($1.0 \pm 0.5 \times 10^6\,M^{-1}$). While all three complexes are stabilized by H bonding between the two C=O groups of the guests to the four amide N–H residues of the host, the complex of diamide **22** finds extra stabilization through favorable N–H/π contacts (Figure 19). Indeed, the X-ray crystal structure of the **19**·**22** complex was later determined and showed clearly that the amide N–H groups of **22** are pointing directly into aromatic rings of the receptor.[214] The complexation of **22** was sufficiently strong that it was even observed in water ($70\,M^{-1}$). From chemical double mutant cycles, Hunter and co-workers estimated the Gibbs free energy contribution of individual N–H/π interactions as $\Delta\Delta G = -1.1 \pm 0.1$ kcal mol^{-1},[215] a higher value than deduced for C–H/π interactions (0.35 ± 0.2 kcal mol^{-1}) in similar experiments (see Section 4.3.2). This result reflects the higher acidity of the N–H donor (pyrrole in this case) relative to C–H.

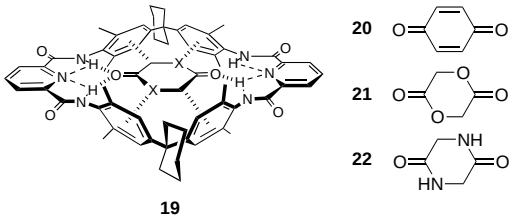

Figure 19. Inclusion complexation of cyclic 1,4-dicarbonyls by the macrocyclic tetramide receptor **19**. The complex formed by diamide **22** is additionally stabilized by N–H/π interactions.[213,214]

Another example for N–H/π interactions in a supramolecular complex has been provided by Cloninger and Whitlock[216] who prepared the complex of a serotonin mimic (methyl 5-hydroxy-3-indolecarboxylate) with a macrobicyclic cyclophane receptor ($K_a = 4840 \pm 1280\,M^{-1}$, $CDCl_3$, 298 K; Figure 20). The very large complexation-induced downfield shift of the NH proton of the guest ($\Delta\delta = 5.46$ ppm) observed in the ^{1}H NMR spectrum strongly supports the proposed T-shaped N–H/π interaction geometry.

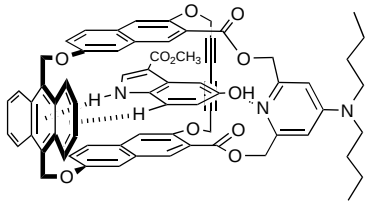

Figure 20. N–H/π interaction in the complex formed between a macrobicyclic cyclophane receptor with a serotonin mimic.[216]

6. Cation–π Interactions

6.1. Introductory Remarks

The cation–π interaction between a protonated HEPES buffer molecule (*N*-2-hydroxyethylpiperazine-*N*′-2-ethanesulfonic acid) and Trp in the acetylcholine (ACh) binding site of an ACh binding protein (Figure 21)[217] more than suggests these contacts to be important contributors to the structure and function of biomolecules.[7,218,219] This study represents a perceptible advance from the earliest structural studies that elucidated the "amino–arene" interaction between positively polarized N–H groups and aromatic amino acid side chains in proteins.[181,190,220] The protonated tertiary ammonium center is snugly located in a "box" of four aromatic residues where it comes into contact with Trp 143 (4.1 Å) and makes cation–π interactions, as shown for a variety of nicotinic ACh receptor agonists.[221–223]

While these and other discoveries in structural biology[218,224] continue to inspire research on the cation–π interactions, early solution studies with chemical systems in the Dougherty research group were responsible for defining its energetic features and establishing the interaction as a general one among the well-known noncovalent forces.[7] The use of elaborate mass-spectrometric techniques, computational protocols, and the possibility to routinely manipulate biological systems has enabled our ability to dissect this and other weak, noncovalent binding forces to burgeon in the past few years.

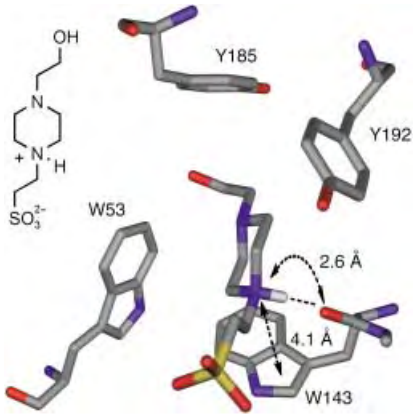

Figure 21. Cation/π interactions between a HEPES molecule and Trp 143 in the ACh binding site of an ACh-binding protein.[217] Most H atoms have been omitted for clarity (PDB code: 1I9B).

The key review of Ma and Dougherty[7] outlines the essential features of the cation–π interactions (namely, its structure and energetics, applications, and biological implications). Subsequent accounts have since appeared which focus on its consequences in structural biology,[218] contribution to ligand structure and catalysis,[224] theoretical investigations,[178] and applications in host–guest chemistry.[225–230] We have chosen to limit our discussion to recent contributions that describe the energetic features of the cation–π interaction; emphasis will be placed on experimental studies using synthetic receptors and biological macromolecules, although essential contributions of gas-phase, solid-state, and theoretical investigations will also be highlighted.

6.2. Cation–π Interactions with Ammonium and Iminium Ions

6.2.1. Energetic Aspects of Host–Guest Chemistry

Dougherty and co-workers found that the anionic cyclophane **23a** (Figure 22) is a better receptor for quaternary ammonium and iminium ions in aqueous borate buffer (pD 9) than for the corresponding neutral molecules.[7,231] Thus, the complex of **23a** with methylquinolinium is 2.2 kcal mol^{-1} more stable than with neutral quinoline (Table 4), even though the cationic guest is better solvated than its neutral counterpart by 46.5 kcal mol^{-1}.[7,232] Host **23a** also complexes the neurotransmitter ACh with $K_a = 20000\,M^{-1}$ ($\Delta G = -5.8$ kcal mol^{-1}). This result prompted the researchers to postulate a similar motif—an aromatic binding site instead of an environment rich in anionic carboxylate or phosphate groups—for the binding of ACh by acetylcholine esterase. The X-ray crystal structure of the enzyme from the Pacific electric ray, *Torpedo Californica*, indeed revealed an onium binding site. The modeling of ACh complexation with this site suggested that its quaternary ammonium ion does not interact with a negatively charged "anionic site" but rather with some of the 14 aromatic residues that line the active site.[233]

Table 4: Free enthalpy of complexation $\Delta G°$ for the 1:1 complexes of **23a** in aqueous deuterated borate buffer (pD = 9) and **23b** in $CDCl_3$ ($T = 295$ K).[231]

Guest	**23a** $-\Delta G°$ [kcal mol^{-1}]	**23b** $-\Delta G°$ [kcal mol^{-1}]
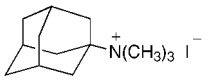	6.7	2.1
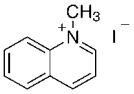	7.6	3.5
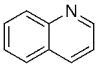	5.4	0.0
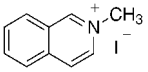	7.2	2.5
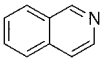	6.3	0.2

The earliest investigations by Ma and Dougherty established the currently accepted "electrostatic model" of the cation/π interaction, namely, the electrostatic attraction between a cation and the permanent quadrupole moment associated with the π system.[7] Replacement of the two *p*-phenylene linkers of **23a** with cyclohexane-1,4-diyl groups indeed reduces its binding to quaternary ammonium guests. However, the contributions of the positively polarized C–H bonds of the onium ion that interact with the negatively polarized π systems should not be ignored (Section 5);[234] in effect, solvation of the positively charged onium ion by the aromatic rings of the host in terms of C–H/π interactions.

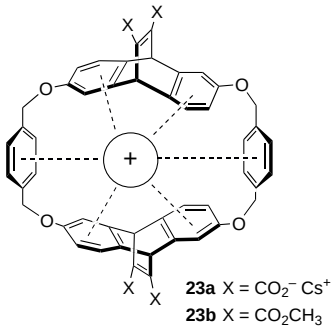

23a X = CO_2^- Cs^+
23b X = CO_2CH_3

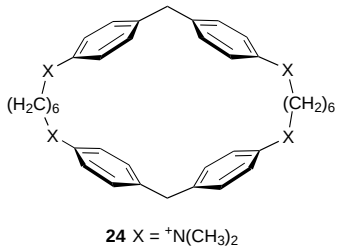

24 X = $^+N(CH_3)_2$

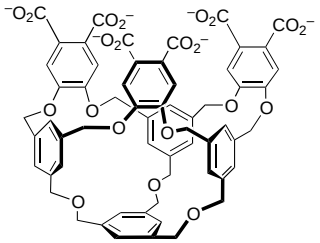

25

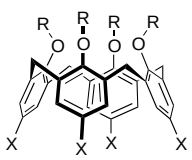

26a R = H; X = SO_3^-
26b R = CH_2CO_2H; X = SO_3^-
26c R = CH_2CO_2H; X = H

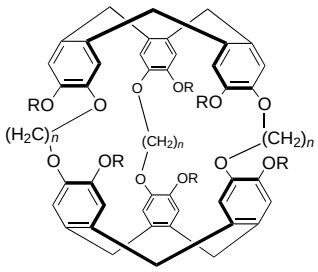

27a R = CH_2CO_2H
27b R = CH_3

Figure 22. Various hosts employed in the study of cation–π interactions.

Binding studies with tetrazoniacyclophane **24** in water by Schneider et al.[235,236] (Figure 22) as well as with other model systems[237–239] reinforced these observations. Linear free energy relationships showed that the binding free enthalpy is proportional to the number of aromatic rings surrounding a cationic center and that the gain in free energy can be as high as 0.5 kcal mol^{-1} per ring. Additional early studies with host–guest systems in aqueous solution, including the cyclophane receptors **25**–**27**,[240–245] have produced the most efficient receptors for onium ions to date. Moreover, these studies demonstrated that multiple cation–π interactions, particularly those involving hosts with electron-rich concave aromatic binding surfaces[126,246] (see Section 4.3.1), are capable of overcoming the desolvation penalty associated with binding various cations or ion pairs (see below) in aqueous media.[247] These investigations have been extensively reviewed.[7,225,226]

While studies of many receptor systems have since been extended to the gas phase[248] and the solid state,[249] the bulk of our knowledge concerning the energetics of cation–π interactions continues to come from solution-phase investigations. Recent calorimetric studies show the binding of quaternary ammonium ions by calixarene hosts to be enthalpy driven ($\Delta H° < 0$) and entropy opposed ($\Delta S° < 0$).[250,251] The data reported for hosts **26b** and **26c** (Table 5) by cation–π interactions and not formation of a salt bridge, which lends further support to the importance of such contacts for the stabilization of protein structures and substrate recognition in biology.

While water is often considered the most "biorelevant" medium for investigating cation–π interactions, measurement of the intrinsic binding affinity between a cation and a π surface is problematic in aqueous solution where competing effects are of some concern.[253] These include significantly different solvation properties of the host and guest, the hydrophobic effect, and may include electrostatic interactions between the cation and a negatively charged host (although this has generally been ruled out through control experiments). Dougherty and co-workers were the first to demonstrate that although the driving forces for apolar complexation (dispersion and desolvation) are too weak in organic solvents such as $CDCl_3$ to ensure binding of neutral guests, cation–π interactions can, and do, induce inclusion complexation of onium ions ($-\Delta G° = 2$–3 kcal mol^{-1}, Table 4). Other work with cryptophanes demonstrated the unprecedented complexation of TMA by **27b** (Figure 22) in $(CDCl_2)_2$ with a $K_a = 225{,}000\ M^{-1}$ ($\Delta G° = -7.4$ kcal mol^{-1}),[244] a value significantly exceeding the gas-phase $\Delta G°$ value of -3.5 kcal mol^{-1} that describes the interaction of TMA with a single benzene ring.[260] The TMA cation clearly prefers solvation by the aromatic rings of host **27b** to the chloroalkane solvent.

Table 5: Thermodynamic parameters describing the complexation of tetramethylammonium (TMA) and *N,N,N*-trimethylanilinium (TMAN) ions (as their chloride salts) by calixarenes **26b** and **26c** in water (pH 7, $T = 298$ K).[a]

Host	Guest	$\log K_a$	$\Delta G°_{298K}$ [kcal mol^{-1}]	$\Delta H°_{293K}$ [kcal mol^{-1}]	$T\Delta S°_{293K}$ [kcal mol^{-1}]
26b	TMA	3.5(1)	−4.8(1)	−5.8(3)	−0.9(3)
26c	TMA	2.1(1)	−2.1(1)	−5.2(3)	−2.4(3)
26c	TMAN	2.2	−3.0	−4.9	−1.9

[a] Standard deviation σ in parentheses; for further details, see ref. [251].

Host–guest complexation in organic solutions based on cation–π interactions continues to be an active research area, where cyclophanes,[261–263] cyclic peptides,[128,254,264,265] and molecular clefts[266] have been among the most versatile receptor scaffolds employed. Remarkable recent examples are the acyclic, "open-phane" receptors by Roelens and Torriti, such as **28** (Figure 23) that are capable of binding the picrate salts of TMA and ACh in $CDCl_3$ without the facilitation of preorganization.[253] The open-chained **28** and cyclic receptor **29** display similar binding free enthalpies for binding tetramethylammonium (TMA) and *N,N,N*-trimethylanilinium (TMAN) ions reveal that the entropies of complexation ($T\Delta S°$) are slightly less unfavorable than for complexation processes involving neutral guest molecules in water (see Section 2, Table 1). This result can be rationalized by a more favorable desolvation entropy for ammonium guests relative to their neutral counterparts (that is, $(CH_3)_4N^+$ versus $(CH_3)_4C$).[252] Additionally, several binding studies have shown that the sulfonate substituents present on host **26b** serve to further desolvate the cationic guest relative to neutral host **26c** ($\Delta(T\Delta S°) = -1.5$ kcal mol^{-1}, Table 5).[253,254]

Recent investigations have employed cation–π interactions in the recognition of a plethora of biologically important cations in aqueous solution. Phosphonate-based amino acid receptors of Schrader and co-workers combine ion-pairing interactions with cation–π contacts to efficiently bind amino acids (for example, Lys, His, and Arg),[255] adrenaline,[256] and small peptides (for example, the RGD sequence).[257] Likewise, the molecular clips of Klärner, Schrader, and co-workers are efficient binders of *N*-alkylpyridinium salts ($-\Delta G = 4.9$–5.5 kcal mol^{-1}), including the sizeable NAD^+ ion, in aqueous solution.[258,259] These hydrophobic binding events are driven

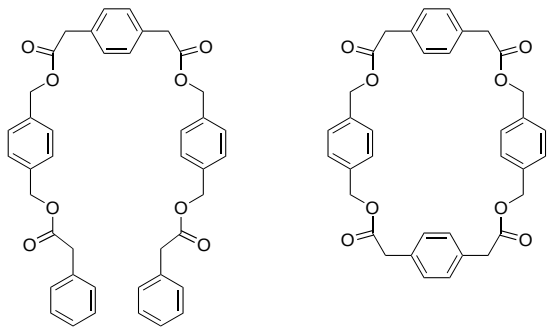

28 **29**

Figure 23. The "open" (**28**) and "closed" (**29**) cyclophane receptors of Roelens and Torriti bind quaternary ammonium species equally well in $CDCl_3$.[253]

tetramethylammonium picrate ($\Delta G° = -7.0$ kcal mol^{-1} and -7.3 kcal mol^{-1}, respectively). The results reiterate that loose association is acceptable, if not required, for strong binding of quaternary ammonium species by aromatic hosts (that is, wherein the contact of the cation with the π surface is maximized).[232] In other words, the solvation requirements of the onium ion determine the conformation of the host in the complex. Free enthalpy increments for the interaction of TMA and ACh with individual aromatic rings were calculated as $\Delta\Delta G = -0.46$ kcal mol^{-1} and -0.45 kcal mol^{-1}, respectively, from the additivity principles based on linear free energy relationships.[238] These results are in excellent agreement with earlier ones determined by Schneider et al.[237,238]

6.2.2. *Substituent Effects and Electrostatics*

Although the electrostatic component does not represent the total binding energy in the cation–π interaction (ca. 60% for many arenes[267,268]), Dougherty and co-workers have shown that molecular electrostatic potential (MEP) maps of aromatic rings are useful for rationalizing cation–π binding trends.[7,268–270] Electrostatics and cation-induced polarization taken together can nearly quantitatively rationalize the variance in binding energy in alkali-metal–π interactions.[271,272] Additionally, while caution is warranted when employing these analyses for ammonium ions, where contributions from dispersive interactions are intensified relative to the "harder" alkali-metal cations,[178,212,234,267,273–275] recent solution-phase studies has reinforced the MEP trend. Modulation of the electrostatic potential (ESP) of the central benzene ring in the receptors **30a–c** (Figure 24) from **30a** (R = H) to **30b** (R = NO_2), for example, results in a decrease in binding of guanidinium derivatives in Me_2SO by 0.2–0.3 kcal mol^{-1}.[276] Likewise, the complexation free enthalpy $-\Delta G$ increases by 0.5–0.6 kcal mol^{-1} upon changing from **30b** (R = NO_2) to **30c** (R = OMe). Similar substituent trends have been reported in the complexation of ammonium salts by cyclic peptide receptors.[128] Incorporation of the naphthalene spacer into **30d** results in a cation affinity equivalent to that exhibited by **30c** (namely, 0.2–0.4 kcal mol^{-1} greater than the one of **30a**), thus demonstrating the effect of aromatic size (that is, polarizability) on binding. This result is in qualitative agreement with recent ab initio[268] and DFT[277] calculations of Na^+/benzene and Na^+/naphthalene complexes.

Hunter et al. have employed their chemical double-mutant cycles (see Section 4) for the investigation of cation–π interactions between pyridinium cations and substituted phenyl rings in chloroform.[278] Again, a clear dependence of the interaction strength is found related to the electrostatics of the individual components; the calculated increment in free enthalpy for the cation–π interaction $-\Delta\Delta G$ decreases by 2.5 kcal mol^{-1} upon changing from electron-rich (-NMe_2) to electron-poor (-NO_2) phenyl rings. This trend was illustrated through a Hammett plot which showed a steep positive slope. It is worth noting that the role of the anion has not been directly addressed in these systems, although the cation is presumably binding as its ion pair.

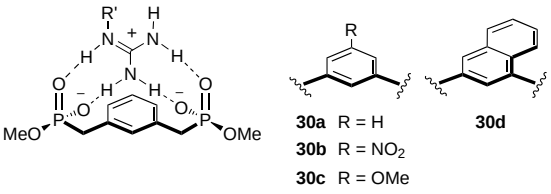

Figure 24. Substituent effects and the size of the aromatic platform modulate the cation-binding ability of synthetic guanidinium receptors.[276]

6.2.3. *Counterion Dependence and Salt Bridges*

Tight ion pairs exist[279] in polar, aprotic media which makes the electrostatic contribution of the anion to cation binding particularly important. While several studies have reported counterion-dependent cation–π binding,[262,280,281] generally in the context of ditopic receptors,[282] it was not until recently that this phenomenon was systematically explored.[253,263,283–285] The stability of aromatic host–cation (TMA, ACh, and *N*-methylpyridinium (NMP)) complexes in $CDCl_3$ and $(CDCl_2)_2$ has been shown in numerous studies to decrease in the following anion sequence: picrate > trifluoroacetate > I^- > Br^- > Cl^- > tosylate ≈ acetate.[263,265,281,284,286] Although this sequence can be seemingly straightforwardly rationalized on the basis of the ion size (for the spherical halides) or ion-pair dissociation energy, Bartoli and Roelens have shown in a detailed study of their cyclophane systems, such as **29** ($CDCl_3$), that there is a linear correlation between the binding free enthalpy ($-\Delta G°$) and solubility of the ammonium salt (lg *S*).[285] The cations of ion pairs, wherein the cation and anion are not strongly interacting (that is, for large charge-diffused cations, such as TMA and ACh, and highly charge dispersed anions), are bound more strongly. These salts (ion pairs) also feature the lowest solubility. Additionally, a definitive linear correlation was found between the calculated electrostatic potential of the ion pair and the experimental binding free enthalpy ($-\Delta G°$). Extrapolation of the $-\Delta G°$ value to that denoting binding of the TMA cation to the aromatic host in the absence of its counterion reveals that more than 80% of the binding energy is lost as a result of the presence of the anion.[287]

The notion of the charge density of the counterion affecting the polarization of the cation charge has been implicated for some time in protein studies; the earliest crystallographic analyses of proteins often revealed aromatic amino acid side chains involving Lys and Arg in the proximity of salt bridges.[188,191,222,288,289] A variety of computational studies have considered ammonium–benzene (see above) and ammonium–carboxylate interactions separately, and have evaluated their intrinsic energies and solvation dependencies.[290] Ab initio calculations have shown that a cation–π interaction in water should be more stabilizing than an analogous salt bridge ($-\Delta\Delta G_{bind} \approx 2.6$ kcal mol^{-1}),[289] while systematic database analysis has revealed the tendency for Lys and Arg to interact with aromatic amino acid side chains.[218,274] An example lies in the preference of Arg to interact with Trp in a facial manner,[218] as shown in the X-ray structure of the human growth hormone receptor (hGHR, Figure 25).[291,292]

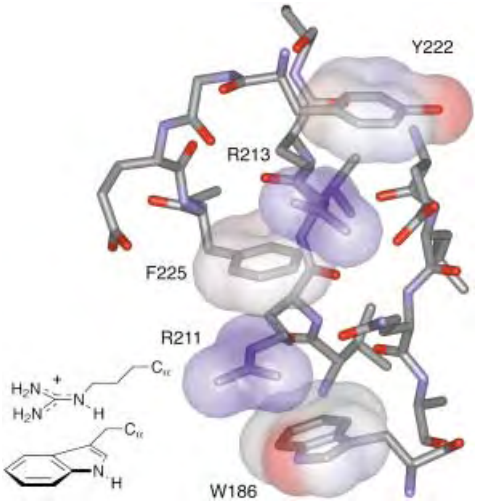

Figure 25. Alternating cationic (Arg, Lys) and aromatic (Tyr, Phe, Trp) amino acid residues shown by X-ray crystallography (2.8 Å) within the human growth hormone receptor (hGHR) extracellular domain (PDB code: 3HHR).[291] The van der Waals and electrostatic potential surfaces (blue: positive, red: negative of the side chains) are shown as generated in WebLabViewer (ViewerPro V. 5.0, Accelyrs, San Diego, CA). Hydrogen atoms have been omitted for clarity.

However, the analysis of ternary complexes involving salt bridges and aromatic compounds has only recently been investigated by computational analysis[289,293] and synthetic studies.[171,294] Dvornikovs and Smithrud, for example, have recently shown for their receptors (Figure 26) that Arg and Lys derivatives, while bound in water (pH 7.5, sodium phosphate buffer) by the carboxylates of **31a** ($-\Delta G^\circ = 1.2$–1.5 kcal mol^{-1}), are not bound when the aromatic surface is absent, as in **31b**.[171][295]

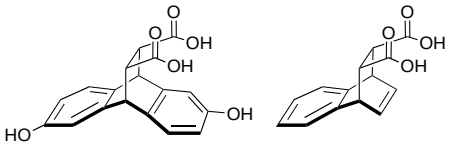

31a **31b**

Figure 26. The role of aromatic groups in stabilizing the formation of a salt bridge: Receptor **31a** binds Arg and Lys derivatives in aqueous phosphate buffer whereas **31b** does not.[171]

6.3. Alkali-Metal-Ion–π Interactions

It is well-established that alkali-metal ions,[296–298] and although not specifically treated here, transition-metal ions,[298,299] form complexes with benzene and other aromatic molecules in the gas phase. The interaction energy is generally high (18.3 kcal mol^{-1} for K^+–benzene[297]) and the ion–molecule binding energy follows the expected electrostatic trend (namely, $K^+ < Na^+ < Li^+$).[300] In aqueous solution, however, an aromatic ring cannot effectively compete with water for solvation of the alkali-metal cation.[301] Alkali-metal-cation–

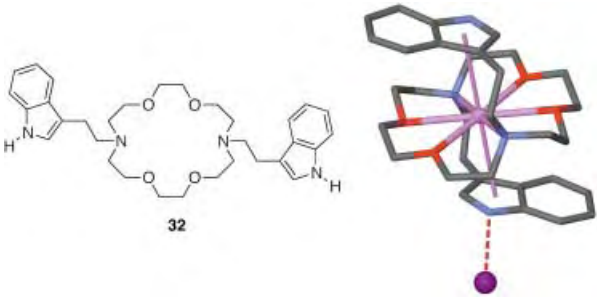

32

Figure 27. Alkali-metal–π interactions in the solid state. Di(indolyl) crown ether receptor **32** binds potassium (iodide) in a "sandwich" complex, with a K^+···arene distance of 3.45 Å.[303] The iodide counterion is shown as the purple sphere.

π interactions have been extensively reviewed by Gokel and co-workers,[228–230,302] who used crown ether derived receptors to study these contacts in solution and the solid state. Figure 27 shows the X-ray crystal structure of di(indolyl) receptor **32** with K^+ that reveals the sandwich complexation motif unique to these structures.[303] The K^+···arene distance in the complex is 3.45 Å. These studies have subsequently provided the chemical basis for understanding interactions between alkali metals and aromatic amino acid side chains in a variety of media.[227,230,304] The interest in these interactions has also been extended to the gas phase[305,306] through advances in mass-spectrometric techniques and computational protocols.[305,307,308]

Many of the fundamental energetic features of the cation–π interaction are applicable to both onium and alkali-metal cations. Extensive theoretical investigations on relatively simple C_6H_6···M^+ complexes are currently providing valuable information on these contacts.[309–312] It is clear that these efforts pave the way for more complete models describing the cation–π interaction in chemistry and biology.

6.4. Energetics from Biological Systems

Experiments designed to quantify cation–π interactions in biological systems, although sparse, have convincingly demonstrated the stabilizing role that such contacts can make within proteins and at their surface.[218,313–320] The most recent studies are summarized in Table 6. On average, the reported interaction energies for positively charged amino acid residues (namely, Lys, His, Arg) and aromatic side chains (Phe, Trp, Tyr) in water lie between -0.4 and -2.4 kcal mol^{-1}. Although these values are somewhat lower than those predicted theoretically (-3.2 to -3.6 kcal mol^{-1}),[274,289] they are surprisingly consistent given the many different systems employed. Known variables include differing intrinsic solvation energies for each amino acid[321] and solvent exposure of the interacting groups (that is, on the surface or buried), as well as indeterminable conformational changes that occur upon substitutions (or protonations) that can markedly affect the entropic and/or enthalpic components of ΔG°. The use of non-natural amino acids to investigate cation–π interactions has been one way to sidestep these uncertainties, as recently

Table 6: Strength of cation–π interactions involving amino acids in water based on biological model systems.

A^+-Ar[a]	$-\Delta G°$ [kcal mol^{-1}][b]	Experimental technique	Biological system	Ref.
His-Trp	ca. 0.9	double-mutant cycles and pH dependence	α-helix (barnase)	[313]
His-Trp (C→N)[c]	0.8 ± 0.1	mutagenesis, AGADIR[d] analysis	*i*,*i*+4 residues in Ala-based α-helices	[314b]
His-Phe	0.5	double-mutant cycles and pH dependence	apoflavodoxin	[316]
Arg–Trp (C→N)[c]	0.4	mutagenesis	*i*,*i*+4 residues in Ala-based α-helices	[317, 320]
S-MeMet-Ar[e]	≤ 2.6[f]	non-natural amino acids, mutagenesis	staphylococcal nuclease	[315]
serotonin-Trp	ca. 4	non-natural amino acids, fluorination plots	serotonin 5-HT_{3A} receptor	[270]
ACh-Trp	ca. 2	non-natural amino acids, fluorination plots	nicotinic acetylcholine receptor	[270]

[a] A^+ = positively charged component, Ar = aromatic component. [b] Generally reported as $\Delta\Delta G°$ between folded proteins/peptides. [c] The directionality (positioning of the residues with respect to the helix termini) appears to be important in these systems. See ref. [320] wherein no interaction was observed in the N→C direction. [d] AGADIR is a computer program described in ref. [314a]. [e] *S*-MeMet = (*S*)-methylmethionine. [f] The exact quantity is unknown as the value reported may represent multiple (1, 2, or 3) interactions; see ref. [315].

shown by the research groups of Schultz[315] and Dougherty[221,270] (Table 6, rows 5–7).

The contribution of the cation–π interaction in proteins can be significant in mixed organic/aqueous solvents, although this has yet to be fully explored. The work of Kostic and co-workers[318] with associating protected single amino acids has shown that Lys–Phe and Lys-Tyr interactions, which are worth (from ^{1}H NMR titration) -2.4 and -2.1 kcal mol^{-1} in water, are magnified to -3.4 and -2.9 kcal mol^{-1} in chloroform/methanol/water mixtures. Likewise, Hamilton and co-workers[322] have recently designed guanidinium receptors for α-helical peptides and postulated that there are significant cation–π interactions between the charged centers of the receptor and a tryptophan residue in the binding site.

6.5. Outlook

Studies of the cation–π interaction, while broad, have reached considerable consensus in describing the basic energetics of the simplest systems. This is a prerequisite, with the aid of advanced computational protocols, superior mass-spectrometric tools, and design creativity, for the continued exploration of these interactions in more complex systems. Particularly exciting are approaches that employ cation–π interactions in the active sites of enzymes for de novo drug design,[8,270] catalysis in both synthetic[323] and biological systems,[324] and organic synthesis (for example, stereocontrol in organic reactions[325]). Cation–π interactions are increasingly observed at protein–DNA interfaces.[326] Although not specifically addressed here, recent reports of anion–arene interactions suggest that these may also be promising contacts for future study.[327,328]

7. Interactions between Aromatic and Perfluoroaromatic Compounds

7.1. Benzene–Hexafluorobenzene

Hints of the unusual properties of perfluoroaromatic compounds came four decades ago from formation of a crystal from an equimolar mixture of hexafluorobenzene and benzene: A solid was formed with a melting point of 23.7 °C, approximately 19 °C higher than either of the two components.[329] Unlike the crystal-packing patterns of benzene and hexafluorobenzene, which feature herringbone arrangements arising from T-shaped interactions (see Section 3), the $C_6H_6 \cdot C_6F_6$ cocrystal shows nearly parallel molecules stacked alternately in infinite columns (Figure 28) with an interplanar distance (r) of about 3.4 Å and an intercentroid distance (d) of 3.7 Å.[330,331] Weak C_{aryl}–H···F contacts help to stabilize neighboring columns (see above). Early calorimetric and NMR studies demonstrated thermodynamic phase transitions for the equimolar mixture at 199 K (most ordered), 247.5, and 272 K (least ordered);[332] the lowest temperature structure (measurement at 30 K) is shown in Figure 28.[331] This general crystal-packing morphology has been reproduced with many complexes of aromatic–perfluoroaromatic compounds,[116,333–335] and has led to the conclusion that the stacking interaction is a general one.[334]

Most, but perhaps not all, of the structural features of the hexafluorobenzene–benzene cocrystal can be rationalized on the basis of the quadrupole moments of the two components[334,336,337]—the values are equal in magnitude but opposite in sign (C_6H_6: -29.0×10^{-40} C m^{-2}; C_6F_6: $+31.7 \times 10^{-40}$ C m^{-2}),[338] as shown schematically in Figure 29.[337,339] Spectroscopic studies have shown that the complexes do not have charge-transfer (π–π*) properties, as demonstrated by the absence of characteristic bands in the UV spectra,[340] and there are only small shifts in the internal vibrational

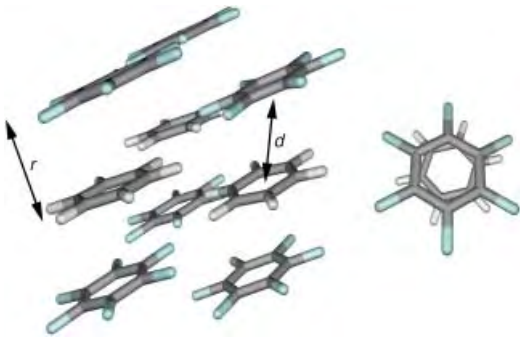

Figure 28. The structure of the lowest temperature phase of the benzene–hexafluorobenzene cocrystal at 30 K.[331] Views along the approximate *b* axis (left) and *c* axis (right) are shown. r = interplanar distance (ca. 3.4 Å); d = intercentroid distance (ca. 3.7 Å); atom coloring: white, H; aqua, F; CSD code: BICVUE01.

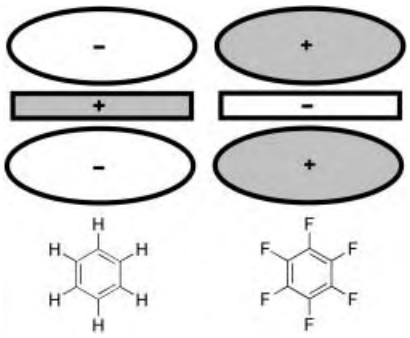

Figure 29. Schematic representations of the quadrupole moments of benzene (left) and hexafluorobenzene (right).

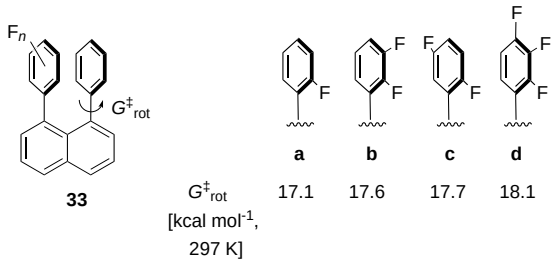

Figure 30. Progressive fluorine substitution results in an increase in the barrier to rotation of the phenyl–naphthalene bond in 1,8-diarylnaphthalenes.[147,352]

frequencies relative to the pure components;[331,341] this is not the case for complexes of C_6F_6 with aromatic amines[342] or metal complexes.[343] The crystal-packing motif indeed reflects the maximizing of favorable quadrupole–quadrupole interactions (distance dependency: r^{-5}) and the minimizing of unfavorable electrostatic repulsions (for example, edge-to-face arrangements).

Estimations of the interaction energy describing the $C_6H_6{\cdot}C_6F_6$ dimer have come from both computational and experimental studies. Ab initio calculations have determined a stabilization energy of $-3.7\,\mathrm{kcal\,mol^{-1}}$ ($r = 3.6$ Å; CP-corrected MP2/6-31G**)[344] and $-4.3\,\mathrm{kcal\,mol^{-1}}$ ($r = 3.7$ Å; SCF-MP2)[345] for the hexafluorobenzene–benzene dimer in the face-to-face eclipsed arrangement. More recent semi-empirical calculations[148] that include extended electron distribution (XED) give a somewhat higher value of $-5.6\,\mathrm{kcal\,mol^{-1}}$ ($r = 3.6$ Å).[346] Finally, a value of $-4.7\,\mathrm{kcal\,mol^{-1}}$[347] has been reported from DFT calculations that consider the eclipsed, offset geometry. In all cases the values for the heterodimer are 1.5–3 times higher than the corresponding interaction energies for the two homodimers. Additionally, and perhaps most importantly, the calculations and crystal-structure analysis[337] have revealed dispersion interactions to be at the very least as large in magnitude (but generally larger, 70–85 %[346,347]) as the electrostatic component in these complexes.[67]

While many solution-based experiments have observed the consequences of the formation of the $C_6H_6{\cdot}C_6F_6$ dimer,[108,348–351] we concern ourselves here with strategies used to quantify interactions between aromatic and perfluoroaromatic compounds. The 1,8-diarylnaphthalenes **33a–d** prepared by Siegel and co-workers have been employed to correlate fluorine substitution with barriers to rotation about aryl–naphthalene bonds (Figure 30; see also Figure 12).[147,352] Each additional fluorine atom in the series **33a** to **33d** increases the $\Delta G^{\ddagger}_{\mathrm{rot}}$ term by $0.5\,\mathrm{kcal\,mol^{-1}}$, which indicates there is a decrease in the repulsion in the stacked ground state upon removal of electron density from the ring. The results are consistent with the so-defined "polar/π" interactions that feature significant electrostatic contributions to π–π stacking (see Section 4.3.4). Experimental[221,270,353,354] and theoretical[221,268,355] investigations of cation–π complexes (see Section 6) with *perfluorinated* aromatic compounds similarly demonstrate electrostatic-dominated interactions. In accordance with this model, the interaction energy decreases strongly in all cases upon incremental substitution of fluorine atoms.[356]

The chemical double-mutant cycles of Hunter and co-workers (Sections 4 and 6) have been employed to investigate interactions between aromatic and perfluoroaromatic compounds.[357] The experiments show a stabilizing interaction between a face-to-face-oriented dimethylamino-substituted aromatic compound and a pentafluorophenyl ring of $0.4\,\mathrm{kcal\,mol^{-1}}$. Coincidentally, this value is similar to the enthalpy of formation calculated for the solid hexafluorobenzene–benzene complex from differential scanning calorimetry (DSC) measurements ($0.24\,\mathrm{kcal\,mol^{-1}}$).[358] Further experiments by Hunter and co-workers revealed the edge-to-face arrangements between the two aromatic rings to be destabilizing, as expected for positively polarized aryl C–H protons directed toward the electron-poor π face of the pentafluorophenyl group. In summary, experimental investigations have nicely demonstrated the important electrostatic contribution to phenyl–perfluorobenzene interactions,[359,360] while theoretical studies have probed the role of dispersion forces in these contacts.

7.2. Stacking Interactions and Molecular Organization

The interaction between phenyl and perfluorophenyl groups fulfills the prerequisites of structural predictability for consideration as a supramolecular synthon.[86] To this end, the interaction has been used elegantly in crystal-engineering studies and the design of novel supramolecular architectures in much the same way as hydrogen-bonding donors and acceptors have been employed for these tasks.[361] A representative example is provided in the stacking of 1,3,5-tris(phenethynyl)benzene (**34**) and 1,3,5-tris(perfluorophenethynyl)benzene (**35**) in the solid state (Figure 31).[362] While **34** and **35** form slipped stacks with their terminal aryl rings twisted with respect to the plane of the central ring (namely, a twisted rotor conformation is formed, not shown) when crystallized separately, the 1:1 heterocomplex is essentially planar with markedly less slippage. These results provide excellent evidence for the structural control attainable when using the phenyl–perfluorophenyl synthon.

Dougherty, Grubbs, and co-workers were the first to use the phenyl–pentafluorophenyl motif to exert topological and

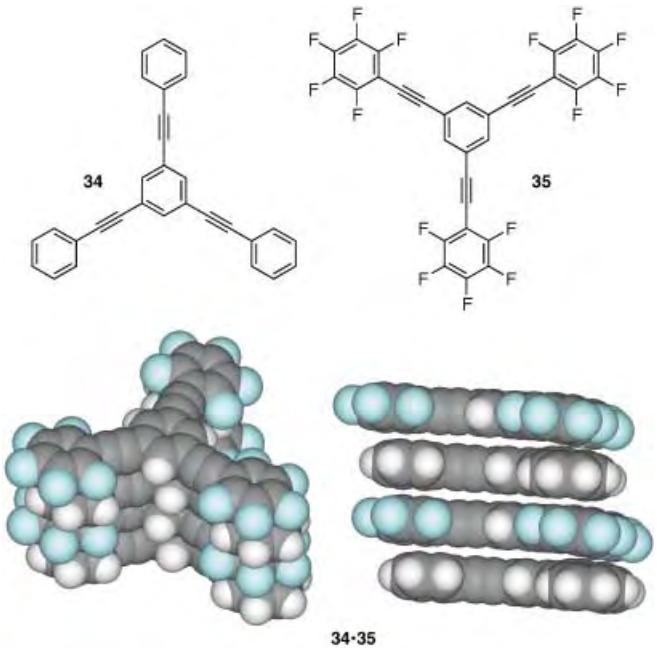

Figure 31. Well-defined solid-state organization that results from the phenyl–perfluorophenyl synthon. Cocrystallization of **34** and **35** gives nearly perfectly aligned alternating layers of the two components.[362] CSD code: WEVYIF.

stereochemical control over the photopolymerization reactions of 1,3-diynes in the condensed phase (Figure 32a).[363] Cocrystallization of **36** with **37** gives a solid (**36**·**37**) that melts at 152 °C, which is considerably higher than either of the two homodimers (87 °C for **36**·**36**, 114 °C for **37**·**37**). Similar to the cocrystal formed from benzene and hexafluorobenzene, the diynes pack alternately into stacked columns where the individual molecules are only slightly longitudinally slipped with respect to one another ($d = 3.69$ Å, not shown). Difunctional **38** packs similarly (although slightly staggered) and in a head-to-tail arrangement (Figure 32b). Both types of complexes ($(\mathbf{36}\cdot\mathbf{37})_n$ and $(\mathbf{38})_n$) are predisposed to form *cis*-polybutadiynes upon irradiation;[364] however, although approximately 20% of the polymerization product has been obtained in each case, its stereochemistry (*cis* or *trans*) has yet to be reported.

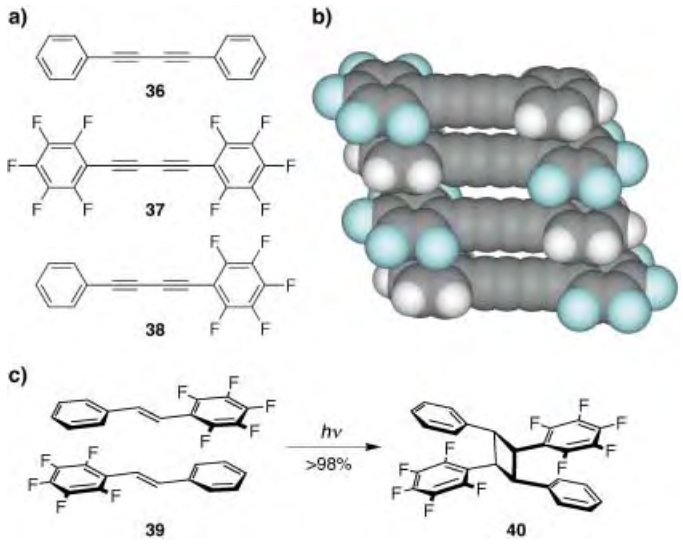

Figure 32. The use of the phenyl–perfluorophenyl synthon to predispose molecules for photochemical reactions in the solid state.[363,365] a) Precursors for *cis*-polybutadiynes. b) The X-ray structure of **38** (ca. 3.7 Å distance between layers, CSD code: RIHGOE). c) The [2+2] photocycloaddition reaction of **39** proceeds with regiochemical and stereochemical control to give **40** quantitatively in the crystal.

Subsequent studies used phenyl–perfluorophenyl interactions to orient distyrylbenzenes in the solid state for photodimerization reactions.[365,366] *trans*-Pentafluorostilbene **39** could be converted into cyclobutane **40** in nearly quantitative yield and with excellent stereocontrol (Figure 32c). There has since been considerable interest in using this motif to control the solid-state packing of distyrylbenzene derivatives for use in optoelectronic technologies.[367] More recent studies, and more are sure to come, have utilized interactions between aromatic and perfluoroaromatic compounds to control supramolecular organization in reversible media; these include modulating the behavior of liquid-crystalline phases,[368] formation of hydrogels,[369] and templation effects in cyclophane synthesis.[370]

7.3. Perfluoroarene Interactions in Biological Recognition

Fluorine-containing compounds have enjoyed a rich history in bioorganic and medicinal chemistry and have been widely studied.[371–373] The function of the fluorine atom in these settings is diverse: from an isosteric and isoelectronic replacement of the hydroxy group,[374] to a means of enhancing the metabolic stability of drugs[371] and modifying electronic and physical properties (for example, lipophilicity, acidity, steric hindrance). Introduction of perfluoroaromatic groups in biological systems, particularly with the intention of exploiting their unique electronic properties, has been somewhat more limited. A few systems are discussed here.[375] Fluorinated tryptophan side chains have been installed in the ligand binding site of acetylcholine receptors to assess the contributions of cation–π interactions to substrate binding.[270,354] A linear correlation in a "fluorination plot" between $\lg(EC_{50})$[376] and the cation–π binding ability of the side chains (as given by their degree of fluorine substitution) provides direct evidence for the presence of a single ammonium–Trp interaction that is essential to ligand binding.

Interactions between Tyr155 and the pentafluorophenyl group of a 1,3,4-thiadiazole-2-thione-based inhibitor of the metalloproteinase stromelysin (Figure 33a) contribute to its high binding affinity ($K_i = 18$ nM) and slowed the rates of ring flip relative to other analogues.[377] Although the familiar quadrupole–quadrupole interaction dominates here, Christianson, Doyon, and co-workers[378–380] have shown with fluorinated inhibitors of carbonic anhydrase II (CAII) that the quadrupolar interaction need not always dominate substrate recognition, but rather a variety of electrostatic forces (for example, dipole–induced dipole, dipole–quadrupole) may contribute differently to the binding depending on the patterns and degree of fluorine substitution in the inhibitor.

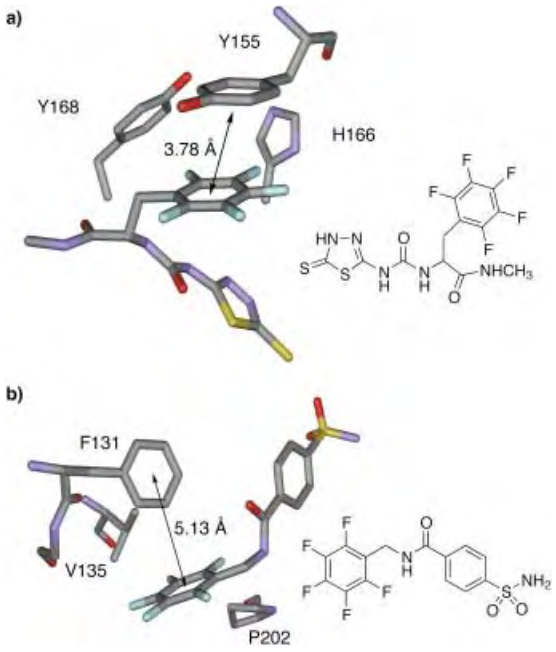

Figure 33. Perfluoroaromatic interactions involving enzymes and their inhibitors. a) Face-to-face interaction between Tyr155 and the pentafluorophenyl group of a 1,3,4-thiadiazole-2-thione inhibitor of a metalloproteinase (PDB code: 1USN).[377] b) A rather unexpected edge-to-face arrangement between the pentafluorophenyl substituent of a carbonic anhydrase II inhibitor and Phe131 of the enzyme (PDB code: 1G54).[379]

Testament to this is the rarely seen edge-to-face orientation between Phe131 of CAII and the pentafluorophenyl derivative of an *N*-(4-sulfamylbenzoyl)benzylamine inhibitor (Figure 33b) in their system.[379]

Finally Kool and co-workers have elegantly shown difluorotoluene, although not a perfluorinated aromatic compound, to be a versatile isostere of the natural nucleobase thymine.[165b,381] In the context of formation of duplex DNA, the fluorinated "base" stacks with its nearest neighbor in a geometry dictated by the helix. The marked increase in DNA stability upon substitution of thymine for difluorotoluene has been attributed to differences in hydrophobicity between the bases (their size, shape, surface area, and polarizability are comparable). However, although not specifically addressed, electronic effects in terms of π–π stacking may also play a role in these interactions.

7.4. Additional Perfluoroarene Interactions

Although there has been considerable debate regarding the effectiveness of organofluorine as a hydrogen-bond acceptor, many of the solid-state studies described above have implicated C_{aryl}–F···H–C interactions[335,373,382] as important intercolumnar and interlayer stabilizing contacts. The conclusion from these studies as well as systematic database analysis[382] is that the C_{aryl}–F···H–C contact may show an orientation dependence and be structure-directing when the C–F carbon atom is sufficiently electropositive and there are no competing H-bond acceptors in the crystal. In general, F···C distances (*d*) lie between 3.3 and 3.6 Å while the C_{aryl}–F···H angle approaches linearity as *d* decreases. Other contacts, such as C_{aryl}–F···M^+ (M^+ is an alkali metal), naturally extend from the polarization of the C_{aryl}–F bond.[383]

The electron deficiency of perfluorinated aromatic compounds makes them excellent acceptors of electron density at their π faces.[384] Hexafluorobenzene has been calculated through DFT and ab initio protocols to form strong complexes with anions (such as Cl^-, Br^-, CN^-, F^-),[385] and calculated interaction energies (−10 to −19 kcal mol^{-1} for the series given) are comparable to those obtained for cation–π interactions with benzene (see Section 6). The contact distances can be quite short (C_6F_6 centroid···F^-: 2.65 Å). Neutral molecules (of various polarity) possessing donor atoms also form complexes with perfluoroaromatic compounds; the interaction with water is the most well-studied.[379,380,386,387] The most stable complex displays a geometry wherein the oxygen lone pairs are directed into the π face, and surprisingly good agreement among computational protocols has been found (ΔE lies between −1.6 and −2.1 kcal mol^{-1}, C_6F_6 centroid···OH_2: 3.2 Å in all cases).[386] The interaction values reported are only slightly higher than the orientationally averaged binding energy for water–hexafluorobenzene calculated from gas-phase calorimetric data (−1.3 kcal mol^{-1}).[387] Finally, as with other donors (for example, molecular oxygen),[388,389] the interactions are generally stronger with C_6F_6 than with the parent C_6H_6.

8. Sulfur–Arene Interactions

8.1. Crystallographic and Computational Analysis

8.1.1. Sulfur–Arene Interactions in Proteins

Close and frequent contacts (< 5 Å from the sulfur center to the center of the ring system) between sulfur-containing amino acid side chains (Met, Cys) and aromatic side chains (Tyr, Trp, Phe) were first recognized in globular protein crystal structures in the late 1970s.[390] Morgan et al. identified eight proteins that contained one or more chains of alternating "sulfur and π-bonded atoms"; a compelling early example is the lysozyme from hen egg-white shown in Figure 34.[391] The distances between the sulfur atoms and ring carbon atoms are 3.5–4.9 Å in this example; this range falls within the distance minimum established by the authors for S···C(sp^2) van der Waals contacts (5 Å).

The nature of the interaction between sulfur and its neighboring aromatic rings could in no way be elucidated from these structures, although the following factors were considered important: 1) the filled 3p and empty 3d orbitals on sulfur, 2) the related enhanced polarizability of sulfur atoms (and C–S or S–S bonds) relative to carbon atoms (or C–C bonds), and 3) the known ability of divalent sulfur-containing molecules (particularly disulfides) to quench the fluorescence of aromatic amino acids (for example, Trp, Tyr),[392] a phenomenon still actively researched.[393] We can add the acidity of the S–H group to this list in the case of cysteine residues, which should interact favorably with π surfaces (see below and Section 5).

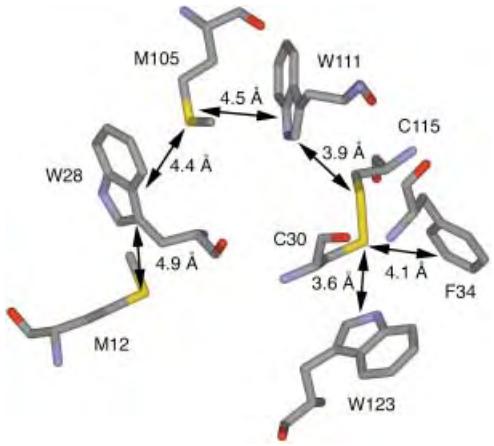

Figure 34. A chain of alternating "sulfur and π-bonded atoms" as identified in hen egg-white lysozyme (PDB code: 6LYZ).[391]

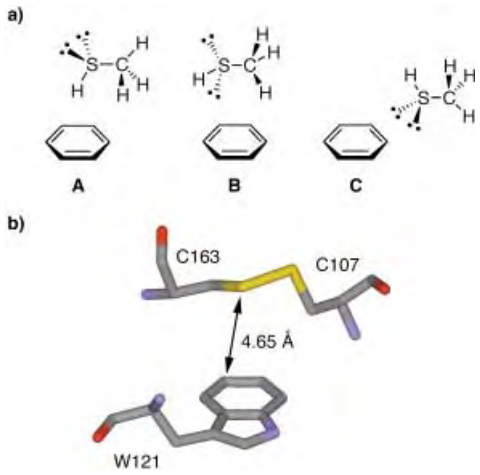

Figure 35. Sulfur–arene interactions involving sulfides and disulfides: a) The three lowest energy arrangements derived from ab initio calculations for methylthiol interacting with benzene (the stability series is **A** > **C** > **B**, least stable);[206] b) an example of the conserved disulfide–tryptophan interaction in immunoglobin (Ig) proteins (PDB code: 1IEA).[403]

Subsequent analysis of 36 proteins by Reid et al. resulted in the first statistical analysis of PDB data and the development of a structural model.[394] A preference was identified for placement of divalent sulfur (-SH, S-S, and -CH_2-S-CH_3) at the edge and slightly above the plane of aromatic rings. The same trend was observed with oxygen in similar analyses and suggested that there were significant electrostatic interactions between the heteroatom and the aromatic hydrogen atoms.

More recent structural studies have considered methionine, cysteine, and cystine (S-S) residues separately, and rightfully so given the different structural and electronic properties of these species. Recent PDB analyses[395] find that methionine is as favored as aromatic amino acids, specifically Tyr and Trp, to be within (distance (d) < 4.0 Å between Met S atom and ring heavy atoms) the environment of the Trp indol ring. In a survey of 1276 Met residues, 9 % were found in contact with an aromatic edge (average d below search cut-off: 3.7(1) Å) and 8 % with an aromatic face (average d below search cut-off: 3.6(1) Å). Despite the statistically equivalent distribution of the geometric signatures of the two interaction types, they were found to be quite different, with more structural regularity and closer distances being associated with facial contacts. However, the orientation of the aromatic partner was not considered in these studies, thus making energetic conclusions tenuous. Similar studies have shown an even stronger preference for cysteine residues to experience facial contacts with aromatic residues.[396]

The recent work of Smith and co-workers on cystine–arene interactions correlates interaction structure with energy values.[206,397,398] Three structural motifs were considered for the interaction of methanethiol with an aromatic ring (Figure 35 a). Initial ab initio calculations (MP2/6-311G(2d,p)) revealed **A** to be the most stable (−3.7 kcal mol^{-1}), followed by **C** (−1.7 kcal mol^{-1}), and **B** (−1.5 kcal mol^{-1}). The sulfur atom in structure **A** is positioned 3.5–4.0 Å above the ring. The S–H/π interaction, a consequence of favorable electrostatic interactions between a positively polarized S–H hydrogen atom and a π system (negatively polarized at this distance),[209,399] and dispersion interactions between the sulfur atom and a π surface account for 2.6 kcal mol^{-1} of the interaction energy (the 1.1 kcal mol^{-1} remaining is attributed to favorable dispersion interactions between the CH_3 group and the arene).[400] Structure **B** is highest in energy since it suffers from a repulsive interaction between an aromatic ring and a lone pair of electrons which is only partially compensated by dispersion contacts between the CH_3 group and the arene. We refer the reader here to computational studies performed on dimethylsulfide–benzene complexes that reveal the importance of such dispersive interactions.[401] Finally, the sulfur atom in structure **C** is positioned slightly above (≤ 2.5 Å) and to the edge (4.5–6.0 Å from ring centroid) of the aromatic ring in a positively polarized region (based on the MEP at this distance).[209] In this arrangement favorable interactions between the lone pair of electrons and the aromatic ring occur, which are calculated to contribute 1.5 kcal mol^{-1} to the interaction energy. These results are in reasonable, but not complete, agreement with earlier ab initio experiments (MP2/6-31G*//HF/3-21G*) performed on the benzene–methanethiol complex.[402] The most stable arrangement in these studies positioned the CH_3 group directly above the ring (for S–CH/π interactions) and the sulfur atom near the ring edge. The S–H hydrogen atom did not participate in the binding at all. An additional finding from these investigations, and one that has yet to be fully explored for sulfur–arene interactions, is a marked dependence of the interaction strength and structure on the local electric field (that is, nearby charge centers).

A subsequent search of the PDB by Smith and co-workers[206] revealed that of 682 cysteine residues (in 609 protein structures) that do not form disulfide bonds, 268 undergo interactions with aromatic rings to give structures such as **A**–**C** in Figure 35. However, of these, 207 involve attractive interactions between arenes and lone pairs of electrons (such as in **C**) and only 4 display the S–H/π-bonding configuration (such as in **A**). It appears that in the majority of cases the protein structure is better served by having the thiol

participate in conventional hydrogen bonding (for example, S–H···O(or N)), and this happens in 82 % of the total residues considered.

Ioerger et al. have studied cysteine–arene interactions in immunoglobin (Ig) proteins.[403] Their results from a survey of over 60 structures have revealed a highly conserved $(Cys)_2$···Trp interaction within the Ig fold motif, an example of which is shown in Figure 35 b.[404] The average distance between the S–S midpoint and the center of the indol ring for the surveyed structures is 4.5 Å, where stabilization of the complexes clearly comes through a combination of favorable dispersion interactions between one of the CH_2 groups and one of the sulfur atoms with the π surface. This geometry is quite similar to the lowest energy structure calculated for 1:1 benzene–dimethyldisulfide complexes by empirical methods[405] that predict direct contacts between one of the sulfur atoms and the benzene ring to make an additional contribution of 0.8 kcal mol^{-1} to the interaction energy.

Statistical analysis of the crystal structures of small molecules in the Cambridge Structural Database has provided convincing evidence for the interaction between divalent sulfur (C-S-C) units and aromatic rings.[406] Local maxima of the probability distributions obtained from the searches were used to define a preferred geometry for the interaction; it was found that the sulfur atom lies essentially in the plane of the aromatic ring approximately 5.0 Å from the center of the aromatic ring.[407] This distance maximum was not identified in analogous searches performed with X-CH_2-X fragments. We have seen in X-ray crystal structures of complexes formed in our own research between Rebek imide-type receptors with appended methylthioether side chains and adenine (Figure 15) an average distance of 4 Å between the heavy atoms of adenine and the sulfur atom located above the heterocycle.[167] However, as discussed in Section 3 and ref. [406], the contribution of crystal-packing forces in these small-molecule structures are likely to be significant and biasing.

8.1.2. *Protein–Ligand Complexes*

Figure 36 shows just two of several results from a PDB search[408] for sulfur–arene contacts between substrates containing divalent sulfur and their enzyme hosts.[409–411] In the first (Figure 36 a), methylmalonyl-CoA mutase employs an S···Ar (Y) contact to stabilize the lipophilic region of its flexible 2-carboxy-(*R*)-propyl-CoA substrate.[409] The second (Figure 36 b) shows a portion of the acyl–enzyme complex solved at 1.95 Å between 6α-(hydroxymethyl)penicillanate and β-lactamase from *Escherichia coli*, wherein a "sub-van der Waals contact" (3.3 Å) is observed between the thiazolidine sulfur atom and the Tyr 105 ring.[410] The sulfur atom is located below and to the edge of the aromatic ring.

The frequency of enzyme binding sites that involve a "sandwiching" of an aromatic substrate between two hydrophobic fragments (particularly Tyr, Phe, Trp, and Met) residues is striking. A poignant example of this motif is seen at the active site of tRNA-guanine transglycosylase (TGT), as shown in Figure 37 a.[412] Here, Tyr 106 undergoes π stacking with the complexed inhibitor on one face while Met 260

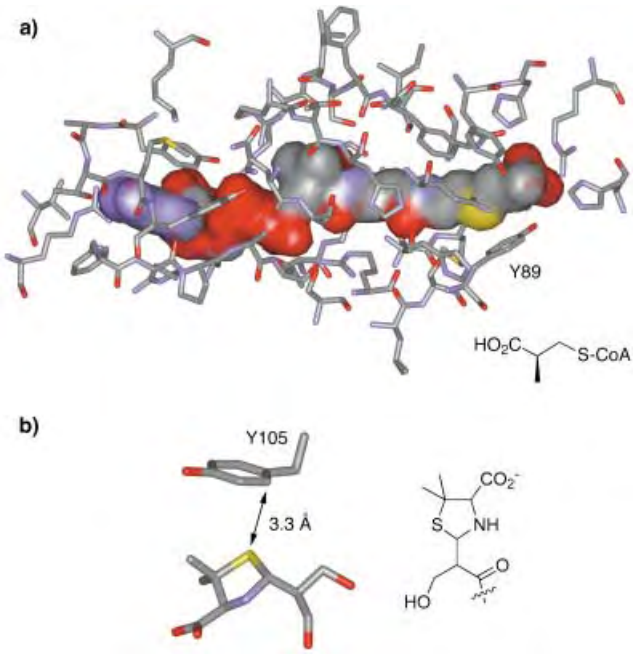

Figure 36. Sulfur–arene contacts between sulfur-bearing substrates and their biological receptors: a) X-ray crystal structure (2.2 Å) of *S*-((*R*)-2-carboxypropyl)-CoA2 bound to methylmalonyl-CoA mutase. The van der Waals surface of the substrate is shown and colored by atom (PDB code: 7REQ).[409] b) A portion of the acyl–enzyme complex formed between 6α-(hydroxymethyl)penicillanate and β-lactamase (PDB code: 1TEM).[410]

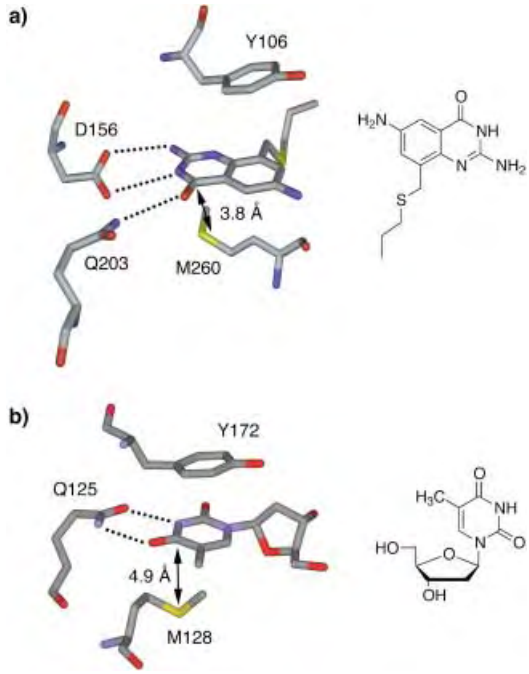

Figure 37. "Sandwich"-type complexation involving methionine. a) A tight-binding quinazoline inhibitor is held between Tyr 106 and Met 260 within the active site of TGT (PDB code: 1K4H).[412] b) Thymidine within the thymidine kinase HSV1 TK (PDB code: 2VTK).[415]

makes a contact distance (sulfur atom to the center of the ring system) of approximately 3.8 Å on the other side. The positioning of the methionine residue in the complex is also notable. Dispersion interactions appear maximized as the planar -CH_2-S-CH_3 fragment lies essentially coplanar with the quinazoline heterocycle.

The role of a highly conserved methionine in substrate binding has been carefully assessed by Folkers and co-workers in their complexes of herpes simplex virus type 1 thymidine kinase (HSV1 TK) with thymidine (Figure 37b).[413,414] The common sandwiching motif of the nucleobase between Met 128 and Tyr 172 in the enzyme active site for this system was revealed by X-ray crystallographic analysis.[415] The sulfur atom is positioned 4.9 Å below the pyrimidine ring, with the terminal methyl group of methionine located within van der Waals distance of the heterocycle (Figure 37b). DFT calculations on a simplified system (dimethylsulfide, thymine, *p*-cresole, and ammonium ion (mimicking the Arg side chain above Tyr 172; not shown)) revealed that the sulfur atom, although polarizable, does not experience any significant inductive effects in this arrangement; hence, the contribution of the sulfur atom to substrate binding comes solely in the form of steric, dispersion, and hydrophobic effects.[413] Subsequent experimental results showed that the mutant with the bio-isosterical modification of methionine to isoleucine indeed exhibited nearly identical activity to that of the wild-type enzyme.[414]

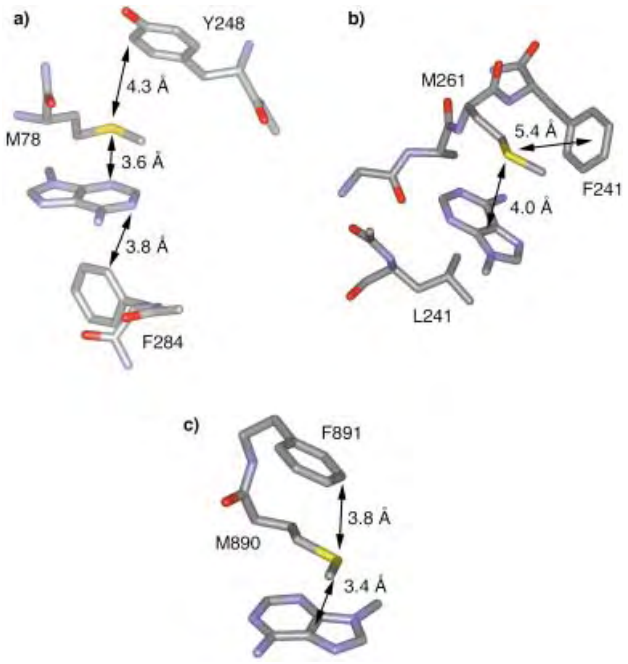

Figure 38. Methionine–adenine interactions in transferases (for a more detailed describtion of the enzymes, see text). PDB codes: a) 1FML;[416] b) 1FP1;[417] c) 1A26.[418]

8.1.3. S_{Met}–Adenine Interactions in Proteins

As with the thymidine kinase discussed above, PDB searches have revealed that adenine substrates or cofactors (ATP, ADP, AMP, FAD, *S*-adenosyl methionine (SAM), etc.) are often stabilized in the binding sites of enzymes (for example, kinases, hydrolases) by methionine side chains. While geometries similar to that shown in Figure 37b for the HSV1 TK complex are also common in these systems, we highlight here the arrangement that is similar to that found in the TGT active site (Figure 37a), namely, one that positions the C-S-C fragment coplanar with and directly above the purine ring, essentially at van der Waals distance (ca. 4.0 Å). Representative examples of S_{Met}–adenine interactions are shown in excerpts from the X-ray crystal structures of a ternary complex of retinol dehydratase (Figure 38a),[416] a ternary complex of chalcone *O*-methyltransferase (Figure 38b),[417] and a NAD^+ analogue complex of poly(ADP-ribose) polymerase (Figure 38c).[418] The common motif is intriguing as it directs one of the sulfur lone pairs into the π system—the distance must represent a subtle balance between repulsive and attractive forces. Analysis of these geometries by high-level computations is underway to shed light on the nature of the interaction. Also apparent from Figure 38 are the sandwich motifs common in these adenine-binding systems.

The bisubstrate inhibitor **41** has been shown to bind to Mg^{2+}-containing catechol *O*-methyltransferase (COMT) with an IC_{50} value of 9 nM; this enzyme is relevant in the treatment of Parkinson's disease.[419] The X-ray crystal structure of the ternary complex of COMT, **41**, and Mg^{2+} ions (Figure 39)[419b] revealed that the adenine moiety (which occupies the *S*-adenosylmethionine (SAM) pocket of the enzyme) experiences favorable sulfur–arene contacts with Met 91, and again depicts a planar C-S-C fragment positioned over the purine ring. The distance between the sulfur atom and the closest ring atom is 3.6 Å. A nearly identical sulfur–arene contact is found in the SAM–enzyme complex between Met 91 and the adenine moiety of the SAM cofactor.[420]

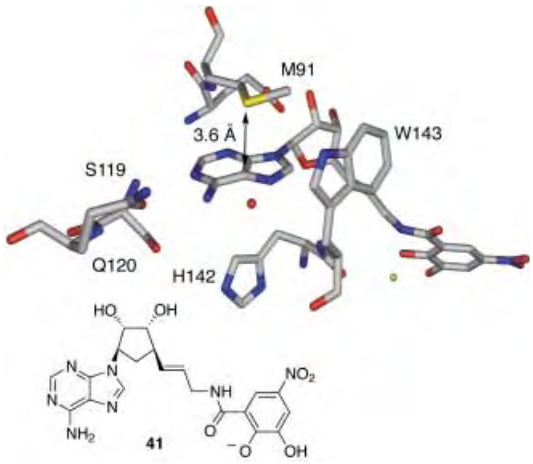

Figure 39. S_{Met}···adenine interaction in the SAM binding pocket of the enzyme catechol *O*-methyltransferase complexed to the bisubstrate inhibitor **41** (PBD code: 1JR4; red sphere: water molecule, green sphere: magnesium ion).[419b]

8.2. Energetic Aspects in Chemical and Biological Systems

8.2.1. Model Studies

The earliest studies by Morgan and co-workers examined the complexation of dimethylsulfide (DMS) by various aromatic compounds (for example, 1-methylnaphthalene) in CCl_4 by analysis of the chemical shifts in the ^1H NMR spectra.[421] Job plots confirmed a 1:1 binding stoichiometry at relatively high concentrations (1.1–3.7 M) of the components, while variable-temperature experiments provided estimates of the binding enthalpies ($\Delta H° \approx -0.8$ kcal mol^{-1}). Complexation-induced changes in the chemical shifts led the authors to conclude that in most cases the methyl group of the DMS molecule was positioned over the aromatic ring center while the sulfur atom was in proximity to the ring edge.[422] This conclusion is in good agreement with the computational experiments described in the previous sections.[423] Subsequent NMR studies performed on deamino-oxytocin analogues by Hruby and co-workers revealed differences in the chemical shifts of aromatic side chain protons in proximity to a disulfide bridge.[424] An "edge-on" interaction was reasoned on the basis of chemical shift data, even though the observed downfield shifts were small ($\Delta\delta \approx 0.06$–$0.08$ ppm).

The receptor shown in Figure 40a has been designed to evaluate the contributions of donor atoms for flavin binding in flavodoxins.[425,426] The xanthene scaffold nicely positions an

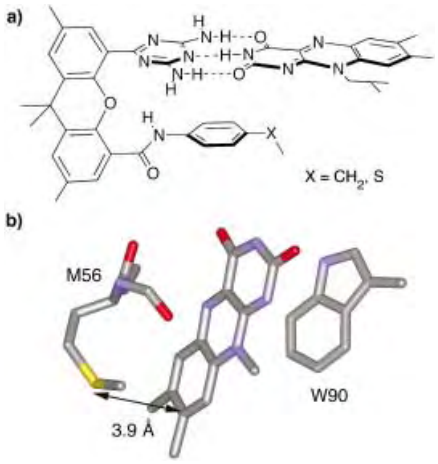

Figure 40. Sulfur–flavin interactions in a) a synthetic model systems[425] and b) flavodoxin from *Clostridium beijerinckii* (PDB code: 5NLL).[430]

aromatic residue below a noncovalently bound flavin substrate; ^1H NMR studies in $CDCl_3$ show a binding free enthalpy difference $-\Delta\Delta G$ of about 1 kcal mol^{-1} for hosts bearing $X = CH_2$ ($K_a = 960$ M^{-1}) versus $X = S$ ($K_a = 4800$ M^{-1}).[425] Further computational studies (DFT methods) have identified a significant electrostatic contribution to the interaction. This observation is consistent with the positioning of sulfur under the electron-deficient pyrimidine moiety of the flavin ring system, however, no detectable overlap of the sulfur and aromatic orbitals or significant inductive effects could be detected.[426]

8.2.2. Employing Biological Systems

Although there have been only a few examples of site-directed mutagenesis experiments in proteins, they have provided compelling evidence for the stabilizing role of S_{Met}–arene interactions. Substitutions between contacting i and $i+4$ residues of α-helical peptides have given $\Delta G°$ values between -0.65 and -0.80 kcal mol^{-1} for Phe···Met interactions in two independent cases.[427] Building on earlier theoretical work of Hirono and co-workers,[428] Spencer and Stites demonstrated protein destabilization (0.8 kcal mol^{-1}) upon mutation of a Met residue (to Leu) situated nearby Phe and Tyr side chains.[429] Swenson and co-workers have shown in comprehensive mutational experiments with flavodoxins that a Met/Ala mutation reduces flavin binding by 0.5 kcal mol^{-1}, wherein the Met residue is known through crystallographic analysis to be positioned approximately 3.9 Å above the flavin ring (Figure 40b).[430,431] While all of these studies do reach some consensus in terms of S_{Met}–arene interaction energies (0.5–0.8 kcal mol^{-1}), the nature of the interaction in each case certainly varies.[432]

8.3. Outlook

Understanding the S···Ar interaction in enzyme–substrate complexes, namely, its contribution to binding strength and geometry, has important consequences for the design of de novo inhibitors. In fact, S···Ar contacts have only recently been considered, a priori, in drug development.[412,419,433] We anticipate intensified contributions along these lines in the future, particularly as modest to significant enhancements in binding can be realized with such a conservative substitution (-S- versus -CH_2-). In closing, we do, however, note that while the "sulfur–arene interaction" implies direct participation of sulfur atoms in binding, it appears that this may only be true in a narrow range of cases, and further theoretical and experimental work is required to elucidate when such contacts are likely to occur.[434]

9. Summary

The accomplishments of more than 20 years of supramolecular chemistry research in advancing the knowledge of structure and energetics of individual intermolecular bonding interactions are now increasingly also recognized in the biomedical community. Examples of investigations with chemical systems that have profoundly influenced biology include the discovery of the cation–π interaction and the revised view of the hydrophobic effect as a driving force for apolar complexation. Nevertheless, it has also become apparent that a single research approach, such as studying solution complexation with artificial receptors, is insufficient for enhancing the knowledge of molecular recognition phenomena up to a level at which it becomes directly useful for application in drug design and lead optimization. This situation has been fully taken into account in this review which presents, in addition to findings from supramolecular

chemistry, quantitative investigations from biostructural research, crystallographic database mining, gas-phase study, and theoretical calculations. In particular, the analysis of the dramatically increasing number of protein crystal structures using modern software is increasingly becoming a fertile ground for advanced molecular recognition study. The more classical interactions involving π–π-stacking and edge-to-face contacts between aromatic rings continue to attract interest in terms of further refined geometries and energy models. The discovery of cation–π interactions has created a "hot" area of research in biology, and these contacts are increasingly finding application in modern drug design. Ample opportunities exist for further exploring fluorine–arene and sulfur–arene interactions; experimental studies targeting H bonding to π surfaces in solution complexes also remain poorly developed. While the complexity of ion pairs and their interactions with aromatic rings has been identified, both experimental and computational studies of these interactions are in their infancy. Add to this the true challenge in future computational chemistry of handling fully solvated chemical and biological complexation processes with acceptable speed at a high level of theory and accuracy. From these few examples, it becomes clear that molecular recognition studies in chemistry and biology will remain a fascinating area of future research.

We thank F. Hoffmann–La Roche Ltd (Basel), the ETH Research Council, the Fonds der Chemischen Industrie, and the U.S. National Science Foundation for their generous support of this research. Continuing fruitful discussions with Prof. Klaus Müller (Roche, Basel), Prof. Jack D. Dunitz (ETH Zürich), and Prof. Gerhard Klebe (Univ. Marburg) are gratefully acknowledged. Furthermore, F.D. wishes to thank all the scientists at Global Roche involved in biostructural research; their findings as discussed in numerous consulting sessions have initiated and stimulated many of the ongoing molecular recognition studies with biological receptors in the Diederich laboratories at ETH Zürich. Contributions of the many enthusiastic co-workers in the Diederich research group are acknowledged through the literature citations. R.K.C. is grateful to the U.S. National Science Foundation (postdoctoral fellowship) and the University of Florida for financial support. Finally, we thank Prof. G. W. Gokel, Prof. F.-G. Klärner, and Dr. K. Deshayes for providing drawings of their receptors and complexes.

Received: November 4, 2002 [A563]

[1] a) G. Kryger, I. Silman, J. L. Sussman, *J. Physiol.* **1998**, *92*, 191 – 194; b) G. Kryger, I. Silman, J. L. Sussman, *Structure* **1999**, *7*, 297 – 307.

[2] a) J.-M. Lehn, *Supramolecular Chemistry: Concepts and Perspectives*, VCH, New York, **1995**; b) *Comprehensive Supramolecular Chemistry, Vols. 1–10* (Eds.: J. L. Atwood, J. E. D. Davies, D. D. MacNicol, F. Vögtle, J.-M. Lehn), Pergamon, Oxford, **1996**; c) *Chem. Rev.* **1997**, *97*, 1231 – 1734 (special issue on molecular recognition (Ed.: S. H. Gellman)); d) H.-J. Schneider, A. Yatsimirsky, *Principles and Methods in Supramolecular Chemistry*, Wiley, Chichester, **2000**; e) J. W. Steed, J. L. Atwood, *Supramolecular Chemistry*, Wiley, Chichester, **2000**; f) *Proc. Natl. Acad. Sci. USA* **2002**, *99*, 4755 – 5750 (special issue on supramolecular chemistry and self-assembly (Ed.: J. Halpern)).

[3] *Curr. Opin. Chem. Biol.* **2002**, *6*, 11 – 12 (special issue on proteomics and genomics (Eds.: J. D. Hoheisel, D. Cahill)).

[4] P. Betschmann, S. Sahli, F. Diederich, U. Obst, V. Gramlich, *Helv. Chim. Acta* **2002**, *85*, 1210 – 1245.

[5] U. Obst, D. W. Banner, L. Weber, F. Diederich, *Chem. Biol.* **1997**, *4*, 287 – 295.

[6] S. K. Burley, G. A. Petsko, *Science* **1985**, *229*, 23 – 28.

[7] J. C. Ma, D. A. Dougherty, *Chem. Rev.* **1997**, *97*, 1303 – 1324.

[8] A. Niedzwiecka, J. Marcotrigiano, J. Stepinski, M. Jankowska-Anyszka, A. Wyslouch-Cieszynska, M. Dadlez, A.-C. Gingras, P. Mak, E. Darzynkiewicz, N. Sonenberg, S. K. Burley, R. Stolarski, *J. Mol. Biol.* **2002**, *319*, 615 – 635.

[9] a) F. Diederich, *Angew. Chem.* **1988**, *100*, 372 – 396; *Angew. Chem. Int. Ed. Engl.* **1988**, *27*, 362 – 386; b) F. Vögtle, *Cyclophane Chemistry*, Teubner, Stuttgart, **1990**; c) C. Seel, F. Vögtle, *Angew. Chem.* **1992**, *104*, 542 – 563; *Angew. Chem. Int. Ed. Engl.* **1992**, *31*, 528 – 549; d) T. H. Webb, C. S. Wilcox, *Chem. Soc. Rev.* **1993**, *22*, 383 – 395; e) *Comprehensive Supramolecular Chemistry, Vol. 2* (Ed.: F. Vögtle), Elsevier/Pergamon, Oxford, **1996**; this volume contains the following chapters on cyclophane complexation: H.-J. Schneider, A. K. Mohammad-Ali, pp. 69–101; A. Pochini, R. Ungaro, pp. 103–142; K. Odashima, K. Koga, pp. 143–194; D. A. Dougherty, pp. 195–209; F. Vögtle, C. Seel, P.-M. Windschief, pp. 211–265; Y. Aoyama, pp. 279–307; B. J. Whitlock, H. W. Whitlock, pp. 309–324; A. Collet, pp. 325–365; Y. Murakami, O. Hayashida, pp. 419–438; f) see also: M. Inouye, K. Fujimoto, M. Furusyo, H. Nakazumi, *J. Am. Chem. Soc.* **1999**, *121*, 1452 – 1458.

[10] F. Diederich, *Cyclophanes*, The Royal Society of Chemistry, Cambridge, **1991**.

[11] a) A. W. Schwabacher, J. Lee, H. Lei, *J. Am. Chem. Soc.* **1992**, *114*, 7597 – 7598; b) M. Fujita, S. Nagao, M. Ida, K. Ogata, K. Ogura, *J. Am. Chem. Soc.* **1993**, *115*, 1574 – 1576; c) H. Chen, S. Ogo, R. H. Fish, *J. Am. Chem. Soc.* **1996**, *118*, 4993 – 5001.

[12] S. B. Ferguson, E. M. Sanford, E. M. Seward, F. Diederich, *J. Am. Chem. Soc.* **1991**, *113*, 5410 – 5419.

[13] D. B. Smithrud, T. B. Wyman, F. Diederich, *J. Am. Chem. Soc.* **1991**, *113*, 5420 – 5426.

[14] F. Diederich, D. B. Smithrud, E. M. Sanford, T. B. Wyman, S. B. Ferguson, D. R. Carcanague, I. Chao, K. N. Houk, *Acta. Chem. Scand.* **1992**, *46*, 205 – 215.

[15] S. B. Ferguson, E. M. Seward, F. Diederich, E. M. Sanford, A. Chou, P. Inocencio-Szweda, C. B. Knobler, *J. Org. Chem.* **1988**, *53*, 5593 – 5595.

[16] For recent applications of cyclophanes such as **1**, see a) S. Anderson, R. T. Aplin, T. D. W. Claridge, T. Goodson III, A. C. Maciel, G. Rumbles, J. F. Ryan, H. L. Anderson, *J. Chem. Soc. Perkin Trans. 2* **1998**, 2383 – 2397; b) J. Huuskonen, J. E. H. Buston, N. D. Scotchmer, H. L. Anderson, *New J. Chem.* **1999**, *23*, 1245 – 1252; c) D. R. Benson, J. Fu, *Tetrahedron Lett.* **1996**, *37*, 4833 – 4836; d) D. R. Benson, J. Fu, C. F. Johnson, S. W. Pauls, D. A. Williamson, *J. Org. Chem.* **1998**, *63*, 9935 – 9945; e) D. A. Williamson, A. M. Barenberg, C. A. Coleman, D. R. Benson, *Chemosphere* **2000**, *40*, 1443 – 1446.

[17] a) W. Kauzmann, *Adv. Protein Chem.* **1959**, *16*, 1 – 63; b) C. Tanford, *The Hydrophobic Effect: Formation of Micelles and Biological Membranes*, 2nd ed., Wiley, New York, **1980**; c) A. Ben-Naim, *Hydrophobic Interactions*, Plenum, New York, **1980**; d) N. T. Southall, K. A. Dill, A. D. J. Haymet, *J. Phys. Chem. B* **2002**, *106*, 521 – 533.

[18] W. Blokzijl, J. B. F. N. Engberts, *Angew. Chem.* **1993**, *105*, 1610 – 1648; *Angew. Chem. Int. Ed. Engl.* **1993**, *32*, 1545 – 1579.

[19] D. A. Stauffer, R. E. Barrans, Jr., D. A. Dougherty, *J. Org. Chem.* **1990**, *55*, 2762 – 2767.
[20] E. L. Piatnitski, R. A. Flowers II, K. Deshayes, *Chem. Eur. J.* **2000**, *6*, 999 – 1006.
[21] For other examples of enthalpy-controlled arene complexation by cyclophanes in water, see a) I. K. Chun, M. W. Lee, *J. Korean Pharm. Sci.* **1989**, *19*, 71 – 75; b) R. M. Izatt, K. Pawlak, J. S. Bradshaw, R. L. Bruening, *Chem. Rev.* **1995**, *95*, 2529 – 2586.
[22] B. R. Peterson, P. Wallimann, D. R. Carcanague, F. Diederich, *Tetrahedron* **1995**, *51*, 401 – 421.
[23] a) K. Harata, *Bull. Chem. Soc. Jpn.* **1979**, *52*, 1807 – 1812; b) K. Harata, K. Tsuda, K. Uekama, M. Otagiri, F. Hirayama, *J. Inclusion Phenom.* **1988**, *6*, 135 – 142; c) G. L. Bertrand, J. R. Faulkner, Jr., S. M. Han, D. W. Armstrong, *J. Phys. Chem. B* **1989**, *93*, 6863 – 6867; d) E. Junquera, V. G. Baonza, E. Aicart, *Can. J. Chem.* **1999**, *77*, 348 – 355.
[24] J. C. Harrison, M. R. Eftink, *Biopolymers* **1982**, *21*, 1153 – 1166.
[25] M. R. Eftink, M. L. Andy, K. Bystrom, H. D. Perlmutter, D. S. Kristol, *J. Am. Chem. Soc.* **1989**, *111*, 6765 – 6772.
[26] E. Junquera, J. Laynez, M. Menéndez, S. Sharma, S. Penadés, *J. Org. Chem.* **1996**, *61*, 6790 – 6798.
[27] K. Kano, T. Kitae, Y. Shimofuri, N. Tanaka, Y. Mineta, *Chem. Eur. J.* **2000**, *6*, 2705 – 2713.
[28] M. V. Rekharsky, Y. Inoue, *Chem. Rev.* **1998**, *98*, 1875 – 1917.
[29] H.-J. Böhm, G. Klebe, *Angew. Chem.* **1996**, *108*, 2750 – 2778; *Angew. Chem. Int. Ed. Engl.* **1996**, *35*, 2588 – 2614.
[30] D. D. F. Shiao, J. M. Sturtevant, *Biochemistry* **1969**, *8*, 4910 – 4917.
[31] a) L. Beres, J. M. Sturtevant, *Biochemistry* **1971**, *10*, 2120 – 2126; b) R. L. Biltonen, N. Langerman, *Methods Enzymol.* **1979**, *61*, 287 – 317; c) P. D. Ross, S. Subramanian, *Biochemistry* **1981**, *20*, 3096 – 3102; d) H.-J. Hinz, *Annu. Rev. Biophys. Bioeng.* **1983**, *12*, 285 – 317.
[32] L. Sebo, B. Schweizer, F. Diederich, *Helv. Chim. Acta* **2000**, *83*, 80 – 92.
[33] R. Talhout, J. B. F. N. Engberts, *Eur. J. Biochem.* **2001**, *268*, 1554 – 1560.
[34] a) W. Y. Chou, L. A. Marky, S. Zaunczkowski, K. J. Breslauer, *J. Biomol. Struct. Dyn.* **1987**, *5*, 345 – 359; b) A. Kagemoto, A. Kunihiro, Y. Baba, *Thermochim. Acta* **1994**, *242*, 65 – 75; c) A. Odani, T. Sekiguchi, H. Okada, S. Ishiguro, O. Yamauchi, *Bull. Chem. Soc. Jpn.* **1995**, *68*, 2093 – 2102; d) J. Ren, T. C. Jenkins, J. B. Chaires, *Biochemistry* **2000**, *39*, 8439 – 8447; e) T.-K. Li, E. Bathory, E. J. LaVoie, A. R. Srinivasan, W. K. Olson, R. R. Sauers, L. F. Liu, D. S. Pilch, *Biochemistry* **2000**, *39*, 7107 – 7116.
[35] H. P. Hopkins, Jr., Y. Ming, W. D. Wilson, D. W. Boykin, *Biopolymers* **1991**, *31*, 1105 – 1114.
[36] D. P. Remeta, C. P. Mudd, R. L. Berger, K. J. Breslauer, *Biochemistry* **1993**, *32*, 5064 – 5073.
[37] Since most of the minor-groove-binding drugs also possess cationic residues for ion pairing with the DNA phosphate backbone and additionally may undergo many H-bonding interactions, both favorable enthalpic and entropic terms are sometimes observed. a) L. A. Marky, K. J. Breslauer, *Proc. Natl. Acad. Sci. USA* **1987**, *84*, 4359 – 4363; b) N. Patel, H. Berglund, L. Nilsson, R. Rigler, L. W. McLaughlin, A. Gräslund, *Eur. J. Biochem.* **1992**, *203*, 361 – 366; c) D. S. Pilch, N. Poklar, C. A. Gelfand, S. M. Law, K. J. Breslauer, E. E. Baird, P. B. Dervan, *Proc. Natl. Acad. Sci. USA* **1996**, *93*, 8206 – 8311; d) D. S. Pilch, N. Poklar, E. E. Baird, P. B. Dervan, K. J. Breslauer, *Biochemistry* **1999**, *38*, 2143 – 2151.
[38] K. J. Breslauer, D. P. Remeta, W.-Y. Chou, R. Ferrante, J. Curry, D. Zaunczkowski, J. G. Snyder, L. A. Marky, *Proc. Natl. Acad. Sci. USA* **1987**, *84*, 8922 – 8926.
[39] Recent investigations show that the thermodynamic quantities for minor-groove intercalation are highly dependent on the structure, solvation, and sequence of the DNA binding site: L. Wang, A. Kumar, D. W. Boykin, C. Bailly, W. D. Wilson, *J. Mol. Biol.* **2002**, *317*, 361 – 374.
[40] I. Jelesarov, L. Leder, H. R. Bosshard, *Methods* **1996**, *9*, 533 – 541.
[41] C. P. Swaminathan, A. Nandi, S. S. Visweswariah, A. Surolia, *J. Biol. Chem.* **1999**, *274*, 31272 – 31278.
[42] P. C. Ackroyd, J. Cleary, G. D. Glick, *Biochemistry* **2001**, *40*, 2911 – 2922.
[43] a) J. Selig, *Biochim. Biophys. Acta* **1997**, *1331*, 103 – 116; b) T. Wieprecht, M. Beyermann, J. Selig, *Biochemistry* **1999**, *38*, 10377 – 10387.
[44] S. R. Vippagunta, A. Dorn, H. Matile, A. K. Bhattacharjee, J. M. Karle, W. Y. Ellis, R. G. Ridley, J. L. Vennerstrom, *J. Med. Chem.* **1999**, *42*, 4630 – 4639.
[45] S. R. Vippagunta, A. Dorn, R. G. Ridley, J. L. Vennerstrom, *Biochim. Biophys. Acta* **2000**, *1475*, 133 – 140.
[46] Y. Inoue, Y. Liu, L.-H. Tong, B.-J. Shen, D.-S. Jin, *J. Am. Chem. Soc.* **1993**, *115*, 10637 – 10644.
[47] a) E. Grunwald, C. Steel, *J. Am. Chem. Soc.* **1995**, *117*, 5687 – 5692; b) M. S. Searle, M. S. Westwell, D. H. Williams, *J. Chem. Soc. Perkin Trans. 1* **1995**, 141 – 151; c) J. D. Dunitz, *Chem. Biol.* **1995**, *2*, 709 – 712; d) L. Liu, Q.-X. Guo, *Chem. Rev.* **2001**, *101*, 673 – 695.
[48] D. B. Smithrud, E. M. Sanford, I. Chao, S. B. Ferguson, D. R. Carcanague, J. Evanseck, K. N. Houk, F. Diederich, *Pure Appl. Chem.* **1990**, *62*, 2227 – 2236.
[49] T. Z. Mordasini Denti, W. F. van Gunsteren, F. Diederich, *J. Am. Chem. Soc.* **1996**, *118*, 6044 – 6051.
[50] C. Reichardt, *Solvent Effects in Organic Chemistry*, 2nd ed., VCH, Weinheim, **1988**, pp. 339 – 405.
[51] a) H. J. Schneider, R. Kramer, S. Simova, U. Schneider, *J. Am. Chem. Soc.* **1988**, *110*, 6442 – 6448; b) A. Mirzoian, A. E. Kaifer, *J. Org. Chem.* **1995**, *60*, 8093 – 8095; c) M. S. Cubberley, B. L. Iverson, *J. Am. Chem. Soc.* **2001**, *123*, 7560 – 7563.
[52] C. A. Berg-Brennan, D. I. Yoon, R. V. Slone, A. P. Kazala, J. T. Hupp, *Inorg. Chem.* **1996**, *35*, 2032 – 2035.
[53] a) B. Zhang, R. Breslow, *J. Am. Chem. Soc.* **1997**, *119*, 1676 – 1681; b) C.-S. Kim, K. C. Russell, *Tetrahedron Lett.* **1999**, *40*, 3835 – 3838.
[54] Ref. [10], p. 253.
[55] W. Saenger, *Angew. Chem.* **1980**, *92*, 343 – 361; *Angew. Chem. Int. Ed. Engl.* **1980**, *19*, 344 – 362.
[56] a) O. Sinanoglu in *Molecular Associations in Biology* (Ed.: B. Pullman), Academic Press, New York, **1968**, pp. 427 – 445; b) O. Sinanoglu in *Molecular Interactions, Vol. 3* (Ed.: W. J. Orville-Thomas), Wiley, Chichester, **1982**, pp. 283 – 342.
[57] a) B. Lee, *Biopolymers* **1985**, *24*, 813 – 823; b) J. Canceill, L. Lacombe, A. Collet, *J. Am. Chem. Soc.* **1986**, *108*, 4230 – 4232; c) R. J. Clarke, J. H. Coates, S. F. Lincoln, *Adv. Carbohydr. Chem. Biochem.* **1988**, *46*, 205 – 249; d) A. Örstan, A. Ross, *J. Phys. Chem.* **1987**, *91*, 2739 – 2745.
[58] C. Carey, Y.-K. Cheng, P. J. Rossky, *Chem. Phys.* **2000**, *258*, 415 – 425.
[59] N. T. Southall, K. A. Dill, *J. Phys. Chem. B* **2000**, *104*, 1326 – 1331.
[60] a) T. Lazaridis, M. E. Paulaitis, *J. Phys. Chem.* **1994**, *98*, 635 – 642; b) R. U. Lemieux, *Acc. Chem. Res.* **1996**, *29*, 373 – 380; c) B. D. Isbister, P. M. St. Hilaire, E. J. Toone, *J. Am. Chem. Soc.* **1995**, *117*, 12877 – 12878.
[61] D. B. Smithrud, F. Diederich, *J. Am. Chem. Soc.* **1990**, *112*, 339 – 343.
[62] a) A. Fersht, *Enzyme Structure and Mechanism*, Freeman, New York, **1985**, pp. 293 – 310; b) A. Fersht, C. Dingwall, *Biochemistry* **1979**, *18*, 1245 – 1249; c) J. A. McCammon, P. G. Wolynes, M. Karplus, *Biochemistry* **1979**, *18*, 927 – 942.
[63] a) R. Castro, M. J. Berardi, E. Cordoba, M. Ochoa de Olza, A. E. Kaifer, J. D. Evanseck, *J. Am. Chem. Soc.* **1996**, *118*,

10257 – 10268; b) V. E. Williams, R. P. Lemieux, *J. Am. Chem. Soc.* **1998**, *120*, 11311 – 11315; c) M. Enescu, B. Levy, V. Gheorghe, *J. Phys. Chem. B* **2000**, *104*, 1073 – 1077; d) T. Liu, H.-J. Schneider, *Angew. Chem.* **2002**, *114*, 1418 – 1420; *Angew. Chem. Int. Ed.* **2002**, *41*, 1368 – 1370.

[64] W. C. Cromwell, K. Bystrom, M. R. Eftink, *J. Phys. Chem.* **1985**, *89*, 326 – 332.

[65] J. Espinosa, S. H. Gellman, *Angew. Chem.* **2000**, *112*, 2420 – 2423; *Angew. Chem. Int. Ed.* **2000**, *39*, 2330 – 2333.

[66] S. Mecozzi, J. Rebek, Jr., *Chem. Eur. J.* **1998**, *4*, 1016 – 1022.

[67] J. Dunitz in *Perspectives in Supramolecular Chemistry: The Crystal as a Supramolecular Entity* (Ed.: G. R. Desiraju), Wiley, Chichester, **1996**, pp. 1 – 30.

[68] H. M. Berman, T. Battistuz, T. N. Bhat, F. Bluhm, P. E. Bourne, K. Burkhardt, Z. Feng, G. L. Gilliland, L. Iype, S. Jain, P. Fagan, J. Marvin, D. Padilla, V. Ravichandran, N. Thanki, H. Weissig, J. D. Westbrook, C. Zardecki, *Acta Crystallogr. Sect. D* **2002**, *58*, 899 – 907.

[69] a) I. J. Bruno, J. C. Cole, J. P. M. Lommerse, R. S. Rowland, R. Taylor, M. L. Verdonk, *J. Comput.-Aided Mol. Des.* **1997**, *11*, 525 – 537; b) D. R. Boer, J. Kroon, J. C. Cole, B. Smith, M. L. Verdonk, *J. Mol. Biol.* **2001**, *312*, 275 – 287; c) A. Bergner, J. Günther, M. Hendlich, G. Klebe, M. Verdonk, *Biopolymers* **2002**, *61*, 99 – 110; Relibase+, V. 1.1., CCDC, Cambridge, **2001**.

[70] a) R. Taylor, *Acta Crystallogr. Sect. D* **2002**, *58*, 879 – 888; b) F. H. Allen, *Acta Crystallogr. Sect. B* **2002**, *58*, 380 – 388; c) I. J. Bruno, J. C. Cole, P. R. Edgington, M. Kessler, C. F. Macrae, P. McCabe, J. Pearson, R. Taylor, *Acta Crystallogr. Sect. B* **2002**, *58*, 389 – 397.

[71] Over 257000 structures have been deposited in the CSD (August 2002) while the last update (August 13, 2002) gave 18464 structures in the PDB.

[72] G. A. Jeffrey, *An Introduction to Hydrogen Bonding*, Oxford University Press, New York, **1997**.

[73] G. A. Jeffrey, W. Saenger, *Hydrogen Bonding in Biological Structures*, Springer, Berlin, **1991**.

[74] G. R. Desiraju, T. Steiner, *The Weak Hydrogen Bond*, Oxford University Press, New York, **1999**.

[75] a) R. Taylor, O. Kennard, *J. Am. Chem. Soc.* **1982**, *104*, 5063 – 5070; b) Z. S. Derewenda, L. Lee, U. Derewenda, *J. Mol. Biol.* **1995**, *252*, 248 – 262; c) G. R. Desiraju, *Acc. Chem. Res.* **1996**, *29*, 441 – 449; d) M. C. Wahl, M. Sundaralingam, *Trends Biochem. Sci.* **1997**, *22*, 97 – 101; e) Y. Mandel-Gutfreund, H. Margalit, R. L. Jernigan, V. B. Zhurkin, *J. Mol. Biol.* **1998**, *277*, 1129 – 1140; f) G. R. Desiraju, *Acc. Chem. Res.* **2002**, *35*, 565 – 573.

[76] J. D. Dunitz, A. Gavezzotti, *Acc. Chem. Res.* **1999**, *32*, 677 – 684.

[77] E. G. Cox, D. W. J. Cruickshank, J. A. S. Smith, *Proc. R. Soc. London Ser. A* **1958**, *247*, 1 – 21.

[78] D. E. Williams, Y. Xiao, *Acta Crystallogr. Sect. A* **1993**, *49*, 1 – 10.

[79] B. P. van Eijck, A. L. Spek, W. T. M. Mooij, J. Kroon, *Acta Crystallogr. Sect. B* **1998**, *54*, 291 – 299, and references therein.

[80] G. Klebe, F. Diederich, *Philos. Trans. R. Soc. London Ser. A* **1993**, *345*, 37 – 48.

[81] a) M. Gurrath, G. Müller, H.-D. Höltje, *Perspect. Drug Discovery Des.* **1998**, *12*, 135 – 157; b) A. Vedani, P. Zbinden, J. P. Snyder, P. A. Greenidge, *J. Am. Chem. Soc.* **1995**, *117*, 4987 – 4994.

[82] D. T. Bong, M. R. Ghadiri, *Angew. Chem.* **2001**, *113*, 2221 – 2224; *Angew. Chem. Int. Ed.* **2001**, *40*, 2163 – 2166.

[83] A. Gavezzotti, *Synlett* **2002**, 201 – 214.

[84] W. D. S. Motherwell, H. L. Ammon, J. D. Dunitz, A. Dzyabchenko, P. Erk, A. Gavezzotti, D. W. M. Hofmann, F. J. J. Leusen, J. P. M. Lommerse, W. T. M. Mooij, S. L. Price, H. Scheraga, B. Schweizer, M. U. Schmidt, B. P. van Eijck, P. Verwer, D. E. Williams, *Acta Crystallogr. Sect. B* **2002**, *58*, 647 – 661.

[85] G. R. Desiraju, A. Gavezzotti, *J. Chem. Soc. Chem. Commun.* **1989**, 621 – 623.

[86] G. R. Desiraju, *Angew. Chem.* **1995**, *107*, 2541 – 2558; *Angew. Chem. Int. Ed. Engl.* **1995**, *34*, 2311 – 2327.

[87] C. V. K. Sharma, K. Panneerselvam, L. Shimoni, H. Katz, H. L. Carrell, G. R. Desiraju, *Chem. Mater.* **1994**, *6*, 1282 – 1292.

[88] a) C. Janiak, *J. Chem. Soc. Dalton Trans.* **2000**, 3885 – 3896; for a recent review on aromatic interactions, see b) C. A. Hunter, K. R. Lawson, J. Perkins, C. J. Urch, *J. Chem. Soc. Perkin Trans. 2* **2001**, 651 – 669.

[89] J. P. Glusker, *Top. Curr. Chem.* **1998**, *198*, 1 – 56.

[90] S. K. Burley, G. A. Petsko, *Adv. Protein Chem.* **1988**, *39*, 125 – 189.

[91] G. B. McGaughey, M. Gagné, A. K. Rappé, *J. Biol. Chem.* **1998**, *273*, 15458 – 15463.

[92] a) J. Singh, J. M. Thornton, *FEBS Lett.* **1985**, *191*, 1 – 6; b) C. A. Hunter, J. Singh, J. M. Thornton, *J. Mol. Biol.* **1991**, *218*, 837 – 846; c) U. Samanta, D. Pal, P. Chakrabarti, *Acta Crystallogr. Sect. D* **1999**, *55*, 1421 – 1427.

[93] R. Bhattacharyya, U. Samanta, P. Chakrabarti, *Protein Eng.* **2002**, *15*, 91 – 100, and references therein.

[94] R. Chelli, F. L. Gervasio, P. Procacci, V. Schettino, *J. Am. Chem. Soc.* **2002**, *124*, 6133 – 6143.

[95] N. Kannan, S. Vishveshwara, *Protein Eng.* **2000**, *13*, 753 – 761.

[96] C. Ibarra, B. S. Nieslanik, W. M. Atkins, *Biochemistry* **2001**, *40*, 10614 – 10624.

[97] F. A. Quiocho, G. Hu, P. D. Gershon, *Curr. Opin. Struct. Biol.* **2000**, *10*, 78 – 86.

[98] a) D. Liu, D. A. Williamson, M. L. Kennedy, T. D. Williams, M. M. Morton, D. R. Benson, *J. Am. Chem. Soc.* **1999**, *121*, 11798 – 11812; b) K. Kano, K. Fukuda, H. Wakami, R. Nishiyabu, R. F. Pasternack, *J. Am. Chem. Soc.* **2000**, *122*, 7494 – 7502.

[99] Y. Wang, X. Hu, *J. Am. Chem. Soc.* **2002**, *124*, 8445 – 8451.

[100] E. Gazit, *FASEB J.* **2002**, *16*, 77 – 83.

[101] S. R. Griffiths-Jones, M. S. Searle, *J. Am. Chem. Soc.* **2000**, *122*, 8350 – 8356.

[102] C. D. Tatko, M. L. Waters, *J. Am. Chem. Soc.* **2002**, *124*, 9372 – 9373.

[103] B. J. Hillier, H. M. Rodriguez, L. M. Gregoret, *Folding Des.* **1998**, *3*, 87 – 93.

[104] L. Serrano, M. Bycroft, A. R. Fersht, *J. Mol. Biol.* **1991**, *218*, 465 – 475.

[105] S. M. Butterfield, P. R. Patel, M. L. Waters, *J. Am. Chem. Soc.* **2002**, *124*, 9751 – 9755.

[106] a) K. C. Janda, J. C. Hemminger, J. S. Winn, S. E. Novick, S. J. Harris, W. Klemperer, *J. Chem. Phys.* **1975**, *63*, 1419 – 1421; b) J. M. Steed, T. A. Dixon, W. Klemperer, *J. Chem. Phys.* **1979**, *70*, 4940 – 4946.

[107] S. Sun, E. R. Bernstein, *J. Phys. Chem.* **1996**, *100*, 13348 – 13366.

[108] R. Laatikainen, J. Ratilainen, R. Sebastian, H. Santa, *J. Am. Chem. Soc.* **1995**, *117*, 11006 – 11010.

[109] G. D. Smith, R. L. Jaffe, *J. Phys. Chem.* **1996**, *100*, 9624 – 9630.

[110] a) R. L. Jaffe, G. D. Smith, *J. Chem. Phys.* **1996**, *105*, 2780 – 2788; b) P. Hobza, H. L. Selzle, E. W. Schlag, *J. Phys. Chem.* **1996**, *100*, 18790 – 18794; c) F. Tran, J. Weber, T. A. Wesolowski, *Helv. Chim. Acta* **2001**, *84*, 1489 – 1503; d) M. O. Sinnokrot, E. F. Valeev, C. D. Sherril, *J. Am. Chem. Soc.* **2002**, *124*, 10887 – 10893.

[111] a) S. Tsuzuki, K. Honda, T. Uchimaru, M. Mikami, K. Tanabe, *J. Am. Chem. Soc.* **2002**, *124*, 104 – 112 D_e/D_0: stabilization energies, are given with a negative sign throughout the review. The zero-point vibration energy (ΔZPV) has been calculated

for the T-shaped dimer, which gives a D_0 value of about -2.2 kcal mol^{-1} ($D_0 = D_e - \Delta ZPV$).

[112] a) H. Krause, B. Ernstberger, H. J. Neusser, *Chem. Phys. Lett.* **1991**, *184*, 411 – 417; b) H. J. Neusser, H. Krause, *Chem. Rev.* **1994**, *94*, 1829 – 1843.

[113] J. R. Grover, E. A. Walters, E. T. Hui, *J. Phys. Chem.* **1987**, *91*, 3233 – 3237.

[114] P. Hobza, H. L. Selzle, E. W. Schlag, *J. Am. Chem. Soc.* **1994**, *116*, 3500 – 3506.

[115] a) C. Gonzalez, E. C. Lim, *J. Phys. Chem. A* **2000**, *104*, 2953 – 2957; b) N. K. Lee, S. Park, S. K. Kim, *J. Chem. Phys.* **2002**, *116*, 7910 – 7917.

[116] M. D. Blanchard, R. P. Hughes, T. E. Concolino, A. L. Rheingold, *Chem. Mater.* **2000**, *12*, 1604 – 1610.

[117] G. R. Dennis, G. L. D. Ritchie, *J. Phys. Chem.* **1991**, *95*, 656 – 660.

[118] C. A. Hunter, *Angew. Chem.* **1993**, *105*, 1653 – 1655; *Angew. Chem. Int. Ed. Engl.* **1993**, *32*, 1584 – 1586. The induction energies arising, for example, from the interaction of polarizable sites with the quadrupole moment, as well as charge-transfer, do not contribute significantly to the overall binding energy.

[119] a) D. H. Rich, *Perspect. Med. Chem.* **1993**, 15 – 25; b) A. M. Davis, S. J. Teague, *Angew. Chem.* **1999**, *111*, 778 – 792; *Angew. Chem. Int. Ed.* **1999**, *38*, 736 – 749.

[120] W. L. Jorgensen, D. L. Severance, *J. Am. Chem. Soc.* **1990**, *112*, 4768 – 4774.

[121] P. Linse, *J. Am. Chem. Soc.* **1992**, *114*, 4366 – 4373.

[122] C. Chipot, R. Jaffe, B. Maigret, D. A. Pearlman, P. A. Kollman, *J. Am. Chem. Soc.* **1996**, *118*, 11217 – 11224.

[123] a) S. Ishikawa, T. Ebata, H. Ishikawa, T. Inoue, N. Mikami, *J. Phys. Chem.* **1996**, *100*, 10531 – 10535; b) F. L. Gervasio, R. Chelli, P. Procacci, V. Schettino, *J. Phys. Chem. A* **2002**, *106*, 2945 – 2948.

[124] S. B. Ferguson, F. Diederich, *Angew. Chem.* **1986**, *98*, 1127 – 1129; *Angew. Chem. Int. Ed. Engl.* **1986**, *25*, 1127 – 1129.

[125] The electron donor/acceptor (EDA) interaction has been introduced to qualitatively describe the attraction between two aromatic rings, one with strong donor and the other with strong acceptor character. This situation affects and introduces polarization as well as a dipole moment in addition to the dispersion and charge-transfer (CT) term. However, this concept can be misleading for describing interactions between aromatic rings, and the use of quadrupoles should be preferred.

[126] a) M. Kamieth, F.-G. Klärner, F. Diederich, *Angew. Chem.* **1998**, *110*, 3497 – 3500; *Angew. Chem. Int. Ed.* **1998**, *37*, 3303 – 3306; b) F.-G. Klärner, U. Burkert, M. Kamieth, R. Boese, J. Benet-Buchholz, *Chem. Eur. J.* **1999**, *5*, 1700 – 1707.

[127] a) C. A. Schalley, R. K. Castellano, M. S. Brody, D. M. Rudkevich, G. Siuzdak, J. Rebek, Jr., *J. Am. Chem. Soc.* **1999**, *121*, 4568 – 4579; b) C. Zonta, S. Cossu, O. De Lucchi, *Eur. J. Org. Chem.* **2000**, 1965 – 1971.

[128] S. Kubik, R. Goddard, *Eur. J. Org. Chem.* **2001**, 311 – 322.

[129] C. A. Hunter, J. K. M. Sanders, *J. Am. Chem. Soc.* **1990**, *112*, 5525 – 5534.

[130] K. Müller-Dethlefs, P. Hobza, *Chem. Rev.* **2000**, *100*, 143 – 167.

[131] a) A. Galán, D. Andreu, A. M. Echavarren, P. Prados, J. de Mendoza, *J. Am. Chem. Soc.* **1992**, *114*, 1511 – 1512; b) C. Raposo, M. Martín, M. L. Mussons, M. Crego, J. Anaya, M. C. Caballero, J. R. Morán, *J. Chem. Soc. Perkin Trans. 1* **1994**, 2113 – 2116; c) A. S. Shetty, J. Zhang, J. S. Moore, *J. Am. Chem. Soc.* **1996**, *118*, 1019 – 1027; d) J. Cuntze, F. Diederich, *Helv. Chim. Acta* **1997**, *80*, 897 – 911; e) J. N. H. Reek, A. H. Priem, H. Engelkamp, A. E. Rowan, J. A. A. W. Elemans, R. J. M. Nolte, *J. Am. Chem. Soc.* **1997**, *119*, 9956 – 9964; f) D. J. Hill, J. S. Moore, *Proc. Natl. Acad. Sci. USA* **2002**, *99*, 5053 – 5057.

[132] F. J. Carver, C. A. Hunter, P. S. Jones, D. J. Livingstone, J. F. McCabe, E. M. Seward, P. Tiger, S. E. Spey, *Chem. Eur. J.* **2001**, *7*, 4854 – 4862.

[133] F. J. Carver, C. A. Hunter, D. J. Livingstone, J. F. McCabe, E. M. Seward, *Chem. Eur. J.* **2002**, *8*, 2848 – 2859.

[134] A. G. Martínez, J. O. Barcina, A. de Fresno Cerezo, *Chem. Eur. J.* **2001**, *7*, 1171 – 1175.

[135] a) S. Paliwal, S. Geib, C. S. Wilcox, *J. Am. Chem. Soc.* **1994**, *116*, 4497 – 4498; b) E. Kim, S. Paliwal, C. S. Wilcox, *J. Am. Chem. Soc.* **1998**, *120*, 11192 – 11193.

[136] For a review on intramolecular edge-to-face interactions, see W. B. Jennings, B. M. Farrell, J. F. Malone, *Acc. Chem. Res.* **2001**, *34*, 885 – 894.

[137] a) T. Ren, Y. Jin, K. S. Kim, D. H. Kim, *J. Biomol. Struct. Dyn.* **1997**, *15*, 401 – 405; b) K. Nakamura, K. N. Houk, *Org. Lett.* **1999**, *1*, 2049 – 2051; c) for a recent theoretical calculation demonstrating backbone effects on the conformational preferences of the molecular torsional balance, see J. Ribas, E. Cubero, F. J. Luque, M. Orozco, *J. Org. Chem.* **2002**, *67*, 7057 – 7065.

[138] U. Obst, P. Betschmann, C. Lerner, P. Seiler, F. Diederich, V. Gramlich, L. Weber, D. W. Banner, P. Schönholzer, *Helv. Chim. Acta* **2000**, *83*, 855 – 909.

[139] J. A. Turk, D. B. Smithrud, *J. Org. Chem.* **2001**, *66*, 8328 – 8335.

[140] a) P. J. Ala, E. E. Huston, R. M. Klabe, D. D. McCabe, J. L. Duke, C. J. Rizzo, B. D. Korant, R. J. DeLoskey, P. Y. S. Lam, C. N. Hodge, C.-H. Chang, *Biochemistry* **1997**, *36*, 1573 – 1580; b) N. O. Concha, C. A. Janson, P. Rowling, S. Pearson, C. A. Cheever, B. P. Clarke, C. Lewis, M. Galleni, J.-M. Frère, D. J. Payne, J. H. Bateson, S. S. Abdel-Meguid, *Biochemistry* **2000**, *39*, 4288 – 4298.

[141] M. Brandl, M. S. Weiss, A. Jabs, J. Sühnel, R. Hilgenfeld, *J. Mol. Biol.* **2001**, *307*, 357 – 377.

[142] Y. Umezawa, S. Tsuboyama, H. Takahashi, J. Uzawa, M. Nishio, *Bioorg. Med. Chem.* **1999**, *7*, 2021 – 2026.

[143] For comparison with other systems, it is noteworthy to mention the methane–benzene complex with a stabilization energy of $D_e = -1.45$ kcal mol^{-1} and a $D_o = -0.98$ kcal mol^{-1}: S. Tsuzuki, K. Honda, T. Uchimaru, M. Mikami, K. Tanabe, *J. Am. Chem. Soc.* **2000**, *122*, 3746 – 3753.

[144] a) M. Nishio, M. Hirota, Y. Umezawa, *The CH/π Interaction*, Wiley, New York, **1998**; b) http://www.tim.hi-ho.ne.jp/dionisio/

[145] H. Suezawa, T. Hashimoto, K. Tsuchinaga, T. Yoshida, T. Yuzuri, K. Sakakibara, M. Hirota, M. Nishio, *J. Chem. Soc. Perkin Trans. 2* **2000**, 1243 – 1249.

[146] N. K. Vyas, M. N. Vyas, F. A. Quiocho, *Science* **1988**, *242*, 1290 – 1295.

[147] F. Cozzi, J. S. Siegel, *Pure Appl. Chem.* **1995**, *67*, 683 – 689.

[148] V. E. Williams, R. P. Lemieux, G. R. J. Thatcher, *J. Org. Chem.* **1996**, *61*, 1927 – 1933.

[149] M. J. Rashkin, M. L. Waters, *J. Am. Chem. Soc.* **2002**, *124*, 1860 – 1861.

[150] N. J. Heaton, P. Bello, B. Herradón, A. Del Campo, J. Jiménez-Barbero, *J. Am. Chem. Soc.* **1998**, *120*, 12371 – 12384.

[151] a) R. S. Lokey, B. L. Iverson, *Nature* **1995**, *375*, 303 – 305; b) J. Q. Nguyen, B. L. Iverson, *J. Am. Chem. Soc.* **1999**, *121*, 2639 – 2640.

[152] a) J. F. Stoddart, *Pure Appl. Chem.* **1988**, *60*, 467 – 472; b) B. Odell, M. V. Reddington, A. M. Z. Slawin, N. Spencer, J. F. Stoddart, D. J. Williams, *Angew. Chem.* **1988**, *100*, 1605 – 1608; *Angew. Chem. Int. Ed. Engl.* **1988**, *27*, 1547 – 1550; c) D. Philp, A. M. Z. Slawin, N. Spencer, J. F. Stoddart, D. J. Williams, *J. Chem. Soc. Chem. Commun.* **1991**, *22*, 1584 – 1586; d) M. C. T. Fyfe, J. F. Stoddart, *Acc. Chem. Res.* **1997**, *30*, 393 – 401; e) C. G. Claessens, J. F. Stoddart, *J. Phys. Org. Chem.* **1997**, *10*, 254 – 272.

[153] a) F. M. Raymo, J. F. Stoddart, *Chem. Rev.* **1999**, *99*, 1643 – 1663; b) F. M. Raymo, J. F. Stoddart in *Templated Organic*

Synthesis (Eds.: F. Diederich, P. J. Stang), Wiley-VCH, Weinheim, **2000**, pp. 75 – 104; c) V. Balzani, A. Credi, F. M. Raymo, J. F. Stoddart, *Angew. Chem.* **2000**, *112*, 3484 – 3530; *Angew. Chem. Int. Ed.* **2000**, *39*, 3348 – 3391; d) S. J. Rowan, S. J. Cantrill, G. R. L. Cousins, J. K. M. Sanders, J. F. Stoddart, *Angew. Chem.* **2002**, *114*, 938 – 993; *Angew. Chem. Int. Ed.* **2002**, *41*, 898 – 952.

[154] For a theoretical analysis on the driving forces for complexation by **16**, see a) R. Castro, M. J. Berardi, E. Córdova, M. Ochoa de Olza, A. E. Kaifer, J. D. Evanseck, *J. Am. Chem. Soc.* **1996**, *118*, 10257 – 10268; b) F. M. Raymo, K. N. Houk, J. F. Stoddart, *J. Am. Chem. Soc.* **1998**, *120*, 9318 – 9322.

[155] The most common approach to describe electrostatic effects in aromatic interactions is the use of atom-centered charges (ACC). A comparison of the various force fields implemented in the program package MacroModel for evaluating ACC effects is available: G. Chessari, C. A. Hunter, C. M. R. Low, M. J. Packer, J. G. Vinter, C. Zonta, *Chem. Eur. J.* **2002**, *8*, 2860 – 2867.

[156] a) A. D. Hamilton, D. Van Engen, *J. Am. Chem. Soc.* **1987**, *109*, 5035 – 5036; b) A. V. Muehldorf, D. Van Engen, J. C. Warner, A. D. Hamilton, *J. Am. Chem. Soc.* **1988**, *110*, 6561 – 6562; c) A. D. Hamilton in *Supramolecular Chemistry, Vol. 371* (Eds.: V. Balzani, L. De Cola), Kluwer, Dordrecht, **1992**, pp. 137 – 144.

[157] A. J. Goodman, E. C. Breinlinger, C. M. McIntosh, L. N. Grimaldi, V. M. Rotello, *Org. Lett.* **2001**, *3*, 1531 – 1534.

[158] A. Weichsel, W. R. Montfort, *Nat. Struct. Biol.* **1995**, *2*, 1095 – 1101.

[159] a) T. Benzing, T. Tjivikua, J. Wolfe, J. Rebek, Jr., *Science* **1988**, *242*, 266 – 268; b) S. C. Zimmerman, W. Wu, Z. Zeng, *J. Am. Chem. Soc.* **1991**, *113*, 196 – 201; c) J. E. Kickham, S. J. Loeb, S. L. Murphy, *Chem. Eur. J.* **1997**, *3*, 1203 – 1213; d) O. Baudoin, F. Gonnet, M.-P. Teulade-Fichou, J.-P. Vigneron, J.-C. Tabet, J.-M. Lehn, *Chem. Eur. J.* **1999**, *5*, 2762 – 2771; e) M. Inouye, M. S. Itoh, H. Nakazumi, *J. Org. Chem.* **1999**, *64*, 9393 – 9398; f) M. Sirish, H.-J. Schneider, *J. Am. Chem. Soc.* **2000**, *122*, 5881 – 5882; g) S. R. Waldvogel, R. Fröhlich, C. A. Schalley, *Angew. Chem.* **2000**, *112*, 2580 – 2583; *Angew. Chem. Int. Ed.* **2000**, *39*, 2472 – 2475.

[160] a) Y. Hamuro, S. J. Geib, A. D. Hamilton, *J. Am. Chem. Soc.* **1997**, *119*, 10587 – 10593; b) A. J. Lovinger, C. Nuckolls, T. J. Katz, *J. Am. Chem. Soc.* **1998**, *120*, 264 – 268; c) J. H. K. K. Hirschberg, L. Brunsveld, A. Ramzi, J. A. J. M. Vekemans, R. P. Sijbesma, E. W. Meijer, *Nature* **2000**, *407*, 167 – 170; d) V. Berl, I. Huc, R. G. Khoury, J.-M. Lehn, *Chem. Eur. J.* **2001**, *7*, 2798 – 2809.

[161] a) W. Saenger, *Principles of Nucleic Acid Structure*, Springer, New York, **1984**; b) A. Eschenmoser, E. Loewenthal, *Chem. Soc. Rev.* **1992**, *21*, 1 – 16; c) I. Detmer, D. Summerer, A. Marx, *Chem. Commun.* **2002**, 2314 – 2315.

[162] a) J. Sponer, J. Leszczynski, P. Hobza, *THEOCHEM* **2001**, *573*, 43 – 53; b) J. Sponer, J. Leszczynski, P. Hobza, *Biopolymers* **2002**, *61*, 3 – 31.

[163] a) S. M. Freier, N. Sugimoto, A. Sinclair, D. Alkema, T. Neilson, R. Kierzek, M. H. Caruthers, D. H. Turner, *Biochemistry* **1986**, *25*, 3214 – 3219; b) S. Bommarito, N. Peyret, J. SantaLucia, Jr., *Nucleic Acids Res.* **2000**, *28*, 1929 – 1934.

[164] a) Y.-P. Pang, J. L. Miller, P. A. Kollman, *J. Am. Chem. Soc.* **1999**, *121*, 1717 – 1725; b) K. M. Guckian, B. A. Schweitzer, R. X.-F. Ren, C. J. Sheils, D. C. Tahmassebi, E. T. Kool, *J. Am. Chem. Soc.* **2000**, *122*, 2213 – 2222; c) S. L. McKay, B. Haptonstall, S. H. Gellman, *J. Am. Chem. Soc.* **2001**, *123*, 1244 – 1245; d) H. Rosemeyer, F. Seela, *J. Chem. Soc. Perkin Trans. 2* **2002**, 746 – 750.

[165] a) D. Barsky, E. T. Kool, M. E. Colvin, *J. Biomol. Struct. Dyn.* **1999**, *16*, 1119 – 1134; b) E. T. Kool, J. C. Morales, K. M. Guckian, *Angew. Chem.* **2000**, *112*, 1046 – 1068; *Angew. Chem. Int. Ed.* **2000**, *39*, 990 – 1009.

[166] a) E. C. Long, J. K. Barton, *Acc. Chem. Res.* **1990**, *23*, 271 – 272; b) F. Gago, *Methods* **1998**, *14*, 277 – 292; c) K. E. Erkkila, D. T. Odom, J. K. Barton, *Chem. Rev.* **1999**, *99*, 2777 – 2795.

[167] R. K. Castellano, V. Gramlich, F. Diederich, *Chem. Eur. J.* **2002**, *8*, 118 – 129.

[168] P. Lustenberger, E. Martinborough, T. Mordasini Denti, F. Diederich, *J. Chem. Soc. Perkin Trans. 2* **1998**, 747 – 761.

[169] J. A. M. Prates, N. Tarbouriech, S. J. Charnock, C. M. G. A. Fontes, L. M. A. Ferreira, G. J. Davies, *Structure* **2001**, *9*, 1183 – 1190.

[170] C.-T. Chen, J. S. Siegel, *J. Am. Chem. Soc.* **1994**, *116*, 5959 – 5960.

[171] S. E. Thompson, D. B. Smithrud, *J. Am. Chem. Soc.* **2002**, *124*, 442 – 449.

[172] G. B. Jones, *Tetrahedron* **2001**, *57*, 7999 – 8016.

[173] W. H. Pirkle, Y. Liu, *J. Chromatogr. A* **1996**, *749*, 19 – 24.

[174] a) I. Dance, M. Scudder, *J. Chem. Soc. Dalton Trans.* **2000**, 1579 – 1585; b) A. Magistrato, P. S. Pregosin, A. Albinati, U. Rothlisberger, *Organometallics* **2001**, *20*, 4178 – 4184.

[175] K. Kishikawa, M. Naruse, S. Kohmoto, M. Yamamoto, K. Yamaguchi, *J. Chem. Soc. Perkin Trans. 1* **2001**, 462 – 468.

[176] a) T. Steiner, *Angew. Chem.* **2002**, *114*, 50 – 80; *Angew. Chem. Int. Ed.* **2002**, *41*, 48 – 76; b) L. J. Prins, D. N. Reinhoudt, P. Timmerman, *Angew. Chem.* **2001**, *113*, 2446 – 2492; *Angew. Chem. Int. Ed.* **2001**, *40*, 2382 – 2426.

[177] D. A. Dixon, K. D. Dobbs, J. J. Valentini, *J. Phys. Chem.* **1994**, *98*, 13435 – 13439.

[178] K. S. Kim, P. Tarakeshwar, J. Y. Lee, *Chem. Rev.* **2000**, *100*, 4145 – 4185.

[179] D. H. Williams, M. S. Westwell, *Chem. Soc. Rev.* **1998**, *27*, 57 – 63.

[180] a) P. Hobza, Z. Havlas, *Chem. Rev.* **2000**, *100*, 4253 – 4264; b) K. Hermansson, *J. Phys. Chem. A* **2002**, *106*, 4695 – 4702.

[181] M. F. Perutz, G. Fermi, D. J. Abraham, C. Poyart, E. Bursaux, *J. Am. Chem. Soc.* **1986**, *108*, 1064 – 1078.

[182] T. Steiner, G. Koellner, *J. Mol. Biol.* **2001**, *305*, 535 – 557.

[183] G. Tóth, R. F. Murphy, S. Lovas, *J. Am. Chem. Soc.* **2001**, *123*, 11782 – 11790, and references therein.

[184] A. Wlodawer, J. Walter, R. Huber, L. Sjölin, *J. Mol. Biol.* **1984**, *180*, 301 – 329.

[185] G. Xiao, S. Liu, X. Ji, W. W. Johnson, J. Chen, J. F. Parsons, W. J. Stevens, G. L. Gilliland, R. N. Armstrong, *Biochemistry* **1996**, *35*, 4753 – 4765.

[186] M. Sulpizi, P. Carloni, *J. Phys. Chem. B* **2000**, *104*, 10087 – 10091.

[187] a) M. F. Perutz, *Philos. Trans. R. Soc. London Ser. A* **1993**, *345*, 105 – 112; b) G. B. Vázquez, X. Ji, C. Fronticelli, G. L. Guilliland, *Acta Crystallogr. Sect. D* **1998**, *54*, 355 – 366; c) M. S. Weiss, M. Brandl, J. Sühnel, D. Pal, R. Hilgenfeld, *Trends Biochem. Sci.* **2001**, *26*, 521 – 523.

[188] J. B. O. Mitchell, C. L. Nandi, I. K. McDonald, J. M. Thornton, S. L. Price, *J. Mol. Biol.* **1994**, *239*, 315 – 331.

[189] K. A. Thomas, G. M. Smith, T. B. Thomas, R. J. Feldmann, *Proc. Natl. Acad. Sci. USA* **1982**, *79*, 4843 – 4847.

[190] S. K. Burley, G. A. Petsko, *FEBS Lett.* **1986**, *203*, 139 – 143.

[191] M. M. Flocco, S. L. Mowbray, *J. Mol. Biol.* **1994**, *235*, 709 – 717.

[192] G. Tóth, C. R. Watts, R. F. Murphy, S. Lovas, *Proteins Struct. Funct. Genet.* **2001**, *43*, 373 – 381.

[193] T. Steiner, A. M. M. Schreurs, J. A. Kanters, J. Kroon, *Acta Crystallogr. Sect. D* **1998**, *54*, 25 – 31.

[194] J. L. Atwood, F. Hamada, K. D. Robinson, G. W. Orr, R. L. Vincent, *Nature* **1991**, *349*, 683 – 684.

[195] G. Hummer, J. C. Rasaiah, J. P. Noworyta, *Nature* **2001**, *414*, 188 – 190.

[196] K. Håkansson, *Int. J. Biol. Macromol.* **1996**, *18*, 189 – 194.

[197] a) T. S. Zwier, *Annu. Rev. Phys. Chem.* **1996**, *47*, 205 – 241; b) B. Brutschy, *Chem. Rev.* **2000**, *100*, 3891 – 3920.
[198] S. Tsuzuki, K. Honda, T. Uchimaru, M. Mikami, K. Tanabe, *J. Am. Chem. Soc.* **2000**, *122*, 11 450 – 11 458.
[199] A. Courty, M. Mons, I. Dimicoli, F. Piuzzi, M.-P. Gaigeot, V. Brenner, P. de Pujo, P. Millié, *J. Phys. Chem. A* **1998**, *102*, 6590 – 6600.
[200] S. Suzuki, P. G. Green, R. E. Bumgarner, S. Dasgupta, W. A. Goddard III, G. A. Blake, *Science* **1992**, *257*, 942 – 945.
[201] P. Ruelle, M. Buchmann, H. Nam-Tran, U. W. Kesselring, *J. Comput.-Aided Mol. Des.* **1992**, *6*, 431 – 448.
[202] M. P. Payne, L. C. Kenny, *J. Toxicol. Environ. Health Part A* **2002**, *65*, 897 – 931.
[203] D. A. Rodham, S. Suzuki, R. D. Suenram, F. J. Lovas, S. Dasgupta, W. A. Goddard III, G. A. Blake, *Nature* **1993**, *362*, 735 – 737.
[204] M. Mons, I. Dimicoli, B. Tardivel, F. Piuzzi, V. Brenner, P. Millié, *Phys. Chem. Chem. Phys.* **2002**, *4*, 571 – 576.
[205] P. Tarakeshwar, H. S. Choi, K. S. Kim, *J. Am. Chem. Soc.* **2001**, *123*, 3323 – 3331.
[206] G. Duan, V. H. Smith, Jr., D. F. Weaver, *Mol. Phys.* **2001**, *99*, 1689 – 1699.
[207] J. F. Malone, C. M. Murray, M. H. Charlton, R. Docherty, A. J. Lavery, *J. Chem. Soc. Faraday Trans.* **1997**, *93*, 3429 – 3436.
[208] a) O. R. Wulf, U. Liddel, S. B. Hendricks, *J. Am. Chem. Soc.* **1936**, *58*, 2287 – 2293; b) W. Klemperer, M. W. Cronyn, A. H. Maki, G. C. Pimentel, *J. Am. Chem. Soc.* **1954**, *76*, 5846 – 5848; c) M. A. Viswamitra, R. Radhakrishnan, J. Bandekar, G. R. Desiraju, *J. Am. Chem. Soc.* **1993**, *115*, 4868 – 4869.
[209] G. Duan, V. H. Smith, Jr., D. F. Weaver, *J. Phys. Chem. A* **2000**, *104*, 4521 – 4532.
[210] G. Duan, V. H. Smith, Jr., D. F. Weaver, *Chem. Phys. Lett.* **1999**, *310*, 323 – 332.
[211] G. Columberg, A. Bauder, *J. Chem. Phys.* **1997**, *106*, 504 – 510.
[212] E. M. Duffy, P. J. Kowalczyk, W. L. Jorgensen, *J. Am. Chem. Soc.* **1993**, *115*, 9271 – 9275.
[213] H. Adams, F. J. Carver, C. A. Hunter, N. J. Osborne, *Chem. Commun.* **1996**, 2529 – 2530.
[214] C. Allot, H. Adams, P. L. Bernad, Jr., C. A. Hunter, C. Rotger, J. A. Thomas, *Chem. Commun.* **1998**, 2449 – 2450.
[215] H. Adams, K. D. M. Harris, G. A. Hembury, C. A. Hunter, D. J. Livingstone, J. F. McCabe, *Chem. Commun.* **1996**, 2531 – 2532.
[216] M. J. Cloninger, H. W. Whitlock, *J. Org. Chem.* **1998**, *63*, 6153 – 6159.
[217] K. Brejc, W. J. van Dijk, R. V. Klaassen, M. Schuurmans, J. van der Oost, A. B. Smit, T. K. Sixma, *Nature* **2001**, *411*, 269 – 276.
[218] J. P. Gallivan, D. A. Dougherty, *Proc. Natl. Acad. Sci. USA* **1999**, *96*, 9459 – 9464.
[219] N. S. Scrutton, A. R. C. Raine, *Biochem. J.* **1996**, *319*, 1 – 8.
[220] M. Levitt, M. F. Perutz, *J. Mol. Biol.* **1988**, *201*, 751 – 754.
[221] W. Zhong, J. P. Gallivan, Y. Zhang, L. Li, H. A. Lester, D. A. Dougherty, *Proc. Natl. Acad. Sci. USA* **1998**, *95*, 12 088 – 12 093.
[222] D. A. Dougherty, *Science* **1996**, *271*, 163 – 168.
[223] M. O. Ortells, G. G. Lunt, *Trends Neurosci.* **1995**, *18*, 121 – 127.
[224] N. Zacharias, D. A. Dougherty, *Trends Pharmacol. Sci.* **2002**, *23*, 281 – 287.
[225] P. Lhoták, S. Shinkai, *J. Phys. Org. Chem.* **1997**, *10*, 273 – 285.
[226] A. Arduini, A. Casnati, A. Pochini, R. Ungaro, *Curr. Opin. Chem. Biol.* **1997**, *1*, 467 – 474.
[227] S. L. De Wall, E. S. Meadows, L. J. Barbour, G. W. Gokel, *Proc. Natl. Acad. Sci. USA* **2000**, *97*, 6271 – 6276.
[228] G. W. Gokel, L. J. Barbour, S. L. De Wall, E. S. Meadows, *Coord. Chem. Rev.* **2001**, *222*, 127 – 154.
[229] G. W. Gokel, L. J. Barbour, R. Ferdani, J. Hu, *Acc. Chem. Res.* **2002**, *35*, 878 – 886.
[230] G. W. Gokel, A. Mukhopadhyay, *Chem. Soc. Rev.* **2001**, *30*, 274 – 286.
[231] D. A. Stauffer, D. A. Dougherty, *Tetrahedron Lett.* **1988**, *29*, 6039 – 6042.
[232] D. A. Dougherty, D. A. Stauffer, *Science* **1990**, *250*, 1558 – 1560.
[233] J. L. Sussman, M. Harel, F. Frolow, C. Oefner, A. Goldman, L. Toker, I. Silman, *Science* **1991**, *253*, 872 – 879.
[234] For a theoretical study, see K. S. Kim, J. Y. Lee, S. J. Lee, T.-K. Ha, D. H. Kim, *J. Am. Chem. Soc.* **1994**, *116*, 7399 – 7400.
[235] H.-J. Schneider, *Angew. Chem.* **1991**, *103*, 1419 – 1439; *Angew. Chem. Int. Ed. Engl.* **1991**, *30*, 1417 – 1436.
[236] H.-J. Schneider, F. Werner, T. Blatter, *J. Phys. Org. Chem.* **1993**, *6*, 590 – 594.
[237] H.-J. Schneider, T. Schiestel, P. Zimmermann, *J. Am. Chem. Soc.* **1992**, *114*, 7698 – 7703.
[238] H.-J. Schneider, *Chem. Soc. Rev.* **1994**, *23*, 227 – 234.
[239] S. Y. Jon, J. Kim, M. Kim, S.-H. Park, W. S. Jeon, J. Heo, K. Kim, *Angew. Chem.* **2001**, *113*, 2174 – 2177; *Angew. Chem. Int. Ed.* **2001**, *40*, 2116 – 2119.
[240] R. Méric, J.-P. Vigneron, J.-M. Lehn, *J. Chem. Soc. Chem. Commun.* **1993**, 129 – 131.
[241] R. Méric, J.-M. Lehn, J.-P. Vigneron, *Bull. Soc. Chim. Fr.* **1994**, *131*, 579 – 583.
[242] a) K. Araki, H. Shimizu, S. Shinkai, *Chem. Lett.* **1993**, 205 – 208; b) K. N. Koh, K. Araki, A. Ikeda, H. Otsuka, S. Shinkai, *J. Am. Chem. Soc.* **1996**, *118*, 755 – 758.
[243] a) J. Canceill, L. Lacombe, A. Collet, *J. Chem. Soc. Chem. Commun.* **1987**, 219 – 221; b) A. Collet, J.-P. Dutasta, B. Lozach, J. Canceill, *Top. Curr. Chem.* **1993**, *165*, 103 – 129.
[244] L. Garel, B. Lozach, J.-P. Dutasta, A. Collet, *J. Am. Chem. Soc.* **1993**, *115*, 11 652 – 11 653.
[245] A. W. Schwabacher, S. Zhang, W. Davy, *J. Am. Chem. Soc.* **1993**, *115*, 6995 – 6996.
[246] A. Sygula, P. W. Rabideau, *J. Chem. Soc. Chem. Commun.* **1994**, 2271 – 2272.
[247] J. Gao, L. W. Chou, A. Auerbach, *Biophys. J.* **1993**, *65*, 43 – 47.
[248] a) C. A. Schalley, *Mass Spectrom. Rev.* **2001**, *20*, 253 – 309; b) for earlier mass-spectrometric studies on ammonium complexes of calixarenes, see F. Inokuchi, Y. Miyahara, T. Inazu, S. Shinkai, *Angew. Chem.* **1995**, *107*, 1459 – 1462; *Angew. Chem. Int. Ed. Engl.* **1995**, *34*, 1364 – 1366.
[249] a) K. Murayama, K. Aoki, *Chem. Commun.* **1997**, 119 – 120; b) K. Murayama, K. Aoki, *Chem. Commun.* **1998**, 607 – 608; c) B. Masci, M. Nierlich, P. Thuéry, *New J. Chem.* **2002**, *26*, 766 – 774.
[250] G. Arena, A. Casnati, A. Contino, G. G. Lombardo, D. Sciotto, R. Ungaro, *Chem. Eur. J.* **1999**, *5*, 738 – 744.
[251] G. Arena, A. Casnati, A. Contino, F. G. Gulino, D. Sciotto, R. Ungaro, *J. Chem. Soc. Perkin Trans. 2* **2000**, 419 – 423.
[252] The Gibbs solvation free energy of $N(CH_3)_4^+$ in water has been calculated to be more favorable by $-70\ kcal\,mol^{-1}$ relative to $C(CH_3)_4$; P. C. Kearney, L. S. Mizoue, R. A. Kumpf, J. E. Forman, A. McCurdy, D. A. Dougherty, *J. Am. Chem. Soc.* **1993**, *115*, 9907 – 9919.
[253] S. Roelens, R. Torriti, *J. Am. Chem. Soc.* **1998**, *120*, 12 443 – 12 452.
[254] S. Kubik, R. Goddard, *J. Org. Chem.* **1999**, *64*, 9475 – 9486.
[255] T. Grawe, T. Schrader, P. Finocchiaro, G. Consiglio, S. Failla, *Org. Lett.* **2001**, *3*, 1597 – 1600.
[256] M. Herm, O. Molt, T. Schrader, *Angew. Chem.* **2001**, *113*, 3248 – 3254; *Angew. Chem. Int. Ed.* **2001**, *40*, 3148 – 3151.
[257] S. Rensing, T. Schrader, *Org. Lett.* **2002**, *4*, 2161 – 2164.
[258] C. Jasper, T. Schrader, J. Panitzky, F.-G. Klärner, *Angew. Chem.* **2002**, *114*, 1411 – 1415; *Angew. Chem. Int. Ed.* **2002**, *41*, 1355 – 1358.

[259] For *N*-alkylpyridinium interactions in rotaxanes and catenanes, see A. R. Pease, J. O. Jeppesen, J. F. Stoddart, Y. Luo, C. P. Collier, J. R. Heath, *Acc. Chem. Res.* **2001**, *34*, 433 – 444.
[260] a) M. Meot-Ner, C. A. Deakyne, *J. Am. Chem. Soc.* **1985**, *107*, 469 – 474; b) C. A. Deakyne, M. Meot-Ner, *J. Am. Chem. Soc.* **1985**, *107*, 474 – 479.
[261] a) B. Masci, M. Finelli, M. Varrone, *Chem. Eur. J.* **1998**, *4*, 2018 – 2030; b) Z. Zhong, A. Ikeda, S. Shinkai, *J. Am. Chem. Soc.* **1999**, *121*, 11 906 – 11 907; c) K. Araki, H. Hayashida, *Tetrahedron Lett.* **2000**, *41*, 1209 – 1213; d) F. Cuevas, S. Di Stefano, J. O. Magrans, P. Prados, L. Mandolini, J. de Mendoza, *Chem. Eur. J.* **2000**, *6*, 3228 – 3234; e) A. Dalla Cort, M. Nissinen, D. Mancinetti, E. Nicoletti, L. Mandolini, K. Rissanen, *J. Phys. Org. Chem.* **2001**, *14*, 425 – 431; f) A. Shivanyuk, J. Rebek, Jr., *Proc. Natl. Acad. Sci. USA* **2001**, *98*, 7662 – 7665; g) L. Frish, M. O. Vysotsky, S. E. Matthews, V. Böhmer, Y. Cohen, *J. Chem. Soc. Perkin Trans. 2* **2002**, 88 – 93.
[262] A. Arduini, A. Pochini, A. Secchi, *Eur. J. Org. Chem.* **2000**, 2325 – 2334.
[263] A. Arduini, G. Giorgi, A. Pochini, A. Secchi, F. Ugozzoli, *J. Org. Chem.* **2001**, *66*, 8302 – 8308.
[264] S. Kubik, *J. Am. Chem. Soc.* **1999**, *121*, 5846 – 5855.
[265] S. Kubik, R. Goddard, *Chem. Commun.* **2000**, 633 – 634.
[266] a) K.-S. Jeong, S. H. Park, J. H. Kim, Y. L. Cho, *Bull. Korean Chem. Soc.* **1997**, *18*, 139 – 141; b) M. Kamieth, F.-G. Klärner, *J. Prakt. Chem.* **1999**, *341*, 245 – 251; c) M. Lämsä, S. Kiviniemi, E.-R. Kettukangas, M. Nissinen, J. Pursiainen, K. Rissanen, *J. Phys. Org. Chem.* **2001**, *14*, 551 – 558.
[267] J. W. Caldwell, P. A. Kollman, *J. Am. Chem. Soc.* **1995**, *117*, 4177 – 4178.
[268] S. Mecozzi, A. P. West, Jr., D. A. Dougherty, *J. Am. Chem. Soc.* **1996**, *118*, 2307 – 2308.
[269] S. Mecozzi, A. P. West, Jr., D. A. Dougherty, *Proc. Natl. Acad. Sci. USA* **1996**, *93*, 10 566 – 10 571.
[270] D. L. Beene, G. S. Brandt, W. Zhong, N. M. Zacharias, H. A. Lester, D. A. Dougherty, *Biochemistry* **2002**, *41*, 10 262 – 10 269.
[271] E. Cubero, F. J. Luque, M. Orozco, *Proc. Natl. Acad. Sci. USA* **1998**, *95*, 5976 – 5980.
[272] E. Cubero, M. Orozco, F. J. Luque, *J. Phys. Chem. A* **1999**, *103*, 315 – 321.
[273] This has been extensively investigated through computational means; see, for example, a) H. Basch, W. J. Stevens, *THEOCHEM* **1995**, *338*, 303 – 315; b) A. Pullman, G. Berthier, R. Savinelli, *J. Am. Chem. Soc.* **1998**, *120*, 8553 – 8554; c) H. Minoux, C. Chipot, *J. Am. Chem. Soc.* **1999**, *121*, 10 366 – 10 372; d) A. Pullman, G. Berthier, R. Savinelli, *THEOCHEM* **2001**, *537*, 163 – 172; e) C. Felder, H.-L. Jiang, W.-L. Zhu, K.-X. Chen, I. Silman, S. A. Botti, J. L. Sussman, *J. Phys. Chem. A* **2001**, *105*, 1326 – 1333; f) T. Liu, J. Gu, X.-J. Tan, W.-L. Zhu, X.-M. Luo, H.-L. Jiang, R.-Y. Ji, K.-X. Chen, I. Silman, J. L. Sussman, *J. Phys. Chem. A* **2001**, *105*, 5431 – 5437; g) T. Liu, J. Gu, X.-J. Tan, W.-L. Zhu, X.-M. Luo, H.-L. Jiang, R.-Y. Ji, K.-X. Chen, I. Silman, J. L. Sussman, *J. Phys. Chem. A* **2002**, *106*, 157 – 164; h) M. Aschi, F. Mazza, A. Di Nola, *THEOCHEM* **2002**, *587*, 177 – 188; i) E. Grunwald, S. Highsmith, T.-P. I in *Ions and Ion Pairs in Organic Reactions, Vol. 2* (Ed.: M. Szwarc), Wiley, New York, **1974**, pp. 447 – 519.
[274] C. Chipot, B. Maigret, D. A. Pearlman, P. A. Kollman, *J. Am. Chem. Soc.* **1996**, *118*, 2998 – 3005.
[275] Y. Mo, G. Subramanian, J. Gao, D. M. Ferguson, *J. Am. Chem. Soc.* **2002**, *124*, 4832 – 4837.
[276] S. Rensing, M. Arendt, A. Springer, T. Grawe, T. Schrader, *J. Org. Chem.* **2001**, *66*, 5814 – 5821.
[277] S. Hashimoto, S. Ikuta, *THEOCHEM* **1999**, *468*, 85 – 94.
[278] C. A. Hunter, C. M. R. Low, C. Rotger, J. G. Vinter, C. Zonta, *Proc. Natl. Acad. Sci. USA* **2002**, *99*, 4873 – 4876.
[279] C. W. Davies, *Ion Association*, Butterworth, London, **1962**.
[280] a) P. B. Savage, S. K. Holmgren, S. H. Gellman, *J. Am. Chem. Soc.* **1994**, *116*, 4069 – 4070; b) R. Arnecke, V. Böhmer, R. Cacciapaglia, A. Dalla Cort, L. Mandolini, *Tetrahedron* **1997**, *53*, 4901 – 4908.
[281] A. Arduini, W. M. McGregor, D. Paganuzzi, A. Pochini, A. Secchi, F. Ugozzoli, R. Ungaro, *J. Chem. Soc. Perkin Trans. 2* **1996**, 839 – 846.
[282] M. T. Reetz in *Comprehensive Supramolecular Chemistry, Vol. 2* (Ed.: F. Vögtle), Pergamon, Oxford, **1996**, pp. 553 – 562.
[283] a) K.-S. Jeong, K.-M. Hahn, Y. L. Cho, *Tetrahedron Lett.* **1998**, *39*, 3779 – 3782; b) V. Böhmer, A. Dalla Cort, L. Mandolini, *J. Org. Chem.* **2001**, *66*, 1900 – 1902.
[284] S. Bartoli, S. Roelens, *J. Am. Chem. Soc.* **1999**, *121*, 11 908 – 11 909.
[285] S. Bartoli, S. Roelens, *J. Am. Chem. Soc.* **2002**, *124*, 8307 – 8315.
[286] G. De Iasi, B. Masci, *Tetrahedron Lett.* **1993**, *34*, 6635 – 6638.
[287] It is worth noting that the anion's role often extends beyond modulating the electrostatics of the cation. Kubik and coworkers have shown that, upon complexation of a variety of *n*-butyltrimethylammonium salts by their cyclic peptide hosts,[128,254,264,265] a remarkable 10^3–10^4-fold cation binding enhancement is observed. This result is attributable to binding of the anion to the host that results in conformational changes that preorganize the host for cation binding, as well as simultaneous binding of the cation and anion to the host in a favorable position for attractive Coulombic interactions. These types of allosteric phenomena appear to be quite universal in cation–π host–guest solution studies.
[288] a) C. L. Nandi, J. Singh, J. M. Thornton, *Protein Eng.* **1993**, *6*, 247 – 259.
[289] J. P. Gallivan, D. A. Dougherty, *J. Am. Chem. Soc.* **2000**, *122*, 870 – 874.
[290] E. C. Meng, P. Cieplak, J. W. Caldwell, P. A. Kollman, *J. Am. Chem. Soc.* **1994**, *116*, 12 061 – 12 062.
[291] A. M. de Vos, M. Ultsch, A. A. Kossiakoff, *Science* **1992**, *255*, 306 – 312.
[292] O. Livnah, E. A. Stura, D. L. Johnson, S. A. Middleton, L. S. Mulcahy, N. C. Wrighton, W. J. Dower, L. K. Jolliffe, I. A. Wilson, *Science* **1996**, *273*, 464 – 471.
[293] a) Y. Inoue, S. Sugio, J. Andzelm, N. Nakamura, *J. Phys. Chem. A* **1998**, *102*, 646 – 648; b) P.-O. Norrby, T. Liljefors, *J. Am. Chem. Soc.* **1999**, *121*, 2303 – 2306; c) many of these polarization effects appear in metalloproteins; see S. D. Zaríc, D. M. Popovic, E.-W. Knapp, *Chem. Eur. J.* **2000**, *6*, 3935 – 3942.
[294] V. Dvornikovs, D. B. Smithrud, *J. Org. Chem.* **2002**, *67*, 2160 – 2167.
[295] For the influence of remote carboxylate groups on cation–π binding in the context of salt bridges, see S. M. Ngola, P. C. Kearney, S. Mecozzi, K. Russell, D. A. Dougherty, *J. Am. Chem. Soc.* **1999**, *121*, 1192 – 1201.
[296] a) R. L. Woodin, J. L. Beauchamp, *J. Am. Chem. Soc.* **1978**, *100*, 501 – 508; b) R. A. Kumpf, D. A. Dougherty, *Science* **1993**, *261*, 1708 – 1710; c) A. Andersen, F. Muntean, D. Walter, C. Rue, P. B. Armentrout, *J. Phys. Chem. A* **2000**, *104*, 692 – 705; d) R. Amunugama, M. T. Rodgers, *J. Phys. Chem. A* **2002**, *106*, 5529 – 5539.
[297] J. Sunner, K. Nishizawa, P. Kebarle, *J. Phys. Chem.* **1981**, *85*, 1814 – 1820.
[298] B. C. Guo, J. W. Purnell, A. W. Castleman, Jr., *Chem. Phys. Lett.* **1990**, *168*, 155 – 160.
[299] A. Gapeev, R. C. Dunbar, *J. Am. Soc. Mass Spectrom.* **2002**, *13*, 477 – 484.
[300] X-ray crystallographic studies of hexasubstituted benzene–cation complexes have shown $M^+\cdots\pi$(arene) contacts with reversed affinity trends (for example, $Cs^+ \approx Rb^+ > K^+ > Na^+$), see G. K. Fukin, S. V. Lindeman, J. K. Kochi, *J. Am. Chem. Soc.* **2002**, *124*, 8329 – 8336.

[301] a) O. M. Cabarcos, C. J. Weinheimer, J. M. Lisy, *J. Chem. Phys.* **1998**, *108*, 5151 – 5154; b) O. M. Cabarcos, C. J. Weinheimer, J. M. Lisy, *J. Chem. Phys.* **1999**, *110*, 8429 – 8435.
[302] G. W. Gokel, S. L. De Wall, E. S. Meadows, *Eur. J. Org. Chem.* **2000**, 2967 – 2978.
[303] E. S. Meadows, S. L. De Wall, L. J. Barbour, G. W. Gokel, *J. Am. Chem. Soc.* **2001**, *123*, 3092 – 3107.
[304] J. Hu, L. J. Barbour, G. W. Gokel, *Proc. Natl. Acad. Sci. USA* **2002**, *99*, 5121 – 5126.
[305] a) V. Ryzhov, R. C. Dunbar, B. Cerda, C. Wesdemiotis, *J. Am. Soc. Mass Spectrom.* **2000**, *11*, 1037 – 1046; b) A. Gapeev, R. C. Dunbar, *J. Am. Chem. Soc.* **2001**, *123*, 8360 – 8365.
[306] J. M. Talley, B. A. Cerda, G. Ohanessian, C. Wesdemiotis, *Chem. Eur. J.* **2002**, *8*, 1377 – 1388.
[307] a) O. Donini, D. F. Weaver, *J. Comput. Chem.* **1998**, *19*, 1515 – 1525; b) J. Wouters, *J. Comput. Chem.* **2000**, *21*, 847 – 855.
[308] a) R. C. Dunbar, *J. Phys. Chem. A* **2000**, *104*, 8067 – 8074; b) F. M. Siu, N. L. Ma, C. W. Tsang, *J. Am. Chem. Soc.* **2001**, *123*, 3397 – 3398.
[309] S. Hoyau, K. Norrman, T. B. McMahon, G. Ohanessian, *J. Am. Chem. Soc.* **1999**, *121*, 8864 – 8875.
[310] a) J. B. Nicholas, B. P. Hay, D. A. Dixon, *J. Phys. Chem. A* **1999**, *103*, 1394 – 1400; b) P. B. Armentrout, M. T. Rodgers, *J. Phys. Chem. A* **2000**, *104*, 2238 – 2247; c) D. Feller, D. A. Dixon, J. B. Nicholas, *J. Phys. Chem. A* **2000**, *104*, 11414 – 11419; d) J. C. Amicangelo, P. B. Armentrout, *J. Phys. Chem. A* **2000**, *104*, 11420 – 11432.
[311] a) M. A. L. Eriksson, P.-Y. Morgantini, P. A. Kollman, *J. Phys. Chem. B* **1999**, *103*, 4474 – 4480; b) W.-L. Zhu, X.-J. Tan, C. M. Puah, J.-D. Gu, H.-L. Jiang, K.-X. Chen, C. E. Felder, I. Silman, J. L. Sussman, *J. Phys. Chem. A* **2000**, *104*, 9573 – 9580.
[312] J. D. Schmitt, C. G. V. Sharples, W. S. Caldwell, *J. Med. Chem.* **1999**, *42*, 3066 – 3074.
[313] R. Loewenthal, J. Sancho, A. R. Fersht, *J. Mol. Biol.* **1992**, *224*, 759 – 770.
[314] a) V. Muñoz, L. Serrano, *Nat. Struct. Biol.* **1994**, *1*, 399 – 409; b) J. Fernández-Recio, A. Vázquez, C. Civera, P. Sevilla, J. Sancho, *J. Mol. Biol.* **1997**, *267*, 184 – 197.
[315] A. Y. Ting, I. Shin, C. Lucero, P. G. Schultz, *J. Am. Chem. Soc.* **1998**, *120*, 7135 – 7136.
[316] J. Fernández-Recio, A. Romero, J. Sancho, *J. Mol. Biol.* **1999**, *290*, 319 – 330.
[317] C. A. Olson, Z. Shi, N. R. Kallenbach, *J. Am. Chem. Soc.* **2001**, *123*, 6451 – 6452.
[318] E. V. Pletneva, A. T. Laederach, D. B. Fulton, N. M. Kostic, *J. Am. Chem. Soc.* **2001**, *123*, 6232 – 6245.
[319] T. P. Burghardt, N. Juranic, S. Macura, K. Ajtai, *Biopolymers* **2002**, *63*, 261 – 272.
[320] Z. Shi, C. A. Olson, N. R. Kallenbach, *J. Am. Chem. Soc.* **2002**, *124*, 3284 – 3291.
[321] B. J. Smith, *J. Comput. Chem.* **1999**, *20*, 428 – 442.
[322] B. P. Orner, X. Salvatella, J. S. Quesada, J. de Mendoza, E. Giralt, A. D. Hamilton, *Angew. Chem.* **2002**, *114*, 125 – 127; *Angew. Chem. Int. Ed.* **2002**, *41*, 117 – 119.
[323] S. M. Ngola, D. A. Dougherty, *J. Org. Chem.* **1996**, *61*, 4355 – 4360.
[324] a) L. C. Hsieh-Wilson, P. G. Schultz, R. C. Stevens, *Proc. Natl. Acad. Sci. USA* **1996**, *93*, 5363 – 5367; b) C. Jenson, W. L. Jorgensen, *J. Am. Chem. Soc.* **1997**, *119*, 10846 – 10854; c) D. Barak, A. Ordentlich, Y. Segall, B. Velan, H. P. Benschop, L. P. A. De Jong, A. Shafferman, *J. Am. Chem. Soc.* **1997**, *119*, 3157 – 3158; d) P. C. Miklis, R. Ditchfield, T. A. Spencer, *J. Am. Chem. Soc.* **1998**, *120*, 10482 – 10489.
[325] a) P. Lakshminarasimhan, R. B. Sunoj, J. Chandrasekhar, V. Ramamurthy, *J. Am. Chem. Soc.* **2000**, *122*, 4815 – 4816; b) S. Yamada, C. Morita, *J. Am. Chem. Soc.* **2002**, *124*, 8184 – 8185.
[326] M. Rooman, J. Liévin, E. Buisine, R. Wintjens, *J. Mol. Biol.* **2002**, *319*, 67 – 76.
[327] H. Ihm, S. Yun, H. G. Kim, J. K. Kim, K. S. Kim, *Org. Lett.* **2002**, *4*, 2897 – 2900.
[328] M. Mascal, A. Armstrong, M. D. Bartberger, *J. Am. Chem. Soc.* **2002**, *124*, 6274 – 6276.
[329] C. R. Patrick, G. S. Prosser, *Nature* **1960**, *187*, 1021.
[330] J. S. W. Overell, G. S. Pawley, *Acta Crystallogr. Sect. B* **1982**, *38*, 1966 – 1972.
[331] J. H. Williams, J. K. Cockcroft, A. N. Fitch, *Angew. Chem.* **1992**, *104*, 1666 – 1669; *Angew. Chem. Int. Ed. Engl.* **1992**, *31*, 1655 – 1657.
[332] J. A. Ripmeester, D. A. Wright, C. A. Fyfe, R. K. Boyd, *J. Chem. Soc. Faraday Trans. 2* **1978**, *74*, 1164 – 1178.
[333] a) V. B. Smith, A. G. Massey, *Tetrahedron* **1969**, *25*, 5495 – 5501; b) J. Potenza, D. Mastropaolo, *Acta Crystallogr. Sect. B* **1975**, *31*, 2527 – 2529; c) D. G. Naae, *Acta Crystallogr. Sect. B* **1979**, *35*, 2765 – 2768; d) M. I. Bruce, M. R. Snow, E. R. T. Tiekink, *Acta Crystallogr. Sect. C* **1987**, *43*, 1640 – 1641; e) T. Dahl, *Acta Chem. Scand. Ser. A* **1988**, *42*, 1 – 7; f) D. J. Parks, W. E. Piers, M. Parvez, R. Atencio, M. J. Zaworotko, *Organometallics* **1998**, *17*, 1369 – 1377; g) C. M. Beck, J. Burdeniuc, R. H. Crabtree, A. L. Rheingold, G. P. A. Yap, *Inorg. Chim. Acta* **1998**, *270*, 559 – 562; h) J. R. Gardinier, F. P. Gabbaï, *J. Chem. Soc. Dalton Trans.* **2000**, 2861 – 2865; i) J. A. C. Clyburne, T. Hamilton, H. A. Jenkins, *Cryst. Eng.* **2001**, *4*, 1 – 9; j) J. C. Collings, A. S. Batsanov, J. A. K. Howard, T. B. Marder, *Acta Crystallogr. Sect. C* **2001**, *57*, 870 – 872; k) A. S. Batsanov, J. C. Collings, J. A. K. Howard, T. B. Marder, D. F. Perepichka, *Acta Crystallogr. Sect. C* **2001**, *57*, 1306 – 1307; l) A. S. Batsanov, J. A. K. Howard, T. B. Marder, E. G. Robins, *Acta Crystallogr. Sect. C* **2001**, *57*, 1303 – 1305; m) J. C. Collings, A. S. Batsanov, J. A. K. Howard, T. B. Marder, *Cryst. Eng.* **2002**, *5*, 37 – 46.
[334] J. C. Collings, K. P. Roscoe, R. L. Thomas, A. S. Batsanov, L. M. Stimson, J. A. K. Howard, T. B. Marder, *New J. Chem.* **2001**, *25*, 1410 – 1417.
[335] V. R. Vangala, A. Nangia, V. M. Lynch, *Chem. Commun.* **2002**, 1304 – 1305.
[336] T. Dahl, *Acta Chem. Scand.* **1994**, *48*, 95 – 106.
[337] J. H. Williams, *Acc. Chem. Res.* **1993**, *26*, 593 – 598.
[338] Not discussed in this chapter, although equally interesting, are the properties and behaviors of 1,3,5-trifluorobenzene derivatives that have negligible quadrupole moments. See, for example, M. I. Cabaco, Y. Danten, M. Besnard, Y. Guissani, B. Guillot, *Chem. Phys. Lett.* **1996**, *262*, 120 – 124.
[339] a) J. Vrbancich, G. L. D. Ritchie, *J. Chem. Soc. Faraday Trans. 2* **1980**, *76*, 648 – 659; b) K. E. Laidig, *Chem. Phys. Lett.* **1991**, *185*, 483 – 489; c) we mostly consider fluoroaromatic compounds with four or more fluorine atoms that have appreciably positive quadrupole moments relative to benzene, see J. Hernández-Trujillo, M. Costas, A. Vela, *J. Chem. Soc. Faraday Trans.* **1993**, *89*, 2441 – 2443.
[340] T. G. Beaumont, K. M. C. Davis, *J. Chem. Soc. B* **1967**, 1131 – 1134.
[341] J. D. Laposa, M. J. McGlinchey, C. Montgomery, *Spectrochim. Acta Part A* **1983**, *39*, 863 – 866.
[342] T. G. Beaumont, K. M. C. Davis, *Nature* **1968**, *218*, 865.
[343] C. J. Aspley, C. Boxwell, M. L. Buil, C. L. Higgitt, C. Long, R. N. Perutz, *Chem. Commun.* **1999**, 1027 – 1028.
[344] A. P. West, Jr., S. Mecozzi, D. A. Dougherty, *J. Phys. Org. Chem.* **1997**, *10*, 347 – 350.
[345] J. Hernández-Trujillo, F. Colmenares, G. Cuevas, M. Costas, *Chem. Phys. Lett.* **1997**, *265*, 503 – 507.
[346] O. R. Lozman, R. J. Bushby, J. G. Vinter, *J. Chem. Soc. Perkin Trans. 2* **2001**, 1446 – 1452.
[347] S. Lorenzo, G. R. Lewis, I. Dance, *New J. Chem.* **2000**, *24*, 295 – 304.

[348] W. J. Gaw, F. L. Swinton, *Nature* **1966**, *212*, 283 – 284.
[349] W. J. Gaw, F. L. Swinton, *Trans. Faraday Soc.* **1968**, *64*, 2023 – 2034.
[350] a) M. E. Baur, C. M. Knobler, D. A. Horsma, P. Perez, *J. Phys. Chem.* **1970**, *74*, 4594 – 4596; b) C. L. Watkins, W. S. Brey, Jr., *J. Phys. Chem.* **1970**, *74*, 235 – 240; c) K. Tanabe, J. Hiraishi, *J. Raman Spectrosc.* **1982**, *12*, 274 – 277; d) E. Bartsch, H. Bertagnolli, P. Chieux, *Ber. Bunsen-Ges.* **1986**, *90*, 34 – 46; e) T. Tassaing, Y. Danten, M. Besnard, E. Zoïdis, J. Yarwood, *Chem. Phys.* **1994**, *184*, 225 – 231.
[351] M. Neelakandan, D. Pant, E. L. Quitevis, *Chem. Phys. Lett.* **1997**, *265*, 283 – 292.
[352] F. Cozzi, F. Ponzini, R. Annunziata, M. Cinquini, J. S. Siegel, *Angew. Chem.* **1995**, *107*, 1092 – 1093; *Angew. Chem. Int. Ed. Engl.* **1995**, *34*, 1019 – 1020.
[353] X. Fei, Y.-Z. Hui, V. Rüdiger, H.-J. Schneider, *J. Phys. Org. Chem.* **1997**, *10*, 305 – 310.
[354] S. M. Ngola, D. A. Dougherty, *J. Org. Chem.* **1998**, *63*, 4566 – 4567.
[355] R. Amunugama, M. T. Rodgers, *J. Phys. Chem. A* **2002**, *106*, 9092 – 9103.
[356] For related effects borne out in catenation formation, see R. Ballardini, V. Balzani, A. Credi, C. L. Brown, R. E. Gillard, M. Montalti, D. Philp, J. F. Stoddart, M. Venturi, A. J. P. White, B. J. Williams, D. J. Williams, *J. Am. Chem. Soc.* **1997**, *119*, 12503 – 12513.
[357] H. Adams, J.-L. J. Blanco, G. Chessari, C. A. Hunter, C. M. R. Low, J. M. Sanderson, J. G. Vinter, *Chem. Eur. J.* **2001**, *7*, 3494 – 3503.
[358] J. S. Brennan, N. M. D. Brown, F. L. Swinton, *J. Chem. Soc. Faraday Trans. 1* **1974**, *70*, 1965 – 1970.
[359] U. H. F. Bunz, V. Enkelmann, *Chem. Eur. J.* **1999**, *5*, 263 – 266.
[360] R. E. Gillard, J. F. Stoddart, A. J. P. White, B. J. Williams, D. J. Williams, *J. Org. Chem.* **1996**, *61*, 4504 – 4505.
[361] M. C. Etter, *Acc. Chem. Res.* **1990**, *23*, 120 – 126.
[362] F. Ponzini, R. Zagha, K. Hardcastle, J. S. Siegel, *Angew. Chem.* **2000**, *112*, 2413 – 2415; *Angew. Chem. Int. Ed.* **2000**, *39*, 2323 – 2325.
[363] G. W. Coates, A. R. Dunn, L. M. Henling, D. A. Dougherty, R. H. Grubbs, *Angew. Chem.* **1997**, *109*, 290 – 293; *Angew. Chem. Int. Ed. Engl.* **1997**, *36*, 248 – 251.
[364] a) G. Wegner, *Z. Naturforsch. B* **1969**, *24*, 824 – 832; b) V. Enkelmann, *Adv. Polym. Sci.* **1984**, *63*, 91 – 136.
[365] G. W. Coates, A. R. Dunn, L. M. Henling, J. W. Ziller, E. B. Lobkovsky, R. H. Grubbs, *J. Am. Chem. Soc.* **1998**, *120*, 3641 – 3649.
[366] For related recent studies on the photodimerization of (1*E*,3*E*)-1-phenyl-4-pentafluorophenylbuta-1,3-dienes, see K. Vishnumurthy, T. N. G. Row, K. Venkatesan, *Photochem. Photobiol. Sci.* **2002**, *1*, 427 – 430.
[367] a) M. L. Renak, G. P. Bartholomew, S. Wang, P. J. Ricatto, R. J. Lachicotte, G. C. Bazan, *J. Am. Chem. Soc.* **1999**, *121*, 7787 – 7799; b) G. P. Bartholomew, X. Bu, G. C. Bazan, *Chem. Mater.* **2000**, *12*, 2311 – 2318; c) W. J. Feast, P. W. Lövenich, H. Puschmann, C. Taliani, *Chem. Commun.* **2001**, 505 – 506.
[368] a) P. Kirsch, K. Tarumi, *Angew. Chem.* **1998**, *110*, 501 – 506; *Angew. Chem. Int. Ed.* **1998**, *37*, 484 – 489; b) M. Weck, A. R. Dunn, K. Matsumoto, G. W. Coates, E. B. Lobkovsky, R. H. Grubbs, *Angew. Chem.* **1999**, *111*, 2909 – 2912; *Angew. Chem. Int. Ed.* **1999**, *38*, 2741 – 2745; c) C. Dai, P. Nguyen, T. B. Marder, A. J. Scott, W. Clegg, C. Viney, *Chem. Commun.* **1999**, 2493 – 2494.
[369] A. F. M. Kilbinger, R. H. Grubbs, *Angew. Chem.* **2002**, *114*, 1633 – 1636; *Angew. Chem. Int. Ed.* **2002**, *41*, 1563 – 1566.
[370] M. J. Marsella, Z.-Q. Wang, R. J. Reid, K. Yoon, *Org. Lett.* **2001**, *3*, 885 – 887.
[371] J. T. Welch, *Tetrahedron* **1987**, *43*, 3123 – 3197.
[372] D. O'Hagan, H. S. Rzepa, *Chem. Commun.* **1997**, 645 – 652.
[373] B. E. Smart, *J. Fluorine Chem.* **2001**, *109*, 3 – 11.
[374] M. Hoffmann, J. Rychlewski, *Int. J. Quantum Chem.* **2002**, *89*, 419 – 427.
[375] Numerous other perfluoroaromatic substituted inhibitors have been generated in various systems. Recent examples include: a) A. Scozzafava, C. T. Supuran, *J. Med. Chem.* **2000**, *43*, 1858 – 1865; b) A. Scozzafava, L. Menabuoni, F. Mincione, F. Briganti, G. Mincione, C. T. Supuran, *J. Med. Chem.* **2000**, *43*, 4542 – 4551; c) J. A. Watts, A. Watts, D. A. Middleton, *J. Biol. Chem.* **2001**, *276*, 43197 – 43204.
[376] The EC_{50} value is a measure of functional binding affinity; see T. Kenakin, *Trends Pharmacol. Sci.* **1999**, *20*, 400 – 405.
[377] B. C. Finzel, E. T. Baldwin, G. L. Bryant, G. F. Hess, J. W. Wilks, C. M. Trepod, J. E. Mott, V. P. Marshall, G. L. Petzold, R. A. Poorman, T. J. O'Sullivan, H. J. Schostarez, M. A. Mitchell, *Protein Sci.* **1998**, *7*, 2118 – 2126.
[378] a) J. B. Doyon, A. Jain, *Org. Lett.* **1999**, *1*, 183 – 185; b) J. B. Doyon, E. A. M. Hansen, C.-Y. Kim, J. S. Chang, D. W. Christianson, R. D. Madder, J. G. Voet, T. A. Baird, Jr., C. A. Fierke, A. Jain, *Org. Lett.* **2000**, *2*, 1189 – 1192.
[379] C.-Y. Kim, J. S. Chang, J. B. Doyon, T. T. Baird, Jr., C. A. Fierke, A. Jain, D. W. Christianson, *J. Am. Chem. Soc.* **2000**, *122*, 12125 – 12134.
[380] C.-Y. Kim, P. P. Chandra, A. Jain, D. W. Christianson, *J. Am. Chem. Soc.* **2001**, *123*, 9620 – 9627.
[381] K. M. Guckian, B. A. Schweitzer, R. X. F. Ren, C. J. Sheils, P. L. Paris, D. C. Tahmassebi, E. T. Kool, *J. Am. Chem. Soc.* **1996**, *118*, 8182 – 8183.
[382] V. R. Thalladi, H.-C. Weiss, D. Bläser, R. Boese, A. Nangia, G. R. Desiraju, *J. Am. Chem. Soc.* **1998**, *120*, 8702 – 8710.
[383] a) H. Plenio, *Chem. Rev.* **1997**, *97*, 3363 – 3384; b) H. Takemura, H. Kariyazono, M. Yasutake, N. Kon, K. Tani, K. Sako, T. Shinmyozu, T. Inazu, *Eur. J. Org. Chem.* **2000**, 141 – 148.
[384] I. Alkorta, I. Rozas, J. Elguero, *J. Org. Chem.* **1997**, *62*, 4687 – 4691.
[385] I. Alkorta, I. Rozas, J. Elguero, *J. Am. Chem. Soc.* **2002**, *124*, 8593 – 8598.
[386] a) J. P. Gallivan, D. A. Dougherty, *Org. Lett.* **1999**, *1*, 103 – 105; b) Y. Danten, T. Tassaing, M. Besnard, *J. Phys. Chem. A* **1999**, *103*, 3530 – 3534; c) I. Alkorta, I. Rozas, M. L. Jimeno, J. Elguero, *Struct. Chem.* **2001**, *12*, 459 – 464.
[387] C. J. Wormald, B. Wurzberger, *Phys. Chem. Chem. Phys.* **2000**, *2*, 5133 – 5137.
[388] N. Kato, K. Endo, T. Tada, *J. Mol. Struct.* **2002**, *602*, 373 – 379.
[389] J. R. Grover, G. Hagenow, E. A. Walters, *J. Chem. Phys.* **1992**, *97*, 628 – 642.
[390] R. S. Morgan, C. E. Tatsch, R. H. Gushard, J. M. McAdon, P. K. Warme, *Int. J. Peptide Protein Res.* **1978**, *11*, 209 – 217.
[391] R. Diamond, *J. Mol. Biol.* **1974**, *82*, 371 – 391.
[392] a) L. G. Augenstine, C. A. Ghiron, *Proc. Natl. Acad. Sci. USA* **1961**, *47*, 1530 – 1547; b) K. Dose, B. Rajewsky, *Photochem. Photobiol.* **1962**, *1*, 181 – 189; c) L. Augenstein, P. Riley, *Photochem. Photobiol.* **1964**, *3*, 353 – 367; d) K. L. Grist, T. Taylor, L. G. Augenstein, *Radiat. Res.* **1965**, *26*, 198 – 210; e) K. Dose, *Photochem. Photobiol.* **1967**, *6*, 437 – 443; f) S. Risi, K. Dose, T. K. Rathinasamy, L. Augenstein, *Photochem. Photobiol.* **1967**, *6*, 423 – 436; g) S. Arian, M. Benjamini, J. Feitelson, G. Stein, *Photochem. Photobiol.* **1970**, *12*, 481 – 487; h) J. Feitelson, E. Hayon, *Photochem. Photobiol.* **1973**, *17*, 265 – 274; i) D. V. Bent, E. Hayon, *J. Am. Chem. Soc.* **1975**, *97*, 2599 – 2606.
[393] a) Z. Li, W. E. Lee, W. C. Galley, *Biophys. J.* **1989**, *56*, 361 – 367; b) G. Krause, A. Holmgren, *J. Biol. Chem.* **1991**, *266*, 4056 – 4066; c) Y. Chen, M. D. Barkley, *Biochemistry* **1998**, *37*, 9976 – 9982; d) M. T. Neves-Petersen, Z. Gryczynski, J. Lakowicz, P. Fojan, S. Pedersen, E. Petersen, S. B. Petersen, *Protein Sci.* **2002**, *11*, 588 – 600.

[394] K. S. C. Reid, P. F. Lindley, J. M. Thornton, *FEBS Lett.* **1985**, *190*, 209 – 213.
[395] a) U. Samanta, D. Pal, P. Chakrabarti, *Proteins Struct. Funct. Genet.* **2000**, *38*, 288 – 300; b) D. Pal, P. Chakrabarti, *J. Biomol. Struct. Dyn.* **2001**, *19*, 115 – 128.
[396] D. Pal, P. Chakrabarti, *J. Biomol. Struct. Dyn.* **1998**, *15*, 1059 – 1072.
[397] For S–H/π interactions in crystal structures, see ref. [74], pp. 253–265.
[398] For a general structural and conformational analysis of cysteines in proteins, see M. T. N. Petersen, P. H. Jonson, S. B. Petersen, *Protein Eng.* **1999**, *12*, 535 – 548.
[399] W. D. Cornell, P. Cieplak, C. I. Bayly, I. R. Gould, K. M. Merz, Jr., D. M. Ferguson, D. C. Spellmeyer, T. Fox, J. W. Caldwell, P. A. Kollman, *J. Am. Chem. Soc.* **1995**, *117*, 5179 – 5197.
[400] The value of 2.6 kcal mol^{-1} is greater than for either N–H or O–H/π interactions (see Section 5) because of the increased polarizability of the sulfur atom and the enhanced acidity of the S–H group.
[401] J. Pranata, *Bioorg. Chem.* **1997**, *25*, 213 – 219.
[402] B. V. Cheney, M. W. Schulz, J. Cheney, *Biochim. Biophys. Acta* **1989**, *996*, 116 – 124.
[403] T. R. Ioerger, C. Du, D. S. Linthicum, *Mol. Immunol.* **1999**, *36*, 373 – 386.
[404] D. H. Fremont, W. A. Hendrickson, P. Marrack, J. Kappler, *Science* **1996**, *272*, 1001 – 1004.
[405] G. Némethy, H. A. Scheraga, *Biochem. Biophys. Res. Commun.* **1981**, *98*, 482 – 487.
[406] R. J. Zauhar, C. L. Colbert, R. S. Morgan, W. J. Welsh, *Biopolymers* **2000**, *53*, 233 – 248.
[407] This orientation differs from those commonly found from model computational experiments and in protein crystal structures.
[408] Searches were performed using Relibase V. 1.1 (see ref. [69]). Results will be reported in more detail in a future publication.
[409] F. Mancia, G. A. Smith, P. R. Evans, *Biochemistry* **1999**, *38*, 7999 – 8005.
[410] L. Maveyraud, I. Massova, C. Birck, K. Miyashita, J.-P. Samama, S. Mobashery, *J. Am. Chem. Soc.* **1996**, *118*, 7435 – 7440.
[411] M. Yun, C.-G. Park, J.-Y. Kim, C. O. Rock, S. Jackowski, H.-W. Park, *J. Biol. Chem.* **2000**, *275*, 28093 – 28099.
[412] E. A. Meyer, R. Brenk, R. K. Castellano, M. Furler, G. Klebe, F. Diederich, *ChemBioChem* **2002**, *3*, 250 – 253.
[413] F. Alber, O. Kuonen, L. Scapozza, G. Folkers, P. Carloni, *Proteins Struct. Funct. Genet.* **1998**, *31*, 453 – 459.
[414] B. D. Pilger, R. Perozzo, F. Alber, C. Wurth, G. Folkers, L. Scapozza, *J. Biol. Chem.* **1999**, *274*, 31967 – 31973.
[415] a) K. Wild, T. Bohner, A. Aubry, G. Folkers, G. E. Schulz, *FEBS Lett.* **1995**, *368*, 289 – 292; b) K. Wild, T. Bohner, G. Folkers, G. E. Schulz, *Protein Sci.* **1997**, *6*, 2097 – 2106.
[416] S. Pakhomova, M. Kobayashi, J. Buck, M. E. Newcomer, *Nat. Struct. Biol.* **2001**, *8*, 447 – 451.
[417] C. Zubieta, X.-Z. He, R. A. Dixon, J. P. Noel, *Nat. Struct. Biol.* **2001**, *8*, 271 – 279.
[418] A. Ruf, V. Rolli, G. de Murcia, G. E. Schulz, *J. Mol. Biol.* **1998**, *278*, 57 – 65.
[419] a) B. Masjost, P. Ballmer, E. Borroni, G. Zürcher, F. K. Winkler, R. Jakob-Roetne, F. Diederich, *Chem. Eur. J.* **2000**, *6*, 971 – 982; b) C. Lerner, A. Ruf, V. Gramlich, B. Masjost, G. Zürcher, R. Jakob-Roetne, E. Borroni, F. Diederich, *Angew. Chem.* **2001**, *113*, 4164 – 4166; *Angew. Chem. Int. Ed.* **2001**, *40*, 4040 – 4042.
[420] J. Vidgren, L. A. Svensson, A. Liljas, *Nature* **1994**, *368*, 354 – 358.
[421] a) B. L. Bodner, L. M. Jackman, R. S. Morgan, *Biophys. J.* **1977**, *17*, A57; b) B. L. Bodner, L. M. Jackman, R. S. Morgan, *Biochem. Biophys. Res. Commun.* **1980**, *94*, 807 – 813.
[422] The similar association strength demonstrated for THF and 1-methylnaphthalene ($\Delta H \approx -0.9$ kcal mol^{-1}) also suggests that the sulfur atom does not participate in the binding; the oxygen atom is considerably more electronegative and less polarizable than the sulfur atom, which suggests that the main attractive interactions involved are between the polarized CH_2 groups and the aromatic ring.
[423] For an intriguing example of a short sulfur–arene contact that influences the reactivity in disubstituted dibenzothiophene chemistry, see T. Kimura, N. Furukawa, *Tetrahedron Lett.* **1995**, *36*, 1079 – 1080.
[424] M. Lebl, E. E. Sugg, V. J. Hruby, *Int. J. Pept. Protein Res.* **1987**, *29*, 40 – 45.
[425] E. C. Breinlinger, C. J. Keenan, V. M. Rotello, *J. Am. Chem. Soc.* **1998**, *120*, 8606 – 8609.
[426] V. M. Rotello, *Heteroat. Chem.* **1998**, *9*, 605 – 606.
[427] a) A. R. Viguera, L. Serrano, *Biochemistry* **1995**, *34*, 8771 – 8779; b) B. J. Stapley, C. A. Rohl, A. J. Doig, *Protein Sci.* **1995**, *4*, 2383 – 2391.
[428] N. Yamaotsu, I. Moriguchi, S. Hirono, *Biochim. Biophys. Acta* **1993**, *1203*, 243 – 250.
[429] D. S. Spencer, W. E. Stites, *J. Mol. Biol.* **1996**, *257*, 497 – 499.
[430] M. L. Ludwig, K. A. Pattridge, A. L. Metzger, M. M. Dixon, M. Eren, Y. Feng, R. P. Swenson, *Biochemistry* **1997**, *36*, 1259 – 1280.
[431] L. J. Druhan, R. P. Swenson, *Biochemistry* **1998**, *37*, 9668 – 9678.
[432] For an example of a mutational study involving a cytochrome c enzyme that does not show a binding enhancement upon sulfur introduction, see D. S. Auld, G. B. Young, A. J. Saunders, D. F. Doyle, S. F. Betz, G. J. Pielak, *Protein Sci.* **1993**, *2*, 2187 – 2197.
[433] a) B. D. Palmer, S. Trumpp-Kallmeyer, D. W. Fry, J. M. Nelson, H. D. Hollis Showalter, W. A. Denny, *J. Med. Chem.* **1997**, *40*, 1519 – 1529; b) P. Traxler, J. Green, H. Mett, U. Séquin, P. Furet, *J. Med. Chem.* **1999**, *42*, 1018 – 1026; c) J. Ren, C. Nichols, L. E. Bird, T. Fujiwara, H. Sugimoto, D. I. Stuart, D. K. Stammers, *J. Biol. Chem.* **2000**, *275*, 14316 – 14320.
[434] Since submission of the manuscript several new articles related to this review have appeared: a) "Anion–π Interactions: Do They Exist?": D. Quiñonero, C. Garau, C. Rotger, A. Frontera, P. Ballester, A. Costa, P. M. Deya, *Angew. Chem.* **2002**, *114*, 3539 – 3542; *Angew. Chem. Int. Ed.* **2002**, *41*, 3389 – 3392; b) "σ-Donor, π-Donor, and anion complexation in π-complexation of alkali metal cations": J. Hu, L. J. Barbour, G. W. Gokel, *Chem. Commun.* **2002**, 1808 – 1809; c) "Aromatic interactions in model systems": M. L. Waters, *Curr. Opin. Chem. Biol.* **2002**, *6*, 736 – 741; d) "Comparison of the nature of π and conventional H-bonds: a theoretical investigation": P. Tarakeshwar, K. S. Kim, *J. Mol. Struct.* **2002**, *615*, 227 – 238; e) "Anion Effects on the Recognition of Ion Pairs by Calix[4]arene-Based Heteroditopic Receptors": A. Arduini, E. Brindani, G. Giorgi, A. Pochini, A. Secchi, *J. Org. Chem.* **2002**, *67*, 6188 – 6194; f) "The Influence of Substituents on Cation-π Interactions. 4. Absolute Binding Energies of Alkali Metal Cation-Phenol Complexes Determined by Threshold Collision-Induced Dissociation and Theoretical Studies": R. Amunugama, M. T. Rodgers, *J. Phys. Chem. A* **2002**, *106*, 9718 – 9728; g) "The Indole Side Chain of Tryptophan as a Versatile π-Donor": J. Hu, L. J. Barbour, G. W. Gokel, *J. Am. Chem. Soc.* **2002**, *124*, 10940 – 10941; h) "A Perturbed pK_a at the Binding Site of the Nicotinic Acetylcholine Receptor: Implications for Nicotinic Binding": E. J. Petersson, A. Choi, D. S. Dahan, H. A. Lester, D. A. Dougherty, *J. Am. Chem. Soc.* **2002**, *124*, 12662 – 12663; i) "Comparison of Various Types of Hydrogen Bonds Involving Aromatic Amino Acids": S. Scheiner, T. Kar, J. Pattanayak, *J. Am. Chem. Soc.* **2002**, *124*, 13257 – 13264; j) "Simple Cation–π Interaction between a Phenyl Ring and a Protonated Amine Stabilizes an α-Helix in Water": L. K. Tsou,

C. D. Tatko, M. L. Waters, *J. Am. Chem. Soc.* **2002**, *124*, 14917–14921; k) "Arene–perfluoroarene interactions in crystal engineering 8: structures of 1:1 complexes of hexafluorobenzene with fused-ring polyaromatic hydrocarbons": J. C. Collings, K. P. Roscoe, E. G. Robins, A. S. Batsanov, L. M. Stimson, J. A. K. Howard, S. J. Clark, T. B. Marder, *New J. Chem.* **2002**, *26*, 1740–1746; l) "Analysis of the π-π Stacking Interactions between the Aminoglycoside Antibiotic Kinase APH(3′)-IIIa and Its Nucleotide Ligands": D. B. Boehr, A. R. Farley, G. D. Wright, J. R. Cox, *Chem. Biol.* **2002**, *9*, 1209–1217; m) "Aromatic Side-Chain Interactions in Proteins. 1. Main Structural Features": A. Thomas, R. Meurisse, B. Charloteaux, R. Brasseur, *Proteins Struct. Funct. Genet.* **2002**, *48*, 628–634; n) "The C–H/π bonds: Strength, identification, and hydrogen-bonded nature: a theoretical study" J. J. Novoa, F. Mota, *Chem. Phys. Lett.* **2000**, *318*, 345—354.

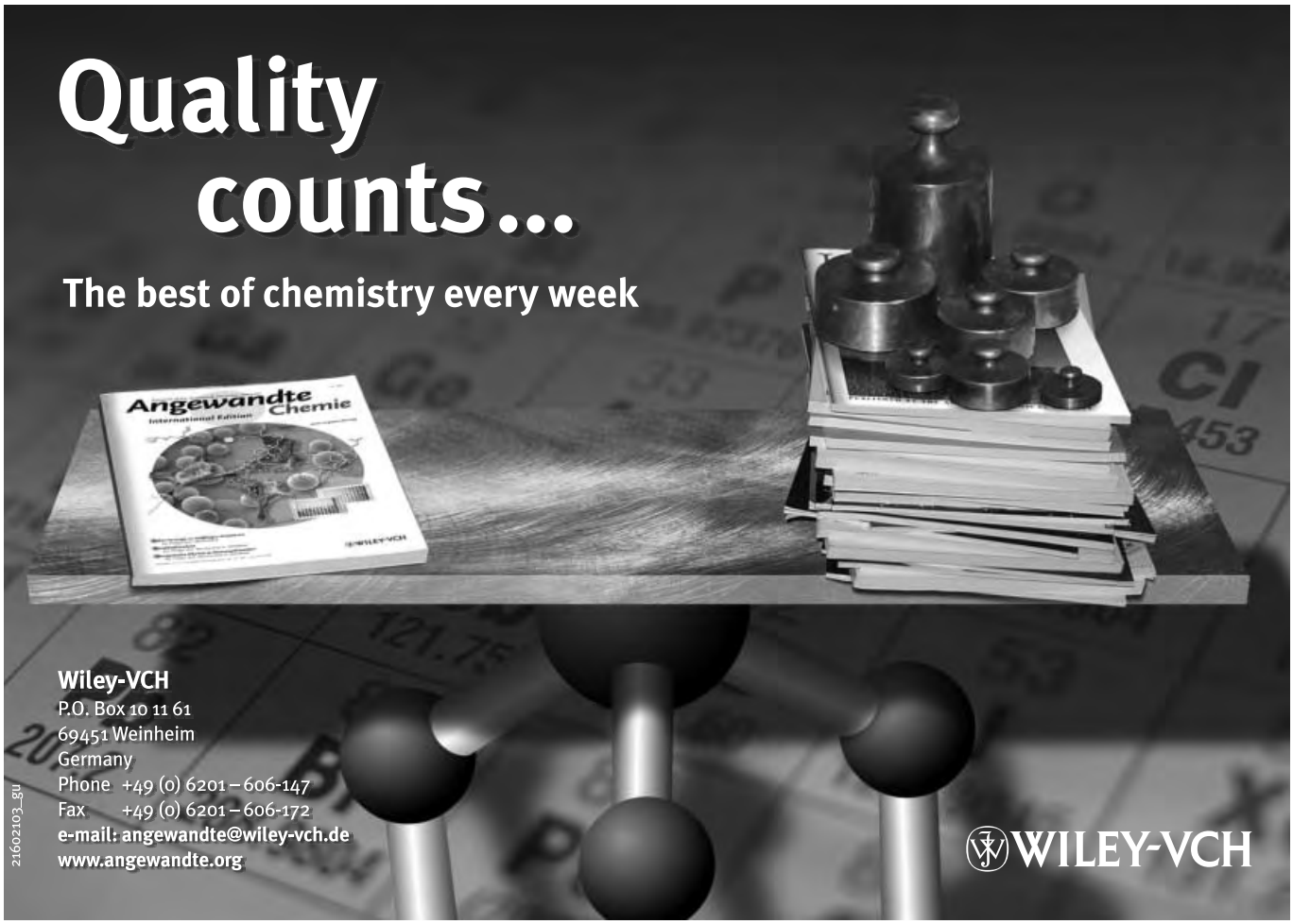

Communications

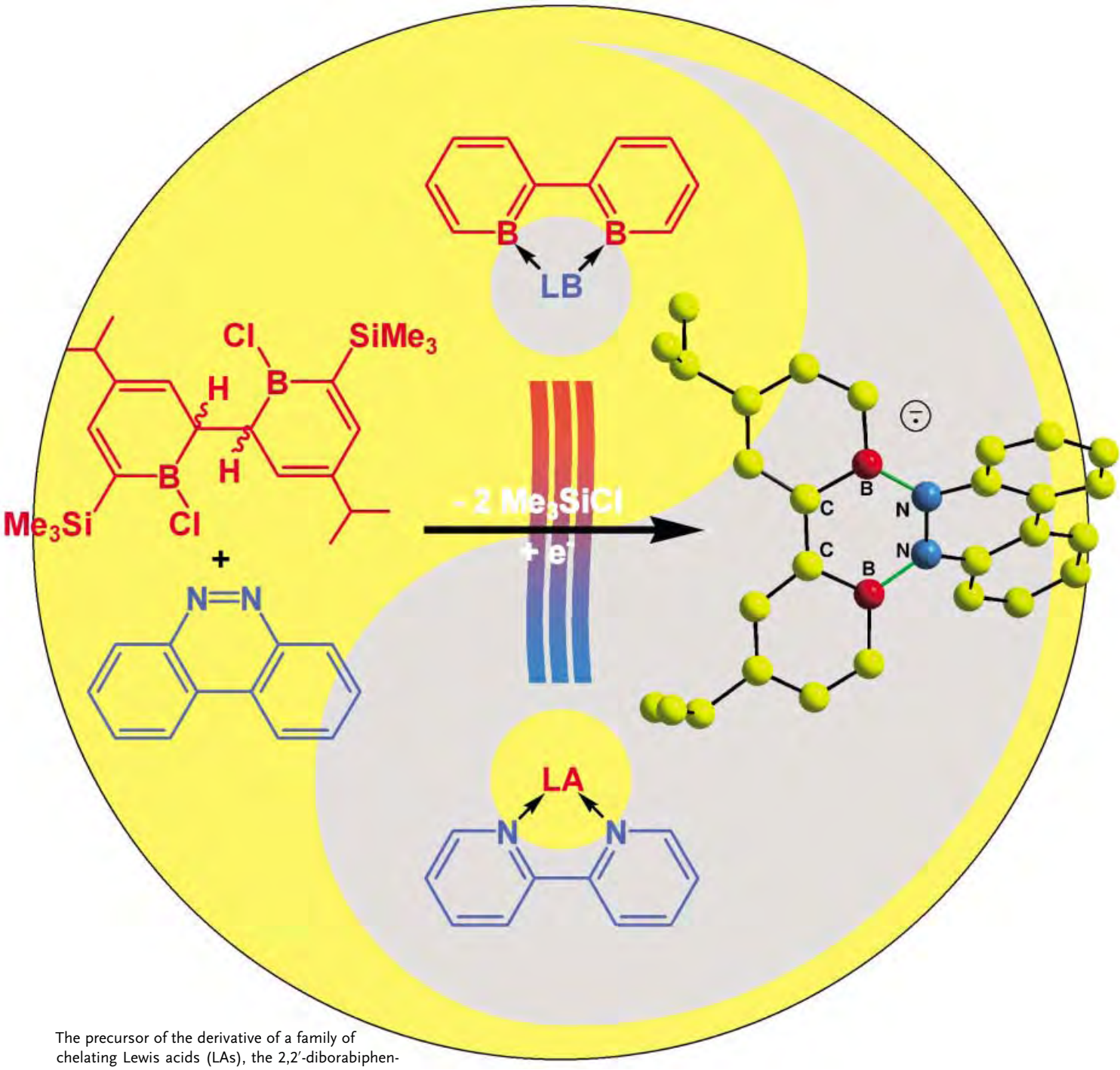

The precursor of the derivative of a family of chelating Lewis acids (LAs), the 2,2′-diborabiphenyls, is shown. These boron analogues of the quintessential Lewis base 2,2′-bipyridine form neutral B_2N_2 heterocycles upon treatment with a difunctional Lewis base (LB), and can be reduced to give a radical anion salt that has been structurally characterized. For more information see the Communication by Piers and co-workers on the following pages...

 © 2003 Wiley-VCH Verlag GmbH & Co. KGaA, Weinheim 1433-7851/03/4211-1251 $ 20.00+.50/0

Lewis Acid Analogues of Bipyridine

2,2′-Diborabiphenyl: A Lewis Acid Analogue of 2,2′-Bipyridine**

David J. H. Emslie, Warren E. Piers, and Masood Parvez*

Chelating Lewis bases are indispensable chemical tools as ligands for Lewis acidic transition metals, and the 2,2′-bipyridine family of ligands (**I**) is among the most important.[1] Conversely, chelating Lewis acids that act as reverse ligands

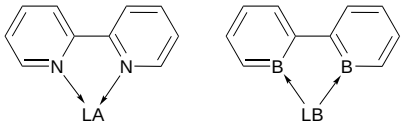

I **II**

for anionic centers or bifunctional Lewis bases are less common.[2] Given the success of **I** as a bidentate ligand, we became interested in its boron analogue **II** as a potential chelating Lewis acid towards anionic and neutral Lewis bases. While the former holds promise for preparing novel anionic heterocycles and boratabiphenyl ligands for transition metals,[3] use of neutral bifunctional nitrogen Lewis bases could lead to B_2N_2 diboraarene adducts which are isoelectronic with all-carbon polycyclic aromatic hydrocarbons (PAHs).[4] Although PAHs are of fundamental interest for probing aromaticity,[5] recent interest in PAHs stems from potential applications in materials chemistry.[6] B_2N_2 analogues would, in all likelihood, exhibit optical and redox properties that are markedly different from their parent hydrocarbons, because of the polarization inherent to such structures. Herein we report the synthesis of some Lewis base adducts of a derivative of **II** that includes bifunctional pyridazine donors, which lead to novel heterocyclic analogues of polycyclic aromatic hydrocarbons that contain a $\{C_2B_2N_2\}$ core.

Synthesis of the precursor to the Lewis base adducts of the title molecule, the silated chlorodiborane compound **1**, was accomplished according to the chemistry shown in Scheme 1.

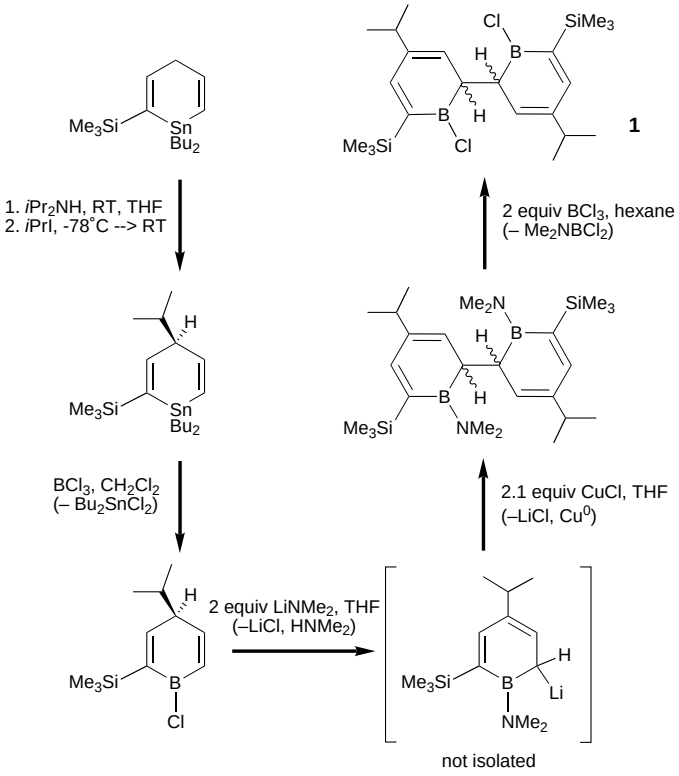

Scheme 1.

The route involves the construction and deprotonation of a six-membered boron heterocycle, followed by a C–C bond-forming coupling reaction to give the desired molecular framework. Building on methodology first used by Maier et al.[7] and then developed by Fu and co-workers,[8] the silated stannacycle shown was used as the precursor to the desired boracycle. To direct the crucial C–C bond-forming step to the position *ortho* to the boron atom, it was necessary to first block the *para* position. This was executed by quenching the lithium salt of the stannacycle with isopropyl iodide.[7b,9] This reaction proceeded with high regioselectivity (in 81 % yield), and transmetalation of the resulting isopropyl substituted stannacycle with excess BCl_3 proceeded smoothly to give the *para*-substituted chloroboracyclohexadiene in excellent yield (98 %). This material was then deprotonated to generate the organolithium species that was to be coupled in situ; treatment with two equivalents of $LiNMe_2$ is necessary to deprotonate the boracycle since one equivalent only leads to the nucleophilic displacement of the chloro group on the boron center. Although this lithium salt was not isolated, its ^{1}H NMR spectrum was very clean and consistent with the formulation given in the Scheme. Treatment with a slight excess of CuCl[10] leads to coupling in the position *ortho* to boron, and gives the diamido diborane in an 89 % overall yield (for the two steps) as a mixture of the *meso* and *rac* diastereomers. This material is readily converted back to a dichloro diborane by treatment with BCl_3, to give precursor compound **1** in 93 % yield as a dark-red oil, again consisting of a diastereomeric mixture of isomers. This oil was stable for long periods at room temperature under dry, inert atmos-

[*] Prof. W. E. Piers, Dr. D. J. H. Emslie, Dr. M. Parvez
Department of Chemistry
University of Calgary, 2500 University Drive N.W.
Calgary, Alberta, T2N 1N4 (Canada)
Fax: (+1) 403-289-9488
E-mail: wpiers@ucalgary.ca

[**] Funding for this work came from the Natural Sciences and Engineering Research Council of Canada in the form of a Discovery Grant (to W.E.P.), and an E.W.R. Steacie Fellowship (2001–2003; to W.E.P.). D.J.H.E. thanks the Alberta Ingenuity Fund for a Postdoctoral Fellowship (2002–2004). W.E.P. is the S. Robert Blair Professor of Chemistry.

Supporting information for this article is available on the WWW under http://www.angewandte.org or from the author.

 © 2003 Wiley-VCH Verlag GmbH & Co. KGaA, Weinheim 1433-7851/03/4211-1252 $ 20.00+.50/0

pheric conditions and proved a convenient starting material for subsequent transformations. Although synthetically intensive, the reactions of Scheme 1 are generally high yielding and we were able to prepare and store quantities of **1** on the gram scale. Each compound, with the exception of the lithium salts generated in situ, was isolated and fully characterized; full details can be found in the Supporting Information.

In chemistry analogous to that reported by Fu and coworkers for the preparation of borabenzenes,[4d,8] treatment of dichlorodiborane **1** with Lewis bases such as PMe_3 or pyridine leads to elimination of Me_3SiCl and a 1,3-shift of the 1,1′ hydrogen atom to give adducts **2** and **3** [Eq. (1)]. The

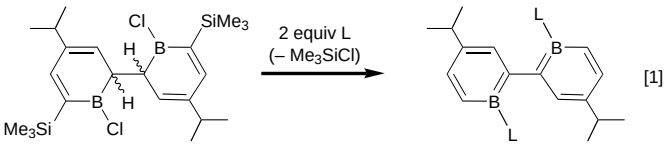

1 L = PMe_3, **2**; L = C_5H_5N, **3** [1]

bistrimethylphosphane adduct **2** is a crystalline solid and crystals suitable for X-ray analysis were obtained, which allowed us to firmly establish that the desired heterocyclic framework had been constructed. The molecular structure of **2**, along with selected metrical parameters, is given in Figure 1.[11] There are three independent molecules in the unit cell, which differ mainly in the torsion angles about the C–C bond linking the two borabenzene rings; other metrical parameters are essentially identical, so only values from one of the molecules are presented. The phosphane ligands are bonded to the trigonal-planar boron nuclei through bonds

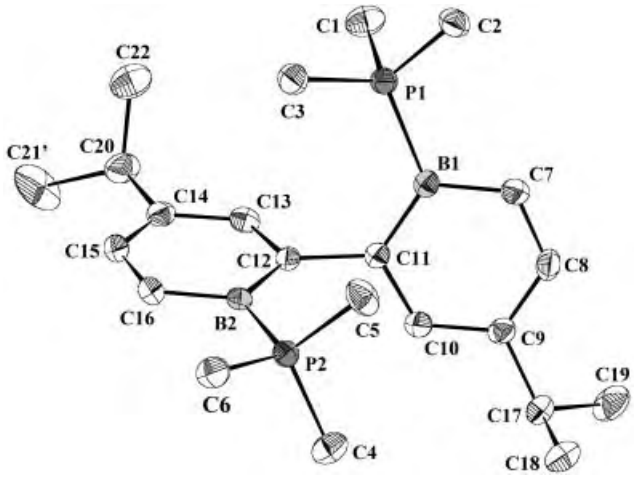

Figure 1. Molecular structure of **2**. Selected bond lengths [Å]: P1-B1 1.925(3), C7-C8 1.396(4), C7-B1 1.491(4), C8-C9 1.393(4), C9-C10 1.404(4), C10-C11 1.393(4), C11-B1 1.494(4), C11-C12 1.505(4); selected bond angles [°]: C8-C7-B1 118.6(3), C9-C8-C7 122.8(3), C8-C9-C10 118.9(3), C11-C10-C9 124.7(3), C10-C11-B1 116.6(2), C10-C11-C12 118.1(2), B1-C11-C12 125.3(2), C7-B1-C11 118.4(3), C7-B1-P1 117.0(2), C11-B1-P1 124.6(2); selected torsion angles [°]: B1-C11-C12-C13 70.5(4), B1-C11-C12-B2 −107.0(3).

which are slightly longer (1.925(4) Å) than that found in the trimethylphosphane adduct of borabenzene (1.900(8) Å).[4] The two borabenzene rings are joined at C11 and C12, which places the boron atoms in the 2 and 2′ positions as desired. The rings are twisted by about 107° such that the boron atoms are pointing in opposite directions, which is the most sensible steric arrangement for the monodentate phosphane base.

The pyridine adduct **3** is also easily prepared and is a B_2N_2 analogue of the aromatic hydrocarbon *ortho*-quaterphenyl. In contrast to yellow **2**, bispyridine adduct **3** is strongly purple in color ($\lambda_{max}(CH_2Cl_2) = 504$ nm, $\varepsilon = 2 \times 10^3\ mol^{-1}\,dm^3\,cm^{-1}$), which suggests extended conjugation throughout the four contiguous aromatic rings. The synthesis of other B_2N_2 congeners of aromatic hydrocarbons can be realized by making use of the chelating ability of the 2,2′-diborabiphenyl framework. Reaction of **1** with bifunctional nitrogen bases such as pyridazine or benzo[*c*]cinnoline similarly leads to the loss of Me_3SiCl and the generation of the novel heterocyclic compounds **4** and **5**, which contain a $\{C_2B_2N_2\}$ molecular core, in good yields (Scheme 2). These compounds are analogues of the polycyclic aromatic hydrocarbons triphenylene and dibenzo[*g*,*p*]chrysene, respectively, and are intensely colored with strong charge-transfer absorptions (**4**: deep red, $\lambda_{max}(CH_2Cl_2) = 509$ and 545 nm, $\varepsilon = 1.6 \times 10^4$ and $2.0 \times 10^4\ mol^{-1}\,dm^3\,cm^{-1}$; **5**: deep red, $\lambda_{max}(CH_2Cl_2) = 501$ nm, $\varepsilon = 1.8 \times 10^4\ mol^{-1}\,dm^3\,cm^{-1}$). Ab initio molecular-orbital computations carried out using MacSpartan Plus at the 6-31G* level on the unsubstituted parent of triphenylene analogue **4** indicate that the HOMO is associated with the pyridazine part of the molecule, while the LUMO is localized largely on the 2,2′-diborabiphenyl moiety. These absorptions thus presumably arise through charge transfer of an electron from the HOMO to the LUMO, a notion supported by the observed shift in the value of λ_{max} to higher energies when the spectrum of **5** was acquired in less polar solvents ($\lambda_{max} = 499$ and 493 nm in THF and hexane, respectively).

The synthesis of compounds **4** and **5** demonstrates the ability of **1** to act as a precursor for a potentially wide variety of PAH analogues with novel optical[12] and redox[13] proper-

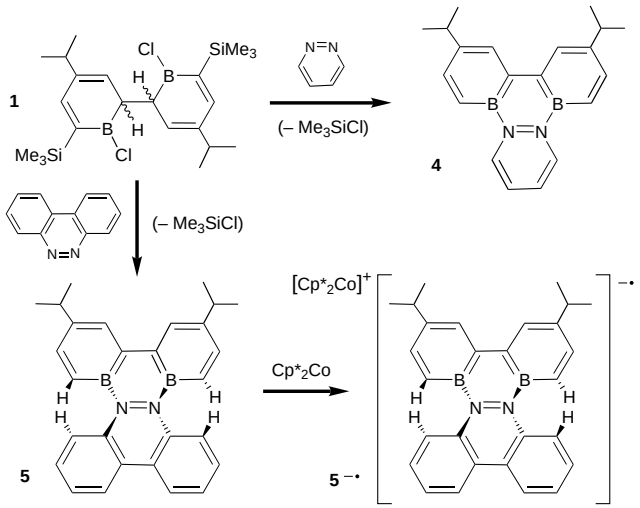

Scheme 2.

 © 2003 Wiley-VCH Verlag GmbH & Co. KGaA, Weinheim 1433-7851/03/4211-1253 $ 20.00+.50/0

ties. For example, cyclic voltammetry experiments on these compounds (1 mM **4** (or **5**); 0.1M NBu_4PF_6, THF, 20 $mV\,s^{-1}$, potentials relative to a saturated calomel electrode (SCE) using Cp^*_2Fe as an internal standard ($Cp^* = \eta^5$-C_5Me_5)) show two reversible one-electron reductions for each compound (**4**: $E_{1/2} = -1.25$ V, -1.85 V; **5**: $E_{1/2} = -1.03$ V, -1.45 V). The former compound is harder to reduce than the dibenzo[*g,p*]-chrysene analogue as it most likely has a planar geometry, whereas **5** probably assumes a less aromatic, twisted geometry resulting from steric interactions between the 3,3′ protons of the diborabenzene moiety and the opposing 3,3′ protons of the benzo[*c*]cinnoline fragment, in analogy to the structure of the parent hydrocarbon.[14] Since addition of electrons disrupts the aromaticity of the molecules, reduction of **5** is inherently more facile than for the (presumably) planar triphenylene analogue **4**.

Indeed, compound **5** can be chemically reduced by the one-electron source Cp^*_2Co, to selectively form the radical anion of **5**, as shown in Scheme 2. The ESR spectrum of this paramagnetic species exhibits a broad signal with a g_{iso} value of 2.003 and little discernable hyperfine structure at either room temperature or 100 K. Its structure was confirmed crystallographically, and is shown in Figure 2.[15] As expected, the framework is twisted considerably about the $\{C_2B_2N_2\}$ core (note the torsion angles associated with this part of the molecule) to alleviate steric interactions between the C–H groups of C22/C33 and C31/C42. The B–N bond lengths of 1.466(4) and 1.482(4) Å are shorter than that found for the pyridine adduct of borabenzene (1.56 Å)[4e] but similar to those found for amide derivatives of boratabenzene (for example, 1.45 Å for NMe_2 derivatives of boratabenzenes[16]). This suggests that some of the aromatic character of the $\{C_2B_2N_2\}$ core of the molecule is retained when an electron populates the LUMO. However, the N1–N2 bond length of 1.430(4) Å is considerably longer than this bond in free benzo[*c*]cinnoline (1.292(3) Å). While some lengthening of this bond should be expected upon coordination to a Lewis acid,[17] we note that the LUMO in the neutral complexes is slightly N–N antibonding in character. More meaningful analysis of this data will follow with structural characterization of **5** and $[\mathbf{5}]^{2-}$.

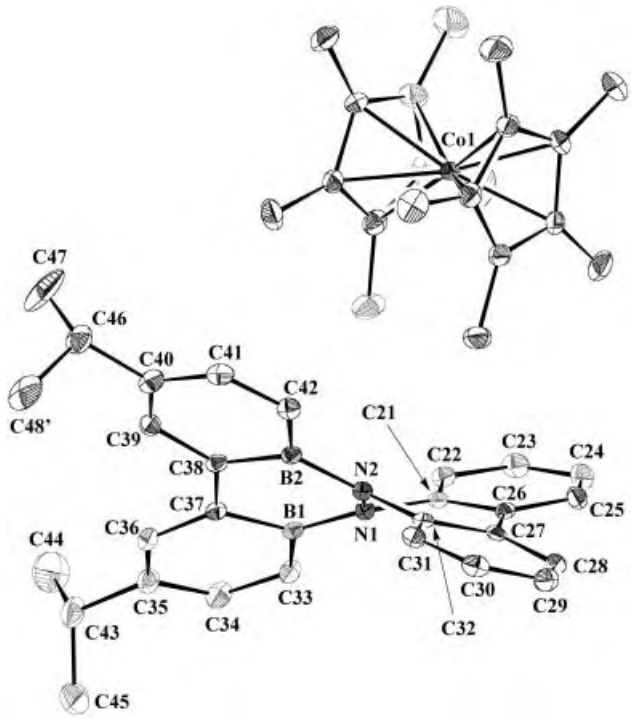

Figure 2. Molecular structure of radical anion $[\mathbf{5}]^{\cdot-}$. Selected bond lengths [Å]: B1-N1 1.466(4), B1-C33 1.519(5), B1-C37 1.527(5), B2-N2 1.482(4), B2-C38 1.511(5), B2-C42 1.513(5), N1-C21 1.413(4), N1-N2 1.430(3), N2-C32 1.402(4), C21-C26 1.405(4), C26-C27 1.460(4), C27-C32 1.412(4), C37-C38 1.444(4); selected bond angles [°]: N1-B1-C33 123.8(3), N1-B1-C37 119.2(3), C33-B1-C37 116.9(3), N2-B2-C38 119.3(3), N2-B2-C42 123.6(3), C38-B2-C42 117.1(3), C21-N1-N2 114.1(2), C21-N1-B1 126.4(3), N2-N1-B1 119.1(2), C32-N2-N1 114.8(2), C32-N2-B2 126.0(3), N1-N2-B2 118.2(2); selected torsion angles [°]: B1-C37-C38-B2 −19.3(4), B1-N1-N2-B2 −29.5(4), C21-N1-N2-C32 −46.9(3), C21-C26-C27-C32 −18.5(4), C33-B1-N1-C21 24.5(5), C42-B2-N2-C32 32.5(4).

In conclusion, we have developed a reliable synthetic route to a precursor of the novel chelating Lewis acid 2,2′-diborabiphenyl and examined its complexation chemistry with simple monodentate Lewis bases, and the bifunctional dinitrogen bases pyridazine and benzo[*c*]cinnoline. Adducts of the latter are isoelectronic with polycyclic aromatic hydrocarbons, which have many applications in materials chemistry.[18] In addition to further development of this theme of research, the propensity of 2,2′-diborabiphenyl to chelate anionic Lewis bases, and the coordination chemistry of the resulting 2,2′-diboratabiphenyl derivatives is being developed.

Complete experimental details including synthesis and characterization of all new compounds can be found in the Supporting Information.

Received: November 14, 2002 [Z50555]

Keywords: boraarenes · boron · chelates · Lewis acids · radical ions

[1] C. Kaes, A. Katz, M. W. Hosseini, *Chem. Rev.* **2000**, *100*, 3553.
[2] a) W. E. Piers, G. J. Irvine, V. C. Williams, *Eur. J. Inorg. Chem.* **2000**, 2131; b) J. D. Wuest, *Acc. Chem. Res.* **1999**, *32*, 81; c) J. Vaugeois, M. Simard, J. D. Wuest, *Coord. Chem. Rev.* **1995**, *145*, 55; d) M. F. Hawthorne, Z. Zheng, *Acc. Chem. Res.* **1997**, *30*, 267; e) J. D. Hoefelmeyer, M. Schult, M. Tschinkl, F. P. Gabbai, *Coord. Chem. Rev.* **2002**, *235*, 93.
[3] a) G. E. Herberich, H. Ohst, *Adv. Organomet. Chem.* **1986**, *25*, 199; b) G. C. Fu, *Adv. Organomet. Chem.* **2001**, *47*, 101.
[4] a) P. I. Paetzold, G. Stohr, H. Maisch, H. Lenz, *Chem. Ber.* **1968**, *101*, 2881; b) A. J. Ashe III, H. Yang, X. Fang, J. W. Kampf, *Organometallics* **2002**, *21*, 4578; c) S.-Y. Liu, M. M.-C. Lo, G. C. Fu, *Angew. Chem.* **2002**, *114*, 182; *Angew. Chem. Int. Ed.* **2002**, *41*, 174; d) S. Qiao, D. A. Hoic, G. C. Fu, *Organometallics* **1997**, *16*, 1501; e) R. Boese, N. Finke, J. Henkelmann, G. Maier, P. Paetzold, H. P. Reisenauer, G. Schmid, *Chem. Ber.* **1985**, *118*, 1644.
[5] P. von R. Schleyer (Guest Editor), *Chem. Rev.* **2001**, *101*, 1115.
[6] a) M. D. Watson, A. Fechtenkötter, K. Müllen, *Chem. Rev.* **2001**, *101*, 1267; b) A. J. Berresheim, M. Müller, K. Müllen, *Chem. Rev.* **1999**, *99*, 1747.

 © 2003 Wiley-VCH Verlag GmbH & Co. KGaA, Weinheim 1433-7851/03/4211-1254 $ 20.00+.50/0

[7] a) G. Maier, H. P. Reisenauer, J. Henkelmann, C. Kliche, *Angew. Chem.* **1988**, *100*, 303; *Angew. Chem. Int. Ed. Engl.* **1988**, *27*, 295; b) G. Maier, H. Wolf, R. Boese, *Chem. Ber.* **1990**, *123*, 505.
[8] D. A. Hoic, J. Robbins-Wolf, W. M. Davis, G. C. Fu, *Organometallics* **1996**, *15*, 1315.
[9] a) J. Tweddell, D. A. Hoic, G. C. Fu, *J. Org. Chem.* **1997**, *62*, 8286; b) A. J. Ashe III, S. Al-Ahmad, X. Fang, J. W. Kampf, *Organometallics*, **1998**, *17*, 3883, and references therein.
[10] a) J. Hassan, M. Sevignon, C. Gozzi, E, Schulz, M. Lemaire, *Chem. Rev.* **2002**, *102*, 1359; b) G. E. Herberich, U. Engert, B. Ganter, M. Pons, R. Wang, *Organometallics* **1999**, *18*, 3406.
[11] Crystal data for **2**: $C_{22}H_{38}B_2P_2$, $M_r = 386.08$, monoclinic, space group $P2_1/c$, $a = 16.6747(2)$, $b = 14.1980(2)$, $c = 30.4768(4)$ Å, $\beta = 91.7737(10)°$, $V = 7211.85(16)$ Å^3, $Z = 12$, $\rho_{calcd} = 1.067$ g cm^{-3}, $Mo_{K\alpha}$ radiation ($\lambda = 0.71073$ Å), $T = 173(2)$ K, 23909 measured reflections, 12615 unique, $R_{int} = 0.065$, 7222 reflections with $I_{net} > 2\sigma(I_{net})$, $\mu = 0.18$ mm^{-1}, min./max. transmission = 0.973 and 0.985, $R1$ $(I > 2\sigma) = 0.053$, $wR2 = 0.117$, GOF = 1.00, No. of parameters = 713, final difference map within +0.24 and −0.30 e Å^3. CCDC-197380 contains the supplementary crystallographic data for this paper. These data can be obtained free of charge via www.ccdc.cam.ac.uk/conts/retrieving.html (or from the Cambridge Crystallographic Data Centre, 12, Union Road, Cambridge CB21EZ, UK; fax: (+44) 1223-336-033; or deposit@ccdc.cam.ac.uk).
[12] a) B. Y. Lee, S. Wang, M. Putzer, G. P. Bartholomew, X. Bu, G. C. Bazan, *J. Am. Chem. Soc.* **2000**, *122*, 3969; b) J. Abe, Y. Shirai, *J. Am. Chem. Soc.* **1996**, *118*, 4705.
[13] a) K. Meerholz, J. Heinze, *Electrochim. Acta* **1996**, *41*, 1839; b) V. D. Parker, *J. Am. Chem. Soc.* **1976**, *98*, 98.
[14] a) F. H. Herbstein, *Acta Crystallogr. Sect. B* **1979**, *35*, 1661; b) D. A. Klumpp, D. N. Back, G. K. S. Prakash, G. A. Olah, *J. Org. Chem.* **1997**, *62*, 6666.
[15] Crystal data for $[\mathbf{5}]^-$: $C_{50}H_{62}B_2Cl_4CoN_2$, $M_r = 913.37$, monoclinic, space group $P2_1/c$, $a = 16.562(3)$, $b = 12.371(2)$, $c = 23.779(6)$ Å, $\beta = 101.927(7)°$, $V = 4766.9(17)$ Å^3, $Z = 4$, $\rho_{calcd} = 1.273$ g cm^{-3}, $Mo_{K\alpha}$ radiation ($\lambda = 0.71073$ Å), $T = 173(2)$ K, 31354 measured reflections, 8807 unique, $R_{int} = 0.0951$, $\mu = 0.620$ mm^{-1}, min./max. transmission = 0.7721 and 0.9406, $R1$ $(I > 2\sigma) = 0.0626$, $wR2 = 0.1256$, GOF = 1.058, No. of parameters = 554, final difference map within +0.661 and −0.613 e Å^3. CCDC-197381 contains the supplementary crystallographic data for this paper. These data can be obtained free of charge via www.ccdc.cam.ac.uk/conts/retrieving.html (or from the Cambridge Crystallographic Data Centre, 12, Union Road, Cambridge CB21EZ, UK; fax: (+44) 1223-336-033; or deposit@ccdc.cam.ac.uk).
[16] a) G. E. Herberich, B. Schmidt, U. Englert, T. Wagner, *Organometallics* **1993**, *12*, 2891; b) G. E. Herberich, U. Englert, M. U. Schmidt, R. Standt, *Organometallics* **1996**, *15*, 2707.
[17] Y. Nakayama, A. Nakamura, K. Mashima, *Chem. Lett.* **1997**, 803.
[18] A. M. van de Craats, J. M. Warman, *Adv. Mater.* **2001**, *13*, 130, and references therein.

 © 2003 Wiley-VCH Verlag GmbH & Co. KGaA, Weinheim 1433-7851/03/4211-1255 $ 20.00+.50/0

Macrolide Synthesis

A Convergent Total Synthesis of Phorboxazole A**

*Miguel A. González and Gerald Pattenden**

Marine organisms have delivered a fascinating variety of structurally novel and biologically important secondary metabolites in recent years, many of which are now beginning to provide leads for the development of new chemotherapeutic agents. Phorboxazole A (**1**) and B (**2**) are unique oxane–oxazole-based macrolide structures isolated from the Indian Ocean sponge *Phorbas* sp,[1] which exhibit extraordinary cytostatic activity ($GI_{50} < 8 \times 10^{-10}$ M) against the entire panel of human tumor cell lines in the NCI database. Not surprisingly, therefore, these compounds have aroused con-

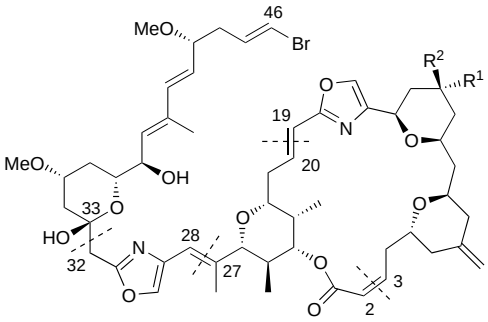

1, R^1= OH, R^2= H
2, R^1= H, R^2= OH

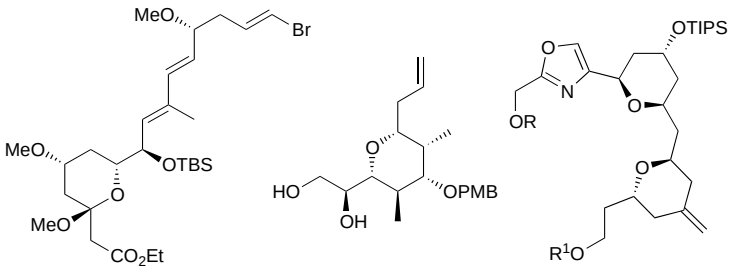

3 **4** **5**

a R= PMB, R^1= H
b R= Ms, R^1= TBS

[*] Prof. G. Pattenden, Dr. M. A. González
School of Chemistry, University of Nottingham
Nottingham, NG72RD (UK)
Fax: (+44) 115-951-3535
E-mail: GP@nottingham.ac.uk

[**] We thank the EPSRC and The University of Nottingham for support of this work. We also thank Dr. P. Little and Dr. D. S. Millan, in particular, for their contributions, as well as Merck Sharp and Dohme and Pfizer Ltd for continued financial support of our work.

Supporting information for this article is available on the WWW under http://www.angewandte.org or from the author.

 © 2003 Wiley-VCH Verlag GmbH & Co. KGaA, Weinheim 1433-7851/03/4211-1255 $ 20.00+.50/0

siderable interest within the medicinal and synthetic chemistry communities. Already three total syntheses of the phorboxazoles have been reported,[2–4] and the results of several structure–activity studies are beginning to emerge.[5] In previous publications we described synthetic routes to the key fragments **3**,[6] **4**,[7] and **5a**[8] in phorboxazole A.[9] We now show how we have brought these fragments together, leading to a new and convergent total synthesis of the natural product itself.

With two disubstituted double bonds (C2=C3 and C19=C20), and one trisubstituted double bond (C27=C28), separating the structural units **3, 4**, and **5**, it was clear from the outset of our studies that the ordered, stereocontrolled synthesis of these three double bonds would play a crucial role in any successful synthesis of phorboxazole A. After some initial disappointing forays,[10] we ultimately decided on a strategy to phorboxazole A whereby the C28–C46 side chain was first attached to the oxane **4**, then the bisoxane **5** was added, and finally the macrolide C2–C3 double bond was elaborated in a final key step (see Schemes 1 and 2). To this end, we envisaged coupling the oxane **4** to the phorboxazole side chain via the corresponding oxane–oxazole **11** and the lactone **8** by using the metalated oxazole chemistry developed by Evans et al.[3b]

Thus, the lactone **8** was first elaborated from the known aldehyde **6**[6] and the sulfone **7**[11] in four relatively straightforward steps, and the oxane–oxazole **11** was prepared through an *E*-selective Wadsworth–Emmons olefination between the oxane methyl ketone **9**, derived from **4**,[7] and the oxazole phosphonate ester **10**,[12] as highlighted in Scheme 1. To our satisfaction, when the oxane-substituted 2-methyloxazole **11** was deprotonated with lithium diethylamide generated in situ at −78 °C, and treated with the lactone **8**, the desired cyclic hemiketal **12a** was obtained in high yield and was immediately protected as its corresponding triethylsilyl ketal **12b** in 66% overall yield (Scheme 1). After selective cleavage of the dimethylacetal unit in **12b** with dimethylboron bromide[13] at −78 °C, an *E*-selective Wittig reaction between the resulting aldehyde **13** and the phosphonium salt obtained from the substituted bisoxane **5b**,[8] in the presence of DBU,[14] then led

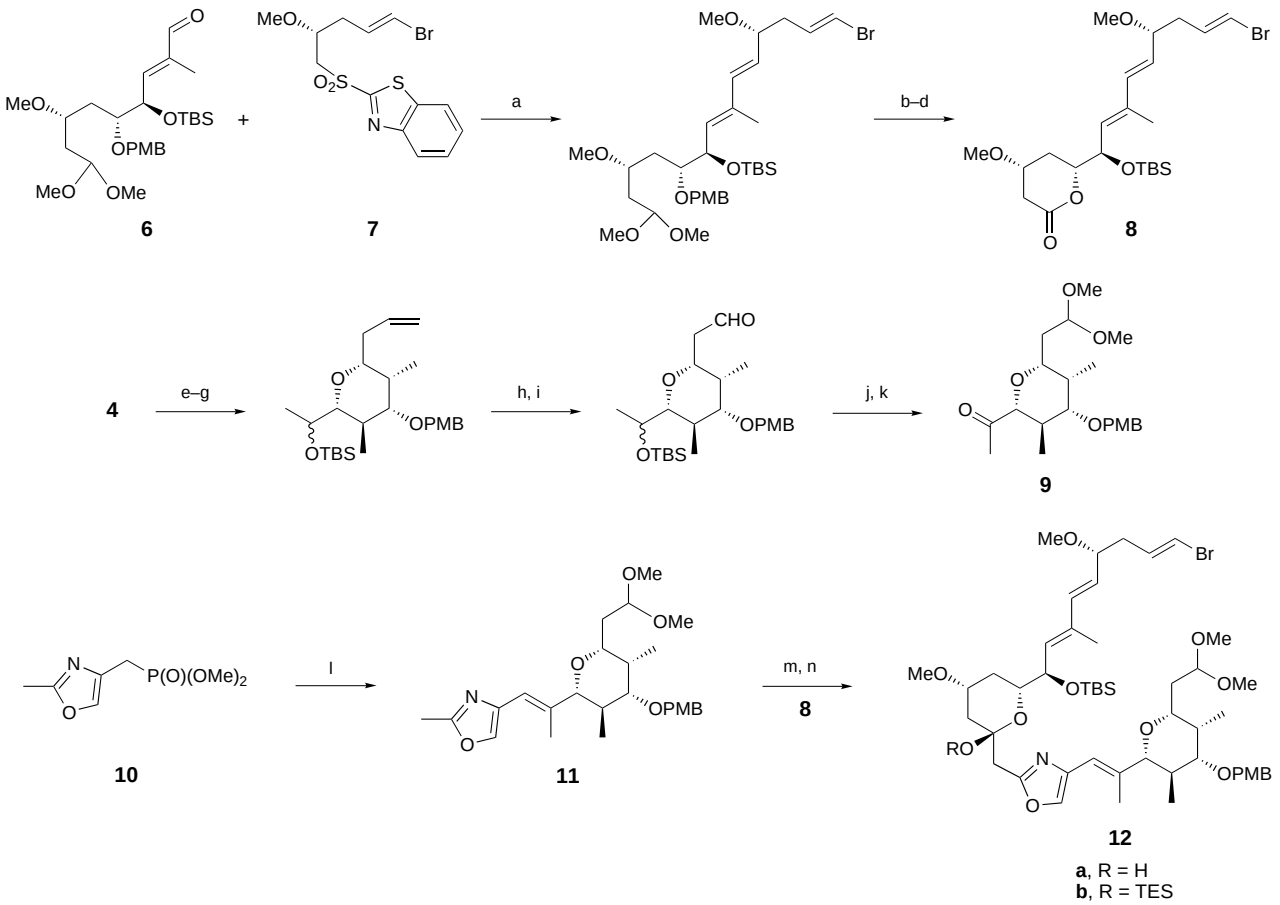

Scheme 1. Synthesis of the side chain **8** and oxazole–pyran **11** and coupling. a) NaHMDS, THF, −78 °C→RT, 93% pure *all-E* isomer; b) Me_2BBr, Et_2O, −78 °C, 98%; c) DDQ, CH_2Cl_2/H_2O (10:1), 0 °C, 85%; d) TPAP, NMO, powdered 4-Å molecular sieves, CH_2Cl_2, 82%; e) Ts–imidazole, NaH, Et_2O, −78 °C→0 °C; f) $LiAlH_4$, Et_2O; g) TBSOTf, 2,6-lutidine, CH_2Cl_2, −78 °C→RT; h) OsO_4, NMO, acetone/water; i) $NaIO_4$ on silica, CH_2Cl_2; j) CSA, $MeOH/CH_2Cl_2$; k) DMP, 2,6-lutidine, CH_2Cl_2, 43% overall yield from **4**; l) LDA, −78 °C, 30 min, then **9**, 89% (49% conversion); m) Et_2NH, *n*BuLi, THF, −78 °C, then **8**; n) TESOTf, pyridine, $MeCN/Et_2O$ (10:1), −47 °C, 36 h, 74% (66% conversion, two steps); HMDS = hexamethyldisilazide, DDQ = 2,3-dichloro-5,6-dicyano-1,4-benzoquinone, TPAP = tetrapropylammonium perruthenate, NMO = 4-methylmorpholine *N*-oxide, Ts = *p*-toluenesulfonyl, Tf = Trifluoromethanesulfonyl, CSA = camphorsulfonic acid, DMP = Dess–Martin periodinane, TBS = *tert*-butyldimethylsilyl, LDA = lithium diisopropylamide, TES = triethylsilyl, PMB = *p*-methoxybenzyl

 © 2003 Wiley-VCH Verlag GmbH & Co. KGaA, Weinheim 1433-7851/03/4211-1256 $ 20.00+.50/0

to the advanced bisoxazole–trisoxane intermediate **14**, as a single stereoisomer in excellent overall yield (Scheme 2).

The stage was now set to complete our synthesis of phorboxazole A through an intramolecular Wadsworth–Emmons reaction of **17** as the penultimate step. Thus, selective cleavage of the primary TBS ether in **14** with HF·pyr[3] at 0 °C proceeded smoothly and the resulting alcohol was then oxidized to the corresponding aldehyde **15** under Dess–Martin conditions[15] (Scheme 2). Removal of the PMB protecting group in **15** with DDQ next led to the secondary alcohol **16**, which was converted into the corresponding fluorophosphonate ester **17**.[2] Intramolecular cyclization of

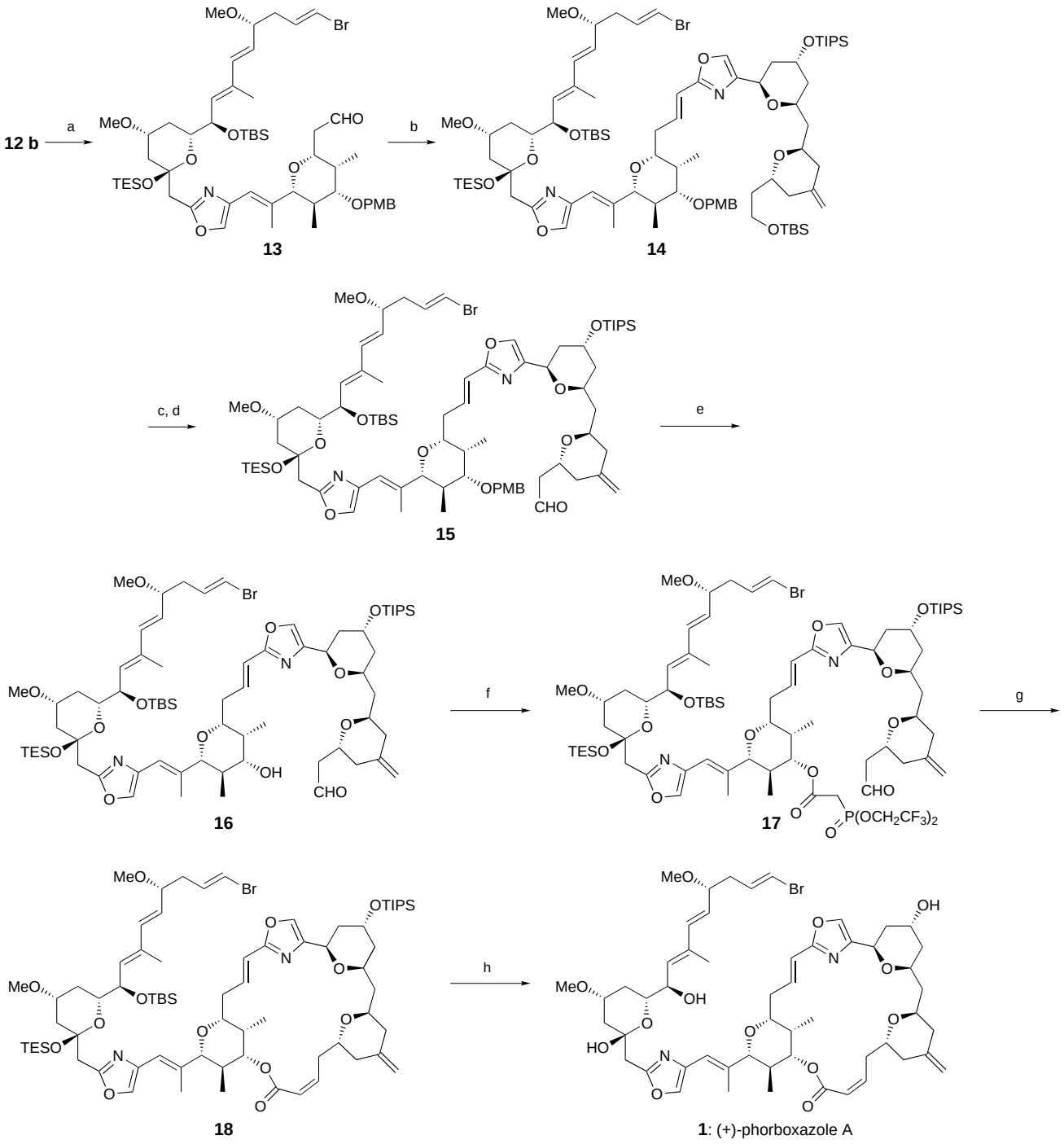

Scheme 2. Completion of the synthesis of **1**. a) Me_2BBr, Et_2O, −78 °C, 85 %; b) **5b**, Bu_3P, DMF, then **13** and DBU, room temperature or 0 °C, 85–87 %; c) HF·pyr, pyridine, THF, 0 °C→RT, 65–70 %; d) DMP, pyridine, CH_2Cl_2, 94 %; e) DDQ, CH_2Cl_2–pH 7 buffer, 85 %; f) EDCI·MeI, HOBT, $HO_2CCH_2PO(OCH_2CF_3)_2$, CH_2Cl_2, >80 %; g) K_2CO_3, [18]crown-6, toluene, room temperature, 82 % (3:1 *Z*/*E*); h) TBAF, THF, 0 °C→RT, 75 %; reversed-phase HPLC purification; DMF = *N*,*N*-dimethylformamide, DBU = 1,8-diazabicyclo[5.4.0]undec-7-ene, pyr = pyridine, DMP = Dess–Martin periodinane, EDCI = 1-ethyl-3-(3-dimethylaminopropyl)carbodiimide chloride, HOBT = 1-hydroxybenzotriazole, TBAF = tetrabutylammonium fluoride, TIPS = triisopropylsilyl.

 © 2003 Wiley-VCH Verlag GmbH & Co. KGaA, Weinheim 1433-7851/03/4211-1257 $ 20.00+.50/0

the aldehyde–phosphonate **17** under the conditions of Still and Gennari[16] gave the *Z*-α,β-unsaturated macrolide **18**, containing approximately 25% of the corresponding *E* isomer.[17] Removal of the three silyl protecting groups in **18** with tetrabutylammonium fluoride in THF at 0°C, followed by chromatography, finally produced (+)-phorboxazole A (**1**), contaminated with its C2–C3 *E* isomer. Further purification by reversed-phase HPLC provided pure (+)-phorboxazole A, whose ^{1}H and ^{13}C NMR spectra, together with high-resolution mass spectrometric data (calcd for $C_{53}H_{71}N_2O_{13}{}^{79}BrNa$ $[M+Na, {}^{79}Br]^+$: 1045.4037; found: 1045.4053 (100%) (ESI)) and optical rotation data ($[\alpha]_D^{20} = +43.3$, $c = 0.12$, $CHCl_3$) corresponded to those reported for the natural product.[1a,18]

Received: October 28, 2002 [Z50447]

Keywords: antifungal agents · antitumor agents · natural products · olefination · total synthesis

[1] a) P. A. Searle, T. F. Molinski, *J. Am. Chem. Soc.* **1995**, *117*, 8126–8131; b) P. A. Searle, T. F. Molinski, L. J. Brzezinski, J. W. Leahy, *J. Am. Chem. Soc.* **1996**, *118*, 9422–9423; c) T. F. Molinski, *Tetrahedron Lett.* **1996**, *37*, 7879–7880.

[2] C. J. Forsyth, F. Ahmed, R. D. Cink, C. S. Lee, *J. Am. Chem. Soc.* **1998**, *120*, 5597–5598.

[3] a) D. A. Evans, D. M. Fitch, T. E. Smith, *J. Am. Chem. Soc.* **2000**, *122*, 10033–10046; b) D. A. Evans, V. J. Cee, T. E. Smith, K. J. Santiago, *Org. Lett.* **1999**, *1*, 87–90.

[4] a) A. B. Smith III, P. R. Verhoest, K. P. Minbiole, M. Schelhaas, *J. Am. Chem. Soc.* **2001**, *123*, 10942–10953. b) After the submission of this paper another total synthesis of phorboxazole A was completed. See the next paper in this issue: D. R. Williams, A. A. Kiryanov, U. Emde, M. P. Clark, M. A. Berliner, J. T. Reeves, *Angew. Chem.* **2003**, *115*, 1296–1300; *Angew. Chem. Int. Ed.* **2003**, *42*, 1258–1262.

[5] a) P. Wolbers, H. M. R. Hoffmann, F. Sasse, *Synlett* **1999**, *11*, 1808–1810; b) F. M. Uckun, C. J. Forsyth, *Bioorg. Med. Chem. Lett.* **2001**, *11*, 1181–1183; c) T. F. Molinski, L. J. Brzezinski, J. W. Leahy, *Tetrahedron: Asymmetry* **2002**, *13*, 1013–1016.

[6] G. Pattenden, A. T. Plowright, J. A. Tornos, T. Ye, *Tetrahedron Lett.* **1998**, *39*, 6099–6102.

[7] G. Pattenden, T. Ye, *Tetrahedron Lett.* **1998**, *39*, 319–322.

[8] G. Pattenden, A. T. Plowright, *Tetrahedron Lett.* **2000**, *41*, 983–986.

[9] Several other synthetic approaches to the phorboxazoles have been described by other research groups. For a full bibliography, see: P. B. Greer, W. A. Donaldson, *Tetrahedron* **2002**, *58*, 6009–6018.

[10] P. Little, D. S. Millan, unpublished results.

[11] The sulfone was prepared by using similar chemistry to that described earlier in reference [6]. For the use of benzothiazolyl sulfones in olefination reactions, see: a) J. B. Baudin, G. Hareau, S. A. Julia, O. Ruel, *Bull. Soc. Chim. Fr.* **1993**, *130*, 336–357; b) J. B. Baudin, G. Hareau, S. A. Julia, R. Lorne, O. Ruel, *Bull. Soc. Chim. Fr.* **1993**, *130*, 856–878.

[12] The oxazole phosphonate **10** was prepared by using standard procedures from the known 4-hydroxymethyl-2-methyloxazole; see: D. A. Entwistle, S. I. Jordan, J. Montgomery, G. Pattenden, *Synthesis* **1998**, 603–612.

[13] Y. Guindon, C. Yoakin, H. E. Morton, *J. Org. Chem.* **1984**, *49*, 3912–3920.

[14] Similar conditions were used earlier by Evans et al; see reference [3a].

[15] D. B. Dess, J. C. Martin, *J. Am. Chem. Soc.* **1991**, *113*, 7277–7287.

[16] W. C. Still, C. Gennari, *Tetrahedron Lett.* **1983**, *24*, 4405–4408. This macrocyclization tactic had earlier been used by Forsyth et al.[2] and Smith et al.[4] in their total synthesis of phorboxazole A.

[17] The *Z*/*E* ratio followed from examination of the absorptions associated with the *Z* ($\delta = 5.92$ ppm) and *E* ($\delta = 6.90$ and 5.85 ppm) olefinic H atoms in the ^{1}H NMR spectrum of the mixture.

[18] Naturally derived phorboxazole A had $[\alpha]_D = +44.8°$ ($c = 1.0$, MeOH). All new compounds reported in this study showed satisfactory spectroscopic and mass spectrometric data.

 © 2003 Wiley-VCH Verlag GmbH & Co. KGaA, Weinheim 1433-7851/03/4211-1258 $ 20.00+.50/0

Macrolide Synthesis

Total Synthesis of Phorboxazole A**

David R. Williams, Andre A. Kiryanov, Ulrich Emde, Michael P. Clark, Martin A. Berliner, and Jonathan T. Reeves*

Phorboxazole A (**1**; see Scheme 1), and its C13 diastereoisomer phorboxazole B, are novel 21-membered macrolides isolated from the rare Indian Ocean sponge *Phorbas* sp.[1] These substances have demonstrated extraordinary potency against the National Cancer Institute (NCI) panel of 60 human tumor cell cultures (mean $GI_{50} < 1.6$ nM).[2] Moreover, phorboxazole A has been shown to arrest the cell cycle in the S phase without affecting tubulin polymerization, suggesting a unique mechanism of action.[2a] While biological studies are severely limited by the scarcity of these natural products, the unprecedented structural features and remarkable antitumor activity have provided the impetus for several synthesis studies.[3] Recently, total syntheses of phorboxazole A[4,5] and phorboxazole B[6] have been reported. Herein, we describe the culmination of our efforts[3d–f] leading to a convergent, enantiocontrolled total synthesis of **1**.

[*] Prof. D. R. Williams, Dr. A. A. Kiryanov, Dr. U. Emde, M. P. Clark, Dr. M. A. Berliner, Dr. J. T. Reeves
Indiana University
Department of Chemistry
800 E. Kirkwood Ave., Bloomington, IN, 47405 (USA)
Fax: (+1) 812-855-8300
E-mail: williamd@indiana.edu

[**] Generous financial support for this research was provided by the NIH (GM-41560). We acknowledge Prof. Craig J. Forsyth for providing us with detailed conditions for reproducing HRMS data for phorboxazole A and ^{1}H NMR spectra of natural and synthetic material. We also thank Prof. Amos B. Smith for ^{1}H NMR spectra of synthetic phorboxazole A for our comparison.

 © 2003 Wiley-VCH Verlag GmbH & Co. KGaA, Weinheim 1433-7851/03/4211-1258 $ 20.00+.50/0

We envisioned in our retrosynthetic analysis the preparation of four nonracemic components **2**–**5** for the convergent assembly of the target macrolide (Scheme 1). Stereoselective formation of the C22–C26 tetrahydropyran moiety of **1** was a central issue for the design strategy that featured the union of components **3** and **4**. Thus, the Horner–Wadsworth–Emmons reaction would precede formation of the fully substituted pyran through retention of the stereochemistry at C22 of component **3** in the π-allyl cation cyclization event. Incorporation of the intact bispyran component **5** utilized the Wittig reaction for construction of the (*E*)-C19–C20 alkene, and was followed by the subsequent attachment of the labile C42–C46 segment by a modified Julia olefination. Finally, our strategy culminated in a late-stage macrocyclization by installation of the (*Z*)-C2–C3 enoate.

Synthesis of the C28–C41 aldehyde **4** began with nonracemic β,γ-unsaturated aldehyde **6** (Scheme 2).[7] Asymmetric allylation of **6** was effected following the tin-to-boron transmetalation of allylstannane **7**[8] using the boron bromide reagent derived from (*R,R*)-1,2-diamino-1,2-diphenylethane bis(sulfonamide) and boron tribromide.[9] Nucleophilic addition provided the homoallylic alcohol **8** as the major component of a mixture (96% yield) of C37 diastereomers (d.r. 7.2:1),[10] demonstrating anti-Felkin stereocontrol as imparted by the chiral auxiliary. Selective oxidative cleavage of the 1,1-disubstituted olefin (OsO_4, $K_3Fe(CN)_6$; $NaIO_4$), and internally directed reduction[11] of the resultant β-hydroxy ketone with $Me_4NBH(OAc)_3$ yielded 1,3-diol **9** with excellent diastereoselectivity (d.r. > 95:5). Protection of **9** as the corresponding acetonide (**10**) led to the expected diagnostic NMR evidence in support of the 1,3-anti relationship.[12]

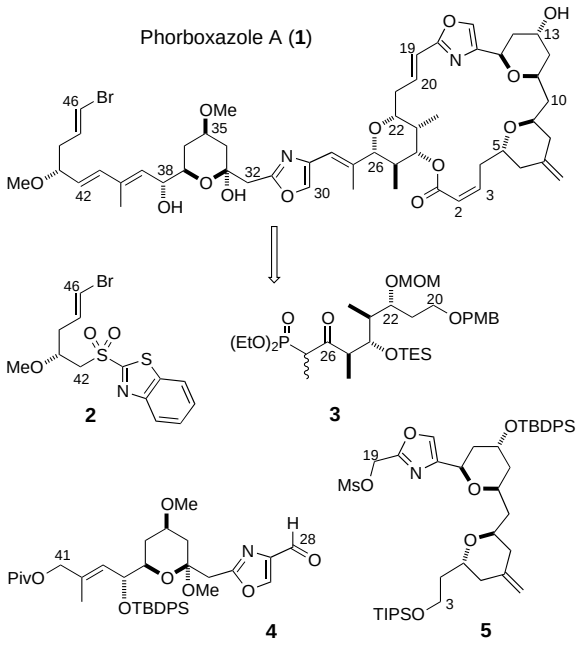

Scheme 1. Components **2**–**5** of phorboxazole A (**1**). MOM = methoxymethyl, Ms = methanesulfonyl, Piv = pivaloyl, PMB = *p*-methoxybenzyl, TBDPS = *tert*-butyldiphenylsilyl, TES = triethylsiyl, TIPS = triisopropylsilyl.

Cleavage of the silyl ether and oxidation of the resultant primary alcohol **11** under Swern conditions[13] furnished the aldehyde **12**.

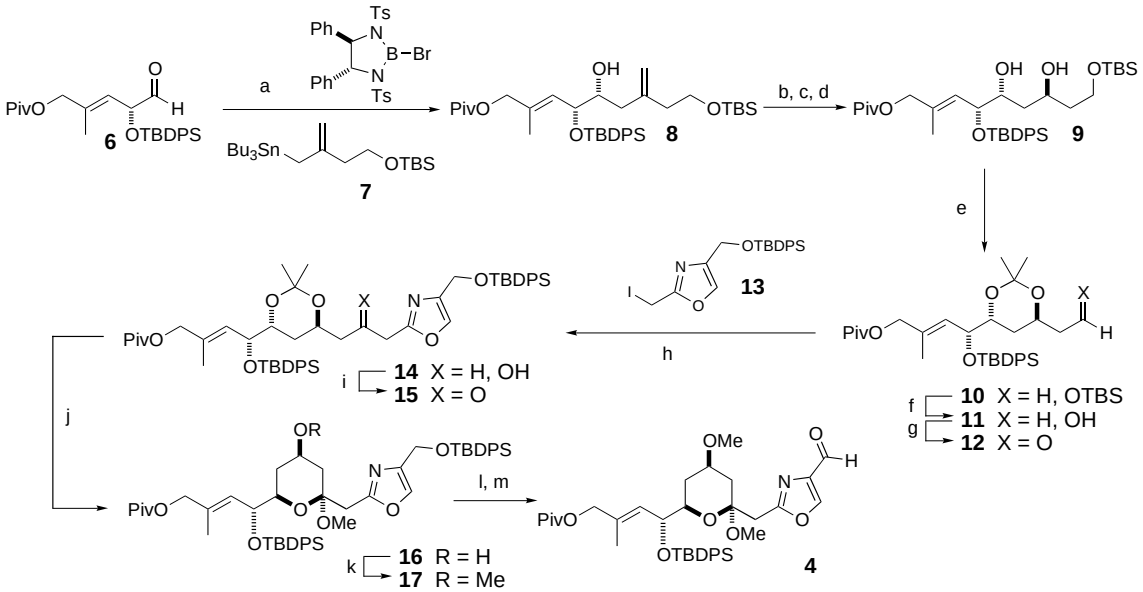

Scheme 2. a) (*S,S*)-1,2-Diamino-1,2-diphenylethane bis(sulfonamide), BBr_3, CH_2Cl_2, 0°C, 1 h; then **7**, RT, 10 h; then **6**, −78°C, 1 h; 96%, 7.2:1 d.r.; b) OsO_4, $K_3Fe(CN)_6$, K_2CO_3, $NaHCO_3$, DABCO, *t*BuOH/H_2O (1:1); c) $NaIO_4$, THF/H_2O (1:1); 95% (two steps); d) $Me_4NBH(OAc)_3$, HOAc/CH_3CN (1:1), −20°C, 10 h; 94%, > 95:5 d.r.; e) 2,2-dimethoxypropane, cat. CSA, RT, 16 h; f) HF·pyr, THF; 87% for two steps; g) $(COCl)_2$, DMSO, CH_2Cl_2, −78°C, then Et_3N; h) **13**, SmI_2, THF, RT; 92% for two steps, 1:1 dr; i) TFAA, DMSO, CH_2Cl_2, −78°C; then acetylacetone, Et_3N, −60° to −40°C; 88%; j) cat. CSA, MeOH, RT, 1.5 h; 82%, 7.2:1 mixture of separable C37 epimers; k) MeI, $CaSO_4$, Ag_2O, 3 d; 90%; l) TBAF, THF, 0°C, 2 h; 92%; m) Dess–Martin periodinane, pyridine, CH_2Cl_2, 1 h; 95%. CSA = camphorsulfonic acid, DABCO = 1,4-diazabicyclo[2.2.2]octane, pyr = pyridine, TBAF = tetra-*n*-butylammonium fluoride, TBS = *tert*-butyldimethylsilyl, TFAA = trifluoroacetic anhydride, Ts = *p*-toluenesulfonyl.

 © 2003 Wiley-VCH Verlag GmbH & Co. KGaA, Weinheim 1433-7851/03/4211-1259 $ 20.00+.50/0

We have previously explored direct incorporation of the intact oxazole nucleus by the use of a Barbier coupling of aldehydes and 2-iodomethyl oxazoles in the presence of SmI_2.[3f] Application of improved conditions using iodide **13** and aldehyde **12** gave the desired alcohol adduct **14** as a 1:1 mixture of diastereomers in 92% yield (over two steps). Oxidation of this mixture using a modification of the trifluoroacetic anhydride–DMSO–NEt_3 protocol[14] provided the corresponding ketone **15** in 88% yield. The inclusion of acetylacetone (3–5 equiv) in the reaction mixture at −60°C immediately prior to addition of triethylamine was necessary to prevent C32-α-methylthiomethylation of the product ketone. In fact, the ease of enolization of **15** was undoubtedly responsible for problems encountered in IBX[15] and Dess–Martin oxidation[16] attempts, which led to varying amounts of further oxidation to aldehydes produced by cleavage of the C32–C33 bond. Subjecting ketone **15** to conditions of acetal exchange with methanol in the presence of a catalytic amount of camphorsulfonic acid provided tetrahydropyran **16** in 82% yield as a 7.2:1 mixture of readily separable C37,C35 epimers, resulting from the original allylation reaction of **6**. Methylation of the C35 alcohol of **16** followed by desilylation of **17** with TBAF and Dess–Martin oxidation delivered the key C28–C41 aldehyde **4** in 39% overall yield from **6**.

Coupling of the β-ketophosphonate **3**, which was synthesized as previously described,[3f] with oxazole carboxaldehyde **4** led to the desired C27-C28 *E*-trisubstituted alkene in 88% yield with excellent selectivity (>95:5 *E*/*Z*; Scheme 3). Reduction of this α,β-unsaturated ketone under Luche conditions gave the C26 alcohol **18** (d.r. 9:1).[17,18] Subsequent treatment of **18** with triflic anhydride (2 equiv) and anhydrous pyridine (5 equiv) in CH_2Cl_2 (−20°C, 12 h) produced a single tetrahydropyran **19** in 55% yield. The mechanism for product formation is consistent with the production of an intermediate transoid allyl cation for internal capture via participation of the β-methoxymethyl ether at C22 with *Re*-face addition followed by dealkylation of the oxonium species.[19] Stereochemical assignments of the fully substituted pyran were supported by one- and two-dimensional NMR experiments (COSY and NOESY). Removal of the PMB ether of **19** followed by Dess–Martin oxidation yielded the C20 aldehyde **20**.

Enantiocontrolled preparation of the C3–C19 bispyran component **5** (Scheme 1) proceeded by a pathway featuring our asymmetric allylation methodology as previously described.[3f] In situ displacement of the reactive mesylate of **5**[20] with tri-*n*-butylphosphane in DMF at room temperature provided an intermediate phosphorane for direct condensation with aldehyde **20** (Scheme 3). The resulting C19–C20 alkene **21** was isolated in nearly quantitative yield with excellent *E* stereoselectivity (*E*:*Z* > 95:5). Reductive removal of the allylic pivaloate and oxidation of the resulting primary

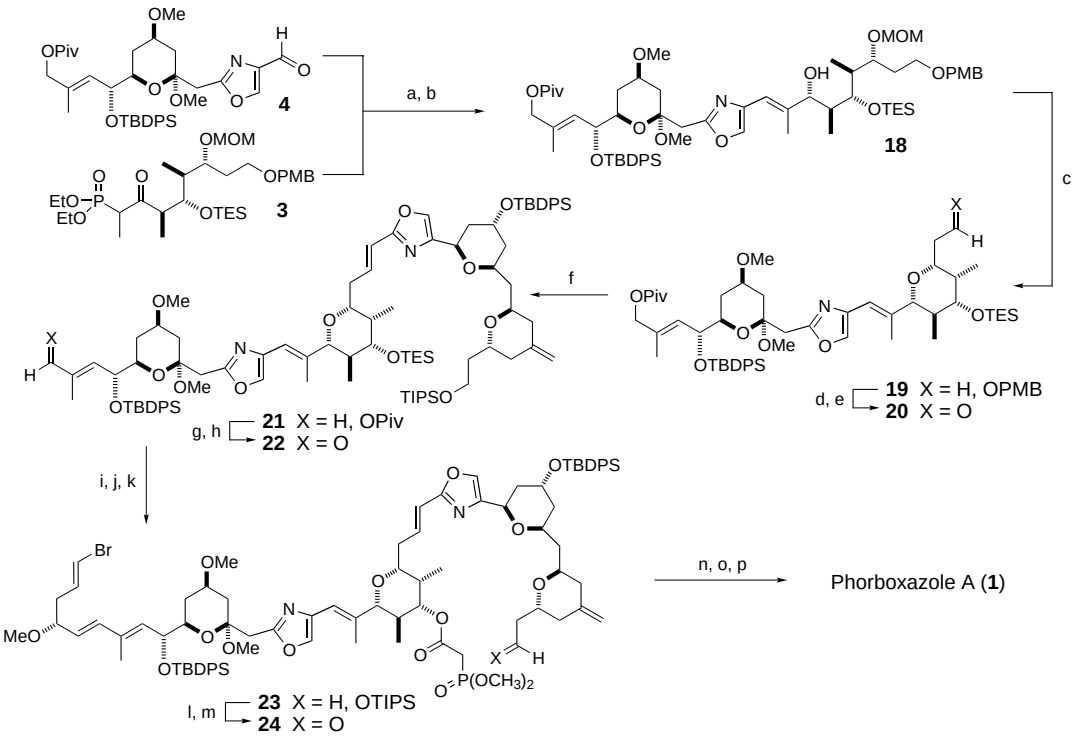

Scheme 3. a) NaH, THF, RT, 0.5 h; 88%, >95:5 *E*:*Z*; b) $NaBH_4$, $CeCl_3 \cdot 7H_20$, MeOH, 0°C, 1 h; 98%, >95:5 d.r.; c) Tf_2O, pyr, CH_2Cl_2, −20°C, 12 h; 55%; d) DDQ, CH_2Cl_2, pH 7 buffer, RT, 1 h; 94%; e) Dess–Martin periodinane, pyr, CH_2Cl_2, RT, 2.5 h; 87%; f) **5**, PBu_3, CH_2Cl_2, RT, 16 h, then add **14**, DBU, RT, 1 h; quant.; g) DIBAL-H, CH_2Cl_2, −78°C, 2 min; 98%; h) Dess–Martin periodinane, pyr, CH_2Cl_2, 1.5 h; 90%; i) **2**, NaHMDS, THF, −78°C to RT; 98%, >95:5 *E*:*Z*; j) CH_2Cl_2/MeOH/HOAc 2:1:1, 2 d, 86%; k) dimethylphosphonoacetic acid, DCC, CH_2Cl_2; l) CSA, MeOH; m) Dess-Martin periodinane, CH_2Cl_2; 76% for three steps; n) K_2CO_3, [18]crown-6, toluene, −20°C, two days; quant., 4:1 *Z*:*E*; o) TBAF, THF; 53%; p) 6% HCl, THF; 80%. DDQ = 2,3-dichloro-5,6-dicyano-1,4-benzoquinone, DBU = 1,8-diazabicyclo[5.4.0]undec-7-ene, DIBAL-H = diisobutylaluminum hydride, HMDS = bis(trimethylsilyl)amide, DCC = *N*,*N*′-dicyclohexylcarbodiimide.

 © 2003 Wiley-VCH Verlag GmbH & Co. KGaA, Weinheim 1433-7851/03/4211-1260 $ 20.00+.50/0

allylic alcohol gave the unsaturated aldehyde **22** for attachment of the remaining C42–C46 carbon chain. In this regard, our previous studies have examined the adaptation of the Kocienski modification of the Julia olefination.[21] Intriguingly, use of the corresponding *N*-phenyltetrazole sulfone of **2** resulted predominantly in the formation of the *Z* olefin. On the other hand, the carbanion of the benzothiazole[22] sulfone **2**, previously reported by Evans and co-workers,[6] cleanly reacted with **22** under similar reaction conditions yielding the desired *E,E* diene (98%; >95:5 *E*:*Z*). Removal of the TES ether at C24 (HOAc, CH_2Cl_2, MeOH, 86%) and esterification of the alcohol at C24 with dimethylphosphonoacetic acid (DCC, CH_2Cl_2) provided phosphonate **23**. Selective removal of the TIPS protecting group at C3 under mildly acidic conditions (CSA, MeOH) followed by Dess–Martin oxidation furnished the key aldehyde **24** in 76% yield over three steps. Intramolecular Horner–Wadsworth–Emmons macrocyclization in toluene (K_2CO_3, [18]crown-6, −20°C) gave the macrocycle as a 4:1 mixture of C2–C3 *Z*:*E* olefin isomers. Deprotection of both TBDPS ethers with TBAF in THF provided a diol (53% yield), which permitted the separation of the minor (*E*)-C2–C3 isomer by silica gel chromatography. Finally, hydrolysis of the methyl ketal moiety under acidic conditions (6% aqueous HCl, THF)[4a] furnished phorboxazole A (**1**) in 80% yield. Our synthetic material was identical in all respects with physical and spectroscopic data provided for the natural product.[1]

In summary, we have reported a highly convergent, stereocontrolled total synthesis of phorboxazole A (**1**). Asymmetric allylation reactions of stannyl-derived allyldiazaborolanes are demonstrated as a powerful protocol for the enantiocontrolled assembly of functionally complex components. Key features of the overall scheme include a stereoselective cationic cyclization reaction for formation of the fully substituted C22–C26 tetrahydropyran, and the use of a Julia olefination for incorporation of the sensitive C37–C46 dienyl system. The novel Barbier-type coupling of an iodomethyl oxazole provides a promising methodology for the incorporation of the intact oxazole heterocycle. Full details of this study will be reported in due course.

Received: December 20, 2002 [Z50817]

Keywords: antitumor agents · asymmetric allylation · macrolides · natural products · total synthesis

[1] P. A. Searle, T. F. Molinski, *J. Am. Chem. Soc.* **1995**, *117*, 8126.
[2] a) P. A. Searle, T. F. Molinski, L. J. Brzezinski, J. W. Leahy, *J. Am. Chem. Soc.* **1996**, *118*, 9422; b) T. F. Molinski, J. Antonio, *J. Nat. Prod.* **1993**, *56*, 54; c) T. F. Molinski, *Tetrahedron Lett.* **1996**, *37*, 7879.
[3] a) C. S. Lee, C. J. Forsyth, *Tetrahedron Lett.* **1996**, *37*, 6449; b) R. D. Cink, C. J. Forsyth, *J. Org. Chem.* **1997**, *62*, 5672; c) F. Ahmed, C. J. Forsyth, *Tetrahedron Lett.* **1998**, *39*, 183; d) D. R. Williams, M. P. Clark, M. A. Berliner, *Tetrahedron Lett.* **1999**, *40*, 2287; e) D. R. Williams, M. P. Clark, *Tetrahedron Lett.* **1999**, *40*, 2291; f) D. R. Williams, M. P. Clark, U. Emde, M. A. Berliner, *Org. Lett.* **2000**, *2*, 3023; g) G. Pattenden, T. Ye, *Tetrahedron Lett.* **1998**, *39*, 319; h) G. Pattenden, A. T. Plowright, J. A. Tornos, T. Ye, *Tetrahedron Lett.* **1998**, *39*, 6099; i) I. Paterson, E. A. Arnott, *Tetrahedron Lett.* **1998**, *39*, 7185; j) A. B. Smith III, P. R. Verhoest, K. P. Minbiole, J. J. Lim, *Org. Lett.* **1999**, *1*, 909; k) A. B. Smith III, K. P. Minbiole, P. R. Verhoest, T. J. Beauchamp, *Org. Lett.* **1999**, *1*, 913; l) D. A. Evans, V. J. Cee, T. E. Smith, K. J. Santiago, *Org. Lett.* **1999**, *1*, 87; m) P. Wolbers, H. M. R. Hoffmann, *Tetrahedron* **1999**, *55*, 1905; n) P. Wolbers, A. M. Misske, H. M. R. Hoffmann, *Tetrahedron Lett.* **1999**, *40*, 4527; o) J. Schaus, J. S. Panek, *Org. Lett.* **2000**, *2*, 469; p) G. Pattenden, A. Plowright, *Tetrahedron Lett.* **2000**, *41*, 983; q) S. Rychnovsky, C. Thomas, *Org. Lett.* **2000**, *2*, 1217.
[4] C. J. Forsyth, F. Ahmed, R. D. Cink, C. S. Lee, *J. Am. Chem. Soc.* **1998**, *120*, 5597.
[5] a) A. B. Smith III, P. R. Verhoest, K. P. Minbiole, M. Schelhaas, *J. Am. Chem. Soc.* **2001**, *123*, 4834; b) A. B. Smith III, P. R. Verhoest, K. P. Minbiole, M. Schelhaas, *J. Am. Chem. Soc.* **2001**, *123*, 10942; c) After submission of this manuscript for publication, we were informed that Prof. G. Pattenden et al. have also completed a synthesis of phorboxazole A. See preceding paper; M. A. Gonzalez, G. Pattenden, *Angew. Chem.* **2003**, *115*, 1293; *Angew. Chem. Int. Ed.* **2003**, *42*, 1255.
[6] a) D. A. Evans, V. J. Cee, T. E. Smith, D. M. Fitch, P. S. Cho, *Angew. Chem.* **2000**, *112*, 2633; *Angew. Chem. Int. Ed.* **2000**, *39*, 2533; b) D. A. Evans, D. M. Fitch, *Angew. Chem.* **2000**, *112*, 2636; *Angew. Chem. Int. Ed.* **2000**, *39*, 2536.
[7] The aldehyde **6**, which bears the primary pivaloate, was prepared by the same route as previously described for the corresponding MOM ether in 62% overall yield.[3f]
[8] Stannane **7** is conveniently prepared by deprotonation of 3-methyl-3-buten-1-ol with two equivalents of Schlosser's base, quenching the resulting dianion with tributyltin iodide, and protection of the resultant alcohol (TBSCl, imidazole).
[9] E. J. Corey, C. M. Yu, S. S. Kim, *J. Am. Chem. Soc.* **1989**, *111*, 5495. For development of this asymmetric allylation methodology, see: D. R. Williams, D. A. Brooks, K. G. Meyer, M. P. Clark, *Tetrahedron Lett.* **1998**, *39*, 7251.
[10] Small-scale reactions permitted the chromatographic separation of homoallylic alcohol diastereomers for individual characterization. Preparative multigram reactions were conveniently carried forward to acetal **16**, where the desired C37 isomer was easily purified by flash chromatography.
[11] D. A. Evans, E. Carreira, *J. Am. Chem. Soc.* **1988**, *110*, 3560.
[12] S. D. Rychnovsky, D. J. Skalitzky, *Tetrahedron Lett.* **1990**, *31*, 945; D. A. Evans, D. L. Rieger, J. R. Gage, *Tetrahedron Lett.* **1990**, *31*, 7099.
[13] A. J. Mancuso, S. L. Huang, D. Swern, *J. Org. Chem.* **1978**, *43*, 2480.
[14] S. L. Huang, K. Omura, D. Swern, *Synthesis* **1978**, 297.
[15] J. D. More, N. S. Finney, *Org. Lett.* **2002**, *4*, 3001–3003.
[16] D. B. Dess, J. C. Martin, *J. Org. Chem.* **1983**, *48*, 4155; D. B. Dess, J. C. Martin, *J. Am. Chem. Soc.* **1991**, *113*, 7277.
[17] J.-L. Luche, *J. Am. Chem. Soc.* **1978**, *100*, 2226.
[18] The relative stereocontrol of the reduction was established on a related compound by conversion (2,2′-dimethoxypropane (2,2-DMP)) into the six-membered acetonide and application of ^{13}C NMR spectroscopic analysis.[12]

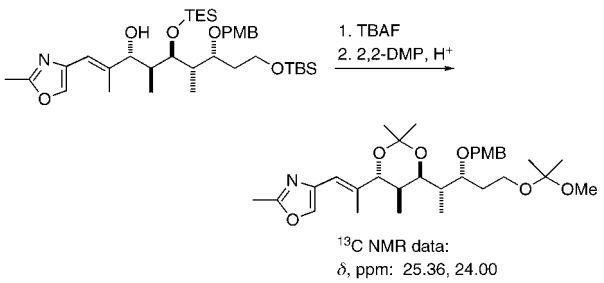

[19] Model studies had shown that individual diastereomeric allylic alcohols were cyclized under these conditions to afford the same tetrahydropyran product.

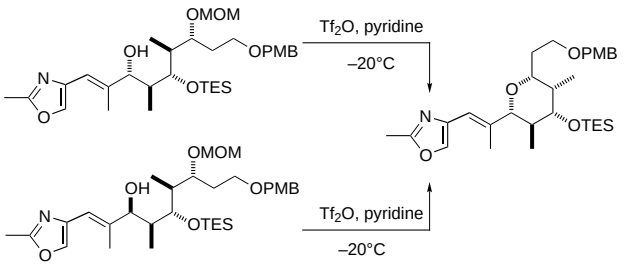

[20] Methanesulfonate **5** was prepared from the previously reported C3 pivaloate/C19 PMB ether[3d] by the following four-step sequence: 1) LiOH, THF/MeOH/H_2O; 2) TIPSOTf, 2,6-lutidine; 3) DDQ, CH_2Cl_2/pH 7 buffer; 4) MsCl, Et_3N.

[21] P. R. Blakemore, W. J. Cole, P. J. Kocienski, A. Morley, *Synlett* **1998**, 26.

[22] J. B. Baudin, G. Hareau, S. A. Julia, O. Ruel, *Bull. Soc. Chim. Fr.* **1993**, *130,* 336.

 © 2003 Wiley-VCH Verlag GmbH & Co. KGaA, Weinheim 1433-7851/03/4211-1262 $ 20.00+.50/0

Microfabrication of 3D Structures

Simple, Three-Dimensional Microfabrication of Electrodeposited Structures**

*David A. LaVan, Paul M. George, and Robert Langer**

Making three-dimensional (3D) micromachined objects is difficult using current techniques; there are few alternatives to using a large number of process steps and masks. We present a new approach to generate 3D microfabricated structures using very few steps and a single photolithographic mask. This new approach relies on a conductive template, which can be produced using conventional lift-off microfabrication, or by other means such as self-assembly or printing, and then an electrodeposition step to produce the full structure. The design of the conductive template determines the full 3D structure—gaps between regions of the template are intentionally introduced. As material is deposited, it expands both vertically and horizontally; the horizontal expansion bridges the spaces between the conductive regions. Once that space is bridged, the electrodeposited material forms an electrical connection with the new region and deposition continues on the existing structure, as well as initiating at the newly connected region. Figure 1 provides a schematic illustration of this process. If a small difference in height were desired between adjacent structures (regions), the gap would be small; a large difference in height is created with a larger gap. We have created a series of test structures, as well as a prototype master pattern to cast a soft microfluidic device.

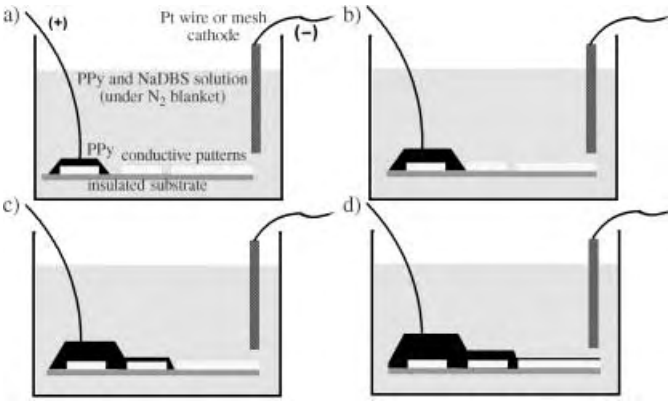

Figure 1. Schematic representation of the deposition technique for polypyrrole (the method is similar for metal films, but they are deposited on the cathode). a) Starting with isolated conductive patterns on a surface, the deposition initiates at region(s) connected to the anode, illustrated here with a wire; b) the deposited film grows horizontally and vertically from the initial region(s); c) the deposited film bridges to new regions, with deposition continuing over the larger surface; d) the deposited film bridges to another region; the relative heights of each region are determined by the spaces between them.

The formation of poly(dimethyl siloxane) (PDMS) replicas of micromachined master patterns for soft lithography[1] and for the creation of microfluidic devices is well known.[2,3] The fabrication of these microfluidic devices relies on bulk micromachining of silicon wafers or a thick layer of patterned photoresist to generate a master pattern—the reversed sense of the pattern is generated by casting a soft replica over this master. There is much interest in producing 3D structures using surface or bulk micromachining techniques[4–6] for the creation of more complex masters for microfluidic devices, as well as for other uses. Much of the published work that describes 3D microfluidic devices relies on the layer-by-layer construction of these structures, which requires a large number of masks and process steps, and the awkward alignment and assembly of the individual layers. The master pattern shown in Figure 2 demonstrates how easily a 3D microfluidic master can be formed. The technique can create

[*] Prof. R. Langer
Department of Chemical Engineering
Massachusetts Institute of Technology
Cambridge, MA 02139 (USA)
Fax: (+1) 617-258-6843
E-mail: rlanger@mit.edu
Dr. D. A. LaVan, P. M. George
Division of Health Science and Technology
Massachusetts Institute of Technology
Cambridge, MA 02139 (USA)

[**] The authors gratefully acknowledge the assistance of Gwen Donahue. This work was supported by a HSDM–MIT Biomaterials Fellowship, a Whitaker Foundation Fellowship, and the Dupont–MIT Alliance. Work was performed, in part, in the MTL and EMSEF facilities at MIT.

 © 2003 Wiley-VCH Verlag GmbH & Co. KGaA, Weinheim 1433-7851/03/4211-1262 $ 20.00+.50/0

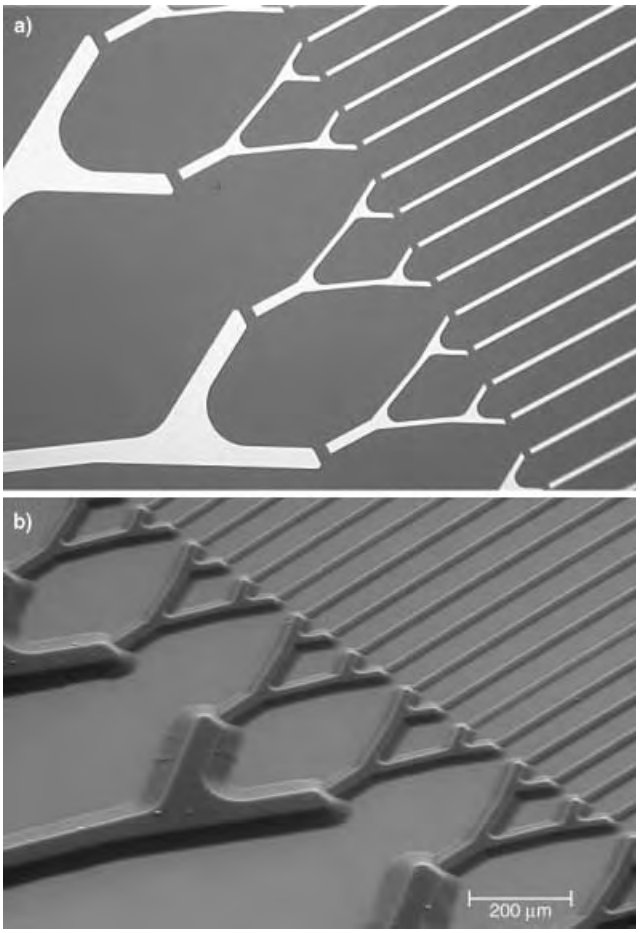

Figure 2. A 3D master pattern to cast a microfluidic mimic of a vascular network. The gaps in the original pattern determine the height of each section. a) The original two-dimensional conductive pattern—a gold film patterned onto a silicon nitride covered wafer; b) SEM image of the resulting 3D structure, the smallest lines are 10 µm high, the tallest are 80 µm. The deposition originated from the left side of the image.

devices with a large ratio between the thickest and thinnest structures (a ratio of 50:1 has been fabricated).

Pyrrole films have been extensively electrodeposited for more than twenty years,[7] and various dopants have been used;[8] of special interest for this technique are those that are highly chemically resistant, since microfabrication often involves aggressive cleaning and etching steps. For this reason, the sodium salt of dodecylbenzenesulfonic acid (NaDBS) was chosen here as the dopant.[9] Other dopants can create polymers that erode in water,[10] which may be of use for creating water-soluble sacrificial structures. Although the exact mechanism for electrodeposition of polypyrrole (PPy) is not fully understood, it involves the oxidation of the pyrrole monomer followed by several chemical and electron-transfer reactions.[8] Pyrrole electropolymerization propagates with a 3D nucleation/growth pattern under charge-transfer control. The film grows with different time constants in the upward and lateral directions.[11] The time constants vary as a function of current density, temperature, dopants, etc.

After studying the characteristics of a variety of PPy films, and observing the well-defined and adherent borders on the films, we believed that it would be possible to form stepped 3D structures by intentionally leaving spaces in the electrode pattern. The uncertainty was whether the film, as it grew, would bridge across the patterns and reliably make an electrical connection to each subsequent unattached pattern. A series of test structures were produced, which included some that were intended as a microfluidic mimic of a vascular network (Figure 2). The original experiments demonstrated that the lateral growth of the film would indeed bridge from the original anode to unattached conductive regions on the surface, and once the gap was bridged, the polymerization process would continue over the entire area.

Electroforming and molding (referred to by its German acronym, LIthography, Galvanoformung, Abformung, or LIGA)[12] of microelectromechanical systems (MEMS) using metal electroplated into an X-ray-defined poly(methyl methacrylate) (PMMA) mold provides a route to the preparation of planar microdevices with critical features of tens to thousands of micrometers. Since many LIGA MEMS are produced from nickel, experiments were also performed using nickel to address the question of whether the gap-bridging process could also be used to directly produce 3D electroplated structures from metals. The results were similar, except for significantly slower deposition rates and a radial expansion of the front, rather than a distinctly faceted surface. For the deposition conditions reported, the surface roughness of the nickel is significantly greater than that of PPy. Nickel LIGA wafers are routinely lapped to remove this roughness, however, this option is not available for the multilevel structures.

Comparing the two materials, there is a noticeable difference in the growth rates and growth behavior of PPy and nickel. The rate of electropolymerization for PPy is 780 nm min^{-1} vertically and 1000 nm min^{-1} horizontally, under the conditions described below. Nickel, under the conditions described below, had a deposition rate of 105 nm min^{-1}, both vertically and horizontally. The 4:3 lateral-to-vertical growth ratio for PPy creates a well-defined faceted profile with the polymer growing slightly faster outward than upward (Figure 3a). The nickel grows uniformly in all directions, which results in the edges of the pattern having a radius equal to the film thickness (Figure 3b). Depending on the application, one or the other of the materials may be more desirable. The PPy surface appears smoother than the nickel surface, and it deposits more rapidly. The sidewalls of the nickel structures, however, are closer to vertical than the corresponding PPy patterns. Vertical sidewalls, or a limit on horizontal expansion, could be obtained by introducing a sacrificial boundary, such as one made from photoresist, around the conductive patterns.

This approach has been demonstrated with a variety of test structures—we have been able to form tapered lines, branched structures, and concave and convex features. Very tall features such as mechanical barriers or sealing rings around a critical region of a device could also be produced. Concave and convex devices were created by a series of concentric patterns—the curvature is a function of the spacing

 © 2003 Wiley-VCH Verlag GmbH & Co. KGaA, Weinheim 1433-7851/03/4211-1263 $ 20.00+.50/0

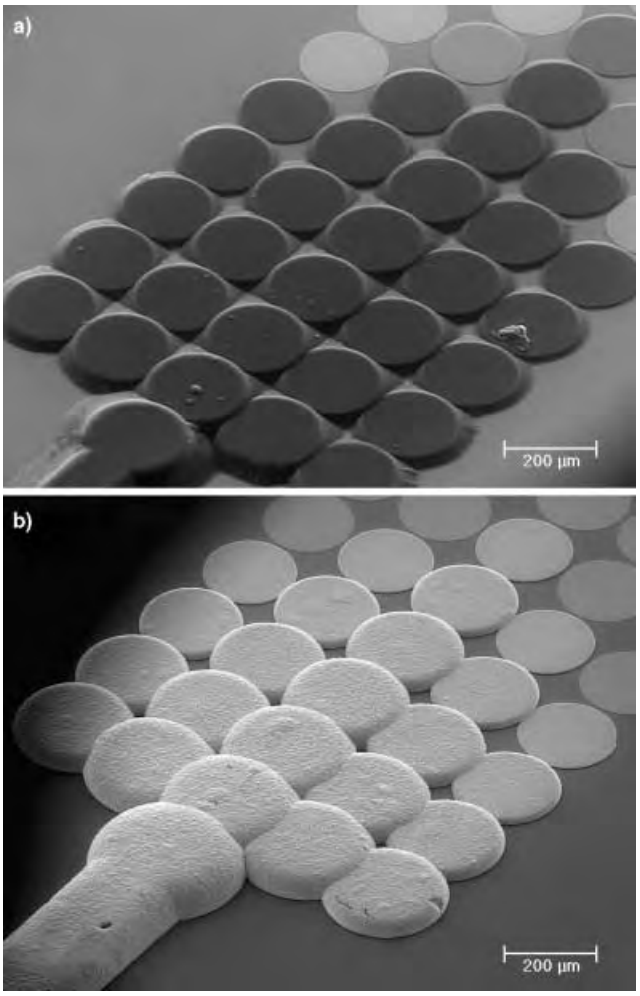

Figure 3. Test patterns in the form of an array of unattached circles. The original patterns are 200 μm in diameter, and 10 μm apart. In each case, deposition originated in the lower left corner of the image, from the circle attached to the anode. a) PPy pattern grown at 3 mA cm^{-2} for 48 min—the middle column has bridged eight gaps; b) nickel structure electroplated at 3 mA cm^{-2} for 14 h—the middle column has bridged six gaps.

of the pattern, and whether the deposition initiates from the inner or outer edge. It was observed that a series of finely spaced lines or arcs provides a more uniform deposition front than those with greater separation; each time the deposited material bridges from one conductive pattern to the next, the expanding front is smoothed. By varying the width of a line pattern, a 3D structure can be produced that varies in thickness and width, or the pattern can be designed so that the final structure maintains a constant width while varying only in thickness.

This technique opens the possibility of new methods to fabricate multilevel structures such as electrodes, interconnects, gratings, and photonic lattices. The next step is to develop approaches to augment these structures with additional films patterned over the first layer. An additional area to explore is the ability of this method to bridge gaps to form low-impedance connections between devices and substrates produced by self-assembly or fluidic self-assembly.[13,14] Lastly, this approach could be used to modify the LIGA process where regions of a microdevice are deposited to regulate the effect of current densities or to create composite or gradient materials from a single mold or pattern.

Experimental Methods

The layouts were generated with AutoCAD software, and DXF files were converted into a chrome-on-glass mask (International Phototool Company). The plating template was formed on 4-inch (10-cm) silicon wafers with a 3000-Å insulating layer of silicon nitride grown by low-pressure chemical vapor deposition (LPCVD). A standard lift-off process was used to pattern the gold electrodes: photoresist was patterned onto the wafer, 200 Å of titanium was deposited as an adhesion layer, after which 3000 Å of gold was deposited to form the conductive pattern. The photoresist was removed, which only left behind the gold in regions deposited directly onto the wafer. The wafers were cut into dies using a flood-cooled die saw. The patterns were protected using an additional layer of photoresist during die sawing; after sawing, the individual dies were cleaned in acetone, ethanol, and deionized water before use—it should be noted that greater adhesion could be achieved using more advanced cleaning procedures, or the addition of a titanium adhesion layer over the conductive layer.

The electrodeposition of PPy occurred at 25 °C using a constant-current power supply (HP 6614C). The current density was 3 mA cm^{-2}. The temperature and current density were varied to find the conditions that gave the smoothest deposited films. Other conditions can produce particularly rough surfaces. Solutions of 0.2 M pyrrole with 0.2 M NaDBS (both Aldrich) as a dopant were prepared more than 24 h in advance to ensure complete dissolution of the constituents. They were stored at 4 °C under nitrogen. Achieving uniform deposition over a large area was difficult, therefore, a platinum wire-mesh cathode was used with an area equal to that of the patterned area of the die, and stirring was adjusted so that the flow across the surface appeared uniform; deposition occurred under a nitrogen blanket. After deposition, the devices were ultrasonically cleaned in deionized water to remove loosely adherent deposits.

The nickel was electroplated using standard procedures.[15,16] The gold pattern acted as the cathode along with a pure nickel anode, and the plating bath was a commercially available nickel sulfamate solution (Mechanical Nickel Sulfamate, Technic Inc.). Current density was regulated to 3 mA cm^{-2}. These dies were also ultrasonically cleaned in deionized water after deposition.

Received: October 22, 2002
Revised: December 18, 2002 [Z50410]

Keywords: electrodeposition · nickel · photolithography · polypyrrole · self-assembly

[1] A. Kumar, N. L. Abbott, H. A. Biebuyck, E. Kim, G. M. Whitesides, *Acc. Chem. Res.* **1995**, *28*, 219.
[2] E. Kim, Y. Xia, G. M. Whitesides, *J. Am. Chem. Soc.* **1996**, *118*, 5722.
[3] D. C. Duffy, J. C. McDonald, O. J. A. Schueller, G. M. Whitesides, *Anal. Chem.* **1998**, *70*, 4974.
[4] B.-H. Jo, D. J. Beebe, *Proc. SPIE-Int. Soc. Opt. Eng.* **1999**, *3877*, 222.
[5] O. Hofmann, G. Voirin, P. Niedermann, A. Manz, *Anal. Chem.* **2002**, *74*, 5243.
[6] L. Griscom, P. Degenaar, B. LePioufle, E. Tamiya, H. Fujita, *Jpn. J. Appl. Phys. Part 1* **2001**, *40*, 5485.
[7] A. F. Diaz, K. K. Kanazawa, G. P. Gardini, *J. Chem. Soc. Chem. Commun.* **1979**, 635.

 © 2003 Wiley-VCH Verlag GmbH & Co. KGaA, Weinheim 1433-7851/03/4211-1264 $ 20.00+.50/0

[8] G. Sabouraud, S. Sadki, N. Brodie, *Chem. Soc. Rev.* **2000**, *29*, 283.
[9] L. F. Warren, D. P. Anderson, *J. Electrochem. Soc.* **1987**, *134*, 101.
[10] A. N. Zelikin, D. M. Lynn, J. Farhadi, I. Martin, V. Shastri, R. Langer, *Angew. Chem.* **2002**, *114*, 149; *Angew. Chem. Int. Ed.* **2002**, *41*, 141.
[11] M. E. G. Lyons, *Adv. Chem. Phys.* **1996**, *94*, 297.
[12] E. W. Becker, W. Ehrfeld, P. Hagmann, A. Maner, D. Münchmeyer, *Microelectron. Eng.* **1986**, *4*, 35.
[13] H.-J. J. Yeh, J. S. Smith, *Sens. Mater.* **1994**, *6*, 319.
[14] J. S. Smith (Alien Technology Corporation), US Pat. 6291896 **2001**.
[15] T. E. Buchheit, D. A. LaVan, J. R. Michael, T. R. Christenson, S. D. Leith, *Metall. Mater. Trans. A* **2002**, *33*, 539.
[16] W. H. Safranek, *The Properties of Electrodeposited Metals and Alloys: a Handbook*, 2nd ed., American Electroplaters and Surface Finishers Society, Orlando, FL, **1986**.

 © 2003 Wiley-VCH Verlag GmbH & Co. KGaA, Weinheim 1433-7851/03/4211-1265 $ 20.00+.50/0

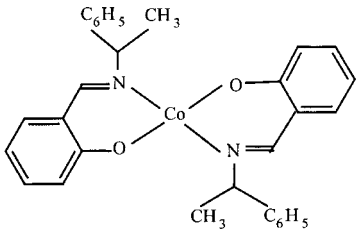

1

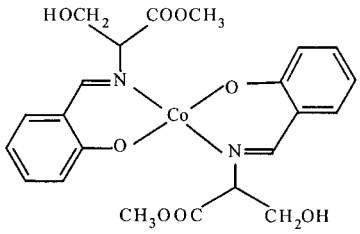

2

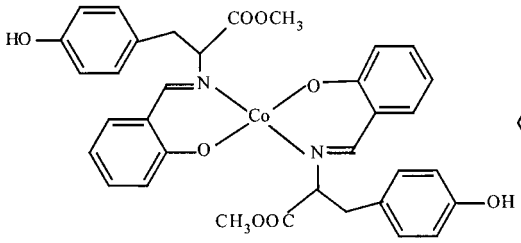

3

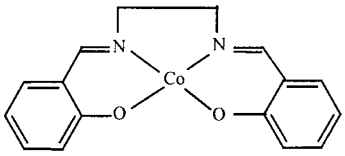

4

Aerobic Oxidation of Amines

An Unconventional Cobalt-Catalyzed Aerobic Oxidation of Tertiary Nitrogen Compounds to *N*-Oxides

*Suman L. Jain and Bir Sain**

The propensity of cobalt complexes to bind with molecular oxygen[1] and the use of such dioxygen–cobalt complexes as catalysts for various oxidation reactions have been subjects of intensive research in recent years.[2] The oxygenation of organic compounds catalyzed by such dioxygen–cobalt complexes and with aldehyde as a sacrificial agent[3] has led to several important methodologies for the epoxidation of olefins,[4] oxidation of sulfides to sulfones,[5] and oxidation of imines to oxaziridines.[6] However, the oxygenation of organic compounds, in which molecular oxygen serves as the oxidant and cobalt complexes as catalysts under ambient conditions without the sacrificial agent, although a desirable goal, has not been very successful. To the best of our knowledge there are only two relevant literature reports describing the oxygenation of trialkylphosphanes[7] and olefins, and cyclic ethers.[8]

[*] Dr. B. Sain, S. L. Jain
Chemical and Biosciences Division
Indian Institute of Petroleum, Dehradun 248005 (India)
Fax: (+91) 135-660202/660098
E-mail: birsain@iip.res.in

The cobalt Schiff base complexes **1**,[4b] **2**,[9] **3**,[10] and **4**[11] are well known to bind with molecular oxygen[4b,9,10] and show very high reactivity in oxygenation reactions with molecular oxygen as the oxidant along with an aldehyde as a sacrificial agent, but there are no reports on the oxygenation of organic compounds with these complexes as catalysts and molecular oxygen as the sole oxidant.

Oxidation of tertiary nitrogen compounds to *N*-oxides is an important synthetic transformation. In the search for environmentally friendly methods for this transformation the use of hydrogen peroxide with the catalysts methyltrioxorhenium(VII),[12] manganese porphyrin,[13] flavin,[14] TS-1,[15] molecular sieves,[16] and tungstate-exchanged Mg/Al-layered double hydroxide[17] has been reported. In continuation of our studies on oxidation with molecular oxygen as the primary oxidant[18] we report here on the first successful oxidation of tertiary nitrogen compounds **5** to *N*-oxides **6** catalyzed by cobalt(II) Schiff base complexes (Scheme 1).

A wide variety of tertiary nitrogen compounds were oxidized to give their corresponding *N*-oxides in nearly quantitative yields by simply bubbling molecular oxygen into a solution of the tertiary nitrogen compound in 1,2-dichloroethane at room temperature in the presence of 5-Å molecular sieves and with the cobalt Schiff base complex **1** as the catalyst. These results are summarized in Table 1. Pyridines containing electron-donating groups (Table 1, entries 2, 3, and 6) were found to react faster than pyridines bearing electron-withdrawing groups (Table 1, entries 4 and

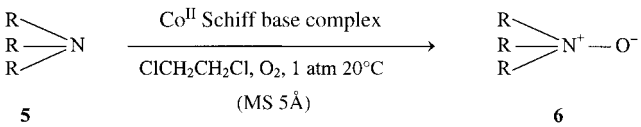

5 6

Scheme 1. Oxidation of tertiary nitrogen compounds **5** to *N*-oxides **6** catalyzed by a cobalt(II) Schiff base.

 © 2003 Wiley-VCH Verlag GmbH & Co. KGaA, Weinheim 1433-7851/03/4211-1265 $ 20.00+.50/0

Table 1: Oxidation of tertiary nitrogen compounds to *N*-oxides.[a]

Entry	Substrate	*t* [h]	Yield [%]
1		8	80
2	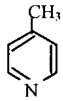	8	85
3	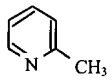	10	75
4	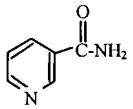	14	55
5	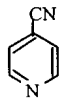	12	50
6	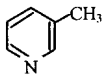	10	65
7	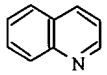	12	50
8	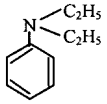	6	92
9	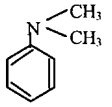	6	90
10	$(C_2H_5)_3N$	5	92

[a] All reactions were conducted with substrate (10 mmol) and Co^{II} Schiff base complex **1** (0.5 mol%) in 1,2-dichloroethane (10 mL) at room temperature under an oxygen atmosphere in the presence of 5-Å molecular sieves (see Experimental Section).

5). To evaluate the relative efficiency of various Co^{II} Schiff base complexes, we prepared complexes **2**–**4** and studied the oxidation of 4-picoline under similar conditions with 0.5 mol% of these catalysts. All of these complexes were found to be efficient catalysts for this transformation; however, compound **1**[19] was found to be most efficient probably as a consequence of the effect of the ligands, which are known to affect the oxidation potential.[20] In a control experiment in the absence of catalyst no oxidation was observed. Although these reactions could also be performed without 5-Å molecular sieves, their presence was found to enhance the reaction rate. We assume the molecular sieves remove the moisture in the reaction system and that added with the oxygen gas.

Although the mechanism of this reaction is not yet clear, it probably involves the coordination of the tertiary nitrogen compound and molecular oxygen with the cobalt complex (→**7**), formation of the binuclear μ-peroxocobalt complex **8,** homolytic cleavage of the O–O bond followed by the formation of reactive oxometal species **9,** and intramolecular transfer of oxygen to the nitrogen atom to yield the *N*-oxide (Scheme 2). The formation of superoxocobalt complexes such as **7** have been assumed earlier for cobalt Schiff base complexes in the presence of tertiary amines.[21] The formation of the binuclear μ-peroxocobalt complex **8** and the oxometal species **9**, and intramolecular oxygen transfer to the tertiary amine are analogous to steps in the mechanistic pathway for the oxidation of tributylphosphane to tributylphosphane oxide with molecular oxygen catalyzed by bis(acetylacetonato)cobalt(II).[7]

In summary, we have demonstrated for the first time that cobalt Schiff base complexes can catalyze the oxidation of tertiary nitrogen compounds with molecular oxygen as the sole oxidant to afford *N*-oxides in excellent yields under mild conditions. The simplicity of the system, simple workup, and excellent yields make this method an attractive, environmentally acceptable synthetic tool.

Experimental Section

All the reagents and solvents used were laboratory reagent grade and purified before use. Cobalt Schiff base complexes **1**,[4b] **2**,[9] **3**,[10] and **4**[11] were prepared according to literature procedures.

A typical procedure for the oxidation of tertiary nitrogen compounds to *N*-oxides: Molecular oxygen was bubbled at room temperature (20°C) into a stirred solution of 4-picoline (0.93 g, 10 mmol) and cobalt Schiff base complex **1** (25 mg, 0.5 mol%) in dichloroethane (10 mL), which contained 5-Å molecular sieves (1 g). The progress of reaction was monitored by TLC (SiO_2). At the end of reaction the molecular sieves were removed by filtration, and the reaction mixture was passed through a silica gel column with dichloromethane/MeOH (95:5) as the eluent. Removal of solvent and standard workup gave 4-picoline *N*-oxide (0.93 g, 85%). Other *N*-oxides were prepared by this procedure; their reaction times and yields are given in Table 1. The products were identified by comparing their physical and spectroscopic data with literature data.

For comparing the efficiency of various Co^{II} Schiff base complexes, experiments were carried out with 4-picoline under similar conditions, and the residue obtained after passage through the silica

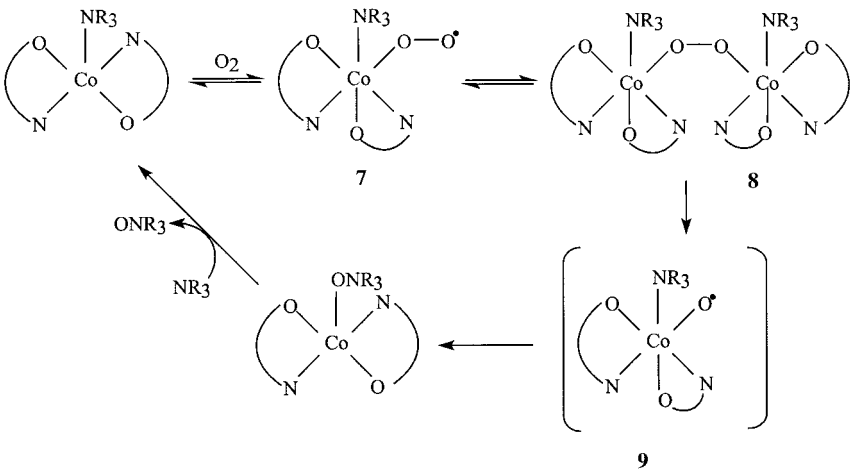

Scheme 2. Proposed mechanism for the oxidation.

 © 2003 Wiley-VCH Verlag GmbH & Co. KGaA, Weinheim 1433-7851/03/4211-1266 $ 20.00+.50/0

gel column was analyzed by HPLC for conversion of 4-picoline to 4-picoline *N*-oxide.

Received: October 1, 2002 [Z50272]

Keywords: cobalt · homogeneous catalysis · N oxides · oxidation · Schiff bases

[1] a) L. I. Simandi, *Catalytic Activation of Dioxygen by Metal Complexes*, Kluwer Academic Publishers, Dordrecht, **1992**; b) A. L. Gavrilova, C. J. Qin, R. D. Sommer, A. L. Rheingold, B. Bosnich, *J. Am. Chem. Soc.* **2002**, *124*, 1714.

[2] a) R. A. Sheldon, J. K. Kochi, *Metal Catalyzed Oxidations of Organic Compounds*, Academic Press, New York, **1981**; b) *The Activation of Dioxygen and Homogeneous Catalytic Oxidation* (Eds.: D. H. R. Barton, A. E. Martell, D. T. Sawyer), Plenum Press, New York, **1993**; c) S. Leonard, P. M. Gannett, Y. Rojana Sakul, D. Schwegler-Berry, V. Castranova, V. Vallyathan, X. Shi, *J. Inorg. Biochem.* **1998**, *70*, 239.

[3] a) T. Mukaiyama, T. Yamada, *Bull. Chem. Soc. Jpn.* **1995**, *68*, 17; b) A. K. Mandal, J. Iqbal, *Tetrahedron* **1997**, *53*, 7641; c) A. K. Mandal, V. Khanna, J. Iqbal, *Tetrahedron Lett.* **1996**, *37*, 3769.

[4] a) S. Bhatia, T. Punniyamurthy, B. Bhatia, J. Iqbal, *Tetrahedron* **1993**, *49*, 6101; b) T. Punniyamurthy, B. Bhatia, J. Iqbal, *J. Org. Chem.* **1994**, *59*, 850; c) P. Li, Y. H. Lin, I. D. Williams, *Appl. Catal. A* **1997**, *150*, 221; d) R. Giannandrea, P. Mastrorilli, C. F. Nobile, G. P. Surauna, *J. Mol. Catal.* **1994**, *94*, 27; e) T. Mukaiyama, T. Yorozu, T. Yamada, *Chem. Lett.* **1993**, 439; f) E. Paez-Mozo, N. Gabriunas, R. Maggi, D. Acosta, P. Ruiz, B. Delmon, *J. Mol. Catal.* **1994**, *91*, 251; g) E. M. Gaigneaux, M. P. Ruiz, B. Delmon, *J. Mol. Catal. A: Chem.* **1996**, *109*, 67.

[5] a) C. F. Nobile, M. M. Dell'Anna, P. Mastrorilli, *J. Mol. Catal. A: Chem.* **1996**, *108*, 57; b) V. Iliev, L. Prahov, L. Bilyarska, H. Fischer, G. Schulz-Ekloff, D. Whrole, L. Petrov, *J. Mol. Catal. A: Chem.* **2000**, *151*, 161.

[6] L. Martiny, K. A. Jorgensen, *J. Chem. Soc. Perkin Trans. 1* **1995**, 699.

[7] R. P. Hanzlik, D. Williamson, *J. Am. Chem. Soc.* **1976**, *98*, 6570.

[8] M. T. Reetz, K. Tollner, *Tetrahedron Lett.* **1995**, *36*, 9461.

[9] S. J. S. Kalra, T. Punniyamurthy, J. Iqbal, *Tetrahedron Lett.* **1994**, *35*, 4847.

[10] G. C. Maikap, D. Guhathakurta, J. Iqbal, *Synlett* **1995**, 189.

[11] H. Diehl, C. C. Hach, *Inorg. Synth.* **1950**, *3*, 196.

[12] a) C. Coperet, H. Adolfsson, T. A. V. Khuong, A. K. Yudin, K. B. Sharpless, *J. Org. Chem.* **1998**, *63*, 1740; b) Z. Zhu, J. H. Espenson, *J. Org. Chem.* **1995**, *60*, 1326; c) Y. Jiao, H. Yu, *Synlett* **2001**, 73.

[13] A. Thellend, P. Battioni, W. Sanderson, D. Mansuy, *Synthesis* **1997**, 1387.

[14] a) K. Bergstad, J. E. Bäckvall, *J. Org. Chem.* **1998**, *63*, 6650; b) S. Ball, C. Bruice, *J. Am. Chem. Soc.* **1980**, *102*, 6498.

[15] D. J. Robinson, P. McMom, D. Bethell, P. C. Bulmanpage, C. Sly, F. King, F. E. Hangcock. , G. J. Hutching, *Catal. Lett.* **2001**, *72*, 233.

[16] M. R. Prasad, G. Kamalkar, G. Madhavi, S. J. Kulkarni, K. V. Raghvan, *Chem. Commun.* **2000**, 1577.

[17] B. M. Choudhary, B. Bharathi, C. V. Reddy, K. M. Lakshmi, K. V. Raghavan, *Chem. Commun.* **2001**, 1736.

[18] a) S. L. Jain, B. Sain, *Chem. Commun.* **2002**, 1040; b) S. L. Jain, B. Sain, *J. Mol. Catal.* **2001**, *176*, 101; c) T. V. Rao, B. Sain, K. Kumar, P. S. Murthy, T. S. R. Prasada Rao, G. C. Goshi, *Synth. Commun.* **1998**, *28*, 319; d) B. Sain, P. S. Murthy, T. V. Rao, T. S. R. Prasada Rao, G. C. Goshi, *Tetrahedron Lett.* **1994**, *35*, 5083; e) T. V. Rao, B. Sain, P. S. Murthy, T. S. R. Prasada Rao, A. K. Jain, G. C. Joshi, *J. Chem. Res. Synop.* **1997**, 300; f) T. V. Rao, B. Sain, P. S. N. Murthy, G. C. Joshi, T. S. R. Prasada Rao, *Stud. Surf. Sci. Catal.* **1998**, *113*, 921.

[19] As suggested by one of the referees, we carried out experiments on the oxidation of a secondary amine (dicyclohexylamine) and a primary amine (4-methoxyaniline) with complex **1** as the catalyst under similar conditions and observed the formation of dicyclohexyl nitrone and 4-nitroanisole, respectively. However, olefins (norbornylene and styrene) did not react under similar conditions.

[20] D. L. Tomaja, L. H. Vogt, J. G. Wirth, *J. Org. Chem.* **1970**, *35*, 2029.

[21] A. L. Crumbliss, F. Basolo, *J. Am. Chem. Soc.* **1970**, *92*, 55.

 © 2003 Wiley-VCH Verlag GmbH & Co. KGaA, Weinheim 1433-7851/03/4211-1267 $ 20.00+.50/0

Diterpene Anti-tuberculosis Agents

Unified Strategy for the Synthesis of (−)-Elisapterosin B and (−)-Colombiasin A**

*Angie I. Kim and Scott D. Rychnovsky**

Elisapterosin B (**1**) is a polycyclic diterpene isolated and characterized by Rodriguez and co-workers from the West Indian sea whip *Pseudopterogorgia elisabethae* (Bayer).[1] Among its cogeners, it showed the most potent inhibitory activity against *Mycobacterium tuberculosis* H37Rv. Rodriguez and co-workers proposed that the uncommon cagelike skeleton of **1** might arise by cyclization of a serrulatane diterpene such as **2**, which was isolated from the same organism (Scheme 1).[2] An alternative biosynthetic cyclization of a serrulatane core leads to colombiasin A (**3**), another unusual structure isolated from the *P. elisabethae*.[3] We became interested in the possible [5+2] and [4+2] cyclizations of a serrulatane skeleton as biomimetic routes to elisapterosin B (**1**) and colombiasin A (**3**), respectively. Nicolaou and co-workers recently reported the synthesis of **3** by an intramolecular Diels–Alder cyclization of a serrulatane diene.[4,5] The [5+2] cycloaddition was discovered by Joseph-Nathan many years ago[6] but has only rarely found use in synthesis.[7,8] Herein we outline the first synthesis of elisapterosin B (**1**) using an intramolecular [5+2] cycloaddition as well as an efficient route to colombiasin A (**3**).

[*] Prof. S. D. Rychnovsky, A. I. Kim
Department of Chemistry
University of California, Irvine
516 Rowland Hall
Irvine, CA 92697-2025 (USA)
Fax: (+1) 949-824-6379
E-mail: srychnov@uci.edu

[**] This work was supported by the National Institutes of Health and a generous gift from Schering–Plough Corporation.

Supporting information for this article is available on the WWW under http://www.angewandte.org or from the author.

 © 2003 Wiley-VCH Verlag GmbH & Co. KGaA, Weinheim 1433-7851/03/4211-1267 $ 20.00+.50/0

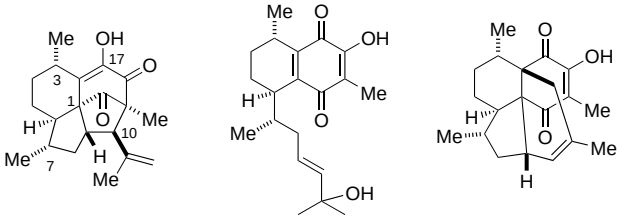

Scheme 1. The structures of (−)-elisapterosin B (**1**), (−)-colombiasin A (**3**), and a serrulatane diterpene **2**, which were each isolated from the sea whip *Pseudopterogorgia elisabethae*.

Synthesis of the *cis*-decaline serrulatane skeleton was based on a Diels–Alder addition (Scheme 2). The chiral diene **7** was prepared beginning with Myers' pseudoephedrine auxiliary.[9] Alkylation of **4**, followed by reduction and hydrolysis produced the enantiomerically pure aldehyde **5**.

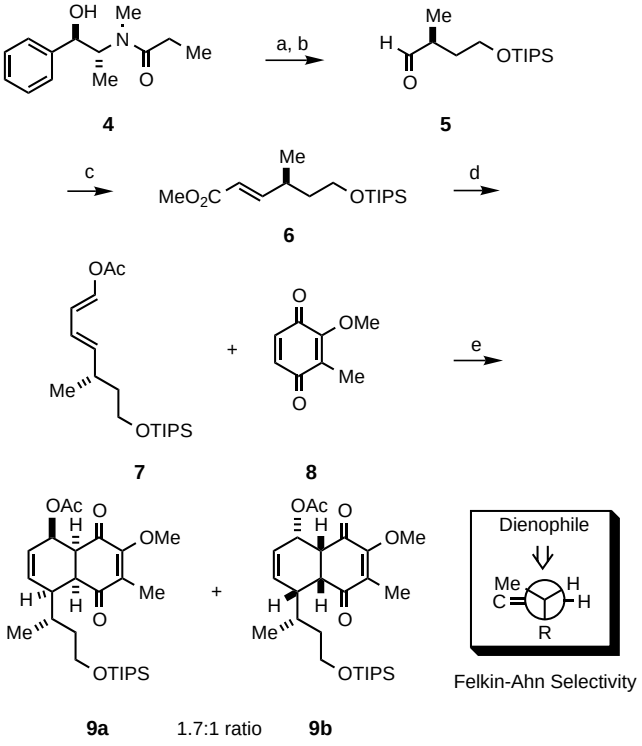

Scheme 2. Synthesis of the decaline **9**. a) LDA, LiCl, ICH_2CH_2OTIPS, 94%, >97% *de*; b) $LiAlH(OEt)_3$, then H^+, 77%; c) $Ph_3P{=}CHCO_2Me$, CH_3CN, reflux, 85%; d) 1. $LiCH_2Br$, THF, −78°C; 2. *n*BuLi, −78 to 23°C; 3. LiH, reflux; 4. Ac_2O, 79%; e) 5 M $LiClO_4$, Et_2O, 24 h, 75%, 1.7:1 ratio. LDA = lithium diisopropylamide, TIPS = triisopropylsilyl.

Wittig olefination of **5** gave the ester **6**. Conversion of **6** into the diene **7** followed precedent from Kowalski's group.[10] Homologation to the lithium ynolate followed by treatment with LiH and acetylation produced the acetoxy diene **7** as a single isomer in 79% yield. The dienophile **8** was prepared by using the strategy developed by Knolker and co-workers.[11] The key Diels–Alder reaction between **7** and **8** was unsuccessful under thermal conditions, and use of Lewis acids such as $ZnBr_2$ led to very low yields. Lithium perchlorate in diethyl ether was uniquely effective in promoting this cycloaddition.[12] Treatment of the diene and dienophile for one day at ambient temperature generated the desired adduct **9** in 75% yield. The Diels–Alder adduct **9** was a 1.7:1 mixture of inseparable diastereomers. Attempts to improve the diastereoselectivity using chiral Lewis acids were unsuccessful,[13,14] and so the mixture of diastereomers was carried on through the synthesis. Ultimately the major isomer was shown to have the configuration **9a** by correlation with the natural product. The minor isomer was shown to have the structure **9b** by correlation with a previously synthesized compound.[15] The stereoselectivity arises from a Felkin–Ahn like approach of the dienophile to the diene as shown in Scheme 2. Thus, overall, decaline **9** was prepared in only five steps from the pseudoephedrine amide **4**.

The acetate substituent on diene **7** controlled the regioselectivity in the cycloaddition to **9** but must be replaced by a methyl group. Several strategies were considered, but a simple dimethylcuprate displacement turned out to be the best approach (Scheme 3). Reduction of the ketone group at C17 with $NaBH_4$ prevented aromatization in the subsequent steps. Treatment with lithium dimethylcuprate cleanly replaced the acetate group with a methyl group. COSY experiments suggested that the position of the C4–C5 alkene had not changed in the reaction, and correlation with the

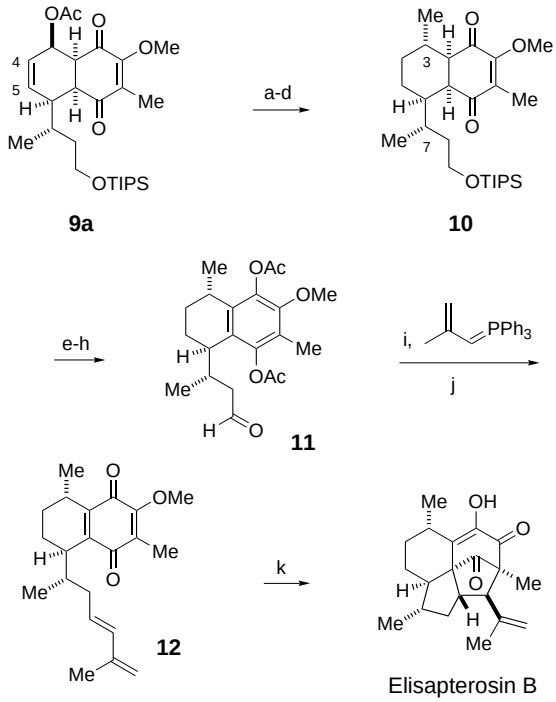

Scheme 3. Synthesis of elisapterosin B (**1**). a) $NaBH_4$, $CeCl_3$, MeOH, 93%; b) $LiCuMe_2$, Et_2O, 0 to 23°C, 89%; c) H_2, Pd/C, EtOH, 95%; d) Dess–Martin, CH_2Cl_2, 92%; e) DBU, CH_2Cl_2, (air), 70%; f) Zn, Ac_2O, NaOAc, then Ac_2O, pyridine, 96%; g) HF–pyridine, THF, 94%; h) Dess–Martin, CH_2Cl_2, 99%; i) Wittig reagent, THF, 78% 3:1 *E*/*Z*; j) K_2CO_3, MeOH (air), 79%, k) 25 equiv $BF_3{\cdot}OEt_2$, CH_2Cl_2, −78°C, 41%. All the intermediates in this scheme are a 1.7:1 diastereomeric ratio derived from the mixture **9a** and **9b**. The diastereomers were separated after the final step in the sequence to produce pure (−)-elisapterosin B (**1**). DBU = 1,8-diazabicyclo[5.4.0]undec-7-ene.

 © 2003 Wiley-VCH Verlag GmbH & Co. KGaA, Weinheim 1433-7851/03/4211-1268 $ 20.00+.50/0

natural product confirmed that S_N2 rather than S_N2' displacement of the acetate had taken place. This felicitous outcome was unexpected.[16] Hydrogenation and Dess–Martin oxidation returned enedione **10** in excellent yield. Treatment of **10** with DBU and air gave the corresponding quinone. Zinc reduction and acetylation produced the hydroquinone diacetate. In theory, deprotonation and acetylation of **10** would give the same product, but all such attempts to effect this transformation produced only the quinone. Deprotection, oxidation, and Wittig reaction generated the diene side chain as a 3:1 mixture of *E* and *Z* isomers. Treatment of the hydroquinone diacetate with K_2CO_3 in methanol led directly to the quinone **12** by a facile air oxidation. Diene **12** is set up to test the key [5+2] cycloaddition.

The proposed [5+2] cycloaddition had good precedent from work of Joseph-Nathan's group, who showed that Lewis acid catalysis promoted intramolecular [5+2] additions.[6] Grieco's group also reported several [5+2] cycloadditions catalyzed by $LiClO_4$.[8] We found that treatment of diene **12** with a modest excess of $BF_3{\cdot}OEt_2$ at 0 °C did not promote the cyclization efficiently, but a large excess of $BF_3{\cdot}OEt_2$ at lower temperature produced the [5+2] cycloadduct. The best conditions involved the use of 25 equivalents of $BF_3{\cdot}OEt_2$ at −78 °C for one hour. Elisapterosin B (**1**) was isolated as a 1.7:1 mixture of diastereomers (from **9a** and **9b**) in 41% yield. The product was accompanied by 22% of *O*-methyl colombiasin A. Attempted cyclization with trimethylsilyl trifluoromethanesulfonate (TMSOTf) led to decomposition, and addition of 2,6-di-*tert*-butylpyridine lowered the yield in the $BF_3{\cdot}OEt_2$ cyclization. Presumably, the [5+2] cycloaddition proceeded from a conformation of **12** with an axial diene side chain that was reinforced by a peri interaction in the alternative chair conformation. The [5+2] cycloaddition is favored by Lewis acid coordination to the quinone, which polarizes the carbonyl π bond. The resulting complex contains a five-carbon, four-electron π system that can undergo a thermally allowed cycloaddition with the pendant alkene. This analysis is related to the explanation for Lewis acid catalysis of a Nazarov cyclization.[17] The synthesis of elisapterosin B was completed by chromatographic separation of the C7 methyl epimers to provide pure (−)-elisapterosin B, which was identical to the natural product by ^{1}H NMR and ^{13}C NMR spectroscopy, high-resolution mass spectrometry (HRMS), and optical rotation.[1,18] Elisapterosin B (**1**) was synthesized from pseudoephedrine amide **4** in 16 steps and 2.6% overall yield.

Colombiasin A methyl ether was isolated as a minor side product in the Lewis acid promoted cyclization of diene **12**. Nicolaou and co-workers had previously shown that the intramolecular Diels–Alder route to colombiasin A (**3**) was viable under thermal conditions.[4] When diene **12** was heated to 180 °C in toluene, the colombiasin A methyl ether was isolated in 83% yield (Scheme 4). The diene **12** was a 3:1 *E*/*Z* mixture, which suggested that *E*/*Z* isomerization was taking place under the reaction conditions and that the (*E*)-diene cyclized preferentially. Synthesis of colombiasin A (**3**) was completed by demethylation using $AlCl_3$ buffered with *N*,*N*-dimethylaniline.[19] Synthetic colombiasin A was isolated in 73% yield as a 1.7:1 mixture of diastereomers (from **9a** and **9b**). Chromatographic separation gave pure (−)-colombiasin A, which was identical to the natural product by ^{1}H NMR and ^{13}C NMR spectroscopy, and HRMS.[3,4] Colombiasin A was prepared in 17 steps and 3.9% yield from pseudoephedrine amide **4**.

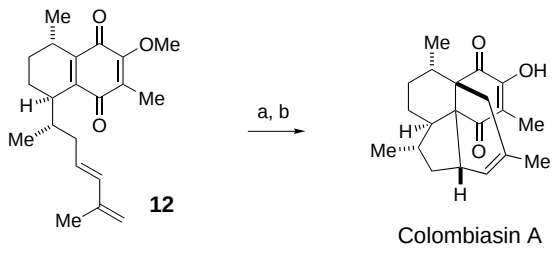

Scheme 4. Synthesis of colombiasin A (**3**). a) 180 °C, toluene, 83%; b) $AlCl_3$, $PhNMe_2$, CH_2Cl_2, 0 to 23 °C, 73%.

We have developed an efficient route to the elisapterosin and colombiasin natural products based on [5+2] and [4+2] intramolecular cyclizations of a common serrulatane diene. These syntheses provide support for biosynthetic proposal developed by Rodriguez's group and provide access to these interesting anti-tuberculosis agents.

Received: November 26, 2002 [Z50636]

Keywords: cycloaddition · natural products · total synthesis

[1] A. D. Rodriguez, C. Ramirez, I. I. Rodriguez, C. L. Barnes, *J. Org. Chem.* **2000**, *65,* 1390–1398.
[2] A. D. Rodriguez, Y. P. Shi, *Tetrahedron* **2000**, *56,* 9015–9023.
[3] A. D. Rodriguez, C. Ramirez, *Org. Lett.* **2000**, *2,* 507–510.
[4] a) K. C. Nicolaou, G. Vassilikogiannakis, W. Magerlein, R. Kranich, *Angew. Chem.* **2001**, *113*, 2543–2547; *Angew. Chem. Int. Ed.* **2001**, *40,* 2482–2486; b) K. C. Nicolaou, G. Vassilikogiannakis, W. Magerlein, R. Kranich, *Chem. Eur. J.* **2001**, *7,* 5359–5371.
[5] D. C. Harrowven, M. J. Tyte, *Tetrahedron Lett.* **2001**, *42,* 8709–8711.
[6] a) P. Joseph-Nathan, M. E. Garibay, R. L. Santillan, *J. Org. Chem.* **1987**, *52,* 759–763; b) P. Joseph-Nathan, V. Mendoza, E. Garcia, *Tetrahedron* **1977**, *33,* 1573–1576; c) I. H. Sanchez, R. Yanez, R. Enriquez, P. Joseph-Nathan, *J. Org. Chem.* **1981**, *46,* 2818–2819.
[7] a) G. Büchi, C.-P. Mak, *J. Am. Chem. Soc.* **1977**, *99,* 8073–8075; b) T. A. Engler, C. M. Scheibe, R. Iyengar, *J. Org. Chem.* **1997**, *62,* 8274–8275; c) T. A. Engler, M. A. Letavic, R. Iyengar, K. O. LaTessa, J. P. Reddy, *J. Org. Chem.* **1999**, *64,* 2391–2405; d) H. Takakura, S. Yamamura, *Tetrahedron Lett.* **1998**, *39,* 3717–3720.
[8] a) J. L. Collins, P. A. Grieco, J. K. Walker, *Tetrahedron Lett.* **1997**, *38,* 1321–1324; b) P. A. Grieco, J. K. Walker, *Tetrahedron* **1997**, *53,* 8975–8996.
[9] A. G. Myers, B. H. Yang, H. Chen, L. McKinstry, D. J. Kopecky, J. L. Gleason, *J. Am. Chem. Soc.* **1997**, *119,* 6496–6511.
[10] a) C. J. Kowalski, M. S. Haque, *J. Am. Chem. Soc.* **1986**, *108,* 1325–1327; b) C. J. Kowalski, G. S. Lal, *J. Am. Chem. Soc.* **1986**, *108,* 5356–5357; c) C. J. Kowalski, G. S. Lal, *Tetrahedron Lett.* **1987**, *28,* 2463–2466; d) C. J. Kowalski, R. E. Reddy, *J. Org. Chem.* **1992**, *57,* 7194–7208.
[11] a) H.-J. Knölker, W. Fröhner, K. R. Reddy, *Synthesis* **2002**, 557–564; b) J. R. Luly, H. Rapoport, *J. Org. Chem.* **1981**, *46,* 2745–2752.

 © 2003 Wiley-VCH Verlag GmbH & Co. KGaA, Weinheim 1433-7851/03/4211-1269 $ 20.00+.50/0

[12] P. A. Grieco, J. J. Nunes, M. D. Gaul, *J. Am. Chem. Soc.* **1990**, *112,* 4595 – 4596.
[13] The use of chiral Lewis acid [Cl_2Ti((*R*)-BINOL)] ((*R*)-BINOL = (*R*)-2,2′-dihydroxy-1,1′-binaphthyl) did not lead to product: a) K. Mikami, M. Terada, Y. Motoyama, T. Nakai, *Tetrahedron: Asymmetry* **1991**, *2,* 643 – 646; b) K. Mikami, Y. Motoyama, M. Terada, *J. Am. Chem. Soc.* **1994**, *116,* 2812 – 2820.
[14] Attempts to use the corresponding quinone monoketals and a chiral Lewis acid also failed to produce Diels–Alder adducts: M. Breuning, E. J. Corey, *Org. Lett.* **2001**, *3,* 1559 – 1562.
[15] Compound **9b** was carried through the remainder of the syntheses, and the epimeric mixture was only separated at the final step. The structure of **9b** was confirmed at the penultimate step of the colombiasin A synthesis, where the minor isomer present in the mixture was compared with the (±)-7-*epi*-*O*-methyl colombiasin A prepared by Nicolaou and co-workers.[4] The two compounds showed identical ^{1}H and ^{13}C NMR data, confirming the structure of our minor component as *ent*-7-*epi*-*O*-methyl colombiasin A.
[16] R. M. Magid, *Tetrahedron* **1980**, *36,* 1901 – 1930.
[17] K. L. Habermas, S. E. Denmark, T. K. Jones, *Org. React.* **1994**, *45,* 1 – 158.
[18] Synthetic elisapterosin B had a rotation of $[\alpha]_D^{23} = -31.5$ (c = 0.16, $CHCl_3$). The natural product had a reported rotation of $[\alpha]_D^{25} = -3.0$ ($c = 4.4$, $CHCl_3$).[1] Professor Rodriguez was able to resolve the discrepancy by finding an error in the original calculation. The correct rotation for the natural product is $[\alpha]_D^{25} = -29.8$ ($c = 0.44$, $CHCl_3$). We thank Professor Rodriguez for his prompt assistance in this matter.
[19] T. Akiyama, H. Hirofuji, S. Ozaki, *Tetrahedron Lett.* **1991**, *32,* 1321 – 1324.

 © 2003 Wiley-VCH Verlag GmbH & Co. KGaA, Weinheim 1433-7851/03/4211-1270 $ 20.00+.50/0

Dynamic Combinatorial Libraries

Selection and Amplification of a Catalyst from a Dynamic Combinatorial Library**

*Barbara Brisig, Jeremy K. M. Sanders, and Sijbren Otto**

The development of catalysts that rival the efficiency and selectivity of enzymes is one of the holy grails in chemistry. To date, success in the design and synthesis of such systems is limited by an imperfect understanding of the host–guest interactions underlying efficient activity. As an alternative, several selection-based approaches to the discovery of new catalytic systems are being developed.[1] Selection can be based on activity such as in the in vitro evolutionary screening and selection of ribozymes,[2] while another approach involves selection of receptors on the basis of the affinity for the transition state of a given reaction. In practice, screening is based on the affinity for a stable transition-state analogue (TSA). In molecular imprinting, a polymer is formed around a TSA that is subsequently removed to generate catalytically active molecular-sized cavities.[3] The catalytic potential of antibodies raised against a TSA has also been explored.[4] Although catalysts have been produced using these methods, success has been relatively rare, whereas the experimental difficulties, time, and expense associated with these methods are considerable. Herein we introduce an alternative approach based on dynamic combinatorial chemistry.[5]

In dynamic combinatorial chemistry, a mixture of compounds is generated by linking small building blocks together through a reversible reaction. Reversibility ensures that the dynamic combinatorial library (DCL) is in thermodynamic equilibrium and responsive to external influences. Upon exposure of a DCL to a molecular target, those library members that bind to the target are stabilized; the equilibrium shifts, and strong binders are amplified at the expense of the poor binders in the library.[6] After the exchange of building blocks has been turned off, the amplified compound(s) can be isolated directly from the frozen library.[7] Thus dynamic combinatorial chemistry is not only a method of selection but also provides a synthetic route towards the selected compounds.

We have demonstrated that disulfide chemistry is well-suited for the generation of DCLs of macrocycles in water.[8] Disulfide formation occurs readily by oxidation of thiols upon exposure to air. Exchange takes place under mild conditions (pH 7–9) in the presence of thiolate, and is switched off either under acidic conditions or after removal of the thiolate. Thiol oxidation is sufficiently slow under the conditions we use to allow equilibration to occur.[8] We recently reported a DCL made by mixing dithiol building blocks **1, 2**, and **3** and showed how exposure of this library to two guest molecules led to the amplification of two receptors for hydrophobic ammonium ions.[6j] Given the high affinity of the selected library members for cationic hydrophobic molecules, we have now used the same library to search for catalysts for the Diels–Alder reaction between acridizinium bromide (**4**) and cyclopentadiene (**5**; Scheme 1).[9] As the transition state of the Diels–Alder reaction is similar to the product **6**, we reasoned that **6** would be a good TSA. Thus we stirred equimolar amounts of

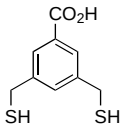

1

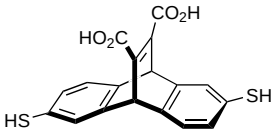

2

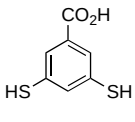

3

[*] Dr. S. Otto, Prof. J. K. M. Sanders
Department of Chemistry, University of Cambridge
Lensfield Road, Cambridge CB2 1EW (UK)
Fax: (+44) 1223-336017
E-mail: so230@cam.ac.uk
B. Brisig
Department of Inorganic Chemistry, University of Basel
Spitalstrasse 51, 4056 Basel (Switzerland)

[**] We thank Prof. A. R. Fersht and Dr. C. M. Johnson for the use of their isothermal titration microcalorimeter and for technical assistance. We also thank Prof. J. B. F. N. Engberts for an initial gift of **4** and for stimulating discussions. We acknowledge support from the European Union (Marie Curie Fellowship) and the Royal Society (University Research Fellowship) to S.O. and from the EPSRC to J.K.M.S.

Supporting information for this article is available on the WWW under http://www.angewandte.org or from the author.

 © 2003 Wiley-VCH Verlag GmbH & Co. KGaA, Weinheim 1433-7851/03/4211-1270 $ 20.00+.50/0

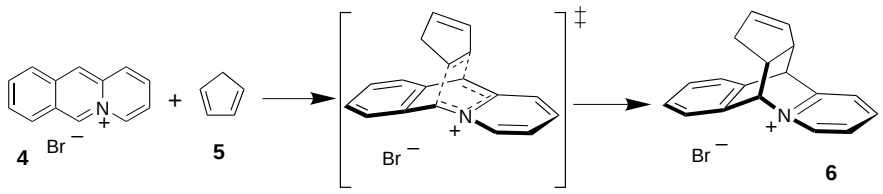

Scheme 1. Diels–Alder reaction demonstrating the similarity between transition state and product.

1, **2**, and **3** in water at pH 8.5 in the presence of atmospheric oxygen for 3–5 days. The product distributions of the resulting DCL in the absence of any template (Figure 1 A) and after addition of **6** (Figure 1 B) were analyzed by HPLC and mass spectrometry. Addition of the TSA results in the selection and amplification of two macrocycles, which were identified by mass spectrometry as **7** and **8** (Figure 1), the same receptors selected in our previous study.[6j] Both macrocycles are formed as mixtures of stereoisomers since racemic **2** was used as a building block. Macrocycles **7** and **8** can be obtained from a biased DCL made from **2** and **3** in the ratio in which they are incorporated in the selected macrocycles. Together, the two macrocycles of interest make up 79% of the library material in the presence of TSA **6** (Figure 2 B), whereas they constitute only 12% in the absence of template (Figure 2 A).

We have studied the binding of diene **4** and Diels–Alder product **6** to hosts **7** and **8** by means of isothermal titration microcalorimetry (ITC; Table 1). Heterotrimer **8** was found to bind the diene starting material more strongly than it binds the Diels–Alder product. In contrast, homotrimer **7** binds the product more strongly than it does the starting material. This suggests that heterotrimer **8** will be catalytically inactive, as the incorporation of cyclopentadiene (**5**), and the subsequent Diels–Alder addition, would lead to a less stable complex. In contrast, incorporation of **5** into the **7**·**4** complex would lead to a more stable species, indicating that **7** could be catalytically active.

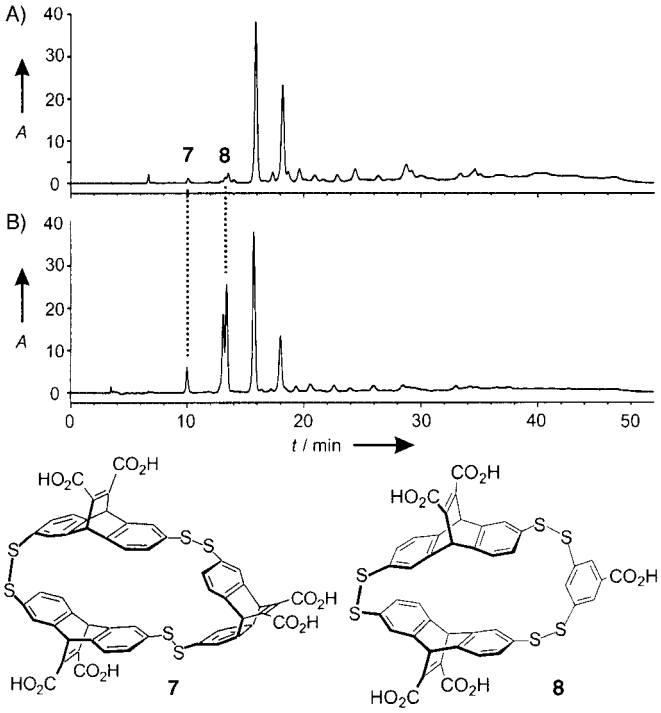

Figure 1. HPLC analyses of the DCL made from dithiols **1, 2**, and **3** (3.3 mM each): A) in the absence of any template, and B) in the presence of TSA **6**, which induced the amplification of macrocycles **7** and **8** (as mixtures of stereoisomers). HPLC analyses were carried out on a 250×4.6 mm 5-μm Hypersil SAX anion-exchange column with a gradient of 0.025–0.5 M ammonium formate in 2-propanol/acetonitrile/water (55:35:10).

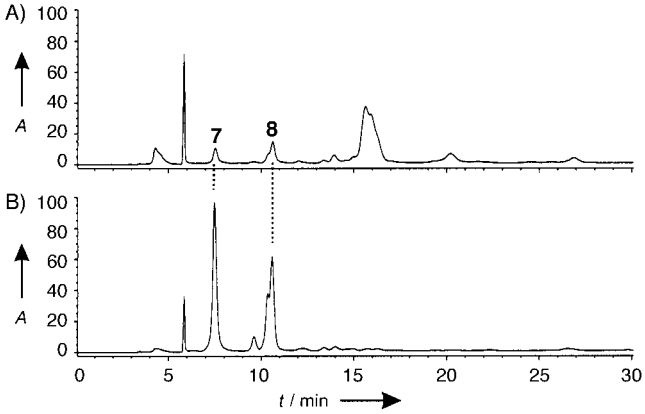

Figure 2. HPLC analyses of a DCL made from dithiols **2** (8.1 mM) and **3** (1.9 mM): A) in the absence, and B) in the presence of TSA **6** (5 mM). HPLC conditions as described in Figure 1.

Table 1: Thermodynamic data for the binding of **4** and **6** with **7** and **8**.[a]

		7	**8**
4	K_1 [M^{-1}]	1.3×10^5	6.4×10^5
	$\Delta G°$ [kJ mol^{-1}]	−29.1	−33.1
	$\Delta H°$ [kJ mol^{-1}]	−23.7	−40.6
	$T\Delta S°$ [kJ mol^{-1}]	5.4	−7.5
6	K_1 [M^{-1}]	2.4×10^5	3.9×10^5
	$\Delta G°$ [kJ mol^{-1}]	−30.7	−31.9
	$\Delta H°$ [kJ mol^{-1}]	−25.8	−38.5
	$T\Delta S°$ [kJ mol^{-1}]	4.9	−6.6

[a] Equilibrium constants (K_1), Gibbs energies ($\Delta G°$), enthalpies ($\Delta H°$), and entropies $T\Delta S°$ of the binding of **4** and **6** to hosts **7** (mixture of stereoisomers) and **8** (major diastereomer) at 298 K were determined by using isothermal titration microcalorimetry. Guest solutions (0.85 mM) were titrated into host solutions (0.075 mM), all prepared in 10 mM borate buffer (pH 9.0).

We have measured the rates of the Diels–Alder reaction of **4** with excess **5** in the absence and the presence of 1.2 equivalents of **7** and **8**. Indeed, **7** induced a modest acceleration of the Diels–Alder reaction, whereas **8** turned out to be catalytically inactive. Figure 3 shows the observed (pseudo) first-order rate constants for the uncatalyzed reaction and the cycloaddition catalyzed by **7** as a function of the concentration of dienophile **5**.

 © 2003 Wiley-VCH Verlag GmbH & Co. KGaA, Weinheim 1433-7851/03/4211-1271 $ 20.00+.50/0

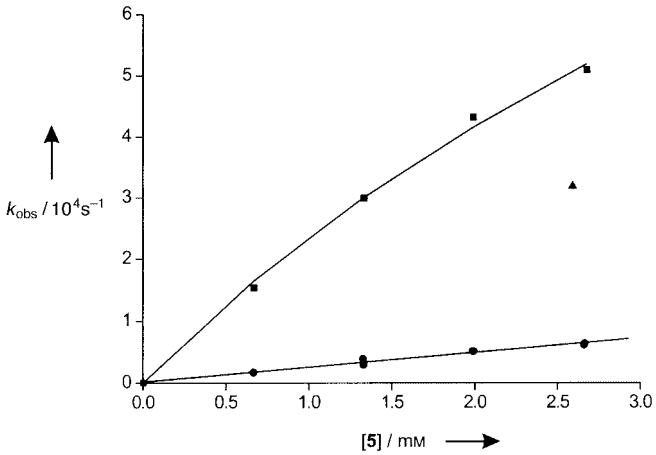

Figure 3. Observed rate constants (k_{obs}) for the Diels–Alder reaction between **4** and **5** in the absence (●) and presence (■) of macrocycle **7** as a function of the concentration of **5**. The solid lines represent fits of the data to a linear function (uncatalyzed reaction) or to Equation (1) (catalyzed reaction). The observed rate constant for the Diels–Alder reaction in the presence of **7** and product **6** (1 equiv) is also shown (▲).

The binding constant data suggest a catalytic mechanism in which the macrocycle strongly binds diene **4**, leaving enough space to simultaneously bind dienophile **5** in the same cavity. Thus the Diels–Alder reactants are in proximity, increasing the rate of their reaction. It can be shown (see Supporting Information) that when using excess **5** and assuming complete binding of **4** to **7**:

$$k_{obs} = \frac{K_2[\mathbf{5}]_t}{1 + K_2[\mathbf{5}]_t} k_{cat} \quad (1)$$

In [Eq. (1)], k_{obs} is the observed pseudo-first-order rate constant at a given concentration of **5**, k_{cat} is the first-order rate constant for the Diels–Alder reaction of the ternary **4**·**5**·**7** complex, $[\mathbf{5}]_t$ is the total concentration of **5** in solution, and K_2 is the equilibrium constant for the binding of **5** to the binary **4**·**7** complex. Using this equation to fit the kinetic data, we obtained values for K_2 and k_{cat} of $1.4(\pm 0.5) \times 10^2\,\text{M}^{-1}$ and $1.9(\pm 0.5) \times 10^{-3}\,\text{s}^{-1}$, respectively. Comparing the values of k_{cat} with the second-order rate constant of the uncatalyzed reaction yields an effective molarity of 0.08 M for **5** at the site of reaction.

We did not expect **7** to exhibit efficient turnover because we have used the reaction product as the TSA. Any catalyst selected this way is bound to be inhibited by the product. However, the binding constants of starting material **4** and product **6** to catalyst **7** (Table 1) are of the same order of magnitude, suggesting that **4** is able to compete with **6** for binding to the catalyst, so that some turnover should be possible. Indeed, when we added 1 equivalent of **6** to the reaction mixture, **7** still accelerated the Diels–Alder reaction (Figure 3).

Although the efficiency of **7** is modest when compared with other noncovalent catalysts for Diels–Alder reactions,[10] we have established that dynamic combinatorial chemistry has potential as a tool for catalyst development. The method is more controllable and experimentally less demanding than the catalytic antibody approach and generates better-defined systems than imprinted polymers.[11] Whereas our current building blocks only provide nonspecific hydrophobic aromatic surfaces, incorporating functional groups capable of specific recognition and activation of the substrate should improve catalytic efficiency.

Experimental Section

Acridizinium bromide (**4**) and its cyclopentadiene adduct **6** were prepared as described in the literature.[9] Cyclopentadiene (**5**) was prepared by thermal cracking of dicyclopentadiene immediately before use.

In a typical experiment the dithiols (10 mM overall) were suspended in water (1–10 mL) and a NaOH solution (1.0 M; 1 equiv with respect to the number of carboxylic acid groups) was added. After all the dithiol had dissolved, the pH value was adjusted to 8.5. Where appropriate, the TSA **6** (5 mM) was added and the mixtures were allowed to oxidize and equilibrate for 3–5 days by stirring in an open vial. Evaporated water was replenished every day.

Rate constants for the cycloaddition between **4** and **5** were determined by UV/Vis spectroscopy: the decrease of the absorbance of diene **4** was monitored at 396 nm using initial rate kinetics.[12] Measurements were performed in cuvettes (1 mm path length) initially containing the appropriate concentrations of **4, 6**, and **7** in 10 mM borate buffer at pH 9.0 at $25 \pm 0.1\,^{\circ}\text{C}$. After thermal equilibration, a solution of **5** (48–143 mM, 5 μL) in 1-propanol was injected and the solution was homogenized. The cuvettes were stoppered carefully to prevent evaporation of **5**. Four reactions were followed simultaneously in each run. Observed rate constants (k_{obs}) were obtained by using the following expression:[12] $k_{obs} = \mathrm{d}(Abs)/\mathrm{d}t(d(\varepsilon_{\mathbf{4}} - \varepsilon_{\mathbf{6}})[\mathbf{4}]_0)^{-1}$. In this equation, $\mathrm{d}(Abs)/\mathrm{d}t$ is the change in absorbance during the first 10 % of the reaction, d is the path length of the cuvette, and $\varepsilon_{\mathbf{4}}$ and $\varepsilon_{\mathbf{6}}$ are the extinction coefficients of **4** and **6**, respectively. These extinction coefficients were determined separately under the same conditions as those used in the kinetic runs.

Received: November 28, 2002 [Z50657]

Keywords: catalysis · combinatorial chemistry · host–guest chemistry · supramolecular chemistry · thermodynamic control

[1] a) P. A. Brady, J. K. M. Sanders, *Chem. Soc. Rev.* **1997**, *26*, 327–336; b) J. K. M. Sanders, *Chem. Eur. J.* **1998**, *4*, 1378–1383; c) W. B. Motherwell, M. J. Bingham, Y. Six, *Tetrahedron* **2001**, *57*, 4663–4686.

[2] a) A. A. Beaudry, G. F. Joyce, *Science* **1992**, *257*, 635–641; b) D. S. Wilson, J. W. Szostak, *Annu. Rev. Biochem.* **1999**, *68*, 611–647.

[3] G. Wulff, *Chem. Rev.* **2002**, *102*, 1–27.

[4] a) A. Tramontano, K. D. Janda, R. A. Lerner, *Science* **1986**, *234*, 1566–1570; b) S. J. Pollack, J. W. Jacobs, P. G. Schultz, *Science* **1986**, *234*, 1570–1573; c) M. M. Mader, P. A. Bartlett, *Chem. Rev.* **1997**, *97*, 1281–1301.

[5] a) S. Otto, R. L. E. Furlan, J. K. M. Sanders, *Drug Discovery Today* **2002**, *7*, 117–125; b) S. Otto, R. L. E. Furlan, J. K. M. Sanders, *Curr. Opin. Chem. Biol.* **2002**, *6*, 321–327; c) J.-M. Lehn, A. V. Eliseev, *Science* **2001**, *291*, 2331–2332; d) S. J. Rowan, S. J. Cantrill, G. R. L. Cousins, J. K. M. Sanders, J. F. Stoddart, *Angew. Chem.* **2002**, *114*, 938–993; *Angew. Chem. Int. Ed.* **2002**, *41*, 898–952; Corrigendum: S. J. Rowan, S. J. Cantrill, G. R. L. Cousins, J. K. M. Sanders, J. F. Stoddart, *Angew. Chem.* **2002**, *114*, 1528; *Angew. Chem. Int. Ed.* **2002**, *41*, 1460

 © 2003 Wiley-VCH Verlag GmbH & Co. KGaA, Weinheim 1433-7851/03/4211-1272 $ 20.00+.50/0

[6] a) I. Huc, J.-M. Lehn, *Proc. Natl. Acad. Sci. USA* **1997**, *94*, 2106 – 2110; b) H. Hioki, W. C. Still, *J. Org. Chem.* **1998**, *63*, 904 – 905; c) R. L. E. Furlan, G. R. L. Cousins, J. K. M. Sanders, *Chem. Commun.* **2000**, 1761 – 1762; d) R. L. E. Furlan, Y.-F. Ng, G. R. L. Cousins, J. E. Redman, J. K. M. Sanders, *Tetrahedron* **2002**, *58*, 771 – 778; e) R. L. E. Furlan, Y.-F. Ng, S. Otto, J. K. M. Sanders, *J. Am. Chem. Soc.* **2001**, *123*, 8876 – 8877; f) E. Stulz, Y.-F. Ng, S. M. Scott, J. K. M. Sanders, *Chem. Commun.* **2002**, 524 – 525; g) C. Karan, B. L. Miller, *J. Am. Chem. Soc.* **2001**, *123*, 7455 – 7456; h) V. Berl, I. Huc, J.-M. Lehn, A. DeCian, J. Fischer, *Eur. J. Org. Chem.* **1999**, 3089 – 3094; i) M. Hochgürtel, H. Kroth, D. Piecha, M. W. Hofmann, C. Nicolau, S. Krause, O. Schaaf, G. Sonnenmoser, A. V. Eliseev, *Proc. Natl. Acad. Sci. USA* **2002**, *99*, 3382 – 3387; j) S. Otto, R. L. E. Furlan, J. K. M. Sanders, *Science* **2002**, *297*, 590 – 593.

[7] S. L. Roberts, R. L. E. Furlan, G. R. L. Cousins, J. K. M. Sanders, *Chem. Commun.* **2002**, 938 – 939.

[8] S. Otto, R. L. E. Furlan, J. K. M. Sanders, *J. Am. Chem. Soc.* **2000**, *122*, 12 063 – 12 064.

[9] G. K. van der Wel, J. W. Wijnen, J. B. F. N. Engberts, *J. Org. Chem.* **1996**, *61*, 9001 – 9005.

[10] S. K. Kim, A. G. Leach, K. N. Houk, *J. Org. Chem.* **2002**, *67*, 4250 – 4260.

[11] For a recent approach to better-defined receptors by molecular imprinting, see: S. C. Zimmerman, M. S. Wendland, N. A. Rakow, I. Zharov, K. S. Suslick, *Nature* **2002**, *418*, 399 – 403.

[12] A. A. Frost, R. G. Pearson, *Kinetics and Mechanism*, Wiley, New York, **1980**.

 © 2003 Wiley-VCH Verlag GmbH & Co. KGaA, Weinheim 1433-7851/03/4211-1273 $ 20.00+.50/0

Allyl-Transfer Reactions

Highly Enantioselective Alk-2-enylation of Aldehydes through an Allyl-Transfer Reaction**

Junzo Nokami, Kenta Nomiyama, Seiji Matsuda, Nobuyuki Imai, and Kazuhide Kataoka*

The enantioselective allylation of aldehydes to prepare optically pure homoallylic alcohols is one of the most attractive and popular methods for the construction of stereogenic centers [Eq. (1)].[1,2d] Not only can this type of reaction provide homoallylic alcohols with high enantiomeric purity, it can also provide modified chiral building blocks after suitable functionalization of the C–C double bond in the introduced allylic unit.

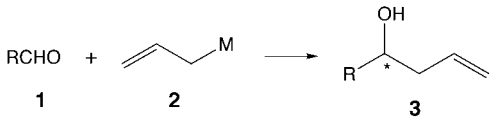

(1)

Highly enantiopure homoallylic alcohols have been prepared by using allylic organometallic reagents ($MCH_2CH{=}CH_2$; M = metal) and a stoichiometric amount of a chiral auxiliary[3] or a catalytic amount of a chiral promoter.[4] Furthermore, allylation reactions with γ-substituted organometallic reagents **4** in the presence of a chiral auxiliary or catalyst afford the γ adduct **5** diastereo- and enantioselectively.[5] This C–C-bond-formation reaction is particularly useful for the construction of vicinal stereogenic centers in a flexible hydrocarbon chain [Eq. (2)].

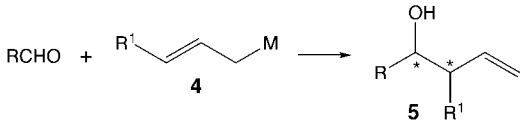

(2)

However, to the best of our knowledge, no asymmetric alk-2-enylation reaction (e.g. crotylation) of aldehydes to give 4-substituted homoallylic alcohols **6** (α adduct) has yet been reported [Eq. (3)]. This is because the allylation reactions by alk-2-enyl metal reagents **4** proceed, without exception, with allylic transposition via a six-membered cyclic transition state, affording exclusively the γ adduct **5**.[6]

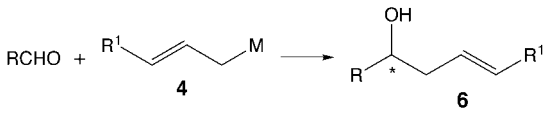

(3)

Recently we discovered an efficient and stereoselective nucleophilic alk-2-enylation reaction of aldehydes that produces the desired α adduct **6**. In this procedure, no allylic metal nucleophiles are involved, and a homoallylic alcohol **7** acts as an allyl donor. This unusual allylation reaction appears to proceed through a 2-oxonium [3,3] sigmatropic rearrangement, as shown in Scheme 1.[2a] The acid-catalyzed reaction of aldehyde **1** with the homoallylic alcohol (γ adduct) **7** stereoselectively gave the homoallylic alcohol α adduct **6** by an allyl transfer from **7** via hemiacetal ($\mathbf{H}_1$) and oxonium cations $\mathbf{T}_1$ and $\mathbf{T}_2$.

More importantly, the $Sn(OTf)_2$-catalyzed (10 mol%) reaction of 3-phenylpropanal (**1a**) with optically pure allyl donor (3*R*,4*S*)-1-phenyl-4-methylhex-5-en-3-ol (**5a**; >99% *ee*) gave (3*S*)-1-phenylhept-5-en-3-ol (**6a**) in 85% yield with >98% *ee* (Scheme 2).[2b,c]

[*] Prof. Dr. J. Nokami, K. Nomiyama, S. Matsuda, Dr. N. Imai, K. Kataoka
Department of Applied Chemistry
Okayama University of Science
1-1 Ridai-cho, Okayama 700-0005 (Japan)
Fax: (+81) 86-252-6891
E-mail: nogami@dac.ous.ac.jp

[**] We gratefully acknowledge Prof. I. E. Markó, Belgium, for his kind discussion during this work. This work was financially supported by the Nagase Science and Technology Foundation, a Grant for Cooperative Research administered by the Japan Private School Promotion Foundation, and a Grant in Aid for Scientific Research from the Ministry of Education, Science, Culture, and Sports, Japan (No. 12450357).

Supporting information for this article is available on the WWW under http://www.angewandte.org or from the author.

 © 2003 Wiley-VCH Verlag GmbH & Co. KGaA, Weinheim 1433-7851/03/4211-1273 $ 20.00+.50/0

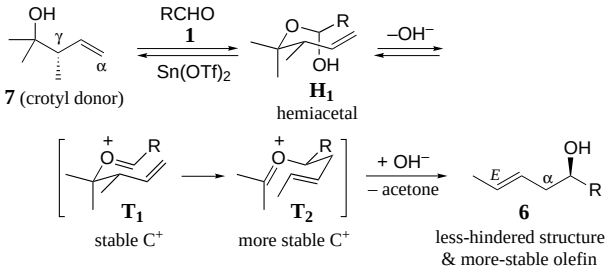

Scheme 1. Crotylation of aldehydes by an allyl-transfer reaction from crotyl donor **7** to aldehyde **1**.

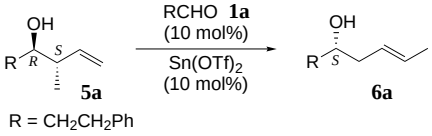

Scheme 2. Conversion of a γ adduct into the α adduct through an allyl-transfer reaction.

This result suggested that more broadly applicable chiral alk-2-enyl donors could be prepared from cheap and readily available optically pure ketones such as (−)- or (+)-menthone. Thus, reaction of (*E*)-but-2-enylmagnesium chloride **4a** (R^1 = Me) with (2*S*,5*R*)-(−)-menthone gave a mixture of 1-substituted menthols in good yield. Based on the reported stereochemistry of the addition of Grignard reagents to menthone,[7,8] the major product, isolated in 70–77%, was determined to be one of the diastereomers of axial alcohols (*R*)- or (*S*)-**8a** (Scheme 3).

Both the diastereomers of **8a** were readily separated and independently used as crotyl donors in the allyl-transfer reaction with 3-phenylpropanal **1a** in the presence of *p*-toluenesulfonic acid monohydrate (*p*TSA·H_2O) as the catalyst. Remarkably, whilst the major isomer gave (5*E*,3*R*)-1-phenylhept-5-en-3-ol **6a** in good yield with >99% *ee*, the minor isomer did not react at all. Therefore, the configuration of the major isomer could be assigned as (*R*)-**8a** as shown in Scheme 4.[2d]

To investigate this asymmetric allylation further, we prepared other chiral alk-2-enyl-donors, from (−)-menthone[9] as shown in Table 1. These chiral alk-2-enyl-donors have substituents R^1 (R^1 = Et, *n*Pent, $(CH_2)_3Cl$, CH=CH_2 in **8** in place of the methyl substituent (R^1 = Me) in crotyl donor **8a**.

In all cases, the addition of the allylic metal reagent to the carbonyl of (−)-menthone involved an equatorial attack (favoring the carbonyl face *trans* to the isopropyl group) to give the corresponding

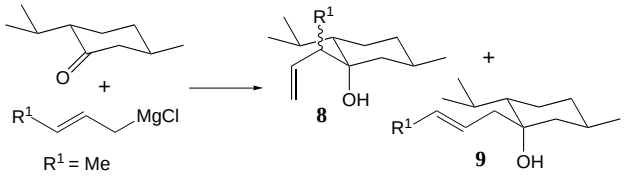

Scheme 3. Stereoselctive reaction of (−)-menthone with alk-2-enylmagnesium chloride.

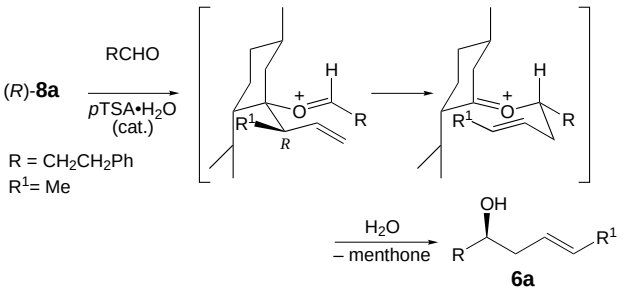

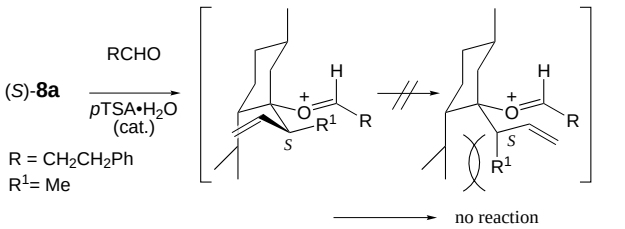

Scheme 4. Stereospecific allyl-transfer reaction from (*R*)-**8a** to aldehyde **1a**.

homoallylic alcohol γ adducts **8b–e** selectively. Moreover, stereochemically pure **8b–d** were readily isolated in good yields by chromatography on silica gel. The structures of the minor by-products were assigned as the corresponding

Table 1: Preparation of chiral allyl donors **8** from (−)-menthone.

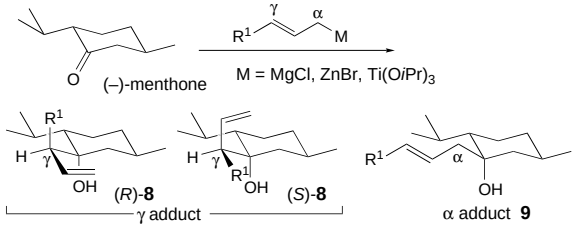

Entry	Allylic nucleophile			*T* [°C]		Yield [%][a]		
	R^1	M	[equiv]			(*R*)-**8**	(*S*)-**8**	**9**
1[b]	Et	MgCl	1.5	0	**b**	79	11	trace
2[b]	*n*Pent	MgCl	1.5	0	**c**	82	11	1.3
3[c]	$Cl(CH_2)_3$	ZnBr	2.0	0	**d**	66	0	21
4[d]	CH_2=CH	$Ti(OiPr)_3$	2.0	−78	**e**	70[e]		5.0

[a] Yield of isolated product. [b] The reaction was performed with (−)-menthone (10 mmol) and alk-2-enylmagnesium chloride (derived from magnesium (15 mmol) and 1-chloroalk-2-ene (15 mmol)) in THF at 0°C for 2 h. [c] The reaction was performed with (−)-menthone (0.5 mmol) and 1-bromo-6-chlorooct-2-ene (1 mmol), Zn (1 mmol), NH_4Ac (1 mmol), in THF (2 mL) at 0°C for 4 h. [d] The reaction was performed with (−)-menthone (5 mmol) and pentadienyltitanium reagent (derived from KO*t*Bu (10 mmol), *n*BuLi (10 mmol), penta-1,3-diene (15 mmol), and $ClTi(OiPr)_3$ (10 mol) in hexane) in THF at −78°C. [e] The allylic carbon atom is not stereogenic.

 © 2003 Wiley-VCH Verlag GmbH & Co. KGaA, Weinheim 1433-7851/03/4211-1274 $ 20.00+.50/0

Table 2: Homoallylic alcohol α adducts **6** by allyl-transfer reaction from allyl-donors **8**.[a]

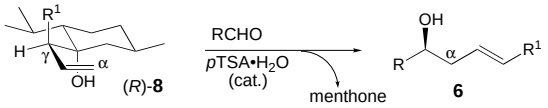

Entry	Allyl donor **8**			Aldehyde		Product **6**[b]	
		R^1	[equiv]	R		Yield [%][c]	*ee* [%][d]
1	**a**	Me	2	$Ph(CH_2)_2$	**a**	83 (70)	>99 (97.0)
2	**a**	Me	1	$Ph(CH_2)_2$	**a**	75	>99
3	**b**	Et	1	$Ph(CH_2)_2$	**b**	85	>99
4	**b**	Et	2	Ph	**c**	61	>99
5	**b**	Et	1	$BnO(CH_2)_5$	**d**	88	>99
6	**b**	Et	2	PhCHMe	**e**	68	>99
7	**b**	Et	1	$PhS(CH_2)_2$	**f**	90	>99
8	**b**	Et	2	Et_2CH	**g**	71	>99[e]
9	**b**	Et	1	$CH_2{=}CH(CH_2)_8$	**h**	75	>99[e]
10	**c**	*n*Pent	1	$Ph(CH_2)_2$	**i**	92 (89)	>99 (99.2)
11	**c**	*n*Pent	2	Ph	**j**	72	99.4
12	**c**	*n*Pent	1	$BnO(CH_2)_5$	**k**	93	>99
13	**c**	*n*Pent	1	$PhS(CH_2)_2$	**L**	88	>99
14	**d**	$Cl(CH_2)_3$	1	$Ph(CH_2)_2$	**m**	92	>99
15	**d**	$Cl(CH_2)_3$	1	$BnO(CH_2)_5$	**n**	96	>99
16	**d**	$Cl(CH_2)_3$	1	$PhS(CH_2)_2$	**o**	95	>99
17	**e**	$CH_2{=}CH$	2	$Ph(CH_2)_2$	**p**	83	>99
18	**e**	$CH_2{=}CH$	2	$BnO(CH_2)_5$	**q**	83	>99
19	**e**	$CH_2{=}CH$	2	$PhS(CH_2)_2$	**r**	63	>99

[a] The reactions were performed with allyl donor **8**, (1 mmol, 2 equiv or 0.5 mmol, 1 equiv), aldehyde (0.5 mmol), and pTSA·H_2O (10 mol%) in CH_2Cl_2 (1 mL), at 20°C for 20 h, unless otherwise noted. [b] Yield and *ee* value of the corresponding product derived from the crude **8** are shown in parentheses. [c] Yield of isolated product. [d] Determined by HPLC analysis (CHIRALCEL OD, *i*PrOH (5%) in hexane as eluent) unless otherwise noted. >99 means that no signal of the corresponding enantiomer. [e] Determined by HPLC analysis (CHIRALPAK AD, *i*PrOH (5%) in hexane as eluent) of the corresponding MTPA ester derived from (+)-MTPA. MTPA = α-methoxy-α-(trifluoromethyl)benzeneacetyl chloride.

diastereoisomer (*S*)-**8** and α-adducts (−)-menthol derivative **9**. A trace of a γ adduct formed by axial attack of (−)-menthone could also be detected.

Asymmetric 2-alkenylation of aldehydes by the allyl transfer reaction from these chiral allyl donors **8b–e** was successfully carried out using pTSA·H_2O as the catalyst. In all cases, the desired, optically pure α adducts were obtained in excellent yields.[2d] These results are summarized in Table 2.

Notably, allyl-transfer reactions using a crude mixture of **8** (containing all the other stereoisomers) and 3-phenylpropanal gave the desired product in good yield and with high *ee* values (Table 2, entries 1, 10). This result suggests that the major isomer is far more reactive than the other stereoisomers.

Finally, highly enantioselective 2,4-pentadienylation of aldehydes with **8e** were carried out (Table 2, entries 17–19).[10] Although the allylic carbon atom of **8e** is not stereogenic, only the *E* isomer of the final adduct is obtained. These results show that only one of the diastereotopic vinyl groups of **8e** is transferred. This observation reinforces even further our proposed transition state, implying the *R* absolute stereochemistry at the γ-stereogenic center of allyl-donors **8**.

In summary, we have discovered a novel asymmetric alk-2-enylation reaction, using (−)- and (+)-menthone as the chiral auxiliaries, which gives the homoallylic alcohols in a pTSA·H_2O-catalyzed allyl-transfer reaction in good yield and with >99% *ee*. To the best of our knowledge, this is the first report of such an asymmetric alk-2-enylation of aldehydes.[3] The chiral allyl donors are conveniently prepared from simple alk-2-enyl metal reagents (e.g. Grignard reagents) and inexpensive (−)- and (+)-menthone. Finally, the absolute stereochemistry of the final adducts can be readily predicted from the conformational analysis of the six-membered-ring chair-like transition state depicted in Scheme 4.

Received: December 2, 2002 [Z50682]

Keywords: alcohols · aldehydes · allylation · asymmetric synthesis · homogeneous catalysis

[1] For reviews on the reaction using allyl(ic) metals, see: a) Y. Yamamoto, N. Asao, *Chem. Rev.* **1993**, *93*, 2207–2293; b) J. A. Marshall in *Lewis Acids in Organic Synthesis, Vol. 1*. (Ed.: H. Yamamoto), Wiley-VCH, New York, **2000**; for reviews on asymmetric allylation and related reactions, see: c) S. E. Denmark, N. G. Almstead in *Modern Carbonyl Chemistry* (Ed.: J. Otera), Wiley-VCH, New York, **2000**; d) S. R. Chemler, W. R. Roush in *Modern Carbonyl Chemistry* (Ed.: J. Otera), Wiley-VCH, New York, **2000**.

[2] a) J. Nokami, K. Yoshizane, H. Matsuura, S. Sumida, *J. Am. Chem. Soc.* **1998**, *120*, 6609–6610; b) S. Sumida, M. Ohga, J. Mitani, J. Nokami, *J. Am. Chem. Soc.* **2000**, *122*, 1310–1313; c) J. Nokami, L. Anthony, S. Sumida, *Chem. Eur. J.* **2000**, *6*, 2909–2913; d) J. Nokami, M. Ohga, H. Nakamoto, T. Matsubara, I. Hussain, H. Ktaoka, *J. Am. Chem. Soc.* **2001**, *123*, 9168–9169; e) I. Hussain, T. Komasaka, M. Ohga, J. Nokami, *Synlett* **2002**, 640–642.

[3] For chiral *B*-allylborane, see: reference [1d] and a) D. R. Williams, M. P. Clark, U. Emde, M. A. Berliner, *Org. Lett.* **2000**, *2*, 3023–3026; for allyltin reagents with a chiral ligand, see: b) J. Otera, Y. Yoshinaga, T. Yamaji, T. Yoshioka, Y. Kawasaki, Y. *Organometal.* **1985**, *4*, 1213–1218; for allyltin reagents with a chiral auxiliary, see: c) T. Mukaiyama, N. Minowa, T. Oriyama, K. Narasaka, *Chem. Lett.* **1986**, 97–100; d) G. P. Boldrini, L. Lodi, E. Tagliavini, C. Tarasco, C. Trombini, A. Umani-Ronchi, *J. Org. Chem.* **1987**, *52*, 5447–5452; e) C. Boga, D. Savoia, E. Tagliavini, C. Trombini, A. Umani-Ronchi, *J. Organomet. Chem.* **1988**, *353*, 177–183; f) S. Kobayashi, K. Nishio, *Tetrahedron Lett.* **1995**, *36*, 6729–6732; g) K. Yamada, T. Tozawa, M. Nishida, T. Mukaiyama, *Bull. Chem. Soc. Jpn.* **1997**, *70*, 2301–2308; for allyl bromide and metallic In with a chiral auxiliary, see: h) T.-P. Loh, J.-R. Zhou, Z. Yin, *Org. Lett.* **1999**, *1*, 1855–1857; i) T.-P. Loh, J.-R. Zhou, *Tetrahedron Lett.* **1999**, *40*, 9115–9118; j) T.-P. Loh, J.-R. Zhou, *Tetrahedron Lett.* **1999**, *40*, 9333–9336; for allyltitanium complexed with a chiral auxiliary, see: k) S. Bouzbouz, J.

 © 2003 Wiley-VCH Verlag GmbH & Co. KGaA, Weinheim 1433-7851/03/4211-1275 $ 20.00+.50/0

Cossy, *Org. Lett.* **2000**, *2*, 501 – 504; l) S. Bouzbouz, M. P. Popkin, J. Cossy, J. *Org. Lett.* **2000**, *2*, 3449 – 3451; m) J. Cossy, C. Willis, V. Bellosta, S. Bouzbouz, *Synlett* **2000**, 1461 – 1463; for allylsilane with a chiral auxiliary, see: n) S. E. Denmark, D. M. Coe, N. E. Pratt, B. D. Griedel, *J. Org. Chem.* **1994**, *59*, 6161 – 6163; o) L. C. Zhang, H. Sakurai, M. Kira, *Chem. Lett.* **1997**, 129 – 130.

[4] For allyltributyltin with a chiral catalyst, see: a) H. Doucet, M. Santelli, *Tetrahedron: Asymmetry* **2000**, *11*, 4163 – 4169; b) T.-P. Loh, I.-R. Zhou, *Tetrahedron Lett.* **2000**, *41*, 5261 – 5264; c) Y. Motoyama, H. Narusawa, H. Nishiyama, *Chem. Commun.* **1999**, 131 – 132; for excess allyltributyltin or tetraallyltin with a chiral catalyst (allylation of ketones), see: d) S. Casolari, D. D'Addario, E. Tagliavini, *Org. Lett.* **1999**, *1*, 1061 – 1063, for allylsilane with a chiral catalyst, see: e) S. E. Denmark, J. Fu, *J. Am. Chem. Soc.* **2000**, *122*, 12021 – 12022; f) A. Yanagisawa, H. Kageyama, Y. Nakatsuka, K. Asakawa, Y. Matsumoto, H. Yamamoto, *Angew. Chem.* **1999**, *111*, 3916 – 3919; *Angew. Chem. Int. Ed.* **1999**, *38*, 3701 – 3703; g) K. Iseki, S. Mizuno, Y. Kuroki, Y. Kobayashi, *Tetrahedron Lett.* **1998**, *39*, 2767 – 2770; h) M. Nakajima, M. Saito, *J. Am. Chem. Soc.* **1998**, *120*, 6419 – 6420; for allyl bromide and metallic Mn with chiral Cr^{II}–salen catalyst, see: i) M. Bandini, P. G. Cozzi, P. Melchiorre, A. Umani-Ronchi, *Angew. Chem.* **1999**, *111*, 3558 – 3561; *Angew. Chem. Int. Ed.* **1999**, *38*, 3357 – 3359.

[5] Asymmetric 1-methylallylation and related reactions: by chiral catalyst with tributylcrotyltin, see: a) J. A. Marshall, Y. Tang, *Synlett* **1992**, 653 – 654; by chiral catalyst with crotylsilane, see: b) S. Aoki, K. Mikami, M. Terada, T. Nakai, *Tetrahedron* **1993**, *49*, 1783 – 1792; c) K. Furuta, M. Mouri, H. Yamamoto, *Synlett* **1991**, 561 – 562; d) K. Iseki, S. Mizuno, Y. Kuroki, Y. Kobayashi, *Tetrahedron Lett.* **1998**, *39*, 2767 – 2770; e) M. Nakajima, M. Saito, *J. Am. Chem. Soc.* **1998**, *120*, 6419 – 6420; see also reference [4f]; by Cr^{II}–salen catalyst with crotyl bromide and metallic Mn, see: f) M. Bandini, P. G. Cozzi, A. Umani-Ronchi, *Angew. Chem.* **2000**, *112*, 2417 – 2420; *Angew. Chem. Int. Ed.* **2000**, *39*, 2327 – 2330; for noncatalytic reactions with a stoichiometric amount of chiral *B*-crotylborane reagents, see: g) W. R. Roush, R. L. Halterman, *J. Am. Chem. Soc.* **1986**, *108*, 294 – 296; h) W. R. Roush, K. Ando, D. B. Powers, R. L. Halterman, A. D. Palkowitz, *Tetrahedron Lett.* **1988**, *29*, 5579 – 5582; i) J. Garcia, B. M. Kim, S. Masamune, *J. Org. Chem.* **1987**, *52*, 4831 – 4832; j) H. C. Brown, R. K. Jadhav, *Tetrahedron Lett.* **1984**, *25*, 1215 – 1218; k) H. C. Brown, K. S. Bhat, *J. Am. Chem. Soc.* **1986**, *108*, 293 – 294.

[6] In various allylation reactions of aldehydes with allylic metal reagents, an allylic barium compound seems to be one of the most exceptional reagents that selectively gives 3-substituted allyl adducts (α adducts): a) A. Yanagisawa, S. Habaue, H. Yamamoto, *J. Am. Chem. Soc.* **1991**, *113*, 8955 – 8956; b) A. Yanagisawa, S. Habaue, K. Yasue, H. Yamamoto, *J. Am. Chem. Soc.* **1994**, *116*, 6130 – 6141.

[7] The diastereoselective addition of carbon nucleophiles to optically active ketones (e.g. menthone) and its application in asymmetric synthesis has been reported; see: a) C. R. Johnson, C. J. Stark, Jr., *Tetrahedron Lett.* **1979**, 4713 – 4716; b) S. E. Chillous, D. J. Hart, D. K. Hutchinson, *J. Org. Chem.* **1982**, *47*, 5418 – 5420; c) J. Jauch, V. Schurig, *Tetrahedron: Asymmetry* **1997**, *8*, 169 – 172; d) C. Spino, C. Beaulieu, *Angew. Chem.* **2000**, *112*, 2006 – 2008; *Angew. Chem. Int. Ed.* **2000**, *39*, 1930 – 1932; e) A. P. Davis, *Angew. Chem.* **1997**, *109*, 609 – 612; *Angew. Chem. Int. Ed. Engl.* **1997**, *36*, 591 – 593; f) T. Harada, T. Hayashiya, I. Wada, N. Iwa-ake, A. Oku, *J. Am. Chem. Soc.* **1987**, *109*, 527 – 532; g) T. Harada, A. Oku, *Synlett* **1994**, 95 – 104, and references therein.

[8] Commercially available (−)-menthone (90% purity, containing ca. 5% of isomenthone) was not suitable for our purpose, because it reacted with crotylmagnesium chloride to give a mixture of inseparable stereoisomers of the crotyl donors **5**, which gave **3a** in 90–95% *ee*.

[9] Both enantiomers are prepared by PCC or Dess–Martin oxidation of the corresponding menthols (> 99%), which are not expensive to produce: K. Tani, T. Yamagata, S. Otsuka, S. Akutagawa, H. Kumobayashi, T. Taketomi, H. Takaya, A. Miyashita, R. Noyori, *J. Chem. Soc. Chem. Commun.* **1982**, 600.

[10] Reaction of 2,4-pentadienylmetal reagents with aldehydes. Li: a) E. Gérard, P. Miginiac, *Bull. Soc. Chim. Fr.* **1974**, 1924; B: b) K. Fujita, M. Schlosser, *Helv. Chim. Acta* **1982**, *65*, 1258 – 1263; c) M. Suginome, Y. Yamamoto, K. Fujii, Y. Ito, *J. Am. Chem. Soc.* **1995**, *117*, 9608 – 9609; Mg: d) H. Yasuda, M. Yamauchi, A. Nakamura, T. Sei, Y. Kai, N. Yasuoka, N. Kasai, *Bull. Chem. Soc. Jpn.* **1980**, *53*, 1089; Si: e) S. Kobayashi, K. Nishio, *Chem. Lett.* **1994**, 1773 – 1776; f) F. Minassian, N. Pelloux-Léon, Y. Vallée, *Synlett* **2000**, 242 – 244; Ti: g) A. Zellner, M. Schlosser, *Synlett* **2001**, 1016 – 1018; Zn: h) L. Ghosez, I. Markó, A. Hesbain-Frisque, *Tetrahedron Lett.* **1986**, *27*, 5211 – 5214; i) L. Chen, L. Ghosez, *Tetrahedron: Asymmetry* **1991**, *2*, 1181 – 1184; j) M. E. Jung, C. J. Nichols, *Tetrahedron Lett.* **1996**, *37*, 7667 – 7670; Zr: k) P. Bertus, F. Cherouvrier, J. Szymoniak, *Tetrahedron Lett.* **2001**, *42*, 1677 – 1680; In: l) T. Hirashita, S. Inoue, H. Yamamura, M. Kawai, S. Araki, *J. Organomet. Chem.* **1997**, *549*, 305 – 309; m) S. Woo, N. Squires, A. G. Fallis, *Org. Lett.* **1999**, *1*, 573 – 575; n) A. Melekhov, A. G. Fallis, *Tetrahedron Lett.* **1999**, *40*, 7867 – 7870; **Sn**: o) Y. Nishigaichi, M. Fujimoto, A. Takuwa, *Synlett* **1994**, 731 – 732. Although almost all these reactions gave selectively γ adduct, there are a few exceptions. For example, reaction of aldehydes with a penta-2,4-dienylsilyl compound with Lewis acids gave the corresponding α adduct. We assumed that the products will be prepared by an allyl-transfer reaction from the γ adduct to the α adduct. This will be discussed elsewhere.

 © 2003 Wiley-VCH Verlag GmbH & Co. KGaA, Weinheim 1433-7851/03/4211-1276 $ 20.00+.50/0

Asymmetric Conjugate Addition

Cu-Catalyzed Enantioselective Conjugate Additions of Alkyl Zinc Reagents to Unsaturated *N*-Acyloxazolidinones Promoted by a Chiral Triamide Phosphane**

*Alexander W. Hird and Amir H. Hoveyda**

An area of recent interest in organic synthesis involves the development of protocols for efficient catalytic asymmetric conjugate additions (ACAs) of alkyl metal compounds to

[*] Prof. A. H. Hoveyda, A. W. Hird
Department of Chemistry, Merkert Chemistry Center
Boston College
Chestnut Hill, MA 02467 (USA)
Fax: (+1) 617-552-1442
E-mail: amir.hoveyda@bc.edu

[**] This research was supported by the United States National Institutes of Health (GM-47480).

Supporting information for this article is available on the WWW under http://www.angewandte.org or from the author.

 © 2003 Wiley-VCH Verlag GmbH & Co. KGaA, Weinheim 1433-7851/03/4211-1276 $ 20.00+.50/0

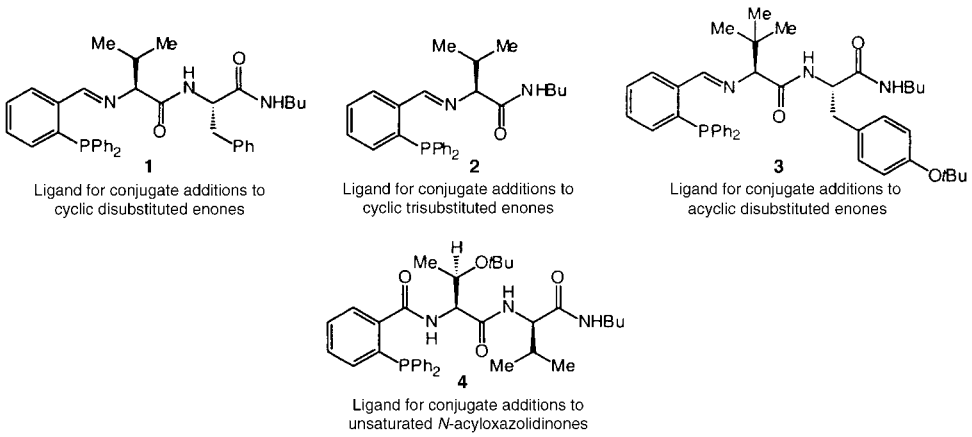

Scheme 1. Chiral amino acid-based phosphane ligands for Cu-catalyzed asymmetric conjugate additions (ACAs) to unsaturated carbonyls.

unsaturated carbonyls.[1] In these laboratories, we have been able to introduce methods for uniquely efficient and enantioselective catalytic ACAs of alkyl zinc reagents (not only [$ZnEt_2$]) to cyclic enones including unactivated cyclopentenones,[2] acyclic enones,[3] and trisubstituted exocyclic unsaturated ketones.[4] These investigations benefited from the modularity of the amino acid based ligands and parallel screening strategies,[5] as each of the above three sets of enone substrates requires a different optimal ligand (Scheme 1).

From the point of synthetic utility, in spite of recent advances outlined by various research groups, several critical problems remain to be addressed. One is in connection to the availability of a general approach to catalytic ACAs of alkyl groups to unsaturated esters,[6] amides, acids, or aldehydes. It was towards this end that we set out to develop catalytic ACAs of alkyl zinc reagents to unsaturated *N*-acyloxazolidinones;[7] the lure of such an approach is that enantioenriched β-alkyl carbonyls can be converted into an assortment of carboxylic acid and related derivatives. An efficient Cu-catalyzed method for ACA of alkyl zinc compounds to α,β-unsaturated oxazolidinones is disclosed herein.

To initiate our studies, we examined the ability of **1**–**3** (Scheme 1), the three chiral ligands that effect the aforementioned catalytic ACA,[2–4] in promoting additions to oxazolidinone **5a** (Scheme 2). As the data in Scheme 2 indicate, these Schiff bases promote facile but relatively nonselective reactions. We then conducted a brief survey of different forms for the phosphane attachment to the amino acid moieties (that is, the derived amines and amides). This led us to determine that, in contrast to the previous studies, it is a triamide ligand (**7**, Scheme 2) that delivers product **6** with appreciable enantioselectivity.

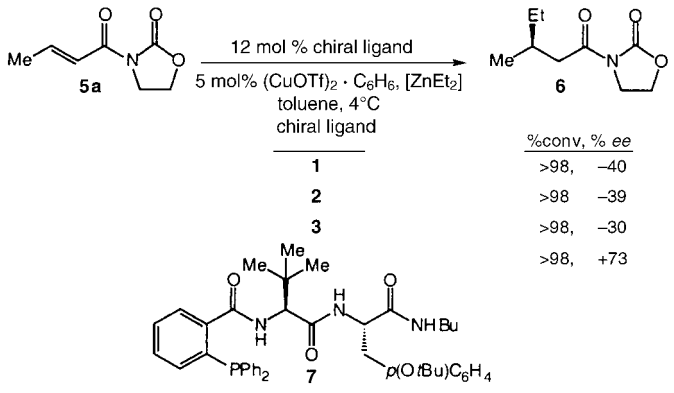

Scheme 2. Results of initial ligand screening.

We then performed screening studies to identify the optimal amino acid moieties of amide phosphanes (**5a**→**6** used as the representative process).[8] These investigations indicated that subtle amino acid modifications can lead to substantial variations in enantioselection (for example, see entries 1–2, Table 1) and that a comprehensive screening process should be carried out to find a more optimal ligand. More importantly, and somewhat to our surprise, we also established that peptidic ligands bearing a D and an L amino acid may prove to be superior (see entries 3–4, Table 1).

Table 1: Amino acid modifications to **5a**.[a]

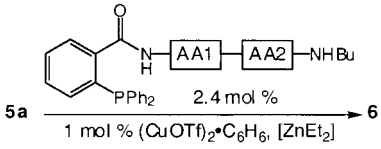

Entry	AA1	AA2	% *ee*
1	L-Phe	L-Phe	−34
2	L-Cha	L-Phe	+45
3	L-Val	L-Phe	+12
4	D-Val	L-Phe	−74

[a] All reactions have >98% conversion.

Subsequent screening of parallel libraries of ligands bearing both L,L- and D,L-dipeptides (approximately 100 ligands) led us to determine that treatment of **5a** with 1.0 mol% $(CuOTf)_2{\cdot}C_6H_6$, 2.4 mol% phosphane amide **4** (Scheme 1) and [$ZnEt_2$] (0°C, 1.3 h) leads to the formation of **6** in 95% *ee* and 95% yield (entry 1, Table 2).[9] It should be noted that ligand **4** has two unique structural attributes compared to the previous ligands used in reactions promoted by related peptidic systems.[2–4,10] Phosphane **4** is a triamide (not a diamide Schiff base or amine), and bears an L and a D amino

 © 2003 Wiley-VCH Verlag GmbH & Co. KGaA, Weinheim 1433-7851/03/4211-1277 $ 20.00+.50/0

Table 2: Cu-catalyzed ACA of alkyl zinc reagents to unsaturated oxazolidinones.[a]

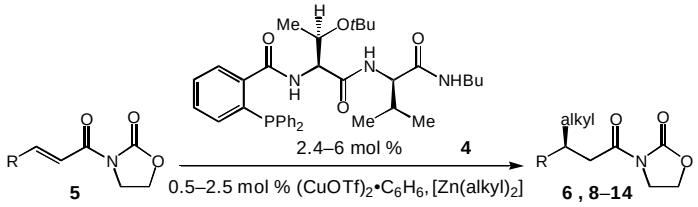

Entry	R	$[Zn(alkyl)_2]$	Product	Mol% **4**	Mol% Cu salt	*t* [h]	Yield [%][b]	*ee* [%][c]
1	Me **a**	$[ZnEt_2]$	**6**	2.4	1.0	1.3	95	95
2	Me **a**	$[Zn\{iPr(CH_2)_3\}_2]$	**8**	5.0	1.0	12	61	93
3	Me **a**	$[Zn(iPr)_2]$	**9**	2.4	0.5	15	95	76
4	*n*Pr **b**	$[ZnEt_2]$	**10**	2.4	1.0	3	86	94
5	*n*Pr **b**	$[Zn\{iPr(CH_2)_3\}_2]$	**11**	2.4	1.0	24	89	95
6[d]	*n*Pr **b**	$[ZnMe_2]$	**12**	6.0	2.5	144	68	97
7	$(CH_2)_3$OTBS **c**	$[ZnEt_2]$	**13**	2.4	1.0	6	95	>98
8	*i*Pr **d**	$[ZnEt_2]$	**14**	2.4	1.0	24	88	92

[a] Conditions: 3 equiv dialkyl zinc reagent (10 equiv in entry 6), toluene, 0°C (−15°C for entry 6). [b] Yields after silica gel chromatography. All reactions proceeded to at least 95% conversion (GLC analysis). [c] All enantioselectivities determined by chiral GLC (β-DEX column for entries 1–6 and 8, CDGTA column for entry 7). [d] Phosphane **15** used as ligand.

acid (not two L or D amino acids). The highest selectivity obtained for formation of **6** from an L,L ligand was 82% *ee* (AA1 = L-Asn(Trt), AA2 = L-Phe).

As indicated by the results summarized in Table 2, a range of unsaturated carbonyls and various alkyl zinc reagents can be used to access β-alkyl *N*-acyloxazolidinones in high yield and excellent enantioselectivity. The requisite unsaturated carbonyl substrates are accessed through olefin cross-metathesis promoted by a commercially available (Aldrich) catalyst developed in these laboratories.[11] As an example, **5c** (entry 7, Table 2) was prepared in this fashion in 94% yield. Furthermore, Cu-catalyzed ACA reactions can be carried out with the commercially available $(CuOTf)_2$·PhMe (Aldrich, used without purification). Conversion of **5a** into **6** is effected in the presence of 1 mol% $(CuOTf)_2$·PhMe and 2.4 mol% **4** to give **6** in 91% *ee* and 88% yield (>98% conversion, 4 h).[12] However, conjugate additions with $[ZnMe_2]$ (for example, entry 6, Table 2) are slower than those with longer chain alkyl zinc reagents and extended reaction times are needed.[13] In transformations involving $[ZnMe_2]$, superior efficiency is observed when **15** is used as the chiral ligand instead of **4** (68% versus 43% yield under identical conditions, shown in entry 6 of Table 2).

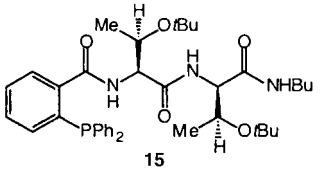

As shown in Equation (1), substrate **16** is inert to Cu-catalyzed ACA conditions. The derived dimethyloxazolidinone **17** can however be converted, albeit slowly, into **18** in 86% *ee* and 91% yield [Eq. (2)]. Control experiments[14] indicate that this difference in reactivity is most likely to

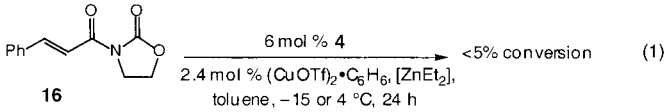

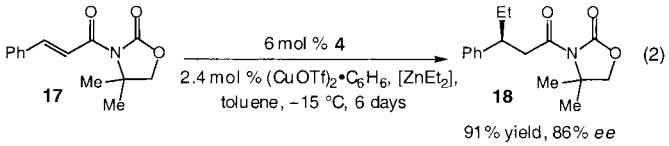

arise from the higher solubility of **17** under the reaction conditions and not as a result of variations in equilibrium between *s-cis* and *s-trans* conformers.[7]

Optically enriched β-alkyl *N*-acyloxazolidinones may be converted into other carbonyl derivatives that are not yet accessible directly through catalytic ACA reactions. Three representative examples are given below. Ketone **19** is formed in 93% *ee* through treatment of **8** (entry 2, Table 2) with *t*BuLi (THF, −20 to 0°C). It should be noted that Cu-catalyzed ACAs to acyclic *tert*-butyl enones proceed with only moderate levels of enantioselectivity (no greater than 75% *ee*).[4] Weinreb amide **20**, also obtained from **8** ($[AlMe_3]$, MeONHMe·HCl)[15] and acid **21** derived from **6**

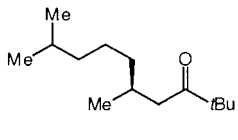

19 81% (93% *ee*) from **8**

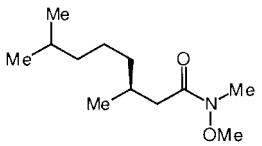

20 74% (93% *ee*) from **8**

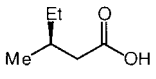

21 >98% (95% *ee*) from **6**

 © 2003 Wiley-VCH Verlag GmbH & Co. KGaA, Weinheim 1433-7851/03/4211-1278 $ 20.00+.50/0

($LiOH$, H_2O_2, THF)[16] can be converted into the corresponding aldehydes and a number of other carbonyl derivatives.

In conclusion, we have developed efficient Cu-catalyzed ACA reactions that are promoted by no more than 5 mol % of a readily accessible catalyst and deliver, in high enantiomeric purity, compounds that cannot be easily prepared by alternative catalytic protocols. This study introduces an amino acid based phosphane amide (versus Schiff base or amine systems) as an effective chiral ligand for asymmetric conjugate addition, and further demonstrates the important utility of this class of modular ligands.[17] The present method complements the previously reported catalytic ACA protocols[1–4,6] and should find utility in enantioselective organic synthesis.

Received: December 4, 2002 [Z50699]

Keywords: alkyl metal compounds · asymmetric catalysis · conjugate addition · copper · enantioselectivity

[1] For reviews on asymmetric conjugate additions of alkyl metal compounds to unsaturated carbonyls, see: a) N. Krause, A. Hoffmann-Roder, *Synthesis* **2001**, 171 – 196; b) A. Alexakis, C. Benhaim, *Eur. J. Org. Chem.* **2002**, 3221 – 3236; c) B. L. Feringa, R. Naasz, R. Imbos, L. A. Arnold, *Modern Organocopper Chemistry* (Ed.: N. Krause), Wiley-VCH, Weinheim, **2002**, pp. 224 – 258; for representative recent advances, see: d) X. Hu, H. Chen, X. Zhang, *Angew. Chem.* **1999**, *111*, 3720 – 3723; *Angew. Chem. Int. Ed.* **1999**, *38*, 3518 – 3521; e) Y. Yamanoi, T. Imamoto, *J. Org. Chem.* **1999**, *64*, 2988 – 2989; f) L. A. Arnold, R. Imbos, A. Mandoli, A. H. M. de Vries, R. Naasz, B. L. Feringa, *Tetrahedron* **2000**, *56*, 2865 – 2878; g) I. H. Escher, A. Pfaltz, *Tetrahedron* **2000**, *56*, 2879 – 2888; h) C. Borner, M. R. Dennis, E. Sinn, S. Woodward, *Eur. J. Org. Chem.* **2001**, 2435 – 2446; i) I. Chataigner, C. Gennari, S. Ongeri, U. Piarulli, S. Ceccarelli, *Chem. Eur. J.* **2001**, *7*, 2628 – 2634; j) A. Alexakis, G. P. Trevitt, G. Bernardinelli, *J. Am. Chem. Soc.* **2001**, *123*, 4358 – 4359; k) R. Shintani, G. C. Fu, *Org. Lett.* **2002**, *4*, 3699 – 3702; l) L. A. Arnold, R. Naasz, A. Minaard, B. L. Feringa, *J. Org. Chem.* **2002**, *67*, 7244 – 7254; m) L. Liang, T. T. L. Au-Yeung, A. S. C. Chan, *Org. Lett.* **2002**, *4*, 3799 – 3801.

[2] S. J. Degrado, H. Mizutani, A. H. Hoveyda, *J. Am. Chem. Soc.* **2001**, *123*, 755 – 756.

[3] H. Mizutani, S. J. Degrado, A. H. Hoveyda, *J. Am. Chem. Soc.* **2002**, *124*, 779 – 781.

[4] a) S. J. Degrado, H. Mizutani, A. H. Hoveyda, *J. Am. Chem. Soc.* **2002**, *124*, 13362 – 13363; for a related process involving cyclic nitroalkenes, see: b) C. A. Luchaco-Cullis, A. H. Hoveyda, *J. Am. Chem. Soc.* **2002**, *124*, 8192 – 8193.

[5] a) K. D. Shimizu, M. L. Snapper, A. H. Hoveyda, *Chem. Eur. J.* **1998**, *4*, 1885 – 1889; for reviews regarding screening strategies for optimal catalyst identification, see: b) M. B. Francis, T. F. Jamison, E. N. Jacobsen, *Curr. Opin. Chem. Biol.* **1998**, *2*, 422 – 428; c) H. B. Kagan, *J. Organomet. Chem.* **1998**, *567*, 3 – 6; d) K. W. Kuntz, M. L. Snapper, A. H. Hoveyda, *Curr. Opin. Chem. Biol.* **1999**, *3*, 313 – 319; e) B. Jandeleit, D. J. Schaefer, T. S. Powers, H. W. Turner, W. H. Weinberg, *Angew. Chem.* **1999**, *111*, 2648 – 2689; *Angew. Chem. Int. Ed.* **1999**, *38*, 2494 – 2532; f) M. L. Snapper, A. H. Hoveyda, *Combinatorial Chemistry* (Ed.: H. Fenniri), Oxford University Press, Oxford, **2000**, pp. 433 – 455.

[6] For a study on Cu-catalyzed asymmetric conjugate additions to alkylidene malonates, where only low-to-moderate selectivities (5–73 % *ee*) are obtained, see: A. Alexakis, C. Benhaim, *Tetrahedron: Asymmetry* **2001**, *12*, 1151 – 1157.

[7] For enantioselective conjugate additions of sterically hindered (*t*Bu and cyclohexyl) radicals to unsaturated *N*-acyloxazolidinones, see: a) M. P. Sibi, J. Ji, J. H. Wu, S. Gurtler, N. A. Porter, *J. Am. Chem. Soc.* **1996**, *118*, 9200 – 9201; b) M. P. Sibi, J. Ji, *J. Org. Chem.* **1997**, *62*, 3800 – 3801.

[8] Since control experiments showed that with Gly as AA3, the phosphane corresponding to **7** affords less than 20 % *ee* (**5a**→**6**), a new route for synthesis of ligand libraries with *n*Bu termini was developed and utilized. See the Supporting Information for details.

[9] See the Supporting Information for details of the screening studies.

[10] For example, see: a) B. M. Cole, K. D. Shimizu, C. A. Krueger, J. P. A. Harrity, M. L. Snapper, A. H. Hoveyda, *Angew. Chem.* **1996**, *108*, 1776 – 1779; *Angew. Chem. Int. Ed. Engl.* **1996**, *35*, 1668 – 1671; b) C. A. Krueger, K. W. Kuntz, C. D. Dzierba, W. G. Wirschun, J. D. Gleason, M. L. Snapper, A. H. Hoveyda, *J. Am. Chem. Soc.* **1999**, *121*, 4284 – 4285; c) C. A. Luchaco-Cullis, H. Mizutani, K. E. Murphy, A. H. Hoveyda, *Angew. Chem.* **2001**, *113*, 1504 – 1508; *Angew. Chem. Int. Ed.* **2001**, *40*, 1456 – 1460; d) J. R. Porter, J. F. Traverse, A. H. Hoveyda, M. L. Snapper, *J. Am. Chem. Soc.* **2001**, *123*, 984 – 985; e) H. Deng, M. P. Isler, M. L. Snapper, A. H. Hoveyda, *Angew. Chem.* **2002**, *114*, 1051 – 1054; *Angew. Chem. Int. Ed.* **2002**, *41*, 1009 – 1012.

[11] a) S. B. Garber, J. S. Kingsbury, B. L. Gray, A. H. Hoveyda, *J. Am. Chem. Soc.* **2000**, *122*, 8168 – 8179, and references therein; for applications to catalytic cross-metathesis, see: b) J. Cossy, S. BouzBouz, A. H. Hoveyda, *J. Organomet. Chem.* **2001**, *624*, 327 – 332; c) S. Randl, S. Gessler, H. Wakamatsu, S. Blechert, *Synlett* **2001**, 430 – 432.

[12] Cu-catalyzed ACA of the *cis* isomer of **5a** with [$ZnEt_2$] affords the opposite enantiomer of **6** in 69 % yield and only 64 % *ee*.

[13] Reactions with [$ZnMe_2$] are carried out at lower temperatures, since transformations performed at 4 °C, which also proceed at a significantly slower pace than other alkyl zinc reagents, lead to the formation of unidentified products.

[14] Reactions of various unsaturated dimethyl oxazolidinones corresponding to substrates in Table 2 leads to significantly slower rates of reaction.

[15] A. Basha, M. Lipton, S. M. Weinreb, *Tetrahedron Lett.* **1977**, *18*, 4171 – 4172.

[16] D. A. Evans, T. C. Britton, J. A. Ellman, *Tetrahedron Lett.* **1987**, *28*, 6141 – 6144.

[17] A. H. Hoveyda, *Handbook of Combinatorial Chemistry*, (Eds.: K. C. Nicolaou, R. Hanko, W. Hartwig), Wiley-VCH, Weinheim, **2002**, pp. 991 – 1016.

 © 2003 Wiley-VCH Verlag GmbH & Co. KGaA, Weinheim 1433-7851/03/4211-1279 $ 20.00+.50/0

Synthesis of Antitumor Agents

Total Synthesis as a Resource in the Discovery of Potentially Valuable Antitumor Agents: Cycloproparadicicol**

*Kana Yamamoto, Robert M. Garbaccio, Shawn J. Stachel, David B. Solit, Gabriela Chiosis, Neal Rosen, and Samuel J. Danishefsky**

Hsp90 is a molecular chaperone required for the refolding of proteins in cells exposed to environmental stress. It governs the conformational maturation of a subset of proteins critical in regulating mitotic signal transduction and cellular survival.[1] These client proteins include steroid receptors, transcription factors, mutant p53, Hif1α, soluble kinases such as Akt, Raf-1, transmembrane kinases such as HER2, as well as cdk4 protein kinases. Hsp90 contains an ATP-binding pocket in its amino terminus. Several natural products, including geldanamycin, herbimycin A, and radicicol bind to this pocket and inhibit its chaperone function. This inhibition is mirrored in enhanced intracellular proteasomal degradation of Hsp90 client proteins. An encouraging consequence of this effect is an attenuation in the proliferation of cancer cells. In animal models, geldanamycin congeners exhibit antitumor activity at nontoxic doses.[2] The novel mechanism of action of geldanamycin-related drugs and the demonstration that they have, in principle, exploitable in vivo therapeutic indices have served to heighten interest in Hsp90 as a target for oncology.[3,4]

Radicicol (**1**),[5] originally isolated from *M. bonorden*, has a high affinity for Hsp90 ($K_d = 20$ nM) and is particularly potent in inhibiting its functions.[6] However, translation of the very promising in vitro profiles of radicicol and radicicol oxime to the in vivo realm has not been accomplished,[7] apparently as a result of unfavorable pharmakokinetics and nonspecific toxicities.

These early findings notwithstanding, we felt it worthwhile to persist in seeking a useful radicicol-based drug that is not subject to the potential liabilities arising from quinone-containing substructures such as those found in the geldanamycin series. We previously developed a highly convergent, three-stage total synthesis of radicicol,[8] which was crucial to the work described herein.

Our investigation of the radicicol series focused on two aspects. The first was directed to the effect, if any, of the stereochemistry of the system on its biological properties. We hoped to examine binding to Hsp90 as well as cytotoxicity. We saw such a study as a way to probe the areas of the drug that make important contacts with the chaperone. Assessing the consequences of altering the stereochemistry at particular points in a complex drug may be a more subtle probe of the stringency of presumably required molecular contacts, than gross deletion of functional groups.

We also became interested in a cyclopropane derivative of radicicol, that is, one in which the oxido linkage that connects C7′ and C8′ is replaced by a methylene group (i.e., a cyclopropane analogue, see Scheme 4, **21**–**24**).[9,10] The thought was that the lack of in vivo efficacy of radicicol might arise from its degradation ($k_{1/2} < 2$ hrs) or undirected cytotoxicity emanating from the ω-epoxydienone. Given the structural information available[11] on the binding of radicicol to the N-terminal ATP/ADP-binding domain of Hsp90, which seems to identify a hydrogen bond between the epoxide and Lys44, there was concern that the cyclopropane derivative might suffer an unacceptable loss of affinity to its intended target. In essence, both aims of this inquiry focused on a careful assessment of Lys44 contact in the action of the drug.

Our previous total synthesis of **1** provided a method for the preparation of compounds **2**–**4**. As before, the synthesis

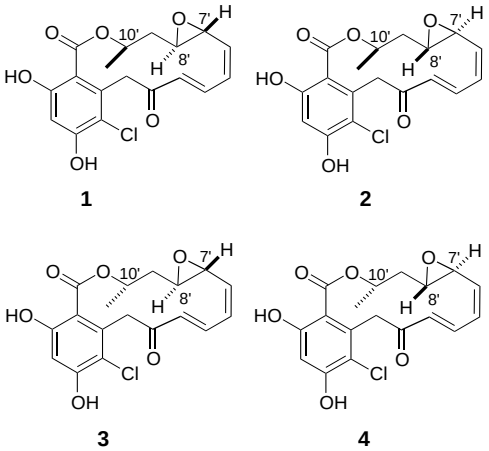

1 **2**

3 **4**

[*] Prof. Dr. S. J. Danishefsky, Dr. K. Yamamoto, Dr. R. M. Garbaccio,[+] Dr. S. J. Stachel
Laboratory for Bioorganic Chemistry
Sloan-Kettering Institute for Cancer Research
1275 York Avenue, New York, NY 10021 (USA)
Fax: (+1) 212-772-8691
E-mail: s-danishefsky@ski.mskcc.org
Prof. Dr. S. J. Danishefsky
Department of Chemistry, Columbia University
Havemeyer Hall, New York, NY 10027 (USA)
Dr. D. B. Solit, Dr. G. Chiosis, Prof. N. Rosen
Program in Cell Biology and Department of Medicine
Sloan-Kettering Institute for Cancer Research
1275 York Avenue, New York, NY 10021 (USA)
[+] Current address:
Merck Research Laboratories
West Point, PA 19486 (USA)

[**] Support for this research was provided by the National Institutes of Health (CA28824). Postdoctoral Fellowship support is gratefully acknowledged by K.Y. (The Helen Hay Whitney Foundation), R.M.G. (NIH, 1 F32 CA85894-01), and S.J.S. (NIH, 1 F32 CA81704). Dr. George Sukenick (NMR Core Facility, Sloan-Kettering Institute) is acknowledged for NMR and mass spectrometric analyses. We thank Dr. Louis J. Todaro (The CUNY X-ray Facility, Hunter College) and Dr. David G. Churchill (Department of Chemistry, Columbia University) for X-ray analyses.

Supporting information for this article is available on the WWW under http://www.angewandte.org or from the author. Experimental details include the description of experimental procedures and spectral data for all new compounds.

 © 2003 Wiley-VCH Verlag GmbH & Co. KGaA, Weinheim 1433-7851/03/4211-1280 $ 20.00+.50/0

featured a novel ring-closing olefin metathesis of a vinyl epoxide.[12,13] Thus, alcohol **5** was converted into **6** or **7** by the sequence described earlier (Scheme 1).[8] Coupling of **6** with acid **8** under either Mitsunobu (C10′ inversion) or acylation (C10′ retention) experimental protocols afforded esters **9** and **11**, respectively. Similarly, when the two senses of coupling were applied to alcohol **7**, esters **10** and **12** were obtained. The strategy used in the total syntheses of radicicol allowed access to stereocongeners **2, 3** (*ent*-**2**), and **4** (*ent*-**1**), as shown in Scheme 2.

The syntheses of the cyclopropane analogues commenced with the same allylic alcohol precursor **5** used in our earlier synthesis of radicicol and its stereocongeners. We now took advantage of the asymmetric cyclopropanation chemistry reported by Charette et al.[14,15] for the conversion of **5** into **13**. Alcohol **13** was converted into vinyl compound **14** (Scheme 3). Again acylation of **14** with **8** by using the two stereodifferentiating protocols led to **17** and **19** in high enantiomeric and diastereomeric purity. The conversion of **17** into the carba version of radicicol (cf. **21**) was carried out as shown. Conversion of **19** into **23** followed an identical route (Scheme 4).

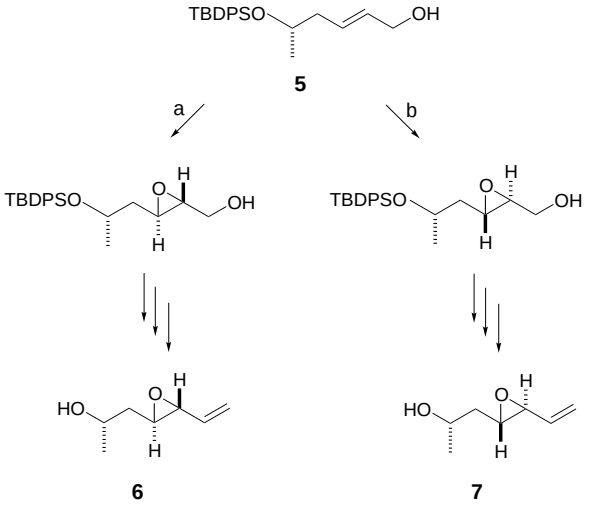

Scheme 1. Synthesis of the enantiopure epoxide side chains. a) (*R,R*)-diisopropyltartrate, $TiCl_4$, CH_2Cl_2, molecular sieves (4 Å), 71%; b) (*S,S*)-diisopropyltartrate, $TiCl_4$, molecular sieves (4 Å), 76%. TBDPS = *tert*-butyldiphenylsilyl.

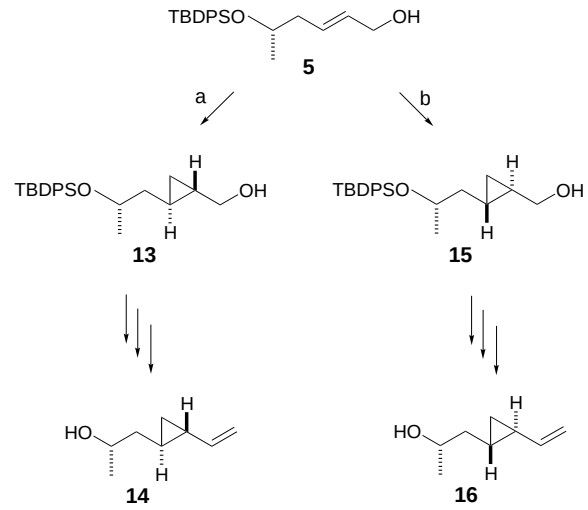

Scheme 3. Synthesis of the enantiopure cyclopropyl side chains. a) (*R,R*)-dioxaborolane, Et_2Zn, CH_2I_2, 69%; b) (*S,S*)-dioxaborolane, Et_2Zn, CH_2I_2, 72%.

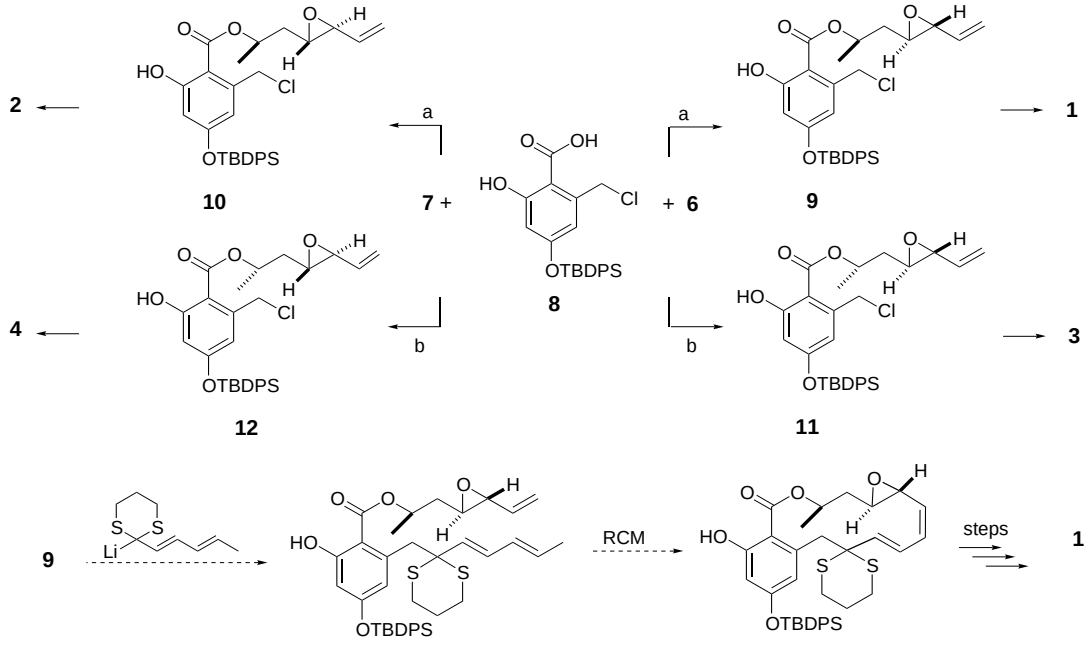

Scheme 2. Divergent synthesis of radicicols. a) DIAD, $P(fur)_3$, benzene, 75% (**9**), 76% (**10**); b) EDCI, DMAP, CH_2Cl_2, 41% (**11**), 44% (**12**). DIAD = diisopropylazodicarboxylate, fur = furyl, EDCI = 1-(3-dimethylaminopropyl)-3-ethylcarbodiimide hydrochloride, DMAP = 4-dimethylaminopyridine, RCM = ring-closing olefin metathesis.

 © 2003 Wiley-VCH Verlag GmbH & Co. KGaA, Weinheim 1433-7851/03/4211-1281 $ 20.00+.50/0

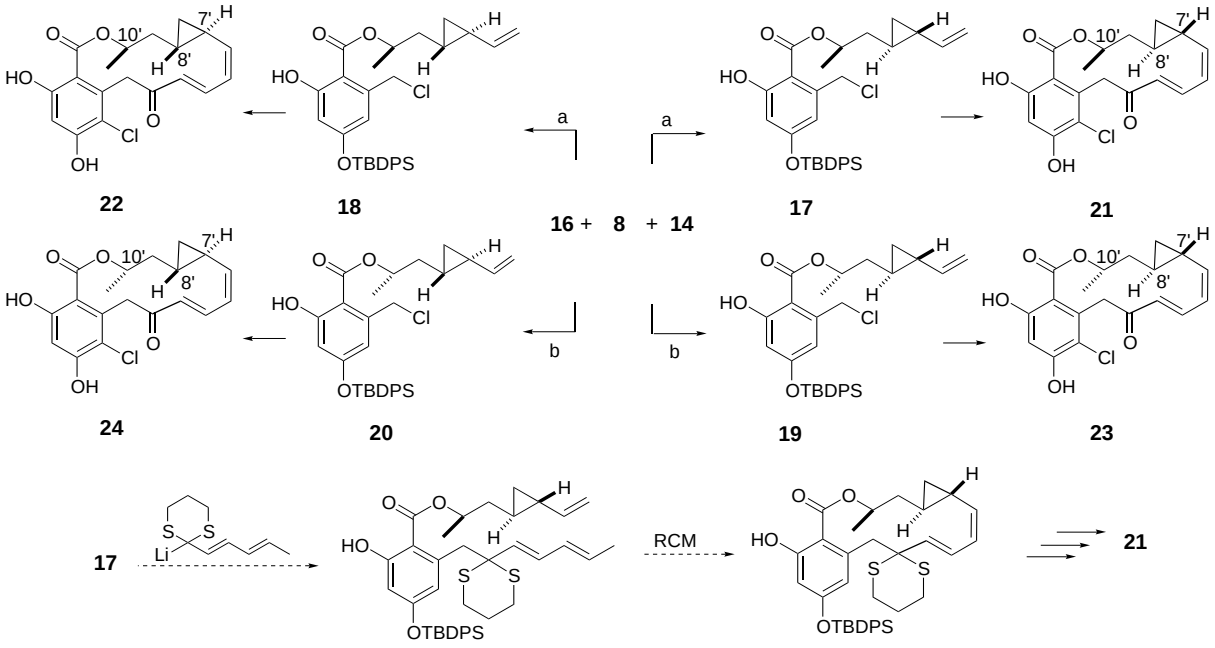

Scheme 4. Divergent synthesis of cycloproparadicicols. a) DIAD, $P(fur)_3$, benzene, 48% (**17**), 39% (**28**); b) EDCI, DMAP, CH_2Cl_2, 54% (**19**), 61% (**20**).

In a similar way **16** was obtained from **5** by using the enantiotopic Charette catalyst (Scheme 3). The conversion of **16** into **18** and **20** followed the same pathway. These, in turn, gave rise to **22** and **24**, respectively, again following closely the strategy and protocols used to reach **21**. Thus the four radicicol stereocongeners **1**–**4** as well as their respective carba variants **21**–**24** became available.

The radicicol congeners were tested for binding with Hsp90 by means of a binding-competition assay.[4] The parent natural product **1** binds with high affinity to Hsp90 (ED_{50} = 45 nM) as reported previously. When **21**, the carba version of the radicicol series, was tested for Hsp90 binding, it was found to still retain high affinity (ED_{50} = 160 nM), that is, a fourfold reduction from **1**. Therefore the hydrogen bond found between the epoxide and the Lys44 of the chaperone in the X-ray structure, while possibly useful, is not critical. Compound **22**, in which the C7′ and C8′ stereocenters are inverted, exhibits binding to a much lower extent (ED_{50} = 2 μM). Compound **23** with inversion at the C10′ stereocenter suffered a further decrease in its binding (ED_{50} = 5 μM). Inversion of all these stereocenters (see **24** = *ent*-**21**), undermines the affinity to Hsp90 still further (ED_{50} = > 10 mM).[16] It would be tempting to argue that in the cycloproparadicicols, and probably in the radicicol series, the protein Hsp90 target recognizes the gross substructure of the 14-membered lactone fused to the resorcinol. Supporting recognition elements are found in the methyl group at C10′ and at the cyclopropyl (epoxide) group, in the "natural" series when these elements are in an optimal stereochemical setting. Inversion of either of these loci, diminishes binding and biological activity. Inversion at both of the supporting sectors leads to severe loss of recognition.

As previously reported, the inhibition of Hsp90 induces the proteasomal degradation of a subset of proteins that require Hsp90 for maturation or stability. The expression levels of Raf1 and HER2, two of the most sensitive protein targets, was analyzed with the above radicicol variants (Figure 1). The radicicol-like action of **21** is also reflected in its potent degradation of oncogenic proteins. Interestingly, the stereochemical trend found in the Hsp90-binding assay, was also observed in the degradation level of the oncogenic proteins in both series. It seems that the actions of **1** and **21** on Hsp90 appear to occur in the same recognition setting.

Subsequently, these radicicol variants were evaluated for their growth-inhibition activity towards MCF-7 breast-cancer cells (Table 1). As expected, the same configurational trend

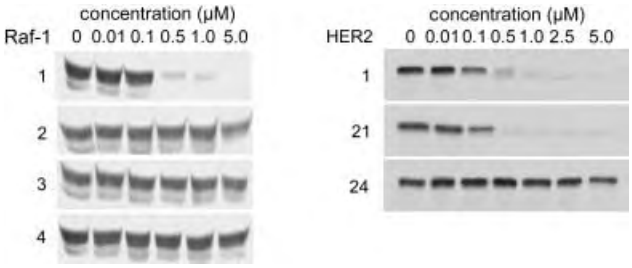

Figure 1. Immunoblot of Raf1 and HER2 expression of MCF-7 cells following 24 h of exposure to the indicated drugs.

Table 1: IC_{50} (nM) values of radicicol and cycloproparadicicol analogues in MCF7 cells.

Entry	Epoxide	IC_{50} [nM][a]	Cyclopropyl	IC_{50} [nM][a]
1	**1**	23	**21**	43
2	**2**	902	**22**	836
3	**3**	1720	**23**	2142
4	**4**	2172	**24**	3364

[a] Determined after 96 h of exposure to the indicated drugs.

 © 2003 Wiley-VCH Verlag GmbH & Co. KGaA, Weinheim 1433-7851/03/4211-1282 $ 20.00+.50/0

was also observed in this assay. Thus, **2** exhibits intermediate cell-growth inhibition (20-fold less), whereas **3** showed further decrease in their potency (50-fold less), and **4** was found to be even less active (~100-fold less). Most significantly, cyclopropane analogue **21**, which has the same stereochemical motif as radicicol (**1**), *retains* the potent cytotoxicity of **1** within a factor of two.

As previously reported for ansamycins, growth inhibition by radicicol (**1**) is a result of an Rb-dependent (Rb = retinoblastoma) arrest in the G1 phase of the cell cycle (Figure 2). Thus, MDA-468 breast cancer, which lacks Rb function, does

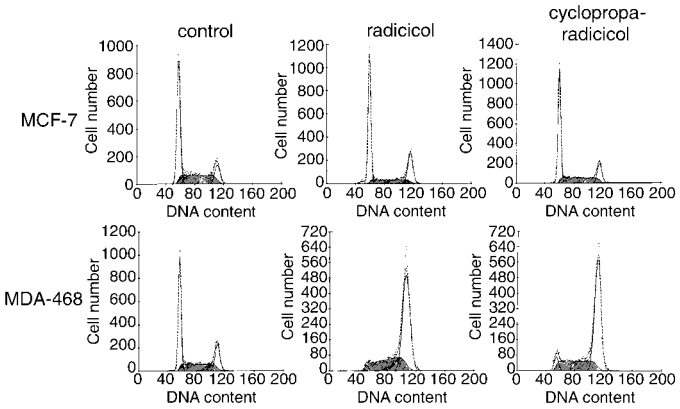

Figure 2. Cell cycle distribution of MCF-7 or MDA-468 cell lines assessed by fluorescence-activated cell sorter (FACS) analysis.

not arrest in G1, but instead is blocked in prometaphase prior to undergoing apoptosis.[17] Inhibition of Rb-dependent growth occurred at concentrations that correlate with those required for protein degradation. Cells with intact Rb (MCF-7) arrested in G1 and then underwent differentiation. Importantly, Rb-negative cells (MDA-468) also underwent apoptosis, in this case upon arrest in prometaphase. The same propensity was observed with cyclopropradicicol **21**.

In summary, these stereo and "carba" radicicol variants were designed and first prepared in our laboratory following the outlines of our concise total synthesis of radicicol.[8] The in vitro biological testing of these compounds revealed previously unrecognized structure–activity relationships. Notably, the oxygen atom of the epoxide of radicicol (**1**), in spite of its apparent Lys44–epoxide hydrogen bonding in the governing crystal structure in the radicicol field, is demonstrated to be non-essential for its activity.[18] A qualitative though instructive recognition model can now be proposed to focus future discovery-oriented investigations in this rather promising series of anticancer agents. The work described above serves to chart a direction by which organic synthesis in conjunction with cell biology can be mutually enhancing in the quest for novel drugs.

Received: December 13, 2002 [Z50769]

Keywords: antitumor agents · chaperone proteins · natural products · structure–activity relationships · synthesis design

[1] For general reviews of Hsp90, see: a) S. Walter, J. Buchner, *Angew. Chem.* **2002**, *114*, 1142–1158; *Angew. Chem. Int. Ed.* **2002**, *41*, 1098–1113; b) L. H. Pearl, C. Prodromou, *Curr. Opin. Struct. Biol.* **2000**, *10*, 1, 46–51; c) J. Buchner, *Trends Biochem. Sci.* **1999**, *24*, 136–141.

[2] For our efforts involving geldanamycin, another natural product which also binds to Hsp90, see: a) S. D. Kuduk, F. F. Zheng, L. Sepp-Lorenzino, N. Rosen, S. J. Danishefsky, *Bioorg. Med. Chem. Lett.* **1999**, *9*, 1233–1238; b) S. D. Kuduk, C. R. Harris, F. F. Zheng, L. Sepp-Lorenzino, Q. Ouerfelli, N. Rosen, S. J. Danishefsky, *Bioorg. Med. Chem. Lett.* **2000**, *10*, 1303–1306.

[3] a) L. Neckers, *Trends Mol. Med.* **2002**, *8*, 4, S55-S61; b) M. V. Blagosklonny, *Leukemia* **2002**, *16*(4), 455–462; c) T. Scheibel, J. Buchner, *Biochem. Pharmacol.* **1998**, *56*, 675–682; D. J. Newman, G. M. Cragg, S. Holbeck, E. A. Sausville, *Curr. Cancer Drug Targets* **2002**, *2*, 279–308.

[4] A novel class of synthetic nucleotide analogues was shown to bind to Hsp90 and inhibit the proliferation of cancer cells; see: a) G. Chiosis, M. N. Timaul, B. Lucas, P. N. Munster, F. F. Zheng, L. Sepp-Lorenzino, N. Rosen, *Chem. Biol.* **2001**, *8*, 289–299; b) G. Chiosis, B. Lucas, A. Shtil, H. Huezo, N. Rosen, *Bioorg. Med. Chem. Lett.* **2002**, *10*, 3555–3564.

[5] P. Delmontte, J. Delmontte-Plaquée, *Nature* **1953**, *171*, 344–347.

[6] a) S. V. Sharma, T. Agatsuma, H. Nakano, *Oncogene* **1998**, *16*, 20, 2639–2645; b) T. W. Schulte, S. Akinaga, T. Murakata, T. Agarsuma, S. Sugimoto, H. Nakano, Y. S. Lee, B. B. Simen, Y. Argon, S. Felts, D. O. Toft, L. M. Neckers, S. V. Sharma, *Mol. Endocrinol.* **1999**, *13*(9), 1435–1448.

[7] Some derivatives of microbial radicicol were reported to exhibit efficacy in animal models: a) Y. Shiotsu, L. M. Neckers, I. Wortman, W. G. An, T. W. Schulte, S. Soga, C. Murakata, T. Tamaoki, S. Akinaga, *Neoplasia* **2000**, *96*, 6, 2284–2291; b) S. Soga, S. V. Sharma, Y. Shiotsu, M. Shimizu, H. Tahara, K. Yamaguchi, Y. Ikuina, C. Murakata, T. Tamaoki, J. Kurebayashi, T. W. Schulte, L. M. Neckers, S. Akinaga, *Cancer Chemother. Pharmacol.* **2001**, *48*, 435–445; c) S. Soga, L. M. Neckers, T. W. Schulte, Y. Shiotsu, K. Akasaka, H. Narumi, T. Agatsuma, Y. Ikuina, C. Murakata, T. Tamaoki, S. Akinaga, *Cancer Res.* **1999**, *59*, 2931–2938; d) T. Agatsuma, H. Ogawa, K. Akasaka, A. Asai, Y. Yamashita, T. Mizukami, S. Akinaga, Y. Saitoh, *Bioorg. Med. Chem.* **2002**, *10*, 3445–3454.

[8] a) R. M. Garbaccio, S. J. Danishefsky, *Org. Lett.* **2000**, *2*, 20, 3127–3129; b) R. M. Garbaccio, S. J. Stachel, D. K. Baeschlin, S. J. Danishefsky, *J. Am. Chem. Soc.* **2001**, *123*, 10903–10908.

[9] The electophilicity of this system would allow Michael addition of a bionucleophile to the dienone or attack of the nucleophile at the epoxide linkage.[7b,d] Esterase action on the macrolactone is still another potential site of vulnerability. In the epothilone series, we found that agents lacking the epoxide manifest a much improved biological profile.[10]

[10] a) T. C. Chou, X. G. Zhang, C. R. Harris, S. D. Kuduk, A. Balog, K. Savin, J. R. Bertino, S. J. Danishefsky, *Proc. Natl. Acad. Sci. USA* **1998**, *95*, 15798–15802; b) T. C. Chou, X. G. Zhang, A. Balog, D. Su, D. F. Meng, K. Savin, J. R. Bertino, S. J. Danishefsky, *Proc. Natl. Acad. Sci. USA* **1998**, *95*, 9642–9647.

[11] S. M. Roe, C. Prodromou, R. O'Brien, J. E. Ladbury, P. W. Piper, L. H. Pearl, *J. Med. Chem.* **1999**, *42*, 260–266.

[12] a) M. S. Stanford, J. A. Love, R. H. Grubbs, *J. Am. Chem. Soc.* **2001**, *123*, 6543–6554, and references therein; b) for reviews, see: A. Fürstner, L. Ackermann, B. Gabor, R. Goddard, C. W. Lehmann, R. Mynott, F. Stelzer, O. R. Thiel, *Chem. Eur. J.* **2001**, *7*, 3236–3253; c) A. Fürstner, *Angew. Chem.* **2000**, *112*, 3140–3172; *Angew. Chem. Int. Ed.* **2000**, *39*, 3012–3043; d) for an important early example of the use of olefin metathesis for macrocyclization in a functionally complex setting, see: Z. Xu,

 © 2003 Wiley-VCH Verlag GmbH & Co. KGaA, Weinheim 1433-7851/03/4211-1283 $ 20.00+.50/0

C. W. Johannes, S. S. Salman, A. H. Hoveyda, *J. Am. Chem. Soc.* **1996**, *118*, 10926 – 10927.
[13] K. Yamamoto, K. Biswas, C. Gaul, S. J. Danishefsky, unpublished results.
[14] a) A. B. Charette, S. Prescott, C. Brochu, *J. Org. Chem.* **1995**, *60*, 1081 – 1083; b) A. B. Charette, H. Juteau, *J. Am. Chem. Soc.* **1994**, *116*, 2651 – 2652; c) A. B. Charette, H. Juteau, H. Lebel, C. Molinaro, *J. Am. Chem. Soc.* **1998**, *120*, 11943 – 11952; d) A. B. Charette, H. Lebel, *Org. Synth.* **1999**, *76*, 86 – 100.
[15] The configuration of the cyclopropane was initially assigned based on Charette's empirical rule and later confirmed by X-ray analysis of the derivative of **14** (see Supporting Information).
[16] This trend is consistent with molecular modeling (MOE 2001.01) results (Chiosis, unpublished data).
[17] Importantly, the small-cell lung cancer, which is not effected by geldanamycin variant are found to be Rb-negative.
[18] On the other hand, other hydrogen bonds in X-ray data appear to be critical as the dimethyl ethers of **1** and its derivatives lost their activities (data not shown).

 © 2003 Wiley-VCH Verlag GmbH & Co. KGaA, Weinheim 1433-7851/03/4211-1284 $ 20.00+.50/0

trans-*Coordinating Diphosphane*

SPANphos: A C_2-Symmetric *trans*-Coordinating Diphosphane Ligand**

*Zoraida Freixa, Mark S. Beentjes, Guido D. Batema, Cedric B. Dieleman, Gino P. F. van Strijdonck, Joost N. H. Reek, Paul C. J. Kamer, Jan Fraanje, Kees Goubitz, and Piet W. N. M. van Leeuwen**

In the last few decades much effort has been devoted to the development of sophisticated ligands for specific applications. Among these, chelating diphosphanes could be considered to be the most popular class of ligands for catalysis. Surprisingly, an overview on the vast number of known diphosphanes revealed that only a limited number of *trans*-chelating diphosphanes has been reported, and even fewer asymmetric variants thereof.[1] Diphosphanes that coordinate only in a *trans* fashion that is not achieved through coordination of an additional heteroatom (i.e., in fact tridentate ligands), are very rare. The TRANSphos ligand, developed by Venanzi et al.,[2] is a flexible ligand that can achieve chelation angles of 175.7°, but *cis* structures have also been reported. In 1991, Ito et al. introduced a new family of *trans*-diphosphanes, namely, the TRAP ligands,[3] which already proved to be active in several asymmetric catalytic reactions in which *cis*-coordinating ligands failed to give enantioselectivity.

The synthesis of new, purely *trans*-diphosphanes is still a worthwhile challenge, because they will provide access to scarcely explored catalysts with unusual dispositions of ligands around the active metal center. By using *trans*-chelating ligands, some coordination positions that are traditionally available when *cis*-diphosphanes are used can be inhibited, and new families of catalysts with new properties could thus be discovered.[1]

We report here the synthesis of a new *trans*-coordinating diphosphane, which is readily available in three steps from cheap reagents, characterization of Rh, Pd, and Pt complexes thereof, and some preliminary catalytic experiments.

Scheme 1 shows the synthetic path to SPANphos (**3**). Racemic 4,4,4′,4′,6,6′-hexamethylspiro-2,2′-bichroman (**1**) was obtained on a 10 g scale by acid-catalyzed reaction of *p*-cresol with acetone.[4] Spirane **1** was brominated with *N*-bromosuccinimide (NBS) to obtain 8,8′-dibromo-4,4,4′,4′,6,6′-hexamethylspiro-2,2′-bichroman (**2**), which was treated with *n*BuLi and chlorodiphenylphosphane to give SPANphos in about 80% overall yield. Optically pure samples of **3** were obtained by racemic resolution by chiral HPLC.[5]

The molecular structure of **3** was determined by X-ray crystallographic analysis (Figure 1).[6] It has an intramolecular P···P distance of 4.991 Å. All atoms in each chroman fragment are nearly in a single plane, except for the spiro carbon atom

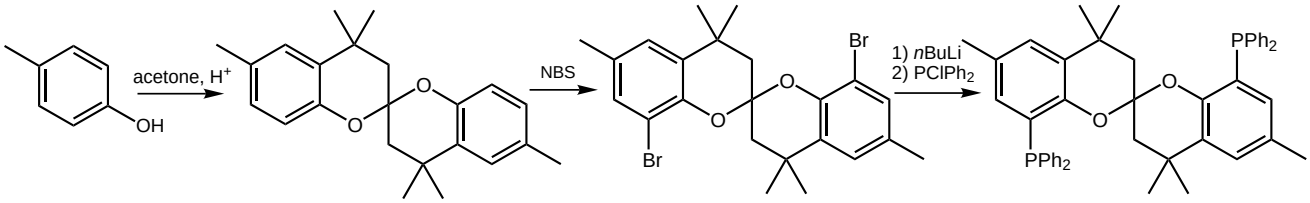

1 **2** SPANphos(**3**)

Scheme 1. Synthetic route to SPANphos **3**.

on the idealized C_2 axis, which lies about 0.7 Å above either plane. The dihedral angle between the two mean planes of 43.9(1)° results in an "*anti*" disposition of the lone pairs of the P atoms, which seems incompatible with a chelating coordination mode of the ligand.

Reaction of **3** with stoichiometric amounts of $[PtCl_2(CH_3CN)_2]$ and $[PdCl_2(cod)]$ (cod = 1,5-cyclooctadiene) gave *trans*-$[PtCl_2(\mathbf{3})]$ (**4**) and *trans*-$[PdCl_2(\mathbf{3})]$ (**5**).

[*] Prof. Dr. P. W. N. M. van Leeuwen, Dr. Z. Freixa, M. S. Beentjes, G. D. Batema, Dr. C. B. Dieleman, Dr. G. P. F. van Strijdonck, Dr. J. N. H. Reek, Dr. P. C. J. Kamer, J. Fraanje, K. Goubitz
Institute of Molecular Chemistry, University of Amsterdam
Nieuwe Achtergracht 166, 1018 WV Amsterdam (The Netherlands)
Fax: (+31) 20-525-6456
E-mail: pwnm@science.uva.nl

[**] The NRSCC is kindly acknowledged for financial support.

 © 2003 Wiley-VCH Verlag GmbH & Co. KGaA, Weinheim 1433-7851/03/4211-1284 $ 20.00+.50/0

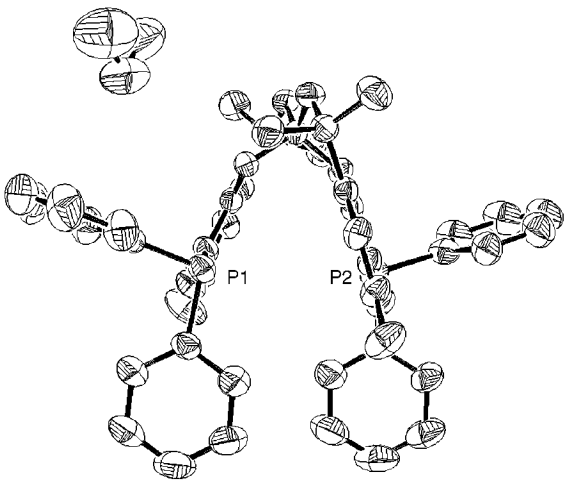

Figure 1. Molecular structure of **3** (ORTEP plot).

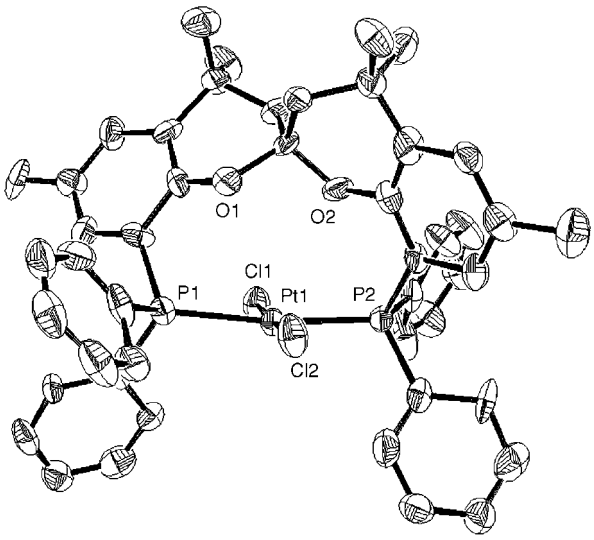

Figure 2. Molecular structure of **4** (ORTEP plot). Selected bond lengths [Å] and angles [°] for **4**. Pt1–Cl1 2.294(8), Pt1–Cl2 2.338(9), Pt1–P1 2.315(5), Pt1–P2 2.293(4), Cl1-Pt1-Cl2 176.4(3); Cl1-Pt1-P1 89.3(2), Cl1-Pt1-P2 92.9(2), Cl2-Pt1-P1 91.1(3), Cl2-Pt1-P2 86.2(2), P1-Pt1-P2 171.9(4).

Figure 2 shows the molecular structure of **4**.[7] The structure confirms the *trans* coordination of the diphosphane ligand, with a P-Pt-P angle of 171.9°. This angle is about 10° wider than those reported for square-planar Pd and Rh complexes of TRAP derivatives.[8] This wider bite angle is likely related to the larger P···P distance enforced by the bichroman backbone, as opposed to the highly congested biferrocenyl backbone of TRAP ligands. In contrast to the free ligand, in complex **4**, the oxygen atom and the carbon atom adjacent to the spiro center lie above and below the plane defined by the aromatic ring of the chroman fragment. This brings the phosphorous atoms 0.40 Å closer to one another than in the free ligand (P···P in **4**: 4.591 versus 4.991 Å in the free ligand) and appropriately orientates the lone pairs of these atoms for *trans* chelation.

The ^{31}P NMR spectrum of **4** shows a single signal with Pt satellites ($\delta = 17.6$ ppm, $^1J(\mathrm{Pt,P}) = 2723$ Hz), which strongly suggests that the mononuclear *trans* complex is the only species in solution. The ^{31}P NMR spectrum of **5** also shows a single signal with the same chemical shift as the Pt complex, which indicates the same molecular structure for both complexes. Furthermore, the related [PdClMe(**3**)] (**6**) shows a singlet at $\delta = 24.7$ ppm in the ^{31}P NMR spectrum and a triplet ($\delta = -0.27$ ppm, $^2J(\mathrm{P,H}) = 6.1$ Hz) in the ^{1}H NMR spectrum, indicative of the *trans* disposition of the bidentate ligand.[9]

The reaction of [Rh(acac)(CO)$_2$] with a stoichiometric quantity of **3** produced the mononuclear complex [Rh(acac)(CO)(η^1-**3**)] (**7**; Scheme 2); this indicates that the ligand cannot achieve a 90° chelation angle. This was also confirmed when complex **7** was treated with 20 bar of CO in a high-pressure (HP) NMR tube. Formation of the new binuclear complex [Rh$_2$(μ-CO)$_2$(CO)$_4$(η^1-**3**)$_2$] (**8**) was observed, as demonstrated by the ^{31}P NMR signals ($\delta =$ 21.1, m, 1P; −15.6 ppm, brs, 1P) as well as by HP-IR experiments. Complex **8** slowly evolves under 20 bar of H$_2$ into a new species characterized by a doublet ($\delta =$ 33.3 ppm, $^1J(\mathrm{Rh,P}) = 143.7$ Hz) in the ^{31}P NMR spectrum and a triplet of doublets in the ^{1}H NMR spectrum ($\delta =$ −9.5 ppm, $^1J(\mathrm{Rh,P}) = 6.2$, $^1J(\mathrm{Rh,H}) = 3.7$ Hz). These signals are consistent both with a mononuclear complex [RhH(CO)$_2$(**3**)] (**9**) and a binuclear species **10** with two bridging diphosphane ligands. Both spectra are consistent with bisequatorial coordination of the P-donor ligand, as was corroborated by HP-IR spectroscopy under CO/H$_2$ and CO/D$_2$. Further investigations to distinguish between these two species by using DOSY techniques are planned.

The catalytic activity of metal complexes containing *rac*-**3** was tested in several reactions. It was shown to be an efficient ligand for rhodium-catalyzed hydroformylation of 1-octene and styrene, palladium-catalyzed allylic alkylation of 1,3-

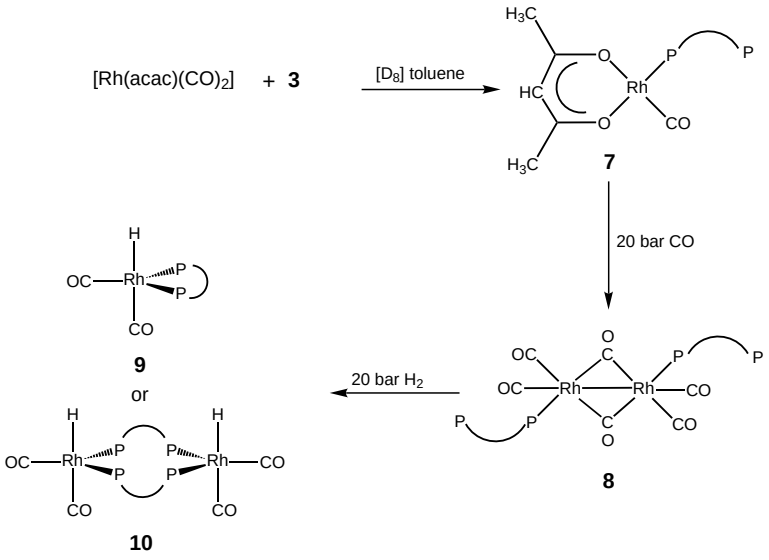

Scheme 2. Rhodium complexes of **3**, which were confirmed by NMR and IR experiments.

 © 2003 Wiley-VCH Verlag GmbH & Co. KGaA, Weinheim 1433-7851/03/4211-1285 $ 20.00+.50/0

diphenylprop-2-ene-1-yl acetate and Michael reaction of ethyl α-cyanopropionate with methyl vinyl ketone.

No activity was observed for palladium-catalyzed CO/ethene oligomerization under different conditions, and not even the formation of methyl propanoate was detected. Recent results suggest that a *cis* arrangement of the diphosphane ligand is necessary to enable solvolysis of the acyl group, which is the main chain-transfer mechanism in CO/ethene oligomerization cycles starting with a palladium hydride species.[10] Hence, these results reinforce the idea that **3** neither forms *cis* compounds, nor undergoes dissociation of one of the phosphorus atoms during the catalytic cycle.

In conclusion, we have synthesized a new C_2-symmetric *trans*-diphosphane ligand that is readily accessible from cheap reagents. Neither *cis–trans* isomerization nor decoordination of one of the P atoms appears to occur under CO/ethene oligomerization conditions. In Pd or Pt complexes SPANphos acts as a purely *trans*-coordinating diphosphane ligand. This is corroborated by NMR studies on rhodium complexes, which showed that chelation angles close to 90° cannot be achieved by this ligand.

As we mentioned before, the introduction by Ito et al. of the TRAP type ligands showed that these chiral *trans*-coordinating diphosphanes provide excellent enantiomeric excesses in some reactions in which *cis*-diphosphanes are inefficient.[3] From the viewpoint of enantioselective discrimination, the main difference between *cis*-and *trans*-diphosphanes is the role of their chiral backbone. For instance, in a square-planar complex, when a *trans*-chelating diphosphane is used, both the backbone and the substituents on the P atoms directly contribute to the formation of a chiral cavity around the metal center. This represents an advantage over the classical *cis*-chelating ligands, in which the backbone is not directly exposed to the active sites of the metal, and the chiral environment is mainly produced by the substituents on the phosphorus atoms by chirality-transfer mechanisms. The potential of the chiral cavity generated by TRAP ligands is evidenced by the remote stereoselective formation of C–C bonds on atoms not directly attached to the metal center.[11]

Investigations on SPANphos derivatives containing the same or related backbones will lead us to a family of potentially chiral, easily accessible *trans* ligands. Catalytic experiments on asymmetric reactions with enantiopure samples of the **3** are currently under development.

Experimental Section

Bichroman **1** was prepared according to a modified literature procedure.[4]

2: A solution of NBS (3.23 g) in DMF (40 mL) was added dropwise to a solution of **1** (2.56 g, 7.25×10^{-3} mol) in DMF (125 mL). The reaction mixture was monitored by GC-MS. After five days, it was quenched with water and extracted with Et_2O. The combined organic layers were dried over magnesium sulfate, and the solvent was evaporated. The product was crystallized from methanol to give a white solid (yield 84%). ^{1}H NMR (500 MHz, $CDCl_3$): $\delta = 7.11$, 7.09 (s, s, 2H, 2H; H5, H5′, H7, H7′), 2.29 (s, 6H; $CH_3$6, $CH_3$6′), 2.21 (d, ^2J(H,H) = 14.0 Hz, 2H; H3a, H3a′), 2.10 (d, ^2J(H,H) = 14.0 Hz, 2H; H3b, H3b′), 1.78 (s, 6H; $CH_3$4a, $CH_3$4a′), 1.38 ppm (s, 6H; $CH_3$4b, $CH_3$4b′); ^{13}C NMR (125.7 MHz, $CDCl_3$): $\delta = 144.94$, 133.53, 131.86, (CH arom.), 131.09, 126.15, (CH arom.), 111.22 (CH arom.), 98.60 (C2), 46.86 ($CH_2$3, $CH_2$3′), 33.07 (CH_3), 32.21 (CH_3), 31.18 (C4, C4′), 20.54 ppm (CH_3).

3: *n*BuLi (2.5 mL, 2.5 M in hexane, 1.2×10^{-2} mol) was added dropwise to a refluxing solution of **2** (2.99 g, 5.8×10^{-3} mol) in THF (150 mL). Upon completion of the reaction, monitored by GC-MS, $ClPPh_2$ (2.3 mL, 1.2×10^{-2} mol) was added, and the reaction mixture stirred at room temperature for 16 h. The reaction was quenched with degassed water and extracted with Et_2O. The combined organic layers were dried over magnesium sulfate, and the solvent was evaporated. The product was crystallized from methanol (yield 89%). ^{1}H NMR (300 MHz, $CDCl_3$): $\delta = 7.42$–7.00 (m, 22H; CH arom), 6.64 (m, 2H; CH arom.), 2.00 (s, 6H; $CH_3$6, $CH_3$6′), 1.82 (d, ^2J(H,H) = 14.1 Hz, 2H; H3a, H3a′), 1.82 (s, 6H; $CH_3$4a, $CH_3$4a′),1.62 (d, ^2J(H,H) = 14.1 Hz, 2H; H3b, H3b′), 1.22 ppm (s, 6H; $CH_3$4b, $CH_3$4b′): ^{13}C NMR (75.4 MHz, $CDCl_3$): $\delta = 151.80$ (d, J(P,C) = 10.8 Hz; C arom.), 139.26 (d, J(P,C) = 8.4 Hz; C arom.), 138.56 (d, J(P,C) = 8.1 Hz; C arom.), 134.92 (d, J(P,C) = 12.4 Hz; CH arom.), 134.44 (d, J(P,C) = 11.6 Hz; CH arom.), 133.24 (s; CH arom.), 131.79 (s; C arom.), 131.25 (s; C arom.), 129.14–128.20 (m, C; CH arom.), 125.55 (d, J(P,C) = 8.8 Hz; C arom.), 98.80 (s; C2), 47.65 (s; $CH_2$3, $CH_2$3′), 34.29 (CH_3), 33.08 (CH_3), 30.94 (C4, C4′), 21.35 ppm (CH_3). ^{31}P NMR (121.5 MHz; $CDCl_3$): $\delta = -14.6$ ppm (s).

CCDC-196129 and CCDC-196130 contain the supplementary crystallographic data for this paper. These data can be obtained free of charge via www.ccdc.cam.ac.uk/conts/retrieving.html (or from the Cambridge Crystallographic Data Centre, 12, Union Road, Cambridge CB21EZ, UK; fax: (+44) 1223-336-033; or deposit@ccdc.cam.ac.uk).

Received: October 25, 2002 [Z50435]

Keywords: homogeneous catalysis · ligand design · platinum · P ligands

[1] a) C. A. Bessel, P. Aggarwal, A. C. Maerschilok, K. J. Takeuchi, *Chem. Rev.* **2001**, *101*, 1031–1066; b) W. Winter, *Angew. Chem.* **1976**, *88*, 260; *Angew. Chem. Int. Ed. Engl.* **1976**, *15*, 241; c) A. Kless, C. Lefeber, A. Spannenberg, R. Kempe, W. Baumann, J. Holz, A. Börner, *Tetrahedron* **1996**, *52*, 14599–14606.

[2] a) N. J. DeStefano, D. K. Johnson, R. M. Lane, L. M. Venanzi, *Helv. Chim. Acta* **1976**, *59*, 2674–2682; b) P. N. Kapoor, L. M. Venanzi, *Helv. Chim. Acta* **1977**, *60*, 2824–2829.

[3] a) M. Sawamura, H. Hamashima, Y. Ito, *Tetrahedron: Asymmetry* **1991**, *2*, 593; b) M. Sawamura, H. Hamashima, Y. Ito, *J. Am. Chem. Soc.* **1992**, *114*, 8295–8296; c) M. Sawamura, H. Hamashima, Y. Ito, *Tetrahedron* **1994**, *50*, 4439–4454; d) R. Kuwano, K. Sato, T. Kurokawa, D. Karube, Y. Ito, *J. Am. Chem. Soc.* **2000**, *122*, 7614–7615; e) R. Kuwano, M. Sawamura, Y. Ito, *Bull. Chem. Soc. Jpn.* **2000**, *73*, 2571–2578; f) R. Kuwano, M. Sawamura, J. Shirai, M. Takahashi, Y. Ito, *Bull. Chem. Soc. Jpn.* **2000**, *73*, 485–496.

[4] This product was obtained by an improved procedure with respect to that already described: a) A. Ryabov, *Neftekhimiya* **1987**, *27*, 215–218; b) A. J. Caruso, J. L. Lee, *J. Org. Chem.* **1997**, *62*, 1058–1063.

[5] Authors are indebted to DSM Research for the enantiomeric separation of a sample of **3**.

[6] $C_{47}H_{46}O_2P_2{\cdot}CH_2Cl_2$, $M_r = 704.8$, triclinic, $P\bar{1}$, $a = 11.9743(5)$, $b = 13.240(1)$, $c = 14.808(1$ Å, $\alpha = 73.807(7)$, $\beta = 79.854(8)$, $\gamma = 71369(7)°$, $V = 2126.6(3)$ Å^3, $Z = 2$, $\rho_{calcd} = 1.23$ g cm^{-3}, $\lambda(Cu_{K\alpha}) = 1.5418$ Å, $\mu(Cu_{K\alpha}) = 2.37$ mm^{-1}, $F(000) = 832$, room temperature, final $R = 0.061$ for 6974 observed reflections.

[7] $C_{47}H_{46}Cl_2O_2P_2Pt$, $M_r = 487.2$, orthorhombic, $Pbn2_1$, $a = 13.167(1)$, $b = 17.369(1)$, $c = 17.735(2)$ Å, $V = 4056.0(6)$ Å^3, $Z =$

 © 2003 Wiley-VCH Verlag GmbH & Co. KGaA, Weinheim 1433-7851/03/4211-1286 $ 20.00+.50/0

4, $\rho_{calcd} = 1.59\ g\,cm^{-3}$, $\lambda(Cu_{K\alpha}) = 1.5418$ Å, $\mu(Cu_{K\alpha}) = 8.73\ mm^{-1}$, $F(000) = 1944$, room temperature, final $R = 0.059$ for 3641 observed reflections.

[8] M. Sawamura, H. Hamashima, M. Sugawara, R. Kuwano, Y. Ito, *Organometallics* **1995**, *14*, 4549 – 4558.

[9] M. A. Zuideveld, B. H. G. Swennenhuis, D. K. Maarten, Y. Guari, G. P. F. van Strijdonck, J. N. H. Reek, P. C. J. Kamer, K. Goubitz, J. Fraanje, M. Lutz, A. L. Spek, P. W. N. M. van Leeuwen, *J. Chem. Soc. Dalton Trans.* **2002**, *11*, 2308 – 2317.

[10] P. W. N. M van Leeuwen, M. A. Zuideveld, B. H. G. Swennenhuis, Z. Freixa, P. C. J. Kamer, K. Goubitz, J. Fraanje, M. Lutz, A. Spek, unpublished results.

[11] a) M. Sawamura, H. Hamashima, H. Shinoto, Y. Ito, *Tetrahedron Lett.* **1995**, *36*, 6479 – 6482; b) M. Sawamura, M. Sudoh, Y. Ito, *J. Am. Chem. Soc.* **1996**, *118*, 3309 – 3310; c) R. Kuwano, H. Miyazaki, Y. Ito, *Chem. Commun.* **1998**, 71 – 72.

 © 2003 Wiley-VCH Verlag GmbH & Co. KGaA, Weinheim 1433-7851/03/4211-1287 $ 20.00+.50/0

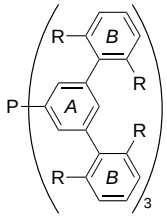

R= Me: P(tm-tp)$_3$
R= H: P(tp)$_3$

High-Speed Hydrosilylation

Rate Enhancement with a Bowl-Shaped Phosphane in the Rhodium-Catalyzed Hydrosilylation of Ketones**

*Osamu Niyomura, Makoto Tokunaga, Yasushi Obora, Tetsuo Iwasawa, and Yasushi Tsuji**

Since the nature of P ligands is very important in transition-metal-catalyzed reactions, a wide variety of these ligands has been designed to realize high catalytic activity and selectivity.[1] So far, most P ligands are rather small, and their design and modification have hitherto been performed within close proximity of the P atom. Recently, several large (nanosized) phosphorus ligands were developed for transition-metal-catalyzed reactions.[2,3] In the course of our studies,[3] we found that a bowl-shaped[4] phosphane ligand markedly enhances the rate of rhodium-catalyzed hydrosilylation of ketones.[5]

The two triarylphosphanes tris(2,2″,6,6″-tetramethyl-*m*-terphenyl-5′-yl)phosphane[6] (denoted as P(tm-tp)$_3$) and tris(*m*-terphenyl-5′-yl)phosphane (denoted as P(tp)$_3$) were prepared and compared with common phosphanes in the rhodium-catalyzed hydrosilylation of cyclohexanone with a trisubstituted silane (Table 1). P(tm-tp)$_3$ was first prepared in 2001[6a] and its Pd^0 complex [Pd{P(tm-tp)$_3$}$_2$] was reported in 2002.[6b] In the presence of catalytic amounts of P(tm-tp)$_3$ and [{RhCl(C$_2$H$_4$)$_2$}$_2$] (P/Rh = 2), the reaction proceeded smoothly in benzene at room temperature over 3 h, and cyclohexanol was obtained in 97% yield after desilylation (Table 1, entry 1). In contrast, the same reaction with P(tp)$_3$ afforded the product in only 25% yield (entry 2). Furthermore, other representative triarylphosphanes (entries 3–6) and trialkylphosphanes (entries 7–9) were also much less effective than P(tm-tp)$_3$. With these ligands (entries 2–9), the reactions were sluggish at room temperature, and much longer reaction times (40–500 h) were required to obtain the products in good yields (70–95%). A kinetic study indicated that the P(tm-tp)$_3$ catalyst system (entry 1) realized 154, 31, and 28 times faster reactions than PPh$_3$ (entry 3), P(tp)$_3$ (entry 2), and P(*o*-tol)$_3$ (entry 5), respectively.[7] Benzene is a better solvent than CH$_2$Cl$_2$ in the reactions of entries 1–3.

Table 1: Effects of ligands in the hydrosilylation of cyclohexanone.[a]

Entry	Ligand[b]	Yield [%][c]
1	P(tm-tp)$_3$	97 (13)[d]
2	P(tp)$_3$	25 (<1)[d]
3	PPh$_3$	7 (<1)[d]
4	P(2-furyl)$_3$	22
5	P(*o*-tol)$_3$	32
6	PMes$_3$	25
7	PEt$_3$	<2
8	PCy$_3$	<2
9	P*t*Bu$_3$	31

[a] Reaction conditions: cyclohexanone (1.0 mmol), HSiMe$_2$Ph (1.2 mmol), [{RhCl(C$_2$H$_4$)$_2$}$_2$] (0.0050 mmol), ligand (0.020 mmol), tridecane (0.25 mmol, as an internal standard), benzene (1.0 mL), RT, 3 h. [b] tol = tolyl, Mes = mesityl, Cy = cyclohexyl. [c] Yield of cyclohexanol by GC after desilylation with HCl/MeOH. [d] In CH$_2$Cl$_2$ as solvent.

The rate enhancement with P(tm-tp)$_3$ was further confirmed with various silanes and ketones, and compared with P(tp)$_3$ and PPh$_3$ (Table 2). With HSiEt$_3$ (Table 2, entries 1–3) or HSiMePh$_2$ (entries 4–6), the hydrosilylation of cyclohexanone proceeded much faster with P(tm-tp)$_3$ (entries 1 and 4) than with P(tp)$_3$ (entries 2 and 5) and PPh$_3$ (entries 3 and 6). Furthermore, in the hydrosilylation of various ketones such as acetophenone (entries 7–9), 2-octanone (entries 10–12), and (−)-menthone (entries 13–15), rate enhancement with P(tm-tp)$_3$ was also evident. As catalyst precursor, the cationic rhodium complex [Rh(cod)$_2$]BF$_4$ (cod = cyclooctadiene) showed a similar rate enhancement with P(tm-tp)$_3$ (entries 16–18).

P(tm-tp)$_3$ is a much more efficient than P(tp)$_3$, although the two ligands strongly resemble each other. The structures of P(tm-tp)$_3$ and P(tp)$_3$ were optimized by HF/6-31G(d) calculations[8a] on initial structures generated by CON-

[*] Prof. Dr. Y. Tsuji, Dr. O. Niyomura, Dr. M. Tokunaga, Dr. Y. Obora, T. Iwasawa
Catalysis Research Center and Division of Chemistry
Graduate School of Science
Hokkaido University
Sapporo 060-0811 (Japan)
Fax: (+081) 11-706-3698
E-mail: tsuji@cat.hokudai.ac.jp

[**] Financial support from the Asahi Glass Foundation is gratefully acknowledged. O.N. is grateful to the JSPS Research Fellowships for Young Scientists.

 © 2003 Wiley-VCH Verlag GmbH & Co. KGaA, Weinheim 1433-7851/03/4211-1287 $ 20.00+.50/0

Table 2: Hydrosilylation with various substrates.[a]

Entry	Ketone	Silane	Ligand	*t* [h]	Yield [%][b]
1	cyclohexanone	$HSiEt_3$	$P(tm\text{-}tp)_3$	21	81
2			$P(tp)_3$	21	36
3			PPh_3	21	13
4	cyclohexanone	$HSiMePh_2$	$P(tm\text{-}tp)_3$	20	97
5			$P(tp)_3$	20	37
6			PPh_3	20	27
7	acetophenone	$HSiMe_2Ph$	$P(tm\text{-}tp)_3$	5	96
8			$P(tp)_3$	5	15
9			PPh_3	5	15
10[c]	2-octanone	$HSiMe_2Ph$	$P(tm\text{-}tp)_3$	6	91
11[c]			$P(tp)_3$	6	41
12[c]			PPh_3	6	31
13	(−)-menthone	$HSiMe_2Ph$	$P(tm\text{-}tp)_3$	20	92 (45/55)[d]
14			$P(tp)_3$	20	8 (43/57)[d]
15			PPh_3	20	12 (38/62)[d]
16[e]	cyclohexanone	$HSiMe_2Ph$	$P(tm\text{-}tp)_3$	6	95
17[e]			$P(tp)_3$	6	65
18[e]			PPh_3	6	9

[a] Reaction conditions: ketone (1.0 mmol), silane (1.2 mmol), $[\{RhCl(C_2H_4)_2\}_2]$ (0.0050 mmol), ligand (0.020 mmol), tridecane (0.25 mmol, as internal standard), benzene (1.0 mL), RT. [b] Yield of alcohol by GC after desilylation with HCl/MeOH. [c] At 50 °C. [d] Product ratio (neomenthol/menthol). [e] $[Rh(cod)_2]BF_4$ (0.010 mmol) was used instead of $[\{RhCl(C_2H_4)_2\}_2]$, in CH_2Cl_2 as solvent.

FLEX[8b]/MM3.[8c] They showed that $P(tm\text{-}tp)_3$ and $P(tp)_3$ both have nanosized bowl-shaped structures with the phosphorus atom at the bottom and diameters of 1.99 and 1.95 nm, respectively (Figure 1). The cone angles of $P(tm\text{-}tp)_3$ and $P(tp)_3$, determined for the optimized structures in Figure 1,

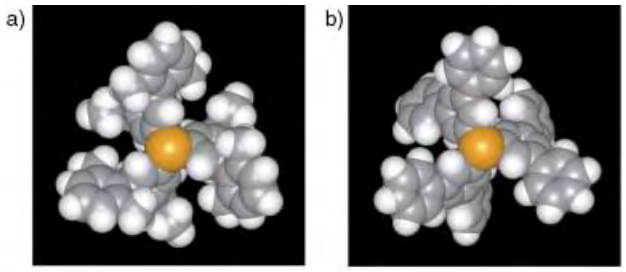

Figure 1. Optimized structures of a) $P(tm\text{-}tp)_3$ and b) $P(tp)_3$.

are 205 and 193°, respectively.[9a] Hence, they are more bulky than PCy_3 and $PtBu_3$, and less congested than $P(o\text{-tol})_3$ and $PMes_3$.[9a] It is well-known that $^1J(^{31}P,^{77}Se)$ coupling constants of phosphane selenides $Se{=}PR_3$ are reliable measures of the basicity of the parent phosphane PR_3: larger coupling constants mean lower basicities.[10a–c] The $^1J(^{31}P,^{77}Se)$ coupling constants of $Se{=}P(tm\text{-}tp)_3$ and $Se{=}P(tp)_3$ of 769.7[10d] and 765.5 Hz,[10d] respectively, indicate that $P(tm\text{-}tp)_3$ and $P(tp)_3$ have comparable basicities. They are less basic than PPh_3 (735 Hz)[10b] and $P(o\text{-tol})_3$ (732 Hz),[10d] and more basic than $P(2\text{-furyl})_3$ (793 Hz).[10a]

Thus, the cone angles and basicities cannot explain the difference in reactivity between $P(tm\text{-}tp)_3$ and $P(tp)_3$. The most important difference between $P(tm\text{-}tp)_3$ and $P(tp)_3$ is the depth of the bowl: $P(tm\text{-}tp)_3$ (depth: 0.208 nm) is a much deeper bowl than $P(tp)_3$ (0.132 nm). The dihedral angles between the phosphanated phenyl ring (ring A) and the phenyl rings in the *meta* position (rings B) are $85.3 \pm 0.5°$ for $P(tm\text{-}tp)_3$ and $44.7 \pm 0.3°$ for $P(tp)_3$. This difference in dihedral angle alters the depth of the bowl.

While the mechanism of the rate enhancement is not completely understood, the high catalytic activity realized with $P(tm\text{-}tp)_3$ might be attributable to the prevalence of the monophosphane species. In rhodium-catalyzed hydrosilylation of alkenes, the rate of the reaction also increased in the order $P/Rh = 3 < 2 < 1$.[11] Bulky phosphanes such as PCy_3 and $PtBu_3$ are also known to afford low-coordinate species.[12] However, severe congestion around the phosphorus atom must lower the efficiency of ligands in the hydrosilylation reaction. In contrast, the deeper bowl-shaped $P(tm\text{-}tp)_3$ ensures substantial empty space around the phosphorus atom and, at the same time, is bulky enough to provide low-coordinate species (long-range steric effect). This unique bowl-shaped structure could facilitate the rate enhancement.

Further studies are now in progress to elucidate the mechanism of the acceleration and to explore the benefit of nanosized well-defined phosphane ligands in transition-metal-catalyzed reactions.

Experimental Section

Synthesis of $P(tp)_3$: *n*-Butyllithium (1.59 M in *n*-hexane, 0.982 mL, 1.56 mmol) was added to a solution of 5′-bromo-*m*-terphenyl[13] (0.482 g, 1.56 mmol) in THF (9 mL) at −78 °C over 10 min. The solution was maintained at this temperature for an additional 1 h. Trichlorophosphane (0.071 g, 0.52 mmol) in toluene (1.4 mL) was added dropwise to the cooled solution over 15 min. The reaction mixture was further stirred at −78 °C for 1.5 h, and at room temperature for 15 h. After evaporation of the solvent, toluene (8 mL) and water (3 mL) were added to the residue and the mixture was stirred vigorously. The organic layer was separated, and the aqueous layer was extracted with toluene (4×2 mL). The organic extracts were combined and dried over anhydrous $MgSO_4$, and then filtered through a glass filter under argon. The solvent was removed from the filtrate in vacuo to give a wet solid. Recrystallization of the residue from $CHCl_3$/MeOH (1/4) yielded white microfine crystals. Yield: 0.310 g, 83 %. M.p. 219–220 °C; FD-MS: *m*/*z* 718 [*M*+]; ^1H NMR (400.13 Hz, $CDCl_3$, 23 °C): $\delta = 7.83$ (t, $^4J(H,H) = 1.5$ Hz, 3H; H2′), 7.75 (dd, $^3J(P,H) = 7.9$ Hz, $^4J(H,H) = 1.5$ Hz, 6H; H4′,6′), 7.61–7.59 (m, 12H; H2,2″,6,6″), 7.46–7.41 (m, 12H; H3,3″5,5″), 7.37–7.33 ppm (m, 6H; H4,4″); $^{13}C\{^1H\}$ NMR (100.61 Hz, $CDCl_3$, 23 °C): $\delta = 142.0$ (d, $^3J(C,P) = 7.2$ Hz; C1′,3′), 140.7 (C1,1″), 138.0 (d, $^1J(C,P) = 11.5$ Hz; C5′), 131.5 (d, $^2J(C,P) = 20.0$ Hz; C4′,6′), 128.8 (C3,3″,5,5″), 127.6 (C4,4″), 127.3 (C2,2″,6,6″), 127.0 ppm (C2′); $^{31}P\{^1H\}$ NMR (161.98 Hz, $CDCl_3$, 23 °C, H_3PO_4): $\delta = -2.0$ ppm; elemental analysis (%) calcd for $C_{54}H_{39}P$: C 90.22, H 5.47; found: C 90.21, H 5.51.

General procedure for hydrosilylation of ketones (Tables 1 and 2): A typical reaction procedure is described for entry 1 in Table 1. $[\{RhCl(C_2H_4)_2\}_2]$ (1.9 mg, 0.0050 mmol) and $P(tm\text{-}tp)_3$ (18 mg, 0.020 mmol) were placed in a 5-mL flask under argon. Anhydrous benzene (1.0 mL) was added by syringe, and then the mixture was stirred at room temperature in a water bath for 2 h. Cyclohexanone (98 mg, 1.0 mmol), tridecane (46 mg, 0.25 mmol), and dimethylphenylsilane (163 mg, 1.2 mmol) were then added by syringe. The reaction mixture was stirred at room temperature. Hydrolysis was performed by adding 1 % HCl/MeOH, and yields of cyclohexanol

 © 2003 Wiley-VCH Verlag GmbH & Co. KGaA, Weinheim 1433-7851/03/4211-1288 $ 20.00+.50/0

were determined by GC analysis relative to an internal standard (tridecane).

Received: October 7, 2002 [Z50320]

Keywords: homogeneous catalysis · hydrosilylation · ligand effects · P ligands · rhodium

[1] a) L. Brandsma, S. F. Vasilevsky, H. D. Verkruijsse, *Applications of Transition Metal Catalysts in Organic Synthesis*, Springer, Berlin, **1999**; b) *Homogeneous Catalysis with Metal Phosphine Complexes* (Ed.: L. H. Pignolet), Plenum, New York, **1983**.

[2] a) A.-M. Caminade, V. Maraval, R. Laurent, J.-P. Majoral, *Curr. Org. Chem.* **2002**, *6*, 739 – 774; b) D. de Groot, B. F. M. de Waal, J. N. H. Reek, A. P. H. J. Schenning, P. C. J. Kamer, E. W. Meijer, P. W. N. M. van Leeuwen, *J. Am. Chem. Soc.* **2001**, *123*, 8453 – 8458; c) T. Mizugaki, M. Murata, M. Ooe, K. Ebitani, K. Kaneda, *Chem. Commun.* **2002**, 52 – 53; d) V. Maraval, R. Laurent, A.-M. Caminade, J.-P. Majoral, *Organometallics* **2000**, *19*, 4025 – 4029; e) Q.-H. Fan, Y.-M. Chen, X.-M. Chen, D.-Z. Jiang, F. Xi, A. S. C. Chan, *Chem. Commun.* **2000**, 789 – 790; f) V. F. Slagt, J. N. H. Reek, P. C. J. Kamer, P. W. N. M. van Leeuwen, *Angew. Chem.* **2001**, *113*, 4401 – 4404; *Angew. Chem. Int. Ed.* **2001**, *40*, 4271 – 4274.

[3] a) B. S. Balaji, Y. Obora, D. Ohara, S. Koide, Y. Tsuji, *Organometallics* **2001**, *20*, 5342 – 5350; b) K. Takenaka, Y. Obora, L. H. Jiang, Y. Tsuji, *Organometallics* **2002**, *21*, 1158 – 1166; c) K. Takenaka, Y. Obora, L. H. Jiang, Y. Tsuji, *Bull. Chem. Soc. Jpn.* **2001**, *74*, 1709 – 1715.

[4] For utilization of bowl-shaped molecules and moieties, see: a) E. Maverick, D. J. Cram in *Comprehensive Supramolecular Chemistry, Vol. 2* (Eds.: J. L. Atwood, J. E. D. Davies, D. D. MacNicol, F. Vögtle), Elsevier, Oxford, **1996**, pp. 367 – 418; b) K. Goto, T. Okumura, T. Kawashima, *Chem. Lett.* **2001**, 1258 – 1259; c) K. Goto, M. Nagahama, T. Mizushima, K. Shimada, T. Kawashima, R. Okazaki, *Org. Lett.* **2001**, *3*, 3569 – 3572; d) M. Naiki, S. Shirakawa, K. Kon-i, Y. Kondo, K. Maruoka, *Tetrahedron Lett.* **2001**, *42*, 5467 – 5471.

[5] H. Brunner in *Transition Metals for Organic Synthesis, Vol. 2* (Eds.: M. Beller, C. Bolm), Wiley-VCH, Weinheim, **1998**, pp. 131 – 140.

[6] a) K. Goto, Y. Ohzu, H. Sato, T. Kawashima, *Abstr. Pap. 15th Int. Conf. of Phosphorus Chemistry* (Sendai, Japan) **2001**, p. 236; b) T. Matsumoto, T. Kasai, K. Tatsumi, *Chem. Lett.* **2002**, 346 – 347.

[7] The rate is first order in both the ketone and the silane: rate = k_{obs}[ketone][silane]. Selected observed rate constants k_{obs} at 24 °C: 4.79 ± 0.36 for P(tm-tp)$_3$ (Table 1, entry 1), 0.154 ± 0.004 for P(tp)$_3$ (entry 2), 0.0311 ± 0.0013 for PPh_3 (entry 3), and 0.169 ± 0.003 mol^{-1} dm^3 h^{-1} for P(*o*-tol)$_3$ (entry 5).

[8] a) Gaussian 98 (Revision A.7), M. J. Frisch, G. W. Trucks, H. B. Schlegel, G. E. Scuseria, M. A. Robb, J. R. Cheeseman, V. G. Zakrzewski, J. A. Montgomery, R. E. Stratmann, J. C. Burant, S. Dapprich, J. M. Millam, A. D. Daniels, K. N. Kudin, M. C. Strain, O. Farkas, J. Tomasi, V. Barone, M. Cossi, R. Cammi, B. Mennucci, C. Pomelli, C. Adamo, S. Clifford, J. Ochterski, G. A. Petersson, P. Y. Ayala, Q. Cui, K. Morokuma, D. K. Malick, A. D. Rabuck, K. Raghavachari, J. B. Foresman, J. Cioslowski, J. V. Ortiz, B. B. Stefanov, G. Liu, A. Liashenko, P. Piskorz, I. Komaromi, R. Gomperts, R. L. Martin, D. J. Fox, T. Keith, M. A. Al-Laham, C. Y. Peng, A. Nanayakkara, C. Gonzalez, M. Challacombe, P. M. W. Gill, B. G. Johnson, W. Chen, M. W. Wong, J. L. Andres, M. Head-Gordon, E. S. Replogle, J. A. Pople, Gaussian, Inc., Pittsburgh, PA, **1998**; b) H. Goto, *J. Am. Chem. Soc.* **1989**, *111*, 8950 – 8951; H. Goto, E. Osawa, *J. Chem. Soc. Perkin Trans. 2* **1993**, 187 – 198; c) J.-H. Lii, N. L. Allinger, *J. Am. Chem. Soc.* **1989**, *111*, 8566 – 8575; J.-H. Lii, N. L. Allinger, *J. Am. Chem. Soc.* **1989**, *111*, 8576 – 8582.

[9] a) Tolman determined the cone angles using "folded-back" CPK molecular models.[9b] Therefore, they are considerably smaller than those of the corresponding real free ligands or ligands in metal complexes. In the present study, we determined the cone angles using structures optimized by CONFLEX/MM3 and HF/6-31G(d).[8] The cone angles of the representative phosphanes thus determined are: PPh_3 (168°), P(*o*-tol)$_3$ (218°), $PMes_3$ (243°), PCy_3 (181°), and P*t*Bu$_3$ (188°); b) C. A. Tolman, *Chem. Rev.* **1977**, *77*, 313 – 348.

[10] a) D. W. Allen, B. F. Taylor, *J. Chem. Soc. Dalton Trans.* **1982**, 51 – 54; b) S. M. Socol, J. G. Verkade, *Inorg. Chem.* **1984**, *23*, 3487 – 3493; c) N. G. Andersen, B. A. Keay, *Chem. Rev.* **2001**, *101*, 997 – 1030. d) The corresponding phosphane selenides were prepared by a literature method,[10a] and the $^1J(^{31}P,^{77}Se)$ values were measured in ^{31}P NMR spectra.

[11] H. M. Dickers, R. N. Haszeldine, L. S. Malkin, A. P. Mather, R. V. Parish, *J. Chem. Soc. Dalton Trans.* **1980**, 308 – 313.

[12] a) H. L. M. Van Gaal, F. L. A. Van Den Bekerom, *J. Organomet. Chem.* **1977**, *134*, 237 – 248; b) T. Yoshida, T. Okano, S. Otsuka, *J. Chem. Soc. Chem. Commun.* **1978**, 855 – 856.

[13] C.-J. F. Du, H. Hart, K.-K. D. Ng, *J. Org. Chem.* **1986**, *51*, 3162 – 3165.

 © 2003 Wiley-VCH Verlag GmbH & Co. KGaA, Weinheim 1433-7851/03/4211-1289 $ 20.00+.50/0

Radioactive Isotope Complexation

Norbadione A: Synthetic Approach to the Bis(pulvinic acid) Moiety and Cesium-Complexation Studies

Marine Desage-El Murr, Stéphanie Nowaczyk, Thierry Le Gall, Charles Mioskowski,* Badia Amekraz,* and Christophe Moulin*

Following the reactor accident in Chernobyl in 1986, it was noted that several species of fungi contained high levels of

[*] Dr. T. Le Gall, Dr. C. Mioskowski,[+] M. Desage-El Murr, Dr. S. Nowaczyk
CEA-Saclay
Service de Marquage Moléculaire et de Chimie Bioorganique
Bât. 547, 91191 Gif-sur-Yvette (France)
Fax: (+33) 1-6908-7991
E-mail: legall@dsvidf.cea.fr
mioskowski@aspirine.u-strasbg.fr

Dr. B. Amekraz, Dr. C. Moulin
CEA-Saclay, DEN/DPC/SECR/LSRM
Bât. 391, 91191 Gif-sur-Yvette (France)
Fax: (+33) 1-6908-5411
E-mail: amekraz@cea.fr

[+] Other address: Laboratoire de Synthèse Bioorganique
UMR CNRS 7514, Faculté de Pharmacie, Université Louis Pasteur
74 route du Rhin, B.P. 24, 67401 Illkirch (France)
Fax: (+33) 3-9024-4306

Supporting information for this article is available on the WWW under http://www.angewandte.org or from the author.

 © 2003 Wiley-VCH Verlag GmbH & Co. KGaA, Weinheim 1433-7851/03/4211-1289 $ 20.00+.50/0

radioactivity, mainly as a result of the radioisotope ^{137}Cs.[1] Among these species was the edible mushroom bay boletus (*Xerocomus badius* (Fr.) Kühn. ex Gilb.). A study by Steglich and co-workers, who had previously isolated badione A and norbadione A (two pigments of the cap cuticle of bay boletus) as their dipotassium salts, showed that these compounds formed complexes with cesium 137.[2,3] A key observation was

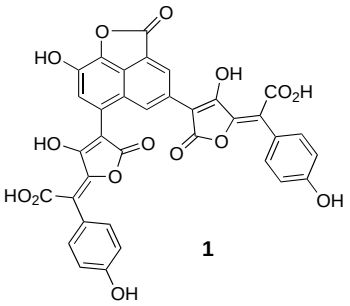

1

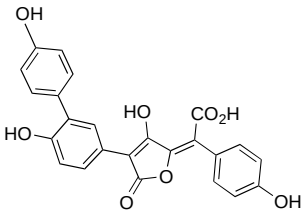

2

that norbadione A (**1**) is a much better ligand than the simple pulvinic acid derivative atromentic acid (**2**), a characteristic that could be attributed to the presence in its structure of two pulvinic acid chains that are able to participate jointly in the binding of the cesium cation.[4]

Selective complexation of cesium could be of great value for such purposes as the separation of the radionuclide ^{137}Cs from nuclear waste[5] or its removal from contaminated persons.[6] The evaluation of norbadione A and structurally related analogues in these applications was envisaged. Herein we first report a synthetic approach to the bis(pulvinic acid) backbone characteristic of the pigments of the badione group, as illustrated by the synthesis of permethylated analogue **3** (Scheme 1). Second, the complexation properties of the dipotassium salt of norbadione A and of compound **3** were investigated by electrospray tandem MS (ESI MS/MS).[7] The utilization of compound **3** was of particular interest for the evaluation of the degree of cesium complexation specifically by the pulvinic acid moieties, as complexation by the carboxylate moieties could not interfere in this case. Full-scan simple ESI MS spectra were used to investigate the stoichiometries and stability constants of the cesium complexes. Structural information on the cesium complexes was then assessed from neutral loss experiments. Such data are reported for the first time.

Our approach to the synthesis of **3** was based on the palladium-catalyzed double Suzuki–Miyaura cross coupling of triflate **5** and diboronate **4** (Scheme 1).[8] Such a strategy has the advantage that it should be amenable to the preparation of other analogues in which the distance between the two pulvinic acid chains could be modified simply by changing the diboronate.

The preparation of triflate **5**, described in Scheme 2, relied mainly on the Lewis acid catalyzed Langer cyclization of 1,3-bis(trimethylsilyloxy)-1,3-butadiene derivative **8** with oxalyl chloride.[9,10] α-Aryl-β-ketoester **7** was obtained in good yield from the reaction of 2 equivalents of the lithium enolate derived from methyl *para*-anisylacetate (**6**) and methyl

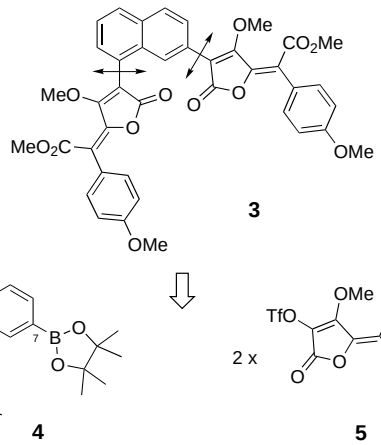

3

4

5

Scheme 1. Retrosynthetic analysis of permethylated analogue **3**. Tf = trifluoromethanesulfonyl.

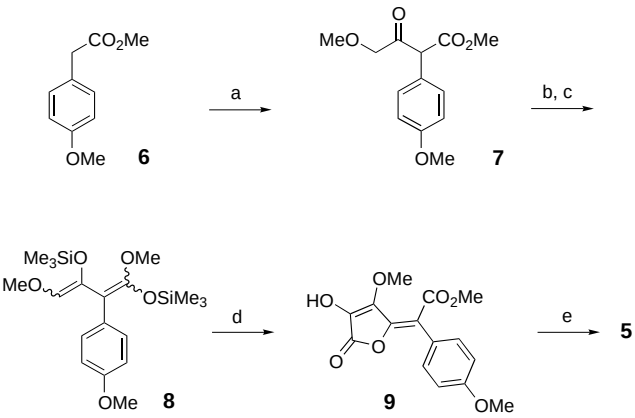

6 **7** **8** **9**

Scheme 2. Synthesis of triflate **5**. a) **6** (2 equiv), *i*Pr_2NLi (2 equiv), THF, −78 °C, then $MeOCH_2CO_2Me$ (1 equiv), −78 °C→RT, 77%; b) Et_3N, Me_3SiCl, THF, room temperature; c) *i*Pr_2NLi, THF, −78 °C, then Me_3SiCl, −78 °C→RT, 95%; d) oxalyl chloride (1.3 equiv), Me_3SiOTf (0.3 equiv), CH_2Cl_2, −78 °C→RT, 54%; e) Tf_2O, pyridine, CH_2Cl_2, −78 °C→RT, 68%.

methoxyacetate. Ketoester **7** was converted into the bis(silylated) diene **8** in two steps, which proceeded in very good yield on a multigram scale. However, compound **8** did not withstand distillation and was therefore used in the next step without purification. The cyclization of **8** with oxalyl chloride was then carried out under a variety of conditions. The best yield of lactone **9** (54%) was obtained with 1.3 equivalents of oxalyl chloride in the presence of 0.3 equivalents of trimethylsilyl triflate, upon allowing the reaction mixture to warm from −78 °C to room temperature overnight. Only one stereoisomer was obtained. The attribution of the indicated *E* configuration is based on general observations by Langer et al.[9] on the stereochemical outcome of related cyclization reactions and on the preparation of the known compound **10** (see below). Alcohol **9** was readily converted into the corresponding triflate **5** by treatment with triflic anhydride in the presence of pyridine.

A Suzuki–Miyaura reaction of triflate **5** was then carried out using phenylboronic acid in the presence of the catalyst

 © 2003 Wiley-VCH Verlag GmbH & Co. KGaA, Weinheim 1433-7851/03/4211-1290 $ 20.00+.50/0

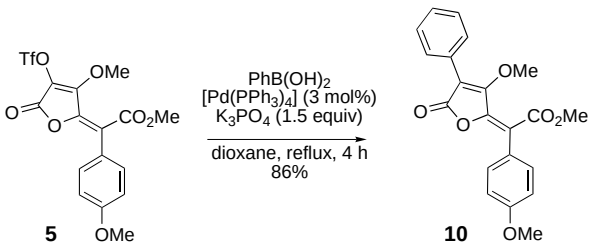

Scheme 3. Preparation of pulvinic acid derivative **10** by the Suzuki–Miyaura reaction of phenylboronic acid with triflate **5**.

$[Pd(PPh_3)_4]$ and the base K_3PO_4 at reflux in dioxane,[11] to afford compound **10** in 86% yield (Scheme 3). The ^1H NMR spectrum of compound **10** was identical to that reported for the *E* isomer of *O*-methylisopinastric acid, which is quite different from that of the *Z* isomer.[12] This allowed us to determine the *E* configuration of the central double bond in alcohol **9** unambiguously.

The preparation of diboronate **4** was carried out in two steps from 1,7-dihydroxynaphthalene (**11**; Scheme 4). Treatment with triflic anhydride in pyridine converted **11** into the corresponding known ditriflate.[13] The procedure described by Masuda and co-workers.[14] for the palladium-catalyzed borylation of aryl triflates with pinacolborane enabled the preparation of diboronate **4** in 45% yield.

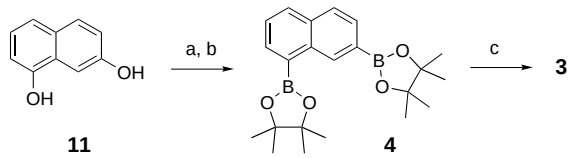

Scheme 4. Preparation of permethylated analogue **3** by double Suzuki–Miyaura reaction of diboronate **4** and triflate **5**. a) Tf_2O, pyridine, 95%; b) pinacolborane (6 equiv), $[PdCl_2(dppf)]$ (0.06 equiv), Et_3N (12 equiv), dioxane, 80°C, 13 h, 45%; c) **5** (2 equiv), $[PdCl_2(PPh_3)_2]$ (cat.), aqueous Na_2CO_3, THF, reflux, 3 h, 63%. dppf = 1,1′-bis(diphenylphosphanyl)ferrocene.

Our initial idea for the preparation of compound **3** through a double Suzuki–Miyaura reaction was to make use of the corresponding diboronic acid as the starting material. However, several attempts to hydrolyze the boronate groups of **4** were unsuccessful. Fortunately, conditions recently described for the palladium-catalyzed cross coupling of vinyl triflates with boronic esters, in the presence of $[PdCl_2(PPh_3)_2]$ as the catalyst and aqueous Na_2CO_3 as the base,[15] were found to be successful for the conversion of diboronate **4** and triflate **5** (2 equiv) into the desired norbadione A analogue **3**, obtained in 63% yield.

ESI MS has been applied previously to the study of metal-ion complexation by a variety of ligands to provide the structures, stoichiometries, and oxidation states of ligand–metal complexes.[16] Several reports have shown the potential of ESI MS for studying the interactions between alkaline cations and ligands.[17] It also appears that ESI MS can be used as a reliable technique for the direct determination of solution binding constants for such noncovalent complexes.[18] These studies have shown good agreement between relative solution-phase and gas-phase ionic abundances of metal complexes present in thermodynamic equilibrium in solution. Recently, ESI MS has allowed the acquisition of solution data such as stoichiometries and stability constants of Ln^{III} complexes of the whole lanthanide series with various di(dialkyltriazinyl)pyridine ligands.[19] ESI MS thus seemed appropriate for the study of the complexation of cesium by the potassium salt of norbadione A or by methylated compound **3**. There have been no reports published that deal with the stability constants of Cs^+ complexes of the potassium salt of norbadione A, which is the naturally occurring form of this compound.

We first studied the complexation behavior of the dipotassium salt of norbadione A (hereafter denoted $NboK_2$) by means of a speciation study. A 10^{-4} M solution of $NboK_2$ in methanol was treated with increasing quantities of cesium chloride.[20] Three different species were identified: free $NboK_2$, observed as the potassium complex $[Nbo+2K+K]^+$ (and as the sodium complex $[Nbo+2K+Na]^+$ of weaker relative intensity),[21] and cesium complexes $[Nbo+2K+Cs]^+$ and $[Nbo+K+2Cs]^+$. The species $[Nbo+3Cs]^+$ was not observed. Its formation might be prevented for steric reasons. Based on the assumption that the ion current in the gas phase quantitatively represents the solution equilibrium, the species distribution was obtained from the total signal response of these singly charged ions in spectra taken at each cesium/norbadione A ratio (see Supporting Information). By doing so, it was possible to plot the speciation curves shown in Figure 1.

As CsCl was added, the quantity of complex $[Nbo+2K+Cs]^+$ present reached a maximum at a 1.2 molar ratio of cesium to ligand, while the quantity of complex $[Nbo+K+2Cs]^+$ increased regularly. The formation of the latter complex is observed even when only small amounts of cesium are present, thus showing that this species is favored.

Neutral loss experiments were also performed to provide structural information about the cesium complexes. The neutral loss of the component $NboK_2$ was only seen from $[Nbo+2K+Cs]^+$ and the neutral loss of the component NboKCs was only seen from $[Nbo+K+2Cs]^+$. This suggests

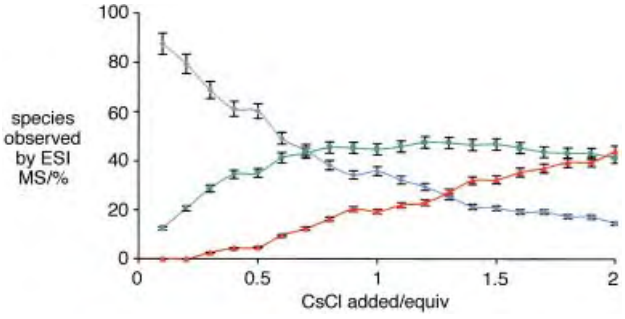

Figure 1. ESI–MS speciation curves of norbadione A dipotassium salt in the presence of cesium chloride in methanol. ◆: free ligand, ■: $[Nbo+2K+Cs]^+$ complex, ▲: $[Nbo+K+2Cs]^+$ complex. Relative abundances are reproducible within 5% from run to run.

 © 2003 Wiley-VCH Verlag GmbH & Co. KGaA, Weinheim 1433-7851/03/4211-1291 $ 20.00+.50/0

that the norbadione A potassium salt binds to Cs^+ through the pulvinic acid moieties, and that the second Cs^+ binding involves one of the carboxylate groups.

The complexation constant determined by ESI MS for the formation of the complex that contains one cesium cation, as represented in Scheme 5, is $\lg\beta = 4.9 \pm 0.4$.

$$NboK_2 + Cs^+ \xrightarrow{\beta} NboK_2{\cdot}Cs^+ \qquad \beta = \frac{[NboK_2{\cdot}Cs^+]}{[NboK_2][Cs^+]}$$

Scheme 5. Formation of the $NboK_2{\cdot}Cs^+$ complex from norbadione A dipotassium salt.

We also undertook a speciation study on the permethylated analogue **3** by using the same experimental procedure as described above. For reasons of coherence with the first speciation study, 1.2 equivalents of potassium were added to each sample to express the competitive influence of potassium on Cs^+–**3** complex formation (Figure 2). Two different

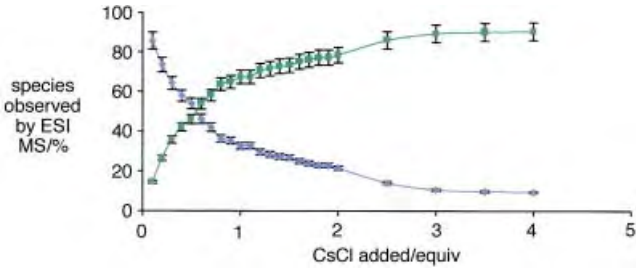

Figure 2. ESI–MS speciation curves of the permethylated analogue **3** in the presence of cesium chloride in methanol. ◆: free ligand, ■: complex $[\mathbf{3}+Cs]^+$. Relative abundances are reproducible within 5% from run to run.

species were identified: free **3**, observed as the potassium complex $[\mathbf{3}+K]^+$, and the cesium complex $[\mathbf{3}+Cs]^+$. The stability constant calculated for the 1:1 complex is $\lg\beta' = 4.6 \pm 0.4$ (Scheme 6). The stability constants of the 1:1 complexes that contain ligands **3** and norbadione A are thus quite similar. These results are in agreement with the structural hypothesis made from the neutral loss experiments whereby the neutral component of the $[Nbo+2K+Cs]^+$ complex is $NboK_2$. We also briefly evaluated the binding selectivity of **3** for Na^+, K^+, and Cs^+. In the presence of 0.8 equivalents of each alkali cation (in total, 2.4 equivalents), we observed a distribution of 60% cesium complex, 24% potassium complex, and 16% sodium complex. This distribution clearly indicates selectivity for cesium over potassium and sodium.

In summary, these results suggest that the complex formed by the dipotassium salt of norbadione A and one cesium cation results from an interaction between this cation and the pulvinic acid moieties of norbadione A. Thus, the structure depicted in Figure 3 might be favored: the cesium ion is held

$$\mathbf{3} + Cs^+ \xrightarrow{\beta'} \mathbf{3}{\cdot}Cs^+$$

Scheme 6. Formation of the $\mathbf{3}{\cdot}Cs^+$ complex from compound **3**.

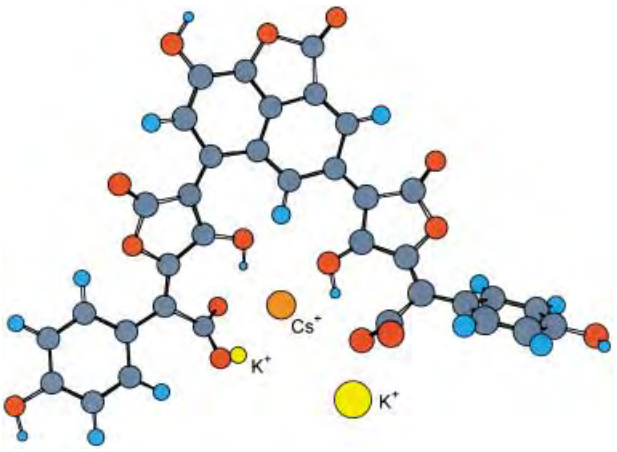

Figure 3. Structural hypothesis for the cesium complex of $NboK_2$ (Chem3D model). One potassium ion is located above the plane of the naphthalene moiety, the other one is located underneath that plane.

in a pseudocavity formed by a special arrangement of the two pulvinic acid moieties. Further work will include a decorporation study of radioactive cesium on animals, by treatment with norbadione A, the development of our synthetic approach towards a total synthesis of norbadione A, and the preparation of analogues designed for the selective complexation of different metal cations.

Received: October 10, 2002 [Z50332]

Keywords: C–C coupling · cesium · mass spectrometry · metal complexation

[1] For a review, see: P. Kalač, *Food Chem.* **2001**, *75*, 29–35.
[2] a) B. Steffan, W. Steglich, *Angew. Chem.* **1984**, *96*, 435; *Angew. Chem. Int. Ed. Engl.* **1984**, *23*, 445–447; b) D. C. Aumann, G. Clooth, B. Steffan, W. Steglich, *Angew. Chem.* **1989**, *101*, 495; *Angew. Chem. Int. Ed. Engl.* **1989**, *28*, 453–454.
[3] Norbadione A was also isolated from the mushroom *Pisolithus tinctorius* (Pers.) Coker et Couch; see: a) M. Gill, D. A. Lally, *Phytochemistry* **1985**, *24*, 1351–1354; b) M. Gill, M. J. Kiefel, *Aust. J. Chem.* **1994**, *47*, 1967–1977; the dipotassium salt of norbadione A employed in this study was provided by Dr. Melvyn Gill, University of Melbourne, Australia.
[4] For a recently reported physicochemical study of the diacid corresponding to norbadione A, see: S. Garaudée, M. Elhabiri, D. Kalny, C. Robiolle, J.-M. Trendel, R. Hueber, A. Van Dorsselaer, P. Albrecht, A.-M. Albrecht-Gary, *Chem. Commun.* **2002**, 944–945.
[5] J. F. Dozol, M. Dozol, R. M. Macias, *J. Inclusion Phenom. Macrocyclic Chem.* **2000**, *38*, 1–22.
[6] For articles on the decorporation of radionuclides from the human body, see: M. H. Henge-Napoli, G. N. Stradling, D. M. Taylor, *Radiat. Prot. Dosim.* **2000**, *87*, 3–57.
[7] P. Kebarle, *J. Mass Spectrom.* **2000**, *35*, 804–817.
[8] For reviews, see: a) A. Suzuki, *J. Organomet. Chem.* **1999**, *576*, 147–168; b) N. Miyaura, A. Suzuki, *Chem. Rev.* **1995**, *95*, 2457–2483; c) S. R. Chemler, D. Trauner, S. J. Danishefsky, *Angew. Chem.* **2001**, *113*, 4676–4701; *Angew. Chem. Int. Ed.* **2001**, *40*, 4545–4568.
[9] a) P. Langer, T. Schneider, M. Stoll, *Chem. Eur. J.* **2000**, *6*, 3204–3214; b) P. Langer, T. Eckardt, *Synlett* **2000**, *6*, 844–846; c) P.

 © 2003 Wiley-VCH Verlag GmbH & Co. KGaA, Weinheim 1433-7851/03/4211-1292 $ 20.00+.50/0

Langer, T. Eckardt, T. Schneider, C. Göbel, R. Herbst-Irmer, *J. Org. Chem.* **2001**, *66*, 2222 – 2226.
[10] For a review, see: P. Langer, *Synthesis* **2002**, 441 – 459.
[11] T. Oh-e, N. Miyaura, A. Suzuki, *J. Org. Chem.* **1993**, *58*, 2201 – 2208.
[12] G. Pattenden, M. W. Turvill, A. P. Chorlton, *J. Chem. Soc. Perkin Trans. 1* **1991**, 2357 – 2361.
[13] M. Takeuchi, T. Tuihiji, J. Nishimura, *J. Org. Chem.* **1993**, *58*, 7388 – 7392.
[14] M. Murata, T. Oyama, S. Watanabe, Y. Masuda, *J. Org. Chem.* **2000**, *65*, 164 – 168.
[15] E. G. Occhiato, A. Trabocchi, A. Guarna, *J. Org. Chem.* **2001**, *66*, 2459 – 2465.
[16] a) C. A. Schalley, *Mass Spectrom. Rev.* **2001**, *20*, 253 – 309; b) R. Colton, A. D'Agostino, J. C. Traeger, *Mass Spectrom. Rev.* **1995**, *14*, 79 – 106.
[17] a) W. Z. Shou, R. F. Browner, *Anal. Chem.* **1999**, *71*, 3365 – 3373; b) G. A. Lawrance, M. J. Robertson, Sutrisno, E. I. von Nagy-Felsobuki, *Inorg. Chim. Acta* **2002**, *328*, 159 – 168; c) M. L. Reyzer, J. S. Brodbelt, A. P. Marchand, Z. Chen, Z. Huang, I. N. N. Namboothiri, *Int. J. Mass Spectrom.* **2001**, *204*, 133 – 142.
[18] a) K. Wang, G. W. Gokel, *J. Org. Chem.* **1996**, *61*, 4693 – 4697; b) P. A. Brady, J. K. M. Sanders, *New J. Chem.* **1998**, *22*, 411 – 417; c) E. C. Kempen, J. S. Brodbelt, *Anal. Chem.* **2000**, *72*, 5411 – 5416.
[19] S. Colette, B. Amekraz, C. Madic, L. Berthon, G. Cote, C. Moulin, *Inorg. Chem.*, **2003**, in press.
[20] Methanol was preferred to water as the solvent, since decarboxylation reactions readily occur in the ESI source with aqueous solutions.
[21] Sodium adducts detected in the spectra result from the background concentration of Na^+ present in the samples.

 © 2003 Wiley-VCH Verlag GmbH & Co. KGaA, Weinheim 1433-7851/03/4211-1293 $ 20.00+.50/0

Parity-Violation Effects

Large Parity-Violation Effects in Heavy-Metal-Containing Chiral Compounds**

Peter Schwerdtfeger, Johannes Gierlich, and Tobias Bollwein*

The weak neutral current (Z-boson exchange)[1–3] between electrons and nucleons (quarks) introduces a small energy difference (ΔE_{PV}) between enantiomers of a chiral molecule owing to parity violation (P-odd effects).[4,5] There have been several attempts to measure the parity-violation (PV) difference between enantiomers,[6–7] however, such effects are estimated to be of the order of a few millihertz[8–10] for currently known molecules, and several orders of magnitude too low for the present ability of high-resolution spectroscopy. Here we report relativistic calculations of PV effects for several chiral compounds that contain a heavy-metal center; shifts in ΔE_{PV} of up to 4.8×10^{-14} au (300 Hz) are recorded for such compounds as $[(\eta^5\text{-}C_5H_5)Re(CO)(NO)I]$, which can easily be prepared. The high ΔE_{PV} value is an indication that future P-odd experiments for chiral molecules should be directed towards heavy-transition-metal complexes.

Since the creation of the unified electroweak theory by Weinberg, Salam, and Glashow, the investigation of PV effects has become one of the most exciting areas in particle physics.[1–3] Precise measurements of PV in atoms are now accurate enough for the standard model to be tested successfully.[11] Electroweak theory also predicts a small energy difference (ΔE_{PV}) between pairs of enantiomers, and thus a breakdown of mirror-image symmetry. The search for such effects currently involves vibrational,[5,12–14] NMR,[15,16] electronic,[17,18] and Mössbauer[6,19] spectroscopy, electric-field optical activity,[20] and preferred crystallization.[21] Most notably, Chardonnet and co-workers performed a saturation spectroscopy experiment for CHFClBr in the 9.3 μm spectral range using a tunable CO_2 laser that provided a spectral purity of 6 Hz.[12] They obtained $\Delta\nu_{PV}=\nu_{R-}-\nu_{S+}=9.4\pm5.1\pm12.7$ Hz between the two enantiomers, where the first value of uncertainty is derived from statistical error and the second is determined by systematic effects. More recently, the same group reduced these uncertainties and obtained $\Delta\nu_{PV}=-4.2\pm0.6\pm1.6$ Hz.[22] Thus the search for the breakdown of mirror-image symmetry in chiral molecules remains one of the most challenging tasks in molecular chemistry and physics.

It is a nontrivial issue to find chiral compounds suitable for high-resolution spectroscopic measurements of parity nonconservation effects.[23] P-odd effects scale approximately like Z^n ($n\approx5$; $Z=$ nuclear charge of the atom),[24] which limits the choice to heavy-element-containing compounds. Furthermore, in accordance with the single-center theorem of Hegstroem, the substance should contain more than one heavy element (either as ligands or chiral centers).[25] A detailed analysis of P-odd effects, with respect to the environment around a center of chirality, has been given by Faglioni and Lazzeretti.[26] Very recently they also proposed the hypothetical molecule [BiHFX] (X = Br, I) as a suitable candidate with PV effects, with the $\Delta\nu_{PV}$ value of the inversion vibrational mode in the Hz range.[27] Here we propose a number of molecules that are known in the literature, each of them containing a heavy-element center leading to large P-odd effects.

The structures of these molecules, as shown in Scheme 1, were fully optimized using density functional theory[28] followed by four-component all-electron Dirac–Fock calculations, which result in an energy shift of $\Delta E_{PV}=2\,E_{PV}$ for a molecule, as an expectation value of the parity-violation-operator (see Computational Details). Changes in spectroscopic properties ($\Delta\nu_{PV}$) are directly related to $\Delta E_{PV}(\boldsymbol{R})$ (or

[*] Prof. Dr. P. Schwerdtfeger, J. Gierlich, Dr. T. Bollwein
Department of Chemistry
University of Auckland
Private Bag 92019, Auckland (New Zealand)
Fax: (+64) 9-373-7422
E-mail: p.schwerdtfeger@auckland.ac.nz

[**] This work was supported by the Alexander von Humboldt Foundation and the Royal Society of New Zealand through a James Cook Fellowship. We are grateful to the Auckland University Research Committee for granting large amounts of computer time.

 © 2003 Wiley-VCH Verlag GmbH & Co. KGaA, Weinheim 1433-7851/03/4211-1293 $ 20.00+.50/0

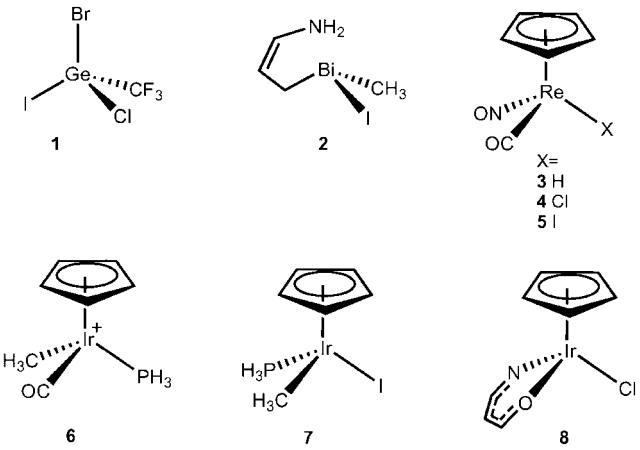

Scheme 1. The calculated compounds containing chiral metal centers.

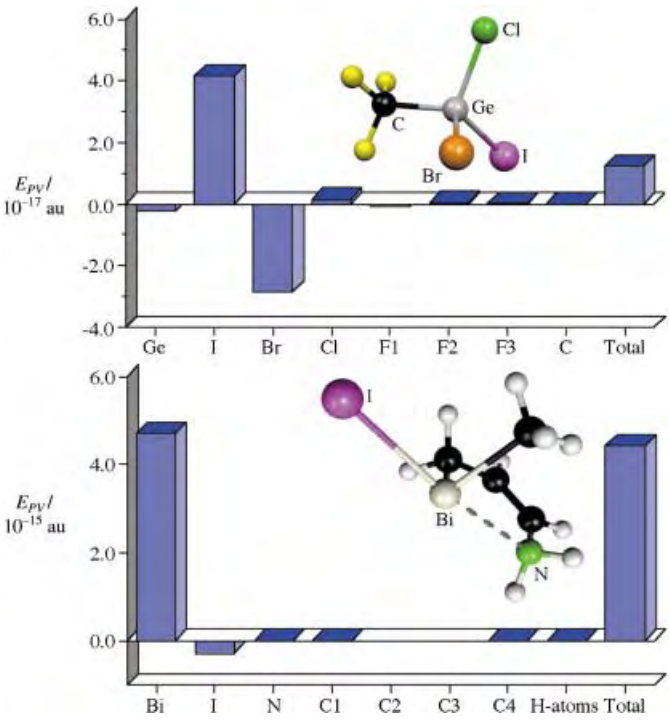

Figure 1. Atomic and total E_{PV} contributions for compounds **1** and **2**.

its derivatives, with respect to the nuclear coordinates $\boldsymbol{R}$), that is, $|\Delta\nu_{PV}| \sim |\Delta E_{PV}|$, and the search for large P-odd effects were therefore initially focused on large $|\Delta E_{PV}|$ values. For example, for a series of chiral carbon compounds, P-odd effects in the C–F stretching mode ($\Delta\nu_{PV}^{C\text{-}F}$) have been examined in detail.[8,23,29] The ratio $|\Delta\nu_{PV}^{C\text{-}F}/\Delta E_{PV}|$ is similar for all such compounds, and ranges between 0.05 and 0.09. Even for the C–Br stretch in CHFBrI, $|\Delta\nu_{PV}^{C\text{-}Br}/\Delta E_{PV}| = 0.09$. By examination, it can be revealed that the major contribution to the E_{PV} value originates from the valence electrons close to the nucleus. This is not unexpected since core orbitals are almost spherical, and hence only contribute to a small degree; or in other words, chirality is revealed in the outer valence shells of a molecule, as one might naively expect.

One of the major problems in the search for P-odd effects in molecules containing main-group heavy elements is to find thermodynamically stable, optically active compounds. For example, [PbHFClBr] displays a $|\Delta E_{PV}|$ value that is more than two orders of magnitude larger than the analogous carbon compound CHFClBr,[8] however, the lead compound, in which the metal center is formally Pb^{IV}, would be easily reduced to give a Pb^{II} species. There are, however, two relatively stable known chiral compounds: [Ge(CF_3)ClBrI] (**1**),[30] which is similar to the already calculated chiral halogen compounds of group 14,[8–10] and [$BiCH_3I(\kappa^2\text{-}CH_2(CH)_2NH_2)$] (**2**), a model compound for a bismuthane species synthesized recently by Murafuji et al.,[31] and similar to the bismuth compound mentioned above.[26] The E_{PV} contributions of the individual atoms are shown in Figure 1 and the total energy shifts ΔE_{PV} are listed in Table 1.

There is no guarantee that values for ΔE_{PV} would reach the current limit of high-resolution spectroscopy once suitable enantiomers containing heavy elements are identified. This is nicely demonstrated for compound **1** where the Ge atom yields only a small PV contribution, while the heavy Br and I ligands show larger effects but of opposite sign and, therefore, cancel each other out; it is currently not known what determines the sign of E_{PV}. The bismuth complex is stabilized by additional coordination of the amino group. Here the total E_{PV} value originates almost entirely from the central Bi atom, which gives a net contribution of $\Delta E_{PV} = 8.88 \times 10^{-15}$ au (58 Hz). Thus, compound **2** is of particular interest for high-resolution spectroscopy.

A large number of thermodynamically stable, optically active heavy-transition-element compounds are known.[32] Of those containing relatively simple ligands are the "piano-stool" compounds containing the $C_5H_5^-$ (Cp) ligand, as shown in Scheme 1. To demonstrate the single-center theorem, we varied one of the ligands in the complex [CpRe(CO)(NO)X] (**3**–**5**; X = H, Cl, and I; Figure 2). The value of E_{PV} increases along with an increase in the mass of the ligand X, with X = H giving a negligible contribution of only 1.8×10^{-22} au. Interestingly, the ligand X gives an E_{PV} value of the same sign as the central atom. For the heaviest ligand (I), E_{PV} is of the same order of magnitude as Re, which results in an unprecedented

Table 1: Parity violation energy differences ($\Delta E_{PV} = 2\,E_{PV}$) for the compounds shown in Scheme 1. A negative sign indicates that the enantiomer shown in Scheme 1 is the P-odd-stabilized form.

Compound	ΔE_{PV} [au]	ΔE_{PV} [Hz]
[Ge(CF_3)ClBrI] (**1**)	2.466×10^{-17}	0.162
[$BiCH_3I(\kappa^2\text{-}CH_2CHNH_2)$] (**2**)	8.881×10^{-15}	58.4
[CpReH(CO)(NO)] (**3**)	-2.642×10^{-16}	−1.74
[CpReCl(CO)(NO)] (**4**)	1.752×10^{-14}	115
[CpReI(CO)(NO)] (**5**)	4.807×10^{-14}	316
[CpIr(CO)(CH_3)(PH_3)]$^+$ (**6**)	-3.525×10^{-14}	−232
[CpIrI(CH_3)(PH_3)] (**7**)	4.007×10^{-14}	264
[CpIrCl(κ^2-HN$(CH)_3$O)] (**8**)	4.069×10^{-15}	26.8

 © 2003 Wiley-VCH Verlag GmbH & Co. KGaA, Weinheim 1433-7851/03/4211-1294 $ 20.00+.50/0

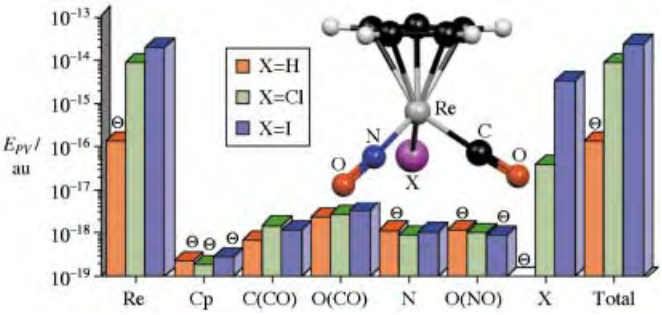

Figure 2. Atomic and total E_{PV} contributions for compounds **3** to **5** shown on the logarithmic scale. Cp denotes all the contributions from the C_5H_5 ligand. If required, the corresponding ligand is given in parentheses along with the coordinate labels of the elements. The label Θ above the bar denotes that E_{PV} is of negative magnitude.

large total value of 2.4×10^{-14} au, which makes compound **5** an ideal candidate for high-resolution measurements.

For the iridium compounds[33–36] studied herein, the main contribution to E_{PV} comes from the central atom. Even for [CpIrI(CH_3)(PH_3)] (**7**) the E_{PV} contribution of iodine (9.5×10^{-16} au) is one order of magnitude below that for the central iridium atom (1.9×10^{-14} au). Table 1 shows that the two isoelectronic compounds $[CpIr(CO)(CH_3)(PH_3)]^+$ (**6**) and [CpIrI(CH_3)(PH_3)] (**7**) show the largest P-odd effect, which are similar in magnitude to the rhenium compound (**5**).

With a few exceptions,[6] the search for P-odd effects in molecules have concentrated on main-group elements.[12,15] In our opinion, transition-metal complexes, especially those of the 6th row, are very good candidates for high-resolution spectroscopy. The compounds investigated here (or some of their derivatives) can be easily synthesized, and the separation of enantiomers may not be as a difficult[37] as it is for the chiral carbon species currently investigated elsewhere.[12,38] We propose high-resolution experiments in both electronic and vibrational spectroscopy for the iridium, rhenium, and bismuth compounds shown in Scheme 1, although current experiments in vibrational spectroscopy are tuned to the CO_2 laser frequency range between 878 and 1108 cm^{-1}.[12] Inclusion of overtones would allow observation of stretching or bending modes in the lower frequency range (450–550 cm^{-1}), which involve transition-metal–ligand stretching modes where larger effects in $\Delta\nu_{PV}$ are expected. Considering electronic transitions, a significant change in P-odd effects from the ground to the excited electronic state is required. It should not be too difficult to identify suitable occupied and unoccupied molecular orbitals by analyzing the matrix elements shown in Equation (1) (see Computational Details), which may result in large changes in $\Delta\nu_{PV}$ for the corresponding electronic transition, for example, excitations involving metal-to-ligand charge transfer. NMR[15] or Mössbauer spectroscopy are also viable alternatives, although in the latter case, strong magnetic fields are required to break the symmetry of Kramers pairs of electrons in a closed-shell system.[6] Here, the use of paramagnetic chiral transition-element compounds is preferred. For theoretical studies of NMR and Mössbauer P-odd effects, the nuclear-spin-dependent parity-violation operator is required. This operator is more difficult to implement into relativistic program packages, as compared to the nuclear-spin-independent operator used here, and work in this direction is in progress.

Computational Details

All structures were fully optimized using the Gaussian 98 program package[28] with scalar relativistic Stuttgart pseudopotentials[39] and corresponding valence basis sets for the heavy elements and cc-pVDZ for the lighter elements at the B3LYP level of theory.[40] Subsequent four-component all-electron Dirac–Fock calculations at optimized geometries[41] gave the energy shift for a molecule with n nuclei and i electrons as an expectation value of the parity-violation operator originating from the time-like contribution of the (A_eV_n) exchange of the weak neutral current between electrons and quarks,[42]

$$\Delta E_{PV} = 2\,E_{PV} = G_F/\sqrt{2}\langle\Psi|\sum\nolimits_{n,i} Q_{w,n}\gamma_i^5\rho_n(\mathbf{r}_i)|\Psi\rangle \qquad (1)$$

where $G_F = 1.6637\cdot10^{-11}\,\mathrm{MeV}^{-2} = 2.22255\times10^{-14}$ au is the Fermi coupling constant and γ^5 is one of the Dirac matrices (the 4×4 pseudoscalar chirality operator).[28] ρ_n is the normalized nucleon density of nucleus n. The weak charge $Q_{w,n} = -N_n + Z_n(1-4\sin^2\theta_W)$ depends on the number of protons (Z) and neutrons (N), and the Weinberg mixing angle ($\sin^2\theta_W = 0.2319$). Consequently, if one enantiomer becomes stabilized by E_{PV} its mirror image then becomes destabilized by the same amount and we obtain the difference between both enantiomeric forms [Eq. (2)],

$$\Delta E_{PV} = \Delta E_{L\text{-}D} = E_{PV,L} - E_{PV,D} = 2\,E_{PV,L} \qquad (2)$$

For the heavy elements, the dual-type basis sets of Faegri were adopted[43] and double-zeta-quality basis sets with added tight s and p functions for the lighter elements were employed. The Dirac small component was produced by restricted kinetic balance.[44] Because of their expected small contribution, the p orbitals for the hydrogen atoms were omitted, as also were two-electron integrals between small components. For the calculation of the weak charge and in the Dirac–Hartree–Fock calculations, the finite nucleus model of the most stable isotope of each element was used: ^{1}H, ^{12}C, ^{14}N, ^{16}O, ^{19}F, ^{35}Cl, ^{74}Ge, ^{79}Br, ^{127}I, ^{187}Re, ^{193}Ir, and ^{209}Bi. Some of these calculations took several weeks of computer time on an IBM Regatta multiprocessor supercomputer. For the compounds shown in Scheme 1 the inversion splitting ($\Delta E_{\pm}$) arising from a double-minimum potential connecting the two enantiomers is far less than the parity-violation energy difference (ΔE_{PV}) because of the large masses and high barriers involved, that is, $|\Delta E_{\pm}| \ll |\Delta E_{PV}|$, and inversion splitting can therefore be neglected.[45]

Received: October 25, 2002 [Z50441]

Keywords: ab initio calculations · chirality · density functional calculations · isomerism · parity violation

[1] S. Weinberg, *Rev. Mod. Phys.* **1980**, *52*, 515–523.
[2] A. Salam, *Rev. Mod. Phys.* **1980**, *52*, 525–538.
[3] S. L. Glashow, *Rev. Mod. Phys.* **1980**, *52*, 539–543.
[4] D. W. Rein, *J. Mol. Evol.* **1974**, *4*, 15–22.
[5] V. S. Letokhov, *Phys. Lett. A* **1975**, 53, 275–276.
[6] A. S. Lahamer, S. M. Mahurin, R. N. Compton, D. House, J. K. Laerdahl, M. Lein, P. Schwerdtfeger, *Phys. Rev. Lett.* **2000**, *85*, 4470–4473.
[7] E. Arimondo, P. Glorieux, T. Oka, *Opt. Commun.* **1977**, *23*, 369–372.
[8] J. K. Laerdahl, P. Schwerdtfeger, H. M. Quiney, *Phys. Rev. Lett.* **2000**, *84*, 3811–3814.

 © 2003 Wiley-VCH Verlag GmbH & Co. KGaA, Weinheim 1433-7851/03/4211-1295 $ 20.00+.50/0

[9] M. Quack, J. Stohner, *Phys. Rev. Lett.* **2000**, *84*, 3807 – 3810.
[10] A. Soncini, A. Ligabue, P. Lazzaretti, R. Zanasi, *Phys. Rev. E* **2000**, *62*, 8395 – 8399.
[11] A. Derevianko, *Phys. Rev. A* **2002**, *65*, 012106/1 – 13.
[12] C. Daussy, T. Marrel, A. Amy-Klein, C. T. Nguyen, C. J. Bordé, C. Chardonnet, *Phys. Rev. Lett.* **1999**, *83*, 1554 – 1557.
[13] O. N. Kompanets, A. R. Kukudzhanov, V. S. Letokhov, L. L. Gervits, *Opt. Commun.* **1976**, *19*, 414 – 416.
[14] M. Quack, J. Stohner, *Chirality* **2001**, *13*, 745 – 753.
[15] J. B. Robert, A. L. Barra, *Chirality* **2001**, *13*, 699 – 702.
[16] M. Fujiki, *Macromol. Rapid Commun.* **2001**, *22*, 669 – 674; Erratum: M. Fujiki, *Macromol. Rapid Commun.* **2001**, *22*, 864.
[17] L. N. Ivanov, V. S. Letokhov, *J. Chem. Phys.* **1997**, *106*, 6045 – 6050.
[18] M. Quack, *Chem. Phys. Lett.* **1986**, *132*, 147 – 153.
[19] A. V. Baluev, L. V. Inzhechik, E. V. Melnikov, B. I. Rogozev, A. S. Khlebnikov, V. G. Tsinoev, V. M. Cherepanov, *JETP Lett.* **1986**, *43*, 656 – 658.
[20] R. A. Harris, *Chem. Phys. Lett.* **2002**, *365*, 343 – 346.
[21] A. Szabó-Nagy, L. Keszthelyi, *Proc. Natl. Acad. Sci. USA* **1999**, *96*, 4252 – 4255.
[22] M. Ziskind, C. Daussy, T. Marrel, C. Chardonnet, *Eur. Phys. J. D* **2002**, *20*, 219 – 225.
[23] P. Schwerdtfeger, J. K. Laerdahl, C. Chardonnet, *Phys. Rev. A* **2002**, *65*, 042508/1 – 7.
[24] M. A. Bouchiat, C. Bouchiat, *J. Phys. (Paris)* **1974**, *35*, 899 – 927.
[25] R. A. Hegstrom, D. W. Rein, P. G. H. Sandars, *J. Chem. Phys.* **1980**, 73, 2329 – 2341.
[26] F. Faglioni, P. Lazzeretti, *Phys. Rev. E* **2002**, *65*, 011901/1 – 11.
[27] F. Faglioni, P. Lazzeretti, unpublished results.
[28] Gaussian 98 (Revision A.7), M. J. Frisch, G. W. Trucks, H. B. Schlegel, G. E. Scuseria, M. A. Robb, J. R. Cheeseman, V. G. Zakrzewski, J. A. Montgomery, R. E. Stratmann, J. C. Burant, S. Dapprich, J. M. Millam, A. D. Daniels, K. N. Kudin, M. C. Strain, O. Farkas, J. Tomasi, V. Barone, M. Cossi, R. Cammi, B. Mennucci, C. Pomelli, C. Adamo, S. Clifford, J. Ochterski, G. A. Petersson, P. Y. Ayala, Q. Cui, K. Morokuma, D. K. Malick, A. D. Rabuck, K. Raghavachari, J. B. Foresman, J. Cioslowski, J. V. Ortiz, B. B. Stefanov, G. Liu, A. Liashenko, P. Piskorz, I. Komaromi, R. Gomperts, R. L. Martin, D. J. Fox, T. Keith, M. A. Al-Laham, C. Y. Peng, A. Nanayakkara, C. Gonzalez, M. Challacombe, P. M. W. Gill, B. G. Johnson, W. Chen, M. W. Wong, J. L. Andres, M. Head-Gordon, E. S. Replogle, J. A. Pople, Gaussian, Inc., Pittsburgh, PA, **1998**.
[29] A. Soncini, A. Ligabue, P. Lazzeretti, R. Zanasi, *Phys. Rev. E* **2000**, *62*, 8395 – 8399.
[30] M. R. Eujen, R. Mellies, *J. Fluorine Chem.* **1983**, *22*, 263 – 280.
[31] T. Murafuji, K. Satoh, Y. Sugihara, N. Azuma, *Organometallics* **1998**, *17*, 1711 – 1715; T. Murafuji, N. Azuma, H. Suzuki, *Organometallics* **1995**, *14*, 1542 – 1544.
[32] H. Brunner, *Angew. Chem.* **1999**, *111*, 1248 – 1263; *Angew. Chem. Int. Ed.* **1999**, *38*, 1194 – 1208.
[33] R. P. Hughes, J. M. Smith, L. M. Liable-Sands, T. E. Concolino, K.-C. Lam, C. Invarvito, A. L. Rheingold, *J. Chem. Soc. Dalton Trans.* **2000**, 873 – 879; R. P. Hughes, D. C. Lindner, J. M. Smith, D. Zhang, C. Invarvito, K.-C. Lam, L. M. Liable-Sands, R. D. Sommer, A. L. Rheingold, *J. Chem. Soc. Dalton Trans.* **2001**, 2270 – 2278.
[34] S. R. Klei, J. T. Golden, T. D. Tilley, R. G. Bergman, *J. Am. Chem. Soc.* **2002**, *124*, 2092 – 2093.
[35] P. J. Alaimo, B. A. Arndtsen, R. G. Bergman, *Organometallics* **2000**, *19*, 2130 – 2143.
[36] M. L. Loza, J. Parr, A. M. Z. Slawin, *Polyhedron* **1997**, *16*, 2321 – 2322; W. Bauer, M. Prem, K. Polborn, K. Sünkel, W. Steglich, W. Beck, *Eur. J. Inorg. Chem.* **1998**, 485 – 493.
[37] S. N. Paisner, R. G. Bergman, *J. Organomet. Chem.* **2001**, *621*, 242 – 245.
[38] D. B. Li, S.-C. Ng, I. Novak, *Tetrahedron* **2002**, *58*, 5923 – 5926.
[39] The Stuttgart group pseudopotentials and valence basis sets of Stoll and co-workers can be obtained from: http://www.theochem.uni-stuttgart.de/pseudopotentials/.
[40] A. D. Becke, *Phys. Rev. A* **1988**, *38*, 3098 – 3100; C. Lee, W. Yang, R. G. Parr, *Phys. Rev. B* **1988**, *37*, 785 – 789.
[41] T. Saue, T. Enveldson, T. Helgaker, H. J. A. Jensen, J. K. Laerdahl, K. Ruud, J. Thyssen, L. Visscher, *Dirac—A relativistic ab initio electronic structure program*, Release 3.2.1, **2000**.
[42] J. K. Laerdahl, P. Schwerdtfeger, *Phys. Rev. A* **1999**, *60*, 4439 – 4453.
[43] K. J. Faegri, *Theor. Chem. Acc.* **2001**, *105*, 252 – 258.
[44] I. P. Grant, H. M. Quiney, *Adv. At. Mol. Phys.* **1988**, *23*, 37 – 86.
[45] M. Quack, *Angew. Chem.* **1989**, *101*, 588 – 604; *Angew. Chem. Int. Ed. Engl.* **1989**, *28*, 571 – 586.

 © 2003 Wiley-VCH Verlag GmbH & Co. KGaA, Weinheim 1433-7851/03/4211-1296 $ 20.00+.50/0

Cluster-Dependent Catalysis

Structural, Electronic, and Impurity-Doping Effects in Nanoscale Chemistry: Supported Gold Nanoclusters**

Hannu Häkkinen, Stéphane Abbet, Antonio Sanchez, Ulrich Heiz,* and Uzi Landman*

Metal clusters exhibit unique size-dependent physical[1] and chemical properties[2] that differ from those of bulk materials. While inert as a bulk material, gold nanoparticles and clusters have attracted considerable interest lately as active catalysts for a number of industrially relevant reactions.[3–6] Unlike supported particles of larger size or extended solid surfaces,[7–10] size-selected small metal clusters adsorbed at specific sites of a support material (e.g. oxygen vacancies in the case of a MgO(100) surface) exhibit unique properties that originate from the highly reduced dimensions of the individual metal aggregates. These properties underlie the remarkable, newly found catalytic activity of small gold clusters, and they include: 1) dynamic structural fluxionality that exhibits itself through the propensity of small clusters to transform, in the course of chemical reactions, between various energetically accessible structural isomers, thus enhancing the rates for overcoming reaction barriers, 2) quantum size effects that are reflected in size-dependent characteristics of the electronic spectra of small gold clusters, and in charge transfer from the support to the clusters, 3) impurity-doping effects that allow modification and control of the electronic structure, and consequently the chemical reactivity, of small supported clusters, through incorporation of judiciously chosen impurity atoms in otherwise inert clusters. Herein, we focus on gaining fundamental insights into the above size-dependent "nanocatalytic factors", and illustrate through experimental and theoretical investigations the manner in which such fundamental understanding may guide the design and atomic-scale modifications of nanocatalysts.

Recently, a set of model catalysts have been prepared by soft-landing[11] of mass-selected Au_n and Au_nSr cluster ions onto well-characterized MgO(100) thin films. These substrate films contained a low concentration (typically 5×10^{13} cm^{-1}) of oxygen vacancies (surface F-centers, FC), that act as strong trapping sites for the clusters at low temperatures.[12–14] Temperature-programmed reaction (TPR) measurements of CO oxidation ($CO+{}^1/_2O_2\rightarrow CO_2$) have shown that the smallest gold cluster that catalyzes the reaction is Au_8. Furthermore, it has been found that while Au_4 is catalytically inert, the doped cluster Au_3Sr is active. These findings, in conjunction with ab initio calculations, have revealed that underlying the aforementioned remarkable chemical size-sensitivity is the nature of bonding and the activation of molecular oxygen by these nanocluster catalysts.

The measured chemical activity is summarized in Figure 1, which shows typical TPR spectra for selected samples (a–e). The total CO_2 yield per cluster obtained in a one-cycle heating experiment for Au_n and Au_nSr with $1\le n\le 9$ is shown in the inset. The active model systems ($n\ge 8$ for the pure Au_n and

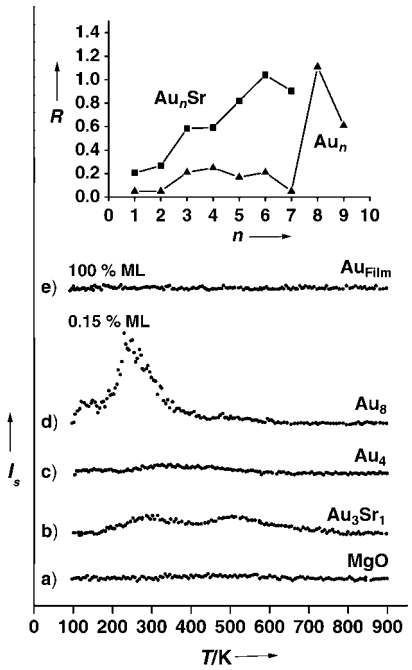

Figure 1. TPR spectra of CO_2 formation on: a) MgO(100) film, b) Au_3Sr/MgO(FC), c) Au_4/MgO(FC), d) Au_8/MgO(FC), and e) multilayer Au film grown on MgO(100). The Au_4/MgO(FC), pure MgO film, and the multilayer Au film are catalytically inert. The inset shows the chemical reactivity R of pure Au_n and doped Au_nSr clusters, with $1\le n\le 9$, expressed by the number of product CO_2 molecules per deposited cluster. The TPR spectra are recorded after exposure of the model catalyst to isotopically labeled $^{18}O_2$ and $^{13}C^{16}O$ at 90 K. Only the production of the $^{13}C^{16}O^{18}O$ isotopomer was detected (by measuring its ion current (I_s)), which indicates that no oxygen from the MgO substrate is involved.

[*] Prof. Dr. U. Heiz, Dr. S. Abbet
Abteilung für Oberflächenchemie und Katalyse
Albert-Einstein-Allee 47
University of Ulm
89069 Ulm (Germany)
E-mail: ulrich.heiz@chemie.uni-ulm.de
Dr. H. Häkkinen, Prof. Dr. U. Landman
School of Physics, Georgia Institute of Technology
Atlanta, Georgia 30332-0430 (USA)
E-mail: hannu.hakkinen@physics.gatecs.edu
Dr. A. Sanchez
Credit Suisse
Paradeplatz 8, 8070 Zürich (Switzerland)

[**] The experimental work was supported by the Swiss National Science Foundation and by the "Deutsche Forschungsgemeinshaft". The theoretical work was supported by the U.S. Air Force Office of Scientific Research and by the Academy of Finland. Simulations were performed at the National Energy Research Scientific Computing Center (NERSC), Berkeley, CA, and in the Georgia Tech Center for Computational Materials Science. We thank J.-F Jeanneret for the fabrication of the AuSr targets, Bokwon Yoon for his contribution to the graphical work, and W.-D. Schneider for his support at the early stages of this research.

Supporting information (experimental and theoretical details) for this article is available on the WWW under http://www.angewandte.org or from the author.

 © 2003 Wiley-VCH Verlag GmbH & Co. KGaA, Weinheim 1433-7851/03/4211-1297 $ 20.00+.50/0

$n \geq 3$ for mixed Au_nSr clusters) yield the same TPR spectra regardless of the order of deposition of O_2 and CO, that is, no CO poisoning occurs. The reproducibility of the TPR cycle has been verified, which indicates that these model systems are thermally stable up to 450 K, that is, no agglomeration to larger particles occurs during the heating phase. The clean MgO(100) surface as well as multilayer gold films grown on MgO(100) are catalytically inert, the latter reflecting the noble character of bulk gold.

The atomic structure and the electronic spectra of these model catalysts were studied by ab initio calculations (see ref. [15] and the Supporting Information). The optimized structures of Au_8 (with two relevant isomers), Au_4, and Au_3Sr adsorbed on MgO(FC) are shown in Figure 2. The Figures 2a–d show the structures before, and Figures 2e–h after O_2 adsorption. These clusters bind to the MgO(FC) surface quite strongly (calculated binding energy of 2.65 eV to 4.06 eV), and their binding is significantly enhanced (typically by about 2 eV) by the F-center defects. These high binding energies and the "anchoring" effect of the F-centers correlate well with the observed thermal stability of the supported clusters. Another important finding pertains to the charge state of the adsorbed clusters—in particular, our calculations predict that the interaction with the surface is accompanied by a charge transfer[6] of 0.5 e, 0.3 e, and 0.3 e to the adsorbed Au_8, Au_4, and Au_3Sr clusters, respectively.

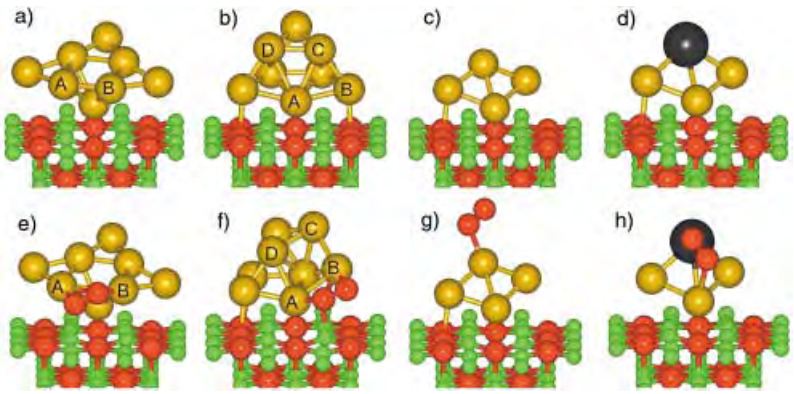

Figure 2. The optimized atomic structures of model catalysts comprising a) and b) Au_8, c) Au_4, and d) Au_3Sr clusters adsorbed at a F center (FC) defect on MgO(100). For Au_8 two relevant isomers, separated by an energy difference of 0.29 eV, are shown, with the more stable cluster (a) having a quasi-planar geometry with one atom bound to the F center and the remaining seven atoms defining a plane tilted slightly away from the MgO-surface plane. The higher-energy isomer (b) has a "two-layer structure" where the bottom layer consists of five atoms with one of the atoms strongly interacting with the F center. The adsorption energies of these clusters are 3.92 eV (a) and 3.45 eV (b). The adsorbed Au_4 and Au_3Sr clusters have rhombic structures, with adsorption energies of 4.06 eV and 2.65 eV, respectively. The adsorption induces an average strain of 3% (Au_8), 3% (Au_4), and 5% (Au_3Sr) in the bond lengths of the clusters, compared to their corresponding gas-phase structures. The optimal geometries for the adsorption of the O_2 molecule on these model catalysts are shown in the panels e–h. Although the dissociation of O_2 is thermodynamically favored, the dissociation process involves a large activation barrier (of the order of 1.5 eV) and is thus kinetically precluded. The corresponding O–O bond lengths and adsorption energies are: e) 1.45 Å and 0.28 eV, f) 1.43 Å and 0.47 eV, g) 1.28 Å and 0.18 eV, and h) 1.37 Å and 1.94 eV. Selected interatomic distances [Å]: a) A-B 2.62, b) A-B 2.94, A-C, A-D 3.14, e) A-B 3.48, f) A-B 2.90, A-C 4.28, A-D 2.95. Note the significant structural rearrangement of the more reactive Au_8 cluster (b) upon oxygen adsorption, reflected in the modified bond lengths d(A-C) and d(A-D) in (b) and (f). Mg green, O red, Au yellow, and Sr black.

Binding and activation of molecular O_2 by the model catalyst are necessary elementary steps in the CO oxidation process,[16,17] and thus understanding the structural, dynamic, electronic, and compositional factors that govern these processes is the key to explaining the observed size-dependent activity of the Au_n/MgO(FC) and Au_nSr/MgO(FC) model catalysts. Indeed, our ab initio calculations show that the binding energy of O_2 to the supported Au_n and Au_nSr clusters and the degree of O–O bond activation are strongly dependent on the cluster size (see below). In contrast, the adsorption energy of CO to the supported clusters is higher than that of oxygen and is relatively insensitive to the cluster size (0.7–1.0 eV per CO molecule, depending on coverage). Consequently, we focus on the adsorption and activation of O_2 by the supported gold nanoclusters, and illustrate the aforementioned nanocatalytic factors that govern this key reaction step.

1) Dynamic structural fluxionality: The capability of small clusters to exhibit several structural forms (isomers) of comparable energies, and to interconvert between such isomers at finite temperature, is one of the hallmarks of cluster science. This unique structural variability may influence the chemical reactivity of nanocatalytic systems in two main ways. First, at finite temperature, the model catalyst (and in particular the cluster component) will form an equilibrium of coexisting structural configurations, with various isomers exhibiting different chemical reactivities. This situation is illustrated here by the properties of two structural isomers of the Au_8 cluster. One isomer has a two-layered structure (Figure 2b) and is thermodynamically less stable (by 0.29 eV) than the other isomer which has a quasi-planar structure (Figure 2a). The two-layered structure binds an oxygen molecule more strongly (energy gain upon oxygen adsorption 0.47 eV compared to 0.28 eV for the latter isomer). Second, and most importantly, is the dynamic structural fluxionality of clusters which is the ability of a given isomer to adapt its structure so as to allow the reaction to evolve on the most favorable free-energy path. Such fluxionality is illustrated in Figures 2b and 2f where the more reactive two-layered Au_8 cluster is shown to undergo a large structural transformation upon adsorption of molecular oxygen at the "periphery site". The approximate bicapped octahedral geometry (Figure 2b) is transformed to a bicapped trigonal-prismatic structure (Figure 2f). This structural fluxionality is essential for the reaction to occur, since we have found that constraining the cluster to maintain its original geometry (Figure 2b) prevents the adsorption and activation of O_2.
2) Electronic size effects: Understanding the size-dependent electronic structure of the

 © 2003 Wiley-VCH Verlag GmbH & Co. KGaA, Weinheim 1433-7851/03/4211-1298 $ 20.00+.50/0

Au_n/MgO(FC) model catalysts, which is fundamental for elucidation of their size-dependant reactivity, is facilitated by analysis of the spectra of the local density of electronic states (LDOS) of the oxygen molecule and the metal cluster. A similar analysis is often employed in the context of the interaction of adsorbates with extended surfaces.[18] Figure 3a shows the LDOS of the O_2 molecule which is adsorbed at the periphery site (Figure 2f) of the more reactive isomer of the Au_8/MgO(FC) model catalyst. All the prominent peaks of the LDOS spectrum in Figure 3a can be unambiguously assigned to orbitals of the (free) molecular oxygen. In addition, these states overlap with the entire d band of the Au_8 cluster (shown in Figure 3b) in the range of $-7\,\text{eV} \le E \le E_F$, where E_F is the Fermi energy. Bonding of the oxygen molecule to the gold octamer mainly involves hybridization of the 5σ, $1\pi_\parallel$, and $1\pi_\perp$ oxygen states with the gold d band (Figure 3b). Most importantly, all the antibonding $2\pi^*$ spin-states of O_2 are located below the E_F, which results in strong activation of the absorbed O_2 molecule through occupation of the antibonding orbitals. This leads to weakening of the O–O bond that is reflected in a significant increase of its length (1.43 Å in Figure 2f) compared to that of the free molecule (1.25 Å). Accompanying the activation process is a change in the spin state of the molecule from a triplet state in the gas phase to a peroxo-like adsorbed state with a zero net spin. A drastically different scenario is found for the interaction of O_2 with the smaller gold cluster, Au_4/MgO(FC), where molecular oxygen adsorbs in an "on-top" configuration, with one oxygen atom binding to a single gold atom (Figure 2g). This system exhibits rather weak binding of the molecule to the metal cluster (0.18 eV), an almost unperturbed O–O bond length (1.28 Å), and, like the free molecule, is in a triplet spin state (see Figure 3c). The weak binding is attributed to the narrower d band of the adsorbed Au_4 cluster compared to that of Au_8 (see Figures 3b and 3d), with a consequent lack of overlap between the states at the bottom of the d band of the gold cluster (Figure 3d) and the molecular-oxygen states ($E < -5$ eV). Moreover, the spin-down antibonding $2\pi^*_\perp$ and $2\pi^*_\parallel$ orbitals of the adsorbed oxygen molecule are located above the E_F (unlike the case of the larger cluster, compare Figures 3c and 3a) which results in no activation of the adsorbed molecule by the Au_4 cluster.

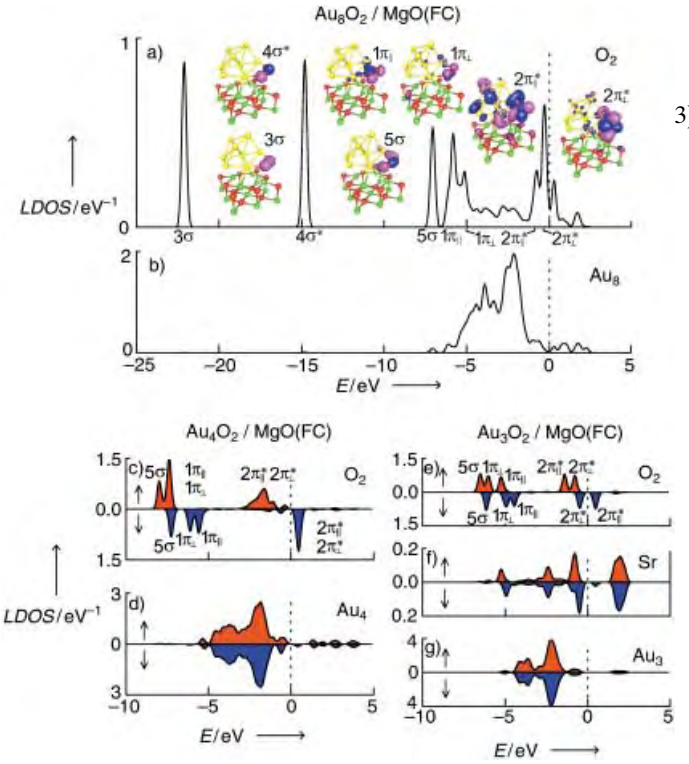

Figure 3. Local density of spin-up and spin-down electronic states (LDOS) of the model catalysts shown in Figure 2f–h for oxygen (a,c,e) and the metal cluster (b,d,f,g). The total spin is 0 in a and b, 1 in c and d and $^1/_2$ in e–g, and only spin-up states are shown in a and b since they are degenerate with the spin-down states. The prominent peaks of the oxygen LDOS are labeled following the conventional nomenclature for the molecular orbitals of the gas-phase O_2 molecule; assignment is by comparison with the free-oxygen orbitals (panel a). In (a) the notations $2\pi^*_\perp$ and $2\pi^*_\parallel$ denote, respectively, the perpendicular and parallel orientation with respect to the plane defined by the two atoms of the O_2 and the Au atoms closest to the FC. In (c) and (e) the orientation is given with respect to the plane defined by the atoms of the O_2 molecule and the metal atom closest to this molecule. The Fermi energy is at 0 eV.

3) Impurity-doping effects: The possibility of enhancing the catalytic activity of a nanocluster by designed incorporation (doping) of an impurity is demonstrated here by the catalyzed oxidation of CO on Au_3Sr/MgO(FC) (see Figure 1b and the inset). The LDOS spectra of the oxygen molecule, the Sr atom, and the Au_3 part of the metal cluster, are displayed in Figures 3e–g, respectively. Doping by a single impurity atom changes significantly the bonding and activation of O_2 compared to that in the pure gold tetramer, Au_4. The O_2 bonds mainly to the strontium atom of the Au_3Sr cluster (Figure 2h), and this bonding is characterized by a substantially higher adsorption energy (1.94 eV compared to 0.18 eV for the configuration shown in Figure 2g) and a significant activation of the O–O bond that is reflected in an increased bond length of 1.37 Å. This activation results from occupation of the spin-down $2\pi^*_\perp$ oxygen orbital (compare Figure 3e and 3c), which results in a superoxo-like state of the adsorbate. Bonding of the oxygen molecule to Au_3Sr/MgO(FC) occurs through resonances formed between the Sr states in the energy intervals (5–6) eV and (0–1) eV below the E_F, with the spin-up $1\pi_\parallel$ and $2\pi^*_\perp$ states, as well as with the spin-down $1\pi_\perp$ and $2\pi^*_\perp$ orbitals, of the adsorbed activated O_2.

In summary, we have identified and illustrated some of the key physical factors that underlie the chemical activity of supported nanoclusters, with a particular focus on the adsorption and activation step of molecular oxygen, that is essential for the oxidation of CO on supported gold model nanocatalysts. First, the metal-oxide support, and in particular surface oxygen vacancy sites, were found to play a dominant role in anchoring the metal clusters, and in activating the clusters by (partial) charge-transfer. Second, the structural fluxionality of the model catalyst (and in particular the

 © 2003 Wiley-VCH Verlag GmbH & Co. KGaA, Weinheim 1433-7851/03/4211-1299 $ 20.00+.50/0

isomerization propensity of the metal-cluster component) is predicted to enable and promote binding and activation of the reactants and to allow propagation of the catalyzed reaction along an optimal path through concurrent structural rearrangements of the model catalyst. Third, size-dependent activation of the reactants by the model catalyst and the resulting reactivity, correlate with subtle features in the electronic structure of the catalyst (in particular the width and positioning of the d band of the model gold catalyst). Finally, we have shown that catalytically inert clusters (e.g., supported gold tetramers) can be activated by doping with impurity atoms (e.g. Sr) that strongly bind and activate the reactants. These results may form guiding principles for further endeavors in the growing field of nanocatalysis, aiming at atomic-scale design of nanocatalysts with desired chemical activity, specificity, and selectivity.

Received: August 22, 2002
Revised: December 10, 2002 [Z50026]

Keywords: CO oxidation · density functional calculations · gold clusters · magnesium oxide · nanocatalysis

[1] *Metal Clusters* (Ed.: W. Ekardt), Wiley, Chichester, **1999**.
[2] U. Heiz, S. Abbet, A. Sanchez, W.-D. Schneider, H. Häkkinen, U. Landman, *Phys. Chem. Clusters Proc. Nobel Symp. 117th* **2001**, 87 – 98.
[3] M. Haruta, *Catal. Today* **1997**, *36*, 153.
[4] M. Valden, X. Lai, D. W. Goodman, *Science* **1998**, *281,* 1647.
[5] G. C. Bond, D. T. Thompson, *Catal. Rev. Sci. Eng.* **1999**, *41,* 319.
[6] A. Sanchez, S. Abbet, U. Heiz, W.-D. Schneider, H. Häkkinen, R. N. Barnett, U. Landman, *J. Phys. Chem. A* **1999**, *103,* 9573.
[7] G. A. Somorjai, *Introduction to Surface Science and Catalysis*, Wiley-VCH, New York, **1994**.
[8] C. T. Campbell, *Surf. Sci. Rep.* **1997**, *27*, 1.
[9] C. R. Henry, *Surf. Sci. Rep.* **1998**, *31*, 231.
[10] G. Ertl, H.-J. Freund, *Phys. Today* **1999**, *52*(1), 32.
[11] H.-P. Cheng, U. Landman, *Science* **1993**, *260*, 1304.
[12] U. Heiz, W.-D. Schneider, *J. Phys. D* **2000**, *33*, R85.
[13] S. Abbet, E. Riedo, H. Brune, U. Heiz, A. M. Ferrari, L. Giordano, G. Pacchioni, *J. Am. Chem. Soc.* **2001**, *123*, 6172.
[14] M. Moseler, H. Häkkinen, U. Landman, *Phys. Rev. Lett.* **2002**, *89*, 176103.
[15] Simulations were performed using the Born-Oppenheimer local-spin-density-functional simulations (BO-LSD-MD, see R. N. Barnett, U. Landman, *Phys. Rev. B* **1993**, *48*, 2081) with self-consistent generalized gradient corrections[19] and employing pseudopotentials[20] with a scalar-relativistic treatment for gold.[21,22] The Kohn–Sham electronic states are expanded in a plane-wave basis set with a kinetic energy cutoff of 62 Ry. The relaxed configurations of the bare adsorbed clusters, and the clusters with O_2, have been obtained by a spatial- and spin-unconstrained gradient-optimization method; in the relaxation process the substrate Mg^{2+} ions which are nearest neighbors to the oxygen vacancy F-center (FC), the metal cluster, and the adsorbed O_2 molecule are treated dynamically. The metal clusters were initially placed about 4 Å above the surface plane and the system was relaxed to the nearest energy minimum; this procedure was repeated several times to explore the isomer space of the adsorbed clusters. In addition, the stability of the lowest energy structures was checked by short-time (a few ps) ab initio molecular-dynamics simulations. It is worth noting that while it was recently found that gas-phase gold clusters (particularly anions) favor planar (2D) optimal structures up to sizes beyond 10 atoms (see ref. [22] and ref. [15] therein), the strong attraction by the FC always anchors one gold atom close to it and distorts the planar structures; in fact, the Au_8/MgO(FC) catalysts shown in Figure 2a and 2b correspond to low-energy 3D isomers of Au_8 in the gas phase.
[16] A. Eichler, J. Hafner, *Phys. Rev. B* **1999**, *59*, 5960.
[17] K.-H. Allers, H. Pfnür, P. Feulner, D. Menzel, *J. Chem. Phys.* **1994**, *100*, 3985.
[18] M. Scheffler, C. Stampfl in *Handbook of Surface Science, Vol. 2* (Eds.: K. Horn, M. Scheffler), Elsevier, Amsterdam, **1999**.
[19] J. P. Perdew, K. Burke, M. Ernzerhof, *Phys. Rev. Lett.* **1996**, *77*, 3865.
[20] N. Troullier, J. L. Martins, *Phys. Rev. B* **1991**, *43*, 1993.
[21] H. Häkkinen, U. Landman, *Phys. Rev. B* **2000**, *62*, R2287.
[22] H. Häkkinen, M. Moseler, U. Landman, *Phys. Rev. Lett.* **2002**, *89*, 033401.

 © 2003 Wiley-VCH Verlag GmbH & Co. KGaA, Weinheim 1433-7851/03/4211-1300 $ 20.00+.50/0

NMR Techniques

Optimized NMR Spectroscopic Method for the Configurational Analysis of Chemically Equivalent Vicinal Protons**

*Burkhard Luy, Gerd Hauser, Andreas Kirschning, and Steffen J. Glaser**

The analysis of the *Z*/*E* configuration of C–C double bonds is an important aspect in determining the structure of natural and synthetic products. Besides the configurational analysis from X-ray structures, the NMR spectroscopy derived ^{3}J(H,H) coupling constants of the vicinal protons play a major role in distinguishing the *Z*- and *E* configurations.[1] However, in the case of symmetrically 1,2-disubstituted alkenes this coupling constant is not directly accessible because of the identical chemical shifts of the alkene protons.[1] A solution to this problem is provided by methods which use the low natural abundance of the NMR-active ^{13}C isotope to break the symmetry of the carbon-bound vicinal protons. In favorable cases, the coupling constant can be extracted from the ^{13}C satellite signals in 1D ^{1}H NMR spectra. But in many cases the overlap with other signals and

[*] Prof. Dr. S. J. Glaser, Dr. B. Luy, Dipl.-Chem. G. Hauser
Institut für Organische Chemie und Biochemie II
Technische Universität München
Lichtenbergstrasse 4, 85747 Garching (Germany)
Fax: (+49) 89-289-13210
E-mail: glaser@ch.tum.de

Prof. Dr. A. Kirschning
Institut für Organische Chemie, Universität Hannover
Schneiderberg 1b, 30167 Hannover (Germany)

[**] B.L. thanks the Fonds der Chemischen Industrie and the DFG (Emmy Noether fellowship LU 835/1-1) for financial support. S.J.G. and A.K. also thank the DFG for financial support (GL 203/3-1,4-1, SFB 416). We thank Dr. G.-W. Chen, Dr. T. Diercks, and Dipl.-Chem. F. Kramer for their help.

 © 2003 Wiley-VCH Verlag GmbH & Co. KGaA, Weinheim 1433-7851/03/4211-1300 $ 20.00+.50/0

the sometimes complicated multiplet patterns do not allow this simple approach. Most of the multi-dimensional experiments that were developed to solve this problem, detect the ^{13}C nuclei[2–5] which leads to a low signal-to-noise ratio especially with inverse detecting probe heads. A significant improvement is achieved by proton-detecting HMQC (heteronuclear multiple-quantum coherence) methods[6–8] applied without ^{13}C decoupling. However, in all these experiments the interpretation of the experimental data is complicated by the presence of additional ^{1}H–^{1}H couplings. Herein, we present a new experiment that combines a good signal-to-noise ratio arising from to ^{1}H detection[9] with improved resolution because of the faster evolution of couplings under selective, isotropic mixing conditions. In the resulting 2D spectra, the double ^3J(H,H) coupling can be directly observed as the only splitting in the ω_1 dimension, which leads to greatly simplified spectra and an additional sensitivity gain.

The selective detection of ^{13}C-bound protons makes it necessary to suppress the approximately 400-fold more intense signal of the ^{12}C-bound protons in samples containing a natural abundance of ^{13}C. An effective solution for this problem is a modified version of a pulse sequence originally developed for water suppression:[10] With a refocused INEPT step[11,12] the magnetization of the ^{13}C-bound protons is transferred to the carbon nuclei and stored along the z-axis. The remaining ^{1}H magnetization is completely dephased by a ^{1}H spinlock pulse and gradient combination before the unaffected carbon magnetization is transferred back to the protons (by another refocused INEPT-step) for the acquisition (Figure 1). With this filter element, a proton-detected 2D J spectrum, similar to the ^{13}C-detected version published in ref. [3] can be acquired, but with the drawback that, as in the HMQC-derived method, all the ^{1}H–^{1}H couplings will be active during the J-evolution period and complex multiplet patterns can result. A simpler spectrum with enhanced coupling-resolution can be obtained through J-evolution under isotropic mixing conditions during t_1[13–16] by applying a selective TOCSY multiple-pulse sequence.[16–18]

If the state $I_{1x}-I_{2x}$ is prepared in a two-spin system, under isotropic mixing conditions[19] the magnetization of the spin I_1 evolves according to $\langle I_{1x}\rangle^{iso} = \cos 2\pi J t_1$.[16] This is twice the frequency of the oscillation during evolution in the weak-coupling limit of the same spin system ($\langle I_{1x}\rangle^{weak} = \cos\pi J t_1$). Hence, the identical resolution of the coupling constant can be obtained in half the evolution time. This is an advantage, especially for larger molecules with faster relaxation rates, which is significant for determining the coupling.

Experimentally, the state $I_{1x}-I_{2x}$ is prepared by a selective inversion of the ^{13}C-bound proton spins using a BIRD element[20] (see Figure 1). The evolution of the desired ^3J(H,H) coupling is achieved by the irradiation of a selective TOCSY sequence with a bandwidth that only covers the two vicinal protons and therefore decouples ^{13}C and additional ^{1}H spins. This approach is particularly straight forward to use for chemically equivalent protons. A suitable, selective TOCSY sequence is an MLEV-16 expanded 180° pulse.[19,21] With a radio frequency of 500 Hz, which corresponds to a 180° pulse of 1 ms, the multiple-pulse sequence has an effective bandwidth of about 360 Hz which is large enough to create isotropic mixing conditions for the desired protons and selective enough to decouple all the additional ^{1}H–^{1}H and ^{13}C–^{1}H couplings. The complete pulse sequence with experimental details is given in Figure 1.

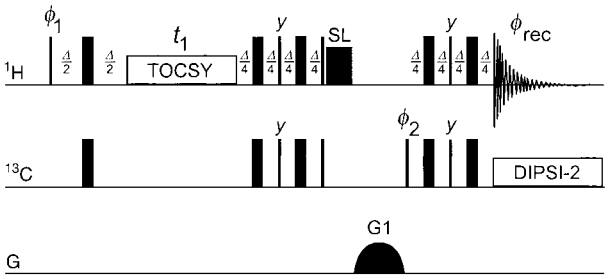

Figure 1. Pulse sequence for the determination of ^3J(H,H) coupling constants of chemically equivalent vicinal protons. After the selective inversion of the magnetization of ^{13}C-bound protons by a BIRD filter,[20] an incremented band-selective TOCSY period is used to monitor the selective evolution of the ^3J(H,H) coupling under isotropic mixing conditions. The subsequent ^{13}C filter element effectively suppresses the central signal of the ^{12}C-bound protons. All pulses are irradiated with phase x unless otherwise indicated. The ^{1}H and ^{13}C emitter frequencies should be positioned at the ^{1}H and ^{13}C resonance frequencies of the vicinal olefinic protons and the directly bound carbon atom, respectively. The phases are cycled: $\varphi_1 = x, -x$; $\varphi_2 = 2(x), 2(-x)$; $\varphi_{rec} = x, 2(-x), x$; $\Delta = 1/(^1J(C,H))$. The evolution under isotropic mixing conditions during t_1 is accomplished by a MLEV-16 expanded 180° pulse with a radio frequency amplitude of 500 Hz. With the supercycle used the minimal t_1 increment is 16 ms and the resulting spectral width is 62.5 Hz. The amplitude of the 2-ms spin-lock pulse (SL) should be chosen roughly 6 dB lower than the hard power ^{1}H pulse to minimize the irradiated radio frequency power. The sine-shaped gradient G1 of 5 ms duration should be applied with high amplitude. Efficient ^{13}C-decoupling during acquisition is achieved by using a DIPSI-2 multiple-pulse sequence with a radio frequency amplitude of 500 Hz.

We applied this method to the Z/E mixture of a linker-bridged homodimeric aminoglycoside **1** (Scheme 1) that resulted from metathesis olefination.[22,23] In the proton spectra, two signals with relative intensities of about 70:30 result from the two configurational isomers. From literature data[1,24] ^3J(H,H) coupling constants for the Z and E configuration of 6–14 Hz (mostly ≈10 Hz) and 14–20 Hz (mostly ≈ 16 Hz), respectively, are expected. However, this coupling could not be measured directly from standard ^{1}H NMR spectra. For an approximately 50 mM NMR sample only the stronger signal was visible in the ^{13}C NMR spectra after

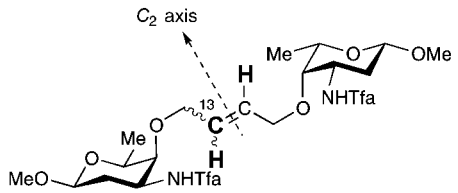

Scheme 1. Linker-bridged bis-daunosaminide **1** (Tfa = trifluoroacetyl). The symmetric dimer is a Z/E mixture, indicated by the wavy bonds. Because of the ^{13}C filtering, only compounds with a ^{13}C spin in the double bond are observed. Only the atoms printed in boldface contribute to the measurement of the ^3J(H,H) coupling in the presented experiment.

 © 2003 Wiley-VCH Verlag GmbH & Co. KGaA, Weinheim 1433-7851/03/4211-1301 $ 20.00+.50/0

1024 scans on a Bruker Avance DMX600 spectrometer equipped with a HCN-TXI-probe head. Hence, ^{13}C-detected methods were not applicable in a reasonable time frame. However, with the ^{1}H-detected pulse sequence shown in Figure 1, we were able to record a 2D spectrum in less than 6 h, from which we could determine the ^{3}J(H,H) coupling constants of 11.1 and 15.2 Hz (Figure 2). Hence, the mixture contains 30 % *Z* and 70 % *E* configuration.[1]

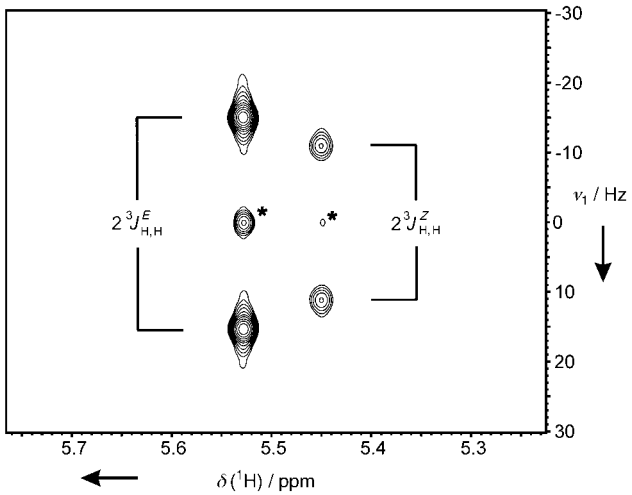

Figure 2. The experiment shown in Figure 1 applied to the configurational mixture **1** yields the double ^{3}J(H,H) couplings of the vicinal olefinic protons as a splitting in the indirect frequency dimension. The relatively weak axial signals (*) are artifacts from imperfect pulses. The spectrum was processed using the software package nmrPipe.[25] In the directly detected dimension 1024 complex points with a spectral width of 10 ppm were acquired, exponentially apodized, and Fourier transformed. To improve the signal-to-noise ratio and to simplify the spectrum, the apodization function was chosen so that the multiplet pattern caused by additional ^{1}H–^{1}H couplings (doublet of doublets) is not resolved in the directly detected dimension. A zero-filled imaginary part was added to the 57 real t_1 increments prior to exponential apodization and Fourier transformation. The spectrum was 0th- and 1st-order phase corrected in both dimensions.

The new experiment allows the straight forward determination of the configuration of double bonds in symmetric molecules. In contrast to conventional methods,[2–8] the ^{13}C spin is not used to produce a nonsymmetrical AA′X spin system during the t_1 evolution, but rather to allow for the selective inversion and detection of the ^{13}C-bound olefinic proton spins. During the isotropic *J* evolution in t_1, the ^{13}C-spins are decoupled and an effective A_2 system is created. The underlying principle of this method is not limited to symmetric molecules with chemically or magnetically equivalent spins, but can also be applied to olefinic protons that have similar resonance frequencies. It reveals crucial structural information about unsaturated natural products and for the synthesis of complex compounds. In particular, the method is very useful for the configurational analysis of metathesis products.

Received: June 27, 2002
Revised: January 17, 2003 [Z19627]

Keywords: alkenes · configurational analysis · NMR spectroscopy · spin—spin coupling · symmetry

[1] H. Günther, *NMR-Spektroskopie*, 2nd ed., Georg Thieme, Stuttgart, **1983**.
[2] R. Radeglia, H. Poleschner, M. Heydenreich, *Magn. Reson. Chem.* **1991**, *29*, 1028–1035.
[3] R. Radeglia, *J. Prakt. Chem.* **1993**, *335*, 291–293.
[4] V. Rutar, *J. Am. Chem. Soc.* **1983**, *105*, 4496–4497.
[5] V. Rutar, *J. Phys. Chem.* **1983**, *87*, 1669–1670.
[6] L. Müller, *J. Am. Chem. Soc.* **1979**, *101*, 4481–4484.
[7] M. R. Bendall, D. T. Pegg, D. M. Doddrell, *J. Magn. Reson.* **1983**, *52*, 81–117.
[8] A. Bax, R. H. Griffey, B. L. Hawkins, *J. Magn. Reson.* **1983**, *55*, 301–315.
[9] C. Griesinger, H. Schwalbe, J. Schleucher, M. Sattler in *Two dimensional NMR-Spectroscopy* (Eds.: W. R. Croasmun, R. M. K. Carlson), VCH, New York, **1994**.
[10] L. E. Kay, G. Y. Xu, A. U. Singer, D. R. Muhandiram, J. D. Forman-Kay, *J. Magn. Reson. Ser. B* **1993**, *101*, 333–337.
[11] G. A. Morris, R. Freeman, *J. Am. Chem. Soc.* **1979**, *101*, 760–762.
[12] D. P. Burum, R. R. Ernst, *J. Magn. Reson.* **1980**, *39*, 163–168.
[13] N. Chandrakumar, A. Ramamoorthy, *J. Magn. Reson.* **1992**, *99*, 372–376.
[14] M. Pfuhl, F. Fogolari, G. Esposito, P. Viglino, A. Pastore, *Q. Magn. Reson. Biol. Med.* **1994**, *1*, 53–60.
[15] M. Ravikumar, A. A. Bothner-By, *J. Am. Chem. Soc.* **1993**, *115*, 7537–7538.
[16] S. J. Glaser, J. J. Quant, *Adv. Magn. Opt. Reson.* **1996**, *19*, 59–252.
[17] J. Quant, T. Prasch, S. Ihringer, S. J. Glaser, *J. Magn. Reson. Ser. B* **1995**, *106*, 116–121.
[18] T. Prasch, P. Gröschke, S. J. Glaser, *Angew. Chem.* **1998**, *110*, 817–821; *Angew. Chem. Int. Ed.* **1998**, *37*, 802–806.
[19] L. Braunschweiler, R. R. Ernst, *J. Magn. Reson.* **1983**, *53*, 521–528.
[20] M. R. Bendall, D. T. Pegg, D. M. Doddrell, J. Field, *J. Am. Chem. Soc.* **1981**, *103*, 934–936.
[21] B. Luy , S. J. Glaser, *J. Magn. Reson.* **2000**, *142*, 369–371.
[22] A. Kirschning, G.-W. Chen, *Tetrahedron Lett.* **1999**, *40*, 4665–4668.
[23] G.-W. Chen, A. Kirschning, *Chem. Eur. J.* **2002**, *8*, 2717–2729.
[24] H. Friebolin, *Ein und zweidimensionale NMR-Spektroskopie: eine Einführung*, 2nd ed., VCH, Weinheim, **1992**.
[25] F. Delaglio, S. Grzesiek, G. W. Vuister, G. Zhu, J. Pfeiffer, A. Bax, *J. Biomol. NMR* **1995**, *6*, 277–293.

 © 2003 Wiley-VCH Verlag GmbH & Co. KGaA, Weinheim 1433-7851/03/4211-1302 $ 20.00+.50/0

Inorganic Cp Analogues

A Novel Class of Aromatic Compounds: Metal-Centered Planar Cations $[Fe(Sb_5)]^+$ and $[Fe(Bi_5)]^+$**

*Matthias Lein, Jan Frunzke, and Gernot Frenking**

Recent theoretical studies have shown that planar molecules $A(X_n)$ which contain a central atom A that is homoleptically bonded to a five- or six-membered ring X_n have unusual bonding situations which can be explained with the help of orbital interaction diagrams.[1–3] A particularly intriguing example is the work by Exner and Schleyer[3a] who reported that the D_{6h} form of the CB_6^{2-} ion, which has a planar hexacoordinate carbon atom, is a minimum on the potential energy surface (PES). Inspection of the molecular orbitals revealed that the compound is a six-π-electron aromatic species and was declared to be a viable possibility for experimental work.[3a] This species is to our knowledge the first example of a six-π-aromate which has an atom in the center of the ring.

Herein we report the molecules $[Fe(E_5)]^+$ (E = Sb, Bi) which also have a central atom that is bonded to an aromatic cyclic ligand but in a different way to in the CB_6^{2-} ion. The finding that the cations $[Fe(Sb_5)]^+$ and $[Fe(Bi_5)]^+$ have planar D_{5h} equilibrium geometries is the serendipitous result of a theoretical study where we investigated the structures and bonding situation of heteroatomic analogues of ferrocene $[Fe(E_5)_2]$ (E = N, P, As, Sb).[4] To analyze the nature of the iron–ligand interactions we optimized the geometries of the fragments $[Fe(E_5)]^+$ and $(E_5)^-$.[5] The calculations gave pyramidal (C_{5v}) equilibrium geometries for $[Fe(E_5)]^+$ (E = N, P, As) but the pyramidal structure of $[Fe(Sb_5)]^+$ collapsed during the optimization and yielded the planar D_{5h} form shown in Figure 1. Then we optimized the geometry of $[Fe(Bi_5)]^+$ which also has a planar equilibrium geometry. Both D_{5h} structures are minima on the singlet PES (number of imaginary frequencies $i = 0$).[15] The theoretically predicted vibrational frequencies are given in the Supporting Information.

The calculated Fe–E separations of $[Fe(E_5)]^+$ (E = Sb, Bi) are very short while the E–E bond lengths are quite long. This situation is clear when the interatomic distances of $[Fe(E_5)]^+$ are compared with the values of $[Fe(E_5)_2]$, also shown in Figure 1. Note that the Fe–E bond lengths in $[Fe(E_5)]^+$ are over 0.4 Å shorter than in $[Fe(E_5)_2]$. The calculated geometries suggest that the Fe–$(E_5)^+$ interactions are rather strong.

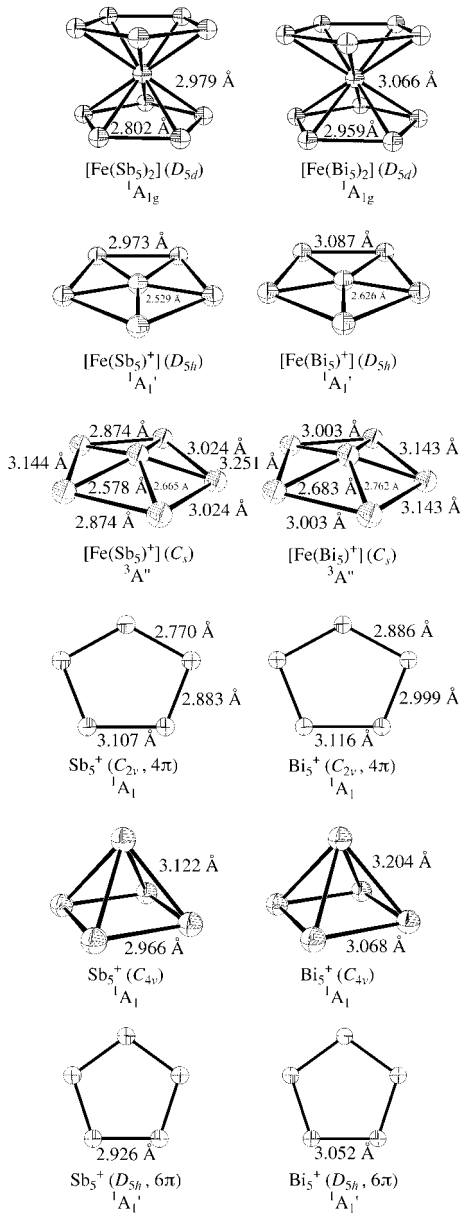

Figure 1. Calculated geometries of $[Fe(E_5)_2]$, $[Fe(E_5)]$, and E_5 (E = Sb, Bi) at BP86/TZ2P along with the symmetry groups and electronic configurations. All structures are minima on the PES except E_5^+ (D_{5h}, six π electrons) which has two imaginary frequencies.

To gain insight into the electronic structure of the molecules we analyzed the molecular orbitals of the $[Fe(E_5)]^+$ ion. Density plots of the occupied valence MOs of the $[Fe(Sb_5)]^+$ ion are shown in Figure 2. The orbitals of the $[Fe(Bi_5)]^+$ ion are very similar and therefore are not shown here. The $[Fe(Sb_5)]^+$ ion (D_{5h}) has eight occupied valence orbitals which have σ symmetry and two orbitals which have π symmetry. The HOMO (a_1') and the double-degenerate HOMO−1 (e_2') are nonbonding σ orbitals which are mainly iron lone-pair atomic orbitals (AOs), that is, $3d_{z^2}$, $3d_{xy}$ and

[*] Prof. Dr. G. Frenking, Dipl.-Chem. M. Lein, Dipl.-Chem. J. Frunzke
Fachbereich Chemie
Philipps-Universität Marburg
Hans-Meerwein-Strasse, 35039 Marburg (Germany)
Fax: (+49) 6421-282-5566
E-mail: frenking@chemie.uni-marburg.de

[**] Theoretical Studies of Inorganic Compounds. Part 23. This work has been supported by the Deutsche Forschungsgemeinschaft and the Fonds der Chemischen Industrie. Part 22: D. S. Nemcsok, A. Kovács, V. M. Rayón, G. Frenking, *Organometallics*, **2002**, *21*, 5803.

Supporting information for this article is available on the WWW under http://www.angewandte.org or from the author.

 © 2003 Wiley-VCH Verlag GmbH & Co. KGaA, Weinheim 1433-7851/03/4211-1303 $ 20.00+.50/0

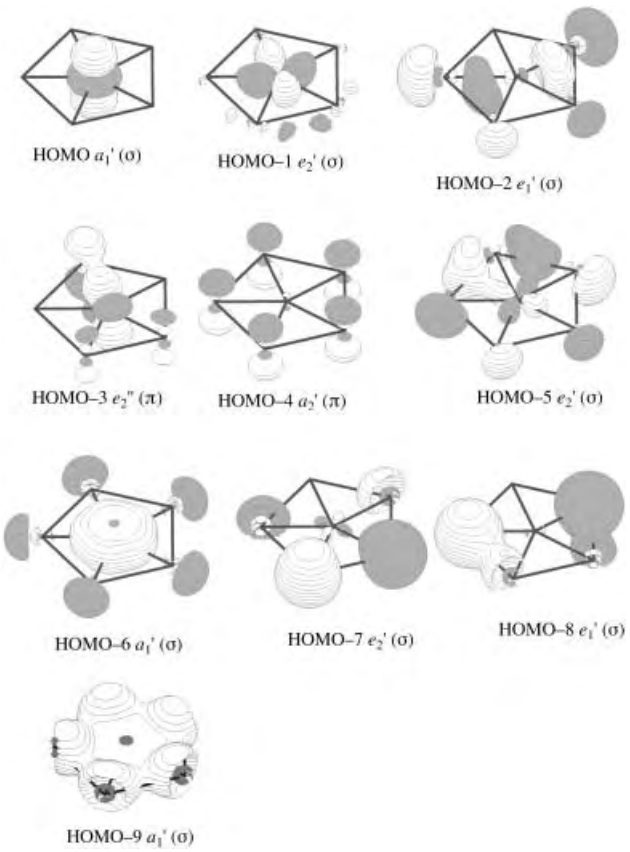

Figure 2. Graphical representation of the occupied valence orbitals of $[Fe(Sb)_5]^+$ (D_{5h}).

$3d_{x^2-y^2}$ where x and y define the molecular plane. The next lower-lying HOMO−2 (e_1') is a degenerate σ orbital which is mainly Sb–Sb bonding in character for two pairs of adjacent Sb atoms with negligible contributions by the Fe p-AOs. The degenerate HOMO−3 (e_1'') and the HOMO−4 (a_2'') are π orbitals which exhibit the typical pattern of a cyclic aromatic molecule with six π electrons. The lower-lying HOMO−4 is a totally bonding orbital of the p_z valence AOs of Sb with negligible contributions of the Fe AOs. However, the HOMO−3 is mainly a Fe–Sb π-bonding MO which has large contributions of the iron $3d_{xz}$ and $3d_{yz}$ AOs. This is a unique bonding pattern which distinguishes the $[Fe(Sb_5)]^+$ and $[Fe(Bi_5)]^+$ ions from the aromatic system CB_6^{2-}.[3a] The latter compound has the main-group element carbon as the central atom which does not have a valence orbital that can mix with the degenerate π orbital of the ring.

The next lower-lying orbitals HOMO−5 (e_2') and HOMO−6 (a_1') are σ-bonding orbitals between Fe and the Sb_5^+ ligand which have contributions from the iron $3d_{xy}$ and $3d_{x^2-y^2}$ AOs (HOMO−5) and the iron 4s AO (HOMO−6). The lowest-lying valence orbitals HOMO−7 (e_2'), HOMO−8 (e_1'), and HOMO−9 (a_1') are ligand-centered orbitals with little contribution from the iron AOs.

We carried out an energy decomposition analysis (EDA) of the $[Fe(Sb_5)]^+$ and $[Fe(Bi_5)]^+$ ions to get a deeper and more quantitative insight into the nature of the iron–ligand bonding situation.[6] The decomposition of the interaction energy into quantities which can be physically interpreted has proven to be a powerful tool for addressing questions about the most important contributions to the chemical bond between a donor and an acceptor moiety, because the strength of the covalent and the electrostatic (ionic) bonding can directly be estimated in a well defined way which makes it also possible to determine the strength of the σ and π bonding.[7] The EDA results of $[Fe(Sb_5)]^+$ and $[Fe(Bi_5)]^+$ which was carried out by choosing Fe in the electronic reference state $(core)^{18}(4s)^2(3d_{z^2})^2(3d_{xy})^2(3d_{x^2-y^2})^2$ and E_5^+ with six π electrons as interacting fragments are given in Table 1.[8]

Table 1: Results of the EDA of $[Fe(Sb_5)]^+$ and $[Fe(Bi_5)]^+$ ions by using the fragments $Fe(3s)^2(3d\sigma)^6$ and $E_5^+(6\pi)$ energy values in [kcal mol^{-1}]. Calculated atomic partial charges q (in units of the elementary charge e) given by the Hirshfeld method.[9]

Parameter	$[Fe(Sb_5)]^+$	$[Fe(Bi_5)]^+$
ΔE_{int}	−297.6	−286.9
ΔE_{Pauli}	493.8	413.9
ΔE_{elstat}	−353.6 (44.7%)[a]	−335.8 (47.9%)[a]
ΔE_{orb}	−437.8 (55.3%)[a]	−365.1 (52.1%)[a]
$\Delta A_1'$	−170.1 (38.9%)[b]	−139.4 (38.2%)[b]
$\Delta A_2'$	0.0	0.0
$\Delta E_1'$	−23.0 (5.3%)[b]	−15.8 (4.3%)[b]
$\Delta E_2'$	−61.4 (14.0%)[b]	−55.6 (15.2%)[b]
$\Delta A_1''$	0.0	0.0
$\Delta A_2''$	−13.2 (3.0%)[b]	−6.2 (1.7%)[b]
$\Delta E_1''$	−170.1 (38.9%)[b]	−148.1 (40.6%)[b]
$\Delta E_2''$	0.0	0.0
ΔE_σ	−254.5 (58.1%)[b]	−210.8 (57.7%)[b]
ΔE_π	−183.3 (41.9%)[b]	−154.3 (42.3%)[b]
q(Fe)	−0.31	−0.29
q(E)	+0.26	+0.26

[a] Percentage of the total attractive interactions $\Delta E_{elstat} + \Delta E_{orb}$. [b] Percentage of the total orbital interactions ΔE_{orb}.

The calculations give a very high interaction energy between the Fe center and the E_5^+ unit in the promoted electronic reference states (−297.6 kcal mol^{-1} for E = Sb and −286.9 kcal mol^{-1} for E = Bi). The Fe−E_5^+ bonding in both molecules is slightly more covalent (55.3% for E = Sn, 52.1% for E = Bi) than electrostatic (44.7% for E = Sb, 47.9% for E = Bi). The π orbitals make a very large contribution to the covalent term ΔE_{orb} (41.9% for E = Sb and 42.3% for E = Bi) which comes mainly from the e_1'' MOs. This result is in agreement with the shape of the HOMO−3 (e_1'') orbital shown in Figure 2. The largest contribution of the σ orbitals to ΔE_{orb} comes from the a_1' orbitals.

How large is the thermodynamic stability of the planar cations $[Fe(Sb_5)]^+$ and $[Fe(Bi_5)]^+$ with respect to dissociation into Fe and E_5^+ in the electronic ground states? The interacting fragments are in electronically highly excited states and it remains to be seen if the $[Fe(E_5)]^+$ species are thermodynamically stable. Table 2 gives calculated energies for ligand-exchange reactions, of the metal cations, which

 © 2003 Wiley-VCH Verlag GmbH & Co. KGaA, Weinheim 1433-7851/03/4211-1304 $ 20.00+.50/0

Table 2: Calculated reaction energies at BP86/TZ2P [kcal mol^{-1}]. The ZPE corrected values D_0 are given in parentheses.

No.	Reaction	E = Sb	E = Bi
1	$[Fe(E_5)]^+ + 5\ CO \rightarrow [Fe(CO)_5] + E_5^+$ (6π, D_{5h})[a]	−37.5 (−24.4)	−47.9 (−34.5)
2	$[Fe(E_5)]^+ + 5\ CO \rightarrow [Fe(CO)_5] + E_5^+$ (4π, C_{2v})[b]	−111.8 (−99.4)	−123.1 (−110.6)
3	$[Fe(E_5)]^+ + 5\ CO \rightarrow [Fe(CO)_5] + E_5^+$ (C_{4v})[c]	−146.5 (−133.8)	−167.9 (−155.1)

[a] Not an energy minimum structure ($i = 2$). [b] Energy minimum structure ($i = 0$). [c] Global energy minimum, pyramidal structure ($i = 0$).

yield $[Fe(CO)_5]$. The first reaction gives the free ligand E_5^+ with D_{5h} symmetry and six π electrons which is the electronically excited reference state. The reaction is exothermic for E = Sb ($D_o = -24.4$ kcal mol^{-1}) and E = Bi ($D_o = -34.5$ kcal mol^{-1}). The experimentally derived total binding energy of the CO ligands in $[Fe(CO)_5]$ is $D_o = 150.1$ kcal mol^{-1}.[21] Thus, the binding energy of the Fe atom in the ^{5}D ground state with the electronically excited E_5^+ (D_{5h}, six π electrons) ligand is 125.7 kcal mol^{-1} for E = Sb and 115.6 kcal mol^{-1} for E = Bi. However, the species E_5^+ (D_{5h}, six π electrons) does not correspond to minima on the PES but to higher-order saddle points ($i = 2$). The energetically lowest lying planar form of the cyclic E_5^+ ion has C_{2v} symmetry (four π electrons).[10] Table 2 shows that the ligand-exchange reaction number 2 yielding E_5^+(C_{2v}, four π electrons) is significantly more exothermic than reaction 1. The energies of the latter reaction and the total binding energy of $[Fe(CO)_5]$ give, for the dissociation of $[Fe(E_5)]^+$ into E_5^+ and Fe in the electronic ground states, the values $D_o = 50.7$ kcal mol^{-1} (E = Sb) and $D_o = 39.5$ kcal mol^{-1} (E = Bi) as reaction energies. The planar isomer of E_5^+ is not the global energy minimum. The most stable structures of Sb_5^+ and Bi_5^+ are the square-pyramidal forms with C_{4v} symmetry which are shown in Figure 1.[10] The calculated ligand-exchange reaction 3 (Table 2) yielding the C_{4v} form of E_5^+ is exothermic by 133.8 kcal mol^{-1} (E = Sb) and 155.1 kcal mol^{-1} (E = Bi). Thus, the calculations predict that $[Fe(Sb_5)]^+$ is thermodynamically more stable by 16.3 kcal mol^{-1} with regard to the energetically lowest lying fragments Fe and Sb_5^+ while $[Fe(Bi_5)]^+$ is −5.0 kcal mol^{-1} more unstable than the fragments Fe and Bi_5^+. However, the dissociation of $[Fe(E_5)]^+$ into the C_{4v} form of E_5^+ should have a significant energy barrier because of the required rearrangement of the ligand.

We speculated that an atom that is placed in the center of an aromatic ring should exhibit an unusual NMR chemical shift because of the ring current of the π electrons. Calculations of NMR chemical shifts at the center of an aromatic ring have been carried out by Schleyer et al. who found that the theoretical values can be used as a probe for aromaticity.[11] The NICS (Nuclear Independent Chemical Shifts) values have been obtained, however, without an atom being present in the ring center. We were curious to find out about the effect of an atom that is not only placed in the middle of the ring, but which in addition is strongly π-bonded to the aromatic system. In this context it is noteworthy that the ^{57}Fe resonance signal of ferrocene $[FeCp_2]$ has a very large paramagnetic shift of $\delta = 1532$ ppm relative to $[Fe(CO)_5]$.[12] It is conceivable that an Fe atom in the *center* of an aromatic ring might even be more deshielded.

Pioneering calculations of ^{57}Fe NMR chemical shifts have been made by Bühl et al. using the SOS-DFPT method.[13] They showed that the calculated ^{57}Fe NMR chemical shifts of several iron complexes have a good correlation with the experimental values, but the slope of the regression line between theoretical and experimental values depends critically on whether hybrid-type exchange correlation functionals were used instead of pure gradient-corrected functionals.[13b] In particular, the ^{57}Fe NMR signal of ferrocene is calculated to be too strongly shielded when BP86 is used. A better correlation between theory and experiment is obtained when the B3LYP-GIAO approach is used.[13,14]

Table 3 gives calculated ^{57}Fe NMR chemical shifts of $[Fe(CO)_5]$, $[FeCp_2]$, $[Fe(Sb_5)]^+$ and $[Fe(Bi_5)]^+$ at two levels of theory, that is, BP86/GIAO and B3LYP/GIAO. The calcu-

Table 3: Calculated and experimental ^{57}Fe NMR chemical shifts in ppm.

	BP86/QZ4P/GIAO		B3LYP/TZP/GIAO		Experimental[a]
	σ	δ	σ	δ	δ
$[Fe(Sb_5)]^+$	−17487	15642	−19091	16479	
$[Fe(Bi_5)]^+$	−20692	18847	n.c.[a]		
$[FeCp_2]$	−2711	866	−4324	1613	1532
$[Fe(CO)_5]$	−1845	0	−2612	0	0

[a] Not converged.

lation of $[Fe(Bi_5)]^+$ at B3LYP/GIAO did not converge and therefore, only the value at BP86/GIAO is given. The computed shift of $[FeCp_2]$ relative to $[Fe(CO)_5]$ at BP86/GIAO ($\delta = 866$ ppm) is significantly lower than the experimental value ($\delta = 1532$ ppm). A better agreement is obtained when the B3LYP/GIAO approach is used ($\delta = 1613$ ppm). The BP86/GIAO calculations predict that the ^{57}Fe NMR chemical shifts of the novel aromatic complexes $[Fe(Sb_5)]^+$ and $[Fe(Bi_5)]^+$ are dramatically shifted towards much larger δ values, that is, the iron nucleus is highly deshielded. The calculated values are $\delta[Fe(Sb_5)]^+ = 15642$ ppm and $\delta[Fe(Bi_5)]^+ = 18847$ ppm. The B3LYP/GIAO calculation gives $\delta[Fe(Sb_5)]^+ = 16479$ ppm. The theoretical data indicate that in experimental NMR studies of such compounds the measurement scale needs to be adjusted to accommodate such unusual numbers.

So far we have only reported the $[Fe(Sb_5)]^+$ and $[Fe(Bi_5)]^+$ ions in the electronic singlet state. We have carried out preliminary calculations of the molecules in electronic triplet states. Geometry optimizations at BP86 of planar triplet species with D_{5h} geometry gave structures which are 0.8 and 3.5 kcal mol^{-1} lower in energy than the singlet states of $[Fe(Sb_5)]^+$ and $[Fe(Bi_5)]^+$, respectively, but they are not minima on the PES. A theoretical search for triplet minima of $[Fe(Sb_5)]^+$ and $[Fe(Bi_5)]^+$ yielded slightly pyramidal structures which have C_s symmetry (^{3}A″ Figure 1; the complete geometry is given as Supporting Information). The latter species are 4.1 and 6.4 kcal mol^{-1} lower in energy than the planar singlet species. We did not carry out further calculations

 © 2003 Wiley-VCH Verlag GmbH & Co. KGaA, Weinheim 1433-7851/03/4211-1305 $ 20.00+.50/0

because a reliable theoretical study of the triplet states of $[Fe(Sb_5)]^+$ and $[Fe(Bi_5)]^+$ requires the use of the multiconfigurational self-consistent field method, which it is not possible for us to carry out as this would need all the valence orbitals of Fe and Sb_5, not just the π orbitals to be included.

The most important result of this work is the prediction that there is a novel type of transition-metal-centered aromatic compound which has strong π bonds between the aromatic ring and the metal atom d(π) AOs. The compounds $[Fe(Sb_5)]^+$ and $[Fe(Bi_5)]^+$ are the first examples of such molecules with the general formula $[TM(E)_n]^q$. The variation of TM (transition metal), *E*, *n*, and *q* should lead to other metal-centered aromatic compounds. We are currently exploring the structures and stabilities of the molecules by quantum-chemical methods.

Received: September 4, 2002 [Z50102]

Keywords: antimony · aromaticity · bond theory · density functional calculations · iron

[1] a) R. Ahlrichs, D. Fenske, H. Oesen, U. Schneider, *Angew. Chem.* **1992**, *104*, 312; *Angew. Chem. Int. Ed. Engl.* **1992**, *31*, 323; b) H. Tang, D. M. Hoffman, T. A. Albright, H. Deng, R. Hoffmann, *Angew. Chem.* **1993**, *105*, 1682; *Angew. Chem. Int. Ed. Engl.* **1993**, *32*, 1616; c) The compounds which are described in the two papers have also a transition metal in the center of a cyclic ligand which is planar. Unlike the aromatic ligands in our study, the cyclic ligands are electronically saturated.

[2] a) F.-W. Cheung, Z. Lin, *Angew. Chem.* **1997**, *109*, 1933; *Angew. Chem. Int. Ed. Engl.* **1997**, *36*, 1847; b) Z. Xu, Z. Lin, *Angew. Chem.* **1998**, *110*, 1815; *Angew. Chem. Int. Ed.* **1998**, *37*, 1686; c) Z. Xu, Z. Lin, *Chem. Eur. J.* **1998**, *4*, 28.

[3] a) K. Exner, P. von R. Schleyer, *Science* **2000**, *290*, 1937; b) R. W. A. Havenith, P. W. Fowler, E. Steiner, *Chem. Eur. J.* **2002**, *8*, 1068.

[4] a) M. Lein, J. Frunzke, A. Y. Timoshkin, G. Frenking, *Chem. Eur. J.* **2001**, *7*, 4155; b) J. Frunzke, M. Lein, G. Frenking, *Organometallics* **2002**, *21*, 3351.

[5] The geometries were optimized using gradient-corrected DFT (BP86)[16] in conjunction with uncontracted Slater-type orbitals (STOs) as basis functions.[17] Relativistic effects have been considered by the zero-order regular approximation (ZORA).[18] The basis set for Fe has triple-ζ quality augmented by one set of six p functions. Triple-ζ basis sets augmented by two sets of d-type polarization functions have been used for the main-group elements. The $(n-1s)^2$ and $(n-1)p^6$ core electrons of the main-group elements and the $(1s2s2p)^{10}$ core electrons of Fe were treated by the frozen-core approximation.[19a] An auxiliary set of s, p, d, f, and g STOs was used to fit the molecular densities and to represent the Coulomb and exchange potentials accurately in each SCF cycle.[19b] All calculations were carried out with the program package ADF.[20]

[6] a) K. Morokuma, *J. Chem. Phys.* **1971**, *55*, 1236; b) T. Ziegler, A. Rauk, *Theor. Chim. Acta* **1977**, *46*, 1.

[7] a) A. Diefenbach, F. M. Bickelhaupt, G. Frenking, *J. Am. Chem. Soc.* **2000**, *122*, 6449; b) J. Uddin, G. Frenking, *J. Am. Chem. Soc.* **2001**, *123*, 1683; c) M. Doerr, G. Frenking, *Z. Anorg. Allg. Chem.* **2002**, *628*, 843; d) Y. Chen, G. Frenking, *J. Chem. Soc. Dalton Trans.* **2001**, 434; e) C. Loschen, K. Voigt, J. Frunzke, A. Diefenbach, M. Diedenhofen, G. Frenking, *Z. Anorg. Allg. Chem.* **2002**, *628*, 1294; f) G. Frenking, K. Wichmann, N. Fröhlich, J. Grobe, W. Golla, D. L. Van, B. Krebs, M. Läge, M. *Organometallics* **2002**, *21*, 2921; g) V. M. Rayón, G. Frenking, *Chem. Eur. J.*, **2002**, *8*, 4693; h) G. Frenking, K. Wichmann, N. Fröhlich, C. Loschen, M. Lein, J. Frunzke, V. M. Rayón, *Coord. Chem. Rev.*, in print.

[8] The choice of the electronic states of the interacting fragments has been made according to the shape of the molecular orbitals. The choice is also supported by the calculated atomic partial charges *q* which are given by the Hirshfeld partitioning method (Table 1).[9] Alternatively, we could have chosen $Fe^{2+}(core)^{18}(4s)^0(3d_{z^2})^2(3d_{xy})^2(3d_{x^2-y^2})^2$ and E_5^- as interacting fragments but this would involve a much higher charge separation.

[9] F. Hirshfeld, *Isr. J. Chem.* **1977**, *16*, 198.

[10] Our calculations of E_5^+ are in agreement with a previous theoretical study of Sb_5^+ which showed that the planar C_{2v} form is an energy minimum and that the square-pyramidal C_{4v} species is probably the global energy minimum: V. Sundararajan, V. Kumar, *J. Chem. Phys.* **1995**, *102*, 9631.

[11] P. von R. Schleyer, C. Maerker, A. Dransfeld, H. J. Jiao, N. Hommes, *J. Am. Chem. Soc.* **1996**, *118*, 6317.

[12] R. Benn in *Transition Metal Nuclear Magnetic Resonance* (Ed.: P. S. Pregosin), Elsevier, Amsterdam, **1991**, p. 103.

[13] a) M. Bühl, O. L. Malkina, V. G. Malkin, *Helv. Chim. Acta* **1996**, *79*, 741; b) M. Bühl, *Chem. Phys. Lett.* **1997**, *267*, 251.

[14] M. Kaupp, V. G. Malkin, O. L. Malkina in *Encyclopedia of Computational Chemistry, Vol. 3* (Eds.: P. von R. Schleyer, N. L. Allinger, T. Clark, J. Gasteiger, P. A. Kollmann, H. F. Schaefer - III, P. R. Schreiner), Wiley, New York, **1998**, p. 1857.

[15] We also optimized the geometries of $[Fe(N_5)]^+$, $[Fe(P_5)]^+$, and $[Fe(As_5)]^+$ with the constraint of planar (D_{5h}) symmetry. The calculated structures are 237.4 ($[Fe(N_5)]^+$, $i=5$), 54.8 ($[Fe(P_5)]^+$, $i=3$), and 24.5 kcal mol^{-1} ($[Fe(As_5)]^+$, $i=3$) higher in energy than the pyramidal form.

[16] a) A. D. Becke, *Phys. Rev. A* **1988**, *38*, 3098; b) J. P. Perdew, *Phys. Rev. B* **1986**, *33*, 8822.

[17] J. G. Snijders, E. J. Baerends, P. Vernooijs, *At. Data Nucl. Data Tables* **1982**, *26*, 483.

[18] a) C. Chang, M. Pelissier, P. Durand, *Phys. Scr.* **1986**, *34*, 394; b) J.-L. Heully, I. Lindgren, E. Lindroth, S. Lundquist, A.-M. Martensson-Pendrill, *J. Phys. B* **1986**, *19*, 2799; c) E. van Lenthe, E. J. Baerends, J. G. Snijders, *J. Chem. Phys.* **1993**, *99*, 4597; d) E. van Lenthe, E. J. Baerends, J. G. Snijders, *J. Chem. Phys.* **1996**, *105*, 6505; e) E. van Lenthe, R. van Leeuwen, E. J. Baerends, J. G. Snijders, *Int. J. Quantum Chem.* **1996**, *57*, 281.

[19] a) E. J. Baerends, D. E. Ellis, P. Ros, *Chem. Phys.* **1973**, *2*, 41; b) J. Krijn, E. J. Baerends, *Fit Functions in the HFS-Method*, Internal Report (in niederländisch), Vrije Universiteit Amsterdam, Amsterdam, The Netherlands, **1984**.

[20] a) F. M. Bickelhaupt, E. J. Baerends, *Rev. Comput. Chem.* **2000**, *15*, 1; b) G. te Velde, F. M. Bickelhaupt, E. J. Baerends, S. J. A. van Gisbergen, C. Fonseca Guerra, J. G. Snijders, T. Ziegler, *J. Comput. Chem.* **2001**, *22*, 931.

[21] The value $D_o = 150.1$ kcal mol^{-1} for the total metal–ligand bond dissociation energy of $[Fe(CO)_5]$ has been calculated from the latest experimental values for the heats of formation $\Delta H_f^0([Fe(CO)_5]) = -187.1$ kcal mol^{-1},[22a] $\Delta H_f^0(CO) = -27.2$ kcal mol^{-1}, and $\Delta H_f^0(Fe) = 99$ kcal mol^{-1}.[22b]

[22] a) K. Norwood, A. Ali, G. D. Flesch, C. Y. Ng, *J. Am. Chem. Soc.* **1990**, *112*, 7502; b) S. G. Lias, J. E. Bartmess, J. F. Liebman, J. L. Holmes, R. D. Levin, W. G. Mallard, *J. Phys. Chem. Ref. Data* **1988**, *17*, Suppl. 1.

 © 2003 Wiley-VCH Verlag GmbH & Co. KGaA, Weinheim 1433-7851/03/4211-1306 $ 20.00+.50/0

Manganese-Based Initiators

Highly Reactive Polyisobutenes Prepared with Manganese(II) Complexes as Initiators**

Mario Vierle, Yanmei Zhang, Eberhardt Herdtweck, Martin Bohnenpoll, Oskar Nuyken, and Fritz E. Kühn**

High-molecular polyisobutenes are known for a long time and have found numerous applications.[1] Low-molecular-weight polyisobutenes are available by means of Lewis acidic initiators, for example, aluminum alkyl chlorides or aluminum(III) chloride.[1,2] Usually, polyisobutenes prepared this way contain less than 10% terminal double bonds and display a polydispersity index (PDI) between 2 and 5. The so called highly reactive polyisobutenes differ from these conventional polyisobutenes described above, they contain more than 60% terminal double bonds and have found applications as intermediates in the preparation of additives for lubricants and fuels.[3] Since mainly the terminal double bonds are involved in these functionalization reactions, a high number of terminal double bonds is an important quality criterion for such polyisobutenes. Adjustable medium molecular weights, of 500–5000 g mol^{-1}, and molecular weight distributions are of importance for the industrial application of the highly reactive polyisobutenes. Several approaches towards the desired products have been described and patented,[3,4] but in all cases they can only be obtained in good yield and with more than 80% terminal double bonds at reaction temperatures below 0°C. The cooling of the reaction mixtures, however, is combined with considerable costs, which greatly reduce the economy of the process.

Herein, we present a novel catalytic method to prepare polyisobutenes with a medium molecular weight, between 2000 and 7000 g mol^{-1}, a content of terminal double bonds over 95 mol%, and at temperatures between 20 and 60°C.[5]

Recently we have shown that first-row transition-metal complexes of the formula $[M(NCCH_3)_4][BF_4]_2$ (M^{II} = V, Cr, Mn, Fe, Co, Ni, Cu, Zn) and some of their second- and third-row congeners show good activities as initiators in the cationic polymerization of cyclopentadiene and methylcyclopentadiene, both in the homogeneous and the heterogeneous phase.[6] These initiators, however, are not active in the polymerization of other monomers even at elevated temperatures.[6b]

Replacing the $[BF_4]^-$ counterions, which coordinate to the metal units by one of their fluorine atoms,[7] by more weakly coordinating ions not only leads to an extremely high activity in cyclopentadiene polymerization, but also enables the polymerization and copolymerization of other monomers,

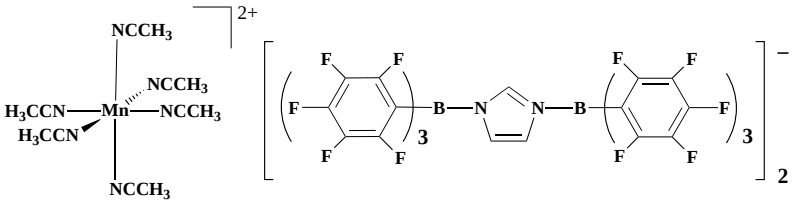

1

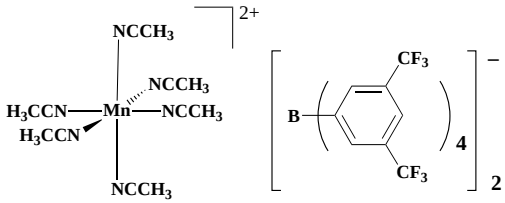

2

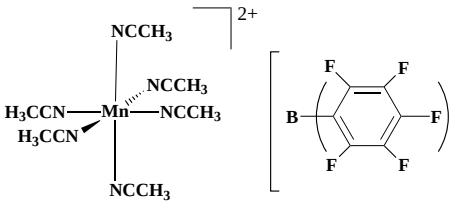

3

among them isobutene. The best initiator activities observed so far display manganese(II) complexes of the general formulae $[Mn(NCCH_3)_6][N_2C_3H_3\{B(C_6F_5)_3\}_2]_2$ (**1**), $[Mn(NCCH_3)_6][B(C_6F_5)_4]_2$ (**2**), and $[Mn(NCCH_3)_6][B\{C_6H_3(m\text{-}CF_3)_2\}_4]_2$ (**3**). These complexes are paramagnetic, as are their $[BF_4]^-$ congeners and their vibrational spectra and elemental analyses are in accord with the structures depicted. The X-ray structure of the propionitrile derivative of compound **2** (compound **2a**) has been determined (Figure 1).[8]

The compounds **1**–**3** can easily be obtained by the reaction of $MnCl_2$ with AgX (X = counteranion) in a solution of the appropriate nitrile. Related compounds with different (usually significantly more strongly coordinating) counterions have been reported since the 1960s.[7,9] Preparation strategies for the anions **1**–**3** have been established only much more recently.[10] The complexes **1**–**3** tend to lose one or two acetonitrile molecules when put under vacuum (oil pump) for prolonged periods of time or heated above 80°C without

[*] Prof. Dr.-Ing. O. Nuyken, Dipl.-Chem. M. Vierle
Lehrstuhl für Makromolekulare Stoffe
Technischen Universität München
Lichtenbergstrasse 4, 85747 Garching (Germany)
Fax: (+49) 89-289-13563
E-mail: oskar.nuyken@ch.tum.de

Priv.-Doz. Dr. F. E. Kühn, Dipl.-Chem. Y. Zhang, Dr. E. Herdtweck
Anorganisch-chemisches Institut
Technischen Universität München
Lichtenbergstrasse 4, 85747 Garching (Germany)
Fax: (+49) 89-289-13473
E-mail: fritz.kuehn@ch.tum.de

Dr. M. Bohnenpoll
BAYER AG, ZF-PK, 51378 Leverkusen (Germany)

[**] The Fonds der Chemischen Industrie and the Deutsche Forschungsgemeinschaft (DFG; Ph.D. grant to Y.Z) are acknowledged for financial support, and Dr. G. Langstein and Dr. W. Obrecht (BAYER AG) for helpful discussions. We are particularly grateful to the BAYER AG for continuous financial support and for permission to publish.

 © 2003 Wiley-VCH Verlag GmbH & Co. KGaA, Weinheim 1433-7851/03/4211-1307 $ 20.00+.50/0

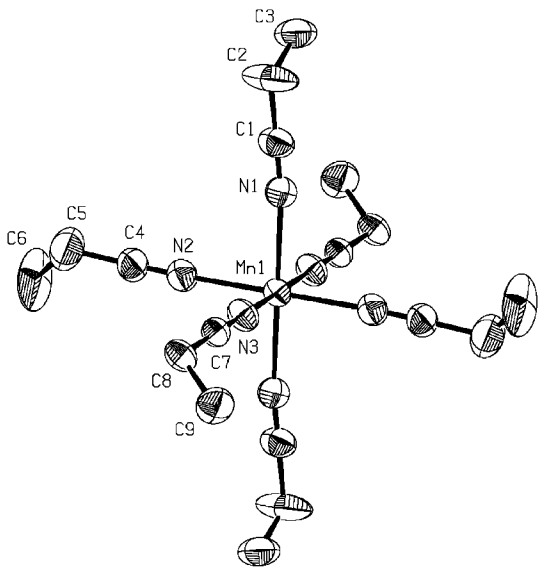

Figure 1. ORTEP drawing of the dicationic part of the solid-state structure of compound **2a**·propionitrile. Thermal ellipsoids are set at 50% probability. The hydrogen atoms are omitted for clarity. Selected bond lengths [Å] and angles [°]: Mn1-N1 2.247(4), Mn1-N2 2.213(4), Mn1-N3 2.214(3); N1-Mn1-N2 86.18(12), N1-Mn1-N3 91.03(11), N1-Mn1-N1′ 180, N1-Mn1-N2′ 93.82(12), N1-Mn1-N3′ 88.97(11), N2-Mn1-N3 87.52(12), N2-Mn1-N2′ 180, N2-Mn1-N3′ 92.48(12), N3-Mn1-N3′ 180. The symmetry code for the translation N→N′ is $(1-x, 1-y, -z)$.

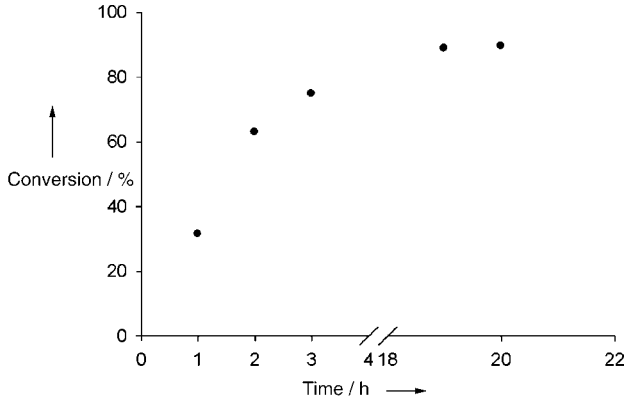

Figure 2. Time-dependent conversion of isobutene into polyisobutene. Initiator: compound **2**; $c(\mathbf{2}) = 1.35 \cdot 10^{-4}$ mol L^{-1}; c(isobutene) = 1.78 mol L^{-1}; solvent: 186 mL CH_2Cl_2; reaction temperature $T = 30$ °C.

excess acetonitrile being present. Complexes **1–3** are moderately stable to air and moisture and can easily be handled in the laboratory atmosphere. For prolonged storage they have to be kept in an inert gas atmosphere at low temperatures. Using such conditions they do not lose their initiator activity even after months.

For the polymerization reactions the reaction temperature was varied between 0–80 °C. Dichloromethane and binary dichloromethane/hexane mixtures with various proportions were used as solvents. The best results with respect to polymer yields were obtained in the temperature interval of 20–60 °C. Below room temperature the reaction is relatively slow, above 60 °C initiator deactivation seems to play a significant role (NMR spectroscopy and thermogravimetry (TG) evidence). The most active initiator for isobutene polymerization, regardless of the reaction temperature and initiator concentration, is complex **1**, the least active complex **3**. Table 1 gives a comparison of the activities of the initiators **1–3** at different initiator concentrations; a typical time/conversion curve is shown in Figure 2. Homopolymerization of isobutene in CH_2Cl_2, initiated by the compounds **1**—**3**, yields polymers of relatively low molecular weight, which is likely to be the result of proton-transfer reactions. However, ^{1}H NMR spectroscopy analysis reveals a high degree of olefinic end groups (ratio terminal:internal olefin 25:1), which makes these polymers very interesting as potential intermediates, for example, for oil additives and lubricants. In all cases it is possible to convert isobutene into polymers quantitatively.

The complexes **1–3** are also able to initiate the copolymerization of isobutene and isoprene (see Table 1). As expected, the rate of polymerization decreases with increasing amount of isoprene in the feedstock and the content of isoprene in the copolymer is lower than in the feedstock (Table 2). The molecular weight decreases with increasing amount of isoprene in the feedstock, which is an indication for a cationic polymerization mechanism with isoprene acting as molecular-weight control agent through the formation of a relatively stable allylic cation.[11,12] Nevertheless, in the cases of initiators **1** and **3**, it was also possible to initiate the homopolymerization of isoprene. As shown in Figure 3, the highest molecular weight of the copolymer was obtained by using initiator **2**. All homo- and copolymers described here are soluble in polar, aprotic solvents.

Several homopolymerization experiments of isobutene were carried out in dichloromethane/*n*-hexane solvent mix-

Table 1: Polymerization of isobutene and copolymerization of isobutene/isoprene with the initiators **1**—**3**.[a]

	Homopolymerization of isobutene				Copolymerization of isobutene/isoprene			
Initiator	c(initiator) [10^{-4} mol L^{-1}]	Conv. [%]	M_n [g mol^{-1}]	PDI [Mol%]	Isoprene [%]	Conv. [g mol^{-1}]	M_n	PDI
1	0.5	76	2820	2.3	4	7	3620	1.9
1	2.5	88	2530	2.4	50	1	1200	1.7
2	0.5	46	4900	1.8	4	16	8030	1.8
2	2.5	70	4100	2.1	50	–	–	–
3	0.5	13	4160	1.9	4	14	5940	1.5
3	2.5	22	4820	1.8	50	<1	2560	1.7

[a] Solvent CH_2Cl_2; c(isobutene) = 1.38 mol L^{-1}; $T = 40$ °C; $t = 16$ h.

 © 2003 Wiley-VCH Verlag GmbH & Co. KGaA, Weinheim 1433-7851/03/4211-1308 $ 20.00+.50/0

Table 2: Copolymerization of isobutene/isopropene (IB/IP) with compound **3** as the initiator.[a]

IB:IP [Mol%:Mol%]	Conv. [%]	M_n [g mol^{-1}]	IP in polymer [Mol%]
100:0	33	6400	0
96:4	15	5900	2.3
92:8	20	4500	3.6
90:10	6	2800	7.7
80:20	2	3300	6.0

[a] 5×10^{-6} mol; $T=30$ °C, $t=16$ h, 20 mL CH_2Cl_2. All polymers are completely soluble in toluene and chloroform and are colorless, highly viscous liquids.

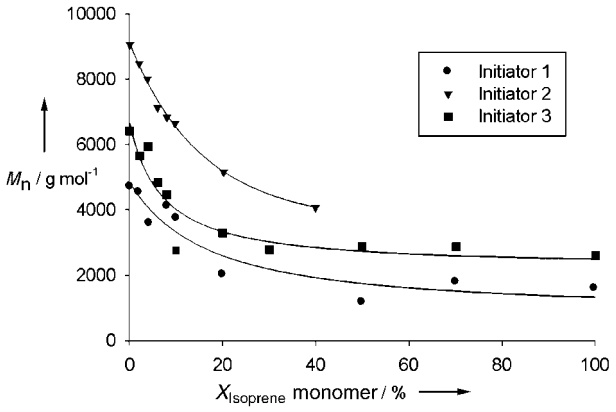

Figure 3. Dependence of the average molecular weight of the isobutene/isoprene copolymer on the composition of the reaction mixture. Conditions: Reaction time $t=16$ h, c(initiator) $=2.5\cdot10^{-4}$ mol L^{-1}, c(isobutene) $=1.38$ mol L^{-1}, $T=30$ °C, solvent CH_2Cl_2.

tures. Mainly, because of the solubility problems of the initiators **1**–**3** in *n*-hexane, the polymer yield, as well as the molecular weight, decreases with the increasing amount of *n*-hexane in the mixture. This also supports a cationic polymerization mechanism, as stabilization of the propagating cationic species by apolar solvents is lower, this causes higher proton-transfer rates, which result in lower molecular weight products. Using more than 60 vol.% of *n*-hexane in the mixture, no polymerization can be observed.

In summary, complexes of the type $[Mn(NCCH_3)_6][A]_2$, in which A is a noncoordinating anion, can be used as initiators for the synthesis of highly reactive polyisobutenes and the copolymerization of isobutene and isoprene at temperatures between 20–60 °C. Being able to carry out the isobutene polymerization at room temperature or slightly above is a major advantage in comparison to the usual process, which only works at temperatures significantly below 0 °C and therefore requires cooling. It is an additional advantage that products with a high degree of unsaturation (> 95%, determined by ^{1}H NMR spectroscopy) are produced by this reaction. Furthermore, the comparatively high amount of incorporated isoprene into the isobutene/isoprene copolymers is an important feature for the preparation of butyl rubber.

Experimental Section

1: $MnCl_2$ (74 mg, 0.44 mmol) was added to a solution of $Ag[(F_5C_6)_3B\text{-}C_3H_3N_2\text{-}B(C_6F_5)_3]$ (0.95 g, 0.87 mmol) in dry MeCN (10 ml) and the mixture stirred at room temperature for 12 h in the darkness. The solution was collected by filtration leaving a pale pink residue. The filtrate was concentrated under vacuum (oil pump) to 3 mL and cooled to −35 °C. 0.89 g of compound **1** formed (81% yield). The product was stored at −35 °C. IR (KBr): $\tilde{\nu}=2312$, 2286 cm^{-1} (CN); elemental analysis calcd (%) for $B_4C_{90}F_{60}H_{24}MnN_{10}$ (2483.3116) C 43.53, H 0.97, N 5.64; found: C 42.96, H 1.00, N 5.41.

Polymerization of Isobutene: A polymerization autoclave (Büchi Ecoclave 3500, equipped with 250-mL glass pressure tube, gas inlet, and septa) was dried and purged with argon. Dry CH_2Cl_2 (185 mL) was added and tempered to the adjusted temperature. By use of liquid nitrogen, isobutene (17 g) was condensed into a separate metal pressure tube and weighed. Afterwards, the isobutene was allowed to thaw and added to the solvent in the autoclave until saturation (reflected by a constant pressure of ca. 3 bar). Then the initiator, dissolved in CH_2Cl_2 (5 mL) is injected by pressure into the reaction mixture. The injecting system was washed with CH_2Cl_2 (10 mL) ($V(CH_2Cl_2)_{tot}=200$ mL, c(initiator) $=1.25\times10^{-4}$ mol L^{-1}). After a short induction period, which depended on the initiator used, the polymerization started which raised the temperature of the reaction mixture to 32 °C. Samples were taken with metal syringes during the whole polymerization process for monitoring the progression of the polymerization. After the pressure in the autoclave had reduced to nearly atmospheric pressure, the reaction was quenched with 50 mL of MeOH. For stabilization against oxidation 2,2′-methylene-bis(4-methyl-6-di-*tert*-butylphenol) (1 g) was added. The remaining reaction mixture was removed from the autoclave and the solvents evaporated to dryness in an oil-pump vacuum. The remaining polymer was dried in vacuum until constant weight. After 5 h of polymerization, 15.18 g of polyisobutene (overall conversion of 90%, calculated by weight percentages). ^{1}H NMR spectra showed an internal to external ratio olefin of about 1:25).

Copolymerization of isobutene/isoprene: For a higher efficiency, the copolymerization was performed in pressure tubes in a dry box. 12 tubes can be prepared at same time. Each tube was filled with dry CH_2Cl_2 (20 mL) at −40 °C and the initiator added (c(initiator) $=2.5\times10^{-4}$ mol L^{-1}). A magnetic stir bar is added to each tube, a variable ratio of isobutene, which had been condensed into a separate tube, and freshly distilled isoprene were added. The pressure tubes were sealed and quickly removed from the dry box. The polymerization was performed in a thermostatically controlled water bath equipped with a magnetic stirrer. The polymerization was quenched with MeOH (5 mL) and 2,2′-methylene-bis(4-methyl-6-di-*tert*-butylphenol (0.2 g) was added to prevent oxidation. The solvents were removed under oil-pump vacuum, the remaining polymer dried under vacuum at 30 °C until constant weight. The polymeric products were kept under inert-gas atmosphere afterwards. For detailed conversions see Tables 1 and 2.

Received: October 18, 2002 [Z50393]

Keywords: copolymerization · homogeneous catalysis · homopolymerization · manganese · polyisobutene

[1] H. Güterbock, *Polyisobutylen und Mischpolymerisate*, Springer, Berlin, **1959**, pp. 77–104.
[2] W. Immel in *Ullmann's Enzyklopädie der Technischen Chemie, Vol. 19*, 4th ed., VCH, Weinheim, **1980**, p. 216.
[3] P. Börzel, K. Bronstert, F. Hovermann (BASF AG), DE 2,702,604 **1978** [*Chem. Abstr.* **1978**, *89*, 130182].
[4] a) H.-P. Rath (BASF AG), WO 99/64482 **1999** [*Chem. Abstr.* **1999**, *113*, 23299]; b) J. T. Nolan, Jr., H. Chafetz (Texaco Inc.),

 © 2003 Wiley-VCH Verlag GmbH & Co. KGaA, Weinheim 1433-7851/03/4211-1309 $ 20.00+.50/0

US 3166546 **1965** [*Chem. Abstr.* **1965**, 62, 44376]; c) J. T. Nolan Jr. , H. Chafetz (Texaco Inc.), US 3024226 **1962** [*Chem. Abstr* **1962**, *56*, 74115]; d) R. E. Booth, F. E. Evans, R. E. Eibeck, M. A. Robinson (Allied Chem. Corp.), US 4227027 **1980** [*Chem. Abstr.* **1981**, *94*, 30326]; e) J. P. Kennedy, B. L. Goodall, A. V. Lubnin (Univ. of Akron), US 5340881 **1994** [*Chem. Abstr.* **1995**, *122*, 32399].

[5] M. Vierle, D. Schön, M. Bohnenpoll, F. E. Kühn, O. Nuyken (BAYER AG), Patent Application submitted DE 10211418.8 (15.03.2002).

[6] a) F. E. Kühn, J. R. Ismeier, D. Schön, W. M. Xue, G. Zhang, O. Nuyken, *Macromol. Rapid Commun.* **1999**, *20*, 555; b) F. E. Kühn, D. Schön, G. Zhang, O. Nuyken, *J. Macromol. Sci. Pure Appl. Chem.* **2000**, *37*, 971; c) M. Pillinger, I. S. Gonçalves, A. A. Valente, P. Ferreira, D. Schön, O. Nuyken, F. E. Kühn, *Des. Monomers Polym.* **2001**, *4*, 269; d) M. Pillinger, I. S. Gonçalves, P. Ferreira, J. Rocha, M. Schäfer, D. Schön, O. Nuyken, F. E. Kühn, *Macromol. Rapid Commun.* **2001**, *22*, 1306; e) M. Pillinger, I. S. Gonçalves, A. D. Lopes, P. Ferreira, J. Rocha, G. Zhang, M. Schäfer, O. Nuyken, F. E. Kühn, *Phys. Chem. Chem. Phys.* **2002**, *4*, 696.

[7] R. T. Henriques, E. Herdtweck, F. E. Kühn, A. D. Lopes, J. Mink, C. C. Romão, *J. Chem. Soc. Dalton Trans.* **1998**, 1293.

[8] a) Crystal-structure analysis of compound **2a**·propionitrile: $C_{18}H_{30}MnN_6 \cdot 2(C_{24}BF_{20}) \cdot C_3H_5N$, $M_r = 1798.60$, monoclinic, space group $P2_1/a$, $a = 17.9484(4)$, $b = 18.6777(5)$, $c = 23.9134(6)$ Å, $\beta = 90.660(1)°$, $V = 8016.1(3)$ Å^3; $Z = 4$; $\rho_{calcd} = 1.490\ g\,cm^{-3}$, $F_{000} = 3572$, $\mu = 0.302\ mm^{-1}$. Data collection was carried out on a kappa-CCD device (NONIUS MACH3) at the window of a rotating anode (NONIUS FR591) with graphite monochromated $Mo_{K\alpha}$ radiation ($\lambda = 0.71073$ Å) at 153 K; $2.31° < \Theta < 25.35°$. 23890 reflections were integrated, corrected for LP, and absorption effects and/or decay during the scaling procedure ($(R_{int} = 0.044)$, 10762 [5979: $I_o > 2\sigma(I_o)$] independent reflections (1094 refining parameters; $R1 = 0.0487$ [$I_o > 2\sigma(I_o)$], $wR2 = 0.1145$ [all data], GOF = 0.972, shift/error < 0.001). The asymmetric unit cell contains two crystallographically independent Mn dications, both located around a center of inversion. At Mn2 a disorder of one methylene carbon atom over two positions (72:28) could be resolved. The two anions and one C_3H_5N solvent molecule are well ordered. In addition, two solvent molecules could not be modeled properly and were rejected using the SQUEEZE procedure. Neutral atom scattering factors for all atoms and anomalous dispersion corrections for the non-hydrogen atoms were taken from the *International Tables for Crystallography*. CCDC 195403 (**2a**·propionitrile) contains the supplementary crystallographic data for this paper. These data can be obtained free of charge via www.ccdc.cam.ac.uk/conts/retrieving.html (or from the Cambridge Crystallographic Data Centre, 12 Union Road, Cambridge CB2 1EZ, UK; fax: (+44) 1223-336-033; or deposit@ccdc.cam.ac.uk); b) Data Collection Software for Nonius kappa-CCD devices, Delft (The Netherlands), **2001**; c) Z. Otwinowski, W. Minor, *Methods Enzymol.* **1997**, *276*, 307; d) SIR92: A. Altomare, G. Cascarano, C. Giacovazzo, A. Guagliardi, M. C. Burla, G. Polidori, M. Camalli, *J. Appl. Crystallogr.* **1994**, *27*, 435–436; e) *International Tables for Crystallography, Vol. C* (Ed.: A. J. C. Wilson), Kluwer Academic Publishers, Dordrecht, **1992**, Tables 6.1.1.4, 4.2.6.8, and 4.2.4.2; f) A. L. Spek, PLATON, *A Multipurpose Crystallographic Tool*, Utrecht University, Utrecht (The Netherlands), **2001**; g) G. M. Sheldrick, SHELXS-97, Program for the Solution of Crystal Structures, University of Göttingen, Göttingen (Germany), **1998**.

[9] a) B. J. Hathaway, D. G. Holah, A. E. Underhill, *J. Chem. Soc.* **1962**, 2444; b) B. J. Hathaway, D. G. Holah, *J. Chem. Soc.* **1964**, 2400; c) J. P. Fackler, D. G. Holah, *Inorg. Chem.* **1965**, *4*, 945; d) W. E. Buschmann, J. S. Miller, *Chem. Eur. J.* **1998**, *4*, 1731.

[10] a) B. H. Lipshutz, W. Vaccuro, B. Huff, *Tetrahedron Lett.* **1986**, *27*, 4095; b) H. S. Kasmai, *J. Chem. Educ.* **1996**, *76*, 830; c) F. Castellanos, J. P. Fouassier, C. Priou, J. Cavezzan, *J. Appl. Polym. Sci.* **1996**, *60*, 705; d) R. E. LaPointe, G. R. Roof, K. A. Abbound, J. Klosin, *J. Am. Chem. Soc.* **2000**, *122*, 9560.

[11] J. P. Kennedy, B. Ivan, *Designed Polymers by Carbocationic Macromolecular Engineering*, Hanser, New York, **1992**, p. 103.

[12] J. Si, J. P. Kennedy, *J. Polym. Sci. Part A* **1994**, *32*, 2011.

 © 2003 Wiley-VCH Verlag GmbH & Co. KGaA, Weinheim 1433-7851/03/4211-1310 $ 20.00+.50/0

Cover Picture

Nicholas E. Leadbeater* and Maria Marco

Biaryl compounds can be prepared in an aqueous Suzuki-type coupling reaction without the need for a transition-metal catalyst. The Suzuki coupling reaction (palladium-catalyzed coupling of aryl halides with boronic acids) has virtually become the method of choice for the synthesis of biaryl compounds. Under the right conditions, however, it is possible to perform catalyst-free Suzuki-type couplings. Further details are reported in the Communication by N. E. Leadbeater and M. Marco on page 1407 ff.

Contents

News

Protein Engineering: Alan Fersht Knighted ——— 1330

Polymers: Klaus Müllen Recognized ——— 1330

Cover Pictures 2002: The Winners ——— 1330

Books

Carbene Chemistry ——— 1331 Guy Bertrand *reviewed by W. Kirmse*

Highlights

Controlled Cycloadditions

F. Zaragoza Dörwald* ——— 1332 – 1334

Solvent-Controlled Selectivity in the Synthesis of Five-Membered Carbocycles from Carbene Complexes

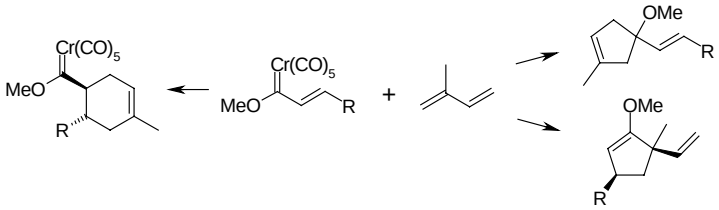

Surprisingly different products can be obtained from Fischer-type alkenyl carbene complexes and 1,3-dienes. The choice of solvent and reaction temperature is of critical importance for the outcome of these reactions, but the reasons for the variable results remain far from being understood.

Agostic Interactions

G. I. Nikonov* ——— 1335 – 1337

Complexation of Si–Si σ Bonds to Metals

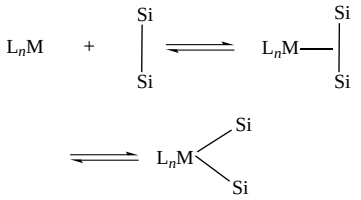

The long-known class of nonclassical complexes containing agostic interactions, X–H→M, and coordinated σ bonds, (X–H)→M, has recently been joined by a new group of "hydrogen-free" compounds that exhibit (X–Y)→M interactions. In addition to those complexes with agostic C–C and C–Si bonding, the first Si–Si σ complexes (see scheme) of group 5 and group 10 transition-metal elements have been prepared, and their relevance towards Si–Si bond-coupling reactions has been established.

Reviews

Rare-Earth Elements

K. Dehnicke,* A. Greiner ——— 1340 – 1354

Unusual Complex Chemistry of Rare-Earth Elements: Large Ionic Radii—Small Coordination Numbers

Ligands slim down: Complexes of rare-earth elements with low coordination numbers for the metal centers can be obtained in the "classical way" by using bulky ligand groups. Recently, they were prepared in a reaction with the slender phosphoraneiminato ligand NPR_3^- (see picture) which protects the metal center on account of metal-nitrogen multiple bonding. These complexes are very efficient catalysts for ring-opening polymerization of lactones.

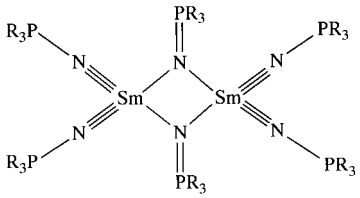

© 2003 Wiley-VCH Verlag GmbH & Co. KGaA, Weinheim

1433-7851/03/4212-1322 $ 20.00+.50/0

Communications

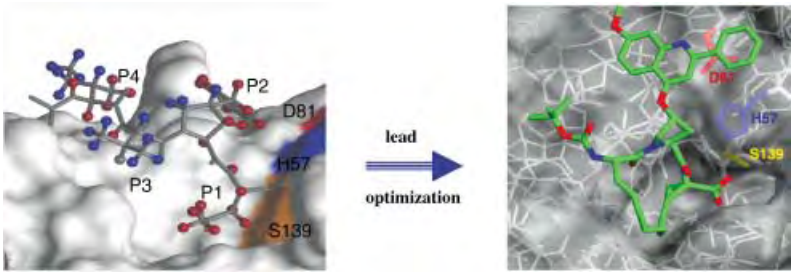

Clinically useful antiviral agents for the treatment of hepatitis C viral infections might be derived from the here presented macrocyclic inhibitors (right) of the hepatitis C virus (HCV) NS3 protease. The NMR-derived conformation of a substrate-based enzyme-bound hexapeptide (left) was used to design these inhibitors. These are the first inhibitors of NS3 protease which block HCV RNA replication in the cell-based replicon assay, they are orally absorbed, and they are stable to metabolic breakdown.

Protease Inhibitors

Y. S. Tsantrizos,* G. Bolger, P. Bonneau, D. R. Cameron, N. Goudreau, G. Kukolj, S. R. LaPlante, M. Llinàs-Brunet, H. Nar, D. Lamarre ——— **1356 – 1360**

Macrocyclic Inhibitors of the NS3 Protease as Potential Therapeutic Agents of Hepatitis C Virus Infection

Be my guest: A new family of supramolecular inclusion compounds is introduced which relies upon second-sphere hydrogen-bonding interactions to assemble highly stable layered networks (see picture). These solids have great potential for structural variation. They are possibly inorganic analogues of a well-studied host family, the guanidinium sulfonates.

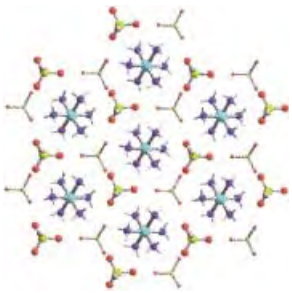

Supramolecular Inclusion Compounds

D. S. Reddy, S. Duncan, G. K. H. Shimizu* ——— **1360 – 1364**

A Family of Supramolecular Inclusion Solids Based Upon Second-Sphere Interactions

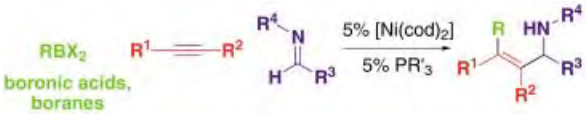

An unusual degree of functional group compatibility for imine addition reactions was observed in the assembly of allylic amines from alkynes, imines, and organoboron reagents (boronic acids or boranes) by using a catalyst derived from $[Ni(cod)_2]$ and $(c\text{-}C_5H_9)_3P$—this catalytic three-component process (see scheme) is tolerant of ketones, esters, and hydroxylic solvents.

Ni-Catalyzed Multicomponent Reaction

S. J. Patel, T. F. Jamison* ——— **1364 – 1367**

Catalytic Three-Component Coupling of Alkynes, Imines, and Organoboron Reagents

For the USA and Canada:
ANGEWANDTE CHEMIE International Edition (ISSN 1433-7851) is published weekly by Wiley-VCH PO Box 191161, D 69451 Weinheim, Germany. Air freight and mailing in the USA by Publications Expediting Inc. 200 Meacham Ave., Elmont, NY 11003. Periodicals postage paid at Jamaica NY 11431. US POSTMASTER: send address changes to *Angewandte Chemie*, Wiley-VCH, 111 River Street, Hoboken, NJ 07030. Annual institutional subscription price for institutions: Europe € 2998.00/3148.00. Outside Europe US$ 3718.00/3904.00 (valid for print or electronic/print and electronic delivery); for individuals who are personal members of a national chemical society, or whose institution already subscribes, or who are retired or self-employed consultants, print only (including postage and handling charges): Europe € 248.00/Outside Europe US$ 348.00.

 © 2003 Wiley-VCH Verlag GmbH & Co. KGaA, Weinheim 1433-7851/03/4212-1323 $ 20.00+.50/0

Contents

Asymmetric Amination

M. Marigo, K. Juhl, K. A. Jørgensen* ——— 1367 – 1369

Catalytic, Highly Enantioselective, Direct Amination of β-Ketoesters

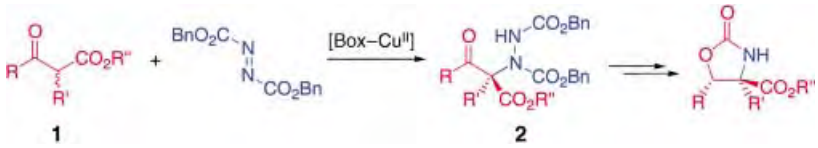

Optically active α-amino acid derivatives were accessed through the direct asymmetric α-amination of α-substituted β-ketoesters **1**, catalyzed by chiral Cu^{II}–bisoxazoline (BOX) complexes. The reaction proceeds with dibenzyl azodicarboxylate in the presence of only 0.2 mol% of the catalyst to give the desired products **2** in high yield with excellent enantioselectivity (up to 99% *ee*).

DNA-Templated Synthesis

Z. J. Gartner, R. Grubina, C. T. Calderone, D. R. Liu* ——— 1370 – 1375

Two Enabling Architectures for DNA-Templated Organic Synthesis

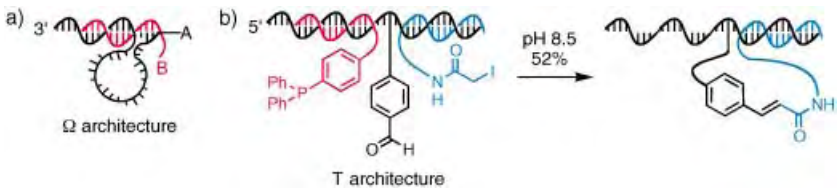

Reactivity can be rationally manipulated in DNA-templated synthesis by altering the design of template architectures: a) The omega (Ω) architecture enables DNA-templated reactions to be encoded by bases distal from the reactive end of the template, regardless of the distance dependence of the reaction. b) The T architecture enables two DNA-templated reactions to take place on a single template in one solution, as illustrated.

Superparamagnetic Nanosensors

M. Zhao, L. Josephson, Y. Tang, R. Weissleder* ——— 1375 – 1378

Magnetic Sensors for Protease Assays

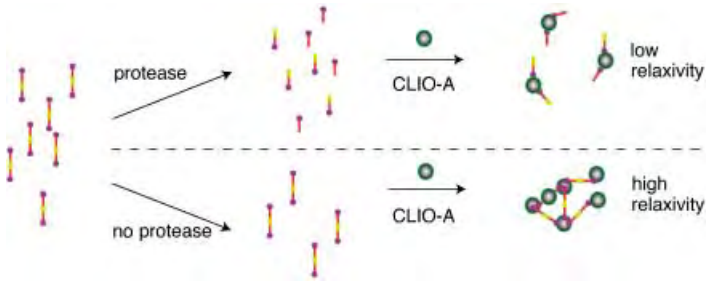

Superparamagnetic nanosensors conjugated to avidin (CLIO-A) can be used to measure sensitively and quantitively the proteolytic cleavage of bi-biotinylated peptide substrates (rods in the scheme) by changes in magnetic resonance properties. This approach may be generalized to determine the activity of a wide range of hydrolytic enzymes.

Biocatalysis in Photochemistry

S. Saphier, S. C. Sinha, E. Keinan* ——— 1378 – 1381

Antibody-Catalyzed Enantioselective Norrish Type II Cyclization

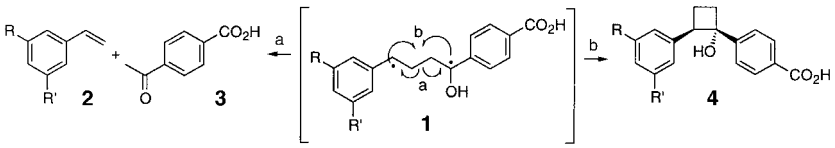

Excellent enantioselectivity (up to 96% *ee*) was attained in an antibody-catalyzed photochemical Norrish type II reaction, which proceeded via the intermediate diradical **1** to produce the cyclobutanols **4** (absolute stereochemistry unknown). Use of the antibody was shown to alter the course of the reaction by favoring formation of the cyclization product **4** over the fragmentation products **2** and **3**.

 © 2003 Wiley-VCH Verlag GmbH & Co. KGaA, Weinheim 1433-7851/03/4212-1324 $ 20.00+.50/0

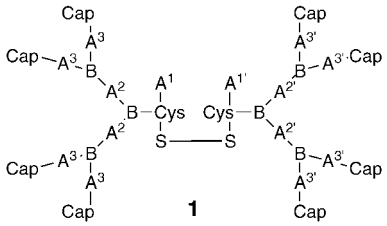

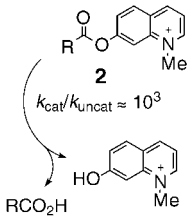

Enzymelike kinetics were observed in the hydrolysis of 7-hydroxy-1-methylquinolium esters **2** under the catalysis of three of a family of synthetic peptide dendrimers **1**. Their synthesis was based on a symmetrical branching diamino acid (B), three variable amino acid positions (A^1, A^2, A^3 = His, Asp, Ser), and a disulfide bond dimerization strategy. All possible permutations of the catalytic triad of the amino acids aspartate, histidine, and serine at the variable positions gave a family of 21 peptide dendrimers.

Biocatalyst Design

A. Esposito, E. Delort, D. Lagnoux, F. Djojo, J.-L. Reymond* — **1381 – 1383**

Catalytic Peptide Dendrimers

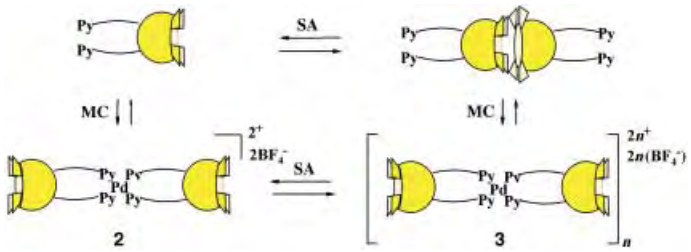

A dual-coded dynamic material was created by the bimodal self-assembly protocol sketched in the scheme. The combination of two orthogonal and reversible interactions, namely solvophobic aggregation (SA) and metal coordination (MC), allows precise control at each step of the self-assembly cycle, leading to the formation of rodlike supramolecular architectures.

Dynamic Self-Assembled Materials

L. Pirondini, A. G. Stendardo, S. Geremia, M. Campagnolo, P. Samorì, J. P. Rabe, R. Fokkens, E. Dalcanale* — **1384 – 1387**

Dynamic Materials through Metal-Directed and Solvent-Driven Self-Assembly of Cavitands

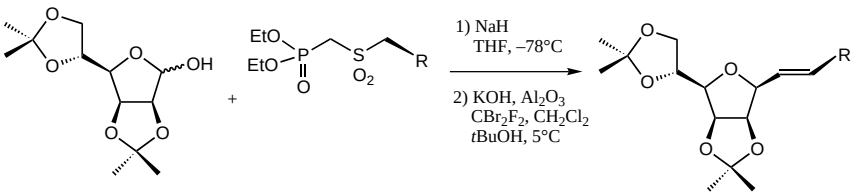

Eight illustrious organic chemists in one pot! A route from protected monosaccharides to novel C-glycosides and C-linked disaccharides is described which involves tandem Horner–Wadsworth–Emmons/conjugate addition (Michael-type), followed by tandem halogenation/Ramberg–Bäcklund reaction using the Meyers–Chan procedure (see scheme, R = protected saccharide).

Preparing C-Linked Disaccharides

G. D. McAllister, D. E. Paterson, R. J. K. Taylor* — **1387 – 1391**

A Simplified Ramberg–Bäcklund Approach to Novel C-Glycosides and C-Linked Disaccharides

 © 2003 Wiley-VCH Verlag GmbH & Co. KGaA, Weinheim 1433-7851/03/4212-1325 $ 20.00+.50/0

Contents

Supported Cluster Calculations

G. N. Vayssilov, B. C. Gates, N. Rösch* ——— **1391 – 1394**

Oxidation of Supported Rhodium Clusters by Support Hydroxy Groups

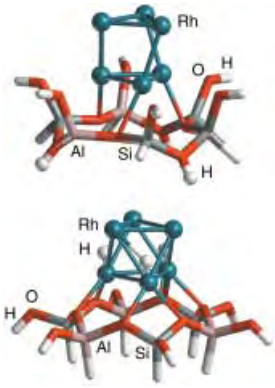

The calculated structures of a supported Rh_6 cluster (depicted) demonstrate that protons of surface OH groups of the oxide support migrate onto the cluster. This migration results in the oxidation of metal atoms that are in close contact with the support. The energy released by this reverse hydrogen spillover is estimated to be 120 kJ mol^{-1} per OH group.

NMR Studies of Glycopeptides

S. Ilin, C. Bosques, C. Turner, H. Schwalbe* ——— **1394 – 1397**

Γ-HMBC: An NMR Experiment for the Conformational Analysis of the *o*-Glycosidic Linkage in Glycopeptides

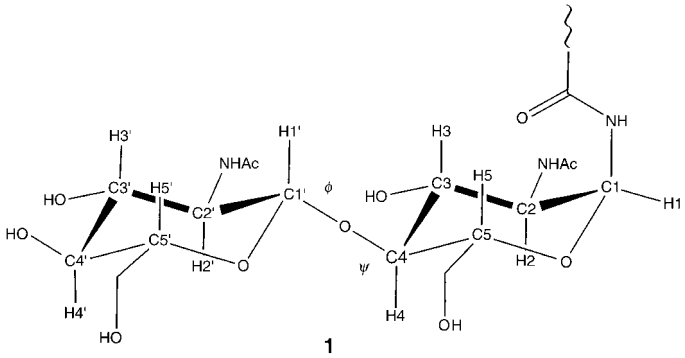

1

A more sensitive approach: A variation on the heteronuclear multiple-bond correlation technique has been devised which can determine the conformation around the glycosidic bonds in oligosaccharides and glycopeptides. The key section of the studied glycopeptide **1** is shown, for which measurements of the torsion angles ϕ and ψ, derived from ^3J(C,H) coupling constants and cross-correlated relaxation rates, compare favorably with those determined by X-ray diffraction or molecular dynamic analysis.

Unsaturated Bicyclic Lactones

A. Kamitani, N. Chatani,* S. Murai ——— **1397 – 1399**

Palladium-Catalyzed Carbonylation of 2-(Propargyl)allyl Phosphates Leading to Highly Unsaturated γ-Lactones

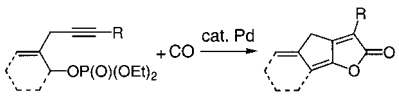

Highly unsaturated γ-lactones are formed in good to high yields from 2-(propargyl)-allyl phosphates and carbon monoxide in the presence of a palladium catalyst (see scheme). The reaction proceeds efficiently under mild reaction conditions (at 80 °C under an ambient pressure of CO).

Pt-Capped C-Rich Molecular Rods

V. W.-W. Yam,* K. M.-C. Wong, N. Zhu ——— **1400 – 1403**

Luminescent Platinum(II) Terpyridyl-Capped Carbon-Rich Molecular Rods—An Extension from Molecular- to Nanometer-Scale Dimensions

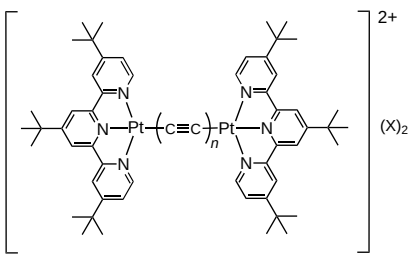

1: $n = 1$, X = OTf^-
2: $n = 2$, X = OTf^-
3: $n = 4$, X = PF_6^-

A change in shift! In contrast to the red shift commonly found in organic polyynes and other metal–alkynyl systems, a blue shift in the transition energy was observed in electronic absorption and emission studies on a novel series of structurally characterized dinuclear platinum(II)–terpyridyl complexes [{Pt(*t*Bu$_3$-tpy)}$_2$-(C≡C)$_n$](X)$_2$ (**1**–**3**; *t*Bu$_3$-tpy = 4,4′,4″-tri-*tert*-butyl-2,2′:6′,2″-terpyridine) upon increasing the extent of π conjugation of the alkynyl bridge.

© 2003 Wiley-VCH Verlag GmbH & Co. KGaA, Weinheim
1433-7851/03/4212-1326 $ 20.00+.50/0

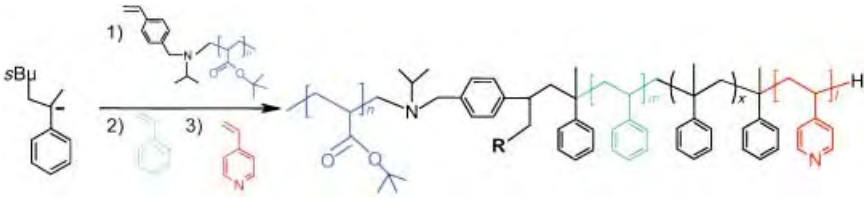

Breathing new life into anionic polymerization: A novel ABC triblock, poly(*tert*-butyl acrylate)-*block*-polystyrene-*block*-poly(4-vinylpyridine) (depicted), was synthesized by living anionic polymerization. A functional macromonomer, poly(*tert*-butyl acrylate) (blue) with a styrene end group (black) was first prepared by anionic polymerization, and then used in the initiation of the anionic polymerization of styrene (green). As the styryl anion remained "alive" in the presence of the poly(*tert*-butyl acrylate) block, the 4-vinylpyridine (red) polymerization could proceed after monomer addition.

ABC Triblock Copolymers

F. Liu, A. Eisenberg* ——— **1404 – 1407**

Synthesis of Poly(*tert*-butyl acrylate)-*block*-Polystyrene-*block*-Poly(4-vinylpyridine) by Living Anionic Polymerization

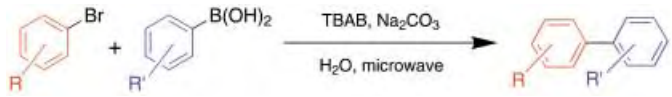

No metal required: The first transition-metal-free Suzuki-type coupling reaction was carried out in water by using tetrabutylammonium bromide (TBAB) as an additive (see scheme). Products were obtained in high yields with a wide range of aryl bromide substrates.

Biaryl Coupling Reactions

N. E. Leadbeater,*
M. Marco ——— **1407 – 1409**

Transition-Metal-Free Suzuki-Type Coupling Reactions

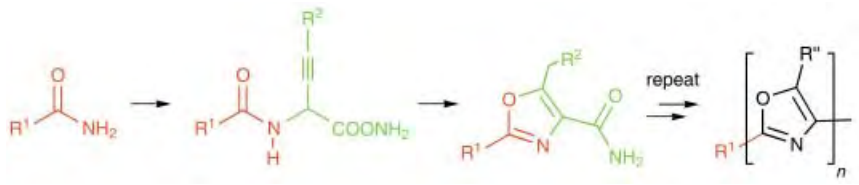

An efficient iterative synthesis of oxazoles involves the cyclization of 2-alkynyl glycinates (see scheme) formed from the reaction of 1-alkynyl aluminum reagents with α-chloroglycinates. This approach was used in the total synthesis of the bisoxazole natural product, (−)-muscoride A.

Synthesis of Oxazoles

P.-Y. Coqueron, C. Didier, M. A. Ciufolini* ——— **1411 – 1414**

Iterative Oxazole Assembly via α-Chloroglycinates: Total Synthesis of (−)-Muscoride A

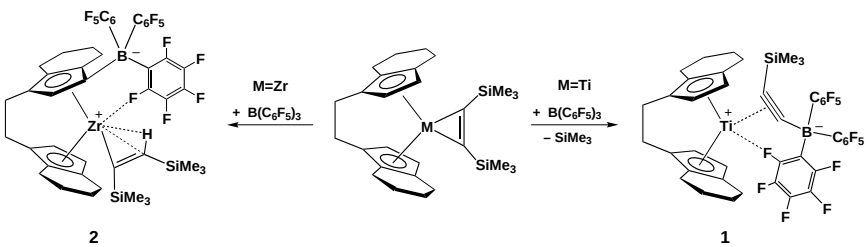

Stabilization by coordination: A long sought after intermediate is stabilized by complexation: $B(C_6F_5)_3$ reacts at a bis(trimethylsilyl)acetylene titanium complex with C–Si bond cleavage and B–C bond formation to give the coordinatively stabilized (trimethylsilyl)alkynylborane **1**. The reaction of the corresponding zirconium complex proceeds totally different giving the agostic complex **2**.

Olefin Polymerization Catalysts

P. Arndt, W. Baumann, A. Spannenberg, U. Rosenthal,* V. V. Burlakov, V. B. Shur ——— **1414 – 1418**

Reactions of Titanium and Zirconium Derivatives of Bis(trimethylsilyl)acetylene with Tris(pentafluorophenyl)borane: A Titanium(III) Complex of an Alkynylboranate

 © 2003 Wiley-VCH Verlag GmbH & Co. KGaA, Weinheim 1433-7851/03/4212-1327 $ 20.00+.50/0

Contents

High-Throughput Enzyme Assay

M. Konarzycka-Bessler, U. T. Bornscheuer* ——— **1418 – 1420**

A High-Throughput-Screening Method for Determining the Synthetic Activity of Hydrolases

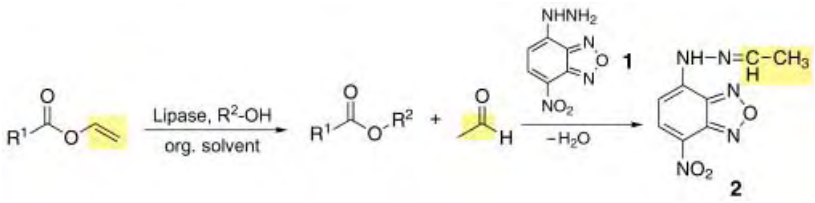

A glowing success in enzyme assay: The first high-throughput format for the determination of synthetic activity of lipases and esterases in organic solvents is described. Acetaldehyde released by enzyme-catalyzed esterification between a vinyl ester and an alcohol is derivatized in situ with a hydrazine **1** to give a highly fluorescent product **2**. Thus, active and stable enzymes can be easily identified in a microtiter plate format.

Communications labeled with this symbol have been judged by two referees as being "very important papers".

The publication of Communications labeled with this symbol has been accelerated because of their topical or highly competitive nature.

Supporting information for articles labeled with this symbol can be found at www.angewandte.org or www.interscience.wiley.com.

Looking for outstanding employees?

Do you need another expert for your excellent team?
... Chemists, PhD Students, Managers, Professors, Sales Representatives...

Place an advert in the printed version and have it made available online for 1 month, free of charge!

Angewandte Chemie International Edition
Advertising Sales Department: Marion Schulz
Phone: 0 62 01 - 60 65 65
Fax: 0 62 01 - 60 65 50
E-Mail: MSchulz@wiley-vch.de

Service

Keywords ——— ***1422***

Authors ——— ***1423***

Events ——— ***1426***

Vacancies ——— ***1339***

Preview ——— ***1425***

Corrigendum

In the Communication by **J.-M. Zen et al.** published in *Angew. Chem. Int. Ed.* **2003**, *5*, 577–579, the reduction of $[Ru(bpy)_3]^{3+}$ to $[Ru(bpy)_3]^{2+}$ in Scheme 1 (as well as in the graphical abstract) should be accompanied by an oxidation of $RSCH_3$ with H_2O_2 to $RSOCH_3$. There were also some ambiguities as to which isomer was used. The footnote to Table 1 should read: [a] +: presence, −: absence, [$RC_6H_4SCH_3$: R = H, *p*-$COCH_3$, *p*-OCH_3] = 17 mM of each separately, Entries 1–8 tested with $PhSCH_3$.

© 2003 Wiley-VCH Verlag GmbH & Co. KGaA, Weinheim

1433-7851/03/4212-1328 $ 20.00+.50/0

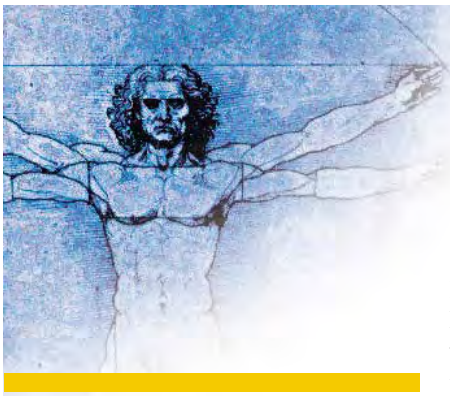

Advisory Board Member A. Fersht Knighted

Alan R. Fersht

Alan R. Fersht, member of the International Advisory Board of *Angewandte Chemie* and co-chairman of *ChemBioChem*'s Editorial Board with Nobel Prize winner Jean-Marie Lehn, was knighted for his scientific achievements by the British government because he "almost singlehandedly opened up the field of protein engineering."

Fersht read natural sciences in Cambridge (UK) and obtained a doctorate in physical organic chemistry under A. J. Kirby. After a post-doc time with W. P. Jenks 1968–69 in organic reaction mechanisms, he returned to a staff position at MRC Laboratory of Molecular Biology in Cambridge. Since then, he has devoted his research to studying problems at the interface of chemistry and biology by combining the techniques and philosophy of chemistry with those of molecular biology. From 1978 to 1988, he was a Royal Society Research Professor at Imperial College in London, and then again returned to Cambridge as a Herchel Smith Professor of Organic Chemistry and Director of the Centre for Protein Engineering.

The key experiments in protein engineering are associated with his name:

- the first systematic mutation of residues in a known structure to understand the principles of enzyme catalysis,
- the refinement of the tool for the analysis of protein activity and structure, and
- Φ-value analysis to monitor the pathway and stability of protein folding at near atomic resolution.

K. Müllen Recognized for Polymer Pigments

Klaus Müllen (Max Planck Institute for Polymer Research, Mainz, Germany) was awarded the Science Prize 2002 of the German Stifterverband (Donors' Association for the Promotion of the Sciences and Humanities). The prize is worth 50000 € and was presented for a successful combination of basic and applied research. Müllen was recognized for his research on pigments on the basis of perylene, terrylene, and perylene polymers which may be used in a variety of applications, such as flat-panel displays and bioassays. His recent Communication on "Shape-Persistent, Fluorescent Polyphenylene Dyads and a Triad for Efficient Vectorial Transduction of Excitation Energy" was featured on the cover of Issue 11/2002 of *Angewandte Chemie*.[1]

Klaus Müllen

Müllen received his doctorate in 1972 from the University of Basel for research on EPR spectroscopy of radical anions of twisted π systems with F. Gerson. He then moved to ETH Zurich to work on dynamic NMR spektroscopy and electrochemistry with J. F. M. Oth to obtain his habilitation in 1977. In 1979, he accepted a professorship for Organic Chemistry at the University of Cologne (Germany). In 1983, he was appointed full professor at the University of Mainz (Germany) and assumed his current position as a director at the MPI in 1989. The research of his group is devoted to new methods of polycondensation and polymers with high structural perfection, processability, and electric conductivity.

Müllen is a member of the editorial board of *European Journal of Organic Chemistry*.

Cover Picture of the Year 2002: And the Winners are...

... Georg Süss-Fink and co-workers (Neuchâtel, Switzerland) who submitted the cover picture of Issue 1 to emphasize supramolecular cluster catalysis, which is commonly regarded as a field lying at the interface of homogeneous and heterogeneous catalysis (artwork: T. Ward and C. Thomas). As an example, their Communication reports "[...] Benzene Hydrogenation Catalyzed by a Cationic Triruthenium Cluster under Biphasic Conditions."[2]

The covers of Issues 10 (Nicolaou/Corey, artwork: R. Echon, S. Snyder), 17 (Vollhardt), and 02 (Waldmann, artwork: P. Herter, G. Schulte) were also very popular among voters.

On the voters' side, the winner drawn among about 1500 participants is Stijn Wuyts, a PhD student at the Catholic University of Leuven, Belgium, who works on racemization reactions, dynamic kinetic resolution, heterogeneous catalysis, enzyme catalysis, and chirality under the supervision of Pierre Jacobs and Dirk De Vos. He will receive a copy of "World Records in Chemistry" by R. Faust et al.

Thank you very much to all participants and congratulations to the winners!

[1] T. Weil, E. Reuther, K. Müllen, *Angew. Chem.* **2002**, *114*, 1980; *Angew. Chem. Int. Ed.* **2002**, *41*, 1900.
[2] G. Süss-Fink, M. Faure, T. R. Ward, *Angew. Chem.* **2002**, *114*, 105; *Angew. Chem. Int. Ed.* **2002**, *41*, 99.

 © 2003 Wiley-VCH Verlag GmbH & Co. KGaA, Weinheim 1433-7851/03/4212-1330 $ 20.00+.50/0

Controlled Cycloadditions

Solvent-Controlled Selectivity in the Synthesis of Five-Membered Carbocycles from Carbene Complexes

*Florencio Zaragoza Dörwald**

Keywords:
carbene ligands · cyclization · cycloaddition · cyclopentenes · diene ligands · solvent effects

Substituted cyclopentanones are both important synthetic intermediates and key structural elements in various natural products, such as terpenes, steroids, and prostaglandins. Cyclopentanones and cyclopentenones have traditionally been prepared by Nazarov, Weiss, Pauson–Khand, or Dieckmann cyclizations or other, related intramolecular condensation reactions. Furthermore, a number of reagents have been described that enable the addition of a C_3 fragment to alkenes to yield five-membered carbocycles.[1]

In recent years new types of substituted cyclopentanones or cyclopentenones have become synthetically accessible by reactions involving Fischer-type carbene complexes, that is, carbene complexes of the type $[(CO)_5M{=}C(XR)R']$ (M = Cr, Mo, W; X = O, NR).[2] These reactions yield either cyclopentanones directly, or lead to the formation of the corresponding enol ethers (1-alkoxy cyclopentenes), which can readily be hydrolyzed to the corresponding cyclopentanones by treatment with aqueous acid. Most of the reported examples of the preparation of five-membered carbocycles from Fischer-type carbene complexes belong to one of the following three reaction types (Scheme 1): a) electrocyclizations of 1-metalla-1,3,5-trienes, which can be easily obtained from alkenyl carbene complexes and alkynes, followed by reductive elimination of the metal,[3] b) formation of ketenes by CO insertion in alkenyl carbene complexes, followed by intramolecular C-acylation,[3f,4] and c) metalla-Diels–Alder reaction of alkenyl carbene complexes with dienophiles, followed by reductive elimination of the metal.[5]

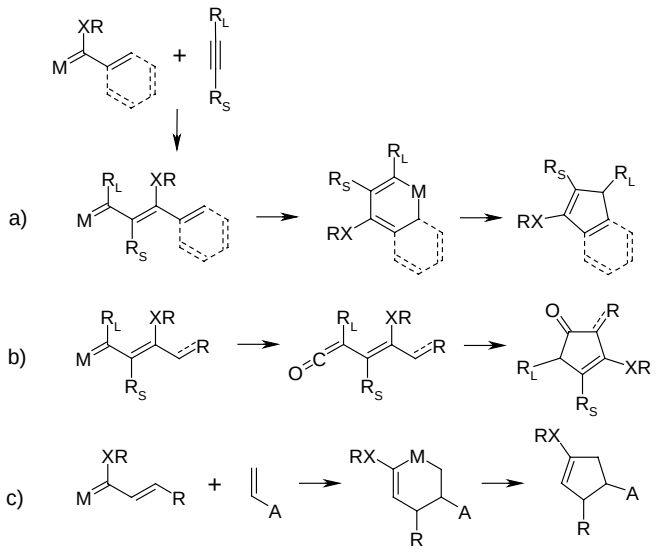

Scheme 1. Different reaction types for the synthesis of cyclopentanones from Fischer carbene complexes. X = O, NR; M: $(CO)_5Cr$, $(CO)_5Mo$, $(CO)_5W$; A = NR_2, CO_2R; R_L = larger group, R_S = smaller group.

Some further methods that do not belong to any of the types of reaction given above (Scheme 1) include the conversion of alkynes into cyclopentenones by treatment with alkoxy(cyclopropyl)carbene–Cr complexes,[6] and the preparation of substituted cyclopentadienes from enamines and alkoxy(alkynyl)carbene–W complexes.[7]

Unfortunately, the outcome of most of these reactions is highly dependent on the precise substitution pattern of the starting materials involved, on the type of solvent used, and on the reaction temperature chosen, and is not easy to predict. Moreover, many of the reactions reported until now lead to product mixtures, which has severely restricted the applicability of this chemistry to target-directed syntheses. This has also been the case for the reaction of alkenyl carbene complexes with 1,3-dienes, which can yield a broad spectrum of products (Scheme 2). The main types of product observed result from Diels–Alder reactions in which either the alkenyl group of the carbene complex acts as the dienophile to yield cyclohexenes **A**,[8] or in which the M=C double bond or one of the double bonds of the diene acts as a dienophile to yield metallacyclohexenes, and, after reductive elimination, cyclopentenes such as **B** and **C**.[9] Cyclopropanation of the diene, followed by a Cope rearrangement to yield cycloheptadienes **D** has also been reported.[9b,10]

[*] Dr. F. Zaragoza Dörwald
Medicinal Chemistry, Novo Nordisk A/S
Novo Nordisk Park, 2760 Måløv (Denmark)
Fax: (+45) 4466-3450
E-mail: flo@novonordisk.com

 © 2003 Wiley-VCH Verlag GmbH & Co. KGaA, Weinheim 1433-7851/03/4212-1332 $ 20.00+.50/0

From the results reported it seems that the outcome of these reactions depends to a large extent on the type of solvent chosen. Although significant solvent effects have been reported for the Dötz reaction,[11] only a few systematic studies concerning solvent effects in cyclopentannulations with Fischer-type carbene complexes have been undertaken.[3e,5c]

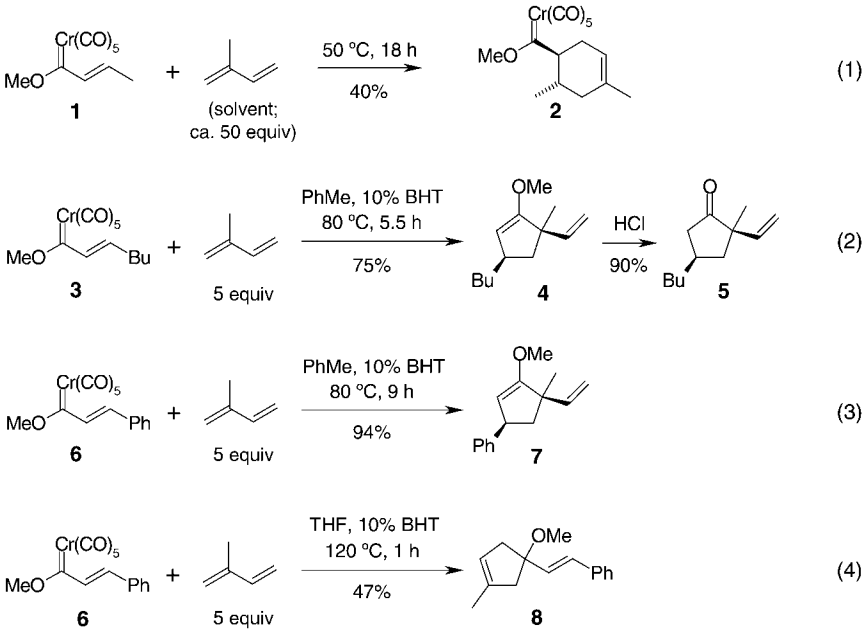

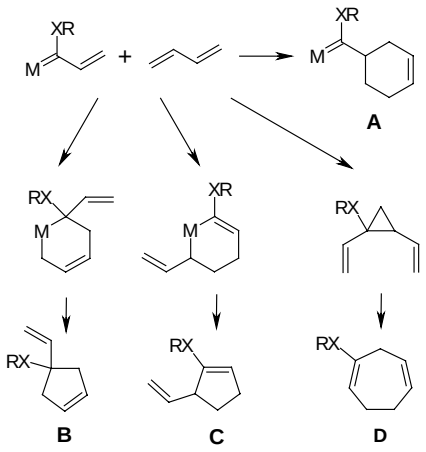

Scheme 2. Observed pathways for the reaction of alkenyl carbene complexes with 1,3-dienes. X = O, NR; M = $(CO)_5Cr$, $(CO)_5Mo$, $(CO)_5W$.

The strong influence of the solvent on reactions between alkenyl carbene complexes and 1,3-dienes is further illustrated by the recent work of the group of Barluenga,[12] who investigated the reactions of alkenyl carbene complexes with simple alkyl-substituted 1,3-butadienes. In contrast to earlier results reported by Wulff et al.,[8b] who found that alkenyl carbene complexes act as dienophiles when using the deoxygenated diene as solvent [Eq. (1)], Barluenga mainly obtained five-membered carbocycles when using toluene or THF as solvents together with the radical scavenger BHT (2,6-di-*tert*-butyl-4-methylphenol; [Eq. (2)–(4)]). Barluenga and co-workers were also able to control the outcome of the reaction by the choice of solvent and by varying the reaction temperature [Eq. (3) and (4)]. Interestingly, under optimized conditions the enol ethers (e.g. **4** and **7**) could be obtained in high yield and diastereoselectivity. Acid-catalyzed hydrolysis of these enol ethers cleanly yielded highly substituted cyclopentanones such as **5**. Only in the reaction of an alkenylcarbene–tungsten complex and 2,3-dimethyl-1,3-butadiene, did Barluenga observe in one instance the formation of small amounts of a cyclohexene derivative analogous to the products prepared by Wulff et al. [Eq. (1)].

The high diastereoselectivity with which enol ethers such as **4** and **7** are formed strongly points towards the mechanism outlined in Scheme 2 for the formation of enol ethers **C**, namely an *endo*-metalla-Diels–Alder reaction with inverse electron demand, followed by a reductive elimination of the metallic fragment in which the stereochemistry is conserved (Scheme 3).

Barluenga et al. also examined the reactions of enantiomerically pure 8-phenylmenthyloxy(alkenyl)carbene–Cr complexes with dienes, with the aim of preparing enantiomerically enriched cyclopentanones.[12] In the case of unsubstituted 1,3-butadiene the cycloaddition reaction proceeded with high diastereoselectivity (> 99 % *de*, Scheme 4), whereas somewhat lower stereocontrol was observed with isoprene as dienophile (74 % *de*). The resulting enol ethers could be cleanly hydrolyzed to cyclopentanones without racemization.

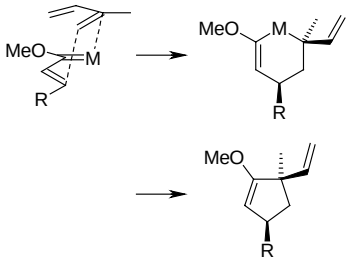

Scheme 3. Possible mechanism for the formation of enol ethers such as **7**. M = $(CO)_5Cr$, $(CO)_5W$.

The results presented above demonstrate that Fischer-type carbene complexes are useful intermediates for the stereoselective preparation of highly substituted cyclopentanones. As in the case of the Dötz reaction, the outcome of these reactions is critically dependent on the solvent and on the precise reaction conditions. The different outcomes of Equations (1) and (2), despite

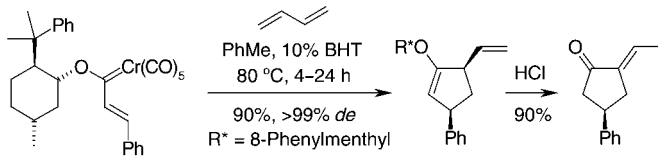

Scheme 4. Cycloaddition of an enantiomerically pure alkenyl carbene complex to 1,3-butadiene.[12]

 © 2003 Wiley-VCH Verlag GmbH & Co. KGaA, Weinheim 1433-7851/03/4212-1333 $ 20.00+.50/0

the almost identical starting materials and reaction conditions, is rather curious, and both reactions should be reexamined carefully to establish the crucial selectivity-controlling factors. A deeper understanding of the parameters that govern the outcome of these reactions will be necessary to enable a more accurate prediction of potential products and therewith the application of these elegant transformations to target-directed syntheses.

[1] a) B. M. Trost, *Angew. Chem.* **1986**, *98*, 1–20; *Angew. Chem. Int. Ed. Engl.* **1986**, *25*, 1–20; b) P. Beak, K. D. Wilson, *J. Org. Chem.* **1987**, *52*, 218–225; c) D. A. Singleton, B. E. Schulmeier, *J. Am. Chem. Soc.* **1999**, *121*, 9313–9317; B. M. Trost, J. R. Paquette, A. L. Marquart, *J. Am. Chem. Soc.* **1995**, *117*, 3284–3285.

[2] a) A. de Meijere, H. Schirmer, M. Duetsch, *Angew. Chem.* **2000**, *112*, 4124–4162; *Angew. Chem. Int. Ed.* **2000**, *39*, 3964–4002; b) F. Zaragoza Dörwald, *Metal Carbenes in Organic Synthesis*, Wiley-VCH, Weinheim, **1999**.

[3] a) K. H. Dötz, C. Christoffers, *Chem. Ber.* **1995**, *128*, 163–166; b) D. F. Harvey, E. M. Grenzer, *J. Org. Chem.* **1996**, *61*, 159–165; c) K. H. Dötz, T. O. Schäfer, K. Harms, *Synthesis* **1992**, 146–150; d) R. Aumann, B. Jasper, R. Fröhlich, *Organometallics* **1995**, *14*, 231–237; e) B. L. Flynn, F. J. Funke, C. C. Silveira, A. de Meijere, *Synlett* **1995**, 1007–1010; f) B. L. Flynn, H. Schirmer, M. Duetsch, A. de Meijere, *J. Org. Chem.* **2001**, *66*, 1747-1754; g) H. Schirmer, B. L. Flynn, A. de Meijere, *Tetrahedron* **2000**, *56*, 4977-4984.

[4] a) C. A. Challener, W. D. Wulff, B. A. Anderson, S. Chamberlin, K. L. Faron, O. K. Kim, C. K. Murray, Y. C. Xu, D. C. Yang, S. D. Darling, *J. Am. Chem. Soc.* **1993**, *115*, 1359–1376; b) B. L. Flynn, C. C. Silveira, A. de Meijere, *Synlett* **1995**, 812–814;c) B. L. Flynn, F. J. Funke, M. Noltemeyer, A. de Meijere, *Tetrahedron* **1995**, *51*, 11141-11148..

[5] a) J. Barluenga, M. Tomás, A. Ballesteros, J. Santamaria, C. Brillet, S. García-Granda, A. Pinera-Nicolas, J. T. Vazquez, *J. Am. Chem. Soc.* **1999**, *121*, 4516–4517; b) J. Barluenga, M. Tomás, A. L. Suárez-Sobrino, *Synthesis* **2000**, 935–940; c) M. Hoffmann, H.-U. Reissig, *Synlett* **1995**, 625–627; d) A. Wienand, H.-U. Reissig, *Chem. Ber.* **1991**, *124*, 957–965.

[6] a) J. W. Herndon, S. U. Tumer, W. F. K. Schnatter, *J. Am. Chem. Soc.* **1988**, *110*, 3334–3335; b) S. U. Tumer, J. W. Herndon, L. A. McMullen, *J. Am. Chem. Soc.* **1992**, *114*, 8394–8404; c) J. W. Herndon, J. Zhu, D. Sampedro, *Tetrahedron* **2000**, *56*, 4985–4993.

[7] R. Aumann, A. G. Meyer, R. Fröhlich, *Organometallics* **1996**, *15*, 5018–5027.

[8] a) J. Barluenga, F. Aznar, A. Martín, S. Barluenga, *Tetrahedron* **1997**, *53*, 9323–9340; b) W. D. Wulff, W. E. Bauta, R. W. Kaesler, P. J. Lankford, R. A. Miller, C. K. Murray, D. C. Yang, *J. Am. Chem. Soc.* **1990**, *112*, 3642–3659; c) J. Christoffers, K. H. Dötz, *Chem. Ber.* **1995**, *128*, 157–161; d) B. A. Anderson, W. D. Wulff, T. S. Powers, S. Tribbitt, A. L. Rheingold, *J. Am. Chem. Soc.* **1992**, *114*, 10784–10798; e) T. S. Powers, W. Jiang, J. Su, W. D. Wulff, *J. Am. Chem. Soc.* **1997**, *119*, 6438–6439.

[9] a) M. Hoffmann, M. Buchert, H.-U. Reissig, *Angew. Chem.* **1997**, *109*, 281–283; *Angew. Chem. Int. Ed. Engl.* **1997**, *36*, 283–285; b) M. Hoffmann, M. Buchert, H.-U. Reissig, *Chem. Eur. J.* **1999**, *5*, 876–882.

[10] a) J. Barluenga, F. Aznar, A. Martín, J. T. Vázquez, *J. Am. Chem. Soc.* **1995**, *117*, 9419–9426; b) J. Barluenga, F. Aznar, M. Fernández, *Chem. Eur. J.* **1997**, *3*, 1629–1637; c) D. F. Harvey, E. M. Grenzer, P. K. Gantzel, *J. Am. Chem. Soc.* **1994**, *116*, 6719–6732; d) J. Barluenga, F. Aznar, C. Valdés, A. Martín, S. García-Granda, E. Martín, *J. Am. Chem. Soc.* **1993**, *115*, 4403–4404; e) J. Barluenga, F. Aznar, A. Martín, *Organometallics* **1995**, *14*, 1429–1433.

[11] a) W. D. Wulff, B. M. Bax, T. A. Brandvold, K. S. Chan, A. M. Gilbert, R. P. Hsung, J. Mitchell, J. Clardy, *Organometallics* **1994**, *13*, 102–126; b) K. S. Chan, G. A. Peterson, T. A. Brandvold, K. L. Faron, C. A. Challener, C. Hyldahl, W. D. Wulff, *J. Organomet. Chem.* **1987**, *334*, 9–56; c) M. E. Bos, W. D. Wulff, R. A. Miller, S. Chamberlin, T. A. Brandvold, *J. Am. Chem. Soc.* **1991**, *113*, 9293–9319.

[12] J. Barluenga, S. López, J. Flórez, *Angew. Chem.* **2003**, *115*, 241–243; *Angew. Chem. Int. Ed.* **2003**, *42*, 231–233.

Agostic Interactions

Complexation of Si–Si σ Bonds to Metals**

*Georgii I. Nikonov**

Keywords:
agostic interactions · bond theory · density functional calculations · electronic structure · Si ligands

Transition-metal-mediated X–Y σ-bond-breaking and bond-formation reactions (X and Y = group 3–6 elements, Scheme 1) are among the current highlights of organometallic chemistry.[1] It is

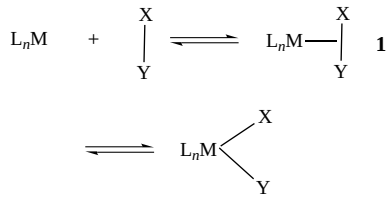

Scheme 1. Reversible behavior of transition metal X–Y σ complexes.

generally assumed that these reactions occur through formation of the intermediate X–Y σ complexes **1**, and therefore the study of such species might allow an insight into the bond formation/rupture processes within the coordination sphere of a transition metal.[2] Much of the work has been carried out with complexes that have at least one hydrogen atom (X = H), which provokes questions regarding whether the isolation of "hydrogen-free" X–Y σ complexes is achievable.[2b] The unique propensity of hydrogen to participate in the complexation of σ bonds is attributed to the spherical symmetry of its 1s orbital, whereas for other elements complexation of an X–Y σ bond composed of highly directed sp^x-hybridized orbitals would require a substantial reorganization energy.[1b] This simple argument suggests that the best candidates for σ-bond complexation are heavy elements of groups 3–6, as a result of the more diffuse nature and steric accessibility of their σ bonds.

Surprisingly, the first evidence for "hydrogen-free" σ-bond complexation was observed with the small and relatively rigid carbon atom. It has been reported recently that the long-known β-agostic C–H bonding motif is not derived from C–H→M electron donation, but rather from a M···C$_\beta$ interaction with a metal.[3] In addition, the weak complexation of a C–C bond to a metal atom has been proposed for a Ti complex.[4] Very recently, agostic C–C interactions have been discovered in a rhodium complex,[5] where the effect is promoted by steric strain, and there have also been reports regarding the occurrence of agostic C–Si bonds.[6] Although providing some hope, these earlier studies were inconclusive as to whether a genuinely hydrogen-free σ complex was possible. It was perhaps not surprising that a breakthrough came from the field of transition-metal silicon chemistry, as the Si–Si bond is much weaker and more accessible than the C–C bond.

In 2001, the research group of Tanaka reported that the 1,2-disilylbenzene **2** reacts with [Ni(dmpe)$_2$] (dmpe = 1,2-bis(dimethylphosphanyl)ethane) to give the dimeric bis(silyl)nickel(II) complex **3**, which upon heating at 110 °C rear-

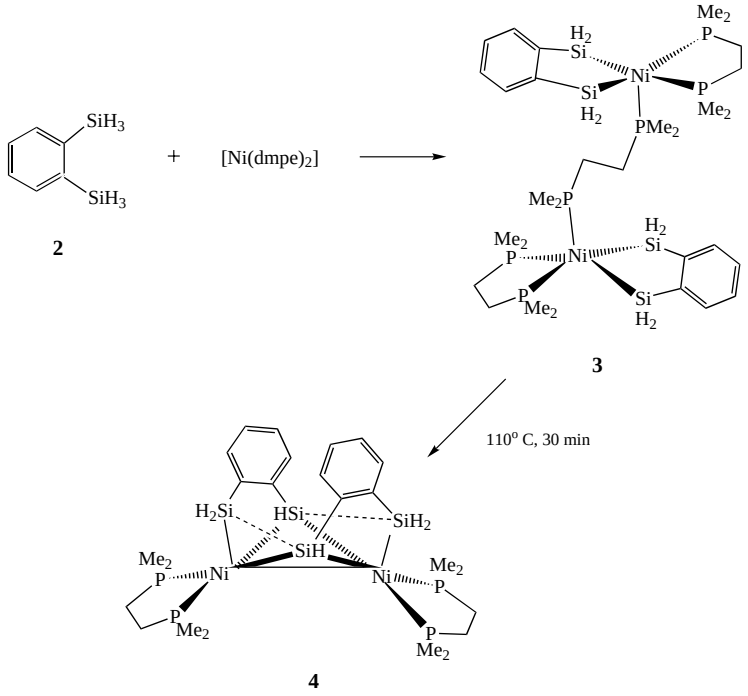

Scheme 2. Reaction of 1,2-didilylbenzene with [Ni(dmpe)$_2$] and subsequent formation of bridged Ni dimer **4**.

[*] Dr. G. I. Nikonov
Department of Chemistry
Moscow State University
Vorob'evy Gory, 119899, Moscow (Russia)
Fax: (+7) 094-932-88-46
E-mail: nikonov@org.chem.msu.su

[**] Financial support from the Russian Fund for Basic Research is gratefully acknowledged.

 © 2003 Wiley-VCH Verlag GmbH & Co. KGaA, Weinheim 1433-7851/03/4212-1335 $ 20.00+.50/0

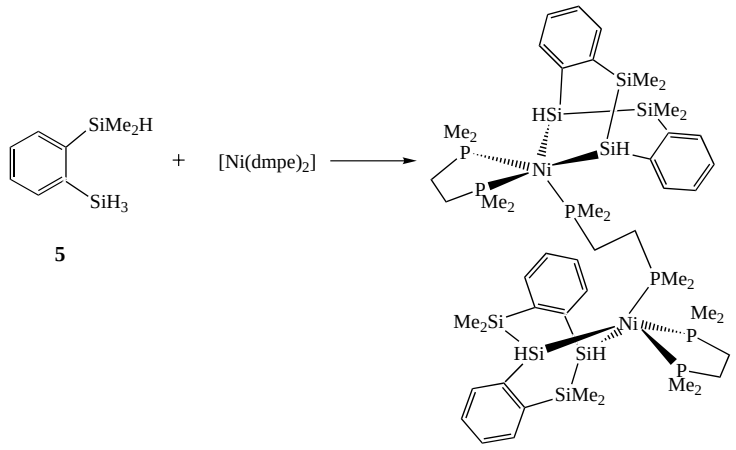

5 **6**

Scheme 3. Reaction of 1-(dimethylsilyl)-2-silylbenzene with [Ni(dmpe)$_2$].

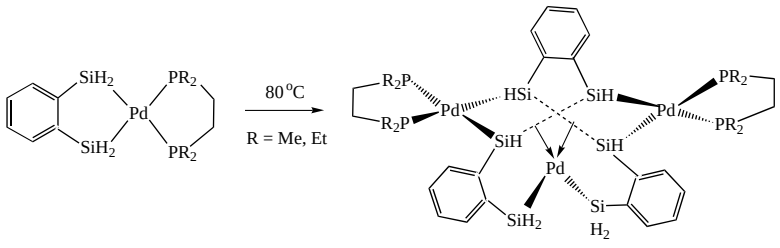

7 **8**

Scheme 4. Formation of the first genuine Si–Si σ complex.

ranges to give the bis(silylene)-bridged Ni^{III} dimer **4** (Scheme 2).[7] A related complex, in which the dmpe ligand was replaced by depe, has also been prepared (depe = 1,2-bis(diethylphosphanyl)ethane).[7] The molecular structure of compound **4** is unusual in that there are short contacts of 2.693(2) and 2.685(1) Å between the silyl and silylene ligands, which compare quite favorably with the length of the longest Si–Si single bonds, and are suggestive of the possibility of a Si–Si interaction.[7] This structure can be viewed either as a stretched Si–Si σ complex of a formal nickel(I) center, or alternatively as having an incipient Si–Si bond on a nickel(III) center. This formulation is further supported by the observation that a closely related reaction of the 1-(dimethylsilyl)-2-silylbenzene **5** with [Ni(dmpe)$_2$] does give the coupled Si–Si-bonded product **6** (Scheme 3).[7]

These fascinating findings have recently been followed by the preparation of the first genuine Si–Si σ complexes. Tanaka and co-workers reported that heating the mononuclear bis(silyl)palladium complex **7** at 80 °C yields a unique tripalladium complex **8**, the central core of which has six silicon atoms in the coordination sphere of the central palladium ion (Scheme 4).[8] This unusual coordination environment was interpreted as being representative of a formal Pd^{VI} complex, an unprecedented oxidation state for palladium,[9] particularly when considering that the metal is ligated by electron-donating silyl ligands rather than electron-withdrawing groups, such as fluorides or oxides, which are more suitable for the stabilization of higher oxidation states. The peripheral bis(silyl) moieties of **8** have Pd^{II} ions at their centers. Several structural features suggested an alternative description of the bonding in **8** [8] in terms of the complexation of two Si–Si σ bonds to the central Pd ion, thus retaining the common Pd^{II} oxidation state. First, the geometry around the central Pd ion is highly distorted, and might be better described as square-planar, if one thinks of the Pd ion interacting with the centers of the two pairs of silylene groups (that is, with Si–Si bonds). Second, the lengths of the Si–Si interactions are very small (2.539(4) Å), even shorter than in the nickel complex **3**, which suggests bonding interactions are involved. Third, the silylene ligands form normal Pd–Si bonds (av. 2.388(3) Å) to the peripheral metal ions but elongated bonds (2.483(3) Å) to the central palladium ion, which is in accordance with the description of **8** as being a bis σ complex.

Both possible formulations of complex **8** (Pd^{VI} versus a Pd^{II} Si–Si σ complex) were unprecedented.[9] The uncertainty in the assignment of bonding modes and a formal oxidation state have now been resolved by two independent DFT studies by the research groups of Alvarez[10] and Cramer.[11] In addition to the structural data listed above, the arguments based on aspects of symmetry (closer to square-planar than octahedral geometry), considerations of possible spin states (diamagnetic Pd^{II} versus paramagnetic Pd^{VI}), calculation of bond orders (high values for the Si–Si contacts), and orbital structure considerations conclusively establish the correct structure of **8** as a bis Si–Si σ complex. This discovery further supports the analogous formulation of the nickel complex **4**, and thus provides a link between Si–Si σ-bond complexation (static form) and the Si–Si σ bond-formation reaction (dynamic form) discussed above.

In both **4** and **8**, the complexation of the Si–Si σ bond to the metal must be supported to some extent by the chelate effect as additional bonding from the ligands to the metal is evident. In contrast, this additional bonding is absent in the niobocene complex **9**, which

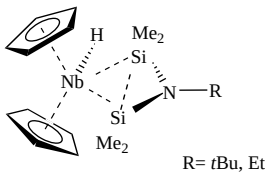

9

also exhibits a number of unusual structural features that suggest its formulation as a Si–Si σ complex.[12] First of all, there are no expected central and lateral silyl groups in the formal trisubstituted

 © 2003 Wiley-VCH Verlag GmbH & Co. KGaA, Weinheim 1433-7851/03/4212-1336 $ 20.00+.50/0

metallocene complex, rather the $\{(SiMe_2)_2NtBu\}$ fragment, as a single unit, is shifted to the central position. Second, the Si–Si contact of 2.654(2) Å is short, in comparison with the values found in complex **4**. Third, as in complex **8**, the Nb–Si bonds are unexpectedly long (2.680(2) and 2.685(1) Å), and are longer than typical Nb–Si bonds in trialkylsilyl derivatives (av. 2.65 Å); however, shorter Nb–Si bonds resulting from the presence of nitrogen substituents on the silicon centers were expected. Fourth, the ^{1}H NMR signal of the hydride ligand was found at surprisingly high field ($\delta = -7.79$ ppm), which is far distant from the normal d^0 trisubstituted niobocene range ($\delta = -2$ to -5 ppm) but typical for d^2 Nb^{III} hydrides, and suggests the presence of partial d^n ($0 < n < 2$) character. Finally, the presence of a direct Si–Si interaction in **9** follows from calculation of a high value for the Wiberg bond index (0.21) and NBO bond order (0.33). These values are comparable with the corresponding parameters found for the Nb–H bond, and are no less than half of those for Nb–Si bonds. These unusual features of **9** are apparently caused by the presence of the nitrogen bridge between the two silyl groups, which distorts the Si–Si bond and prevents effective back-donation from the metal to the (Si–Si)* antibonding orbital, thus leading to some residual Si–Si bonding.[12]

These recent results suggest that the complexation of other "hydrogen-free" X–Y σ bonds to metals is possible. Studying this phenomenon is a fascinating and rewarding field of research which, as the formation of complex **6** shows, exhibits not only a distinct theoretical importance, but also has a strong relevance towards transition-metal-mediated transformations of organic molecules.

[1] a) M. Suginome, Y. Ito, *J. Chem. Soc. Dalton Trans.* **1998**, 1925; b) U. Schubert, *Angew. Chem.* **1994**, *106*, 435; *Angew. Chem. Int. Ed. Engl.* **1994**, *33*, 419.c) H. K. Sharma, K. H. Pannell, *Chem. Rev.* **1995**, *95*, 1351.

[2] a) G. J. Kubas, *Metal Dihydrogen and σ-Bond Complexes*, Kluwer Academic/Plenum, New York, **2001**; b) R. H. Crabtree, *Angew. Chem.* **1993**, *105*, 805; *Angew. Chem. Int. Ed. Engl.* **1993**, *32*, 789; c) U. Schubert, *Adv. Organomet. Chem.* **1990**, *30*, 151; d) J. Y. Corey, J. Braddock-Wilking, *Chem. Rev.* **1999**, *99*, 175; e) G. I. Nikonov, *J. Organomet. Chem.* **2001**, *635*, 24; f) G. I. Nikonov, *Angew. Chem.* **2001**, *113*, 3457; *Angew. Chem. Int. Ed.* **2001**, *40*, 3353; g) Z. Lin, *Chem. Soc. Rev.* **2002**, *31*, 239.

[3] A. Haaland, W. Scherer, K. Ruud, G. S. McGrady, A. J. Downs, O. Swang, *J. Am. Chem. Soc.* **1998**, *120*, 3762.

[4] R. Tomaszewski, I. Hyla-Krypsin, C. L. Mayne, A. M. Arif, R. Gleiter, R. Ernst, *J. Am. Chem. Soc.* **1998**, *120*, 2959.

[5] B. Rybtchinski, S. Oevers, M. Montag, A. Vigalok, H. Rozenberg, J. M. L. Martin, D. Milstein, *J. Am. Chem. Soc.* **2001**, *123*, 9064, and references therein.

[6] a) W. T. Klooster, L. Brammer, C. J. Scharverien, P. H. M. Budzelaar, *J. Am. Chem. Soc.* **1999**, *121*, 1381; b) C. Qian, W. Nie, Y. Chen, J. Sun, *J. Organomet. Chem.* **2002**, *645*, 82.

[7] S. Shimada, M. L. N. Rao, T. Hayashi, M. Tanaka, *Angew. Chem.* **2001**, *113*, 219; *Angew. Chem. Int. Ed.* **2001**, *40*, 213.

[8] W. Chen, S. Shimada, M. Tanaka, *Science* **2002**, *295*, 308.

[9] R. H. Crabtree, *Science* **2002**, *295*, 288.

[10] G. Aullon, A. Lledos, S. Alvarez, *Angew. Chem.* **2002**, *114*, 2036; *Angew. Chem. Int. Ed.* **2002**, *41*, 1956.

[11] E. C. Scherer, C. R. Kinsinger, B. L. Kormos, J. D. Thompson, C. J. Cramer, *Angew. Chem.* **2002**, *114*, 2033; *Angew. Chem. Int. Ed.* **2002**, *41*, 1953.

[12] G. I. Nikonov, S. F. Vyboishchikov, L. G. Kuzmina, J. A. K. Howard, *Chem. Commun.* **2002**, 568.

 © 2003 Wiley-VCH Verlag GmbH & Co. KGaA, Weinheim 1433-7851/03/4212-1337 $ 20.00+.50/0

Rare-Earth Elements

Unusual Complex Chemistry of Rare-Earth Elements: Large Ionic Radii—Small Coordination Numbers

Kurt Dehnicke and Andreas Greiner*

Keywords:
coordination chemistry · ligand effects · N ligands · polymerization · rare-earth elements

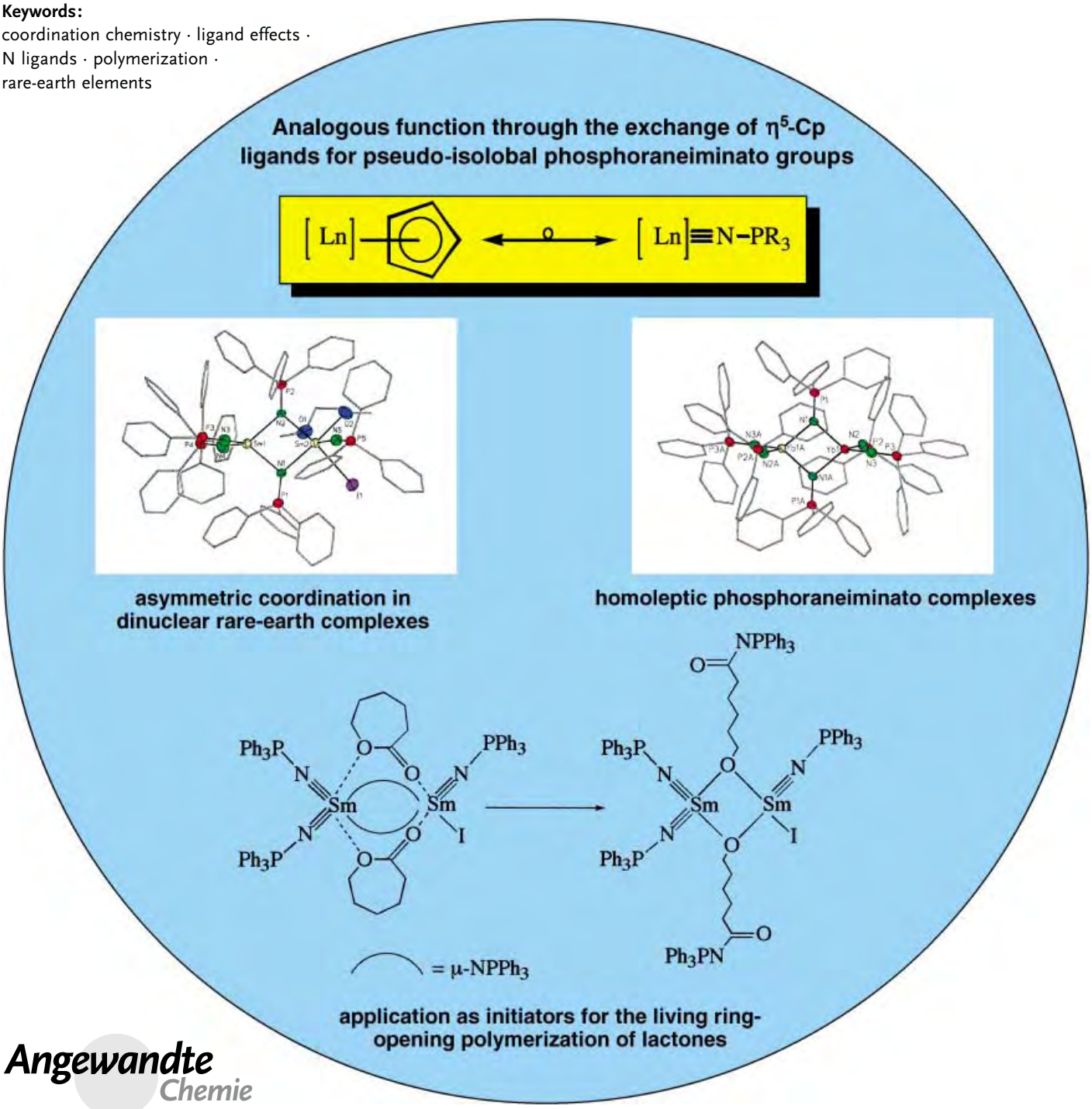

 © 2003 Wiley-VCH Verlag GmbH & Co. KGaA, Weinheim 1433-7851/03/4212-1340 $ 20.00+.50/0

Because of their large ionic radii and relatively low oxidation states rare-earth elements generally form complexes which have high coordination numbers and weak metal–ligand bonds. They are often not suitable for homogeneous catalysis on account of their instability of configuration in solution. Complexes of the corresponding metal atoms with low coordination numbers may be an improvement. This type of complex can be obtained in the classical way by the introduction of bulky ligands, and recently, they were also prepared in reactions with ligand groups which offer remarkable metal–ligand bond features. This concept is demonstrated for complexes with bulky bis(trimethylsilyl)amido ligands $\{N(SiMe_3)_2\}^-$ and "slim" phosphoraneiminato ligands (NPR_3^-). Their suitability as catalysts for the ring-opening polymerization of lactones is reported as well.

From the Contents

1. Introduction 1341

2. Complexes of Rare-Earth Ions Ln^{3+} with Low Coordination Numbers 1341

3. Outlook 1351

1. Introduction

Rare-earth elements, which in addition to the lanthanoides (Ln) cerium to lutetium (f-electron number 1–14), include scandium, yttrium, and lanthanum, in general realize large coordination numbers (CNs) in their complex chemistry because of their large ionic radii. Typically transition-metal and main-group elements have coordination numbers 2–6, while rare-earth metals have CNs > 6. The resulting coordination polyhedra include trigonal prisms (CN = 6) or its variation by stepwise capping of the prism face up to CN = 9. In addition, square antiprisms (CN = 8) and dodecahedra (CN = 12) are also known, as well as complexes with CN = 16. Table 1 shows the effective ionic radii of the rare-earth elements for trivalent metal ions as obtained by Shannon[1] as well as selected main-group elements with CN = 6. As shown, even scandium, the smallest rare-earth element, has a larger ionic radius than gallium, which is positioned ten units higher in the Periodic Table of Elements. Nearly all other rare-earth metal ions show ionic radii larger than Tl^{3+}. The resulting large coordination numbers lead, depending on the ionic radius of the central ion, to long and therefore unstable metal–ligand bonds. As the contribution of the 4f-electrons to stabilization of the ligand field is small, structural transformation in solution is possible, for example, octahedral → trigonal prism. Therefore complexes of this type are too unspecific for homogeneous catalysis.

Table 1: Effective ionic radii [pm] of 3+ metal ions for CN = 6 according to Shannon.[1]

Sc^{3+}	88.5			Al^{3+}	67.5
Y^{3+}	104			Ga^{3+}	76.0
La^{3+}	117.2	Ce^{3+} 115	Lu^{3+} 100	In^{3+}	94.0
				Tl^{3+}	102.5

Table 2 shows examples of rare-earth elements with coordination numbers 3–16. Coordination number 3 is realized only under extreme conditions, for example, in the trichloride or tribromide species at high temperatures in the gas phase.[2,3] Compounds with very bulky ligands also show CN 3, for example, with the isoelectronic groups, $[N(SiMe_3)_2]^-$ and $[CH(SiMe_3)_2]^-$.[4,5] The conditions required for compounds with CN = 4 are similar, as seen in trihalides, such as $(ErBr_3)_2$, which is in equilibrium with monomeric $ErBr_3$ at high temperatures in the gas phase.[3] Recently, CN = 4 was noticed in $[\{Y[P(SiMe_3)_2]_3\}_2]$,[7] a phosphido complex that is stable at room temperature. The yttrium atoms achieve the low coordination numbers with phosphorus atoms, which are about the same size as chloro ligands, through the steric bulk of the $SiMe_3$ (TMS) groups. CN = 4 complexes of the type $[Ln(CMe_3)_4]^-$,[6] with voluminous *tert*-butyl ligands, are also known, whereas the methyl ligands in $[LnMe_6]^{3-}$ ions lead to octahedral coordination.[10] Coordination numbers 8 and 9 are found in crystalline trihalides, which form bi- and tricapped trigonal-prismatic coordination polyhedra.[14,15] Larger coordination numbers are realized in nitrato complexes in which the NO_3^- ion functions as a chelate ligand.[16,17,19,20] Rare-earth arene complexes are characterized by large coordination numbers as shown by complexes formed with η^5-bonded cyclopentadienyl ligands[21] and η^8-bonded cyclooctadienyl ligands.[22] Similar coordination chemistry is reported for trivalent bismuth species. Its effective ionic radius for hexacoordination (117 pm) is equivalent to that of the La^{3+} ion and since the s-electron pair of the Bi^{3+} ion is usually steric ineffective the analogous complexes of bismuth are often enlisted for comparison purposes.

2. Complexes of Rare-Earth Ions Ln^{3+} with Low Coordination Numbers

The interest in development of rare-earth element complexes, which have a stable configuration, is based not just on their attractive coordination and bonding modes but more importantly on their application in homogeneous catalysis. Several groups have generated divalent, tetradentate, rigid ligands, which are able to form highly asymmetric complex

[*] Prof. Dr. K. Dehnicke, Prof. Dr. A. Greiner
Fachbereich Chemie
Philipps-Universität Marburg
Hans-Meerwein-Strasse, 35032 Marburg (Germany)
Fax: (+49) 6421-282-5653
E-mail: greiner@mailer.uni-marburg.de

 © 2003 Wiley-VCH Verlag GmbH & Co. KGaA, Weinheim 1433-7851/03/4212-1341 $ 20.00+.50/0

Table 2: Selected complexes of lanthanides for 3+ central ions.

Complex	CN	Coordination polyhedra	Ref.
$[ErCl_3]$	3	pyramidal, gas phase	[2]
$[ErBr_3]$	3	planar, gas phase 1095 K	[3]
$[Ln\{N(SiMe_3)_2\}_3]$	3	pyramidal	[4]
$[La\{CH(SiMe_3)_2\}_3]$	3	pyramidal, agostic βSiC···LaH interactions	[5]
$[(ErBr_3)_2]$	4	tetrahedral, gas phase 1095 K, equilibrium with $ErBr_3$	[3]
$[Lu(CMe_3)_4]^-$	4	tetrahedral	[6]
$[\{Y[P(SiMe_3)_2]_3\}_2]$	4	tetrahedral	[7]
$[Ln(CH_2SiMe_3)_3(thf)_2]$ (Ln = Sc, Y, Er, Tm, Yb, Lu)	5	trigonal bipyramidal, thf in axial positions	[8]
[Sm(Schiff Base O,O′-N,N′) $\{N(SiMe_3)_2\}$]	5	tetragonal-bipyramidal	[9]
$[HoMe_6]^{3-}$	6	octahedral	[10]
ScF_3	6	octahedral, ReO_3 variation	[11]
$[Gd_2Br_4(\mu\text{-}NHPh)_2(thf)_5]$	6 and 7	octahedral and pentagonal-bipyramidal; Br atoms in apical positions	[12]
$[EuCl_3(thf)_4]$	7	pentagonal-bipyramidal; two Cl atoms in apical positions	[13]
LaI_3	8	$PuBr_3$ type; layered structure	[14]
$LaCl_3$, $LaBr_3$	9	VCl_3 type; tricapped trigonal prism	[15]
$[La(NO_3)_3(bipy)_2]$	10	irregular polyhedra	[16]
$[Sm\{2.2.2\}crypt(NO_3)]^{2+}$ $[Sm(NO_3)_5(H_2O)]^{2-}$	10 and 12	cation distorted antiprism, capped with two N atoms; complex anion	[17]
LaF_3	11 (7+2+2)	trigonal prism, all-planes capped	[18]
$[Gd(NO_3)_2(18C\text{-}6)]_3$ $[Gd(NO_3)_6]$	10 and 12	polyhedra complex	[19]
$[(C_4H_9)_3NH]_3[La(NO_3)_6]$	12	icosahedral with O_2N planes tilted towards each other	[20]
$[\{(\eta^5\text{-}C_5H_5)_2Sc(\mu\text{-}Cl)\}_2]$	12	pseudo-tetrahedral with centroid Sc-Cp bonding	[21]
$[Li(thf)_4][Ce(\eta^8\text{-}C_8H_8)_2]$	16	D_{8h} symmetry of the anion	[23]

fragments $\{L_4Ln\}^+$ that are considered to be stable catalysts.[19,23–26] Rare-earth complexes do not only catalyze olefin polymerization but also ring-opening polymerization (ROP) of lactones, such as ε-caprolactone and lactides.[27,28] To achieve consistent molecular weights (M_w) the catalyst complexes have to have a highly stable configuration as well as allowing the primary step in Lewis acid–base attack. Rare-earth complexes possessing central ions with low coordination numbers are ideal for this purpose.

In the following we describe two different ways to prepare complexes showing these properties. The first and classical way is to use bulky ligand groups with low charge. In addition to saturating the three charges of the Ln^{3+} ion these ligands provide a substantial steric shielding effect. The bis(trimethylsilyl)amido $[N(SiMe_3)_2]^-$ ligand was found to be acceptable.

The second way makes use of the far more slender phosphoraneiminato ligand $[NPR_3]^-$ which has a single negative charge, like the amido ligand, but the physical shielding effect for the rare-earth central ion is based on the special features of the Ln–N bonds. Complexes of this type are able to support the primary step of the coordination of polymerizable monomers.

2.1 Low Coordination Numbers as a Result of Bulky Ligands

Amido ligands with large organic groups, such as the *tert*-butyl ligand in $[Ln(CMe_3)_4]^-$, are useful for the synthesis of rare-earth complexes with low coordination numbers. Complexes with bis(trimethylsilyl)amido groups are well stud-

Kurt Dehnicke was born 1931 in Köln. He studied chemistry in Leipzig and Stuttgart, where he was awarded a PhD in 1957 for work with Professor Josef Goubeau. He habilitated in Stuttgart and then became professor of inorganic chemistry at the Philipps-Universität Marburg. His main scope of work is the chemistry of halideazides, and of nitrido, phosphoraneiminato and polychalcogenide complexes of main-group and transition-metal elements. In 1989 he received the Wilhelm-Klemm Award of the Gesellschaft Deutscher Chemiker.

Andreas Greiner was born 1959 in Hanau. He studied chemistry in Marburg, where he was awarded a PhD 1988 for work carried out with Professor Walter Heitz. After a postdoc in 1989 at the University of California, Santa Barbara he habilitated in 1995 in Marburg and was appointed in 1999 associate professor for organic chemistry and macromolecular chemistry at the Johannes Gutenberg University of Mainz. In 2000 he was appointed full professor for macromolecular chemistry and technology at the Philipps-University of Marburg. His main research interests are in the field of metal-catalyzed polymerizations and polycondensations, polymers by vapor-phase deposition, functional polymers for optical, electronic, and medical applications and nano structured polymeric materials (e.g. polymer fibers and polymer tubes). 2001 he received the Arthur K. Dolittle Award of the ACS PMSE division and in 2002 he was the Steinhofer Lecturer at the University of Freiburg.

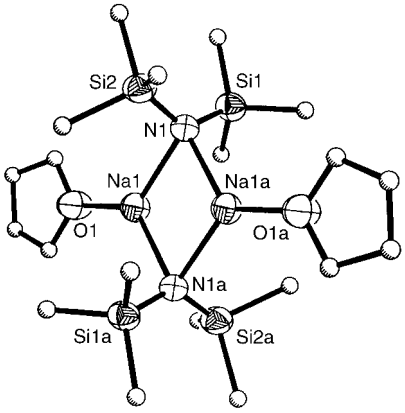

1

Figure 1. Structure of $[\{NaN(SiMe_3)_2(thf)\}_2]$ (**1**).

ied.[29] The bulkiness of such species is revealed in the crystal structure of the THF-solvated sodium derivative **1** (Figure 1), a species which is often used as a synthetic reagent.[30]

The sodium ions have the extremely low coordination number of 3. Reactions with anhydrous trihalides of rare-earth elements LnX_3 (X = Cl, Br)[31] or with triflates $Ln(OTf)_3$[9] yielded monomeric trisamides **2**, which crystallize without any solvent [Eq. (1)].

$$LnCl_3 + 3\,NaN(SiMe_3)_2 \cdot THF \rightarrow [Ln\{N(SiMe_3)_3\}] + 3\,NaCl + 3\,THF \quad (1)$$

2

All the crystal structures of the trisamides of rare-earth elements **2** show trigonal pyramidal coordination[4,32,33] unlike the trisamides of transition-metal complexes of this type which are exclusively trigonal planar. Figure 2 shows the recently obtained structure of the ytterbium complex $[Yb\{N(SiMe_3)_2\}_3]$.[33]

In all cases the rare-earth atom is disordered along the threefold symmetry axis in two positions each with an occupation factor of 0.5. The reason for the formation of the pyramidal shape is still uncertain.[34,35] After the influence of stereochemically active nonbonding electrons as well as charge-induced dipole interactions was shown not to be significant the markedly short intraatomic Ln···Si distances were discussed.[32] The crystal-structure analysis of $[Yb\{N(SiMe_3)_2\}_3]$[33] shows three strikingly short Yb···C separations of 297.6(6) pm to one carbon atom of each of the three bis(trimethylsilyl)amido ligands. At the same time the torsion angle Yb-N-Si-C of 2.6° is small and the Yb-N-Si bonding angle of 107.4(1)° for the participating groups is correspondingly narrow. Nevertheless, a decision about the existence of a Yb···β_{SiC} or a Yb···γ_{CH} interaction is still not possible.[33] However, such agostic interactions would agree with a (3+3) coordination at the lanthanoid atoms, as found in analogous complexes of $[Ln\{CH(SiMe_3)_2\}_3]$ which contain agostic interactions.[5]

Neutron-diffraction analysis of $[Cp^*La\{CH(SiMe_3)_2\}_2]$ ($Cp^* = C_5Me_5$) at 15 K showed that agostic β_{SiC} interactions dominate at the lanthanum atom whereas γ_{CH}···La bonds are precluded; La···C separations are 296.4(8) and 297.3(9) pm.[36]

From the pyramidal structure of rare-earth trisamide compounds the metal atoms would be expected to show Lewis acidity. However, it is not possible to obtain an "ate" complex $[Ln\{N(SiMe_3)_2\}_4]^-$ by introducing a fourth amido ligand. Only partial substitution of $[N(SiMe_3)_2]^-$ ligands for slender $[NPh_2]^-$ ligands yields ate complexes of the type $[Ln(NPh_2)_2\{N(SiMe_3)_2\}_2]^-$ (see below). In contrast to more slender Lewis bases, rare-earth trisamide compounds are capable of generating stable donor–acceptor complexes. The contact ion pair $[(thf)_3LiClY\{N(SiMe_3)_2\}_3]$ with a linear Li-Cl-Y axis was prepared in THF by addition of solvated lithium chloride to the trisamide of yttrium.[4] Also, the stable donor–acceptor complex $[(C_6H_5CN)Y\{N(SiMe_3)_2\}_3]$ was prepared with a linear benzonitrile C≡N–Y axis and tetrahedral coordination at the yttrium atom.[4] In contrast to this reaction phenylacetylide, which is isoelectronic (and isolobal) to benzonitrile, coordinates to give the samarium complex **3**. The bonding angle of the axis C≡C–Sm is bent to 151.4° which can be explained by coordination of the solvated sodium ion at the C≡C triple bond (Figure 3).[30] The Sm–C1 bond in **3** at

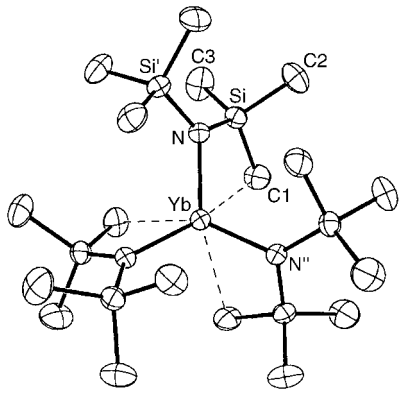

2

Figure 2. Structure of $[Yb\{N(SiMe_3)_2\}_3]$[33] illustrating the agostic Yb···C interaction. Only one of the two disordered Yb atoms is depicted.

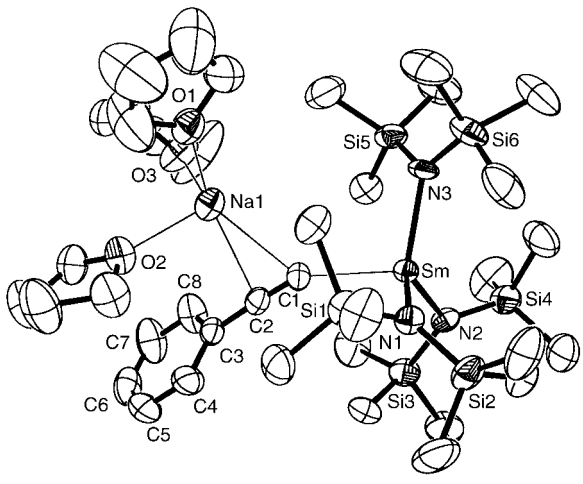

3

Figure 3. Structure of $[(thf)_3Na][(Ph–C{\equiv}C)Sm\{N(SiMe_3)_2\}_3]$.

248.5 pm is slightly shorter than that in the molecular complex $[Cp^*_2Sm(C{\equiv}C\text{-}Ph)(thf)]$ 250.1 pm.[37]

The addition of $[N(SiMe_3)_2]^-$ to silylated trisamides **2** failed due to the bulkiness of this ligand. However, using $[OSiMe_3]^-$ which has one less silyl group as a ligand yielded the corresponding heteroleptic ate complexes $[Ln\{N(SiMe_3)_2\}_3(OSiMe_3)]^-$[30,38] in solvating solvents [Eq. (2), (3)].

$$[Nd\{N(SiMe_3)_2\}_3] + LiOSiMe_3 \xrightarrow{THF} \underset{\mathbf{4}}{[Li(thf)_4][Nd\{N(SiMe_3)_2\}_3(OSiMe_3)]} \quad (2)$$

$$\{Ln\{N(SiMe_3)_2\}_3] + NaOSiMe_3 \xrightarrow{[12]crown\text{-}4} \underset{\begin{array}{c}\mathbf{5a}\ Ln = Sm\\ \mathbf{5b}\ Ln = Eu\\ \mathbf{5c}\ Ln = Yb\\ \mathbf{5d}\ Ln = Lu\end{array}}{[Na([12]crown\text{-}4)_2][Ln\{N(SiMe_3)_2\}_3(OSiMe_3)]} \quad (3)$$

Because of the structures of the alkali-metal siloxanes the sequence of the reaction depends greatly on the solvation properties of the applied donor-solvents, thus, for example, $[(NaOSiMe_3)_4]$ does not react with trisamides in toluene; the reaction occurs spontaneously after addition of crown ether. Structural investigations of the complex anion indicate the unusual coordination of the $[OSiMe_3]^-$ ligand which has almost linear Ln-O-Si bonding axes[30,38] forced by steric effects (Figure 4).

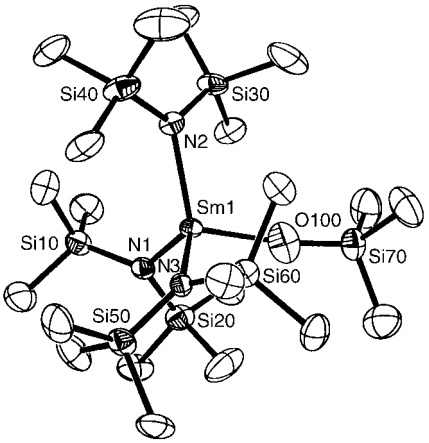

Figure 4. Structure of the $[Sm\{N(SiMe_3)_2\}_3(OSiMe_3)]^-$ ion in **5a**.

The unusual linear metal-O-Si arrangement is also known for transition metal compounds, but in these cases it is explained by metal–oxygen multiple bonds.[39] The bonding angles O-Sm-N in **5a** are almost tetrahedral with an average value of 104.9°,a result of the different demands of space of the two ligand groups. On the other hand, the N-Sm-N angles with an average value of 113.9° are noticeably larger than the ideal tetrahedral angle. It is interesting that the N-Ln-N bonding angles of all the discussed complexes vary negligibly compared to the parameters of the trisamides **2**. This effect may be a be an additional reason for the pyramidal structure of the trisamides $[Ln\{(NSiMe_3)_2\}_3]$ (**2**).

Although the silylated trisamides of rare-earth elements are not able to form homoleptic "ate" complexes, tetrakisamido complexes can be obtained if the demand for space is slightly diminished. The synthetic concept is based on the proton transfer from diphenylamine to the strongly basic sodium bis(trimethylsilyl)amide [Eq. (4)].[40,41] All complexes

$$[Ln\{N(SiMe_3)_2\}_3] + NaN(SiMe_3)_2 + 2\ HNPh_2 \xrightarrow{THF} \underset{\begin{array}{c}\mathbf{6a}\ Ln = Sc\\ \mathbf{6b}\ Ln = Sm\\ \mathbf{6c}\ Ln = Gd\\ \mathbf{6d}\ Ln = Yb\end{array}}{[(thf)_2Na][(Ph_2N)_2Ln\{N(SiMe_3)_2\}_2] + 2\ HN(SiMe_3)_2} \quad (4)$$

of this type crystallize in the monoclinic space group *C*2/*c*. The ion-pair structure is achieved by the sandwich-like coordination of the sodium ions between two phenyl rings of the diphenylamido ligands of the ions $[(Ph_2N)_2Ln\{N(SiMe_3)_2\}_2]^-$ (**6**; Figure 5).[40,41] As a result of the two bridging diphenyl-

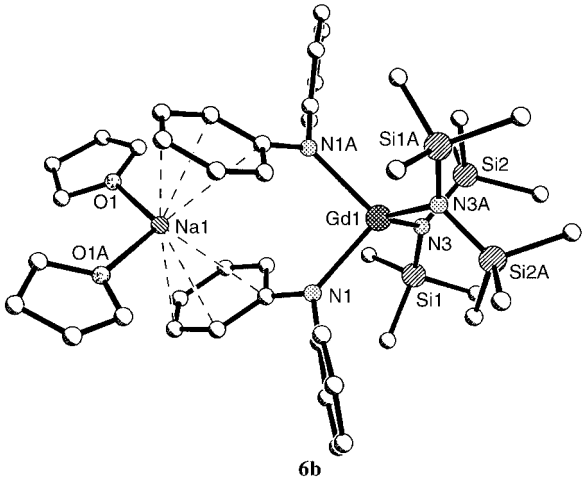

Figure 5. Structure of the ion pair $[(thf)_2Na][(Ph_2N)_2Sm\{N(SiMe_3)_2\}_2]$.

amido groups the Ln–N separations are 5 to 6 pm longer than the Ln–N separations of the silylated amido groups. The N-Ln-N angles of the diphenylamido ligands (95°) are smaller than those of the silylated amido ligands, which reflects the different space demands of the two ligand groups.

The strong basicity of $NaN(SiMe_3)_2$ is responsible for the deprotonation of silylated trisamides, yet only under more extreme conditions. The trisamides **2** of the smaller rare-earth elements scandium, ytterbium, and lutetium react in boiling THF [Eq. (5)] to give the cyclic product **7** (Figure 6).[42]

According to crystal structure determinations the complexes **7** contain linear Na-C-Ln axes and a distorted trigonal bipyramidal environment at the CH_2 carbon atom. The H atoms of the CH_2 group in the scandium complex **7a** deviate further from the trigonal plane than those in the ytterbium complex **7b** this being a result of the different bond lengths

$$\left[Ln\{N(SiMe_3)_2\}_3\right] + NaN(SiMe_3)_2 \xrightarrow[75°C]{THF} \left[(thf)_3Na{-}CH_2{-}Ln\{N(SiMe_3)_2\}_2 \;(Me_2Si{-}N{-}SiMe_3)\right] + HN(SiMe_3)_2 \quad (5)$$

7a Ln = Sc
7b Ln = Yb
7c Ln = Lu

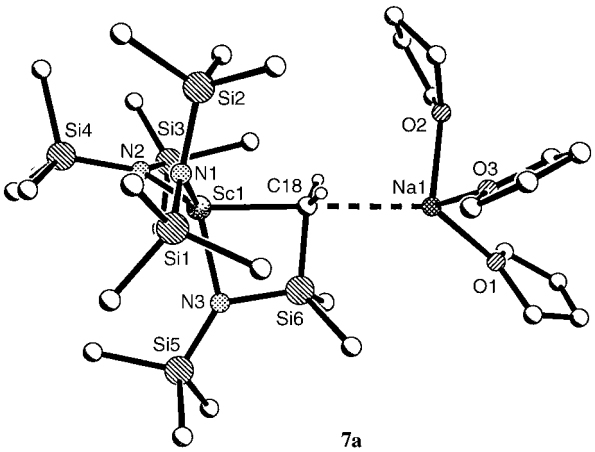

7a

Figure 6. Structure of the cyclization product **7a**.

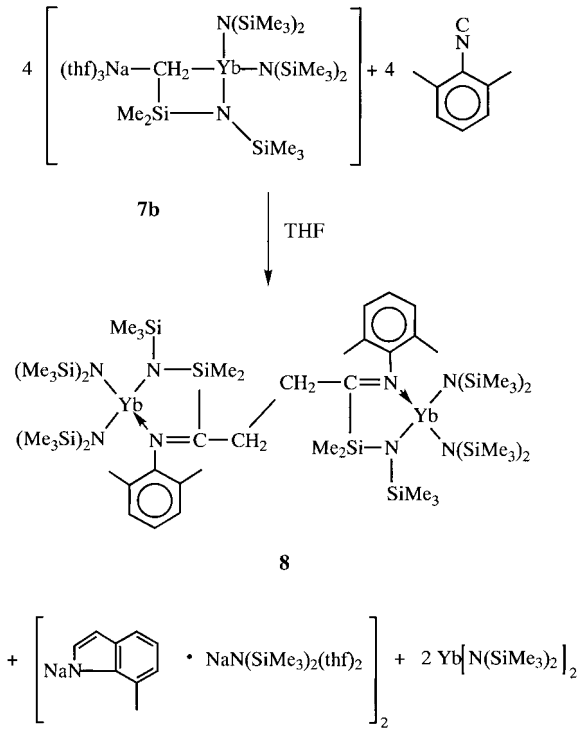

Scheme 1. Reaction pathway of the cyclization product **7b** with 2,6-dimethylbenzoisocyanide.

Sc-CH_2 227.1 pm and Yb-CH_2 238.6 pm. The preparative potential of these reactive complexes is not yet revealed. On account of the possibility to adjust the length of the Ln–C bonds by variation of the lanthanide element different reactivities are expected. For instance the binuclear Yb^{III} complex **8** was generated by the insert of 2,6-dimethylbenzoisocyanide into the Yb–CH_2 bond, concurrent with partial reduction of Yb^{III} to Yb^{II} and C–C coupling[41] (Scheme 1).

Quantum-chemical DFT calculations of the scandium model compound **9** show the strong negative charge of −1.50 at the five coordinate carbon atom in the four-membered ring.

$$\left[Na(OMe_2)_3\overline{ScCH_2SiMe_2NSiH_3}\;\{N(SiH_3)_2\}_2\right] \quad \mathbf{9}$$

It has an almost "pure" p-orbital and is connected by a strong Coulomb interaction to the positively charged scandium atom (+1.63).[42]

Coordination number four is retained on the metal atoms of the binuclear anionic lutetium complex **10**, which are bridged with an amido and an imido ligand (Figure 7). The complex can be obtained in a reaction of $LuBr_3$ with four equivalents of $NaN(SiMe_3)_2$ in boiling THF which also forms the counterion $[Na(thf)_6]^+$. In **10** the Lu atoms are linked to give a planar Lu_2N_2 four-membered ring with an acute internal angle at the Lu atoms of about 81°.[30]

The steric pressure on the metal atoms is relieved if one of the three silylated amido ligands in the trisamides **2** is replaced with a halide ligand. Therefore the coordination number rises to five as a result of dimerization of the halide-

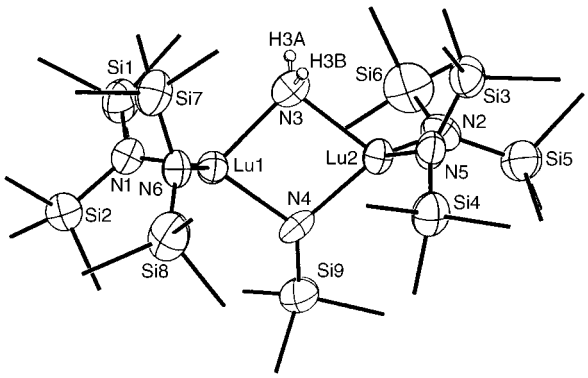

Figure 7. Structure of the $[Lu_2(\mu\text{-}NH_2)(\mu\text{-}NSiMe_3)\{N(SiMe_3)_2\}_4]^-$ ion in **10**.

bridges and because of solvation. Compounds of this type are easy to prepare by comproportionation in THF [Eq. (6)].[43]

The crystals of the chloride **11b** and the bromide **11c** are not isotypic but their molecular structures are similar, that of the bromo derivative **11c** is shown in Figure 8. The samarium

$$4\,Ln[N(SiMe_3)_2]_3 + 2\,LnX_3 \xrightarrow{THF} 3[LnX\{N(SiMe_3)_2\}_2(thf)]_2 \quad (6)$$

11a Ln = Nd, X = Cl
11b Ln = Sm, X = Cl
11c Ln = Sm, X = Br
11d Ln = Eu, X = Cl
11e Ln = Gd, X = Cl
11f Ln = Yb, X = Cl

atoms are linked by two μ_2-halide-bridges to give centrosymmetrical dimers which have similar Sm–X bond lengths. The unusual fivefold coordination of the samarium atoms results in a distorted trigonal-bipyramidal arrangement with one of the halogen atoms (Br) and an oxygen atom in the apical positions and Br′, N1, and N2 in the equatorial positions. The great spatial demands of the amido ligands leads to THF molecules being orientated towards the Sm_2X_2 ring centers. Using less spatially demanding ligands enlarges the coordination number up to seven, as for example, in $[SmCl_3(thf)_4]$.[44]

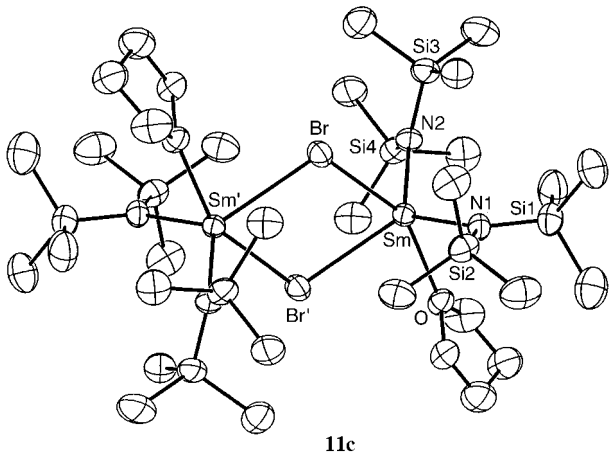

11c

Figure 8. Structure of $[\{Sm(\mu\text{-}Br)\{N(SiMe_3)_2\}_2(thf)\}_2]$ (**11c**).

The dimeric samarium complexes **11** are catalysts for the ROP of ε-caprolactone and δ-valerolactone.[28] The corresponding homopolymers are obtained in high yields in short reaction times. Although these polymerizations are not strictly speaking "living", the chain ends are still active, so block copolymers can be prepared by sequential monomer addition of lactones and/or lactides.[45] The experimental molecular weights differ considerably from the theoretical ones, this effect is probably the result of side reactions.

A further example for coordination number five at the metal atom is the monoamide complex **12**. This compound was obtained in a reaction of scandium trichloride, in THF suspension, according to Equation (7);[46] the reaction cannot

$$ScCl_3 + NaN(SiMe_3)_2 \xrightarrow[-NaCl]{THF} \underset{\mathbf{12}}{[ScCl_2\{N(SiMe_3)_2\}(thf)_2]} \quad (7)$$

be applied to other lanthanoid chlorides. The rest of the rare-earth trichlorides, with larger metal ionic radii than Sc^{3+}, react under these conditions to give bis(amido)halogeno complexes of the type **11**.[43]

The molecular structure shows compound **12** to be a monomer with distorted trigonal-bipyramidal coordination at the scandium atom (Figure 9). The two coordinated THF molecules occupy the axial positions but as a result of the bulky amido ligand the corresponding O-Sc-O angle of 170.9° differs widely from linearity. The Cl1-Sc-Cl2 plane makes a dihedral angle of 22° with the Si1-N1-Si2 plane, which results

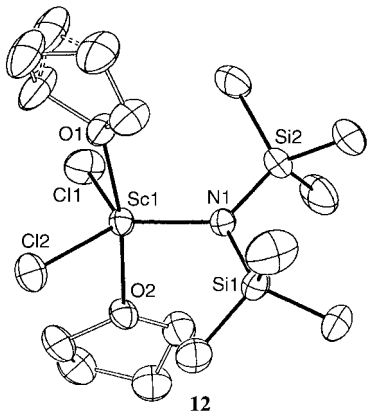

12

Figure 9. Structure of $[ScCl_2\{N(SiMe_3)_2\}(thf)_2]$ (**12**).

in a short Sc–N bond of 203.9 pm. This bond is even slightly shorter than the Sc–N bonds of 204.9 pm in $[Sc\{N(SiMe_3)_2\}_3]$[47] with CN = 3 at the Sc atom.

Exchange of the amido ligand in **12** for another chloro ligand yielded $[ScCl_3(thf)_3]$ with an octahedral structure and meridional arrangement of ligands.[48] The number of chloro ligands in compound **12** corresponds to the number of $SiMe_3$ groups lost so this complex is a perfect precursor to synthesize scandium nitride. Thermolysis proceeds in two steps in vacuum. First the two thf-molecules are split off at 100 °C, then trimethylchlorsilane is eliminated at 400 °C [Eq. (8)].

$$[ScCl_2\{N(SiMe_3)_2\}(thf)_2] \xrightarrow[-THF]{100\,^\circ C} [ScCl_2\{N(SiMe_3)_2\}] \xrightarrow[-ClSiMe_3]{400\,^\circ C} ScN \quad (8)$$

The established procedures for the synthesis of scandium nitride are the direct nitridation of the metal with either nitrogen (700–1500 °C), ammonia, or alkali-metal azides, as well as the ammonolysis of $ScCl_3$ or trisamide **2** at 500–900 °C.[49] Compared to these methods the reaction in Equation (8) offers the considerable advantage of condensation at thermo-sensitive surfaces.

2.2 Low Coordination Numbers as a Result of Metal–Nitrogen Multiple Bonds

A great variety of transition-metal complexes with metal centers in high oxidation states and metal–nitrogen multiple bonds are known.[50–55] Three different groups of them are summarized in Scheme 2, the nitrido-type **A**, the imido-

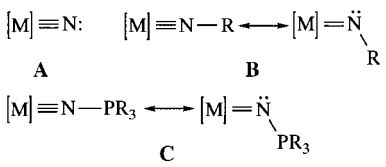

Scheme 2. Formal bonding representation of nitrido (**A**), imido (**B**), and phosphoraneiminato ligands (**C**).

type **B** and the phosphoraneiminato-type **C**. The R group is enormously variable. In all cases the short M–N bonds, which arise from the overlap of unoccupied d orbitals of metal atoms with s and p electrons of the nitrogen atoms, require a considerable amount of space as a result of their multiple-bond character. In addition to the well known *trans*-influence this situation also forces the *cis*-positioned ligand atoms out of the ideal polyhedral arrangement. This effect is so substantial that it is reminiscent of the impact of the bulky η^5-bonded cyclopentadienyl ($C_5H_5^-$) ligand. There are also bonding-theory parallels with respect to the $C_5H_5^-$ ligand. The $C_5H_5^-$ ligand, as well as the NPR_3^- ligand, show a (σ, 2π) set of orbitals which can be described as a pseudo-isolobal phenomenon.[56,57] Pairs of compounds of both ligand types with the same metal atom show amazing analogies in structure and bonding modes seen from this point of view:

$$[Cl_3Ti(\eta^5\text{-}C_5H_5)] \leftrightarrow [Cl_3Ti(\equiv NPPh_3)]$$
$$[O_3Re(\eta^5\text{-}C_5H_5)] \leftrightarrow [O_3Re(\equiv NPPh_3)]$$
$$[Cl_2Ti(\eta^5\text{-}C_5H_5)_2] \leftrightarrow [Cl_2Ti(\equiv NPPh_3)_2]$$

The idea was first expressed to compare the η^5-$C_5H_5^-$ ligand and the double negatively charged (NR^{2-}) imido ligand.[58] However, a direct comparison requires a shifting of a transition-metal atom in the Periodic Table:

$$[Cl_4Nb(\eta^5\text{-}C_5H_5)] \leftrightarrow [Cl_4Mo(\equiv NR)]$$
$$[Cl_2Zr(\eta^5\text{-}C_5H_5)_2] \leftrightarrow [Cl_2Mo(\equiv NR)_2]$$

Finally the principle should also be valid for the bonding pair η^5-$C_5H_5^-$ and N^{3-}, which requires at least a shifting of two positions for the metal atom for straight comparison:

$$[Cl_3Hf(\eta^5\text{-}C_5H_5)] \leftrightarrow [Cl_3W(\equiv N\colon)]$$
$$[Cl_4Ta(\eta^5\text{-}C_5H_5)] \leftrightarrow [Cl_4Re(\equiv N\colon)]$$

The metal atoms must be in the highest possible oxidation state in compounds of the types **A, B**, and **C** for metal–nitrogen triple bonds to be realized. Therefore, only a small selection of transition metals of Groups 5–8 can be considered for this purpose.[50–55] Surprisingly, the bonding mode [M]≡N–PR_3 **C** is also found for phosphoraneiminato complexes of the trivalent rare-earth elements.

2.2.1. *Rare-Earth Element Complexes with η^5-$C_5H_5^-$ and NPR_3^- Ligands*

Rare-earth element compounds **13** of yttrium, dysprosium, erbium, and ytterbium are convincing examples for the pseudo-isolobal principle of η^5-$C_5H_5^-$/NPR_3^- ligands. They crystallize isotypically with each other and were obtained in boiling toluene in almost quantitative yield according to Equation (9).[59,60]

$$3[LnCp_2Cl] + 3\,LiNPPh_3 \rightarrow [LnCp_3] + [Ln_2Cp_3(NPPh_3)_3] + 3\,LiCl \quad (9)$$

13a Ln = Y
13b Ln = Dy
13c Ln = Er
13d Ln = Yb

Figure 10 shows the structure of the dysprosium compound **13b**. The two metal atoms are linked with μ_2-N bridges of two $NPPh_3^-$ groups to create a nonplanar Ln_2N_2 four-membered ring with a butterfly arrangement. This arrangement permits short Ln···Ln separations between the metal atoms, for example, 347.4 pm for compound **13b**. Nevertheless, measurements of the magnetic susceptibility between 1.7 and 300 K and 0.001 and 5 T, respectively, do not show appreciable spin–spin coupling between the metal atoms.[59]

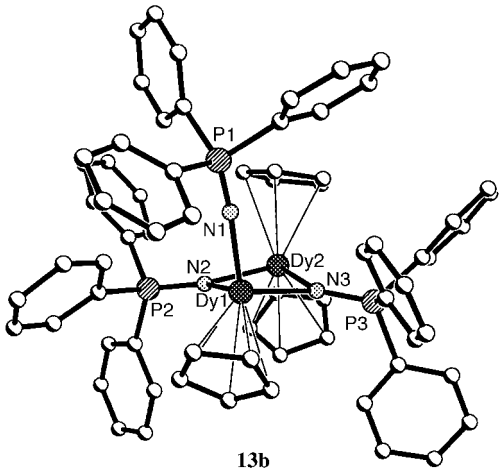

13b

Figure 10. Structure of the dinuclear dysprosium compound $[Dy_2Cp_3(NPPh_3)_3]$ (**13b**).

Direct Ln···Ln interactions can be excluded. One of the Ln atoms is bound to two η^5-$C_5H_5^-$ ligands, while the second Ln atom has a terminal phosphoraneiminato ligand instead of an η^5-$C_5H_5^-$ ligand. Specific features of this ligand are the linear Ln-N-P arrangement and the very short Ln–N bond, which is the shortest Ln–N bond yet known. These parameters are summarized in Table 3. They permit the pseudo-isolobal arrangement of η^5-bonded $C_5H_5^-$ ligand and the phosphoraneiminato ligand:.

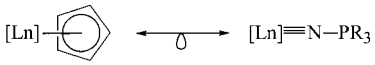

Table 3: Comparison of structural parameters of complexes **13**.

	Y	Dy	Er	Yb
angle Ln-N-P [°]	168.0(6)	167.9(5)	169.6(7)	171.2(4)
separation Ln–N [pm]	213.9(9)	215.4(7)	215.1(9)	214.2(6)

Similar to cyclopentadienyl complexes, Coulomb interactions in phosphoraneiminato compounds contribute to Ln–N triple bonds. The magnetochemical analysis of the dysprosium complex **13b** reveals little difference between the two dysprosium atoms, which supports the analysis of bonding features of the two ligand groups.[59] The similarity in the bonding is reflected in the bonding angles of the participating ligand groups, which differ only slightly despite the ligands very different demands for space (Scheme 3).

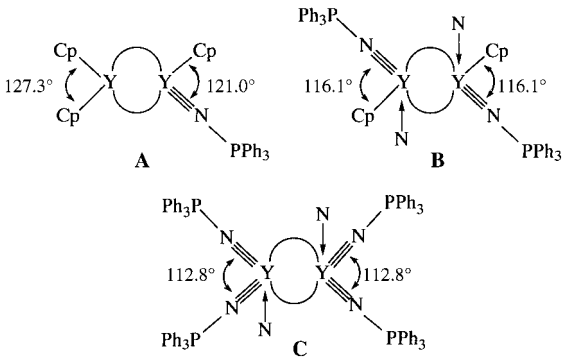

Scheme 3. Bonding angles Cp-Y-Cp, Cp-Y≡N-PPh_3 (always centroid), and Ph_3P-N≡Y≡N-PPh_3 demonstrated for the yttrium complexes **13a** (A), **19** (B), and **18a** (C). The signs N→ symbolize the N donor atoms of the $OSiMe_2$-$NPPh_3$ groups.

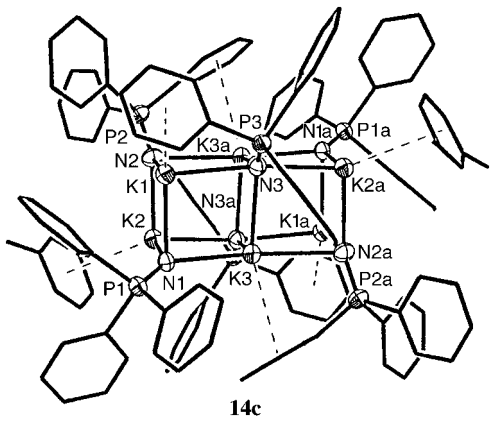

14c

Figure 11. Structure of $[KNPPh_3]_6 \cdot 4\,C_7H_8$. Two of four toluene molecules are coordinate to K2 and K2a by their π systems, the rest of the potassium ions each coordinate to a phenyl ring.

Within the series [CpLnCp], $[CpLnNPPh_3]$, $[Ph_3PNLnNPPh_3]$ the bonding angles decrease at the Ln atoms, thus demonstrating a smaller demand of space on changing the cyclopentadienyl for phosphoraneiminato ligands. This behavior is significant for using phosphoraneiminato complexes as catalysts in the ROP of lactones. Thus, the first step of a donor—acceptor interaction is favored with a declining steric-shielding effect. Comparative studies of $[YbCp_3]$ and $[\{Yb(NPPh_3)_3\}_2]$ verify this impressively.[61] ROP of ε-caprolactone, initiated by $[\{Yb(NPPh_3)_3\}_2]$, require significantly shorter reaction times for quantitative polymerization than ROP of ε-caprolactone initiated by $[YbCp_3]$. However, neither the phosphoraneiminato complex nor the analogous Cp complex gives a living polymerization.

2.2.2. *Homoleptic Phosphoraneiminato Complexes of Rare-Earth Elements*

A very efficient initiator system for ROP was obtained in a reaction of anhydrous rare-earth-element trichlorides with pure phosphoraneiminates of the heavy alkaline metals (Na, K, Rb, Cs) which have recently become available.[59,62] The cores of these compounds are very well shielded by the surrounding organic groups, which leads to high solubility of the reagents even in nonsolvating solvents. For instance, the phenyl derivatives are soluble in toluene, the cyclohexyl derivative $[\{KNPCy_3\}_4]$ in *n*-pentane. Consequently, fast reaction is observed with the very sparingly insoluble rare-earth-element halides. The alkaline-metal phosphoraneiminate compounds are also structurally interesting. Metal atoms and nitrogen atoms in compounds $[\{LiNPPh_3\}_6]$ (**14a**)[59] and $[\{NaNPPh_3\}_6]$ (**14b**)[62a] form hexagonal-prismatic frameworks, and doublecubes with a shared M_2N_2 plane in $[\{RbNPPh_3\}_6]$ (**14d**)[62c] and $[\{KNPPh_3\}_6]$ (**14c**)[62b] (see Figure 11) as well as heterocubane M_4N_4 skeletons in $[\{CsNPPh_3\}_4]$ (**14e**)[62c] and $[\{KNPCy_3\}_4]$ (**14f**; Cy = Cyclohexyl).[62d]

Reactions of rare-earth-element trichlorides or triflates with alkaline-metal phosphaniminates take place in THF suspension and give almost quantitative yields [Eq. (10)].[63]

$$2\,LnCl_3 + [\{NaNPPh_3\}_6] \rightarrow [\{Ln(NPPh_3)_3\}_2] + 6\,NaCl \qquad (10)$$

15a Ln = Y
15b Ln = Yb

The solvent-free complexes **15** crystallize from THF solution to yield centrosymmetric dimers (Figure 12) with slightly differing Ln–N bond lengths in the Ln_2N_2 four-membered ring (225.0 and 226.2(4) pm for **15b**). As a result the μ_2-N bridges these bond lengths are noticeably longer than those of the terminally bonded ($NPPh_3^-$) ligands which have Yb–N bonds of 210.7 and 213.7 (4) pm. The latter are slightly shorter than that in the mixed-ligand complex **13d** of 214.2 (6) pm.

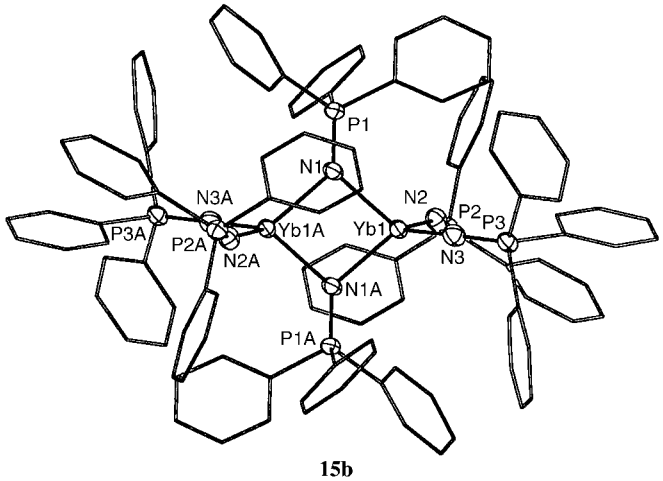

15b

Figure 12. Structure of $[\{Yb(NPPh_3)_3\}_2]$ (**15b**).

Unlike complexes **15** which crystallize without solvent, the complex with the larger ion, lanthanum, forms the THF solvate $[\{La(NPPh_3)_3\}_2(thf)]$ (**16**). In addition the oxygen atom of the THF molecule bridges the two lanthanum ions to give a trigonal-bipyramidal coordination environment with O1 and N1 or N1A, respectively, in axial position (Figure 13).[63]

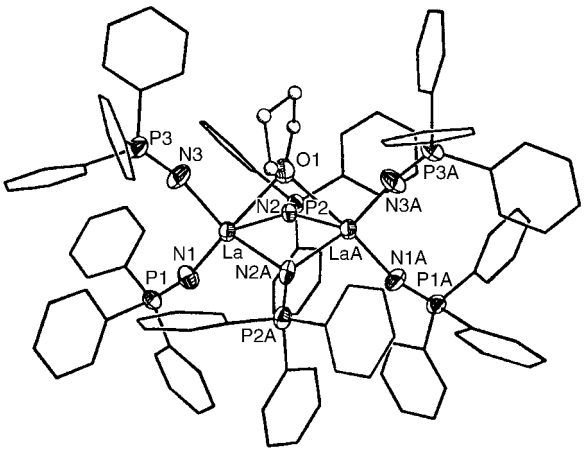

16

Figure 13. Structure of $[La_2(NPPh_3)_6(thf)]$ (**16**).

In complex **16** the La–N bonds of the terminal ($NPPh_3^-$) groups with almost stretched La-N-P bonding axes of 163.9° and 168.1° and bond lengths of 228.4 and 231.6 pm are the shortest La–N bonds found to date.

The attempt to synthesize a homoleptic "ate" complex $[Ln(NPPh_3)_4]^-$ was only successful with Ln = Yb. It does not succeed with Ln = La because of the lower Lewis acidity of the La^{3+} ion (ionic radius 117.2 pm) compared to that of the Yb^{3+} ion (100.8 pm). The synthesis follows Equation (11) in a reaction with cesium phosphoraneiminate in THF.[64]

$$[\{Yb(NPPh_3)_3\}_2] + 2\ CsNPPh_3 \rightarrow 2\ Cs[Yb(NPPh_3)_4] \quad (11)$$

17

Complex **17** has the structure of a dimeric centrosymmetric ion assembly. The $[Yb(NPPh_3)_4]^-$ ions are connected by two Cs^+ ions (Figure 14).

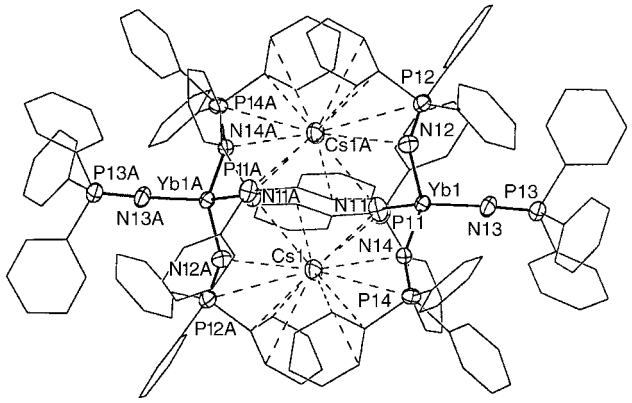

17

Figure 14. Structure of $Cs[Yb(NPPh_3)_4]$ (**17**).

These cations form Cs···N bonding contacts with three of the four $NPPh_3^-$ ligands resulting in bent Yb-N-P axes (147.0°; average value). The fourth terminal Yb-N-P axis retains a more-or-less linear arrangement with 170.2°. This arrangement corresponds to the unchanged Yb–N separation of that group with 213.7 pm, whereas the bent $NPPh_3^-$ ligands show slightly lengthened bond lengths of 215.9 pm (average value). Nevertheless all the Yb–N bonds in compound **17** are significantly shorter than in the homoleptic complex $[Li(thf)_4][Yb(NPh_2)_4]$[65] with Yb–N bonds of 218.8 to 224.1 pm. The perfect physical shielding of the Yb atoms in complex **17** accounts for its ineffective catalytic behavior in the ROP of lactones, which is in sharp contrast to the extremely active molecular complexes **15** and **16**.

The synthesis of the ate complex $[Yb(NPPh_3)_4]^-$ introduces the first representatives of rare-earth-element compounds into the series of valence-isoelectronic homoleptic phosphoraneiminato complexes:

Compound	M–N separation [pm] (average values)
$[Yb(NPPh_3)_4]^-$[64]	214.6
$[Hf(NPPh_3)_4]$[66]	200.9
$[Ta(NPPh_3)_4]^+$[67]	185.0
$[W(NPPh_3)_4]^{2+}$[68]	180.9

All the species in this series have qualitatively the same multiple-bonding mode for the metal–nitrogen bonding although the M–N separations differ significantly. It has to be remembered that increasing the oxidation state of the central atom is accompanied by a decrease in the atomic radius on going from ytterbium(III) to tungsten(VI). The increasing the positive charge across the same series also shortens the M–N bonds; both effects are mutually amplifying.

The phosphoraneiminato complexes of the rare-earth elements have proved to be remarkably reactive. They are able to break down linear arranged silicones $(\text{-}OSiMe_2)_n$ or hexamethyltrisiloxane $(OSiMe_2)_3$ by insertion of monomeric $OSiMe_2$ groups into the Ln–N bond [Eq. (12)].[60]

$$[Ln(\{NPPh_3\}_3\}_2] + 2/n\,(OSiMe_2)_n \rightarrow [\{Ln(NPPh_3)_2(\mu\text{-}OSiMe_2NPPh_3)\}_2] \quad (12)$$

18a Ln = Y
18b Ln = Sm

The N atoms of the Ln_2N_2 bridge of the educt are thus replaced with the more electronegative O atoms of the $OSiMe_2NPPh_3^-$ groups yielding planar centrosymmetrical Ln_2O_2 four-membered rings with different Ln–O bond lengths. This effect is explained by the additional N-donor function of the phosphoraneimine rest of the $OSiMe_2NPPh_3^-$ group resulting in the formation of two four-membered LnOSiN rings with fivefold coordination at the metal atom (Figure 15).

It should be interesting to apply this arrangement in homogeneous catalysis. The Ln–N bond lengths with values of 250.3 pm (**18a**) and 259.8 pm (**18b**) confirm the donor–acceptor character of this group. These bonds should open and close easily and are therefore available for the primary step in the formation of a substrate bond.

The miscellaneous complex $[YCp(NPPh_3)_2]$, which is pseudo-isolobal to complex **18** is able to insert an $OSiMe_2$

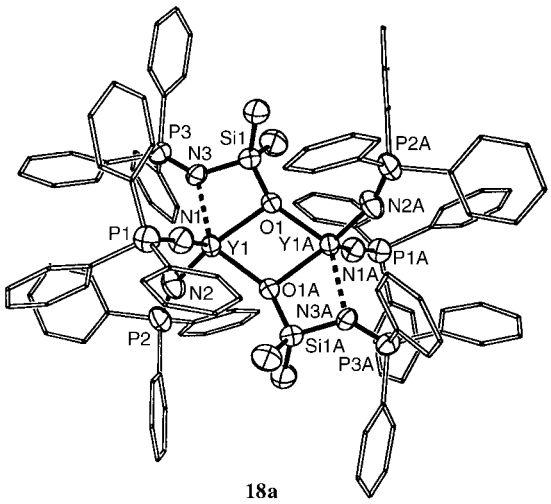

18a

Figure 15. Structure of $[\{Y(NPPh_3)_2(\mu\text{-}OSiMe_2NPPh_3)\}_2]$ (**18a**).

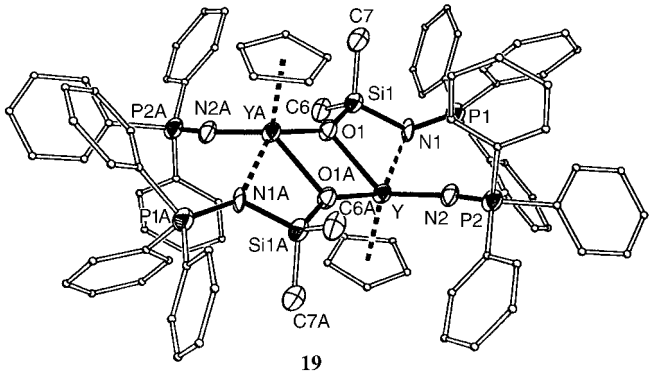

19

Figure 16. Structure of $[\{YCp(NPPh_3)(\mu\text{-}OSiMe_2NPPh_3)\}_2]$ (**19**).

unit to one of the Y–N bonds, as in Equation (12). The product $[\{YCp(NPPh_3)(\mu\text{-}OSiMe_2NPPh_3)\}_2]$ (**19**) was obtained from the reaction of $[YCpCl_2]$ and $[\{LiNPPh_3\}_6]$ with $(OSiMe_2)_3$ in boiling toluene in one step.[60] The structure (Figure 16) shows a planar Y_2O_2 four-membered ring and a (4+1) coordination at the yttrium atom corresponding to the isolobal complex **18a**.

It should be interesting to compare the catalytic properties of compounds **18** and **19** which differ only in the steric subtlety of a $NPPh_3^-$ and a $\eta^5\text{-}C_5H_5^-$ group, respectively.

2.2.3. *Iodo-Phosphoraneiminato Complexes of Rare-Earth Elements*

Reactions of $INPPh_3$ with finely spread metal powder in suspension of solvating solvents using ultrasound reaction conditions are an alternative to the synthesis of phosphoraneiminato complexes using metathesis reaction of rare-earth element halides with alkali-metal phosphoraneiminates [Eq. (9), (10)]. $INPPh_3$ is easily accessible from $Me_3SiNPPh_3$ and iodine in dichloromethane in the presence of cesium fluoride. The behavior of $INPPh_3$ in redox reactions is similar to that of iodine[69] and therefore it reacts depending on metal, agent of suspension, and the conditions of the reactants according to the examples in Equations (13)–(15).

$$7\,Yb + 8\,INPPh_3 \xrightarrow{THF} 2\,[Yb_2I(NPPh_3)_4(thf)_2] + 3\,[YbI_2(thf)_4] \quad (13)$$

20

$$4\,Sm + 5\,INPPh_3 \xrightarrow{DME} [Sm_2I(NPPh_3)_5(dme)] + 2\,[SmI_2(dme)_3] \quad (14)$$

21

$$2\,Y + 4\,INPPh_3 \xrightarrow{THF} [Y_2I(NPPh_3)_4(thf)_2]^+I_3^- \quad (15)$$

22

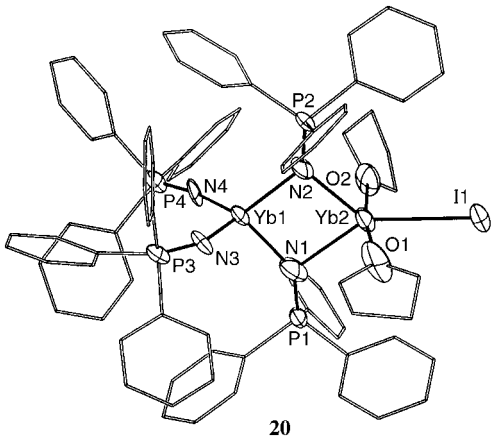

20

Figure 17. Structure of $[Yb_2I(NPPh_3)_4(thf)_2]$ (**20**).

The mixed-valence ytterbium complex **20**,[70] obtained in a reaction following Equation (13) has interesting coordination chemistry. From the crystal structure (Figure 17) it can be described as being an ionic pair consisting of the highly anisotropic ion $[IYb^{II}(thf)_2]^+$ and the "ate"-complex $[Yb^{III}(NPPh_3)_4]^-$, the latter being similar to compound $[\{Cs[Yb(NPPh_3)_4]\}_2]$ (**17**). The Yb^{II} atom of the cation forms long Yb–N bonds (average value of 214.6 pm) to two N atoms of the anion, which results in a distorted trigonal-bipyramidal arrangement with the THF molecules in axial positions.

The binuclear samarium complex **21** (Figure 18), accessible through a reaction of the type in Equation (14), has proved to be an efficient initiator for the ROP of lactones, such as ε-caprolactone and δ-valerolactone.[71,72] The excellent catalytic properties are attributed to the asymmetrical coordination of the two samarium atoms. Removing of the solvating DME molecule allows a primary step in which the

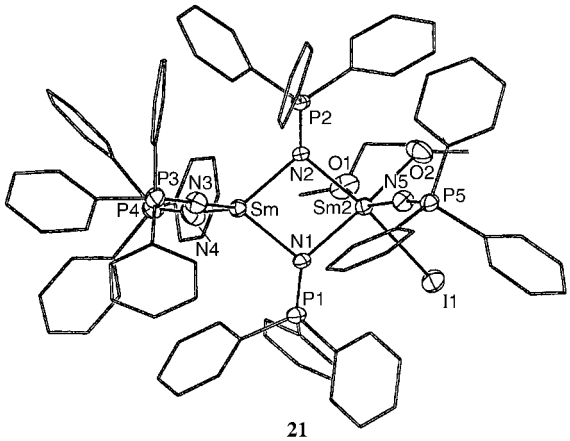

21

Figure 18. Structure of $[Sm_2I(NPPh_3)_5(dme)]$ (**21**).

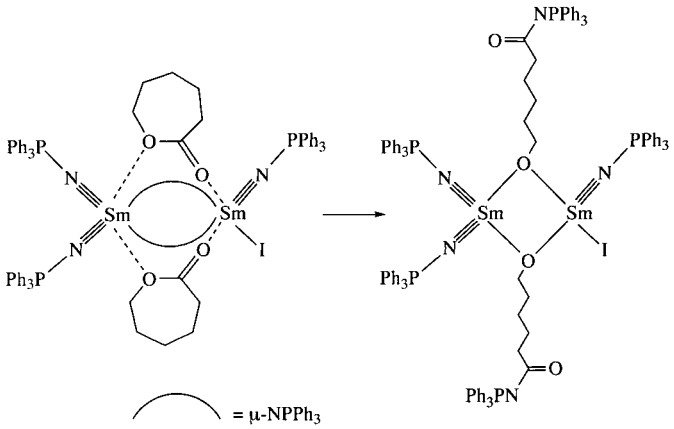

Scheme 4. Coordination of ε-caprolactone after replacing DME in **21** and primary, ring-opening step of polymerization.

asymmetrical donor qualities of lactones are accommodated in that the lactone is bound in a bridging fashion (Scheme 4).

Living ROP of ε-caprolactone and δ-valerolactone is observed for a wide range of $[monomer]_0/[\mathbf{21}]_0$ ratios. Experimental and theoretical molecular weights are consistent, and sequential addition of monomers result in corresponded block copolymers. Participation of coordinating solvent molecules reduces the rate of polymerization compared to the rate of initiation so that the corresponding polymers show relatively narrow M_W distribution ($M_w/M_n = 1.09–1.35$).

The subsequent ring-opening step starts, as for the Si–O bond cleavage for silicones (see above), at the μ_2-N bridging phosphoraneiminato groups which results in the replacement of the Sm_2N_2 four-membered ring with the Sm_2O_2 ring. The resulting $C(O)NPPh_3$ end groups proved to be active too in the polymer so that copolymerization and synthesis of block copolymers is possible.[72]

The ytterbium complex **22** accessible from the reaction given in Equation (15) has ionic structure (Figure 19).[73] Only two $NPPh_3^-$ groups are available per metal atom, which results in an increase of the coordination number up to six, and is achieved by solvation.

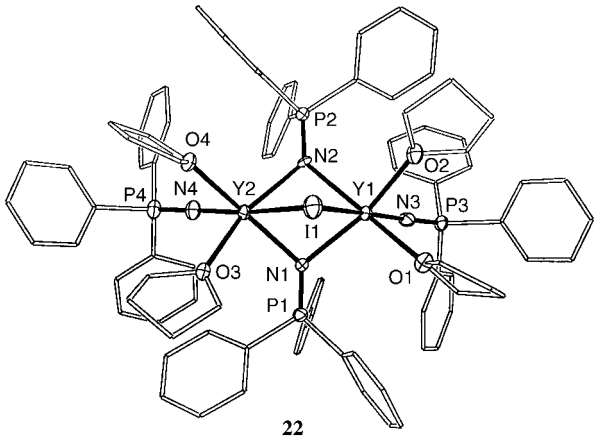

22

Figure 19. Structure of the $[Y_2I(NPPh_3)_4]^+$ ion (without I_3^- counterion) of **22**.

Typically both of the terminal phosphoraneiminato groups, which have a strong *trans*-influence which originates from the Y–N multiple bonds, are located in the positions *trans* to the iodo ligand. The Y–I separations are correspondingly large with average values of 328.7 pm. The complex cation $[Y_2I(NPPh_3)_4(thf)_4]^+$ shows a significant similarity to the cation of the bismuth complex $[Bi_2I(NPPh_3)_4]^+I_3^-$ (**23**;[74] Figure 20). The terminal $NPPh_3^-$ groups are also in the positions *trans* to the μ-iodo ligand.

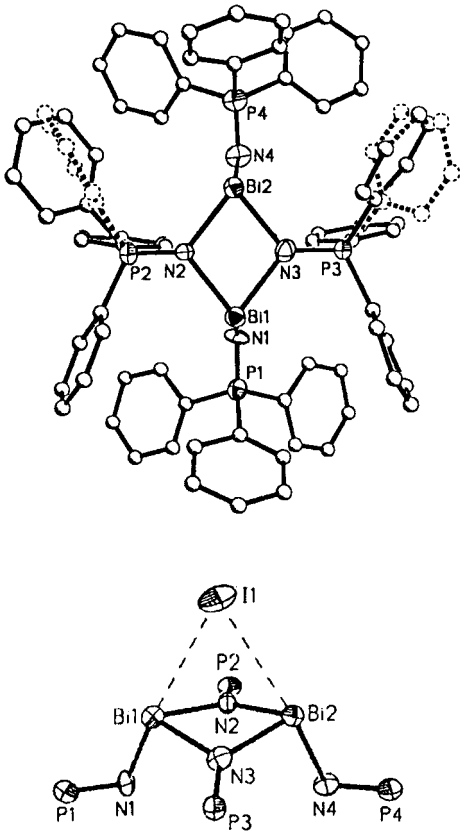

Figure 20. Structure of the $[Bi_2(NPPh_3)_4]^{2+}$ unit in the crystal structure of $[Bi_2I(NPPh_3)_4]^+I_3^-$ (top) and the skeleton atoms of the $[Bi_2I(NPPh_3)_4]^+$ ion (bottom).

It is interesting that the coordination sites of the yttrium complex, occupied with THF molecules, are replaced with steric active free electron pairs of the bismuth atoms in the corresponding bismuth compound, which results in a pseudo-trigonal bipyramidal arrangement.[74]

3. Outlook

The phosphoraneiminato complexes are promising candidates as catalysts for the polymerization of olefins and lactones. From the pseudo-isolobal relationship between cyclopentadienyl complexes and with complexes of phosphoraneiminato ligands:

$$[M]-Cp \quad \leftrightarrow \quad [M]\equiv N-PR_3$$

interesting parallels arise with numerous applications for catalysis. The R_3PN^- ligand shows almost the same demand for space as the η^5-bonded Cp^- ligand although it is significantly smaller. It easily allows the first step of a of metal-atom–substrate interaction because of its high stability of configuration. As with the Cp complexes, a great many phosphoraneiminato complexes of transition metals are known, in addition to the derivatives of rare-earth elements described here.[75] A large number of catalysts should be available by selection of the metal atom as well as variation of the organic moiety, the chirality of the phosphorus atom, and the remaining ligand sphere. With such a choice of variables, quantum-chemical calculations are essential for developing the most efficient and appropriate complexes in an adequate amount of time. As a result of their graduated ionic radii the rare-earth elements in particular offer the opportunity to design optimum catalysts.

The same applies to the highly efficient catalysts of the metallocene-type[76] of zirconium and hafnium. Their corresponding bis(phosphoraneiminato)complexes are also available. Recently, the synthesis of the first ferrocenyl-substituted bis(phosphoraneiminatochelate) compound **24** opens up in

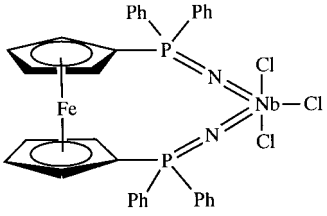

24

this row the parallel to the ansa-bounded metallocene species of titanium, zirconium, and hafnium.

The first promising results using phosphoraneiminato complexes as pre-catalysts (together with methyl alumoxane (MAO) or boranes) for the polymerization of olefins[78,79] shows the beginning of an exciting new development.

Metal complexes with phosphoraneiminato substituted carbanionic ligands for example, **25**[80] and **26**[81] are promising variations.

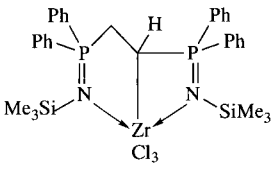

25

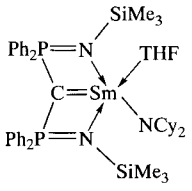

26

Finally, because of their pronounced oxophilic nature, the phosphoraneiminato complexes of rare-earth elements, analogous to the insertion reactions of silicon fragments (R_2Si-O) into Ln–N bonds,[60] can be used as anchor groups for immobilization on SiO_2 supports. Thus, they should be also find use in heterogeneous catalysis.

The authors are grateful to the co-workers for their contributions, their names appear in the work cited. We are grateful to Ms Edith Schmidt for her support to provide the manuscript.

Received: June 17, 2002 [A543]

[1] R. D. Shannon, C. T. Prewitt, *Acta Crystallogr. Sect. B* **1969**, *25*, 925–946; R. D. Shannon, *Acta Crystallogr. Sect. A* **1976**, *32*, 751–767.
[2] N. I. Giricheva, G. V. Girichev, S. A. Shlykov, O. V. Pelipets, *J. Struct. Chem.* **2000**, *41*, 231–237.
[3] A. V. Zakharov, N. I. Giricheva, N. Vogt, S. A. Shlykov, J. Vogt, G. V. Girichev, *J. Chem. Soc. Dalton Trans.* **2001**, 3160–3162.
[4] Rewiew: M. Westerhausen, M. Hartmann, A. Pfitzner, W. Schwarz, *Z. Anorg. Allg. Chem.* **1995**, *621*, 837–850.
[5] P. B. Hitchcock, M. F. Lappert, R. G. Smith, R. A. Bartlett, P. P. Power, *J. Chem. Soc. Chem. Commun.* **1988**, 1007–1009; M. Niemeyer, *Acta Crystallogr. Sect. E* **2001**, *57*, m553-m555; H. Schumann, D. M. M. Freckmann, S. Dechert, *Z. Anorg. Allg. Chem.* **2002**, *628*, 2422–2426.
[6] H. Schumann, W. Genthe, E. Hahn, J. Pickardt, H. Schwarz, K. Eckart, *J. Organomet. Chem.* **1986**, *306*, 215–225.
[7] M. Westerhausen, S. Schneiderbauer, M. Hartmann, M. Warchhold, H. Nöth, *Z. Anorg. Allg. Chem.* **2002**, *628*, 330–332.
[8] H. Schumann, J. Müller, *J. Organomet. Chem.* **1979**, *169*, C1–C4; M. F. Lappert, R. Pearce, *J. Chem. Soc. Chem. Commun.* **1973**, 126–127.
[9] S. A. Schuetz, V. W. Day, R. D. Sommer, A. L. Rheingold, J. A. Belot, *Inorg. Chem.* **2001**, *40*, 5292–5295.
[10] H. Schumann, J. Müller, *Angew. Chem.* **1978**, *90*, 307–308; *Angew. Chem. Int. Ed. Engl.* **1978**, *17*, 276–277; H. Schumann, J. Müller, N. Bruncks, H. Lauke, J. Pickardt, H. Schwarz, K. Eckart, *Organometallics* **1984**, *3*, 69–74.
[11] A. F. Wells, *Structural Inorganic Chemistry*, Clarendon, Oxford, **1984**.
[12] S. Kraut, J. Magull, V. Schaller, M. Karl, K. Harms, K. Dehnicke, *Z. Anorg. Allg. Chem.* **1998**, *624*, 1193–1201.
[13] S.-H. Lin, Z.-C. Dong, J.-S. Huang, Q.-E. Zhang, X.-L. Lu, *Acta Crystallogr. Sect. C* **1991**, *47*, 426–427.
[14] L. B. Asprey, T. K. Keenan, F. H. Kruse, *Inorg. Chem.* **1964**, *3*, 1137–1140.
[15] J. D. Forrester, A. Zalkin, D. H. Templeton, J. C. Wallmann, *Inorg. Chem.* **1964**, *3*, 185–188.
[16] A. R. Al-Karaghouli, J. S. Wood, *J. Am. Chem. Soc.* **1968**, *90*, 6548–6549.
[17] J. H. Burns, *Inorg. Chem.* **1979**, *18*, 3044–3047.
[18] R. E. Thoma, G. D. Brunton, *Inorg. Chem.* **1966**, *5*, 1937–1939.
[19] F. Nicolò, J.-C. G. Bünzli, G. Chapuis, *Acta Crystallogr. Sect. C* **1988**, *44*, 1733–1738.
[20] C. Yan, Y. Zhang, S. Gao, B. Li, C. Huang, G. Xu, *J. Alloys Compd.* **1995**, *225*, 385–389.
[21] H. Schumann, J. A. Meese-Marktscheffel, L. Esser, *Chem. Rev.* **1995**, *95*, 865–986; K. D. Smith, J. L. Atwood, *J. Chem. Soc. Chem. Commun.* **1972**, 593–594; J. L. Atwood, K. D. Smith, *J. Chem. Soc. Dalton Trans.* **1973**, 2487–2490.
[22] V. Kilimann, M. Schäfer, R. Herbst-Irmer, F. T. Edelmann, *J. Organomet. Chem.* **1994**, *469*, C15-C18.
[23] H. W. Görlitzer, M. Spiegler, R. Anwander, *J. Chem. Soc. Dalton Trans.* **1999**, 4287–4288; R. Anwander, O. Runte, J. Eppinger, G. Gerstberger, E. Herdtweck, M. Spiegler, *J. Chem. Soc. Dalton Trans.* **1998**, 847–858; O. Runte, T. Priermeier, R. Anwander, *Chem. Commun.* **1996**, 1385–1386.
[24] P. W. Roesky, *Chem. Soc. Rev.* **2000**, *29*, 335–345, and references therein.
[25] Q. Liu, M. Ding, Y. Lin, Y. Xing, *Polyhedron* **1998**, *17*, 2327–2330; Q. Liu, M. Ding, *J. Organomet. Chem.* **1998**, *553*, 179–181;

Q. Liu, M. Ding, Y. Lin, Y. Xing, *Polyhedron* **1998**, *17*, 555 – 559; Q. Liu, M. Ding, Y. Lin, Y. Xing, *J. Organomet. Chem.* **1997**, *548*, 139 – 142.

[26] W. J. Evans, C. H. Fujimoto, J. W. Ziller, *Chem. Commun.* **1999**, 311 – 312.

[27] H. Yasuda, E. Ihara, *Adv. Polym. Sci.* **1997**, *133*, 53 – 101.

[28] S. Agarwal, C. Mast, K. Dehnicke, A. Greiner, *Makromol. Chem. Rapid Commun.* **2000**, *21*, 195 – 212.

[29] W. J. Evans, M. A. Johnston, R. D. Clark, R. Anwander, J. W. Ziller, *Polyhedron* **2001**, *20*, 2483 – 2490, and references therein; R. Anwander, *Top. Curr. Chem.* **1996**, *179*, 33 – 122, and references therein.

[30] M. Karl, G. Seybert, W. Massa, K. Harms, S. Agarwal, R. Maleika, W. Stelter, A. Greiner, W. Heitz, B. Neumüller, K. Dehnicke, *Z. Anorg. Allg. Chem.* **1999**, *625*, 1301 – 1309.

[31] P. G. Eller, D. C. Bradley, M. B. Hursthouse, D. W. Meek, *Coord. Chem. Rev.* **1977**, *24*, 1 – 95.

[32] W. A. Herrmann, R. Anwander, F. C. Munck, W. Scherer, V. Dufaud, N. W. Huber, G. R. J. Artus, *Z. Naturforsch. B* **1994**, *49*, 1789 – 1797.

[33] M. Niemeyer, *Z. Anorg. Allg. Chem.* **2002**, *628*, 647 – 657.

[34] T. Fjeldberg, R. A. Andersen, *J. Mol. Struct.* **1985**, *129*, 93 – 105.

[35] K. N. Raymond, C. W. Eigenbrot, Jr., *Acc. Chem. Res.* **1980**, *13*, 276 – 283.

[36] W. T. Kloster, L. Brammer, C. J. Schaverien, P. H. M. Budzelaar, *J. Am. Chem. Soc.* **1999**, *121*, 1381 – 1382.

[37] W. J. Evans, T. A. Ulibarri, L. R. Chamberlain, J. W. Ziller, D. Alvarez, Jr., *Organometallics* **1990**, *9*, 2124 – 2130.

[38] F. T. Edelmann, A. Steiner, D. Stalke, *Polyhedron* **1994**, *13*, 539 – 546.

[39] W. G. Klemperer, V. V. Mainz, R.-C. Wang, W. Shum, *Inorg. Chem.* **1985**, *24*, 1968 – 1970; F. J. Feher, J. F. Walzer, *Inorg. Chem.* **1991**, *30*, 1689 – 1694; B. Stensland, P. Kierkegaard, *Acta Chem. Scand.***1970**, *24*, 211 – 220; W. H. Leung, A. A. Danopoulos, G. Wilkinson, B. Hussain-Bates, M. B. Hursthouse, *J. Chem. Soc. Dalton Trans.* **1991**, 2051 – 2061; E. A. Babaian, D. C. Hrncir, S. G. Bott, J. L. Atwood, *Inorg. Chem.* **1986**, *25*, 4818 – 4821; W. M. P. B. Menge, J. G. Kerkade, *Inorg. Chem.* **1991**, *30*, 4628 – 4631; D. Wolff von Gudenberg, H.-C. Kang, W. Massa, K. Dehnicke, C. Maichle-Mössmer, J. Strähle, *Z. Anorg. Allg. Chem.* **1994**, *620*, 1719 – 1724.

[40] M. Karl, K. Harms, K. Dehnicke, *Z. Anorg. Allg. Chem.* **1999**, *625*, 1774 – 1776.

[41] M. Karl, A. Dashti-Mommertz, B. Neumüller, K. Dehnicke, *Z. Anorg. Allg. Chem.* **1998**, *624*, 355 – 356.

[42] M. Karl, K. Harms, G. Seybert, W. Massa, S. Fau, G. Frenking, K. Dehnicke, *Z. Anorg. Allg. Chem.* **1999**, *625*, 2055 – 2063.

[43] **11a**: D. J. Berg, R. A. L. Gendron, *Can. J. Chem.* **2000**, *78*, 454 – 458; **11b, 11c**: M. Karl, G. Seybert, W. Massa, S. Agarwal, A. Greiner, K. Dehnicke, *Z. Anorg. Allg. Chem.* **1999**, *625*, 1405 – 1407; **11d**: T. D. Tilley, A. Zalkin, R. A. Andersen, D. H. Templeton, *Inorg. Chem.* **1981**, *20*, 551 – 554; **11d–f**: H. C. Aspinall, D. C. Bradley, M. B. Hursthouse, K. D. Sales, N. P. C. Walker, B. Hussain, *J. Chem. Soc. Dalton Trans.* **1989**, 623 – 626.

[44] W. J. Evans, I. Bloom, J. W. Grate, L. A. Hughes, W. E. Hunter, J. L. Atwood, *Inorg. Chem.* **1985**, *24*, 4620 – 4623; S. Anfang, M. Karl, N. Faza, W. Massa, J. Magull, K. Dehnicke, *Z. Anorg. Allg. Chem.* **1997**, *623*, 1425 – 1432.

[45] S. Agarwal, M. Karl, K. Dehnicke, A. Greiner, *Polym. Prepr. (Am. Chem. Soc. Div. Polym. Chem.)* **1998**, *39*, 361 – 362.

[46] M. Karl, G. Seybert, W. Massa, K. Dehnicke, *Z. Anorg. Allg. Chem.* **1999**, *625*, 375 – 376.

[47] J. S. Ghotra, M. B. Hursthouse, A. J. Welch, *J. Chem. Soc. Chem. Commun.* **1973**, 669 – 670.

[48] J. L. Atwood, K. D. Smith, *J. Chem. Soc. Dalton Trans.* **1974**, 921 – 923.

[49] B. Hajek, V. Brozek, P. H. Duvigneaud, *J. Less-Common Met.* **1973**, *33*, 385 – 386; M. D. Lyutaya, A. B. Goucharuk, I. I. Timofeeva, *Zh. Prikl. Khim.* **1975**, *48*, 721 – 724; W. Lengauer, *J. Solid State Chem.* **1988**, *76*, 412 – 415; J. P. Dismukes, W. M. Yim, V. S. Ban, *J. Cryst. Growth* **1972**, *13–14*, 365 – 370; R. L. LaDuca, P. T. Wolczanski, *Inorg. Chem.* **1992**, *31*, 1311 – 1313.

[50] W. A. Nugent, J. M. Mayer, *Metal-Ligand Multiple Bonds*, Wiley, New York, **1988**.

[51] K. Dehnicke, J. Strähle, *Angew. Chem.* **1981**, *93*, 451 – 464; *Angew. Chem. Int. Ed. Engl.* **1981**, *20*, 413 – 426.

[52] K. Dehnicke, J. Strähle, *Angew. Chem.* **1992**, *104*, 978 – 1000; *Angew. Chem. Int. Ed. Engl.* **1992**, *31*, 955 – 978.

[53] P. Mountford, *Chem. Commun.* **1997**, 2127 – 2134.

[54] K. Dehnicke, J. Strähle, *Chem. Rev.* **1993**, *93*, 981 – 994.

[55] K. Dehnicke, J. Strähle, *Polyhedron* **1989**, *8*, 707 – 726; K. Dehnicke, M. Krieger, W. Massa, *Coord. Chem. Rev.* **1999**, *182*, 19 – 65.

[56] T. Rübenstahl, F. Weller, S. Wocadlo, W. Massa, K. Dehnicke, *Z. Anorg. Allg. Chem.* **1995**, *621*, 953 – 958.

[57] A. Diefenbach, F. M. Bickelhaupt, *Z. Anorg. Allg. Chem.* **1999**, *625*, 892 – 900.

[58] D. S. Williams, M. H. Schofield, J. T. Anhaus, R. R. Schrock, *J. Am. Chem. Soc.* **1990**, *112*, 6728 – 6729; D. S. Williams, J. T. Anhaus, M. H. Schofield, R. R. Schrock, *J. Am. Chem. Soc.* **1991**, *113*, 5480 – 5481.

[59] S. Anfang, K. Harms, F. Weller, O. Borgmeier, H. Lueken, H. Schilder, K. Dehnicke, *Z. Anorg. Allg. Chem.* **1998**, *624*, 159 – 166.

[60] S. Anfang, T. Gröb, K. Harms, G. Seybert, W. Massa, A. Greiner, K. Dehnicke, *Z. Anorg. Allg. Chem.* **1999**, *625*, 1853 – 1859.

[61] P. Ravi, T. Gröb, K. Dehnicke, A. Greiner, *Macromol. Chem. Phys.* **2001**, *202*, 2641 – 2647.

[62] a) T. Gröb, C. Müller, W. Massa, T. Miekisch, G. Seybert, K. Harms, K. Dehnicke, *Z. Anorg. Allg. Chem.* **2001**, *627*, 2191 – 2197; b) S. Chitsaz, B. Neumüller, K. Dehnicke, *Z. Anorg. Allg. Chem.* **1999**, *625*, 9 – 10; c) T. Gröb, K. Harms, K. Dehnicke, *Z. Anorg. Allg. Chem.* **2000**, *626*, 1065 – 1072; d) T. Gröb, S. Chitsaz, K. Harms, K. Dehnicke, *Z. Anorg. Allg. Chem.* **2002**, *628*, 473 – 479.

[63] T. Gröb, G. Seybert, W. Massa, F. Weller, P. Ravi, A. Greiner, K. Dehnicke, *Angew. Chem.* **2000**, *112*, 4542 – 4544; *Angew. Chem. Int. Ed.* **2000**, *39*, 4373 – 4375.

[64] T. Gröb, G. Seybert, W. Massa, K. Dehnicke, *Z. Anorg. Allg. Chem.* **2001**, *627*, 304 – 306.

[65] W. K. Wong, L. Zhang, F. Xue, T. C. W. Mak, *Polyhedron* **1997**, *16*, 345 – 347.

[66] T. Gröb, K. Harms, K. Dehnicke, *Z. Anorg. Allg. Chem.* **2001**, *627*, 1801 – 1806.

[67] D. Nußhär, F. Weller, A. Neuhaus, G. Frenking, K. Dehnicke, *Z. Anorg. Allg. Chem.* **1992**, *615*, 86 – 92.

[68] E. Rentschler, D. Nußhär, F. Weller, K. Dehnicke, *Z. Anorg. Allg. Chem.* **1993**, *619*, 999 – 1003.

[69] J. Grebe, F. Weller, K. Dehnicke, *Z. Naturforsch. B* **1996**, *51*, 1739 – 1743.

[70] T. Gröb, G. Seybert, W. Massa, K. Dehnicke, *Z. Anorg. Allg. Chem.* **2000**, *626*, 349 – 353.

[71] T. Gröb, G. Seybert, W. Massa, K. Dehnicke, *Z. Anorg. Allg. Chem.* **1999**, *625*, 1897 – 1903.

[72] P. Ravi, T. Gröb, K. Dehnicke, A. Greiner, *Macromolecules* **2001**, *34*, 8649 – 8653.

[73] T. Gröb, G. Seybert, W. Massa, K. Harms, K. Dehnicke, *Z. Anorg. Allg. Chem.* **2000**, *626*, 1361 – 1366.

[74] S. Chitsaz, K. Harms, B. Neumüller, K. Dehnicke, *Z. Anorg. Allg. Chem.* **1999**, *625*, 939 – 944.

[75] K. Dehnicke, M. Krieger, W. Massa, *Coord. Chem. Rev.* **1999**, *182*, 19 – 65.

[76] Selected recent review articles: a) H. H. Brintzinger, D. Fischer, R. Mülhaupt, B. Rieger, R. M. Waymouth, *Angew. Chem.* **1995**, *107*, 1255 – 1283; *Angew. Chem. Int. Ed. Engl.* **1995**, *34*, 1143 – 1181; b) W. Kaminsky, *J. Chem. Soc. Dalton Trans.* **1998**, 1413 – 1418; c) C. Janiak in *Metallocenes* (Eds.: A. Togni, R. L. Halterman), Wiley-VCH, Weinheim, **1998**, chap. 9, pp. 547 – 624; d) G. G. Hlatky, *Coord. Chem. Rev.* **1999**, *181*, 243 – 296; e) H. G. Alt, A. Köppl, *Chem. Rev.* **2000**, *100*, 1205 – 1222; f) G. Fink, B. Steinmetz, J. Zechlin, C. Przybyla, B. Tesche, *Chem. Rev.* **2000**, *100*, 1377 – 1390; g) L. Resconi, L. Cavallo, A. Fait, F. Piemontesi, *Chem. Rev.* **2000**, *100*, 1253 – 1346; h) K. Angermund, G. Fink, V. R. Jensen, R. Kleinschmidt, *Chem. Rev.* **2000**, *100*, 1457 – 1470; i) C. Janiak, P. G. Lassahn, *J. Mol. Catal. A* **2001**, *166*, 193 – 209.

[77] U. Siemeling, B. Neumann, H.-G. Stammler, O. Kuhnert, *Z. Anorg. Allg. Chem.* **2000**, *626*, 825 – 826.

[78] D. W. Stephan, J. C. Stewart, F. Guérin, R. E. v. H. Spence, W. Xu, D. G. Harrison, *Organometallics* **1999**, *18*, 1116 – 1118.

[79] D. W. Stephan, F. Guérin, R. E. v. H. Spence, L. Koch, X. Gao, S. J. Brown, J. W. Swabey, Q. Wang, W. Xu, P. Zoricak, D. G. Harrison, *Organometallics* **1999**, *18*, 2046 – 2048.

[80] M. J. Sarsfield, M. Said, M. Thornton-Pett, L. A. Gerrard, M. Bochmann, *J. Chem. Soc. Dalton Trans.* **2001**, 822 – 827.

[81] K. Aparna, M. Ferguson, R. G. Cavell, *J. Am. Chem. Soc.* **2000**, *122*, 726 – 727.

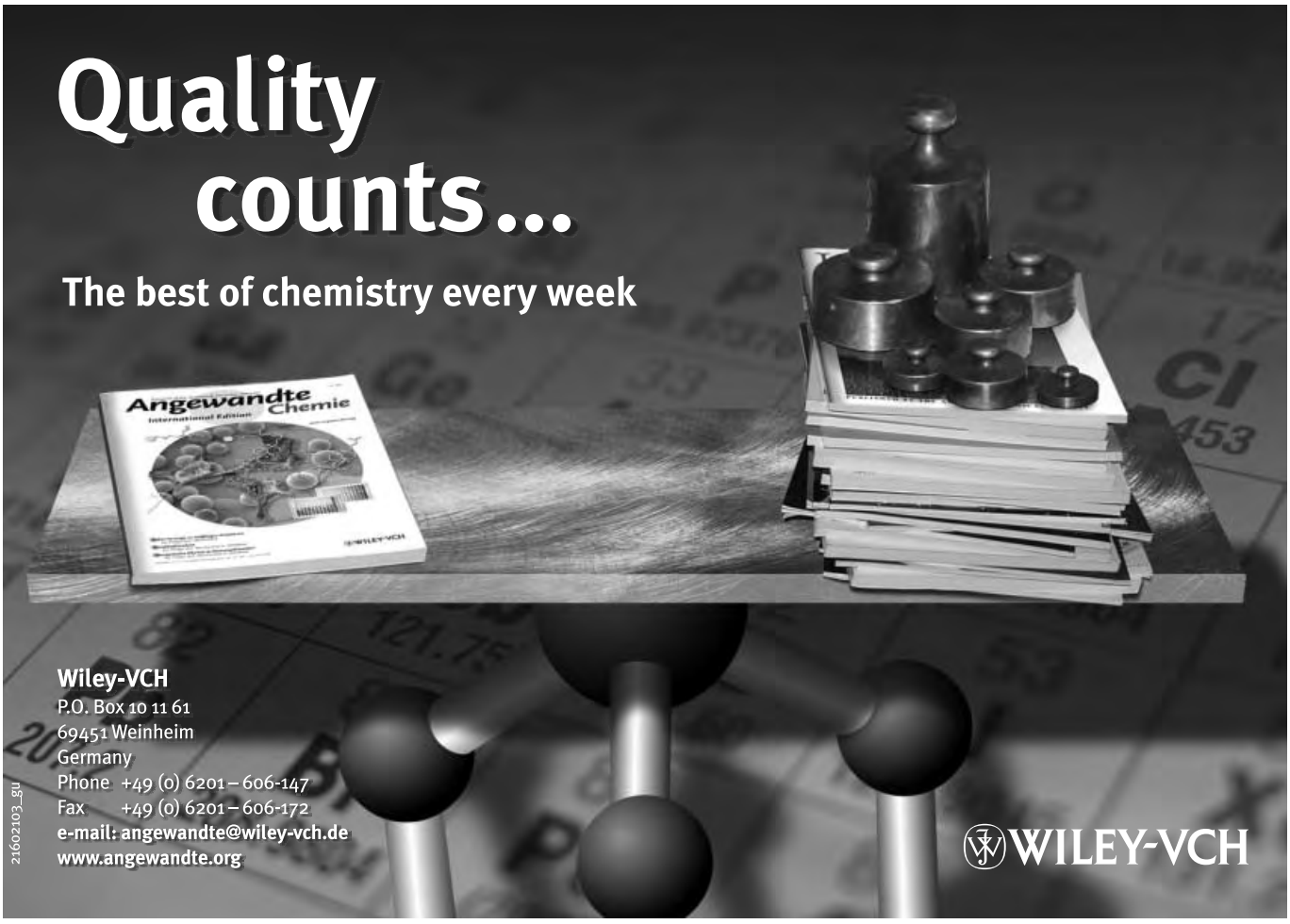

Communications

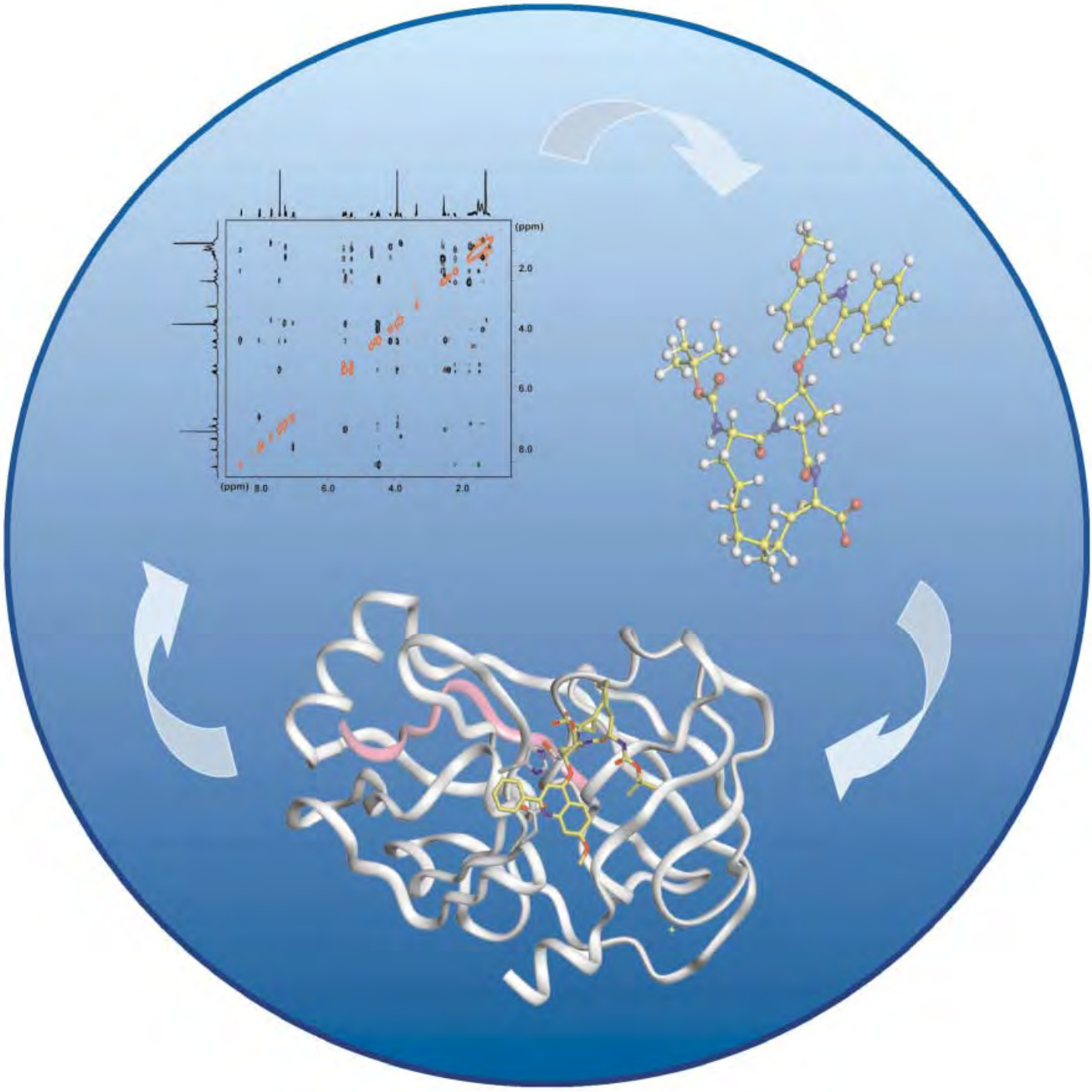

Potent and selective macrocyclic inhibitors of the hepatitis C virus NS3 serine protease based on the conformation of a enzyme-bound substratelike hexapeptide demonstrate many of the desirable properties of a druglike archetype, which could lead to an antiviral agent for the treatment of hepatitis C in man. For more details see the following communication by Tsantrizos et al.

 © 2003 Wiley-VCH Verlag GmbH & Co. KGaA, Weinheim 1433-7851/03/4200-1355 $ 20.00+.50/0

Protease Inhibitors

Macrocyclic Inhibitors of the NS3 Protease as Potential Therapeutic Agents of Hepatitis C Virus Infection**

Youla S. Tsantrizos, Gordon Bolger, Pierre Bonneau, Dale R. Cameron, Nathalie Goudreau, George Kukolj, Steven R. LaPlante, Montse Llinàs-Brunet, Herbert Nar, and Daniel Lamarre*

The hepatitis C virus (HCV) is the etiologic agent of chronic hepatitis C infection, an important health problem that can lead to cirrhosis of the liver and hepatocellular carcinoma in humans.[1] The number of infected individuals is estimated to exceed 170 million people worldwide and the current available treatments (interferon α alone or in combination with ribavirin) are of limited efficacy.[2] In spite of intensive efforts, many aspects of the disease and the biology of the hepatitis C virus remain unclear, making drug discovery an extremely challenging endeavor. We present herein the design of a novel class of selective inhibitors of the HCV NS3 protease, an enzyme which is essential for viral replication in vivo.[3] These compounds exhibit many of the desirable biopharmaceutical properties of antiviral agents and represent a significant advancement towards the discovery of a therapeutic agent for the treatment of hepatitis C in humans.

[*] Dr. Y. S. Tsantrizos, Dr. G. Bolger, Dr. P. Bonneau, Dr. D. R. Cameron, Dr. N. Goudreau, Dr. G. Kukolj, Dr. S. R. LaPlante, Dr. M. Llinàs-Brunet, Dr. D. Lamarre
Departments of Chemistry and Biological Sciences
Boehringer Ingelheim (Canada) Ltd.
Research and Development
2100 Cunard Street, Laval, PQ H7S2G5 (Canada)
Fax: (+1) 450-682-4189
E-mail: ytsantrizos@lav.boehringer-ingelheim.com
Dr. H. Nar
Chemische Forschung und Leitstrukturfindung
Boehringer Ingelheim Pharma KG
Birkendorfer Strasse 65, 88397 Biberach (Germany)

[**] Numerous scientists from Boehringer Ingelheim have contributed to the success of this project. In particular, we wish to acknowledge M. Poirier and J.-M. Ferland (for the synthesis of the macrocyclic inhibitors), N. Aubry (for assistance with the NMR studies), M. Marquis, A. Pause, and C. Pellerin (for their contribution to the replicon assay), D. Thibeault and R. Maurice (for the in vitro enzymatic assays and K_i determinations), C. Plouffe, S. Lefebvre, and H. Li (for purification of the NS3 protease and the specificity assays), A. Schmid (for expert help in crystallization and data collection), H. Bartunik (for access to the beamline BW6 at DESY), and F. Liard, M. Rhéaume, and M. Yazdanian (for their contributions to the metabolism, cell permeability, and PK studies). Finally, we are grateful to P. C. Anderson, M. Bös, M. G. Cordingley for their support, and to J. Duan and S. Kawai for valuable discussions concerning this manuscript. The frontispiece was designed by Dr. Lynn Amon, Boehringer Ingelheim (Canada).

Supporting information for this article is available on the WWW under http://www.angewandte.org or from the author.

The HCV RNA genome contains a long open reading frame, encoding a polyprotein of about 3011 amino acids which must be proteolytically processed into four structural and six nonstructural (NS) polypeptides.[1] The structural polypeptides are cleaved from the polyprotein by host enzymes, whereas the nonstructural proteins are processed by two virally encoded enzymes, the NS2/NS3 and the NS3 proteases;[2] the latter enzyme is responsible for processing four out of the five cleavage sites of the nonstructural region, thus it represents a particularly important target for drug discovery.

Initial investigations revealed that the N-terminal peptide products derived from sequences of the HCV NS3 protease substrates are competitive inhibitors of this enzyme, and these peptides became leads for the design of peptidomimetic inhibitors.[4,5] Similar peptides were used for exploring the interactions between substrate-based ligands and the NS3 protease by NMR spectroscopy,[6–9] molecular modeling, and crystallography.[10] However, the inherent conformational flexibility of these peptides, in addition to the solvent exposure of the shallow S1–S3 binding region of the NS3 protease,[11] posed a significant challenge to the design of relatively small peptidomimetic compounds that could penetrate cell membranes and block replication of the HCV RNA genome in cell culture.

To design of a novel class of inhibitors which could potentially provide a therapeutic agent for the treatment of hepatitis C in humans, the bimolecular recognition elements involved in an NS3–ligand complex were evaluated extensively by NMR spectroscopy and molecular modeling. The HCV NS3 enzyme is fairly unique amongst serine proteases in that it is activated by its structure-modifying cofactor NS4A[12] and by its ligands.[13] Interactions between NS3 and its NS4A cofactor induce conformational changes that significantly reduce (but not entirely eliminate) the plasticity of the enzyme.[13] In addition, stabilization of the NS3 active site upon binding of a substrate-based ligand has been proposed.[8] We explored the interactions of the NS3 protease domain with the substrate-based inhibitor **1** (Figure 1a) by NMR spectroscopy.[6,9,14]

Transferred nuclear Overhauser effects and transferred ^{13}C spin–lattice relaxation NMR experiments indicate that peptide **1** binds to the protease in an extended conformation and undergoes extensive rigidification upon binding. Studies on protease-induced differential line broadening suggested that the P5 and P6 residues are solvent-exposed and interact only weakly with the protease,[6] consistent with reports by other investigators.[7,15] In the inhibitor–protein complex, the P3 side chain lies on the solvent-exposed surface of the protein and close to the P1 norvaline side chain. This latter group is folded, placing the δ CH_3 group close to α H of P1 (Figure 1b).

On the basis of this data and literature precedence,[16] we speculated that intramolecular linking of the P1 side chain to the P3 side chain with a hydrocarbon bridge would lead to a macrocyclic inhibitor which would, in the free state, preferentially adopt the conformation of NS3-bound peptide **1**. A rigid macrocyclic scaffold would also assure that the P2–P3 amide bond would adopt exclusively the *trans* geometry

 © 2003 Wiley-VCH Verlag GmbH & Co. KGaA, Weinheim 1433-7851/03/4212-1356 $ 20.00+.50/0

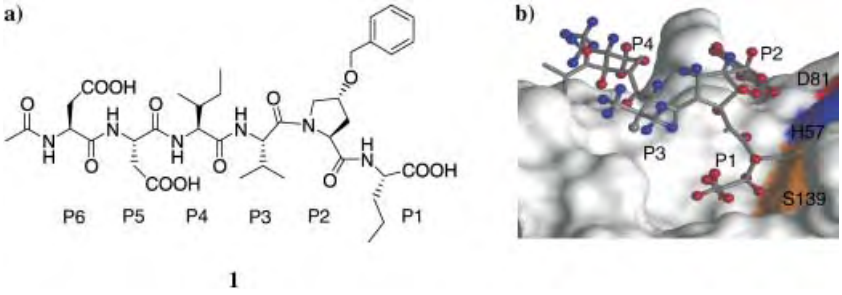

Figure 1. a) Structure of hexapeptide **1**; b) model of P1–P4 moieties of **1** docked in the active site of the apo form of the NS3 protease.[17] Differential line broadening (DLB) NMR data (blue = negative DLB, red = positive DLB) of NS3-bound **1**.

observed in the bound conformation, unlike linear peptides which exist as mixtures of *cis* and *trans* rotamers. The anticipated reduction of the conformational entropic penalty, paid upon binding of this inhibitor, could lead to an increase in the overall binding energy. A model of an inhibitor–enzyme complex was created by simply inserting the NMR-derived structure of NS3-bound **1** into the active site of the apoenzyme (Figure 1 b).[17] This model supported our hypothesis and suggested that additional interactions could be gained between the hydrocarbon bridge of the cyclic inhibitor and the S1–S3 binding pocket of the enzyme. Furthermore, as a consequence of the net reduction in the peptidic nature of the macrocyclic inhibitors, we speculated that these molecules may exhibit more desirable biopharmaceutical properties than their corresponding linear peptides.

The design and synthesis of the rigid macrocyclic inhibitors began with an evaluation of the interactions between the NS3 protease and the basic peptidic scaffold of previously developed tetrapeptide inhibitors, typified by compound **2** (Scheme 1).[18] During these studies, we observed that the tetrapeptide scaffold **2a** and its truncated analogue **3a** are poor inhibitors of the NS3 enzyme in vitro (Table 1, $<20\,\%$ inhibition at 1000 μM was observed). However, we discovered that the 15-membered macrocyclic peptide **4a**, where the double bond is *Z* configured, is more potent than either of the two linear peptides (Table 1, $IC_{50} = 400$ μM).[19] Optimization of **4a** by substitution of the proline with a 4-hydroxy-7-methoxyquinoline moiety (X^1), as previously reported,[18] led to inhibitor **4b** with an approximate 16600-fold increase in potency over the "naked" scaffold **4a**, a close to 50-fold increase in potency over the linear tetrapeptide **2b**, and a 2-fold increase in potency over **2c** which has a vinyl substituent at the cyclopropyl ring (Table 1).[20] Addition of a phenyl substituent to X^1 ($\rightarrow X^2$) led to a doubling of the potency in the in vitro assay (Table 1, **4b** vs **4c**).[21] However, a more than 36-fold drop in potency was observed upon cleaving the bridge of inhibitor **4c** to produce the corresponding open-chain analogue **3b** (Table 1), which confirms the importance of macrocyclization. Predictably, the binding affinity and potency of these inhibitors is highly dependent on the ring size and the stereochemistry of each chiral center.[19] For example, peptide **4c** is 180-fold more potent than its epimer **5**, which further validates the specificity of these inhibitors for their intended molecular target.

Steady-state kinetic analysis of the mode of inhibition by compound **4c** demonstrated competitive inhibition of the NS3–NS4A protease heterodimer of genotype 1b with a K_i of 1.0 nM. For the

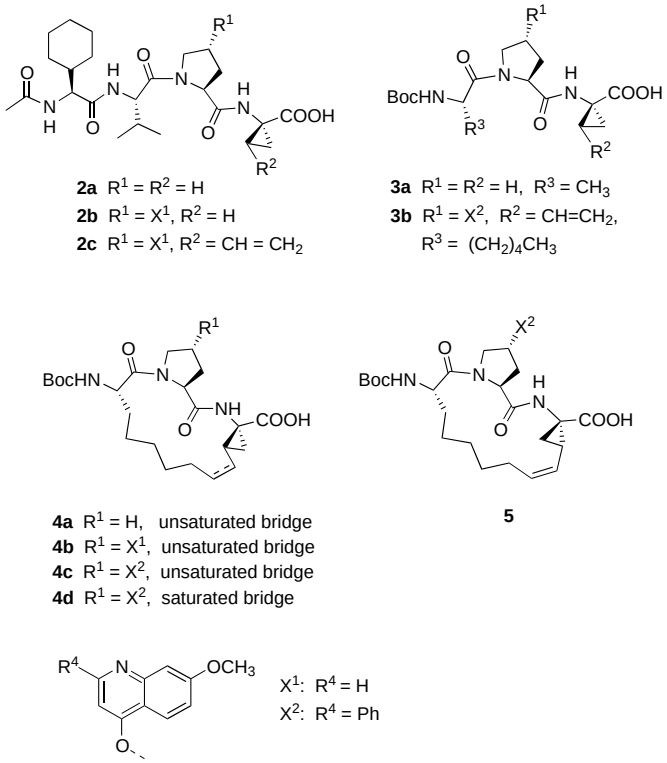

Scheme 1. Structures of tested inhibitors for the NS3 protease.

Table 1: Potency and specificity of the HCV NS3 protease inhibitors **2**–**5** in enzymatic (IC_{50}[a]) and cell-based assays (EC_{50}[b]); n.d. not determined.[29]

Compound	IC_{50}	EC_{50}	IC_{50}(HLE[c])	IC_{50}(HLCatB[d])	IC_{50}(BPChym[e])
2a	>1000				
2b	1.4	>20.0			
2c	0.047	>5.0			
3a	>1000				
3b	0.400	n.d.	>30	n.d.	>30
4a	400.0				
4b	0.024	1.20	>30	n.d.	>30
4c	0.011	0.077	>30	>30	>30
4d	0.028	0.12	>75	>75	>75
5	2.00				

[a] In vitro IC_{50} [μM] determination in enzymatic assays using an NS3–NS4A heterodimer protein of genotype 1b. [b] EC_{50} [μM] determination in Huh-7 cells harboring the bicistronic subgenomic HCV RNA replicon. [c]–[e] In vitro specificity assays used: human leukocyte elastase, human liver cathepsin B, bovine pancreatic chymotrypsin.

 © 2003 Wiley-VCH Verlag GmbH & Co. KGaA, Weinheim 1433-7851/03/4212-1357 $ 20.00+.50/0

heterodimer of genotype 1a a K_i of 1.4 nM was obtained. The compounds **4** were also highly selective in inhibiting the HCV NS3 protease without inhibiting mammalian proteases, even at concentrations exceeding 30 μM (Table 1).[29]

Inhibition of the HCV NS3 protease by the macrocyclic inhibitors **4** was subsequently confirmed in a cell-based assay,[22] using human hepatoma (Huh-7) cells transfected with a selectable subgenomic HCV RNA.[23] In this assay, RNA replication is dependent on the key virally encoded enzymes and is sensitive to compounds which specifically inhibit these enzymes.[24] Negligible reduction in the HCV RNA levels was observed with tetrapeptides **2b** and **2c** even at their solubility limits. In contrast, a median effective concentration (EC_{50}) of 1.2 μM and 0.077 μM was measured for the macrocyclic inhibitors **4b** and **4c**, respectively (Table 1). Saturation of the P1–P3 olefinic bridge of inhibitor **4c** resulted in compound **4d**, which was almost equipotent to its precursor in both the enzymatic and the cell-based assay (Table 1, $IC_{50} = 0.028$ μM, $EC_{50} = 0.120$ μM). Thus, the electronic properties (π character) and rigidification elements of the olefin moiety did not significantly impact the overall stability of the NS3 protease–inhibitor complex.

Binding of the macrocyclic inhibitors in the active site of the NS3 protease was also confirmed by X-ray crystallography. Previously reported crystallographic data revealed the typical chymotrypsin-like fold of the NS3 protease, complexed with the key central segment of its NS4A cofactor (a peptide composed of residues 21–34 of the NS4A and known as $NS4A_{peptide}$).[25,26] The $NS4A_{peptide}$ was shown to intercalate within the N-terminal domain of the protease, forming a β sheet with the enzyme. More recently, X-ray and NMR data of α-keto acid inhibitors covalently bound to the NS3 protease were reported.[8,10] In addition, a crystal structure analysis of an engineered single polypeptide, containing the C-terminal helicase domain and the N-terminal protease covalently linked to the NS4A cofactor, revealed the binding of the C-terminal carboxylic acid moiety of the helicase to the active site of the protease.[27] This is the only earlier report of a C-terminal carboxylate bound to the active site of the NS3–NS4A complex and the system represents a model of product inhibition for this enzyme. However, with the **4c**–NS3–$NS4A_{peptide}$ complex (Figure 2) we present the first X-ray structure analysis of a small-molecule carboxylic acid bound to the active site of this enzyme.

We were successful in obtaining small needlelike co-crystals of the wild-type BK* NS3 protease–$NS4A_{peptide}$ complexed with inhibitor **4c** that diffracted X-rays to 3.0 Å resolution (Figure 2). The macrocyclic compound **4c** was found at the NS3 active site and was clearly defined in the difference electron density. This structure revealed how the carboxylate group interacts with the active site and provided additional insight into the mechanism of product inhibition observed with natural substrates of the HCV NS3 protease. The heteroatom-to-heteroatom distances suggest that one of the carboxylate oxygen atoms of the inhibitor binds in the oxyanion hole of NS3 (NH of G137 and S139), while the other forms a hydrogen bond with the H57 (δ N) residue (Figure 2b). In addition, the side chain (γ O) of S139 appears to form weak asymmetric bifurcated hydrogen bonds with both carboxylate oxygen atoms of the inhibitor. The binding affinities of **4c** toward a wild-type 1b HCV NS3 protease and its corresponding S139A and H57A (catalytically inactive) single amino acid mutants were determined by using a fluorescence polarization assay. We obtained K_D values of 0.04 μM with wild-type NS3 and of 0.007 μM with the S139A mutant,[28,29] whereas a dramatically lower affinity ($K_D >$ 10 μM) was estimated for the H57A mutant. These results suggest that the H57 side chain plays a crucial role in stabilizing the enzyme–inhibitor complex, whereas the net contributions of S139 (γ O) are modulated by many other factors, including perhaps the energy penalty associated with dehydration and disruption of the hydrogen bond with H57.

Formation of canonical hydrogen bonds between the amide moieties of the inhibitor and the NS3 main chain hydrogen bond donor/acceptor residues R155 and A157 was also observed. The *tert*-butyl group was well defined and

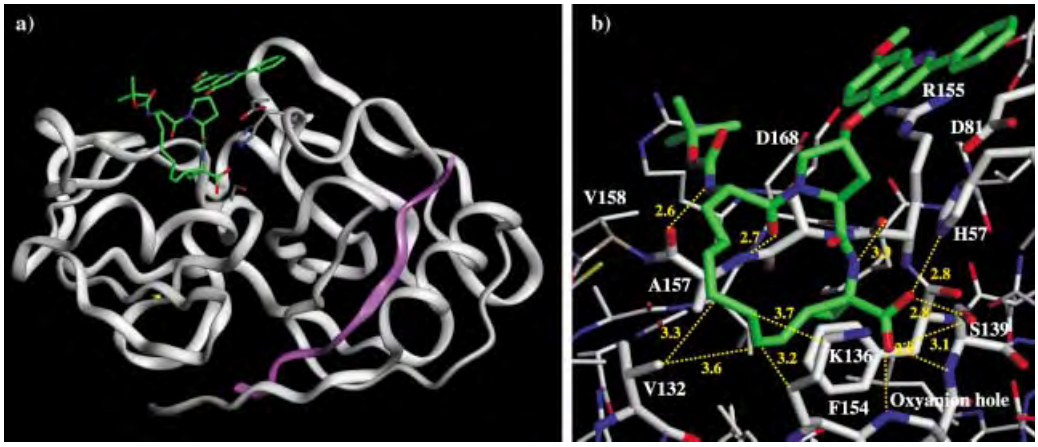

Figure 2. Structure of **4c** bound to the HCV NS3–$NS4A_{peptide}$ complex as determined by X-ray structure analysis. a) **4c** bound in the active site of the complex of BK* NS3 protease (white ribbon with Zn^{2+} ion shown as a yellow ball) with $NS4A_{peptide}$ (purple). b) Key interactions of **4c** with the active site; figures at dashed yellow lines are distances in Å, measured from heteroatom to heteroatom that may be implicated in hydrogen-bond or van der Waals interactions. NS3 residues distal from the binding pocket are shown in thinner lines. Carbon atoms of the inhibitor are colored in green, those of NS3 in white. All nitrogen and oxygen atoms are colored in blue and red, respectively.

 © 2003 Wiley-VCH Verlag GmbH & Co. KGaA, Weinheim 1433-7851/03/4212-1358 $ 20.00+.50/0

positioned above V158 of the protein surface. The aliphatic bridge between P1 and P3 of the inhibitor was clearly visible in the electron density, which indicates that the bridge is conformationally fixed within the S1–S3 pocket. The NS3 residue V132 appears to be within van der Waals distance of this bridge and may contribute to the overall binding energy in the inhibitor–enzyme complex (Figure 2b). Furthermore, inhibitor-induced conformational changes of the R155 and D168 side chains leads to the formation of a salt bridge between these residues and facilitates an interaction of the guanidine group of R155 with the methoxy quinoline unit (Figure 2b).

A comparison of the X-ray data of our inhibitor–enzyme complex with those of the previously reported complex between the apo form of the NS3 protease and $NS4A_{peptide}$ of the BK-strain hepatitis C virus reveals a similar overall structure with only modest differences at the active site.[25] However, our structure provides strong evidence for the molecular basis of the interactions between a potent and selective druglike inhibitor and the NS3 protease, which lead to the distortion of the catalytic triad and the disruption of the hydrogen bond between S139 and H57. Furthermore, the hydrogen bond between H57 and one of the carboxylate oxygen atoms of the inhibitor appears to be forcing a side chain rotation of S139, which places γ O deeper into the core of the protein.

Data from preliminary pharmacokinetic studies on the macrocyclic inhibitors **4c** and **4d** were also encouraging.[29] Both inhibitors were found to be relatively stable to in vitro metabolism in human and rat liver microsomes. After i.v. (intra venous) administration (5.0 $mg\,kg^{-1}$) in rat, both inhibitors were excreted in the bile, which suggests that the liver is the main clearance organ. However, compound **4c** was cleared more rapidly than **4d** and gave a lower volume of distribution at steady state (V_{dss}) (this indicates lower general tissue distribution of **4c**). Oral administration of the inhibitors at a dose of 25 $mg\,kg^{-1}$ to conscious male rats resulted in a peak plasma concentration (c_{max}) of about 0.2 (**4c**) and 1.3 μM (**4d**) and a bioavailability (*F*, calculated by comparison between the i.v. and oral profile) of 2 (**4c**) and 22% (**4d**). Based on the Caco-2 model, the cell membrane permeability for inhibitor **4c** was also significantly lower (~10-fold lower) than that for **4d,** a fact that might contribute to the overall differences in oral bioavailability between the two compounds.[29]

In summary, we have elucidated the subtle details governing the structure–activity relationship between a substrate-based peptidomimetic ligand and the HCV NS3 serine protease. We have used this knowledge to design a novel class of highly specific and potent inhibitors of the HCV NS3 protease for the most prevalent HCV genotypes 1a and 1b, which are also the most resistant to chemotherapy with interferon α. Compound **4c** and its saturated analogue **4d** are the first inhibitors of the NS3 protease which inhibit HCV RNA replication in the cell-based replicon assay. In addition, they are orally absorbed and stable to metabolic breakdown. Thus, these compounds show many of the desirable properties of a druglike archetype and could lead to a clinically useful antiviral agent for the treatment of hepatitis C viral infections in humans.

Experimental Section

Confirmation of the structure and purity of all inhibitors and details on the biological assays and pharmacokinetic studies are provided in the Supporting Information.

The BK* NS3 protease was derived from a construct which encoded a modified BK strain sequence that spanned amino acids 1–180 and contained the C-terminal solubilization motif ASKKKK as previously reported.[9] The protease was complexed with $NS4A_{peptide}$ (KK-^{21}GSVVIVGRIILSGR^{34}-K) and exposed to the inhibitor **4c**. Crystal data: Space group: $P3_221$, cell constants: 76.5, 76.5, 169.2 Å. Data to 3.0 Å resolution were collected at the MPI wiggler beamline BW6B at DESY Hamburg using monochromatic X-radiation with a wavelength of 1.05 Å. Data were integrated, scaled, and merged with the HKL package.[30] Structure solution was done by molecular replacement using 1JXP coordinates from PDB as the search model.[25] Two crystallographically independent molecules were found in each asymmetric unit. An initial difference electron density map unambiguously showed the entire structure of the bound inhibitor. The model was refined with CNS,[31] using data between 20.0 and 3.0 Å resolution and applying noncrystallographic symmetry restraints. (Data collection statistics: resolution limits 100.0–3.0 Å, total observations 41980, unique reflections 11050, completeness 92.7%, *R* merge 0.065; refinement statistics: number of atoms in model: protein 2774, inhibitors 102, zinc ions 2, number of reflections (free set) 10493 (527), rms deviation from ideal geometry: bond lengths 0.01 Å, bond angles 1.59°, temperature factors [$Å^2$]: all protein atoms 60.9 $Å^2$, rms bonded 1.2 $Å^2$, *R* 0.271, R_{free} 0.327.)

Received: October 1, 2002 [Z50274]

Keywords: hepatitis C · inhibitors · NMR spectroscopy · structure elucidation · structure–activity relationships

[1] Q.-L. Choo, G. Kuo, A. J. Weiner, L. R. Overby, D. W. Bradley, M. Houghton, *Science* **1989**, *244*, 359.
[2] A. M. Di Bisceglie, J. McHutchison, C. M. Rice, *Hepatology* **2002**, *35*, 224.
[3] A. A. Kolykhalov, K. Mihalik, S. M. Feinstone, C. M. Rice, *J. Virol.* **2000**, *74*, 2046.
[4] P. Ingallinella, S. Altamura, E. Bianchi, M. Taliani, R. Ingenito, R. Cortese, R. De Francesco, C. Steinkühler, A. Pessi, *Biochemistry* **1998**, *37*, 8906, and references therein.
[5] M. Llinàs-Brunet, M. Bailey, G. Fazal, E. Ghiro, V. Gorys, S. Goulet, T. Halmos, R. Maurice, M. Poirier, M.-A. Poupart, J. Rancourt, D. Thibeault, D. Wernic, D. Lamarre, *Bioorg. Med. Chem. Lett.* **2000**, *10*, 2267, and references therein.
[6] S. R. LaPlante, D. R. Cameron, N. Aubry, S. Lefebvre, G. Kukolj, R. Maurice, D. Thibeault, D. Lamarre, M. Llinàs-Brunet, *J. Biol. Chem.* **1999**, *274*, 18618.
[7] D. O. Cicero, G. Barbato, U. Koch, P. Ingallinella, E. Bianchi, M. C. Nardi, C. Steinkühler, R. Cortese, V. Matassa, R. De Francesco, A. Pessi, R. Bazzo, *J. Mol. Biol.* **1999**, *289*, 385.
[8] G. Barbato, D. O. Cicero, F. Cordier, F. Narjes, B. Gerlach, S. Sambucini, S. Grzesiek, V. G. Matassa, R. De Francesco, R. Bazzo, *EMBO J.* **2000**, *19*, 1195.
[9] S. R. LaPlante, N. Aubry, P. R. Bonneau, G. Kukolj, D. Lamarre, S. Lefebvre, H. Li, M. Llinàs-Brunet, C. Plouffe, D. R. Cameron, *Bioorg. Med. Chem. Lett.* **2000**, *10*, 2271.
[10] S. Di Marco, M. Rizzi, C. Volpari, M. A. Walsh, F. Narjes, S. Colarusso, R. De Francesco, V. G. Matassa, M. Sollazzo, *J. Biol. Chem.* **2000**, *275*, 7152.
[11] Protease subsite nonmenclature: I. Schechter, A. Berger, *Biochem. Biophys. Res. Commun.* **1967**, *27*, 157.
[12] R. Bartenschlager, *J. Viral Hepat.* **1999**, *6*, 165.

 © 2003 Wiley-VCH Verlag GmbH & Co. KGaA, Weinheim 1433-7851/03/4212-1359 $ 20.00+.50/0

[13] E. Bianchi, S. Orrû, F. Dal Piaz, R. Ingenito, A. Casbarra, G. Biasiol, U. Koch, P. Pucci, A. Pessi, *Biochemistry* **1999**, *38*, 13844.
[14] S. R. LaPlante, N. Aubry, R. Déziel, F. Ni, P. Xu, *J. Am. Chem. Soc.* **2000**, *122*, 12530.
[15] U. Koch, G. Biasiol, M. Brunetti, D. Fattoti, M. Pallaoro, C. Steinkühler, *Biochemistry* **2001**, *40*, 631.
[16] J. D. A. Tyndall, D. P. Fairlie, *Curr. Med. Chem.* **2001**, *8*, 893.
[17] R. A. Love, H. E. Parge, J. A. Wickersham, Z. Hostomsky, N. Habuka, E. W. Moomaw, T. Adachi, Z. Hostomska, *Cell* **1996**, *87*, 331.
[18] M.-A. Poupart, D. R. Cameron, C. Chabot, E. Ghiro, N. Goudreau, S. Goulet, M. Poirier, Y. S. Tsantrizos, *J. Org. Chem.* **2001**, *66*, 4743.
[19] Y. S. Tsantrizos, D. R. Cameron, A.-M. Faucher, E. Ghiro, N. Goudreau, T. Halmos, M. Llinàs-Brunet, *PTC Int. Appl.* [Boehringer Ingelheim (Canada) Ltd.] WO 00/59929 **2000**.
[20] J. Rancour, unpublished results.
[21] N. Goudreau, unpublished results.
[22] V. Lohmann, F. Körner, J.-O. Koch, U. Herian, L. Theilmann, R. Bartenschlager, *Science* **1999**, *285*, 110.
[23] G. Kukolj, A. Pause, *PTC Int. Appl.* [Boehringer Ingelheim (Canada) Ltd.] WO 02/052015A2 **2002**.
[24] D. Dhanak, K. J. Duffy, V. K. Johnston, J. Lin-Goerke, M. Darcy, A. N. Shaw, B. Gu, C. Silverman, A. T. Gates, M. R. Nonnemacher, D. L. Earnshaw, D. J. Casper, A. Kaura, A. Baker, C. Greenwood, L. L. Gutshall, D. Maley, A. DelVecchio, R. Macarron, G. A. Hofmann, Z. Alnoah, H.-Y. Cheng, G. Chan, S. Khandekar, R. M. Keenan, R. T. Sarisky, *J. Biol. Chem.* **2002**, *277*, 38322.
[25] Y. Yan, Y. Li, S. Munshi, V. Sardana, J. L. Cole, M. Sardana, C. Steinkühler, L. Tomei, R. De Francesco, L. C. Kuo, Z. Chen, *Protein Sci.* **1998**, *7*, 837.
[26] J. L. Kim, K. A. Morgenstern, C. Lin, T. Fox, M. D. Dwyer, J. A. Landro, S. P. Chambers, W. Markland, C. A. Lepre, E. T. O'Malley, S. L. Harbeson, C. M. Rice, M. A. Murcko, P. R. Caron, J. A. Thomson, *Cell* **1996**, *87*, 343.
[27] N. Yao, P. Reichert, S. S. Taremi, W. W. Prosise, P. C. Weber, *Structure* **1999**, *7*, 1353.
[28] D. Fattori, A. Urbani, M. Brunetti, R. Ingenito, A. Pessi, K. Prendergast, F. Narjes, V. G. Matassa, R. De Francesco, C. Steinkühler, *J. Biol.* Chem. **2000**, *275*, 15106.
[29] Supporting Information to this paper is available on: cloning, expression, enzyme purification, in vitro enzymatic asays, cell-based assay, and fluorescence polarization assay (Appendix I), pharmacokinetic studies (Appendix II), NMR and MS data of inhibitors (Appendix III).
[30] D. Gewirth, *The HKL Manual*, 3rd ed., Yale University, New Haven, CT, **1994**.
[31] A. T. Brünger, P. D. Adams, G. M. Clore, W. L. DeLano, P. Gros, R. W. Grosse-Kunstleve, J.-S. Jiang, J. Kuszewski, M. Nilges, N. S. Pannu, R. J. Read, L. M. Rice, T. Simonson, G. L. Warren, *Acta Crystallogr. Sect. D* **1998**, *54*, 905.

 © 2003 Wiley-VCH Verlag GmbH & Co. KGaA, Weinheim 1433-7851/03/4212-1360 $ 20.00+.50/0

Supramolecular Inclusion Compounds

A Family of Supramolecular Inclusion Solids Based Upon Second-Sphere Interactions**

*D. Shekhar Reddy, Scott Duncan, and George K. H. Shimizu**

The ability to include and order molecules in the solid state is of fundamental importance in the design of new functional solids.[1] Layered solids with porous interlayer regions have long offered an attractive route to such compounds.[2] The focus of these studies has ranged from wholly inorganic solids, such as pillared clays,[3] to hybrid inorganic–organic solids, such as metal phosphonates (RPO_3^{2-})[4] and sulfonates (RSO_3^-).[5] For the metal phosphonates and sulfonates, in simple $[M^{n+}(XO_3^{m-})_{n/m}]$ (X = P, S) complexes, adjacent organic pendant groups are oriented in an efficiently packed manner by the metal ions and yield nonporous interlayer regions (Figure 1a). For metal phosphonates, a typical approach to remedy this problem is to alternate a "pillaring" phosphonate group with either a methylphosphonate or with phosphate ion[6] (Figure 1b). The evolution of layered solids continued to systems sustained by weaker interactions, such

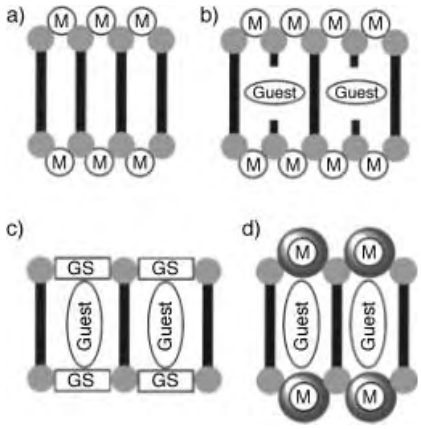

Figure 1. Representations of pillared layered solids: a) a simple metal diphosphonate with no space for guest inclusion, b) a mixed diphosphonate/phosphate with guests, c) a guanidinium disulfonate with guest inclusion, d) a second-sphere metal hexaamine disulfonate structure with guest inclusion.

[*] Dr. G. K. H. Shimizu, Dr. D. S. Reddy
Department of Chemistry
University of Calgary
Calgary, AB T2N 1N4 (Canada)
Fax: (+1) 403-289-9488
E-mail: gshimizu@ucalgary.ca
Dr. S. Duncan
Defence Research and Development Canada—Suffield
Medicine Hat, AB T1A 8K6 (Canada)

[**] This work was funded by a grant from the Technology Investment Fund administered by the Canadian Department of National Defence.

 © 2003 Wiley-VCH Verlag GmbH & Co. KGaA, Weinheim 1433-7851/03/4212-1360 $ 20.00+.50/0

as charge-assisted hydrogen bonding. Notable examples in this domain include the complexes of secondary ammonium salts and polycarboxylate anions, studied by Zaworotko and co-workers,[7] and the layered networks formed between guanidinium (G) cations and organosulfonate (S) anions, extensively studied by Ward and co-workers and also by Masson and co-workers.[8,9] In contrast to $[M^{n+}(XO_3^{m-})_{n/m}]$ systems, the organic pillars in GS networks are oriented in a less densely packed manner, a result of the larger size of a guanidinium cation relative to a metal ion, which allows for guest inclusion in the interlayer region (Figure 1c). The vast array of inclusion phenomena observed for this family of compounds (> 350 structures) owe their existence to the ability of the GS framework to adjust to different guests by puckering of the layers and "turnstile-like" rotation of the pillars. The insights provided by this library have enabled the generation a framework containing highly ordered polar guest molecules for nonlinear optical applications.[8b] Our approach, shown in Figure 1d, extends our recent work on second-sphere aqua complexes of organosulfonate ligands[10] and represents an inorganic analogue of guanidinium sulfonates. In essence, an octahedral hexaamine metal complex should provide two triangular triamine faces with divergent N–H bonds to act as hydrogen-bond donors. Thus, each face would be similar to a guanidinium cation and could possibly form highly complementary hydrogen-bond pairs with sulfonate anions. Significantly, the larger radius of a second-sphere complex relative to a single metal ion would further distance the pendant organic groups on the sulfonates and facilitate guest inclusion. Herein, we present two complexes, formed from $[Co(NH_3)_6]Cl_3$ and disulfonate anions, which form pillared layered structures and include guest molecules, $[\{[Co(NH_3)_6Cl](PIPES)(H_2O)_6\}_\infty]$ (**1**, PIPES = 1,4-piperazine-bis(ethanesulfonate) and $[\{[Co(NH_3)_6](NDS)_{1.5}(H_2O)_2\text{-}(dioxane)\}_\infty]$ (**2**, NDS = 2,6-naphthalenedisulfonate). The networks are sustained by charge-assisted hydrogen bonding and show two different assembly motifs, one based on the complementarity of the edges of the triangular triamine faces with sulfonate groups, this is the GS analogue, and the other on hydrogen-bond complementarity with the centroids of the triangular faces.

Compound **1** forms a hexagonal hydrogen-bonding motif with complementarity between the periphery of the triangular $\{Co(NH_3)_3\}$ faces and two sulfonate oxygen atoms as shown in Figure 2a and b.[11] The N···O hydrogen bonds between the amine groups and sulfonate ions are in the range 2.94–3.17 Å with N–H···O angles between 128–167°. The $[Co(NH_3)_6]^{3+}$ ions align in a plane with their C_3 axes perpendicular to the layer. The layers in **1** are pillared by the bis(ethyl)piperazine moieties at a distance of 14.12(1) Å. The distances between neighboring S atoms, which anchor the pillars, in a given layer are between 7.376(3)–7.975(3) Å. Thus, this structural motif is well organized for guest inclusion. The greater separation between pillars allows for the inclusion of approximately 7.5 molecules of water in the interlayer region for each disulfonate unit. With the substitution of guanidinium cations for the pyramidalized $\{Co(NH_3)_3\}$ units, this hydrogen-bonding motif is identical to that observed in GS networks. For an octahedral hexaamine metal complex to function as two

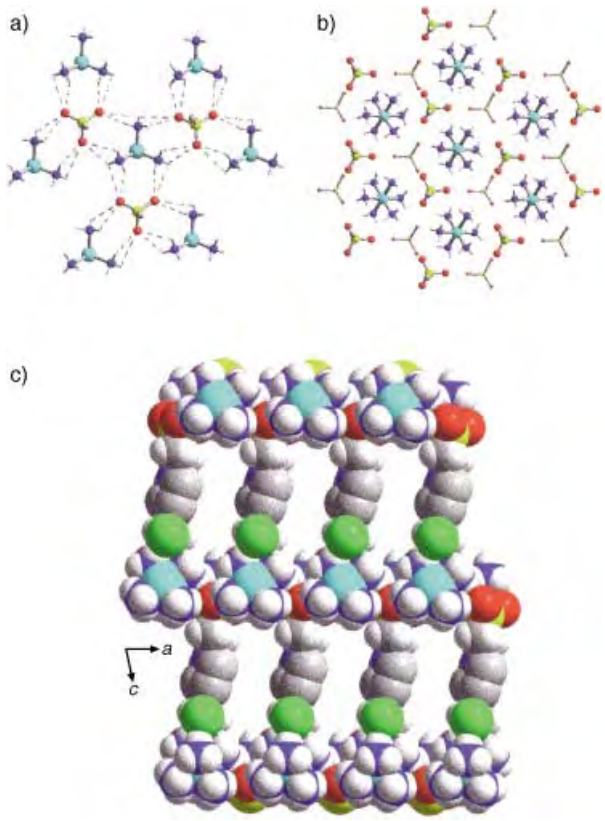

Figure 2. Structure of **1** showing: a) the hydrogen-bonding pattern about each triangular $\{Co(NH_3)_3\}$ face, b) the hexagonal assembly of a single layer, and c) space-filling representation, perpendicular to the layers, showing the spatial arrangement of the pillars and the "nesting" of the Cl^- ions (green). One NH_3 molecule in the top layer (to show the Co centers) and guest water molecules have been deleted. Co light blue, N dark blue, S yellow, O red, H gray.

(monovalent) guanidinium cations and form a similar hydrogen-bonding motif with sulfonate anions, the metal ion would be expected to be divalent. Interestingly, with respect to its hydrogen-bonding pattern, the Co^{3+} center in structure **1** behaves effectively as a divalent center by the incorporation of a chloride ion which "nests" atop one triamine face of each metal complex (Figure 2c). The N···Cl hydrogen bonds between the amine groups and chloride ions are between 3.32–3.35 Å.

Compound **2** also forms a perfectly flat layered structure based upon hydrogen bonding between $[Co(NH_3)_6]^{3+}$ units and pillaring sulfonate anions.[12] In this case, with a 2,6-naphthyl unit as the pillar, no chloride ion is incorporated and the hydrogen-bonding complementarity is shifted. In **2**, the metal octahedra align with their C_4 axes perpendicular to the layers (Figure 3a and 3b). The predominant hydrogen-bonding interaction of each $[Co(NH_3)_6]^{3+}$ unit with neighboring sulfonate groups is then between the centroids of each triangular triamine face and single sulfonate oxygen atoms (N···O distances from 2.90–3.33 Å with N–H···O angles from 112–163°). The layers in **2** are separated at a distance of 13.987(6) Å by the naphthyl spacers, which is half the length of the *a* axis. As in **1**, the second-sphere approach results in the orientation of the organic pillars in a less densely packed

 © 2003 Wiley-VCH Verlag GmbH & Co. KGaA, Weinheim 1433-7851/03/4212-1361 $ 20.00+.50/0

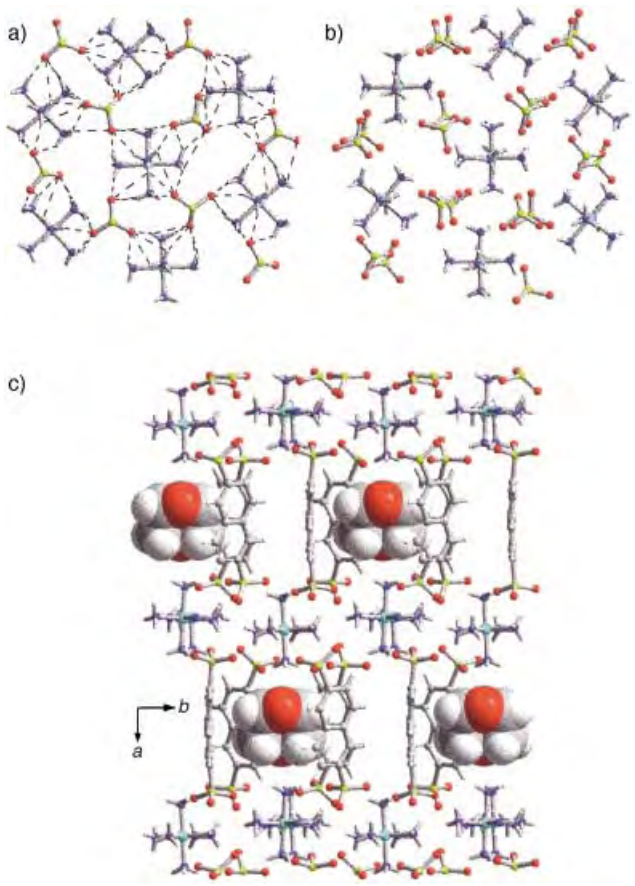

Figure 3. Structure of **2** showing: a) the hydrogen-bonding pattern about the fourfold axis of each $[Co(NH_3)_6]$ octahedron, b) the view down onto a single layer, c) the view perpendicular to the layers showing the 2,6-naphthyl pillars and, in space-filling representation, the included dioxane molecules. Colors as in Figure 2.

manner to enable guest inclusion. In **2**, two molecules of water and one dioxane molecule are included for each 2,6-naphthyl unit (Figure 3c).

Thermogravimetric analyses (TGA) and powder X-ray diffraction (PXRD) data of the two structures show very different features. The PXRD studies confirmed that bulk powders of both compounds **1** and **2** were indeed the same phases as those observed in the respective single-crystal structures. In the TGA, **1** shows a fairly rapid mass loss from 25–60 °C, which corresponds to the loss of the guest water molecules from the interlayer region. A steadier decline in mass is then observed from 60–200 °C. The PXRD of **1** revealed changes in intensities but not in peak positions upon drying for 44 h at room temperature (or for 30 min at 50 °C). In both these cases, exposure to water vapor generated a solid with the same PXRD as the original solid. Heating **1** to 140 °C for 30 min gave a PXRD pattern with weak signal relative to the background albeit with small peaks which did correlate with the original sample. At this temperature, as supported by the TGA data, NH_3 is being lost from the primary coordination sphere, which results in the disruption of the hydrogen-bonded framework. In this case, resolvation did not regenerate the original PXRD pattern. In light of the behavior of **1**, the results for 2,6-naphthyl analogue are quite striking (see below).

PXRD studies of a bulk aqueous precipitate from sodium 2,6-naphthalenedisulfonate and $[Co(NH_3)_6]Cl_3$ in the absence of dioxane showed this sample to possess the same framework as that of structure **2**. Figure 4a and b show the simulated PXRD pattern from **2** and the pattern for the dioxane-free bulk precipitate **2a**, respectively. Compound **2a** is formulated as $[\{[Co(NH_3)_6](NDS)_{1.5}(H_2O)_x\}_\infty]$ (**2a**). As a sufficient quantity of **2** in single-crystal form was not obtainable for all required TGA and PXRD experiments, further characterization was performed on the bulk aqueous precipitate, **2a**.[13] TGA measurements reveal that **2a** loses included water molecules up to roughly 100 °C. From this temperature, the compound is completely stable until loss of the coordinated NH_3 molecules at about 270 °C. As shown in Figure 4c, a PXRD pattern of **2a** acquired after heating to 140 °C for 90 min is virtually identical to the original solid, not only with respect to the positions of the peaks, but also the sharpness of the lines. Remarkably, the differential scanning calorimetry

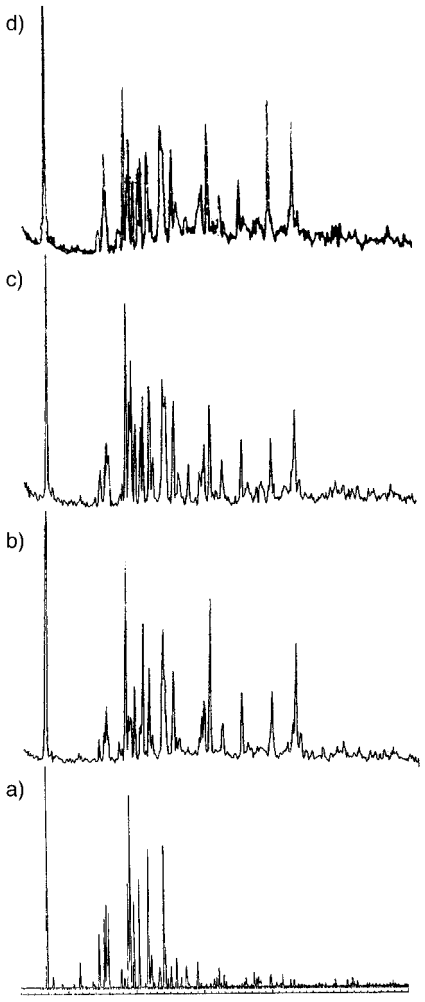

Figure 4. a) PXRD simulation from the single-crystal data of **2**. PXRD data of compound **2a**, b) run at room temperature without drying, c) run after heating at 140 °C for 90 min, DSC/TGA indicate this phase persists until ≈270 °C, and d) after resolvation of the sample in (c) with water.

 © 2003 Wiley-VCH Verlag GmbH & Co. KGaA, Weinheim 1433-7851/03/4212-1362 $ 20.00+.50/0

(DSC)/TGA data indicate that this phase is stable until around 270 °C. For a sample sustained by charge-assisted hydrogen bonding, this is a surprising degree of stability. Upon resolvation of the heated sample with water, there is again little change in the observed PXRD pattern (Figure 4d).

The difference in stability of compounds **1** and **2a** can be rationalized by two factors. The first is the nature of the pillaring group. In compound **2a**, the 2,6-naphthyl unit is much more rigid as it has a fused aromatic skeleton and is locked into a plane with the sulfonate groups perfectly antiparallel. Thus, one sulfonate group in a highly favorable hydrogen-bonding orientation with a layer would necessarily orient the other sulfonate group in a similar manner with the next layer resulting in a mutual stabilizing effect. We have documented these effects for the stabilization of a primary hexaaqua coordination sphere.[10] In comparison, the bis-(ethyl)piperazine unit in **1** is a not-at-all rigid pillar and the enhanced stabilization effects through cooperative bonding by the disulfonates are not optimized. Second, in **1**, in addition to the sulfonate anions, there is incorporation of a chloride ion which also hydrogen bonds to the amine groups of the Co^{3+} center. This interaction would serve to neutralize some of the positive charge on the metal amine unit. Thus, effectively, the hydrogen bonds to the sulfonate groups in **1** are not as charge-assisted as those in **2**.

The compounds presented here, beyond being two examples of supramolecular inclusion compounds, are members of an entire new family of hosts.[14] Significantly, these compounds can be considered as inorganic analogues of guanidinium sulfonates, the single most structurally characterized supramolecular host family.[1,8] The breadth of structures possible with the second-sphere approach should, in principle, be even greater than with the GS structures. This statement is based on the fact that all the pillaring options with the GS structures are equally available to be employed with the second-sphere approach, however, both the identity and charge of the metal center can also be varied. As may be discerned from the structure of compound **1**, the GS motif should also occur for divalent hexaamine metal centers.

Experimental Section

1: The Na salt of piperazinebis(ethanedisulfonate) (292 mg, 0.843 mmol) and hexaamminecobalt(III) chloride (150 mg, 0.561 mmol) were dissolved separately in a minimum amount of water. The dissolved components were added to 10-mL round-bottom flask and stirred at room temperature for 12 h. The pale yellow solid which precipitated was collected by filtration and dried. Yield: 0.246 g, 0.320 mmol (77 % with respect to Co). Crystals suitable for an X-ray analysis were grown by slow evaporation of an aqueous solution. Elemental analysis calcd (%) for $C_8H_{34}ClCoN_8O_6S_2$ (dehydrated) C 18.17, H 6.46, N 21.19; found C 18.46, H 7.01, N 20.54. IR (KBr): $\tilde{\nu} = 3448, 3261, 1356, 1326, 1250, 1211, 836, 587\ cm^{-1}$.

2: The Na salt of naphthalene-2,6-disulfonate (200 mg, 0.602 mmol) and hexaamminecobalt(III) chloride (107 mg, 0.401 mmol) were dissolved separately in water (25 mL). The dissolved components were placed in a H-tube and pure water added to fill the linking bridge. A small amount of p-dioxane was added to the H-tube and the tube allowed to stand at room temperature. A small sampling (≈ 10) of light brown crystals of **2** suitable for an X-ray analysis were observed after 10 days. Elemental analysis calcd (%) for $CoS_3O_{11}N_6C_{19}H_{35}$: C 32.16, H 4.92, N 13.24; found C 32.61, H 4.97, N, 13.26. IR (KBr): $\tilde{\nu} = 3295, 1330, 1306, 1224, 1179, 1087, 1032, 869, 662, 544\ cm^{-1}$.

The differences in O and H stoichiometries between samples employed for elemental analyses and the crystal data reflect loss of water and that the H atoms on the free water molecules in the channels were not included in the single-crystal refinement.

Received: October 1, 2002 [Z50275]

Keywords: cobalt · crystal engineering · host–guest systems · layered compounds · supramolecular chemistry

[1] D. J. Plaut, K. T. Holman, A. M. Pivovar, M. D. Ward, *J. Phys. Org. Chem.* **2000**, *13*, 858.

[2] a) R. S. Taylor, *Pillared Layered Structures* (Ed.: I. V. Mitchell), Elsevier, New York, **1990**, pp. 3–12; b) K. Ohtsuka, *Chem. Mater.* **1997**, *9*, 2039.

[3] a) J. T. Kloprogge, *J. Porous Mater.* **1998**, *5*, 5; b) A. Vaccari, *Catal. Today* **1998**, *41*, 51.

[4] a) G. Alberti, U. Costantino, *Comprehensive Supramolecular Chemistry, Vol. 7* (Eds.: J. L. Atwood, J. E. D. Davies, D. D. MacNicol, F. Vögtle), Elsevier Science, New York, **1996**, chap. 1, pp. 1–24; b) A. Clearfield, *Prog. Inorg. Chem.* **1998**, *47*, 371; c) T. E. Mallouk, J. A. Gavin, *Acc. Chem. Res.* **1998**, *31*, 209; d) M. E. Thompson, *Chem. Mater.* **1994**, *6*, 1168.

[5] a) A. P. Côté, G. K. H. Shimizu, *Chem. Commun.* **2001**, 251; b) S. A. Dalrymple, G. K. H. Shimizu, *Chem. Eur. J.* **2002**, *8*, 3010; c) A. P. Côté, M. J. Ferguson, K. A. Khan, G. D. Enright, A. D. Kulynych, S. A. Dalrymple, G. K. H. Shimizu, *Inorg. Chem.* **2002**, *41*, 287.

[6] a) G. Alberti, U. Costantino, F. Marmottini, R. Vivani, P. Zappelli, *Angew. Chem.* **1993**, *105*, 1396; *Angew. Chem. Int. Ed. Engl.* **1993**, *32*, 1357; b) G. Alberti, F. Marmottini, S. Murcia-Mascarós, R. Vivani, *Angew. Chem.* **1994**, *106*, 1655; *Angew. Chem. Int. Ed. Engl.* **1994**, *33*, 1594; c) N. J. Clayden, *J. Chem. Soc. Dalton Trans.* **1987**, 1877.

[7] a) R. E. Melendez, C. V. K. Sharma, M. J. Zaworotko, C. Bauer, R. D. Rogers, *Angew. Chem.* **1996**, *108*, 2357; *Angew. Chem. Int. Ed. Engl.* **1996**, *35*, 2213; b) K. Biradha, D. Dennis, V. A. MacKinnon, C. V. K. Sharma, M. J. Zaworotko, *J. Am. Chem. Soc.* **1998**, *120*, 11894.

[8] a) K. T. Holman, A. M. Pivovar, J. A. Swift, M. D. Ward, *Acc. Chem. Res.* **2001**, *34*, 107, and references therein; b) K. T. Holman, A. M. Pivovar, M. D. Ward, *Science* **2001**, *294*, 1907; c) A. M. Pivovar, K. T. Holman, M. D. Ward, *Chem. Mater.* **2001**, *13*, 3018; d) V. A. Russell, C. C. Evans, W. Li, M. D. Ward, *Science* **1997**, *276*, 575.

[9] Masson and co-workers have also employed the GS tectons to generate liquid-crystalline solids, F. Mathevet, P. Masson, J.-F. Nicoud, A. Skoulios, *Chem. Eur. J.* **2002**, *8*, 2248.

[10] a) S. A. Dalrymple, M. Parvez, G. K. H. Shimizu, *Chem. Commun.* **2001**, 2672; b) S. A. Dalrymple, G. K. H. Shimizu, *Chem. Commun.* **2002**, 2224.

[11] Crystal data for **1**, $[\{[Co(NH_3)_6Cl](PIPES)(H_2O)_6\}_\infty]$: $C_8H_{38}ClCoN_8O_{12}S_2$: M_r596.96, triclinic, space group $P\bar{1}$ (No. 1), $a = 7.247(1)$, $b = 7.281(1)$, $c = 14.493(3)$ Å, $\alpha = 78.62(3)$, $\beta = 83.60(3)$, $\gamma = 69.40(3)°$, $V = 701.0(2)$ Å^3, $Z = 1$, $\rho_{calcd} = 1.414\ Mg\,m^{-3}$, $\mu(Mo_{K\alpha}) = 0.915\ mm^{-1}$, crystal size $0.01 \times 0.01 \times 0.02$ mm. Data were collected on a Nonius Kappa CCD diffractometer using $Mo_{K\alpha}$ radiation. A total of 4939 reflections ($1.43° < \theta < 26.03°$) were processed and considered significant with $I_{net} > 2\sigma(I_{net})$. Structure solution, refinement and molecular graphics were carried out with the SHELXTL software package, release 5.1.[15] Final residuals for $I_{net} > 2\sigma(I_{net})$ were $R1 = 0.0606$

 © 2003 Wiley-VCH Verlag GmbH & Co. KGaA, Weinheim 1433-7851/03/4212-1363 $ 20.00+.50/0

and $wR_2 = 0.1545$ (GoF = 1.088) for 258 parameters. CCDC-194474 (**1**) CCDC-194475 (**2**) contains the supplementary crystallographic data for this paper. These data can be obtained free of charge via www.ccdc.cam.ac.uk/conts/retrieving.html (or from the Cambridge Crystallographic Data Centre, 12 Union Road, Cambridge CB21EZ, UK; fax: (+44) 1223-336-033; or deposit@ccdc.cam.ac.uk).

[12] Crystal data for **2**, $[\{[Co(NH_3)_6](NDS)(H_2O)_2(dioxane)\}_\infty]$: $C_{19}H_{35}CoN_6O_{12.25}S_3$, $M_r = 698.64$, monoclinic, space group $C2/c$ (No. 15), $a = 27.973(6)$, $b = 12.701(3)$, $c = 15.338(3)$ Å, $\alpha = \gamma = 90$, $\beta = 113.14(3)°$, $V = 5011(2)$ Å^3, $Z = 8$, $\rho_{calcd} = 1.852$ Mg m^{-3}, $\mu(Mo_{K\alpha}) = 1.016$ mm^{-1}, crystal size $0.01 \times 0.015 \times 0.02$ mm. Data were collected on a Nonius Kappa CCD diffractometer using $Mo_{K\alpha}$ radiation. A total of 20678 reflections ($3.12° < \theta < 27.72°$) were processed of which 5775 were considered significant with $I_{net} > 2\sigma(I_{net})$. Structure solution, refinement and molecular graphics were carried out with the SHELXTL software package, release 5.1.[15] Final residuals for $I_{net} > 2\sigma(I_{net})$ were $R1 = 0.0428$ and $wR_2 = 0.0875$ (GoF = 1.004) for 340 parameters.[12]

[13] This is because crops of single crystals of **2** were grown by diffusion in H-shaped tubes. Each preparation yielded no more than 8–10 small crystals.

[14] To date, we have characterized some 20 members of this family. Whereas the hydrogen-bonding patterns observed are not as regular as with the GS networks (some incorporate Cl^- ions and adopt C_3-symmetric structures and others adopt the C_4 orientation) the structures are all 2D. A more extensive study will be reported as a full paper in due course.

[15] SHEXTL Version 5.1, Bruker AXS Inc., Madison, Wisconsin, **1997**.

 © 2003 Wiley-VCH Verlag GmbH & Co. KGaA, Weinheim 1433-7851/03/4212-1364 $ 20.00+.50/0

Ni-Catalyzed Multicomponent Reaction

Catalytic Three-Component Coupling of Alkynes, Imines, and Organoboron Reagents**

*Sejal J. Patel and Timothy F. Jamison**

As part of our interest in selective, catalytic multicomponent reactions,[1] we report an unprecedented catalytic assembly of allylic amines from three simple precursors—alkynes, imines, and organoboron reagents (boronic acids or organoboranes). As allylic amines are key structural elements in a variety of important naturally occurring molecules[2] and pharmaceuticals[3] and are among the most versatile intermediates in the synthesis of other important molecules,[4] they have attracted much attention.[5] Previously, several Ni-catalyzed multicomponent coupling reactions involving additions to carbonyl compounds have been described.[1a,6] The process described herein is the first such example involving imines and also the first that utilizes boronic acids (Scheme 1).[7] Our preliminary investigations also support a mechanistic framework that accounts for the high selectivities observed in these reactions.

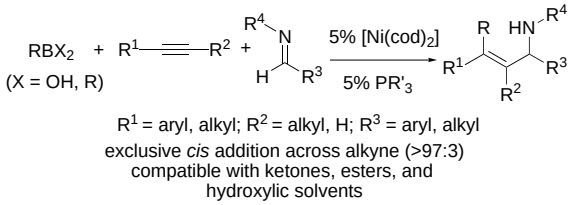

Scheme 1. Catalytic assembly of allylic amines from alkynes, imines, and organoboron reagents.

The markedly diminished electrophilicity of imines relative to aldehydes[8] presented significant challenges in our initial experiments. After extensive studies with different imines,[9] solvents,[10] and organometallic reagents,[11] we observed exceptional results when both organoboron reagents and hydroxylic solvents were employed.[12] Methanol in particular provided substantial increases in yield, and also displayed high selectivity for alkylative coupling product **1** over reductive coupling product **2** (Table 1).[13] Best results were obtained when methyl acetate was used as a cosolvent and electron-rich, tri-(*sec*-alkyl)-phosphane ligands were employed (Table 1, entries 3 and 4).[14] As summarized in Table 2, reactions involving internal alkynes with at least one alkyl substituent are typically highly selective, and nearly quantitative yields are observed in some cases (**1c** and **1f**). Imines derived from aliphatic aldehydes also undergo three-

Table 1: Ligand effects in catalytic three-component assembly of allylic amines.

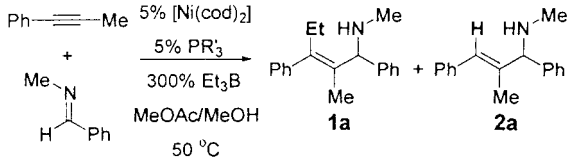

Entry	PR'_3[a]	Yield [%]	**1a**:**2a**[b]	Regioselectivity[c]
1	Bu_3P	80	94:6	96:4
2	Bn_3P	72	97:3	93:7
3	Cy_3P	88	89:11	91:9
4	Cyp_3P	85	92:8	91:9
5	tBu_3P	9	93:7	80:20
6	Ph_3P	34	95:5	91:9

[a] $Cy_3P = (c\text{-}C_6H_{11})_3P$, $Cyp_3P = (c\text{-}C_5H_9)_3P$. [b] Ratio determined by ^1H NMR. [c] Regioselectivity of **1a** (determined by ^1H NMR).

[*] Prof. Dr. T. F. Jamison, S. J. Patel
Department of Chemistry
Massachusetts Institute of Technology
Cambridge, MA 02139 (USA)
Fax: (+1) 617-258-7500
E-mail: tfj@mit.edu

[**] We thank the NIGMS (GM063755), the NSF (CAREER CHE-0134704), Merck Research Laboratories, Pfizer, Boehringer-Ingelheim, 3M, Johnson & Johnson, The Donors of the PRF, and MIT for generous financial support. NSF grants CHE-9809061 and DBI-9729592 and NIH grant 1S10RR13886-01 provided partial support for the MIT Department of Chemistry Instrumentation Facility (DCIF).

Supporting information for this article is available on the WWW under http://www.angewandte.org or from the author.

 © 2003 Wiley-VCH Verlag GmbH & Co. KGaA, Weinheim 1433-7851/03/4212-1364 $ 20.00+.50/0

Table 2: Allylic amines prepared by catalytic three-component couplings of alkynes, imines, and organoboranes.[a]

	Product	Yield [%][b]	**1**:**2**[c]	Regioselectivity[c,d]
1b	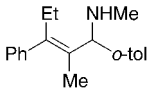	85	94:6	90:10
1c	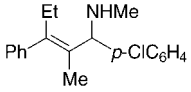	95	96:4	90:10
1d	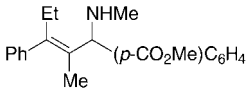	82	>96:4	90:10
1e	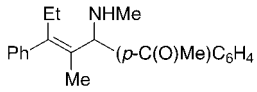	78	>96:4	91:9
1f	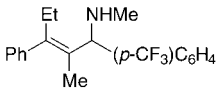	98	96:4	89:11
1g	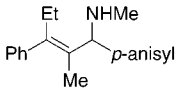	64	86:14	91:9
1h	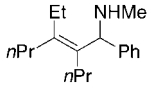	91	94:6	–
1i	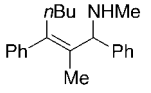	70	90:10	91:9
1j	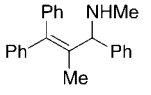	65	–	93:7
1k	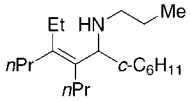	52	>96:4	–
1l	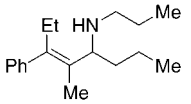	30	90:10	91:9
1m	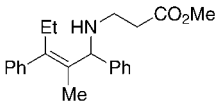	75	94:6	91:9
1n	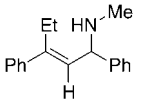	35[e]	>95:5	>98:2

[a] $[Ni(cod)_2]$ (5%) and $(c\text{-}C_5H_9)_3P$ (5%) used in all cases. [b] Combined yield of alkylative (**1**) and reductive (**2**) coupling products. [c] Determined by ^1H NMR. [d] Regioselectivity of major product. [e] Reaction performed at 25°C.

component coupling (**1k** and **1l**). Notably, esters (**1d** and **1m**) and ketones (**1e**) are tolerated, as are aryl chlorides (**1c**). Phenylacetylene affords trisubstituted allylic amine **1n** in moderate yield as a result of competitive cyclotrimerization of the alkyne under the reaction conditions.[15]

Of even greater significance is that both alkenylboronic and arylboronic acids are of equal or better efficacy in these reactions (Scheme 2). The scope and utility of this method is dramatically enhanced owing to the greater availability,

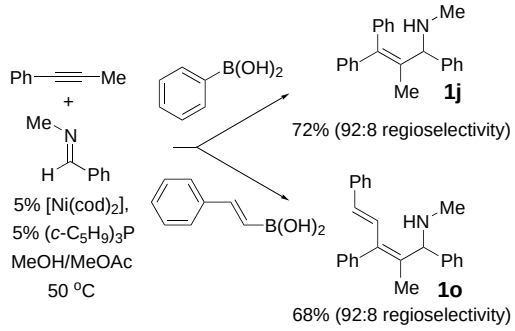

Scheme 2. Boronic acids in catalytic three-component couplings.

stability, and functional group tolerance of boronic acids relative to organozinc reagents and organoboranes.[1a,6]

Contrasting mechanisms have been reported for Ni-catalyzed coupling reactions involving carbonyl compounds,[6,16] yet imines have to be studied in this regard. With the aim of eliminating some of the possible mechanistic frameworks, we conducted several catalytic couplings by using (*S*)-(+)-(neomenthyl)diphenylphosphane as a chiral phosphane. Most notably, we observed that the enantiomeric excess of the alkylative coupling product **1** is *identical* to that of the corresponding reductive coupling product **2** in every case (Table 3). In addition, in cases where the amount of the minor regioisomer of the reductive coupling product **2** is detectable in the unpurified product mixtures by ^1H NMR spectroscopy, the regioselectivity is also *identical* for coupling products **1** and **2**.

These findings are consistent with the mechanistic pathway shown in Scheme 3, in which enantioselectivity and regioselectivity are determined in the same step and *before* a common intermediate **A** partitions into two pathways to lead to either **1** or **2**. Furthermore, this mechanism accounts for the high selectivity for alkylative coupling (→**1**) imparted by methanol: occupation of coordination sites required for a β-H elimination step that would lead to reductive coupling (→**2**).[17] At this juncture, we have no direct evidence for azametallacyclopentene **A**; nevertheless, it is analogous to azametallacyclopentenes of early transition metals[5a–d] and related to oxametallacyclopentenes proposed for other Ni-catalyzed couplings of alkynes and aldehydes.[16]

Table 3: Enantioselectivities observed for alkylative (**1**) and reductive (**2**) coupling products by using (*S*)-(+)-(neomenthyl)diphenylphosphane ((*S*)-NMDPP).

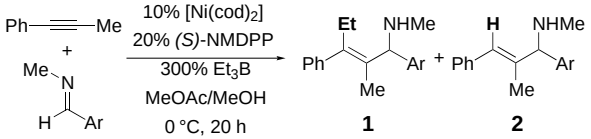

Entry	Ar	*ee* **1** [%][a]	*ee* **2** [%][a]
1	Ph	41	42
2	*p*-ClC_6H_4	33	33
3	(*p*-CF_3)C_6H_4	40	39

[a] Enantiomeric excess determined for the corresponding acetamides (Ac_2O, Et_3N, cat. DMAP), Chiralcel OD column.

 © 2003 Wiley-VCH Verlag GmbH & Co. KGaA, Weinheim 1433-7851/03/4212-1365 $ 20.00+.50/0

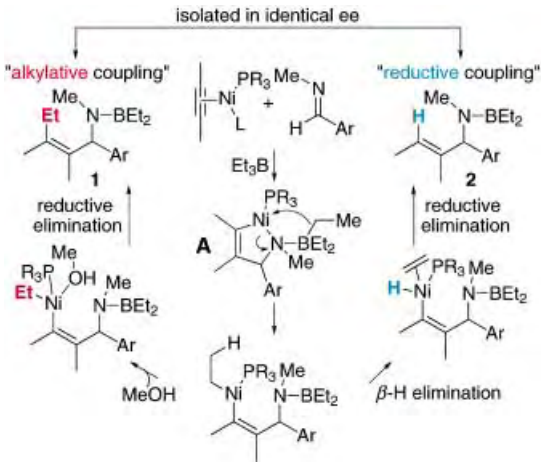

Scheme 3. A mechanistic framework for a novel Ni-catalyzed three-component coupling reaction that accounts for the selectivities observed.

In conclusion, the above catalytic transformation provides a significant amplification of molecular complexity and tolerates ketones, esters, and even unprotected hydroxy groups—three functional groups that are typically problematic in imine addition reactions.[18] Direct addition of the organoboron reagent to the imine is not observed,[19] and the mode of addition across the alkyne is exclusively *cis* (>97:3), thereby establishing the configuration of the double bond in the course of two carbon–carbon bond-forming events. Since the phosphane is involved in the enantio- and regioselectivity-determining steps, and methanol appears to be critical for catalytic turnover and for alkylative/reductive selectivity, efficient and highly selective asymmetric catalytic three-component coupling may be achieved by using chiral monodentate phosphanes with an appropriately placed hydroxy group. We are currently investigating ligands of this type and will report our findings of these and related studies in due course.

Experimental Section

General Procedure: The imine (1.0 mmol) and alkyne (0.40 mmol) were added to a solution of R_3B (0.60 mmol, 3 M in solvent specified), [Ni(cod)$_2$] (0.05 mmol), phosphane ligand (0.05 mmol), and MeOH (5 mL) and heated (50 °C) under Ar. Four equal portions of additional R_3B (4 × 0.60 mmol) and alkyne (4 × 0.40 mmol) were added over 4 h, and the solution was heated (50 °C) for 12 h. Concentration in vacuo and silica gel purification (hexanes/EtOAc) afforded the allylic amine products.

Received: November 13, 2002 [Z50542]

Keywords: alkynes · allylic amines · boronic acids · imines · nickel

[1] a) W.-S. Huang, J. Chan, T. F. Jamison, *Org. Lett.* **2000**, *2*, 4221; b) A. J. Skaggs, E. Y. Lin, T. F. Jamison, *Org. Lett.* **2002**, *4*, 2277.
[2] a) Microcystins: K. L. Reinhart, K.-i. Harada, M. Namikoshi, C. Chen, C. A. Harvis, M. H. G. Munro, J. W. Blunt, P. E. Mulligan, V. R. Beasley, A. M. Dahlem, W. W. Carmichael, *J. Am. Chem. Soc.* **1988**, *110*, 8557; b) motuporin: E. D. de Silva, D. E. Williams, R. J. Anderson, H. Klix, C. F. B. Holmes, T. M. Allen, *Tetrahedron Lett.* **1992**, *33*, 1561; c) cyclotheonamides: N. Fusetani, S. Matsunaga, H. Matsumoto, Y. Takebayashi, *J. Am. Chem. Soc.* **1990**, *112*, 7053; d) criamides: J. E. Coleman, E. D. de Silva, F. Kong, R. J. Andersen, T. M. Allen, *Tetrahedron* **1995**, *51*, 10653; e) leucascandrolide A: M. D'Ambrosio, A. Guerriero, C. Debitus, F. Pietra, *Helv. Chim. Acta* **1996**, *79*, 51.
[3] G. Petranyi, N. S. Ryder, A. Stütz, *Science* **1984**, *224*, 1239.
[4] Examples: a) K. Burgess, M. J. Ohlmeyer, *J. Org. Chem.* **1991**, *56*, 1027; b) M. Hagihara, N. J. Anthony, T. J. Stout, J. Clardy, S. L. Schreiber, *J. Am. Chem. Soc.* **1992**, *114*, 6568; c) E. Vedejs, M. Gringras, *J. Am. Chem. Soc.* **1994**, *116*, 579; d) T. A. Johnson, M. D. Curtis, P. Beak, *J. Am. Chem. Soc.* **2001**, *123*, 1004; e) Takasago process: R. Noyori, *Asymmetric Catalysis in Organic Synthesis*, Wiley, New York, **1994**.
[5] Reductive coupling of alkynes and imines by using early transition metal complexes: a) S. L. Buchwald, B. T. Watson, M. W. Wannamaker, J. C. Dewan, *J. Am. Chem. Soc.* **1989**, *111*, 4486; b) M. Jensen, T. Livinghouse, *J. Am. Chem. Soc.* **1989**, *111*, 4495; c) K. Takai, S. Miwatashi, Y. Kataoka, K. Utimoto, *Chem. Lett.* **1992**, 99; d) Y. Gao, K. Harada, F. Sato, *Tetrahedron Lett.* **1995**, *36*, 5913; alkenylmetal additions to imines and related electrophiles: e) S. E. Denmark, N. Nakajima, O. J.-C. Nicaise, *J. Am. Chem. Soc.* **1994**, *116*, 8797; f) N. A. Petasis, I. A. Zavialov, *J. Am. Chem. Soc.* **1997**, *119*, 445; g) N. A. Petasis, I. A. Zavialov, *J. Am. Chem. Soc.* **1998**, *120*, 11798; h) R. A. Batey, D. B. MacKay, V. Santhakumar, *J. Am. Chem. Soc.* **1999**, *121*, 5075; i) P. Wipf, C. Kendall, C. R. J. Stephenson, *J. Am. Chem. Soc.* **2001**, *123*, 5122; j) review: M. Johannsen, K. A. Jørgensen, *Chem. Rev.* **1998**, *98*, 1689.
[6] a) Y. Sato, M. Takimoto, K. Hayashi, T. Katsuhara, K. Takagi, M. Mori, *J. Am. Chem. Soc.* **1994**, *116*, 9771; b) E. Oblinger, J. Montgomery, *J. Am. Chem. Soc.* **1997**, *119*, 9065; c) M. Kimura, A. Ezoe, K. Shibata, Y. Tamaru, *J. Am. Chem. Soc.* **1998**, *120*, 4033; d) J. Montgomery, *Acc. Chem. Res.* **2000**, *33*, 467, and references therein; e) S. Ikeda, *Acc. Chem. Res.* **2000**, *33*, 511, and references therein; f) Y. Ni, K. K. D. Amarasinghe, J. Montgomery, *Org. Lett.* **2002**, *4*, 1743.
[7] See references [5f–i] for other multicomponent couplings that afford allylic amines.
[8] a) S. Kobayashi, H. Ishitani, *Chem. Rev.* **1999**, *99*, 1069; b) P. Wipf, C. Kendall, *Org. Lett.* **2001**, *3*, 2773, and references therein.
[9] For example, more electrophilic imines (NSO_2R and $NP(O)Ph_2$) did not undergo coupling.
[10] Reactions with toluene, THF, hexanes, CH_3CN, or EtOAc as solvent gave mixtures of **1a** and **2a** in <10% yield.
[11] Et_2Zn, polymethylhydrosiloxane (PMHS), and Et_3SiH gave complex mixtures of undesired products corresponding to imine addition and/or reduction.
[12] M. Kimura, A. Ezoe, S. Tanaka, Y. Tamaru, *Angew. Chem.* **2001**, *113*, 3712; *Angew. Chem. Int. Ed.* **2001**, *40*, 3600.
[13] This phenomenon probably does not result from water, as substoichiometric, stoichiometric, or excess amounts depreciate yield. EtOH and *i*PrOH gave significantly lower yields.
[14] Reactions conducted with diphosphanes as ligands (BINAP, dppe, dppb) gave trace amounts of allylic amines.
[15] With 1-phenyl-2-(trimethylsilyl)acetylene, allylic amine **1n** is formed in 22% yield (regioselectivity >98:2) under the standard reaction conditions.
[16] a) T. Tsuda, T. Kiyoi, T. Saegusa, *J. Org. Chem.* **1990**, *55*, 2554; b) Y. Sato, T. Takanashi, M. Mori, *Organometallics* **1999**, *18*, 4891; c) Y. Sato, N. Saito, M. Mori, *J. Am. Chem. Soc.* **2000**, *122*, 2371; d) S. K. Chowdhury, K. K. D. Amarasinghe, M. J. Heeg, J. Montgomery, *J. Am. Chem. Soc.* **2000**, *122*, 6775; e) K. K. D.

 © 2003 Wiley-VCH Verlag GmbH & Co. KGaA, Weinheim 1433-7851/03/4212-1366 $ 20.00+.50/0

Amarasinghe, S. K. Chowdhury, M. J. Heeg, J. Montgomery, *Organometallics* **2001**, *20*, 370. See also Refs [6b, d].

[17] MeOH may also promote group transfer from B to Ni, in analogy to Suzuki reaction additives, but this hypothesis does not account for alkylative/reductive selectivity (i.e., **1** vs. **2**). Extended storage of Et_3B in MeOH results in formation of Et_2BOMe and $EtB(OMe)_2$ which, based on other experiments, do not undergo coupling reactions. See: K.-M. Chen, K. G. Gunderson, G. E. Hardtmann, K. Prasad, O. Repic, M. J. Shapiro, *Chem. Lett.* **1987**, *10*, 1923.

[18] The Strecker and Mannich reactions are also examples of this unusual functional group tolerance. For examples of imine additions in the presence of aldehydes, see: a) H. Nakamura, H. Iwama, Y. Yamamoto, *J. Am. Chem. Soc.* **1996**, *118*, 6641; b) S. Kobayashi, S. Nagayama, *J. Org. Chem.* **1997**, *62*, 232.

[19] K. Shibata, M. Kimura, K. Kojima, S. Tanaka, Y. Tamaru, *J. Organomet. Chem.* **2001**, *624*, 348. Also see references [5f–h].

 © 2003 Wiley-VCH Verlag GmbH & Co. KGaA, Weinheim 1433-7851/03/4212-1367 $ 20.00+.50/0

Asymmetric Amination

Catalytic, Highly Enantioselective, Direct Amination of β-Ketoesters**

*Mauro Marigo, Karsten Juhl, and Karl Anker Jørgensen**

Optically active α-amino acid derivatives are fundamental constituents of numerous natural products and of other highly valuable compounds of importance for our daily life. Many different approaches for the synthesis of optically active α-amino acids are available.[1] However, the development of stereoselective transformations for the synthesis of optically active non-natural α-amino acid derivatives from simple and readily available starting compounds in the presence of a chiral catalyst is an ongoing challenge for chemists. The importance of these molecules has led to extensive development of synthetic methods that use catalytic enantioselective reactions. The majority of the procedures developed for the formation of optically active α-amino acid derivatives are C–C-bond-forming reactions and include catalytic enantioselective addition to imines using Strecker[2] and Mannich[3] reactions.

[*] Dr. K. A. Jørgensen, M. Marigo, Dr. K. Juhl
The Danish National Research Foundation: Center for Catalysis
Department of Chemistry, Aarhus University
DK-8000 Aarhus C (Denmark)
Fax: (+45) 8919-6199
E-mail: kaj@chem.au.dk

[**] This work was made possible by a grant from The Danish National Research Foundation and the EU: HMPT-CT-2001-00317. We are grateful to Dr. R. G. Hazell for X-ray crystallographic analysis.

Supporting information for this article is available on the WWW under http://www.angewandte.org or from the author.

The synthesis of optically active α-amino acid derivatives by a catalytic, enantioselective, direct C–N-bond-forming reaction is probably among the simplest procedures for the formation of an asymmetric carbon center attached to a nitrogen atom.[4] Recently, we presented the first direct enantioselective α-amination of 2-ketoesters catalyzed by chiral copper(II)–bisoxazoline complexes,[5,6] and later both List and we developed the first direct organocatalytic α-amination of aldehydes[7,8] and ketones.[9] These developments led to simple procedures for the synthesis of optically active *syn*-β-amino-α-hydroxy esters, α-amino acid derivatives, α-amino aldehydes and ketones, and α-amino alcohols.

Herein we present the first direct α-amination of α-substituted β-ketoesters[10] **1** catalyzed by a chiral copper(II)–bisoxazoline (BOX)[11] complex with azodicarboxylates **2** as the nitrogen fragment source. This new reaction gives access to β-hydroxy-α-amino acids such as oxazolidinone derivatives. Some representative screening results for the catalytic enantioselective α-amination of the β-ketoester **1a** with the azodicarboxylates **2a** and **2b** in the presence of [(*S*)-Ph-BOX–Cu(OTf)$_2$] as the catalyst (10 mol%) are presented in Table 1.

The ethyl β-ketoester **1a** reacted with dibenzyl azodicarboxylate (**2a**) under the catalysis of [(*S*)-Ph-BOX–Cu(OTf)$_2$] (10 mol%) to give the α-aminated product **3a** in high yield with excellent enantioselectivity (97–98% *ee*) in a variety of solvents (Table 1, entries 1–3). The catalyst loading is remarkable for this direct α-amination reaction, which proceeds in excellent yield and enantioselectivity in the presence of just 0.2 mol% of catalyst (Table 1, entry 5). When diethyl azodi-

Table 1: Enantioselective direct α-amination of **1a** with **2a** and **2b**, catalyzed by [(*S*)-Ph-BOX–Cu(OTf)$_2$].[a]

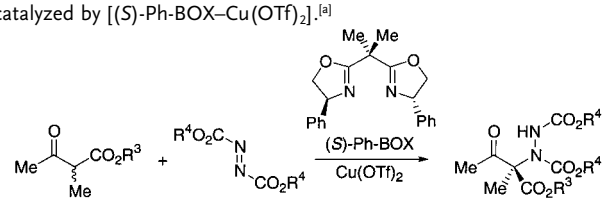

1a: R^3 = Et **2a:** R^4 = Bn **2b:** R^4 = Et **3a:** R^3 = Et, R^4 = Bn **3ab:** R^3 = Et, R^4 = Et

Entry	R^3	R^4	Catalyst loading [%]	Solvent	Product	Yield[b] [%]	*ee*[c] [%]
1	Et (**1a**)	Bn (**2a**)	10	CH_2Cl_2	**3a**	98	98
2	Et (**1a**)	Bn (**2a**)	10	Et_2O	**3a**	90	97
3	Et (**1a**)	Bn (**2a**)	10	THF	**3a**	82	97
4	Et (**1a**)	Bn (**2a**)	1	CH_2Cl_2	**3a**	92	98
5	Et (**1a**)	Bn (**2a**)	0.2	CH_2Cl_2	**3a**	91	96
6	Et (**1a**)	Bn (**2a**)	0.05	CH_2Cl_2	**3a**	65	55
7	Et (**1a**)	Et (**2b**)	10	CH_2Cl_2	**3ab**	87	>95

[a] Experimental conditions: Cu(OTf)$_2$ (9 mg, 25 μmol) and (*S*)-(−)-2,2′-isopropylidene-bis(4-phenyl-2-oxazoline) (9.2 mg, 26 μmol) were stirred under vacuum in an oven-dried Schlenk tube for 2 h. The tube was then filled with N_2, dry CH_2Cl_2 (2 mL) was added, and the resulting solution was stirred for 1 h. The β-ketoester **1a** (0.25 mmol) was then added, followed by dibenzyl azodicarboxylate (**2a**) (90 mg, 0.30 mmol), and the product **3a** was isolated by flash chromatography after 16 h (see Supporting Information). [b] Yield of isolated product. [c] Chiral HPLC with AD or AS Daicel Chiralpack columns was used to determine the *ee* value.

 © 2003 Wiley-VCH Verlag GmbH & Co. KGaA, Weinheim 1433-7851/03/4212-1367 $ 20.00+.50/0

carboxylate (**2b**) was used, the α-aminated adduct **3ab** was also produced in high yield and with >95% *ee* (Table 1, entry 7). The use of other β-ketoesters is also possible. The phenyl ester (R^3 = Ph) reacted highly enantioselectively with **2b**, and the corresponding α-aminated adduct was isolated in 91% yield and with 96% *ee*. Catalysts containing other chiral bisoxazoline ligands gave rise to lower yields and enantiomeric excesses of the α-aminated adducts than did the [(*S*)-Ph-BOX–Cu(OTf)$_2$] catalyst.

The excellent catalytic enantioselective direct α-amination properties of [(*S*)-Ph-BOX–Cu(OTf)$_2$] were demonstrated for a series of acyclic and cyclic β-ketoesters. The β-ketoesters **1a–j** were all treated with dibenzyl azodicarboxylate (**2a**) under the catalysis of [(*S*)-Ph-BOX–Cu(OTf)$_2$] (10 mol% and 0.5 mol%) in CH_2Cl_2 at room temperature to show the scope of the reaction (Table 2).

Table 2: Catalytic enantioselective direct α-amination of **1a–j** with **2a**, catalyzed by [(*S*)-Ph-BOX–Cu(OTf)$_2$].[a]

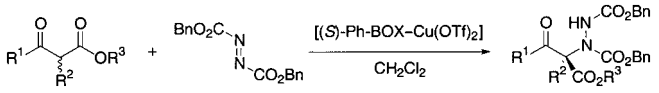

1a–j **2a** **3a–j**

Entry	β-Ketoester			Product	Catalyst loading			
					10 mol%		0.5 mol%	
	R^1	R^2	R^3		Yield[b] [%]	*ee*[c] [%]	Yield[b] [%]	*ee*[c] [%]
1	Me	Me	Et (**1a**)	**3a**	98	98	91	96[d]
2	Et	Me	Et (**1b**)	**3b**	94	98	98	98
3	Ph	Me	Et (**1c**)	**3c**	85	95	81	87
4	*i*Pr	Me	*t*Bu (**1d**)	**3d**	96	98	89	98
5	Bn	Me	*t*Bu (**1e**)	**3e**	84	98	79	98
6	Me	allyl	*t*Bu (**1f**)	**3f**	–	–	80	98
7	Me	Me	*t*Bu (**1g**)	**3g**	86	98	–	–
8	$(CH_2)_3$		Et (**1h**)	**3h**	98	99	96	99
9	$(CH_2)_4$		Et (**1i**)	**3i**	98	99	96	99
10	$(CH_2)_5$		Et (**1j**)	**3j**	76	98	70	99

[a] Experimental conditions (0.5 mol% of catalyst): A mixture of Cu(OTf)$_2$ (9 mg, 25 μmol) and (*S*)-(−)-2,2′-isopropylidene-bis(4-phenyl-2-oxazoline) (9.2 mg, 26 μmol) was stirred under vacuum in an oven-dried Schlenk tube for 2 h. The tube was then filled with N_2, dry CH_2Cl_2 (10 mL) was added, and the solution was stirred for a further 1 h. An aliquot of the solution (1 mL) was transferred to another oven-dried Schlenk tube and dry CH_2Cl_2 (1 mL) was added. The β-ketoester **1b** (0.50 mmol) was then added, followed by dibenzyl azodicarboxylate (**2a**) (180 mg, 0.60 mmol). After 16 h the product **3b** was isolated by flash chromatography (see Supporting Information). [b] Yield of isolated product. [c] Chiral HPLC with AD or AS Daicel Chiralpack or OD-Daicel Chiralgel columns was used to determine the *ee* value. [d] Reaction performed with 0.2 mol% catalyst loading.

1f reacted with **2a** in the presence of 0.5 mol% of the catalyst and the α-aminated adduct **3f** was formed in 80% yield and 98% *ee* (Table 2, entry 6). The cyclic β-ketoesters **1h–j** underwent a particularly highly enantioselective α-amination reaction. For all three ring sizes (five-, six-, and seven-membered) 99% *ee* was observed when only 0.5 mol% of the catalyst was used (Table 2, entries 7–9). Furthermore, the α-aminated adducts were isolated in excellent yields. The catalytic enantioselective α-amination reaction of α-substituted β-ketoesters with dibenzyl azodicarboxylate as the nitrogen fragment source and catalyzed by [(*S*)-Ph-BOX–Cu(OTf)$_2$] seems to be a general reaction and gives the desired products in high yield with excellent enantioselectivity.

The absolute configuration of the α-aminated adducts was solved by X-ray crystal-structure analysis of a derivative of **3a** and showed that the stereogenic carbon center formed in the reaction is of *R* stereochemistry.[12] On the basis of the absolute configuration of the products and the results we have obtained in our investigations to date, we propose a reaction mechanism that involves the approach of dibenzyl azodicarboxylate to the catalyst-coordinated β-ketoester, as outlined in **5**.[13]

A variety of possible product modifications can be envisaged, for example, as shown in the reaction sequence in Scheme 1: Reduction of the β-keto functionality in **3a** proceeded in a highly diastereoselective manner and the *N*-amino

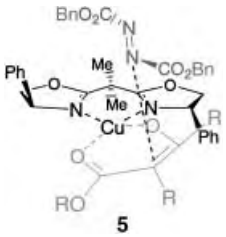

5

This catalytic enantioselective direct α-amination of the α-substituted β-ketoesters is remarkable in that there is virtually no change in yield or enantioselectivity when the loading of the [(*S*)-Ph-BOX–Cu(OTf)$_2$] catalyst is decreased from 10 to 0.5 mol%. Acyclic β-ketoesters with alkyl, branched alkyl, benzyl, or phenyl substituents as R^1 (**1a–e**, and **1g**) all reacted with dibenzyl azodicarboxylate (**2a**) to give the corresponding α-aminated adducts **3a–e**, and **3g** in high yields with excellent enantioselectivity (Table 2, entries 1–5,7). The enantiomeric excesses observed were generally >95% *ee*, with the exception of **1c** in the presence of 0.5 mol% of the catalyst, in which case 87% *ee* was found. However, an improvement to 95% *ee* occurred when 10 mol% of the catalyst was used. The α-allyl-β-ketoester oxazolidinone **6** was formed with a d.r. of 24:1. Cleavage of the N–N bond gave the oxazolidinone derivative **7** in an overall yield of 25% (unoptimized conditions). Thus, this direct α-amination reaction can be used as a new synthetic procedure for the formation of optically active β-hydroxy-α-amino acid derivatives.

In conclusion, the first direct α-amination of α-substituted β-ketoesters with dibenzyl azodicarboxylate as the nitrogen fragment source has been developed. The reactions are catalyzed by [Ph-BOX–Cu(OTf)$_2$] and proceed with only 0.2–0.5 mol% of the catalyst to give the desired products in high yields and excellent enantiomeric excesses. Both acyclic and cyclic β-ketoesters undergo this highly selective α-amination reaction and the products obtained can be converted, for

 © 2003 Wiley-VCH Verlag GmbH & Co. KGaA, Weinheim 1433-7851/03/4212-1368 $ 20.00+.50/0

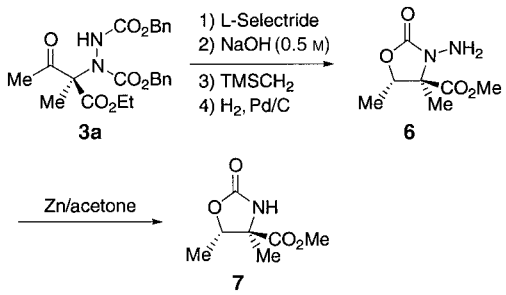

Scheme 1. Reduction of the β-keto functionality in **3a** and conversion into the optically active β-hydroxy-α-amino acid derivative **7**. TMS = trimethylsilyl.

example, into optically active functionalized oxazolidinone derivatives by standard chemistry.

Received: November 28, 2002 [Z50655]

Keywords: β-ketoesters · amination · asymmetric catalysis · copper · synthetic methods

[1] See, for example: a) R. M. Williams, *Synthesis of Optically Active α-Amino Acids*, Pergamon, Oxford, **1989**; b) R. M. Williams, J. A. Hendrix, *Chem. Rev.* **1992**, *92*, 889; c) M. Arend, *Angew. Chem.* **1999**, *111*, 3047; *Angew. Chem. Int. Ed.* **1999**, *38*, 2873; d) L. Yet, *Angew. Chem.* **2001**, *113*, 900; *Angew. Chem. Int. Ed.* **2001**, *40*, 875; e) R. O. Duthaler, *Tetrahedron* **1994**, *50*, 1539; f) S. C. Bergmeier, *Tetrahedron* **2000**, *56*, 2561.

[2] See, for example: a) M. S. Sigman, E. N. Jacobsen, *J. Am. Chem. Soc.* **1998**, *120*, 5315; b) M. S. Sigman, P. Vachal, E. N. Jacobsen, *Angew. Chem.* **2000**, *112*, 1336; *Angew. Chem. Int. Ed.* **2000**, *39*, 1279; c) M. S. Sigman, E. N. Jacobsen, *J. Am. Chem. Soc.* **1998**, *120*, 4901; d) C. A. Krueger, K. W. Kuntz, C. D. Dzierba, W. G. Wirschun, J. D. Gleason, M. L. Snapper, A. H. Hoveyda, *J. Am. Chem. Soc.* **1999**, *121*, 4284; e) M. Takamura, Y. Hamashima, H. Usuda, M. Kanai, M. Shibasaki, *Angew. Chem.* **2000**, *112*, 1716; *Angew. Chem. Int. Ed.* **2000**, *39*, 1650; f) E. J. Corey, M. J. Grogan, *Org. Lett.* **1999**, *1*, 157; g) H. Ishitani, S. Komiyama, S. Kobayashi, *Angew. Chem.* **1998**, *110*, 3369; *Angew. Chem. Int. Ed.* **1998**, *37*, 3186; f) H. Ishitani, S. Komiyama, Y. Hasegawa, S. Kobayashi, *J. Am. Chem. Soc.* **2000**, *122*, 762.

[3] See, for example: a) H. Ishitani, M. Ueno, S. Kobayashi, *J. Am. Chem. Soc.* **1997**, *119*, 7153; b) S. Kobayashi, T. Hamada, K. Manabe, *J. Am. Chem. Soc.* **2002**, *124*, 5640; c) H. Ishitani, M. Ueno, S. Kobayashi, *J. Am. Chem. Soc.* **2000**, *122*, 8180; d) E. Hagiwara, A. Fujii, M. Sodeoka, *J. Am. Chem. Soc.* **1998**, *120*, 2474; e) A. Fujii, E. Hagiwara, M. Sodeoka, *J. Am. Chem. Soc.* **1999**, *121*, 5450; f) D. Ferraris, B. Young, T. Dudding, T. Lectka, *J. Am. Chem. Soc.* **1998**, *120*, 4548; g) D. Ferraris, B. Young, C. Cox, T. Dudding, W. J. Drury, L. Ryzhkov, A. E. Taggi, T. Lectka, *J. Am. Chem. Soc.* **2002**, *124*, 67; h) A. Córdova, S.-I. Watanabe, F. Tanaka, W. Notz, C. F. Barbas III, *J. Am. Chem. Soc.* **2002**, *124*, 1842; i) A. Córdova, W. Notz, G. Zhong, J. M. Betancort, C. F. Barbas III, *J. Am. Chem. Soc.* **2002**, *124*, 1866; j) B. List, *J. Am. Chem. Soc.* **2000**, *122*, 9336; k) B. List, P. Pojarliev, W. T. Biller, H. J. Martin, *J. Am. Chem. Soc.* **2002**, *124*, 827; l) A. G. Wenzel, E. N. Jacobsen, *J. Am. Chem. Soc.* **2002**, *124*, 12964; m) S. Yamasaki, T. Iida, M. Shibasaki, *Tetrahedron* **1999**, *55*, 8857; n) K. Juhl, N. Gathergood, K. A. Jørgensen, *Angew. Chem.* **2001**, *113*, 3083; *Angew. Chem. Int. Ed.* **2001**, *40*, 2995.

[4] For a review on asymmetric α-amination reactions, see: J.-P. Genet, C. Greck, D. Lavergne, *Modern Amination Methods* (Ed.: A. Ricci), Wiley-VCH, Weinheim, **2000**, chap. 3.

[5] K. Juhl, K. A. Jørgensen, *J. Am. Chem. Soc.* **2002**, *124*, 2420.

[6] See also: D. A. Evans, S. G. Nelson, *J. Am. Chem. Soc.* **1997**, *119*, 6452.

[7] A. Bøgevig, K. Juhl, N. Kumaragurubaran, W. Zhuang, K. A. Jørgensen, *Angew. Chem.* **2002**, *114*, 1868; *Angew. Chem. Int. Ed.* **2002**, *41*, 1790.

[8] B. List, *J. Am. Chem. Soc.* **2002**, *124*, 5656.

[9] N. Kumaragurubaran, K. Juhl, W. Zhuang, A. Bøgevig, K. A. Jørgensen, *J. Am. Chem. Soc.* **2002**, *124*, 6254.

[10] For metal-catalyzed direct α-amination reactions leading to racemic products, see: a) S. Fioravanti, A. Morreale, L. Pellacani, P. A. Tardella, *Tetrahedron Lett.* **2001**, *42*, 1171; b) J. Clarine, N. Gálvez, C. Marchi, M. Moreno-Manas, A. Vallribera, E. Molins, *Tetrahedron* **1999**, *55*, 7331.

[11] For reviews of C_2-symmetric bisoxazoline–Lewis acid complexes as catalysts, see, for example: a) A. K. Ghosh, P. Mathivanen, J. Cappiello, *Tetrahedron: Asymmetry* **1998**, *9*, 1; b) K. A. Jørgensen, M. Johannsen, S. Yao, H. Audrain, J. Thorhauge, *Acc. Chem. Res.* **1999**, *32*, 605; c) J. S. Johnson, D. A. Evans, *Acc. Chem. Res.* **2000**, *33*, 325.

[12] The absolute configuration was determined by X-ray crystal structure analysis of the oxazolidinone product **8** formed with a diastereomeric ratio of 24:1. CCDC 198364 contains the supplementary crystallographic data for this paper. These data

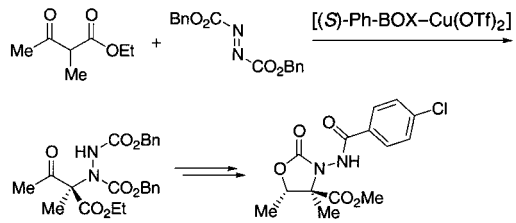

can be obtained free of charge via www.ccdc.cam.ac.uk/conts/retrieving.html (or from the Cambridge Crystallographic Data Centre, 12, Union Road, Cambridge CB21EZ, UK; fax: (+44) 1223-336-033; or deposit@ccdc.cam.ac.uk).

[13] For a study of intermediates, see: J. Thorhauge, M. Roberson, R. G. Hazell, K. A. Jørgensen, *Chem. Eur. J.* **2002**, *8*, 1888.

DNA-Templated Synthesis

Two Enabling Architectures for DNA-Templated Organic Synthesis**

*Zev J. Gartner, Rozalina Grubina, Christopher T. Calderone, and David R. Liu**

DNA templates can direct a wide variety of chemical reactions[1–24] without obvious structural requirements[23–25] by sequence specifically recruiting reactants linked to complementary oligonucleotides. The generality of DNA-templated synthesis raises the possibility of applying powerful processes such as in vitro selection and PCR (polymerase chain reaction) amplification to the discovery of synthetic molecules with desired properties.[23] In addition, the scope of DNA-templated synthesis provides an experimental basis for models of prebiotic chemistry[26–32] in which nucleic acid templates may have mediated the earliest translation of replicable information into a variety of functional structures. The DNA-templated format also enables modes of reaction that are not possible using conventional synthetic approaches.[33]

A DNA-templated chemical reaction is mediated by a specific architecture in which a portion of a DNA template anneals to a complementary DNA-linked reagent. Annealing places functional groups on the template and reagent in reactive proximity. The structure of this architecture could profoundly affect the nature of the resulting reaction, and it may therefore be possible to manipulate reaction conditions by rationally designing template–reagent complexes with different secondary structures. We previously used the end-of-helix (E) and hairpin (H) architectures (Figure 1) to mediate a variety of DNA-templated reactions.[23–25,33] During the course of these studies, two challenges emerged. First, some DNA-templated reactions do not proceed efficiently when the annealed reactive groups on the template and reagent are separated by even a small number of bases.[24] When the E or H architectures are used, these "distance-dependent" reactions can only be encoded by template bases at the reactive end of the template. Second, the presence of double-stranded DNA between annealed reactive groups can greatly reduce the efficiency of templated reactions because the flexibility of a single-stranded template is required.[23] This precludes the possibility of performing two or more reactions in a single DNA-templated step with the E or H architectures, even though the template oligonucleotide may contain enough bases to encode multiple reactions. Herein we describe two new architectures for DNA-templated synthesis that overcome each of these challenges.

We hypothesized that the distance dependence of certain DNA-templated reactions such as 1,3-dipolar cycloaddition and reductive amination could be overcome through the design of a new architecture that enables a reagent to anneal simultaneously to two widely separated regions of the template. In this omega (Ω) architecture (Figure 1), the template oligonucleotide contains a small number of constant bases at the reactive 5′ end of the template in addition to distal coding regions. A reagent oligonucleotide for the Ω architecture contains at its reactive 3′ end the bases that complement the constant region of the template followed by bases that complement a coding region anywhere on the template. The constant regions are designed to be of insufficient length to anneal in the absence of a complementary coding region. When the coding region of the template and reagent are complementary and anneal, however, the elevated effective molarity of the constant regions induces their annealing. Annealing of the constant regions forms a bulge (resembling an Ω) in the otherwise double-stranded template–reagent complex and places groups at the ends of the template and of the reagent in reactive proximity. In theory, this design would enable distance-dependent DNA-templated reactions to be encoded for the first time by bases distal from the reactive end of the template (Figure 1).

We compared the efficiency of the Ω architecture in DNA-templated synthesis with that of the standard E and H architectures. The Ω architectures studied consisted of a) three to five constant bases at the 5′ end of the template, followed by b) a 5- to 17-base loop, and c) a ten-base coding region. As a basis for comparison, we performed four different DNA-templated reactions that collectively span the range of distance dependence that we have observed to date.

Amine acylation reactions are representative of distance-independent reactions that proceed efficiently even when considerable distances (e.g. 30 bases) separate the amine and carboxylate groups.[24,25] As expected, amine acylation (20 mM DMT-MM,[34] 30 °C, pH 7.0, 12 h) proceeded efficiently (46–96 % yield) in all architectures regardless of the distance between reactive groups on the reagent and template (Figure 2, lanes 1–5, and Figure 3a). The Ω architecture mediated efficient amine acylation with three, four, or five constant bases at the reactive ends of the template and reagent and 10 or 20 bases between annealed reactants ($n =$ 10 or 20). Importantly, control reactions in which the distal coding region contained three sequence mismatches failed to generate significant product despite the presence of the complementary three- to five-base constant regions at the ends of the template and reagent (see Figure 2, lane 5 for a representative example). The Ω architecture therefore did not impede the efficiency or sequence specificity of the distance-independent amine acylation reaction.

DNA-templated Wittig olefination proceeds at a significantly lower rate when the aldehyde and phosphorane are separated by larger numbers of template bases, even though product yields are typically excellent after >12 h of reaction

[*] Prof. D. R. Liu, Z. J. Gartner, R. Grubina, C. T. Calderone
Department of Chemistry and Chemical Biology, Harvard University
12 Oxford Street, Cambridge, MA 02138 (USA)
Fax: (+1) 617-496-5688
E-mail: drliu@fas.harvard.edu

[**] Funding was generously provided by the Searle Scholars Program (00-C-101), an Office of Naval Research Young Investigator Award (N0014-00-1-0596), an Arnold and Mabel Beckman Foundation Young Investigator Award, and an Alfred P. Sloan Foundation Research Fellowship (BR-4141). Z.J.G. is an NSF Graduate Research Fellow. C.T.C. is an NDSEG Graduate Research Fellow.

 © 2003 Wiley-VCH Verlag GmbH & Co. KGaA, Weinheim 1433-7851/03/4212-1370 $ 20.00+.50/0

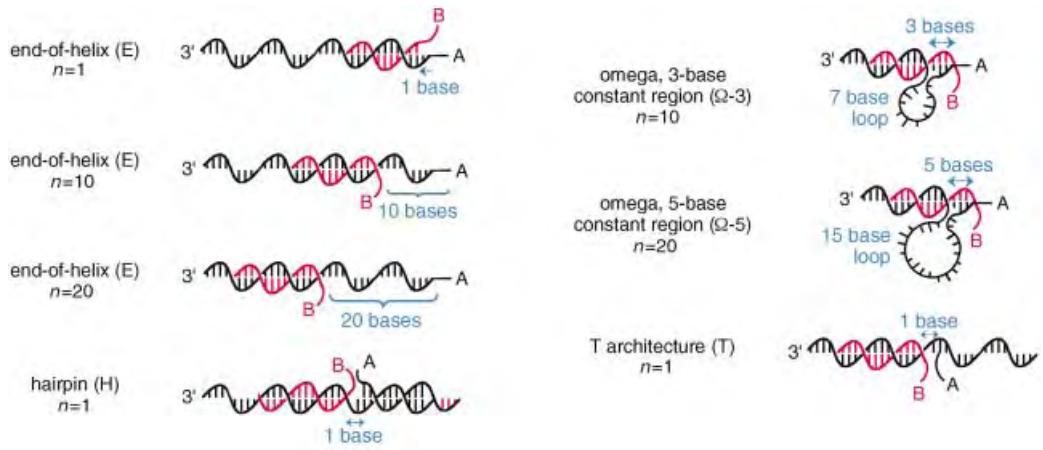

Figure 1. Four architectures for DNA-templated synthesis. The Ω and T architectures are presented in this work. Templates are colored black and reagents are colored red. The number of single-stranded-template bases that separate the reactive groups of the template and the reagent is designated "*n*". For the Ω architectures, the number of fixed bases at the reactive end of the template is shown following the Ω symbol.

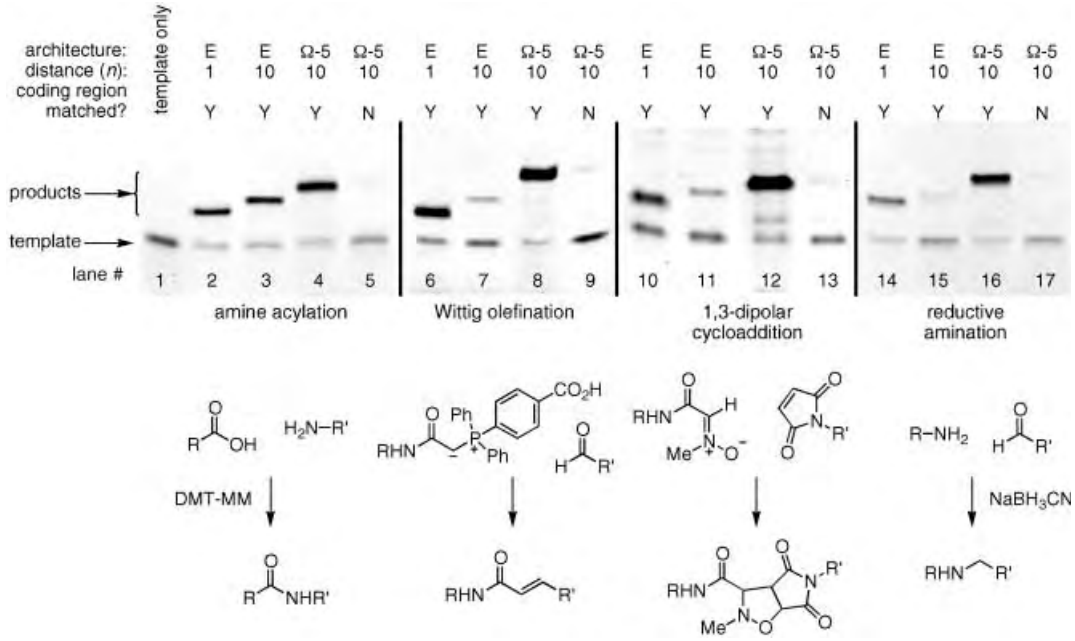

Figure 2. Denaturing polyacrylamide-gel electrophoresis analysis of representative DNA-templated amine acylation, Wittig olefination, 1,3-dipolar cycloaddition, and reductive amination reactions with the end-of-helix (E) and Ω architectures. For lanes 5, 9, 13, and 17, reagents with coding region sequences containing three mismatches were used. R = template oligonucleotide, R′ = reagent oligonucleotide.

regardless of the intervening distance.[24] After only 2 h of reaction (pH 7.5, 30 °C) in the E or H architectures, yields of olefin products are three- to sixfold lower when the reactants are separated by ten or more bases ($n = 10$ or 20) than when reactants are separated by only one base ($n = 1$) (Figure 2, lanes 6 and 7, and Figure 3b). In contrast, the Ω architecture with four or five constant bases at the reactive end results in efficient and sequence-specific Wittig product formation after 2 h even when 10 or 20 bases separate the coding region and the reactive end of the template (Figure 2, lanes 8 and 9, and Figure 3b). These results suggest that the constant regions at the reactive ends of the template and reagent in the Ω architecture enable the aldehyde and phosphorane to react at an effective concentration comparable to that in the E architecture when $n = 1$ (Figure 1).

Of the many DNA-templated reactions that we have studied to date, the 1,3-dipolar cycloaddition and reductive amination reactions[24] demonstrate the most pronounced distance dependence. Both reactions proceed with low to modest efficiency (7–44 % yield) in the E or H architectures when 10 or 20 bases separate the annealed reactive groups (Figure 2, lanes 10, 11, 14, and 15, and Figure 3c–d). This distance dependence limits the positions on a DNA template that can encode these or other distance-dependent reactions. In contrast, both 1,3-dipolar cycloaddition and reductive amination proceed efficiently (up to 97 % yield) and sequence

 © 2003 Wiley-VCH Verlag GmbH & Co. KGaA, Weinheim 1433-7851/03/4212-1371 $ 20.00+.50/0

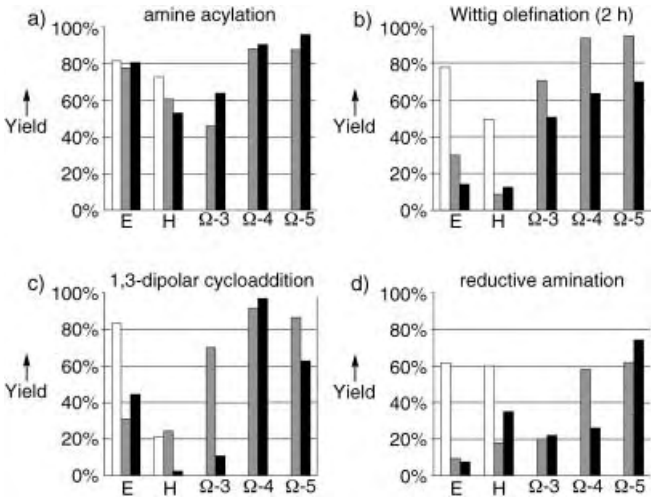

Figure 3. Comparison of end-of-helix (E), hairpin (H), and Ω architectures for mediating DNA-templated a) amine acylation, b) Wittig olefination, c) 1,3-dipolar cycloaddition, and d) reductive amination reactions. □ $n=1$, ■ $n=10$, ■ $n=20$. See Experimental Section for reaction conditions. In each case $<5\%$ product was generated under these reaction conditions when reagent coding region sequences contained three mismatches.

specifically when encoded by template bases 15–25 bases away from the functionalized end of the template in the Ω architecture with four or five constant bases (Figure 2, lanes 12, 13, 16, and 17, and Figure 3c–d). These results demonstrate that the Ω architecture enables distance-dependent reactions to be efficiently mediated by DNA bases far from the reactive end of the template. By overcoming the distance dependence of these reactions while preserving the efficiency of distant independent reactions, the Ω architecture should enable virtually any contiguous subset of bases in a single-stranded 30-base template to encode any viable DNA-templated reaction. Interestingly, the Ω templates with only three constant bases at their reactive ends do not consistently improve the efficiency of these reactions relative to the E architecture (Figure 3c–d), which suggests that four or five constant bases may be required in the Ω architecture to fully realize favorable proximity effects.

To probe the structural features underlying the observed properties of the Ω architecture, we characterized the thermal denaturation of template–reagent complexes in the Ω-5 and E architectures when $n=10$ or $n=20$. For all template–reagent combinations, only a single cooperative melting transition was observed. Compared to the E-architecture reagent lacking the five-base constant region, the Ω-5 reagent increased hypochromicity upon annealing by $\approx 50\%$ but did not significantly affect melting temperature (Table 1). These results are consistent with a model in which template–reagent annealing in the Ω architecture is dominated by coding-region interactions, even though the constant region forms a secondary structure once the coding region is annealed. The entropic cost of partially ordering the loop between the coding and constant regions may therefore be barely offset by the favorable interactions that arise upon annealing of the constant region.

Table 1: Melting temperatures of selected template–reagent combinations using the Ω and end-of-helix (E) architectures.[a]

Architecture	Buffer	T_m [°C]
E ($n=10$)	PBS	45
Ω ($n=10$)	PBS	46
E ($n=10$)	HSP	55
Ω ($n=10$)	HSP	54
E ($n=20$)	PBS	40
Ω ($n=20$)	PBS	39

[a] For conditions, see Experimental Section. PBS = phosphate-buffered saline, HSP = high salt phosphate buffer.

DNA templates of arbitrary length are easy to synthesize and undesired cross-reactivity in a given solution is avoided by using concentrations that are too low to allow noncomplementary reactants to react intermolecularly.[33] These features of DNA-templated synthesis in theory enable more than one DNA-templated reaction to take place on a single template in one solution, eliminating the effort associated with additional DNA-templated steps and product purification. However, multiple DNA-templated reactions per step are difficult to achieve with the E, H, or Ω architectures because the reagent oligonucleotide that remains annealed to the template following the first reaction forms a relatively rigid double helix that can prevent a second reagent, annealed further away along the template, from encountering the reactive end of the template.[23] To overcome this difficulty, we moved the reactive group on the template from the end to the middle of the oligonucleotide, and attached the reactive group to the non-Watson–Crick face of a base. We hypothesized that this T architecture (Figure 1) would enable two DNA-templated reactions, one with a reagent annealed between the reactive group and the 5′ end of the template, and one with a reagent annealed between the reactive group and the 3′ end of the template, to take place sequence specifically in the same solution on a single template.

To test the viability of the T architecture in DNA-templated reactions, we evaluated the efficiency of the amine acylation, Wittig olefination, 1,3-dipolar cycloaddition, and reductive amination reactions in the T architecture with one to five bases between the annealed reactants. The T architecture directed these four reactions sequence specifically with efficiencies comparable to or greater than those of the E or H architectures (Figure 4, 69–100% yield when $n=1$ or when $n=-1$. The observed degree of distance dependence in the T architecture for each of the four reactions is consistent with the findings described above (compare Figure 4 and Figure 3). Together these results demonstrate that the T architecture can mediate sequence-specific and efficient DNA-templated synthesis.

Once the ability of the T architecture to support efficient DNA-templated synthesis had been established, we tested its ability to direct two DNA-templated reactions on one template in one solution. We performed two different two-reaction sequences with the T architecture. In the first of these, a benzaldehyde-linked T template **1** was combined with a phosphane-linked reagent **2** and an α-iodoamide-linked reagent **3** in a single solution (pH 8.5, 1M NaCl, 25°C, 1 h)

 © 2003 Wiley-VCH Verlag GmbH & Co. KGaA, Weinheim 1433-7851/03/4212-1372 $ 20.00+.50/0

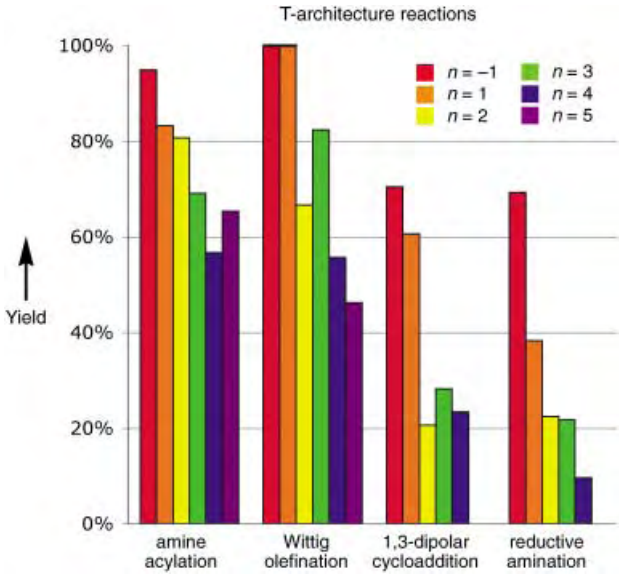

Figure 4. Efficiencies of DNA-templated reactions mediated by the T architecture. See Experimental Section for reaction conditions. Positive values of *n* refer to reagents annealing to the 3′ side of the reactive group on the template, while $n = -1$ refers to a reagent that anneals leaving one unpaired base 5′ of the reactive group on the template.

(Figure 5a). The phosphane-linked oligonucleotide complemented ten bases of the template between its 5′ end and the aldehyde ($n = -4$), while the iodide-linked oligonucleotide complemented ten bases between the aldehyde and the 3′ end of the template ($n = 0$). DNA-templated S_N2 reaction between the phosphane and α-iodoamide generated the corresponding phosphorane, which then participated in a DNA-templated Wittig reaction to generate cinnanamide **4** in 52% overall yield after 1 h (Figure 5b, lanes 9 and 10). Control reactions containing sequence mismatches in either reagent generated no detectable product. An additional control reaction in which there was no aldehyde group linked to the template generated only the S_N2 reaction product (Figure 5b, lanes 3 and 4), and control reactions in the absence of either the phosphane group or the α-iodoamide group did not generate any detectable products (Figure 5b, lanes 5–8).

In a second two-reaction sequence mediated by the T architecture, we combined an amine-linked T template **5** with a propargylglycine-linked 5′ reagent **6** at $n = -1$ and a phenylazide-linked 3′ reagent **7** at $n = 1$. The addition of 20 mM DMT-MM at pH 7.0 to induce amide formation,

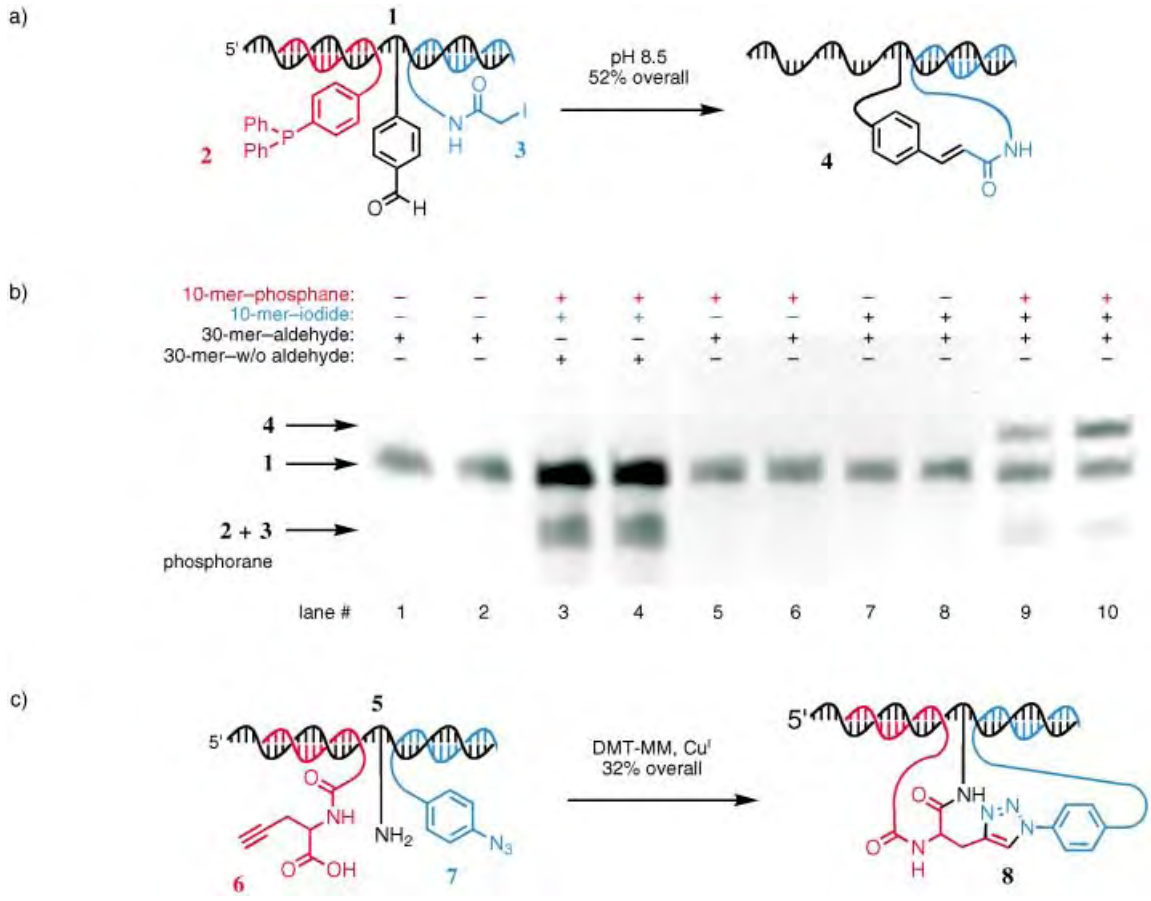

Figure 5. Two DNA-templated steps on a single template in one solution, mediated by the T architecture. a) S_N2 reaction–Wittig olefination sequence. b) Analysis of the reactions in (a) by denaturing polyacrylamide-gel electrophoresis. The 30-base T architecture template **1** with an aldehyde group was present in lanes 1, 2, and 5–10. A template lacking the aldehyde group but otherwise identical to **1** was present in lanes 3 and 4. DNA-linked phosphane reagent **2** was present in lanes 3–6, 9, and 10. DNA-linked α-iodoamide reagent **3** was present in lanes 3, 4, and 7–10. Lanes 1, 3, 5, 7, and 9 show reactions after 30 min; lanes 2, 4, 6, 8, and 10 show reactions after 1 h. c) Amine acylation–Huisgen cycloaddition sequence. For reaction conditions, see Experimental Section.

 © 2003 Wiley-VCH Verlag GmbH & Co. KGaA, Weinheim 1433-7851/03/4212-1373 $ 20.00+.50/0

followed by the addition of 500 μM copper(II) sulfate and sodium ascorbate to induce the recently reported Sharpless-modified Huisgen 1,3-dipolar cycloaddition,[35] provided 1,4-disubstituted triazoylalanine adduct **8** in 32% overall yield (Figure 5c). We conclude from these results that the T architecture enables two sequence-specific DNA-templated reactions to take place on one template in one solution. Importantly, the T-architecture templates described above were accepted as efficient templates for both a single cycle of primer extension as well as standard PCR amplification by *Taq* DNA polymerase, consistent with the known tolerance[36] of several DNA polymerases for modifications to the non-Watson–Crick face of DNA templates. In addition to reducing the number of separate DNA-templated steps required for the synthesis of a target structure, this architecture may enable three-component reactions,[37,38] commonly used to build structural complexity into synthetic libraries, to be performed in a DNA-templated format.

The Ω and T architectures developed in this work significantly expand the scope of DNA-templated synthesis. Our findings also demonstrate how reactivity can be rationally manipulated in a DNA-templated format by altering the design of template and reagent architectures, rather than by the traditional approach of changing global reaction conditions. By enabling distance-dependent DNA-templated reactions to be encoded by bases located far away from the reactive end of the template, the Ω architecture expands the types of reactions that can be encoded anywhere on a DNA template. The T architecture enables two DNA-templated reactions to take place on a single template in one step. Together these new architectures are proving to be useful in ongoing efforts to synthesize new compounds translated from corresponding DNA sequences.

Experimental Section

Unless otherwise specified, DNA oligonucleotides were synthesized and functionalized as previously described,[33] by using 2-[2-(4-monomethoxytrityl)aminoethoxy]ethyl-(2-cyanoethyl)-*N,N*-diisopropylphosphoramidite (Glen Research, Sterling, Virginia, USA) for 5′-functionalized oligonucleotides, and by using 2-dimethoxytrityloxymethyl-6-fluorenylmethoxycarbonylaminohexane-1-succinoyl long chain alkylamino-CPG (Glen Research) for 3′-functionalized oligonucleotides. In the case of templates for the T architecture, the amine groups were installed by using 5′-dimethoxytrityl-5-[*N*-(trifluoroacetylaminohexyl)-3-acrylimido]-2′-deoxyuridine-3′-(2-cyanoethyl-*N,N*-diisopropyl)phosphoramidite (Glen Research) and then acylated as reported previously.[33]

Amine acylation: Amine-labeled and carboxylic acid labeled DNA were combined in aqueous *N*-[3-morpholinopropane]sulfonic acid (MOPS) buffer (100 mM), NaCl (1M), pH 7.0 (60 nM in template DNA, 120 nM in reagent DNA) in the presence of 4-(4,6-dimethoxy-1,3,5-triazin-2-yl)-4-methylmorpholinium chloride (DMT-MM; 20 mM). The reactions were carried out for 12 h at 25°C.

Wittig olefination: Aldehyde-labeled and phosphorane-labeled DNA were combined in aqueous MOPS (100 mM), NaCl (1M), pH 7.5 (60 nM in template DNA, 120 nM in reagent DNA). The reactions were carried out for 2 h at 30°C.

1,3-Dipolar cycloaddition: Glyoxamide-linked DNA[25] was incubated in *N*-methylhydroxylamine hydrochloride (260 mM) for 1 h at room temperature. It was subsequently combined with maleimide-labeled DNA in aqueous MOPS (50 mM), NaCl (2.8M), pH 7.5 (final concentration of *N*-methylhydroxylamine hydrochloride 0.75 mM, 60 nM in template DNA and 90 nM in reagent DNA). The reactions were carried out for 12 h at 37°C.

Reductive amination: Amine-labeled and aldehyde-labeled DNA were combined in aqueous *N*-[2-morpholinoethane]sulfonic acid (MES) buffer (100 mM), NaCl (1M), pH 6.0 (60 nM in template DNA, 120 nM in reagent DNA). Sodium cyanoborohydride was added as a 5M stock solution in NaOH (1M) to a final concentration of 38 mM, and reactions were carried out for 2 h at 25°C. Reactions were quenched by ethanol precipitation in the presence of 15 mM methylamine.

1→**4** (T architecture): The 5′-phosphane-linked oligonucleotide **2** was generated by coupling 4-(diphenylphosphanyl)benzoic acid to the T ($n=-4$) oligonucleotide listed below as described previously.[25] The 3′-α-iodoamide-linked reagent **3** was prepared by treating the T ($n=1$) oligonucleotide (see below) with SIA as described previously.[23] The aldehyde-labeled template **1** was prepared by treating the "T template" oligonucleotide (see below) with *para*-formylbenzoic acid *N*-hydroxysuccinimidyl ester as described previously.[24] Template **1** was combined with reagents **2** and **3** in aqueous *N*-(2-hydroxyethyl)piperazine-*N*′-(2-ethanesulfonic acid) (HEPES) buffer (200 mM) at pH 8.5 with NaCl (1M), (63 nM template and 125 nM of each reagent). The reactions were carried out for up to 1 h at 25°C.

5→**8** (T architecture): The 5′-propargylglycine-linked oligonucleotide **6** was generated by combining the corresponding T ($n=-1$) 5′-amine-linked reagent oligonucleotide (see below) with bis(sulfosuccinimidyl)suberate (2 mg mL^{-1}) in sodium phosphate (200 mM, pH 7.2)/DMF (9:1) for 10 min at 25°C, followed by treatment with racemic propargylglycine (300 mM, 0.3 vol) in NaOH (300 mM) for 2 h at 25°C. The 3′-azido-linked oligonucleotide **7** was generated by combining the T ($n=1$) amine-linked reagent oligonucleotide (see below) with *N*-hydroxysuccinimidyl-4-azidobenzoate (2 mg mL^{-1}) in sodium phosphate (200 mM, pH 7.2)/DMF (9:1) for 2 h at 25°C. Reagents **6** and **7** were purified by gel filtration and reversed-phase HPLC. Template **5** and reagents **6** and **7** were combined in aqueous MOPS (100 mM, pH 7.0) in the presence of NaCl (1M) and DMT-MM (20 mM) for 12 h (60 nM in template, 120 nM in reagents) at 25°C. Copper(II) sulfate pentahydrate and sodium ascorbate were then added to 500 μM each. After 1 h at 25°C, the reactions were quenched by ethanol precipitation.

DNA oligonucleotide sequences used: E or Ω template: 5′-H_2N-GGT ACG AAT TCG ACT CGG GAA TAC CAC CTT; H template: 5′-H_2N-CGC GAG CGT ACG CTC GCG GGT ACG AAT TCG ACT CGG GAA TAC CAC CTT; T template: 5′-GGT ACG AAT TCG AC(dT-NH_2) CGG GAA TAC CAC CTT; E or H reagent ($n=1$): 5′-AAT TCG TAC C-NH_2; E or H reagent ($n=10$): 5′-TCC CGA GTC G-NH_2; E or H reagent ($n=20$): 5′-AAG GTG GTA T-NH_2; mismatched E or H reagent: 5′-TCC CTG ATC G-NH_2; Ω-3 reagent ($n=10$): 5′-TCC CGA GTC GAC C-NH_2; Ω-4 reagent ($n=10$): 5′-TCC CGA GTC GTA CC-NH_2; Ω-5 reagent ($n=10$): 5′-TCC CGA GTC GGT ACC-NH_2; Ω-3 reagent ($n=20$): 5′-AAG GTG GTA TAC C-NH_2; Ω-4 reagent ($n=20$): 5′-AAG GTG GTA TTA CC-NH_2; Ω-5 reagent ($n=20$): 5′-AAG GTG GTA TGT ACC-NH_2; mismatched Ω-3 reagent: 5′-TCC CTG ATC GAC C-NH_2; mismatched Ω-4 reagent: 5′-TCC CTG ATC GTA CC-NH_2; mismatched Ω-5 reagent: 5′-TCC CTG ATC GGT ACC-NH_2; T reagent ($n=1$): 5′-GGT ATT CCC G-NH_2; T reagent ($n=2$): 5′-TGG TAT TCC C-NH_2; T reagent ($n=3$): 5′-GTG GTA TTC C-NH_2; T reagent ($n=4$): 5′-GGT GGT ATT C-NH_2; T reagent ($n=5$): 5′-AGG TGG TAT T-NH_2; T reagent ($n=-1$): 5′-NH_2-GTC GAA TTC G; T reagent ($n=-4$) for **2**: 5′-[C_{12}-amine linker]-AAT TCG TAC C.

Reaction yields were quantified by denaturing polyacrylamide gel electrophoresis followed by ethidium bromide staining, UV visualization, and densitometry of product and template starting material bands. Yield calculations assumed that templates and products were denatured and therefore stained with comparable intensity per base; for those cases in which products are partially

 © 2003 Wiley-VCH Verlag GmbH & Co. KGaA, Weinheim 1433-7851/03/4212-1374 $ 20.00+.50/0

double-stranded during quantification, changes in staining intensity may result in higher apparent yields. Representative reaction products were characterized by MALDI (matrix-assisted laser desorption/ionization) mass spectrometry in addition to denaturing polyacrylamide gel electrophoresis.

Melting curves were obtained on a Hewlett-Packard 8453 UV/Vis spectrophotometer using a Hewlett-Packard 89090A Peltier thermocontroller. Absorptions of template–reagent pairs (1.5 μM each) at 260 nm were measured every 1 °C from 20 °C to 80 °C, holding for 1 min at each temperature, in either phosphate-buffered saline (NaCl (137 mM), KCl (2.7 mM), potassium phosphate (1.4 mM), sodium phosphate (10 mM), pH 7.4) or in high salt phosphate buffer (sodium phosphate (50 mM), NaCl (1M), pH 7.2).

Received: December 19, 2002 [Z50806]

Keywords: bioorganic chemistry · combinatorial chemistry · DNA · template synthesis

[1] D. Summerer, A. Marx, *Angew. Chem.* **2002**, *114*, 93; *Angew. Chem. Int. Ed.* **2002**, *41*, 89.
[2] L. E. Orgel, *Acc. Chem. Res.* **1995**, *28*, 109.
[3] X. Li, Z. Y. Zhan, R. Knipe, D. G. Lynn, *J. Am. Chem. Soc.* **2002**, *124*, 746.
[4] Y. Gat, D. G. Lynn, *Biopolymers* **1998**, *48*, 19.
[5] J. T. Goodwin, D. G. Lynn, *J. Am. Chem. Soc.* **1992**, *114*, 9197.
[6] J. G. Schmidt, L. Christensen, P. E. Nielsen, L. E. Orgel, *Nucleic Acids Res.* **1997**, *25*, 4792.
[7] R. K. Bruick, P. E. Dawson, S. B. H. Kent, N. Usman, G. F. Joyce, *Chem. Biol.* **1996**, *3*, 49.
[8] J. L. Czlapinski, T. L. Sheppard, *J. Am. Chem. Soc.* **2001**, *123*, 8618.
[9] Y. Z. Xu, E. T. Kool, *Tetrahedron Lett.* **1997**, *38*, 5595.
[10] Y. Xu, E. T. Kool, *J. Am. Chem. Soc.* **2000**, *122*, 9040.
[11] Y. Xu, N. B. Karalkar, E. T. Kool, *Nat. Biotechnol.* **2001**, *19*, 148.
[12] M. K. Herrlein, J. S. Nelson, R. L. Letsinger, *J. Am. Chem. Soc.* **1995**, *117*, 10151.
[13] A. Luther, R. Brandsch, G. von Kiedrowski, *Nature* **1998**, *396*, 245.
[14] J. Liu, J. S. Taylor, *Nucleic Acids Res.* **1998**, *26*, 3300.
[15] K. Fujimoto, S. Matsuda, N. Takahashi, I. Saito, *J. Am. Chem. Soc.* **2000**, *122*, 5646.
[16] N. G. Dolinnaya, M. Blumenfeld, I. N. Merenkova, T. S. Oretskaya, N. F. Krynetskaya, M. G. Ivanovskaya, M. Vasseur, Z. A. Shabarova, *Nucleic Acids Res.* **1993**, *21*, 5403.
[17] R. L. Letsinger, T. Wu, R. Elghanian, *Nucleosides Nucleotides* **1997**, *16*, 643.
[18] D. Albagli, R. V. Atta, P. Cheng, B. F. Huan, M. L. Wood, *J. Am. Chem. Soc.* **1999**, *121*, 6954.
[19] A. Mattes, O. Seitz, *Angew. Chem.* **2001**, *113*, 3277; *Angew. Chem. Int. Ed.* **2001**, *40*, 3178.
[20] C. Hartel, M. W. Göbel, *Helv. Chim. Acta* **2000**, *83*, 2541.
[21] X. Wu, G. Delgado, R. Krishnamurthy, A. Eschenmoser, *Org. Lett.* **2002**, *4*, 1283.
[22] L. H. Eckardt, K. Naumann, W. M. Pankau, M. Rein, M. Schweitzer, N. Windhab, G. von Kiedrowski, *Nature* **2002**, *420*, 286.
[23] Z. J. Gartner, D. R. Liu, *J. Am. Chem. Soc.* **2001**, *123*, 6961.
[24] Z. J. Gartner, M. W. Kanan, D. R. Liu, *Angew. Chem.* **2002**, *114*, 1874; *Angew. Chem. Int. Ed.* **2002**, *41*, 1796.
[25] Z. J. Gartner, M. W. Kanan, D. R. Liu, *J. Am. Chem. Soc.* **2002**, *124*, 10304.
[26] A. I. Scott, *Tetrahedron Lett.* **1997**, *38*, 4961.
[27] K. Tamura, P. Schimmel, *Proc. Natl. Acad. Sci. USA* **2001**, *98*, 1393.
[28] E. Szathmary, *Proc. Natl. Acad. Sci. USA* **1993**, *90*, 9916.
[29] M. Yarus, *J. Mol. Evol.* **1998**, *47*, 109.
[30] T. Li, K. C. Nicolaou, *Nature* **1994**, *369*, 218.
[31] C. Bohler, P. E. Nielsen, L. E. Orgel, *Nature* **1995**, *376*, 578.
[32] R. R. Breaker, G. F. Joyce, *J. Mol. Evol.* **1995**, *40*, 551.
[33] C. T. Calderone, J. W. Puckett, Z. J. Gartner, D. R. Liu, *Angew. Chem.* **2002**, *114*, 4278; *Angew. Chem. Int. Ed.* **2002**, *41*, 4104.
[34] M. Kunishima, C. Kawachi, K. Hioki, K. Terao, S. Tani, *Tetrahedron* **2001**, *57*, 1551.
[35] V. V. Rostovtsev, L. G. Green, V. V. Fokin, K. B. Sharpless, *Angew. Chem.* **2002**, *114*, 2708; *Angew. Chem. Int. Ed.* **2002**, *41*, 2596.
[36] J. A. Bittker, K. J. Phillips, D. R. Liu, *Curr. Opin. Chem. Biol.* **2002**, *6*, 367.
[37] A. Domling, *Curr. Opin. Chem. Biol.* **2002**, *6*, 306.
[38] A. Domling, I. I. Ugi, *Angew. Chem.* **2000**, *112*, 3300; *Angew. Chem. Int. Ed.* **2000**, *39*, 3168.

 © 2003 Wiley-VCH Verlag GmbH & Co. KGaA, Weinheim 1433-7851/03/4212-1375 $ 20.00+.50/0

Superparamagnetic Nanosensors

Magnetic Sensors for Protease Assays

*Ming Zhao, Lee Josephson, Yi Tang, and Ralph Weissleder**

Sensitive protease assays play an important role in elucidating protease function and in developing effective and selective anti-protease therapeutics. Although assays based on radioisotopes excel in sensitivity, the use of ionizing radiation often impedes a more general adaptation. Fluorogenic substrates with an internally quenched fluorophore are designed to produce fluorescent emission upon cleavage in assays based on fluorescence resonance energy transfer (FRET).[1,2] While the widespread application of such assays underscores their usefulness and practicality, issues intrinsic or secondary to the quenching mechanism must be resolved for each substrate.[1,3]

Here we describe a protease assay system that uses superparamagnetic nanoparticles as magnetic relaxation switches (MRS)[4] and determines protease activity from the spin–spin relaxation time (T_2) of water. The MRS approach differs from the method based on paramagnetic agents, in which enzyme activity is measured through changes in the spin–lattice relaxation time (T_1) of water.[5,6] The current assay employs peptide substrates that consist of a central sequence for protease recognition and cleavage, flanked by a biotinylated residue on each terminal. The bi-biotinylated peptide (BBP) substrates interact with avidin-magnetic nanoparticles (CLIO-A) and induce a clustered state with high T_2 relaxivity (Figure 1). When present, proteases cleave the

[*] Prof. R. Weissleder, M. Zhao, L. Josephson, Y. Tang
Center For Molecular Imaging Research
Massachusetts General Hospital, Harvard Medical School
Building 149, 13th Street, Room 5403, Charlestown, MA 02129 (USA)
Fax: (+1) 617-726-5709
E-mail: weissleder@helix.mgh.harvard.edu

 © 2003 Wiley-VCH Verlag GmbH & Co. KGaA, Weinheim 1433-7851/03/4212-1375 $ 20.00+.50/0

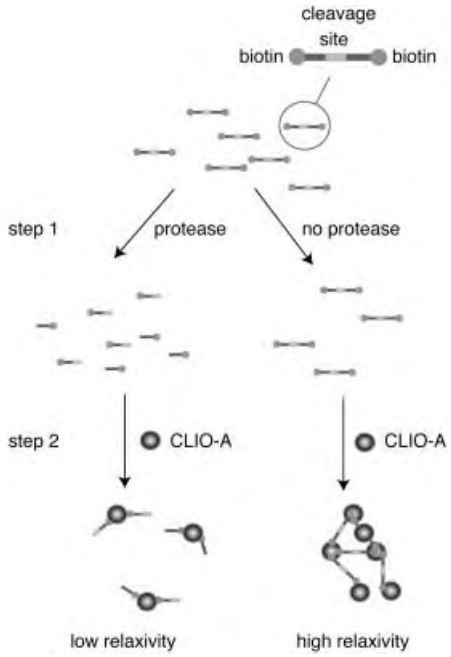

Figure 1. Schematic view of the BBP-MRS assay. The BBP substrate contains a central sequence with a cleavage site and flanking terminal biotins (insert). BBP induces cluster formation among CLIO-A nanoparticles, which results in high T_2 relaxivity (right). A protease converts BBP into mono-biotinylated fragments, abolishing the cluster-inducing activity; this is accompanied by low T_2 relaxivity (left).

substrate sequence between the two biotins (Btns), which results in mono-biotinylated fragments that interact with CLIO-A nanoparticles without inducing aggregation. Such a substrate design obviates the necessity of fluorescent quenching, and the magnetic resonance measurements can be conducted with optically opaque media such as tissue culture medium and tissue extracts.

To demonstrate the principle of the BBP-MRS assay, cluster formation in CLIO-A was induced by using various amounts of the generic substrate Btn-$(G)_4$RRRR$(G)_3$K(Btn). The transformation of the nanoparticle conjugates from a monodispersed to higher order clustered state was accompanied by a linear increase in the T_2 relaxivity R_2 (which is defined as the slope of the plot of the relaxation rate ($1/t$, s^{-1}) against nanosensor concentration (Fe, mM); Figure 2a). Subsequently, when we synthesized a more specific substrate for trypsin, Btn-GPARLAIK(Btn),[7,8] and used quantitative HPLC as a reference for the BBP-MRS assay, the changes in T_2 were correlated to the extent of substrate hydrolysis. The enzyme kinetics constants k_{cat} and K_m were determined to be 71.6 s^{-1} and 80.4 μM, respectively, which are in the same range as previously published values for both native peptide and FRET substrates for trypsin.[7,8] According to the HPLC profile and MS data, the site of hydrolysis is between positions P_1 and P_1', also consistent with the literature.[8,9] These observations strongly indicate that the BBP substrates retain native activities to proteolytic recognition and hydrolysis, while carrying molecular ligands designed for magnetic resonance readout. To demonstrate the feasibility of using the BBP-MRS assay in a high-throughput fashion, we imaged a 96-well microtiter plate (200 μL per well) with a 1.5 T clinical MR imaging system as described previously (Figure 2b).[10] With this methodology we have shown that stacked microtiter plates with up to 1536 wells per plate and 10 μL per well can be imaged simultaneously, providing data on thousands of samples in tens of minutes.[10]

Next, we investigated whether this technique could be used to quantitate a clinically relevant protease such as renin and how sensitive the magnetic assay would be. Renin is a protease secreted by juxtaglomerular cells in the kidney and plays an important role in blood pressure regulation.[11] Figure 3 summarizes the direct comparison of the assays against purified enzyme with FRET[12] and BBP substrates. The detection limit of the current method was calculated to be 69 ng mL^{-1} h^{-1} (equivalent to 31 nM h^{-1} of BBP hydrolyzed), which is in a range similar to that of published values obtained with FRET substrates for renin assay.[12] In comparison, FRET assays have the advantage of being continuous measurements. However, while the inner filter effect often limits the useful substrate concentration of FRET assays to micromolar range,[3] a given BBP substrate may be used at much higher concentrations. The ability to use a wide range of substrate concentrations facilitates measurements for the maximal rate of hydrolysis in enzyme kinetics studies. Another demonstration of the indifference of MRS to interferences was performed with renin in the presence of

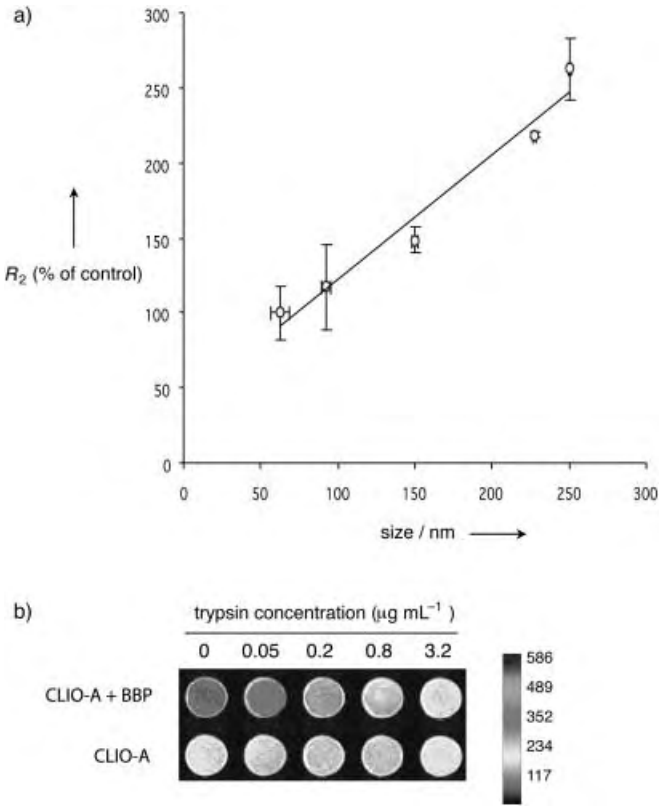

Figure 2. a) Plot of the increase in the average cluster size and the increase in relaxivity R_2 among CLIO-A nanoparticles, in the presence of BBP. b) T_2 mapping of 96-well plate samples measuring trypsin activity. The upper row contains CLIO-A and trypsin from 0 to 3.2 μg mL^{-1}. In the lower row are reference wells with CLIO-A only. T_2 values are coded according to the bar on the right.

 © 2003 Wiley-VCH Verlag GmbH & Co. KGaA, Weinheim 1433-7851/03/4212-1376 $ 20.00+.50/0

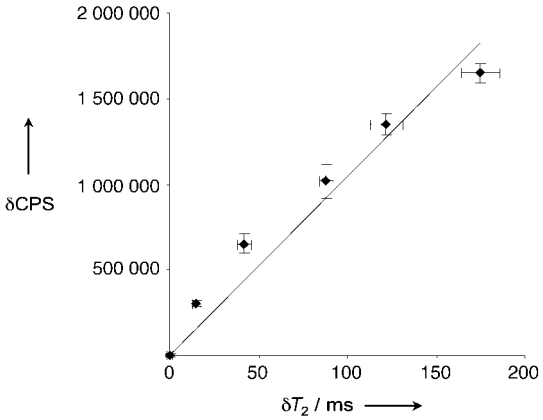

Figure 3. Direct comparison between FRET (*y* axis) and magnetic (*x* axis) assays. CPS = counts per second.

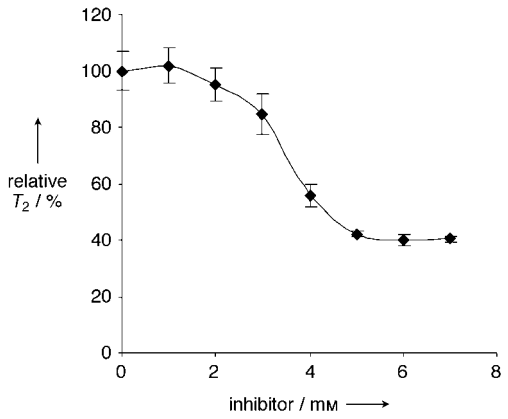

Figure 4. MMP-2 activity from the cell culture media of HT1080 fibrosarcoma cells was shown by the BBP-MRS assay to be inhibited by the presence of EDTA in a dose-dependent manner.

red blood cells. A solution of 2% whole blood in buffer reduced the fluorescence of the FRET substrate to near background levels, which makes it imposssible to perform FRET measurements. In contrast, the MRS assay was unaffected.

Proteases play key roles in diverse diseases.[13–17] In subsequent studies we wished to explore whether the BBP-MRS assay could be used to measure inhibition of matrix metalloproteinase 2 (MMP-2), a protease linked to metastasis and tumor angiogenesis.[13] The substrate Btn-GGPLGVRGK(Btn) was incubated with purified, active MMP-2, which led to hydrolysis at the expected cleavage site,[18] as confirmed by HPLC and mass spectrometry. Subsequently, we measured the concentration of MMP-2 in cell-culture supernatant from HT1080 fibrosarcoma cells without any purification.[19] Apart from MMP-2, the collected media also contained a host of biomolecules that contribute to a broad range of background absorbance at wavelengths less than 600 nm, which can be problematic to fluorescent measurements. However, with the MRS-BBP method, MMP-2 activity could be determined in unpurified samples (19 ng mL^{-1} from 24 h growth media), whereas fluorescence measurements under similar conditions required the assay to be run in buffer. Since MMP-2 activity is zinc dependent,[20] EDTA (ethylenediaminetetraacetate) as a model inhibitor was able to inhibit MMP-2 activity in a dose-dependent fashion (Figure 4). Similar results were also observed with other more specific MMP inhibitors (data not shown).

The MRS protease assay we describe utilizes bi-biotinylated peptides readily made by solid-phase peptide synthesis. Yet the assay format could, in theory, be extended to other hydrolytic enzymes (nucleases, polysaccharidases, lipases). Since the protease recognizes the bi-biotinylated peptide in solution, immobilization of the peptide is not required. Unlike fluorescence-based protease assays, the MRS method can accommodate a range of assay conditions, including high turbidity and extreme pH and temperatures.[21] Owing to the penetrating nature of the radio-frequency radiation it employs, the method is also free from light interferences. Finally, in terms of instrumentation, T_2 measurements can be conducted with individual samples in single tubes by using MR relaxometers or with microtiter plates in a high-throughput format.

Experimental Section

BBP synthesis: Fmoc amino acids were obtained from Calbiochem, NovaBiochem (San Diego, CA). BBPs were synthesized by using an automated peptide synthesizer (PS3, Rainin, Woburn, MA), and biotinylated at the N-terminal NH_2 and C-terminal lysine by reaction with NHS-biotin (Pierce) after removal of the Fmoc and 2-(4,4-dimethyl-2,6-dioxocyclohexylidene)ethyl (Dde) protecting groups. A second method for making BBPs employed Fmoc-Lys(Btn)-OH in automated peptide synthesis. BBPs were cleaved from the resin and purified by HPLC, and their molecular weights were determined by mass spectrometry. The following BBPs were synthesized: BTN-$(G)_4$RRRR$(G)_3$K(BTN) (M_w calcd: 1622.9, found: 1622.9); trypsin substrate BTN-GPARLAIK(BTN) (M_w calcd: 1276.6, found: 1276.6); MMP-2 substrate BTN-GGPLGVRGK(BTN) (M_w calcd: 1291.4, found: 1291.4), and renin substrate RK(Btn)IHPFHL-VIHTK(Btn)R (M_w calcd: 2233.6, found: 2233.6).

CLIO-A synthesis: Aminated CLIO (CLIO-NH_2) was prepared as described elsewhere.[22] *N*-Succinimidyl *S*-acetylthioacetate (SATA), *N*-succinimidyl 6-[3′-(2-pyridyldithio)propionamido]hexanoate (Lc-SPDP), and neutravidin were obtained from Pierce. Neutravidin is a modified form of avidin with a near-neutral isoelectric point and is free of carbohydrate units to minimize nonspecific binding. To neutravidin (10 mg mL^{-1}, 0.1 mL) was added SATA (11 mg mL^{-1}, 10 μL), and the mixture was allowed to stand for 2 h at room temperature before it was dialyzed and deacetylated with hydroxylamine HCl (Sigma). Thiolated neutravidin was incubated with Lc-SPDP activated CLIO-NH_2. The average number of neutravidin per CLIO particle was determined as described,[23] and CLIO-A was purified by using a magnetic separation column. The hydrodynamic size was determined by using a Zetasizer 1000 SHA (Malvern Instruments).

Protease assays: A solution of the BBP substrate was subjected to protease digestion. Aliquots were removed at defined time intervals and added to CLIO-A, typically at 15 μg Fe per mL, in the presence of protease inhibitors to prevent neutravidin degradation. After 1 h at room temperature, T_2 was measured on a 0.47 T benchtop spectrometer (Bruker). When appropriate, reverse-phase (C18) HPLC was employed as a reference method (a gradient from 10 to 80% solvent A (0.1% trifluoroacetic acid in H_2O as solvent A; 10% solvent A and 90% acetonitrile as solvent B)). The percentage of hydrolysis was calculated from the peak areas and correlated to T_2. K_m was estimated by using the Lineweaver–Burk plot; k_{cat} was deduced from the

 © 2003 Wiley-VCH Verlag GmbH & Co. KGaA, Weinheim 1433-7851/03/4212-1377 $ 20.00+.50/0

equation $k_{cat}/K_m = K_{obs}/Et$, given that substrate concentration was substantially lower than the estimated K_m value.

Comparison with FRET: BBP and FRET (Molecular Probes) substrates were incubated in the same cuvettes (0.5 mL, 1 cm) at 2 μM, with final concentrations of renin (CalBiochem) of 0.78, 1.56, and 3.13 mU. After 8 h, emission at 490 nm (excitation 340 nm) was measured with a Fluorolog spectrofluorometer (Jobin Yuon Inc.). Immediately following fluorescent measurements, T_2 values were obtained. In addition, both assays were repeated in the presence of 2% mouse whole blood.

MMP-2 assay: A solution of MMP-2 BBP substrate (10 $\mu g\,mL^{-1}$) was incubated with various amounts of active recombinant MMP-2 (CalBiochem) at 37°C (50 mM HEPES, 10 mM of $CaCl_2$ and 0.005% Brij (Sigma), pH 7.4). T_2 measurements were performed as described above. HT1080 fibrosarcoma cells were cultured in MEM (Gibco) to confluence, with 10% fetal calf serum. The cells were washed twice, and cultured in serum-free MEM for 24 h. The media were collected and centrifuged, and MMP-2 BBP substrate was added to give a final concentration of 10 $\mu g\,mL^{-1}$. EDTA (0–5 mM) was included as an MMP-2 inhibitor in some of the samples. After incubation for 12 h at 37°C, magnetic resonance measurements were conducted as described above.

MR imaging: Samples of 200 μL were loaded into a 96-well plate and imaged on a 1.5 T superconducting magnet (Signa 5.0; GE Medical Systems, Milwaukee, WI) using a 5-inch surface coil and a T_2-weighted spin echo sequence: 3000/85 (TR/TE), 1 mm slice thickness, 6 × 6 cm field of view, 256 × 256 imaging matrix. To obtain a T_2 map, echo time (TE) values between 20 to 400 ms were used; the T_2 maps were calculated by using Matlab (Matlab 6.0; The MathWorks, Natick, MA).

Received: September 23, 2002
Revised: December 19, 2002 [Z50213]

Keywords: biosensors · biotin · enzymes · magnetic properties · proteases

[1] E. D. Matayoshi, G. T. Wang, G. A. Krafft, J. Erickson, *Science* **1990**, *247*, 954.
[2] G. B. Irvine, M. Ennis, C. H. Williams, *Anal. Biochem.* **1990**, *85*, 304.
[3] B. P. Holskin, M. Bukhtiyarova, B. M. Dunn, P. Baur, J. de Chastonay, M. W. Pennington, *Anal. Biochem.* **1995**, *226*, 148.
[4] L. Josephson, J. M. Perez, R. Weissleder, *Angew. Chem.* **2001**, *113*, 3304; *Angew. Chem. Int. Ed.* **2001**, *40*, 3204.
[5] A. Y. Louie, M. M. Hüber, E. T. Ahrens, U. Rothbächer, R. Moats, R. E. Jacobs, S. E. Fraser, T. J. Meade, *Nat. Biotechnol.* **2000**, *18*, 321.
[6] A. Bogdanov, L. Matuszewski, C. Bremer, A. Petrovsky, R. Weissleder, *Mol. Imaging* **2002**, *1*, 16.
[7] V. Schellenberger, C. W. Turck, L. Hedstrom, W. J. Rutter, *Biochemistry* **1993**, *32*, 4349.
[8] S. Grahn, D. Ullmann, H. D. Jakubke, *Anal. Biochem.* **1998**, *265*, 225.
[9] I. Schechter, A. Berger, *Biochem. Biophys. Res. Commun.* **1967**, *27*, 157.
[10] D. Hogemann, V. Ntziachristos, L. Josephson, R. Weissleder, *Bioconjugate Chem.* **2002**, *13*, 116.
[11] L. M. Resnick, J. H. Laragh, *Am. J. Cardiol.* **1985**, *56*, 68.
[12] G. T. Wang, C. C. Chung, T. F. Holzman, G. A. Krafft, *Anal. Biochem.* **1993**, *210*, 351.
[13] A. John, B. Tuszynski, *Pathol. Oncol. Res.* **2001**, *7*, 14.
[14] Z. S. Galis, J. J. Khatri, *Circ. Res.* **2002**, *90*, 251.
[15] R. A. Nixon, *Ann. N. Y. Acad. Sci.* **2000**, *924*, 117.
[16] J. A. Tavel, *Expert Opin. Invest. Drugs* **2000**, *9*, 917.
[17] G. Giannelli, S. Antonaci, *Histol. Histopathol.* **2002**, *17*, 339.
[18] E. I. Chen, S. J. Kridel, E. W. Howard, W. Li, A. Godzik, J. W. Smith, *J. Biol. Chem.* **2002**, *277*, 4485.
[19] H. J. Cha, S. K. Bae, H. Y. Lee, O. H. Lee, H. Sato, M. Seiki, B. C. Park, K. W. Kim, *Cancer Res.* **1996**, *56*, 2281.
[20] B. Isaksen, M. K. Fagerhol, *Mol. Pathol.* **2001**, *54*, 289.
[21] J. Perez, L. Josephson, T. O'Loughlin, D. Hoegeman, R. Weissleder, *Nat. Biotechnol.* **2002**, *20*, 816
[22] L. Josephson, C. H. Tung, A. Moore, R. Weissleder, *Bioconjugate Chem.* **1999**, *10*, 186.
[23] M. Zhao, M. F. Kircher, L. Josephson, R. Weissleder, *Bioconjugate Chem.* **2002**, *13*, 840.

 © 2003 Wiley-VCH Verlag GmbH & Co. KGaA, Weinheim 1433-7851/03/4212-1378 $ 20.00+.50/0

Biocatalysis in Photochemistry

Antibody-Catalyzed Enantioselective Norrish Type II Cyclization**

*Sigal Saphier, Subhash C. Sinha, and Ehud Keinan**

The Norrish type II photochemical reaction involves abstraction of a γ hydrogen atom by an excited carbonyl oxygen atom (e.g. in **1**) to produce a 1,4-diradical intermediate, such as **A**.[1] The latter can undergo three possible reactions: a) reverse hydrogen transfer to regenerate the ground state of **1**; b) C–C-bond cleavage to form an alkene **2** and an enol that tautomerizes to the carbonyl compound **3**; or c) radical recombination (Yang cyclization[2]) to produce the cyclobutanols **4** and **5** (Scheme 1). Usually, pathway b is the most common route, while c) represents a minor side reaction. Intense mechanistic studies over the past three decades have made the Norrish type II reaction one of the most well-understood photochemical reactions.[1] Unfortunately, this important reaction has not yet enjoyed comparable status in synthetic chemistry, mainly as a result of a lack of control over product selectivity and, in particular, stereoselectivity.[3]

The most successful approach to limiting the broad variety of possible photoproducts has been based on solid-state reactions, in which the crystal-packing forces severely restrict the range of available conformations.[4] However, for syn-

[*] Prof. E. Keinan, S. Saphier, Prof. S. C. Sinha
Department of Chemistry and
Institute of Catalysis Science and Technology
Technion - Israel Institute of Technology
Technion City, Haifa 32000 (Israel)
Fax: (+972) 4-829-3913
E-mail: keinan@techunix.technion.ac.il
Prof. E. Keinan, Prof. S. C. Sinha
Department of Molecular Biology and
the Skaggs Institute for Chemical Biology
The Scripps Research Institute
10550 North Torrey Pines Road
La Jolla, CA 92037 (USA)
Fax: (+1) 858-784-8732

[**] We thank the Israel Science Foundation and the Skaggs Institute for Chemical Biology for financial support.

Supporting information for this article is available on the WWW under http://www.angewandte.org or from the author.

 © 2003 Wiley-VCH Verlag GmbH & Co. KGaA, Weinheim 1433-7851/03/4212-1378 $ 20.00+.50/0

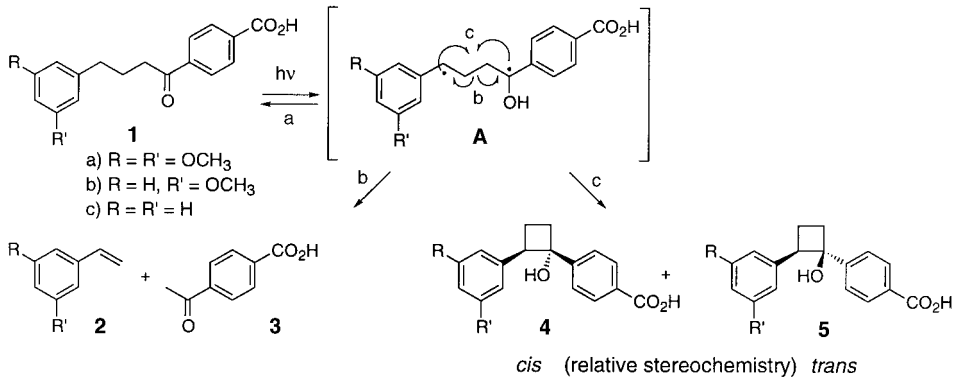

Scheme 1. Norrish type II reaction with possible reaction pathways of the 1,4-diradical intermediate.

thetic purposes this approach is limited to cases in which the reactant conformation is photochemically productive. Moreover, it is difficult to predict the preferred solid-state conformation of a given compound. Other attempts to control the reaction by using various organized media that restrict the conformational flexibility of the diradical intermediate have enjoyed limited success.[5]

Biocatalysis with enzymes represents an attractive strategy to restrain mechanistic manifolds and channel a reactive intermediate into a single product.[6] Unfortunately, the natural diversity of enzymes that catalyze photochemical reactions is rather limited. Aside from the highly complex protein assemblies involved in light-harvesting systems,[7] only three enzymes that catalyze a specific photoreaction have been reported.[8] These include protochlorophylide reductase[9] and two enzymes that catalyze the fragmentation of thymine dimers in the DNA-repair mechanism: DNA photolyase[10] and [6-4]-photoproduct lyase.[11] It is clear that evolution has selected against photoenzymes, particularly in multicellular organisms.

The deficiency in natural catalysts calls for the design of new ones, for example, catalytic antibodies. The three reported attempts to catalyze photoreactions with antibodies are the dimerization of methyl *p*-nitrocinnamate,[12] the cleavage of thymine and uracil cyclobutane dimers,[13] and intramolecular hydrogen transfer in an α-ketoamide.[14]

Scheffer reported the successful photocyclization of ketones in the solid state.[4] We envisioned that antibodies elicited against the *cis* and *trans* oxetanes **6** and **7** would

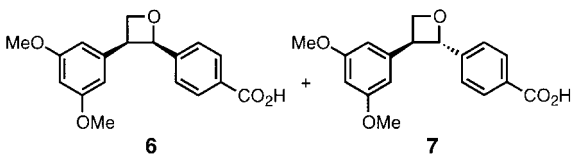

Scheme 2. Haptens used for immunization.

restrict the conformational flexibility of **1** and stabilize its productive conformation for photochemical cyclization. Herein we report that antibodies that were elicited against **6** and **7** (Scheme 2) do indeed selectively catalyze the formation of a cyclobutanol product in the Norrish type II reaction. Furthermore, we show that the resultant photoproduct is obtained as a single stereoisomer with very high enantioselectivity.

Each of the isomeric haptens **6** and **7** were synthesized as racemic mixtures and fully characterized (see Supporting Information). They were then mixed in a 1:1 ratio and the mixture was conjugated to KLH (keyhole limpet hemocyanin) and to BSA (bovine serum albunin) using known procedures.[15a] The KLH conjugate was used to elicit monoclonal antibodies by standard hybridoma technology.[15b] Preliminary ELISA (enzyme-linked immunosorbent assay) screening for the best binders of **6** and **7** using the BSA conjugate[15c] afforded 800 antibody-producing hybridoma cell lines. As we were interested in antibodies that bind the entire substrate molecule in the desired conformation, we selected the 60 best binders based on their selective recognition of either **6** or **7**. Assuming that the desired catalysts should also bind the substrate, we carried out further ELISA selection for binders of the **1**-BSA conjugate and thus narrowed the library down to ten antibodies. Our assumption was corroborated later by the fact that all three catalysts discovered for the reaction were in the narrow library of the ten anti-**1** antibodies, while no catalyst was found in the remaining group of 50 antibodies that bind **6** and/or **7** well, but do not bind **1**.

Antibodies were tested for catalysis by irradiation in solution in the presence of **1** (with either a xenon or a mercury UV lamp). Three antibodies, 12B4, 20F10, and 21H9, catalyzed the formation of the *cis*-cyclobutanols **4**, the structure and relative stereochemistry of which were determined by comparison (^{1}H NMR, MS, UV and HPLC) with authentic synthetic samples (see Supporting Information). No reaction was observed in the dark, either in the presence or absence of antibodies.

The possibility of carrying out such an enantioselective cyclization is of particular interest because it is generally difficult to achieve stereochemical control over reactions that involve radical intermediates. We used HPLC with a chiral column to measure the enantioselectivity of the antibody-catalyzed photochemical cyclization. The chromatograms were compared with those of authentic racemic samples of **4**, which was synthesized independently (see Supporting Information). Interestingly, all three antibodies produced the

 © 2003 Wiley-VCH Verlag GmbH & Co. KGaA, Weinheim 1433-7851/03/4212-1379 $ 20.00+.50/0

same enantiomer of **4**, the absolute configuration of which is yet unknown (antibody, *ee*): 20F10, 96%; 12B4, 80%; 21H9, 78%; for R = R' = OMe.

The most enantioselective antibody, 20F10, also yielded the highest cyclization/fragmentation ratio (70:30) at 312 nm. Therefore, we selected 20F10 for kinetic studies and further characterization. At low antibody concentrations, the background photochemical cleavage reaction becomes dominant. This precluded measurements of the initial rates for the cyclization under Michaelis–Menten approximation, in which low catalyst concentrations relative to substrate loadings are normally used to determine the kinetic parameters (k_{cat} and K_M). To circumvent this problem we turned to an alternative model, which uses excess catalyst with constant substrate concentration. Under these conditions, rate constants were obtained from a series of pseudo-first-order kinetic data (see Supporting Information). Data were modeled according to the general format of Michaelis–Menten as described by Klotz and co-workers.[16] As expected, the rate constant is highly dependent on the flux of light. For example, when a 150-W Xenon lamp was used the reaction was complete within 10 s. This high k_{cat} made it technically difficult to obtain accurate results. We therefore used a weaker, 75-W Xenon lamp to delay the reaction over a time span of 20 min. Under these conditions, we obtained the values of $k_{cat} = 0.008 \pm 0.001$ min^{-1} and $K_M = 58 \pm 13$ μM. Much higher values of k_{cat} would be obtained with more intense UV lamps. No cyclization products were detected in the absence of the antibody.

To evaluate the catalytic efficiency of the antibody over multiple turnovers, the antibody was recycled several times by dialysis and its activity was examined. The photochemical reaction was performed in each cycle with equal concentrations of antibody and substrate. No reduction in activity was observed after five cycles, indicating that the active site of the protein is remarkably stable under the photochemical conditions. The stability of antibodies under UV radiation seems to be a general phenomenon.[17] Moreover, the ability of the active sites of antibodies to handle reactive intermediates, including free radicals, carbonium ions[18] and reactive oxygen species,[17] is of particular significance to the general field of biocatalysis. Total product formation amounted to more than three times the initial concentration of the antibody. This observation, together with the stability of the catalyst, suggest that, in principle, the catalyst could be immobilized and used in a flow system for continuous synthesis of the photoproduct.[19]

The dependence of cyclization efficiency on the irradiation wavelength within the range of 245–320 nm was examined (see Supporting Information). The relative rates followed the antibody absorption spectrum quite faithfully, with a red shift of approximately 10 nm (maximal activity at 290 nm). This suggests the presence of a possible active site tryptophan, which acts as a sensitizer and transfers the light energy to the substrate.[13a] By contrast, the fragmentation efficiency was found to follow the absorption spectrum of the substrate ($\lambda_{max} = 250$ nm). The different wavelength dependence of the two reaction routes could be exploited to optimize the cyclization yield. Indeed, the cyclization/fragmentation ratio was increased from 37:63 at 240 nm to 70:30 at 312 nm.

As substrate **1** is inert in the dark, it is possible to measure its binding constants to the antibody directly. Isothermal titration calorimetry (ITC) measurements afforded the binding constants of substrates and haptens (compound, K_a (M^{-1})): **6**, 5.89×10^4; **7**, 2.10×10^5; **1a**, 1.92×10^6; **1b**, 1.2×10^4; **1c**, $< 5 \times 10^3$. Interestingly, the methoxy groups in the substrate play a crucial role in binding, as reflected by the significant drop in binding upon removal of one or two methoxy groups. The trend in substrate binding was found to parallel the relative efficiency in forming the corresponding *cis* cyclobutanol product in the presence of antibody 20F10 (substrate, relative rate): **1a**, 8; **1b**, 2; **1c**, 1.

Remarkably, 20F10 binds substrate **1a** more strongly than it binds either of the two haptens. Furthermore, 20F10 catalyzes the formation of a *cis*-diaryl cyclobutanol **4**, and yet it binds the *trans* oxetane **7** more tightly than the *cis* isomer **6**. Apparently, **1a** is sufficiently flexible to assume the optimal binding conformation, which seems to be an intermediate structure between **6** and **7**. It has been proposed that the cleavage of 1,4-biradicals requires good overlap between the radical-containing p orbitals and the C2–C3 bond.[4a] Failing that, and provided that C1 and C4 are within reasonable bonding distance, cyclization will predominate. Thus, it is conceivable that the protein imposes conformational constraints on the substrate, which enforce preferential cyclization.

In conclusion, the first antibody-catalyzed Yang cyclization has been developed, producing a single stereoisomeric product with very high enantioselectivity. Catalysis by the antibody probably involves the dual effects of stabilizing the productive conformation as well as light harvesting and energy transferal. Further work towards a better understanding of these effects is currently underway.

Received: September 30, 2002 [Z50267]

Keywords: catalytic antibodies · cyclization · enantioselectivity · photochemistry · radical reactions

[1] P. J. Wagner in *CRC Handbook of Organic Photochemistry and Photobiology*, CRC, Boca Raton, FL, **1995**, p. 449.
[2] N. C. Yang, D. H. Yang, *J. Am. Chem. Soc.* **1958**, *80*, 2913.
[3] A. G. Griesbeck, H. Heckroth, *Res. Chem. Intermed.* **1999**, *25*, 599.
[4] a) M. Leibovitch, G. Olovsson, J. R. Scheffer, J. Trotter, *J. Am. Chem. Soc.* **1998**, *120*, 12755, and references therein; b) J. R. Scheffer, M. Garcia-Garibay, O. Nalamasu in *Organic Photochemistry, Vol. 8* (Ed.: A. Padwa), Marcel Dekker, **1987**, chap. 4, pp. 249–347.
[5] Y. Inoue, *Chem. Rev.* **1992**, *92*, 741.
[6] a) J. Rétey, *Angew. Chem.* **1990**, *102*, 373; *Angew. Chem. Int. Ed. Engl.* **1990**, *29*, 355; b) C. Walsh, *Enzymatic Reaction Mechanisms*, W. H. Freeman, New York, **1979**.
[7] J. Deisenhofer, H. Michel, R. Huber, *Trends Biochem. Sci.* **1985**, *10*, 243, and references therein.
[8] L. A. Tai, K. C. Hwang, *Angew. Chem.* **2000**, *112*, 4044; *Angew. Chem. Int. Ed.* **2000**, *39*, 3886.
[9] T. P. Begley, *Acc. Chem. Res.* **1994**, *27*, 394.
[10] A. P. M. Eker, J. K. C. Hessels, R. H. Dekker, *Photochem. Photobiol.* **1986**, *44*, 197.

 © 2003 Wiley-VCH Verlag GmbH & Co. KGaA, Weinheim 1433-7851/03/4212-1380 $ 20.00+.50/0

[11] T. Todo, H. Takemori, H. Ryo, M. Ihara, T. Marsunaga, O. Nikaido, K. Sato, T. Nomura, *Nature* **1993**, *361*, 371.
[12] A. Balan, B. P. Docto, B. S. Green, M. Torten, H. Ziffer, *Chem. Commun.* **1998**, 106.
[13] a) A. G. Cochran, R. Sugasawara, P. G. Schultz, *J. Am. Chem. Soc.* **1998**, *110*, 7888; b) J. R. Jacobsen, A. G. Cochran, J. C. Stephans, D. S. King, P. G. Schultz, *J. Am. Chem. Soc.* **1995**, *117*, 5453.
[14] M. J. Taylor, T. Z. Hoffman, J. T. Yli-Kauhaluoma, R. A. Lerner, K. D. Janda, *J. Am. Chem. Soc.* **1998**, *120*, 12783.
[15] a) J. V. Staros, R. W. Wright, D. M. Swingle, *Anal. Biochem.* **1986**, *156*, 220; b) J. W. Goding, *Monoclonal Antibodies: Principles and Practice*, 2nd ed., Academic Press, New York, **1986**; c) B. Clark, E. Eengvali in *ELISA: Theoretical and Practical Aspects in Enzyme-Immunoassay*, Mggio (Ed.: E. T. Ed), CRC, Boca Raton, FL, **1980**, chap. 8.
[16] J. Suh, I. S. Scarpa, I. M. Klotz, *J. Am. Chem. Soc.* **1976**, *98*, 7060.
[17] A. D. Wentworth, L. H. Jones, P. Wentworth, Jr., K. D. Janda, R. A. Lerner, *Proc. Natl. Acad. Sci. USA* **2000**, *97*, 10930.
[18] J. Hasserodt, K. D. Janda, R. A. Lerner, *J. Am. Chem. Soc.* **2000**, *122*, 40.
[19] D. Shabat, F. Grynszpan, S. Saphier, A. Turniansky, D. Avnir, E. Keinan, *Chem. Mater.* **1997**, *9*, 2258.

 © 2003 Wiley-VCH Verlag GmbH & Co. KGaA, Weinheim 1433-7851/03/4212-1381 $ 20.00+.50/0

Biocatalyst Design

Catalytic Peptide Dendrimers**

*Annamaria Esposito, Estelle Delort, David Lagnoux, Françis Djojo, and Jean-Louis Reymond**

Enzyme catalysis is made possible by the folding of linear peptide chains into well-defined three-dimensional structures. The aim of de novo enzyme design is to create selective catalysts through the catalytically productive combination of amino acids.[1] A variety of α-helical peptides have been designed that are catalytically active.[2] Thus, the spatial proximity of amino acid side chains placed one turn apart in an α helix were shown to induce catalysis. Protected β-turn peptides have been found to be selective catalysts in organic solvents.[3] Such approaches have required the linear peptides to form a properly folded structure for catalysis to be observed. Alternatively one can design three-dimensional structures by chemical synthesis using a dendrimeric architecture, which enforces a globular shape by steric crowding and therefore obviates the folding requirement and greatly simplifies design.[4] Whereas catalytic dendrimers based on ether linkages and incorporating catalytically active subunits such as metal complexes and cofactors are known,[5] peptide dendrimers have to date only been reported as antigen-display units (multiple antigenic peptides)[6] or in structural studies.[7] Herein we report the preparation of the first catalytic peptide dendrimers. The peptide dendrimers exhibit enzymelike kinetic properties, including selective substrate binding and rate acceleration in aqueous media.

We prepared dendrimeric peptides with the sequence $((CapCONH\text{-}A^3)_2BA^2)_2B\text{-}Cys\text{-}A^1\text{-}NH_2$ (Scheme 1). The symmetrical, achiral diamino acid (1,3-diaminoisopropyloxy)acetic acid was chosen as the branching unit B, which provides the dendrimeric architecture. The sequences were terminated by acylation with the 3-dimethylaminoisophthaloyl group (= Cap, introduced as the mono-*tert*-butyl ester), which provided a spectroscopic signature and allowed the homogeneous solubility of the dendrimers under both the acidic conditions of HPLC purification and the neutral conditions of aqueous buffers. Permutations of the catalytic triad of the amino acids histidine (His), aspartate (Asp), and serine (Ser) were chosen as the variable positions A^1, A^2, and A^3 to generate a family of esterolytic peptide dendrimers. The solid-phase peptide synthesis was carried out on a Rink amide resin with Fmoc-

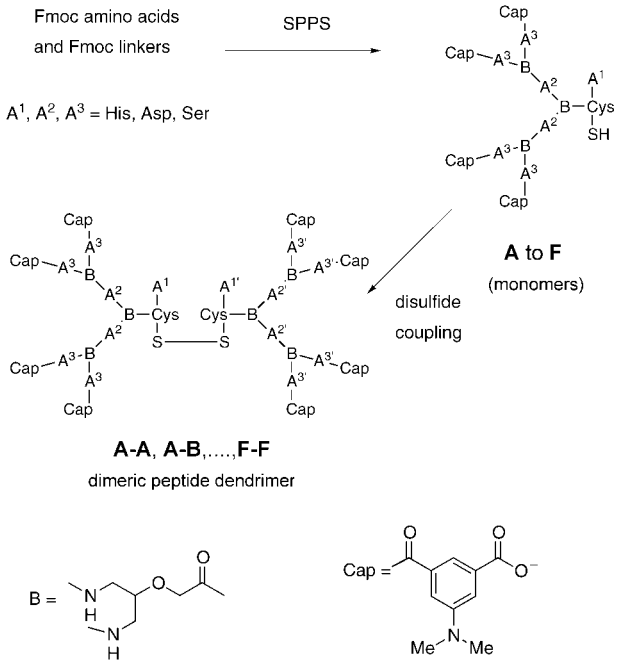

Scheme 1. Synthesis of catalytic peptide dendrimers. SPPS = solid-phase peptide synthesis.

[*] Prof. Dr. J.-L. Reymond, Dr. A. Esposito, E. Delort, D. Lagnoux, Dr. F. Djojo
Department of Chemistry and Biochemistry, University of Bern
Freiestrasse 3, 3012 Bern (Switzerland)
Fax: (+41) 31-631-8057
E-mail: reymond@ioc.unibe.ch

[**] This work was supported by the Swiss National Science Foundation, the Swiss Office Fédéral de L'Education et de la Science, and the Novartis Foundation (postdoctoral grant to A.E.).

Supporting information for this article is available on the WWW under http://www.angewandte.org or from the author.

 © 2003 Wiley-VCH Verlag GmbH & Co. KGaA, Weinheim 1433-7851/03/4212-1381 $ 20.00+.50/0

protected building blocks. Each of the six resulting dendrimeric peptides were then used to prepare all possible dimeric combinations by disulfide-bond formation with aldrithiol,[8] resulting in a family of 21 different peptide dendrimers. Each of the dimeric peptides was prepared on a milligram scale and purified by semipreparative reversed-phase HPLC.

The dendrimers were assayed for the catalysis of ester hydrolysis in both a neutral (pH 7.4) and a slightly acidic (pH 6.0) aqueous buffer, using chromogenic and fluorogenic acetyl esters and acetoxymethyl ethers of umbelliferone,[9] 8-acetoxypyrene-1,3,6-trisulfonate,[10] and 7-acetoxy-1-methylquinolinium sulfate,[11] with 200 μM substrate and 5 μM catalyst (2.5 mol%).[12] While there was no detectable activity with most substrates, several dendrimers catalyzed the hydrolysis of 7-acetoxy-1-methylquinolinium sulfate **1** (Scheme 2, Table 1). The activity pattern indicated that

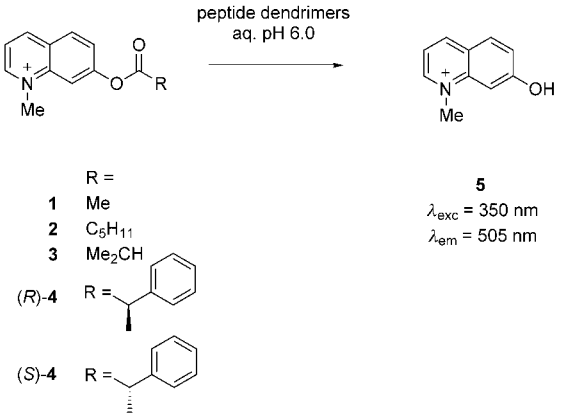

Scheme 2. Peptide-dendrimer-catalyzed ester hydrolysis.

catalysis was correlated with the presence of histidine residues at the outermost positions A^3 of the dendrimers. The three most active dendrimers were selected for further characterization.

All three of the most active catalytic peptide dendrimers, **E-E, E-F**, and **F-F**, catalyzed the hydrolysis of **1**, the related hexanoyl ester **2**, and isobutyroyl ester **3** with enzymelike kinetics, with a Michaelis–Menten constant of $K_M \sim 200$ μM, turnover numbers of $k_{cat} \sim 0.25\ min^{-1}$, and specific rate acceleration over background of up to $k_{cat}/k_{uncat} \sim 10^3$ (Figure 1 and Table 2). A pH-profile analysis between pH 5.5 and 8.5 showed that catalysis was most efficient at pH 6.0. The specific rate acceleration over that of 4-methylimidazole (MeIm), as a model for the catalytic histidine side chain, amounted to $k_{cat}/K_M/k_2 \sim 350$. The catalytic effect observed corresponds to a 40-fold reactivity increase per histidine side chain, which might be caused by productive interactions at the surface of the dendrimer. These results are similar to those observed by Baltzer and co-workers

Table 1: Apparent hydrolysis rates measured with 200 μM ester **1** and 5 μM dendrimer at 25 °C in 20 mM aqueous Bis-Tris buffer pH 6.0.[a]

A^3, A^2, A^1		–	**A**	**B**	**C**	**D**	**E**	**F**
Ser, Asp, His	**A**	0.5	0.2					
Asp, Ser, His	**B**	0.0	0.7	0.5				
Asp, His, Ser	**C**	0.6	0.3	0.6	0.4			
Ser, His, Asp	**D**	0.4	0.2	0.5	0.7	0.4		
His, Asp, Ser	**E**	2.1	3.1	1.9	1.6	1.4	**9.2**	
His, Ser, Asp	**F**	1.7	2.1	0.7	1.8	1	**12**	**6.4**

[a] The ratio V_{net}/V_{uncat} is reported for monomeric dendrimers **A** to **F** (column 1) and all combinations of dimers. V_{uncat} is the apparent spontaneous rate of formation of **5** in buffer alone, and $V_{net} = V_{app} - V_{uncat}$ (V_{app} is the apparent rate of formation of **5** in the presence of dendrimer). The reactions were run in 96-well polystyrene half-area microtiter plates and monitored by a SpectraMAX fluorescence detector with $\lambda_{exc} = 350$ nm, $\lambda_{em} = 505$ nm. Fluorescence was converted into product concentration by using a calibration curve, which was linear in the concentration range used.

with a four-helix-bundle peptide catalyst of their design, containing six histidine residues,[2d] which suggests that histidine catalysis occurs without direct participation of the serine and aspartate residues. The reaction of α-methylphenacetyl ester **4** was also catalyzed by the dendrimers. Reaction with the pure enantiomeric substrates showed modest yet significant enantioselectivity, with the best dendrimer (**E-F**) showing an E value of 2.0 in favor of the (*S*)-**4** enantiomer (Table 2).

In summary, peptide dendrimers were assembled from a branching diamino acid building block by means of a disulfide-dimerization strategy. The synthetic strategy chosen defines a broad structural family in which structural variations are readily accessible by changing the amino acids, branching diamino acids, and capping components. Out of a total of 32 million possible dimeric peptide dendrimers with the given branching and capping units, and 20 proteinogenic amino acids ($n = 20^3$ monomers, $n(n+1)/2$ dimers), a subset of 21 dendrimers incorporating a catalytic triad of amino acids at the variable positions was prepared and tested for ester hydrolysis. Dendrimers bearing histidine residues at the outermost position in the sequence showed selective substrate recognition and enzymelike catalytic behavior in an aqueous

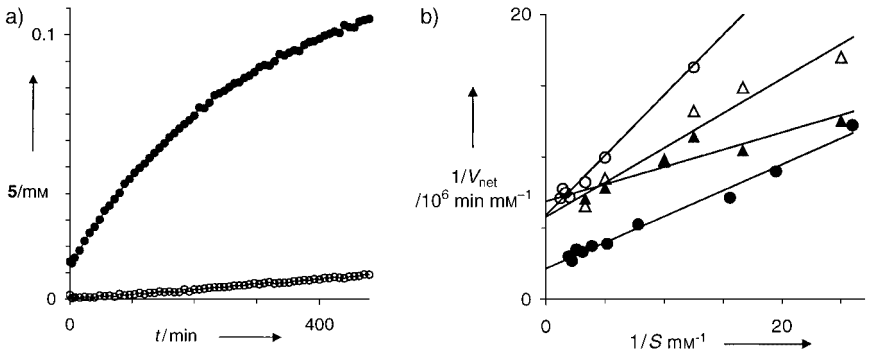

Figure 1. a) Hydrolysis of **3** to form **5** in the presence (●) or absence (○) of dendrimer **E-F**, with 200 μM substrate and 5 μM catalyst; b) double reciprocal plot for ester hydrolysis catalyzed by peptide dendrimer **E-F**. (○) acetate ester **1**; (△) α-methylphenacetyl ester (*S*)-**4**; (▲) α-methylphenacetyl ester (*R*)-**4**; (●) isobutyroyl ester **3**; *S* = substrate concentration. Conditions as in Tables 1 and 2.

 © 2003 Wiley-VCH Verlag GmbH & Co. KGaA, Weinheim 1433-7851/03/4212-1382 $ 20.00+.50/0

Table 2: Michaelis–Menten parameters for the three most active dendrimers on substrates **1**–**4**.[a]

		1	**2**	**3**	(*S*)-**4**	(*R*)-**4**	E[b]
	k_{uncat} [min^{-1}]	3.6×10^{-4}	2.4×10^{-4}	2.0×10^{-4}	3.7×10^{-4}	3.7×10^{-4}	
4-MeIm	k_2 [mM^{-1} min^{-1}]	6.7×10^{-3}	5.6×10^{-3}	7.0×10^{-3}	8.4×10^{-3}	8.0×10^{-3}	
E-E	K_M [mM]	0.20	0.21	0.11	0.10	0.13	
	k_{cat} [min^{-1}]	0.31	0.26	0.28	0.21	0.20	
	k_{cat}/k_{uncat}	860	1050	1380	570	540	
	$k_{cat}/K_M/k_2$	230	220	350	240	190	1.27
	v_{net}/v_{uncat}[c]	9.2	12.5	23.3	9.2	8.3	
F-F	K_M [mM]	0.52	0.34	0.27	0.021	0.016	
	k_{cat} [min^{-1}]	0.28	0.22	0.20	0.037	0.035	
	k_{cat}/k_{uncat}	770	890	1020	102	97	
	$k_{cat}/K_M/k_2$	80	110	110	210	270	0.77
	v_{net}/v_{uncat}[c]	6.4	8.4	12	2.3	2.2	
E-F	K_M [mM]	0.14	0.12	0.17	0.030	0.080	
	k_{cat} [min^{-1}]	0.12	0.33	0.33	0.10	0.12	
	k_{cat}/k_{uncat}	340	1380	1680	290	340	
	$k_{cat}/K_M/k_2$	130	360	280	360	180	2.00
	v_{net}/v_{uncat}[c]	12.0	18.8	31.5	6.2	6.1	

[a] Conditions and measurement method as in Table 1 with 5 μM dendrimer and 40–700 μM substrate. The kinetic constants given are derived from the linear double-reciprocal plots of $1/V_{net}$ versus 1/S (Figure 1b), with $r^2 > 0.95$ (r = correlation coefficient); [b] $E = (k_{cat}/K_M((S)\text{-}\mathbf{4}))/(k_{cat}/K_M((R)\text{-}\mathbf{4}))$; [c] V_{net}/V_{uncat} observed with S = 200 μM and 5 μM dendrimer (see footnote Table 1).

medium. Although the catalytic activities observed occur with a relatively labile class of ester substrates, this work opens the way for further development of peptide dendrimers as enzyme mimics. Further structural characterization and mechanistic studies and the exploration of building-block variations to improve the activity and diversity of catalytic peptide dendrimers are underway.

Received: October 9, 2002
Revised: December 11, 2002 [Z50330]

Keywords: dendrimers · enantioselectivity · enzyme catalysis · hydrolysis · peptides

[1] a) J. W. Bryson, S. F. Betz, H. S. Lu, D. J. Suich, H. X. Zhou, K. T. O'Neill, W. F. DeGrado, *Science* **1995**, *270*, 935; b) L. Baltzer, H. Nilsson, J. Nilsson, *Chem. Rev.* **2001**, *101*, 3153; c) M. Mutter, S. Vuilleumier, *Angew. Chem.* **1989**, *101*, 551; *Angew. Chem. Int. Ed. Engl.* **1989**, *28*, 535; d) A. J. Kirby, *Angew. Chem.* **1996**, *108*, 770; *Angew. Chem. Int. Ed. Engl.* **1996**, *35*, 707.

[2] a) B. Gutte, M. Daeumigen, E. Wittschieber, *Nature* **1979**, *281*, 650; b) K. Johnsson, R. K. Allemann, H. Widmer, S. A. Benner, *Nature* **1993**, *365*, 530; c) K. S. Broo, L. Brive, P. Ahlberg, L. Baltzer, *J. Am. Chem. Soc.* **1997**, *119*, 11362; d) S. Kerstin, H. Nilsson, J. Nilsson, L. Baltzer, *J. Am. Chem. Soc.* **1998**, *120*, 10287.

[3] a) G. T. Copeland, E. R. Jarvo, S. J. Miller *J. Org. Chem.* **1998**, *63*, 6784; b) M. M. Vasbinder, R. J. Elizabeth, S. J. Miller, *Angew. Chem.* **2001**, *113*, 2906; *Angew. Chem. Int. Ed.* **2001**, *40*, 2824; c) T. E. Horstmann, D. J. Guerin, S. J. Miller, *Angew. Chem.* **2000**, *112*, 3781; *Angew. Chem. Int. Ed.* **2000**, *39*, 3635; d) T. E. Hortstmann, D. J. Guerin, S. J. Miller, *Org. Lett.* **1999**, *1*, 1247; e) B. R. Sculimbrene, S. J. Miller, *J. Am. Chem. Soc.* **2001**, *123*, 10125.

[4] For selected references on dendrimers, see: a) S. Hecht, J. M. J. Fréchet, *Angew. Chem.* **2001**, *113*, 76, *Angew. Chem. Int. Ed.* **2001**, *40*, 74; b) S. M. Grayson, J. M. J. Fréchet, *Chem. Rev.* **2001**, *101*, 3819; c) G. R. Newkome, C. N. Moorefield, F. Vögtle, *Dendritic Molecules: Concepts, Synthesis, Perspectives*, VCH, Weinheim, **1996**; d) A. W. Bosman, H. M. Janssen, *Chem. Rev.* **1999**, *99*, 1665; e) D. A. Tomalia, *Adv. Mater.* **1994**, *6*, 529; f) H.-F. Chow, T. K.-K. Monga, M. F. Nongruma, C.-W. Wan, *Tetrahedron* **1998**, *54*, 8543.

[5] a) D. A. Tomalia, P. R. Dvornic, *Nature* **1994**, *372*, 617; b) J. W. J. Knapen, A. W. Van der Made, J. C. De Wilde, P. W. N. M. van Leeuwen, P. Wijkens, D. M. Grove, G. van Koten, *Nature* **1994**, *372*, 659; c) L. Balogh, D. A. Tomalia, *J. Am. Chem. Soc.* **1998**, *120*, 7355; d) M. Zhao, R. M. Crooks, *Angew. Chem.* **1999**, *111*, 375; *Angew. Chem. Int. Ed.* **1999**, *38*, 364; e) B. Bhyrappa, G. Vaijayanthimala, *J. Am. Chem. Soc.* **1999**, *121*, 262; f) S. Nlate, J. Ruiz, V. Sartor, R. Navarro, J. C. Blais, D. Astruc, *Chem. Eur. J.* **2000**, *6*, 2544; g) P. Weyermann, F. Diederich, *Helv. Chim. Acta* **2002**, *85*, 599; h) H. Sellner, P. B. Rheiner, D. Seebach, *Helv. Chim. Acta* **2002**, *85*, 352; i) L. J. Twyman, A. S. H. King, I. K. Martin, *Chem. Soc. Rev.* **2002**, *31*, 69.

[6] K. Sadler, J. P. Tam, *Mol. Biotechnol.* **2002**, *90*, 195.

[7] a) R. G. Denkelwalter, W. J. Lukasavage, , US Pat. 44101081 **1983**; b) T. M. Chapman, G. L. Hillyert, E. J. Mahan, K. A. Shaffer, *J. Am. Chem. Soc.* **1994**, *116*, 11195; c) Y. Kim, F. Zeng, S. C. Zimmermann, *Chem. Eur. J.* **1999**, *5*, 2133.

[8] G. Sengle, A. Jenne, P. S. Arora, B. Seelig, J. S. Nowick, A. Jäschke, M. Famulok, *Bioorg. Med. Chem.* **2000**, *8*, 1317.

[9] N. Bensel, M. T. Reymond, J.-L. Reymond, *Chem. Eur. J.* **2001**, *7*, 4604.

[10] J. E. Whitaker, R. P. Haugland, P. L. Moore, P. C. Hewitt, M. Reese, R. P. Haugland, *Anal. Biochem.* **1991**, *198*, 119.

[11] F. M. Menger, K. H. Nelson, Y. Guo, *Chem. Commun.* **1998**, *18*, 2001.

[12] These ester substrates all have similar uncatalyzed reaction rates, for example, at pH 6.0 (20 mM aqueous Bis-Tris buffer): umbelliferyl acetate: $k_{uncat} = 2\times10^{-5}\,s^{-1}$; umbelliferyl acetoxymethyl ether: $k_{uncat} = 6\times10^{-6}\,s^{-1}$; 8-acetoxypyrene-1,3,6-trisulfonate: $k_{uncat} = 2\times10^{-6}\,s^{-1}$, 7-acetoxy-1-methylquinolinium sulfate: $k_{uncat} = 6\times10^{-6}\,s^{-1}$.

 © 2003 Wiley-VCH Verlag GmbH & Co. KGaA, Weinheim 1433-7851/03/4212-1383 $ 20.00+.50/0

Dynamic Self-Assembled Materials

Dynamic Materials through Metal-Directed and Solvent-Driven Self-Assembly of Cavitands**

*Laura Pirondini, Anna G. Stendardo, Silvano Geremia, Mara Campagnolo, Paolo Samorì, Jürgen P. Rabe, Roel Fokkens, and Enrico Dalcanale**

Reversibility constitutes one of the hallmarks of self-assembly.[1] This feature of self-assembled structures conveys many interesting properties, among which responsiveness to external stimuli is pivotal to the development of dynamic materials.[2] For this reason noncovalent interactions are being used increasingly in polymer science.[3] So far hydrogen bonding has been the workhorse of interactions, because it combines directionality with simplicity.[4] Metal–ligand coordination is another highly directional interaction that can lead to supramolecular polymeric architectures such as linear polymers[5] and dendrimers.[6] Hydrophobic interactions have also been exploited to form nanotube aggregates in aqueous solution.[7] However, to generate highly adaptive dynamic materials, systems operating in multimodal fashion through the implementation of several self-assembly codes are required.[8]

As a first step in this direction we report on the design, preparation, and properties of cavitand **1**, which is capable of bimodal, independent self-assembling interactions, namely solvophobic aggregation and metal coordination. The self-assembly cycle in Scheme 1 was devised to test the workability and orthogonality of the two interactions. For the first interaction the dimerization properties of quinoxaline kite velcrands have been exploited: the driving forces for dimerization are dipole–dipole, van der Waals, and solvophobic interactions.[9] For metal complexation two pyridine ligands have been introduced at the lower rim of **1** to induce dimerization through coordination to a metal center.[10] The two interactions operate under totally different sets of conditions allowing the independent activation/deactivation of each of them.

The kite monomer **1** was synthesized by condensing 2,3-dichloroquinoxaline with a tetramethylhydroxyl-footed resorcinarene[10,11] to afford the corresponding quinoxaline-bridged cavitand, which was then treated with 3,5-bis(chlorocarbonyl)pyridine in pyridine (see Supporting Information for experimental details and characterization of new compounds). The reaction led to the formation of **1** in 28% yield. Cavitand **1** is soluble only in chlorinated and aromatic hydrocarbons at relatively high dilution ($c < 2.2$ mM). Of the two possible isomers, only that in which the pyridyl moieties are under the *out*-phenyls of the resorcinarene skeleton is formed.[12]

Kite-to-kite dimerization in CD_2Cl_2 solution was monitored by ^{1}H NMR spectroscopy by following the splitting of several diagnostic signals (see Supporting Information). The association–dissociation rates for the monomer and dimer are fast on the ^{1}H NMR timescale at room temperature but slow below 240 K. At that temperature two different sets of signals appear, belonging to the monomer and dimer in slow exchange. The populations of the two species can be determined directly by integration of their respective signals, which provides a convenient means of determining association constants (K_a) and free energies of association over a range of temperatures (235–205 K).[13] The following thermodynamic parameters were determined: $K_{a273K} = 1.91 \times 10^3\,\text{M}^{-1}$; $\Delta G^{\circ}_{273K} = -4.10$ kcal mol^{-1}; $\Delta H = -0.66$ kcal mol^{-1}, $\Delta S = 12.6$ cal mol^{-1} K^{-1} (correlation factor in van't Hoff plot: 0.9523).

These data, compared with those of the related tetrapentyl-footed kite velcrand **HQx**,[9] indicate a reduced tendency of **1** to dimerize ($\Delta G^{\circ}_{\mathbf{HQx}} = -6.81$ kcal mol^{-1} versus $\Delta G^{\circ}_{\mathbf{1}} = -4.10$ kcal mol^{-1} calculated at 273 K). As shown by the X-ray crystal structure[14] (Figure 1) a **1**·**1** velcrand dimer forms in the solid state, in which the two cavitands are rotated reciprocally by 90°: two methyl groups are oriented outward and the other two point upward, fitting into the cavities formed by the sloping aryl faces and the "out" methyl groups. When two molecules are fitted to one another they share a large common surface formed by their large rectangular areas in roughly parallel planes. The introduction of two pyridyl-based connecting units at the lower rim rigidifies the structure, affecting the spatial orientation of the quinoxaline wings and therefore reducing the tendency to dimerize. This is confirmed by the crystal structure of **1**·**1**, which evidences only 77 short intermolecular atomic distances, remarkably less than the 132 short distances observed in **HQx**·**HQx** (see Supporting Information).[15] Besides, the crystal packing reveals that in the solid state the pyridyl terminal groups act as clips, forming linear chains of **1**·**1** dimers through stacking interactions (Scheme 1).

Metal-directed dimerization has been already performed on the corresponding methylene-bridged cavitand, by using

[*] Prof. E. Dalcanale, Dr. L. Pirondini, Dr. A. G. Stendardo
Dipartimento di Chimica Organica ed Industriale and Unità INSTM
Università degli Studi di Parma
Parco Area delle Scienze 17/A, 43100 Parma (Italy)
Fax: (+39) 0521-905-472
E-mail: enrico.dalcanale@unipr.it

Prof. S. Geremia, Dr. M. Campagnolo
Centro di Eccellenza in Biocristallografia
Dipartimento di Scienze Chimiche, Università di Trieste
Via L. Giorgieri 1, 34127 Trieste (Italy)

Dr. P. Samorì, Prof. J. P. Rabe
Humboldt University Berlin, Department of Physics
10099 Berlin (Germany)

Dr. R. Fokkens
Laboratory of Supramolecular Chemistry and Technology
MESA+ Research Institute, University of Twente
P.O. Box 217, 7500 AE Enschede (The Netherlands)

[+] Present address:
Istituto per la Sintesi Organica e la Fotoreattività
C.N.R. Bologna, Via Gobetti 101
40129 Bologna (Italy)

[**] We acknowledge the CNR Nanotechnology Programme for financial support. We thank Dr. Nikolai Severin for help in preparing the thin films.

Supporting information for this article is available on the WWW under http://www.angewandte.org or from the author.

 © 2003 Wiley-VCH Verlag GmbH & Co. KGaA, Weinheim 1433-7851/03/4212-1384 $ 20.00+.50/0

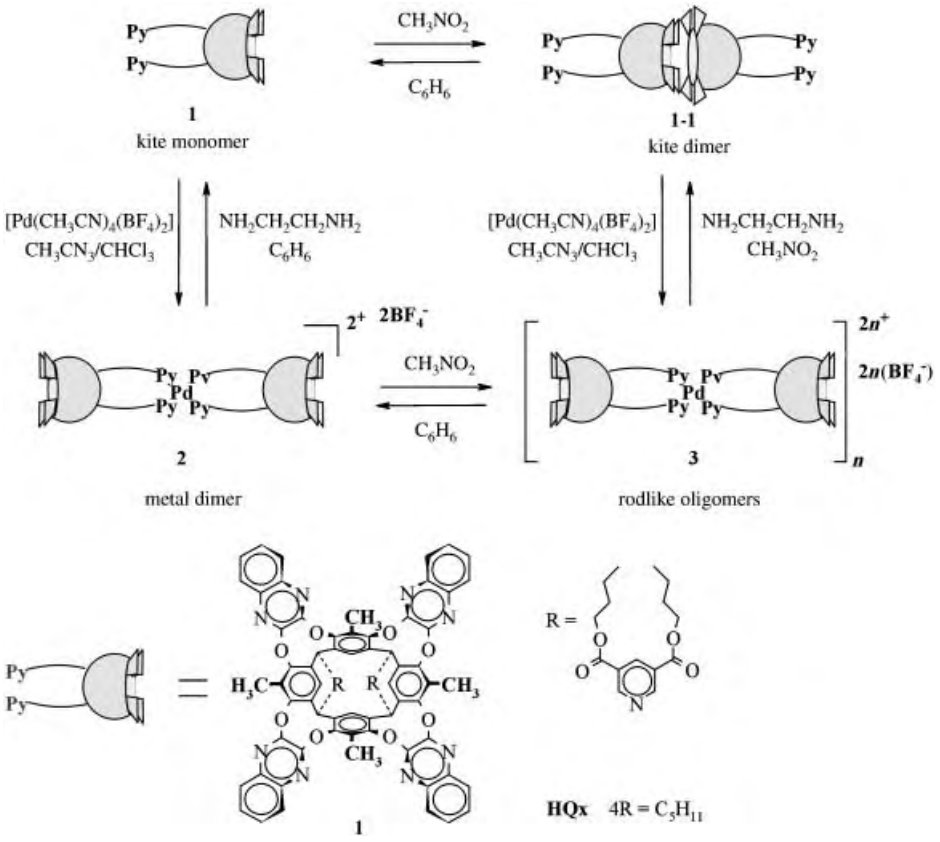

Scheme 1. Bimodal self-assembly cycle.

$[Pd(CH_3CN)_4](BF_4)_2$ as the metal precursor (see Supporting Information).[10] Addition of a small excess of a bidentate competitive ligand such as ethylenediamine to the preformed complex led to complete and clean disassembly of the coordination dimer, which proves the reversibility of the metal-directed dimerization process.

The two self-assembly protocols were combined to generate new oligomeric structures by mixing **1** and $[Pd(CH_3CN)_4](BF_4)_2$ in a 2:1 molar ratio in $CHCl_3/CH_3CN$.

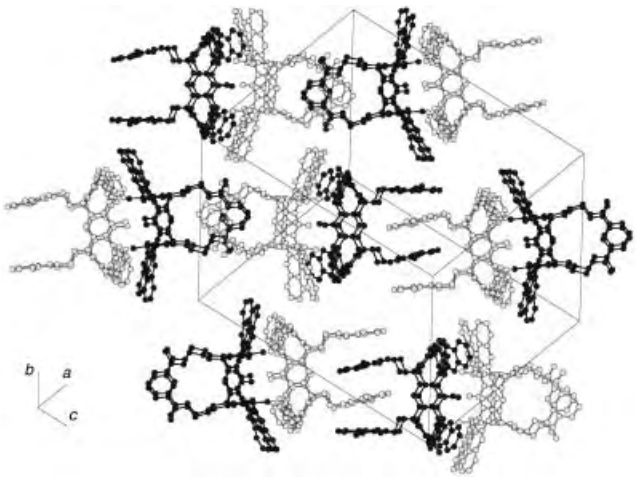

Figure 1. X-ray crystal structure of the **1**·**1** dimer.

Complex **3** precipitated as a yellow powder, soluble only in nitromethane. The ^1H NMR spectrum of **3** in CD_3NO_2 shows both a broadening and an increased number of peaks, indicative of the formation of oligomeric species. A downfield shift of the peaks relative to the pyridine protons from $\delta = 9.20$ ppm (**1** in CD_2Cl_2) to $\delta = 9.80$ ppm (**3** in CD_3NO_2) was observed, which is diagnostic of coordination to the metal center. The MALDI-TOF mass spectrum of **3**[16] in CH_3NO_2 shows three singly charged ion peaks at *m*/*z* 3279.2, 6648.6, and 10016.3 attributable to $[\mathbf{1}\cdot Pd(BF_4)_2\cdot\mathbf{1}\text{-}BF_4^-]^+$, $[(\mathbf{1}\cdot Pd(BF_4)_2\cdot\mathbf{1})_2\text{-}BF_4^-]^+$, and $[(\mathbf{1}\cdot Pd(BF_4)_2\cdot\mathbf{1})_3\text{-}BF_4^-]^+$, which belong to the species with $n = 1$, $n = 2$, and $n = 3$, respectively (see Supporting Information). The laser ionization process was kept at threshold level to avoid molecular clustering in the gas phase.

Clean solvophobic disassembly was observed by dissolving complex **3** in [D_6]benzene.[17] The resulting ^1H NMR spectrum shows sharp and easily assignable peaks belonging to the dimeric species **2**. This attribution was confirmed by a MALDI-TOF MS experiment performed on a solution of complex **3** in benzene,[16] in which only the single charged ion peak at *m*/*z* 3279.2 ($[\mathbf{1}\cdot Pd(BF_4)_2\cdot\mathbf{1}\text{-}BF_4^-]^+$) attributable to dimer **2**, is revealed.

Coordinative disassembly of **3** has been carried out through addition of ethylenediamine to break selectively the oligomeric species at the metal coordination sites. Depending on the solvent used, either **1** (in benzene) or **1**·**1** (as a precipitate from nitromethane) were recovered, proving

 © 2003 Wiley-VCH Verlag GmbH & Co. KGaA, Weinheim 1433-7851/03/4212-1385 $ 20.00+.50/0

the complete reversibility of the metal-directed self-assembly at the lower rim.

The self-assembly of these supramolecular architectures on surfaces has also been explored, by making use of tapping mode scanning force microscopy (TM-SFM). When **3** was deposited from dilute solution in CH_3NO_2 onto the basal plane of highly oriented pyrolytic graphite (HOPG), large disordered assemblies were obtained (image not shown). To avoid lateral aggregation between individual self-assembled objects, a linear alkane ($C_{32}H_{64}$) was added to the dilute solution (ca. 10^{-3} M) of **3** in CH_3NO_2 up to saturation. Upon application of this solution to a graphite surface the two solutes are codeposited.[5d] Due to the strong affinity between the alkanes and the HOPG surface,[18] the alkanes pack in lamellar 2D single crystals, with the long molecular axes parallel to the substrate and extended over several hundreds of nanometers. After the liquid was removed by spinning off in a spin-coater, the films were thermally annealed at 40 °C for 15 min, which led to complete solvent evaporation. The SFM image in Figure 2a shows different types of nanostructures

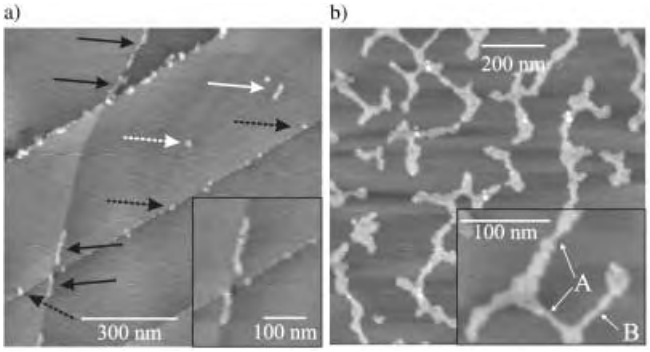

Figure 2. Trapping mode STM images of self-assembled **3** codeposited with linear alkanes from a CH_3NO_2 solution.

coexisting on the graphite surface. Rodlike (solid arrows) and grainlike objects (dashed arrows) can be recognized. Both of them are preferentially packed at the graphite steps (black arrows), although they can also exist on a flat graphite terrace (white arrows). The inset in Figure 2a gives a closer look at two rodlike objects at a graphite step. A single self-assembled object is expected to exhibit a rodlike shape with a cross-section diameter ranging from 0.8 (coordination site) to 1.5 nm (solvophobic site).

The observed anisotropic objects exhibit heights of roughly (0.8 ± 0.2) nm, lengths of up to 150 nm, and widths of (7 ± 3) nm,[19] which is consistent with the lateral aggregation of five to seven supramolecular rods.[20] Different areas of the same film are characterized by a higher degree of coverage, leading to networks with heights of (0.8 ± 0.2) nm or multiples thereof. The inset in Figure 2b exhibits some narrow arms with constant widths of 1.5 nm, which is compatible with a single rod having a height of about 0.8 nm (monolayer, marked with A) or 1.5 nm (bilayer, indicated with B).[21,22]

In summary we have devised and tested a bimodal self-assembly protocol for the generation of a dual-coded dynamic supramolecular species, which has been transferred and amplified on surfaces. The two interaction modes are both orthogonal and reversible, as proven by the self-assembly cycle of Scheme 1, where the formation/dissolution of either dimers or oligomers has been triggered by solvent polarity, metal coordination, and ligand exchange. This result can be of importance in the frame of the implementation of new materials with the peculiar properties of adaptability, healing, and response to external stimuli.

Received: October 14, 2002 [Z50352]

Keywords: cavitands · dynamic materials · nanostructures · self-assembly · supramolecular chemistry

[1] J. S. Lindsey, *New J. Chem.* **1995**, *15*, 153 – 180.
[2] a) J.-M. Lehn in *Supramolecular Science: Where It Is and Where It Is Going* (Eds.: R. Ungaro, E. Dalcanale), Kluwer Academic Publishers, Dordrecht, **1999**, 287 – 304; b) J.-M. Lehn, *Chem. Eur. J.* **1999**, *5*, 2455 – 2463.
[3] a) N. Zimmerman, J. S. Moore, S. C. Zimmerman, *Chem. Ind.* **1998**, 604 – 610; b) *Supramolecular Polymers* (Ed.: A. Ciferri), Dekker, New York, **2000**.
[4] a) R. P. Sijbesma, F. H. Beijer, L. Brunsveld, B. J. B. Folmer, J. H. K. K. Hirschberg, R. F. M. Lange, J. K. L. Lowe, E. W. Meijer, *Science* **1997**, *278*, 1601 – 1604; b) R. K. Castellano, D. M. Rudkevich, J. Rebek, Jr., *Proc. Natl. Acad. Sci. USA* **1997**, *94*, 7132 – 7137; c) R. K. Castellano, J. Rebek, Jr., *J. Am. Chem. Soc.* **1998**, *120*, 3657 – 3663.
[5] a) U. Michelsen, C. A. Hunter, *Angew. Chem.* **2000**, *112*, 780 – 783; *Angew. Chem. Int. Ed.* **2000**, *39*, 764 – 767; b) L. Brunsveld, B. J. B. Folmer, E. W. Meijer, R. P. Sijbesma, *Chem. Rev.* **2001**, *101*, 4071 – 4097; c) U. S. Schubert, C. Eschbaumer, *Angew. Chem.* **2002**, *114*, 3016 – 3050; *Angew. Chem. Int. Ed.* **2002**, *41*, 2892 – 2926; d) D. G. Kurth, N. Severin, J. P. Rabe, *Angew. Chem.* **2002**, *114*, 3833 – 3835; *Angew. Chem. Int. Ed.* **2002**, *41*, 3681 – 3683.
[6] a) W. T. S. Huck, F. C. J. M. van Veggel, B. L. Kropman, D. H. A. Blank, E. G. Keim, M. M. A. Smithers, D. N. Reinhoudt, *J. Am. Chem. Soc.* **1995**, *117*, 8293 – 8294; b) W. T. S. Huck, F. C. J. M. van Veggel, D. N. Reinhoudt, *Angew. Chem.* **1996**, *108*, 1304 – 1306; *Angew. Chem. Int. Ed. Engl.* **1996**, *35*, 1213 – 1215.
[7] G. Li, L. B. McGown, *Science* **1994**, *264*, 249 – 251.
[8] J.-M. Lehn, *Science* **2002**, *295*, 2400 – 2403.
[9] a) J. R. Moran, J. L. Ericson, E. Dalcanale, J. A. Bryant, C. B. Knobler, D. J. Cram, *J. Am. Chem. Soc.* **1991**, *113*, 5707 – 5714; b) D. J. Cram, H.-J. Choi, J. A. Bryant, C. B. Knobler, *J. Am. Chem. Soc.* **1992**, *114*, 7748 – 7765.
[10] L. Pirondini, D. Bonifazi, E. Menozzi, E. Wegelius, K. Rissanen, C. Massera, E. Dalcanale, *Eur. J. Org. Chem.* **2001**, 2311 – 2320.
[11] B. C. Gibb, R. G. Chapman, J. C. Sherman, *J. Org. Chem.* **1996**, *61*, 1505 – 1509.
[12] No kite-to-kite interconversion to give the other isomer has been observed by dynamic ^{1}H NMR spectroscopy up to 373 K.
[13] K_a can be calculated by $K_a = R(2R+1)/[M]_i$, where $R =$ 0.5 (integral value of dimer)/(integral value of monomer), and $[M]_i$ is the initial concentration of monomer.
[14] Crystals of **1** suitable for X-ray analysis were grown in EtOH/CH_2Cl_2 solution. Crystal data: $2(C_{90}H_{66}N_{10}O_{16})\cdot 0.5(C_6H_{14}O_4)\cdot 1.5(C_4H_{10}O_3)\cdot 8.5\,C_2H_6O\cdot 6H_2O$, $M_r = 3821$, monoclinic, space group $P2_1/n$, $a = 25.525(5)$, $b = 25.003(5)$, $c = 33.306(5)$ Å, $\beta = 91.58(5)°$, $V = 21248(7)$ Å^3, $Z = 4$, $\rho_{calcd} = 1.194$ mg m^{-3}, $\mu = 0.72$ mm^{-1}, $F(000) = 8068$, $\lambda/2\theta_{max} = 0.95$ Å. A total of 81624 reflections were measured, of which 23203 were

 © 2003 Wiley-VCH Verlag GmbH & Co. KGaA, Weinheim 1433-7851/03/4212-1386 $ 20.00+.50/0

unique ($R_{int} = 0.053$). To solve the structure 19441 reflections were used (parameters = 2338, $R1[I > 2\sigma(I)] = 0.1541$, $wR2 = 0.4125$). Data collection was performed at the X-ray diffraction beamline of Elettra Synchrotron, Trieste (Italy) (monochromatic wavelength $\lambda = 1.0000$ Å), by using a Mar CCD detector with the rotating crystal method. The crystal was soaked with an aqueous solution of PEG 1000 (100% g mL^{-1}) (used as cryoprotectant), mounted in a loop, and flash-frozen to 100 K. The diffraction data were indexed and integrated using MOSFLM and scaled with SCALA. The structure was solved by direct methods (SIR97) and Fourier analyses, and refined by full-matrix least-squares based on F^2 (SHELXL-97). Several solvent molecules were detected in the asymmetric unit: 0.5 molecules of triethyleneglycol, 1.5 molecules of diethyleneglycol, 8.5 molecules of ethanol, and 6 water molecules. CCDC-194186 contains the supplementary crystallographic data for this paper. These data can be obtained free of charge via www.ccdc.cam.ac.uk/conts/retrieving.html (or from the Cambridge Crystallographic Data Centre, 12, Union Road, Cambridge CB2 1EZ, UK; fax: (+44) 1223-336-033; or deposit@ccdc.cam.ac.uk).

[15] The average contribution to the free energy of each contact is 0.053 kcal mol^{-1}, which is in full agreement with the reported value for Cram's **HQx**·**HQx** system (0.053 kcal mol^{-1}).

[16] The spot wells of the MALDI-TOF sample plate containing millimolar solutions of the assemblies in different solvents were covered with a thin poly(ethyleneglycol) film. In this way the original constitution of the sample solutions is mostly preserved, and evaporation is kept to a minimum.

[17] For the opposite behavior in hydrogen-bonded velcrands see: F. C. Tucci, D. M. Rudkevich, J. Rebek, Jr., *Chem. Eur. J.* **2000**, *6*, 1007 – 1016.

[18] J. P. Rabe, S. Buchholz, *Science* **1991**, *253*, 424 – 427.

[19] The rod widths were determined by taking into account the broadening due to the convolution with the SFM tip, as described in: P. Samorí, V. Francke, K. Müllen, J. P. Rabe, *Chem. Eur. J.* **1999**, *5*, 2312 – 2317.

[20] The individual supramolecular rods could not be resolved due to the limitation in the SFM resolution and to their tight packing.

[21] As in the case of polyelectrolyte–amphiphile complexes,[5d] the cavitand-based supramolecular polymer is very likely lying on the top of an alkane monolayer (SAM) self-assembled on HOPG, taking advantage of the high surface potential ripple of the underlying SAM.

[22] The apparent rod thickness of 0.8 nm is at the lower end of the expected range. This can be due to both the flattening at surfaces occurring upon adsorption and to imaging artifacts. The latter can include indentation of the supramolecular object by the probing tip as well as the adhesion of the tip to the surface as discussed in: P. Samorí, C. Ecker, I. Gössl, P. A. J. de Witte, J. J. L. M. Cornelissen, G. A. Metselaar, M. B. J. Otten, A. E. Rowan, R. J. M. Nolte, J. P. Rabe, *Macromolecules* **2002**, *35*, 5290 – 5294.

 © 2003 Wiley-VCH Verlag GmbH & Co. KGaA, Weinheim 1433-7851/03/4212-1387 $ 20.00+.50/0

Preparing C-Linked Disaccharides

A Simplified Ramberg–Bäcklund Approach to Novel C-Glycosides and C-Linked Disaccharides**

*Graeme D. McAllister, Duncan E. Paterson, and Richard J. K. Taylor**

Dedicated to Dr. Alan H. Haines

In recent years, there has been increasing interest in the preparation and properties of C-disaccharides. Their hydrolytic stability and potential enzyme-inhibitory properties make such compounds attractive as unnatural mimetics and therefore as synthetic targets.[1] As a result, a number of methodologies have been developed for the synthesis of this class of compound.[2,3] As part of an ongoing program[3,4] to investigate applications of the Ramberg–Bäcklund Reaction (RBR),[5] we recently reported a RBR approach to C-linked disaccharides and employed it to prepare C-isotrehalose, C-homoisotrehalose, and methyl C-gentiobioside.[3] However, the route involved the initial preparation of protected monosaccharides and their subsequent conversion into thioglycosides and then thioglycoside dioxides and was therefore rather lengthy. Herein we report the rapid synthesis of a range of novel C-glycosides and C-disaccharides which commences from readily available protected monosaccharides **1** and involves a tandem Horner–Wadsworth–Emmons (HWE)/conjugate-addition C-glycosidation followed by a tandem halogenation–RBR sequence, utilizing Meyers variant of the RBR[6] (Scheme 1). Thus, the plan was to prepare glycosylsulfonylmethyl-HWE reagents **2** and then carry out the condensation giving the vinyl sulfone intermediate **3** which would be expected[7] to undergo conjugate cyclization in situ to produce sulfone **4**. Subsequent Meyers-type in situ α-sulfonyl halogenation followed by tandem RBR should then produce alkene **5** which could be elaborated/deprotected to provide a range of novel C-disaccharides.

Proof-of-principle studies were carried out using the benzylsulfonylphosphonate reagent **6**[8] and diisopropylidene mannofuranose **7** (Scheme 2). We were delighted to find that the HWE/conjugate-addition process proceeded in a reasonable 64% unoptimized yield using sodium hydride in THF giving the C-glycoside **8** stereoselectively as the β-isomer ($J_{1,2} = 3.6$ Hz). Sulfone **8** was next subjected to the halogenation-RBR sequence. The standard Meyers conditions[6a] only gave a 48% yield of **9** but use of the supported KOH-CBr_2F_2

[*] Prof. R. J. K. Taylor, G. D. McAllister, D. E. Paterson
Department of Chemistry
University of York
Heslington, York YO10 5DD (UK)
Fax: (+44) 1904-434523
E-mail: rjkt1@york.ac.uk

[**] We thank the EPSRC for postdoctoral funding (G.D.M.) and the University of York for studentship support (D.E.P.). Dedicated to Dr. Alan H. Haines, to mark his retirement from the University of East Anglia and his many contributions to carbohydrate chemistry.

 © 2003 Wiley-VCH Verlag GmbH & Co. KGaA, Weinheim 1433-7851/03/4212-1387 $ 20.00+.50/0

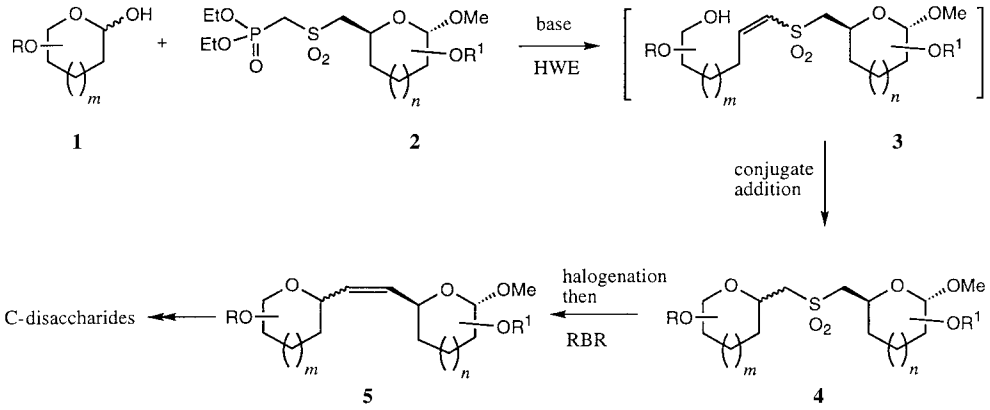

Scheme 1. Summary of overall transformation ($m,n = 0,1$).

conditions devised by Chan et al.[6b] produced alkene **9** in 88% yield, exclusively as the 1,2-*cis*-diastereomer with the β-anomeric configuration, and the *E*-geometry ($J_{vinyl} = 16.0$ Hz). The thermodynamic preference for the 1,2-*cis*-relationship in 2,3-*O*-isopropylidene derivatives of furanosyl C-glycosides has precedent.[7,9]

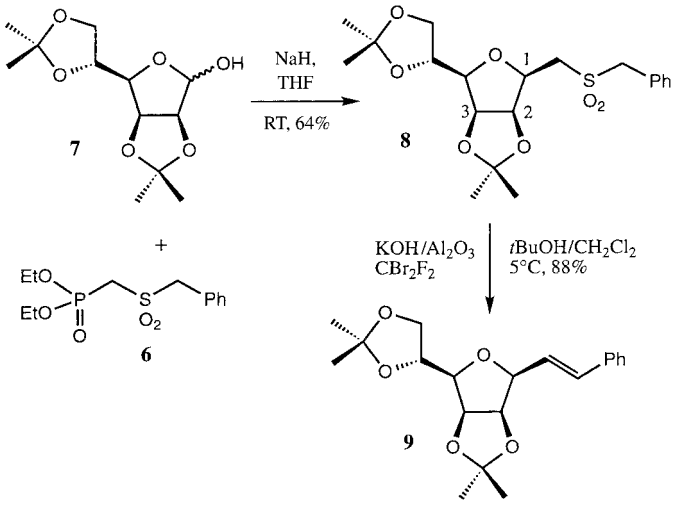

Scheme 2. Proof-of-principle studies using benzylsulfonylphosphonate **6**.

The multiple roles of the sulfonyl group in this sequence are noteworthy: it provides the stabilizing group needed for the HWE reaction, the activating group which facilitates the conjugate addition, and the key functionality for the RBR—and its removal does not require a separate step, it is lost in a cheleotropic manner during the key carbon–carbon bond forming reaction.

We extended these studies to ribose derivatives and investigated the compatibility of a range of protecting groups (Table 1). As can be seen, benzyl (Bn), acetonide, and *tert*-butyldimethylsilyl (TBS) protecting groups were all accommodated within this methodology. Noteworthy is that epimerization at the anomeric position occurs under these conditions: this is most apparent in the conversion of the 1,2-*trans*-system **18** into the predominantly 1,2-*cis*-C-glycoside **20** ($J_{1,2} = 6.0$ Hz for **20α**, 4.0 Hz for **20β**; the larger coupling constants for the *cis*-1,2-protons is in accord with previous[9] observations).

Having succeeded with the model studies, the next step was to prepare a carbohydrate-derived phosphonate reagent. The glucose-derived phosphonate **2a** was chosen in view of the reported efficient five-step preparation of thiol **22** from methyl α-D-glucopyranoside (**21**).[3] As shown in Scheme 3, *S*-alkylation of thiol **22** with diethyl iodomethylphosphonate followed by oxidation produced the required HWE reagent **2a** in 40% overall yield from **21**.

With HWE reagent **2a** in hand, we investigated its reaction with diisopropylidene mannofuranose **7** (Scheme 4). We were delighted to discover that the HWE/conjugate-addition sequence proceeded in high yield (86%) to produce the adduct sulfone **23** (as a mixture of diastereomers). The key halogenation-RBR was again carried out using the conditions devised by Chan et al.[6b] giving *E*-alkene **24** ($J_{vinyl} = 15.9$ Hz) as the only isolable product. Alkene hydrogenation and concomitant debenzylation, followed by acetylation for characterization purposes, gave the novel disaccharide **25** in 69% yield over the two reactions. The four-pot sequence shown in Scheme 4 involves 11 transformations (HWE, conjugate addition, halogenation, RBR, reduction, 3 × debenzylations, 3 × acetylations); the overall yield of 30% is noteworthy, though capable of improvement.

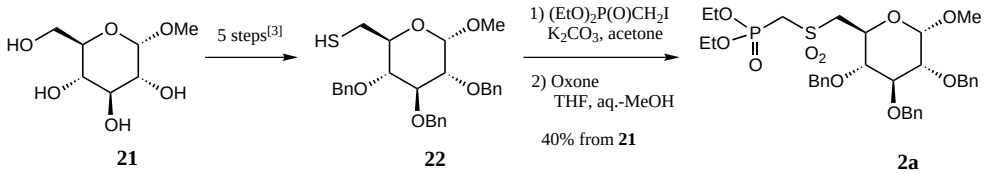

Scheme 3. Preparation of glucose-derived phosphonate **2a**.

 © 2003 Wiley-VCH Verlag GmbH & Co. KGaA, Weinheim 1433-7851/03/4212-1388 $ 20.00+.50/0

Table 1: HWE/conjugate-addition/RBR sequence with phosphonate **6** and a range of protected carbohydrates[a,b]

Monosaccharide	HWE/conjugate-addition adduct	RBR product
1) 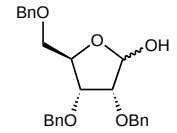 **10**	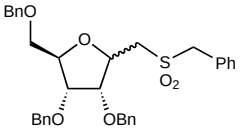 **11** 74% (α:β = 1:1)	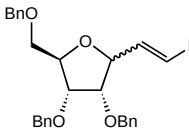 **12** 83% (α:β = 1:2.4)
2) 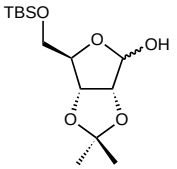 **13**	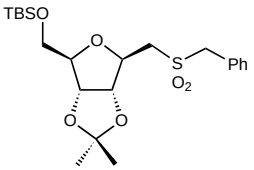 + **14** (22%)[c]	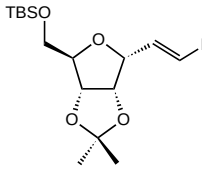 **16** 77% (α:β = 4:1)
	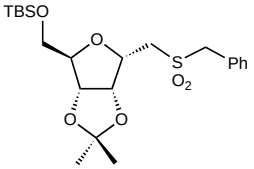 **15** (32%)[c]	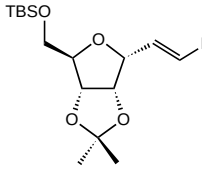 **16** 81% (α:β = 6:1)
3) 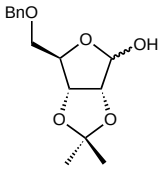 **17**	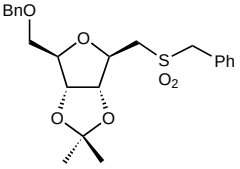 + **18** (32%)[c]	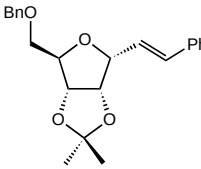 **20** 78% (α:β = 7:1)
	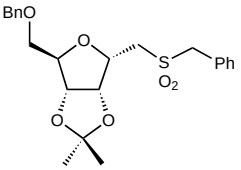 **19** (30%)[c]	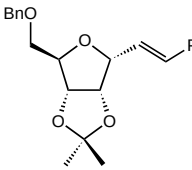 **20** 70% (α:β = 8:1)

[a] 1) NaH (1.1 equiv), phosphonate **6** (1.1 equiv) in THF at RT and then add lactol (1 equiv) and stir for 6–18 h; 2) Sulfone (1 equiv) in *tert*-butyl alcohol–CH_2Cl_2 at 0 °C then add KOH-Al_2O_3 (14 g mmol^{-1} sulfone) and then CBr_2F_2 (10 equiv) and stir at 0 °C for 30 min; 3) Dilute with CH_2Cl_2, stir for 10 min, filter through Celite, concentrate and purify by column chromatography on silica. [b] all alkenes > 99% *E*. [c] **14**/**15** and **18**/**19** were readily separated by chromatography.

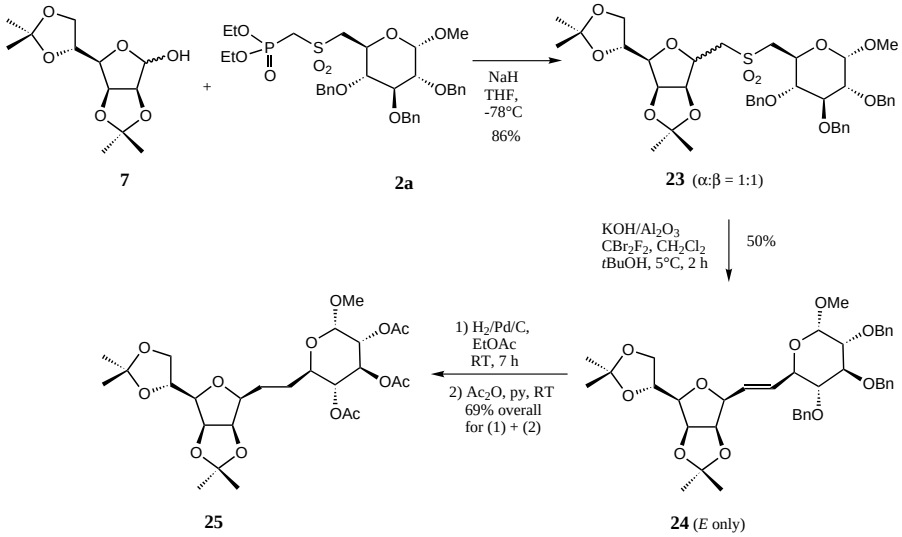

Scheme 4. C-disaccharide synthesis using phosphonate **2a**; py = pyridine.

 © 2003 Wiley-VCH Verlag GmbH & Co. KGaA, Weinheim 1433-7851/03/4212-1389 $ 20.00+.50/0

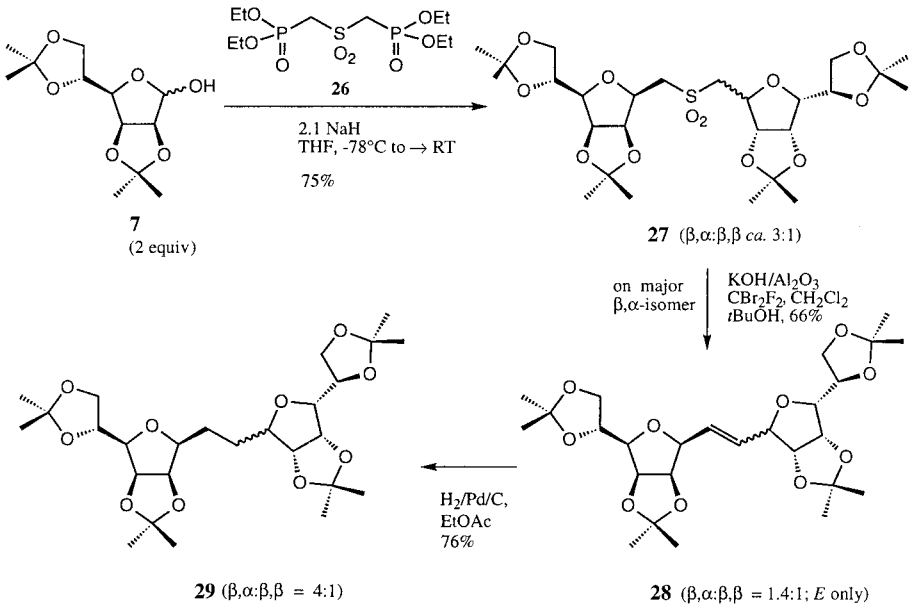

Scheme 5. Two-directional C-disaccharide synthesis using bisphosphonate **26**.

We have also shown that a two-directional variant of this methodology can be used to prepare symmetrical C-disaccharides, as shown in Scheme 5. The requisite bisphosphonate **26** has been described for the synthesis of distyryl sulfones.[10] The double HWE reaction using **26** and diisopropylidene mannofuranose **7** worked extremely well in the HWE/conjugate-addition C-glycosidation sequence giving diastereomeric sulfones **27**, in a combined yield of 75 %. RBR on the major stereoisomer (β,α-**27**) using the Meyers–Chan procedure gave alkene **28** in 66 % unoptimized yield, and hydrogenation produced the novel C-linked bisfuranose disaccharide **29** in 76 % yield.

Finally, we have established that the original model study involving the Horner–Wadsworth–Emmons/conjugate addition sequence with substrates **6** and **7** followed by tandem halogenation-Ramberg–Bäcklund reaction can be carried out as a "one-pot" transformation (Scheme 6). Thus, **7** was added to the deprotonated phosphonate **6** and the mixture stirred at RT overnight. After cooling the mixture to 0 °C, the base and halogenating agent (KOH-Al_2O_3, CBr_2F_2) were added and the mixture stirred for about 30 minutes. A standard work-up (see Experimental Section) produced C-glycoside **9** in 78 % purified yield, a considerable increase on the two-step method (56 % overall yield). It should be noted that the Meyers–Chan procedure was successful in THF–CH_2Cl_2 and that *tert*-butanol, which is normally employed as a cosolvent,[6b] was not required.

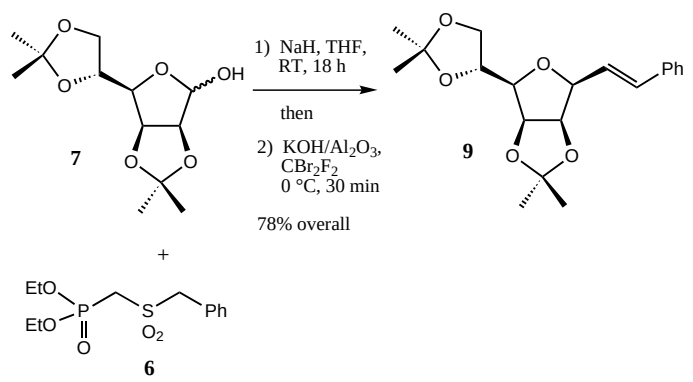

Scheme 6. One-pot variant of the C-glycoside synthesis.

In summary, we have established that a range of protected furanoses undergo a HWE/conjugate-addition/RBR sequence with benzylsulfonylphosphonate reagent **6** to produce the corresponding 2-styrenyl C-glycosides, and shown that this sequence can be performed in a "one-pot" variant in excellent yield. We have also demonstrated that monosaccharide-derived phosphonates can be employed in this methodology by utilizing the glucose-derived phosphonate **2a** to produce the mixed furanose–pyranose C-linked system **24**. Of course, by variation of the monosaccharide and the glycosyl phosphonate (**1** and **2** respectively, in Scheme 1), a range of other C-disaccharides becomes available. In addition, we have shown that a symmetrical C-linked bisfuranose system **29** is available by a double HWE sequence. Further work is in progress to optimize and apply this new methodology, initially to prepare C-linked analogues of furanose-pyranose disaccharides.[11] It should also be noted that the HWE reaction has been shown[7] to proceed efficiently on unprotected monosaccharides and studies in this area are in progress.

Experimental Section

All new compounds were fully characterized spectroscopically and by HRMS or elemental analysis.

Preparation of C-glycoside **9** by a "one-pot" procedure: A solution of phosphonate **6** (139 mg, 0.45 mmol) in THF (2 mL) was added dropwise to a suspension of NaH (18 mg, 60 % dispersion in oil, 0.45 mmol) in dry THF (6 mL) under nitrogen at RT. After stirring at RT for 10 min, a solution of 2,3:5,6-diisopropylidene D-mannofuranose (**7**) (107 mg, 0.41 mmol) in THF (2 mL) was added, and the reaction stirred at RT. After 18 h, the reaction was cooled to 0 °C, KOH-Al_2O_3[6b] (5.8 g) added and the suspension stirred for 10 min. CBr_2F_2 (0.37 mL) was added with stirring at 0 °C and the flask sealed, the stirring continued at this temperature for 30 min. The suspension was then warmed to RT and CH_2Cl_2 (10 mL) added. After stirring for 15 min, the reaction mixture was filtered through Celite, washing with CH_2Cl_2, and then the combined organic washings were concentrated in vacuo. Chromatography on silica (petroleum ether:EtOAc, 3:1) gave alkene **9** (111 mg, 78 %) as a colorless semi-solid, R_f (petroleum ether:EtOAc, 3:1) 0.49, $[\alpha]_D = +91$ (*c.* 1.2, $CHCl_3$), Found: 347.1858. $C_{20}H_{26}O_5$ requires $[MH]^+$ 347.1858 (0 ppm error). Consistent ^{1}H NMR, ^{13}C NMR, IR spectroscopy, and MS data were also obtained.

Received: October 21, 2002 [Z50403]

 © 2003 Wiley-VCH Verlag GmbH & Co. KGaA, Weinheim 1433-7851/03/4212-1390 $ 20.00+.50/0

Keywords: C–C coupling · disaccharides · glycosides · synthetic methods · tandem processes

[1] For recent reviews see: Y. Kishi, *Tetrahedron* **2002**, *58*, 6239 – 6258; T. Skrydstrup, B. Vauzeilles, J.-M. Beau, in *Carbohydrates in Chemistry and Biology, Vol. I*, Part I (Eds.: B. Ernst, G. W. Hart, P. Sinaÿ), Wiley-VCH, Weinheim, **2000**, chap. 20; Y. Du, R. J. Linhardt, I. R. Vlahov, *Tetrahedron* **1998**, *54*, 9913 – 9959; D. E. Levy, C. Tang, *The Chemistry of C-Glycosides*, Pergamon, Oxford, **1995**; M. H. D. Postema, *C-Glycoside Synthesis*, CRC, Boca Raton, FL, **1995**.

[2] For recent references see: M. K. Gurjar, R. Nagaprasad, C. V. Ramana, *Tetrahedron Lett.* **2002**, *43,* 7577 – 7579; L. M. Mikkelsen, S. L. Krintel, J. Jiménez-Barbero, T. Skrydstrup, *J. Org. Chem.* **2002**, *67,* 6297 – 6308; A. Dondoni, A. Marra, M. Mizuno, P. P. Giovannini, *J. Org. Chem.* **2002**, *67,* 4186 – 4199; W.-B. Yang, Y.-Y. Yang, Y.-F. Gu, S.-H. Wang, C.-C. Chang, C.-H. Lin, *J. Org. Chem.* **2002**, *67,* 3773 – 3782; A. M. Gómez, A. Pedregosa, S. Valverde, J. C. López, *Chem. Commun.* **2002**, 2022 – 2023; A. M. Gómez, G. O. Danelón, A. Pedregosa, S. Valverde, J. C. López, *Chem. Commun.* **2002**, 2024 – 2025; R. Hodgson, T. Mahid, A. Nelson, *Chem. Commun.* **2001**, 2076 – 2077; P. Pasetto, X. Chen, C. M. Drain, R. W. Franck, *Chem. Commun.* **2001**, 81 – 82; X. Li, O. Ohtake, H. Takahashi, S. Ikegami, *Tetrahedron* **2001**, *57,* 4283 – 4295.

[3] F. K. Griffin, D. E. Paterson, R. J. K. Taylor, *Angew. Chem.* **1999**, *111*, 3123 – 3125; *Angew. Chem. Int. Ed.* **1999**, *38*, 2939 – 2942.

[4] a) F. K. Griffin, P. V. Murphy, D. E. Paterson, R. J. K. Taylor, *Tetrahedron Lett.* **1998**, *39,* 8179 – 8182; b) M.-L. Alcaraz, F. K. Griffin, D. E. Paterson, R. J. K. Taylor, *Tetrahedron Lett.* **1998**, *39*, 8183 – 8186; c) R. J. K. Taylor, *Chem. Commun.* **1999**, 217 – 227, and references therein; d) A. D. Campbell, D. E. Paterson, T. M. Raynham, R. J. K. Taylor, *Chem. Commun.* **1999**, 1599 – 1600; e) G. D. McAllister, R. J. K. Taylor, *Tetrahedron Lett.* **2001**, *42*, 1197 – 1200.

[5] L. Ramberg, B. Bäcklund, *Ark. Kemi Mineral. Geol.* **1940**, *13A, 27*, 1 – 50 [*Chem. Abstr.* **1940**, *34*, 4725]; for reviews see L. A. Paquette, *Org. React.* **1977**, *25*, 1 – 71; J. M. Clough, *Comprehensive Organic Synthesis, Vol. 3*, Pergamon, Oxford, **1991**, chap. 3.8, pp. 880–886.

[6] a) C. Y. Meyers, A. M. Malte, W. S. Matthews, *J. Am. Chem. Soc.* **1969**, *91*, 7510 – 7512; b) T.-L. Chan, S. Fong, Y. Li, T.-O. Man, C.-D. Poon, *Chem. Commun.* **1994**, 1771 – 1772.

[7] A. H. Davidson, L. R. Hughes, S. S. Qureshi, B. Wright, *Tetrahedron Lett.* **1988**, *29*, 693 – 696, and references therein.

[8] Prepared by *S*-alkylation of benzyl thiol with diethyl iodomethylphosphonate followed by oxidation using Oxone. This compound has recently been described: M. Sindt, S. B. Schneider, J. L. Mieloszynski, *Phosphorus Sulfur Silicon Relat. Elem.* **2001**, *174*, 163 – 176.

[9] H. Ohrui, G. H. Jones, J. G. Moffatt, M. L. Maddox, A. T. Christensen, S. K. Byram, *J. Am. Chem. Soc.* **1975**, *97*, 4602 – 4613, and references therein.

[10] M. Mikolajczyk, M. Popielarczyk, S. Grzejszczak, *Phosphorus Sulfur Relat. Elem.* **1981**, *10*, 369 – 374.

[11] M. Wang, Y. Shao, N. Zhu, M. Rangarajan, E. J. LaVoie, C.-T. Ho, *J. Nat. Prod.* **1999**, *62*, 454 – 456; H. Matsuda, A. Ishikado, N. Nishida, K. Ninomiya, H. Fujiwara, Y. Kobayashi, M. Yoshikawa, *Bioorg. Med. Chem. Lett.* **1998**, *8*, 2939 – 2944.

 © 2003 Wiley-VCH Verlag GmbH & Co. KGaA, Weinheim 1433-7851/03/4212-1391 $ 20.00+.50/0

Supported Cluster Calculations

Oxidation of Supported Rhodium Clusters by Support Hydroxy Groups**

*Georgi N. Vayssilov, Bruce C. Gates, and Notker Rösch**

Metal clusters or particles on porous-oxide and zeolite supports are important industrial catalysts, with the role of the support often going beyond that of a mere platform for the stable dispersion of the metal.[1–3] The metal–support interaction involves support ligands, inferred to be surface oxygen or OH groups. How the bonding, reactivity, and catalytic properties of the metal depend on these ligands is essentially unresolved. Furthermore, supported metal catalysts often facilitate "spillover", whereby an adsorbate, typically H_2, reacts with the metal to give species that migrate onto the support. Molecular hydrogen dissociates on metals, and some of the H_2 ultimately forms OH groups on the support. Spillover has been demonstrated,[4] but its chemistry is ill defined; it must involve redox processes, since H_2 is converted into a hydride bound to the metal and the protons in OH groups.

To help clarify metal–support interactions and spillover effects, we modeled computationally the interaction of the bridging OH groups of zeolites with a supported cluster, Rh_6, and compared the theoretical results with the experimental results. The model system was selected because of its close correspondence[5] to the EXAFS-derived structure parameters for zeolite-supported Rh_6 clusters.[6] Our calculations show that the interaction of the hexanuclear cluster with OH groups from the support leads to the oxidation of Rh atoms that are in close contact with the support; the energy released per OH group is estimated to be about 120 $kJ\,mol^{-1}$. The results demonstrate the redox character of hydrogen spillover, which includes changes in the oxidation state of the supported metal.

[*] Prof. N. Rösch
Institut für Physikalische und Theoretische Chemie
Technische Universität München
85747 Garching (Germany)
Fax: (+49) 89-289-13468
E-mail: roesch@ch.tum.de

Dr. G. N. Vayssilov
Faculty of Chemistry
University of Sofia
Sofia 1126 (Bulgaria)

Prof. B. C. Gates
Department of Chemical Engineering and Materials Science
University of California
Davis, CA 95616 (USA)

[**] We thank Drs. K. M. Neyman and S. Krüger for helpful comments. This work was supported by Deutsche Forschungsgemeinschaft and Fonds der Chemischen Industrie. G.N.V. gratefully acknowledges an equipment donation from the Alexander von Humboldt Foundation and B.C.G. support from the U.S. Department of Energy, Office of Energy Research, Office of Basic Energy Sciences, Division of Chemical Sciences, Contract FG02-87ER13790, and a fellowship from the Alexander von Humboldt Foundation.

 © 2003 Wiley-VCH Verlag GmbH & Co. KGaA, Weinheim 1433-7851/03/4212-1391 $ 20.00+.50/0

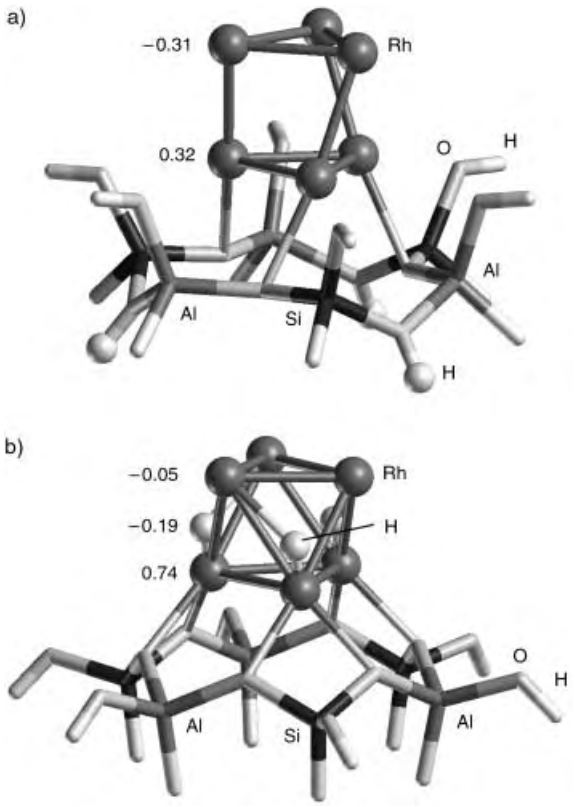

Figure 1. Calculated structures of Rh_6 clusters supported on a zeolite fragment (Zeo): a) nonreactive adsorption, Rh_6/Zeo(3H); b) reactive adsorption, Rh_6(3H)/Zeo. Also shown are Mulliken charges (in e) of the atoms in the supported cluster.

The structural model represents an Rh_6 cluster adsorbed at a six-ring model cluster of the faujasite structure with C_3 symmetry that contains three Al and three Si T atoms (Figure 1); the representation of the zeolite is as in our previous work.[7] The electronic-structure calculations were carried out with a density-functional method.[8–13] To evaluate the reaction energy for reverse hydrogen spillover from the OH groups of the zeolite to the supported Rh_6 cluster, we considered two systems: a) Rh_6/Zeo(3H), in which the cluster is adsorbed on the model zeolite fragment with three bridging OH groups (Figure 1a) corresponds to "nonreactive" adsorption of the Rh_6 cluster on the zeolite, and b) Rh_6(3H)/Zeo, formed by reverse spillover from a), in which the hydrogen atoms are bound to the Rh_6 (Figure 1b).

In Rh_6/Zeo(3H), the zeolite fragment is formally neutral; the negative charge of the six-ring, which arises from the presence of three Al atoms, is compensated by the three protons of the bridging OH groups (Figure 1a). Accordingly, the Rh_6 moiety is also formally neutral. The optimized geometry of the supported Rh_6 unit is a triangular prism twisted by 34° (compared to 60° of an octahedron); the shortest Rh–O bonds are 237 pm (Table 1), that is, ~20 pm longer than the experimental values determined by EXAFS spectroscopy,[6] 210–217 pm. The difference is far greater than the errors of current DF methods for such systems[14]

In Rh_6(3H)/Zeo, the three H atoms bridge metal atoms of the supported Rh_6 cluster. (Bridge-bonding of H atoms in the gas-phase Rh_6 was found to give the most stable conformation.[5]) In this structure, the zeolite fragment can be considered to bear a formal charge of −3 e, whereas the supported Rh_6(3H) cluster bears a formal charge of +3 e. The Rh atoms of this cluster form a triangular prism twisted by 58°, that is, close to an octahedron (Figure 1b). A comparison of the Rh_6(3H)/Zeo model cluster with the EXAFS data, which were interpreted as being indicative of octahedral clusters,[6] suggests[5] that the structural parameters of the theoretical model are in satisfactory agreement with the experimental results characterizing the zeolite-supported Rh_6,[6] namely, 1) the average calculated Rh–Rh bond of 262 pm is close to the experimental values, 267–269 pm (allowing for a typical experimental error of 1%); 2) the difference between the smallest and largest calculated Rh–Rh bond length is only 7 pm, consistent with the high quality of the EXAFS data[6] and the estimated experimental accuracy of 10 pm;[15] and 3) the optimized distances between of the "lower-layer" rhodium atoms and the zeolite oxygen centers, Rh_z–O_z, 218 and 220 pm, agree well with the EXAFS values, 210–217 pm.

Table 1: Interatomic distances [pm] in zeolite-supported Rh_6 clusters.

Model	Separations				
	Rh–Rh	$\langle R\rangle$[a]	ΔR[b]	Rh–H	Rh–O_z
experiment[c]	267–269	-	-	-	210–217
Rh_6/Zeo(3H)	251–307	265	56	-	237
Rh_6(3H)/Zeo	260–267	262	7	176	218, 220

[a] Average value of the Rh–Rh bond lengths in the cluster. [b] Difference between the smallest and largest nearest-neighbor Rh–Rh separation in the cluster. [c] Experimental value for zeolite-supported rhodium clusters, reference [6]. O_z = zeolite oxygen atom.

On the basis of these comparisons, we conclude that the zeolite-supported Rh_6 clusters prepared experimentally were not actually Rh_6, but instead were clusters decorated by H atoms. These clusters, which form by the migration of protons of the zeolite OH groups onto the cluster by reverse hydrogen spillover, are consistent with the calculated relative energies of the two model structures. The structure Rh_6(3H)/Zeo (Figure 1b) with three H atoms on the cluster is more stable (by 370 kJ mol^{-1}) than Rh_6/Zeo(3H) (Figure 1a).[16]

In addition to the structural and energetic aspects of the interaction of the Rh_6 cluster with the support, our results characterize significant chemical changes in the supported cluster. These changes were diagnosed by an analysis of the charge distribution in the model systems, which combined a Mulliken population analysis with core level binding energy shifts ΔE(Rh 3d).[17] Nonreactive adsorption of the Rh_6 cluster on a Zeo(3H) fragment is not accompanied by transfer of electron density between the metal cluster and the support; $q(Rh_6) = 0.03$ e. However, the support polarizes the electron density of the Rh_6 cluster, and two different types of Rh center result. The first type are the metal atoms, Rh_z, close to the zeolite support; they have a slightly cationic character,[18] with a positive charge of 0.32 e per atom and ΔE(Rh 3d) = −0.1 eV. The second type are the metal atoms, Rh_t, in the "top" layer of the cluster, which are negatively charged, −0.31 e per atom; correspondingly, their ΔE(Rh 3d) value is

 © 2003 Wiley-VCH Verlag GmbH & Co. KGaA, Weinheim 1433-7851/03/4212-1392 $ 20.00+.50/0

more negative, −0.6 eV. The redistribution of electron density in metal clusters is expected to be important for the reactivity and catalytic activity of such species on supports.

The charge distribution in the other model cluster, $Rh_6(3H)/Zeo$, clearly shows oxidation of the lower layer of the rhodium atoms, probably to Rh^I; the charge of these Rh_z centers is 0.74 e, and $\Delta E(Rh\,3d) = 2.1$ eV. The charges of the Rh_t atoms are close to zero, $q(Rh_t) = -0.05$ e, but their core levels are also strongly stabilized compared to those of the neutral gas-phase Rh_6 cluster, $\Delta E(Rh\,3d) = 1.7$ eV. This high positive value of $\Delta E(Rh\,3d)$ of the Rh_t atoms is ascribed to the large overall positive charge of the moiety $Rh_6(3H)$, + 1.50 e. This value compares to the formal charge +3 e. The difference in the $\Delta E(Rh\,3d)$ values characterizing Rh_t and Rh_z atoms is essentially the same for nonreactive and reactive adsorption; the core levels of the Rh_t atoms are 0.4–0.5 eV less stable than those of Rh_z. Reactive adsorption of the metal cluster decreases the electron density in both layers of rhodium atoms with respect to nonreactive adsorption, as shown by the charges in Figure 1.

An additional argument for the oxidation of the supported Rh_6 cluster as a result of an interaction with surface OH groups relies on a comparison of the Rh−O distances. Both experimentally measured (210–217 pm) and calculated[20] (218, 220 pm) Rh_z−O_z distances for the zeolite-supported hexarhodium cluster are close to the corresponding experimental and calculated values of the cationic dicarbonyl complex $Rh^I(CO)_2$ supported on a zeolite, 216 pm and 219–220 pm, respectively.[21] This observation suggests that the nature of the metal centers in the two types of supported species is similar, namely, the Rh centers bound to zeolite oxygen atoms in the supported hexarhodium cluster are oxidized with an effective charge similar to that of the Rh^I center in the supported dicarbonyl species, 0.53 e (Mulliken charge).[21]

Thus, our computational modeling suggests that transition-metal particles are oxidized by surface OH groups. This inference invites comparison with relevant experimental results. When metal clusters are prepared, for example, by the aggregation of smaller metal-containing species, or the decarbonylation of supported metal carbonyl clusters,[6,22] OH groups are necessary for successful syntheses, at least for those that give nearly uniform clusters. Hence, reference studies of samples without surface OH groups seemingly cannot be performed. However, when the supported particles are produced by vapor deposition, the experiments can be performed with a controlled density of surface OH groups. Because this technique is not appropriate for the preparation of metal clusters in zeolite cavities, we use experimental results obtained for rhodium particles supported on alumina films.[2] Freund and co-workers[2] have shown by infrared spectroscopy and X-ray photoelectron spectroscopy (XPS; O1s, Al2p) that the deposition of rhodium particles on hydroxylated alumina involved a consumption of surface OH groups. Simultaneously, the XPS of the Rh 3d level shows a concomitant positive binding energy shift by 0.3 eV, that is, a stabilization of the corresponding core level. This result can be rationalized by a direct interaction of the metal particles with surface OH groups, including oxidation of some of the metal atoms to Rh^I. This argument is in line with trends of our computational models.

The quantitative difference between our calculated $\Delta E(Rh\,3d)$ values, ≈ 2.0 eV, and experimental XPS results, 0.3 eV, is not entirely surprising. First, in our calculations, we used only a rather approximate estimate of core-level energy shifts.[17] More importantly, the small $\Delta E(Rh\,3d)$ value could be a consequence of the different sizes of the metal particles. In the experiment, relatively large particles, consisting of about 100 Rh atoms per island,[2] were used, in contrast to our six-atom clusters; therefore, only a small fraction of the Rh atoms in the particles interacted with the support and were oxidized. Furthermore, such large metal particles exhibit screening effects. It is evident that the cluster oxidation and effects of such a charge redistribution would be most pronounced for the smallest metal clusters, becoming negligible for increasingly larger clusters, which, in the limit (i.e. the largest clusters), have properties approaching those of bulk metals.[23]

Thus, we suggest that the redox processes of spillover shown by our results may be quite general for supported metal species, but the changes in the metal centers may be too small to detect, except when the clusters are small. A related inference is that bare metal clusters may not even exist on hydroxylated surfaces, because of reverse spillover. This suggestion is consistent with EXAFS data for small, nearly uniform supported clusters of Rh and of Ir, for which the metal–metal separations are larger than those of the free clusters.[7c,22a] Another consequence is related to the interpretation of hydrogen chemisorption data, which are often used to determine dispersions of supported metal clusters. The stoichiometry of adsorption of hydrogen on platinum, for example, was shown to a good approximation to be 1:1, even for clusters as small as those containing several tens of atoms.[24] But successful measurements of the amount of hydrogen chemisorbed require that the metal surface be cleaned before the adsorption. When supported metal clusters are sufficiently small, this cleaning may not be possible without reverse spillover replenishing the metal with hydrogen.[25] It remains to be determined how these effects depend quantitatively on the metal, support, and metal cluster size.

Received: October 23, 2002 [Z50412]

Keywords: density functional calculations · rhodium · supported catalysts · surface chemistry · zeolites

[1] a) M. Zaki, G. Kunzmann, B. C. Gates, H. Knözinger, *J. Phys. Chem.* **1987**, *91*, 1486; b) P. Basu, D. Panayotov, J. T. Yates, Jr., *J. Am. Chem. Soc.* **1988**, *110*, 2074; c) H. Miessner, I. Burkhardt, D. Gutschick, A. Zecchina, C. Morterra, G. Spoto, *J. Chem. Soc. Faraday Trans. 1* **1989**, *85*, 2113.

[2] a) J. Libuda, M. Frank, A. Sandell, S. Andersson, P. A. Brühwiler, M. Bäumer, N. Mårtensson, H.-J. Freund, *Surf. Sci.* **1997**, *384*, 106; b) M. Heemeier, M. Frank, J. Libuda, K. Wolter, H. Kuhlenbeck, M. Bäumer, H.-J. Freund, *Catal. Lett.* **2000**, *68*, 19.

[3] K. I. Hadjiivanov, G. N. Vayssilov, *Adv. Catal.* **2002**, *47*, 307.

 © 2003 Wiley-VCH Verlag GmbH & Co. KGaA, Weinheim 1433-7851/03/4212-1393 $ 20.00+.50/0

[4] W. C. Conner, Jr., J. L. Falconer, *Chem. Rev.* **1995**, *95*, 759.

[5] G. N. Vayssilov, N. Rösch, unpublished results. This density-functional study explores the effect of C, O, and H impurity atoms on the structure of gas-phase and zeolite-supported Rh_6 clusters. Calculated structures are compared to EXAFS-derived metal–metal separations in Rh_6 clusters on a zeolite support. Model clusters with C or O impurities show large differences between the calculated Rh–Rh separations in the clusters and those determined experimentally; thus, these models were not considered pertinent to the experimentally studied supported metal clusters. A structure with three H atoms as impurities bridging the Rh–Rh bonds of a Rh_6 cluster supported on zeolite, denoted here as Rh_6(3H)/Zeo, was found to agree best with the EXAFS data.

[6] W. A. Weber, B. C. Gates, *J. Phys. Chem. B* **1997**, *101*, 10423.

[7] a) G. N. Vayssilov, J. A. Lercher, N. Rösch, *J. Phys. Chem. B* **2000**, *104*, 8614; b) G. N. Vayssilov, N. Rösch, *J. Phys. Chem. B* **2001**, *105*, 4277; c) A. M. Ferrari, K. M. Neyman, M. Mayer, M. Staufer, B. C. Gates, N. Rösch, *J. Phys. Chem. B* **1999**, *103*, 5311.

[8] We employed the program PARAGAUSS[9,10] for parallel computers to perform Kohn-Sham calculations with a gradient-corrected exchange-correlation functional.[11] The program PARAGAUSS implements the LCGTO-FF-DF method (linear combination of Gaussian-type orbitals fitting-functions density functional).[12,13] Further computational details are given in ref. [5].

[9] "Lecture Notes in Computational Science and Engineering": T. Belling, T. Grauschopf, S. Krüger, M. Mayer, F. Nörtemann, M. Staufer, C. Zenger, N. Rösch in *High Performance Scientific and Engineering Computing, Vol. 8* (Eds.: H.-J. Bungartz, F. Durst, C. Zenger), Springer, Heidelberg, **1999**, p. 439.

[10] PARAGAUSS version 2.1, T. Belling, T. Grauschopf, S. Krüger, F. Nörtemann, M. Staufer, M. Mayer, V. P. Nasluzov, U. Birkenheuer, A. Hu, A. V. Matveev, N. Rösch, Technische Universität München, **1999**.

[11] a) A. D. Becke, *Phys. Rev. A* **1988**, *38*, 3098; b) J. P. Perdew, *Phys. Rev. B* **1986**, *33*, 8822; J. P. Perdew, *Phys. Rev. B* **1986**, *34*, 7406.

[12] B. I. Dunlap, N. Rösch, *Adv. Quantum Chem.* **1990**, *21*, 317.

[13] N. Rösch, S. Krüger, M. Mayer, V. A. Nasluzov in *Recent Development and Applications of Modern Density Functional Theory. Theoretical and Computational Chemistry, Vol. 4* (Ed.: J. M. Seminario), Elsevier, Amsterdam, **1996**, p. 497.

[14] A. Görling, S. B. Trickey, P. Gisdakis, N. Rösch in *Topics in Organometallic Chemistry, Vol. 4* (Eds.: J. Brown, P. Hofmann), Springer, Heidelberg, **1999**, p. 109.

[15] B. K. Teo, *Acc. Chem. Res.* **1980**, *13*, 412, and references therein.

[16] A rigorous analysis of the different contributions to the considerable stabilization of the structure with the reactive adsorption of the Rh_6 cluster is not possible because the Rh_6/Zeo(3H) system is constructed from neutral fragments, Rh_6 and Zeo(3H), whereas the other model, Rh_6(3H)/Zeo, is formally composed of highly charged fragments, $Rh_6(3H)^{3+}$ and Zeo^{3-}. We can only estimate the binding energy of nonreactive adsorption of the Rh_6 cluster on the zeolite fragment, Rh_6/Zeo(3H); it is 77 kJ mol^{-1} with respect to a Rh_6 cluster in the gas phase, separated from a neutral zeolite fragment.

[17] The value of ΔE(Rh 3d) is estimated from calculated Kohn–Sham orbital energies as the corresponding energy-difference shift with respect to an Rh_6 cluster in the gas phase. A positive value of ΔE(Rh 3d) corresponds to a stabilization of Rh 3d levels.

[18] Such a polarization of small supported metal clusters was anticipated in early work,[19] but was not clearly evident in the calculated results representing Ir_4 on a zeolite support.[7c]

[19] J.-R. Chang, L. U. Gron, A. Honji, K. M. Sanchez, B. C. Gates, *J. Phys. Chem.* **1991**, *95*, 9944.

[20] For the model Rh_6(3H)/Zeo that corresponds to the experimentally observed species, as discussed above, ref. [6].

[21] a) J. F. Goellner, B. C. Gates, G. N. Vayssilov, N. Rösch, *J. Am. Chem. Soc.* **2000**, *122*, 8056; b) G. N. Vayssilov, N. Rösch, *J. Am. Chem. Soc.* **2002**, *124*, 3783.

[22] a) O. Alexeev, B. C. Gates, *Top. Catal.* **2000**, *10*, 273; b) W. M. H. Sachtler, *Acc. Chem. Res.* **1993**, *26*, 383; c) W. M. H. Sachtler, Z. Zhang, *Adv. Catal.* **1993**, *39*, 129; d) L. Kubelkova, J. Vylita, L. Brabec, L. Drozdova, T. Bolom, J. Novakova, G. Schulz-Ekloff, N. I. Jaeger, *J. Chem. Soc. Faraday Trans.* **1996**, *92*, 2035.

[23] a) S. Krüger, S. Vent, N. Rösch, *Ber. Bunsen-Ges.* **1997**, *101*, 1640; b) S. Krüger, S. Vent, F. Nörtemann, M. Staufer, N. Rösch, *J. Chem. Phys.* **2001**, *115*, 2082; c) I. V. Yudanov, R. Sahnoun, K. M. Neyman, N. Rösch, *J. Chem. Phys.* **2002**, *117*, 9887.

[24] O. Alexeev, D.-W. Kim, G. W. Graham, M. Shelef, B. C. Gates, *J. Catal.* **1999**, *185*, 170.

[25] The question arises as to whether sufficient cycles of pumping would remove all the support OH groups and ultimately prevent reverse spillover, but it is also questionable whether this can be done successfully without sintering the metal.

 © 2003 Wiley-VCH Verlag GmbH & Co. KGaA, Weinheim 1433-7851/03/4212-1394 $ 20.00+.50/0

NMR Studies of Glycopeptides

Γ-HMBC: An NMR Experiment for the Conformational Analysis of the *o*-Glycosidic Linkage in Glycopeptides**

*Sergey Ilin, Carlos Bosques, Christopher Turner, and Harald Schwalbe**

Carbohydrates play a major role in many processes, such as the immunological response, and in cellular recognition events in general.[1] The structural characterization of carbohydrates by NMR spectroscopy has been a challenge because of the lack of experimental parameters and the intrinsic high mobility and resulting conformational averaging of oligosaccharides in solution. For example, the conformation around

[*] Prof. Dr. H. Schwalbe
Institut für Organische Chemie und Chemische Biologie
Zentrum für Biomolekulare Magnetische Resonanz
Johann Wolfgang Goethe-Universität Frankfurt am Main
Marie-Curie-Str. 11, 60439 Frankfurt am Main (Germany)
Fax: (+49) 69-7982-9515
E-mail: schwalbe@nmr.uni-frankfurt.de

S. Ilin, Dr. C. Bosques, Dr. C. Turner
Department of Chemistry and MIT/Harvard Center for Magnetic Resonance at the Francis Bitter Magnet Laboratory
Massachusetts Institute of Technology, Department of Chemistry
170 Albany Street, Bldg. NW14, Cambridge, MA 02139 (USA)

[**] We thank M.I.T., the Winnacker Foundation, and the Sloan Foundation for financial support. Spectra were recorded at the Bitter Laboratory (supported by NIH grant RR-00995) and the Spectroscopy Facilities at M.I.T. We thank Dr. J. Klein-Seetharaman for stimulating discussions.

Supporting information for this article is available on the WWW under http://www.angewandte.org or from the author.

 © 2003 Wiley-VCH Verlag GmbH & Co. KGaA, Weinheim 1433-7851/03/4212-1394 $ 20.00+.50/0

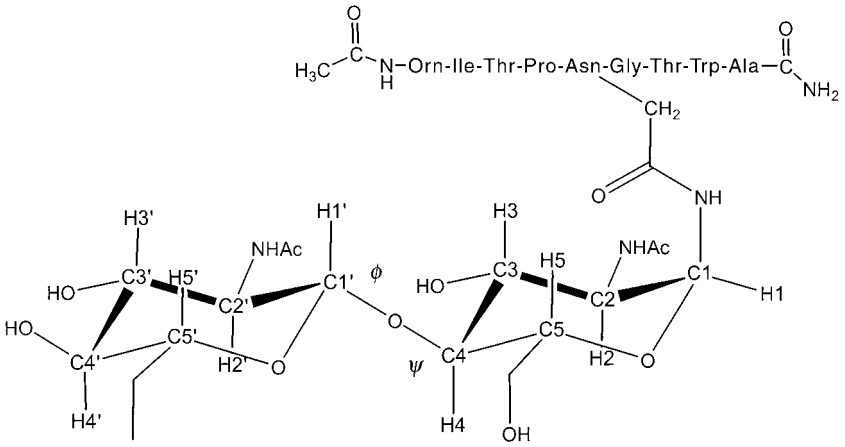

Figure 1. {[GlcNAc-β(1-4)-GlcNAc-α-]Asn}$^{286}_{281-290}$-hemagglutinin peptide **1** used as a model substance for a glycopeptide. The nomenclature follows IUPAC recommendations for carbohydrates, where φ and ψ are the O5-C1-OX-CX and C3-C4-OX-CX torsion angles, respectively; three-letter codes are used for amino acids.

the exocyclic glycosidic bonds cannot unambiguously be determined from measurement of inter-residue ^{1}H–^{1}H NOE measurements.[2] For oligosaccharides in solution, residual dipolar couplings that are partially oriented in bicelles [3] are not very sensitive to conformational averaging, as shown by NOE experiments. Only two ^3J(C,H) coupling constants can be observed as a result of varying the exocyclic torsion angles, and current methods for their measurement are insensitive for larger molecules.

We have therefore developed a new experiment, the *Γ*-HMBC (HMBC = heteronuclear multiple-bond correlation), in which four NMR parameters, ^3J(C,H) couplings, and cross-correlated relaxation rates $\Gamma^c_{C_iH_i,C_iH_j}$ are measured that can describe the conformation of the glycosidic torsion angles ϕ and ψ in oligosaccharides.[4] It relies on a correlation developed by Vincent et al.[5] in which coherence transfer between hydrogen and carbon atoms across the glycosidic linkage is achieved by C–H-dipolar cross-correlated relaxation. In the experiment, an initial antiphase operator $2H1'_zC1'_x$ (representing the annotated atoms in Figure 1) evolves into the operator $2H4_zC1'_x$ during a constant time delay CT (Figure S1 in Supporting Information). Correlation peaks in the experiment are generated through cross-correlated relaxation[6] between two dipoles centered on the same carbon atom. The cross-correlated relaxation rate is given by Equation (1):

$$\Gamma^c_{C_iH_i,C_iH_j} = \frac{2}{5}\frac{\gamma_H^2\gamma_C^2}{r^3_{C_iH_i}r^3_{C_iH_j}}\left(\frac{\mu_0}{4\pi}\right)^2\hbar^2\left(S^c_{ij}\right)^2\left(\frac{3\cos^2\theta_{ij}-1}{2}\right)\tau_c \qquad (1)$$

In this equation, γ_C and γ_H are the gyromagnetic ratios, μ_0 is the susceptibility of the vacuum, $r_{C_iH_i}$ and $r_{C_iH_j}$ are the carbon–proton separations, $\hbar$ is the Planck constant, S^c_{ij} is the order parameter, and τ_c is the overall correlation time. This variable depends on the projection angle (θ_{ij}) between the two dipole tensors which, in turn, depends on the torsion angles ϕ and ψ.

The operator $2H4_yC1'_z$ generated prior to t_2 can be detected by NMR and is modulated by the ^3J(C1′,H4) coupling. Therefore, ^3J(C,H) coupling constants can be determined from the spectra shown in Figure 2a–d by fitting spectral peaks with simulated multiplets with Lorentzian line shapes. This approach is related to the Keeler–Neuhaus–Titman approach for the determination of ^3J(C,H) coupling constants from ω_2-coupled HMBC-spectra.[7] However, in the original HMBC experiment, cross-peaks are phase-modulated by evolution of homonuclear ^3J(H,H) couplings during a fixed delay, which causes a complex line shape. The phase distortion in the HMBC requires the acquisition of two separate experiments to simulate the line shape of the target multiplet.

In contrast, in the experiments described here, the signal detected in t_2 is not phase distorted and split only by a single J(H,C) coupling in antiphase.[8] Experimental and simulated multiplets for H1′C1′ and H1′C4 cross-peaks in the glycopeptide **1** (Figure 1) are shown in Figure 2. The cross-peak H1′C4 (Figure 2b) is modulated by the same ^3J(H,H) couplings and transverse relaxation rate as either the upfield or downfield part of the related, direct cross-peak (H1′C1′) (Figure 2a); it differs only by its magnitude and by convolution with an antiphase long-range ^3J(C,H) coupling. Homonuclear ^3J(H,H) coupling constants and proton transverse relaxation rates were determined by fitting to both the upfield and downfield components of the cross-peak H1′C1′ that is observed with a high signal-to-noise ratio. These parameters were kept fixed in the simulation for the long-range ^3J(C,H)

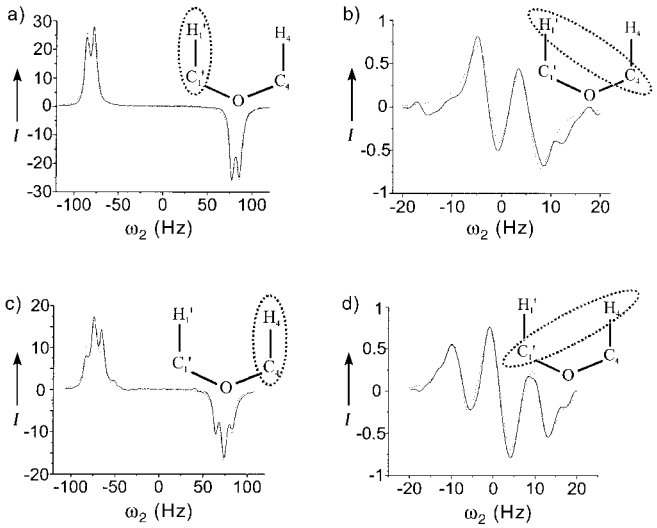

Figure 2. Experimental (-----) and simulated (•••••) multiplets. a) H1′C1′; b) H1′C4, ^3J(C,H) = 3.3 ± 0.2 Hz; c) H4C4; d) H4C1′, ^3J(C,H) = 1.2 ± 0.2 Hz. The measurement time was 48 h, and the sample concentration was 4 mM. Experimental parameters are given in Figure S1 of the Supporting Information.

 © 2003 Wiley-VCH Verlag GmbH & Co. KGaA, Weinheim 1433-7851/03/4212-1395 $ 20.00+.50/0

Table 1: Experimental transverse relaxation rates R_2, ^3J(H,C) and ^3J(H,H) coupling constants, and regression coefficient R^2 fit to the multiplets shown in Figure 2 a–d.

	H4C1′	H1′C4	H1C5
R_2 [s^{-1}]	6.9	6.5	6.7
^3J(H,H) [Hz]	8.3, 10.4	8.2	5.1
^3J(H,C) [Hz][a]	1.2 ± 0.2	3.3 ± 0.2	6.5 ± 0.2
R^2	0.97	0.93	0.97

[a] Active heteronuclear ^3J(C,H) coupling constant leading to the indicated cross-peak.

couplings in the H1′C4 cross-peak, as shown in Figure 2 b and d for the fits with the lowest χ^2 value. The complete statistics on the calculations of cross-peak parameters are given in Table 1. The torsion angles ϕ and ψ were calculated using the Karplus equation for ^3J(C,H) in oligosaccharides, polysaccharides, and glycoconjugates;[9] the results are listed in Table 2. The angles determined by this method are ambiguous because each coupling (J) can arise from up to four different torsion angles, and the conformation around the glycosidic bond is described by the two torsion angles ϕ and ψ. This ambiguity can be resolved by calculating the cross-correlated relaxation rates from the experimental intensities of the multiplets (Figure 2) according to Equation (2).

$$\frac{\sinh(\Gamma^{c}_{C_1H_1',C_1'H_4}CT)}{\sinh(\Gamma^{c}_{C_5H_5,C_5H_1}CT)} = \frac{I_{C_1H_1',C_1'H_4}}{I_{C_5H_5,C_5H_1}} \qquad (2)$$

The cross-correlated relaxation rate measured for cross-peaks across the glycosidic bond was internally referenced to the known cross-correlated relaxation rate $\Gamma^{c}_{C_5H_5,C_5H_1}$ observed within the sugar ring.[10] Variation of the relaxation rates, as a function of the torsion angles ϕ and ψ, is shown in Figure 3 using standard parameters (bond lengths: C–H 1.09 Å, C–O 1.42 Å; bond angles: H-C-O 109.7°, glycosidic C-O-C 115.5°, internal C-O-C 112.0°). The H1C5 cross-peak was used as a reference (torsion angle of −175°).

Out of sixteen possible combinations of ϕ and ψ angles based on coupling data, the cross-correlated relaxation data support two pairs of angles, where $\phi = 10°$ or 110°, and $\psi = 12°$ (Figure 3). Molecular dynamics (MD) simulations and an X-ray crystal structure are available for an analogue (GlcNAc-β(1-4)-GlcNAc) of the sugar moiety in the glycopeptide **1** investigated here. The MD simulation shows considerable flexibility (with $0° \le \phi \le 70°$ and $-75° \le \psi \le 15°$) and average torsion angles of $\phi = 46 \pm 13°$ and $\psi = -10 \pm 16°$.[11] In the crystal structure, ϕ and ψ assume values

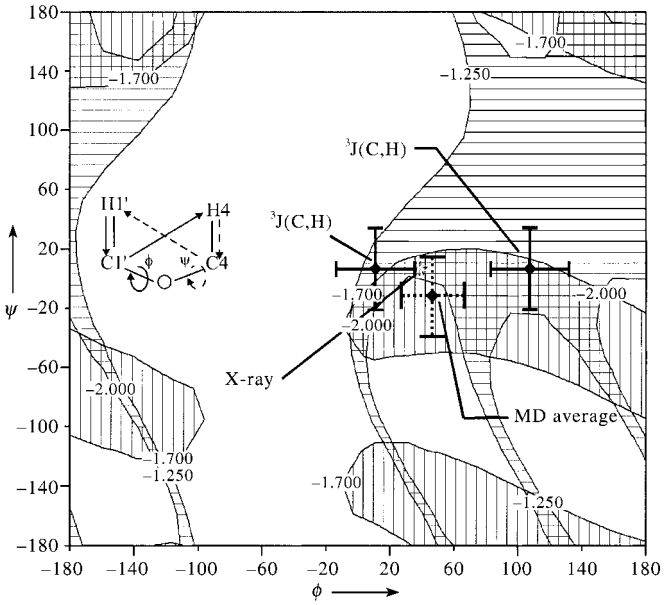

Figure 3. Overlay of simulated cross-correlated relaxation rates $\Gamma^{DD,DD}_{C_4H_1',C_4H_4}$ (horizontal line) and $\Gamma^{DD,DD}_{C_1'H_4,C_1'H_1'}$ (vertical line) as a function of φ and ψ. Crossover indicates experimentally allowed combinations. Single points with error bars indicate torsion angles derived from ^3J(C,H) coupling constants; "X-ray" and and "MD average" indicate angles derived from the crystal structure and MD simulations, respectively.

of 36.3° and 11.7°, respectively.[12]. NMR data of the species in solution supports a similar region of preferred conformation ($\phi = 10 \pm 20°$ and $\psi = 12 \pm 20°$). While identical values are found for ψ in the crystal and in solution, the torsion angle ϕ is shifted both in the MD and in the NMR data. Values of angle ϕ of approximately 40° are in agreement with predictions based on the exo-anomeric effect.

In conclusion, a novel method is introduced to determine the conformation around glycosidic bonds based on ^3J(C,H) couplings and C–H-dipolar cross-correlated relaxation by solution NMR spectroscopy. Using conventional NMR probes, the data can be obtained for glycopeptides without ^{13}C labeling at a concentration of 5 mM. The experiment is shorter than normal HMBC experiments as long periods with transverse proton magnetization are avoided. Extension of the method to the study of large polysaccharides is expected to add to a structural understanding of the role of carbohydrates in cell recognition[13] and may aid in the design of novel carbohydrate-based drugs.[14]

Table 2: A summary of coupling constants, torsion angles, and relaxation times.

	J [Hz][a]	φ,ψ [°][b]	$\Gamma^{DD,DD}$ [s^{-1}][c]
^3J(H1′,C4)	3.3 ± 0.2	ϕ:10 ± 20,110 ± 20,79 ± 20,-162 ± 20	$\Gamma_{C_4H_1',C_4H_4} = -1.4$
^3J(H4,C1′)	1.2 ± 0.2	ψ:12 ± 20,55 ± 20,-132 ± 20,-175 ± 20	$\Gamma_{C_1'H_4,C_1'H_1'} = -4.4$
^3J(H1,C5)	6.5 ± 0.2	±175 ± 5	$\Gamma_{C_5H_1,C_5H_5} = -1.5$

[a] ^3J(H,C) coupling constants. [b] Torsion angles from ^3J(H,C) coupling constants based on Karplus equation: $^3J(H,C) = 5.7\cos^2\alpha - 0.6\cos\alpha + 0.5$. Estimated torsion angle uncertainties are given. [c] Cross-correlated relaxation rates.

Experimental Section

Sample preparation: Glycopeptide **1** {[GlcNAc-β(1-4)-GlcNAc-α-]Asn}$^{286}_{281-290}$-hemagglutinin was synthesized using standard 9-fluorenyl methoxycarbonyl (Fmoc) chemistry and solid-phase peptide synthesis techniques. The α-linked chitobiose moiety was introduced as the Fmoc-Asn (TBDMS-chitobiose)-OH building block. The predicted mass for glycopeptide **1** (1421.5) was confirmed by ESI-MS. Although GlcNAc-β(1-4)-GlcNAc is the natural core in N-linked glycopro-

 © 2003 Wiley-VCH Verlag GmbH & Co. KGaA, Weinheim 1433-7851/03/4212-1396 $ 20.00+.50/0

teins, the anomeric center on the first sugar moiety in glycopeptide **1** investigated here was in the α conformation. All data were acquired on Bruker DRX 600 and Homebuilt 600 spectrometers with a 5 mm Bruker TXI ^{1}H {$^{15}N/^{13}C$} z-grad probe and Nalorac triple resonance probes, respectively. Information about the pulse sequence shown is given in the Supporting Information. The concentration of glycopeptide **1** was 4.5 mM (6 mg mL^{-1}) in a volume of 300 μL using a Shigemi tube. The sample temperature was 278 K.

Received: November 15, 2002 [Z50564]

Keywords: conformational analysis · glycosides · NMR spectroscopy · oligosaccharides · structural biology

[1] *Polysaccharides: Structural Diversity and Functional Versatility* (Ed.: S. E. Dumitriu), Marcel Dekker, New York, **1998**; P. M. Rudd, T. Elliot, P. Cresswell, I. A. Wilson, R. A. Dwek, *Science* **2001**, *291*, 2370 – 2375; S. E. O'Connor, B. Imperiali, *J. Am. Chem. Soc.* **1997**, *119*, 2295 – 2296; *NMR Spectroscopy of Glycoconjugates* (Ed.: J. Jiménez-Barbero, T. Peters), Wiley-VCH, Weinheim, **2002**.

[2] S. W. Homans, *Prog. Nucl. Magn. Reson. Spectrosc.* **1990**, *22*, 55 – 81; C. A. Bush, M. M. Pastor, *Annu. Rev. Biophys. Biomol. Struct.* **1999**, *28*, 269 – 293.

[3] F. Tian, H. M. Al-Hashimi, J. L. Craighead, J. H. Prestegard, *J. Am. Chem. Soc.* **2001**, *123*, 485 – 492; H. Neubauer, J. Meiler, W. Peti, C. Griesinger, *Helv. Chim. Acta* **2001**, *84*, 243 – 258.

[4] O. Jardetzky, *Biochim. Biophys. Acta* **1980**, *621*, 227 – 232; A. Parfondry, N. Cyr, A. S. Perlin, *Carbohydr. Res.* **1977**, *59*, 299 – 309; M. L. Hayes, A. S. Serianni, R. Barker, *Carbohydr. Res.* **1982**, *100*, 87 – 101; J. M. Duker, A. S. Serianni, *Carbohydr. Res.* **1993**, *249*, 281 – 303.

[5] S. J. F. Vincent, C. Zwahlen, *J. Am. Chem. Soc.* **2000**, *122*, 8307 – 8308.

[6] B. Reif, M. Hennig, C. Griesinger, *Science* **1997**, *276*, 1230 – 1233; H. Schwalbe, T. Carlomagno, M. Hennig, J. Junker, B. Reif, C. Richter, C. Griesinger, *Methods Enzymol.* **2001**, *338*, 35 – 81.

[7] J. J. Titman, D. Neuhaus, J. Keeler, *J. Magn. Reson.* **1989**, *85*, 111 – 131; J. M. Richardson, J. J. Titman, J. Keeler, *J. Magn. Reson.* **1991**, *93*, 533 – 553.

[8] H. Schwalbe, W. Samstag, J. W. Engels, W. Bermel, C. Griesinger, *J. Biomol. NMR* **1993**, *3(4)*, 479 – 486.

[9] I. Tvaroska, M. Hricovinin, E. Petrakova, *Carbohydr. Res.* **1989**, *189*, 359 – 362; S. A. Wacowich-Sgarbi, C. C. Ling, A. Otter, D. R. Bundle, *J. Am. Chem. Soc.* **2001**, *123*, 4362 – 4363.

[10] Uniform ^{13}C-T_1 relaxation times of 0.32 ± 0.02 s were measured for **1**. s^c_{ij} values were therefore assumed to be similar for the corresponding peaks generated through cross-correlated relaxation.

[11] R. J. Woods, A. Pathiaseril, M. R. Wormald, C. J. Edge, R. A. Dwek, *Eur. J. Biochem.* **1998**, *258*, 372 – 386.

[12] F. Mo, L. H. Jensen, *Acta Crystallogr. Sect. B* **1978**, *34*, 1562 – 1569.

[13] A. Varki, *Glycobiology* **1993**, *3*, 97 – 130.

[14] J. McAuliffe, O. Hindsgaul, *Chem. Ind.* **1997**, *5*, 14 – 26.

 © 2003 Wiley-VCH Verlag GmbH & Co. KGaA, Weinheim 1433-7851/03/4212-1397 $ 20.00+.50/0

Palladium-Catalyzed Carbonylation of 2-(Propargyl)allyl Phosphates Leading to Highly Unsaturated γ-Lactones**

Akihito Kamitani, Naoto Chatani, and Shinji Murai*

Unsaturated lactones are an intensively studied family of heterocycles, which are important subunits in naturally occurring, as well as biologically active compounds.[1,2] While numerous approaches have been developed for the synthesis of such skeletons,[1] a simple and straightforward method for the construction of highly functionalized γ-lactones continues to be a challenge. We have previously reported on a new method for the construction of γ-lactone skeletons.[3–5] This methodology involves a carbonylative [2+2+1] cycloaddition reaction (Scheme 1a). If one uses

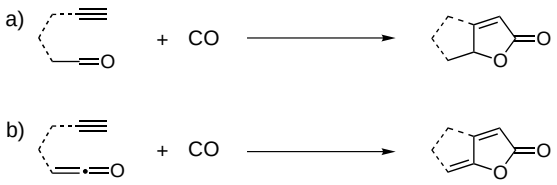

Scheme 1. Cycloaddition of alkynes, CO, and carbonyl functionality; see text for details.

acetylene–ketenes as the substrate in place of acetylene–aldehydes, the formation of γ-alkylidene-α,β-unsaturated lactones would be expected, through the [2+2+1] cycloaddition of alkynes, ketene–carbonyl, and CO (Scheme 1b). The transformation would provide a new route to unsaturated lactones; however, such a transformation has not been reported thus far.[6] Herein we report on the realization of this approach for the construction of polyunsaturated, fused bicyclic γ-lactones by the Pd-catalyzed carbonylation of 2-(propargyl)allyl phosphates.

Ketenes are versatile, well-known substrates in organic synthesis, but they are most often produced in situ from acid chlorides through dehydrochlorination reactions with tertiary amines.[7] Although various reaction conditions were explored

[*] Prof. N. Chatani, A. Kamitani, Prof. S. Murai
Department of Applied Chemistry
Faculty of Engineering, Osaka University
Suita, Osaka 565-0871 (Japan)
Fax: (+81) 6-6879-7396
E-mail: chatani@chem.eng.osaka-u.ac.jp

[**] This work was supported by a Grant-in-Aid for Scientific Research on Priority Areas (A) "Exploitation of Multi-Element Cyclic Molecules" from the Ministry of Education, Culture, Sports, Science and Technology, Japan. Thanks are given to the Instrumental Analysis Center, Faculty of Engineering, Osaka University, for assistance in obtaining MS, HRMS, 600 MHz NMR, and elemental analyses.

Supporting information for this article is available on the WWW under http://www.angewandte.org or from the author.

 © 2003 Wiley-VCH Verlag GmbH & Co. KGaA, Weinheim 1433-7851/03/4212-1397 $ 20.00+.50/0

to achieve the reaction of intramolecular acetylene–acid chlorides with CO, the expected lactones were not formed. We then examined π-allyl palladium complexes and CO as the ketene source. Torii et al. reported that the Pd-catalyzed reaction of allyl phosphates with imines led to β-lactams, a reaction in which a [2+2] cycloaddition of in situ generated vinylketenes and imines was proposed as the key step.[8] Negishi et al. also proposed the generation of phenylketene derivatives from the reaction of benzylpalladium complexes and CO.[9] A preliminary screening of potential substrates indicated that 2-(propargy)allyl phosphate provided high reactivity. Thus, treatment of 2-methylene-4-hexyn-1-yl diethyl phosphate (**1a**) (0.5 mmol) with CO (1 atm) in THF (2 mL) in the presence of $[\{(\eta^3\text{-allyl})PdCl\}_2]$ (0.01 mmol) and Cy_2NMe (1 mmol) for 12 h led to the formation of the expected bicyclic lactone **2a**[10] in 52% yield [Eq. (1)]. Among

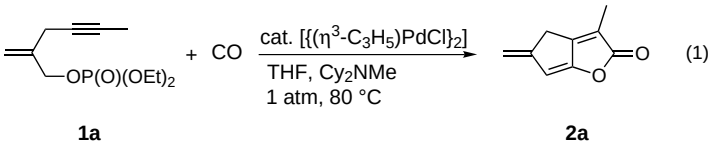

1a **2a**

the solvents examined, THF was found to be the best solvent and gave the highest yield; toluene (47%), DMF (39%), cyclohexane (16%), and CH_2Cl_2 (no reaction). While tertiary aliphatic amines were effective, *N,N*-dimethylaniline, pyridine, and K_2CO_3 were not. In place of phosphate, acetate and carbonate did not function as a leaving group, but the use of a chloride gave **2a** in 45% yield. Some phosphane-free palladium complexes, such as $PdCl_2$ (61% yield), $PdCl_2(PhCN)_2$ (64%), and $Pd(acac)_2$ (40%) were active. When the reaction given in Equation (1) was carried out for 40 h, the product yield increased to 73%.

The reaction was also appplicable to various derivatives of **1** (Table 1). Altering the steric character of an alkyl substituent at the acetylenic carbon atom had little effect on the efficiency of the reaction (Table 1, entries 1–3). However, substitution with trimethylsilyl and H resulted in no observable products, as evidenced by GC and TLC, although the starting materials were completely consumed. The substitution of a phenyl group gave the expected product in only 17% yield, along with a large variety of impurities (data not shown). The substitution of a butyl group at the olefinic carbon atom, as in **1e**, gave **2e** in 80% yield (Table 1, entry 4). The stereochemistry of the starting material **1e** was exclusively *E*, but the products obtained were a 2:1 mixture of *E* and *Z* isomers. The reaction of **1e** and **1f** gave the same product **2e**, indicating that the reaction proceeds via a common intermediate (Table 1, entries 4 and 5). Tricyclic lactones **2i** and **2j** were produced in high yield from a cyclic phosphonate (Table 1, entries 8 and 9).

Scheme 2 shows the proposed reaction mechanism. Reaction of **1** with Pd^0 gives a π-allyl palladium complex **3**, in which the insertion of CO followed by deprotonation takes place to generate the ketene **5**. Oxidative cyclization of **5** at a Pd^0 center gives the metallacycle **6**. The insertion of CO[11] in **6**

Table 1: Pd-catalyzed reaction of 2-propargylallyl phosphates with CO.[a]

Entry	Allyl phosphate	Product	Yield [%][b]
	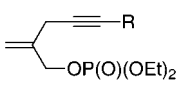	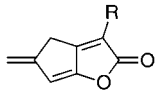	
1	**1b** (R = Bu)	**2b**	73
2	**1c** (R = Cy)	**2c**	94
3	**1d** (R = *t*Bu)	**2d**	87
4	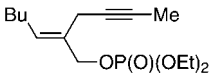 **1e**	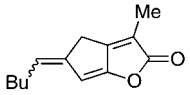 **2e**	80 (*Z*/*E* = 2/1)
5[c]	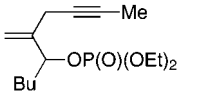 **1f**	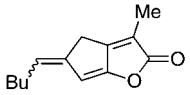 **2e**	88 (*Z*/*E* = 2/1)
6	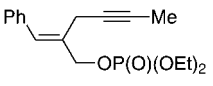 **1g**	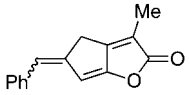 **2g**	50 (*Z*/*E* = 1/1)
7	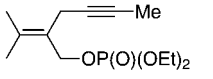 **1h**	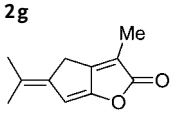 **2h**	73
8[c]	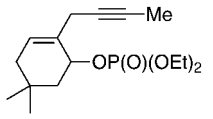 **1i**	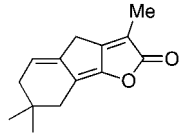 **2i**	72
9[c,d]	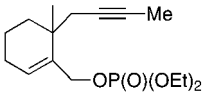 **1j**	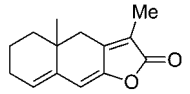 **2j**	64

[a] Reaction conditions: substrate (0.5 mmol), $[\{(\eta^3\text{-}C_3H_5)PdCl\}_2]$ (0.01 mmol), Cy_2NMe (1 mmol), CO (1 atm), THF (2 mL) at 80°C for 12 h. [b] Yields of isolated products. The ratio in the parentheses was determined by NMR analysis. [c] 0.025 mmol of catalyst was used. [d] Reaction time 40 h.

followed by reductive elimination gives the final product **2**. An alternative mechanism, which does not involve the intermediacy of ketene **5**, should also be considered. Here, complex **4** undergoes carbometalation to give the vinyl palladium complex **7**, in which CO is inserted to give an acyl complex **8**. The cyclization of **8** gives the π-allyl palladium complex **9**,[12] which is then deprotonated to give the final product **2**.[13] The loss of stereochemistry at the olefinic part in the starting phosphonates is rationalized by the formation of π-allyl palladium complex **3** (Table 1, entries 4 and 6). The reaction of **1e** and **1f** gave the same product **2e**, indicating that both reactions proceed via the π-allyl palladium complex **3**.

In summary, the present reaction provides a new method for the construction of highly unsaturated bicyclic lactones,[14] which are difficult to access by conventional methods, by the Pd-catalyzed carbonylation of 2-proparygylallyl phosphonates. The reaction proceeds smoothly even under mild

 © 2003 Wiley-VCH Verlag GmbH & Co. KGaA, Weinheim 1433-7851/03/4212-1398 $ 20.00+.50/0

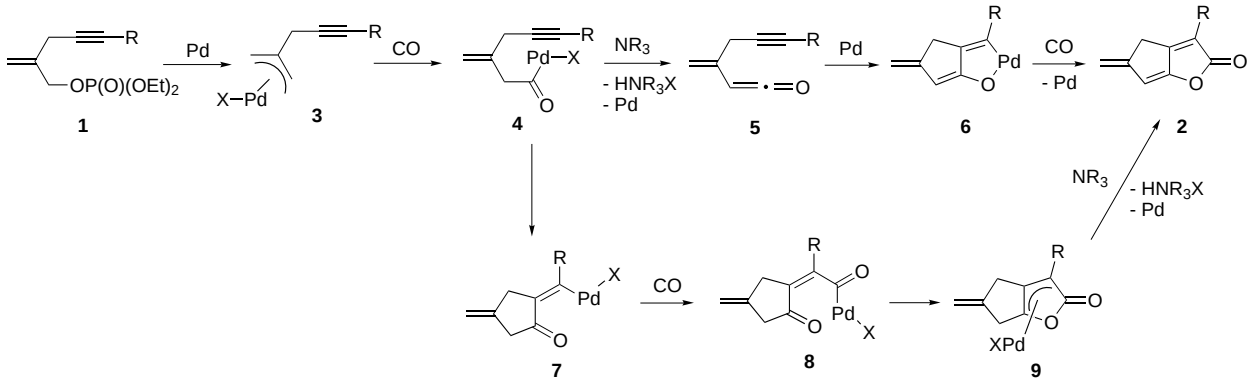

Scheme 2. Proposed reaction mechanism for the formation of **2**.

reaction conditions. Studies of the synthetic applications of these compounds and the reaction mechanism are currently underway.

Experimental Section

Full procedures and chracterization data are given in the Supporting Information.

Representative procedure [Eq. (1)]: A 50-mL resealable Schlenk tube was flame-dried under a stream of nitrogen. The flask was charged with **1a** (0.5 mmol, 123 mg), $[\{(\pi\text{-}C_3H_5)PdCl\}_2]$ (0.01 mmol, 3.7 mg), dicyclohexylmethylamine (1.0 mmol, 0.2 mL), and THF (2 mL), and a three-way stopcock, which was connected to a vacuum line and a balloon filled with carbon monoxide, was attached to the flask. The system was carefully evacuated and refilled with carbon monoxide four times and then filled with carbon monoxide (1 atm). Finally the system was sealed and immersed in an oil bath at 80 °C. After 40 h, the flask was removed from the oil bath and allowed to cool for 1 h, after which the CO was released. The contents were transferred to a 100-mL round-bottomed flask and volatiles were removed in vacuo. The residue was subjected to column chromatography on silica gel (eluent; hexane/EtOAc = 20/1) to give **2a** (54 mg, 73 % yield) as a white solid. Mp 69–73 °C (hexane); $R_f = 0.47$ (hexane/EtOAc = 3/1); ^{1}H NMR (270 MHz, $CDCl_3$, TMS): $\delta = 1.95$ (s, 3H), 3.31 (m, 2H), 5.09 (s, 1H), 5.24 (s, 1H), 6.07 ppm (s, 1H); ^{13}C NMR (68 MHz, $CDCl_3$): $\delta = 9.2$, 29.3, 108.6, 112.2, 113.7, 148.2, 157.8, 159.8, 173.4 ppm; IR (KBr): $\tilde{\nu} = 3524$ w, 2936 w, 1944 w, 1922 w, 1770 s, 1660 s, 1614 s, 1498 w, 1406 m, 1374 m, 1306 m, 1246 w, 1232 m, 1184 m, 1106 w, 1050 w, 972 m, 918 w, 858 s, 748 m, 722 w, 674 w, 660 w, 646 cm^{-1} w; MS: *m*/*z* (%): 148 (80) [M^+], 120 (26), 91 (100), 67 (49), 65 (15), 53 (25), 51 (24), 50 (16); elemental analysis calcd (%) for $C_9H_8O_2$: C 72.96, H 5.44; found: C 72.72, H 5.55.

Received: November 21, 2002 [Z50602]

Keywords: carbonylation · cyclization · homogeneous catalysis · lactones · palladium

[1] E. Negishi, M. Kotora, *Tetrahedron* **1997**, *53*, 6707.
[2] Y. S. Rao, *Chem. Rev.* **1976**, *76*, 625; S. V. Ley, L. R. Cox, G. Meek, *Chem. Rev.* **1996**, *96*, 423; I. Collins, *J. Chem. Soc. Perkin Trans. 1* **1998**, 1869; I. Collins, *J. Chem. Soc. Perkin Trans. 1* **1999**, 1377.
[3] N. Chatani, T. Morimoto, Y. Fukumoto, S. Murai, *J. Am. Chem. Soc.* **1998**, *120*, 5335.
[4] N. Chatani, M. Tobisu, T. Asaumi, Y. Fukumoto, S. Murai, *J. Am. Chem. Soc.* **1999**, *121*, 7160; M. Tobisu, N. Chatani, T. Asaumi, K. Amako, Y. Ie, Y. Fukumoto, S. Murai, *J. Am. Chem. Soc.* **2000**, *122*, 12663.
[5] For applications to the construction of lactams, see: N. Chatani, T. Morimoto, A. Kamitani, Y. Fukumot, S. Murai, *J. Organomet. Chem.* **1999**, *579*, 177; N. Chatani, M. Tobisu, T. Asaumi, S. Murai, *Synthesis* **2000**, 925; A. Göbel, W. Imhof, *Chem. Commun.* **2001**, 593.
[6] The reaction of diphenylketene with alkynes in the presence of a stoichiometric amount of $Fe(CO)_5$ resulted in a [2+2+1] cycloaddition, leading to cyclopentediones, in which the ketene carbonyl group had not been incorporated. K. Kinugawa, T. Agawa, *Organomet. Chem. Synth.* **1972**, *1*, 427.
[7] T. T. Tidwell, *Ketenes*, Wiley, New York, **1995**; T. T. Tidwell, *Acc. Chem. Res.* **1990**, *23*, 273.
[8] S. Torii, H. Okumoto, M. Sadakane, A. K. M. A. Hai, H. Tanaka, *Tetrahedron Lett.* **1993**, *34*, 6553; H. Tanaka, A. K. M. A. Hai, M. Sadakane, H. Okumoto, S. Torii, *J. Org. Chem.* **1994**, *59*, 3040. See also: Z. Zhou, H. Alper, *J. Org. Chem.* **1996**, *61*, 1256; C. S. Cho, J. C. Park, L. H. Jiang, T.-J. Kim, S. C. Shim, M. C. Kim, *Bull. Korean Chem. Soc.* **2000**, *21*, 541.
[9] G. Wu, I. Shimoyama, E. Negishi, *J. Org. Chem.* **1991**, *56*, 6506.
[10] All new compounds were characterized by NMR, IR, mass spectral data, and by elemental analyses or high-resolution mass spectra. See Supporting Information.
[11] We do not know whether CO insertion takes place into a C–Pd bond or a O–Pd bond in complex **6**.
[12] Related Pd or Rh complexes were proposed. C. Coperet, T. Sugihara, G. Wu, L. Shimoyama, E. Negishi, *J. Am. Chem. Soc.* **1995**, *117*, 3422; B. Van den Hoven, B. El Ali, H. Alper, *J. Org. Chem.* **2000**, *65*, 4131.
[13] An alternative path, as shown below, also exists. See ref. [9].

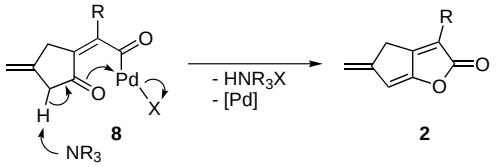

[14] Negishi et al. reported a new synthesis of polyunsaturated lactones by a carbometalation–carbonylation cascade, which is closely related to our system. T. Sugihara, C. Coperet, Z. Owczarczyk, L. Harring, E. Negishi, *J. Am. Chem. Soc.* **1994**, *116*, 7923.

 © 2003 Wiley-VCH Verlag GmbH & Co. KGaA, Weinheim 1433-7851/03/4212-1399 $ 20.00+.50/0

Pt-Capped C-Rich Molecular Rods

Luminescent Platinum(II) Terpyridyl-Capped Carbon-Rich Molecular Rods—An Extension from Molecular- to Nanometer-Scale Dimensions**

Vivian Wing-Wah Yam, Keith Man-Chung Wong, and Nianyong Zhu*

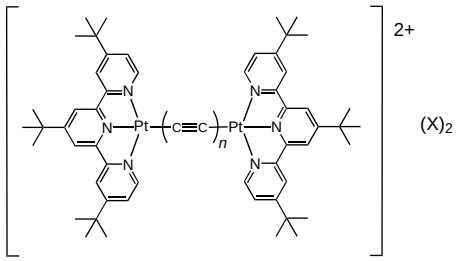

1: $n = 1$, X = OTf
2: $n = 2$, X = OTf
3: $n = 4$, X = PF_6

There has been a growing interest in the chemistry of carbon-rich metal-containing systems, in particular those of metal-containing polyynes. Examples include the transition-metal end-capped [M]-$(C{\equiv}C)_n$-[M] systems ([M] = Re(Cp*)(NO)-(PPh_3),[1] *trans*-$[Pt(C_6F_5)(PR_3)_2]$,[2] Fe(Cp*)(dppe),[3] $Fe(Cp^*)(CO)_2$,[4] Ru(Cp)$(PPh_3)_2$,[5] $Mn(dppe)_2I$,[6] Re(tBu$_2$-bpy)$(CO)_3$,[7] Au(PCy_3)[8]). Some of them have recently been shown to display interesting luminescence behavior.[7,8] Despite platinum-containing polyynes being known, most of them are confined to platinum phosphane complexes, with corresponding studies on the nitrogen donor analogues unexplored. These, together with the numerous studies on the luminescence behavior of platinum(II)–polypyridine systems,[9,10] in particular those of the platinum(II)–terpyridyl complexes,[9f,10] and our recent report on the novel solvatochromic properties of platinum(II)–terpyridyl complexes[11] as well as our interest in luminescent carbon-rich molecular materials,[12] have prompted us to investigate the luminescence properties of the [Pt]-$(C{\equiv}C)_n$-[Pt] system of various alkynyl chain lengths with platinum(II)–terpyridyl groups as the transition-metal end-capped termini. Herein we report the synthesis, electronic absorption, photophysical properties, and structural characterization of a series of alkynyl-bridged dinuclear platinum(II)–terpyridyl complexes, [Pt(tBu$_3$-tpy)-$(C{\equiv}C)_n$Pt(tBu$_3$-tpy)](X)$_2$ (**1**–**3**; tBu$_3$-tpy = 4,4′,4″-tri-*tert*-butyl-2,2′:6′,2″-terpyridine). The bulky trisubstituted terpyridine ligand was chosen to eliminate the influence of Pt···Pt and π–π interactions on the luminescence behavior. The luminescence behavior together with the structure–property relationship of the complexes have been studied.

Figure 1 depicts the structures of the complex cations of **1**–**3**. In all cases, the platinum(II) metal center adopts an essentially square-planar geometry with slight distortion due to the coordination constraints imposed by the terpyridyl ligand (N1-Pt1-N3 160.2–160.4°; N1-Pt1-N2 and N2-Pt1-N3 79.8–80.6°). The two platinum(II)–terpyridyl ends are connected by the alkynyl chain in a linear [Pt]-$(C{\equiv}C)_n$-[Pt] fashion ($n = 1$, 2, and 4) with Pt-C≡C angles in the range of 173.8–178.5°. The Pt–C (2.026 Å in **1**; 1.934–1.935 Å in **2** and **3**) and C≡C (1.118 Å in **1**; 1.191–1.210 Å in **2** and **3**) bond lengths are comparable to that found in the related mononuclear counterpart [Pt(tBu$_3$-tpy)(C≡C-C≡CH)](OTf)[11] and in other platinum(II)–alkynyl systems.[2,10c] Upon increasing the $(C{\equiv}C)_n$ unit, the dimensions of these rigid rodlike complexes are found to extend from the molecular scale to nanoscale; the separation between the two platinum(II) termini ranges from 5.16 Å in **1** to 7.71 Å in **2** and 12.83 Å in **3**. Unlike other related platinum(II) systems, no significant Pt–Pt or π–π interaction is observed from the crystal packing of **1**–**3** owing to the presence of the sterically bulky *tert*-butyl groups on the terpyridyl ligands, which hinder the molecules from coming into close proximity with each other. Similar observations have been reported in other 4,4′,4″-tri-*tert*-butyl-2,2′:6′,2″-terpyridine-containing platinum(II) complexes.[11] In contrast to **2** and **3** in which the square planes about the platinum(II)–terpyridyl termini are essentially coplanar, the two platinum(II)–terpyridyl moieties in **1** are twisted with respect to each other with an interplanar angle of 35.83°. This may be rationalized by the fact that the length of the C_2 carbon bridge in **1**, unlike the C_4 and C_8 bridges in **2** and **3**, respectively, is rather short and a slight twisting of the square planes containing the two platinum(II)–terpyridyl units may help to relieve the steric strain arising from the coplanar arrangement of the two adjacent platinum(II)–terpyridyl units.

Complexes **1**–**3** show intense absorptions at about 308–342 nm and 428–522 nm in acetonitrile at 298 K (Figure 2) and their photophysical data are summarized in Table 1. With reference to previous spectroscopic studies on the mononuclear [Pt(tBu$_3$-tpy)(C≡C–C≡CH)](OTf)[11] and related complexes,[10] the high-energy structured absorption bands at about 308–342 nm are ascribed to intra-ligand (IL) π→π*[$(C{\equiv}C)_n$] and π→π*(tBu$_3$-tpy) transitions of the alkynyl bridge and the substituted terpyridine ligand, while the low-energy band in the visible region is assigned to a [dπ(Pt)→π*(tBu$_3$-tpy)] metal-to-ligand charge transfer (MLCT) transition, probably mixed with an [π(C≡C)→π*(tBu$_3$-tpy)] alkynyl-to-terpyridine ligand-to-ligand charge transfer

[*] Prof. V. W.-W. Yam, Dr. K. M.-C. Wong, Dr. N. Zhu
Centre for Carbon-Rich Molecular and Nano-Scale Metal-Based Materials Research, Department of Chemistry and HKU-CAS Joint Laboratory on New Materials
The University of Hong Kong
Pokfulam Road, Hong Kong (P. R. China)
Fax: (+852) 2857-1586
E-mail: wwyam@hku.hk

[**] V.W.-W.Y. acknowledges support from The University of Hong Kong Foundation for Educational Development and Research Limited, and the receipt of a Croucher Senior Research Fellowship from the Croucher Foundation. This work has been supported by a CERG Grant from the Research Grants Council of Hong Kong Special Administrative Region, China (Project No. HKU 7123/00P). K.M.-C.W. and N.Z. acknowledge the receipt of University Postdoctoral Fellowships from The University of Hong Kong.

 © 2003 Wiley-VCH Verlag GmbH & Co. KGaA, Weinheim 1433-7851/03/4212-1400 $ 20.00+.50/0

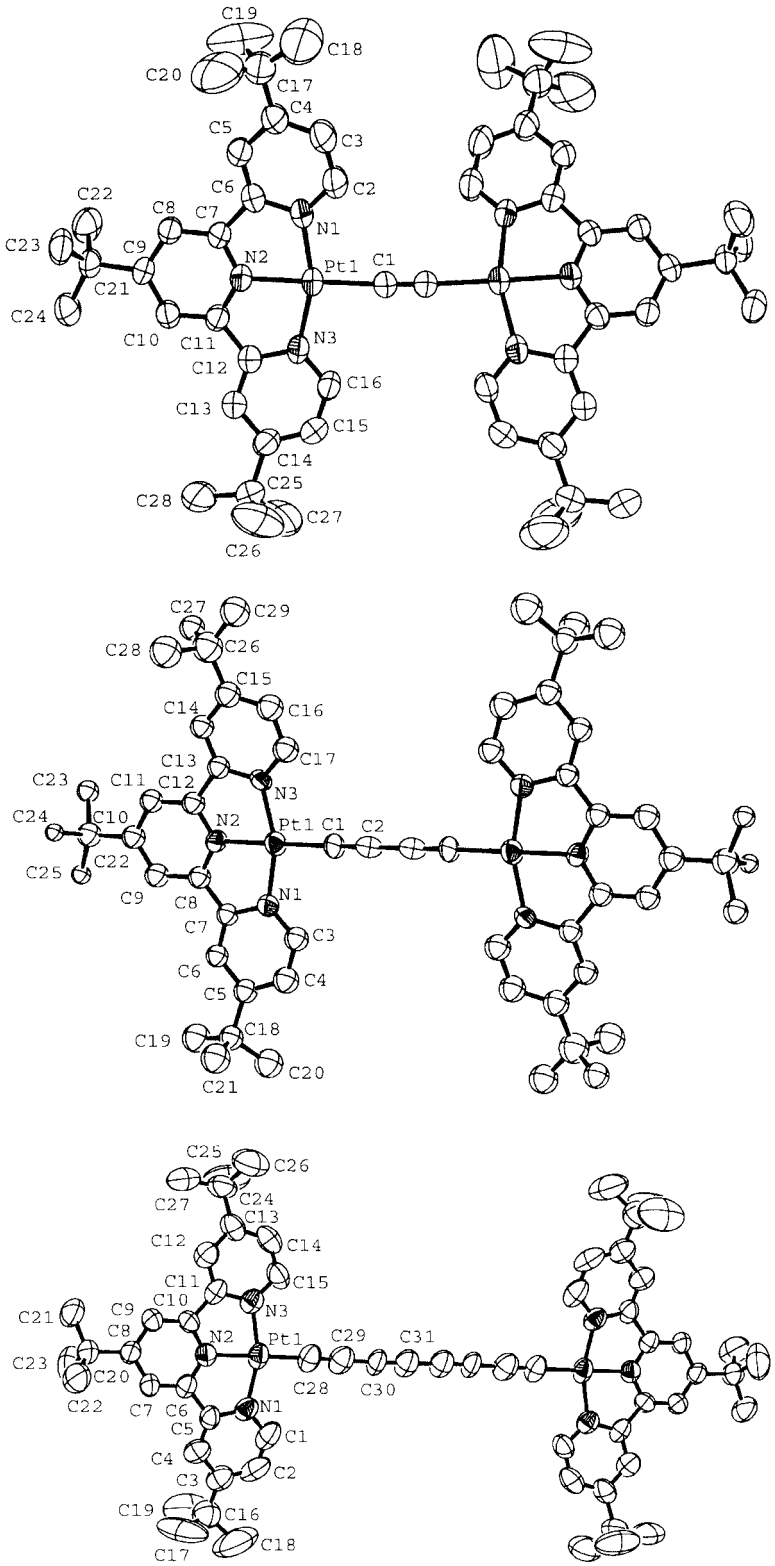

Figure 1. Structures of the complex cations of **1** (top), **2** (middle), and **3** (bottom). Hydrogen atoms are omitted for clarity. Thermal ellipsoids are drawn at the 50% probability level.

(LLCT) character. Interestingly, the low-energy absorption band of **2** shows an extinction coefficient that is almost double that of the 382–400 nm band of the related mononuclear complex, [Pt(tBu$_3$-tpy)(C≡C–C≡CH)](OTf). The low-energy absorption band was found to shift to higher energy upon going from **1** (484–522 nm) to **2** (436–466 nm) and **3** (428–452 nm) with an increasing number of C≡C units. This is rather unusual as one would have expected a shift to lower energy with increasing C≡C units as is commonly found in organic polyynes[13] and in other metal–alkynyl systems.[8] The blue shift observed on going from **1** to **2** to **3** is likely to be a result of the greater stabilization of the dπ orbital on platinum(II) upon increasing the length of the conjugated alkynyl chain. Two effects may account for the observed trend. 1) The π-donor ability exhibited by the alkynyl chain, which gives rise to a filled–filled pπ–dπ overlap. 2) The π-accepting ability of the alkynyl chain, which results in a dπ–π* interaction. Given the similar σ-donating ability of the monoynyl, diynyl, and tetraynyl bridges, the π-donor orbital energy of the $(C{\equiv}C)_n$ bridge should follow the order: $n = 4 > 2 > 1$. Despite the fact that a better energy match between the dπ(Pt) and the $\pi(C{\equiv}C)_n$ orbitals upon increasing the C≡C chain length is expected to raise the dπ(Pt) orbital energy, the decreased overlap integral between the dπ(Pt) and the $\pi(C{\equiv}C)_n$ orbitals resulting from the delocalizaion of electron density across the C≡C unit would, on the other hand, lead to a net overall decrease in the dπ(Pt) orbital energy, rendering the dπ(Pt) orbital on **3**, which has the longest $(C{\equiv}C)_n$ unit, lowest-lying in energy, and hence giving rise to the highest MLCT absorption energy. An alternative rationale arises from the increased π-accepting ability of the alkynyl unit upon increasing the $(C{\equiv}C)_n$ chain, that is, the $\pi^*(C{\equiv}C)_n$ orbital energy follows the order: $n = 4 < 2 < 1$, which would stabilize the dπ(Pt) orbital through dπ–π overlap. The higher MLCT energy in **3** is likely to be a result of the greater stabilization of the dπ(Pt) orbital energy. Similar observations have been reported by us in the related rhenium(I)–alkynyl system.[12f]

Upon excitation at $\lambda > 400$ nm, **1**–**3** both in the solid state and in solution exhibit intense luminescence at about 550–625 nm (Table 1). With reference to the spectroscopic studies on other platinum(II)–terpyridyl systems[10] and the occurrence of the emission at similar energies to that found in the related mononuclear complex [Pt(tBu$_3$-tpy)(C≡C-C≡CH)](OTf),[11] the origin of the luminescence is assigned as derived from states of predominantly ^{3}MLCT [dπ(Pt)→π*(tBu$_3$-tpy)] character, probably mixed with some intraligand ^{3}IL [π→π*$(C{\equiv}C)_n$], and ligand-to-ligand charge transfer ^{3}LLCT [π$(C{\equiv}C)_n$ →π*(tBu$_3$-tpy)] character. The excitation spectra of **1**–**3** (Figure 3a) show excitation bands at about 425–525 nm, which closely resemble that of the low-energy MLCT bands in

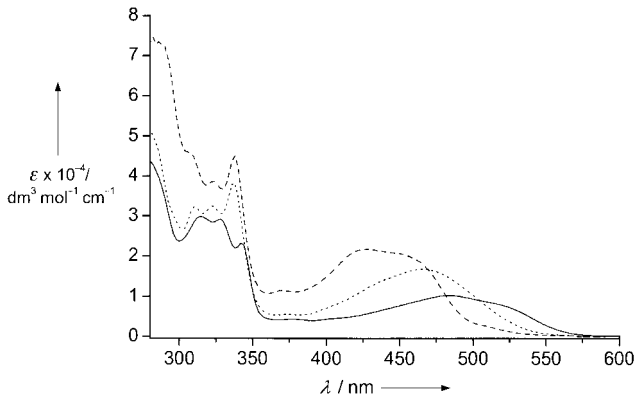

Figure 2. Electronic absorption spectra of **1** (——), **2** (••••), and **3** (-----) in acetonitrile at room temperature.

Table 1: Photophysical data for **1**–**3**.

Complex	Medium (T [K])	Absorption λ_{max} [nm] (ε_{max} [dm^3 mol^{-1} cm^{-1}])	Emission λ_{max} [nm] (τ_o [μs])
1	MeCN (298)	314 (29820), 328 (29180), 342 (23155), 484 (10175), 522 (7615)	625
	solid (298)		615 (0.2)
	solid (77)		604 (2.6) {1270}[a]
	glass (77)		572 (8.1) {1250}[a]
2	MeCN (298)	310 (32210), 322 (32475), 338 (38110), 436 (13510), 466 (16670)	625
	solid (298)		606 (0.2)
	solid (77)		604 (1.1) {1270}[a]
	glass (77)		550 (6.5) {1230}[a]
3	MeCN (298)	308 (45705), 324 (38590), 338 (44980), 428 (21690), 452 (20480)	589 {2050}[a]
	solid (298)		605 (0.2) {2020}[a]
	solid (77)		607 (1.0) {2060}[a]
	glass (77)		582 (1.1) {2100}[a]

[a] Vibrational progressional spacings [cm^{-1}].

their respective electronic absorption spectra, further supportive of an assignment of a ^{3}MLCT band mixed with some of ^{3}IL/^{3}LLCT character. The emission band of **3** is vibronically structured with vibrational progressional spacings of about 2052 cm^{-1}; such spacings are typical of a ν(C≡C) stretch in the ground state. This observation indicates the involvement of the alkynyl bridge, and the possible mixing of a ^{3}LLCT [π(C≡C)$_n$→π*(tBu$_3$-tpy)] state and an ^{3}IL [π→π*(C≡C)$_n$] state into the ^{3}MLCT [dπ(Pt)→π*(tBu$_3$-tpy)] character. Similarly, the emission spectra of **1** and **2** in glass at 77 K exhibit vibronically structured bands with vibrational progressional spacings of about 1250 cm^{-1}, typical of the ν(C=C) and ν(C=N) stretching modes of the terpyridyl ligand. It is likely that the origin of the emission has in addition to a ^{3}MLCT origin, mixing of a ^{3}LLCT and ^{3}IL character, with the mixing being more important in **3** with the increasing π conjugation in the C_8 chain. The observation of a Huang–Rhys factor of less than 1 in the emission spectra of **1** and **2** in butyronitrile glass at 77 K is in line with an assignment of predominantly ^{3}MLCT character. Similar to that observed in the electronic absorption spectroscopy, a blue shift of the emission band was observed upon going from **1** (572 nm) to **2** (550 nm) in butyronitrile glass at 77 K (Figure 3b). Arguments similar to that discussed for the trend in the electronic absorption energy have been made to explain the observed trend in the emission energies of **1** and **2**. On the other hand, the emission spectrum of **3** in butyronitrile glass at 77 K shows a vibronically structured emission band at about 582 nm with vibrational progressional spacings of about 2100 cm^{-1}, typical of the ν(C≡C) stretch in the ground state. It is likely that upon increasing the π conjugation of the C_n chain, the origin of the emission changes in character, with an increasing contribution from the ^{3}IL [π→π*(C≡C)$_n$] excited state, leading to an emission that is predominantly ^{3}IL in character.

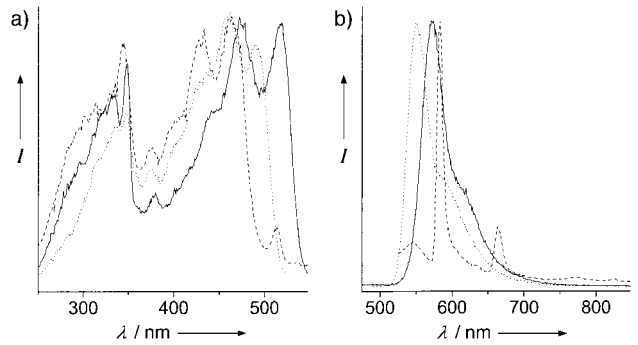

Figure 3. a) Excitation and b) emission spectra of **1** (——), **2** (••••), and **3** (-----) in butyronitrile at 77 K. I = normalized emission intensity.

Experimental Section

Complexes **1** and **2** were synthesized by the reaction of [Pt(tBu$_3$-tpy)(MeCN)](OTf)$_2$ with TMS-C≡CH and TMS-C≡C–C≡C-TMS, respectively, in the presence of KF in methanol. Orange-red crystals of **1** and **2** were obtained from an *n*-hexane/acetonitrile mixture after column chromatography on silica gel by using dichloromethane–acetone as eluent. Complex **3** was prepared by the oxidative coupling reaction of [Pt(tBu$_3$-tpy)(C≡C–C≡CH)](OTf)[11] in the presence of a catalytic amount of copper(II) acetate in pyridine. Metathesis reaction with NH_4PF_6, followed by column chromatography on silica gel, and recrystallization from slow diffusion of *n*-hexane into a solution of **3** in dichloromethane yielded the pure forms of **3** as orange-red crystals.

1: ^{1}H NMR (400 MHz, CD_3CN, 298 K, relative to Me_4Si): $\delta = 9.36$ (d with Pt satellites, 4H; terpyridyl H), 8.48 (s, 4H; terpyridyl H), 8.42 (d, 4H; terpyridyl H), 7.78 (dd, 4H; terpyridyl H), 1.58 (s, 18H; *tert*-butyl H), 1.48 ppm (s, 36H; *tert*-butyl H); ^{13}C NMR (125.8 MHz, CD_3CN, 298 K, relative to Me_4Si): $\delta = 167.6$, 167.5, 160.1, and 55.3 (quaternary C on terpyridine), 154.9, 126.7, 124.1, and 122.3 (tertiary C on terpyridine), 113.4 (Pt–C), 38.1 and 37.1 (quaternary C on *tert*-butyl group), 30.7 and 30.4 ppm (primary C on *tert*-butyl group); positive ESI-MS: m/z 1365 [M−OTf]$^+$, 609 [M−2OTf]$^{2+}$; elemental analyses calcd (%) for $C_{58}H_{70}F_6N_6O_6Pt_2S_2 \cdot 1.5\,CH_2Cl_2$: C 43.50, H 4.45, N 5.12; found: C 43.50, H 4.50, 5.16.

2: ^{1}H NMR (400 MHz, CD_3CN, 298 K, relative to Me_4Si): $\delta = 9.04$ (d with Pt satellites, 4H; terpyridyl H), 8.36 (s, 4H; terpyridyl H), 8,32 (d, 4H; terpyridyl H), 7.80 (dd, 4H; terpyridyl H), 1.54 (s, 18H; *tert*-butyl H), 1.46 ppm (s, 36H; *tert*-butyl H); ^{13}C NMR (125.8 MHz,

 © 2003 Wiley-VCH Verlag GmbH & Co. KGaA, Weinheim 1433-7851/03/4212-1402 $ 20.00+.50/0

CD_3CN, 298 K, relative to Me_4Si): $\delta = 168.5$, 168.1, 159.9, and 155.3 (quaternary C on terpyridine), 155.0, 127.0, 124.4, and 122.5 (tertiary C on terpyridine), 91.1 (Pt−*C*≡C−), 87.4 (Pt−C≡*C*−), 38.1 and 37.2 (quaternary C on *tert*-butyl group), 30.6 and 30.3 ppm (primary C on *tert*-butyl group); positive ESI-MS: *m*/*z* 1389 $[M-OTf]^+$, 620 $[M-2OTf]^{2+}$; elemental analyses calcd (%) for $C_{60}H_{70}F_6N_6O_6Pt_2S_2\cdot CH_2Cl_2$: C 45.10, H 4.44, N 5.18; found: C 45.36, H 4.48, N 5.01.

3: ^{1}H NMR (400 MHz, CD_3CN, 298 K, relative to Me_4Si): $\delta = 8.84$ (d with Pt satellites, 4H; terpyridyl H), 8.36 (s, 4H; terpyridyl H), 8.32 (d, 4H; terpyridyl H), 7.76 (dd, 4H; terpyridyl H), 1.54 (s, 18H; *tert*-butyl H), 1.46 ppm (s, 36H; *tert*-butyl H); ^{13}C NMR (125.8 MHz, CD_3CN, 298 K, relative to Me_4Si): $\delta = 169.4$, 168.6, 159.7 and 155.4 (quaternary C on terpyridine), 154.8, 127.2, 124.6 and 122.7 (tertiary C on terpyridine), 97.2 (Pt−*C*≡C−C≡C−), 87.1 (Pt−C≡*C*−C≡C−), 64.5 (Pt−C≡C−*C*≡C−), 59.3 ppm (Pt−C≡C−C≡*C*−); positive ESI-MS: *m*/*z* 1434 $[M-PF_6]^+$, 645 $[M-2PF_6]^{2+}$; elemental analyses calcd for $C_{62}H_{70}F_{12}N_6P_2Pt_2$: C 47.15, H 4.44, N 5.32; found: C 47.19, H 4.41, N 4.94.

Crystal data for **1**·$(C_2H_5)_2O$: $C_{58}H_{70}F_6N_6O_6Pt_2S_2\cdot C_4H_{10}O$; $M_r = 1589.62$, crystal dimensions $0.4\times0.1\times0.05$ mm^3, monoclinic, space group *C*2/*c*, $a = 24.224(5)$, $b = 17.755(4)$, $c = 16.529(3)$ Å, $\beta = 108.25(3)°$, $V = 6751(2)$ Å^3, $Z = 4$, $\rho_{calcd} = 1.564$ g cm^{-3}, $\mu(Mo_{K\alpha}) = 4.271$ mm^{-1}, $F(000) = 3168$, $T = 293$ K; $R = 0.0308$, $wR = 0.0756$ for 5435 reflections with $I > 2\sigma(I)$. MAR diffractometer, $Mo_{K\alpha}$ radiation ($\lambda = 0.71073$ Å); collection range $2\theta_{max} = 50.69°$ with 2° oscillation step of φ, 420 s exposure time and scanner distance at 120 mm; 88 images were collected. For **2**·2$(CH_3)_2CO$: $C_{60}H_{70}F_6N_6O_6Pt_2\cdot S_2\cdot 2C_3H_6O$; $M_r = 1655.68$, crystal dimensions $0.2\times0.1\times0.02$ mm^3, monoclinic, space group $P2_1/c$, $a = 16.348(3)$, $b = 10.540.(2)$, $c = 20.594(4)$ Å, $\beta = 92.72(3)°$, $V = 3544.5(12)$ Å^3, $Z = 2$, $\rho_{calcd} = 1.551$ g cm^{-3}, $\mu(Mo_{K\alpha}) = 4.072$ mm^{-1}, $F(000) = 1652$, $T = 301$ K; $R = 0.0489$, $wR = 0.1088$ for 3837 reflections with $I > 2\sigma(I)$. MAR diffractometer, $Mo_{K\alpha}$ radiation ($\lambda = 0.71073$ Å); collection range $2\theta_{max} = 49.82$ ° with 2° oscillation step of φ, 1200 s exposure time and scanner distance at 120 mm; 53 images were collected. For **3**·4$(CH_3)_2CO$: $C_{62}H_{70}F_{12}N_6P_2Pt_2\cdot 4C_3H_6O$; $M_r = 1811.67$, crystal dimensions $0.3\times0.1\times0.05$ mm^3, monoclinic, space group $C2_1/c$, $a = 14.220(3)$, $b = 14.158(3)$, $c = 20.329(4)$ Å, $\beta = 95.44(3)°$, $V = 4074.3(14)$ Å^3, $Z = 2$, $\rho_{calcd} = 1.477$ g cm^{-3}, $\mu(Mo_{K\alpha}) = 3.544$ mm^{-1}, $F(000) = 1812$, $T = 301$ K; $R = 0.0403$, $wR = 0.0916$ for 4637 reflections with $I > 2\sigma(I)$. MAR diffractometer, $Mo_{K\alpha}$ radiation ($\lambda = 0.71073$ Å); collection range $2\theta_{max} = 50.66°$ with 2° oscillation step of φ, 900 s exposure time and scanner distance at 120 mm; 80 images were collected. CCDC-198503 (**1**·$(C_2H_5)_2O$), CCDC-198504 (**2**·2$(CH_3)_2CO$), and CCDC-198505 (**3**·4$(CH_3)_2CO$) contain the supplementary crystallographic data for this paper. These data can be obtained free of charge via www.ccdc.cam.ac.uk/conts/retrieving.html (or from the Cambridge Crystallographic Data Centre, 12, Union Road, Cambridge CB2 1EZ, UK; fax: (+44) 1223-336-033; or deposit@ccdc.cam.ac.uk).

Received: November 25, 2002 [Z50627]

Keywords: alkynes · luminescence · molecular rods · N ligands · platinum

[1] a) R. Dembinski, B. Bartik, T. Bartik, M. Jaeger, J. A. Gladysz, *J. Am. Chem. Soc.* **2000**, *122*, 810; b) W. E. Meyer, A. J. Amoroso, C. R. Horn, M. Jaeger, J. A. Gladysz, *Organometallics* **2001**, *20*, 1115.

[2] a) T. B. Peters, J. C. Bohling, A. M. Arif, J. A. Gladysz, *Organometallics* **1999**, *18*, 3261; b) W. Mohr, J. Stahl, F. Hampel, J. A. Gladysz, *Inorg. Chem.* **2001**, *40*, 3263; c) J. Stahl, J. C. Bohling, E. B. Bauer, T. B. Peters, W. Mohr, J. M. Martín-Alvarez, F. Hampel, J. A. Gladysz, *Angew. Chem.* **2002**, *114*, 1951; *Angew. Chem. Int. Ed.* **2002**, *41*, 1871.

[3] a) F. Paul, C. Lapinte, *Coord. Chem. Rev.* **1998**, *178–180*, 431; b) N. Le Narvor, C. Lapinte, *J. Chem. Soc. Chem. Commun.* **1993**, 357; c) N. Le Narvor, L. Toupet, C. Lapinte, *J. Am. Chem. Soc.* **1995**, *117*, 7129.

[4] M. Akita, M. C. Chung, A. Sakurai, S. Sugimoto, M. Terada, M. Tanaka, Y. Moro-oka, *Organometallics* **1997**, *16*, 4882.

[5] a) M. I. Bruce, *Coord. Chem. Rev.* **1997**, *166*, 91; b) M. I. Bruce, P. J. Low, K. Costuas, J. F. Halet, S. P. Best, G. A. Heath, *J. Am. Chem. Soc.* **2000**, *122*, 1949.

[6] S. Kheradmandan, K. Heinze, H. W. Schmalle, H. Berke, *Angew. Chem.* **1999**, *111*, 2412; *Angew. Chem. Int. Ed.* **1999**, *38*, 2270.

[7] a) V. W. W. Yam, *Chem. Commun.* **2001**, 789; b) V. W. W. Yam, V. C. Y. Lau, K. K. Cheung, *Organometallics* **1995**, *14*, 2749; c) V. W. W. Yam, V. C. Y. Lau, K. K. Cheung, *Organometallics* **1996**, *15*, 1740.

[8] a) C. M. Che, H. Y. Chao, V. M. Miskowski, Y. Li, K. K. Cheung, *J. Am. Chem. Soc.* **2001**, *123*, 4985; b) W. Lu, H. F. Xiang, N. Zhu, C. M. Che, *Organometallics* **2002**, *21*, 2343.

[9] a) *Extended Linear Chain Compounds* (Ed.: J. S. Miller), Plenum, New York, **1982**; b) D. M. Roundhill, H. B. Gray, C. M. Che, *Acc. Chem. Res.* **1989**, *22*, 55; c) V. H. Miskowski, V. H. Houlding, *Coord. Chem. Rev.* **1991**, *111*, 145; d) C. W. Chan, L. K. Cheng, C. M. Che, *Coord. Chem. Rev.* **1994**, *132*, 87; e) H. Yersin, D. Donges, *Top. Curr. Chem.* **2001**, *214*, 82; f) D. R. McMillin, J. J. Moore, *Coord. Chem. Rev.* **2002**, *229*, 113.

[10] a) J. A. Bailey, M. G. Hill, R. E. Marsh, V. M. Miskowski, W. P. Schaefer, H. B. Gray, *Inorg. Chem.* **1995**, *34*, 4591; b) R. Büchner, C. T. Cunningham, J. S. Field, R. J. Haines, D. R. McMillin, G. C. Summerton, *J. Chem. Soc. Dalton Trans.* **1999**, 711; c) V. W. W. Yam, R. P. L. Tang, K. M. C. Wong, K. K. Cheung, *Organometallics* **2001**, *20*, 4476.

[11] V. W. W. Yam, K. M. C. Wong, N. Zhu, *J. Am. Chem. Soc.* **2002**, *124*, 6506.

[12] a) V. W. W. Yam, *Acc. Chem. Res.* **2002**, *35*, 555; b) V. W. W. Yam, K. K. W. Lo, K. M. C. Wong, *J. Organomet. Chem.* **1999**, *578*, 3; c) V. W. W. Yam, K. K. W. Lo, *Chem. Soc. Rev.* **1999**, *28*, 323; d) V. W. W. Yam, K. L. Cheung, L. H. Yuan, K. M. C. Wong, K. K. Cheung, *Chem. Commun.* **2000**, 1513; e) V. W. W. Yam, S. H. F. Chong, C. C. Ko, K. K. Cheung, *Organometallics* **2000**, *19*, 5092.

[13] a) R. Eastmond, T. R. Johnson, D. R. M. Walton, *Tetrahedron* **1972**, *28*, 4601; b) G. Schermann, T. Grösser, F. Hampel, A. Hirsch, *Chem. Eur. J.* **1997**, *3*, 1105.

 © 2003 Wiley-VCH Verlag GmbH & Co. KGaA, Weinheim 1433-7851/03/4212-1403 $ 20.00+.50/0

ABC Triblock Copolymers

Synthesis of Poly(*tert*-butyl acrylate)-*block*-Polystyrene-*block*-Poly(4-vinylpyridine) by Living Anionic Polymerization**

*Futian Liu and Adi Eisenberg**

Amphiphilic block copolymers, such as polystyrene-*b*-poly(acrylic acid) (PS-*b*-PAA) and polystyrene-*b*-poly(4-vinylpyridine) (PS-*b*-P4VP), can self-assemble to form various aggregates, which include vesicles, in aqueous solutions.[1] It was demonstrated recently that vesicles were formed from a mixture of PS-*b*-PAA (with a relatively short PAA block) and PS-*b*-P4VP (with a longer P4VP block) in which the PAA was on the inner interface of the vesicle while P4VP was on the outer interface.[2] Recently, our interests have focused on the study of triblock copolymers with the composition PAA-*b*-PS-*b*-P4VP, which contain the hydrophobic PS block between two hydrophilic blocks, and might yield the same types of aggregates as those formed with amphiphilic block copolymers. The precursor for PAA-*b*-PS-*b*-P4VP is PtBA-*b*-PS-*b*-P4VP (PtBA = poly(*tert*-butyl acrylate)). Many methods, such as living anionic polymerization,[3] group-transfer polymerization (GTP),[4] and atom-transfer radical polymerization (ATRP)[5] have been employed in the preparation of ABC triblock copolymers. However, the synthesis of the PtBA-*b*-PS-*b*-P4VP triblock is very difficult because of the significantly different reactivities of the monomers in that neither PtBA nor P4VP ions can initiate styrene polymerization, especially in anionic polymerization reactions, and because the PS is located between the PtBA and P4VP blocks. *tert*-Butylacrylate and 4-vinylpyridine are much more reactive than styrene; therefore, styrene has to be polymerized first, followed by the polymerization of either *tert*-butyl acrylate or 4-vinylpyridine.[6] This method was employed by Giebeler and Stadler[3d] to prepare a PS-*b*-PVP-*b*-PtBMA triblock in which styrene was polymerized first; however, the sequence in this triblock is different from that needed in our polymer. Techniques, such as GTP[4] and living cationic polymerization,[7] allow only the polymerization of monomers with similar chemistry, and consequently similar reactivities, and therefore are not suitable for the preparation this particular triblock copolymer. ATRP was used by Davis and Matyjaszewski[5a] in the preparation of ABC triblock copolymers, which includes an example of a similar polymer, PtBA-*b*-PMMA-*b*-P4VP (PMMA = polymethyl methacrylate), in which there is a hydrophobic PMMA sequence between hydrophilic blocks. This polymer was prepared with a 16% conversion of 4VP and a polydispersity of 1.43. Herein, we report a new method for preparing PtBA-*b*-PS-*b*-P4VP triblock copolymers starting with a PtBA macromonomer that contains a styrene end group. The macromonomer is used in the initiation of the anionic polymerization of styrene (st), followed by 4VP polymerization by sequential monomer addition (Figure 1). Polymers prepared by this method have a well-defined structure, low polydispersity, and quantitative conversion.

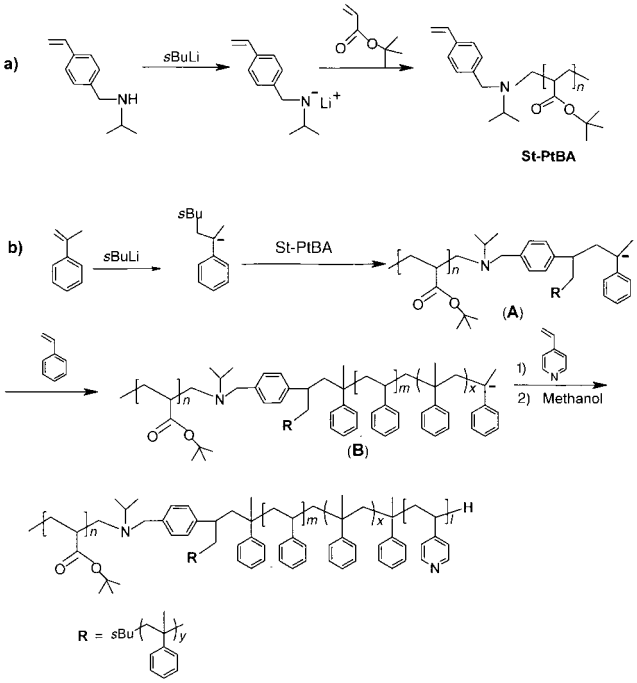

Figure 1. a) Reaction scheme for the synthesis of macromonomer poly(*tert*-butyl acrylate) with a styrene end group. b) Schematic representation for the synthesis of triblock poly(*tert*-butyl acrylate)-*b*-polystyrene-*b*-poly(4-vinylpyridine).

The PtBA macromonomer with a styrene functional end group (St-PtBA) was prepared by the living anionic polymerization of tBA and was initiated with a nitro ion (Figure 1a), by using a published procedure.[8] Three different samples ($\bar{M}_n = 3380$, $\bar{M}_w/\bar{M}_n = 1.07$; $\bar{M}_n = 2320$, $\bar{M}_w/\bar{M}_n = 1.13$; and $\bar{M}_n = 2270$, $\bar{M}_w/\bar{M}_n = 1.16$; $\bar{M}_n$ = number-average molar mass, $\bar{M}_w$ = weight-average molar mass) were prepared. An analysis

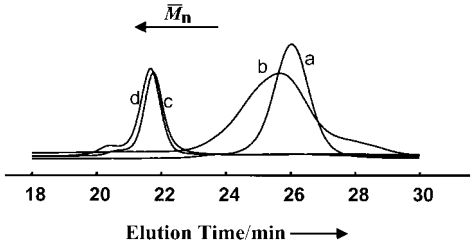

Figure 2. GPC traces: a) PtBA macromonomer; b) the reaction product of macromonomer with α-methylstyryllithium; c) PtBA-*b*-PS diblock copolymer; and d) PtBA-*b*-PS-P4VP triblock copolymer.

[*] Prof. A. Eisenberg, Dr. F. Liu
Department of Chemistry
McGill University
801 Sherbrooke Street West
Montreal, PQ H3A 2K6 (Canada)
Fax: (+1) 514-398-3797
E-mail: adi.eisenberg@mcgill.ca

[**] We thank the Natural Science and Engineering Research Council of Canada (NSERC) for supporting this research. Owen Terreau is thanked for valuable discussions.

 © 2003 Wiley-VCH Verlag GmbH & Co. KGaA, Weinheim 1433-7851/03/4212-1404 $ 20.00+.50/0

of the product by gel-permeation chromatography (GPC; Figure 2 trace a) shows a narrow molecular-weight distribution for the first sample ($\bar{M}_n = 3280$, equivalent to 26 repeat units with $\bar{M}_W/\bar{M}_n = 1.07$), the other two samples, not shown, are similar. Resonance signals arising from protons of the vinyl functional group in this macromonomer are seen in the range between 5.0 and 7.0 ppm of the ^{1}H NMR spectrum, while resonance signals from *tert*-butyl protons (-C(CH_3)$_3$) appear at 1.44 ppm (Figure 3 A). The number of repeat units of tBA in this sample was calculated to be 25, based on integrated values for protons in the vinyl group and the *tert*-butyl group and this number is in good agreement with the result obtained by GPC. This sample was used for the next step of the polymerization. For the macromonomer/styrene polymerization, an attempt was made to initiate the vinyl group on the macromonomer with *s*BuLi. Unfortunately, the anions generated by this reaction "died" quickly, their deactivation being attributed mostly to side reactions of the butyl ion with the acrylate ester of PtBA. α-Methylstyryllithium (α-MS$^-$Li$^+$), the reaction product of *s*BuLi with a few units of α-methylstyrene, is less reactive than the styryl ion, and has been employed to prepare diblock copolymers such as PS-*b*-PtBA[9] and PS-*b*-P4VP;[1d] thus, α-MS$^-$Li$^+$ was used to react with the vinyl group of the macromonomer. The GPC trace of the resulting product (Figure 2, trace b) shows a broader peak compared with that of the macromonomer. A lower-molecular-weight peak, corresponding to an elution time of 28 min, is evident. The peak arises, most likely, from short α-methylstyrene chains that were formed by the reaction of the *s*BuLi with α-methylstyrene and terminated by impurities from the macromomoner solution prior to the initiation of the styrene terminated macromonomer. The primary peak in trace b is broader than that in trace a and reflects the higher-molecular-weight component. The increased molecular weight for **A** (Figure 1 b) arises from the reaction of the activated macromonomer with some additional α-methyl styrene.

A fast polymerization occurred upon the addition of styrene to the reaction mixture, as seen from the increased viscosity and successive color changes (red to yellow to red). The results of GPC analysis showed a sharp peak (Figure 2 trace c) and a complete peak shift from trace b, which indicates the effective initiation and polymerization of styrene. The length of the second block (PS) can be controlled by a further addition of styrene. The third block (P4VP) can be formed by the addition of 4-vinylpyridine to the reaction diblock copolymer (**B** in Figure 1 b); a sharp single GPC peak was observed for this triblock (Figure 2 trace d). The small shoulders representing a high molar-mass component were observed in trace c and trace d (especially the latter) of Figure 2. These shoulders might arise from infrequent coupling of polymer anions during the withdrawal of the samples for GPC analysis.[6b] The increased molecular weight between the diblock and triblock (trace c versus trace d) is very small because only a short vinylpyridine segment was wanted. The length of the PVP segment was estimated from chemical compositions by ^{1}H NMR spectroscopy and the molecular weight of the precursor PtBA by GPC; see below.

Notably, the presence of α-methylstyrene is essential to the success of the polymerization. If the α-methylstyrene had been polymerized completely before the addition of the styrene, the styrene could still be polymerized. However, in this reaction, the yellow from the polystyryl anions was found to fade gradually, and no further polymerization of vinylpyridine was detected by GPC or by ^{1}H NMR analysis of the final product. This fact suggests the existence of interfering side reactions of the polystyryl anions in the presence of PtBA. To guarantee that α-methylstyrene monomer is present throughout the whole polymerization in sufficient amounts to provide a short-chain segment at the end of the styrene polymerization, the α-methylstyrene should be present in excess and the reaction of the macromomer with the α-MS$^-$Li$^+$ should not be allowed to proceed for too long. A direct indication for the existence of free α-methylstyrene is obtained by observing the reaction mixture, as the poly(α-methylstyryl) anions are deep red, while the polystyryl anions are yellow. As long as the PS chain is capped by an α-methylstyrene molecule, the polymerization of 4VP can proceed.

The PtBA-*b*-PS-*b*-P4VP triblock copolymers were further characterized by ^{1}H NMR spectroscopy. The presence of the different components in the triblock copolymer is shown for a typical sample, PtBA$_{26}$-*b*-PS$_{450}$-*b*-P4VP$_{23}$, in Figure 3 B (^{1}H NMR (CDCl$_3$, 300 HMz): $\delta = 1.44$, (-C(CH_3)$_3$), 6.5, 7.0 (C$_6H_5$ and C$_6H_4$N), 8.5 (C$_6H_4$N)). The compositions were calculated from the integrated values of the proton peaks. For the molecular-weight calculation, the method used by Gieb-eler and Stadler[3d] was employed. The molecular weights were calculated from the molecular weight of the PtBA

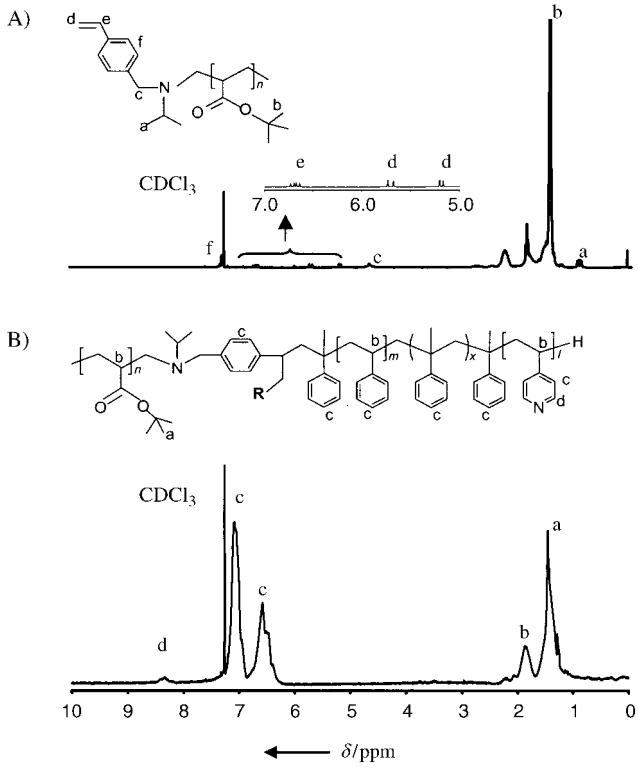

Figure 3. ^{1}H NMR spectra for a) PtBA macromonomer in CDCl$_3$; b) triblock PtBA$_{26}$-PS$_{450}$-P4VP$_{23}$ in CDCl$_3$.

 © 2003 Wiley-VCH Verlag GmbH & Co. KGaA, Weinheim 1433-7851/03/4212-1405 $ 20.00+.50/0

Table 1: Molecular weights and molecular distributions of triblock copolymers and their corresponding precursors.

Sample[a]	StPtBA		[StPtBA][b]		PtBA-*b*-PS		PtBA-PS-P4VP	
	$\bar{M}_n$[c]	$\bar{M}_w/\bar{M}_n$[c]	$\bar{M}_n$[c]	$\bar{M}_w/\bar{M}_n$[c]	$\bar{M}_n$[d]	$\bar{M}_w/\bar{M}_n$[e]	$\bar{M}_n$[d]	$\bar{M}_w/\bar{M}_n$[e]
$PtBA_{26}$-*b*-PS_{450}-*b*-$P4VP_{23}$	3280	1.07	3890	1.18	50200	1.07	52600	1.11
$PtBA_{26}$-*b*-PS_{370}-*b*-$P4VP_{11}$	3280	1.07	4140	1.20	41900	1.14	43000	1.18
$PtBA_{26}$-*b*-PS_{890}-*b*-$P4VP_{25}$	3280	1.07	3900	1.16	96000	1.06	98600	1.09

[a] The numbers refer to the final compositions determined by methods shown below.[b] [StPtBA] refers to the reaction product of PtBA macromonomer with α-methylstyryllithium. The broadened molecular-weight distribution reflects the presence of some low molecular-weight poly(α-methylstyrene). [c] Determined by GPC, calibrated against PtBA standards. For the StPtBA, the molecular weight of the styrene end group was subtracted. [d] Determined from the molecular weight of the PtBA precursor and the composition from ^{1}H NMR spectroscopy. The α-methylstyrene is counted as styrene because its chemical shifts are similar to those of styrene and its low triblock content. [e] Determined by GPC, calibrated against PS standards.

precursor along with the chemical compositions obtained from ^{1}H NMR spectra. The molecular characteristics are shown in Table 1; narrow molecular weight distributions ($\bar{M}_w/\bar{M}_n = 1.07$–$1.20$ were obtained for the PtBA-*b*-PS-*b*-P4VP triblock copolymer and their PtBA and PtBA-*b*-PS precursors.

In conclusion, we have developed a method to prepare PtBA-*b*-PS-*b*-P4VP triblock copolymers. These are examples of ABC or asymmetric ABA triblock copolymers in which A does not initiate B, but B does initiate A and C. The advantage of this method is that the polymers have controlled block lengths and narrow polydispersity, and the conversion of monomers is quantitative. The novelty of this method is that polystyrene can be formed as the second block by a two-step anionic polymerization. This method can be used to prepare a range of ABC or ABA triblock copolymers.

Received: November 27, 2002 [Z50643]

Keywords: block copolymers · copolymerization · living polymerization · polystyrenes

Experimental Section

Reagents and solvents: LiCl and monomers, such as *tert*-butyl acrylate, styrene, α-methylstyrene, and 4-vinylpyridine were purified by standard procedures.[9] The initiator used in this study was the reaction product of *s*BuLi with a few units of α-methylstyrene, which gave a red solution, and was prepared in the glass reactor that was to be used for the polymerization.

Macromonomer (St-PtBA) preparation and purification: The poly(*tert*-butyl acrylate) macromonomer with the vinyl functional group was prepared according to literature procedures,[8] and purified as follows: Macromonomer (0.66 g, 0.19 mmol of vinyl groups) was dissolved in benzene, then freeze dried in the presence of P_2O_5 for 6 h. The macromonomer was further dried under vacuum at 60 °C for 3 h, then dissolved by introducing freshly distilled THF (10 mL) under nitrogen. It was then ready for polymerization.

Polymerization: THF (≈ 800 mL) and α-methylstyrene (2 mL) were added to a flask containing LiCl (0.2 g, 4.7 mmol). After the LiCl had completely dissolved, the solution was titrated with *s*BuLi until the solution turned light red, then a further portion of *s*BuLi was added (0.15 mL, 0.19 mmol). After 15 min, this solution was cooled to −78 °C, and the solution of macromonomer was quickly added through a stainless steel capillary. The deep-red solution changed rapidly to deep yellow and then changed to red, which indicated the completion of the reaction between the macromonomer and initiator. After 15 min, the calculated amount of pure styrene was introduced to the reaction mixture; again, the reaction mixture changed from red to deep yellow to red, which indicated the end of styrene polymerization. The polymerization was allowed to proceed for another 10 min, and then 10 mL of the reaction medium was extracted for GPC analysis to determine the degree of polymerization of the polystyrene block. Upon the addition of a few drops of 4VP to the reaction medium, the red from the poly(α-methylstyryllithium) anions changed instantaneously to yellow. The polymerization was allowed to proceed for another 1 h, before being terminated by the addition of degassed methanol (1 mL). As we reported previously,[1d] the precise degrees of polymerization of the P4VP blocks can not be determined by GPC because of some absorption of the P4VP block in the GPC column. The polydispersities determined by GPC for the triblocks containing P4VP should be broader than the real polydispersities, and thus should be considered as the upper limits. ^{1}H NMR spectroscopy was used to measure the degree of polymerization of the P4VP blocks by referring to the PtBA and PS blocks. The final triblock copolymers were recovered by precipitation into cold petroleum ether and dried under vacuum for 48 h.

[1] a) L. Zhang, A. Eisenberg, *Science* **1995**, *268*, 1728; b) L. Zhang, K. Yu, A. Eisenberg, *Science* **1996**, *272*, 1777; c) D. E. Discher, A. Eisenberg, *Science* **2002**, *297*, 967; d) H. Shen, L. Zhang, A. Eisenberg, *J. Am. Chem. Soc.* **1999**, *121*, 2728; e) J. Ding, G. Liu, *Macromolecules* **1997**, *30*, 655; f) J. Ding, G. Liu, *J. Phys. Chem. B* **1998**, *102*, 6107; g) B. M. Discher, Y. Won, D. S. Ege, J. C.-M. Lee, F. S. Bates, D. E. Discher, D. A. Hammer, *Science* **1999**, *284*, 1143.

[2] L. Luo, A. Eisenberg, *Angew. Chem.* **2002**, *114,* 1043; *Angew. Chem. Int. Ed.* **2002**, *41*, 1001.

[3] a) C. Auschra, R. Stadler, *Polym. Bull.* **1993**, *30*, 257; b) K. Jung, V. Abetz, R. Stadler, *Macromolecules* **1996**, *29*, 1076; c) H. Elbs, K. Fukunaga, R. Stadler, G. Sauer, R. Magerle, G. Krausch, *Macromolecules* **1999**, *32*, 1204; d) E. Giebeler, R. Stadler, *Macromol. Chem. Phys.* **1997**, *198*, 3815; e) H. Elbs, C. Drummer, V. Abetz, G. Krausch, *Macromolecules* **2002**, *35*, 5570; f) G. Yu, A. Eisenberg, *Macromolecules* **1998**, *31*, 5546; g) X. Yan, G. Liu, F. Liu, B. Tang, H. Peng, A. Pakhomov, C. Wong, *Angew. Chem.* **2001**, *113,* 3705; *Angew. Chem. Int. Ed.* **2001**, *40*, 3593.

[4] C. S. Patrickios, A. B. Lowe, S. P. Armes, N. C. Billingham, *J. Polym. Sci. Part A* **1998**, *36*, 617.

[5] a) K. A. Davis, K. Matyjaszewski, *Macromolecules* **2001**, *34*, 2101; b) K. A. Davis, K. Matyjaszewski, *Macromolecules* **2000**, *33*, 4039; c) U. Tunca, T. Erdogan, G. Hizal, *J. Polym. Sci. Part A* **2002**, *40,* 2025.

[6] a) M. Moller, R. W. Lenz, *Makromol. Chem.* **1989**, *190*, 1151; b) A. Noshay, J. E. McGrath, *Block Copolymers-Overview and Critical Survey,* Academic Press, **1977**, p. 105, p. 55–56; c) G. Odian, *Principles of Polymerization*, 2nd ed., Wiley, New York,

 © 2003 Wiley-VCH Verlag GmbH & Co. KGaA, Weinheim 1433-7851/03/4212-1406 $ 20.00+.50/0

1981, p. 399; d) H. L. Hsieh, R. P. Quirk, *Anionic Polymerization: Principles and Practical Applications,* New York, **1996**, p. 307.
[7] M. Miyamoto, M. Sawamoto, T. Higashimura, *Macromolecules* **1984**, *17*, 265.
[8] F. Zeng, Y. Shen, S. Zhu, *Macromol. Rapid Commun.* **2001**, *22*, 1399.
[9] X. F. Zhong, S. K. Varshney, A. Eisenberg, *Macromolecules* **1992**, *25*, 7160.

 © 2003 Wiley-VCH Verlag GmbH & Co. KGaA, Weinheim 1433-7851/03/4212-1407 $ 20.00+.50/0

Biaryl Coupling Reactions

Transition-Metal-Free Suzuki-Type Coupling Reactions**

Nicholas E. Leadbeater and Maria Marco*

The Suzuki reaction (palladium-catalyzed cross coupling of aryl halides with boronic acids) is one of the most versatile and utilized reactions for the selective construction of C–C bonds, in particular for the formation of biaryl compounds.[1] As the biaryl motif is found in a range of pharmaceuticals, herbicides, and natural products, as well as in conducting polymers and liquid-crystalline materials, development of improved conditions for the Suzuki reaction has received much recent attention. Indeed, in the last ten years, there have been over 700 publications on the area of aryl–aryl bond formation. A wide range of metal complexes have been used as catalysts in these coupling reactions, attention particularly being focused on palladium. In addition to a range of organic solvents, there has been considerable recent interest in the use of water as a reaction medium. Water, which is cheap, readily available, nontoxic, and nonflammable, has clear advantages as a solvent for use in chemistry.[2,3] Suzuki coupling reactions of water-soluble aryl iodides have been performed in water with simple palladium salts[4,5] or amphiphilic polymer-supported palladium catalysts.[6] Badone and co-workers have investigated the effects of solvent, including water, on the rate of the ligand-free palladium acetate catalyzed Suzuki reaction of a range of aryl bromides, iodides, and triflates.[7] They report that when using water as a solvent, the addition of 1 equivalent of tetrabutylammonium bromide (TBAB) to the reaction mixture greatly accelerates the reaction.[8] They find that aryl bromides can be coupled with phenylboronic acid to yield biaryl compounds fairly rapidly (1 h) and in good yields, whereas with aryl iodides the reaction does not reach completion. The role of the ammonium salts is thought to be twofold: first, they facilitate solvation of the organic substrates in the solvent medium; second, they are thought to enhance the rate of the coupling reaction by activating the boronic acid to reaction by formation of $[ArB(OH)_3]^-[R_4N]^+$. TBAB has been used recently in conjunction with a palladium oxime catalyst for the Suzuki coupling of aryl chlorides with phenylboronic acid in water.[9] We recently reported that it is possible to couple a range of aryl halides, including chlorides, with phenylboronic acid in neat water using microwave heating with palladium acetate as the catalyst and TBAB as an additive.[10] The total reaction time is between 5 and 10 min, and low palladium loadings are used. Like Badone and co-workers, we attribute much of the success of our methodology to the use of TBAB as additive. In our studies to understand further the role of this additive, we have found that, using the appropriate conditions, it is possible to perform Suzuki-type coupling reactions without the need for a transition-metal catalyst, which we report herein.

As a starting point for the development of our transition-metal-free aryl-coupling methodology, we chose to study the microwave-promoted coupling of phenylboronic acid with 4-bromoacetophenone, as this would act as a sharpening stone for optimizing reaction conditions. The results from our optimization studies are presented in Table 1.

Performing the reaction at 150 °C in a sealed tube, we found that optimum yields of product are obtained when a ratio of aryl bromide to boronic acid of 1:1.3 is used. The reason that excess boronic acid is required is because, at the elevated temperatures used in the reactions, there is competitive protodeboronation of the boronic acid to produce benzene. We found that a microwave power of 100 W is optimum. Since we were not concerned about deactivation of a metal catalyst, we used a higher power than that normally

Table 1: Microwave-promoted Suzuki-type coupling of 4-bromoacetophenone and phenylboronic acid in water.[a]

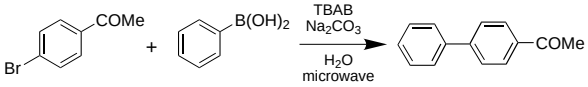

Entry	Reaction conditions[b]						Yield[c]
	$PhB(OH)_2$ [equiv]	TBAB [equiv]	Na_2CO_3 [equiv]	Power [W]	T [°C]	t [min]	[%]
1	1.3	1.0	3.8	60	150	5	97
2	1.3	1.0	3.8	**150**	150	5	100
3	1.3	1.0	3.8	**100**	150	5	100
4	**1.0**	1.0	3.8	**100**	150	5	82
5	**1.1**	1.0	3.8	**100**	150	5	95
6	**1.2**	1.0	3.8	**100**	150	5	100 (98)[d]
7	**1.2**	**0.5**	3.8	**100**	150	5	58
8	**1.2**	1.0	**1.9**	**100**	150	5	84[d]
9	**1.2**	1.0	3.8	**oil bath**	150	120	94[d]

[a] Aryl halide (1 mmol), water (2 mL). Temperature ramped to that stated and held there for the allotted time. [b] Conditions changed from entry 1 are highlighted in **bold**. [c] Determined by ^1H NMR spectroscopic analysis. [d] Yield of isolated product.

[*] Dr. N. E. Leadbeater, M. Marco
Department of Chemistry, King's College London
Strand, London, WC2R 2LS (UK)
Fax: (+44) 20-7848-2810
E-mail: nicholas.leadbeater@kcl.ac.uk

[**] We thank the Royal Society for a University Research Fellowship (N.E.L.) and King's College London for a PhD studentship (M.M.). Funding from the Royal Society and King's College London is acknowledged.

Supporting information for this article (NMR data and experimental details) is available on the WWW under http://www.angewandte.org or from the author.

 © 2003 Wiley-VCH Verlag GmbH & Co. KGaA, Weinheim 1433-7851/03/4212-1407 $ 20.00+.50/0

used in the palladium-mediated couplings (60 W). We found that the amount of base used in the reaction affects the yield considerably, the optimum quantity being 3.8 equivalents. The reaction reaches completion in 5 min. To show that the reaction is indeed metal-free, we used new glassware, apparatus, and reagents and analyzed the entire crude product mixture for palladium content. We found that there was no palladium in the product mixture to the level of detection of the analysis apparatus.[11] This, and the fact that the reaction is reproducible argues against catalytic contaminants. We also checked the levels of other metals in the product mixture that could possibly be acting as catalysts by inductively coupled plasma atomic absorption (ICP AA) spectroscopy. None of them were present in the product mixture in concentrations above the level of detection of the apparatus of 0.5–1 ppm.[12]

In an attempt to broaden the scope of the methodology, we investigated the possibility of performing the reaction with conventional heating. We found that placing a sealed tube in an oil bath at 150 °C offers an easy way to perform the reaction with 4-bromoacetophenone, a 91 % yield of product being obtained after heating for 2 h. However, the reaction of unactivated and deactivated aryl bromide substrates is not so efficient under conventional heating, even after heating for extended periods of time (16 h).

Table 2: Suzuki-type coupling of aryl halides and aryl boronic acids in water.[a]

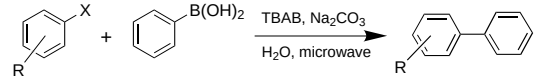

X = Cl, Br, I

Entry	Aryl halide	Yield [%]	Entry	Aryl halide	Yield [%]
1		90[b]	11	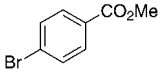	71[c]
2	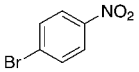	99[b]	12	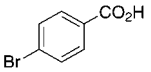	99[b]
3	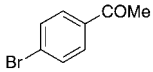	98 (91)[b]	13		50[b]
4	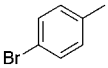	82[b]	14		76[c]
5		61[b]	15	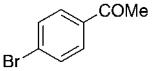	99[b,d]
6	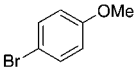	53[c]	16	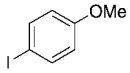	3[c]
7	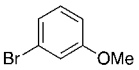	73[b]	17		79[c]
8	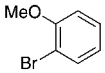	55[b]	18	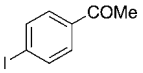	25[c]
9	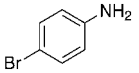	82[c]	19	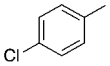	0[c]
10	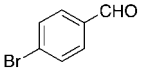	96[c]	20		0[c]

[a] Aryl halide (1 mmol), boronic acid (1.3 mmol), Na_2CO_3 (3.8 mmol), TBAB (1.0 mmol), water (2 mL). Yields quoted are for microwave promotion using a microwave power of 100 W. The temperature was ramped to 150 °C and held for 5 min. The yield quoted in parentheses was obtained when using conventional heating. The sealed tube was placed in an oil bath at 150 °C and held for 5 h. [b] Yields of isolated product. [c] Determined by ^{1}H NMR spectroscopic analysis. [d] Reaction using 4-methylbenzeneboronic acid as the coupling partner.

The methodology is applicable to a wide range of aryl bromide substrates (Table 2, entries 1–15), with good yields being obtained in the reaction with phenylboronic acid. A wide range of functional groups are tolerated in the reaction and are not affected by the high temperature and aqueous conditions used. Furthermore, sterically demanding aryl bromides can be coupled with phenylboronic acid to give good yields of product (Table 2, entries 8 and 13). To show that the reaction is regiospecific with respect to both the aryl bromide and the boronic acid, we screened the reaction of 4-bromoacetophenone with 4-methylbenzeneboronic acid and obtained the desired coupling product in excellent yield (Table 2, entry 15). Representative aryl iodides were also screened in the coupling reaction using our methodology (Table 2, entries 16–18), but product yields were lower those with their bromo counterparts. Aryl chlorides cannot be coupled by this method (Table 2, entries 19 and 20).

In conclusion, we have shown that the Suzuki-type coupling of boronic acids and aryl halides is possible without the need for a transition-metal catalyst. The methodology is immediately viable for use both in small research and larger industrial scales. Since the use of transition metals leads to the generation of waste and has a number of hazards associated with it, such as the handling of toxic, air- and moisture-sensitive complexes, the eradication of the transition-metal catalyst from the Suzuki reaction offers significant advantages. Work is currently underway to investigate the mechanism of the coupling reaction.

Received: December 16, 2002 [Z50773]

Keywords: aqueous chemistry · biaryl compounds · boron · cross-coupling · microwave chemistry

 © 2003 Wiley-VCH Verlag GmbH & Co. KGaA, Weinheim 1433-7851/03/4212-1408 $ 20.00+.50/0

[1] For recent reviews, see: a) J. Hassan, M. Sévignon, C. Gozzi, E. Schulz, M. Lemaire, *Chem. Rev.* **2002**, *102*, 1359; b) A. Suzuki, *J. Organomet. Chem.* **1999**, *576*, 147; c) N. Miyaura, A. Suzuki, *Chem. Rev.* **1995**, *95*, 2457.
[2] For an introduction to the use of water as a solvent in organic synthesis, see: a) *Organic Synthesis in Water* (Ed.: P. A. Grieco), Klewer Academic Publishers, Dordrecht, **1998**; b) C.-J. Li, T.-H. Chan, *Organic Reactions in Aqueous Media*, Wiley, New York, **1997**.
[3] For an introduction to the use of organometallic catalysts in aqueous-phase catalysis, see: *Aqueous-Phase Organometallic Catalysis, Concepts and Applications* (Eds.: B. Cornils, W. A. Herrmann), Wiley-VCH, Weinheim, **1998**.
[4] N. A. Bumagin, V. V. Bykov, *Tetrahedron* **1997**, *53*, 14437.
[5] H. Sakurai, T. Tsukuda, T. Hirao, *J. Org. Chem.* **2002**, *67*, 2721.
[6] Y. Uozumi, H. Danjo, T. Hayashi, *J. Org. Chem.* **1999**, *64*, 3384.
[7] D. Badone, M. Baroni, R. Cardamone, A. Ielmini, U. Guzzi, *J. Org. Chem.* **1997**, *62*, 7170.
[8] The use of TBAB in palladium-mediated catalysis has been reported on a number of occasions, in particular for the Heck reaction; see, for example: T. Jeffery, *Tetrahedron Lett.* **1994**, *35*, 3051.
[9] L. Botella, C. Nájera, *Angew. Chem.* **2002**, *114*, 187; *Angew. Chem. Int. Ed.* **2002**, *41*, 179.
[10] N. E. Leadbeater, M. Marco, *Org. Lett.* **2002**, *4*, 2973. We have subsequently shown that it is possible to perform the reaction conventionally: N. E. Leadbeater, M. Marco *J. Org. Chem.* **2003**, *68*, 888
[11] No Pd found down to below 0.1 ppm Pd.
[12] Elements screened: As, Bi, Be, Cd, Ce, Co, Cr, Cu, Dy, Eu, Gd, Ge, Hf, Hg, Ir, K, La, Li, Mn, Mo, Nd, Ni, Os, P, Pb, Pr, Pt, Re, Rh, Ru, Sb, Sc, Se, Sm, Sn, Tb, Th, Ti, Tl, Tm, V, Y, Yb, Zn, Zr.

 © 2003 Wiley-VCH Verlag GmbH & Co. KGaA, Weinheim 1433-7851/03/4212-1409 $ 20.00+.50/0

Synthesis of Oxazoles

Iterative Oxazole Assembly via α-Chloroglycinates: Total Synthesis of (−)-Muscoride A**

*Pierre-Yves Coqueron, Charles Didier, and Marco A. Ciufolini**

Ongoing work directed toward the synthesis of oxazole-containing natural products revealed the desirability for a mild method for iterative oxazole construction based on the approach shown in Scheme 1.[1] A generic primary amide **1** (possibly derived from an α-amino acid) would be advanced to oxazole-4-carboxamide **2**, which upon subjection to the same reaction sequence leads to bisoxazole **3**. A polyoxazole **4** bearing diverse substituents R would materialize after *n* such iterations.

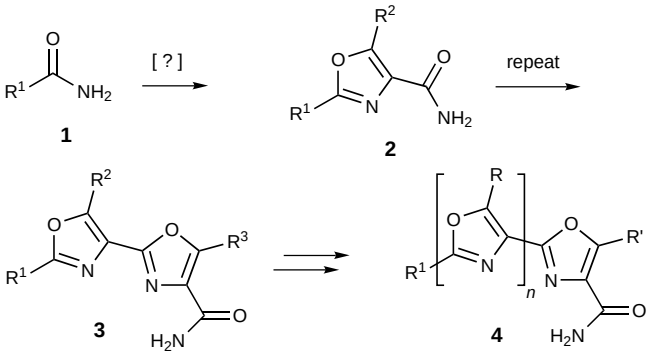

Scheme 1. Iterative approach to oxazole construction.

The documented cyclization of simple *N*-acyl propargylamines (e.g. **5a**→**6a**, Scheme 2)[2] offered an attractive solution to the issue of oxazole assembly, provided that the transformation could be effected with alkynylglycine-type substrates **5b**, in which R^1 may contain potentially labile stereocenters. Furthermore, this logic requires that intermediate **5b** be built de novo from amides **1**. Herein, we provide details of how these principles were translated into practice and we demonstrate an application of the new chemistry to the synthesis of the bisoxazole natural product (−)-muscoride A (**26**, see Scheme 5).

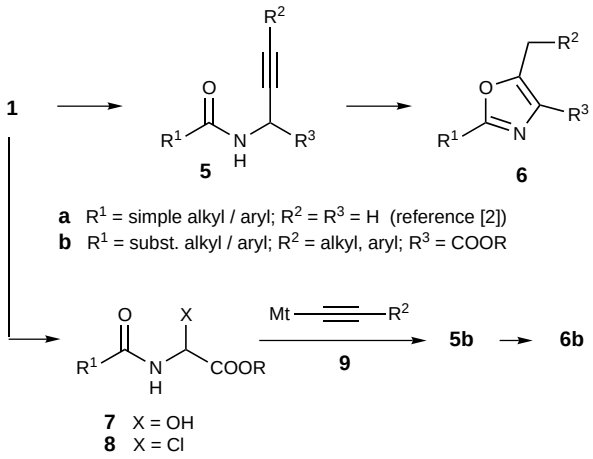

Scheme 2. Cyclization of *N*-acyl propargylamines in oxazole formation.

Alkynyl glycine derivatives can be prepared by the method of Williams and co-workers,[3] which involves the reaction of 1-stannylalkynes (e.g. **9**, Mt = Bu_3Sn) with α-chloroglycinates **8**, readily obtained, in turn, by treatment of α-hydroxyglycinates **7** with $SOCl_2$.[4] This approach was readily reproduced, but we found it more practical to use alkynyl dimethylaluminum reagents generated in situ (e.g. **9**, Mt = $AlMe_2$)[5] for the crucial C–C-bond-forming step, especially during large-scale operations.[6,7]

Addition of a primary amide to a glyoxylate ester and dissolution of the resulting α-hydroxyglycinates **7** in $SOCl_2$ resulted in conversion into essentially pure (by NMR spectroscopic analysis) **8**,[8] which reacted rapidly with dimethylaluminum acetylides to form the corresponding alkynyl glycinates **5b**. These intermediates were isolated and characterized in several instances, but we found that prolonged reaction times (> 2 h) induce a considerable degree of in situ cyclization to form oxazoles **6b**. However, complete cyclization may require an inconveniently long contact time, which may also result in side reactions. Fortunately, gentle basic treatment (aqueous $NaHCO_3$) of **5b** was found to induce rapid conversion into **6b**. Complete oxazole formation is thus best achieved during a mild basic workup of the reaction mixture.[9]

Table 1 lists representative oxazoles **10** synthesized by the new procedure. Yields are uniformly good to excellent. Heterocycles **10** often need to be converted into the corresponding free acids as a prelude to subsequent operations. In this case, it is expedient to employ the stronger base LiOH in the workup/cyclization step, whereupon the desired acids are obtained directly (Table 1, **10b**). Treatment of silylated products of the type **10g** (or of their alkynyl glycine forerunners) with LiOH results in loss of the TMS group as well.[10]

[*] Prof. Dr. M. A. Ciufolini, P.-Y. Coqueron, C. Didier
Laboratoire de Synthèse et Méthodologie Organiques
CNRS UMR 5078, Université Claude Bernard Lyon 1
and
École Supérieure de Chimie, Physique, Electronique de Lyon
43 Bd. du 11 Novembre 1918
69622 Villeurbanne cedex (France)
Fax: (+33) 4-72-43-29-63
E-mail: ciufi@cpe.fr

[**] We thank Aventis CropScience and the CNRS (BDI Fellowship to P.-Y.C.), the MENRT, the CNRS, and the Région Rhône-Alpes for support of our research. We are grateful to Ms. Laurence Rousset, Mr. Aymeric Morla, and Dr. Denis Bouchu for the mass spectrometric data. M.A.C. is the recipient of a Merck&Co Academic Development Award.

Supporting information for this article is available on the WWW under http://www.angewandte.org or from the author.

Table 1:

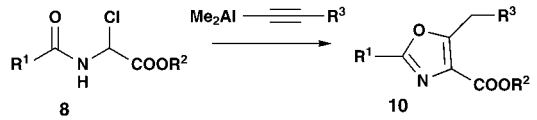

	R^1	R^2	R^3	Yield [%]
a	Ph	*n*Bu	*n*-C_6H_{13}	91
b	Ph	H[a]	*n*-C_6H_{13}	81
c	Ph	*n*Bu	Ph	90
d	Ph	Et	*n*-C_6H_{13}	89
e	Me	*n*Bu	Ph	77
f	*cyclo*-C_6H_{11}	*n*Bu	Ph	84
g	*cyclo*-C_6H_{11}	*n*Bu	TMS[c]	84
h	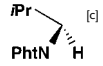	allyl	CH_2OMe	51[b]

[a] The butyl ester of **8** was used as in this experiment, as in entry **a**; however, the reaction was worked up with aqueous LiOH (see text), resulting in saponification of the ester. [b] The corresponding vinyloxazole resulting from elimination of MeOH was also formed in 21% yield (see text). [c] PhtN = phthalimido, TMS = trimethylsilyl.

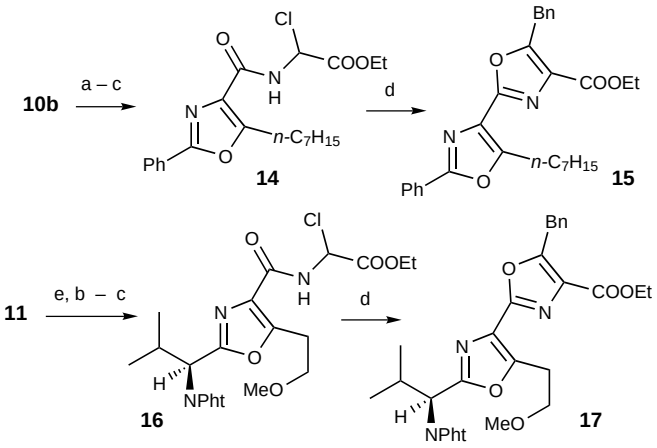

Scheme 4. Reagents and conditions: a) $SOCl_2$, reflux, 20 min, then gaseous NH_3, room temperature, 71%; b) CHOCOOEt, THF, reflux, 12 h; c) $SOCl_2$, room temperature, 90% (steps b, c for **14**), 68% (steps b, c for **16**); d) PhC≡CAlMe_2, Et_2O/THF, 0°C→RT, 2 h, 79% (**15**), 65% (**17**); e) EtOOCCl, Et_3N, 0°C, then gaseous NH_3, room temperature, 44%.

Products **8** derived from α-amino acids behaved normally in the oxazole-forming sequence (e.g. Table 1, with L-valine-derived **8h**). Best results were obtained when the α-amino group of the initial amino acid was blocked as an imide or a tertiary amide, that is, when no N–H bonds remained in the intermediates leading to **10**. Notably, a phthalimide segment (e.g. **8h**) is resistant to the action of the acetylenic organometallic compound. On the other hand, selective ester saponification in oxazoles that bear an *N*-phthalimido group was problematic as a result of competing semihydrolysis of the protecting group and consequent formation of highly polar materials. This difficulty may be circumvented by use of allyl glyoxylate in the synthetic scheme. The emerging allyl esters of the type **10h** are then selectively cleaved under catalysis by Pd^0 to form **11** (Scheme 3).[11] This is apparent in the conversion of **10h** into (*R*)-(+)-α-methylbenzylamide **12**, NMR spectra of which revealed the presence of only one diastereomer, indicating no erosion of stereochemical integrity during oxazole formation. Finally, the cyclization of alkynyl glycines derived from propargyl ethers proceeded with partial elimination of a molecule of alcohol to give vinyloxazoles: In the case of **5h**, by-product **13** (21% yield) accompanied oxazole **10h**.[12]

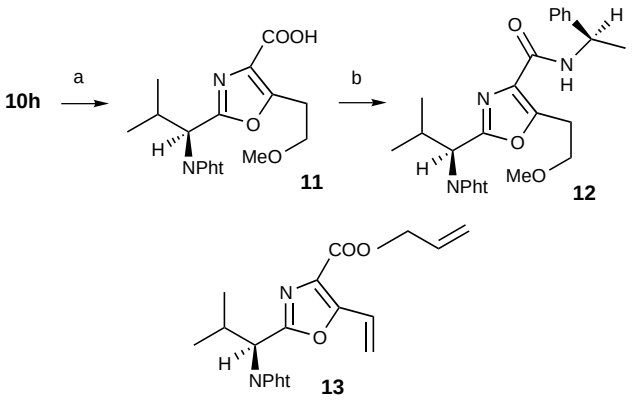

Scheme 3. Reagents and conditions: a) dimedone, $[Pd(PPh_3)_4]$, THF, room temperature, 91%; b) (*R*)-(+)-α-methylbenzylamine, EDCI, DMAP, CH_2Cl_2, room temperature, 63%. EDCI = 3-(3-dimethylaminopropyl)-1-ethylcarbodiimide, DMAP = 4-dimethylaminopyridine.

The iterative mode of oxazole construction is exemplified herein with substrates **10b** and **11** (Scheme 4). Overall yields were comparable to those of monooxazoles described in Table 1.

As an application of the new findings, we describe a total synthesis of (−)-muscoride A (**26**),[13] a secondary metabolite of the freshwater cyanobacterium *Nostoc muscorum*, as outlined in Scheme 5. This bisoxazole natural product displays only modest antibiotic activity, but it has served as a useful platform to test methods of oxazole construction.[14] Our synthesis commenced with the reaction of L-*N*-Troc-prolinamide (**18**)[15] with ethyl glyoxylate. Chlorination of the resulting **19** furnished **20**, which upon sequential exposure to the dimethylaluminum derivative of TMS acetylene and aqueous LiOH workup, afforded oxazole carboxylic acid **21** through cyclization, ester hydrolysis, and desilylation.[16] The corresponding amide **22**[17] was subjected to the same sequence. The resulting acid **23** was esterified (prenyl alcohol, BOP), and the Troc group was cleaved with Cd/Pb couple.[18] *N*-Acylation of the emerging **25** with the pentafluorophenyl ester of L-*N*-(3,3-dimethyl-1-propenyl)valine, as described by Wipf and Venkatraman, led to the formation of (−)-muscoride A, $[\alpha]_D^{25} = -80.2$ ($c = 0.5$, MeOH; ref. [13]: −89, $c = 0.7$, MeOH) in 23% yield, consistent with previous work.[14a] The overall yield of **26** from **18** was thus 3.5% over ten steps.

In conclusion, the new oxazole-forming reaction appears to be generally applicable to the preparation of heterocycles

 © 2003 Wiley-VCH Verlag GmbH & Co. KGaA, Weinheim 1433-7851/03/4212-1412 $ 20.00+.50/0

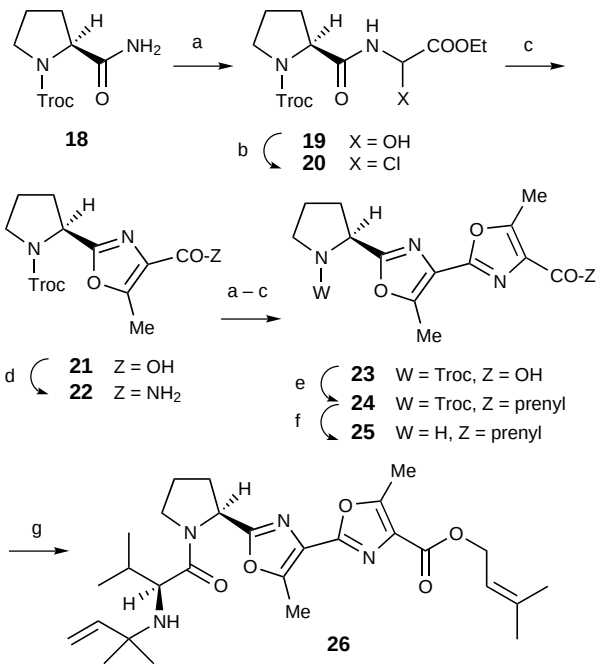

Scheme 5. Reagents and conditions: a) CHOCOOEt (1.2 equiv), THF, reflux, 12 h, 95% (**19**), 75% (**23**); b) $SOCl_2$ (neat), 10 min, room temperature, quant. (crude); c) $Me_2AlC{\equiv}CSiMe_3$ (1 equiv), Et_2O/THF, 0 °C→RT, 2 h, then workup with aqueous LiOH (2 equiv), aqueous THF, 72% (**20**, crude), 60% (**24**, crude); d) EtOOCCl (2 equiv), Et_3N (2 equiv), CH_2Cl_2, 0 °C, then gaseous NH_3, room temperature, 85%; e) prenyl alcohol (2 equiv), BOP (1.5 equiv), Et_3N (3 equiv), CH_2Cl_2, room temperature, 12 h, 65%; f) Cd/Pb couple, THF, aqueous NH_4OAc buffer, room temperature, 80%; g) **25** (1.5 equiv relative to the activated valine derivative), DMAP (1 equiv), $CHCl_3$, reflux, 24 h, 23%. Troc = trichloroethoxycarbonyl; BOP = (benzotriazol-1-yloxy)tris-(dimethylamino)phosphonium hexafluorophosphate.[14a]

of type **10**. The technique lends itself to an iterative mode of polyoxazole construction and appears to be fully compatible with multistep synthetic operations.

Received: October 10, 2002 [Z50331]

Keywords: alkynes · aluminum · natural products · oxazoles · polyoxazoles

[1] For general methods of oxazole synthesis, see: a) A. R. Katritzky, A. F. Pozharskii in *Handbook of Heterocyclic Chemistry*, 2nd ed., Pergamon, Oxford, **2000**, p. 569; b) F. W. Hartner, Jr. in *Comprehensive Heterocyclic Chemistry II, Vol. 3* (Eds.: A. R. Katritzky, C. W. Rees), Elsevier, New York, **1996**, p. 261; for more recent methods, see: c) S. Swaminathan, A. K. Singh, W. S. Li, J. J. Venit, K. J. Natalie, Jr., J. H. Simpson, R. E. Weaver, L. J. Silverberg, *Tetrahedron Lett.* **1998**, *39*, 4769; d) M. C. Begley, R. T. Buck, S. L. Hind, C. J. Moody, *J. Chem. Soc. Perkin Trans. 1* **1998**, 591; e) M. Falorni, G. Dettori, G. Giacomelli, *Tetrahedron: Asymmetry* **1998**, *9*, 1419; f) R. S. Varma, D. Kumar, *J. Heterocycl. Chem.* **1998**, *35*, 1533; g) W. W. Pei, S. H. Li, X. P. Nie, Y. W. Li, J. Pei, B. Z. Chen, J. Wu, X. L. Ye, *Synthesis* **1998**, 1298; h) C. M. Shafer, T. F. Molinski, *J. Org. Chem.* **1999**, *64*, 4995; i) B. A. Kulkarni, A. Ganesan, *Tetrahedron Lett.* **1999**, *40*, 5633; j) L. M. Martin, B. H. Hu, *Tetrahedron Lett.* **1999**, *40*, 7951; k) C. M. Shafer, T. F. Molinski, *Heterocycles* **2000**, *53*, 1167; l) M. Lautens, A. Roy, *Org. Lett.* **2000**, *2*, 555; m) J. Sisko, A. J. Kassick, M. Mellinger, J. J. Filan, A. Allen, M. A. Olsen, *J. Org. Chem.* **2000**, *65*, 1516; n) U. Grabowska, A. Rizzo, K. Farnell, M. Quibell, *J. Comb. Chem.* **2000**, *2*, 475; o) M. S. Addie, R. J. K. Taylor, *J. Chem. Soc. Perkin Trans. 1* **2000**, 527; p) M. C. Bagley, S. L. Hind, C. H. Moody, *Tetrahedron Lett.* **2000**, *41*, 6897; q) A. J. Phillips, Y. Uto, P. Wipf, M. J. Reno, D. R. Williams, *Org. Lett.* **2000**, *2*, 1165; r) P. Wipf, J. L. Methot, *Org. Lett.* **2001**, *3*, 1261; s) F. Yokokawa, T. Asano, T. Shioiri, *Tetrahedron* **2001**, *57*, 6311; t) A. Radspieler, J. Liebscher, *Synthesis* **2001**, 745; u) C. Saitz, H. Rodriguez, A. Marquez, A. Canete, C. Jullian, A. Zanocco, *Synth. Commun.* **2001**, *31*, 135; v) A. B. Smith III, P. R. Verhoest, K. P. Minbiole, M. Schelhaas, *J. Am. Chem. Soc.* **2001**, *123*, 4834; w) A. G. M. Barrett, S. M. Cramp, A. J. Hennessy, P. A. Procopiou, R. S. Roberts, *Org. Lett.* **2001**, *3*, 271; x) A. Arcadi, S. Cacchi, L. Cascia, G. Fabrizi, F. Marinelli, *Org. Lett.* **2001**, *3*, 2501; y) R. Berger, W. S. Shoop, J. V. Pivnichny, L. M. Warmke, M. Zakson-Aiken, K. A. Owens, P. deMontigny, S. M. Schmatz, M. J. Wyvratt, M. H. Fischer, P. T. Meinke, S. L. Colletti, *Org. Lett.* **2001**, *3*, 3715; z) A. Couture, P. Grandclaudon, C. Hoarau, J. Cornet, J. P. Hénichart, R. Houssin, *J. Org. Chem.* **2002**, *67*, 3601; aa) K. J. Hodgetts, M. T. Kershaw, *Org. Lett.* **2002**, *4*, 2904; ab) K.-I. Itoh, S. Takahashi, T. Ueki, T. Sugiyama, T. T. Takahashi, C. A. Horiuchi, *Tetrahedron Lett.* **2002**, *43*, 7035; ac) J. D. Kreisberg, P. Magnus, S. Shinde, *Tetrahedron Lett.* **2002**, *43*, 7393, and references therein; see also reference [12].

[2] a) B. M. Nilsson, U. Hacksell, *J. Heterocycl. Chem.* **1989**, *26*, 269; b) F. Eloy, A. Deryckere, *Chim. Ther.* **1973**, 437; c) Y. Yura, *Chem. Pharm. Bull. Jpn.* **1962**, *10*, 1087; d) P. Wipf, L. T. Rahman, S. R. Rector, *J. Org. Chem.* **1998**, *63*, 7132; e) A. Arcadi, S. Cacchi, L. Cascia, G. Fabrizi, F. Marinelli, *Org. Lett.* **2001**, *3*, 2501.

[3] R. M. Williams, D. J. Aldous, S. C. Aldous, *J. Org. Chem.* **1990**, *55*, 4657.

[4] a) U. Zoller, D. Ben-Ishai, *Tetrahedron* **1975**, *31*, 863; b) D. Ben-Ishai, I. Sataty, Z. Bernstein, *Tetrahedron* **1976**, *32*, 1571; c) Z. Bernstein, D. Ben-Ishai, *Tetrahedron* **1977**, *33*, 881; an alternative route to **8** is described in reference [3]; see also reference [8].

[5] The use of alkynyl aluminum reagents was inspired by: A. R. Katritzky, D. C. Oniciu, N. M. Yoon, *J. Org. Chem.* **1999**, *64*, 488.

[6] Application of the method of Williams and co-workers[3] was complicated by the poor solubility of several intermediates of the type **8** in CCl_4 or other nonpolar solvents, which are required for best results.

[7] Other acetylenic organometallic compounds produced poor results. Thus, we failed to induce conversion of **8** into **5b** with Li or Na acetylides (complex mixtures). Base-promoted formation of the imine corresponding to **8** (see conversion of compound **5** into **3** in: J. Vidal, J.-C. Hannachi, G. Hourdin, J.-C. Mulatier, A. Collet, *Tetrahedron Lett.* **1998**, *39*, 8845) prior to exposure to an alkynyl organometallic compound did not solve the problem. Trimethylsilylacetylenes proved to be unreactive toward **8** under a variety of conditions. The facile reaction of vinylboronic acids with iminium-type electrophiles (see N. A. Petasis, I. A. Zavialov, *J. Am. Chem. Soc.* **1997**, *119*, 7703) prompted us to explore alkynyl boronic acids as acetylide donors. Results were unsatisfactory.

[8] The following modification of the procedure of Ben-Ishai and co-workers[4] was used: α-hydroxyglycinate **7** was dissolved in $SOCl_2$ (30 equiv) and stirred at room temperature for 10 min. The mixture was diluted with an equal volume of CH_2Cl_2 and concentrated to afford the crude α-chloroglycinate **8**.

[9] Representative procedure for the preparation of oxazoles: commercial *n*BuLi (1.2 mmol) was added dropwise to a solution

 © 2003 Wiley-VCH Verlag GmbH & Co. KGaA, Weinheim 1433-7851/03/4212-1413 $ 20.00+.50/0

of 1-octyne (1.2 mmol) in THF (0.9 mL) at −78 °C under Ar. After stirring for 5 min, the mixture was transferred through a cannula into a cold (0 °C) solution of commercial dimethylaluminum chloride (solution in hexane, 1.2 mmol) in diethyl ether (0.9 mL). The mixture was stirred at 0 °C for 1 h and was then transferred dropwise through a cannula into a cold (0 °C) solution of chloroglycinate **8a** (1.2 mmol) in THF (2 mL). The cold bath was removed and the mixture was stirred for 2 h. The mixture was then was carefully concentrated *in vacuo* to about 1/3 of the original volume. Dilution with chloroform (5 mL), filtration through a plug of silica gel (elution with neat EtOAc), concentration, treatment with solid $NaHCO_3$ (2.4 mmol) in THF/H_2O (1:1, 5 mL) for 2 h, extraction with diethyl ether, and concentration provided the crude oxazole. Purification by silica-gel column chromatography with cyclohexane/EtOAc (6:1) gave pure **10a** (1.1 mmol).

[10] Desilylation without ester hydrolysis may be induced in essentially quantitative yield by treatment of, for example, **10g**, with tetrabutylammonium fluoride (TBAF) (2 equiv) in CH_2Cl_2 (1 h, room temperature).

[11] For reviews of allyl-type blocking groups, see: a) H. Kunz, *Angew. Chem.* **1987**, *99*, 297; *Angew. Chem. Int. Ed. Engl.* **1987**, *26*, 294; b) T. W. Greene, P. G. M. Wuts, *Protective Groups in Organic Synthesis*, Wiley Interscience, New York, NY, **1999**, p. 409, and references therein.

[12] A similar reaction has been described in P. Wipf, L. T. Rahman, S. R. Rector, *J. Org. Chem.* **1998**, *63*, 7132.

[13] A. Nagatsu, H. Kajitani, J. Sakakibara, *Tetrahedron Lett.* **1995**, *36*, 4097.

[14] For previous syntheses, see: a) P. Wipf, S. Venkatraman, *J. Org. Chem.* **1996**, *61*, 6517; b) J. C. Muir, G. Pattenden, R. Thomas, *Synthesis* **1998**, 613.

[15] Prepared from *N*-Troc-L-proline (96 mmol) (see S. A. Boys, W. J. Thompson, *J. Org. Chem.* **1987**, *52*, 1790) by reaction with $SOCl_2$ (10 equiv) in CH_2Cl_2 (200 mL) at reflux (20 min), concentration to dryness, dissolution into more CH_2Cl_2 (200 mL), and treatment with gaseous ammonia (room temperature, 90 min). Partitioning with water (100 mL), washing with brine, and concentration gave an orange residue, which was triturated with diethyl ether to furnish **18** as a white solid, $[\alpha]_D^{25} = -72$ ($c = 2.85$, $CHCl_3$).

[16] Scrutiny of the NMR spectra of the crude (*R*)-(+)-α-methylbenzylamide derivative of **21** revealed the presence of only one diastereomer (1:1 mixture of Troc rotamers) signifying that stereochemical integrity had once again been preserved.

[17] The structure of **22** was confirmed by single-crystal X-ray crystallographic analysis.

[18] Q. Dong, C. A. Anderson, M. A. Ciufolini, *Tetrahedron Lett.* **1995**, *36*, 5681.

 © 2003 Wiley-VCH Verlag GmbH & Co. KGaA, Weinheim 1433-7851/03/4212-1414 $ 20.00+.50/0

Olefin Polymerization Catalysts

Reactions of Titanium and Zirconium Derivatives of Bis(trimethylsilyl)acetylene with Tris(pentafluorophenyl)borane: A Titanium(III) Complex of an Alkynylboranate **

Perdita Arndt, Wolfgang Baumann, Anke Spannenberg, Uwe Rosenthal, Vladimir V. Burlakov, and Vladimir B. Shur*

Dedicated to D. habil. Erhard Kurras on the occasion of his 75th birthday

Special cations, formed by the formal abstraction of a methyl anion from zirconocene dimethyl complexes with the help of the strong Lewis acid $B(C_6F_5)_3$, introduced by Ewen and Marks, are highly active catalysts for the polymerization of α-olefins.[1] It has become evident that other zirconocene complexes (for example, of olefins, alkynes, butadienes) can also undergo a similar activation and thus may be suitable precursors for polymerization catalysts.[2]

Recently we described[3] that titanocene and zirconocene complexes of silylalkynes, such as $[Cp'_2M(\eta^2\text{-}Me_3SiC_2SiMe_3)]$ ($Cp' =$ substituted or unsubstituted $\eta^5\text{-}C_5H_5$) offer a rich chemistry of this type with boron-containing reagents. Especially interesting are the titanium complexes because dissociation of the alkyne ligands and C–H activation of the Cp ligands are possible (Scheme 1). Cationic complexes of type **A** were formed with $[HNMe_3][BPh_4]$,[3a] whereas an electrophilic substitution of an H atom of one $\eta^5\text{-}C_5H_5$ ring or of one methyl group of a Cp* ligand ($Cp^* = C_5Me_5$) occurred with $B(C_6F_5)_3$, and paramagnetic zwitterionic Ti^{III} complexes of types **B**[3b,c] or **C**[3d,e] were formed.

Similar compounds,[2] such as $[Cp\{C_5H_4B(C_6F_5)_3\}Zr(acac)]$ (acac = 2,4-pentanedione (acetylacetone))[4] or $[Cp\{C_5H_4BH(C_6F_5)_2\}Zr\{\sigma\text{-}C(Et)=CHEt\}]$,[5] were described also. The functionalization of the Cp* ligands is the same in reactions of Cp* silylalkyne zirconocene complexes as for the titanium compounds of type **C**. However, the alkyne does not

[*] Prof. Dr. U. Rosenthal, Dr. P. Arndt, Dr. W. Baumann, Dr. A. Spannenberg
Leibniz-Institut für Organische Katalyse an der Universität Rostock e.V.
Buchbinderstrasse 5–6, 18055 Rostock (Germany)
Fax: (+49) 381-466-9376
E-mail: uwe.rosenthal@ifok.uni-rostock.de

Dr. V. V. Burlakov, Prof. V. B. Shur
A.N. Nesmeyanov Institute of Organoelement Compounds
Russian Academy of Sciences
Vavilov Street 28, 117813 Moscow (Russia)

[**] We thank Prof. Karel Mach, Prague, for ESR measurements. This work was supported by the Deutsche Forschungsgemeinschaft (No. AR 321/1-1), the Fonds der Chemischen Industrie, and the Russian Foundation for Basic Research (code 02-03-32589).

Supporting information (syntheses and details of X-ray structure investigations) for this article is available on the WWW under http://www.angewandte.org or from the author.

 © 2003 Wiley-VCH Verlag GmbH & Co. KGaA, Weinheim 1433-7851/03/4212-1414 $ 20.00+.50/0

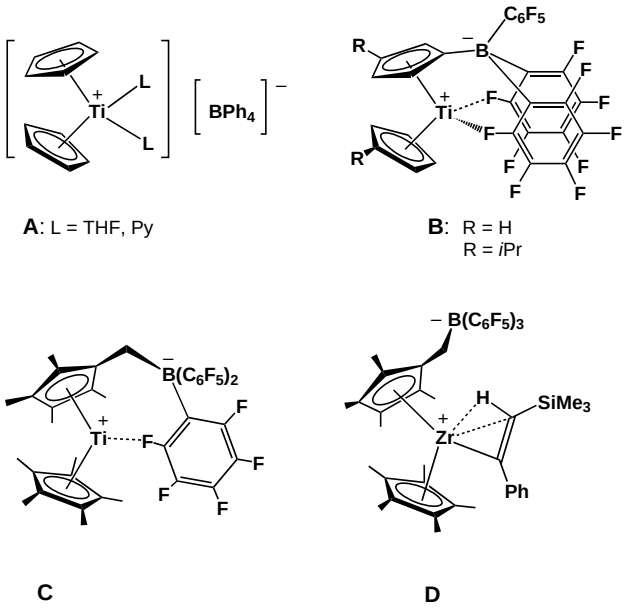

Scheme 1. Typical structures of boron-containing titanocene and zirconocene complexes

dissociate but binds the H atom under formation of an agostic alkenyl compound of type **D**.[3d]

Herein we report the reactions of complexes *rac*-[(ebthi)M(η^2-$Me_3SiC_2SiMe_3$)],[6] (ebthi = 1,2-ethylene-1,1′-bis(η^5-tetrahydroindenyl)) with $B(C_6F_5)_3$,[1] which proceed totally differently for Ti and Zr complexes.[7] The reaction of the Zr complex occurs as for the type **D** complexes with an electrophilic substitution at an H atom of the Cp ring to give an alkenyl compound **1** (Scheme 2). At room temperature the ^{1}H NMR spectra of **1** display at very broad resonance signals, which become sharp on cooling to 252 K and broaden again at lower temperatures. The poor solubility (crystallization upon cooling) prevents a deeper insight into the dynamics of the molecule, but at 252 K two species in a 2:1 ratio are evident. They undergo chemical exchange and exhibit the number of NMR signals expected from their solid state structures (see below). One plausible explanation of this dynamic behavior could be a hindered rotation of the alkenyl group around the C–Zr bond. A reason for the hindered rotation could be the agostic Zr-H-C interaction or the proximity of one silyl group to one C_6F_5 group.

The molecular structure of **1**[8] (Figure 1) shows the typical (ebthi)Zr-part, which is substituted in 3-position by the boranate. One *ortho* F atom coordinates to the zirconium center, therefore the corresponding F–C_{ring} bond is elongated. This coordination is also evident from the ^{19}F NMR signal which, at $\delta = -200.2$ ppm, is shifted to extremely high field.

The alkenyl group is σ bonded to the Zr center and has an additional agostic interaction,[9] indicated by the typical Zr-C14-C13 angle of 87.4 (4)°, similar to that found in **D** (86.5°).[3d] Additionally, the small coupling constant ^1J(C,H) of 91 Hz at C13 is characteristic for an agostic interaction.[9]

The preparation of complex **1** demonstrates the importance of the proper sequence when adding reagents to achieve catalytic activity. If the alkyne complex *rac*-[(ebthi)Zr-(η^2-$Me_3SiC_2SiMe_3$)] is first treated with ethene to yield the zirconacyclopentane *rac*-[(ebthi)Zr(C_4H_8)] and this is subsequently activated by $B(C_6F_5)_3$, an active catalyst for polymerization results.[10a] But if the borane is added to the alkyne

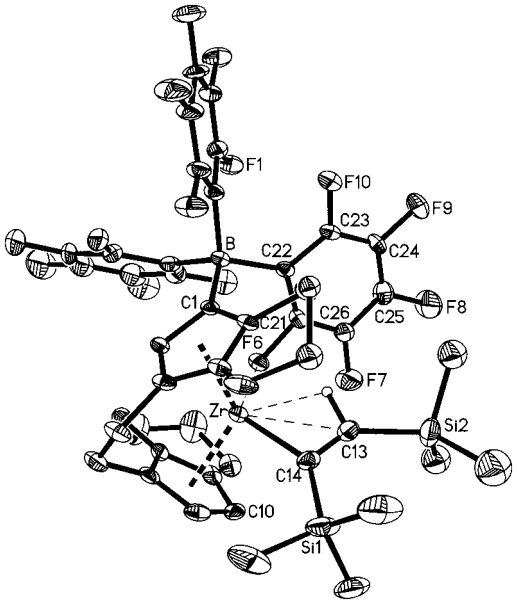

Figure 1. ORTEP plot of **1**. The thermal ellipsoids are set at 30% probability. For clarity the hydrogen atoms (with exception of H13) and one position of the disordered groups are omitted. Selected bond lengths [Å] and angles [°]: C1-B 1.640(9), Zr-F6 2.379(3), C21-F6 1.421(6), C26-F7 1.332 (8), C25-F8 1.377(8), C24-F9 1.361(7), C23-F10 1.343(7), Zr-C14 2.259(7); C1-B-C22 108.2(5), Zr-C14-C13 87.4(4).

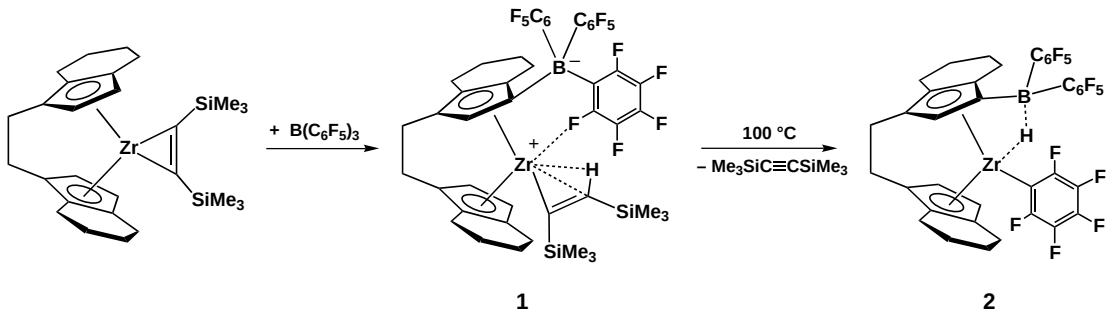

Scheme 2. Formation and reaction of **1**.

 © 2003 Wiley-VCH Verlag GmbH & Co. KGaA, Weinheim 1433-7851/03/4212-1415 $ 20.00+.50/0

compound first, complex **1** is formed, which does not react with ethene and, accordingly, is inactive in polymerization. The similar complex **D** is active in ethene polymerization, presumably because it has no Zr–F interaction.

If solutions of **1** are heated to 100 °C, the alkyne is eliminated and one B–C bond is cleaved with a subsequent transfer of a pentafluorophenyl group from boron to zirconium, whereupon complex **2** with one μ-H atom between boron and the zirconium center is formed (Scheme 2) Such a transfer of C_6F_5 from boron to zirconium[10b] is known, as is the μ-H atom type of structure.[10c] It is possible to describe compound **2** either as Zr^{IV} σ-C_6F_5 hydrido complex with an electroneutral borane ligand or alternatively as a zwitterionic betaine-boranate.

The resonance signal of the hydride unit is located in the same region of the ^{1}H NMR spectra as the signals of the ebthi groups and was identified only by ^{11}B-decoupling experiments ($\delta = 0.82$ ppm). During the thermal interconversion of **1** into **2** the high-field shifted ^{19}F NMR signal disappeared, which indicates that there is no F–Zr interaction in **2**.

The molecular structure of **2**[11] (Figure 2) displays the typical (ebthi)Zr-part, substituted by the diaryl boron unit $B(C_6F_5)_2$. The Zr-H-B bridge of **2** has atomic distances typical for this type of structure.[10c]

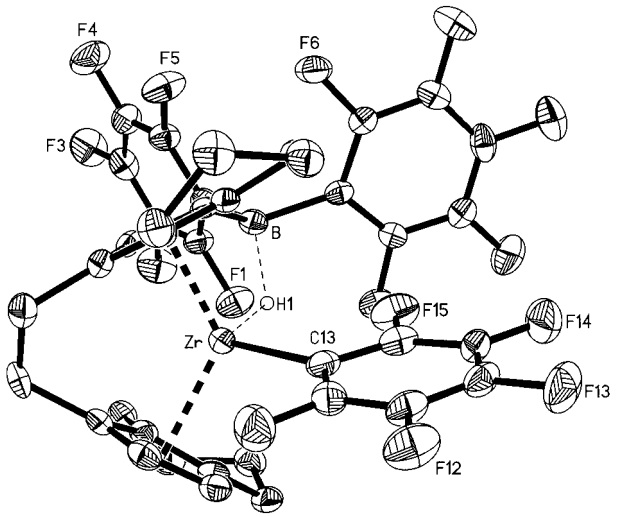

Figure 2. ORTEP plot of **2**. The thermal ellipsoids are set at 30% probability. For clarity the hydrogen atoms (with exception of H1) are omitted. Selected bond lengths [Å]: Zr-C13 2.334(6), B-H1 1.481, Zr-H1 2.113.

The Ti complex *rac*-[(ebthi)Ti(η^2-$Me_3SiC_2SiMe_3$)] reacts, surprisingly, in a totally different way with $B(C_6F_5)_3$ to the Zr compound (Scheme 3). Neither an electrophilic substitution of an H atom nor an elimination of the alkyne were observed, but after a C–Si bond cleavage and a subsequent B–C bond formation the first zwitterionic titanocene(III) η^2-(trimethylsilyl)alkynylboranate complex *rac*-[{(ebthi)Ti}$^+${η^2-$Me_3SiC_2B(C_6F_5)_3$}$^-$] (**3**) was obtained. Similar Si–C bond cleavage reactions of silylalkynes $Me_3SiC{\equiv}CR$ by transition-metal complexes under formation of σ-alkynyl complexes [$L_nM(SiMe_3)(C{\equiv}CR)$] are known for late-transition-metal compounds.[12]

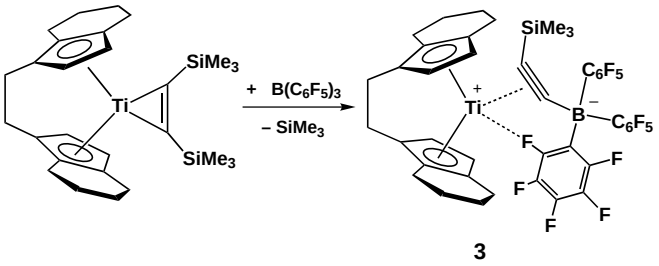

Scheme 3. Conversion of *rac*-[(ebthi)Ti(η^2-$Me_3SiC_2SiMe_3$)] into **3**.

The green compound **3** is paramagnetic (EPR in toluene at 20 °C: $g = 1.980$, $\Delta H = 6.7$ G, $a_{Ti} = 11.0$ G). A large number of lines indicate an unpaired electron, which interacts with one or two F-atoms. The IR spectrum (nujol mull) displays the absorption for the C≡C bond at 1988 cm^{-1} which indicates very weak alkyne complexation. In the starting complex which can be described as a Ti^{II} alkyne complex or alternatively as a Ti^{IV} metallacyclopropene, this absorption was found at 1594 cm^{-1},[6] a result of stronger backbonding effects. This interpretation is also supported by the X-ray crystal structure (Figure 3).

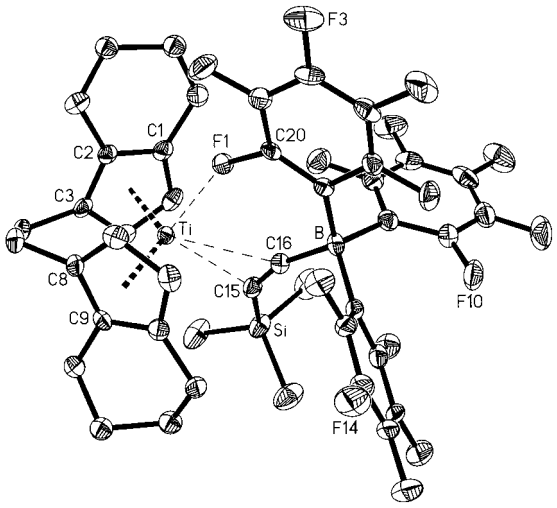

Figure 3. ORTEP plot of **3**. The thermal ellipsoids are set at 30% probability. For clarity the hydrogen atoms and one position of the disordered groups are omitted. Selected bond lengths [Å] and angles [°]: C15-C16 1.226(5), C15-Si 1.866(4), C16-B 1.617(5), Ti-C16 2.639(4), Ti-C15 2.515(4), Ti-F1 2.260(2), C20-F1 1.389(4); C15-C16-B 161.1(4), C16-C15-Si 144.3(3).

The molecular structure of **3**[13] (Figure 3) shows the typical (ebthi)Ti structure, but in contrast to **1** is unsubstituted. The $[Me_3SiC{\equiv}CB(C_6F_5)_3]^-$ ligand is complexed unsymmetrically and weakly as expected. A comparably weak coordination was also found in the dimeric σ,π-alkynyl-bridged titanocene(III) complexes [{$Cp_2Ti(C{\equiv}CSiMe_3)$}$_2$] (C-C 1.244(3), Ti-C(Ti) 2.393(1), Ti-C(Si) 2.318(2) Å; C-C-Ti 176.4(1), C-C-Si 141.5(2)°).[14] A stronger complexation is found in [Cp^*_2Ti(η^2-$Me_3SiC_2SiMe_3$)] (C-C 1.309(4), Ti-C 2.122(3) and 2.126(3) Å; Si-C-C 134.8(3) and 136.8(3)°).[15] One *ortho* F atom in **3** coordinates to the titanium center and

 © 2003 Wiley-VCH Verlag GmbH & Co. KGaA, Weinheim 1433-7851/03/4212-1416 $ 20.00+.50/0

thus lies farther from the ring carbon atoms than all the other F atoms.

Compound **3**, to our knowledge, is the first Ti^{III} alkyne complex, if one leaves out the very special cases of dimeric σ,π-alkynyl-bridged complexes $[\{Cp_2Ti(C{\equiv}CSiMe_3)\}_2]$[14] and $[\{Cp_2Ti(C{\equiv}CSnMe_3)\}_2]$.[16] In addition metallocene complexes of alkynylboranates $[RC{\equiv}C\text{-}BR_3]^-$ have not been isolated or characterized before, though they were assumed frequently as reactive intermediates.[17,18] One example for this is the $B(C_6F_5)_3$-catalyzed C–C coupling of alkynyl groups to 1,3-butadiynes from zirconocene(IV)-bisalkynyl complexes $[Cp_2Zr(C{\equiv}CR)_2]$ described by Erker et al. which was proposed to proceed via the not-isolated $[RC{\equiv}CB(C_6F_5)_3]^-$ complexes of zirconocene(IV) monoalkynyl cations $[Cp_2Zr(C{\equiv}CR)]^+$.[17] Complexes of the type $[Cp_2Zr\{\eta^2\text{-}RC_2B(C_6F_5)_2\}]$ were isolated by Piers et al. from neutral alkynylboranes $RC{\equiv}C{-}BR_2$ with metallocenes.[19] Compounds with alkynylboranates were proposed also by Wrackmeyer et al. in the reaction of stannylalkynes $Me_3SnC{\equiv}CR$ with triethylborane (BEt_3), where not-isolated intermediates, such as $[Me_3Sn]^+[RC{\equiv}CBEt_3]^-$ react under formation of stannylolefines $Me_3SnC(Et){=}CR(BEt_2)$.[18]

The reaction which generates **3** may be understood as an oxidative Si–C bond cleavage in $Me_3SiC{\equiv}CSiMe_3$ (in analogy to ref. [12]) under formation of the σ-alkynyl complex *rac*-$[(ebthi)Ti(SiMe_3)(C{\equiv}CSiMe_3)]$, which gives (by reduction) Me_3Si radicals and the dimeric σ,π-alkynyl-bridged complex *rac*-$[\{(ebthi)Ti(C{\equiv}CSiMe_3)\}_2]$ (in analogy to ref. [14]). With $B(C_6F_5)_3$, this complex would generate **3**. Similar reaction steps were described for $Me_3SnC{\equiv}CSnMe_3$, via $[Cp_2Ti(SnMe_3)(C{\equiv}CR)]$, to Me_3Sn radicals and $[\{Cp_2Ti(C{\equiv}C\text{-}SnMe_3)\}_2]$.[16] An NMR-spectroscopy investigation of the reaction was prevented by the presence of paramagnetic complexes, and the fate of the Me_3Si group remains unknown. Pure complex **3** crystallizes from the mixture but after evaporation of all the *n*-hexane, only amorphous mixtures of undefined compounds remained.

With utmost exclusion of moisture,[20a] the green complex **3** was formed in a yield of approximately 35% along with trace amounts of blue crystals, which are a mixture of *rac*-$[\{(ebthi)Ti\}^+\{HO\text{-}B(C_6F_5)_3\}]^-$ (**4**) and *rac*-$[\{(ebthi)Ti\}^+\{H\text{-}B(C_6F_5)_3\}]^-$ (**5**).[20b] If water is present (as the Brönsted acid $B(C_6F_5)_3{\cdot}H_2O$[21]), **4** and **5** were isolated as the only products,[20b] and bis(trimethylsilyl)acetylene was detected in the reaction solution by NMR spectroscopy. Complex **3** was not formed in the reaction of *rac*-$[(ebthi)Ti(\eta^2\text{-}Me_3SiC_2SiMe_3)]$ with a mixture of **4** and **5** in *n*-hexane.

The compounds described here form a series of complexes of the type *rac*-$[\{(ebthi)Ti\}^+\{X\text{-}B(C_6F_5)_3\}^-]$ (X = $C{\equiv}CSiMe_3$ (**3**), OH (**4**) or H (**5**)). To date, we failed to synthesize similar complexes by the reaction of the recently published stable permethyltitanocene monoalkynyl complexes $[Cp^*_2Ti\text{-}C{\equiv}C\text{-}tBu]$[22] with $B(C_6F_5)_3$. Whether this is because of the specific properties of the Cp ligands (Cp* vs. ebthi) or of the alkynyl substituents (Me_3Si vs. *t*Bu) or because of the reaction path itself is being investigated.

Received: October 23, 2002
Revised: November 29, 2002 [Z50421]

Keywords: borate ligands · lewis acids · titanium · zirconium · zwitterions

[1] H. H. Brintzinger, D. Fischer, R. Mülhaupt, B. Rieger, R. Waymouth, *Angew. Chem.* **1995**, *107*, 1255–1283; *Angew. Chem. Int. Ed. Engl.* **1995**, *34*, 1143–1171, and references therein.

[2] a) W. E. Piers, *Chem. Eur. J.* **1998**, *4*, 13–18; b) G. Erker, *Acc. Chem. Res.* **2001**, *34*, 309–317, and references therein.

[3] a) A. Ohff, R. Kempe, W. Baumann, U. Rosenthal, *J. Organomet. Chem.* **1996**, *520*, 241–244; b) V. V. Burlakov, S. I. Troyanov, A. V. Letov, E. I. Mysov, G. G. Furin, V. B. Shur, *Izv. Akad. Nauk Ser. Khim.* **1999**, *48,* 1022–1023; (Engl. Transl.) *Russ. Chem. Bull.* **1999**, *48*, 1012–1013; c) V. V. Burlakov, S. I. Troyanov, A. V. Letov, L. I. Strunkina, M. Kh. Minacheva, G. G. Furin, U. Rosenthal, V. B. Shur, *J. Organomet. Chem.* **2000**, *598*, 243–247; d) V. V. Burlakov, P.-M. Pellny, P. Arndt, W. Baumann, A. Spannenberg, V. B. Shur, U. Rosenthal, *Chem. Commun.* **2000**, 241–242; e) V. V. Burlakov, P. Arndt, W. Baumann, A. Spannenberg, U. Rosenthal, A. V. Letov, K. A. Lyssenko, A. A. Korlyukov, L. I. Strunkina, M. Kh. Minacheva, V. B. Shur, *Organometallics* **2001**, *20*, 4072–4079.

[4] J. Ruwwe, G. Erker, R. Fröhlich, *Angew. Chem.* **1996**, *108*, 108–110; *Angew. Chem. Int. Ed. Engl.* **1996**, *35*, 80–82.

[5] L. Somlai, W. E. Piers, unpublished results, citat [22] in ref. [2a].

[6] C. Lefeber, W. Baumann, A. Tillack, R. Kempe, H. Görls, U. Rosenthal, *Organometallics* **1996**, *15*, 3486–3490.

[7] P. Arndt, V. V. Burlakov, A. Spannenberg, W. Baumann, U. Rosenthal, *50 Years Catalysis Research in Rostock*, **2002**, P24.

[8] Crystal structure of **1**: crystal size $0.4\times0.3\times0.2$ mm, colorless prism, space group $P\bar{1}$, triclinic, $a=13.186(3)$, $b=13.822(3)$, $c=16.300(3)$ Å, $\alpha=85.44(3)$, $\beta=88.65(3)$, $\gamma=83.00(3)°$, $V=2939.0(11)$ Å^3, $Z=2$, $\rho_{calcd}=1.270$ g cm^{-3}, 7137 reflections measured, 7137 were independent of symmetry and 3913 were observed ($I>2\sigma(I)$), $R1=0.058$, wR^2 (all data) $=0.178$, 633 parameters.

[9] D. Thomas, N. Peulecke, V. V. Burlakov, B. Heller, A. Spannenberg, R. Kempe, U. Rosenthal, R. Beckhaus, *Z. Anorg. Allg. Chem.* **1998**, *624*, 919–924.

[10] a) S. Mansel, D. Thomas, C. Lefeber, D. Heller, R. Kempe, W. Baumann, U. Rosenthal, *Organometallics* **1997**, *16*, 2886–2890; b) X. Yang, C. L. Stern, T. J. Marks, *J. Am. Chem. Soc.* **1994**, *116*, 10015–10031, and references therein; c) Y. Sun, R. E. v. H. Spence, W. E. Piers, M. Parvez, G. P. A. Yap, *J. Am. Chem. Soc.* **1997**, *119*, 5132–5143.

[11] Crystal structure of **2**: crystal size $0.4\times0.3\times0.2$ mm, yellow prism, space group $P2_1/n$, monoclinic, $a=9.331(2)$, $b=21.371(4)$, $c=18.188(4)$ Å, $\beta=95.04(3)°$, $V=3612.9(13)$ Å^3, $Z=4$, $\rho_{calcd}=1.635$ g cm^{-3}, 12779 reflections measured, 4514 were independent of symmetry and 2629 were observed ($I>2\sigma(I)$), $R1=0.044$, wR^2 (all data) $=0.112$, 515 parameters.

[12] C. Müller, R. J. Lachicotte, W. D. Jones, *Organometallics* **2002**, *21*, 1190–1196, and references therein.

[13] Crystal structure of **3**: crystal size $0.5\times0.4\times0.4$ mm, dark green prism, space group $P2_1/n$, monoclinic, $a=13.373(3)$, $b=12.206(2)$, $c=24.584(5)$ Å, $\beta=102.72(3)°$, $V=3914.4(13)$ Å^3, $Z=4$, $\rho_{calcd}=1.564$ g cm^{-3}, 11406 reflections measured, 5892 were independent of symmetry and 3358 were observed ($I>2\sigma(I)$), $R1=0.048$, wR^2 (all data) $=0.112$, 546 parameters. CCDC-195461 (**1**), CCDC-195462 (**2**), CCDC-195463 (**3**) contain the supplementary crystallographic data for this paper. These data can be obtained free of charge via www.ccdc.cam.ac.uk/conts/retrieving.html (or from the Cambridge Crystallographic Data Centre, 12 Union Road, Cambridge CB2 1EZ, UK; fax: (+44) 1223-336-033; or deposit@ccdc.cam.ac.uk).

[14] a) G. L. Wood, C. B. Knobler, M. F. Hawthorne, *Inorg. Chem.* **1989**, *28*, 382; b) U. Rosenthal, H. Görls, *J. Organomet. Chem.* **1992**, *439*, C36-C41.
[15] a) V. V. Burlakov, U. Rosenthal, R. Beckhaus, A. V. Polyakov, Yu. T. Struchkov, G. Oehme, V. B. Shur, M. E. Vol'pin, *Metalloorg. Khim.* **1990**, *3*, 476–477; *Organomet. Chem. USSR* **1990**, *3*, 273–274; b) V. V. Burlakov, A. V. Polyakov, A. I. Yanovsky, Yu. T. Struchkov, V. B. Shur, M. E. Vol'pin, U. Rosenthal, H. Görls, *J. Organomet. Chem.* **1994**, *476*, 197–206.
[16] V. Varga, K. Mach, J. Hiller, U. Thewalt, P. Sedmera, M. Polasek, *Organometallics* **1995**, *14*, 1410–1416.
[17] a) B. Temme, G. Erker, R. Fröhlich, M. Grehl, *Angew. Chem.* **1994**, *106*, 1570–1572; *Angew. Chem. Int. Ed. Engl.* **1994**, *33*, 1480–1482; b) W. Ahlers, B. Temme, G. Erker, R. Fröhlich, T. Fox, *J. Organomet. Chem.* **1997**, *527*, 191–201; c) W. Ahlers, G. Erker, R. Fröhlich, U. Peuchert, *J. Organomet. Chem.* **1999**, *578*, 115–124; d) W. Ahlers, B. Temme, G. Erker, R. Fröhlich, F. Zippel, *Organometallics* **1997**, *16*, 1440–1444.
[18] B. Wrackmeyer, G. Kehr, S. Willbold, S. Ali, *J. Organomet. Chem.* **2002**, *646*, 125–133.
[19] K. Köhler, W. E. Piers, A. P. Jarvis, S. Xin, Y. Feng, A. M. Bravakis, S. Collins, W. Clegg, G. P. A. Yap, T. B. Marder, *Organometallics* **1998**, *17*, 3557–3566.
[20] a) An *absolute* exclusion of moisture seems impossible also in heated glassware and with carefully dried $B(C_6F_5)_3$ because of the formation of stable adducts with water $B(C_6F_5)_3{\cdot}H_2O$[21] (see also ref. [10c]); b) A. Spannenberg, V. V. Burlakov, P. Arndt, W. Baumann, V. B. Shur, U. Rosenthal, *Z. Kristallogr. New Cryst. Struct.* **2002**, *217*, 546–548.
[21] C. Bergquist, B. M. Bridgewater, C. J. Harlan, J. R. Norton, R. A. Friesner, G. Parkin, *J. Am. Chem. Soc.* **2000**, *122*, 10581–10590.
[22] F. G. Kirchbauer, P.-M. Pellny H. Sun, V. V. Burlakov, P. Arndt, W. Baumann, A. Spannenberg, U. Rosenthal, *Organometallics* **2001**, *20*, 5289–5296.

 © 2003 Wiley-VCH Verlag GmbH & Co. KGaA, Weinheim 1433-7851/03/4212-1418 $ 20.00+.50/0

High-Throughput Enzyme Assay

A High-Throughput-Screening Method for Determining the Synthetic Activity of Hydrolases**

*Monika Konarzycka-Bessler and Uwe T. Bornscheuer**

Lipases and esterases are versatile biocatalysts and find increasing application in organic syntheses.[1] The main interest stems for their broad substrate specificity and exceptionally high stability in organic solvents. Thus, not only hydrolysis, but also synthesis reactions are possible. Indeed, numerous reactions have been performed in organic media and many of them have been commercialized. These include the synthesis of optically pure building blocks, flavors and fragrances, lipid modification, and also simple esters, such as myristyl myristate for cosmetic applications.

Active (and stereoselective) biocatalysts can be identified by means of hydrolytic assays, for which a considerable number of useful high-throughput methods have been developed.[2] However, it often turns out that enzymes identified by these methods are not suitable for the desired synthetic reactions. An alternative can be small-scale esterification reactions in organic solvents, for which conversion (and optical purity) is then determined by GC or HPLC analysis. Broad investigations of a large number of enzymes and the identification of best reaction conditions (different alcohols or acyl donors, solvents, carriers for immobilization, temperature) easily can lead to several hundred individual experiments and are therefore very time-consuming.

Herein we describe an assay format, which allows high-throughput determination of synthetic activity of hydrolases. This method is based on lipase- or esterase-catalyzed transesterification reactions between a vinyl ester and an alcohol. Acetaldehyde released stoechiometrically by keto–enol tautomerization of the vinyl alcohol released during ester synthesis,[3] reacts in situ with hydrazine **1** to produce a fluorogenic derivative **2**, which can be quantified by fluorescence measurements (Scheme 1).

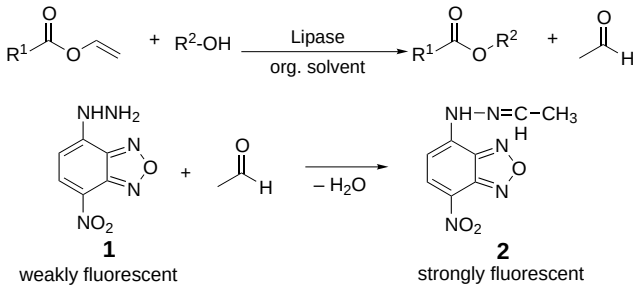

Scheme 1. Model reaction for the evaluation of the assay.

Crucial for success is the choice of a suitable derivatizing reagent. A considerable number of compounds have been described for the trapping of volatile carbonyl compounds, for example, in environmental analysis hydrazine compounds, such as the classical dinitrophenylhydrazine are often used.[4] Unfortunately, the derivatization step takes places under conditions which are not compatible with enzymatic reactions. Also, excess reagent must be separated, for example, by HPLC from the product to allow a reliable quantification. We identified the commercially available 4-hydrazino-7-nitro-2,1,3-benzoxadiazole (**1**; NBD-H)[5] as a promising reagent, as it shows very low fluorescence (≈300 relative fluorescence units, RFU), whereas the corresponding hydrazone **2** shows very high fluorescence (≈30000 RFU). Moreover, the derivatization can be performed in organic solvents at ambient temperatures.[6]

[*] Prof. Dr. U. T. Bornscheuer, M. Konarzycka-Bessler
Institute of Chemistry and Biochemistry
Department of Technical Chemistry and Biotechnology
Greifswald University
Soldmannstrasse 16, 17487 Greifswald (Germany)
Fax: (+49) 3834-86-4346
E-mail: uwe.bornscheuer@uni-greifswald.de

[**] We thank the Degussa AG (Project House Biotechnology and Business Unit Care Specialties) for financial support and PD. Dr. Uwe Karst, University of Münster (Germany), for valuable discussions.

 © 2003 Wiley-VCH Verlag GmbH & Co. KGaA, Weinheim 1433-7851/03/4212-1418 $ 20.00+.50/0

As a model reaction, the esterification between vinyl laurate and 1-propanol, in the presence of NBD-H (**1**), was studied in microtiterplates (MTP),[7] several lipases and esterases were investigated with this reaction. Figure 1 shows a typical time course of this reaction as monitored by fluorescence measurements, and clearly shows, that the progress of the reaction can be easily monitored. Although the reaction is performed in a heterogeneous system composed of solid enzyme and liquid reactants, this does not seem to disturb the measurement of synthetic activity. Thus, Chirazyme L9 (RML, lipase from *Rhizomucor miehei*) and Chirazyme L2 (lipase B from *Candida antarctica*) were identified as very active biocatalysts, Chirazyme L5 (Lipase A from *C. antarctica*) and L6 (lipase from *Pseudomonas* sp.) show modest synthetic activity, and an esterase from *Streptomyces diastatochromogenes* (SDE), a lipase from *Aspergillus niger* (Amano A), and lipase from *Candida rugosa* (Amano AY) are almost inactive.

After determining the standard curve (Figure 2) to correlate fluorescence intensity with the concentration of **2**, it was possible to calculate the conversion for each reaction. For very active enzymes, this turned out to be less accurate,[8] as the linear range of the standard curve levels off at around 0.02 mM (> 12000 RFU) and conversion must be calculated by regression analysis. On the other hand, most data shown in Figure 3 correlate well with the conversion determined by conventional GC analysis. Furthermore, this assay works also in other organic solvents (e.g., *n*-hexane, ethers), which are used for lipase- or esterase-catalyzed reactions (data not shown).

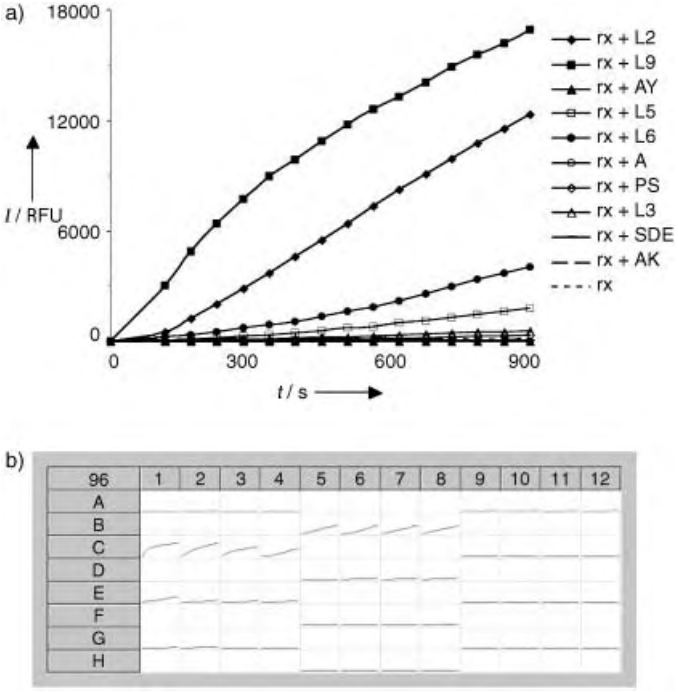

Figure 1. a) Combination of lipase-catalyzed esterification of vinyl laurate with 1-propanol in isooctane and in situ derivatization of acetaldehyde with NBD-H using several hydrolases: rx = control without enzyme; L2–L9 = Chirazyme L2–L9; for other enzyme abbreviations, see text and Experimental Section. b) results from the microtiter plate analysis: wells A1–A4: reaction mixture (vinyl laurate + 1-propanol) in isooctane (control 1), A9–A12: reaction mixture in isooctane with **1** (control 2), B5–B8: Chirazyme L2, C1–C4: Chirazyme L9, C9–C12: Amano AY, D5–D8: Chirazyme L5, E1–E4: Chirazyme L6, E9–E12: Amano A, F5–F8: Amano PS, G1–G4: Chirazyme L3, G9–G12: SDE, H5–H8: Amano AK.

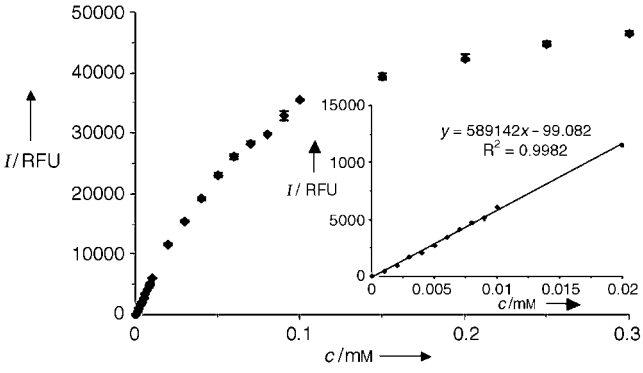

Figure 2. Calibration curve for **2** as determined in isooctane:1-propanol (10:1). The insert shows the linear range of the measurement.

Despite the few limitations mentioned above, this assay format is extremely versatile for the determination of the synthetic activity of lipases or esterases in a high-throughput format and thus enables the rapid identification of active enzymes and/or appropriate reaction conditions.

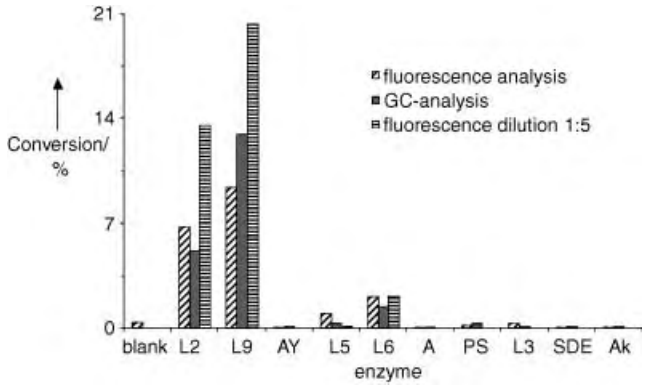

Figure 3. Comparison of conversion determined by fluorescence measurement and GC analysis. For highly active enzymes, the reaction media was diluted fivefold.

Experimental Section

NBD-H (**1**) was purchased from Fluka. All other chemicals were obtained at the highest purity available from common commercial suppliers. For enzymatic reactions ten different non-immobilized enzymes were selected: Chirazyme L2 (CAL-B), L3 (CRL), L5 (CAL-A), L6 (PSL), L9 (RML), Amano PS (PCL), Amano A (ANL), Amano AK (PFL), Amano AY (CRL), and SDE.[9]

Fluorimetric analysis was performed with the FLUOstar Galaxy from BMG Labtechnologies GmbH (Offenburg, Germany). Gaschromatographic analysis was performed on a Hewlett Packard GC

 © 2003 Wiley-VCH Verlag GmbH & Co. KGaA, Weinheim 1433-7851/03/4212-1419 $ 20.00+.50/0

(5890 Series II) equipped with a Permabond FFAP column (25 m × 0.25 mm, Macherey & Nagel, Düren, Germany) under isothermal (140 °C) conditions with hydrogen as carrier gas.

Conventional lipase-catalyzed synthesis of 1-propyl laurate: vinyl laurate (77.5 μL, 0.3 mmol), 1-propanol (22.5 μL, 0.3 mmol), and solvent (900 μL; *n*-hexane, isooctane, petroleum ether) were combined in an eppendorf tube (1.5 mL) and CAL-B (Chirazyme L2; 1 mg) was added. The mixture was shaken at 900 rpm at 60 °C. Samples were diluted with chloroform, vortexted, centrifuged, and analyzed by GC.

Synthesis and fluorescence of **2**: **1** (20.3 mg 0.104 mmol) was dissolved in dichloromethane (4 mL) in a round bottom flask and acetaldehyde (12 μL, 0.213 mmol) was added. The reaction mixture was stirred for 10 min at room temperature in the dark under nitrogen atmosphere. Then, more acetaldehyde (0.213 mmol) was added and the reaction was continued for 20 min. After removal of excess solvent, the product was crystallized from benzene:cyclohexane (1:1) yielding **2** (12.5 mg, 54.4 %) as confirmed by NMR spectroscopy and fluorescence spectra. For the standard curve, a 0.3-mM stock solution of **2** in isooctane:1-propanol (10:1, v/v) was prepared and then diluted to obtain solutions in the range of 0.001–0.25 mM. 150 μL of each solution were transferred into a MTP which was sealed with tape. Fluorescence was determined at 45 °C, excitation at 485 nm and emission 520 nm (gain 0). All measurements were performed in triplicate.

Determination of enzymatic synthetic activity in MTP: As accurate weighing of small amounts of solid enzyme (≈0.01–0.02 mg) is very difficult, a known amount of enzyme was dissolved in phosphate buffer (pH 7.5, 50 mM), transferred to a MTP, and freeze-dried. Then a mixture of vinyl laurate (15 μmol), 1-propanol (150 μmol), and **1** in organic solvent (e.g., 1-propanol, *n*-hexane, isooctane, petroleum ether, DMSO) was added, the plates (total volume: 150 μL per well) were tape-sealed and inserted into the fluorimeter (shaken at 45 °C at 170 rpm) and the increase of fluorescence was monitored as described above. As controls, the same format was used without enzyme, or alternatively, **1** was incubated with enzyme or solvent only. To avoid undesired hydrolysis by the presence of water, it is recommended to dry all reactants and solvent over activated molecular sieves before the reaction.

Received: July 8, 2002
Revised: October 25, 2002 [Z19674]

Keywords: enzyme catalysis · high-throughput screening · hydrazine · lipase · transesterification

[1] a) U. T. Bornscheuer, R. J. Kazlauskas, *Hydrolases in organic synthesis—regio- and stereoselective biotransformations*, Wiley-VCH, Weinheim, **1999**; b) K. Faber, *Biotransformations in Organic Chemistry*, 4th ed., Springer, Berlin, **2000**.

[2] a) M. Baumann, R. Stürmer, U. T. Bornscheuer, *Angew. Chem.* **2001**, *113*, 4329–4333; *Angew. Chem. Int. Ed.* **2001**, *40*, 4201–4204; b) F. Badalassi, D. Wahler, G. Klein, P. Crotti, J.-L. Reymond, *Angew. Chem.* **2000**, *112*, 4233–4236; *Angew. Chem. Int. Ed.* **2000**, *39*, 4067–4070; c) L. E. Janes, R. J. Kazlauskas, *J. Org. Chem.* **1997**, *62*, 4560–4561; L. E. Janes, A. C. Löwendahl, R. J. Kazlauskas, *Chem. Eur. J.* **1998**, *4*, 2324–2331; d) M. T. Reetz, M. T. Reetz, *Angew. Chem.* **2001**, *113*, 292–320; *Angew. Chem. Int. Ed.* **2001**, *40*, 284–310; e) D. Wahler, J. L. Reymond, *Curr. Opin. Chem. Biol.* **2001**, *5*, 152–158.

[3] Y. F. Wang, J. J. Lalonde, M. Momongan, D. E. Bergbreiter, C.-H. Wong, *J. Am. Chem. Soc.* **1988**, *110*, 7200–7205.

[4] M. Vogel, A. Büldt, U. Karst, *Fresenius J. Anal. Chem.* **2000**, *366*, 781–791.

[5] H. Koizumi, Y. Suzuki, *J. Chromatogr.* **1988**, *457*, 299–307.

[6] Compound **1** shows only fast reaction with aldehydes, but not with ketones. In addition, hydrazones derived from ketones (e.g. acetone, acetophenone) show significantly lower fluorescence. Thus, the use of isopropenyl acetate as acyl donor, for example, is less feasible.

[7] It is recommended to use tape-sealed MTPs to avoid evaporation of the highly volatile acetaldehyde. Fluorescence is measured preferentially from the top of the MTP to avoid interactions with solid enzyme particles.

[8] The deviation in the data can also be caused by the time required for GC sample preparation, as it takes a few minutes to remove the enzyme by centrifugation.

[9] V. Khalameyzer, U. T. Bornscheuer, *Biotechnol. Lett.* **1999**, *21*, 101–104.

 © 2003 Wiley-VCH Verlag GmbH & Co. KGaA, Weinheim 1433-7851/03/4212-1420 $ 20.00+.50/0